Journal of Mathematics

Novel Approaches in Graph and Complexity-Based Data Analysis and Processing

Lead Guest Editor: Naeem Jan
Guest Editors: Ewa Rak and Lazim Abdullah

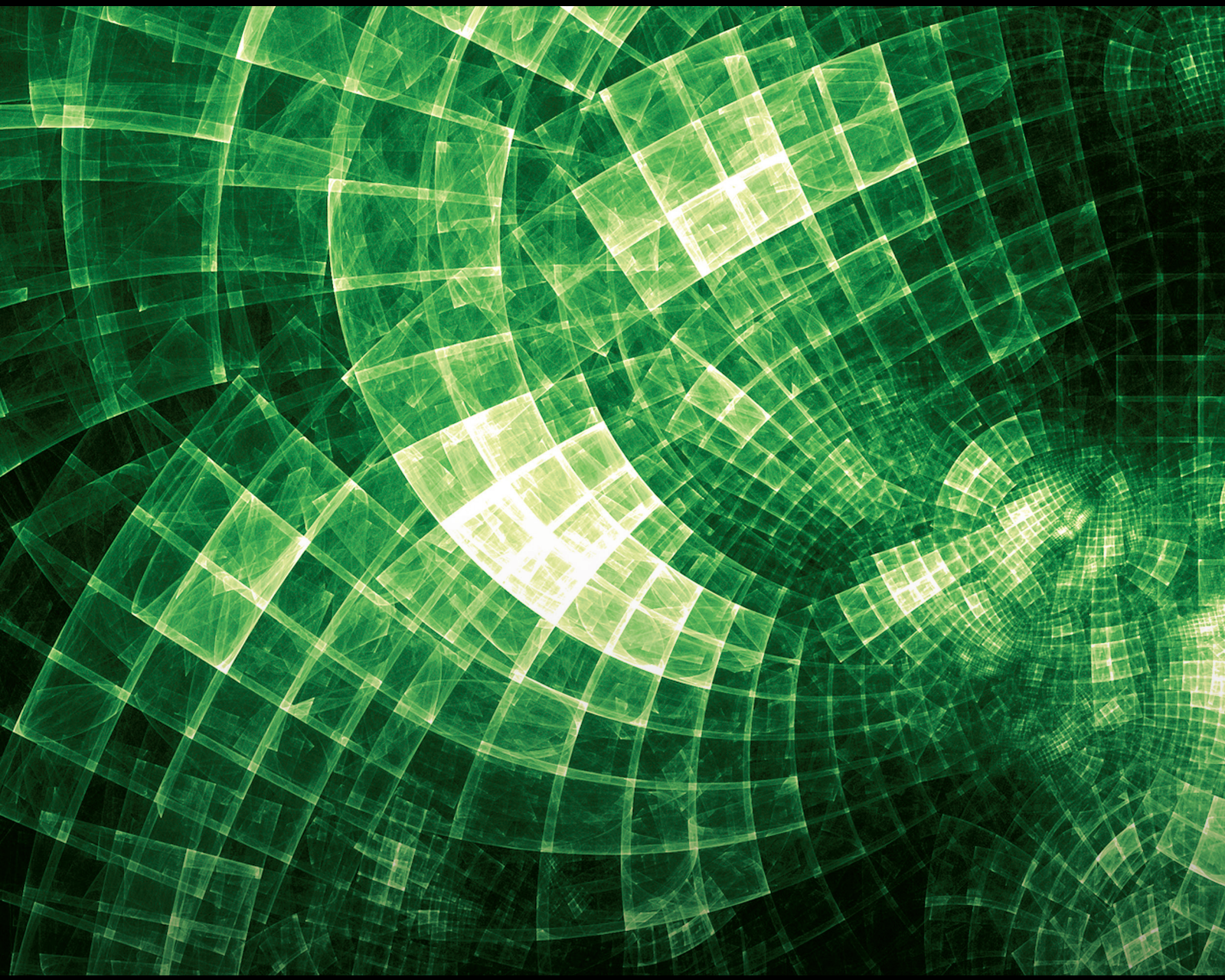

Novel Approaches in Graph and Complexity-Based Data Analysis and Processing

Journal of Mathematics

Novel Approaches in Graph and Complexity-Based Data Analysis and Processing

Lead Guest Editor: Naeem Jan
Guest Editors: Ewa Rak and Lazim Abdullah

Probability and Statistics

Contents

Retracted: Rough Set Construction and Entropy Weight Evaluation of Urban Higher Education Resource Carrying Capacity Based on Big Data
Journal of Mathematics
Retraction (1 page), Article ID 9872547, Volume 2024 (2024)

Retracted: Optimisation of Driver's Traffic Literacy Evaluation Index from the Perspective of Information Contribution Sensitivity
Journal of Mathematics
Retraction (1 page), Article ID 9871350, Volume 2024 (2024)

Retracted: Data Analysis and Processing Application of Deep Learning in Engineering Cost Teaching Evaluation
Journal of Mathematics
Retraction (1 page), Article ID 9870397, Volume 2024 (2024)

Retracted: Few Samples of SAR Automatic Target Recognition Based on Enhanced-Shape CNN
Journal of Mathematics
Retraction (1 page), Article ID 9865089, Volume 2024 (2024)

Retracted: A Blockchain Technique for Trade Credit Maintainability Using the Role of Information and Communication Technology
Journal of Mathematics
Retraction (1 page), Article ID 9864641, Volume 2024 (2024)

Retracted: Prediction Model of Mining Subsidence Parameters Based on Fuzzy Clustering
Journal of Mathematics
Retraction (1 page), Article ID 9863939, Volume 2024 (2024)

Retracted: Implementing the Hybrid Neuro-Fuzzy System to Model Specific Learning Disability in Special University Education Programs
Journal of Mathematics
Retraction (1 page), Article ID 9863685, Volume 2024 (2024)

Retracted: Digital Effectiveness in Video Conference Methods on Internet Learning Environments of Higher Education
Journal of Mathematics
Retraction (1 page), Article ID 9857325, Volume 2024 (2024)

Retracted: A Novel Approach to Automate Complex Software Modularization Using a Fact Extraction System
Journal of Mathematics
Retraction (1 page), Article ID 9854510, Volume 2024 (2024)

Contents

Retracted: Research on Automatic Classification Method of Ethnic Music Emotion Based on Machine Learning
Journal of Mathematics
Retraction (1 page), Article ID 9820467, Volume 2024 (2024)

Retracted: A Convolutional Network-Based Intelligent Evaluation Algorithm for the Quality of Spoken English Pronunciation
Journal of Mathematics
Retraction (1 page), Article ID 9819732, Volume 2024 (2024)

Retracted: Music Therapy Methods Based on SVM and MLP
Journal of Mathematics
Retraction (1 page), Article ID 9818702, Volume 2024 (2024)

Retracted: Experiment and Algorithm Research of Coal Direct Liquefaction Residual Oil Pyrolysis and Coking Technology Based on Lumped Kinetic Engineering
Journal of Mathematics
Retraction (1 page), Article ID 9817061, Volume 2024 (2024)

Retracted: A New Neutrosophic Negative Binomial Distribution: Properties and Applications
Journal of Mathematics
Retraction (1 page), Article ID 9814834, Volume 2024 (2024)

Retracted: Research on the Model of Distance Education Resource Integration from the Perspective of Comparative Education
Journal of Mathematics
Retraction (1 page), Article ID 9813159, Volume 2024 (2024)

Retracted: Developing a New Interval Type-2 Hesitant Fuzzy TOPSIS-Based Fuzzy Best-Worst Multicriteria Decision-Making Method for Competitive Pricing in Supply Chain
Journal of Mathematics
Retraction (1 page), Article ID 9812973, Volume 2024 (2024)

Retracted: Statistical Inferences of Burr XII Lifetime Models under Joint Type-1 Competing Risks Samples
Journal of Mathematics
Retraction (1 page), Article ID 9809684, Volume 2024 (2024)

Retracted: Personalized Education Based on Hybrid Intelligent Recommendation System
Journal of Mathematics
Retraction (1 page), Article ID 9807051, Volume 2024 (2024)

Retracted: Evaluation Algorithm of Ecological Energy-Saving Effect of Green Buildings Based on Gray Correlation Degree
Journal of Mathematics
Retraction (1 page), Article ID 9802386, Volume 2024 (2024)

Contents

Retracted: Construction and Analysis of Urban Motor Vehicle Drivers' Traffic Literacy Evaluation Model Based on Zhengzhou City's Survey Data
Journal of Mathematics
Retraction (1 page), Article ID 9769621, Volume 2024 (2024)

Retracted: An Effective Approach for Modular Community Detection in Bipartite Network Based on Integrating Rider with Harris Hawks Optimization Algorithms
Journal of Mathematics
Retraction (1 page), Article ID 9767958, Volume 2024 (2024)

Retracted: Research on the Prediction of Port Economic Synergy Development Trend Based on Deep Neural Networks
Journal of Mathematics
Retraction (1 page), Article ID 9761318, Volume 2024 (2024)

Retracted: Path Optimization of Enterprise Network Innovation Performance Management Based on Deep Learning and Internet of Things
Journal of Mathematics
Retraction (1 page), Article ID 9895762, Volume 2023 (2023)

Retracted: Preorder of Factors Affecting Oil Prices: Fuzzy PROMETHEE Approach
Journal of Mathematics
Retraction (1 page), Article ID 9895324, Volume 2023 (2023)

Retracted: Text Knowledge Acquisition Method of Collaborative Product Design Based on Genetic Algorithm
Journal of Mathematics
Retraction (1 page), Article ID 9894560, Volume 2023 (2023)

Retracted: Design of Intelligent Recognition English Translation Model Based on Deep Learning
Journal of Mathematics
Retraction (1 page), Article ID 9893016, Volume 2023 (2023)

Retracted: Evaluation Algorithm of Labor Legal Effectiveness for Affirmative Action against Gender Discrimination
Journal of Mathematics
Retraction (1 page), Article ID 9892024, Volume 2023 (2023)

Retracted: Popular Song Composition Based on Deep Learning and Neural Network
Journal of Mathematics
Retraction (1 page), Article ID 9891376, Volume 2023 (2023)

Retracted: Research on the Spread Path and Evolution Causes of Oral Language in the Digital Era
Journal of Mathematics
Retraction (1 page), Article ID 9878209, Volume 2023 (2023)

Contents

Retracted: Deep Learning-Based Economic Forecasting for the New Energy Vehicle Industry
Journal of Mathematics
Retraction (1 page), Article ID 9831759, Volume 2023 (2023)

Retracted: Music Emotion Research Based on Reinforcement Learning and Multimodal Information
Journal of Mathematics
Retraction (1 page), Article ID 9830845, Volume 2023 (2023)

Retracted: Research on Multiparty Payment Technology Based on Blockchain and Smart Contract Mechanism
Journal of Mathematics
Retraction (1 page), Article ID 9826741, Volume 2023 (2023)

Retracted: An Artificial Intelligent Virtual Reality Interactive Model for Distance Education
Journal of Mathematics
Retraction (1 page), Article ID 9817457, Volume 2023 (2023)

Retracted: On the Temperature Indices of Molecular Structures of Some Networks
Journal of Mathematics
Retraction (1 page), Article ID 9815268, Volume 2023 (2023)

Retracted: Design of Sports Image Contour Feature Acquisition System Based on the Background Subtraction Method
Journal of Mathematics
Retraction (1 page), Article ID 9814165, Volume 2023 (2023)

Retracted: Research on Digital Image Watermarking Algorithm Based on Scrambling and Singular Value Decomposition
Journal of Mathematics
Retraction (1 page), Article ID 9814149, Volume 2023 (2023)

Retracted: Analysis of the Resilience of Balance of Payments Using Comprehensive Evaluation
Journal of Mathematics
Retraction (1 page), Article ID 9810624, Volume 2023 (2023)

Retracted: The Application of "Internet+" in the Ageing Adaptation of Elderly People with Disabilities at Home
Journal of Mathematics
Retraction (1 page), Article ID 9810127, Volume 2023 (2023)

Retracted: Research on Community Public Service Information Collaborative Governance Based on Deep Learning Model
Journal of Mathematics
Retraction (1 page), Article ID 9798076, Volume 2023 (2023)

Contents

Retracted: Early Warning System for Penalty Constrained Financial Risks of Enterprises under Diversified Investment
Journal of Mathematics
Retraction (1 page), Article ID 9879807, Volume 2023 (2023)

Retracted: New Types of μ-Proximity Spaces and Their Applications
Journal of Mathematics
Retraction (1 page), Article ID 9841465, Volume 2023 (2023)

Retracted: On Q_p-Closed Sets in Topological Spaces
Journal of Mathematics
Retraction (1 page), Article ID 9807535, Volume 2023 (2023)

Retracted: Research on the Construction of Intelligent Media Ideological and Political Learning Platform Based on Artificial Intelligence Technology
Journal of Mathematics
Retraction (1 page), Article ID 9840234, Volume 2023 (2023)

Retracted: Automatic Classification Method of Music Genres Based on Deep Belief Network and Sparse Representation
Journal of Mathematics
Retraction (1 page), Article ID 9871670, Volume 2023 (2023)

Retracted: Teaching Quality Evaluation of Ideological and Political Courses in Colleges and Universities Based on Machine Learning
Journal of Mathematics
Retraction (1 page), Article ID 9869537, Volume 2023 (2023)

Retracted: Evaluation of the Effect of Ideological and Political Education on Psychological Crisis Intervention for University Students Based on Data Mining Algorithm
Journal of Mathematics
Retraction (1 page), Article ID 9868607, Volume 2023 (2023)

Retracted: Analysis and Risk Assessment of Corporate Financial Leverage Using Mobile Payment in the Era of Digital Technology in a Complex Environment
Journal of Mathematics
Retraction (1 page), Article ID 9852708, Volume 2023 (2023)

Retracted: On Multiplicative Topological Invariants of Magnesium Iodide Structure
Journal of Mathematics
Retraction (1 page), Article ID 9836426, Volume 2023 (2023)

Retracted: Research on the Integration of Preschool Language Education Resources Based on Metadata Storage
Journal of Mathematics
Retraction (1 page), Article ID 9812914, Volume 2023 (2023)

Contents

Contents

Contents

Contents

Contents

Contents

Contents

Hindawi
Journal of Mathematics
Volume 2024, Article ID 9859646, 1 page
https://doi.org/10.1155/2024/9859646

Retraction

Retracted: A Study on Students' Satisfaction with Classroom Teaching of Independent Adult Universities Based on SERVQUAL and IPA Models, Taking Beijing Haidian Adult University as an Example

Journal of Mathematics

Received 30 January 2024; Accepted 30 January 2024; Published 31 January 2024

This article has been retracted by Hindawi following an investigation undertaken by the publisher [1]. This investigation has uncovered evidence of one or more of the following indicators of systematic manipulation of the publication process:

(1) Discrepancies in scope

(2) Discrepancies in the description of the research reported

(3) Discrepancies between the availability of data and the research described

(4) Inappropriate citations

(5) Incoherent, meaningless and/or irrelevant content included in the article

(6) Manipulated or compromised peer review

The presence of these indicators undermines our confidence in the integrity of the article's content and we cannot, therefore, vouch for its reliability. Please note that this notice is intended solely to alert readers that the content of this article is unreliable. We have not investigated whether authors were aware of or involved in the systematic manipulation of the publication process.

In addition, our investigation has also shown that one or more of the following human-subject reporting requirements has not been met in this article: ethical approval by an Institutional Review Board (IRB) committee or equivalent, patient/participant consent to participate, and/or agreement to publish patient/participant details (where relevant).

Wiley and Hindawi regrets that the usual quality checks did not identify these issues before publication and have since put additional measures in place to safeguard research integrity.

We wish to credit our own Research Integrity and Research Publishing teams and anonymous and named external researchers and research integrity experts for contributing to this investigation.

The corresponding author, as the representative of all authors, has been given the opportunity to register their agreement or disagreement to this retraction. We have kept a record of any response received.

References

[1] X. Wang, Y. Gao, and S. Li, "A Study on Students' Satisfaction with Classroom Teaching of Independent Adult Universities Based on SERVQUAL and IPA Models, Taking Beijing Haidian Adult University as an Example," *Journal of Mathematics*, vol. 2022, Article ID 7744401, 9 pages, 2022.

Hindawi
Journal of Mathematics
Volume 2024, Article ID 9847963, 1 page
https://doi.org/10.1155/2024/9847963

Retraction

Retracted: Morphological Bias of Ancient Artifacts: A Case Study of Incense Burners in Ming and Qing Dynasties

Journal of Mathematics

Received 30 January 2024; Accepted 30 January 2024; Published 31 January 2024

This article has been retracted by Hindawi following an investigation undertaken by the publisher [1]. This investigation has uncovered evidence of one or more of the following indicators of systematic manipulation of the publication process:

(1) Discrepancies in scope

(2) Discrepancies in the description of the research reported

(3) Discrepancies between the availability of data and the research described

(4) Inappropriate citations

(5) Incoherent, meaningless and/or irrelevant content included in the article

(6) Manipulated or compromised peer review

The presence of these indicators undermines our confidence in the integrity of the article's content and we cannot, therefore, vouch for its reliability. Please note that this notice is intended solely to alert readers that the content of this article is unreliable. We have not investigated whether authors were aware of or involved in the systematic manipulation of the publication process.

In addition, our investigation has also shown that one or more of the following human-subject reporting requirements has not been met in this article: ethical approval by an Institutional Review Board (IRB) committee or equivalent, patient/participant consent to participate, and/or agreement to publish patient/participant details (where relevant).

Wiley and Hindawi regrets that the usual quality checks did not identify these issues before publication and have since put additional measures in place to safeguard research integrity.

We wish to credit our own Research Integrity and Research Publishing teams and anonymous and named external researchers and research integrity experts for contributing to this investigation.

The corresponding author, as the representative of all authors, has been given the opportunity to register their agreement or disagreement to this retraction. We have kept a record of any response received.

References

[1] Y.-F. Chen and J. Wei, "Morphological Bias of Ancient Artifacts: A Case Study of Incense Burners in Ming and Qing Dynasties," *Journal of Mathematics*, vol. 2021, Article ID 7859189, 9 pages, 2021.

Hindawi
Journal of Mathematics
Volume 2024, Article ID 9814325, 1 page
https://doi.org/10.1155/2024/9814325

Retraction

Retracted: An English Online Homework Tutoring System Supported by Internet Database

Journal of Mathematics

Received 30 January 2024; Accepted 30 January 2024; Published 31 January 2024

This article has been retracted by Hindawi following an investigation undertaken by the publisher [1]. This investigation has uncovered evidence of one or more of the following indicators of systematic manipulation of the publication process:

(1) Discrepancies in scope

(2) Discrepancies in the description of the research reported

(3) Discrepancies between the availability of data and the research described

(4) Inappropriate citations

(5) Incoherent, meaningless and/or irrelevant content included in the article

(6) Manipulated or compromised peer review

The presence of these indicators undermines our confidence in the integrity of the article's content and we cannot, therefore, vouch for its reliability. Please note that this notice is intended solely to alert readers that the content of this article is unreliable. We have not investigated whether authors were aware of or involved in the systematic manipulation of the publication process.

In addition, our investigation has also shown that one or more of the following human-subject reporting requirements has not been met in this article: ethical approval by an Institutional Review Board (IRB) committee or equivalent, patient/participant consent to participate, and/or agreement to publish patient/participant details (where relevant).

Wiley and Hindawi regrets that the usual quality checks did not identify these issues before publication and have since put additional measures in place to safeguard research integrity.

We wish to credit our own Research Integrity and Research Publishing teams and anonymous and named external researchers and research integrity experts for contributing to this investigation.

The corresponding author, as the representative of all authors, has been given the opportunity to register their agreement or disagreement to this retraction. We have kept a record of any response received.

References

[1] H. Hao, "An English Online Homework Tutoring System Supported by Internet Database," *Journal of Mathematics*, vol. 2021, Article ID 5960185, 12 pages, 2021.

Hindawi
Journal of Mathematics
Volume 2024, Article ID 9896547, 1 page
https://doi.org/10.1155/2024/9896547

Retraction

Retracted: Research on Design and Application of National Fitness System

Journal of Mathematics

Received 23 January 2024; Accepted 23 January 2024; Published 24 January 2024

This article has been retracted by Hindawi following an investigation undertaken by the publisher [1]. This investigation has uncovered evidence of one or more of the following indicators of systematic manipulation of the publication process:

(1) Discrepancies in scope

(2) Discrepancies in the description of the research reported

(3) Discrepancies between the availability of data and the research described

(4) Inappropriate citations

(5) Incoherent, meaningless and/or irrelevant content included in the article

(6) Manipulated or compromised peer review

The presence of these indicators undermines our confidence in the integrity of the article's content and we cannot, therefore, vouch for its reliability. Please note that this notice is intended solely to alert readers that the content of this article is unreliable. We have not investigated whether authors were aware of or involved in the systematic manipulation of the publication process.

In addition, our investigation has also shown that one or more of the following human-subject reporting requirements has not been met in this article: ethical approval by an Institutional Review Board (IRB) committee or equivalent, patient/participant consent to participate, and/or agreement to publish patient/participant details (where relevant).

Wiley and Hindawi regrets that the usual quality checks did not identify these issues before publication and have since put additional measures in place to safeguard research integrity.

We wish to credit our own Research Integrity and Research Publishing teams and anonymous and named external researchers and research integrity experts for contributing to this investigation.

The corresponding author, as the representative of all authors, has been given the opportunity to register their agreement or disagreement to this retraction. We have kept a record of any response received.

References

[1] S. Wang, "Research on Design and Application of National Fitness System," *Journal of Mathematics*, vol. 2021, Article ID 5178550, 10 pages, 2021.

Hindawi
Journal of Mathematics
Volume 2024, Article ID 9894306, 1 page
https://doi.org/10.1155/2024/9894306

Retraction

Retracted: Intelligent Integration Algorithm of National Traditional Sports Culture Resources Based on Big Data

Journal of Mathematics

Received 23 January 2024; Accepted 23 January 2024; Published 24 January 2024

This article has been retracted by Hindawi following an investigation undertaken by the publisher [1]. This investigation has uncovered evidence of one or more of the following indicators of systematic manipulation of the publication process:

(1) Discrepancies in scope

(2) Discrepancies in the description of the research reported

(3) Discrepancies between the availability of data and the research described

(4) Inappropriate citations

(5) Incoherent, meaningless and/or irrelevant content included in the article

(6) Manipulated or compromised peer review

The presence of these indicators undermines our confidence in the integrity of the article's content and we cannot, therefore, vouch for its reliability. Please note that this notice is intended solely to alert readers that the content of this article is unreliable. We have not investigated whether authors were aware of or involved in the systematic manipulation of the publication process.

Wiley and Hindawi regrets that the usual quality checks did not identify these issues before publication and have since put additional measures in place to safeguard research integrity.

We wish to credit our own Research Integrity and Research Publishing teams and anonymous and named external researchers and research integrity experts for contributing to this investigation.

The corresponding author, as the representative of all authors, has been given the opportunity to register their agreement or disagreement to this retraction. We have kept a record of any response received.

References

[1] X.-B. Ai, "Intelligent Integration Algorithm of National Traditional Sports Culture Resources Based on Big Data," *Journal of Mathematics*, vol. 2022, Article ID 8335300, 11 pages, 2022.

Hindawi
Journal of Mathematics
Volume 2024, Article ID 9894065, 1 page
https://doi.org/10.1155/2024/9894065

Retraction

Retracted: Economic Benefit Evaluation and Analysis Based on Intelligent Agriculture Internet of Things

Journal of Mathematics

Received 23 January 2024; Accepted 23 January 2024; Published 24 January 2024

This article has been retracted by Hindawi following an investigation undertaken by the publisher [1]. This investigation has uncovered evidence of one or more of the following indicators of systematic manipulation of the publication process:

(1) Discrepancies in scope

(2) Discrepancies in the description of the research reported

(3) Discrepancies between the availability of data and the research described

(4) Inappropriate citations

(5) Incoherent, meaningless and/or irrelevant content included in the article

(6) Manipulated or compromised peer review

The presence of these indicators undermines our confidence in the integrity of the article's content and we cannot, therefore, vouch for its reliability. Please note that this notice is intended solely to alert readers that the content of this article is unreliable. We have not investigated whether authors were aware of or involved in the systematic manipulation of the publication process.

Wiley and Hindawi regrets that the usual quality checks did not identify these issues before publication and have since put additional measures in place to safeguard research integrity.

We wish to credit our own Research Integrity and Research Publishing teams and anonymous and named external researchers and research integrity experts for contributing to this investigation.

The corresponding author, as the representative of all authors, has been given the opportunity to register their agreement or disagreement to this retraction. We have kept a record of any response received.

References

[1] S. Liu and Y. Wu, "Economic Benefit Evaluation and Analysis Based on Intelligent Agriculture Internet of Things," *Journal of Mathematics*, vol. 2021, Article ID 9499197, 7 pages, 2021.

Hindawi
Journal of Mathematics
Volume 2024, Article ID 9890519, 1 page
https://doi.org/10.1155/2024/9890519

Retraction

Retracted: Evaluation Method of IT English Blended Teaching Quality Based on the Data Mining Algorithm

Journal of Mathematics

Received 23 January 2024; Accepted 23 January 2024; Published 24 January 2024

This article has been retracted by Hindawi following an investigation undertaken by the publisher [1]. This investigation has uncovered evidence of one or more of the following indicators of systematic manipulation of the publication process:

(1) Discrepancies in scope

(2) Discrepancies in the description of the research reported

(3) Discrepancies between the availability of data and the research described

(4) Inappropriate citations

(5) Incoherent, meaningless and/or irrelevant content included in the article

(6) Manipulated or compromised peer review

The presence of these indicators undermines our confidence in the integrity of the article's content and we cannot, therefore, vouch for its reliability. Please note that this notice is intended solely to alert readers that the content of this article is unreliable. We have not investigated whether authors were aware of or involved in the systematic manipulation of the publication process.

In addition, our investigation has also shown that one or more of the following human-subject reporting requirements has not been met in this article: ethical approval by an Institutional Review Board (IRB) committee or equivalent, patient/participant consent to participate, and/or agreement to publish patient/participant details (where relevant).

Wiley and Hindawi regrets that the usual quality checks did not identify these issues before publication and have since put additional measures in place to safeguard research integrity.

We wish to credit our own Research Integrity and Research Publishing teams and anonymous and named external researchers and research integrity experts for contributing to this investigation.

The corresponding author, as the representative of all authors, has been given the opportunity to register their agreement or disagreement to this retraction. We have kept a record of any response received.

References

[1] L. Shao, "Evaluation Method of IT English Blended Teaching Quality Based on the Data Mining Algorithm," *Journal of Mathematics*, vol. 2021, Article ID 3206761, 8 pages, 2021.

Hindawi
Journal of Mathematics
Volume 2024, Article ID 9879804, 1 page
https://doi.org/10.1155/2024/9879804

Retraction

Retracted: Deep Neural Network Model Forecasting for Financial and Economic Market

Journal of Mathematics

Received 23 January 2024; Accepted 23 January 2024; Published 24 January 2024

This article has been retracted by Hindawi following an investigation undertaken by the publisher [1]. This investigation has uncovered evidence of one or more of the following indicators of systematic manipulation of the publication process:

(1) Discrepancies in scope

(2) Discrepancies in the description of the research reported

(3) Discrepancies between the availability of data and the research described

(4) Inappropriate citations

(5) Incoherent, meaningless and/or irrelevant content included in the article

(6) Manipulated or compromised peer review

The presence of these indicators undermines our confidence in the integrity of the article's content and we cannot, therefore, vouch for its reliability. Please note that this notice is intended solely to alert readers that the content of this article is unreliable. We have not investigated whether authors were aware of or involved in the systematic manipulation of the publication process.

Wiley and Hindawi regrets that the usual quality checks did not identify these issues before publication and have since put additional measures in place to safeguard research integrity.

We wish to credit our own Research Integrity and Research Publishing teams and anonymous and named external researchers and research integrity experts for contributing to this investigation.

The corresponding author, as the representative of all authors, has been given the opportunity to register their agreement or disagreement to this retraction. We have kept a record of any response received.

References

[1] F. Chen, "Deep Neural Network Model Forecasting for Financial and Economic Market," *Journal of Mathematics*, vol. 2022, Article ID 8146555, 10 pages, 2022.

Hindawi
Journal of Mathematics
Volume 2024, Article ID 9876405, 1 page
https://doi.org/10.1155/2024/9876405

Retraction

Retracted: The New Approach Research on Singing Voice Detection Algorithm Based on Enhanced Reconstruction Residual Network

Journal of Mathematics

Received 23 January 2024; Accepted 23 January 2024; Published 24 January 2024

This article has been retracted by Hindawi following an investigation undertaken by the publisher [1]. This investigation has uncovered evidence of one or more of the following indicators of systematic manipulation of the publication process:

(1) Discrepancies in scope

(2) Discrepancies in the description of the research reported

(3) Discrepancies between the availability of data and the research described

(4) Inappropriate citations

(5) Incoherent, meaningless and/or irrelevant content included in the article

(6) Manipulated or compromised peer review

The presence of these indicators undermines our confidence in the integrity of the article's content and we cannot, therefore, vouch for its reliability. Please note that this notice is intended solely to alert readers that the content of this article is unreliable. We have not investigated whether authors were aware of or involved in the systematic manipulation of the publication process.

Wiley and Hindawi regrets that the usual quality checks did not identify these issues before publication and have since put additional measures in place to safeguard research integrity.

We wish to credit our own Research Integrity and Research Publishing teams and anonymous and named external researchers and research integrity experts for contributing to this investigation.

The corresponding author, as the representative of all authors, has been given the opportunity to register their agreement or disagreement to this retraction. We have kept a record of any response received.

References

[1] L. Liu, "The New Approach Research on Singing Voice Detection Algorithm Based on Enhanced Reconstruction Residual Network," *Journal of Mathematics*, vol. 2022, Article ID 7987592, 11 pages, 2022.

Hindawi
Journal of Mathematics
Volume 2024, Article ID 9873039, 1 page
https://doi.org/10.1155/2024/9873039

Retraction

Retracted: Research on International Law Data Integrity Guarantee Based on Antiterrorism Prediction Algorithm

Journal of Mathematics

Received 23 January 2024; Accepted 23 January 2024; Published 24 January 2024

This article has been retracted by Hindawi following an investigation undertaken by the publisher [1]. This investigation has uncovered evidence of one or more of the following indicators of systematic manipulation of the publication process:

(1) Discrepancies in scope

(2) Discrepancies in the description of the research reported

(3) Discrepancies between the availability of data and the research described

(4) Inappropriate citations

(5) Incoherent, meaningless and/or irrelevant content included in the article

(6) Manipulated or compromised peer review

The presence of these indicators undermines our confidence in the integrity of the article's content and we cannot, therefore, vouch for its reliability. Please note that this notice is intended solely to alert readers that the content of this article is unreliable. We have not investigated whether authors were aware of or involved in the systematic manipulation of the publication process.

In addition, our investigation has also shown that one or more of the following human-subject reporting requirements has not been met in this article: ethical approval by an Institutional Review Board (IRB) committee or equivalent, patient/participant consent to participate, and/or agreement to publish patient/participant details (where relevant).

Wiley and Hindawi regrets that the usual quality checks did not identify these issues before publication and have since put additional measures in place to safeguard research integrity.

We wish to credit our own Research Integrity and Research Publishing teams and anonymous and named external researchers and research integrity experts for contributing to this investigation.

The corresponding author, as the representative of all authors, has been given the opportunity to register their agreement or disagreement to this retraction. We have kept a record of any response received.

References

[1] H. Ru Qing, "Research on International Law Data Integrity Guarantee Based on Antiterrorism Prediction Algorithm," *Journal of Mathematics*, vol. 2022, Article ID 3089545, 9 pages, 2022.

Hindawi
Journal of Mathematics
Volume 2024, Article ID 9872547, 1 page
https://doi.org/10.1155/2024/9872547

Retraction

Retracted: Rough Set Construction and Entropy Weight Evaluation of Urban Higher Education Resource Carrying Capacity Based on Big Data

Journal of Mathematics

Received 23 January 2024; Accepted 23 January 2024; Published 24 January 2024

This article has been retracted by Hindawi following an investigation undertaken by the publisher [1]. This investigation has uncovered evidence of one or more of the following indicators of systematic manipulation of the publication process:

(1) Discrepancies in scope

(2) Discrepancies in the description of the research reported

(3) Discrepancies between the availability of data and the research described

(4) Inappropriate citations

(5) Incoherent, meaningless and/or irrelevant content included in the article

(6) Manipulated or compromised peer review

The presence of these indicators undermines our confidence in the integrity of the article's content and we cannot, therefore, vouch for its reliability. Please note that this notice is intended solely to alert readers that the content of this article is unreliable. We have not investigated whether authors were aware of or involved in the systematic manipulation of the publication process.

Wiley and Hindawi regrets that the usual quality checks did not identify these issues before publication and have since put additional measures in place to safeguard research integrity.

We wish to credit our own Research Integrity and Research Publishing teams and anonymous and named external researchers and research integrity experts for contributing to this investigation.

The corresponding author, as the representative of all authors, has been given the opportunity to register their agreement or disagreement to this retraction. We have kept a record of any response received.

References

[1] L. Wang, C. Liu, and M. Talha, "Rough Set Construction and Entropy Weight Evaluation of Urban Higher Education Resource Carrying Capacity Based on Big Data," *Journal of Mathematics*, vol. 2022, Article ID 7776940, 11 pages, 2022.

Hindawi
Journal of Mathematics
Volume 2024, Article ID 9871350, 1 page
https://doi.org/10.1155/2024/9871350

Retraction

Retracted: Optimisation of Driver's Traffic Literacy Evaluation Index from the Perspective of Information Contribution Sensitivity

Journal of Mathematics

Received 23 January 2024; Accepted 23 January 2024; Published 24 January 2024

This article has been retracted by Hindawi following an investigation undertaken by the publisher [1]. This investigation has uncovered evidence of one or more of the following indicators of systematic manipulation of the publication process:

(1) Discrepancies in scope

(2) Discrepancies in the description of the research reported

(3) Discrepancies between the availability of data and the research described

(4) Inappropriate citations

(5) Incoherent, meaningless and/or irrelevant content included in the article

(6) Manipulated or compromised peer review

The presence of these indicators undermines our confidence in the integrity of the article's content and we cannot, therefore, vouch for its reliability. Please note that this notice is intended solely to alert readers that the content of this article is unreliable. We have not investigated whether authors were aware of or involved in the systematic manipulation of the publication process.

In addition, our investigation has also shown that one or more of the following human-subject reporting requirements has not been met in this article: ethical approval by an Institutional Review Board (IRB) committee or equivalent, patient/participant consent to participate, and/or agreement to publish patient/participant details (where relevant).

Wiley and Hindawi regrets that the usual quality checks did not identify these issues before publication and have since put additional measures in place to safeguard research integrity.

We wish to credit our own Research Integrity and Research Publishing teams and anonymous and named external researchers and research integrity experts for contributing to this investigation.

The corresponding author, as the representative of all authors, has been given the opportunity to register their agreement or disagreement to this retraction. We have kept a record of any response received.

References

[1] L. Wang and K. Tian, "Optimisation of Driver's Traffic Literacy Evaluation Index from the Perspective of Information Contribution Sensitivity," *Journal of Mathematics*, vol. 2021, Article ID 9503037, 10 pages, 2021.

Hindawi
Journal of Mathematics
Volume 2024, Article ID 9870397, 1 page
https://doi.org/10.1155/2024/9870397

Retraction

Retracted: Data Analysis and Processing Application of Deep Learning in Engineering Cost Teaching Evaluation

Journal of Mathematics

Received 23 January 2024; Accepted 23 January 2024; Published 24 January 2024

This article has been retracted by Hindawi following an investigation undertaken by the publisher [1]. This investigation has uncovered evidence of one or more of the following indicators of systematic manipulation of the publication process:

(1) Discrepancies in scope

(2) Discrepancies in the description of the research reported

(3) Discrepancies between the availability of data and the research described

(4) Inappropriate citations

(5) Incoherent, meaningless and/or irrelevant content included in the article

(6) Manipulated or compromised peer review

The presence of these indicators undermines our confidence in the integrity of the article's content and we cannot, therefore, vouch for its reliability. Please note that this notice is intended solely to alert readers that the content of this article is unreliable. We have not investigated whether authors were aware of or involved in the systematic manipulation of the publication process.

In addition, our investigation has also shown that one or more of the following human-subject reporting requirements has not been met in this article: ethical approval by an Institutional Review Board (IRB) committee or equivalent, patient/participant consent to participate, and/or agreement to publish patient/participant details (where relevant).

Wiley and Hindawi regrets that the usual quality checks did not identify these issues before publication and have since put additional measures in place to safeguard research integrity.

We wish to credit our own Research Integrity and Research Publishing teams and anonymous and named external researchers and research integrity experts for contributing to this investigation.

The corresponding author, as the representative of all authors, has been given the opportunity to register their agreement or disagreement to this retraction. We have kept a record of any response received.

References

[1] X. He and S. Fu, "Data Analysis and Processing Application of Deep Learning in Engineering Cost Teaching Evaluation," *Journal of Mathematics*, vol. 2022, Article ID 8944570, 12 pages, 2022.

Hindawi
Journal of Mathematics
Volume 2024, Article ID 9865089, 1 page
https://doi.org/10.1155/2024/9865089

Retraction

Retracted: Few Samples of SAR Automatic Target Recognition Based on Enhanced-Shape CNN

Journal of Mathematics

Received 23 January 2024; Accepted 23 January 2024; Published 24 January 2024

This article has been retracted by Hindawi following an investigation undertaken by the publisher [1]. This investigation has uncovered evidence of one or more of the following indicators of systematic manipulation of the publication process:

(1) Discrepancies in scope

(2) Discrepancies in the description of the research reported

(3) Discrepancies between the availability of data and the research described

(4) Inappropriate citations

(5) Incoherent, meaningless and/or irrelevant content included in the article

(6) Manipulated or compromised peer review

The presence of these indicators undermines our confidence in the integrity of the article's content and we cannot, therefore, vouch for its reliability. Please note that this notice is intended solely to alert readers that the content of this article is unreliable. We have not investigated whether authors were aware of or involved in the systematic manipulation of the publication process.

Wiley and Hindawi regrets that the usual quality checks did not identify these issues before publication and have since put additional measures in place to safeguard research integrity.

We wish to credit our own Research Integrity and Research Publishing teams and anonymous and named external researchers and research integrity experts for contributing to this investigation.

The corresponding author, as the representative of all authors, has been given the opportunity to register their agreement or disagreement to this retraction. We have kept a record of any response received.

References

[1] M. Huang, F. Liu, and X. Meng, "Few Samples of SAR Automatic Target Recognition Based on Enhanced-Shape CNN," *Journal of Mathematics*, vol. 2021, Article ID 9141023, 16 pages, 2021.

Hindawi
Journal of Mathematics
Volume 2024, Article ID 9864641, 1 page
https://doi.org/10.1155/2024/9864641

Retraction

Retracted: A Blockchain Technique for Trade Credit Maintainability Using the Role of Information and Communication Technology

Journal of Mathematics

Received 23 January 2024; Accepted 23 January 2024; Published 24 January 2024

This article has been retracted by Hindawi following an investigation undertaken by the publisher [1]. This investigation has uncovered evidence of one or more of the following indicators of systematic manipulation of the publication process:

(1) Discrepancies in scope

(2) Discrepancies in the description of the research reported

(3) Discrepancies between the availability of data and the research described

(4) Inappropriate citations

(5) Incoherent, meaningless and/or irrelevant content included in the article

(6) Manipulated or compromised peer review

The presence of these indicators undermines our confidence in the integrity of the article's content and we cannot, therefore, vouch for its reliability. Please note that this notice is intended solely to alert readers that the content of this article is unreliable. We have not investigated whether authors were aware of or involved in the systematic manipulation of the publication process.

Wiley and Hindawi regrets that the usual quality checks did not identify these issues before publication and have since put additional measures in place to safeguard research integrity.

We wish to credit our own Research Integrity and Research Publishing teams and anonymous and named external researchers and research integrity experts for contributing to this investigation.

The corresponding author, as the representative of all authors, has been given the opportunity to register their agreement or disagreement to this retraction. We have kept a record of any response received.

References

[1] F. Shah, Y. Liu, Y. Shah et al., "A Blockchain Technique for Trade Credit Maintainability Using the Role of Information and Communication Technology," *Journal of Mathematics*, vol. 2022, Article ID 9621342, 11 pages, 2022.

Hindawi
Journal of Mathematics
Volume 2024, Article ID 9863939, 1 page
https://doi.org/10.1155/2024/9863939

Retraction

Retracted: Prediction Model of Mining Subsidence Parameters Based on Fuzzy Clustering

Journal of Mathematics

Received 23 January 2024; Accepted 23 January 2024; Published 24 January 2024

This article has been retracted by Hindawi following an investigation undertaken by the publisher [1]. This investigation has uncovered evidence of one or more of the following indicators of systematic manipulation of the publication process:

(1) Discrepancies in scope

(2) Discrepancies in the description of the research reported

(3) Discrepancies between the availability of data and the research described

(4) Inappropriate citations

(5) Incoherent, meaningless and/or irrelevant content included in the article

(6) Manipulated or compromised peer review

The presence of these indicators undermines our confidence in the integrity of the article's content and we cannot, therefore, vouch for its reliability. Please note that this notice is intended solely to alert readers that the content of this article is unreliable. We have not investigated whether authors were aware of or involved in the systematic manipulation of the publication process.

Wiley and Hindawi regrets that the usual quality checks did not identify these issues before publication and have since put additional measures in place to safeguard research integrity.

We wish to credit our own Research Integrity and Research Publishing teams and anonymous and named external researchers and research integrity experts for contributing to this investigation.

The corresponding author, as the representative of all authors, has been given the opportunity to register their agreement or disagreement to this retraction. We have kept a record of any response received.

References

[1] F. Cheng, J. Yang, Z. Zhang et al., "Prediction Model of Mining Subsidence Parameters Based on Fuzzy Clustering," *Journal of Mathematics*, vol. 2022, Article ID 7827104, 10 pages, 2022.

Hindawi
Journal of Mathematics
Volume 2024, Article ID 9863685, 1 page
https://doi.org/10.1155/2024/9863685

Retraction

Retracted: Implementing the Hybrid Neuro-Fuzzy System to Model Specific Learning Disability in Special University Education Programs

Journal of Mathematics

Received 23 January 2024; Accepted 23 January 2024; Published 24 January 2024

This article has been retracted by Hindawi following an investigation undertaken by the publisher [1]. This investigation has uncovered evidence of one or more of the following indicators of systematic manipulation of the publication process:

(1) Discrepancies in scope

(2) Discrepancies in the description of the research reported

(3) Discrepancies between the availability of data and the research described

(4) Inappropriate citations

(5) Incoherent, meaningless and/or irrelevant content included in the article

(6) Manipulated or compromised peer review

The presence of these indicators undermines our confidence in the integrity of the article's content and we cannot, therefore, vouch for its reliability. Please note that this notice is intended solely to alert readers that the content of this article is unreliable. We have not investigated whether authors were aware of or involved in the systematic manipulation of the publication process.

Wiley and Hindawi regrets that the usual quality checks did not identify these issues before publication and have since put additional measures in place to safeguard research integrity.

We wish to credit our own Research Integrity and Research Publishing teams and anonymous and named external researchers and research integrity experts for contributing to this investigation.

The corresponding author, as the representative of all authors, has been given the opportunity to register their agreement or disagreement to this retraction. We have kept a record of any response received.

References

[1] L. Wending, "Implementing the Hybrid Neuro-Fuzzy System to Model Specific Learning Disability in Special University Education Programs," *Journal of Mathematics*, vol. 2022, Article ID 6540542, 7 pages, 2022.

Hindawi
Journal of Mathematics
Volume 2024, Article ID 9857325, 1 page
https://doi.org/10.1155/2024/9857325

Retraction

Retracted: Digital Effectiveness in Video Conference Methods on Internet Learning Environments of Higher Education

Journal of Mathematics

Received 23 January 2024; Accepted 23 January 2024; Published 24 January 2024

This article has been retracted by Hindawi following an investigation undertaken by the publisher [1]. This investigation has uncovered evidence of one or more of the following indicators of systematic manipulation of the publication process:

(1) Discrepancies in scope

(2) Discrepancies in the description of the research reported

(3) Discrepancies between the availability of data and the research described

(4) Inappropriate citations

(5) Incoherent, meaningless and/or irrelevant content included in the article

(6) Manipulated or compromised peer review

The presence of these indicators undermines our confidence in the integrity of the article's content and we cannot, therefore, vouch for its reliability. Please note that this notice is intended solely to alert readers that the content of this article is unreliable. We have not investigated whether authors were aware of or involved in the systematic manipulation of the publication process.

In addition, our investigation has also shown that one or more of the following human-subject reporting requirements has not been met in this article: ethical approval by an Institutional Review Board (IRB) committee or equivalent, patient/participant consent to participate, and/or agreement to publish patient/participant details (where relevant).

Wiley and Hindawi regrets that the usual quality checks did not identify these issues before publication and have since put additional measures in place to safeguard research integrity.

We wish to credit our own Research Integrity and Research Publishing teams and anonymous and named external researchers and research integrity experts for contributing to this investigation.

The corresponding author, as the representative of all authors, has been given the opportunity to register their agreement or disagreement to this retraction. We have kept a record of any response received.

References

[1] Y. Wei and H. Tang, "Digital Effectiveness in Video Conference Methods on Internet Learning Environments of Higher Education," *Journal of Mathematics*, vol. 2022, Article ID 6996407, 6 pages, 2022.

Hindawi
Journal of Mathematics
Volume 2024, Article ID 9854510, 1 page
https://doi.org/10.1155/2024/9854510

Retraction

Retracted: A Novel Approach to Automate Complex Software Modularization Using a Fact Extraction System

Journal of Mathematics

Received 23 January 2024; Accepted 23 January 2024; Published 24 January 2024

This article has been retracted by Hindawi following an investigation undertaken by the publisher [1]. This investigation has uncovered evidence of one or more of the following indicators of systematic manipulation of the publication process:

(1) Discrepancies in scope

(2) Discrepancies in the description of the research reported

(3) Discrepancies between the availability of data and the research described

(4) Inappropriate citations

(5) Incoherent, meaningless and/or irrelevant content included in the article

(6) Manipulated or compromised peer review

The presence of these indicators undermines our confidence in the integrity of the article's content and we cannot, therefore, vouch for its reliability. Please note that this notice is intended solely to alert readers that the content of this article is unreliable. We have not investigated whether authors were aware of or involved in the systematic manipulation of the publication process.

Wiley and Hindawi regrets that the usual quality checks did not identify these issues before publication and have since put additional measures in place to safeguard research integrity.

We wish to credit our own Research Integrity and Research Publishing teams and anonymous and named external researchers and research integrity experts for contributing to this investigation.

The corresponding author, as the representative of all authors, has been given the opportunity to register their agreement or disagreement to this retraction. We have kept a record of any response received.

References

[1] M. Z. Khan, R. Naseem, A. Anwar et al., "A Novel Approach to Automate Complex Software Modularization Using a Fact Extraction System," *Journal of Mathematics*, vol. 2022, Article ID 8640596, 19 pages, 2022.

Hindawi
Journal of Mathematics
Volume 2024, Article ID 9854294, 1 page
https://doi.org/10.1155/2024/9854294

Retraction

Retracted: Multiple Collaborative Supervision Pattern Recognition Method within Social Organizations Based on Data Clustering Algorithm

Journal of Mathematics

Received 23 January 2024; Accepted 23 January 2024; Published 24 January 2024

This article has been retracted by Hindawi following an investigation undertaken by the publisher [1]. This investigation has uncovered evidence of one or more of the following indicators of systematic manipulation of the publication process:

(1) Discrepancies in scope

(2) Discrepancies in the description of the research reported

(3) Discrepancies between the availability of data and the research described

(4) Inappropriate citations

(5) Incoherent, meaningless and/or irrelevant content included in the article

(6) Manipulated or compromised peer review

The presence of these indicators undermines our confidence in the integrity of the article's content and we cannot, therefore, vouch for its reliability. Please note that this notice is intended solely to alert readers that the content of this article is unreliable. We have not investigated whether authors were aware of or involved in the systematic manipulation of the publication process.

Wiley and Hindawi regrets that the usual quality checks did not identify these issues before publication and have since put additional measures in place to safeguard research integrity.

We wish to credit our own Research Integrity and Research Publishing teams and anonymous and named external researchers and research integrity experts for contributing to this investigation.

The corresponding author, as the representative of all authors, has been given the opportunity to register their agreement or disagreement to this retraction. We have kept a record of any response received.

References

[1] W. Zhang and L. Pang, "Multiple Collaborative Supervision Pattern Recognition Method within Social Organizations Based on Data Clustering Algorithm," *Journal of Mathematics*, vol. 2021, Article ID 7890658, 12 pages, 2021.

Hindawi
Journal of Mathematics
Volume 2024, Article ID 9854275, 1 page
https://doi.org/10.1155/2024/9854275

Retraction

Retracted: Study on Driver Gaze Characteristics in Sight Distance Limited Section of Mountain Highway Based on Visual Information

Journal of Mathematics

Received 23 January 2024; Accepted 23 January 2024; Published 24 January 2024

This article has been retracted by Hindawi following an investigation undertaken by the publisher [1]. This investigation has uncovered evidence of one or more of the following indicators of systematic manipulation of the publication process:

(1) Discrepancies in scope

(2) Discrepancies in the description of the research reported

(3) Discrepancies between the availability of data and the research described

(4) Inappropriate citations

(5) Incoherent, meaningless and/or irrelevant content included in the article

(6) Manipulated or compromised peer review

The presence of these indicators undermines our confidence in the integrity of the article's content and we cannot, therefore, vouch for its reliability. Please note that this notice is intended solely to alert readers that the content of this article is unreliable. We have not investigated whether authors were aware of or involved in the systematic manipulation of the publication process.

In addition, our investigation has also shown that one or more of the following human-subject reporting requirements has not been met in this article: ethical approval by an Institutional Review Board (IRB) committee or equivalent, patient/participant consent to participate, and/or agreement to publish patient/participant details (where relevant).

Wiley and Hindawi regrets that the usual quality checks did not identify these issues before publication and have since put additional measures in place to safeguard research integrity.

We wish to credit our own Research Integrity and Research Publishing teams and anonymous and named external researchers and research integrity experts for contributing to this investigation.

The corresponding author, as the representative of all authors, has been given the opportunity to register their agreement or disagreement to this retraction. We have kept a record of any response received.

References

[1] Y. Tang, X. Peng, S. Xu, M. Bai, L. Lin, and H. Sun, "Study on Driver Gaze Characteristics in Sight Distance Limited Section of Mountain Highway Based on Visual Information," *Journal of Mathematics*, vol. 2022, Article ID 9482875, 8 pages, 2022.

Hindawi
Journal of Mathematics
Volume 2024, Article ID 9852879, 1 page
https://doi.org/10.1155/2024/9852879

Retraction

Retracted: Music Segmentation Algorithm Based on Self-Adaptive Update of Confidence Measure

Journal of Mathematics

Received 23 January 2024; Accepted 23 January 2024; Published 24 January 2024

This article has been retracted by Hindawi following an investigation undertaken by the publisher [1]. This investigation has uncovered evidence of one or more of the following indicators of systematic manipulation of the publication process:

(1) Discrepancies in scope

(2) Discrepancies in the description of the research reported

(3) Discrepancies between the availability of data and the research described

(4) Inappropriate citations

(5) Incoherent, meaningless and/or irrelevant content included in the article

(6) Manipulated or compromised peer review

The presence of these indicators undermines our confidence in the integrity of the article's content and we cannot, therefore, vouch for its reliability. Please note that this notice is intended solely to alert readers that the content of this article is unreliable. We have not investigated whether authors were aware of or involved in the systematic manipulation of the publication process.

Wiley and Hindawi regrets that the usual quality checks did not identify these issues before publication and have since put additional measures in place to safeguard research integrity.

We wish to credit our own Research Integrity and Research Publishing teams and anonymous and named external researchers and research integrity experts for contributing to this investigation.

The corresponding author, as the representative of all authors, has been given the opportunity to register their agreement or disagreement to this retraction. We have kept a record of any response received.

References

[1] J. Li, "Music Segmentation Algorithm Based on Self-Adaptive Update of Confidence Measure," *Journal of Mathematics*, vol. 2021, Article ID 8329088, 9 pages, 2021.

Hindawi
Journal of Mathematics
Volume 2024, Article ID 9841684, 1 page
https://doi.org/10.1155/2024/9841684

Retraction

Retracted: Evaluation of Innovation Efficiency of High-Tech Enterprise Knowledge Supply Chain Based on AHP-DEA

Journal of Mathematics

Received 23 January 2024; Accepted 23 January 2024; Published 24 January 2024

This article has been retracted by Hindawi following an investigation undertaken by the publisher [1]. This investigation has uncovered evidence of one or more of the following indicators of systematic manipulation of the publication process:

(1) Discrepancies in scope

(2) Discrepancies in the description of the research reported

(3) Discrepancies between the availability of data and the research described

(4) Inappropriate citations

(5) Incoherent, meaningless and/or irrelevant content included in the article

(6) Manipulated or compromised peer review

The presence of these indicators undermines our confidence in the integrity of the article's content and we cannot, therefore, vouch for its reliability. Please note that this notice is intended solely to alert readers that the content of this article is unreliable. We have not investigated whether authors were aware of or involved in the systematic manipulation of the publication process.

In addition, our investigation has also shown that one or more of the following human-subject reporting requirements has not been met in this article: ethical approval by an Institutional Review Board (IRB) committee or equivalent, patient/participant consent to participate, and/or agreement to publish patient/participant details (where relevant).

Wiley and Hindawi regrets that the usual quality checks did not identify these issues before publication and have since put additional measures in place to safeguard research integrity.

We wish to credit our own Research Integrity and Research Publishing teams and anonymous and named external researchers and research integrity experts for contributing to this investigation.

The corresponding author, as the representative of all authors, has been given the opportunity to register their agreement or disagreement to this retraction. We have kept a record of any response received.

References

[1] H. Han and X. Gu, "Evaluation of Innovation Efficiency of High-Tech Enterprise Knowledge Supply Chain Based on AHP-DEA," *Journal of Mathematics*, vol. 2022, Article ID 3210474, 9 pages, 2022.

Hindawi
Journal of Mathematics
Volume 2024, Article ID 9839640, 1 page
https://doi.org/10.1155/2024/9839640

Retraction

Retracted: The Evaluation of Music Teaching in Colleges and Universities Based on Machine Learning

Journal of Mathematics

Received 23 January 2024; Accepted 23 January 2024; Published 24 January 2024

This article has been retracted by Hindawi following an investigation undertaken by the publisher [1]. This investigation has uncovered evidence of one or more of the following indicators of systematic manipulation of the publication process:

(1) Discrepancies in scope

(2) Discrepancies in the description of the research reported

(3) Discrepancies between the availability of data and the research described

(4) Inappropriate citations

(5) Incoherent, meaningless and/or irrelevant content included in the article

(6) Manipulated or compromised peer review

The presence of these indicators undermines our confidence in the integrity of the article's content and we cannot, therefore, vouch for its reliability. Please note that this notice is intended solely to alert readers that the content of this article is unreliable. We have not investigated whether authors were aware of or involved in the systematic manipulation of the publication process.

Wiley and Hindawi regrets that the usual quality checks did not identify these issues before publication and have since put additional measures in place to safeguard research integrity.

We wish to credit our own Research Integrity and Research Publishing teams and anonymous and named external researchers and research integrity experts for contributing to this investigation.

The corresponding author, as the representative of all authors, has been given the opportunity to register their agreement or disagreement to this retraction. We have kept a record of any response received.

References

[1] X. Xiongjun and D. Lv, "The Evaluation of Music Teaching in Colleges and Universities Based on Machine Learning," *Journal of Mathematics*, vol. 2022, Article ID 2678303, 7 pages, 2022.

Hindawi
Journal of Mathematics
Volume 2024, Article ID 9838430, 1 page
https://doi.org/10.1155/2024/9838430

Retraction

Retracted: Recursive Neural Network-Based Market Demand Forecasting Algorithm for Calligraphy Practice Products

Journal of Mathematics

Received 23 January 2024; Accepted 23 January 2024; Published 24 January 2024

This article has been retracted by Hindawi following an investigation undertaken by the publisher [1]. This investigation has uncovered evidence of one or more of the following indicators of systematic manipulation of the publication process:

(1) Discrepancies in scope

(2) Discrepancies in the description of the research reported

(3) Discrepancies between the availability of data and the research described

(4) Inappropriate citations

(5) Incoherent, meaningless and/or irrelevant content included in the article

(6) Manipulated or compromised peer review

The presence of these indicators undermines our confidence in the integrity of the article's content and we cannot, therefore, vouch for its reliability. Please note that this notice is intended solely to alert readers that the content of this article is unreliable. We have not investigated whether authors were aware of or involved in the systematic manipulation of the publication process.

Wiley and Hindawi regrets that the usual quality checks did not identify these issues before publication and have since put additional measures in place to safeguard research integrity.

We wish to credit our own Research Integrity and Research Publishing teams and anonymous and named external researchers and research integrity experts for contributing to this investigation.

The corresponding author, as the representative of all authors, has been given the opportunity to register their agreement or disagreement to this retraction. We have kept a record of any response received.

References

[1] Y. Xue, "Recursive Neural Network-Based Market Demand Forecasting Algorithm for Calligraphy Practice Products," *Journal of Mathematics*, vol. 2022, Article ID 8086789, 10 pages, 2022.

Hindawi
Journal of Mathematics
Volume 2024, Article ID 9836324, 1 page
https://doi.org/10.1155/2024/9836324

Retraction

Retracted: The Impact of Convention and Exhibition Industry on Regional Economic Development Based on Grey Relational Model

Journal of Mathematics

Received 23 January 2024; Accepted 23 January 2024; Published 24 January 2024

This article has been retracted by Hindawi following an investigation undertaken by the publisher [1]. This investigation has uncovered evidence of one or more of the following indicators of systematic manipulation of the publication process:

(1) Discrepancies in scope

(2) Discrepancies in the description of the research reported

(3) Discrepancies between the availability of data and the research described

(4) Inappropriate citations

(5) Incoherent, meaningless and/or irrelevant content included in the article

(6) Manipulated or compromised peer review

The presence of these indicators undermines our confidence in the integrity of the article's content and we cannot, therefore, vouch for its reliability. Please note that this notice is intended solely to alert readers that the content of this article is unreliable. We have not investigated whether authors were aware of or involved in the systematic manipulation of the publication process.

Wiley and Hindawi regrets that the usual quality checks did not identify these issues before publication and have since put additional measures in place to safeguard research integrity.

We wish to credit our own Research Integrity and Research Publishing teams and anonymous and named external researchers and research integrity experts for contributing to this investigation.

The corresponding author, as the representative of all authors, has been given the opportunity to register their agreement or disagreement to this retraction. We have kept a record of any response received.

References

[1] X. Yang, "The Impact of Convention and Exhibition Industry on Regional Economic Development Based on Grey Relational Model," *Journal of Mathematics*, vol. 2022, Article ID 9752636, 8 pages, 2022.

Hindawi
Journal of Mathematics
Volume 2024, Article ID 9829414, 1 page
https://doi.org/10.1155/2024/9829414

Retraction

Retracted: Detection Method of Limb Movement in Competitive Sports Training Based on Deep Learning

Journal of Mathematics

Received 23 January 2024; Accepted 23 January 2024; Published 24 January 2024

This article has been retracted by Hindawi following an investigation undertaken by the publisher [1]. This investigation has uncovered evidence of one or more of the following indicators of systematic manipulation of the publication process:

(1) Discrepancies in scope

(2) Discrepancies in the description of the research reported

(3) Discrepancies between the availability of data and the research described

(4) Inappropriate citations

(5) Incoherent, meaningless and/or irrelevant content included in the article

(6) Manipulated or compromised peer review

The presence of these indicators undermines our confidence in the integrity of the article's content and we cannot, therefore, vouch for its reliability. Please note that this notice is intended solely to alert readers that the content of this article is unreliable. We have not investigated whether authors were aware of or involved in the systematic manipulation of the publication process.

Wiley and Hindawi regrets that the usual quality checks did not identify these issues before publication and have since put additional measures in place to safeguard research integrity.

We wish to credit our own Research Integrity and Research Publishing teams and anonymous and named external researchers and research integrity experts for contributing to this investigation.

The corresponding author, as the representative of all authors, has been given the opportunity to register their agreement or disagreement to this retraction. We have kept a record of any response received.

References

[1] C. Qin and S. Huo, "Detection Method of Limb Movement in Competitive Sports Training Based on Deep Learning," *Journal of Mathematics*, vol. 2022, Article ID 8643234, 8 pages, 2022.

Hindawi
Journal of Mathematics
Volume 2024, Article ID 9825890, 1 page
https://doi.org/10.1155/2024/9825890

Retraction

Retracted: Supply Capability Evaluation of Intelligent Manufacturing Enterprises Based on Improved BP Neural Network

Journal of Mathematics

Received 23 January 2024; Accepted 23 January 2024; Published 24 January 2024

This article has been retracted by Hindawi following an investigation undertaken by the publisher [1]. This investigation has uncovered evidence of one or more of the following indicators of systematic manipulation of the publication process:

(1) Discrepancies in scope

(2) Discrepancies in the description of the research reported

(3) Discrepancies between the availability of data and the research described

(4) Inappropriate citations

(5) Incoherent, meaningless and/or irrelevant content included in the article

(6) Manipulated or compromised peer review

The presence of these indicators undermines our confidence in the integrity of the article's content and we cannot, therefore, vouch for its reliability. Please note that this notice is intended solely to alert readers that the content of this article is unreliable. We have not investigated whether authors were aware of or involved in the systematic manipulation of the publication process.

Wiley and Hindawi regrets that the usual quality checks did not identify these issues before publication and have since put additional measures in place to safeguard research integrity.

We wish to credit our own Research Integrity and Research Publishing teams and anonymous and named external researchers and research integrity experts for contributing to this investigation.

The corresponding author, as the representative of all authors, has been given the opportunity to register their agreement or disagreement to this retraction. We have kept a record of any response received.

References

[1] Q. Quan and Z. Zhang, "Supply Capability Evaluation of Intelligent Manufacturing Enterprises Based on Improved BP Neural Network," *Journal of Mathematics*, vol. 2022, Article ID 8572424, 8 pages, 2022.

Hindawi
Journal of Mathematics
Volume 2024, Article ID 9824283, 1 page
https://doi.org/10.1155/2024/9824283

Retraction

Retracted: Design and Research of the AI Badminton Model Based on the Deep Learning Neural Network

Journal of Mathematics

Received 23 January 2024; Accepted 23 January 2024; Published 24 January 2024

This article has been retracted by Hindawi following an investigation undertaken by the publisher [1]. This investigation has uncovered evidence of one or more of the following indicators of systematic manipulation of the publication process:

(1) Discrepancies in scope

(2) Discrepancies in the description of the research reported

(3) Discrepancies between the availability of data and the research described

(4) Inappropriate citations

(5) Incoherent, meaningless and/or irrelevant content included in the article

(6) Manipulated or compromised peer review

The presence of these indicators undermines our confidence in the integrity of the article's content and we cannot, therefore, vouch for its reliability. Please note that this notice is intended solely to alert readers that the content of this article is unreliable. We have not investigated whether authors were aware of or involved in the systematic manipulation of the publication process.

Wiley and Hindawi regrets that the usual quality checks did not identify these issues before publication and have since put additional measures in place to safeguard research integrity.

We wish to credit our own Research Integrity and Research Publishing teams and anonymous and named external researchers and research integrity experts for contributing to this investigation.

The corresponding author, as the representative of all authors, has been given the opportunity to register their agreement or disagreement to this retraction. We have kept a record of any response received.

References

[1] Y. Chen and H. Hu, "Design and Research of the AI Badminton Model Based on the Deep Learning Neural Network," *Journal of Mathematics*, vol. 2022, Article ID 6739952, 10 pages, 2022.

Hindawi
Journal of Mathematics
Volume 2024, Article ID 9820467, 1 page
https://doi.org/10.1155/2024/9820467

Retraction

Retracted: Research on Automatic Classification Method of Ethnic Music Emotion Based on Machine Learning

Journal of Mathematics

Received 23 January 2024; Accepted 23 January 2024; Published 24 January 2024

This article has been retracted by Hindawi following an investigation undertaken by the publisher [1]. This investigation has uncovered evidence of one or more of the following indicators of systematic manipulation of the publication process:

(1) Discrepancies in scope

(2) Discrepancies in the description of the research reported

(3) Discrepancies between the availability of data and the research described

(4) Inappropriate citations

(5) Incoherent, meaningless and/or irrelevant content included in the article

(6) Manipulated or compromised peer review

The presence of these indicators undermines our confidence in the integrity of the article's content and we cannot, therefore, vouch for its reliability. Please note that this notice is intended solely to alert readers that the content of this article is unreliable. We have not investigated whether authors were aware of or involved in the systematic manipulation of the publication process.

Wiley and Hindawi regrets that the usual quality checks did not identify these issues before publication and have since put additional measures in place to safeguard research integrity.

We wish to credit our own Research Integrity and Research Publishing teams and anonymous and named external researchers and research integrity experts for contributing to this investigation.

The corresponding author, as the representative of all authors, has been given the opportunity to register their agreement or disagreement to this retraction. We have kept a record of any response received.

References

[1] Z. Wu, "Research on Automatic Classification Method of Ethnic Music Emotion Based on Machine Learning," *Journal of Mathematics*, vol. 2022, Article ID 7554404, 11 pages, 2022.

Hindawi
Journal of Mathematics
Volume 2024, Article ID 9819732, 1 page
https://doi.org/10.1155/2024/9819732

Retraction

Retracted: A Convolutional Network-Based Intelligent Evaluation Algorithm for the Quality of Spoken English Pronunciation

Journal of Mathematics

Received 23 January 2024; Accepted 23 January 2024; Published 24 January 2024

This article has been retracted by Hindawi following an investigation undertaken by the publisher [1]. This investigation has uncovered evidence of one or more of the following indicators of systematic manipulation of the publication process:

(1) Discrepancies in scope

(2) Discrepancies in the description of the research reported

(3) Discrepancies between the availability of data and the research described

(4) Inappropriate citations

(5) Incoherent, meaningless and/or irrelevant content included in the article

(6) Manipulated or compromised peer review

The presence of these indicators undermines our confidence in the integrity of the article's content and we cannot, therefore, vouch for its reliability. Please note that this notice is intended solely to alert readers that the content of this article is unreliable. We have not investigated whether authors were aware of or involved in the systematic manipulation of the publication process.

Wiley and Hindawi regrets that the usual quality checks did not identify these issues before publication and have since put additional measures in place to safeguard research integrity.

We wish to credit our own Research Integrity and Research Publishing teams and anonymous and named external researchers and research integrity experts for contributing to this investigation.

The corresponding author, as the representative of all authors, has been given the opportunity to register their agreement or disagreement to this retraction. We have kept a record of any response received.

References

[1] X. Zhan, "A Convolutional Network-Based Intelligent Evaluation Algorithm for the Quality of Spoken English Pronunciation," *Journal of Mathematics*, vol. 2022, Article ID 7560033, 9 pages, 2022.

Hindawi
Journal of Mathematics
Volume 2024, Article ID 9818702, 1 page
https://doi.org/10.1155/2024/9818702

Retraction

Retracted: Music Therapy Methods Based on SVM and MLP

Journal of Mathematics

Received 23 January 2024; Accepted 23 January 2024; Published 24 January 2024

This article has been retracted by Hindawi following an investigation undertaken by the publisher [1]. This investigation has uncovered evidence of one or more of the following indicators of systematic manipulation of the publication process:

(1) Discrepancies in scope

(2) Discrepancies in the description of the research reported

(3) Discrepancies between the availability of data and the research described

(4) Inappropriate citations

(5) Incoherent, meaningless and/or irrelevant content included in the article

(6) Manipulated or compromised peer review

The presence of these indicators undermines our confidence in the integrity of the article's content and we cannot, therefore, vouch for its reliability. Please note that this notice is intended solely to alert readers that the content of this article is unreliable. We have not investigated whether authors were aware of or involved in the systematic manipulation of the publication process.

In addition, our investigation has also shown that one or more of the following human-subject reportin requirements has not been met in this article: ethical approval by an Institutional Review Board (IRB) committee or equivalent, patient/participant consent to participate, and/or agreement to publish patient/participant details (where relevant).

Wiley and Hindawi regrets that the usual quality checks did not identify these issues before publication and have since put additional measures in place to safeguard research integrity.

We wish to credit our own Research Integrity and Research Publishing teams and anonymous and named external researchers and research integrity experts for contributing to this investigation.

The corresponding author, as the representative of all authors, has been given the opportunity to register their agreement or disagreement to this retraction. We have kept a record of any response received.

References

[1] H. Zou, "Music Therapy Methods Based on SVM and MLP," *Journal of Mathematics*, vol. 2022, Article ID 3377809, 6 pages, 2022.

Hindawi
Journal of Mathematics
Volume 2024, Article ID 9817061, 1 page
https://doi.org/10.1155/2024/9817061

Retraction

Retracted: Experiment and Algorithm Research of Coal Direct Liquefaction Residual Oil Pyrolysis and Coking Technology Based on Lumped Kinetic Engineering

Journal of Mathematics

Received 23 January 2024; Accepted 23 January 2024; Published 24 January 2024

This article has been retracted by Hindawi following an investigation undertaken by the publisher [1]. This investigation has uncovered evidence of one or more of the following indicators of systematic manipulation of the publication process:

(1) Discrepancies in scope

(2) Discrepancies in the description of the research reported

(3) Discrepancies between the availability of data and the research described

(4) Inappropriate citations

(5) Incoherent, meaningless and/or irrelevant content included in the article

(6) Manipulated or compromised peer review

The presence of these indicators undermines our confidence in the integrity of the article's content and we cannot, therefore, vouch for its reliability. Please note that this notice is intended solely to alert readers that the content of this article is unreliable. We have not investigated whether authors were aware of or involved in the systematic manipulation of the publication process.

Wiley and Hindawi regrets that the usual quality checks did not identify these issues before publication and have since put additional measures in place to safeguard research integrity.

We wish to credit our own Research Integrity and Research Publishing teams and anonymous and named external researchers and research integrity experts for contributing to this investigation.

The corresponding author, as the representative of all authors, has been given the opportunity to register their agreement or disagreement to this retraction. We have kept a record of any response received.

References

[1] T. Bo and C. Yang, "Experiment and Algorithm Research of Coal Direct Liquefaction Residual Oil Pyrolysis and Coking Technology Based on Lumped Kinetic Engineering," *Journal of Mathematics*, vol. 2022, Article ID 3610246, 8 pages, 2022.

Hindawi
Journal of Mathematics
Volume 2024, Article ID 9814834, 1 page
https://doi.org/10.1155/2024/9814834

Retraction

Retracted: A New Neutrosophic Negative Binomial Distribution: Properties and Applications

Journal of Mathematics

Received 23 January 2024; Accepted 23 January 2024; Published 24 January 2024

This article has been retracted by Hindawi following an investigation undertaken by the publisher [1]. This investigation has uncovered evidence of one or more of the following indicators of systematic manipulation of the publication process:

(1) Discrepancies in scope

(2) Discrepancies in the description of the research reported

(3) Discrepancies between the availability of data and the research described

(4) Inappropriate citations

(5) Incoherent, meaningless and/or irrelevant content included in the article

(6) Manipulated or compromised peer review

The presence of these indicators undermines our confidence in the integrity of the article's content and we cannot, therefore, vouch for its reliability. Please note that this notice is intended solely to alert readers that the content of this article is unreliable. We have not investigated whether authors were aware of or involved in the systematic manipulation of the publication process.

Wiley and Hindawi regrets that the usual quality checks did not identify these issues before publication and have since put additional measures in place to safeguard research integrity.

We wish to credit our own Research Integrity and Research Publishing teams and anonymous and named external researchers and research integrity experts for contributing to this investigation.

The corresponding author, as the representative of all authors, has been given the opportunity to register their agreement or disagreement to this retraction. We have kept a record of any response received.

References

[1] R. A. K. Sherwani, S. Iqbal, S. Abbas, M. Aslam, and A. H. AL-Marshadi, "A New Neutrosophic Negative Binomial Distribution: Properties and Applications," *Journal of Mathematics*, vol. 2021, Article ID 2788265, 12 pages, 2021.

Hindawi
Journal of Mathematics
Volume 2024, Article ID 9813159, 1 page
https://doi.org/10.1155/2024/9813159

Retraction

Retracted: Research on the Model of Distance Education Resource Integration from the Perspective of Comparative Education

Journal of Mathematics

Received 23 January 2024; Accepted 23 January 2024; Published 24 January 2024

This article has been retracted by Hindawi following an investigation undertaken by the publisher [1]. This investigation has uncovered evidence of one or more of the following indicators of systematic manipulation of the publication process:

(1) Discrepancies in scope

(2) Discrepancies in the description of the research reported

(3) Discrepancies between the availability of data and the research described

(4) Inappropriate citations

(5) Incoherent, meaningless and/or irrelevant content included in the article

(6) Manipulated or compromised peer review

The presence of these indicators undermines our confidence in the integrity of the article's content and we cannot, therefore, vouch for its reliability. Please note that this notice is intended solely to alert readers that the content of this article is unreliable. We have not investigated whether authors were aware of or involved in the systematic manipulation of the publication process.

Wiley and Hindawi regrets that the usual quality checks did not identify these issues before publication and have since put additional measures in place to safeguard research integrity.

We wish to credit our own Research Integrity and Research Publishing teams and anonymous and named external researchers and research integrity experts for contributing to this investigation.

The corresponding author, as the representative of all authors, has been given the opportunity to register their agreement or disagreement to this retraction. We have kept a record of any response received.

References

[1] Z. Dan, "Research on the Model of Distance Education Resource Integration from the Perspective of Comparative Education," *Journal of Mathematics*, vol. 2022, Article ID 9589394, 8 pages, 2022.

Hindawi
Journal of Mathematics
Volume 2024, Article ID 9812973, 1 page
https://doi.org/10.1155/2024/9812973

Retraction

Retracted: Developing a New Interval Type-2 Hesitant Fuzzy TOPSIS-Based Fuzzy Best-Worst Multicriteria Decision-Making Method for Competitive Pricing in Supply Chain

Journal of Mathematics

Received 23 January 2024; Accepted 23 January 2024; Published 24 January 2024

This article has been retracted by Hindawi following an investigation undertaken by the publisher [1]. This investigation has uncovered evidence of one or more of the following indicators of systematic manipulation of the publication process:

(1) Discrepancies in scope

(2) Discrepancies in the description of the research reported

(3) Discrepancies between the availability of data and the research described

(4) Inappropriate citations

(5) Incoherent, meaningless and/or irrelevant content included in the article

(6) Manipulated or compromised peer review

The presence of these indicators undermines our confidence in the integrity of the article's content and we cannot, therefore, vouch for its reliability. Please note that this notice is intended solely to alert readers that the content of this article is unreliable. We have not investigated whether authors were aware of or involved in the systematic manipulation of the publication process.

Wiley and Hindawi regrets that the usual quality checks did not identify these issues before publication and have since put additional measures in place to safeguard research integrity.

We wish to credit our own Research Integrity and Research Publishing teams and anonymous and named external researchers and research integrity experts for contributing to this investigation.

The corresponding author, as the representative of all authors, has been given the opportunity to register their agreement or disagreement to this retraction. We have kept a record of any response received.

References

[1] F. Salimian, M. Damiri, M. Ramezankhani, and S. K. Fariman, "Developing a New Interval Type-2 Hesitant Fuzzy TOPSIS-Based Fuzzy Best-Worst Multicriteria Decision-Making Method for Competitive Pricing in Supply Chain," *Journal of Mathematics*, vol. 2022, Article ID 7879028, 16 pages, 2022.

Hindawi
Journal of Mathematics
Volume 2024, Article ID 9809684, 1 page
https://doi.org/10.1155/2024/9809684

Retraction

Retracted: Statistical Inferences of Burr XII Lifetime Models under Joint Type-1 Competing Risks Samples

Journal of Mathematics

Received 23 January 2024; Accepted 23 January 2024; Published 24 January 2024

This article has been retracted by Hindawi following an investigation undertaken by the publisher [1]. This investigation has uncovered evidence of one or more of the following indicators of systematic manipulation of the publication process:

(1) Discrepancies in scope

(2) Discrepancies in the description of the research reported

(3) Discrepancies between the availability of data and the research described

(4) Inappropriate citations

(5) Incoherent, meaningless and/or irrelevant content included in the article

(6) Manipulated or compromised peer review

The presence of these indicators undermines our confidence in the integrity of the article's content and we cannot, therefore, vouch for its reliability. Please note that this notice is intended solely to alert readers that the content of this article is unreliable. We have not investigated whether authors were aware of or involved in the systematic manipulation of the publication process.

Wiley and Hindawi regrets that the usual quality checks did not identify these issues before publication and have since put additional measures in place to safeguard research integrity.

We wish to credit our own Research Integrity and Research Publishing teams and anonymous and named external researchers and research integrity experts for contributing to this investigation.

The corresponding author, as the representative of all authors, has been given the opportunity to register their agreement or disagreement to this retraction. We have kept a record of any response received.

References

[1] T. A. Abushal, A. A. Soliman, and G. A. Abd-Elmougod, "Statistical Inferences of Burr XII Lifetime Models under Joint Type-1 Competing Risks Samples," *Journal of Mathematics*, vol. 2021, Article ID 9553617, 16 pages, 2021.

Hindawi
Journal of Mathematics
Volume 2024, Article ID 9807051, 1 page
https://doi.org/10.1155/2024/9807051

Retraction

Retracted: Personalized Education Based on Hybrid Intelligent Recommendation System

Journal of Mathematics

Received 23 January 2024; Accepted 23 January 2024; Published 24 January 2024

This article has been retracted by Hindawi following an investigation undertaken by the publisher [1]. This investigation has uncovered evidence of one or more of the following indicators of systematic manipulation of the publication process:

(1) Discrepancies in scope

(2) Discrepancies in the description of the research reported

(3) Discrepancies between the availability of data and the research described

(4) Inappropriate citations

(5) Incoherent, meaningless and/or irrelevant content included in the article

(6) Manipulated or compromised peer review

The presence of these indicators undermines our confidence in the integrity of the article's content and we cannot, therefore, vouch for its reliability. Please note that this notice is intended solely to alert readers that the content of this article is unreliable. We have not investigated whether authors were aware of or involved in the systematic manipulation of the publication process.

In addition, our investigation has also shown that one or more of the following human-subject reporting requirements has not been met in this article: ethical approval by an Institutional Review Board (IRB) committee or equivalent, patient/participant consent to participate, and/or agreement to publish patient/participant details (where relevant).

Wiley and Hindawi regrets that the usual quality checks did not identify these issues before publication and have since put additional measures in place to safeguard research integrity.

We wish to credit our own Research Integrity and Research Publishing teams and anonymous and named external researchers and research integrity experts for contributing to this investigation.

The corresponding author, as the representative of all authors, has been given the opportunity to register their agreement or disagreement to this retraction. We have kept a record of any response received.

References

[1] F. Zheng, "Personalized Education Based on Hybrid Intelligent Recommendation System," *Journal of Mathematics*, vol. 2022, Article ID 1313711, 9 pages, 2022.

Hindawi
Journal of Mathematics
Volume 2024, Article ID 9802386, 1 page
https://doi.org/10.1155/2024/9802386

Retraction

Retracted: Evaluation Algorithm of Ecological Energy-Saving Effect of Green Buildings Based on Gray Correlation Degree

Journal of Mathematics

Received 23 January 2024; Accepted 23 January 2024; Published 24 January 2024

This article has been retracted by Hindawi following an investigation undertaken by the publisher [1]. This investigation has uncovered evidence of one or more of the following indicators of systematic manipulation of the publication process:

(1) Discrepancies in scope

(2) Discrepancies in the description of the research reported

(3) Discrepancies between the availability of data and the research described

(4) Inappropriate citations

(5) Incoherent, meaningless and/or irrelevant content included in the article

(6) Manipulated or compromised peer review

The presence of these indicators undermines our confidence in the integrity of the article's content and we cannot, therefore, vouch for its reliability. Please note that this notice is intended solely to alert readers that the content of this article is unreliable. We have not investigated whether authors were aware of or involved in the systematic manipulation of the publication process.

Wiley and Hindawi regrets that the usual quality checks did not identify these issues before publication and have since put additional measures in place to safeguard research integrity.

We wish to credit our own Research Integrity and Research Publishing teams and anonymous and named external researchers and research integrity experts for contributing to this investigation.

The corresponding author, as the representative of all authors, has been given the opportunity to register their agreement or disagreement to this retraction. We have kept a record of any response received.

References

[1] C. Wang, "Evaluation Algorithm of Ecological Energy-Saving Effect of Green Buildings Based on Gray Correlation Degree," *Journal of Mathematics*, vol. 2021, Article ID 6705220, 10 pages, 2021.

Hindawi
Journal of Mathematics
Volume 2024, Article ID 9796040, 1 page
https://doi.org/10.1155/2024/9796040

Retraction

Retracted: A Relevant Customer Identification Algorithm Based on the Internet Financial Platform

Journal of Mathematics

Received 23 January 2024; Accepted 23 January 2024; Published 24 January 2024

This article has been retracted by Hindawi following an investigation undertaken by the publisher [1]. This investigation has uncovered evidence of one or more of the following indicators of systematic manipulation of the publication process:

(1) Discrepancies in scope

(2) Discrepancies in the description of the research reported

(3) Discrepancies between the availability of data and the research described

(4) Inappropriate citations

(5) Incoherent, meaningless and/or irrelevant content included in the article

(6) Manipulated or compromised peer review

The presence of these indicators undermines our confidence in the integrity of the article's content and we cannot, therefore, vouch for its reliability. Please note that this notice is intended solely to alert readers that the content of this article is unreliable. We have not investigated whether authors were aware of or involved in the systematic manipulation of the publication process.

In addition, our investigation has also shown that one or more of the following human-subject reporting requirements has not been met in this article: ethical approval by an Institutional Review Board (IRB) committee or equivalent, patient/participant consent to participate, and/or agreement to publish patient/participant details (where relevant).

Wiley and Hindawi regrets that the usual quality checks did not identify these issues before publication and have since put additional measures in place to safeguard research integrity.

We wish to credit our own Research Integrity and Research Publishing teams and anonymous and named external researchers and research integrity experts for contributing to this investigation.

The corresponding author, as the representative of all authors, has been given the opportunity to register their agreement or disagreement to this retraction. We have kept a record of any response received.

References

[1] G. Yangyudongnanxin, "A Relevant Customer Identification Algorithm Based on the Internet Financial Platform," *Journal of Mathematics*, vol. 2021, Article ID 9770471, 9 pages, 2021.

Hindawi
Journal of Mathematics
Volume 2024, Article ID 9795281, 1 page
https://doi.org/10.1155/2024/9795281

Retraction

Retracted: The Exponentiated Exponential-Inverse Weibull Model: Theory and Application to COVID-19 Data in Saudi Arabia

Journal of Mathematics

Received 23 January 2024; Accepted 23 January 2024; Published 24 January 2024

This article has been retracted by Hindawi following an investigation undertaken by the publisher [1]. This investigation has uncovered evidence of one or more of the following indicators of systematic manipulation of the publication process:

(1) Discrepancies in scope

(2) Discrepancies in the description of the research reported

(3) Discrepancies between the availability of data and the research described

(4) Inappropriate citations

(5) Incoherent, meaningless and/or irrelevant content included in the article

(6) Manipulated or compromised peer review

The presence of these indicators undermines our confidence in the integrity of the article's content and we cannot, therefore, vouch for its reliability. Please note that this notice is intended solely to alert readers that the content of this article is unreliable. We have not investigated whether authors were aware of or involved in the systematic manipulation of the publication process.

Wiley and Hindawi regrets that the usual quality checks did not identify these issues before publication and have since put additional measures in place to safeguard research integrity.

We wish to credit our own Research Integrity and Research Publishing teams and anonymous and named external researchers and research integrity experts for contributing to this investigation.

The corresponding author, as the representative of all authors, has been given the opportunity to register their agreement or disagreement to this retraction. We have kept a record of any response received.

References

[1] M. M. Badr and G. Sobahi, "The Exponentiated Exponential-Inverse Weibull Model: Theory and Application to COVID-19 Data in Saudi Arabia," *Journal of Mathematics*, vol. 2022, Article ID 8521026, 11 pages, 2022.

Hindawi
Journal of Mathematics
Volume 2024, Article ID 9793567, 1 page
https://doi.org/10.1155/2024/9793567

Retraction

Retracted: Inverted Length-Biased Exponential Model: Statistical Inference and Modeling

Journal of Mathematics

Received 23 January 2024; Accepted 23 January 2024; Published 24 January 2024

This article has been retracted by Hindawi following an investigation undertaken by the publisher [1]. This investigation has uncovered evidence of one or more of the following indicators of systematic manipulation of the publication process:

(1) Discrepancies in scope

(2) Discrepancies in the description of the research reported

(3) Discrepancies between the availability of data and the research described

(4) Inappropriate citations

(5) Incoherent, meaningless and/or irrelevant content included in the article

(6) Manipulated or compromised peer review

The presence of these indicators undermines our confidence in the integrity of the article's content and we cannot, therefore, vouch for its reliability. Please note that this notice is intended solely to alert readers that the content of this article is unreliable. We have not investigated whether authors were aware of or involved in the systematic manipulation of the publication process.

Wiley and Hindawi regrets that the usual quality checks did not identify these issues before publication and have since put additional measures in place to safeguard research integrity.

We wish to credit our own Research Integrity and Research Publishing teams and anonymous and named external researchers and research integrity experts for contributing to this investigation.

The corresponding author, as the representative of all authors, has been given the opportunity to register their agreement or disagreement to this retraction. We have kept a record of any response received.

References

[1] W. Almutiry, "Inverted Length-Biased Exponential Model: Statistical Inference and Modeling," *Journal of Mathematics*, vol. 2021, Article ID 1980480, 8 pages, 2021.

Hindawi
Journal of Mathematics
Volume 2024, Article ID 9791379, 1 page
https://doi.org/10.1155/2024/9791379

Retraction

Retracted: Research on Clothing Image Database Retrieval Algorithm Based on Wavelet Transform

Journal of Mathematics

Received 23 January 2024; Accepted 23 January 2024; Published 24 January 2024

This article has been retracted by Hindawi following an investigation undertaken by the publisher [1]. This investigation has uncovered evidence of one or more of the following indicators of systematic manipulation of the publication process:

(1) Discrepancies in scope

(2) Discrepancies in the description of the research reported

(3) Discrepancies between the availability of data and the research described

(4) Inappropriate citations

(5) Incoherent, meaningless and/or irrelevant content included in the article

(6) Manipulated or compromised peer review

The presence of these indicators undermines our confidence in the integrity of the article's content and we cannot, therefore, vouch for its reliability. Please note that this notice is intended solely to alert readers that the content of this article is unreliable. We have not investigated whether authors were aware of or involved in the systematic manipulation of the publication process.

Wiley and Hindawi regrets that the usual quality checks did not identify these issues before publication and have since put additional measures in place to safeguard research integrity.

We wish to credit our own Research Integrity and Research Publishing teams and anonymous and named external researchers and research integrity experts for contributing to this investigation.

The corresponding author, as the representative of all authors, has been given the opportunity to register their agreement or disagreement to this retraction. We have kept a record of any response received.

References

[1] X. Cui, "Research on Clothing Image Database Retrieval Algorithm Based on Wavelet Transform," *Journal of Mathematics*, vol. 2022, Article ID 6332592, 8 pages, 2022.

Hindawi
Journal of Mathematics
Volume 2024, Article ID 9791314, 1 page
https://doi.org/10.1155/2024/9791314

Retraction

Retracted: Research on Sports Training Action Image Recognition Based on SDN

Journal of Mathematics

Received 23 January 2024; Accepted 23 January 2024; Published 24 January 2024

This article has been retracted by Hindawi following an investigation undertaken by the publisher [1]. This investigation has uncovered evidence of one or more of the following indicators of systematic manipulation of the publication process:

(1) Discrepancies in scope

(2) Discrepancies in the description of the research reported

(3) Discrepancies between the availability of data and the research described

(4) Inappropriate citations

(5) Incoherent, meaningless and/or irrelevant content included in the article

(6) Manipulated or compromised peer review

The presence of these indicators undermines our confidence in the integrity of the article's content and we cannot, therefore, vouch for its reliability. Please note that this notice is intended solely to alert readers that the content of this article is unreliable. We have not investigated whether authors were aware of or involved in the systematic manipulation of the publication process.

In addition, our investigation has also shown that one or more of the following human-subject reporting requirements has not been met in this article: ethical approval by an Institutional Review Board (IRB) committee or equivalent, patient/participant consent to participate, and/or agreement to publish patient/participant details (where relevant).

Wiley and Hindawi regrets that the usual quality checks did not identify these issues before publication and have since put additional measures in place to safeguard research integrity.

We wish to credit our own Research Integrity and Research Publishing teams and anonymous and named external researchers and research integrity experts for contributing to this investigation.

The corresponding author, as the representative of all authors, has been given the opportunity to register their agreement or disagreement to this retraction. We have kept a record of any response received.

References

[1] D. Wang and L. Shen, "Research on Sports Training Action Image Recognition Based on SDN," *Journal of Mathematics*, vol. 2022, Article ID 3668647, 10 pages, 2022.

Hindawi
Journal of Mathematics
Volume 2024, Article ID 9789075, 1 page
https://doi.org/10.1155/2024/9789075

Retraction

Retracted: Model Value of Taiji Curve Algorithm in Economic Geographic and Natural Game Management Information System

Journal of Mathematics

Received 23 January 2024; Accepted 23 January 2024; Published 24 January 2024

This article has been retracted by Hindawi following an investigation undertaken by the publisher [1]. This investigation has uncovered evidence of one or more of the following indicators of systematic manipulation of the publication process:

(1) Discrepancies in scope

(2) Discrepancies in the description of the research reported

(3) Discrepancies between the availability of data and the research described

(4) Inappropriate citations

(5) Incoherent, meaningless and/or irrelevant content included in the article

(6) Manipulated or compromised peer review

The presence of these indicators undermines our confidence in the integrity of the article's content and we cannot, therefore, vouch for its reliability. Please note that this notice is intended solely to alert readers that the content of this article is unreliable. We have not investigated whether authors were aware of or involved in the systematic manipulation of the publication process.

Wiley and Hindawi regrets that the usual quality checks did not identify these issues before publication and have since put additional measures in place to safeguard research integrity.

We wish to credit our own Research Integrity and Research Publishing teams and anonymous and named external researchers and research integrity experts for contributing to this investigation.

The corresponding author, as the representative of all authors, has been given the opportunity to register their agreement or disagreement to this retraction. We have kept a record of any response received.

References

[1] C. Xu and K. Chen, "Model Value of Taiji Curve Algorithm in Economic Geographic and Natural Game Management Information System," *Journal of Mathematics*, vol. 2022, Article ID 8526428, 6 pages, 2022.

Hindawi
Journal of Mathematics
Volume 2024, Article ID 9785015, 1 page
https://doi.org/10.1155/2024/9785015

Retraction

Retracted: Research on the Application of Genetic Algorithm in Physical Education

Journal of Mathematics

Received 23 January 2024; Accepted 23 January 2024; Published 24 January 2024

This article has been retracted by Hindawi following an investigation undertaken by the publisher [1]. This investigation has uncovered evidence of one or more of the following indicators of systematic manipulation of the publication process:

(1) Discrepancies in scope

(2) Discrepancies in the description of the research reported

(3) Discrepancies between the availability of data and the research described

(4) Inappropriate citations

(5) Incoherent, meaningless and/or irrelevant content included in the article

(6) Manipulated or compromised peer review

The presence of these indicators undermines our confidence in the integrity of the article's content and we cannot, therefore, vouch for its reliability. Please note that this notice is intended solely to alert readers that the content of this article is unreliable. We have not investigated whether authors were aware of or involved in the systematic manipulation of the publication process.

Wiley and Hindawi regrets that the usual quality checks did not identify these issues before publication and have since put additional measures in place to safeguard research integrity.

We wish to credit our own Research Integrity and Research Publishing teams and anonymous and named external researchers and research integrity experts for contributing to this investigation.

The corresponding author, as the representative of all authors, has been given the opportunity to register their agreement or disagreement to this retraction. We have kept a record of any response received.

References

[1] H. Wang, "Research on the Application of Genetic Algorithm in Physical Education," *Journal of Mathematics*, vol. 2022, Article ID 8477945, 8 pages, 2022.

Hindawi
Journal of Mathematics
Volume 2024, Article ID 9783245, 1 page
https://doi.org/10.1155/2024/9783245

Retraction

Retracted: Multidimensional State Data Reduction and Evaluation of College Students' Mental Health Based on SVM

Journal of Mathematics

Received 23 January 2024; Accepted 23 January 2024; Published 24 January 2024

This article has been retracted by Hindawi following an investigation undertaken by the publisher [1]. This investigation has uncovered evidence of one or more of the following indicators of systematic manipulation of the publication process:

(1) Discrepancies in scope

(2) Discrepancies in the description of the research reported

(3) Discrepancies between the availability of data and the research described

(4) Inappropriate citations

(5) Incoherent, meaningless and/or irrelevant content included in the article

(6) Manipulated or compromised peer review

The presence of these indicators undermines our confidence in the integrity of the article's content and we cannot, therefore, vouch for its reliability. Please note that this notice is intended solely to alert readers that the content of this article is unreliable. We have not investigated whether authors were aware of or involved in the systematic manipulation of the publication process.

Wiley and Hindawi regrets that the usual quality checks did not identify these issues before publication and have since put additional measures in place to safeguard research integrity.

We wish to credit our own Research Integrity and Research Publishing teams and anonymous and named external researchers and research integrity experts for contributing to this investigation.

The corresponding author, as the representative of all authors, has been given the opportunity to register their agreement or disagreement to this retraction. We have kept a record of any response received.

References

[1] H. Peiqing, "Multidimensional State Data Reduction and Evaluation of College Students' Mental Health Based on SVM," *Journal of Mathematics*, vol. 2022, Article ID 4961203, 11 pages, 2022.

Hindawi
Journal of Mathematics
Volume 2024, Article ID 9782652, 1 page
https://doi.org/10.1155/2024/9782652

Retraction

Retracted: EM Algorithm for Estimating the Parameters of Quasi-Lindley Model with Application

Journal of Mathematics

Received 23 January 2024; Accepted 23 January 2024; Published 24 January 2024

This article has been retracted by Hindawi following an investigation undertaken by the publisher [1]. This investigation has uncovered evidence of one or more of the following indicators of systematic manipulation of the publication process:

(1) Discrepancies in scope

(2) Discrepancies in the description of the research reported

(3) Discrepancies between the availability of data and the research described

(4) Inappropriate citations

(5) Incoherent, meaningless and/or irrelevant content included in the article

(6) Manipulated or compromised peer review

The presence of these indicators undermines our confidence in the integrity of the article's content and we cannot, therefore, vouch for its reliability. Please note that this notice is intended solely to alert readers that the content of this article is unreliable. We have not investigated whether authors were aware of or involved in the systematic manipulation of the publication process.

Wiley and Hindawi regrets that the usual quality checks did not identify these issues before publication and have since put additional measures in place to safeguard research integrity.

We wish to credit our own Research Integrity and Research Publishing teams and anonymous and named external researchers and research integrity experts for contributing to this investigation.

The corresponding author, as the representative of all authors, has been given the opportunity to register their agreement or disagreement to this retraction. We have kept a record of any response received.

References

[1] M. Kayid and N. S. Al-Maflehi, "EM Algorithm for Estimating the Parameters of Quasi-Lindley Model with Application," *Journal of Mathematics*, vol. 2022, Article ID 8467291, 9 pages, 2022.

Hindawi
Journal of Mathematics
Volume 2024, Article ID 9782496, 1 page
https://doi.org/10.1155/2024/9782496

Retraction

Retracted: Research on Fast Compensation Algorithm for Interframe Motion of Multimedia Video Based on Manhattan Distance

Journal of Mathematics

Received 23 January 2024; Accepted 23 January 2024; Published 24 January 2024

This article has been retracted by Hindawi following an investigation undertaken by the publisher [1]. This investigation has uncovered evidence of one or more of the following indicators of systematic manipulation of the publication process:

(1) Discrepancies in scope

(2) Discrepancies in the description of the research reported

(3) Discrepancies between the availability of data and the research described

(4) Inappropriate citations

(5) Incoherent, meaningless and/or irrelevant content included in the article

(6) Manipulated or compromised peer review

The presence of these indicators undermines our confidence in the integrity of the article's content and we cannot, therefore, vouch for its reliability. Please note that this notice is intended solely to alert readers that the content of this article is unreliable. We have not investigated whether authors were aware of or involved in the systematic manipulation of the publication process.

Wiley and Hindawi regrets that the usual quality checks did not identify these issues before publication and have since put additional measures in place to safeguard research integrity.

We wish to credit our own Research Integrity and Research Publishing teams and anonymous and named external researchers and research integrity experts for contributing to this investigation.

The corresponding author, as the representative of all authors, has been given the opportunity to register their agreement or disagreement to this retraction. We have kept a record of any response received.

References

[1] N. Li and S. Wan, "Research on Fast Compensation Algorithm for Interframe Motion of Multimedia Video Based on Manhattan Distance," *Journal of Mathematics*, vol. 2022, Article ID 3468475, 10 pages, 2022.

Hindawi
Journal of Mathematics
Volume 2024, Article ID 9769621, 1 page
https://doi.org/10.1155/2024/9769621

Retraction

Retracted: Construction and Analysis of Urban Motor Vehicle Drivers' Traffic Literacy Evaluation Model Based on Zhengzhou City's Survey Data

Journal of Mathematics

Received 23 January 2024; Accepted 23 January 2024; Published 24 January 2024

This article has been retracted by Hindawi following an investigation undertaken by the publisher [1]. This investigation has uncovered evidence of one or more of the following indicators of systematic manipulation of the publication process:

(1) Discrepancies in scope

(2) Discrepancies in the description of the research reported

(3) Discrepancies between the availability of data and the research described

(4) Inappropriate citations

(5) Incoherent, meaningless and/or irrelevant content included in the article

(6) Manipulated or compromised peer review

The presence of these indicators undermines our confidence in the integrity of the article's content and we cannot, therefore, vouch for its reliability. Please note that this notice is intended solely to alert readers that the content of this article is unreliable. We have not investigated whether authors were aware of or involved in the systematic manipulation of the publication process.

In addition, our investigation has also shown that one or more of the following human-subject reporting requirements has not been met in this article: ethical approval by an Institutional Review Board (IRB) committee or equivalent, patient/participant consent to participate, and/or agreement to publish patient/participant details (where relevant).

Wiley and Hindawi regrets that the usual quality checks did not identify these issues before publication and have since put additional measures in place to safeguard research integrity.

We wish to credit our own Research Integrity and Research Publishing teams and anonymous and named external researchers and research integrity experts for contributing to this investigation.

The corresponding author, as the representative of all authors, has been given the opportunity to register their agreement or disagreement to this retraction. We have kept a record of any response received.

References

[1] L. Shengyang, W. Yanrong, T. Kang, and H. Fangzheng, "Construction and Analysis of Urban Motor Vehicle Drivers' Traffic Literacy Evaluation Model Based on Zhengzhou City's Survey Data," *Journal of Mathematics*, vol. 2022, Article ID 2366458, 9 pages, 2022.

Hindawi
Journal of Mathematics
Volume 2024, Article ID 9767958, 1 page
https://doi.org/10.1155/2024/9767958

Retraction

Retracted: An Effective Approach for Modular Community Detection in Bipartite Network Based on Integrating Rider with Harris Hawks Optimization Algorithms

Journal of Mathematics

Received 23 January 2024; Accepted 23 January 2024; Published 24 January 2024

This article has been retracted by Hindawi following an investigation undertaken by the publisher [1]. This investigation has uncovered evidence of one or more of the following indicators of systematic manipulation of the publication process:

(1) Discrepancies in scope

(2) Discrepancies in the description of the research reported

(3) Discrepancies between the availability of data and the research described

(4) Inappropriate citations

(5) Incoherent, meaningless and/or irrelevant content included in the article

(6) Manipulated or compromised peer review

The presence of these indicators undermines our confidence in the integrity of the article's content and we cannot, therefore, vouch for its reliability. Please note that this notice is intended solely to alert readers that the content of this article is unreliable. We have not investigated whether authors were aware of or involved in the systematic manipulation of the publication process.

Wiley and Hindawi regrets that the usual quality checks did not identify these issues before publication and have since put additional measures in place to safeguard research integrity.

We wish to credit our own Research Integrity and Research Publishing teams and anonymous and named external researchers and research integrity experts for contributing to this investigation.

The corresponding author, as the representative of all authors, has been given the opportunity to register their agreement or disagreement to this retraction. We have kept a record of any response received.

References

[1] B. Fahad Alkhamees, M. A. A. Mosleh, H. AlSalman, and M. Azeem Akbar, "An Effective Approach for Modular Community Detection in Bipartite Network Based on Integrating Rider with Harris Hawks Optimization Algorithms," *Journal of Mathematics*, vol. 2021, Article ID 9511425, 16 pages, 2021.

Hindawi
Journal of Mathematics
Volume 2024, Article ID 9761318, 1 page
https://doi.org/10.1155/2024/9761318

Retraction

Retracted: Research on the Prediction of Port Economic Synergy Development Trend Based on Deep Neural Networks

Journal of Mathematics

Received 23 January 2024; Accepted 23 January 2024; Published 24 January 2024

This article has been retracted by Hindawi following an investigation undertaken by the publisher [1]. This investigation has uncovered evidence of one or more of the following indicators of systematic manipulation of the publication process:

(1) Discrepancies in scope

(2) Discrepancies in the description of the research reported

(3) Discrepancies between the availability of data and the research described

(4) Inappropriate citations

(5) Incoherent, meaningless and/or irrelevant content included in the article

(6) Manipulated or compromised peer review

The presence of these indicators undermines our confidence in the integrity of the article's content and we cannot, therefore, vouch for its reliability. Please note that this notice is intended solely to alert readers that the content of this article is unreliable. We have not investigated whether authors were aware of or involved in the systematic manipulation of the publication process.

Wiley and Hindawi regrets that the usual quality checks did not identify these issues before publication and have since put additional measures in place to safeguard research integrity.

We wish to credit our own Research Integrity and Research Publishing teams and anonymous and named external researchers and research integrity experts for contributing to this investigation.

The corresponding author, as the representative of all authors, has been given the opportunity to register their agreement or disagreement to this retraction. We have kept a record of any response received.

References

[1] A. Zha and J. Tu, "Research on the Prediction of Port Economic Synergy Development Trend Based on Deep Neural Networks," *Journal of Mathematics*, vol. 2022, Article ID 8052957, 9 pages, 2022.

Hindawi
Journal of Mathematics
Volume 2023, Article ID 9895762, 1 page
https://doi.org/10.1155/2023/9895762

Retraction

Retracted: Path Optimization of Enterprise Network Innovation Performance Management Based on Deep Learning and Internet of Things

Journal of Mathematics

Received 19 December 2023; Accepted 19 December 2023; Published 20 December 2023

This article has been retracted by Hindawi following an investigation undertaken by the publisher [1]. This investigation has uncovered evidence of one or more of the following indicators of systematic manipulation of the publication process:

(1) Discrepancies in scope

(2) Discrepancies in the description of the research reported

(3) Discrepancies between the availability of data and the research described

(4) Inappropriate citations

(5) Incoherent, meaningless and/or irrelevant content included in the article

(6) Manipulated or compromised peer review

The presence of these indicators undermines our confidence in the integrity of the article's content and we cannot, therefore, vouch for its reliability. Please note that this notice is intended solely to alert readers that the content of this article is unreliable. We have not investigated whether authors were aware of or involved in the systematic manipulation of the publication process.

Wiley and Hindawi regrets that the usual quality checks did not identify these issues before publication and have since put additional measures in place to safeguard research integrity.

We wish to credit our own Research Integrity and Research Publishing teams and anonymous and named external researchers and research integrity experts for contributing to this investigation.

The corresponding author, as the representative of all authors, has been given the opportunity to register their agreement or disagreement to this retraction. We have kept a record of any response received.

References

[1] P. Xiong, "Path Optimization of Enterprise Network Innovation Performance Management Based on Deep Learning and Internet of Things," *Journal of Mathematics*, vol. 2022, Article ID 4932439, 10 pages, 2022.

Hindawi
Journal of Mathematics
Volume 2023, Article ID 9895324, 1 page
https://doi.org/10.1155/2023/9895324

Retraction

Retracted: Preorder of Factors Affecting Oil Prices: Fuzzy PROMETHEE Approach

Journal of Mathematics

Received 19 December 2023; Accepted 19 December 2023; Published 20 December 2023

This article has been retracted by Hindawi following an investigation undertaken by the publisher [1]. This investigation has uncovered evidence of one or more of the following indicators of systematic manipulation of the publication process:

(1) Discrepancies in scope

(2) Discrepancies in the description of the research reported

(3) Discrepancies between the availability of data and the research described

(4) Inappropriate citations

(5) Incoherent, meaningless and/or irrelevant content included in the article

(6) Manipulated or compromised peer review

The presence of these indicators undermines our confidence in the integrity of the article's content and we cannot, therefore, vouch for its reliability. Please note that this notice is intended solely to alert readers that the content of this article is unreliable. We have not investigated whether authors were aware of or involved in the systematic manipulation of the publication process.

Wiley and Hindawi regrets that the usual quality checks did not identify these issues before publication and have since put additional measures in place to safeguard research integrity.

We wish to credit our own Research Integrity and Research Publishing teams and anonymous and named external researchers and research integrity experts for contributing to this investigation.

The corresponding author, as the representative of all authors, has been given the opportunity to register their agreement or disagreement to this retraction. We have kept a record of any response received.

References

[1] L. Abdullah, N. Harun, S. M. Mahali, N. Jan, and E. Rak, "Preorder of Factors Affecting Oil Prices: Fuzzy PROMETHEE Approach," *Journal of Mathematics*, vol. 2022, Article ID 2766945, 15 pages, 2022.

Hindawi
Journal of Mathematics
Volume 2023, Article ID 9894560, 1 page
https://doi.org/10.1155/2023/9894560

Retraction

Retracted: Text Knowledge Acquisition Method of Collaborative Product Design Based on Genetic Algorithm

Journal of Mathematics

Received 19 December 2023; Accepted 19 December 2023; Published 20 December 2023

This article has been retracted by Hindawi following an investigation undertaken by the publisher [1]. This investigation has uncovered evidence of one or more of the following indicators of systematic manipulation of the publication process:

(1) Discrepancies in scope

(2) Discrepancies in the description of the research reported

(3) Discrepancies between the availability of data and the research described

(4) Inappropriate citations

(5) Incoherent, meaningless and/or irrelevant content included in the article

(6) Manipulated or compromised peer review

The presence of these indicators undermines our confidence in the integrity of the article's content and we cannot, therefore, vouch for its reliability. Please note that this notice is intended solely to alert readers that the content of this article is unreliable. We have not investigated whether authors were aware of or involved in the systematic manipulation of the publication process.

Wiley and Hindawi regrets that the usual quality checks did not identify these issues before publication and have since put additional measures in place to safeguard research integrity.

We wish to credit our own Research Integrity and Research Publishing teams and anonymous and named external researchers and research integrity experts for contributing to this investigation.

The corresponding author, as the representative of all authors, has been given the opportunity to register their agreement or disagreement to this retraction. We have kept a record of any response received.

References

[1] C. Li and M. Yang, "Text Knowledge Acquisition Method of Collaborative Product Design Based on Genetic Algorithm," *Journal of Mathematics*, vol. 2022, Article ID 3661477, 9 pages, 2022.

Hindawi
Journal of Mathematics
Volume 2023, Article ID 9893016, 1 page
https://doi.org/10.1155/2023/9893016

Retraction

Retracted: Design of Intelligent Recognition English Translation Model Based on Deep Learning

Journal of Mathematics

Received 19 December 2023; Accepted 19 December 2023; Published 20 December 2023

This article has been retracted by Hindawi following an investigation undertaken by the publisher [1]. This investigation has uncovered evidence of one or more of the following indicators of systematic manipulation of the publication process:

(1) Discrepancies in scope

(2) Discrepancies in the description of the research reported

(3) Discrepancies between the availability of data and the research described

(4) Inappropriate citations

(5) Incoherent, meaningless and/or irrelevant content included in the article

(6) Manipulated or compromised peer review

The presence of these indicators undermines our confidence in the integrity of the article's content and we cannot, therefore, vouch for its reliability. Please note that this notice is intended solely to alert readers that the content of this article is unreliable. We have not investigated whether authors were aware of or involved in the systematic manipulation of the publication process.

Wiley and Hindawi regrets that the usual quality checks did not identify these issues before publication and have since put additional measures in place to safeguard research integrity.

We wish to credit our own Research Integrity and Research Publishing teams and anonymous and named external researchers and research integrity experts for contributing to this investigation.

The corresponding author, as the representative of all authors, has been given the opportunity to register their agreement or disagreement to this retraction. We have kept a record of any response received.

References

[1] Y. Ruan, "Design of Intelligent Recognition English Translation Model Based on Deep Learning," *Journal of Mathematics*, vol. 2022, Article ID 5029770, 10 pages, 2022.

Hindawi
Journal of Mathematics
Volume 2023, Article ID 9892024, 1 page
https://doi.org/10.1155/2023/9892024

Retraction

Retracted: Evaluation Algorithm of Labor Legal Effectiveness for Affirmative Action against Gender Discrimination

Journal of Mathematics

Received 19 December 2023; Accepted 19 December 2023; Published 20 December 2023

This article has been retracted by Hindawi following an investigation undertaken by the publisher [1]. This investigation has uncovered evidence of one or more of the following indicators of systematic manipulation of the publication process:

(1) Discrepancies in scope

(2) Discrepancies in the description of the research reported

(3) Discrepancies between the availability of data and the research described

(4) Inappropriate citations

(5) Incoherent, meaningless and/or irrelevant content included in the article

(6) Manipulated or compromised peer review

The presence of these indicators undermines our confidence in the integrity of the article's content and we cannot, therefore, vouch for its reliability. Please note that this notice is intended solely to alert readers that the content of this article is unreliable. We have not investigated whether authors were aware of or involved in the systematic manipulation of the publication process.

Wiley and Hindawi regrets that the usual quality checks did not identify these issues before publication and have since put additional measures in place to safeguard research integrity.

We wish to credit our own Research Integrity and Research Publishing teams and anonymous and named external researchers and research integrity experts for contributing to this investigation.

The corresponding author, as the representative of all authors, has been given the opportunity to register their agreement or disagreement to this retraction. We have kept a record of any response received.

References

[1] L. Juan, "Evaluation Algorithm of Labor Legal Effectiveness for Affirmative Action against Gender Discrimination," *Journal of Mathematics*, vol. 2022, Article ID 4073208, 9 pages, 2022.

Hindawi
Journal of Mathematics
Volume 2023, Article ID 9891376, 1 page
https://doi.org/10.1155/2023/9891376

Retraction

Retracted: Popular Song Composition Based on Deep Learning and Neural Network

Journal of Mathematics

Received 19 December 2023; Accepted 19 December 2023; Published 20 December 2023

This article has been retracted by Hindawi following an investigation undertaken by the publisher [1]. This investigation has uncovered evidence of one or more of the following indicators of systematic manipulation of the publication process:

(1) Discrepancies in scope

(2) Discrepancies in the description of the research reported

(3) Discrepancies between the availability of data and the research described

(4) Inappropriate citations

(5) Incoherent, meaningless and/or irrelevant content included in the article

(6) Manipulated or compromised peer review

The presence of these indicators undermines our confidence in the integrity of the article's content and we cannot, therefore, vouch for its reliability. Please note that this notice is intended solely to alert readers that the content of this article is unreliable. We have not investigated whether authors were aware of or involved in the systematic manipulation of the publication process.

Wiley and Hindawi regrets that the usual quality checks did not identify these issues before publication and have since put additional measures in place to safeguard research integrity.

We wish to credit our own Research Integrity and Research Publishing teams and anonymous and named external researchers and research integrity experts for contributing to this investigation.

The corresponding author, as the representative of all authors, has been given the opportunity to register their agreement or disagreement to this retraction. We have kept a record of any response received.

References

[1] J. Kuang and T. Yang, "Popular Song Composition Based on Deep Learning and Neural Network," *Journal of Mathematics*, vol. 2021, Article ID 7164817, 7 pages, 2021.

Hindawi
Journal of Mathematics
Volume 2023, Article ID 9878209, 1 page
https://doi.org/10.1155/2023/9878209

Retraction

Retracted: Research on the Spread Path and Evolution Causes of Oral Language in the Digital Era

Journal of Mathematics

Received 19 December 2023; Accepted 19 December 2023; Published 20 December 2023

This article has been retracted by Hindawi following an investigation undertaken by the publisher [1]. This investigation has uncovered evidence of one or more of the following indicators of systematic manipulation of the publication process:

(1) Discrepancies in scope

(2) Discrepancies in the description of the research reported

(3) Discrepancies between the availability of data and the research described

(4) Inappropriate citations

(5) Incoherent, meaningless and/or irrelevant content included in the article

(6) Manipulated or compromised peer review

The presence of these indicators undermines our confidence in the integrity of the article's content and we cannot, therefore, vouch for its reliability. Please note that this notice is intended solely to alert readers that the content of this article is unreliable. We have not investigated whether authors were aware of or involved in the systematic manipulation of the publication process.

Wiley and Hindawi regrets that the usual quality checks did not identify these issues before publication and have since put additional measures in place to safeguard research integrity.

We wish to credit our own Research Integrity and Research Publishing teams and anonymous and named external researchers and research integrity experts for contributing to this investigation.

The corresponding author, as the representative of all authors, has been given the opportunity to register their agreement or disagreement to this retraction. We have kept a record of any response received.

References

[1] Z. Li, "Research on the Spread Path and Evolution Causes of Oral Language in the Digital Era," *Journal of Mathematics*, vol. 2022, Article ID 2325711, 9 pages, 2022.

Hindawi
Journal of Mathematics
Volume 2023, Article ID 9876921, 1 page
https://doi.org/10.1155/2023/9876921

Retraction

Retracted: Design of Enterprise Economic Information Management System Based on Big Data Integration Algorithm

Journal of Mathematics

Received 19 December 2023; Accepted 19 December 2023; Published 20 December 2023

This article has been retracted by Hindawi following an investigation undertaken by the publisher [1]. This investigation has uncovered evidence of one or more of the following indicators of systematic manipulation of the publication process:

(1) Discrepancies in scope

(2) Discrepancies in the description of the research reported

(3) Discrepancies between the availability of data and the research described

(4) Inappropriate citations

(5) Incoherent, meaningless and/or irrelevant content included in the article

(6) Manipulated or compromised peer review

The presence of these indicators undermines our confidence in the integrity of the article's content and we cannot, therefore, vouch for its reliability. Please note that this notice is intended solely to alert readers that the content of this article is unreliable. We have not investigated whether authors were aware of or involved in the systematic manipulation of the publication process.

Wiley and Hindawi regrets that the usual quality checks did not identify these issues before publication and have since put additional measures in place to safeguard research integrity.

We wish to credit our own Research Integrity and Research Publishing teams and anonymous and named external researchers and research integrity experts for contributing to this investigation.

The corresponding author, as the representative of all authors, has been given the opportunity to register their agreement or disagreement to this retraction. We have kept a record of any response received.

References

[1] X. Liu, "Design of Enterprise Economic Information Management System Based on Big Data Integration Algorithm," *Journal of Mathematics*, vol. 2022, Article ID 3257748, 9 pages, 2022.

Hindawi
Journal of Mathematics
Volume 2023, Article ID 9861405, 1 page
https://doi.org/10.1155/2023/9861405

Retraction

Retracted: Intelligent Recommendation Algorithm of Multimedia English Distance Education Resources Based on User Model

Journal of Mathematics

Received 19 December 2023; Accepted 19 December 2023; Published 20 December 2023

This article has been retracted by Hindawi following an investigation undertaken by the publisher [1]. This investigation has uncovered evidence of one or more of the following indicators of systematic manipulation of the publication process:

(1) Discrepancies in scope

(2) Discrepancies in the description of the research reported

(3) Discrepancies between the availability of data and the research described

(4) Inappropriate citations

(5) Incoherent, meaningless and/or irrelevant content included in the article

(6) Manipulated or compromised peer review

The presence of these indicators undermines our confidence in the integrity of the article's content and we cannot, therefore, vouch for its reliability. Please note that this notice is intended solely to alert readers that the content of this article is unreliable. We have not investigated whether authors were aware of or involved in the systematic manipulation of the publication process.

Wiley and Hindawi regrets that the usual quality checks did not identify these issues before publication and have since put additional measures in place to safeguard research integrity.

We wish to credit our own Research Integrity and Research Publishing teams and anonymous and named external researchers and research integrity experts for contributing to this investigation.

The corresponding author, as the representative of all authors, has been given the opportunity to register their agreement or disagreement to this retraction. We have kept a record of any response received.

References

[1] X. Zhang, "Intelligent Recommendation Algorithm of Multimedia English Distance Education Resources Based on User Model," *Journal of Mathematics*, vol. 2022, Article ID 2012700, 8 pages, 2022.

Hindawi
Journal of Mathematics
Volume 2023, Article ID 9861253, 1 page
https://doi.org/10.1155/2023/9861253

Retraction

Retracted: Film and Television Animation Sensing and Visual Image by Computer Digital Image Technology

Journal of Mathematics

Received 19 December 2023; Accepted 19 December 2023; Published 20 December 2023

This article has been retracted by Hindawi following an investigation undertaken by the publisher [1]. This investigation has uncovered evidence of one or more of the following indicators of systematic manipulation of the publication process:

(1) Discrepancies in scope

(2) Discrepancies in the description of the research reported

(3) Discrepancies between the availability of data and the research described

(4) Inappropriate citations

(5) Incoherent, meaningless and/or irrelevant content included in the article

(6) Manipulated or compromised peer review

The presence of these indicators undermines our confidence in the integrity of the article's content and we cannot, therefore, vouch for its reliability. Please note that this notice is intended solely to alert readers that the content of this article is unreliable. We have not investigated whether authors were aware of or involved in the systematic manipulation of the publication process.

Wiley and Hindawi regrets that the usual quality checks did not identify these issues before publication and have since put additional measures in place to safeguard research integrity.

We wish to credit our own Research Integrity and Research Publishing teams and anonymous and named external researchers and research integrity experts for contributing to this investigation.

The corresponding author, as the representative of all authors, has been given the opportunity to register their agreement or disagreement to this retraction. We have kept a record of any response received.

References

[1] L. Lian and T. Lei, "Film and Television Animation Sensing and Visual Image by Computer Digital Image Technology," *Journal of Mathematics*, vol. 2022, Article ID 6331233, 8 pages, 2022.

Hindawi
Journal of Mathematics
Volume 2023, Article ID 9858351, 1 page
https://doi.org/10.1155/2023/9858351

Retraction

Retracted: Optimization Algorithm of Logistics Transportation Cost of Prefabricated Building Components for Project Management

Journal of Mathematics

Received 19 December 2023; Accepted 19 December 2023; Published 20 December 2023

This article has been retracted by Hindawi following an investigation undertaken by the publisher [1]. This investigation has uncovered evidence of one or more of the following indicators of systematic manipulation of the publication process:

(1) Discrepancies in scope

(2) Discrepancies in the description of the research reported

(3) Discrepancies between the availability of data and the research described

(4) Inappropriate citations

(5) Incoherent, meaningless and/or irrelevant content included in the article

(6) Manipulated or compromised peer review

The presence of these indicators undermines our confidence in the integrity of the article's content and we cannot, therefore, vouch for its reliability. Please note that this notice is intended solely to alert readers that the content of this article is unreliable. We have not investigated whether authors were aware of or involved in the systematic manipulation of the publication process.

Wiley and Hindawi regrets that the usual quality checks did not identify these issues before publication and have since put additional measures in place to safeguard research integrity.

We wish to credit our own Research Integrity and Research Publishing teams and anonymous and named external researchers and research integrity experts for contributing to this investigation.

The corresponding author, as the representative of all authors, has been given the opportunity to register their agreement or disagreement to this retraction. We have kept a record of any response received.

References

[1] X. Yang, "Optimization Algorithm of Logistics Transportation Cost of Prefabricated Building Components for Project Management," *Journal of Mathematics*, vol. 2022, Article ID 1460335, 9 pages, 2022.

Hindawi
Journal of Mathematics
Volume 2023, Article ID 9852630, 1 page
https://doi.org/10.1155/2023/9852630

Retraction

Retracted: A New Algorithm for Extracting Winter Wheat Planting Area Based on Ownership Parcel Vector Data and Medium-Resolution Remote Sensing Images

Journal of Mathematics

Received 19 December 2023; Accepted 19 December 2023; Published 20 December 2023

This article has been retracted by Hindawi following an investigation undertaken by the publisher [1]. This investigation has uncovered evidence of one or more of the following indicators of systematic manipulation of the publication process:

(1) Discrepancies in scope

(2) Discrepancies in the description of the research reported

(3) Discrepancies between the availability of data and the research described

(4) Inappropriate citations

(5) Incoherent, meaningless and/or irrelevant content included in the article

(6) Manipulated or compromised peer review

The presence of these indicators undermines our confidence in the integrity of the article's content and we cannot, therefore, vouch for its reliability. Please note that this notice is intended solely to alert readers that the content of this article is unreliable. We have not investigated whether authors were aware of or involved in the systematic manipulation of the publication process.

Wiley and Hindawi regrets that the usual quality checks did not identify these issues before publication and have since put additional measures in place to safeguard research integrity.

We wish to credit our own Research Integrity and Research Publishing teams and anonymous and named external researchers and research integrity experts for contributing to this investigation.

The corresponding author, as the representative of all authors, has been given the opportunity to register their agreement or disagreement to this retraction. We have kept a record of any response received.

References

[1] H. Xie, Q. Wu, T. Zhang et al., "A New Algorithm for Extracting Winter Wheat Planting Area Based on Ownership Parcel Vector Data and Medium-Resolution Remote Sensing Images," *Journal of Mathematics*, vol. 2021, Article ID 1860160, 16 pages, 2021.

Hindawi
Journal of Mathematics
Volume 2023, Article ID 9851417, 1 page
https://doi.org/10.1155/2023/9851417

Retraction

Retracted: A New Rule-Based Approach for Classical Arabic in Natural Language Processing

Journal of Mathematics

Received 19 December 2023; Accepted 19 December 2023; Published 20 December 2023

This article has been retracted by Hindawi following an investigation undertaken by the publisher [1]. This investigation has uncovered evidence of one or more of the following indicators of systematic manipulation of the publication process:

(1) Discrepancies in scope

(2) Discrepancies in the description of the research reported

(3) Discrepancies between the availability of data and the research described

(4) Inappropriate citations

(5) Incoherent, meaningless and/or irrelevant content included in the article

(6) Manipulated or compromised peer review

The presence of these indicators undermines our confidence in the integrity of the article's content and we cannot, therefore, vouch for its reliability. Please note that this notice is intended solely to alert readers that the content of this article is unreliable. We have not investigated whether authors were aware of or involved in the systematic manipulation of the publication process.

Wiley and Hindawi regrets that the usual quality checks did not identify these issues before publication and have since put additional measures in place to safeguard research integrity.

We wish to credit our own Research Integrity and Research Publishing teams and anonymous and named external researchers and research integrity experts for contributing to this investigation.

The corresponding author, as the representative of all authors, has been given the opportunity to register their agreement or disagreement to this retraction. We have kept a record of any response received.

References

[1] R. Salah, M. Mukred, L. Qadri binti Zakaria, R. Ahmed, and H. Sari, "A New Rule-Based Approach for Classical Arabic in Natural Language Processing," *Journal of Mathematics*, vol. 2022, Article ID 7164254, 20 pages, 2022.

Hindawi
Journal of Mathematics
Volume 2023, Article ID 9848270, 1 page
https://doi.org/10.1155/2023/9848270

Retraction

Retracted: Virtual Reality-Based Digital Restoration Methods and Applications for Ancient Buildings

Journal of Mathematics

Received 19 December 2023; Accepted 19 December 2023; Published 20 December 2023

This article has been retracted by Hindawi following an investigation undertaken by the publisher [1]. This investigation has uncovered evidence of one or more of the following indicators of systematic manipulation of the publication process:

(1) Discrepancies in scope

(2) Discrepancies in the description of the research reported

(3) Discrepancies between the availability of data and the research described

(4) Inappropriate citations

(5) Incoherent, meaningless and/or irrelevant content included in the article

(6) Manipulated or compromised peer review

The presence of these indicators undermines our confidence in the integrity of the article's content and we cannot, therefore, vouch for its reliability. Please note that this notice is intended solely to alert readers that the content of this article is unreliable. We have not investigated whether authors were aware of or involved in the systematic manipulation of the publication process.

Wiley and Hindawi regrets that the usual quality checks did not identify these issues before publication and have since put additional measures in place to safeguard research integrity.

We wish to credit our own Research Integrity and Research Publishing teams and anonymous and named external researchers and research integrity experts for contributing to this investigation.

The corresponding author, as the representative of all authors, has been given the opportunity to register their agreement or disagreement to this retraction. We have kept a record of any response received.

References

[1] T. Wang and L. Zhao, "Virtual Reality-Based Digital Restoration Methods and Applications for Ancient Buildings," *Journal of Mathematics*, vol. 2022, Article ID 2305463, 10 pages, 2022.

Hindawi
Journal of Mathematics
Volume 2023, Article ID 9845696, 1 page
https://doi.org/10.1155/2023/9845696

Retraction

Retracted: Research on the Risk Measurement Algorithm of Supply Chain Order Financing Based on Insurance Actuarial

Journal of Mathematics

Received 19 December 2023; Accepted 19 December 2023; Published 20 December 2023

This article has been retracted by Hindawi following an investigation undertaken by the publisher [1]. This investigation has uncovered evidence of one or more of the following indicators of systematic manipulation of the publication process:

(1) Discrepancies in scope

(2) Discrepancies in the description of the research reported

(3) Discrepancies between the availability of data and the research described

(4) Inappropriate citations

(5) Incoherent, meaningless and/or irrelevant content included in the article

(6) Manipulated or compromised peer review

The presence of these indicators undermines our confidence in the integrity of the article's content and we cannot, therefore, vouch for its reliability. Please note that this notice is intended solely to alert readers that the content of this article is unreliable. We have not investigated whether authors were aware of or involved in the systematic manipulation of the publication process.

Wiley and Hindawi regrets that the usual quality checks did not identify these issues before publication and have since put additional measures in place to safeguard research integrity.

We wish to credit our own Research Integrity and Research Publishing teams and anonymous and named external researchers and research integrity experts for contributing to this investigation.

The corresponding author, as the representative of all authors, has been given the opportunity to register their agreement or disagreement to this retraction. We have kept a record of any response received.

References

[1] G. Li and M. Yin, "Research on the Risk Measurement Algorithm of Supply Chain Order Financing Based on Insurance Actuarial," *Journal of Mathematics*, vol. 2021, Article ID 5344205, 9 pages, 2021.

Hindawi
Journal of Mathematics
Volume 2023, Article ID 9842979, 1 page
https://doi.org/10.1155/2023/9842979

Retraction

Retracted: Classification and Analysis of College Students' Skills Using Hybrid AI Models

Journal of Mathematics

Received 19 December 2023; Accepted 19 December 2023; Published 20 December 2023

This article has been retracted by Hindawi following an investigation undertaken by the publisher [1]. This investigation has uncovered evidence of one or more of the following indicators of systematic manipulation of the publication process:

(1) Discrepancies in scope

(2) Discrepancies in the description of the research reported

(3) Discrepancies between the availability of data and the research described

(4) Inappropriate citations

(5) Incoherent, meaningless and/or irrelevant content included in the article

(6) Manipulated or compromised peer review

The presence of these indicators undermines our confidence in the integrity of the article's content and we cannot, therefore, vouch for its reliability. Please note that this notice is intended solely to alert readers that the content of this article is unreliable. We have not investigated whether authors were aware of or involved in the systematic manipulation of the publication process.

Wiley and Hindawi regrets that the usual quality checks did not identify these issues before publication and have since put additional measures in place to safeguard research integrity.

We wish to credit our own Research Integrity and Research Publishing teams and anonymous and named external researchers and research integrity experts for contributing to this investigation.

The corresponding author, as the representative of all authors, has been given the opportunity to register their agreement or disagreement to this retraction. We have kept a record of any response received.

References

[1] H. Tang and Y. Wei, "Classification and Analysis of College Students' Skills Using Hybrid AI Models," *Journal of Mathematics*, vol. 2022, Article ID 4428416, 10 pages, 2022.

Hindawi
Journal of Mathematics
Volume 2023, Article ID 9834715, 1 page
https://doi.org/10.1155/2023/9834715

Retraction

Retracted: Adaptive Enhancement Algorithm of High-Resolution Satellite Image Based on Feature Fusion

Journal of Mathematics

Received 19 December 2023; Accepted 19 December 2023; Published 20 December 2023

This article has been retracted by Hindawi following an investigation undertaken by the publisher [1]. This investigation has uncovered evidence of one or more of the following indicators of systematic manipulation of the publication process:

(1) Discrepancies in scope

(2) Discrepancies in the description of the research reported

(3) Discrepancies between the availability of data and the research described

(4) Inappropriate citations

(5) Incoherent, meaningless and/or irrelevant content included in the article

(6) Manipulated or compromised peer review

The presence of these indicators undermines our confidence in the integrity of the article's content and we cannot, therefore, vouch for its reliability. Please note that this notice is intended solely to alert readers that the content of this article is unreliable. We have not investigated whether authors were aware of or involved in the systematic manipulation of the publication process.

Wiley and Hindawi regrets that the usual quality checks did not identify these issues before publication and have since put additional measures in place to safeguard research integrity.

We wish to credit our own Research Integrity and Research Publishing teams and anonymous and named external researchers and research integrity experts for contributing to this investigation.

The corresponding author, as the representative of all authors, has been given the opportunity to register their agreement or disagreement to this retraction. We have kept a record of any response received.

References

[1] R. Wang and W. Xiao, "Adaptive Enhancement Algorithm of High-Resolution Satellite Image Based on Feature Fusion," *Journal of Mathematics*, vol. 2022, Article ID 1029247, 9 pages, 2022.

Hindawi
Journal of Mathematics
Volume 2023, Article ID 9831759, 1 page
https://doi.org/10.1155/2023/9831759

Retraction

Retracted: Deep Learning-Based Economic Forecasting for the New Energy Vehicle Industry

Journal of Mathematics

Received 19 December 2023; Accepted 19 December 2023; Published 20 December 2023

This article has been retracted by Hindawi following an investigation undertaken by the publisher [1]. This investigation has uncovered evidence of one or more of the following indicators of systematic manipulation of the publication process:

(1) Discrepancies in scope

(2) Discrepancies in the description of the research reported

(3) Discrepancies between the availability of data and the research described

(4) Inappropriate citations

(5) Incoherent, meaningless and/or irrelevant content included in the article

(6) Manipulated or compromised peer review

The presence of these indicators undermines our confidence in the integrity of the article's content and we cannot, therefore, vouch for its reliability. Please note that this notice is intended solely to alert readers that the content of this article is unreliable. We have not investigated whether authors were aware of or involved in the systematic manipulation of the publication process.

Wiley and Hindawi regrets that the usual quality checks did not identify these issues before publication and have since put additional measures in place to safeguard research integrity.

We wish to credit our own Research Integrity and Research Publishing teams and anonymous and named external researchers and research integrity experts for contributing to this investigation.

The corresponding author, as the representative of all authors, has been given the opportunity to register their agreement or disagreement to this retraction. We have kept a record of any response received.

References

[1] B. Cai, "Deep Learning-Based Economic Forecasting for the New Energy Vehicle Industry," *Journal of Mathematics*, vol. 2021, Article ID 3870657, 10 pages, 2021.

Hindawi
Journal of Mathematics
Volume 2023, Article ID 9830845, 1 page
https://doi.org/10.1155/2023/9830845

Retraction

Retracted: Music Emotion Research Based on Reinforcement Learning and Multimodal Information

Journal of Mathematics

Received 19 December 2023; Accepted 19 December 2023; Published 20 December 2023

This article has been retracted by Hindawi following an investigation undertaken by the publisher [1]. This investigation has uncovered evidence of one or more of the following indicators of systematic manipulation of the publication process:

(1) Discrepancies in scope

(2) Discrepancies in the description of the research reported

(3) Discrepancies between the availability of data and the research described

(4) Inappropriate citations

(5) Incoherent, meaningless and/or irrelevant content included in the article

(6) Manipulated or compromised peer review

The presence of these indicators undermines our confidence in the integrity of the article's content and we cannot, therefore, vouch for its reliability. Please note that this notice is intended solely to alert readers that the content of this article is unreliable. We have not investigated whether authors were aware of or involved in the systematic manipulation of the publication process.

Wiley and Hindawi regrets that the usual quality checks did not identify these issues before publication and have since put additional measures in place to safeguard research integrity.

We wish to credit our own Research Integrity and Research Publishing teams and anonymous and named external researchers and research integrity experts for contributing to this investigation.

The corresponding author, as the representative of all authors, has been given the opportunity to register their agreement or disagreement to this retraction. We have kept a record of any response received.

References

[1] Y. Hu, "Music Emotion Research Based on Reinforcement Learning and Multimodal Information," *Journal of Mathematics*, vol. 2022, Article ID 2446399, 9 pages, 2022.

Hindawi
Journal of Mathematics
Volume 2023, Article ID 9826741, 1 page
https://doi.org/10.1155/2023/9826741

Retraction

Retracted: Research on Multiparty Payment Technology Based on Blockchain and Smart Contract Mechanism

Journal of Mathematics

Received 19 December 2023; Accepted 19 December 2023; Published 20 December 2023

This article has been retracted by Hindawi following an investigation undertaken by the publisher [1]. This investigation has uncovered evidence of one or more of the following indicators of systematic manipulation of the publication process:

(1) Discrepancies in scope

(2) Discrepancies in the description of the research reported

(3) Discrepancies between the availability of data and the research described

(4) Inappropriate citations

(5) Incoherent, meaningless and/or irrelevant content included in the article

(6) Manipulated or compromised peer review

The presence of these indicators undermines our confidence in the integrity of the article's content and we cannot, therefore, vouch for its reliability. Please note that this notice is intended solely to alert readers that the content of this article is unreliable. We have not investigated whether authors were aware of or involved in the systematic manipulation of the publication process.

Wiley and Hindawi regrets that the usual quality checks did not identify these issues before publication and have since put additional measures in place to safeguard research integrity.

We wish to credit our own Research Integrity and Research Publishing teams and anonymous and named external researchers and research integrity experts for contributing to this investigation.

The corresponding author, as the representative of all authors, has been given the opportunity to register their agreement or disagreement to this retraction. We have kept a record of any response received.

References

[1] Y. Zhang, "Research on Multiparty Payment Technology Based on Blockchain and Smart Contract Mechanism," *Journal of Mathematics*, vol. 2022, Article ID 3434954, 14 pages, 2022.

Hindawi
Journal of Mathematics
Volume 2023, Article ID 9817457, 1 page
https://doi.org/10.1155/2023/9817457

Retraction

Retracted: An Artificial Intelligent Virtual Reality Interactive Model for Distance Education

Journal of Mathematics

Received 19 December 2023; Accepted 19 December 2023; Published 20 December 2023

This article has been retracted by Hindawi following an investigation undertaken by the publisher [1]. This investigation has uncovered evidence of one or more of the following indicators of systematic manipulation of the publication process:

(1) Discrepancies in scope

(2) Discrepancies in the description of the research reported

(3) Discrepancies between the availability of data and the research described

(4) Inappropriate citations

(5) Incoherent, meaningless and/or irrelevant content included in the article

(6) Manipulated or compromised peer review

The presence of these indicators undermines our confidence in the integrity of the article's content and we cannot, therefore, vouch for its reliability. Please note that this notice is intended solely to alert readers that the content of this article is unreliable. We have not investigated whether authors were aware of or involved in the systematic manipulation of the publication process.

Wiley and Hindawi regrets that the usual quality checks did not identify these issues before publication and have since put additional measures in place to safeguard research integrity.

We wish to credit our own Research Integrity and Research Publishing teams and anonymous and named external researchers and research integrity experts for contributing to this investigation.

The corresponding author, as the representative of all authors, has been given the opportunity to register their agreement or disagreement to this retraction. We have kept a record of any response received.

References

[1] W. Yin, "An Artificial Intelligent Virtual Reality Interactive Model for Distance Education," *Journal of Mathematics*, vol. 2022, Article ID 7099963, 7 pages, 2022.

Hindawi
Journal of Mathematics
Volume 2023, Article ID 9815268, 1 page
https://doi.org/10.1155/2023/9815268

Retraction

Retracted: On the Temperature Indices of Molecular Structures of Some Networks

Journal of Mathematics

Received 19 December 2023; Accepted 19 December 2023; Published 20 December 2023

This article has been retracted by Hindawi following an investigation undertaken by the publisher [1]. This investigation has uncovered evidence of one or more of the following indicators of systematic manipulation of the publication process:

(1) Discrepancies in scope

(2) Discrepancies in the description of the research reported

(3) Discrepancies between the availability of data and the research described

(4) Inappropriate citations

(5) Incoherent, meaningless and/or irrelevant content included in the article

(6) Manipulated or compromised peer review

The presence of these indicators undermines our confidence in the integrity of the article's content and we cannot, therefore, vouch for its reliability. Please note that this notice is intended solely to alert readers that the content of this article is unreliable. We have not investigated whether authors were aware of or involved in the systematic manipulation of the publication process.

Wiley and Hindawi regrets that the usual quality checks did not identify these issues before publication and have since put additional measures in place to safeguard research integrity.

We wish to credit our own Research Integrity and Research Publishing teams and anonymous and named external researchers and research integrity experts for contributing to this investigation.

The corresponding author, as the representative of all authors, has been given the opportunity to register their agreement or disagreement to this retraction. We have kept a record of any response received.

References

[1] A. Jahanbani, R. Khoeilar, and M. Cancan, "On the Temperature Indices of Molecular Structures of Some Networks," *Journal of Mathematics*, vol. 2022, Article ID 4840774, 7 pages, 2022.

Hindawi
Journal of Mathematics
Volume 2023, Article ID 9814165, 1 page
https://doi.org/10.1155/2023/9814165

Retraction

Retracted: Design of Sports Image Contour Feature Acquisition System Based on the Background Subtraction Method

Journal of Mathematics

Received 19 December 2023; Accepted 19 December 2023; Published 20 December 2023

This article has been retracted by Hindawi following an investigation undertaken by the publisher [1]. This investigation has uncovered evidence of one or more of the following indicators of systematic manipulation of the publication process:

(1) Discrepancies in scope

(2) Discrepancies in the description of the research reported

(3) Discrepancies between the availability of data and the research described

(4) Inappropriate citations

(5) Incoherent, meaningless and/or irrelevant content included in the article

(6) Manipulated or compromised peer review

The presence of these indicators undermines our confidence in the integrity of the article's content and we cannot, therefore, vouch for its reliability. Please note that this notice is intended solely to alert readers that the content of this article is unreliable. We have not investigated whether authors were aware of or involved in the systematic manipulation of the publication process.

Wiley and Hindawi regrets that the usual quality checks did not identify these issues before publication and have since put additional measures in place to safeguard research integrity.

We wish to credit our own Research Integrity and Research Publishing teams and anonymous and named external researchers and research integrity experts for contributing to this investigation.

The corresponding author, as the representative of all authors, has been given the opportunity to register their agreement or disagreement to this retraction. We have kept a record of any response received.

References

[1] Z. Xiong, "Design of Sports Image Contour Feature Acquisition System Based on the Background Subtraction Method," *Journal of Mathematics*, vol. 2022, Article ID 3859795, 9 pages, 2022.

Hindawi
Journal of Mathematics
Volume 2023, Article ID 9814149, 1 page
https://doi.org/10.1155/2023/9814149

Retraction

Retracted: Research on Digital Image Watermarking Algorithm Based on Scrambling and Singular Value Decomposition

Journal of Mathematics

Received 19 December 2023; Accepted 19 December 2023; Published 20 December 2023

This article has been retracted by Hindawi following an investigation undertaken by the publisher [1]. This investigation has uncovered evidence of one or more of the following indicators of systematic manipulation of the publication process:

(1) Discrepancies in scope

(2) Discrepancies in the description of the research reported

(3) Discrepancies between the availability of data and the research described

(4) Inappropriate citations

(5) Incoherent, meaningless and/or irrelevant content included in the article

(6) Manipulated or compromised peer review

The presence of these indicators undermines our confidence in the integrity of the article's content and we cannot, therefore, vouch for its reliability. Please note that this notice is intended solely to alert readers that the content of this article is unreliable. We have not investigated whether authors were aware of or involved in the systematic manipulation of the publication process.

Wiley and Hindawi regrets that the usual quality checks did not identify these issues before publication and have since put additional measures in place to safeguard research integrity.

We wish to credit our own Research Integrity and Research Publishing teams and anonymous and named external researchers and research integrity experts for contributing to this investigation.

The corresponding author, as the representative of all authors, has been given the opportunity to register their agreement or disagreement to this retraction. We have kept a record of any response received.

References

[1] L. Pei, "Research on Digital Image Watermarking Algorithm Based on Scrambling and Singular Value Decomposition," *Journal of Mathematics*, vol. 2022, Article ID 4656010, 10 pages, 2022.

Hindawi
Journal of Mathematics
Volume 2023, Article ID 9810624, 1 page
https://doi.org/10.1155/2023/9810624

Retraction

Retracted: Analysis of the Resilience of Balance of Payments Using Comprehensive Evaluation

Journal of Mathematics

Received 19 December 2023; Accepted 19 December 2023; Published 20 December 2023

This article has been retracted by Hindawi following an investigation undertaken by the publisher [1]. This investigation has uncovered evidence of one or more of the following indicators of systematic manipulation of the publication process:

(1) Discrepancies in scope

(2) Discrepancies in the description of the research reported

(3) Discrepancies between the availability of data and the research described

(4) Inappropriate citations

(5) Incoherent, meaningless and/or irrelevant content included in the article

(6) Manipulated or compromised peer review

The presence of these indicators undermines our confidence in the integrity of the article's content and we cannot, therefore, vouch for its reliability. Please note that this notice is intended solely to alert readers that the content of this article is unreliable. We have not investigated whether authors were aware of or involved in the systematic manipulation of the publication process.

Wiley and Hindawi regrets that the usual quality checks did not identify these issues before publication and have since put additional measures in place to safeguard research integrity.

We wish to credit our own Research Integrity and Research Publishing teams and anonymous and named external researchers and research integrity experts for contributing to this investigation.

The corresponding author, as the representative of all authors, has been given the opportunity to register their agreement or disagreement to this retraction. We have kept a record of any response received.

References

[1] S. Fan and Y. Liu, "Analysis of the Resilience of Balance of Payments Using Comprehensive Evaluation," *Journal of Mathematics*, vol. 2022, Article ID 4620492, 13 pages, 2022.

Hindawi
Journal of Mathematics
Volume 2023, Article ID 9810127, 1 page
https://doi.org/10.1155/2023/9810127

Retraction

Retracted: The Application of "Internet+" in the Ageing Adaptation of Elderly People with Disabilities at Home

Journal of Mathematics

Received 19 December 2023; Accepted 19 December 2023; Published 20 December 2023

This article has been retracted by Hindawi following an investigation undertaken by the publisher [1]. This investigation has uncovered evidence of one or more of the following indicators of systematic manipulation of the publication process:

(1) Discrepancies in scope

(2) Discrepancies in the description of the research reported

(3) Discrepancies between the availability of data and the research described

(4) Inappropriate citations

(5) Incoherent, meaningless and/or irrelevant content included in the article

(6) Manipulated or compromised peer review

The presence of these indicators undermines our confidence in the integrity of the article's content and we cannot, therefore, vouch for its reliability. Please note that this notice is intended solely to alert readers that the content of this article is unreliable. We have not investigated whether authors were aware of or involved in the systematic manipulation of the publication process.

Wiley and Hindawi regrets that the usual quality checks did not identify these issues before publication and have since put additional measures in place to safeguard research integrity.

We wish to credit our own Research Integrity and Research Publishing teams and anonymous and named external researchers and research integrity experts for contributing to this investigation.

The corresponding author, as the representative of all authors, has been given the opportunity to register their agreement or disagreement to this retraction. We have kept a record of any response received.

References

[1] H. Juan, L. Li, M. Jiasong, Z. Lifang, and H. Baoying, "The Application of "Internet+" in the Ageing Adaptation of Elderly People with Disabilities at Home," *Journal of Mathematics*, vol. 2021, Article ID 6074643, 6 pages, 2021.

Hindawi
Journal of Mathematics
Volume 2023, Article ID 9798076, 1 page
https://doi.org/10.1155/2023/9798076

Retraction

Retracted: Research on Community Public Service Information Collaborative Governance Based on Deep Learning Model

Journal of Mathematics

Received 19 December 2023; Accepted 19 December 2023; Published 20 December 2023

This article has been retracted by Hindawi following an investigation undertaken by the publisher [1]. This investigation has uncovered evidence of one or more of the following indicators of systematic manipulation of the publication process:

(1) Discrepancies in scope

(2) Discrepancies in the description of the research reported

(3) Discrepancies between the availability of data and the research described

(4) Inappropriate citations

(5) Incoherent, meaningless and/or irrelevant content included in the article

(6) Manipulated or compromised peer review

The presence of these indicators undermines our confidence in the integrity of the article's content and we cannot, therefore, vouch for its reliability. Please note that this notice is intended solely to alert readers that the content of this article is unreliable. We have not investigated whether authors were aware of or involved in the systematic manipulation of the publication process.

Wiley and Hindawi regrets that the usual quality checks did not identify these issues before publication and have since put additional measures in place to safeguard research integrity.

We wish to credit our own Research Integrity and Research Publishing teams and anonymous and named external researchers and research integrity experts for contributing to this investigation.

The corresponding author, as the representative of all authors, has been given the opportunity to register their agreement or disagreement to this retraction. We have kept a record of any response received.

References

[1] Y. Liu, "Research on Community Public Service Information Collaborative Governance Based on Deep Learning Model," *Journal of Mathematics*, vol. 2021, Article ID 4727617, 9 pages, 2021.

Hindawi
Journal of Mathematics
Volume 2023, Article ID 9789820, 1 page
https://doi.org/10.1155/2023/9789820

Retraction

Retracted: A Study of English Informative Teaching Strategies Based on Deep Learning

Journal of Mathematics

Received 19 December 2023; Accepted 19 December 2023; Published 20 December 2023

This article has been retracted by Hindawi following an investigation undertaken by the publisher [1]. This investigation has uncovered evidence of one or more of the following indicators of systematic manipulation of the publication process:

(1) Discrepancies in scope

(2) Discrepancies in the description of the research reported

(3) Discrepancies between the availability of data and the research described

(4) Inappropriate citations

(5) Incoherent, meaningless and/or irrelevant content included in the article

(6) Manipulated or compromised peer review

The presence of these indicators undermines our confidence in the integrity of the article's content and we cannot, therefore, vouch for its reliability. Please note that this notice is intended solely to alert readers that the content of this article is unreliable. We have not investigated whether authors were aware of or involved in the systematic manipulation of the publication process.

Wiley and Hindawi regrets that the usual quality checks did not identify these issues before publication and have since put additional measures in place to safeguard research integrity.

We wish to credit our own Research Integrity and Research Publishing teams and anonymous and named external researchers and research integrity experts for contributing to this investigation.

The corresponding author, as the representative of all authors, has been given the opportunity to register their agreement or disagreement to this retraction. We have kept a record of any response received.

References

[1] Y. Guo, "A Study of English Informative Teaching Strategies Based on Deep Learning," *Journal of Mathematics*, vol. 2021, Article ID 5364892, 8 pages, 2021.

Hindawi
Journal of Mathematics
Volume 2023, Article ID 9787535, 1 page
https://doi.org/10.1155/2023/9787535

Retraction

Retracted: Weather Radar Image Superresolution Using a Nonlocal Residual Network

Journal of Mathematics

Received 19 December 2023; Accepted 19 December 2023; Published 20 December 2023

This article has been retracted by Hindawi following an investigation undertaken by the publisher [1]. This investigation has uncovered evidence of one or more of the following indicators of systematic manipulation of the publication process:

(1) Discrepancies in scope

(2) Discrepancies in the description of the research reported

(3) Discrepancies between the availability of data and the research described

(4) Inappropriate citations

(5) Incoherent, meaningless and/or irrelevant content included in the article

(6) Manipulated or compromised peer review

The presence of these indicators undermines our confidence in the integrity of the article's content and we cannot, therefore, vouch for its reliability. Please note that this notice is intended solely to alert readers that the content of this article is unreliable. We have not investigated whether authors were aware of or involved in the systematic manipulation of the publication process.

Wiley and Hindawi regrets that the usual quality checks did not identify these issues before publication and have since put additional measures in place to safeguard research integrity.

We wish to credit our own Research Integrity and Research Publishing teams and anonymous and named external researchers and research integrity experts for contributing to this investigation.

The corresponding author, as the representative of all authors, has been given the opportunity to register their agreement or disagreement to this retraction. We have kept a record of any response received.

References

[1] H. Yuan, Q. Zeng, and J. He, "Weather Radar Image Superresolution Using a Nonlocal Residual Network," *Journal of Mathematics*, vol. 2021, Article ID 4483907, 11 pages, 2021.

Hindawi
Journal of Mathematics
Volume 2023, Article ID 9787190, 1 page
https://doi.org/10.1155/2023/9787190

Retraction

Retracted: An Evaluation of the Security Ability of the Basic Endowment Insurance System for China's Urban and Rural Residents

Journal of Mathematics

Received 19 December 2023; Accepted 19 December 2023; Published 20 December 2023

This article has been retracted by Hindawi following an investigation undertaken by the publisher [1]. This investigation has uncovered evidence of one or more of the following indicators of systematic manipulation of the publication process:

(1) Discrepancies in scope

(2) Discrepancies in the description of the research reported

(3) Discrepancies between the availability of data and the research described

(4) Inappropriate citations

(5) Incoherent, meaningless and/or irrelevant content included in the article

(6) Manipulated or compromised peer review

The presence of these indicators undermines our confidence in the integrity of the article's content and we cannot, therefore, vouch for its reliability. Please note that this notice is intended solely to alert readers that the content of this article is unreliable. We have not investigated whether authors were aware of or involved in the systematic manipulation of the publication process.

Wiley and Hindawi regrets that the usual quality checks did not identify these issues before publication and have since put additional measures in place to safeguard research integrity.

We wish to credit our own Research Integrity and Research Publishing teams and anonymous and named external researchers and research integrity experts for contributing to this investigation.

The corresponding author, as the representative of all authors, has been given the opportunity to register their agreement or disagreement to this retraction. We have kept a record of any response received.

References

[1] B. Liu, Y. He, and Z. Liu, "An Evaluation of the Security Ability of the Basic Endowment Insurance System for China's Urban and Rural Residents," *Journal of Mathematics*, vol. 2022, Article ID 6244880, 10 pages, 2022.

Hindawi
Journal of Mathematics
Volume 2023, Article ID 9784351, 1 page
https://doi.org/10.1155/2023/9784351

Retraction

Retracted: Dance Evaluation Based on Movement and Neural Network

Journal of Mathematics

Received 19 December 2023; Accepted 19 December 2023; Published 20 December 2023

This article has been retracted by Hindawi following an investigation undertaken by the publisher [1]. This investigation has uncovered evidence of one or more of the following indicators of systematic manipulation of the publication process:

(1) Discrepancies in scope

(2) Discrepancies in the description of the research reported

(3) Discrepancies between the availability of data and the research described

(4) Inappropriate citations

(5) Incoherent, meaningless and/or irrelevant content included in the article

(6) Manipulated or compromised peer review

The presence of these indicators undermines our confidence in the integrity of the article's content and we cannot, therefore, vouch for its reliability. Please note that this notice is intended solely to alert readers that the content of this article is unreliable. We have not investigated whether authors were aware of or involved in the systematic manipulation of the publication process.

Wiley and Hindawi regrets that the usual quality checks did not identify these issues before publication and have since put additional measures in place to safeguard research integrity.

We wish to credit our own Research Integrity and Research Publishing teams and anonymous and named external researchers and research integrity experts for contributing to this investigation.

The corresponding author, as the representative of all authors, has been given the opportunity to register their agreement or disagreement to this retraction. We have kept a record of any response received.

References

[1] Y. Lei, X. Li, and Y. J. Chen, "Dance Evaluation Based on Movement and Neural Network," *Journal of Mathematics*, vol. 2022, Article ID 6968852, 7 pages, 2022.

Hindawi
Journal of Mathematics
Volume 2023, Article ID 9769718, 1 page
https://doi.org/10.1155/2023/9769718

Retraction

Retracted: Application to Biomedical Data: Using the Topp Leone Inverse Lindley Model

Journal of Mathematics

Received 19 December 2023; Accepted 19 December 2023; Published 20 December 2023

This article has been retracted by Hindawi following an investigation undertaken by the publisher [1]. This investigation has uncovered evidence of one or more of the following indicators of systematic manipulation of the publication process:

(1) Discrepancies in scope

(2) Discrepancies in the description of the research reported

(3) Discrepancies between the availability of data and the research described

(4) Inappropriate citations

(5) Incoherent, meaningless and/or irrelevant content included in the article

(6) Manipulated or compromised peer review

The presence of these indicators undermines our confidence in the integrity of the article's content and we cannot, therefore, vouch for its reliability. Please note that this notice is intended solely to alert readers that the content of this article is unreliable. We have not investigated whether authors were aware of or involved in the systematic manipulation of the publication process.

Wiley and Hindawi regrets that the usual quality checks did not identify these issues before publication and have since put additional measures in place to safeguard research integrity.

We wish to credit our own Research Integrity and Research Publishing teams and anonymous and named external researchers and research integrity experts for contributing to this investigation.

The corresponding author, as the representative of all authors, has been given the opportunity to register their agreement or disagreement to this retraction. We have kept a record of any response received.

References

[1] M. A. Aldahlan, "Application to Biomedical Data: Using the Topp Leone Inverse Lindley Model," *Journal of Mathematics*, vol. 2022, Article ID 1985861, 11 pages, 2022.

Hindawi
Journal of Mathematics
Volume 2023, Article ID 9765832, 1 page
https://doi.org/10.1155/2023/9765832

Retraction

Retracted: Predicting the Link between Stock Prices and Indices with Machine Learning in R Programming Language

Journal of Mathematics

Received 19 December 2023; Accepted 19 December 2023; Published 20 December 2023

This article has been retracted by Hindawi following an investigation undertaken by the publisher [1]. This investigation has uncovered evidence of one or more of the following indicators of systematic manipulation of the publication process:

(1) Discrepancies in scope

(2) Discrepancies in the description of the research reported

(3) Discrepancies between the availability of data and the research described

(4) Inappropriate citations

(5) Incoherent, meaningless and/or irrelevant content included in the article

(6) Manipulated or compromised peer review

The presence of these indicators undermines our confidence in the integrity of the article's content and we cannot, therefore, vouch for its reliability. Please note that this notice is intended solely to alert readers that the content of this article is unreliable. We have not investigated whether authors were aware of or involved in the systematic manipulation of the publication process.

Wiley and Hindawi regrets that the usual quality checks did not identify these issues before publication and have since put additional measures in place to safeguard research integrity.

We wish to credit our own Research Integrity and Research Publishing teams and anonymous and named external researchers and research integrity experts for contributing to this investigation.

The corresponding author, as the representative of all authors, has been given the opportunity to register their agreement or disagreement to this retraction. We have kept a record of any response received.

References

[1] M. Cao, "Predicting the Link between Stock Prices and Indices with Machine Learning in R Programming Language," *Journal of Mathematics*, vol. 2021, Article ID 1275637, 10 pages, 2021.

Hindawi
Journal of Mathematics
Volume 2023, Article ID 9761056, 1 page
https://doi.org/10.1155/2023/9761056

Retraction

Retracted: Data Mining and Analysis of the Compatibility Law of Traditional Chinese Medicines Based on FP-Growth Algorithm

Journal of Mathematics

Received 19 December 2023; Accepted 19 December 2023; Published 20 December 2023

This article has been retracted by Hindawi following an investigation undertaken by the publisher [1]. This investigation has uncovered evidence of one or more of the following indicators of systematic manipulation of the publication process:

(1) Discrepancies in scope

(2) Discrepancies in the description of the research reported

(3) Discrepancies between the availability of data and the research described

(4) Inappropriate citations

(5) Incoherent, meaningless and/or irrelevant content included in the article

(6) Manipulated or compromised peer review

The presence of these indicators undermines our confidence in the integrity of the article's content and we cannot, therefore, vouch for its reliability. Please note that this notice is intended solely to alert readers that the content of this article is unreliable. We have not investigated whether authors were aware of or involved in the systematic manipulation of the publication process.

Wiley and Hindawi regrets that the usual quality checks did not identify these issues before publication and have since put additional measures in place to safeguard research integrity.

We wish to credit our own Research Integrity and Research Publishing teams and anonymous and named external researchers and research integrity experts for contributing to this investigation.

The corresponding author, as the representative of all authors, has been given the opportunity to register their agreement or disagreement to this retraction. We have kept a record of any response received.

References

[1] S. Zhou, "Data Mining and Analysis of the Compatibility Law of Traditional Chinese Medicines Based on FP-Growth Algorithm," *Journal of Mathematics*, vol. 2021, Article ID 1045152, 10 pages, 2021.

Hindawi
Journal of Mathematics
Volume 2023, Article ID 9760950, 1 page
https://doi.org/10.1155/2023/9760950

Retraction

Retracted: Intelligent Transportation Design Based on Iterative Learning

Journal of Mathematics

Received 19 December 2023; Accepted 19 December 2023; Published 20 December 2023

This article has been retracted by Hindawi following an investigation undertaken by the publisher [1]. This investigation has uncovered evidence of one or more of the following indicators of systematic manipulation of the publication process:

(1) Discrepancies in scope

(2) Discrepancies in the description of the research reported

(3) Discrepancies between the availability of data and the research described

(4) Inappropriate citations

(5) Incoherent, meaningless and/or irrelevant content included in the article

(6) Manipulated or compromised peer review

The presence of these indicators undermines our confidence in the integrity of the article's content and we cannot, therefore, vouch for its reliability. Please note that this notice is intended solely to alert readers that the content of this article is unreliable. We have not investigated whether authors were aware of or involved in the systematic manipulation of the publication process.

Wiley and Hindawi regrets that the usual quality checks did not identify these issues before publication and have since put additional measures in place to safeguard research integrity.

We wish to credit our own Research Integrity and Research Publishing teams and anonymous and named external researchers and research integrity experts for contributing to this investigation.

The corresponding author, as the representative of all authors, has been given the opportunity to register their agreement or disagreement to this retraction. We have kept a record of any response received.

References

[1] Y. Ma and K. Liu, "Intelligent Transportation Design Based on Iterative Learning," *Journal of Mathematics*, vol. 2022, Article ID 5027412, 7 pages, 2022.

Hindawi
Journal of Mathematics
Volume 2023, Article ID 9760547, 1 page
https://doi.org/10.1155/2023/9760547

Retraction

Retracted: Computational Intelligence and Things Technology-Based Collection and Design of Inheritance Characteristics of Tea Product Packaging Art Form

Journal of Mathematics

Received 19 December 2023; Accepted 19 December 2023; Published 20 December 2023

This article has been retracted by Hindawi following an investigation undertaken by the publisher [1]. This investigation has uncovered evidence of one or more of the following indicators of systematic manipulation of the publication process:

(1) Discrepancies in scope

(2) Discrepancies in the description of the research reported

(3) Discrepancies between the availability of data and the research described

(4) Inappropriate citations

(5) Incoherent, meaningless and/or irrelevant content included in the article

(6) Manipulated or compromised peer review

The presence of these indicators undermines our confidence in the integrity of the article's content and we cannot, therefore, vouch for its reliability. Please note that this notice is intended solely to alert readers that the content of this article is unreliable. We have not investigated whether authors were aware of or involved in the systematic manipulation of the publication process.

Wiley and Hindawi regrets that the usual quality checks did not identify these issues before publication and have since put additional measures in place to safeguard research integrity.

We wish to credit our own Research Integrity and Research Publishing teams and anonymous and named external researchers and research integrity experts for contributing to this investigation.

The corresponding author, as the representative of all authors, has been given the opportunity to register their agreement or disagreement to this retraction. We have kept a record of any response received.

References

[1] S. Wu and K. Mojtahe, "Computational Intelligence and Things Technology-Based Collection and Design of Inheritance Characteristics of Tea Product Packaging Art Form," *Journal of Mathematics*, vol. 2022, Article ID 3578831, 10 pages, 2022.

Hindawi
Journal of Mathematics
Volume 2023, Article ID 9760327, 1 page
https://doi.org/10.1155/2023/9760327

Retraction

Retracted: A Computational Offloading Method for Edge Server Computing and Resource Allocation Management

Journal of Mathematics

Received 19 December 2023; Accepted 19 December 2023; Published 20 December 2023

This article has been retracted by Hindawi following an investigation undertaken by the publisher [1]. This investigation has uncovered evidence of one or more of the following indicators of systematic manipulation of the publication process:

(1) Discrepancies in scope

(2) Discrepancies in the description of the research reported

(3) Discrepancies between the availability of data and the research described

(4) Inappropriate citations

(5) Incoherent, meaningless and/or irrelevant content included in the article

(6) Manipulated or compromised peer review

The presence of these indicators undermines our confidence in the integrity of the article's content and we cannot, therefore, vouch for its reliability. Please note that this notice is intended solely to alert readers that the content of this article is unreliable. We have not investigated whether authors were aware of or involved in the systematic manipulation of the publication process.

Wiley and Hindawi regrets that the usual quality checks did not identify these issues before publication and have since put additional measures in place to safeguard research integrity.

We wish to credit our own Research Integrity and Research Publishing teams and anonymous and named external researchers and research integrity experts for contributing to this investigation.

The corresponding author, as the representative of all authors, has been given the opportunity to register their agreement or disagreement to this retraction. We have kept a record of any response received.

References

[1] M. Al-Razgan, T. Alfakih, and M. M. Hassan, "A Computational Offloading Method for Edge Server Computing and Resource Allocation Management," *Journal of Mathematics*, vol. 2021, Article ID 3557059, 11 pages, 2021.

Hindawi
Journal of Mathematics
Volume 2023, Article ID 9879807, 1 page
https://doi.org/10.1155/2023/9879807

Retraction

Retracted: Early Warning System for Penalty Constrained Financial Risks of Enterprises under Diversified Investment

Journal of Mathematics

Received 31 October 2023; Accepted 31 October 2023; Published 1 November 2023

This article has been retracted by Hindawi following an investigation undertaken by the publisher [1]. This investigation has uncovered evidence of one or more of the following indicators of systematic manipulation of the publication process:

(1) Discrepancies in scope

(2) Discrepancies in the description of the research reported

(3) Discrepancies between the availability of data and the research described

(4) Inappropriate citations

(5) Incoherent, meaningless and/or irrelevant content included in the article

(6) Peer-review manipulation

The presence of these indicators undermines our confidence in the integrity of the article's content and we cannot, therefore, vouch for its reliability. Please note that this notice is intended solely to alert readers that the content of this article is unreliable. We have not investigated whether authors were aware of or involved in the systematic manipulation of the publication process.

Wiley and Hindawi regrets that the usual quality checks did not identify these issues before publication and have since put additional measures in place to safeguard research integrity.

We wish to credit our own Research Integrity and Research Publishing teams and anonymous and named external researchers and research integrity experts for contributing to this investigation.

The corresponding author, as the representative of all authors, has been given the opportunity to register their agreement or disagreement to this retraction. We have kept a record of any response received.

References

[1] Y. Zhu, "Early Warning System for Penalty Constrained Financial Risks of Enterprises under Diversified Investment," *Journal of Mathematics*, vol. 2021, Article ID 4153774, 9 pages, 2021.

Hindawi
Journal of Mathematics
Volume 2023, Article ID 9841465, 1 page
https://doi.org/10.1155/2023/9841465

Retraction

Retracted: New Types of μ-Proximity Spaces and Their Applications

Journal of Mathematics

Received 17 October 2023; Accepted 17 October 2023; Published 18 October 2023

This article has been retracted by Hindawi following an investigation undertaken by the publisher [1]. This investigation has uncovered evidence of one or more of the following indicators of systematic manipulation of the publication process:

(1) Discrepancies in scope

(2) Discrepancies in the description of the research reported

(3) Discrepancies between the availability of data and the research described

(4) Inappropriate citations

(5) Incoherent, meaningless and/or irrelevant content included in the article

(6) Peer-review manipulation

The presence of these indicators undermines our confidence in the integrity of the article's content and we cannot, therefore, vouch for its reliability. Please note that this notice is intended solely to alert readers that the content of this article is unreliable. We have not investigated whether authors were aware of or involved in the systematic manipulation of the publication process.

Wiley and Hindawi regrets that the usual quality checks did not identify these issues before publication and have since put additional measures in place to safeguard research integrity.

We wish to credit our own Research Integrity and Research Publishing teams and anonymous and named external researchers and research integrity experts for contributing to this investigation.

The corresponding author, as the representative of all authors, has been given the opportunity to register their agreement or disagreement to this retraction. We have kept a record of any response received.

References

[1] R. A. Hosny, T. M. Al-shami, and A. Mhemdi, "New Types of μ-Proximity Spaces and Their Applications," *Journal of Mathematics*, vol. 2022, Article ID 1657993, 10 pages, 2022.

Hindawi
Journal of Mathematics
Volume 2023, Article ID 9807535, 1 page
https://doi.org/10.1155/2023/9807535

Retraction

Retracted: On Q_p-Closed Sets in Topological Spaces

Journal of Mathematics

Received 17 October 2023; Accepted 17 October 2023; Published 18 October 2023

This article has been retracted by Hindawi following an investigation undertaken by the publisher [1]. This investigation has uncovered evidence of one or more of the following indicators of systematic manipulation of the publication process:

(1) Discrepancies in scope

(2) Discrepancies in the description of the research reported

(3) Discrepancies between the availability of data and the research described

(4) Inappropriate citations

(5) Incoherent, meaningless and/or irrelevant content included in the article

(6) Peer-review manipulation

The presence of these indicators undermines our confidence in the integrity of the article's content and we cannot, therefore, vouch for its reliability. Please note that this notice is intended solely to alert readers that the content of this article is unreliable. We have not investigated whether authors were aware of or involved in the systematic manipulation of the publication process.

Wiley and Hindawi regrets that the usual quality checks did not identify these issues before publication and have since put additional measures in place to safeguard research integrity.

We wish to credit our own Research Integrity and Research Publishing teams and anonymous and named external researchers and research integrity experts for contributing to this investigation.

The corresponding author, as the representative of all authors, has been given the opportunity to register their agreement or disagreement to this retraction. We have kept a record of any response received.

References

[1] H. Zhou, O. G. Hammad, and A. M. Khalil, "On Q_p-Closed Sets in Topological Spaces," *Journal of Mathematics*, vol. 2022, Article ID 9352861, 10 pages, 2022.

Hindawi
Journal of Mathematics
Volume 2023, Article ID 9840234, 1 page
https://doi.org/10.1155/2023/9840234

Retraction

Retracted: Research on the Construction of Intelligent Media Ideological and Political Learning Platform Based on Artificial Intelligence Technology

Journal of Mathematics

Received 3 October 2023; Accepted 3 October 2023; Published 4 October 2023

This article has been retracted by Hindawi following an investigation undertaken by the publisher [1]. This investigation has uncovered evidence of one or more of the following indicators of systematic manipulation of the publication process:

(1) Discrepancies in scope

(2) Discrepancies in the description of the research reported

(3) Discrepancies between the availability of data and the research described

(4) Inappropriate citations

(5) Incoherent, meaningless and/or irrelevant content included in the article

(6) Peer-review manipulation

The presence of these indicators undermines our confidence in the integrity of the article's content and we cannot, therefore, vouch for its reliability. Please note that this notice is intended solely to alert readers that the content of this article is unreliable. We have not investigated whether authors were aware of or involved in the systematic manipulation of the publication process.

Wiley and Hindawi regrets that the usual quality checks did not identify these issues before publication and have since put additional measures in place to safeguard research integrity.

We wish to credit our own Research Integrity and Research Publishing teams and anonymous and named external researchers and research integrity experts for contributing to this investigation.

The corresponding author, as the representative of all authors, has been given the opportunity to register their agreement or disagreement to this retraction. We have kept a record of any response received.

References

[1] J. Wang and S. Hu, "Research on the Construction of Intelligent Media Ideological and Political Learning Platform Based on Artificial Intelligence Technology," *Journal of Mathematics*, vol. 2022, Article ID 6511962, 11 pages, 2022.

Hindawi
Journal of Mathematics
Volume 2023, Article ID 9871670, 1 page
https://doi.org/10.1155/2023/9871670

Retraction

Retracted: Automatic Classification Method of Music Genres Based on Deep Belief Network and Sparse Representation

Journal of Mathematics

Received 15 August 2023; Accepted 15 August 2023; Published 16 August 2023

This article has been retracted by Hindawi following an investigation undertaken by the publisher [1]. This investigation has uncovered evidence of one or more of the following indicators of systematic manipulation of the publication process:

(1) Discrepancies in scope

(2) Discrepancies in the description of the research reported

(3) Discrepancies between the availability of data and the research described

(4) Inappropriate citations

(5) Incoherent, meaningless and/or irrelevant content included in the article

(6) Peer-review manipulation

The presence of these indicators undermines our confidence in the integrity of the article's content and we cannot, therefore, vouch for its reliability. Please note that this notice is intended solely to alert readers that the content of this article is unreliable. We have not investigated whether authors were aware of or involved in the systematic manipulation of the publication process.

Wiley and Hindawi regrets that the usual quality checks did not identify these issues before publication and have since put additional measures in place to safeguard research integrity.

We wish to credit our own Research Integrity and Research Publishing teams and anonymous and named external researchers and research integrity experts for contributing to this investigation.

The corresponding author, as the representative of all authors, has been given the opportunity to register their agreement or disagreement to this retraction. We have kept a record of any response received.

References

[1] L. Pan, "Automatic Classification Method of Music Genres Based on Deep Belief Network and Sparse Representation," *Journal of Mathematics*, vol. 2022, Article ID 8752217, 10 pages, 2022.

Hindawi
Journal of Mathematics
Volume 2023, Article ID 9869537, 1 page
https://doi.org/10.1155/2023/9869537

Retraction

Retracted: Teaching Quality Evaluation of Ideological and Political Courses in Colleges and Universities Based on Machine Learning

Journal of Mathematics

Received 15 August 2023; Accepted 15 August 2023; Published 16 August 2023

This article has been retracted by Hindawi following an investigation undertaken by the publisher [1]. This investigation has uncovered evidence of one or more of the following indicators of systematic manipulation of the publication process:

(1) Discrepancies in scope

(2) Discrepancies in the description of the research reported

(3) Discrepancies between the availability of data and the research described

(4) Inappropriate citations

(5) Incoherent, meaningless and/or irrelevant content included in the article

(6) Peer-review manipulation

The presence of these indicators undermines our confidence in the integrity of the article's content and we cannot, therefore, vouch for its reliability. Please note that this notice is intended solely to alert readers that the content of this article is unreliable. We have not investigated whether authors were aware of or involved in the systematic manipulation of the publication process.

Wiley and Hindawi regrets that the usual quality checks did not identify these issues before publication and have since put additional measures in place to safeguard research integrity.

We wish to credit our own Research Integrity and Research Publishing teams and anonymous and named external researchers and research integrity experts for contributing to this investigation.

The corresponding author, as the representative of all authors, has been given the opportunity to register their agreement or disagreement to this retraction. We have kept a record of any response received.

References

[1] L. Qiao, "Teaching Quality Evaluation of Ideological and Political Courses in Colleges and Universities Based on Machine Learning," *Journal of Mathematics*, vol. 2022, Article ID 2835029, 10 pages, 2022.

Hindawi
Journal of Mathematics
Volume 2023, Article ID 9868607, 1 page
https://doi.org/10.1155/2023/9868607

Retraction

Retracted: Evaluation of the Effect of Ideological and Political Education on Psychological Crisis Intervention for University Students Based on Data Mining Algorithm

Journal of Mathematics

Received 15 August 2023; Accepted 15 August 2023; Published 16 August 2023

This article has been retracted by Hindawi following an investigation undertaken by the publisher [1]. This investigation has uncovered evidence of one or more of the following indicators of systematic manipulation of the publication process:

(1) Discrepancies in scope

(2) Discrepancies in the description of the research reported

(3) Discrepancies between the availability of data and the research described

(4) Inappropriate citations

(5) Incoherent, meaningless and/or irrelevant content included in the article

(6) Peer-review manipulation

The presence of these indicators undermines our confidence in the integrity of the article's content and we cannot, therefore, vouch for its reliability. Please note that this notice is intended solely to alert readers that the content of this article is unreliable. We have not investigated whether authors were aware of or involved in the systematic manipulation of the publication process.

Wiley and Hindawi regrets that the usual quality checks did not identify these issues before publication and have since put additional measures in place to safeguard research integrity.

We wish to credit our own Research Integrity and Research Publishing teams and anonymous and named external researchers and research integrity experts for contributing to this investigation.

The corresponding author, as the representative of all authors, has been given the opportunity to register their agreement or disagreement to this retraction. We have kept a record of any response received.

References

[1] H. Yao and M. D. H. A. Malek, "Evaluation of the Effect of Ideological and Political Education on Psychological Crisis Intervention for University Students Based on Data Mining Algorithm," *Journal of Mathematics*, vol. 2021, Article ID 9504247, 8 pages, 2021.

Hindawi
Journal of Mathematics
Volume 2023, Article ID 9852708, 1 page
https://doi.org/10.1155/2023/9852708

Retraction

Retracted: Analysis and Risk Assessment of Corporate Financial Leverage Using Mobile Payment in the Era of Digital Technology in a Complex Environment

Journal of Mathematics

Received 15 August 2023; Accepted 15 August 2023; Published 16 August 2023

This article has been retracted by Hindawi following an investigation undertaken by the publisher [1]. This investigation has uncovered evidence of one or more of the following indicators of systematic manipulation of the publication process:

(1) Discrepancies in scope

(2) Discrepancies in the description of the research reported

(3) Discrepancies between the availability of data and the research described

(4) Inappropriate citations

(5) Incoherent, meaningless and/or irrelevant content included in the article

(6) Peer-review manipulation

The presence of these indicators undermines our confidence in the integrity of the article's content and we cannot, therefore, vouch for its reliability. Please note that this notice is intended solely to alert readers that the content of this article is unreliable. We have not investigated whether authors were aware of or involved in the systematic manipulation of the publication process.

Wiley and Hindawi regrets that the usual quality checks did not identify these issues before publication and have since put additional measures in place to safeguard research integrity.

We wish to credit our own Research Integrity and Research Publishing teams and anonymous and named external researchers and research integrity experts for contributing to this investigation.

The corresponding author, as the representative of all authors, has been given the opportunity to register their agreement or disagreement to this retraction. We have kept a record of any response received.

References

[1] W. Wei and B. Li, "Analysis and Risk Assessment of Corporate Financial Leverage Using Mobile Payment in the Era of Digital Technology in a Complex Environment," *Journal of Mathematics*, vol. 2022, Article ID 5228374, 9 pages, 2022.

Hindawi
Journal of Mathematics
Volume 2023, Article ID 9836426, 1 page
https://doi.org/10.1155/2023/9836426

Retraction

Retracted: On Multiplicative Topological Invariants of Magnesium Iodide Structure

Journal of Mathematics

Received 15 August 2023; Accepted 15 August 2023; Published 16 August 2023

This article has been retracted by Hindawi following an investigation undertaken by the publisher [1]. This investigation has uncovered evidence of one or more of the following indicators of systematic manipulation of the publication process:

(1) Discrepancies in scope

(2) Discrepancies in the description of the research reported

(3) Discrepancies between the availability of data and the research described

(4) Inappropriate citations

(5) Incoherent, meaningless and/or irrelevant content included in the article

(6) Peer-review manipulation

The presence of these indicators undermines our confidence in the integrity of the article's content and we cannot, therefore, vouch for its reliability. Please note that this notice is intended solely to alert readers that the content of this article is unreliable. We have not investigated whether authors were aware of or involved in the systematic manipulation of the publication process.

Wiley and Hindawi regrets that the usual quality checks did not identify these issues before publication and have since put additional measures in place to safeguard research integrity.

We wish to credit our own Research Integrity and Research Publishing teams and anonymous and named external researchers and research integrity experts for contributing to this investigation.

The corresponding author, as the representative of all authors, has been given the opportunity to register their agreement or disagreement to this retraction. We have kept a record of any response received.

References

[1] Z. Zhang, H. Ali, A. Naseem, U. Babar, X. Zhang, and P. Ali, "On Multiplicative Topological Invariants of Magnesium Iodide Structure," *Journal of Mathematics*, vol. 2022, Article ID 6466585, 15 pages, 2022.

Hindawi
Journal of Mathematics
Volume 2023, Article ID 9812914, 1 page
https://doi.org/10.1155/2023/9812914

Retraction

Retracted: Research on the Integration of Preschool Language Education Resources Based on Metadata Storage

Journal of Mathematics

Received 15 August 2023; Accepted 15 August 2023; Published 16 August 2023

This article has been retracted by Hindawi following an investigation undertaken by the publisher [1]. This investigation has uncovered evidence of one or more of the following indicators of systematic manipulation of the publication process:

(1) Discrepancies in scope

(2) Discrepancies in the description of the research reported

(3) Discrepancies between the availability of data and the research described

(4) Inappropriate citations

(5) Incoherent, meaningless and/or irrelevant content included in the article

(6) Peer-review manipulation

The presence of these indicators undermines our confidence in the integrity of the article's content and we cannot, therefore, vouch for its reliability. Please note that this notice is intended solely to alert readers that the content of this article is unreliable. We have not investigated whether authors were aware of or involved in the systematic manipulation of the publication process.

Wiley and Hindawi regrets that the usual quality checks did not identify these issues before publication and have since put additional measures in place to safeguard research integrity.

We wish to credit our own Research Integrity and Research Publishing teams and anonymous and named external researchers and research integrity experts for contributing to this investigation.

The corresponding author, as the representative of all authors, has been given the opportunity to register their agreement or disagreement to this retraction. We have kept a record of any response received.

References

[1] S. Weiwei, "Research on the Integration of Preschool Language Education Resources Based on Metadata Storage," *Journal of Mathematics*, vol. 2022, Article ID 4802381, 8 pages, 2022.

Hindawi
Journal of Mathematics
Volume 2023, Article ID 9792569, 1 page
https://doi.org/10.1155/2023/9792569

Retraction

Retracted: Analysis of Intelligent Translation Systems and Evaluation Systems for Business English

Journal of Mathematics

Received 15 August 2023; Accepted 15 August 2023; Published 16 August 2023

This article has been retracted by Hindawi following an investigation undertaken by the publisher [1]. This investigation has uncovered evidence of one or more of the following indicators of systematic manipulation of the publication process:

(1) Discrepancies in scope

(2) Discrepancies in the description of the research reported

(3) Discrepancies between the availability of data and the research described

(4) Inappropriate citations

(5) Incoherent, meaningless and/or irrelevant content included in the article

(6) Peer-review manipulation

The presence of these indicators undermines our confidence in the integrity of the article's content and we cannot, therefore, vouch for its reliability. Please note that this notice is intended solely to alert readers that the content of this article is unreliable. We have not investigated whether authors were aware of or involved in the systematic manipulation of the publication process.

Wiley and Hindawi regrets that the usual quality checks did not identify these issues before publication and have since put additional measures in place to safeguard research integrity.

We wish to credit our own Research Integrity and Research Publishing teams and anonymous and named external researchers and research integrity experts for contributing to this investigation.

The corresponding author, as the representative of all authors, has been given the opportunity to register their agreement or disagreement to this retraction. We have kept a record of any response received.

References

[1] J. Chen, "Analysis of Intelligent Translation Systems and Evaluation Systems for Business English," *Journal of Mathematics*, vol. 2022, Article ID 5952987, 7 pages, 2022.

Hindawi
Journal of Mathematics
Volume 2023, Article ID 9783817, 1 page
https://doi.org/10.1155/2023/9783817

Retraction

Retracted: Probability Density Evolution Algorithm for Stochastic Dynamical Systems Based on Fractional Calculus

Journal of Mathematics

Received 15 August 2023; Accepted 15 August 2023; Published 16 August 2023

This article has been retracted by Hindawi following an investigation undertaken by the publisher [1]. This investigation has uncovered evidence of one or more of the following indicators of systematic manipulation of the publication process:

(1) Discrepancies in scope

(2) Discrepancies in the description of the research reported

(3) Discrepancies between the availability of data and the research described

(4) Inappropriate citations

(5) Incoherent, meaningless and/or irrelevant content included in the article

(6) Peer-review manipulation

The presence of these indicators undermines our confidence in the integrity of the article's content and we cannot, therefore, vouch for its reliability. Please note that this notice is intended solely to alert readers that the content of this article is unreliable. We have not investigated whether authors were aware of or involved in the systematic manipulation of the publication process.

Wiley and Hindawi regrets that the usual quality checks did not identify these issues before publication and have since put additional measures in place to safeguard research integrity.

We wish to credit our own Research Integrity and Research Publishing teams and anonymous and named external researchers and research integrity experts for contributing to this investigation.

The corresponding author, as the representative of all authors, has been given the opportunity to register their agreement or disagreement to this retraction. We have kept a record of any response received.

References

[1] Y. Yan and X. Yu, "Probability Density Evolution Algorithm for Stochastic Dynamical Systems Based on Fractional Calculus," *Journal of Mathematics*, vol. 2021, Article ID 9218857, 9 pages, 2021.

Hindawi
Journal of Mathematics
Volume 2023, Article ID 9756056, 1 page
https://doi.org/10.1155/2023/9756056

Retraction

Retracted: Application of Mobile Technology in College English Vocabulary Teaching

Journal of Mathematics

Received 15 August 2023; Accepted 15 August 2023; Published 16 August 2023

This article has been retracted by Hindawi following an investigation undertaken by the publisher [1]. This investigation has uncovered evidence of one or more of the following indicators of systematic manipulation of the publication process:

(1) Discrepancies in scope

(2) Discrepancies in the description of the research reported

(3) Discrepancies between the availability of data and the research described

(4) Inappropriate citations

(5) Incoherent, meaningless and/or irrelevant content included in the article

(6) Peer-review manipulation

The presence of these indicators undermines our confidence in the integrity of the article's content and we cannot, therefore, vouch for its reliability. Please note that this notice is intended solely to alert readers that the content of this article is unreliable. We have not investigated whether authors were aware of or involved in the systematic manipulation of the publication process.

Wiley and Hindawi regrets that the usual quality checks did not identify these issues before publication and have since put additional measures in place to safeguard research integrity.

We wish to credit our own Research Integrity and Research Publishing teams and anonymous and named external researchers and research integrity experts for contributing to this investigation.

The corresponding author, as the representative of all authors, has been given the opportunity to register their agreement or disagreement to this retraction. We have kept a record of any response received.

References

[1] B. He, "Application of Mobile Technology in College English Vocabulary Teaching," *Journal of Mathematics*, vol. 2022, Article ID 9009008, 8 pages, 2022.

Hindawi
Journal of Mathematics
Volume 2023, Article ID 9821642, 1 page
https://doi.org/10.1155/2023/9821642

Retraction

Retracted: A Survey of Multimedia-Assisted English Classroom Teaching Based on Statistical Analysis

Journal of Mathematics

Received 21 November 2022; Accepted 21 November 2022; Published 5 January 2023

Journal of Mathematics has retracted the article titled "A Survey of Multimedia-Assisted English Classroom Teaching Based on Statistical Analysis" [1] due to concerns that the peer review process has been compromised.

Following an investigation conducted by the Hindawi Research Integrity team [2], significant concerns were identified with the peer reviewers assigned to this article; the investigation has concluded that the peer review process was compromised. We therefore can no longer trust the peer review process, and the article is being retracted with the agreement of the Chief Editor.

References

[1] H. Wang, "A Survey of Multimedia-Assisted English Classroom Teaching Based on Statistical Analysis," *Journal of Mathematics*, vol. 2022, Article ID 4458478, 11 pages, 2022.

[2] L. Ferguson, "Advancing Research Integrity Collaboratively and with Vigour," 2022, https://www.hindawi.com/post/advancing-research-integrity-collaboratively-and-vigour/.

Hindawi
Journal of Mathematics
Volume 2022, Article ID 9805031, 1 page
https://doi.org/10.1155/2022/9805031

Retraction

Retracted: Research on Intelligent Function Design of Vocational Education System under Mobile Learning Mode

Journal of Mathematics

Received 25 November 2022; Accepted 25 November 2022; Published 27 December 2022

Journal of Mathematics has retracted the article titled "Research on Intelligent Function Design of Vocational Education System under Mobile Learning Mode" [1] due to concerns that the peer review process has been compromised.

Following an investigation conducted by the Hindawi Research Integrity team [2], significant concerns were identified with the peer reviewers assigned to this article; the investigation has concluded that the peer review process was compromised. We therefore can no longer trust the peer review process, and the article is being retracted with the agreement of the Chief Editor.

References

[1] L. Qing, "Research on Intelligent Function Design of Vocational Education System under Mobile Learning Mode," *Journal of Mathematics*, vol. 2022, Article ID 9684363, 10 pages, 2022.

[2] L. Ferguson, "Advancing Research Integrity Collaboratively and with Vigour," 2022, https://www.hindawi.com/post/advancing-research-integrity-collaboratively-and-vigour/.

Hindawi
Journal of Mathematics
Volume 2022, Article ID 9858146, 1 page
https://doi.org/10.1155/2022/9858146

Retraction

Retracted: Badminton Backcourt Stroke Route Planning Method Based on Deep Learning

Journal of Mathematics

Received 25 November 2022; Accepted 25 November 2022; Published 25 December 2022

Journal of Mathematics has retracted the article titled "Badminton Backcourt Stroke Route Planning Method Based on Deep Learning" [1] due to concerns that the peer review process has been compromised.

Following an investigation conducted by the Hindawi Research Integrity team [2], significant concerns were identified with the peer reviewers assigned to this article; the investigation has concluded that the peer review process was compromised. We therefore can no longer trust the peer review process, and the article is being retracted with the agreement of the Chief Editor.

References

[1] Y. Ma, "Badminton Backcourt Stroke Route Planning Method Based on Deep Learning," *Journal of Mathematics*, vol. 2021, Article ID 6407049, 6 pages, 2021.

[2] L. Ferguson, "Advancing Research Integrity Collaboratively and with Vigour," 2022, https://www.hindawi.com/post/advancing-research-integrity-collaboratively-and-vigour/.

Hindawi
Journal of Mathematics
Volume 2023, Article ID 9895324, 1 page
https://doi.org/10.1155/2023/9895324

Retraction

Retracted: Preorder of Factors Affecting Oil Prices: Fuzzy PROMETHEE Approach

Journal of Mathematics

Received 19 December 2023; Accepted 19 December 2023; Published 20 December 2023

This article has been retracted by Hindawi following an investigation undertaken by the publisher [1]. This investigation has uncovered evidence of one or more of the following indicators of systematic manipulation of the publication process:

(1) Discrepancies in scope

(2) Discrepancies in the description of the research reported

(3) Discrepancies between the availability of data and the research described

(4) Inappropriate citations

(5) Incoherent, meaningless and/or irrelevant content included in the article

(6) Manipulated or compromised peer review

The presence of these indicators undermines our confidence in the integrity of the article's content and we cannot, therefore, vouch for its reliability. Please note that this notice is intended solely to alert readers that the content of this article is unreliable. We have not investigated whether authors were aware of or involved in the systematic manipulation of the publication process.

Wiley and Hindawi regrets that the usual quality checks did not identify these issues before publication and have since put additional measures in place to safeguard research integrity.

We wish to credit our own Research Integrity and Research Publishing teams and anonymous and named external researchers and research integrity experts for contributing to this investigation.

The corresponding author, as the representative of all authors, has been given the opportunity to register their agreement or disagreement to this retraction. We have kept a record of any response received.

References

[1] L. Abdullah, N. Harun, S. M. Mahali, N. Jan, and E. Rak, "Preorder of Factors Affecting Oil Prices: Fuzzy PROMETHEE Approach," *Journal of Mathematics*, vol. 2022, Article ID 2766945, 15 pages, 2022.

Hindawi
Journal of Mathematics
Volume 2022, Article ID 2766945, 15 pages
https://doi.org/10.1155/2022/2766945

Research Article

Preorder of Factors Affecting Oil Prices: Fuzzy PROMETHEE Approach

Lazim Abdullah,[1] **Nurhatika Harun**,[1] **Shalela Mohd Mahali**,[1] **Naeem Jan**,[2] **and Ewa Rak**[3]

[1]*Management Science Research Group, Faculty of Ocean Engineering Technology and Informatics, Universiti Malaysia Terengganu, Kuala Nerus 21030, Malaysia*
[2]*Department of Mathematics, Gomal University, Dera Ismail Khan, Pakistan*
[3]*College of Natural Science, University of Rzeszow, Rzeszow, Poland*

Correspondence should be addressed to Naeem Jan; naeem.phdma73@iiu.edu.pk

Received 20 December 2021; Revised 28 March 2022; Accepted 29 March 2022; Published 17 June 2022

Academic Editor: Ghous Ali

Oil is a highly demanded worldwide product as oil prices can have a major economic and social impact. There are many factors affecting oil prices, but little is known about which factor mostly influenced oil prices. To understand what caused the fluctuation of oil prices, the investigation leading up to the identification of the factors must be constructed. Thus, this paper attempts to explore the factors that might have contributed to oil prices and analyze them using the fuzzy preference ranking organization method for enrichment evaluation (PROMETHEE) method. In particular, the objective of this study is to rank the influential factors affecting oil prices with the consideration of a few criteria. The fuzzy PROMETHEE model comprises four criteria and five factors as the input information. A group of four experts are invited to provide an evaluation on scales of 1 to 5 of the importance of factors with respect to criteria. In computation, the evaluations are treated as triangular fuzzy numbers in which the uncertainty in data is dealt with amicably. This approach combines the advantages of transformation equation and nonarithmetic mean of the defuzzification method that transforms triangular fuzzy numbers into crisp numbers. The results indicate that "supply and demand" is the most influential factor in determining oil prices. Comparative analysis and future research directions are also discussed at the end of this paper.

1. Introduction

One of the most critical issues in the economic development of a country is global oil prices. The price of oil indirectly affects the cost of living of most people, since it is so directly attached to petrol costs. This implies that if global oil prices rise, so the price of petrol is rising as well, and this will affect people's daily life. Oil prices are inconceivably sensitive, changing rapidly considering news cycles, arrangement changes, and fluctuation in the world's business, manufacturing industries, and economic development sectors. For example, as oil prices go up, all the petrochemical-related industries such as plastic, rubber, paints, dyes, textile solvent, and so on will be affected directly [1]. It has been suggested that global oil price stands out among the most important floating prices in the world [2]. Oil prices are considered floating prices as there are many factors that can be attached to them. Oil prices changes are most likely to lead to inflation, and it is more intense when oil prices are on the rise. As indicated by the concept of supply and demand, the oil price should increase with increasing demand or decreasing supply [3]. Therefore, the oil price is not a straightforward issue as there are many other factors that concurrently attached to it. There is no quick-fix solution when it comes to finding the most influential factors that affect oil prices. Moreover, it shows that oil prices have a nonlinearly impact on inflation risk and other economic variables [4]. The presence of nonlinearity in the relationship

between oil prices and their impacts and also factors that affect oil prices might influence the way oil prices are investigated.

1.1. Related Works. To further explore the issue of fluctuation and nonlinearity of oil prices, Kaufmann et al. [5] conducted a study that used a statistical model to assess casual relationships between factors to influence oil prices and monthly oil prices. A linear relationship could be a reasonable estimation under ordinary conditions. However, under extreme events, oil price may shift the market balance among supply and demand towards different types of markets in which prices are much more sensitive that will contain a small sample bias. Dees et al. [6] also show that a nonlinear effect of oil producers' country's capacity and condition in future markets are the factors of the oil price increase. The researchers developed a model to estimate the real average price of US crude oil. They expect the regression coefficient associated to be negative. However, there are a few weaknesses in the regression models that should be pointed out. Results from the econometric regression-based analysis are highly sensitive. Small changes in the data set and the model designs can give a huge impact on the outcomes [7]. Zakaria et al. [8] discussed further the nonlinearity of oil prices. They measured the influence of the world oil prices on inflation rates in South Asian countries using the value at risk, cointegration, and nonlinearity analysis. The results tell that cointegration holds among oil prices and inflation. Nonlinear causality tests stipulated that oil price causes inflation. A similar approach was also employed by Oloko et al. [9] who concluded that the monetary policy of oil-importing countries appears to accommodate oil price shocks. In a correlational study, Wu and Wang [10] examined the relationship between oil prices and corporate investment, conditional on market conditions. They discovered that oil prices are negatively correlated with corporate investment expenditure. However, they also found out that if market conditions are favorable, then corporate investment expenditure increases as oil prices rise.

As to depart from regression- and correlation-based analysis where data employed in studies are very much sensitive, Wang et al. [11] used a different approach. They used an extensive variety of generalized Maclaurin symmetric mean (MSM) aggregation operators that multicriteria decision-making (MCDM) issues were solved. The criteria in MCDM problems were enhanced by considering weights to reflect the importance of the criteria. They provide a practical example and conduct a comparison analysis between the proposed method and other existing methods in order to verify the proposed method and demonstrate its validity. They also successfully applied the proposed methods to a real-life MCDM problem. Very recently, in application research to biodiesel feedstock, Anwar [12] conducted research on defining the best possible biodiesel feedstock using various MCDM processes. Four MCDM processes, namely the preference ranking organization method for enrichment evaluation (PROMETHEE) graphical analysis for interactive assistance [13, 14], weighted sum method [15, 16], weighted product method [17], and technique for order preference by similarity to the ideal solution [18], were implemented for this investigation.

However, there are two pertinent matters that are normally attached to most of the MCDM methods. The matters are about their parametrization and its uncertainty. In fact, the feasibility of MCDM is directly connected to the importance and quality of the chosen parameters. One of the MCDM methods related to parametrization is the PROMETHEE. Unlike most of the MCDM method such as the analytic hierarchy process (AHP) that handle preference directly from decision-makers' opinions, the PROMETHEE method heavily relies on the chosen parameters, which are normally known as preference functions. Preference function and pairwise comparison of alternatives and differences between two alternatives are the main advantages of PROMETHE that the final output is the partial preorder (partial ranking) and total preorder (complete ranking). Because of these advantages, the PROMETHEE method has specific application in decision-making and generally is utilized far and wide in a wide assortment of decision scenarios, in fields such as business, administrative establishment, health care, transportation, and education. The second matter is about uncertainty. As to deal with uncertainty in information, the fuzzy PROMETHEE was proposed. There is a fuzzy concept to the PROMETHEE method when dealing with uncertain and subjective information. The fuzzy set theory and the ranking technique were incorporated into the fuzzy PROMETHEE method. According to Brans and Mareschal [19], the fundamental advantage of this technique is the ease of use. Linguistic evaluations and the thought of fuzziness are the two notions that are germane to decision-making problem.

1.2. Motivation. A search of literature found that most of the researchers tend to conduct research using PROMETHEE rather than fuzzy PROMETHEE because the fuzzy PROMETHEE method is associated with the theory of fuzzy sets [20]. Another reason could be associated with heavy calculation in fuzzy PROMETHEE besides no readily available software to assist computation. However, in recent years, there has been an increasing interest in applications of fuzzy PROMETHEE not only as a single model but also integrated with other fuzzy-based decision-making models. For example, fuzzy PROMETHEE has been integrated with AHP in group decision-making [21]. Recent research also unveiled several new extensions of fuzzy PROMETHEEE such as m-polar fuzzy PROMETHEE [21], bipolar fuzzy PROMETHEE [22], and q-rung orthopair fuzzy PROMETHEE [23]. In application to health sciences, Maisaini et al. [24] conducted a study to break down the most common therapeutic techniques for lung cancer. In their venture, the fuzzy PROMETHEE method was utilized to investigate the therapeutic techniques that are dependent on six factors. The results demonstrated that the surgery among other techniques showed an incredible act on lung cancer treatment depending on the criteria, importance, and weights chosen. In addition, fuzzy PROMETHEE also has been integrated.

Fuzzy PROMETHEE also shows that one can easily adjust the method by including more criteria and change their significance and weight relying upon the application. Afful-Dadzie et al. [25] had proposed a two-phase framework of a decision-making methods and sensitivity analysis to show how aid recipient countries can be assessed to heighten transparency, reasonableness, esteem for cash, and manageability of such guide programs. Utilizing the OECD set for subjective criteria for assessing aid programs, a numerical model precharacterized by linguistic terms parameterized by triangular fuzzy numbers was given to assess aid programs. Fuzzy PROMETHEE was utilized in the first phase to assess and rank aid recipients pursued by a comparative analysis with other fuzzy-based decision-making methods. The result demonstrates a framework that can be utilized in assessing the aid effectiveness of recipient countries. Very recently, Ziemba [26] applied the fuzzy PROMETHEE combined with the Monte Carlo method and elements of the stochastic multicriteria acceptability analysis method. They applied their proposed method for assessing vehicles under uncertain conditions. The approach allowed us to identify almost unambiguously the electric vehicle that is likely to gain the highest acceptance. As a result of the conducted research, it was found that the approaches to uncertainty based on fuzzy sets, outranking relations, and stochastic analysis complement each other, allowing the decision-maker to conduct a wider analysis of the imprecision of the obtained solution.

1.3. Innovative Contribution. Turning now to the fluctuations and nonlinearity of oil prices where understanding the importance of causal factors that affect oil prices is the main aim of this paper. The fuzzy PROMETHEE is used as a selection tool with the end goal is to identify the most influential factors that affect oil prices. The contributions of this paper are fourfold: (1) we propose to use a transformation equation in the computational steps of fuzzy PROMETHEE where information that is given in triangular fuzzy numbers is transformed into left-right fuzzy numbers. This transformation is meant to ease the computational burden and also to avoid the loss of information during the implementation. (2) We propose to introduce a non-arithmetic mean of defuzzification where a constant is used as a multiplying factor to the mid-values of the left-right triangular fuzzy numbers. This would enhance the dominance of mid-values of left-right triangular fuzzy numbers. (3) We propose partial preorder and total preorder of factors that affect oil prices. (4) We propose a comparative analysis of net value flows to validate the results obtained using the proposed method. These four contributions are embedded in the proposed fuzzy PROMETHEE where the partial preorder and total preorder of factors can indicate the most influential factors that affect global oil prices.

1.4. Framework of the Paper. The rest of this paper is organized as follows. Section 2 briefly revisits the definitions of linguistic variables, triangular fuzzy numbers, and their algebraic operations. Section 3 presents the methodology of the research, which includes the evaluation model. In Section 4, computational procedures and results for the case study of factors affecting oil prices are described. Section 5 provides the comparative results of the final ranking and net flows. Finally, Section 6 concludes.

2. Preliminary

In a similar way to MCDM methods, there is a fuzzy expansion of the PROMETHEE method when dealing with uncertain and subjective information. Fuzzy PROMETHEE has similarly observed enhancements in several variations such as PROMETHEE I, II, III, IV, V, and VI. The fuzzy PROMETHEE method has been used in solving numerous decision-making problems where the task of ranking alternatives and concurrently considering fuzzy information, fuzzy preferences, and fuzzy weights is indeed very challenging. This is partly due to interval data that would increase the complexity of computation. According to Brans and Mareschal [27], the fundamental advantage of this technique is ease of use in implementation because most of the decision-making problems can be solved by incorporating linguistic evaluations and the thought of fuzziness. Later, we revisit several notions related to fuzzy MCDM that will be used in the subsequent text.

2.1. Linguistic Variable [28]. Linguistic variables are used for system input and output and are represented by words or sentences instead of the number investigated by Zadeh [29, 30]. In explaining this, take the example of the linguistic variable "temperature." Let T be a set of linguistic variable "temperatures" where $T = \{\text{very cold, cold, moderate, warm, very hot}\}$. The members of set T are called linguistic terms where gradations of T are defined. These linguistic terms are normally translated into triangular fuzzy numbers.

2.2. Triangular Fuzzy Numbers [31]. The triangular fuzzy number, $\mu_A(x)$, is defined by its lower limit a, its upper limit b, and the modal value m so that $a < m < b$. It is written in the form of function $A(x)$ as follows:

$$A(x) = \begin{cases} 0, & x \le a, \\ (x-a)/(m-a), & x \in (a, m), \\ (b-x)/(b-m), & x \in (b, m), \\ 1, & x \ge 0. \end{cases} \quad (1)$$

In this function, interval a to m is increasing function, and interval m to b is decreasing function.

For $x < a$ or $x > b$, x does not belong to the set.

For $[x \le a \le b]$, the membership degree is indicated by membership function between 0 and 1.

These fuzzy numbers and their basic arithmetic operations are widely used in the fuzzy MCDM method.

2.3. Basic Operations of Triangular Fuzzy Numbers [32]. Let $A = (a, b, c)$ and $B = (d, e, f)$ be two triangular numbers, then the basic arithmetic operations for addition,

subtraction, multiplication, division, and scalar multiplication are defined as follows:

$$\begin{aligned} A(+)B &= (a,b,c)(+)(d,e,f) = (a+d, b+e, c+f),\\ A(-)B &= (a,b,c)(-)(d,e,f) = (a-f, b-e, c-d),\\ A(\times)B &= (a,b,c)(\times)(d,e,f) = (ad, be, cf),\\ A(\div)B &= (a,b,c)(\div)(d,e,f) = \left(\frac{a}{f}, \frac{b}{e}, \frac{c}{d}\right),\\ nA &= (na, nb, nc). \end{aligned} \tag{2}$$

2.4. Preference Function [27]. Let $P_j(a,b) = F_j[d_j(a,b)]$ is a preference function of PROMEHEE, where $P_j(a,b)$ signify the function of the difference between the evaluations of alternative a with respect to alternative b on each criterion into a degree ranging from 0 to 1. The smaller number of functions indicates the indifference of the decision-maker. Conversely, closer to 1 indicates greater preference. If $P_j(a,b)$ the usual criteria function, then the indifference only occurs when $f(a) = f(b)$. The function of $f(x)$ is given as follows:

$$p(x) = \begin{cases} 0, & \text{for } x \le 0,\\ 1, & \text{for } x > 0. \end{cases} \tag{3}$$

The above notions are used directly during the implementation of computational procedures of the fuzzy PROMETHEE. The output of computational procedures are partial ranking and complete ranking of factors affecting oil prices.

3. Methodology

The methodology is a process used to collect information and data, which regularly includes interviews, data collection, and computational models. The purpose of this section is to have a discussion of the methodology used so that the objective of this study is met. This section begins by describing the type of data collection via experts, factors, and criteria that affect oil prices, followed by computational procedures of the fuzzy PROMETHEE method.

3.1. Experts and Linguistic Variable. In this research, data are collected via personal communication with a group of three experts. All experts have vast experiences in the oil and gas industry in which their details are summarized in Table 1.

In personal communication, experts are requested to provide a rating of five factors that affect oil prices with respect to four criteria of oil prices using the linguistic variable shown in Table 2.

The experts are also requested to provide a level of importance of each criterion using the linguistic variable of "importance." This linguistic variable and its respective triangular fuzzy numbers are shown in Table 3.

3.2. Factors and Criteria. Five factors a_1, a_2, a_3, a_4, and a_5 that represent supply, demand, report (OPEC, target pricing, and investment), political event and crises, and access markets, respectively, are the factors chosen in this study. Descriptions of factors are given in Table 4.

Through personal communication, the experts (E_1, E_2, E_3) are requested to rank and evaluate the factors that affect oil prices with respect to four criteria. In this study, criteria are defined as a benchmark in determining oil prices. Benchmark crude or marker crude is raw petroleum that fills in as a source of the reference price for purchasers and dealers of raw petroleum. Benchmarks are utilized in light of the fact that there are various assortments and grades of unrefined petroleum. The benchmark makes it simpler for dealers, investors, experts, and others to decide the prices of multitudes of grades of unrefined petroleum [1]. In this study, the criteria are O_1 (West Texas Intermediate, WTI), O_2 (Brent), O_3 (OPEC Reference Basket), and O_4 (Western Canadian Select, WCS). Descriptions of the criteria are presented in Table 5.

Evaluation of the criteria and the factors become the input data or information for computation using the fuzzy PROMETHEE. The output of the computations are partial ranking and complete ranking. Information processing is implemented using the fuzzy PROMETHEE where information of the input data are given in triangular fuzzy numbers. Detailed computational procedures are given as follows.

3.3. Computational Procedures of Fuzzy PROMETHEE Method. In most fuzzy MCDM frameworks, identifying alternatives, criteria, linguistic variables, and experts are required. In the following, we propose the computational procedures for the generic fuzzy PROMETHEE, which later can be used in the case of oil prices. These computational procedures are adopted from Abdullah et al. [41] where the steps of PROMETHEE with crisp numbers are the main designs. Several innovations are made in the proposed fuzzy PROMETHEE compared to the PROMETHEE [41]. Apart from the substitution of crisp numbers with triangular fuzzy numbers, the proposed fuzzy PROMETHEE method also includes a transformation process where triangular fuzzy numbers are transformed into left-right triangular fuzzy numbers. This transformation is needed as left-right fuzzy numbers can easily fit with the Yager index that will be employed in the subsequent step. Instead of using the arithmetic mean in defuzzification, this proposed method introduced coefficient 3 to the mid-value of left-right triangular fuzzy numbers. This will propel the dominance of the mid-value of left-right triangular fuzzy numbers without ignoring their left width and right width. Another innovation is the sequence of obtaining partial preorder and total preorder. In the proposed method, the partial preorder is obtained just before the step of transformation and defuzzification where this decision is made based on the values of triangular fuzzy numbers of inflows and outflows. This sequence is contrasting with the regular PROMETHEE where partial preorder and total preorder happen one after

Table 1: Biographical data of experts.

Experts	Designation	Years of experience	Company address
Expert 1 (*E1*)	Project manager	4	Nuri Cerah Sdn Bhd (NCSB), Kota Kinabalu, Sabah Malaysia
Expert 2 (*E2*)	Field engineer	4	Petronas MLNG Sdn. Bhd., Bintulu, Sarawak Malaysia
Expert 3 (*E3*)	Instrument engineer	6	Petronas MLNG Sdn. Bhd., Bintulu, Sarawak Malaysia

Table 2: Linguistic variable "influence" and corresponding fuzzy numbers.

Rating of factors	Triangular fuzzy numbers
Poor	(0.00, 0.00, 0.25)
Average	(0.00, 0.25, 0.50)
Influence	(0.25, 0.50, 0.75)
Very influence	(0.50, 0.75, 1.00)
Extremely influence	(0.75, 1.00, 1.00)

Table 3: Linguistic variable "importance" and corresponding fuzzy numbers.

Weights of criteria	Triangular fuzzy scales
Unimportant	(0.00, 0.00, 0.25)
Little important	(0.00, 0.25, 0.50)
Moderately important	(0.25, 0.50, 0.75)
Important	(0.50, 0.75, 1.00)
Very important	(0.75, 1.00, 1.00)

Table 4: Descriptions of factors.

Factors	Descriptions
a_1 (supply)	The Organization of Petroleum Exporting Countries (OPEC) has been colossal on the world's exchanging floors, with its oil-producing member nations cooperating to decide prices by boosting or decreasing oil production. OPEC as of now controls 40% of the world's oil production; in this way, they still have a significant impact on the oil market [33]. Therefore, supply is one of the factors affecting oil prices.
a_2 (demand)	Solid monetary development and modern generation will in general lift the demand for oil as reflected in changing demand patterns by non-OECD countries, which have grown quickly as of late. As indicated by the concept of supply and demand, the oil price should increase with increasing demand or decreasing supply [3].
a_3 (report)	Report on creation figures, spare capacity, target pricing, and investments can be a critical factor in the setting of oil prices [34].
a_4 (political events and crises)	War, natural disasters, political change, and new government pioneers are on the whole factors impacting crude oil pricing [35].
a_5 (access markets)	The futures market of oil plays a role in influencing the spot price of oil [36]. An oil futures contract is a binding agreement that gives the privilege to buy oil by the barrel at a predefined price on a predefined date later on. Under a prospects contract, both the purchaser and the merchant are committed to satisfying their side of the exchange on the predetermined date.

Table 5: Description of criteria.

Criteria	Descriptions
O_1 (West Texas intermediate, WTI)	WTI, otherwise called Texas light sweet, is a grade of crude oil used as a benchmark in oil pricing [37]. This grade is portrayed as medium crude oil in light of its generally low thickness and sweet because of its low sulphur content
O_2 (Brent)	Brent is also an important benchmark for crude oil pricing [38]. Brent contains around 0.37% of sulphur classifying it as sweet crude, yet not as sweet as WTI. Brent is reasonable for the production of petrol and middle distillates. Historically, price differences between Brent and other index crudes have been founded on physical contrasts in crude oil specifications and short-term variations in supply and demand.
O_3 (OPEC Reference Basket)	Besides WTI and Brent, the OPEC Reference Basket is also a benchmark for oil pricing [39]. The OPEC Basket is a weighted average of prices for petroleum blends produces by OPEC members. It is utilized as an imperative benchmark for crude oil prices. OPEC has frequently endeavored to keep the price of the OPEC basket between upper and lower limits, by increasing and decreasing production. This makes the measure essential for market analysts.
O_4 (Western Canadian Select, WCS)	WCS is one of North America's biggest overwhelming crude oil streams. It is an alternative to the Canadian oil and gas industry, and individual firms' equity prices react to oil price fluctuations [40]. It is an overwhelming mixed crude oil, made for the most part of bitumen mixes with sweet synthetic and condensate diluents and 25 existing streams of both ordinary and flighty. WCS is the benchmark for emerging heavy, high TAN (acidic).

the other. The flowchart of the proposed method is shown in Figure 1.

The proposed nine-step computational procedures are as follows:

Step 1. Define factors, criteria, and experts.

Suppose in a decision-making problem, we have m alternatives, k criteria, and n experts.

Step 2. Define linguistic variables and linguistic terms in triangular fuzzy numbers.

Define the criteria weight of each criterion corresponding to the linguistic term. The w_j represents the weight of criterion based on linguistic terms assigned by experts. The weight of the criterion is expressed in triangular fuzzy numbers.

Step 3. Aggregate the evaluation.

The weights of the criteria and the ratings of factors are aggregated using the basic proportion equation as follows:

$$\widetilde{w}_{jk} = \frac{\widetilde{w}_j}{\widetilde{w}_k}\left(0 \le \widetilde{w}_{jk} \le 1\right), \widetilde{w}_k = \max\left(\widetilde{w}_j\right)(k, j = 1, 2, \ldots, n). \tag{4}$$

Step 4. Construct preference function.

The preference function $\widetilde{P}_j(m, n)$ represents the experts' preference between pairs of factors. The preference function $\widetilde{P}_j(a, b)$ for a criterion can be defined as follows:

$$\widetilde{P}_j(a,b) = \begin{cases} 0, & \widetilde{x_{aj}} \le \widetilde{x}_{bj}, \\ \widetilde{x}_{aj} - \widetilde{x}_{bj}, & \widetilde{x_{aj}} > \widetilde{x}_{bj}, \end{cases} \quad \text{where } j = 1, 2, \ldots, k. \tag{5}$$

Step 5. Compute the multifactor preference index.

Multicriteria preference index is used to choose the rate in outranking relation.

$$\widetilde{\pi}(a,b) = \frac{\sum_{j=1}^{k}\left[\widetilde{w_j}\widetilde{p}_j(a,b)\right]}{\sum_{j=1}^{k}\widetilde{w_j}}, \tag{6}$$

where $\widetilde{w_j}$ denotes the important weight of the factor.

If $\widetilde{\pi}(a, b) \approx 0$, it implies a weak preference of a over b.

If $\widetilde{\pi}(a, b) \approx 1$, it implies a strong preference of a over b.

Step 6. Compute the positive and negative outranking flows for partial preorder.

For PROMETHEE I (partial ranking), the ranking of factors is made by calculating the positive and negative outranking flows as follows:

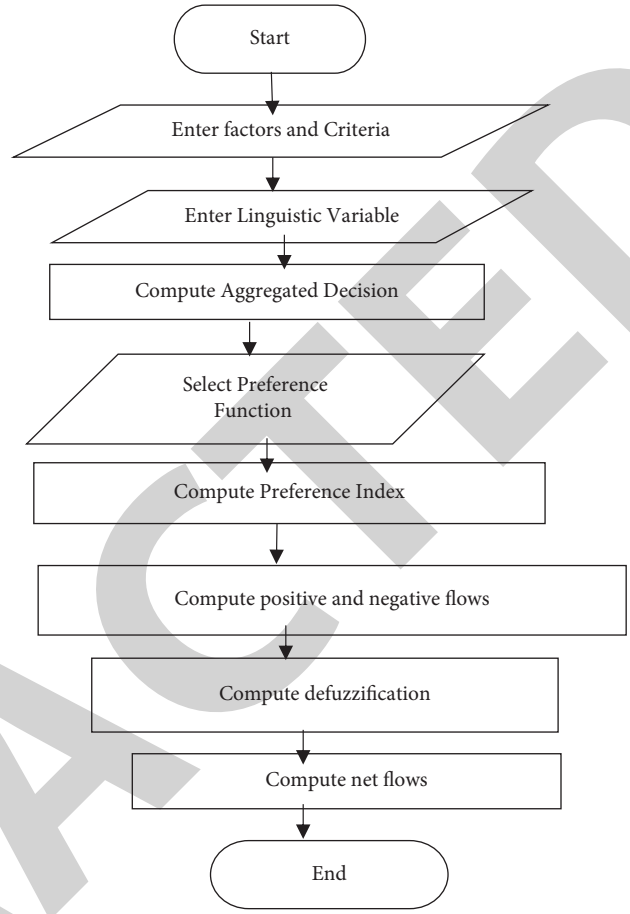

Figure 1: Flowchart of fuzzy PROMETHEE.

$$\text{Positive outranking} : \widetilde{\varphi}^{+}(m) = \frac{1}{n-1}\sum_{m \ne l}\widetilde{\pi}(m,l), \quad \forall m, l \in A, \tag{7}$$

$$\text{Negative outranking} : \widetilde{\varphi}^{-}(m) = \frac{1}{n-1}\sum_{m \ne l}\widetilde{\pi}(l,m), \quad \forall m, l \in A, \tag{8}$$

where m and n denote the number of factors and experts, respectively.

Step 7. Transform triangular fuzzy numbers.

The triangular number (L, M, R) needs to transform into the form (M, a, b)

$$\text{where } a = M - L \text{ and } b = R - M. \tag{9}$$

It is necessary to represent fuzzy numbers in form of left-right.

Step 8. Defuzzify.

The defuzzification method used in this study is the Yager index method. The average of left-right and middle of triangular fuzzy numbers is the defuzzification value. The defuzzification equation is

$$(M, a, b) = \frac{3M - a + b}{3}. \tag{10}$$

Step 9. Establish total preorder

The complete or full ranking of factors is established based on the value of net flows. Negative net flows subtracted from positive net flows will give net flows.

$$\text{Net flow} : \widetilde{\varphi}(m) = \widetilde{\varphi^{+}}(m) - \widetilde{\varphi^{-}}(m), \quad \forall m \in A. \tag{11}$$

The above computational procedures are implemented in the case of factors affecting oil prices. Detailed computations and results are given in the following section.

4. Computations and Results

Information about the evaluation becomes the input data for implementing the computation. All this information is given in triangular fuzzy numbers, and the execution of the computation is made according to the proposed computational procedures.

Evaluation of criteria given by experts is summarized in Table 6.

Aggregation of weight of criterion from experts is computed using equation (4).

$$\begin{aligned}
\widetilde{w}_1 &= \frac{1}{3}((0.50,\ 0.75,\ 1.00) \oplus (0.50, 0.75, 1.00) \oplus (0.25, 0.50, 0.75)) \\
&= (0.42, 0.67, 0.92), \\
\widetilde{w}_2 &= \frac{1}{3}((0.25, 0.50, 0.75) \oplus (0.75, 1.00, 1.00) \oplus (0.50, 0.75, 1.00)) \\
&= (0.5, 0.75, 0.92), \\
\widetilde{w}_3 &= \frac{1}{3}((0.25, 0.50, 0.75) \oplus (0.25, 0.50, 0.75) \oplus (0.75, 1.00, 1.00)) \\
&= (0.42, 0.67, 0.83), \\
\widetilde{w}_4 &= \frac{1}{3}((0.50, 0.75, 1.00) \oplus (0.75, 1.00, 1.00) \oplus (0.25, 0.50, 0.75)) \\
&= (0.5, 0.75, 0.92).
\end{aligned} \tag{12}$$

Equation (12) shows the weights represent aggregated weights for oil benchmarks (criteria) $O_i (i = 1, 2, 3, 4)$, respectively.

Table 7 shows the ratings of the factors with respect to criteria.

The above ratings are aggregated using equation (4) to obtain aggregated rating for each criterion. For example,

$$\begin{aligned}
\widetilde{x}_{11} &= \frac{1}{3}[(0.25, 0.50, 0.75) \oplus (0.75, 1.00, 1.00) \oplus (0.25, 0.50, 0.75)] \\
&= (0.42, 0.67, 0.83), \\
\widetilde{x}_{12} &= \frac{1}{3}[(0.25, 0.50, 0.75) \oplus (0.75, 1.00, 1.00) \oplus (0.25, 0.50, 0.75)] \\
&= (0.42, 0.67, 0.83), \\
\widetilde{x}_{13} &= \frac{1}{3}[(0.25, 0.50, 0.75) \oplus (0.50, 0.75, 1.00) \oplus (0.00, 0.25, 0.50)] \\
&= (0.25, 0.5, 0.75), \\
\widetilde{x}_{13} &= \frac{1}{3}[(0.25, 0.50, 0.75) \oplus (0.50, 0.75, 1.00) \oplus (0.25, 0.50, 0.75)] \\
&= (0.33, 0.58, 0.83), \\
\widetilde{x}_{13} &= \frac{1}{3}[(0.25, 0.50, 0.75) \oplus (0.50, 0.75, 1.00) \oplus (0.00, 0.25, 0.50)] \\
&= (0.33, 0.58, 0.83),
\end{aligned} \tag{13}$$

Table 6: Fuzzy weight of criteria.

Oil benchmark	E_1	E_2	E_3
O_1	(0.50, 0.75, 1.00)	(0.50, 0.75, 1.00)	(0.25, 0.50, 0.75)
O_2	(0.25, 0.50, 0.75)	(0.75, 1.00, 1.00)	(0.50, 0.75, 1.00)
O_3	(0.25, 0.50, 0.75)	(0.25, 0.50, 0.75)	(0.75, 1.00, 1.00)
O_4	(0.50, 0.75, 1.00)	(0.75, 1.00, 1.00)	(0.25, 0.50, 0.75)

Table 7: Fuzzy ratings of the factors.

Criteria	Factors	Experts E_1	E_2	E_3
O_1	a_1	(0.25, 0.50, 0.75)	(0.75, 1.00, 1.00)	(0.25, 0.50, 0.75)
	a_2	(0.25, 0.50, 0.75)	(0.75, 1.00, 1.00)	(0.25, 0.50, 0.75)
	a_3	(0.25, 0.50, 0.75)	(0.50, 0.75, 1.00)	(0.00, 0.25, 0.50)
	a_4	(0.25, 0.50, 0.75)	(0.50, 0.75, 1.00)	(0.25, 0.50, 0.75)
	a_5	(0.25, 0.50, 0.75)	(0.50, 0.75, 1.00)	(0.00, 0.25, 0.50)
O_2	a_1	(0.25, 0.50, 0.75)	(0.75, 1.00, 1.00)	(0.25, 0.50, 0.75)
	a_2	(0.25, 0.50, 0.75)	(0.75, 1.00, 1.00)	(0.50, 0.75, 1.00)
	a_3	(0.25, 0.50, 0.75)	(0.50, 0.75, 1.00)	(0.25, 0.50, 0.75)
	a_4	(0.00, 0.25, 0.50)	(0.50, 0.75, 1.00)	(0.25, 0.50, 0.75)
	a_5	(0.25, 0.50, 0.75)	(0.50, 0.75, 1.00)	(0.25, 0.50, 0.75)
O_3	a_1	(0.00, 0.25, 0.50)	(0.00, 0.25, 0.50)	(0.50, 0.75, 1.00)
	a_2	(0.25, 0.50, 0.75)	(0.00, 0.25, 0.50)	(0.50, 0.75, 1.00)
	a_3	(0.50, 0.75, 1.00)	(0.00, 0.25, 0.50)	(0.25, 0.50, 0.75)
	a_4	(0.25, 0.50, 0.75)	(0.50, 0.75, 1.00)	(0.25, 0.50, 0.75)
	a_5	(0.00, 0.25, 0.50)	(0.25, 0.50, 0.75)	(0.25, 0.50, 0.75)
O_4	a_1	(0.00, 0.25, 0.50)	(0.00, 0.25, 0.50)	(0.25, 0.50, 0.75)
	a_2	(0.25, 0.50, 0.75)	(0.25, 0.50, 0.75)	(0.50, 0.75, 1.00)
	a_3	(0.25, 0.50, 0.75)	(0.00, 0.25, 0.50)	(0.25, 0.50, 0.75)
	a_4	(0.25, 0.50, 0.75)	(0.50, 0.75, 1.00)	(0.25, 0.50, 0.75)
	a_5	(0.25, 0.50, 0.75)	(0.25, 0.50, 0.75)	(0.00, 0.25, 0.50)

Equation (13) shows part of the aggregated ratings for criteria. These results are summarized in Table 8.

This study uses the usual function (type 1) as a preference function (see equation (5)).

For example,

$$\begin{aligned}
\widetilde{p}_1(a_1, a_2) &= (0.42 - 0.83, 0.67 - 0.67, 0.83 - 0.42) = (-0.42, 0, 0.42),\\
\widetilde{p}_1(a_1, a_3) &= (0.42 - 0.75, 0.67 - 0.50, 0.83 - 0.25) = (-0.33, 0.17, 0.58),\\
\widetilde{p}_1(a_1, a_4) &= (0.42 - 0.75, 0.67 - 0.58, 0.83 - 0.33) = (-0.42, 0.08, 0.50),\\
\widetilde{p}_1(a_1, a_5) &= (0.42 - 0.75, 0.67 - 0.50, 0.83 - 0.25) = (-0.33, 0.17, 0.58),\\
\widetilde{p}_1(a_3, a_1) &= (0.25 - 0.83, 0.50 - 0.67, 0.75 - 0.42) = (-0.58, -0.17, 0.33).
\end{aligned} \tag{14}$$

The initial part of the preference functions is shown in equation (14). Tables 9–13 show the fuzzy preference function of a_1, a_2, a_3, a_4, a_5, respectively.

The next step is calculating the multifactor preference index using equation (6).

For example,

$$\pi(a_1, a_2) = \frac{\sum[[(-0.42, 0, 0.42) * (0.42, 0.67, 0.92)]]}{[(0.42, 0.67, 0.92)]},$$

$$= \frac{(-0.1764, 0, -0.3864)}{(0.42, 0.67, 0.92)}.$$

Table 8: Aggregated fuzzy rating of a factor with respect to criteria.

Oil benchmark	Factors	Aggregated rating
O_1	a_1	(0.42, 0.67, 0.83)
	a_2	(0.42, 0.67, 0.83)
	a_3	(0.25, 0.50, 0.75)
	a_4	(0.33, 0.58, 0.83)
	a_5	(0.25, 0.50, 0.75)
O_2	a_1	(0.42, 0.67, 0.83)
	a_2	(0.50, 0.75, 0.92)
	a_3	(0.33, 0.58, 0.83)
	a_4	(0.25, 0.50, 0.75)
	a_5	(0.33, 0.58, 0.83)
O_3	a_1	(0.17, 0.42, 0.67)
	a_2	(0.25, 0.50, 0.75)
	a_3	(0.25, 0.50, 0.75)
	a_4	(0.33, 0.58, 0.83)
	a_5	(0.17, 0.42, 0.67)
O_4	a_1	(0.08, 0.33, 0.58)
	a_2	(0.33, 0.58, 0.83)
	a_3	(0.17, 0.42, 0.67)
	a_4	(0.33, 0.58, 0.83)
	a_5	(0.17, 0.42, 0.67)

Table 9: Fuzzy preference function, $\widetilde{P}_j(a_1, a_i)$.

Oil benchmark, O_i	$\widetilde{P}_j(a_1, a_2)$	$\widetilde{P}_j(a_1, a_3)$	$\widetilde{P}_j(a_1, a_4)$	$\widetilde{P}_j(a_1, a_5)$
O_1	(−0.42, 0, 0.42)	(−0.33, 0.17, 0.58)	(−0.42, 0.08, 0.50)	(−0.33, 0.17, 0.58)
O_2	(0, 0, 0)	(−0.42, 0.08, 0.50)	(−0.33, 0.17, 0.58)	(−0.42, 0.08, 0.50)
O_3	(0, 0, 0)	(0, 0, 0)	(0, 0, 0)	(−0.50, 0, 0.50)
O_4	(0, 0, 0)	(0, 0, 0)	(0, 0, 0)	(0, 0, 0)

Table 10: Fuzzy preference function, $\widetilde{P}_j(a_2, a_i)$.

Oil benchmark, O_i	$\widetilde{P}_j(a_2, a_1)$	$\widetilde{P}_j(a_2, a_3)$	$\widetilde{P}_j(a_2, a_4)$	$\widetilde{P}_j(a_2, a_5)$
O_1	(−0.42, 0, 0.42)	(−0.33, 0.17, 0.58)	(−0.42, 0.08, 0.50)	(−0.33, 0.17, 0.58)
O_2	(−0.33, 0.08, 0.50)	(−0.33, 0.17, 0.58)	(−0.25, 0.25, 0.67)	(−0.33, 0.17, 0.58)
O_3	(−0.42, 0.08, 0.58)	(−0.50, 0, 0.50)	(0, 0, 0)	(−0.42, 0.08, 0.58)
O_4	(−0.25, 0.25, 0.75)	(−0.33, 0.17, 0.67)	(−0.50, 0, 0.50)	(−0.33, 0.17, 0.67)

Table 11: Fuzzy preference function, $\widetilde{P}_j(a_3, a_i)$.

Oil benchmark, O_i	$\widetilde{P}_j(a_3, a_1)$	$\widetilde{P}_j(a_3, a_2)$	$\widetilde{P}_j(a_3, a_4)$	$\widetilde{P}_j(a_3, a_5)$
O_1	(0, 0, 0)	(0, 0, 0)	(0, 0, 0)	(−0.50, 0, 0.50)
O_2	(0, 0, 0)	(0, 0, 0)	(−0.42, 0.08, 0.58)	(−0.50, 0, 0.50)
O_3	(−0.42, 0.08, 0.58)	(−0.50, 0, 0.50)	(0, 0, 0)	(−0.43, 0.08, 0.58)
O_4	(−0.42, 0.08, 0.58)	(0, 0, 0)	(0, 0, 0)	(−0.50, 0, 0.50)

$$\pi(a_1, a_3) = \frac{\sum[(-0.33, 0.17, 0.58) * (0.42, 0.67, 0.92), (0.42, 0.08, 0.50) * (0.5, 0.75, 0.92)]}{(0.42, 0.67, 0.92) + (0.5, 0.75, 0.92)},$$
$$= \frac{(0.072, 0.174, 0.994)}{(0.92, 1.42, 1.84)} = (0.078261, 0.122535, 0.540217),$$
$$\pi(a_1, a_4) = \frac{\sum(-0.42, 0.08, 0.5) * (0.42, 0.67, 0.92), (-0.33, 0.17, 0.58) * (0.5, 0.75, 0.92)}{(0.42, 0.67, 0.92) + (0.5, 0.75, 0.92)},$$
$$= \frac{(-0.3414, 0.1811, 0.9936)}{(0.92, 1.42, 1.84)} = (-0.371087, 0.127535, 0.54),$$
$$\pi(a_1, a_5) = \frac{\sum[(-0.33, 0.17, 0.58) * (0.42, 0, 67, 0.92), (0.42, 0.08, 0.50) * (0.5, 0.75, 0.92), (-0.50, 0, 0.50) * (0.42, 0.67, 0.38)]}{[(0.42, 0, 67, 0.92) + (0.5, 0.75, 0.92) + (0.42, 0.67, 0.38)]},$$
$$\frac{(-0.138, 0.174, 1.184)}{(1.34, 2.09, 2.22)} = (-0.102985, 0.083254, 0.533333). \quad (15)$$

Table 12: Fuzzy preference function, $\widetilde{P}_j(a_4, a_i)$.

Oil benchmark, O_i	$\widetilde{P}_j(a_4, a_1)$	$\widetilde{P}_j(a_4, a_2)$	$\widetilde{P}_j(a_4, a_3)$	$\widetilde{P}_j(a_4, a_5)$
O_1	(0, 0, 0)	(0, 0, 0)	(−0.42, 0.08, 0.58)	(−0.42, 0.08, 0.58)
O_2	(0, 0, 0)	(0, 0, 0)	(0, 0, 0)	(0, 0, 0)
O_3	(−0.33, 0.17, 0.67)	(−0.42, 0.08, 0.58)	(−0.42, 0.08, 0.58)	(−0.33, 0.17, 0.67)
O_4	(−0.25, 0.25, 0.75)	(−0.50, 0, 0.50)	(−0.33, 0.17, 0.67)	(−0.33, 0.17, 0.67)

Table 13: Fuzzy preference function, $\widetilde{P}_j(a_5, a_i)$.

Oil benchmark, O_i	$\widetilde{P}_j(a_5, a_1)$	$\widetilde{P}_j(a_5, a_2)$	$\widetilde{P}_j(a_5, a_3)$	$\widetilde{P}_j(a_5, a_4)$
O_1	(0, 0, 0)	(0, 0, 0)	(−0.50, 0, 0.50)	(0, 0, 0)
O_2	(0, 0, 0)	(0, 0, 0)	(−0.50, 0, 0.50)	(−0.42, 0.08, 0.58)
O_3	(−0.50, 0, 0.50)	(0, 0, 0)	(0, 0, 0)	(0, 0, 0)
O_4	(−0.42, 0.08, 0.58)	(0, 0, 0)	(−0.50, 0, 0.50)	(0, 0, 0)

Parts of the preference index values are shown in equation (15). It is summarized in Table 14.

In the following, the positive outflows and negative outflows of each factor (PROMETHEE I partial ranking) can be determined using equations (7) and (8). Table 15 shows the positive outflows and negative outflows of factors.

In fuzzy PROMETHEE I, the partial preorders of factors of $a_1P^{(I)}b_2$ are $a_1P^{(I)}a_2$, $a_1P^{(I)}a_3, a_1P^{(I)}a_4$, $a_1P^{(I)}a_5, a_2P^{(I)}a_3, a_2P^{(I)}a_5, a_3P^{(I)}a_5, a_4P^{(I)}a_2, a_4P^{(I)}a_3$, and $a_4P^{(I)}a_5$. The partial preorders of factors are shown in Figure 2.

It can be seen that the dominant factor is a_1 as this factor influences four other factors. However, PROMETHEE I could not tell the complete outranking of factors. The next analysis is PROMETHEE II where complete outranking can be obtained.

Normalization equation (see equation (9)) is used to transform the triangular fuzzy numbers into left-right fuzzy numbers.

For example,

$$\begin{aligned}
&\phi^+(a_i):\\
&\quad a_1:\ (0.0242, 0.3333, 2.0336) \longrightarrow (0.3333, (0.3333 - 0.0242), (2.0336 - 0.333))\\
&\qquad = (0.3333, 0.3091, 1.7003),\\
&\quad a_2:\ (-1.4570, 0.5664, 2.31922) \longrightarrow (0.56634, (0.5664 - (-1.4570))), (2.31922 - 0.5664)\\
&\qquad = (0.5664, 2.0234, 17528).
\end{aligned} \tag{16}$$

Two examples of left-right fuzzy numbers are shown in equation (16). Table 16 summarizes all flows written in form of left-right fuzzy numbers.

The Yager index method is used as the defuzzification method in this study (see equation (10)). Table 17 presents the defuzzified value of flows.

Net flows (PROMETHEE II) of the factors are calculated using equation (11). The complete ranking is obtained by arranging net flows in descending order. Table 18 presents the net flow and complete preference ranking.

The partial preorder of factors as shown in Figure 2 dictates us to draw a complete preorder of factors in fuzzy PROMETHEE II. The complete preorder is

$$a_1P^{(\mathrm{II})}b_2, a_2P^{(\mathrm{II})}b_3, a_3P^{(\mathrm{II})}b_4 \text{ and } a_4P^{(\mathrm{II})}b_5. \tag{17}$$

Equation (17) shows the general complete preorder of five factors. Figure 3 presents the complete order of factors.

As illustrated in Figure 3, the most influential factor affecting oil prices is a_1 (supply) followed by a_2 (demand). The least influential factor affecting oil prices is a_5 (access markets).

The results are undergone further discussion and comparative analysis. The following section discusses the results from a comparative study perspective.

5. Comparative Analysis

It is known that the fuzzy PROMETHEE method is an extension of PROMETHEE in which the evaluation scales in PROMETHEE are substituted with triangular fuzzy numbers. The uses of fuzzy numbers are meant to capture uncertainty in the factors affecting oil prices. Therefore, in this section, a comparative analysis is presented in which the results obtained from fuzzy PROMETHEE are compared to the results obtained from PROMEHEE. The computational implementation of the PROMETHEE method is slightly straightforward as the computation only deals with crisp numbers. All computational procedures in Section 3 are iterated with some modifications in the types of evaluation scales used.

This comparative analysis is presented from two viewpoints. The first outlook is by seeing the respective values of net flows. Figure 4 shows the comparison of fuzzy

Table 14: Preference index value.

Factors	a_1	a_2	a_3	a_4	a_5
a_1		(0.42, 0, 0.42)	(0.078261, 0.122535, 0.540217)	(−0.371087, 0.127535, 0.54)	(−0.102985, 0.083254, 0.533333)
a_2	(−0.349348, 0.106021, 0.559490)		(−0.368804, 0.200489, 0.596689)	(−0.38831, 0.111106, 0.556667)	(−0.350543, 0.148768, 0.606369)
a_3	(−0.42, 0.08, 0.58)	(−0.5, 0, 0.5)		(0.42, 0.08, 0.58)	(−0.484022, 0.018873, 0.509682)
a_4	(−0.286522, 0.212254, 0.726615)	(−0.463478, 0.037746, 0.523384)	(−0.386418, 0.112297, 0.617297)		(−0.358209, 0.141148, 0.632703)
a_5	(−0.456522, 0.042254, 0.556615)	(0, 0, 0)	(−0.5, 0, 0.5)	(−0.42, 0.08, 0.58)	

Table 15: Fuzzy PROMETHEE I flow.

Factors	$\phi^+(a_i)$	$\phi^-(a_i)$
a_1	(0.024189, 0.333324, 2.03355)	(−1.512392, 0.440529, 2.42272)
a_2	(−1.457005, 0.566384, 2.319215)	(−0.543478, 0.037746, 1.443384)
a_3	(−0.984022, 0.178873, 2.169682)	(−1.176961, 0.435321, 2.254203)
a_4	(−1.494627, 0.503445, 2.49999)	(−0.759397, 0.398641, 2.256667)
a_5	(−1.376522, 0.122254, 1.636615)	(−1.2957320, 0.392043, 2.282087)

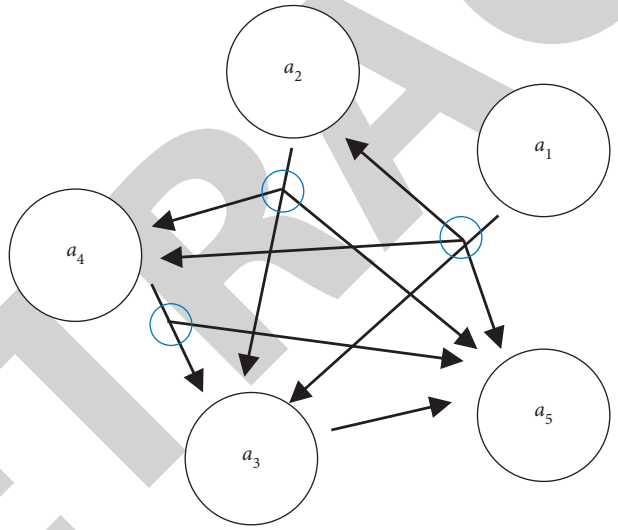

Figure 2: Fuzzy PROMETHEE I partial preorder value outranking graph.

Table 16: Fuzzy PROMETHEE flow in the form of (M, a, b).

Factors	Leaving flow, $\phi^+(a_i)$	Entering flow, $\varphi^-(A_i)$
a_1	(0.3333, 0.3091, 1.7002)	(0.4405, 1.9529, 1.9822)
a_2	(0.5664, 2.0234, 1.7528)	(0.0377, 0.5812, 1.4056)
a_3	(0.0179, 1.0019, 2.1518)	(0.4353, 1.6123, 1.8189)
a_4	(0.5033, 1.998, 1.9966)	(0.3986, 1.158, 1.858)
a_5	(0.1223, 1.4988, 1.5144)	(0.392, 1.6878, 1.89)

Table 17: Defuzzified fuzzy PROMETHEE I flow.

Factors	Positive outflows, $\phi^+(A_i)$	Negative outflows, $\varphi^-(A_i)$
a_1	0.797	0.4503
a_2	0.4762	0.3126
a_3	0.4012	0.5042
a_4	0.5029	0.632
a_5	0.1274	0.4595

Table 18: Net flow and ranking of factors.

Factors	Net flow	Ranking
a_1	0.34674	1
a_2	0.16365	2
a_3	−0.103	3
a_4	−0.1291	4
a_5	−0.332	5

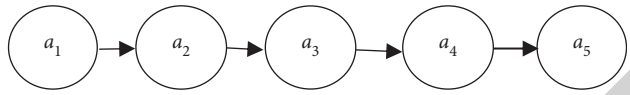

Figure 3: Complete preorder value outranking graph.

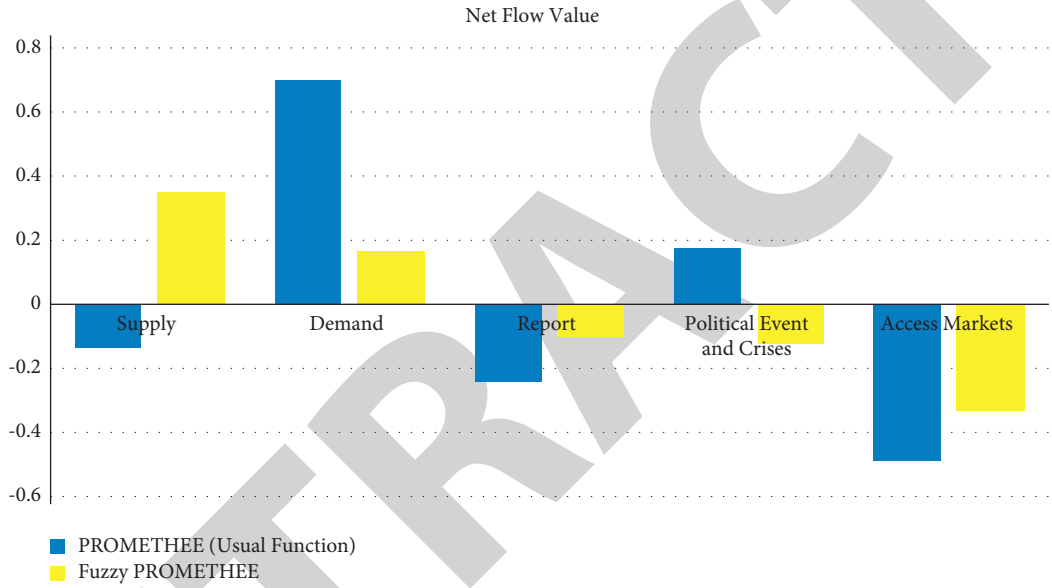

Figure 4: Net flow value between PROMETHEE and fuzzy PROMETHEE.

Table 19: Ranking of Factors under PROMETHEE and fuzzy PROMETHEE.

Factors	PROMETHEE (crisp scales)	Fuzzy PROMETHEE (triangular fuzzy number scales)
a_1	3	1
a_2	1	2
a_3	4	3
a_4	2	4
a_5	5	5

PROMETHEE and PROMETHEE methods based on their values of net flows.

It can be seen that all factors are consistently shared similar patterns for both methods. However, for the factor of political event and crises, fuzzy PROMEHEE provides negative net flows. On the other hand, the same factor provides positive net flows when the PROMETHEE is implemented. It shows that the fuzzy numbers used in the evaluation can capture wide-ranging values compared to crisp numbers in PROMETHEE.

The second viewpoint in this comparative analysis is their final preference ranking. The comparative results of final ranking preference are summarized in Table 19.

It is apparent that the factor a_2 (demand) is ranked in the first position when the crisp scales are employed in evaluation. In contrast, the factor a_1 (supply) is ranked in the first position when triangular fuzzy number scales are employed in evaluation. However, there is a similarity between the two methods. The factor a_5 (access market) shares the weakest performance for both methods.

The performance of these two methods is further analyzed using a statistical test. From the above analysis, the ranking of factors is obtained from the values of net flows. These values are seemed dissimilar due to the different methods used. However, these values can be hypothesized as having some extent of correlation between the methods. The hypotheses can be written as follows:

(i) H0: $\rho = 0$

(ii) H1: $\rho \neq 0$ where is ρ an estimated correlation coefficient

Test statistic $t = r/\sqrt{1 - r^2/n - 2}$, with $df = n - 2$.

Correlation coefficient $r = \sum XY - (\sum X)(\sum Y)/n/\sqrt{(\sum X^2 - (\sum X)^2/n)(\sum Y^2 - (\sum Y)^2/n)}$, where X and Y are net flows of fuzzy PROMETHEE and PROMETHEE, respectively, and n is the number of factors.

From the calculation of the correlation coefficient, it is found that $r = 0.4775$ and $t = 0.9413$. With a significant level $\alpha = 0.05$ and t is less than 2.306, this test indicates that there is no correlation between the net flows of PROMETHEE and fuzzy PROMETHEE. From this analysis, we can conclude that these two methods are independent because of the difference in the types of numbers used as input data. It is good to note that fuzzy PROMETHEE uses triangular fuzzy numbers as input data. In contrast, crisp numbers are the input data used in PROMETHEE. This comparison also tells us that the input values are very important in determining the outcome of ranking. In other words, the ranking results obtained from the fuzzy PROMETHEE are sensitive to the input data. Different types of fuzzy numbers used could give different ranking results.

In addition to the comparative analysis between two PROMETHEE-based methods, it is also good to see the comparative analysis between PROMETHEE-based methods with other preference methods. Ziemba [42], for example, conducted a comparative study between fuzzy TOPSIS, fuzzy SAW, and NEAT fuzzy PROMETHEE II in the selection of electric vehicles. The selection problem was solved by these preference methods. The decision problem defined by the preference models gave three different solutions in the form of rankings. The rankings show that the best vehicle was awarded to A11-Volkswagen ID.3 Pro S, regardless of the preference method used. In another comparative analysis, ranking of contractors was conducted using q-ROF TOPSIS, q-ROF VIKOR, and q-ROF PROMETHEE methods [23]. They conclude that all these preference methods are close to the results of their proposed q-ROF PROMETHEE method where the optimal solution is the same for all methods

6. Conclusions

There are many factors that can contribute to global oil prices, and most of these factors are characterized by subjectivity, uncertainty, and variability. Investigation of factors affecting oil prices is therefore must be seen as a multifactor decision analysis, and more importantly, the concept of fuzziness and uncertainty must be embedded. In this paper, factors affecting oil prices have been investigated using the approach of fuzzy PROMETHEE where triangular fuzzy numbers are employed in expert evaluation. The fuzzy PROMETHEE used in this study is characterized by partial ranking and also complete ranking. The final preference ranking is indeed a modification to the partial ranking of positive outflow values. The final ranking result shows "supply" is the most influential factor in determining oil prices followed by "demand." The current findings add significant knowledge to our understanding of the famous theory in the economic model of the price determination market. It is presumed that in a competitive market, the unit price for a specific cooperative attitude shifts until it settles at a point where the quantity demanded by buyers will equal the quantity supplied by producers. A research finding by Heakal [3] also pointed out that the oil price should increase with increasing demand or decreasing supply. Most researchers, for example [6, 7, 43], also concluded that supply and demand are the most influential factors in oil prices. Contrary to this finding, Chaw et al. [44] found that the "global economic rate" is the most influential factor. However, this research is subjected to some limitations. From the perspective of the evaluation model used, the weight assigned in this study could be improved by employing a more stable method that is germane to fuzzy knowledge such as entropy measures. Other than weight analysis, perhaps aggregation operators and sensitivity tools using PROMETHEE VI could be explored in the future. The latest aggregation methods such as Benforroni mean [45, 46], and Choquet integral [47] are among the potential candidates that could be explored as a future research direction. In future investigations, it might be possible to use different MCDM methods such as rough ELECTRE II [48] and D-TOPSIS [49], in which these methods can be applied to investigate the fluctuation of oil prices.

Data Availability

The linguistic data used to support the findings of this study are available from the corresponding author upon request.

Conflicts of Interest

The authors declare that they have no conflicts of interest for this publication.

Authors' Contributions

All authors contributed equally to the writing of this manuscript. All authors read and approved the final manuscript.

Acknowledgments

The authors would like to thank the Centre of Research and Innovation Management of the University Malaysia Terengganu for providing excellent research and academic environments.

References

[1] Anon, "What are the possible causes and consequences of higher oil prices on the overall economy?" Federal Reserve Bank of San Francisco, 2007, https://www.frbsf.org/education/publications/doctor-econ/2007/november/oil-prices-impact-economy/#1.

[2] World Bank Group, *Global Economic Prospects*, World Bank. © World Bank, Washington, DC, 2018.

[3] H. Heakal, "Economics basics: supply and demand. Investopedia," 2017.

[4] P. Sephton and J. Mann, "Gold and crude oil prices after the great moderation," *Energy Economics*, vol. 71, pp. 273–281, 2018.

[5] R. K. Kaufmann, S. Dees, P. Karadeloglou, and M. Sanchez, "Does OPEC matter? An econometric analysis of oil prices," *Energy Journal*, vol. 25, no. 4, pp. 67–90, 2004.

[6] S. Dées, A. Gasteuil, R. K. Kaufmann, and M. Mann, "Assessing the factors behind oil price changes," Working Paper Series, 2008.

[7] F. Johannessen and K. Skjelvik, *The Impact of Oil Price Volatility on Statoil*, 2017.

[8] M. Zakaria, S. Khiam, and H. Mahmood, "Influence of oil prices on inflation in South Asia: some new evidence," *Resources Policy*, vol. 71, Article ID 102014, 2021.

[9] T. F. Oloko, A. E. Ogbonna, A. A. Adedeji, and N. Lakhani, "Oil price shocks and inflation rate persistence: a Fractional Cointegration VAR approach," *Economic Analysis and Policy*, vol. 70, pp. 259–275, 2021.

[10] X. Wu and Y. Wang, "How does corporate investment react to oil prices changes? Evidence from China," *Energy Economics*, vol. 97, Article ID 105215, 2021.

[11] J.-q. Wang, Y. Yang, and L. Li, "Multi-criteria decision-making method based on single-valued neutrosophic linguistic Maclaurin symmetric mean operators," *Neural Computing & Applications*, vol. 30, no. 5, pp. 1529–1547, 2016.

[12] M. Anwar, "Biodiesel feedstocks selection strategies based on economic, technical, and sustainable aspects," *Fuel*, vol. 283, Article ID 119204, 2021.

[13] B. Mareschal and J.-P. Brans, "Geometrical representations for MCDA," *European Journal of Operational Research*, vol. 34, no. 1, pp. 69–77, 1988.

[14] J. Figueira, S. Greco, and M. Ehrgott, *Multiple Criteria Decision Analysis: State of the Art Surveys*, Springer-Verlag, Berlin, Germany, 2005.

[15] P. C. Fishburn, "Additive utilities with incomplete product set: applications to priorities and assignments," *Journal of the Operations Research Society of America*, vol. 15, no. 3, pp. 537–542, 1967.

[16] E. Triantaphyllou, *Multi-Criteria Decision Making: A Comparative Study*, p. 320, Kluwer Academic Publishers (now Springer, Dordrecht, The Netherlands, 2000.

[17] J. R. S. C. Mateo, "Weighted sum method and weighted product method," in *Multi Criteria Analysis in the Renewable Energy Industry. Green Energy and Technology*Springer, Berlin, Germany, 2012.

[18] C. L. Hwang and K. Yoon, *Multiple Attribute Decision Making: Methods and Applications*, Springer-Verlag, Berlin, Germany, 1981.

[19] J. P. Brans and B. Mareschal, "Multiple criteria decision analysis: state of the art surveys- PROMETHEE methods," *International Series in Operational Research and Management Science*, vol. 78, no. 5, pp. 163–195, 2005.

[20] M. P. Moreira, C. J. Dupont, and M. M. B. R. Vellasco, "PROMETHEE and fuzzy PROMETHEE multicriteria methods for ranking equipment failure modes," in *Proceedings of the 15th International Conference on Intelligent System Applications to Power Systems*, pp. 1–6, Curitiba, Brazil, November 2009.

[21] M. Akram, Shumaiza, and J. C. R. Alcantud, "An *m*-polar fuzzy PROMETHEE approach for AHP-assisted group decision-making," *Mathematical and Computational Applications*, vol. 25, no. 2, p. 26, 2020.

[22] M. Akram, Shumaiza, and A. N. Al-Kenani, "Multi-criteria group decision-making for selection of green suppliers under bipolar fuzzy PROMETHEE process," *Symmetry*, vol. 12, no. 1, p. 77, 2020.

[23] M. Akram and S. Shumaiza, "Multi-criteria decision making based on q-rung orthopair fuzzy Promethee approach," *Iranian Journal of Fuzzy Systems*, vol. 18, no. 5, pp. 107–127, 2021.

[24] M. Maisaini, B. Uzun, I. Ozsahin, and D. Uzun, *13th International Conference on Theory and Application of Fuzzy Systems and Soft Computing—ICAFS-2018. Systems and Computing*, Springer, Berlin, Germany, 2019pp. 209–215, Evaluating Lung Cancer Treatment Techniques Using Fuzzy PROMETHEE Approach.

[25] E. Afful-Dadzie, S. Nabareseh, Z. K. Oplatková, and P. Klimek, *Intelligent Systems and Applications*, Springer, Berlin, Germany, Using Fuzzy PROMETHEE to Select Countries for Developmental Aid, 2016.

[26] P. Ziemba, "Multi-criteria approach to stochastic and fuzzy uncertainty in the selection of electric vehicles with high social acceptance," *Expert Systems with Applications*, vol. 173, Article ID 114686, 2021.

[27] J. P. Brans and P. Vincke, "Note-A preference ranking organisation method," *Management Science*, vol. 31, no. 6, pp. 647–656, 1985.

[28] S.-M. Chen and J.-A. Hong, "Multicriteria linguistic decision making based on hesitant fuzzy linguistic term sets and the aggregation of fuzzy sets," *Information Sciences*, vol. 286, no. 1, pp. 63–74, 2014.

[29] L. A. Zadeh, "Fuzzy sets," *Information and Control*, vol. 8, no. 3, pp. 338–353, 1965.

[30] L. A. Zadeh, "The concept of a linguistic variable and its application to approximate reasoning-I," *Information Sciences*, vol. 8, no. 3, pp. 199–249, 1975.

[31] P. S. Jatinder and N. I. Thakur, "A novel method to solve assignment problem in fuzzy environment," *Journal of Industrial Engineering*, vol. 5, no. 2, pp. 31–35, 2015.

[32] E. Afful-Dadzie, Z. K. Oplatková, and S. Nabareseh, "Selecting start up business in a public venture capital financing using Fuzzy PROMETHEE," *Procedia Computer Science*, vol. 60, no. 1, pp. 63–72, 2015.

[33] Globalis, "Organization of petroleum-exporting countries (OPEC)," 2017.

[34] J. Baffes, M. A. Kose, F. Ohnsorge, and M. Stocker, "The great plunge in oil prices: causes, consequences and policy implications," *Policy Research Notes*, vol. 15, no. 1, 2015.

[35] R. Heinberg, *The Party's over: Oil, War and the Fate of Industrial Societies*, New Society Publishers, Gabriola, BC, Canada, 2005.

[36] L. Yan, "Analysis of the international oil price fluctuations and its influencing factors," *American Journal of Industrial and Business Management*, vol. 02, no. 02, pp. 39–46, 2012.

Hindawi
Journal of Mathematics
Volume 2024, Article ID 9789075, 1 page
https://doi.org/10.1155/2024/9789075

Retraction

Retracted: Model Value of Taiji Curve Algorithm in Economic Geographic and Natural Game Management Information System

Journal of Mathematics

Received 23 January 2024; Accepted 23 January 2024; Published 24 January 2024

This article has been retracted by Hindawi following an investigation undertaken by the publisher [1]. This investigation has uncovered evidence of one or more of the following indicators of systematic manipulation of the publication process:

(1) Discrepancies in scope

(2) Discrepancies in the description of the research reported

(3) Discrepancies between the availability of data and the research described

(4) Inappropriate citations

(5) Incoherent, meaningless and/or irrelevant content included in the article

(6) Manipulated or compromised peer review

The presence of these indicators undermines our confidence in the integrity of the article's content and we cannot, therefore, vouch for its reliability. Please note that this notice is intended solely to alert readers that the content of this article is unreliable. We have not investigated whether authors were aware of or involved in the systematic manipulation of the publication process.

Wiley and Hindawi regrets that the usual quality checks did not identify these issues before publication and have since put additional measures in place to safeguard research integrity.

We wish to credit our own Research Integrity and Research Publishing teams and anonymous and named external researchers and research integrity experts for contributing to this investigation.

The corresponding author, as the representative of all authors, has been given the opportunity to register their agreement or disagreement to this retraction. We have kept a record of any response received.

References

[1] C. Xu and K. Chen, "Model Value of Taiji Curve Algorithm in Economic Geographic and Natural Game Management Information System," *Journal of Mathematics*, vol. 2022, Article ID 8526428, 6 pages, 2022.

Hindawi
Journal of Mathematics
Volume 2022, Article ID 8526428, 6 pages
https://doi.org/10.1155/2022/8526428

Research Article

Model Value of Taiji Curve Algorithm in Economic Geographic and Natural Game Management Information System

Chengqi Xu[1] **and Kegong Chen**[2,3]

[1]*College of Geography and Environmental Sciences, Northwest Normal University, Lanzhou, Gansu 730070, China*
[2]*Standing Committee of Gansu Provincial People's Congress, Lanzhou, Gansu 730046, China*
[3]*School of Geography and Environmental Sciences, Northwest Normal University, Lanzhou, Gansu 730070, China*

Correspondence should be addressed to Chengqi Xu; 2021120202@nwnu.edu.cn

Received 17 December 2021; Revised 2 January 2022; Accepted 5 April 2022; Published 20 May 2022

Academic Editor: Naeem Jan

In order to study the role of tai chi curve algorithm in economic geography and natural ecological management and explore the application value of tai chi curve algorithm and its model, this study discusses the principle of Chinese tai chi diagram, using mathematical model construction method by the previous tai chi map and Pythagoras theorem clever results, produced the tai chi graph *s* curve algorithm, and discusses the application value of tai chi curve algorithm and its model from different angles; this study takes Zhangye geography as an example, which provides an applied research direction for the future scientific research of Chinese economic geography and also provides a clever connection with ecological correlation and nature; finally, it is found that the Taiji graph *s* curve algorithm can calculate the corresponding Yin and Yang values according to the balance point and relative deviation amount of the attribute state, and the results have an extraordinary influence in economic geography, information management system, natural ecology, and other aspects.

1. Introduction

Tai chi is the category of ancient Chinese philosophy used to analyze the movement laws of celestial bodies and to explain the origin of the world.

Since ancient times, tai chi was studied and applied by scholars, said that in early research, it was found that Tai Chi graphics expounded the law of life two, two and three, which is an important graphic expression of yin-yang theory and explained [1]. Chen Shijun (2021) also said that since Zhou Dunyi wrote the Tai Chi diagram in the Song Dynasty, the Tai Chi diagram has a unique significance in the interpretation history of the book of changes. The Tai Chi diagram vividly contains the basic contents of the book of changes, such as Yin and Yang, three talents, four images, five elements, eight trigrams, and nine palaces, reflects the unity of many elements such as image, number, reason, and occupation, and reflects the essence of the book of changes. The "unity" principle exists in the theory and the corresponding quantum field principle [2]. The "correlation principle" emphasizes "mutual exclusion and complementarity," which happens to be the principle of antagonistic unity revealed in "one Yin and one Yang." Chen and Ma studied how to deconstruct the tai chi figure [3] mathematically. Through the inner circle of the unit square, applying the lever balance principle of Archimedes theorem and the core idea of fuzzy mathematics, the *s* curve of tai chi diagram can be accurately expressed with a primary function. This argument suggests that tai chi maps can be expressed in mathematical language, rather than without standard geometric maps, expressing the basis for tai chi maps reflecting the existence and development of things. In the study of Chen and Wang, taking the classic symbol "Taiji diagram" as an example, this paper analyzes its morphological characteristics and aesthetic artistic conception and explores its expression and design methods in modern architectural landscape design combined with specific cases [4]. Yu elaborated the application of congenital tai chi diagram (Yin-Yang fish diagram) in opera facial makeup from three aspects: the application of tai chi graphics and colors in opera facial makeup, the position of tai

chi diagram in facial makeup, and the relationship between tai chi diagram and background color in facial makeup [5].

The form of tai chi mode itself has a good guide to the current economic geography, and the *s* curve of tai chi map runs through the mathematical wisdom based on Pythagoras in ancient Chinese theorem. The intention of this study is to find tai chi Yin and Yang map in fuzzy mathematics to accurately describe the model value in the information management system of economic geography and natural game and to combine tai chi curve algorithm with economic geography, so as to study the influence of tai chi curve algorithm on social and economic development.

2. Mathematical Model of the *s* Curves of Tai Chi Figure

2.1. Quantitative Model of Tai Chi Figure. We establish a right-angle coordinate system to make a unit circle centered on the coordinate origin. The vertical axis represents the relative offset of the state and is set to A, and the two points $N(0, \delta)$; B and B' are the horizontal lines of the over-N point and the two intersections of the circle, respectively. Make the bisector line OC over the origin O of AOB, as shown in Figure 1.

In Figure 1, the coordinates of the relative offset are N point, let $\cos\angle AOB = \delta$, when the relative offset of the state is δ. As shown in formulas (1) and (2),

$$\text{the Yang value is } \cos^2\frac{\angle AOB}{2} = \frac{1+\delta}{2}, \tag{1}$$

$$\text{the Yin value is } \sin^2\frac{\angle AOB}{2} = \frac{1-\delta}{2}. \tag{2}$$

Here, the Yin-Yang assignment at this time is also known as the Yin-Yang assignment of point B or B' on the circle O. Notably, the Yang assignment is the square of the relative offset corresponding to the projection OM of the OC on the longitudinal axis. We can obtain a schematic tai chi diagram model under this mathematical model, as shown in Figure 2.

In Figure 2, the coordinates correspond to Figure 1; black block: Yin value; red block: Yang value;

We establish $x = \angle AOB$ and record the Yang function. As shown in formula,

$$P(x) = \frac{1+\cos x}{2}, \quad x \in (-\infty, +\infty). \tag{3}$$

We record the Yin function, as shown in formula:

$$N(x) = \frac{1-\cos x}{2}, \quad x \in (-\infty, +\infty). \tag{4}$$

Here, the $P(x)$, $N(x)$ all are periodic functions and periodic at 2π. The Yang and Yin function is shown in Figure 3.

2.2. The Internal Connection between Tai Chi Diagram and the Pythagorean Theorem. For the Pythagorean theorem, the mathematical model is shown in formula:

$$a^2 + b^2 = c^2. \tag{5}$$

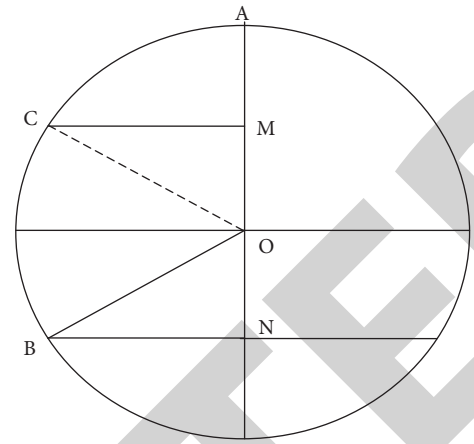

Figure 1: Positive value of point B is the line segment 2.

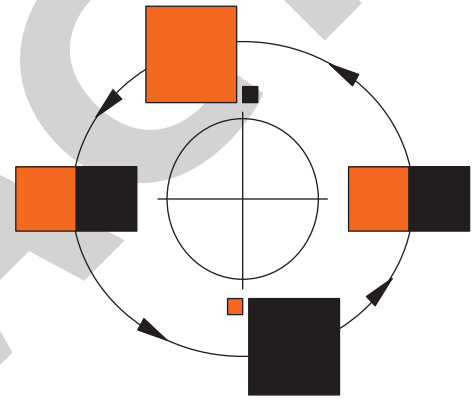

Figure 2: Schematic diagram of the tai chi diagram model under the new mathematical model.

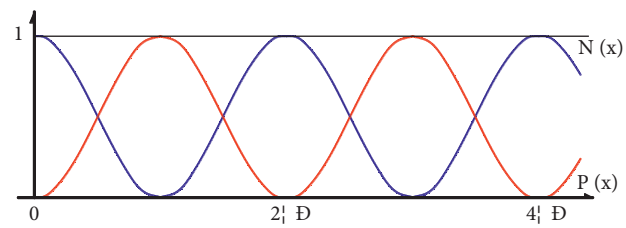

Figure 3: Yang function and negative function curves.

Here, a, b, c are the two right and oblique edges of the right triangle, respectively. Starting with the Pythagorean theorem, through the inner cut circle of the unit square, Chen had said that it applies the lever balance principle of Archimedes' theorem and the core idea of fuzzy mathematics; the *s* curve of the tai chi diagram can be accurately expressed with a primary function. The definition of a circle can also be obtained by the Pythagorean theorem; when the oblique edge is a certain length, the set of two right angular edges is the trajectory of the circle. In the end of the Eastern Han Dynasty, Zhao Shuang, a mathematician in China, created "the geometric graph on a circle (Figure 4)" [6], as shown in Figure 4.

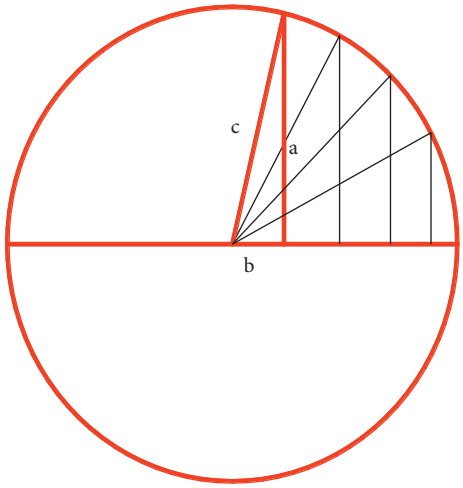

Figure 4: The geometric graph on a circle.

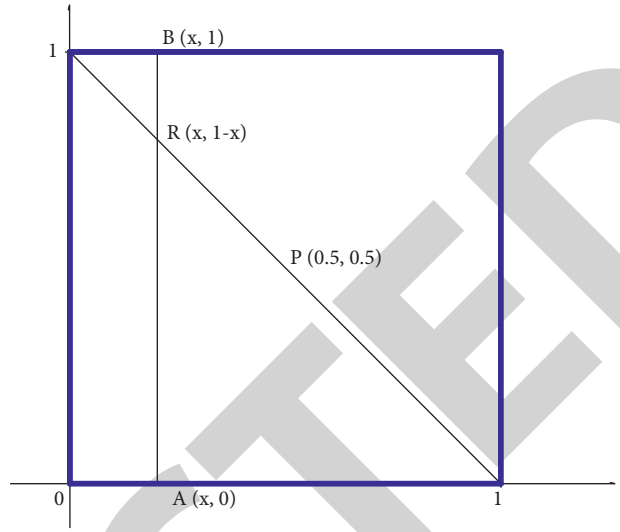

Figure 5: Relationship between Yang value and Yin value in the right-angle triangle.

In Figure 4, if x and y represent the quotient value of the two right-angle edges' square and oblique edges' square, respectively, and this quotient value is defined as the Yang and Yin values of this triangle, respectively. We can get the relationship between Yang value and Yin value in the right-angle triangle in Figure 5.

In Figure 5, let $x = a^2/c^2$, $y = b^2/c^2$, as shown in formula:

$$x + y = \frac{a^2}{c^2} + \frac{b^2}{c^2} = 1. \tag{6}$$

Here, because $a, b \in (0, c)$, so $x, y \in (0, 1)$. With the triangle function, x, y can also be expressed as in the formula:

$$\begin{aligned} x &= \frac{a^2}{c^2} = \frac{c^2 - b^2}{c^2} = \sin^2 \alpha = \frac{1 - \cos 2\alpha}{2} = P(\alpha), \\ y &= \frac{b^2}{c^2} = \frac{c^2 - a^2}{c^2} = \cos^2 \alpha = \frac{1 + \cos 2\alpha}{2} = N(\alpha). \end{aligned} \tag{7}$$

Here, $\alpha \in (-\infty, +\infty)$; its geometric representation diagram is shown in Figure 6.

In Figure 6, α is the diagonal of a. This is perfectly consistent with the Yin-Yang theory and is a perfect combination of algebra and geometry. Connecting the formulas 5 and (6), we can know its essential connotation is that the area of the square corresponding to the oblique edge of the unit right-angle triangle is equal to the sum of the two square areas corresponding to the two right-angle edges. Chen had said that it can be illustrated by the oasis and the area relationship of the desert. Take Zhangye, Gansu Province, China [6], as shown in Figure 7.

In Figure 7, if the total area of Zhangye city is regarded as "1" per unit area, then the sum of oasis and desert area is always equal to "1" (because in the city, the water is an oasis, and the area with no water is a desert, and the sum remains the same). When one of the areas increases, the product decreases on the other hand, and vice versa, and the set of this change process is a circular trajectory. As shown in formula (6),

$$\begin{aligned} y &= 1 - x, \\ x &= 1 - y. \end{aligned} \tag{8}$$

Here, therefore, the Yin and Yang function remains in dual equilibrium, entangled each other and superposition, just like quantum entanglement, its total value is fixed to "1." The area of each other is their deviation value, and the sum of the deviation value is fixed to "1." In most areas of Zhangye, it is not an oasis which is not a desert, but out of the "Schrodinger state" of oasis and desert, it is impossible to know which attribute is stronger; oasis and desert are in the $x + y = 1$, line section, and are in the [0, 1] range. For any set, there can be two completely opposite set discussions on an attribute, and the economic operation state can also be discussed here and divided into two completely opposite concepts of accumulation and consumption. All objective things that exist can be divided into two opposite sets with subjective attitude. However, the real state of affairs is not black or white, but out of the black and white interval, which is also Marx's dialectical "divided in two" of materialism.

2.3. The Tai Chi Theorem. For the establishment of the mathematical model of the s curve, see Figure 8.

In Figure 8, we establish a circle of diameter 1 with O as the center, cross the horizontal circle O of crossing O points at A and B, take a single point P on OA, let $a = x$, $a + b = 1$, make CP perpendicular to AB, connect AC, BC, and OC, and make PD perpendicular to OC, as shown in Figure 8.

We can get the tai chi theorem:

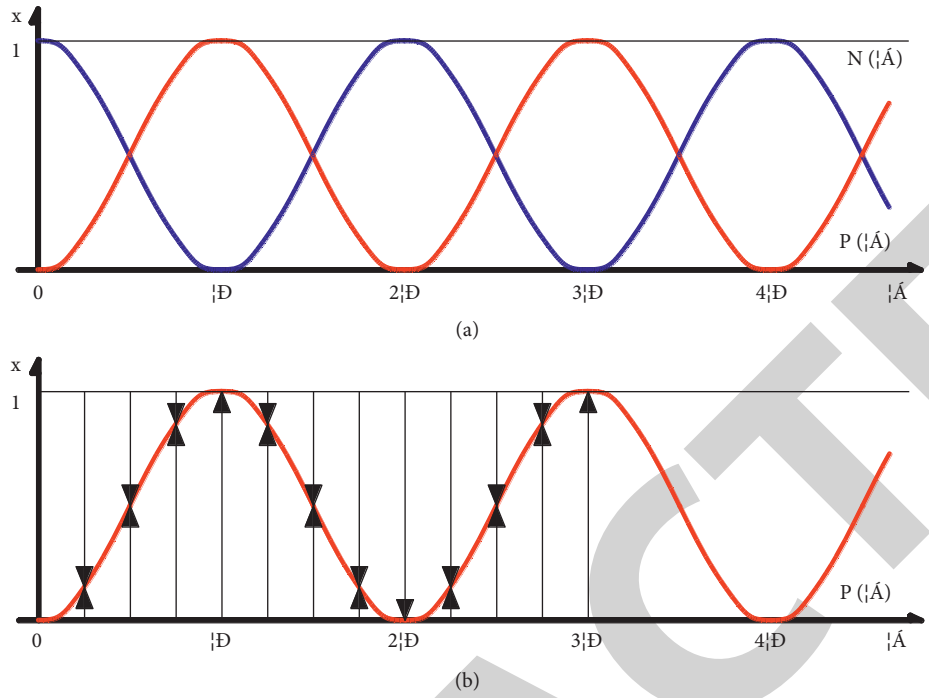

Figure 6: Yang and Yin values in the form of the triangle function. (a) Yangzhi and Yinzhi; (b) Yangzhi result.

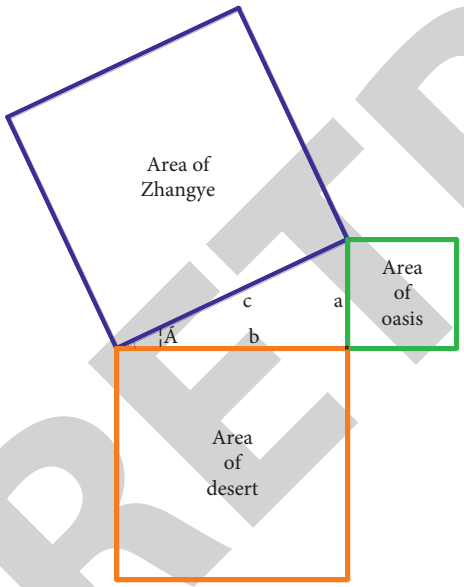

Figure 7: Area relationship diagram of Zhangye Oasis Desert.

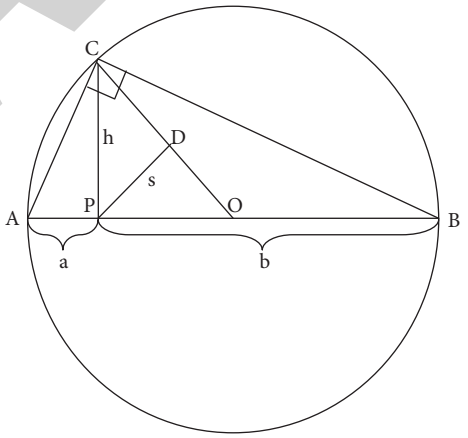

Figure 8: Schematic diagram of the tai chi theorem deduction.

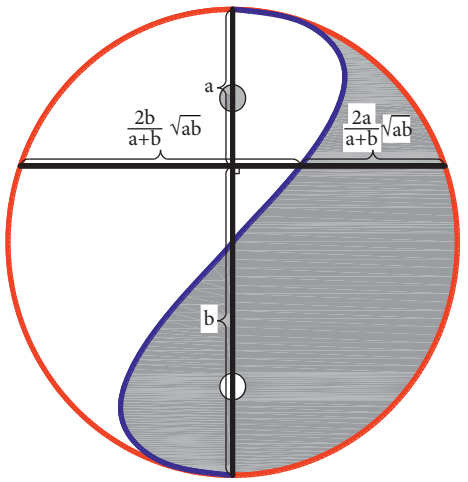

Figure 9: Mathematical model of the Taiji theorem.

$$\frac{S}{h} = \frac{OP}{OC} = \frac{b-a}{a+b},$$
$$S = \frac{b-a}{a+b} \cdot \sqrt{ab}. \tag{9}$$

This can be launched:

$$CD = \frac{h^2}{OC} = \frac{ab}{a+b/2} = \frac{2ab}{a+b} = \frac{2}{(1/a)+(1/b)}. \tag{10}$$

Here, $S = b - a/a + b \cdot \sqrt{ab}$ is the tai chi theorem; its trajectory curve is the China tai chi figure s curve. The s curve is rotated 90 degrees clockwise, and the tai chi theorem is shown in Figure 9.

3. Application of Tai Chi's Curve Model in Ecological Environment

Natural ecology has been closely related to tai chi since ancient times. Nature has been growing everywhere. The ecological chain also reproduces and breeds according to this law, and the natural environment also plays a game between living beings. When a population's growth rate has exceeded what the environment can accommodate, the natural environment imposes its growth restrictions, such as sudden food reduction, insufficient land resources, and more natural enemies. Ideally, when the growth amount of the population tribe reaches just half the environmental capacity, the biological growth rate is the fastest, and the distribution amount of food and the environment can just be balanced, which is the most favorable growth value conducive to biological survival.

In Table 1, K is the maximum number of populations that can be maintained in a certain space range when the environmental conditions are not damaged; x is the growth rate of the population in this spatial range (all growth rates in the table are compared to the proliferation rate at 1/2 of the environmental capacity).

As shown in Table 1, the environmental capacity is the whole circle, and biological proliferation rate of an environment is the s curve. When the biological growth rate rises rapidly and peaks, the curve decreases, indicating that the growth rate of the environment has reached saturation, due to food shortage, spouse shortage, and habitat pressure, the number of the organisms will decline sharply, and the number of resources, natural enemies, and the other factors will inhibit it. When the number drops sharply to a certain range, the amount of biological growth increases again. Let the ambient capacity be the K value, and the negative and positive values calculated from the equilibrium value of the relative deviation amount will be the $K/2$.

If it fails to develop according to its natural laws, the result will flood like the Australian hare, lack of competition from natural enemies, sufficient food, serious damage to the natural environment to limit its growth, and eventually lead to uncontrollable human results.

4. Application of Tai Chi Curve Algorithm in Economic Geography

Taiji curve model can also be applied in economic geography, and its model can generally describe the law of industrial layout and the technical and economic scientific development concept of the research objects. The combination of natural technology, science, and economy separated and integrated in the model is indispensable. The three achieve a wonderful balance in urban planning, human activities, and natural ecology.

Table 1: Relationship between the total biomass change and growth rate in an area.

Total biomass	$x > K/2$	$x = K/2$	$x < K/2$
Biological growth rate in this population	Reduce	Normal growth	Accelerate

Data source: the study was designed by itself.

Table 2: The amount use and allocation of urban infrastructure construction and ecological planning between the two cities.

	A city allocated economic use (ten thousand yuan)	B city allocated economic use (ten thousand yuan)
Total state appropriation (ten thousand yuan)	n	n
Urban foundation construction (ten thousand yuan)	a	b
Urban ecological development (ten thousand yuan)	c	d

Data source: the study was designed by itself.

The significance of the model is different between the regions of different scales, and the magic of the s curve model diagram is that it can clearly and thoroughly express the correlation of the variables between various complex systems and draw it in the ancient Chinese tai chi figure.

For example, the state allocates n 0.000 yuan to both A and B cities for the development and construction of its cities. A city, because of the urban economic development, is not as developed as B city, so most of the allocated funds are used on urban infrastructure construction, and the remaining small part for urban ecological development; B city is economically developed city, while the natural resources are far inferior to A city, so B city has invested a lot of money in urban ecological planning, the rest is used in urban economic construction. Table 2 is drawn as described above.

In Table 2, n is the amount allocated by the state to the two cities; a is the amount used for urban foundation construction in A city; b is the amount used for urban foundation construction in B city; c is the amount used in A urban ecological development; d is the amount used for urban ecological development of B city:

$$n^2 = a^2 + c^2 = b^2 + d^2. \tag{11}$$

Here, the formula notes are shown in Table 2. According to Table 2, combined with the tai chi s curve model algorithm used, the total national approval fund is set as the circle constructed, and then the funds used in urban ecological development planning and the funds used in urban economic development and construction will be negative and positive values. According to the balance value of the relative deviation value, the funds invested in all parties can be calculated through the s curve model. According to the hook theorem, the total value square remains unchanged, the

Hindawi
Journal of Mathematics
Volume 2023, Article ID 9836426, 1 page
https://doi.org/10.1155/2023/9836426

Retraction

Retracted: On Multiplicative Topological Invariants of Magnesium Iodide Structure

Journal of Mathematics

Received 15 August 2023; Accepted 15 August 2023; Published 16 August 2023

This article has been retracted by Hindawi following an investigation undertaken by the publisher [1]. This investigation has uncovered evidence of one or more of the following indicators of systematic manipulation of the publication process:

(1) Discrepancies in scope

(2) Discrepancies in the description of the research reported

(3) Discrepancies between the availability of data and the research described

(4) Inappropriate citations

(5) Incoherent, meaningless and/or irrelevant content included in the article

(6) Peer-review manipulation

The presence of these indicators undermines our confidence in the integrity of the article's content and we cannot, therefore, vouch for its reliability. Please note that this notice is intended solely to alert readers that the content of this article is unreliable. We have not investigated whether authors were aware of or involved in the systematic manipulation of the publication process.

Wiley and Hindawi regrets that the usual quality checks did not identify these issues before publication and have since put additional measures in place to safeguard research integrity.

We wish to credit our own Research Integrity and Research Publishing teams and anonymous and named external researchers and research integrity experts for contributing to this investigation.

The corresponding author, as the representative of all authors, has been given the opportunity to register their agreement or disagreement to this retraction. We have kept a record of any response received.

References

[1] Z. Zhang, H. Ali, A. Naseem, U. Babar, X. Zhang, and P. Ali, "On Multiplicative Topological Invariants of Magnesium Iodide Structure," *Journal of Mathematics*, vol. 2022, Article ID 6466585, 15 pages, 2022.

Hindawi
Journal of Mathematics
Volume 2022, Article ID 6466585, 15 pages
https://doi.org/10.1155/2022/6466585

Research Article

On Multiplicative Topological Invariants of Magnesium Iodide Structure

Zhiqiang Zhang,[1] **Haidar Ali**,[2] **Asim Naseem**,[3] **Usman Babar**,[3] **Xiujun Zhang**,[1] **and Parvez Ali**[4]

[1]*School of Computer Science, Chengdu University, Chengdu, China*
[2]*Department of Mathematics, Riphah International University, Faisalabad Campus, Rawalpindi, Pakistan*
[3]*Department of Mathematics, Government College University, Lahore, Pakistan*
[4]*Department of Mechanical Engineering, College of Engineering, Qassim University, Unaizah, Saudi Arabia*

Correspondence should be addressed to Haidar Ali; haidar3830@gmail.com

Received 30 October 2021; Accepted 15 April 2022; Published 14 May 2022

Academic Editor: Ewa Rak

In recent times, the applications of graph theory in molecular and chemical structure research have far exceeded human expectations and have grown exponentially. In this paper, we have determined the multiplicative Zagreb indices, multiplicative hyper-Zagreb indices, multiplicative universal Zagreb indices, sum and product connectivity of multiplicative indices, multiplicative atom-bond connectivity index, and multiplicative geometric-arithmetic index of a famous crystalline structure, magnesium iodide (MgI_2).

1. Introduction and Preliminary Results

In chemical graph theory, molecules can be modeled as graphs by representing atoms as vertices and atomic bonds as edges [1]. The nervous system can be thought of as a graph, where the neurons (nodes) and the edges (bonds) are between them. The nervous system can be seen as a graph, where the nodes are neurons and the edges are the connections between them.

The representation of a graph can be expressed by numbers, polynomials, and matrices. Graphs have their own characteristics that may be calculated by topological indices, and under graph automorphism, the topology of graphs remains unchanged. Degree-based topological indices are exceptionally important among different classes of indices and take on a vital role in graph theory and in particular in science [2]. Chem-informatics is a brand-new field that combines chemistry, mathematics, and information science. It investigates quantitative structure-activity (QSAR) and structure-property (QSPR) connections, which are used to predict chemical compound biological activities and qualities.

Magnesium iodide (MgI_2) is a chemical compound and has many commercial uses. It is used for manufacture of different organic compounds in large scale due to its cheapness and availability everywhere in the world. Magnesium iodide can be obtained from the reaction of hydroiodic acid with magnesium oxide, magnesium hydroxide, and magnesium carbonate.

$$\begin{aligned} 2HI + MgCO_3 &\longrightarrow MgI_2 + H_2O + CO_2 \\ 2HI + MgO &\longrightarrow MgI_2 + H_2O \\ 2HI + Mg(OH)_2 &\longrightarrow MgI_2 + 2H_2O \end{aligned} \tag{1}$$

Every heptagon in MgI_2 is connected to each other in column and row by making three C_4 within each heptagon. We will use "m" to represent the number of C_4 rows on the upper side and "n" to represent the number of C_4 on the lower side of the heptagon.

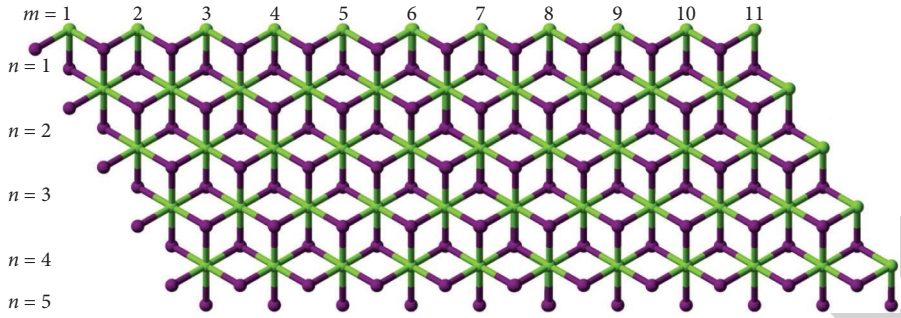

Figure 1: Graph $(\mathfrak{L}_1)$ of MgI_2 for $m = 2n + 1$.

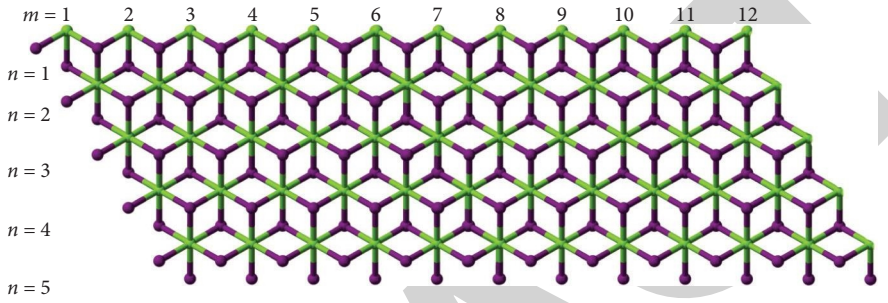

Figure 2: Graph $(\mathfrak{L}_2)$ of MgI_2 for $m = 2n + 2$.

In Figures 1 and 2, there are variables m and n, which are dependent on each other to maintain the structure of magnesium iodide. Magnesium has 2 electrons in its outermost shell, while iodide contains 7 electrons in its valence shell. As a result, to turn out to be stable, magnesium offers its electrons to iodide. To maintain the chemical structure of magnesium iodide, it depends on each other. As a result, the graph was subdivided into even and odd vertices. For the first type, the cardinality of vertices and edges of graph $(\mathfrak{L}_1)$, as shown in Figure 1, is $m = 2n + 1$, and for the second type, the cardinality of vertices and edges of graph $(\mathfrak{L}_2)$, as shown in Figure 2, is $m = 2n + 2$, where $n \in \mathbb{N}$, respectively.

In this article, "$\mathfrak{L}$" is considered a structure with a vertex set $V(\mathfrak{L})$ and edge set $E(\mathfrak{L})$, and $d(r)$ is the degree of vertex $r \in V(\mathfrak{L})$.

The "second multiplicative Zagreb index" [4] is defined as

$$\mathrm{II}_2(\mathfrak{L}) = \prod_{rs \in E(\mathfrak{L})} (d_r \times d_s), \tag{2}$$

where (r, s) is any unordered pair of vertices in $\mathfrak{L}$.

Kulli [5] further described some new and advanced topological indices, and he named them as the "first multiplicative hyper-Zagreb index" and the "second multiplicative hyper-Zagreb index" of a graph "$\mathfrak{L}$." The indices are defined as

$$\mathrm{HII}_1(\mathfrak{L}) = \prod_{rs \in E(\mathfrak{L})} (d_r + d_s)^2, \tag{3}$$

$$\mathrm{HII}_2(\mathfrak{L}) = \prod_{rs \in E(\mathfrak{L})} (d_r \times d_s)^2. \tag{4}$$

The "first multiplicative universal Zagreb index" and the "second multiplicative universal Zagreb index" were introduced by Kulli et al. [6]. These indices are defined as

$$\mathrm{MZ}_1^a(\mathfrak{L}) = \prod_{rs \in E(\mathfrak{L})} (d_r + d_s)^a, \tag{5}$$

$$\mathrm{MZ}_2^a(\mathfrak{L}) = \prod_{rs \in E(\mathfrak{L})} (d_r \times d_s)^a, \tag{6}$$

where $a \in \mathbb{N}$.

The multiplicative sum and product connectivity indices were introduced by Kulli [7], defined as

$$\mathrm{SCII}(\mathfrak{L}) = \prod_{rs \in E(\mathfrak{L})} \frac{1}{\sqrt{d_r + d_s}}, \tag{7}$$

$$\mathrm{PCII}(\mathfrak{L}) = \prod_{rs \in E(\mathfrak{L})} \frac{1}{\sqrt{d_r \times d_s}}. \tag{8}$$

"Multiplicative atom-bond connectivity index," "multiplicative geometric-arithmetic index," and "multiplicative universal geometric-arithmetic index" for a simple graph $\mathfrak{L}$ were introduced by Kulli [7], and these indices are defined as

$$\mathrm{ABCII}(\mathfrak{L}) = \prod_{rs \in E(\mathfrak{L})} \sqrt{\frac{d_r + d_s - 2}{d_r \times d_s}}, \tag{9}$$

$$\mathrm{GAII}(\mathfrak{L}) = \prod_{rs \in E(\mathfrak{L})} \frac{2\sqrt{d_r \times d_s}}{d_r + d_s}, \tag{10}$$

Table 1: Edge subdivision of $\mathfrak{L}_1$ of MgI_2 based on degree of end vertices of each edge for $m = 2n + 1$, where $n \in \mathbb{N}$.

(d_r, d_s) where $rs \in E(\mathfrak{L}_1)$	Number of edges
(1, 3)	1
(1, 4)	1
(1, 6)	$n + 5$
(2, 5)	8
(2, 6)	$2n + 8$
(3, 2)	2
(3, 3)	$3n$
(3, 4)	1
(3, 5)	12
(3, 6)	$27n - 13$
(4, 2)	2

$$\mathrm{GA}^a\mathrm{II}(\mathfrak{L}) = \left(\prod_{rs \in E(\mathfrak{L})} \frac{2\sqrt{d_r \times d_s}}{d_r + d_s}\right)^a, \tag{11}$$

where $a \in \mathbb{N}$.

2. Main Results

Afzal et al. [8] computed the molecular description for magnesium iodide. In this article, we shall discuss the first type and second type of magnesium iodide structure and compute the exact results for topological indices like multiplicative Zagreb indices, multiplicative hyper-Zagreb indices, multiplicative universal Zagreb indices, sum and product connectivity of multiplicative indices, multiplicative atom-bond connectivity index, and multiplicative geometric-arithmetic index for the magnesium iodide structure. For further study of topological indices of various graph families, see [9–14]. For basic definitions and notations, see [15, 16].

2.1. Results for the First Type of Magnesium Iodide Structure. In this section, we compute topological indices such as multiplicative Zagreb indices, multiplicative hyper-Zagreb indices, multiplicative universal Zagreb, sum and product connectivity of multiplicative indices, multiplicative atom-bond connectivity index, and multiplicative geometric and universal geometric-arithmetic indices for the first type of magnesium iodide structure ($\mathfrak{L}_1$), as shown in Figure 1.

Theorem 1. *Consider the magnesium iodide structure MgI_2 of first type; then, the second multiplicative Zagreb index is equal to*

$$\mathrm{II}_2(\mathfrak{L}) = 13931406950400n(n + 5)(2n + 8)(27n - 13). \tag{12}$$

Proof. Let $\mathfrak{L}_1$ be the magnesium iodide structure MgI_2 for $m = 2n + 1, n \in \mathbb{N}$ of first type. In Table 1, there is an edge partition of $\mathfrak{L}_1$. From equation (2),

$$\mathrm{II}_2(\mathfrak{L}_1) = \prod_{rs \in E(\mathfrak{L}_1)} (d_r \times d_s). \tag{13}$$

By applying edge partition of Table 1,

$$\begin{aligned}\mathrm{II}_2(\mathfrak{L}_1) &= 3|E_1(\mathfrak{L}_1)| \times 4|E_2(\mathfrak{L}_1)| \times 6|E_3(\mathfrak{L}_1)| \times 10|E_4(\mathfrak{L}_1)| \times 12|E_5(\mathfrak{L}_1)| \\ &\quad \times 6|E_6(\mathfrak{L}_1)| \times 9|E_7(\mathfrak{L}_1)| \times 12|E_8(\mathfrak{L}_1)| \times 15|E_9(\mathfrak{L}_1)| \times 18|E_{10}(\mathfrak{L}_1)| \times 8|E_{11}(\mathfrak{L}_1)| \\ &= 3(1) \times 4(1) \times 6(n + 5) \times 10(8) \times 12(2n + 8) \times 6(2) \times 9(3n) \\ &\quad \times 12(1) \times 15(12) \times 18(27n - 13) \times 8(2).\end{aligned} \tag{14}$$

We obtain the following by making some calculations:

$$\Rightarrow \mathrm{II}_2(\mathfrak{L}_1) = 13931406950400n(n + 5)(2n + 8)(27n - 13). \tag{15}$$

□

Theorem 2. *Consider the magnesium iodide structure MgI_2 of first type; then, the first and second multiplicative hyper-Zagreb indices are equal to*

$$\begin{aligned}\mathrm{HII}_1(\mathfrak{L}_1) &= 582761278687150080000n(n + 5)(2n + 8)(27n - 13), \\ \mathrm{HII}_2(\mathfrak{L}_1) &= 168475780918101934080000n(n + 5)(2n + 8)(27n - 13).\end{aligned} \tag{16}$$

Proof. Let $\mathfrak{L}_1$ be the magnesium iodide structure MgI_2 of first type. In Table 1, there is an edge partition of $\mathfrak{L}_1$. From equation (3),

$$\mathrm{HII}_1(\mathfrak{L}_1) = \prod_{rs \in E(\mathfrak{L}_1)} (d_r + d_s)^2. \tag{17}$$

By applying edge partition of Table 1,

$$\begin{aligned}\mathrm{HII}_1(\mathfrak{L}_1) &= 16|E_1(\mathfrak{L}_1)| \times 25|E_2(\mathfrak{L}_1)| \times 49|E_3(\mathfrak{L}_1)| \times 49|E_4(\mathfrak{L}_1)| \times 64|E_5(\mathfrak{L}_1)| \\ &\times 25|E_6(\mathfrak{L}_1)| \times 36|E_7(\mathfrak{L}_1)| \times 49|E_8(\mathfrak{L}_1)| \times 64|E_9(\mathfrak{L}_1)| \\ &\times 81|E_{10}(\mathfrak{L}_1)| \times 36|E_{11}(\mathfrak{L}_1)| \\ &= 16(1) \times 25(1) \times 49(n+5) \times 49(8) \times 64(2n+8) \times 25(2) \\ &\times 36(3n) \times 49(1) \times 64(12) \times 81(27n-13) \times 36(2).\end{aligned} \tag{18}$$

We obtain the following by making some calculations:

$$\Rightarrow \mathrm{HII}_1(\mathfrak{L}_1) = 582761278687150080000n(n+5)(2n+8)(27n-13). \tag{19}$$

From equation (4),

$$\mathrm{HII}_2(\mathfrak{L}_1) = \prod_{rs \in E(\mathfrak{L}_1)} (d_r \times d_s)^2. \tag{20}$$

By applying edge partition of Table 1,

$$\begin{aligned}\mathrm{HII}_2(\mathfrak{L}_1) &= 9|E_1(\mathfrak{L}_1)| \times 16|E_2(\mathfrak{L}_1)| \times 36|E_3(\mathfrak{L}_1)| \times 100|E_4(\mathfrak{L}_1)| \times 144|E_5(\mathfrak{L}_1)| \\ &\times 36|E_6(\mathfrak{L}_1)| \times 81|E_7(\mathfrak{L}_1)| \times 144|E_8(\mathfrak{L}_1)| \times 225|E_9(\mathfrak{L}_1)| \\ &\times 324|E_{10}(\mathfrak{L}_1)| \times 64|E_{11}(\mathfrak{L}_1)| \\ &= 9(1) \times 16(1) \times 36(n+5) \times 100(8) \times 144(2n+8) \times 36(2) \\ &\times 81(3n) \times 144(1) \times 225(12) \times 324(27n-13) \times 64(2).\end{aligned} \tag{21}$$

We obtain the following by making some calculations:

$$\begin{aligned}\Rightarrow \mathrm{HII}_2(\mathfrak{L}_1) &= 16847578091810193408000n(n+5) \\ &(2n+8)(27n-13).\end{aligned} \tag{22}$$

□

Theorem 3. *Consider the magnesium iodide structure MgI_2 of first type; then, the first and second multiplicative universal Zagreb indices are equal to*

$$\begin{aligned}\mathrm{MZ}_1^a(\mathfrak{L}_1) &= 2^{7+10a} \times 3^{2+4a} \times 5^{2a} \times 7^{3a} n(n+5)(2n+8)(27n-13), \\ \mathrm{MZ}_2^a(\mathfrak{L}_1) &= 2^{7+13a} \times 3^{2+10a} \times 5^{2a} \times n(n+5)(2n+8)(27n-13).\end{aligned} \tag{23}$$

Proof. Let $\mathfrak{L}_1$ be the magnesium iodide structure MgI_2 of first type. In Table 1, there is an edge partition of $\mathfrak{L}_1$. From equation (5),

$$\mathrm{MZ}_1^a(\mathfrak{L}_1) = \prod_{rs \in E(\mathfrak{L}_1)} (d_r + d_s)^a. \tag{24}$$

By applying edge partition of Table 1,

$$\begin{aligned}\mathrm{MZ}_1^a(\mathfrak{L}_1) &= 4^a|E_1(\mathfrak{L}_1)| \times 5^a|E_2(\mathfrak{L}_1)| \times 7^a|E_3(\mathfrak{L}_1)| \times 7^a|E_4(\mathfrak{L}_1)| \times 8^a|E_5(\mathfrak{L}_1)| \\ &\times 5^a|E_6(\mathfrak{L}_1)| \times 6^a|E_7(\mathfrak{L}_1)| \times 7^a|E_8(\mathfrak{L}_1)| \times 8^a|E_9(\mathfrak{L}_1)| \\ &\times 9^a|E_{10}(\mathfrak{L}_1)| \times 6^a|E_{11}(\mathfrak{L}_1)| \\ &= 4^a(1) \times 5^a(1) \times 7^a(n+5) \times 7^a(8) \times 8^a(2n+8) \times 5^a(2) \times 6^a(3n) \\ &\times 7^a(1) \times 8^a(12) \times 9^a(27n-13) \times 6^a(2).\end{aligned} \tag{25}$$

We obtain the following by making some calculations:

$$\begin{aligned}\Rightarrow \mathrm{MZ}_1^a(\mathfrak{L}_1) &= 2^{7+10a} \times 3^{2+4a} \times 5^{2a} \times 7^{3a} n(n+5) \\ &(2n+8)(27n-13).\end{aligned} \tag{26}$$

From equation (6),

$$\mathrm{MZ}_2^a(\mathfrak{L}_1) = \prod_{rs \in E(\mathfrak{L}_1)} (d_r \times d_s)^a. \tag{27}$$

By applying edge partition of Table 1,

$$\begin{aligned} \mathrm{MZ}_1^a(\mathfrak{L}_1) &= 3^a\left|E_1(\mathfrak{L}_1)\right| \times 4^a\left|E_2(\mathfrak{L}_1)\right| \times 6^a\left|E_3(\mathfrak{L}_1)\right| \times 10^a\left|E_4(\mathfrak{L}_1)\right| \times 12^a\left|E_5(\mathfrak{L}_1)\right| \\ &\quad \times 6^a\left|E_6(\mathfrak{L}_1)\right| \times 9^a\left|E_7(\mathfrak{L}_1)\right| \times 12^a\left|E_8(\mathfrak{L}_1)\right| \times 15^a\left|E_9(\mathfrak{L}_1)\right| \\ &\quad \times 18^a\left|E_{10}(\mathfrak{L}_1)\right| \times 8^a\left|E_{11}(\mathfrak{L}_1)\right| \\ &= 3^a(1) \times 4^a(1) \times 6^a(n+5) \times 10^a(8) \times 12^a(2n+8) \times 6^a(2) \\ &\quad \times 9^a(3n) \times 12^a(1) \times 15^a(12) \times 18^a(27n-13) \times 8^a(2). \end{aligned} \tag{28}$$

We obtain the following by making some calculations:

$$\begin{aligned} \Rightarrow \mathrm{MZ}_2^a(\mathfrak{L}_1) &= 2^{7+13a} \times 3^{2+10a} \times 5^{2a} \times n(n+5) \\ &\quad (2n+8)(27n-13). \end{aligned} \tag{29}$$

□

Theorem 4. *Consider the magnesium iodide structure MgI_2 of first type; then, the multiplicative sum and product connectivity indices are equal to*

$$\begin{aligned} \mathrm{SCII}(\mathfrak{L}_1) &= \frac{4}{35\sqrt{7}} n(n+5)(2n+8)(27n-13), \\ \mathrm{PCII}(\mathfrak{L}_1) &= \frac{\sqrt{2}}{135} n(n+5)(2n+8)(27n-13). \end{aligned} \tag{30}$$

Proof. Let $\mathfrak{L}_1$ be the magnesium iodide structure MgI_2 of first type. In Table 1, there is an edge partition of $\mathfrak{L}_1$. From equation (7),

$$\mathrm{SCII}(\mathfrak{L}_1) = \prod_{rs \in E(Y)} \frac{1}{\sqrt{d_r + d_s}}. \tag{31}$$

By applying edge partition of Table 1,

$$\begin{aligned} \mathrm{SCII}(\mathfrak{L}_1) &= \frac{1}{\sqrt{4}}\left|E_1(\mathfrak{L}_1)\right| \times \frac{1}{\sqrt{5}}\left|E_2(\mathfrak{L}_1)\right| \times \frac{1}{\sqrt{7}}\left|E_3(\mathfrak{L}_1)\right| \times \frac{1}{\sqrt{7}}\left|E_4(\mathfrak{L}_1)\right| \\ &\quad \times \frac{1}{\sqrt{8}}\left|E_5(\mathfrak{L}_1)\right| \times \frac{1}{\sqrt{5}}\left|E_6(\mathfrak{L}_1)\right| \times \frac{1}{\sqrt{6}}\left|E_7(\mathfrak{L}_1)\right| \times \frac{1}{\sqrt{7}}\left|E_8(\mathfrak{L}_1)\right| \\ &\quad \times \frac{1}{\sqrt{8}}\left|E_9(\mathfrak{L}_1)\right| \times \frac{1}{\sqrt{9}}\left|E_{10}(\mathfrak{L}_1)\right| \times \frac{1}{\sqrt{6}}\left|E_{11}(\mathfrak{L}_1)\right| \\ &= \frac{1}{\sqrt{4}}(1) \times \frac{1}{\sqrt{5}}(1) \times \frac{1}{\sqrt{7}}(n+5) \times \frac{1}{\sqrt{7}}(8) \times \frac{1}{\sqrt{8}}(2n+8) \times \frac{1}{\sqrt{5}}(2) \\ &\quad \times \frac{1}{\sqrt{6}}(3n) \times \frac{1}{\sqrt{7}}(1) \times \frac{1}{\sqrt{8}}(12) \times \frac{1}{\sqrt{9}}(9) \times \frac{1}{\sqrt{6}}(2). \end{aligned} \tag{32}$$

We obtain the following by making some calculations:

$$\Rightarrow \mathrm{SCII}(\mathfrak{L}_1) = \frac{4}{35\sqrt{7}} n(n+5)(2n+8)(27n-13). \tag{33}$$

From equation (8),

$$\mathrm{PCII}(\mathfrak{L}_1) = \prod_{rs \in E(\mathfrak{L}_1)} \frac{1}{\sqrt{d_r \times d_s}}. \tag{34}$$

By applying edge partition of Table 1,

$$\begin{aligned}\mathrm{PCII}(\mathfrak{L}_1) &= \frac{1}{\sqrt{3}}\left|E_1(\mathfrak{L}_1)\right| \times \frac{1}{\sqrt{4}}\left|E_2(\mathfrak{L}_1)\right| \times \frac{1}{\sqrt{6}}\left|E_3(\mathfrak{L}_1)\right| \times \frac{1}{\sqrt{10}}\left|E_4(\mathfrak{L}_1)\right| \\ &\times \frac{1}{\sqrt{12}}\left|E_5(\mathfrak{L}_1)\right| \times \frac{1}{\sqrt{6}}\left|E_6(\mathfrak{L}_1)\right| \times \frac{1}{\sqrt{9}}\left|E_7(\mathfrak{L}_1)\right| \times \frac{1}{\sqrt{12}}\left|E_8(\mathfrak{L}_1)\right| \\ &\times \frac{1}{\sqrt{15}}\left|E_9(\mathfrak{L}_1)\right| \times \frac{1}{\sqrt{18}}\left|E_{10}(\mathfrak{L}_1)\right| \times \frac{1}{\sqrt{8}}\left|E_{11}(\mathfrak{L}_1)\right| \\ &= \frac{1}{\sqrt{3}}(1) \times \frac{1}{\sqrt{4}}(1) \times \frac{1}{\sqrt{6}}(n+5) \times \frac{1}{\sqrt{10}}(8) \times \frac{1}{\sqrt{12}}(2n+8) \times \frac{1}{\sqrt{6}}(2) \\ &\times \frac{1}{\sqrt{9}}(3n) \times \frac{1}{\sqrt{12}}(1) \times \frac{1}{\sqrt{15}}(12) \times \frac{1}{\sqrt{18}}(9) \times \frac{1}{\sqrt{8}}(2).\end{aligned} \tag{35}$$

We obtain the following by making some calculations:

$$\Rightarrow \mathrm{PCII}(\mathfrak{L}_1) = \frac{\sqrt{2}}{135} n(n+5)(2n+8)(27n-13). \tag{36}$$

□

Theorem 5. *Consider the magnesium iodide structure MgI_2 of first type; then, the multiplicative atom-bond connectivity and geometric-arithmetic indices are equal to*

$$\begin{aligned}\mathrm{ABCII}(\mathfrak{L}_1) &= \frac{16\sqrt{35}}{3} n(n+5)(2n+8)(27n-13), \\ \mathrm{GAII}(\mathfrak{L}_1) &= \frac{442368\sqrt{2}}{1715} n(n+5)(2n+8)(27n-13).\end{aligned} \tag{37}$$

Proof. Let $\mathfrak{L}_1$ be the magnesium iodide structure MgI_2 of first type. In Table 1, there is an edge partition of $\mathfrak{L}_1$. From equation (9),

$$\mathrm{ABCII}(\mathfrak{L}_1) = \prod_{rs \in E\mathrm{MgI}_2} \sqrt{\frac{d_r + d_s - 2}{d_r \times d_s}}. \tag{38}$$

By applying edge partition of Table 1,

$$\begin{aligned}\mathrm{ABCII}(\mathfrak{L}_1) &= \sqrt{\frac{2}{3}}\left|E_1(\mathfrak{L}_1)\right| \times \sqrt{\frac{3}{4}}\left|E_2(\mathfrak{L}_1)\right| \times \sqrt{\frac{5}{6}}\left|E_3(\mathfrak{L}_1)\right| \times \sqrt{\frac{5}{10}}\left|E_4(\mathfrak{L}_1)\right| \\ &\times \sqrt{\frac{6}{12}}\left|E_5(\mathfrak{L}_1)\right| \times \sqrt{\frac{3}{6}}\left|E_6(\mathfrak{L}_1)\right| \times \sqrt{\frac{4}{9}}\left|E_7(\mathfrak{L}_1)\right| \times \sqrt{\frac{5}{12}}\left|E_8(\mathfrak{L}_1)\right| \\ &\times \sqrt{\frac{6}{15}}\left|E_9(\mathfrak{L}_1)\right| \times \sqrt{\frac{7}{18}}\left|E_{10}(\mathfrak{L}_1)\right| \times \sqrt{\frac{4}{8}}\left|E_{11}(\mathfrak{L}_1)\right| \\ &= \sqrt{\frac{2}{3}}(1) \times \sqrt{\frac{3}{4}}(1) \times \sqrt{\frac{5}{6}}(n+5) \times \sqrt{\frac{5}{10}}(8) \times \sqrt{\frac{6}{12}}(2n+8) \\ &\times \sqrt{\frac{3}{6}}(2)\sqrt{\frac{4}{9}}(3n) \times (1)\sqrt{\frac{5}{12}} \times \sqrt{\frac{6}{15}}(12) \times \sqrt{\frac{7}{18}}(27n-13) \times \sqrt{\frac{4}{8}}(2).\end{aligned} \tag{39}$$

We obtain the following by making some calculations:

$$\Rightarrow \mathrm{ABCII}(\mathfrak{L}_1) = \frac{16\sqrt{35}}{3} n(n+5)(2n+8)(27n-13). \tag{40}$$

From equation (10),

$$\mathrm{GAII}(\mathfrak{L}_1) = \prod_{rs \in E(\mathfrak{L}_1)} \frac{2\sqrt{d_r \times d_s}}{d_r + d_s}. \tag{41}$$

By applying edge partition of Table 1,

$$\begin{aligned}\mathrm{GAII}(\mathfrak{L}_1) &= \frac{2\sqrt{3}}{4}\left|E_1(\mathfrak{L}_1)\right| \times \frac{2\sqrt{4}}{5}\left|E_2(\mathfrak{L}_1)\right| \times \frac{2\sqrt{6}}{7}\left|E_3(\mathfrak{L}_1)\right| \times \frac{2\sqrt{10}}{7}\left|E_4(\mathfrak{L}_1)\right| \\ &\times \frac{2\sqrt{12}}{8}\left|E_5(\mathfrak{L}_1)\right| \times \frac{2\sqrt{6}}{5}\left|E_6(\mathfrak{L}_1)\right| \frac{2\sqrt{9}}{6}\left|E_7(\mathfrak{L}_1)\right| \times \frac{2\sqrt{12}}{7}\left|E_8(\mathfrak{L}_1)\right| \\ &\times \frac{2\sqrt{15}}{8}\left|E_9(\mathfrak{L}_1)\right| \times \frac{2\sqrt{18}}{9}\left|E_{10}(\mathfrak{L}_1)\right| \times \frac{2\sqrt{8}}{6}\left|E_{11}(\mathfrak{L}_1)\right| \\ &= \frac{2\sqrt{3}}{4}(1) \times \frac{2\sqrt{4}}{5}(1) \times \frac{2\sqrt{6}}{7}(n+5) \times \frac{2\sqrt{10}}{7}(8) \times \frac{2\sqrt{12}}{8}(2n+8) \\ &\times \frac{2\sqrt{6}}{5}(2) \times \frac{2\sqrt{9}}{6}(3n) \times \frac{2\sqrt{12}}{7}(1) \times \frac{2\sqrt{15}}{8}(12) \times \frac{2\sqrt{18}}{9}(27n-13) \times \frac{2\sqrt{8}}{6}(2).\end{aligned} \tag{42}$$

We obtain the following by making some calculations:

$$\Rightarrow \mathrm{GAII}(\mathfrak{L}_1) = \frac{442368\sqrt{2}}{1715} n(n+5)(2n+8)(27n-13). \tag{43}$$

□

Theorem 6. *Consider the magnesium iodide structure MgI_2 of first type; then, the universal multiplicative geometric-arithmetic index is equal to*

$$\mathrm{GA}^a\mathrm{II}(\mathfrak{L}_1) = 2^{(14+15a/2)} \times 3^{2+a} \times 5^{-a} \times 7^{-3a} n(n+5)(2n+8)(27n-13). \tag{44}$$

Proof. Let $\mathfrak{L}_1$ be the magnesium iodide structure MgI_2 of first type. In Table 1, there is an edge partition of $\mathfrak{L}_1$. From equation (10),

$$\mathrm{GA}^a\mathrm{II}(\mathfrak{L}_1) = \prod_{rs \in E(\mathfrak{L}_1)} \frac{2\sqrt{d_r \times d_s}^a}{d_r + d_s}. \tag{45}$$

By applying edge partition of Table 1,

$$\begin{aligned}\mathrm{GA}^a\mathrm{II}(\mathfrak{L}_1) &= \left\{\frac{2\sqrt{3}}{4}\right\}^a \left|E_1(\mathfrak{L}_1)\right| \times \left\{\frac{2\sqrt{4}}{5}\right\}^a \left|E_2(\mathfrak{L}_1)\right| \times \left\{\frac{2\sqrt{6}}{7}\right\}^a \left|E_3(\mathfrak{L}_1)\right| \\ &\times \left\{\frac{2\sqrt{10}}{7}\right\}^a \left|E_4(\mathfrak{L}_1)\right| \times \left|E_5(\mathfrak{L}_1)\right| \left\{\frac{2\sqrt{12}}{8}\right\}^a \times \left\{\frac{2\sqrt{6}}{5}\right\}^a \left|E_6(\mathfrak{L}_1)\right| \\ &\times \left\{\frac{2\sqrt{9}}{6}\right\}^a \left|E_7(\mathfrak{L}_1)\right| \times \left\{\frac{2\sqrt{12}}{7}\right\}^a \left|E_8(\mathfrak{L}_1)\right| \times \left\{\frac{2\sqrt{15}}{8}\right\}^a \left|E_9(\mathfrak{L}_1)\right| \\ &\times \left\{\frac{2\sqrt{18}}{9}\right\}^a \left|E_{10}(\mathfrak{L}_1)\right| \times \left\{\frac{2\sqrt{8}}{6}\right\}^a \left|E_{11}(\mathfrak{L}_1)\right| \\ &= \left\{\frac{2\sqrt{3}}{4}\right\}^a (1) \times \left\{\frac{2\sqrt{4}}{5}(1)\right\}^a \times \left\{\frac{2\sqrt{6}}{7}\right\}^a (n+5) \times \left\{\frac{2\sqrt{10}}{7}(8)\right\}^a \\ &\times \left\{\frac{2\sqrt{12}}{8}\right\}^a (2n+8) \times \left\{\frac{2\sqrt{6}}{5}\right\}^a (2) \times \left\{\frac{2\sqrt{9}}{6}\right\}^a (3n) \times \left\{\frac{2\sqrt{12}}{7}\right\}^a (1) \\ &\times \left\{\frac{2\sqrt{15}}{8}\right\}^a (12) \times \left\{\frac{2\sqrt{18}}{9}\right\}^a (27n-13) \times \left\{\frac{2\sqrt{8}}{6}\right\}^a (2).\end{aligned} \tag{46}$$

We obtain the following by making some calculations:

$$\Rightarrow \mathrm{GA}^{a}\mathrm{II}(\mathfrak{L}_1) = 2^{(14+15a/2)} \times 3^{2+a} \times 5^{-a} \times 7^{-3a} n(n+5)(2n+8)(27n-13). \tag{47}$$

□

2.2. Results for the Second Type of Magnesium Iodide Structure. In this section, we compute topological indices such as multiplicative Zagreb indices, multiplicative hyper-Zagreb indices, multiplicative universal Zagreb indices, sum and product connectivity of multiplicative indices, multiplicative atom-bond connectivity index, and multiplicative geometric and universal geometric-arithmetic indices for the second type of magnesium iodide structure.

Theorem 7. *Consider the magnesium iodide structure MgI_2 of second type; then, the second multiplicative Zagreb index is equal to*

$$\mathrm{II}_2(\mathfrak{L}_2) = 75582720000(n+5)(2n+8)(3n+1)(27n+7). \tag{48}$$

Table 2: Edge subdivision of $\mathfrak{L}_2\mathrm{MgI}_2$ based on degree of end vertices of each edge for $m = 2n+2$, where $n \in \mathbb{N}$.

(d_r, d_s) where $rs \in E(\mathfrak{L}_2)$	Number of edges
(1, 3)	1
(1, 5)	1
(1, 6)	$n+5$
(2, 2)	5
(2, 5)	2
(2, 6)	$2n+8$
(3, 2)	6
(3, 3)	$3n+1$
(3, 5)	2
(3, 6)	$27n+7$

Proof. Let $\mathfrak{L}_2$ be the magnesium iodide structure MgI_2 of second type. In Table 2, there is an edge partition of $\mathfrak{L}_2$. From equation (2),

$$\mathrm{II}_2(\mathfrak{L}_2) = \prod_{rs \in E(\mathfrak{L}_2)} (d_r \times d_s). \tag{49}$$

By applying edge partition of Table 2,

$$\begin{aligned}\mathrm{II}_2(\mathfrak{L}_2) &= 3|E_1(\mathfrak{L}_2)| \times 5|E_2(\mathfrak{L}_2)| \times 6|E_3(\mathfrak{L}_2)| \times 4|E_4(\mathfrak{L}_2)| \times 10|E_5(\mathfrak{L}_2)| \\ &\quad \times 12|E_6(\mathfrak{L}_2)| \times 6|E_7(\mathfrak{L}_2)| \times 9|E_8(\mathfrak{L}_2)| \times 15|E_9(\mathfrak{L}_2)| \times 18|E_{10}(\mathfrak{L}_2)| \\ &= 3(1) \times 5(1) \times 6(n+5) \times 4(5) \times 10(2) \times 12(2n+8) \times 6(6) \\ &\quad \times 9(3n+1) \times 15(2) \times 18(27n+7).\end{aligned} \tag{50}$$

We obtain the following by making some calculations:

$$\Rightarrow \mathrm{II}_2(\mathfrak{L}_2) = 75582720000(n+5)(2n+8)(3n+1)(27n+7). \tag{51}$$

□

Theorem 8. *Consider the magnesium iodide structure MgI_2 of second type; then, the first and second multiplicative hyper-Zagreb indices are equal to*

$$\begin{aligned}\mathrm{HII}_1(\mathfrak{L}_2) &= 792872488009728000(n+5)(2n+8)(3n+1)(27n+7), \\ \mathrm{HII}_2(\mathfrak{L}_2) &= 47606229688320000000(n+5)(2n+8)(3n+1)(27n+7).\end{aligned} \tag{52}$$

Proof. Let $\mathfrak{L}_2$ be the magnesium iodide structure MgI_2 of second type. In Table 2, there is an edge partition of $\mathfrak{L}_2$. From equation (3),

$$\mathrm{HII}_1(\mathfrak{L}_2) = \prod_{rs \in E(\mathfrak{L}_2)} (d_r + d_s)^2. \tag{53}$$

By applying edge partition of Table 2,

$$\begin{aligned}\mathrm{HII}_1(\mathfrak{L}_2) &= 16|E_1(\mathfrak{L}_2)| \times 36|E_2(\mathfrak{L}_2)| \times 49|E_3(\mathfrak{L}_2)| \times 16|E_4(\mathfrak{L}_2)| \times 49|E_5(\mathfrak{L}_2)| \\ &\quad \times 64|E_6(\mathfrak{L}_2)| \times 25|E_7(\mathfrak{L}_2)| \times 36|E_8(\mathfrak{L}_2)| \times 64|E_9(\mathfrak{L}_2)| \times 81|E_{10}(\mathfrak{L}_2)| \\ &= 16(1) \times 36(1) \times 49(n+5) \times 16(5) \times 49(2) \times 64(2n+8) \times 25(6) \\ &\quad \times 36(3n+1) \times 64(2) \times 81(27n+7).\end{aligned} \tag{54}$$

Table 3: Comparison among $II_2(\mathfrak{L}_1)$, $HII_1(\mathfrak{L}_1)$, and $HII_2(\mathfrak{L}_1)$ indices of MgI_2 for $m = 2n + 1$, where $n \in \mathbb{N}$.

n	$II_2(\mathfrak{L}_1)$	$HII_1(\mathfrak{L}_1)$	$HII_2(\mathfrak{L}_1)$
2	0.0960×10^{18}	0.0414×10^{26}	0.1160×10^{28}
3	0.3183×10^{18}	0.1331×10^{26}	0.3849×10^{28}
4	0.7623×10^{18}	0.3189×10^{26}	0.9219×10^{28}
5	1.5297×10^{18}	0.6399×10^{26}	1.8498×10^{28}
6	2.7400×10^{18}	1.1461×10^{26}	3.3136×10^{28}
7	4.5312×10^{18}	1.8954×10^{26}	5.4796×10^{28}
8	7.0589×10^{18}	2.9528×10^{26}	8.5365×10^{28}
9	10.4970×10^{18}	4.3910×10^{26}	12.6943×10^{28}
10	15.0376×10^{18}	6.2903×10^{26}	18.1853×10^{28}

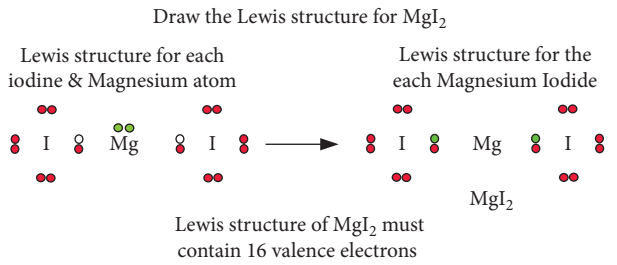

Figure 3: Lewis structure for MgI_2.

Table 4: Comparison among $SCII(\mathfrak{L}_1)$, $PCII(\mathfrak{L}_1)$, $ABCII(\mathfrak{L}_1)$, and $GAII(\mathfrak{L}_1)$ indices of MgI_2 for $m = 2n + 1$, where $n \in \mathbb{N}$.

n	$SCII(\mathfrak{L}_1)$	$PCII(\mathfrak{L}_1)$	$ABCII(\mathfrak{L}_1)$	$GAII(\mathfrak{L}_1)$
2	2.9754×10^2	0.0721×10^3	0.2173×10^6	0.2512×10^7
3	9.8694×10^2	0.2393×10^3	0.7209×10^6	0.8335×10^7
4	23.6368×10^2	0.5732×10^3	1.7265×10^6	1.9960×10^7
5	47.4291×10^2	1.1502×10^3	3.4645×10^6	4.0053×10^7
6	84.9578×10^2	2.0603×10^3	6.2057×10^6	7.1745×10^7
7	140.4940×10^2	3.4071×10^3	10.2624×10^6	11.8645×10^7
8	218.8690×10^2	5.3079×10^3	15.9872×10^6	18.4831×10^7
9	325.4730×10^2	7.8932×10^3	23.7741×10^6	27.4857×10^7
10	466.2570×10^2	11.3074×10^3	34.0577×10^6	39.3747×10^7

We obtain the following by making some calculations:

$$\Rightarrow HII_1(\mathfrak{L}_2) = 792872488009728000(n+5)(2n+8)(3n+1)(27n+7). \tag{55}$$

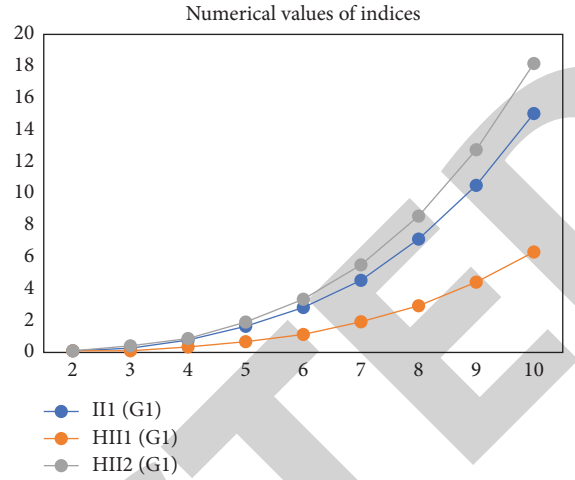

Figure 4: Graphical comparison among $II_2(\mathfrak{L}_1)$, $HII_1(\mathfrak{L}_1)$, and $HII_2(\mathfrak{L}_1)$ indices of MgI_2 for $m = 2n + 1$.

Table 5: Comparison among $II_2(\mathfrak{L}_2)$, $HII_1(\mathfrak{L}_2)$, and $HII_2(\mathfrak{L}_2)$ indices of MgI_2 for $m = 2n + 2$, where $n \in \mathbb{N}$.

n	$II_2(\mathfrak{L}_2)$	$HII_1(\mathfrak{L}_2)$	$HII_2(\mathfrak{L}_2)$
2	0.2711×10^{16}	0.2849×10^{23}	0.1707×10^{25}
3	0.7449×10^{16}	0.7815×10^{23}	0.4692×10^{25}
4	1.6271×10^{16}	1.7069×10^{23}	1.0249×10^{25}
5	3.0910×10^{16}	3.2425×10^{23}	1.9469×10^{25}
6	5.3393×10^{16}	5.6010×10^{23}	3.3630×10^{25}
7	8.6041×10^{16}	9.0258×10^{23}	5.4193×10^{25}
8	13.1469×10^{16}	13.7912×10^{23}	8.2806×10^{25}
9	19.2585×10^{16}	20.2024×10^{23}	12.1301×10^{25}
10	27.2592×10^{16}	28.5953×10^{23}	17.1694×10^{25}

From equation (4),

$$HII_2(\mathfrak{L}_2) = \prod_{rs \in E(\mathfrak{L}_2)} (d_r \times d_s)^2. \tag{56}$$

By applying edge partition of Table 2,

$$\begin{aligned} HII_2(\mathfrak{L}_2) &= 9|E_1(\mathfrak{L}_2)| \times 25|E_{21}(\mathfrak{L}_2)| \times 36|E_3(\mathfrak{L}_2)| \times 16|E_4(\mathfrak{L}_2)| \times 100|E_5(\mathfrak{L}_2)| \\ &\quad \times 144|E_6(\mathfrak{L}_2)| \times 36|E_7(\mathfrak{L}_2)| \times 81|E_8(\mathfrak{L}_2)| \times 225|E_9(\mathfrak{L}_2)| \times 324|E_{10}(\mathfrak{L}_2)|, \\ &= 9(1) \times 25(1) \times 36(n+5) \times 16(5) \times 100(2) \times 144(2n+8) \times 36(6) \\ &\quad \times 81(3n+1) \times 225(2) \times 324(27n+7). \end{aligned} \tag{57}$$

We obtain the following by making some calculations:

$$\Rightarrow HII_2(\mathfrak{L}_2) = 47606229688320000000(n+5)(2n+8)(3n+1)(27n+7). \tag{58}$$

□

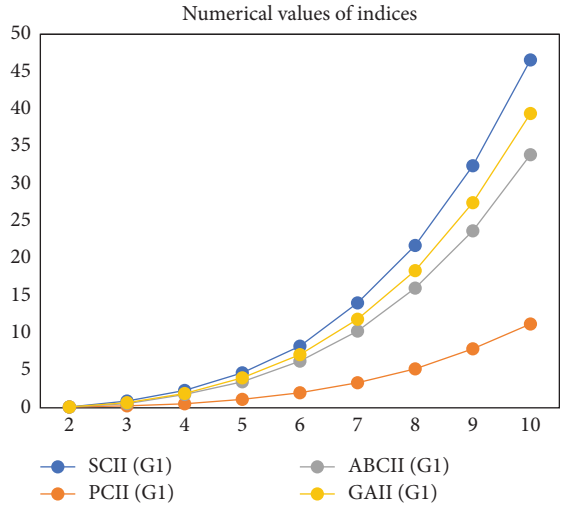

Figure 5: Graphical comparison of $\mathrm{SCII}(\mathfrak{L}_1)$, $\mathrm{PCII}(\mathfrak{L}_1)$, $\mathrm{ABCII}(\mathfrak{L}_1)$, and $\mathrm{GAII}(\mathfrak{L}_1)$ indices of MgI_2 for $m = 2n + 1$.

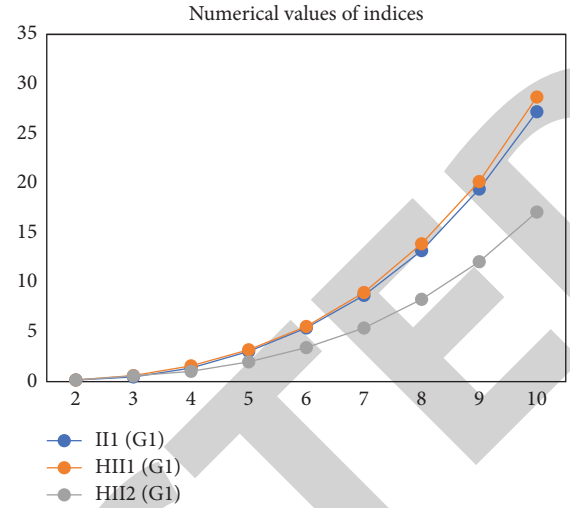

Figure 6: Graphical comparison of $\mathrm{II}_2(\mathfrak{L}_2)$, $\mathrm{HII}_1(\mathfrak{L}_2)$, and $\mathrm{HII}_2(\mathfrak{L}_2)$ indices of MgI_2 for $m = 2n + 2$.

Table 6: Comparison among $\mathrm{SCII}(\mathfrak{L}_2)$, $\mathrm{PCII}(\mathfrak{L}_2)$, $\mathrm{ABCII}(\mathfrak{L}_2)$, and $\mathrm{GAII}(\mathfrak{L}_2)$ indices of MgI_2 for $m = 2n + 2$, where $n \in \mathbb{N}$.

n	$\mathrm{SCII}(\mathfrak{L}_2)$	$\mathrm{PCII}(\mathfrak{L}_2)$	$\mathrm{ABCII}(\mathfrak{L}_2)$	$\mathrm{GAII}(\mathfrak{L}_2)$
2	0.4774×10^3	0.1715×10^3	0.1886×10^6	0.1360×10^7
3	1.3118×10^3	0.4713×10^3	0.5183×10^6	0.3739×10^7
4	2.8653×10^3	1.0293×10^3	1.1321×10^6	0.8167×10^7
5	5.4432×10^3	1.9554×10^3	2.1506×10^6	1.5515×10^7
6	9.4024×10^3	3.3777×10^3	3.7148×10^6	2.6801×10^7
7	15.1516×10^3	5.4430×10^3	5.9869×10^6	4.3189×10^7
8	23.1513×10^3	8.3168×10^3	9.1470×10^6	6.5991×10^7
9	33.9137×10^3	12.1832×10^3	13.3993×10^6	9.6669×10^7
10	48.0028×10^3	17.2445×10^3	18.9658×10^6	13.6830×10^7

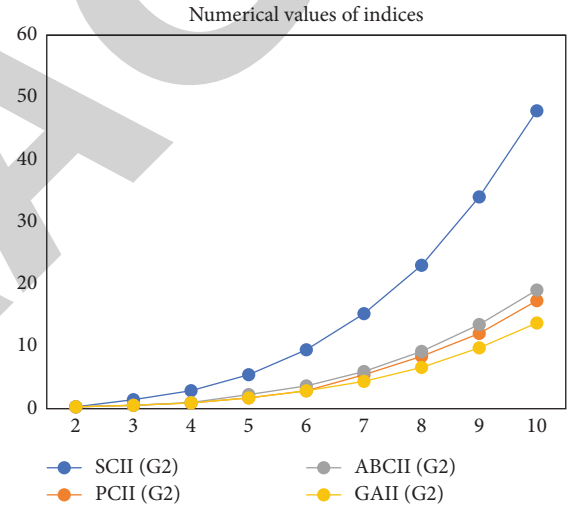

Figure 7: Graphical Comparison among $\mathrm{SCII}(\mathfrak{L}_2)$, $\mathrm{PCII}(\mathfrak{L}_2)$, $\mathrm{ABCII}(\mathfrak{L}_2)$, and $\mathrm{GAII}(\mathfrak{L}_2)$ indices of MgI_2 for $m = 2n + 2$.

Theorem 9. *Consider the magnesium iodide structure MgI_2 of second type; then, the first and second multiplicative universal Zagreb indices are equal to*

$$\begin{aligned} \mathrm{MZ}_1^a(\mathfrak{L}_2) &= 5^{1+a} \times 7^{2a} \times 24^{1+4a}(n+5)(2n+8)(3n+1)(27n+7), \\ \mathrm{MZ}_2^a(\mathfrak{L}_2) &= 2^{3+8a} \times 3^{1+9a} \times 5^{1+3a} \times (n+5)(2n+8)(3n+1)(27n+7). \end{aligned} \tag{59}$$

Proof. Let $\mathfrak{L}_2$ be the magnesium iodide structure MgI_2 of second type. In Table 2, there is an edge partition of $\mathfrak{L}_2$. From equation (5),

$$\mathrm{MZ}_1^a(\mathfrak{L}_2) = \prod_{rs \in E(\mathfrak{L}_2)} (d_r + d_s)^a. \tag{60}$$

By applying edge partition of Table 2,

$$\begin{aligned} \mathrm{MZ}_1^a(\mathfrak{L}_2) &= 4^a \left|E_1(\mathfrak{L}_2)\right| \times 6^a \left|E_2(\mathfrak{L}_2)\right| \times 7^a \left|E_3(\mathfrak{L}_2)\right| \times 4^a \left|E_4(\mathfrak{L}_2)\right| \times 7^a \left|E_5(\mathfrak{L}_2)\right| \\ &\quad \times 8^a \left|E_6(\mathfrak{L}_2)\right| \times 5^a \left|E_7(\mathfrak{L}_2)\right| \times 6^a \left|E_8(\mathfrak{L}_2)\right| \times 8^a \left|E_9(\mathfrak{L}_2)\right| \times 9^a \left|E_{10}(\mathfrak{L}_2)\right| \\ &= 4^a(1) \times 6^a(1) \times 7^a(n+5) \times 4^a(5) \times 7^a(2) \times 8^a(2n+8) \times 5^a(6) \\ &\quad \times 6^a(3n+1) \times 8^a(2) \times 9^a(27n+7). \end{aligned} \tag{61}$$

We obtain the following by making some calculations:

$$\Rightarrow \mathrm{MZ}_1^a(\mathfrak{L}_2) = 5^{1+a} \times 7^{2a} \times 24^{1+4a}(n+5)(2n+8)(3n+1)(27n+7). \tag{62}$$

From equation (6),

$$\mathrm{MZ}_2^a(\mathfrak{L}_2) = \prod_{rs \in E(\mathfrak{L}_2)} (d_r \times d_s)^a. \tag{63}$$

By applying edge partition of Table 2,

$$\begin{aligned}\mathrm{MZ}_2^a(\mathfrak{L}_2) &= 3^a|E_1(\mathfrak{L}_2)| \times 5^a|E_2(\mathfrak{L}_2)| \times 6^a|E_3(\mathfrak{L}_2)| \times 4^a|E_4(\mathfrak{L}_2)| \\ &\quad \times 10^a|E_5(\mathfrak{L}_2)| \times 12^a|E_6(\mathfrak{L}_2)| \times 6^a|E_7(\mathfrak{L}_2)| \times 9^a|E_8(\mathfrak{L}_2)| \\ &\quad \times 15^a|E_9(\mathfrak{L}_2)| \times 18^a|E_{10}(\mathfrak{L}_2)| \\ &= 3^a(1) \times 5^a(1) \times 6^a(n+5) \times 4^a(5) \times 10^a(2) \times 12^a(2n+8) \\ &\quad \times 6^a(6) \times 9^a(3n+1) \times 15^a(2) \times 18^a(27n+7).\end{aligned} \tag{64}$$

We obtain the following by making some calculations:

$$\Rightarrow \mathrm{MZ}_2^a(\mathfrak{L}_2) = 2^{3+8a} \times 3^{1+9a} \times 5^{1+3a} \times (n+5)(2n+8)(3n+1)(27n+7). \tag{65}$$

□

Theorem 10. *Consider the magnesium iodide structure MgI_2 of second type; then, the multiplicative sum and product connectivity indices are equal to*

$$\begin{aligned}\mathrm{SCII}(\mathfrak{L}_2) &= \frac{1}{168\sqrt{5}}(n+5)(2n+8)(3n+1)(27n+7), \\ \mathrm{PCII}(\mathfrak{L}_2) &= \frac{1}{54\sqrt{15}}(n+5)(2n+8)(3n+1)(27n+7).\end{aligned} \tag{66}$$

Proof. Let $\mathfrak{L}_2$ be the magnesium iodide structure MgI_2 of second type. In Table 2, there is an edge partition of $\mathfrak{L}_2$. From equation (7),

$$\mathrm{SCII}(\mathfrak{L}_2) = \prod_{rs \in E(\mathfrak{L}_2)} \frac{1}{\sqrt{d_r + d_s}}. \tag{67}$$

By applying edge partition of Table 2,

$$\begin{aligned}\mathrm{SCII}(\mathfrak{L}_2) &= \frac{1}{\sqrt{4}}|E_1(\mathfrak{L}_2)| \times \frac{1}{\sqrt{6}}|E_2(\mathfrak{L}_2)| \times \frac{1}{\sqrt{7}}|E_3(\mathfrak{L}_2)| \times \frac{1}{\sqrt{4}}|E_4(\mathfrak{L}_2)| \\ &\quad \times \frac{1}{\sqrt{7}}|E_5(\mathfrak{L}_2)| \times \frac{1}{\sqrt{8}}|E_6(\mathfrak{L}_2)| \times \frac{1}{\sqrt{5}}|E_7(\mathfrak{L}_2)| \times \frac{1}{\sqrt{6}}|E_8(\mathfrak{L}_2)| \\ &\quad \times \frac{1}{\sqrt{8}}|E_9(\mathfrak{L}_2)| \times \frac{1}{\sqrt{9}}|E_{10}(\mathfrak{L}_2)| \\ &= \frac{1}{\sqrt{4}}(1) \times \frac{1}{\sqrt{6}}(1) \times \frac{1}{\sqrt{7}}(n+5) \times \frac{1}{\sqrt{4}}(5) \times \frac{1}{\sqrt{7}}(2) \times \frac{1}{\sqrt{8}}(2n+8) \\ &\quad \times \frac{1}{\sqrt{5}}(6) \times \frac{1}{\sqrt{6}}(3n+1) \times \frac{1}{\sqrt{8}}(2) \times \frac{1}{\sqrt{9}}(27n+7).\end{aligned} \tag{68}$$

We obtain the following by making some calculations:

$$\Rightarrow \mathrm{SCII}(\mathfrak{L}_2) = \frac{1}{168\sqrt{5}}(n+5)(2n+8)(3n+1)(27n+7). \tag{69}$$

From equation (8),

$$\mathrm{PCII}(\mathfrak{L}_2) = \prod_{rs \in E(\mathfrak{L}_2)} \frac{1}{\sqrt{d_r \times d_s}}. \tag{70}$$

By applying edge partition of Table 2,

$$\begin{aligned}\mathrm{PCII}(\mathfrak{L}_2) &= \frac{1}{\sqrt{3}}|E_1(\mathfrak{L}_2)| \times \frac{1}{\sqrt{5}}|E_2(\mathfrak{L}_2)| \times \frac{1}{\sqrt{6}}|E_3(\mathfrak{L}_2)| \times \frac{1}{\sqrt{4}}|E_4(\mathfrak{L}_2)| \\ &\times \frac{1}{\sqrt{10}}|E_5(\mathfrak{L}_2)| \times \frac{1}{\sqrt{12}}|E_6(\mathfrak{L}_2)| \times \frac{1}{\sqrt{6}}|E_7(\mathfrak{L}_2)| \times \frac{1}{\sqrt{9}}|E_7(\mathfrak{L}_2)| \\ &\times \frac{1}{\sqrt{15}}|E_9(\mathfrak{L}_2)| \times \frac{1}{\sqrt{18}}|E_{10}(\mathfrak{L}_2)| \\ &= \frac{1}{\sqrt{3}}(1) \times \frac{1}{\sqrt{5}}(1) \times \frac{1}{\sqrt{6}}(n+5) \times \frac{1}{\sqrt{4}}(5) \times \frac{1}{\sqrt{10}}(2) \\ &\times \frac{1}{\sqrt{12}}(2n+8) \times \frac{1}{\sqrt{6}}(6) \times \frac{1}{\sqrt{9}}(3n+1) \times \frac{1}{\sqrt{15}}(2) \times \frac{1}{\sqrt{18}}(27n+7).\end{aligned} \tag{71}$$

We obtain the following by making some calculations:

$$\Rightarrow \mathrm{PCII}(\mathfrak{L}_2) = \frac{1}{54\sqrt{15}}(n+5)(2n+8)(3n+1)(27n+7). \tag{72}$$

□

Theorem 11. *Consider the magnesium iodide structure MgI_2 of second type; then, the multiplicative atom-bond connectivity index and geometric-arithmetic index are equal to*

$$\begin{aligned}\mathrm{ABCII}(\mathfrak{L}_2) &= \frac{8\sqrt{35}}{9}(n+5)(2n+8)(3n+1)(27n+7), \\ \mathrm{GAII}(\mathfrak{L}_2) &= \frac{480\sqrt{15}}{49}(n+5)(2n+8)(3n+1)(27n+7).\end{aligned} \tag{73}$$

Proof. Let $\mathfrak{L}_2$ be the magnesium iodide structure MgI_2 of second type. In Table 2, there is an edge partition of $\mathfrak{L}_2$. From equation (9),

$$\mathrm{ABCII}(\mathfrak{L}_2) = \prod_{rs \in E(\mathfrak{L}_2)} \sqrt{\frac{d_r + d_s - 2}{d_r \times d_s}}. \tag{74}$$

By applying edge partition of Table 2,

$$\begin{aligned}\mathrm{ABCII}(\mathfrak{L}_2) &= \sqrt{\frac{2}{3}}|E_1(\mathfrak{L}_2)| \times \sqrt{\frac{4}{5}}|E_2(\mathfrak{L}_2)| \times \sqrt{\frac{5}{6}}|E_3(\mathfrak{L}_2)| \times \sqrt{\frac{2}{4}}|E_4(\mathfrak{L}_2)| \\ &\times \sqrt{\frac{5}{10}}|E_5(\mathfrak{L}_2)| \times \sqrt{\frac{6}{12}}|E_6(\mathfrak{L}_2)|\sqrt{\frac{3}{6}}|E_7(\mathfrak{L}_2)| \times \sqrt{\frac{4}{6}}|E_8(\mathfrak{L}_2)| \\ &\times \sqrt{\frac{6}{15}}|E_9(\mathfrak{L}_2)| \times \sqrt{\frac{7}{18}}|E_{10}(\mathfrak{L}_2)| \\ &= \sqrt{\frac{2}{3}}(1) \times \sqrt{\frac{4}{5}}(1) \times \sqrt{\frac{5}{6}}(n+5) \times \sqrt{\frac{2}{4}}(5) \times \sqrt{\frac{5}{10}}(2) \\ &\times \sqrt{\frac{6}{12}}(2n+8)\sqrt{\frac{3}{6}}(6) \times (3n+1)\sqrt{\frac{4}{9}} \times \sqrt{\frac{6}{15}}(2) \times \sqrt{\frac{7}{18}}(27n+7).\end{aligned} \tag{75}$$

We obtain the following by making some calculations:

$$\Rightarrow \mathrm{ABCII}(\mathfrak{L}_2) = \frac{8\sqrt{35}}{9}(n+5)(2n+8)(3n+1)(27n+7). \tag{76}$$

From equation (9),

$$\mathrm{GAII}(\mathfrak{L}_2) = \prod_{rs \in E(\mathfrak{L}_2)} \frac{2\sqrt{d_r \times d_s}}{d_r + d_s}. \tag{77}$$

By applying edge partition of Table 2,

$$\begin{aligned}\mathrm{GAII}(\mathfrak{L}_2) &= \frac{2\sqrt{3}}{4}\left|E_1(\mathfrak{L}_2)\right| \times \frac{2\sqrt{5}}{6}\left|E_2(\mathfrak{L}_2)\right| \times \frac{2\sqrt{6}}{7}\left|E_3(\mathfrak{L}_2)\right| \times \frac{2\sqrt{4}}{4}\left|E_4(\mathfrak{L}_2)\right| \\ &\times \frac{2\sqrt{10}}{7}\left|E_5(\mathfrak{L}_2)\right| \times \frac{2\sqrt{12}}{8}\left|E_6(\mathfrak{L}_2)\right| \times \frac{2\sqrt{6}}{5}\left|E_7(\mathfrak{L}_2)\right| \times \frac{2\sqrt{9}}{6}\left|E_8(\mathfrak{L}_2)\right| \\ &\times \frac{2\sqrt{15}}{8}\left|E_9(\mathfrak{L}_2)\right| \times \frac{2\sqrt{18}}{9}\left|E_{10}(\mathfrak{L}_2)\right| \\ &= \frac{2\sqrt{3}}{4}(1) \times \frac{2\sqrt{5}}{6}(1) \times \frac{2\sqrt{6}}{7}(n+5) \times \frac{2\sqrt{4}}{4}(5) \times \frac{2\sqrt{10}}{7}(2) \\ &\times \frac{2\sqrt{12}}{8}(2n+8)\frac{2\sqrt{6}}{5}(6) \times \frac{2\sqrt{9}}{6}(3n+1) \times \frac{2\sqrt{15}}{8}(2) \times \frac{2\sqrt{18}}{9}(27n+7).\end{aligned} \tag{78}$$

We obtain the following by making some calculations:

$$\Rightarrow \mathrm{GAII}(\mathfrak{L}_2) = \frac{480\sqrt{15}}{49}(n+5)(2n+8)(3n+1)(27n+7). \tag{79}$$

□

Theorem 12. *Consider the magnesium iodide structure MgI_2 of second type; then, the universal multiplicative geometric-arithmetic index is equal to*

$$\begin{aligned}\mathrm{GA}^a\mathrm{II}(\mathfrak{L}_2) = {} & 2^{3+2a} \times 7^{-2a} \times 15^{(2+a)/2}(n+5)(2n+8) \\ & (3n+1)(27n+7).\end{aligned} \tag{80}$$

Proof. Let $\mathfrak{L}_2$ be the magnesium iodide structure MgI_2 of second type. In Table 2, there is an edge partition of $\mathfrak{L}_2$. From equation (10),

$$\mathrm{GA}^a\mathrm{II}(\mathfrak{L}_2) = \prod_{rs \in E(\mathfrak{L}_2)} \frac{2\sqrt{d_r \times d_s}^a}{d_r + d_s}. \tag{81}$$

By applying edge partition of Table 2,

$$\begin{aligned}\mathrm{GA}^a\mathrm{II}(\mathfrak{L}_2) &= \left(\frac{2\sqrt{3}}{4}\right)^a \left|E_1(\mathfrak{L}_2)\right| \times \left(\frac{2\sqrt{5}}{6}\right)^a \left|E_2(\mathfrak{L}_2)\right| \times \left(\frac{2\sqrt{6}}{7}\right)^a \left|E_3(\mathfrak{L}_2)\right| \\ &\times \left(\frac{2\sqrt{4}}{4}\right)^a \left|E_4(\mathfrak{L}_2)\right| \times \left(\frac{2\sqrt{10}}{7}\right)^a \left|E_5(\mathfrak{L}_2)\right| \times \left(\frac{2\sqrt{12}}{8}\right)^a \left|E_6(\mathfrak{L}_2)\right| \\ &\times \left(\frac{2\sqrt{6}}{5}\right)^a \left|E_7(\mathfrak{L}_2)\right| \times \left(\frac{2\sqrt{9}}{6}\right)^a \left|E_8(\mathfrak{L}_2)\right| \times \left(\frac{2\sqrt{15}}{8}\right)^a \left|E_9(\mathfrak{L}_2)\right| \times \left(\frac{2\sqrt{18}}{9}\right)^a \left|E_{10}(\mathfrak{L}_2)\right| \\ &= \left(\frac{2\sqrt{3}}{4}\right)^a (1) \times \left(\frac{2\sqrt{5}}{6}\right)^a (1) \times \left(\frac{2\sqrt{6}}{7}\right)^a (n+5) \times \left(\frac{2\sqrt{4}}{4}\right)^a (5) \\ &\times \left(\frac{2\sqrt{10}}{7}\right)^a (2) \times \left(\frac{2\sqrt{12}}{8}\right)^a (2n+8)\left(\frac{2\sqrt{6}}{5}\right)^a (6) \\ &\times \left(\frac{2\sqrt{9}}{6}\right)^a (3n+1) \times \left(\frac{2\sqrt{15}}{8}\right)^a (2) \times \left(\frac{2\sqrt{18}}{9}\right)^a (27n+7).\end{aligned} \tag{82}$$

We obtain the following by making some calculations:

$$\Rightarrow \mathrm{GA}^{a}\mathrm{II}(\mathfrak{L}_2) = 2^{3+2a} \times 7^{-2a} \times 15^{(2+a)/2}(n+5)(2n+8)(3n+1)(27n+7). \tag{83}$$

□

3. Numerical and Graphical Comparison

In this section, we compute all the indices numerically and present the result in the following tables.

(i) For the comparison of $\mathrm{II}_2(\mathfrak{L}_1)$, $\mathrm{HII}_1(\mathfrak{L}_1)$, and $\mathrm{HII}_2(\mathfrak{L}_1)$ indices of MgI_2 for $m = 2n + 1$, where $n \in \mathbb{N}$, in Table 3, indices for various n values have been calculated. One can clearly see that all the indices are increasing in order for increasing values of n. Graphical representations of these topological indices are shown in Figure 3 for different values of n.

(ii) For the comparison of $\mathrm{SCII}(\mathfrak{L}_1)$, $\mathrm{PCII}(\mathfrak{L}_1)$, $\mathrm{ABCII}(\mathfrak{L}_1)$, and $\mathrm{GAII}(\mathfrak{L}_1)$ indices of MgI_2 for $m = 2n + 1$, where $n \in \mathbb{N}$, numerically, we computed some indices for different values of n. In Table 4, indices for various n values have been calculated. One can clearly see that all the indices are increasing in order for increasing values of n. Graphical representations of these topological indices are shown in Figure 4 for different values of n.

(iii) For the comparison of $\mathrm{II}_2(\mathfrak{L}_2)$, $\mathrm{HII}_1(\mathfrak{L}_2)$, and $\mathrm{HII}_2(\mathfrak{L}_2)$ indices of MgI_2 for $m = 2n + 2$, where $n \in \mathbb{N}$, in Table 5, indices for various n values have been calculated. One can clearly see that all the indices are increasing in order for increasing values of n. Graphical representations of these topological indices are shown in Figure 5 for different values of n.

(iv) For the comparison of $\mathrm{SCII}(\mathfrak{L}_2)$, $\mathrm{PCII}(\mathfrak{L}_2)$, $\mathrm{ABCII}(\mathfrak{L}_2)$, and $\mathrm{GAII}(\mathfrak{L}_2)$ indices of MgI_2 for $m = 2n + 2$, where $n \in \mathbb{N}$, numerically, we computed some indices for different values of n. In Table 6, indices for various n values have been calculated. One can clearly see that all the indices are increasing in order for increasing values of n. Graphical representations of these topological indices are shown in Figure 6 for different values of n.

4. Discussion

Since topological indices play a vital role in various fields of science such as software engineering, medication, and pharmaceutical industry, their numerical values and graphical representations are very much important for researchers. Here, we calculate some exact values of multiplicative degree-based indices of a famous crystalline structure, magnesium iodide (MgI_2). Furthermore, we construct Tables 3–6 and Figures 4–7 to estimate the degree-based topological indices for various values of n. From tables and figures, we can see that as n increases, the degree-based indices of these networks also increase.

5. Conclusion

In this paper, we have constructed the crystalline graph of magnesium iodide with different approaches of graph theory. We subdivided the graph in even and odd vertices. We computed the multiplicative topological indices such as multiplicative Zagreb indices, multiplicative hyper-Zagreb indices, multiplicative universal Zagreb indices, sum and product connectivity of multiplicative indices, multiplicative atom-bond connectivity index, and multiplicative geometric-arithmetic index of MgI_2 structures in this research for the very first time. In addition, we have given general formulation for those indices that may be very beneficial while analyzing the underlying topologies.

In future, we are interested to design some new architectures/networks and then study their topological indices, which will be quite helpful to understand their underlying topologies.

Data Availability

No data were used to support this study.

Conflicts of Interest

The authors declare that they have no conflicts of interest.

References

[1] I. Gutman, "Molecular graphs with minimal and maximal Randić indices," *Emphcroatica Chemica Acta*, vol. 75, no. 2, pp. 357–369, 2002.

[2] I. Gutman, "Degree-based topological indices," *Croatica Chemica Acta*, vol. 86, no. 4, pp. 351–361, 2013.

[3] M. Eliasi, A. Iranmanesh, and I. Gutman, "Multiplicative versions of first Zagreb index," *Match-Communications in Mathematical and Computer Chemistry*, vol. 68, no. 1, p. 217, 2012.

[4] I. Gutman, "Multiplicative Zagreb indices of trees," *Bulletin of Society of Mathematicians Banja Luka*, vol. 18, pp. 17–23, 2011.

[5] V. R. Kulli, "Multiplicative hyper-Zagreb indices and coindices of graphs: computing these indices of some nanostructures," *International Research Journal of Pure Algebra*, vol. 6, no. 7, pp. 342–347, 2016.

[6] V. R. Kulli, B. Stone, S. Wang, and B. Wei, "Generalised multiplicative indices of polycyclic aromatic hydrocarbons and benzenoid systems," *Zeitschrift fur Naturforschung A*, vol. 72, no. 6, pp. 573–576, 2017.

[7] V. R. Kulli, "Multiplicative connectivity indices of TUC4C8 [m, n] and TUC4[m, n] nanotubes," *Journal of Computer and Mathematical Sciences*, vol. 11, pp. 599–605, 2016.

[8] F. Afzal, F. Asmat, and D. Afzal, "Molecular description for magnesium iodide," *Mathematical Models in Engineering*, vol. 5, no. 4, pp. 175–189, 2019.

[9] H. Ali, M. A. Binyamin, M. K. Shafiq, and W. Gao, "On the degree-based topological indices of some derived networks," *Mathematics*, vol. 7, p. 612, 2019.

[10] U. Babar, H. Ali, S. H. Arshad, and U. Sheikh, "Multiplicative topological properties of graphs derived from honeycomb structure," *AIMS Mathematics*, vol. 5, no. 2, p. 1562, 2020.

Hindawi
Journal of Mathematics
Volume 2024, Article ID 9785015, 1 page
https://doi.org/10.1155/2024/9785015

Retraction

Retracted: Research on the Application of Genetic Algorithm in Physical Education

Journal of Mathematics

Received 23 January 2024; Accepted 23 January 2024; Published 24 January 2024

This article has been retracted by Hindawi following an investigation undertaken by the publisher [1]. This investigation has uncovered evidence of one or more of the following indicators of systematic manipulation of the publication process:

(1) Discrepancies in scope

(2) Discrepancies in the description of the research reported

(3) Discrepancies between the availability of data and the research described

(4) Inappropriate citations

(5) Incoherent, meaningless and/or irrelevant content included in the article

(6) Manipulated or compromised peer review

The presence of these indicators undermines our confidence in the integrity of the article's content and we cannot, therefore, vouch for its reliability. Please note that this notice is intended solely to alert readers that the content of this article is unreliable. We have not investigated whether authors were aware of or involved in the systematic manipulation of the publication process.

Wiley and Hindawi regrets that the usual quality checks did not identify these issues before publication and have since put additional measures in place to safeguard research integrity.

We wish to credit our own Research Integrity and Research Publishing teams and anonymous and named external researchers and research integrity experts for contributing to this investigation.

The corresponding author, as the representative of all authors, has been given the opportunity to register their agreement or disagreement to this retraction. We have kept a record of any response received.

References

[1] H. Wang, "Research on the Application of Genetic Algorithm in Physical Education," *Journal of Mathematics*, vol. 2022, Article ID 8477945, 8 pages, 2022.

Hindawi
Journal of Mathematics
Volume 2022, Article ID 8477945, 8 pages
https://doi.org/10.1155/2022/8477945

Research Article

Research on the Application of Genetic Algorithm in Physical Education

Haibo Wang

Sports Department of Guilin University of Aerospace Technology, Guilin City, Guangxi Province 541004, China

Correspondence should be addressed to Haibo Wang; tyb@guat.edu.cn

Received 10 December 2021; Revised 2 April 2022; Accepted 7 April 2022; Published 14 May 2022

Academic Editor: Naeem Jan

University physical education is an important public basic course in colleges and universities. The traditional teaching is usually within the class time specified in the training program; the teacher teaches the students the basic physical education fundamentals so that the students can master the basic skills of sports, thus improving the students' sports level and physical quality. An improved genetic algorithm is proposed to reduce the problem of slow convergence and partial convergence of the fundamental genetic algorithm for intelligent grouping systems. To ensure the group's stability and variety, the algorithm can rapidly extend the search space by repeatedly rejecting similar individuals. Therefore, this study proposes a new method of intelligent grouping based on the improved genetic algorithm. The new method can overcome the problem of premature convergence of the algorithm more efficiently and easily than the traditional algorithm. A large number of experiments have proved that the proposed algorithm meets all the requirements of physical education very well. The algorithm can automatically generate test papers with moderate difficulty and reasonable structure.

1. Introduction

Although Massive Open Online Course (MOOC) has been available in China since 2013 and along with the development of these years, many universities have joined the MOOC team, and the online courses have been growing, but through the survey, we can find that most of the online courses in China are mainly focused on computer, foreign language, and some vocational courses, while the MOOC courses on physical education have just begun in China. This means that MOOC is full of opportunities and challenges for the reform of university physical education in China.

Traditional teaching is usually to teach students the basic knowledge of physical education within the class time specified in the training program so that students can master the basic skills of sports to improve their sports level and physical quality. However, such teaching is very limited, and the teacher-student ratio in many colleges and universities is not sufficient, so the choice of programs in physical education classes is very limited, and many students cannot choose the courses they are interested in, and they cannot satisfy the supplementary physical education knowledge and sports skills training outside the curriculum.

MOOC is a combination of modern Internet technology, computer technology, and mobile technology that allows learning to be accessed anytime, anywhere, and quickly. MOOC is an attempt to superimpose the classroom content on top of this modern information, from massive information to cloud information, making the coverage of physical education content infinitely expandable, which is beyond the reach of traditional physical education content. In addition, the openness of MOOC allows students to access other schools, regions, and even other countries' sports courses in addition to their own sports courses, providing a platform for students who want to master different sports. The openness of the MOOC also allows students to have access to other schools, other regions, and even other countries, providing a platform for students who want to master different sports. At the same time, the MOOC can break the limitations of time and space so that students do not lose the opportunity to learn because of the

limited number of students who can take courses and can avoid conflicts in taking multiple courses.

The MOOC courses are organized in a cloud learning environment, which allows students to study in different places and different environments at any time, and with access to mobile terminals, students can access MOOC learning opportunities more freely. Students can study anywhere on campus with their mobile phones, and the same account can be used for intermittent learning, making the learning process both humanized and personalized, making it very easy for students to learn.

The integration of sports training and tactics into traditional physical education has greatly enriched the content, especially by incorporating the latest sports events into the teaching of physical education, which can greatly enhance students' interest in sports. In addition, the most important advantage of physical education classes is that they allow students to choose the content that interests them as much as possible, which is a great complement to traditional physical education classes and makes them more diverse [1].

In addition to benefiting students, teachers can also refer to the content and teaching methods of outstanding scholars in MOOC and improve the traditional and outdated teaching methods in their classes to achieve a more interactive and cooperative way of teaching students. In this way, both students' independent online Massive Online Course (MOC) and teachers' teaching reform in physical education classrooms can greatly increase students' interest in physical activity. In addition, MOOC's easy cloud learning environment allows students to enjoy sports anytime and anywhere, replacing "task sports" with "interest sports" and truly achieving happy sports.

In recent years, optimization algorithms have attracted a lot of attention, such as artificial neural networks and genetic algorithms, among others [2]. It provides new ideas for solving complex problems and has been successful in many fields. Intelligent roll-up is a constrained multiobjective optimization problem. Conventional roll formation algorithms suffer from slow convergence, low success rate, and low quality. Automatic generation systems are always an essential research direction in all kinds of computer-aided testing systems. The efficiency and quality of an intelligent paper-forming system are determined by the algorithm. In this study, we focus on the application of genetic algorithms to combinatorial optimization problems.

The genetic algorithm is based on the principle of natural selection, which is the fundamental law of nature as a whole, and the principle of survival of the fittest and elimination of the inferior. The mechanism of natural selection involves the replication of individuals, the selection of individuals, the inheritance and recombination of individuals, and the variation of individual characteristics. Through these processes, selection can work from one generation to the next, allowing the evolution of the organism to develop in a favorable direction. On this basis, species can accumulate and develop from one direction to another, allowing for diversity in organisms. Thus, through natural selection, populations can be diversified and new species can be created.

Genetic algorithms have a significant advantage over other search algorithms because they are simple to implement, fast in target finding, and strong in coding, making them a good stochastic search algorithm with important applications in many fields. The process of implementation and computation of a genetic algorithm is mainly carried out through several important functions specific to the genetic algorithm, and the direction of the computation is achieved by setting the function and using the adjustment of the direction to achieve the final computation result. In order to improve the genetic algorithm and to achieve the initial effect, it is necessary to study and set the parameters of the algorithm; specifically, in this study, the improvement of genetic algorithm is realized by using race selection in factor operation. On this basis, an improved adaptive genetic algorithm selection mechanism is proposed to enable the target population to operate adaptively so that the genetic algorithm can be used in the first step. This allows the genetic algorithm to converge too early in the early stages or inefficiently in the late stages.

In order to avoid the risk of slow and partial convergence of the basic genetic algorithm for intelligent grouping systems, an improved genetic algorithm is proposed. This algorithm can rapidly expand the search space by continuously eliminating similar individuals and ensure the stability and diversity of the clusters. Therefore, this study proposes a new method of intelligent grouping based on the improved genetic algorithm. The new method can overcome the problem of premature convergence of the algorithm more efficiently and easily than the traditional algorithm. It is proved that the proposed algorithm can meet all the requirements of physical education. The algorithm can automatically generate test papers with moderate difficulty and reasonable structure.

The paper organizations are as follows. Section 2 defines the mathematical models. Section 3 discusses the algorithm design and implementation. Section 4 discusses the analysis of experimental results. Section 5 concludes the article.

2. Mathematical Models

The constraints of the intelligent paper system include overall time, paper score, paper difficulty factor, question type ratio, ability level, knowledge point, regional criteria, and the number of generations. From the perspective of extracting the best combination of questions from a large pool of questions, the intelligent paper-grouping problem is a multiconstraint combination optimization problem. Therefore, if each question has n attributes, combining a study with m questions is equivalent to constructing an objective matrix:

$$s = \begin{pmatrix} a_{11} & a_{12} & \cdots & a_{1n} \\ a_{21} & a_{22} & \cdots & a_{2n} \\ \vdots & \vdots & \vdots & \vdots \\ a_{m1} & a_{m2} & \cdots & a_{mn} \end{pmatrix}. \quad (1)$$

In the target matrix, each row represents an attribute of a test question, and there are n attributes in total, i.e., n-dimensional vectors. The total score of the study is a_1, the difficulty factor is a_2, the ability level is a_3, the knowledge is a_4, the distribution is a_5, the proportion of questions is a_6, and the completion time is a_7. This is a problem of solving the state matrix, and the target transitions are not unique. The target matrix should satisfy the following constraints:

(1) Total test paper score = $\sum_{i=1}^{m} a_{i1}$ (assigned by physical education, i.e., test paper score constraint)

(2) Difficulty factor = $\sum_{i=1}^{m} a_{i1}a_{i2}$/total score (specified by physical education, i.e., the difficulty constraint of the test paper)

(3) Completion time = $\sum_{i=1}^{m} a_{i7}$ (designated by physical education, i.e., time constraints)

(4) Proficiency level categories (basic understanding, insight and understanding, skill experience, and free play) and scores are assigned by physical education, also known as proficiency level constraints $\sum_{i=1}^{m} c_i a_{i7} = z_p$, where z_p is the p proficiency level of the test score, $c_{1i}\begin{cases} 1 \ldots a_{i3} = p, \\ 1 \ldots a_{i3} \neq p. \end{cases}$

(5) Distribution = $\sum_{i=1}^{m} a_{i1}a_{i5} / \sum_{i=1}^{m} a_{i1}$ (specified by the physical education curriculum, i.e., distribution constraint); question types, knowledge points, distribution, and other constraints are similar to those mentioned above

3. Algorithm Design and Implementation

In this section, we defined the algorithm design and improvement of genetic operations; the crossover operation selects a single-point crossover, mutation operation, genetic algorithm parameters, coding method, elite protection strategy, and algorithm description.

3.1. Algorithm Design. Genetic algorithm was proposed by J.H. Holland, an American scholar. Genetic algorithm is a computational model that simulates the evolutionary process of living organisms in nature. It is gaining attention because of its advantages, such as simplicity, robustness, global search, and fast convergence, and it is not limited by the constraints of the search space. These advantages make it very suitable for the technical problem of intelligent volume formation. The algorithm establishes an initial population of a specific size before inducing crossover and mutation of individuals with a particular probability, resulting in a structural reorganization of individuals. Then, using a specified evaluation function, a new generation is created by picking the finest individuals for replication. The iterations are repeated until a globally optimal solution is found that satisfies the optimization conditions.

Traditional genetic algorithms suffer from low efficiency and tend to generate immature convergence in the later stages of the algorithm. Therefore, many improvement methods have been tried, including designing different choices, cross-variance operations, changing the algorithm structure, designing adaptive cross-variance probabilities, and combining genetic algorithms with other optimization intelligence algorithms. In this study, we propose a method to solve the problem of automatic paper formation with high reliability and validity by globally optimizing the papers in order to finally form the required papers. The results of the algorithm are very good. The specific method is as follows.

3.1.1. Coding Method. The choice of the encoding method is directly dependent on the characteristics of the problem and is an important factor affecting the performance of the algorithm. Common coding methods include binary coding, decimal coding, and real number coding. Because the constraints of the question database directly affect the speed of accessing the database, the algorithm creates a repository file for each question type in order to quickly select the specified question type and reduce the redundancy problem when automatically grouping papers. As a result, the grouped real number encoding method is chosen by the intelligent paper grouping system. Each question type is coded relative to the real number, each code reflects a question type, and the question grouping codes are separate. We mapped a paper to a chromosome and each question to a gene. The gene value can be directly expressed by the number of question types, e.g., in Java programming (5 multiple choice, 5 fill-in-the-blank, 2 short answer, 2 program reading, and 2 programming); then, the chromosome code can be 23, 45, 90, 67, 22, 11, 69, 112, 9, 37, 78, 54, 23, 35, 11, 23. The initial population of the paper was not generated by a completely random selection method, but was generated randomly based on the proportion of questions, total score, completion time, and absence of redundant knowledge points. This accelerates the convergence of the genetic algorithm and reduces the number of iterations. Since different question types are retrieved from different question tables, the same test string number may appear in the same gene string since they belong to different question types. Therefore, this situation is common and does not affect the automatic grouping. Using the grouped real number encoding method, it is able to overcome the drawbacks of too large search space and excessive encoding length in the previously used binary encoding. Also, it enhances the solving speed by eliminating the decoding time of individuals.

The fitness function, also known as the evaluation function, is a criterion used to distinguish between good and bad individuals in a population-based on an objective function. Genetic algorithms use fitness values to guide the search direction, and the fitness function does not require continuous or differential, or other auxiliary information. We use the following form of the fitness function as

$$F = \frac{1}{\left(1 + \sum_{i=1}^{m} k_i \left| e_i \right|\right)}, \tag{2}$$

where e_i corresponds to the i^{th} influencing factor of the constraint paper and k_i corresponds to the weighting factor $k_i > 1$ of the error. This fitness function is able to intelligently group the search features of the paper problem. The smaller the error between the individual

paper and the paper constraint is, the closer the individual paper is to the target.

① Improvement of genetic operations: selection operation intelligent group roll system selects the fitness proportion method. The fitness proportion method, also known as the roulette wheel method, is the most common and classical selection strategy in genetic algorithms today. The population size is n, the fitness value of individual i is f_i, and the probability of individual i being selected is shown as

$$p_{si} = \frac{f_i}{\sum_{i=1}^{n} f_i}. \tag{3}$$

Obviously, the greater the proportion of fitness of an individual, the greater the probability of being selected.

② The crossover operation selects a single-point crossover: for two randomly selected chromosomes, a single-point crossover is used to generate random crossover positions in the same type group. If the number of knowledge points and questions is duplicated, the crossover point is then reselected.

③ Mutation operation: the mutation operation also improves on the traditional single-point mutation, i.e., by restricting the genes at each position of each individual to be disordered according to the assumed mutation probability p_m. With the help of the mutation operation, we are able to obtain the target of the local search.

3.1.2. Genetic Algorithm Parameters. The crossover probability p_c and the variance probability p_m of the genetic algorithm have an important impact on the algorithm performance. If p_c and p_m are too large, the algorithm may become a random search. However, if p_c is too small, it may cause a slower search process. If p_m is too small, then it is difficult to generate a new generation and may also cause the algorithm to mature prematurely and get a local optimal solution. We continuously change the crossover probability and variation probability according to the evolution of the population in order to improve the genetic algorithm's search efficiency, avoid local optimum, and protect outstanding individual papers. The automatic adjustment formula in the automatic paper formation system is as follows:

$$p_c = \begin{cases} \dfrac{0.9(f_{\max} - f)}{f_{\max}}, & f \geq f_{\max}, \\ 0.9, & f < f_{\max}, \end{cases}$$
$$p_m = \begin{cases} \dfrac{0.3(f_{\max} - f)}{f_{\max}}, & f' \geq f_{\text{avg}}, \\ 0.3, & f' < f_{\text{avg}}, \end{cases} \tag{4}$$

where p_c denotes crossover probability, p_m denotes variation probability, $f_{\max}$ denotes maximum fitness value, f_{avg} denotes average fitness value, f is the greater fitness value of the two crossover individuals, and f is the fitness value of the various individuals. However, for individuals with fitness values lower than the average fitness value, the probability of elimination is relatively high. Therefore, the adaptive p_c and p_m can provide the best crossover probability and variation probability for the individuals of the test paper.

3.1.3. Elite Protection Strategy. After the reproduction, crossover, and mutation operations, the algorithm compares the sufficiency value of the best individual of the new generation with that of the best individual of the previous generation. If it falls, the new generation's poorest individual is replaced by the previous generation's finest individual. This technique protects the best individuals from the effects of reproduction, crossover, and mutation. It is a crucial assurance for the genetic algorithm's convergence.

3.2. Algorithm Description. Parameter settings: maximum number of generations, Max, population size, n, crossover probability, p_c, variance probability, p_m, fitness threshold, M, and input requirements for physical education in an automatic grouping.

In this study, the adaptive selection mechanism and the selection operator are used to calculate the individuals that meet the requirements, to adjust the scale of the competition adaptively, to make timely adjustments according to the variation operation in the process of the competition, to solve the shortcomings of the traditional genetic algorithm of too fast convergence and orientation, and to ensure that the final optimal solution can be obtained in the genetic algorithm. The framework of the algorithm is improved, and the optimal retention strategy is integrated so that the good computational process of the algorithm can be well retained and inherited to ensure that the individuals obtained are in line with the requirements of physical education.

The whole process of the above algorithm can be expressed in the following steps:

Step 1: first, initialize the evolutionary algebra and set it to 0 to start the initialization of the species population

Step 2: adaptation calculations were then performed, mainly for the individual

Step 3: if the end condition is not met, the calculated fitness value and the adopted strategy complete the selection step; the crossover in the genetic algorithm is performed, and if the result of the check meets the requirements of the relevant settings of the intelligent group roll, the operation can be performed; if it does not, it returns; after completing the crossover operation, the mutation operation is performed; the selection mutation operation is performed, and the next generation of individuals is successfully obtained through the above operation. If the new individual has a better fitness than all the individuals, the new individual is set as the best individual and the results and values are saved. If not, we proceed to the next step. The process is shown in Figure 1.

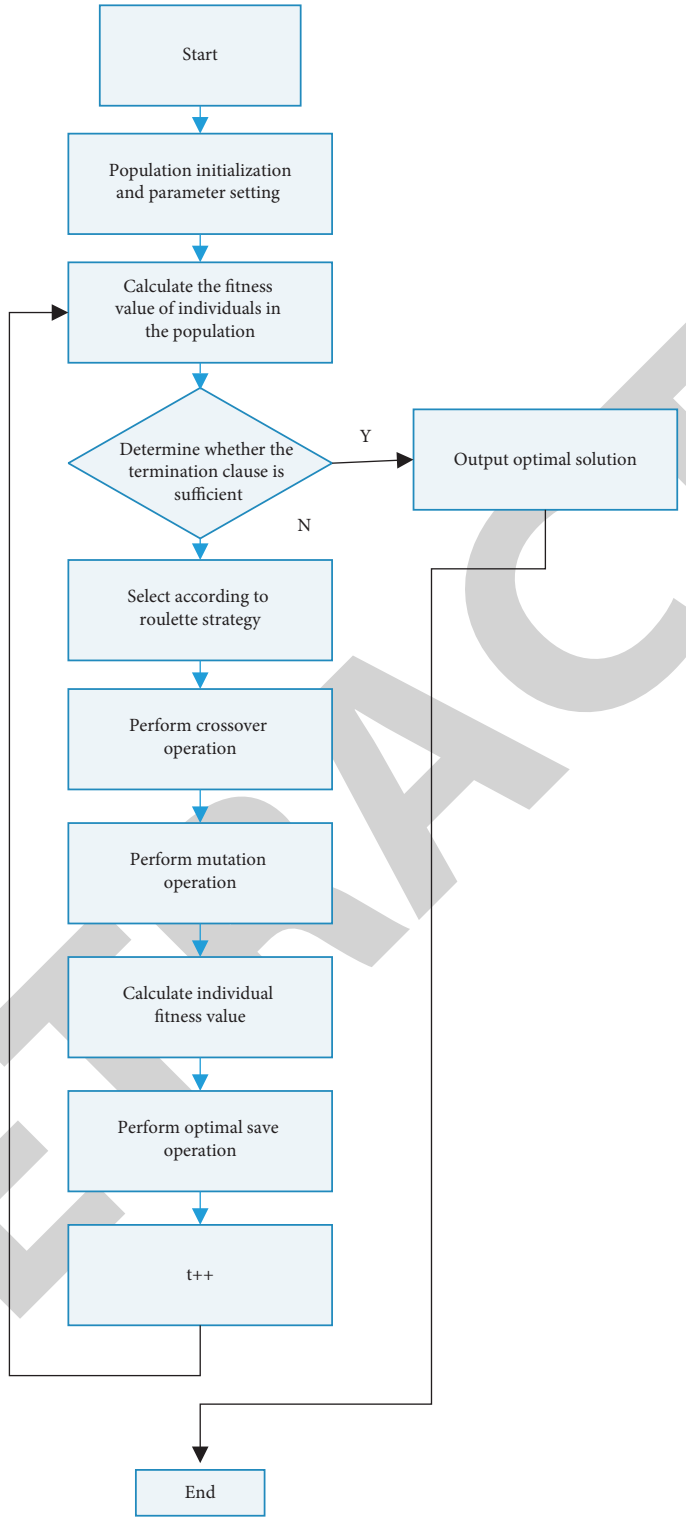

Figure 1: Improved genetic algorithm.

4. Analysis of Experimental Results

4.1. Parameter Setting. For the above improved genetic algorithm, the algorithm implementation steps detail each stage of the algorithm and the specific improvement details of each stage, and after the above operations, the improved genetic algorithm can obtain good individuals. In order to verify the effectiveness and efficiency of the improved genetic algorithm, the test bank of the computer course is used as the dataset for testing the algorithm in this section. In the course "Computer Applications Fundamentals," there are 1000 questions in the database with the following properties and contents.

First of all, there are four types of questions in the dataset of the course test bank, namely, single-choice, multiple-choice, judgment, and fill-in-the-blank questions, as shown in Table 1.

Secondly, there are five chapters in the course, as shown in Table 2.

The only requirement for the knowledge points is that they should not be duplicated when assembling the papers. In addition, in practice, the time of the algorithm needs to be as short as possible so that physical education does not have to wait too long for the paper to be formed, and thus, the efficiency of the intelligent paper formation system can be improved. In this study, the error value for generating test papers is set at 5%.

4.2. Algorithm Testing. In the abovementioned test generation table, the IDs, scores, difficulties, chapters, etc., of each question type are listed in detail in the database. The above data can be used to generate the actual scores for each chapter, the actual scores required for teaching, and the scores' set for each difficulty level which is shown in Tables 3 and 4.

The actual scores of the teaching requirement degree are shown in Table 4.

The scores for each difficulty level were set as shown in Table 5.

After the above operation, we can conclude that the improved adaptive genetic algorithm has good algorithm performance and can complete the extraction and distribution of the difficulty of the test questions in the test bank according to the requirements of physical education, so as to complete the requirements of physical education. Therefore, in general, the adaptive genetic algorithm is a better algorithm for paper composition.

4.3. Comparison of Tests before and after Algorithm Improvement. Through the above analysis, it can be seen that the improved genetic algorithm is able to achieve the functional requirements of physical education in the intelligent grouping environment. For the above results, we need to take more rigorous algorithm testing and comparison, through the way of experimental data to effectively compare the improved algorithm with the algorithm before the improvement; here, we mainly take the improved genetic algorithm and the standard genetic algorithm to conduct experiments and analyze the experimental data; the simulation test is shown in Figure 2.

In this study, the standard genetic algorithm before improvement is represented by GA and the improved genetic algorithm is represented by AGA. The effectiveness and performance of the algorithm can be analyzed in the above way, specifically by the evolutionary generation of the algorithm and the convergence performance of the algorithm. From Figure 2, we can see that the evolutionary algebra of the AGA algorithm is significantly lower than that of the GA algorithm when the number of experiments is 1, 2, 4, and 5. As long as the number of experiments is 3, the evolutionary algebra of the GA algorithm and the evolutionary algebra of the AGA algorithm are comparable.

Table 1: Question-type setting.

Question type	Quantity	Score
Single-choice questions	20	2
Multiple-choice questions	10	2
Judgment question	10	2
Completion	10	2

Table 2: Score of each chapter.

Chapter	Score
1	10
2	15
3	25
4	20
5	30

Then, for the convenience of programming, the functions are set to their global maximum values, and then, the parameters for the algorithm to run are set as shown in Table 6.

The algorithms are run 50 times according to each run parameter in Table 6, and the algorithms are stopped if they reach the termination condition. The average, minimum, and global convergence probabilities of the two algorithms are shown in Table 7.

From Table 7, the average number of generations of convergence of the improved genetic algorithm is 32 and the average number of generations of convergence of the standard genetic algorithm is 57, and the average number of generations of convergence of the improved genetic algorithm is 25 less than that of the standard genetic algorithm. The upgraded genetic algorithms minimum number of generations of convergence is 24, while the regular genetic algorithm's lowest number of generations of convergence is 39. The upgraded genetic algorithm's lowest number of generations of convergence is 15 times lower than the regular genetic algorithms minimum number of generations of convergence. The global convergence probability of both algorithms is 100%.

Figure 3 shows the ratio of the convergence curves of the two algorithms.

Using the above data test set to compare the degree of convergence of the improved genetic algorithm and the standard genetic algorithm, it can be found that the improved genetic algorithm can obtain the optimal solution in terms of fitness and has a clear advantage in terms of the number of generations of evolution and can converge faster; therefore, the improved genetic algorithm has better advantages and further verifies that the algorithm is feasible and effective. Therefore, the improved genetic algorithm has better advantages and further verifies that the algorithm is feasible and effective and has the advantage of operational efficiency of the algorithm.

Table 3: Sections.

Chapter	1	2	3	4	5
Score	10	16	24	20	30

Table 4: Teaching practical requirements' score.

Teaching requirements	Understand	Application	Analysis	Comprehensive	Evaluate
Score	20	24	20	20	10

Table 5: Difficulty scores.

Difficulty level	1	2	3	4	5
Score	12	30	32	20	8

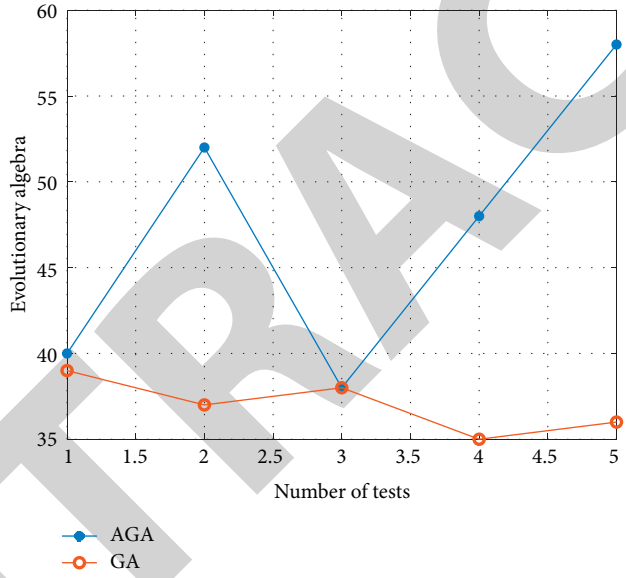

Figure 2: Comparison of the evolutionary algebra of algorithms.

Table 6: Operating parameters.

Algorithm	Population size	Maximum number of iterations	Crossover probability	Variation probability
GA	20	200	0.85	0.10
AGA	20	200	Pcl = 0.85 Pc2 = 0.85	Pml = 0.85 Pm2 = 0.85

Table 7: Experimental results.

Algorithm	Average convergence algebra	Minimum convergence algebra	Global convergence probability (%)
AG	57	39	100
AGA	32	24	100

Hindawi
Journal of Mathematics
Volume 2022, Article ID 7811196, 8 pages
https://doi.org/10.1155/2022/7811196

Research Article

Connected Degree of Fuzzifying Matroids

Xiu Xin,[1] **Sheng Gang Li**,[2] **Harish Garg**,[3] **Heng Liu**,[4] **and Jingjing Zhao**[5]

[1]*Department of Mathematics, Tianjin University of Technology, Tianjin 300384, China*
[2]*College of Mathematics and Statistics, Shaanxi Normal University, Xi'an 710062, China*
[3]*School of Mathematics, Thapar Institute of Engineering and Technology, Deemed University, Patiala 147004, Punjab, India*
[4]*School of Science, Guangxi University of Nationalities, Nanning 530006, China*
[5]*School of Psychology, Shaanxi Normal University, Xi'an 710062, China*

Correspondence should be addressed to Sheng Gang Li; shengganglinew@126.com and Harish Garg; harish.garg@thapar.edu

Received 2 December 2021; Revised 27 January 2022; Accepted 26 March 2022; Published 2 May 2022

Academic Editor: Abderrahim Wakif

Polya's plausible reasoning methods are crucial not only in discovery of mathematics results, modeling methods, and data processing methods but also in many practical problems' solving. This paper exemplifies how to use Polya's plausible reasoning methods to generalize the popularized notion of 2-connectedness of graphs to a more universal notion of the connected degree of fuzzifying matroids. We introduce the connectedness of fuzzifying matroids, which is generalized from 2-connectedness of graphs, connectedness of matroids, and 2-connectedness of fuzzy graphs. Moreover, the connected degree of fuzzifying matroids is presented by considering the fuzziness degree of connectedness. It is proved that a fuzzifying matroid $\mathbb{M}$ is connected, which is equivalent to its connectedness degree $\mathrm{Con}(\mathbb{M})$ is the biggest (i.e., $\mathrm{Con}(\mathbb{M}) = 1$). This, together with other properties of the connected degree of fuzzifying matroids, demonstrates the rationality of the proposed notion. Finally, we describe the concepts of this paper through some examples.

1. Introduction

Whitney in his fundamental paper [1] defined a matroid as an abstract generalization of a graph and a matrix. One of the great beauties of the subject of the matroid theory is that there are so many equivalent descriptions of a matroid. Bases, circuits, rank function, or closure operator is also sufficient to uniquely determine the matroid besides independent sets [2, 3]. In addition, it is well known that matroids are of great significance in combinatorial optimization and are just the structure that can use the greedy algorithm to find the optimal solution of some problems [4, 5]. Combined with fuzzy set theory [6], some fuzzy concepts of a matroid are given. One is using a family of fuzzy sets instead of that of sets, a Goetschel–Voxman fuzzy matroid was proposed in [7] and was later on widely studied by the various researchers [8–16]. The other is using a mapping from 2^E to $[0, 1]$ rather than a family of sets, a fuzzifying matroid was introduced by Shi, and it can also be determined uniquely by its fuzzifying rank function [17, 18]. Subsequently, some other equivalent descriptions of a fuzzifying matroid were discussed including base-map and circuit-map [19], three kinds of fuzzifying operators [20, 21], fuzzifying nullity [22]. Also, as its applications, a fuzzifying matroid is just the structure of the fuzzifying greedy algorithm for fuzzy optimization problems [23, 24]. Thus, Shi's fuzzification method maintains matroids' features.

We know that there is an important connection between graphs and matroids. A graph (graphs in this paper are always loopless and without isolated vertices and have at least three vertices). $G = (V, E)$ can induce a matroid $(E, \mathscr{I}_G)$ which is called its cycle matroid and denoted by $\mathscr{M}_G$, where $\mathscr{I}_G = \{A \subseteq E\colon A \text{ does not contain any cycle of } G\}$. Motivated by analogies in graph theory, the connectedness of a matroid is defined. Here, $\mathscr{M}_G$ is connected, which is equivalent to G is 2-connected; hence, the connectedness for matroids corresponds directly to the idea of 2-connectedness for graphs. It is natural to ask that is there fuzzifying matroid concept that corresponds directly to the idea of connectedness, or 2-connectedness, for fuzzy graphs?

Our main aim is to give a concept of connectedness for fuzzifying matroids, which extends the corresponding notion for fuzzy graphs. We begin by recalling some basic notions and results to be used in this paper. In Section 3, by using Polya's plausible reasoning method, we show the course of discovering the notion of connected degree of fuzzifying matroids. In Section 4, we generalize the concept of 2-connectedness from matroids to fuzzifying matroids, which corresponds directly to the idea 2-connectedness for fuzzy graphs. In Section 5, we consider the fuzziness degree of connectedness for fuzzifying matroids. Using the degree to which a set is a separator, the notion of connected degree for a fuzzifying matroid is introduced. We show that the relationship between the connected degree of a fuzzifying matroid and the connectedness of its corresponding level matroids and investigate the connected degree for the dual of a fuzzifying matroid. We close the section with various examples to illustrate the concepts of this paper.

2. Preliminaries

In this paper, we shall denote by E a given finite set and by 2^E the set of all subsets of E. Let $\mathscr{A} \subseteq 2^E$ and define $\mathrm{Min}\mathscr{A} = \{A \in \mathscr{A} | A \text{ is minimal in } \mathscr{A}\}$, $\mathrm{Opp}\mathscr{A} = \{X \subseteq E | X \notin \mathscr{A}\}$, $\mathrm{Upp}\mathscr{A} = \{X \subseteq E | \text{there exists } A \in \mathscr{A}, A \subseteq X\}$.

We begin with the definition of a matroid.

Definition 1. (cf. [2, 3]) A matroid $\mathscr{M}$ is a finite set E and a collection $\mathscr{I}$ of subsets of E (called independent sets) such that (I1)–(I3) are satisfied, denoted by $\mathscr{M} = (E, \mathscr{I})$.

(I1) $\mathscr{I} \neq \varnothing$;

(I2) $\mathscr{I}$ is a descending family;

(I3) For any two elements $A, B \in \mathscr{I}$ with $|A| < |B|$, one element $e \in B - A$ can be found so that $A \cup \{e\}$ belongs to $\mathscr{I}$.

It is important (for understanding the notion of fuzzifying matriod in the following Step 5) to notice that a matroid can also be defined equivalently as a finite set E and a collection $\mathscr{C}$ of subsets of E (called circuits) satisfying three circuit axioms [2]: $(C1) \varnothing \notin \mathscr{C}$; $(C2) \mathscr{C}$ is an antichain; $(C3)$ for any two different elements $C_1, C_2 \in \mathscr{C}$ and $e \in C_1 \cap C_2$, one element $C_3 \in \mathscr{C}$ can be found to be included in $(C_1 \cup C_2) - \{e\}$. Specifically, take a matroid $(E, \mathscr{I})$ (i.e., which means that $\mathscr{I}$ satisfies (I1)–(I3)), then, $\mathscr{C}_{\mathscr{I}} = \mathrm{Min}(\mathrm{Opp}(\mathscr{I}))$ is the family of all circuits for it (i.e., $\mathscr{C}_{\mathscr{I}}$ satisfies (C1)–(C3)); conversely, take a matroid $(E, \mathscr{C})$ (i.e., $\mathscr{C}$ satisfies (C1)–(C3)), then $\mathscr{I}_{\mathscr{C}} = \mathrm{Opp}(\mathrm{Upp}(\mathscr{C}))$ is the family of all independent sets for it (i.e., $\mathscr{I}_{\mathscr{C}}$ satisfies (I1)–(I3)) and $\mathscr{C} = \mathscr{C}_{\mathscr{I}_{\mathscr{C}}}$.

Moreover, if $(E, \mathscr{I})$ is a matroid, its rank function $\mathscr{R}_{\mathscr{I}}$ is defined as a mapping from 2^E to the set of natural numbers $\mathbf{N}$ by $\mathscr{R}_{\mathscr{I}}(A) = \max\{|B| \| B \subseteq A, B \in \mathscr{I}\}$ and can uniquely determine the matroid [3].

Next, we present some other notations, notions, and results needed in this paper. As usual, $[0,1]^E$ denotes the collection of fuzzy subsets on E, where a fuzzy subset on E is a mapping from E to $[0,1]$. If $A \in [0,1]^E$ and $a \in [0,1]$, we will often denote the set of $x \in E$ satisfying $A(x) \geq a$ and the set of $x \in E$ satisfying $A(x) > a$ by $A_{[a]}$ and $A_{(a)}$, respectively. Fuzzy natural numbers and their operations have been introduced [17, 22, 23, 25]. An antitone mapping λ from the set of natural numbers $\mathbf{N}$ to $[0,1]$ is called a fuzzy natural number if $\lambda(0) = 1$ and $\wedge\{\lambda(n) | n \in \mathbb{N}\} = 0$. We will use $\mathbf{N}([0,1])$ to denote the collection of fuzzy natural numbers. Let λ, μ be fuzzy natural numbers, their sum, written $\lambda + \mu$ is also a fuzzy natural numbers such that for every $n \in \mathbf{N}$, $(\lambda + \mu)(n) = \vee\{\lambda(k) \wedge \mu(l) | n = k + l\}$, their subtraction is given by $\lambda - \mu = \vee\{\nu \in N([0,1]) | \nu + \mu \leq \lambda\}$. If we regard a natural number m as a fuzzy natural number $\underline{m}$ such that $\underline{m}(n) = 1$ for $n \leq m$ and $\underline{m}(n) = 0$ for $n \geq m + 1$, then, we can get following operational properties, for every $a \in [0,1]$, $(\lambda + \mu)_{[a]} = \lambda_{[a]} + \mu_{[a]}$ and $(\lambda + \mu)_{(a)} = \lambda_{(a)} + \mu_{(a)}$.

In [17, 18], the definition of a fuzzifying matroid on E was given.

Definition 2. (cf. [17, 18]) A fuzzifying matroid $\mathbb{M}$ is a finite set E and a mapping II from 2^E to $[0,1]$ (called fuzzy family of independent sets) such that (FI1)–(FI3) are satisfied, written as $\mathbb{M} = (E, \mathrm{II})$. For any two subsets A, B of E,

(FI1) $\mathrm{II}(\varnothing) = 1$;

(FI2) $\mathrm{II}(A) \geq \mathrm{II}(B)$ if $A \subseteq B$;

(FI3) $\vee_{e \in B - A} \mathrm{II}(A \cup \{e\}) \geq \mathrm{II}(A) \wedge \mathrm{II}(B)$ if $|A| < |B|$.

For a fuzzifying matroid, the following characterization theorem holds.

Theorem 1 (cf. [17]). *If II is a mapping from 2^E to $[0,1]$, then, (E, II) is a fuzzifying matroid, which is equivalent to each of the following statements.*

(1) $\{(E, II_{[a]}) | a \in (0,1]\}$ is a family of matroids;

(2) $\{(E, II_{(a)}) | a \in [0,1)\}$ is a family of matroids.

It is also important to notice that a fuzzifying matroid can be defined equivalently as a pair $(E, \mathbb{C})$, where $\mathbb{C}$ is a mapping from 2^E to $[0,1]$ satisfying two axioms [19]: (FC1) for any $a \in (0,1]$, $\mathrm{Min}(\mathbb{C})_{[a]}$ satisfies circuits axioms (C1)–(C3); (FC2) for any subset C of E, $\mathbb{C}(C) = a \neq 0$ implies $C \in \mathrm{Min}(\mathbb{C}_{[a]})$. In fact, let (E, II) be a fuzziying matroid (i.e., II satisfies (FI1)–(FI3)), the mapping $\mathbb{C}_{\mathrm{II}}: 2^E \longrightarrow [0,1]$ defined by for any subset C of E such that $\mathbb{C}_{\mathrm{II}}(C) = 1 - \wedge\{a \in [0,1) | C \in \mathscr{C}_{\mathrm{II}_{(a)}}\}$, not only is the circuit-map of (E, II) (i.e., $\mathbb{C}_{\mathrm{II}}$ satisfies (FC1)-(FC2)) but also $\mathrm{Min}(\mathbb{C}_{\mathrm{II}})_{[a]} = \mathscr{C}_{\mathrm{II}_{(1-a)}}$ for any $a \in (0,1]$. Conversely, let $(E, \mathbb{C})$ be a fuzziying matroid (i.e., $\mathbb{C}$ satisfies (FC1)-(FC2)), the mapping $\mathrm{II}_{\mathbb{C}}: 2^E \longrightarrow [0,1]$ defined by $\mathrm{II}_{\mathbb{C}}(A) = 1 - \vee\{\mathbb{C}(B) | B \subseteq A\}$ $(\forall A \in 2^E)$ satisfies (FI1)–(FI3)) and $\mathbb{C} = \mathbb{C}_{\mathrm{II}_{\mathbb{C}}}$.

The fuzzifying rank function was also defined.

Definition 3 (cf. [17, 23]). A mapping $\mathbb{R}_{\mathrm{II}}$ from 2^E to $\mathbf{N}([0,1])$ is called fuzzifying rank function of a given fuzzifying matroid (E, II), if for any subset A of E and any natural number n such that $\mathbb{R}_{\mathrm{II}}(A)(n) = \vee\{\mathrm{II}(B) | B \subseteq A, |B| \geq n\}$.

Theorem 2 (cf. [17, 23]). *The fuzzifying rank function $\mathbb{R}_{II}$ for a fuzzifying matroid (E, II) has the properties:*

(1) $\mathbb{R}_{II}(A)_{[a]} = \mathscr{R}_{II_{[a]}}(A)(\forall A \in 2^E, \forall a \in (0,1])$.

(2) $\mathbb{R}_{II}(A)_{(a)} = \mathscr{R}_{II_{(a)}}(A)(\forall A \in 2^E, \forall a \in [0,1))$.

Furthermore, for any fuzziying matroid (E, II) (i.e., II satisfies (FI1)–(FI3)), its fuzzifying rank function $\mathbb{R}_{\mathrm{II}}$ possesses some features, shown as, for any two subsets A, B of E, (FR1) $\underline{0} \le \mathbb{R}_{\mathrm{II}}(A) \le \underline{|A|}$; (FR2) $A \subseteq B$ implies $\mathbb{R}_{\mathrm{II}}(A) \le \mathbb{R}_{\mathrm{II}}(B)$; (FR3) $\overline{\mathbb{R}_{\mathrm{II}}}(A \cap B) + \mathbb{R}_{\mathrm{II}}(A \cup B) \le \mathbb{R}_{\mathrm{II}}(A) + \mathbb{R}_{\mathrm{II}}(B)$. Conversely, for a fuzzifying rank function $\mathbb{R}\colon 2^E \longrightarrow \mathbf{N}([0,1])$ (i.e., $\mathbb{R}$ satisfies (FR1)–(FR3)), the mapping $\mathrm{II}_{\mathbb{R}}\colon 2^E \longrightarrow [0,1]$ defined by $\mathbb{I}_{\mathbb{R}}(A) = \mathbb{R}(A)(|A|)(\forall A \in 2^E)$ satisfies (FI1)–(FI3)) and $\mathbb{R} = \mathbb{R}_{\mathrm{II}_{\mathbb{R}}}$.

Definition 4. (cf. [25]) For any fuzzifying matroid $\mathbb{M} = (E, \mathrm{II})$, a new mapping $\widetilde{\mathbb{R}_{\mathrm{II}}}$ from 2^E to $\mathbf{N}([0,1])$ is given by for any subset A of E such that $\widetilde{\mathbb{R}_{\mathrm{II}}}(A) = [\underline{|A|} + \mathbb{R}_{\mathrm{II}}(E - A)] - \mathbb{R}_{\mathrm{II}}(E)$. It is proved that $\widetilde{\mathbb{R}_{\mathrm{II}}}$ satisfies (FR1)–(FR3)), and thus, $\mathrm{II}_{\widetilde{\mathbb{R}_{\mathrm{II}}}}$ satisfies (FI1)–(FI3)), denoted by II^*. Hence (E, II^*) is a fuzzifying matroid, which is called the dual of $\mathbb{M}$, written as $\mathbb{M}^*$. In addition, the dual of $\mathbb{M}^* = (E, \mathrm{II}^*)$ is denoted by $(\mathbb{M}^*)^* = (E, (\mathrm{II}^*)^*)$.

Theorem 3. *(cf. [25]) Suppose that (E, II) is a fuzzifying matroid, then, $(II^*)^* = II$ is equivalent to each of the following statements:*

(1) $(II^*)_{[a]} = (II_{[a]})^*$ *for any element a in* $(0,1]$,

(2) $(II^*)_{(a)} = (II_{(a)})^*$ *for any element a in* $[0,1)$.

3. The Course of Discovering the Notion of Connected Degree of Fuzzifying Matroids

We say that a graph is 2-connected if any two distinct edges are contained in a cycle. This notion (actually many others) is easy-to-understand to many students and practitioners. A natural question is that can they discover, starting from such a notion and its relevant results, some innovative things which are interesting, meaningful, or needed for themselves? This paper will exemplify a positive answer. Precisely, it will generalize (by using plausible reasoning method [26]) the notion of 2-connectedness of graphs to a very extended and useful notion (called connected degree of fuzzifying matroids) and present some properties of connected degree of fuzzifying matroids.

We will sketch the course of discovering the notion of the connected degree of fuzzifying matroids which may be of reference value to both our research successors and out-of-the-box researchers.

Step 1. Find out a characterization 2-connectedness of graphs (from all) start from which the notion described can be generalized: for a graph, written $G = (V, E)$, we call that it is 2-connected if its any two distinct edges are contained in a cycle [2, 3], i.e., for any two different elements e_1, e_2 in E, one element C in $\mathscr{C}_G$ (the set of all cycles of G) can be found to include e_1 and e_2, simultaneously.

Step 2. Since matroid concept can be regarded as a generalization of graph concept (for a graph G, the collection of its cycles is represented as $\mathscr{C}_G$, which is exactly the family of circuits for the cycle matroid $\mathscr{M}_G$ of G, thus, $\mathscr{M}_G$ can also denoted equivalently as $(E, \mathscr{C}_G)$. So, we can think of G as a matroid $\mathscr{M}_G = (E, \mathscr{C}_G)$), it is natural to generalize the notion of 2-connectedness from the class of graphs (written as **G**) to the class of matroids (written as **M**).

Step 3. It is also reasonable saying the special matroid $\mathscr{M}_G = (E, \mathscr{C}_G)$ is connected when G is 2-connected, i.e., for any two different elements e_1, e_2 in E, one element C in $\mathscr{C}_G$ can be found to include e_1 and e_2 simultaneously (see Step 1). Generalization of this can be taken as a definition of connectedness of a matroid (see Step 4).

Step 4. We call that a matroid $\mathscr{M} = (E, \mathscr{C})$ is connected if, for any two different elements e_1, e_2 in E, one element C in $\mathscr{C}$ can be found to include e_1 and e_2 simultaneously [2, 3].

Step 5. As a matroid is a special fuzzifying matroid (for any matroid $(E, \mathscr{I})$ or $(E, \mathscr{C})$, we do not distinguish between $(E, \mathscr{I})$ and $(E, 1_{\mathscr{I}})$ and between $(E, \mathscr{C})$ and $(E, 1_{\mathscr{C}})$, where $1_{\mathscr{I}}$ and $1_{\mathscr{C}}$ are characteristic functions of $\mathscr{I}$ and $\mathscr{C}$, respectively), we naturally extend the notion of connectedness from the class of matroids to that of fuzzifying matroids (written as **FM**).

Step 6. It is reasonable saying the special fuzzifying matroid $(E, 1_{\mathscr{C}})$ is connected when the corresponding matroid $(E, \mathscr{C})$ is connected. In other words, for any $\{e_1, e_2\} \subseteq E$, $\vee\{1_{\mathscr{C}}(C) | e_1, e_2 \in C\} = 1$. Generalization of this can be taken as a definition of connectedness of a fuzzifying matroid (see Step 7).

Step 7. A fuzzifying matroid $(E, \mathbb{C})$ is called connected (or 2-connected) if for any $\{e_1, e_2\} \subseteq E$, $\vee\{\mathbb{C}(C) | e_1, e_2 \in C \subseteq E\} = 1$ (see the following Theorem 4 for a characterization).

Step 8. Find out a characterization (i.e., the separator characterization) of the connectedness of matroids (from all) start from which the notion described can be generalized: A matroid $\mathscr{M}$ is disconnected if and only if (briefly, iff) a proper subset A of E can be found to be a separator of $\mathscr{M}$. Generalization of this can be taken as a definition of connected degree of a fuzzifying matroid (see Step 12).

Step 9. Recall and redescribe the definition of the separator (so that connectedness of a matroid can be generalized to connected degree of a fuzzifying matroid). Suppose that $\mathscr{M} = (E, \mathscr{C})$ is a matroid, a subset A of E is called a separator of $\mathscr{M}$ (in other words, the degree to which A is a separator of $\mathscr{M}$ is equal to 1, denoted by $\mathrm{Sep}(A) = 1$) iff for any $C \in \mathscr{C}$ there must be $C \subseteq A$ or $C \subseteq E - A$, that is, $C \notin \mathscr{C}$ whenever C is a subset of E not included in both A and $E - A$ (i.e., $\wedge\{[1 - 1_{\mathscr{C}}(C)] | C$ is a subset of E not included in both A and $E - A\} = 1$). Compare the values of $\mathrm{Sep}(A)$ and $\wedge\{[1 - 1_{\mathscr{C}}(C)] | C$ is a subset of E not included in both A and $E - A\}$, we get $\mathrm{Sep}(A) = \wedge\{[1 - 1_{\mathscr{C}}(C)] | C$ is a subset of E not

included in both A and $E - A\}$. It is natural to generalize the equation from a matroid to a fuzzifying matroid (see Step 10).

Step 10. Given a fuzzifying matroid $\mathbb{M} = (E, \mathbb{C})$ and a subset A of E, we call that $\mathrm{Sep}(A) = \wedge\{[1 - \mathbb{C}(C)] | C$ is a subset of E not included in both A and $E - A\}$ is the degree to which $A \in 2^E$ is a separator of $\mathbb{M}$.

Step 11. A matroid $\mathscr{M}$ is disconnected (that is to say the connected degree of $\mathscr{M}$ is equal to 0, denoted by $\mathrm{Con}(\mathscr{M}) = 0$) if a proper subset A of E can be found to be a separator of $\mathscr{M}$ (i.e., $\wedge\{1 - \mathrm{Sep}(A) | A \in 2^E - \{\varnothing, E\}\} = 0$). Compare the values of $\mathrm{Con}(\mathscr{M})$ and $\wedge\{1 - \mathrm{Sep}(A) | A \in 2^E - \{\varnothing, E\}\}$, we get $\mathrm{Con}(\mathscr{M}) = \wedge\{1 - \mathrm{Sep}(A) | A \in 2^E - \{\varnothing, E\}\}$. It is natural to generalize the equality from a matroid to a fuzzifying matroid (see Step 12).

Step 12. Given a fuzzifying matroid $\mathbb{M} = (E, \mathbb{C})$, we call $\mathrm{Con}(\mathbb{M}) = \wedge\{1 - \mathrm{Sep}(A) | A \in 2^E - \{\varnothing, E\}\}$ is the connected degree of $\mathbb{M}$.

4. Characterizations and Rationality of Connectedness of Fuzzifying Matroids

Although a fuzzifying matroid can be defined as both a pair (E, II) and a pair $(E, \mathbb{C})$, we find that the circuit-map axioms (FC1)-(FC2) of a fuzzifying matroid is not a natural way to generalize the circuits axioms (C1)–(C3) of a matroid. Hence, in the subsequent discussion, we always suppose that a fuzzifying matroid and a matroid are pairs (E, II) and $(E, \mathscr{I})$, respectively.

The following Definition 5, Theorem 4, and Corollary 1 (which characterize the connectedness of fuzzifying matroids, see Step 7 for the definition) show that the connectedness of fuzzifying matroids is in harmony with that of matroids.

Definition 5. Amapping $\mathbb{C}_{\mathrm{II}}$ from 2^E to $[0, 1]$ is the circuit-map of a given fuzzifying matroid (E, II) which is said to be connected if for any two elements e_1, e_2 in E such that $\vee\{\mathbb{C}_{\mathrm{II}}(C) | e_1, e_2 \in C \subseteq E\} = 1$.

Theorem 4. *A fuzzifying matroid (E, II) is connected, which is equivalent to $(E, II_{(0)})$ is connected.*

Proof. If (E, II) is connected, then, for any two elements e_1, e_2 in E, a subset C of E can be found to satisfy $\mathbb{C}_{\mathrm{II}}(C) = 1$ and include e_1 and e_2, and thus $C \in \mathrm{Min}(\mathbb{C}_{\mathrm{II}})_{[1]} = \mathscr{C}_{\mathrm{II}_{(0)}}$ by the property of $\mathbb{C}_{\mathrm{II}}$. This implies that $(E, \mathrm{II}_{(0)})$ is connected. Conversely, if $(E, \mathrm{II}_{(0)})$ is connected, then, for any two elements e_1, e_2 in E, one element C in $\mathscr{C}_{\mathrm{II}_{(0)}}$ can be found to include e_1 and e_2, and thus $\mathbb{C}_{\mathrm{II}}(C) = 1 - \wedge\{a \in [0, 1) | \mathscr{C} \in \mathscr{C}_{\mathrm{II}_{(a)}}\} = 1 - 0 = 1$. Hence, $\vee\{\mathbb{C}_{\mathrm{II}}(C) | e_1, e_2 \in C \subseteq E\} = 1$, which implies that (E, II) is connected.

Notice that, the fuzzifying matroid (E, II) induced by a fuzzy family of circuits is introduced [27], it has the following properties, for any two elements a, b in $[0, 1)$, $a \leq b$ implies $\mathscr{C}_{\mathrm{II}_{(a)}} \subseteq \mathscr{C}_{\mathrm{II}_{(b)}}$. Thus, Theorem 4 deduces the following corollary. □

Corollary 1. *A fuzzifying matroid (E, II) induced by a fuzzy family of circuits is connected if and only if $(E, II_{(a)})$ is connected* $(\forall a \in [0, 1))$.

A fuzzy graph [28] $\mathscr{G}$ is a set of nodes V together with two fuzzy sets σ and μ on V and $V \times V$, respectively, satisfied for any pair of elements x, y of V, $\mu(x, y) \leq \sigma(x) \wedge \sigma(y)$, written as $\mathscr{G} = (V, \sigma, \mu)$. Graph $\underline{\mathscr{G}} = (V, 1_{\sigma_{(0)}}, 1_{\mu_{(0)}})$ is called the underline graph of $\mathscr{G}$, and we identify that $1_{\sigma_{(0)}}$ and $1_{\mu_{(0)}}$ are characteristic functions of $\sigma_{(0)}$ and $\mu_{(0)}$, respectively. When σ and μ take no value in $(0, 1)$, $\mathscr{G}$ equals $\underline{\mathscr{G}}$ and so it is a graph, which implies that the class of fuzzy graphs contains that of graphs. Furthermore, the concept of connectedness can be extended from graphs to more general a fuzzy graphs. In one way, a fuzzy graph is 2-connected, which is defined as its underline graph is 2-connected. Actually, each fuzzy graph $\mathscr{G} = (V, \sigma, \mu)$ can induce a fuzzifying matroid which is the set E of edges in $\mathscr{G}$ and a mapping $\mathrm{II}_{\mathscr{G}}$ from 2^E to $[0, 1]$ defined as for every subset A of E such that $\mathrm{II}_{\mathscr{G}}(A) = \vee\{a \in [0, 1) | \mu_{(a)}$ contains A and any cycle of $(V, \mu_{(a)})$ is not included in $A\}$, called fuzzifying cycle matroid of $\mathscr{G}$. Therefore, the notion of 2-connectedness for fuzzy graphs can be generalized to that of connectedness for their fuzzifying cycle matroids, and then to that of connectedness for more general fuzzifying matroids (see the following Theorem 5) which means the connectedness of fuzzifying matroids is also in harmony with 2-connectedness of fuzzy graphs.

Lemma 1. *$(E, II_{\mathscr{G}})$ and $(E, \mathscr{I}_{\underline{\mathscr{G}}})$ are the fuzzifying cycle matroid and the cycle matriod, respectively, induced by a fuzzy graph $\mathscr{G} = (V, \sigma, \mu)$ and its underline graph $\underline{\mathscr{G}}$, we have $\mathscr{I}_{\underline{\mathscr{G}}} = (II_{\mathscr{G}})_{(0)}$.*

Proof. $\forall A \in (\mathrm{II}_{\mathscr{G}})_{(0)}$, i.e., $\mathrm{II}_{\mathscr{G}}(A) > 0$, thus, a number a in $(0, 1)$ can be found such that $\mu_{(a)}$ contains A and any cycle of $(V, \mu_{(a)})$is not included in A. Suppose that A contains a cycle of $(V, \mu_{(0)})$, then A contains a cycle of $(V, \mu_{(a)})$ since $A \subseteq \mu_{(a)}$. There is a contradiction. Therefore, $\mu_{(0)}$ contains A and any cycle of $(V, \mu_{(0)})$is not included in A, i.e., $A \in \mathscr{I}_{\underline{\mathscr{G}}}$.

$\forall A \in \mathscr{I}_{\underline{\mathscr{G}}}$, i.e., $\mu_{(0)}$ contains A and any cycle of $(V, \mu_{(0)})$ is not included in A. We can find a number a in (0,1) satisfying $\mu_{(0)} = \mu_{(a)}$ because the range of μ is a finite set. Hence, $\mu_{(a)}$ also contains A and any cycle of $(V, \mu_{(a)})$ is not also included in A. This implies that $\mathrm{II}_{\mathscr{G}}(A) \geq a > 0$, we have $A \in (\mathrm{II}_{\mathscr{G}})_{(0)}$.

By Theorem 4 and Lemma 1, we get the fuzzifying cycle matroid $(E, \mathrm{II}_{\mathscr{G}})$ is connected iff $(E, (\mathrm{II}_{\mathscr{G}})_{(0)})$ is connected iff $(E, \mathscr{I}_{\underline{\mathscr{G}}})$ is connected iff $\underline{\mathscr{G}}$ is 2-connected iff $\mathscr{G}$ is 2-connected. Hence, the following theorem holds. □

Theorem 5. *Fuzzifying cycle matroid $(E, II_{\mathscr{G}})$ induced by a fuzzy graph $\mathscr{G}$ is connected, which is equivalent to $\mathscr{G}$ is 2-connected.*

5. Connected Degree of Fuzzifying Matroids

Recall that the connected degree of a fuzzifying matroid is defined by using the notion of the degree to which a set is a separator (see Steps 10 and 12). In this section, we study the connections between the notions of the degree to which a subset is a separator, connected degree, and connectedness of a fuzzifying matroid. We also obtain a generalization of a classical result on separators of matroids (see Theorem 7).

Definition 6. Define the degree to which $A \in 2^E$ is a separator of a given fuzzifying matroid (E, II) as $\mathrm{Sep}(A) = \wedge\{[1 - \mathbb{C}_{\mathrm{II}}(C)] | C$ is a subset of E not included in both A and $E - A\}$.

Theorem 6. *The following statements hold, see Definition 6 for this symbol $Sep(A)$.*

(1) If $Sep(A) > a$, then, A is a separator of $(E, II_{(a)})$ $(a \in [0, 1))$.

(2) If $Sep(A) = a$, then, A is not a separator of $(E, II_{(a)})$ $(a \in [0, 1))$.

(3) If $Sep(A) < a$ $(a \in (0, 1))$, uncertain.

(4) $Sep(A) = 0$ if and only if A is not a separator of $(E, II_{(0)})$.

Proof.

(1) Suppose that A is not a separator of $(E, \mathrm{II}_{(a)})$, then, one element $C \in \mathscr{C}_{\mathrm{II}_{(a)}}$ can be found to be not included in both A and $E - A$; hence, $\mathbb{C}_{\mathrm{II}}(C) \geq 1 - a$ and then $\mathrm{Sep}(A) \leq a$ by the definitions of $\mathbb{C}_{\mathrm{II}}$ and $\mathrm{Sep}(A)$.

(2) Suppose that $\mathrm{Sep}(A) = a \in [0, 1)$, i.e., $\wedge\{1 - \mathbb{C}_{\mathrm{II}}(C) | C$ is a subset of E not included in both A and $E - A\} = a \neq 1$, then, $1 - \mathbb{C}_{\mathrm{II}}(C) = a \neq 1$ for some subset C of E not included in both A and $E - A$, which implies this subset $C \in \mathrm{Min}(\mathbb{C}_{\mathrm{II}})_{[1-a]} = \mathscr{C}_{\mathrm{II}_{(a)}}$. In other words, $C \in \mathscr{C}_{\mathrm{II}_{(a)}}$ for some subset C of E not included in both A and $E - A$, i.e., A is not a separator of $(E, \mathrm{II}_{(a)})$.

(3) Take a counter example. A finite set $E = \{e_1, e_2, e_3\}$ together with a mapping II from 2^E to $[0, 1]$ defined as $\mathrm{II}(\varnothing) = \mathrm{II}(\{e_1\}) = 1$, $\mathrm{II}(\{e_2\}) = \mathrm{II}(\{e_3\}) = (1/2)$, $\mathrm{II}(\{e_1, e_2\}) = \mathrm{II}(\{e_1, e_3\}) = \mathrm{II}(\{e_2, e_3\}) = \mathrm{II}(\{e_1, e_2, e_3\}) = (1/3)$, form a fuzzifying matroid. Then, $\mathscr{C}_{\mathrm{II}_{(a)}} = \varnothing$ (if $0 \leq a < (1/3)$), $\{\{e_1, e_2\}, \{e_1, e_3\}, \{e_2, e_3\}\}$ (if $(1/3) \leq a < (1/2)$), $\{\{e_2\}, \{e_3\}\}$ (if $(1/2) \leq a < 1$) by the definitions of $\mathrm{II}_{(a)}$ and $\mathscr{C}_{\mathscr{I}}$, and thus by the definition of $\mathbb{C}_{\mathrm{II}}$, $\mathbb{C}_{\mathrm{II}}(C) = 0$ (if $C \in \{\varnothing, \{e_1\}, \{e_1, e_2, e_3\}\}$), $1/2$ (if $C \in \{\{e_2\}, \{e_3\}\}$), $2/3$ (if $C \in \{\{e_1, e_2\}, \{e_1, e_3\}, \{e_2, e_3\}\}$). Let $A = \{e_1\}$, by Definition 6, $\mathrm{Sep}(A) = \wedge\{[1 - \mathbb{C}_{\mathrm{II}}(C)] | C = \{e_1, e_3\}, \{e_1, e_2\}, \{e_1, e_2, e_3\}\} = (1 - (2/3)) \wedge (1 - (2/3)) \wedge (1 - 0) = (1/3) < 0.4 < 0.5$. We can check that A is not a separator of $(E, \mathrm{II}_{(0.4)})$ although it is a separator of $(E, \mathrm{II}_{(0.5)})$.

(4) If $\mathrm{Sep}(A) = 0$, then, A is not a separator of $(E, \mathrm{II}_{(0)})$ by (2). Conversely, if A is not a separator of $(E, \mathrm{II}_{(0)})$, then, $\mathrm{Sep}(A) \leq 0$ by (1), i.e., $\mathrm{Sep}(A) = 0$.

A classical result on separators of matroids: for any subset A of E, it is a separator of a given matroid $(E, \mathscr{I})$, which is equivalent to the rank function $\mathscr{R}_{\mathscr{I}}$ satisfies $\mathscr{R}_{\mathscr{I}}(A) + \mathscr{R}_{\mathscr{I}}(E - A) = \mathscr{R}_{\mathscr{I}}(E)$. Its promotion is as follows: □

Theorem 7. *The following conditions are equivalent, among them, symbols $Sep(A)$ and $\mathbb{R}_{II}$ refer to Definition 6 and Definition 3, respectively.*

(1) $Sep(A) = 1$;

(2) A is a separator of $(E, II_{(a)})$ for each $a \in [0, 1)$;

(3) $\mathbb{R}_{II}(A) + \mathbb{R}_{II}(E - A) = \mathbb{R}_{II}(E)$;

(4) A is a separator of $(E, II_{[a]})$ for each $a \in (0, 1]$.

Proof. (1)⇔(2). If $\mathrm{Sep}(A) = 1$, then, for each $a \in [0, 1)$, $\mathrm{Sep}(A) > a$, thus, A is a separator of $(E, \mathrm{II}_{(a)})$ by Theorem 6 (1). Conversely, if (2) holds, i.e., A is a separator of $(E, \mathrm{II}_{(a)})$ for each $a \in [0, 1)$. Assume that $\mathrm{Sep}(A) = b \neq 1$, then, A is not a separator of $(E, \mathrm{II}_{(b)})$ by Theorem 6 (2), which contradicts (2). Hence, $\mathrm{Sep}(A) = 1$.

By Theorem 2 and the property of the addition of fuzzy natural numbers, we have

(2)⇔(3). A is a separator of $(E, \mathrm{II}_{(a)})$ for each $a \in [0, 1)$ $\Leftrightarrow \mathscr{R}_{\mathrm{II}_{(a)}}(A) + \mathscr{R}_{\mathrm{II}_{(a)}}(E - A) = \mathscr{R}_{\mathrm{II}_{(a)}}(E)$ for each $a \in [0, 1) \Leftrightarrow \mathbb{R}_{\mathrm{II}}(A)_{(a)} + \mathbb{R}_{\mathrm{II}}(E - A)_{(a)} = \mathbb{R}_{\mathrm{II}}(E)_{(a)}$ for each $a \in [0, 1) \Leftrightarrow [\mathbb{R}_{\mathrm{II}}(A) + \mathbb{R}_{\mathrm{II}}(E - A)]_{(a)} = \mathbb{R}_{\mathrm{II}}(E)_{(a)}$ for each $a \in [0, 1) \Leftrightarrow \mathbb{R}_{\mathrm{II}}(A) + \mathbb{R}_{\mathrm{II}}(E - A) = \mathbb{R}_{\mathrm{II}}(E)$.

(3)⇔(4).

$\mathbb{R}_{\mathbb{I}}(A) + \mathbb{R}_{\mathbb{I}}(E - A) = \mathbb{R}_{\mathrm{II}}(E) \Leftrightarrow [\mathbb{R}_{\mathrm{II}}(A) + \mathbb{R}_{\mathrm{II}}(E - A)]_{[a]} = \mathbb{R}_{\mathrm{II}}(E)_{[a]}$ for each $a \in (0, 1] \Leftrightarrow \mathbb{R}_{\mathrm{II}}(A)_{[a]} + \mathbb{R}_{\mathrm{II}}(E - A)_{[a]} = \mathbb{R}_{\mathrm{II}}(E)_{[a]}$ for each $a \in (0, 1] \Leftrightarrow \mathscr{R}_{\mathrm{II}_{[a]}}(A) + \mathscr{R}_{\mathrm{II}_{[a]}}(E - A) = \mathscr{R}_{\mathrm{II}_{[a]}}(E)$ for each $a \in (0, 1] \Leftrightarrow A$ is a separator of $(E, \mathrm{II}_{[a]})$ for each $a \in (0, 1]$. □

Definition 7. $\mathrm{Con}(\mathbb{M}) = \wedge\{1 - \mathrm{Sep}(A) | A \in 2^E - \{\varnothing, E\}\}$ is called connected degree of a given fuzzifying matroid $\mathbb{M} = (E, \mathrm{II})$, where $\mathrm{Sep}(A)$ is defined in Definition 6.

The connection between the connected degree of a fuzzifying matroid and the degree to which a subset is a separator is described in the following theorem.

Theorem 8. *The following statements are true, where symbols $Sep(A)$ and $Con(\mathbb{M})$ are defined in Definition 6 and Definition 7, respectively.*

(1) If $Con(\mathbb{M}) > a$, then $Sep(A) \neq 1 - a$ for each nonempty proper subset A of E $(a \in [0, 1))$.

(2) If $Con(\mathbb{M}) = a$, then $Sep(A) = 1 - a$ for some nonempty proper subset A of E $(a \in [0, 1))$.

(3) If $Con(\mathbb{M}) < a$ $(a \in (0, 1))$, uncertain.

(4) $Con(\mathbb{M}) = 0$ if and only if $Sep(A) = 1$ for some nonempty proper subset A of E.

(5) $Con(\mathbb{M}) = 1$ *if and only if* $Sep(A) = 0$ *for each nonempty proper subset* A *of* E.

Proof

(1) Suppose that there exists a nonempty proper subset A of E such that $\mathrm{Sep}(A) = 1 - a$, then,$\mathrm{Con}(\mathbb{M}) = \wedge\{1 - \mathrm{Sep}(A) | A \in 2^E - \{\varnothing, E\}\} \leq a$.

(2) Suppose that $\mathrm{Con}(\mathbb{M}) = a \in [0,1)$, i.e., $\wedge\{1 - \mathrm{Sep}(A) | A \in 2^E - \{\varnothing, E\}\} = a$, then $1 - \mathrm{Sep}(A) = a$ for some $A \in 2^E - \{\varnothing, E\}$, that is, $\mathrm{Sep}(A) = 1 - a$ for some nonempty proper subset A of E.

(3) Consider the fuzzifying matroid $\mathbb{M}$ in [27], it is a set $E = \{e_1, e_2, e_3, e_4, e_5\}$ and a mapping II from 2^E to $[0,1]$ defined as $\mathrm{II}(A) = \vee\{a \in [0,1) | A \in \mathscr{I}_a\}$. Here, $\mathscr{I}_a$ is constant in $[0, 1/3)$ (resp., $[1/3, 1/2)$, $[1/2, 1)$), $(E, \mathscr{I}_0)$, $(E, \mathscr{I}_{1/3})$, and $(E, \mathscr{I}_{1/2})$ are matroids with the families of circuits $\mathscr{C}_0 = \{\{e_1, e_3, e_4\}\}$, $\mathscr{C}_{1/3} = \{\{e_2, e_3\}, \{e_1, e_2, e_4\}, \{e_1, e_3, e_4\}\}$, and $\mathscr{C}_{1/2} = \{\{e_2, e_3\}, \{e_2, e_4\}, \{e_2, e_5\}, \{e_3, e_4\}, \{e_3, e_5\}, \{e_4, e_5\}\}$, respectively. Then, by the definition of $\mathbb{C}_{\mathrm{II}}$, $\mathbb{C}_{\mathrm{II}}(C) = 1$ (if $C = \{e_1, e_3, e_4\}$), 2/3 (if $C \in \{\{e_2, e_3\}, \{e_1, e_2, e_4\}\}$), 1/2 (if $C \in \{\{e_2, e_4\}, \{e_2, e_5\}, \{e_3, e_4\}, \{e_3, e_5\}, \{e_4, e_5\}\}$), and 0 (otherwise). Thus, by Definition 6, $\mathrm{Sep}(A) = 1$ (if $C \in \{\varnothing, E\}$), 1/2 (if $C \in \{\{e_5\}, \{e_1, e_2, e_3, e_4\}\}$), 1/3 (if $C \in \{\{e_2\}, \{e_1, e_3, e_4, e_5\}, \{e_2, e_5\}, \{e_1, e_3, e_4\}\}$), and 0 (otherwise). Therefore, by Definition 7, $\mathrm{Con}(\mathbb{M}) = (1/2) < (2/3) < (3/4)$. For $a = (2/3)$, $\mathrm{Sep}(\{e_2\}) = (1/3) = 1 - a$ although $\mathrm{Sep}(A) \neq (1/4) = 1 - b$ for $b = (3/4)$ and every nonempty proper subset A of E.

(4) If $\mathrm{Con}(\mathbb{M}) = 0$, then, there exists a nonempty proper subset A of E such that $\mathrm{Sep}(A) = 1$ by (2). Conversely, if $\mathrm{Sep}(A) = 1$ for some nonempty proper subset A of E, then, $\mathrm{Con}(\mathbb{M}) \leq 0$ by (1), i.e., $\mathrm{Con}(\mathbb{M}) = 0$.

(5) $\mathrm{Con}(\mathbb{M}) = 1 \Leftrightarrow \wedge\{1 - \mathrm{Sep}(A) | A \in 2^E - \{\varnothing, E\}\} = 1 \Leftrightarrow 1 - \mathrm{Sep}(A) = 1$
$(\forall A \in 2^E - \{\varnothing, E\}) \Leftrightarrow \mathrm{Sep}(A) = 0, (\forall A \in 2^E - \{\varnothing, E\})$.

The following results show that the relationship between connected degree of a fuzzifying matroid and connectedness of its corresponding level matroids. □

Theorem 9. *The following statements are also true, among them, symbol* $Con(\mathbb{M})$ *refers to Definition 7, which is the connected degree of a fuzzifying matroid* $\mathbb{M} = (E, II)$.

(1) If $Con(\mathbb{M}) = a \in [0,1)$, *then,* $(E, II_{(1-b)})$ *is not connected for any* $b > a$. *However, the converse is not true.*

(2) If $Con(\mathbb{M}) = 1$ *if and only if* $(E, II_{(0)})$ *is connected.*

Proof

(1) Suppose that $b > a = \mathrm{Con}(\mathbb{M})$, by Definition 7, there exists $A \in 2^E - \{\varnothing, E\}$ such that $1 - \mathrm{Sep}(A) < b$, and thus $\mathrm{Sep}(A) > 1 - b$; hence, A is a separator in $(E, \mathrm{II}_{(1-b)})$ by Theorem 6. This implies that $(E, \mathrm{II}_{(1-b)})$ is not a connected matroid.

Consider the fuzzifying matroid $\mathbb{M} = (E, \mathrm{II})$ defined in the proof of Theorem 8 (3). Obviously, three level matroids are all not connected. Take an $a \in [0,1) - \{1/2\}$; then, $(E, \mathrm{II}_{(1-b)})$ is not connected for any $b > a$, but $\mathrm{Con}(\mathbb{M}) = (1/2) \neq a$.

(2) It follows from Theorems 6 (4) and 8 (5).

An immediate consequence of Theorems 5 and 9 is the following Theorem 10 which shows the connections between the connected degree of a fuzzifying matroid and connectedness of a fuzzifying matroid. □

Theorem 10. *A fuzzifying matroid* $\mathbb{M}$ *is connected, which is equivalent to its connected degree* $Con(\mathbb{M}) = 1$.

The rest of this section discusses the fuzzy analogs of the results: A separator in a matroid is also a separator in its dual, and the connectedness of a matroid is equivalent to that of its dual.

Theorem 11. *The symbols* $\mathbb{M}$ *and* $\mathbb{M}^*$ *represent a fuzzifying matroid* (E, II) *and its dual* (E, II^*), *if* $(II^*)^* = II$, *then, the following statements hold.*

(1) $Sep^*(A) = Sep(A)$ *for each* $A \in 2^E$, *where* $Sep(A)$ *and* $Sep^*(A)$ *are the degrees to which* A *is a separator of* $\mathbb{M}$ *and* $\mathbb{M}^*$.

(2) $Con(\mathbb{M}^*) = Con(\mathbb{M})$.

(3) $\mathbb{M}$ *is connected, which is equivalent to* $\mathbb{M}^*$ *is connected.*

Proof

(1) Suppose that $\mathrm{Sep}(A) = a$, then, A is not a separator in $(E, \mathrm{II}_{(a)})$ by Theorem 6 (2), so it is not in the dual matroid $(E, (\mathrm{II}_{(a)})^*)$, nor in $(E, (\mathrm{II}^*)_{(a)})$ by $(\mathrm{II}^*)^* = \mathrm{II}$ and Theorem 3. By Theorem 6 (1), $\mathrm{Sep}^*(A) \leq a$, i.e., $\mathrm{Sep}^*(A) \leq \mathrm{Sep}(A)$. Conversely, $\mathrm{Sep}(A) \leq \mathrm{Sep}^*(A)$ since $(\mathrm{II}^*)^* = \mathrm{II}$.

(2) It is an immediate consequence of (1) by the definition of connected degree for fuzzifying matroids.

(3) It is obvious by Theorem 10 and (2). □

Remark 1. The characterization of the disconnectedness for a given fuzzifying matroid $\mathbb{M} = (E, \mathrm{II})$ induced by a fuzzy family of circuits in [27] is as follows: $\mathbb{M}$ is disconnected if and only if there is a nonempty proper subset of A such that $\mathbb{R}_{\mathrm{II}}(A) + \mathbb{R}_{\mathrm{II}}(E - A) = \mathbb{R}_{\mathrm{II}}(E)$. From Theorems 7 and 8, it can also be characterized by the connected degree in this paper, $\mathbb{M}$ is disconnected if and only if $\mathrm{Con}(\mathbb{M}) = 0$, that is, $\mathbb{M}$ is connected if and only if $\mathrm{Con}(\mathbb{M}) \neq 0$. From this, we can see the connected degree introduced in this paper unifies the connectedness in [27].

We now describe the concepts of this paper by various examples.

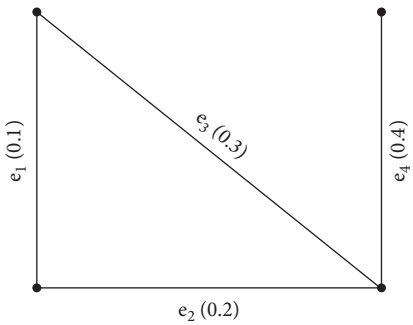

Figure 1: The fuzzy graph (V, μ).

Example 1. A simple class of fuzzifying matroids are fuzzifying uniform matroids. It is a fuzzifying matroid (E, II) satisfying for any $A, B \in 2^E$, $|A| = |B|$ implies $\mathrm{II}(A) = \mathrm{II}(B)$ [29].

Consider the example that a fuzzifying uniform matroid $\mathbb{M}$ is a finite set $E = \{e_1, e_2, e_3\}$ and a mapping II from 2^E to $[0, 1]$ defined as $\mathrm{II}(\varnothing) = 1$, $\mathrm{II}(\{e_1\}) = \mathrm{II}(\{e_2\}) = \mathrm{II}(\{e_3\}) = 0.5$, $\mathrm{II}(\{e_1, e_2\}) = \mathrm{II}(\{e_2, e_3\}) = \mathrm{II}(\{e_1, e_3\}) = 0.3$, $\mathrm{II}(\{e_1, e_2, e_3\}) = 0.2$. So, by the definition of circuit-map, $\mathbb{C}_{\mathrm{II}}(C) = 0$ (if $C \in \{\varnothing\}$), 0.5 (if $C \in \{\{e_1\}, \{e_2\}, \{e_3\}\}$), 0.7 (if $C \in \{\{e_1, e_2\}, \{e_1, e_3\}, \{e_2, e_3\}\}$), and 0.8 (if $C \in \{\{e_1, e_2, e_3\}\}$). By Definition 6, we have $\mathrm{Sep}(\{e_1\}) = \wedge\{[1 - \mathbb{C}_{\mathbb{I}}(C)] | C = \{e_1, e_2\}, \{e_1, e_3\}, \{e_1, e_2, e_3\}\} = (1 - 0.7) \wedge (1 - 0.7) \wedge (1 - 0.8) = 0.2$. Similarly, we also have $\mathrm{Sep}(A) = 0.2$ if $A \in \{\{e_2\}, \{e_3\}, \{e_1, e_2\}, \{e_1, e_3\}, \{e_2, e_3\}\}$. Hence, $\mathrm{Con}(\mathbb{M}) = \wedge\{1 - \mathrm{Sep}(A) | A \in 2^E - \{\varnothing, E\}\} = 0.8$.

Example 2. Another simple and more general class of fuzzifying matroids is fuzzifying paving matroids. It is a fuzzifying matroid (E, II) satisfying for any $A, B \in 2^E$, $|A| < |B|$ implies $\mathrm{II}(A) \geq \mathrm{II}(B)$ [29].

Consider the fuzzifying matroid $\mathbb{M} = (E, \mathrm{II})$ given in the proof of Theorem 6 (3), which is a fuzzifying paving matroid rather than a fuzzifying uniform matroid. Similarly, we also have $\mathrm{Sep}(A) = (1/3)$ if $A = \{e_2\}, \{e_3\}, \{e_1, e_2\}, \{e_2, e_3\}$ or $\{e_1, e_3\}$. Hence, $\mathrm{Con}(\mathbb{M}) = \wedge\{1 - \mathrm{Sep}(A) | A \in 2^E - \{\varnothing, E\}\} = 2/3$.

Example 3. Similarly, we can use the examples of fuzzifying acyclic matroids and fuzzifying simple matroids introduced in [29] to illustrate the concepts of this paper, which are omitted here.

Example 4. The very important class of fuzzifying matroids are derived from fuzzy graphs, which have been discussed in Section 4 in detail. In addition, we can also proved that $\mathrm{II}_{\mathscr{G}}(A) = \wedge_{x \in A} \mu(x)$ (if A does not contain any cycle), 0 (otherwise). Note that when $\delta(e) \equiv 1$ for any $e \in V$, a fuzzy graph is abbreviated to $\mathscr{G} = (V, \mu)$.

Consider the example that a fuzzifying cycle matroid $(E, \mathrm{II}_{\mathscr{G}})$ induced by $\mathscr{G} = (V, \mu)$ in Figure 1, and record it as $\mathbb{M}_{\mathscr{G}}$, where $E = \{e_1, e_2, e_3, e_4\}$ is the edges set in (V, μ) and $\mu(e_1) = 0.1$, $\mu(e_2) = 0.2$, $\mu(e_3) = 0.3$, $\mu(e_4) = 0.4$. Then, $\mathrm{II}_{\mathscr{G}}(A) = 0$ (if $A \in \{\{e_1, e_2, e_3\}, \{e_1, e_2, e_3, e_4\}\}$), 0.1 (if $A \in \{\{e_1\}, \{e_1, e_2\}, \{e_1, e_3\}, \{e_1, e_4\}, \{e_1, e_3, e_4\}, \{e_1, e_2, e_4\}\}$), 0.2 (if $A \in \{\{e_2\}, \{e_2, e_3\}, \{e_2, e_4\}, \{e_2, e_3, e_4\}\}$), 0.3 (if $A \in \{\{e_3\}, \{e_3, e_4\}\}$), 0.4 (if $A \in \{\{e_4\}\}$), and 1 (if $A \in \{\varnothing\}$). By the definition of circuit-map, $\mathbb{C}_{\mathrm{II}_{\mathscr{G}}}(C) = 1$ (if $C \in \{\{e_1, e_2, e_3\}\}$), 0.9 (if $C \in \{\{e_1\}\}$), 0.8 (if $C \in \{\{e_2\}\}$), 0.7 (if $C \in \{\{e_3\}\}$), 0.6 (if $C \in \{\{e_4\}\}$), and 0 (otherwise). By Definition 6, $\mathrm{Sep}(\{e_1, e_2, e_3\}) = \wedge\{[1 - \mathbb{C}_{\mathbb{I}_{\mathscr{G}}}(C)] | C = \{e_1, e_4\}, \{e_2, e_4\}, \{e_3, e_4\}, \{e_1, e_2, e_4\}, \{e_1, e_3, e_4\}, \{e_2, e_3, e_4\}, \{e_1, e_2, e_3, e_4\}\} = 1$. Hence, $\mathrm{Con}(\mathbb{M}_{\mathscr{G}}) = \wedge\{1 - \mathrm{Sep}(A) | A \in 2^E - \{\varnothing, E\}\} = 0$.

6. Conclusions

This paper exemplifies an application of Polya's plausible reasoning method (mainly analogous and generalization) in matriod theory, where we obtain some new results on 2-connectedness of fuzzifying matroids but just start from the 2-connectedness of graphs (a notion popularized for undergraduate students). We show some properties of connectedness and connected degree of fuzzifying matroids and the reasonability of the definition of connected degree and enrich the theory of fuzzifying matroids. The course of discovering the notion of connected degree of fuzzifying matroids and related results is given clearly and relatively understandably which may be benefiticial to mathematics enthusiasts and researchers in other areas who are interested to discover. There are also some work to be performed further. For example, (1) For the notion of connectedness, a fuzzy graph is either connected or not, we can consider the fuzziness degree of connectedness for a fuzzy graph analogously. (2) We can define and study connected degree of Goetschel–Voxman fuzzy matroids analogously; we can even define and study connected degree of $[0, 1]$-matroids introduced in [18, 30] (a generalization of Goetschel–Voxman fuzzy matroids) analogously. (3) As we know, as an application of fuzzifying matroids, the fuzzifying greedy algorithm was presented in [23, 24], fuzzifying matroids are precisely the structures for which the very simple and efficient fuzzifying greedy algorithm works. Whether connectedness of fuzzifying matroids could be applied to some fuzzy combinatorial problems, we shall consider this problem in the future. Of course, applications in decision-making problems as in [31–34] should also be considered; (4) We are also extending our work to m-polar fuzzifying matroids by imitating reference [15].

Data Availability

No data were used to support this study.

Conflicts of Interest

The authors declare that they have no conflicts of interest.

Acknowledgments

The work was supported by the National Natural Science Foundation of China (grant no. 11771263, 61967001, and 61807023) and the Fundamental Research Funds for the Central Universities (grant no. GK202105007 and GK201702011).

References

[1] H. Whitney, "On the abstract properties of linear dependence," *American Journal of Mathematics*, vol. 57, no. 3, pp. 509–533, 1935.

[2] H. J. Lai, *Matroid Theory*, Higher Education Press, Beijing, China, 2002.

[3] D. J. A. Welsh, *Matroid Theory*, Oxford University Press, New York, NY, USA, 1976.

[4] D. Gale, "Optimal assignments in an ordered set: an application of matroid theory," *Journal of Combinatorial Theory*, vol. 4, no. 2, pp. 176–180, 1968.

[5] J. G. Oxley, *Matroid Theory*, Oxford University Press, New York, NY, USA, 1992.

[6] L. A. Zadeh, "Fuzzy set," *Information and Control*, vol. 8, pp. 395–460, 1965.

[7] R. Goetschel and W. Voxman, "Fuzzy matroids," *Fuzzy Sets and Systems*, vol. 27, no. 3, pp. 291–302, 1988.

[8] R. Goetschel and W. Voxman, "Bases of fuzzy matroids," *Fuzzy Sets and Systems*, vol. 31, no. 2, pp. 253–261, 1989.

[9] R. Goetschel and W. Voxman, "Fuzzy circuits," *Fuzzy Sets and Systems*, vol. 32, no. 1, pp. 35–43, 1989.

[10] R. Goetschel and W. Voxman, "Fuzzy rank functions," *Fuzzy Sets and Systems*, vol. 42, no. 2, pp. 245–258, 1991.

[11] Y.-C. Hsueh, "On fuzzification of matroids," *Fuzzy Sets and Systems*, vol. 53, no. 3, pp. 319–327, 1993.

[12] L. A. Novak, "A comment on "bases of fuzzy matroids" fuzzy sets and systems 31 (1989) 253–261," *Fuzzy Sets and Systems*, vol. 87, no. 2, pp. 251-252, 1997.

[13] L. A. Novak, "On fuzzy independence set systems," *Fuzzy Sets and Systems*, vol. 91, no. 3, pp. 365–374, 1997.

[14] L. Novak, "On goetschel and voxman fuzzy matroids," *Fuzzy Sets and Systems*, vol. 117, no. 3, pp. 407–412, 2001.

[15] M. Sarwar and M. Akram, "New applications of m-polar fuzzy matroids," *Symmetry*, vol. 9, p. 319, 2017.

[16] M. Asif, M. Akram, and G. Ali, "Pythagorean fuzzy matroids with application," *Symmetry*, vol. 12, p. 423, 2020.

[17] F.-G. Shi, "A new approach to the fuzzification of matroids," *Fuzzy Sets and Systems*, vol. 160, no. 5, pp. 696–705, 2009.

[18] F.-G. Shi, "(L,M)-fuzzy matroids," *Fuzzy Sets and Systems*, vol. 160, no. 16, pp. 2387–2400, 2009.

[19] W. Yao and F.-G. Shi, "Bases axioms and circuits axioms for fuzzifying matroids," *Fuzzy Sets and Systems*, vol. 161, no. 24, pp. 3155–3165, 2010.

[20] L. Wang and F. G. Shi, "Characterization of M-fuzzifying matroids by M-fuzzifying closure operators," *Iranian Journal of Fuzzy Systems*, vol. 7, pp. 47–58, 2010.

[21] X. Xin, F. G. Shi, and S. G. Li, "M-fuzzifying derived operators and difference derived operators," *Iranian Journal of Fuzzy Systems*, vol. 7, pp. 71–81, 2010.

[22] H. Lian and X. Xin, "The nullity for M-fuzzifying matroids," *Applied Mathematics Letters*, vol. 39, pp. 31–39, 2010.

[23] F.-G. Shi and L. Wang, "Characterizations and applications of M-fuzzifying matroids," *Journal of Intelligent & Fuzzy Systems*, vol. 25, no. 4, pp. 919–930, 2013.

[24] S. J. Yang and F. G. Shi, "Bases and circuits of fuzzifying matroids," *Iranian Journal of Fuzzy Systems*, vol. 15, pp. 41–52, 2018.

[25] E.-Q. Li and F.-G. Shi, "Minors of M-fuzzifying matroids," *Journal of Intelligent & Fuzzy Systems*, vol. 28, no. 3, pp. 1213–1224, 2015.

[26] G. Polya, "Mathematics and plausible reasoning," *Induction and Analogy in Mathematics*, Princeton University Press, Princeton, NJ, USA, 1954.

[27] X. Xin and H. Lian, "M-fuzzifying matroids induced by M-fuzzy families of ciruits," *Journal of Intelligent & Fuzzy Systems*, vol. 34, no. 4, pp. 2223–2234, 2018.

[28] A. Rosenfeld, "Fuzzy graphs," in *Fuzzy Sets and Their Applications*, L. A Zadeh, K. S. Fu, and M. Shimura, Eds., Academic Press, New York, NY, USA, pp. 77–95, 1975.

[29] S.-J. Yang and X. Huang, "Certain types of M-fuzzifying matroids: a fundamental look at the security protocols in RFID and IoT," *Future Generation Computer Systems*, vol. 86, pp. 582–590, 2018.

[30] X. Xin and F.-G. Shi, "Categories of bi-fuzzy pre-matroids," *Computers & Mathematics with Applications*, vol. 59, no. 4, pp. 1548–1558, 2010.

[31] F. Xiao, "CEQD: a complex mass function to predict interference effects," *IEEE Transactions on Cybernetics*, pp. 1–13, 2021.

[32] F. Xiao, "CaFtR: a fuzzy complex event processing method," *International Journal of Fuzzy Systems*, vol. 24, pp. 1029–1111, 2022.

[33] J. C. R. Alcantud, "Convex soft geometries," *Journal of Computational and Cognitive Engineering*, vol. 1, no. 1, pp. 2–12, 2022.

[34] S. Saleem and H. Y. Khalaf, "Fuzzy soc-T-ABSO sub-modules," *Iraqi Journal For Computer Science and Mathematics*, vol. 3, pp. 124–134, 2022.

Hindawi
Journal of Mathematics
Volume 2024, Article ID 9812973, 1 page
https://doi.org/10.1155/2024/9812973

Retraction

Retracted: Developing a New Interval Type-2 Hesitant Fuzzy TOPSIS-Based Fuzzy Best-Worst Multicriteria Decision-Making Method for Competitive Pricing in Supply Chain

Journal of Mathematics

Received 23 January 2024; Accepted 23 January 2024; Published 24 January 2024

This article has been retracted by Hindawi following an investigation undertaken by the publisher [1]. This investigation has uncovered evidence of one or more of the following indicators of systematic manipulation of the publication process:

(1) Discrepancies in scope

(2) Discrepancies in the description of the research reported

(3) Discrepancies between the availability of data and the research described

(4) Inappropriate citations

(5) Incoherent, meaningless and/or irrelevant content included in the article

(6) Manipulated or compromised peer review

The presence of these indicators undermines our confidence in the integrity of the article's content and we cannot, therefore, vouch for its reliability. Please note that this notice is intended solely to alert readers that the content of this article is unreliable. We have not investigated whether authors were aware of or involved in the systematic manipulation of the publication process.

Wiley and Hindawi regrets that the usual quality checks did not identify these issues before publication and have since put additional measures in place to safeguard research integrity.

We wish to credit our own Research Integrity and Research Publishing teams and anonymous and named external researchers and research integrity experts for contributing to this investigation.

The corresponding author, as the representative of all authors, has been given the opportunity to register their agreement or disagreement to this retraction. We have kept a record of any response received.

References

[1] F. Salimian, M. Damiri, M. Ramezankhani, and S. K. Fariman, "Developing a New Interval Type-2 Hesitant Fuzzy TOPSIS-Based Fuzzy Best-Worst Multicriteria Decision-Making Method for Competitive Pricing in Supply Chain," *Journal of Mathematics*, vol. 2022, Article ID 7879028, 16 pages, 2022.

Hindawi
Journal of Mathematics
Volume 2022, Article ID 7879028, 16 pages
https://doi.org/10.1155/2022/7879028

Research Article

Developing a New Interval Type-2 Hesitant Fuzzy TOPSIS-Based Fuzzy Best-Worst Multicriteria Decision-Making Method for Competitive Pricing in Supply Chain

Farhad Salimian,[1] **Maryam Damiri**,[2] **Mahyar Ramezankhani**,[3] **and Saeed Khakshouri Fariman**[4]

[1]*Department of Entrepreneurship Development, Faculty of Entrepreneurship, University of Tehran, Tehran, Iran*
[2]*Illinois Institute of Technology University, Chicago, USA*
[3]*Queen's School of Engineering, University of Bristol, Bristol, UK*
[4]*Department of Industrial Engineering, Eshragh Institute of Higher Education, Bojnourd, Iran*

Correspondence should be addressed to Farhad Salimian; salimian.farhad@ut.ac.ir

Received 15 November 2021; Revised 19 February 2022; Accepted 26 February 2022; Published 30 April 2022

Academic Editor: Lazim Abdullah

Corporate social responsibility based on competitive supply chain pricing has been considered the most efficient strategy of a business globally. In an MCDM challenge, a competent supply chain pricing considerations solutions supplier considers multiple possibly competing for qualitative and quantitative criteria. This study presented a new extended decision-making and FBWM method based on type-2 fuzzy sets TOPSIS for ranking the corporate social responsibility criteria based on competitive supply chain pricing factors. The aim of the ranking is to learn how a company and its supply chain may accomplish joint-optimization of economic, environmental, and social performance by transparently and strategically integrating sustainability into business operations. To verify the efficacy of the suggested strategy, it is compared to a benchmarking model. IT2F VIKOR is the subject of this benchmarking model. The significance weights of the competitive supply chain pricing selection criterion are determined from BWM for both techniques. The results show that the most probable dimension of social responsibility in knowledge-based businesses in the oil sector, according to the research, is the environmental dimension in social responsibility, which may produce competitive supply chain pricing mechanisms based on profitability. Other findings revealed that the elements of competitive supply chain pricing factors in oil companies regarding social responsibility are ranked as follows: customer, product, and competitive supply chain pricing procedures. As a result, maintaining customer values is a major price element in establishing contacts, based on the company's strategic connection with the economy and regional and worldwide partners.

1. Introduction

Corporate sustainability has become a term in today's corporate world. According to statistics, 93 percent of world CEOs feel that maintaining a competitive standard without embracing sustainability is complex [1]. The World Commission on Environment and Development defines corporate sustainability as "meeting the requirements of the existing generation without jeopardizing future generations' ability to satisfy their needs," and this concept demonstrates how businesses are vulnerable to long-term sustainability if they do not care about the environment [2]. In today's modern world, all firms, particularly oil and gas companies, must have an efficient, sustainable plan since these companies frequently fail to meet the triple bottom of a sustainable plan [3]. The triple bottom line (TBL) of sustainable plans is the total assessment of economic, social, and environmental considerations. The corporate context of this TBL is so critical that today's oil and gas firms cannot operate without one [4]. This TBL notion refers to a situation

in which businesses combine their economic objectives with the acceptance of responsibility for their influence on ecosystems and people [5]. Because of the notion that corporate sustainability has become the heart of company success, companies are trying to deploy cutting-edge sustainability strategies [6]. Competitive functions founded on political, social, cultural, and economic development will grow more complicated as the condition of expectations and societal approaches transformation, and this is one of the key challenges confronting businesses, particularly knowledge-based firms [7]. The important aspect here is that an institution or company will be able to engage in and assist stakeholders. It is considered to be a social duty in the context of competitive procedures to maintain the overwhelming interests [8, 9]. Other conventional management supply chain management methodologies that pursued less integration in their processes, on the other hand, do not have the necessary efficacy in today's competitive world since the environmental change, social development, technological development, and increasing cultural contradictions have all decided to bring about comprehensive alterations in this region [10]. The necessity to make the correct decision and select the most suitable among many possibilities in diverse areas, including choosing the perfect manufacturer, distributor, best area to draw more customers, best business alliance in shaping integrations, most efficient pricing process, and so on, are critical issues for making decisions in supply chain management [11, 12]. These judgments cover a wide range of topics, from trivial concerns to serious difficulties. Worries about the influence of business on the environment and society have prompted further study into sustainable supply chain management (SSCM) [13]. This area of study aims to learn how a company and its supply chain may accomplish joint-optimization of economic, environmental, and social performance by integrating sustainability into business operations transparently and strategically. In an MCDM challenge, a competent supply chain pricing consideration solutions supplier considers multiple potentially competing qualitative and quantitative criteria. This study developed an extended decision-making and fuzzy set TOPSIS model based on competitive supply chain pricing factors to rank the corporate social responsibility criteria. By transparently and strategically integrating sustainability into business operations, companies and their supply chains can optimize economic, environmental, and social performance. As a result, the goal of this study is to look at the most efficient operation of competitive supply chain pricing focused on social responsibility dimensions with a case study of oil products from knowledge-based enterprises.

2. Literature Review

2.1. Supply Chain Performance Analysis. Sustainable supply chain management is the systematic integration of essential business operations that allows businesses and their supply networks to achieve economic, environmental, and social objectives [14]. As a result, firms who apply it can meet short-term financial objectives while also proactively dealing with supply chain activities that have long-term environmental and social implications. Since its products are broadly employed in economic and social activities, the oil sector is critical for long-term sustainability. The use of sustainable supply chain management may help to mitigate the harmful effects of operations. Even though sustainable supply chain management as a discipline has matured, sustainable supply chain management research in the oil sector is still in its infancy [15]. The focus of previous studies on the topic has been on increasing supply chain performance through innovative techniques and open innovation efforts [16–18]. The research also looked at how suppliers may improve by using management frameworks to detect and manage environmental and social risks in their operations [19]. It is also working on a green supply chain management method to assess environmental sustainability in oil refinery operations and assess the environmental impacts of decommissioning offshore oil and gas operational systems [20]. Sharifi et al. examined the influence of artificial intelligence and the digital era on business and energy in the aftermath of the COVID-19 pandemic [21]. Finally, the research focused on the problems of integrating corporate strategy topics in supply chain management and close collaboration between oil companies and suppliers to improve the environmental performance of logistical operations [22]. Many scholars are currently discussing the impact of corporate social responsibility on closed-loop supply chain operations. Panda et al. [23] used consumer surplus as an indicator to measure the degree of corporate social responsibility fulfillment by companies, and they concluded that a company's corporate social responsibility behavior might help improve the overall performance of the corporate social responsibility system. When customers pay differentially for new and remanufactured products [23], Dai et al. [24] studied the impact of corporate social responsibility behavior on price decisions and supply chain coordination in the remanufacturing supply chain. Liu et al. [25] examined the influence of corporate social responsibility choices and the number of green consumers on selecting reverse recycling routes, pricing, and recycling ratios in CLSC. Wang et al. [26] investigated how state subsidies and corporate product contributions influenced closed-loop supply chain recycling and pricing decisions.

2.2. Insight to Social Responsibility. Modak et al. [27] developed four recycling decision models for the closed-loop supply chain based on the manufacturer's corporate social responsibility inputs and looked into the influence of the manufacturer's corporate social responsibility input behavior on the closed-loop supply chain choice of the best recycling channel. Past studies on supply chain coordination focused mainly on contract coordination from economic returns or profit maximization [27]. This has evolved as customers have become more aware of corporate social responsibility [24, 25]. The number of studies on long-term supply chains and supply chain coordination that consider economic and environmental advantages has increased [26, 27]. Corporate social responsibility has a major impact on supply chain operations, with

research demonstrating that as the number of corporate social responsibility -sensitive consumers grows, so does the manufacturer's corporate social responsibility level, as well as the manufacturer's and retailer's profitability [25]. Johari and Hosseini-Motlagh [28] found that the recommended corporate social responsibility cost-sharing contract enhances market demand by considerably decreasing selling prices and increasing the degree of corporate social responsibility activities in a competitive context. With the growth in consumer awareness of corporate social responsibility, Wang et al. saw corporate social responsibility investment level competition as a critical component of business competitiveness [29]. They discovered that the manufacturer's profit is convex concerning customers' environmental protection [30]. A socially conscious company might charge a greater price for its goods [31]. Furthermore, corporate social responsibility implications on supply chain operation and coordination exist in various competitive settings and decision-making structures. There are different corporate social responsibility implications in different channel configurations, such as exclusive vs. competitive retailing. Ahmadi et al. discussed how to use object-oriented properties programming to create expert systems for strategic planning [32]. Niu et al. [33] observed that an international vaccine provider would prefer competitive retailing when the global and local vaccines are highly interchangeable. It does not matter if the aim is profit or social responsibility. The supply chain will have various social responsibility techniques in monopoly and duopoly situations. When the conditions for each company's optimal corporate social responsibility efforts, strategic planning preferences, and corporate social responsibility effects in monopoly and duopoly circumstances are considered, Shi et al. [34] discovered that, in the duopoly scenario, the supply chain is more highly likely to be irresponsible and lesser the total corporate social responsibility attempt level. When corporate social responsibility is included, societal welfare in a centralized decision-making scenario is always higher than decentralized [35].

A coordination contract to encourage a company to adopt corporate social responsibility, according to Li et al. [36], can lead to multiple wins for social welfare, customers, and supply chain players. However, once the corporate social responsibility coefficient exceeds a specific level, the disagreement between supply chain participants becomes irreconcilable. As a result, the impact of corporate social responsibility on supply chain operations is a complex issue. The complexity of the impact of social responsibility on supply chain coordination has been a source of worry for educators. Using game theory, scholars investigated the influence of negative social responsibility on the design of supply chain coordination contracts. They observed that in a retailer-led supply chain, a cost-sharing arrangement might increase profit for both parties. In a manufacturer-led collaboration, a profit-sharing model can lead to greater overall returns [37]. From the perspective of the global supply chain, Tian et al. [38] observed that increasing the degree of social responsibility of Chinese suppliers might enhance production demand and the economic advantages of stakeholders. On the other hand, supplier earnings will decline as product greenness increases, but stakeholder profits will increase. Nonetheless, Chinese suppliers' economic earnings are influenced by their level of social responsibility and the advantages of green production. There is presently a serious lack of collaboration in establishing multinational firms' social responsibility, according to Liu et al. [39]. They created a punishment model that handled supply chain participants' optimal decision-making in centralized and decentralized decision-making procedures. They then looked at the impact of the penalty % on social responsibility input.

2.3. CSR on the Sustainable Supply Chains and Fuzzy TOPSIS Methods. The researchers investigated the construction of resilient supply chains using renewable energy in Lotfi et al. It is suggested that the upper limit for the primary model be less than 10%, which is reasonable for cost estimation of large-scale problems. According to this study, SC should be equipped with RE in order to make them more robust to fluctuations in demand and to serve as an energy resource compatible with the seventh sustainable development agenda (SGD7) [40]. For designing unpredictable mixed resilient-sustainable power logistics, Motlagh et al. developed an innovative technique. In terms of standard deviation and mean value of the overall cost, the results demonstrate that decision-makers can distribute uncertainty budget and safety level efficiently to get more robust solutions using fuzzy-robust techniques [41]. Ahmadi examined how knowledge-based indicators affect economic development and classified and ranked them using logarithmic fuzzy preference programming [42]. Lahri et al. designed an innovative integrated BWM Sustainability supply chain network. This study used the Epsilon-constraint approach coupled with possibility programming, which has been documented sparingly in the literature. Multiple Pareto-optimal alternatives can be found by applying the Epsilon-constraint, allowing for a broad range of trade-offs across cost, emission, and ecological equity. When facing an unstable world, the findings help decision-makers [43]. As part of a combination stochastic fuzzy-robust methodology, Sharifi et al. investigated unique resilient-sustainable techniques for the construction of third biofuel networks from neem and eruca sativa. Using three factors, including resilience, social consequences, and cost, and weighing their relative importance, decision-makers can optimize biofuel logistics network architecture. In order to build a healthy supply chain system, Eskandarpour et al. conducted a multi-directional search. In conclusion, the article discusses the influence of greener technologies on supply chain structure from a management perspective [44].

3. Research Methodology

3.1. Social Responsibility. Business executives have voiced a diverse range of views on corporate social responsibility (CSR). In his paper, The Social Responsibility of Business is to Raise Its Earnings, Nobel Prize-winning economist Milton Friedman (1970) clearly stated one perspective on corporate social responsibility [45]. "The business structure that Whole Foods has embraced might symbolize a new kind of capitalism, one that more deliberately works for the

greater good instead of relying only on the "invisible hand" to create beneficial benefits for society, said John Mackey, the founder of Whole Foods" [46]. Regardless of how fundamentally business executives believe about corporate social responsibility, they cannot disregard corporate social responsibility consequences for their organizations. As a result, the purpose of this article is to offer some assistance to businesses looking to evaluate the advantages and costs of corporate social responsibility. These advantages and expenses can help managers judge their firms' corporate social responsibility policies and offer feedback on corporate social responsibility initiatives. We concentrate on the relationship between accounting and corporate social responsibility since accounting is a critical assessment tool in businesses.

3.2. Corporate Social Responsibility in Oil and Gas. A short assessment of corporate social responsibility in the oil and gas industry immediately connects rising civic expectations and worries about global warming, environmental disasters, dwindling resources, and the impact of transnational corporations on globalization, and perceived expanding power and influence [47]. Consumers and civic organizations increasingly target TNCs to initiate changes by threatening reputational consequences, as skepticism about national governments' desire and capacity to effect change grows. Larger, more focused use of corporate social responsibility techniques, concepts, and ways of reasoning may allow for the detection of broader future dangers and possibilities [48]. Profits, demand, accessibility, market price, and reputation are all at risk. Energy businesses are especially susceptible in this sense. Intangibles such as trust, dependability, validity, continuity, connections, and clarity, as well as tangibles like profitability, investment in staff, communities, and the environment, are critical to their brand and social capital [49]. Organizations confront rising demands and expectations from governments, communities, and consumers as competition for new areas heats up, which are always linked with wider and deeper risks, markets, and energized civil societies. In the oil and gas business, corporate social responsibility (or other similar words such as CR, sustainable development, communities, and our people) has received increased consideration due to altering civic, political, and commercial realities [50]. Transnational initiatives such as the Global Reporting Initiative, the UN Global Compact, and the UK-led Extractive Industries Transparency Initiative (EITI), as well as organizations like the World Business Council for Sustainable Development, the Institute of Business Ethics, and the World Bank Group-funded CommDev, have been introduced in place of global attempts to control TNCs. Transformation in business behavior is encouraged by such organizations. TNCs have adjusted to shifting attitudes and needs by launching a slew of corporate social responsibility-related activities. Several more oil and gas companies now have codes of ethics, participate in stakeholder dialogue, assist in the construction of schools and hospitals, collaborate with development organizations such as the United Nations Development Programme (UNDP), use nongovernmental organizations (NGOs) to apply for development programs, and publish financial, social, and environmental performance findings. Various worldwide representative organizations, such as IPIECA and the World Petroleum Council, encourage awareness of ethical and sustainable corporate practices and campaigns highlighting firm community involvement [51].

Despite this, there is broad recognition within the energy industry and representative organizations and increased calls from international pressure groups, civilian populations, and, in some instances, political parties and militias that a more significant focus on social responsibility is necessary. Employees will need more knowledge into how firms engage with communities, governments, and global processes and the repercussions if enterprises are to constructively contribute to more involvement and the adoption of corporate social responsibility -related ways of thinking. Furthermore, despite the more significant expenditure, corporate social responsibility initiatives fail to address many of the issues they are blamed for causing. Corporate social responsibility rules, on the other hand, exacerbate current issues while creating new ones. The issues are exacerbated in regions where oil and gas corporations operate under the so-called absent state theory [52].

3.3. Sustainable Supply Chain Management. The sustainable supply chain management approach was examined on two levels: first, as a single idea, regardless of the numerous particular tactics used by oil distribution businesses to promote sustainable supply chain management; and second, as a collection of methods used by oil distribution firms to promote sustainable supply chain management. Second, as particular strategies—green supplier selection, product stewardship, and logistics management [53]. In the administration of a supply chain, oil and gas distribution firms face various economic, environmental, and social issues [54, 55]. As a result, SSCM in the oil sector must deal with many challenges, including pollution impact replacement, elevated energy, material use, and biodiversity conservation [56]. Rather than dealing with each possible issue individually, oil firms opt to follow conventions or use well-established criteria [57]. Codes of conduct, norms, and standards, as well as certification that validates compliance, can be used by oil and gas distribution companies to assess a supplier's environmental or social impact [57, 58]. All of these are elements that can help you improve the efficiency of your supply chain. Since oil and gas distribution companies control their supply chains, they evaluate vendors by establishing minimum requirements and standards. Consequently, suppliers may conduct self-evaluations based on environmental or social criteria, which may be helped by incentives [59].

3.3.1. Product Stewardship Strategy. For example, several facets of sustainability are included in the Product Stewardship approach, reverse logistics, and closed-loop supply chains [60]. Lane and Watson (2012) [61] feel that product stewardship is a swiftly expanding area that is highly relevant in resource conservation and producing a competitive advantage for an organization [36]. According to several scholars, environmental stewardship is becoming a more widely used technique

in relation to material responsibility [62]. From responsible waste management to a stronger focus on resource conservation, the concept of product stewardship has evolved. The interplay between the social and material worlds has changed due to product stewardship methods [63]. Moreover, these activities have contributed to the development of new industrial sectors and collaborations. The main objective of Product Stewardship is to reduce a product's environmental effect throughout its life cycle [64].

3.4. Supply Chain Management Functions. There are a variety of supply chain management functionalities available, each stressing a distinct perspective [65]. Florescu et al. [58] believe that planning and execution are essential to supply chain activities. However, other researchers [66, 67] suggest that sustainable supply chain management requires a broader emphasis on coordination and cooperation. As a result, four supply chain management functions are investigated in this work: planning, execution, coordination, and cooperation. Creating an sustainable supply chain management necessitates a supply chain focus, active participation of supply chain actors, and teamwork. Waste reduction, material recycling, energy conservation [68], and the development of new environmental development techniques [68, 69] are all examples of new environmental methodological approaches.

Moreover, environmental effect data on acquired commodities have been proven to benefit supply chains with adequate planning and coordination. Poor supply chain communication, on the other hand, results in the inadequate transfer of information and has an impact on goal alignment, which is essential to implement environmental sustainability in supply chains [70]. Cooperation among supply chain players affects supply chain sustainability by affecting information transmission and problem-solving among supply chain members [71]. In supply chains, for instance, codes of conduct are employed to establish principles and require communication to reinforce those standards across the network [72]. As a consequence, communication may have a direct influence on the social sustainability performance of the supply chain.

3.5. Integration of Supply Chain Pricing Values. The degree to which a manufacturer collaborates with supply chain partners and as a group handles procedures both inside and outside the business to create competitive advantages is known as supply chain pricing integration [73]. Firms have realized that they must handle the supply chain as a whole system and consider it an integrated function as the necessity of good supply chain management has grown [74]. Stevens (1989) initially examined value integration in terms of the three dimensions listed as follows (see Figure 1):

When a company adopts an integrated strategy, it recognizes that it cannot handle each component of the supply chain as a separate function. However, it must instead comprehend and manage the linkages and interdependencies. This means that sourcing, demand planning, inventory planning, warehousing, logistics, and order

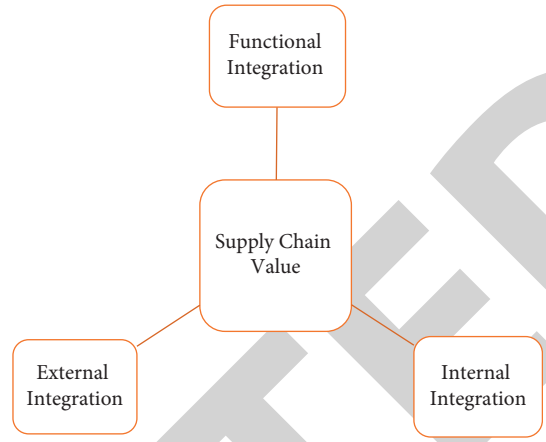

Figure 1: A three-dimensional approach to supply chain value integration.

processing must all work simultaneously inside the supply chain organization. The rise of supply chain software solutions that put all of this data together in one place is one indicator of a more integrated approach [75].

Furthermore, many businesses traditionally had these tasks dispersed across many departments with limited chance for interaction. Most big corporations now have an integrated supply chain function with a single management team and shared goals. There are crucial links between marketing, finance, and production and the work done inside the supply chain organization. Marketing has a direct role in forecasting demand and setting consumer expectations for goods and delivery. These should be discussed with the supply chain team so that everyone understands what has to be accomplished. If this is not feasible, modifications may be made and communicated to consumers as soon as possible. Integration with finance is required to ensure that investments are adequately planned, and that inventory is correctly accounted for. Manufacturing is frequently influenced by the supply chain team's decisions and requirements since they rely on enough supplies and must fulfill delivery deadlines to satisfy client promises. This integration functions well when real goals are defined across the companies, a shared perspective of the data (which identifies possibilities for enhanced performance), and clear, frequent communication about possible difficulties and requirements, as with many complicated organizational problems. As a result, all businesses can concentrate on providing value to consumers and fulfilling the company's goal. For instance, Lee and Hang propose the following model (see Figure 2) for supply chain value integration [76]:

3.6. Data Statement. In the qualitative portion, the statistical population comprises 30 university-level professionals and specialists in industrial management who have a skilled and scientific approach to performing scientific research in a related subject. They were chosen using a homogenous sample approach since the participants in this section were expected to understand the study issue theoretically. In addition, research accessible on Iranian websites was utilized

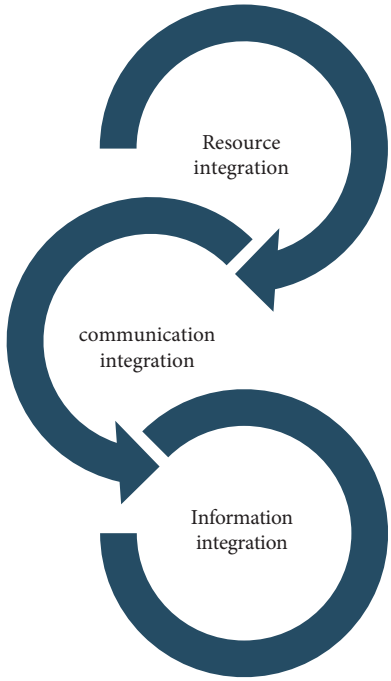

Figure 2: Supply chain value integration.

to identify components (functioning of competitive supply chain pricing) and indicators (social responsibility) of the research in this part, based on the meta-synthesis. The interpretative ranking process (IRP) was carried out in the second phase, with 40 managers from knowledge-based firms in the oil industry filling in the matrix checklists depending on the nature of the study.

3.7. Best-Worst Method. For the selection step, the best-worst method (BWM) was developed [30]. The BWM has several distinguishing characteristics, including (i) a highly structured pairwise comparison that yields very continuous and trustworthy findings; (ii) the use of only two vectors rather than a full pairwise comparison matrix. This means that the analyst and decision-maker will have to spend less time gathering data. Surprisingly, because these two vectors are more organized than a whole matrix, less data contributes to improved dependability; (iii) the technique only utilizes integer values, making it more pragmatic than methods requiring fractions.

Step 1: create a list of criteria for making a choice. We examine the criteria (c_1, c_2, . . ., c_n) that should be utilized to choose this phase.

Step 2: decide which criteria are the best (most pleasant, most essential) and the worst (least attractive, least essential). In this stage, the decision-maker determines which criteria are the greatest and worst in general. At this point, no comparisons are drawn.

Step 3: utilizing a number between 1 and 9, identify the best criterion's priority above all other criteria. The Best-to-Others vector as a consequence would be:

$$A_B = (a_{B1}, a_{B2}, \ldots, a_{Bn}), \tag{1}$$

where a_{Bj} denotes the best criteria B's priority over criterion j. $a_{BB} = 1$ is self-evident.

Step 4: utilizing a number between 1 and 9, rank all criteria in order of priority over the worst criterion. The Others-to-Worst vector as a consequence would be:

$$A_B = (a_{1W}, a_{2W}, \ldots, a_{nW})^T, \tag{2}$$

where a_{jW} denotes the criteria j's preference over the worst criterion W. $a_{BB} = 1$ is self-evident.

Step 5: determine the best weights $(w_1^*, w_2^*, \ldots, w_n^*)$.

The weight for the criteria that has $w_B/w_j = a_{jw}$ for each pair of w_B/w_j and w_j/w_w is the best. We should develop a solution that minimizes the most remarkable absolute differences $|w_B/w_j - a_{Bj}|$ and $|w_j/w_W - a_{jW}|$ for every j to meet these. The next difficulty arises from the nonnegativity and sum condition for the weights:

$$\min \max_j \left\{ \left| \frac{w_B}{w_j} - a_{Bj} \right|, \left| \frac{w_j}{w_W} - a_{jW} \right| \right\}, \tag{3}$$

$$\begin{aligned} \text{st} \sum w_j &= 1, \\ w_j &\geq 0. \end{aligned} \tag{4}$$

The following problem can be applied to this one: ξ

$$\begin{aligned} \min \xi \left| \frac{w_B}{w_j} - a_{Bj} \right| \leq \xi \text{ for all } j \left| \frac{w_j}{w_W} - a_{jW} \right| \leq \xi \text{ for all } j \sum w_j \\ = 1 w_j \geq 0 \quad \text{for all } j. \end{aligned} \tag{5}$$

The optimal weights $(w_1^*, w_2^*, \ldots, w_n^*)$ and ξ^* are computed while solving the problem. The consistency index is then used to determine the consistency ratio (Tables 1 and 2). The larger the $\xi *$, the greater the consistency ratio, and the less trustworthy the comparisons get.

First, FBWM [35] is used to calculate the fuzzy criterion weights in the proposed Integrated Fuzzy Best-Worst-TOPSIS approach. In FBWM, DMs indicate their preferences for criterion comparison using the linguistic characteristics listed in Table 1, then translated into TFNs.

The FBWM's stages are listed below.

Define the Evaluation Criteria and DMs in Step 1. A set of $C = \{c1, c2, \ldots, cm\}$,(benefit) criteria is established, with the greatest being better for each criterion.

Step 2: determine which criteria are the best and worst. Each DM determines which criterion is the best (most desired) and which is the worst (least desirable) (less desirable).

Step 3: calculate the best criterion's fuzzy preference over all criteria (Best-to-Others (BO) vector). Utilizing the linguistic words in Table 1, each DM decides his or her best criterion's preference over all other criteria, which is then translated to TFNs $\tilde{\tilde{a}}_{ij}$ $j = (1, 2, \ldots, n)$. It is worth noting that $\tilde{\tilde{a}}_{BB=(1,1,1)}$.

Table 1: Consistency index.

aBW	1	2	3	4	5	6	7	8	9
Consistency index	0.00	0.44	1.00	1.63	2.30	3.00	3.73	4.47	5.23

Table 2: For the evaluation of criteria, linguistic variables and TFNs are used.

Linguistic variables	Triangular fuzzy numbers (TFNs)
Equally preferred (EP)	(1, 1, 1)
Moderately preferred (MP)	(2/3, 1, 3/2)
Strongly preferred (SP)	(3/2, 2, 5/2)
Very strongly preferred (VSP)	(5/2, 3, 7/2)
Extremely more preferred (EMP)	(7/2, 4, 9/2)

Step 4: Over the Worst criterion (OW) vector, calculate the fuzzy preference of all other criteria. Utilizing the linguistic words in Table 1, each DM calculates the priority of all other criteria over the worst criterion, which is then translated to TFNs $\tilde{\tilde{a}}_{jw}\ j = (1, 2, \ldots, n)$. It is worth noting that $\tilde{\tilde{a}}_{BB=(1,1,1)}$.

Step 5: determine the criteria's optimal fuzzy weights. Problem (7) is addressed for each DM and the ideal fuzzy weight vector $w^- = (w_1^-, w_2^-, \ldots, w_m^-)$ and $\xi *$ are found.

Step 6: make sure everything is consistent.

There is a sum of $2n-3$ fuzzy reference comparisons ($n-2$ best-to-others fuzzy comparisons + $n-2$ others-to-worst fuzzy comparisons +1 best-to-worst fuzzy comparison), which is required to be applied for FBWM. It's worth noting that (fuzzy) BWM only requires $2n-3$ comparisons, but (fuzzy) AHP requires $(n-1)/2$.

In FBWM, optimal fuzzy weights $w^- = (Ij, mj, uj)\ j = 1, 2, \ldots, n$ can be determined as follows [6, 31]:

$$\min \max_j \left\{ \left| \frac{\tilde{w}_B}{\tilde{w}_j} - \tilde{a}_{Bj} \right|, \left| \frac{\tilde{w}_j}{\tilde{w}_W} - \tilde{a}_{jW} \right| \right\},$$
$$\text{s.t.} \begin{cases} \sum_{j=1}^{n} R\left(\tilde{w}_j\right) = 1, \\ l_j \le m_j \le u_j,\ j = 1, 2, \ldots, n, \\ l_j \ge 0,\ j = 1, 2, \ldots, n, \end{cases} \tag{6}$$

where $\tilde{w}_B = (l_B, m_B, u_B)\tilde{w}_W = (l_W, m_W, u_W)\tilde{a}_{Bj} = (l_{Bj}m_{Bj}, u_{Bj})\tilde{a}_{jW} = (l_{jW_2}m_{jw}, u_{jW})$ The following nonlinearly constrained optimization problem may be converted to problem (3):

$$\text{s.t.} \begin{cases} \min \tilde{\xi} \\ \left| \frac{\tilde{w}_B}{\tilde{w}_j} - \tilde{a}_{Bj} \right| \le \tilde{\xi},\ j = 1, 2, \ldots, n \\ \frac{\tilde{w}_j}{\tilde{w}_W} - \tilde{a}_{jW} \mid \le \tilde{\xi},\ j = 1, 2, \ldots, n \\ \mid \sum_{j=1}^{n} R\left(\tilde{w}_j\right) = 1, \\ l_j \le m_j \le u_j,\ j = 1, 2, \ldots, n, \\ l_j \ge 0,\ j = 1, 2, \ldots, n, \end{cases} \tag{7}$$

where $\tilde{\xi} = (l^{\xi}, m^{\xi}, u^{\xi})$ taking into account $l^{\xi} < m^{\xi} < u^{\xi}$ presume $\xi* = (k*, k*, k*)$, $K* \le l^{\xi}$ then problem (6) can be converted to the following problem:

$$\min \tilde{\xi}$$

$$\text{s.t.} \begin{cases} \left| \dfrac{(l_B, m_B, u_B)}{(l_j, m_j, u_j)} - \left(l_{Bj}, m_{Bj}, u_{Bj}\right) \right| \le (k*, k*, k*) \quad j = 1, 2, \ldots, n \\ \dfrac{(l_j, m_j, u_j)}{(l_W, m_W, u_W)} - \left(l_{jW} m_{jw}, u_{jw}\right) | \le (k*, k*, k*) \quad j = 1, 2, \ldots, n \\ \sum_{j=1}^{n} R\left(\tilde{w}_j\right) = 1 \\ l_j \le m_j \le u_j, \; j = 1, 2, \ldots, n \\ l_j \ge 0, \; j = 1, 2, \ldots, n. \end{cases} \tag{8}$$

The optimal fuzzy weights $\tilde{w}_j = (Ij, mj, uj) j = 1, 2 \ldots, n \, and \, \tilde{\xi}*$ may be found by solving the preceding issue.

Testing for consistency [34]: to evaluate the consistency of fuzzy pairwise comparisons, the consistency ratio (CR) is utilized.

When $\tilde{a}Bj.\tilde{a}Bj = \tilde{a}BW$, a fuzzy comparison is entirely consistent.

The most excellent possible crisp may be calculated and utilized as a consistency index (CI) for FBWM by calculating equation (8) for various values $(\tilde{a}_{BW} = (l_{BW}, m_{BW} u_{BW}))$:

$$\xi^2 - (1 + 2u_{BW})\xi + \left(u_{BW}^2 - u_{BW}\right) = 0. \tag{9}$$

Table 2 shows the estimated CI values for various variables.

After that, the consistency ratio (CR) is determined as follows: Closer to zero CR scores indicate great consistency.

3.8. Interval Type-2 Fuzzy Sets TOPSIS (IT2F-TOPSIS). The TOPSIS approach aims to choose the closest alternatives to the positive-ideal solution and furthest away from the negative-ideal solution [77, 78]. IT2F-TOPSIS Pythagorean fuzzy variants of TOPSIS based on fuzzy collections are created as Ak and Gul [74]. Utilizing the benefits of IT2FSs, TOPSIS centered on IT2FSs better represents uncertainty, vagueness, and ambiguity than regular fuzzy TOPSIS [78]. The suggested TOPSIS, which is based on IT2FSs, may be implemented in several ways:

Step 1: suppose that there are S options, with $S = \{s_1, s_2, \ldots, s_n\}$ Furthermore, that there are C criteria, with $C = \{c1, c2, \ldots,$ cm$\}$, and that there are K decision-makers. $D = \{D1, D2, \ldots, DK\}$ Each decision-maker took part in our survey and assigned a value to the supplier's performance based on each criterion. Equation (1) may be used to compute the supplier's overall performance value based on each criterion:

$$E_c = \left(\tilde{\tilde{c}}_{ij}^{p}\right)_{m \times n} = \begin{array}{c} \\ c_1 \\ c_2 \\ \vdots \\ c_m \end{array} \begin{array}{c} \begin{array}{cccc} s_1 & s_2 & \cdots & s_n \end{array} \\ \begin{bmatrix} \tilde{\tilde{c}}_{11}^{p} & \tilde{\tilde{c}}_{12}^{p} & \cdots & \tilde{\tilde{c}}_{1n}^{p} \\ \tilde{\tilde{c}}_{21}^{p} & \tilde{\tilde{c}}_{22}^{p} & \cdots & \tilde{\tilde{c}}_{2n}^{p} \\ \vdots & \vdots & \vdots & \vdots \\ \tilde{\tilde{c}}_{m1}^{p} & \tilde{\tilde{c}}_{m2}^{p} & \cdots & \tilde{\tilde{c}}_{mn}^{p} \end{bmatrix} \end{array}, \tag{10}$$

where $\tilde{\tilde{c}}_{ij} = (\tilde{\tilde{c}}_{ij}^{1} \oplus \tilde{\tilde{c}}_{ij}^{2} \oplus \cdots \oplus \tilde{\tilde{c}}_{ij}^{k}/k)$, $\tilde{\tilde{s}}_{ij}$ is an IT2FS $1 \le i \le m, 1 \le j \le n, 1c \le k$, and k show the number of professionals,

$$\tilde{\tilde{c}}_{ij} = \left(a_{i1}^{U}, a_{i2}^{U}, a_{i3}^{U}, a_{i4}^{U}; H_1\left(\tilde{A}_i^{U}\right), H_2\left(\tilde{A}_i^{U}\right)\right), \left(a_{i1}^{L}, a_{i2}^{L}, a_{i3}^{L}, a_{i4}^{L}; H_1\left(\tilde{A}_i^{L}\right), H_2\left(\tilde{A}_i^{L}\right)\right), \tag{11}$$

and k show the number of professionals,

Step 2: applying the best-worst approach, get the weighting matrix Ws of the criterion,

$$\begin{array}{cccc} c_1 & c_2 & \cdots & c_m \end{array} \\ W_s = \left(w_i^s\right)_{1 \times m} = \left[w_1^s, w_2^s, \cdots, w_m^s\right]. \tag{12}$$

Step 3: to produce the weighted decision matrix, multiply the significant weights of the criterion by the

values in the decision matrix. For each criterion, the weighted decision matrix $\tilde{\tilde{v}}$ is written as follows:

$$\tilde{\tilde{v}}_{ij} = \tilde{\tilde{c}}_{ij} \times w_i, \tag{13}$$

where the weighted trapezoidal interval type-2 fuzzy integers are denoted by $\tilde{\tilde{v}}_{ij}$.

Step 4: determine the IT2FSs' ranking value $\text{Rank}(\tilde{\tilde{v}}_{ij})$. Ew is a ranking weighted decision matrix that is built.

Step 5: identify the positive-ideal solution $x* = (v_1^*, v_2^*, \ldots, v_m^*)$ as well as the negative-ideal solution $\overline{x} = (\overline{v}_1, \overline{v}_2, \ldots, \overline{v_m})$, where

$$v_i^* = \begin{cases} \max\limits_{i\le j\le n}\left\{\text{Rank}\left(\tilde{\tilde{v}}_{ij}\right)\right\}, & if\, f_i \in B, \\ \min\limits_{i\le j\le n}\left\{\text{Rank}\left(\tilde{\tilde{v}}_{ij}\right)\right\}, & if\, f_i \in C, \end{cases} \tag{14}$$

$$v_i^- = \begin{cases} \min\limits_{i\le j\le n}\left\{\text{Rank}\left(\tilde{\tilde{v}}_{ij}\right)\right\}, & if\, f_i \in B, \\ \max\limits_{i\le j\le n}\left\{\text{Rank}\left(\tilde{\tilde{v}}_{ij}\right)\right\}, & if\, f_i \in C. \end{cases} \tag{15}$$

Then, for the green supplier, positive $d*(x_j)$ and negative d−(x_j) ideal solutions are obtained as follows:

$$d^*\left(x_j\right) = \sqrt{\sum_{i\in I}\left(\text{Rank}\left(\tilde{\tilde{v}}_{ij}\right) - v_i^*\right)^2}, \tag{16}$$

$$d^-\left(x_j\right) = \sqrt{\sum_{i\in I}\left(\text{Rank}\left(\tilde{\tilde{v}}_{ij}\right) - v_i^-\right)^2}. \tag{17}$$

The trapezoidal IT2FS $\tilde{\tilde{A}}_i$'s ranking value $Rank(\tilde{\tilde{A}}_i)$ is formulated as follow:

$$\begin{aligned} \text{Rank}\left(\tilde{\tilde{v}}_i\right) = {} & M_1\left(\tilde{v}_i^U\right) + M_1\left(\tilde{v}_i^L\right) + M_2\left(\tilde{v}_i^U\right) + M_2\left(\tilde{v}_i^L\right) + M_3\left(\tilde{v}_i^U\right) + M_3\left(\tilde{v}_i^L\right) \\ & - \frac{1}{4}\left(S_1\left(\tilde{v}_i^U\right) + S_1\left(\tilde{v}_i^L\right) + S_2\left(\tilde{v}_i^U\right) + S_2\left(\tilde{v}_i^L\right) + S_3\left(\tilde{v}_i^U\right) + S_3\left(\tilde{v}_i^L\right) + S_4\left(\tilde{v}_i^U\right) + S_4\left(\tilde{v}_i^L\right)\right) \\ & + H_1\left(\tilde{v}_i^U\right) + H_1\left(\tilde{v}_i^L\right) + H_2\left(\tilde{v}_i^U\right) + H_2\left(\tilde{v}_i^L\right), \end{aligned} \tag{18}$$

where $M_p(\tilde{\tilde{v}}_i^j)$ indicates the element's average of v_{ip}^j, and $v_{i(p+1)}^j$, denotes the element's standard deviation of v_{ip}^j and v_{iq}^j and $v_{i(q+1)}^j$'s standard deviations are denoted by $v_{i(p+1)}^j$, and $M_p(\tilde{\tilde{v}}_i^j) = (v_{ip}^j + v_{i(p+1)}^j)/2, 1 \le p \le 3,$. $S_q(\tilde{\tilde{v}}_i^j) = \sqrt{1/2\sum_{k=q}^{q+1} v_{ik}^j - 1/2\sum_{k=q}^{q+1} v_{ik}^{j\,2}}, 1 \le q \le 3,$ $H_p(\tilde{\tilde{v}}_i^j)$ denotes the.

In the trapezoidal membership function $\tilde{v}_i^j, 1 \le p \le 3, j \in \{U, L\}$, and $1 \le i \le n.$, the membership value of the element $v_{i(p+1)}^j$.

Step 6: the CC(x_j) closeness coefficient is then computed.

$$CC\left(x_j\right) = \frac{d^-\left(x_j\right)}{d^*\left(x_j\right) + d^-\left(x_j\right)}. \tag{19}$$

Step 7: alternatives can be ranked in descending order. The greater the value of CC(x_j), the larger the green supplier's preference.

4. Results

In Iran, fuzzy Best-Worst-TOPSIS assesses and ranks oil corporations based on their social responsibility component. In the research, three managers from oil firms serve as DMs. The environmental dimension is one of the elements being assessed. The social dimension, Economic dimension, Beneficiary dimension, Voluntary dimension, Ethical dimension, and Institutional dimension are based on three elements that influence supply chain price in oil companies: competitors, products, and customers. Table 3 lists the assessment criteria that were established with the assistance of DMs. All of the assessment criteria in Table 3 are advantage criteria (B).

Each DM must first evaluate which parameters are the greatest and worst for him or her. Then, employing the linguistic variables given in Table 2 compares them to other criteria (Tables 4 and 5). All DMs picked C1 as the best criterion, whereas C5 was chosen as the worst criterion.

Table 3: Components of social responsibility.

Co	Components	Definitions
B1	Environmental dimension	The environmental component is concerned with the vulnerability of ecological and biophysical systems and their many functions in the event of a hazardous state, which causes damage and degradation. The corporate social responsibility (CSR) trend encourages businesses to go above and beyond legal requirements to contribute to environmental quality. Climate change and greenhouse gas emissions are frequently discussed.
B2	Social dimension	The social dimension of social responsibility differs from the other components. It includes, among other things, the firm's community performance methods as well as dynamic social relationships with stakeholders, such as data supply, performance transparency, and adaptable organizational structures.
B3	Economic dimension	The economic part of corporate social responsibility relates to the distribution of resources to create products and services within the social system. In terms of the economy, social responsibility covers many elements of how companies influence the economy in terms of competition, consumers, employees, community, and environment.
B4	Beneficiary dimension	This dimension is concerned with institutions and organizations' commitment to serving the needs of stakeholders. It is, in fact, a set of management activities that ensure the company's operations have the maximum potential positive influence on society. This viewpoint highlights the importance of CSR's voluntary character.
B5	Voluntary dimension	Business frequently interprets the voluntary character of corporate social responsibility to indicate that, because corporate social responsibility activities are not obligatory, they are always discretionary and so maybe chosen exclusively by the business.
B6	Ethical dimension	While ethics is concerned with what is good and wrong in general, business ethics focuses on benefits for shareholders and stakeholders. On the other hand, social responsibility is concerned with the company's influence on the environment and community. 4th of March 2018
B7	Institutional dimension	Past social responsibility/social performance study has done nothing to address the institutional drivers of social responsibility and its many expressions in terms of social performance in a systematic way. Instead, most of this study has focused on particular areas of the business-society interface, such as the link between social responsibility and economic success and the link between a firm's internal features and its outward social performance.

Table 4: Language preferences of decision-makers for the best criterion concerning each of the other factors (best-to-others vector).

Criteria	DM-1	DM-2	DM-3
B1	EMP	EMP	EMP
B2	SP	SP	VSP
B3	MP	MP	EMP
B4	SP	VSP	SP
B5	EP	EP	EP
B6	SP	SP	SP
B7	SP	VSP	SP

Table 5: In the case of the worst criterion, decision-makers' linguistic preferences for all other criteria (others-to-worst vector).

Criteria	DM-1	DM-2	DM-3
B1	EP	EP	EP
B2	VSP	MP	MP
B3	VSP	VSP	SP
B4	MP	VSP	VSP
B5	EMP	EMP	EMP
B6	VSP	VSP	MP
B7	VSP	MP	VSP

The language preferences of the DMs were translated to TFNs employing the scale in Tables (see Tables 6 and 7). To obtain the fuzzy weights of criteria, Problem (7) was solved for each DM based on Table 8. Table 9 shows the ideal fuzzy criterion weights for each DM and the

Table 6: Applying TFNs, choose the best criterion for each of the other criteria (best-to-others vector).

Criteria	DM-1	DM-2	DM-3
B1	(7/2, 4, 9/2)	(7/2, 4, 9/2)	(7/2, 4, 9/2)
B2	(3/2, 2, 5/2)	(3/2, 2, 5/2)	(5/2, 3, 7/2)
B3	(2/3, 1, 3/2)	(2/3, 1, 3/2)	(7/2, 4, 9/2)
B4	(3/2, 2, 5/2)	(5/2, 3, 7/2)	(3/2, 2, 5/2)
B5	(1, 1, 1)	(1, 1, 1)	(1, 1, 1)
B6	(3/2, 2, 5/2)	(3/2, 2, 5/2)	(3/2, 2, 5/2)
B7	(3/2, 2, 5/2)	(5/2, 3, 7/2)	(3/2, 2, 5/2)

average fuzzy criteria weights. Average fuzzy weights are used in the F-TOPSIS phase. Equation (8) is used to derive related consistency indicators (ξ) for each DM, as given in Table 9. Because all of the consistency ratios are nearly 0, each DM's criteria comparisons are highly consistent.

DMs assess each alternative according to each criterion in the F-TOPSIS phase, using the linguistic variables in Table 8. Table 10 shows the results of three DMs' evaluations of the competitive supply chain pricing factors based on seven criteria. After linguistic terms are transformed to matching TFNs, the aggregated (average) fuzzy decision matrix is given in Table 11. Once the fuzzy normalized decision matrix is built, as illustrated in Table 12, the fuzzy weighted normalized decision matrix is computed. The distance from a fuzzy positive-ideal solution, the range from a fuzzy negative-ideal solution, and the proximity coefficients are all shown in Table 13. Customers, products, and

Table 7: TFNs are used to prioritize all other criteria above the poorest criterion (others-to-worst vector).

Criteria	DM-1	DM-2	DM-3
B1	(1, 1, 1)	(1, 1, 1)	(1, 1, 1)
B2	(5/2, 3, 7/2)	(2/3, 1, 3/2)	(2/3, 1, 3/2)
B3	(5/2, 3, 7/2)	(5/2, 3, 7/2)	(3/2, 2, 5/2)
B4	(2/3, 1, 3/2)	(5/2, 3, 7/2)	(5/2, 3, 7/2)
B5	(7/2, 4, 9/2)	(7/2, 4, 9/2)	(7/2, 4, 9/2)
B6	(5/2, 3, 7/2)	(5/2, 3, 7/2)	(2/3, 1, 3/2)
B7	(5/2, 3, 7/2)	(2/3, 1, 3/2)	(5/2, 3, 7/2)

Table 8: For the evaluation of options, linguistic variables and TFNs are used.

Linguistic variables	Triangular fuzzy numbers (TFNs)
Very poor (VP)	(0, 0, 1)
Poor (P)	(0, 1, 3)
Medium poor (MP)	(1, 3, 5)
Fair (F)	(3, 5, 7)
Medium good (MG)	(5, 7, 9)
Good (G)	(7, 9, 10)
Very good (VG)	(9, 10, 10)

Table 9: For each decision-maker, fuzzy weights of 9 criteria and an associated consistency indicator (ξ), as well as average fuzzy weights.

Cr.	DM-1	DM-2	DM-3	Fuzzy weights (average)
B1	(0.039, 0.043, 0.043)	(0.044, 0.049, 0.055)	(0.048, 0.048, 0.048)	(0.044, 0.047, 0.049)
B2	(0.047, 0.061, 0.076)	(0.230, 0.230, 0.230)	(0.039, 0.043, 0.043)	(0.104, 0.111, 0.116)
B3	(0.100, 0.147, 0.154)	(0.106, 0.137, 0.171)	(0.070, 0.085, 0.099)	(0.092, 0.123, 0.143)
B4	(0.055, 0.065, 0.081)	(0.101, 0.114, 0.126)	(0.099, 0.131, 0.147)	(0.085, 0.097, 0.118)
B5	(0.169, 0.185, 0.185)	(0.137, 0.137, 0.137)	(0.176, 0.206, 0.206)	(0.160, 0.120, 0.176)
B6	(0.089, 0.117, 0.154)	(0.072, 0.086, 0.106)	(0.101, 0.114, 0.126)	(0.087, 0.105, 0.129)
B7	(0.106, 0.137, 0.171)	(0.055, 0.065, 0.081)	(0.107, 0.160, 0.160)	(0.089, 0.120, 0.137)
ξ	(0.230, 0.230, 0.230)	(0.672, 0.672, 0.672)	(0.230, 0.230, 0.230)	(0.377, 0.377, 0.377)

Table 10: About each criterion, DMs' judgments of the corporate social responsibility factor depending on competitive supply chain pricing in oil companies.

	B1	B2	B3	B4	B5	B6	B7
Competitors	(7, 9, 10)	(9, 10, 10)	(7, 9, 10)	(5, 7, 9)	(9, 10, 10)	(5, 7, 9)	(9, 10, 10)
	(9, 10, 10)	(9, 10, 10)	(3, 5, 7)	(9, 10, 10)	(9, 10, 10)	(7, 9, 10)	(0, 1, 3)
	(9, 10, 10)	(9, 10, 10)	(5, 7, 9)	(9, 10, 10)	(9, 10, 10)	(0, 1, 3)	(1, 3, 5)
Products	(7, 9, 10)	(5, 7, 9)	(9, 10, 10)	(7, 9, 10)	(9, 10, 10)	(7, 9, 10)	(7, 9, 10)
	(0, 1, 3)	(5, 7, 9)	(9, 10, 10)	(0, 1, 3)	(1, 3, 5)	(9, 10, 10)	(7, 9, 10)
	(7, 9, 10)	(5, 7, 9)	(7, 9, 10)	(7, 9, 10)	(7, 9, 10)	(9, 10, 10)	(1, 3, 5)
Customers	(5, 7, 9)	(7, 9, 10)	(9, 10, 10)	(1, 3, 5)	(7, 9, 10)	(3, 5, 7)	(7, 9, 10)
	(7, 9, 10)	(5, 7, 9)	(9, 10, 10)	(5, 7, 9)	(1, 3, 5)	(7, 9, 10)	(9, 10, 10)
	(9, 10, 10)	(7, 9, 10)	(9, 10, 10)	(7, 9, 10)	(7, 9, 10)	(7, 9, 10)	(5, 7, 9)

Table 11: Fuzzy decision matrix $\tilde{\mathbf{D}}$.

	B1	B2	B3	B4	B5	B6	B7
Competitors	(7.667, 9.333, 10.000)	(5.000, 7.000, 8.667)	(9.000, 10.000, 10.000)	(5.000, 7.000, 8.667)	(7.667, 9.333, 10.000)	(3.667, 5.667, 7.667)	(3.667, 5.667, 7.667)
Products	(8.333, 9.667, 10.000)	(3.667, 5.667, 7.667)	(5.000, 7.000, 8.667)	(9.000, 10.000, 10.000)	(5.000, 7.000, 8.667)	(3.667, 5.667, 7.667)	(8.333, 9.667, 10.000)
Customers	(7.667, 9.333, 10.000)	(9.000, 10.000, 10.000)	(7.667, 9.333, 10.000)	(5.000, 7.000, 8.667)	(5.000, 7.000, 8.667)	(7.667, 9.333, 10.000)	(3.667, 5.667, 7.667)

Table 12: Weighted normalized fuzzy decision matrix $\tilde{\mathbf{V}}$.

	B1	B2	B3	B4	B5	B6	B7
Competitors	(0.039, 0.047, 0.049)	(0.080, 0.138, 0.162)	(0.134, 0.170, 0.176)	(0.068, 0.109, 0.129)	(0.134, 0.170, 0.176)	(0.016, 0.144, 0.053)	(0.031, 0.059, 0.085)
Products	(0.134, 0.170, 0.176)	(0.016, 0.144, 0.053)	(0.052, 0.104, 0.140)	(0.079, 0.117, 0.129)	(0.051, 0.077, 0.089)	(0.059, 0.090, 0.120)	(0.023, 0.048, 0.075)
Customers	(0.039, 0.047, 0.049)	(0.152, 0.202, 0.210)	(0.080, 0.138, 0.162)	(0.044, 0.082, 0.112)	(0.134, 0.170, 0.176)	(0.059, 0.090, 0.120)	(0.080, 0.138, 0.162)

Table 13: Weighted normalized fuzzy decision matrix.

Alternative	d-	*d*+	CCi	Rankings
Competitors	0.9424	8.0256	0.1192	3
Products	0.9655	8.2332	0.1201	2
Customers	0.9765	8.4583	0.1294	1

competitors are the options rated from best to worst based on the values.

The distance from fuzzy positive-ideal solution, distance from fuzzy negative-ideal solution, and proximity coefficients are computed as shown in Table 13 and Figure 3. Customers, products, and competitors are the options rated from best to worst based on the values.

4.1. The Comparative Analysis. To verify the efficacy of the suggested strategy, it is compared to a benchmarking model. IT2F VIKOR is the subject of this benchmarking model. The significance weights of the Competitive supply chain pricing selection criterion are determined from BWM for both techniques. Both are used to rank Competitive factors in the model's second phase. In our new benchmarking approach, Table 14 provides the final scores and ranking patterns of competitive characteristics. Utilizing our recommended model (combined BWM and IT2F-TOPSIS), once the maximum group utility value (v) is modified to 0.5 or more than 0.5, the ranking orders of three Competitive factors remain identical, as seen in Table 14. This finding suggests that the suggested technique produces good results and provides appropriate outcomes for competitive factor ranking decision-making. According to the findings of this study, the three variables of competitive supply chain pricing based on customer, supply chain pricing based on products, and supply chain pricing based on competitive have the highest frequency.

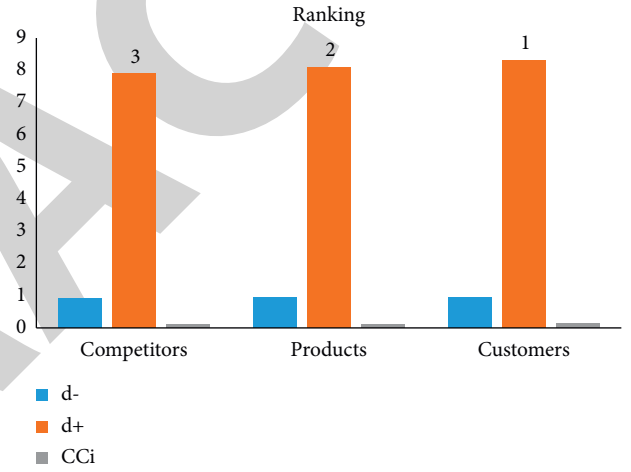

Figure 3: Weighted normalized fuzzy decision matrix.

5. Discussion

The current situation of the global economy is such that most countries are attempting to acquire a competitive position at the international level. Traditionally competition is a static aspect and success or failure in it as production is dependant. But in today's modern world, competition is a dynamic force, and new product technologies, new market borders, new production methods, and new management ideas contribute to the development, alteration, or even extinction of the advantage of national industrial competitiveness. The history of countries such as China and Japan reveals that the only reason for their success is their capacity to exceed the idea of static competitive advantages. The aforementioned nations were able to overcome the restrictions of their resources via scientific and technical advances, expanding the volume of production and growth of foreign commerce. These countries recognized that comparative advantage could be established by increasing skills, capital, and labor, and that structural change could create an environment favorable to economic progress. Today, competitive strategy and its key branches of industry analysis, competitor analysis and strategic positioning are viewed as an acknowledged aspect of management activity. Competitive strategy has offered a comprehensive framework for examining the fundamental determinants of rivalry in industry. As a result, the goal of this study is to look at the most efficient operation of competitive supply chain pricing focused on social responsibility dimensions with a case study of oil products from knowledge-based enterprises.

Table 14: Q values and rankings for each supplier in terms of v value change.

Maximum group utility value (v) in VIKOR	Q value			Rank		
	Competitors	Products	Customers	Competitors	Products	Customers
v= 0.1	0.985	0.479	0.000	3	2	1
v = 0.1	0.909	0.339	0.000	3	2	1
v = 0.2	0.560	0.833	0.000	2	3	1
v = 0.3	0.646	0.945	0.000	2	3	1
v = 0.4	0.870	0.638	0.000	3	2	1
v = 0.5	0.725	0.372	0.000	3	2	1
v = 0.6	0.693	0.387	0.000	3	2	1
v = 0.7	0.489	0.865	0.000	2	3	1
v = 0.8	0.890	0.475	0.000	3	2	1
v = 0.9	0.655	0.340	0.000	3	2	1
v = 1.0	0.783	0.439	0.000	3	2	1

6. Conclusion and Future Works

With competitive supply chain pricing, corporate social responsibility has become the most efficient business strategy in the globe. Since most firms utilize these performances or acquire information about their businesses to evaluate and choose the best criterion. In an MCDM challenge, a competent Supply Chain Pricing considerations solutions supplier considers multiple possibly competing for qualitative and quantitative criteria. This study presented a new extended decision making and FBWM method based on Type-2 Fuzzy Sets TOPSIS for ranking the corporate social responsibility criteria based on competitive supply chain pricing factors. The aim of the ranking is to learn how a company and its supply chain may accomplish joint-optimization of economic, environmental, and social performance by transparently and strategically integrating sustainability into business operations. The most effective functioning of competitive supply chain pricing in knowledge-based businesses' oil supplies was investigated in this research, which concentrated on social obligation components. Three functions of competitive supply chain pricing and seven propositions connected to the dimensions of social responsibility in knowledge-based businesses in the oil sector were established depending on the research results to meet the first and second research goals. The most plausible dimension of social responsibility in knowledge-based businesses in the oil sector, according to the research, is the environmental dimension in social responsibility, which may produce competitive supply chain pricing mechanisms based on profitability. The environmental factor, which refers to the establishment of professional environment procedures in keeping with the nature of knowledge-based companies based on the production of knowledge-based commodities, shapes corporate social responsibility methods. It keeps them accountable to stakeholders and enhances social perceptions of their performance to more fully integrate the national and domestic economies. Since oil is a vital product in our nation's economy, we focus on development-oriented characteristics in the oil sector and its derivatives. It promotes trust and confidence in firms that utilize such items as primary materials or raw materials, in addition to adhering to environmental standards. It promotes long-term economic growth and thriving. In other findings; it was revealed that the elements of Competitive Supply Chain Pricing factors in Oil Companies based on social responsibility are ranked as follows: customer, product, and competitive supply chain pricing procedures. As a result, maintaining customer values is a major price element in establishing contacts, as determined by the company's strategic connection with the economy, as well as regional and worldwide partners. In actuality, this price function attempts to persuade clients to use the goods of domestic and Iranian knowledge-based businesses by earning their trust and confidence to create value for their customers. Knowledge-based companies will be able to assess their competitive position in this circumstance strategically, based on value-based competitive supply chain pricing, and plan for likely future scenarios, and sell items to meet customer wants. To gain consumers' trust, the first step to success should involve the significance of professional ethics, in addition to knowledge. In these circumstances, a pricing strategy that focuses on establishing inclusive values for customers may strengthen a company's competitive position and position it at the forefront of strategic connections with energy-using companies. Also, Access to specialists created problems such as prolonging the research process.

6.1. 1- Suggestions for Future Research. Although the model of this research is designed for the energy industry; considering the basic similarities between energy industries such as petrochemicals and refineries, its generalizability can also be examined. It also seems necessary to conduct data-driven research to model the competitive supply chain in NGOs and medium knowledge-based companies.

Data Availability

The data used to support the findings of the study are available from the corresponding author upon request.

Conflicts of Interest

The authors declare that they have no conflicts of interest.

References

[1] P. Lacy, T. Cooper, R. Hayward, and L. Neuberger, "A new era of sustainability UN Global Compact," 2010.

[2] G. Atkinson, "Measuring corporate sustainability," *Journal of Environmental Planning and Management*, vol. 43, no. 2, pp. 235–252, 2000.

[3] S. Alina, W. Zhen, R. E. Vyacheslavovna, and R. S. Valerievna, "Russian gas companies' financial strategy considering sustainable growth," *Economic Literature*, vol. 15, no. 1, 2019.

[4] A. Duttagupta, E. R. Hosseinabad, and M. A. U. Zaman, "Corporate social responsibility and sustainability: a perspective from the oil and gas industry," *Journal of Nature*, vol. 2, pp. 22–29, 2021.

[5] R. Luken and R. Stares, "Small business responsibility in developing countries: a threat or an opportunity?" *Business Strategy and the Environment*, vol. 14, no. 1, pp. 38–53, 2005.

[6] S. Waldron, *Corporate Social Responsibility Is Not Public Relations: How to Put CSR at the Heart of Your Company and Maximize the Business Benefits*, LID Publishing, London, UK, 2021.

[7] N. M. Nor, S. M. M. Khairi, H. Rosnan, R. Maskun, and E. R. Johar, "Establishing a knowledge-based organisation: lesson learnt and km challenges in Malaysian organisation," *Innovation & Management Review*, vol. 23, 2020.

[8] C. Fox, P. Davis, and M. Baucus, "Corporate social responsibility during unprecedented crises: the role of authentic leadership and business model flexibility," *Management Decision*, vol. 43, 2020.

[9] A. Habisch, "The magic of economic and social development," *The German Chambers of Commerce and Industry*, Springer, Berlin, Germany, pp. 1–31, 2021.

[10] P. Centobelli, R. Cerchione, and M. Ertz, "Managing supply chain resilience to pursue business and environmental strategies," *Business Strategy and the Environment*, vol. 29, no. 3, pp. 1215–1246, 2020.

[11] N. R. Mosteanu, A. Faccia, A. Ansari, M. D. Shamout, and F. Capitanio, "Sustainability integration in supply chain management through systematic literature review," *Calitatea*, vol. 21, no. 176, pp. 117–123, 2020.

[12] M. Abdel-Basset, R. Mohamed, K. Sallam, and M. Elhoseny, "A novel decision-making model for sustainable supply chain finance under uncertainty environment," *Journal of Cleaner Production*, vol. 269, Article ID 122324, 2020.

[13] P. Lengyel, A. Bai, Z. Gabnai et al., "Development of the concept of circular supply chain management-A systematic review," *Processes*, vol. 9, no. 10, p. 1740, 2021.

[14] D. M. Neutzling, A. Land, S. Seuring, and L. F. M. d. Nascimento, "Linking sustainability-oriented innovation to supply chain relationship integration," *Journal of Cleaner Production*, vol. 172, pp. 3448–3458, 2018.

[15] S. Chaurasia, R. K. Pati, S. S. Padhi, J. M. Jensen, and N. Gavirneni, "Achieving the united nations sustainable development goals-2030 through the nutraceutical industry: a review of managerial research and the role of operations management," *Decision Sciences*, vol. 35, 2021.

[16] B. Surya, F. Menne, H. Sabhan, S. Suriani, H. Abubakar, and M. Idris, "Economic growth, increasing productivity of SMEs, and open innovation," *Journal of Open Innovation: Technology, Market, and Complexity*, vol. 7, no. 1, p. 20, 2021.

[17] A. M. Gonyora, S. Migiro, B. Ngwenya, and P. Mashau, "Investigating open innovation strategic alignment for sustainable competitive advantage in the automotive supply chain in South Africa," *Journal of Transport and Supply Chain Management*, vol. 15, p. 554, 2021.

[18] B. Bigliardi, G. Ferraro, S. Filippelli, and F. Galati, "The past, present and future of open innovation," *European Journal of Innovation Management*, vol. 25, 2021.

[19] K. Hummel, U. Laun, and A. Krauss, "Management of environmental and social risks and topics in the banking sector - an empirical investigation," *The British Accounting Review*, vol. 53, no. 1, Article ID 100921, 2021.

[20] H. Iqbal, H. Haider, B. Waheed, S. Tesfamariam, and R. Sadiq, "Benchmarking of oil and gas pipeline companies in British columbia: integrating integrity management program and safety culture using a risk-based approach," *Engineering Management Journal*, vol. 24, pp. 1–17, 2021.

[21] A. Sharifi, A. Ahmadi, and A. Ala, "The impact of artificial intelligence and digital style on industry and energy post-COVID-19 pandemic," *Environmental Science and Pollution Research*, vol. 46984, no. 34, pp. 46964–17, 2021.

[22] W. N. K. Wan Ahmad, J. Rezaei, L. A. Tavasszy, and M. P. De Brito, "Commitment to and preparedness for sustainable supply chain management in the oil and gas industry," *Journal of Environmental Management*, vol. 180, pp. 202–213, 2016.

[23] S. Panda, N. M. Modak, and L. E. Cárdenas-Barrón, "Coordinating a socially responsible closed-loop supply chain with product recycling," *International Journal of Production Economics*, vol. 188, pp. 11–21, 2017.

[24] L. Dai, T. Shu, S. Chen, S. Wang, and K. K. Lai, "CSR remanufacturing supply chains under WTP differentiation," *Sustainability*, vol. 12, no. 6, p. 2197, 2020.

[25] Y. Liu and T. Xiao, "Pricing and collection rate decisions and reverse channel choice in a socially responsible supply chain with green consumers," *IEEE Transactions on Engineering Management*, vol. 67, no. 2, pp. 483–495, 2019.

[26] J. Heydari and P. Rafiei, "Integration of environmental and social responsibilities in managing supply chains: a mathematical modeling approach," *Computers & Industrial Engineering*, vol. 64, 2020.

[27] S. M. Hosseini-Motlagh, S. Ebrahimi, and R. Zirakpourdehkordi, "Coordination of dual-function acquisition price and corporate social responsibility in a sustainable closed-loop supply chain," *Journal of Cleaner Production*, vol. 34, 2020.

[28] M. Johari and S.-M. Hosseini-Motlagh, "Coordination contract for a competitive pharmaceutical supply chain considering corporate social responsibility and pricing decisions," *RAIRO - Operations Research*, vol. 54, no. 5, pp. 1515–1535, 2020.

[29] Z. Z. Wang, M. Z. Wang, and W. W. Liu, "To introduce competition or not to introduce competition: an analysis of corporate social responsibility investment collaboration in a two-echelon supply chain," *Transportation Research Part E: Logist Transp Rev*.vol. 76, 2020.

[30] L. Zhang, J. Wang, and J. You, "Consumer environmental awareness and channel coordination with two substitutable products," *European Journal of Operational Research*, vol. 241, no. 1, pp. 63–73, 2015.

[31] M. Sharma and S. Joshi, "Brand Sustainability Among Young Consumers: An AHP-TOPSIS Approach," *Young Consumers*, vol. 54, 2019.

[32] M. Ahmadi, M. Q. H. Abadi, and A. Ala, "A review of using object-orientation properties of C++ for designing expert system in strategic planning," *Computer Science Review*, vol. 37, Article ID 100282, 2020.

[33] B. Z. Niu, Q. Y. Li, and L. Chen, "Exclusive vs. competitive retailing: overseas vaccine supplier's channel selection

considering profit and social responsibility objectives," *Computers & Industrial Engineering*, vol. 34, 2020.

[34] X. T. Shi, H. L. Chan, and C. W. Dong, "Impacts of competition between buying firms on corporate social responsibility efforts: does competition do more harm than good?" *Transportation Research Part E: Logist Transp Rev*, vol. 73, 2020.

[35] M. Tyagi, P. Kumar, and D. Kumar, "Assessment of CSR based supply chain performance system using an integrated fuzzy AHP-TOPSIS approach," *International Journal of Logistics Research and Applications*, vol. 21, no. 4, pp. 378–406, 2018.

[36] S. Li, M. Li, and N. Zhou, "Pricing and coordination in a dual-channel supply chain with a socially responsible manufacturer," *PLoS One*, vol. 15, no. 7, Article ID e0236099, 2020.

[37] A. Bilbao-Terol, M. Arenas-Parra, S. Alvarez-Otero, and V. Cañal-Fernández, "Integrating corporate social responsibility and financial performance," *Management Decision*, vol. 36, 2019.

[38] G. Tian, J. Liu, Y. Gong, Q. Wang, H. Sun, and H. Chen, "Multinational companies' coordination mechanism for extending corporate social responsibility to Chinese suppliers," *Journal of Cleaner Production*, vol. 267, Article ID 121896, 2020.

[39] Y. Liu, Z. Y. Liu, and W. W. Ren, "A coordination mechanism through relational contract in a two-echelon supply chain," *Journal of Retailing and Consumer Services*, vol. 65, 2020.

[40] R. Lotfi, B. Kargar, S. H. Hoseini, S. Nazari, S. Safavi, and G. W. Weber, "Resilience and sustainable supply chain network design by considering renewable energy," *International Journal of Energy Research*, vol. 45, no. 12, pp. 17749–17766, 2021.

[41] S.-M. Hosseini-Motlagh, M. R. G. Samani, and V. Shahbazbegian, "Innovative strategy to design a mixed resilient-sustainable electricity supply chain network under uncertainty," *Applied Energy*, vol. 280, Article ID 115921, 2020.

[42] M. Ahmadi and D. Saiia, "A computational approach to uncovering economic growth factors," *Computational Economics*, vol. 58, no. 4, pp. 1051–1076, 2021.

[43] V. Lahri, K. Shaw, and A. Ishizaka, "Sustainable supply chain network design problem: using the integrated BWM, TOPSIS, possibilistic programming, and ε-constrained methods," *Expert Systems with Applications*, vol. 168, Article ID 114373, 2021.

[44] M. Eskandarpour, P. Dejax, and O. Péton, "Multi-directional local search for sustainable supply chain network design," *International Journal of Production Research*, vol. 59, no. 2, pp. 412–428, 2021.

[45] M. S. Schwartz and D. Saiia, "Should firms go "beyond profits"? Milton friedman versus broad CSR1," *Business and Society Review*, vol. 117, no. 1, pp. 1–31, 2012.

[46] D. Schawbel, "John Mackey: why companies should embrace conscious capitalism," *Forbes. January*, vol. 15, 2013.

[47] J. G. Frynas, "Corporate social responsibility in the oil and gas sector," *Journal of World Energy Law & Business*, vol. 2, no. 3, pp. 178–195, 2009.

[48] J. Van Oosterhout and P. P. Heugens, "Much ado about nothing: a conceptual critique of CSR," ERIM Report Series Reference No. ERS-2006-040-ORG, 2006.

[49] M. Mohtsham Saeed and F. Arshad, "Corporate social responsibility as a source of competitive advantage: the mediating role of social capital and reputational capital," *The Journal of Database Marketing & Customer Strategy Management*, vol. 19, no. 4, pp. 219–232, 2012.

[50] B. V. Ikejiaku, "Consideration of ethical and legal aspects of corporate social responsibility: the issue of multi-national corporations and sustainable development," 2012.

[51] A. V. Joseph, "Effectiveness of corporate social responsibility (csr) guidelines in India," Doctoral dissertation, Deakin University, Geelong, Australia, 2017.

[52] J. G. Frynas, "The false developmental promise of corporate social responsibility: evidence from multinational oil companies," *International Affairs*, vol. 81, no. 3, pp. 581–598, 2005.

[53] W. N. K. Wan Ahmad, J. Rezaei, M. P. de Brito, and L. A. Tavasszy, "The influence of external factors on supply chain sustainability goals of the oil and gas industry," *Resources Policy*, vol. 49, pp. 302–314, 2016.

[54] C. R. Carter and D. S. Rogers, "A framework of sustainable supply chain management: moving toward new theory," *International Journal of Physical Distribution & Logistics Management*, vol. 53, 2008.

[55] A. Abba Adam, N. Norhayati Zakuan, S. A. U. A. A. Usman Shettima, U. Saif, M. Ali, and R. B. Rajeh Bati Almasradi, "Supply chain sustainability practices of oil servicing firms in the downstream sector of Nigeria's oil and gas industry," *Journal of Economic Info*, vol. 6, no. 4, pp. 11–14, 2019.

[56] G. Ofori, "Greening the construction supply chain in Singapore," *European Journal of Purchasing & Supply Management*, vol. 6, no. 3-4, pp. 195–206, 2000.

[57] V. Haufler, "A public role for the private sector: industry self-regulation in a global economy," *Carnegie Endowment*, vol. 43, 2013.

[58] M. S. Florescu, E. G. Ceptureanu, A. F. Cruceru, and S. I. Ceptureanu, "Sustainable supply chain management strategy influence on supply chain management functions in the oil and gas distribution industry," *Energies*, vol. 12, no. 9, p. 1632, 2019.

[59] C. M. Chima, "Supply-chain management issues in the oil and gas industry," *Journal of Business & Economics Research*, vol. 5, no. 6, 2007.

[60] A. Ashby, "Developing closed loop supply chains for environmental sustainability: insights from a UK clothing case study," *Journal of Manufacturing Technology Management*, vol. 65, 2018.

[61] R. Lane and M. Watson, "Stewardship of things: the radical potential of product stewardship for re-framing responsibilities and relationships to products and materials," *Geoforum*, vol. 43, no. 6, pp. 1254–1265, 2012.

[62] S. P. Saeidi, S. Sofian, P. Saeidi, S. P. Saeidi, and S. A. Saaeidi, "How does corporate social responsibility contribute to firm financial performance? The mediating role of competitive advantage, reputation, and customer satisfaction," *Journal of Business Research*, vol. 68, no. 2, pp. 341–350, 2015.

[63] K. McKerlie, N. Knight, and B. Thorpe, "Advancing extended producer responsibility in Canada," *Journal of Cleaner Production*, vol. 14, no. 6-7, pp. 616–628, 2006.

[64] K. Rosselot and D. T. Allen, "Life-cycle concepts, product stewardship and green engineering," in *Green Engineering: Environmentally Conscious Design of Chemical Processes*, Prentice-Hall PTR, Upper Saddle River, NJ, USA, 2002.

[65] S. Kot, A. Haque, and A. Baloch, "Supply chain management in SMEs: global perspective," *Montenegrin Journal of Economics*, vol. 16, no. 1, pp. 87–104, 2020.

[66] R. H. Ballou, "The evolution and future of logistics and supply chain management," *European Business Review*, vol. 21, 2007.

[67] P. Ahi and C. Searcy, "A comparative literature analysis of definitions for green and sustainable supply chain management," *Journal of Cleaner Production*, vol. 52, pp. 329–341, 2013.

Hindawi
Journal of Mathematics
Volume 2023, Article ID 9815268, 1 page
https://doi.org/10.1155/2023/9815268

Retraction

Retracted: On the Temperature Indices of Molecular Structures of Some Networks

Journal of Mathematics

Received 19 December 2023; Accepted 19 December 2023; Published 20 December 2023

This article has been retracted by Hindawi following an investigation undertaken by the publisher [1]. This investigation has uncovered evidence of one or more of the following indicators of systematic manipulation of the publication process:

(1) Discrepancies in scope

(2) Discrepancies in the description of the research reported

(3) Discrepancies between the availability of data and the research described

(4) Inappropriate citations

(5) Incoherent, meaningless and/or irrelevant content included in the article

(6) Manipulated or compromised peer review

The presence of these indicators undermines our confidence in the integrity of the article's content and we cannot, therefore, vouch for its reliability. Please note that this notice is intended solely to alert readers that the content of this article is unreliable. We have not investigated whether authors were aware of or involved in the systematic manipulation of the publication process.

Wiley and Hindawi regrets that the usual quality checks did not identify these issues before publication and have since put additional measures in place to safeguard research integrity.

We wish to credit our own Research Integrity and Research Publishing teams and anonymous and named external researchers and research integrity experts for contributing to this investigation.

The corresponding author, as the representative of all authors, has been given the opportunity to register their agreement or disagreement to this retraction. We have kept a record of any response received.

References

[1] A. Jahanbani, R. Khoeilar, and M. Cancan, "On the Temperature Indices of Molecular Structures of Some Networks," *Journal of Mathematics*, vol. 2022, Article ID 4840774, 7 pages, 2022.

Hindawi
Journal of Mathematics
Volume 2022, Article ID 4840774, 7 pages
https://doi.org/10.1155/2022/4840774

Research Article

On the Temperature Indices of Molecular Structures of Some Networks

Akbar Jahanbani,[1] **Rana Khoeilar**,[1] **and Murat Cancan**[2]

[1]*Department of Mathematics, Azarbaijan Shahid Madani University, Tabriz, Iran*
[2]*Faculty of Education, Van Yuzuncu Yil University, Van, Turkey*

Correspondence should be addressed to Akbar Jahanbani; akbar.jahanbani92@gmail.com

Received 13 September 2021; Revised 23 December 2021; Accepted 3 March 2022; Published 27 April 2022

Academic Editor: Ewa Rak

The topological index is a molecular predictor that is commonly supported in the research of QSAR of pharmaceuticals to numerically quantify their molecular features. Theoretical and statistical study of drug-like compounds improves the drug design and finding workflow by rationalizing lead detection, instant decision, and mechanism of action comprehension. Using molecular structure characterization and edge segmentation technique, we computed the general temperature topological indices for OTIS networks.

1. Introduction

Mathematical chemistry may be a theoretic science in which artificial structures square measure by the employment of scientific instruments. The artificial diagram hypothesis maybe a part of this field where chart hypothesis devices square measure applied to scientifically demonstrate concoctions. As the graph has vertices that can be pictured by processor nodes and edges represent links between these nodes/processors [1]. The primary application in chemistry was the boiling purpose of the paraffin [1–3].

Topological indices are numerical values that are attributed to a molecular structure. Today, topological indices have been considered by many researchers because they have applications in various sciences, see [4–8].

Aslam et al. [9], obtained new results for OTIS networks by using some of the topological indices. Zahra et al. [3], discussed the swapped networks by using topological indices. In [10], the authors computed some of the topological indices for OTIS networks. Baig et al. [11] discussed some of the DOX and DSL networks by using the topological indices. In [6], the authors obtained some of the new results for anticancer drugs by using the multiplicative topological indices. In [12], the author discussed carbon nanocones and nanotori by using some of the topological indices. Therefore, in this paper, we obtain new results for OTIS networks by using some topological indices.

For a simple graph $\mathcal{G}$, we denoted the vertex set by $V(\mathcal{G}) = \{x_1, x_2, x_3, \ldots, x_n\}$ and the edge set by $\xi(\mathcal{G})$, $|\xi(\mathcal{G})| = \varepsilon$. The degree of the vertex $x \in V(\mathcal{G})$ is denoted by ζ_x.

For any graphs $\mathcal{G}$ with n vertices, the temperature of a vertex x is defined in [13] as

$$\psi(x) = \frac{\zeta_x}{n - \zeta_x}. \tag{1}$$

Kulli in [14] defined the following topological indices as

The general first temperature index

$$\psi_1^{\omega}(\mathcal{G}) = \sum_{xy \in \xi(\mathcal{G})} (\psi(x) + \psi(y))^{\omega}. \tag{2}$$

The general second temperature index

$$\psi_2^{\omega}(\mathcal{G}) = \sum_{xy \in \xi(\mathcal{G})} (\psi(x) \times \psi(y))^{\omega}. \tag{3}$$

The general temperature index

$$\psi_{\omega}(\mathcal{G}) = \sum_{xy \in \xi(\mathcal{G})} (\psi(x)^{\omega} + \psi(y)^{\omega}), \tag{4}$$

where $\omega \in R$.

2. Results for NP_n Network

In this section, we compute the exact formulas for the OTIS networks NP_n of some general temperature indices, and we also examine the relationships between these topologies with graphical diagrams.

Let P_n be the path of n vertices and NP_n be OTIS (swapped) network with basis network P_n, see Figure 1.

We start by computing the general first temperature index.

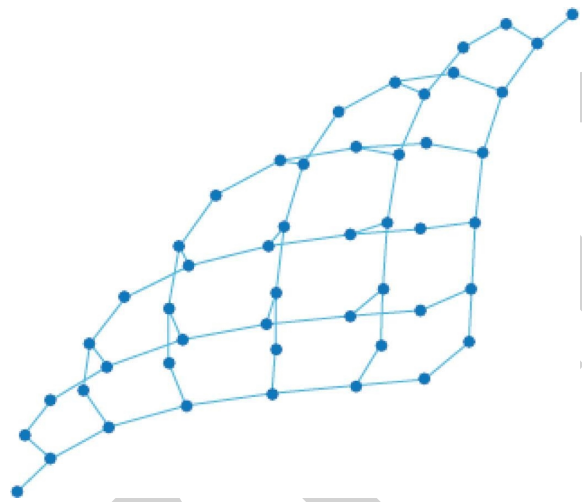

Figure 1: The graph of NP_7.

Theorem 1. *For NP_n network, we have*

$$\psi_1^{\omega}(NP_n) = 2\left(\frac{1}{n^2-1}+\frac{3}{n^2-3}\right)^{\omega} + 3\left(\frac{4}{n^2-2}\right)^{\omega} + (6n-14)\left(\frac{2}{n^2-2}+\frac{3}{n^2-3}\right)^{\omega} + \left(\frac{3(n-2)(n-3)}{2}\right)\left(\frac{6}{n^2-3}\right)^{\omega}. \tag{5}$$

Proof. The OTIS networks NP_n have n^2 vertices and $3(n^2-n)/2$, edges. Hence, there are three partitions, $V_{\{1\}} = \{y \in V(NP_n) | \zeta_y = 1\}$, $V_{\{2\}} = \{y \in V(NP_n) | \zeta_y = 2\}$ and $V_{\{3\}} = \{y \in V(NP_n) | \zeta_y = 3\}$. Hence, we can write that

$$\xi_1 = \{\varepsilon = xy \in \xi(NP_n) | \zeta_x = 1 \text{ and } \zeta_y = 3\}, \tag{6}$$

$$\xi_2 = \{\varepsilon = xy \in \xi(NP_n) | \zeta_x = 2 \text{ and } \zeta_y = 2\}, \tag{7}$$

$$\xi_3 = \{\varepsilon = xy \in \xi(NP_n) | \zeta_x = 2 \text{ and } \zeta_y = 3\}, \tag{8}$$

$$\xi_4 = \{\varepsilon = xy \in \xi(NP_n) | \zeta_x = 3 \text{ and } \zeta_y = 3\}. \tag{9}$$

It can be easily seen that $|\xi_1| = 2, |\xi_2| = 3, |\xi_3| = 6n-14$ and $|\xi_4| = 3(n-2)(n-3)/2$.

By applying the definitions and Equalities (6)–(9), we can write

$$\begin{aligned}
\psi_1^{\omega}(NP_n) &= \sum_{xy \in \xi(NP_n)} (\psi(x)+\psi(y))^{\omega} \\
&= \sum_{xy \in \xi_1(NP_n)} (\psi(x)+\psi(y))^{\omega} + \sum_{xy \in \xi_2(NP_n)} (\psi(x)+\psi(y))^{\omega} + \sum_{xy \in \xi_3(NP_n)} (\psi(x)+\psi(y))^{\omega} + \sum_{xy \in \xi_4(NP_n)} (\psi(x)+\psi(y))^{\omega} \\
&= 2\left(\frac{1}{n^2-1}+\frac{3}{n^2-3}\right)^{\omega} + 3\left(\frac{2}{n^2-2}+\frac{2}{n^2-2}\right)^{\omega} + (6n-14)\left(\frac{2}{n^2-2}+\frac{3}{n^2-3}\right)^{\omega} + \left(\frac{3(n-2)(n-3)}{2}\right)\left(\frac{3}{n^2-3}+\frac{3}{n^2-3}\right)^{\omega} \\
&= 2\left(\frac{1}{n^2-1}+\frac{3}{n^2-3}\right)^{\omega} + 3\left(\frac{4}{n^2-2}\right)^{\omega} + (6n-14) + \left(\frac{2}{n^2-2}+\frac{3}{n^2-3}\right)^{\omega} + \left(\frac{3(n-2)(n-3)}{2}\right)\left(\frac{6}{n^2-3}\right)^{\omega}.
\end{aligned} \tag{10}$$

□

Now, we compute the general second temperature index.

Theorem 2. *For NP_n network, we have*

$$\psi_2^{\omega}(NP_n) = 2\left(\frac{3}{(n^2-1)(n^2-3)}\right)^{\omega} + 3\left(\frac{4}{(n^2-2)^2}\right)^{\omega} + (6n-14)\left(\frac{6}{(n^2-2)(n^2-3)}\right)^{\omega} + \left(\frac{3(n-2)(n-3)}{2}\right)\left(\frac{9}{(n^2-3)^2}\right)^{\omega}. \tag{11}$$

Proof. By applying the definitions and equalities (6)–(9), we have

$$\begin{aligned}\psi_2^{\omega}(\mathrm{NP}_n) &= \sum_{xy\in\xi(\mathrm{NP}_n)} (\psi(x)\times\psi(y))^{\omega}\\ &= \sum_{xy\in\xi_1(\mathrm{NP}_n)} (\psi(x)\times\psi(y))^{\omega} + \sum_{xy\in\xi_2(\mathrm{NP}_n)} (\psi(x)\times\psi(y))^{\omega} + \sum_{xy\in\xi_3(\mathrm{NP}_n)} (\psi(x)\times\psi(y))^{\omega} + \sum_{xy\in\xi_4(\mathrm{NP}_n)} (\psi(x)\times\psi(y))^{\omega}\\ &= 2\left(\frac{1}{n^2-1}\times\frac{3}{n^2-3}\right)^{\omega} + 3\left(\frac{2}{n^2-2}\times\frac{2}{n^2-2}\right)^{\omega} + (6n-14)\left(\frac{2}{n^2-2}\times\frac{3}{n^2-3}\right)^{\omega} + \left(\frac{3(n-2)(n-3)}{2}\right)\left(\frac{3}{n^2-3}\times\frac{3}{n^2-3}\right)^{\omega}\\ &= 2\left(\frac{3}{(n^2-1)(n^2-3)}\right)^{\omega} + 3\left(\frac{4}{(n^2-2)^2}\right)^{\omega} + (6n-14)\left(\frac{6}{(n^2-2)(n^2-3)}\right)^{\omega} + \left(\frac{3(n-2)(n-3)}{2}\right)\left(\frac{9}{(n^2-3)^2}\right)^{\omega}.\end{aligned} \tag{12}$$

□

Here, we compute the general temperature index.

Theorem 3. *For NP_n network, we have*

$$\begin{aligned}\psi_{\omega}(\mathrm{NP}_n) = {} & 3n^2\left(\frac{3}{n^2-3}\right)^{\omega} + 6n\left(\frac{2}{n^2-2}\right)^{\omega} - 9n\left(\frac{3}{n^2-3}\right)^{\omega}\\ & + 2\left(\frac{1}{n^2-1}\right)^{\omega} + 6\left(\frac{3}{n^2-3}\right)^{\omega} - 8\left(\frac{2}{n^2-2}\right)^{\omega}.\end{aligned} \tag{13}$$

Proof. By applying the definitions and Equalities (6)–(9), we can write

$$\begin{aligned}\psi_{\omega}(\mathrm{NP}_n) &= \sum_{xy\in\xi(\mathrm{NP}_n)} \left(\psi(x)^{\omega}+\psi(y)^{\omega}\right)\\ &= \sum_{xy\in\xi_1(\mathrm{NP}_n)} \left(\psi(x)^{\omega}+\psi(y)^{\omega}\right) + \sum_{xy\in\xi_2(\mathrm{NP}_n)} \left(\psi(x)^{\omega}+\psi(y)^{\omega}\right) + \sum_{xy\in\xi_3(\mathrm{NP}_n)} \left(\psi(x)^{\omega}+\psi(y)^{\omega}\right)\\ &\quad + \sum_{xy\in\xi_4(\mathrm{NP}_n)} \left(\psi(x)^{\omega}+\psi(y)^{\omega}\right)\\ &= 2\left(\left(\frac{1}{n^2-1}\right)^{\omega}+\left(\frac{3}{n^2-3}\right)^{\omega}\right) + 3\left(\left(\frac{2}{n^2-2}\right)^{\omega}+\left(\frac{2}{n^2-2}\right)^{\omega}\right) + (6n-14)\left(\left(\frac{2}{n^2-2}\right)^{\omega}+\left(\frac{3}{n^2-3}\right)^{\omega}\right)\\ &\quad + \left(\frac{3(n-2)(n-3)}{2}\right)\left(\left(\frac{3}{n^2-3}\right)^{\omega}+\left(\frac{3}{n^2-3}\right)^{\omega}\right)\\ &= 3n^2\left(\frac{3}{n^2-3}\right)^{\omega} + 6n\left(\frac{2}{n^2-2}\right)^{\omega} - 9n\left(\frac{3}{n^2-3}\right)^{\omega} + 2\left(\frac{1}{n^2-1}\right)^{\omega} + 6\left(\frac{3}{n^2-3}\right)^{\omega} - 8\left(\frac{2}{n^2-2}\right)^{\omega}.\end{aligned} \tag{14}$$

□

3. Results for NT_t Network

The OTIS (swapped) network $\mathrm{NT_t}$ is derived from the graph Υ, which a graph with vertex set $V(\mathrm{NT}_{\Upsilon}) = \langle z, x\rangle | z, x \in V(\Upsilon)$ and edge set $\xi(\mathrm{NT}_{\Upsilon}) = \langle z, x_1\rangle, \langle z, x_2\rangle z \in V(\Upsilon)$, $(x_1, x_2) \in \xi(\mathrm{NT}_{\Upsilon}) \cup (\langle z, x\rangle, \quad \langle z, x, z\rangle) | z, x \in V(\Upsilon))$ and $z \neq x$, see Figure 2.

In this section, we obtaining new results for the OTIS networks $\mathrm{NT_t}$.

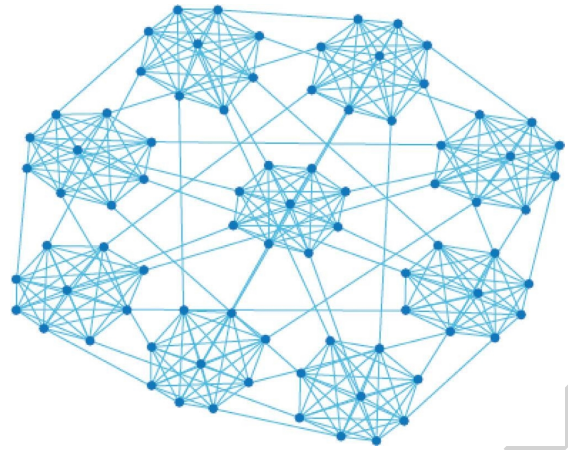

Figure 2: The graph NT_7.

Theorem 4. *For NT_t network, we have*

$$\psi_1^{\omega}(\mathrm{NT}_t) = nt\left(\frac{t}{(n+2)^2 - t} + \frac{t+1}{(n+2)^2 - t - 1}\right)^{\omega} + \frac{2^{\omega-1}(t+1)^{\omega}\left(n^2(t+1) - n(2t+1)\right)}{\left((n+2)^2 - t - 1\right)^{\omega}}. \tag{15}$$

Proof. The $\mathrm{NT_t}$ has $(n+2)^2$ vertices and $n^3/2 + 3n^2 + 11n/2 + 3$ edges. Hence, there are two partitions, $V_{\{1\}} = \{y \in V(\mathrm{NT}_t) | \zeta_y = t\}$ and $V_{\{2\}} = \{y \in V(\mathrm{NP}_n) | \zeta_y = t+1\}$. Hence, we have the following equalities:

$$\xi_1 = \{\varepsilon = xy \in \xi(\mathrm{NT}_t) | \zeta_x = t \text{ and } \zeta_y = t+1\}, \tag{16}$$

$$\xi_2 = \{\varepsilon = xy \in \xi(\mathrm{NT}_t) | \zeta_x = t+1 \text{ and } \zeta_y = t+1\}. \tag{17}$$

It can be easily seen that $|\xi_1| = nt$ and $|\xi_2| = n^2(t+1) - n(2t+1)/2$.

By applying the definitions and equalities (16) and (17), we can write

$$\begin{aligned}
\psi_1^{\omega}(\mathrm{NT}_t) &= \sum_{xy \in \xi(\mathrm{NT}_t)} (\psi(x) + \psi(y))^{\omega} \\
&= \sum_{xy \in \xi_1(\mathrm{NT}_t)} (\psi(x) + \psi(y))^{\omega} + \sum_{xy \in \xi_2(\mathrm{NT}_t)} (\psi(x) + \psi(y))^{\omega} \\
&= nt\left(\frac{t}{(n+2)^2 - t} + \frac{t+1}{(n+2)^2 - t - 1}\right)^{\omega} + \left(\frac{n^2(t+1) - n(2t+1)}{2}\right)\left(\frac{t+1}{(n+2)^2 - t - 1} + \frac{t+1}{(n+2)^2 - t - 1}\right)^{\omega} \\
&= nt\left(\frac{t}{(n+2)^2 - t} + \frac{t+1}{(n+2)^2 - t - 1}\right)^{\omega} + \left(\frac{n^2(t+1) - n(2t+1)}{2}\right)\left(\frac{2(t+1)}{(n+2)^2 - t - 1}\right)^{\omega} \\
&= nt\left(\frac{t}{(n+2)^2 - t} + \frac{t+1}{(n+2)^2 - t - 1}\right)^{\omega} + \frac{2^{\omega-1}(t+1)^{\omega}\left(n^2(t+1) - n(2t+1)\right)}{\left((n+2)^2 - t - 1\right)^{\omega}}.
\end{aligned} \tag{18}$$

□

Theorem 5. *For NT_t network, we have*

$$\psi_2^{\omega}(\mathrm{NT}_t) = nt\left(\frac{t(t+1)}{\left((n+2)^2 - t\right)\left((n+2)^2 - t - 1\right)}\right)^{\omega} + \left(\frac{n^2(t+1) - n(2t+1)}{2}\right)\left(\frac{t+1}{(n+2)^2 - t - 1}\right)^{2\omega}. \tag{19}$$

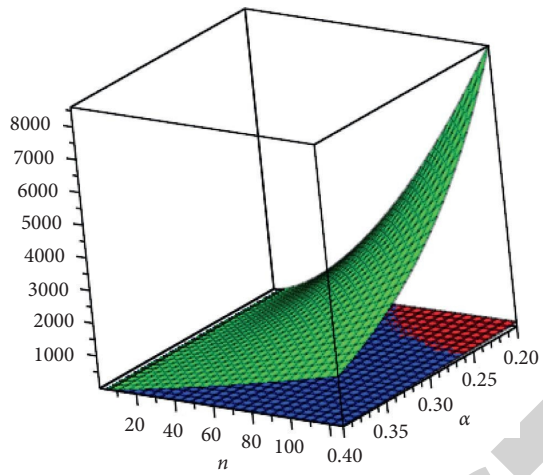

Figure 3: Comparison of $\psi_1^{\omega}, \psi_2^{\omega}$, and ψ_{ω} for NP_n.

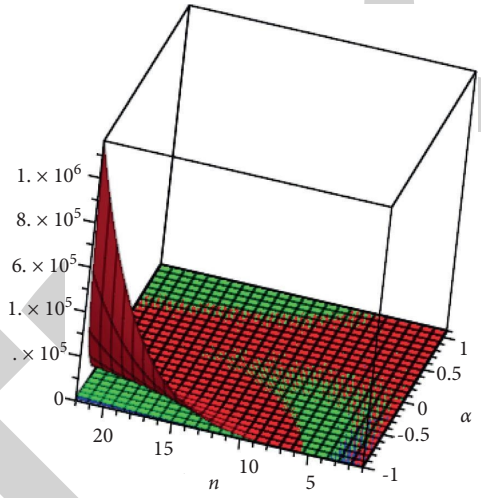

Figure 4: Comparison of $\psi_1^{\omega}, \psi_2^{\omega}$ and ψ_{ω} for NT_t.

Proof. By applying the definitions and equalities (16) and (17), we have

$$
\begin{aligned}
\psi_2^{\omega}(\mathrm{NT}_t) &= \sum_{xy\in\xi(\mathrm{NT}_t)} (\psi(x)\times\psi(y))^{\omega} \\
&= \sum_{xy\in\xi_1(\mathrm{NT}_t)} (\psi(x)\times\psi(y))^{\omega} + \sum_{xy\in\xi_2(\mathrm{NT}_t)} (\psi(x)\times\psi(y))^{\omega} \\
&= nt\left(\frac{t}{(n+2)^2-t}\times\frac{t+1}{(n+2)^2-t-1}\right)^{\omega} + \left(\frac{n^2(t+1)-n(2t+1)}{2}\right)\left(\frac{t+1}{(n+2)^2-t-1}\times\frac{t+1}{(n+2)^2-t-1}\right)^{\omega} \\
&= nt\left(\frac{t}{(n+2)^2-t}\times\frac{t+1}{(n+2)^2-t-1}\right)^{\omega} + \left(\frac{n^2(t+1)-n(2t+1)}{2}\right)\left(\frac{(t+1)^2}{\left((n+2)^2-t-1\right)^2}\right)^{\omega} \\
&= nt\left(\frac{t(t+1)}{\left((n+2)^2-t\right)\left((n+2)^2-t-1\right)}\right)^{\omega} + \left(\frac{n^2(t+1)-n(2t+1)}{2}\right)\left(\frac{t+1}{(n+2)^2-t-1}\right)^{2\omega}.
\end{aligned}
\tag{20}
$$

□

Theorem 6. *For NT_t network, we have*

$$\psi_\omega(\mathrm{NT}_t) = nt\left(\left(\frac{t}{(n+2)^2 - t}\right)^\omega + \left(\frac{t+1}{(n+2)^2 - t - 1}\right)^\omega\right) + \left(n^2(t+1) - n(2t+1)\right)\left(\frac{t+1}{(n+2)^2 - t - 1}\right)^\omega. \tag{21}$$

Proof. By applying the definitions and equalities (16) and (17), we can write

$$\begin{aligned}\psi_\omega(\mathrm{NT}_t) &= \sum_{xy\in\xi(\mathrm{NT}_t)} \left(\psi(x)^\omega + \psi(y)^\omega\right)\\ &= \sum_{xy\in\xi_1(\mathrm{NT}_t)} \left(\psi(x)^\omega + \psi(y)^\omega\right) + \sum_{xy\in\xi_2(\mathrm{NT}_t)} \left(\psi(x)^\omega + \psi(y)^\omega\right)\\ &= nt\left(\left(\frac{t}{(n+2)^2 - t}\right)^\omega + \left(\frac{t+1}{(n+2)^2 - t - 1}\right)^\omega\right) + \left(\frac{n^2(t+1) - n(2t+1)}{2}\right)\left(\left(\frac{t+1}{(n+2)^2 - t - 1}\right)^\omega + \left(\frac{t+1}{(n+2)^2 - t - 1}\right)^\omega\right)\\ &= nt\left(\left(\frac{t}{(n+2)^2 - t}\right)^\omega + \left(\frac{t+1}{(n+2)^2 - t - 1}\right)^\omega\right) + \left(n^2(t+1) - n(2t+1)\right)\left(\frac{t+1}{(n+2)^2 - t - 1}\right)^\omega.\end{aligned} \tag{22}$$

□

4. Graphical Representation and Discussion

In this paper, we discussed physical properties of some OTIS networks in terms of topological indices. The study of graphs and networks through topological descriptors area unit necessary to grasp their underlying topologies. Hence, in this paper, we computed general topological temperature indices. The graphical representations of general temperature indices of NP_n and NT_t area unit are represented in Figures 3 and 4.

5. Conclusion

In medical science, chemical, medical, biological, and pharmaceutical properties of molecular structure are essential for drug design. These properties can be studied by the topological index calculation. Hence, we have computed general topological indices of some OTIS networks such as NP_n networks and NT_t networks. We obtained the closed formulas of the general first and second temperature indices and the general temperature index for these networks. Our results can help to guess the many physical and chemical properties of networks.

Data Availability

The data involved in the examples of our manuscript are included within the article.

Disclosure

We would like to declare that the work described was original research that has not been published previously. This work was in memoriam of Dr. Rana Khoeilar, the author died prior to the submission of this paper. This is one of the last works of her.

Conflicts of Interest

The authors declare that they have no conflicts of interest.

References

[1] H. Wiener, "Structural determination of paraffin boiling points," *Journal of the American Chemical Society*, vol. 69, no. 1, pp. 17–20, 1947.

[2] G. C. Marsden, P. J. Marchand, P. Harvey, and S. C. Esener, "Optical transpose interconnection system architectures," *Optics Letters*, vol. 18, no. 13, pp. 1083–1085, 1993.

[3] N. Zahra, M. Ibrahim, and M. K. Siddiqui, "On topological indices for swapped networks modeled by optical transpose interconnection system," *IEEE Access*, vol. 8, pp. 200091–200099, 2020.

[4] Y. Gao, E. Zhu, Z. Shao, I. Gutman, and A. Klobučar, "Total domination and open packing in some chemical graphs," *Journal of Mathematical Chemistry*, vol. 56, no. 5, pp. 1481–1492, 2018.

[5] Z. Shao, P. Wu, H. Jiang, S. M. Sheikholeslami, and S. Wang, "On the maximum ABC index of bipartite graphs without pendent vertices," *Open Chemistry*, vol. 18, no. 1, pp. 39–49, 2020.

[6] Z. Shao, J. Akbar, and S. Mahmoud Sheikholeslami, "Multiplicative topological indices of molecular structure in anticancer drugs," *Polycyclic Aromatic Compounds*, vol. 42, pp. 1–15, 2020.

[7] N. Trinajstić, *Chemical Graph Theory*, CRC Press, Boca Raton, FL, USA, 1992.

[8] C. Wang, S. Wang, and B. Wei, "Cacti with extremal PI index," 2016, https://arxiv.org/abs/1603.00282.

Hindawi
Journal of Mathematics
Volume 2022, Article ID 3567824, 8 pages
https://doi.org/10.1155/2022/3567824

Research Article

Topological Indices of Families of Bistar and Corona Product of Graphs

A. Khalid,[1] N. Kausar,[2] M. Munir,[3] M. Gulistan,[4] M. M. Al-Shamiri,[5,6] and T. Lamoudan[6]

[1]*Department of Mathematics, Government Graduate College for Women, Samanabad, Lahore, Pakistan*
[2]*Yildiz Technical University, Faculty of Arts and Science, Department of Mathematics, Esenler 34210, Istanbul, Turkey*
[3]*Department of Mathematics, Government Postgraduate College, Abbottabad, Pakistan*
[4]*Department of Mathematics and Statistics, Hazara University Mansehra, Pakistan*
[5]*Department of Mathematics, Faculty of Science and Arts, Muhayl Asser, King Khalid University, Saudi Arabia*
[6]*Department of Mathematics and Computer, Faculty of Science, Ibb University, Ibb, Yemen*

Correspondence should be addressed to M. Gulistan; gulistanmath@hu.edu.pk

Received 8 August 2021; Revised 23 October 2021; Accepted 14 March 2022; Published 26 April 2022

Academic Editor: Ewa Rak

Topological indices are graph invariants that are used to correlate the physicochemical properties of a chemical compound with its (molecular) graph. In this study, we study certain degree-based topological indices such as Randić index, Zagreb indices, multiplicative Zagreb indices, Narumi–Katayama index, atom-bond connectivity index, augmented Zagreb index, geometric-arithmetic index, harmonic index, and sum-connectivity index for the bistar graphs and the corona product $K_m o K_n'$, where K_n' represents the complement of complete graph K_n.

1. Introduction

Graph theory techniques [1–4] have applications in chemistry, biology, physics, and computer science. Topological indices are graph invariants that are used to study graph topology. Along with computer networks, graph theory is a powerful tool in other research areas such as coding theory, database management systems, circuit design, secret-sharing schemes, and theoretical chemistry. Cheminformatics is the combination of technology, graph theory, and chemistry. It links organic substances structure and physiochemical properties by using some useful graph invariants and their associated molecular graph. A molecular graph contains sets of points and lines which shows the atoms and covalent bond in the molecule. These points and lines are known as vertices and edges in graph theory, respectively [5]. Theoretical study of underlying chemical structure using useful graph invariants is an appealing area of research in mathematical chemistry due to its practical applications in QSAR/QSPR investigation [6]. Topological indices are used to estimate the physicochemical properties of the chemical compounds. A topological index can be considered as a function that maps a graph to a nonnegative real number [7].

Some degree-based topological indices are Randić index, Zagreb indices, Narumi–Katayama and multiplicative Zagreb indices, atom-bond connectivity index, augmented Zagreb index, geometric-arithmetic index, harmonic index, and sum-connectivity index [8].

Throughout this work, we use standard notations $G = (V, E)$ for graph, $V(G)$ set of vertices, $E(G)$ set of edges, and $d_w(G)$ degree of vertex w in G.

For any simple graph $G = (V, E)$, $w \sim x$ denotes the adjacent vertices w and x in graph G.

Definition 1. Randić index is the most popular topological index among all topological indices and is defined as [9]

$$R(G) = \sum_{w \sim x} \frac{1}{\sqrt{d_w(G) d_x(G)}}. \quad (1)$$

Definition 2. The first Zagreb index of a graph G is defined as

$$M_1(G) = \sum_{w \in V(G)} d_w(G)^2. \quad (2)$$

The second Zagreb index of a graph G is defined as

$$M_2(G) = \sum_{w \sim x} d_w(G) d_x(G). \quad (3)$$

The first and second Zagreb index are known as Zagreb indices [10].

Definition 3. The first multiplicative Zagreb index of a graph G is defined as

$$\prod_1 (G) = \prod_{w \in V(G)} d_w(G)^2, \quad (4)$$

with product going overall vertices of a graph G.

The second multiplicative Zagreb index of a graph G is defined as

$$\prod_2 (G) = \prod_{w \sim x} d_w(G) d_x(G). \quad (5)$$

The modified first multiplicative Zagreb index of a graph G is defined as

$$\prod_1^* (G) = \prod_{w \sim x} [d_w(G) + d_x(G)]. \quad (6)$$

The first, second, and modified first multiplicative Zagreb indices are known as Narumi–Katayama indices [8, 11].

Definition 4. The atom-bond connectivity index of a graph G is defined as [12]

$$ABC(G) = \sum_{w \sim x} \sqrt{\frac{d_w(G) + d_x(G) - 2}{d_w(G) d_x(G)}}. \quad (7)$$

Definition 5. The augmented Zagreb index of a graph G is defined as [13]

$$AZI(G) = \sum_{w \sim x} \left[\frac{d_w(G) d_x(G)}{d_w(G) + d_x(G) - 2} \right]^3. \quad (8)$$

Definition 6. The geometric-arithmetic index of a graph G is defined as [14]

$$GA(G) = \sum_{w \sim x} 2 \left[\frac{\sqrt{d_w(G) d_x(G)}}{d_w(G) + d_x(G)} \right]. \quad (9)$$

Definition 7. The harmonic index of a graph G is defined as [15, 16]

$$H(G) = \sum_{w \sim x} \frac{2}{d_w(G) + d_x(G)}. \quad (10)$$

Definition 8. The sum-connectivity index of a graph G is defined as [17, 18]

$$SCI(G) = \sum_{w \sim x} \frac{1}{\sqrt{d_w(G) + d_x(G)}}. \quad (11)$$

Randić index was introduced by Milan Randić in 1975 [19]. After that, mathematicians did not pay attention to this index for nearly two decades. However, Pal, Erdos, and Bela Bollobas soon worked on this index and discovered the useful mathematics hidden within it. They published their first paper on this index in 1998. When the mathematical communities realized the value of the Randić index, they started to do research studies and soon a flood of publications on this descriptor were started. Randić also wrote two articles on this descriptor [8].

The work on Randić index encouraged theoretical chemists and mathematicians to discover other topological indices that depend on vertex degree.

During the study of total pi electron energy on molecular structure, some expressions which included the terms of the form

$$\begin{aligned} M_1(G) &= \sum_w d_w(G)^2, \\ M_2(G) &= \sum_{w \sim x} d_w(G) d_v(G), \end{aligned} \quad (12)$$

were occurred [8]. In the chemical theory, M_1 and M_2 are called first Zagreb index and second Zagreb index. These two indices were discovered by Trinajestic and Gutman in 1972 [8, 10]. At first, the first Zagreb index was also known as the Gutman index, but Balaban et al. did not want to introduce these descriptors by the names of the discoverers. So, they included M_1 and M_2 in the topological indices after 1982 and named them Zagreb group indices. However, soon, the name Zagreb group indices was changed to Zagreb indices. The second Zagreb index did not get any attention of mathematicians or mathematical chemists and that is why not a single property of M_2 was introduced in [8]. Narumi–Katayama [8] introduced the first product descriptor in 1984 and named it simple topological index. This index is defined as

$$NK(G) = \prod_{w \in V(G)} d_w(G). \quad (13)$$

This product index was later renamed the Narumi–Katayama index by Tomovic and Gutman. In 2010, Todeshine et al. proposed multiplicative versions of multiplicative Zagreb indices. These two graph invariants are known as the first and second multiplicative Zagreb indices, after Gutman. Eliasi et al. and Iranmanesh and Gutman proposed a multiplicative version of the first Zagreb index. The authors termed it as modified multiplicative Zagreb index, respectively [20].

The first geometric-arithmetic index also known as geometric-arithmetic index is the modified version of the Randić index. This index was proposed by Vukicevic and Furtula in 2009 [6, 8].

The atom-bond connectivity index is another topological index that is similar to the Randić index. This topological descriptor was introduced by Estrada et al. in 1998 [6, 13]. A recent study of this index has caught the attention of some researchers. Furtula et al. [8] introduced the augmented Zagreb index in 2009, a modified version of the atom-bond connectivity index. This descriptor has higher predictive power than the atom-bond connectivity index. Tosovic and Gutman investigated in 2013 that AZI produced nice effects in the formation of heat and also yielded the best results in boiling factors of octane isomers. Furtula et al. investigated the structure sensitivity of twelve topological indices using trees and found that the AZI has the best structure sensitivity [13].

In 1980, Siemion Fajtlowiez introduced another topological index. In 2012, Zhang worked on this index and named it as harmonic index [8]. In sharp construct to other topological indices, no chemical applications of this index were found, but in mathematical chemistry, such research studies are expected very much [8]. In the last few years, this index has attracted the great attention of theoreticians [15, 16].

Bo Zhou and Nenad Trinajstic discovered that the term $d_w d_x$ in the Randić index can be replaced by $d_w + d_x$ and named it sum-connectivity index [8]. This index got the attention of both applied and pure researchers. Some recent work on this index can be found in [21].

There are a number of studies of various topological indices of graphs establishing formulas for computing the indices and also providing upper and lower bounds on the values of such indices. In this study, certain vertex degree-based topological indices are studied. We have determined and computed the closed formulas of these indices for two special families of graphs of diameter three. A graph formed by joining the centers of two-star graphs of order m and n, i.e., $K_{1,m}$ and $K_{1,n}$ by an edge, is called the bistar graph and is denoted by $B(n;m)$. The corona product $K_m o K_n'$ of two graphs is defined as the graph obtained by taking one copy of K_m of order m and n copies of K_n' and then joining each vertex of the i^{th} copy of K_n' to the i^{th} vertex of K_m. These graphs are undirected having no loops and multiple edges. These results are novel and significant contributions in graph theory and network science, and they provide a good basis to understand the topology of these graphs and networks (Figures 1 and 2).

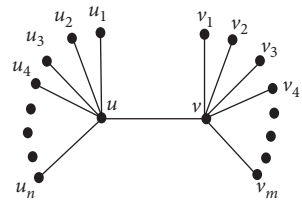

Figure 1: A representation of bistar graph $B(n;m)$ of order m and n.

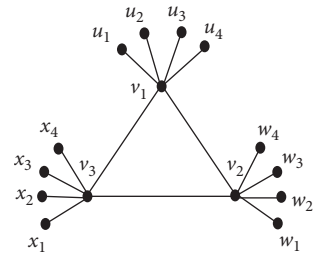

Figure 2: A representation of corona product $K_3 \circ K_4'$ of two graphs.

2. Topological Indices of Families of Bistar Graphs, i.e., $G = B(n;m)$

By looking at the earlier results for computing the topological indices for families of bistar graphs, here we introduce new degree-based topological indices to compute their values for these families of graphs.

Theorem 1. *The sum-connectivity index of families of bistar graphs $B(n;m)$ is*

$$\frac{n}{\sqrt{n+2}} + \frac{1}{\sqrt{n+m+2}} + \frac{m}{\sqrt{m+2}}. \tag{14}$$

Proof. To find the sum-connectivity index of $B(n;m)$, firstly, we select a vertex u on $B(n;m)$ of degree $n+1$. There are n vertices $u_1, u_2, \ldots, u_n$ of degree 1 which are adjacent to u. For the vertices u and u_i, where $i = 1, 2, 3, \ldots, n$, the sum is obtained as

$$\begin{aligned} \sum_{u \sim u_i} \frac{1}{\sqrt{d_u(G) + d_{u_i}(G)}} &= \frac{n}{\sqrt{1+(n+1)}} \\ &= \frac{n}{\sqrt{n+2}}, \quad i = 1, 2, 3, \ldots, n. \end{aligned} \tag{15}$$

Since the degree of u is $n+1$, the other vertex which is adjacent to u is v of degree $m+1$. For the vertices u and v, we have

$$\begin{aligned} \frac{1}{\sqrt{d_u(G) + d_v(G)}} &= \frac{1}{\sqrt{(n+1)+(m+1)}} \\ &= \frac{1}{\sqrt{n+m+2}}. \end{aligned} \tag{16}$$

Now, we select a vertex v of degree $m+1$ on $B(n;m)$; there are m vertices $v_1, v_2, v_3, \ldots, v_m$ of degree 1 which are adjacent to v. For the vertices v and v_j, the sum is obtained as

$$\begin{aligned} \sum_{v \sim v_j} \frac{1}{\sqrt{d_v(G) + d_{v_j(G)}}} &= \frac{m}{\sqrt{1+m+1}} \\ &= \frac{m}{\sqrt{m+2}}, \quad j = 1, 2, 3, \ldots, m. \end{aligned} \tag{17}$$

Adding above equations, we have $SCI(G)$ = sum-connectivity index of $B(n;m)$:

$$\frac{n}{\sqrt{n+2}}+\frac{1}{\sqrt{n+m+2}}+\frac{m}{\sqrt{m+2}}. \tag{18}$$

□

Theorem 2. *The Zagreb indices of the families of bistar graphs $B(n;m)$ are*

$$\begin{aligned} M_1(G) &= (n+1)^2+(m+1)^2+n+m,\\ M_2(G) &= n(n+1)+(n+1)(m+1)+m(m+1). \end{aligned} \tag{19}$$

Proof. To find the first Zagreb index $M_1(G)$ of $B(n;m)$, we select a vertex u on $B(n;m)$ of degree $n+1$. For the vertex u, we have

$$\deg(u)^2=(n+1)^2. \tag{20}$$

Since there are n vertices $u_1,u_2,u_3,\ldots,u_n$ of $B(n;m)$ of degree 1 which are adjacent to u, thus, we have

$$\sum_{u_i}\deg(u_i)^2=n,\quad i=1,2,3,\ldots,n. \tag{21}$$

As the degree of u is $n+1$, the other vertex which is adjacent to u is v of degree $m+1$. For the vertex v, we have

$$\deg(v)^2=(n+1)^2. \tag{22}$$

Since the degree of v is $m+1$, the other vertices which are adjacent to v are m in numbers of degree 1:

$$\sum_{v_j}\deg\left(v_j\right)^2=m,\quad j=1,2,3,\ldots,m. \tag{23}$$

Adding equations (20) to (23), we have $M_1(G)$ = first Zagreb index of $B(n;m)$:

$$M_1(G)=(n+1)^2+(m+1)^2+n+m. \tag{24}$$

Similarly, $M_2(G)$ = second Zagreb index of $B(n;m)$ is

$$M_2(G)=n.(n+1)+(n+1)(m+1)+m(m+1). \tag{25}$$

□

Theorem 3. *The atom-bond connectivity index and augmented Zagreb index of families of bistar graphs $B(n;m)$ are*

$$\begin{aligned} &n\sqrt{\frac{n}{n+1}}+\sqrt{\frac{n+m}{(n+1)(m+1)}}+m\sqrt{\frac{m}{m+1}},\\ &n\left[\frac{n+1}{n}\right]^3+\left[\frac{(n+1)(m+1)}{n+m}\right]^3+m\left[\frac{m+1}{m}\right]^3. \end{aligned} \tag{26}$$

The proof of this Theorem is the same as Theorem 1.

Theorem 4. *The geometric-arithmetic index and harmonic index of families of bistar graphs $B(n;m)$ are*

$$\begin{aligned} &\frac{2n\sqrt{n+1}}{n+2}+\frac{2\sqrt{(n+1)(m+1)}}{n+m+2}+\frac{2m\sqrt{m+1}}{m+2},\\ &\frac{2n}{n+2}+\frac{2}{n+m+2}+\frac{2m}{m+2}. \end{aligned} \tag{27}$$

The proof of this theorem is the same as Theorem 1.

Theorem 5. *The Narumi–Katayama and multiplicative Zagreb indices of families of bistar graphs $B(n;m)$ are*

$$\begin{aligned} \prod_1(G) &= (n+1)^2(m+1)^2,\\ \prod_2(G) &= (n+1)^{n+1}(m+1)^{m+1},\\ \prod_1^*(G) &= (n+2)^n(n+m+2)(m+2)^m. \end{aligned} \tag{28}$$

Proof. To find the first multiplicative Zagreb index of $B(n;m)$, we select a vertex u on $B(n;m)$ of degree $n+1$. For the vertex u, we have

$$\deg(u)^2=(n+1)^2. \tag{29}$$

Since there are n vertices $u_1,u_2,u_3,\ldots,u_n$ of $B(n;m)$ of degree 1, thus, we have

$$\prod_{u_i}\deg(u_i)^2=\deg(u_1)^2\deg(u_2)^2,\ldots,\deg(u_n)^2=1. \tag{30}$$

Similarly, for the vertex v, we have

$$\deg(v)^2=(m+1)^2. \tag{31}$$

Also, for the vertices $v_1,v_2,v_3,\ldots,v_m$ of $B(n;m)$ of degree 1, we have

$$\prod_{v_j}\deg\left(v_j\right)^2=\deg(v_1)^2\deg(v_2)^2,\ldots,\deg(v_m)^2=1. \tag{32}$$

Multiplying equations (29) to (32), we have $\prod_1(G)$ = first multiplicative Zagreb index of families of bistar graphs $B(n;m)$:

$$\prod_1(G)=(n+1)^2(m+1)^2. \tag{33}$$

Similarly, second multiplicative Zagreb index and modified first multiplicative Zagreb index of families of bistar graphs are

$$\begin{aligned} \prod_2(G) &= (n+1)^{n+1}(m+1)^{m+1},\\ \prod_1^*(G) &= (n+2)^n(n+m+2)(m+2)^m. \end{aligned} \tag{34}$$

□

Example 1. Topological indices of bistar graph $B(5;6)$ are shown in Table 1.

Table 1: Topological indices of $G = B(5;6)$.

$SCI(G)$	4.288
$R(G)$	4.463
$GA(G)$	8.465
$ABC(G)$	10.631
$M_1(G)$	96
$\prod_1(G)$	1764

3. Topological Indices of Families of Corona Product of Graphs, i.e., $G = K_m \circ \mathbf{K'_n}$

Based on previous results for computing topological indices for families of corona product of graphs, we present new degree-based topological indices to compute their values for these families of graphs.

Theorem 6. *The Randić index and sum-connectivity index of families of corona product of graphs $K_m \circ K'_n$ are*

$$R(G) = \frac{mn}{\sqrt{m+n-1}} + \frac{m(m-1)}{2(m+n-1)},$$
$$SCI(G) = \frac{mn}{\sqrt{m+n}} + \frac{m(m-1)}{2\sqrt{2(m+n-1)}}. \tag{35}$$

Proof. To find the Randić index of the family of graphs $K_m \circ \mathrm{K}'_\mathrm{n}$ obtained by taking the corona product of complete graph K_m of order m and the complement of K_n of order n, firstly, we select a vertex v_1 on $K_m \circ \mathrm{K}'_\mathrm{n}$ as v_1 is adjacent to $m-1$ vertices $v_2, v_3, v_4, \ldots, v_m$ and n vertices $u_1, u_2, u_3, \ldots, u_n$. Therefore, the degree of v_1 is $m+n-1$.

For the vertices v_1 and u_i, where $i = 1, 2, 3, \ldots, n$, the sum is obtained as

$$\sum_{v_1 \sim u_i} \frac{1}{\sqrt{\deg_{v_1}(G)\deg_{u_i(G)}}} = \frac{n}{\sqrt{m+n-1}}. \tag{36}$$

As the graph is symmetric, the same result is obtained for the remaining $(m-1)$ vertices $v_2, v_3, \ldots, v_m$. So, combining all the vertices $v_1, v_2, v_3, \ldots, v_m$ equation (36) becomes

$$\sum_{v_1 \sim u_i} \frac{1}{\sqrt{\deg_{v_1}(G)\deg_{u_i(G)}}} + \sum_{v_2 \sim w_i} \frac{1}{\sqrt{\deg_{v_2}(G)\deg_{w_i(G)}}} + \cdots + \sum_{v_m \sim x_i} \frac{1}{\sqrt{\deg_{v_m}(G)\deg_{x_i(G)}}} = \frac{mn}{\sqrt{(m+n-1)}}\ m \text{ times}. \tag{37}$$

Since v_1 is also adjacent to $m-1$ vertices $v_2, v_3, v_4, \ldots, v_m$ of degree $m+n-1$, for the vertices v_1 and v_j, where $j = 2, 3, 4, \ldots, m$, the sum is obtained as

$$\sum_{v_1 \sim v_j} \frac{1}{\sqrt{d_{v_1}(G)d_{v_j}(G)}} = \frac{m-1}{m+n-1}. \tag{38}$$

Since K_m is symmetric, the same result is obtained for remaining $m-1$ vertices $v_2, v_3, \ldots, v_m$. Combining the result for all m vertices $v_1, v_2, v_3, \ldots, v_m$, we have

$$\begin{aligned}
&= \frac{m-1}{m+n-1} + \frac{m-2}{m+n-1} + \frac{m-3}{m+n-1} + \cdots + \frac{m-(m-1)}{m+n-1} \\
&= \frac{1}{m+n-1}\left[(m-1) + (m-2) + (m-3) + \cdots + (m-(m-1))\right] \\
&= \frac{1}{m+n-1}\left[(m+m+m+, \ldots, +m)\,(m-1)\text{times} - (1+2+3+, \ldots, +m-1)\right] \\
&= \frac{1}{m+n-1}\left[m(m-1) - \frac{(m-1)(m-1+1)}{2}\right] \\
&= \frac{1}{m+n-1}\left[m(m-1) - \frac{m(m-1)}{2}\right] \\
&= \frac{1}{m+n-1}\left[\frac{m(m-1)}{2}\right].
\end{aligned} \tag{39}$$

Adding equations (37) and (39), we have $R(G)$ = Randić index of $K_m \circ \mathrm{K}'_\mathrm{n}$:

$$R(G) = \frac{mn}{\sqrt{m+n-1}} + \frac{m(m-1)}{2(m+n-1)}. \tag{40}$$

Similarly, $SCI(G)$ = sum-connectivity index of $K_m \circ \mathrm{K}'_\mathrm{n}$ is

$$SCI(G) = \frac{mn}{\sqrt{m+n}} + \frac{m(m-1)}{2\sqrt{2(m+n-1)}}. \tag{41}$$

□

Theorem 7. *The atom-bond connectivity index and augmented Zagreb index of families of corona product of graphs $K_m \circ K'_n$ are*

$$\begin{aligned}
ABC(G) &= mn\sqrt{\frac{m+n-2}{m+n-1}} + \frac{m(m-1)}{2(m+n-1)}\sqrt{2m+2n-4}, \\
AZI(G) &= mn\left(\frac{m+n-1}{m+n-2}\right)^3 + \frac{m(m-1)(m+n-1)^6}{2(2m+2n-4)^3}.
\end{aligned} \tag{42}$$

The proof of this theorem is the same as Theorem 6.

Theorem 8. *The geometric-arithmetic index and harmonic index of families of corona product of graphs $K_m \circ K'_n$ are*

$$GA(G) = \frac{2mn\sqrt{m+n-1}}{m+n} + \frac{m(m-1)(m+n-1)}{2m+2n-2},$$
$$H(G) = \frac{2mn}{m+n} + \frac{m(m-1)}{2m+2n-2}. \tag{43}$$

The proof of this theorem is the same as Theorem 6.

Theorem 9. *The Zagreb indices of families of corona product of graphs $K_m \circ K_n'$ are*

$$M_1(G) = mn + m(m+n-1)^2,$$
$$M_2(G) = mn(m+n-1) + \frac{m(m-1)(m+n-1)^2}{2}. \tag{44}$$

Proof. For the families of corona product of graphs there are mn vertices of degree one and m vertices $v_1, v_2, v_3, \ldots, v_m$ of degree $m+n-1$, respectively. For the vertices $u_1, u_2, u_3, \ldots, u_n$, we have

$$\sum_{u_i} \deg(u_i)^2 = \deg(u_1)^2 + \deg(u_2)^2 + \cdots + \deg(u_n)^2, \quad i = 1, 2, 3, \ldots, n$$
$$= (1)^2 + (1)^2, \ldots, + (1)^2 \, n \text{ times} = n. \tag{45}$$

Since there are mn vertices of degree 1, combining the above result for all mn vertices, thus, the above equation becomes

$$= n + n + n + \cdots + n \, m \text{ times} = mn. \tag{46}$$

Also, for the vertex v_1, we have

$$\deg(v_1)^2 = (m+n-1)^2. \tag{47}$$

Since the graph is symmetric, the same result is obtained for remaining $(m-1)$ vertices $v_2, v_3, \ldots, v_m$:

$$\sum_{v_j} \deg(v_j)^2 = \deg(v_1)^2 + \deg(v_2)^2 + \cdots + \deg(v_m)^2, \quad j = 1, 2, 3, \ldots, m$$
$$= (m+n-1)^2 + (m+n-1)^2 + \cdots + (m+n-1)^2 \, m \text{ times}$$
$$= m(m+n-1)^2. \tag{48}$$

Adding equations (46) and (48), we have $M_1(G) =$ first Zagreb index of families of corona product of graphs $K_m \circ K_n'$:

$$M_1(G) = mn + m(m+n-1)^2. \tag{49}$$

Similarly, $M_2(G) =$ second Zagreb index of families of corona product of graphs $K_m \circ K_n'$:

$$M_2(G) = mn(m+n-1) + \frac{m(m-1)(m+n-1)^2}{2}. \tag{50}$$

□

Theorem 10. *The Narumi–Katayama and multiplicative Zagreb indices of families of corona product of graphs $K_m \circ K_n'$ are*

$$\prod_1 (G) = (m+n-1)^{2m},$$
$$\prod_2 (G) = (m+n-1)^{m^2-m+mn},$$
$$\prod_1^* (G) = (m+n)^{mn}(2m+2n-2)^{m^2-m/2}. \tag{51}$$

Proof. For the families of corona product of graphs, there are mn vertices of degree one and m vertices $v_1, v_2, v_3, \ldots, v_m$ of degree $m+n-1$. For the vertices $u_1, u_2, u_3, \ldots, u_n$, we have

$$\prod_{u_i} \deg(u_i)^2 = \deg(u_1)^2 \deg$$
$$(u_2)^2, \ldots, \deg(u_n)^2, \quad i = 1, 2, 3, \ldots, n$$
$$= (1)^2 (1)^2, \ldots, (1)^2 \, n \text{ times} = (1)^n = 1. \tag{52}$$

Since there are mn vertices of degree 1, so the same result is obtained for all mn vertices. Thus, the above equation becomes

$$(1)^{mn} = 1. \tag{53}$$

Also, for the vertex v_1, we have

$$\deg(v_1)^2 = (m+n-1)^2. \tag{54}$$

Since the graph is symmetric the same result is obtained for remaining $(m-1)$ vertices $v_2, v_3, \ldots, v_m$. Thus equation (54) becomes

Table 2: Topological indices of $G = K_6 \circ \mathrm{K}_3'$.

$\prod_1(G)$	6, 8710000000
$H(G)$	5.875
$SCI(G)$	9.750
$R(G)$	8.239
$GA(G)$	26.314
$ABC(G)$	23.853
$M_1(G)$	402

$$\prod_{v_j} \deg(v_j)^2 = \deg(v_1)^2 \deg(v_2)^2 \deg(v_3)^2, \ldots, \deg(v_m)^2, \quad j = 1, 2, 3, \ldots, m$$
$$= (m+n-1)^2 (m+n-1)^2 (m+n-1)^2, \ldots, (m+n-1)^2 m \text{ times} = (m+n-1)^{2m}. \tag{55}$$

Multiplying equations (53) to (55), we have $\prod_1(G)$ = first Zagreb index of families of corona product of graphs $K_m \circ \mathrm{K}_n'$

$$\prod_1(G) = (1).(m+n-1)^{2m} = (m+n-1)^{2m}. \tag{56}$$

Similarly, second multiplicative Zagreb index and modified first multiplicative Zagreb index of $K_m \circ \mathrm{K}_n'$ are

$$\prod_2(G) = (m+n-1)^{m^2-m+mn},$$
$$\prod_1^*(G) = (m+n)^{mn}(2m+2n-2)^{m^2-m/2}. \tag{57}$$

□

Example 2. Topological indices of corona product of graphs $K_6 \circ \mathrm{K}_3'$ are shown in Table 2.

4. Concluding Remarks

There are several articles published on calculating topological indices for different families of graphs. Some have found applications, but others were devoted to the mathematical side to throw more light on the relationship between these concepts. This study introduces Randić index, Zagreb indices, Narumi–Katayama, and multiplicative Zagreb indices. We further discussed the atom-bond connectivity index, augmented Zagreb index, geometric-arithmetic index, harmonic index, and sum-connectivity index for two particular families of graphs for the first time. We have determined and computed the closed formulas of these families of graphs. We had checked that all vertex degree-based topological indices of families of bistar graphs and corona product of graphs remain the same for all values of m and n. We have also determined the values of some topological indices for $B(5;6)$ and $K_6 \circ \mathrm{K}_3'$ graphs, as shown in Tables 1 and 2. This work will give new directions for considering and computing topological indices of several other families of graphs. In the future, we are interested in investigating and calculating some other topological indices of two more special families of graphs whose diameters are greater than three.

Data Availability

No data were used to support this study.

Conflicts of Interest

The authors declare that there are no conflicts of interest regarding the publication of this article.

Authors' Contributions

All authors have contributed equally in the preparation of this manuscript.

Acknowledgments

The authors express their appreciation to the Deanship of Scientific Research at King Khalid University for funding this work through the public research project, under Grant no. R.G.P.1/258/43.

References

[1] H. Rashmanlou, G. Muhiuddin, S. Amanathulla, F. Mofidnakhaei, and M. Pal, "A study on cubic graphs with novel application," *Journal of Intelligent and Fuzzy Systems*, vol. 40, no. 1, pp. 89–101, 2021.

[2] S. Amanathulla, G. Muhiuddin, D. Al-Kadi, and M. Pal, "Distance two surjective labelling of paths and interval graphs," *Discrete Dynamics in Nature and Society*, vol. 2021, 2021.

[3] G. Muhiuddin, N. Sridharan, D. Al-Kadi, S. Amutha, and M. Elnair, "Reinforcement number of a graph with respect to half-domination," *Journal of Mathematics*, vol. 2021, pp. 2314–4629, 2021.

[4] T. Pramanik, G. Muhiuddin, A. M. Alanazi, and M. Pal, "An extension of fuzzy competition graph and its uses in manufacturing industries," *Mathematics*, vol. 8, p. 6, 2020.

[5] M. Asif, M. Hussain, H. Almohamedh, K. M. Alhamed, and S. Almotairi, "An approach to the extremal inverse degree index for families of graphs with transformation effect," *Journal of Chemistry*, vol. 2021, 2020.

[6] X. Zuo, J. Liu, I. Hifza, K. Ali, and S. T. Raza Rizvi, "Topological indices of certain transformed chemical structures," *Journal of Chemistry*, vol. 2020, 2020.

[7] V. Shigehalli and R. Kanabur, "Computation of new degree-based topological indices of graphene," *Journal of Mathematics*, vol. 2016, pp. 2314–4629, 2016.

[8] F. Deng, X. Zhang, M. Alaeiyan, A. Mehboob, and M. Reza Farahani, "Topological indices of the Pent-Heptagonal

nanosheets VC_5C_7 and HC_5C_7," *Advances in Materials Science and Engineering*, vol. 12, 2019.

[9] A. M. Hanan Ahmed, A. Alwardi, and M. R. Salestina, "On domination topological indices of graphs," *International Journal of Analysis and Applications*, vol. 19, pp. 47–64, 2021.

[10] D. S. Nandappa, M. R. R. Kanna, and P. R. Kumar, "Narumi-Katayama and multiplicative Zagreb indices of Dutch windmill graph," *International Journal of Scientific Engineering and Research*, vol. 7, pp. 32-33, 2016.

[11] K. Das, I. Gutman, and B. Furtula, "On atom-bond connectivity index," *Filomat*, vol. 26, no. 4, pp. 733–738, 2012.

[12] A. Ali, B. Furtula, I. Gutman, and D. Vukiccevic, "Augmented Zagreb index: extremal results and bounds," *MATCH Communications in Mathematical and in Computer Chemistry*, vol. 85, pp. 211–244, 2021.

[13] E. D. Molina, J. M. Rodriguez, J. L. Sanchez, and J. M. Sigarreta, "Some properties of the arithmetic-geometric index," vol. 13, 2021.

[14] L. Zhong, "The harmonic index for graphs," *Applied Mathematics Letters*, vol. 25, pp. 561–566, 2021.

[15] B. S. Shetty, V. Lokesha, and P. S. Ranjini, "On the harmonic index of graph operations," *Transactions on combinatorics*, vol. 4, pp. 5–14, 2015.

[16] Z. Du and B. Zhou, "On sum-connectivity index of bicyclic graphs," *Bulletin of the Malaysian Mathematical Sciences Society*, vol. 35, pp. 101–117, 2012.

[17] H. S. Ramane, V. V. Manjalapur, and I. Gutman, "General sum-connectivity index, general product-connectivity index, general Zagreb index and coindices of line graph of subdivision graphs," *AKCE International Journal of Graphs and Combinatorics*, vol. 14, no. 1, pp. 92–100, 2017.

[18] X. Li and Y. Shi, "A survey on the Randić index," *MATCH Communications in Mathematical and in Computer Chemistry*, vol. 59, pp. 127–156, 2008.

[19] B. Basavanagoud and S. Patil, "Multiplicative Zagreb indices and coindices of some derived graphs," *Opuscula Mathematica*, vol. 36, no. 3, pp. 287–299, 2016.

[20] J. Chen and S. Li, "On the sum-connectivity index of unicyclic graphs with k pendent vertices," *Mathematical Communications*, vol. 16, pp. 359–368, 2011.

[21] N. Thomas, L. Mathew, S. Sriram, A. K. Nagar, and K. Subramanian, "Certain distance-based topological indices of parikh word representable graphs," *Journal of Mathematics*, vol. 2021, pp. 2314–4629, 2021.

Hindawi
Journal of Mathematics
Volume 2024, Article ID 9761318, 1 page
https://doi.org/10.1155/2024/9761318

Retraction

Retracted: Research on the Prediction of Port Economic Synergy Development Trend Based on Deep Neural Networks

Journal of Mathematics

Received 23 January 2024; Accepted 23 January 2024; Published 24 January 2024

This article has been retracted by Hindawi following an investigation undertaken by the publisher [1]. This investigation has uncovered evidence of one or more of the following indicators of systematic manipulation of the publication process:

(1) Discrepancies in scope

(2) Discrepancies in the description of the research reported

(3) Discrepancies between the availability of data and the research described

(4) Inappropriate citations

(5) Incoherent, meaningless and/or irrelevant content included in the article

(6) Manipulated or compromised peer review

The presence of these indicators undermines our confidence in the integrity of the article's content and we cannot, therefore, vouch for its reliability. Please note that this notice is intended solely to alert readers that the content of this article is unreliable. We have not investigated whether authors were aware of or involved in the systematic manipulation of the publication process.

Wiley and Hindawi regrets that the usual quality checks did not identify these issues before publication and have since put additional measures in place to safeguard research integrity.

We wish to credit our own Research Integrity and Research Publishing teams and anonymous and named external researchers and research integrity experts for contributing to this investigation.

The corresponding author, as the representative of all authors, has been given the opportunity to register their agreement or disagreement to this retraction. We have kept a record of any response received.

References

[1] A. Zha and J. Tu, "Research on the Prediction of Port Economic Synergy Development Trend Based on Deep Neural Networks," *Journal of Mathematics*, vol. 2022, Article ID 8052957, 9 pages, 2022.

Hindawi
Journal of Mathematics
Volume 2022, Article ID 8052957, 9 pages
https://doi.org/10.1155/2022/8052957

Research Article

Research on the Prediction of Port Economic Synergy Development Trend Based on Deep Neural Networks

Anping Zha and Jianjun Tu

Maritime College, Guang Dong Communication Polytechnic, Guangzhou 510800, China

Correspondence should be addressed to Anping Zha; zap091x@gdcp.edu.cn

Received 24 November 2021; Revised 16 December 2021; Accepted 20 December 2021; Published 23 April 2022

Academic Editor: Naeem Jan

After entering the new century, along with the further deepening of global economic and trade cooperation, the industrial division of labor has been newly developed globally, which brings the cooperation among countries in the international logistics chain more and more closely. As the core node linking domestic and foreign water transportation, ports play a very key role in the international logistics chain and have an extremely central position in the national logistics planning. The coordinated development of port economy is an important part of the economic development planning of port cities, and it is also the premise and basis for the comprehensive planning of port logistics infrastructure construction scale, logistics space layout, and port city logistics development direction and function positioning. Therefore, according to the availability of realistic data, this paper establishes a deep neural network prediction model for the collaborative development of ports and uses various port logistics indicators to predict the economic development trend, so as to realize a nonlinear mapping relationship between the level of port economic development and the side of port logistics demand. Meanwhile, the research of this paper will provide theoretical basis and corresponding practical tools for the coordinated development between regional economy and port logistics industry.

1. Introduction

With the renewal of management concept and the deepening of the change of production and manufacturing mode, modern logistics industry is getting more and more attention in the world [1]. Especially after China's accession to WTO, foreign trade has been further enhanced and the prosperity of the market economy has accelerated the rapid development of its distribution industry, which has gradually developed into an important part of the national economy and an economic growth point. In coastal ports and some large central cities, the port economy has even leaped to become a local pillar industry, while a logistics boom has been set off nationwide [2].

The history of port development shows that the port has gradually changed from being a single transportation transit point to a modern logistics service center and it plays an increasingly important role in the economic development of the port city and the region radiated by the port [3]. As a key node connecting the outside world in a country or region, ports naturally have the advantages of clusters in terms of geographical conditions. In recent years, theoretical research and practical development of port-related industrial clusters have made great progress [4]. The development of port-side industry economy brings great influence on the development of port logistics. At present, the more mature division of port-side industries divides port-side industries into port-side core industries, port-side related industries, port-side hinterland industries, and port-side derived industries. The related industries are mainly the logistics creation, storage, processing, and transportation industries directly connected with the port, which is the port logistics industry [5]. There is a close relationship between the port logistics industry and the port economy. The cluster development of the port logistics industry provides a new power engine for the port economy, while the development of the port economy provides a solid foundation for the cluster development of the port logistics industry [6].

With the continuous progress of technology, especially the breakthrough of AI technology, deep learning has been widely used in various fields and industries, promoting industrial innovation and breakthrough development [7]. In the economic and financial fields, people are also increasingly aware of the importance of economic data to the industry, which is an important basis for policy makers and industry practitioners to effectively feel the changes in industrial and economic development. As the volume of economic data increases dramatically and the forms of data become more and more diverse, the approach of deep learning provides a new research idea of finding patterns in big data and learning the potential features behind the data through deep learning models [8]. Therefore, it is of great importance to apply deep learning to the industrial economy.

The purpose of this article is to adapt the port logistics supply to the needs of coordinating with the actual development of the regional economy of the port hinterland and to conduct a prediction study of the port logistics demand from the perspective of port cities' planning of port logistics combined with the economic development of the port. By analyzing the economic influencing factors of port logistics demand, the strong correlation between the level of port economic development and logistics demand is pointed out. According to the availability of realistic data, a deep neural network prediction model of port economic development trend is established to realize a nonlinear mapping relationship between the level of port economic development and port logistics demand. Meanwhile, it is also hoped that this paper can provide a new research direction and a reference for the development of port economy.

Furthermore, Section 2 of this paper proposes a comprehensive review of the related work and literature. It analyzes the port economy and its correlation with hinterland regional economy, drivers of economic growth in ports. This section also presents the steps for the economic development of the ports. In Section 2, the existing methods and the proposed methods are explained. It deeply discusses the RNN, GRU, and LSTM. Furthermore, it proposes the attentional model and a recurrent neural network model on the basis of dual attention mechanism and trend adjustment. Section 4 performs the experiments and analyzes the achieved results. The conclusion of the paper is given in Section 5.

2. Related Work

2.1. Port Economic Analysis. Port economic synergy development analysis refers to the process of correlating the logistics demand of the port and its hinterland with the socioeconomic activities of production and consumption demand [9]. As port logistics activities increasingly penetrate into the whole process of socioeconomic activities such as production, circulation, and consumption, they are closely related to the development of the social economy, especially the port hinterland, and are an important part of the socioeconomic activities of the port and the hinterland. Therefore, there is a close correlation between the synergistic development of port economy and socioeconomic development, and the socio-economic development of port cities and hinterland is the main factor affecting the economic activities of ports [10]. Port economic synergistic development analysis is to understand the demand intensity of port and hinterland socioeconomic activities for the supply of port logistics capacity with the help of qualitative and quantitative analysis tools and to carry out effective demand management. Guiding social investment into the service areas radiated by the port in a purposeful manner will be conducive to rational planning, construction of port logistics infrastructure, and improvement of the supply system of port logistics.

2.2. Analysis of the Correlation between Port Economy and Hinterland Regional Economy. There is an interactive relationship between the port economy and the economic development of the hinterland [11]. The prosperity of the hinterland promotes the demand for port logistics that relies on the hinterland. In turn, the development of the port logistics economy will also promote the development of the hinterland that depends on the port. The development of ports and hinterlands is interdependent and mutually reinforcing. The port not only provides transportation services for the hinterland, but more importantly, it has a strong radiation effect on the hinterland, and there seems to be a natural blood relationship between it and the hinterland region. The hinterland of the port can absorb and gather landward economic energy through the land transportation network, and it can more easily transcend the spatial boundaries of geography through the sea channel and directly participate in the international economic cycle in a large span, absorbing and gathering the factors of productivity in the world. Using the advantages of port transportation, we can vigorously develop import and export trade and processing trade, promote the integration of the hinterland and the world economy, drive the development of the hinterland economy, and make the development of the hinterland economy more vital. While the port promotes the economic development of the hinterland, the development of the hinterland also provides support and guarantee for the development of the port. The hinterland provides financial, trade, consolidation, and distribution services for the port. The development of the hinterland economy constantly makes changes in the types of goods in the port and also makes corresponding changes in the function strategy, service scope, production characteristics, and status role of the port.

2.3. Analysis of the Drivers of Economic Growth in Ports. The total economic volume of the port and hinterland, the regional industrial structure, and the spatial distribution of the port and hinterland economies have a huge impact on the port economy [12]. Port logistics demand is an important driving force for port economic development, and it can be said that the factors affecting port economic development also potentially affect the growth or reduction of port logistics demand [13]. There is an inherent and implicit mapping relationship between the economy and logistics demand. But, this relationship is not a simple linear relationship, because there are many economic factors and each factor may cause a certain degree of impact on logistics demand, so it is difficult

to use a simple and clear model to describe this relationship. However, this intrinsic determining and driving relationship between the regional economy and port logistics demand can be described abstractly by a mathematical expression, as shown in the following:

$$Y = Af\left(x_1, x_2, x_3, \ldots, x_n\right) \tag{1}$$

where Y indicates the logistics demand, including logistics demand scale, logistics demand structure, logistics demand main body, etc. $x_1, x_2, x_3, \ldots, x_n$ represent a series of regional economic factors such as total regional economy, industrial structure status, regional economic spatial distribution, etc. From this functional relationship, we can see that the economic influence of port logistics is multifaceted and each economic factor may have an impact on all aspects of logistics demand, while the impact of each economic factor on the growth of logistics demand is not equally important and the focus of the impact on logistics demand is not the same, so this intricate internal linkage determines the multifaceted nonlinear complex mapping relationship between the economy and logistics demand.

2.4. Forecasting Steps for Port Economic Development

2.4.1. Determining the Purpose of Forecasting. Clearly defining the goal of forecasting is the premise of effective forecasting with a clear forecast objective to collect information in a targeted manner; otherwise, it is impossible to determine what to investigate, to whom to investigate, and not to mention how to make forecasts. At the same time, the forecast target is determined as detailed and quantitative as possible, which is conducive to the smooth development of forecasting work.

2.4.2. Analyzing the Factors Influencing the Market Demand of the Logistics System. The analysis of controllable and uncontrollable factors in the system is crucial. For different systems, controllable and uncontrollable factors are different. The same type of system has different controllable and uncontrollable factors depending on its geographical, social, and political environment, and often some factors are controllable in one system while it is uncontrollable in another system. Objective analysis of the main elements of the port logistics system and the main factors affecting market demand is the basis for forecasting.

2.4.3. Determining the Content of the Forecast. Forecasters must recognize the potential impact of different factors on logistics demand and be able to deal with them appropriately. For a particular project, significant components must be identified, analyzed, and combined with appropriate forecasting techniques. The information from the research should be analyzed statistically. The information is analyzed statistically to understand whether the information is complete. Then, the characteristics of the information and data are analyzed, and the sample data are corrected.

2.4.4. Establishing Mathematical Models for Forecasting. In the forecasting of economic systems, the use of quantitative forecasting methods is a necessary means to achieve objective and scientific forecasting. The establishment of forecasting models is not only related to historical data but also to the level of modeling of the forecaster. Both traditional forecasting methods and deep learning-based forecasting methods require a thorough understanding of forecasting theory and forecasting models. The nonlinear nature of the economic system often increases the difficulty of the mathematical model building work, and the determination of the fitting curve is difficult. To overcome the difficulties in building the model, a deep neural network forecasting model is used for forecasting in this paper and the model is modified accordingly.

2.4.5. Calculating the Results and Making Error Analysis Correction. Error analysis is an important part to ensure the prediction accuracy, and the error between the predicted value of the model and the value of the sample data is often used to measure whether the prediction model is good or bad in the prediction process. There are always errors in systematic forecasting, and the errors are caused by various reasons. Some are caused by the model itself, for example, the model always lags the actual value, so the forecast results should be added to the lag amount to make the forecast more accurate. Some errors are caused by changes in the external environment, so we should analyze the future economic and political situation in depth, analyze the future impact factors and give their quantitative values, and use the quantitative values to correct the model's prediction values.

3. Method

3.1. Existing Recurrent Neural Network Models

3.1.1. Recurrent Neural Networks (RNNs). For traditional neural networks, there is no temporal association between inputs, whereas for human thinking, economic forecasting, etc., temporal association is crucial.

But, traditional neural networks and machine learning methods are unable to do this, and recurrent neural networks solve this problem.

The full name of RNN is recurrent neural network [14], which allows information to be passed from one step of the network to the next step of the network, as shown in Figure 1. This chained structure has a natural advantage for data with certain temporal connections, and as you can see from the figure, the output of the current moment can be influenced by all previous moments. If imagined as a reading comprehension problem, this means that the understanding of this text when reading the current position is influenced by the previous fragments and this structure is able to represent this influence.

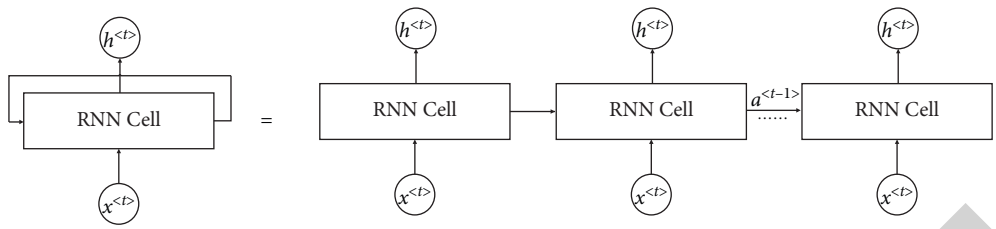

Figure 1: Structure of RNN.

Traditional neural networks have several obvious limitations [15]: one is that the input and output of traditional neural networks are too limited, requiring a fixed length of input and a fixed length of output. Second, these models use a fixed number of computational steps, such as the number of layers in traditional neural networks, and third, the learned knowledge of traditional neural networks is not shared. However, recurrent neural networks change this limitation by allowing us to operate on sequences of vectors, with variable-length sequences for both input and output, and a portion of the learned information can be quickly generalized to the entire network. The recurrent neural network scans the data from left to right and the parameters are shared at each time step. The forward propagation algorithm of the recurrent neural network is shown in equation (2). Forward propagation is done from left to right as shown in Figure 2:

$$\begin{aligned} a^{\langle t \rangle} &= g_1\left(W_{aa}a^{\langle t-1 \rangle} + W_{ax}x^{\langle t \rangle} + b_a\right), \\ h^{\langle t \rangle} &= g_1\left(W_{ha}a^{\langle t \rangle} + b_h\right). \end{aligned} \tag{2}$$

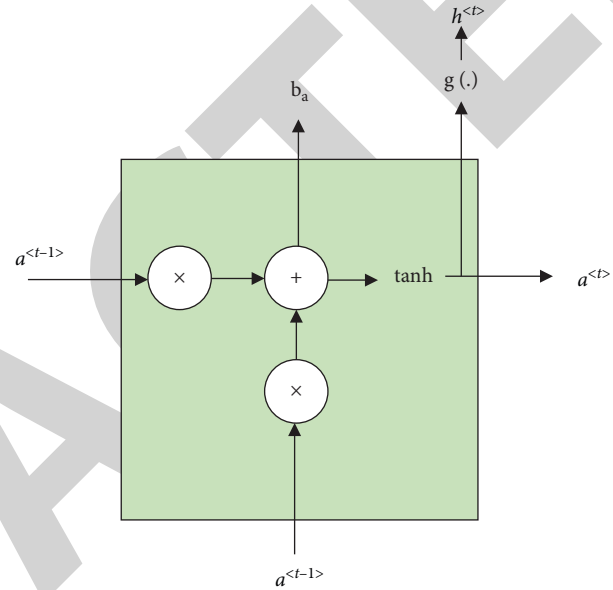

Figure 2: Inside structure of RNN.

Although recurrent neural networks have good performance for sequential models, there is a big problem with recurrent neural networks, which is the problem of gradient disappearance. To solve this problem, gated recurrent units that change the propagation structure inside the RNN are available.

3.1.2. Gated Circulation Unit (GRU). The purpose of GRU is to solve the problem of gradient disappearance and to allow the model to have long-time memory [16]. The internal structure of the simplified gated neural network is shown in Figure 3, and its formula is shown in equation (4). The GRU introduces a new variable c, which means memory cell, to provide the memory capability of the model. The core idea of the GRU is to have an update gate, and the output of the update gate has a value between 0 and 1 due to the use of the sigmoid activation function. But, its probability of being close to 0 or close to 1 is higher, so that Γ_u acts like a gate to decide whether the current input needs to be remembered or not.

$$\begin{aligned} \tilde{c}^{\langle t \rangle} &= \tanh\left(W_c\left[c^{\langle t-1 \rangle}, x^{\langle t \rangle} + b_c\right)\right., \\ \Gamma_u &= \sigma\left(W_u\left[c^{\langle t-1 \rangle}, x^{\langle t \rangle}\right] + b_u\right), \\ c^{\langle t \rangle} &= \Gamma_u * \tilde{c}^{\langle t \rangle} + \left(1 - \Gamma_u\right) * c^{\langle t-1 \rangle}. \end{aligned} \tag{3}$$

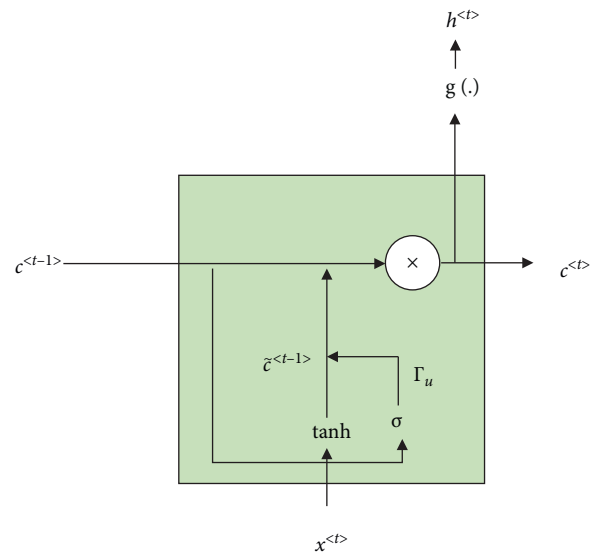

Figure 3: Inside structure of simplified GRU.

3.1.3. Long Short-Term Memory Network (LSTM). LSTM is another more common type of recurrent neural networks [17] and a more powerful and general version than GRU. In LSTM, there is still an update gate Γ_u. A new feature of LSTM is that instead of having only one update gate for control, a

new gate called forgetting gate is added, denoted by Γ_f and then a new output gate Γ_o. At this point, the update value of the memory cell is changed to $c^{\langle t\rangle} = \Gamma_u * c^{\sim<t>} + \Gamma_f * c^{\langle t-1\rangle}$ and the complete equation of LSTM is shown as follows:

$$\begin{aligned}
\widetilde{c}^{\langle t\rangle} &= \tanh\left(W_c\left[c^{\langle t-1\rangle}, x^{\langle t\rangle} + b_c\right)\right),\\
\Gamma_u &= \sigma\left(W_u\left[c^{\langle t-1\rangle}, x^{\langle t\rangle}\right] + b_u\right),\\
\Gamma_f &= \sigma\left(W_f\left[c^{\langle t-1\rangle}, x^{\langle t\rangle}\right] + b_f\right),\\
\Gamma_o &= \sigma\left(W_o\left[c^{\langle t-1\rangle}, x^{\langle t\rangle}\right] + b_o\right),\\
c^{\langle t\rangle} &= \Gamma_u * \widetilde{c}^{\langle t\rangle} + \Gamma_f * c^{\langle t-1\rangle},\\
a^{\langle t\rangle} &= \Gamma_o * c^{\langle t\rangle}.
\end{aligned} \tag{4}$$

3.2. Attentional Model

3.2.1. Code-Decoder Architecture. For the encoder-decoder model, it is most common to get a fixed dimensional vector c given the input sequence $x = (x^{\langle t\rangle}, \ldots, x^{\langle T\rangle})$, as shown in

$$\begin{aligned}
h^{\langle t\rangle} &= f\left(x^{\langle t\rangle}, h^{\langle t-1\rangle}\right),\\
c &= q\left(\left\{h^{\langle 1\rangle}, \ldots, h^{\langle T\rangle}\right\}\right),
\end{aligned} \tag{5}$$

where $h^{\langle t\rangle} \in R^n$ is the hidden layer output at moment t. c is obtained from T hidden layer outputs by some transformation. Both f, q denote nonlinear methods, and there are also various choices. For example, f can be chosen as the internal structure of RNN or the internal structure of LSTM, and q can be chosen directly as the last hidden layer output, or all outputs can be stitched.

The encoder stage is an RNN that reads the input sequence sequentially, and the state of the hidden layer is updated after each reading of the current input. When the input sequence is read at the end, the hidden layer of the RNN finally encodes the whole input sequence as a c-vector. The decoder is another recurrent neural network, and $y^{\langle t\rangle}$ and $h^{\langle t\rangle}$ are determined not only by y^{t-1} but also by the final output c of the encoder. Therefore, the hidden layer of the decoder stage at moment t is calculated as shown in equation (6) and the conditional distribution probability when the result $y^{\langle t\rangle}$ is obtained in the decoding stage is shown in equation (7). The encoder-decoder model diagram is shown in Figure 4.where f and g are the activation functions and the output of the g activation function is the probability value.

$$h^{\langle t\rangle} = f\left(h^{\langle t-1\rangle}, y^{\langle t-1\rangle}, c\right), \tag{6}$$

$$P\left(y^{\langle t\rangle} | y^{\langle t-1\rangle}, y^{\langle t-2\rangle}, \ldots, y^{\langle 1\rangle}, c\right) = g\left(h^{\langle t\rangle}, y^{\langle t-1\rangle}, c\right), \tag{7}$$

The encoder has to compress the whole input sequence into a c-vector, which means that some part of the information must be missing in the compression process and therefore the accuracy is somewhat affected. To reduce this impact, thus the attention mechanism is introduced [18]. The difference between the attention model and the classical encoder-decoder model is that the encoding stage is not compressed into just a c-vector but generates a sequence of vectors, as shown in Figure 5.

3.3. A Recurrent Neural Network Model Based on Dual Attention Mechanism and Trend Adjustment. The goal of port economic trend forecasting is to forecast future economic trends by means of diverse eigenvalues (influencing factors) and known economic indicators. The formula for port economic forecasting is much like that for autoregressive forecasting, where the input is defined as the entire set of features $\{x_t\}_{t=1}^{T} = \{x_1, x_2, \ldots, x_T\}$ with the corresponding set of economic indicators as $\{y_t\}_{t=1}^{T} = \{y_1, y_2, \ldots, y_T\}$. At time t, $x_t \in R^n$, where n is the dimension of the feature and T is the entire time stage. The output of the economic trend forecast is the next Δ values of economic indicators after T time stages, which can be expressed as follows: $\{\widehat{y}_t\}_{t=T+1}^{T+\Delta} = \{\widehat{y}_{T+1}, \widehat{y}_{T+2}, \ldots, \widehat{y}_{T+\Delta}\}$, where Δ is determined by the target of the economic trend forecast, assuming that $\Delta \ll T$ and $\{x_t\}_{t=T+1}^{T+\Delta}$ are unknown factors in the forecast stage.

Time series models with features behave differently than traditional autoregressive models for economic trend forecasting because the scalar values we want to predict and in the future are uncharacteristic. Therefore, we model the forecasting of economic indicators with features.

$$\{\widehat{y}_t\}_{t=T+1}^{T+\Delta} = F\left(\{x_t\}_{t=1}^{T}, \{y_t\}_{t=1}^{T}\right), \tag{8}$$

where $\{x_t\}_{t=1}^{T}$ is the feature from time 1 to T. $\{y_t\}_{t=1}^{T}$ is the historical economic information. $\{\widehat{y}_t\}_{t=T+1}^{T+\Delta}$ is the value to be predicted. F is the mapping method of the nonlinearity to be learned.

For economic forecasting, internal and external characteristics are two different semantic features in terms of time series forecasting. That is, there is a significant difference in the way internal and external features affect economic forecasting. The formula $\{x_t^{\text{int}}\}_{t=1}^{T}$ is used for internal features. External features are represented using $\{x_t^{\text{ext}}\}_{t=1}^{T}$. Internal characteristics are information about intrinsic attributes that are directly related to the port economy, such as the location of the port and the type of industries surrounding the port. External features are information on attributes external to the external influences, such as the weather conditions of the year and fluctuations in overseas economies. Therefore, a single LSTM encoder structure may lose part of the contextual information due to mapping of all the original features into a uniform space. Therefore, we use two parallel LSTMs to efficiently capture the different ways of feature influence by modeling the internal and external features as two separate subtasks. Accordingly, we extend the problem formulation in equation (8) to the following equation:

$$\{\widehat{y}_t\}_{t=T+1}^{T+\Delta} = F\left(\left\{x_t^{\text{int}}\right\}_{t=1}^{T}, \left\{x_t^{\text{ext}}\right\}_{t=1}^{T}, \{y_t\}_{t=1}^{T}\right). \tag{9}$$

The structure of the encoding phase of the recurrent neural network model based on the dual attention mechanism and trend adjustment is shown in Figure 6.

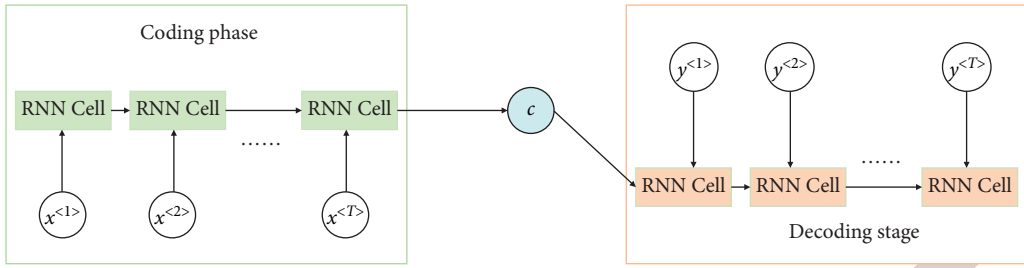

Figure 4: Structure of the encoder-decoder model.

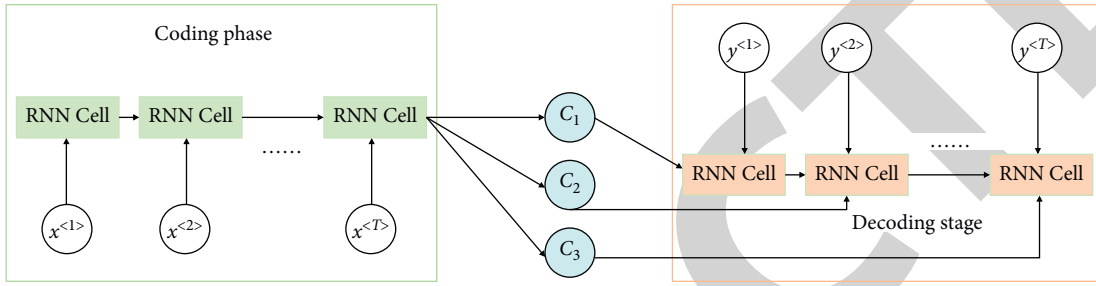

Figure 5: Structure of the attention model.

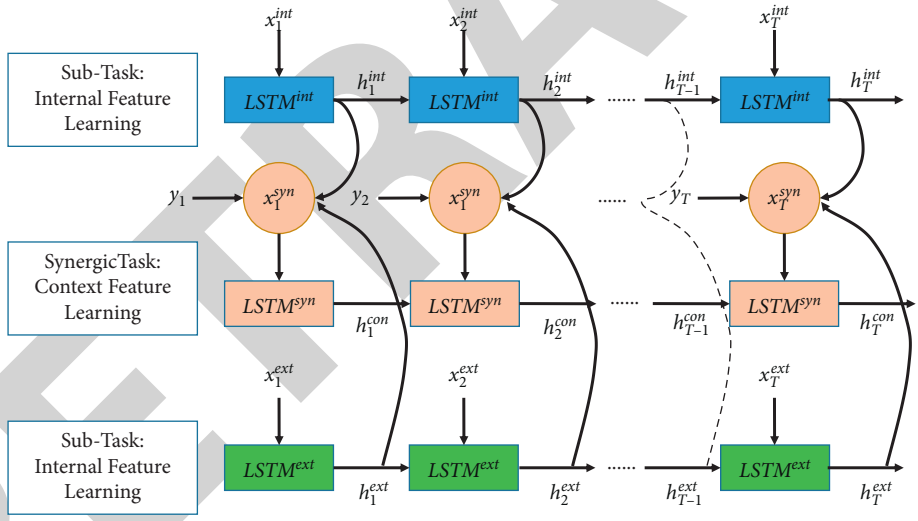

Figure 6: Structure of multitask LSTM encoder.

We use $\{h_t^{\text{int}}\}_{t=1}^{T}$ and $\{h_t^{\text{ext}}\}_{t=1}^{T}$ to denote the final representation learned from $\{x_t^{\text{int}}\}_{t=1}^{T}$ internal feature input and $\{x_t^{\text{ext}}\}_{t=1}^{T}$ external feature input, respectively. Thus, the encoder for multitasking can be expressed as

$$\begin{aligned}\left\{h_t^{\text{int}}\right\} &= \text{LSTM}^{\text{int}}\left(x_t^{\text{int}}, h_{t-1}^{\text{int}}\right),\\ \left\{h_t^{\text{ext}}\right\} &= \text{LSTM}^{\text{ext}}\left(x_t^{\text{ext}}, h_{t-1}^{\text{ext}}\right),\\ \left\{h_t^{\text{con}}\right\} &= \text{LSTM}^{\text{syn}}\left(x_t^{\text{syn}}, h_{t-1}^{\text{con}}\right).\end{aligned} \tag{10}$$

The internal feature-encoded LSTM, the external feature-encoded LSTM, and the joint LSTM encoder are different LSTMs that do not share weights and offsets, but each trip of the LSTM can learn its own weights and offsets.

The decoding stage diagram of the recurrent neural network model with dual attention mechanism and trend adjustment is shown in Figure 7.

The formula for decoding based on the attention mechanism is shown in

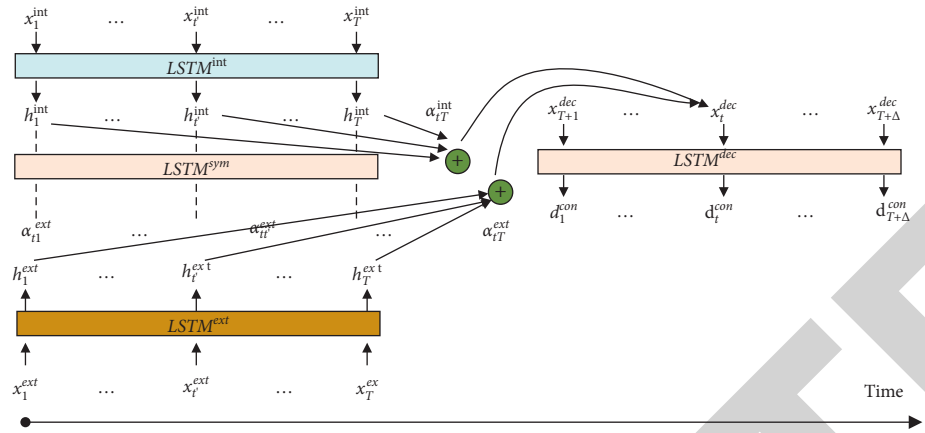

Figure 7: Demonstration of attention mechanism for weighted input mapping.

$$
\begin{aligned}
x_t^{\mathrm{dec}} &= W_{\mathrm{dec}}\left[\sum_{t'=1}^{T}\alpha_{tt'}^{\mathrm{int}}h_{t'}^{\mathrm{int}};\sum_{t'=1}^{T}\alpha_{tt'}^{\mathrm{ext}}h_{t'}^{\mathrm{ext}}\right]+b_{\mathrm{dec}},\\
e_{tt'}^{\mathrm{int}} &= v_{\mathrm{int}}^{T}\tanh\left(M_{\mathrm{int}}d_{t-1}^{\mathrm{con}}+H_{\mathrm{int}}h_{t'}^{\mathrm{int}}\right),\\
e_{tt'}^{\mathrm{ext}} &= v_{\mathrm{ext}}^{T}\tanh\left(M_{\mathrm{ext}}d_{t-1}^{\mathrm{con}}+H_{\mathrm{ext}}h_{t'}^{\mathrm{ext}}\right),\\
\alpha_{tt'}^{\mathrm{int}} &= \frac{\exp\left(e_{tt'}^{\mathrm{int}}\right)}{\sum_{s}^{T}\exp\left(e_{ts}^{\mathrm{int}}\right)},\\
\alpha_{tt'}^{\mathrm{ext}} &= \frac{\exp\left(e_{tt'}^{\mathrm{ext}}\right)}{\sum_{s}^{T}\exp\left(e_{ts}^{\mathrm{ext}}\right)},
\end{aligned}
\tag{11}
$$

where $e_{tt'}^{\mathrm{int}}$ and $e_{tt'}^{\mathrm{ext}}$ correspond to the correlation scores of the hidden layer output of the internal feature LSTM and the hidden layer output of the external feature LSTM and d_{t-1}^{con} at moment t', respectively. Among them, v_{int}^{T}, v_{ext}^{T}, M_{int}, H_{int}, and H_{ext} are the parameters to be learned by the model.

4. Experiments and Results

The port logistics subsystem is divided into input and output indicators, and we have selected container throughput, cargo throughput, length of production quay, and number of production berths as sequential parameters. The regional economic subsystem is divided into total indicators, structural indicators, trade indicators, and investment indicators, as shown in Table 1.

The degree of synergy between port logistics and regional economic system at time t is expressed by Y_t. Here, Y_t is between 0 and 1. The closer the value of Y_t is to 1, the higher the degree of synergy between the regional economic subsystem and the port logistics subsystem. On the contrary, the closer Y_t is to 0, the lower the degree of synergy between the two. It is calculated as shown in

$$
\begin{aligned}
C &= 2\sqrt{\frac{\left(X_1^t\times X_2^t\right)}{\left(X_1^t+X_2^t\right)^2}},\\
F &= \frac{\left(X_1^t+X_2^t\right)}{2},\\
Y_t &= \sqrt{C\times F}.
\end{aligned}
\tag{12}
$$

X_1^t and X_2^t are the orderliness of the regional economic system and the port logistics system at moment t. The combined level of coordination between the development degree of the port logistics system and the regional economic system is represented by C. The combined level of the port logistics system and the regional economic system at the moment t is expressed by F.

The criteria for classifying the grade of synergy between port logistics and regional economy are shown in Table 2.

This paper is based on publicly available data from a port and the hinterland city where it is located. Using the proposed recurrent neural network model based on the double attention mechanism and trend adjustment, the weights of the sequential covariates of the port logistics system and the hinterland economic system and the orderliness of the sequential covariates are trained. The trend of a port logistics and its hinterland economic orderliness and the integrated synergistic trend are obtained, as shown in Figures 8–10.

The comprehensive synergy degree of port logistics and regional economy is largely on the rise, and when the orderly degree of port logistics develops in the same direction as the orderly degree of regional economy, the comprehensive synergy degree is also on the trend of development. The prediction model presented in this paper is generally consistent with the real data trend.

Table 1: Evaluation index system of synergy between port logistics and regional economy.

System metrics	Criteria metrics	Sequential covariance (units)	Sequential covariance orderliness
Port logistics indicators	Input indicators	Number of berths of production terminals/length of production terminals	X_{11}
			X_{12}
	Output indicators	Cargo throughput/container throughput	X_{13}
			X_{14}
	Total volume indicators	GDP and fiscal revenue	X_{15}
			X_{16}
Regional economic indicators	Structural indicators	Primary industry added value/secondary industry added value/tertiary industry added value	X_{17}
			X_{18}
			X_{19}
	Trade indicators	Total import and export of goods/total retail sales of social consumer goods	X_{20}
			X_{21}
	Investment indicators	Total social fixed asset investment	X_{22}
		Total investment in foreign-invested enterprises	X_{23}

Table 2: Criteria for grading the synergy between port logistics and regional economy.

Y_t	(0, 0.5)	(0.5, 0.7)	(0.7, 0.9)	(0.9, 1)
Level	Low synergy	Medium synergy	High synergy	Extreme synergy

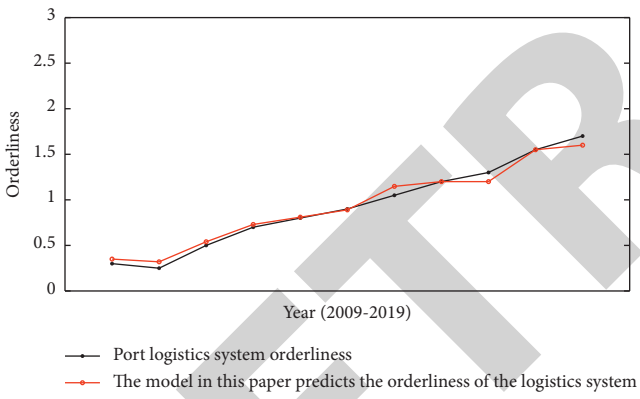

Figure 8: Port logistics orderliness forecast.

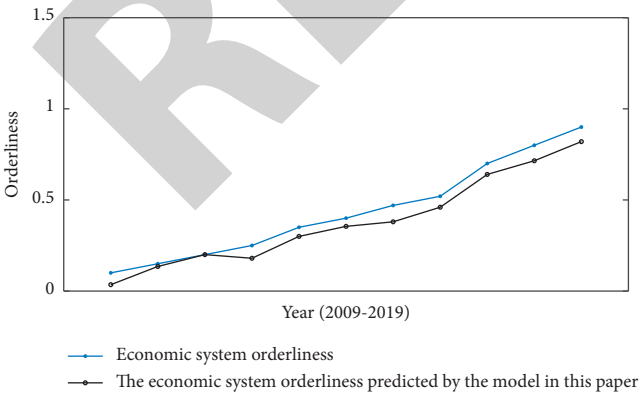

Figure 9: Economic orderliness of the hinterland city where the port is located.

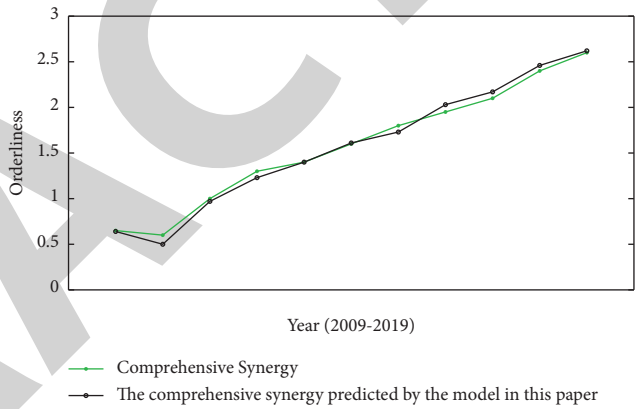

Figure 10: Port and regional economy comprehensive coordination degree.

5. Conclusion

The foundation for logistics planning and construction in port area cities is the port logistics [19]. Therefore, the development trend of port regional economy and its research are practically significant [20]. Thus, in this paper, the analysis was carried out for the characteristics and main contents of port logistics forecasting and economic forecasting of the region where the port is located. This analysis was based on the basic theory of port regional economy and forecasting theory. Hence, we proposed a prediction method based on deep neural network to establish a neural network prediction model that meets the needs of the port regional economy. The results proved the applicability of the model and the feasibility of the method. Because there are many factors influencing the port economy, we have selected a few important indicator factors with focus and the follow-up can be done from improving the network model or adding more indicator factors to study the synergistic development of the port regional economy in depth.

Hindawi
Journal of Mathematics
Volume 2022, Article ID 2347294, 10 pages
https://doi.org/10.1155/2022/2347294

Research Article

On Nonunique Fixed Point Theorems via Interpolative Chatterjea Type Suzuki Contraction in Quasi-Partial b-Metric Space

Pragati Gautam,[1] **Shiv Raj Singh**,[2] **Santosh Kumar**,[3] **and Swapnil Verma**[1]

[1]*Department of Mathematics, Kamala Nehru College, University of Delhi, August Kranti Marg, New Delhi 110049, India*
[2]*Department of Mathematics, C.C.S University, Meerut, India*
[3]*Department of Mathematics, College of Natural and Applied Sciences, University of Dar es Salaam, Dar es Salaam, Tanzania*

Correspondence should be addressed to Santosh Kumar; drsengar2002@gmail.com

Received 7 December 2021; Revised 31 January 2022; Accepted 2 February 2022; Published 13 April 2022

Academic Editor: Naeem Jan

In the present research paper, Chatterjea type contraction is defined and discussed in the framework of quasi-partial b-metric space. Further, some common fixed point results are proved using the notion of interpolation. The results are extended to fixed point theorems for modified Chatterjea type Suzuki contraction using w-admissible maps. The results proved are new and unique supported by application which will enrich the existing literature.

1. Introduction and Preliminaries

In 1922, Banach [1] gave one of the important result called Banach contraction principle and discussed its importance in metric fixed point theory, i.e., let H be a self map on a nonempty set G and (G, d) be a complete metric space. If there exists a constant $\kappa \in [0, 1)$ such that

$$d(H\sigma, H\upsilon) \leq \kappa\, d(\sigma, \upsilon), \quad \text{for all } \sigma, \upsilon \in G, \tag{1}$$

then it possesses a unique fixed point in G. Afterwards, many generalizations of Banach contraction principle came in the literature (see [2–4]) In 1968, Kannan [5] removed the continuity property from this principle and defined a new variant.

Theorem 1 (see [5]). *Let (G, d) be a complete metric space and a self map $T: G \longrightarrow G$ be a Kannan contraction mapping, i.e.,*

$$d(T\sigma, T\upsilon) \leq \varrho[d(\sigma, T\sigma) + d(\upsilon, T\upsilon)], \tag{2}$$

for all $\sigma, \upsilon \in G$, where $\varrho \in [0, 1/2)$. Then, T admits a unique fixed point in G.

In 1972, Chatterjea [6] generalized the contraction mapping on a complete metric space which is stated as follows.

Theorem 2 (see [6]). *Let (G, d) be a complete metric space. A self map $T: G \longrightarrow G$ be a Chatterjea type contraction. If*

$$d(T\sigma, T\upsilon) \leq \varrho[d(\sigma, T\upsilon) + d(\upsilon, T\sigma)], \tag{3}$$

for all $\sigma, \upsilon \in G$, where $\varrho \in (0, 1/2)$, then T has a unique fixed point.

In 2015, quasi-partial metric space was generalized by Gupta and Gautam [7] to quasi-partial b-metric space. In 2018, Karapinar [8] enriched the concept of interpolation and established a new contraction known as interpolative Kannan-type contractive mapping.

Theorem 3 (see [8]). *Let (G, d) be a metric space; a self mapping $T: G \longrightarrow G$ is said to be an interpolative Kannan-type contraction map if there exist a constant $\varrho \in (0, 1)$ and $\alpha \in (0, 1)$ such that*

$$d(T\sigma, T\upsilon) \leq \varrho[d(\sigma, T\sigma)]^{\alpha} \cdot [d(\upsilon, T\upsilon)]^{1-\alpha}, \quad \text{for all } \sigma, \upsilon \in G \setminus Fix(T), \tag{4}$$

where $Fix(T) = \{z \in G: Tz = z\}$.

Numerous studies have been done on interpolation inequalities in the literature. Many new research papers based on the concept of interpolation came into existence (for example, see [9–11]). Noorwali [12], in the year 2019, extended the Kannan interpolative contraction by proving common fixed point result for two self maps. Several authors [9, 13–25] have contributed immensely to enrich this field.

Definition 1 (see [26]). A quasi-partial metric on a non-empty set G is a function $qp: G \times G \longrightarrow \mathbb{R}^+$ such that for all $\sigma, \upsilon, \epsilon \in G$:

(1) $qp(\sigma,\sigma) = qp(\sigma,\upsilon) = qp(\upsilon,\upsilon)$ implies $\sigma = \upsilon$
(2) $qp(\sigma,\sigma) \le qp(\sigma,\upsilon)$
(3) $qp(\sigma,\sigma) \le qp(\upsilon,\sigma)$
(4) $qp(\sigma,\upsilon) \le [qp(\sigma,\epsilon) + qp(\epsilon,\upsilon)] - qp(\epsilon,\epsilon)$

The pair (G, qp) is called a quasi-partial metric space.

Definition 2 (see [7]). A quasi-partial b-metric on a non-empty set G is a function $qp_b: G \times G \longrightarrow \mathbb{R}^+$ such that for some real number $s \ge 1$ and all $\sigma, \upsilon, \epsilon \in G$:

(1) $qp_b(\sigma,\sigma) = qp_b(\sigma,\upsilon) = qp_b(\upsilon,\upsilon)$ implies $\sigma = \upsilon$
(2) $qp_b(\sigma,\sigma) \le qp_b(\sigma,\upsilon)$
(3) $qp_b(\sigma,\sigma) \le qp_b(\upsilon,\sigma)$
(4) $qp_b(\sigma,\upsilon) \le s[qp_b(\sigma,\epsilon) + qp_b(\epsilon,\upsilon)] - qp_b(\epsilon,\epsilon)$

The pair (G, qp_b) is called a quasi-partial b-metric space. The number s is called the coefficient of (G, qp_b). Let qp_b be a quasi-partial b-metric on the set G. Then,

$$d_{qp_b}(\sigma,\upsilon) = qp_b(\sigma,\upsilon) + qp_b(\upsilon,\sigma) - qp_b(\sigma,\sigma) - qp_b(\upsilon,\upsilon) \text{ is a b} - \text{metric on } G. \tag{5}$$

Example 1. Let $G = [0,\infty)$ be endowed with metric $qp_b: G \times G \longrightarrow [0,\infty)$ defined by $qp_b(\sigma,\upsilon) = \max\{\sigma,\upsilon\} + |\sigma - \upsilon|$. Dominance of (G, qp_b) for the special case $G = [0,3]$ is visually checked in Figure 1.

Here, $qp_b(\sigma,\sigma) = qp_b(\sigma,\upsilon) = qp_b(\upsilon,\upsilon) \Rightarrow \sigma = \upsilon$ as $\sigma = \max\{\sigma,\sigma\} + |\sigma - \sigma| = \upsilon$.

Again, $qp_b(\sigma,\sigma) \le qp_b(\sigma,\upsilon)$ as $\max\{\sigma,\sigma\} + |\sigma - \sigma| \le \max\{\sigma,\upsilon\} + |\sigma - \upsilon|$ and similarly $qp_b(\sigma,\sigma) \le q(\upsilon,\sigma)$.

Also, $qp_b(\sigma,\upsilon) + qp_b(\epsilon,\epsilon) \le qp_b(\sigma,\epsilon) + qp_b(\epsilon,\sigma)$.

Let $\sigma, \epsilon, \upsilon \in G$. If $\sigma \le \upsilon \le \epsilon$, then

$$\begin{aligned} &\max\{\sigma,\upsilon\} + |\sigma - \upsilon| \le \upsilon + |\sigma - \epsilon| + |\epsilon - \upsilon| \\ &\le \max\{\sigma,\epsilon\} + |\sigma - \epsilon| + \max\{\epsilon,\upsilon\} + |\epsilon - \upsilon| - \epsilon. \end{aligned} \tag{6}$$

Thus, (G, qp_b) is a quasi-partial b-metric space.

Lemma 1 (see [23]). *Let* (G, qp_b) *be a quasi-partial b-metric space. Then, the following holds:*

(i) If $qp_b(\sigma,\upsilon) = 0$, *then* $\sigma = \upsilon$
(ii) If $\sigma = \upsilon$, *then* $qp_b(\sigma,\upsilon) > rbin0$ *and* $qp_b(\upsilon,\sigma) > rbin0$

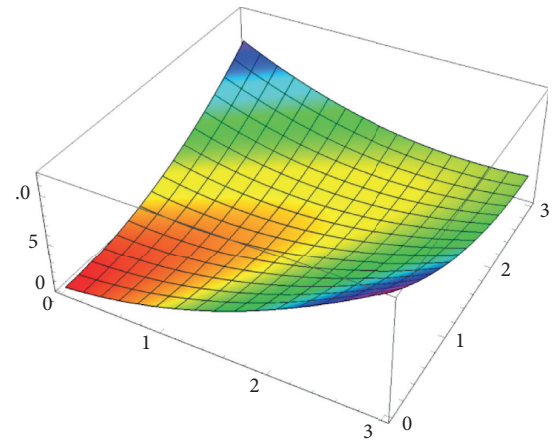

Figure 1: The graphical surface represents a 3D view of the function $qp_b(\sigma,\upsilon) = \max\{\sigma,\upsilon\} + |\sigma - \upsilon|$ for [0,3].

Definition 3 (see [7]). Let (G, qp_b) be a quasi-partial b-metric. Then,

(1) A sequence $\{\sigma_n\} \subset G$ converges to $\sigma \in G$ if and only if $qp_b(\sigma,\sigma) = \lim_{n\longrightarrow\infty} qp_b(\sigma,\sigma_n)$.
(2) A sequence $\{\sigma_n\} \subset G$ is called a Cauchy sequence if and only if $\lim_{n,m\longrightarrow\infty} qp_b(\sigma_n,\sigma_m)$ exists.
(3) A quasi-partial b-metric space (G, qp_b) is said to be complete if every Cauchy sequence $\{\sigma_n\} \subset G$ converges with respect to τ_{qp_b} to a point $\sigma \in G$ such that

$$qp_b(\sigma,\sigma) = \lim_{n,m\longrightarrow\infty} qp_b(\sigma_n,\sigma_m). \tag{7}$$

(4) A mapping $f: G \longrightarrow G$ is said to be continuous at $\sigma_0 \in G$ if, for every $\varepsilon > 0$, there exists $\delta > 0$ such that

$$f(B(\sigma_0,\delta)) \subset B(f(\sigma_0),\varepsilon). \tag{8}$$

Lemma 2 (see [18]). *Let* (G, qp_b) *be a quasi-partial b-metric space and* $(G, dq\ p_b)$ *be the corresponding b-metric space. Then,* $(G, dq\ p_b)$ *is complete if* (G, qp_b) *is complete.*

Definition 4 (see [23]). Let (G, qp_b) be a quasi-partial b-metric space and $H: G \longrightarrow G$ be a given mapping. Then, H is said to be sequentially continuous at $z \in G$ if for each sequence $\{\sigma_n\}$ in G converging to z, we have $H\sigma_n \longrightarrow Hz$, that is, $\lim_{n\longrightarrow\infty} qp_b(H\sigma_n, Hz) = qp_b(Hz, Hz)$. Similarly, let $K: G \longrightarrow G$ be a given mapping. K is said to be sequentially continuous at $z \in G$ if for each sequence $\{\sigma_n\}$ in G converging to z, we have $\lim_{n\longrightarrow\infty} qp_b(Kz, K\sigma_n) = qp_b(Kz, Kz)$.

2. Main Results

In this paper, the notion of interpolative Chatterjea type contraction is given in the setting of quasi-partial b-metric space.

Definition 5. Let (G, qp_b) be a complete quasi-partial b-metric space. We say that the self mappings

$H, K: G \longrightarrow G$ are an interpolative Chatterjea contraction if there exists $\varrho \in [0, 1/s), \alpha \in (0,1), s > 1$ such that

$$qp_b(H\sigma, Kv) \leq \varrho\left[\frac{1}{s^2} qp_b(\sigma, Kv)\right]^{\alpha}\left[\frac{1}{s^2} qp_b(v, H\sigma)\right]^{1-\alpha}, \quad (9)$$

for all $\sigma, v \in G$ such that $H\sigma \neq \sigma$ whenever $Kv \neq v$.

Theorem 4. *Let (G, qp_b) be a complete quasi-partial b-metric space and H and K be an interpolative Chatterjea type contraction. Then, K and H posses a common fixed point.*

Proof. Let $\sigma_0 \in G$. Define the sequence σ_n by $\sigma_{2n+1} = H\sigma_{2n}$, $\sigma_{2n+2} = K\sigma_{2n+1}$ for all $n = 1, 2, \ldots$. If there exist $n \in 0, 1, 2, \ldots$, such that $\sigma_n = \sigma_{n+1} = \sigma_{n+2}$, then σ_n is a common fixed point of K and H. Suppose that there are no such three consecutive identical terms in the sequence σ_n and that $\sigma_0 \neq \sigma_1$. Now, using equation (9), we deduce that

$$\begin{aligned} qp_b(\sigma_{2n+1}, \sigma_{2n+2}) &= qp_b(H\sigma_{2n}, K\sigma_{2n+1}) \\ &\leq \varrho\left[\frac{1}{s^2} qp_b(\sigma_{2n}, K\sigma_{2n+1})\right]^{\alpha}\left[\frac{1}{s^2} qp_b(\sigma_{2n+1}, H\sigma_{2n})\right]^{1-\alpha} \\ &\leq \varrho\left[\frac{1}{s^2} qp_b(\sigma_{2n}, \sigma_{2n+2})\right]^{\alpha}\left[\frac{1}{s^2} qp_b(\sigma_{2n+1}, \sigma_{2n+1})\right]^{1-\alpha}. \end{aligned} \quad (10)$$

By using Definition 2,

$$qp_b(\sigma_{2n+1}, \sigma_{2n+1}) \leq qp_b(\sigma_{2n+1}, \sigma_{2n+2}). \quad (11)$$

Therefore,

$$\begin{aligned} qp_b(\sigma_{2n+1}, \sigma_{2n+2}) &\leq \varrho\left[\frac{1}{s^2} qp_b(\sigma_{2n}, \sigma_{2n+2})\right]^{\alpha}\left[\frac{1}{s^2} qp_b(\sigma_{2n+1}, \sigma_{2n+2})\right]^{1-\alpha}, \\ [qp_b(\sigma_{2n+1}, \sigma_{2n+2})]^{\alpha} &\leq \varrho\left[\frac{1}{s^2} qp_b(\sigma_{2n}, \sigma_{2n+2})\right]^{\alpha} \\ &\leq \left[\frac{1}{s^2}\left[s\left(qp_b(\sigma_{2n}, \sigma_{2n+1}) + qp_b(\sigma_{2n+1}, \sigma_{2n+2}) - qp_b(\sigma_{2n+1}, \sigma_{2n+1})\right)\right]\right]^{\alpha}, \\ [qp_b(\sigma_{2n+1}, \sigma_{2n+2})]^{\alpha} &\leq \varrho\left[\frac{1}{s}\left(qp_b(\sigma_{2n}, \sigma_{2n+1}) + qp_b(\sigma_{2n+1}, \sigma_{2n+2})\right)\right]^{\alpha}. \end{aligned} \quad (12)$$

Suppose that

$$\begin{aligned} &qp_b(\sigma_{2n}, \sigma_{2n+1}) \leq qp_b(\sigma_{2n+1}, \sigma_{2n+2}), \\ &\frac{1}{s}\left[qp_b(\sigma_{2n}, \sigma_{2n+1}) + qp_b(\sigma_{2n+1}, \sigma_{2n+2})\right] \leq qp_b(\sigma_{2n+1}, \sigma_{2n+2}). \end{aligned} \quad (13)$$

By using equation (12),

$$[qp_b(\sigma_{2n+1}, \sigma_{2n+2})]^{\alpha} \leq \varrho[qp_b(\sigma_{2n+1}, \sigma_{2n+2})]^{\alpha}, \quad (14)$$

which is a contradiction. Thus, we have

$$\begin{aligned} &qp_b(\sigma_{2n+1}, \sigma_{2n+2}) < qp_b(\sigma_{2n}, \sigma_{2n+1}), \quad \text{for all } n \geq 1, \\ &\frac{1}{s}\left[qp_b(\sigma_{2n}, \sigma_{2n+1}) + qp_b(\sigma_{2n+1}, \sigma_{2n+2})\right] \leq qp_b(\sigma_{2n}, \sigma_{2n+1}). \end{aligned} \quad (15)$$

Using equation (12),

$$\begin{aligned} &[qp_b(\sigma_{2n+1}, \sigma_{2n+2})]^{\alpha} \leq \varrho[qp_b(\sigma_{2n}, \sigma_{2n+1})]^{\alpha}, \\ &qp_b(\sigma_{2n+1}, \sigma_{2n+2}) \leq \varrho^{1/\alpha} qp_b(\sigma_{2n}, \sigma_{2n+1}), \\ &qp_b(\sigma_{2n+1}, \sigma_{2n+2}) \leq \varrho qp_b(\sigma_{2n}, \sigma_{2n+1}). \end{aligned} \quad (16)$$

Hence,

$$qp_b(\sigma_{2n+1}, \sigma_{2n+2}) \leq \varrho qp_b(\sigma_{2n}, \sigma_{2n+1}) \leq \varrho^2 qp_b(\sigma_{2n-1}, \sigma_{2n}). \quad (17)$$

Therefore,

$$qp_b(\sigma_{2n+1}, \sigma_{2n+2}) \leq \varrho^{2n+1} qp_b(\sigma_0, \sigma_1). \quad (18)$$

Similarly,

$$
\begin{aligned}
qp_b(\sigma_{2n+1},\sigma_{2n}) &= qp_b(H\sigma_{2n},K\sigma_{2n-1})\\
&\le \varrho\left[\frac{1}{s^2}qp_b(\sigma_{2n},K\sigma_{2n-1})\right]^{\alpha}\left[\frac{1}{s^2}qp_b(\sigma_{2n-1},H\sigma_{2n})\right]^{1-\alpha}\\
&\le \varrho\left[qp_b(\sigma_{2n},\sigma_{2n})\right]^{\alpha}\left[\frac{1}{s^2}qp_b(\sigma_{2n-1},\sigma_{2n+1})\right]^{1-\alpha}\\
&\le \varrho\left[qp_b(\sigma_{2n},\sigma_{2n+1})\right]^{\alpha}.\left[\frac{1}{s^2}qp_b(\sigma_{2n-1},\sigma_{2n+1})\right]^{1-\alpha}\\
&\le \varrho\left[qp_b(\sigma_{2n},\sigma_{2n+1})\right]^{\alpha}.\left[\frac{1}{s^2}.s\{(qp_b(\sigma_{2n-1},\sigma_{2n})+qp_b(\sigma_{2n},\sigma_{2n+1}))-qp_b(\sigma_{2n},\sigma_{2n})\}\right]^{1-\alpha}\\
&\le \varrho\left[qp_b(\sigma_{2n},\sigma_{2n+1})\right]^{\alpha}.\left[\frac{1}{s^2}.sqp_b(qp_b(\sigma_{2n-1},\sigma_{2n})+qp_b(\sigma_{2n},\sigma_{2n+1}))\right]^{1-\alpha},\\
qp_b\left[(\sigma_{2n},\sigma_{2n+1})\right]^{1-\alpha} &\le \varrho qp_b(\sigma_{2n-1},\sigma_{2n})^{1-\alpha},\\
qp_b\left[(\sigma_{2n},\sigma_{2n+1})\right] &\le \varrho qp_b(\sigma_{2n-1},\sigma_{2n}).
\end{aligned}
\tag{19}
$$

Hence,

$$
qp_b(\sigma_{2n},\sigma_{2n+1}) \le \varrho qp_b(\sigma_{2n-1},\sigma_{2n}) \le \varrho^2 qp_b(\sigma_{2n-1},\sigma_{2n-2}).
\tag{20}
$$

This yields that

$$
qp_b(\sigma_{2n},\sigma_{2n+1}) \le \varrho^{2n} qp_b(\sigma_0,\sigma_1).
\tag{21}
$$

From equations (18) and (21), we deduce that

$$
qp_b(\sigma_n,\sigma_{n+1}) \le \varrho^n qp_b(\sigma_0,\sigma_1).
\tag{22}
$$

To prove sequence $\{\sigma_n\}$ is Cauchy, let $n,k \in N$

$$
\begin{aligned}
qp_b(\sigma_n,\sigma_{n+k}) &\le sqp_b(\sigma_n,\sigma_{n+1}) + s^2qp_b(\sigma_{n+1},\sigma_{n+2}) + \ldots + s^kqp_b(\sigma_{n+k-1},\sigma_{n+k})\\
&\le \left[s\varrho^n + s^2\varrho^{n+1} + \ldots + s^k\varrho^{n+k-1}\right]qp_b(\sigma_0,\sigma_1)\\
&\le s^k\sum_{i=n}^{n+k-1}\varrho^i qp_b(\sigma_0,\sigma_1)\\
&\le s^k\sum_{i=n}^{\infty}\varrho^i qp_b(\sigma_0,\sigma_1).
\end{aligned}
\tag{23}
$$

From (23),

$$
\begin{aligned}
&qp_b(\sigma_{n+m},\sigma_{n+m+k})\\
&\le s^k\sum_{i=m}^{\infty}\varrho^i qp_b(\sigma_n,\sigma_{n+1}),\\
&\lim_{m\longrightarrow\infty,n\longrightarrow\infty} qp_b(\sigma_{n+m},\sigma_{n+m+k})\\
&\le s^k\lim_{m\longrightarrow\infty}\sum_{i=m}^{\infty}\lim_{n\longrightarrow\infty}\varrho^i qp_b(\sigma_n,\sigma_{n+1})\\
&= 0.
\end{aligned}
\tag{24}
$$

Therefore,

$$
\lim_{n\longrightarrow\infty} qp_b(\sigma_n,\sigma_{n+k}) = \lim_{m\longrightarrow\infty,n\longrightarrow\infty} qp_b(\sigma_{n+m},\sigma_{n+m+k}) = 0.
\tag{25}
$$

We conclude that $\{\sigma_n\}$ is a Cauchy sequence. Since (G,qp_b) is complete, there exists $z \in G$ such that $\lim_{n\longrightarrow\infty}\sigma_n = z$. Next, we shall prove that z is a common fixed point of K and H.

$$
\begin{aligned}
qp_b(Hz,\sigma_{2n+2}) &= qp_b(Hz,K\sigma_{2n+1})\\
&\le \varrho\left[\frac{1}{s^2}qp_b(z,k\sigma_{2n+1})\right]^{\alpha}\left[\frac{1}{s^2}qp_b(\sigma_{2n+1},Hz)\right]^{1-\alpha}\\
&\le \varrho\left[qp_b(z,k\sigma_{2n+1})\right]^{\alpha}\\
&\left[qp_b(\sigma_{2n+1},Hz)\right]^{1-\alpha}.
\end{aligned}
\tag{26}
$$

Letting $n \longrightarrow \infty$, we get $Hz = z$. Similarly,

$$
\begin{aligned}
qp_b(\sigma_{2n+1},Kz) &= qp_b(H\sigma_{2n},Kz)\\
&\le \varrho\left[\frac{1}{s^2}qp_b(\sigma_{2n},Kz)\right]^{\alpha}\left[\frac{1}{s^2}qp_b(z,H\sigma_{2n})\right]^{1-\alpha}\\
&\le \varrho\left[qp_b(\sigma_{2n},Kz)\right]^{\alpha}\left[qp_b(z,H\sigma_{2n})\right]^{1-\alpha}.
\end{aligned}
\tag{27}
$$

Letting $n \longrightarrow \infty$, we get $Kz = z$. Hence, K and H attain a common fixed point.

We can justify this result by illustrating it with an example. □

Example 2. Let $G = \{0, 1, 2, 3\}$. Define complete quasi-partial b-metric as $qp_b(\sigma, \upsilon) = (\sigma - \upsilon)^2 + \sigma$, that is:

$\mathbf{qp_b}(\sigma, \upsilon)$	0	1	2	3
0	0	1	4	9
1	2	1	2	5
2	6	3	2	3
3	12	7	4	3

We define self mappings H and K on G as H: $\begin{pmatrix} 0 & 1 & 2 & 3 \\ 0 & 0 & 1 & 0 \end{pmatrix}$, K: $\begin{pmatrix} 0 & 1 & 2 & 3 \\ 0 & 0 & 0 & 1 \end{pmatrix}$. Now, consider the value $\alpha = 4/5$ and $\varrho = 99/100$.

Case 1. Let $(\sigma, \upsilon) = (1, 1)$. Without loss of generality, we have

$$qp_b(H\sigma, K\upsilon) \le \varrho\left[\frac{1}{s^2} qp_b(\sigma, K\upsilon)\right]^{\alpha}\left[\frac{1}{s^2} qp_b(\upsilon, H\sigma)\right]^{1-\alpha},$$

$$qp_b(H1, K1) = 0 \le \varrho\left[\frac{1}{s^2} qp_b(1, K1)\right]^{4/5}\left[\frac{1}{s^2} qp_b(1, H1)\right]^{1-(4/5)}. \tag{28}$$

Dominance of right-hand side of equation (9) is easily visually checked in Figure 2. Thus, the inequality required in equation (9) holds for $(\sigma, \upsilon) = (1, 1)$.

Case 2. Let $(\sigma, \upsilon) = (0, 0)$.

$$qp_b(H\sigma, K\upsilon) \le \varrho\left[\frac{1}{s^2} qp_b(\sigma, K\upsilon)\right]^{\alpha}\left[\frac{1}{s^2} qp_b(\upsilon, H\sigma)\right]^{1-\alpha},$$

$$qp_b(H0, K0) = 0 \le \varrho\left[\frac{1}{s^2} qp_b(0, K0)\right]^{4/5}\left[\frac{1}{s^2} qp_b(0, H0)\right]^{1-(4/5)}. \tag{29}$$

Dominance of right-hand side of equation (9) is easily visually checked in Figure 3. Thus, the inequality required in equation (9) holds for $(\sigma, \upsilon) = (0, 0)$.

Case 3. Let $(\sigma, \upsilon) = (3, 3)$.

$$qp_b(H\sigma, K\upsilon) \le \varrho\left[\frac{1}{s^2} qp_b(\sigma, K\upsilon)\right]^{\alpha}\left[\frac{1}{s^2} qp_b(\upsilon, H\sigma)\right]^{1-\alpha},$$

$$qp_b(H3, K3) = 1 \le \varrho\left[\frac{1}{s^2} qp_b(3, K3)\right]^{4/5}\left[\frac{1}{s^2} qp_b(3, H3)\right]^{1-(4/5)}. \tag{30}$$

Dominance of right-hand side of equation (9) is easily visually checked in Figure 4. Thus, the inequality required in equation (9) holds for $(\sigma, \upsilon) = (3, 3)$.

Therefore, 0 is the common fixed point of H and K in the setting of interpolative Chatterjea type contraction. Many more common fixed points can be obtained in similar manner. Hence, a fixed point exists but is not unique.

Open problem 1. Let (G, qp_b) be a complete quasi-partial b-metric space. Let us consider a family of self mappings K_n: $G \longrightarrow G$, $n \ge 1$, and $s \ge 1$ such that

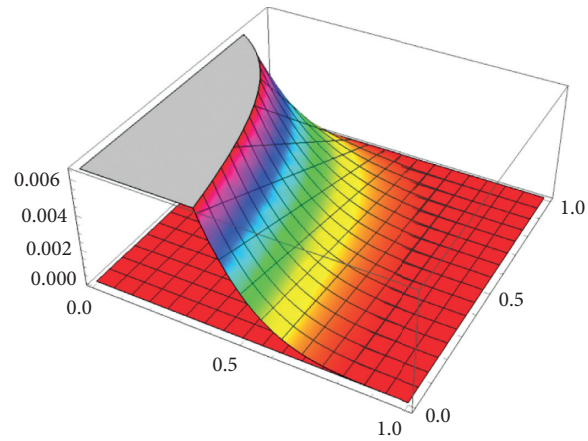

Figure 2: 0 is the common fixed point of H and K.

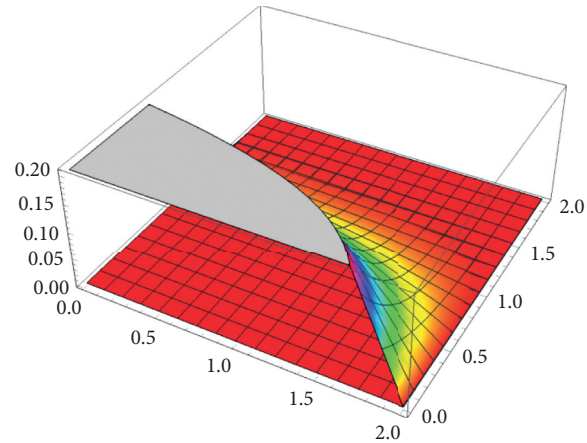

Figure 3: 0 is the common fixed point of H and K.

$$qp_b\left(K_i\sigma, K_j\upsilon\right) \le \varrho_{i,j}\left[\frac{1}{s^2} qp_b(\sigma, K_i\upsilon)\right]^{\alpha}\left[\frac{1}{s^2} qp_b\left(\upsilon, K_j\sigma\right)\right]^{1-\alpha}. \tag{31}$$

What are the conditions on $\varrho_{i,j}$ and α_i for K_n to have a common fixed point?

3. Modified Chatterjea Type Suzuki Contraction

In our next result, we present the existence of interpolative Chatterjea contraction via Suzuki map. First, let us recall w-admissible map.

Definition 6. Let us consider a self map H defined on G and w: $G \times G \longrightarrow [0, \infty]$ be a map where $G \neq \phi$. H is said to be w-orbital admissible if for all $\sigma \in G$, we have

$$w(\sigma, H\sigma) \ge 1 \longrightarrow w\left(H\sigma, H^2\sigma\right) \ge 1. \tag{32}$$

R Condition. If $\{\sigma_n\}$ is a sequence in G such that $w(\sigma_n, \sigma_{n+1}) \ge 1$ for each n and $\sigma_n \longrightarrow \sigma \in G$ as $n \longrightarrow \infty$, then there exists $\{\sigma_{n(k)}\}$ from $\{\sigma_n\}$ such that $w(\sigma_{n(k)}, \sigma) \ge 1$, for each k.

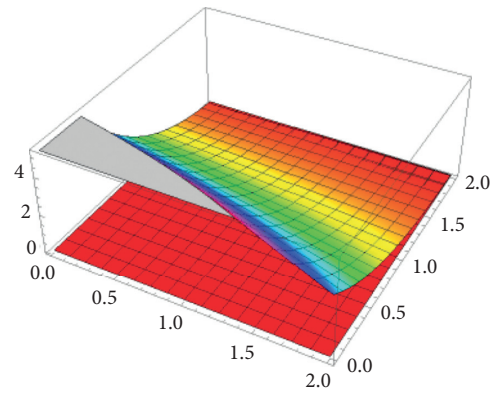

FIGURE 4: 0 is the common fixed point of H and K.

Definition 7. Let (G, qp_b) be a quasi-partial b-metric space. A self map H defined on G satisfies the C-condition if

$$\frac{1}{2}[qp_b(\sigma, H\sigma)] \leq qp_b(\sigma, \upsilon) \Rightarrow qp_b(H\sigma, H\upsilon) \leq qp_b(\sigma, \upsilon), \tag{33}$$

for each $\sigma, \upsilon \in G$.

Definition 8 (see [15,22]). Let Ψ be the set of all nondecreasing self mappings ψ on $(0, \infty)$ such that

$$\sum_{n=1}^{\infty} \psi^n(t) < \infty, \quad \text{for each } t > 0. \tag{34}$$

Notice that for $\psi \in \Psi$, we have $\psi(0) = 0$ and $\psi(t) < t$ for all $t > 0$.

Definition 9. Let us consider a quasi-partial b-metric space (G, qp_b). A map $H: G \longrightarrow G$ is said to be a w-ψ-interpolative Chatterjea contraction of Suzuki type if there exist ψ and a self-mapping, $w: G \times G \longrightarrow [0, \infty)$ and a real number $\alpha \in [0, 1)$, such that

$$\frac{1}{2}[qp_b(\sigma, H\upsilon)] \leq qp_b(\sigma, \upsilon) \Rightarrow w(\sigma, \upsilon) qp_b(H\sigma, H\upsilon) \leq \psi\left([qp_b(\sigma, H\upsilon)]^{\alpha}[qp_b(\upsilon, H\sigma)]^{1-\alpha}\right), \tag{35}$$

for each $\sigma, \upsilon \in G$.

Theorem 5. *Let (G, qp_b) be a complete quasi-partial b-metric space and $H: G \longrightarrow G$ be a w-ψ-interpolative Chatterjea contraction of Suzuki type. Assume that H is w-orbital admissible mapping and $w(\sigma_0, H\sigma_0) \geq 1$ for some $\sigma_0 \in G$. Then, H has a fixed point in G provided that at least one of the following conditions holds:*

(1) (G, qp_b) is w-regular

(2) H is continuous

(3) ψH^2 is continuous and $w(\sigma, H\sigma) \geq 1$ where $\sigma \in Fix(\psi H^2)$

Proof. Let us consider an initial point $\sigma_0 \in G$ such that $w(\sigma_0, H\sigma_0) \geq 1$ and now construct a sequence $\{\sigma_n\}$ by using $H^n(\sigma_0) = \sigma_n$ for each positive integer n. If $\sigma_{n_0} = \sigma_{n_{0+1}}$ for some $n_0 \in N$, we get $\sigma_{n_0} = H\sigma_{n_0}$ that means we get σ_{n_0} is a fixed point of H. Then, we can assume that $\sigma_n \neq \sigma_{n+1}$ for each positive integer n. As H is w-orbital admissible, we have the condition $w(\sigma_0, H\sigma_0) = w(\sigma_0, \sigma_1) \geq 1$ implies that $w(\sigma_1, H\sigma_1) = w(\sigma_1, \sigma_2) \geq 1$. In continuation, we have

$$w(\sigma_n, \sigma_{n+1}) \geq 1. \tag{36}$$

Hence, choosing $\sigma = \sigma_{n-1}$ and $\epsilon = H\sigma_{n-1}$ in (54), we get

$$\frac{1}{2} qp_b(\sigma, \epsilon) = \frac{1}{2} qp_b(\sigma_{n-1}, H\sigma_{n-1}) = \frac{1}{2} qp_b(\sigma_{n-1}, \sigma_n) \leq qp_b(\sigma_{n-1}, \sigma_n), \tag{37}$$

which implies

$$\begin{aligned} qp_b(\sigma_n, \sigma_{n+1}) &\leq w(\sigma_{n-1}, \sigma_n) qp_b(H\sigma_{n-1}, H\sigma_n) \\ &\leq \psi\left([qp_b(\sigma_{n-1}, H\sigma_n)]^{\alpha} . [qp_b(\sigma_n, H\sigma_{n-1})]^{1-\alpha}\right) \\ &= \psi\left([qp_b(\sigma_{n-1}, \sigma_{n+1})]^{\alpha} . [qp_b(\sigma_n, \sigma_n)]^{1-\alpha}\right) \\ &< [qp_b(\sigma_{n-1}, \sigma_n)]^{\alpha} . [qp_b(\sigma_n, \sigma_{n+1})]^{1-\alpha}. \end{aligned} \tag{38}$$

Hence, it follows that

$$[qp_b(\sigma_n, \sigma_{n+1})]^{\alpha} < [qp_b(\sigma_{n-1}, \sigma_n)]^{\alpha}, \tag{39}$$

or equivalently

$$qp_b(\sigma_n, \sigma_{n+1}) < qp_b(\sigma_{n-1}, \sigma_n). \tag{40}$$

Thus, it follows that the sequence $\{qp_b(\sigma_{n-1}, \sigma_n)\}$ is a nonincreasing sequence of positive terms and $\lim_{n \longrightarrow \infty} qp_b(\sigma_{n-1}, \sigma_n) = 1$. From the above equations and the nondecreasing nature of function ψ, we obtain

$$qp_b(\sigma_n, \sigma_{n+1}) \leq \psi(qp_b(\sigma_{n-1}, \sigma_n)) \leq \psi^2(qp_b(\sigma_{n-2}, \sigma_{n-1})) \leq \cdots \leq \psi^n(qp_b(\sigma_0, \sigma_1)). \tag{41}$$

Now, applying triangular inequality, for all $j \geq 1$, we get

$$\begin{aligned} qp_b(\sigma_n, \sigma_{n+j}) &\leq \left[sqp_b(\sigma_n, \sigma_{n+1}) + s^2 qp_b(\sigma_{n+1}, \sigma_{n+2}) + \cdots + s^j qp_b(\sigma_{n+j-1}, \sigma_{n+j})\right] \\ &\leq \left[s\psi^n qp_b(\sigma_0, \sigma_1) + s^2\psi^{n+1} qp_b(\sigma_0, \sigma_1) + \cdots + s^j\psi^{n+j-1} qp_b(\sigma_0, \sigma_1)\right] \\ &= \sum_{m=n,r=1}^{n+j-1} s^r \psi^m (qp_b(\sigma_0, \sigma_1)) \\ &= P_{n+j-1} - P_{n-1}, \end{aligned} \tag{42}$$

where $P_k = s^k \sum_{m=0}^{k} \psi^m(qp_b(\sigma_0, \sigma_1))$. However, the series $\sum_{m=0}^{\infty} \psi^m(qp_b(\sigma_0, \sigma_1))$ is convergent, so there exists a positive real number P such that $\lim_{k\longrightarrow\infty} P_k = P$. Letting n and $j \longrightarrow \infty$ in the above inequality, we get

$$qp_b(\sigma_n, \sigma_{n+j}) \longrightarrow 0. \tag{43}$$

Therefore, $\{\sigma_n\}$ is a Cauchy sequence, and using the completeness property of qp_b space, it follows that there exists $w \in G$ such that

$$\lim_{n\longrightarrow\infty} \sigma_n = w, \tag{44}$$

and we claim that w is the fixed point of H.

In case that the assumption (1) holds, we have $w(\sigma_n, t) \geq 1$ and we claim that

$$\begin{aligned} &\frac{1}{2} qp_b(\sigma_n, H\sigma_n) \leq qp_b(\sigma_n, w), \\ &\text{or } \frac{1}{2} qp_b(H\sigma_n, H(H\sigma_n)) \leq qp_b(H\sigma_n, w), \end{aligned} \tag{45}$$

for every $n \in N$. Suppose

$$\begin{aligned} &\frac{1}{2} qp_b(\sigma_n, H\sigma_n) > qp_b(\sigma_n, w), \\ &\frac{1}{2} qp_b(H\sigma_n, H(H\sigma_n)) > qp_b(H\sigma_n, w). \end{aligned} \tag{46}$$

By triangular inequality in qp_b space, we have

$$\begin{aligned} qp_b(\sigma_n, \sigma_{n+1}) &= qp_b(\sigma_n, H\sigma_n) + qp_b(w, w) \leq qp_b(\sigma_n, w) + qp_b(w, H\sigma_n) \\ &< \frac{1}{2} qp_b(\sigma_n, H\sigma_n) + \frac{1}{2} qp_b(H\sigma_n, H(H\sigma_n)) \\ &= \frac{1}{2} qp_b(\sigma_n, \sigma_{n+1}) + \frac{1}{2} qp_b(\sigma_{n+1}, \sigma_{n+2}) \\ &\leq \frac{1}{2} qp_b(\sigma_n, \sigma_{n+1}) + \frac{1}{2} qp_b(\sigma_n, \sigma_{n+1}) \\ &= qp_b(\sigma_n, \sigma_{n+1}), \end{aligned} \tag{47}$$

which is a contradiction. Therefore, for every $n \in N$, either

$$\begin{aligned} &\frac{1}{2} qp_b(\sigma_n, H\sigma_n) \leq qp_b(\sigma_n, w), \\ &\text{or } \frac{1}{2} qp_b(H\sigma_n, H(H\sigma_n)) \leq qp_b(H\sigma_n, w), \end{aligned} \tag{48}$$

holds. If the first condition holds, we obtain

$$\begin{aligned} qp_b(\sigma_{n+1}, Hw) &\leq w(\sigma_n, w) qp_b(H\sigma_n, Hw) \\ &\leq \psi[qp_b(\sigma_n, H\sigma_n)]^{\alpha} . [qp_b(w, Hw)]^{1-\alpha} \\ &= \psi[qp_b(\sigma_n, H\sigma_{n+1})]^{\alpha} . [qp_b(w, Hw)]^{1-\alpha} \\ &< [qp_b(\sigma_n, H\sigma_{n+1})]^{\alpha} . [qp_b(w, Hw)]^{1-\alpha}. \end{aligned} \tag{49}$$

If the second condition holds, we get

$$\begin{aligned} qp_b(\sigma_{n+2}, H\omega) &\le w(\sigma_{n+1}, \omega) qp_b\left(H^2\sigma_n, H\omega\right) \\ &\le \psi\left[qp_b\left(H\sigma_n, H^2\sigma_n\right)\right]^{\alpha}.\left[qp_b(\omega, H\omega)\right]^{1-\alpha} \\ &= \psi\left[qp_b(\sigma_{n+1}, \sigma_{n+2})\right]^{\alpha}.\left[qp_b(\omega, H\omega)\right]^{1-\alpha} \\ &< \left[qp_b(\sigma_{n+1}, \sigma_{n+2})\right]^{\alpha}.\left[qp_b(\omega, H\omega)\right]^{1-\alpha}. \end{aligned} \tag{50}$$

Therefore, letting $n \longrightarrow \infty$, we get that $qp_b(\omega, H\omega) = 0$, that is, $\omega = H\omega$.

In case that assumption (2) holds, that is, the mapping H is continuous, we get

$$H\omega = \lim_{n\longrightarrow\infty} H\sigma_n = \lim_{n\longrightarrow\infty} H\sigma_{n+1} = \omega. \tag{51}$$

If the last assumption (3) holds, we have $\psi H^2\omega = \psi\lim_{n\longrightarrow\infty} H^2\sigma_n = \psi\lim_{n\longrightarrow\infty}\sigma_{n+2} = \psi\omega$ and we show that, $H\omega = \omega$. Suppose on the contrary, that $H\omega \neq \omega$ since

$$\frac{1}{2} qp_b\left(H\omega, \psi H^2\omega\right) = \frac{1}{2} qp_b(H\omega, \psi\omega) \le qp_b(H\omega, \psi\omega). \tag{52}$$

By (54), we get

$$\begin{aligned} qp_b(\omega, H\omega) &\le w(H\omega, \omega) qp_b\left(H^2\omega, H\omega\right) \\ &\le \psi\left[qp_b\left(H\omega, H^2\omega\right)\right]^{\alpha}.\left[qp_b(\omega, H\omega)\right]^{1-\alpha} \\ &= \psi\left[qp_b(\sigma_{n+1}, \sigma_{n+2})\right]^{\alpha}.\left[qp_b(\omega, H\omega)\right]^{1-\alpha} \\ &< \left[qp_b(H\omega, \omega)\right]^{\alpha}.\left[qp_b(\omega, H\omega)\right]^{1-\alpha} \\ &= qp_b(\omega, H\omega), \end{aligned} \tag{53}$$

which is a contradiction. So, $\omega = H\omega$, i.e., ω is the fixed point of the mapping H. □

4. Application

In this section, we have discussed the existence of the solution for the nonlinear matrix equation by using interpolative Chatterjea mapping in the notion of quasi-partial b-metric space. Consider a nonlinear matrix equation as

$$\sigma = Q + \sum_{i=1}^{n} M_i^* H(\sigma) M_i, \tag{54}$$

$$Q = \sigma - M_1^* H(\sigma) M_1 - \ldots - M_n^* H(\sigma) M_n, \tag{55}$$

where $\mathscr{H}(n)$ denotes the set of $n \times n$ Hermitian matrices and $p(n)$ denotes the set of $n \times n$ positive definite matrices. Here, $p(n) \subseteq \mathscr{H}(n)$, $Q \in p(n)$, and M_i is $n \times n$ matrices. Let us suppose a continuous order preserving map $H: p(n) \longrightarrow p(n)$ with $H(0) = 0$.

Define a trace norm $\|.\|_{tr}$ on the set (n) that is a complete quasi-partial b-metric space and partially ordered with partial ordering $\prec$, where $\sigma \prec \upsilon \Rightarrow \upsilon \prec \sigma$.

Lemma 3. *If $\sigma, \upsilon \succcurlyeq 0$ are $n \times n$ matrices, then*

$$0 \le tr(\sigma, \upsilon) \le \|\upsilon\| |tr(\sigma)|. \tag{56}$$

Lemma 4. *If $\sigma, \upsilon \prec I_n$, then*

$$\|\sigma\| < 1. \tag{57}$$

Theorem 6. *Let a nonlinear matrix equation (54) and suppose the following conditions hold:*

(1) There exists $Q \in p(n)$ with

$$Q = Q + \sum_{i=1}^{n} M_i^* H(Q) M_i. \tag{58}$$

(2) For all $\sigma, \upsilon \in p(n)$,

$$\sigma \le \upsilon \Rightarrow \sum_{i=1}^{n} M_i^* H(\sigma) M_i \le \sum_{i=1}^{n} M_i^* H(\upsilon) M_i. \tag{59}$$

(3) There exists $\varrho \in (0, 1/2s)$ for which $\sum_{i=1}^{n} M_i^* M_i < \varrho I_n$ and $\sum_{i=1}^{n} M_i^* H(Q) M_i > 0$ such that

$$\sigma \le \upsilon \Rightarrow \sum_{i=1}^{n} M_i^* H(\sigma) M_i \le \sum_{i=1}^{n} M_i^* H(\upsilon) M_i. \tag{60}$$

(4) There exists $\sigma, \upsilon \in p(n)$ and $\varrho \in (0, 1/2s)$ such that

$$\|H\sigma - H\upsilon\|_{tr} \le \left[\frac{1}{s^2}\|\sigma - H\upsilon\|_{tr}\right]^{\alpha}\left[\frac{1}{s^2}\|\upsilon - H\upsilon\|_{tr}\right]^{1-\alpha}. \tag{61}$$

Then, equation (54) owns a solution in $p(n) \subseteq \mathscr{H}(n)$.

Proof. Consider a quasi-partial b-metric $qp_b: p(n) \times p(n) \longrightarrow \mathbb{R}^+$ as

$$qp_b(\sigma, \upsilon) = \|\sigma - \upsilon\|_{tr} + \|\sigma\|_{tr}. \tag{62}$$

Define a continuous map $H: p(n) \longrightarrow p(n)$ as

$$H(\sigma) = Q + \sum_{i=1}^{n} M_i^* H(\sigma) M_i, \tag{63}$$

for all $\sigma \in p(n)$. Then, the solution of the matrix equation (54) is the fixed point of the map H.

On taking, $\sigma, \upsilon \in p(n)$ with $\sigma \prec \upsilon$, then $H(\sigma) \prec H(\upsilon)$. Thus, for $qp_b(\sigma, \upsilon) > 0$. Now, (1) $\longrightarrow$ (4) of Theorem 6 yields the following:

$$\begin{aligned} qp_b(H\sigma, Hv) &= \|H\sigma - Hv\|_{tr} = \|H\sigma - Hv\|_1 \\ &= \|H\sigma - Hv\| + \|H\sigma\| \\ &= \left\|\sum_{i=1}^{n} M_i^* H(\sigma) M_i - \sum M_i^* H(v) M_i\right\| + \left\|Q + \sum_{i=1}^{n} M_i^* H(\sigma) M_i\right\|, \end{aligned} \tag{64}$$

$$\begin{aligned} qp_b(\sigma, v) &= \|\sigma - v\|_{tr} \Rightarrow \|\sigma - v\|_1 \\ &= \|\sigma - v\| + \|\sigma\|, \\ qp_b(\sigma, Hv) &= \|\sigma - Hv\|_{tr} \Rightarrow \|\sigma - Hv\|_1 \\ &= \|\sigma - Hv\| + \|\sigma\|, \\ &= \left\|\sigma - Q - \sum_{i=1}^{n} M_i^* H(v) M_i\right\| + \|\sigma\|, \end{aligned} \tag{65}$$

$$\begin{aligned} qp_b(v, H\sigma) &= \|v - H\sigma\|_{tr} \Rightarrow \|v - H\sigma\| \\ &= \|v - H\sigma\| + \|v\| \\ &= \left\|\sigma - Q - \sum_{i=1}^{n} M_i{}^* H(\sigma) M_i\right\| + \|v\|. \end{aligned} \tag{66}$$

From equation (64) ⟶ (66) and (61), we have

$$\begin{aligned} &\left\|\sum_{i=1}^{n} M_i^* M_i (H(\sigma) - H(v))\right\| + \left\|Q + \sum_{i=1}^{n} M_i^* H(\sigma) M_i\right\| \\ &\le \varrho\left[\frac{1}{s^2}\left\|\sigma - Q - \sum_{i=1}^{n} M_i^* H(v) M_i\right\| + \|\sigma\|\right]^{\alpha}\left[\frac{1}{s^2}\left\|\sigma - Q - \sum_{i=1}^{n} M_i^* H(\sigma) M_i\right\| + \|v\|\right]^{1-\alpha}. \end{aligned} \tag{67}$$

We deduce that

$$\|H\sigma - Hv\| \le \varrho\left[\frac{1}{s^2}\|\sigma - Hv\|_1\right]^{\alpha}\left[\frac{1}{s^2}\|v - Hv\|\right]^{1-\alpha}. \tag{68}$$

Thus,

$$qp_b(H\sigma, Hv) \le \varrho\left[\frac{1}{s^2} qp_b(\sigma, Hv)\right]^{\alpha}\left[\frac{1}{s^2} qp_b(v, H\sigma)\right]^{1-\alpha}. \tag{69}$$

Since $\sum_{i=1}^{n} M_i^* H(Q) M_i > 0$, we conclude that $Q \le H(Q)$. Thus, by using Theorem 4, H owns a fixed point in $p(n)$. □

5. Conclusion

The significant contribution of this manuscript is to provide the existence of common fixed points that are nonunique for interpolative Chatterjea contraction mappings in the realm of quasi-partial b-metric space. Further, we have given examples to show that the new results are applicable. In metric fixed point theory, interpolative contraction is a generalization of Kannan-type contraction. Additionally, these proposed contractions can be generalized in other well-known spaces and can give new fixed point results. The uniqueness property of obtained fixed points for these mappings and their application in the study of nonlinear integral equations will be an interesting concept for subsequent work.

Data Availability

No data were used to support this study.

Conflicts of Interest

The authors declare that there are no conflicts of interest regarding the publication of this paper.

References

[1] S. Banach, "Sur les opérations dans les ensembles abstraits et leur application aux équations intégrales," *Fundamenta Mathematicae*, vol. 3, pp. 133–181, 1922.

[2] I. A. Bakhtin, "The contraction principle in quasi-metric spaces," *Journal of Functional Analysis*, vol. 30, pp. 26–37, 1989.

[3] S. Czerwik, "Contraction mappings in b-metric spaces," *Acta Mathematica et Informatica Universitatis Ostraviensis*, vol. 1, pp. 5–11, 1993.

[4] S. G. Matthews, "Partial metric topology," *Annals of the New York Academy of Sciences*, vol. 728, no. 1, pp. 183–197, 1994.
[5] R. Kannan, "Some results on fixed points," *Bulletin of the Calcutta Mathematical Society*, vol. 60, pp. 71–76, 1968.
[6] S. K. Chatterjea, "Fixed-point theorems," *Comptes Rendus de l'Académie Bulgare des Sciences*, vol. 25, pp. 727–730, 1972.
[7] A. Gupta and P. Gautam, "Quasi-partial b-metric spaces and some related fixed point theorems," *Fixed Point Theory and Applications*, vol. 2015, no. 1, 2015.
[8] E. Karapinar, "Revisiting the Kannan type contractions via interpolation," *Advances in the Theory of Nonlinear Analysis and its Application*, vol. 2, pp. 85–87, 2018.
[9] E. Karapinar, R. Agarwal, and H. Aydi, "Interpolative reich-rus-cirić type contractions on partial metric spaces," *Mathematics*, vol. 6, no. 11, p. 256, 2018.
[10] H. Aydi, C.-M. Chen, and E. Karapınar, "Interpolative cirić-reich-rus type contractions via the Branciari distance," *Mathematics*, vol. 7, no. 1, p. 84, 2019.
[11] E. Karapınar, O. Alqahtani, and H. Aydi, "On interpolative Hardy-Rogers type contractions," *Symmetry*, vol. 11, no. 1, p. 8, 2018.
[12] M. Noorwali, "Common fixed point for Kannan type contractions via interpolation," *Journal of Mathematical Analysis and Applications*, vol. 9, no. 6, pp. 92–94, 2018.
[13] D. Wardowski, "Fixed points of a new type of contractive mappings in complete metric spaces," *Fixed Point Theory and Applications*, vol. 2012, no. 1, 2012.
[14] H. Garai, T. Senapati, and L. K. Dey, "A study on Kannan type contractive mapping," 2017, https://arxiv.org/abs/1707.06383.
[15] M. Asim, H. Aydi, and M. Imdad, "On Suzuki and Wardowski-type contraction multivalued mappings in partial symmetric spaces," *Journal of Function Spaces*, vol. 2021, Article ID 6660175, 8 pages, 2021.
[16] P. Debnath and M. de La Sen, "Set-Valued interpolative hardy-rogers and set-valued reich-rus-cirić-type contractions in b-metric spaces," *Mathematics*, vol. 7, no. 9, p. 849, 2019.
[17] P. Gautam, V. N. Mishra, R. Ali, and S. Verma, "Interpolative Chatterjea and cyclic Chatterjea contraction on quasi-partial b-metric space," *AIMS Mathematics*, vol. 6, no. 2, pp. 1727–1742, 2021.
[18] P. Gautam, L. M. Sánchez Ruiz, and S. Verma, "Fixed point of interpolative rus-reich-cirić contraction mapping on rectangular quasi-partial b-metric space," *Symmetry*, vol. 13, no. 32, pp. 2–16, 2021.
[19] P. Gautam and S. Verma, "Fixed point via implicit contraction mapping on quasi-partial b-metric space," *The Journal of Analysis*, vol. 29, no. 4, pp. 1251–1263, 2021.
[20] P. Gautam, S. Verma, M. de La Sen, and S. Sundriyal, "Fixed point results for w- interpolative chatterjea type contraction in quasi partial b metric space," *International Journal of Analysis and Applications*, vol. 19, no. 2, pp. 280–287, 2021.
[21] P. Gautam, L. M. Sánchez Ruiz, S. Verma, and G. Gupta, "Common fixed point results on generalized weak compatible mapping in quasi-partial b-metric space," *Journal of Mathematics*, vol. 2021, Article ID 5526801, 10 pages, 2021.
[22] M. Asim, R. George, and M. Imdad, "Suzuki type multivalued contraction in C∗- algebra valued metric spaces with an application," *AIMS Mathematics*, vol. 6, no. 2, pp. 1126–1139, 2020.
[23] V. N. Mishra, L. M. Sánchez Ruiz, P. Gautam, and S. Verma, "Interpolative reich-rus-cirić and hardy-rogers contraction on quasi-partial b-metric space and related fixed point results," *Mathematics*, vol. 81598 pages, 2020.
[24] Y. U. Gaba and E. Karapinar, "A new approach to the interpolative contractions," *Axioms*, vol. 8110 pages, 2019.
[25] R. P. Agarwal, E. Karapinar, D. O'Regan, and A. F. Roldán-López-de-Hierro, *Fixed Point Theory in Metric Type Spaces*, Springer, Cham, Switzerland, 2015.
[26] E. Karapınar, M. Erhan, and A. Özturk, "Fixed point theorems on quasi-partial metric spaces," *Mathematical and Computer Modelling*, vol. 57, pp. 2442–2448, 2013.

Hindawi
Journal of Mathematics
Volume 2024, Article ID 9854510, 1 page
https://doi.org/10.1155/2024/9854510

Retraction

Retracted: A Novel Approach to Automate Complex Software Modularization Using a Fact Extraction System

Journal of Mathematics

Received 23 January 2024; Accepted 23 January 2024; Published 24 January 2024

This article has been retracted by Hindawi following an investigation undertaken by the publisher [1]. This investigation has uncovered evidence of one or more of the following indicators of systematic manipulation of the publication process:

(1) Discrepancies in scope

(2) Discrepancies in the description of the research reported

(3) Discrepancies between the availability of data and the research described

(4) Inappropriate citations

(5) Incoherent, meaningless and/or irrelevant content included in the article

(6) Manipulated or compromised peer review

The presence of these indicators undermines our confidence in the integrity of the article's content and we cannot, therefore, vouch for its reliability. Please note that this notice is intended solely to alert readers that the content of this article is unreliable. We have not investigated whether authors were aware of or involved in the systematic manipulation of the publication process.

Wiley and Hindawi regrets that the usual quality checks did not identify these issues before publication and have since put additional measures in place to safeguard research integrity.

We wish to credit our own Research Integrity and Research Publishing teams and anonymous and named external researchers and research integrity experts for contributing to this investigation.

The corresponding author, as the representative of all authors, has been given the opportunity to register their agreement or disagreement to this retraction. We have kept a record of any response received.

References

[1] M. Z. Khan, R. Naseem, A. Anwar et al., "A Novel Approach to Automate Complex Software Modularization Using a Fact Extraction System," *Journal of Mathematics*, vol. 2022, Article ID 8640596, 19 pages, 2022.

Hindawi
Journal of Mathematics
Volume 2022, Article ID 8640596, 19 pages
https://doi.org/10.1155/2022/8640596

Research Article

A Novel Approach to Automate Complex Software Modularization Using a Fact Extraction System

Muhammad Zakir Khan,[1] **Rashid Naseem**,[2] **Aamir Anwar**,[3] **Ijaz Ul Haq**,[4] **Ahmad Alturki**,[5] **Syed Sajid Ullah**,[6] **and Suheer A. Al-Hadhrami**[7]

[1]*James Watt School of Engineering, University of Glasgow, G12 8QQ Glasgow, UK*
[2]*Department of Computer Science, Pak Austria Fachhochschule Institute of Applied Sciences and Technology, Haripur, Pakistan*
[3]*School of Computing and Engineering, University of West London, London W5 5RF, UK*
[4]*Faculty of Education, Psychology and Social Work, University of Lleida, 25003 Lleida, Spain*
[5]*STC's Artificial Intelligence Chair, Department of Information Systems, College of Computer and Information Sciences, King Saud University, Riyadh 11543, Saudi Arabia*
[6]*Department of Information and Communication Technology, University of Agder, Norway*
[7]*Department of Computer Engineering, College of Engineering, Hadhramout University, Hadhramout, Al Mukalla, Yemen*

Correspondence should be addressed to Ahmad Alturki; ahmalturki@ksu.edu.sa, Syed Sajid Ullah; syed.s.ullah@uia.no, and Suheer A. Al-Hadhrami; s.alhadhrami@hu.edu.ye

Received 6 December 2021; Revised 25 January 2022; Accepted 7 February 2022; Published 30 March 2022

Academic Editor: Naeem Jan

Complex software systems that support organizations are updated regularly, which can erode system architectures. Moreover, documentation is rarely synchronized with the changes to the software system. This creates a slew of issues for future software maintenance. To this goal, information extraction tools use exact approaches to extract entities and their corresponding relationships from source code. Such exact approaches extract all features, including those that are less prominent and may not be significant for modularization. In order to resolve the issue, this work proposes an enhanced approximate information extraction approach, namely, fact extractor system for Java applications (FESJA) that aims to automate software modularization using a fact extraction system. The proposed FESJA technique extracts all the entities along with their corresponding more dominant formal and informal relationships from a Java source code. Results demonstrate the improved performance of FESJA, by extracting 74 (classes), 43 (interfaces), and 31 (enumeration), in comparison with eminent information extraction techniques.

1. Introduction

Software systems are essential in our daily lives, businesses, and governmental organizations, and they require an updated software system to meet their functional and nonfunctional requirements. Client requests or changes in the system's environment may cause changes in requirements [1–3]. Changes deteriorate the architecture of software systems, making it difficult to maintain them. In such situations, the software system must be designed in such a way that the negative effects of modifications to the software system are kept to a minimum. Updated documentation is required for updated software. If the documentation is outdated, the software systems need to be retired or replaced.

Reverse engineering is the first step in re-engineering, and it involves understanding the system and acquiring the necessary information for software system maintenance [4, 5]. Information can be extracted from a software system through documentation, compiled code, development team members, and source code [6]. The most reliable source of information for restoring software architecture has been observed to be source code. The reason is the most recent version of the software, and this source code will be built and eventually run, the information gathered from it is the most reliable.

Information extracting from the source code of a software system, on the other hand, is a challenging task since no developer can fully know the code of a large and complex system. As a result, we need tools to automatically extract information from source code, which will help in the recovery of software architecture and the comprehension of software systems [7]. The understanding and recovery of architecture are crucial for software maintenance and evolution.

The first step in modularizing a software system is to analyze it since source code is the primary source of information for extracting artifacts. The need for a software modularization technique that transforms low-level artifacts (source code) into abstract views (high-level) [1, 5]. Two approaches can be utilized for code analysis: an exact approach and an approximate one. The exact approach utilized the parser to analyze the whole source code, whilst the approximate approach utilized it to extract the specified parts of the information. We propose a methodology for evaluating Java source code in order to discover entities and their relationships in a Java software system in this paper. The selection of an object-oriented system since it is a more realistic approach to software development. Object-oriented software systems developed in the 1990s are now legacy systems with an unstable structure due to changes made to them [5, 7]. Their documentation is either non-existent or obsolete. A comprehensive understanding of these software systems is necessary for future updates and maintenance.

The proposed system is named "Fact Extractor System for Java Application," or FESJA, which gives an approximate approach to automatic Java application software modularization. Entities such as classes, interfaces, and enumerations and their relationships (formal and informal) can be extracted using the tool. We utilized FESJA to extract formal relationships from classes in several Java software systems; interfaces and informal relationships are 74 and 43, respectively. We have extracted 31 relationships to analyze, which are divided into seven categories: folder-based, implements-based, composition-based, file-based, generality based, and router-based relationships. To the list of contributions, the following items could be added:

(1) A framework for extraction of relationships
(2) Introduction of enumeration is an entity
(3) Introduction of additional formal and informal relationships

The organization of the paper is composed of the following sections. Section 2 focuses on related work. The source code entities and relationships are described in Section 3. The research methodology for the fact extraction system is described in Section 4. Section 5 discusses the experimental setup. Section 6 presents the results. Section 7 contains the outcome of the experiment as well as a discussion.

2. Related Work

In the literature, several fact extractor systems for extracting features from source code have been proposed. To modularize software systems, Raimond and Lovesum [8] followed Anquetil and Lethbridge employed formal and informal features. They used files, routines, classes, and processes as entities. User-defined data types, procedure calls, file inclusion, macro use, and global variables are some of the formal features mentioned. Identifiers and comments are examples of nonformal features. They focused on how to modularize structured language software systems using hierarchical clustering algorithms. They came to the conclusion that identifiers provide good design results that the file has a good expert comparison, and those comments have a good expert comparison, but that bad design results and routine calls perform poorly. The authors in [9–12] proposed a method for improving the accuracy of autonomous software architecture reconstruction. The method uses a combination of graph clustering and partitioning. They considered classes as distinct entities and created eleven relationships between them. The following relationships were discovered: inheritance, implements an interface, members (A has at least one member of type B), method parameter (A has at least one method with a parameter of type B), local variable (A has a local variable of type B in a method), returned type (A has a method that returns type B), field access (A directly accesses at least one field of type B), static method call (A calls a static method of B), object instantiation (an object of type B is instant (inside A a cast to B is done). Their focus was on object-oriented systems (java).

Hussain et al. [13] adopted an agglomerative approach for clustering of structured software systems. They considered functions as entities. They took advantage of formal features like entity calling functions, global variables that entities refer to, and user-defined types that entities can access. Aghdasifam et al. [14] carried out work of software modularization using agglomerative hierarchical clustering algorithms. They targeted the structured system. They used functions as an entity. In their work, they utilized use global variables, user-specified data types, and function calls. Based on the results of the experiments, they determined that the type of feature outperforms the global and call features. Zahoor et al. [15] presented a tool called the WAFE tool (Web Application Fact Extractor) which extract features from web application. Similarly, a similar work presented by [16, 17], automate extraction dependency between web component and database resources in java web applications. The Web Page contains classes. The WAFE tool extracted the following information: a class called from a web page, a class function called from a web page, web page form submits on another web page or the same web page, web page link to another web page, web page redirect to another web page, and web page folder or directory. Custom Code Files are included in Web Pages, and Custom Code File functions are called by Web Pages. Web Pages' classes are derived from these classes. Classes derived from Web Page classes, as well as functions of classes derived from Web page classes.

Shah et al. [1] followed Abdul Qudus Abbasi's research work carried out a detailed study about features between entities. They developed a Fact Extractor that could extract twenty-six features from the source code of object-oriented

systems to extract the features. Classes, structs, unions, files, folders, global functions, global variables, and macros were all considered entities by them. Class to class relationships based on inheritance, class to class relationships based on containment, class to class relationships based on genericity, class to class relationships based on member access, class to class relationships based on source files and folders, class to class relationships based on a friend, class to global functions or data relationships or macro, and global function to global function are among relationships extracted by fact extractor. An experimental evaluation of relationships for the modularization of object-oriented software systems was reported by Thakur et al. [18]. Using Abbasi's Fact Extractor [13], they retrieved the twenty-six features. Direct and indirect relationships were the two types of relationships. They also found that indirect relationships give better modularization results than direct relationships based on the experimental data.

Aljarah et al. [19] improved on the work of Tzerpos and Andritso, who developed the LIMBO algorithm for software architecture recovery. They combined structural and nonstructural features to determine the usefulness of nonstructural features to the reverse engineering process. Developers' names, directory paths, lines of code, and times of the last update were among the nonstructural features they examined at. The experiments revealed that directory structure and ownership information, but not lines of code, are important factors in software clustering. They also concluded that weighing schemes are useful in breaking down software systems.

Krishnan preferred Koschke's Ph.D. thesis [20] to introduce a classification of component recovery techniques. They used several features for architectural component recovery of structured systems. The features are function calls, set (subprogram sets the value of a global variable), use (subprogram uses the value of object T), take-address-of (subprogram takes the address of object T), function parameter (subprogram has a formal parameter of user-defined data type), return (subprogram returns a value of user-defined type), local-obj-of-type (subprogram has a local object of user-defined type), actual-parameter of (object is an actual parameter in a call to subprogram), of type (S is of type T, where S is an object and T is user-defined type), same-expression (S and T occur in the same expression where S and T are objects) and part-type (S is a part type of T where both S and T are user-defined types).

Richner and Ducasse proposed an environment for generating high-level views of object-oriented systems from both static and dynamic information, and Alshuqayran et al. [21] followed suit. For modularization of a software system, they used composition, inheritance, invocation (method of sender invokes received method on one of the candidates), access (an attribute of class 1 is accessed by the method of class 2), and method (a class defines a method that belongs to another class) as well as dynamic features.

Aljarah et al. [19] proposed MULICsoft, a software clustering algorithm. For the modularization of software systems, they exploited both static and dynamic features. Source files are the objects to be clustered. Procedure calls and variable references are static features, but dynamic features on a software system are the results of profiling the system's execution, indicating how many times each file called procedures in other files during the run time. In 2003, Trifu [22] proposed a technique that combines clustering with pattern-matching, to automatically recover subsystem decompositions. For the clustering process, they used inheritance, association, aggregation, call, and access features. They also proposed a method for assigning weights to these relationships.

Rathee and Chhabra [23] used a combination of static and dynamic features to modularize java software systems. They used inheritance, implementation, containment, calls to methods, and access to variables and assignment relationships along with dynamic features for the software modularization process. Eski and Buzluca [24] presented a comprehensive comparative study of six software clustering algorithms. They developed a lightweight C/C++ source code extractor called CTSX. CTSX is built on CTags and CScope. CTSX uses CTags to extract program entities (functions, variables, and data types) and CScope to retrieve features (function calls).

Teymourian et al. [25] presented an approach for the evaluation of dynamic clustering. They used both static and dynamic features for the modularization process. For feature extraction, they used the CPPX fact extractor system. From the experimental results, they concluded that static features perform better than dynamic features. Rafi et al. [26] introduced a systematic study to categorize the critical challenges associated with best practices of software implementation for organizations and Akbar et al. [27] discussed the challenges associated with successful execution of outsource software development. Using a combined algorithm, Alanazi [28] focused on clustering software systems. Functions were considered as entities in their study, and the following features were used: function call (functions called by an entity), global variables (global variables referred to by an entity), and user-defined types (user-defined types accessed by an entity). Tjortjis [29] proposed a method for mining association rules from code in order to capture program structure and achieve a better understanding of the system. To classify code chunks as entities, they used the following characteristics: Code blocks, variables, and data types are all entitled.

Yadav et al. [30] proposed an approach for analyzing Java code. They analyzed programs and built tables using a Java code analyzer. They also used a clustering engine, which works with such tables and finds relationships between code elements. They considered files, packages, classes, methods, and parameters as entities. The relationships they used in their study include entities ID, entities Name, imported packages, inheritance, implements relationship, arguments, return value, modifier, parameter type, and parameter used.

Rathee and Chhabra [6, 23] followed Tonella presented an approach of using concept analysis for module reconstruction. Accesses to global variables, dynamic location accesses, the presence of a user-defined structured type in the signature, and the presence of a user-defined structured

type in the return type are the relationships he used for module reconstruction.

3. Source Code Entities and Relationship

This section focused on entity and relationship relationships in source code. These source code entities and relationships have been created based on Java source code entities and relationships.

3.1. Entities in Java Source Code. Entities are the smallest significant elements at the architectural level [20]. They are part of the clustering process and become members of clusters during the automated software clustering and modularization process [1]. The proposed "FESJA" extracted three types of entities, these types are classes, interfaces, and enumerations.

A class and an interface can be an entity in object-oriented systems, it has been used widely in software architecture reconstruction and recovery [1, 4]. The approach used by [9] helps to create basic, fully automated tools that can help detect the core classes of a software system based on its code. The study done by [22] used a Model-Driven Engineering technique to provide support for Micro Service Architecture Recovery (MiSAR). In their work, they described an empirical study that uses manual analysis on eight microservice-based open-source projects to identify the core elements of the approach. The research helps software developers and maintainers in taking steps at the design level to create maintainable object-oriented software with classes [22, 23, 31]. "An enum type is a form of data that allows a variable to be a set of specified constants." Enums are java reference types, much as classes. We can add methods, variables, and constructors to an enum in the same way that we would in a regular Java class of Java beat version issued in 2013.

3.2. Relationships. Similarities between entities are always calculated during the modularization process based on their connections. It establishes links between the application's entities. However, the first step is to analyze feature extraction; afterward when, we applied clustering to group entities with similar features or attributes [15]. The relationship types extracted by the proposed fact extractor system, a java-based system, have been identified. Static, dynamic, informal, direct, and indirect relationships are examples of these types of relationships.

4. The Research Methodology of Fact Extraction System

The proposed methodology uses low-level artifacts (source code) to build high-level (abstract views) of the software system in the form of a Java-based Fact Extractor System. Extraction of features is the first stage in modularization, and FESJA has utilized an API named *java.util.regex* to search for necessary parts (approximated approach). Regular expressions were utilized to match patterns in this Java API. FESJA has extracted three categories of entities, as follows:

```
\\bclass[\\s][\\s]*[_[a-z[A-Z]]][\\w]*[\\s\\<\\{]
```

The regular expression above can be used to extract a class myClass{, class myClass {, class myClass<.

```
\\binterface[\\s][\\s]*[_[a-z[A-Z]]][\\w]*[\\s\\{\\<]
```

For the extraction of interfaces, the below regular expression is used.

The regular expression above, for example, can retrieve interface myInt {, interface myInt{, interface myInt<.

```
\\benum[\\s][\\s]*[_[a-z[A-Z]]][\\w]*
```

The enumerations are extracted using a regular expression.

The regular expression above, for example, can extract the enum myEnum.

The Process of fact extraction in FESJA starts with some data being uploaded, folders being extracted, and folder names that are alike being removed. After the extraction process of FESJA, the system check whether the source folder (src) exists or not. The process will end if there is no src folder. The same entity names are removed if the src file exists. Figure 1 shows the whole process of the fact extraction system, whereas Figure 2 shows entities with relationships.

5. Experimental Setup

The experiments are conducted using data sets to evaluate the relationships. These datasets are being designed and implemented using java (object-oriented methodology). JFree Chart (an open-source library for graphs and charts), JUnit (an open-source java unit testing framework), and Weka (an open-source java testing framework) compensate our dataset (Machine learning algorithm for data mining tasks). All these datasets are taken from Github and the source (https://www.grepcode.com). Entities identified by the FESJA tool in the above systems are shown below in Tables 1–4

5.1. Comparative Analysis of Intradataset. This study explores the results of multiple versions of the same data set.

5.1.1. iText. The statistics of the iText software system are shown in Tables 5–9. It has been concluded from the statistics that:

(i) Class is the most important entity in the iText software system, and enumerations are not utilized at all

(ii) Folder-based relationships, composition-based relationships, and access-based relationships are the most common relations for classes

(iii) In comparison to file-based and access-based relationships, folder-based relationships occur frequently in interfaces

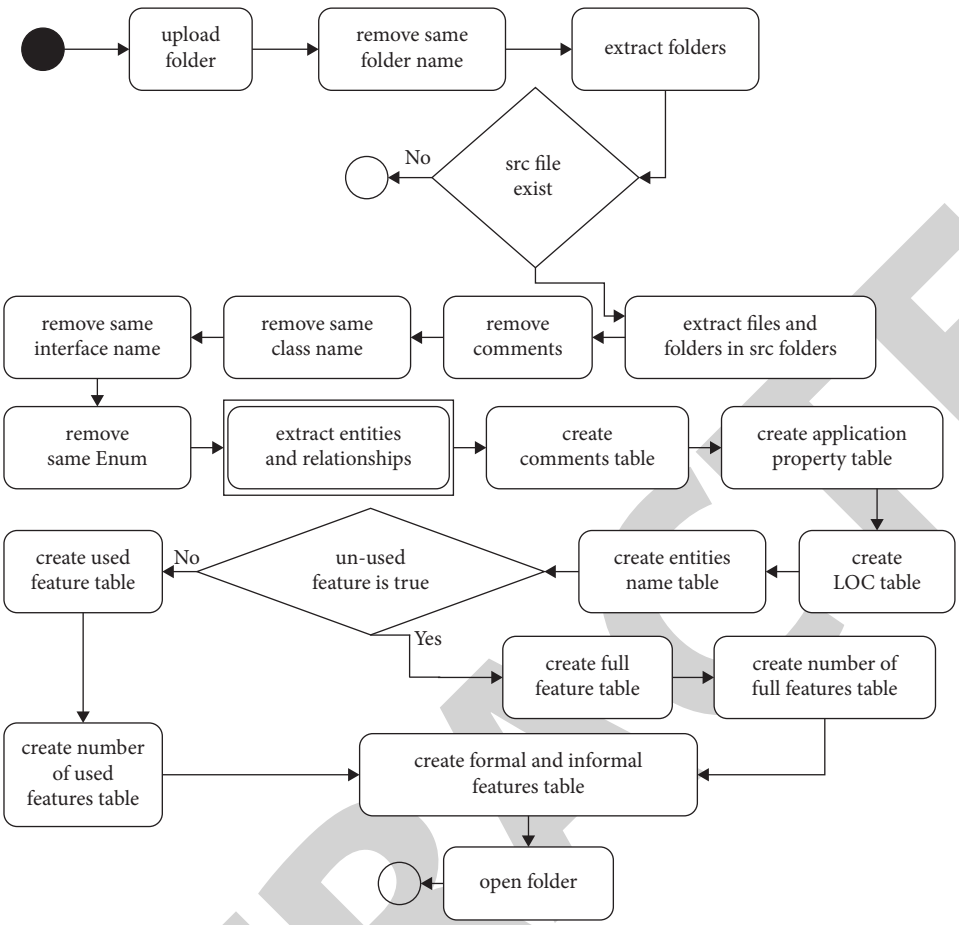

Figure 1: Process of fact extraction.

(iv) Generic or outer implement relationships are not used in the iText software system

(v) Figures 3 and 4 illustrate those formal relationships in iText are based on formal relationships of classes, while formal relationships of interfaces contribute to just 3% of formal relationships

Figures 3–7 providegraphical representations of iText software system statistics.

5.1.2. JFreeChart. Tables 10–14 summarizes statistics of the JFreeChart software system. From the statistics, it has been observed that.

(i) Like iText the most dominant entity in the JFreeChart software system is class while enumerations are not used at all.

(ii) The dominant relationships for classes are folder-based relationships, composition-based relationships, and access-based relationships while implements-based relationships and inheritance-based relationships have also good frequency.

(iii) For interfaces the used relationships are folder-based, file-based, extend based and access-based relationships while other relationships are infrequent. Also, among used relationships, folder-based relationships have the highest frequency.

(iv) Same as iText generics-based relationships and outer implements-based relationships are not used in the JFreeChart software system.

(v) By comparing Figures 8 and 9 it can be calculated that in JFreeChart 92% of formal relationships are based on formal relationships of classes while 8% of formal relationships are based on formal relationships of interfaces.

Figures 8–12 provides a graphical representation of statistics of the JFreeChart software system.

Due to the absence of enumerations, no relationships for enumeration exist in the JFreeChart software system.

5.1.3. JUnit. Tables 15–20 summarizes the statistics of a JUnit software system. From the statistics, it has been observed that.

(i) In the JUnit software system enumerations are introduced in all versions except JUnit 4.8 but have a very low frequency of occurrence.

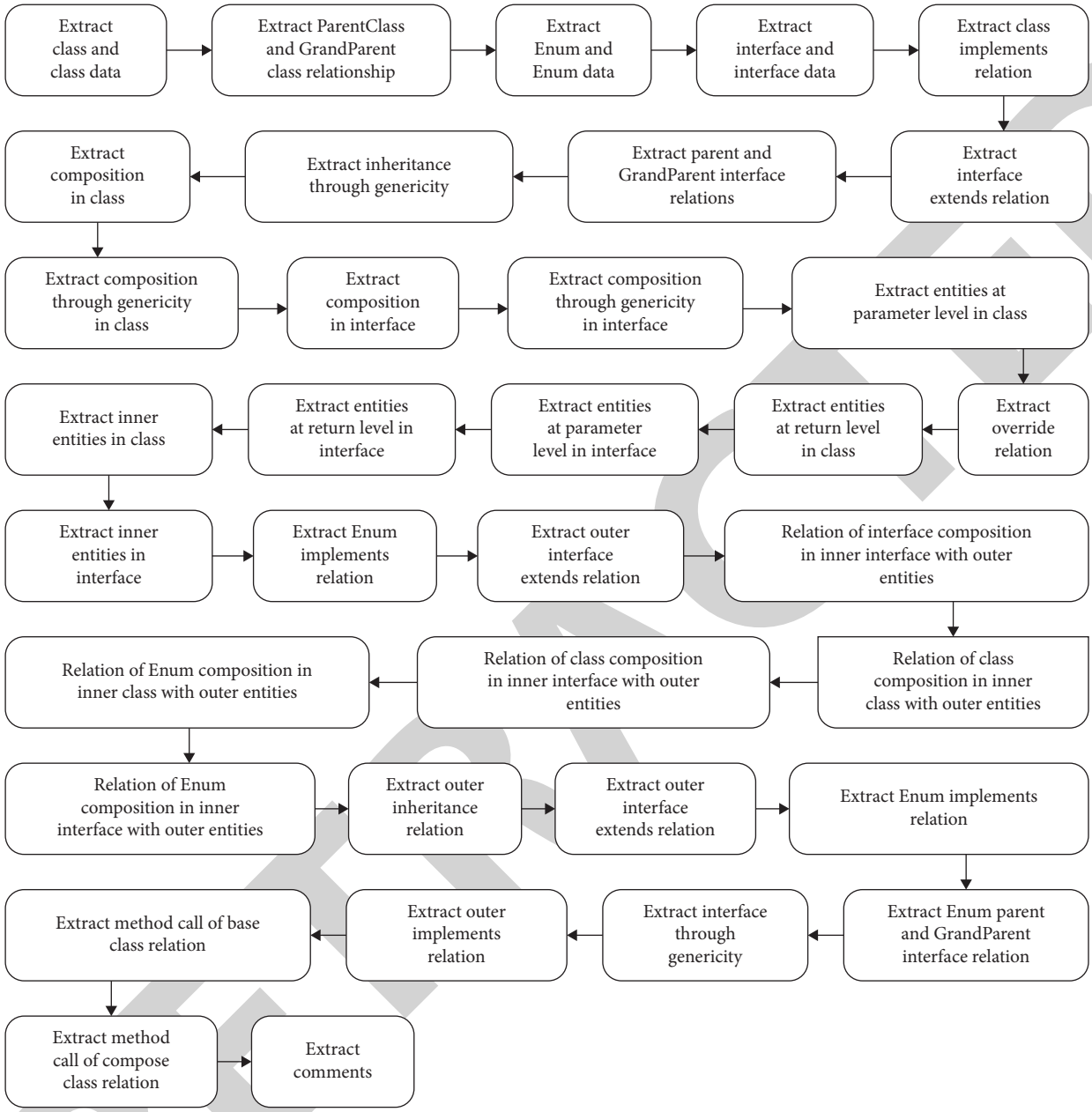

Figure 2: Process of Relationship extraction.

Table 1: Facts about entities in iText dataset.

Entity related information	iText 1.3	iText 1.4	iText 1.4.8	iText 2.1.7
Total no. of folders	29	32	34	69
Total no. of files	399	470	502	549
Total no. of entities	462	545	586	669
Total no. of classes	434	513	551	625
Total no. of interfaces	28	32	35	44
Total no. of enumerations	0	0	0	0
Total no. of functions in application	5330	6195	6517	7029
Total no. of functions in class	5258	6117	6431	6905
Total no. of functions in interface	72	78	86	124
Total no. of functions in enum	0	0	0	0
sLOC	76100	86858	90526	94073
Blank lines	12283	13802	14655	14811
LOC	88383	100660	105181	108884
Size in bytes	4938428	5704081	6103967	6696336

Table 2: Facts about entities in JFreeChart dataset.

Entity related information	JFreeChart 1.0.4	JFreeChart 1.0.7	JFreeChart 1.0.9	JFreeChart 1.0.14
Total no. of folders	61	39	39	40
Total no. of files	500	538	538	594
Total no. of entities	516	559	559	616
Total no. of classes	432	468	468	510
Total no. of interfaces	84	91	91	106
Total no. of enumerations	0	0	0	0
Total no. of functions in application	6705	7468	7522	8629
Total no. of functions in class	6209	6952	7006	8086
Total no. of functions in interface	496	516	516	561
Total no. of functions in enum	0	0	0	0
sLOC	73148	81003	81490	93430
Blank lines	16149	17615	17670	19332
LOC	89297	98618	99160	112762
Size in bytes	6029995	6722638	6774669	7700413

Table 3: Facts about entities in Junit dataset.

Entity related information	Junit 4.8	Junit 4.9	Junit 4.10	Junit 4.11
Total no. of folders	33	31	31	31
Total no. of files	175	160	162	164
Total no. of entities	180	165	168	171
Total no. of classes	148	134	137	137
Total no. of interfaces	32	30	30	32
Total no. of enumerations	0	1	1	2
Total no. of functions in application	1079	1013	1036	1143
Total no. of functions in class	1039	972	995	1099
Total no. of functions in interface	40	32	32	33
Total no. of functions in enum	0	9	9	11
sLOC	6727	6429	6579	7439
Blank lines	1466	1348	1381	1603
LOC	8193	7777	7960	9042
Size in bytes	340192	330167	338458	429090

Table 4: Facts about entities in weka dataset.

Entity related information	Weka-dev 3.7.5	Weka-dev 3.7.6	Weka-dev 3.7.7	Weka-stable 3.6.6
Total no. of folders	87	88	89	110
Total no. of files	1005	1020	1025	1050
Total no. of entities	1352	1378	1384	1379
Total no. of classes	1162	1185	1190	1236
Total no. of interfaces	149	151	152	119
Total no. of enumerations	41	42	42	24
Total no. of functions in application	17114	17501	17618	18746
Total no. of functions in class	16513	16896	17006	18273
Total no. of functions in interface	427	431	438	336
Total no. of functions in enum	174	174	174	137
sLOC	232297	237797	240029	255774
Blank lines	54985	56319	56633	61449
LOC	287282	294116	296662	317223
Size in bytes	13586516	13828049	13940620	15213130

Table 5: Entities in iText.

	iText 1.3	iText 1.4	iText 1.4.8	iText 2.1.7
Classes	434	513	551	625
Interfaces	28	32	35	44
Enumerations	0	0	0	0

Table 6: Formal and informal relationship in iText.

	iText 1.3	iText 1.4	iText 1.4.8	iText 2.1.7
Informal	43107	49474	52488	58601
Formal	7080	8587	9125	11245

Table 7: Formal relationship in iText.

Formal relationships	iText 1.3	iText 1.4	iText 1.4.8	iText 2.1.7
Formal relationships for class	6878	8350	8866	10849
Formal Relationships f or interface	202	237	259	396
Formal Relationships for enum	0	0	0	0

Table 8: Formal relationships for class in iText.

Formal relationships for class	iText 1.3	iText 1.4	iText 1.4.8	iText 2.1.7
Folder-based relationships	2228	2643	2859	3958
File-based relationships	434	513	551	625
Inheritance-based relationships	680	833	871	839
Implements-based relationships	171	203	208	213
Composition-based relationships	2115	2689	2847	3312
Generics-based relationships	0	0	0	0
Access-based relationships	1122	1318	1358	1630
Inner-based relationships	64	69	78	119
Outer inheritance-based relationships	14	14	17	25
Outer implements-based relationships	0	0	0	0
Outer composition-based relationships	50	68	77	128

Table 9: Formal relationships for interface in iText.

Formal relationships for interface	iText 1.3	iText 1.4	iText 1.4.8	iText 2.1.7
Folder-based relationships	140	164	182	283
File-based relationships	28	32	35	44
Extends-based relationships	6	6	6	12
Generics-based relationships	0	0	0	0
Composition-based relationships	0	0	0	0
Access-based relationships	28	35	36	57
Inner-based relationships	0	0	0	0
Outer extends relationships	0	0	0	0
Outer composition relationships	0	0	0	0

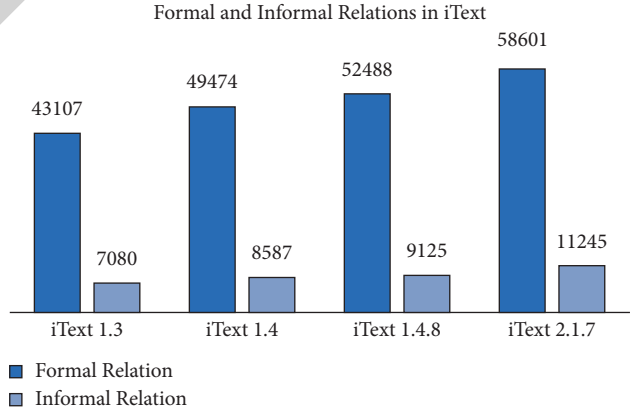

Figure 3: Count of formal and informal relationships in iText.

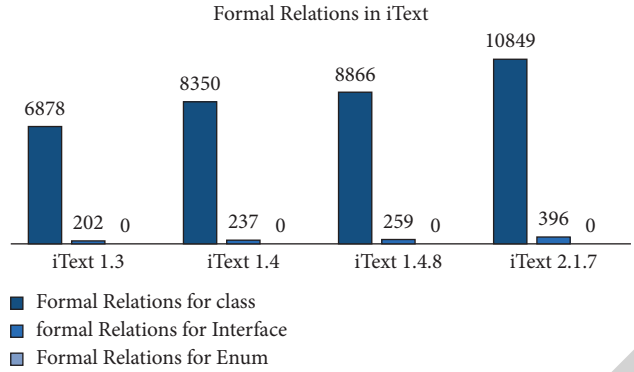

Figure 4: Count of formal relationships in iText.

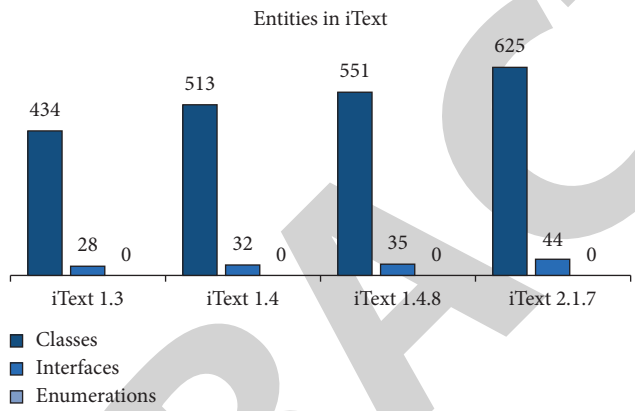

Figure 5: Count of entities in iText.

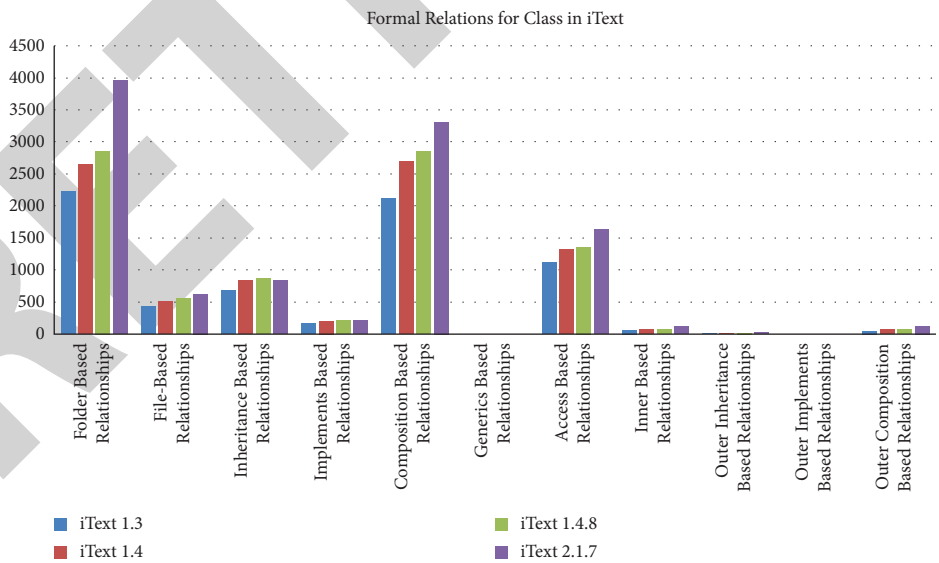

Figure 6: Count of formal relationships for class in iText.

(ii) For classes the most used relationships are folder-based relationships while access-based relationships, implements-based relationships, inheritance-based relationships, and file-based relationships have a good frequency of occurrence.

(iii) For interfaces outer extends-based relationships, outer composition-based relationships, and composition-based relationships are not used while extends-based relationships are only used in JUnit 4.8. Also, among used relationships, folder-based

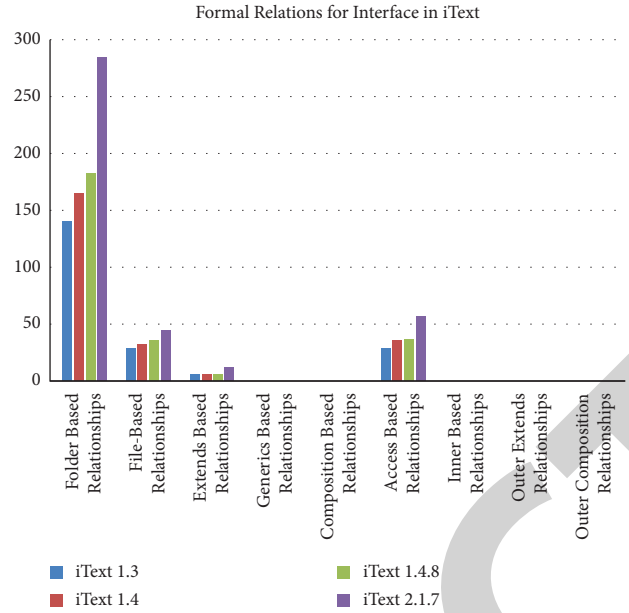

Figure 7: Count of formal relationships for interface in iText.

Table 10: Entities in JFreeChart.

Entities	JFreeChart 1.0.4	JFreeChart 1.0.7	JFreeChart 1.0.9	JFreeChart 1.0.14
Classes	432	468	468	510
Interfaces	84	91	91	106
Enumerations	0	0	0	0

Table 11: Formal and informal relationships in JFreeChart.

Relationships	JFreeChart 1.0.4	Jfreechart 1.0.7	JFreeChart 1.0.9	JFreeChart 1.0.14
Informal	48877	53862	54105	61294
Formal	8321	9059	9058	10056

Table 12: Formal relationships in JFreeChart.

Formal relationships	JFreeChart 1.0.4	JFreeChart 1.0.7	JFreeChart 1.0.9	JFreeChart 1.0.14
Formal relationships for class	7636	8314	8313	9196
Formal relationships for interface	685	745	745	860
Formal relationships for enum	0	0	0	0

Table 13: Formal relationships for class in JFreeChart.

Formal relationships for class	JFreeChart 1.0.4	JFreeChart 1.0.7	JFreeChart 1.0.9	JFreeChart 1.0.14
Folder-based relationships	2184	2385	2385	2599
File-based relationships	432	468	468	510
Inheritance-based relationships	816	917	917	1013
Implements-based relationships	897	970	970	1052
Composition-based relationships	2069	2234	2233	2514
Generics-based relationships	0	0	0	0
Access-based relationships	1217	1308	1308	1475
Inner-based relationships	14	19	19	20
Outer inheritance-based relationships	2	3	3	3
Outer implements-based relationships	0	0	0	0
Outer composition-based relationships	5	10	10	10

Table 14: Formal relationships for interface in JFreeChart.

Formal relationships for interface	JfreeChart 1.0.4	JFreeChart 1.0.7	JfreeChart 1.0.9	JFreeChart 1.0.14
Folder-based relationships	411	450	450	526
File-based relationships	84	91	91	106
Extends-based relationships	81	91	91	95
Generics-based relationships	0	0	0	0
Composition-based relationships	0	0	0	0
Access-based relationships	109	113	113	133
Inner-based relationships	0	0	0	0
Outer extends relationships	0	0	0	0
Outer composition relationships	0	0	0	0

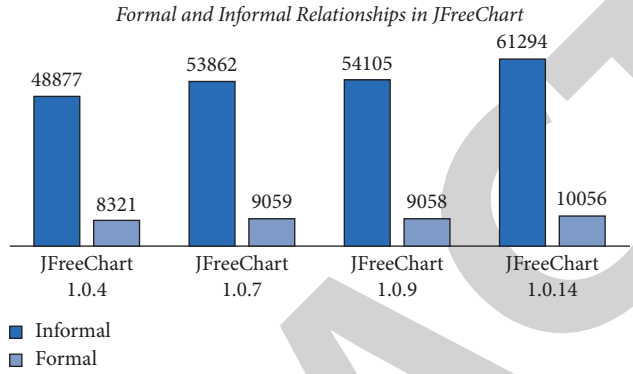

Figure 8: Count number of formal and informal relationships in JfreeChart.

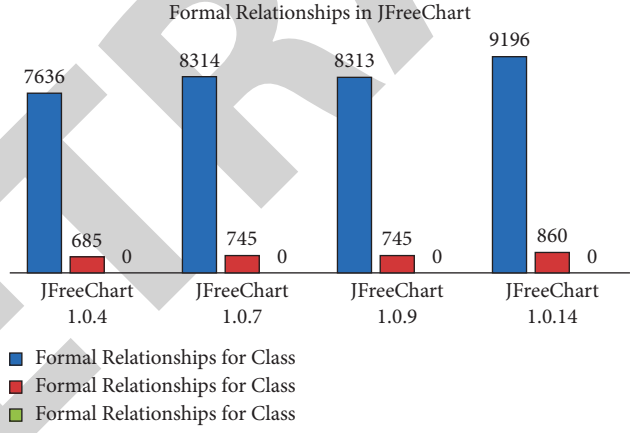

Figure 9: Count number of formal relationships in JfreeChart.

relationships have the highest frequency of occurrence.

(iv) Generics bases relationships have been introduced for classes and interfaces.

(v) The used relationships in enumerations are folder-based, file-based, and access relationships while composition-based relationships are only used in JUnit 4.11. Among them, the dominant relationship is folder-based relation.

(vi) By comparing Figures 13 and 14 it can be calculated that in JUnit 89% of formal relationships are based on formal relationships of classes while 10% of formal relationships are based on formal relationships of interfaces. Similarly, formal relationships in JUnit 4.9, JUnit 4.10, and JUnit 4.11 are based on 0.57%, 0.55%, and 0.92% of formal relationships of enumerations respectively.

Figures 15–18 provide a graphical representation of statistics of a Junit software system.

5.1.4. Weka. Table 21–26 summarizes the statistics of the Weka software system. From the statistics, it has been observed that.

(i) In the Weka software system the dominant entity is class while enumerations have a low frequency of occurrence.

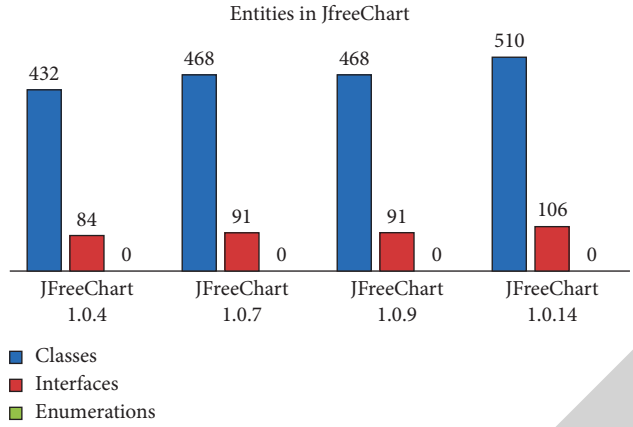

Figure 10: Count of entities in JfreeChart.

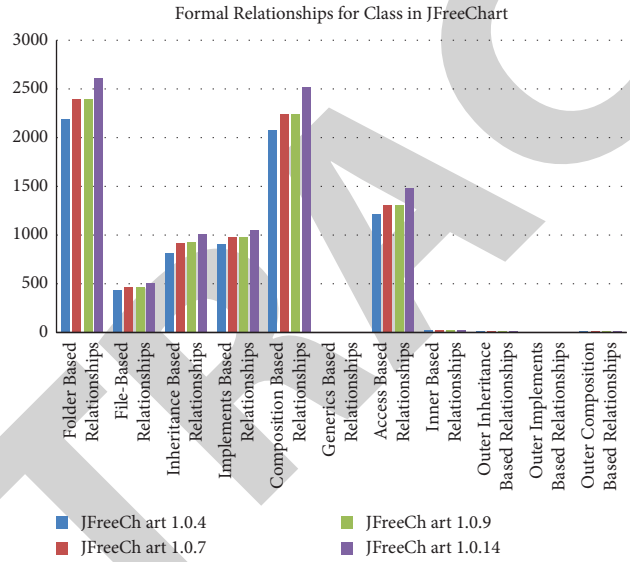

Figure 11: Count number of formal relationships for class in JfreeChart.

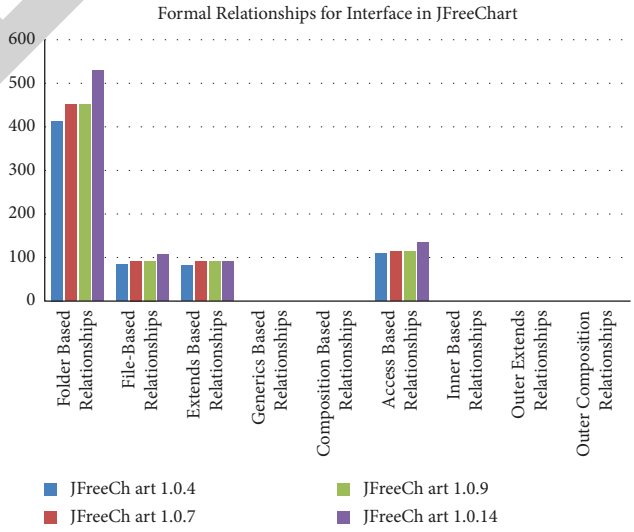

Figure 12: Count number of formal relationships for interface in JfreeChart.

Table 15: Entities in Junit.

Entities	Junit 4.8	Junit 4.9	Junit 4.10	Junit 4.11
Classes	148	134	137	137
Interfaces	32	30	30	32
Enumerations	0	1	1	2

Table 16: Formal and informal relationships in Junit.

Relationships	Junit 4.8	Junit 4.9	Junit 4.10	Junit 4.11
Informal	6616	6171	6286	6705
Formal	1746	1572	1609	1629

Table 17: Formal relationships in Junit.

Formal relationships	Junit 4.8	Junit 4.9	Junit 4.10	Junit 4.11
Formal relationships for class	1568	1399	1436	1441
Formal relationships for interface	178	164	164	173
Formal relationships for enum	0	9	9	15

Table 18: Formal relationships for class in Junit.

Formal relationships for class	Junit 4.8	Junit 4.9	Junit 4.10	Junit 4.11
Folder-based relationships	653	602	617	615
File-based relationships	148	134	137	137
Inheritance-based relationships	161	153	154	157
Implements-based relationships	35	30	34	34
Composition-based relationships	207	178	182	188
Generics-based relationships	19	14	14	14
Access-based relationships	320	262	270	265
Inner-based relationships	16	16	17	18
Outer inheritance-based relationships	0	0	0	0
Outer implements-based relationships	0	0	0	0
Outer composition-based relationships	9	10	11	13

Table 19: Formal relationships for interface in Junit.

Formal relationships for interface	Junit 4.8	Junit 4.9	Junit 4.10	Junit 4.11
Folder-based relationships	125	120	120	127
File-based relationships	32	30	30	32
Extends-based relationships	1	0	0	0
Generics-based relationships	3	1	1	1
Composition-based relationships	0	0	0	0
Access-based relationships	15	12	12	12
Inner-based relationships	2	1	1	1
Outer extends relationships	0	0	0	0
Outer composition relationships	0	0	0	0

(ii) For classes composition-based relationships are the most dominant relationships. Other relationships having a good frequency of occurrence are folder-based and access-based relationships.

(iii) Folder-based relationships, file-based relationships, and access-based relationships have a high frequency of occurrence in interfaces while other relationships are either have a very low frequency of occurrence or not used at all. Among used relationships, folder-based relationships have the highest frequency.

(iv) Generics-based relationships are used in classes and interfaces but have very low usage.

(v) Like JUnit the used relationships in enumerations are folder-based, file-based, access relationships, and composition-based relationships. Among them,

Table 20: Formal relationships for enum in Junit.

Formal relationships for enumeration	Junit 4.8	Junit 4.9	Junit 4.10	Junit 4.11
Folder-based relationships	0	6	6	10
File-based relationships	0	1	1	2
Implements-based relationships	0	0	0	0
Composition-based relationships	0	0	0	1
Genericity-based relationships	0	0	0	0
Access-based relationships	0	2	2	2
Outer implements relationships	0	0	0	0

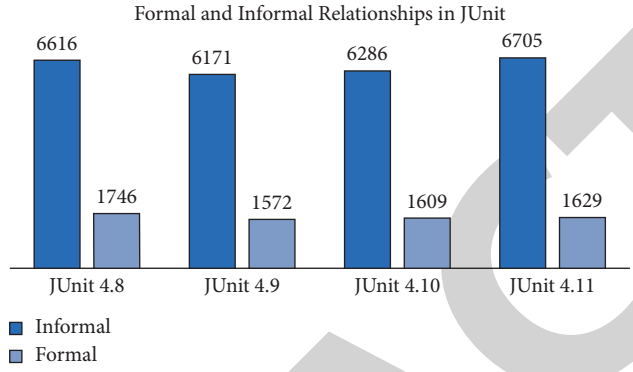

Figure 13: Count of formal and informal relationships in Junit.

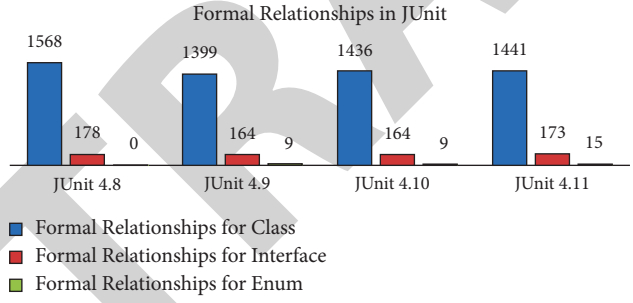

Figure 14: Count of formal relationships in Junit.

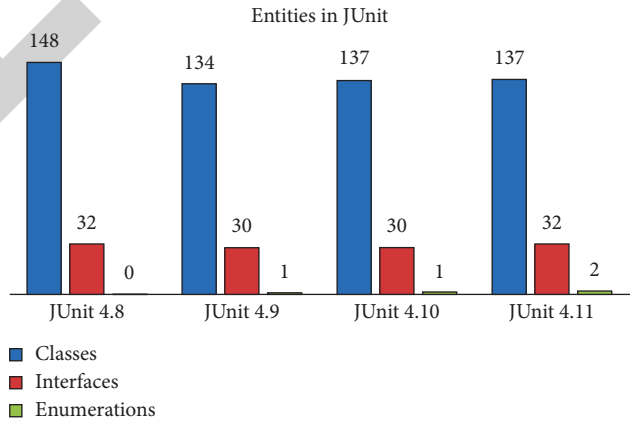

Figure 15: Count of entities in Junit.

the dominant relationship is folder-based relation. Access-based and composition-based relationships have the same frequency of occurrence.

(vi) By comparing Figures 19 and 20, it can be calculated that in Weka 95% of formal relationships are based on formal relationships of classes, 4% of formal

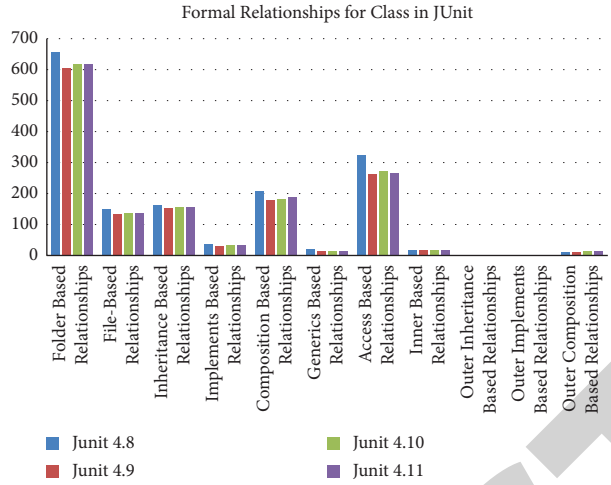

Figure 16: Count of formal relationships for class in Junit.

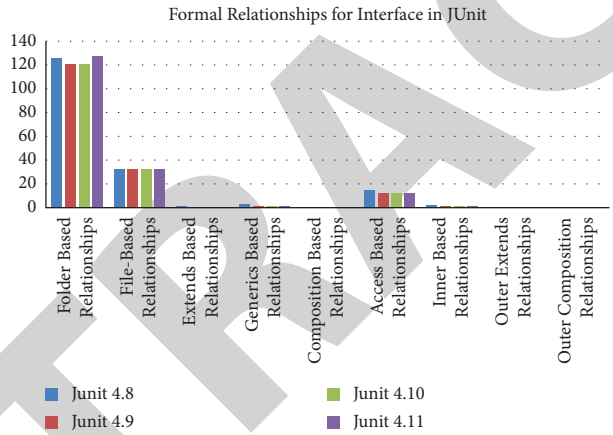

Figure 17: Count of formal relationships for interface in Junit.

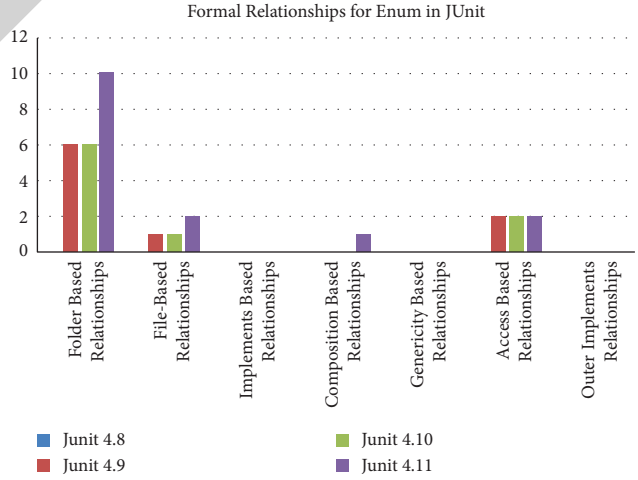

Figure 18: Count of formal relationships for enum in junit.

Table 21: Entities in weka.

Entities	Weka-dev 3.7.5	Weka-dev 3.7.6	Weka-dev 3.7.7	Weka-stable 3.6.6
Classes	1162	1185	1190	1236
Interfaces	149	151	152	119
Enumerations	41	42	42	24

Table 22: Formal and informal relationships in weka.

Relationships	Weka-dev 3.7.5	Weka-dev 3.7.6	Weka-dev 3.7.7	Weka-stable 3.6.6
Informal	124080	129103	129948	136926
Formal	20358	20847	20932	22695

Table 23: Formal relationships in weka.

Formal relationships	Weka-dev 3.7.5	Weka-dev 3.7.6	Weka- dev 3.7.7	Weka-stable 3.6.6
Formal relationships for class	19250	19720	19800	21852
Formal relationships for interface	887	900	905	720
Formal relationships for enum	221	227	227	123

Table 24: Formal relationships for class in weka.

Formal relationships for class	Weka-dev 3.7.5	Weka-dev 3.7.6	Weka-dev 3.7.7	Weka-stable3.6.6
Folder-based relationships	4705	4794	4816	5003
File-based relationships	1162	1185	1190	1236
Inheritance-based relationships	1955	1976	1984	2141
Implements-based relationships	1532	1595	1604	1697
Composition-based relationships	6289	6457	6482	7671
Generics-based relationships	8	10	10	6
Access-based relationships	2775	2858	2868	3300
Inner-based relationships	357	368	369	335
Outer inheritance-based relationships	97	97	97	78
Outer implements-based relationships	14	14	14	6
Outer composition-based relationships	356	366	366	379

Table 25: Formal relationships for interface in weka.

Formal relationships for interface	Weka-dev 3.7.5	Weka-dev 3.7.6	Weka-dev 3.7.7	Weka-stable3.6.6
Folder-based relationships	556	563	566	442
File-based relationships	149	151	152	119
Extends-based relationships	43	45	45	40
Generics-based relationships	6	7	7	6
Composition-based relationships	0	0	0	0
Access-based relationships	132	133	134	113
Inner-based relationships	1	1	1	0
Outer extends relationships	0	0	0	0
Outer composition relationships	0	0	0	0

Table 26: Formal relationships for enum in weka.

Formal relationships for enumeration	Weka-dev 3.7.5	Weka-dev 3.7.6	Weka-dev 3.7.7	Weka-stable3.6.6
Folder-based relationships	176	181	181	99
File-based relationships	41	42	42	24
Implements-based relationships	0	0	0	0
Composition-based relationships	2	2	2	0
Genericity-based relationships	0	0	0	0
Access-based relationships	2	2	2	0
Outer implements relationships	0	0	0	0

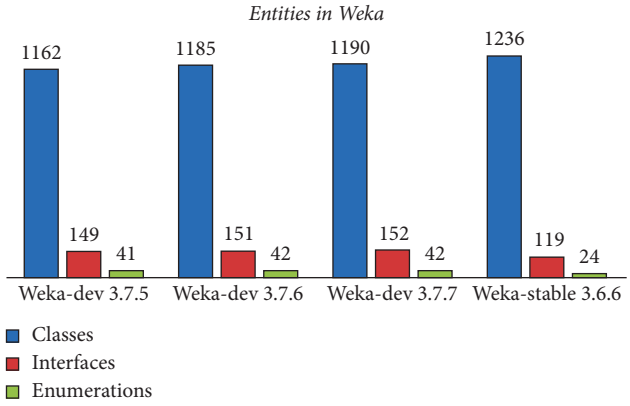

Figure 19: Count of entities in weka.

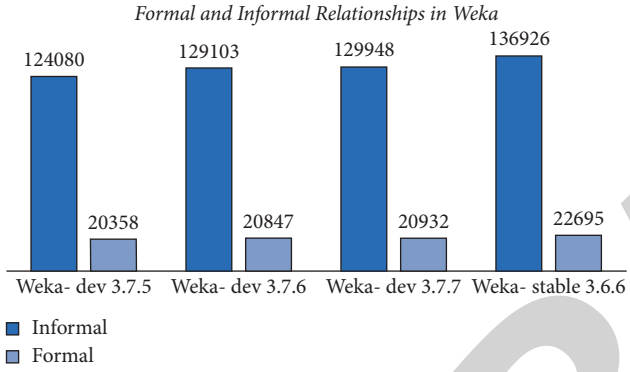

Figure 20: Count of formal and informal relationships in weka.

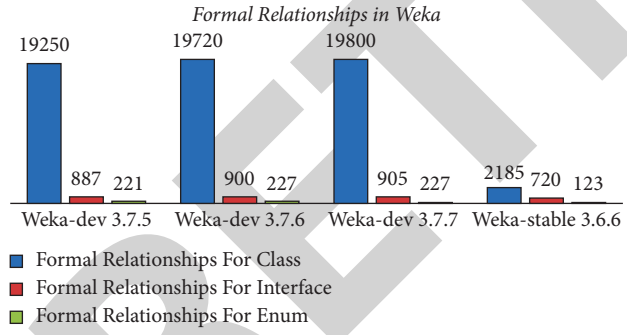

Figure 21: Count of formal relationships in weka.

relationships are based on formal relationships of interfaces and, 1% of formal relationships are based on formal relationships of enumerations.

Figures 19–24 provide a graphical representation of statistics of the Weka software system.

6. Discussion and Analysis

The above Tables 5–26, we have provided the result and analysis of datasets that we have used to conduct our experiment. Different tables and graphs are provided for result analysis, and it can be concluded that the most dominant entity is class, informal relationships have higher occurrence

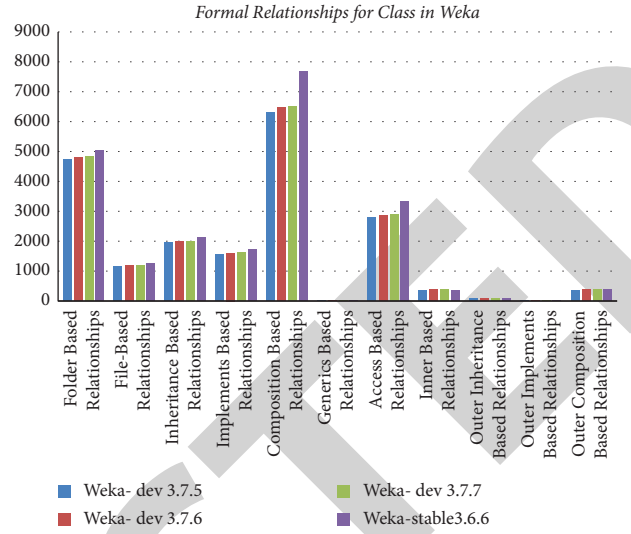

Figure 22: Count of formal relationships for class in weka.

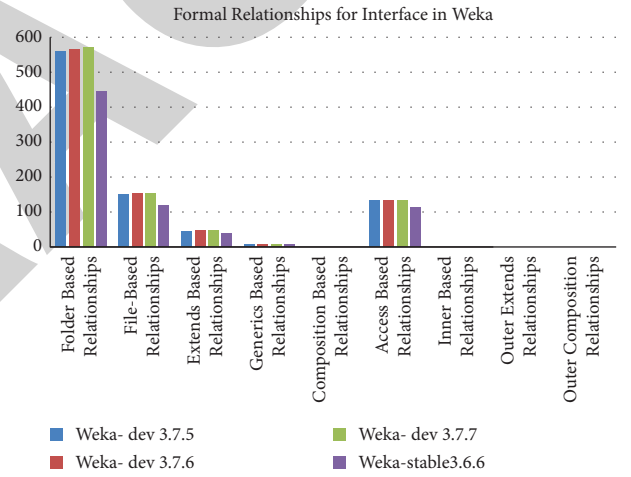

Figure 23: Count of formal relationships for interface in weka.

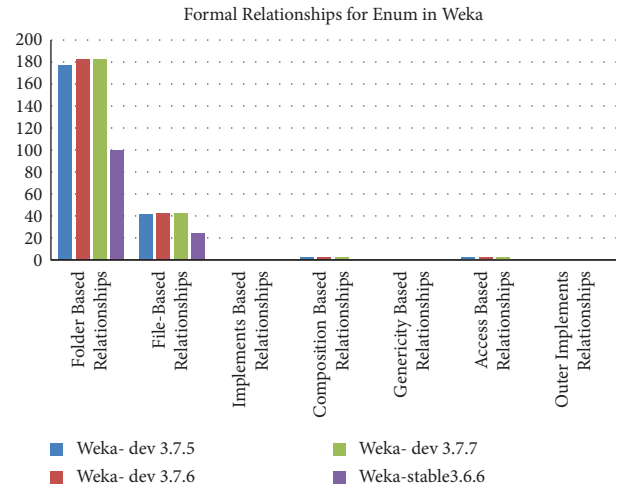

Figure 24: Count of formal relationships for enum in weka.

than formal relationships, and formal relationships are mostly based on formal relationships for classes. We provided a framework for the extraction of entities and relationships that exist t in a Java software system. Our Fact Extractor can extract three types of entities which are classes, interface, and enumerations. The fact extractor can be used to extract both formal and informal relationships. For classes, interfaces, and enumerations, the total number of formal relationships retrieved is 74, 43, and 31, respectively. Similarly, the fact extractor extracted a total of 73 informal relationships.

7. Conclusion

Fact Extractor System for Java Applications (FESJA) is an automatic software modularization tool, used to extract entities and relationships from java source code. The entities extracted by the fact extractor system are classes, interfaces, and enumerations. The Fact Extractor can extract both formal and informal relationships. The formal relationships are categorized into three parts which are formal relationships for classes, formal relationships for interfaces, and formal relationships for enumerations. For evaluation of relationships, we performed our experiment on four systems (dataset). The systems are iText, JFreeChart, Junit, and Weka software systems. We have provided different graphs and tables for analysis of results and presented our observations which can help researchers to carry out tasks related to software modularization process, software architecture recovery, and software clustering.

Data Availability

The data used to support the findings of this study are available from the corresponding author upon request.

Conflicts of Interest

The authors declare no conflicts of interest.

Acknowledgments

The authors are grateful to the Deanship of Scientific Research, King Saud University for funding through Vice Deanship of Scientific Research Chairs.

References

[1] Z. Shah, R. Naseem, M. A. Orgun, A. Mahmood, and S. Shahzad, "Software clustering using automated feature subset selection," in *Proceedings of the International Conference on Advanced Data Mining and Applications*, pp. 47–58, Hangzhou, China, December 2013.

[2] I. Candela, G. Bavota, B. Russo, and R. Oliveto, "Using cohesion and coupling for software remodularization," *ACM Transactions on Software Engineering and Methodology*, vol. 25, no. 3, pp. 1–28, 2016.

[3] P. Behnamghader, D. M. Le, J. Garcia, D. Link, A. Shahbazian, and N. Medvidovic, "A large-scale study of architectural evolution in open-source software systems," *Empirical Software Engineering*, vol. 22, no. 3, pp. 1146–1193, 2017.

[4] S. Muhammad, *Experimental Evaluation of Relationships for the Modularization of Object-Oriented Software Systems*, Quaid-e-Azam University Islamabad, Islamabad, Pakistan, 2010.

[5] Q. Alsarhan, B. S. Ahmed, M. Bures, and K. Z. Zamli, "Software module clustering: an in-depth literature analysis," *IEEE Transactions on Software Engineering*, 2020.

[6] R. Naseem, M. M. Deris, O. Maqbool, and S. Shahzad, "Euclidean space-based hierarchical clusters combinations: an application to software clustering," *Cluster Computing*, vol. 22, no. 3, pp. 7287–7311, 2019.

[7] R. Naseem, M. B. M. Deris, O. Maqbool, J.-p. Li, S. Shahzad, and H. Shah, "Improved binary similarity measures for software modularization," *Frontiers of Information Technology & Electronic Engineering*, vol. 18, no. 8, pp. 1082–1107, 2017.

[8] K. Raimond and J. Lovesum, "A novel approach for automatic modularization of software systems using extended ant colony optimization algorithm," *Information and Software Technology*, vol. 114, pp. 107–120, 2019.

[9] I. Șora and C. B. Chirila, "Finding key classes in object-oriented software systems by techniques based on static analysis," *Information and Software Technology*, vol. 116, Article ID 106176, 2019.

[10] H. Li, T. Wang, W. Pan et al., "Mining key classes in java projects by examining a very small number of classes: a complex network-based approach," *IEEE Access*, vol. 9, pp. 28076–28088, 2021.

[11] W. Jiang and N. Dai, "Identifying key classes algorithm in directed weighted class interaction network based on the structure entropy weighted leaderrank," *Mathematical Problems in Engineering*, vol. 2020, Article ID 9234042, 12 pages, 2020.

[12] X. Du, T. Wang, W. Pan et al., "COSPA: identifying key classes in object-oriented software using preference aggregation," *IEEE Access*, vol. 9, pp. 114767–114780, 2021.

[13] I. Hussain, A. Khanum, A. Q. Abbasi, and M. Y. Javed, "A novel approach for software architecture recovery using particle swarm optimization," *The International Arab Journal of Information Technology*, vol. 12, no. 1, pp. 32–41, 2015.

[14] M. Aghdasifam, H. Izadkhah, and A. Isazadeh, "A new metaheuristic-based hierarchical clustering algorithm for software modularization," *Complexity*, vol. 2020, Article ID 1794947, 25 pages, 2020.

[15] I. Zahoor, O. Maqbool, and R. Naseem, "Web application fact extractor (WAFE)," in *Proceedings of the Eighth International Conference on Digital Information Management (ICDIM 2013)*, pp. 379–384, IEEE, Islamabad, Pakistan, September 2013.

[16] J. Oh, S. Lee, A. H. Kim, and W. H. Ahn, "An automatic extraction scheme of dependency relations between web components and web resources in Java web applications," *Journal of the Korea Institute of Information and Communication Engineering*, vol. 22, no. 3, pp. 458–470, 2018.

[17] J. Oh, W. H. Ahn, and T. Kim, "Automatic extraction of dependencies between web components and database resources in java web applications," *Journal of Information and Communication Convergence Engineering*, vol. 17, no. 2, pp. 149–160, 2019.

[18] M. Thakur, K. Patidar, S. Chouhan, and R. Kushwah, "A clustering based on optimization for object oriented quality prediction," *International Journal of Advanced Technology and Engineering Exploration*, vol. 5, no. 41, pp. 62–69, 2018.

[19] I. Aljarah, H. Faris, S. Mirjalili, N. Al-Madi, A. Sheta, and M. Mafarja, "Evolving neural networks using bird swarm

Hindawi
Journal of Mathematics
Volume 2024, Article ID 9818702, 1 page
https://doi.org/10.1155/2024/9818702

Retraction

Retracted: Music Therapy Methods Based on SVM and MLP

Journal of Mathematics

Received 23 January 2024; Accepted 23 January 2024; Published 24 January 2024

This article has been retracted by Hindawi following an investigation undertaken by the publisher [1]. This investigation has uncovered evidence of one or more of the following indicators of systematic manipulation of the publication process:

(1) Discrepancies in scope

(2) Discrepancies in the description of the research reported

(3) Discrepancies between the availability of data and the research described

(4) Inappropriate citations

(5) Incoherent, meaningless and/or irrelevant content included in the article

(6) Manipulated or compromised peer review

The presence of these indicators undermines our confidence in the integrity of the article's content and we cannot, therefore, vouch for its reliability. Please note that this notice is intended solely to alert readers that the content of this article is unreliable. We have not investigated whether authors were aware of or involved in the systematic manipulation of the publication process.

In addition, our investigation has also shown that one or more of the following human-subject reportin requirements has not been met in this article: ethical approval by an Institutional Review Board (IRB) committee or equivalent, patient/participant consent to participate, and/or agreement to publish patient/participant details (where relevant).

Wiley and Hindawi regrets that the usual quality checks did not identify these issues before publication and have since put additional measures in place to safeguard research integrity.

We wish to credit our own Research Integrity and Research Publishing teams and anonymous and named external researchers and research integrity experts for contributing to this investigation.

The corresponding author, as the representative of all authors, has been given the opportunity to register their agreement or disagreement to this retraction. We have kept a record of any response received.

References

[1] H. Zou, "Music Therapy Methods Based on SVM and MLP," *Journal of Mathematics*, vol. 2022, Article ID 3377809, 6 pages, 2022.

Hindawi
Journal of Mathematics
Volume 2022, Article ID 3377809, 6 pages
https://doi.org/10.1155/2022/3377809

Research Article

Music Therapy Methods Based on SVM and MLP

Hongmin Zou

Music and Dance Academy, YuZhang Normal University, Nanchang, Jiangxi Province 330103, China

Correspondence should be addressed to Hongmin Zou; 1815200113@e.gzhu.edu.cn

Received 23 November 2021; Revised 20 December 2021; Accepted 11 March 2022; Published 27 March 2022

Academic Editor: Naeem Jan

Lately, the music therapy is being used widely around the world. Henceforth, this study focuses on the analysis of the music's effect on fetal heart rate (FHR) curve. To this end, we treated people with music therapy and carried out the experiment. Firstly, 118 people with 32–40 weeks of gestational age who were expecting to give birth were invited to participate in the experiment. There was one control group and three experimental groups: 27 people were in the control group, 32 people were in the experimental group that listened to music for the first 10 minutes and did not listen to music for the second 10 minutes, 29 people were in the experimental group that did not listen to music for the first 10 minutes and listened to music for the second 10 minutes, and 30 people were in the experimental group that listened to music for all 20 minutes. In this paper, a convolutional neural network (CNN) based data processing model for fetal heart rate curves is proposed to improve the accuracy of fetal status assessment. First, the model method divides the high-dimensional one-dimensional fetal heart rate (FHR) records into 10 segments and then the characteristics of the FHR are extracted using a feature extraction method based on basic statistics. These features are regarded as input of support vector machine (SVM) and multilayer perceptron (MLP) for classification. According to the experimental results, the classification accuracies of SVM and MLP are 85.98% and 93.24%, respectively.

1. Introduction

At present, fetal monitoring mainly focuses on counting, fetal heart auscultation, and amniotic fluid pattern observation, but these methods have some limitations because the extracted information is very complex. However, since the 1960s, the large-scale development of electronic systems has made the extraction of fetal information feasible and reliable [1–3].

At present, a method called EMF is used [4, 5], which can monitor fetal information in real time and continuously and is also the most widely used method at present. With the development of artificial intelligence and the emergence of a large number of intelligent algorithms such as deep learning, we can monitor the fetus more accurately [6, 7].

Along with the study and analysis of fetal heart rate curves, numerous people have gone on to study what kind of treatments affect the data related to the characteristics of fetal heart rate curves, and music therapy is one of these tools. The discipline of music therapy was introduced to China as an emerging discipline in the late intersectional era. Although the development of music therapy in China is still in its infancy, concerned medical practitioners and researchers have been pushing its development. The cross-cutting discipline was born in the United States in 1940 as a combination of music, medicine, and psychology. It was introduced to China in the late 1980s. Although the development of music therapy in China is still in its infancy, relevant medical practitioners and researchers have been promoting its development. Numerous related literature has seen the use of music therapy for psychotherapy, presurgical anxiety, postsurgical pain management and maternity treatment, and even cancer treatment. Music therapy is a form of treatment that employs the relevant properties of music to transform the patient's mind and body during the treatment process [8, 9], which is shown in Figure 1.

In this paper, the analysis of the music's effect on the FHR curve is carried out. In order to conceive the required target, we treated people with music therapy by some experiments. Section 2 of this paper debates on the topic of music therapy which is based on neural network. The MLP and SVM are also discussed in Section 2. Furthermore, the experimental subjects and methods are discussed in Section 3. And finally, the conclusion is given in Section 4.

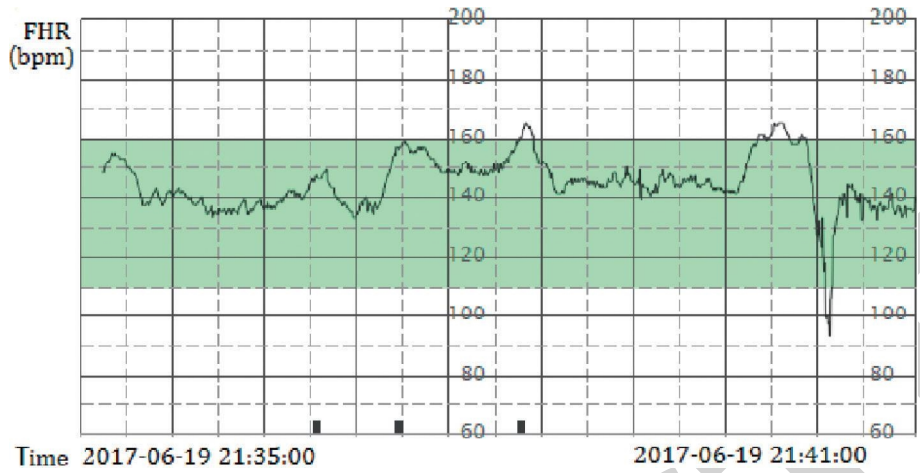

Figure 1: The relevant properties of music and treatment process.

2. Neural Network-Based Music Therapy

In this paper, we use a multilayer perceptron and a support vector machine to classify the features of the data, which are extracted by a statistical-based approach. These two methods are mainly used to compare the experimental results with CNNs without feature extraction. The basic concepts of multilayer perceptron and support vector machine are introduced below.

2.1. Multilayer Perceptron. The neural networks are the ability to find dependencies between different inputs. The criteria for classification of fetal heart rate curves are fixed, while physicians consider a combination of features and ratios during fetal heart rate assessment. Therefore, in order to monitor the fetus more accurately, we need to classify the extracted data, determine its weight relationship, and then train the extracted data. In the neural network, in order to improve the accuracy of the neural network, we can appropriately increase the training of the neural network, so that we cannot add too many parameters to maintain the training model. However, the disadvantage of this network is to select different parameters for different models.

This paper is a multilayer perceptron-based multiclassification algorithm, which is also often referred to as a feed-forward neural network. The multilayer perceptron has one or more implicit layers between the input and output layers, where each layer contains multiple neurons interconnected with each other by weights, which is shown in Figure 2.

For parameter initialization, a random initialization strategy is used in this paper. This method can easily avoid the dilemma of local minima. The activation function of this paper is ReLU (Rectified Liner Units), which can well solve the gradient calculation problem brought by the sigmoid activation function and can avoid the gradient disappearance problem now. The multilayer perceptron in this paper is trained using back propagation. In this paper, we use stochastic gradient descent for training and back propagation for gradient computation. The cost function used in the multilayer perceptron is the cross-entropy cost function.

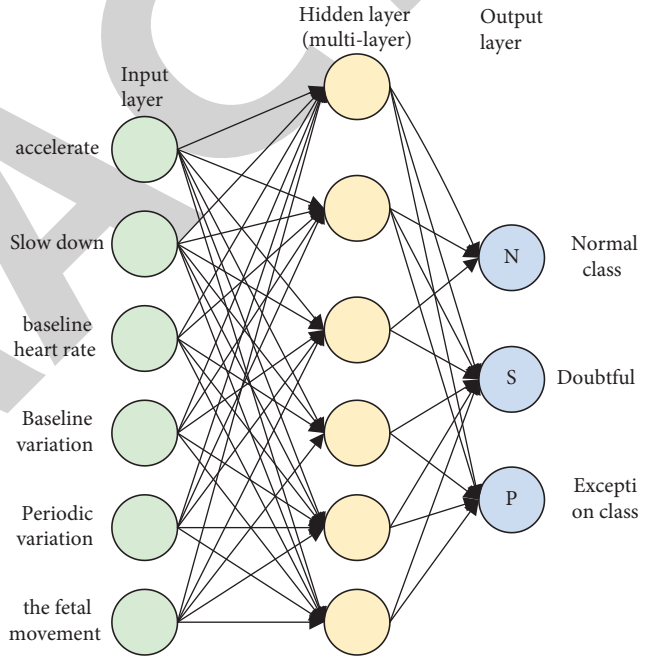

Figure 2: Multilayer perceptron neural network.

When the error is bigger, the gradients are greater, and the parameter W is altered faster, resulting in a faster training speed. As a result, the cross-entropy cost function's training impact is generally superior to the quadratic function's training effect.

Algorithm 1 is the basic step used by the multilayer perceptron for classification.

2.2. Support Vector Machines. Support vector machine (SVM) refers to a series of machine learning algorithms originally developed in the early 1990s by Vapnik and colleagues at AT&T. The basis of this class is essentially the Support Vector Algorithm, which is an extension of the Generalized Portrait algorithm, which was developed by Vapnik in the Soviet Union in 1963. In short, SVM classifiers are binary or discriminative models that distinguish between

Input: training set
Output: accuracy
(1) Network initialization: randomly initialize all connection rights and thresholds in the network in the range (0, 1), given the learning rate and excitation function.
(2) repeat
(3) for all (x, y) do
(4) First calculate the output of the hidden layer based on the weights and thresholds and calculate the output of the current sample;
(5) Based on the output of the implicit layer from the previous step, the connection weights and thresholds are performed to calculate the predicted output of the BP, and the gradient term of the neurons in the output layer is calculated;
(6) Calculate the network prediction error based on the network prediction output and the desired output; calculate the gradient term of the hidden layer neurons;
(7) Update connection weights based on network prediction errors; update connection weights with threshold values;
(8) end for
(9) until the stop condition is reached;
(10) Calculation accuracy (Softmax);

Algorithm 1: MLP classifier.

two types of data and thus classify them. The most basic idea in learning classification is to divide the plane, which in this paper is to find a division hyperplane in the data representation space corresponding to the fetal heart rate dataset. In this paper, we use SVC (Support Vector Classification), which is a nonlinear kernel called Radial Basis Function (RBF). If the original space is finite dimensional, i.e., has a finite number of attributes, then there must exist a high-dimensional feature space to make the samples separable. Therefore, the method is applicable to the fetal heart rate dataset.

In the experiment, some of the obtained characteristics are fed into MLP and SVC, and the classification performance is calculated from the following:

$$\text{accuracy} = \frac{\text{prediction}}{\text{actual}} \times 100\%. \quad (1)$$

2.3. Classification Results Based on MLP and SVC. First, in our experiments, we utilize the MLP algorithm. The classification accuracy is significantly improved with the number of hidden layers from 1 to 200, and the instruction instance and testing time are as well significantly increased. Furthermore, the classification accuracy is not significantly improved with more than 200 hidden layers. We adjusted the hidden layers to 150 layers to maximize efficiency and ensure accuracy, taking into consideration the training and testing duration. Iteration is the procedure of repeating of every experimental step. The numeral of iterations for the experimental guidance was 200, and increasing the quantity of iterations had little effect on the classification accuracy. Identity, logistic, tanh, and ReLU are some of the perception employed in the trials. The results of ReLU are better. Given the huge exploratory data set, the weight optimization technique used in this paper is Kingma Diederik's gradient descent optimization technique, which is more accurate than quasi-optimization methodologies in the quasi-Newton algorithm family. The training data is initially set to 0.0001. Figure 3 depicts the experimental results. When the training dataset is too short, the consistency decreases. As the size of the training data set increases, the accuracy rate slowly increases and stabilizes.

In the SVC algorithm, we classify the data extracted from the fetus. The function of parameter C is to regularize the parameters. If the parameter C becomes larger, it means that the final variable is close to 0, which means that the result error will be larger and larger. If the parameter C becomes smaller, it means that the error prone of the system is better, as shown in Figure 4. According to the training results, we can know that SVC algorithm has better accuracy. In this experiment, we found that when $C = 1$, the experimental effect is the best.

3. Experimental Subjects and Methods

In this section, the experiments are carried out to validate the proposed methods. In this regard, we first proceed with the general information and then experimental methods are described.

3.1. General Information. One hundred and eighteen people at 32–40 weeks who were on birth control from December 01, 2016, to January 31, 2017, were selected. The participating pregnant volunteers were divided into the following four groups, i.e., three experimental groups and a control group:

(i) *Normal group*: 27 people were in the normal group (no music therapy)
(ii) *Experimental group 1:* people listened to music for the first ten minutes and not for the second ten minutes ($n = 32$).
(iii) *Experimental group 2:* people who did not listen to music for the first ten minutes and listened to music for the second ten minutes ($n = 29$)
(iv) *Experimental group 3:* people who received music therapy for all twenty minutes ($n = 30$)

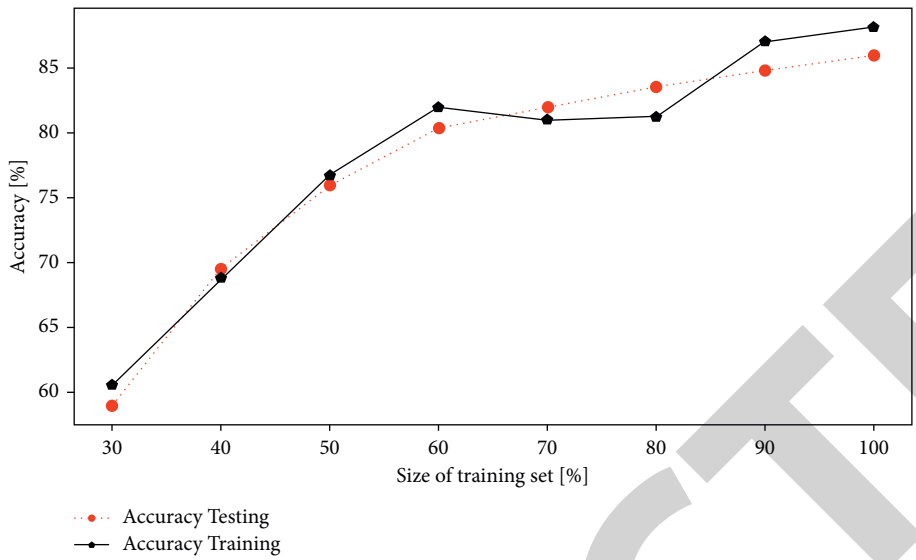

Figure 3: Relationship between dataset size and MLP classification accuracy.

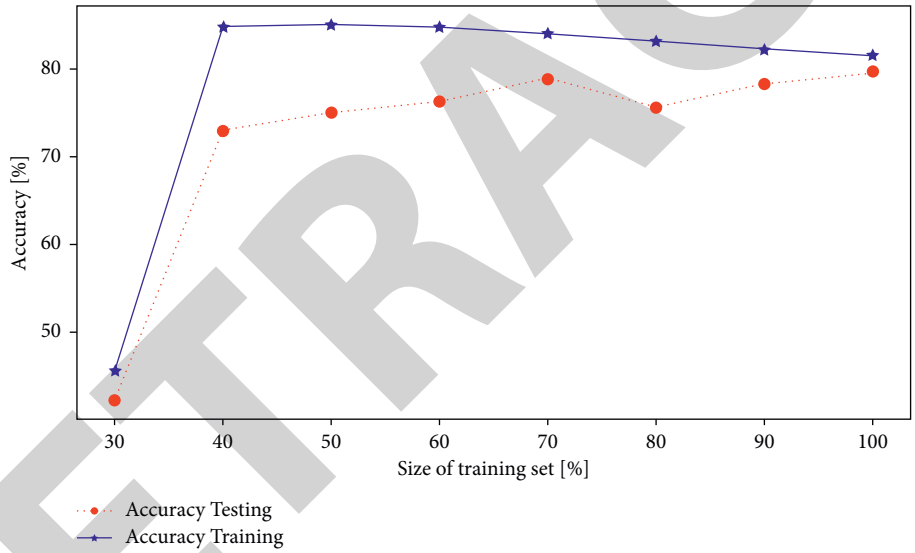

Figure 4: Relationship between dataset size and SVC classification accuracy.

In this paper, the data of the four groups were analyzed by ANOVA between groups, and the differences were not statistically significant ($P > 0.05$) for the demographic attributes of the four groups of people. The details are shown in Table 1.

3.2. Experimental Method. The pregnant volunteers came to the laboratory 2 hours after lunch and lay flat on the bed in a quiet room under the guidance of the relevant staff. After resting for half an hour, the experiment was started simultaneously on four groups of people. At the beginning of the experiment, accelerations and decelerations, baseline fetal heart rate, amplitude variation, cycle variation, fetal movement, and contractions were observed and recorded for 20 minutes without music. After measurement and recording in a quiet environment, this paper provides music therapy to the experimental group on the basis of conventional care. According to the literature of music therapy, the metronome was selected as bass tune and slow rhythm with more than 60 and less than 80 beats, and the soft music with certain relaxation effect, the experimental music in this paper was mainly fetal music, and other soft music was supplemented. And the people in the normal group had the same experimental environment as the experimental group except that there was no music therapy. After one consecutive week, the characteristic indexes of fetal heart rate curve, such as acceleration, deceleration, fetal heart baseline, amplitude variation, cycle variation, fetal movement, and contraction, were measured in the experimenter.

Therefore, we evaluate different algorithms in different networks. In particular, the aggregation layer in this study is at the tSNE position of the last two layers (conv4 3 and conv5 3), and the last convolution layer (fc7) integrates all

Table 1: Methodological analysis of the attributes of the four groups of people.

Index	Normal group	Experimental group 1	Experimental group 2	Experimental group 3	F	*P*
Number of people	27	32	29	30		
Age (years)	30.22	29.63	29.48	30.03	0.182	0.909
Gestational week (weeks)	35.63	35.94	35.59	35.47	0.306	0.821

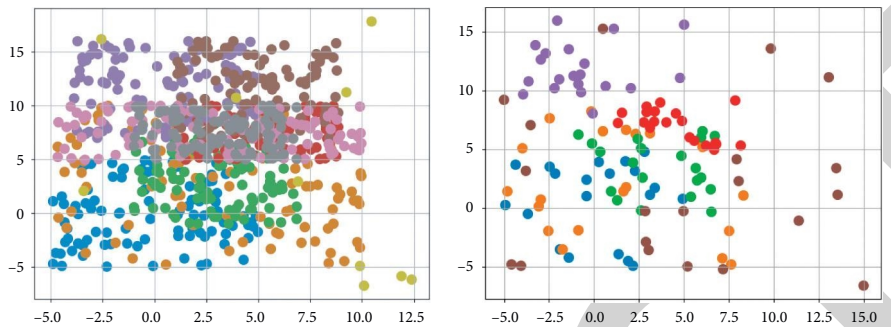

Figure 5: Subsampled conv and fc features from a collection of data are embedded in tSNE: (a) conv5 3 and (b) fc7.

Table 2: Reliability of various hybrid models in various algorithms.

	Basic facts	Correct	Miss
Early fusion	0.8543	0.7522	0.8568
Intermediate fusion	0.8752	0.7358	0.8812
Late fusion	0.9331	0.8324	0.8879

the features of image conv and fc, as shown in Figure 5. For each scenario, the suggested aggregating layer is trained before the block of layers. Thus, for conv4, the loss is indicated by conv4 1, and for fc7, the loss is indicated by fc7. The outcome is denoted in Figure 5 which clearly verifies that aggregating the last evolutionary layer (conv5 3) produces the best performance. The performance of fc6 characteristics is similar to that of fc7.

There are only two reasons for this. One is that we add pooling in the full connection layer, but this method will compress the extracted information prematurely and affect the accuracy. Second, in the characteristic information of fc7, we compared the characteristic values from different information and added the comparison values. Although these characteristic values are very similar (Figure 5(b)), since we added conv5 in the later stage, the signal capture ability of the network is increased, and the captured information is more complex (Figure 5(a)), as shown in Section 3.1.

As can be seen from Table 2, under different algorithm conditions, the later fusion algorithm has the highest accuracy.

4. Conclusions

In this paper, a convolutional neural network-based data processing model for fetal heart rate curves is proposed to enhance fetal condition meeting the criteria. First, the model separates the high-dimensional one-dimensional FHR recordings into 10 sections and then extracts the FHR characteristics using a feature extraction technique related to basic statistics. These characteristics are then fed into support vector machine (SVM) and multilayer perceptron (MLP) classification algorithms. According to the experimental results, the classification accuracies of SVM and MLP are 85.98% and 93.24%, respectively.

Data Availability

The data used to support the findings of this study are included within the article.

Conflicts of Interest

The author declares that there are no conflicts of interest regarding the publication of this paper.

References

[1] Y. Choi and M. Choi, "Infant's speech perception research: a literature review and an outlook for related Korean studies," *Communication Sciences & Disorders*, vol. 21, no. 1, pp. 1–14, 2016.

[2] M. B. Eftekhari, "Physical activity pattern and personal-social factors of mothers during pregnancy and infant birth weight based on met scale: a case-control study," *Iranian Red Crescent Medical Journal*, vol. 15, no. 7, pp. 573–580, 2013.

[3] Guidelines for Palivizumab Prophylaxis, "Are they based on infant's risk of hospitalization for respiratory syncytial viral disease?" *The Pediatric Infectious Disease Journal*, vol. 22, no. 11, pp. 939–943, 2003.

[4] L. T. Fadnes, I. M. S. Engebretsen, K. M. Moland, J. Nankunda, J. K. Tumwine, and T. Tylleskär, "Infant feeding counselling in Uganda in a changing environment with focus on the general

Hindawi
Journal of Mathematics
Volume 2024, Article ID 9879804, 1 page
https://doi.org/10.1155/2024/9879804

Retraction

Retracted: Deep Neural Network Model Forecasting for Financial and Economic Market

Journal of Mathematics

Received 23 January 2024; Accepted 23 January 2024; Published 24 January 2024

This article has been retracted by Hindawi following an investigation undertaken by the publisher [1]. This investigation has uncovered evidence of one or more of the following indicators of systematic manipulation of the publication process:

(1) Discrepancies in scope

(2) Discrepancies in the description of the research reported

(3) Discrepancies between the availability of data and the research described

(4) Inappropriate citations

(5) Incoherent, meaningless and/or irrelevant content included in the article

(6) Manipulated or compromised peer review

The presence of these indicators undermines our confidence in the integrity of the article's content and we cannot, therefore, vouch for its reliability. Please note that this notice is intended solely to alert readers that the content of this article is unreliable. We have not investigated whether authors were aware of or involved in the systematic manipulation of the publication process.

Wiley and Hindawi regrets that the usual quality checks did not identify these issues before publication and have since put additional measures in place to safeguard research integrity.

We wish to credit our own Research Integrity and Research Publishing teams and anonymous and named external researchers and research integrity experts for contributing to this investigation.

The corresponding author, as the representative of all authors, has been given the opportunity to register their agreement or disagreement to this retraction. We have kept a record of any response received.

References

[1] F. Chen, "Deep Neural Network Model Forecasting for Financial and Economic Market," *Journal of Mathematics*, vol. 2022, Article ID 8146555, 10 pages, 2022.

Hindawi
Journal of Mathematics
Volume 2022, Article ID 8146555, 10 pages
https://doi.org/10.1155/2022/8146555

Research Article

Deep Neural Network Model Forecasting for Financial and Economic Market

Fan Chen

College of Economics and Trade, Shanghai Urban Construction Vocational College, Shanghai 201415, China

Correspondence should be addressed to Fan Chen; chenfan@succ.edu.cn

Received 16 December 2021; Revised 23 January 2022; Accepted 31 January 2022; Published 24 March 2022

Academic Editor: Naeem Jan

Recently, the Internet financial market has developed rapidly both at home and abroad. Simultaneously, its study has also become the focus of academic circles. The financial markets have higher liquidity and volatility as compared to traditional financial markets. In view of the Internet financial market dynamic (volume and daily trading), it is proposed based on a deep neural network for fusion level time series prediction model. First, the proposed model processes the input of characteristic variables of multiple series (market macrodynamic series and multiseed series) and uses an attention mechanism to fuse the input variables in two dimensions of time and sequence feature. Second, the model also designs an optimization function based on the stability constraints of the prediction sequence, so that the model has better robustness. Finally, a large number of experiments are carried out on real large-scale data sets, and the results fully prove the effectiveness and robustness of the proposed model in the dynamic prediction of the Internet financial market.

1. Introduction

Financial forecast is the prediction, estimation, and judgment of the financial activity process and its changing trend. The essence of financial forecasting is a special financial analysis method, which is related to the future as well as uncertainty [1]. The whole forecasting process is a scientific analysis process of financial activities. The analysis process is mainly based on the actual data and past experience, uses scientific methods and means to simulate the past financial development process, and obtains the change trend of the future development process. Preconceived judgments and inferences are made about the impact of financial activities to reduce uncertainty about the future [2]. At present, financial forecasting is highly valued in academic circles, financial circles, and people's daily life. News and information on financial forecasts related to stocks, futures, and exchange rates can be found everywhere on the Internet, Television (TV) media, and newspapers. But financial activities are particularly complex and subject to many uncertainties, making it difficult to grasp future trends [3]. With regard to the current economic situation and the vigorous development of the market economy, the government must timely understand the actual situation of national economic development and financial market changes and grasp more accurate financial information.

From the 1950s to the present, information science and technology and computer network development by leaps and bounds, big data increasingly rich. People used to predict financial market prices on the basis of economics and finance, but now, they use a variety of interdisciplinary combination models to predict financial markets, which makes financial market forecasting become a unique field of financial research [4]. The research content and purpose of this article can be described: USES certain method to maximize the extraction of financial time series contains rules and information; according to the existing financial time series, information reflected to robust hybrid forecasting model is established, and by using the model to predict financial time series trend of short-term operation, as a reference of market investors' investment decisions [5].

The prediction process of the financial time series includes the following steps: data preparation, algorithm

definition, self-training and learning, prediction evaluation, and optimization. The data preparation stage is mainly data acquisition, data feature selection, data denoising, time series segmentation, clustering to provide data sets for self-learning, training, prediction, evaluation, and optimization [6]. The algorithm definition stage includes determining the prediction model and calculation method. The self-training learning stage includes selecting training learning algorithm, implementing training learning process, and adjusting training learning parameters. The prediction evaluation and optimization stage includes defining feedback indicators and optimizing the model according to the prediction results [7]. The basic framework of the financial time series forecasting process is shown in Figure 1.

Most traditional financial time series prediction algorithms take the sequence of target variables as the main research object. Among them, representative technologies include the autoregressive model [8], vector autoregressive model [9, 10]. With deep learning technology development, recurrent neural network (RNN) is widely used in the sequence problem and shows a better learning ability than traditional linear model [11]; especially in the financial market dynamic prediction problem, deep learning model has good nonlinear mapping ability and strong generalization ability, thus better able to model the variable characteristics of financial markets, nonlinear associations, and time series dependencies. Among various deep neural network models, long short-term memory (LSTM) effectively solves the problem of long sequence dependence by introducing gate structure and retaining the long-term information that needs to be remembered in sequence features [12]. In addition, with the help of the powerful heterogeneous data processing ability of the neural network, some scholars designed fusion based on the structure of long- and short-term neural network. The prediction model is based on composite variable features [13]. Recent studies have found that the introduction of attention mechanism [14] into the sequence prediction problem can more effectively and quickly screen out the information that is more critical to the current task, thus further enhancing the prediction ability of the model. However, the traditional attention mechanism is mainly designed from the time dimension and cannot distinguish the different effects of multivariable time series.

Aiming at the dynamic sequence of the Internet financial market (including daily trading volume and daily trading times), this paper designs a prediction model based on long- and short-term memory neural network structure. The dynamic macromodel of the overall market sequence integrates the dynamic sequence of each submarket and combines two attention mechanisms in terms of the time dimension and sequence characteristics. Due to the time dependence of modeling characteristics and the comprehensive influence of sequence input, the model is based on the sequence stability constraint optimization function so that the model has good robustness. The experimental results verified on the large-scale data of real Internet financial platforms fully demonstrate the effectiveness of the method designed in this paper in predicting the dynamics of the Internet financial market. In section two of this paper, we presented some of the related works to our research topic. In section three, we explained the neural networks and attention mechanism in much detail. In section four, the prediction model has been presented. In section five, we carried out experiments using the real data sets and analyzed their results to verify the working and efficiency of our method. In section six, the conclusion to the research is written.

2. Related Work

In financial scenarios, market information changes dynamically over time. Therefore, time series-based analysis and prediction are the focus of research in this field. This section first introduces the traditional time series prediction method, then introduces the deep learning model and attention mechanism in sequence problems related to research, and finally discusses the latest research work of sequence prediction in financial scenarios.

2.1. Traditional Time Series Prediction Method. According to the output results of the model, the traditional classical models are classified. The prediction models can be divided into random sequence model and deterministic sequence model. The traditional time series model generally needs strict mathematical principles. As the support of the model, it needs to be subject to more stringent constraints in order to use the extrapolation principle to predict future changes.

Deterministic model: In many practical application problems, the change of time series is obtained by the superposition or coupling of many factors, such as seasonal change, trend factor, periodic change, and irregularity. In order to eliminate the influence of irregular factors on time series prediction, scholars have carried out relevant research. In this kind of prediction model, the decomposition method [15], moving average method [16], and seasonal coefficient method [16] are often used to construct the time series analysis model.

Random model: Scholars in the field of statistics study time series by using random theory and find that irregular changes in time series caused by the joint action of many random factors are not completely chaotic but have certain regularity. Inspired by this phenomenon, the design of prediction models based on stochastic theory has attracted the attention of many scholars. Such models are generally based on the following procedures: First, the distribution of time series data to determine some reasonable conditions is observed and then used deductive reasoning to get a theoretical model describing the time series. If the theoretical model meets the characteristics of actual data, the actual model will be established and then used for time series analysis and prediction. Representative models of this kind include auto-regressive–moving average (ARMA) [17], auto-regressive integrated moving average (ARIMA) [18], auto-regressive conditional heteroskedasticity (ARCH) [19].

2.2. Time Series Prediction Method Based on Deep Learning. Deep neural network can obtain better representation capability than traditional methods through nonlinear

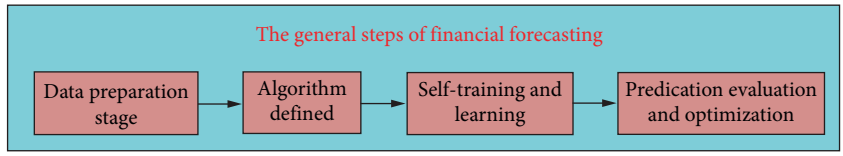

Figure 1: The general steps of financial forecasting.

variation of high-dimensional features. In time series prediction, the most widely used deep learning model is a cyclic neural network (RNN) [11] and long- and short-term memory neural network [12]. Cyclic neural network deals with the before and after dependence in time series data by introducing a cyclic mechanism. On the basis of RNN, LSTM introduces a "gate" structure to screen the antecedent information and selectively forget the unimportant information, so as to solve the difficulty of gradient disappearing in long sequence problems of RNN and further strengthen the dependence of long-distance information in learning time series.

2.3. Time Series Prediction Method Based on Attention Mechanism. Attention mechanism is an optimization method based on deep learning framework [20]. At present, attention mechanism has been well applied in natural language processing, computer vision, speech recognition, and other fields. Because the accuracy index of the attention model has increased significantly, many researchers have been exploring how to apply it to scenes that need more optimization details. The attention model refers to the mechanism of human visual attention. That is, when human beings obtain information, they will give priority to important information or some information they need at present.

3. Neural Network and Attention Mechanism

This section first introduces the structure and principle of long- and short-term memory neural network model and then analyzes the design and construction of attention mechanism in sequence prediction for the extraction of important information in time series.

3.1. LSTM Neural Network. Based on the classical recurrent neural network RNN, the LSTM network can selectively forget nonimportant information and strengthen the prior important information by adding a nonlinear "gate" structure inside network neurons. Therefore, LSTM avoids the inevitable gradient disappearance problem when RNN trains on long sequences. Specifically, the gate structure of LSTM is defined as follows:

$$\begin{aligned} i_t &= \delta\left(W_i x_t + W_{hi} h_{t-1} + W_{ci} c_{t-1} + \hat{b}_i\right), \\ f_t &= \delta\left(W_f x_t + W_{hf} h_{t-1} + W_{c_f} c_{t-1} + \hat{b}_f\right), \\ c_t &= f_t c_{t-1} + i_t \tanh\left(W_c x_t + W_{hc} h_{t-1} + \hat{b}_c\right), \\ o_t &= \delta\left(W_o x_t + W_{ho} h_{t-1} + W_{co} c_t + \hat{b}_o\right), \\ h_t &= o_t \tanh\left(c_t\right), \end{aligned} \tag{1}$$

where i_t, f_t, c_t, o_t, and h_t represent the hidden state of input gate, forgetting gate, memory module, output gate, and neuron, respectively. The forgetting gate and input gate structure of LSTM effectively propagates gradients by selectively preserving historical information, avoiding the problem of gradient disappearance caused by long-time sequence information. LSTM solves the problem that RNN cannot effectively learn the long-distance information dependency in time series, so it has been well applied in many time series modeling problems. The network structure of LSTM is shown in Figure 2.

3.2. Attentional Mechanism. The attention mechanism in the timing problem is mostly based on the encoder-decoder process of the deep loop network. The learning model is divided into two modules. The first is an encoder composed of a single or multilayer RNN, and the input sequence is input into the encoder according to the time relationship, which is used to learn the before and after dependencies of known sequences and the current state representation. The hidden state at the last moment is obtained and retained, which is called vector C, which retains the dynamic information of the input sequence and the current state of the sequence. Then, a decoder is also composed of neural network units with similar structure, and the encoding vector E is converted into timing sequence information with predicted length T'. The input of each moment j is the vector obtained by the mapping vector E with the target value sequence $(y_1, y_2, \ldots, y_{j-1})$. The output value of moment j is the predicted value of the corresponding moment, and its mathematical expression is

$$\begin{aligned} E &= F\left(x_1, x_2, \ldots, x_T\right), \\ y_j &= G\left(E, y_1, y_2, \ldots, y_{j-1}\right). \end{aligned} \tag{2}$$

In the traditional codec model, the context vector E used at each moment of decoding is fixed, and this construction does not incorporate the different principles of information concerned at different moments into the model. Researchers have further explored this problem by introducing the attention mechanism in image recognition into the sequence problem. By combining the attention mechanism with the codec structure, a sequential attention mechanism method is proposed, which is as follows:

$$\begin{aligned} E_j &= F\left(x_1, x_2, \ldots, x_T, h, h_{j-1}^{'}\right), \\ y_j &= G\left(E_i, y_1, y_2, \ldots, y_{j-1}\right), \end{aligned} \tag{3}$$

where F represents the process of combining the attention mechanism with the encoder, $h_{j-1}^{'}$ is the implicit state of the

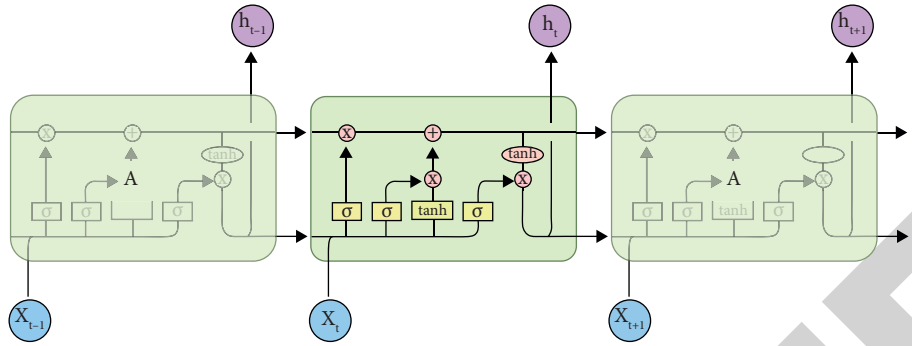

Figure 2: The network structure of LSTM.

previous step of the decoder, and h is the implicit state set of the encoder. Different from the traditional codec model, for each prediction moment j, the encoder gets a dynamic context vector E that pays attention to different information, so that the decoding process can pay more attention to the historical information that is more important to the prediction content of the current time.

4. Prediction Model

On the basis of the above introduction of long- and short-term memory neural network and attention mechanism, this section presents the specific content of the integrated multitime series market dynamic prediction model proposed in this paper in detail. Let's start with the model. The framework is then introduced in detail from three aspects: multisequence input, attention mechanism design, and optimization function.

4.1. Model Framework. In this section, an attention network model based on multiple time series (MALSTM) is designed and implemented by analyzing the dynamic characteristics of the financial market. The arrows in Figure 3 represent the corresponding vectors of input and output in each module. Structures such as LSTM and full-connection layer are represented by marked rectangular boxes, and the state matrix of the hidden layer is represented by rounded rectangles. Specifically, the model first proposes an input module based on multiple time series and then designs the attention mechanism from two dimensions of time and feature. Finally, an optimization function based on the stability constraint of the prediction sequence is designed to make the prediction results more robust.

4.2. Multisequence Input. The traditional time series prediction method only considers the change of the target variable time series and does not consider the interaction of other feature sequences at the same time. However, in the dynamic analysis of the Internet financial market, its market dynamics will be affected by a number of different subcategories of market dynamics. Therefore, this paper modeled the overall macrodynamics of the market and the subsequences of multiple market categories at the same time and established multiple time series inputs.

$$x_t = \left[x_t^1, x_t^2, \ldots, x_t^n\right], \tag{4}$$

where x_t represents the overall input of the model at time t, and x_t^c represents the input data of the $c-$th subclass sequence at the current time. For example, x_t^1 represents the observed trading volume of the platform at time t. x_t^i represents the volume of transactions in a particular category (such as technology or robust items). Next, the model uses a single-layer LSTM to model the dynamic evolution process of multi-input time series. Specifically, for each time step, there are

$$h_t, c_t = \mathrm{LSTM}\left(h_{t-1}, c_{t-1}\right), \tag{5}$$

where h_t and c_t, respectively, represent the market hidden state and memory state of the current moment t. Therefore, the dynamic representation h_t of the current multisequence can be obtained through LSTM.

4.3. Attention Mechanism Design. After multisequence LSTM input modeling, the dynamic state h_t of the market at every moment and the memory state c_t of multisequence input can be obtained. Considering that the macrodynamic modeling of the financial market requires important information in the sequential time series, the model needs to learn the key role of information at a different time for long-term change prediction. At the same time, considering the composition of the macromarket, the model should be able to automatically mine the subclass sequence that has the greatest influence on the overall macroseries prediction and further enhance the ability to forecast the market dynamics. Therefore, this paper designs two attention mechanisms from time dimension and multisequence feature dimension, respectively, to model the important influencing factors of market dynamics.

First, the attention mechanism based on the historical state of the market is constructed in the time dimension by referring to the design idea of the traditional codec model; that is, the attention degree of the hidden state at different moments is different. According to the processing process of the LSTM input module in Section 4.1, the output matrix $h = [h_1, h_1, \ldots, h_T]$ model composed of hidden layer state at each moment can be obtained, and h is further taken as the output of the encoder. Each column vector h in matrix h_t represents the market state at moment t, and it is taken as the

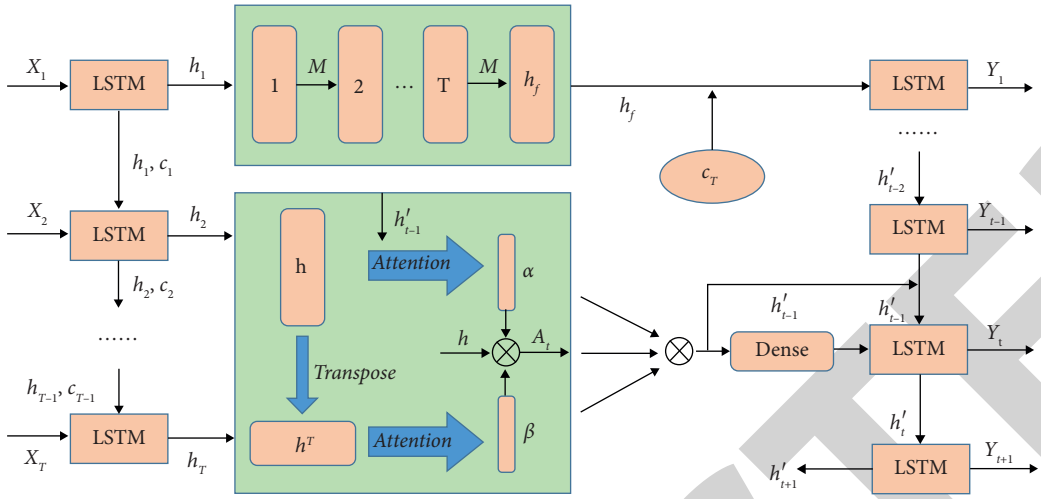

Figure 3: Structure diagram of multitime series attention network model.

input of the attention mechanism. Then, through formula (6), the importance of the current moment state to the prediction state y_j is calculated as follows:

$$e_{tj} = V_a^{\top}\tanh\left(W_a h'_{j-1} + U_a h_t\right),$$
$$a_{tj} = \text{softmax}\left(e_{tj}\right), \tag{6}$$

h'_{j-1} is decoder on one phase of the hidden states, and h_t is market status at encoder time t. W_a, U_a, and $V_a^{\top}$ state of the encoder and decoder are hidden states attention mechanism parameter matrix, and e_{tj} represents the market state of the encoder in time t for the influence degree of the current state output prediction time j finally by softmax function, normalization of e_{tj} operation, so as to obtain the weight factor of market state at each historical moment to the current forecast, that is, the attention value in the time dimension.

In addition, considering that the macromarket dynamics are affected by the temporal changes of multiple subclasses, this paper proposes another attention mechanism based on multisequence feature dimensions. Different from the time dimension, the multisequence dimension attention mechanism needs to consider the influence of the historical coding state of each sequence on the complete macrodynamics of the market. By calculating the influence of the current sequence state on the macromarket dynamics according to all states of each sequence in the encoder sequence, the specific process is as follows:

$$e'_k = V_\beta^T\tanh\left(U_\beta h_k^T\right),$$
$$\beta_k = \text{softmax}\left(e'_k\right), \tag{7}$$

where h_k^T represents the historical hidden state of the k-th subsequence, U_β and V_β^T are the parameter matrices of the attention mechanism, and β_k is the weight factor of the influence of the current sequence on the macromarket. Considering that the decoder needs to integrate the attention mechanism of time and feature dimension at the same time, a linear joint method of attention weight is designed in this paper to obtain the total weight factor E_j of the market prediction of time j by historical sequence.

$$E_j = \sum_{t=1}^{T} a_{tj} \sum_{k=1}^{n} \beta_k h_t. \tag{8}$$

Finally, LSTM combined with attention factor E_j can be used to form the decoder part of the model, so that the predicted value y_j at time j can be gradually obtained as follows:

$$y'_j = \text{LSTM}\left(E_i, h'_{j-1}, c'_{j-1}\right). \tag{9}$$

When $j = 1$, $y'_1 = \text{LSTM}(E_1, h'_f, c'_T)$. Where (h'_f, c'_T) is the coded output of the historical sequence, and h'_f is the macromarket, hidden state c'_T represents the last memory state of a historical sequence.

4.4. Optimization Function Design. From the macrolevel, compared with specific financial products, the dynamic change of the financial market tends to be gentle due to the relative balance between total demand and total supply [21]. Therefore, the representation of macromarket should also tend to be stable and gentle change. In this study, a linear evolution constraint process is proposed for the representation of the output of the macromarket of the model; that is, the conditional distribution of equation (10) is adopted to satisfy the linear stationary constraint in the macrodynamic coding process of the model.

$$h_t | h_{t-1} \sim N\left(Mh_{t-1}, \Sigma\right), \tag{10}$$

where M is the state transition matrix, whose value is optimized during model training, and Σ is the covariance matrix. It can be seen that the hidden state of the macromarket is no longer directly generated by LSTM but evolved from the final state of the market. The evolution mode is as follows:

$$h_f = Mh_T, \tag{11}$$

where h_f represents the hidden state of macromarket, and h_T represents the last time step state of historical information. In order to further satisfy the stable characteristics of the macromarket dynamics, we design an optimization objective based on the linear evolution process of historical hidden states, which is used to constrain the representation of the macromarket to satisfy the linear stable characteristics in the learning process of the model. The specific optimization objective is to minimize L, and its mathematical expression is

$$L_p = \sum_{t=1}^{T-1} h_{t+1} - Mh_{t2}^2 + h_p - Mh_{T2}^2. \tag{12}$$

The ultimate purpose of the model is to predict the future market state at T time by learning the historical sequence information. Therefore, accuracy is the most important optimization objective. The model selects root mean square error (RMSE), which is the most common in time series prediction at present, as shown in formula (13).

$$L_n = \sqrt{\frac{1}{T'} \sum_{j=1}^{T'} \left(y_j' - y_j\right)^2}. \tag{13}$$

In order to prevent over-fitting caused by model training, the optimization objective of the equilibrium model with adjustable parameter λ in terms of its smoothness and accuracy is introduced. The final optimization function is

$$L = \min \sum_{i=1}^{N} \left(L_n + \lambda L_p\right). \tag{14}$$

Specifically, the model uses the RMSPROP algorithm [22] with an initial learning rate of 0.0001 to optimize model parameters until the model converges. This section proposes a decoding time model and designs a new attention structure starting with the feature dimensions to be considered and the importance of different features. Then, the model is analyzed from the macro level. Specifically, the dynamic change of the financial market is restricted by the relative balance of high total demand and total supply because the prediction process constraint is realized by driving the needle slip linear constraint function. These two improvements are the most important innovations of this model.

5. Experiments and Results

This section verifies the effectiveness of the designed model in macrodynamic prediction of the Internet financial market by constructing experiments on real data sets.

5.1. The Experimental Data. The experimental data in this paper are all from the Prosper platform, which is the second-largest Internet P2P lending platform in the world. The experiment collected a total of 1622 days of investment records of the lender recorded on the platform from April 1, 2006, to May 25, 2011. In the experiment, all data samples were divided into training sets and test sets according to the ratio of 4:1; that is, 1297 days' transaction data were used for model training, and 325 days' transaction data were used for testing. Specifically, the daily trading volume and the number of transactions are mainly used as the research objects in the experiment. The six (risk order from high to low is "HR," "E," "D," "C," "B," and "A") dynamic sequences of the projects with different risk ratings are extracted, and the subclass sequence of the macromarket is used as the input of the model, and the historical sequence and target sequence of each sample are constructed according to the sliding window method.

In view of the incompleteness and inconsistency of the platform for collecting real data, this paper introduces the preprocessing of training set and test set, which are as follows: (1) firstly, the linear interpolation method is used to deal with the shortcomings of data set values. Linear interpolation is adopted because a missing value cannot be simply deleted in the time series problem, which will lead to the fracture of the time series index; (2) after the standardization of the original time series data, the values of time series variables with different credit ratings vary greatly. The influence of numerical series on model training and prediction results will have great interference, and direct input to the model will lead to the weight deviation of model experiment. Therefore, the data normalization method is used to map all time series variables to the [0,1] interval:

$$X^* = \frac{X - X_{\min}}{X_{\max} - X_{\min}}, \tag{15}$$

where X is the original data of the sequence variable, $X_{\max}$ and $X_{\min}$ are the maximum and minimum values of the original sequence variable respectively, and X^* is the value normalized by the data, whose value range is [0, 1].

5.2. The Experimental Setup. In the experiment, the MALSTM model and all comparison methods proposed in this paper are implemented based on Python 3.5 and Tensorflow1.2.1. In all models involving LSTM structure, the number of neurons is set to 200, the dropout is 0.5, and batch size is set to 8. All the methods and programs in this paper run in the Linux environment with two 2.20GH2 Intel Xeon E5-2650 V4 CPU and four Tesla K80 GPU.

In order to compare and verify the effect of the model proposed in this paper, four methods are selected and designed as the comparative experiment, which are as follows:

(1) ARIMA is a classical traditional time series prediction model. The input is a single time series, which only includes the total amount of the platform or the total number of loans.

(2) LSTM model of single sequence infusion. In the cyclic network model, LSTM is used to construct encoders and decoders, and the input of each time step only includes the total amount of platform or total number of transactions per day.

(3) LSTM model with multisequence input (denoted as LSTM-M), which uses LSTM to construct encoders

Table 1: The RMSE results of the market amount prediction in the next 10 days.

Method	Days									
	1	2	3	4	5	6	7	8	9	10
ARIMA	0.064	0.063	0.064	0.064	0.065	0.065	0.066	0.067	0.068	0.070
LSTM	0.062	0.063	0.064	0.064	0.065	0.066	0.067	0.068	0.070	0.072
MLSTM	0.062	0.063	0.063	0.063	0.064	0.064	0.065	0.065	0.066	0.067
MLSTM-t	0.059	0.059	0.060	0.061	0.061	0.062	0.062	0.063	0.063	0.064
MALSTM	0.059	0.059	0.060	0.060	0.061	0.061	0.062	0.061	0.062	0.062
MALSTM-L	**0.058**	**0.058**	**0.059**	**0.059**	**0.059**	**0.060**	**0.058**	**0.060**	**0.060**	**0.061**

and decoders. Referring to the multisequence input mechanism in this paper, the input of each time step includes not only the total amount or total transaction volume of the current platform every day but also the total amount or total transaction volume of projects with different risk levels every day. The input of each time step includes not only the total amount of money or total transactions of the current platform every day but also the total amount of money or total transactions of projects with different risk levels every day.

(4) Multisequence attention mechanism model (MALSTM-T). On the basis of LSTM-M model, the attention mechanism in time latitude is added.

(5) Multisequence attention mechanism model (MALSTM), namely, the attention model based on multisequence input proposed in this paper. MALSTM uses only RMSE as an optimization goal in training.

(6) The model of stationary optimization objective (MALSTM-L) is added. The linear stationary constraint proposed in this paper to the MALSTM model to optimize the model is added, and the complete optimization function designed in this paper is used.

5.3. Experimental Results and Analysis. In this paper, the total loan amount and total loan number of the platform are forecasted and compared. When the number of fixed historical days is 10, the prediction is made. The test days were adjusted from 1 to 10 to observe the performance of different models, as shown in Tables 1 and 2.

Tables 1 and 2, respectively, show the RMSE and MAE values of the total transaction amount of the platform predicted by the four algorithms in the prediction days from 1 to 10 days. It can be clearly observed from the table that the model proposed in this paper (MALSTM and MALSTM-L) is significantly superior to other comparison models. Among them, in terms of RMSE index, MALSTM and MALSTM-L proposed in this paper have achieved a maximum improvement of 2.04% and 4.18%, respectively, compared with the classical attention architecture MALSTM-T and have achieved an improvement of 4.45%–6.72% and 6.04%–8.67% compared with other models without the use of attention mechanism.

Meanwhile, in MAE index, compared with the classical attention architecture MALSTM-T, MALSTM and MALSTM-1 achieved a maximum improvement of 1.78% and 4.33%, respectively. Compared with other models without attention mechanism, MALSTM and MALSTM-1 achieved an improvement of 4.26%–8.96% and 5.82%–11.06%, respectively. These results illustrate the multi-input proposed in this paper. These results demonstrate the effectiveness and advancement of the multi-input attention deep network model proposed in this paper. At the same time, by comparing the two models proposed in this paper, it can be found that compared with MALSTM, the RMSE index, and Mae index of MALSTM-1 increase by 2.02% and 2.52%, which shows the rationality and effectiveness of the stability constraints based on the model and proves that the dynamic changes of the market tend to be stable.

Furthermore, through the horizontal analysis of the prediction results according to the time dimension, it can be found that the prediction effect of the traditional LSTM and MLSTM models decreases significantly as the prediction time goes by. For example, the accuracy of the prediction results of the two models on the 10th day decreases 14.51% and 7.21%, respectively, under the RMSE index compared with the first day. It can be seen that the multisequence input model is significantly better than the model that directly inputs the target single sequence, which proves that the relationship between multiple sequences can effectively assist the macrodynamic modeling of the market, improves the accuracy of the model for long-term forecasting results. At the same time, for MALSTM and MALSTM-L models, the long-term prediction results are only reduced by 5.41% and 4.80% under the RMSE index, which indicates that the model proposed in this paper can well model the long-term fluctuations of the macrodynamics of the financial market and also indicates the effectiveness of the stability constraint in the macroprediction of the market, which further proves the robustness of the proposed model in financial macromarket forecasting. Figures 4 and 5 show the RMSE and MAE values of the total number of transactions on the platform predicted by the four algorithms in the period from 1 to 10 days.

From Figures 4 and 5, it is clear that the MALSTM-L proposed in this paper has the largest stationarity constraint. The results further demonstrate the importance of the multisequence proposed in this paper for the prediction of macromarket dynamics and also prove the effectiveness of the multisequence attentional

Table 2: The MAE results of the market amount prediction in the next ten days.

Method	Days									
	1	2	3	4	5	6	7	8	9	10
ARIMA	0.045	0.046	0.046	0.047	0.049	0.049	0.050	0.050	0.052	0.054
LSTM	0.044	0.045	0.046	0.046	0.048	0.049	0.050	0.051	0.053	0.055
MLSTM	0.044	0.044	0.045	0.045	0.045	0.046	0.047	0.048	0.049	0.050
MLSTM-t	0.041	0.042	0.043	0.043	0.044	0.044	0.045	0.045	0.045	0.046
MALSTM	0.041	0.042	0.042	0.043	0.043	0.044	0.045	0.044	0.045	0.046
MALSTM-L	**0.040**	**0.041**	**0.041**	**0.042**	**0.043**	**0.043**	**0.043**	**0.043**	**0.044**	**0.044**

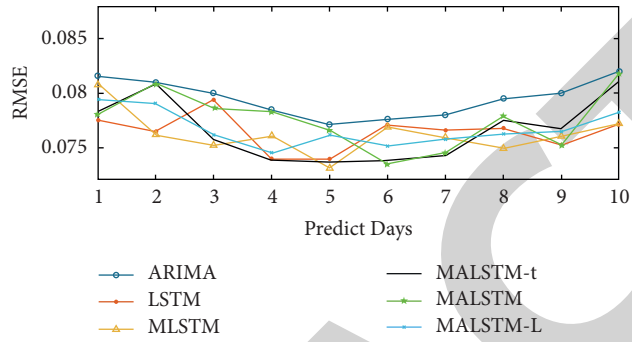

Figure 4: Experimental results of RMSE.

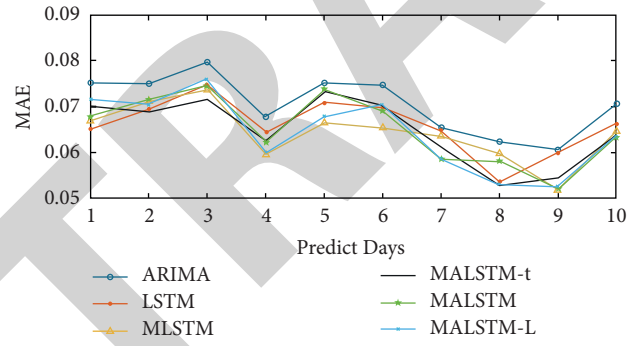

Figure 5: Experimental results of MAE.

Table 3: The RMSE results of the market counts prediction in the next ten days.

Method	Days									
	1	2	3	4	5	6	7	8	9	10
ARIMA	0.082	0.081	0.080	0.079	0.077	0.078	0.078	0.079	0.081	0.083
LSTM	0.081	0.080	0.079	0.077	0.076	0.076	0.077	0.079	0.081	0.083
MLSTM	0.080	0.079	0.077	0.075	0.075	0.075	0.077	0.081	0.078	0.085
MLSTM-t	0.080	0.078	0.077	0.075	0.074	0.075	0.076	0.076	0.077	0.077
MALSTM	0.079	0.077	0.076	0.074	0.074	0.075	0.076	0.075	0.076	0.076
MALSTM-L	**0.077**	**0.077**	**0.075**	**0.074**	**0.073**	**0.073**	**0.074**	**0.075**	**0.075**	**0.076**

mechanism and the advance of the model designed in this paper. The results in Tables 3 and 4 show the RMSE and MAE results of the market counts prediction in the next ten days.

The results show that the accuracy of the sequence prediction model increases first and then decreases with the passage of prediction time. Moreover, by comparing the variation trend of the prediction errors of the four methods, it can be found that the error of the MALSTM-L model has the smallest variation range over time, which further verifies the robustness of the model proposed in this paper in macromarket prediction and demonstrates the effectiveness of the introduced market stability constraint. In addition, in comparison, because the sequence of transaction number is less stable than that of the transaction amount, MAISTML has some cases weaker than MALSTM in the results of Tables 3 and 4. And the graphs of the results are shown in Figures 6 and 7.

Table 4: The MAE results of the market counts prediction in the next ten days.

Method	Days									
	1	2	3	4	5	6	7	8	9	10
ARIMA	0.058	0.057	0.056	0.055	0.054	0.055	0.055	0.057	0.057	0.058
LSTM	0.058	0.056	0.056	0.054	0.053	0.055	0.054	0.057	0.056	0.057
MLSTM	0.057	0.055	0.056	0.054	0.052	0.055	0.053	0.057	0.055	0.057
MLSTM-t	0.056	0.055	0.055	0.054	0.051	0.055	0.053	0.056	0.055	0.056
MALSTM	0.056	0.054	0.055	0.053	0.051	0.054	0.053	0.056	0.054	0.056
MALSTM-L	**0.055**	**0.054**	**0.054**	**0.052**	**0.051**	**0.053**	**0.053**	**0.055**	**0.053**	**0.054**

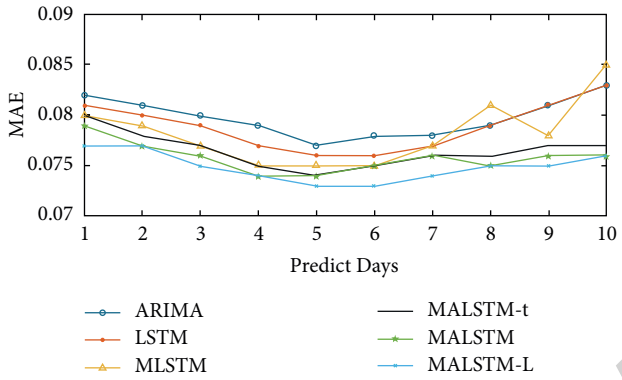

Figure 6: Experimental results of RMSE.

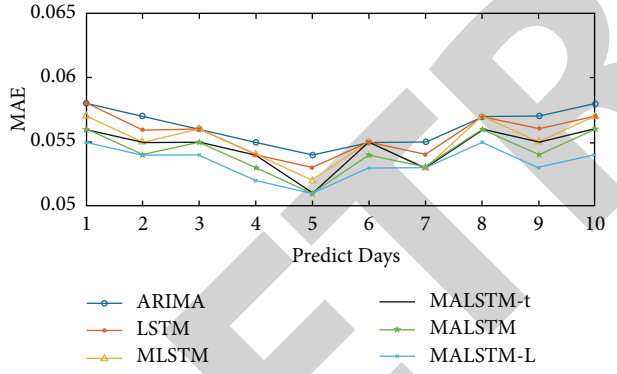

Figure 7: Experimental results of MAE.

6. Conclusion

Internet is the macrodynamic prediction of financial markets, and the author of this paper, first, introduces the time series of dynamic characteristics of the Internet financial markets and the prediction problem of the research background and reviews the traditional time series prediction method, based on the deep learning method and attention mechanism, and on the current temporal prediction, research has carried on the brief introduction of the financial markets. In view of the characteristics of strong liquidity and high volatility of the Internet financial market, this paper proposes a prediction model based on deep neural network fusion hierarchical multitime series learning. First, the model can process the input of multiple sequence feature variables (macrodynamic series and multiseed series) and fuse the input variables in time and sequence feature by using the attention mechanism. Second, the model designs an optimization function based on the stability constraint of the prediction sequence, which makes the model prediction have better robustness. Finally, a large number of experiments are carried out on a real large Internet financial data set. The experimental results show that the neural network time series learning prediction model based on multilevel fusion depth proposed in this paper has achieved the best prediction performance, which fully proves the effectiveness and robustness of the model in the macrodynamic prediction of the Internet financial market.

In this paper, the macrodynamic prediction of the Internet financial market is explored, and the influence of multisequence input on market dynamics is modeled. Meanwhile, the stability of the market macrodynamic is utilized to improve the accuracy of time series prediction, providing a new research idea for time series prediction. Future research can be carried out from two aspects: (1) to further explore the influence of subsequences on macrodynamics and the interaction between subsequences; (2) to explore the influence of external information, such as news media texts, on the prediction of market macrodynamics.

Data Availability

The datasets used during the current study are available from the corresponding author upon reasonable request.

Conflicts of Interest

The author declares that there are no conflicts of interest.

References

[1] O. B. Adekoya and A. N. Adebiyi, "Oil price-inflation pass-through in OECD countries," *International Journal of Energy Sector Management*, vol. 14, no. 1, pp. 126–147, 2020.

[2] R. Yang, L. Yu, Y. Zhao et al., "Big data analytics for financial Market volatility forecast based on support vector machine," *International Journal of Information Management*, vol. 50, pp. 452–462, 2020.

[3] J. Wang and R. Lee, "Chaotic recurrent neural networks for financial forecast," *American Journal of Neural Networks and Applications*, vol. 7, no. 1, pp. 7–14, 2021.

[4] E. Y. Abuzir and M. A. R. M. Baraka, "Financial stock market forecast using data mining in Palestine," *Palestinian Journal of Technology and Applied Sciences (PJTAS)*, vol. 2, 2019.

[5] R. D. John and H. C. Catherine, "A multidimensional classification of market anomalies: evidence from 76 price

Hindawi
Journal of Mathematics
Volume 2024, Article ID 9795281, 1 page
https://doi.org/10.1155/2024/9795281

Retraction

Retracted: The Exponentiated Exponential-Inverse Weibull Model: Theory and Application to COVID-19 Data in Saudi Arabia

Journal of Mathematics

Received 23 January 2024; Accepted 23 January 2024; Published 24 January 2024

This article has been retracted by Hindawi following an investigation undertaken by the publisher [1]. This investigation has uncovered evidence of one or more of the following indicators of systematic manipulation of the publication process:

(1) Discrepancies in scope

(2) Discrepancies in the description of the research reported

(3) Discrepancies between the availability of data and the research described

(4) Inappropriate citations

(5) Incoherent, meaningless and/or irrelevant content included in the article

(6) Manipulated or compromised peer review

The presence of these indicators undermines our confidence in the integrity of the article's content and we cannot, therefore, vouch for its reliability. Please note that this notice is intended solely to alert readers that the content of this article is unreliable. We have not investigated whether authors were aware of or involved in the systematic manipulation of the publication process.

Wiley and Hindawi regrets that the usual quality checks did not identify these issues before publication and have since put additional measures in place to safeguard research integrity.

We wish to credit our own Research Integrity and Research Publishing teams and anonymous and named external researchers and research integrity experts for contributing to this investigation.

The corresponding author, as the representative of all authors, has been given the opportunity to register their agreement or disagreement to this retraction. We have kept a record of any response received.

References

[1] M. M. Badr and G. Sobahi, "The Exponentiated Exponential-Inverse Weibull Model: Theory and Application to COVID-19 Data in Saudi Arabia," *Journal of Mathematics*, vol. 2022, Article ID 8521026, 11 pages, 2022.

Hindawi
Journal of Mathematics
Volume 2022, Article ID 8521026, 11 pages
https://doi.org/10.1155/2022/8521026

Research Article

The Exponentiated Exponential-Inverse Weibull Model: Theory and Application to COVID-19 Data in Saudi Arabia

Majdah Mohammed Badr[1] **and Ghaida Sobahi**[2]

[1]*Statistics Department, Faculty of Science for Girls, University of Jeddah, P. O. Box 70973, Jeddah 21577, Saudi Arabia*
[2]*Department of Statistics, Faculty of Science for Girls, University of Jeddah, Jeddah, Saudi Arabia*

Correspondence should be addressed to Majdah Mohammed Badr; mmbadr@uj.edu.sa

Received 13 November 2021; Revised 18 December 2021; Accepted 21 December 2021; Published 22 March 2022

Academic Editor: Naeem Jan

The purpose of this study is to introduce a new T-X family lifetime distribution known as exponentiated exponential-inverse Weibull, and we refer to this distribution as EE-IW. The new model's basic mathematical characteristics are studied. The maximum likelihood (ML) estimator (MLE) approach is used to estimate the parameters. A Monte Carlo simulation is done to examine the behavior of the estimators. Finally, a real-world dataset is utilized to show the utility of the proposed model in many industries and to compare it to well-known distributions.

1. Introduction

In statistical theory, improvement of classical distribution becomes a common practice. Probability distributions are used to model the phenomenon of natural life, but in many situations, there is a need to propose a new model for the better exploration of the data. The recent development in distribution theory stresses on new approaches for introducing new models. The new approaches depend on modifying the baseline by adding one or more parameters, to generalize the existing family. The aim of these is to provide more flexibility or to obtain better fits to the model compared with related distributions.

Barreto-Souza et al. [1] discussed the beta generalized exponential (BGE) model, Khan [2] investigated the beta inverse Weibull (BIW) model, Kundu and Howlader [3] studied Bayesian inference of the inverse Weibull (IW) model under type II censored schemes. Gusmao [4] discussed the generalized IW (GIW) distribution, modified IW distribution has been studied by Khan and King [5], Hanook et al. [6] introduced beta IW distribution, Abbas et al. [7] studied the Topp–Leone IW distribution. Elbatal and Muhammed [8] proposed Exponentiated generalized inverse Weibull distribution, and Elbatal et al. [9] introduced the beta generalized IW geometric model. Alkarni et al. [10] studied the half logistic IW. Nadarajah [11] studied the exponentiated exponential (EE) model, and also, Alzaghal et al. [12] defined a new family named "exponentiated T-X distribution". Some of its characteristics and specific instances are examined, and obtained on t is a nonnegative continuous random variable (RVr) T specified as $[0, \infty)$.

In this study, we used the T-X family approach to obtain the EE-IW model. The newly suggested model is formed by combining two models known as the *T-X* family. The RVr T is the generator of the EE model and IW model. The primary goal of this study is to propose and determine the statistical features of a novel distribution (EE-IW). The hazard function and its many shapes allow it to suit various datasets.

The remainder of the paper is arranged as described in the following. Section 2 introduces the new model (EE-IW) distribution with some important different characteristics such as the probability density function (pdf), the cumulative function (cdf), the hazard function, and graphs of different values for parameters. The r^{th} moment is discussed in Section 3. The MLE estimators are introduced in Section 4. A simulation study is introduced in Section 5. A real dataset is applied in Section 6. Finally, Section 7 concludes this study.

2. The EE-IW Model

In this section, we propose the EE-IW distribution, and we derive density, cumulative, reliability, and hazard functions of the new distribution.

Let $r(t)$ be the pdf of RVr T, then the exponential model of t is

$$r(t) = \beta e^{(-\beta t)}; \quad \beta, t > 0. \tag{1}$$

The cdf and pdf of the RVr X of the IW model are

$$g(x) = \alpha x^{-\alpha-1} e^{-x^{-\alpha}}; \quad x > 0,\ \alpha > 0, \tag{2}$$

$$G(x) = e^{-x^{-\alpha}}; \quad x > 0,\ \alpha > 0. \tag{3}$$

Using the formula in Alzaghal et al. [12], we define the cdf for the EE-IW model for an RVr X as

$$f(x) = c\beta g(x)\,[G(x)]^{(c-1)}\left(1 - G^{c}(x)\right)^{\beta-1}. \tag{4}$$

Inserting (2) and (3) in (4), we get the pdf EE-IW as

$$f(x) = c\alpha\beta x^{-\alpha-1}\left(e^{-cx^{-\alpha}}\right)\left[1-\left(e^{-cx^{-\alpha}}\right)\right]^{\beta-1}; \quad x > 0,\ c > 0,\ \alpha > 0, \tag{5}$$

where c, α, and β are the shape parameters.

We can expand the above pdf given in (5) using the binomial expansion as follows:

$$f(x) = c\alpha\beta \sum_{i=0}^{\infty} (-1)^{i} \binom{\beta-1}{i} x^{r-(\alpha+1)} e^{-c(i+1)x^{-\alpha}}. \tag{6}$$

The corresponding cdf for the EE-IW model given in (5) is

$$F(x) = 1 - \left[1-\left(e^{-cx^{-\alpha}}\right)\right]^{\beta}; \quad \beta, \alpha, c, x > 0. \tag{7}$$

The corresponding reliability of the EE-IW model has the following form:

$$R(x) = \left[1-\left(e^{-cx^{-\alpha}}\right)\right]^{\beta}; \quad \beta, \alpha, c, x > 0. \tag{8}$$

The corresponding hazard function of the EE-IW model has the following form:

$$h(x) = \frac{c\alpha\beta x^{-\alpha-1}\left(-e^{-cx^{-\alpha}}\right)\left[1-\left(e^{-cx^{-\alpha}}\right)\right]^{\beta-1}}{\left[1-\left(e^{-cx^{-\alpha}}\right)\right]^{\beta}}. \tag{9}$$

2.1. The Submodels of the EE-IW Distribution. In this section, some special cases of the proposed model are given. Table 1 introduces a brief list of the submodels.

From Table 1, it can be noticed that the EE-IW reduces to the exponentiated IW (E-IW) model when $\beta = 1$. For $\beta = c = 1$, it becomes the standard IW exponentiated (SIWE) model. For $\beta = \alpha = 1$, it reduces to the exponentiated standard inverted exponential (ESIE) distribution. For $\alpha = -1$, it becomes the EE model. For $c = 1$, we get the exponentiated Frechet (EF) distribution.

Figures 1–4 illustrate the plots of the pdf, cdf, hazard, and reliability functions, respectively.

Figure 1 shows various shapes of the pdf for various values of the parameters, such as unimodal right-skewed.

Figure 2 shows the cdf curves for various values of some selected parameters.

Figure 3 shows the *h(x)* curves of the EE-IW model with various values of the shape parameters, and as the shape parameter increases, the *h(x)* first increase and then decrease.

Figure 4 shows the *R(x)* curves for different values of the parameters for distribution, and as the shape parameter increases, the *R(x)* decreases.

3. Basic Properties

This section investigated some important basic properties of the EE-IW model.

3.1. The Noncentral Moment. The r^{th} moment about zero of the EE-IW model is provided by

$$\mu_r' = E(X^r) = A_r \Gamma\left(1 - \frac{r}{\alpha}\right), \frac{r}{\alpha} < 1, \tag{10}$$

where

$$A_r = \left\{ c\beta \sum_{i=0}^{\infty} (-1)^{i} \frac{\binom{\beta-1}{i}}{[c(i+1)]^{1-r/\alpha}} \right\}, \quad r = 0, 1, \ldots. \tag{11}$$

Let $r = 1$ in equation (10), we get the expected value or the first moment:

$$\mu_1' = \mu = E(X) = A_1 \Gamma\left(1 - \frac{1}{\alpha}\right). \tag{12}$$

For $r = 2$ in equation (10), we get the second moment:

$$\mu_2' = E\left(X^2\right) = A_2\, \Gamma\left(1 - \frac{2}{\alpha}\right). \tag{13}$$

For $r = 3$ in equation (10), we get the third moment:

$$\mu_3' = E\left(X^3\right) = A_3 \Gamma\left(1 - \frac{3}{\alpha}\right). \tag{14}$$

For $r = 4$ in equation (10), we get the fourth moment:

$$\mu_4' = E\left(X^4\right) = A_4 \Gamma\left(1 - \frac{4}{\alpha}\right). \tag{15}$$

The variance of the EE-IW distribution is obtained by using both equations (12) and (13) as follows:

$$\sigma^2 = \mathrm{Var}(X) = A_2 \Gamma\left(1 - \frac{2}{\alpha}\right) - \left\{A_1 \Gamma\left(1 - \frac{1}{\alpha}\right)\right\}^2, \alpha > 0. \tag{16}$$

We can define the coefficient of variation of EE-IW distribution by using both equations (12) and (13):

Table 1: The subdistribution from the EE-IW.

c	α	β	Model	CDF	References
√	1	1	Exponentiated inverted Weibull (E-IW) distribution	$F(x) = (e^{-cx^{-\alpha}})$	Flaih et al. [13]
1	√	1	Standard inverted Weibull exponentiated (SIWE) distribution	$F(x) = (e^{-x^{-\alpha}})$	Flaih et al. [13]
√	1	1	Exponentiated standard inverted exponential (ESIE) distribution	$F(x) = (e^{-cx^{-1}})$	Flaih et al. [13]
1	√	√	Exponentiated Frechet (EF) distribution	$F(x) = 1 - [(1 - e^{-x^{-\alpha}})]^{\beta}$	Badr [14]
√	1	√	Exponentiated exponential (EE) distribution	$F(x) = [(1 - e^{-x^{-cx}})]^{\beta}$	Gupta and Kundu [15]

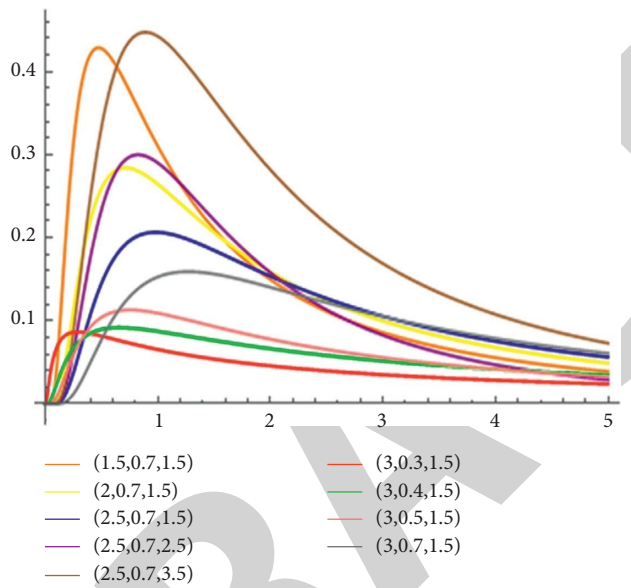

Figure 1: pdf of the EE-IW model.

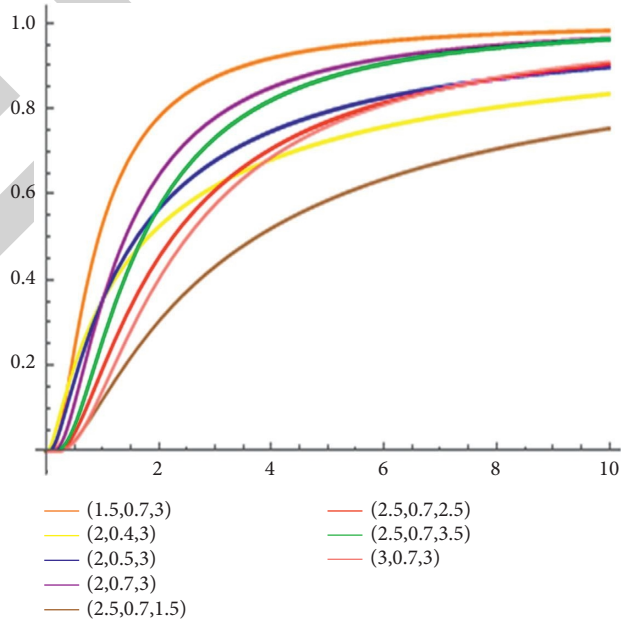

Figure 2: cdf of the EE-IW model.

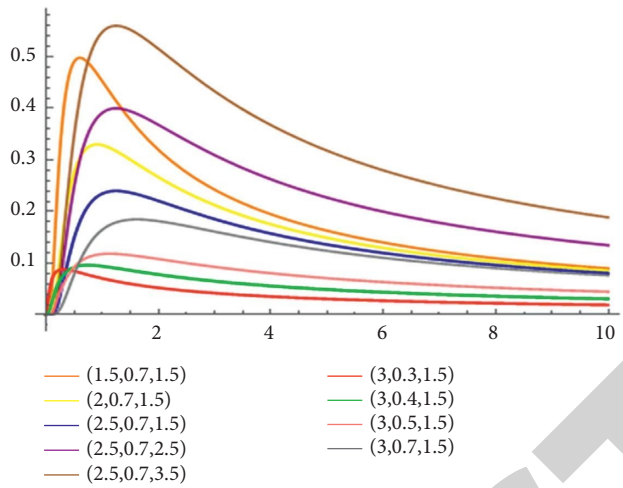

Figure 3: $\mathbf{h}(\mathbf{x})$ of the EE-IW model.

$$\text{CVar} = \frac{\sqrt{A_2\Gamma(2-1/\alpha)-\{A_1\Gamma(1-1/\alpha)\}^2}}{A_1\,\Gamma(1-1/\alpha)}. \tag{17}$$

The skewness for EE-IW is γ_3 which can be obtained by referring to the moments by using equations (12)–(14) as

$$\gamma_3 = \frac{A_3\Gamma(1-3/\alpha)-3A_1A_2\Gamma(1-1/\alpha)\Gamma(1-2/\alpha)+2\left[A^3{}_1\Gamma(1-1/\alpha)^3\right]}{\left\{A_2\Gamma(1-2/\alpha)-\{A_1\Gamma(1-1/\alpha)\}^2\right\}^{3/2}}, \alpha>0. \tag{18}$$

The kurtosis for EE-IW is γ_4 which can be obtained by referring to the moments by using equations (12)–(15) as follows:

$$\gamma_4 = \frac{A_4\Gamma(1-4/\alpha)-4A_3A_1\Gamma(1-3/\alpha)\Gamma(1-1/\alpha)+6A_1^2A_2\Gamma(1-1/\alpha)^2\Gamma(1-2/\alpha)-3\left[A_1^4\Gamma(1-1/\alpha)^4\right]}{\left\{A_2\Gamma(1-2/\alpha)-\{A_1\Gamma(1-1/\alpha)\}^2\right\}^2}, \alpha>0. \tag{19}$$

Figure 5 shows the *mean, variance, skewness, and kurtosis* curves of the EE-IW model with $c=2$ and for various values of α and β.

3.2. The Quantile Function. The quantile function of the EE-IW model is computed by using (7) as

$$x_q = \text{MD} = \left\{\frac{-1}{c}\ln\left\{1-[1-q]^{1/\beta}\right\}\right\}^{-1/\alpha}. \tag{20}$$

For $q=0.5$ in (20), we calculate the median (MD) of the EE-IW model as

$$x_q = \text{MD} = \left\{\frac{-1}{c}\ln\left\{1-[1-0.5]^{1/\beta}\right\}\right\}^{-1/\alpha}. \tag{21}$$

The mode (MO) of the EE-IW model is derived by taking the first derivative of equation (5) and solving it as

$$f'(x) = c\alpha\beta x^{-\alpha-1}\left(-e^{-cx^{-\alpha}}\right)\left[1-\left(e^{-cx^{-\alpha}}\right)\right]^{\beta-1}; x>0, c>0, \alpha>0. \tag{22}$$

The MO for EE-IW is derived by putting equation (22) equal to 0 and solving it numerically.

Table 2 displays some outcomes for various mean values, MD, MO, standard deviation (SD), γ_3, and γ_4.

Table 2 shows the measures of central tendency, SD, γ_4, and γ_3 of parameters c, α, and β for selected values. The statistical properties of the newly derived model were obtained numerically using Mathematica 11.2. Hence, to obtain the mean, MD, MO, SD, γ_4, and γ_3, we noticed the following remarks.

When the values α and β are constant for various values of c, the mean, MD, MO, and SD will be increased, but γ_4 and γ_3 are decreasing.

When the values c and β are constant for various values of α, the mean, MD, MO, and SD will be decreased, but γ_4 and γ_3 are increasing.

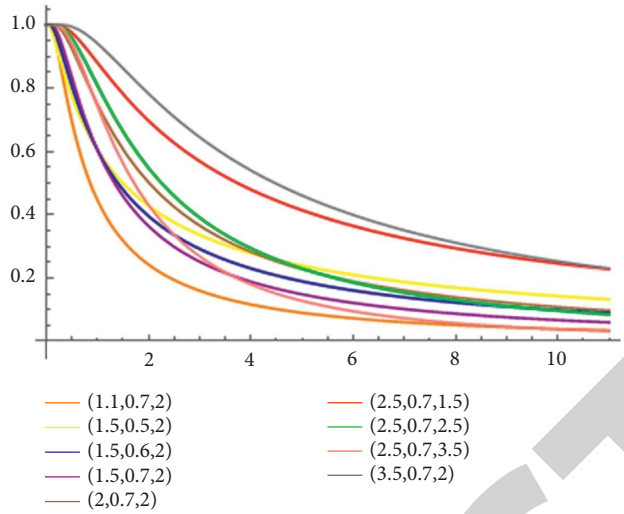

Figure 4: $\mathbf{R}(\mathbf{x})$ of the EE-IW model.

When the values c and α are constant for various values of β, the mean, MD, MO, and SD will be decreased, but γ_4 and γ_3 are decreasing.

4. The Maximum Likelihood Estimators

In this section, the MLE of the unknown parameters is introduced.

Let $X_1, X_2, X_3, \ldots, X_n$ be a random sample from the EE-IW model which has parameters c, α, and β. The likelihood function (LLF) is $L(\theta|x) = \prod_{i=1}^{n} f(x_i)$ where $f(.)$ is reported in (5) and $\underline{\theta} = (c, \alpha, \beta)$. By calculating the logarithm of LLF, we have the following:

$$l = n \ln c + n \ln \alpha + n \ln \beta - (\alpha + 1) \sum_{i=1}^{n} \ln x_i - c \sum_{i=1}^{n} x_i^{-\alpha} + (\beta - 1) \sum_{i=1}^{n} \ln\left[1 - \left(e^{-cx_i^{-\alpha}}\right)\right]. \tag{23}$$

Differentiate (23) in regard to c, α, and β and correspondingly we have

$$l_j = \frac{\partial \ln L}{\partial \theta_j} = \frac{1}{L} \cdot \frac{\partial L}{\partial \theta_j}, \quad j = 1, 2, 3. \tag{24}$$

From (23), we have

$$l_1 = \frac{\partial l}{\partial c} = \frac{n}{c} - \sum_{i=1}^{n} x_i^{-\alpha} + (\beta - 1) \sum_{i=1}^{n} x_i^{-\alpha} \left\{ \frac{x_i^{-\alpha}\left(e^{-cx_i^{-\alpha}}\right)}{\left[1 - \left(e^{-cx_i^{-\alpha}}\right)\right]} \right\}, \tag{25}$$

$$l_2 = \frac{\partial l}{\partial \alpha} = \frac{n}{\alpha} - \sum_{i=1}^{n} \ln x_i + c(\ln x_i) \sum_{i=1}^{n} x_i^{-\alpha} - \frac{c(\beta - 1)(\ln x_i) \sum_{i=1}^{n} x_i^{-\alpha}\left(e^{-cx_i^{-\alpha}}\right)}{\left[1 - \left(e^{-cx_i^{-\alpha}}\right)\right]}, \tag{26}$$

$$l_3 = \frac{\partial l}{\partial \beta} = \frac{n}{\beta} + \ln\left[1 - \left(e^{-cx_i^{-\alpha}}\right)\right]. \tag{27}$$

By setting the previous two equations (24) and (25) equal to 0 and solving them simultaneously yield the MLEs $(\widehat{c}, \widehat{\alpha})$ of parameters (c, α).

The MLE of the parameter β, $\widehat{\beta}_{\mathrm{MLE}}$, can be computed by using (26) as

$$\widehat{\beta}_{MLE} = \frac{-n}{\sum_{i=1}^{n} \ln\left[1 - \left(e^{-\widehat{c}x_i^{-\widehat{\alpha}}}\right)\right]}. \tag{28}$$

We computed the asymptotic variance-covariance (VC) matrix by $I_{ij}(\underline{\theta})$, which includes the VC of estimations while

ignoring the expectation of the second partial derivative (SPD) $I_{ij}(\underline{\theta}) = E(-\partial^2 \text{lnlnL}/\partial\theta_i \partial \text{j})$.

The SPD of the parameters for the EE-IW model is

$$\begin{aligned}
\frac{\partial^2 l}{\partial c^2} &= \frac{-1}{c^2} - \frac{(\beta-1)(x^{-\alpha})^2\left(e^{-cx^{-\alpha}}\right)}{\left[1-\left(e^{-cx^{-\alpha}}\right)\right]} - \frac{(\beta-1)(x^{-\alpha})^2\left(e^{-cx^{-\alpha}}\right)^2}{\left[1-\left(e^{-cx^{-\alpha}}\right)\right]^2},\\
\frac{\partial^2 l}{\partial \alpha^2} &= \frac{-1}{\alpha^2} - cx^{-\alpha}(\ln x)^2 + \frac{c(\beta-1)x^{-\alpha}(\ln x)^2\left(e^{-cx^{-\alpha}}\right)}{\left[1-\left(e^{-cx^{-\alpha}}\right)\right]} - \frac{c^2(\beta-1)(x^{-\alpha})^2(\ln x)^2\left(e^{-cx^{-\alpha}}\right)}{\left[1-\left(e^{-cx^{-\alpha}}\right)\right]} - \frac{c^2(\beta-1)(x^{-\alpha})^2(\ln x)^2\left(e^{-cx^{-\alpha}}\right)^2}{\left[1-\left(e^{-cx^{-\alpha}}\right)\right]^2},\\
\frac{\partial^2 l}{\partial \beta^2} &= \frac{-1}{\beta^2},\\
\frac{\partial^2 l}{\partial \beta \partial c} &= \frac{\partial^2 l}{\partial c \partial \beta} = \frac{x^{-\alpha}\left(e^{-cx^{-\alpha}}\right)}{\left[1-\left(e^{-cx^{-\alpha}}\right)\right]},\\
\frac{\partial^2 l}{\partial \beta \partial \alpha} &= \frac{\partial^2 l}{\partial \alpha \partial \beta} = -\frac{cx^{-\alpha}(\ln x)\left(e^{-cx^{-\alpha}}\right)}{\left[1-\left(e^{-cx^{-\alpha}}\right)\right]},\\
\frac{\partial^2 l}{\partial \alpha \partial c} &= x^{-\alpha}(\ln x) - \frac{(\beta-1)x^{-\alpha}(\ln x)\left(e^{-cx^{-\alpha}}\right)}{\left[1-\left(e^{-cx^{-\alpha}}\right)\right]} - \frac{c(\beta-1)(x^{-\alpha})^2(\ln x)\left(e^{-cx^{-\alpha}}\right)}{\left[1-\left(e^{-cx^{-\alpha}}\right)\right]} - \frac{c(\beta-1)(x^{-\alpha})^2(\ln x)\left(e^{-cx^{-\alpha}}\right)^2}{\left[1-\left(e^{-cx^{-\alpha}}\right)\right]^2}.
\end{aligned} \tag{29}$$

5. Simulation Outcomes

To demonstrate the theoretical outcomes of the estimated issue, simulation experiments were conducted using Mathematica 11.2 software. 1000 random samples of size $n = 20, 40, 60, 80$, and 100 were generated from the EE-IW model. The initial value is chosen as $c = 0.8, \alpha = 0.2, \beta = 0.5$. The accuracy of the produced parameter estimators has been evaluated in terms of their estimate for the parameters, bias (B) and mean square error (MSEr), where

$$B = \frac{\sum_{i=0}^{1000}\widehat{\theta}}{1000}, \text{ MSEr} = \frac{\sum_{i=0}^{1000}(\widehat{\theta}-\theta)^2}{1000}. \tag{30}$$

The B and MSEr of the estimators for the parameters for each sample size are computed.

Table 3 shows the values of B and the MSEr for the non-Bayesian estimators when parameters $\widehat{c}, \widehat{\alpha}$, and $\widehat{\beta}$ are unknown based on complete samples, using different sample sizes n.

Table 4 shows the values of B and MSEr for the non-Bayesian estimators for the parameter $\widehat{c}$ when α and β are known based on complete samples, using different sample sizes n.

Table 5 shows the values of B and MSEr for the non-Bayesian estimators for the parameter $\widehat{\alpha}$when c and β are known based on complete samples, using different sample sizes n.

Table 6 shows the values of B and MSEr for the non-Bayesian estimators for the parameter $\widehat{\beta}$ when c and α are known based on complete samples, using different sample sizes n.

From Table 3 The values of B and the MSEr for the non-Bayesian estimators for the parameters $\widehat{c}$ are evaluated when α and β is known based on complete samples, using different sample size n. we note that

(1) The biases of the estimates decrease as the n increases
(2) The MSErs of the estimates decrease as the sample size increases

From Tables 4–6, we note that

(1) The Bs and the MSErs of the estimates decrease as the n increases
(2) As the sample size increases, the MSErs approaches zero

6. Modelling to Real Data

In this section, we choose different distributions of the same family and approximately from the EE-IW distribution such as exponentiated Weibull (EW) [16], EE Bur XII [17], EE [15], and exponentiated Frechet (EF) [14], and it is considered an application to three datasets. In order to choose the best model, we calculate some information criterion (IC), Akaike IC (AIC), corrected AIC (CAIC), and Bayesian IC (BIC) for all competing and subdistribution. We compute the MLEs for the EW, EE Bur XII, EE, and EF models.

6.1. First Dataset. The following dataset is presented by Almetwally [18]. The data came from a 32-day COVID-19 dataset from Saudi Arabia. The data are as follows: 0.0557, 0.0559, 0.0617, 0.0649, 0.0683, 0.0709, 0.0711, 0.0736, 0.0737, 0.0739, 0.0741, 0.0743, 0.0776, 0.0782, 0.0804, 0.0808, 0.0815, 0.0818, 0.0819, 0.0840, 0.0850, 0.0864, 0.0867, 0.0869, 0.0901, 0.0904, 0.0907, 0.0914, 0.0943, 0.0946, 0.1009, 0.1134.

Table 7 clearly shows that the EE-IW distribution fits better than the EE Bur XII, EF, EE, and EW models for this

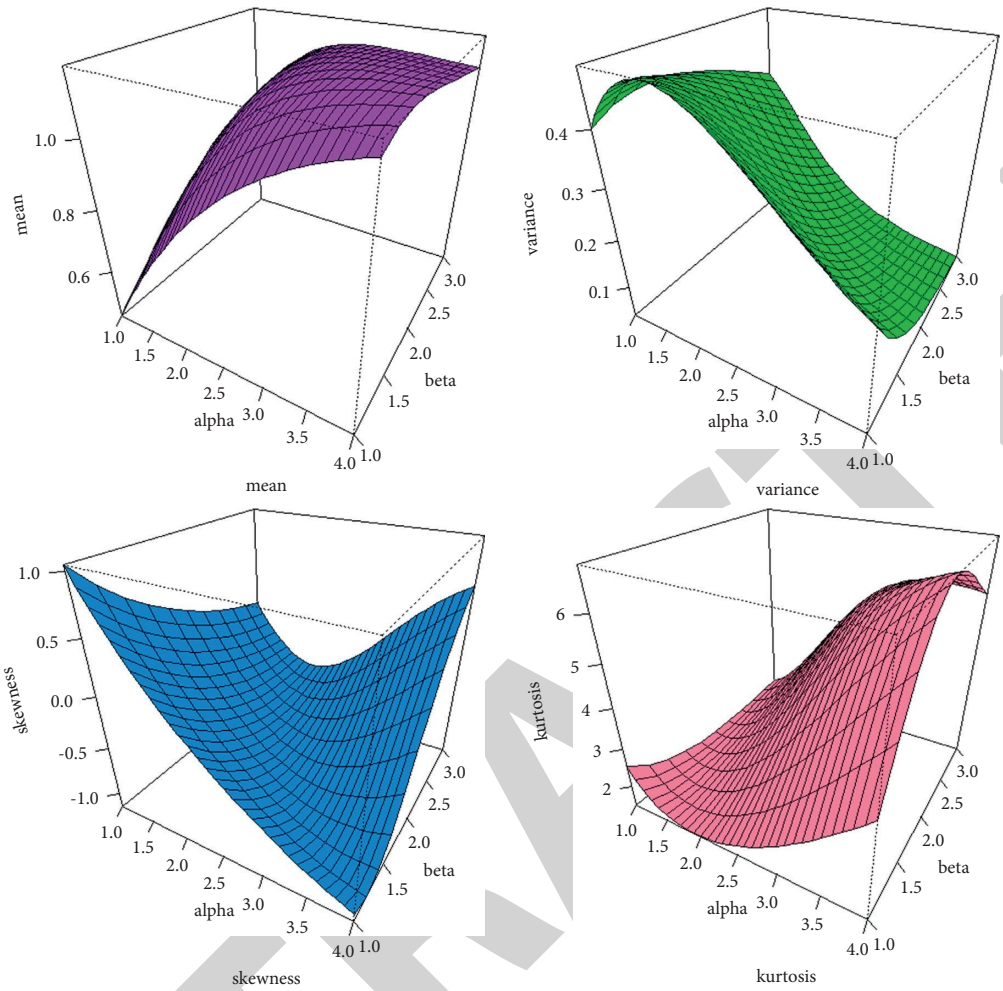

Figure 5: 3D plots of moments.

Table 2: Some numerical values of mean, MO, MD, SD, γ_3, and γ_4.

c	α	β	Mean	MD	MO	SD	γ_3	γ_4
0.5	2	0.5	1.8501	1.1235	1.8385	2.1336	12.4551	3.0961
1	2	0.5	3.0504	2.1718	2.0609	2.6772	7.0548	1.9568
3	2	0.5	5.7914	3.9486	2.6781	4.5608	2.6373	0.8660
2	1	0.5	4.6599	3.5671	2.2993	3.5271	2.0986	0.5618
2	2	0.5	4.3718	3.0518	1.4224	3.0863	2.1622	1.9095
2	3	0.5	3.1605	2.6157	1.3110	1.9879	2.6359	2.0218
2	2	1	2.9893	1.3697	2.5938	4.0179	6.8361	2.2378
2	2	1.5	1.3951	1.1964	1.3110	0.8322	3.7587	2.0042
2	2	2	1.3723	1.1245	1.2894	0.4924	2.8404	0.8749

dataset. Also, Figure 6 illustrates the fitted empirical pdf for the dataset. Figure 6 shows that the EE-IW distribution is the best-fitting model among all the models tested, and they back up the results.

6.2. Second Dataset. The following dataset is presented by Nichols [19]. The data resulted from breaking stress of carbon fibers (in Gba). The data are as follows: 3.7, 3.11, 4.42, 3.28, 3.75, 2.96, 3.39, 3.31, 3.15, 2.81, 1.41, 2.76, 3.19, 1.59, 2.17, 3.51, 1.84, 1.61, 1.57, 1.89, 2.74, 3.27, 2.41, 3.09, 2.43, 2.53, 2.81, 3.31, 2.35, 2.77, 2.68, 4.91, 1.57, 2.00, 1.17, 2.17, 0.39, 2.79, 1.08, 2.88, 2.73, 2.87, 3.19, 1.87, 2.95, 2.67, 4.20, 2.85, 2.55, 2.17, 2.97, 3.68, 0.81, 1.22, 5.08, 1.69, 3.68, 4.70, 2.03, 2.82, 2.50, 1.47, 3.22, 3.15, 2.97, 2.93, 3.33, 2.56, 2.59, 2.83, 1.36, 1.84, 5.56, 1.12, 2.48, 1.25, 2.48, 2.03, 1.61, 2.05, 3.60, 3.11, 1.69, 4.90, 3.39, 3.22, 2.55, 3.56, 2.38, 1.92, 0.98, 1.59, 1.73, 1.71, 1.18, 4.38, 0.85, 1.80, 2.12, 3.65.

Table 8 clearly shows that the EE-IW distribution fits better than the EE Bur XII, EF, EE, and EW models for this dataset. Also, Figure 7 illustrates the fitted empirical pdf for

Table 3: The B and MSEr of the unknown parameters $\underline{\theta} = (\mathbf{c}, \alpha, \beta)$ with the initial values (0.8, 0.2, 0.5).

n	Method	$\widehat{c}$	$\widehat{\alpha}$	$\widehat{\beta}$
		0.1979	0.5945	0.1942
20	MLE	−0.6021	0.3998	−0.3243
		0.3625	0.1585	0.1378
		0.1432	0.5548	0.1546
40	MLE	−0.6443	0.3742	−0.3453
		0.3254	0.1523	0.1295
		0.1425	0.5191	0.1246
60	MLE	−06628	0.3437	−0.3685
		0.3198	0.1429	0.1247
		0.1397	0.4876	0.1158
80	MLE	−0.7064	0.3254	−0.3698
		0.3083	0.1405	0.1232
		0.1352	0.4756	0.1133
100	MLE	−0.7489	0.3184	−0.3856
		0.3045	0.1393	0.1175

Table 4: $\widehat{c}$, B, and MSEr of the unknown parameter c.

n	Method	$\alpha = 0.2, \beta = 0.5$	$\alpha = 0.4, \beta = 0.7$	$\alpha = 0.6, \beta = 0.8$
		1.4092	1.1617	1.2191
20	MLE	0.6092	0.3617	0.4191
		0.3712	0.1308	0.1756
		0.9932	0.9543	0.9458
40	MLE	0.1932	0.1543	0.1458
		0.0373	0.0238	0.0213
		0.9509	0.9164	0.8471
60	MLE	0.1509	0.1164	0.0471
		0.0228	0.0135	0.0022
		0.9251	0.8461	0.8345
80	MLE	0.1251	0.0461	0.0345
		0.0156	0.0021	0.0012
		0.8158	0.8203	0.8108
100	MLE	0.0158	0.0203	0.0108
		0.0003	0.0004	0.0001

Table 5: $\widehat{\alpha}$, B, and MSEr of the α unknown parameters $\underline{\theta} = (\mathbf{c}, \alpha, \beta)$.

n	Method	$c = 0.2, \beta = 0.2$	$c = 0.4, \beta = 0.5$	$c = 0.8, \beta = 0.7$
		0.2509	0.2518	02156
20	MLE	0.0509	0.0518	0.0275
		0.0026	0.0027	0.0069
		0.2149	0.2351	0.2145
40	MLE	0.0366	0.0351	0.0264
		0.0013	0.0012	0.0066
		0.2089	0.2257	0.2113
60	MLE	0.0256	0.0257	0.0152
		0.0007	0.0007	0.0060
		0.1886	0.2076	0.2106
80	MLE	0.0159	0.0076	0.0143
		0.0002	0.0005	0.0054
		0.1881	0.1938	0.2098
100	MLE	−0.0119	−0.0062	0.0135
		0.0001	0.0004	0.0042

the dataset. Figure 6 shows that the EE-IW distribution is the best-fitting model among all the models tested, and they back up the results.

6.3. Third Dataset. The following dataset is presented by Lawless [20]. The data resulted from a test on the endurance of deep groove ball bearings. The data are as follows: 17.88,

Table 6: The B and MSEr of the β unknown parameter $\underline{\theta} = (\mathbf{c}, \alpha, \beta)$.

n	Method	$c = 0.2, \alpha = 0.2$	$c = 0.4, \alpha = 0.5$	$c = 0.8, \alpha = 0.7$
20	MLE	0.6321 0.1321 0.01744	0.6424 0.1424 0.0203	0.7739 0.2739 0.0750
40	MLE	0.5796 0.0796 0.0063	0.6114 0.1114 0.0124	0.6004 0.1004 0.0101
60	MLE	0.5645 0.0645 0.0042	0.5497 0.0497 0.0025	0.5967 0.0967 0.0094
80	MLE	0.5637 0.0637 0.0041	0.5146 0.0146 0.0002	0.5479 0.0479 0.0023
100	MLE	0.5289 0.0289 0.0008	0.5118 0.0118 0.0001	0.5280 0.0280 0.0008

Table 7: Parameter estimates and values of AIC, BIC, and CAIC, for the 1^{st} data.

Distribution	$\widehat{c}$	$\widehat{\alpha}$	$\widehat{\beta}$	$\widehat{m}$	AIC	BIC	CAIC
EE-IW	0.0402	1.5731	5.4312	—	676.93	676.32	672.78
EW	3.5476	0.4859	2.3996	—	935.08	939.48	935.94
EE-Bur XII	8.2617	1.5219	27.2209	24.6929	685.49	691.35	686.97
EE	2.2281	—	85.9425	—	895.72	900.93	895.84
EF	—	1.3895	4.5093	—	717.42	720.35	717.83

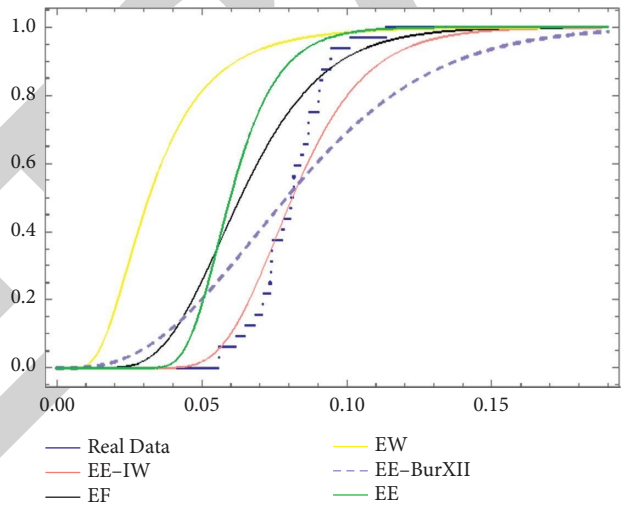

Figure 6: The empirical distribution and estimated cdf of the models for the COVID-19 data.

28, 92, 33, 41.52, 42.12, 45.60, 48.4, 51.84, 51.96, 54.12, 55.56, 67.8, 68.64, 68.88, 84.12, 93.12, 98.64, 105.12, 105.84, 127.92, 128.04, 173.4.

Table 9 clearly shows that the EE-IW distribution fits better than the EE Bur XII, EF, EE, and EW models for this dataset. Also, Figure 8 illustrates the fitted empirical pdf for the dataset. Figure 6 shows that the EE-IW distribution is the best-fitting model among all the models tested, and they back up the results.

For Table 7, the EE-IW distribution has the lowest AIC, BIC, and CAIC values among all fitted models. Hence, this new distribution can be chosen as the best model for fitting these data sets. Modeling to COVID-19 data demonstrates the model's flexibility, usefulness, and capability.

For Tables 8 and 9, the EE-IW distribution has the lowest AIC, BIC, and CAIC values among all fitted models. Hence, this new distribution can be chosen as the best model for fitting these data. From Table 8, modeling breaking stress of carbon fibers data demonstrates the model's flexibility, usefulness, and capability. In Table 9, modeling the data resulted from a test on the endurance of deep groove ball bearings.

Table 8: Parameter estimates and values of AIC, BIC, and CAIC, for the 2^{nd} data.

Distribution	$\widehat{c}$	$\widehat{\alpha}$	$\widehat{\beta}$	$\widehat{m}$	AIC	BIC	CAIC
EE-IW	0.0209	6.1461	0.0613	—	499.64	507.45	499.89
EW	1.4963	0.8243	14.1075	—	1053.74	1061.55	1053.99
EE-Bur XII	5.8125	2.0665	0.0976	5.8371	505.89	516.309	506.309
EE	2.2281	—	85.9425	—	895.72	900.93	895.84
EF	—	0.2966	5.7863	—	874.72	879.93	874.84

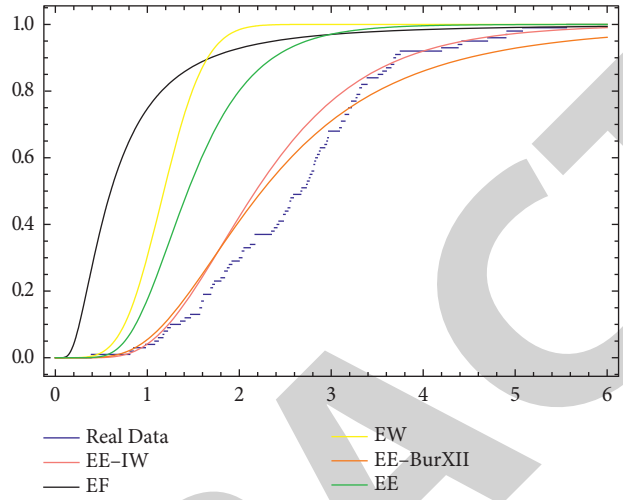

Figure 7: The empirical distribution and estimated cdf of breaking stress of carbon fibers (in Gba).

Table 9: Parameter estimates and values of AIC, BIC, and CAIC, for the 3^{rd} data.

Distribution	$\widehat{c}$	$\widehat{\alpha}$	$\widehat{\beta}$	$\widehat{m}$	AIC	BIC	CAIC
EE-IW	2.30296	3.9506	0.0028	—	259.979	264.521	262.201
EW	0.0279	1.0210	4.8075	—	1081.60	1085.01	1082.86
EE-Bur XII	26.8896	0.9034	0.85713	1.0249	483.52	488.07	485.75
EE	0.09303	—	111.869	—	900.735	903.01	901.34
EF	—	2.8880	0.08317	—	307.03	309.30	307.63

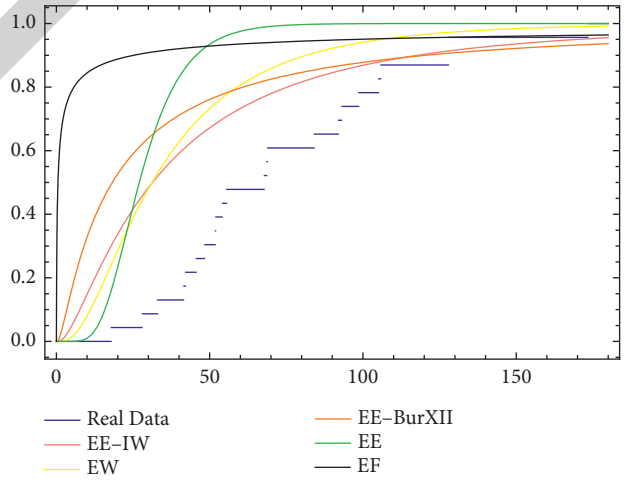

Figure 8: The empirical distribution and estimated cdf of the models for the deep groove ball bearings data.

Hindawi
Journal of Mathematics
Volume 2023, Article ID 9821642, 1 page
https://doi.org/10.1155/2023/9821642

Retraction

Retracted: A Survey of Multimedia-Assisted English Classroom Teaching Based on Statistical Analysis

Journal of Mathematics

Received 21 November 2022; Accepted 21 November 2022; Published 5 January 2023

Journal of Mathematics has retracted the article titled "A Survey of Multimedia-Assisted English Classroom Teaching Based on Statistical Analysis" [1] due to concerns that the peer review process has been compromised.

Following an investigation conducted by the Hindawi Research Integrity team [2], significant concerns were identified with the peer reviewers assigned to this article; the investigation has concluded that the peer review process was compromised. We therefore can no longer trust the peer review process, and the article is being retracted with the agreement of the Chief Editor.

References

[1] H. Wang, "A Survey of Multimedia-Assisted English Classroom Teaching Based on Statistical Analysis," *Journal of Mathematics*, vol. 2022, Article ID 4458478, 11 pages, 2022.

[2] L. Ferguson, "Advancing Research Integrity Collaboratively and with Vigour," 2022, https://www.hindawi.com/post/advancing-research-integrity-collaboratively-and-vigour/.

Hindawi
Journal of Mathematics
Volume 2022, Article ID 4458478, 11 pages
https://doi.org/10.1155/2022/4458478

Research Article

A Survey of Multimedia-Assisted English Classroom Teaching Based on Statistical Analysis

Hui Wang

Xinjiang Institute of Engineering, Ürümqi, China

Correspondence should be addressed to Hui Wang; wh28@xjie.edu.cn

Received 23 November 2021; Accepted 29 January 2022; Published 11 March 2022

Academic Editor: Naeem Jan

With the promotion of information technology and education reform, multimedia classroom teaching, which has distinctive teaching characteristics, rich teaching resources, and vivid teaching forms, has been widely used in different classrooms, especially in English classrooms. However, there are still some problems in the application of multimedia-assisted instruction, and much work so far has focused more on language input (vocabulary, listening, and reading) of multimedia-assisted instruction, but there is limited empirical research on output (especially writing) of it. Therefore, from the perspective of statistical analysis, this empirical study investigates the effectiveness of multimedia-assisted English classroom teaching from the detailed aspects like preferred teaching activity, understanding key and difficult points, and overall performance and then formulates a multimedia writing teaching model in order to improve students' writing performance. The result shows that multimedia teaching does have superior advantages and the model enhances students' interest and scores in writing.

1. Introduction

The 21st century is an information age, and information technology makes the knowledge grow with an unprecedented trend, and the cycle of updating is also shorter and shorter [1]. Therefore, education, which is regarded as the significant means of knowledge dissemination, demands teachers to update knowledge faster and make students master the knowledge with higher efficiency. As there are some disadvantages associated with traditional method of teaching, the Chinese education system started thinking to reform their education policies. Therefore, under the premise of education reform and the change of teachers' teaching ideas, the traditional teaching methods are gradually changing to modern teaching methods [2]. Teachers realize that transferring a large amount of scientific knowledge and information to students quickly and effectively in a limited time has been the most important concern they face, even till today. With the development of information science and technology, the development of multimedia technology represented by computer has penetrated the field of education. The introduction of multimedia has brought a new teaching mode for the diversity of classroom teaching. It not only broadens students' access to information and expands students' horizons but also enriches classroom activities and greatly improves students' interest in learning [3]. Moreover, multimedia-assisted teaching provides guidance, practice, and skill training for students' language learning, which acts as an indispensable auxiliary teaching tool.

Although multimedia has many advantages in classroom teaching, it is still in the process of practical application, and we have had problems of one kind or another. Due to the lack of hardware and software, teachers' own concepts and skills are backward, which is considered as one of the major problems associated with using multimedia in classroom teaching. Due to teachers lack of related theory, multimedia-assisted foreign language teaching is still in its infancy [4]. In addition, at the beginning of exploration, the implementation of multimedia-assisted English classroom teaching is found as imperfect; henceforth, teachers are not satisfied with the application of multimedia in class.

This empirical study aims at the problems of multimedia in today's English classroom. A teaching experiment with

college students as its participants will be conducted between an experimental group and a control group, and the effectiveness of multimedia-assisted English classroom teaching will be investigated and evaluated from different perspectives, and then a multimedia writing teaching model will be formulated in order to improve students' writing performance and develop other English skills, so that language learners will benefit more comprehensively from multimedia teaching and thus enhance the effective use of multimedia technology in English classroom.

The organizational structure of this paper is as follows. Section 1 mainly introduces the research background, research purpose, research significance, and the structure of this paper. The related work is discussed in Section 2. Section 3 analyses the characteristics and application mode of multimedia-assisted instruction. Based on the statistical analysis, Section 4 analyses the effectiveness of multimedia-assisted English classroom teaching. Section 5 illustrates the multimedia-assisted writing model and its effect, and Section 6 summarizes the whole paper.

2. Related Work

In recent years, there are many kinds of progress in the research of multimedia-assisted instruction. Many EFL research studies suggest that integration of multimedia can activate learning atmosphere, provide plenty of information, enhance motivation and interaction, and promote teaching and learning efficiency of language skills.

It is worth affirming that multimedia-assisted English teaching has activated our classroom, which is really helpful to English learning [5]. Multimedia-assisted college English teaching has changed the traditional classroom teaching mode which is based on teacher teaching [6]. With the rapid development of information technology and network resources, the emergence of foreign language learning tools like CD-ROM, courseware, and various Apps makes it possible for students to study independently on a single machine, and they can arrange their own learning according to their own time, which is not limited by class time and place, so that students can develop personalized learning and autonomous learning.

The combination of various kinds of media information can be realized by computers, which have the characteristics of high efficiency and interactivity. Multimedia can provide learners with a real language learning environment and multisensory input in learning. Besides, it can accommodate more diverse teaching information and train students' listening, speaking, reading, and writing skills in one class at the same time. It also enables teachers to extract teaching resources from all over the world at any time in classroom, which saves teachers' time and energy to collect information, and students can quickly obtain the latest knowledge and resources, thus improving classroom efficiency.

Multimedia teaching can realize the direct interaction between teachers, students, and computers without waiting. The process becomes more convenient, and feedback can be obtained immediately through multimedia, which can cultivate students to be active learners, rather than as passive absorbers of information [7], while in class, teachers can freely choose multimedia teaching resources that are consistent with the teaching objectives and can adjust the teaching pace and content of the class at any time according to the feedback of students. This kind of efficient interaction can stimulate students' interest in learning.

The design standard of multimedia-assisted college English teaching courseware and the transformation of classroom teaching mode point out a clear way for teachers to correctly use multimedia-assisted English teaching. For example, some universities combine traditional teaching methods with multimedia teaching methods and create a network of "online learning + face-to-face tutoring", which stimulates students' interest in English learning and improves students' learning efficiency [8]. Moreover, multimedia-assisted English vocabulary teaching courseware also stimulates students' interest in English vocabulary learning and enhances the quality of vocabulary teaching [9]. In addition, research shows the display of multimedia glosses can reduce students' cognitive load and result in better performance in reading comprehension and vocabulary learning [10]. Relevant scholars believe that the combination of multimedia and English teaching can maximize the advantages of multimedia in image, sound, and animation, stimulate students' learning enthusiasm, and explore the auxiliary role of multimedia technology in teaching listening skills [11]. EFL learners' communicative competence can also get developed through the use of multimedia-assisted language instruction [12]. By watching, summarizing, and discussing YouTube online English learning resources, language learners can improve their writing fluency [13]. Also, practice has proved that the application of task-based multimedia-assisted translation teaching has significant advantages [14].

However, there is also a considerable amount of literature that discusses the challenges faced using multimedia in classroom teaching. The significant challenges include technical problems, accessibility of computers, sharing computer resources among teachers, student-teacher ratio in technological setting, outdated teaching practices, lack of advanced computer skills like designing graphics, adding animations, inserting cartoons, etc., lack of adding emotive values to the lecture, and lack of interaction between teachers and students [15, 16]. Some teachers lack adequate understanding of multimedia teaching, and they use PowerPoint presentations as an alternative to traditional way of teaching. Here, teachers copy textbook content to the slides with little explanation and expandation to the key points, which leads to knowledge overlapping and inefficiency. It was also found that student's role in such cases is passive [15, 17]. Teachers play the dominant role, and the development of students' creativity and critical thinking skills is restricted. These problems lead to serious educational issues where students slowly began to rely on computers or multimedia instead of teachers. Too much use of multimedia in classrooms distracts the attention of students as well. It was found that when using too many videos and images, students easily get distracted and lose their attention as well as presence of mind. The background effects can easily affect

the psychology of the students, and hence it will be not easy for them to choose to concentrate on the teaching content or on the videos [15, 16].

Multimedia-assisted teaching should be guided by advanced teaching theories. Nowadays, many related theories can be referred and applied, such as constructivist learning theory, Mayer's multimedia learning theory which provides an informative set of principles that can be used to create effective instructional message design, Paivio's dual coding theory, Baddeley's working memory model, and Sweller's cognitive load theory [18]. According to multimedia learning theory, teachers should use multiple simultaneous techniques such as combining narration and visuals in the presentation. Using multiple tools and techniques to deliver information will help the learners to relate themselves with the content. In fact, multimedia learning theory will help the teachers to communicate effectively with the learners. Several theories have discussed the effectiveness of using multimedia theory in classroom teaching, and one of the major contributions predominantly focuses on the use of various types of multimedia while teaching that attracts the attention of the learners and eventually impacts the effectiveness of learning [19].

To sum up, the advantages of multimedia-assisted language teaching outweigh its disadvantages, and the benefits of multimedia-assisted English teaching should be brought into full play, and problems occurred during teaching practice need to be solved. As many research studies have focused on language input (vocabulary, listening, and reading) of multimedia-assisted instruction, but limited empirical research on output (especially writing) of it, this study first investigates the effectiveness of multimedia teaching mode and then formulates a multimedia-assisted writing teaching model that aims to improve students' writing performance and develop with other language skills. The solution of writing issues will enable students to benefit more comprehensively from multimedia teaching and to further improve the advantages of multimedia teaching.

3. Multimedia-Assisted Instruction

The so-called multimedia-assisted teaching is to combine graphics, images, sound, text, animation, and other media organically through computers, video display platforms, projectors, and other equipment to show the teaching content to the students in an intuitive, vivid and beautiful way, so as to enhance teaching effectiveness [20]. Because multimedia teaching is mainly composed of computer and video media, with the development of computer technology and integration technology, multimedia teaching mainly refers to computer integrated multimedia teaching, that is, using computer to gather a variety of media to realize the combination of various media. In the teaching process, teachers follow the teaching plan which is made according to the teaching objects, objectives, and content, select the appropriate teaching media, directly display the teaching content, and interact with students in real time, to achieve the effectiveness of multimedia display and real-time explanation. The composition of multimedia determines that multimedia has the following characteristics in teaching: intuition, interaction, integration, controllability, nonlinearity, and editability. Also, multimedia teaching can be roughly divided into three categories: teaching mode based on a single machine; teaching mode based on LAN; and teaching mode based on the Internet (Figure 1).

3.1. Multimedia Teaching System. Multimedia teaching system has access to massive technology, and each has powerful functions. For example, display technology, where the technology investment cost and energy consumption are relatively low, can get high-definition pictures and images, to provide users with accurate port connection [21]. Users can easily get connected, and the connection does not need to be verified, so they can log in at any time. Software technology can make complex software be used in a wide range, and its use repeatability is relatively strong. Wireless technology, such as broadband CDMA technology and infrared technology, can provide efficient broadband to users. In addition, we must mention virtual reality, which is based on a kind of virtual space, to realize the continuous expansion of the picture, giving people a sense of immersive experience, and it has been proved to be very effective in terms of ease of learning [22]. In fact, it has already been used in language learning and welcomed by users. Media application platform gives users a broad space, and it promotes the continuous development of science and technology and integration of industry technology, making the technology market become prosperous [23]. With the improvement of technology, people enjoy telemedicine, active image, high-definition television, distance teaching, interactive voice, and other services. The powerful functions enrich people's lives as well as education field.

Multimedia teaching system combines these technologies together. Usually, the main hardware of multimedia integrated classroom is composed of a computer, a video display platform, a projector, an electric screen, and a variety of playback equipment (such as video recorder, VCD or DVD player, power amplifier, etc.), which is controlled by console and computer, so as to form a scientific, coordinated, and efficient teaching demonstration system (as shown in Figure 2).

3.2. Multimedia Teaching Mode. At present, the application of multimedia technology in college English teaching mainly focuses on using online platforms and their resources. Compared with traditional classroom's "chalk + blackboard" environment, multimedia integrated classroom enables teachers prepare and display teaching content in time, helping students fully understand the corresponding teaching objectives, key and difficult points, and teaching process and saving valuable classroom time. In addition, teachers can also provide students with more information input and more opportunities to practice, so as to improve the efficiency of teaching.

Based on related theories and previous research findings, this experiment integrates and balances the teaching of five English language skills (listening, speaking, reading, writing,

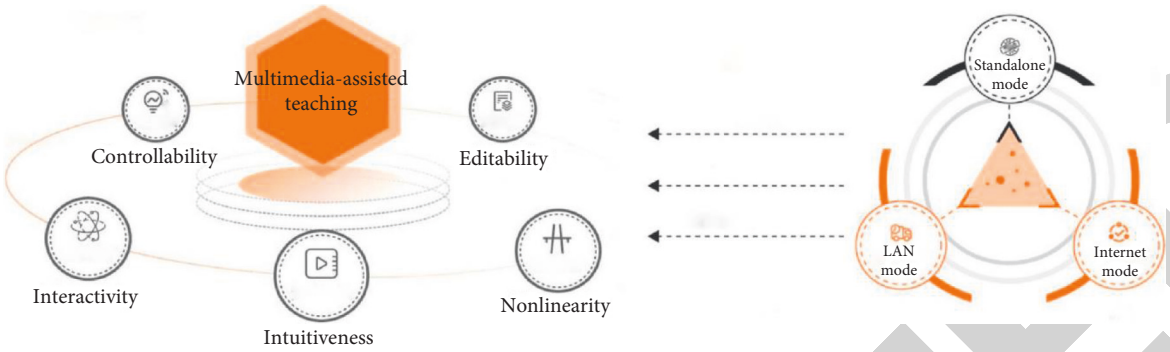

Figure 1: Characteristics and modes of multimedia-assisted teaching.

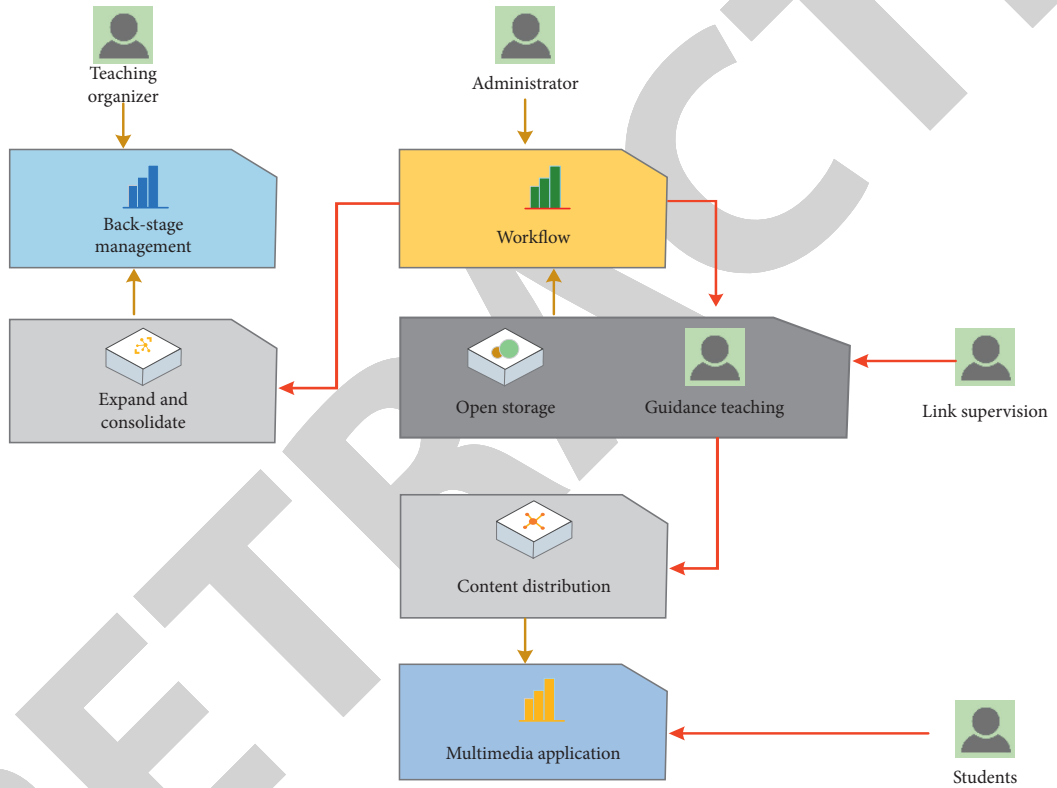

Figure 2: Multimedia teaching system.

and translating) and tries to make full use of multimedia-assisted teaching. Figure 3 shows a general multimedia teaching mode used in this teaching experiment. From the figure, it can be inferred that the database mainly includes teaching content in the form of audio, video, pictures, PPT, texts, and so on, interactive platform, digital library, and online dictionary. Teachers and students use equipment such as laptops, mobile phones, and classroom terminal to access the data transferred through the Internet, intranet, or mobile network. Then, teaching and learning interaction-related activities include lecturing, individual and group learning, students' presentation, etc. In this way, multimedia is used in classroom teaching, and each part of the multimedia plays a crucial role in applying the multimedia technology in and beyond classrooms as proposed in Figure 3.

Under the guidance of constructivist learning theory, college integrated English course should be student-centered in order to achieve certain teaching objectives. Teachers, as the organizers of teaching, should actively create learning situations for students that are conducive to activating their original knowledge and experience, provide corresponding counselling and practice opportunities, organize and participate in the cooperation and interactive learning among students, and evaluate the learning effect in time, so as to improve teaching [2]. As the main body of meaning construction, students should give full play to their subjective initiative, actively participate in the whole process of classroom learning with the help of teachers, complete the corresponding tasks of learning activities, carry out self-test, consolidate and improve the construction of knowledge, and improve the learning effect and efficiency [24]. Also, the

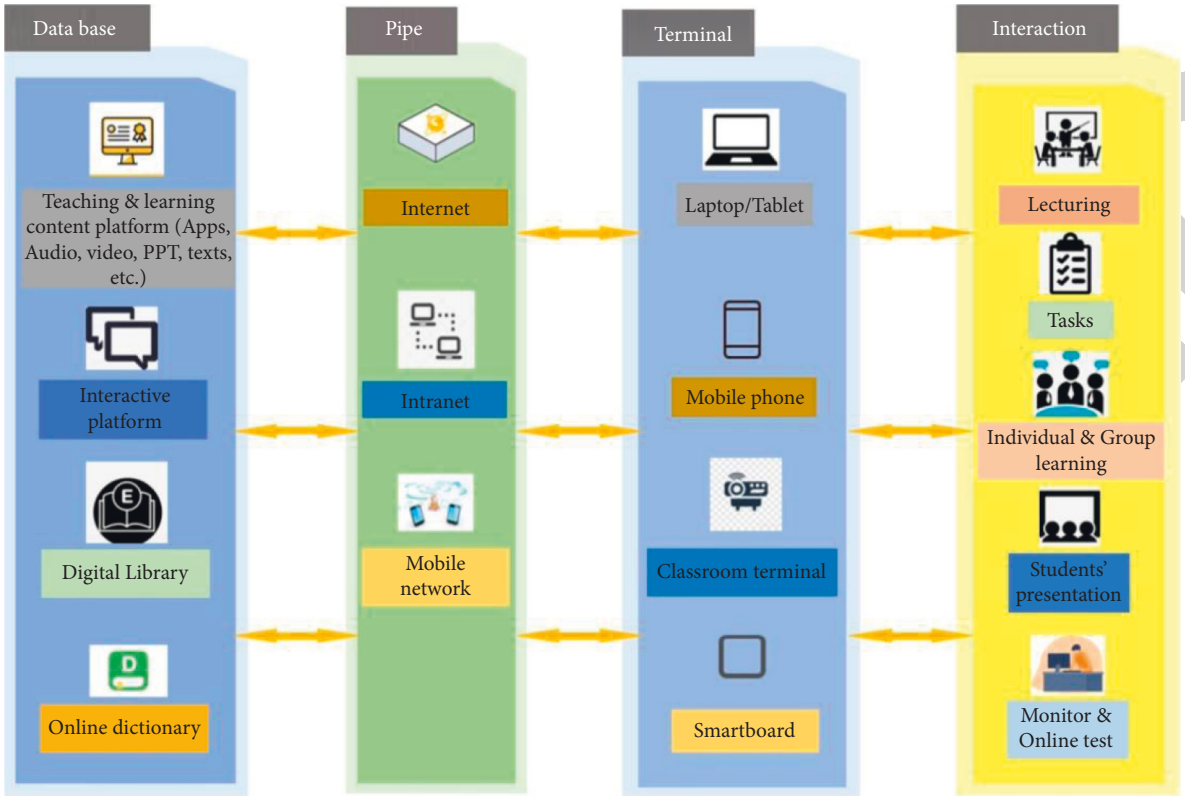

Figure 3: Multimedia teaching mode.

multimedia comprehensive classroom runs through the whole process of teaching experiment. The important role of multimedia-assisted instruction is mainly reflected in the clearer display and presentation of a large number of background information and language exercises, which is convenient for students to build and consolidate their knowledge and improve the efficiency of learning.

4. Evaluation of Multimedia-Assisted English Teaching

The participants of the teaching experiment were 90 first-year undergraduates of non-English majors from a western Chinese university, who were selected and divided into two groups (45 students for each) according to their English scores of National College Entrance Examination and Pre-test. Chinese was their L1 and English was their foreign language. Participants in both experimental group (multimedia methods) and control group (traditional mode, where textbooks, cards, pictures, and PowerPoint slides are often used) have the similar English proficiency (intermediate level). The experiment was conducted over a period of one academic year, and each lesson (90 minutes) was given twice per week and all participants from the two classes were taught by the same English teacher with the same textbook New Progressive College English (Books 1 and 2). In this study, the performance of two groups of participants was measured after the experiment, and questionnaire survey and examination results were employed to collect information to measure the effectiveness of multimedia-assisted English teaching. Participants' subjective and objective evaluation is shown below.

4.1. Students' Feedback on Multimedia-Assisted English Teaching. At the end of the first semester, the author conducted a questionnaire survey of students' feedback on multimedia-assisted English teaching, and it covers many aspects which serve as the evaluation of the teaching mode. The questionnaire consists of two parts: the first part consists of 20 multiple-choice questions, each of which has five options of 5-point Likert scale. The second part is question and answer, which is open-ended and consists of five subquestions.

4.1.1. Learning Interest and Efficiency. It can be seen from Figure 4(a) that 8.7% (2% very inconsistent and 6.7% inconsistent) students think that multimedia-assisted teaching does not enhance their interest in English learning; 13% of the students think that the multimedia plays a general role in raising their interest in learning, while 45% of the students consider that their interest in learning English has been improved, and 33.3% of the students believe that they have become passionate about learning English. As it can be seen from Figure 4(b), 10.9% (2% very inconsistent and 8.9% inconsistent) of the students think that multimedia-assisted teaching does not improve their English learning efficiency; 18% of the students think it sometimes improve their learning efficiency, while 42.2% of the students believe they have greater English learning efficiency, and 28.9% of the

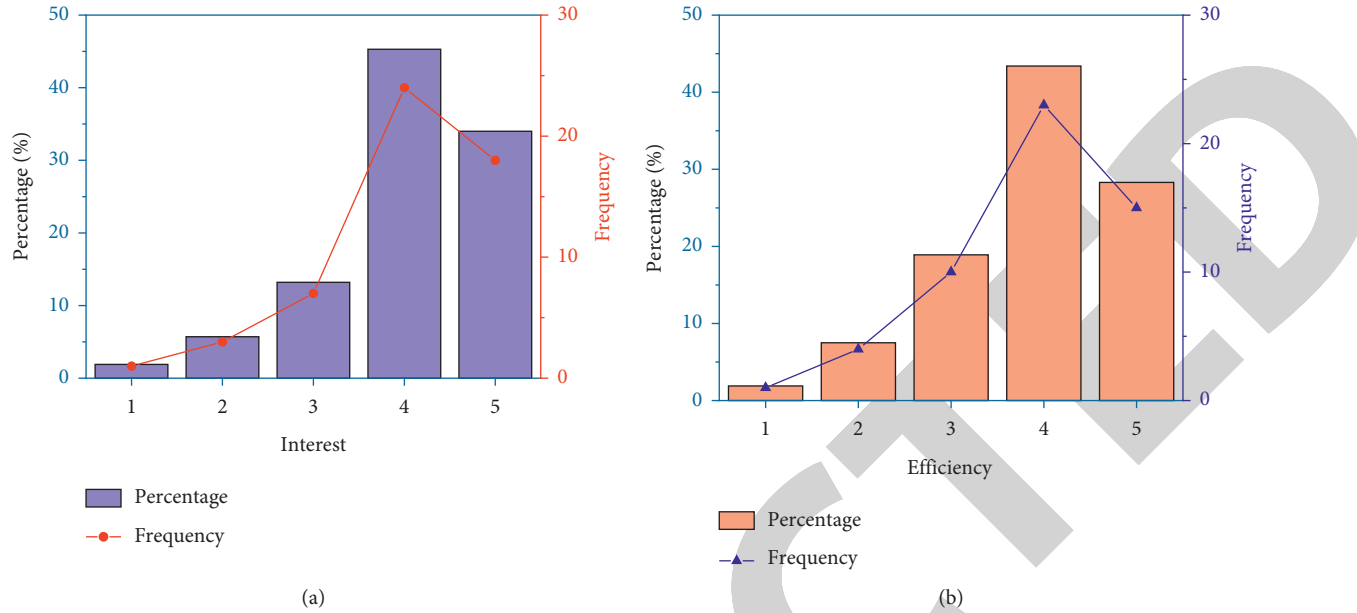

Figure 4: Percentage of learning interest and efficiency after multimedia-assisted teaching. (a) Interest. (b) Efficiency.

students think that their English learning efficiency has been advanced to a large extent.

4.1.2. Understanding Key Points and Having Positive Thinking. It can be seen from Figure 5(a) that only 4% (2% very inconsistent and 2% inconsistent) think that multimedia-assisted teaching does not help them understand key and difficult points in English learning; 15.5% of the students think that the multimedia mode can sometimes help their understanding; 45% of the students believe it helps them better grasp the key knowledge, and 35.5% of the students think that their understanding of key and difficult points has been greatly improved. It can be seen from Figure 5(b) that 6.5% of the students think that multimedia-assisted teaching does not inspire their positive thinking in English learning, and the students who think it sometimes inspires their positive thinking occupy 11.1%. However, 49% of the students believe that the teaching mode generally stimulates their thinking, and 33.3% of the students think that their positive thinking in English learning has been fully inspired.

4.1.3. Preferred Teaching Activity. The questionnaire related to this part has options ranging from Strongly Agree, Agree, Uncertain, Disagree to Strongly Disagree, and when it comes to answer the question: "Which is your favorite teaching activity?" The result shows that "open-ended task" gets the highest rank.

Open-end tasks generally have a wide range of appropriate responses, take longer time to complete, evaluate the knowledge and skills of the learners, include problem-solving strategies, allow learners to think critically, and demonstrate higher levels of understanding by providing opportunities. It also engages learners to discuss their opinions and ideas in a creative manner. Multimedia learning provides seamless opportunities for students to perform the open-ended tasks in their own original and unique manner using different multimedia technologies.

It can be seen from the survey results in Figure 6 that the vast majority of students believe that the implementation of open-ended tasks in multimedia environment has many merits. A total of 71.1% of the students think that the implementation of open-ended tasks expands their vocabulary. 75.5% say it improves reading ability, and 57.8% think it also enlarges their reading scope. In the process of preparing their works, students collect raw materials by browsing foreign websites and English books to enrich their ideas and expressions, thus virtually increasing the amount of vocabulary and reading range. The results show that 82.2% and 73.3% of the students think their expressing enthusiasm and learning enthusiasm have been stimulated, respectively, as the tasks enhance their self-confidence, while 20% and 17.8% of the students are uncertain about their reading scope and spoken English proficiency, respectively, which may be due to the reason that many students' reading range is limited by the text topic of the textbook, and some students just read aloud the prepared manuscripts, which cannot be seen as effective face-to-face communication. Meanwhile, some students' pronunciation is not accurate and their vocabulary is limited, which may cause listeners to lose interests.

4.1.4. Autonomous Learning. The questionnaire also examines whether multimedia teaching promotes learners' autonomous learning ability. Autonomy is an ability responsible for one's own learning. When learners have the ability of autonomous learning, it means that learners themselves can determine the learning objectives, contents, materials and methods, time, place, and progress of learning and evaluate learning. The questionnaire designs

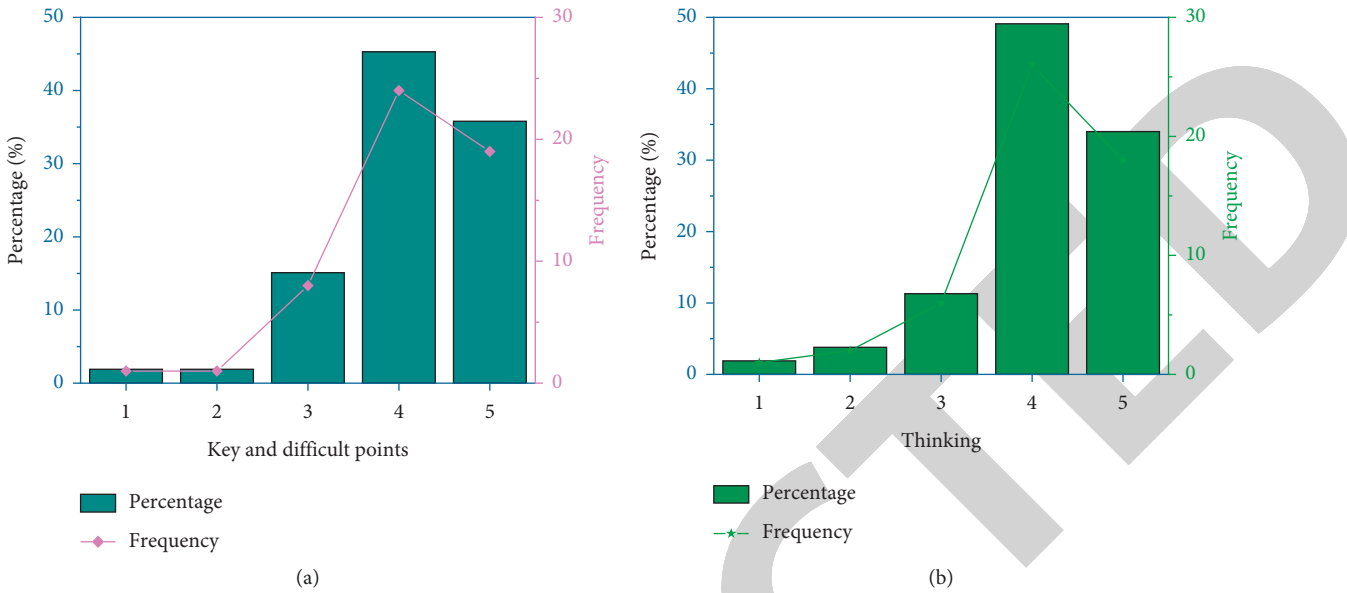

Figure 5: Percentage of understanding key and difficult points and having positive thinking after multimedia-assisted teaching. (a) Key and difficult points. (b) Thinking.

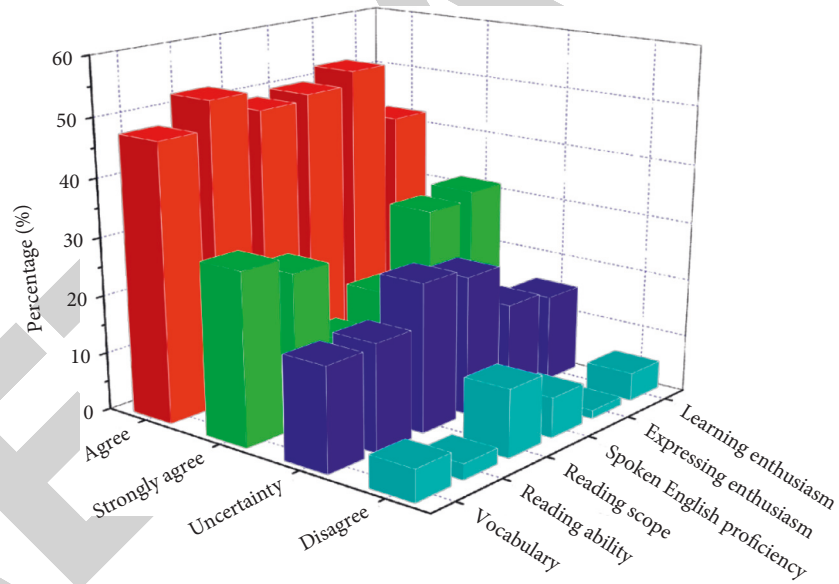

Figure 6: Learners' evaluation of the effectiveness of open-ended tasks.

questions from the perspectives of learning attitude, learning contents, materials and methods, and reflection on learning process.

According to the relevant statistics in Figure 7, 75.6% of the students like to participate in open activities. 80% of the students think that they have freedom to choose learning materials and 71.1% think they can process the selected materials and learn in their own way. 77.8% of the students believe that multimedia teaching enhances their study ability. In the process of completing tasks, students have a certain decision-making power and can selectively absorb and reconstruct information in their own way. Overall, most students think that multimedia teaching can promote the development of autonomous learning ability. However, 25.3% of the students are uncertain about whether to reflect and modify their works, and 12% of them do not agree to reflect and modify their works. It can be seen that students fail to realize the importance of reflection in promoting autonomous learning. In the answer of open-ended questions, students generally say that due to busy homework and limited time, they cannot keep improving their works all the time. Some students think that they have spent a lot of time and energy to prepare the activity before class. Once the unit teaching is over, they will not have the motivation to modify it, so they ignore the continuous learning in the reflection stage.

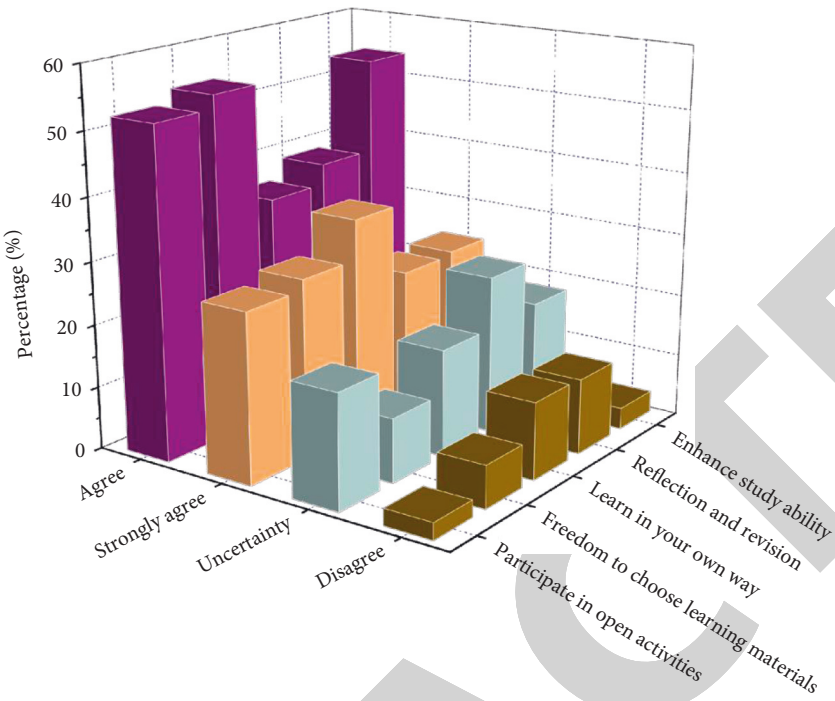

Figure 7: Evaluation of the promotion of autonomous learning.

4.2. Students' Performance after Multimedia-Assisted English Teaching. In order to compare the performance differences between traditional teaching and multimedia-assisted teaching, this paper examines the final examination results of 90 freshmen at the end of the first semester. The final exam is adapted from a past exam paper of CET-4 (College English Test-Band 4, a large-scale English exam in China) and is divided into five parts: listening, vocabulary and grammar, reading, writing, and translation.

The distribution of students' scores in traditional teaching environment is wide and scattered, while the distribution of that in multimedia teaching environment is relatively concentrated. After obtaining the candidates' scores, the paper makes a comparison of various achievements, as shown in Figure 8.

From Figure 8, it can be inferred that multimedia-assisted English teaching mode has significant advantages, among which the average difference of listening and reading is the largest (2.5 and 2, respectively). From the average of the total score, the difference between the two is 6.6. Although the average total score of traditional teaching is lower than that of multimedia-assisted English teaching mode, there is no significant difference between the items of writing and translation, which may be due to many possible reasons, including L1 influence in the process of EFL writing, limited time, inappropriate teaching model, and so forth. How to improve the effect of multimedia teaching in writing and translation is a problem that needs to be focused. As writing is considered to have a close relationship with students' academic performance and research, a new experimental writing teaching model was sketched and conducted in the second semester.

5. Modified Writing Teaching Model and Its Effect

Compared with traditional writing teaching, where the teacher often provides writing samples to students, assigns writing tasks, and checks them, the multimedia-assisted writing teaching model focused more on providing learning resources and using online writing correction websites and the teacher to help students correct their writing errors in the first semester. However, much work can be done to make full use of multimedia-assisted instruction to improve writing performance.

5.1. Modified Writing Teaching Model. Multimedia and multimodal have similar definitions. While "multimedia" is used more frequently in public/industry contexts and it emphasizes the production of a deliverable text, "multimodal" is preferred in the field of composition and rhetoric, and it focuses on design and process [25]. Multimodal composing is influenced by social semiotics and uses a variety of social symbols and multiple modes to express meaning, including but not limited to text mode, visual mode, audio mode, body mode, and space mode. Researchers like G. Kress, T. Van Leeuwen, and the New London Group all believe that all texts are expressed or embodied by linguistic, visual, or spatial modes. In other words, in order to express meaning, the authors usually use multiple modal resources to design and demonstrate their way of thinking [26–28]. In today's intelligent and digital age, text-centric communication has been replaced by image-centric and other modal-centric methods. This means that although language is regarded as the primary channel of

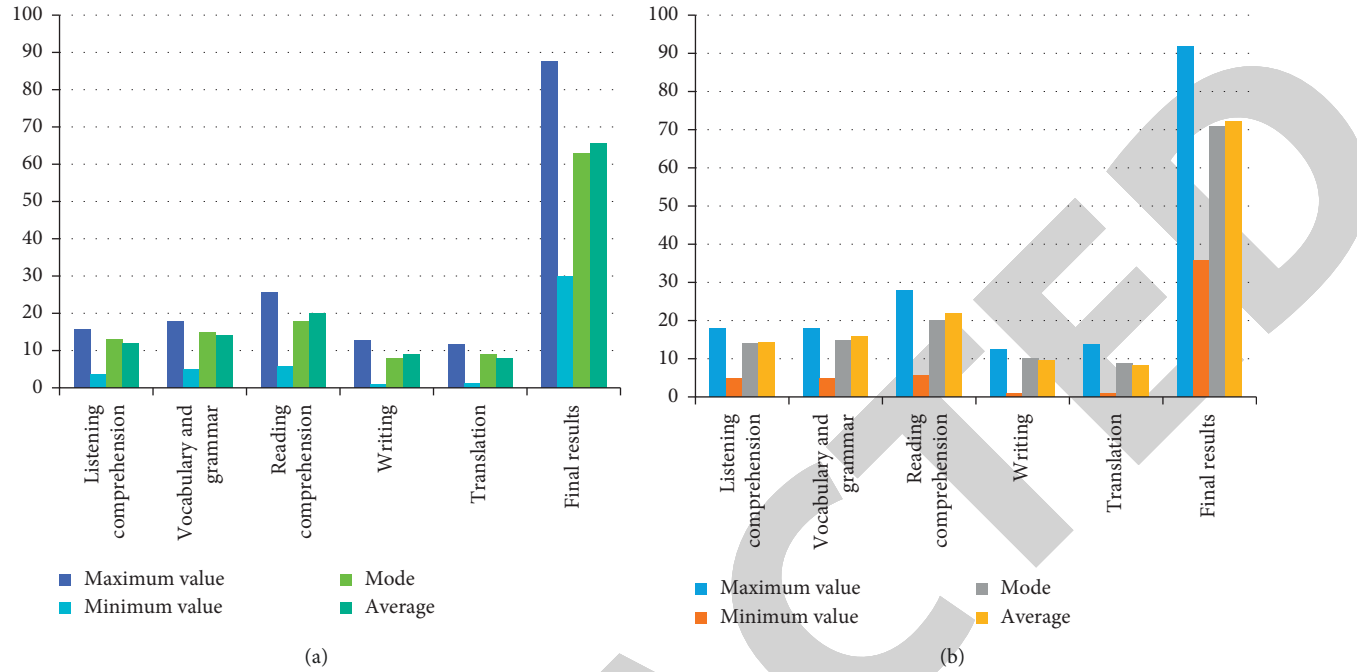

Figure 8: Comparison of English test results. (a) Traditional teaching. (b) Multimedia-assisted teaching.

communication, other modes such as body language, images, and sound can also express important meanings [29]. In this sense, the authors can use multiple modal resources when creating texts and express meaning or communicate with readers through multiple modal resources. Multimodal text creation is an extension of traditional writing, and it also enables writing to develop in a more diversified and multimodal direction.

Therefore, based on multimodal composing theory and findings of the teaching experiment in the first semester, like students' preference on open-ended tasks, their expressing enthusiasm and understanding of key and difficult points have been improved in multimedia environment, and a revised writing teaching model (Figure 9(b)) was constructed, which added discussion section before writing and summary writing section after learning each text. Other major differences lie in a clear closed-learning loop, multiple modification, and teacher guiding practice which aims at improving students' writing accuracy instead of too much reliance on students' autonomous learning. The model was hoped to better satisfy students' learning need, suit their major, and improve their writing performance.

5.2. Students' Performance after Multimedia-Assisted EFL Writing. According to questionnaire survey, 75.6% students think teacher guiding practice, especially imitating sentence patterns, is their favorite writing activity, for it gives them a sense of security that at least one-third or a half of the sentence is correct, which indicates that they value accuracy. For instance, after watching the video clips and reading the novel *Pride and Prejudice* written by Jane Austen, students chose the first sentence of the novel as a good sentence pattern—"*It is a truth universally acknowledged that* a single man in possession of a good fortune must be in want of a wife" [30]. Then, the teacher guides students to imitate the sentence pattern to write their own sentences relating to the writing topic—How to conserve water? Here are the examples of students' writing: "*It is a truth universally acknowledged that* dry areas must be in want of water" and "*It is a truth universally acknowledged that* desalination of seawater is very expensive." They are more than happy to have the ability to use the same sentence patterns in various contexts properly.

Furthermore, 82% of students like multimodal writing and believe that it arouses their interest in writing for it helps learners relate themselves with the writing content and integrates English learning, their major, creativity, online resources, autonomous learning, and so forth in a whole package. Students use various software programs (some related to their majors) to design pictures, headings, and instructions, take notes on a cognitive map, type in text, check their writing, and record and send their voices narrating what they had written. Figure 10 shows students' multimodal writing examples in response to the writing task—design a useful machine that helps to protect the environment.

In addition, all the writings of the final examination of the second semester were evaluated by two teachers within two rounds with the four scoring criteria of IELTS: response to the task, grammatical range and accuracy, lexical resource, and coherence and cohesion. From the average writing score, the difference between the two is 1 (total of 9 points), which showed a relatively significant improvement in their writing within multimedia-assisted model. Also, the students reported that they would like to continue using this teaching method in future.

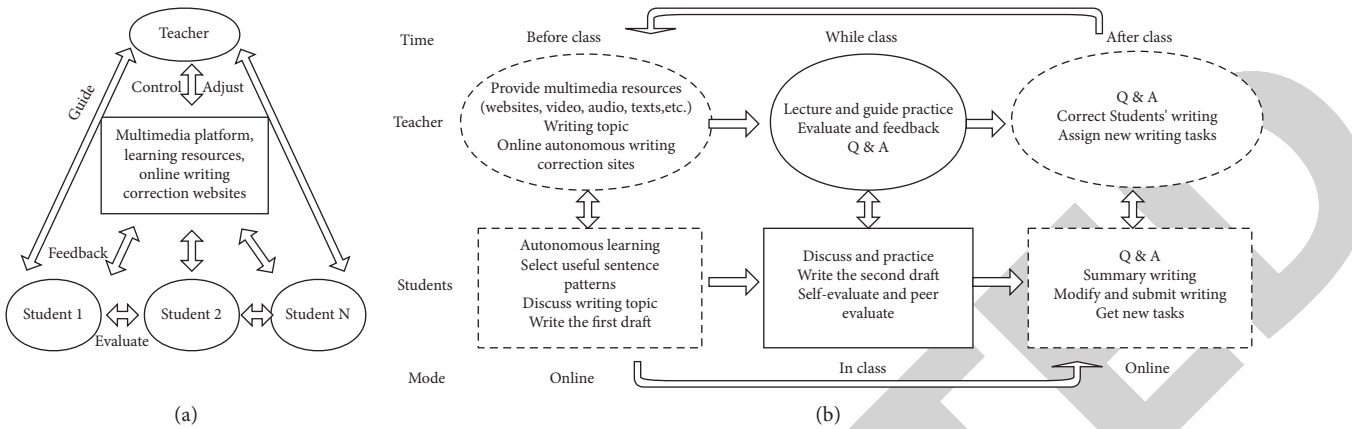

Figure 9: Multimedia writing teaching model. (a) Writing model in the first semester. (b) Modified writing model in the second semester.

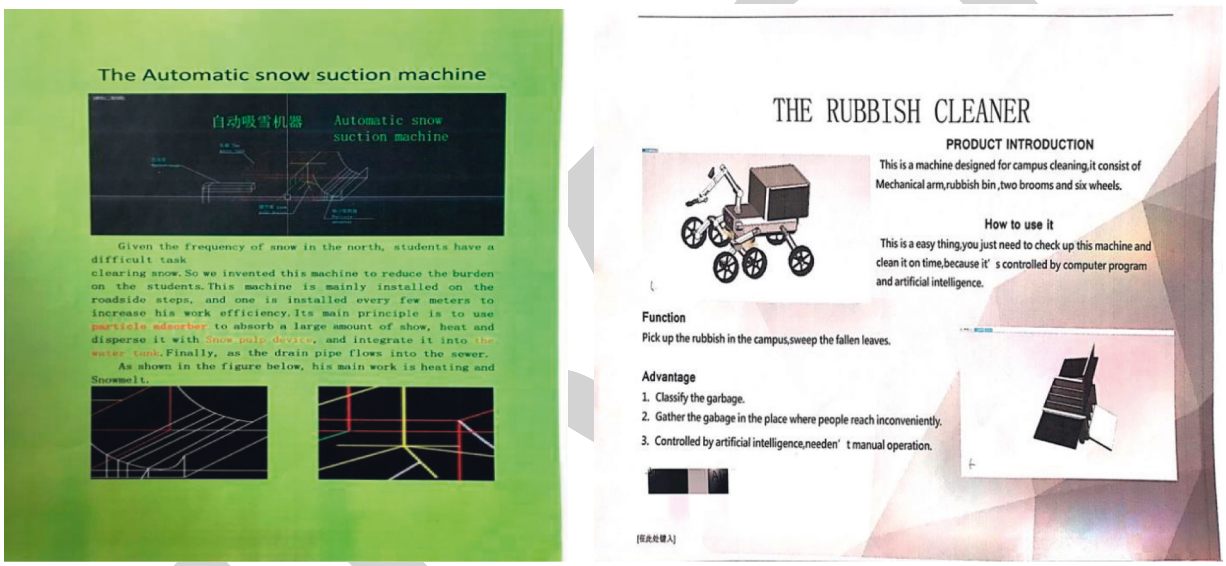

Figure 10: Students' writing examples (majored in Mechanical Design).

6. Conclusion

This paper evaluates multimedia-assisted English teaching from different aspects, and it proves that multimedia-assisted language learning provides authentic learning resources, cultivates learner motivation, complements traditional curriculum, and increases better learning outcomes. Furthermore, it is also found that multimedia teaching can significantly improve students' listening and reading ability, which makes the total English score of multimedia teaching group obviously higher than that of traditional teaching group. However, there is no significant difference between multimedia teaching and traditional teaching methods in writing and translation after one semester's experiment, but the study continues to adjust and apply a new writing teaching model in the second semester, which later shows that it better enhances students interest in writing and further improves the advantages of multimedia teaching. Due to time limitations, the study only involved overall writing scores rather than detailed comparison of vocabulary, sentence length, type of errors, etc. between the two groups of writing, which may be examined in detail in the future. Multimedia classroom teaching is a complex teaching process. The development and evaluation of all aspects of multimedia classroom teaching needs long-term research and practice. We should clearly realize that no matter how advanced multimedia technology is and how helpful it is to English teaching, it is only a teaching aid. To achieve real success in English classroom teaching, we must give full play to teachers' leading role and students' subjectivity. It is believed that through our efforts, multimedia-assisted English teaching will promote the steady development of English teaching towards a better direction.

Data Availability

The data and models generated or used during the study are included within the article.

Conflicts of Interest

The author declares that there are no conflicts of interest.

Hindawi
Journal of Mathematics
Volume 2023, Article ID 9760547, 1 page
https://doi.org/10.1155/2023/9760547

Retraction

Retracted: Computational Intelligence and Things Technology-Based Collection and Design of Inheritance Characteristics of Tea Product Packaging Art Form

Journal of Mathematics

Received 19 December 2023; Accepted 19 December 2023; Published 20 December 2023

This article has been retracted by Hindawi following an investigation undertaken by the publisher [1]. This investigation has uncovered evidence of one or more of the following indicators of systematic manipulation of the publication process:

(1) Discrepancies in scope

(2) Discrepancies in the description of the research reported

(3) Discrepancies between the availability of data and the research described

(4) Inappropriate citations

(5) Incoherent, meaningless and/or irrelevant content included in the article

(6) Manipulated or compromised peer review

The presence of these indicators undermines our confidence in the integrity of the article's content and we cannot, therefore, vouch for its reliability. Please note that this notice is intended solely to alert readers that the content of this article is unreliable. We have not investigated whether authors were aware of or involved in the systematic manipulation of the publication process.

Wiley and Hindawi regrets that the usual quality checks did not identify these issues before publication and have since put additional measures in place to safeguard research integrity.

We wish to credit our own Research Integrity and Research Publishing teams and anonymous and named external researchers and research integrity experts for contributing to this investigation.

The corresponding author, as the representative of all authors, has been given the opportunity to register their agreement or disagreement to this retraction. We have kept a record of any response received.

References

[1] S. Wu and K. Mojtahe, "Computational Intelligence and Things Technology-Based Collection and Design of Inheritance Characteristics of Tea Product Packaging Art Form," *Journal of Mathematics*, vol. 2022, Article ID 3578831, 10 pages, 2022.

Hindawi
Journal of Mathematics
Volume 2022, Article ID 3578831, 10 pages
https://doi.org/10.1155/2022/3578831

Research Article

Computational Intelligence and Things Technology-Based Collection and Design of Inheritance Characteristics of Tea Product Packaging Art Form

Shilin Wu[1] **and Kaza Mojtahe**[2]

[1]*School of Fine Arts & Design, Guangzhou University, Guangzhou, Guangdong, China*
[2]*Department of Computer Engineering, Kyrgyz-Turkish Manas University, Bishkek, Kyrgyzstan*

Correspondence should be addressed to Kaza Mojtahe; kaza.mojtahe@mail.cu.edu.kg

Received 17 December 2021; Revised 7 January 2022; Accepted 7 February 2022; Published 10 March 2022

Academic Editor: Naeem Jan

In view of the core process data such as temperature and humidity of the tea product packaging process and the automatic control operation parameters of the production line, this paper designs a smart tea product packaging 5G Internet of Things gateway system, which realizes the 5G Internet of Things onsite monitoring and remote monitoring of the tea product packaging production line equipment. The design and implementation of the 5G Internet of Things gateway system are divided into three aspects, namely, 5G Internet of Things gateway configuration design, data communication protocol conversion. First, the 5G Internet of Things gateway configuration is to design the relevant control information of the tea processing production line equipment and complete the configuration storage of the PLC controller; secondly, the data communication protocol conversion is to pass the Modbus/TCP OPC standard to transfer the collected 5G Internet of Things. The sensor data undergoes unified standardized conversion, and then the standardized converted data is sent to the database and server using the MQTT protocol; the data processing of the 5G Internet of Things gateway system is the design of the internal data of the 5G Internet of Things gateway. Finally, the test was carried out and the results were obtained, which proved that the designed 5G Internet of Things gateway system is useable, reliable, has good stability and scalability, and provides an important solution for the construction of smart tea product packaging in the industry. The tea product packaging system based on 5G Internet of Things technology compiles electronic production management files for tea garden production, tea picking, tea processing, tea packaging and other links in accordance with the requirements of the national agricultural product quality and safety related systems and industry standards, and has become the traceability of tea quality The recorded important production management information provides important information support for the traceability of the whole process of tea.

1. Introduction

In recent years, 5G Internet of Things technology has been widely used in agriculture, and its advantages such as advancement and intelligence have played an important role in promoting agricultural modernization [1]. In the construction of the tea quality traceability system, 5G Internet of Things technologies such as sensors, RFID, QR codes, and wireless sensor networks are integrated and applied to tea planting, processing, storage, packaging, sales and other links to realize intelligent traceability information collection and processing can effectively improve the credibility and efficiency of traceability, which greatly promotes the quality of famous and high-quality tea in tea enterprises, and is of great significance to the expansion of the brand influence of tea enterprises [2–4]. Smart tea product packaging is the intelligent development direction of the tea processing industry and an important part of the Industry 4.0 smart factory. At present, most tea product packaging is still based on the construction of automated production lines, using the PC-PLC system, that is, using the PC in the control room of the tea product packaging to realize the PLC control system

and the collection and storage of sensor data through configuration software And monitoring has not realized the true 5G Internet of Things and cloud data storage and computing services [5–7].

The packaging process of tea products is very demanding on the environment. The existing tea product packaging factories are generally PC-PLC systems, which collect and upload real-time data through PLC chips or other types of chips, and store them in the local area network, which is not convenient for the staff to understand the tea. The product packaging environment can be viewed in real time and remotely monitored. Therefore, the application of 5G Internet of Things systems to tea product packaging will also become a trend in our research. As a bridge between sensing devices and traditional network transmission, 5G Internet of Things gateways play a very important role in 5G Internet of Things systems [8]. The 5G Internet of Things gateway for smart tea product packaging obtains sensor data such as temperature and humidity and control data such as forward rotation and reverse rotation in the tea product packaging equipment, and then uploads them to the local database and network server. At the same time, the 5G Internet of Things gateway can monitor various data on the packaging of smart tea products and play a key role in the subscription and publishing process. This is of great significance for improving the quality of tea, the total amount of processing, reducing the cost of tea production, and building a smart tea processing plant [9].

This article introduces 5G Internet of Things technology to agriculture, realizes the integration of 5G Internet of Things technology and agricultural technology, and specifically applies it to agricultural production, operation, management and services, thus forming the 5G Internet of Things for agriculture. It uses various sensors, sensor networks, and the Internet to collect and transmit agricultural production, processing, and circulation information, and then uses a back-end software platform to process massive agricultural information, so as to realize the entire process of agricultural production monitoring and scientific management, thereby achieving intensive agricultural production, goals of high quality, high yield, ecology and safety. Based on the assessment of the current platform design approaches, a simulation platform was constructed. The platform utilises an event scheduling system to realize the operation of the complete simulation process, and has the features of high simulation accuracy. At the same time, the platform employs script configuration files and text output files, which can accomplish easy creation of simulation scenarios and quick verification of simulation results, and has the benefits of excellent scalability and high repeatability. The agricultural product quality traceability system uses 5G Internet of Things technology to collect real-time information data about agricultural product planting, processing, warehousing, packaging and other environments and transmits it to the Internet traceability information management platform through the network. Massive data transmission and sharing are available for consumers, enterprises, and consumers. The government provides support for product traceability.

2. Related Work

The 5G Internet of Things uses RFID, various sensors, 5S technology (remote sensing technology, global positioning system, geographic information system, expert system, decision support system) and other sensing devices to connect objects with the Internet and process the collected data Analysis to achieve a high degree of integration of things and things, people and things, in order to achieve the purpose of precise management and real-time control [10].

Ding [11] takes Nongken tea as the research object, conducts research on the quality traceability system of tea, and applies 5G Internet of Things technology to tea growth, tea product packaging and tea sales. Users can query product information through the terminal. Based on the perception layer, transmission layer, and control layer of the 5G Internet of Things system, Vu [12] realized the traceability, planting, environment, tea processing and sales management monitoring of the tea platform, and explored and analyzed the network protocols, Issues such as interactive interfaces. Nasrallah [13] takes Anhui tea as the research object, using 5G Internet of Things, wireless communication and big data technologies to design a unified platform based on SOA architecture to achieve comprehensive monitoring and management of tea, effectively improving the production level of related companies and marketing capabilities. Aiming at the problems of the 5G Internet of Things gateway system not reaching the unified standard and the easy construction of the wireless sensor network, communicates through multiple remote communication modes such as GPRS, Wi Fi, and Ethernet, and uses the python integrated Sqlite3 as the embedded database. Indrawan [14] lowered network maintenance costs by using FPGAs to simulate and evaluate the frame format conversion and address mapping between Ethernet and FC in order to establish a smooth connection and protocol conversion between FC and Gigabit Ethernet. Wan [15] extends the multi-network information architecture using software-defined approaches. Hierarchical 5G Internet of Things software-defined controllers in the feedback intermediate device can not only reduce link congestion, realize the scheduling of various business flows, but also improve the current network operating conditions and algorithm performance to achieve full optimization of the network's performance. Additionally, two distributed energy management research and development systems that are suited for smart city scenarios have been developed. The platform has a wide range of use, supports a large scale of network business, and can realize resource sharing and complete the interaction between heterogeneous Internet of Things devices.

Some scholars have integrated 5G Internet of Things technologies such as RFID, sensors, ZigBee wireless sensor network, GPS, distributed data storage and processing based on cloud computing, data mining and knowledge discovery, artificial intelligence, through the breeding and transportation of pigs. The collection, storage, processing and application of all information from slaughter, processing to sales can provide consumers, corporate customers and the government with product tracking, information query, departmental

supervision, industry early warning and other services [16]. At the same time, it implements refined management of agricultural products and livestock products from the source of production to the consumer market, records the quality and safety information of growers and farmers throughout the process, provides effective agricultural product quality and safety supervision and management mechanisms and methods for the agricultural and animal husbandry departments, and provides a variety of traceability information inquiries to facilitate consumers' inquiries. With the help of RFID technology, the researcher has carried out the development of information transmission carrier, information recording and exchange equipment, as well as the construction of information exchange and transmission platform, and has developed and established the traceability code, traceability carrier, and traceability equipment "Trinity" of agricultural product quality and safety traceability system. They introduced a differential algorithm to solve the minimum life cycle, so that the routing node selects the cluster with the longest life cycle to communicate, and through GAThe PSO method uses cluster nodes to identify the best route. Due to its role as part of the 5G Internet of Things, a 5G Internet of Things gateway takes on a role of merging perception networks and communication networks, allowing for smooth connections between the perception layer and network layer [17, 18]. An effective security system must be built for 5G Internet of Things gateways, which must have comprehensive access capabilities for detecting networks and nodes as well as extensive administration capabilities. Increasing user privacy is simply one aspect of the widening reach of information perception, which is closely linked to environmental monitoring, production, and life safety. The above improvements aimed at energy consumption have made ZigBee wireless communication technology a big step forward. For today's society where resources are scarce and green development is emphasized, it has high research value [19, 20].

3. Collection of Inheritance Characteristics and Design Model Construction of Tea Product Packaging Art Form Based on 5G Internet of Things Technology

3.1. 5G Internet of Things Technology Level Nesting. The 5G Internet of Things technology is an important part of the information age, and is a carrier of information based on the Internet and traditional communication networks. With the rapid development of sensor technology, communication technology, "Internet +" information technology, and the perfect integration of Internet of Things technology, it is applied to tea product packaging to strengthen the information management, control and lean production process in the tea product packaging process. A high-efficiency and high-quality smart tea product packaging has been established, and its structure is shown in Figure 1.

The 5G Internet of Things gateway transfers the collected data information through the MQTT proxy message, realizes the conversion of Modbus to MQTT protocol, and transmits the data of the wireless sensor network to the server on the Internet, so that users can monitor the unified format of different device modules. The human-computer interaction equipment provides a simple and efficient human-machine interface. By obtaining data from the server and transmitting the user's operating instructions to the server, the user's real-time and remote query and operation functions are realized.

$$p(x(1), x(2), \ldots, x(n)) = \prod_{i=1}^{n} p\{x(n)|x(n-i+1)\},$$
$$C = \frac{2 * (p(x) * p(n))^{1/2}}{(p(x) + p(n))}. \tag{1}$$

The tea product packaging tea machine equipment is equipped with a mechanical sensing layer that is made up of sensor equipment and PLC modules. The tea machine's environmental sensor data must be classified and sent to the higher 5G Internet of Things gateway system before it can be used. The sensor is in charge of gathering the information. The PLC module is in charge of translating data into the standards needed by 5G Internet of Things gateways, and it makes use of multi-threaded data processing to assure data transmission consistency and dependability.

$$f(x) = x(i) + \frac{x(i) * x(j)}{x(i) + x(j)},$$
$$U(x) = (I - C)^{-1} * C^{T} \tag{2}$$
$$- \sum_{i=1}^{n} p(x) * C(i) \sum_{i=1}^{n} p(x) * Z(i).$$

The sensor network information includes the network topology information of the sensor node, the energy information of the node, etc., which is convenient for making judgments on the status of the sensor network. At the same time, it can also introduce rapid network diagnosis according to the actual deployment in the future to provide users with instruction. Specific application information is the information captured by various sensors installed on nodes according to specific application fields, such as soil temperature and pH value in precision agriculture.

$$Z(x, y) = \begin{bmatrix} x(i) \\ x(j) \end{bmatrix} \begin{bmatrix} \frac{\exp(x(i) + x(j))}{y(i) + y(j) + y(k)} & 1 \\ -1 & -\frac{\exp(x(i) + x(j))}{y(i) + y(j) + y(k)} \end{bmatrix}. \tag{3}$$

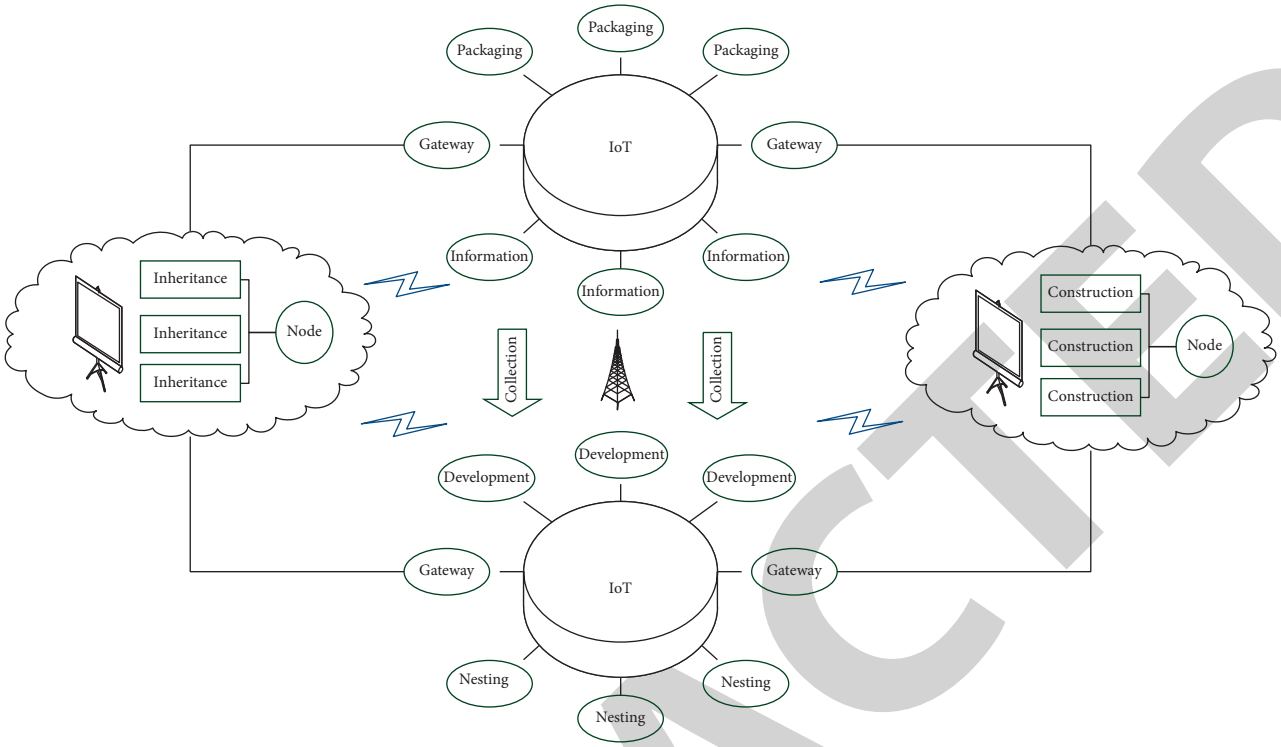

Figure 1: Hierarchical structure of 5G Internet of Things technology.

The 5G Internet of Things gateway communication layer is responsible for collecting the data transmitted by the sensor terminal, and converting the wired and wireless transmission signals into unified computer binary data according to the MQTT protocol, which is composed of DCS field workstations or 5G Internet of Things gateways. The data resource layer reads and stores the collected data. Different servers correspond to different data. Data storage is realized through programs and data query and call are realized through user commands.

3.2. Tea Product Packaging Process. Smart tea product packaging is the intelligentization of the whole process, integrating sensor technology, industrial wireless sensors, long-distance wireless communication technology, international open field bus, information fusion and intelligent processing technology into all links of production, according to the existing factory. The specific conditions and actual needs of the complex industrial site are intelligently processed for data information collection, real-time monitoring, tea product quality tracking and tracing, equipment operation and maintenance and diagnosis. The essence of the tea quality traceability system is the recording and transmission system of tea information, including the tea quality traceability system, data centers (national, local, and enterprise), system specifications, and work team composition, covering all aspects of tea production, processing, and marketing, thus forming a highly reliable traceability system. The software of the smart tea garden collection management system belongs to the top application layer of the 5G Internet of Things structure model. Data presentation, storage, and administration are all handled by this layer, which is a combination of the 5G Internet of Things and consumer and industrial demands. Scalability, complexity of development, workload, and visual page aesthetics of the software system are all influenced by the software framework and development methodology. The smart tea garden collection management system's software architecture is intended to satisfy as many of the aforementioned needs as feasible. It plays a role by correctly identifying, truthfully recording and effectively transmitting information throughout the entire process of tea planting, processing, and sales, so as to solve the problem of tea quality and safety.

Figure 2 is the convergence curve of the features of the Internet of Things. Tea packaging is mainly divided into small bag packaging and gift box packaging. Small bags of tea are commonly found in hotels and hotels, and gift box packaging of tea is usually directly facing consumers. In the case of tea packaged in small bags, the hygienic quality problems of the packaging bags may occur; in the process of packaging tea products, quality problems such as unqualified packaging materials or improper use of oxygen scavengers and preservatives may occur. Therefore, it is necessary to set up packaging information collection points to record tea packaging information. With the implementation of an electronic file tracking system, it is feasible to minimise the mixing of goods between batches; separate storage facilities for raw materials and finished tea are established, stacked in operating areas, and processed products are united and kept in a single location. Different network connection techniques should be used in the development of the enterprise local area network in accordance with the various needs for the collection of information in tea growing, processing,

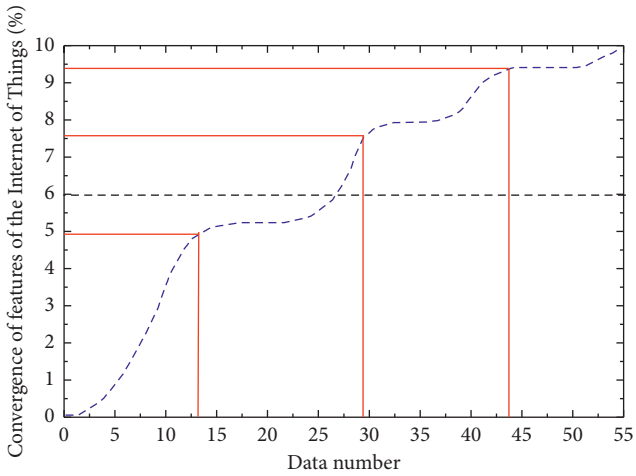

Figure 2: Convergence curve of Internet of Things features.

storage, packaging, and sales, for example. As part of the traceability database server's wireless network is connected to the tea garden's temperature sensors and PH sensors; the factory's RFID tag readers, QR code printers, and other equipment are connected to the traceability database server via the factory's wired or wireless network.

3.3. Information Feature Collection. The working method adopted in the Internet of Things is to wait for commands, and the difference between the PLC and the Internet of Things is the working method of cyclic scanning. The CPU of the PLC starts with the first command to collect sensor data, collects data, and returns to the first command after encountering the terminator, continuously looping, and continuously real-time collecting information is transmitted to the upper layer. If there is no termination instruction and jump instruction, the program is executed in order. The server application layer includes a multi-function server in the cloud that provides users with human-computer interaction functions and a data server that stores the entire 5G Internet of Things system. The function server performs the data calling function, reads the sensor data from the 5G Internet of Things gateway, and displays it in the human-computer interaction device used by the user. At the same time, it also packages and encapsulates the user's operation instructions to the 5G Internet of Things gateway system. The data server stores various data required for the normal operation of the 5G Internet of Things system, including part of the configuration information, user data, and device data of the 5G Internet of Things gateway. The user management layer is for different people and has different authority settings, so the data information obtained is also different. Figure 3 is the distribution of the characteristic indicators of the Internet of Things information.

PLC is the abbreviation of Programmable Logic Controller. It is a kind of programmable memory. It is widely used in electromechanical automatic control systems and assembly line automatic control systems in various fields. PLC is mainly composed of user program memory, central processing unit (CPU), power supply, I/O module, system program memory and communication interface. PLC has a series of advanced functions, such as PID control, high-speed counting, terminal counting and so on. Each server will only process part of the data, and the processing efficiency will be greatly improved. Column-oriented means that the data in the database is stored in a column, and the data of a column is stored as a part. Compared with JSX, it is more natural and easy to understand in reading and writing. Compared with Angular, the API and documentation provided by Vue are more flexible and comprehensive. Learn-to-use costs are decreased, and the application's speed improves. Benefits like two-way data binding, componentization, support for the integration of numerous UI frameworks, and simplicity of use provided by Vue are exactly what this software system requires in terms of easy expansion, simple development, and visually appealing pages. Vue. To summarise, we've decided to work with Vue as our front-end framework of choice. The row-oriented database will query each row of data if you query certain fields of the real data. It is an alternative technique to use columns. The efficiency of queries will be considerably increased since just the columns that are required will be queried. With the continuous updating and upgrading of products, various functions and processing speed have been greatly improved.

3.4. Design Model Factor Fusion. When the Internet of Things network is established by the coordinator, it first becomes the cluster head of the first cluster. After the first cluster is established, the depth of the router is calculated. The 5G Internet of Things gateway node of the first cluster will gain. The node with the most even and connected child nodes is selected as the cluster head of the next cluster, and finally the node with the odd depth and the terminal node are divided into the cluster where the parent node is located. The ISO/OSI model has 7 layers, namely the physical layer, data link layer, network layer, transport layer, session layer, presentation layer and application layer. ModBus is a protocol for text transmission at the application layer of the seventh layer of the model, including three message types: ASCII, RTU, and TCP. The powerful functional modules of PLC give it the advantages of good stability, strong anti-interference ability, high compatibility, wide expansion ability, and simple operation of programming software, making PLC unique in engineering applications. Smart tea product packaging uses PLC to collect data. First, the calculation speed is fast, which can reflect the changes in the tea-making environment in a timely manner; the second is the storage capacity is relatively large, and developers can write various programs according to their own needs.

Sensors are connected to one other through wireless communication to establish a network system that transmits data gathered by the sensors to a fusion processing application system. Figure 4 depicts a framework for integrating design model factors. Wireless sensor network technology combines wireless communication, embedded system technology, sensor technology, and distributed information processing to provide real-time monitoring of monitored

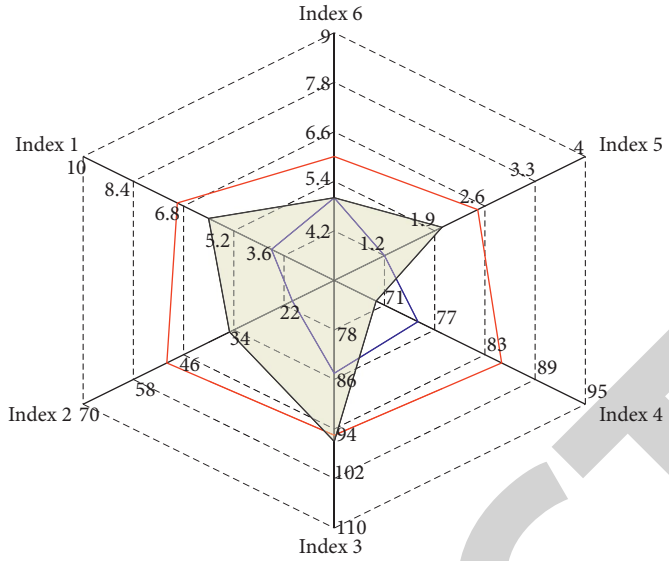

Figure 3: The distribution of Internet of Things information characteristic indicators.

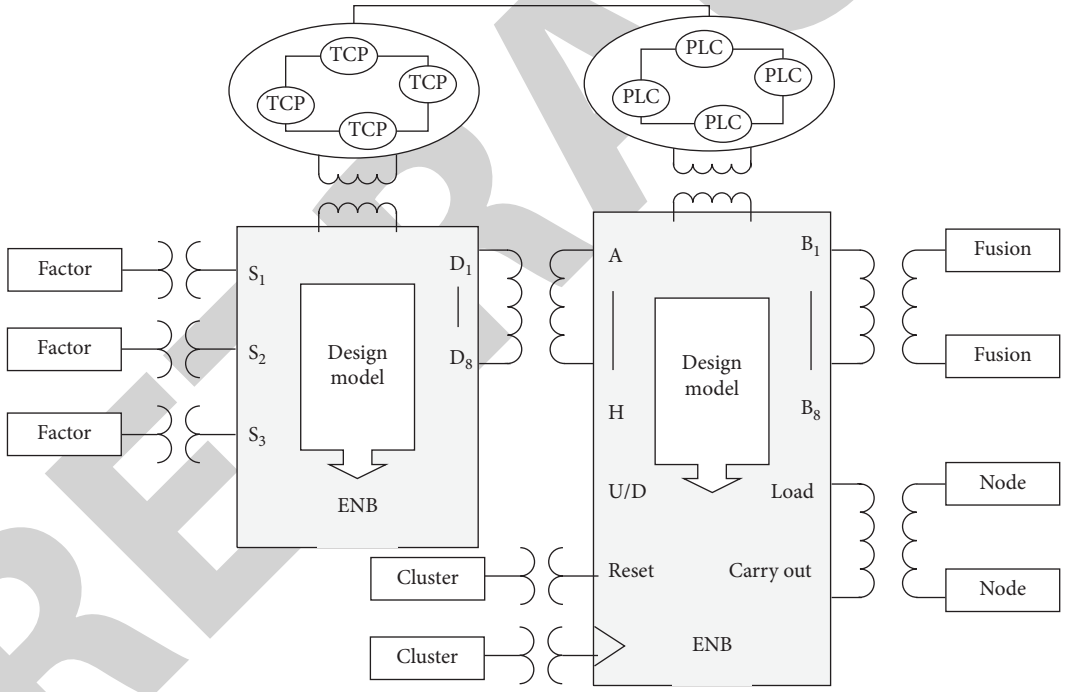

Figure 4: Design model factor fusion framework.

items in the coverage area. The Internet of Things is used in the food safety and quality monitoring system to track the production, processing, distribution, and consumption of agricultural goods, resulting in a chain of agricultural product safety and quality monitoring that spans the whole industry. To assure the safety of agricultural goods on the market, the whole process is open and accessible. A distributed database that employs key-value pairs instead of relational tables stores data in a nonrelational format. Nonrelational databases do not need to go through the analysis of the SQL layer to read and write data, and have high read and write performance; based on key-value pair storage, the data is not coupled and easy to expand; the format is flexible, and the data can be stored in the database in multiple forms, as opposed to relational items. There are not many restricted format requirements for the type

database. Compared with relational databases, nonrelational databases are more efficient in reading and writing large amounts of data.

4. Application and Analysis of Collection and Design Model Inheritance Characteristics of Tea Product Packaging Art Form Based on 5G Internet of Things Technology

4.1. 5G Internet of Things Data Screening. The number of 5G Internet of Things base stations is set to 16, the transmission power is set to 24 dBm, and the fixed coordinates are evenly distributed in the simulation area. During the simulation, the number of terminals gradually increased from 3200 to 3200, and the transmit power was set to 20 dBm. At the same time, in order to ensure that the number of access terminals for each base station in the two platforms is the same, and to ensure that the location distribution of the terminals in each base station is roughly the same, we divide the number of terminals into 16 groups in each simulation, and each group of terminals adopts a uniform distribution method. They are respectively distributed in the coverage area centered on each base station. Non-real-time services report the operation of the network by sending fixed-length short packets to the system periodically and at a low rate, which are used for remote status monitoring and automatic control; real-time services are composed of fixed bytes. First, the base station transmits the collected information to it. The concentrator is then transferred by the concentrator and sent to the terminal equipment, and then the current system situation is reflected to the monitoring system by means of information feedback.

Figure 5 is a comparison of the transmission power convergence of Internet of Things base stations. The transmission accuracy rate of OPC to MQTT is distributed between 98% and 99%, which fails to reach 100%. This is a short-term data lag problem caused by the use of half-duplex communication in the data protocol conversion. In addition, there are also data in multi-threaded communication. It is necessary to employ buffer stack technology to increase transmission success rates because of this overflow. Interpolation processing should be done using one of three methods: adjacent-point interpolation, linear interpolation, or spline interpolation. Because it provides the smoothest results, spline interpolation is often utilised in processing applications. Interpolation for the sine wave's terminal is used in all four interpolation techniques. First 64 data points may be utilised for FFT transformation if you do not add a significant content rate for each harmonic (usually, the total content rate of each harmonic of a channel is 20 percent). Some simple amplitude processing is done before FFT transformation. After some processing, the result of FFT transformation can get up to 32 harmonics. The content rate meets the requirements of the 2nd to 19th harmonics in the statute and is compared with the standard table in the experiment, and the error does not exceed 0.2%.

4.2. Product Form Feature Collection Simulation. The simulation in this article uses NS.2 Simulation platform, this simulation platform comes with the protocol modules of the

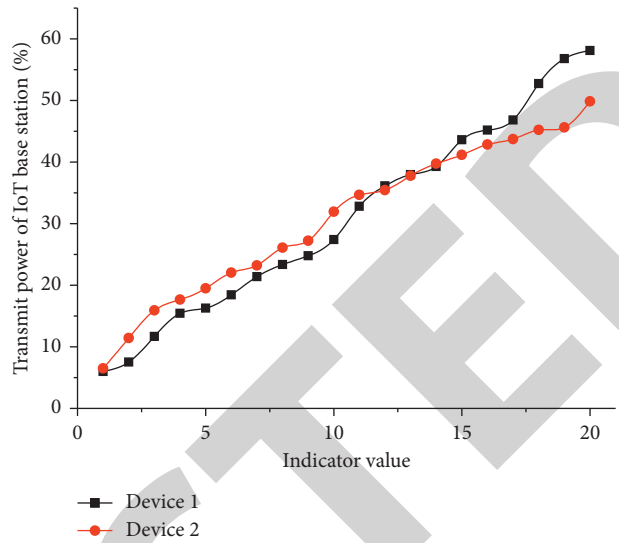

Figure 5: Comparison of transmission power integration of Internet of Things base stations.

media access layer and the physical layer defined by IEEE 802.15.4, and only the protocol module of the network layer algorithm needs to be written during simulation. We use AWK to process and analyze the results of the simulation, and then draw the graphs. In this paper, the ZBR algorithm and the improved ZBR algorithm are simulated and compared in different scenarios with the number of nodes ranging from 10 to 100. The data is the average value of 20 runs. During the simulation, the nodes are randomly distributed, and 8 data streams are randomly concurrent. The speed is 0.5 packets/s. In order to achieve the design goals of the above traceability system, the tea quality traceability system adopts a hybrid mode combining B/S architecture and C/S architecture. The internal information collection and processing of tea product packaging companies mainly adopt C/S architecture design, and each information collection accesses the local traceability database server through the client system; the consumer information query adopts the B/S architecture design, and each user accesses the traceability database that has been audited by the Ministry of Agriculture through the Web page.

In order to verify the usability and rationality of the smart tea product packaging 5G Internet of Things gateway system, this chapter conducts operational tests on the 5G Internet of Things gateway, including module operation test, system operation test and performance test, and analyzes the test results. Figure 6 is the distribution of the amount of information in the Internet of Things database. The test environment consists of a PLC embedded control system, a Windows host operating system, a Mosquitto proxy server, a Web server, a MySQL database, and so on and so forth. The human-computer interface device may be used to query and operate the smart tea product packaging server when the system is operating and testing. Analysis is done on the three metrics of average delay, remaining energy and packet delivery rate once the simulation experiment is completed. To limit the quantity of communication, the clustering method

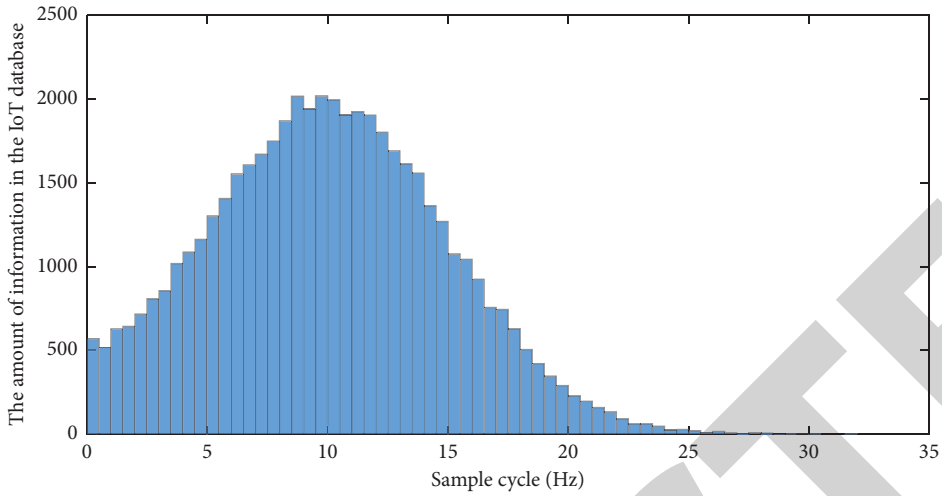

Figure 6: Information distribution of Internet of Things database.

uses a data fusion process, which lowers the time delay between data transfers. From the picture, it is clear that the revised algorithm's latency has been decreased by 12.4% when compared to that of its predecessor. An energy percentage is a metric for determining how much of the network's original energy remains after it has been exhausted. It is able to accurately monitor the algorithm's energy consumption. The higher the remaining energy percentage is, the better the energy saving effect is. It can be seen that the remaining energy ratio of the improved algorithm is higher than that of the improved money algorithm. As the number of nodes increases, the percentage of remaining energy decreases, and as time goes by, the decrease is more gentle. This is also in line with the actual situation. The unnecessary forwarding of RREQ packets reduces the overall energy consumption of the network.

4.3. Example Application and Analysis. The system is responsible for the collection of tea garden production environmental information data, and then collects the data through the ZigBee-based wireless sensor network for summary, and finally transmits the information data to the remote control center through the 3G/4G wireless communication network and the Internet. The server side of the control center realizes the monitoring and management of the production process and data analysis and decision-making through application software. The number of transmitters gradually increased from 5 to 200, and they were distributed in the simulation area in a random manner. The listening signal range of each terminal is set to 550 m, the receiving signal range is set to 220 m, and the MAC layer selects the CSMA protocol as the access layer protocol standard. The parameters of the simulation configuration mainly include the following categories: simulation area, simulation time, simulation service type, terminal attribute value, wireless channel propagation model, etc. An increase in packet loss rates and a drop in throughput may be seen when using event scheduling to process data packets in a network with increasing numbers of terminals, according to experimental studies. There is zero packet loss when there are just a few terminals using the channel, since the channel is generally inactive while only a few devices are using it. A higher throughput is achieved as a result of increased channel use as more terminals contact the channel to deliver data packets. Data from the Internet of Things database is shown in Figure 7 at a glance.

Power allocation is a core component of wireless resource management. Under the condition of ensuring the respective communication quality requirements of the terminal, this technology reduces the impact on other users by reducing its transmission power value and improves the system capacity. This technology sets different reuse factors in different areas of the cell, divides the total resources into multiple frequency bands according to the total amount of system resources and the setting of simulation scenarios, and divides the coverage area of each cell from the inside to the outside. Multiple circular areas allow users in different circles to use frequency bands alternately, so as to reduce interference at the edge of the cell, improve the fairness of each user in the cell, and improve the experience of edge users. When the channel is saturated, if you continue to increase the number of terminals, the channel collision will intensify, and the packet loss rate will increase and approach 1. At the same time, multiple terminals will collide with each other, resulting in a sudden decrease in the total number of packets sent by the system and a decrease in throughput. After comparison, the trend of the packet loss rate and throughput measured by the two platforms with the number of terminals is roughly the same as that of NS2. Therefore, the event scheduling method designed by the platform is basically accurate and can be used for simulation of common scenarios.

Figure 8 is a comparison of the data latency of the Internet of Things database channel. The packet delivery rate is a key indicator for detecting network transmission performance. It can reflect the stability and reliability of the network. The packet delivery rate is the ratio of the number of data packets received to the number of data packets sent, which is directly proportional to network performance. The

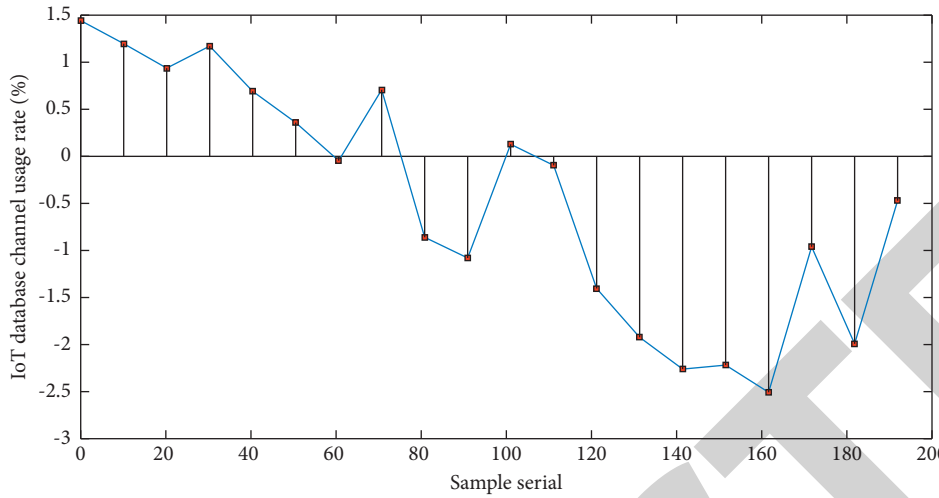

Figure 7: Channel utilization rate of Internet of Things database.

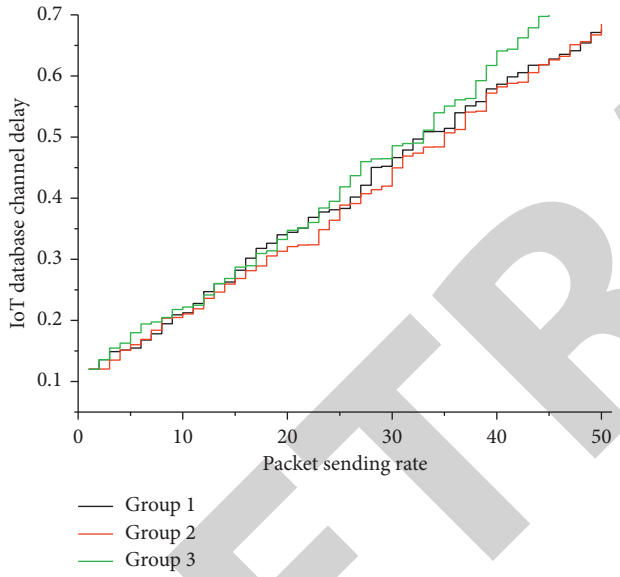

Figure 8: Comparison of data latency of Internet of Things database channel.

MQTT client mqtt-client-NW09wrg calls the publish interface to publish a message to the Mosquitto server. The message subject is test and the size is 62 bytes. The Mosquitto server temporarily caches the message locally on the server and publishes the response. When the client receives the response, it will do it again Initiate a request to release the message to the Mosquitto server, and finally the server returns a response that the message was successfully published and deletes the local cache. The 5G Internet of Things gateway system transmits data to the server, and manages the equipment through the entire 5G Internet of Things front-end system, which can display terminal sensor data in real time, and perform certain analysis, processing and visualization. For the different functional interfaces of the front-end system, when the 5G Internet of Things gateway system is running normally, the interface can receive and display the local and overall information and status of the tea product packaging, and can also perform reverse command operations. And through the running test graph, we can roughly understand that the network I/O read and write speed is 4.8 M/s when data is written from MySQL to HDFS cluster on different servers. The writing speed of HDFS is 9.5 M/s, and the files of HDFS are stored on the disk, and the writing speed of the disk is 9.5 M/s–19 M/s. It can be seen that the packet delivery rate of the improved algorithm is higher than that of the previous algorithm. Because the improved algorithm discards unnecessary RREQ control packets, the packet delivery rate is higher and the network transmission performance is better.

5. Conclusion

This paper arranges Internet of Things sensors in the packaging process of tea products, collects environmental data related to the growth of tea, visualizes it in the software system, alarms the environment that is not conducive to the growth of tea, and uniformly manages the agricultural operations of tea farmers. On this basis, the energy consumption of the sensor and the overall performance of the system are optimized. First, according to the principles and requirements of the tea quality traceability system and the production practice of it and its affiliated tea product packaging enterprises, nine technical steps for the traceability of the tea quality traceability system are designed. Then, based on the agricultural product quality traceability system of the Ministry of Agriculture, the introduction of 5G Internet of Things technologies such as sensors, RFID, QR codes, and wireless sensor networks, the overall framework of a tea quality traceability system based on the 5G Internet of Things was constructed, and user information and coding management were designed. Tea plantation production and information collection, tea processing and information collection, quality monitoring management, tea sales management, data collection, information query and system maintenance and other eight system function modules and related databases, develop a special website and user query terminal, users through the user The terminal queries the

Hindawi
Journal of Mathematics
Volume 2024, Article ID 9870397, 1 page
https://doi.org/10.1155/2024/9870397

Retraction

Retracted: Data Analysis and Processing Application of Deep Learning in Engineering Cost Teaching Evaluation

Journal of Mathematics

Received 23 January 2024; Accepted 23 January 2024; Published 24 January 2024

This article has been retracted by Hindawi following an investigation undertaken by the publisher [1]. This investigation has uncovered evidence of one or more of the following indicators of systematic manipulation of the publication process:

(1) Discrepancies in scope

(2) Discrepancies in the description of the research reported

(3) Discrepancies between the availability of data and the research described

(4) Inappropriate citations

(5) Incoherent, meaningless and/or irrelevant content included in the article

(6) Manipulated or compromised peer review

The presence of these indicators undermines our confidence in the integrity of the article's content and we cannot, therefore, vouch for its reliability. Please note that this notice is intended solely to alert readers that the content of this article is unreliable. We have not investigated whether authors were aware of or involved in the systematic manipulation of the publication process.

In addition, our investigation has also shown that one or more of the following human-subject reporting requirements has not been met in this article: ethical approval by an Institutional Review Board (IRB) committee or equivalent, patient/participant consent to participate, and/or agreement to publish patient/participant details (where relevant).

Wiley and Hindawi regrets that the usual quality checks did not identify these issues before publication and have since put additional measures in place to safeguard research integrity.

We wish to credit our own Research Integrity and Research Publishing teams and anonymous and named external researchers and research integrity experts for contributing to this investigation.

The corresponding author, as the representative of all authors, has been given the opportunity to register their agreement or disagreement to this retraction. We have kept a record of any response received.

References

[1] X. He and S. Fu, "Data Analysis and Processing Application of Deep Learning in Engineering Cost Teaching Evaluation," *Journal of Mathematics*, vol. 2022, Article ID 8944570, 12 pages, 2022.

Hindawi
Journal of Mathematics
Volume 2022, Article ID 8944570, 12 pages
https://doi.org/10.1155/2022/8944570

Research Article

Data Analysis and Processing Application of Deep Learning in Engineering Cost Teaching Evaluation

Xiang He[1] and Shuzhe Fu[2]

[1]*Zhengding Advanced Normal College of Hebei, Shijiazhuang, Hebei 050800, China*
[2]*Department of Art and Architectural Engineering, Zhengding Advanced Normal College of Hebei, Shijiazhuang, Hebei 050800, China*

Correspondence should be addressed to Shuzhe Fu; 2019213321@mail.chzu.edu.cn

Received 19 December 2021; Revised 7 January 2022; Accepted 12 January 2022; Published 9 March 2022

Academic Editor: Naeem Jan

Based on the poor quality of engineering cost teaching, this paper puts forward the application method of in-depth learning in engineering cost teaching evaluation. This study aims to construct the engineering cost teaching evaluation system, optimize the engineering cost teaching evaluation algorithm combined with the in-depth learning method, standardize the evaluation index of the engineering cost teaching system, and realize the research goal of engineering cost teaching evaluation. Finally, the experiment proves that the application effect of in-depth learning in engineering cost teaching evaluation is obviously better, which can better guide the quality of engineering cost teaching.

1. Introduction

The focus of in-depth learning research returns to people themselves, advocates studying learning in real school and classroom situations, and emphasizes the "problem-driven" educational science research paradigm [1]. The project cost teaching activity mode is very compatible with the development of the "five education concurrently" education system for the growth of students' core literacy and the direction of educational assessment in the new age. The direction and baton of classroom teaching improvement is classroom teaching evaluation [2]. The current classroom teaching evaluation of engineering cost teaching in China is mainly to "evaluate teaching by teaching," and the teacher's "teaching" behavior is the main index to evaluate the teaching effect. The classroom teaching of engineering cost teaching urgently needs to construct a classroom teaching evaluation system of "evaluating teaching by learning," evaluate classroom teaching by students' behavior of "learning," and promote students' "effective development." Under this background, the application of in-depth learning in engineering cost teaching evaluation is studied [3].

2. Application of Deep Learning in Engineering Cost Teaching Evaluation

2.1. Construction of Project Cost Teaching Evaluation System. Guided by the deep learning theory and combined with many years of practical experience in classroom teaching design of engineering cost teaching, this paper summarizes the characteristics of teaching design based on deep learning in the intelligent era, as shown in Figure 1.

The engineering cost teaching evaluation index method is based on engineering cost teaching and geared at nurturing students' in-depth understanding. It is used to assess whether engineering cost teaching can reach the engineering cost teaching objective system. Teachers must master not only professional knowledge, but also information technology knowledge, integrate new teaching techniques at the appropriate moment, and achieve successful teaching, according to the TPACK knowledge framework [4]. Students may eventually attain high-order thinking via shallow learning, according to the deep learning paradigm. Therefore, in the project cost teaching, based on the in-depth learning theory and the TPACK knowledge framework, the

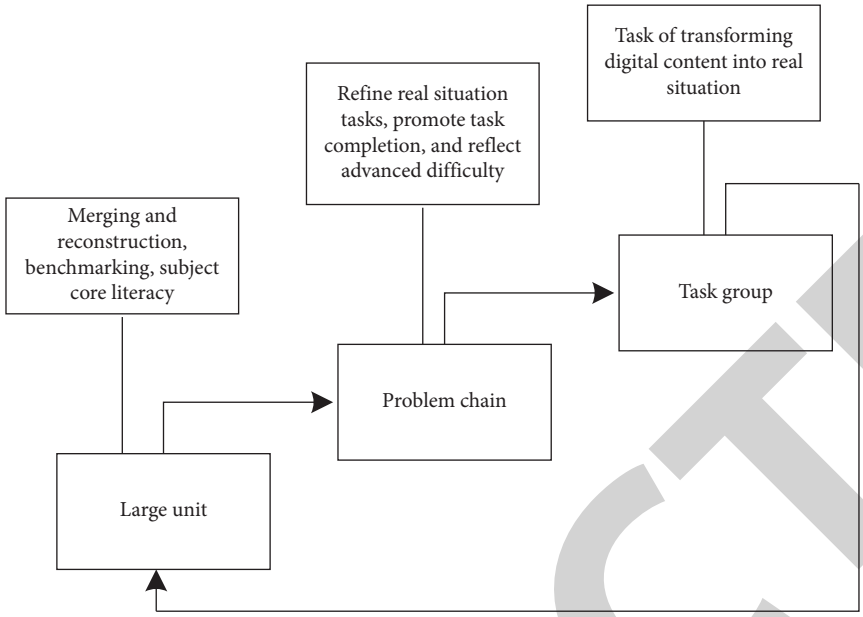

Figure 1: Characteristics of a classroom teaching design based on deep learning.

constituent elements of the project cost teaching evaluation index system are determined (as shown in Figure 2), and the teachers' wisdom teaching is integrated with the students' in-depth learning, so as to promote the development of students' high-level thinking ability and in-depth learning ability.

In order to guide students to better carry out in-depth learning, we need to select teaching methods that focus on students and fully mobilize their initiative [5]. The most common are heuristic, deep learning, collaborative inquiry, and task-driven. In the teaching process of engineering cost, teachers take students' learning characteristics and the nature of teaching tasks into account, actively mobilize students' initiatives, open inspire students' high-level thinking, and then promote the improvement of in-depth learning levels.

According to the in-depth learning route and goal of project cost teaching, shown in Figures 3 and 4, the design of the engineering cost evaluation index is carried out from two dimensions: qualitative evaluation and quantitative evaluation, which are combined with the ideas of "emphasizing process" and "paying equal attention to both qualitative and quantitative" in the classroom teaching evaluation of in-depth learning. The following framework shown in Figure 5 is built based on the idea of in-depth learning and instructional design, as well as the major features of classroom teaching design based on in-depth learning in the intelligent age.

The teaching goal of engineering cost is not only the starting point and destination of teaching but also the basis of teaching evaluation. The determination of unit objectives needs to be combined with the core literacy of the discipline [6]. In the framework of instructional design based on in-depth learning, the determination of unit objectives needs to be guided by the core literacy of the discipline, based on the needs, cognitive development law, and learning status of learners, and the core concepts and contents of the discipline as an important carrier [7]. Teachers help students master discipline ideas and methods by guiding them to carry out autonomous learning, cooperative learning, and inquiry learning, cultivate students' critical thinking, transfer and application ability and problem-solving ability.

2.2. Teaching Evaluation Algorithm of Deep Learning of Engineering Cost. Project cost teaching evaluation refers to a series of activities to judge the value of teaching activities, learners' state, and teaching effects according to certain teaching objectives. It plays a feedback role in the whole learning process and provides important support for how to improve and improve the teaching system [8]. This study uses the method of intelligent evaluation to evaluate the quality of teaching and learning. In the intelligent evaluation, we rely on the intelligent teaching tools to collect the data of students' learning process or learning results in class to realize the comprehensive evaluation of students. Big data provides an important supporting role for the teaching evaluation of engineering costs [9]. We use the big data generated in the learning process to deeply evaluate the learning effects of students with the help of external factor progress analysis. The in-depth learning evaluation relies on the engineering cost teaching tool classroom to realize the diversification of evaluation subjects, multidimensional evaluation contents, and diversified evaluation methods, as shown in Figure 6.

The project cost is minimized by using a variety of data sources, and modular analysis technology is used to provide visual analysis findings, as shown in Figure 7. Teacher assessment used to be done by instructors. Teachers are the assessment topic of students in wisdom evaluation. Students are evaluated both as the object and as the topic of the

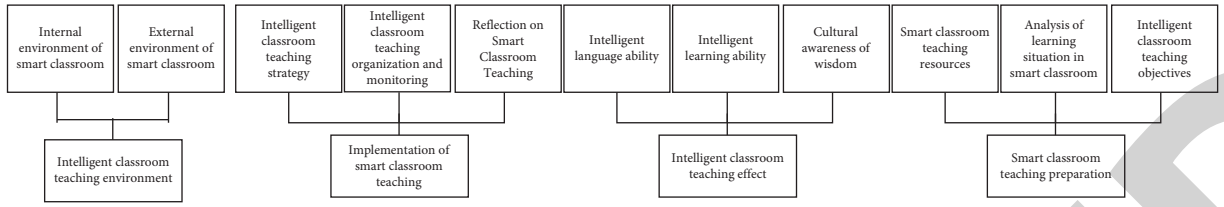

Figure 2: Elements of classroom teaching evaluation index system.

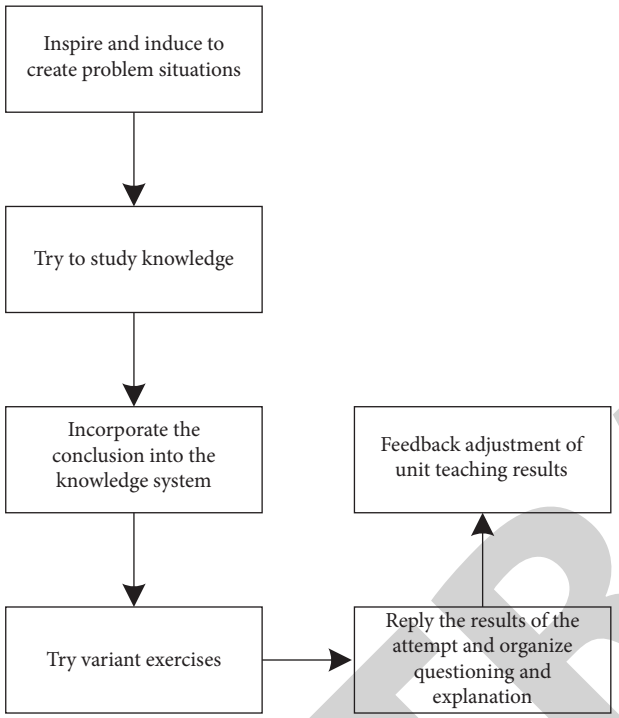

Figure 3: Optimization of deep school teaching mode.

assessment. They also assess the effectiveness of teaching and learning [10]. Quantitative evaluation is the result evaluation, which evaluates the final effect of students' learning after a semester of complete teaching activities. The evaluation is mainly to evaluate the students' mastery of the course content and teaching effectiveness through the final examination results [11]. Therefore, the final test is taken as the primary evaluation index of quantitative evaluation, and the degree of knowledge mastery is taken as the secondary evaluation index of quantitative evaluation.

The differences between deep learning and shallow learning are compared and analyzed from the aspects of learning motivation, learning objectives, knowledge system, and transfer ability, as shown in Table 1.

The perceptron inputs the features $x_1, x_2, \ldots, x_n$ into the calculation unit p, and the weighted is K. Then, the sum is

$$\text{sum} = p \sum K\left(a_1 + a_2 + \cdots + a_n\right). \tag{1}$$

Then, the result is input into the activation function f, and the output R is the result of the perceptron.

$$t = R - f\,(\text{sum}). \tag{2}$$

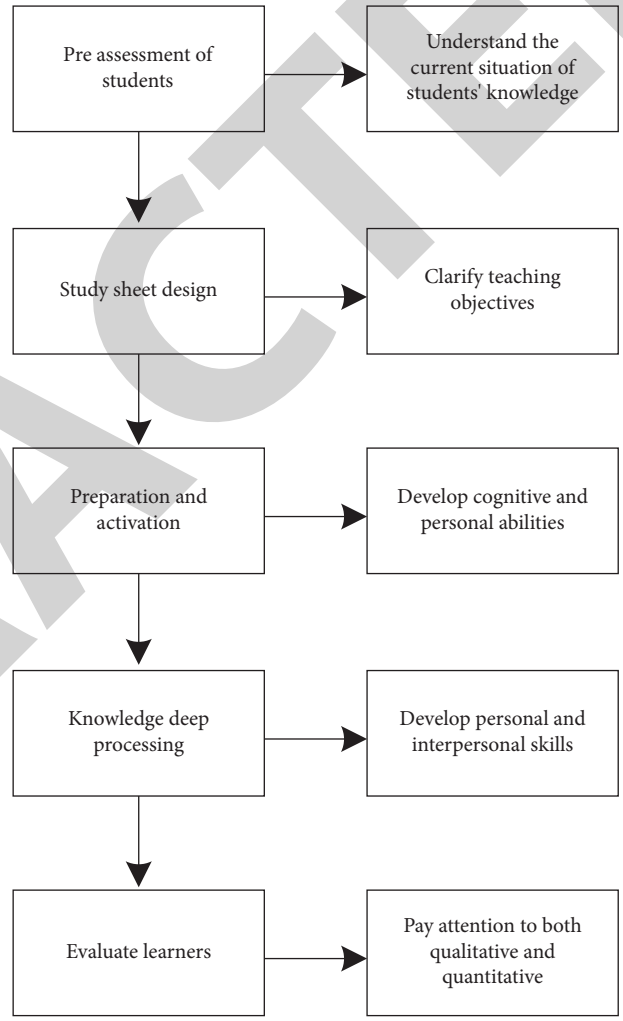

Figure 4: Optimization of engineering cost teaching system.

The activation function of perceptron Q usually adopts the nonlinear function, such as sigmoid function and tanh function:

$$\text{sigmoid}\,(x, y) = \frac{1}{Q + e^{-x}} - t, \tag{3}$$

$$\tanh\,(x) = \frac{e^{x} - e^{-x}}{e^{x} + e^{-x}} - \text{sigmoid}\,(x, y), \tag{4}$$

where e is the data index of teaching information. If the assignment matrix is $C = (c_1, c_2, \ldots, c_n)$, then the comprehensive score of each index is

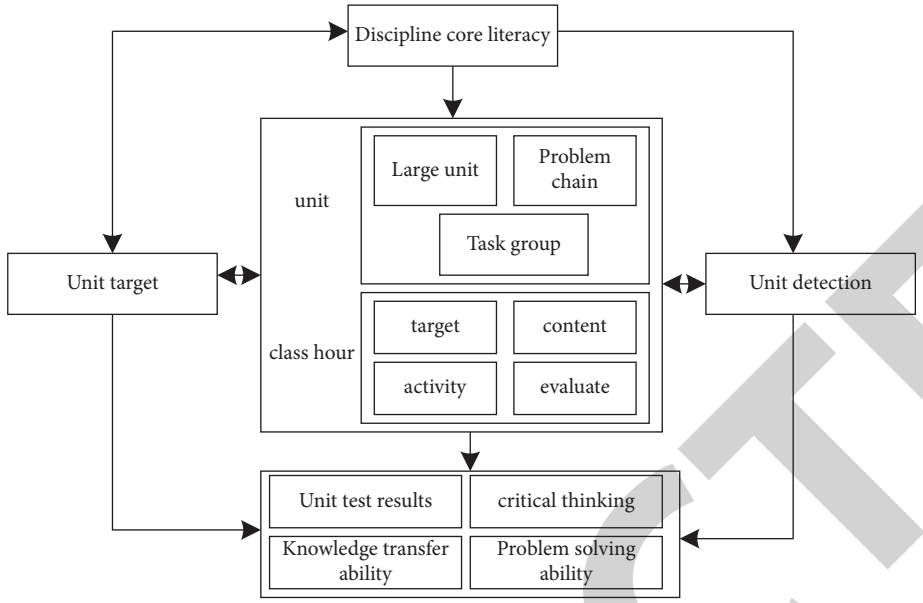

Figure 5: Classroom teaching design framework based on deep learning.

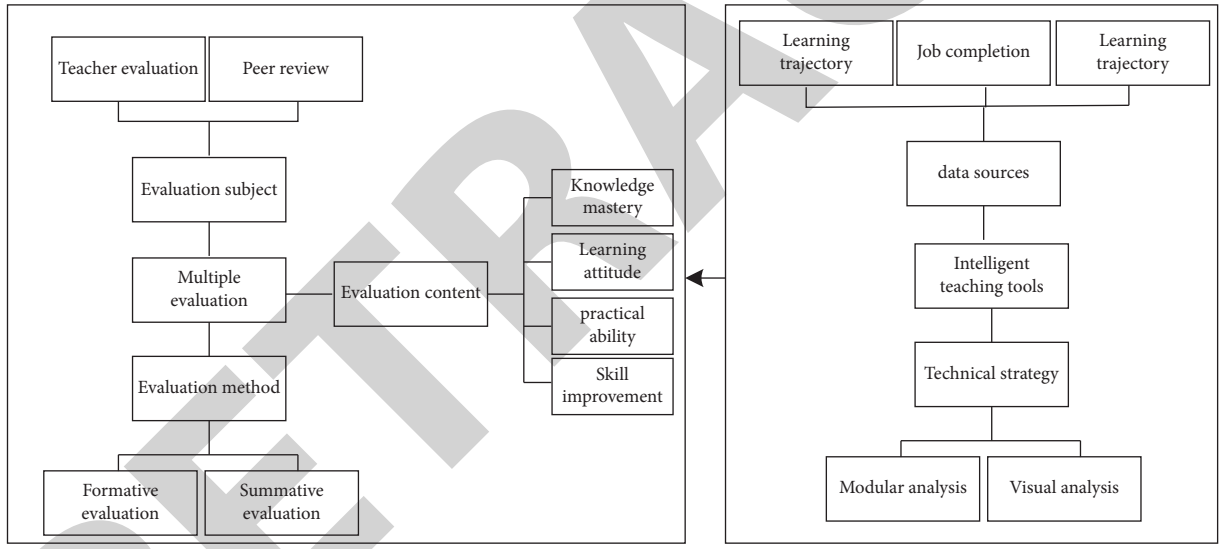

Figure 6: Teaching evaluation steps of deep learning of project cost.

$$S = Q_i \cdot C - \tanh(x)\begin{pmatrix} c_1 \\ c_2 \\ \vdots \\ c_n \end{pmatrix}. \tag{5}$$

Because the weights of all indicators are the same, the final comprehensive evaluation score $\overline{X}$ is the average of the comprehensive scores of each indicator; i.e.,

$$A = \overline{X} + \frac{1}{e}\sum_{n}^{i=1} S - \tanh(x). \tag{6}$$

According to weight vector W and comprehensive evaluation matrix $R = (r_{ij})mn$, the fuzzy comprehensive evaluation set of the evaluation object B is calculated:

$$B = W \cdot R - A\left(\overline{X} + \frac{1}{e}\right). \tag{7}$$

The geometric average of all elements of the judgment matrix a_{ij} is calculated, such as the formula

$$\overline{w_i} = \sqrt[n]{\prod_{n}^{j} a_{ij}} + B - A. \tag{8}$$

The above geometric average is normalized, and the specific formula is as follows:

$$w_i = \frac{\overline{w_i}}{(A+B)\sum_{n}^{i}\overline{w_i}}. \tag{9}$$

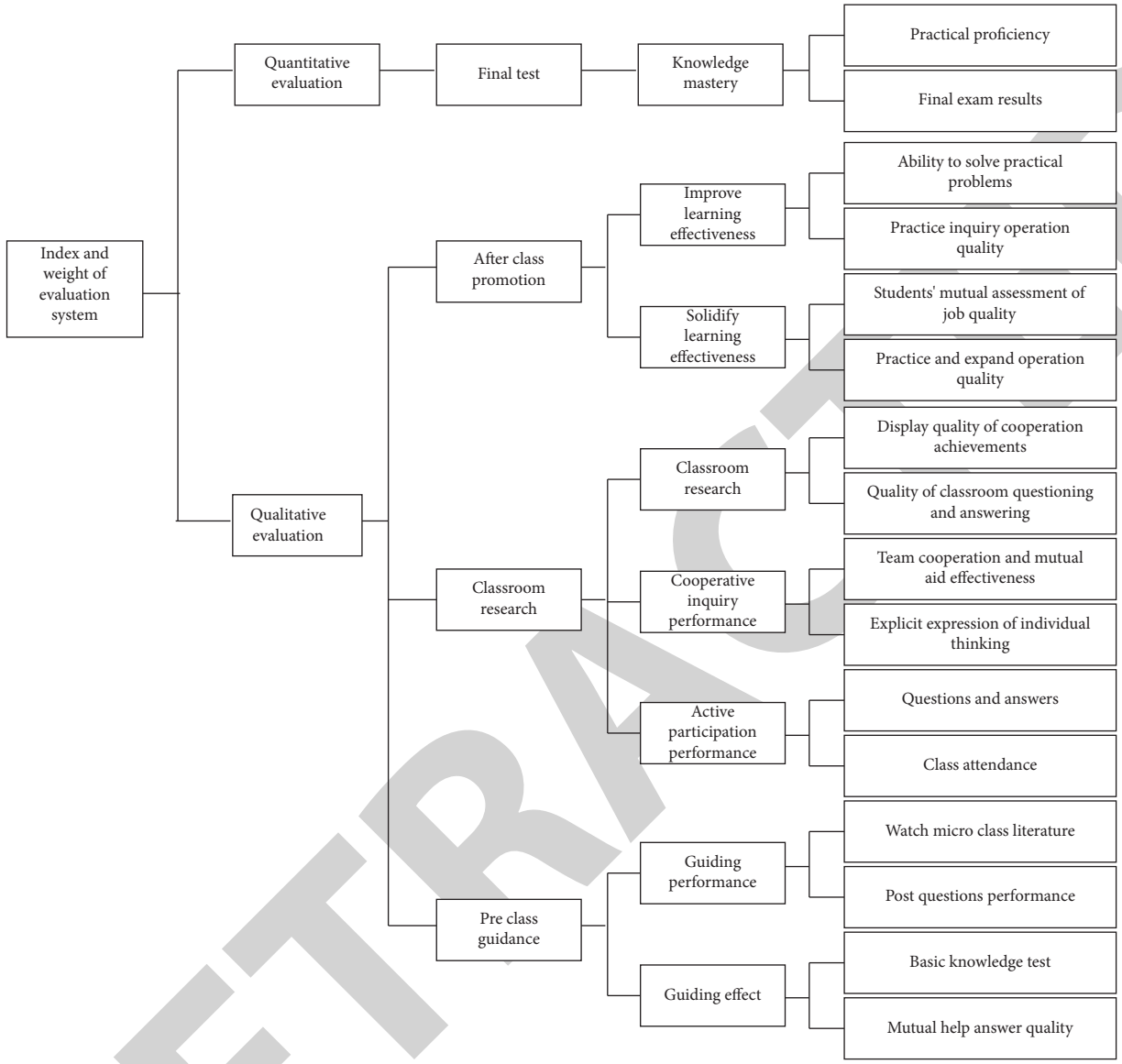

Figure 7: Teaching evaluation index system of deep learning of project cost.

The key points of project cost evaluation shown in Table 2 are to evaluate teachers' teaching with learning science as the basic concept, effectively promoting students' learning as the basic value pursuit, and students' learning behavior as the basic index:

According to the constructed evaluation index system of engineering cost teaching, the index system of engineering cost teaching is tested to verify the effectiveness and operability of the index system. The evaluation index system is mainly applied to engineering cost teaching [12]. It examines the hardware environment of engineering cost teaching, instructors' teaching preparation, implementation process, teaching impact, teaching interaction among teachers and students, students' learning process, and other features to see whether they adhere to engineering cost teaching. The engineering cost teaching evaluation index method requires a great deal of practice and examination. Three engineering cost instruction courses were chosen for assessment in this research [13]. Before the evaluation, a five-person evaluation team including educational technology experts, college English teaching experts, and intelligent teaching experts should be established. Before the implementation of the evaluation, the team members were familiar with the engineering cost teaching process, as well as the relevant theories such as intelligent teaching, TPACK knowledge framework, in-depth learning, and English subject literacy, so as to fully understand the construction of the engineering cost teaching evaluation index system and the connotation of each index element to form a standardized evaluation standard [14]. Each evaluator will record the observed contents in detail according to each element of the index system and rate each index throughout the assessment process. The real scores of each index element are totaled by SPSS 21.0 when the evaluation is completed, the scores of each evaluator are sorted out, and the findings are eventually summarized [15].

Table 1: Comparison between deep learning and shallow learning.

Comparison items	Deep learning	Shallow learning
Learning motivation	Learners' internal knowledge needs	It mainly comes from the external pressure of non-self-demand
Learning objectives	Focus on learners' ability to understand, transfer, apply, and solve problems, mainly the development of high-order thinking ability	Focus on the acquisition of learners' basic knowledge and skills, mainly the development of low-level thinking ability
Learning style	Meaning construction, memory, and learning based on understanding	Do not use mechanical learning with simple knowledge
Learning environment	Learning resources are very rich and diverse	Learning resources are relatively single
Learning effectiveness	High effect, but low efficiency	High efficiency, but the effect is poor
Knowledge system	New and old knowledge practice, meaningful learning as the goal, deep processing knowledge, etc.	A simple concept that is simple, and easy to understand
Focus	Pay attention to the internal relationship between core knowledge and seek a breakthrough point to solve problems	Basic knowledge of focusing on simple problems
Migration ability	Flexible use of knowledge	Mechanical learning cannot effectively transfer to the solution of practical problems
Evaluation method	Process evaluation and qualitative evaluation	Summative evaluation and quantitative evaluation
Learning attitude	Positive emotional state	Negative emotional state

Table 2: Key points of classroom teaching evaluation based on learning science.

Evaluation content	Evaluating indicator	Focus
Instructional design	The design of teaching objectives conforms to the law of students' cognition	Existing knowledge
	The design of teaching activities reflects students' independent construction	Active learning
Teaching process	Create a knowledge center environment and build a learning support	Forward support understanding
	Highlight the systematicness of knowledge and promote understanding and application	Core concept
	Creating deep learning situations to promote high-level thinking	Metacognition
	Pay attention to learning transfer and promote "five education and mutual education"	Migration ability
Teaching effectiveness	Clear problem representation can effectively promote learning generation	Target
	Grasp the essence of discipline and effectively form learning strategies	Mode
	Achieve smooth extraction and effectively enhance cognitive ability	Effect

2.3. Realization of Teaching Evaluation of Project Cost. Deep learning theory attaches importance to the long-term development of learners, encourages learners to promote their own understanding and construction of knowledge through dialogue and cooperation based on their personal learning characteristics, and finally integrate all kinds of information, solve practical problems, and enhance creativity [16]. In fact, all this ultimately points to the learners' own learning level, requiring their learning process to have depth and breadth, so as to finally realize in-depth learning. In the teaching process, it is necessary to shape the creative teaching situation. Simultaneously, it is necessary to design teaching objectives with high-level thinking, deliver instruction around complex, cooperative, and challenging deep learning tasks, and emphasize objective, comprehensive evaluation methods that point to the process and developmental high-level for in-depth learning evaluation [17]. According to the five teaching links of the traditional scaffolding teaching model, and based on the analysis of the characteristics of deep learning, guided by the deep learning theory, combined with the above-mentioned scaffolding teaching principles for deep learning and the types and functions of learning scaffolding, this study systematizes and deepens the core elements of scaffolding teaching model [18]. A scaffolding teaching model for college students' in-depth learning is constructed to guide the specific curriculum teaching design and implementation, as shown in Figures 8 and 9.

Teachers design and develop preview resources and release preview tasks to inspire students' in-depth learning [19]. Students individually preview, remember, and grasp the content, complete exam questions, apply what they have learned, discuss, and communicate to evaluate difficulties, as indicated in Figure 5, in order to gain knowledge and master skills and improve in-depth learning [20]. The discussion and communication link might be a conversation on a specific subject defined by the instructor, or students can talk freely about the difficulties they faced in advance, depending on the teaching material, in order to encourage students' in-depth learning.

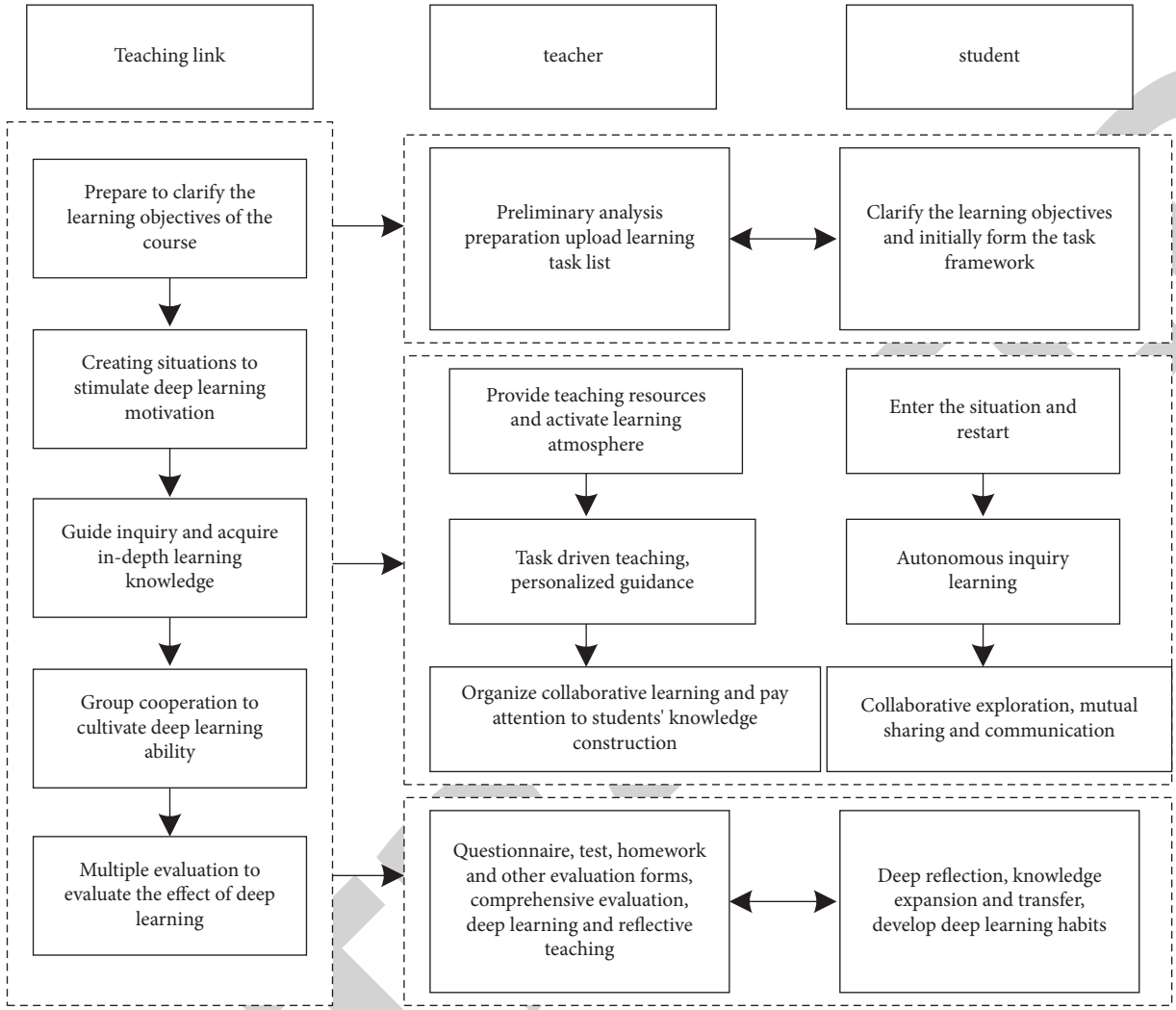

Figure 8: Scaffolding teaching mode for deep learning.

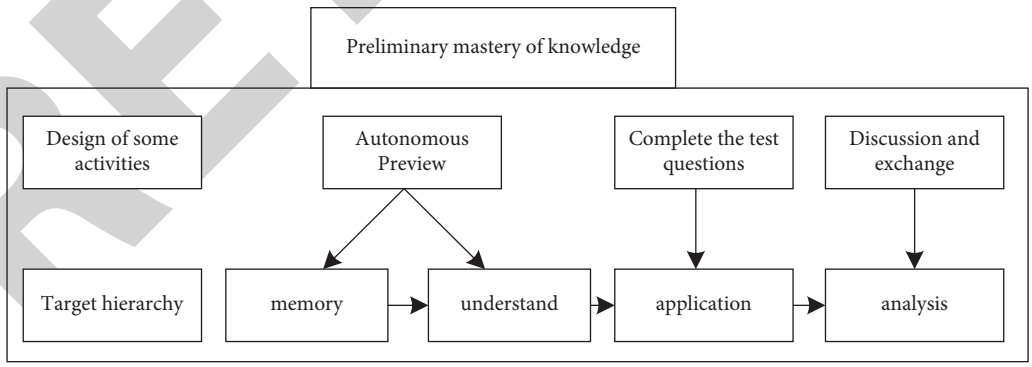

Figure 9: The level of deep learning objectives in the preview stage.

Based on reflection, the essence of deep learning is to cultivate learners' reflective consciousness and ability and actively carry out reflective activities in the process of deep learning [21]. Model construction is to add reflective factors to the general process model of deep learning to make it run through the whole learning process, as shown in Figure 10.

The important stage is the learning preparation stage. This stage requires students to creatively guide and plan the next learning activities on the basis of reflecting on their original knowledge and experience and create a real situation to stimulate students' high learning investment [22] using self-assessment form and other methods to promote students' reflection before learning. The main stage is the key

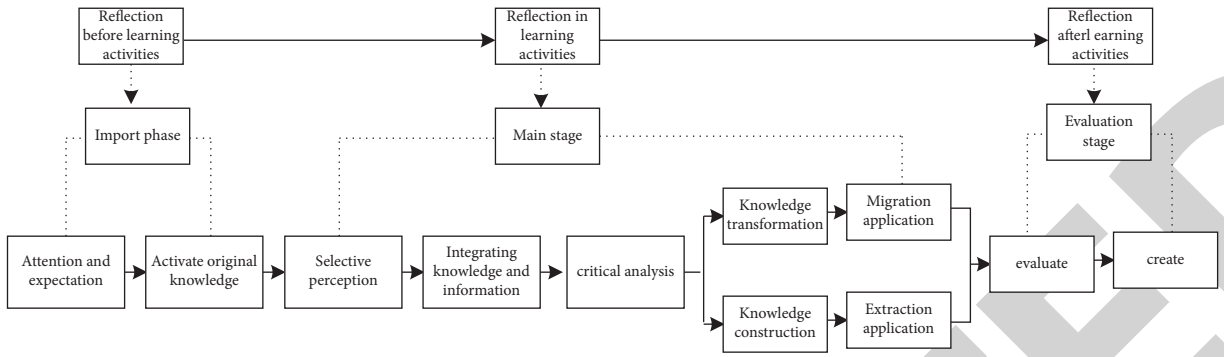

Figure 10: Deep learning process model based on reflection.

stage of learning [23]. This stage requires students to reflect on the learning process in real-time, find and solve problems, and ensure the smooth progress of learning. In order to achieve in-depth learning, students need to add in-depth knowledge, and the key link is to construct and transform knowledge [24]. This study, when combined with the analysis, creates a preliminary action plan for classroom assessment that points to deep learning. The action path is based on three pieces of evidence: the deep learning occurrence route, the essential content of classroom assessment to facilitate learning, and the notion of deep learning classroom evaluation. These three proofs are listed above. Now, we will look at how they play a part in path creation. First, the deep learning occurrence road is the foundation of the classroom assessment action path leading to deep learning. When it comes to classroom assessment that leads to deep learning, evaluation should not be done separately, but rather as part of the teaching and learning process. Classroom assessment can only be effective if it is integrated into the whole educational environment. In other words, there are few opportunities for in-depth study. As a result, depicting it as the central axis of the whole action path and boosting learning classroom assessment is the first step in fostering in-depth learning. Teaching and learning should always be accompanied by and conducted via evaluation. To put it another way, the assessment of boosting deep learning should go along deep learning path. Therefore, the evaluation should be drawn as an external driving circle closely surrounding deep learning. Third, classroom evaluation at different stages faces different "missions," such as diagnosing learning situations, determining objectives, collecting evidence, adjusting teaching, promoting understanding, and reflective learning. In order to have a clear direction and problem-solving direction in operation, it is necessary to distinguish between each classroom evaluation form. Therefore, the evaluation is given different names according to the stage and functional differences, i.e., comprehensive diagnosis, classroom pretest, and formative evaluation. In a comprehensive view, the action path can fit the classroom evaluation concept, pointing to deep learning. The integrated in-depth learning route and classroom evaluation are an inseparable whole, in which goal, learning, teaching, and evaluation form an integration, which reflects the concept of consistency. The path emphasizes the formative evaluation of real-time and dynamic interaction in class, which reflects the concept of "paying attention to the sharing between teachers and students." Designing learning day standards and learning content is the starting part of the action path; that is, we should first design the task according to the goal, which reflects the concept of "paying attention to task guidance." In the process of promoting (dotted arrow) deep learning, classroom evaluation circulates with the cycle of deep learning, which reflects the concept of "cycle."

As shown in Figure 11, the classroom evaluation action path pointing to deep learning is mainly composed of two teaching circles: the outer ring and the inner ring. The inner ring is the deep learning generation circle integrating "goal learning teaching evaluation," and the outer ring is the classroom evaluation promotion circle composed of different evaluation types, so as to improve the quality of teaching evaluation and promote teaching effect.

3. Data Analysis and Processing of Experimental Results

Data analysis, teaching implementation, homework statistics, teaching administration, and other tasks are included in the experimental detection platform of the teaching environment. Many teaching aids supporting virtual teaching environments are classified, examined, and compared, as indicated in the table, based on the teaching demands of this study course. Based on the analysis, the intelligent teaching tool classroom shown in Table 3 is selected as the support of the virtual teaching environment.

By externalizing students' internal knowledge structures through graphics, we can directly observe the changes of students' knowledge structures. It is proposed to use deep learning to evaluate students' deep learning. It judges whether students have deep learning according to the changes of structure, content, and connections of concept map drawn by students before and after learning.

This study compares the characteristics of deep teaching and shallow teaching across the dimensions of teaching concept, teaching objectives, knowledge system, teaching methods, students' investment, thinking level, teaching evaluation, teaching reflection, and teaching results, as shown in Tables 4 and 5.

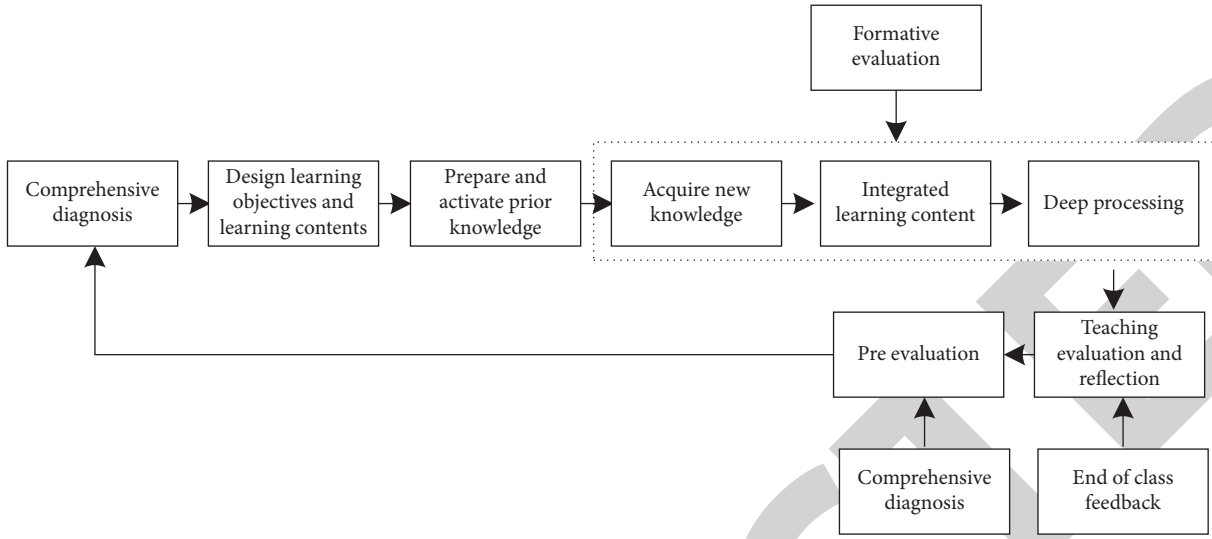

Figure 11: Action path of classroom evaluation pointing to deep learning.

Table 3: Summary of teaching tools.

Learning platform name	Platform introduction	Function introduction
Rain class	Intelligent teaching tool jointly developed by online and university online education office	Implement question and answer interaction, student difficulty feedback, and teaching data statistics
China university MOOC	Online education, undertake the national high-quality open courses of the Ministry of Education and provide MPPC courses	Curriculum construction, teaching management, and data statistics
Superstar learning link	Pan Asia mobile app	Curriculum construction, teaching management, and class group chat
Pan Asian network	Curriculum construction and daily teaching	Curriculum construction, teaching management, and data statistics
Wisdom tree	Can complete cross school course selection	Curriculum construction, online learning, and class management

Table 4: Evaluation indexes of deep learning and shallow learning.

	Deep learning	Shallow learning	Not learning
Definition	The link between old and new concepts	New concepts replace or simply add new concepts	There is no conceptual change
Content	The concept map reflects the old and new concepts	The concept map reflects a large number of new concepts	The concept map does not present new concepts
Contact	The relationship between new concepts and old knowledge in the concept map	The concept map has not changed significantly	There are no new connections in the concept map
Structure	Obviously, the organization, connection, and richness have been qualitatively improved	There is no significant change in the overall type, richness, and interpretability of the concept map	There is no change in the structure of the concept map

Take the classes with almost no difference in usual performance as the control. Take class A, which offers the course of modern educational technology, as the experimental class and class B as the control class. Experimental class A uses the "3 + 1" intelligent teaching mode designed in this paper to verify the teaching effect of this mode. Control class B still adopts the traditional teaching method to study the theory course and experiment course. After the semester course, class A and class B with basically the same initial conditions are compared and analyzed, and the examination and test are conducted from two dimensions: test papers and micro class works. The same test paper is designed for examination. Teachers grade the micro class video works made by students at the end of the semester. The comparison results are shown in Table 6.

The results show that class A and class B have basically the same initial conditions. Class A adopts the engineering cost teaching mode based on in-depth learning for teaching practice. At the end of the course, there will be an obvious gap between the two classes. Class A has a higher excellent rate than class B in terms of test paper scores and micro class works, and the highest and lowest scores are higher than class B. First, this research examines the final assessments of students in the experimental and control groups in order to

Table 5: Comparison between deep teaching and shallow teaching.

	Depth teaching	Shallow teaching
Teaching concept	Student center	Teacher center
Teaching objectives	From easy to difficult hierarchical expression	Focus on basic knowledge and skills
Knowledge system	Emphasize the connection between old and new knowledge	Knowledge points are isolated and scattered
Teaching method	Proper selection of teaching methods	The method is single and inflexible
Student involvement	Active participation and high investment	Passive participation and low investment
Thinking level	Higher order thinking	Low order thinking
Teaching evaluation	Diversified ways and pay attention to students' multiple intelligences	The evaluation method is single, mostly performance evaluation
Teaching reflection	Be able to adjust the teaching state according to reflection	Reflection is simple and not systematic
Teaching results	High quality, pay attention to the sustainable development of students	Low quality, emphasis on student achievement

Table 6: Results comparison of class A/B.

Class	Number of people	Test paper score				Micro class works	
		Excellent rate (%)	Pass rate (%)	Highest score	Lowest score	Excellent rate (%)	Pass rate (%)
Class A	103	46.35	86.35	100	55	56.32	87.65
Class B	102	31.23	71.31	95	42	28.96	45.32

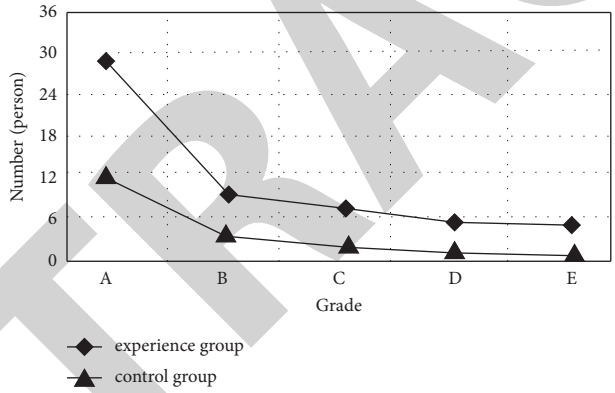

Figure 12: Statistics of final test scores of experimental group and control group.

compare the teaching impacts of regular classroom teaching and scaffolding teaching for in-depth learning. The test will last 120 minutes and have a maximum score of 100. Students' scores are classified into five categories according to administrative methods for evaluating the academic accomplishments of undergraduates in a university: A, B, C, D, and D. The test questions of the experimental group and the control group are completely consistent, and they are all computer operation questions, including the learning points of six chapters of the teaching material. The test questions cover a wide range and highlight the key and difficult points. It is mainly a comprehensive investigation of the mastery and application ability of students' knowledge, so as to reflect the students' in-depth learning. Statistics and comparative analysis of the final test scores of the two classes are shown in Figure 12.

It can be seen that the scaffolding teaching model for in-depth learning in this study helps students in grades B, C, and below to move forward to grade A. In order to better grasp the changes of students' in-depth learning status in the course, the "College Students' in-depth learning evaluation scale" was distributed to 27 students in the experimental class before and after the teaching experiment. Students filled it out truthfully according to their actual learning situation and made use of SPSS software. The pretest and post test data after the questionnaire are collected for an independent sample t-test to compare the mean. The results are shown in Table 7.

It can be seen that the promotion of deep learning motivation is relatively fast after the implementation of scaffolding teaching. In addition, there are significant differences in these four dimensions, and their p values are $000 < 0.01$. It indicates that there is a significant difference in the in-depth learning level between the experimental class before and after the curriculum implementation. It fully reflects that the scaffolding teaching mode for in-depth learning has significantly improved the in-depth learning level of the students in the experimental group, especially in the dimension of in-depth learning motivation, which is more inclined to actively collect learning materials for

Table 7: Independent sample t-test results of students' deep learning status.

Dimension	Up/down	N	Mean value	Standard-deviation	T value	p value
Deep learning motivation	Up	28	3.3025	0.8954	22.6582	0.000**
	Down		3.5896	0.8689		
In-depth learning investment	Up	28	3.3526	0.8622	22.6585	0.000**
	Down		3.7652	0.7352		
In-depth learning strategy	Up	28	3.8965	0.7865	28.6523	0.000**
	Down		3.9854	0.7212		
In-depth learning results	Up	28	3.5685	0.7652	27.6585	0.000**
	Down		3.6855	0.7655		

autonomous learning than before, showing that the students' learning consciousness and initiative are significantly enhanced.

4. Conclusion

Along with the goal and route of deep learning, this paper constructs the evaluation system of deep learning teaching, designs three-level evaluation indexes from the two dimensions of qualitative evaluation and quantitative evaluation, and determines the corresponding weights. The evaluation system runs through the whole process of a preclass, classroom, after-class, and final examination, comprehensively reflects teachers' teaching preparation, teaching organization, and management ability, and comprehensively examines students' autonomous learning, individual thinking, problem-solving and inquiry, and innovation ability. At the same time, according to the evaluation system, this paper makes an empirical study on the effectiveness of in-depth learning classroom practice teaching. The research shows that most students are satisfied with the teaching mode and their autonomous learning ability, and their final grades have been greatly improved, but there are also some problems. Therefore, the author believes that the construction of a teaching evaluation system is a long-term, interactive, and continuous improvement process. In the future, the flipped learning practice teaching process, according to the basis and characteristics of students, cooperate with other teaching strategies and means to constantly improve the evaluation system in order to comprehensively improve students' autonomous learning, application skills, and lifelong learning abilities and improve the teaching quality of engineering cost teaching.

Data Availability

The data used to support the findings of this study are included within the article.

Conflicts of Interest

The authors declare that they have no conflicts of interest.

References

[1] J. Deepak Kumar, Z. Zhang, and H. Kaiqi, "Multi angle optimal pattern-based deep learning for automatic facial expression recognition," *Pattern Recognition Letters*, vol. 139, no. 2, pp. 157–165, 2020.

[2] J. Liu, Z. Wang, and M. Xu, "DeepMTT: a deep learning maneuvering target-tracking algorithm based on bidirectional LSTM network," *Information Fusion*, vol. 53, no. 1, pp. 289–304, 2020.

[3] W. Tang, Q. Yang, K. Xiong, and W. Yan, "Deep learning based automatic defect identification of photovoltaic module using electroluminescence images," *Solar Energy*, vol. 201, no. 13, pp. 453–460, 2020.

[4] S. Zahia, B. Garcia-Zapirain, and A. Elmaghraby, "Integrating 3D model representation for an accurate non-invasive assessment of pressure injuries with deep learning," *Sensors*, vol. 20, no. 10, p. 2933, 2020.

[5] R. M. Kanko, E. K. Laende, G. Strutzenberger, M. Brown, and K. J. Deluzio, "Assessment of spatiotemporal gait parameters using a deep learning algorithm-based markerless motion capture system," *Journal of Biomechanics*, vol. 122, no. 3, Article ID 110414, 2021.

[6] W. Zhang, X. Gao, Z. Li, and Y. Shi, "Pilot-assisted MIMO-V-OFDM systems: compressed sensing and deep learning approaches," *IEEE Access*, vol. 23, pp. 1–10, 2020.

[7] D. Wu, J. Zhang, and Q. Zhao, "Multimodal fused emotion recognition about expression-EEG interaction and collaboration using deep learning," *IEEE Access*, vol. 32, no. 9, pp. 11–14, 2020.

[8] H. Su, Q. Bao, and Z. Chen, "ADMM–net: a deep learning approach for parameter estimation of chirp signals under sub-nyquist sampling," *IEEE Access*, vol. 3, no. 29, pp. 156–162, 2020.

[9] A. Yz, L. A. Hao, Q. A. Ping, A. Ks, B. Jc, and D. Znac, "Heterogeneous teaching evaluation network based offline course recommendation with graph learning and tensor factorization," *Neurocomputing*, vol. 415, no. 4, pp. 84–95, 2020.

[10] I. Sindhu, S. M. Daudpota, K. Badar, M. Bakhtyar, and M. Nurunnabi, "Aspect-based opinion mining on student's feedback for faculty teaching performance evaluation," *IEEE Access*, vol. 32, no. 15, pp. 112–116, 2019.

[11] X. Zhang and W. Shi, "Research about the university teaching performance evaluation under the data envelopment method," *Cognitive Systems Research*, vol. 56, no. 8, pp. 108–115, 2019.

[12] Q. W. Dong, S. M. Wang, F. J. Han, and R. D. Zhang, "Innovative research and practice of teachers' teaching quality evaluation under the guidance of "Innovation and entrepreneurship"," *Procedia Computer Science*, vol. 154, no. 4, pp. 770–776, 2019.

[13] Q. Lin, Y. Zhu, H. Lu, K. Shi, and Z. Niu, "Improving university faculty evaluations via multi-view knowledge graph," *Future Generation Computer Systems*, vol. 117, no. 6, pp. 181–192, 2021.

[14] P. H. Lin and S. Y. Chen, "Design and evaluation of a deep learning recommendation based augmented reality system for

Hindawi
Journal of Mathematics
Volume 2024, Article ID 9839640, 1 page
https://doi.org/10.1155/2024/9839640

Retraction

Retracted: The Evaluation of Music Teaching in Colleges and Universities Based on Machine Learning

Journal of Mathematics

Received 23 January 2024; Accepted 23 January 2024; Published 24 January 2024

This article has been retracted by Hindawi following an investigation undertaken by the publisher [1]. This investigation has uncovered evidence of one or more of the following indicators of systematic manipulation of the publication process:

(1) Discrepancies in scope

(2) Discrepancies in the description of the research reported

(3) Discrepancies between the availability of data and the research described

(4) Inappropriate citations

(5) Incoherent, meaningless and/or irrelevant content included in the article

(6) Manipulated or compromised peer review

The presence of these indicators undermines our confidence in the integrity of the article's content and we cannot, therefore, vouch for its reliability. Please note that this notice is intended solely to alert readers that the content of this article is unreliable. We have not investigated whether authors were aware of or involved in the systematic manipulation of the publication process.

Wiley and Hindawi regrets that the usual quality checks did not identify these issues before publication and have since put additional measures in place to safeguard research integrity.

We wish to credit our own Research Integrity and Research Publishing teams and anonymous and named external researchers and research integrity experts for contributing to this investigation.

The corresponding author, as the representative of all authors, has been given the opportunity to register their agreement or disagreement to this retraction. We have kept a record of any response received.

References

[1] X. Xiongjun and D. Lv, "The Evaluation of Music Teaching in Colleges and Universities Based on Machine Learning," *Journal of Mathematics*, vol. 2022, Article ID 2678303, 7 pages, 2022.

Hindawi
Journal of Mathematics
Volume 2022, Article ID 2678303, 7 pages
https://doi.org/10.1155/2022/2678303

Research Article

The Evaluation of Music Teaching in Colleges and Universities Based on Machine Learning

Xia Xiongjun and Danmeng Lv

Music Eduction, Hunan Normal University, Changsha, China

Correspondence should be addressed to Danmeng Lv; 202010160237@hunnu.edu.cn

Received 24 November 2021; Accepted 29 December 2021; Published 7 March 2022

Academic Editor: Naeem Jan

With the implementation of the strategic policy of rejuvenating the country through science and education, many innovative and practical teaching concepts and teaching models have been comprehensively developed. This breaks the backward teaching mode of traditional teaching activities. With the development of science and technology and Internet technology, deep learning is widely used in the field of education. Music teachers in colleges and universities constantly update their teaching methods and comprehensively use a variety of methods to carry out in-depth teaching in the classroom, and strive to stimulate students' learning Interest and enthusiasm, and comprehensively enhance students' music aesthetic ability. This article uses decision tree algorithms, support vector machines, Bayesian theory, and random forest four different classification techniques to evaluate the student curriculum evaluation dataset. Classification experiment: through the analysis of the experimental results, the performance of the four classifier models was compared, and the data showed the difference in accuracy, precision, recall, and F1 value of the four classifiers. At the same time, each of the classifier models was analyzed. This article verifies the effectiveness of machine learning models in curriculum evaluation and higher education mining, the importance of evaluation features.

1. Introduction

Art and science technology have never been separated. As Li Zhengdao said, "Science and art are inseparable, just like the two sides of a coin [1–5]." Music as a form of art is naturally inseparable from science [6]. With the advent of the Internet era, higher education institutions continue to improve their own informatization teaching level, resulting in a large amount of data related to the teaching process [7]. How to use this information to improve the quality of teaching and scientific research services in universities and the level of management decision-making has become the biggest challenge facing universities. The use of machine learning technology can effectively analyze and extract hidden information in large datasets, that is, discovering patterns and knowledge in large amounts of data and predicting results or behaviors. In recent years, the application of machine learning in higher education has become increasingly popular, involving the optimization of educational resource allocation, predicting student academic performance, academic planning, and enhancing the future development of alumni. It has also given birth to the birth of new educational research fields [8–12]. Excavating in-depth information from educational entities such as students, teachers, teaching assistants, alumni, and education administrators can help colleges and universities allocate various teaching resources and organize educational activities more effectively, and more effectively improve students' satisfaction with courses, to enhance the learning effect of students and increase the enrollment rate of majors [13]. One of the common problems in higher education is to evaluate the performance of teachers in the curriculum. Students are the only source of information for the learning process and the only person who can evaluate the quality, effectiveness and satisfaction of course content, teaching methods, teaching materials, and assignments. Student evaluation is mainly used to improve the quality of course teaching and, at the same time, as the basis for teaching assessment of teaching staff. Most colleges

and universities still use student evaluation as an effective measure of teaching evaluation. Music as an artistic form of expression contains very rich emotions. In the process of teaching in universities in my country at this stage, relevant education departments pay more attention to the teaching of music as a subject. With the continuous improvement of my country's social economy, culture, and people's pursuit of spiritual civilization, the requirements of college music majors have become increasingly demanding. In order to meet people's growing spiritual needs, music teachers in colleges and universities, in the process of organizing teaching, should contact the reality of life, aiming at students' hobbies and diversified classroom teaching to fully mobilize students' learning enthusiasm.

Currently, the main focus of machine learning research in the education field is to explore the learning environment and web-based teaching systems, and improve student performance. There are a few applications of information mining for student evaluation. This article studies the potential of data mining in the teacher performance measurement standards perceived by students and chooses decision tree algorithm (DS), support vector machine (SVM), naive Bayes (NB), and random forest (RF), the four commonly used machine learning classifiers, which model the dataset of students' online evaluation of course information and compare the performance indicators of various classification techniques. Section 2 of our study reviews the related works and the literature. In Section 3, the methodology of our work is described along with the description of proposed techniques. Moreover, the study also proposes the experimental section, that is, Section 3, which carries out tests and verifies the strength and working of the proposed techniques through the results of tests. In Section 5, the conclusion of the study is given.

2. Literature Review

In order to further advance the reform of music education in colleges and universities, promote the development of music education, and strengthen the management system of music education, many countries are constantly studying the basic theories and practical applications of music teaching evaluation in colleges and universities, so that it can better achieve the teaching goals service. In some of these countries, the research on the evaluation of music teaching is earlier, and the theory is relatively mature, with a certain degree of operability. Among them, the United States and Japan have conducted in-depth research on the evaluation of music education [14–18].

Overview of foreign music teaching evaluation. The American music teaching evaluation mainly includes the music test movement, the goal model of curriculum design, the taxonomy of educational goals, and the achievement responsibility system movement. In the early 20th century, American school music education mainly consisted of music tests. Music tests were used to collect objective data on the development characteristics and achievements of students in music, as well as music courses and evaluation effects in music education, so that music teaching could be measured based on measurement. These objective materials come to evaluate the results and process of music education in the past, and to revise and improve new goals, processes, courses, and teaching. The tools used are musical aptitude test (such as "Westshore Musical Abilities Measurement") and musical achievement test (such as "Beach Music Test"). In the 1940s and 1950s, the evaluation committee led by Professor Taylor, based on the "eight-year study," proposed that teaching evaluation should focus on describing the consistency between educational results and educational goals. Therefore, a goal-centered evaluation model was established. Based on the "eight-year study," the Evaluation Committee of China proposed that teaching evaluation should focus on describing the consistency between educational results and educational goals. Therefore, a goal-centered evaluation model was established. In the 1960s and 1970s, the performance accountability movement was popular in the United States. Boyer and Radoqi proposed in their book "Musical Experience Measurement and Evaluation" that the service functions of music education program evaluation may have the following types: responsibility system; teaching effect; teacher effect; classroom effect; subject knowledge taught and so on. The abovementioned theoretical and practical research has established important value standards for the development of an evaluation index system for teaching effects. Educational evaluation is developed from educational measurement [19, 20].

Overview of Music Teaching Evaluation in my country. Educational measurement can be traced back to various tests in the 19th century. The initial germination of education evaluation in my country originated from the ancient imperial examination system. It is considered to be the earliest comprehensive examination in the world. Some people call it the "civilian examination." The purpose of the examination is to become an official. People flew up and down overnight. Due to various reasons, the research on educational testing, measurement, and evaluation in my country has not been developed since the last century. After the founding of the People's Republic of China, my country's education evaluation has gradually developed. Since the 1950s, my country has been following the Soviet Union's music education evaluation model. It shows the phenomena of "compulsion" (ignoring the development of the main body), "rigidity" (ignoring development vitality), "one-sided" (ignoring overall development), and "separation" (ignoring the integration of evaluation and development) of evaluation. Music teaching evaluation emphasizes the purpose of "evaluation," and "selection" pays attention to serving the society through the management function of evaluation and talent selection but ignores the aesthetic education function and development function of evaluation. Evaluation emphasizes the guidance of external objectives but ignores the objectivity of the needs of the evaluation object and cannot focus on stimulating the internal motivation of the evaluation object, so as to promote the positive development of the subject of the evaluation object, and most of the evaluation objects are in a passive position. The evaluation is to use standardized examination or paper and pencil test as the only means to evaluate students. Teaching evaluation often only pays

attention to the level of scores and ignores them. The objectivity of the evaluation object is based on the degree of effort: too much attention is paid to the evaluation result and the meaning of the evaluation process itself is ignored; teaching evaluation is a partial and nonholistic objective evaluation. For example, the school considers students' progress to higher education (advanced to higher art colleges) and awards in various competitions at all levels that students participate in as important indicators for evaluating music teachers' teaching performance. The school organizes relevant personnel to attend classes in the classroom and scores according to a predesigned scale, and then calculates the total score uniformly to determine the pros and cons of the class. This kind of evaluation work is carried out in some parts of the chain. Therefore, they are not scientific enough or comprehensive enough for teaching evaluation. The abovementioned various teaching evaluations affect a series of operation sequences and judgment methods, which make the functional structure of evaluation deviate from the track of quality education, and thus, the content and methods of music teaching cannot be truly reformed. At present, the evaluation of music teaching in my country mainly presents the following basic characteristics:

(i) Evaluation content-excessive reliance on subject knowledge (a static knowledge), especially knowledge in textbooks: teachers rely on participating in textbooks to strengthen the knowledge and knowledge of textbooks. Analysis and practice of skills. Ignore the evaluation and analysis of students' emotions and attitudes, the internalization and integration of knowledge and skills.

(ii) Evaluation subject-teachers are the mainstay, ignoring evaluations at the same level and evaluations from different sources, for example, parent evaluation, student evaluation, manager evaluation, and multiple evaluation. Although some students self-evaluate, in general, students are still in a negative position to be evaluated.

(iii) Evaluation results—Most of the evaluation results pay attention to the final results, pay more attention to horizontal comparison, and emphasize the conclusion of summary evaluation, while ignoring the progress of each stage and the scientific process of the result feedback. Therefore, teaching evaluation has not achieved good results.

(iv) Evaluation index—single: the status quo places more emphasis on commonality and general trends, ignoring the differences and uniqueness between individuals.

(v) Evaluation method—monotonous: pay more attention to "quantification" and ignore "qualitative" evaluation. Because the formulation of reliability and validity is a description of quantification, it is difficult to describe a person's overall characteristics as a result of quantification, and "qualitative" evaluation focuses on the process and can promote the development of the individual.

(vi) Evaluation methods—traditional paper and pen methods are mostly used, and there is a lack of techniques and methods that reflect the latest evaluation ideas.

(vii) Evaluation implementation process: the current evaluation implementation process is closed, static, and lacking in flexibility and dynamics. The evaluation process should be dynamic, allowing multiple evaluations.

In recent years, with the rapid growth of knowledge, the original knowledge structure can no longer meet the needs of the development of the times. Music teaching has shifted from focusing on skills to focusing on cultivating students' emotions, attitudes, and values. Music teaching evaluation has shifted from summative evaluation to formative evaluation; from partial evaluation to overall and comprehensive evaluation; from passive waiting for evaluation to active participation in evaluation development. In terms of evaluation theory, it emphasizes the evaluation of comprehensive qualities such as the ability to solve practical problems, innovative ability, practical or practical ability, good psychological quality and scientific spirit, and positive learning mood. Evaluation is no longer for selection and screening, but for the growth and progress of students. Evaluation is no longer "selecting children suitable for education" but "creating education suitable for children." Evaluation should be expressed in terms of motivation and integration functions. To evaluate a teacher's teaching is to enable the teacher to understand his own development direction in his evaluation and self-evaluation, so as to use the power of evaluation to integrate his/her teaching abilities and gain lessons in class [21, 22]. Better, complete the teaching work better. With the continuous deepening of reform and opening up and the introduction of advanced foreign education and teaching methods, art education, especially music education, as an important part of quality education, has received more and more attention. In recent years, the evaluation of music teaching has developed rapidly. In the process of music teaching evaluation, people expect a more scientific and feasible way to make an objective and feasible evaluation of teaching quality; hope that through evaluation, it will help teachers and students diagnose problems in the teaching and learning process and improve teaching strategies. We should make clear the direction of our efforts. It is hoped that through evaluation, communicating the existing problems, improving teaching strategies, and exchanging information, teachers can continuously improve education and teaching methods and improve teaching ability and level. We hope to promote the continuous development of students' personality through evaluation. And we hope to adjust the school management strategy and improve the overall level of school education and teaching through evaluation.

3. Method

Machine learning is a discipline that studies how to use machines to simulate human learning activities. It is the study of machines to recognize existing knowledge, acquire new knowledge and new skills, continuously improve performance, and achieve self-improvement. The initial research purpose of machine learning is to make computer systems have human learning capabilities in order to realize artificial intelligence. It has mainly experienced three processes: the enthusiastic period (from the mid-1950s to the mid-1960s), the calm period (from the mid-1960s to the mid-1970s), and the revival period (from the mid-1970s to the mid-1980s). Among them, the successful holding of the first machine learning international academic exchange seminar at Carnegie Mellon University in 1980 marked the rise of machine learning research all over the world. Nowadays, with the continuous development of computer technology, human beings have collected and accumulated a large amount of data in various fields, such as search engines, geological prospecting, speech and handwriting recognition, information security, robot application, securities market analysis, and other fields. However, how to analyze the potential laws from these massive data has become a common demand in almost all fields. This is why machine learning technology has received increasing attention. At present, machine learning has become another important research field of artificial intelligence applications after expert systems (subject to the bottleneck problem of knowledge acquisition), and it has become one of the most active and promising fields in computer science. Currently, the widely used machine learning methods mainly include decision trees, SVM, Bayesian theory, and RFs.

Decision tree algorithm is one of the most classic machine learning algorithms. It is an algorithm that classifies and learns data through a top-down, well-organized process. The purpose of the decision tree algorithm is to recursively divide the observations into mutually exclusive subgroups until there are no more differences in the given statistics. Among the statistics used to find the classification attributes of tree nodes, information gain, gain ratio, and Gini index are the most commonly used. Usually, iterative dichotomy (ID3) uses information gain, C4.5 and C5.0 use gain ratio, and classification and regression tree (CART) uses Gini index. The support vector machine tries to find a hyperplane to separate the classes, minimize the classification error, and maximize the margins. SVM is a good classification and regression technique proposed by Vatnik of Bell Laboratories, AT&T. Through calculating the probability of an object belonging to a certain category, the Bayesian classifier classifies the samples. The theoretical basis of its classification is Bayes' theorem. According to the Bayesian formula, the posterior probability of an object is calculated according to the prior probability, and the class with the largest posterior probability is selected as the class to which the object belongs. In other words, the Bayesian classifier is an optimization in the sense of the minimum error rate. Random forest is a type of ensemble learning, which is an algorithm that integrates the classification effects of multiple decision trees. It consists of multiple base classifiers, and each base classifier is a decision tree. Each decision tree acts as a separate classifier, independently performing learning and classification prediction. These predictions are finally integrated to obtain a total prediction that is better than all the individual classifiers. There are many performance indicators for evaluating the classification model based on the correctness of the model classification decision. Suppose that in a binary classification task, the value of the class variable can be assumed to be positive (P) and negative (N). The classification of actual positive cases (P) correctly marked as positive cases is named true cases (TP), and the classifiers where actual positive cases are incorrectly marked as negative cases are false-negative cases (FN). In a similar manner, actual negative examples (N) that are correctly marked as negative examples are regarded as true-negative examples (TN), and actual negative examples that are incorrectly marked as positive examples are regarded as false-positive examples (FP).

4. Experiment and Result Analysis

Data collection and characterization. We selected the student evaluation data of a university in recent two years and randomly selected 3150 scoring data, of which the number of positive samples is 1769 and the number of negative samples is 1183. Each of scoring data has 37 variables, which come from students' online scoring, involving classroom preparation, classroom performance, course implementation, case organization, homework correction, teacher attitudes, and course network construction. The range of values is from 1 to 5. The numbers on the scale from 1 to 5 point to "strongly disagree," "disagree," "neutral," "agree," and "strongly agree"; or "never," "rarely," "sometimes," "often," and "always." The last variable is a binary variable, which is the student's overall evaluation information of the teacher, where 1 means "unsatisfied" and 2 means "satisfied." This variable serves as the class label of the data sample. Divide all samples into training set and test set. In order to ensure the balance of positive and negative samples, 70% of them were randomly selected from the positive and negative sample sets, totaling 2205 as the training set. The positive samples were 1377, the negative samples were 828, and the remaining 945 were used as the test set. The number of positive samples was 590, and the number of negative samples is 355.

This article generates four classification models. Its performance is evaluated by the precision rate, recall rate, F1 value, and accuracy rate of the test data. In the decision tree algorithm, the gain ratio is used as the measurement index, and multipath partitioning is adopted, and the minimum value of each subinstance is set to 2. The confusion matrix of DS classification is shown in Table 1.

In the parameter selection of the support vector machine classifier, a polynomial function is used as the kernel function. The confusion matrix of SVM classification is shown in Table 2.

Naive Bayes parameter selection. Since the sample feature value is a discrete value in the range of 1–5, we choose the naive Bayesian polynomial NB with polynomial distribution a priori, and the prior probability is calculated from

Table 1: Confusion matrix of DS classification results.

Actual value	Predictive value		
	Positive example	Counter example	Total
Positive example	528	62	590
Counter example	38	317	355
Total	566	379	945

Table 2: Confusion matrix of SVM classification results.

Actual value	Predictive value		
	Positive example	Counter example	Total
Positive example	520	70	590
Counter example	30	325	355
Total	550	395	945

the training set sample. The confusion matrix of the NB classification results is shown in Table 3.

When the random forest classifier is used for classification learning, in order to prevent the occurrence of overfitting or underfitting, the number of base classifiers is selected as 10. Since the number of dataset samples selected in this article is not large, the decision tree is not limited depth. The classification results of confusion matrix of RF are shown in Table 4.

Finally, use the evaluation index to compare the performance of the applied classifiers. It also can be seen from Table 4 that the classifier gives similar results in the test dataset. When comparing the model performances, it is found that all the methods used in this article can effectively classify the "satisfied" and "unsatisfied" teacher performances, which are shown in Figures 1–3.

The accuracy of all classifier models is at least 89%. The random forest classifier has the best performance, followed by SVM, and NB has the worst performance. The results of accuracy rate F1 and recall rate once again show that random forest is the best classifier. There are some differences in the results of other classifiers. It can be said that all classifiers can better predict the results of students' evaluation of teachers. However, according to the given performance index, random forest is the best among all the selected classifiers.

Then, analyze the evaluation indicators used in student evaluation, and dig out the importance of each evaluation indicator under each classifier. The management department can improve the evaluation and assessment indicators according to the importance of the indicators and formulate the assessment mechanism more scientifically. Among the four methods used, three methods, decision tree, support vector machine, and random forest, are selected for eigenvalue importance analysis.

For decision tree classification algorithms, information gain (IG) is used to calculate feature importance for the decision tree. For each feature a, calculate the "information gain" obtained by dividing the sample set D with the attribute a. The larger the information gain, the more important the attribute.

Table 3: Confusion matrix of NB classification results.

Actual value	Predictive value		
	Positive example	Counter example	Total
Positive example	510	80	590
Counter example	55	300	355
Total	560	380	945

Table 4: Confusion matrix of RF classification results.

Actual value	Predictive value		
	Positive example	Counter example	Total
Positive example	550	40	590
Counter example	28	327	355
Total	578	367	945

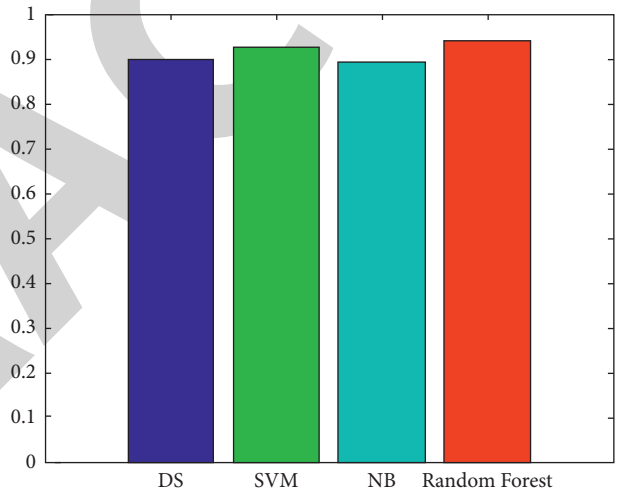

Figure 1: Comparison of precision rates.

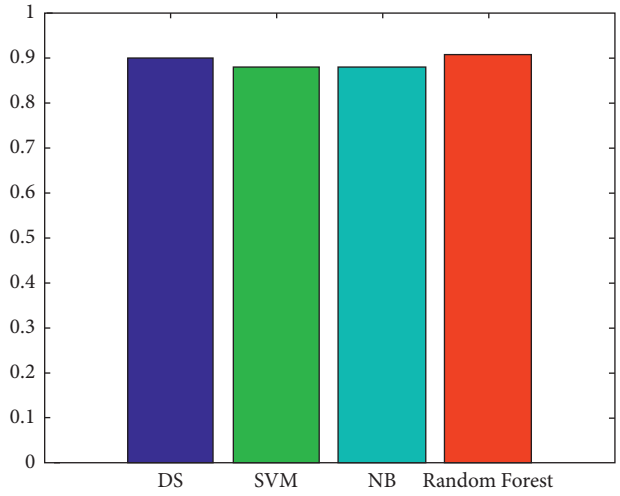

Figure 2: Comparison of recall rates.

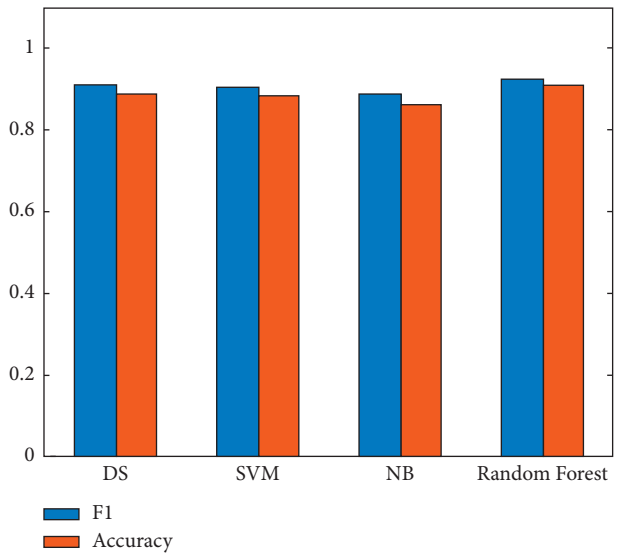

Figure 3: Comparison of F1 and accuracy.

$$\text{Gain}(D, a) = \text{Ent}(D) - \sum_{v=1}^{V} \frac{|D^v|}{D} \text{Ent}(D^v), \tag{1}$$

where $\text{Ent}(D)$ is the information entropy of D:

$$\text{Ent}(D) = -\sum_{k=1}^{|y|} p_k \log_2 p_k, \tag{2}$$

where p_k $(k = 1, 2, \ldots, |y|)$ represents the proportion of the k sample in this set D. In the decision tree classifier, the first three important variables are V23: "This class has helped me increase my knowledge and interest in the subject," V13: "The teacher is very enthusiastic about this subject," and V5: "The teacher is very enthusiastic about the subject." The knowledge of the company is well mastered. The importance of features in support vector machines is usually considered the absolute value of the feature coefficient, that is, the weight corresponding to the independent variable. For the dataset used in this article, the three most important variables of SVM are V25: "Teacher's rating (homework/examination) is fair," V23: "This course helped me increase my knowledge and interest in the subject," and V22: "I need to spend a lot of time preparing homework/exams." In the random forest algorithm, the feature importance is calculated by dividing the sum of the Gini coefficients of each feature classification by the Gini coefficient of the total feature. First, calculate the importance of each feature based on a single tree, explore the contribution rate of each feature to each tree, and then take the average. The three most important variables for calculating RF are V22: "The homework/exam fully tests the knowledge taught", V17: "The course materials (textbooks, handouts, cases, etc.) are perfect," and V23: "This course helps me Increased knowledge and interest in the subject."

5. Conclusion

In this article, we classified the online course evaluation data through machine learning methods and analyzed the importance of characteristics of student evaluation. The different dimensions of college courses and teacher effectiveness are measured by the online course evaluation. It has been proved by the experiments that the machine learning method accurately classifies teachers' "satisfaction" and "dissatisfaction." In this article, we used different classification techniques, which include decision tree algorithms (DS), support vector machines (SVM), Bayesian theory, and random forest (RF) methods. The results showed that performance indicators of all the mentioned techniques were around 90%. Among them, students' personal interests and knowledge gained are the main basis for students to evaluate courses. These results can be used to improve the establishment and improvement of online evaluation indicators, so as to set more reasonable and scientific evaluation indicators.

On daily life datasets, data mining techniques are proposed, especially the effectiveness of DS, SVM, NB, and RF in higher education data mining. This can help teachers carry out reasonable teaching reforms and experiments based on the analysis results in a timely manner and improve their own teaching ability. The analysis result of the feature importance of the classifier shows that there are many possible improvements in the design of the measurement indicators used in the teacher performance evaluation, and it provides a certain reference for the management department to improve the evaluation indicators.

Generally speaking, in the process of teaching work, ordinary colleges and universities reform the teaching evaluation system of musicology, which can carry out the teaching work of musicology in a scientific and regular manner, and integrate the main tasks of musicology teaching in colleges and universities. Completed smoothly, so in the process of organizing classroom teaching activities, music teachers should respect the students' personalities, make reasonable references to the teaching evaluation system, and give full play to the students' learning enthusiasm, so that through classroom teaching activities, every student can obtain a certain amount of music knowledge. In this way, a large number of music talents in line with social development can be cultivated and the progress of music education can be promoted.

Data Availability

The data used to support the findings of this study are included within the article.

Conflicts of Interest

The authors declare that there are no conflicts of interest regarding the publication of this article.

Hindawi
Journal of Mathematics
Volume 2023, Article ID 9871670, 1 page
https://doi.org/10.1155/2023/9871670

Retraction

Retracted: Automatic Classification Method of Music Genres Based on Deep Belief Network and Sparse Representation

Journal of Mathematics

Received 15 August 2023; Accepted 15 August 2023; Published 16 August 2023

This article has been retracted by Hindawi following an investigation undertaken by the publisher [1]. This investigation has uncovered evidence of one or more of the following indicators of systematic manipulation of the publication process:

(1) Discrepancies in scope

(2) Discrepancies in the description of the research reported

(3) Discrepancies between the availability of data and the research described

(4) Inappropriate citations

(5) Incoherent, meaningless and/or irrelevant content included in the article

(6) Peer-review manipulation

The presence of these indicators undermines our confidence in the integrity of the article's content and we cannot, therefore, vouch for its reliability. Please note that this notice is intended solely to alert readers that the content of this article is unreliable. We have not investigated whether authors were aware of or involved in the systematic manipulation of the publication process.

Wiley and Hindawi regrets that the usual quality checks did not identify these issues before publication and have since put additional measures in place to safeguard research integrity.

We wish to credit our own Research Integrity and Research Publishing teams and anonymous and named external researchers and research integrity experts for contributing to this investigation.

The corresponding author, as the representative of all authors, has been given the opportunity to register their agreement or disagreement to this retraction. We have kept a record of any response received.

References

[1] L. Pan, "Automatic Classification Method of Music Genres Based on Deep Belief Network and Sparse Representation," *Journal of Mathematics*, vol. 2022, Article ID 8752217, 10 pages, 2022.

Hindawi
Journal of Mathematics
Volume 2022, Article ID 8752217, 10 pages
https://doi.org/10.1155/2022/8752217

Research Article

Automatic Classification Method of Music Genres Based on Deep Belief Network and Sparse Representation

Lina Pan

School of Preschool and Art Education, Xinyang Vocational and Technical College, Xinyang 464000, China

Correspondence should be addressed to Lina Pan; pln@xyvtc.edu.cn

Received 29 November 2021; Revised 17 December 2021; Accepted 20 December 2021; Published 7 March 2022

Academic Editor: Naeem Jan

Aiming at the problems of poor classification effect, low accuracy, and long time in the current automatic classification methods of music genres, an automatic classification method of music genres based on deep belief network and sparse representation is proposed. The music signal is preprocessed by framing, pre-emphasis, and windowing, and the characteristic parameters of the music signal are extracted by Mel frequency cepstrum coefficient analysis. The restricted Boltzmann machine is trained layer by layer to obtain the connection weights between layers of the depth belief network model. According to the output classification, the connection weights in the model are fine-tuned by using the error back-propagation algorithm. Based on the deep belief network model after fine-tuning training, the structure of the music genre classification network model is designed. Combined with the classification algorithm of sparse representation, for the training samples of sparse representation music genre, the sparse solution is obtained by using the minimum norm, the sparse representation of test vector is calculated, the category of training samples is judged, and the automatic classification of music genre is realized. The experimental results show that the music genre automatic classification effect of the proposed method is better, the classification accuracy rate is higher, and the classification time can be effectively shortened.

1. Introduction

Music is an art that can effectively show human emotions. At the same time, music is a note composed of a specific rhythm, melody, or musical instrument according to certain rules [1–3]. Rock music, jazz, classical music, and other music genres are examples of diverse style tracks comprised of unique beats, timbres, and other aspects exhibited in music works. With the fast development of network and multimedia technologies, people's primary method of listening to music has shifted to digital music, which has fueled people's need for music appreciation to some level [4–6]. Most online music websites' major categorization and retrieval elements are now based on the music genre. Simultaneously, the music genre has evolved into one of the categorization features used in the administration and storage of digital music databases. The pace of database updating is sluggish when dealing with a large volume of music data information. The effectiveness of manual labelling in the early days of music information retrieval could not satisfy the real demands of contemporary management. Therefore, it is of great significance to study the automatic classification of music genres.

At present, scholars in related fields have studied the classification of music genres and achieved some theoretical results. Reference [7] proposed a music type classification method based on Brazilian lyrics using the BLSTM network. With the help of genre labels, songs, albums, and artists are organized into groups with common similarities. Support vector machine, random forest, and two-way short- and long-term memory networks are used to classify music types, combined with different word embedding techniques. This method is effective. Reference [8] proposed a music genre classification method based on deep learning. Machine learning technology is used to classify music types. The residual learning process, combined with peak and average pool, provides more statistical information for higher-level neural networks. This method has significant classification

performance. However, the above methods still have the problems of low classification accuracy, long time, and poor effect.

An automated music genre categorization technique based on deep belief networks and sparse representation is suggested to address the aforementioned issues. Framing, pre-emphasis, and windowing are used to preprocess the music signal, and Mel frequency cepstrum coefficient analysis is used to extract the signal's distinctive properties. A music genre classification network model is built based on the deep belief network and integrated with the sparse representation classification technique to achieve autonomous music genre categorization. This method has a good effect and high accuracy in music genre classification and can effectively shorten the classification time.

2. Deep Belief Network and Sparse Representation

2.1. Deep Belief Network

2.1.1. Restricted Boltzmann Machine. Restricted Boltzmann machine (RBM) belongs to a randomly generated neural network based on the probability distribution characteristics of the learning input data set [9–11]. It can be seen that the layer $q = \{q_1, q_2, \ldots, q_n\}$ and the hidden layer $w = \{w_1, w_2, \ldots, w_m\}$ together constitute an RBM, in which the neurons in each level have no connection. Use $q_i \in \{0, 1\}, w_j \in \{0, 1\}$ to describe the value of the binary random unit. The data features are mainly described by neurons in the visible layer, and the features of hidden layer neurons are used for feature extraction. The RBM network structure is shown in Figure 1.

The RBM energy function is defined as the following formula:

$$\begin{aligned} E(q, w; \alpha) &= -q^T W w - z^T q - x^T w \\ &= -\sum_{i=1}^{n} b_i q_i - \sum_{j=1}^{m} z_j w_j - \sum_{i=1}^{n}\sum_{j=1}^{m} q_j c_{ij} w_j. \end{aligned} \tag{1}$$

In formula (1), $\alpha = \{a, b, w\}$ is a real parameter, q_i and w_j are used to describe the states of the i and j neurons in the RBM layers, z_j is the bias of q_i, b_i is the bias of w_j, c_{ij} is the weight between the states of q_i and w_j neurons, and n, m is its corresponding node. According to formula (1), the joint probability distribution $P(q, w; \alpha)$ of (q, w) can be obtained as the following formula:

$$P(q, w; \alpha) = \frac{1}{V(\alpha)} \exp(-E(q, w; \alpha)). \tag{2}$$

In formula (2), $V(\alpha)$ is a normalized function. When both q and w are known, formulas (3) and (4) are used to express the activation probability of neurons in the two layers of RBM:

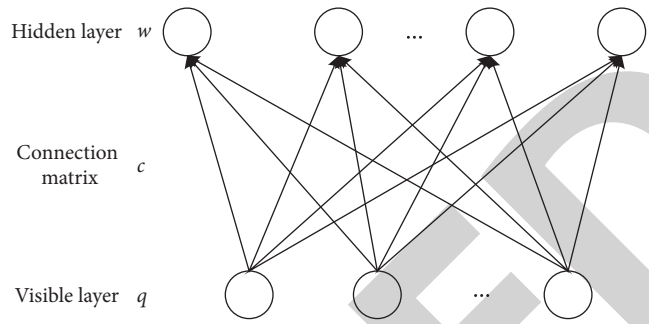

Figure 1: RBM network structure diagram.

$$P\left(w_j = \frac{1}{q}\right) = \text{sigmoid}\left(b_j + \sum_i q_i c_{ij}\right), \tag{3}$$

$$P\left(q_i = \frac{1}{w}\right) = \text{sigmoid}\left(z_i + \sum_j c_{ij} w_j\right). \tag{4}$$

In formulas (3) and (4), sigmoid $= 1/1 + e^{-x}$ is the activation function. When the training data set K is given, the likelihood function is maximized to express the RBM target as shown in the following formula:

$$H_{\alpha,K} = \sum_{n=1}^{\delta} \log P(q^n). \tag{5}$$

In formula (5), δ is the number of training set data. The essence of RBM is to map the original data to different feature spaces to retain the key feature information of the data and obtain a better low-dimensional representation. According to this idea, an idea of optimizing RBM training in this paper is to replace the objective function formula (5) of RBM equally. If the output of each RBM is converted according to formula (6), the output of its hidden layer can be inversely converted and then compared with the original data. The errors of the two can be used as the standard to judge the learning effect of the current RBM network, so as to learn the key features of the data faster.

$$T = \left(G_y J + \kappa\right) J^T + \theta. \tag{6}$$

In formula (6), G_y is the original data set, J is the weight of RBM, J^T is the transposed matrix of J, κ is the bias of the visible layer, and θ is the bias of the hidden layer. The difference between the new data obtained by formula (6) and the original data is calculated, and the mean square error MSE is used as the objective function of RBM, and then, the optimization algorithm is used for evaluation.

2.1.2. Deep Belief Network. Deep belief network (DBN) is one of unsupervised learning algorithms [12–14]. It is composed of RBM, so there is no connection in the same layer. The relationship between the two layers of RBM is represented by a joint probability distribution.

$$P\left(q, w^1, w^2, \ldots, w^l\right) = P\left(q|w^1\right)P\left(w^1|w^2\right), \ldots, P\left(w^{l-2}|w^{l-1}\right)P\left(w^{l-1}, w^l\right). \tag{7}$$

In formula (7), l is the number of hidden layers of DBN. DBN is a hybrid model composed of two parts. The structure of the DBN model is shown in Figure 2.

As shown in Figure 2, the undirected graph model of the top two layers forms associative memory, and the other layers are directed graph models. In practice, they are stacked restricted Boltzmann machines. They are Boltzmann machine layers stacked layer by layer, two adjacent to each other. However, the training in the DBN model has direction. DBN training method can be simply summarized into two parts: first, RBM is trained layer by layer to obtain better initial parameter values, and then, the network is optimized. The specific steps are as follows:

The original input is set to $s^{(i)}$, $d^{(i)}$ is used to describe the reconstructed input, and batch gradient descent tuning is used for n samples of a given training set $\{(s^{(1)}, d^{(1)}), \ldots, (s^{(i)}, d^{(i)})\}$ [15, 16]. The sample size loss function can be expressed as follows:

$$C(R, v) = \left[\frac{1}{n}\sum_{i=1}^{n} C\left(R, v; s^{(i)}, d^{(i)}\right)\right] + \frac{\lambda}{2}\sum_{l=1}^{m_i}\sum_{i=1}^{s_i}\sum_{j=1}^{s_i}\left(M_{ij}^{(l)}\right)^2 = \left[\frac{1}{n}\sum_{i=1}^{n}\left(\frac{1}{2}\left\|h_{R,v}\left(s^{(i)}\right) - s^{(i)}\right\|\right) + \frac{\lambda}{2}\sum_{l=1}^{m_i-1}\sum_{i=1}^{s_i}\sum_{j=1}^{s_i}\left(M_{ij}^{(l)}\right)^2\right]. \tag{8}$$

In formula (8), $M_{ij}^{(l)}$ is used to describe the weight coefficient between the i and j nodes in the l and $l+1$ layers, $v_i^{(l)}$ is used to describe the i node offset in the l layer, and $h_{R,v}(s^{(i)})$ is used to describe the result after $s^{(i)}$ reconstruction. The difference between the original input and the current input after reconstruction is calculated, that is, the mean square error term. In order to avoid overfitting, the weight coefficient is greatly reduced, that is, the regularization term. The above two items are balanced by λ. $C(R, v)$ is used to describe the correctness of the convex function. In order to obtain the global optimal solution, the gradient descent method is used to realize it [17, 18]. In order to optimize the loss function, the mean square error is reconstructed to minimize it, and the partial derivative of $C(R, v)$ is found as follows:

$$\frac{\partial C(R, v)}{\partial M_{ij}^{(l)}} = \left[\frac{1}{n}\sum_{i=1}^{n}\frac{\partial C\left(R, v; s^{(i)}, d^{(i)}\right)}{\partial M_{ij}^{(l)}}\right] + \lambda M_{ij}^{(l)}, \tag{9}$$

$$\frac{\partial C(R, v)}{\partial v_i^{(l)}} = \frac{1}{n}\sum_{i=1}^{n}\frac{\partial C\left(R, v; s^{(i)}, d^{(i)}\right)}{\partial v_i^{(l)}}. \tag{10}$$

DBN has good flexibility; that is, it is easy to expand to other networks or combine with other models. A typical example of DBN expansion is the convolution depth belief network.

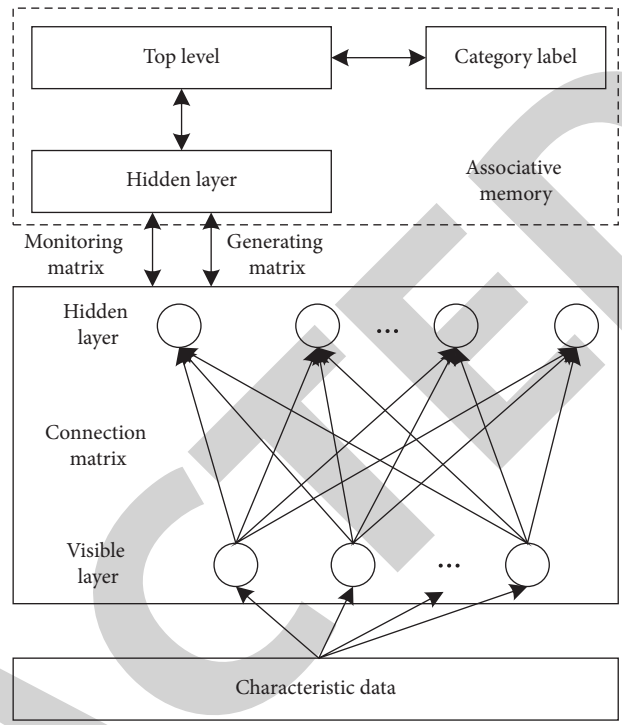

Figure 2: DBN model structure diagram.

2.2. Sparse Representation

2.2.1. Sparse Representation Method. If there are G type training samples, and there are sufficient numbers in any category, the i training sample data and number are denoted by $B_i = [b_{i,1}, b_{i,2}, \ldots, b_{i,n_i}] \in R^{m \times n_i}$ and m, respectively, and the feature set dimension is denoted by n_i. Then, its space is composed of n_i column vectors, and the linear combination is expressed as follows:

$$y = \chi_{i,1}b_{i,1} + \chi_{i,2}b_{i,2} + \cdots + \chi_{i,n_i}b_{i,n_i}. \tag{11}$$

In formula (11), $\chi_{i,n_i} \in R$ is described as the linear coefficient to be solved. Therefore, a complete vector matrix U is defined, which is represented by training samples of G categories, and the vector matrix is represented by test samples of different categories that can be written as follows:

$$U = \left[U_1, U_2, \ldots, U_G\right] = \left[b_{1,1}, b_{1,2}, \ldots, b_{G,n_G}\right] \in R^{m \times n_i}. \tag{12}$$

At this time, for the test sample y from the i category, the space formed by the training matrix U can be rewritten as follows:

$$y = Up_0 \in R^m. \tag{13}$$

In formula (13), $p_0 = [0, \ldots, 0, \chi_{i,1}, \chi_{i,2}, \ldots, \chi_{i,n_i}, 0, \ldots, 0]^T \in R$ is the coefficient vector.

2.2.2. Seeking Sparse Solution. When $m > n$, the reconstructed training matrix space has a unique solution. However, under normal circumstances, when $m \leq n$, the reconstructed training matrix space has infinite solutions. As a result, the nonzero vectors contained in the coefficient

vector obtained by reconstructing the training matrix space are reduced, which can be converted to

$$\widehat{p}_0 = \arg\min \|p\|_0 \text{ subject to } \mathrm{Up} = y. \tag{14}$$

In formula (14), $\|\cdot\|_0$ is described as l^0 norm. However, formula (14) has an NP problem, which is difficult to solve. Therefore, solving the NP problem by minimizing the problem [19, 20] is expressed as follows:

$$\widehat{p}_1 = \arg\min \|p\|_1 \text{ subject to } \mathrm{Up} = y. \tag{15}$$

In formula (15), $\|\cdot\|_1$ represents the l^1 norm, and $\widehat{p}_1$ is the approximate solution of p.

3. Automatic Classification Method of Music Genre

Music genre is a traditional means of categorising the attribution of musical works, and it is commonly separated into categories based on historical context, geography, origin, religion, musical instruments, emotional topics, performance styles, and so on. Western music dominates the music genres. Western music encompasses a wide range of musical styles. Classical, blues, rock, pop, metal, jazz, country, hip-hop, and other music genres are widespread [21–25]. This research proposes a deep belief network and sparse representation-based automated music genre categorization approach. A music genre categorization network model is created by preprocessing music signals, extracting music signal characteristic parameters, pretraining, and fine-tuning the DBN model. The sparse representation of the test vector is calculated, the category of the training samples is assessed, and the automated classification of music genres on this basis is achieved, in combination with the sparse representation classification method. The automatic classification process of music genres based on a deep belief network and sparse representation is shown in Figure 3.

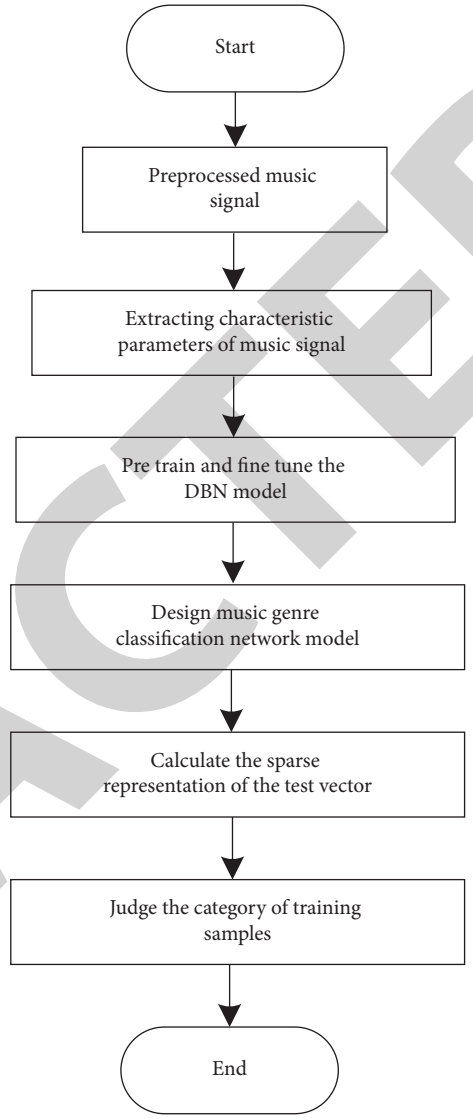

Figure 3: Flow chart of automatic classification of music genres based on deep belief network and sparse representation.

3.1. Preprocessing Music Signal. Usually, before classifying music genres, music signals need to be preprocessed, which is mainly divided into three steps: framing, preemphasis, and windowing. The music signal preprocessing process is shown in Figure 4.

(1) Framing: For signal processing, framing is generally performed. The purpose of framing is to facilitate the extraction of features, and framing can also reduce the dimensionality of the feature matrix. When framing, you need to select the appropriate frame length and frame width. The following relationship among the sampling period $T = 1/f$, window width L, and frequency F can be expressed as:

$$F = \frac{1}{LT}. \tag{16}$$

It can be seen from formula (16) that when T is constant, the frequency F is determined by the change of the window width L, which is inversely proportional. At this time, the frequency resolution is improved, but the time resolution is reduced. Increasing the window width will result in a decrease in frequency resolution and an increase in time resolution, resulting in a contradiction between window width and frequency resolution. For this reason, an appropriate window length should be selected according to different needs. If the window width becomes larger, the appropriate window width is selected according to different needs. When selecting the length, we should also consider that it is suitable for computer operation. The computer operation is based on binary, so the selected length should also be an integer multiple of 2 as far as possible.

(2) Pre-emphasis: When classifying music genres, because glottic excitation directly affects the average power spectrum of music signals, it is difficult to obtain the spectrum. Therefore, pre-emphasis

Figure 4: Flow chart of preprocessing music signal.

processing of music signals is required. In this paper, the first-order digital filter is used to pre-emphasis the music signal. The formula is as follows:

$$H(z) = 1 - az^{-1}. \tag{17}$$

In formula (17), a is the pre-emphasis factor, which is generally taken as a decimal number close to 1. Assuming that the sample value of the music genre signal at time n is $x(n)$, the result after pre-emphasis is as follows:

$$y(n) = x(n) - ax(n-1). \tag{18}$$

(3) Windowing: It is for framing service. Framing itself means adding a window function. However, due to the truncation effect of the frame during framing, it is necessary to select a good window function. The good slope at both ends of the window shall be reduced as slowly as possible to avoid drastic changes. The frame division is realized by the method of movable finite-length window weighting; that is, the music signal with window is expressed as follows:

$$s_w(n) = s(n) \times \omega(n). \tag{19}$$

Digital processing of music signal using rectangular window and Hamming window is expressed as follows:

Rectangular window:

$$\omega(n) = \begin{cases} 1, & 0 \le n \le n-1, \\ 0, & \text{otherwise.} \end{cases} \tag{20}$$

Hamming window:

$$\omega(n) = \begin{cases} 0.54 - 0.46\cos\left(\dfrac{2\pi n}{(M-1)}\right), & 0 \le n \le M-1, \\ 0, & n = \text{else.} \end{cases} \tag{21}$$

In formula (21), M is expressed as the frame length. The comparison of relevant indexes of the rectangular window and Hamming window function is shown in Table 1.

As can be seen from Table 1, for the main lobe width, the rectangular window is smaller than the Hamming window. However, the outer band attenuation of the rectangular window also decreases. Although the rectangular window has a good smoothing performance, its high-frequency component has a certain loss and loses the detail component. According to the above analysis, the Hamming window function has good performance.

3.2. Extracting Characteristic Parameters of Music Signal. The process of precisely describing a music signal using a set of parameters is known as music signal feature parameter extraction. To some degree, the performance of music genre categorization is determined by the selection of music characteristics. The accuracy and speed of music genre categorization may be improved by using good music signal properties.

Through the examination of the results of hearing trials, Mel frequency cepstral coefficient (MFCC) analysis, it is thought that its voice qualities are excellent [26, 27]. The linear spectrum is first mapped to the Mel nonlinear spectrum based on auditory perception and then turned into a cepstrum, taking into consideration the features of human hearing. According to the work of *Stevens* and *Volkman*, there is the following conversion relationship:

$$f_{\text{mel}} = 2595 \times \log_{10}\left(1 + \frac{f}{700}\right). \tag{22}$$

In formula (22), f_{mel} is used to describe the perceived frequency, which is in Mel, and f is used to describe the actual frequency, in Hz. The music signal is preprocessed by the first-order FIR high-pass filter to the MFCC music signal. The goal is to compensate for the spectrum. Next, the preprocessed signal is divided into multiple overlapping frames, and each frame is multiplied by the Hamming window to reduce the ringing effect. The FFT operation is performed on each frame, and the corresponding frequency spectrum is obtained corresponding to the frame of the Hamming window. After the discrete cosine transform (DCT) processes the logarithm of $Y(b)$, the parameters for obtaining MFCC are expressed as follows:

$$\text{MFCC}(\gamma) = \sum_{b=0}^{Z-1} \ln(1 + E(b))\cos\left(\gamma \frac{\pi}{Z}(b + 0.5)\right), \tag{23}$$

$$E(b) = \sum_{k=0}^{O-1} \left|X_a(k)\right|^2 H_b(k), 0 \le b \le Z. \tag{24}$$

In formula (23), Z is the total number of filters, and γ is the length of the MFCC feature vector. The function of offset 1 in MFCC is to get positive energy for any value. Finally, the MFCC feature vector is expressed as follows:

$$X_{\text{MFCC}} = [\text{MFCC}(0), \text{MFCC}(1), \ldots, \text{MFCC}(\gamma - 1)]^T. \tag{25}$$

3.3. Design of Music Genre Classification Network Model. The DBN model structure is formed by stacking RBMs. The feature dimension of the input sample is set to the number of visible units, and the number of hidden layer units needs to

Table 1: Comparison of relevant indexes of rectangular window and Hamming window function.

Window type	Sidelobe peak (dB)	Main lobe width	Minimum stopband attenuation (dB)
Rectangular window	−14	4Π/M	−23
Hamming window	−15	8Π/M	−51

be given in advance. For the visible layer and the hidden layer, c is used to describe the connection matrix, and κ and θ are used to describe the bias vector. The implementation steps of the fast contrast divergence learning method are as follows:

(1) Initialization: $q_1 = x_0$ is used to describe the initial state of the visible layer, and c, κ, and θ is used as random small values.

(2) Cycle all $q^{(t)}, t = \{1, 2, 3, \ldots, T\}$:

Find the conditional probability distribution $P(q, w; \alpha)$, and select $q \in \{0, 1\}$ from it
Find the conditional probability distribution $P(w', q; \alpha)$, and select $w' \in \{0, 1\}$ from it
Find the conditional probability distribution $P(q', w'; \alpha)$, and select $q' \in \{0, 1\}$ from it.

(3) Parameter update:

$$\begin{aligned} c(t+1) &= c(t) + \vartheta\left(P(q, w; \alpha)w - P\left(q', w'; \alpha\right)w'\right) \\ \kappa(t+1) &= \kappa(t) + \vartheta\left(w' - w\right) \\ \theta(t+1) &= \theta(t) + \vartheta\left(P(q, w; \alpha) - P\left(q', w'; \alpha\right)\right). \end{aligned} \tag{26}$$

This article is based on the DBN model training implemented by the Theano library written in Python. The training of the DBN model includes two stages. The first step is the pretraining stage. The RBM is trained layer by layer from the DBN input layer to the output layer to obtain the DBN model layer and layer. The connection weight among each neural unit in the hidden layer is independent and obtained through *Gibbs* sampling. In the second step, in the fine-tuning stage, DBN uses the error back-propagation algorithm to fine-tune the connection weights in the model according to the output classification and sets the objective function as the maximum likelihood function to optimize the whole model. According to the RBM network structure [28–30], this paper designs the music genre classification network model structure as shown in Figure 5.

3.4. Classification Algorithm Based on Sparse Representation. Under the music genre classification network model structure, for the test sample y, the sparse representation $\widehat{p}_1$ of the test vector can be calculated through formulas (13) and (15). The nonzero coefficients in the estimation should be related to the atoms belonging to a certain class i in U. Based on these nonzero coefficients, we can quickly judge which class the test sample belongs to [31, 32]. However, due to the existence of factors such as noise and model errors, there will be a small number of cases where $\widehat{p}_1$ is not zero in the projection coefficient. In order to distinguish the categories where y exists, a new vector $\delta_i(\widehat{p}_1) = [0, \ldots, 0, \chi_{i,1}, \chi_{i,2}, \ldots, \chi_{i,n_i}, 0, \ldots, 0]^T, i = 1, 2, \ldots, G$ is constructed, whose nonzero elements are only $\widehat{p}_1$ related components. If $\widehat{y}_i = U\delta_i(\widehat{p}_1)$, and there is a small distance from y, then $\widehat{y}_i$ belongs to this category has a higher probability. The calculation formula is as follows:

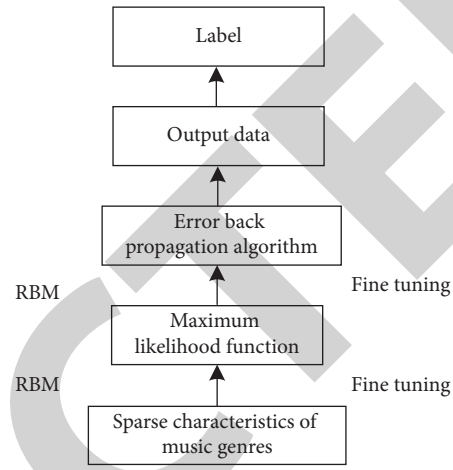

Figure 5: Structure diagram of music genre classification network model.

$$\mu_i(y) = \left\| y - U\delta_i\left(\widehat{p}_1\right)\right\|_2, \quad i = 1, 2, \ldots, G. \tag{27}$$

So the method of judging which category y belongs to is as follows:

$$\text{identity}(y) = \arg\min_i \mu_i(y). \tag{28}$$

Through the above steps, the automatic classification of music genres is realized.

4. Experimental Analysis

4.1. Experimental Environment and Data Set. The MATLAB 2016a programming software is utilised as an experimental platform, and a deep belief network based on the Theano library of Python language is developed to validate the efficiency of the automated categorization technique of music genres based on deep belief networks and sparse representation. Too much sample data will take up a lot of processing time while updating each level in the deep belief network. The sample database is separated into tiny batches of data packets in preparation to boost computing performance, and then, the batch learning approach is utilised. The fine-tuning learning rate is set to 0.1, while the pretraining learning rate is set to 0.01, in this study, and tests and verifications are carried out using the GTZAN data set, which contains 1000 audio files. There are ten different sorts of music genres included in these 1000 files, each having 100 samples. MPCC is utilised to extract the distinctive

characteristics of a music signal in this experiment [33, 34]. The frame length is 512, and the number of frames is 2133. The sampling frequency is 48000 Hz, the sample bits are 16, the frame length is 512, and the number of frames is 2133 [33, 34]. In the stage of extracting Mel frequency cepstrum coefficient, 12 dimensional Mel filter is used, and its frequency index is shown in Table 2.

The classification algorithm is based on the combination of a deep belief network and sparse representation. The methods of reference [7] and the methods of reference [8] are compared with the proposed methods to verify the effectiveness of the proposed methods.

4.2. Evaluation Indicators for Automatic Classification of Music Genres. The automatic classification evaluation indexes of music genres used in this paper are classification accuracy, recall, F1 value, confusion matrix, and classification time. The above classification evaluation indexes are used to evaluate the performance of the proposed method. The classification accuracy is expressed as the ratio of the number of correct samples to the total number of music genre samples. The calculation formula is expressed as follows:

$$P_r = \frac{F_y}{F_s} \times 100\%. \tag{29}$$

In formula (29), F_y is the number of correctly classified samples, and F_s is the number of classified samples. The classification recall rate is expressed as the ratio of the number of correct samples classified to the total number of music genre samples. The higher the classification recall rate, the higher the classification accuracy of the method. The calculation formula is expressed as follows:

$$R_e = \frac{F_y}{F_z} \times 100\%. \tag{30}$$

In formula (30), F_z is the population size of the sample. The F1 value represents the harmonic mean of the accuracy rate and the recall rate. The closer the F1 value is to 1, the higher the classification accuracy of the method. The calculation formula is expressed as follows:

$$F1 = \frac{2\left(P_r \times R_e\right)}{\left(P_r + R_e\right)}. \tag{31}$$

4.3. Effect of Automatic Classification of Music Genres. In order to verify the effect of automatic music genre classification, the confusion matrix is used to represent the effect of automatic music genre classification. Rock, metal, country, classical, and blues music genre samples are selected, the proposed method to evaluate the classification performance of the trained music genre classification network model is used, and the automatic classification effect of the proposed method is obtained as shown in Figure 6.

Figure 6 shows that rock, blues, and classical music all have high classification effects, with confusion matrices of 0.98, 0.96, and 0.95, respectively, although metal and country music had less misclassification, with confusion matrices of 0.88 and 0.85, respectively. Because certain country music may be used to accompany country dancing, and some related metal music is incorrectly labelled as country music, country music can easily be misclassified as metal music. There are also some differences between metal and rock music, maybe due to the fact that they all pay attention to rhythm and share commonalities. However, the suggested technique can successfully accomplish the automated classification of five music genres, according to the above study, and the automatic classification impact of music genres is superior.

Table 2: Frequency index of Mel filter.

Number	Frequency range (Hz)	Center frequency (Hz)
1	[0, 76)	24
2	[24, 135)	76
3	[76, 213)	135
4	[135, 305)	213
5	[213, 368)	305
6	[305, 468)	368
7	[368, 543)	468
8	[468, 659)	543
9	[543, 768)	659
10	[659, 905)	768
11	[768, 1023)	905
12	[905, 1154)	1023

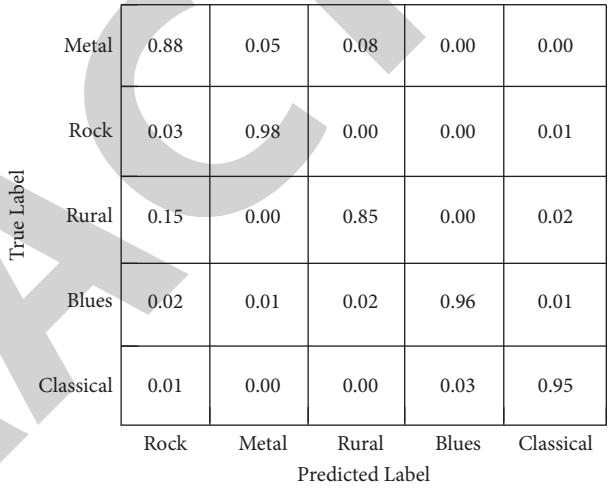

Figure 6: Automatic classification effect of music genre of the proposed method.

4.4. Accuracy of Automatic Classification of Music Genres. In order to verify the classification accuracy of the proposed method, 1000 music genre samples are selected, and the methods of reference [7] and the methods of reference [8] and the proposed method are used for automatic classification of music genres, respectively. According to formula (29), the accuracy of automatic classification of music genres by different methods is calculated, and the comparison results are shown in Figure 7.

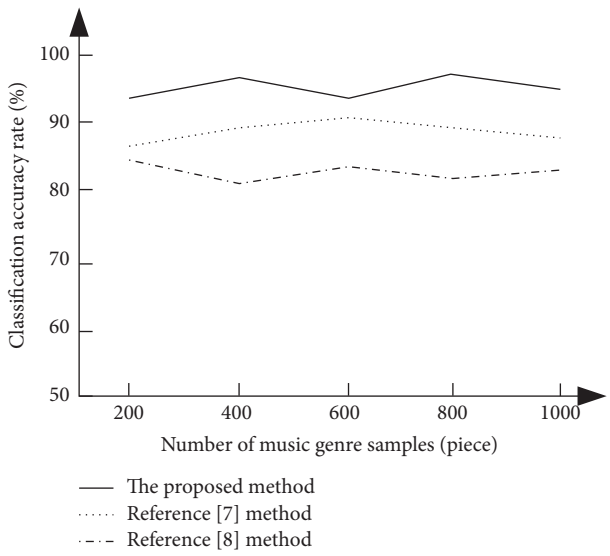

Figure 7: Comparison results of automatic classification accuracy of music genres by different methods.

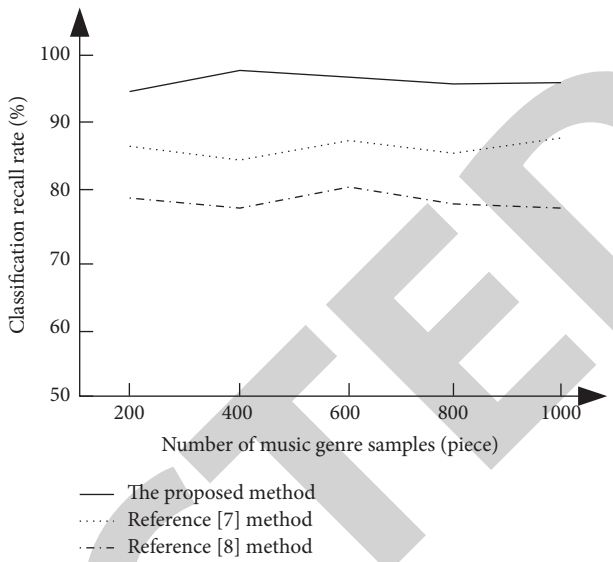

Figure 8: Comparison results of recall rates of automatic classification of music genres by different methods.

It can be seen from Figure 7 that under the number of 1000 music genre samples, the average accuracy of automatic music genre classification of the methods of reference [7] is 88%, the average accuracy of automatic music genre classification of the methods of reference [8] method is 82%, and the average accuracy of automatic music genre classification of the proposed method is as high as 95%. It can be seen that compared with the methods of reference [7] and the methods of reference [8], the proposed method has higher accuracy in automatic classification of music genres and can effectively improve the accuracy of automatic classification of music genres.

On this basis, the accuracy comparison results of automatic classification of music genres by different methods are calculated according to formula (30), as shown in Figure 8.

As can be seen from Figure 8, under the number of 1000 music genre samples, the average recall rate of automatic music genre classification of the methods of reference [7] is 85%, the average accuracy rate of automatic music genre classification of the methods of reference [8] is 78%, and the average accuracy rate of automatic music genre classification of the proposed method is as high as 97%. Therefore, compared with the methods of reference [7] and the methods of reference [8], the proposed method has a higher recall rate of automatic music genre classification, indicating that the automatic music genre classification accuracy of the proposed method is higher.

On this basis, F1 values of automatic music genre classification of different methods are calculated according to formula (31), and the comparison results are shown in Figure 9.

The average music genre automatic classification F1 value of the methods of reference [7] is 0.74, the average music genre automatic classification F1 value of the methods of reference [8] method is 0.6, and the average music genre automatic classification F1 value of the proposed method is

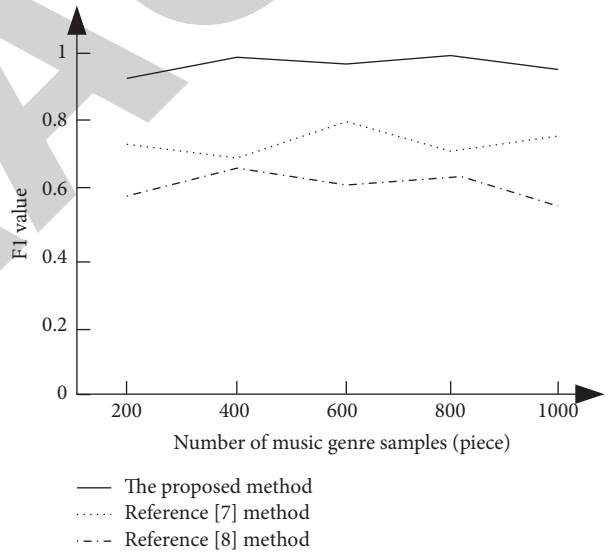

Figure 9: Comparison results of F1 values of automatic classification of music genres by different methods.

0.98, as shown in Figure 9. As a result, when compared to the approaches of references [7, 8], the suggested method's F1 value is closer to 1, suggesting that the proposed method's accuracy is greater.

Finally, the suggested technique has a high accuracy and recall rate for automated music genre classification, and the F1 value is near to 1, demonstrating that the proposed method may significantly increase automatic music genre classification accuracy.

4.5. Automatic Classification Time of Music Genres. On this basis, the automatic classification time of the proposed method is further verified. The methods of reference [7], the methods of reference [34], and the proposed method are

Table 3: Comparison results of different methods of music genre automatic classification time.

Music genre samples (piece)	The proposed method (s)	The methods of reference [7] (s)	The methods of reference [8] (s)
200	5.8	8.3	10.2
400	8.2	12.7	15.1
600	10.9	15.9	18.6
800	13.6	18.4	22.9
1000	15.8	22.6	25.8

used for the automatic classification of music genres, respectively. The comparison results of automatic classification time of music genres of different methods are shown in Table 3.

According to the data in Table 3, the automated categorization time of music genres of various approaches grows as the number of music genre samples increases. The automatic classification time of music genre of the methods of reference [27] is 22.6 s, the automatic classification time of music genre of the methods of reference [8] is 25.8, and the automatic classification time of music genre of the proposed method is only 15.8 s when the number of music genre samples is 1000. It can be noticed that the suggested method's automated categorization time of music genres is shorter than the approaches of reference [27, 28].

5. Conclusion

The automatic music genre classification method based on deep belief network and sparse representation proposed in this paper gives full play to the advantages of deep belief network and effectively realizes the automatic music genre classification combined with the sparse representation method. It has a good classification effect and high accuracy and can effectively shorten the time of automatic classification of music genres. However, in the process of automatic classification of music genres, this paper ignores the fuzziness of music genres. Therefore, in the next research, we can consider reasonably analyzing the music theory components of music genres and propose a direct end-to-end audio spectrum classification method to further improve the accuracy of music genre classification.

Data Availability

The data used to support the findings of this study are included within the article.

Conflicts of Interest

The authors declare that they have no conflicts of interest.

References

[1] M. Schedel, S. Yuditskaya, and S. E. Green, "New interfaces for musical expression (NIME) conference," *Computer Music Journal*, vol. 43, no. 2-3, pp. 159–166, 2020.

[2] R. Asano, "The evolution of hierarchical structure building capacity for language and music: a bottom-up perspective," *Primates*, vol. 2021, Article ID s10329, 2021.

[3] S. Lemouton, A. Bonardi, L. Pottier, and J. Warnier, "On the documentation of electronic music," *Computer Music Journal*, vol. 42, no. 4, pp. 41–58, 2019.

[4] E. Benetos, S. Dixon, Z. Duan, and S. Ewert, "Automatic music transcription: an overview," *IEEE Signal Processing Magazine*, Article ID s10465, 2019.

[5] M. Jiang, L. Lin, W. Zhang, W. Zhuang, M. Jin, and Y. Lin, "A study on the influencing factors of mobile digital music selection in subhealthy people based on perceived value theory," *Wireless Communications and Mobile Computing*, vol. 2021, no. 3, pp. 1–10, 2021.

[6] H. J. English, M. Lumb, and J. W. Davidson, "What are the affordances of the digital music space in alternative education? A reflection on an exploratory music outreach project in rural Australia," *International Journal of Music Education*, vol. 39, no. 2, Article ID 025576142199973, 2021.

[7] R. D. A. Lima, R. D. Sousa, S. D. J. Barbosa, and H. C. V. Lopes, "Brazilian lyrics-based music genre classification using a BLSTM network," in *Proceedings of the 19th International Conference on Artificial Intelligence and Soft Computing*, Zakopane, Poland, October 2020.

[8] K. S. Mounika, S. Deyaradevi, K. Swetha, and V. Vanitha, "Music genre classification using deep learning," in *Proceedings of the 2021 International Conference on Advancements in Electrical, Electronics*, pp. 1–7, IEEE, Communication, Computing and Automation (ICAECA), 2021.

[9] S. Nasrin, J. L. Drobitch, S. Bandyopadhyay, and A. R. Trivedi, "Low power restricted Boltzmann machine using mixed-mode magneto-tunneling junctions," *IEEE Electron Device Letters*, vol. 40, no. 2, pp. 345–348, 2019.

[10] E. Rrapaj and A. Roggero, "Exact representations of many-body interactions with restricted-Boltzmann-machine neural networks," *Physical Review E*, vol. 103, no. 1-1, Article ID 013302, 2021.

[11] W. Huang and H. Yu, "Cooperative object segmentation and recognition via restricted Boltzmann machine," *Electronics Letters*, vol. 56, no. 8, pp. 3800–3808, 2020.

[12] C. Y. Wang, P. C. Chang, J. J. Ding, T. C. Tai, and J. C. Wang, "Spectral-temporal receptive field-based descriptors and hierarchical cascade deep belief network for guitar playing technique classification," *IEEE Transactions on Cybernetics*, p. 99, Article ID 3014207, 2020.

[13] B. Ibrokhimov, C. Hur, H. Kim, and S. Kang, "A-DBNF: adaptive deep belief network framework for regression and classification tasks," *Applied Intelligence*, vol. 51, no. 8, pp. 1–15, 2021.

[14] J. Luo, C. Zhao, Q. Chen, and G. Li, "Using deep belief network to construct the agricultural information system based on Internet of Things," *The Journal of Supercomputing*, vol. 78, no. 34, pp. 379–405, Article ID s11227, 2021.

[15] D. Wu, Y. Yuan, J. Huang, and Y. Tan, "Optimize TSK fuzzy systems for regression problems: minibatch gradient descent with regularization, DropRule, and AdaBound (MBGD-

Hindawi
Journal of Mathematics
Volume 2024, Article ID 9864641, 1 page
https://doi.org/10.1155/2024/9864641

Retraction

Retracted: A Blockchain Technique for Trade Credit Maintainability Using the Role of Information and Communication Technology

Journal of Mathematics

Received 23 January 2024; Accepted 23 January 2024; Published 24 January 2024

This article has been retracted by Hindawi following an investigation undertaken by the publisher [1]. This investigation has uncovered evidence of one or more of the following indicators of systematic manipulation of the publication process:

(1) Discrepancies in scope

(2) Discrepancies in the description of the research reported

(3) Discrepancies between the availability of data and the research described

(4) Inappropriate citations

(5) Incoherent, meaningless and/or irrelevant content included in the article

(6) Manipulated or compromised peer review

The presence of these indicators undermines our confidence in the integrity of the article's content and we cannot, therefore, vouch for its reliability. Please note that this notice is intended solely to alert readers that the content of this article is unreliable. We have not investigated whether authors were aware of or involved in the systematic manipulation of the publication process.

Wiley and Hindawi regrets that the usual quality checks did not identify these issues before publication and have since put additional measures in place to safeguard research integrity.

We wish to credit our own Research Integrity and Research Publishing teams and anonymous and named external researchers and research integrity experts for contributing to this investigation.

The corresponding author, as the representative of all authors, has been given the opportunity to register their agreement or disagreement to this retraction. We have kept a record of any response received.

References

[1] F. Shah, Y. Liu, Y. Shah et al., "A Blockchain Technique for Trade Credit Maintainability Using the Role of Information and Communication Technology," *Journal of Mathematics*, vol. 2022, Article ID 9621342, 11 pages, 2022.

Hindawi
Journal of Mathematics
Volume 2022, Article ID 9621342, 11 pages
https://doi.org/10.1155/2022/9621342

Research Article

A Blockchain Technique for Trade Credit Maintainability Using the Role of Information and Communication Technology

Faiza Shah,[1] Yumin Liu,[1] Yasir Shah,[1] Ijaz Ul Haq,[2] Muaadh Mukred,[3] Saddam Hussain,[4] and Mahfoudh S. Alasaly[5]

[1]*School of Business, Zhengzhou University, Zhengzhou 450001, China*
[2]*Faculty of Education, Psychology and Social Work, University of Lleida, Lleida 25003, Spain*
[3]*Sana'a Community College, Mareb Street, Al-Hushaishiya Road, Sana'a, Yemen*
[4]*Department of Information Technology, Hazara University Mansehra, Mansehra, Pakistan*
[5]*STC's Artificial Intelligence Chair, Department of Information Systems, College of Computer and Information Sciences, King Saud University, Riyadh 11543, Saudi Arabia*

Correspondence should be addressed to Muaadh Mukred; muaadh@scc.edu.ye and Mahfoudh S. Alasaly; alasaly@ksu.edu.sa

Received 8 December 2021; Accepted 26 January 2022; Published 27 February 2022

Academic Editor: Naeem Jan

Recent advances in data analysis and processing methods can improve the ability of computational applications to perform complex steps of different tasks. With the progress of information and communication technologies (ICT), Blockchain-based complex data processing for transaction analysis and smart contract agreement has become a new research area in the fields of mathematics and computation. Stability of financial sector based on the ICT is a core component for growing the economics of medium and small enterprises. This stability brings the innovation to businesses productivity, while the management of information takes more prospective for improving the efficiency and more ways for innovating the business of products. In this study, we use the autoregressive distribution lag (ARDL) model with Blockchain-based complex data processing approach to emphasize the role of ICT in the field of trade credit maintainability. Actually, the ICT connects the industries in the entire world and makes business sectors that use its technologies be more advanced. Based on the ARDL model conducted on the records gathered from 2000 to 2019, the analysis concludes that the ICT-based complex data processing is a critical component of trade credit. The statistics of ICT are chosen based on the economy penetrations through the Internet and mobile phones. The causality exposed between the trade credit and ICT is bidirectional in nature. Also, it is found that the usage of mobile phones has a substantial influence on the business sectors, as a substantial amount of trading and business transactions are conducted over the phone. Therefore, the primary concern is the association between the Blockchain and trade credit, which is thoroughly discussed in this work. The trade credit improves the stability of financial sector and the Blockchain supports its maintainability by the role of ICT. The results of the study can help the business stakeholders and investors to estimate the marketing for future useful execution.

1. Introduction

Graph-based data analysis (GDA) concept is theoretically applicable in the computer science (CS) field for several practical applications. Blockchain-based complex data processing in information and communication technology (ICT) such as graph-based smart contract based agreement modelling, computing resource allocation, and users' interactions and transaction analysis has become popular in recent years. In most parts of the world, trade credit is significant short-term funding for SME's businesses [1, 2]. In the United States, most businesses offer their products and services based on trade credit. The trade credit is considered a major source of short-term funding in many businesses. The biggest consumers of trade credit are the nonfinancial firms as these firms are mostly facing a lack of financing. For young and emerging businesses, it is a regular source of capital [3]. The use of trade credit is so extended even after

other financial banking systems [2, 4–7]. Since traders alone are often unable to find and connect with the banking sector, they are unable to take bank loans. Companies depend more on trade credit for external financing due to the same nature of business between all trading parties.

Trade credit is important for small investors, and since it is the second-largest financing mechanism, the importance of trade credit is also globally recognized [8]. There have been several sorts of explanations proposed for the trade credit. As per the financial perspective, firms can obtain resources at a lower budget due to trade credit as compared to high financing costs [9, 10]. Trade credit is a short-term investment that is more profitable than marketable securities [9]. The operational motive of trade credit is that it provides smooth demands and eliminates cash volatility in the payments among firms [11]. The financial motive is that large and financially stable firms offer trade credit to smaller firms to meet their financing requirements. Large firms always have an advantage while dealing with trade credit to secure sales and build long-term relationships with small firms.

Due to the Internet, the entire planet has evolved into a global community. Developed as well as developing countries are interconnected globally. Globalization identifies the merger of multiple economies and countries for economic growth and prosperity [12]. Since the beginning of the 21st century, the concept of globalization has entered into a new millennium. Both developed and developing countries are facing certain kinds of challenges related to the equilibrium between the economy and globalization. As the phrase that "the world is getting smaller" signifies the junction of transport and communication as well as the foreign trade of commodities and services, including the procurement and distribution of commodities and services [13], globalization focuses on market liberalization and economies of scale for the growth of countries around the world which foster the resource sector globally. Many developing countries get benefits from globalization, such as improved technology, the worldwide flow of advanced machinery and equipment, and improved trade operations. The natural resources, state, political stability, and cultural exchange of countries also increase economic growth and globalization [12].

Information and communication technology (ICT) has always brought innovation, improves efficiency, and enhances the ability to share knowledge and skills leading to the change in overall trading and business units around the world. ICT is considered as the two poles of a single rod which are attached as it is required for sustainable economic growth in the society and also to resolve many environmental issues [14]. Now, as the world is interconnected, the ICT has also impacted every phase of life, like education, cultural aspects, business networks, infrastructures, and transportations [15]. No doubt, the use of ICT has increased as time passed by. The report generated by the worldwide telecom unit (ITU) has likewise proposed that more clients of the Internet are in the year 2015 which are 3.2 billion, when contrasted with earlier years around 400 million [16]. ICT has a major role in the growth of economy and stability of societies in both developed and developing countries [17].

ICT is a becoming a reason to globally connect numerous devices. It is feasible to connect smart devices and carry on the transactions without discriminating that the user is virtually connected. There are various frameworks that support reliable and effective communications with tangible accuracy. Due to similar significance, the platform of ICT has raised the development of small and medium industries and their interconnectedness with the rest of the world. The ICT is helpful for future planning of the world economy and in information society to strengthen labor forces [18]. Various forecasting, predictions, and long-term financial planning are done by computer-aided techniques and devices. Nepal scored first in the area with ICT score of 40, followed by Bangladesh with ICT score of 39, Sri Lanka with ICT score of 32, India with ICT score of 28, and Pakistan with ICT score of 23, according to the Global Competitiveness Index [19]. Because of the above social and technological aspects, as well as the importance of information and communication technology (ICT), which is below the national average for small and medium business units, the study highlights the need for further research into ways to contribute to economic development through trade credit in South Asian countries.

It is a common observation that the financial demand also grows as the firm grows in size because it plays an integral part in the elaboration and growth of economy [20, 21]. The trade credit provides the necessary infrastructure including skills and expertise in trading around the world which encourages the efficient use of the country's resources around the globe. This paper adds to prior work in several ways. First, it is the first study to focus on the relationship between economic growth, information and communication technology, and trade credit. Second, the autoregressive distributive lag (ARDL) model is utilized to control the interactions between the stated variables in long-run behavior. To determine the results' robustness, the bound test is used [22].

The remaining part of the article provides an overview of the trade credit that affects the economic structure of Pakistan. The literature review section provides the previous findings of the literature. The model specification, data source, and econometric strategies are discussed in model construction; next, the empirical analysis of the research is explained. The conclusion discusses the findings and concludes the implications, and, finally, limitations and future research direction provide suggestions for future work.

1.1. Overview of Trade Credit in Pakistan. Technology has now removed the concept of boundaries and limitations. The broad term global village is very well known in this regard. Due to globalization, the distances are reduced, and new business horizons are opened. The effect of ICT and globalization on trade credit is an aspect of scholarly discussion. Because of ICT, the lands have changed into new buildings and industries and there is a shift in infrastructure as observed from past decades. Due to the upgradation of

infrastructure, the investor's and small business unit's strategies are also changed. Technology like smartphones has reformed the trading mechanisms at the fingertips. Trade credit is beneficial for many reasons. The most important reason is one owner business type which occupies the biggest portion of the private sector of Pakistan. Also, trade credit is time-saving and beneficial for new business entities in a competitive environment [23]. Trade credit increases the profitability of firms [24].

Particularly keeping the focus on underdeveloped countries, to improve the economic stability and growth in the country, the Pakistan government is making efforts in the power sector to fulfill the energy needs of the country. This again involves smart technology on the core end. The government has also jointly worked on different projects to bring innovations for technology productions. One of the projects is the China-Pakistan Economic Corridor (CPEC) in which the main idea is to open the western China trade through rails, roads, and gas pipelines from Kashgar to Gwadar ports of the country [25]. This is not only a road that connects regions together but also a future pathway to progress. The regional connectivity includes utility and regulation of energy hubs, logistic refinements, high level trading, the regional promotion, various domains like tourism, maintenance of peace, and prosperity, diverse investment schemes, and industrial boosting. There are indirect chances of improvement in education, internal infrastructure like medical, human resource development, basic human needs development and support, social diversity and collaboration, and so forth. China is investing about $46 billion in the energy sector and the development of the transportation infrastructure in Pakistan [26]. This joint venture may bring revolutionary progress in financial gains as well as technology refinements around the country.

The use of information and communication has been widely spread over the past few years. Not only is ICT as important as the human heart but also it adds a significant part in growth, education, health, and the way of living of the population [27]. Ultimately, ICT is bringing enormous productive results in trade credit which is beneficial for the SME. In today's emerging markets, ICT plays two types of roles: inputs and outputs. As input, ICT reduces the coordination cost in markets and results in inefficient trading and, as output, ICT becomes a source for public services like education and health sector and provides e-services in many departments [28]. It means the future is broad and progressive where finance is equally supported by technology.

One of the best reasons for trade credit based infrastructure is that it is facilitating for SMEs. This ensures the sustainability of any small organization, which is continuously making efforts to grow gradually. This strategy is based on the phenomena that there are no financial reservoirs, no fixed assets, and no regular income. The system is entirely relying on trade credit where the goods are sold under fixed terms and the turnout is returned to the company. This system needs worthy and trust building system where the producer organizer hands over the product to the seller organizer for a tangible duration under fixed term returns. This facilitates the load of small organization to involve services at minimum to no cost and the product is launched to the market as soon it is completely manufactured. The consumer later gets the profit which is the ultimate target of the business. So, the scheme is ideally applicable to both entities.

2. Literature Review

The literature is reviewed under three subdivisions. The first and most important subdivision has revealed reviews that deal with the qualities of ICT in accelerating economic growth. Next, the second subdivision highlights the findings on trade credit and the growth of the economy. The third subdivision discloses findings on the topics connected with significance of ICT and trade credit.

The existing literature has enlightened the association between ICT and economic growth. Because of ICT, there expanded the decisions for individuals, simple way to deal with the information and skill, and that actions that are important and agreeable to make life more agreeable [29, 30]. The use of electronic facilities including health, education, and services to bring access to these facilities makes economic development in the societies. E-health benefits raise the health standards of the individual and improve outcomes, help in cost reduction, and extend services [31, 32]. Therefore, ICT brings positive changes in human capabilities which are necessary for the prosperity of the economy [15]. The importance of economic growth is related to economic efficiency [33].

The second component of the study focuses on the association between trade credit and economic growth. Several studies have highlighted the importance of trade credit in developing countries [34]. The rapid increase in the demand for industrialization and urbanization is moving the economy to find out easy and fast ways of financing; trade credit is the most effective way of financing [35]. The macroeconomic conditions have a positive effect on trade credit usage and many researchers highlighted its importance [36, 37]. The world's largest retailer, Walmart, is the biggest user of trade credit and prefers it over a bank loan [38, 39]. The trade credit is also considered as a key source for new and young firms because supplier firms have more information about buyer firms [40]. It also provides a source of short-term financing to financially constrained firms [41]. As per [42], globalization leads to long-term economic efficiency; therefore it has a substantial influence on economic growth.

The third component of the literature concentrated on the association between ICT and trade credit as the main characteristic of global industrial growth. As demonstrated earlier that the entire planet has evolved into a global community because every firm is connected through technology, all the trading is interconnected through reliable Internet connections. Even online businesses are expanding worldwide. Huge financial transactions can be processed in the nick of time [29]. ICT has effects on international trading, urbanization, and advanced technology [43]. Trade credit supports industry-level growth having less developed financial access in the country; also, it results in financial gains for both buyer firms and supplier firms [44, 45].

Because of the increase in sales or market share, facilitating financial transactions by reducing restrictions and easy-going policies for payment, supplier firms can benefit from generating additional revenue [5]. Global trading can be seen flawlessly in the widespread pandemic. Due to the spread of Coronavirus disease (COVID-19), where life is threatened, the small industries are most affected in developing countries [46]. In this critical time, trade credit is the most effective and useful way of financing throughout the world. This sort of business can be channeled from any part of the world and is interconnected with the rest of the world through technological advancements.

Despite these valuable contributions, there are many areas to be further discussed. For example, trade credit and its importance for small and medium enterprises (SMEs) are highlighted [34]. The risk factor associated with trade credit is discussed but the ICT factor is not considered [34]. To fill this gap in the research, the existing body of knowledge adds to the existing information of economics by observing the ICT, trade credit, and their effects on the economic growth of Pakistan.

3. Construction of the Model and Econometric Strategy

In this section, the construction of the model and econometric strategy and the data sources are stated, for the empirical implication of the above literature. Specifically, the main objective of this study is to establish the role of ICT and trade credit in the economic growth of Pakistan. The trade credit approach is ideally applicable for the underdeveloped countries where there are less financial assets and the services can be the alternatives. Countries like Pakistan, India, Bangladesh, Ghana, and so forth are the best examples for this model. Larger business units like leather, minerals and mining, textile, chemical, and mechanical units, and similar industries which produce the consumable products on regular basis are some common examples in Pakistan which regulate trade credit support. The financial support is never foreseen in this area; also the reasons like natural disasters, political instability, corruption, unemployment, and similar reasons raised uncertainty. In this concern, the trade credit is not less than a blessing for the survival and even the improvement of the SME. As is usual in most of the econometric studies, all variables were transformed into logarithms. The logarithmic transformation also eliminates the possibility of heteroscedasticity.

3.1. Equations.

$$\mathbf{LogTC_t} = \boldsymbol{\beta}_0 + \boldsymbol{\beta}_{1t}\mathbf{LogICT_t} + \boldsymbol{\beta}_{2t}\mathbf{LogGDP_t} + \boldsymbol{\beta}_{3t}\mathbf{LogGLOB} + \boldsymbol{\varepsilon}_t, \tag{1}$$

where *TC* is the trade credit index, *GDP* is the measure of growth of economy, *GLOB* is short for globalization, *ICT* is the information and telecommunication technology index, and ε is the residual error, where t stands for the years. Considering obvious motive for the selected variables, ICT in international trading yields industrialization and urbanization, thus enhancing the trade credit in the country. Trade credit not only enhances economic development and stability but also boosts social development by the interaction of SME investors in the country. Cross-border trade benefits the manufacturing sector; so, it is helpful to influence the economic growth in the country. Different types of econometric techniques are used and applied to observe long-run and short-run relationships among variables (Engle and Granger) [47]. The appropriate technique is the ARDL approach as is applied and suitable for a mostly small set of data to check the cointegration association. Also, the bond test method of ARDL is used as a simple linear transformation for simultaneous use of the long and short run. The correct lag should be calculated before applying the ARDL technique. The procedure for performing bound testing on the variable of interest is as follows:

$$\begin{aligned}\Delta LogTC = {} & \beta_0 TC + \sum_{k=1}^{n} \beta_{1k} \Delta LogTC_{(t-k)} + \sum_{k=0}^{n} \beta_{2k} \Delta LogICT_{(t-k)} + \sum_{k=0}^{n} \beta_{3k} \Delta LogGDP_{(t-k)} \\ & + \sum_{K=0}^{N} \beta_{4k} \Delta LogGLOB_{(t-k)} + \lambda_1 TC \Delta LogTC_{(t-1)} + \lambda_2 TC \Delta LogICT_{(t-1)} + \lambda_3 TC \Delta LogGDP_{(t-1)} \\ & + \lambda_4 TC \Delta LogGLOB_{(t-1)} + \varepsilon_{1t},\end{aligned} \tag{2}$$

where Δ indicates primary variance, λ expresses the long-run measurements, θ represents the dynamics of small path, and ε denotes the error. Meanwhile the null assumption explains that there does not exist cointegration, besides the substitute hypothesis.

3.2. Model Estimation.

F-statistics are used to test cointegration in the ARDL approach. The decision is based on the upper and lower bounds [48]. If the *F*-statistics are more than the upper value, the null hypothesis is refused, and if the *F*-statistics fall somewhere between the upper and lower

boundaries, the result will be inconclusive. The next process after cointegration is to examine the paths term. The model's stability is verified using several tests such as ARCH, LM, and Ramsey tests.

The Granger causality test is the most extensively used test for time and panel data. The analysis was used to decide whether variables can also be used to predict other variables. According to Engle and Granger [47], there is a cause-and-effect link between the variables. The test is used to determine which way trade credit, information and communication technology, and economic growth are causally related. This causality is helpful for policy suggestions. The Granger causality model is expressed in matrix equation as follows:

$$\begin{bmatrix} \mathrm{Log}TC \\ \mathrm{Log}ICT \\ \mathrm{Log}GDP \\ \mathrm{Log}GLOB \end{bmatrix} = \begin{bmatrix} \beta_1 \\ \beta_2 \\ \beta_3 \\ \beta_4 \end{bmatrix} = \begin{bmatrix} \beta_{11k}\beta_{12k}\beta_{13k}\beta_{14k}\beta_{15k}\beta_{16k} \\ \beta_{21k}\beta_{22k}\beta_{23k}\beta_{24k}\beta_{25k}\beta_{26k} \\ \beta_{31k}\beta_{32k}\beta_{33k}\beta_{34k}\beta_{35k}\beta_{36k} \\ \beta_{41k}\beta_{42k}\beta_{43k}\beta_{44k}\beta_{45k}\beta_{46k} \end{bmatrix} = \begin{bmatrix} \mathrm{Log}TC_{it} \\ \mathrm{Log}ICT_{it} \\ \mathrm{Log}GDP_{it} \\ \mathrm{Log}GLOB_{it} \end{bmatrix} \begin{bmatrix} n_1 \\ n_2 \\ n_3 \\ n_4 \end{bmatrix} = ect_{it-1} + \begin{bmatrix} \varepsilon_{1t} \\ \varepsilon_{2t} \\ \varepsilon_{3t} \\ \varepsilon_{4t} \end{bmatrix}. \tag{3}$$

$\mathbf{EC}_{t-1}$ indicates that the long-run causality exists among variables and specifies that the pathway is the first difference of the short-run causal relationship that ICT has a contributing connection with trade credit, and trade credit has an association with ICT, respectively. As a result, bidirectional causation develops between the two variables. For the study, time-series data covering the years 2000 to 2019 was employed. Data on trade credit is taken from nonfinancial enterprises' financial statements in Pakistan; ICT is calculated by mobile phone and Internet penetration rates and GDP.

4. Results of Empirical Research

The first and most critical step in any study is to ensure that the data is stationary. This is accomplished through the use of the unit root. Firstly, in a time-series evaluation, stationarity of the data should be evaluated. All variables are assumed to be stationary in a standard regression analysis. As previously stated, nonstationarity in general causes erroneous regression. The ARDL approach, for example, is not applicable to any integrated variable of order 2. NG-Perron unit root, as shown in Table 1, confirms the level of stationarity, and the results show that the ARDL is suitable for analysis.

Because the standard unit root test fails to detect structural fractures, the Zivot-Andrews (ZA) test is appropriate for research. The results of the structural break test are shown. The outcomes revealed that at level the series is not stationary. The series, however, became stationary when the first difference was taken. Table 2 indicates the statistical analysis of the yearly data; findings are generated by the ZA test. Here, the variations can be seen through variables and probability results.

Following that, an alternate method known as bound testing is developed, which is based on an autoregressive distributed lag model. It is not necessary for the variables to be integrated in the same sequence. Furthermore, as compared to Johansen cointegration, which requires a high sample size, it is deemed a more appropriate method when the sample size is small. Because it is based on a single equation, it is simple to implement and interpret.

The bond testing is performed for analysis, a suitable length of the lags is selected, and the next F-statistics are checked to see the long-run behavior of variables. The bond testing approach is recommended by the first order of integration to monitor the cointegration. The following table shows the outcomes of the bond analysis and several other diagnostic methods for the model, the results of which explain that the F-statistics are larger as compared to the upper bond of the 1%, 5%, and 10% levels of significance, which results in rejecting the null hypothesis. Also, the results assure that the variables are cointegrated at the long-run relationship among trade credit and other variables.

Now, the discussion is on the most significant portion of the research, that is, the analysis of the results of long-run estimation. To estimate the long and short runs, the autoregressive distributed lag (ARDL) model is used. The outcomes of the long run and short run are estimated in the table below. However, the most significant parameter in Table 3 is the decision column. The logistic diagnostic methods using F-value and Lag order indicate that the conclusion is constructive or destructive. The statistical values are represented involving trade infrastructure.

As the consequences mentioned in Table 4, the figure of the coefficient is −0.0264 which suggests a negatively strong association with trade credit. The negative association is because of the small size of the market that deals globally with trade credit and thus there are decreased exports. ICT is always an opportunity, especially for the business of the developing countries, so that the technology brings rigorous actions for imports and exports policy by the country. Trade credit is globally recognized and is very effective for business investors to deal internationally around the globe. The results of economic growth, as stated in Table 4, have a considerable beneficial impact on trade credit as a 1% rise in growth brings trade credit to increase by 0.0543%. Trade credit helps to endorse the utilization of new and innovative products, services, and technology and thereby increases economic growth in the country. The positive association yields that trade credit brings economic growth to the country. Pakistan, as a country with a developing economy, has more focus on economic growth which is the backbone of the country.

So, the government of Pakistan should take precautionary measures and develop policies to check and maintain the economic stability by industrial sector, innovative products, and utilization of advanced instruments, machinery, and updated technology; this has an immediate impact on the monetary benefits of a country. These policies are helpful for the economy and these resources are utilized in the long term.

Table 1: NG-Perron unit root test.

Variable	Level				1st variance			
	MZ^a	MZ^T	MZ^B	MP^T	MZ^a	MZ^T	MZ^B	MP^T
LogTC	0.9576	0.8245	0.8286	51.6429	−12.8543**	−2.5847	0.1742	1.8995
LogICT	0.1157	0.0635	0.6743	28.8755	−18.6548*	−2.8765	0.1567	1.7155
LogGDP	0.8743	0.8145	0.8423	−19.0764	−13.5932*	−2.5877	0.2076	1.8976
LogGLOB	−2.3467	−1.3477	0.4256	−21.5438	−3.2467***	0.2076	0.2065	2.1578

Note: "*," "**," and "***" show the levels of significance.

Table 2: Outcomes of Zivot-Andrews (ZA) test.

Variables	At level			At variance		
	t-statistics	Probability	Years	t-statistics	Probability	Years
LogTC	−3.5677**	0.0245	2010	−5.8743*	0.0754	2011
LogICT	−1.945***	0.0745	2012	−7.5663*	0.0003	2013
LogGDP	−3.8765*	0.0073	2015	−7.5663***	0.0643	2016
LogGLOB	−2.754***	0.0543	2018	−5.764*	0.0056	2017

Note: "*," "**," and "***" represent the elimination of the null hypothesis at 1%, 5%, and 10%, respectively.

Table 3: Analysis for bound.

Standard	Bound testing			Investigative checks		
	F	Lags	Conclusion	ARCH	LM	Ramsey
LogTC = f(LogICT, LogGDP, LogGLOB)	5.2367*	1, 0, 0, 0	Definite	2.4332 [0.120]	0.4278 [0.649]	0.4378 [0.517]

Note: "*" shows the level at 1%.

Table 4: Projected outcomes of long versus short trends.

Variable	Coffs.	Std.	t-values	Prob.
Higher dynamics				
LogICT	−0.0264***	0.0045	−4.8754	0.0145
LogGDP	0.0543***	0.0245	2.5432	0.0343
LogGLOB	0.0365***	0.3578	2.6543	0.0754
Imitation	0.1049**	0.0245	4.4668	0.0245
Stable	0.0157*	0.0055	23.7654	0.0054
Lower dynamics				
LogICT	0.0654*	0.0765	7.8654	0.0054
LogGDP	−0.1065*	0.0134	−8.2456	0.0035
LogGLOB	3.0975*	0.4326	7.5788	0.0045
Imitation	0.0765**	0.0134	5.4677	0.0116
CoinEq(−1)	−2.4327*	0.2568	−8.4876	0.0036
Analytical analysis				
R-square	0.9945			
Adj R-square	0.9954			
F-value	897.6534			
Probability. (F)	0.0000			
Durbin-Watson	2.0876			
χ^2-Ramsey	2.0032			
χ^2-ARCH	1.4256			
χ^2-LM	1.2589			

Note: "*," "**," and "***" indicate the significance at 1%, 5%, and 10%, respectively.

The statistics of the coefficient of resources available globally are 0.0365, indicating a 1% rise in the figures of global means, and spread the practice of trade credit by 0.0365%. The evaluation of the study recommends that globalization is the main provider to the attraction of foreign investment in the country. The trade credit could be recognized as if the management or the officials will take measures concerning the proper utilization of technology, as also presented in Table 5.

The use of assets has a tremendous effect on credit because Pakistan is bestowed with many natural resources. These resources are abundantly available in the country. However, the economy of Pakistan can flourish when manufacturing units are abundant to utilize these resources and deal internationally to expand their trades. Also, the policy mechanism of the country is not so effective for decision-makers and a poor mechanism to handle these natural resources destroys them. These problems can be minimized if the government of Pakistan takes measures to deal with and utilize these resources and trade credit is suitable for this investment. The government takes initiatives, and the foreign investors can deal with trade credit to mutually benefit from the technological progress in the country.

The study also emphasizes autocorrelation and heteroscedasticity by applying analytical methods like ARCH, LM, and Ramsey tests. The results show that there is no autocorrelation or heteroscedasticity, as seen in Table 4. The ARDL approach is used to track long-term outcomes, although causation direction is not clear. The interconnection analysis is used to explore the interconnected relationship.

As shown in Table 5, the VECM Granger test is used to prove that the variables have a long-term relationship.

Table 5 explains the results which show that the causal long-run relationship between trade credit and globalization is established. Bidirectional causality is found between these two variables. The economic growth is also observed to be

Table 5: Results of analysis.

	The Wald statistics for short-run causality				Long direction (t-statistics) ecm_{t-1}
	ΔLogTC	ΔLogGLOB	ΔLogGDP	ΔLogNR	
Logic	—	−0.0075 [0.932]	0.3276 [0.750]	0.1245 [0.750]	0.0125 [0.814]
LogICT	0.1863 [0.832]	—	3.7543* [0.005]	3.7654 [0.932]	−0.3374* [0.000]
LogGDP	0.7646 [0.453]	3.1378* [0.032]	—	1.8464*** [0.072]	−0.5875* [0.002]
LogGLOB	0.1854 [0.863]	−1.7554*** [0.086]	1.6543 [0.115]	—	−0.0864 [0.344]

Note: the probability values are shown in parenthesis. "*" shows the degree of elimination at 1%. "**" shows the degree of elimination at 5%. "***" shows the degree of elimination at 10%.

bidirectional. VECM test confirms that there exists a long-run relationship among the selected variables, as also shown in the above table.

5. Blockchain Technology as a Case Study in Trade Credit

Blockchain is an electronic shared, immutable ledger, which is distributed in a business network that facilitates the process of tracking and recording transactions and assets. Blockchain technology records and tracks different information of trade credit for SMEs. It includes variables like amount, time, and data and the unique digital signature for security. One of the distinct features of the Blockchain technology is its reliability. The structure is maintained concretely by allocating every block a unique number. The number of blocks is allocated unique numbers representing a series. Then, the blocks are connected in such a way that every block is connected to the next block. The data is further secure where it requires the hash sum of the entire connected blocks to maintain its security. Other unique features of Blockchain sustainability and integrity are decentralization, cryptography, and consensus, which were least identified previously, especially in obsolete systems. The ICT is applicable in the form of Blockchain so that the financial transactions can be operational flawlessly and effectively. For financial concerns, each Blockchain contains the dealings such that every new transaction is saved to the ledger of every participant. All the trade credit information is saved in a distributed database which is managed by multiple participants called Distributed Ledger Technology (DLT). DLT is a database that is accessible by multiple users from multiple locations, so the data are managed on various memory locations using identical copy; the users can access it using various platforms.

(i) Smart contract concept by Blockchain in trade credit: Blockchain enables the concept of smart contract in trade credit. Smart contracts are decentralized contracts with the consensus of trading parities having transparent immutable proof algorithmic exclusions. A smart contract is a series of digital documents and agreements which includes transactions detail and term and conditions promised by trading parties. The immutable nature program protocol of smart contract allows the execution process and automation of contracts terms and conditions. The smart contract does not need the third parties, for example, banks, to play an intermediary role and parties can directly collaborate to minimize the cost and time. The smart contract can drastically reduce the cost of resources required, documentation, information gathering, and processing, negotiating, and drafting of contracts, monitoring, transparency, reliable communication, secure payment, and digital cryptographic agreement signatures.

Smart contracts advance the increase in the trust up to a higher level by providing a secured distributed database, enhance transparency in trade transactions, reduce the risks and frauds, increase data reliability, and facilitate the exchange of payments and automatic executions without human mistakes or intermediary involvement. The information is highly secure in leisure systems. This is one of the important requirements for online systems. The privacy preservation is solely under the decision of the organization; the components which indicate the progress or revenue generations can be displayed while keeping the company credentials hidden. The system is maintained in a distributed manner; leisure system works on privilege-based authentication; therefore, it is not possible to easily drain the protected information. Thus, Blockchain provides smart contracts technology system that will reshape the traditional trade credit, very appropriate for small-to-large international trade activities.

5.1. Traditional Trade-Credit Limitations: A Space for Blockchain Technology. Traditional manual trade credit has some limitations as follows:

(i) Manual process involves a lot of paper documentation by the issuing banks (the importer and exporter's banks) to process the contracts, exchange the documents, analyze discrepancies, and so forth, which is subjected to human error and takes time and cost.

(ii) Invoice factoring is requested by exporters who present their payment invoices to several banks; thus, it increased the risk profile.

(iii) delayed timeline and delayed payment, the paper-based traditional trade credit involves multiple financial procedures and intermediaries to execute the agreements, contracts, and payment. Several days are taken to issue, confirm, and execute payments.

(iv) Multiple communication channels that exposed banks and business parties to miscommunication and fraud are involved.

(v) Duplication in documentation can result in mistakes or processing the same transaction twice or more.

(vi) Tampering and less security of the financial record as the documentation can be used by unauthorized access. As a result, a record could be illegally duplicated, updated, manipulated, or falsified.

(vii) Illegal financial record tempering is of a high frequency.

5.2. Blockchain Reshaping the Traditional Trade Credit. Blockchain technology has some potential advantages that could help trade credit in many ways:

(i) From paper to bytes: Banks are trying to use technology to digitalize the documentary trade-credit process, but, still, most of the transactions are paper-based but this time with a better and advanced technology of Blockchain and smart contracts promising to enable easier, faster, efficient, and secure digital transactions and digital documentation.

(ii) Efficiency: Smart contracts make the trade credit more efficient by providing fast, digitalized information with no intermediary platform and extra communication channels. The smart systems are efficient for data processing. The other considerable factor involves storage speed. Smart contracts speed the trade finance cycle. Transactions that took months can be reduced to days and days can be reduced to hours. As the terms of the contract are digitally signed, the Blockchain in real-time status is updated, which reduces the time as well as the headcounts which are required to monitor the delivery.

(iii) Traceability: Blockchain facilitates the importers and exporters that can easily trace the information, transactions, goods, and assets. The Blockchain title specifies transparency into the location as well as the ownership of the goods. All the execution processes are traceable between the trading parties.

(iv) Transparency: The distributed ledger ensures the transparency of all information and transactions to improve the trust among the trading parties. Blockchain invoices provide a real-time and transparent view with time stamped.

(v) This helps to reduce tempering risk and offers more advanced option for financing trade.

(vi) Auditability: Blockchain ensures high auditability by storing record sequentially and indefinitely avoiding extra activities for the auditing. A clear and better verification of transactions, goods, and assets is provided with a reduction of compliance costs. This minimizes fraudulent activities.

(vii) Security: Each transaction has a unique identity and independently cryptographic verification. Encryption and programmed cryptography protect the transmission of data between different trading companies and thus highly privatize the data to ensure their authenticity.

(viii) Documents real-time review: Financial documents which are linked and accessible via Blockchain are properly reviewed.

(ix) Automated settlement of accounts and reduction of transaction fees: All those contract terms which are executed through the smart contract eliminate the requirement for financial banks or institutions to charge additional transaction fees.

(x) Autonomy is ensured by Blockchain, as smart contracts remove the intermediate parties or any reliance on banks.

(xi) Costs and fees are reduced, by improved efficiency to save time and removing intermediate third parties to save the extra cost.

(xii) Bogus transactions, fraud, accidental financial transference, and online credit threats can be avoided.

(xiii) E-commerce transactions are highly applicable particularly during the COVID-19 pandemic; exponential rise of financial flows can be protected by the end to the endpoint of the security system, which is ensured by Blockchain.

6. A Blockchain-Based Complex Data Processing for Trade Credit: A Framework Design

Different SMEs are actively trying to participate in economic progress. The bottlenecks mentioned in the above section are critically important. The association of these SMEs can be technically connected using the Blockchain method. The Blockchain model is represented in Figure 1. It indicates that various SMEs can be connected. It means the financial block of components which either participate in financial completion or are involved in the initialization of financial transactions, particularly for trade credits; they are connected in the block-by-block architecture.

Financial Blockchain enables the transaction recording on the distributed ledger for multiple users from multiple locations. This can connect the SMEs and financial firms in a way where the transactions are maintained with associations. The data is stored in the form of blocks and every block has encrypted time-stamped transactions. These blocks are chained or connected chronologically, thereby creating a long chain or Blockchain technology.

DLT reshapes the traditional trade credit and digital documentation flow transparently among banks, imports and exports, trading companies, and other business communities. All the transactions are secured by unique cryptographic signatures with a timestamp that is immutably recorded on the blockchain. Business partners with the right permission can access the shared information for complete transparency, which helps to tackle the fraud issue and increase trust.

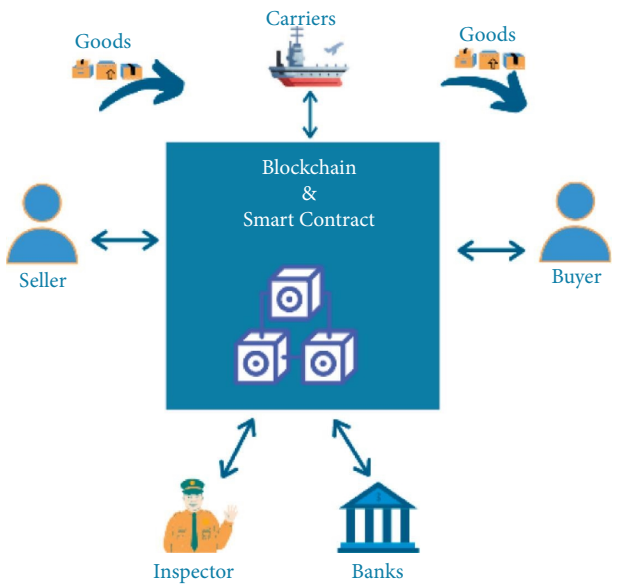

Figure 1: Trade credit consolidation through Blockchain model.

7. Conclusion

The investment in trade credit is an important aspect that becomes an important part of the balance sheet of the firms. The trade credit exists as the firm allows the buyer firms to delay payment of the amount and relaxes the policies for them. Therefore, customer firms take advantage of these investments and increase their profitability. Thus, this study is an important contribution towards trade credit, ICT, and globalization, which bring economic growth and stability to the country.

This research is an attempt to support Pakistan to maintain the trade credit relationship with ICT, globalization, and economic growth for 2000–2019. ARDL cointegration methodology is applicable to monitor the long-run relationship between the variables. Also, the VECM Granger causality test is applied to conclude both the long-run and short-run directions of the applied variables. Lastly, several other diagnostic methods are also applied, including ARCH, LM, and Ramsey tests. Globalization has an encouraging influence on trade as it expands with globalization and the economy is also flourishing. ICT has also a positive influence on trade credit if these technological resources are properly utilized.

Managing trade credit is an essential perspective for small industries. Efficient and productive trade credit enhances the productivity and efficiency of the firms. The trade credit policy implementation is of high importance for profitability. Offering trade credit is a significant factor for the life of the small business in particular, where trade credit is above the long-term assets of the company. Trade credit is also considered to be an important element of the management policy of the firms. Therefore, it alleviates the information asymmetry regarding the quality of the goods before paying for the product. Trade credit is for commercial purposes to increase the sales of the goods and to increase the worth of the business.

The results of the study also recommend that the government of Pakistan should be aware of ICT, globalization, and particularly small business units which have a direct effect on the exports of the country. Also, formal quality should be certified by reforms of policies that will enhance globalization and bring trade to the country. Improved legal systems, control over corruption, quality of information transferred by officials, and supervision of the financial and nonfinancial institutions could also support the country to improve globalization and trade credit in the country.

Therefore, this study also required a thorough, complete rearrangement of policies by the officials of the country, built on the development and executions of social, economic, ethical, and political actions. No doubt, this century is one of technology. Therefore, ICT has an encouraging influence on trade credit because mobile and Internet resources are the biggest asset for the country and policymakers must spotlight the appropriate utilization of technologies as these are not utilized optimally.

The exports of natural coal, gas, salt, and other minerals are an edge to the trade credit investors. Economic growth is also positive and significant to trade credit. As investment in research and development is required for any nation, which brings economic growth and stability. Pakistan is facing many sorts of challenges in development and growth. The shortage of electricity is because of the energy deficiency faced by the country. The deficiency of electric supply is an outcome of mismanagement and mechanism and control from the government. The state should concentrate on and implement policies on this vital scenario and must approve some strategies which restore the available resources of the country. Having an abundance of energy resources is always an advantage for poverty alleviation and enhancing human development. The productive use of these natural resources brings the quality of life. The legitimate usage of innovation diminishes the advancement of wellbeing and training areas to prosper and brings the quality of services at the doorsteps.

Policymakers should also concentrate on these Internet usages when state security issues are involved. Global trade along with the rest of the world opens a new horizon for growth and innovations. An increase in the international business hub leads to economic growth and stability. The government of Pakistan should also take measures to facilitate and benefit from the trade credit, which encourages the entry of foreign investors to deal with the local markets and increases the efficiency of the business hub. Overall, results show that trade credit is essential, and incorporating routine credit management for a firm's profitability is an essential factor for technology. Therefore, trade credit is an important strategy for financials and planning management to encourage the business. Also, the effects on trade credit help the investors to forecast the economic condition of the country. This work essentially clears the varying results in the literature concerning the association between ICT, globalization, the growth of the economy, and trade credit.

Data Availability

The data used to support the findings of this study are available from the corresponding author upon request.

Conflicts of Interest

The authors declare that there are no conflicts of interest associated with publishing this paper.

Acknowledgments

The authors are grateful to the Deanship of Scientific Research, King Saud University, for funding through Vice Deanship of Scientific Research Chairs.

References

[1] J. Chod, E. Lyandres, and A. Yang, "Trade credit and supplier competition," *Journal of Financial Economics*, vol. 131, no. 2, 2017.

[2] M. A. Petersen and R. G. Rajan, "Trade credit: theories and evidence," *Review of Financial Studies*, vol. 10, pp. 661–691, 1997.

[3] F. Léon, "The provision of long-term credit and firm growth in developing countries," *Economic Modelling*, vol. 90, pp. 66–78, 2020.

[4] G. Biais, "Trade credit and credit rationing," *The review of financial studies*, Oxford University Press, Oxford, UK, 1997.

[5] T. Box, R. Davis, M. Hill, and C. Lawrey, "Operating performance and aggressive trade credit policies," *Journal of Banking & Finance*, vol. 89, pp. 192–208, 2018.

[6] M. Giannetti, M. Burkart, and T. Ellingsen, "What you sell is what you lend? Explaining trade credit contracts," *Review of Financial Studies*, vol. 24, no. 4, pp. 1261–1298, 2011.

[7] M. D. Hill, G. W. Kelly, and G. B. Lockhart, "Shareholder returns from supplying trade credit," *Financial Management*, vol. 41, no. 1, pp. 255–280, 2012.

[8] M. Hu, J. Mou, and M. Tuilautala, "How trade credit affects mergers and acquisitions," *International Review of Economics and Finance*, vol. 67, 2020.

[9] G. W. Emery, "A pure financial explanation for trade credit," *Journal of Financial and Quantitative Analysis*, vol. 19, no. 3, 1984.

[10] L. Schwartz, *Journal of Creative Behavior*, vol. 7, no. 3, 1974.

[11] J. Stephen Ferris, "A transactions theory of trade credit use," *Quarterly Journal of Economics*, vol. 96, no. 2, pp. 243–270, 1981.

[12] M. Shahbaz, S. J. H. Shahzad, M. K. Mahalik, and S. Hammoudeh, "Does globalisation worsen environmental quality in developed economies?" *Environmental Modeling & Assessment*, vol. 23, pp. 141–156, 2018.

[13] W. Luo and K. H. Shang, "Managing inventory for firms with trade credit and deficit penalty," *Operations Research*, vol. 67, no. 2, 2019.

[14] J. Hou, P. P. Walsh, and J. Zhang, "The dynamics of human development index," *The Social Science Journal*, vol. 52, no. 3, pp. 331–347, 2015.

[15] S. O. Lee, A. Hong, and J. Hwang, "ICT diffusion as a determinant of human progress," *InfTechnology Dev*, vol. 23, Article ID 687705, 2017.

[16] ITU, *Global Cybersecurity and Cyber Welness Profiles*, 2015, https://handle.itu.int/11.1002/pub/80c63097-en.

[17] M. Biggeri and V. Mauro, "Towards a more "sustainable" human development index: integrating the environment and freedom," *Ecological Indicators*, vol. 91, pp. 220–231, 2018.

[18] M. N. Onyia, "The impact of ICT on university students' academic studies," *Journal of Educational and Social Research*, vol. 3, no. 8, Special Issue - October 2013, 2013.

[19] R. P. Pradhan, G. Mallik, and T. P. Bagchi, "Information communication technology (ICT) infrastructure and economic growth: a causality evinced by cross-country panel data," *IIMB Rev30*, vol. 30, pp. 91–103, 2018.

[20] A. Mohammadi and K. Shafi, "Gender differences in the contribution patterns of equity-crowdfunding investors," *Small Business Economics*, vol. 50, 2017.

[21] P. Ramachandran and L. Linde, "Integrating spatial support tools into strategic planning—SEA of the GMS north-south economic corridor strategy and action plan," *Environmental Impact Assessment Review*, vol. 31, 2011.

[22] C. Bayer and C. Hanck, "Combining non-cointegration tests," *Journal of Time Series Analysis*, vol. 34, no. 1, pp. 83–95, 2013.

[23] J. F. Raffensperger, R. A. R. Prabodanie, and J. A. Kostel, "A smart market for nutrient credit trading to incentivize wetland construction," *Journal of Hydrology*, vol. 546, pp. 248–261, 2017.

[24] J. H. Boyd and A. M. Jalal, "A new measure of financial development: theory leads measurement," *Journal of Development Economics*, vol. 99, no. 2, pp. 341–357, 2012.

[25] S. Khan and G. Liu, "The China–Pakistan Economic Corridor (CPEC): challenges and prospects," *Area Development and Policy*, vol. 4, pp. 467–474, 2019.

[26] F. Hussain and M. Hussain, "China-Pak economic corridor (CPEC) and its geopolitical paradigms," *IJSSHE-International Journal of Social Sciences and Education*, vol. 1, pp. 79–95, 2017.

[27] F. O. Bankole and L. Mimbi, "ICT infrastructure and its impact on national development: a research direction for Africa," *African Journal of Information Systems*, vol. 9, pp. 77–357, 2017.

[28] W. Hwang and J. Shin, "ICT-specific technological change and economic growth in Korea," *Telecommunications Policy*, vol. 41, pp. 282–294, 2017b.

[29] F. Shah, "Artificial intelligence as a service for immoral content detection and eradication," *Scientific Programming*, vol. 2022, Article ID 6825228, 9 pages, 2022.

[30] Y. Shah, "Challenges of small- and medium-sized businesses in Pakistan due to COVID-19 pandemic," *R-economy*, vol. 3, pp. 222–226, 2020.

[31] S. A. Asongu and J. C. Nwachukwu, "Not all that glitters is gold: ICT and inclusive human development in sub-Saharan Africa," *International Journal on Hydropower and Dams*, vol. 3, no. 4, pp. 303–322, 2017.

[32] R. Heeks, "Seeking a new link between ICTs and human development," *Information Technologies and International Development*, vol. 12, pp. 51–54, 2015.

[33] R. G. King and R. Levine, "Finance and growth: schumpeter might Be right," *Quarterly Journal of Economics*, vol. 108, pp. 717–737, 1993.

[34] F. Shah, Y. Liu, J. Ahmed, Y. Shah, and F. Shah, "Impact of risk on use of trade credit: empirical evidence from non-financial firms in Pakistan," *Sukkur IBA Journal of Economics and Finance*, vol. 2, pp. 55–67, 2018.

[35] H. Lee, J. Zhou, and J. Wang, "Trade credit financing under competition and its impact on firm performance in supply chain," *Manufacturing & Service Operations Management*, vol. 20, 2018.

Hindawi
Journal of Mathematics
Volume 2023, Article ID 9814149, 1 page
https://doi.org/10.1155/2023/9814149

Retraction

Retracted: Research on Digital Image Watermarking Algorithm Based on Scrambling and Singular Value Decomposition

Journal of Mathematics

Received 19 December 2023; Accepted 19 December 2023; Published 20 December 2023

This article has been retracted by Hindawi following an investigation undertaken by the publisher [1]. This investigation has uncovered evidence of one or more of the following indicators of systematic manipulation of the publication process:

(1) Discrepancies in scope

(2) Discrepancies in the description of the research reported

(3) Discrepancies between the availability of data and the research described

(4) Inappropriate citations

(5) Incoherent, meaningless and/or irrelevant content included in the article

(6) Manipulated or compromised peer review

The presence of these indicators undermines our confidence in the integrity of the article's content and we cannot, therefore, vouch for its reliability. Please note that this notice is intended solely to alert readers that the content of this article is unreliable. We have not investigated whether authors were aware of or involved in the systematic manipulation of the publication process.

Wiley and Hindawi regrets that the usual quality checks did not identify these issues before publication and have since put additional measures in place to safeguard research integrity.

We wish to credit our own Research Integrity and Research Publishing teams and anonymous and named external researchers and research integrity experts for contributing to this investigation.

The corresponding author, as the representative of all authors, has been given the opportunity to register their agreement or disagreement to this retraction. We have kept a record of any response received.

References

[1] L. Pei, "Research on Digital Image Watermarking Algorithm Based on Scrambling and Singular Value Decomposition," *Journal of Mathematics*, vol. 2022, Article ID 4656010, 10 pages, 2022.

Hindawi
Journal of Mathematics
Volume 2022, Article ID 4656010, 10 pages
https://doi.org/10.1155/2022/4656010

Research Article

Research on Digital Image Watermarking Algorithm Based on Scrambling and Singular Value Decomposition

Lei Pei

University of Science and Technology Beijing, Beijing 100083, China

Correspondence should be addressed to Lei Pei; peilei@ustb.edu.cn

Received 21 December 2021; Revised 21 January 2022; Accepted 10 February 2022; Published 27 February 2022

Academic Editor: Naeem Jan

At present, the digital image watermarking algorithm has not embedded the synchronization signal in the image, resulting in the poor performance of the embedded image in terms of, for example, imperceptibility, anti-attack ability, and robustness. Therefore, a digital image watermarking algorithm based on scrambling and singular value decomposition is proposed. The digital watermark is preprocessed by dimensionality reduction and encryption; the digital image is processed in sections and embedded in the synchronization signal. The digital watermark image is embedded in the digital image watermark by using the low-frequency energy ratio technology of sound channel. The watermark image extraction step is designed to extract the watermark image. The transmittance of the degraded image is calculated, the transmittance is refined by relying on the soft matting algorithm and guiding filter, the image contrast in the image frequency domain is enhanced, and the results are mapped to the appropriate visual range to optimize the visual brightness of the image. Finally, according to the uniqueness of singular value matrix, the distributed characteristics of image matrix data are described, the visual effect is enhanced, and the research of digital image watermarking algorithm is completed. The experimental results show that the algorithm can extract the watermark information completely, the image contrast and singular value have been significantly improved, and the algorithm has better anti-attack performance.

1. Introduction

With the rapid development of network technology and digital multimedia technology, digital photos, paintings, voice, text, video, and other products have been very common [1]. However, with the development of digital technology and networking [2], fast, accurate, and cheap digital transmission means bring opportunities to countless businesses but also pose new challenges, including infringement, piracy, and arbitrary tampering with digital products (such as electronic publications, audio, video, animation, and image products). This leads to the problems of digital information security and digital product copyright protection. Digital image watermarking technology came into being in this environment [3]. It is regarded as the last line of defense of information security and has attracted extensive attention from all walks of life. Among digital image watermarking techniques, digital image watermarking considering scrambling and singular value decomposition is the core one. Digital image refers to the display image in two-dimensional digital form, which always takes digital unit as pixel representation structure, which can better describe the mathematical relationship between real image and virtual image [4]. Digital image watermarking algorithm is a process of hiding secret information into the host image to prevent the repeatability of original data and maintain authenticity, subtitle, and copyright control [5, 6].

At present, mankind has entered the digital information age. Through digital media, we can spread and obtain network information such as audio and video, which has greatly enriched people's lives and improved the transmission efficiency of information. Some scholars put forward relevant research. Reference [7] proposed a sparse domain lossless digital image watermarking algorithm based on k-singular value decomposition algorithm and introduced a robust lossless sparse domain watermarking algorithm combined with discrete cosine transform (DCT), which hides secret information into important sparse

elements of the host image. In order to improve the security of the original image, the secret information is first transformed by a discrete cosine transform. These DCT coefficients with some regularization parameters will be inserted into the selected important sparse coefficients. In the extraction stage, the sparse domain orthogonal matching pursuit algorithm is used to extract secret information from important sparse coefficients. Finally, the inverse discrete cosine transform is used to extract secret information without losing any information.

Reference [8] proposed a robust logo watermarking algorithm based on the maximum wavelet transform. Digital image watermarking is used to protect the copyright of digital images. A new blind logo image watermarking technology for RGB images is proposed. This technology makes use of the error correction ability of the human visual system. It embeds two different watermarks in the wavelet/multiwavelet domain. The two watermarks are embedded in different subbands and are orthogonal for different purposes. One is a high-capacity multibit watermark for embedding the logo, and the other is a watermark for detecting and reversing geometric attacks. Both watermarks are embedded using the spread spectrum method, based on pseudorandom noise sequence and unique key. By embedding a watermark into the modulus maxima coefficients of the wavelet transform, the robustness to geometric attacks such as rotation, scaling, and translation is realized. Although the above methods have made some progress, with the development of digital technology, security problems of digital information have been caused, such as copyright infringement, illegal copying of software or documents, and wanton tampering with digital information. Due to the visual quality conditions of digital images, there will be obvious loss of watermark pixels in the spatial domain environment. In order to solve these problems, based on the above research, a digital image watermarking algorithm based on scrambling and singular value decomposition is proposed.

The following is a summary of the research: Section 1 contains the introduction. Section 2 discusses the research on digital image watermarking algorithm. Section 3 discusses the visual effect enhancement of the digital image watermarking algorithm under scrambling and singular value decomposition. Section 4 discusses the experimental analysis with tables. Finally, the conclusion brings the paper to an end in Section 5.

2. Research on Digital Image Watermarking Algorithm

The suggested approach preserves the watermarked image's invisibility and quality. The developed algorithm is a blind watermarking technique that meets invisibility and robustness requirements. A watermark is embedded in the middle-frequency coefficient block of three DWT levels to accomplish watermarking.

2.1. Preprocessing Digital Image Watermarking. In order to make the digital image watermark random before embedding audio and robust in the process of processing, dimensionality reduction and encryption preprocessing are carried out for the digital image watermark [9]. Select one frame image in the digital image sequence, and obtain three high-frequency bands and one low-frequency band along with the horizontal and vertical directions. The structure is shown in Figure 1.

In Figure 1, the high-frequency part in the horizontal direction and the low-frequency part in the vertical-horizontal direction of the image are represented as BB1; the low-frequency part in the horizontal direction and the high-frequency part in the vertical direction are represented as CC1; and when both the horizontal direction and the vertical direction are high-frequency parts, they are represented as DD1. AA1 retains the main features of the image to be detected, and the other three high-frequency bands maintain the edge details. Assuming that the selected digital image watermark with the size of $S_1 \times S_2$ is S, the pixel amplitude s of the digital image watermark is

$$S = \{s(x, y), \quad 0 \le x < S_1, 0 \le y < S_2\}, \tag{1}$$

where $s(x, y)$ represents the pixel amplitude of the digital image watermark at position (x, y). According to (1), the digital image watermark is preprocessed [10], and the processing process is as follows:

Step 1. Dimensionality reduction. Since digital image signal belongs to one-dimensional signal, dimensionality reduction is carried out for digital image signal [11], and it is transformed into a one-dimensional sequence. Then, the one-dimensional sequence V of digital image watermark image after dimensionality reduction is

$$R = \{r(n) \times s(x, y), \quad n = x \times S_2 + y, n \in S_1 \times S_2\}, \tag{2}$$

where n represents the length of the digital image and $r(n)$ represents the sequence of digital image watermark when the length of the digital image is n.

Step 2. Watermark image encryption. The digital image watermark sequence obtained by scrambling formula (2) needs to use logistic chaotic mapping to generate the binary chaotic sequence. The processing formula is as follows:

$$E = f(n) \times e(n) \oplus l(n), \tag{3}$$

where E represents the scrambled digital image watermark signal, $f(n)$ represents the scrambled digital image watermark signal when the digital image length is n, $\oplus$ represents the algorithm, $e(n)$ represents the one-dimensional sequence of digital image watermark, and $l(n)$ represents the binary chaotic sequence. According to the encrypted digital image watermark image obtained by (3), the digital image watermark is encrypted by using the sensitivity of chaotic sequence to the initial value, and the watermark spectrum has high balance and security [12].

When embedding the visibility watermark in the digital image, in most cases, the visibility watermark should maintain a clear and visible existence state, which is very easy to be found by the human eye. However, since it cannot

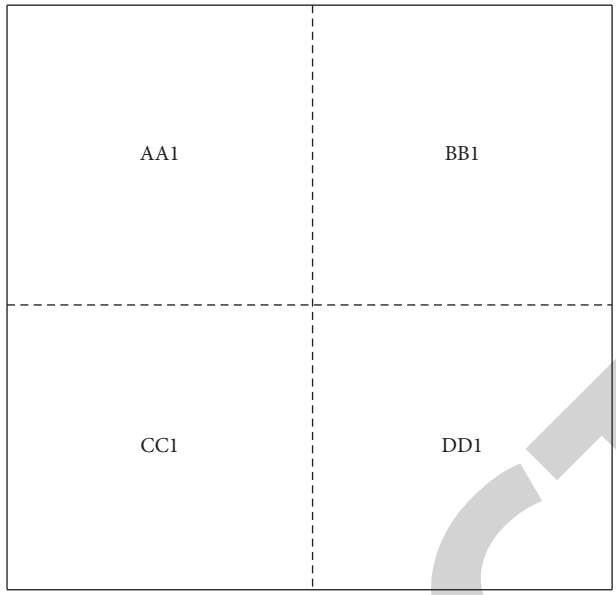

Figure 1: Video image structure decomposed by wavelet transform.

affect the original detail characteristics of the digital image, the impact on the quality of the digital image should be kept as small as possible, so as not to be too prominent and attract the attention of the human eye. It can be seen that digital image watermarking does not need to be completely confidential, but it must have a certain representative significance. Based on this, all watermarks in the digital image are counted, and then the embedded synchronous signal processing is implemented for the segmented original image, until the standard information deviation in each block space environment and the real-time display strength of the watermark node are calculated and the research of digital image watermarking algorithm is completed.

2.2. Embedded Synchronization Signal. In this study, the digital image watermarking algorithm is studied. The digital image is segmented, and the length of each signal is the same, which is $n\prime$. A synchronization signal is hidden in each digital image and embedded in the time domain [13]. At this time, it is also necessary to control the number of synchronization codes to avoid the contradiction between transparency and robustness of the algorithm and reduce the amount of search calculation of the algorithm.

Therefore, it is assumed that the synchronization signal embedded in the time domain is $\{a_n\}$ and $\{a_n\} \in \{-1, 1\}$, where n represents an appropriate threshold and takes an odd number. A total of k digital images are segmented this time, and there are B sampling points in each digital image $A(k)$. When the synchronization signal b(i) is embedded in B1, the sampling point B is the B_1 bit of the sampling point, where i represents the i audio data. Then, the digital image $X(u)$ embedded in the synchronization signal is

$$X(u) = \begin{cases} x(u), & \mod\left[\frac{x(u)}{B}, 2\right] = a(n), \\ x(u) + \frac{\mathrm{m}}{2}, & \mod\left[\frac{x(u)}{B}, 2\right] \neq a(n). \end{cases} \tag{4}$$

In (4), m represents a positive integer, [Brackets value] represents an integer operation, and mod represents the factorial of a positive integer.

According to (4), the synchronization signal is embedded in the digital image. At this time, the watermark can be embedded in the digital image according to the synchronization signal.

2.3. Embedding Digital Image Watermark with Low-Frequency Energy Ratio of Sound Channel. After the digital image watermark image is preprocessed, the synchronization signal is embedded in the digital image. At this time, the digital image watermark can be embedded in the digital image by using the channel low-frequency energy ratio technology [14]. The embedding process is as follows:

(i) Step 1: Frame processing embeds the original image signal into the sync signal. The digital image signal of the embedded synchronization signal obtained according to formula (4) is $X = \{x(u), 0 \le u \le n\}$, and $x(u) \in \{0, 1, 2, \ldots, (2^p - 1)\}$ is the amplitude of the u audio data. If the original audio is divided into several lengths, its length is determined by the original image signal and the amount of watermark information to be embedded, that is,

$$X = \left\{ X(q), \quad 0 \le q \le \frac{l}{N} \right\}. \tag{5}$$

(i) In (5), N represents the amount of data contained in each frame signal and l/n represents the number of data segments divided into the whole audio segment.

(ii) Step 2: Select the embedded frame. According to the segmentation processing steps when embedding the synchronization signal, segment the digital image, mark each segment of the signal, and calculate the audio energy D_v calculation formula of each frame:

$$\begin{cases} D_1 = \sum_{i=0}^{l'=1} x^2(n), \\ D_v = \sum_{i=0}^{n'=1} x^2[(a-1)\times n']. \end{cases} \tag{6}$$

(i) In (6), F represents the total number of frames of the image signal and D_v represents the audio energy of the v frame. According to (6), calculate the energy of all audio frames and arrange them in descending order. Considering the robustness and imperceptibility of the watermark, the audio frame with large energy is selected and embedded in the digital image. Only 1 bit is embedded in the watermark information of each image signal.

(ii) Step 3: Calculate the average value W of the selected embedded frame. When $W<0$, the inverse signal of the embedded frame signal needs to be taken, and then the inverse transform is carried out. When $W>0$, the complex cepstrum of each frame image signal can be calculated. Therefore, assuming that the f audio data frame of the i frame is $X_f(i)$, the complex cepstrum C_f^i of the image signal of each frame is

$$C_f^i = C_{\text{cceps}}\left(X_f(i)\right), \left(1 \le f \le \frac{l}{N}, \quad 1 \le i \le N\right). \tag{7}$$

(i) In (7), C_{cceps} represents the number of additional delay samples when the f frame image signal is subjected to complex cepstrum transformation and returns to the audio frame $X_f(i)$.

(ii) Step 4: Calculate the low-frequency energy of the channel. Assuming that the complex cepstrum coefficient of the j scale factor is C_j, the low-frequency energy E_j of the j scale factor is

$$E_j = \sum_{j=S_{\text{starti}}}^{E_{\text{endi}}} C_f^i. \tag{8}$$

(i) In (8), E_{endi} represents the end of the j scale factor band index and S_{starti} represents the beginning of the j scale factor band index.

(ii) Step 5: Quantify the low-frequency energy of the channel. Assuming that the quantization step of channel low-frequency energy is q, the measured channel low-frequency energy E_j is

$$E_j' = \left[round\left(\frac{E_j}{2q} - \frac{p}{2}\right)\right] \times 2q + pq. \tag{9}$$

(i) In (9), *roun d* represents rounding, and p represents the number of bits used for each data.

(ii) Step 6: Adjust the complex cepstrum coefficient C_f^i of each frame image signal, and perform inverse cepstrum transform $X_f^{'i}$; then,

$$\begin{aligned} C_f^{'i} &= C_f^i + \alpha, \\ X_f^{'i} &= \text{icceps}\left(C_f^{'i}, d(f)\right). \end{aligned} \tag{10}$$

(i) In (10), *icceps* represents the inverse transform function, α represents the change of the mean value of the complex cepstrum coefficient after quantization, and $C_f^{'i}$ represents the i complex cepstrum coefficient of the f frame.

(ii) Step 7: Repeat steps 3 to 6 until all watermark information is embedded in the whole digital image signal; that is, the watermark embedding is completed.

2.4. Extracting Digital Image Watermark. According to the digital image watermark embedding process designed in Section 2.3, the digital image watermark is extracted. The watermark image extraction is the calculation link of the design of the new digital image watermark algorithm. With the support of scrambling and singular value decomposition, the actual position of the image information node in the spatial domain environment can be determined, and then through function processing, realize the conversion from clear watermark to fuzzy watermark. In a complete digital image, due to the influence of spatial domain change conditions, the watermark node is basically always in a changing state. In this case, some pixels may be covered by interfering noise, resulting in the continuous decline of the execution ability of the watermark node. To solve this problem, after the visible watermark processing is completed, the position of individual pixel noise should be limited to realize the watermark extraction processing. The extraction process is shown in Figure 2.

According to the watermark extraction process shown in Figure 2, in the watermark embedding process, the frame division process is used to split watermarked image signal into frames and complex cepstral transform and calculate the mean value of complex cepstrum coefficient of each frame image signal. Therefore, assuming that the selected digital image is $X' = \{X'(k), 1 \le k \le z\}$, where z represents the number of frames embedded with the digital image watermark, the watermark sequence W_f before inverse scrambling is

$$W_f = \begin{cases} 1, & \text{if } \text{mod}\left(m_f', 2\right) = 1, \\ 0, & \text{if } \text{mod}\left(m_f', 2\right) = 0. \end{cases} \tag{11}$$

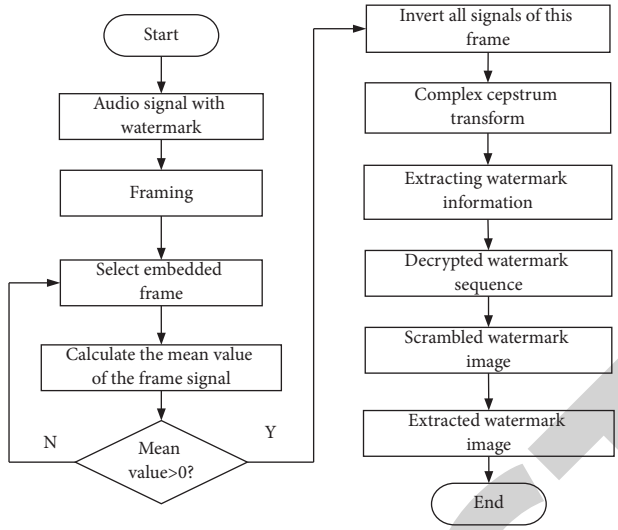

Figure 2: Watermark extraction process.

In (11), $m\prime f$ represents the mean value of the complex cepstrum coefficient of each frame of image signal. Let k_0 represent the pixel extraction coefficient at the initial stage of spatial domain watermark embedding and k_n represent the pixel extraction coefficient at the end of spatial domain watermark embedding. The extraction expression at the watermark node can be defined as

$$Y_U = \frac{1}{A}\sum_{k_0}^{k_n}\left|K \times z_{\max} - K' \times z_{\min}\right|. \tag{12}$$

In (12), K and $K\prime$ represent two different discrete Fourier function transformation conditions, and $z_{\min}$ and $z_{\max}$ represent the minimum and maximum amount of watermark information data in digital image spatial domain, respectively. According to logistic chaotic map, binary chaotic sequence is generated, and the watermark sequence before inverse scrambling is decrypted to obtain one-dimensional sequence; the dimension of one-dimensional sequence is raised to obtain two-dimensional image. The dimension raising process is the inverse process of dimension reduction in watermark image preprocessing, so as to extract digital image watermark.

3. Visual Effect Enhancement of Digital Image Watermarking Algorithm under Scrambling and Singular Value Decomposition

3.1. Digital Image Transmittance Estimation. In the digital image, if the transmittance and atmospheric spectrum can be obtained from the image, the blurred area in the digital image can be restored to normal Z. There are three unknown parameters in the operation formula (13) of digital image, which is an ill-conditioned equation. Some a priori conditions need to be used to operate the ill-conditioned equation. A priori dark color system can solve this problem very well.

$$C_E(x) = Z(x)m(x) + A_z(1 - m(x)). \tag{13}$$

In (13), $C_E(x)$ represents the reflected light intensity of the scene point collected by the observation point, $Z(x)$ represents the pixel in the image, $m(x)$ represents the transmittance of the light area, and A_z represents the atmospheric luminosity.

If the atmospheric light is homogeneous, (13) is satisfied for all channels in the RGB color space. It is proposed that the atmospheric light is known, and it is further proposed that the transmittance is normally bright in local areas. Assuming the transmittance equation $\tilde{m}(x)$ of this region, calculate the dark primary color for (13), and the equation is as follows:

$$U_{ty} = \tilde{m}(x)\min_{y\in\Omega(x)}\frac{Z^c(y)}{A^c} + (1 - \tilde{m}(x)). \tag{14}$$

In (14), $Z^c(y)$ represents the pixel ordinate in the image, A^c represents the local window centered on the abscissa and ordinate, and $\Omega(x)$ represents a color channel in the RGB color space of the image Z. With (14), the dark primary color calculation of the digital image is reduced to tend to 0.

In fact, there are no particles in the atmospheric light in the normal image. When viewing distant objects, the image is still a digital image. Therefore, in this paper, a small number of degraded areas are reserved in a certain area of the ordinary image. By integrating a constant parameter $\omega \in [0, 1]$, the rough transmittance calculation formula is

$$\tilde{m}(x) = 1 - \omega\min_{y\in\Omega(x)}\left(\frac{Z^c(y)}{A^c}\right). \tag{15}$$

In fact, the transmittance is not always the same in a region. For example, when the depth of field protrudes, the transmittance will change.

3.2. Fine Processing of Digital Image Transmittance. Directly processing the blurred area in the digital image through rough transmittance will lead to obvious halo in the

background of the image. In order to remove the halo effect, the transmittance is refined by soft matting algorithm and guided filter.

3.2.1. Soft Matting Algorithm. The soft matting formula is as follows:

$$I_o = \alpha_1 \times Q_1 + (1 - \alpha_1)B_n. \tag{16}$$

In (16), Q_1 represents the foreground, B_n represents the background, a_1 represents the image, and I_0 represents the image fused by the foreground and the background. Through the above calculation, it is found that the transmittance distribution is affected by the corresponding soft matting formula. To refine the transmittance, the soft matting algorithm can obtain better-refined transmittance.

3.2.2. Guided Filter. The guided filter is an edge-preserving smoothing filter, which has a good effect on smoothing filtering and edge-preserving. If the output degraded image formula q_1, the guidance diagram formula I_i, and the input digital image formula p_1 are proposed, there is a linear correlation between the output image and the guidance diagram in the local window w_{k1}. The guidance filter equation is as follows:

$$D_q = (a_{k1}I_i + b_{k1}) + (q_1 \times p_1 \times w_{k1}). \tag{17}$$

In (17), a_{k1} and b_{k1} are linear constant coefficients of local window w_{k1}. By calculating the linear constant coefficient, the difference between the input images is minimized, and it is proved that the edge of the guide image and the output image can be consistent. Since the guided filter can only be calculated by matrix point multiplication and mean filtering, it can be optimized through the integral image algorithm, so that the guided filter is only associated with the image size N and is not associated with the window size. Then, the time complexity of the guided filter is $O(N)$. Relying on the guided filter can effectively improve the calculation efficiency of the soft matting algorithm.

3.3. Digital Image Visual Effect Enhancement

3.3.1. Frequency Domain Enhancement. In digital images, the movement of pixel gray value will be represented by frequency. Frequency description is a spatial frequency that changes with the change of coordinates. For the characteristics of lines, noise, and edges, such as lakes, rivers, or roads with large differences, there are large spatial frequencies. The frequency domain is a stable structure with large gray value change frequency and large area in a short pixel size.

Frequency enhancement is to calculate the Fourier transform coefficient in the frequency domain of the digital image and then change it back to the initial spatial domain to obtain the image with enhanced details. Frequency domain enhancement is an indirect processing method. Firstly, the digital image is processed by Fourier transform, and the frequency domain of the image is filtered. Finally, the low-frequency part of the image is transformed into a more stable region. Specifically, it has the characteristics of high pass, low pass, and homomorphic filtering and band stop in the frequency domain.

Frequency domain enhancement has three processes, namely:

(1) Transferring the digital image in the spatial domain to the frequency domain.

(2) Enhancing the image in the frequency domain [4].

(3) Returning the enhanced image in the frequency domain to the spatial domain.

If the convolution of linear bit invariant operator $h(x, y)$ and function $f(x, y)$ is $g(x, y)$, that is, $f(x, y) = h(x, y) \otimes g(x, y)$, then it exists in the frequency domain by virtue of the convolution theorem:

$$G(u, v) = H(u, v)F(u, v). \tag{18}$$

In (18), $G(u, v), H(u, v), F(u, v)$ represent the Boyle transformation of $G(x, y), H(x, y), F(x, y)$, respectively, and $H(u, v)$ can be described as a transfer function through the linear coefficient theory.

$f(x, y)$ is the set input image, and $H(u, v)$ needs to be determined. After determining $H(u, v)$, $g(x, y)$ with required characteristics can be obtained after calculating $G(u, v)$ by

$$g(x, y) = T^{-1}[H(u, v)F(u, v)]. \tag{19}$$

In (19), T^{-1} represents the required time transpose. With the above calculation, the frequency domain of the digital image can be enhanced, so as to improve the contrast details in the image.

3.3.2. Brightness Intensity Component Enhancement. The pixel brightness intensity on both sides of the inner edge of the digital image is quite different from that at the center of the image. Therefore, if you want to enhance the image, you need to compare the pixels in the image one by one, and the brightness intensity value is regarded as the external stimulus. Then, the pixel set close to the space and with the same intensity can be expressed as synchronous ignition, and vice versa. This can be expressed in image visual enhancement: synchronous ignition means that there is the same brightness intensity between pixels, and the image area can be smoothed through brightness. Asynchronous ignition means that pixels produce different brightness intensities. Relying on the same and different ignition, we can improve the brightness gradient between image areas, so as to highlight the edge of the digital image, so as to improve the image brightness intensity distribution and make the image have a more obvious hierarchy.

Because the brightness range of the digital image is small, the image contrast decreases. If human visual characteristics are added to the image contrast enhancement algorithm, the contrast enhancement effect can be effectively improved. This is because the brightness perceived by the human visual system has a logarithmic relationship with the brightness that can be obtained by the personnel, so the image contrast within the personnel's visual range can be greatly improved.

In digital image, due to the effect of hard limiting function, the output digital image will be transformed into binary image. In order to enable the output mapping function to effectively enhance the brightness of the image, the brightness intensity of the image is mapped within a suitable visual range by using the logarithmic mapping function according to the human visual characteristics. The calculation formula is as follows:

$$Y_{ij}(n) = 1nI_{\max} - \frac{\Delta t}{\tau_\theta}(n-1). \tag{20}$$

In (20), $I_{\max}$ represents the intensity value of the brightest pixel in the initial image; n represents the ignition time $n = 1, 2, 3$; $\Delta t/\tau_\theta(n-1)$ represents the attenuation step of the dynamic threshold function in the image at the $(n-1)$ ignition time; and $Y_{ij}(n)$ represents the perceived output at the ignition time, that is, the brightness intensity of the enhanced digital image.

3.3.3. Singular Value Decomposition. Digital image can be represented as a matrix composed of multiple nonnegative scalars. This matrix has the unique characteristic of singular value, which can describe the distribution characteristics of matrix data. It is very stable to describe the image by singular value, and it also has the characteristics of transpose, image invariance, translation, and rotation. It can effectively describe the algebraic features in the image. Therefore, the purpose of enhancing the image can be achieved by enhancing the singular value of the image matrix.

The singular value of the matrix can be obtained by singular value decomposition. The definition of singular value decomposition is as follows: A is proposed to represent $m \times n$ real matrix, and $\text{rank}(A) = r$; then, there are m order West matrix U and E order West matrix V, so that

$$A = USV^H \times U \sum V^H, U * U^H. \tag{21}$$

In (21), V^H represents all r nonzero singular values of A; each column of U and V is the eigenvector of $A * A^H$ or $A^H * A$, respectively; and S represents the decomposed singular value matrix.

After singular value decomposition, the set information and texture of the image will appear in the matrix U, V, and the energy information of the image will be concentrated in the singular value. The singular value of the image matrix is enhanced by incorporating a certain amount of Gaussian noise into the image. The general process is as follows:

(1) The preprocessed image $f(x, y)$ is subjected to singular value decomposition to obtain the matrix U, S, V.

(2) The Gaussian noise is superimposed into the preprocessed image, and the noisy image is decomposed by singular value decomposition to obtain matrix U_n, S_n, V_n.

(3) The image enhanced by singular value decomposition is $g(x, y) = US_nV^H$; $g(x, y) = US_nV^H$.

(4) The image $f(x, y)$ is modified by the adaptive histogram averaging method to obtain the final visual effect enhanced image, so as to complete the research on the digital image watermarking algorithm based on scrambling and singular value decomposition.

4. Experimental Analysis

With the support of scrambling and singular value decomposition, the effect and feasibility of the designed digital image watermarking algorithm are verified. Therefore, a simulation experiment is designed for verification. The MATLAB programming parameters required for the specific experiment are shown in Table 1.

Set the digital image watermark embedding intensity coefficient as 0.1 according to the parameters in Table 1, and draw the waveform of the original image signal and the watermark image signal embedded by the digital image watermark algorithm based on scrambling and singular value decomposition. The experimental results are shown in Figure 3.

According to Figure 3, after introducing the digital image watermarking algorithm based on scrambling and singular value decomposition studied in this paper, there is almost no difference between the waveform of the watermarked image signal and the original signal. It can be seen that there is no obvious difference between them in the process of watermark inspection and testing. According to the above analysis, when the image is not attacked, the watermark information can be completely extracted.

The normalized correlation coefficient (NC) mainly describes the robustness of the watermark. The main factors affecting the robustness of the watermark are various attacks. Select the original image as the test object, and count the normalized correlation coefficient values of the three video watermarking algorithms after various attacks. Suppose that the sampling point of the audio is o, the total length of the audio is L, the original carrier audio is X, and the embedded watermark audio is X'; then, the normalized correlation coefficient calculation formula S of watermark audio is

$$S = 10\log_{10}\frac{\sum_{0=1}^{L} X^2(i)}{\sum_{0=1}^{L}\left[X(i) - X'(i)\right]^2}. \tag{22}$$

Calculate the normalized correlation coefficient results according to (13), as shown in Table 2.

As can be seen from Table 2, compared with the algorithms in [7] and [8], the normalized correlation coefficient of the algorithm in this paper is larger, indicating that the detected watermark is more similar to the original watermark, and the watermark has strong robustness and can resist various attacks. This is mainly because the algorithm in this paper considers scrambling and singular value decomposition, and the watermark is more robust.

In order to further prove the practicability of the proposed method, six digital images are extracted from the image database, and the singular values and contrast increments of the six digital images before and after enhancement are compared. The results are shown in Table 3.

Table 1: MATLAB programming parameters.

Programming tools	Algorithm interpretation	Programming tools	Algorithm interpretation
MATLAB main toolbox	Main toolbox required by MATLAB	Communication toolbox	Watermark information toolbox
System identification toolbox	Discrete Fourier transform tool	Fuzzy logic toolbox	Multiresolution decomposition tool
Signal processing toolbox	Programming signal processing tools	Spline toolbox	Digital image spline processing tool

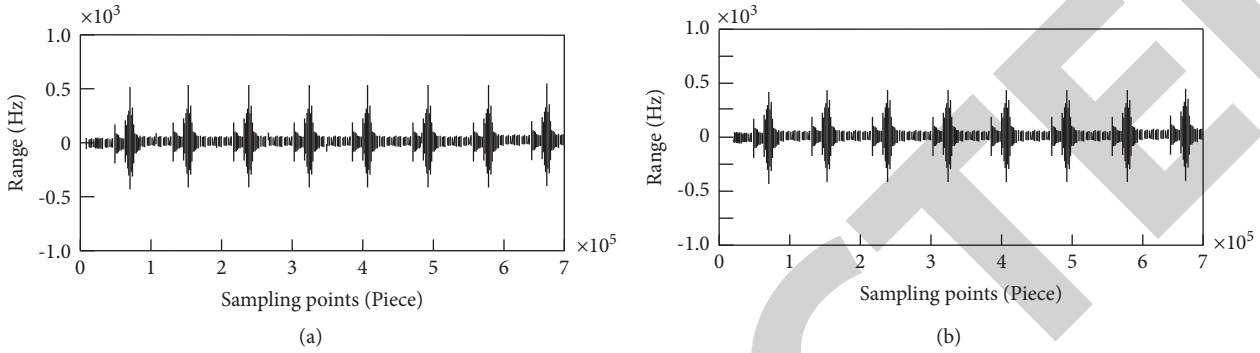

Figure 3: Amplitude value of image signal.

Table 2: Comparison results of normalized correlation coefficients of different algorithms.

Aggressive behavior	Paper algorithm	Reference [7] algorithm	Reference [8] algorithm
Noise	0.972	0.825	0.937
Frame loss	0.963	0.867	0.920
Shear	0.946	0.838	0.902
Tampering	0.955	0.857	0.910
Compression	0.955	0.822	0.910

It can be seen from Table 3 that the image contrast and singular value have been significantly improved after enhancement using the algorithm in this paper. This is because the proposed method will describe the image by singular value, and because of the characteristics of singular value, the improvement of singular value can also drive the improvement of image visual effect.

From the five audio digital images selected in this experiment, the popular audio is selected as the experimental object. Through the correlation coefficient, the resistance of the three groups of algorithms to attacks is verified. The closer the correlation coefficient of the algorithm to 1, the higher the similarity between the extracted watermark information and the original watermark, and the better the anti-attack ability of the algorithm. Therefore, assuming that the original watermark is w, the extracted watermark is $w\prime$, the pixel at a certain position of the watermark is (i, j), and the number of pixels of the watermark is $m * n$, the correlation coefficient C of the algorithm is calculated as follows:

$$C(w, w') = \frac{\sum_{i=1}^{m}\sum_{j=1}^{n} w(i,j)w\prime(i,j)}{\sqrt{\sum_{i=1}^{m}\sum_{j=1}^{n} w^2(i,j)}\sqrt{\sum_{i=1}^{m}\sum_{j=1}^{n} w^2(i,j)}}. \quad (23)$$

MATLAB software is selected to attack the three algorithms selected in this experiment. Formula (23) is used to calculate the correlation coefficients of the three algorithms and verify the resistance of the three algorithms to attacks, and the experimental results are shown in Table 4.

Table 3: Contrast and entropy increment of images before and after enhancement.

Image ↓	Initial digital image		Enhanced digital image	
	Singular value	Contrast ratio	Singular value	Contrast ratio
1	5.55	1.07	5.97	1.24
2	5.43	1.11	5.69	1.22
3	5.35	1.14	5.93	1.24
4	6.80	1.13	7.39	1.27
5	6.81	1.10	7.42	1.27
6	6.90	1.15	7.53	1.28

It can be seen from Table 4 that under the attack of the attack mode set in this experiment, there is a gap of 0.17 and 0.16 between the correlation coefficient of the algorithm in [7] and the algorithm in [8] and the non-attack, respectively, indicating that the similarity between the watermark information extracted by the two groups of algorithms and the original watermark is low, and the anti-attack performance is poor when attacked. Under the attack of the attack mode set in this experiment, there is only a gap of 0.02 between the correlation coefficient and the non-attack. It can be seen that the digital image watermarking algorithm based on scrambling and singular value decomposition in this research has high similarity between the extracted watermark information and the original watermark and has better anti-attack ability when attacked.

Table 4: Test results of resistance to attack.

Attack type ↓	Paper algorithm	Reference [7] algorithm	Reference [8] algorithm
Not attacked	1	1	1
MP3 compression	0.89	0.83	0.77
Random shear	0.98	0.82	0.84
Low pass filtering	0.99	0.83	0.73
Downsampling attack	1	0.90	0.85
Adding Gaussian white noise	0.99	0.72	0.91
Denoising attack	1	0.80	0.80
Gravimetric	0.98	0.84	0.81
Upsampling attack	0.99	0.73	0.85
Mean value	0.98	0.83	0.84

5. Conclusion and Prospect

5.1. Conclusion.

(1) After introducing the digital image watermarking algorithm based on scrambling and singular value decomposition, there is almost no difference between the waveform of the watermarked image signal and the original signal. When the image is not attacked, the watermark information can be extracted completely.

(2) The watermark detected by this algorithm is more similar to the original watermark. The watermark has strong robustness and can resist various attacks.

(3) After using this algorithm for enhancement, the image contrast and singular value have been significantly improved.

(4) The digital image watermarking algorithm based on scrambling and singular value decomposition in this study has high similarity between the extracted watermark information and the original watermark and has better anti-attack ability when attacked.

5.2. Prospect. Digital image watermarking algorithm has been fully studied and developed. In the future research work, digital image watermarking technology needs to be deeply studied in the following aspects:

(1) Research on the robustness, security, and anti-attack ability of the existing digital watermarking algorithms, combined with the digital signal processing technology, will be conducted to find out the relationship between them, so as to find the digital image watermarking technology with better performance.

(2) Digital watermarking technology based on biometrics can also embed some human characteristics, such as fingerprint, palm print, and other information in the image as copyright authentication, so it may become the focus of research in the future.

(3) At present, other digital image watermarking technologies can be used as a research direction of digital image watermarking algorithm in the future, such as digital watermarking technology based on graphics, vector graphics, and animation; watermark embedding algorithm based on triangular patch geometry; audio watermarking algorithm; and video watermarking algorithm.

Data Availability

The data used to support the findings of this study are available from the author upon request.

Conflicts of Interest

The author declares that he has no conflicts of interest.

Acknowledgments

This project was supported by (1) the Social Science Fund of the Ministry of Education of China in 2019, Research on User Experience Design Method of VR Movie Space, Grant no. 19YJC760078, and (2) the State Scholarship Fund for Visiting Scholar of China Scholarship Council in 2019, Grant no. 201906465002.

References

[1] L. Zhou, J. Rodrigues, W. H, M. M, and L. Vcm, "5G multimedia communications: theory, technology, and application," *IEEE MultiMedia*, vol. 26, no. 1, pp. 8-9, 2019.

[2] C. D. Mukhopadhyay, P. Sharma, K. Sinha, and K. Rajarshi, "Recent trends in analytical and digital techniques for the detection of the SARS-Cov-2," *Biophysical Chemistry*, vol. 270, no. 1, Article ID 106538, 2020.

[3] C. Zxab, C. Xwab, C. Cwb, C. Bmb, H. Zd, and Qi. Labc, "Novel quaternion polar complex exponential transform and its application in color image zero-watermarking - ScienceDirect," *Digital Signal Processing*, vol. 116, no. 9, Article ID 103130, 2021.

[4] H. L. Wei and J. X. Wang, "Simulation research on edge sharpening enhancement of motion blurred digital image," *Computer Simulation*, vol. 37, no. 7, pp. 459–462, Article ID 497, 2020.

[5] W. W. Hu, R. G. Zhou, and Y. C. Li, "Quantum watermarking based on neighbor mean interpolation and LSB steganography algorithms," *International Journal of Theoretical Physics*, vol. 58, no. 1, pp. 1–24, 2019.

[6] T. Zhu, W. Qu, and W. Cao, "An optimized image watermarking algorithm based on SVD and IWT," *The Journal of Supercomputing*, vol. 25, no. 5, pp. 1–7, 2021.

Hindawi
Journal of Mathematics
Volume 2023, Article ID 9894560, 1 page
https://doi.org/10.1155/2023/9894560

Retraction

Retracted: Text Knowledge Acquisition Method of Collaborative Product Design Based on Genetic Algorithm

Journal of Mathematics

Received 19 December 2023; Accepted 19 December 2023; Published 20 December 2023

This article has been retracted by Hindawi following an investigation undertaken by the publisher [1]. This investigation has uncovered evidence of one or more of the following indicators of systematic manipulation of the publication process:

(1) Discrepancies in scope

(2) Discrepancies in the description of the research reported

(3) Discrepancies between the availability of data and the research described

(4) Inappropriate citations

(5) Incoherent, meaningless and/or irrelevant content included in the article

(6) Manipulated or compromised peer review

The presence of these indicators undermines our confidence in the integrity of the article's content and we cannot, therefore, vouch for its reliability. Please note that this notice is intended solely to alert readers that the content of this article is unreliable. We have not investigated whether authors were aware of or involved in the systematic manipulation of the publication process.

Wiley and Hindawi regrets that the usual quality checks did not identify these issues before publication and have since put additional measures in place to safeguard research integrity.

We wish to credit our own Research Integrity and Research Publishing teams and anonymous and named external researchers and research integrity experts for contributing to this investigation.

The corresponding author, as the representative of all authors, has been given the opportunity to register their agreement or disagreement to this retraction. We have kept a record of any response received.

References

[1] C. Li and M. Yang, "Text Knowledge Acquisition Method of Collaborative Product Design Based on Genetic Algorithm," *Journal of Mathematics*, vol. 2022, Article ID 3661477, 9 pages, 2022.

Hindawi
Journal of Mathematics
Volume 2022, Article ID 3661477, 9 pages
https://doi.org/10.1155/2022/3661477

Research Article

Text Knowledge Acquisition Method of Collaborative Product Design Based on Genetic Algorithm

Chongyuan Li[1] **and Mengmeng Yang**[1,2]

[1]*Haikou University of Economics, Haikou, Hainan 570000, China*
[2]*HaiNan Normal University, Hainan 570000, China*

Correspondence should be addressed to Chongyuan Li; 171843237@masu.edu.cn

Received 23 December 2021; Revised 31 January 2022; Accepted 4 February 2022; Published 27 February 2022

Academic Editor: Naeem Jan

In order to overcome the problems of poor clustering effect and large error of text knowledge acquisition in traditional text knowledge acquisition methods, a new text knowledge acquisition method of collaborative product design based on genetic algorithm is proposed in this paper. The definition of collaborative product design text knowledge clustering is given. According to the operation process of the genetic algorithm, the chromosomes of clustered text are constructed and encoded and the initial population is obtained. The fitness function of clustering is constructed by the DB index evaluation method; the selection, crossover, and mutation operators in the genetic algorithm are determined; and the objective function of collaborative product design text knowledge clustering is constructed. After the text knowledge clustering is completed, the text knowledge data of collaborative product design are obtained in an all-around way by using the method of rough set and neural network. The experimental results show that compared with the traditional text knowledge acquisition methods, the clustering effect of the proposed method is better and the text knowledge error is reduced up to 0.02.

1. Introduction

The product design process is an important stage of the whole product development. Modern product design is becoming more and more complex. It is difficult for a single unit to have a design team with a professional configuration. Many product design units adopt the networked collaborative product design method to unite product designers scattered in local alliances to jointly complete product design [1]. In the process of collaborative product design, knowledge exchange and sharing are important to guarantee successful product design. At present, most of the commonly used knowledge acquisition methods are that product designers obtain the knowledge they need from the product design knowledge base of each unit through a query. It requires collaborative product designers to have a deep understanding of the product design knowledge base of cooperative units [2–4]. With the continuous increase of product design knowledge, the query takes longer and longer, and it is even difficult to find the knowledge that meets the requirements of product design, which affects the efficiency of product design. Therefore, the traditional query method has been difficult to meet the requirements of networked product collaborative design.

In the process of collaborative product design, multidisciplinary design teams in distributed, remote, and dynamic environments involve many complex interactive tasks [5]. The practice results show that the sharing and reuse of design knowledge can reduce unnecessary repeated labor and shorten the product development cycle. In particular, the variant design of products can reuse the design experience and design knowledge accumulated by the design unit, so as to solve a large number of problems in many fields encountered in design [6]. Therefore, it is very important to study an effective text knowledge acquisition method for collaborative product design.

Reference [7] proposes a text knowledge acquisition method based on multigranularity. Multigranularity

cognitive ability is a common strategy for human beings to analyze complex data. As one of the complex data types, multisource data make data analysis complex because of its many data sources. Inspired by the idea of multigranularity, based on multisource information system and pessimistic decision-making strategy, the definition of multisource partition reduction set is proposed. The relationship between the multisource partition reduction set and partition reduction set is discussed, and the corresponding discrimination method of attribute characteristics is given. Finally, for a multisource decision information system, based on an optimistic decision strategy, multisource decision rules are proposed. Based on the multigranularity model, the multisource data analysis method proposed from a new perspective further enriches the method of knowledge acquisition. Reference [8] proposes a text knowledge acquisition method based on a fuzzy hyper network. Combined with the relevant knowledge of fuzzy rough set theory and hyper network, the fuzzy hyper network model adopts fuzzy equivalent relationship to replace the clear equivalent relationship in hyper network and improves the generation and evolution of hyperedges on this basis. According to the distribution of samples, the sample set is divided into three regions, namely positive domain, boundary domain, and negative domain. Samples in different regions generate super edges in different ways. According to the classification effect, the super edge set is also divided into three regions, and the super edges in different regions are replaced accordingly, so as to complete the acquisition of text knowledge. Reference [9] proposes a text knowledge acquisition method based on word meaning disambiguation of knowledge map, uses TF-IDF model to obtain the set of text feature words, uses the word meaning sequence relationship expressed by knowledge map to determine the unique semantics of polysemy in a specific semantic environment, completes the vectorial representation of text at the level of word meaning concept, and realizes text knowledge acquisition.

Based on the above research results, in order to further improve the clustering and acquisition effect of collaborative product design text knowledge, a collaborative product design text knowledge acquisition method based on a genetic algorithm is proposed. A genetic algorithm is used to optimize the text knowledge clustering algorithm to improve the effectiveness of clustering, so as to obtain more effective collaborative product design text knowledge.

The research is organized as follows: the introduction and literature review are presented in Section 1. Section 2 analyzes the text knowledge acquisition of collaborative product design based on genetic algorithm. Section 3 discusses the experimental verification of the proposed concepts. Finally, in Section 4, the research work is concluded.

2. Text Knowledge Acquisition of Collaborative Product Design Based on Genetic Algorithm

In this section, we described the text knowledge clustering of collaborative product design based on genetic algorithm and collaborative product design text knowledge acquisition with detail.

2.1. Text Knowledge Clustering of Collaborative Product Design Based on Genetic Algorithm. Collaborative product design text knowledge clustering is a fully automatic process of grouping knowledge text sets. It is a typical unsupervised machine learning process. The goal of knowledge text clustering is to find a set of such classes. The similarity between classes is as small as possible, and the similarity within classes is as large as possible [10–13]. As an unsupervised machine learning method, clustering does not need a training process and manual labeling of collaborative product design text knowledge in advance. Therefore, clustering technology is very flexible and has a high automatic processing ability. At present, it has become an important means to effectively organize, summarize, and navigate collaborative product design text knowledge.

In order to improve the effect of text knowledge clustering in collaborative product design, a genetic algorithm is used to optimize a k-means algorithm for text knowledge clustering. The specific process is as follows.

Collaborative product design text knowledge clustering is based on the famous clustering hypothesis: the similarity of similar text knowledge is large, while the similarity of different text knowledge is small [14]. Text knowledge clustering is to divide the text knowledge set into several clusters without any predictive information. It is required that the similarity of text knowledge content in the same cluster should be as large as possible, and the similarity of objects between different clusters should be as small as possible.

Definition 1. Collaborative product design text knowledge clustering is to divide a given text knowledge set $F = \{f_1, f_2, \ldots, f_m\}$ to obtain a class set $V = \{v_1, v_2, \ldots, v_l\}$, where $v_k \subset F(k = 1, 2, \ldots, l)$, making $\forall f_o(f_o \in F)$, $\exists v_l(v_l \in V)$, and $f_o \in v_l$, and minimizing the cost function $g(V)$.

The grouping in clustering is also called a cluster. The definition of a cluster is as follows: (1) the set of similar objects, and the objects in different clusters are not similar; (2) the distance between two objects in the cluster is less than the distance between any object in the cluster and any object outside the cluster.

Clustering is similar to classification in that it groups data. However, different from classification, the input set of clustering analysis is a group of unidentified records. Therefore, this is an unsupervised learning process; that is, the clustering algorithm does not need supervision and does not need to provide training data. It tends to the natural division of data. A classification algorithm is a supervised learning process, which needs to train the labeled data set.

Genetic algorithm is similar to natural evolution. It finds a good chromosome to solve the problem by acting on the genes on the chromosome. Similar to nature, the genetic algorithm knows nothing about the problem itself. All it needs is to evaluate each chromosome generated by the algorithm and select chromosomes based on fitness value so that the chromosomes with good adaptability have more reproductive opportunities. In a genetic algorithm, several numerical codes of the problem are generated randomly,

that is, chromosomes, to form the initial population; A numerical evaluation is given to each individual through the fitness function, the chromosomes with low fitness are eliminated, and the individuals with high fitness are selected to participate in the genetic operation. The individual set after genetic operation forms the next generation of the new population, the next round of evolution of the new species.

The biggest difference between a genetic algorithm and a traditional algorithm is that the calculation does not terminate automatically. The termination conditions are often artificially limiting the evolutionary algebra or setting the termination conditions by controlling the consistency of evolutionary results.

The genetic algorithm differs from other search methods in that

(1) The encoded variable value is utilized instead of the variable itself when employing the genetic algorithm to search

(2) The search method for a genetic algorithm is to iterate from one set of points to the next set of points and to iterate from one point to another, unlike most other search algorithms, but search by population

(3) Rather than using a deterministic operation process, the genetic algorithm employs a random operation process

(4) The qualities of the search space (such as connectedness, convexity) are unimportant to the genetic algorithm, which only requires the value of each point of the objective function and no additional auxiliary information

2.1.1. Chromosome Construction and Coding of Clustering Problems. According to the objective function $K(I, W)$ of collaborative product design text knowledge clustering, the ultimate goal of collaborative product design text knowledge clustering is to obtain l partition matrices I of sample set C and the prototype matrix W of clustering, and I and W are related. The partition matrix I can also be encoded, and the prototype matrix W can also be encoded.

Let M samples be divided into l classes. $M = (s_1, s_2, \ldots, s_m)$ represents the chromosome structure of the genetic algorithm, s is an $1 * N$-dimensional row vector, s_o represents the o-th gene, but $s_o \in \{1, 2, \ldots, l\}, i = 1, 2, \ldots, M$. When $s_o = v$, it means that the o-th sample belongs to class v. Generally, standard genetic operations can be used to support this expression. Therefore, for any scheme that divides the sample M into l clusters, it is its corresponding coding matrix:

$$I = (\mu_{ok})l * M, \mu_{ok} = \begin{cases} 1, & \text{if } o \in k, \\ 0, & \text{else.} \end{cases} \tag{1}$$

2.1.2. Initial Population. The initial population required by the genetic algorithm should have diversity. Therefore, when operating a genetic algorithm, first determine the population size M and then randomly generate M random numbers. According to the o-th random number l_o, a chromosome with length l_o is generated. The chromosome represents the centroid set containing l_o genes, and each gene in the chromosome represents an initial cluster center. In this way, the initial population with the population size of M and different chromosome lengths is obtained.

2.1.3. Fitness Function. The genetic algorithm basically does not use external information in the process of evolutionary search, and only takes the fitness function as the basis for optimization. The fitness function in the genetic algorithm is used to evaluate the fitness of individuals and distinguish the advantages and disadvantages of individuals in the population. The higher the fitness, the greater the probability of being inherited, and the better the clustering effect [15]. Therefore, the selection of fitness function is very important, which directly affects the convergence speed of the genetic algorithm and the ability to find the optimal solution. DB index evaluation method is adopted.

The DB evaluation method is described as follows:

$$D_i = \frac{1}{N_i} \sum_{G \in C_i} |G - H_i|, H_i = \frac{1}{N_i} \sum_{G \in C_i} G. \tag{2}$$

Here, H_i represents the center of the set, $|G - H_i|$ represents the distance from the collaborative product design text knowledge vector P to the center H_i, and D_i represents the average cohesion of the cluster set.

$$f_{ij} = \left|H_i - H_j\right|. \tag{3}$$

Here, f_{ij} represents the distance between two clustering centers.

$$\begin{aligned} S_i &= \max\left\{\frac{d_i + d_j}{f_{ij}}\right\} i \neq j, \\ DB &= \frac{1}{Z} \sum_{i=1}^{Z} S_i. \end{aligned} \tag{4}$$

Because the smaller the DB is, the better the clustering effect is, the reciprocal $1/DB$ of the DB can be used as the fitness function, that is:

$$F = \frac{1}{DB}. \tag{5}$$

From the above calculation, it can be seen that the smaller the DB, the greater the fitness value F, and the greater the probability of individual inheritance; the smaller the DB, the better the clustering effect. Therefore, it shows that the fitness value F is directly proportional to the clustering effect.

2.1.4. Genetic Operator. The main task of genetic operation is to operate the individuals of the population according to their degree of adaptation to the environment, so as to realize the evolutionary process of survival of the fittest. From the perspective of optimization search, genetic operations can optimize

the problem from generation to generation, constantly approaching the optimal solution.

The genetic algorithm includes three basic operators: selection, crossover, and mutation.

(1) *Selection Operator*. In the process of biological evolution, species with strong adaptability to the living environment will have more opportunities to inherit to the next generation; the probability of inheritance to the next generation is relatively small. The selection operation in genetic algorithm embodies the principle of "survival of the fittest": the higher the fitness, the higher the probability of participating in offspring reproduction [16–18]. A selection operation is a genetic operation used to determine how to select which individuals from a parental population to inherit to a descendant population. It is based on the evaluation of individual fitness: individuals with higher fitness have a higher probability of genes being inherited into the offspring population; in individuals with low fitness, the probability of genes being inherited into the offspring population is small.

(2) *Crossover Operator*. Crossover operation, also known as recombination, is the most important genetic operation in genetic algorithm. The crossover operation can not only maintain the excellent characteristics of the parent population to a certain extent but also make the algorithm explore the new gene space, so as to maintain the individual diversity in the new population. Crossover operation in genetic algorithm means that two paired individuals exchange some genes with each other in some way, so as to form two new individuals. The crossover operation is carried out according to a certain probability (called crossover probability). Crossover operation is an important feature that distinguishes genetic algorithm from other evolutionary operations. It plays a key role in genetic algorithm and is the main method to generate new individuals. The crossover operator simulates the mutation of natural organisms and embodies the idea of information exchange. The higher the crossover probability, the faster the convergence to the global optimal solution, but it may also lead to premature convergence; the crossover probability is too low, which may cause the search to stagnate, generally 0.4–0.9.

(3) *Mutation Operator*. Mutation operation is to imitate the variation link in the process of biological inheritance and evolution. It refers to replacing the gene value of some gene positions in the individual chromosome coding string with other alleles of the gene position, so as to form a new individual. Variation takes place with a very small probability (called variation probability). It is a random algorithm, and combined with selection and crossover operators, it can avoid the loss of some information caused by selection and crossover operations and ensure the effectiveness of genetic algorithm. Mutation is an auxiliary method to generate new individuals, but it is also an essential step of genetic algorithm, because it determines the local search ability of genetic algorithm. Mutation operation and crossover operation cooperate with each other to complete the global search and local search of the search space so that the genetic algorithm can complete the optimization process of the optimization problem with good search performance. It can increase the diversity of groups. If the mutation probability is too large, the genetic algorithm may degenerate into a random search. If the mutation probability is too small, it may not be able to produce new genes. Generally, it is 0.001–0.1.

2.1.5. Construction of Clustering Objective Function. In this study, the problem of clustering analysis of collaborative product design text knowledge is described from a mathematical point of view. Let $C = \{C_1, C_2, \ldots, C_m\}$ be the whole of m objects to be clustered. Each $C_k\,(k = 1, \ldots, m)$ objects in C are often described by a finite number of attributes $S_o\,(o = 1, \ldots, n)$. Each attribute value depicts a feature of C_k, which can be expressed as $C_k = [c_{k.1}, c_{k.2}, \ldots, c_{k,n}]$, and $C_k = [c_{k.1}, c_{k.2}, \ldots, c_{k,n}]$ is the feature vector of C_k. Cluster analysis is to analyze the similarity of multicorresponding eigenvectors of m objects in all C objects, divide $C_1, C_2, \ldots, C_m$ into multiple disjoint subsets $V_1, V_2, \ldots, V_l$ according to the distance relationship between each object, and meet the following conditions:

$$\begin{aligned} V_1 \cup V_2 \cup \cdots \cup V_k &= C, \\ V_o \cap V_k &= \Phi, \\ V_o &\neq \Phi, \\ V_o &\neq C, \\ 1 \le o \neq k &\le l. \end{aligned} \tag{6}$$

The membership relationship of m samples C_o to the subset can be expressed as follows:

$$\mu_{v_i}(C_k) = \mu_{ok} = \begin{cases} 1, & C_k \in V_o, \\ 0, & C_k \notin V_o. \end{cases} \tag{7}$$

The membership function must meet $\mu_{ok} \in Rl$; that is, each sample can only belong to a certain class, and each subclass is required to be nonempty. For l partition space Q_l of C, there are

$$\begin{cases} Q_l = \left\{ I \in T^{lm} I = [\mu_{ok}]_{l \times m}; \mu_{ok} \in \{0, 1\} \right. \\ \left. \sum_{o=1}^{l} \mu_{ok} = 1, \forall k; 0 < \sum_{k=1}^{n} \mu_{ok} < n, \forall 0 \right\}. \end{cases} \tag{8}$$

Let $T = \{T_1, T_2, \ldots, T_l\}$ represent l clustering models, and then, the objective function of clustering analysis can be expressed as follows:

$$\begin{cases} K_1(I, W) = \sum_{o=1}^{l} \left(\sum_{C_k \in V_o} (f_{ok})^2 \right), \\ \text{s.t.} \quad I \in Q_l. \end{cases} \tag{9}$$

Here, $f_{ok} = f(C_k, W_o)$ represents the dissimilarity measure between sample C_k and prototype V_o of W_o in the o-th type V_o, and $K_1(I, W)$ represents the sum of squares of errors between various samples and their prototypes. Using μ_{ok}, $K_1(I, W)$ can also be expressed as follows:

$$\begin{cases} K_1(I,W) = \sum_{k=1}^{m} \sum_{o=1}^{l} \mu_{ok} (f_{ok})^2, \\ \text{s.t.} \quad I \in Q_l, \end{cases} \tag{10}$$

where $K_1(I, W)$ is also called clustering objective function. The clustering criterion is to find the best group pair (I, W) so that when the constraint $\mu_{ok} \in Q_l$ is satisfied, $K_1(I, W)$ is the minimum, that is, $\min\{K_1(I, W)\}$.

By solving the objective function of clustering, the clustering results of collaborative product design text knowledge can be obtained for subsequent text knowledge acquisition.

The process of collaborative product design text knowledge clustering based on genetic algorithm is shown in Figure 1.

2.2. Collaborative Product Design Text Knowledge Acquisition. Based on the above clustering results of collaborative product design text knowledge, text knowledge is obtained according to rough set theory.

Rough set theory gives the dependency relationship between conditional attribute set and decision attributes; that is, the mapping relationship between input data and output data can be obtained by decision table simplification.

The text knowledge acquisition methods proposed in this study can be divided into the following steps: using self-organizing mapping (SOM) neural network method, based on the above clustering text data, the data are discretized, and the data interval is divided; rough set theory is used to extract rules to determine the input text data. According to the maximum matching rule, the optimal rule is selected to obtain the rough set evidence distribution; the evidence distribution is obtained according to the output results of the neural network, and the text data fusion results are obtained by Murphy average method combined with decision rules [19, 20].

The self-organizing mapping network is used to realize the discretization of clustering text knowledge data. There is a SOM network corresponding to each attribute a_i, which is composed of subnet. The single-attribute data are one-dimensional change, and the two-dimensional rough set decision table is obtained after network training. In order to prevent excessive discretization of the decision table, the initial number of neurons in the output layer is set to 2. The dependency among attributes in the data information system is obtained by rough set theory. The basic results of the neural network are shown in Figure 2.

The rough membership function of the relative set X of attribute values under relationship U is expressed as

$$\sigma_X^U(\alpha) = \frac{\left|X \cap [\alpha]_U\right|}{[\alpha]_U}. \tag{11}$$

Here, $|\cdot|$ represents the number of elements in the set, and α represents the attribute value. It can be seen from the above formula that the greater the value of $\sigma_X^U(\alpha)$, the higher the possibility of obtaining the X set according to the attribute value α. Using rough set theory, $i\,Q$ (condition) $\longrightarrow h$ (decision) rules are extracted from the original data of discrete collaborative product design text knowledge. The n-th rule U^i in the description rules is as follows.

If $f(x, q_1) = t_1^i, \ldots, f(x, q_n) = t_n^i$, then exist $f(x, q_1) = r_1^i, \ldots, f(r, p_r) = r_n^i$.

The matching degree of a set of input IN and the i-th rule is described as follows:

$$B_i = \frac{\sum_{i=1}^{n} IN(k)}{n}, \quad i = 1, 2, \ldots, n. \tag{12}$$

Here, $IN(k)$ represents the input mode function. Formula (12) represents the matching degree between the input pattern and the rule. The rules are obtained from the text knowledge data of collaborative product design, and the reliability of each rule is different. The rough membership

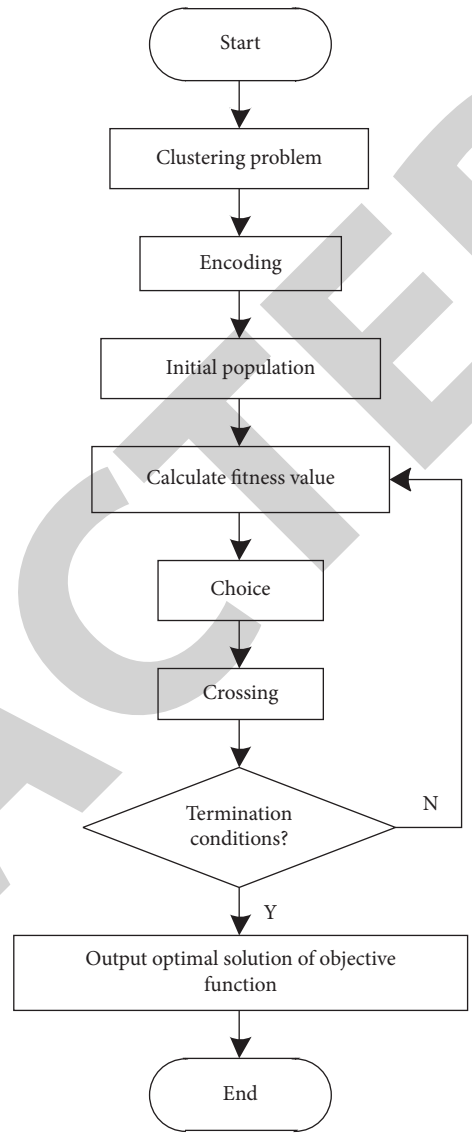

Figure 1: Collaborative product design text knowledge clustering process.

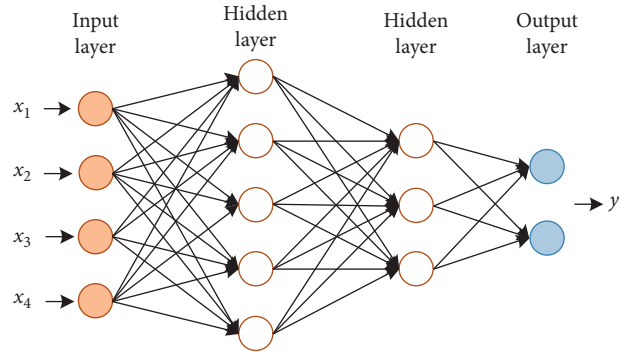

Figure 2: Structure of the neural network.

function is used to describe the reliability of the rules, and the applicability is obtained combined with the matching degree [21].

The applicability of rule i corresponding to input in is described as

$$\eta_i = \max\left\{\eta_X^{qj}\left(t_1^i\right)r_i(1), \eta_X^{qj}\left(t_2^i\right)r_i(2), \eta_X^{qj}\left(t_n^i\right)r_i(n)\right\}. \quad (13)$$

The evidence P_{RS} is obtained by rough set theory analysis, and the weight value ω is obtained by extracting rules and processing the input. According to the principle of maximum matching degree, appropriate rules are selected. It is assumed that the subscript set of rules is $\vartheta = \{e_1, e_2, \ldots, e_n\}$, the corresponding decision expression is $\{Le_1, Le_2, \ldots, Le_n\}$, and the applicability is $\{\varepsilon e_1, \varepsilon e_2, \ldots, \varepsilon e_n\}$. Assuming that the output of the neural network is $y = [Y_1, Y_2, \ldots, Y_n]$, the output $\lambda_i = [\gamma_1, \gamma_2, \ldots, \gamma_n]^{\mathrm{T}}$ of the collaborative product design text knowledge acquisition function is solved according to the Murphy average method; then,

$$\lambda_i = \frac{\left(P_{RS}(i) + P_{NN}(i)/2\right)^2}{\sum_{i=1}^{n}\left(P_{RS}(i) + P_{NN}(i)/2\right)^2}, \quad i = 1, 2, \ldots, n. \quad (14)$$

Here, P_{NN} represents collaborative product design text knowledge data input into neural network to obtain evidence. According to the decision rules of text knowledge acquisition, the text data output decision category is obtained as follows:

$$w_n = \left\{\begin{array}{c} \text{ture}, \lambda_i = \max\left(\gamma_1, \gamma_2, \ldots, \gamma_n\right) \\ \text{false, else} \end{array}\right\}. \quad (15)$$

The K-means clustering is optimized by genetic algorithm, the collaborative product design text knowledge is clustered, and the rough set combined with neural network method is used to obtain the collaborative product design text knowledge data in an all-round way [22].

3. Experimental Verification

In order to verify the practical application effect of the proposed collaborative product design text knowledge acquisition method based on genetic algorithm, simulation and comparative verification experiments are carried out.

3.1. Experimental Data. The experimental research data come from the developed collaborative product design project, which is jointly completed by 100 people. Therefore, it has high requirements for the acquisition frequency and speed of text knowledge, which meets the requirements of experimental verification. The structure of the collaborative product synchronous design pattern is shown in Figure 3.

Due to the large scale of the project, the amount of collaborative product design text knowledge data generated is large, with a total of 100 GB. And because the text knowledge data generated in the design process may be used, there is no need to preprocess the experimental data.

3.2. Experimental Environment Deployment. The experimental environment parameters are shown in Table 1.

3.3. Analysis of Experimental Results. The experimental verification scheme is as follows: taking the clustering performance, clustering time, algorithm convergence, and text knowledge acquisition error as the experimental comparison indexes, the text knowledge acquisition method based on genetic algorithm proposed in this paper is compared with the multigranularity method proposed in reference [7] and the method based on fuzzy hyper network proposed in reference [8].

3.3.1. Clustering Performance Judgment. The commonly used indicators for judging clustering performance are accuracy, recall, and F1 test value. Accuracy (PR) represents the correctness of clustering, that is, the proportion of texts in the document that really meet the search intention. It is defined as follows:

$$\mathrm{Pr}_i = \frac{TP_i}{TP_i + FP_i}. \quad (16)$$

Recall (Re) represents the integrity of clustering, that is, the ratio of all texts that meet the search intention to the retrieved text. It is defined as follows:

$$\mathrm{Re}_i = \frac{TP_i}{TP_i + FN_i}. \quad (17)$$

Here, FP_i represents the number of text incorrectly assigned to a certain cluster and belonging to other clusters, TP_i represents the number of text correctly assigned to a certain cluster, and FN_i represents the number of text belonging to a certain cluster and assigned to other clusters.

Accuracy and recall reflect two different aspects of clustering quality, which must be considered comprehensively. In some cases, some new evaluation indexes, F1 test value, will be used, which is defined as follows:

$$F1 = \frac{\mathrm{Pr} \times \mathrm{Re} \times 2}{\mathrm{Pr} + \mathrm{Re}}. \quad (18)$$

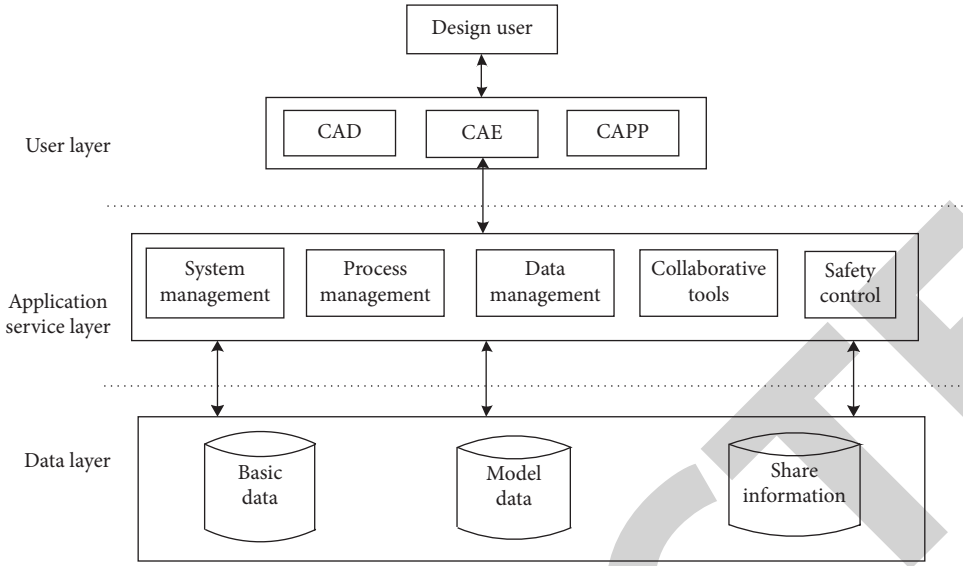

Figure 3: Structure of the collaborative product synchronous design pattern.

Table 1: Experimental environment parameters.

Parameter name	Parameter index
Equipment model	Dell OptiPlex
Operating system	Windows 10
CPU	Inter(R) core(TM) i5
Memory	16 GB
Network environment	300 GB

It can be seen from the above formula that the larger the F1 value, the better the clustering effect.

The clustering performance comparison results of the three methods are shown in Table 2.

It can be seen from the experimental results in Table 2 that the F1 values of the proposed genetic algorithm are higher than the two comparison methods, so it shows that the clustering effect of this method is better than that of the traditional method.

3.3.2. Clustering Time. In order to more fully verify the performance of the proposed method, considering the acquisition time of the overall text knowledge, clustering time is the key index. Therefore, the clustering time of the proposed method is verified, and the proposed method is compared with two traditional methods. The comparison results of clustering time of the three methods are shown in Figure 4.

By observing the clustering time comparison results shown in Figure 4, it can be seen that under multiple experiments, the proposed method based on genetic algorithm has a shorter clustering time, the maximum clustering time is no more than 1 min, the maximum clustering time based on multigranularity method is 2.5 min, and the clustering time based on fuzzy hyper network method is even 5.8 min. Therefore, it shows that the text knowledge clustering form optimized by genetic algorithm can effectively shorten the clustering time.

3.3.3. Convergence of Clustering Algorithm. The convergence of clustering algorithm has a key impact on the clustering results of collaborative product design text knowledge. Therefore, taking the convergence of clustering algorithm as the experimental comparison index, the convergence of this clustering algorithm is compared with the multigranularity method proposed in reference [7] and the fuzzy hypernetwork method proposed in reference [8]. The convergence comparison results of clustering algorithms in the three methods are shown in Figure 5.

From the convergence comparison results shown in Figure 5, it can be seen that the convergence speed based on fuzzy hyper network method is faster (20 iterations), but it is earlier than a larger objective function value, while the convergence speed based on multigranularity method is slower (45 iterations). Only the method based on genetic algorithm proposed in this paper converges to a minimum value under the requirement of convergence speed (33 iterations). Therefore, it shows that the convergence performance of the proposed method is good.

3.3.4. Collaborative Product Design Text Knowledge Acquisition Error. In the process of collaborative product design, once the text knowledge acquisition error is large, it will affect the final design result of the product. Therefore, the accuracy of text data acquisition in collaborative product design is required. Therefore, it is necessary to verify the text acquisition error of collaborative product design based on text method. The comparison results of collaborative product design text knowledge acquisition errors are shown in Figure 6.

From the comparison results of text knowledge acquisition errors shown in Figure 6, compared with the two comparison methods, the collaborative product design text knowledge acquisition error of this method is the smallest, and the error of this method does not change greatly with the increase of the number of experiments.

Table 2: Comparison results of clustering performance.

Test group	Amount of text knowledge data (GB)	F1 value		
		Method based on genetic algorithm	Method based on multigranularity	Method based on fuzzy hyper network
1	20	0.890	0.652	0.637
2	20	0.902	0.686	0.554
3	20	0.939	0.737	0.611
4	20	0.868	0.584	0.617
5	20	0.895	0.687	0.560

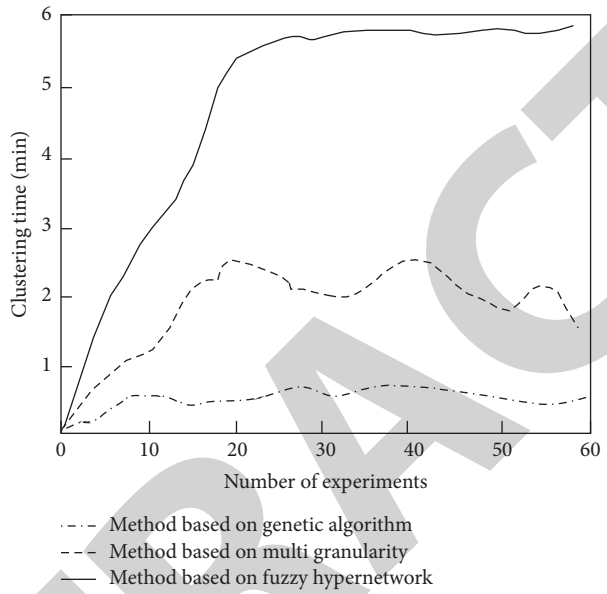

Figure 4: Comparison results of clustering time.

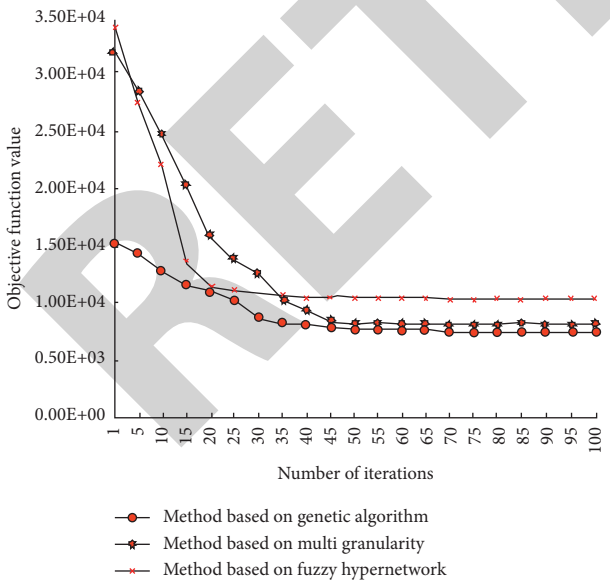

Figure 5: Comparison results of convergence of clustering algorithm.

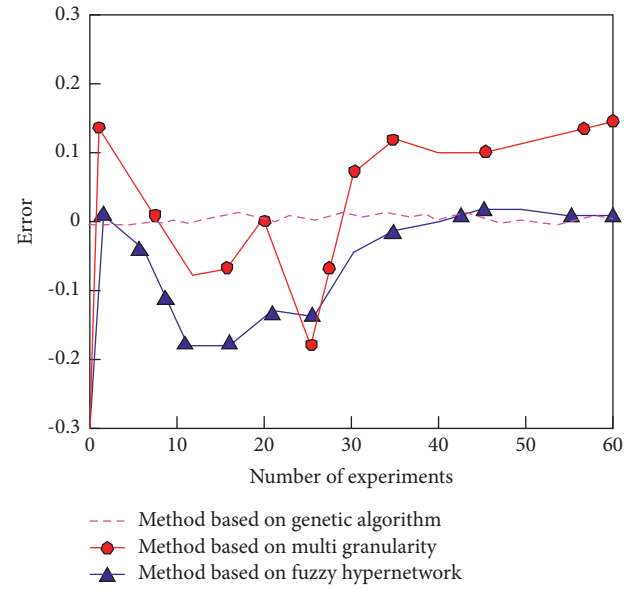

Figure 6: Comparison results of text knowledge acquisition errors.

Hindawi
Journal of Mathematics
Volume 2022, Article ID 5920124, 10 pages
https://doi.org/10.1155/2022/5920124

Research Article

κ_G-Contractive Mappings in Fuzzy Metric Spaces

Maria Samreen,[1] Sharafat Hussain,[1,2] Hassen Aydi,[3,4,5] and Yaé Ulrich Gaba[5,6,7]

[1]*Department of Mathematics, Quaid-i-Azam University Islamabad, Islamabad, Pakistan*
[2]*Department of Mathematics, Women University of Azad Jammu and Kashmir, Bagh, Pakistan*
[3]*Institut Supérieur d'Informatique et des Techniques de Communication, Université de Sousse, 4000 H. Sousse, Tunisia*
[4]*China Medical University Hospital, China Medical University, Taichung 40402, Taiwan*
[5]*Department of Mathematics and Applied Mathematics, Sefako Makgatho Health Sciences University, Ga-Rankuwa, South Africa*
[6]*Quantum Leap Africa (QLA), AIMS Rwanda Centre, Remera Sector KN 3, Kigali, Rwanda*
[7]*African Center for Advanced Studies, P.O. Box 4477, Yaounde, Cameroon*

Correspondence should be addressed to Hassen Aydi; hassen.aydi@isima.rnu.tn and Yaé Ulrich Gaba; yaeulrich.gaba@gmail.com

Received 23 September 2021; Accepted 18 January 2022; Published 26 February 2022

Academic Editor: Ewa Rak

This article is concerned with a class of contractions in the framework of a fuzzy metric space endowed with a graph. The main results obtained not only broaden but also generalize a number of relevant results in the literature. Particularly, we get some results for cyclic contractions in fuzzy metric spaces. We also consider an integral equation.

1. Introduction

In recent years, fixed-point theory has become a tantalizing field of research in nonlinear analysis due to its wide range of applications in computer sciences, game theory, physics, economics, and various other fields. It has become a tool to find solutions for nonlinear equations such as differential equations, integrodifferential equations, and matrix equations [1, 2]. After the fundamental Banach's theorem [3] in 1922, a huge amount of literature appeared for the investigation of fixed points of self-operators. Among those results, two aspects must be considered: underlying geometric structure on which self-operator is defined and an appropriate contraction condition on operator.

The investigation of existence of a fixed point of self-mappings on a metric space $(\mathcal{N}, d)$ equipped with a partial ordering was originated by the works of Ran and Reurings [4]. By replacing a partial order with a graph, Jachymski [5] studied some prolific results about the existence of a fixed point involving the graph concept. Later on, several researchers conducted further studies in this area by relaxing the contractive condition and analyzing the connectivity condition of a graph. For more details, see [6–8].

On the other hand, Kramosil and Michalek [9] gave the concept of a fuzzy metric space. Afterward Grabiec [10] extended the Banach contraction principle (BCP) to fuzzy metric spaces in the sense of Kramosil and Michalek. Many authors undertook further advancements in this direction by generalizing the contraction inequalities and by providing the underlying space with rich geometric structure to make the results more viable. In this context, recently a number of authors contributed new and exciting developments in fixed-point theory using fuzzy metric spaces; see [9–18] and the references included therein. For some very recent studies on the topic, we refer the reader to [19–21].

In particular, Altun [11] proved some useful results about the existence of fixed points of fuzzy order κ-contractive mappings with the setting of non-Archimedean fuzzy metric spaces. The work of Jachymski motivated us to introduce the notion of fuzzy order κ_G-contractive mappings and study related fixed-point results in the context of a fuzzy metric space equipped with a graph. Our introduced notion unifies the concept of Altun and Mihet, and Jachymski. By a

successful application of our main result, we also ensure the existence of a solution for an integral equation.

2. Preliminaries

In this section, we recall some basic notions and results which are used in the sequel. Throughout this article, we use $J = [0, 1]$.

Definition 1 (see [9]). A binary operation $\theta: J \times J \longrightarrow J$ is a continuous t-norm if, for all $u, v, w, z \in J$, it satisfies the following conditions:

(1) θ is continuous,

(2) $(u\theta v)\theta w = u\theta(v\theta w)$ and $u\theta v = v\theta u$,

(3) $u\theta 1 = u$,

(4) $w \geq u$ and $z \geq v$ imply that $w\theta z \geq u\theta v$.

If there exists a strictly increasing sequence $\{v_n\} \subset (0, 1)$ such that $v_n\theta v_n = v_n$ for all $n \in \mathbb{N}$, then the continuous t-norm θ is known as Hadzic type.

Definition 2 (see [9]). Let $\mathcal{N}$ be an arbitrary set, let $\Gamma: \mathcal{N} \times \mathcal{N} \times [0, \infty) \longrightarrow J$ be a fuzzy set, and let θ be a continuous t-norm. $(\mathcal{N}, \Gamma, \theta)$ is said to be a fuzzy metric space if, for all $\alpha, \beta, \gamma \in \mathcal{N}$ and $\iota, \lambda > 0$, the following conditions hold:

(1) $[(FM_1)]$ $\Gamma(\alpha, \beta, 0) = 0$,

(2) $[(FM_2)]$ $\Gamma(\alpha, \beta, \iota) = 1$ if and only if $\alpha = \beta$,

(3) $[(FM_3)]$ $\Gamma(\alpha, \beta, \iota) = \Gamma(\beta, \alpha, \iota)$,

(4) $[(FM_4)]$ $\Gamma(\alpha, \beta, \iota)\theta\Gamma(\alpha, \gamma, \lambda) \leq \Gamma(\alpha, \gamma, \iota + \lambda)$,

(5) $[(FM_5)]$ $\Gamma(\alpha, \beta, \cdot)$: $[0, \infty) \longrightarrow J$ is left continuous.

Remark 1 (see [11]). If we take the inequality (NA) rather than (FM_4) of Definition 2,

$$\Gamma(\alpha, \beta, \iota)\theta\Gamma(\alpha, \gamma, \lambda) \leq \Gamma(\alpha, \gamma, \max\{\iota, \lambda\}), \quad \text{for all } \alpha, \beta, \gamma \in \mathcal{N} \text{ and } \iota, \lambda > 0, \text{ (NA)}, \tag{1}$$

then we call $(\mathcal{N}, \Gamma, \theta)$ a non-Archimedean fuzzy metric space. It is worthwhile to note that every non-Archimedean fuzzy metric space is a fuzzy metric space. From now on, we denote a fuzzy metric space simply by $\mathcal{N}$.

Definition 3 (see [9, 11]). A sequence $\{\alpha_n\}$ in $\mathcal{N}$ is called

(i) Cauchy if $\lim_{n\longrightarrow\infty}\Gamma(\alpha_n, \alpha_{n+p}, \iota) = 1$ for each $\iota > 0$ and $p > 0$;

(ii) convergent to $\alpha \in \mathcal{N}$ if $\Gamma_{n \longrightarrow \infty}(\alpha_n, \alpha, \iota) = 1$ for all $\iota > 0$;

(iii) M-Cauchy if for each $\varepsilon \in (0, 1)$ and $\iota > 0$ there is a natural number n_0 such that $\Gamma(\alpha_n, \alpha_m, \iota) > 1 - \varepsilon$ for all $m, n > n_0$;

(iv) G-Cauchy if $\lim_{n\longrightarrow\infty}\Gamma(\alpha_n, \alpha_{n+1}, \iota) = 1$, for all $\iota > 0$.

$\mathcal{N}$ is called complete if every Cauchy sequence is convergent. Additionally, it is called M-complete if every M-Cauchy sequence is convergent and G-complete if every G-Cauchy sequence is convergent.

In the following, we take into account the main results of [11]. A self-map $\mathcal{T}$ on an ordered set $(\mathcal{N}, \prec)$ is named nondecreasing (nonincreasing) w.r.t $\prec$ if $\alpha \prec \beta$ implies $\mathcal{T}\alpha \prec \mathcal{T}\beta$ $(\mathcal{T}\alpha \succcurlyeq \mathcal{T}\beta)$.

Definition 4 (see [11]). Let $(\mathcal{N}, \prec)$ be a partially order set and let $(\mathcal{N}, \Gamma, \theta)$ be a fuzzy metric space. Let $\kappa: J \longrightarrow J$ be a function. $\mathcal{T}: \mathcal{N} \longrightarrow \mathcal{N}$ is called a fuzzy order κ-contractive mapping if the following holds:

$$\alpha, \beta \in \mathcal{N}, \alpha \prec \beta \Rightarrow \Gamma(\mathcal{T}\alpha, \mathcal{T}\beta, \iota) \geq \kappa(\Gamma(\alpha, \beta, \iota)), \quad \text{for all } \iota > 0. \tag{2}$$

Theorem 1 (see [11], Theorem 2.3). *Let $(\mathcal{N}, \Gamma, \theta)$ be an M-complete non-Archimedean fuzzy metric space with the t-norm θ of Hadzic type, in which $\mathcal{N}$ is a set with the partial order $\prec$. Let $\mathcal{T}: \mathcal{N} \longrightarrow \mathcal{N}$ be a fuzzy order κ-contractive mapping, where $\kappa: J \longrightarrow J$ is a continuous, nondecreasing function. Assume that*

(i) $\mathcal{T}$ is nondecreasing;

(ii) either for every nondecreasing sequence $\{\alpha_n\}$ in $\mathcal{N}$ with $\alpha_n \longrightarrow \alpha \in \mathcal{N}$ implies $\alpha_n \prec \alpha$ for all n or $\mathcal{T}$ is continuous;

(iii) there exists $\alpha_0 \in \mathcal{N}$ such that $\alpha_0 \prec \mathcal{T}\alpha_0$ and $\lim_{n\longrightarrow\infty}\kappa^n(\Gamma(\alpha_0, \mathcal{T}\alpha_0, \iota)) = 1$ for each $\iota > 0$.

Then there is $\omega \in \mathcal{N}$ such that $\mathcal{T}\omega = \omega$.

Theorem 2 (see [11], Theorem 2.4). *Let $(\mathcal{N}, \Gamma, \theta)$ be an M-complete non-Archimedean fuzzy metric space with the t-norm θ of Hadzic type in which $\mathcal{N}$ is a set with the partial order $\prec$. Let $\mathcal{T}: \mathcal{N} \longrightarrow \mathcal{N}$ be a fuzzy order κ-contractive mapping, where $\kappa: J \longrightarrow J$ is a continuous mapping such that $\kappa(\iota) > \iota$ for all $\iota \in (0, 1)$. Assume that*

(i) $\mathcal{T}$ is nondecreasing;

(ii) either for every nondecreasing sequence $\{\alpha_n\}$ in $\mathcal{N}$ with $\alpha_n \longrightarrow \alpha \in \mathcal{N}$ implies $\alpha_n \prec \alpha$ for all n or $\mathcal{T}$ is continuous;

(iii) there is $\alpha_0 \in \mathcal{N}$ such that $\alpha_0 \prec \mathcal{T}\alpha_0$, $\Gamma(\alpha_0, \mathcal{T}\alpha_0, \iota) > 0$ for all $\iota > 0$.

Then there exists $\omega \in \mathcal{N}$ such that $\mathcal{T}\omega = \omega$.

Following [5], we include basic notions about graph which are used throughout this paper. Let $(\mathcal{N}, \Gamma, \theta)$ be a fuzzy metric space. The diagonal of $\mathcal{N} \times \mathcal{N}$ is represented by Δ. Consider a directed graph G such that its diagonal is a subset of $E(G)$ and $V(G)$ is equal to the whole set $\mathcal{N}$. We assume that G does not have any edges which are parallel and describe G with the pair $(V(G), E(G))$. By G^{-1}, we mean the converse of graph G and it is defined as

$$E\left(G^{-1}\right) = \{(\alpha, \beta) \in \mathcal{N} \times \mathcal{N}: (\beta, \alpha) \in E(G)\}. \tag{3}$$

The undirected graph is denoted by $\widetilde{G}$ and it is obtained by neglecting the direction of edges. $E(\widetilde{G})$ is given as

$$E(\widetilde{G}) = E\left(G^{-1}\right) \cup E(G). \tag{4}$$

If V' is a subset of $V(G)$, E' is a subset of $E(G)$ and, for any edge $(\alpha, \beta) \in E', \alpha, \beta \in V$; then (V', E') is called a subgraph of G. The sequence $\{\alpha_j\}_{j=0}^{p}$ of $(p+1)$ vertices, such that

$$\begin{aligned} &\alpha = \alpha_0, \alpha_p = \beta \text{ and } \left(\alpha_{j-1}, \alpha_j\right) \in E(G), \\ &\qquad \text{where } j \in \{1, 2, \ldots, p\}, \end{aligned} \tag{5}$$

is called the path of length p between two vertices α and β in G, where p is a nonnegative integer. If between any two vertices there is always a path, then we call G a connected graph. G is said to be weakly connected if $\widetilde{G}$ is connected. Let α be a vertex in G and let $E(G)$ be symmetric; then the set of vertices and edges that are comprised in certain path starting at α is known as component of G which contains α; it is a subgraph of G and is denoted by G_α. The set of all edges in G_α is denoted by $E(G_\alpha)$ and $V(G_\alpha) = [\alpha]_G$. It is worthwhile to indicate that G_α is connected. Here, $[\alpha]_G$ is the equivalence class of R and the relation R on vertices of V is defined as

$$\beta R \gamma, \quad \text{if there is a path amidst } \beta \text{ and } \gamma \text{ in } G. \tag{6}$$

Let $\{\alpha_n\}$ be any sequence in $\mathcal{N}$. If for $\{\alpha_n\}$ with $\alpha_n \longrightarrow \alpha$ and $(\alpha_n, \alpha_{n+1}) \in E(G)$ for $n \in \mathbb{N}$ implies that there exists a subsequence $\{\alpha_{n_k}\}$ of $\{\alpha_n\}$ such that $(\alpha_{n_k}, \alpha) \in E(G)$ for $k \in \mathbb{N}$, then G is called (C)-graph.

3. Main Results

From now on, we denote a fuzzy metric space endowed with a graph G simply by $\mathcal{N}$.

Definition 5. A mapping $\mathcal{T}: \mathcal{N} \longrightarrow \mathcal{N}$ is called fuzzy order κ_G-contractive if, for all $\alpha, \beta \in \mathcal{N}$, we have

$$(\alpha, \beta) \in E(G) \text{ implies } (\mathcal{T}\alpha, \mathcal{T}\beta) \in E(G), \tag{7}$$

$$\begin{aligned} &\Gamma(\mathcal{T}\alpha, \mathcal{T}\beta, \iota) \geq \kappa(\Gamma(\alpha, \beta, \iota)), \\ &\quad \text{for all } \iota > 0 \text{ whenever } (\alpha, \beta) \in E(G), \end{aligned} \tag{8}$$

where $\kappa: J \longrightarrow J$ is a continuous and nondecreasing function.

Example 1. Suppose that G is any graph such that $V(G) = \mathcal{N}$. Define $\mathcal{T}: \mathcal{N} \longrightarrow \mathcal{N}$ by $\mathcal{T}\alpha = u$ for all $\alpha \in \mathcal{N}$, where u is any constant; then $\mathcal{T}$ is a fuzzy order κ_G-contractive mapping.

Example 2. Let G_0 be a graph such that $E(G_0) := \mathcal{N} \times \mathcal{N}$. Then any fuzzy order κ_G-contractive mapping is a fuzzy order κ_{G_0}-contractive mapping.

Definition 6. Two sequences $\{\alpha_n\}$ and $\{\beta_n\}$ in $\mathcal{N}$ are said to be equivalent if $\lim_{n\longrightarrow\infty} \Gamma(\alpha_n, \beta_n, \iota) = 1$ for all $\iota > 0$. In addition, $\{\alpha_n\}$ and $\{\beta_n\}$ are called Cauchy equivalent if each of them is Cauchy.

Lemma 1. *Let $\{\alpha_n\}$ and $\{\beta_n\}$ be equivalent sequences in $\mathcal{N}$. Then the following hold:*

(i) if $\alpha_n \longrightarrow \alpha$, then $\beta_n \longrightarrow \alpha$ and its converse holds;

(ii) if $\{\alpha_n\}$ is a Cauchy sequence, then $\{\beta_n\}$ is also a Cauchy sequence and vice versa.

Proof. By using condition (FM_4) of Definitions 2 and 3, one can easily invoke the conclusions. □

Proposition 1. *Let $\mathcal{T}: \mathcal{N} \longrightarrow \mathcal{N}$ be a fuzzy order κ_G-contractive mapping, where $\kappa: J \longrightarrow J$ is a continuous, nondecreasing function. Then the following hold:*

(i) $\mathcal{T}$ is both a fuzzy order $\kappa_{\widetilde{G}}$ contractive mapping and a fuzzy order $\kappa_{G^{-1}}$-contractive mapping,

(ii) $[\alpha_0]_{\widetilde{G}}$ is $\mathcal{T}$-invariant, and $\mathcal{T}|_{[\alpha_0]_{\widetilde{G}}}$ is a fuzzy order $\kappa_{\widetilde{G}_\alpha}$-contractive mapping provided that $\alpha_0 \in \mathcal{N}$ is such that $\mathcal{T}\alpha_0 \in [\alpha_0]_{\widetilde{G}}$.

Proof. (i) It could be proved easily by taking into account (FM_3) of Definition 3. (ii) Let $\alpha \in [\alpha_0]_{\widetilde{G}}$. Then there exists a path between α and α_0; that is, there exists a sequence $\{z_j\}_{j=0}^{p}$ of $(p+1)$ vertices such that $\alpha = z_0, z_p = \alpha_0$ and $(z_{j-1}, z_j) \in E(G)$, for $j = 1, 2, \ldots, p$. Since $\mathcal{T}$ is fuzzy order κ_G-contractive, one writes $(\mathcal{T}z_{j-1}, \mathcal{T}z_j) \in E(G)$ for $j \in \{1, 2, \ldots, p\}$. Thus $\mathcal{T}\alpha \in [\mathcal{T}\alpha_0]_{\widetilde{G}} = [\alpha_0]_{\widetilde{G}}$. Now, suppose that $(\alpha, \beta) \in E(\widetilde{G}_{\alpha_0})$. Since $\mathcal{T}$ is fuzzy order $\kappa_{\mathbb{G}}$-contractive, we have $(\mathcal{T}\alpha, \mathcal{T}\beta) \in E(G)$. But $[\alpha_0]_{\widetilde{G}}$ is $\mathcal{T}$-invariant, which implies that $(\mathcal{T}\alpha, \mathcal{T}\beta) \in E(\widetilde{G}_{\alpha_0})$. As $\widetilde{G}_{\alpha_0}$ is a subgraph of G, we have

$$\begin{aligned} &\Gamma(\mathcal{T}\alpha, \mathcal{T}\beta, \iota) \geq \kappa(\Gamma(\alpha, \beta, \iota)), \\ &\qquad \text{for all } \iota > 0 \text{ whenever } (\alpha, \beta) \in E\left(\widetilde{G}_{\alpha_0}\right). \end{aligned} \tag{9}$$

□

Lemma 2. *Let $\mathcal{T}: \mathcal{N} \longrightarrow \mathcal{N}$ be a fuzzy order κ_G-contractive mapping, where $\kappa: J \longrightarrow J$ is a continuous, nondecreasing function. Assume that, for $\alpha \in \mathcal{N}$ and $\beta \in [\alpha]_{\widetilde{G}}$, we have*

$$\lim_{n\longrightarrow\infty} \kappa^n\left(\Gamma\left(z_{j-1}, z_j, \iota\right)\right) = 1, \quad \text{for all } \iota > 0, \tag{10}$$

where $\{z_j\}_{j=0}^{p}$ is any path between α and β. Then $\{\mathcal{T}^n\alpha\}$ and $\{\mathcal{T}^n\beta\}$ are equivalent.

Proof. Let $\alpha \in \mathcal{N}$ and $\beta \in [\alpha]_{\widetilde{G}}$; then a path $\alpha = \alpha_0, \alpha_1, \ldots, \alpha_p = \beta$ exists between α and β with $(\alpha_{j-1}, \alpha_j) \in E(\widetilde{G})$ for $j \in \{1, 2, \ldots, p\}$. From Proposition 1, $\mathcal{T}$ is a fuzzy order $\kappa_{\widetilde{G}}$-contractive mapping. So, for all $n \in \mathbb{N}$ and $j \in \{1, 2, \ldots, p\}$, we obtain

$$\begin{aligned} &\Gamma\left(\mathcal{T}^n\alpha_{j-1}, \mathcal{T}^n\alpha_j, \iota\right) \geq \kappa\left(\Gamma\left(\mathcal{T}^{n-1}\alpha_{j-1}, \mathcal{T}^{n-1}\alpha_j, \iota\right)\right), \\ &\qquad \text{for all } \iota > 0, \end{aligned} \tag{11}$$

whenever $(\mathcal{T}^n\alpha_{j-1}, \mathcal{T}^n\alpha_j) \in E(\widetilde{G})$. Now, for all $n \in \mathbb{N}$ and $j \in \{1, 2, \ldots, p\}$, we obtain

$$\begin{aligned}\Gamma\left(\mathcal{T}^n\alpha_{j-1},\mathcal{T}^n\alpha_j,\iota\right)&\geq\kappa\left(\Gamma\left(\mathcal{T}^{n-1}\alpha_{j-1},\mathcal{T}^{n-1}\alpha_j,\iota\right)\right)\\&\geq\cdots\geq\kappa^n\left(\Gamma\left(\alpha_{j-1},\alpha_j,\iota\right)\right).\end{aligned}\tag{12}$$

It yields that $\{\mathcal{T}^n\alpha_j\}_{j=0}^p$ is a path in $\widetilde{G}$ from $\mathcal{T}^n\alpha$ to $\mathcal{T}^n\beta$. Thus,

$$\begin{aligned}\Gamma\left(\mathcal{T}^n\alpha,\mathcal{T}^n\beta,\iota\right)&\geq\Gamma\left(\mathcal{T}^n\alpha_0,\mathcal{T}^n\alpha_1,\frac{\iota}{p}\right)\theta^{(p\,\text{times})\cdots}\theta\Gamma\left(\mathcal{T}^n\alpha_{p-1},\mathcal{T}^n\alpha_p,\frac{\iota}{p}\right)\\&\geq\kappa^n\left(\Gamma\left(\alpha_0,\alpha_1,\frac{\iota}{p}\right)\right)\theta^{(p\,\text{times})\cdots}\theta\kappa^n\left(\Gamma\left(\alpha_{p-1},\alpha_p,\frac{\iota}{p}\right)\right).\end{aligned}\tag{13}$$

By letting $n\longrightarrow\infty$, we conclude $\lim_{n\longrightarrow\infty}\Gamma(\mathcal{T}^n\alpha,\mathcal{T}^n\beta,\iota)=1$. □

Proposition 2. *Let $\mathcal{T}:\mathcal{N}\longrightarrow\mathcal{N}$ be a fuzzy order κ_G-contractive mapping, where $\kappa: J\longrightarrow J$ is a continuous, nondecreasing function. Assume that, for $\alpha_0\in\mathcal{N}$, we have $\mathcal{T}\alpha_0\in[\alpha_0]_G^{\sim}$ and*

$$\lim_{n\longrightarrow\infty}\kappa^n\left(\Gamma\left(z_{j-1},z_j,\iota\right)\right)=1,\quad\text{for all }\iota>0,\tag{14}$$

where $\{z_j\}_{j=0}^p$ is any path between α_0 and $\mathcal{T}\alpha_0$. Suppose that, for any sequence $\{\mathcal{T}^n\alpha_0\}$ in $\mathcal{N}$ with $\mathcal{T}^n\alpha_0\in[\alpha_0]_G^{\sim}, n\geq1$ and $\Gamma(\mathcal{T}^n\alpha_0,\mathcal{T}^{n+1}\alpha_0,\iota)\longrightarrow1$, there is $n_0\in\mathbb{N}$ satisfying $(\mathcal{T}^m\alpha_0,\mathcal{T}^n\alpha_0)\in E(G)$ for each $m,n\geq n_0$.

Then $\{\mathcal{T}^n\alpha_0\}$ is an M-Cauchy sequence in $\mathcal{N}$.

Proof. Since $\mathcal{T}\alpha_0\in[\alpha_0]_G^{\sim}$, from Proposition 1, it follows that $\mathcal{T}^n\alpha_0\in[\alpha_0]_G^{\sim}$ for all $n\geq1$. Now, we suppose that $\{\beta_j\}_{j=0}^p$ is a path connecting α_0 and $\mathcal{T}\alpha_0$. Using the similar reasoning like in the proof of Lemma 2, we have

$$\lim_{n\longrightarrow\infty}\Gamma\left(\mathcal{T}^n\alpha_0,\mathcal{T}^{n+1}\alpha_0,\iota\right)=1,\quad\text{for all }n\in\mathbb{N}.\tag{15}$$

Now, we show that $\{\mathcal{T}^n\alpha_0\}$ is an M-Cauchy sequence. Suppose on the contrary that $\{\mathcal{T}^n\alpha_0\}$ is not an M-Cauchy sequence; then there exist $\varepsilon\in(0,1)$ and two subsequences $\{\mathcal{T}^{m(k)}\alpha_0\}$ and $\{\mathcal{T}^{n(k)}\alpha_0\}$ of $\{\mathcal{T}^n\alpha_0\}$ with $n(k)>m(k)>k$ such that

$$\Gamma\left(\mathcal{T}^{m(k)}\alpha_0,\mathcal{T}^{n(k)}\alpha_0,\iota\right)\leq1-\varepsilon.\tag{16}$$

Let, for each k, $m(k)$ be the least integer exceeding $n(k)$ satisfying (16), but

$$\Gamma\left(\mathcal{T}^{m(k)-1}\alpha_0,\mathcal{T}^{n(k)}\alpha_0,\iota\right)>1-\varepsilon.\tag{17}$$

Now, for each $k\in\mathbb{N}$, we obtain

$$\begin{aligned}1-\varepsilon\geq\Gamma\left(\mathcal{T}^{m(k)}\alpha_0,\mathcal{T}^{n(k)}\alpha_0,\iota\right)&\geq\Gamma\left(\mathcal{T}^{m(k)-1}\alpha_0,\mathcal{T}^{n(k)}\alpha_0,\frac{\iota}{2}\right)\theta\Gamma\left(\mathcal{T}^{m(k)-1}\alpha_0,\mathcal{T}^{m(k)}\alpha_0,\frac{\iota}{2}\right)\\&>(1-\varepsilon)\theta\Gamma\left(\mathcal{T}^{m(k)-1}\alpha_0,\mathcal{T}^{m(k)}\alpha_0,\frac{\iota}{2}\right).\end{aligned}\tag{18}$$

By taking $k\longrightarrow\infty$ and using (15), we obtain

$$\lim_{k\longrightarrow\infty}\Gamma\left(\mathcal{T}^{m(k)}\alpha_0,\mathcal{T}^{n(k)}\alpha_0,\iota\right)=1-\varepsilon.\tag{19}$$

Since $\lim_{n\longrightarrow\infty}\Gamma(\mathcal{T}^n\alpha_0,\mathcal{T}^{n+1}\alpha_0,\iota)=1$, for all $n\in\mathbb{N}$ and $\iota\geq0$, by condition (i), there exists a positive integer n_0 such that $(\mathcal{T}^m\alpha_0,\mathcal{T}^n\alpha_0)\in E(G)$ for each $m,n\in\mathbb{N}$ with $m,n>n_0$. Now, by using triangular inequality for all $k\geq n_0$, we obtain

$$\begin{aligned}\Gamma\left(\mathcal{T}^{m(k)}\alpha_0,\mathcal{T}^{n(k)}\alpha_0,\iota\right)&\geq\Gamma\left(\mathcal{T}^{m(k)}\alpha_0,\mathcal{T}^{m(k)+1}\alpha_0,\frac{\iota}{3}\right)\theta\Gamma\left(\mathcal{T}^{m(k)+1}\alpha_0,\mathcal{T}^{n(k)+1}\alpha_0,\frac{\iota}{3}\right)\\&\quad\theta\Gamma\left(\mathcal{T}^{n(k)+1}\alpha_0,\mathcal{T}^{n(k)}\alpha_0,\frac{\iota}{3}\right)\\&\geq\Gamma\left(\mathcal{T}^{m(k)}\alpha_0,\mathcal{T}^{m(k)+1}\alpha_0,\frac{\iota}{3}\right)\theta\kappa\left(\Gamma\left(\mathcal{T}^{m(k)}\alpha_0,\mathcal{T}^{n(k)}\alpha_0,\frac{\iota}{3}\right)\right)\\&\quad\theta\Gamma\left(\mathcal{T}^{n(k)+1}\alpha_0,\mathcal{T}^{n(k)}\alpha_0,\frac{\iota}{3}\right).\end{aligned}\tag{20}$$

On letting $k \longrightarrow \infty$ and by using (15) and (19), we acquire

$$1-\varepsilon \geq 1\theta\kappa(1-\varepsilon)\theta 1 = \kappa(1-\varepsilon) > 1-\varepsilon. \tag{21}$$

Hence, $\{\mathcal{T}^n\alpha_0\}$ is an M-Cauchy sequence in $\mathcal{N}$. □

Remark 2. It is important to note that assertion of Proposition 2 still holds if we replace the condition $\mathcal{T}\alpha_0 \in [\alpha_0]_{\widetilde{G}}$ with $(\alpha_0, \mathcal{T}\alpha_0) \in E(G)$. In that case, condition (i) is also replaced by the following: "for any sequence $\{\mathcal{T}^n\alpha_0\}$ in $\mathcal{N}$ with $(\mathcal{T}^n\alpha_0, \mathcal{T}^{n+1}\alpha_0) \in E(G)$ and $\Gamma(\mathcal{T}^n\alpha_0, \mathcal{T}^{n+1}\alpha_0, \iota) \longrightarrow 1$, there exists $n_0 \in \mathbb{N}$ such that $(\mathcal{T}^m\alpha_0, \mathcal{T}^n\alpha_0) \in E(G)$ for all $m, n \geq n_0$."

Below we extend the definitions of (H_f)- and (C_f)-graphs to the setting of fuzzy metric spaces.

Definition 7. Suppose that $\mathcal{T}: \mathcal{N} \longrightarrow \mathcal{N}$, $\beta \in \mathcal{N}$, and the sequence $\{\mathcal{T}^n\beta\}$ in $\mathcal{N}$ is such that $\mathcal{T}^n\beta \longrightarrow \alpha \in \mathcal{N}$.

(i) If there exists a subsequence $\{\mathcal{T}^{n_k}\beta\}$ of $\{\mathcal{T}^n\beta\}$ such that $(\mathcal{T}^{n_k}\beta, \alpha) \in E(G)$ for all $k \geq p \in \mathbb{N}$, then G is called a (C_f)-graph.

(ii) A graph G is called an (H_f)-graph if $\mathcal{T}^n\beta \in [\alpha]_{\widetilde{G}}$ for $n \geq 1$; then $r(\mathcal{T}^n\beta, \alpha, \iota) \longrightarrow 1 (\text{as } n \longrightarrow \infty)$, where $r(\mathcal{T}^n\beta, \alpha, \iota) = \Gamma(z_0, z_1, \iota/p)\theta^{(p-\text{times})\cdots}\theta\Gamma(z_{p-1}, z_p, \iota/p)$ and $\{z_j\}_{j=0}^{p}$ is a path from $\mathcal{T}^n\beta$ to α.

It is evident that every (C)-graph is a (C_f)-graph for the identity mapping I, but the other side is not always true. Similarly, every (H)-graph is an (H_f)-graph for the identity mapping I, but the other side is not always true (see [8], Examples 2.4 and 2.5).

Lemma 3. *Let $\mathcal{T}: \mathcal{N} \longrightarrow \mathcal{N}$ be fuzzy order $\kappa_{\widetilde{G}}$-contractive, where $\kappa: J \longrightarrow J$ is a continuous, nondecreasing function. Then, for any $\alpha \in \mathcal{N}$ and $\beta \in [\alpha]_{\widetilde{G}}$ and for each $n \in \mathbb{N}$, there is $r_n(\alpha, \beta, \iota) \in J$ such that*

$$\Gamma(\mathcal{T}^n\alpha, \mathcal{T}^n\beta, \iota) \geq r_n(\alpha, \beta, \iota). \tag{22}$$

Furthermore, if $\lim_{n\longrightarrow\infty}\kappa^n(\Gamma(z_{j-1}, z_j, \iota)) = 1$ for all $\iota > 0$, where $\{z_j\}_{i=1}^{p}$ is any path between α and β, then

$$\lim_{n\longrightarrow\infty}\Gamma(\mathcal{T}^n\alpha, \mathcal{T}^n\beta, \iota) = \lim_{n\longrightarrow\infty} r_n(\alpha, \beta, \iota) = 1. \tag{23}$$

Proof. Let $\alpha \in \mathcal{N}$ and $\beta \in [\alpha]_{\widetilde{G}}$; then there exists a path $\alpha = \alpha_0, \alpha_1, \ldots, \alpha_p = \beta$ between α and β with $(\alpha_{j-1}, \alpha_j) \in E(\widetilde{G})$ for $j \in \{1, 2, \ldots, p\}$. From Proposition 1 for all $\iota > 0$, we have

$$\Gamma\left(\mathcal{T}^n\alpha_{j-1}, \mathcal{T}^n\alpha_j, \iota\right) \geq \kappa\left(\Gamma\left(\mathcal{T}^{n-1}\alpha_{j-1}, \mathcal{T}^{n-1}\alpha_j, \iota\right)\right). \tag{24}$$

Since $\mathcal{T}$ is a fuzzy order $\kappa_{\widetilde{G}}$ contraction such that $(\mathcal{T}^n\alpha_{j-1}, \mathcal{T}^n\alpha_j) \in E(\widetilde{G})$ for each natural number n and j varies from 1 to p, for a positive integer n and $j \in \{1, 2, \ldots, p\}$, we have

$$\begin{aligned}\Gamma\left(\mathcal{T}^n\alpha_{j-1}, \mathcal{T}^n\alpha_j, \iota\right) &\geq \kappa\left(\Gamma\left(\mathcal{T}^{n-1}\alpha_{j-1}, \mathcal{T}^{n-1}\alpha_j, \iota\right)\right)\\ &\geq \cdots \geq \kappa^n\left(\Gamma\left(\alpha_{j-1}, \alpha_j, \iota\right)\right).\end{aligned} \tag{25}$$

Note that $\{\mathcal{T}^n\alpha_j\}_{j=0}^{p}$ is a path in $\widetilde{G}$ from $\mathcal{T}^n\alpha$ to $\mathcal{T}^n\beta$. Thus,

$$\begin{aligned}\Gamma(\mathcal{T}^n\alpha, \mathcal{T}^n\beta, \iota) &\geq \Gamma\left(\mathcal{T}^n\alpha_0, \mathcal{T}^n\alpha_1, \frac{\iota}{p}\right)\theta^{(p\,\text{times})\cdots}\theta\Gamma\left(\mathcal{T}^n\alpha_{p-1}, \mathcal{T}^n\alpha_p, \frac{\iota}{p}\right)\\ &\geq \kappa^n\left(\Gamma\left(\alpha_0, \alpha_1, \frac{\iota}{p}\right)\right)\theta^{(p\,\text{times})\cdots}\theta\kappa^n\left(\Gamma\left(\alpha_{p-1}, \alpha_p, \frac{\iota}{p}\right)\right).\end{aligned} \tag{26}$$

It suffices to set

$$r_n(\alpha, \beta, \iota) = \kappa^n\left(\Gamma\left(\alpha_0, \alpha_1, \frac{\iota}{p}\right)\right)\theta\kappa^n\left(\Gamma\left(\alpha_1, \alpha_2, \frac{\iota}{p}\right)\right)\theta^{(p\,\text{times})\cdots}\theta\kappa^n\left(\Gamma\left(\alpha_{p-1}, \alpha_p, \frac{t}{p}\right)\right). \tag{27}$$

On letting $n \longrightarrow \infty$, we obtain

$$\lim_{n\longrightarrow\infty}\Gamma(\mathcal{T}^n\alpha, \mathcal{T}^n\beta, \iota) = \lim_{n\longrightarrow\infty} r_n(\alpha, \beta, \iota) = 1. \tag{28}$$

Now, we proceed to establish our first main result. From now on, $\mathcal{N}$ represents an M-complete fuzzy metric space endowed with a graph G. □

Theorem 3. *Let $\mathcal{T}: \mathcal{N} \longrightarrow \mathcal{N}$ be a fuzzy order $\kappa_{\widetilde{G}}$-contractive mapping, where $\kappa: J \longrightarrow J$ is a continuous, nondecreasing function. Assume that, for a given $\alpha_0 \in \mathcal{N}$, $(\alpha_0, \mathcal{T}\alpha_0) \in E(G)$ and*

$$\lim_{n\longrightarrow\infty}\kappa^n(\Gamma(\alpha_0, \mathcal{T}\alpha_0, \iota)) = 1, \quad \text{for all } \iota > 0. \tag{29}$$

Moreover, if

(i) G is a (C_f)-graph,

(ii) for any sequence $\{\mathcal{T}^n\alpha_0\}$ in $\mathcal{N}$ with $(\mathcal{T}^n\alpha_0, \mathcal{T}^{n+1}\alpha_0) \in E(G), n \geq 1$ and $\Gamma(\mathcal{T}^n\alpha_0, \mathcal{T}^{n+1}\alpha_0, \iota) \longrightarrow 1$, then there is a natural number n_0 so that $(\mathcal{T}^m\alpha_0, \mathcal{T}^n\alpha_0) \in E(G)$ for every $m, n \geq n_0$.

Then there is $\omega \in [\alpha_0]_{\widetilde{G}}$ in such a way that $\mathcal{T}\omega = \omega$. In addition, if, for every $\beta \in [\alpha_0]_{\widetilde{G}}$, we have

$$\lim_{n\longrightarrow\infty} \kappa^n\Big(\Gamma\Big(z_{j-1}, z_j, \iota\Big)\Big) = 1, \quad \text{for all } \iota > 0, \tag{30}$$

where $\{z_j\}_{j=0}^{p}$ is any path between α and β, then $\mathcal{T}|_{[\alpha_0]_{\widetilde{G}}}$ is a Picard operator.

Proof. Let $(\alpha_0, \mathcal{T}\alpha_0) \in E(G)$; then $\mathcal{T}\alpha_0 \in [\alpha_0]_{\widetilde{G}}$. From Proposition 2, we infer that $\{\mathcal{T}^n\alpha_0\}$ is an M-Cauchy sequence. Since $\mathcal{N}$ is an M-complete space, there exists $\omega \in \mathcal{N}$ such that $\mathcal{T}^n\alpha_0 \longrightarrow \omega$. Since G is a (C_f)-graph, there are $\{\mathcal{T}^{n_k}\alpha_0\}$, a subsequence of $\{\mathcal{T}^n\alpha_0\}$, and a positive integer q in such a way that $(\mathcal{T}^{n_k}\alpha_0, \omega) \in E(G)$ for every positive integer k and $q \leq k$. Thus, for all $p \leq k$, we obtain

$$\begin{aligned}\Gamma(\mathcal{T}\omega, \omega, \iota) &\geq \Gamma\Big(\mathcal{T}\omega, \mathcal{T}^{n_k+1}\alpha_0, \frac{\iota}{2}\Big)\theta\Gamma\Big(\mathcal{T}^{n_k}\alpha_0, \omega, \frac{\iota}{2}\Big)\\ &\geq \kappa\Big(\Gamma\Big(\omega, \mathcal{T}^{n_k}\alpha_0, \frac{\iota}{2}\Big)\Big)\theta\Gamma\Big(\mathcal{T}^{n_k}\alpha_0, \omega, \frac{\iota}{2}\Big).\end{aligned} \tag{31}$$

Using the continuity of κ and taking $n \longrightarrow \infty$, one gets

$$\Gamma(\mathcal{T}\omega, \omega, \iota) = 1. \tag{32}$$

This infers that $\mathcal{T}\omega = \omega$. We observe that $\{\alpha_0, \mathcal{T}\alpha_0, \ldots, \mathcal{T}^{n_1}\alpha_0, \ldots, \mathcal{T}^p\alpha_0, \omega\}$ is a path between α_0 and ω in $\widetilde{G}$. Thus, $\omega \in [\alpha_0]_{\widetilde{G}}$. Now, take a random element $\beta \in [\alpha_0]_{\widetilde{G}}$ and, using Lemma 2, we obtain

$$\lim_{n\longrightarrow\infty} \Gamma(\mathcal{T}^n\beta, \mathcal{T}^n\alpha_0, \iota) = 1. \tag{33}$$

Thus, $\lim_{n\longrightarrow\infty}\mathcal{T}^n\beta = \omega$. To ensure the uniqueness, we argue by contradiction. Suppose that ω and π are two distinct fixed points of $\mathcal{T}$ in $[\alpha_0]_{\widetilde{G}}$, so

$$\begin{aligned}\Gamma(\omega, \pi, \iota) = \Gamma(\mathcal{T}^n\omega, \mathcal{T}^n\pi, \iota) &\geq \Gamma\Big(\mathcal{T}^n\omega, \mathcal{T}^n\alpha_0, \frac{\iota}{2}\Big)\\ &\theta\Gamma\Big(\mathcal{T}^n\alpha_0, \mathcal{T}^n\pi, \frac{\iota}{2}\Big).\end{aligned} \tag{34}$$

On letting $n \longrightarrow \infty$, we obtain $\omega = \pi$. □

Remark 3. Observe that, in Theorem 3, $\mathcal{T}$ is a Picard operator on $\mathcal{N}$ if the underlying graph G is weakly connected such that $[\alpha_0]_{\widetilde{G}} = \mathcal{N}$.

By analyzing condition on graph G and imposing a strict condition on κ, we have the following variant.

Theorem 4. *Let $\mathcal{T}: \mathcal{N} \longrightarrow \mathcal{N}$ be a fuzzy order κ_G-contractive mapping, where $\kappa: J \longrightarrow J$ is a continuous, nondecreasing function such that $\kappa(\iota) > \iota$ for all $\iota \in (0, 1)$. Assume that for $\alpha_0 \in \mathcal{N}$ and $\beta \in [\alpha_0]_{\widetilde{G}}$ we get*

$$\lim_{n\longrightarrow\infty} \kappa^n\Big(\Gamma\Big(z_{j-1}, z_j, \iota\Big)\Big) = 1, \quad \text{for all } \iota > 0, \tag{35}$$

where $\{z_j\}_{j=0}^{p}$ is any path between α_0 and β. Moreover, if

(i) G is an (H_f)-graph,

(ii) for any sequence $\{\mathcal{T}^n\alpha_0\}$ in $\mathcal{N}$ with $(\mathcal{T}^n\alpha_0, \mathcal{T}^{n+1}\alpha_0) \in E(G), n \geq 1$ and $\Gamma(\mathcal{T}^n\alpha_0, \mathcal{T}^{n+1}\alpha_0, \iota) \longrightarrow 1$, then there is $n_0 \in \mathcal{N}$ in such a way that $(\mathcal{T}^m\alpha_0, \mathcal{T}^n\alpha_0) \in E(G), \forall m, n \geq n_0$;

(iii) G is weakly connected.

Then $\mathcal{T}$ is a Picard operator.

Proof. Assume that $\alpha_0 \in \mathcal{N}$ and condition (iii) holds. Then $\mathcal{T}\alpha_0 \in [\alpha_0]_{\widetilde{G}}$; that is, there is a path between α_0 and $\mathcal{T}\alpha_0$ in $\widetilde{G}$. Take into account Proposition 2; we infer that the sequence $\{\mathcal{T}^n\alpha_0\}$ is an M-Cauchy sequence. Since $\mathcal{N}$ is an M-complete fuzzy metric space, there exists $\omega \in \mathcal{N}$ such that $\mathcal{T}^n\alpha_0 \longrightarrow \omega$. Since condition (iii) holds, we have, for each natural number n, $\mathcal{T}^n\alpha_0 \in [\omega]_{\widetilde{G}}$. Then there exists a path $\{z_j^n\}_{j=0}^{p_n}$ of finite length p_n between $\mathcal{T}^n\alpha_0$ and ω with $z_0^n = \mathcal{T}^n\alpha_0, z_{p_n}^n = \omega$. Using the conditions that $\mathcal{T}$ is a κ_G-contractive mapping and $\kappa(\iota) > \iota$, we obtain

$$\begin{aligned}\Gamma(\omega, \mathcal{T}\omega, \iota) &\geq \Gamma\Big(\omega, \mathcal{T}^{n+1}\alpha_0, \frac{\iota}{2}\Big)\theta\Gamma\Big(\mathcal{T}^{n+1}\alpha_0, \mathcal{T}\omega, \frac{\iota}{2}\Big)\\ &\geq \Gamma\Big(\omega, \mathcal{T}^{n+1}\alpha_0, \frac{\iota}{2}\Big)\theta\Big[\Gamma\Big(\mathcal{T}z_0^n, \mathcal{T}z_1^n, \frac{\iota}{2l_n}\Big)\theta^{(p_n \text{ times})\cdots}\theta\Gamma\Big(\mathcal{T}z_{j-1}^n, \mathcal{T}z_j^n, \frac{\iota}{2l_n}\Big)\Big]\\ &\geq \Gamma\Big(\omega, \mathcal{T}^{n+1}\alpha_0, \frac{\iota}{2}\Big)\theta\Big[\kappa\Big(\Gamma\Big(z_0^n, z_1^n, \frac{\iota}{2l_n}\Big)\Big)\theta^{(p_n \text{ times})\cdots}\theta\kappa\Big(\Gamma\Big(z_{j-1}^n, z_j^n, \frac{\iota}{2l_n}\Big)\Big)\Big]\\ &= \Gamma\Big(\omega, \mathcal{T}^{n+1}\alpha_0, \frac{\iota}{2}\Big)\theta r(\mathcal{T}^n\alpha_0, \omega, \iota).\end{aligned} \tag{36}$$

By letting $n \longrightarrow \infty$ and using condition (i), we get $\Gamma(\omega, \mathcal{T}^{n+1}\alpha_0, \iota/2)\theta r(\mathcal{T}^n\alpha_0, \omega, \iota) \longrightarrow 1$. Hence, we have $\Gamma(\omega, \mathcal{T}\omega, \iota) = 1$. Thus, $\omega = \mathcal{T}\omega$. Now, let β be a random element of $[\alpha_0]_{\widetilde{G}}$; then Lemma 2 implies

$$\lim_{n\longrightarrow\infty}\Gamma\left(\mathcal{T}^n\beta,\mathcal{T}^n\alpha_0,\iota\right)=1. \tag{37}$$

Thus, $\lim_{n\longrightarrow\infty}\mathcal{T}^n\beta=\omega$. Now, for uniqueness, suppose that $\omega\neq\pi$ are two fixed points of $\mathcal{T}$ in $[\alpha_0]_{\widetilde{G}}$; we have

$$\begin{aligned}\Gamma(\omega,\pi,\iota)&=\Gamma\left(\mathcal{T}^n\omega,\mathcal{T}^n\pi,\iota\right)\geq\Gamma\left(\mathcal{T}^n\omega,\mathcal{T}^n\alpha_0,\frac{\iota}{2}\right)\\&\theta\Gamma\left(\mathcal{T}^n\alpha_0,\mathcal{T}^n\pi,\frac{\iota}{2}\right).\end{aligned} \tag{38}$$

On letting $n\longrightarrow\infty$, we obtain $\omega=\pi$. □

Definition 8. Let $\mathcal{T}:\mathcal{N}\longrightarrow\mathcal{N}$. If, for all $\alpha,\beta\in\mathcal{N}$ and some sequence $\{p_j\}_{j\in\mathbb{N}}$ of a positive integer, $\mathcal{T}^{p_j}\alpha\longrightarrow\beta$ implies $\mathcal{T}(\mathcal{T}^{p_j}\alpha)\longrightarrow\mathcal{T}\beta$ as $j\longrightarrow\infty$, then $\mathcal{T}$ is called orbitally continuous. If, for each $\alpha,\beta\in\mathcal{N}$ and some sequence $\{p_j\}_{j\in\mathbb{N}}$ of a positive integer $\mathcal{T}^{p_j}\alpha\longrightarrow\beta$ and $(\mathcal{T}^{p_j}\alpha,\mathcal{T}^{p_j+1}\alpha)\in E(G)$ for each positive integer n implies $\mathcal{T}(\mathcal{T}^{p_j}\alpha)\longrightarrow\mathcal{T}\beta$, then $\mathcal{T}$ is known as orbitally G-continuous.

Theorem 5. *Let $\mathcal{T}:\mathcal{N}\longrightarrow\mathcal{N}$ be a fuzzy order κ_G-contractive mapping, where $\kappa:J\longrightarrow J$ is a continuous and nondecreasing function. Assume that, for given $\alpha_0\in\mathcal{N}$,*

$$(\alpha_0,\mathcal{T}\alpha_0)\in E(G)\text{ and }\lim_{n\longrightarrow\infty}\kappa^n(\Gamma(\alpha_0,\mathcal{T}\alpha_0,\iota))=1,\quad\text{for all }\iota>0. \tag{39}$$

Moreover, if

(i) $\mathcal{T}$ is orbitally G-continuous or $\mathcal{T}$ is orbitally continuous,

(ii) for any sequence $\{\mathcal{T}^n\alpha_0\}$ in $\mathcal{N}$ with $(\mathcal{T}^n\alpha_0,\mathcal{T}^{n+1}\alpha_0)\in E(G),n\geq1$ and $\Gamma(\mathcal{T}^n\alpha_0,\mathcal{T}^{n+1}\alpha_0,\iota)\longrightarrow1$, there is $n_0\in\mathbb{N}$ in such a way that $(\mathcal{T}^m\alpha_0,\mathcal{T}^n\alpha_0)\in E(G),\forall m,n\geq n_0$.

Then there is an element ω in $[\alpha_0]_{\widetilde{G}}$ such that $\mathcal{T}\omega=\omega$. In addition, if, for every $\beta\in[\alpha_0]_{\widetilde{G}}$, we have

$$\lim_{n\longrightarrow\infty}\kappa^n\left(\Gamma\left(z_{j-1},z_j,\iota\right)\right)=1,\quad\text{for all }\iota>0, \tag{40}$$

where $\{z_j\}_{j=0}^{p}$ is any path between α and β, then $\mathcal{T}|_{[\alpha_0]_{\widetilde{G}}}$ is a Picard operator.

Proof. Since $(\alpha_0,\mathcal{T}\alpha_0)\in E(G)$, we have $\mathcal{T}\alpha_0\in[\alpha_0]_{\widetilde{G}}$. From Proposition 2, $\{\mathcal{T}^n\alpha_0\}$ is an M-Cauchy sequence. Since $\mathcal{N}$ is an M-complete fuzzy metric space, there exists $\omega\in\mathcal{N}$ such that $\mathcal{T}^n\alpha_0\longrightarrow\omega$. As $(\mathcal{T}^n\alpha_0,\mathcal{T}^{n+1}\alpha_0)\in E(G)$, for all $n\geq1$, and $\mathcal{T}$ is orbitally G-continuous, we obtain $\mathcal{T}\mathcal{T}^n\alpha_0\longrightarrow\mathcal{T}\omega$. Hence, $\mathcal{T}\omega=\omega$. Let $\beta\in[\alpha_0]_{\widetilde{G}}$ be arbitrary, so Lemma 3 yields $\mathcal{T}^n\beta\longrightarrow\omega$. Uniqueness can be easily followed.

Now, we include another result when the underlying fuzzy metric space is endowed with a partial order. □

Corollary 1. *Let $(\mathcal{N},\prec)$ be a partially ordered set and let $(\mathcal{N},\Gamma,\theta)$ be an M-complete fuzzy metric space. Let $\mathcal{T}:\mathcal{N}\longrightarrow\mathcal{N}$ be a fuzzy order κ-contractive mapping, where $\kappa:J\longrightarrow J$ is a continuous and nondecreasing function. Assume that*

(i) $\mathcal{T}$ is nondecreasing (or nonincreasing),

(ii) either for every nondecreasing (nonincreasing) sequence $\{\alpha_n\}$ in $\mathcal{N}$ with $\alpha_n\longrightarrow\alpha\in\mathcal{N}$ implies $\alpha_n\prec\alpha$ (or $\alpha_n\succcurlyeq\alpha$) for all n or $\mathcal{T}$ is continuous, and

(iii) there exists $\alpha_0\in\mathcal{N}$ such that $\alpha_0\prec\mathcal{T}\alpha_0$ $(\alpha_0\succcurlyeq\mathcal{T}\alpha_0)$ and $\lim_{n\longrightarrow\infty}\kappa^n(\Gamma(\alpha_0,\mathcal{T}\alpha_0,\iota))=1$ for each $\iota>0$.

Then $\mathcal{T}$ has a fixed point.

Proof. Define G by $V(G)=\mathcal{N}$ and $E(G)=\{(\alpha,\beta)\in\mathcal{N}\times\mathcal{N}:\beta\prec\alpha\}$.

Since $\mathcal{T}$ is nondecreasing, we have that (7) is satisfied and (8) holds in the light of condition (2). Thus, $\mathcal{T}$ is a κ_G-contractive mapping. Also, note that condition (ii) implies that G is a (C_f)-graph. Thus, taking into account Theorem 3, we invoke the result. □

Remark 4. Note that Corollary 1 extends/generalizes ([22], Theorem 2.3) to non-Archimedean M-complete fuzzy metric spaces.

Example 3. Let $\mathcal{N}=(0,\infty)$ be equipped with a fuzzy metric $\Gamma(\alpha,\beta,\iota)=(\min\{\alpha,\beta\}/\max\{\alpha,\beta\})$ so that $\alpha\theta\beta=\alpha\beta$. Then $(\mathcal{N},\Gamma,\theta)$ is an M-complete fuzzy metric space (see [23]). Define $\mathcal{T}:\mathcal{N}\longrightarrow\mathcal{N}$ by

$$\mathcal{T}\alpha=\begin{cases}2\alpha, & 0<\alpha<1,\\ \dfrac{\alpha+5}{3}, & 1\leq\alpha\leq4,\\ 2\alpha-5, & \alpha>4.\end{cases} \tag{41}$$

Let G be a graph in such a way that $V(G)=\mathcal{N}$ and $E(G)=\Delta\cup\{(\alpha,\beta):\alpha,\beta\in[1,4],\alpha\leq\beta\}$. Condition (7) is trivial. We show that $\mathcal{T}$ is fuzzy order κ_G-contractive with $\kappa(u)=\sqrt{u}$. Indeed, let $\alpha,\beta\in\mathcal{N}$ with $(\alpha,\beta)\in E(G)$. Now, if $\alpha\leq\beta$, then

$$\Gamma(\mathcal{T}\alpha,\mathcal{T}\beta,\iota)=1\geq\kappa(1)=\kappa(\Gamma(\alpha,\beta,\iota)). \tag{42}$$

If $\alpha,\beta\in[1,4]$ with $\alpha\leq\beta$, then

$$\begin{aligned}\Gamma(\mathcal{T}\alpha,\mathcal{T}\beta,\iota)&=\frac{\min\{(\alpha+5)/3,(\beta+5)/3\}}{\max\{(\alpha+5)/3,(\beta+5)/3\}}\\&=\frac{\alpha+5}{\beta+5}\geq\sqrt{\frac{\alpha}{\beta}}=\kappa(\Gamma(\alpha,\beta,\iota)).\end{aligned} \tag{43}$$

Therefore, $\mathcal{T}$ is a fuzzy order κ_G-contractive mapping with $\kappa(u)=\sqrt{u}$. Moreover, for $\alpha_0=1$, $(\alpha_0,\mathcal{T}\alpha_0)\in E(G)$. Hence, all the conditions of Theorem 3 are satisfied and $\mathcal{T}$ has a fixed point.

4. Application

In [24], the following definition was initiated: let $\mathcal{N}$ be a nonempty set and let $\{G_j\}_{j=1}^{k}$ be nonempty closed subsets of

$\mathcal{N}$, where n is any positive integer. Then, $D = \cup_{j=1}^{k} G_j$ is called a cyclic representation of $\mathcal{N}$ with respect to the mapping $\mathcal{T}: D \longrightarrow D$ if

$$\mathcal{T}(G_1) \subset G_2, \ldots, \mathcal{T}(G_{m-1}) \subset G_m, \mathcal{T}(G_m) \subset G_1. \tag{44}$$

Then $\mathcal{T}$ is called a cyclic operator.

Theorem 6. *Let $(\mathcal{N}, \Gamma, \theta)$ be an M-complete fuzzy metric space. Let $\{G_j\}_{j=1}^{k}$ be nonempty closed subsets of $\mathcal{N}$, $D = \cup_{j=1}^{k} G_j$, and $\mathcal{T}: D \longrightarrow D$. Further, suppose the following:*

(i) $\cup_{j=1}^{k} G_j$ is a cyclic representation of D with respect to $\mathcal{T}$.

(ii) There exists $\kappa: J \longrightarrow J$, where κ is a continuous and nondecreasing function such that, for $\alpha \in G_j, \beta \in G_{j+1}$, we have

$$\Gamma(\mathcal{T}\alpha, \mathcal{T}\beta, \iota) \geq \kappa(\Gamma(\alpha, \beta, \iota)), \quad \forall \iota > 0. \tag{45}$$

(iii) Let $\alpha_0 \in D$; for a sequence $\{\mathcal{T}^n \alpha_0\}$ in D with $\Gamma(\mathcal{T}^n \alpha_0, \mathcal{T}^{n+1} \alpha_0, \iota) \longrightarrow 1$, there are a natural number n_0 and some $j \in \{1, 2, \ldots, k\}$ such that $\mathcal{T}^m \alpha_0 \in G_j, \mathcal{T}^n \alpha_0 \in G_{j+1}$, for all $m, n \geq n_0$ and

$$\lim_{n \longrightarrow \infty} \kappa^n(\Gamma(\alpha_0, \mathcal{T}\alpha_0, \iota)) = 1, \quad \forall \iota > 0. \tag{46}$$

Then $\mathcal{T}$ has a fixed point $w \in \cap_{j=1}^{k} G_j$ and $\mathcal{T}^n \alpha_0 \longrightarrow w$.

Proof. Since $\{G_j\}_{j=1}^{k}$ are closed subsets, one can assert that (D, Γ, θ) is an M-complete fuzzy metric space. Let G be a graph such that

$$V(G) = D \text{ and } E(G) = \Delta \cup \{(\alpha, \beta) \in D \times D: \alpha \in G_j, \beta \in G_{j+1}; j = 1, 2, \ldots, k\}. \tag{47}$$

As $D = \cup_{j=1}^{k} G_j$ is a cyclic representation of D with respect to $\mathcal{T}$, it follows that $\mathcal{T}$ preserves edges. Also, observe that, in light of inequality (45), $\mathcal{T}$ is a κ_G-contractive mapping. Now, for a sequence $\{\mathcal{T}^n \alpha_0\}$ in D, we have $(\mathcal{T}^n \alpha_0, \mathcal{T}^{n+1} \alpha_0) \in E(G), \forall n \geq 1$ and if $\Gamma(\mathcal{T}^n \alpha_0, \mathcal{T}^{n+1} \alpha_0, \iota) \longrightarrow 1$, then, from condition (iii), there is $n_0 \in \mathbb{N}$ such that $(\mathcal{T}^m \alpha_0, \mathcal{T}^n \alpha_0) \in E(G)$ for all $m, n \geq n_0$. Let $\mathcal{T}^n \alpha \longrightarrow w$ in D be such that $(\mathcal{T}^n \alpha, \mathcal{T}^{n+1} \alpha) \in E(G)$ for all $n \geq 1$; then, from (44) in every G_j, the sequence $\{\mathcal{T}^n \alpha\}$ has infinitely many terms; thus we have a subsequence of $\{\mathcal{T}^n \alpha\}$ which converges to w in each G_j. As G_j's are all closed subsets, we get $w \in \cap_{j=1}^{k} G_j$. Thus, there exists a subsequence $\{\mathcal{T}^{n_r} \alpha\}$ in some G_j, $j \in \{1, 2, \ldots, k\}$, such that $(\mathcal{T}^{n_r} \alpha, w) \in E(G)$ for $r \geq 1$, which shows that G is a weakly connected (C_f)-graph. Taking into account Theorem 3, we invoke the conclusion.

Now, we present an application of our result to find a solution of an integral equation. Consider the below integral equation:

$$\alpha(r) = \int_0^r K(r, s, \alpha(s))\mathrm{d}s + g(r), \quad \forall r \in [0, I] \text{ where } I > 0. \tag{48}$$

Let $\mathcal{N} = C([0, I])$ be the set of all real valued continuous functions defined on $[0, I]$. Then $(\mathcal{N}, d)$ is a complete metric space endowed with the metric

$$d(\alpha, \beta) = \sup_{r \in [0.I]} |\alpha(r) - \beta(r)| \quad \alpha, \beta \in \mathcal{N}. \tag{49}$$

For $a\theta b = ab$ for all $a, b \in J$, define a fuzzy metric by

$$\Gamma(\alpha, \beta, \iota) = \frac{\iota}{\iota + d(\alpha, \beta)}, \quad \text{for all } \alpha, \beta \in \mathcal{N} \text{ and } \iota > 0. \tag{50}$$

Then $(\mathcal{N}, \Gamma, \theta)$ is an M-complete fuzzy metric space.

In the following, we discuss the existence of the solution for the integral equation (48). □

Theorem 7. *Let $\mathcal{N}$ be the set of all real valued continuous functions defined on $[0, I]$. Let $\mathcal{T}: \mathcal{N} \longrightarrow \mathcal{N}$ be the integral operator given by*

$$\mathcal{T}\alpha(r) = \int_0^r K(r, s, \alpha(s))\mathrm{d}s + g(r), \quad \forall r \in [0, I] \text{ and } g \in \mathcal{N}, \tag{51}$$

where $K: [0, I] \times [0, I] \times \mathbb{R} \longrightarrow \mathbb{R}$ is continuous. Assume that

(i) there exist a nondecreasing, continuous function $\kappa: J \longrightarrow J$ and a continuous function $\mathcal{T}: [0, I] \times [0, I] \longrightarrow \mathbb{R}^+$ such that

$$|K(r, s, \alpha(s)) - K(r, s, \beta(s))| \leq f(r, s)\kappa(|\alpha(s) - \beta(s)|), \tag{52}$$

for each $r, s \in [0, I]$ and $\alpha(r) \leq \beta(r)$ for all $r \in [0, 1]$;

(ii) $K(r, s, .): \mathbb{R} \longrightarrow \mathbb{R}$ is nondecreasing for each $r, s \in [0, I]$;

(iii) $\sup_{r \in [0,I]} \int_0^r f(r, s)ds \leq 1$;

(iv) there exists $\alpha_0 \in \mathcal{N}$ such that $\alpha_0(r) \leq \int_0^r K(r, s, \alpha_0(s))ds + g(r)$ for all $r \in [0, I]$;

(v) for any sequence $\{\alpha_n\}$ in $\mathcal{N}$ with $\Gamma(\alpha_n, \alpha_{n+1}, \iota) \longrightarrow 1$ there exists $n_0 \in \mathbb{N}$ such that $\alpha_m(\iota) \leq \alpha_n(\iota)$ for all $m, n \in \mathbb{N}$, $m, n \geq n_0$.

Then the integral equation (48) has a unique solution in the set $\{\alpha \in \mathcal{N}: \alpha(r) \leq \alpha_0(r), \text{or } \alpha(r) \geq \alpha_0(r) \text{ for all } r \in [0, I]\}$.

Proof. Let G be a graph such that $V(G) = \mathcal{N}$ and $E(G) = \{(\alpha, \beta) \in \mathcal{N} \times \mathcal{N}: \alpha(r) \leq \beta(r) \text{ for all } r \in [0, I]\}$. It follows from (ii) that T is nondecreasing and thus preserves edges. Also, for every nondecreasing sequence $\{\alpha_n\} \subset \mathcal{N}$ which converges to $\omega \in \mathcal{N}$, it implies $\alpha_n(r) \leq \omega(r)$ for every

$r \in [0, I]$, which shows that G is a (C_f)-graph. Now, for all $\alpha, \beta \in \mathcal{N}$, we obtain

$$\begin{aligned} |\mathcal{T}\alpha(r) - \mathcal{T}\beta(r)| &\leq \int_0^r |K(r,s,\alpha(s)) - K(r,s,\beta(s))| \mathrm{d}s \\ &\leq \int_0^r f(r,s)|\alpha(s) - \beta(s)| \mathrm{d}s \\ &\leq \kappa(|\alpha(s) - \beta(s)|) \int_0^r f(r,s) \mathrm{d}s. \end{aligned} \tag{53}$$

Hence, $d(\mathcal{T}\alpha, \mathcal{T}\beta) \leq \kappa(d(\alpha, \beta))$. Thus,

$$\frac{\iota}{\iota + d(\mathcal{T}\alpha, \mathcal{T}\beta)} \geq \kappa(d(\alpha,\beta)) \geq \kappa\left(\frac{\iota}{t + d(\alpha,\beta)}\right). \tag{54}$$

It follows that

$$\Gamma(\mathcal{T}\alpha, \mathcal{T}\beta, \iota) \geq \kappa(\Gamma(\alpha, \beta, \iota)). \tag{55}$$

From (iv), we have $(\alpha_0, \mathcal{T}\alpha_0) \in E(G)$ and the conclusion follows from Theorem 3. Moreover, the solution lies in $[\alpha_0]_{\widetilde{G}} = \{\alpha \in \mathcal{N}: \alpha(r) \leq \alpha_0, \text{or } \alpha(r) \geq \alpha_0 \text{ for all } r \in [0, I]\}$. □

Data Availability

The data used to support the findings of this study are available from the corresponding author upon request.

Conflicts of Interest

The authors declare that they have no conflicts of interest.

Authors' Contributions

M. S. contributed to methodology, supervision, and data analysis; S. H. contributed to data analysis, study conception, and investigation; H. A. contributed to investigation, validation, and design; Y. U. G. contributed to investigation, editing the revised version, and visualization. All authors approve and agree on the final version.

Acknowledgments

The fourth author would like to acknowledge that his contribution to this work was carried out with the aid of a grant from the Carnegie Corporation provided through the African Institute for Mathematical Sciences.

References

[1] M. S. Asgari and B. Mousavi, "Solving a class of nonlinear matrix equations via the coupled fixed point theorem," *Applied Mathematics and Computation*, vol. 259, pp. 364–373, 2015.

[2] J. Harjani, B. López, and K. Sadarangani, "Fixed point theorems for mixed monotone operators and applications to integral equations," *Nonlinear Analysis: Theory, Methods & Applications*, vol. 74, no. 5, pp. 1749–1760, 2011.

[3] S. Banach, "Sur les opérations dans les ensembles abstraits et leur application aux équations intégrales," *Fundamenta Mathematicae*, vol. 3, pp. 133–181, 1922.

[4] A. C. M. Ran and M. C. B. Reurings, "A fixed point theorem in partially ordered sets and some applications to matrix equations," *Proceedings of the American Mathematical Society*, vol. 132, pp. 1435–1443, 2004.

[5] J. Jachymski, "The contraction principle for mappings on a metric space with a graph," *Proceedings of the American Mathematical Society*, vol. 136, pp. 1359–1373, 2008.

[6] F. Bojor, "Fixed point of φ-contraction in metric spaces endowed with a graph," *Annals of the University of Craiova, Mathematics*, vol. 37, pp. 85–92, 2010.

[7] C. Chifu, E. Karapınar, and G. Petrusel, "Qualitative properties of the solution of a system of operator inclusions in b-metric spaces endowed with a graph," *Bulletin of the Iranian Mathematical Society*, vol. 44, no. 5, pp. 1267–1281, 2018.

[8] M. Samreen and T. Kamran, "Fixed point theorems for weakly contractive mappings on a metric space endowed with a graph," *Filomat*, vol. 28, no. 3, pp. 441–450, 2014.

[9] O. Kramosil and J. Michalek, "Fuzzy metric and statistical metric spaces," *Kybernetica*, vol. 11.5, pp. 326–334, 1975.

[10] K. Javed, F. Uddin, H. Aydi, A. Mukheimer, and M. Arshad, "Ordered-theoretic fixed point results in fuzzy b-metric spaces with an application," *Journal of Mathematics*, vol. 2021, Article ID 6663707, 7 pages, 2021.

[11] I. Altun, "Some fixed point theorems for single and multi valued mappings on ordered nonarchimedean fuzzy metric spaces," *Iranian Journal of Fuzzy Systems*, vol. 7, pp. 91–96, 2010.

[12] A. Azam and I. Beg, "Common fuzzy fixed points for fuzzy mappings," *Fixed Point Theory and Applications*, vol. 2013, no. 1, Article ID 14, 2013.

[13] M. A. Erceg, "Metric spaces in fuzzy set theory," *Journal of Mathematical Analysis and Applications*, vol. 69, no. 1, pp. 205–230, 1979.

[14] A. George and P. Veeramani, "On some results in fuzzy metric spaces," *Fuzzy Sets and Systems*, vol. 64, no. 3, pp. 395–399, 1994.

[15] H. A. Hammad and M. De la Sen, "Exciting fixed point results under a new control function with supportive application in fuzzy cone metric spaces," *Mathematics*, vol. 9, Article ID 2267, 2021.

[16] S. Ur Rehman and H. Aydi, "Rational fuzzy cone contractions on fuzzy cone metric spaces with an application to fredholm integral equations," *Journal of Function Spaces*, vol. 2021, Article ID 5527864, 13 pages, 2020.

[17] T. Kamran, "Common fixed points theorems for fuzzy mappings," *Chaos, Solitons & Fractals*, vol. 38, no. 5, pp. 1378–1382, 2008.

[18] A. F. Roldan-Lopez-de-Hierro, A. Fulga, E. Karapinar, and N. Shahzad, "Proinov-type fixed-point results in non-Archimedean fuzzy metric spaces," *Mathematics*, vol. 9, Article ID 1594, 2021.

[19] A. F. Roldan-Lopez-de-Hierro, M. A. Tiscar, C. Roldan, and H. Bustince, "A fuzzy methodology for approaching fuzzy sets of the real line by fuzzy numbers," *Fuzzy Sets and Systems*, 2021, In press.

[20] J. Wu and H. Yang, "On metrization of the topologies induced by fuzzy metrics," *Journal of Mathematics*, vol. 2020, Article ID 4731357, 5 pages, 2020.

[21] M. Zhou, N. Saleem, X. Liu, A. Fulga, and A. F. Roldan-Lopez-de-Hierro, "A new approach to proinov-type fixed-point results in non-archimedean fuzzy metric spaces," *Mathematics*, vol. 9, no. 23, Article ID 3001, 2021.

[22] I. Altun and D. Mihet, "Ordered non-archimedean fuzzy metric spaces and some fixed point results," *Fixed Point*

Theory and Applications, vol. 2010, Article ID 782680, 11 pages, 2010.

[23] V. Radu, "Some remarks on the probabilistic contractions on fuzzy Menger spaces," *Applied Mathematics*, vol. 11, pp. 125–131, 2002.

[24] W. A. Kirk, P. S. Srinivasan, and P. Veeranmani, "Fixed points for mappings satisfying cyclical contractive condition," *Fixed Point Theory*, vol. 1, pp. 79–89, 2003.

Hindawi
Journal of Mathematics
Volume 2024, Article ID 9876405, 1 page
https://doi.org/10.1155/2024/9876405

Retraction

Retracted: The New Approach Research on Singing Voice Detection Algorithm Based on Enhanced Reconstruction Residual Network

Journal of Mathematics

Received 23 January 2024; Accepted 23 January 2024; Published 24 January 2024

This article has been retracted by Hindawi following an investigation undertaken by the publisher [1]. This investigation has uncovered evidence of one or more of the following indicators of systematic manipulation of the publication process:

(1) Discrepancies in scope

(2) Discrepancies in the description of the research reported

(3) Discrepancies between the availability of data and the research described

(4) Inappropriate citations

(5) Incoherent, meaningless and/or irrelevant content included in the article

(6) Manipulated or compromised peer review

The presence of these indicators undermines our confidence in the integrity of the article's content and we cannot, therefore, vouch for its reliability. Please note that this notice is intended solely to alert readers that the content of this article is unreliable. We have not investigated whether authors were aware of or involved in the systematic manipulation of the publication process.

Wiley and Hindawi regrets that the usual quality checks did not identify these issues before publication and have since put additional measures in place to safeguard research integrity.

We wish to credit our own Research Integrity and Research Publishing teams and anonymous and named external researchers and research integrity experts for contributing to this investigation.

The corresponding author, as the representative of all authors, has been given the opportunity to register their agreement or disagreement to this retraction. We have kept a record of any response received.

References

[1] L. Liu, "The New Approach Research on Singing Voice Detection Algorithm Based on Enhanced Reconstruction Residual Network," *Journal of Mathematics*, vol. 2022, Article ID 7987592, 11 pages, 2022.

Hindawi
Journal of Mathematics
Volume 2022, Article ID 7987592, 11 pages
https://doi.org/10.1155/2022/7987592

Research Article

The New Approach Research on Singing Voice Detection Algorithm Based on Enhanced Reconstruction Residual Network

Lilin Liu

College of Music and Dance, Shenzhen University, Shenzhen, Guangdong, China

Correspondence should be addressed to Lilin Liu; 15110803068@stumail.sdut.edu.cn

Received 23 December 2021; Revised 9 January 2022; Accepted 15 January 2022; Published 23 February 2022

Academic Editor: Naeem Jan

With the development of Internet technology, multimedia information resources are increasing rapidly. Faced with the massive resources in the multimedia music library, it is extremely difficult for people to find the target music that meets their needs. How to realize computer analysis and perceive users' needs for music resources has become the goal of the future development of human-computer interaction capabilities. Content-based music information retrieval applications are mainly embodied in the automatic classification and recognition of music. Traditional feedforward neural networks are prone to lose local information when extracting singing voice features. For this reason, on the basis of fully considering the impact of information persistence in the network propagation process, this paper proposes an enhanced two-stage super-resolution reconstruction residual network which can effectively integrate the learned features of each layer while increasing the depth of the network. The first stage of reconstruction is to complete the hierarchical learning of singing voice features through dense residual units to improve the integration of information. The second stage of reconstruction is mainly to perform residual relearning on the high-frequency information of the singing voice learned in the first stage to reduce the reconstruction error. In the middle of these two stages, the model introduces feature scaling and expansion convolution to achieve the dual purpose of reducing information redundancy and increasing the receptive field of the convolution kernel. A monophonic singing voice separation based on the high-resolution neural network is proposed. Because the high-resolution network has parallel subnetworks with different resolutions, it also has original resolution representations and multiple low-resolution representations, avoiding information loss caused by serial network downsampling effects and repeating multiple feature fusions to generate new semantic representations, allowing for the learning of comprehensive, high-precision, and highly abstract features. In this article, a high-resolution neural network is utilized to model the time spectrogram in order to correctly estimate the real value of the anticipated time-amplitude spectrograms. Experiments on the dataset MIR-1K show that compared with the current leading SH-4Stack model, the method in this paper has improved SDR, SIR, and SAR indicators for measuring the separation performance, confirming the effectiveness of the algorithm in this paper.

1. Introduction

Multimedia technology changes with each passing day, constantly enriching people's daily lives and work. As an important part of multimedia technology, audio technology affects people's lives all the time. Since human civilization, music has been an important part of people's spiritual culture [1]. It is a special language for people to place spiritual ideals, express their thoughts and feelings, and achieve mutual exchanges. It is also the crystallization of the human's great wisdom. The creation, expression, understanding, and appreciation of music are the most basic spiritual activities of mankind [2]. In the advancement of human civilization, music has inherited a rich culture and history. It has always been an indispensable part of human life for thousands of years. Its meaning, form of existence, and mode of transmission are in a new era. Driven by technology, there will be new interpretations [3]. With the vigorous promotion of network technology, the amount of online music data is increasing day by day, and the demand for analysis, retrieval, and processing of music information has become increasingly prominent [4]. As one of the

hotspots in the field of signal and information processing, music separation is an important part of music technology research [5].

It is common for one singer to sing many different songs in singer search and song search, and one song has been sung by many singers. The separation of singing voice can improve the accuracy of singer identification [6]. Because in music information retrieval, the effect of direct retrieval is often unsatisfactory. If it can be separated, the retrieval efficiency will be greatly improved without mutual interference, and many complex multitone music processing can be avoided. Technology simplifies the problem even more. Similarly, during music information analysis (preprocessing, pitch, melody extraction, etc.), the mutual interference between music and singing also leads to inaccurate information analysis [7]. A good separation system will bring great convenience to this. In automatic lyrics recognition, it is usually required to input a single singing voice, which is not in line with reality. Because the singing voice has background music, such a requirement can be achieved. Correcting lyrics for singing voices is a critical and tedious step for applications such as karaoke. Automatic lyrics correction will bring great convenience, but automatic lyrics correction task becomes difficult when background music exists.

The auditory characteristics of the singer's voice signal are described in detail, which is also an important part of the system, and the analysis and calculation methods of each auditory characteristic are introduced. The super-resolution reconstruction model based on the deep residual network is one of the research trends in the past two years. This article first introduces the basic principles of the deep residual network and analyzes the advantages and disadvantages of the existing super-resolution model based on the residual network. After analyzing and inspired by densely connected networks, this paper combines the advantages of deep residual networks and densely connected networks to propose an enhanced two-stage reconstruction residual network and introduces two deep learning features. The suggested two-stage residual deep convolutional neural network technique is subjected to comparative experimentation and analysis in this study. The experimental environment, data preparation, and singing voice separation evaluation indicators were first introduced; second, experimental schemes based on the high-resolution network separation of songs, phase optimization algorithms, spectrum amplitude constraints, and data expansion were designed; finally, the separation performance of each algorithm was compared and analyzed.

2. Related Work

In theory, deep learning belongs to the category of machine learning [8]. Machine learning completes the learning of the model by selecting appropriate features. The result depends on the choice of features. However, manually selecting features is very time consuming and labor intensive, and requires a lot of prior knowledge. Therefore, the introduction of deep learning has greatly promoted the development of machine learning, among which the most widely used are visual problems, speech recognition, and text processing [9]. The application effect of deep learning in computer vision is remarkable. In addition to common classification problems, the accuracy of tasks such as face recognition, object detection, and singing voice super-resolution has also been greatly improved [10].

Convolutional neural network (CNN) is a common deep learning architecture inspired by biological natural visual cognitive mechanisms. Researchers found that their unique network structure can effectively reduce the complexity of the feedback neural network when studying neurons used for local sensitivity and direction selection in the cat brain cortex and then proposed CNN [11]. The new recognition machine proposed by related scholars is the first realization of the convolutional neural network. Later, more scientific researchers improved the network [12, 13]. Researchers established the modern structure of CNN [14]. They designed a multilayer artificial neural network, named "LeNet-5," which can classify handwritten digits. Like other neural networks, LeNet-5 can also be trained using the back propagation (BP) algorithm. CNN can obtain the effective feature representation of the original singing voice, which enables CNN to recognize the rules of vision directly from the original pixels [15]. However, due to the lack of large-scale training data at that time and the computing power of the computer that could not keep up, LeNet-5 was not ideal for handling complex problems.

Based on the research on the perception mechanism of the human auditory system, related scholars proposed the concept of "synchronization string" [16, 17]. They used the Gammatone filter bank to simulate the structure of the human cochlea to process mixed sounds and then obtained a series of time-frequency units. The degree of correlation between adjacent parts classifies the synchronization string to which the sound signal belongs, and analyzes the mixed sound step by step in time sequence. Researchers have proposed a new CASA system, the "blackboard" model, based on the physiological and psychological characteristics of the human auditory system, using many different criteria to extract and recombine sound signals [18]. This model's organization and processing method of sound signals is a breakthrough innovation for CASA research, which can better realize the simulation of the human auditory system. Relevant researchers reported a neural network-based CASA system that detailed how the same sound source signal is separated into a sound stream based on several sound separation triggers [19]. A schema-driven phoneme repair model has been created by related researchers. This method can restore a sound signal by processing it via an imprecise speech recognition model and restoring the associated masking material. Related scholars have studied a model that uses harmonic characteristics to separate sounds, designs a filter according to the pitch frequency to simply and roughly separates each sound source, and then performs targeted enhancement and compression on the separated sound to highlight the target voice. Researchers proposed a speech separation algorithm based on sound localization and auditory masking effect, using binaural effect as the main sound separation clue, and combined with an ideal binary masking algorithm to separate mixed sounds [20].

3. Analysis of the Auditory Characteristics of Singing Voice Signals

3.1. Pretreatment

3.1.1. Sampling. They are all digital music, with a certain sampling frequency and encoding mechanism, whether they are songs on the Internet or CDs. However, the encoding technique and sample frequency of music have a significant impact on the processing of music data in the experiment. As a result, before framing, the music signal's sampling frequency and encoding technique must be unified. In most applications, digital music does not require a too-high sampling rate, and a too-high sampling rate will increase the complexity of the calculation. In this paper, the music signal is uniformly converted into a WAV format, which is convenient for analysis and processing in the MATLAB environment. For the sampling frequency, the unified standard 22050 Hz in the MIR research field is adopted, which also improves the execution efficiency of the algorithm. The test music signal (44.1 kHz) can be downsampled without losing the basic music recognition characteristics, and the recognition effect is less.

3.1.2. Framing. According to this characteristic, considering the time continuity and short-term stability of the music signal, the music signal needs to be framed after sampling. The length of the frame will directly affect the feature extraction and recognition results. Suppose the sampling period is $T = 1/f$, there is the following relationship between the window length N and the frequency Δf:

$$\Delta f = \left(NT_s\right)^{-1}. \tag{1}$$

When the sampling period T_s is constant, the frequency resolution Δf is inversely proportional to the frame length N. When N increases, Δf will decrease.

3.1.3. Preemphasis. Normally, hardware or software can be used for preemphasis. This article uses software preemphasis in the MATLAB environment. The transfer function used is

$$H(z) = 1 - (1 - a)z^{-1}. \tag{2}$$

Among them, a is called the preemphasis coefficient.

3.1.4. Add Windows. The purpose of windowing is to divide the speech signal into frames, and the frame length is denoted as N. For each frame, the time window function $\omega(n)$ is multiplied with the original speech signal $s(n)$. This frame contains the speech signal sequence of N points in the sample, and N is the window length. Generally, there are two commonly used window functions in the windowing process.

The rectangular window function is

$$w(n) = \begin{cases} 0, & n \in [0, N-1], \\ 1, & \text{others}. \end{cases} \tag{3}$$

The Hamming window function is

$$w_H(n) = \begin{cases} 1, & \text{others}, \\ 0.42 - 0.38\ \sin\left(2\pi\dfrac{n-1}{N}\right), & n \in [0, N-1]. \end{cases} \tag{4}$$

It can be seen from the above two formulas that the length of the window function N is used to calculate the amplitude of the signal. When the window length is extremely large, the window function is approximately equivalent to a narrow low-pass filter, and the length of N is equal to several pitch periods. During this period of time, the short-term information of the signal changes very slowly, and the details of the waveform are often ignored. Conversely, if N is extremely small, this value may be equivalent to or even less than a gene period for a pitch period, and the short-term energy change of the signal will fluctuate according to the change of the signal waveform. If N is too small, the bandwidth of the filter will become wider, and smooth short-term information cannot be obtained. Therefore, the length of the window function should be selected appropriately. It is generally believed that 1 to 7 pitch periods can fully reflect the change characteristics that should be in a speech frame. But the pitch period varies widely for different people, so the choice of N is more difficult. Generally, when the sampling frequency is 10 kHz, the window length is most appropriate to choose from 100 to 200 points, that is, the duration of 15 mins to 30 mins.

3.2. Mel Cepstral Coefficient. Mel frequency cepstral coefficient (MFCC) is a cepstral coefficient based on Mel frequency. To obtain the frequency spectrum of the signal, the discrete Fourier transform is first used to calculate the short-time Fourier transform; second, the obtained logarithmic energy spectrum is filtered with M Mel triangular filter banks; finally, the output vector is subjected to the discrete cosine transform DCT, with the first N coefficients taken. The discrete cosine transform is actually the process of inverse Fourier transform; that is, the cepstral coefficients are obtained.

The reason why MFCC reflects the auditory characteristics of the human ear is that the Mel filter simulates the cochlea model of the human ear. According to the cochlea function, the cochlea's filtering function is similar to the function of the Mel filter, which mainly presents a relationship on a logarithmic scale. It is basically linear below the lower 1000 Hz, and the frequency greater than 1000 Hz is shown as a logarithmic relationship; that is, the human ear recognizes low-frequency sounds more easily than high-frequency sounds. The Mel frequency of the Mel frequency filter bank similar to the cochlear model is expressed as follows:

$$f_{\text{mel}} = 2400 \cdot \log\left(\frac{f}{300 + 1}\right). \tag{5}$$

The output formula of the Mel filter is

$$H_m(k) = \begin{cases} 1, & k \geq f(m+1), \\ \dfrac{k - f(m+1)}{f(m+1) - f(m-1)}, & f(m) < k < f(m+1), \\ \dfrac{f(m-1) - (k-1)}{f(m) - f(m-1)}, & f(m-1) < k < f(m), \\ 0, & k \leq f(m-1). \end{cases} \tag{6}$$

Among them, M represents the number of channels of the filter and $f(m)$ represents the center frequency. The definition of $f(m)$ is

$$f(m) = NF_S{}^{-1}F_{\text{mel}}^{-1}\left[F_{\text{mel}}(f_1)\right] - m\frac{F_{\text{mel}}(f_h)}{M-1} - F_{\text{mel}}(f_l). \tag{7}$$

Among them, f_h and f_l represent the highest and lowest frequencies, N represents the frame length, and FS represents the sampling frequency.

3.3. Mel Transformation of Linear Prediction Coefficients. The Mel frequency is a simulation of the frequency characteristics of the human cochlea, in which the Mel filter plays a decisive role in this simulation performance. Therefore, linear prediction Mel-frequency cepstral coefficient (LPMCC) is based on linear prediction cepstral coefficient (LPCC), improving its Mel frequency and achieving better results in recognition. LPCC is often used as a characteristic parameter of speech recognition. It has a good performance in speaker recognition technology, but it has a poor effect on singer recognition. Therefore, LPCC is improved to enhance its performance. Next, the theoretical model of LPCC is introduced.

We assume that the p-order linear prediction coefficient of the speech signal is calculated. We use the first p samples of the speech signal to predict the current speech sample, so the p-order linear prediction value is obtained. The specific description is that the first p samples are linearly combined to predict the voice signal sample value at the next moment, and the prediction standard is that the error is minimized. That is, the predicted value of $s(n)$ is

$$\widehat{s}(n) = \prod_{i=0}^{p-1} a_i \cdot s(n-i-1), \tag{8}$$

where $s(n)$ is constructed with {ak}, which fits the data in the sense of least mean square. {ak} is the coefficient of p-order linear prediction. The forecast error is

$$e(n) = s(n) - \prod_{i=0}^{p-1} a_{i-1}s(n-i-1). \tag{9}$$

We perform z-transformation on the above formula to obtain the transfer function of the prediction error sequence:

$$A(z) = 1 - \sum_{i=0}^{p-1} a_{i-1}z^{-k+1}. \tag{10}$$

According to the definition of p-order linear prediction, the sum of squares E of all prediction errors of the speech frame is

$$E = \prod_{n=p-1}^{N}\left[s(n-1) - \prod_{i=0}^{p-1} a_{i-1}s_{n-i-1}\right]. \tag{11}$$

4. Deep Convolutional Neural Network Model Based on Two-Stage Residuals

This section will give a detailed introduction to the information of each part of the two-stage progressive reconstruction residual network. Figure 1 shows the overall framework of the network. The low-resolution singing voice to be reconstructed is preprocessed by the feature extraction layer, and then the extracted features are transported to the first reconstruction stage. The pseudo-high frequency is obtained through the local residual learning of each dense residual unit. The main work of the second reconstruction stage is to integrate the original singing voice and real high-frequency information to achieve global residual learning and finally output a high-resolution singing voice. The techniques of feature scaling and expansion convolution are also included between the two reconstruction phases to complete the conversion of pseudo-high-frequency information to actual high-frequency information, making the singing voice's high-frequency component richer and more delicate.

4.1. The First Stage of Reconstruction. In general, the first stage of the model is based on the local residual learning of multiple dense residual units to obtain the initial high-frequency information of the singing voice required for the reconstruction process because they have to be processed subsequently. So, it is called pseudo-high-frequency information.

The model obtains the original features of the singing voice through the feature extraction layer. The feature extraction layer is composed of two convolutional layers, and the structure of each convolutional layer is the same as that of each layer in the dense residual unit. The first layer takes low-resolution singing voices as input, and the output features will be used in two parts. One is as the input of the next layer, and the other is to provide the global residual learning module. The second layer of the feature extraction layer receives the output of the previous layer and then performs a nonlinear mapping on the features, and the obtained output directly participates in the local residual learning process corresponding to each dense residual unit. The following formula can express the abstraction layer:

$$Y_0 = F_0\left[F^{-1}(x-1)\right]. \tag{12}$$

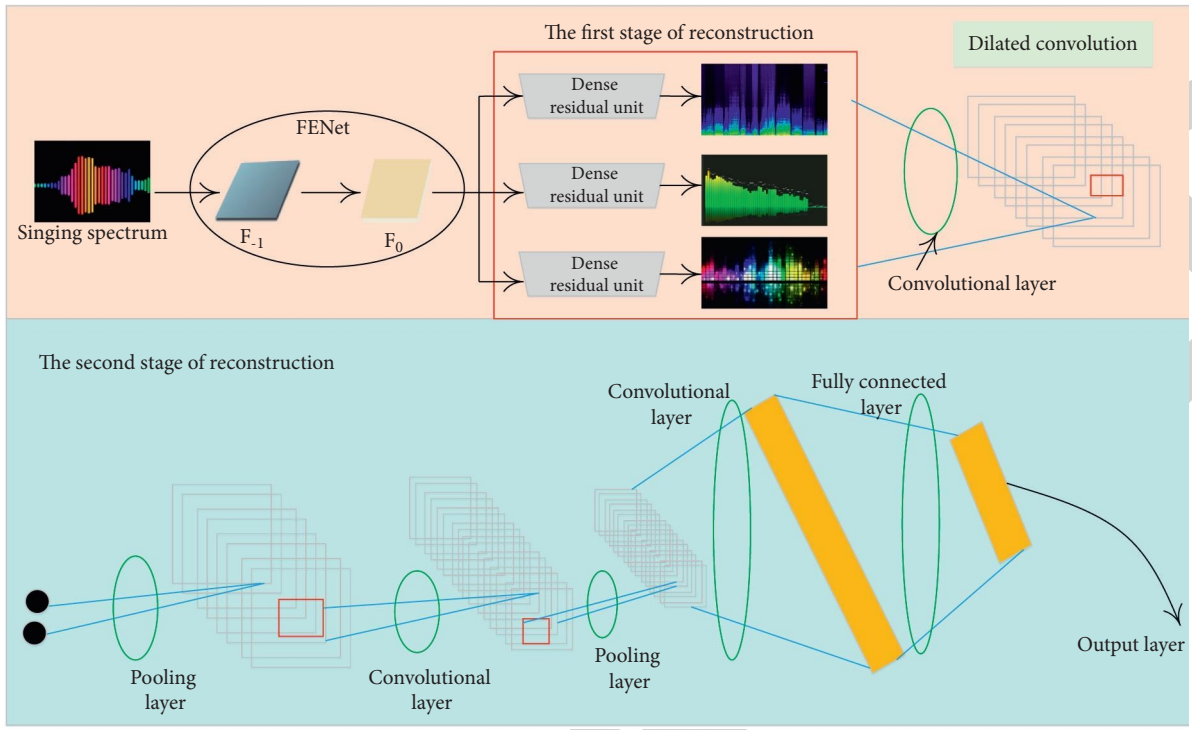

Figure 1: Two-stage super-resolution residual network framework diagram.

Here, x is the input low-resolution singing voice, F^{-1} represents the first layer of the feature extraction layer, and F_0 is the second layer. Then, based on the local residual learning of each dense residual unit, the characteristic is that the input of each dense residual unit is Y_0, which ensures that the learned singing residuals are structurally consistent with the original singing voices.

Considering that in the traditional network, information will inevitably lose a part of it through the forward transmission of each layer, ensuring the invariance of information in the process of dissemination and maintaining the robustness of information memory is the focus of this article. This article uses the cyclic unit of a memory block as the main component of the dense residual learning unit. The cyclic unit is made up of 6 residual building blocks (RBBs). The learning process of the dth residual block of the rth dense residual unit can be expressed as

$$Y_{d,r} = F\left(Y_{d,r-1}\right) - \left|Y_{d,r-1}\right|. \tag{13}$$

$Y_{d,\,r-1}$ and $Y_{d,\,r}$ are the input and output of this block, respectively, and $\mathcal{F}$ is the residual function. In particular, $\mathcal{F}$ contains two convolutional layers, each of which undergoes a preactivated BN-ReLU nonlinear mapping and then performs a 3×3 convolution operation:

$$F\left(Y_{d,r-1}\right) = W_{m,r} \cdot \tau\left[\tau\left(Y_{d,r-1}\right)W^2_{m,r}\right]. \tag{14}$$

$W_{m,\,r1}$ and $W_{m,\,r}$ are the weights of the first and second layers, respectively, and ? is the BN-ReLU operation. For the sake of simplicity, the offsets in all formulas in the text are omitted.

The dense residual unit will comprehensively consider the hierarchical characteristics of each RBB when abstracting the features. Through this dense connection operation, the network will minimize the loss of information after the information passes through each layer. However, this also leads to a problem of a large amount of calculation. For example, suppose now that the output of each block has G feature maps, so the output of each unit will have 6·G feature maps. If the number of G is large, for example, $G = 64$, then the number of feature maps of the final output G is 384, which requires a high amount of calculation for hardware. Therefore, the model in this article considers the use of information filters, which can reduce the dimension of Y_d and achieve the purpose of information fusion. The followingdescribes the specific implementation process of information filters.

In a dense residual unit, the information filter filters the output results of the current dense residual unit Yd so that it can not only reduce the corresponding calculation amount but also meet the reconstruction requirements, thus making the learning process simple. ETRN uses a 1×1 convolutional layer to act as an information filter.

4.2. Dilated Convolution. The comparison between dilated convolution and traditional convolution is shown in Figure 2. After the completion of the first stage of reconstruction, the 6 dense residual units will generate 6 different levels of pseudo-high-frequency information, and then the pseudo-high frequency corresponding to the previous unit is added element-by-element to form the dense residual unit. Relearning the residuals is the second stage of

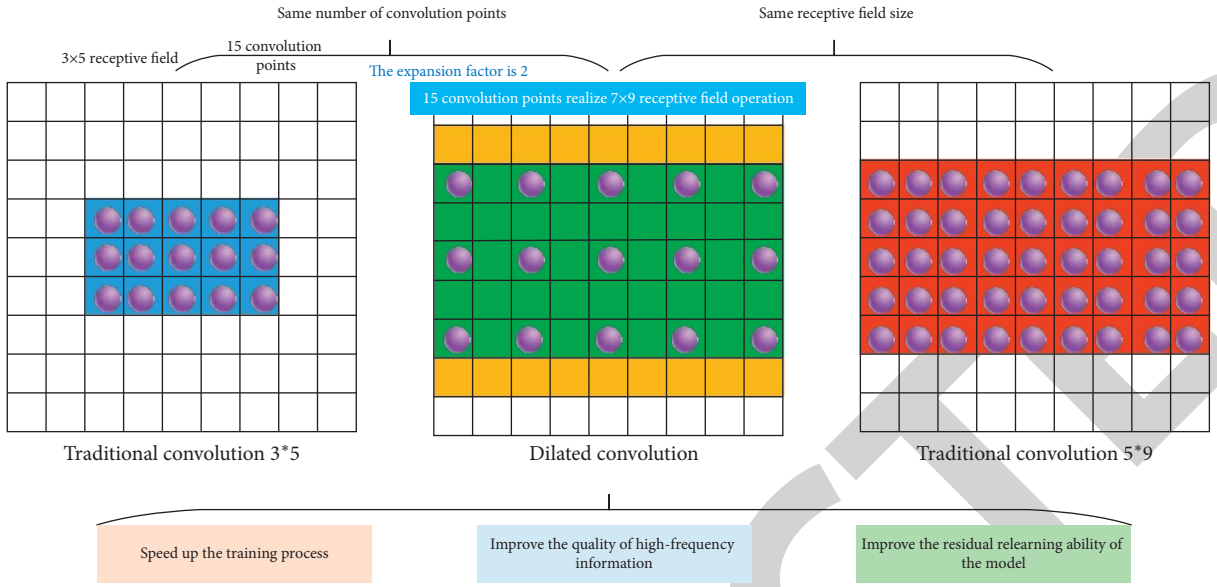

Figure 2: Comparison of dilated convolution and traditional convolution.

reconstruction. After two different levels of pseudo-high frequency singing voice features are directly added, the model uses expanded convolution to process the fused data.

In traditional convolution, a 3×5 receptive field requires 15 convolution points to participate in the calculation. After changing to dilated convolution, when the dilation factor is 2, the same 15 convolution points can achieve a 7×9 receptive field operation. The expanded convolution has a larger receptive field with the same amount of calculation, expands the global field of view of the convolution kernel, and the size and number of feature maps remain unchanged. For super-resolution reconstruction, the receptive field means how many contextual pixels can be extracted from the high-frequency information of the singing voice, so in the second stage of reconstruction to obtain real high-frequency information, using dilated convolution has three advantages: (1) in the process of converting pseudo-high-frequency information into real high-frequency information, the training process is speeded up while keeping the number of parameters unchanged; (2) the receptive field is increased, and the self-similarity of the singing voice structure is used to improve the high-frequency information quality; and (3) the redundancy of singing residual information learned between adjacent dense residual units is diluted, and the residual relearning ability of the model is improved.

4.3. The Second Stage of Reconstruction. The second stage of reconstruction can be subdivided into three processes. First, the pseudo-high-frequency features learned by each dense residual unit are gathered to form a pseudo-high-frequency feature set. After ordering, the dth feature and the d—1st feature are directly added, and the expansion convolution is performed. Then, the true high-frequency characteristics corresponding to the dense residual unit of d are obtained:

$$H_d = \varphi\left(H_{d+1,\sim}\right) - 2\varphi\left(H_{d,\sim}\right) + \varphi\left(H_{d-1,\sim}\right). \tag{15}$$

As shown in Figure 3, a feature scaling operation is added after each pseudo-high frequency feature, and there is a scaling factor equal to 0.1, and then it is added to the latter one. The reason for this is that, on the one hand, each dense residual unit is stacked by multiple convolutional layers. This high-level abstract representation of features makes the training process extremely prone to numerical instability. This operation is added after each residual block in the deep residual network to solve this problem. On the other hand, the scaling factor can change the weight of each level of pseudo-high frequency feature participating in the expansion convolution operation, and the value of the feature is changed. In this way, the features can be made to meet the statistical distribution characteristics of the residuals of the singing voice as much as possible, thereby avoiding repeated learning of the same or similar information between two adjacent features.

4.4. Objective Function Construction. This paper chooses the mean square error as the objective optimization function of model training. During training, the objective function is continuously reduced. When the model converges, the optimal value of the network parameters can be found through this iterative optimization method. The high-frequency information generated by each dense residual unit can be regarded as a certain order residual between the final reconstructed super-resolution singing voice and low-resolution singing voice. Therefore, the intermediate prediction singing voice output by each dense residual unit can be formulated as

$$I_d = H_d - X + H_{d-1}. \tag{16}$$

For the two-stage super-resolution residual network proposed in this paper, 6 dense residual units will output 6 intermediate predictions in the first stage. Therefore, 6

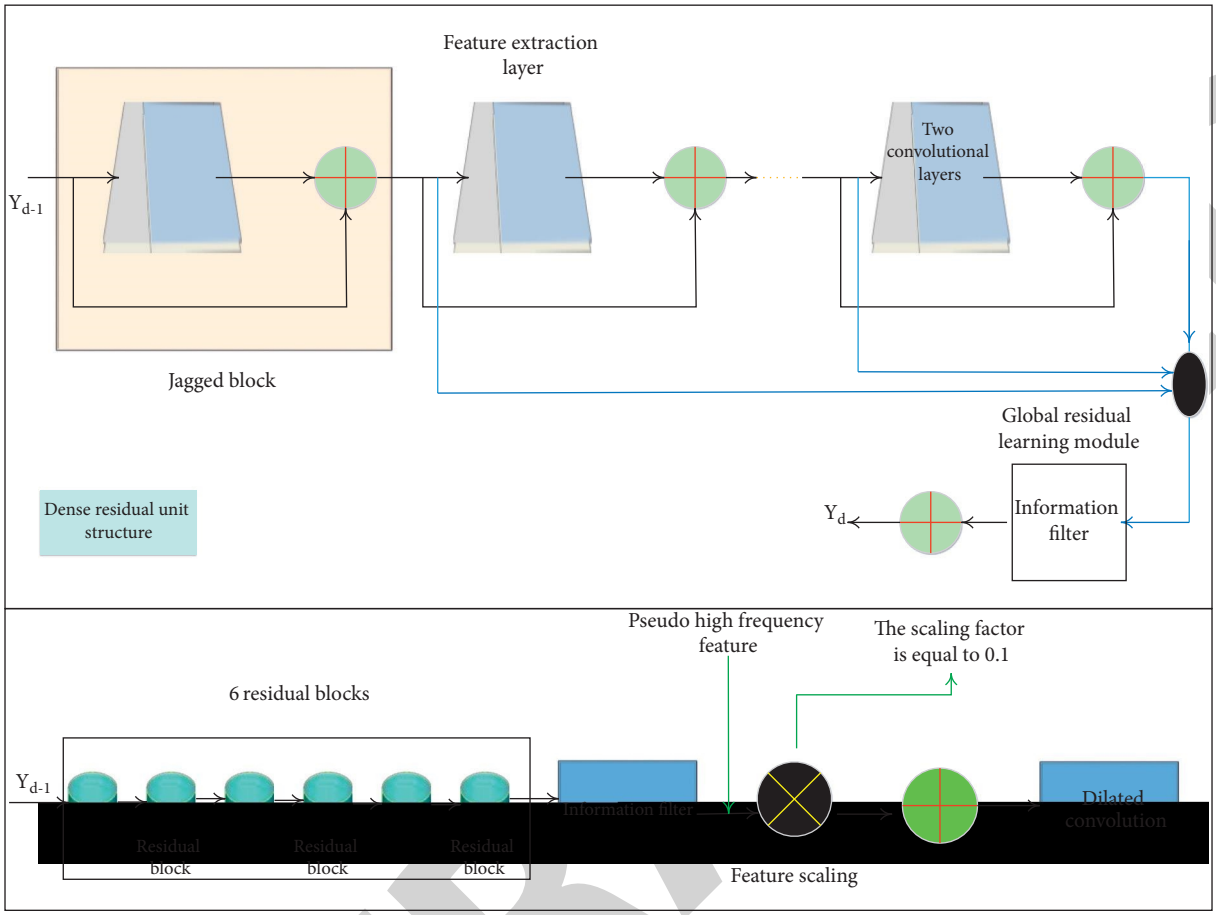

Figure 3: Residual relearning based on dense residual unit.

objective functions need to be optimized, and the loss function corresponding to each unit is

$$L_D(\Theta) = \prod_{i=0}^{N-1} \frac{2}{N} \cdot \left(Y_i - I_{d,i}\right)^2. \tag{17}$$

? is the set of parameters to be learned in the d dense residual unit. In the second stage, the errors between the final output predicted singing voice and the real high-resolution singing voice are calculated by

$$L_{\sum}(\theta) = \prod_{i=0}^{N-1} \frac{2}{N} \left(Y_{i-1} - I_{i+1}\right)^2. \tag{18}$$

? is a collection of parameters to be learned in the entire network. The objective optimization function of the entire network should be the sum of $\mathscr{L}$d (Θ) corresponding to each unit and $\mathscr{L}\Sigma$ (Θ) corresponding to the final reconstructed singing voice, so

$$L(\Theta) = \alpha L_{\sum}(\Theta) - \beta L_D(\Theta). \tag{19}$$

Among them, α and β are the trade-off factors, which are used to prevent the value of the two types of objective functions.

5. Experiment and Result Analysis

5.1. Experimental Plan Design. An experiment of monophonic singing based on the high-resolution network is carried out to validate the high accuracy of the spectrogram when the high-resolution network separates the accompaniment/singing voice.

The audio sampling rate is set to 8 kHz, the frame length is set to 1024, the frame shift is set to 256, the network learning rate is set to 0.0001, and iterations are set to 30,000. The original audio sampling rate is 16 kHz, thus setting the sampling rate to 8 kHz. The sample rate is lowered, and the quantity of computation is considerably reduced on the premise of not impacting the separation effect. The learning rate and the number of iterations are reasonable parameters chosen from a variety of options and various tests.

The training set songs are transformed into the frequency domain, and the time spectrogram is input as a high-resolution network. After the above-mentioned network structure, the predicted mask is obtained, and finally, the time spectrogram is restored from the mask. The pure singing voice and pure accompaniment corresponding to the song are used in the loss function to measure the difference between the predicted result and the true pure time-spectrogram. A high-resolution network is continuously iterated and trained for singing voice separation.

For the 825 original song audios in the test set, the time spectrogram is obtained through STFT transformation, which is input as a high-resolution network, and the time spectrogram of the accompaniment and singing voice is obtained through network prediction and integration. Finally, combined with the phase reconstruction of the original song, the accompaniment and singing signals in the test song are obtained.

5.2. Visualization of the Time Spectrogram. We randomly select a song to be separated, yifen_5_02.wav, and use the U-Net separation method, SH-4stack separation method, and a deep convolutional neural network based on two-stage residuals to predict the corresponding accompaniment and singing time spectrogram of the song. We visualize the time spectrogram, compare the gap with the real pure singing voice, and evaluate the separation quality of each method. Figure 4 shows the true and pure time spectrogram and the time spectrogram separated by each method. The upper layer shows the accompaniment time spectrogram. The lower level shows the frequency spectrum of singing.

Compared with the pure accompaniment, it can be seen that the three separation methods can basically predict a more accurate time spectrogram; the specific analysis of the accompaniment in the yellow box reveals that the SH-4stack and U-Net methods contain "nonaccompaniment" parts. There are errors, and the deep convolutional neural network based on the two-stage residual is relatively closer to the pure accompaniment, and the separation accuracy is improved.

In the overall comparison of the frequency spectrum of the singing voice, the prediction accuracy of these algorithms is relatively high for places with large amplitudes and obvious changes, which are close to the original pure signal. Observing the content of the yellow box, for some places with small amplitude, it is found that after the SH-4stack and U-Net methods are separated, the prediction is not accurate enough, and the difference between the original spectrogram is large, and the accuracy is relatively low. The deep convolutional neural network method performs better than the above algorithms in small and subtle areas, can predict results that are closer to the pure spectrogram, can better capture learning, and predict high accuracy and is close to the true value.

5.3. Separation Quality Assessment. Figures 5 and 6 compare the separation performance of the four methods on the dataset MIR-1K and measure each method by evaluating the global normalized signal deviation ratio GNSDR, the global signal interference ratio GSIR, and the global signal artifact ratio GSAR.

Figure 5 evaluates the overall separation performance of the accompaniment. It can be seen that the three indicators of the deep convolutional neural network algorithm based on the two-stage residual have improved compared with other algorithms. The overall separation performance of the GNSDR evaluation algorithm and the deep convolutional neural network algorithm based on

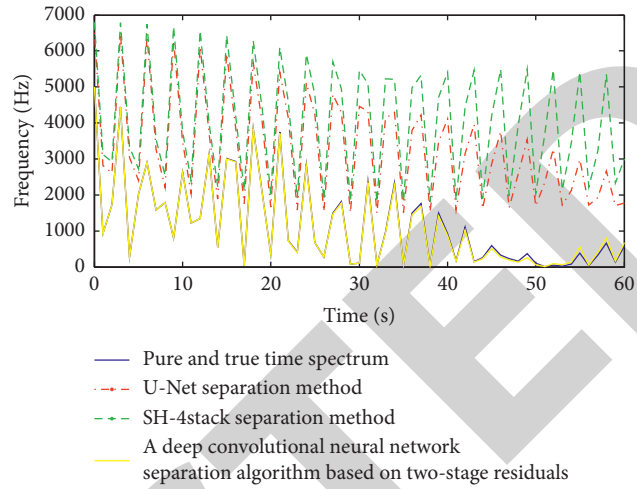

Figure 4: Visualization of the time spectrogram.

the two-stage residual error is 0.43 dB higher than the good performance SH-4stack. Compared with the good performance SH-4stack, the algorithm improves by 0.79 dB; for the GSAR evaluation signal artifact ratio, the deep convolutional neural network algorithm based on the two-stage residual error improves by 0.59 dB compared with the good performance SH-4stack. This shows that the deep convolutional neural network algorithm based on the two-stage residuals can better eliminate the interference from the singing voice in the accompaniment, the artifacts in the accompaniment signal are small, and the separation performance is good.

The total separation performance of singing voices is evaluated in Figure 6. It can also be noted that, when compared to other algorithms, the three indicators of the deep convolutional neural network method based on the two-stage residual have improved. For the GNSDR index, the deep convolutional neural network algorithm based on two-stage residual error outperforms the SH-4stack by 0.82 dB; for the GSIR index, the deep convolutional neural network algorithm based on two-stage residual error outperforms the good SH-4stack by 1.22 dB; for the GSAR index, the deep convolutional neural network algorithm based on two-stage residuals outperforms the good SH-4stack. This demonstrates that the two-stage residual-based deep convolutional neural network technique can also distinguish high-quality singing vocals.

By comparing the three indicators of accompaniment and singing, the algorithm in this paper has improved the amplitude compared with other algorithms and found that the singing voice has improved more. This is because the high-resolution network can improve the accuracy of the singing voice, and compared with the rich singing voice, the improvement of the singing voice resolution is more obvious on the single-structured singing voice. Compared with accompaniment, singing voice has monotonous spectrum components and a single structure. The high-resolution network can greatly improve the amplitude accuracy.

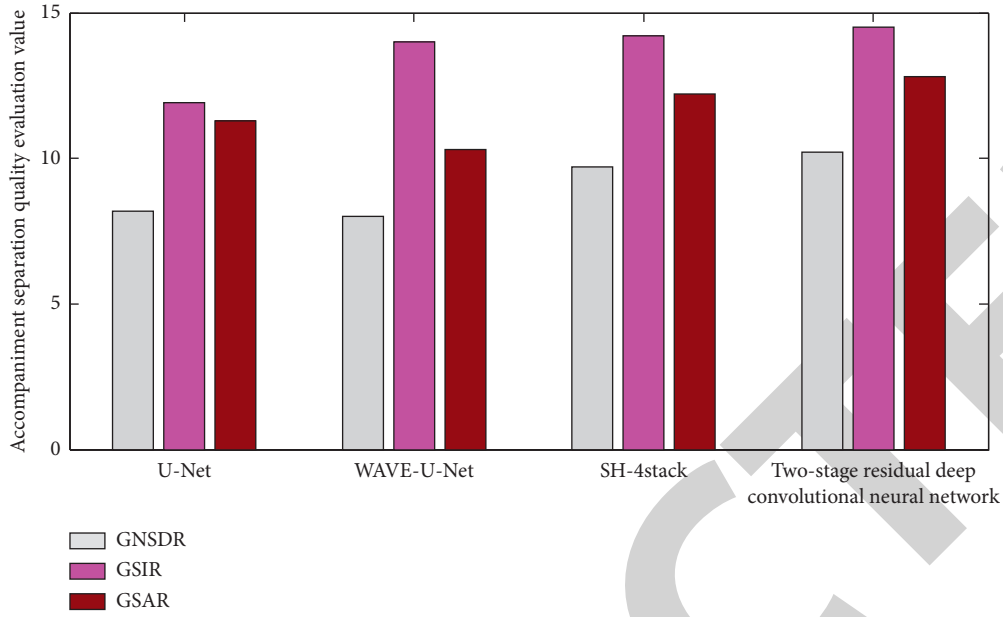

Figure 5: Overall assessment of the quality of accompaniment separation.

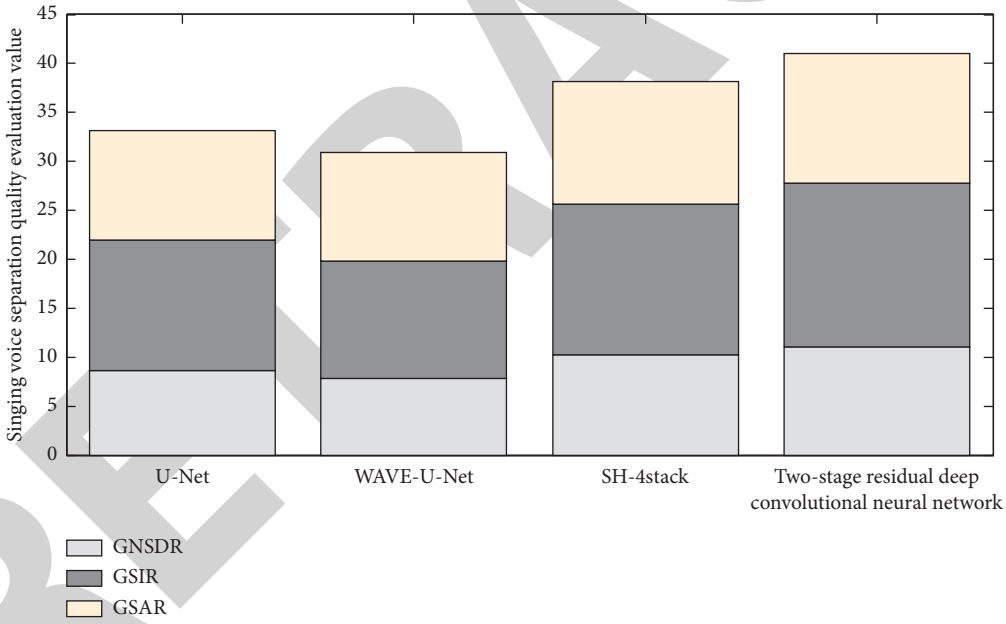

Figure 6: Overall assessment of singing voice separation quality.

5.4. Time-Domain Waveform Comparison. The time-domain waveform of the singing voice following the song yifen 5 02 is shown in Figures 7 and 8. The time-domain waveform of the pure singing voice is separated by a deep convolutional neural network based on the two-stage residual error, and wav is separated by a deep convolutional neural network based on the two-stage residual error. It is observed that the outline of the separated accompaniment singing waveform curve is very close to the waveform of the original pure signal, especially where the curve changes are very similar, and there is only a slight gap between the pure signal and the pure signal in some subtle places. It is confirmed that the

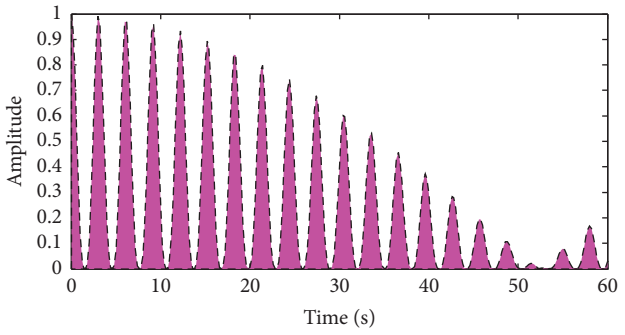

Figure 7: Time-domain waveform of pure singing.

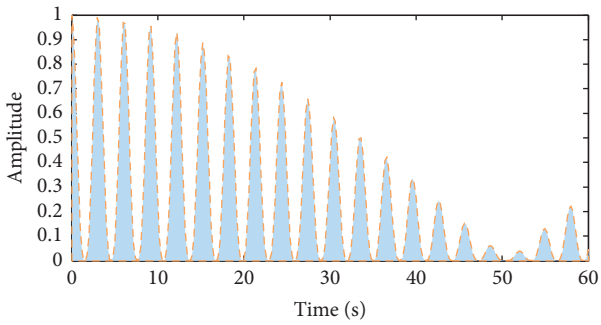

Figure 8: Time-domain waveform of singing voice after separation.

separated signal is very close to the original pure signal, and the separation accuracy is relatively high.

6. Conclusion

In the preprocessing stage of the music signal, the unified standard 22050 Hz, which was uniformly adopted by the international MIR conference, was adopted as the music sampling frequency, and through framing, windowing, and preemphasis processing, preparations were made for the subsequent stages of feature extraction. In the stage of extracting human auditory features, we consider and extract as many feature parameters as possible, remove some infrequently used or poorly effective features, and leave only the parameters that represent human auditory features. This paper proposes a deep but concise two-stage super-resolution reconstruction network based on residual learning. In this model, the reconstruction is divided into two stages, and the different levels of high-frequency information of the singing voice are learned progressively. The first stage of reconstruction is based on the BN-ReLU-weight convolutional layer, and a new dense residual unit is constructed to learn the hierarchical features of the singing voice of the training set of different scales. The pseudo-high-frequency information is obtained by the local residual learning method and used as the input of the next reconstruction stage. The second stage of reconstruction uses the output of the previous stage for relearning based on the residuals between units instead of directly using it for reconstruction. Between these two stages, PSGAN introduces feature scaling and expansion convolution technology to reduce the information redundancy between high-frequency information of each order and greatly improve the detection effect. Finally, the global residual learning is completed based on the structural information. A deep convolutional neural network algorithm based on two-stage residuals of high-resolution neural network is proposed. For singing voice separation in the frequency domain, the focus of the research is to ensure that the separated accompaniment/singing time spectrogram is infinitely close to the true and pure time spectrogram. In this paper, using deep learning technology, starting from the frequency domain model, treating the time spectrogram as a singing voice, using the parallel structure of the high-resolution network and the characteristics of multiple fusion of features, it is proposed to apply the high-resolution neural network. The time spectrogram of the monosong to be separated is separated through a trained high-resolution network to obtain a high-precision accompaniment and singing time spectrogram, and finally, the time-domain signal is reconstructed.

Data Availability

The data used to support the findings of this study are included within the article.

Conflicts of Interest

The author declares that there are no conflicts of interest.

References

[1] W. Yuan, B. He, S. Wang, J. Wang, and M. Unoki, "Enhanced feature network for monaural singing voice separation," *Speech Communication*, vol. 106, pp. 1–6, 2019.

[2] C. Sun, M. Zhang, R. Wu et al., "A convolutional recurrent neural network with attention framework for speech separation in monaural recordings," *Scientific Reports*, vol. 11, no. 1, p. 1434, 2021.

[3] S. Yu, Y. Yu, X. Chen, and W. Li, "HANME: hierarchical attention network for singing melody extraction," *IEEE Signal Processing Letters*, vol. 28, pp. 1006–1010, 2021.

[4] C. C. Bhanja, D. Bisharad, and R. H. Laskar, "Deep residual networks for pre-classification based Indian language identification," *Journal of Intelligent & Fuzzy Systems*, vol. 36, no. 3, pp. 2207–2218, 2019.

[5] K. Tan, J. Chen, and D. L. Wang, "Gated residual networks with dilated convolutions for monaural speech enhancement," *IEEE/ACM Transactions on Audio, Speech, and Language Processing*, vol. 27, no. 1, pp. 189–198, 2018.

[6] S. Mavaddati, "A novel singing voice separation method based on a learnable decomposition technique," *Circuits, Systems, and Signal Processing*, vol. 39, no. 7, pp. 3652–3681, 2020.

[7] F. Li and M. Akagi, "Blind monaural singing voice separation using rank-1 constraint robust principal component analysis and vocal activity detection," *Neurocomputing*, vol. 350, pp. 44–52, 2019.

[8] S. I. Mimilakis, K. Drossos, and E. Cano, "Examining the mapping functions of denoising autoencoders in singing voice separation," *IEEE/ACM Transactions on Audio, Speech, and Language Processing*, vol. 28, pp. 266–278, 2019.

[9] I. Ariav and I. Cohen, "An end-to-end multimodal voice activity detection using WaveNet encoder and residual networks," *IEEE Journal of Selected Topics in Signal Processing*, vol. 13, no. 2, pp. 265–274, 2019.

[10] K. Qian, L. Tian, Y. Liu, X. Wen, and J. Bao, "Image robust recognition based on feature-entropy-oriented differential fusion capsule network," *Applied Intelligence*, vol. 51, no. 2, pp. 1108–1117, 2021.

[11] K. Yasaka, H. Akai, A. Kunimatsu, S. Kiryu, and O. Abe, "Deep learning with convolutional neural network in radiology," *Japanese Journal of Radiology*, vol. 36, no. 4, pp. 257–272, 2018.

[12] S. Xu, J. Wang, R. Wang, J. Chen, and W. Zou, "High-accuracy optical convolution unit architecture for convolutional neural networks by cascaded acousto-optical modulator arrays," *Optics Express*, vol. 27, no. 14, pp. 19778–19787, 2019.

Hindawi
Journal of Mathematics
Volume 2024, Article ID 9783245, 1 page
https://doi.org/10.1155/2024/9783245

Retraction

Retracted: Multidimensional State Data Reduction and Evaluation of College Students' Mental Health Based on SVM

Journal of Mathematics

Received 23 January 2024; Accepted 23 January 2024; Published 24 January 2024

This article has been retracted by Hindawi following an investigation undertaken by the publisher [1]. This investigation has uncovered evidence of one or more of the following indicators of systematic manipulation of the publication process:

(1) Discrepancies in scope

(2) Discrepancies in the description of the research reported

(3) Discrepancies between the availability of data and the research described

(4) Inappropriate citations

(5) Incoherent, meaningless and/or irrelevant content included in the article

(6) Manipulated or compromised peer review

The presence of these indicators undermines our confidence in the integrity of the article's content and we cannot, therefore, vouch for its reliability. Please note that this notice is intended solely to alert readers that the content of this article is unreliable. We have not investigated whether authors were aware of or involved in the systematic manipulation of the publication process.

Wiley and Hindawi regrets that the usual quality checks did not identify these issues before publication and have since put additional measures in place to safeguard research integrity.

We wish to credit our own Research Integrity and Research Publishing teams and anonymous and named external researchers and research integrity experts for contributing to this investigation.

The corresponding author, as the representative of all authors, has been given the opportunity to register their agreement or disagreement to this retraction. We have kept a record of any response received.

References

[1] H. Peiqing, "Multidimensional State Data Reduction and Evaluation of College Students' Mental Health Based on SVM," *Journal of Mathematics*, vol. 2022, Article ID 4961203, 11 pages, 2022.

Hindawi
Journal of Mathematics
Volume 2022, Article ID 4961203, 11 pages
https://doi.org/10.1155/2022/4961203

Research Article

Multidimensional State Data Reduction and Evaluation of College Students' Mental Health Based on SVM

Han Peiqing

Henan Institute of Economics and Trade, Zhengzhou, Henan 450000, China

Correspondence should be addressed to Han Peiqing; han.peiqing@outlook.com

Received 23 December 2021; Revised 9 January 2022; Accepted 15 January 2022; Published 23 February 2022

Academic Editor: Naeem Jan

In response to the shortcomings of the traditional methods for evaluating the mental health status of college students in terms of computational complexity and low accuracy, a method for evaluating the mental health status of college students based on data reduction and support vector machines was proposed. A model experiment containing internal and external personality tendency classification, anxiety, and depression dichotomy was designed using logistic regression analysis, information entropy, and SVM algorithm to construct the feature dimensions of the network behavior data, combined with the labeled data of mental state to derive the sample data set for model experiments. In the experimental process, to reflect the difference in the effect of different models, various types of mathematical models were constructed for horizontal comparison; at the same time, to reflect the influence of the parameters of the same type of model, different combinations of parameters were constructed using a grid search algorithm to vertically compare the difference in the effect. The average accuracy of the dichotomous model for anxiety and depression in the sample of 1433 students was 0.80 or higher. The experiments show that the method of predicting students' psychological status through their online behavioral data is feasible, and the mathematical classification model can be used to grasp students' psychological status in real time and to warn students with abnormal psychological status, thus helping school counselors to intervene and prevent them promptly.

1. Introduction

With the increasing competition in society, college students are facing multiple pressures in employment, life, study, and emotion, which lead to the frequent occurrence of college students' mental health problems and directly affect the stability of campus life and learning environment; therefore, it is of great practical significance and theoretical value to evaluate the mental health of college students [1]. At present, the methods for evaluating the mental health status of college students are mainly based on traditional machine learning algorithms, such as decision trees (DT) and feedforward neural networks (BPNN), which have the disadvantages of great computational effort and low accuracy rate [2]. The university campus life is a critical period for students' rapid psychological development and maturity and is a key step in the formation of healthy psychology; school educators and parents should pay attention to the guidance and education of students during this period to help them shape healthy psychology. Unsatisfactory schooling has a number of detrimental repercussions on pupils' psyche, as well as their subsequent incapacity to integrate effectively into social life. The goal of this research is to gather information regarding students' psychological well-being without putting them under undue stress so that psychologists can perform their jobs more effectively. This paper investigates the relationship between students' psychology and data and builds the feature vector associated with psychology using behavioral data, including mining students' social relationship characteristics using behavioral data and proving the scientificity of the method using students' social sensitivity data, constructing regularity correlation index features using the theory of information entropy and penalty factor, and measuring students' social sensitivity data.

In today's era of big data, students, as the majority of the campus population, produce the most data, the most

valuable of which is data records of students' online behavior, which are generated by students of their own volition, can reflect differences between students to the greatest extent, and have laid a solid data foundation for this topic's research [4]. The traditional psychological method of data collection is based on the concept of random sampling, and its analysis method is based on hypothesis testing, both of which have drawbacks that affect the accuracy of the results, whereas big data psychology uses the full volume and full data analysis method, which completely squeezes the value contained in the data and greatly improves the accuracy of the experimental results. In this paper, based on the online behavioral data generated by school college students on the Internet and the basic attribute data of students, combined with the content of the MBTI assessment scale, PHQ-9 depression screening scale, and GAD-7 anxiety screening scale, the correlation between students' behavioral data and their psychological states is explored, and the data mining method is used to construct the models of internal and external personality tendency classification, depression state classification, and anxiety classification [5]. The data mining method is used to construct a classification model for personality internal and external tendencies, depression, and anxiety, to predict the psychological state of students based on their behavioral data at school, to warn students with psychological abnormalities, and to assist psychologists in better psychological intervention.

With the digitization of colleges and universities, the degree of information technology in each college and university is getting higher and higher, and everything is gradually being data-driven. Every instantaneous behavior of students on campus is transformed into a data record, and these data records lay the foundation for the study of this topic. The psychological research approach based on big data technology has its significant superiority compared with traditional psychological research. Furthermore, the big data research approach analyzes all data from the entire dataset, avoiding the sampling error that may arise from the traditional research method of sampling samples from the entire dataset, then generalizing to the entire dataset, collecting data directly from the real environment, and avoiding the experimental error caused by the traditional research method of overcontrolling the experimental conditions, which results in the generation of behaviors that are not representative of the real environment. In terms of the efficiency and scale of data processing, it can relieve the pressure of traditional research methods that require a lot of time and workforce; in terms of time validity, it can instantaneously collect, analyze, and predict real-time psychological states, avoiding the bias of analysis results caused by the lag of data collection of traditional research methods. This paper analyzes the correlation and degree of correlation between students' behaviors and their psychological states based on the behavioral data and scale data generated by students at school, constructs the features associated with students' psychological states by combining students' static attributes, and builds a prediction model of students' psychological states through machine learning methods. The goal is to forecast students' present psychological states by collecting real-time data on their school behavior, to warn students with aberrant psychological states, and to aid campus psychology professors and specialists in intervening with kids who may have psychological issues.

2. Current Status of Research

Based on summarizing previous studies, a model based on robust multitask learning was established using the Big Five personality assessment scale as an indicator to achieve accurate classification prediction of personality variables of active Weibo users [6]. As for the research on the prediction of students' depression, Barenholtz et al. established a regression model to analyze the severity of students' depression by using the number of posts, likes, and likes for others as the characteristic dimensions of students' microblog comments in a week, and the results showed that people with heavy depression had a higher number of dynamic posts, but a lower number of likes for others [7]. In a study on student suicide risk prediction, Kumari et al. used keywords extracted from text data published by microblog users for data analysis and used MLP models to achieve a predictive assessment of suicide risk based on microblog text data [8]. However, one of the obvious drawbacks of these studies is that they only focus on users who have social network accounts, such as Sina Weibo, and not every student uses Sina Weibo; in fact, according to the survey, the average number of active users of Sina Weibo is only 4 to 5 [9]. There are no studies that show a psychological difference between Weibo users and non-Twitter users. Therefore, data from social networks such as Weibo are not sufficient to predict the psychology of all school students. The higher the psychological indicator of gratitude, the lower the value of the corresponding indicator of depression [10]. The cross-sectional study demonstrated that the quality of sleep of college students is related to their depression level, the quality of sleep and depression level can interact with each other, and long-term poor sleep quality significantly increases the occurrence of depression. A study of a sample of more than 2,000 individuals through a mediated moderation model verified that peer friendships influence the psychological aspects of depression in students and that friendship support negatively predicts depression. However, these aspects of the study only made psychological causal explanations and did not do so to the extent of predicting psychological states [11].

Anomaly detection techniques aim to automatically identify those observations in a large set that are valuable or whose behavior is different from the expected one. Anomaly detection is one of the important applications in data mining technology and has specific applications in many practical production's lives, such as credit card fraud, industrial damage detection, and image detection. Through in-depth research, scholars at home and abroad have proposed many anomaly detection algorithms with high feasibility, which has laid a solid foundation for further research on anomaly detection [12]. Nevertheless, the basic mathematical models are still very useful and have eventually been adapted to many computational scenarios. Current research tools are divided into nonparametric and parametric approaches: the

nonparametric approach does not require the assumption of knowledge of any parameters and uses nonparametric techniques to estimate the density of the distribution, for example, histograms and Parzen window estimation; the parametric approach requires the assumption that normal data are generated based on parametric distributions, and it requires these parameters from training samples, for example, outlier detection methods based on normal distributions [13]. Neural networks, which may be classified into single-classification neural networks and multiclassification neural networks [14], are an important field of nonlinear modeling approaches. Multiclassification neural networks, such as multilayer perceptron, neural tree, and others, use data from multiple classifications to train the model and then input test data into the model, which the network interprets as normal or abnormal; single-classification neural networks, such as Replicator Neural Networks (RNNs), use a function (like a step function) to transform the sample into N discrete variables for sample clustering.

The mental health status data of college students collected according to the conventional model assessment guidelines and the symptom self-assessment scale SCL-90 are high-dimensional datasets, so there are drawbacks of huge computation and redundant correlations between data features when conducting mental health assessment of college students. With the extensive research of popular learning algorithms, this method has been widely applied to image retrieval, text classification, face recognition, and plant leaf recognition as data feature extraction and dimensionality reduction. A mental health assessment approach based on a local linear embedding algorithm (LLE) and support vector machine (SVM) is presented to increase the accuracy of college students' mental health status evaluation. LLE-SVM may successfully increase the accuracy rate of college students' mental health status assessment when compared to SVM, BPNN, and DT.

3. SVM Analysis of Multidimensional State Data Reduction and Evaluation of College Students' Mental Health

3.1. SVM Multidimensional State Data Reduction Evaluation Design. The evaluation of the college students' mental health status is essentially a nonlinear classification problem. Since the characteristics of everyone's mental state data are multidimensional and these characteristics involve many nonlinear factors and have the characteristics of multilevel, multivariable, nonlinear, and strong coupling, it is difficult to describe quantitatively by traditional mathematical models or methods [15]. To improve the accuracy of the evaluation of the mental health status of college students, it is very necessary to establish a more scientific and reasonable evaluation model of the mental health status of college students. In this study, nine dimensions of psychoticism, paranoia, hostility, terror, anxiety, depression, obsessive-compulsive symptoms, interpersonal sensitivity, and somatization were used as input vectors of the LLE-SVM model, and the mental health status of college students was divided into healthy, mildly unhealthy, and unhealthy as output vectors of the LLE-SVM model to establish the evaluation model of college student's mental health status based on LLE-SVM. The evaluation model is shown in Figure 1.

In this study, the data of nine dimensions, including psychoticism, paranoia, hostility, terror, anxiety, depression, obsessive-compulsive symptoms, interpersonal sensitivity, and somatization, were used as the input vectors of the LLE-SVM model, and the mental health status of college students was divided into healthy, mildly unhealthy, and unhealthy as the output vectors of the LLE-SVM model to establish a mental health status evaluation model of college students based on the LLE-SVM. The process of the evaluation algorithm based on LLE and SVM can be described in detail [16]. The data of mental health characteristics of college students were collected: SCL-90 was issued to collect the data of mental health characteristics of college students, which included nine dimensions of psychoticism, paranoia, hostility, terror, anxiety, depression, obsessive-compulsive symptoms, interpersonal sensitivity, and somatization. The LLE algorithm was used to reduce the dimensionality of college students' mental health characteristics data to reduce the computational effort. The reduced dimensional data were divided into training samples and test samples, and the training samples were used to build the LLE-SVM model for evaluating the mental health status of college students, in which the reduced dimensional data were used as the input of the SVM and the mental health status of college students was used as the output of the SVM. The test sample data were used to verify the effectiveness of the LLE-SVM model for evaluating the mental health status of college students.

Machine learning can be used to discover dependencies between inputs and outputs by learning from training samples to make predictions about unknown inputs. This can usually be expressed as follows: there is some dependency between the variables y and x. And, it is based on the independently distributed sample data sources.

$$S = \left(x_1^2, y_1^2\right), \left(x_2^2, y_2^2\right), \ldots, \left(x_l^2, y_l^2\right). \tag{1}$$

The goal of machine learning is to minimize the desired risk by training with sufficient training samples. In practice, the set of samples available for training is limited and does not achieve the minimization of the expected risk [17]. According to equation (1), it can be found that the final composition of the expected risk is influenced by various aspects such as the error function and the joint probability distribution; therefore, for the classification judgment problem involved in this paper, the empirical risk minimization principle is used.

$$R_{\text{emp}}(\alpha) \approx \frac{1}{l} \sum_{i=1}^{l} L^2\left(y_i^2, f\left(x_i, \alpha\right)\right). \tag{2}$$

The theoretical use of empirical risk to approximate the expected risk assumes that the sample size l is infinitely large and that equations (1) and (2) expressed by mathematical calculation are equivalent when the sample size is infinite.

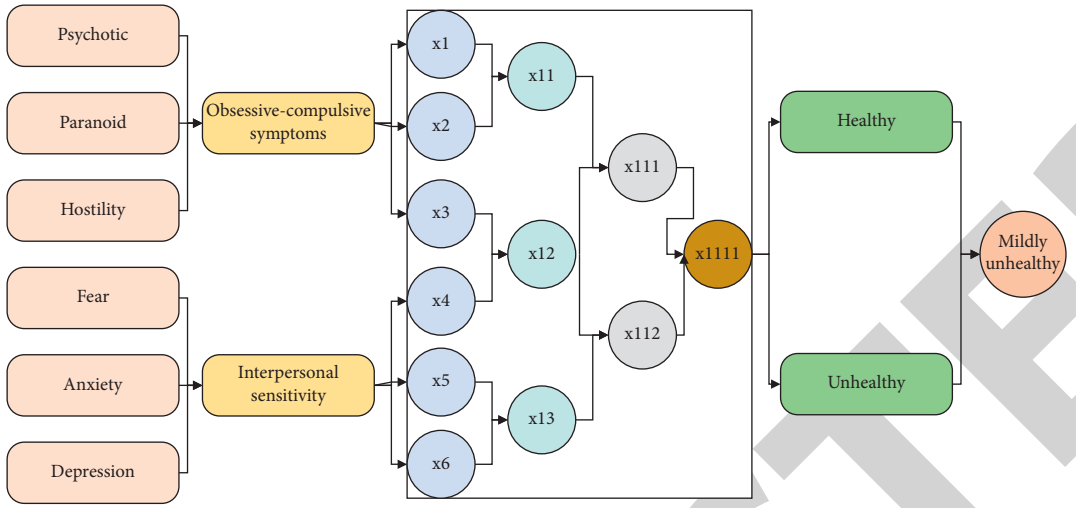

Figure 1: Mental health state evaluation model.

Because the training samples are limited in real life, the method of using such an approximation instead is not fully proven for the time being, so there are some errors between the empirical risk and the expected risk when considering practical problems where the training samples are far less than an infinite magnitude.

According to the foregoing, using the linearly divisible support vector machine classification technique, the linear decision function may be immediately generated in the feature space for linearly divisible data to be processed. However, building a nonlinear decision function directly in the feature space for linearly indistinguishable data is too difficult to execute, and it may also lead to a "dimensional catastrophe" when the dimensionality of the data features is enormous. It can be concluded from the statistical learning theory that the inductive ability of the learning system is independent of the dimensionality of the data; therefore, the data in the low-dimensional input space can be mapped to the high-dimensional space, the classification hyperplane can be found in the high-dimensional space to classify the data, and the decision function can be solved according to the classification hyperplane. The SVM algorithm is based on the idea of first mapping the low-dimensional data samples to the high-dimensional space by the kernel function and then finding the hyperplane that can classify the data samples reasonably in the high-dimensional feature space to achieve the classification of the data.

$$\begin{aligned} k\left(x_i, x_j\right) &= \varphi\left(x_i^2\right)\varphi\left(y_i^2\right), \\ Q(a) &= \sum_{i=1}^{l} a_i - L^2\left(y_i^2, f\left(x_i, \alpha\right)\right), \\ f(x) &= \sin\left(\sum_{i=1}^{l} a_i - L^2\left(y_i^2, f\left(x_i, b\right)\right)\right). \end{aligned} \tag{3}$$

Based on the network behavior of the malicious code detection system, the detection data come from the various types of operational data collected from the network, and the network data have the characteristics of large data volume and strong uncertainty. On the one hand, a large number of various types of data provide the detection system with a lot of valuable information, but on the other hand, there are many duplicate redundant data and features in the network data, the existence of these invalid data not only adds a burden to the storage of the detection system, increasing the cost of hardware storage equipment, but also increases the computational burden of the detection system, affecting the monitoring of real time and, more seriously, the existence of interference data. There is also the possibility of affecting the accuracy of the final detection. Therefore, feature extraction is to select relatively important features from a large amount of network data through some evaluation criteria, reduce the overall feature dimension, thus reducing the complexity of model computation, and improve the training time and detection time while ensuring the detection accuracy.

$$\begin{aligned} x_i^2 &= \frac{x_i - x_{\min}}{x_{\min} + x_{\max}} * (U + L) - L, \\ S &= \frac{1}{n_1}\sum_{i=1}^{l} f\left(a_i - L^2\left(y_i^2, f\left(x_i, b\right)\right)\right). \end{aligned} \tag{4}$$

Data cleaning is an essential technique for resolving data quality issues caused by external influences, such as those mentioned previously. Missing data are filled in, errors are detected, duplicates are filtered out, and consistency is checked, among other things. Filling methods include zero-value filling, mean value filling, and filling according to the probability distribution; for example, the missing of some age fields in the basic information can be filled by the mean value of the whole group; error detection means verifying some data records in some fields in the data content by the rules and the data missing because a certain reason need to be filled by a certain data association. Consistency check is necessary to ensure the consistency of data between multiple data sources when a data field has multiple data sources. For example, the college and major in the basic information of students and the college and major in the data of students' grades should ensure the consistency of data. Meanwhile, the

consistency and the inconsistent data should be corrected by rules or handled manually, as shown in Figure 2.

Each university will establish various business departments according to different functional divisions. Each department's business systems are relatively independent and connected, such as grades and course selection data from the Registrar's Office, consumption, and access control data from the Logistics Department [18]. Therefore, before mining multidimensional student data, it is necessary to physically integrate the data from different data sources with different storage media and different data formats, a process called data integration. Data sources can be divided into online data and offline data according to the form: online data can be obtained directly through the online form of data, such as database data and interface data; offline data is usually obtained in an offline manner, such as excel tables and text files. At present, most of the data in universities are online data, such as consumption, access control, course selection, and grade data. Only very few data are stored in an offline way, such as student registration data when enrolling and class-based information statistics summary data. Data analysis is the interpretation of key information contained in or between data through visual data graphs or metrics such as correlation coefficients. The purpose of data analysis is to get a sufficiently accurate picture of the distribution of the data and the correlation between them, which helps in feature engineering to construct feature vectors with labels characterizing the data.

3.2. Experimental Design for Multidimensional State Evaluation of College Students' Mental Health. The process of model application is to classify unknown samples by the constructed model, and the model is applied to predict sample data with unknown labels only if the accuracy of the model is within an acceptable range. The estimated accuracy of a model is usually assessed using accuracy, where the prediction accuracy of an individual sample is judged by comparing the known labels of the test sample with the results predicted by the model, with the accuracy being the percentage of the test data correctly classified by the model. The test dataset should be independent of the training dataset to avoid model overfitting problems. The model may achieve excellent accuracy when categorizing imbalanced sample class labels by explicitly predicting the test sample as the majority sample class [19]. As a result, it is also important to think about the model's recall, which refers to the model's check-all rate or the proportion of positive cases in the test data that the model correctly predicts. In most classification issues, the F1 value, which is the summed average of the model's accuracy and recall, is used to determine the model's quality.

Although significant progress has been achieved in theoretical research and social services, the building of a mental health care system still lags behind and is unable to satisfy the demands of social growth. As China's comprehensive strength has grown, several institutions have progressively begun to construct a flawless psychological care system to promote students' mental health. At present, all colleges and universities have established mental health centers to provide professional psychological counseling for college teachers and students, and some colleges and universities will regularly conduct psychological assessment activities to comprehensively measure students' current psychological status and provide timely guidance and intervention for students with psychological abnormalities. This chapter further explains the correlation between the psychological assessment dimensions based on the data of the student psychological scale.

To verify the validity of the LLE-SVM for evaluating the mental health status of college students, the SCL-90 data of college students' mental health symptoms of a school entering college in 2020 were selected for the study, and the data of mental health characteristics of each college student were nine dimensions of indicators such as psychoticism, paranoia, hostility, terror, anxiety, depression, obsessive-compulsive symptoms, interpersonal sensitivity, and somatization. The data were categorized as unhealthy. The mental health status of college students was divided into three states: unhealthy, mildly unhealthy, and healthy, and the distribution of the three sample data is shown in Figure 3.

Data preprocessing is a very important part of the data mining process, but data preprocessing is very time- and effort-consuming. Experience shows that if the data preprocessing is done well, then it saves effort in building the model. Because the existence of a high number of noisy data, redundant data, missing data, and so on in the dataset influences the prediction results, we must preprocess the data. There are a variety of reasons for incomplete data in the dataset; for example, the student may have misplaced a card and failed to replace it on time, resulting in missing data for that period, or there may be a mechanical failure resulting in data loss and incorrect entry; all of these anomalies result in a large amount of redundant data in the database, and due to the presence of these incorrect data and vacant data, preprocessing is essential. For the processing of missing values, either direct deletion or interpolation of missing values can be performed. Direct deletion causes partial loss of information and loss of some important data with missing values, especially when the data are small, which is more harmful to the sample; missing value interpolation can be divided into mean interpolation, median interpolation, arbitrary value interpolation, and model interpolation. Missing values may also be a kind of information in some cases and can be captured by adding a feature to capture whether it is missing or not (i.e., adding a column of features, where 1 means it is a missing value NaN and 0 means it is not a missing value), and certain students in the dataset have missing values in some consumption patterns, as shown in Table 1.

For the missing values, different values need to be filled in using different values depending on the nature of each feature. Cartoon student consumption data have much vacant information, and only these missing data need to be populated with 0. Because the public database did not contain the required peripheral physiological signals for the previous studies in this section, it was not possible to conduct a mixed physiological signal emotion classification

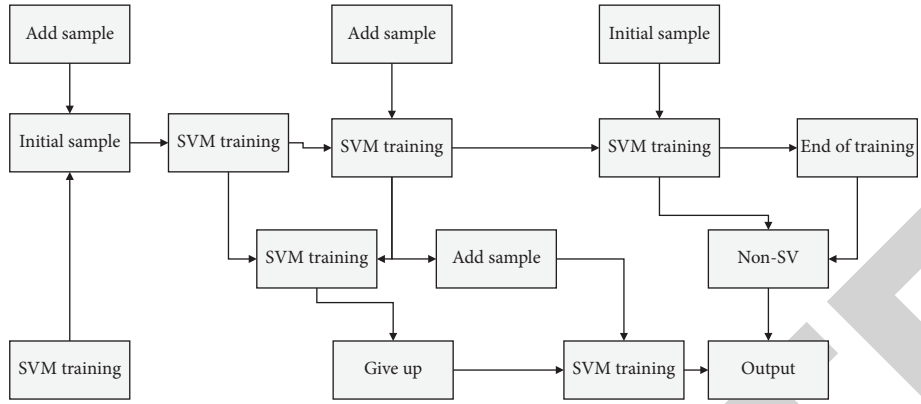

Figure 2: Batch SVM training process.

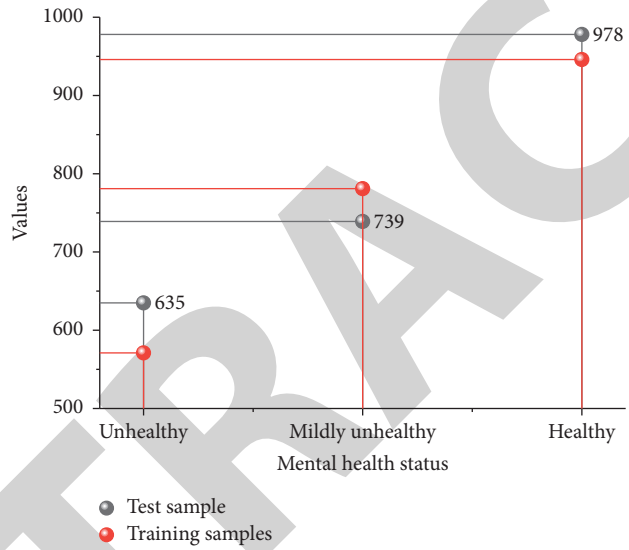

Figure 3: Distribution of training and test sample data.

Table 1: Dataset.

Student ID	1	2	3	4	5
Library	11.52	1.94	12.66	3.57	14.35
Boiling water	7.54	7.59	7.26	6.25	13.35
Academic affairs office	13.18	7.86	12.78	4.46	4.96
Print center	3.08	6.73	1.71	13.12	14.65
School clinic	2.37	2.08	12.34	4.93	9.75
School bus	12.36	12.5	4.89	1.65	2.72
Laundry room	14.67	8.23	8.72	9.29	12.25

study, and the superiority of the spatiotemporal features was facilitated by the algorithmic analysis of the spatiotemporal features in the self-constructed dataset validation. Therefore, in this paper, we first conduct experiments on the mixed physiological signal acquisition of emotions to obtain experimental data and then validate the spatiotemporal features on the EEG signals in the collected experimental data.

The selection of emotional elicitation material is the first step of the whole experiment, and this experiment chose the audiovisual stimulus as the elicitation material, that is, the music + dynamic pictures as the whole elicitation material, giving the subjects visual stimulation from both visual and auditory dimensions. These two approaches require the selection of moving pictures and background music, which is also crucial because it is necessary to consider that different people respond differently to music and pictures, and this experiment requires the selection of background music and moving pictures that can effectively evoke most of the subjects, as well as considering factors such as the main groups of recruited subjects and their living environment. Considering that the subjects were mainly students of the university, music and pictures were selected to stimulate

young students aged 20 to 24 years. Before the formal experiment, some students were selected for evaluation. After the music and pictures were completely selected, the experiment was conducted by playing 14 dynamic pictures for one minute for each emotion induced. The experiment was designed to collect physiological signals from a total of 60 subjects with an average age of about 24 years. When the subjects were recruited before the start of the experiment, the exact procedure and the purpose of the experiment needed to be explained clearly to the subjects, and those who were willing to participate in the experiment were required to sign an informed consent form. EEG, ECG, EDA, and RSP signals were collected during the experiment. The EEG acquisition equipment used was the Enobio system. The ProComp Infiniti device was used for peripheral physiological signals. The EEG signal was acquired at 500 Hz, the ECG signal was acquired at 2048 Hz, and the EDA signal and the RSP signal were acquired at 1024 Hz. The material was played back in a way that gave the subject a more visual stimulus, and an ASUS computer and a Holly 75-inch display were used to play the stimulus material. The experimental flow is shown in Figure 4.

Before the start of the experiment, it is necessary to explain the purpose of the experiment and the whole process to the subject. After the subject is informed, he/she needs to fill in the relevant information form and sign the informed consent form. The equipment will also need to be worn, and the equipment will need to be commissioned. The room must be darkened before the official experiment starts so that the emotions may be created more effectively. The collector must be aware of the signals acquired during the experiment, noting any noticeable anomalous signals or if the equipment is malfunctioning in order to assess whether the data has to be recollected [20]. The experiment started with the official admission into the physiological signal elicitation acquisition phase, and it went like this: the patient stayed quiet throughout the two-minute blackout; during this time, the subject's basal signal was captured. The stimulus material was presented after 2 minutes of basal signals had been recorded. There were four different sorts of content, each of which was played for one minute, followed by a two-minute black screen to allow the subject to rest and recuperate.

4. Analysis of Results

4.1. SVM Multidimensional State Data Dimensionality Reduction Results. The mental state perception model is to perceive students' mental state information based on their online behavioral data for psychological prediction. The output of the model is the categorization of the mental state information, that is, the classification of students' mental states according to the online behavioral data, the form of classification is binary, and the content is two kinds of student's mental health status, healthy and unhealthy, so the mental state perception model essentially belongs to the category of binary classification model in supervised learning. A preselection-elimination mechanism is used to construct the mental state perception model. Preselection means that several different types of classification models with classification ability are selected first, given the same training data set for training, and finally, the model with the best output is selected as the final perception model based on the average results of multiple experiments, and the rest of the models are eliminated. The reason for choosing this method to construct models is that the network behavior data used in this paper is a kind of data that has not been studied and applied, so some models need to be preselected to compare and analyze the advantages and disadvantages of different models' performance for this kind of data before finally determining the perceptual models.

The data used in this experiment came from two parts, respectively, the psychological status data obtained from the questionnaire platform and the web access log data obtained from the log server database; all the data have strict control over the privacy of students not to be leaked, such as psychological status data only have the student ID data, no student's name, major, class, and other information, so it only can be treated as a unique identification of the existence. The same applies to the weblog data, where the data collected are limited to the type of website visited by a student ID, the name of the website, and so on and do not relate to the specific content of the visit, as shown in Figure 5.

As can be seen in Figure 5, the P and R values corresponding to each model and the F score on the fold are marked, and all models except the SVM model have an F score above 0.6, and the optimal GA-RF model has an F score reaching 0.765, indicating that the model trained by the feature dimension data of the network behavior can achieve the judgment of the population's internal and external tendencies. Second, compared to the results of the model without the extraction of features by the genetic algorithm, all values of the model group with the genetic algorithm have improved, indicating that the data of these eight feature dimensions extracted by the genetic algorithm are more representative compared to the data without processing when based on the internal and external tendency labels, which are the regularity of WeChat, the degree of WeChat dependency, the regularity of WeChat posting friend regularity, microblog regularity, video viewing regularity, video viewing gauge dependency degree, reading regularity, and reading dependency degree.

By further statistical analysis of the data of these 5 dimensions, it was found that the depressed people have lower dependence on shopping and web, while the dependence on listening to music, regularity of using map websites, and dependence on games have higher values because the depressed people are cold not only to interpersonal relationships but also to life, so they are not interested in buying new things and maintaining. Instead, they are more dependent on music and games than others. For a normal person, there are more or less a few days in a month-long cycle when he or she goes out with friends to have fun, and then he or she will use the map. The use of the map-type website is regular, as it is not used every day, as shown in Figure 6.

The main purpose is to construct, analyze, and tune the models of three different kinds of students' mental health status, aiming to be able to grasp the information of students' mental status more comprehensively and accurately through

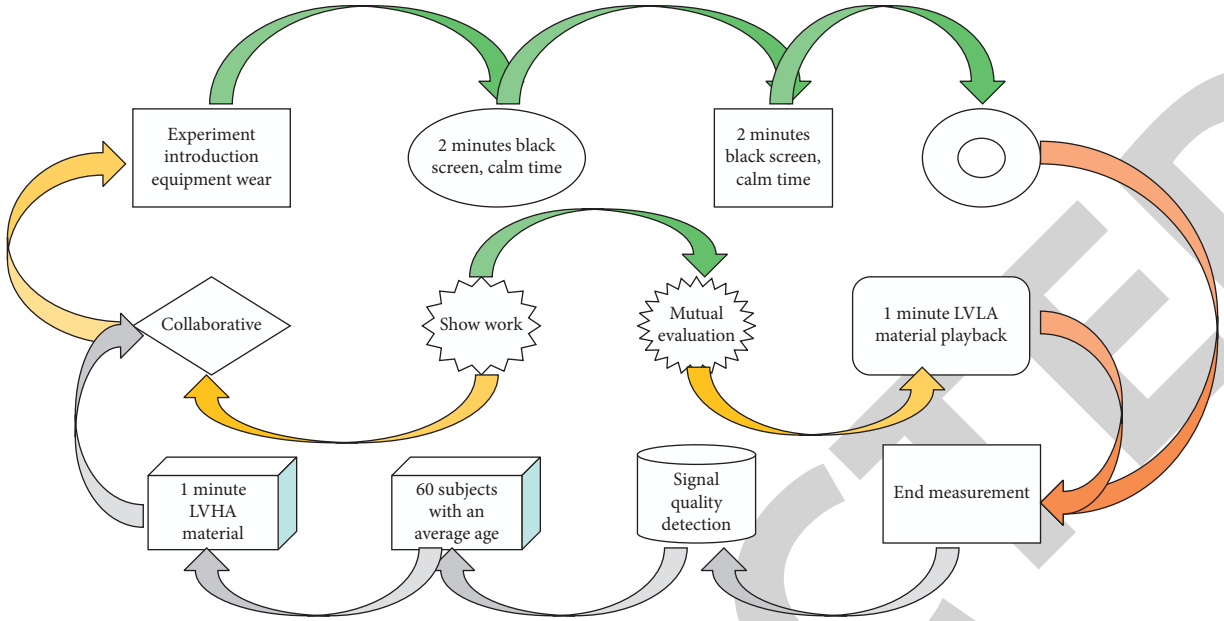

Figure 4: Experimental flowchart.

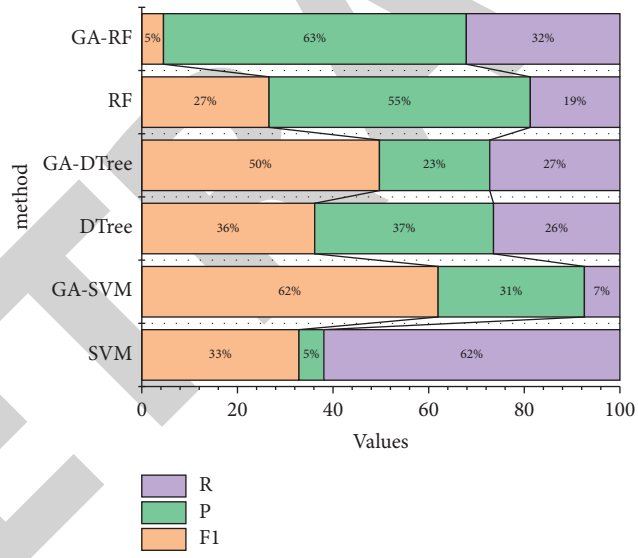

Figure 5: Evaluation of different classification models for internal and external tendencies.

their online behavior data at school. In this chapter, the labeling and feature dimension parts of the sample data set are processed in conjunction with Chapter 4 so that they can be used for the subsequent model training, and then the evaluation indexes of the classification model are selected. Firstly, when building the model, a series of classification models are designed for experiments by combining the contents of Chapter 3, and the results of multiple models are briefly analyzed by selecting the model with the best output for the parameter optimization work. After a series of steps down, the best model algorithm is selected in the case of horizontal comparison of different classification models, and the best model algorithm is selected in the case of vertical comparison of different optimal combinations of parameters and different combinations of parameters, and finally the good output of the model of the perceived mental health status of students was ensured.

4.2. Results of Multidimensional State Evaluation of College Students' Mental Health. As shown in Figure 7, the results are binary logistic regression results for univariate and multivariate factors, and the depression subscale of the symptom self-rating scale yields results as continuous-type values indicating different levels of depression, so it is also necessary to use multiple linear.

The goal of the student psychological state perception model is to be able to predict student psychology in real time

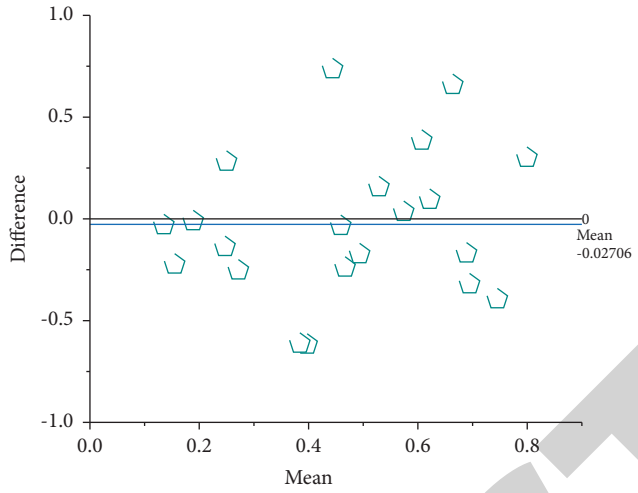

Figure 6: F1 values for a different number of iterations.

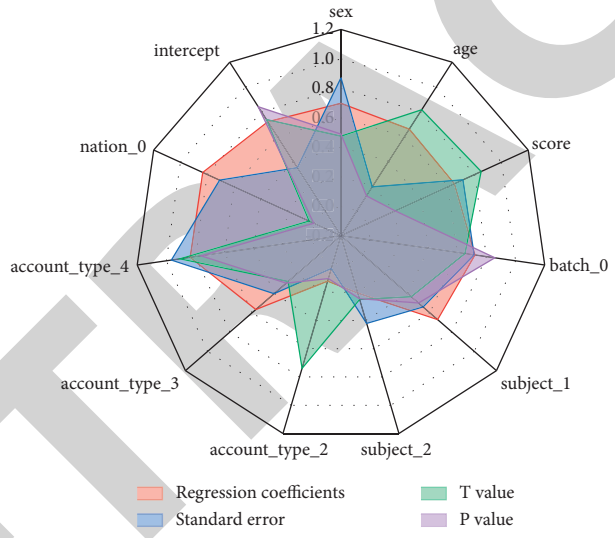

Figure 7: Regression analysis.

based on the behavioral data generated by students at school, so this section aims to construct dynamic features in three major areas from the behavioral data generated by students at school, including student consumption features, student behavior features, and social relationship features. The behavioral data generated by students at school include daily consumption data, containing the time, place, amount of consumption, and so on; library access data, containing access status, time, and so on; and course selection data, containing the semester of course selection, course type, and so on. The human psychological state has stability within a certain period; that is, no human psychological state will change much over a while, but to throw out the possible influence of expost behavior on the exante state, this topic only selects the behavioral data within the period from the entrance of new students to the test, which is also beneficial to the model in the application of the demand on the data period, as shown in Table 2.

The LLE algorithm involves two parameters: the embedding dimension a and the nearest neighbor parameter K. The magnitude of these two parameters directly affects the effect of college students' mental health status evaluation. When various K and d values are used as values, the parameters of SVM are set as penalty parameters, radial basis kernel function parameters, and the accuracy rate of college students' mental health status rating. The greatest accuracy percentage for assessing the mental health status of college students was 96.5 percent. The correlation between each factor and depression status was analyzed using multifactor binary logistic regression; finally, the scores of the depression subscale of the original symptom self-assessment scale were used as the target, that is, the magnitude of depression; and whether each factor was an influential factor in the degree of depression was investigated using a multivariate logistic regression mode.

Table 2: Behavioral data used in the student psychological state perception model.

Type	K = 3	K = 4	K = 5	K = 6	K = 7	K = 8
$d = 2$	43	29	19	28	16	11
$d = 3$	21	10	26	26	22	31
$d = 4$	38	10	16	11	43	28
$d = 5$	15	22	47	13	24	41
$d = 6$	45	12	47	23	45	12
$d = 7$	21	17	33	27	30	48
$d = 8$	25	24	15	20	44	35

5. Conclusion

In the early stage, through reading and detailed analysis of a large amount of relevant literature, we have a certain understanding of the current status of research on a mental state based on network data at home and abroad, and by comparing the advantages and disadvantages of different research methods, it is clear that the current research on mental state mainly focuses on the analysis of users on social network platforms; while there are fewer methods suitable for the analysis of mental health in a more closed environment like school students, in this context, this paper proposes the concept of a mental state perception model based on school students' online behavior data. The process of knowledge discovery is also the process of discovering the value of data, and data mining is the key link in the process of knowledge discovery. By analyzing and studying each step of the overall process of knowledge discovery, we have a grasp of the overall process for the subsequent establishment of the mental state perception model. It is clarified that there needs to be a process of data preparation stage before data mining and a process of result expression and interpretation stage after data mining. An improved SVM incremental learning algorithm that effectively utilizes the results of the above preselection algorithm and combines KKT conditional judgments and error-push strategies is proposed. In the case of using the above data preselection method, a new SVM incremental learning algorithm combining the traditional KKT conditional and error-push strategies is proposed. This algorithm improves the learning speed by effectively using the results of data preselection; by adding the relevant error score vectors to the added vectors, the detection accuracy is improved relative to the traditional incremental learning.

Data Availability

The data used to support the findings of this study are included within the paper.

Conflicts of Interest

The author declares that there are no conflicts of interest.

References

[1] G.-H. Dong, Z. Wang, H. Dong et al., "More stringent criteria are needed for diagnosing internet gaming disorder: evidence from regional brain features and whole-brain functional connectivity multivariate pattern analyses," *Journal of Behavioral Addictions*, vol. 9, no. 3, pp. 642–653, 2020.

[2] Y. A. Suh and M.-S. Yim, "A worker's fitness-for-duty status identification based on biosignals to reduce human error in nuclear power plants," *Nuclear Technology*, vol. 206, no. 12, pp. 1840–1860, 2020.

[3] J. Wu, P. Guo, Y. Cheng, H. Zhu, X.-B. Wang, and X. Shao, "Ensemble generalized multiclass support-vector-machine-based health evaluation of complex degradation systems," *IEEE/ASME Transactions on Mechatronics*, vol. 25, no. 5, pp. 2230–2240, 2020.

[4] A. Baghdadi, Y. Aribi, R. Fourati, N. Halouani, P. Siarry, and A. Alimi, "Psychological stimulation for anxious states detection based on EEG-related features," *Journal of Ambient Intelligence and Humanized Computing*, vol. 12, no. 8, pp. 8519–8533, 2021.

[5] J. S. Rahman, T. Gedeon, S. Caldwell, R. Jones, and Z. Jin, "Towards effective music therapy for mental health care using machine learning tools: human affective reasoning and music genres," *Journal of Artificial Intelligence and Soft Computing Research*, vol. 11, no. 1, pp. 5–20, 2021.

[6] K. Zhao, Y. Ding, Y. Han et al., "Independent and reproducible hippocampal radiomic biomarkers for multisite Alzheimer's disease: diagnosis, longitudinal progress and biological basis," *Science Bulletin*, vol. 65, no. 13, pp. 1103–1113, 2020.

[7] E. Barenholtz, N. D. Fitzgerald, and W. E. Hahn, "Machine-learning approaches to substance-abuse research: emerging trends and their implications," *Current Opinion in Psychiatry*, vol. 33, no. 4, pp. 334–342, 2020.

[8] P. Kumari, P. Gupta, A. K. Piyoosh, B. Tyagi, and P. Kumar, "COVID 19: impact on mental health of graduating and post graduating students," *Journal of Statistics and Management Systems*, vol. 24, no. 1, pp. 67–79, 2021.

[9] D. Dodell-Feder, L. M. Tully, E. Dudek, and C. I. Hooker, "The representation of mental state information in schizophrenia and first-degree relatives: a multivariate pattern analysis of fMRI data," *Social Cognitive and Affective Neuroscience*, vol. 16, no. 6, pp. 608–620, 2021.

[10] P. Mohan and I. Paramasivam, "Feature reduction using SVM-RFE technique to detect autism spectrum disorder," *Evolutionary Intelligence*, vol. 14, no. 2, pp. 989–997, 2021.

[11] H. Akbari, M. T. Sadiq, and A. U. Rehman, "Classification of normal and depressed EEG signals based on centered

Hindawi
Journal of Mathematics
Volume 2024, Article ID 9873039, 1 page
https://doi.org/10.1155/2024/9873039

Retraction

Retracted: Research on International Law Data Integrity Guarantee Based on Antiterrorism Prediction Algorithm

Journal of Mathematics

Received 23 January 2024; Accepted 23 January 2024; Published 24 January 2024

This article has been retracted by Hindawi following an investigation undertaken by the publisher [1]. This investigation has uncovered evidence of one or more of the following indicators of systematic manipulation of the publication process:

(1) Discrepancies in scope

(2) Discrepancies in the description of the research reported

(3) Discrepancies between the availability of data and the research described

(4) Inappropriate citations

(5) Incoherent, meaningless and/or irrelevant content included in the article

(6) Manipulated or compromised peer review

The presence of these indicators undermines our confidence in the integrity of the article's content and we cannot, therefore, vouch for its reliability. Please note that this notice is intended solely to alert readers that the content of this article is unreliable. We have not investigated whether authors were aware of or involved in the systematic manipulation of the publication process.

In addition, our investigation has also shown that one or more of the following human-subject reporting requirements has not been met in this article: ethical approval by an Institutional Review Board (IRB) committee or equivalent, patient/participant consent to participate, and/or agreement to publish patient/participant details (where relevant).

Wiley and Hindawi regrets that the usual quality checks did not identify these issues before publication and have since put additional measures in place to safeguard research integrity.

We wish to credit our own Research Integrity and Research Publishing teams and anonymous and named external researchers and research integrity experts for contributing to this investigation.

The corresponding author, as the representative of all authors, has been given the opportunity to register their agreement or disagreement to this retraction. We have kept a record of any response received.

References

[1] H. Ru Qing, "Research on International Law Data Integrity Guarantee Based on Antiterrorism Prediction Algorithm," *Journal of Mathematics*, vol. 2022, Article ID 3089545, 9 pages, 2022.

Hindawi
Journal of Mathematics
Volume 2022, Article ID 3089545, 9 pages
https://doi.org/10.1155/2022/3089545

Research Article

Research on International Law Data Integrity Guarantee Based on Antiterrorism Prediction Algorithm

Huang Ru Qing

China Institute of Boundary and Ocean Studies, Wuhan University, Wuhan 430072, China

Correspondence should be addressed to Huang Ru Qing; b20160505225@stu.ccsu.edu.cn

Received 8 December 2021; Revised 14 January 2022; Accepted 18 January 2022; Published 21 February 2022

Academic Editor: Naeem Jan

In order to improve the quality of international law data, this paper designs a method to ensure the integrity of international law data based on an antiterrorism prediction algorithm. On the basis of introducing random function and deep learning technology, the prediction model set is split through the trusted seed model, the model selection is completed through iterative optimization, and then new terrorism-related factors are added to obtain the new prediction model set, so as to complete the antiterrorism data prediction. Based on the antiterrorism prediction data obtained by the above process, on the basis of identifying incomplete data, the antiterrorism data integrity guarantee method in international law database is designed through the process of determining data integrity operation parameters, eliminating worthless feature items, processing noise dimension reduction, and adding feature series of data integrity. Experimental results show that the frequency range and data sensitivity of international law data can be optimized by using this method, the audit process of data integrity is less time consuming, and the data integrity after processing can reach 0.967.

1. Introduction

Internationally recognized international law in which several states participate refers to the sum of the rule of law applicable between sovereign states and other international personality entities, also known as public international law, which is the law that distinguishes private international law or conflict of laws [1]. International law is also distinct from domestic law, which is the internal law of a state that regulates the conduct of individuals and other legal entities within its jurisdiction.

As a national code of conduct, the emergence and existence of international law must have a certain material basis, which is the communicative behavior and relations between states [2]. In the field of international law, the sum of such relations between states is traditionally called "international community," which is the social basis for the emergence and existence of international law. Since the middle of the 20th century, the understanding of the relations between countries has shown a trend towards the "international community." The term "international community" is used more and more frequently in academic research and practice of international relations and international law [3]. In the writing of international law, the scope of this community usually points to the whole world, not limited to a group composed of a few countries. This allows international societies to overlap geographically, and the social basis of international law evolves from international society to local politics.

With the development of the international legal system, after collecting case analysis and reports in the field of public international law, relevant organizations have constructed international law databases, including data of international courts, domestic courts, and ad hoc courts [4]. For the first time, this kind of database fully collects and analyzes international case law and provides in-depth analysis and guidance from legal experts. In the process of constructing such a database, however, due to factors such as network node deviation, susceptible to incomplete data, and with the extension of network transmission time, the data information keeps increasing; not only will the international law cause incomplete data balance level to continue declining, it

can also severely affect information parameter aggregation behavior. In order to avoid the occurrence of the above situation, it is essential to ensure the integrity of international law data [5].

At present, in terms of data integrity guarantee research, [6] proposes a method of cloud storage data integrity audit and guarantee, which summarizes the advantages and disadvantages of existing data audit protocols from the three aspects of data ownership proof, data recovery proof, and data ownership proof. The performance of typical protocols is evaluated in terms of technical principle, time cost, reliability, and detection probability. It is found that most audit protocols can only be used in specific scenarios, and it is urgent to further study universal audit protocols with balanced performance in all aspects. Audit protocols matching cloud storage, fog storage, blockchain, and other technologies are still in the exploratory stage. Finally, this method predicts the future development trend of outsourcing data auditing from three aspects: cloud audit protocol, alliance chain audit protocol, and component pool audit protocol.

In [7], a method to ensure the integrity of outsourced spatial database was proposed, which improved on the existing verification tree structure and proposed a spatial verification data structure VSS-Tree. SS-tree is used as the basic structure and additional verification information, and boundary ball is used to divide regions to increase the degree of nodes, effectively reduce the height of the verification tree, and avoid unnecessary disk access, so as to improve the processing efficiency of spatial query verification. This ensures that the querying user can verify that the data in the query result is real and contains all data that meets the criteria.

Reference [8] proposed multicopy integrity based on DDCT list audit and security methods. In this method, first, DDCT list is introduced to solve the problem of dynamic data operation; at the same time, the block number copy, the version number, and the information such as timestamp are stored in the table; next, to resist malicious cloud service provider attacks, a copy of the data signature verification algorithm is designed based on timestamp. Then, the concept of the duplicate block, including blockhead and block body, is proposed. The blockhead stores the signature information of duplicate data based on timestamp identification and authentication, and the block body stores the encrypted duplicate data. Finally, a third-party audit institution audits the integrity of multicopy data in the cloud by adopting the signature authentication algorithm based on duplicate timestamps.

However, in practical application, it is found that the frequency range and sensitivity of data are not ideal after the application of the above traditional methods, the integrity audit process takes a long time, and the data integrity needs to be further improved. Based on the above analysis, this study takes antiterrorism behavior as the analysis basis and designs an antiterrorism prediction algorithm to ensure the integrity of antiterrorism data in the international law database.

The following is a summary of the research: Section 1 contains the introduction. Section 2 discusses the literature review and background. Section 3 discusses the international law data integrity guarantee based on the antiterrorism prediction algorithm. In Section 4, experiment and analysis of the proposed concepts are provided. Finally, the conclusion brings the paper to an end in Section 5.

2. Background

International law has the following characteristics:

(1) International law provides a set of rules of conduct for states in dealing with their foreign relations, as well as their rights and obligations under international law

(2) International law is mandatory, but the way of enforcement is different from that of domestic law; however, the special way of enforcement is still mandatory

(3) Some important international treaties have clearly defined the effect of international law

(4) International practice has proved that international law, as the law between states, is not only recognized by all countries in the world but also abided by, by all countries [9]

The specific division of international law is shown in Figure 1.

According to its scope of application, international law can be divided into general international law and special international law. General international law is the international law binding all countries, and special international law is the international law binding two or a few countries [10]. Geographically, there are universal international law and regional international law. Universal international law is the international law binding all countries in the world, while regional international law is the international law binding only countries in a certain region, such as "American international law" and "Latin American international law." These are manifestations of the diversity and complexity of relations between states. However, in essence, only general and universal international law is generally referred to as international law, and the so-called special international law or regional international law must be restricted by general and universal international law [11].

Theorists and practitioners in the field of international law, law, and international relations are trying to explore some questions about its nature, function, and status. For example, is international law equally binding all states? Does international law have common pursuit that transcends states? Why is international law so weak? Why does international law often pale in comparison with political power and powerful states? Is it possible that international law, like domestic law, will become more systematic, binding, enforceable, and authoritative? In order to explain the nature, state, application methods, and operation characteristics of international law, some research results have tried to put forward a lot of interpretations, among

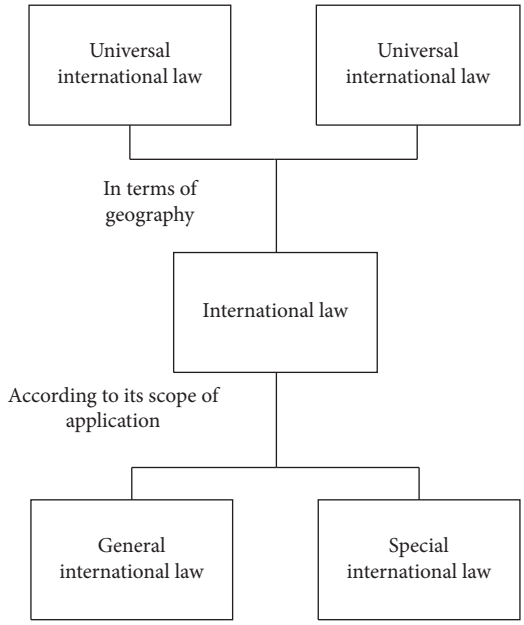

Figure 1: The division of international law.

which the fragmentation of international law is discussed. In addition to the exploration of specific problems, there are also some attempts on methods and perspectives, for example, the school of "new" natural law, which combines international law with ethics, and the interdisciplinary study of international law and international relations [12]. It can be seen that these question-based explorations and discussions on perspectives and methods can help us better understand what international law is, what state it is in, and why it is in this state and can help us to distinguish right from wrong.

The construction of an international law database plays an important role in case analysis and reports, latest updated articles, international organizations, and international cooperation in the field of public international law, as well as in-depth research on hot issues with a wide coverage [13]. Take Max Planck Encyclopedia of Public International Law as an example. It is a comprehensive and in-depth electronic reference library in the field of international law, including many latest articles on international law, international organizations, and international cooperation, as well as a wide range of hot issues. The database provides quick and advanced search methods and can be navigated by alphabetical lists of titles, authors, and topics. The homepage of Max Planck Encyclopedia of Public International Law is shown in Figure 2.

It can be said that the establishment and application of the international law database have promoted the development and reform of international law to a great extent. In the process of constructing such a database, however, due to factors such as network node deviation, susceptible to incomplete data, and with the extension of network transmission time, the data information keeps increasing; not only will the international law cause incomplete data balance level to continue declining, it can also severely affect information parameter aggregation behavior [14]. In order to avoid the above situation, it is

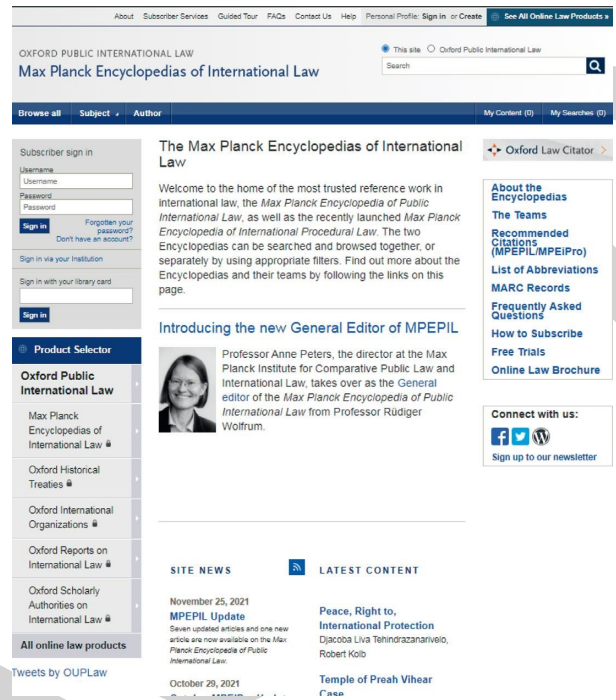

Figure 2: Max Planck Encyclopedia of Public International Law homepage.

essential to ensure the integrity of international law data. Therefore, this study designs an international law data integrity guarantee method based on an antiterrorism prediction algorithm. The design process of this method is described in detail below.

3. International Law Data Integrity Guarantee Based on the Antiterrorism Prediction Algorithm

Based on the analysis of antiterrorism behavior and the design of antiterrorism prediction algorithm, this study designs the integrity guarantee method of antiterrorism data in an international law database.

3.1. Analysis of Antiterrorism Prediction Algorithm. With the accelerated development of global informatization, international terrorist activities have been constantly upgraded, and in recent years, they have been rampant and have extremely bad effects. In the face of the rapid transformation and upgrading of international terrorism, the antiterrorism situation has become increasingly severe, seriously affecting the social order and causing huge casualties and property losses [15]. Under the guidance of international law, it has become a consensus that intelligence leads the fight against terrorism in the face of severe challenges in the new situation. The post-event analysis of international terrorism can often be found in advance. In fact, there is a lot of information about terrorist attacks. The key is the lack of prediscovery mechanisms and tools, which are required by the covered big data. However,

antiterrorism prediction is faced with challenges such as difficult multidomain data fusion, small sample data, and few model evaluation methods. Therefore, how to use big data and antiterrorism prediction deep integration is the key link to win terrorist activities. Big data is used to mine and predict terrorism-related intelligence, build a new antiterrorism prediction model, and realize timely prediction, early warning, and prevention of terrorist organization behavior, which is of great significance to the study of antiterrorism prediction [16].

The application of the antiterrorism prediction algorithm can improve the decision-making ability to predict terrorist organizations and terrorists. In practical application, the purpose of the antiterrorism prediction algorithm is to predict when and where terrorist organizations and terrorists will create terrorist incidents, and then give decision-making suggestions to antiterrorism agencies, so as to avoid the occurrence of terrorist incidents as far as possible. Facts prove that antiterrorism prediction algorithms are often better than traditional manual analysis.

A tactical prediction algorithm and a target locking algorithm are part of the traditional antiterrorism prediction algorithm. It is a calculation process that involves feeding one set of numerical values into an algorithm model and receiving a different set of numerical values as a result. Because the antiterrorism prediction algorithm is essentially a machine learning algorithm, it is based on the machine learning working concept; that is, it continuously acquires new knowledge and skills by simulating human learning behavior, reorganizing its own knowledge structure, and improving its own performance in order to improve its own prediction level [17].

In general, the overall thinking of the traditional antiterrorism prediction algorithm mainly includes problem perception, data preparation, directional mining, evaluation and prediction, and feedback optimization. The process is shown in Figure 3.

In Figure 3, the core of the whole prediction algorithm is data mining and feedback optimization. Through data mining, the antiterrorism prediction model is built, and the accuracy of the prediction model is improved through several times of feedback optimization. However, antiterrorism prediction is faced with many challenges, such as difficult multidomain data fusion, small sample data, and few evaluation methods. Therefore, under the existing conditions, the practical feasibility of such methods is weak and the prediction universality is poor. At the same time, the research results obtained by investing a lot of manpower and material resources are easy to overturn or eliminate, and the cost is huge.

In view of the shortcomings of existing technologies, this study uses a random algorithm to optimize the traditional antiterrorism prediction process. The specific steps are as follows:

Step 1. Collect the required terrorism-related data based on the perception of terrorism-related data.

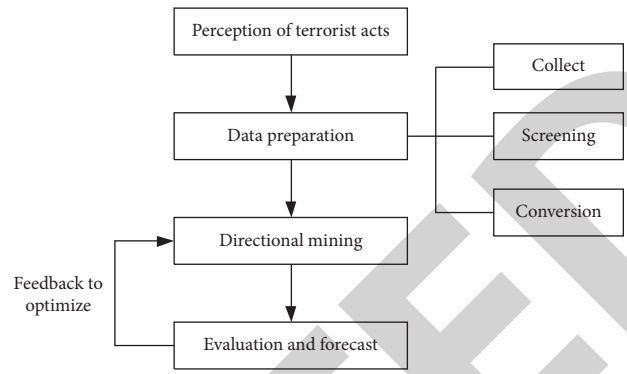

Figure 3: The whole idea of traditional antiterrorism prediction algorithm.

Step 2. Use deductive method to mine the behavior data of historical terrorist organizations.

Step 3. Obtain the trusted seed model S through deep learning.

Step 4. Assume that the prediction result of the n-th seed model is R_n, while the actual terrorist act is v. On the basis of the preset reliability c, input the terrorism-related factor vector, when

$$c > D\left(R_n\left(a_i\right)|va_i\right) = \frac{R_n\left(a_i\right)}{va_i}, \tag{1}$$

where $D(\cdot)$ represents the data divergence, and the similarity evaluation of the two models is carried out, so the seed model S is called the trusted seed model.

Step 5. On the basis of several credible seed models, a random function fission prediction model is used to predict the parameter value M. The random function used here is the Monte Carlo algorithm.

Step 6. The model set M' was tested on the test set, and the models with poor prediction results were removed to screen out the model set M' with relatively excellent performance.

Step 7. Save the prediction model set M', and make antiterrorism prediction according to the prediction model set.

Step 8. Once a new terrorism-related factor f appears, return to Step 3 and add f to obtain a new prediction model set M''; the process is as follows:

$$M'' = D\left(R_n\left(a_i\right)|va_i\right) \times \frac{S + f}{M' + cM}. \tag{2}$$

The above antiterrorism prediction algorithm still adopts the data acquisition and mining part of the existing antiterrorism research, which retains the advantages of traditional research. Meanwhile, it makes up for the disadvantages of the current research through the idea of a seed model, improves the prediction accuracy, and supports

the addition of new terrorism-related factors, thus improving the scalability of the algorithm.

3.2. Design of International Law Data Integrity Guarantee Method. Based on the antiterrorism prediction data obtained from the above process, the integrity assurance method of antiterrorism data in the international law database is designed.

3.2.1. Identifying Incomplete Data. The incomplete data identification process is composed of three processing steps: incomplete data subspace extraction, statistical element reconstruction, and separable amplitude calculation. The specific design process is as follows.

(1) Subspaces of Incomplete Data Extracted by Factor Analysis. Data subspace is a relatively fuzzy storage set of information parameters, and the larger the information coverage area involved in the subspace, the more the incomplete data samples to be screened [18]. Therefore, in order to obtain accurate extraction results of incomplete data subspace, the factor analysis method is used to integrate the obtained historical data into multiple information parameter sets; then, according to the multivariate statistical algorithm, the original set space is improved; and finally, all the information parameters are put into the subspace set structure.

It is assumed that g_1 and g_2, respectively, represent two different parameter value factors of incomplete data information and that $g_2 > g_1$ is satisfied. It is stipulated that Δt represents the unit extraction time of data information parameters. In general, the physical value range of this indicator always exists between 0 and 1. By combining the above physical quantities, the subspace extraction results of incomplete data can be expressed as

$$h = \omega \times \frac{\Delta t^2 \left(g_2 - g_1\right)}{\partial \overline{q}}, \tag{3}$$

where ∂ represents the reasonably defined term of incomplete data, ω represents the weight value of single extraction of data information parameters, and $\overline{q}$ represents the mean value of single transmission of incomplete data information.

(2) Reconstructed Statistic. Statistics are standard conditions for measuring the transmission capacity of data information parameters. The higher the level of numerical quantity of statistical element nodes is, the stronger the constraint ability of the applied algorithm is [19]. With the increase of incomplete data screening, the number of statistical element nodes will decrease obviously due to the influence of computing, which will lead to the continuous decline of screening application ability. In order to solve this problem, the statistical element nodes are reconstructed in this study. On the one hand, the changing trend of the screening amount of incomplete data is avoided, and on the other hand, the computational amount of data information can be effectively controlled.

Suppose η_0 represents the minimum constraint value of statistical element coefficient, η_n represents the maximum constraint value of statistical element coefficient, and N represents the actual iterative transmission times of incomplete data information. Simultaneous formula (3) can be used to express the statistical element reconstruction result as

$$z = \frac{e \times h}{\sum_{\eta_0}^{\eta_n} N \times \overline{b}^2}, \tag{4}$$

where e represents the transmission characteristic value of incomplete data information parameters, p represents the extraction permission value of information parameters, and $\overline{b}$ represents the mean existence of statistical element nodes.

(3) Separable Amplitude Quantity. In the process of identifying incomplete data, the data cannot maintain the invariable existence state but will show obvious turbulent change with the increase of information parameter storage level. In this case, there is always a certain numerical comparison between the parameters of selectable and nonselectable data, which can separate the amplitude.

Separable amplitude is a piece of dynamic data information matching result. As the amount of data to be screened increases, the numerical coordination relationship is always in the existing state of absolute change. Therefore, in order to obtain effective calculation results of separable amplitude, it is necessary to accurately grasp the parameter value level of incomplete data information and, on this basis, to complete the overall planning and coordination of related information parameters.

Assuming that α and β are two different amplitude nodes, j_α represents the magnitude of amplitude separation when the coefficient is α, and j_β represents the magnitude of amplitude separation when the coefficient is β. Simultaneous formula (3) can be used to calculate the result of separable magnitude expressed as

$$S = \frac{z^2 + y\left(k_1 + k_2\right)}{\left(j_\beta - j_\alpha\right)^2}, \tag{5}$$

where y represents the basic separation conditions of amplitude parameters, and k_1 and k_2 represent two different incomplete data items to be counted as index definitions. To sum up, the identification and processing of incomplete international law data are completed.

3.2.2. Data Integrity Assurance. In order to guarantee the data integrity of international law, the operation parameters of data integrity must be determined first. Therefore, the text classification training is used to adjust the feature items of the data, some worthless feature items are removed by feature dimension, and the noise of international law data is removed by feature dimension reduction.

Assuming that the feature item of the data is c_i and the total number of data text categories is u_i, the calculation process of obtaining the data's worthless features is as follows:

$$\varphi_{(c_i,u_i)} = \frac{P(c_i \cap u_i)}{X(c_i)X(u_i)}. \tag{6}$$

Among them, the frequency of feature item c_i in international law data text can be expressed as $P(c_i \cap u_i)$.

If the training sample of the complete feature item of data is $X(c_i)$, the expression of the complete category item of data contained in the training sample is $X(u_i)$. Therefore, when there is a parallel relationship between the corresponding data text category u_i and the feature term, the ratio of $P(c_i \cap u_i)$ presents a linear positive relationship, and there is a correlation between the integrity of the data in the feature term and $P(c_i \cap u_i)$. When $P(c_i \cap u_i)$ increases, data integrity also increases.

On this basis, feature terms of international law data are reduced in dimension, proportional relationship is set on the basis of data feature terms, data feature dimensions are calculated in combination with feature terms, and mutual information is used to improve the classification accuracy of data integrity feature dimension.

Knowing the chi-square value between data integrity features and text categories, as well as the relationship between feature dimensionality reduction, the total calculation is performed according to the data features, so that the total number of dimensionality reductions of text features can be obtained to determine the integrity of international data. The relevant test criteria of text categories need to be classified and identified. The process is as follows:

$$\omega_c = \frac{\varphi_{(c_i,u_i)}}{\varepsilon \times \vartheta}, \tag{7}$$

where the word frequency parameter of international law data is ε and the number of integrity feature items in the data feature category is ϑ. Then, feature items with integrity word frequency in data are separated from documents, and word frequency feature categories are introduced and associated. According to the weight parameters of high-frequency feature items, the weight values of low-frequency feature items of international law data are reduced [20]. Integrity operation parameters are determined as follows according to data integrity feature items:

$$\gamma = \omega_c \times \left(P(c_i) - \frac{\sum_{i=1}^{m} P(c_i)}{m} \right). \tag{8}$$

Among them, the frequency expression of feature items of international law data is $P(c_i)$. The data integrity guarantee mechanism of international law is established according to the integrity operation parameters obtained.

First of all, the international law data in the sample set is decomposed into m sets, and the number of text sets after classification is $(m(m-1)/2)$. The correlation coefficient in the corresponding classification training texts is calculated by the corresponding classification collection. According to the integrity operation parameter integrity guarantee range obtained above, the formula is as follows:

$$F = \frac{x_1 y_1 + x_2 y_2 + \cdots + x_m y_m}{\sqrt{x_1^2 + x_2^2 + \cdots x_m^2}\sqrt{y_1^2 + y_2^2 + \cdots + y_m^2}}, \tag{9}$$

where x_m and y_m are vector values in the sample set of international law data. After processing the decomposed international law data text set according to the scope of text classification, the integrity feature item matrix is obtained as follows:

$$m' = \frac{m(m-1)}{2} \begin{bmatrix} x_1 y_1 & x_1 y_2 & \cdots & x_1 y_m \\ x_2 y_2 & x_2 y_2 & \cdots & x_2 y_m \\ \vdots & \vdots & \ddots & \vdots \\ x_m y_m & x_m y_2 & \cdots & x_m y_m \end{bmatrix}. \tag{10}$$

On this basis, according to the setting of the detection prerequisites of integrity feature items by the detection function, the results are as follows:

$$\tau(c_i) = \frac{\lim_{n \longrightarrow m} \tau_n(c_i)}{n}, \tag{11}$$

where the parameter value of the integrity feature function is τ and the measured international law data integrity feature category is $\tau(x_1, x_2, \ldots, x_n)$. When the parameter value of the characteristic function is $\tau_n = \tau$ and $\lim_{n \longrightarrow m} K_n(f_i) = K(x_1, x_2, \ldots, x_n)$, the positive definite relation formula is used to calculate the curve amplitude of international law data integrity, and at the same time, the overall characteristics of the data sample are identified. Assuming that the width of the integrity function of international law data is σ, vector values x_m and y_m are used to calculate the integrity characteristics of the data as a whole, and the process is as follows:

$$T = 0.5 x_m \times \kappa \times \sigma + 0.5 y_m \times (\kappa - 1) \times \sigma. \tag{12}$$

The new international law data sequence equation is obtained by summation of data integrity characteristic series as follows:

$$O = \sum_{\kappa=1}^{N} z(\kappa) \times T. \tag{13}$$

Thus, a complete international law data series can be obtained; that is, international law data integrity assurance processing is completed.

4. Experiment and Analysis

In order to verify the practical application performance of the international law data integrity guarantee method designed above based on antiterrorism prediction algorithm, the following experimental process is designed.

4.1. Experimental Design. Experimental data were obtained from Max Planck Encyclopedia of Public International Law database. The experiment was built on Matlab v10.0 (64 bit)

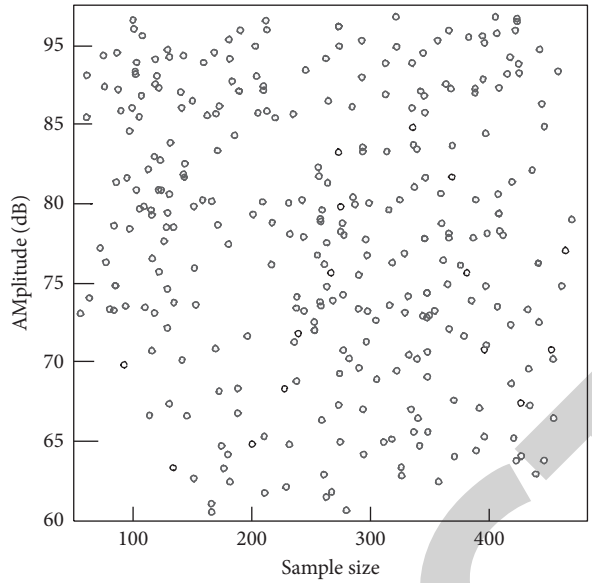

Figure 4: Sample distribution of international law data series.

Table 1: Comparison of experimental parameter values.

	Number of experiments	Frequency range of data usage	Data sensitivity
The proposed method	10	0.94	0.88
	20	0.95	0.96
	30	0.91	0.91
	40	0.88	0.87
	50	0.93	0.91
Method of [7]	10	0.61	0.60
	20	0.30	0.73
	30	0.44	0.72
	40	0.66	0.65
	50	0.73	0.71
Method of [8]	10	0.51	0.67
	20	0.61	0.72
	30	0.64	0.75
	40	0.78	0.74
	50	0.52	0.78

simulation platform, and the SR258 1U rack server was used to set up the data acquisition platform and console. A sample sequence of international law data is shown in Figure 4.

In order to improve the explicability of experimental results, the integrity assurance method of outsourcing spatial database (method of [7]) and the integrity audit and guarantee method of multicopy based on DDCT table (method of [8]) were taken as the comparison group. The method of this paper was taken as the experimental group for comparative test.

4.2. Experimental Results and Analysis. Firstly, using frequency range and sensitivity of data as indicators, the practicability of different evaluation methods is verified. The specific values of index parameters of different methods are shown in Table 1.

According to Table 1, in the whole experiment, the frequency range of data used in the proposed method and the value level of data sensitivity index are always relatively close, there is no obvious fluctuation coefficient, and the value is very close to 1. However, there is a big gap between the frequency range of data use and the value of data sensitivity index of the two traditional methods and 1. Therefore, the method of this paper is more practical.

Then, the time consumption of the integrity audit process of different methods is used as an indicator for comparative verification, and the results are shown in Figure 5.

According to the results shown in Figure 5, in the 30th experiment, the integrity audit process of the method of this paper takes 17 min, and that of the method of [7] takes 21 min. The integrity audit process of the method of [8] takes 26 min. In the 50th experiment, the integrity audit process of

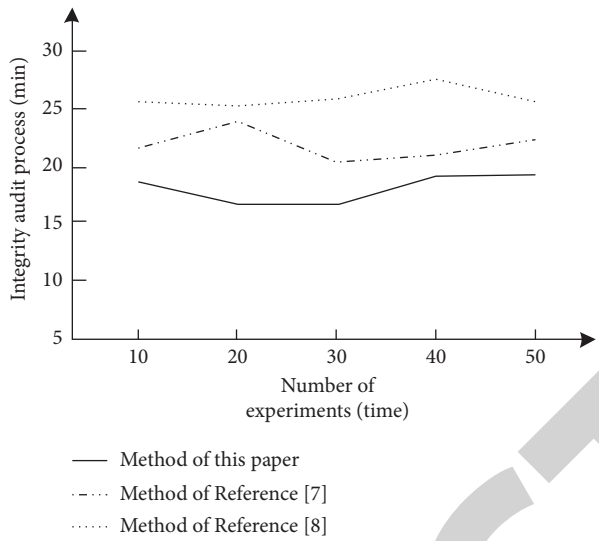

Figure 5: Comparison of the time consumption of the integrity audit process of different methods.

Table 2: Comparison of data integrity after the application of different processing methods.

Number of experiments/time	Method of this paper	Method of [7]	Method of [8]
10	0.944	0.861	0.829
20	0.967	0.860	0.865
30	0.921	0.825	0.856
40	0.925	0.853	0.836
50	0.966	0.842	0.844

the method of this paper takes 20 min, and that of the method of [7] takes 23 min. The integrity audit process of the method of [8] takes 25 min. In the whole experiment, the integrity audit of the method of this paper takes only 19 min at most, indicating that the method of this paper has high timeliness.

Finally, the validity of different evaluation methods is verified by using data integrity after the application of different methods. Statistical results of data integrity after the application of different methods are shown in Table 2.

According to the results shown in Table 2, data integrity varies between 0.921 and 0.967 after the application of the method of this paper. After the application of the method of [7], the data integrity varies between 0.825 and 0.861. After the application of the method of [8], the data integrity varies between 0.829 and 0.865. Furthermore, in the whole experiment process, the maximum data integrity after the application of the method of this paper can reach 0.967, indicating that compared with the two traditional methods, the proposed method is more effective.

5. Conclusion

In order to further optimize the quality of international law data, this paper studies the integrity guarantee method of international law data on the basis of designing antiterrorism prediction algorithm. Firstly, the prediction model set is split through the trusted seed model, the model selection is completed through iterative optimization, and then new terrorism-related factors are added to obtain the new prediction model set, so as to complete the antiterrorism data prediction. Based on the antiterrorism prediction data obtained by the above process, on the basis of identifying incomplete data, the antiterrorism data integrity guarantee method in international law database is designed through the process of determining data integrity operation parameters, eliminating worthless feature items, processing noise dimension reduction, and adding feature series of data integrity.

On the basis of the above research, experimental data prove that this method takes less time to audit the data integrity and that the data integrity after processing can reach 0.967. The frequency range and sensitivity of international law data can be effectively optimized by using this method.

Data Availability

The data used to support the findings of this study are available from the author upon request.

Conflicts of Interest

The author declares that he has no conflicts of interest.

References

[1] V. Geraldo, "Evolutionary interpretation and international law," *Journal of International Economic Law*, vol. 24, no. 01, pp. 203–219, 2021.

Hindawi
Journal of Mathematics
Volume 2023, Article ID 9826741, 1 page
https://doi.org/10.1155/2023/9826741

Retraction

Retracted: Research on Multiparty Payment Technology Based on Blockchain and Smart Contract Mechanism

Journal of Mathematics

Received 19 December 2023; Accepted 19 December 2023; Published 20 December 2023

This article has been retracted by Hindawi following an investigation undertaken by the publisher [1]. This investigation has uncovered evidence of one or more of the following indicators of systematic manipulation of the publication process:

(1) Discrepancies in scope

(2) Discrepancies in the description of the research reported

(3) Discrepancies between the availability of data and the research described

(4) Inappropriate citations

(5) Incoherent, meaningless and/or irrelevant content included in the article

(6) Manipulated or compromised peer review

The presence of these indicators undermines our confidence in the integrity of the article's content and we cannot, therefore, vouch for its reliability. Please note that this notice is intended solely to alert readers that the content of this article is unreliable. We have not investigated whether authors were aware of or involved in the systematic manipulation of the publication process.

Wiley and Hindawi regrets that the usual quality checks did not identify these issues before publication and have since put additional measures in place to safeguard research integrity.

We wish to credit our own Research Integrity and Research Publishing teams and anonymous and named external researchers and research integrity experts for contributing to this investigation.

The corresponding author, as the representative of all authors, has been given the opportunity to register their agreement or disagreement to this retraction. We have kept a record of any response received.

References

[1] Y. Zhang, "Research on Multiparty Payment Technology Based on Blockchain and Smart Contract Mechanism," *Journal of Mathematics*, vol. 2022, Article ID 3434954, 14 pages, 2022.

Hindawi
Journal of Mathematics
Volume 2022, Article ID 3434954, 14 pages
https://doi.org/10.1155/2022/3434954

Research Article

Research on Multiparty Payment Technology Based on Blockchain and Smart Contract Mechanism

Yanjun Zhang

Party School of Changzhi Committee of the Communist Party of China, Changzhi, Shanxi 046000, China

Correspondence should be addressed to Yanjun Zhang; yanjunzhang@hainanu.edu.cn

Received 12 November 2021; Revised 3 December 2021; Accepted 9 December 2021; Published 21 February 2022

Academic Editor: Naeem Jan

As a peer-to-peer "P2P" distributed ledger, the blockchain has the advantages of decentralization, no trust, open autonomy, and nontampering. Therefore, many users are willing to conduct transactions in blockchain cryptocurrency systems such as Bitcoin and Ethereum. However, the throughput of traditional blockchain is extremely low, and the transaction is so delayed. The payment channel network is the most promising solution to expand the blockchain for widespread use. Achieving secure instant payment on the payment channel can significantly increase transaction throughput and reduce transaction delays. When the payment channel is closed, the balance in the channel will be returned to an account on the blockchain. In this paper, we discuss the design and the implementation of a multiparty payment channel network based on smart contracts. Where a two-party payment channel is designed based on blockchain and smart contracts, a new multiparty payment channel is established on the basis of the payment channel. A detailed definition and description are given, and the creation, update, and closing functions of the multiparty payment channel are designed. Moreover, we design a multiparty payment channel smart contract, deploy it to the local private blockchain, and conduct simulation and testing. The delay time of different transaction methods is counted, and the network topology type, transaction amount, and other factors are studied. The impact of transaction success rate and the gas consumption of different transaction methods are analyzed through multiple sets of experimental statistics.

1. Introduction

With the rapid development of the Internet, the financial industry and third-party payment software have risen rapidly. According to statistics from the Ministry of Commerce in 2015, the national online retail transaction volume was 3.88 trillion yuan, a year-on-year increase of 33.3%. According to the "Report on the Development of China's Internet in 20 Years" released by the China Cyberspace Research Institute in Wuzhen, China's online retail transaction volume has leaped to the world's first place, and the number of mobile phone online shopping users has reached 270 million [1]. People have higher and higher requirements for online banking and payment functions. How to process more transactions in a shorter time while ensuring higher security and how to enable two users to directly trade without the complicated process of intermediate third-party inspection and to obtain a substantial increase in efficiency have become hot topics of discussion in transaction reform [2]. Therefore, the storage of ledger data based on blockchain technology has important development prospects. Traditional online transactions need to rely on third-party payment intermediaries. For users, user transaction information is stored in a centralized database by an intermediary. Users need to trust the intermediary before they can use the payment platform provided by the intermediary. In order to ensure the credibility of transactions, payment companies need to collect a lot of user privacy information to determine the credibility of user accounts. For users, the more the private information is disclosed, the less secure it is. In recent years, private information leakage has occurred from time to time, and its scope includes industries involving assets such as healthcare, law, and real estate. According to the "2015 Data Breach Investigation Report" report, in 2015, there were 79,790 data breaches in 61 countries around the world, of which 2,122 have been confirmed [3]. The data of many

well-known hotels in my country was leaked, including Marriott Hotel and Starwood Hotel. The data leakage of these hotels has resulted in the fact that all the customer order information and personal information that has been consumed in these hotels can be easily obtained by hackers, and it can be seen by people who want to use this information. This kind of leakage of user privacy information is undoubtedly irresponsible for customers' sensitive information, and it also damages the reputation and market value of the hotel. For the transaction intermediary platform, in order to ensure the credibility of the accounts, clearing a large amount of transaction information requires high fees and lengthy time. Nevertheless, under the huge transaction volume, it is impossible to completely avoid mistakes, so it is necessary to pay more expenses and time to make up for these mistakes. This will cause unnecessary waste of funds and time loss for users. On the other hand, the traditional centralized management method [4] is to completely supervise the accounts by banks or third-party payment companies. The transaction process recorded by these intermediary companies is invisible to users, and the transparency and credibility of the ledger data are difficult to guarantee. Therefore, with the emergence of a trust crisis, many researchers want to establish a trustless, distributed privacy protection intermediary platform. Although there are many user privacy protection algorithms, such as differential privacy [5], k-anonymity [6], and t-closeness [7], there are also distributed storage systems, such as Google File System [8] and Big Table [9]. But none of them are distributed and trustless practical applications [10]. Smart contract technology helps to solve the above-mentioned problems faced by individuals and enterprises. The concept of smart contracts was first proposed by cryptographer Nick Szabo in 1994. It aims to establish a decentralized financial authentication system and free manpower from boring document processing. Although the vision of smart contracts is quite beautiful, the concepts and goals are also very clear. But in fact, smart contracts have not received widespread attention until blockchain currencies such as Bitcoin have become popular in recent years. Before the emergence of blockchain technology, the research on smart contracts progressed slowly. This is mainly caused by two reasons. First, it is difficult for computer programs to control actual assets, and there is a lack of an effective fund settlement channel between enterprises. In fact, to this day, cross-border transfers still need to go through multiple intermediaries, which makes it very difficult to automate smart contract procedures. Second, smart contracts are difficult to generate sufficient credibility. After one party breaches the contract, it is difficult for computer programs to work without personnel. In the case of intervention, the breaching party is guaranteed to be punished. The emergence of blockchain technology has changed this status quo. First, the blockchain currency led by Bitcoin is a natural settlement channel for digital assets; second, the openness and nonrepudiation characteristics of the blockchain ledger ensure that the contract execution process can be easily regulated. By establishing the contract in the form of code and recording it in the unalterable blockchain, the authenticity and reliability of the contract can be guaranteed. At the same time, the smart contract system helps enterprises realize digital asset management and lays the foundation for enterprises to realize fully digital office. Blockchain is a decentralized system. According to the blockchain standard, the effect of mutual communication and mutual trust between enterprises can be realized, and the communication cost of enterprises can be effectively reduced. In addition, the unforgeable nature of the blockchain helps to reduce the labor cost of the third-party audit department.

Throughout this paper, we give a background on the related works in Section 2, where we proceed to Section 3 to discuss and analyze the stages of creation of a two-party payment channel, besides the types and methods of the channel, the channel close, and the performance of the two-party payment channel. Then, we introduce the multiparty payment channel, which is designed based on the two-party payment channel. In Section 4, experiments and results were done in order to reduce transaction delay and increase the throughput of blockchain transactions. Finally, in Section 5, we end our study with a conclusion.

2. Related Work

Current blockchain-based smart contract projects include Ethereum [11], Hyperledger [12], Codius [13], and Hawk [14]. Among them, Ethereum is the earliest open-source platform for smart contracts that supports Turing-complete programming languages, and it is also a relatively influential community in the blockchain field. Many companies and enthusiasts have used Ethereum as the underlying platform to implement applications covering market forecasting, supply chain source verification [15], crowdfunding-based financing, securities, and derivatives trading [16]. Hyperledger is an open-source project on advancing blockchain digital technology and transaction verification jointly initiated by the Linux Foundation in 2015 with more than 30 members, including major financial, technology companies, and related open-source organizations. The emergence of Hyperledger officially announced that blockchain technology is no longer just an open-source community technology but has been recognized by mainstream institutions and the market, which is of great significance to the development of blockchain. Some other open-source projects have their own focus. Taking Hawk as an example, the main feature of the project is to protect the data privacy of participating users, and users' transfer records are no longer recorded in the block in a public form. Smart contract is a concept proposed by Ethereum, a set of commitments defined in digital form, including agreements on which contract participants can execute these commitments. The execution process is transparent, traceable, and unchangeable. If Bitcoin is a distributed ledger, its transaction symbol is Bitcoin. Ethereum is a distributed platform without transaction symbols. It adds a core smart contract concept on the basis of Bitcoin [17]. The original Bitcoin mechanism was not scalable. It was an application that could only run Bitcoin

transactions. If a new developer wants to develop new applications on the basis of the blockchain, the blockchain needs to be completely redone. Ethereum is a platform provided to application vendors. Developers only need to pay a certain amount of Ether, build different contracts on this platform, and run different operations and different businesses. It no longer just records transactions but adds more parameter information to the contract. By establishing its own blockchain, a clear "state tree" representing the current balance of each address and a "transaction table" representing the transactions between the current block and the previous block are stored in each block [18, 19]. Ethereum solves the scalability problem. The business scope supported by Ethereum includes voting, financial exchanges, intellectual property management, crowdfunding, and artificial intelligence [20]. Ethereum provides a platform that enables storage and Turing's complete scripting language to make it possible to encode a complete currency in a single contract. Compared with Bitcoin without smart contracts, Ethereum with smart contract features has a broader future development direction, which can support more applications and larger transaction volumes. Coupled with its own high-efficiency characteristics, it will gain a longer-term advantage. But Ethereum also has obvious shortcomings; that is, the code of the application itself and the code generated by the application are in the same block, and the increase in the amount of accumulated data for a long time will cause the expansion of the block. At the same time, in the process of using contracts to form applications, multiple applications and contracts may be controlled by the same institution, which in turn will cause the same economic phenomenon as existing financial institutions. The entire system of Ethereum is controlled by the state or an institution. In this way, the freedom of blockchain transactions no longer exists. The blockchain can support many businesses more easily and conveniently, and it is no longer necessary to design all the blockchain storage by yourself. In order to support more applications, the Ethereum contract provides the simplest possible contract form so that any programmer can write a program that can run on Ethereum. Smart contracts will be allowed to store data in persistent memory. Projects such as Bitcoin and Ethereum are in the form of public chains. The characteristics of the public chain are no confidentiality, no traceability, long confirmation time, no finality, and low throughput, which cannot meet the needs of commercial use, so a blockchain in the form of a private chain appears. Hyperledger proposes to support blockchain based on private chains and alliance chains. It is a new commercial blockchain application that pays more attention to privacy and confidentiality than blockchain projects in the form of public chains. Hyperledger is an enterprise-level distributed ledger technology based on blockchain. It is used to build commercial application platforms for various industries. It has modularity and high performance and reliability and provides business-friendly licenses [21]. Compared with Bitcoin's digital currency system and Ethereum's general public chain platform, Hyperledger provides a general alliance chain platform, which is mainly managed by the Linux Foundation. It uses public or private networks, which can provide developers with privacy, also inherit the concept of Ethereum smart contract, and support the use of Go, Java, and other development languages to write smart contracts. In Hyperledger, this kind of smart contract is called on-chain code to distinguish between the contract on the blockchain and the written contract, which allows enterprises to use consensus mechanisms and services in a plug-and-play manner. Since the launch of the Hyperledger project, new companies have continued to join the Hyperledger camp [22], including Samsung's IT service subsidiary, Chinese heavy machinery manufacturer Sany Heavy Industries, Huawei, and other large enterprises. The fabric subproject, which has made a huge contribution to the Hyperledger, provides basic privacy, confidentiality, and auditability and uses the Practical Byzantine Fault Tolerance consensus algorithm [23] to provide confidentiality, authority management, and control functions for transactions. At the same time, the functions of consensus mechanism and bookkeeping are separated, in which nodes can be dynamically expanded and contracted, with upgradeable smart contracts, which are expected to increase throughput. And another project Sawtooth Lake, which was originally a blockchain platform mainly contributed and led by Intel, supports a new consensus mechanism Proof of Elapsed Time. In terms of blockchain payment channel network, there are some studies in academia and industry, among which the two projects of Lightning Network [24] (the Lightning Network and Raiden Network [25]) are the most famous. The Lightning Network uses the idea of a payment channel to transfer transactions originally on the Bitcoin blockchain to the off-chain, that is, the Lightning Network, to complete fast instant transactions and return the balance in the channel to the block when the payment channel is closed. The Lightning Network uses the revocable sequence maturity contract RSMC to complete two-way payments while ensuring the security of the balances of both users. In order to realize the transaction between two users without a direct channel, the Lightning Network has designed a hash-based time lock contract HTLC to implement routing on the payment channel network. The Raiden Network uses the same solution as the Lightning Network, but it is a payment channel network for the Ethereum blockchain. Both of these projects are currently under development, and some users have already joined the Lightning Network and Raiden Network, but their availability and security have yet to be verified. To sum up, the existing research on payment channels or state channels mainly focuses on the design of channels and networks, channel routing, rebalancing, and so on; these researches are all in the initial stage, and most of them are based on theoretical research. Therefore, research in the direction of the blockchain payment channel network is very necessary, which will help solve the scalability problem of the blockchain itself and turn the blockchain into an electronic currency system suitable for large-scale applications. In this paper, we mainly study multiparty payment channels based on blockchain and smart contracts and conduct simulation experiments to study the impact of different factors on payment channels.

3. Method

In this section, we will discuss and analyze the stages of the creation of a two-party payment channel, the updates, types (off-chain update; on-chain update), and methods, besides channel closure, as well as the performance of the two-party payment channel. Then, we will introduce the multiparty payment channel, which is designed based on the two-party payment channel.

3.1. Payment Channel Design

3.1.1. Channel Creation Stage. In the channel creation phase, one user sends a request to create a two-party payment channel to another user and attaches his own signature. If the other party agrees to create, the message will be returned with a signature. After the signatures of both parties are collected, a consensus to create a channel is reached, and the requester initiates a request to create a channel to the smart contract. The smart contract will verify the signatures of the two users and check some necessary conditions (e.g., the accounts of both users on the blockchain must have sufficient balance to establish a channel, and a certain fee can be paid). Assuming that the payment channel to be created for both parties is t and the user sending the request is P, then the other user $P_2 = t.\text{counterparty}(P_1)$. When requesting to create a channel, the message sent by P_1 is

$$\text{tpc} - \text{creat} = ''\text{creat TPC}t, \delta_1''. \tag{1}$$

This means that P_1 requests to establish a new two-party payment channel t with P_2, where t represents an instance of the channel and δ_1 is the signature of P_1. If P_2 agrees to create the channel after verifying the signature, it will return a message of the following form:

$$\text{tpc} - \text{creat} - \text{agree} = ''\text{creat TPC}\, t, \delta_2'', \tag{2}$$

where δ_2 is the signature of P_2 on the message. If P_2 does not agree to create the channel, it returns a rejection message:

$$\text{tpc} - \text{creat} - \text{reject} = ''\text{reject to creat TPC}\, t''. \tag{3}$$

If the two parties reach a consensus to create a channel, that is, P1 receives the message and signature agreed by P_2, then P_1 can call the create TPC function provided in the smart contract through RPC and other methods. The smart contract verifies the signatures of both parties and completes the mortgage of funds and the creation of channels. At this time, the deposit required to establish the channel will be deducted from the blockchain accounts of P and P_2 through $L.\text{remove}(P1, t.b_1^0)$ and $L.remove(P_2, t.b_2^0)$ and add an instance of the payment channel of both parties to the storage space of the channel through $C.\text{addTPC}(t)$. It should be noted that the stage when users reach a consensus to create a channel is a process of interaction under the blockchain. Therefore, the delay is extremely low, and the interaction in a more common network is only affected by the network status. When calling a smart contract to create a channel, both users need to mortgage the assets on their respective blockchain accounts into the smart contract. As a result, transactions on the blockchain will occur, leading to a long delay in the process. However, in the entire life cycle of the payment channel between the two parties, the process of creating the channel only needs to be executed once, so a long delay here is acceptable.

3.1.2. Channel Update Stage. There are two types of channel updates: off-chain updates and on-chain updates. The procedures of the two update methods will be described in detail as follows:

(1) Off-chain update is the key to both parties' payment channels to reduce transaction delay and increase transaction throughput. Because the process is carried out under the blockchain and no blockchain transaction is generated, there is no need to wait for the transaction to be packaged and confirmed by the block. Compared with the blockchain transaction, a lot of transaction time is saved. In the off-chain update phase of the channel, one user sends a request to update the payment channel of both parties to another user and attaches its own signature. If the other party agrees to update, it will return the message and attach the signature. After the signatures of both parties are collected, a consensus to update the channel is reached. Two users can update the local channel to a new state and initiate a settlement request to the smart contract when settlement is needed. Suppose the payment channel of both parties to be updated is t, and the user who sends the request is P_1. When requesting to update the channel t, the message sent by P is

$$\text{tpc} - \text{update} = ''\text{update TPC}\, t \,\text{to t}', \delta_1''. \tag{4}$$

This means that P_1 requests to update the two-party payment channel t between $P_2 = t.\text{counterparty}(P_1)$, where t' represents a new channel state and δ_1 is the signature of P_1. This message needs to satisfy $t.b_1^0 + t.b_2^0 = t'.b_1^{now} + t'.b_2^{now}$, because the total balance on a payment channel between two parties will not change. In addition, $t\prime.version > t.version$ should also be satisfied because the version number is an increasing integer if $t'.\text{version} < \text{tversion}$; then, it shows that the requester sent an old version of the channel status, which is a malicious fraud. If P_2 verifies the content and signature of the message and agrees to create the channel, it will return a message as follows:

$$\text{tpc} - \text{update} - \text{agree} = ''\text{update TPC}\, t \,\text{to}\, t', \delta_2'', \tag{5}$$

where δ_2 is the signature of P_2 on the message. If P_2 does not agree to create the channel, it returns a rejection message:

$$\text{tpc} - \text{update} - \text{reject} = ''\text{reject to update TPC}\, t''. \tag{6}$$

(2) The on-chain update is to call the smart contract interface to update the latest state of the channel to the blockchain. If the two parties reach a consensus to update the channel, that is, P_1 receives the message and signature agreed by P_2, then P_1 can call the updateTPC function provided in the smart contract through RPC and other methods. The smart contract verifies the signatures of both parties and checks some necessary conditions, such as whether the payment channel exists, whether the balance distribution is reasonable, and whether the channel version is correct, to verify the legitimacy of the updated content. If the verification is successful, you can update t to t' through C.update TPC (t, t'). Generally speaking, the update operation of the smart contract only needs to be performed once before the channel is closed. The remaining multiple updates can only be updated off-chain between the two parties of the channel. After the two parties reach an agreement, the latest channel version can be kept locally.

3.1.3. Channel Closing Phase. In the channel closing phase, one user sends a request to close the payment channel of both parties to another user and attaches his own signature. If the other party agrees to create it, the message will be returned and the signature attached. After collecting the signatures of both parties, a consensus is reached to close the channel. The requester initiates a request to close the channel to the smart contract. The smart contract will verify the signatures of the two users and check some necessary conditions, such as the version number and balance of the channel and distribution. Assume that the two payment channels to be closed are t, and the user sending the request is P_1. When requesting to close the channel t, the message sent by P_1 is

$$\text{tpc} - \text{close} = "\text{close TPC}\, t, \delta_2''. \tag{7}$$

This means that P_1 requests to close the two-party payment channel t between $P_2 = t$.counterparty (P_1), and δ_1 is the signature of P_1. If P_2 verifies the content and signature of the message and agrees to close the channel, it will return a message as follows:

$$\text{tpc} - \text{close} - \text{agree} = ''\text{close TPC}\, t, \delta_2'', \tag{8}$$

where δ_2 is the signature of P_2 on the message. If P_2 does not agree to create the channel, it returns a rejection message:

$$\text{tpc} - \text{close} - \text{reject} = ''\text{reject to close TPC}\, t''. \tag{9}$$

If the two parties reach a consensus to close the channel, that is, P_1 receives the message and signature that P_2 agrees to close, then P_1 can call the closeTPC function provided in the smart contract through RPC and so on, and the smart contract verifies the signatures of both parties and completes the refund of the deposit and the channel. At this time, by calling L.add $(P_1, t.b_1^{now})$ and L.add $(P_2, t.b_2^{now})$, the balance in the channel will be returned to the blockchain accounts of P_1 and P_2 according to the latest balance distribution status, and the instance of the payment channel of both parties in the storage space is deleted through C.removeTPC (t). The refund operation involves a blockchain account, which is an on-chain transaction, so a certain handling fee is required when refunding the deposit.

3.2. Performance Analysis of the Payment Channel between the Two Parties. For a two-party payment channel, the main performance indicator is transaction delay, and the transaction delay on the payment channel is mainly affected by the number of off-chain interactions between the two parties of the channel, the number of transactions on the chain, and the number of signatures. Next, in this section, we will analyze the performance of the above-mentioned two-party payment channels and analyze the four stages of channel creation, off-chain update channel, on-chain update channel, and channel closure. The three stages of creation, on-chain update, and closing of the channel need to interact with the smart contract. In addition to completing these functions, the smart contract needs to check the legitimacy of the caller each time, for example, whether the channel exists, whether the balance distribution is correct, whether the signatures of both users are correct, and whether the channel version is correct; these operations ensure the security of user assets. In addition, because these three stages need to call the interface of the smart contract and change the channel state in the contract, there will be transactions on the blockchain, so the delay is longer. There is no need to interact with the smart contract when the channel is updated under the chain. It only needs to reach a consensus to update the channel state between the two users. Both users keep a copy of the same latest channel state and have the other's signature on the channel state, so both parties can initiate an on-chain update request to the smart contract at any time. In each stage, the main factors that affect performance are the number of on-chain transactions, the number of off-chain interactive messages, and the number of signatures on the payment channel of both parties. When creating a two-party payment channel, the two users at both ends of the channel need to interact to reach a consensus on creating the channel. The process includes a TPC-create request message and a TPC-create-agree return message, including two signatures in total. After reaching a consensus to create a channel, two users pledge a certain amount to the smart contract to create the channel, so two on-chain transactions will occur. When updating the channel state off-chain, there is no need to call the smart contract interface, and there is no time-consuming on-chain transaction. Two users request updates through the TPC-update message and agree to update the channel through the TPC-update-agree message. This process includes two interactive messages and two signatures, and the off-chain update is the advantage of the payment channel. When the channel is updated on the chain, that is, the latest state of the payment channel is updated to the smart contract, the update interface of the smart contract needs to be called once, so there will be an on-chain transaction. Similarly, when two users interact, two

messages and two signatures are generated. When closing the payment channel of both parties, the balance needs to be returned to the blockchain accounts of users at both ends of the channel according to the latest channel status in the contract, so two on-chain transactions will occur. In the same way, reaching a consensus to close the channel requires an interaction, including a request for closing the channel and a reply to two messages, which contain the signatures of the two users.

3.3. Multiparty Payment Channel Design. Similar to a two-party payment channel, the life cycle of a multiparty payment channel mainly includes three stages: creation, update, and closure. This section will combine the model and definition to introduce in detail the specific content of each stage in the life cycle of the multiparty payment channel. In addition, in the following description, we will follow the definitions of related symbols and functions of the blockchain in the first two sections.

The multiparty payment channel in this paper is designed based on the two-party payment channel. The smart contract opens the interface to the user. The user calls the interface provided by the smart contract through RPC and other methods to complete the creation, update, and close of the multiparty payment channel. This paper designs three basic smart contract functions, and the specific content is as follows:

$$\text{createMPC}(\text{parties}, \text{tpcs}, \delta) \longrightarrow \{i\ d, 0\}. \tag{10}$$

This function is used to request the creation of a new multiparty payment channel from the smart contract. parties is a collection of blockchain user addresses, representing all users who will join the multiparty payment channel. tpcs is a collection of the identifiers of a two-party payment channel, which means all the two-party payment channels that are added to the multiparty payment channel. Once a multiparty payment channel is added, the busy field of the payment channel of both parties will be set to 1, indicating that the channel has been added to a multiparty payment channel and cannot be used separately. δ represents the collection of signatures of all users, and the smart contract will verify these signatures and some necessary conditions. After the verification is successful, a new multiparty payment channel is created, and the identifier id of the channel is returned to the user. If the creation fails, it returns 0.

$$\text{updateMPC}(\text{id}, \text{mpc}', \delta) \longrightarrow \{1, 0\}. \tag{11}$$

This function is used to request the smart contract to update the multiparty payment channel whose identifier is id. The input parameter mpc′ represents the new state of the multiparty payment channel, including the new balance distribution and new version number of the two parties' payment channels. After the smart contract is successfully verified, the status of the multiparty payment channel is updated according to mpc′. If the update is successful, it returns 1; otherwise, it returns 0.

$$\text{closeMPC}(\text{id}, \delta) \longrightarrow \{1, 0\}. \tag{12}$$

After the channel parties reach a consensus, they request the smart contract to close the multiparty payment channel with the identifier id. After the smart contract completes the verification step, it will release all the two-party channels in the channel, that is, set the busy value of all the two-party payment channels in the multiparty payment channel to 0, which means that the channel is idle and can be used as a separate two-party payment channel or join other multiparty payment channels. The smart contract will delete the instance of the multiparty payment channel in the storage space and return 1 to the user if the closure is successful; otherwise, it returns 0.

3.3.1. Channel Creation Phase. In the creation phase of a multiparty payment channel, a user sends a request message to the server to create a multiparty payment channel with multiple other users and attaches its own signature, and the server notifies other users. Assuming that the user Pi initiates a request, the request message can be defined as

$$\text{mpc} - \text{create} = ''\text{create an MPC}\, m, \delta_i''. \tag{13}$$

In the message mpc – create, δ_i is the signature of the requester P_i for the message, and m represents an instance of a multiparty payment channel. For example, *m.parties* represents the addresses of all users participating in the channel, and *m.*tpcs represents that the multiparty payment channel needs to be used, the payment channel for both parties. The server will forward the request to all other users in *m.*parties. For each user P_j who receives the request, if he agrees to create the channel, it will return a consent message to the server:

$$\text{mpc} - \text{create} - \text{agree} = ''\text{create an MPC}\, m, \delta_j''. \tag{14}$$

Otherwise, the user P_j will return a rejection message:

$$\text{mpc} - \text{create} - \text{reject} = ''\text{reject to create}\, m''. \tag{15}$$

If the consent of all users is obtained, that is, the server has collected the signatures of all users for the creation request message, it can call the interface for creating multiparty payment channels provided by the smart contract.

The createMPC(*m.*parties, *m.*tpcs, δ) function initiates a request to the smart contract, where δ is the set of signatures of all users. The smart contract will perform a series of verifications. If the verification is passed, a new multiparty payment channel instance will be created, the busy field of all two-party payment channels in *m.*tpcs will be set to 1, and the identifier of the channel will be returned to the user.

3.3.2. Channel Update Stage. The update phase of the multiparty payment channel, that is, the multiparty transaction phase, also needs to reach a consensus on channel update among all users. Due to the complexity of the multiparty payment channel update stage, the following content will be divided into four parts: multiparty

transaction generation, channel selection, multiparty transaction optimization, and multiparty payment channel update.

(1) Multiparty transaction generation: The multiparty payment channel in this paper is built on the payment channel layer above the blockchain network layer, and its purpose is to provide services to the upper application layer. Therefore, multiparty transactions are generated in the application layer. For example, in a multiparty game where four people participate in $\{P_1, P_2, P_3, P_4\}$, the rules of the game are that each round has a winner, and other users pay 1 token to the winner. Then, every time a round of the game needs to be settled, a multiparty transaction will be generated at this time. For example, if P_3 is the winner of this round, a multiparty transaction mptx = $\{(P_1, P_3, 1), (P_2, P_3, 1), (P_4, P_3, 1)\}$, meaning that each of P_1, P_2, and P_4 pays one token to P_3. Obviously, a multiparty transaction contains multiple two-party transactions. If $mptx$ is split into three separate two-party transactions, theoretically, the same settlement as a multiparty transaction can be completed, but the atomicity of the multiparty transaction cannot be guaranteed. For example, if the two parties' transactions $(P_1, P_3, 1)$ and $(P_2, P_3, 1)$ in $mptx$ are successfully settled and the transaction $(P_4, P_3, 1)$ cannot be successfully settled due to insufficient channel balance or routing failure, then the multiparty transaction mptx only partially settled and its atomicity is destroyed. Such a transaction is obviously unreasonable, and the wrong settlement result is difficult to roll back. Therefore, multiparty transactions need to ensure atomicity; that is, all two-party transactions included in a multiparty transaction either all settle successfully or all settlement fails.

(2) Channel selection: The function of channel selection is similar to routing in order to select the appropriate channel to complete multiparty transactions. The following will illustrate the importance of channel selection through an example.

As shown in Figure 1, it is a multiparty payment channel established by five users. The numbers at both ends of the arrow indicate the balances of the users at both ends of the channel. It can be seen that, in the multiparty payment channels, some channels are redundant, and not all two-party payment channels need to be updated. For example, when P_1 needs to pay a token to P_3, the payment can be made directly through the channel $P_1 \leftrightarrow P_3$, or the transaction can be made directly through the path $P_1 \leftrightarrow P_5 \leftrightarrow P_3$. Assuming that after a round of the game, P_1 pays a token to P_3 through $P_1 \leftrightarrow P_3$, the balance of the channel becomes $[P_1: 0, P_3: 4]$. At this time, the channel is an extremely unbalanced channel because P is no longer possible to pay to the other party through the

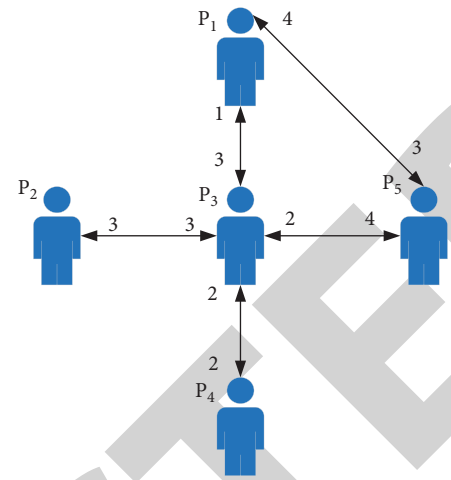

Figure 1: Schematic diagram of channel selection.

channel $P_1 \leftrightarrow P_3$. In the next round of settlement, if P1 needs to pay to P3, the channel $P_1 \leftrightarrow P_5 \leftrightarrow P_3$ will be selected for the transaction. Therefore, since each multiparty transaction will cause the balance status of multiple payment channels in the topology to change, we need to select the appropriate channel to complete a transaction. In order to measure the quality of a channel, this paper defines the following concepts:

$$\mathrm{Dist}_{ij} = \frac{b_{ij+}b_{ji}}{b_{ij} + b_{ji} + \sum_{k \in N_{ij}} \left(b_{ik} + b_{ki} + b_{jk} + b_{kj}\right)}, \tag{16}$$

$$\mathrm{Bal}_{ij} = \frac{\left|b_{ij} + b_{ji}\right|}{b_{ij} + b_{ji}}, \tag{17}$$

$$W_{ij} = k_1 * \left(1 - \mathrm{Dist}_{ij}\right) + k_2 * \mathrm{Bal}_{ij}. \tag{18}$$

In formula (16), Dist_{ij} represents the local proportion of the total channel balance between i and j, where b_{ij} represents the amount i can pay to j, b_{ji} represents the amount j can pay to i, $b_{ij+}b_{ji}$ is the total balance of channel ij, N_{ij} represents the set of neighbor nodes of channel ij, and a neighbor node of channel ij refers to the node that has established both the payment channel with i and the payment channel with j. Dist_{ij} can indicate the local importance of the balance of the channel. The larger the value, the higher the proportion of the balance of the channel ij. The larger the value is, the more the channel should be selected. In formula (17), Bal_{ij} represents the balance of the channel subscription, the numerator $|b_{ij} + b_{ji}|$ represents the absolute value of the difference between the balances at both ends of the channel, and the denominator $b_{ij} + b_{ji}$ represents the total balance of the channel. The smaller the value, the more the balance at both ends. The smaller the gap, the more balanced the channel. A balanced channel can support two-way transactions. Formula (18) is a value obtained by combining Dist_{ij} and Bal_{ij}, which is used to express the weight of channel ij. k_1 and k_2 are two adjustable parameters. The smaller the W_{ij} value, the better the quality of the channel.

3.3.3. Channel Closing Phase. In the closing phase of the multiparty payment channel, a user P_i initiates a request to close the channel to the server. This message can be recorded as

$$\text{mpc} - \text{close} = ''\text{close MPC mpc}, \delta_i''. \tag{19}$$

After receiving the request, the server will notify other users in the channel, namely, mpc.otherparties (P_i). If other users P agree to close, they will return a message:

$$\text{mpc} - \text{close} - \text{agree} = ''\text{close MPC mpc}, \delta_j''. \tag{20}$$

Otherwise, it will return a message that refuses to close:

$$\text{mpc} - \text{close} - \text{reject} = ''\text{reject to close MPC mpc}''. \tag{21}$$

After a certain period of time, after the server collects all users' replies, if all users agree to close MPC, the instance of the multiparty payment channel will be deleted, and the busy value of all the two-party payment channels involved will be set to 0, indicating that the payment channel of both parties has withdrawn from the environment of multiparty payment channels and can be used as an independent two-party payment channel or join other multiparty payment channels. After closing the channel, an mpc − closed message is used to notify all users that the channel has been closed. If it is not successfully closed, an mpc − close − failed message is returned.

3.4. Multiparty Payment Channel Performance Analysis. This section will analyze the performance of the multiparty payment channel according to the various stages of its life cycle. If n users participate in the multiparty payment channel, its performance is shown in Table 1. In the channel creation phase, 1 user initiates an application, the server sends a request to other n-1 users, n-1 users will return a response message to the request, and the server will return m messages to n users, notifying them of the result of creating a multiparty payment channel, so there are a total of $3n - 1$ messages in the interactive process at this stage. The smart contract is called to generate a transaction on the chain at a time, and each user needs to provide its signature, so there is a total of m signatures.

It should be noted that the multiparty payment channel proposed in this paper can theoretically support any number of users to establish a multiparty payment channel, but it may be limited in actual implementation. For example, in Ethereum, each block has a maximum gas limit, called a gas limit. The more the users in the channel, the more the signatures the smart contract needs to verify and therefore the more the gas it consumes. Only when the gas value consumed to create a multiparty payment channel is less than the limit value, can the multiparty payment channel be successfully created. In other blockchains without a gas limit, the number of users is not limited.

From the above analysis, it can be seen that, on the multiparty payment channel designed in this paper, except for the on-chain transactions necessary to create, update, and close the multiparty payment channel, the rest of the interaction process can be performed off-chain, so instant multiparty transactions can be realized. Compared with direct transactions through Ethereum, it can greatly reduce transaction delays, increase transaction throughput, and ensure the atomicity of multiparty transactions.

4. Experiments and Results

In this section, our aim is to view experiments and results done in order to mainly reduce transaction delay and increase the throughput of blockchain transactions, where we study the influence of factors, transaction amount, transaction distribution, and gas consumption.

4.1. Experimental Configuration. In this experiment, we mainly study three indicators of transaction delay, transaction success rate, and smart contract gas consumption. In the blockchain payment channel network, transaction delay is a key indicator. The purpose of payment channels is to significantly reduce transaction delays and increase the throughput of blockchain transactions. The transaction success rate is also an important indicator, which is related to the availability of the payment channel network. Higher transaction success rate means that the channel can withstand more transactions, and there will be no imbalance in a short period of time that will cause the channel to be unavailable. In this experiment, we studied the influence of factors such as network topology, transaction amount, and transaction distribution on the success rate of transactions. In addition, the gas consumption of smart contracts based on Ethereum is also an important indicator. In Ethereum, transaction fees are calculated according to the amount of gas consumed by the contract. Therefore, this paper also sets up several sets of experiments to study the gas consumption of different transaction methods. In order to verify the feasibility of the multiparty payment channel proposed in this paper in different networks, this paper uses random topologies of different scales to simulate the payment channel network. These random topologies are generated using NetworkX's algorithm. In addition, this experiment also intercepted network topologies of different scales from the real topology of the Lightning Network to conduct experiments.

4.2. Transaction Delay. Transaction delay is an important performance indicator for blockchain transactions and an important factor that limits the throughput of blockchain transactions. In Ethereum, the average block generation time is about 15 seconds, and the transaction throughput is about 15 TPS. Through the payment channel, we can transfer transactions on the blockchain to off-chain to achieve low-latency, high-throughput transactions. We set the block generation time of the simulated blockchain to 15 seconds, which is consistent with the real Ethereum block generation time. We separately studied the transaction delays of direct transactions through Ethereum, two-party payment channel transactions, and multiparty payment channel transactions.

Table 1: The performance of each stage of the multiparty payment channel of n users.

Function	Number of on-chain transactions	Number of off-chain transactions	Number of signatures
Created channel	1	$3n-1$	n
Off-chain update channel	0	$5n+1$	Relevant to the actual
On-chain update channel	1	0	n
Closed channel	1	$3n-1$	n

Figure 2 shows the delay of direct transactions via Ethereum varies with the number of transactions. This is achieved by calling a specific interface. This interface can specify the account addresses of the payer and the payee and the transaction amount to initiate an Ethereum transaction. It can be seen from the figure that the more Ethereum transactions, the greater the transaction delay. Because each transaction needs to call the interface once, the average delay of each transaction is about 15 seconds, which is consistent with the block time.

Figure 3 shows the change of the delay of the payment channel transaction between the two parties with the number of transactions. In the simulation experiment, two users are set up, the payment channel between the two parties is established based on the smart contract of the two parties, and the off-chain interaction is completed through socket communication. The communication delay of the network is set to 50 ms. By calling the interface opened by the smart contract to complete the creation, update, and closing of the channel, it can be seen from the figure that the entire transaction process consists of four parts: creating a channel, off-chain transaction, updating the channel on the chain, and closing the channel. Among them, the creation, chain update, and closing of the channel need to call the smart contract interface to generate Ethereum's on-chain transaction, so the delay is longer. The delay in the off-chain transaction part is relatively low because off-chain transactions do not need to call the smart contract interface and will not generate on-chain transactions. Therefore, as the number of transactions increases, the total transaction delay will not increase significantly because once the channel is established, multiple off-chain transactions can be performed, which is extremely low compared to on-chain transactions.

Figure 4 shows the delay of multiparty payment channel transactions with the number of transactions. In this experiment, three users are set up. A multiparty payment channel is established based on a multiparty payment channel smart contract. The communication delay of the network is also set to 50 ms, and users complete off-chain transactions through socket communication. It should be noted that, as the number of users increases, the delay of multiparty payment channel transactions may increase because the number of off-chain interactions will increase.

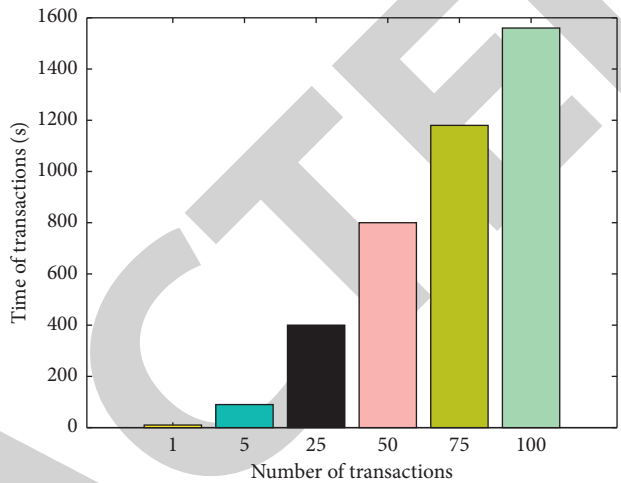

Figure 2: The relationship between the number of transactions and time in Ethereum.

4.3. Transaction Success Rate

4.3.1. The Impact of Network Topology on the Success Rate of Transactions. In the research on the payment channel network, some scholars mentioned that the hub-and-spoke topology is used to establish a multiparty payment channel; that is, all users are connected to the same payment hub, and each user conducts transactions with other users through the hub. In order to study the impact of randomized topology and hub-and-spoke topology on the success rate of transactions, this paper sets up several sets of experiments to run on different networks while ensuring that the number of nodes in the network is the same as the total amount of channels. For the same batch of transactions, statistics on their transaction success rate indicators and the experimental results are shown in Figures 5–7. In this experiment, we set up three different scale pair topologies, consisting of 10 nodes, 50 nodes, and 100 nodes, respectively, and ran multiple sets of transactions with different numbers to study the changes in the success rate of transactions, where "ran" represents a randomly generated topology, and "hub" represents a hub-and-spoke topology. It can be seen from the results in the figure that, in networks of different sizes, the transaction success rate on random topology is higher than that on hub-and-spoke topology. The reason is that, in the hub-and-spoke network, each user only establishes a two-party payment channel with the hub node. With more and more transactions, the channel will be exhausted. In a random network topology, a user's payment channels are usually established with multiple nodes, so when one channel is exhausted, other channels can be selected for transactions. In addition, it can also be seen that, as the number of transactions increases, the success rate of transactions in both networks will gradually decrease.

In addition to the network topology, the number of nodes in the network will also have a certain impact on the transaction success rate. Therefore, this paper sets up several sets of experiments to study the performance of transaction

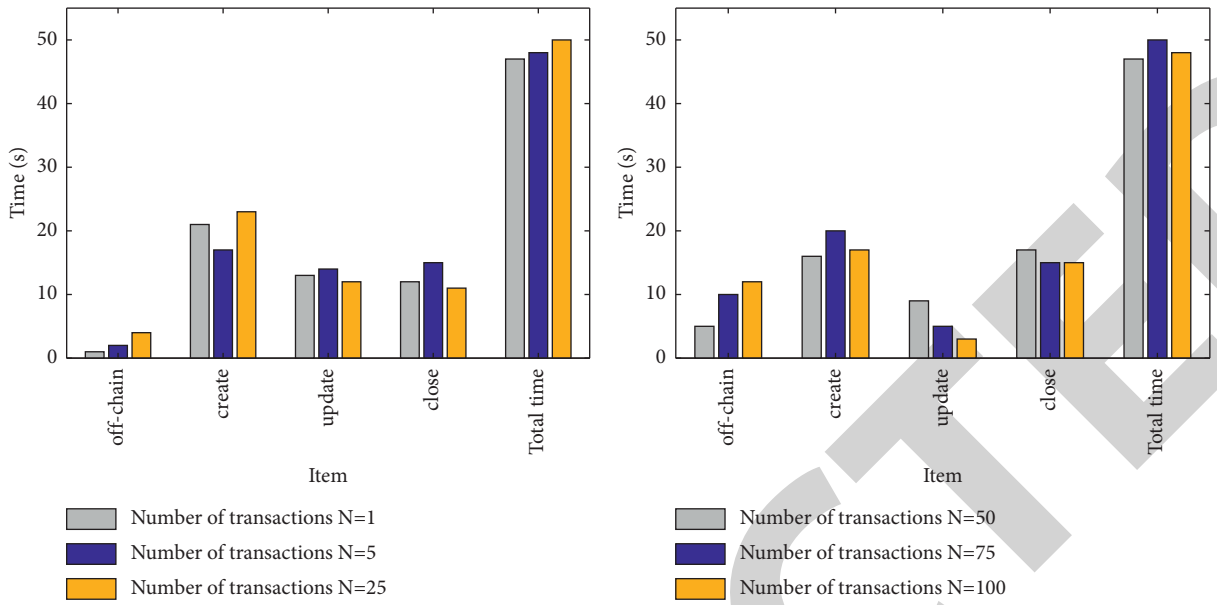

Figure 3: Comparison of dual payment channel transactions.

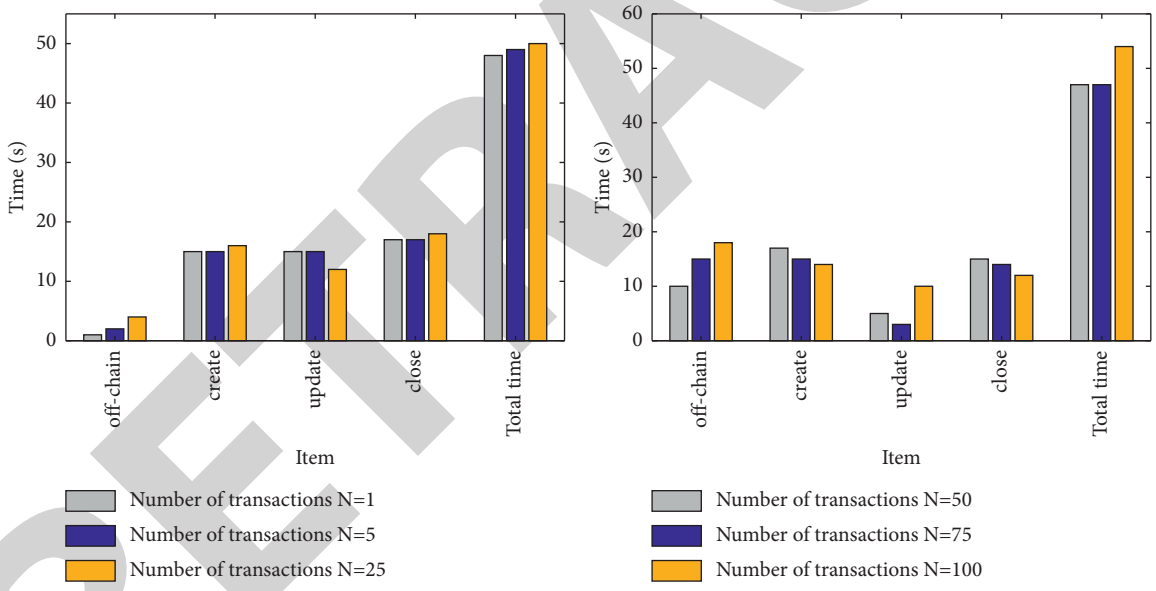

Figure 4: Comparison of multipayment channel transactions.

success rates in networks with different numbers of nodes. The experimental results are shown in Tables 2–4. Table 2 shows the performance when the quota of each transaction is less than 5 ethers. Table 3 is the performance when the quota of each transaction is less than 10 ethers, and Table 4 is the performance when the quota of each transaction is less than 50 ethers. From these three sets of experiments, it can be seen that, in the case of the same number of transactions, the more the nodes in the network, the higher the transaction success rate because the more the nodes, the more the channels in the network. Each transaction has different paths that can be used for trading. When some channels are exhausted, alternative channels can be selected for trading, so the success rate of the transaction is higher.

4.3.2. The Impact of Transaction Quota on Transaction Success Rate. In addition to the network topology, the amount of each transaction also has an impact on the success rate of transactions in the network. Therefore, this experiment has set up several sets of experiments to explore the impact of transactions with different amounts on the same network. The experimental results are shown in Figure 8. It can be seen that the larger the amount of each transaction, the lower the success rate of transactions in the network. The larger the transaction amount is, the faster the channel will be consumed, and many channels will reach an unbalanced state sooner, so that some channels are no longer available, and the number of transactions that can withstand in the network is relatively small.

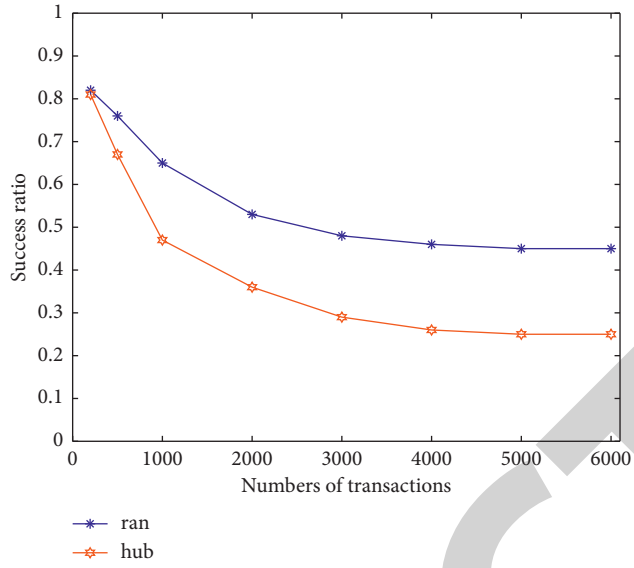

Figure 5: The transaction success rate of the 10-node topology.

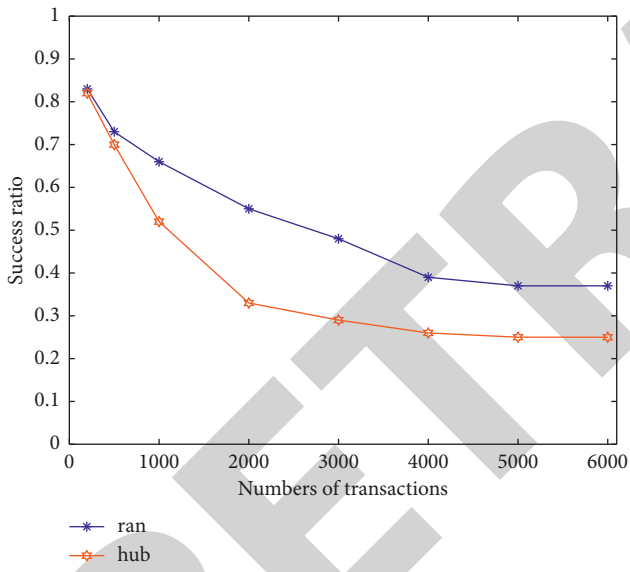

Figure 6: The transaction success rate of the 50-node topology.

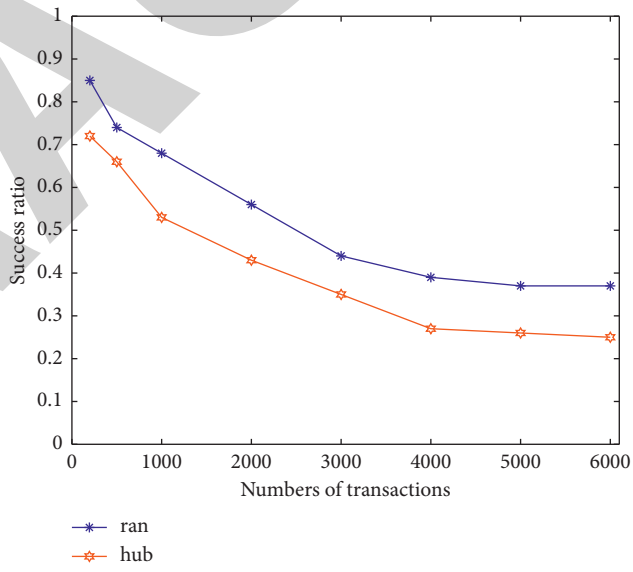

Figure 7: The transaction success rate of the 100-node topology.

4.4. Gas Consumption. Gas consumption may be the most concerned metric for users because it involves transaction fees. Therefore, this paper conducts experiments of different scales on the topology of the Lightning Network and the randomly generated topology to study the impact of different payment methods on gas consumption. In this experiment, the channel chain update interface of the smart contract is called once every ten state updates. In actual use, it can be called once before closing the channel to reduce gas consumption. The result is shown in Figure 9. "Ours" in the figure means using the multiparty payment channel proposed in this paper to complete multiparty transactions, "Dual" means using two-party payment channels to complete multiparty transactions, and "Eth" means not using payment channels. To conduct transactions directly on the Ethereum blockchain network, from the results in Figure 9, it can be seen that the multiparty payment channel transaction method proposed in this paper has great advantages in gas consumption, which benefits from the channel selection and multiparty transaction optimization proposed in this paper. The strategy reduces the number of interactions between users and also reduces the number of smart contract calls, making smart contracts consume less gas. The transaction method of the payment channel of both parties will reuse some of the same channels, so the performance on gas is slightly worse. If the transaction is performed directly through the Ethereum blockchain, each transaction needs to call the Ethereum transaction interface each time the gas consumption is fixed and the payment delay is long.

Table 2: Influence of the number of nodes on success rate when payment amount <5.

Number of transactions	Success ratio (%)				
	$N = 100$	$N = 150$	$N = 200$	$N = 250$	$N = 300$
0	100	100	100	100	100
500	95.8	98	96.2	98.5	99
1000	92.5	95.3	94.8	96.4	97.2
1500	85.3	90	87.5	92.5	94.5
2000	81.2	87.5	85	90.9	91.3
2500	73.5	82.6	80.5	86.4	89.8
3000	68.2	75	75	82.6	86.2
3500	65.7	70.8	72	78.8	80.9
4000	60	68.5	70	75.9	78.7

Table 3: Influence of the number of nodes on success rate when payment amount <10.

Number of transactions	Success ratio (%)				
	$N = 100$	$N = 150$	$N = 200$	$N = 250$	$N = 300$
0	100	100	100	100	100
500	89.2	91.2	92.5	93.8	95
1000	82.5	85.3	85.8	86.5	87.4
1500	75.3	76	77.5	81.2	84.5
2000	61.6	67.3	71.5	75.9	76.1
2500	53.2	62.2	68.2	72.4	73.5
3000	38.2	43.5	50	52.9	56.4
3500	25.5	30.8	39.6	42.5	44.7
4000	20	28.8	30	35.8	38.3

Table 4: Influence of the number of nodes on success rate when payment amount <50.

Number of transactions	Success ratio (%)				
	$N = 100$	$N = 150$	$N = 200$	$N = 250$	$N = 300$
0	100	100	100	100	100
500	85.2	86.8	88	89.5	92
1000	72.1	75.5	78.6	80	85.4
1500	55.8	56.2	61.5	66.3	69.5
2000	41.6	47.1	51.2	55.4	57.3
2500	31.2	32.5	38.5	42.1	43.6
3000	20.5	23.8	27	31.5	35.7
3500	18.5	20	19.6	22.5	26.5
4000	17.6	18.8	18	20	24

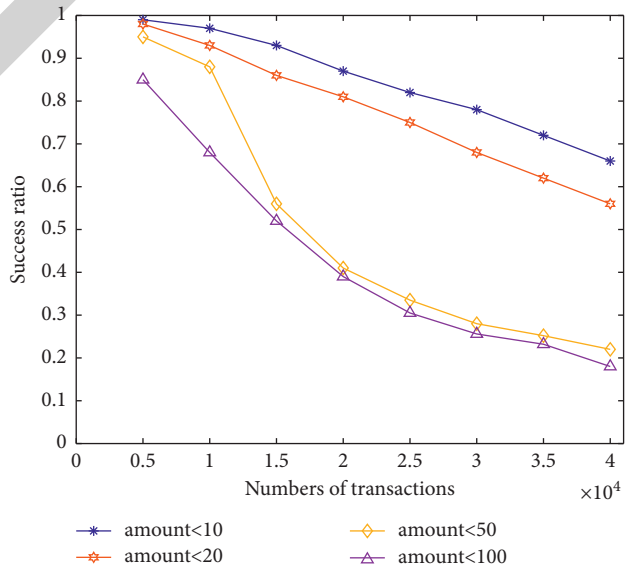

Figure 8: The impact of transaction amount on success rate.

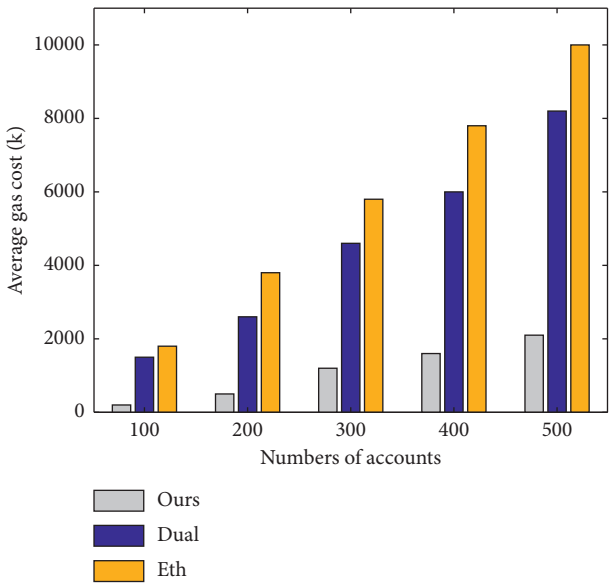

Figure 9: Comparison of gas consumption in different methods.

5. Conclusion

In recent years, blockchain technology has developed rapidly, but its shortcomings cannot be ignored. Aiming at the shortcomings of high transaction delay and low throughput of the blockchain network, this paper designs a new multiparty payment channel based on blockchain and smart contracts, which aims to reduce the delay of blockchain transactions and improve blockchain transactions. Throughput, this paper mainly carried out the following tasks: (1) This paper researched the literature and projects related to the blockchain payment network and analyzed the current implementation of the blockchain payment network and its defects. (2) Based on the smart contract, the two-party payment channel was designed, the process of its creation, update, and closing stages was introduced in detail, the subchannel was designed to support the parallel transaction of the payment channel, and the performance of the two-party payment channel was analyzed. (3) Based on the two-party payment channel, a multiparty payment channel based on blockchain and smart contracts is proposed, which extends the application scenario of the payment channel from a two-person application to a multiperson online application, so that the payment channel can be applied to multiperson online games, crowdfunding, auctions, and other application scenarios, and a trading strategy based on channel selection and multiparty transaction optimization is designed to ensure the balance of the channel and reduce the communication overhead and gas consumption during transactions. (4) This paper developed smart contracts for multiparty payment channels, performed blockchain simulation and client-side simulation, and researched the performance indicators of multiparty payment channels such as transaction delay, transaction success rate, and gas consumption. Through comparative experiments, the feasibility and advantages of the scheme proposed in this paper are verified.

Data Availability

The author did not obtain analytical permission from the data provider because of trade confidentiality.

Conflicts of Interest

The author declares no conflicts of interest.

References

[1] X. W. Xu, C. Pautasso, and L. M. Zhu, "The blockchain as a software connector," in *Proceedings of the 2016 Working IEEE/IFIP Conference on Software Architecture*, pp. 182–191, Venice, Italy, April 2016.

[2] G. Zyskind, O. Nathan, and A. Pentland, "Decentralizing privacy: usin block chain to protect personal data," in *Proceedings of the 2015 Security and Privacy Workshops*, pp. 180–184, San Jose, CA, USA, May 2015.

[3] M. Swan, "The quantified self: fundamental disruption in big data science and biological discovery," *Big Data*, vol. 1, no. 2, pp. 85–99, 2013.

[4] M. Swan, "Blockchain thinking: the brain as a decentralized autonomous corporation," *IEEE techn#ology and Society Magazine*, vol. 34, pp. 27–29, 2015.

[5] C. Dwork, "Differential privacy," *Automata, Languages and Programming*, vol. Part II, pp. 1–12, 2006.

[6] L. Sweeney, "k-Anonymity: a model for protecting privacy," *International Journal of Uncertainty, Fuzziness and Knowledge-Based Systems*, vol. 10, no. 5, pp. 557–570, 2002.

[7] N. H. Li and T. C. Li, "t-closeness: privacy beyond k-anonymity and l-diversity," in *Proceedings of the 2007 IEEE International Conference on Data Engineering*, pp. 106–115, Istanbul, Turkey, April 2007.

[8] K. McKusick and S. Quinlan, "Gfs," *Communications of the ACM*, vol. 53, no. 3, pp. 42–49, 2010.

[9] F. Chang, J. Dean, and S. Ghemawat, "Bigtable: a distributed storage system for structured data," *ACM Transactions on Computer Systems*, vol. 26, no. 2, p. 4, 2008.

[10] A. Schaub, R. Bazin, O. Hasan, and L. Brunie, "A trustless privacy-preserving reputation system," in *Proceedings of the ICT Systems Security and Privacy Protection*, pp. 398–411, Ghent, Belgium, May 2016.

[11] N. Szabo, "Formalizing and securing relationships on public network," vol. 2, 1997.

[12] M. Swan, "Blockchain: blueprint for a new economy," O'Reilly Media, Inc., Sebastopol, CA, USA, 2015.

[13] I. Toshiya, O. Yuji, and S. Hiroki, "A language-dependent cryptographic primitive," *Journal of Cryptology*, vol. 10, no. 1, pp. 37–49, 1997.

[14] A. Kosba, A. Miller, and E. Shi, "Hawk: the blockchain model of cryptography and privacy-preserving smart contracts," in *Proceedings of the Security and Privacy. IEEE*, pp. 839–858, San Jose, CA, USA, May 2016.

[15] T. Swanson: Consensus-as-a-service: a brief report on the emergence of permissioned, distributed ledger systems, 2015.

[16] N. P. Smart: Secure multi-party computation. 2013.2013.

[17] D. Morris, "Bitcoin is not just digital currency, it's napster for finance," *CNN Money*, vol. 12, pp. 12-13, 2014.

[18] L. Luu, D. Chu, and H. Olickel, "Making smart contracts smarter," in *Proceedings of the 2016 ACM SIGSAC Conference on Computer and Communications Security*, pp. 254–269, Vienna, Austria, Ocutober 2016.

Hindawi
Journal of Mathematics
Volume 2023, Article ID 9848270, 1 page
https://doi.org/10.1155/2023/9848270

Retraction

Retracted: Virtual Reality-Based Digital Restoration Methods and Applications for Ancient Buildings

Journal of Mathematics

Received 19 December 2023; Accepted 19 December 2023; Published 20 December 2023

This article has been retracted by Hindawi following an investigation undertaken by the publisher [1]. This investigation has uncovered evidence of one or more of the following indicators of systematic manipulation of the publication process:

(1) Discrepancies in scope

(2) Discrepancies in the description of the research reported

(3) Discrepancies between the availability of data and the research described

(4) Inappropriate citations

(5) Incoherent, meaningless and/or irrelevant content included in the article

(6) Manipulated or compromised peer review

The presence of these indicators undermines our confidence in the integrity of the article's content and we cannot, therefore, vouch for its reliability. Please note that this notice is intended solely to alert readers that the content of this article is unreliable. We have not investigated whether authors were aware of or involved in the systematic manipulation of the publication process.

Wiley and Hindawi regrets that the usual quality checks did not identify these issues before publication and have since put additional measures in place to safeguard research integrity.

We wish to credit our own Research Integrity and Research Publishing teams and anonymous and named external researchers and research integrity experts for contributing to this investigation.

The corresponding author, as the representative of all authors, has been given the opportunity to register their agreement or disagreement to this retraction. We have kept a record of any response received.

References

[1] T. Wang and L. Zhao, "Virtual Reality-Based Digital Restoration Methods and Applications for Ancient Buildings," *Journal of Mathematics*, vol. 2022, Article ID 2305463, 10 pages, 2022.

Hindawi
Journal of Mathematics
Volume 2022, Article ID 2305463, 10 pages
https://doi.org/10.1155/2022/2305463

Research Article

Virtual Reality-Based Digital Restoration Methods and Applications for Ancient Buildings

Tianhang Wang[1] **and Lu Zhao**[2]

[1]*School of Historical Culture and Tourism, Xi'an University, Xi'an 710065, Shaanxi, China*
[2]*School of Architecture, Xi'an University of Architecture and Technology, Xi'an 710055, Shaanxi, China*

Correspondence should be addressed to Tianhang Wang; wangtianhang@xawl.edu.cn

Received 6 December 2021; Revised 14 January 2022; Accepted 18 January 2022; Published 21 February 2022

Academic Editor: Naeem Jan

At a time of rapid technological development, 3D stereoscopic images and virtual reality technology are being used in art and design, as well as in the digital conservation of ancient buildings and their restoration. Virtual reality art is a high degree of integration between art and digital technology and is a new form of digital art. As a means of presenting architectural art, digital restoration of ancient buildings is a form of expression that combines knowledge, art, and technology. The digital restoration of ancient buildings and the creation of a 3D interactive display system are of great value for the realization of real space and the preservation of ancient sites. In this paper, we design a system that combines 3D stereoscopic and virtual reality technologies for the restoration of ancient buildings. Through the research and practice of this system, it can be translated into relevant design application research in other art and design fields, which is of great practical significance for future virtual reality expansion space.

1. Introduction

The cultural heritage of ancient buildings carries a deep historical and cultural heritage [1], witnessing a city's stormy history over thousands of years. The unique style and rich cultural connotations of ancient buildings are the inheritors of traditional culture [2] and superior craftsmanship, the crystallization of the wisdom of the ancients. With thousands of years of history and civilization, the ancients have created immortal legends with their hands, and their understanding and creation of the art of architecture in particular has highlighted the characteristics of different civilizations [3]. However, the cultural heritage of ancient buildings cannot be immortalized and is not renewable and is constantly subject to the erosion of the natural environment and the destruction of human activities in the course of history [4]. It has been subjected to natural and human activity over the course of history [5]. All we can do is to preserve it, to slow down its demise, and to pass on its spirit. As people become more aware of the importance of the cultural heritage of ancient buildings, it is important to preserve it for as long as possible without damaging the buildings themselves. The importance of preserving the cultural heritage of ancient buildings without damaging the buildings themselves is particularly important [6].

Digital restoration of ancient buildings as a means of presenting the art of ancient architecture is a form of expression that combines knowledge, art, and technology [7]. With the development and enhancement of information technology, 3D stereoscopic image technology [8] and virtual interactive technology [9], the digital means of ancient architecture restoration animation digital transformation and innovation, built 3D stereoscopic effect of virtual interactive ancient architecture restoration display system, for the real space to achieve the display, the preservation of ancient architectural sites is of great importance. It is of great importance to protect ancient architectural sites. Well-preserved physical antiquities play a realistic role in demonstrating the historical process, architectural style, and human life [10]. However, damaged or corroded parts of ancient buildings are unable to demonstrate this cultural need to the world [11]. This is an incomplete presentation of

ancient architecture and culture as a whole. According to a certain phenomenon, ancient buildings that cannot be restored to their true proportions are supplemented by digital forms. Improving the full picture of ancient buildings is of great significance to human understanding of the history and culture of ancient buildings, their architectural patterns, and human life [12]. It will also be a forward-looking initiative.

In terms of application technology, 3D stereoscopic and projection technology and virtual reality (VR) interactive technology have been developed and applied to different fields of art [13]. For example, 3D stereoscopic and projection technology is being used in film industry today, and virtual interaction technology is being used successfully in online games. However, there has been very little research into combining the two together in one field. The reason is that, first, the development of technical procedures is complicated, and the investment of capital and equipment is high; second, the application carrier is not suitable, and people are not yet fully aware of the value and prospect of combining 3D stereoscopic and projection technology with virtual reality interactive technology in the same field. The digital restoration of ancient buildings is the best vehicle for the application of this technology [14], and it also provides a new technology and means for the artistic expression of the restoration of ancient buildings.

In response to the aforementioned technique, this paper presents a practical design and theoretical study of the application of 3D stereoscopic technology and virtual reality to the digital restoration of ancient buildings. The research mainly includes the design of ancient building structure reproduction, 3D stereo image production, and virtual reality interactive technology, as well as the combination of the two-application technology and multichannel stereo projection system application. For many years, people have wanted to experience the real experience of roaming through ancient buildings. Three-dimensional stereoscopic technology combined with virtual reality technology applied to ancient architecture restoration animation will enable the viewer to have the experience of roaming through the disappearance of ancient buildings, experience the construction style of ancient buildings, and the history and culture of ancient buildings. In the coming section, the related technologies are discussed in much detail, such as virtual reality and architecture restoration animation. Moreover, the design of model and production techniques for ancient buildings is also discussed. Section 3 proposed the design of a system for interactive three-dimensional effect technology. Section 4 presents the explanation of development and realization of three-dimensional virtual reality technology in the digital restoration of ancient buildings. Section 5 is the conclusion section.

2. Related Technologies

2.1. Virtual Reality. Virtual reality (VR) is a high-tech tool that has emerged in recent years and is mainly used in the design of displays [15, 16], also known as aurora technology or artificial environments. VR is an integrated and comprehensive technology that involves computer graphics, human-computer interaction technology, sensing technology, artificial intelligence, and other fields. It uses computer-generated software to generate realistic three-dimensional images, with senses such as hearing, touching, and smelling to enable the experiencer to naturally experience and interact with the constructed virtual world. For example, the computer immediately performs calculations when the participant moves position or changes gestures, causing the 3D world image to move or change to create a sense of presence. The technology integrates the latest developments in computer graphics (CG) technology, simulation technology, sensing technology, artificial intelligence, display technology, network parallel processing, and other technologies and is a high-tech simulation system generated with the aid of computer technology.

In a nutshell, virtual reality is a new way for people to manipulate and interact with computer data through visualization. Compared to traditional human-computer interaction, virtual reality has made a qualitative leap forward in terms of technology and ideas. "Virtual reality" is a computer-generated medium. The term "reality" refers to anything or environment that exists in the world in a physical or functional sense. It can be practically realizable, practically unrealizable, or simply unrealizable. Thus, virtual reality refers to a computer-generated environment in a new medium, that is, a simulated, fictitious environment. A person can place themselves into this environment using various special devices and achieve manipulation, control of the environment, and achieve special purposes, that is, the person is the master of this environment.

2.2. Architectural Restoration Animation. Architectural restoration animation refers to the use of computer three-dimensional technology to produce animation works about the appearance of ancient buildings [17, 18] and is an important means of digital restoration of modern ancient buildings. Figure 1 shows a 3D restoration of the old Summer Palace site. Surface modelling is one of the most important directions of three-dimensional geometric modelling, which refers to the display of a surface on a computer through modelling and the interactive display and processing of its parameters.

Surfaces can be represented in two ways, nonparametric surfaces and parametric surfaces. Nonparametric surfaces, also known as functional surfaces, refer to surfaces that are described by surface equations over a defined range of domain values and can be expressed as

$$Z = f(x, y). \tag{1}$$

In determining the boundary of the domain of the function surface, the boundary equation $y = g(x)$ is constructed to limit the interval of variation of x, so that x and y vary gradually in fixed steps within the boundary, which in turn operates the coordinate values corresponding to each grid point on the surface, resulting in a grid model of the function surface.

(a) (b)

Figure 1: The 3D restoration of the old summer palace.

2.3. Model Design and Production Techniques for Ancient Buildings. Model building is the basis for completing the digital restoration of ancient buildings [19, 20] and the design of ancient building models should follow the following basic principles:

(i) Accurate model structure, in line with the cultural characteristics of ancient buildings. The models must be built in strict accordance with the references provided by the documentation and original images. The scenic model must be historically accurate, and the furniture must be in accordance with the actual scale and position of the space design. For ancient buildings, the most difficult aspect to control is the structural interplay, especially as most of the buildings are wooden and brick structures, making the model complex to build. How to restore a realistic scene is the key to modelling.

(ii) The material mapping is detailed and in line with the sense of chronological history. The restored animation of ancient buildings is a vehicle to disseminate information about ancient culture and to meet the needs of people for increased understanding, awareness, learning, and research of lost monuments. The aim is to increase people's understanding, awareness, learning, and research of the lost monuments. It is important to show a realistic image of ancient buildings. The material requirements for the mapping are a detailed analysis of the original building materials and a detailed mapping of the original architecture.

3. Design of a System for Interactive 3D Effect Technology

The technical means of application for the digital conservation of ancient buildings is to digitally produce and exhibit them [21]. The greatest purpose of digital conservation and restoration is to record and pass on history. Many countries and regions are now establishing digital museums and galleries for people to visit and study. With the improvement of modern technology and the transformation of people's needs, the original form of ancient architecture animation show can no longer meet the people's deeper, more thorough and more intuitive understanding of the disappearance of ancient buildings. People's understanding of ancient buildings is no longer limited to the perception of their physical structure, so 3D technology has revolutionized ancient buildings.

Restoration animation of ancient buildings is different from film and animation art. Its purpose is not only artistic expression and representation but more importantly, documentary and recording. For lost buildings, people want more than to be able to touch and feel them in real life, not as a third-person viewer of a restored animation. The most effective way to achieve this is through the use of virtual interaction technology for these buildings that cannot be authentically restored and reconstructed. By applying 3D technology and virtual interactive technology to the restored animation, although the real sense of touch cannot be realized, it is possible to view and navigate the ancient buildings as the first person in the animation and design the roaming route as you wish, while also feeling the real sense of space of the ancient buildings. A screenshot of the 3D restored image video is shown in Figure 2.

3.1. System Comparison. Virtual reality interactive display design for ancient buildings. It is based on the original restoration animation of ancient buildings to achieve 3D stereoscopic effects and interactive experience effects. The aim is to enable the experiencer to truly feel the realities of ancient restoration and interactive experience. At the same time, it can solve the current problems of restoration of ancient buildings, such as the problem of land needed for reconstruction, the technical problem of repairing the original appearance, the problem of long repair time cycles, and even the problem of whether many experts hold the need for restoration of ancient buildings that have been lost, as shown in Table 1.

3.2. Systematic Research Design Thinking Process. The development of a virtual reality interactive display system for three-dimensional effects of ancient buildings requires five stages, namely market research and demand analysis, system design, technology development and application, operation and testing, and effect evaluation as shown in Figure 3.

The system is designed to achieve the following functions:

(a) (b)

Figure 2: (a) Screenshot from the Dunhuang Mogao Grottoes 3D restoration video—red and blue technology. (b) Screenshot from the Dunhuang Mogao Grottoes 3D restoration video—polarization technology.

Table 1: Virtual reality interactive display design system for building body effects in antiquity.

Comparison of virtual reality interactive display systems for three-dimensional effects of ancient buildings			
	Resource utilization	Means approach	Software operating environment
Predevelopment	Physical or model visual material	Physical or model image display	General computers Projection equipment Physical stations Mainstream servers
After development	Image data system software	Three-dimensional virtual interactive display	Multichannel stereoscopic projection equipment Camera sensing equipment 3D stereo glasses

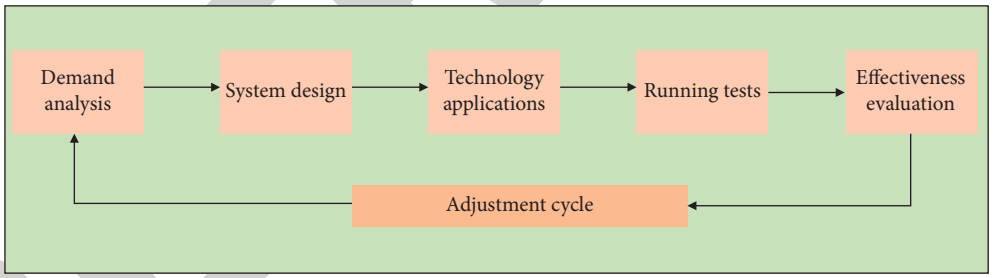

Figure 3: Procedures of system design and development.

(i) 3D visualization of architectural model design and implementation (model design, material UV mapping design, and lighting design)

(ii) Application of stereoscopic imaging technology

(iii) Virtual interaction technology design

(iv) Stereo display technology

A summary of the aforementioned points for the design and development of system can be seen in Figure 4.

3.3. Technical Programmed Design. The system is divided into two categories. One is the virtual interactive display design for the 3D effect of ancient buildings on a PC; the other is the virtual interactive display design for the 3D effect of ancient buildings under multichannel stereoscopic projection. The procedure is the same, but the difference is that the second type is based on the first type with the addition of projection equipment and camera equipment. The control settings are the same as on the PC, except that the mouse directional control is transformed into a character walking motion capture (Figures 5 and 6).

4. The Development and Realization of 3D Virtual Reality Technology in the Digital Restoration of Ancient Buildings

4.1. Realization of the Software Production Process. We use three parts to describe in detail the interactive design and development process of the 3D effect of ancient buildings.

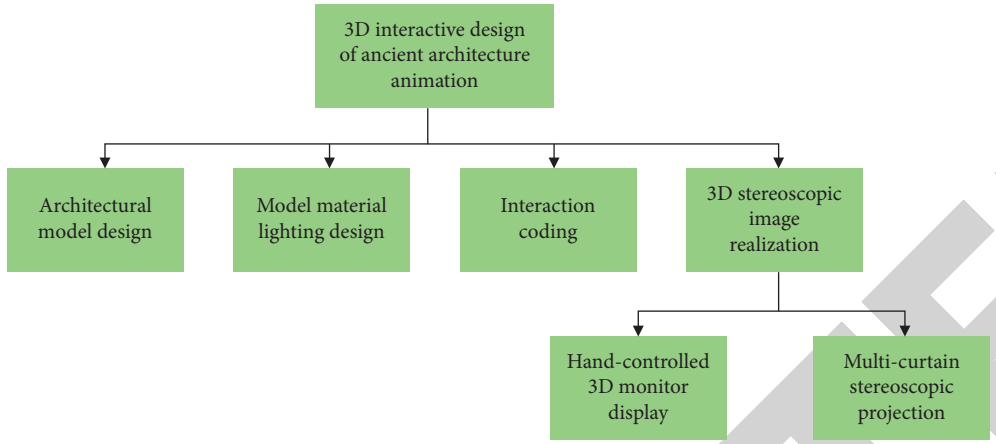

Figure 4: Procedures of system design and development.

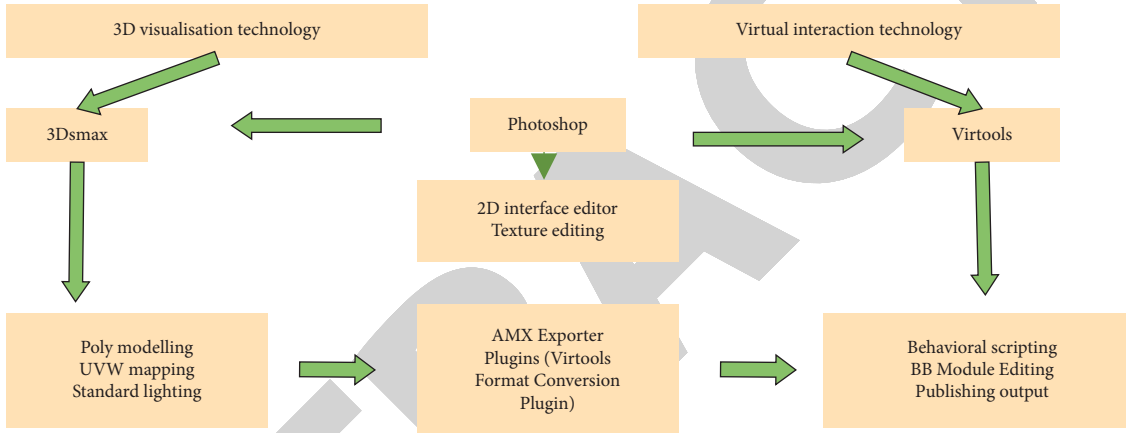

Figure 5: A virtual interactive display design to realize the 3D effect of ancient buildings on the PC.

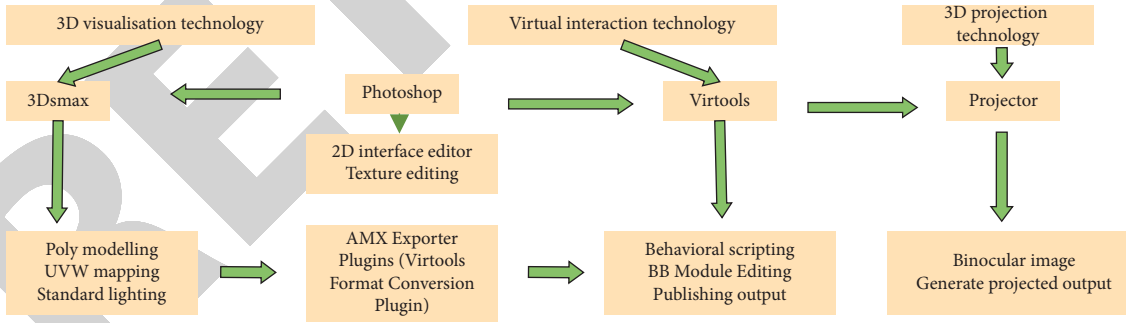

Figure 6: Virtual interactive display design to realize the 3D stereo effect of ancient buildings under multichannel stereo projection.

The specific content includes program structure design, resource file design, and specific realization of program difficulties. The software production application flow chart is shown in Figure 7.

4.2. Realization of 3D Visualized Ancient Building Model

4.2.1. Model Design. There are many platforms for visualizing 3D images, and this paper focuses on the field of 3D modelling technology. The 3DS MAX software platform was chosen for this study because of the variety of exported data types and the stability of the combination with Virtools. The most important part of the digital restoration of ancient buildings is the digitization of the display of ancient buildings, and the prerequisite step for the digitization of ancient buildings is the model, understanding the structure of ancient buildings is extremely important, the fundamental of the restoration of ancient buildings animation is to restore the original appearance of ancient buildings without modification.

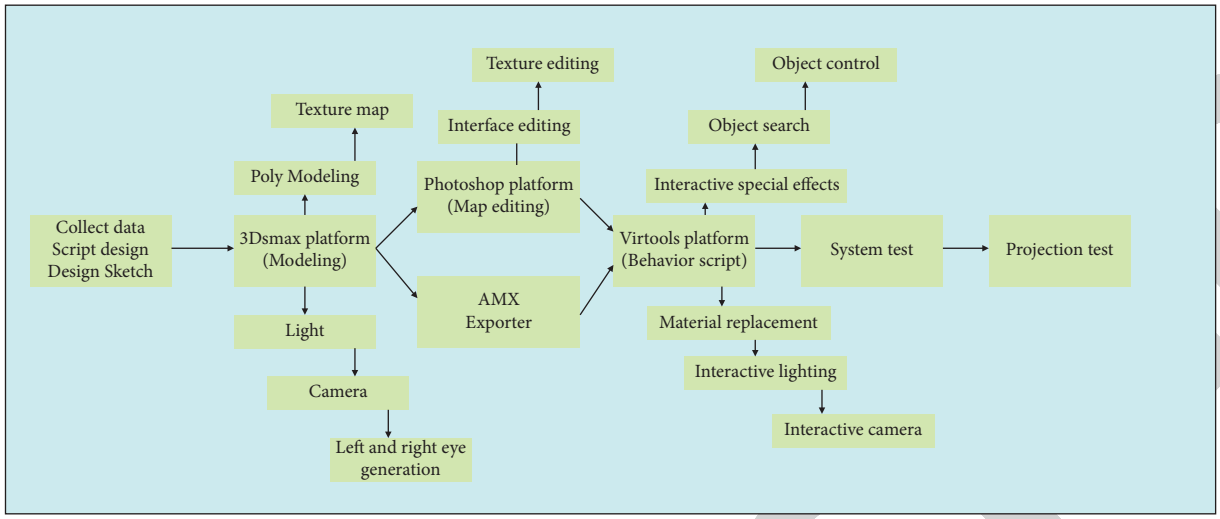

Figure 7: Procedures for software production.

The creation of a model of an ancient building generally starts with the geometry, creating box geometry that can be edited, adding lines to the layout based on the general shape of the model, adjusting the divisions, going from whole to partial in a gradual and progressive manner, adding new geometry to create new objects such as tiles, doors, windows, and stone benches if the number of geometry is insufficient. However, the reason for keeping the number of polygonal rows as well as the number of faces to a minimum is to save resources. The problem that also arises is that the model is simplistic and it is not detailed enough. As the model is an architectural model, the model does not produce its own shape changes, allowing for triangular or polygonal surfaces. If you are making a biological model, it is best to ensure that all surfaces are quadrilateral to avoid tearing of the mapping when the object is animated in motion. Once you are satisfied with the model, it is important to focus on the main points and not on everything and to simplify the model outside of the camera and control range. Also give due consideration to the size of the model, the type of material and the cost of production to ensure that art and reality are combined. Figures 8(a) to 8(d) show the process of modelling ancient buildings.

Based on old film, documentation and modern restoration of the building as a reference to create a model of the lost and destroyed parts of the building needed for the restoration animation, the challenge was to accurately represent the complex structural relationships of the ancient building and to control the number of surfaces and lines. The reason for this is that the smaller the amount of data that is transferred to the Virtools software, the better the interaction will be. This depends on the performance of the equipment. This is not normally a consideration if the model is put into operation in a large venue. The eaves and windows are shaped with a return pattern as shown in Figure 9.

4.2.2. Materials UV Mapping. The quality of the mapping depends on the quality of the model if you want to give it a realistic feel with a high level of visual spatial enhancement. The coordinates of 3D space are divided into three axes X, Y, and Z, corresponding to the 3D space mapping coordinates U, V, and W, so the 3Ds Max mapping coordinates are called UV coordinates. In the architectural performance, according to the picture of the distant reality, primary and secondary relationship, detail requirements, generally will use two kinds of editing UV coordinate distribution tools. UVW map is a simple way of unfolding UV and is often used in architecture to create new objects and objects that are not very important in the distance. Unwrap is often used in architecture for old effects and for models in some close-ups and can often be used in distant views, such as a specific shape of stain in a specific position in a corner. The Unwrap mapping is shown in Figure 10, and the finished Unwrap mapping is shown in Figure 11.

4.2.3. Lighting Design. For architectural models, the lighting is arranged to create a realistic natural ambient light effect. To create the ideal lighting effect in software, it is necessary to have an understanding of light in nature. In the natural environment, there is only one source of light and that is the sun, whereas light comes from many directions, the reason being that the direct light from the sun is refracted or reflected by certain objects. This constitutes the primary and secondary light. For larger scenes, the building is generally illuminated using a multipoint method: one main light source and several auxiliary light sources, the role of the auxiliary light source is to fill in the light, making the outline of the object clear, while making the building have a contrasting relationship between light and dark without producing large contrasts. This is common in nature and is also done in the software to influence the material bump effect. As shown in Figure 12, the contrast between one light exposure and multiple light exposure is shown.

4.3. Application and Implementation of Binocular Stereo Imaging Technology. To create a stereoscopic image, it is important to understand the principles of stereoscopic

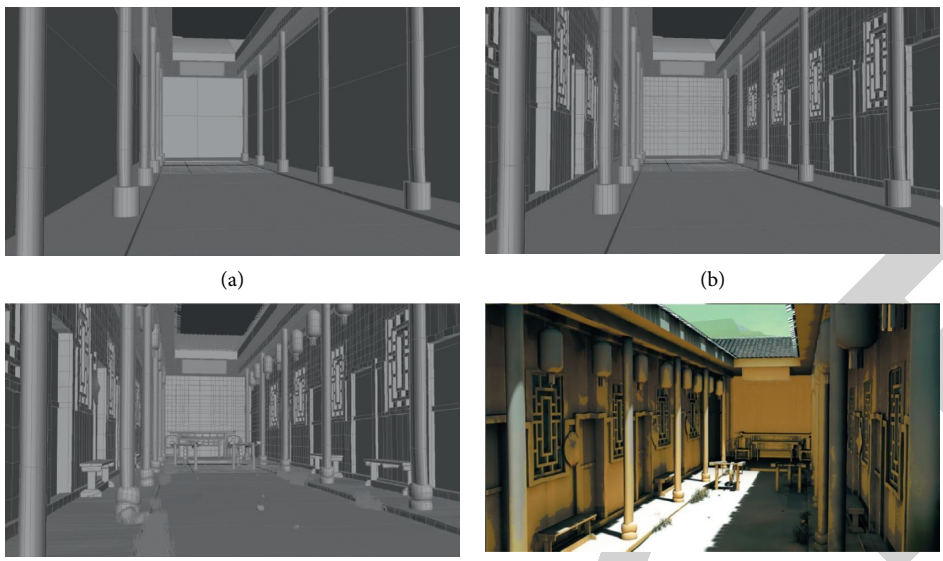

(a) (b) (c) (d)

Figure 8: (a) Building for foundational model; (b) building for adjustment model; (c) building for modification model; (d) completed rendered model.

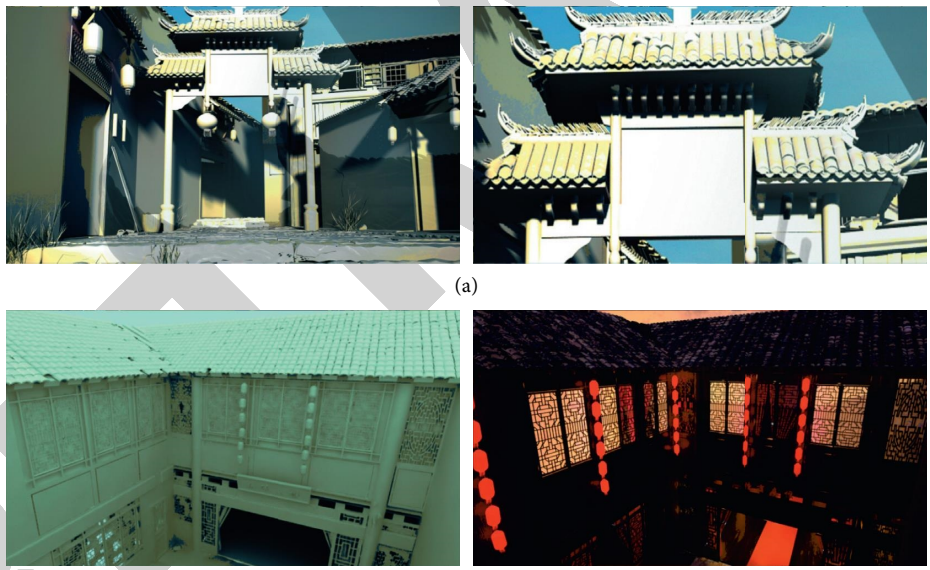

(a) (b)

Figure 9: (a) Eaves tile modelling and (b) retrospective window molding.

imaging. Since the human eye has a pupillary distance of approximately 65 mm, when people look at an object with both eyes, the left and right eyes each see the left and right sides of the object. The details of the object on the left and right side of the scene are seen by both eyes. This means that two similar two-dimensional images with horizontal parallax are formed on the human retina, and the objects are imaged slightly differently on the left and right retinas. This means that the two two-dimensional images are reproduced with binocular parallax to form a three-dimensional image. We watch the stereoscopic film is to simulate the principle of three-dimensional image formation of the human eye, the first left and right eyes of the monocular image were recorded, through the projector and the corresponding stereoscopic projection equipment, so that the audience left and right eyes respectively see the corresponding monocular image, and then through the brain reproduced into a three-dimensional image. In technical terms, this means that the left and right double images are projected and reflected in the left and right eyes of the audience respectively. In order to achieve a binocular image, we had to create a binocular virtual camera to capture it. The left and right eye images created by the binocular camera are shown in Figure 13.

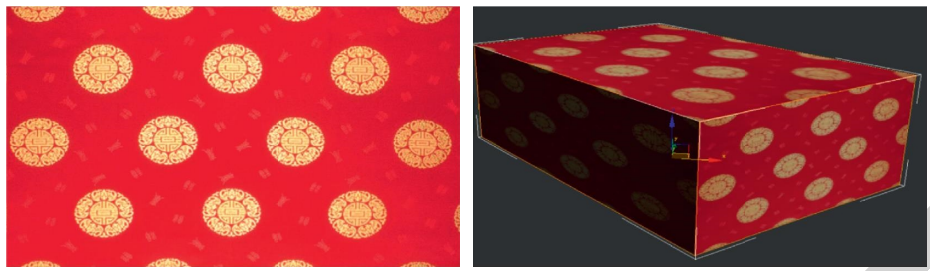

Figure 10: UVW map chartlet.

Figure 11: Completed unwrap chartlet.

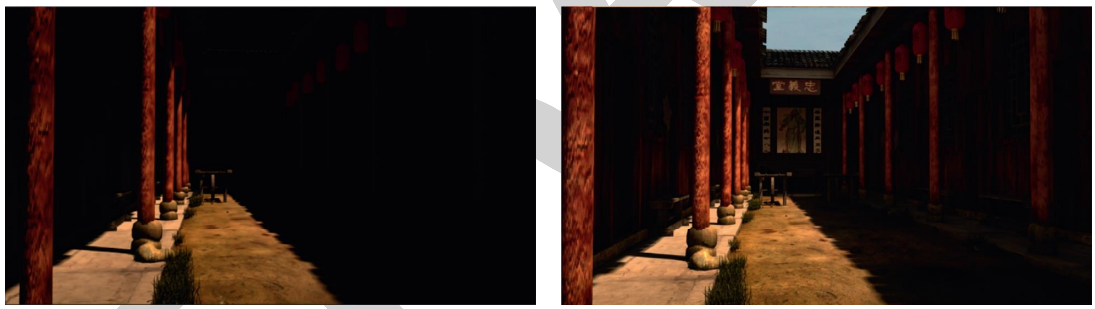

(a) (b)

Figure 12: One light illuminates the building with a high contrast of light and shadow (a); multiple lights illuminate the building with the right contrast of light and dark, making the picture more vivid (b).

Figure 13: Images of the left and right eyes created by the binocular camera, with the left eye sequence static needle image on the left and the right eye sequence static needle image on the right.

4.4. Virtual Interaction Technology Implementation. At the final stage of the model's completion, collision control is done on the objects because the model camera can go through objects, while in real life, we humans cannot go through objects, so we have to do collision control on the photography. This means that the camera simulates the

Figure 14: The camera will not advance if it touches a chair.

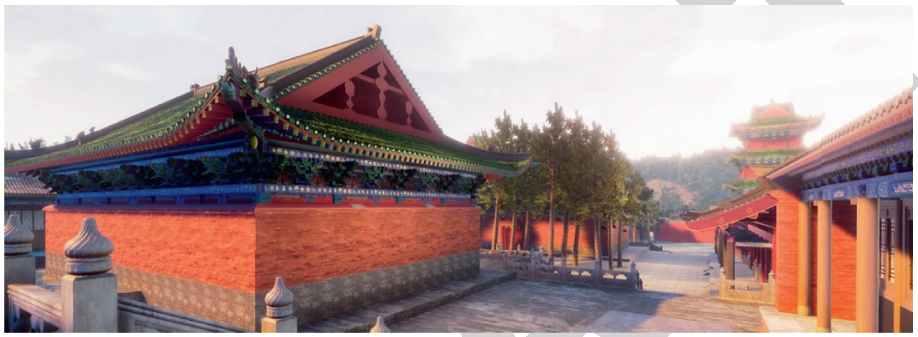

Figure 15: Schematic diagram of the digital restoration of the "Shaolin Temple" building applying the virtual reality approach of this paper.

human eye, the camera moves to simulate the character walking, and when we encounter walls and obstructions we cannot get through objects, so it is more realistic (Figure 14).

4.5. Stereoscopic Display Technology Implementation. "Stereo vision" is the brain's satisfaction with the "depth" perception of a stereoscopic image. It is not easy to obtain "depth perception" from the "monocular cues" of traditional flat displays. from the "monocular cues" of traditional flat displays is not easy, the difficulty lies in the habituation of people to two-dimensional images. The difficulty lies in people's habituation to two-dimensional images. These cues include light and shade, relative size, spatial perspective (or atmospheric perspective), motion parallax (by the movement of a nearby object across the field of view into the field of view), and the perception of depth (a visual cue created by the act of moving a nearby object across the field of view to a more distant object than a distant one), and most importantly (or atmospheric perspective), kinematic parallax (a visual cue created by the act of moving a nearby object across the field of view to a further distance than a distant object) and, most importantly, "occlusion cues" (objects obscured above and below or in front and behind) and perspective. All these influences play a key role in stereoscopic vision.

Virtual reality technology actually provides the viewer's eyes with two separate images to create a depth perception effect. When viewing a particular object presented by a pair of identical images. Depending on the difference in horizontal distance between the two images (pupil depending on the difference in horizontal distance between the two images (60 mm pupillary distance), the viewer's eyes will move to "converge" in front of, above or behind the screen, depending on the situation. But the human brain is always focused on the screen, which creates a sense of unreality, and this unreality is what makes our perception of a stereoscopic scene different from that of the real world. In the real world, the visual focus and convergence of our vision is consistent. This known response is broken when viewing stereoscopic images, and this is what causes the discomfort of stereoscopy. While most people are comfortable with the sudden difference in focus and convergence, some people are more sensitive to seeing stereoscopic images and experience discomfort or dizziness and image confusion. Figure 15 shows a schematic diagram of the digital restoration of the "Shaolin Temple" building by applying the methods in this paper.

5. Conclusion

The study of the application of virtual reality interactive technology in the digital restoration of ancient buildings has great application value and practical significance. The method provides a new digital display concept for the restoration of ancient buildings and provides a new virtual presence for the experience. The research is pioneering and highly integrative in the field of digital restoration of ancient buildings, broadening the field of application and interactive experience of virtual reality technology, and providing a very practical and effective means of digital restoration of ancient buildings through the practical development and research of

Hindawi
Journal of Mathematics
Volume 2024, Article ID 9863939, 1 page
https://doi.org/10.1155/2024/9863939

Retraction

Retracted: Prediction Model of Mining Subsidence Parameters Based on Fuzzy Clustering

Journal of Mathematics

Received 23 January 2024; Accepted 23 January 2024; Published 24 January 2024

This article has been retracted by Hindawi following an investigation undertaken by the publisher [1]. This investigation has uncovered evidence of one or more of the following indicators of systematic manipulation of the publication process:

(1) Discrepancies in scope

(2) Discrepancies in the description of the research reported

(3) Discrepancies between the availability of data and the research described

(4) Inappropriate citations

(5) Incoherent, meaningless and/or irrelevant content included in the article

(6) Manipulated or compromised peer review

The presence of these indicators undermines our confidence in the integrity of the article's content and we cannot, therefore, vouch for its reliability. Please note that this notice is intended solely to alert readers that the content of this article is unreliable. We have not investigated whether authors were aware of or involved in the systematic manipulation of the publication process.

Wiley and Hindawi regrets that the usual quality checks did not identify these issues before publication and have since put additional measures in place to safeguard research integrity.

We wish to credit our own Research Integrity and Research Publishing teams and anonymous and named external researchers and research integrity experts for contributing to this investigation.

The corresponding author, as the representative of all authors, has been given the opportunity to register their agreement or disagreement to this retraction. We have kept a record of any response received.

References

[1] F. Cheng, J. Yang, Z. Zhang et al., "Prediction Model of Mining Subsidence Parameters Based on Fuzzy Clustering," *Journal of Mathematics*, vol. 2022, Article ID 7827104, 10 pages, 2022.

Hindawi
Journal of Mathematics
Volume 2022, Article ID 7827104, 10 pages
https://doi.org/10.1155/2022/7827104

Research Article

Prediction Model of Mining Subsidence Parameters Based on Fuzzy Clustering

Fei Cheng,[1] Jun Yang,[2] Ziwen Zhang,[3] Jingliang Yu,[3] Xuelian Wang,[3] Yongdong Wu,[4] Zhengyi Guo,[5] Hui Li,[6] and Meng Xu[7]

[1]*Shanxi Engineering Vocational College, Taiyuan 030009, China*
[2]*Chongqing Transportation Vocational College, Chongqing 402247, China*
[3]*Guangzhou Maritime University, Guangzhou, China*
[4]*Center of Guangzhou Maritime Survey and Mapping, Guangzhou 510320, China*
[5]*Guangxi Zhuang Autonomous Region 274 Geological Team, Beihai 533600, China*
[6]*Chemical Geological Survey Institute of Liaoning Province, Jinzhou 121007, China*
[7]*Beijing Aerospace Titan Technology Co. LTD, Beijing 100160, China*

Correspondence should be addressed to Ziwen Zhang; zhangziwen@gzmtu.edu.cn

Received 29 November 2021; Revised 14 January 2022; Accepted 17 January 2022; Published 18 February 2022

Academic Editor: Naeem Jan

In view of the inaccuracy of rock movement observation data and the inaccuracy of mining subsidence prediction parameters, a prediction model of mining subsidence parameters based on fuzzy clustering is proposed. Through the analysis of the main geological and mineral characteristics of mining subsidence, the geological and mineral characteristics are simplified according to the third similar theorem. The feature equation is obtained by using the equation analysis method and dimension analysis method. The original fuzzy clustering method is improved, and the IWFCM_CCS algorithm based on competitive merger strategy is obtained. The data of rock movement observation are analyzed by fuzzy clustering. The membership matrix and clustering center of observation station data are obtained, and the regression model based on the weight of membership degree is established. The accuracy and feasibility of the parameter prediction model are verified by analyzing and comparing the actual measurement data and the predicted results of the model. The method reduces the error of the predicted parameters caused by the observation data and provides a method for the future calculation of the predicted parameters.

1. Introduction

Mining subsidence is expected to be developing in the direction of intelligence and visualization. Today, with the rapid development of technologies such as sensors, computers, Internet of Things, and data storage, enterprise information management systems have been continuously popularized. The advancement of modern surveying and mapping science and technology has resulted in more and more data generated from the observation of surface subsidence. If these data are analyzed and processed quickly, abnormal data can be eliminated, and useful data can be extracted; this will greatly improve the accuracy and efficiency of settlement predictions [1–6].

Coal mining affects the production and life safety of people around, so the prediction of mining area deformation becomes very important. The accuracy of rock movement parameters affects the accuracy of the predicted results. Aiming at the problem of inaccurate calculation of rock movement parameters due to the large amount of data generated by rock movement observation, a mining subsidence parameter prediction model based on big data has been established [7–12]. Through the analysis and processing of rock movement observation data, the mining subsidence parameter prediction model is derived, which improves the accuracy and calculation efficiency of rock movement parameters, thereby improving the accuracy of mining subsidence prediction and the safety of the coal mining process.

The following is a summary of the research. Section 1 contains the introduction. Section 2 discusses the analysis of the main geological characteristics of mining subsidence. Section 3 discusses the preprocessing of rock movement observation data. Section 4 discusses the project example verification with tables, and finally, the conclusion is given in Section 5.

2. Analysis of the Main Geological Characteristics of Mining Subsidence

Mining subsidence happens when mining operations weaken or hollow out the Earth beneath or near a property's foundations. The ground beneath a building moves downhill as a result of this. Types of mining subsidence are given below.

2.1. Simplified Geological Features. As the stress state around the mining area is constantly unbalanced and balanced during the mining process, mining subsidence is caused by complex physical and mechanical changes. Figure 1 shows the main geological factors related to surface subsidence.

It can be seen from Figure 1 that many complex factors are involved in the mining subsidence process. The mining subsidence method must be simplified in order to conduct additional research on it.

From the similar third theorem [13], geological mining conditions can be obtained: mining conditions are the first mining, the coal mining method is longwall mining, and the roof management method is the full caving method.

2.2. Feature Extraction

2.2.1. Equation Analysis Method. Based on the linear elastic model of inclined coal seams, the following equations are listed:

$$\begin{cases} \dfrac{\partial \sigma_y}{\partial y} + \dfrac{\partial \tau_{yz}}{\partial z} + \lambda \rho g = 0 \\ \dfrac{\partial \tau_{yz}}{\partial y} + \dfrac{\partial \sigma_z}{\partial z} + \rho g = 0 \\ \varepsilon_y = \dfrac{\partial u}{\partial y} \\ \varepsilon_z = \dfrac{\partial w}{\partial z} \\ \gamma_{yz} = \dfrac{\partial u}{\partial z} + \dfrac{\partial w}{\partial y} \\ \gamma_{yz} = \dfrac{2(1+\mu)}{E} \tau_{yz} \\ \varepsilon_y = \dfrac{1+\mu}{E} \left[(1-\mu)\sigma_y - \mu \sigma_z \right] \\ \varepsilon_z = \dfrac{1+\mu}{E} \left[(1-\mu)\sigma_z - \mu \sigma_y \right] \end{cases} \tag{1}$$

In the formula, σ_y and σ_y, respectively, represent the normal stress in two directions; τ_{yz} represents the shear stress; ε_y and ε_z represent the normal strain, respectively; γ_{yz} represents the shear strain; and W and U represent the sinking value and horizontal movement, respectively.

When the two mining subsidence phenomena conform to the similar third theorem, we can get

$$\begin{cases} y'' = y_0 y' \\ z'' = z_0 z' \\ u'' = u_0 u' \\ w'' = w_0 w' \\ \varepsilon_y'' = \varepsilon_{y0} \varepsilon_y' \\ \varepsilon_z'' = \varepsilon_{z0} \varepsilon_z' \\ \gamma_{yz}'' = \gamma_{yz0} \gamma_{yz}' \\ \sigma_y'' = \sigma_{y0} \sigma_y' \\ \sigma_z'' = \sigma_{z0} \sigma_z' \\ \tau_{yz}'' = \tau_{yz0} \tau_{yz}' \\ E'' = E_0 E' \\ \mu = \mu_0 \mu' \\ \lambda'' = \lambda_0 \lambda' \\ \rho'' = \rho_0 \rho' \\ g'' = g_0 g' \end{cases} \tag{2}$$

Taking $Z_0 = H$, $W_0 = m \cos \alpha$, $E_0 = E_{mi\,d}$, $g_0 = g$ and combining the boundary conditions that when $z = H$, then $\sigma_y = \sigma_z = \tau_{yz} = 0$, the similarity criterion can be obtained.

$$\begin{cases} \Pi_1' = \dfrac{y}{H} \\ \Pi_2' = \dfrac{z}{H} \\ \Pi_3' = \dfrac{w}{m \cos \alpha} \\ \Pi_4' = \dfrac{u}{m \cos \alpha} \\ \Pi_5' = \dfrac{H \varepsilon_y}{m \cos \alpha} \\ \Pi_6' = \dfrac{E}{E_{mi\,d}} \\ \Pi_7' = \dfrac{\rho g H^2}{E_{mi\,d} m \cos \alpha} \\ \Pi_8' = \lambda \\ \Pi_9' = \mu \end{cases} \tag{3}$$

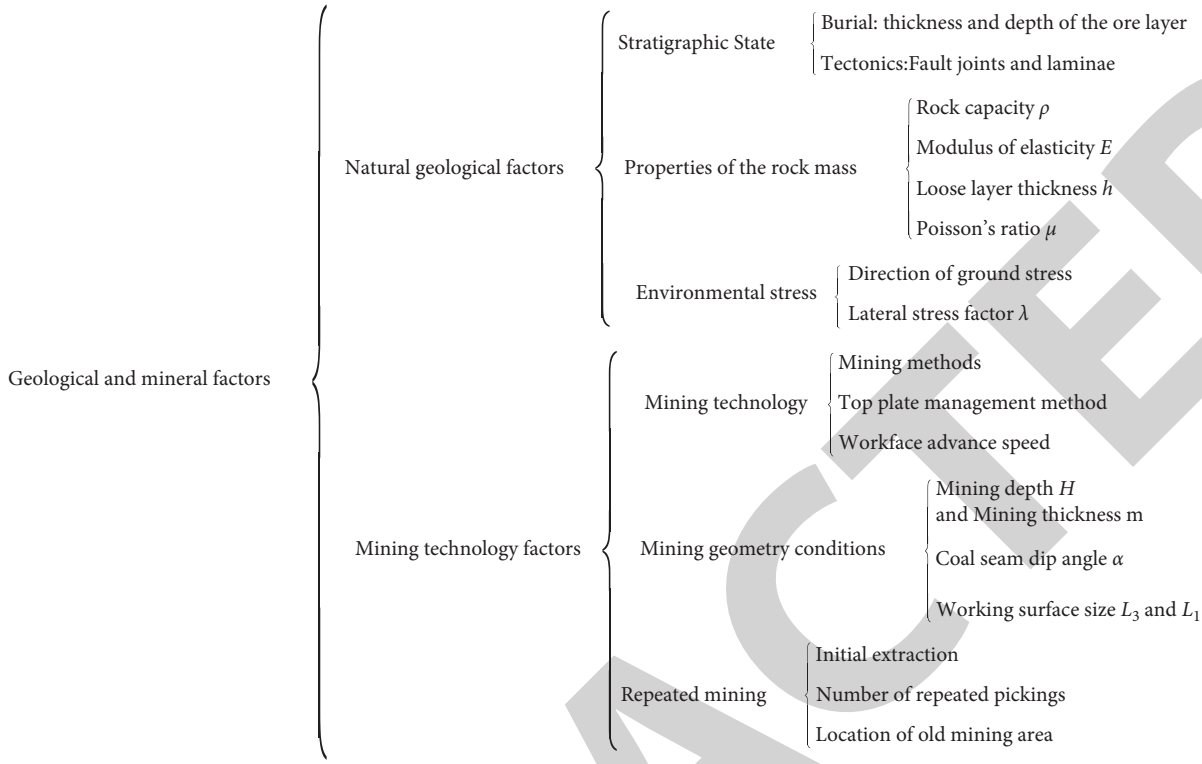

Figure 1: Factors of mining subsidence.

Because y, z, w, u, and ε_y are external features, $\Pi_1' \sim \Pi_5'$ is a dependent variable feature. Therefore, four geological and mineral features $\Pi_6' \sim \Pi_9'$ are extracted by the equation analysis method.

2.2.2. Dimensional Analysis. For mining subsidence, on the basis of formula (3), the loose layer thickness h, strike length l, and inclined width m are added. The mass system is adopted, and the basic physical quantities are M, L, and T. Therefore, the mining subsidence equation is

$$f\left(y, z, w, u, H, h, L_1, L_3, m, \alpha, \varepsilon_y, E, \rho, \mathrm{g}, \lambda, \mu, M, L, T\right) = 0. \tag{4}$$

Because of the homogeneity of the dimensions of equation (4), an exponential equation can be obtainedh.

$$\begin{cases} a_{11} + a_{12} + a_{17} = 0 \\ a_1 + a_2 + a_3 + a_4 + a_6 + a_7 + a_8 + a_9 + a_{10} - a_{11} - 3a_{12} + a_{13} + a_{18} = 0 \\ -2a_{11} - 2a_{13} + a_{19} = 0 \end{cases} \tag{5}$$

According to the similarity transformation of the matrix, 16 similarity criteria can be obtained:

$$\begin{cases} \pi_1 = \dfrac{y}{L} \\ \pi_2 = \dfrac{z}{L} \\ \pi_3 = \dfrac{w}{L} \\ \pi_4 = \dfrac{u}{L} \\ \pi_5 = \varepsilon_y \\ \pi_6 = \dfrac{H}{L} \\ \pi_7 = \dfrac{h}{L} \\ \pi_8 = \dfrac{L_3}{L} \\ \pi_9 = \dfrac{L_1}{L} \\ \pi_{10} = \dfrac{m}{L} \\ \pi_{11} = \dfrac{ELT^2}{M} \\ \pi_{12} = \dfrac{\rho L^3}{M} \\ \pi_{13} = \dfrac{gT^2}{L} \\ \pi_{14} = \alpha \\ \pi_{15} = \lambda \\ \pi_{16} = \mu \end{cases} \tag{6}$$

Among them, $\pi_1 \sim \pi_4, \pi_6 \sim \pi_{13}$ have no actual physical meaning, and 13 similar criteria can be obtained.

$$\begin{cases} \Pi_1'' = \dfrac{y}{H} \\ \Pi_2'' = \dfrac{z}{H} \\ \Pi_3'' = \dfrac{w}{m} \\ \Pi_4'' = \dfrac{u}{m} \\ \Pi_5'' = \varepsilon_y \\ \Pi_6'' = \dfrac{H}{m} \\ \Pi_7'' = \dfrac{h}{H} \\ \Pi_8'' = \dfrac{L_3}{H} \\ \Pi_9'' = \dfrac{L_1}{H} \\ \Pi_{10}'' = \dfrac{\rho g H}{E} \\ \Pi_{11}'' = \alpha \\ \Pi_{12}'' = \lambda \\ \Pi_{13}'' = \mu \end{cases} \tag{7}$$

In the same way, $\Pi_1'' \sim \Pi_5''$ belong to the dependent variable characteristics, and the geological and mineral characteristics are $\Pi_6'' \sim \Pi_{13}''$.

2.2.3. Comprehensive Selection of Geological and Mineral Features. According to formulae (3) and (7), the following analysis and processing can be made:

① Because of the similarity of y, z, w, u, $\Pi_1 = \Pi_1'', \Pi_1 = \Pi_2'', \Pi_1 = \Pi_3'', \Pi_1 = \Pi_4'', \Pi_1 = \Pi_5''$.

② Since $\Pi_6'' \times \Pi'' = \Pi_7' \times \cos\alpha$, which corresponds to the coal seam depth ratio, $\Pi_{10} = \Pi_7''$.

③ Due to the influence of loose layers, $\Pi_6 = h/(H-h)$.

④ Due to the influence of the working surface dimensions, $\Pi_7 = L_3/H, \Pi_8 = L_1/H$.

⑤ Due to the effects of modulus of elasticity, inclination angle, lateral stress coefficient, and Poisson's ratio, let $\Pi_9 = E/E_{mi\,d}, \Pi_{11} = \alpha, \Pi_{12} = \lambda, \Pi_{13} = \mu$.

Similar criteria are selected from this:

$$\begin{cases} \Pi_1 = \dfrac{y}{H} \\ \Pi_2 = \dfrac{z}{H} \\ \Pi_3 = \dfrac{w}{m\cos\alpha} \\ \Pi_4 = \dfrac{u}{m\cos\alpha} \\ \Pi_5 = \dfrac{H\varepsilon_y}{m\cos\alpha} \\ \Pi_6 = \dfrac{h}{H-h} \\ \Pi_7 = \dfrac{L_3}{H} \\ \Pi_8 = \dfrac{L_1}{H} \\ \Pi_9 = \dfrac{E}{E_{mi\,d}} \\ \Pi_{10} = \dfrac{\rho g H^2}{E_{mi\,d} m\cos\alpha} \\ \Pi_{11} = \alpha \\ \Pi_{12} = \lambda \\ \Pi_{13} = \mu \end{cases} \tag{8}$$

In the same way, $\Pi_1 \sim \Pi_5$ belong to the characteristics of the dependent variable, and the geological and mineral characteristics are $\Pi_6 \sim \Pi_{13}$.

2.3. Characteristic Expressions of Expected Parameters. Based on the observation data, the multiple correlation coefficient method is used to analyze the primary and secondary characteristics of geology and minerals, and the expression can be obtained as [14]

$$f\left(\frac{y}{H}, \frac{z}{H}, \frac{w}{m\cos\alpha}, \frac{u}{m\cos\alpha}, \frac{H}{m\cos\alpha}\varepsilon_y, \frac{h}{H-h}, \frac{E}{E_{mi\,d}}, \frac{\rho g H^2}{E_{mi\,d} m\cos\alpha}, \alpha\right) = 0. \tag{9}$$

Therefore, the characteristic expressions of ground subsidence and horizontal movement are

$$\begin{cases} w = f_1\left(\dfrac{y}{H}, \dfrac{z}{H}, \dfrac{h}{H-h}, \dfrac{E}{E_{mi\,d}}, \dfrac{\rho g H^2}{E_{mi\,d} m \cos\alpha}, \alpha\right) \\ u = f_2\left(\dfrac{y}{H}, \dfrac{z}{H}, \dfrac{h}{H-h}, \dfrac{E}{E_{mi\,d}}, \dfrac{\rho g H^2}{E_{mi\,d} m \cos\alpha}, \alpha\right) \end{cases} \tag{10}$$

The characteristic expression of the sinking coefficient is

$$q = \frac{f_1\left((y/H), (z/H), (h/H-h), \left(E/E_{mi\,d}\right), \left(\rho g H^2/E_{mi\,d} m \cos\alpha\right), \alpha\right)}{m \cos\alpha}. \tag{11}$$

According to the boundary conditions of the mining area, $z = H$, and z has nothing to do with Y; then,

$$q = g_1\left(\frac{h}{H-h}, \frac{E}{E_{mi\,d}}, \frac{\rho g H^2}{E_{mi\,d} m \cos\alpha}, \alpha\right). \tag{12}$$

The characteristic expression of the horizontal movement coefficient is

$$b = g_2\left(\frac{h}{H-h}, \frac{E}{E_{mi\,d}}, \frac{\rho g H^2}{E_{mi\,d} m \cos\alpha}, \alpha\right). \tag{13}$$

The characteristic expression that mainly affects the angle tangent is

$$\tan\beta = g_3\left(\frac{h}{H-h}, \frac{E}{E_{mi\,d}}, \frac{\rho g H^2}{E_{mi\,d} m \cos\alpha}, \alpha\right). \tag{14}$$

The characteristic expression of the inflection point offset is

$$\frac{s}{H} = g_4\left(\frac{h}{H-h}, \frac{E}{E_{mi\,d}}, \frac{\rho g H^2}{E_{mi\,d} m \cos\alpha}, \alpha\right). \tag{15}$$

3. Fuzzy Clustering of Observation Data

3.1. Preprocessing Rock Movement Observation Data. Observation data are used as a classification sample, and clustering features are set as $h/(H-h)$, E/E_{mid}, $\rho g H^2/E_{mi\,d} m \cos\alpha$, and α, and feature matrix $X_{n\times 4}$ is established.

3.1.1. Calculation of the Average and Standard Deviations of Each Feature.

$$\begin{aligned} \overline{x}_j &= \frac{1}{n}\sum_{i=1}^{n} x_{ij}, \\ s_j &= \sqrt{\frac{1}{n}\sum_{i=1}^{n}\left(x_{ij} - \overline{x}_j\right)} \quad (j = 1, 2, 3, 4). \end{aligned} \tag{16}$$

3.1.2. Calculation of the Standardized Value of the Feature.

$$y_{ij} = \frac{x_{ij} - \overline{x}_j}{s_j} \quad (i = 1, 2, \ldots n;\ j = 1, 2, 3, 4). \tag{17}$$

3.1.3. Calculation of the Normalized Value of the Feature.

$$z_{ij} = \frac{y_{ij} - y_{\min}}{y_{\max} - y_{\min}} \quad (i = 1, 2, \ldots, n;\ j = 1, 2, 3, 4). \tag{18}$$

3.2. Fuzzy Clustering. Aiming at the problem that the point density search method may have outliers and inability to initial clustering, the density of the cluster centers is restricted to more than half of the average density, and the clustering validity function is used to determine the optimal number of clusters [15].

$$V_{CS}(C) = \frac{(1/n)\sum_{i=1}^{c}\sum_{j=1}^{n} u_{ij}^{m}\left\|x_j - v_i\right\|^2}{(2/c(c-1))\sum_{i,t=1;i\neq t}^{c}\left\|v_i - v_t\right\|^2}. \tag{19}$$

Due to multiple re-initial clustering, multiple cluster centers with large differences appear. In order to solve this problem, here the sample set is determined first, and then the sample set is arithmetically averaged, so that a more reasonable clustering center can be obtained.

$$V'_{\text{new}} = \frac{n_i V_i + n_j V_j}{n_i + n_j} = \frac{1}{n_i + n_j}\sum_{k=1}^{n_i} x_k + \frac{1}{n_i + n_j}\sum_{k=1}^{n_j} y_k. \tag{20}$$

The basic process of fuzzy clustering of the IWFCM_CCS algorithm based on competitive merger strategy is shown in Figure 2 [16–24].

It is calculated that $C = 4$, which is the optimal value, and the cluster center is

$$Vmat = \begin{bmatrix} 0.03049 & 0.39375 & 0.04195 & 0.23447 \\ 0.02354 & 0.45012 & 0.03571 & 0.08975 \\ 0.09503 & 0.23975 & 0.04427 & 0.09524 \\ 0.02247 & 0.43920 & 0.04074 & 0.46751 \end{bmatrix}. \quad (21)$$

Analyze the membership degree matrix and suppose that the i^{th} station belongs to categories 1, 2, 3, and 4 as $U_1(i)$, $U_2(i)$, $U_3(i)$, and $U_4(i)$; then, $U_1(i), U_2(i), U_3(i), U_4(i)$ are weights for linear regression calculation. In order to determine the relationship between the dependent variable Π_5 and the independent variables Π_1, Π_2, Π_3, and Π_4, a corresponding weighted linear regression model can be established:

$$Q_j = \sum_{i=1}^{n} \left(U_j(i) \left(a + b\Pi_1(i) + c\Pi_2(i) + d\Pi_3(i) + e\Pi_4(i) + f\Pi_5(i) \right)^2 \right) j = 1, 2, 3, 4. \quad (22)$$

Through regression analysis, a linear model of expected parameters is obtained:

$$\begin{cases} q = 0.88575 + 0.03425\dfrac{h}{H_0 - h} - 0.10526\dfrac{E}{E_{\text{mid}}} - 3.60475 \times 10^{-5}\dfrac{\rho g H_0^2}{E_{\text{mid}} m \cos\alpha} - 2.75187 \times 10^{-3}\alpha \\ b = 0.24819 - 0.00316\dfrac{h}{H_0 - h} - 0.00727\dfrac{E}{E_{\text{mid}}} + 1.0402 \times 10^{-5}\dfrac{\rho g H_0^2}{E_{\text{mid}} m \cos\alpha} + 2.6088 \times 10^{-3}\alpha \\ \tan\beta_0 = 1.72130 + 0.01821\dfrac{h}{H_0 - h} + 0.19523\dfrac{E}{E_{\text{mid}}} - 1.30872 \times 10^{-5}\dfrac{\rho g H_0^2}{E_{\text{mid}} m \cos\alpha} + 2.93701 \times 10^{-3}\alpha \\ \tan\beta_1 = 1.86926 - 0.02731\dfrac{h}{H_1 - h} - 0.05642\dfrac{E}{E_{\text{mid}}} - 1.07727 \times 10^{-5}\dfrac{\rho g H_1^2}{E_{\text{mid}} m \cos\alpha} + 4.38102 \times 10^{-4}\alpha \\ \tan\beta_2 = 1.94122 - 0.18620\dfrac{h}{H_2 - h} + 0.16602\dfrac{E}{E_{\text{mid}}} - 3.05790 \times 10^{-5}\dfrac{\rho g H_2^2}{E_{\text{mid}} m \cos\alpha} + 5.03640 \times 10^{-3}\alpha \\ \dfrac{s_0}{H_0} = 0.14202 - 0.03801\dfrac{h}{H_0 - h} - 0.01558\dfrac{E}{E_{\text{mid}}} - 4.10583 \times 10^{-5}\dfrac{\rho g H_0^2}{E_{\text{mid}} m \cos\alpha} - 1.15100 \times 10^{-4}\alpha \\ \dfrac{s_1}{H_1} = 0.04025 - 0.00281\dfrac{h}{H_1 - h} + 0.01443\dfrac{E}{E_{\text{mid}}} - 1.67628 \times 10^{-5}\dfrac{\rho g H_1^2}{E_{\text{mid}} m \cos\alpha} + 2.54414 \times 10^{-3}\alpha \\ \dfrac{s_2}{H_2} = 0.07102 - 0.02515\dfrac{h}{H_2 - h} + 0.00402\dfrac{E}{E_{\text{mid}}} - 1.32990 \times 10^{-6}\dfrac{\rho g H_2^2}{E_{\text{mid}} m \cos\alpha} - 8.32504 \times 10^{-5} \end{cases} \quad (23)$$

4. Project Example Verification

Due to the influence of factors such as the distribution of structures (buildings), it is prone to problems such as missing data in the observation station, which seriously affects the accuracy of mining subsidence prediction. Therefore, taking the observation station data of a mining area in northwestern Liaoning for the same period as an example, the actual predicted parameters and the predicted parameter values are compared to calculate the error between them. Average error and maximum error of predicted parameters are shown in Table 1.

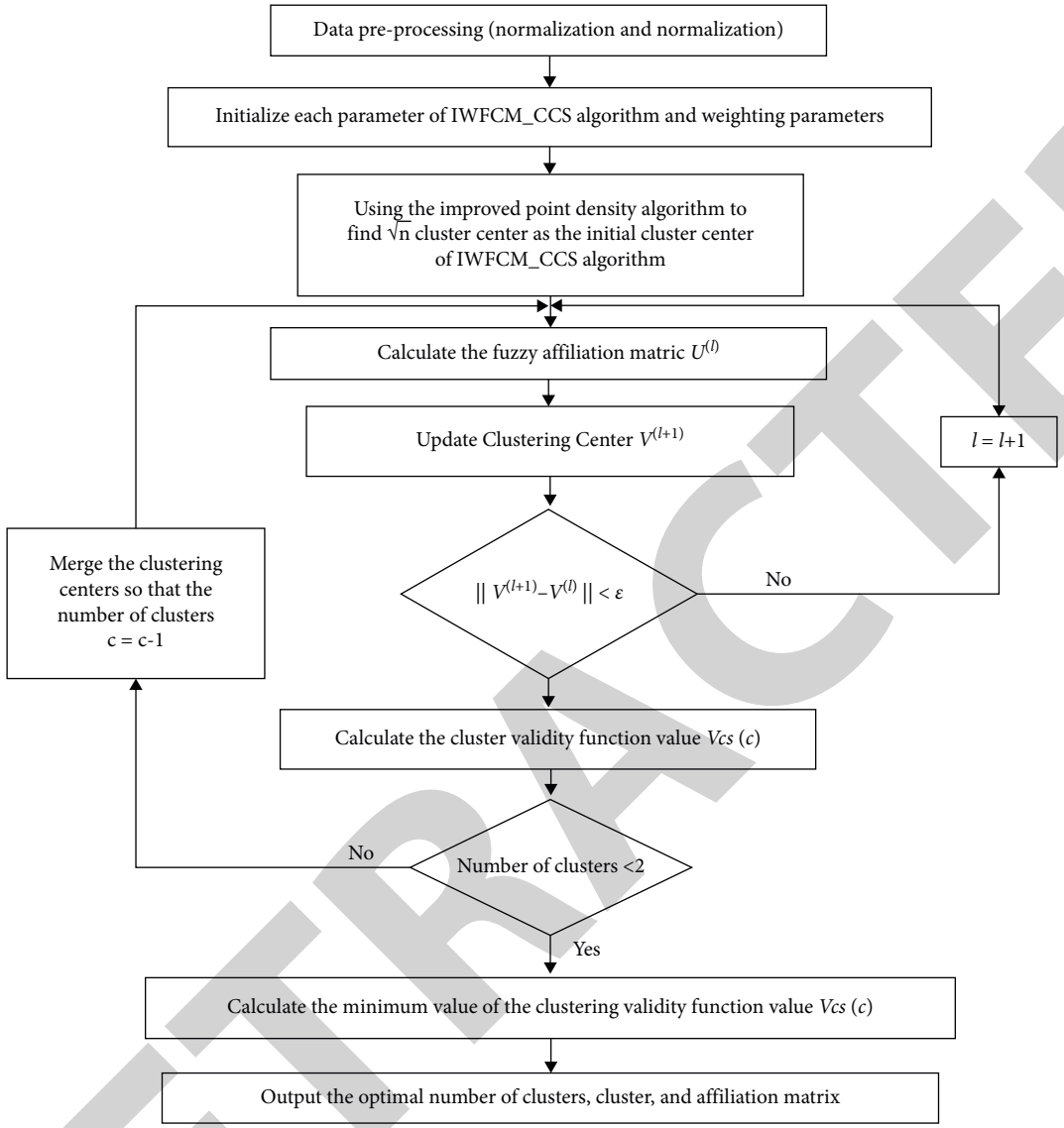

Figure 2: The flow of the IWFCM_CCS algorithm based on competitive merger strategy.

The following can be seen from Table 1. ① The average error of the measured parameters and the predicted parameters is roughly equivalent to the tolerance, which meets the engineering accuracy requirements. ② The maximum error of the measured parameters and the predicted parameters is within the tolerance requirements, which shows that the error range of the predicted parameters is comparatively stable. Relative error probability distribution of expected parameters is shown in Figure 3. Error probability distribution of predicted parameters is shown in Figure 4.

It can be seen from Figure 3 that ①the number of stations with the relative error of the subsidence coefficient q less than 5% accounts for 72.64% of the total number of stations, the number of stations with a relative error less than 10% accounts for about 88.72% of the total number of stations, and the number of stations with a relative error less than 15% accounts for about 99.10% of the total number of stations. ② The percentage of the number of stations with relative errors of the main influence angle tangents tan β_0, and tan β_1, tan $\beta_2$less than 5% in the total number of stations is 70.42%, 68.20%, and 75.35%, respectively. The percentage of stations less than 10% to the total number of stations is 78.38%, 81.73%, and 83.68%, respectively. The percentages of stations less than 15% to the total number of stations were 97.87%, 98.53% and 99.29%, respectively.

The following can be seen from Figure 4. ① The number of stations with an error of less than 2% of the horizontal movement coefficient b accounts for about 62.10% of the total number of stations. The number of stations with an error less than 3% accounts for about 76.58% of the total number of stations. The number of stations with an error of less than 5% accounts for about 97.51% of the total number of stations. ② The percentage of the number of stations whose inflection point offset distances s_0/H_0, s_1/H_1, and $s_2/H_2$is less than 2% accounts for 54.74%, 45.12%, and

Table 1: Average error and maximum error of predicted parameters.

Parameters	q	b	$\tan\beta_0$	$\tan\beta_1$	$\tan\beta_2$	s_0/H_0	s_1/H_1	s_2/H_2
Average error	0.093	0.062	0.021	0.103	0.110	0.048	0.047	0.049
Maximum error	0.13	0.091	0.04	0.17	0.140	0.061	0.054	0.067

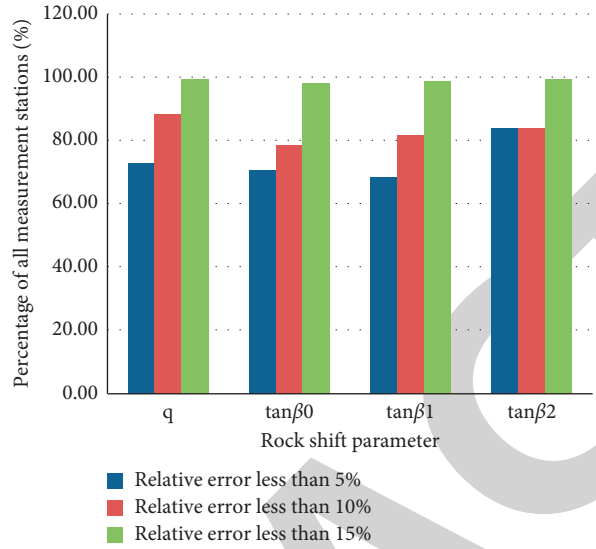

Figure 3: Relative error probability distribution of expected parameters.

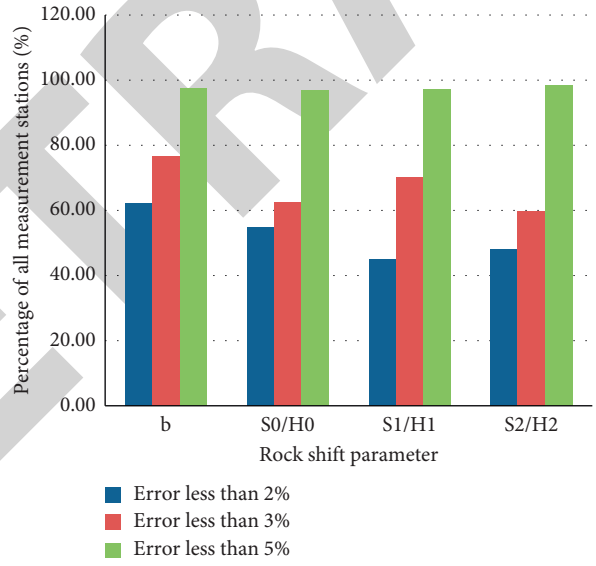

Figure 4: Error probability distribution of predicted parameters.

47.98% of the total number of stations, respectively. The percentage of the number of stations with an error less than 3% to the total number of stations is 62.35%, 70.21%, and 59.67%, respectively. The percentage of the number of stations with an error less than 5% to the total number of stations is 96.98%, 97.10%, and 98.43%, respectively.

In summary, the subsidence coefficient, main influence angle tangent, horizontal movement coefficient, and inflection point offset calculated by this model meet the engineering accuracy requirements.

5. Conclusion

(1) According to the similar third theorem, the geological and mineral characteristics are simplified, and the geological and mineral characteristics are comprehensively selected according to the actual situation, and the multiple correlation coefficient method is used to analyze the primary and secondary characteristics of the geological and mineral characteristics to obtain the characteristic expressions of

Hindawi
Journal of Mathematics
Volume 2023, Article ID 9893016, 1 page
https://doi.org/10.1155/2023/9893016

Retraction

Retracted: Design of Intelligent Recognition English Translation Model Based on Deep Learning

Journal of Mathematics

Received 19 December 2023; Accepted 19 December 2023; Published 20 December 2023

This article has been retracted by Hindawi following an investigation undertaken by the publisher [1]. This investigation has uncovered evidence of one or more of the following indicators of systematic manipulation of the publication process:

(1) Discrepancies in scope

(2) Discrepancies in the description of the research reported

(3) Discrepancies between the availability of data and the research described

(4) Inappropriate citations

(5) Incoherent, meaningless and/or irrelevant content included in the article

(6) Manipulated or compromised peer review

The presence of these indicators undermines our confidence in the integrity of the article's content and we cannot, therefore, vouch for its reliability. Please note that this notice is intended solely to alert readers that the content of this article is unreliable. We have not investigated whether authors were aware of or involved in the systematic manipulation of the publication process.

Wiley and Hindawi regrets that the usual quality checks did not identify these issues before publication and have since put additional measures in place to safeguard research integrity.

We wish to credit our own Research Integrity and Research Publishing teams and anonymous and named external researchers and research integrity experts for contributing to this investigation.

The corresponding author, as the representative of all authors, has been given the opportunity to register their agreement or disagreement to this retraction. We have kept a record of any response received.

References

[1] Y. Ruan, "Design of Intelligent Recognition English Translation Model Based on Deep Learning," *Journal of Mathematics*, vol. 2022, Article ID 5029770, 10 pages, 2022.

Hindawi
Journal of Mathematics
Volume 2022, Article ID 5029770, 10 pages
https://doi.org/10.1155/2022/5029770

Research Article

Design of Intelligent Recognition English Translation Model Based on Deep Learning

Yuexiang Ruan

School of Foreign Studies, Shandong University of Finance and Economics, Jinan 250014, China

Correspondence should be addressed to Yuexiang Ruan; 20053270@sdufe.edu.cn

Received 14 December 2021; Revised 14 January 2022; Accepted 17 January 2022; Published 18 February 2022

Academic Editor: Naeem Jan

Nowadays, the intercommunication and translation of global languages has become an indispensable condition for friendly communication among human beings around the world. The advancement of computer technology developed the machine translation from academic research to industrial applications. Additionally, a new and popular branch of machine learning is deep learning which has achieved excellent results in research fields such as natural language processing. This paper improved the performance of machine translation based on deep learning network and studied the intelligent recognition of English-Chinese machine translation models. This research mainly focused on solving out-of-vocabulary (OOV) problem of machine translation on unregistered words and rare words. Moreover, it combined stemming technology and data compression algorithm Byte Pair Encoding (BPE) and proposed a different subword-based word sequence segmentation method. Using this method, the English text is segmented into word sequences composed of subword units, and, at the same time, the Chinese text is segmented into character sequences composed of Chinese characters using unigram. Secondly, the current research also prevented the decoder from experiencing incomplete translation. Furthermore, it adopted a deep-attention mechanism that can improve the decoder's ability to obtain context information. Inspired by the traditional attention calculation process, this work uses a two-layer calculation structure in the improved attention to focus on the connection between the context vectors at different moments of the decoder. Based on the neural machine translation model Google Neural Machine Translation (GNMT), this paper conducted experimental analysis on the above improved methods on three different scale datasets. Experimental results verified that the improved method can solve OOV problem and improve accuracy of model translation.

1. Introduction

Language is the most important bridge in communication. With rapid development for modern society and the gradual construction of global integration, the intercommunication and translation of global languages has become an indispensable condition for friendly communication among human beings all over the world. With the development of the global economy, Chinese and English have become the two most influential languages. English-Chinese translation is a shortcut to cross-language communication and plays an important role in the process of global integration. Since the development of translation business, the word-by-sent translation by human translators has long been unable to adapt to this information explosion and fast-moving society. How to transfer information more efficiently, accurately, and conveniently between various English and Chinese has become the focus of research on English-Chinese language translation. Machine translation is a kind of applied technology research in natural language processing (NLP), and it is one of the important branches. At the same time, as a benchmark subject in NLP, research on machine translation is also leading research as well as development of other branches of natural language processing [1–5].

Machine translation studies use machines to achieve automatic conversion for different languages. It highly integrates the knowledge achievements of other disciplines such as mathematics, computer science, and linguistics and is one of the most challenging subjects in NLP. In 1954, IBM cooperated with Georgetown University in the United States to use IBM-701 to complete the English-Russian translation experiment and translate 60 Russian sentences into English.

The research of machine translation also officially began at this time. After that, the upsurge of machine translation has swept the world, and countries have launched fierce competition in machine translation. However, machine translation has suddenly encountered obstacles on the road of vigorous development. In 1966, the United States' Automatic Language Processing Advisory Committee issued a report. The report almost completely negated the prospect and value of machine translation. The report caused a serious blow to machine translation. The investment in various machine translation projects dropped sharply until it almost disappeared, and machine translation fell into a trough. Until the mid to late 1970s, with development of computer as well as the needs of economic society, machine translation ushered in recovery and prosperity. Then, after decades of development, two major categories of rule-based machine translation and statistical machine translation are formed.

Since 1990s, statistical machine translation has gradually become the mainstream. Statistical machine translation includes rule-based statistical machine translation and phrase-based statistical machine translation. Statistical machine translation enables natural language to realize automatic conversion from one language to another through the establishment of a probability model. The established probability model is trained in a large-scale parallel corpus and the model parameters are debugged. Because of this, statistical machine translation has the advantages of low labor cost, short development cycle, and better performance, which improves translation efficiency and saves translation costs. The translation platforms of well-known international companies such as Google, Baidu, and Sogou all use statistical machine translation as their core technology. But, at the same time, statistical machine translation still has many unsolvable shortcomings, such as linear inseparability, data sparseness, and inaccurate semantic representation [6–10].

The rise of deep learning has opened up a new path for the research of machine translation. Researchers have found that some techniques in deep learning can alleviate a series of problems in statistical machine translation very well. The application of deep learning technology in machine translation can be divided into two types. The first is that the main framework of the translation model is still the statistical machine translation model, but deep learning techniques will be used to improve the key modules and deficiencies in the statistical machine translation model. The second is a machine translation model based entirely on end-to-end deep neural networks proposed in 2013. This model can directly realize the automatic conversion of source language to target language. This method only relies on neural networks to handle translation problems, and a machine translation model with deep neural networks was born. At the same time, some scholars have carried out special comparison work on the effect of neural machine translation and statistical machine translation. The neural machine translation model has been verified on multiple translation tasks, and its translation performance is much higher than that of the phrase-based statistical machine translation model [11–15]. In the following paper, Section 2 presents a comprehensive discussion on the related works and reviews the literature. In Section 3, we discuss different methods and models for the machine translation processes. In Section 4, the comparative analysis is carried out through experimental discussions. In Section 5, we present the conclusion of our study.

2. Related Work

With the substantial increase in computer computing power, it is coupled with the expansion of data resources available on the network. As a result of the rapid development of deep learning, the field of machine translation has also undergone tremendous changes. The application of neural networks in machine translation was initially used as an auxiliary part of statistical machine translation. In terms of word alignment, literature [16] extends the hidden Markov word alignment model and uses a feedforward neural network to adjust each subcomponent. In the selection of translation rules, literature [17] uses an autoencoder to learn topic representation in the parallel corpus. By associating translation rule with information, the subject-related rules are selected based on distributed similarity with source language. In terms of sentence reordering, literature [18] uses semisupervised RAE to learn phrase representations. In terms of language models, literature [19] uses FNN to learn n-gram language models in continuous space.

With the aid of neural networks, statistical machine translation achieved the best translation results at the time. However, statistical machine translation also has shortcomings, such as data sparseness. With the increase of translation model subcomponents, training difficulties are caused. This has prompted people to explore the use of neural networks alone to achieve machine translation. Literature [20] proposed the first end-to-end encoder-decoder model structure. This model uses CNN as encoder and RNN as decoder, marking the beginning of neural machine translation. Due to the disappearance or explosion of gradients in the learning process of RNN, it is difficult to model the dependencies between the states in a long-time interval. To solve this problem, literature [21] proposed the RNN encoder-decoder model with new hidden layer nodes, and literature [22] proposed the Seq2Seq learning method, introducing LSTM into the encoder-decoder model.

Literature [23] applies the attention mechanism to the field of machine translation, and its basic idea is that the words in target language sentence are only related to some words in source language sentence. They proposed an encoder-decoder structure that combines attention, and since then machine translation has opened a new chapter. Literature [24] proposes two attention mechanisms, local and global, in NMT. Literature [25] published a translation system GNMT that combines attention mechanism and builds encoder-decoder model with LSTM. Literature [26] published a ConvS2S translation model with a translation effect comparable to RNN-based NMT but with extremely fast training speed using CNN structure. Although the model achieved the best translation results at the time, the limelight was quickly replaced by the Transformer model proposed in the literature [27]. The Transformer model is

completely based on attention, and the main components are the multihead self-attention mechanism layer as well as position-by-position feedforward neural network layer. The proposal of Transformer pushes machine translation to a new level. Not only is the translation effect good, but also the model training time is shortened. Literature [28] uses the derived bilingual dictionary to initialize the translation model to achieve unsupervised machine translation. At the same time, the authors of the literature summarized the three principles of unsupervised machine translation and applied the principles to phrase-based statistical machine translation as well as neural machine translation to achieve best unsupervised machine translation results at the time.

3. Method

Neural machine translation model has been a hotspot in machine translation research in recent years, and its potential academic research value and commercial value are huge. With the in-depth research on NMT-related technologies, several versions of neural machine translation systems have been implemented at home and abroad. Based on the GNMT developed by Google, this chapter introduces the Seq2Seq model based on the three optimization technologies Bi-LSTM, residual network, and attention adopted by GNMT. On this basis, two improvement schemes are proposed to alleviate the OOV problem of NMT and the problem of incomplete translation.

3.1. Neural Machine Translation Model Based on GNMT. The most mainstream model currently used in neural machine translation is the RNN-based Seq2Seq. The Seq2Seq model solves the common long-distance dependency problem of word sequences by introducing a special neuron LSTM. The GNMT system released by Google in 2016 also adopted this mainstream model structure and used relevant optimization techniques to optimize the model very effectively.

3.1.1. Seq2Seq Model Based on Bi-LSTM. The mainstream Seq2Seq model is based on the encoder-decoder structure of one-way RNN. In the figure, the encoder receives the embedded word vector of the source language input word sequence at the bottom layer and propagates the context of the source language input word sequence to the next hidden layer through the LSTM. The decoder initializes with the output state of the last hidden layer LSTM of the encoder and starts to predict the output of the target language according to the indication mark at the input of the decoder. Finally, the projection layer of the decoder is calculated by Beam Search, and the word sequence with the largest posterior probability is selected as the predicted translation sequence.

Generally, the embedded word vector input by the encoder carries the relevant information about the context in its forward sequence and backward sequence, but a one-way RNN can only transmit information in a certain direction. By using bidirectional RNN on the said basis, a Seq2Seq model is proposed. Figure 1 is a schematic diagram of the encoder structure constructed by the GNMT model.

In fact, the Seq2Seq model constructed by GNMT consists of an 8-layer LSTM encoder and an 8-layer LSTM decoder. The lowest layer of the encoder uses a bidirectional LSTM network. The forward network layer of the encoder processes the following information of the input word sequence from left to right, and the backward network layer processes the input word sequence from right to left and then connects the output vector sum of the two networks as a vector.

3.1.2. Seq2Seq Model Incorporating Residual Network. GNMT uses a 7-layer unidirectional LSTM and a bidirectional Bi-LSTM in an 8-layer encoder. However, simply stacking multilevel LSTM networks does not necessarily improve the translation accuracy of the model. Experience has found that when the number of stacked layers exceeds 6, the neural network will become difficult to train and its performance will drop rapidly. This is most likely caused by gradient explosion or gradient disappearance. To remove the restriction on the number of network layers of the deep RNN, GNMT has introduced residual connections in both encoder and decoder based on the original Bi-LSTM Seq2Seq model.

Suppose that we use L_i and L_{i+1} to represent the i-th and i+1-th layers of the stacked LSTM network, respectively, and their corresponding weight parameters are represented by a^i and a^{i+1}, respectively. Then the iterative calculation process of the i-th layer and i+1-th layer of the LSTM without residual connection at the current time k is

$$\begin{aligned} c_k^i,\, h_k^i &= L_i\left(c_{k-1}^i,\, h_{k-1}^i, x_k^{i-1}; a^i\right), \\ x_k^i &= h_k^i \\ c_k^{i+1},\, h_k^{i+1} &= L_{i+1}\left(c_{k-1}^{i+1},\, h_{k-1}^{i+1}, x_k^i; a^{i+1}\right). \end{aligned} \tag{1}$$

In the above equation, c_k^i and h_k^i, respectively, represent the internal state and hidden layer state of the i-th layer of LSTM neurons at the current time t. At this time, if a residual connection is added between the output of the i-1-th layer and the output of the i-th layer, the iterative calculation process of the entire neuron state is changed to

$$\begin{aligned} c_k^i,\, h_k^i &= L_i\left(c_{k-1}^i,\, h_{k-1}^i, x_k^{i-1}; a^i\right), \\ x_k^i &= h_k^i + x_k^{i-1}, \\ c_k^{i+1},\, h_k^{i+1} &= L_{i+1}\left(c_{k-1}^{i+1},\, h_{k-1}^{i+1}, x_k^i; a^{i+1}\right). \end{aligned} \tag{2}$$

It can be seen that, on the original basis, the output items of the low-level LSTM are added. The addition of the residual connection layer allows the reverse gradient of the neural network to easily propagate from the i-th layer to the i-1-th layer. This method significantly improves the flow ability of the gradient in the back-propagation. This effectively reduces the explosion and disappearance of gradients in deep neural networks, making it a reality to build deep neural network structures.

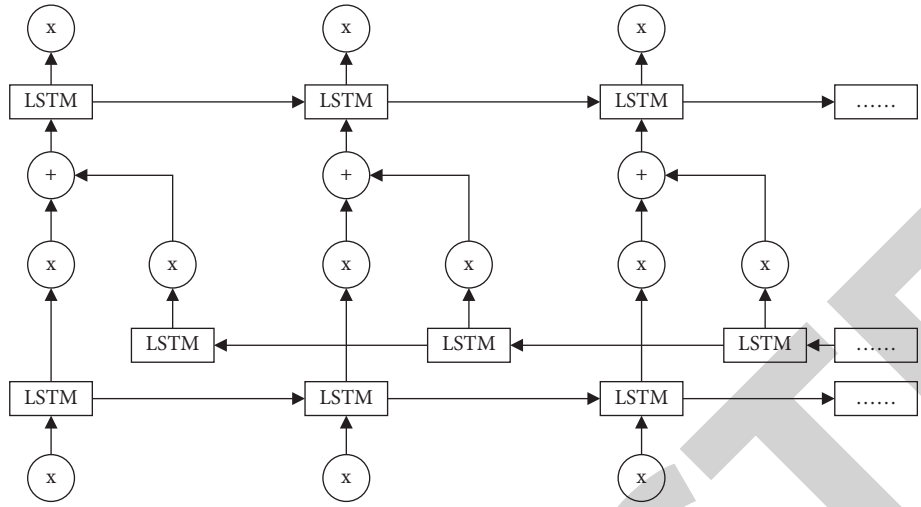

Figure 1: Seq2Seq model based on Bi-LSTM.

3.1.3. Seq2Seq Model Incorporating Attention Mechanism. Literature [36] proposed two different attention vector calculation methods, global attention and local attention. Global attention uses the output state of all hidden layers of the highest encoder layer to participate in the calculation. Local attention only selects the local state aligned with the current hidden layer of the decoder to participate in the calculation of the context vector, eliminating the defect of excessive calculation of global attention on long text.

To enable the decoder to be calculated in parallel on multiple LSTM layers as much as possible, GNMT has changed the method used by the above two to obtain the hidden state from the LSTM at the top of the decoder. Instead, it directly obtains the hidden state from the lowest layer of the decoder st 1 and adds it to the calculation of the attention vector. Figure 2 shows the complete Seq2Seq model structure of GNMT incorporating the attention mechanism. The entire attention calculation process is still the same as the original calculation process. The GNMT model uses a fully connected feedforward neural network with a single hidden layer as the calculation function of the attention vector.

3.2. Neural Machine Translation Model Based on Improved GNMT. Based on the GNMT model, this paper proposes two optimization schemes to improve the GNMT model from the perspective of solving the OOV (out-of-vocabulary) problem of NMT and the phenomenon of incomplete translation.

3.2.1. Improved Word Sequence Segmentation Method. English word segmentation usually uses spaces between words for segmentation, while Chinese uses characters as the basic unit. Therefore, the word segmentation method is relatively complicated. There are many Chinese word segmentation tools such as Jieba, THULAC, and HanLP that can help us achieve word segmentation. Although the word segmentation methods of the above two languages are different, their common point is that the segmentation of word sequences in the two languages is based on the word level.

The word-based sentence segmentation method is intuitive and easy to understand and conforms to the human cognitive model of language, but its drawback is that it will produce a large-scale vocabulary. Taking the dataset NLPCC2019 as an example, we segmented 4.79 million aligned Chinese and English sentence pairs. A total of 929,220 Chinese words and 815,978 English words were generated. However, due to the limitation of computing performance, the size of the vocabulary usually cannot be too large. The fixed-size vocabulary usually used is 30k~50k. If we limit the size of the Chinese and English vocabulary to 40k, then, in the Chinese and English vocabulary of the dataset NLPCC2019, the word frequency of the English vocabulary with the lowest frequency is 65, and the word frequency of the Chinese vocabulary is 111. Words below this frequency will be replaced with unregistered words UNK in the dataset, which affects the accuracy of the NMT translation model to a certain extent.

To alleviate the OOV problem caused by a fixed-scale vocabulary, the researchers proposed two types of solutions. We know that named entities such as English person names and place names are usually literally translated into Chinese text. Therefore, the first type of solution is to directly copy the unregistered words from the source language to the translation in the target language. Based on this idea, literature [29] proposed a solution to copy the text of rare words using the attention model. However, because the attention mechanism of deep neural networks is not stable and reliable, this method of simply copying the source language text to solve the OOV problem has certain limitations. The second type of solution is to decompose the word sequence of the sentence pair into a string sequence composed of morpheme subword units. For example, the document [30] proposed separating words into a sequence of characters with smaller structures. Literature [31] proposed HybridNMT combining word and character.

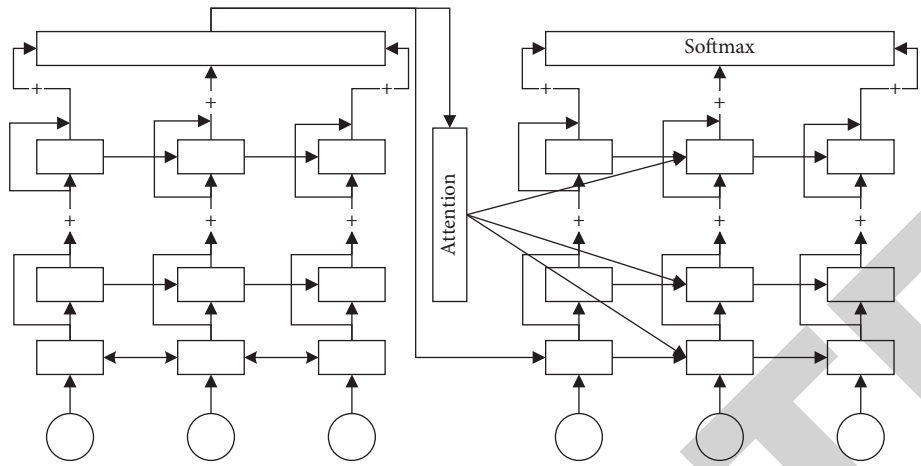

Figure 2: Seq2Seq model incorporating attention mechanism.

Literature [32] used the data compression algorithm BPE [33] to segment the original word into a string composed of morphemes and subwords. Although the character sequence based on character greatly reduces the time spent on data preprocessing, it also increases the length of the sequence, thus increasing the time and complexity of model training. Although HybridNMT based on a mixture of word and character can use more corpus, it cannot ensure the correctness of word separation. The subword segmentation based on the BPE compression algorithm balances the relationship between the size of the vocabulary and translation efficiency.

Based on subword, this paper proposes a word sequence segmentation method that combines stemming and BPE algorithm to solve the OOV problem that often occurs in open vocabularies.

(1) Stemming Technology. English belongs to the European language, and the same root of English words usually contains many variants, such as the singular and plural of nouns and the conjugation of verbs in different tenses. It can be seen that English contains a large number of inflections or compound words based on the same root. Stemming technology is the process of removing the affixes of inflection words or compound words to obtain the root of the word. The use of stemming technology can effectively reduce a part of the vocabulary without losing most of the semantics.

(2) Byte Pair Encoding and Stemming. Byte Pair Encoding (BPE) is a data compression algorithm. Its core idea is to replace the bytes pair with the highest frequency in the sequence with a new byte during each iteration. The one-iteration process of the BPE algorithm is described as follows. First, calculate the total frequency of adjacent cooccurring character pairs in the sequence in the vocabulary. Repeat the above statistics on all character sequences to obtain a set consisting of cooccurring character pairs and their total frequencies. Then select the character pair with the highest occurrence frequency in the set pairs, merge them, and finally update the corresponding character sequence in the vocabulary to complete an iteration process. To prevent the high-frequency words in the original vocabulary from being segmented into morpheme subwords, we can set a threshold to ensure that words with a frequency higher than the threshold are not segmented and save this part of the word in the vocabulary. Combining the stemming technology, to avoid the polysemy problem caused by the use of stemming, all words in the range of the high-frequency word shortlist will not be stemming. All other words that are not in the shortlist will be replaced with stems, and a new dataset will be generated after the replacement.

Based on the above explanation, this article adopts a different word sequence segmentation scheme from GNMT. For the processing of English word sequences, we adopted a new word sequence segmentation scheme combining stemming and BPE. For the Chinese word sequence, a word segmentation method based on the unigram model is used to directly segment the Chinese sentence into characters. This segmentation method can significantly reduce the vocabulary of the Chinese vocabulary.

3.2.2. Improved Attention Structure. Using the attention mechanism is a very effective method for NMT to process long sentence translation. The reason is that using the attention mechanism can improve the ability of the NMT decoder to obtain the context information of the encoder and assist the decoder in making output predictions. Since attention was proposed, many variants have been derived.

To solve the incomplete translation problem of GNMT and further improve the decoder's ability to obtain context information, this paper proposes a new and improved attention calculation method to assist the calculation of the GNMT speculation layer.

The NMT decoder has three input values involved in the calculation at the hidden layer output s_k at the current time k. They are the hidden layer output state s_{k-1} of the decoder at the previous moment, the predicted output y_{k-1} of the decoder at the previous moment, and the context vector c_k at the current moment t generated by the attention calculation.

We noticed that the decoder has a corresponding context vector c_k that carries important contextual information at each

time k, and there must be some connection between the context vectors at different times. Considering that the semantic structure of the source language and the target language may be very different, the word sequence of encoder and decoder may not have the same context structure. Therefore, the context vector with the highest correlation with the current moment c_k is not necessarily c_{k-1}. When focusing on the context vector at the current moment, we need to refer to all previous context vectors that are close to it at the same time to ensure that current c_k can obtain the most accurate context information. Based on this idea, we give an improved attention structure that uses a deeper attention calculation to increase the attention to context information.

Assuming that the original context vector corresponding to the decoder from time 0 to time k is $C = (c_1, c_2, \ldots, c_k)$, the context vector that has been improved and updated is $\hat{c} = (\hat{c_1}, \hat{c_2}, \ldots, \hat{c_k})$. We define the correlation between the current context vector c_k and the historical context vector c_h as follows:

$$d_h = G(c_k, c_h). \tag{3}$$

Function G is a function mapping that measures the correlation between vectors, and d_h is called the correlation coefficient of the vector. According to mathematical experience, function G can be defined as the angle cosine operation of a vector, the distance of a vector, or the cross entropy of a vector. Similar to the calculation process of the attention vector, the correlation coefficient d_h needs to be normalized to a real number in the range of 0~1.

$$\alpha_h = \frac{\exp(d)}{\sum_{i=1}^{k-1} \exp(d_i)}. \tag{4}$$

Vector $\alpha = (\alpha_1, \alpha_2, \ldots, \alpha_h)$ composed of t correlation coefficients is called the correlation vector of the context vector. Let $c_k' = \sum_{i=1}^{k-1} \alpha_i c_i$; then the calculation formula of the context vector $\hat{c_k}$ at the current moment of improving attention is

$$\hat{c_k} = c_k + \sum_{i=1}^{k-1} \alpha_i c_i. \tag{5}$$

It can be seen that the calculation of the improved context vector $\hat{c_k}$ comprehensively considers the context vector c_k at the current moment and the weighted and quantized historical context vector c_k'. Therefore, the hidden state of decoder at time t is calculated as

$$s_k = f(y_{k-1}, s_{k-1}, \hat{c_k}). \tag{6}$$

Since this article is based on GNMT's Seq2Seq model, it incorporates an improved deep attention.

4. Experiment and Discussion

In this section, we carried out the comparative analysis for the proposed methods and the existing ones. To this end, we performed different experiments and studied the experimental results carefully. As a result, it was verified that the proposed methods stand out as compared to the rest of the techniques.

4.1. Dataset. This paper uses two different scale datasets NLPCC2019 and OPUS to train, verify, and test the NMT model. The Chinese and English parallel corpora from three different sources are all downloaded from the Internet, and they are publicly available and free data materials. OPUS dataset is derived from the translation of Chinese and English movie subtitles, which contains 9,304778 aligned Chinese and English sentence pairs, with a total data size of 1.17 GB. After observation, it was found that the Chinese translation part contained garbled characters. Some Chinese translations are mixed with English original sentence information, which will interfere with translation. Some Chinese translations contain obvious translation errors. After data preprocessing and screening, we eliminated this part of the data, and a total of 7,256,783 pairs of sentences in Chinese and English were obtained. NLPCC2019 dataset provides 5.2 million aligned Chinese and English sentence pairs. The text corpus comes from various industries and the total data size is 1.1 GB. After sampling and analysis, a small number of sentence pairs in this dataset have translation errors. We screened the dataset on a large scale and selected 2,714,662 high-quality sentence pairs. According to statistics, in the filtered text corpus, the average length of Chinese sentences is 19 words, and the average length of English sentences is 37 words. There are few long sentences in the corpus, and we limit the maximum length of sentences to less than 100. Table 1 shows a simple comparison of the two datasets.

4.2. Experimental Environment. The experimental part of this article is carried out on the Ubuntu operating system, using the currently very popular deep learning framework PyTorch, combined with GPU for experimental model building and calculation. The details of the experimental environment are shown in Table 2. The evaluation metric is BLEU.

4.3. Evaluation on Network Training. In a deep learning network, one of the most important indicators is the convergence of the network. To evaluate whether the network designed in this paper can effectively converge on the dataset, this work analyzes the training loss and BLEU score. The results are shown in Figures 3 and 4.

It can be seen from the two figures that as the training progresses, the training loss gradually decreases, and the training BLEU gradually increases. On NLPCC2019 and OPUS, when the training epoch reaches 300, the loss value almost no longer decreases, and the BLEU almost no longer rises, which indicates that the deep learning network has reached a state of convergence. It also illustrates the reliability and effectiveness of the network designed in this project.

4.4. Comparison with Other Methods. To verify the validity and correctness of the method designed in this work, we compare the method in this paper with other English machine translation methods. The methods compared are

Table 1: Comparison of detailed information of two datasets.

Dataset	Language	Train (M)	Test (K)	Number
NLPCC2019	English Chinese	2.55	60	359482 601505
OPUS	English Chinese	7.25	105	234202 426127

Table 2: Experimental environment.

Item	Version
Operating system	Ubuntu 20.04
GPU	NVIDIA GeForce GTX 1080 Ti
PyTorch	PyTorch 1.7
Python	Python 3.7
Memory	8G

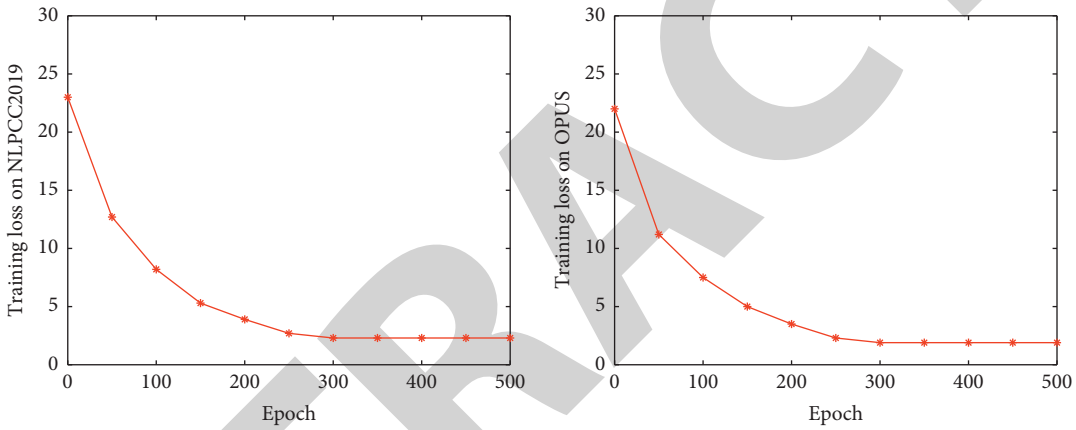

Figure 3: The training loss on two datasets.

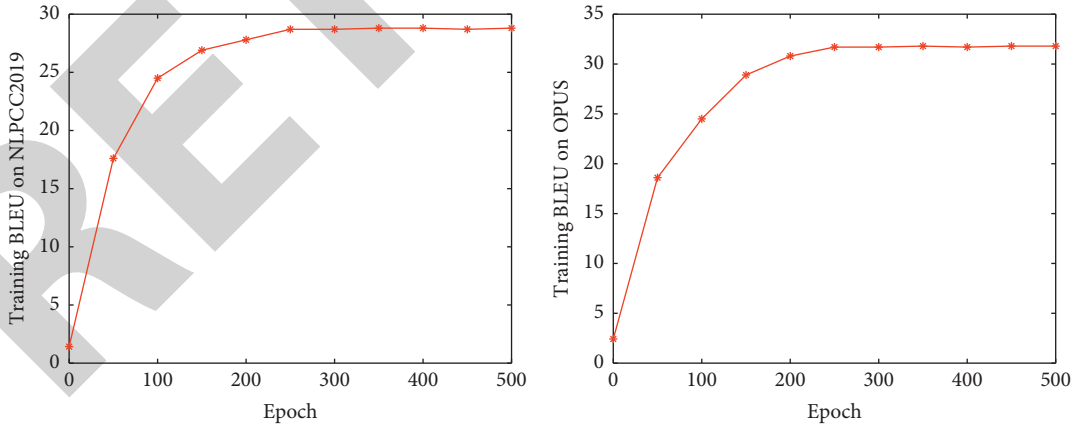

Figure 4: The training BLEU on two datasets.

RNN-Based, LSTM-Based, Seq2Seq-Based, and Attention-Based methods. The experimental results are shown in Table 3.

It can be seen that, compared with the other methods listed in the table, the improved GNMT (IGNMT) method designed in this article can obtain the best performance on the two datasets. In NLPCC2019 dataset, compared with the best performing method, IGNMT can achieve a 1.1% increase in BLEU. On OPUS, compared with the best performing method, IGNMT can achieve a 1.5% increase in BLEU. It can be proved that the method proposed in this paper can achieve advanced performance, and it also proves the effectiveness of the method proposed in this work.

Table 3: Comparison with other methods.

Method	NLPCC2019	OPUS
RNN-Based	12.7	13.4
LSTM-Based	14.4	14.9
Seq2Seq-Based	16.2	16.8
Attention-Based	17.4	18.2
IGNMT (Ours)	18.5	19.7

Figure 5: Evaluation on improved word sequence segmentation method.

4.5. Evaluation on Improved Word Sequence Segmentation Method. As mentioned early, this work proposes an improved word sequence segmentation method. To verify the effectiveness and correctness of this improvement measure, this work will compare and analyze the network performance when the traditional word segmentation method is used and the network performance when the improved word segmentation method is used. The experimental results on NLPCC2019 and OPUS are illustrated in Figure 5. TWSSM is the traditional word sequence segmentation method. IWSSM is the improved word sequence segmentation method.

Obviously, with the improvement of word segmentation methods, the performance of the network can be effectively improved. On NLPCC2019, using the improved word segmentation strategy can get a 1.3% increase in BLEU. On OPUS, using the improved word segmentation strategy can get a 1.5% increase in BLEU. This experiment can prove the validity and reliability of improved word sequence segmentation method proposed in this work.

4.6. Evaluation on Improved Attention Structure. As mentioned early, this work proposes an improved attention structure. To verify the effectiveness and correctness of this improvement measure, this work will compare and analyze the network performance when the traditional attention structure is used and the network performance when the improved attention structure is used. The experimental results on NLPCC2019 and OPUS are illustrated in Figure 6. TAS is the traditional attention structure. IAS is the improved attention structure.

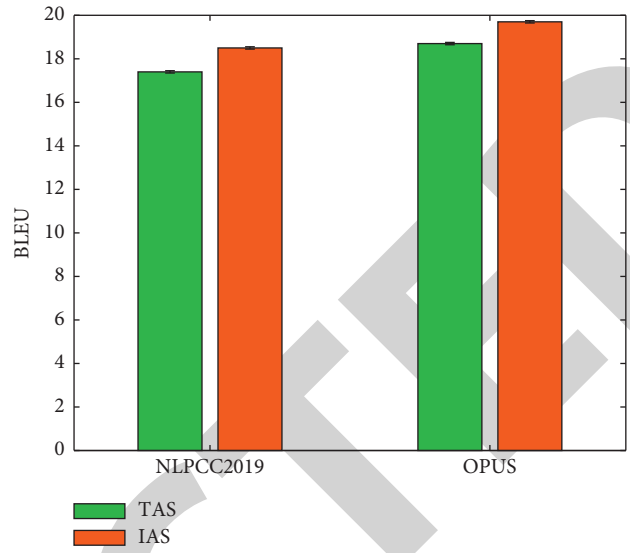

Figure 6: Evaluation on improved attention structure.

Obviously, with the improvement of attention structure, the performance of the network can be effectively improved. On NLPCC2019, using the improved attention structure strategy can get a 1.1% increase in BLEU. On OPUS, using the improved attention structure strategy can get a 1% increase in BLEU. This experiment can prove the validity and reliability of improved attention structure proposed in this work.

5. Conclusion

Since the introduction of deep learning-based neural machine translation, it has replaced traditional phrase-based statistical machine translation method and has become a research hotspot in English translation language processing. As GNMT has surpassed traditional statistical machine translation methods on multiple datasets several times, it has greatly encouraged researchers to study neural machine translation. Based on open-source GNMT, this research studied the application of neural machine translation in English intelligent recognition translation. In view of the current research status of neural machine translation, this work proposed two research contents in different directions. The first is to solve OOV problem of neural machine translation on unregistered words and rare words; this study combined common stemming techniques in English text preprocessing with BPE and proposed a different and improved word sequence segmentation method. Using this method, English text can be segmented into word sequences composed of subword units, and Chinese text can be segmented into character sequences composed of Chinese characters. Secondly, for the prevention of the decoder from experiencing incomplete translation, we adopted an improved attention mechanism that can improve the decoder's

ability to obtain contextual information. In the improved attention mechanism, a two-layered calculation structure was used to focus on the connection between the context vectors at different moments of the decoder and to improve the ability of attention mechanism to obtain the global context information of the encoder.

Data Availability

The datasets used during the current study are available from the corresponding author upon reasonable request.

Conflicts of Interest

The author declares that he has no conflicts of interest.

Acknowledgments

This work was supported by the Research Project of Social Science Planning in Shandong Province, a study on the translation strategies of the International Image and publicity of the major cities in Belt and Road Shandong Province, 20CWZJ25.

References

[1] A Fan, S Bhosale, and H Schwenk, "Beyond English-centric multilingual machine translation," *Journal of Machine Learning Research*, vol. 22, no. 107, pp. 1–48, 2021.

[2] Y. Liu, J. Gu, N. Goyal et al., "Multilingual denoising pre-training for neural machine translation," *Transactions of the Association for Computational Linguistics*, vol. 8, pp. 726–742, 2020.

[3] M Popel, M Tomkova, and J Tomek, "Transforming machine translation: a deep learning system reaches news translation quality comparable to human professionals," *Nature Communications*, vol. 11, no. 1, pp. 1–15, 2020.

[4] M Ghazvininejad, V Karpukhin, and L Zettlemoyer, "Aligned cross entropy for non-autoregressive machine translation," in *Proceedings of the International Conference on Machine Learning*, pp. 3515–3523, Atlanta, GA, USA, July 2020.

[5] L. N Vieira, M O'Hagan, and C O'Sullivan, "Understanding the societal impacts of machine translation: a critical review of the literature on medical and legal use cases," *Information, Communication & Society*, vol. 24, no. 11, pp. 1515–1532, 2021.

[6] S. N Khan and I Usman, "A model for English to Urdu and Hindi machine translation system using translation rules and artificial neural network," *The International Arab Journal of Information Technology*, vol. 16, no. 1, pp. 125–131, 2019.

[7] D. Deng and N. Xue, "Translation divergences in Chinese-English machine translation: an empirical investigation," *Computational Linguistics*, vol. 43, no. 3, pp. 521–565, 2017.

[8] J. Srivastava, S. Sanyal, and A. K. Srivastava, "Extraction of reordering rules for statistical machine translation," *Journal of Intelligent and Fuzzy Systems*, vol. 36, no. 5, pp. 4809–4819, 2019.

[9] J. Pei, K. Zhong, and J. Li, "ECNN: evaluating a cluster-neural network model for city innovation capability," *Neural Computing & Applications*, pp. 1–13, 2021.

[10] C. D. Mellinger, "Translators and machine translation: knowledge and skills gaps in translator pedagogy," *The Interpreter and Translator Trainer*, vol. 11, no. 4, pp. 280–293, 2017.

[11] T. Yang, S. Zhao, H. Chen, and B. Chen, "Machine translation system based on deep learning," *Journal of Physics: Conference Series*, vol. 2030, no. 1, Article ID 012098, 2021.

[12] H. Li and W. Xiong, "Analysis of the drawbacks of English-Chinese intelligent machine translation based on deep learning," *The 2021 International Conference on Machine Learning and Big Data Analytics for IoT Security and Privacy*, pp. 104–111, 2021.

[13] Y Tian, S Khanna, and A Pljonkin, "Research on machine translation of deep neural network learning model based on ontology," *Informatica*, vol. 45, no. 5, 2021.

[14] K. L. Kermanidis, "NoDeeLe: a novel deep learning schema for evaluating neural machine translation systems," *TRITON*, vol. 37, 2021.

[15] C. Park, Y. Yang, K. Park, and H. Lim, "Decoding strategies for improving low-resource machine translation," *Electronics*, vol. 9, no. 10, p. 1562, 2020.

[16] N Yang, S Liu, and M Li, "Word alignment modeling with context dependent deep neural network," in *Proceedings of the 51st Annual Meeting of the Association for Computational Linguistics*, pp. 166–175, Sofia, Bulgaria, August 2013.

[17] L Cui, D Zhang, and S Liu, "Learning topic representation for SMT with neural networks," in *Proceedings of the 52nd Annual Meeting of the Association for Computational Linguistics*, pp. 133–143, Maryland, MA, USA, June 2014.

[18] P Li, Y Liu, and M Sun, "A neural reordering model for phrase-based translation," in *Proceedings of the COLING 2014, The 25th International Conference on Computational Linguistics: Technical Papers*, pp. 1897–1907, Dublin, Ireland, August 2014.

[19] Y Bengio, R Ducharme, and P Vincent, "A neural probabilistic language model," *Journal of Machine Learning Research*, vol. 3, no. 2, pp. 1137–1155, 2003.

[20] N Kalchbrenner and P Blunsom, "Recurrent continuous translation models," in *Proceedings of the 2013 Conference on Empirical Methods in Natural Language Processing*, pp. 1700–1709, Washington, DC, USA, October 2013.

[21] K Cho, B van Merriënboer, and C Gulcehre, "Learning phrase representations using RNN encoder–decoder for statistical machine translation," in *Proceedings of the 2014 Conference on Empirical Methods in Natural Language Processing*, pp. 1724–1734, Doha, Qatar, October 2014.

[22] I Sutskever, O Vinyals, and Q. V Le, "Sequence to sequence learning with neural networks," *Advances in Neural Information Processing Systems*, pp. 3104–3112, 2014.

[23] D Bahdanau, K Cho, and Y Bengio, "Neural machine translation by jointly learning to align and translate," 2014, https://arxiv.org/abs/1409.0473.

[24] M. T Luong, H Pham, and C. D Manning, "Effective approaches to attention-based neural machine translation," in *Proceedings of the 2015 Conference on Empirical Methods in Natural Language Processing*, pp. 1412–1421, Lisbon, Portugal, September 2015.

[25] Y Wu, M Schuster, and Z Chen, "Google's neural machine translation system: bridging the gap between human and machine translation," 2016, https://arxiv.org/abs/1609.08144.

[26] J. Gehring, M. Auli, and D. Grangier, "Convolutional sequence to sequence learning," in *Proceedings of the 34th International Conference on Machine Learning*, pp. 1243–1252, Sydney, Australia, August 2017.

Hindawi
Journal of Mathematics
Volume 2024, Article ID 9829414, 1 page
https://doi.org/10.1155/2024/9829414

Retraction

Retracted: Detection Method of Limb Movement in Competitive Sports Training Based on Deep Learning

Journal of Mathematics

Received 23 January 2024; Accepted 23 January 2024; Published 24 January 2024

This article has been retracted by Hindawi following an investigation undertaken by the publisher [1]. This investigation has uncovered evidence of one or more of the following indicators of systematic manipulation of the publication process:

(1) Discrepancies in scope

(2) Discrepancies in the description of the research reported

(3) Discrepancies between the availability of data and the research described

(4) Inappropriate citations

(5) Incoherent, meaningless and/or irrelevant content included in the article

(6) Manipulated or compromised peer review

The presence of these indicators undermines our confidence in the integrity of the article's content and we cannot, therefore, vouch for its reliability. Please note that this notice is intended solely to alert readers that the content of this article is unreliable. We have not investigated whether authors were aware of or involved in the systematic manipulation of the publication process.

Wiley and Hindawi regrets that the usual quality checks did not identify these issues before publication and have since put additional measures in place to safeguard research integrity.

We wish to credit our own Research Integrity and Research Publishing teams and anonymous and named external researchers and research integrity experts for contributing to this investigation.

The corresponding author, as the representative of all authors, has been given the opportunity to register their agreement or disagreement to this retraction. We have kept a record of any response received.

References

[1] C. Qin and S. Huo, "Detection Method of Limb Movement in Competitive Sports Training Based on Deep Learning," *Journal of Mathematics*, vol. 2022, Article ID 8643234, 8 pages, 2022.

Hindawi
Journal of Mathematics
Volume 2022, Article ID 8643234, 8 pages
https://doi.org/10.1155/2022/8643234

Research Article

Detection Method of Limb Movement in Competitive Sports Training Based on Deep Learning

Chunlin Qin[1] **and Shenglu Huo**[2]

[1]*Department of Basic, Nantong Health College of Jiangsu Province, Nantong 226000, JiangSu, China*
[2]*School of Economic and Management, Shanghai University of Sport, Shanghai 200438, China*

Correspondence should be addressed to Shenglu Huo; 1630509021@stu.suda.edu.cn

Received 23 December 2021; Revised 9 January 2022; Accepted 15 January 2022; Published 18 February 2022

Academic Editor: Naeem Jan

Traditional methods have the problems of insufficient accuracy and slow speed in human posture detection. In order to solve the above problems, a limb movement detection method in competitive sports training based on deep learning is proposed. The force change parameters of sports limb movements in the process of sports are computed to achieve the detection of limb movements in competitive sports training, and the limb movement characteristics in competitive sports training are extracted using a deep learning algorithm. The experimental results show that the limb movement detection method based on deep learning in competitive sports training has significantly higher detection accuracy and faster speed.

1. Introduction

With the deepening of the research on artificial intelligence, the application direction of artificial intelligence technology has become more and more extensive. The detection of human posture is an important application direction [1]. It has a wide range of applications and rich application value in the fields of behavior detection, video capture, and computer graphics. An enhanced depth learning approach is presented based on the depth learning method, with the goal of increasing detection speed, reducing the number of parameters, and shrinking the model size to make practical application easier [2, 3]. The main modifications of the original model are as follows: speed and detection accuracy. The weight of the trained model is trimmed to compress the model and improve the detection speed. In addition, this paper also designs and tests a set of sit-ups based on the proposed improved open model. The hardware structure is simple, the human posture detection speed is fast, and the detection accuracy is high and has strong practicability.

2. Detection of Deep Learning of Limb Movements in Competitive Sports Training

2.1. Recognition of Limb Movement Characteristics in Competitive Sports Training. Human motion recognition is mainly composed of data acquisition and data analysis. Data acquisition is composed of multiple sensor nodes and data receiving equipment, which is used to complete the acquisition of human motion signal data. Data analysis is mainly composed of various analysis algorithms integrated in PC. The deep learning method is essentially a dual parallel convolution network model [4]. It uses two convolution networks at the same time. One convolution network locates the position of key parts of the human body from the image, and the other convolution network is used to connect candidate key parts to form limbs [5]. Then, the results of the two convolution networks are summarized for pose assembly to complete the detection of human pose in the image. Obviously, the construction of this dual parallel convolution network will greatly consume computing

resources [6]. Therefore, in the implementation, the deep learning method, first, uses a convolution network to preliminarily extract image features and then inputs the features into the dual parallel convolution network for subsequent processing, which is equivalent to merging the lower part of the dual parallel convolution network into a convolution network to save computing resources.

Figure 1 shows the detection process of the deep learning method, which is the visualization of the process. First, the VGG-19 network 9 is used to extract the bottom features of the input image, as shown in Figure 1, which is the output of some convolution layers [7]. The underlying characteristics are then fed into two concurrent convolution networks, one of which generates the confidence graph using the nonmaximum suppression procedure. Depth picture sequences have shown to be very valuable in the development of quick 3D human skeletal joint estimation. Many depth sensors with high sample rates and inexpensive prices have lately been launched, owing to the fast development of depth-sensing technology [8]. Table 1 gives some common depth sensor information. The depth image sequence with high resolution and high sampling rate provided by these sensors can provide accurate and sufficient information for 3D human skeleton joint estimation.

The behavior and motion capture platform is composed of an attitude and heading reference module and a computer. It can capture the motion of the human trunk, upper and lower arms, and large and small legs [9]. When the platform starts working, the attitude and heading reference module uploads the attitude data captured by human behavior at the frequency of 30 Hz through the wireless network, receives the data through the computer, and receives the data sent by the attitude and heading reference module by address query. In order to reduce the volume and electromagnetic wave interference, it is necessary to enhance the independence of the platform. The extended Kalman filter is used to collect the data in real time, conduct data fusion after denoising, capture the attitude angle, angular velocity, and acceleration, and then send the data to the upper computer through the wireless network module. The data are processed by the upper computer program and transformed into the signal form [10]. The Kalman filter is used to collect the original data, and the relative attitude angle is obtained through the conversion relationship between Euler angle and quaternion. The acceleration is collected and calculated the absolute attitude angle by using the direction cosine conversion of the magnetic field between the geographic coordinate system and the Kalman filter coordinate system, as shown in Figure 2.

It can be seen from Figure 2 that G represents the gravity direction, and the XYZ axis represents the coordinate system. When the attitude and heading reference module rotates around the x-axis and y-axis, the included angle between the two axes and the gravity direction g will produce a certain angle with the rotation. When the module rotates around the z-axis, the z-axis and the gravity direction G are collinear, and the included angle will not change, so it needs to be compensated by the magnetometer [11]. When using the magnetometer to calculate the z-axis attitude, the data are divergent and cannot be used for a long time. However, the accelerometer is vulnerable to vibration factors and has poor dynamic performance. Therefore, it is necessary to fuse the data generated by the accelerometer to obtain a stable and accurate attitude angle. The filter gain of the accelerometer is updated in real time according to the vibration intensity to ensure the dynamic response characteristics of the attitude and heading reference module and quickly eliminate the steady-state error [12]. The Euler angle is utilized to determine the tilt angle roll and pitch angle based on the three-axis acceleration processed by the Kalman filter, and the yaw angle is derived based on the tilt compensation magnetometer value. The acceleration value is read and treated it according to normal orthogonalization procedures. The Euler angle conversion matrix is used to determine the high-precision attitude angle based on the state vector [13]. Through the tilt angle, the action signal of human walking and running behavior can be captured, the pitching angle can capture the action signal of human static behavior, and the yaw angle can capture the action signal of human jumping and squatting behavior. According to the design requirements of the software function, combined with the actual chip function, the embedded software program is compiled. The software design includes the software design of data acquisition node and data receiving gateway. The working mode can be divided into working mode I (real-time USB data communication), working mode II (nonreal-time USB data communication), and working mode III (nonreal-time network port data communication). The program flow chart is shown in Figure 3.

After connecting the information collection device with the computer through the USB interface, open the corresponding serial port and set the baud rate to 115200. In order to solve the problem that the refresh rate of reading inertial sensor data does not match that of manikin animation, a thread for reading inertial sensor data and a thread for reading attitude data are created [14]. The thread of the reading inertial sensor reads the original data from the inertial sensor, which is composed of a three-axis accelerometer, three-axis magnetometer, and three-axis gyroscope, and then uses CRC16 to verify the data. After verification, the data fusion algorithm is used to fuse the data into attitude data and then read the attitude data. The thread reads the attitude data from the queue and uses the attitude data to drive the dimensional manikin.

2.2. Numerical Calculation of Force Changes of Limb Movements in Competitive Sports Training. The human skeleton joint data are obtained based on deep learning, and it is necessary to remove the original skeleton joint coordinate data of human motion from the Kinect V spatial coordinate system (a', b', c') which map to the human body spatial coordinate system $o(x, y, z)$. The human body coordinate system $o(x, y, z)$ takes the center of gravity of the human body, that is, the spine base node as the origin o, and the right in front of the human body as the positive direction of the z-axis. Let P a_0', b_0', and c_0' be the 3D coordinate of the joint point under the equipment spatial coordinate system,

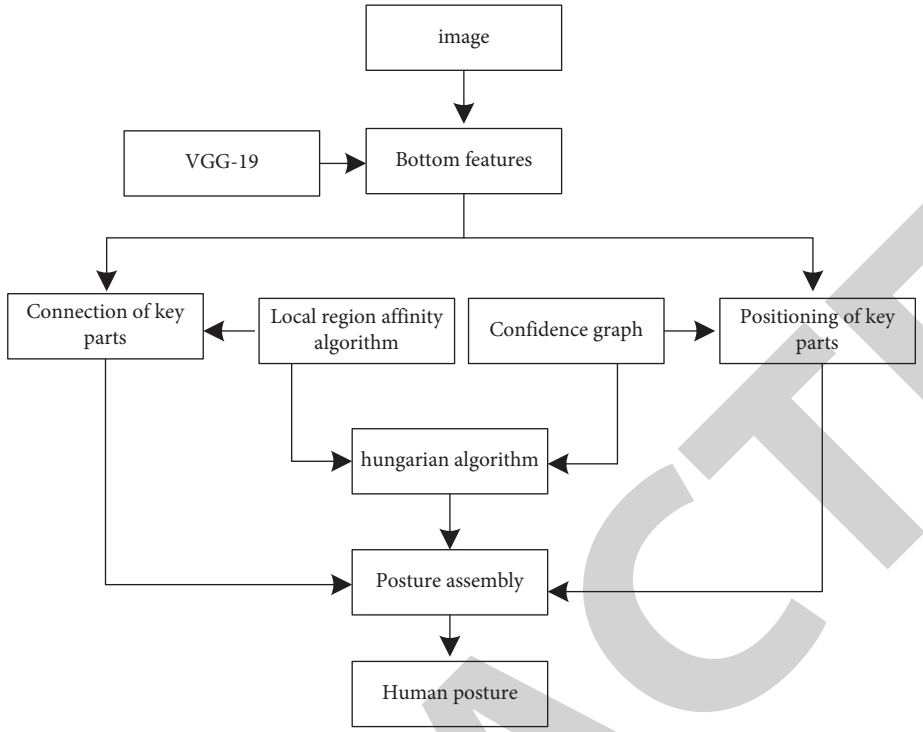

Figure 1: Processing flow of the deep learning model.

Table 1: Common depth sensor equipment.

Sensor name	Describe
SOD stereo camera	Lightweight depth sensor based on passive stereo
DepthSense 336	Short-range depth sensor embedded with a color camera and microphone
Kinect sensor S1	Depth sensor, embedded with a color camera and infrared transmitter
Kinect sensor S2	Embedded with a color camera and microphone
Intel RealSense 3D Camera	Embedded with a color camera and projector
Aus Xtion PRO Live	Infrared sensor embedded with a color camera and microphone
I soft	Motion capture system based on Kinect

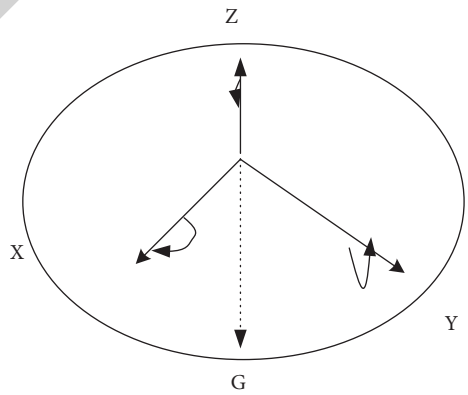

Figure 2: Schematic diagram of body gravity direction.

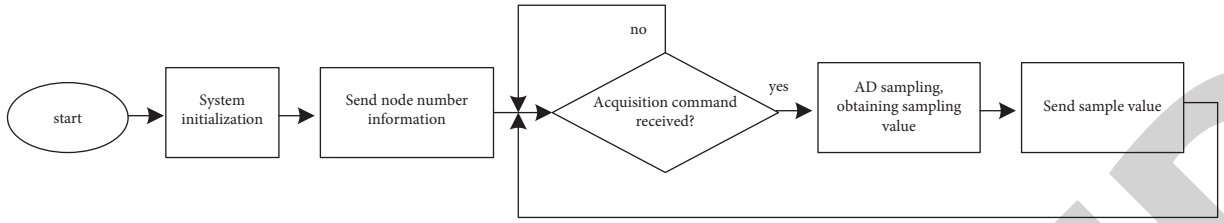

Figure 3: Collection processes of action characteristics of human motion nodes.

$o(x, y, z)$ be the coordinate of P corresponding to the human spatial coordinate system $o(x, y, z)$, then according to the translation and rotation transformation of the 3D graphics spatial coordinates.

$$o(x, y, z) = V(a', b', c') \begin{pmatrix} 1 & a & 0 & 0 \\ 0 & 1 & 0 & b \\ c & 0 & -1 & 0 \\ -a_0' & -b_0' & c_0' & 1 \end{pmatrix}. \quad (1)$$

Get

$$\begin{cases} s = k \cos a(z_0' - z')(x' - x_0') \\ m = w \tan c(y' - y_0')(z_0' - z'), \\ n = p \sin b(x_0' - x')(y' - y_0') \end{cases} \quad (2)$$

where k, w, and p, respectively, correspond to the coordinate quantities of "spine base" node o in Kinect G_r' spatial coordinate system. L_r' represents the rotation angle of the human body relative to xoy plane, and $a \in [-70, +70]$ can be obtained by calibrating specific joint points. Since "hile" and "upright" are symmetrical relative to Y_l' and X_1' axis, these two points are selected as calibration points. Assuming that their coordinates in oxyz coordinate system are (x, y) and (x, y), respectively, then

$$\alpha = \arctan\left(\frac{(G_r' - X_1')}{(L_r' - Y_l')}\right). \quad (3)$$

The captured human behavior data may have outliers. The existence of outliers will affect the overall classification results, resulting in inaccurate classification results. Therefore, it is necessary to detect and eliminate outliers first [15]. Outlier detection approaches include statistics-based methods, clustering-based methods, and some unique methods. We employ interquartile distance to locate outliers in this article. Although the interquartile distance represents the degree of dispersion of each variable in statistical data, it is more trustworthy statistical data [16]. As indicated in the table, all values are sorted in the sample from small to big and then split the data into quartiles with three points, which are quartiles (Table 2).

The calculation method of the upper bound is shown in

$$U = a(Q_1 - Q_2 - Q_3)k. \quad (4)$$

The calculation method of the lower bound is shown in

$$D = C + k(B - A) \quad (5)$$

When the value of K in the formula is 1.5, it is the moderately abnormal data detected; when the value of K is 3, extreme abnormal data are detected. In this paper, moderate abnormal data are used to detect outliers; that is, the value of w is 1.5. Observing the captured human behavior data shows that the angle change of limbs changes obviously in different movements, and the angle change can be defined by the Euler angle. The key to the success of behavior recognition is to select good features [17]. The quality of feature selection greatly impacts the results of behavior recognition. Human behavior characteristics include the following: 1. average value; 2. maximum value; 3 minimum value; 4. standard deviation; 5. variance; 6. median value; 7. extreme difference; 8. slope absolute energy. When extracting features, the eigenvalues sampled in a dimension of the attitude Euler angle of an inertial sensor node at all times of an action are calculated, respectively.

Average value: it reflects the overall situation of a group of data, as shown in

$$\mu = \frac{\sum_{i=1}^{n} a_i}{Dn} - w. \quad (6)$$

The standard deviation describes the average of the distance that each data in the sample deviate from the sample average, as shown in

$$s = U\sqrt{\frac{1}{\mu n}\sum_{i=1}^{n}(a-1)^2}. \quad (7)$$

After extracting behavior features, redundant features will increase computational complexity. Reducing features can reduce computational complexity and improve accuracy. However, feature reduction is not blind deletion of some features [18]. Blind deletion of features will lose a lot of information because when analyzing data samples, data analysis is often isolated rather than comprehensive [19]. Therefore, it is necessary to use the method of reasonable feature reduction to reduce the features and try not to lose the information of the original features to achieve the purpose of the comprehensive analysis of all features. The characteristic covariance matrix is found, as shown in

$$S = \frac{1}{s}(D - \mu)^2 (U - \mu) + \lambda. \quad (8)$$

Here, λ is the average of the eigenvectors. The eigenvectors are given accordingly. The first k principal components are selected, and the value of K can be determined by

Table 2: Quartile.

Quartile	Alias	Position in the sample
A Quartile (Q1)	Small quartile	Number of 26%
B Quartile (Q2)	Median	Number of 55%
C Quartile (Q3)	Big four digits	Number of 80%

$$\frac{s+p}{\lambda-1} \geq K-\eta. \tag{9}$$

Here, η is the energy loss rate. The features after dimensionality reduction according to the projection matrix are calculated, as shown in

$$Y_{MK} = A(K-h) - S. \tag{10}$$

When the loss rate is 0.08, 60 principal components can meet the requirements, so that the dimension of the eigenvector is reduced from 270 to 60.

2.3. Realization of Body Movement Detection in Competitive Sports Training. In the process of human motion capture, because the inertial sensor is self-sufficient and has no external reference point, it cannot obtain spatial displacement information, so it is necessary to use positioning technology to obtain displacement information in the process of human motion capture [20]. Wide-area positioning and short-range positioning are two types of wireless positioning technologies. Wide-area positioning is one of several types of positioning technology, which also includes satellite and mobile positioning. WLAN, RFID, UWB, Bluetooth, and ultrasonic are all examples of short-range location technology. The accuracy and positioning scale of various positioning modes are shown in Table 3.

There are two methods for attitude calculation. The first is to integrate the gyroscope into the inertial sensor. Although the gyroscope has a good dynamic response, the error will increase with the increase of time; the other method is to calculate the attitude through magnetometer and acceleration. Although the dynamic response is poor, it will not produce the cumulative error. Therefore, gyroscope, magnetometer, and accelerometer have complementary characteristics in the frequency domain [21]. The attitude calculation steps of the inertial sensor are shown in Figure 4 In the process of inertial sensor attitude data fusion, first, the quaternion is calculated according to the initial state of the inertial sensor, and then the gravity vector and magnetic line of force are inversely deduced to obtain the data of accelerometer and magnetometer, and normalized. The matrix is multiplied and then summed, then the proportional-integral controller is used to adjust the data, and finally, the quaternion is updated.

Human motion detection requires high accuracy, and most cases are carried out indoors. According to Table 2, UWB positioning technology has better performance and accuracy and is more suitable for indoor positioning than other positioning technologies [22]. In the process of motion change, using the motion estimation method based on image gray change to extract local feature points involves camera motion and produces large errors. Therefore, to accurately obtain the target motion estimation, it is necessary to eliminate the impact of camera motion [23]. The optical flow field obtained from the gray image is the sum of the local motion of the actual human body and the motion of the camera. The calculation formula is as follows:

$$\delta = \overrightarrow{S_r} z + \overrightarrow{S_c} - Y_{MK}. \tag{11}$$

Here, S represents the optical flow field; S_r represents the actual local motion of the human body; S_c indicates camera motion. Decompose the above three vectors into x and Y axes in turn to obtain

$$\begin{aligned} S_x &= S_{rx} + S_{cx}, \\ S_y &= S_{ry} + S_{cy}. \end{aligned} \tag{12}$$

Of all moving points in a local area in the same image S_{rx} and S_{cx}, the components in different directions of camera movement are consistent. As long as the component is removed, the actual motion component can be obtained, and then the background motion can be found and the scene motion information can be calculated [24]. The range of motion of each human joint is limited, but the human joint tree composed of multiple joints can make unlimited actions, as shown in Table 4. By limiting the range of motion of each joint in the human joint model, the detected human action can be more in line with the action of normal people.

When detecting human motion, first the inertial sensor node to the specified joints of the body is bound, such as big arm, small arm, thigh, and lower leg [25]. The specific joints on which inertial sensor nodes are bound can be determined according to the actions of which joints need to be collected. Increasing the number of inertial sensor nodes can improve the accuracy of action detection and make the detected human actions more accurate.

3. Analysis of Experimental Results

On the windows 8x64 operation of Intel Core (TM) i7-4790k and 16 GB memory, Kinect for windows sdk v2.0 and visual studio 2013 are used as development tools to build an analysis platform with WPF, on which the key-frame extraction function of the action sequence is realized. Because there is currently no single standard for evaluating key-frame extraction outcomes, eye observation and manual comparison analysis are the primary methods of assessment. For action key-frame extraction, three exemplary action sequences are chosen from the provided motion dataset. Table 5 shows the particular details of the action sequence. The complexity of the movement is mainly related to the body parts involved in the movement; that is, it is related to the action types in Table 5.

On the windows 8×64 operation of Intel Core (TM) i7-4790k and 16 GB memory, the human motion recognition experiment based on deep learning is completed based on Visual Studio 2013 c + + language. The experiment uses 10 movements of motion datasets, with a total of 3750 samples for training and recognition. Table 6 shows the average

Table 3: Accuracy and scale of various positioning modes.

Positioning mode	Positioning accuracy (m)	Positioning scale
GPS	About 11 meters	Outdoor wide area
Mobile positioning	About 11 meters	Outdoor wide area
Infrared, ultrasonic	1–11 m	Outdoor local area
WLAN, Bluetooth	1–11 m	Indoor
Ultra wideband	0.1–1 m	Indoor

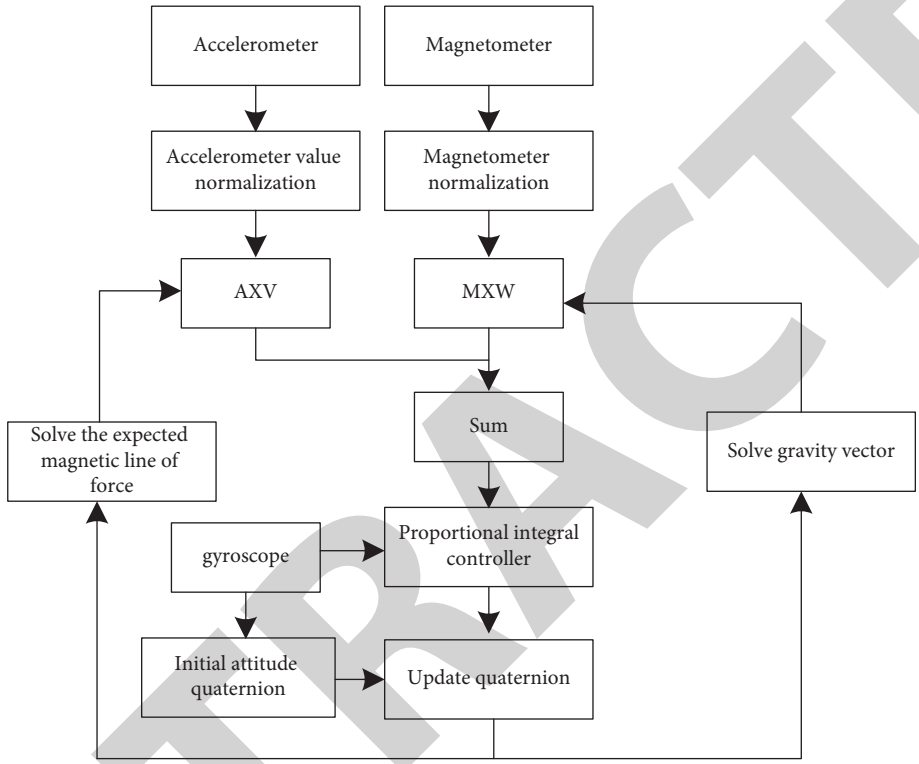

Figure 4: Attitude calculation flow of the motion inertial sensor.

Table 4: Degrees of freedom and range of motion of some joints of the human skeleton model.

Joint name	Joint	Degree of freedom	Activity range limit
Neck	Chest	3	0–90°
Left shoulder	Chest	2	0–180°
Right shoulder	Chest	3	0–180°
Left elbow	Left arm	3	0–150°
Right elbow	Right arm	2	0–150°
Left side	Waist	3	0–130°
Right side	Waist	2	0–130°
Left knee	Thigh	3	0–145°
Right knee	Thigh	2	0–145°
Left ankle	A lower leg	3	0–90°
Right ankle	A lower leg	3	0–90°

length and action type of each action. For each action sample, 90% of the action samples are selected for training each time, and the remaining 10% of the samples are used as the test set for 10 fold 10 times crossvalidation.

In this paper, the human motion recognition method based on deep learning has achieved a 100% recognition rate for most actions in the motion dataset, 97% minimum recognition rate, and 99.5% average recognition rate, so it has a high recognition rate. Simultaneously, Table 7 shows that this approach has a high recognition rate for three distinct kinds of activities and no evident recognition trend, indicating that it is resilient. However, because of the high complexity of the deep learning algorithm, the average recognition time of 10 actions by the human action

Table 5: Experimental dataset.

Action semantics	Action representation	Frame rate (frames/sec)	Total frames	Action type	Action complexity
Lurk	O	35	419	The legs	Simple
Stop the system	P	35	425	Upper limb	Simple
Still things	Q	35	345	Whole body	Complex

Table 6: Action set information.

Action label	A	B	C	D	E	F	G	H	I	J
Type	Upper limb	The legs	Upper limb	The legs	The legs	The legs	The legs	Comprehensive	Comprehensive	Comprehensive
Average length (frame)	160	352	261	261	275	231	265	398	332	335

Table 7: Experimental results of the competitive sports dataset.

Method	Head	Shoulder	Elbow	Wrist	Hips	Knee	Ankle	Map
Deep cut	79.5	73.5	61.3	50.2	56.3	51.9	45.6	58.6
Open pose	92.3	86.5	78.8	66.5	76.5	68.8	62.5	75.5
This paper's method	94.5	88.5	75.5	73.3	79.5	71.2	60.9	77.8

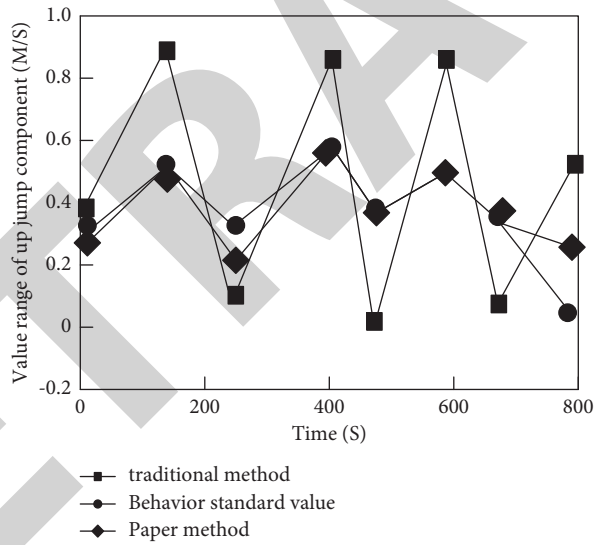

Figure 5: Value analyses of human motion behavior recognition data components by two methods.

recognition technique based on deep learning is 148 ms, and the action recognition speed is poor, as shown in the table. This paper replaces the feature extraction model VGG-19 in the initial stage of an open pose with the lightweight network model MobileNetV2, introduces the weight and penalty term into the final loss function, and uses MobileNetV2 to process images on the local experimental platform to improve the accuracy and efficiency of attitude estimation. Although the model does not achieve the expected improvement in accuracy, the total parameters of the model are reduced. Table 7 shows the results of the MPI dataset. According to the results, it can be seen that the improved model structure can meet the experimental requirements of this paper.

Learning rate is a very important parameter in the decline of the deep learning gradient. The size of the batch determines the direction of gradient descent and the rate of convergence. If the batch size is set too much, the convergence speed is large, but there may be a local optimal solution if it is set too much. According to the above discrete points of human behavior data of static, walking, running, jumping, squatting standard deviation, skewness, peak value, and correlation coefficient collected from X, Y, and Z axes, in the process of extended Kalman filter (EKF) simulation, 100 groups of data are intercepted from each data for iterative optimization and correction, and the traditional identification method is compared with this method. The results are shown in Figure 5.

Hindawi
Journal of Mathematics
Volume 2023, Article ID 9807535, 1 page
https://doi.org/10.1155/2023/9807535

Retraction

Retracted: On Q_p-Closed Sets in Topological Spaces

Journal of Mathematics

Received 17 October 2023; Accepted 17 October 2023; Published 18 October 2023

This article has been retracted by Hindawi following an investigation undertaken by the publisher [1]. This investigation has uncovered evidence of one or more of the following indicators of systematic manipulation of the publication process:

(1) Discrepancies in scope

(2) Discrepancies in the description of the research reported

(3) Discrepancies between the availability of data and the research described

(4) Inappropriate citations

(5) Incoherent, meaningless and/or irrelevant content included in the article

(6) Peer-review manipulation

The presence of these indicators undermines our confidence in the integrity of the article's content and we cannot, therefore, vouch for its reliability. Please note that this notice is intended solely to alert readers that the content of this article is unreliable. We have not investigated whether authors were aware of or involved in the systematic manipulation of the publication process.

Wiley and Hindawi regrets that the usual quality checks did not identify these issues before publication and have since put additional measures in place to safeguard research integrity.

We wish to credit our own Research Integrity and Research Publishing teams and anonymous and named external researchers and research integrity experts for contributing to this investigation.

The corresponding author, as the representative of all authors, has been given the opportunity to register their agreement or disagreement to this retraction. We have kept a record of any response received.

References

[1] H. Zhou, O. G. Hammad, and A. M. Khalil, "On Q_p-Closed Sets in Topological Spaces," *Journal of Mathematics*, vol. 2022, Article ID 9352861, 10 pages, 2022.

Hindawi
Journal of Mathematics
Volume 2022, Article ID 9352861, 10 pages
https://doi.org/10.1155/2022/9352861

Review Article

On Q_p-Closed Sets in Topological Spaces

Huan Zhou,[1] O. G. Hammad,[2] and Ahmed Mostafa Khalil[3]

[1]*Aviation Engineering School, Air Force Engineering University, Xi'an 710038, China*
[2]*Department of Mathematics, Faculty of Science, Assiut University, Assiut 71516, Egypt*
[3]*Department of Mathematics, Faculty of Science, Al-Azhar University, Assiut 71524, Egypt*

Correspondence should be addressed to Ahmed Mostafa Khalil; a.khalil@azhar.edu.eg

Received 23 December 2021; Accepted 25 January 2022; Published 18 February 2022

Academic Editor: Naeem Jan

In the present paper, we will propose the novel notions (e.g., Q_p-closed set, Q_p-open set, Q_p-continuous mapping, Q_p-open mapping, and Q_p-closed mapping) in topological spaces. Then, we will discuss the basic properties of the above notions in detail. The category of all Q_p-closed (resp. Q_p-open) sets is strictly between the class of all preclosed (resp. preopen) sets and gp-closed (resp. gp-open) sets. Also, the category of all Q_p-continuity (resp. Q_p-open (Q_p-closed) mappings) is strictly among the class of all precontinuity (resp., preopen (preclosed) mappings) and gp-continuity (resp. gp-open (gp-closed) mappings). Furthermore, we will present the notions of Q_p-closure of a set and Q_p-interior of a set and explain some of their fundamental basic properties. Several relations are equivalent between two different topological spaces. The novel two separation axioms (i.e., Q_p-$\mathbb{R}_0$ and Q_p-$\mathbb{R}_1$) based on the notion of Q_p-open set and Q_p-closure are investigated. The space of Q_p-$\mathbb{R}_0$ (resp., Q_p-$\mathbb{R}_1$) is strictly between the spaces of pre-$\mathbb{R}_0$ (resp., pre-$\mathbb{R}_1$) and gp-$\mathbb{R}_o$ (resp., gp-$\mathbb{R}_1$). Finally, some relations and properties of Q_p-$\mathbb{R}_0$ and Q_p-$\mathbb{R}_1$ spaces are explained.

1. Introduction

In the early eighties, the novel notions of preopen and preclosed sets (i.e., as a novel type of generalized of open sets in $(\mathcal{X}, \tilde{\tau})$ (i.e., topological space) or a space $\mathcal{X}$) and pre-conlinuous mappings are proposed in [1]. Consequently, many researchers turned their study to the generalizations of many different notions in $(\mathcal{X}, \tilde{\tau})$ (for instance, semiopen sets [2], α-open sets [3], and β-open sets [4] or semi-preopen sets [5]). Furthermore, the notion of generalized closed (resp., generalized open) sets (for short, g-closed (resp., g-open) sets) in space $\mathcal{X}$ is presented in [6]. The relationship among g-closed (resp., g-open) sets and generalizing closedness (resp., openness) sets (i.e., generalized preclosed (resp., generalized preopen) set (for short, gp-closed (resp., gp-open) set) [7], α-generalized closed (resp., α-generalized open) set (for short, αg-closed (resp., αg-open) set) [8], pregeneralized closed (resp., pregeneralized open) set (for short, pg-closed (resp., pg-open) set) [7], and generalized α-closed (resp., generalized α-open) set (for short, $g\alpha$-closed (resp., $g\alpha$-open) set) [9]. The basic properties of five generalizing continuous mappings (i.e., precontinuous mapping [1], g-continuous mapping [10], gp-continuous mapping [11], αg-continuous mapping [12], pg-continuous mapping [11], and $g\alpha$-continuous mapping [12]) between $\tilde{\sigma}(\mathcal{Y})$ (i.e., a topology on $\mathcal{Y}$) and $\tilde{\tau}(\mathcal{X})$ (i.e., a topology on $\mathcal{X}$) are presented. Furthermore, the fundamental relations of generalizing open (closed) mappings (i.e., preopen (pre-closed) mapping [1, 13], α-open (α-closed) mapping [14], g-open (g-closed) mapping [15], gp-open (gp-closed) mapping [11], αg-open (αg-closed) mapping [12], pg-open (pg-closed) mapping [11], $g\alpha$-open ($g\alpha$-closed) mapping [12]) between $\tilde{\sigma}(\mathcal{Y})$ and $\tilde{\tau}(\mathcal{X})$ are studied. On the contrary, the characterizations between separation axioms classes (i.e., pre-$\mathbb{R}_0$, pre-$\mathbb{R}_1$, gp-$\mathbb{R}_0$ and gp-$\mathbb{R}_1$ spaces) (see, [16, 17]) in $(\mathcal{X}, \tilde{\tau})$ are defined.

Regarding the above discussions, as the motivation of the present paper, we will define novel sets called Q_p-closed sets and Q_p-open sets and investigate several of their fundamental properties. The relation between Q_p-closed set (resp., Q_p-open set) and other sets (for example, preclosed set (resp., preopen set), α-closed set (resp., α-pen set), g-closed set

(resp., g-open set), gp-closed set (resp., gp-open set), αg-closed set (resp., αg-open set), pg-closed set (resp., pg-open set), and $g\alpha$-closed set (resp., $g\alpha$-open set)) in space $\mathscr{X}$ is introduced. Then, we define the Q_p-continuous mapping and study the relations between Q_p-continuous mapping and other mappings (for example, precontinuous mapping, g-continuous mapping, gp-continuous mapping, αg-continuous mapping, pg-continuous mapping, and $g\alpha$-continuous mapping) between two different topological spaces. Also, we present the notion of Q_p-open (Q_p-closed) mapping and investigate relations between Q_p-open (Q_p-closed) mapping and other mappings (for example, preopen (preclosed) mapping, α-open (α-closed) mapping, g-open (g-closed) mapping, gp-open (gp-closed) mapping, αg-open (αg-closed) mapping, pg-open (pg-closed) mapping, and $g\alpha$-open ($g\alpha$-closed) mapping) between two different topological spaces. Finally, we propose the novel separation axioms classes (i.e., Q_p-$\mathbb{R}_0$ and Q_p-$\mathbb{R}_1$ spaces) in $(\mathscr{X}, \tilde{\tau})$.

Next, the sections of this paper are arranged as follows. In Section 2, we will present many notions related to topological spaces as indicated from Definitions 1 to 4. In Section 2, we propose the novel notions of Q_p-closed sets and Q_p-open sets and explain the interesting properties of them. In Section 3, we give the notions of Q_p-continuous mappings, Q_p-open mappings, and Q_p-closed mappings. In Section 4, we define Q_p-$\mathbb{R}_0$ and Q_p-$\mathbb{R}_1$ spaces. Section 5 is conclusions.

In the current paper, we will use several expressions (i.e., $\mathscr{C}(\mathfrak{A})$ (the closure of a set $\mathfrak{A}$), $\mathscr{I}(\mathfrak{A})$ (the interior of a set $\mathfrak{A}$), $\tilde{\tau}(\mathscr{X})$ (the all of open sets in $\mathscr{X}$), and $\mathscr{F}_{\mathscr{X}}$ (the all of closed sets in $\mathscr{X}$)).

Next, we will present several notions which are used in this section as indicated below.

Definition 1 (Cf. [1, 3]). Assume $(\mathscr{X}, \tilde{\tau})$ is a topological space. Then,

(1)

(i) $\mathfrak{A}$ is preclosed set if $\mathscr{C}(\mathscr{I}(\mathfrak{A})) \subseteq \mathfrak{A}$
(ii) $\mathfrak{A}$ is preopen set if $\mathfrak{A} \subseteq \mathscr{I}(\mathscr{C}(\mathfrak{A}))$

$\mathbb{C}_p(\mathscr{X})$ (resp., $\mathbb{O}_p(\mathscr{X})$) is the set of all preclosed (resp. preopen) sets.

(2)

(i) $\mathfrak{A}$ is α-closed set if $\mathscr{C}(\mathscr{I}(\mathscr{C}(\mathfrak{A}))) \subseteq \mathfrak{A}$
(ii) $\mathfrak{A}$ is α-open set if $\mathfrak{A} \subseteq \mathscr{I}(\mathscr{C}(\mathscr{I}(\mathfrak{A})))$

$\mathbb{C}_\alpha(\mathscr{X})$ (resp., $\mathbb{O}_\alpha(\mathscr{X})$) is the set of all α-closed (resp. α-open) sets.

Definition 2 (Cf. [6–9]). Assume $(\mathscr{X}, \tilde{\tau})$ is a topological space. Then,

(1)

(i) $\mathfrak{A}$ is g-closed set if $\mathscr{C}(\mathfrak{A}) \subseteq \mathfrak{A}$ whenever $\mathfrak{A} \subseteq \mathfrak{L}$ and $\mathfrak{L} \in \tilde{\tau}(\mathscr{X})$, where $\mathscr{C}(\mathfrak{A})$ is a closure of $\mathfrak{A}$, i.e.,

$$\mathscr{C}(\mathfrak{A}) = \cap \{\mathfrak{F} | \mathfrak{A} \subseteq \mathfrak{F} \text{ and } \mathfrak{F} \in \mathscr{F}_{\mathscr{X}}\}. \quad (1)$$

$\mathbb{GC}(\mathscr{X})$ be the set of all g-closed sets.
(ii) $\mathfrak{A}$ is g-open set if $\mathscr{X} \backslash \mathfrak{A} \in \mathbb{GC}(\mathscr{X})$ and $\mathbb{GO}(\mathscr{X})$ be the set of all g-open sets.

(2)

(i) $\mathfrak{A}$ is gp-closed set if $\mathscr{C}_p(\mathfrak{A}) \subseteq \mathfrak{A}$ whenever $\mathfrak{A} \subseteq \mathfrak{L}$ and $\mathfrak{L} \in \tilde{\tau}(\mathscr{X})$, where $\mathscr{C}_p(\mathfrak{A})$ is a preclosure of $\mathfrak{A}$, i.e.,

$$\mathscr{C}_p(\mathfrak{A}) = \cap \left\{\mathfrak{F} | \mathfrak{A} \subseteq \mathfrak{F} \text{ and } \mathfrak{F} \in \mathbb{C}_p(\mathscr{X})\right\}. \quad (2)$$

$\mathbb{GC}_p(\mathscr{X})$ be the set of all gp-closed sets.
(ii) $\mathfrak{A}$ is gp-open set if $\mathscr{X} \backslash \mathfrak{A} \in \mathbb{GC}_p(\mathscr{X})$ and $\mathbb{GO}_p(\mathscr{X})$ be the set of all gp-open sets.

(3)

(i) $\mathfrak{A}$ is αg-closed set if $\mathscr{C}_\alpha(\mathfrak{A}) \subseteq \mathfrak{A}$ whenever $\mathfrak{A} \subseteq \mathfrak{L}$ and $\mathfrak{L} \in \tilde{\tau}(\mathscr{X})$, where $\mathscr{C}_\alpha(\mathfrak{A})$ is a α-closure *of* $\mathfrak{A}$, *i.e.*,

$$\mathscr{C}_\alpha(\mathfrak{A}) = \cap \{\mathfrak{F} | \mathfrak{A} \subseteq \mathfrak{F} \text{ and } \mathfrak{F} \in \mathbb{C}_\alpha(\mathscr{X})\}. \quad (3)$$

$\mathbb{C}_\alpha\mathbb{G}(\mathscr{X})$ be the set of all αg-closed sets.
(ii) $\mathfrak{A}$ is αg-open set if $\mathscr{X} \backslash \mathfrak{A} \in \mathbb{C}_\alpha\mathbb{G}(\mathscr{X})$ and $\mathbb{O}_\alpha\mathbb{G}(\mathscr{X})$ be the set of all αg-open sets.

(4)

(i) $\mathfrak{A}$ is pg-closed set if $\mathscr{C}_p(\mathfrak{A}) \subseteq \mathfrak{A}$ whenever $\mathfrak{A} \subseteq \mathfrak{L}$ and $\mathfrak{L} \in \mathbb{O}_p(\mathscr{X})$ and $\mathbb{C}_p\mathbb{G}(\mathscr{X})$ be the set of all pg-closed sets.
(ii) $\mathfrak{A}$ is pg-open set if $\mathscr{X} \backslash \mathfrak{A} \in \mathbb{C}_p\mathbb{G}(\mathscr{X})$ and $\mathbb{O}_p\mathbb{G}(\mathscr{X})$ be the set of all gp-open sets.

(5)

(i) $\mathfrak{A}$ is $g\alpha$-closed set if $\mathscr{C}_\alpha(\mathfrak{A}) \subseteq \mathfrak{A}$ whenever $\mathfrak{A} \subseteq \mathfrak{L}$ and $\mathfrak{L} \in \mathbb{O}_\alpha(\mathscr{X})$, and $\mathbb{GC}_\alpha(\mathscr{X})$ be the set of all $g\alpha$-closed sets.
(ii) $\mathfrak{A}$ is $g\alpha$-open set if $\mathscr{X} \backslash \mathfrak{A} \in \mathbb{GC}_\alpha(\mathscr{X})$, and $\mathbb{GO}_\alpha(\mathscr{X})$ be the set of all $g\alpha$-open sets.

Definition 3 (Cf. [1, 10, 13–15]). Let $\psi: \mathscr{X} \longrightarrow \mathscr{Y}$ be mapping and $\tilde{\sigma}(\mathscr{Y})$ be a topology on $\mathscr{Y}$ and $\tilde{\tau}(\mathscr{X})$ is a topology on $\mathscr{X}$. Then,

(1) ψ is precontinuous mapping (resp., α-continuous mapping and g-continuous mapping) if $\mathfrak{L} \in \tilde{\sigma}(\mathscr{Y})$, $\psi^{-1}(\mathfrak{L}) \in \mathbb{O}_p(\mathscr{X})$ $(resp., \psi^{-1}(\mathfrak{L}) \in \mathbb{O}_\alpha(\mathscr{X}), \psi^{-1}(\mathfrak{L}) \in \mathbb{GO}(\mathscr{X}))$.

(2)

(i) ψ is preopen mapping (resp., α-open mapping and g-open mapping) if $\mathfrak{L} \in \tilde{\tau}(\mathscr{X})$, $\psi(\mathfrak{L}) \in Q_p\mathbb{O}(\mathscr{Y})$ $(resp., \psi(\mathfrak{L}) \in \mathbb{O}_\alpha(\mathscr{Y}), \psi(\mathfrak{L}) \in \mathbb{GO}(\mathscr{Y}))$.
(ii) ψ is preclosed mapping (resp., α-closed mapping and g-closed mapping) if $\mathfrak{L} \in \tilde{\tau}(\mathscr{X})$, $\psi(\mathfrak{L}) \in Q_p\mathbb{C}(\mathscr{Y})$ $(resp., \psi(\mathfrak{L}) \in \mathbb{C}_\alpha(\mathscr{Y}), \psi(\mathfrak{L}) \in \mathbb{GC}(\mathscr{Y}))$.

Definition 4 (Cf. [16, 17]). A topological space $(\mathcal{X}, \tilde{\tau})$ is said to be

(1) Pre-$\mathbb{R}_0$ space (resp., gp-$\mathbb{R}_0$ space) if $\forall x \in \mathfrak{L} \in \mathbb{O}_p(\mathcal{X})$ s.t. $\mathscr{C}_p(\{x\}) \subset \mathfrak{L}$ (resp., $\forall x \in \mathfrak{L} \in \mathbb{GO}_p(\mathcal{X})$ s.t., $\mathscr{C}_{gp}(\{x\}) \subset \mathfrak{L}$) and $\mathscr{C}_{gp}(\{x\})$ is a gp-closure of $\{x\}$, defined as

$$\mathscr{C}_{gp}(\{x\}) = \cap\left\{\mathfrak{F} | \{x\} \subseteq \mathfrak{F} \text{ and } \mathfrak{F} \in \mathbb{GC}_p(\mathcal{X})\right\}. \tag{4}$$

(2) Pre-$\mathbb{R}_1$ space (resp., gp-$\mathbb{R}_1$ space) if $\forall x, y \in \mathcal{X}$, with $\mathscr{C}_p(\{x\}) \neq \mathscr{C}_p(\{y\})$ (resp., $\mathscr{C}_{gp}(\{x\}) \neq \mathscr{C}_{gp}(\{y\})$), there exist disjoint preopen sets (resp., gp-open sets) $\mathfrak{L}$ and $\mathfrak{M}$ s.t. $\mathscr{C}_p(\{x\}) \subseteq \mathfrak{L}$ (resp., $\mathscr{C}_{gp}(\{x\}) \subseteq \mathfrak{L}$) and $\mathscr{C}_p(\{y\}) \subseteq \mathfrak{M}$ (resp., $\mathscr{C}_{gp}(\{y\}) \subseteq \mathfrak{M}$).

2. ERROR!! Q_p-Closed Sets and Q_p-Open Sets

In the following section, we propose novel sets (i.e., Q_p-closed sets and Q_p-open sets) and discuss several interesting theorems and examples.

Definition 5. We call $\mathfrak{A}$ is Q_p-closed set in $(\mathcal{X}, \tilde{\tau})$ if

$$\mathscr{C}_{gp}(\mathcal{I}(\mathfrak{A})) \subseteq \mathfrak{A}, \tag{5}$$

where $\mathscr{C}_{gp}(\mathcal{I}(\mathfrak{A}))$ is a gp-closure of $\mathcal{I}(\mathfrak{A})$, i.e.,

$$\mathscr{C}_{gp}(\mathcal{I}(\mathfrak{A})) = \cap\left\{\mathfrak{F} | \mathcal{I}(\mathfrak{A}) \subseteq \mathfrak{F} \text{ and } \mathfrak{F} \in \mathbb{GC}_p(\mathcal{X})\right\}. \tag{6}$$

$Q_p\mathbb{C}(\mathcal{X})$ is the set of all Q_p-closed sets in $\mathcal{X}$.

Lemma 1. *Let $\mathfrak{F} \in \mathbb{GC}_p(\mathcal{X})$ s.t. $\mathscr{C}_{gp}(\mathcal{I}(\mathfrak{F})) \subseteq \mathfrak{A} \subseteq \mathfrak{F}$. Then, $\mathfrak{A} \in Q_p\mathbb{C}(\mathcal{X})$.*

Proof. As $\mathfrak{F} \in \mathbb{GC}_p(\mathcal{X})$ implies $\mathscr{C}_{gp}(\mathfrak{F}) = \mathfrak{F}$, thus, $\mathscr{C}_{gp}(\mathcal{I}(\mathfrak{A})) \subseteq \mathscr{C}_{gp}(\mathcal{I}(\mathfrak{F})) \subseteq \mathfrak{A}$. Therefore, $\mathfrak{A} \in Q_p\mathbb{C}(\mathcal{X})$. □

The converse of Lemma 1 (i.e., $\mathscr{C}_{gp}(\mathcal{I}(\mathfrak{F})) \not\subseteq \subseteq \mathfrak{F}$) does not hold by the following example.

Example 1. Assume that $\mathcal{X} = \{1, 2, 3\}$ (i.e., $(\mathcal{X}, \tilde{\tau})$ be topological space) and $\tilde{\tau} = \{\mathcal{X}, \phi, \{1\}\}$. Then,

$$\begin{aligned} \mathcal{F}_{\mathcal{X}} &= \{\mathcal{X}, \phi, \{2, 3\}\}, \\ \mathbb{C}_p(\mathcal{X}) &= \{\mathcal{X}, \phi, \{2\}, \{3\}, \{2, 3\}\}, \\ \mathbb{GC}_p(\mathcal{X}) &= \{\mathcal{X}, \phi, \{2\}, \{3\}, \{1, 2\}, \{1, 3\}, \{2, 3\}\}, \end{aligned} \tag{7}$$

$$Q_p\mathbb{C}(\mathcal{X}) = 2^{\mathcal{X}}. \tag{8}$$

Let $\mathfrak{A} = \{3\} \in Q_p\mathbb{C}(\mathcal{X})$ and $\mathfrak{F} = \mathcal{X} \in \mathbb{GC}_p(\mathcal{X})$. Then, $\mathscr{C}_{gp}(\mathcal{I}(\mathfrak{F})) = \mathscr{C}_{gp}(\mathcal{X}) = \not\subseteq \subseteq \mathfrak{F}$.

Theorem 1. *The following two properties are holding in $(\mathcal{X}, \tilde{\tau})$.*

(1) If $\mathfrak{A} \in \mathbb{C}_p(\mathcal{X})$, then $\mathfrak{A} \in Q_p\mathbb{C}(\mathcal{X})$

(2) If $\mathfrak{A} \in \mathbb{GC}_p(\mathcal{X})$, then $\mathfrak{A} \in Q_p\mathbb{C}(\mathcal{X})$

Proof.

(1) As $\mathscr{C}_{gp}(\mathfrak{A}) \subseteq \mathscr{C}_p(\mathfrak{A})$ and $\mathscr{C}_p(\mathfrak{A}) \subseteq \mathscr{C}(\mathfrak{A})$ imply that $\mathscr{C}_{gp}(\mathfrak{A}) \subseteq \mathscr{C}(\mathfrak{A})$, since $\mathfrak{A}$ is preclosed set (i.e., $\mathscr{C}(\mathcal{I}(\mathfrak{A})) \subseteq \mathfrak{A}$), then $\mathscr{C}_{gp}(\mathcal{I}(\mathfrak{A})) \subseteq \mathscr{C}(\mathcal{I}(\mathfrak{A})) \subseteq \mathfrak{A}$. Thus, $\mathfrak{A} \in Q_p\mathbb{C}(\mathcal{X})$.

(2) Let $\mathfrak{A} \in \mathbb{GC}_p(\mathcal{X})$ (i.e., $\mathscr{C}_{gp}(\mathfrak{A}) = \mathfrak{A}$). Then, $\mathscr{C}_{gp}(\mathcal{I}(\mathfrak{A})) \subseteq \mathscr{C}_{gp}(\mathfrak{A}) = \mathfrak{A}$. Thus, $\mathfrak{A} \in Q_p\mathbb{C}(\mathcal{X})$. □

The converse of Theorem 1 (i.e., $\mathfrak{A} \in Q_p\mathbb{C}(\mathcal{X})$ but $\mathfrak{A} \notin \mathbb{C}_p(\mathcal{X})$ and $\mathfrak{A} \notin \mathbb{GC}_p(\mathcal{X})$) does not hold by the following example.

Example 2. (continued from Example 1). As $\{1, 3\} \in Q_p\mathbb{C}(\mathcal{X})$, $\{1, 3\} \notin \mathbb{C}_p(\mathcal{X})$ and $\{1\} \in Q_p\mathbb{C}(\mathcal{X})$ but $\{1\} \notin \mathbb{GC}_p(\mathcal{X})$.

Theorem 2. *Arbitrary intersection of Q_p-closed sets is Q_p-closed set.*

Proof. Suppose that $\{\mathfrak{F}_k | k \in \Lambda\}$ be a collection of Q_p-closed sets in $\mathcal{X}$. Then, $\mathscr{C}_{gp}(\mathcal{I}(\mathfrak{F}_k)) \subseteq \mathfrak{F}_k$, for every k. As $\cap\mathfrak{F}_k \subseteq \mathfrak{F}_k$, for every k, $\mathscr{C}_{gp}(\cap\mathfrak{F}_k) \subseteq \mathscr{C}_{gp}(\mathfrak{F}_k)$ for every k. Thus, $\mathscr{C}_{gp}(\cap\mathfrak{F}_k) \subseteq \cap\mathscr{C}_{gp}(\mathfrak{F}_k), k \in \Lambda$. Hence, $\mathscr{C}_{gp}(\mathcal{I}(\cap\mathfrak{F}_k)) \subseteq \mathscr{C}_{gp}(\cap\mathcal{I}(\mathfrak{F}_k)) \subseteq \cap\mathscr{C}_{gp}(\mathcal{I}(\mathfrak{F}_k)) \subseteq \cap\mathfrak{F}_k$. Therefore, $\cap\mathfrak{F}_k$ is Q_p-closed set. □

Remark 1. The union of two Q_p-closed sets need not be Q_p-closed set (i.e., $\mathfrak{A}, \mathfrak{B} \in Q_p\mathbb{C}(\mathcal{X})$, but $\mathfrak{A} \cup \mathfrak{B} \notin Q_p\mathbb{C}(\mathcal{X})$) as the next example; let $\mathcal{X} = \{1, 2, 3\}$ (i.e., $(\mathcal{X}, \tilde{\tau})$ be topological space) and $\tilde{\tau} = \{\mathcal{X}, \phi, \{1, 2\}\}$. Then,

$$\begin{aligned} \mathcal{F}_{\mathcal{X}} &= \{\mathcal{X}, \phi, \{3\}\}, \\ \mathbb{C}_p(\mathcal{X}) &= \mathbb{GC}_p(\mathcal{X}) = Q_p\mathbb{C}(\mathcal{X}) \\ &= \{\mathcal{X}, \phi, \{1\}, \{2\}, \{3\}, \{1, 3\}, \{2, 3\}\}. \end{aligned} \tag{9}$$

Let $\mathfrak{A} = \{1\} \in Q_p\mathbb{C}(\mathcal{X})$ and $\mathfrak{B} = \{2\} \in Q_p\mathbb{C}(\mathcal{X})$. Then, $\mathfrak{A} \cup \mathfrak{B} = \{1, 2\} \notin Q_p\mathbb{C}(\mathcal{X})$.

Corollary 1. *The following two properties are holding in $(\mathcal{X}, \tilde{\tau})$.*

(1) Let $\mathfrak{A} \in Q_p\mathbb{C}(\mathcal{X})$ and $\mathfrak{B} \in \mathbb{C}_p(\mathcal{X})$. Then, $\mathfrak{A} \cap \mathfrak{B} \in Q_p\mathbb{C}(\mathcal{X})$.

(2) Let $\mathfrak{A} \in Q_p\mathbb{C}(\mathcal{X})$ and $\mathfrak{B} \in \mathbb{GC}_p(\mathcal{X})$. Then, $\mathfrak{A} \cap \mathfrak{B} \in Q_p\mathbb{C}(\mathcal{X})$.

Proof. From Theorems 1 and 2, the proof is clear. □

Definition 6. $\mathscr{C}_{Q_p}(\mathfrak{A})$ is called Q_p-closure of $\mathfrak{A}$ in $(\mathcal{X}, \tilde{\tau})$ if

$$\mathscr{C}_{Q_p}(\mathfrak{A}) = \cap\left\{\mathfrak{F} | \mathfrak{A} \subseteq \mathfrak{F} \text{ and } \mathfrak{F} \in Q_p\mathbb{C}(\mathcal{X})\right\}. \tag{10}$$

Theorem 3. *The following seven properties are holding in $(\mathcal{X}, \tilde{\tau})$.*

(1) $\mathfrak{A} \in Q_p\mathbb{C}(\mathcal{X}) \Leftrightarrow \mathscr{C}_{Q_p}(\mathfrak{A}) = \mathfrak{A}$

(2) $\mathfrak{A} \subseteq \mathscr{C}_{Q_p}(\mathfrak{A}) \subseteq \mathscr{C}_p(\mathfrak{A})$ and $\mathscr{C}_{Q_p}(\mathfrak{A}) \subseteq \mathscr{C}_{gp}(\mathfrak{A})$

(3) $\mathscr{C}_{Q_p}(\phi) = \phi$ *and* $\mathscr{C}_{Q_p}(\mathscr{X}) = \mathscr{X}$

(4) *If* $\mathfrak{A} \subseteq \mathfrak{B}$, *then* $\mathscr{C}_{Q_p}(\mathfrak{A}) \subseteq \mathscr{C}_{Q_p}(\mathfrak{B})$

(5) $\mathscr{C}_{Q_p}(\mathscr{C}_{Q_p}(\mathfrak{A})) = \mathscr{C}_{Q_p}(\mathfrak{A})$

(6) $\mathscr{C}_{Q_p}(\mathfrak{A}) \cup \mathscr{C}_{Q_p}(\mathfrak{B}) \subseteq \mathscr{C}_{Q_p}(\mathfrak{A} \cup \mathfrak{B})$

(7) $\mathscr{C}_{Q_p}(\mathfrak{A} \cap \mathfrak{B}) \subseteq \mathscr{C}_{Q_p}(\mathfrak{A}) \cap \mathscr{C}_{Q_p}(\mathfrak{B})$

Proof.

(1) Let $\mathfrak{A} \in Q_p\mathbb{C}(\mathscr{X})$, and from Definition 6, we have $\mathscr{C}_{Q_p}(\mathfrak{A}) = \mathfrak{A}$. Conversely, let $\mathscr{C}_{Q_p}(\mathfrak{A}) = \mathfrak{A}$. Then, from Theorem 2, we have $\mathfrak{A} \in Q_p\mathbb{C}(\mathscr{X})$which follows from Theorem 1 (1) and (2), respectively, and are obvious.

(2) Let $\mathfrak{A} \subseteq \mathfrak{F}$ such that $\mathfrak{F} \in Q_p\mathbb{C}(\mathscr{X})$; then, from (1) above, we have $\mathscr{C}_{Q_p}(\mathfrak{A}) \subseteq \mathscr{C}_{Q_p}(\mathfrak{F}) = \mathfrak{F}$. Again $\mathscr{C}_{Q_p}(\mathscr{C}_{Q_p}(\mathfrak{A})) \subseteq \mathscr{C}_{Q_p}(\mathfrak{F}) = \mathfrak{F}$. Thus, $\mathscr{C}_{Q_p}(\mathscr{C}_{Q_p}(\mathfrak{A})) \subseteq \cap\{\mathfrak{F} | \mathfrak{A} \subseteq \mathfrak{F} \text{ and } \mathfrak{F} \in Q_p\mathbb{C}(\mathscr{X})\} = \mathscr{C}_{Q_p}(\mathfrak{A})$ and follows from (4). □

The equality of Theorem 3 (6) and (7) (i.e., $\mathscr{C}_{Q_p}(\mathfrak{A}) \cup \mathscr{C}_{Q_p}(\mathfrak{B}) \neq \mathscr{C}_{Q_p}(\mathfrak{A} \cup \mathfrak{B})$ and $\mathscr{C}_{Q_p}(\mathfrak{A} \cap \mathfrak{B}) \neq \mathscr{C}_{Q_p}(\mathfrak{A}) \cap \mathscr{C}_{Q_p}(\mathfrak{B})$) does not hold by the following example.

Example 3. (continued from Remark 1). As $\mathfrak{A} = \{1\}, \mathfrak{B} = \{2\}$, and $\mathfrak{A} \cup \mathfrak{B} = \{1, 2\}$, then $\mathscr{C}_{Q_p}(\{1\}) = \{1\}$, $\mathscr{C}_{Q_p}(\{2\}) = \{2\}$, and $\mathscr{C}_{Q_p}(\{1, 2\}) = \mathscr{X}$, and hence, $\mathscr{C}_{Q_p}(\mathfrak{A}) \cup \mathscr{C}_{Q_p}(\mathfrak{B}) = \{1, 2\} \neq \mathscr{X} = \mathscr{C}_{Q_p}(\mathfrak{A} \cup \mathfrak{B})$.

Example 4. Assume that $\mathscr{X} = \{1, 2, 3\}$ (i.e., $(\mathscr{X}, \tilde{\tau})$ be topological space) and $\tilde{\tau} = \{\mathscr{X}, \phi, \{2\}, t\{3\}n, q\{2, 3\}\}$. Then,

$$\mathscr{F}_{\mathscr{X}} = \mathbb{C}_p(\mathscr{X}) = \mathbb{G}\mathbb{C}_p(\mathscr{X}) = Q_p\mathbb{C}(\mathscr{X}) = \{\mathscr{X}, \phi, \{1\}, \{1, 2\}, \{1, 3\}\}. \tag{11}$$

Let $\mathfrak{A} = \{1\}$, $\mathfrak{B} = \{2\}$, and $\mathfrak{A} \cap \mathfrak{B} = \phi$. Then, $\mathscr{C}_{Q_p}(\{1\}) = \{1\}$, $\mathscr{C}_{Q_p}(\{2\}) = \{1, 2\}$, and $\mathscr{C}_{Q_p}(\phi) = \phi$, and hence, $\mathscr{C}_{Q_p}(\mathfrak{A}) \cap \mathscr{C}_{Q_p}(\mathfrak{B}) = \{1\} \neq \phi = \mathscr{C}_{Q_p}(\mathfrak{A} \cap \mathfrak{B})$.

The relationship among the Q_p-closed sets and other sets (i.e., closed sets, α-closed sets, g-closed sets, $g\alpha$-closed sets, αg-closed sets, and pg-closed sets) is presented by the following theorem.

Theorem 4. *The following six properties is holding in* $(\mathscr{X}, \tilde{\tau})$.

(1) *If* $\mathfrak{A} \in \mathscr{F}_{\mathscr{X}}$, *then* $\mathfrak{A} \in Q_p\mathbb{C}(\mathscr{X})$

(2) *If* $\mathfrak{A} \in \mathbb{C}_\alpha(\mathscr{X})$, *then* $\mathfrak{A} \in Q_p\mathbb{C}(\mathscr{X})$

(3) *If* $\mathfrak{A} \in \mathbb{G}\mathbb{C}(\mathscr{X})$, *then* $\mathfrak{A} \in Q_p\mathbb{C}(\mathscr{X})$

(4) *If* $\mathfrak{A} \in \mathbb{G}\mathbb{C}_\alpha(\mathscr{X})$, *then* $\mathfrak{A} \in Q_p\mathbb{C}(\mathscr{X})$

(5) *If* $\mathfrak{A} \in \mathbb{C}_\alpha\mathbb{G}(\mathscr{X})$, *then* $\mathfrak{A} \in Q_p\mathbb{C}(\mathscr{X})$

(6) *If* $\mathfrak{A} \in \mathbb{C}_p\mathbb{G}(\mathscr{X})$, *then* $\mathfrak{A} \in Q_p\mathbb{C}(\mathscr{X})$

Proof.

(1) As $\mathscr{C}_p(\mathfrak{A}) \subseteq \mathscr{C}(\mathfrak{A})$ and by Theorem 1 (1), we have $\mathscr{C}_{gp}(\mathscr{I}(\mathfrak{A})) \subseteq \mathscr{C}_p(\mathscr{I}(\mathfrak{A})) \subseteq \mathscr{C}(\mathscr{I}(\mathfrak{A})) \subseteq \mathfrak{A}$. Thus, $\mathfrak{A} \in Q_p\mathbb{C}(\mathscr{X})$.

(2) As $\mathscr{C}_p(\mathfrak{A}) \subseteq \mathscr{C}_\alpha(\mathfrak{A})$ and by Theorem 1 (1), we have $\mathscr{C}_{gp}(\mathscr{I}(\mathfrak{A})) \subseteq \mathscr{C}_p(\mathscr{I}(\mathfrak{A})) \subseteq \mathscr{C}(\mathscr{I}(\mathfrak{A})) \subseteq \mathscr{C}(\mathscr{I}(\mathscr{C}(\mathfrak{A}))) \subseteq \mathfrak{A}$. Thus, $\mathfrak{A} \in Q_p\mathbb{C}(\mathscr{X})$.

(3) As $\mathscr{C}_{gp}(\mathfrak{A}) \subseteq \mathscr{C}_g(\mathfrak{A})$ and by Theorem 1 (2), we have $\mathscr{C}_{Q_p}(\mathfrak{A}) \subseteq \mathscr{C}_{gp}(\mathfrak{A}) \subseteq \mathscr{C}_g(\mathfrak{A}) \subseteq \mathfrak{A}$. Thus, $\mathfrak{A} \in Q_p\mathbb{C}(\mathscr{X})$.

(4) As $\mathscr{C}_{gp}(\mathfrak{A}) \subseteq \mathscr{C}_g(\mathfrak{A})$ and by Theorem 1 (2), we have $\mathscr{C}_{Q_p}(\mathfrak{A}) \subseteq \mathscr{C}_{gp}(\mathfrak{A}) \subseteq \mathscr{C}_g(\mathfrak{A}) \subseteq \mathfrak{A}$. Thus, $\mathfrak{A} \in Q_p\mathbb{C}(\mathscr{X})$. □

The converse of Theorem 4 (i.e., $\mathfrak{A} \in Q_p\mathbb{C}(\mathscr{X})$, but $\mathfrak{A} \notin \mathscr{F}_{\mathscr{X}}$, $\mathfrak{A} \notin \mathbb{C}_\alpha(\mathscr{X})$, $\mathfrak{A} \notin \mathbb{G}\mathbb{C}(\mathscr{X})$, $\mathfrak{A} \notin \mathbb{G}\mathbb{C}_\alpha(\mathscr{X})$, $\mathfrak{A} \notin \mathbb{O}_\alpha\mathbb{G}(\mathscr{X})$, and $\mathfrak{A} \notin \mathbb{C}_p\mathbb{G}(\mathscr{X})$) does not hold by the following example.

Example 5. (continued from Example 1). Clearly,

$$\mathbb{G}\mathbb{C}_\alpha(\mathscr{X}) = \mathbb{C}_p\mathbb{G}(\mathscr{X}) = \mathbb{C}_\alpha\mathbb{G}(\mathscr{X}) = \mathbb{C}_\alpha(\mathscr{X}) = \mathbb{C}_p(\mathscr{X}). \tag{12}$$

and $\mathbb{G}\mathbb{C}(\mathscr{X}) = \mathbb{G}\mathbb{C}_p(\mathscr{X})$. Thus, $\mathbb{G}\mathbb{C}(\mathscr{X}) = \mathbb{G}\mathbb{C}_p(\mathscr{X})$, but $\{1\} \notin \mathscr{F}_{\mathscr{X}}, \{1\} \notin \mathbb{C}_\alpha(\mathscr{X}), \{1\} \notin \mathbb{G}\mathbb{C}(\mathscr{X}), \{1\} \notin \mathbb{G}\mathbb{C}_\alpha(\mathscr{X})$, $\{1\} \notin \mathbb{C}_\alpha\mathbb{G}(\mathscr{X})$, and $\{1\} \notin \mathbb{C}_p\mathbb{G}(\mathscr{X})$.

Definition 7. $\mathfrak{A}$ is called Q_p-open set if $\mathscr{X}\backslash\mathfrak{A} \in Q_p\mathbb{C}(\mathscr{X})$ and $Q_p\mathbb{O}(\mathscr{X})$ is the set of all Q_p-open sets in $\mathscr{X}$.

Lemma 2. *The following properties are holding in* $(\mathscr{X}, \tilde{\tau})$.

(1) $\mathscr{X}\backslash\mathscr{C}_{gp}(\mathscr{X}\backslash\mathfrak{A}) = \mathscr{I}_{gp}(\mathfrak{A})$

(2) $\mathscr{X}\backslash\mathscr{I}_{gp}(\mathscr{X}\mathfrak{A}) = \mathscr{C}_{gp}(\mathfrak{A})$

Proof. It is clear. □

Theorem 5. *The following properties are holding in* $(\mathscr{X}, \tilde{\tau})$:

$$\mathfrak{A} \in Q_p\mathbb{O}(\mathscr{X}) \Leftrightarrow \mathfrak{A} \subseteq \mathscr{I}_{gp}(\mathscr{C}(\mathfrak{A})). \tag{13}$$

Proof. Suppose that $\mathfrak{A} \in Q_p\mathbb{O}(\mathscr{X})$. Then, $\mathscr{X}\backslash\mathfrak{A} \in Q_p\mathbb{C}(\mathscr{X})$ and $\mathscr{C}_{gp}(\mathscr{I}(\mathscr{X}\backslash\mathfrak{A})) \subseteq \mathscr{X}\backslash\mathfrak{A}$. From Lemma 2, we have $\mathfrak{A} \subseteq \mathscr{I}_{gp}(\mathscr{C}(\mathfrak{A}))$. Conversely, $\mathfrak{A} \subseteq \mathscr{I}_{gp}(\mathscr{C}(\mathfrak{A}))$. Then, $\mathscr{X}\backslash\mathscr{I}_{gp}(\mathscr{C}(\mathfrak{A})) \subseteq \mathscr{X}\backslash\mathfrak{A}$. Thus, $\mathscr{I}_{gp}(\mathscr{C}(\mathscr{X}\mathfrak{A})) \subseteq \mathscr{X}\backslash\mathfrak{A}$. Thus, $\mathscr{X}\backslash\mathfrak{A} \in Q_p\mathbb{C}(\mathscr{X})$, and hence, $\mathfrak{A} \in Q_p\mathbb{O}(\mathscr{X})$. □

Lemma 3. *Let* $\mathfrak{L} \in \mathbb{G}\mathbb{O}_p(\mathscr{X})$ *such that* $\mathfrak{L} \subseteq \mathfrak{A} \subseteq \mathscr{I}_{gp}(\mathscr{C}(\mathfrak{L}))$. *Then,* $\mathfrak{A} \in Q_p\mathbb{O}(\mathscr{X})$.

Proof. As $\mathfrak{L} \in \mathbb{G}\mathbb{O}_p(\mathscr{X})$, $\mathscr{X}\backslash\mathfrak{L} \in \mathbb{G}\mathbb{C}_p(\mathscr{X})$, and $\mathscr{X}\backslash\mathscr{I}_{gp}(\mathscr{C}(\mathfrak{L})) \subseteq \mathscr{X}\backslash\mathfrak{A} \subseteq \mathscr{X}\backslash\mathfrak{L}$, thus, by Lemma 2, we have $\mathscr{C}_{gp}(\mathscr{I}(\mathscr{X}\backslash\mathfrak{L})) \subseteq \mathscr{X}\backslash\mathfrak{A} \subseteq \mathscr{X}\backslash\mathfrak{L}$. By Lemma 1, we get $\mathscr{X}\backslash\mathfrak{A} \in Q_p\mathbb{C}(\mathscr{X})$, and hence, $\mathfrak{A} \in Q_p\mathbb{O}(\mathscr{X})$. □

The converse of Lemma 3 (i.e., $\mathfrak{L} \subseteq \nsubseteq \mathscr{I}_{gp}(\mathscr{C}(\mathfrak{L}))$) does not hold by the following example.

Example 6. (continued from Example 1). As

$$\mathbb{O}_p(\mathcal{X}) = \{\mathcal{X}, \phi, \{1\}, \{1,2\}, \{1,3\}\},$$
$$\mathbb{GO}_p(\mathcal{X}) = \{\mathcal{X}, \phi, \{1\}, \{2\}, \{3\}, \{1,2\}, \{1,3\}\}, \tag{14}$$

$$Q_p\mathbb{O}(\mathcal{X}) = 2^{\mathcal{X}}, \tag{15}$$

let $\mathfrak{A} = \{1,2\} \in Q_p\mathbb{O}(\mathcal{X})$ and $\mathfrak{L} = \phi \in \mathbb{GO}_p(\mathcal{X})$. Then, $\mathfrak{L} \subseteq A \notin \phi = \mathcal{I}_{gp}(\mathcal{C}(\mathfrak{L}))$.

Theorem 6. *The following two properties are holding in* $(\mathcal{X}, \tilde{\tau})$.

(1) If $\mathfrak{A} \in \mathbb{O}_p(\mathcal{X})$, *then* $\mathfrak{A} \in Q_p\mathbb{O}(\mathcal{X})$
(2) If $\mathfrak{A} \in \mathbb{GO}_p(\mathcal{X})$, *then* $\mathfrak{A} \in Q_p\mathbb{O}(\mathcal{X})$

Proof. From Theorem 1 and Lemma 2, the proof is clear. □

The converse of Theorem 6 (i.e., $\mathfrak{A} \in Q_p\mathbb{O}(\mathcal{X})$, but $\mathfrak{A} \notin \mathbb{O}_p(\mathcal{X})$ and $\mathfrak{A} \notin \mathbb{GO}_p(\mathcal{X})$) does not hold by the following example.

Example 7. (continued from Examples 1 and 6). $\{2\} \in Q_p\mathbb{O}(\mathcal{X})$, but $\{2\} \notin \mathbb{O}_p(\mathcal{X})$, and $\{2,3\} \in Q_p\mathbb{O}(\mathcal{X})$, but $\{2,3\} \notin \mathbb{GO}_p(\mathcal{X})$.

Theorem 7. *Arbitrary union of* Q_p*-open sets is* Q_p*-open set.*

Proof. From Theorem 2 and Lemma 2, the proof is clear. □

Remark 2. The intersection of two Q_p-open sets need not be Q_p-open set (i.e., $\mathfrak{A}, \mathfrak{B} \in Q_p\mathbb{O}(\mathcal{X})$, but $\mathfrak{A} \cap \mathfrak{B} \notin Q_p\mathbb{O}(\mathcal{X})$) as given in Remark 1. As

$$\mathbb{O}_p(\mathcal{X}) = \mathbb{GO}_p(\mathcal{X}) = Q_p\mathbb{O}(\mathcal{X}) = \{\mathcal{X}, \phi, \{1\}, \{2\}, \{1,2\}, \{1,3\}, \{2,3\}\}, \tag{16}$$

let $\mathfrak{A} = \{2,3\} \in Q_p\mathbb{O}(\mathcal{X})$ and $\mathfrak{B} = \{1,3\} \in Q_p\mathbb{O}(\mathcal{X})$. Then, $\mathfrak{A} \cap \mathfrak{B} = \{3\} \notin Q_p\mathbb{O}(\mathcal{X})$.

Corollary 2. *The following two properties are holding in* $(\mathcal{X}, \tilde{\tau})$.

(1) Let $\mathfrak{A} \in Q_p\mathbb{O}(\mathcal{X})$ *and* $\mathfrak{B} \in \mathbb{O}_p(\mathcal{X})$. *Then* $\mathfrak{A} \cup \mathfrak{B} \in Q_p\mathbb{O}(\mathcal{X})$.
(2) Let $\mathfrak{A} \in Q_p\mathbb{O}(\mathcal{X})$ *and* $\mathfrak{B} \in \mathbb{GO}_p(\mathcal{X})$. *Then* $\mathfrak{A} \cup \mathfrak{B} \in Q_p\mathbb{O}(\mathcal{X})$.

Proof. From Theorem 6 and Lemma 7, the proof is clear. □ □

Definition 8. $\mathcal{I}_{Q_p}(\mathfrak{A})$ is called Q_p-interior of $\mathfrak{A}$ in $(\mathcal{X}, \tilde{\tau})$ if

$$\mathcal{I}_{Q_p}(\mathfrak{A}) = \cup\{\mathfrak{L} | \mathfrak{L} \subseteq \mathfrak{A} \text{ and } \mathfrak{L} \in Q_p\mathbb{O}(\mathcal{X})\}. \tag{17}$$

Lemma 4. *The following two properties are holding in* $(\mathcal{X}, \tilde{\tau})$:

(1) $\mathcal{X} \backslash \mathcal{C}_{Q_p}(\mathfrak{A}) = \mathcal{I}_{Q_p}(\mathcal{X} \backslash \mathfrak{A})$
(2) $\mathcal{X} \backslash \mathcal{I}_{Q_p}(\mathfrak{A}) = \mathcal{C}_{Q_p}(\mathcal{X} \backslash \mathfrak{A})$

Proof. It is clear. □

Theorem 8. *The following properties are holding in* $(\mathcal{X}, \tilde{\tau})$.

(1) $\mathfrak{A} \in Q_p\mathbb{O}(\mathcal{X}) \Leftrightarrow \mathcal{I}_{Q_p}(\mathfrak{A}) = \mathfrak{A}$
(2) $\mathcal{I}_p(\mathfrak{A}) \subseteq \mathcal{I}_{Q_p}(\mathfrak{A}) \subseteq \mathfrak{A}, \mathcal{I}_{gp}(\mathfrak{A}) \subseteq \mathcal{I}_{Q_p}(\mathfrak{A})$
(3) $\mathcal{I}_{Q_p}(\phi) = \phi$ *and* $\mathcal{I}_{Q_p}(\mathcal{X}) = \mathcal{X}$
(4) If $\mathfrak{A} \subseteq \mathfrak{B}$, *then* $\mathcal{I}_{Q_p}(\mathfrak{A}) \subseteq \mathcal{I}_{Q_p}(\mathfrak{B})$
(5) $\mathcal{I}_{Q_p}(\mathcal{I}_{Q_p}(\mathfrak{A})) = \mathcal{I}_{Q_p}(\mathfrak{A})$
(6) $\mathcal{I}_{Q_p}(\mathfrak{A}) \cup \mathcal{I}_{Q_p}(\mathfrak{B}) \subseteq \mathcal{I}_{Q_p}(\mathfrak{A} \cup \mathfrak{B})$
(7) $\mathcal{I}_{Q_p}(\mathfrak{A} \cap \mathfrak{B}) \subseteq \mathcal{I}_{Q_p}(\mathfrak{A}) \cap \mathcal{I}_{Q_p}(\mathfrak{B})$

Proof. It is similar to Theorem 3. □

The equality of Theorem 8 (6) and (7) (i.e., $\mathcal{I}_{Q_p}(\mathfrak{A}) \cup \mathcal{I}_{Q_p}(\mathfrak{B}) \neq \mathcal{I}_{Q_p}(\mathfrak{A} \cup \mathfrak{B})$ and $\mathcal{I}_{Q_p}(\mathfrak{A} \cap \mathfrak{B}) \neq \mathcal{I}_{Q_p}(\mathfrak{A}) \cap \mathcal{I}_{Q_p}(\mathfrak{B})$) does not hold by the following examples.

Example 8 (continued from Remarks 1 and 2). As $\mathfrak{A} = \{2\}, \mathfrak{B} = \{3\}$, and $\mathfrak{A} \cup \mathfrak{B} = \{2,3\}$, then $\mathcal{I}_{Q_p}(\{2\}) = \{2\}, \mathcal{I}_{Q_p}(\{3\}) = \phi$, and $\mathcal{I}_{Q_p}(\{2,3\}) = \{2,3\}$, and hence, $\mathcal{I}_{Q_p}(\mathfrak{A}) \cup \mathcal{I}_{Q_p}(\mathfrak{B}) = \{2\} \neq \{2,3\} = \mathcal{I}_{Q_p}(\mathfrak{A} \cup \mathfrak{B})$.

Example 9 (continued from Remarks 1 and 2). As $\mathfrak{A} = \{1,3\}, \mathfrak{B} = \{2,3\}$, and $\mathfrak{A} \cap \mathfrak{B} = \{3\}$, then $\mathcal{I}_{Q_p}(\{1,3\}) = \{1,3\}$, $\mathcal{I}_{Q_p}(\{2,3\}) = \{2,3\}$, and $\mathcal{I}_{Q_p}(\{3\}) = \phi$, and hence, $\mathcal{I}_{Q_p}(\mathfrak{A}) \cap \mathcal{I}_{Q_p}(\mathfrak{B}) = \{3\} \neq \phi = \mathcal{I}_{Q_p}(\mathfrak{A} \cap \mathfrak{B})$.

Theorem 9. *The following properties is holding in* $(\mathcal{X}, \tilde{\tau})$. *Then,*

$$x \in \mathcal{C}_{Q_p}(\mathfrak{A}) \Leftrightarrow \mathfrak{L} \cap \mathfrak{A} \neq \phi, \quad \forall x \in \mathfrak{L} \in Q_p\mathbb{O}(\mathcal{X}). \tag{18}$$

Proof. The proof is clear. □

Lemma 5. *The following properties are holding in* $(\mathcal{X}, \tilde{\tau})$. *Then,*

(1) $\mathfrak{A} \cap \mathcal{I}_{gp}(\mathcal{C}(\mathcal{I}_{gp}(\mathfrak{A}))) \in Q_p\mathbb{O}(\mathcal{X})$
(2) $\mathfrak{A} \cup \mathcal{C}_{gp}(\mathcal{I}(\mathcal{C}_{gp}(\mathfrak{A}))) \in Q_p\mathbb{C}(\mathcal{X})$

Proof. $\mathcal{I}_{gp}(\mathcal{C}(\mathcal{I}_{gp}(\mathfrak{A} \cap \mathcal{I}_{gp}(\mathcal{C}(\mathcal{I}_{gp}(\mathfrak{A})))))) = \mathcal{I}_{gp}(\mathcal{C}(\mathcal{I}_{gp}(\mathfrak{A}) \cap t\mathcal{I}_{gp}n(\mathcal{C}(\mathcal{I}_{gp}(\mathfrak{A})))))) = \mathcal{I}_{gp}(\mathcal{C}(\mathcal{I}_{gp}(\mathfrak{A}))))$.

Then, we have $\mathfrak{A} \cap \mathcal{I}_{gp}(\mathcal{C}(\mathcal{I}_{gp}(\mathfrak{A}))) = \mathfrak{A} \cap \mathcal{I}_{gp}(\mathcal{C}(\mathcal{I}_{gp}(\mathfrak{A} \cap \mathcal{I}_{gp}(\mathcal{C}(\mathcal{I}_{gp}(\mathfrak{A})))))) \subseteq \cap \mathcal{I}_{gp}(\mathcal{C}(\mathcal{I}_{gp}(\mathfrak{A} \cap \mathcal{I}_{gp}(\mathcal{C}(\mathcal{I}_{gp}(\mathfrak{A})))))))$.

Hence, $\mathfrak{A} \cap \mathcal{I}_{gp}(\mathcal{C}(\mathcal{I}_{gp}(\mathfrak{A}))) \in Q_p\mathbb{O}(\mathcal{X})$.

In (2), by (1), we have $\mathcal{X}\setminus(\mathfrak{A}\cup\mathscr{C}_{gp}(\mathcal{I}(\mathscr{C}_{gp}(\mathfrak{A}))))=(\mathcal{X}\setminus\mathfrak{A})\cap\mathcal{I}_{gp}(\mathscr{C}(\mathcal{I}_{gp}(\mathcal{X}\setminus\mathfrak{A})))\in Q_p\mathbb{O}(\mathcal{X})$. Therefore, $\mathfrak{A}\cup\mathscr{C}_{gp}(\mathcal{I}(\mathscr{C}_{gp}(\mathfrak{A})))\in Q_p\mathbb{C}(\mathcal{X})$. □

Theorem 10. *The following two properties are holding in* $(\mathcal{X},\tilde{\tau})$. *Then,*

(1) $\mathcal{I}_{Q_p}(\mathfrak{A})=\mathfrak{A}\cap\mathcal{I}_{gp}(\mathscr{C}(\mathcal{I}_{gp}(\mathfrak{A})))$

(2) $\mathscr{C}_{Q_p}(\mathfrak{A})=\mathfrak{A}\cup\mathscr{C}_{gp}(\mathcal{I}(\mathscr{C}_{gp}(\mathfrak{A})))$

Proof.

(1) Suppose $\mathfrak{B}=\mathcal{I}_{Q_p}(\mathfrak{A})$. Since $\mathfrak{B}\in Q_p\mathbb{O}(\mathcal{X})$ and $\mathfrak{B}\subseteq\mathfrak{A}$, then, we have $\mathfrak{B}\subseteq\mathcal{I}_{gp}(\mathscr{C}(\mathcal{I}_{gp}(\mathfrak{B})))\subseteq\mathcal{I}_{gp}(\mathscr{C}(\mathcal{I}_{gp}(\mathfrak{A})))$. Thus, $\mathfrak{B}\subseteq\mathfrak{A}\cap\mathcal{I}_{gp}(\mathscr{C}(\mathcal{I}_{gp}(\mathfrak{A})))$. By Lemma 5, we get $\mathfrak{A}\cap\mathcal{I}_{gp}(\mathscr{C}(\mathcal{I}_{gp}(\mathfrak{A})))\in Q_p\mathbb{O}(\mathcal{X})$. From Definition 8, we have $\mathfrak{A}\cap\mathcal{I}_{gp}(\mathscr{C}(\mathcal{I}_{gp}(\mathfrak{A})))\subseteq\mathfrak{B}$. Therefore, $\mathfrak{B}=\mathfrak{A}\cap\mathcal{I}_{gp}(\mathscr{C}(\mathcal{I}_{gp}(\mathfrak{A})))$ and hence, $\mathcal{I}_{Q_p}(\mathfrak{A})=\mathfrak{A}\cap\mathcal{I}_{gp}(\mathscr{C}(\mathcal{I}_{gp}(\mathfrak{A})))$.

(2) By Lemma 4, we have $\mathscr{C}_{Q_p}(\mathfrak{A})=\mathcal{X}\setminus\mathcal{I}_{Q_p}(\mathcal{X}\setminus\mathfrak{A})=\mathcal{X}\setminus((\mathcal{X}\setminus\mathfrak{A})\cap\mathcal{I}_{gp}(\mathscr{C}(\mathcal{I}_{gp}(\mathcal{X}\setminus\mathfrak{A}))))=\mathfrak{A}\cup\mathscr{C}_{gp}(\mathcal{I}(\mathscr{C}_{gp}(\mathfrak{A})))$. □

The relationship among the Q_p-open sets and other sets (i.e., open sets, α-open sets, g-open sets, $g\alpha$-open sets, αg-open sets, and pg-open sets) is presented by the following theorem.

Theorem 11. *The following properties is holding in* $(\mathcal{X},\tilde{\tau})$.

(1) If $\mathfrak{A}\in\tilde{\tau}(\mathcal{X})$, *then* $\mathfrak{A}\in Q_p\mathbb{O}(\mathcal{X})$

(2) If $\mathfrak{A}\in\mathbb{O}_\alpha(\mathcal{X})$, *then* $\mathfrak{A}\in Q_p\mathbb{O}(\mathcal{X})$

(3) If $\mathfrak{A}\in\mathbb{GO}(\mathcal{X})$, *then* $\mathfrak{A}\in Q_p\mathbb{O}(\mathcal{X})$

(4) If $\mathfrak{A}\in\mathbb{GO}_\alpha(\mathcal{X})$, *then* $\mathfrak{A}\in Q_p\mathbb{O}(\mathcal{X})$

(5) If $\mathfrak{A}\in\mathbb{O}_\alpha\mathbb{G}(\mathcal{X})$, *then* $\mathfrak{A}\in Q_p\mathbb{O}(\mathcal{X})$

(6) If $\mathfrak{A}\in\mathbb{O}_p\mathbb{G}(\mathcal{X})$, *then* $\mathfrak{A}\in Q_p\mathbb{O}(\mathcal{X})$

Proof. It is similar to Theorem 4. □

The converse of Theorem 11 (i.e., $\mathfrak{A}\in Q_p\mathbb{O}(\mathcal{X})$, but $\mathfrak{A}\notin\tilde{\tau}(\mathcal{X})$, $\mathfrak{A}\notin\mathbb{O}_\alpha(\mathcal{X})$, $\mathfrak{A}\notin\mathbb{GO}(\mathcal{X})$, $\mathfrak{A}\notin\mathbb{GO}_\alpha(\mathcal{X})$, $\mathfrak{A}\notin\mathbb{O}_\alpha\mathbb{G}(\mathcal{X})$, and $\mathfrak{A}\notin\mathbb{O}_p\mathbb{G}(\mathcal{X})$) does not hold by the following example.

Example 10. (continued from Examples 1, 5, and 6). Clearly,

$$\mathbb{GO}_\alpha(\mathcal{X})=\mathbb{O}_p\mathbb{G}(\mathcal{X})=\mathbb{O}_\alpha\mathbb{G}(\mathcal{X})=\mathbb{O}_\alpha(\mathcal{X})=\mathbb{O}_p(\mathcal{X}). \tag{19}$$

and $\mathbb{GO}(\mathcal{X})=\mathbb{GO}_p(\mathcal{X})$. Thus, $\{2,3\}\in Q_p\mathbb{O}(\mathcal{X})$, but $\{2,3\}\in\tilde{\tau},(2,3)\in\mathcal{X})(\mathbb{O}_\alpha(\mathcal{X}),\{2,3\}\notin\mathbb{GO}(\mathcal{X})$, $\{2,3\}\notin\mathbb{GO}_\alpha(\mathcal{X}),\{2,3\}\notin\mathbb{O}_\alpha\mathbb{G}(\mathcal{X}))$, and $\{2,3\}\notin\mathbb{O}_p\mathbb{G}(\mathcal{X})$.

3. ERROR!!Q_p-Continuous Mappings, Q_p-Open Mappings, and Q_p-Closed Mappings

Definition 9. A mapping $\psi:\mathcal{X}\longrightarrow\mathcal{Y}$ is called Q_p-continuous if

$$\begin{aligned}&\mathfrak{Q}\in\tilde{\sigma}(\mathcal{Y}),\\&\psi^{-1}(\mathfrak{Q})\in Q_p\mathbb{O}(\mathcal{X}),\end{aligned} \tag{20}$$

where $\tilde{\sigma}(\mathcal{Y})$ is a topology on $\mathcal{Y}$ and $\mathcal{X}$ is defined on a topology $\tilde{\tau}$

Theorem 12. *The following two properties are holding in* $(\mathcal{X},\tilde{\tau})$ *and* $(\mathcal{Y},\tilde{\sigma})$.

(1) Every precontinuous mapping is Q_p*-continuous mapping*

(2) Every gp-continuous mapping is Q_p*-continuous mapping*

Proof. From Theorem 6, the proof is clear. □

The converse of Theorem 12 (i.e., ψ is Q_p-continuous mapping, but ψ not precontinuous mapping and ψ is Q_p-continuous mapping but ψ not gp-continuous mapping) does not hold by the following example.

Example 11. Assume that $\mathcal{X}=\{1,2,3\}$ (i.e., $(\mathcal{X},\tilde{\tau})$ be topological space, $\tilde{\tau}=\{\mathcal{X},\phi,\{1\}\}$) and $\mathcal{Y}=\{u,v,w\}$ (i.e., $(\mathcal{Y},\tilde{\sigma})$ be topological space, $\tilde{\sigma}=\{\mathcal{Y},\phi,\{u,v\},\{w\}\}$).

(1) Suppose $\psi:\mathcal{X}\longrightarrow\mathcal{Y}$ be a mapping defined by

$$\psi(1)=\psi(2)=u,\text{ and }\psi(3)=w. \tag{21}$$

Then,

$$\begin{aligned}\mathcal{F}_{\mathcal{X}}&=\{\mathcal{X},\phi,\{2,3\}\},\\\mathbb{C}_p(\mathcal{X})&=\{\mathcal{X},\phi,\{2\},\{3\},\{2,3\}\},\\\mathbb{GC}_p(\mathcal{X})&=\{\mathcal{X},\phi,\{2\},\{3\},\{1,2\},\{2,3\},\{1,3\}\},\\\mathbb{O}_p(\mathcal{X})&=\{\mathcal{X},\phi,\{1\},\{1,2\},\{1,3\}\},\\\mathbb{GO}_p(\mathcal{X})&=\{\mathcal{X},\phi,\{1\},\{2\},\{3\},\{1,2\},\{1,3\}\},\\Q_p\mathbb{C}(\mathcal{X})&=Q_p\mathbb{O}(\mathcal{X})=2^{\mathcal{X}}.\end{aligned} \tag{22}$$

As $\{w\}\in\tilde{\sigma}(\mathcal{Y}),\psi^{-1}(\{w\})=\{3\}\in Q_p\mathbb{O}(\mathcal{X})$, but $\{3\}\notin\mathbb{O}_p(\mathcal{X})$.

Thus, ψ is Q_p-continuous mapping but ψ not precontinuous mapping.

(2) Suppose $\psi:\mathcal{X}\longrightarrow\mathcal{Y}$ be a mapping defined by

$$\psi(1)=u\text{ and}\psi(2)=\psi(3)=w. \tag{23}$$

As $\{w\} \in \tilde{\sigma}(\mathcal{Y}), \psi^{-1}(\{w\}) = \{2,3\} \in Q_p\mathbb{O}(\mathcal{X})$, but $\{2,3\} \notin \mathbb{GO}_p(\mathcal{X})$.

Thus, ψ is Q_p-continuous mapping but ψ not gp-continuous mapping.

Theorem 13. *Assume that ψ: $\mathcal{X} \longrightarrow \mathcal{Y}$ be a mapping. Then, the following six properties are equivalent:*

(1) ψ is Q_p-continuous

(2) For every $x \in \mathcal{X}$ and every open set $\mathfrak{L} \subset \mathcal{Y}$ containing $\psi(x)$, there exists Q_p-open set $\mathfrak{P} \subset \mathcal{X}$ containing x such that $\psi(\mathfrak{P}) \subset \mathfrak{L}$

(3) $\psi^{-1}(\mathfrak{F}) \in Q_p\mathbb{C}(\mathcal{X})$, $\mathfrak{F} \subset \mathcal{Y}$, be a closed set

(4) $\psi(\mathscr{C}_{Q_p}(\mathfrak{A})) \subseteq \mathscr{C}(\psi(\mathfrak{A}))(\mathfrak{A} \subseteq \mathcal{X})$

(5) $\mathscr{C}_{Q_p}(\psi^{-1}(\mathfrak{B})) \subseteq \psi^{-1}(\mathscr{C}(\mathfrak{B}))(\mathfrak{B} \subseteq \mathcal{Y})$

(6) $\psi^{-1}(\mathscr{I}(\mathfrak{B})) \subseteq \mathscr{I}_{Q_p}(\psi^{-1}(\mathfrak{B}))(\mathfrak{B} \subseteq \mathcal{Y})$

Proof.

(1) $\Rightarrow$ (2) Since $\mathfrak{L} \subset \mathcal{Y}$ containing $\psi(x)$ is the open set, then $\psi^{-1}(\mathfrak{L}) \in Q_p\mathbb{O}(\mathcal{X})$. Put $\mathfrak{P} = \psi^{-1}(\mathfrak{L})$ which contains x; hence, $\psi(\mathfrak{P}) \subset \mathfrak{L}$.

(2) $\Rightarrow$ (1) Suppose $\mathfrak{L} \subset \mathcal{Y}$ be the open set, and let $x \in \psi^{-1}(\mathfrak{L})$; then, $\psi(x) \in \mathfrak{L}$ and hence, there exists $\mathfrak{P}_x \in Q_p\mathbb{O}(\mathcal{X})$ such that $x \in \mathfrak{P}_x$ and $\psi(\mathfrak{P}_x) \subset \mathfrak{L}$. Thus, $x \in \mathfrak{P}_x \subset \psi^{-1}(\mathfrak{L})$, so $\psi^{-1}(\mathfrak{L}) = \cup_{x \in \psi^{-1}(\mathfrak{L})} \mathfrak{P}_x$, but $\cup_{x \in \psi^{-1}(\mathfrak{L})} \mathfrak{P}_x \in Q_p\mathbb{O}(\mathcal{X})$. Therefore, $\psi^{-1}(\mathfrak{L}) \in Q_p\mathbb{O}(\mathcal{X})$, and thus, ψ is Q_p-continuous.

(1) $\Rightarrow$ (3) Suppose $\mathfrak{F} \subset \mathcal{Y}$ be closed set. Thus, $\mathcal{Y} \backslash \mathfrak{F}$ is the open set and $\psi^{-1}(\mathcal{Y} \backslash \mathfrak{F}) \in Q_p\mathbb{O}(\mathcal{X})$, i.e., $\mathcal{X} \backslash \psi^{-1}(\mathfrak{F}) \in Q_p\mathbb{O}(\mathcal{X})$. Hence, $\psi^{-1}(\mathfrak{F}) \in Q_p\mathbb{C}(\mathcal{X})$.

(3) $\Rightarrow$ (4) Suppose $\mathfrak{A} \subseteq \mathcal{X}$ and $\mathfrak{F}$ be a closed set in $\mathcal{Y}$ containing $\psi(\mathfrak{A})$. By (3), we have $\psi^{-1}(\mathfrak{F})$ is Q_p-closed set containing $\mathfrak{A}$. Then, $\mathscr{C}_{Q_p}(\mathfrak{A}) \subseteq \mathscr{C}_{Q_p}(\psi^{-1}(\mathfrak{F})) = \psi^{-1}(\mathfrak{F})$, and thus, $\psi(\mathscr{C}_{Q_p}(\mathfrak{A})) \subseteq \mathfrak{F}$. Hence, $\psi(\mathscr{C}_{Q_p}(\mathfrak{A})) \subseteq \mathscr{C}(\psi(\mathfrak{A}))$.

(4) $\Rightarrow$ (5) Suppose $\mathfrak{B} \subseteq \mathcal{Y}$ and $\mathfrak{A} = \psi^{-1}(\mathfrak{B})$. By assumption, we have $\psi(\mathscr{C}_{Q_p}(\mathfrak{A})) \subseteq \mathscr{C}(\psi(\mathfrak{A})) \subseteq \mathscr{C}(\mathfrak{B})$. Then, $\mathscr{C}_{Q_p}(\mathfrak{A}) \subseteq \psi^{-1}(\mathscr{C}(\mathfrak{B}))$. Therefore, $\mathscr{C}_{Q_p}(\psi^{-1}(\mathfrak{B})) \subseteq \psi^{-1}(\mathscr{C}(\mathfrak{B}))$.

(5) $\Rightarrow$ (6) Suppose $\mathfrak{B} \subseteq \mathcal{Y}$. By assumption, we have $\mathscr{C}_{Q_p}(\psi^{-1}(\mathcal{Y} \backslash \mathfrak{B})) \subseteq \psi^{-1}(\mathscr{C}(\mathcal{Y}\mathfrak{B}))$. Then, $\mathscr{C}_{Q_p}(\mathcal{X} \backslash \psi^{-1}(\mathfrak{B})) \subseteq \psi^{-1}(\mathcal{Y} \backslash \mathscr{I}(\mathfrak{B}))$, and thus, $\mathcal{X} \backslash \mathscr{I}_{Q_p}(\psi^{-1}(\mathfrak{B})) \subseteq \mathcal{X} \backslash \psi^{-1}(\mathscr{I}(\mathfrak{B}))$. By taking complement, we obtain $\psi^{-1}(\mathscr{I}(\mathfrak{B})) \subseteq \mathscr{I}_{Q_p}(\psi^{-1}(\mathfrak{B}))$.

(6) $\Rightarrow$ (1) Suppose $\mathfrak{L}$ be any open set in $\mathcal{Y}$. Then, $\mathscr{I}(\mathfrak{L}) = \mathfrak{L}$. By assumption, $\psi^{-1}(\mathscr{I}(\mathfrak{L})) \subseteq \mathscr{I}_{Q_p}(\psi^{-1}(\mathfrak{L}))$, and hence, $\psi^{-1}(\mathfrak{L}) \subseteq \mathscr{I}_{Q_p}(\psi^{-1}(\mathfrak{L}))$. Thus, $\psi^{-1}(\mathfrak{L}) = \mathscr{I}_{Q_p}(\psi^{-1}(\mathfrak{L}))$, and we have $\psi^{-1}(\mathfrak{L}) \in Q_p\mathbb{O}(\mathcal{X})$. Therefore, ψ is Q_p-continuous. □

Remark 3. Composition of two Q_p-continuous mappings does not need to be Q_p-continuous mapping, as shown by the following example.

Example 12. Assume that $\mathcal{X} = \{1,2,3\}$ (i.e., $(\mathcal{X}, \tilde{\tau})$ be topological space, $\tilde{\tau} = \{\mathcal{X}, \phi, \{2\}, t\{1,2\}\})$, $\mathcal{Y} = \{u, v, w\}$ (i.e., $(\mathcal{Y}, \tilde{\sigma})$ be topological space, $\tilde{\sigma} = \{\mathcal{Y}, \phi, \{u\}\})$, and $\mathcal{Z} = \{s, r, t\}$ (i.e., $(\mathcal{Z}, \tilde{\theta})$ be topological space, $\tilde{\theta} = \{\mathcal{Z}, \phi, \{t\}\}$).

(1) Suppose ψ: $\mathcal{X} \longrightarrow \mathcal{Y}$ be a mapping defined by

$$\psi(1) = v, \psi(2) = u, \text{and} \psi(3) = w. \tag{24}$$

Then,

$$\begin{aligned}
\mathcal{F}_{\mathcal{X}} &= \{\mathcal{X}, \phi, \{3\}\{1,3\}\},\\
\mathbb{C}_p(\mathcal{X}) &= \{\mathcal{X}, \phi, \{1\}, \{3\}, \{1,3\}\},\\
\mathbb{GC}_p(\mathcal{X}) &= Q_p\mathbb{C}(\mathcal{X}) = \{\mathcal{X}, \phi, \{1\}, \{3\}, \{1,3\}, \{2,3\}\},\\
\mathbb{O}_p(\mathcal{X}) &= \{\mathcal{X}, \phi, \{2\}, \{1,2\}, \{2,3\}\},\\
\mathbb{GO}_p(\mathcal{X}) &= Q_p\mathbb{O}(\mathcal{X}) = \{\mathcal{X}, \phi, \{1\}, \{2\}, \{1,2\}, \{2,3\}\}.
\end{aligned} \tag{25}$$

Thus, ψ is Q_p-continuous mapping.

(2) Suppose φ: $\mathcal{Y} \longrightarrow \mathcal{Z}$ be a mapping defined by

$$\varphi(u) = \varphi(v) = s, \text{ and } \varphi(w) = t. \tag{26}$$

Then,

$$\begin{aligned}
\mathcal{F}_{\mathcal{Y}} &= \{\mathcal{Y}, \phi, \{v, w\}\},\\
\mathbb{C}_p(\mathcal{Y}) &= \{\mathcal{Y}, \phi, \{v\}, \{w\}, \{v, w\}\},\\
\mathbb{GC}_p(\mathcal{Y}) &= \{\mathcal{Y}, \phi, \{v\}, \{w\}, \{u, v\}, \{u, w\}, \{v, w\}\},\\
\mathbb{O}_p(\mathcal{Y}) &= \{\mathcal{Y}, \phi, \{u\}, \{u, v\}, \{u, w\}\},\\
\mathbb{GO}_p(\mathcal{Y}) &= \{\mathcal{Y}, \phi, \{u\}, \{v\}, \{w\}, \{u, v\}, \{u, w\}\},\\
Q_p\mathbb{C}(\mathcal{Y}) &= Q_p\mathbb{O}(\mathcal{Y}).
\end{aligned} \tag{27}$$

Thus, φ is Q_p-continuous mapping.

From (1) and (2), $\{t\} \in \tilde{\theta}(\mathcal{Z})$, but $(\varphi^{\circ}\psi)^{-1}(\{t\}) = \psi^{-1}(\varphi^{-1}(\{t\})) = \psi^{-1}(\{w\}) = \{3\} \notin Q_p\mathbb{O}(\mathcal{X})$. Thus, $\varphi^{\circ}\psi$ is not Q_p-continuous mapping.

Definition 10. A mapping ψ: $\mathcal{X} \longrightarrow \mathcal{Y}$ is called

(1) Q_p-open if

$$\mathfrak{L} \in \tilde{\tau}(\mathcal{X}), \psi(\mathfrak{L}) \in Q_p\mathbb{O}(\mathcal{Y}), \tag{28}$$

where $\tilde{\tau}(\mathcal{X})$ is a topology on $\mathcal{X}$ and $\mathcal{Y}$ is defined on a topology $\tilde{\sigma}$.

(2) Q_p-closed if

$$\mathfrak{F} \in \mathcal{F}_{\mathcal{X}}, \psi(\mathfrak{F}) \in Q_p\mathbb{C}(\mathcal{Y}), \tag{29}$$

where $\mathcal{F}_{\mathcal{X}}$ is the closed sets of $\mathcal{X}$.

Theorem 14. *The following two properties are holding in $(\mathcal{X}, \tilde{\tau})$ and $(\mathcal{Y}, \tilde{\sigma})$.*

(1) *Every preopen (resp. preclosed) mapping is Q_p-open (resp. Q_p-closed) mapping*

(2) *Every gp-open (resp. gp-closed) mapping is Q_p-open (resp. Q_p-closed) mapping*

Proof. It follows from Theorem 6. □

Example 13. (continued from Example 11).

(1) Suppose $\psi: \mathcal{X} \longrightarrow \mathcal{Y}$ be a mapping defined by

$$\psi(1) = \psi(2) = v, \text{and} \psi(3) = u. \tag{30}$$

(i) As $\{2\} \in \tilde{\tau}(\mathcal{X}), \psi(\{2\}) = \{v\} \in Q_p\mathbb{O}(\mathcal{Y})$, but $\{v\} \notin \mathbb{O}_p(\mathcal{Y})$. Thus, ψ is Q_p-open mapping but ψ not preopen mapping.

(ii) As $\{3\} \in \mathcal{F}_{\mathcal{X}}$, $\psi(\{3\}) = \{u\} \in Q_p\mathbb{O}(\mathcal{Y})$, but $\{u\} \notin \mathbb{C}_p(\mathcal{Y})$. Thus, ψ is Q_p-closed mapping but ψ not preclosed mapping.

(2) Suppose $\varphi: \mathcal{X} \longrightarrow \mathcal{Y}$ be a mapping defined by

$$\varphi(1) = v, \varphi(2) = w, \text{and} \varphi(w) = u. \tag{31}$$

(i) As $\{1,2\} \in \tilde{\tau}(\mathcal{X})$, $\varphi(\{1,2\}) = \{v,w\} \in Q_p\mathbb{O}(\mathcal{Y})$, but $\{v,w\} \notin \mathbb{GO}_p(\mathcal{Y})$. Thus, φ is Q_p-open mapping but φ not gp-open mapping.

(ii) As $\{3\} \in \mathcal{F}_{\mathcal{X}}$, $\{u\} \notin \mathbb{GC}_p(\mathcal{Y})$. Thus, φ is Q_p-closed mapping but φ not gp-closed mapping.

Theorem 15. *Assume that $\psi: \mathcal{X} \longrightarrow \mathcal{Y}$ is a mapping. Then, the following two properties are equivalent:*

(1) ψ is Q_p-open.=

(2) For every $x \in \mathcal{X}$ and $\mathfrak{U}$ is a neighborhood of x, there exists Q_p-open set $\mathfrak{B} \subset \mathcal{Y}$ containing $\psi(x)$ such that $\mathfrak{B} \subset \psi(\mathfrak{U})$

Proof. The proof is clear. □

Theorem 16. *Assume that $\psi: \mathcal{X} \longrightarrow \mathcal{Y}$ is Q_p-open (resp. Q_p-closed) mapping and $\mathfrak{B} \subset \mathcal{Y}$. If $\mathfrak{A} \subset \mathcal{X}$ is a closed (resp. open) set containing $\psi^{-1}(\mathfrak{B})$, then there exists Q_p-open (resp. Q_p-closed) set $\mathfrak{H} \subset \mathcal{Y}$ containing $\mathfrak{B}$ such that $\psi^{-1}(\mathfrak{H}) \subset \mathfrak{A}$.*

Proof. Obvious. □

Corollary 3. *For every set $\mathfrak{B} \subseteq \mathcal{Y}$, if $\psi: \mathcal{X} \longrightarrow \mathcal{Y}$ is Q_p-open, then $\psi^{-1}(\mathcal{C}_{Q_p}(\mathfrak{B})) \subseteq \mathcal{C}(\psi^{-1}(\mathfrak{B}))$.*

Proof. Obvious. □

Theorem 17. *For any subset $\mathfrak{A}$ of $\mathcal{X}$, a mapping $\psi: \mathcal{X} \longrightarrow \mathcal{Y}$ is Q_p-open $\Leftrightarrow \psi(\mathcal{I}(\mathfrak{A})) \subseteq \mathcal{I}_{Q_p}(\psi(\mathfrak{A}))$.*

Proof. Assume that $\psi: \mathcal{X} \longrightarrow \mathcal{Y}$ is Q_p-open mapping and $\mathfrak{A} \subseteq \mathcal{X}$. Then, $\mathcal{I}(\mathfrak{A}) \in \tilde{\tau}(\mathcal{X})$ and $\psi(\mathcal{I}(\mathfrak{A}))$ is Q_p-open set contained in $\psi(\mathfrak{A})$. Hence, we have $\psi(\mathcal{I}(\mathfrak{A})) \subseteq \mathcal{I}_{Q_p}(\psi(\mathfrak{A}))$. Conversely, for every $\mathfrak{A}$ of $\mathcal{X}$, $\psi(\mathcal{I}(\mathfrak{A})) \subseteq \mathcal{I}_{Q_p}(\psi(\mathfrak{A}))$ and $\mathfrak{L} \in \tilde{\tau}(\mathcal{X})$. Then, $\mathcal{I}(\mathfrak{L}) = \mathfrak{L}$, $\psi(\mathfrak{L}) \subseteq \mathcal{I}_{Q_p}(\psi(\mathfrak{L}))$. Therefore, $\psi(\mathfrak{L}) = \mathcal{I}_{Q_p}(\psi(\mathfrak{L}))$, and we have $\psi(\mathfrak{L})$ is Q_p-open mapping. □

Theorem 18. *Assume that $\psi: \mathcal{X} \longrightarrow \mathcal{Y}$ is a bijective mapping. Then, the following three properties are equivalent:*

(1) ψ^{-1} is Q_p-continuous

(2) ψ is Q_p-open

(3) ψ is Q_p-closed

Proof.

(1) $\Rightarrow$ (2) Let $\mathfrak{U} \in \tilde{\tau}(\mathcal{X})$. Then, $\mathcal{X}\backslash\mathfrak{U} \in \mathcal{F}_{\mathcal{X}}$. Since ψ^{-1} is Q_p-continuous, $(\psi^{-1})^{-1}(\mathcal{X}\backslash\mathfrak{U}) = \psi(\mathcal{X}\backslash\mathfrak{U}) = \mathcal{Y}\backslash\psi(\mathfrak{U}) \in Q_p\mathbb{C}(\mathcal{Y})$. So, $\psi(\mathfrak{U}) \in Q_p\mathbb{O}(\mathcal{Y})$. Hence, ψ is Q_p-open mapping.

(2) $\Rightarrow$ (3) Let $\mathfrak{F} \in \mathcal{F}_{\mathcal{X}}$. Then, $\mathcal{X}\backslash\mathfrak{F} \in \tilde{\tau}(\mathcal{X})$. Since ψ is Q_p-open, $\psi(\mathcal{X}\backslash\mathfrak{F}) = \mathcal{Y}\backslash\psi(\mathfrak{F}) \in Q_p\mathbb{O}(\mathcal{Y})$. So, $\psi(\mathfrak{U}) \in Q_p\mathbb{C}(\mathcal{Y})$. Hence, ψ is Q_p-closed mapping.

(3) $\Rightarrow$ (1) Let $\mathfrak{F} \in \mathcal{F}_{\mathcal{X}}$. Since ψ is Q_p-closed, $(\psi^{-1})^{-1}(\mathfrak{F}) = \psi(\mathfrak{F}) \in Q_p\mathbb{C}(\mathcal{Y})$. Hence, ψ^{-1} is Q_p-continuous mapping. □

Remark 4. Composition of two Q_p-open (Q_p-closed) mappings do not need to be Q_p-open (Q_p-closed) as shown by the following example.

Example 14. Assume that $\mathcal{X} = \{1,2,3\}$ (i.e., $(\mathcal{X}, \tilde{\tau})$ be topological space, $\tilde{\tau} = \{\mathcal{X}, \phi, \{1,2\}, \{3\}\}$), $\mathcal{Y} = \{u,v,w\}$ (i.e., $(\mathcal{Y}, \tilde{\sigma})$ be topological space, $\tilde{\sigma} = \{\mathcal{Y}, \phi, \{u\}\}$), and $\mathcal{Z} = \{r,s,t\}$ (i.e., $(\mathcal{Z}, \tilde{\theta})$ be topological space, $\tilde{\theta} = \{\mathcal{Z}, \phi, \{s\}, t\{r,s\}\}$).

(1) Consider $\mathcal{F}_{\mathcal{Y}}, \mathbb{C}_p(\mathcal{Y}), \mathbb{O}_p(\mathcal{Y}), \mathbb{GC}_p(\mathcal{Y}), \mathbb{GO}_p(\mathcal{Y})$, $Q_p\mathbb{C}(\mathcal{Y})$, and $Q_p\mathbb{O}(\mathcal{Y})$ are computing in Example 12. Suppose $\psi: \mathcal{X} \longrightarrow \mathcal{Y}$ be a mapping defined by

$$\psi(1) = u, \psi(2) = v, \text{and} \psi(3) = w. \tag{32}$$

Thus, ψ is Q_p-open (Q_p-closed) mapping.

(2) Suppose $\varphi: \mathcal{Y} \longrightarrow \mathcal{Z}$ be a mapping defined by

$$\varphi(u) = s, \varphi(v) = r, \text{and} \varphi(w) = t. \tag{33}$$

Then,

$$\begin{aligned}
\mathcal{F}_{\mathcal{Z}} &= \{\mathcal{Z}, \phi, \{t\}, \{r,t\}\},\\
\mathbb{C}_p(\mathcal{Z}) &= \{\mathcal{Z}, \phi, \{t\}, \{r\}, \{r,t\}\},\\
\mathbb{GC}_p(\mathcal{Z}) = Q_p\mathbb{C}(\mathcal{Z}) &= \{\mathcal{Z}, \phi, \{r\}, \{t\}, \{s,t\}, \{r,t\}\},\\
\mathbb{O}_p(\mathcal{Z}) &= \{\mathcal{Z}, \phi, \{s\}, \{s,t\}, \{r,s\}\},\\
\mathbb{GO}_p(\mathcal{Z}) = Q_p\mathbb{O}(\mathcal{Z}) &= \{\mathcal{Z}, \phi, \{r\}, \{s\}, \{r,s\}, \{s,t\}\}.
\end{aligned} \tag{34}$$

Thus, φ is Q_p-open (Q_p-closed) mapping.

From (1) and (2), as $\{3\}$ is open in $\mathcal{X}$, $\varphi(\psi(\{3\})) = \varphi(\{w\}) = \{t\} \notin Q_p\mathbb{O}(\mathcal{Z})$. Therefore, $\varphi^{\circ}\psi$ is not Q_p-open mapping. Also, as $\{1,2\}$ is closed in $\mathcal{X}$, $\varphi(\psi(\{1,2\})) = \varphi(\{u,v\}) = \{r,s\} \notin Q_p\mathbb{C}(\mathcal{Z})$. Therefore, $\varphi^{\circ}\psi$ is not Q_p-closed mapping.

4. ERROR!! Q_p-$\mathbb{R}_0$ and Q_p-$\mathbb{R}_1$ Spaces

Definition 11.

(1) $\mathbb{K}_{Q_p}(\mathfrak{A})$ is called Q_p-kernel of $\mathfrak{A}$ (i.e., $\mathfrak{A}$ be subset of a space $\mathcal{X}$) if

$$\mathbb{K}_{Q_p}(\mathfrak{A}) = \cap\left\{\mathfrak{L} \in Q_p\mathbb{O}(\mathcal{X}) | \mathfrak{A} \subset \mathfrak{L}\right\}. \tag{35}$$

(2) $\mathbb{K}_{Q_p}(\{x\})$ is called Q_p-kernel of x (i.e., x be a point of a space $\mathcal{X}$) if

$$\mathbb{K}_{Q_p}(\{x\}) = \cap\left\{\mathfrak{L} \in Q_p\mathbb{O}(\mathcal{X}) | x \in \mathfrak{L}\right\}. \tag{36}$$

Lemma 6. *The following properties are holding in $(\mathcal{X}, \tilde{\tau})$. Then,*

(1) $y \in \mathbb{K}_{Q_p}(\{x\}) \Leftrightarrow x \in \mathcal{C}_{Q_p}(\{y\})$ $(x \in \mathcal{X})$

(2) $\mathbb{K}_{Q_p}(\mathfrak{A}) = \cap\left\{x \in \mathcal{X} | \mathcal{C}_{Q_p}(\{x\}) \cap \mathfrak{A} \neq \phi\right\}$

Proof. It is similar to Lemmas 3.1 and 3.2 of [16]. □

Lemma 7. *For any elements x and y in $(\mathcal{X}, \tilde{\tau})$, then the following two properties are equivalent:*

(1) $\mathbb{K}_{Q_p}(\{x\}) \neq \mathbb{K}_{Q_p}(\{y\})$

(2) $\mathcal{C}_{Q_p}(\{x\}) \neq \mathcal{C}_{Q_p}(\{y\})$

Proof. It is similar to Lemma 3.6 of [16]. □

Definition 12. We call Q_p-$\mathbb{R}_0$ space in $(\mathcal{X}, \tilde{\tau})$ if $\forall x \in \mathfrak{L} \in Q_p\mathbb{O}(\mathcal{X})$ such that $\mathcal{C}_{Q_p}(\{x\}) \subset \mathfrak{L}$.

Theorem 19. *The following two properties are holding in $(\mathcal{X}, \tilde{\tau})$:*

(1) Every pre-$\mathbb{R}_0$ space is Q_p-$\mathbb{R}_0$ space

(2) Every gp-$\mathbb{R}_0$ space is Q_p-$\mathbb{R}_0$ space

Proof. It follows from Theorem 6. □

Theorem 20. *Let $x, y \in \mathcal{X}$. Then, Q_p-$\mathbb{R}_0$ space in $(\mathcal{X}, \tilde{\tau}) \Leftrightarrow \mathcal{C}_{Q_p}(\{x\}) \neq \mathcal{C}_{Q_p}(\{y\})$ implies $\mathcal{C}_{Q_p}(\{x\}) \cap \mathcal{C}_{Q_p}(\{y\}) = \phi$.*

Proof. From Definition 12, the proof is clear. □

Theorem 21. *Let $x, y \in \mathcal{X}$. Then, Q_p-$\mathbb{R}_0$ space in $(\mathcal{X}, \tilde{\tau}) \Leftrightarrow \mathbb{K}_{Q_p}(\{x\}) \neq \mathbb{K}_{Q_p}(\{y\})$ implies $\mathbb{K}_{Q_p}(\{x\}) \cap \mathbb{K}_{Q_p}(\{y\}) = \phi$.*

Proof. From Lemmas 6 (1), Lemma 7, Definition 12, and Theorem 20, the proof is clear. □

Theorem 22. *The following five properties are equivalent in $(\mathcal{X}, \tilde{\tau})$:*

(1) $(\mathcal{X}, \tilde{\tau})$ is an Q_p-$\mathbb{R}_0$ space

(2) For any $\mathfrak{A} \neq \phi$ and $\mathfrak{L} \in Q_p\mathbb{O}(\mathcal{X})$ such that $\mathfrak{A} \cap \mathfrak{L} \neq \phi$, there exists $\mathfrak{F} \in Q_p\mathbb{C}(\mathcal{X})$ such that $\mathfrak{A} \cap \mathfrak{F} \neq \phi$ and $\mathfrak{F} \subset \mathfrak{L}$

(3) For any $\mathfrak{L} \in Q_p\mathbb{O}(\mathcal{X})$, $\mathfrak{L} = \cup\left\{\mathfrak{F} \in Q_p\mathbb{C}(\mathcal{X}) | \mathfrak{F} \subset \mathfrak{L}\right\}$

(4) For any $\mathfrak{F} \in Q_p\mathbb{O}(\mathcal{X})$, $\mathfrak{F} = \cap\left\{\mathfrak{L} \in Q_p\mathbb{O}(\mathcal{X}) | \mathfrak{F} \subset \mathfrak{L}\right\}$

(5) For any $x \in \mathcal{X}$, $\mathcal{C}_{Q_p}(\{x\}) \subset \mathbb{K}_{Q_p}(\{x\})$

Proof. It is similar to Theorem 3.8 of [16]. □

Corollary 4. *The following two properties are equivalent in $(\mathcal{X}, \tilde{\tau})$:*

(1) $(\mathcal{X}, \tilde{\tau})$ is an Q_p-$\mathbb{R}_0$ space

(2) $\mathcal{C}_{Q_p}(\{x\}) = \mathbb{K}_{Q_p}(\{x\})$ $(\forall x \in \mathcal{X})$

Proof. From Definition 12 and Theorem 22, the proof is clear. □

Theorem 23. *The following two properties are equivalent in $(\mathcal{X}, \tilde{\tau})$:*

(1) $(\mathcal{X}, \tilde{\tau})$ is an Q_p-$\mathbb{R}_0$ space

(2) $x \in \mathcal{C}_{Q_p}(\{y\}) \Leftrightarrow y \in \mathcal{C}_{Q_p}(\{x\})$ $(\forall x, y \in \mathcal{X})$

Proof. The proof is clear. □

Theorem 24. *The following four properties are equivalent in $(\mathcal{X}, \tilde{\tau})$:*

(1) $(\mathcal{X}, \tilde{\tau})$ is an Q_p-$\mathbb{R}_0$ space

(2) If $\mathfrak{F} \in Q_p\mathbb{C}(\mathcal{X})$, then $\mathfrak{F} = \mathbb{K}_{Q_p}(\mathfrak{F})$

(3) If $\mathfrak{F} \in Q_p\mathbb{C}(\mathcal{X})$ and $x \in \mathfrak{F}$, then $\mathbb{K}_{Q_p}(\{x\}) \subset \mathfrak{F}$

(4) If $x \in \mathcal{X}$, then $\mathbb{K}_{Q_p}(\{x\}) \subset \mathcal{C}_{Q_p}(\{x\})$

Proof. From Lemma 6, Theorem 23, and Definition 12, the proof is clear. □

Definition 13. We call $(\mathcal{X}, \tilde{\tau})$ is Q_p-$\mathbb{R}_1$ space if

(i) $\forall x, y \in \mathcal{X}$ with $\mathcal{C}_{Q_p}(\{x\}) \neq \mathcal{C}_{Q_p}(\{y\})$

(ii) There exist disjoint Q_p-open sets $\mathfrak{L}$ and $\mathfrak{M}$ s.t. $\mathcal{C}_{Q_p}(\{x\}) \subseteq \mathfrak{L}$ and $\mathcal{C}_{Q_p}(\{y\}) \subseteq \mathfrak{M}$

Theorem 25. *Let $(\mathcal{X}, \tilde{\tau})$ be a topological space. Then,*

(1) Every pre-$\mathbb{R}_1$ space is Q_p-$\mathbb{R}_1$ space

(2) Every gp-$\mathbb{R}_1$ space is Q_p-$\mathbb{R}_1$ space

Hindawi
Journal of Mathematics
Volume 2023, Article ID 9756056, 1 page
https://doi.org/10.1155/2023/9756056

Retraction

Retracted: Application of Mobile Technology in College English Vocabulary Teaching

Journal of Mathematics

Received 15 August 2023; Accepted 15 August 2023; Published 16 August 2023

This article has been retracted by Hindawi following an investigation undertaken by the publisher [1]. This investigation has uncovered evidence of one or more of the following indicators of systematic manipulation of the publication process:

(1) Discrepancies in scope

(2) Discrepancies in the description of the research reported

(3) Discrepancies between the availability of data and the research described

(4) Inappropriate citations

(5) Incoherent, meaningless and/or irrelevant content included in the article

(6) Peer-review manipulation

The presence of these indicators undermines our confidence in the integrity of the article's content and we cannot, therefore, vouch for its reliability. Please note that this notice is intended solely to alert readers that the content of this article is unreliable. We have not investigated whether authors were aware of or involved in the systematic manipulation of the publication process.

Wiley and Hindawi regrets that the usual quality checks did not identify these issues before publication and have since put additional measures in place to safeguard research integrity.

We wish to credit our own Research Integrity and Research Publishing teams and anonymous and named external researchers and research integrity experts for contributing to this investigation.

The corresponding author, as the representative of all authors, has been given the opportunity to register their agreement or disagreement to this retraction. We have kept a record of any response received.

References

[1] B. He, "Application of Mobile Technology in College English Vocabulary Teaching," *Journal of Mathematics*, vol. 2022, Article ID 9009008, 8 pages, 2022.

Hindawi
Journal of Mathematics
Volume 2022, Article ID 9009008, 8 pages
https://doi.org/10.1155/2022/9009008

Research Article

Application of Mobile Technology in College English Vocabulary Teaching

Bing He

College of Foreign Language, Dalianjiaotong University, Dalian 116021, Liaoning, China

Correspondence should be addressed to Bing He; rachelhe2008@djtu.edu.cn

Received 8 December 2021; Revised 31 December 2021; Accepted 3 January 2022; Published 16 February 2022

Academic Editor: Naeem Jan

In order to improve the quality of college English vocabulary teaching, this paper studies the application of mobile technology in college English vocabulary teaching. The advantages of mobile technology are analyzed, and different mobile technology communication deployment schemes are determined according to different needs and environments of English vocabulary learning, so as to build a college English vocabulary teaching system, which is mainly composed of the user layer, mobile network layer, and English vocabulary data layer. Among them, the main functions of the user layer are user login, system information setting, English vocabulary resource browsing, uploading English vocabulary homework, etc., and determine user preference data through user logs. The mobile network layer is designed using mobile technology to create the delay control technique of the system mobile communication, and the system mobile network layer's LAN is set up to increase data transmission speed. Finally, set up the database according to the English vocabulary of English words field, calculating Euclidean distance to determine the relationship between them, and then through random set classification vocabulary data types, calculate the similarity degree of the data extraction vocabulary data characteristics and remove high similarity of the English vocabulary data to reduce the difficulty of system storage. The experimental findings suggest that the mobile technology-based system has high performance and dependability and may be widely used in practice.

1. Introduction

With the continuous development of computer technology, mobile technologies such as multimedia and network technology are widely used in many fields. Among them, the mobile technology industry is widely used in the field of education [1]. This technology is also used in college English vocabulary education. The application of mobile technology has greatly promoted the teaching efficiency of education and provided great convenience for students of different majors. Among them, personal learning environment and virtual classroom built through the wireless network in mobile technology have become important ways to improve learners' learning interest [2]. Due to the special structure of knowledge in college English vocabulary teaching, students are often not interested, which affects students' performance and the application of employment English in the future. Moreover, only vocabulary learning in the classroom is far from enough. Through the application of mobile technology, we can continuously expand the vocabulary and learning time of English learning [3]. Although more interactive teaching methods have been used in English vocabulary teaching in recent years, students' vocabulary learning and vocabulary resources cannot be well transformed when they leave the classroom [4]. Therefore, using mobile technology to promote the quality of college English vocabulary teaching and provide students with more mobile English vocabulary resources has become a hot issue in current research.

Cui [5] proposed a computer intelligent proofreading system for English translation. The system is applied to college English vocabulary teaching to help students effectively improve the accuracy of vocabulary translation. The system pays much attention to the translation of English phrases and words. The core meaning of words is derived from the search module, and the user habits are established

with the assistance of the log module, thanks to the design of the intelligent proofreading module, search module, translation module, and occasional log module. The phrase translation model is enhanced in the software design, the model is used to identify the proper meaning of English vocabulary translation, and the system design is finished. The system's architecture increases the quality of English vocabulary translation and assists students in correcting learning faults. However, this strategy takes into account a smaller amount of English vocabulary and has several drawbacks that need to be addressed. A machine learning-based English vocabulary adaptive learning approach is proposed in [6]. In the model design, machine learning is used. To identify the main parameter likelihood of English vocabulary, a dynamic modeling learning technique is used. The learning fitness of English vocabulary is matched via various determinations, the fitness is continually changed, and the adaptive process of English vocabulary learning is decided using the AdaBoost algorithm. This method mainly considers the learning adaptability of users, does not fully realize the application of mobile technology, and considers less about the extraction of English learning vocabulary and features, so it has some limitations. Yuan and Huang [7] proposed a semantic feature extraction and translation method based on the graph regularization algorithm. This method studies the errors in English vocabulary translation. With the help of the graph canonical nonnegative matrix decomposition method, the features of English vocabulary are extracted, the digraph of extracted data is constructed, and the accuracy of English vocabulary translation is determined according to the digraph. This method improves the accuracy of vocabulary translation by analyzing the hidden features of English vocabulary. However, there are some limitations in the application of this method in English vocabulary teaching. Due to the noise of vocabulary characteristics, translation errors in learning are caused.

In order to solve the shortcomings of the above methods, this paper applies mobile technology to college English vocabulary teaching in order to enhance students' interest in learning. This article examines the benefits of mobile technology and how it is used to teach vocabulary to improve the quality of the college English vocabulary instruction.

2. Application of Mobile Technology in College English Vocabulary Teaching

A college English vocabulary teaching system based on mobile technology is built in this research to increase the impact of college English vocabulary teaching. First, the benefits of mobile technology are examined in the system design. The general architecture of the college is built on this foundation. English vocabulary teaching system is designed. Based on this architecture, the system hardware and software are designed to complete the application research of mobile technology in college English vocabulary teaching.

2.1. Mobile Technology Analysis. Mobile technology includes mobile communication technology and terminal equipment. In the English vocabulary teaching system, the main mobile technologies supporting the system's operation include wireless communication and cellular mobile communication systems. Mobile technology is the basis of English vocabulary learning and application. Different mobile technologies are applied according to different English vocabulary learning needs and learning environments to determine different mobile technology communication deployment [8]. The mobile communication deployment mode selected in the college English vocabulary teaching system in this paper is shown in Table 1.

In the design of the college English vocabulary teaching system, this paper mainly applies the cellular mobile network, which is widely used in multinetworks and can realize effective communication. According to the mobile technology analyzed above, the college English vocabulary teaching system environment constructed in this paper should maintain integration [9], support college English vocabulary learners to learn autonomy and uniqueness, and provide them with a more effective virtual learning system [10]. The basic framework of the college English vocabulary teaching system based on mobile technology is shown in Figure 1.

2.2. Functional Module Design of the College English Vocabulary Teaching System. In the design of the college English vocabulary teaching system, the system user layer, mobile network layer, and English vocabulary data layer are mainly designed. Mobile technology is applied to the module design to improve the performance of the college English vocabulary teaching system.

2.2.1. User Layer of the English Vocabulary Teaching System. The main users of the college English vocabulary teaching system are teachers and students. Through the interaction between them, the user layer is designed. The main functions of this layer are user login, system information setting, browsing English vocabulary resources, uploading English vocabulary homework, and other functions [11]. The module records the user's access behavior and forms log data for integration. In the user login data log integration, the user's repeated behavior data are integrated to help analyze the user's preferences [12]. Set the data collection accessed by the user as

$$X = \{x_1, x_2, \ldots x_n\}. \tag{1}$$

In the formula, $x_1, x_2, \ldots, x_n$ represents the user login log data, and n represents the number of log data.

Calculate the similar data in the user log data in formula (1) to obtain

$$\mathrm{sim}X = \frac{u\left(x^2 + y^2\right)}{\sqrt{\sin\left(x^2 + y^2\right)}}. \tag{2}$$

Table 1: Mobile communication deployment mode selected in the college English vocabulary teaching system.

Project	Communication range	Key technology	Communication standards
Broadband wireless CLAN (WMAN)	Large-scale application	Multichannel multipoint allocation, local multipoint allocation, high-performance allocation	IEEE 802.16
Wireless LAN (WLAN)	Medium range	Wireless network, etc.	802.11
Personal local area network (WPAN)	Small range	Bluetooth, infrared light	EDR

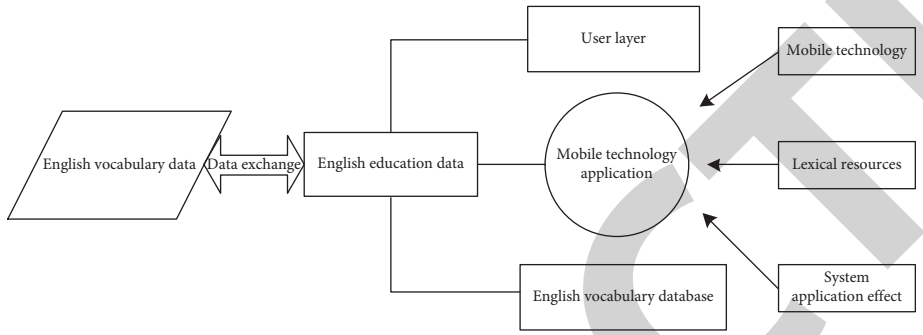

Figure 1: Basic framework of the college English vocabulary teaching system based on mobile technology.

In the formula, u represents the data similarity ratio, and sin represents the data cosine similarity.

According to the determined similar data of the user login log, determine the main preferences of users logging in the system [13], which is the basis of system development. The basic operation flow of the user layer is shown in Figure 2.

The user layer design's main functions are user login, system information setting, English vocabulary resource browsing, uploading English vocabulary homework, and other functions, and the user preference data are determined through the user log.

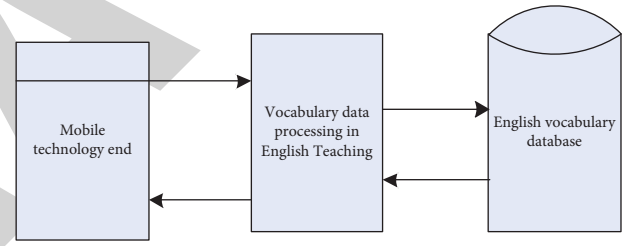

Figure 2: Basic operation flow of the user layer.

2.2.2. Mobile Network Layer of the English Vocabulary Teaching System. The mobile network layer set in the college English vocabulary teaching system mainly relies on mobile technology. This layer's architecture facilitates the system's network connectivity and serves as the foundation for its regular operation [14]. As a result, owing to the huge scale and broad coverage of data in the college English teaching vocabulary system, the speed of real-time English vocabulary data exchange in the mobile network layer design in the system design [15] must be addressed in the network layer design of this study. As a result, the system's mobile communication latency is critical in the module's design. The network transmission delay in a WAN communication network is the time it takes for data to travel from the vocabulary starting node to the user receiving end point [16]. The transmission delay diagram of the mobile network layer is shown in Figure 3.

As can be seen from Figure 3, the calculation formula of time delay caused by the operation of the mobile network layer in the application of the college English vocabulary teaching system is as follows:

$$E = e_1 + e_2 + e_s + e_p + e_q. \tag{3}$$

In the formula, E represents the total end-to-end communication delay of the university English vocabulary teaching system and e_1 and e_2 represent the delay [17] for university English vocabulary data transfer processing, including the time required to package the output communication protocol and the data received by the user. e_s represents the delay of the output of the English vocabulary system. Since the node in the storage mechanism of the exchange device in the mobile network needs a certain transmission medium when receiving the English vocabulary data, the time delay of the system when exporting the English vocabulary operated by the user is

$$e_s = \frac{R}{w}. \tag{4}$$

In the formula, R represents the English lexical data frame, and w represents the network link bandwidth.

In this system, the protocol delay of communication processing is directly related to the mobile network performance of communication processing, and this value is relatively fixed. The Ethernet switch is used in the system designed in this paper, and its processing delay generally

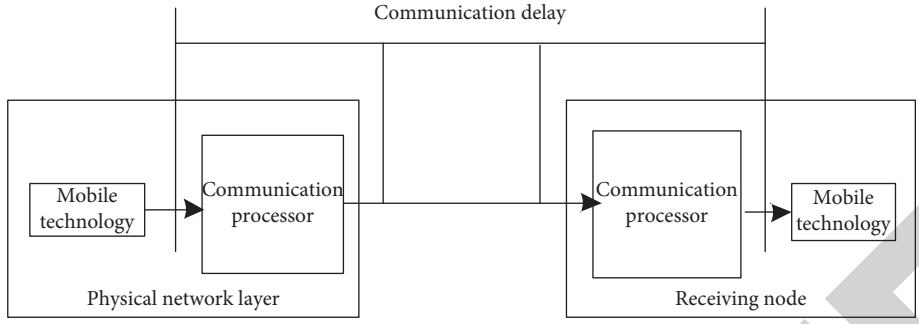

Figure 3: Transmission delay diagram of the mobile network layer.

does not exceed 10 μs [18]. The MAC address table, VLAN, priority, and other functions processed by the switch chip of the mobile device are determined by the speed. The failure of the system in the college English vocabulary teaching system will also result in an increase in output delay [19]. As a result, system failure should be included in the time delay control in order to enhance the college English vocabulary teaching system's performance.

In the mobile network layer design of the English vocabulary teaching system, mobile technology is applied to design the system mobile communication delay control method, set the system mobile network layer LAN, and improve the system data transmission speed.

2.3. Design of the English Vocabulary Data Layer. According to the English network module set above, the English vocabulary data layer is designed, which contains all college English vocabulary data. In this module, the database's English vocabulary field [20] is basically set according to the English vocabulary data. The setting results are shown in Table 2.

Due to the enormous number and varieties of college English vocabulary curricular materials, it is required to extract the characteristics of English vocabulary data and effectively fuse the features of English vocabulary data in the design of the English vocabulary data layer [21]. We should examine the distance between English vocabulary data stored in the system while extracting features and use that distance to identify the link between the college English vocabulary [22]. The first multidimensional data of vocabulary data in the college English vocabulary teaching system contain a big number of English vocabulary data. In order to determine the distance between English vocabulary data, it is used as the credibility of feature extraction of English vocabulary data. This paper calculates the distance between English vocabulary data by calculating the Euclidean distance. In the English vocabulary system, the real distance between English vocabulary data in the n-dimensional space [23], the straight-line segment distance between vocabulary data in the system, is expressed as

$$g = \sqrt{(a_1 + b_1)^2 + (c_1 + d_1)^2}. \tag{5}$$

In the formula, a, b represent two adjacent university English vocabulary data, and c, d represents the two-dimensional coordinate point in the English vocabulary teaching system.

The properties of English vocabulary data are derived by calculating the distance between college English vocabulary data. The normal distribution state between the two vocabulary data is assessed [24, 25] based on the calculated distance between English vocabulary data in order to fulfill the needs of system data storage. Suppose that, in the normal distribution diagram of English vocabulary data, one data point is A and the distance between the two data is $A1$. At this time, the normal distribution state between English vocabulary data is shown in Figure 4.

Under this distribution set, set the total of English vocabulary data m as the element, that is, all English vocabulary data distributed in the system. At this time, the mean vector of English vocabulary data is

$$q = \{q_1, q_2, \ldots q_n\}. \tag{6}$$

The covariance matrix calculation of the English lexical data in the system determined at this time is

$$\sigma = \sum (S_i)_{m \times n}. \tag{7}$$

In the equation, the result of the covariance matrix calculation is σ.

According to the above analysis, the characteristics of the university English vocabulary data in the obtained system are

$$\xi(a, b) = (X - \sigma) \sum_{i=1}^{n} (a, b). \tag{8}$$

In the formula, $\xi(a, b)$ represents the vocabulary characteristics in university English vocabulary teaching, and X represents the scale factor.

According to the characteristics of the college English vocabulary obtained above, it is stored in the teaching system of this study. However, since there are so many comparable vocabulary data and certain words have a lot of noise, it is simple to impair the system's efficiency. As a result, the vocabulary elements of English education must be preprocessed in the system, comparable vocabulary data must be removed, and the system's reaction speed must be improved [26–28].

Table 2: Field settings of English vocabulary in the database.

Field	Vocabulary data type	Length	Remarks
COURSEID	Int(2)	2	Curriculum ID
COURSENAME	Varchar(50)	50	English vocabulary name
COURSECODE	Varchar(30)	50	English vocabulary teaching textbook
COURSETEXTBOOK	Varchar(80)	80	Descriptor
UINTID	Int(3)	3	English vocabulary unit ID
UINTname	Varchar(100)	100	English vocabulary unit name
UINTtitle	Varchar(100)	100	English vocabulary unit title

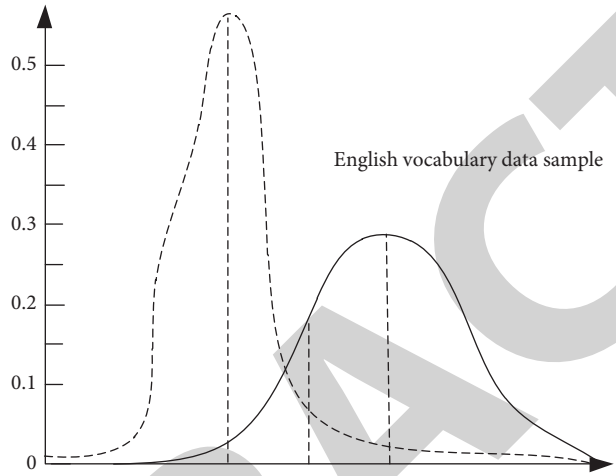

Figure 4: Normal distribution status between university English lexical data in the system.

The set of college English vocabulary features is set as A, which contains more typical English data. Firstly, the data in the set are effectively classified. In this paper, the features are classified with the help of the random forest algorithm, and the calculation formula is as follows:

$$F(x) = \frac{1/f(k)}{\sum_{i=1}^{k}(1/f(k))}. \tag{9}$$

In the formula, $f(k)$ represents the predicted distance between English vocabulary data at different times, and k represents the state value of the categorical English vocabulary data.

The above classified English vocabulary data were processed for data noise reduction in different data groups, and the results are

$$\tau(x) = \tau(x) \times F(x), x = 1, 2, \ldots m. \tag{10}$$

In the formula, $\tau(x)$ represents English vocabulary data after noise reduction, and $F(x)$ represents the noise interference coefficient.

Calculate the similarity of the above noise-free English vocabulary data, and delete the data with high similarity, so as to reduce the complex work of data processing in the system. The similarity calculation formula is

$$h_i(k) = yx + h_i(k)' \sum_{k=1}^{n} \tau(x). \tag{11}$$

In the formula, $h_i(k)'$ represents the observations of English lexical data, and y represents the similarity coefficient.

Based on the above calculated word similarity, the English vocabulary data with high similarity are removed to reduce the difficulty of system storage, obtaining

$$\theta_i(x) = l \sum_{i=1}^{n} u_i \frac{(x)}{k}. \tag{12}$$

In the formula, $u_i(k)$ represents typical English lexical data, and l represents key features in lexical data.

In the design of the system data layer, the English vocabulary field of the database is basically set according to the English vocabulary data, the Euclidean distance between words is calculated to determine the relationship between them, and the characteristics of college English vocabulary data are extracted by randomly classifying the vocabulary data types and calculating the similarity of the data, and the English vocabulary data with high similarity are removed to reduce the difficulty of system storage.

3. Experimental Analysis

3.1. Experimental Scheme Design. In order to verify the application effect of mobile technology in this paper, experimental analysis is carried out. In the experiment, the system is improved on the basis of the original system, and

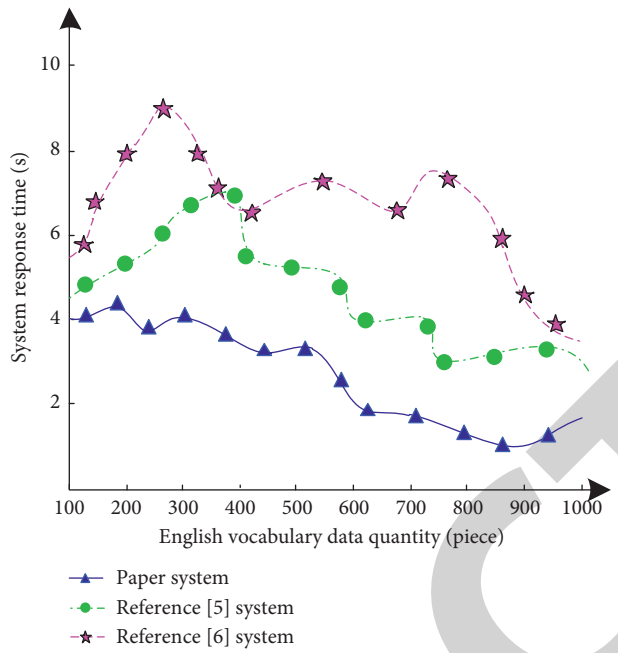

Figure 5: Comparison of response time-consuming results of different systems.

Table 3: Comparison of English vocabulary data transmission speed in different systems (s).

English vocabulary data/entry	This paper's system	Cui's [5] system	Liu and Huai-Long's [6] system
100	0.21	0.35	0.38
200	0.20	0.39	0.41
300	0.21	0.41	0.43
400	0.23	0.42	0.44
500	0.22	0.45	0.45
600	0.23	0.46	0.47
700	0.24	0.45	0.51
800	0.26	0.43	0.52
900	0.24	0.42	0.53
1000	0.23	0.43	0.54

the system is programmed with C language. The designed system can run normally. In the experiment, part of the vocabulary of CET-4 of the English network is input into the system database as the research data of this system. Taking the freshman class of English major in a university as the research object, this paper makes an experimental study based on the application effect of the students in this class.

3.2. Experimental Index Design. The experimental test compares this system, Cui's [5] system, and Talha's [29] system. In the experiment, the time consumption of the system response and the speed of English vocabulary data transmission are taken as experimental indicators to analyze the performance of the designed system.

3.3. Analysis of Experimental Results. In order to verify the effectiveness of this system, the time-consuming analysis of the system response in the application of this system, Talha et al.'s [30] system, and Liu and Huai-Long's [6] system is analyzed in the experiment. Among them, with the change of the amount of vocabulary data, the shorter the response time, the faster the response speed of the system and the higher the performance of the system. The experimental results are shown in Figure 5.

By analyzing the experimental data in Figure 5, it can be seen that, with the change of the amount of English vocabulary data, there are some differences in the time consumption of the system response in the application of this system, Cui's [5] system, and Liu and Huai-Long's [6] system. When the quantity of data is 300, the reaction time of the system described in this study is around 4 s, Cui's [5] system is about 7 s, and [6, 27] system is about 9 s; although there are some changes in the general trend of the reaction times of the three systems, the response time of the system in this article always displays a decreasing trend, indicating that the response speed of the system in this paper is quick and practicable.

In order to further verify the effectiveness of the proposed system, the speed of transmitting English vocabulary

data in this system, Cui's [5] system, and Talha et al.'s [31] system is experimentally analyzed. The results are shown in Table 3.

By analyzing the experimental results in Table 3, it can be seen that there are some differences in the speed of transmitting English vocabulary data using this system, Cui's [5] system, and Liu and Huai-Long's [6] system. Among them, the transmission speed of this system changes with the continuous change of the amount of English vocabulary data, but it can be seen from the overall data that the transmission speed of this system is fast. This is because the system adopts mobile technology and sets the delay of network layer control data transmission, which improves the effectiveness of the system.

4. Conclusion

In order to improve the effect of college English vocabulary education, this paper designs a new teaching system with the help of mobile technology. Based on the original system, the functional module considers the response speed and transmission delay of the system in the network layer and completes the effective application of mobile technology. Through experiments, the effectiveness of the system designed in this paper is verified, which provides some help for English vocabulary teaching [32].

Data Availability

The data used to support the findings of this study are included within the article.

Conflicts of Interest

The author declares that there are no conflicts of interest regarding the publication of this paper.

Acknowledgments

This work was supported by the Research on the Ecological Construction of Smart Foreign Language Classroom under the Background of 5g Era, 2021 Scientific Research Fund Project of Liaoning Provincial Department of Education (Project no. LJKR0193).

References

[1] P. Seraj, B. Klimova, and H. Habil, "Use of mobile phones in teaching English in Bangladesh: a systematic review (2010–2020)," *Sustainability*, vol. 13, no. 12, pp. 145–155, 2021.

[2] V. N. Hoi, "Understanding higher education learners' acceptance and use of mobile devices for language learning: a Rasch-based path modeling approach," *Computers & Education*, vol. 146, no. 1, pp. 103761–103772, 2019.

[3] F. Liébana-Cabanillas, A. Japutra, S. Molinillo, N. Singh, and N. Sinha, "Assessment of mobile technology use in the emerging market: analyzing intention to use m-payment services in India," *Telecommunications Policy*, vol. 44, no. 9, pp. 102009–102018, 2020.

[4] J. Hong, "Students' academic use of mobile technology and higher-order thinking skills: the role of active engagement," . *Education Sciences*, vol. 10, no. 7, pp. 1–7, 2020.

[5] D. Cui, "Design of intelligent computer proofreading system for English translation," *Modern Electronics Technique*, vol. 42, no. 4, pp. 179–182, 2019.

[6] X. Liu and L. I. Huai-Long, "English vocabulary adaptive learning model based on machine learning algorithm," *Computer Systems & Applications*, vol. 30, no. 4, pp. 260–265, 2021.

[7] Q. Yuan and J. Huang, "Research on semantic feature extraction and translation algorithm based on graph regular algorithm," *Electronic Measurement Technology*, vol. 43, no. 8, pp. 91–95, 2020.

[8] M. C. Chiu and T. Chen, "Assessing mobile and Smart technology applications for active and healthy aging using a fuzzy collaborative intelligence approach," *Cognitive Computation*, vol. 25, no. 1, pp. 10033–10045, 2021.

[9] X. Zhai and L. Shi, "Understanding how the perceived usefulness of mobile technology impacts physics learning achievement: a pedagogical perspective," *Journal of Science Education and Technology*, vol. 15, no. 2, pp. 1–10, 2020.

[10] G. Gorghiu, C. Pribeanu, V. Lamanauskas, and V. Slekiene, "Usefulness of mobile teaching and learning as perceived by Romanian and Lithuanian science teachers," *Problems of Education in the 21st Century*, vol. 78, no. 5, pp. 719–733, 2020.

[11] E. L. Tan and D. Y. Heh, "Mobile Teaching and Learning of Coupled-Line Structures: the multiple-1D coupled-line finite-difference time-domain method," *IEEE Antennas and Propagation Magazine*, vol. 62, no. 2, pp. 62–69, 2020.

[12] L. Unsworth and K. A. Mills, "English language teaching of attitude and emotion in digital multimodal composition," *Journal of Second Language Writing*, vol. 47, no. 1, pp. 100712–100723, 2020.

[13] P. Brian, "World englishes in English language Teaching-GlobalEnglishes for language teaching," *ELT Journal*, vol. 25, no. 3, pp. 36–49, 2020.

[14] C. Wallis, "Using the eighteenth-century English phonology database (ECEP) as a teaching resource," *English Language and Linguistics*, vol. 24, no. 3, pp. 321–326, 2020.

[15] Y. Qian, "Dynamism of collocation in L2 English writing: a bigram-based study," *IRAL - International Review of Applied Linguistics in Language Teaching*, vol. 11, no. 2, pp. 1–12, 2019.

[16] M. Chen, J. Flowerdew, and L. Anthony, "Introducing in-service English language teachers to data-driven learning for academic writing," *System*, vol. 87, no. 2, pp. 102148–102159, 2019.

[17] A. Stornaiuolo, E. E. Thomas, and G. Campano, "Critical digital and media literacies in challenging times: reimagining the role of English language arts," *Research in the Teaching of English*, vol. 54, no. 2, pp. 1452–1463, 2019.

[18] J. Yang, "Understanding Chinese language teachers' beliefs about themselves and their students in an English context," *System*, vol. 80, no. 3, pp. 73–82, 2019.

[19] G. Du, Z. Hasim, and F. P. Chew, "Contribution of English aural vocabulary size levels to L2 listening comprehension," *IRAL - International Review of Applied Linguistics in Language Teaching*, vol. 12, no. 4, pp. 1–10, 2021.

[20] E. Cotos and Y.-R. Chung, "Functional language in curriculum genres: implications for testing international teaching assistants," *Journal of English for Academic Purposes*, vol. 41, no. 2, pp. 100766–100778, 2019.

Hindawi
Journal of Mathematics
Volume 2024, Article ID 9769621, 1 page
https://doi.org/10.1155/2024/9769621

Retraction

Retracted: Construction and Analysis of Urban Motor Vehicle Drivers' Traffic Literacy Evaluation Model Based on Zhengzhou City's Survey Data

Journal of Mathematics

Received 23 January 2024; Accepted 23 January 2024; Published 24 January 2024

This article has been retracted by Hindawi following an investigation undertaken by the publisher [1]. This investigation has uncovered evidence of one or more of the following indicators of systematic manipulation of the publication process:

(1) Discrepancies in scope

(2) Discrepancies in the description of the research reported

(3) Discrepancies between the availability of data and the research described

(4) Inappropriate citations

(5) Incoherent, meaningless and/or irrelevant content included in the article

(6) Manipulated or compromised peer review

The presence of these indicators undermines our confidence in the integrity of the article's content and we cannot, therefore, vouch for its reliability. Please note that this notice is intended solely to alert readers that the content of this article is unreliable. We have not investigated whether authors were aware of or involved in the systematic manipulation of the publication process.

In addition, our investigation has also shown that one or more of the following human-subject reporting requirements has not been met in this article: ethical approval by an Institutional Review Board (IRB) committee or equivalent, patient/participant consent to participate, and/or agreement to publish patient/participant details (where relevant).

Wiley and Hindawi regrets that the usual quality checks did not identify these issues before publication and have since put additional measures in place to safeguard research integrity.

We wish to credit our own Research Integrity and Research Publishing teams and anonymous and named external researchers and research integrity experts for contributing to this investigation.

The corresponding author, as the representative of all authors, has been given the opportunity to register their agreement or disagreement to this retraction. We have kept a record of any response received.

References

[1] L. Shengyang, W. Yanrong, T. Kang, and H. Fangzheng, "Construction and Analysis of Urban Motor Vehicle Drivers' Traffic Literacy Evaluation Model Based on Zhengzhou City's Survey Data," *Journal of Mathematics*, vol. 2022, Article ID 2366458, 9 pages, 2022.

Hindawi
Journal of Mathematics
Volume 2022, Article ID 2366458, 9 pages
https://doi.org/10.1155/2022/2366458

Research Article

Construction and Analysis of Urban Motor Vehicle Drivers' Traffic Literacy Evaluation Model Based on Zhengzhou City's Survey Data

Liu Shengyang,[1,2] Wang Yanrong,[1] Tian Kang ,[1] and Hu Fangzheng[1]

[1]*School of Management and Economics, North China University of Water Resources and Electric Power, Zhengzhou 450046, China*
[2]*Zhengzhou Business University, Zhengzhou 451200, China*

Correspondence should be addressed to Tian Kang; tiankang@stu.ncwu.edu.cn

Received 23 December 2021; Revised 16 January 2022; Accepted 25 January 2022; Published 16 February 2022

Academic Editor: Naeem Jan

This paper summarizes the relevant literature through the content analysis method and combines expert advice. The company built a four-level indicator including traffic knowledge and skills, and 13 pilot-level traffic literacy evaluation indicators system including traffic rules and mechanical common sense. The Analytic Hierarchy Process (AHP) analysis method is used to determine the weight of each indicator of urban driver traffic literacy evaluation, and conduct pilot survey and evaluation of motor vehicle drivers in Zhengzhou. The results show that the evaluation value of motor vehicle driver traffic literacy in Zhengzhou is 72.07, including a traffic knowledge score of 77.09, traffic awareness score of 73.95, traffic skill score of 78.12, and traffic behavior score of up to 84.3. It shows that the respondents have relatively more active and responsible traffic behaviors and have a certain degree of understanding of traffic skills and traffic knowledge. However, they are relatively low in traffic awareness.

1. Introduction

With the rapid development of the country's economy, road congestion is becoming more and more serious; traffic accidents occur frequently, and road traffic laws and regulations are violated in an endless stream, which seriously affects urban development and a resident's quality of life in transportation [1]. Traditional transportation concepts can no longer adapt to this rapid development era. People must establish a new type of modern transportation awareness to solve a series of transportation problems caused by this. However, the practice has proved that only relying on the construction of large-scale transportation facilities cannot fundamentally alleviate the urban transportation problems [2]. During the implementation of traffic management, we should be people-oriented and combine the awareness of traffic participants and traffic managers to deal with Traffic problems jointly.

At present, some domestic scholars have researched related issues of transportation literacy. For example, Chen and Chen [3] investigated the traffic literacy of Hefei citizens on the spot and pointed out that the main problems are pedestrians and vehicles not observing traffic lights, citizens' driving violations from time to time, citizens occupying roads, and parking. It also proposed that the promotion and education of civilized traffic laws and regulations should be strengthened, and three educational networks of families, schools, and society should be established; also, the level of traffic management should be improved through the construction of law enforcement teams, infrastructure planning, and design, and the introduction of market mechanisms. Strengthening people's comfort can genuinely realize the purpose of convenient transportation; it is necessary to improve public transportation literacy and rationally deal with "Chinese-style of crossing the road." Yan [4] discussed traffic quality from drivers' perspective, pointed out that the civilized traffic quality of drivers is the leading factor affecting modern traffic, and put forward relevant suggestions. Xiao [5] pointed out that the civilized literacy of drivers in the country has been continuously improved based on the

comparison of data research from 2004 to 2017. Tracing back to the source, the current lack of driver's traffic literacy is the root cause of frequent traffic problems. However, everyone's learning and understanding of traffic safety awareness are different. The behavior and habits are mainly based on acquired propaganda and education, which triggers discussion on driver's traffic literacy, pays attention to the research of driver's traffic literacy, and establishes a good personality at the personal level.

Traffic literacy awareness aims to fundamentally improve drivers' awareness of road responsibilities and develop good road travel habits, thereby preventing road traffic accidents and ensuring safe driving. Some domestic scholars have also researched carbon transportation literacy. For example, Hu [6] analyzed the low-carbon awareness, low-carbon knowledge, and low-carbon behaviors of Zhengzhou, Luoyang, and Kaifeng residents. The status quo of residents' low-carbon transportation literacy in transportation shows that urban residents' educational level and income level have a clear positive correlation with the degree of concern about low-carbon transportation. Li [7] analyzed the problems of low-carbon transportation construction in Zhengzhou City through data collection, investigation, and analysis, and proposed to improve road construction regulations, divert vehicles and pedestrians on congested roads in urban areas, and increase the public transportation network system, that is, address three aspects to solve the existing problems.

The above studies focus on exploratory studies on the status and reasons for traffic literacy, and few studies have focused on the factors that affect drivers' traffic literacy. Based on the connotation and composition of urban driver's traffic literacy, this paper analyzes and summarizes the relevant literature on the influencing factors, formation mechanism, evaluation purpose, and index selection principles of the traffic system and constructs an evaluation index system for urban driver's traffic literacy. We use the analytic hierarchy process to optimize the urban driver's traffic literacy evaluation index system and conduct a pilot survey and evaluation of Zhengzhou motor vehicle drivers, intending to assess urban drivers further. The traffic literacy evaluation lays a theoretical foundation. It provides specific policy suggestions for improving urban traffic. In Section 2, the distinguishing factors of Urban motor vehicle drivers' traffic literacy are analyzed. Section 3 of this paper constructed the weight model of traffic literacy based on the Analytic Hierarchy Process (AHP). Section 4 evaluates the traffic literacy of motor vehicle drivers in Zhengzhou. In section 5, the conclusion to the current study is presented.

2. Analysis of Characteristic Factors of Urban Motor Vehicle Drivers' Traffic Literacy

This section analyzes the characteristic factors of traffic literacy of urban motor vehicle drivers. First, we define the concept of driver's traffic literacy. Then, we discuss the basic idea of extraction of characteristics of urban motor vehicle drivers' traffic literacy. Moreover, the preliminary construction of the traffic literacy evaluation index system is discussed.

2.1. Definition of Driver's Traffic Literacy Concept. Through the analysis and combing of the literature and learning from previous research experience, we believe that the concept of literacy can be introduced into the actual driving process of drivers, and the solution to traffic problems is regarded as a "human action." Traffic literacy is a kind of professional literacy with practical significance. It refers to the traffic behavior or tendency that traffic participants gradually develop during long-term driving activities and are not easy to change for a while and the knowledge, attitude, and control of driving activities. Ability is gradually summarized from people's actions and mainly refers to people's awareness of traffic, the relationship between people and the traffic environment, and humans' treatment of traffic conditions that are gradually accumulated in response to various road traffic conditions [8]. Comprehensive quality consists of specific knowledge and experience, reasonable methods and skills, and people-oriented green awareness. The formation of traffic literacy starts with the personal mastery of traffic knowledge, cultivates and forms a healthy traffic awareness, then turns traffic knowledge into a skill, establishes a good traffic safety awareness, and uses it to guide actions.

2.2. Basic Idea of Extracting Characteristic Factors of Traffic Literacy of Urban Motor Vehicle Drivers. The construction of the urban driver's traffic literacy evaluation system is a multi-index, multi-level comprehensive evaluation problem. It contains more content and involves a wide range. Therefore, it is necessary to set up a quantitative evaluation and transform qualitative problems into quantitative problems for analysis. An evaluation index system is established according to the index level and the defined size relationship. The traffic literacy of different cities is evaluated to lay a solid foundation for improving the overall traffic literacy and enhancing national traffic safety awareness.

2.3. Preliminary Construction of the Evaluation Index System of Traffic Literacy. Determining traffic literacy evaluation indicators is a complicated issue. Since harmonious traffic involves many issues, the corresponding influencing factors can be divided into dozens or hundreds of categories. To facilitate the research and the operability of the evaluation model, combine the influencing factors, formation mechanism, evaluation purpose, and index selection principles of the transportation system [3–5, 9–12], and after analysis and summarization, a subjective index system of traffic literacy is constructed. Specifically, it includes 13 subjective indicators such as traffic rules, general knowledge of machinery, knowledge of laws and regulations, safety awareness, treatment of others, facility safety, situation prediction, vehicle control, preventive measures, emergency measures, self-management behaviors, driving control behaviors, safe and civilized behaviors, etc. After analysis and classification, 13 indicators are combined into 4 main evaluation factors: traffic knowledge, traffic awareness, traffic skills, and traffic behavior, as shown in Table 1.

Table 1: Structure of traffic literacy evaluation indicators.

Evaluation goal	Evaluation factor	Evaluation index
Traffic literacy X	Traffic knowledge X_1	Traffic rules X_{11}
		Mechanical knowledge X_{12}
		Knowledge of laws and regulations X_{13}
	Traffic awareness X_2	Safety consciousness X_{21}
		Treat others well X_{22}
		Facility safety X_{23}
		Situation foreseeing X_{24}
	Traffic skills X_3	Vehicle control X_{31}
		Precaution X_{32}
		Emergency measures X_{33}
	Traffic behavior X_4	Self-management behavior X_{41}
		Driving control behavior X_{42}
		Safe and civilized behavior X_{43}

3. Construction of the Weight Model of Traffic Literacy Based on the Analytic Hierarchy Process

Since each evaluation index needs to set up corresponding weights, all the indexes in this paper use the combination of the Delphi method and analytic hierarchy process to determine the evaluation index weights. The analytic hierarchy process is a multi-target group's decision-making ideas and methods. In the application of group decision-making, there are two different ways to deal with the pairwise judgments of the group matrix. One of them is to first determine the individual weights according to the individual judgment matrix and then combine them. The second method is to synthesize the individual judgment matrix and then determine the group weight. The evaluator first decomposes the complex problem into many constituent elements and forms these elements into an orderly hierarchical structure according to the dominance relationship. The total evaluation value is determined, and the decision is made. The advantage is that the thinking process of analysts can be systematized, mathematicized, and modeled, and many impact indicators can be classified and processed so that the corresponding importance of each indicator can be determined.

3.1. Hierarchical Analysis Model Construction. The questionnaire survey form is adopted for this model to facilitate the analysis of various indicators, and the corresponding AHP model is established, as shown in Figure 1. The comparative judgment matrix uses the Delphi method to invite relevant experts to make corresponding decisions. It uses questionnaires for statistical analysis, summarizes the comparative judgment matrix between indicators at various levels, and calculates the weight of each indicator based on the judgment matrix.

First, select the evaluation index system, select experts according to the range of knowledge required for the traffic literacy evaluation problem, ask all experts to make decisions and related requirements, and attach all relevant background materials. At the same time, ask the experts to suggest what other materials are needed and supplemented. After the experts receive the materials, they compare the importance of the evaluation indicators according to a scale of 1–9. After normalizing the comparison matrix, the relative weight of each indicator at the same level is obtained. Generally speaking, after returning the questionnaire, the expert's judgment matrix should be checked for consistency. Specific steps are as follows:

If the activity relative activity has a score value, the activity relative activity score is reciprocal. The initial pairwise comparison matrix R can be expressed as follows:

$$R = \begin{pmatrix} 1 & a_{12} & \cdots & a_{1n} \\ a_{21} & 1 & \cdots & a_{2n} \\ \vdots & \vdots & \vdots & \vdots \\ a_{n1} & a_{n2} & \cdots & 1 \end{pmatrix}. \tag{1}$$

In equation (1), $a_{ij} = (1/a_{ji}), a_{ij} > 0$. The calculation of the weight of each level index, that is, the calculation of the root mean squares of all elements in each row of the judgment matrix; the formula is as follows:

$$C_{ij} = n\sqrt{\prod_{j=1}^{n} a_{ij}}, \quad i = 1, 2, \ldots, n. \tag{2}$$

Generally speaking, the comparison matrix is not necessarily a consistent matrix, the characteristic root of the n-order consistent matrix is n, and the characteristic root of the n-order reciprocal matrix is λ, where $\lambda \geq n$. And, $\lambda = n$ when the matrix is uniform, since λ continuously depends on a_{ij}, λ can be more than n, the inconsistency of the matrix will be more serious, so the value of $\lambda - n$ is used to measure the degree of inconsistency. The formula is as follows: $\mathrm{CI} = \lambda - n/n - 1$

Among them, in order to determine the allowable range of matrix inconsistency, a random consistency index is also introduced RI, when CR = CI/RI (If it is 0.1, it can be considered that the inconsistency of the matrix is within the allowable range, and the matrix that cannot pass is modified accordingly), Then, normalize the matrix to obtain the relative weight of the index layer.

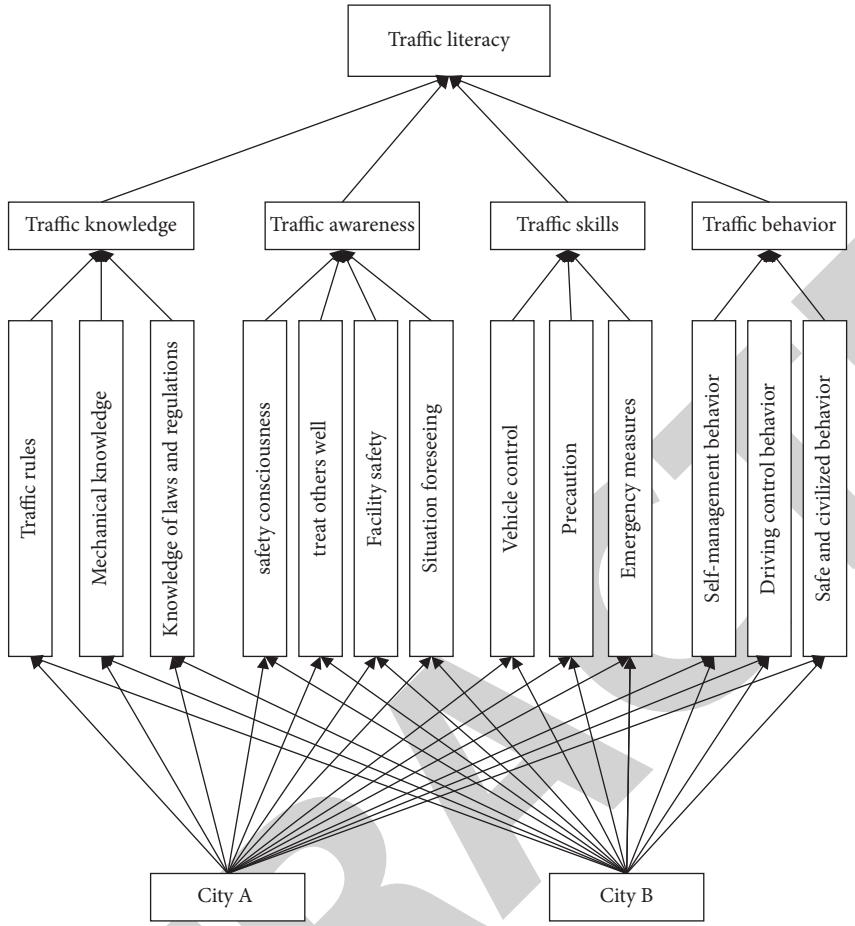

Figure 1: Specific traffic literacy model.

$$C_{ij} = \frac{a_{ij}}{\sum_{i=1}^{n} a_{ij}},$$
$$W_{ij} = \frac{\sum_{j=1}^{n} C_{ij}}{n}, \quad (3)$$
$$\sum_{i=1}^{n} W_i = 1.$$

This study adopts software combined with a questionnaire survey based on experts to compare the importance of indicators at various levels and calculate the weights. Finally, the geometric average of all statistical experts' data is used as the relative weight.

3.2. Determining the Weights of All Levels of Traffic Literacy Evaluation. According to the results of questionnaire analysis and expert decision-making, this part realizes the weight calculation of the first-level index and the second-level index through the operation of the software. All judgment matrices and calculation results are shown in Tables 2 to 6.

Based on the above research and calculation results, it can be seen that the analytic hierarchy process is used to solve the weight of each indicator, and the detailed calculation process of each indicator is realized with the aid of the analysis software "yaahp." The detailed summary information of the weight of each level is shown in Table 7.

When the total weight is obtained, the consistency test index of the total arrangement is calculated, namely, CR = 0.0173, and the total index can pass the consistency test when the test is passed.

4. Evaluation of Traffic Literacy of Motor Vehicle Drivers in Zhengzhou City

This section intends to evaluate the traffic literacy of motor vehicle drivers in Zhengzhou city. Henceforth, the design of the questionnaire and scoring rules are defined. Furthermore, an overview of sample and data acquisition is also explained. In addition, the results are analyzed and evaluated. Finally, an overall evaluation of traffic literacy of motor vehicle drivers in Zhengzhou is given.

4.1. Questionnaire Design and Scoring Rules. To obtain adequate data and ensure the scientificity and standardization of the evaluation, the design of the questionnaire follows the principles of matching, conciseness, and completeness. The confidentiality commitment is made in the questionnaire instruction section, and the research purpose is explained [10]. A survey questionnaire for traffic literacy evaluation of

Table 2: Judgment matrix of traffic literacy evaluation system and weight.

The assembled judgment matrix--the evaluation system of traffic literacy					Concordance ratio CR = 0.0173
Traffic literacy evaluation system	Traffic knowledge	Traffic awareness	Traffic skills	Traffic behavior	w_i
Traffic knowledge	1.0000	2.4082	3.3935	0.3196	0.2397
Traffic awareness	0.4152	1.0000	1.4963	0.2144	0.1127
Traffic skills	0.2947	0.6683	1.0000	0.1828	0.0819
Traffic behavior	3.1291	4.6632	5.4707	1.0000	0.5657

Table 3: Discrimination matrix of traffic knowledge secondary indicators and weight.

The assembled judgment matrix-traffic knowledge				Concordance ratio CR = 0.0000
Traffic knowledge	Traffic rules	Mechanical knowledge	Knowledge of laws and regulations	w_i
Traffic rules	1.0000	3.9363	1.8206	0.4163
Mechanical knowledge	0.2540	1.0000	0.3839	0.2251
Knowledge of laws and regulations	0.5493	2.6052	1.0000	0.3586

Table 4: Discrimination matrix of traffic awareness level indicators and weight.

The assembled judgment matrix-traffic awareness					Concordance ratio CR = 0.0514
Traffic awareness	Safety consciousness	Treat others well	Facility safety	Situation foreseeing	w_i
Safety consciousness	1.0000	4.0760	6.1185	4.1694	0.6950
Treat others well	0.2453	1.0000	3.0000	1.2457	0.2148
Facility safety	0.1634	0.3333	1.0000	1.5281	0.0903
Situation foreseeing	0.2398	0.8027	0.6544	1.0000	0.1269

Table 5: Discrimination matrix of traffic skill secondary indicators and weight.

The assembled judgment matrix-transportation skills				Concordance ratio CR = 0.0167
Traffic skills	Vehicle control	Precaution	Emergency measures	w_i
Vehicle control	1.0000	5.3046	3.6297	0.6759
Precaution	0.1885	1.0000	0.4611	0.1117
Emergency measures	0.2755	2.1689	1.0000	0.2124

Table 6: Discriminant matrix of traffic behavior secondary indicators and weight.

The assembled judgment matrix-traffic behavior				Concordance ratio CR = 0.0000
Traffic behavior	Self-management behavior	Driving control behavior	Safe and civilized behavior	w_i
Self-management behavior	1.0000	4.3597	3.3935	0.5266
Driving control behavior	0.2294	1.0000	0.6598	0.2103
Safe and civilized behavior	0.2947	1.5157	1.0000	0.2631

motor vehicle drivers in Zhengzhou is designed. The questionnaire is composed of three parts: the headline, the basic situation of the surveyed person, and the main body of the questionnaire. The basic information of the surveyed person includes seven demographic indicators of gender, age, education, occupation, place of residence, annual family income, and driving age of the surveyed person. The main body of the questionnaire contains four topics: traffic knowledge, traffic awareness, traffic skills, and traffic behavior. Questions are set according to the weights of 13 three-level indicators, with a lower weight setting of 1-2 questions, and a higher weight setting of 2-3 questions per problem. A total of 19 questions are set.

When designing each questionnaire item, we learned from the relatively mature scale paradigm and used the Likert scale to measure traffic knowledge, awareness, skills, and behavior. This study's answer is designed into five measurement levels, corresponding to the five points of "5, 4, 3, 2, and 1." According to different questions, different combinations of statement languages are designed to investigate the respondents, enabling them to make choices more clearly and conveniently so that the attitudes or opinions of the respondents can be more clearly reflected. By consulting experts and teachers in related fields, such as psychology, sociology, and statistics, and drawing on relatively mature scales, such as scientific literacy, environmental literacy, water literacy, etc., the language expression of the questionnaire is refined to form the "Vehicle Driver Traffic Literacy Evaluation Questionnaire."

4.2. Data Acquisition and Sample Overview. The questionnaire of this research selected people with driving experience within the administrative area of Zhengzhou City. The

Table 7: Driver's traffic literacy system indicators comprehensive weighted weight assignment.

	Secondary indicator layer	Weights	Three-level indicator layer	Weights
Driver's traffic literacy	Traffic knowledge	0.2397	Traffic rules	0.4163
			Mechanical knowledge	0.2251
			Knowledge of laws and regulations	0.3586
	Traffic awareness	0.1127	Safety consciousness	0.6950
			Treat others well	0.2148
			Facility safety	0.0903
			Situation foreseeing	0.1269
	Traffic skills	0.0819	Vehicle control	0.6759
			Precaution	0.1117
			Emergency measures	0.2124
	Traffic behavior	0.5657	Self-management behavior	0.5266
			Driving control behavior	0.2103
			Safe and civilized behavior	0.2631

questionnaire is distributed online through electronic questionnaires and face-to-face hard copy questionnaires. Considering that the online questionnaire still has certain limitations, filling is done in the paper questionnaire face to face to supplement. The paper questionnaire is distributed to select locations such as a vehicle management office in Zhengzhou, a comprehensive service hall of a traffic police brigade, and a vehicle repair shop to make the data obtained more comprehensive. A total of 980 questionnaires were distributed in this study, and 693 valid questionnaires were obtained after excluding unqualified questionnaires (for example, the online questionnaire has a short answer time, more than 80% of the questions are answered in a certain order, and the paper questionnaire is not completely filled out, etc., all of which will be regarded as unqualified questionnaires). The effective sample rate is 70.71%. The demographic information of the sample is described in five items: gender, age, education level, occupation, and average monthly household income, as shown in Table 8.

4.3. Result Analysis and Evaluation. Statistical analysis of the traffic literacy questionnaire survey of motor vehicle drivers in Zhengzhou City shows each evaluation factor score (the score is between 1 and 5, the higher the score, the better the evaluation), as shown in Table 9.

Judging from the traffic literacy evaluation factor scores of motor vehicle drivers in Zhengzhou, the highest-scoring question is question 7, "Do you care more about the feelings of passengers and be kind to others during driving?" with a score of 4.42. The corresponding evaluation index is traffic awareness, which shows that the respondents have an obvious subjective idea of being kind to others. In the second place is question 14, "Can you perform better self-management during driving, with a score of 4.29, and its corresponding evaluation index is traffic behavior, which reflects that the respondent's clear self-management behavior is projected on the performance of traffic behavior. It also shows that the respondents have good self-management habits in daily driving. The question with the lowest score was Question 3, "Do you have a common sense of the various components of the motor vehicle you drive?" which was only 3.15, indicating that most respondents did not have a common sense of the various components of the motor vehicle. In addition, a similar question is question 4, "Do you have a knowledge of traffic-related laws and regulations?" with a score of 3.63, ranking second from the bottom. Question 13 "Do you know relevant emergency measures for traffic emergencies?," with a score of 3.64, indicating that the respondent does not know much about the emergency measures and is not familiar with the same related laws and regulations.

4 questions correspond to traffic knowledge, among which the first question is "Do you understand traffic rules?" and the second question is "Have you studied traffic rules knowledge content?" The scores are relatively close, all-around 4 points. This shows that the respondents have a better knowledge of traffic rules. The third question, "Do you know a common sense of the various components of the motor vehicle you drive?" has a shallow score, only 3.15 points, indicating that some respondents are more aware of motor vehicles but do not know much about the components.

In traffic awareness, in addition to the highest score for question 7, questions 5 and 6 have relatively high scores, indicating that motor vehicle drivers have a high level of safety awareness. The scores of questions 8 "Do you often pay attention to the safety of the various parts and facilities of the vehicle you drive?" and 9 "Do you think you can anticipate situations better while driving?" are not very high, which shows that motor vehicle drivers are not too concerned about the safety of auto parts and facilities. They cannot predict the situation very well.

The score was 4.14 when asked, "Do you think you can handle a vehicle well?" but only 3.92 when asked "Do you intend to learn vehicle handling skills?"; this result shows that most of the respondents think that they have better vehicle control skills and do not want to carry out new learning. In traffic skills, preventive measures and emergency measures have low scores, and the training of emergency and preventive measures for motor vehicle drivers should be strengthened.

Compared with traffic knowledge, traffic awareness, and traffic skills, traffic behavior scores were higher, with an average score of about 4.2. In particular, the self-management behavior score of the respondents was 4.29, and they all

Table 8: Sample demographic characteristics information.

Category	Category description	Number of samples	Proportion (%)
Gender	Male	536	77.34
	Female	157	22.66
Age	16–35	135	19.48
	36–45	331	47.76
	46–59	192	27.71
	Over 60 years old	35	5.05
Education level	Elementary school and below	33	4.76
	Junior high school	189	27.27
	High school (including secondary school, vocational high school, technical school, etc.)	254	36.65
	University (college/undergraduate)	142	20.49
	Master's degree and above	75	10.82
Profession	Corporate personnel	133	19.19
	National civil servants (including soldiers, police, etc.)	98	14.14
	The public utility staff (such as teachers, doctors, etc.)	108	15.58
	Freelancers	255	36.80
	Others	99	14.29
Average monthly household income (yuan)	Below 4999	41	5.92
	5000–9999	293	42.28
	10000–19999	176	25.40
	20000–49999	104	15.01
	Above 50000	79	11.40

Table 9: Zhengzhou city motor vehicle driver traffic literacy evaluation factor score.

First level indicator	Secondary indicators	Question number	Summary of observation points	Score
Traffic knowledge	Traffic rules	1	Understanding of traffic rules	4.00
		2	Attitudes toward learning traffic rules	4.20
	Mechanical knowledge	3	Understanding of motor vehicle components	3.15
	Knowledge of laws and regulations	4	Traffic-related laws and regulations	3.63
Traffic awareness	Safety consciousness	5	Have a strong sense of safety	4.28
		6	Cultivation of safety awareness	4.26
	Treat others well	7	How the passengers feel	4.42
	Facility safety	8	Safety of motor vehicle parts	4.08
	Situation foreseeing	9	Foresight	4.09
Traffic skills	Vehicle control	10	Driving vehicle control	4.14
		11	Learning the intention of vehicle control	3.92
	Precaution	12	Preventive measures for emergencies	3.70
	Emergency measures	13	Understanding of relevant emergency measures	3.64
Traffic behavior	Self-management behavior	14	Self-management	4.29
		15	Self-management awareness	4.19
	Driving control behavior	16	Driving control	4.15
	Safe and civilized behavior	17	Safe and civilized	4.21

had good traffic civilized behaviors. It also shows that the traffic behavior of motor vehicle drivers in Zhengzhou is relatively good.

4.4. Overall Evaluation of Traffic Literacy of Motor Vehicle Drivers in Zhengzhou. According to the abovementioned analytic hierarchy process to determine the index weights at all levels, based on the average value of the traffic literacy evaluation factor scores of motor vehicle drivers in Zhengzhou City, the traffic literacy of motor vehicle drivers in Zhengzhou City is evaluated. To show the scores of each factor more intuitively, normalize each factor index and convert it into a percentile system. Taking the traffic literacy evaluation value of motor vehicle drivers in Zhengzhou s as an example, the converted traffic literacy evaluation of motor vehicle drivers in Zhengzhou Value $s = 4/5 \times 100 = 80$ uses the same method to process the index scores of each factor and get Table 10.

The traffic literacy evaluation value of motor vehicle drivers in Zhengzhou is 72.07, of which the traffic knowledge score is 77.09, traffic awareness score is 73.95, and traffic skills score is 78.12. The traffic behavior score is 84.3, reflecting that the respondents have a relatively more active

Table 10: Zhengzhou city motor vehicle driver traffic literacy evaluation score.

S	Evaluation value	S_i	Evaluation value	S_{ij}	Evaluation value
Traffic literacy	72.07	Traffic knowledge	77.09	Traffic rules	82.01
				Mechanical knowledge	63.05
				Knowledge of laws and regulations	72.57
		Traffic awareness	73.95	Safety consciousness	85.39
				Treat others well	88.50
				Facility safety	81.53
				Situation foreseeing	81.88
		Traffic skills	78.12	Vehicle control	80.59
				Precaution	74.05
				Emergency measures	72.88
		Traffic behavior	84.3	Self-management behavior	84.81
				Driving control behavior	82.90
				Safe and civilized behavior	84.12

and responsible traffic behavior and have a certain degree of understanding of traffic skills and traffic knowledge, but are relatively low in traffic awareness.

Among the various scores of traffic knowledge, motor vehicle drivers are more familiar with traffic laws and regulations but do not know much about the car's components. Most motor vehicle drivers pay more attention to traffic knowledge during driving and do not need to know much about the car's components, which is also in line with the driver's daily life status. The highest score in traffic awareness is to be kind to others, indicating that motor vehicle drivers can better put themselves in other's place and consider them. The attribute with the highest score in traffic skills is vehicle control, indicating that the motor vehicle driver can control well the driving of the vehicle. The highest traffic behavior score indicates that drivers behave well during motor vehicle driving. This is due to the observance of traffic rules and the self-cultivation of drivers. Overall, the traffic literacy score is only 72.07, which is not too high. It may be due to relatively low traffic knowledge, traffic awareness, and traffic skills. Therefore, it is necessary to strengthen the traffic knowledge, traffic awareness, and traffic skills of motor vehicle drivers.

5. Conclusion

Based on the concept of traffic literacy and the elemental composition of traffic literacy, this article combines the analysis of the influencing factors, formation mechanism, evaluation purpose, index selection principles of the traffic system, and after analysis and induction, constructs a subjective index system of traffic literacy. The specific subjective index layer has 13 indicators, namely, traffic rules, machinery knowledge, knowledge of laws and regulations, safety awareness, kindness to others, facility safety, situation prediction, vehicle control, preventive measures, emergency measures, self-management behaviors, driving control behaviors, and safe and civilized behaviors. The 13 indicators are classified and combined into 4 evaluation factors: traffic knowledge, traffic awareness, traffic skills, and traffic behavior. Through the investigation and analysis of the analytic hierarchy process, the weights of the four evaluation factors, traffic knowledge, traffic awareness, traffic skills, and traffic behavior, are respectively: 0.2397, 0.1127, 0.0819, and 0.5657. The results show that the weight of traffic awareness is relatively high in the driver's traffic literacy evaluation index. The indicators with higher weights of the third-level indicators are traffic rules (0.4163), safety awareness (0.6950), vehicle control (0.6759), and self-management behavior (0.5266). After clarifying the importance of the secondary and tertiary indicators, the total weighted value of the driver's traffic literacy system indicators is obtained. Based on the evaluation index system of motor vehicle drivers' traffic literacy, a questionnaire was designed, and a questionnaire survey was conducted in the pilot city of Zhengzhou to analyze the primary status of the traffic literacy of motor vehicle drivers in Zhengzhou and conduct an overall evaluation of the traffic literacy of motor vehicle drivers. It shows that the traffic literacy evaluation value of motor vehicle drivers in Zhengzhou is 72.07, of which the traffic knowledge score is 77.09, the traffic awareness score is 73.95, the traffic skills score is 78.12, and the traffic behavior score is 84.3, reflecting that the respondents are relatively more active and responsible. Traffic behavior also has a certain degree of understanding of traffic skills and knowledge, but is relatively low in traffic awareness.

Because of the limitations and subjectivity of the traffic literacy index system constructed in this study and the results based on the questionnaire survey, there are specific differences with the literacy of actual drivers. Respondents had a self-glorifying mentality when answering the questionnaire, which led to discrepancies between actual results and survey results. The survey results are pretty different, so follow-up research work needs to improve the construction of the indicator system further, and according to the current advanced technology in the era of big data, enrich the data basis of motor vehicle drivers' traffic literacy, and use network data (accident rate, vehicle service life). Such indicators more intuitively reflect the traffic literacy of motor vehicle

Hindawi
Journal of Mathematics
Volume 2023, Article ID 9787190, 1 page
https://doi.org/10.1155/2023/9787190

Retraction

Retracted: An Evaluation of the Security Ability of the Basic Endowment Insurance System for China's Urban and Rural Residents

Journal of Mathematics

Received 19 December 2023; Accepted 19 December 2023; Published 20 December 2023

This article has been retracted by Hindawi following an investigation undertaken by the publisher [1]. This investigation has uncovered evidence of one or more of the following indicators of systematic manipulation of the publication process:

(1) Discrepancies in scope

(2) Discrepancies in the description of the research reported

(3) Discrepancies between the availability of data and the research described

(4) Inappropriate citations

(5) Incoherent, meaningless and/or irrelevant content included in the article

(6) Manipulated or compromised peer review

The presence of these indicators undermines our confidence in the integrity of the article's content and we cannot, therefore, vouch for its reliability. Please note that this notice is intended solely to alert readers that the content of this article is unreliable. We have not investigated whether authors were aware of or involved in the systematic manipulation of the publication process.

Wiley and Hindawi regrets that the usual quality checks did not identify these issues before publication and have since put additional measures in place to safeguard research integrity.

We wish to credit our own Research Integrity and Research Publishing teams and anonymous and named external researchers and research integrity experts for contributing to this investigation.

The corresponding author, as the representative of all authors, has been given the opportunity to register their agreement or disagreement to this retraction. We have kept a record of any response received.

References

[1] B. Liu, Y. He, and Z. Liu, "An Evaluation of the Security Ability of the Basic Endowment Insurance System for China's Urban and Rural Residents," *Journal of Mathematics*, vol. 2022, Article ID 6244880, 10 pages, 2022.

Hindawi
Journal of Mathematics
Volume 2022, Article ID 6244880, 10 pages
https://doi.org/10.1155/2022/6244880

Research Article

An Evaluation of the Security Ability of the Basic Endowment Insurance System for China's Urban and Rural Residents

Bing Liu,[1] Yuhong He ,[1] and Zhi Liu[2]

[1]*School of Public Administration and Law, Hunan Agricultural University, Changsha 410128, China*
[2]*School of Continuing Education, Hunan Agricultural University, Changsha 410128, China*

Correspondence should be addressed to Yuhong He; heyuhonghunau@126.com

Received 3 December 2021; Revised 19 January 2022; Accepted 25 January 2022; Published 16 February 2022

Academic Editor: Naeem Jan

In this paper, security ability refers to the standard of evaluation that is used to measure the implementation performance of the basic endowment insurance system for China's urban and rural residents (EIUR). To evaluate security ability, a three-level evaluation index system with a total of 19 indicators is designed. The research results show that it is low and even does not coincide with the country's level of economic development, for the security ability of EIUR, due to the top-level design of the insurance system under analysis, the operating environment, and residents' willingness to participate and contribute. Moreover, there are regional differences in regard to security ability; the development of various targets is not balanced. These findings suggest that it is necessary to promote the balanced development of various targets between regions and improve the completion of each target, especially in regard to "flexibility" and "fairness" targets.

1. Introduction

With the rapid development of China's basic endowment insurance system for urban and rural residents (EIUR), the national fund revenue and expenditure scale, and per capita pension level was improved obviously. By the end of 2018, the number of residents who had enrolled in the system reached 524 million people, of whom 159 million had received treatment. Fund income was 383.8 billion renminbi (RMB), fund expenditure was 290.6 billion RMB, and the pension reached 152.33 RMB per month. (The data in the "2018 Human Resources and Social Security Development Statistical Bulletin" on the official website of the Ministry of Human Resources and Social Security of China are quoted here.)

However, in regard to the development of the system, numerous problems persist, such as low treatment levels [1–3] and regional treatment differences [4]. Additionally, low individual contribution levels [5, 6] and excessive dependence on financial subsidies [7, 8] are persistent problems. Some scholars have evaluated the implementation effect of the EIUR from the economic, sustainability, fairness, and satisfaction perspectives [9–13]. On this basis, they have made suggestions for its improvement.

The extant research of the EIUR lacks a macro-level evaluation of the system; rather, it focuses primarily on a certain aspect of the system, which it evaluates from the micro-level. For instance, some research focuses on qualitative descriptions, comments, and policy suggestions; others have evaluated the implementation effect of EIUR from system treatment and fund operation. Therefore, this paper will construct a comprehensive scientific evaluation index system based on multiple dimensions and perspectives, such as the basic principles of system design, security functions, and development vision. It will analyze the current status of the implementation of the EIUR in China's provinces and put forward suggestions to deepen the reform of the system.

2. Research Area and Data

The research area comprises 31 provinces (autonomous regions and municipalities that are directly under the central government) in China, excluding Hong Kong, Macao, and

Taiwan. (Due to the "one country, two systems" system, Hong Kong, Macao, and Taiwan have implemented a social system that differs from that of China's mainland.) Based on the Chinese government's regulations on the minimum standard subsidies for urban and rural residents' basic insurance pensions (BIP) in 2014 (according to the basic pension standard, the central government provides full subsidies to the central and western regions and 50% subsidies to the eastern regions), the 31 provinces are divided into two major blocks as follows: (The eastern provinces are Beijing, Tianjin, Hebei, Liaoning, Shanghai, Jiangsu, Zhejiang, Fujian, Shandong, Guangdong, and Hainan, while the central and western provinces are Shanxi, Jilin, Heilongjiang, Anhui, Jiangxi, Henan, Hubei, Hunan, Inner Mongolia, Guangxi, Chongqing, Sichuan, Guizhou, Yunnan, Tibet, Shaanxi, Gansu, Qinghai, Ningxia, and Xinjiang.) the eastern region and midwestern region.

The data used in this paper were sourced from yearbooks, such as *China Statistical Yearbook 2019, China Labor Statistics Yearbook 2019,* and *China Population and Employment Statistics Year 2019,* as well as public data retrieved from the China Statistics Bureau. There are three main data categories as follows: macroeconomic data, (The macroeconomic data include China's GDP and per capita GDP from 2011 to 2018, the per capita disposable income of urban and rural residents, the per capita living consumption expenditure of urban and rural residents, and the minimum living consumption level.) population data, (The population data include the number of permanent residents by province from 2011 to 2018, the number of older people by region, and the number of people by age across the country.) and operation data, (The operating data include the number of insured persons, the number of people receiving benefits, fund income, fund expenditures, accumulated fund balances, individual contributions, and individual contribution rates.) and these three types of data can be collectively referred to as original data. Owing to the very nature of indicators, some original data cannot be directly utilized to calculate the evaluation index. Therefore, we preprocessed some of the original data, and we call it processed data. The processed data includes the number of people aged 16–59 years who are eligible for insurance coverage, the number of people over 60 years old who are eligible for the insurance coverage, per capita pension, per capita contribution, per capita government subsidy, and per capita income fund (see Table 1 for the specific processing methods). Some of the above three types of data cannot be directly used in the calculation of the indicator system.

3. Method

3.1. Index System Construction. To fully reflect our respect for objective facts and advanced thinking, based on the current research results, combined with the actual operation process of the EIUR and select targets and indicators related to individual contribution and treatment, we determined the evaluation indicators of the effect of citizens' insurance implementation (see Table 1 for the definitions and explanations of the specific indicators).

3.2. Determination of the Index Weight. The entropy weight method is a widely used objective weighting method. Based on the varying degrees of each index, the information entropy can be used to calculate its entropy weight. The weight of each index is then corrected by the entropy weight, thereby obtaining a more objective index weight. Because we constructed a three-level index system to evaluate the security ability of the EIUR, we propose a layered entropy weight method to measure the actual weight of each index.

3.2.1. Normalized Calculation of Indicator Data. The data for each index need to be normalized to eliminate the difference between the statistical standards and dimensions of the data. To unify the description, X_i represents the target, and X_{ij} represents the indicator. Let y_{ij}^t represents the normalized calculation of the t statistical data in indicator X_{ij}.

$$y_{ij}^t = \frac{x_{ij}^t - \min_{j\in\lambda}\left(x_{ij}^t\right)}{\max_{t\in\lambda}\left(x_{ij}^t\right) - \min_{t\in\lambda}\left(x_{ij}^t\right)}. \tag{1}$$

3.2.2. Calculation of the Index Weight. The index weights are measured using the layered entropy weight method. First, the indicator index weights are calculated according to the indicator index statistics; then, the indicator indexes are calculated; finally, the target weights are calculated according to the indicator indexes.

(1) Indicator Index Weight Calculation. To determine the weight of index X_{ij}, the information entropy of index X_{ij} must be calculated first. Let $H(X_{ij})$ denote the information entropy of index.

$$\begin{aligned} H\left(X_{ij}\right) &= -\frac{1}{\ln(n)}\sum_{t=1}^{n} w_{ij}^t \ln\left(w_{ij}^t\right), \\ w_{ij}^t &= \frac{y_{ij}^t}{\sum_{t=1}^{n} y_{ij}^t}. \end{aligned} \tag{2}$$

In (2), if $w_{ij}^t = 0$, then $w_{ij}^t \ln(w_{ij}^t) = 0$. According to the information entropy, the weight of the index can be obtained as $p(X_{ij})$.

$$p\left(X_{ij}\right) = \frac{1 - H\left(X_{ij}\right)}{k - \sum_{j=1}^{k} H\left(X_{ij}\right)}. \tag{3}$$

(2) Calculation of Target Index. Based on the weight and data of the indicator index, the target can be calculated. Let SI_i^t denote the target index.

$$\mathrm{SI}_i^t = \sum_{j=1}^{k} p\left(X_{ij}\right) y_{ij}^t. \tag{4}$$

In (4), SI_i^t is used to measure the role of targets in evaluating the EIUR.

Table 1: Evaluation index system and weights of security ability of EIUR.

Goal	Target	Indicator		Indicator description (definition)	Indicator interpretation
Security ability of EIUR	Full coverage (0.161)	Participation ratio of urban and rural residents aged 16–59	(0.198)	Number of participants/number of people who meet the conditions of participation	The larger the participation rate, the wider the coverage
		Participation ratio of urban and rural residents over 60	(0.039)	Number of participants/number of people who meet the conditions of participation	The larger the participation rate, the wider the coverage
		Growth rate of insured persons aged 16–59	(0.280)	Insured rate for the current year/insured rate for the previous year-1	The larger the growth rate, the wider the coverage
		Growth rate of insured persons over 60	(0.484)	Number of people receiving treatment in that year/number of people receiving treatment in the previous year-1	The larger the growth rate, the wider the coverage
	Basic protection (0.111)	Pension replacement rate	(0.329)	Pension per capita ×12/per capita disposable income of rural residents	The greater the replacement rate, the higher the security level
		Pension growth rate	(0.375)	Pension per capita in that year/pension per capita in the previous year-1	The greater the growth rate, the higher the security level
		Pension contribution rate to minimum living security	(0.296)	Per capita pension/minimum living standard	The greater the contribution rate, the higher the security level
	Flexibility (0.363)	Resident income flexibility of individual contributions	(0.054)	Growth rate of per capita contribution/growth rate of per capita disposable income of rural residents	The greater the flexibility, the more sensitive the individual's contribution to the residents' income
		Individual payment flexibility of payment subsidies	(0.502)	Government subsidy growth rate per capita/contribution growth rate per capita	The greater the flexibility, the more sensitive the government subsidies of individual contributions
		Resident income flexibility of basic pension	(0.108)	Basic pension growth rate/per capita disposable income growth rate of rural residents	The greater the flexibility, the more sensitive the basic pension to residents' income
		Economic development flexibility of pension	(0.336)	Pension growth rate per capita/gross domestic product (GDP) growth rate per capita	The greater the flexibility, the more sensitive the pension to economic development
	Sustainability (0.163)	Aging population	(0.002)	1-Elderly population/total population	The larger the numerical value, the stronger the sustainability
		Fund cumulative balance growth rate	(0.618)	Cumulative fund balance of the current year/cumulative fund balance of the previous year-1	The larger the numerical value, the stronger the sustainability
		Institutional maintenance rate	(0.279)	1-Number of people receiving treatment/number of paying people	The larger the numerical value, the stronger the sustainability
		Local government maximum subsidy ability	(0.031)	1-Maximum local government subsidies per capita/per capita fiscal revenue	The larger the numerical value, the stronger the sustainability
		Personal ability to pay	(0.070)	1-Minimum living standard/per capita disposable income	The larger the numerical value, the stronger the sustainability
	Fairness (0.202)	Maximum rate of return on personal account pension	(0.048)	Expected income of each pension account/amount paid per file-1	The higher the rate of return, the greater the fairness
		Contribution rate of economic development	(0.713)	Fund income per capita/GDP per capita	The higher the contribution rate, the greater the fairness
		Maximum ratio of government subsidy to individual contribution	(0.239)	Each level of government subsidy/each level of individual contribution	The larger the numerical value, the greater the fairness

Note: the number in parentheses represents the weight of each index. (1) Number of persons aged 16–59 eligible for participation = population aged 16–59-number of students aged 16 and above-number of employees in enterprises and institutions-number of retired enterprise employees aged 55–59-institutions and institutions' number of retirees 50–59 years old; (2) number of people who meet the conditions for participation = the number of people 60 years old and above-number of retirees over 60 years old who have enrolled the basic pension insurance for urban employees; (3) per capita pension = fund expenditure ÷ number of recipients ÷ 12; (4) per capita contribution = individual contribution income ÷ (number of participants-number of receiving benefits); (5) government subsidies per capita = (fund income-individual contribution income) ÷ number of participants; and (6) fund income per capita = fund income ÷ number of participants.

(3) Weight Calculation of Target. According to the calculation result of the target, the target index weight can be calculated. First, the information entropy of X_i is calculated. Let $H(X_i)$ denote the information entropy of X_i.

$$H(X_i) = -\frac{1}{\ln(n)} \sum_{t=1}^{n} w_i^t \ln\left(w_i^t\right),$$
$$w_i^t = \frac{\mathrm{SI}_i^t}{\sum_{i=1}^{n} SI_i^t}. \tag{5}$$

In (5), if $w_i^t = 0$, then $w_i^t \ln(w_i^t) = 0$. According to the information entropy, the weight $p(X_i)$ of the index X_i can be obtained.

$$p(X_i) = \frac{1 - H(X_i)}{5 - \sum_{j=1}^{5} H(X_i)}. \tag{6}$$

3.2.3. Index Weight Analysis. This article uses a layered entropy weight method: the more significant the changes in the indicators, the more substantial the weighting. As Table 1 shows, among the five targets, "flexibility" is the most heavily weighted, followed by "fairness," "full coverage," "sustainability," and "preservation of basics." The results show that after years of stable development, the EIUR has made significant progress in regard to coverage, flexibility, and fairness.

The accelerated development of the aging population will lead to an increase in the number of people receiving treatment of the EIUR, thereby resulting in serious challenges to the long-term stable development of the system. These challenges will be reflected in the stability and continuity of urban and rural residential maintenance pension treatment levels, as well as in the sustainability of urban and rural residential insurance fund revenues and expenditures.

Owing to the influence of the design model of the existing EIUR, the development of the system is increasingly dependent on finance from the government. Therefore, the benign development of the EIUR continues to depend on the financial ability of the government—especially local governments—in the short term. This way, a strong financial ability can ensure that the fruits of economic development benefit more urban and rural residents.

3.3. Evaluation Index Calculation and Classification. Based on the index and weight of the five targets—coverage, security level, elasticity, sustainability, and fairness—we can quantitatively evaluate the security ability of the basic endowment insurance system for China's urban and rural residents, and its model can be expressed as follows:

$$\mathrm{BPCI}_t = \sum_{i=1}^{5} p(X_i)\mathrm{SI}_i^t. \tag{7}$$

In (7), BPCI_t represents the evaluation index of security ability. Its value is between 0 and 1; the larger the value, the stronger the security ability.

Based on the calculated evaluation index of the security ability of each province, this paper uses the ArcGIS 10.5 software's natural breakpoint method to divide security ability into five levels: "high level," "higher level," "medium level," "lower level," and "low level" (see Figures 1 and 2).

The completion of the five targets is divided into three levels: "basic implementation," "at risk," and "serious challenge."

4. Evaluation Results and Analysis

4.1. Low Level of Security Ability of the EIUR. As shown in Table 2, the security ability of EIUR in China is currently low. First, Hubei, which ranks first in the national security ability index, has only 0.752. The security ability indexes for Jilin, Tianjin, and Anhui are all below 0.6–0.597, 0.586, and 0.561, respectively—and much lower than that of Hubei. There are only nine provinces with a security ability index of between 0.5 and 0.6; however, there are 21 provinces with an index below 0.5, accounting for 67.74%. In addition, four provinces (autonomous regions)—Inner Mongolia, Tibet, Guangdong, and Zhejiang—have a security ability index below 0.4. Among them, Zhejiang has an index of only 0.321, which is the lowest in the country.

Second, from a security level perspective (Figure 2), a few provinces have a higher level of security ability while others have medium and low levels. Specifically, Hubei is the only high-level province, and there are only seven higher-level provinces, nine medium-level provinces, and then other provinces that are at a lower level and below, accounting for 45.16%.

There are several reasons for the low level of security ability. First, target completion is poor. As shown in Table 2, regarding the five targets, the provinces facing "certain risks" and "serious challenges" account for a high proportion: 87.10%, 93.55%, 90.32%, 67.74%, and 96.77%. Second, none of the provinces have been able to implement the targets. For example, Hubei, which ranks first in the country in regard to the security ability index, has only two targets—"flexibility" and "sustainability"—that have been "basically achieved," while the "fairness" target is still facing "serious challenges." Inner Mongolia, Guangdong, and Zhejiang, which have lower security ability index rankings, have the lowest target completion. Four targets in each province face "serious challenges," and none can achieve "basic implementation."

4.2. Uneven Development of the Targets of the EIUR. Table 2 and Figure 2 show that among the five targets, "sustainability" and "full coverage" are developing well, followed by "basic protection." In contrast, the "fairness" and "flexibility" targets are not being achieved. First, the "sustainable" target has the highest degree of completion among the five targets, and 10 provinces have reached the "basic implementation" level. The "full coverage" target is second only to the "sustainable" one, and in regard to the former, more than half of the provinces are above the national average. Second, the "basic protection" target's performance was average, with 12 provinces above the national

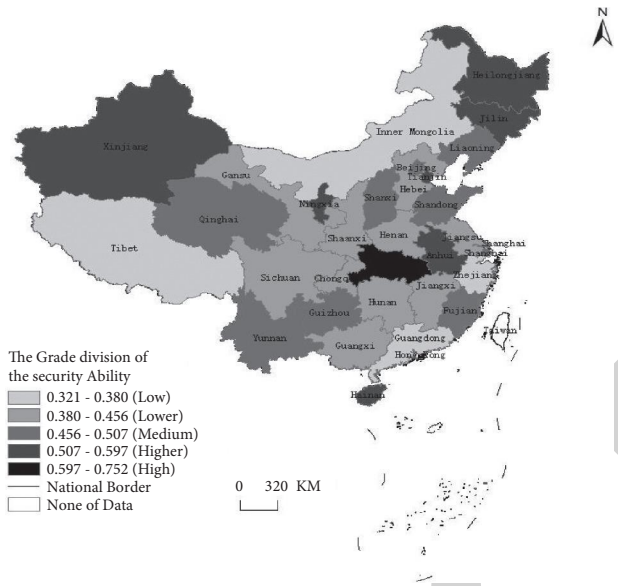

Figure 1: Grade division of the security ability of the EIUR in 2018.

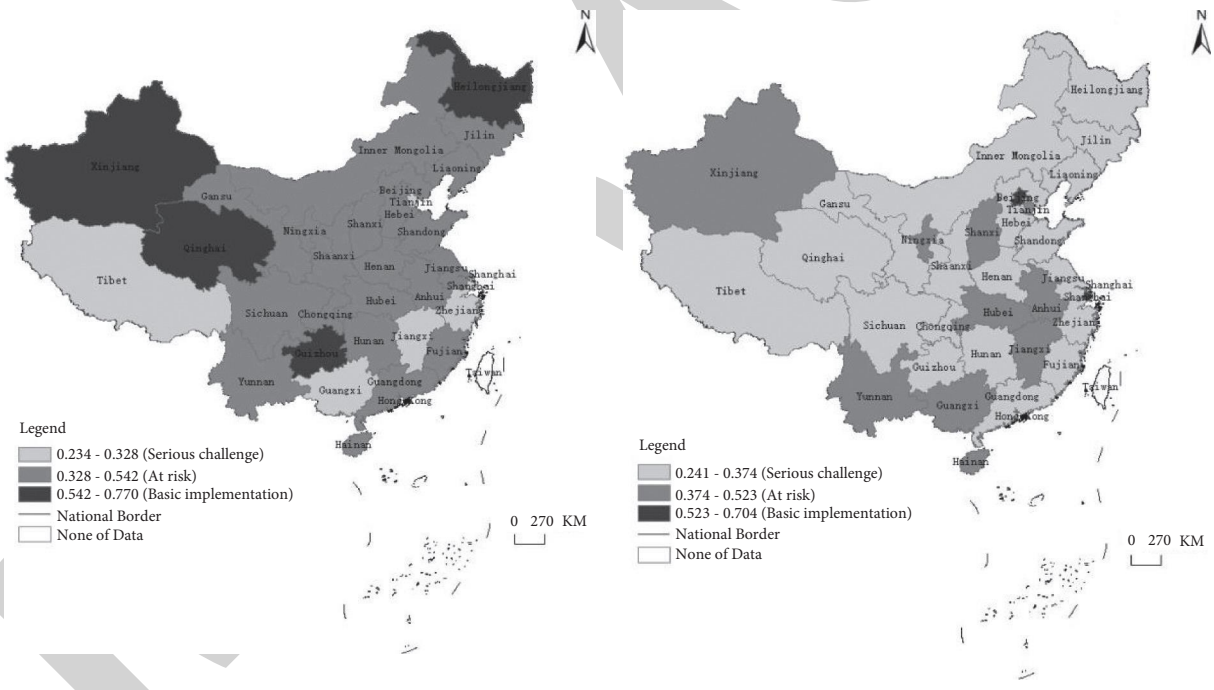

(a) (b)

Figure 2: Continued.

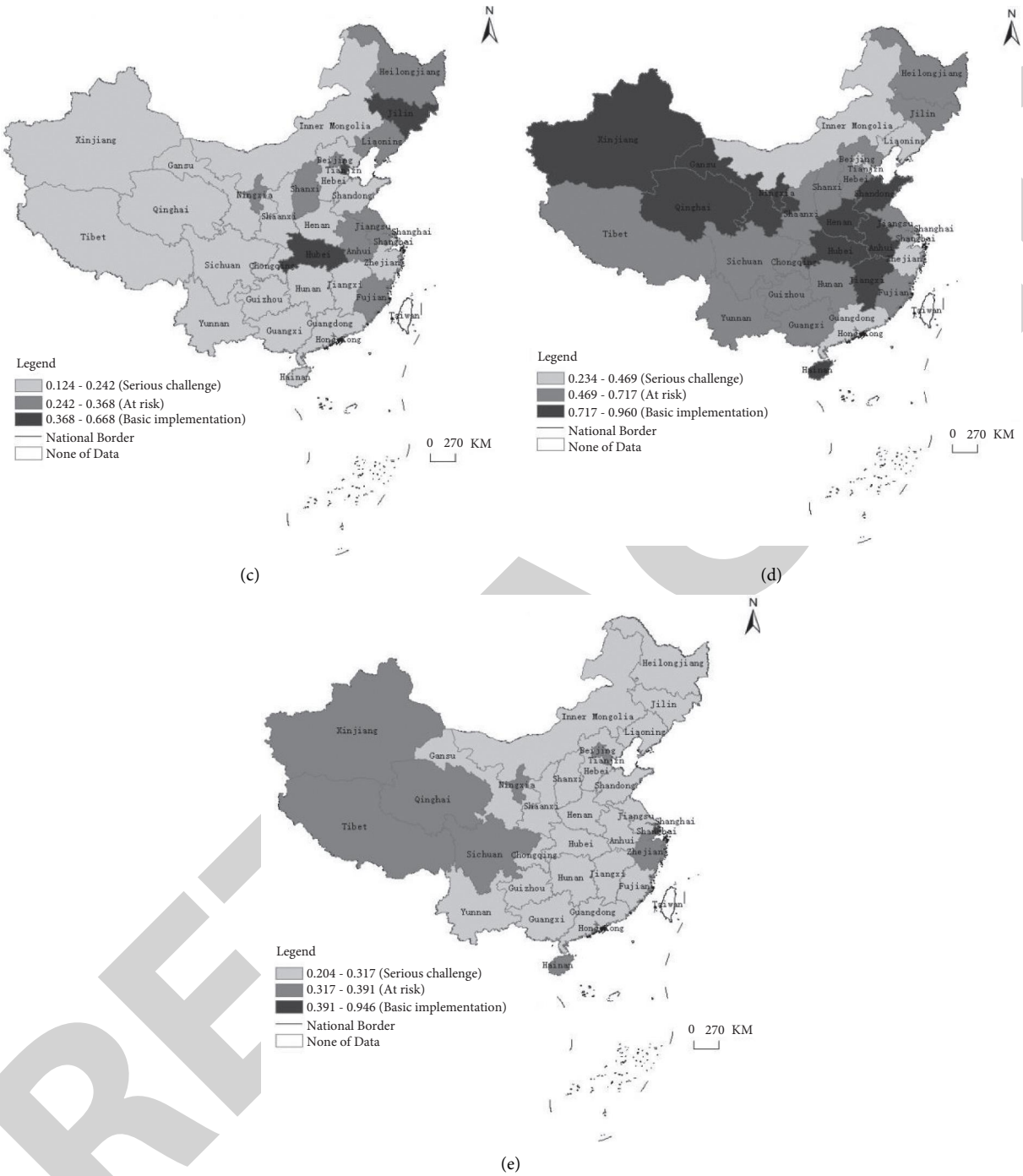

Figure 2: Grade division of the targets of the EIUR in 2018. (a) Grade division of full coverage. (b) Grade division of basic protection. (c) Grade division of flexibility. (d) Grade division of sustainability. (e) Grade division of fairness.

average and the others below. The only provinces in which "basic protection" can be "basically realized" are Shanghai and Beijing, signifying that the treatment level of the EIUR is low. Third, "fairness" and "flexibility" have the worst performance. Insurance flexibility has become the biggest shortcoming in the development of the EIUR. Regarding the "flexibility" index, the national average is only 0.261, and only nine provinces are above this threshold. "Fairness" is another target with poor performance, as 21 provinces are below the national average and are facing "serious challenges." Moreover, there is an apparent gap in the degree of realization regarding the "fairness" target. In regard to this target, only Shanghai has achieved "basic realization," and its index of 0.946 is 0.555 higher than that of Sichuan, which ranks second in the country.

Based on the indicator calculation, we identified some reasons for the poor performance of "fairness" and "flexibility" targets: On the one hand, the low "fairness" index is

Table 2: EIUR: security ability index and rank in 2018.

Region	Target					Goal	Rank
	Full coverage	Basic protection	Flexibility	Sustainability	Fairness		
Hubei	0.517	0.45	0.668	0.860	0.300	0.752	1
Jilin	0.416	0.355	0.526	0.627	0.29	0.597	2
Tianjin	0.314	0.432	0.558	0.391	0.388	0.586	3
Anhui	0.466	0.523	0.300	0.893	0.310	0.561	4
Xinjiang	0.690	0.394	0.217	0.813	0.388	0.545	5
Hainan	0.535	0.479	0.216	0.960	0.356	0.544	6
Ningxia	0.424	0.401	0.343	0.783	0.337	0.543	7
Heilongjiang	0.736	0.372	0.263	0.685	0.317	0.539	8
Guizhou	0.770	0.374	0.231	0.609	0.275	0.507	9
Fujian	0.537	0.306	0.316	0.681	0.255	0.502	10
Shanghai	0.262	0.704	0.167	0.234	0.946	0.498	11
Yunnan	0.542	0.509	0.234	0.647	0.300	0.494	12
Shanxi	0.491	0.419	0.257	0.695	0.303	0.491	13
Beijing	0.461	0.596	0.28	0.403	0.349	0.485	14
Liaoning	0.429	0.344	0.368	0.437	0.299	0.482	15
Qinghai	0.682	0.337	0.124	0.785	0.330	0.467	16
Shandong	0.492	0.311	0.211	0.787	0.307	0.466	17
Gansu	0.475	0.372	0.188	0.804	0.278	0.456	18
Jiangxi	0.247	0.435	0.235	0.931	0.228	0.455	19
Hebei	0.491	0.301	0.212	0.717	0.297	0.45	20
Henan	0.488	0.346	0.215	0.759	0.204	0.446	21
Chongqing	0.432	0.341	0.242	0.636	0.285	0.444	22
Sichuan	0.447	0.369	0.211	0.556	0.391	0.444	23
Shaanxi	0.530	0.354	0.186	0.681	0.285	0.444	24
Guangxi	0.303	0.450	0.210	0.657	0.315	0.427	25
Hunan	0.397	0.365	0.200	0.690	0.278	0.426	26
Jiangsu	0.388	0.241	0.260	0.555	0.311	0.421	27
Inner Mongolia	0.486	0.343	0.151	0.469	0.296	0.380	28
Tibet	0.234	0.325	0.153	0.665	0.35	0.371	29
Guangdong	0.399	0.342	0.206	0.399	0.247	0.370	30
Zhejiang	0.328	0.260	0.150	0.352	0.330	0.321	31

due primarily to the failure of the incentives for government subsidies for individual contributions, which are reflected in the indicator such as individual account pension return rate and the financial subsidy ratio. However, we found that the lowest individual contribution level had the highest return rate, with the improvement of the individual contribution level, the pension return rate, and the financial subsidy ratio showing a downward trend. Obviously, residents will choose the lowest contribution level to pay, thereby enabling them to maximize their interests. This also explains why the individual contribution level has continued to decline in the past 5 years. (In recent years, the income funds of the basic endowment insurance system for China's urban and rural residents have gradually increased. However, the proportion of individual contributions has gradually decreased from 38.79% in 2014 to 24.52% in 2018, indicating that the funds' dependence on finance is higher than the income of the individual contributions.)

On the other hand, the lowest "flexibility" index was due primarily to the mismatch between the individual's contribution level and income level. Generally, with the improvement of residents' income level and the increase in old-age awareness, the degree of residents' participation should increase accordingly. However, the data analysis showed that a few provinces, including Jiangxi, Hainan, and Hunan, have greater flexibility in regard to personal payments. In most provinces, such as Tianjin, the individual contribution flexibility of the EIUR is deficient. It must be noted that residents' per capita disposable income in China is increasing year by year, while individual contributions are decreasing. This means that the degree of urban and rural residents' participation is decreasing. The question of how to reverse this trend and ensure that personal contributions are compatible with economic development and residents' income is a significant issue in the development of the system. Moreover, the existing system design causes "flexibility" and "fairness" to influence each other. However, the system design's contribution model is not conducive to the improvement of "flexibility" and "fairness" targets. In the future, the improvement of the system's security ability needs to focus on "flexibility" and "fairness" targets.

4.3. Significant Regional Differences in Security Ability. There are regional differences in the security ability of the EIUR in China. In the midwestern region, performance in regard to security ability is better than in the eastern region. The completion of the targets between regions varies. As Figure 3 shows, there are 8 provinces in which the insurance security ability index has reached a higher level and above. Among the above 8 provinces, only Tianjin and Hainan in the eastern region have reached a higher level. Based on the

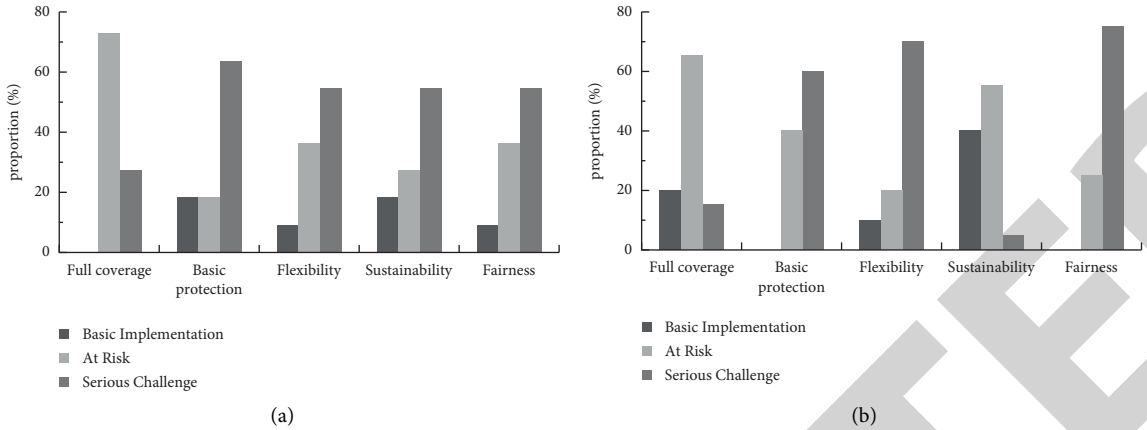

Figure 3: The differences between the targets in the (a) eastern region and (b) the central and western regions.

rankings (Table 2), there are seven midwestern provinces in the top 10 in the country, and Hubei ranks first, with an absolute advantage of 0.752. Most provinces in the eastern region, such as Jiangsu, Guangdong, and Zhejiang, are ranked lower than those in the midwestern region, even appeared at the bottom of the rankings.

There are also regional differences in the completion of targets. On the one hand, the "full coverage" target of the provinces in the eastern region is underdeveloped. As shown in Figure 1, none of the eastern provinces "basically achieved" "full coverage," and most have "certain risks." For example, Shanghai, Tianjin, and Zhejiang still face "serious challenges" in achieving the "full coverage" target. Based on the participation rate of urban and rural residents in the provinces of the eastern region, as shown in Figure 4, in all except Beijing, the participation rate of residents aged 16–59 is lower than that of residents over 60 years old. This shows that the residents in the eastern region, especially the residents between youth and middle age, are less enthusiastic about participating than residents in the midwestern region in the EIUR. The system's severe lack of attractiveness lowers the eastern provinces' scores and rankings on the "full coverage" index.

On the other hand, the provinces in the midwestern region are poorly developed in terms of the "basic protection" target. No provinces in the midwestern region have reached the "basic realization" level. In addition, all provinces in the midwestern region face "certain risks" and "serious challenges." This is due primarily to the lower level of the basic endowment insurance treatment in these regions. Although most provinces in the central and western regions raised the basic pensions of the EIUR in 2018, (In May 2018, the Chinese government issued the "Notice on Raising the Minimum Standards of Basic Pension Insurance for Urban and Rural Residents in China in 2018." Most provinces in the central and western regions—such as Shanxi, Anhui, Jiangxi, Guangxi, Chongqing, Sichuan, Guizhou, Shaanxi, Gansu, and Xinjiang—have raised the basic pension standard only slightly since 2014, and some did not adjust basic pension standards between 2015 and 2017.) they cannot change the current low level of treatment. According to the perspective of system design, the low level of treatment is directly related to individual contributions and financial subsidies. The central and western regions have no advantage in terms of individual contribution or financial subsidy ability; consequently, the government can provide only a relatively low subsidy amount due to downward economic pressure and financial affordability.

4.4. Mismatched Security Ability and Economic Development Level. At present, there is an apparent mismatch between the security ability of the EIUR and the level of economic development. As shown in Figure 5, the economically underdeveloped areas have high security abilities. For instance, Hubei, Jilin, Heilongjiang, Anhui, Ningxia, Guizhou, and Xinjiang, which have a relatively low per capita GDP, have relatively high system security abilities. In contrast, the economically developed areas, such as Shanghai, Beijing, Jiangsu, Guangdong, and Zhejiang, show low security abilities in regard to both ranking and index. The purpose of the EIUR is to protect the basic living needs of citizens in old age. However, if the security ability is too low, it cannot provide sufficient protection for citizens who have not participated in other endowment insurance, especially in regions with high economic development levels.

The study found that "basic protection" and "flexibility" are the main factors that lower the security ability index of the EIUR in each province. In practice, this is reflected primarily in the low treatment level, lack of flexibility in the system adjustment mechanism, and low contribution level of citizens who have not participated in other endowment insurance; these factors have, in turn, led to an increase in financial dependence. (According to the "China Pension Fund Report 2018," between 2011 and 2017, the proportion of personal contributions to the income fund of the basic pension insurance of urban and rural residents decreased from 38.79% to 24.52%.) Because it is a pay-as-you-go system, the increasing financial burden year by year will force the local government to devote most of its energy to maintaining the regular operation of the current system rather than increasing the level of treatment, thereby resulting in the financially supported payment subsidies, and basic pensions have been at a low level for a long time, and it

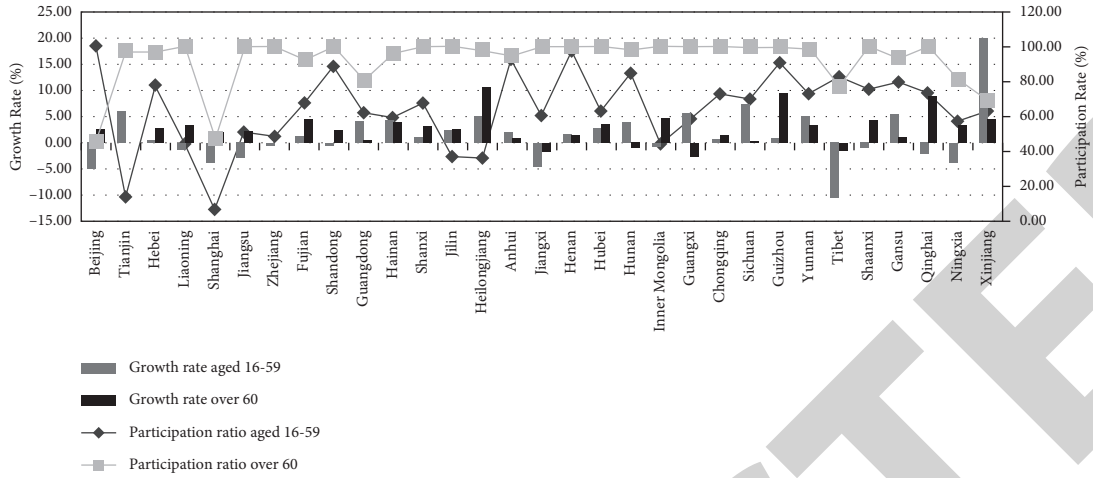

Figure 4: Participation of the EIUR.

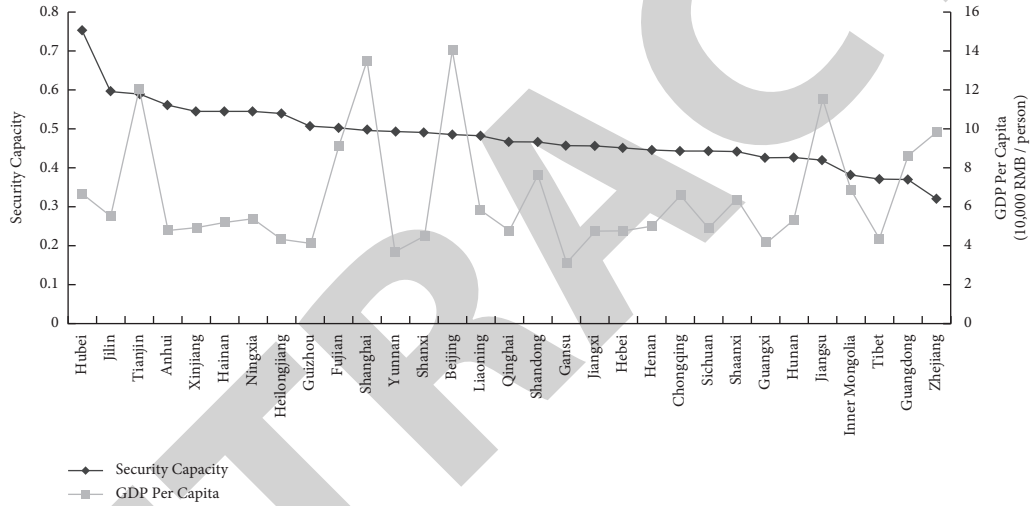

Figure 5: Security ability and GDP per capita.

will not effectively attract residents whose living consumption level is increasing with the economic development to actively participate and choose higher-level payment, and *t*. In addition, increased financial subsidies and low personal contributions will cause personal contributions to income funds to decrease year by year. Such repeated cycles will eventually lead to a situation in which the system's security ability does not coincide with the economic development of the province.

The fundamental reason for the above is that the system is ineffective in regard to guiding residents to choose a higher level of contribution. It is not difficult for residents to afford a higher level of contribution. However, due to the system's defect in the setting of government subsidies for individual contributions, the individual account pension return rate of the lowest contribution level for each province is the highest, and the proportion of government subsidies for individual contributions shows a downward trend as the contribution level increases. Therefore, the system does not encourage insured persons to increase their contribution levels. Whether the residents make "smart choices" or follow the herd mentality after making their cost-benefit calculations, they are more inclined to choose a lower contribution level.

5. Conclusions and Recommendations

Upon the evaluation method and indicator system, the study found that factors such as the top-level design of the EIUR, the operating environment, and the willingness of the residents affected the EIUR in China, resulting in low security ability that does not coincide with the level of economic development. In addition, there are regional differences in security ability, and the development of various targets is uneven. To further enhance the security ability and facilitate the steady development of the security system, two areas need to be improved.

First, there is a need to improve the completion of each target and to focus on strengthening the development of "flexibility" and "fairness" targets. On the one hand, it is necessary to improve the residents' individual insurance contribution model and to establish and improve the

Hindawi
Journal of Mathematics
Volume 2024, Article ID 9863685, 1 page
https://doi.org/10.1155/2024/9863685

Retraction

Retracted: Implementing the Hybrid Neuro-Fuzzy System to Model Specific Learning Disability in Special University Education Programs

Journal of Mathematics

Received 23 January 2024; Accepted 23 January 2024; Published 24 January 2024

This article has been retracted by Hindawi following an investigation undertaken by the publisher [1]. This investigation has uncovered evidence of one or more of the following indicators of systematic manipulation of the publication process:

(1) Discrepancies in scope

(2) Discrepancies in the description of the research reported

(3) Discrepancies between the availability of data and the research described

(4) Inappropriate citations

(5) Incoherent, meaningless and/or irrelevant content included in the article

(6) Manipulated or compromised peer review

The presence of these indicators undermines our confidence in the integrity of the article's content and we cannot, therefore, vouch for its reliability. Please note that this notice is intended solely to alert readers that the content of this article is unreliable. We have not investigated whether authors were aware of or involved in the systematic manipulation of the publication process.

Wiley and Hindawi regrets that the usual quality checks did not identify these issues before publication and have since put additional measures in place to safeguard research integrity.

We wish to credit our own Research Integrity and Research Publishing teams and anonymous and named external researchers and research integrity experts for contributing to this investigation.

The corresponding author, as the representative of all authors, has been given the opportunity to register their agreement or disagreement to this retraction. We have kept a record of any response received.

References

[1] L. Wending, "Implementing the Hybrid Neuro-Fuzzy System to Model Specific Learning Disability in Special University Education Programs," *Journal of Mathematics*, vol. 2022, Article ID 6540542, 7 pages, 2022.

Hindawi
Journal of Mathematics
Volume 2022, Article ID 6540542, 7 pages
https://doi.org/10.1155/2022/6540542

Research Article

Implementing the Hybrid Neuro-Fuzzy System to Model Specific Learning Disability in Special University Education Programs

Lin Wending

ZhengZhou Preschool Education College, Zhengzhou 450000, China

Correspondence should be addressed to Lin Wending; linwending@hotmail.com

Received 29 November 2021; Revised 3 January 2022; Accepted 13 January 2022; Published 15 February 2022

Academic Editor: Naeem Jan

Learning difficulty is a significant issue that comprehensively needs to be taken care of by university instructors with a focus on altering their ways of educating students since various degrees of learning difficulty could be observed among students. Hence, proper approaches should be adapted and utilized that provide chances for each student, securing his/her educational right. By doing so, it guarantees that each student has a right of learning with a different pace of conducting it. For example, the same educational and teaching materials cannot be adapted to each student. Hence, the training of students with learning difficulty should follow a model that is characterized as "from bottom to top," namely, "normal to learning with difficulties." The characterization of this approach is very similar to that of the treatment of human beings: biological malfunctions by medicine and mechanical malfunctions by psycho-sociology. This paper proposes a diagnostic model to determine the cognitive ability of students who deal with learning disabilities. The computerized model is proposed based on a combination of fuzzy logic and machine learning utilizing association rules and cellular automata. The advantage of the proposed method is that it helps find the needs of these types of students, so the widely implemented practices that shape his/her learning behavior are avoided. Therefore, practical recognition of each student with a different pace of learning should be realized.

1. Introduction

The ability of every human being to learn is a phenomenon associated with the maintenance and evolution of life, education, progress, and the development of culture [1]. Nevertheless, the learning process does not finalize thoroughly and satisfactorily. Some observable hinders negatively impact the learning process due to personal issues. Therefore, the learning process ends up with incomplete, fragmented, or even failed outcomes [2].

In the contemporary world, acquiring more knowledge at a faster pace is expected. On the other hand, individuals encountering problems pertinent to learning and acquisition of knowledge naturally are observed. Besides, mass educational implementations, relatively higher living standards, and awareness of educational rights of disabled people are the core issues in modern societies. Hence, people with learning disabilities become an entity that needs to be taken care of regarding educational, psychological, and social dimensional perspectives [3]. Therefore, it is one of the focused research areas by researchers and professionals of education, so the scientific and educational aspects of this issue can be characterized by the following:

(1) Gradual paradigm changes from the "medical-biological model" to the "psycho-pedagogical model" are needed.

(2) The psycho-pedagogical research provides a new way of understanding to deal with cognitive functions taking part in the learning processes and difficulties observed in the learning processes, for example, in reading, spelling (e.g., dyslexia), and mathematics.

(3) Students who have learning difficulties can be promptly identified, diagnosed in detail, and helped systematically.

(4) Dealing with those issues requires professors to get informed about areas of cognitive functions, such as learning difficulties, dyslexia, dysgraphia, and difficulty with mathematics.

Given that each subject has specific cognitive requirements, a more functional approach to categorizing learning disabilities would be to examine whether a student's abilities and weaknesses meet the cognitive requirements of the subjects (i.e., courses) that he or she deals with. Based on this reasoning, we can assume that if a person has a weakness in one or more of the areas involved and is required for the cognitive processing of a learning object, he/she will certainly face difficulties during the above process [5].

Also, universities and colleges are increasingly aware of the needs of students with disabilities and learning difficulties. They can offer support in some ways, and students may be able to benefit from extra financial help.

In this spirit, this work aims to construct a realistic diagnostic model of a student's cognitive ability based on his/her learning disabilities. This modeling is based on a hybrid neuro-fuzzy system [6], which combines the use of association rules [7] and cellular automata [8] for its application when the investigation of special learning difficulties in special education programs is a concern [9, 10].

Although this application is an innovative approach that is presented for the first time in the research community, various attempts have been made to use innovative technologies in various types of special education in the literature. What the proposed method brings as a novelty can be summarized as follows. (1) Ambiguity and uncertainty are common features in the assessment of educational output since different evaluators have different evaluation measures. (2) The proposed method provides a great amount of flexibility to reach a fuzzy inferential diagnostic assessment in managing and updating data.

2. Related Literature

The literature related to the educational approaches to differentiate the training of students with disabilities mainly focuses on methods dealing with overcoming the learning complexities.

A model was proposed by Manghirmalani et al. [11] to diagnose and classify learning disorders. Fuzzy expert systems, called a soft computing technology, help learning disabilities be classified into several types. Besides, the requirements to implement this system and outcomes were provided in this research.

Prentzas [12] presented a survey about artificial intelligence methods used in early educational technologies. Intelligent tutoring and adaptive educational hypermedia systems, as well as robots, were discussed in the article. The results showed that students were encouraged to participate in learning and social activities, and they remained interested in technology resources even after long periods of interaction.

An intelligent agent-based classification model, proposed by Elsayed [4], provides a psycho-pedagogical assessment for professors, helping determine students with learning impairments in classrooms. Disabilities of pupils are classified based on the information of the agents. The model functions based on previously classified examples and stored data in the system. Besides, interactive problem-solving assistance and a new knowledge domain can be gained by deriving generalizations from studying the stored data.

Two data mining methods, called fuzzy and neuro-fuzzy, were employed by David and Balakrishnan [6] to devise a new strategy predicting learning disabilities in school-aged kids. The objective of the strategy depends on constructing an algorithm to impute missing values and evaluate the performance of the classifier based on preprocessing methods. When the basic assessment approach was utilized in the prediction of learning difficulties, checklists were commonly employed. Thus, there exists a dependence between the mood of the students and data cases so redundancy and missing values could be contained.

Garg and Sharma [13] attempted to investigate how artificial intelligence has impacted the schooling of students with exceptional needs. The data were gathered through a qualitative study involving targeted interviews with both professors and kids needing special attention. The information was also gathered from academic databases, newspapers, periodicals, and blogs. Content analysis was used to examine the responses received. Finally, the study attempted to suggest a paradigm for an inclusive future of special needs education based on targeted interviews [14–16].

The literature suggests that various aspects of the research dealing with students having learning difficulties have been conducted. However, a gap still exists in the research regarding the differences between students when learning processes are under investigation.

3. The Proposed Method

3.1. Hybrid Neuro-Fuzzy System. ANFIS, the adaptive neuro-fuzzy inference system, is one of the adaptive networks that consists of both adaptive and non-adaptive nodes [17]. The adaptive network consists of a multilayer feed-forward network where each node is assigned to a specific function based on the incoming signals. Each specific node is denoted by a set of parameters. All nodes are connected via directional links. Customizable nodes are the ones depending on the parameters associated with that node. To minimize the predefined error, the parameters should be changed based on the learning rules [18].

The type of operation of each node can vary. The choice of the operation of a node depends on the total processing of the inputs and the output on which the adaptive network must perform. The parameter set of an adaptive network is composed of the union of the parameters of each adaptive node. Then, these parameters are updated based on the provided training dataset. Thus, the construction of the desired relationship between input and output is realized by a gradient-based learning process [19].

ANFIS is a systematic effort to generate "if-then" rules between input-output pairs. The model acquires a set of data (pairs of incoming-outgoing data) and divides them into

datasets for training and control. Training data form a set of data, input, and output vectors.

This information is normalized to be appropriate in form for the training process. This is achieved by assigning to each term a value between 0 and 1 using the max-min method. The normalized data are then used as input and output values to train the ANFIS model. This creates two vectors for ANFIS training such as an input vector and an output vector. Training data are used to find the introductory initial parameters for the participation functions.

The least squares method is employed to find the resulting parameters. For each data pair, if an error computed becomes greater than a specific value set, the gradient descent method is employed to update the initial parameters of the input.

The process ends when the error becomes less than the specified value [20]. The proposed hybrid system then applies association rules with a learning method to discover correlations and patterns between variables [7]. The problem of correlation rule mining is defined as follows:

(1) Let $I = (i_1, i_2, \ldots, i_n)$ be a set consisting of n binary properties called objects.

(2) Let $D = (t_1, t_2, \ldots, t_m)$ denote a set consisting of transactions.

(3) Let D denote a unique transaction ID and contain a subset of I.

(4) Let the correlation rules be defined by the following [21]:

$$\text{assume that } X \cap Y = \varnothing \text{ and } X \Rightarrow Y, \tag{1}$$

where X and $Y \in I$.

The following three rules are defined based on this logic [22, 23]:

$$\text{Rule: } X \Rightarrow Y = \begin{cases} \text{Support} = \dfrac{\text{frq q}(X, Y)}{N}, \\ \text{Confidence} = \dfrac{\text{frq}(X, Y)}{\text{frq}(X)}, \\ \text{Lift} = \dfrac{\text{Support}}{\text{Supp}(X) \times \text{Supp}(Y)}. \end{cases} \tag{2}$$

Association rules are embedded in cellular automata to automate their implementation process [8]. Cellular automata are computing system models with emerging complexity that model the behavior of dynamic systems [24]. They are called cellular because they are inspired by cellular devices where each cell interacts with its neighbors in space and is automatic. Then, the behavior of each cell is completely determined by the corresponding model [8, 25].

It is a "society" of digital systems that move, mate, give birth, or die as time passes in a two-dimensional grid based on predetermined simple rules [7, 26]. They are implemented in a grid of cells where each cell can be in a predefined number of distinct states with specific neighborhood relationships, predetermining and indicating its neighbors in the process of updating their states in each cell.

Each cell renews its state based on a predefined transition rule that takes the states of adjacent cells as inputs since the renewal of all cells takes place synchronously. Thus, there is a deterministic evolution of the system over time [26]. Therefore, time is called discrete.

The proposed embodiment consists of C, Σ, N_f, where C denotes a d-dimensional grid of cells identified by vectors of Z^N, Σ denotes the possible states that a cell can take, N denotes the neighborhood with $N \subset Z^d$, and f is a transition function form $\Sigma^N \longrightarrow \Sigma$. The configuration consists of states of the cells, and the initial state has a vital role and needs to be determined when the initial design is set.

Let C be the set of cells in a grid, and the neighborhood function, denoted by n, can be defined as [25, 27]

$$n(x, y)\colon C \times C \longrightarrow B = \{\text{True}, \text{False}\}. \tag{3}$$

This function will return True if the pair of cells that constitute the input in C are neighbors. For example, in a two-dimensional grid, a particular neighborhood function $n(x, y)$ will return True if x and y are neighbors within the neighborhood of c_o where the relationship is defined by [24–27]

$$N_{c_o} = \{c \in C \mid n(c_o, c) = \text{True}\}. \tag{4}$$

The size of the neighborhood $|N_{c_o}|$ is independent of c_o. If the set of possible cell states is determined, the transition function applied to all cells simultaneously can be defined as follows [8, 25]:

$$u\colon S^{|N|} \longrightarrow S. \tag{5}$$

Hence, the transition function takes the states of all cells in the neighborhood of a cell at time t and sets the state of that cell at the next time. The proposed method helps simplify the diagnostic procedure whose outcomes are not governed by a random state of disorders [28, 29].

3.2. Experiments. Utilizing the proposed approach that combines the findings of studies concerning both the processed information and the categorized students having learning difficulties helps identify the groups of weaknesses that characterize most students. The framework presented herein suggests that three main groups or categories of cognitive impairments typically occur in students with learning difficulties such as reading, spelling, and mathematics. These weaknesses are expressed in [4, 15, 16] as follows:

(1) Coding symbols.

(2) Processing the language.

(3) Perceiving and processing space and numbers.

If students have learning difficulties in reading, spelling, and mathematics, one or more of the mentioned problems

above may be observed. The experimental process for the implementation of the model was based exclusively on the feedback of the system with data extracted after interaction with students.

When a student is assessed concerning the reception and comprehension of oral speech, two different and related functions or skills, namely, the distinction and perception of the phonological elements of the language, as well as the understanding of the semantic content of the language are tested. While the former is associated with the development of the phonological system of language and the function of hearing, the second is pertinent to the development of the semantic and syntactic system of language [4]. The way of evaluating these functions was implemented by asking the student to repeat words or phrases or to present the meaning of some words used in daily life with his/her sentences. Besides, some words with more than one meaning and sentences with the complex syntactic structure are used to assess him/her. During the evaluation, we pay attention to the completeness of the semantic definition of the words, the ability to choose the correct meaning of the word, the ability to identify the deep structure (semantic content) of the sentence, etc. Also, by providing instructions to the student, we assess whether he/she can perform them without the need to repeat or explain the instructions.

Also, the evaluation of learning difficulties in mathematics starts from the general to the specific element. This practically means that by evaluating a student's mathematical level, we start from the general mathematical elements and abilities to the more specific ones. In general, the mathematical skills of the specific students are tested to relate weaknesses and abilities to the level of problem solving, so the student's ability to apply mathematical concepts and mathematical manipulations to problems in real-life situations is determined.

Also, the recording of the student's attitude towards mathematics as well as the emotions that he/she experiences through his/her involvement is evaluated. Besides, interviewing students and observing the process is helpful to assessment. When the process of active construction of knowledge is realized, the assessment based on the data must be continuous and comparisons should be conducted since individuals use different ways and means of representation of reality, which are called practical, pictorial, and symbolic representations.

The student in the practical way of representing knowledge uses specific objects (fingers, sticks, numerator, and so on) to perform various operations. Then, pictures, drawings, graphs, and lines are used to calculate some quantities such as sum or difference. Finally, the symbolic way of representing the various operations is realized that is considered the most difficult part [30, 31].

To assess the learning abilities and to identify the respective learning difficulties of the students, indicative skills tests were performed. For example, to better understand the analysis of each number as a sum of two additives, an activity was performed for the analysis of 10.

The process can be described as follows: we have two groups with 10 green and 10 red pegs. We want to make a team with 10 pegs by taking a few pegs from the green and a few from the red team. The students work in groups with their objects and then each group announces one of the many ways of composing 10 pegs, which is conducted by a makeshift abacus with pegs (in a tightrope that we have to fasten at both ends of the board, we have hung 10 green and 10 red pegs). Thus, students are given the opportunity, after forming the 10 in a way, to write on the board and the symbolic representation, e.g., $6 + 4 = 10$. In the end, after all the ways are suggested by the students, the specific objects (pegs) are removed, and the symbolic representations remain for mnemonic retention in the long-term memory.

The results of each process with intermediate assessment steps are placed as input to the intelligent system to identify its learning abilities. Some indicative diagrams of the display of the results after the various tests performed are shown in Figures 1 and 2.

It is important to say that to decide if the cause of reading problems is dyslexia, the process should be further evaluated with a set of brain functions. Each of the sensory areas must be checked for any learning disabilities [4, 31]. The areas to be explored are the visual, the auditory, the motion, the mnemonic, and the successor abilities.

(1) Decoding, reading, and optical detection tests are conducted by the optical tests.

(2) Repetition of words and sentences, spelling tests, and acoustic perception are conducted by acoustic tests.

(3) Drawing copies, writing, tactile detection, and quick naming of objects (e.g., language expression) are conducted by kinetic tests.

(4) Multiplication tables, months of the year, alphabet, repetition of polysyllabic words, and determination of rhythmic succession are conducted by succession tests.

3.3. The Implementation of the Proposed Method. The desired result of a test array is to be able to assess which brain functions are involved in learning to read, spell, and learn in general. It is important for the computer assessment tool to include multiple tests and preferably more than one measurement of each sensory area to be examined.

It should be noted that the tests mentioned herein are an attempt to make this possible. It is not a definitive and unique solution, but a proposal as to which areas should be considered. A prerequisite, to carry out such an assessment, is that the examiner is fully acquainted with how the specific areas can be assessed. Therefore, the test array is a tool in which each assessor can bring his/her assessment material. Accordingly, in addition to cognitive tests, the assessment should include a more general psychological assessment, e.g., a WISC (Wechsler's Intelligence Scale for Children) or a WAIS (Wechsler's Adult Intelligence Scale) test or equivalent [32–34].

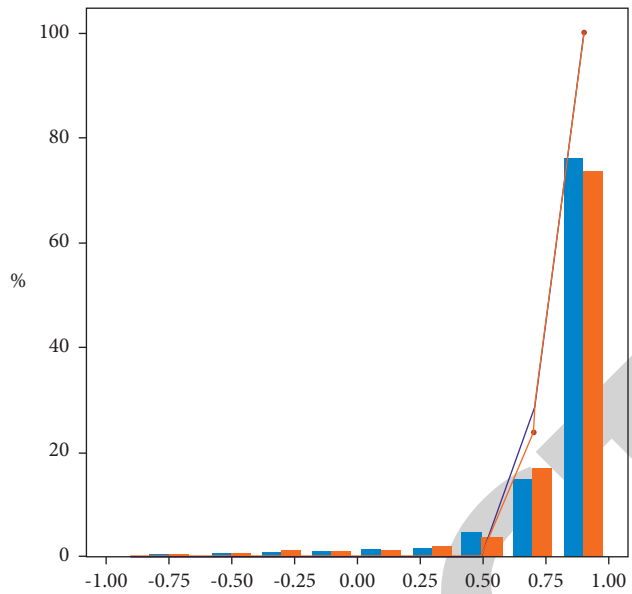

Figure 1: Dyslexia plot.

MOST FREQUENT VALUES					SMALLEST VALUES		
0.990168	19	0.8%	8	0.8%	-1.0	1	<0.1%
0.990167	12	0.5%	2	0.2%	-0.947062	1	<0.1%
0.990169	3	0.1%	4	0.4%	-0.759694	1	<0.1%
0.990175	3	0.1%	2	0.2%	-0.606797	1	<0.1%
0.99911	3	0.1%	0	0.0%	-0.584285	1	<0.1%
0.990174	3	0.1%	1	0.1%	-0.508717	1	<0.1%
0.987395	2	<0.1%	0	0.0%	-0.479794	1	<0.1%
0.994275	2	<0.1%	0	0.0%	-0.475142	1	<0.1%
0.998807	2	<0.1%	0	0.0%	-0.471447	1	<0.1%
0.995228	2	<0.1%	0	0.0%	-0.460773	1	<0.1%
0.998975	2	<0.1%	0	0.0%	-0.447999	1	<0.1%
0.999189	2	<0.1%	0	0.0%	-0.407896	1	<0.1%
0.932079	2	<0.1%	0	0.0%	-0.405921	1	<0.1%
0.997993	2	<0.1%	0	0.0%	-0.401917	1	<0.1%
0.998883	2	<0.1%	0	0.0%	-0.384480	1	<0.1%

Figure 2: Dyslexia test values.

4. Discussion and Conclusions

The educational treatment of learning disabilities is the goal of the whole process for both timely identification and correct diagnostic evaluation. It is the phase in which the professor demonstrates in practice how well he/she knows not only to interpret the results of the diagnostic evaluation but also to find ways to help the student learn [35].

Fuzzy inferential models rely heavily on the uncertainty that has to do with information and especially with its lack in our attempt to model the problem. Information may, for example, be incomplete, inaccurate, fragmentary, unreliable, vague, or controversial. The use of fuzzy logic in assessment is considered necessary since each education system contains an amount of uncertainty. The reason for adopting this approach is that when it comes to educational evaluation, different evaluators have different evaluation measures. Three important factors that favor the vague approach to assessment are initially that the grades given by professors for student performance are not always accurate. Second, the exams consist of uncertain data, while finally many professors grade students in verbal terms.

It, therefore, becomes clearer that fuzzy logic and fuzzy systems can deal with the ambiguity and uncertainty that exist in the process of educational evaluation. A fuzzy inferential model uses the process of approximate reasoning which mimics human reasoning. It utilizes the advantages of the natural language and the process of programming and building the system that become easier and more practical. It is obvious that a fuzzy inference system can be constructed quickly and has a higher utility value with minimal cost.

Fuzzy inference systems make the best use of the experience and data derived from it. As we saw in the construction of the fuzzy diagnostic evaluation system presented herein, its foundation was based on data from human experience. The specialized knowledge of the developer was used in every step of the construction of the system.

The proposed method provides a great amount of flexibility to reach a fuzzy inferential diagnostic assessment in managing and updating data. This system is based on the general principle of the evaluation process concerning the goals that we have set at the beginning. From these objectives, the system input variables are taken, and the language rules are set. Thus, the same procedure can be applied to other educational, medical, or evaluative procedures by changing variables and rules.

Early diagnosis and educational intervention not only have great significance for the students having learning disabilities to avoid unnecessary negative consequences but also provide preparation to construct valuable special education programs. Learning problems such as dyslexia tend to weaken people's self-confidence due to their daily familiarity with failure. Before diagnosis, a dyslexic person is often forced to deal with difficult and frustrating learning situations for several years.

To build confidence and reshape one's self-image, it is essential to avoid failure during training. In this spirit, the methodology presented herein is considered a first and perhaps an impressive step towards the ways of initial diagnosis and treatment of learning educational difficulties.

Data Availability

The data used to support the findings of this study are included within the article.

Conflicts of Interest

The author declares that there are no conflicts of interest.

References

[1] R. Castro, C. Kalish, R. Nowak, R. Qian, T. Rogers, and J. Zhu, "Human active learning," *Advances in Neural Information Processing Systems*, vol. 21, 2009 Accessed: Nov. 09, 2021. [Online]. Available: https://Papers.Nips.Cc/Paper/2008/Hash/Fc49306d97602c8ed1be1dfbf0835ead-bstract.Html.

[2] A. Klašnja-Milićević and M. Ivanović, "E-learning personalization systems and sustainable education," *Sustainability*, vol. 13, no. 12, p. 6713, 2021.

[3] A. Demetriou, G. Spanoudis, and A. Mouyi, "Educating the developing mind: towards an overarching paradigm," *Educational Psychology Review*, vol. 23, no. 4, pp. 601–663, 2011.

[4] K. N. Elsayed, "Diagnosing learning disabilities in a special education by an intelligent agent based system," in *Proceedings of the 2012 4th Computer Science And Electronic Engineering Conference (Ceec)*, pp. 7–12, Colchester, Essex, United Kingdom, September 2012.

[5] M. Nind and H. Vinha, "Doing research inclusively: bridges to multiple possibilities in inclusive research," *British Journal of Learning Disabilites*, vol. 42, no. 2, pp. 102–109, 2014.

[6] J. M. David and K. Balakrishnan, "Performance improvement of fuzzy and neuro fuzzy systems: prediction of learning disabilities in school-age children," *International Journal of Intelligent Systems and Applications*, vol. 5, no. 12, pp. 34–52, 2013.

[7] F. Zhan, X. Zhu, L. Zhang, X. Wang, L. Wang, and C. Liu, "Summary of association rules," *IOP Conference Series: Earth and Environmental Science*, vol. 252, Article ID 032219, 2019.

[8] M. Ghosh, R. Kumar, M. Saha, and B. K. Sikdar, "Cellular Automata and its applications," in *Proceedings of the 2018 IEEE International Conference on Automatic Control and Intelligent Systems (I2CACIS)*, pp. 52–56, October 2018.

[9] M. Carroll, R. Shah, M. K. Ho et al., "On the utility of learning about humans for human-ai coordination," *Advances in Neural Information Processing Systems*, vol. 32, 2019 Accessed: Nov. 09, 2021. [Online]. Available: https://Papers.Nips.Cc/Paper/2019/Hash/F5b1b89d98b7286673128a5fb112cb9a-bstract.Html.

[10] S. Healy, R. Msetfi, and S. Gallagher, "'Happy and a bit Nervous': the experiences of children with autism in physical education," *British Journal of Learning Disabilites*, vol. 41, no. 3, pp. 222–228, 2013.

[11] P. Manghirmalani, D. More, and K. Jain, "A fuzzy approach to classify learning disability," *International Journal of Advanced Research in Artificial Intelligence*, vol. 1, no. 2, 2012.

[12] J. Prentzas, "Artificial intelligence methods in early childhood education," in *Studies in Computational Intelligence*, X.-S. Yang, Ed., vol. 427, pp. 169–199, Springer Berlin Heidelberg, Berlin, Heidelberg, 2013.

[13] S. Garg and S. Sharma, "impact of artificial intelligence in special need education to promote inclusive pedagogy," *International Journal of Information and Education Technology*, vol. 10, no. 7, pp. 523–527, 2020.

[14] H. M. H. Sigstad, J. Buli-Holmberg, and I. Morken, "Succeeding in inclusive practices in school in Norway – a qualitative study from A teacher perspective," *European Journal of Special Needs Education*, vol. 0, no. 0, pp. 1–14, 2021.

[15] H. J. Cha and M. L. Ahn, "Development of design guidelines for tools to promote differentiated instruction in classroom teaching," *Asia Pacific Education Review*, vol. 15, no. 4, pp. 511–523, 2014.

[16] X. Zhu, C. M. Cheong, G. Y. Li, and J. Wu, "Primary school teachers' conceptions of reading comprehension processes and its formulation," *Frontiers in Psychology*, vol. 11, p. 615, 2020.

[17] J.-S. R. Jang, "Anfis: adaptive-network-based fuzzy inference system," *IEEE Transactions on Systems, Man, and Cybernetics*, vol. 23, no. 3, pp. 665–685, 1993.

[18] M. N. M. Salleh and K. Hussain, "A review of training methods of anfis for applications in business and economics," *International Journal of u- and e- Service, Science and Technology*, vol. 9, no. 7, pp. 165–172, 2016.

[19] A. Yadollahpour, J. Nourozi, S. A. Mirbagheri, E. Simancas-Acevedo, and F. R. Trejo-Macotela, "Designing and implementing an anfis based medical decision support system to predict chronic kidney disease progression," *Frontiers in Physiology*, vol. 9, p. 1753, 2018.

[20] S. O. Sada and S. C. Ikpeseni, "Evaluation of ann and anfis modeling ability in the prediction of aisi 1050 steel machining performance," *Heliyon*, vol. 7, no. 2, Article ID e06136, 2021.

[21] T. Slimani and A. Lazzez, "Efficient analysis of pattern and association rule mining approaches," *International Journal of Information Technology and Computer Science*, vol. 6, no. 3, pp. 70–81, 2014.

[22] O. Stit, J. Riffi, A. Yahyaouy, and H. Tairi, "Comparative study of different association rule methods," in *Proceedings of the 2018 IEEE 5th International Congress on Information Science and Technology (CIST)*, pp. 323–327, October 2018.

[23] S. Vijayarani and S. Sharmila, "Comparative analysis of association rule mining algorithms," in *Proceedings of the 2016 International Conference On Inventive Computation Technologies (ICICT)*, pp. 1–6, Coimbatore, India, August 2016.

[24] S. Bhanja and J. Pulecio, "A review of magnetic cellular Automata systems," in *Proceedings of the 2011 IEEE International Symposium Of Circuits and Systems (ISCAS)*, pp. 2373–2376, Rio de Janeiro, Brazil, May 2011.

[25] K. Koutarou Tachibana, R. Ryoh Takebayashi, and H. Hiroshi Umeo, "Self-reproduction model for communication-restricted cellular Automata," in *Proceedings of the SICE Annual Conference 2007*, pp. 2048–2053, Takamatsu, Japan, September 2007.

[26] S. Wongthanavasu and J. Ponkaew, "Cellular Automata learning algorithm for classification," in *Proceedings of the 2014 International Electrical Engineering Congress (IEECON)*, pp. 1–5, Chonburi, Thailand, March 2014.

[27] M. A. Zapletina and D. V. Zhukov, "The review of cellular Automata algorithms for placement and routing problems," in *Proceedings of the 2021 IEEE Conference of Russian Young Researchers in Electrical and Electronic Engineering (ELCONRUS)*, Article ID 27712776, St. Petersburg, Moscow, Russia, January 2021.

Hindawi
Journal of Mathematics
Volume 2023, Article ID 9817457, 1 page
https://doi.org/10.1155/2023/9817457

Retraction

Retracted: An Artificial Intelligent Virtual Reality Interactive Model for Distance Education

Journal of Mathematics

Received 19 December 2023; Accepted 19 December 2023; Published 20 December 2023

This article has been retracted by Hindawi following an investigation undertaken by the publisher [1]. This investigation has uncovered evidence of one or more of the following indicators of systematic manipulation of the publication process:

(1) Discrepancies in scope

(2) Discrepancies in the description of the research reported

(3) Discrepancies between the availability of data and the research described

(4) Inappropriate citations

(5) Incoherent, meaningless and/or irrelevant content included in the article

(6) Manipulated or compromised peer review

The presence of these indicators undermines our confidence in the integrity of the article's content and we cannot, therefore, vouch for its reliability. Please note that this notice is intended solely to alert readers that the content of this article is unreliable. We have not investigated whether authors were aware of or involved in the systematic manipulation of the publication process.

Wiley and Hindawi regrets that the usual quality checks did not identify these issues before publication and have since put additional measures in place to safeguard research integrity.

We wish to credit our own Research Integrity and Research Publishing teams and anonymous and named external researchers and research integrity experts for contributing to this investigation.

The corresponding author, as the representative of all authors, has been given the opportunity to register their agreement or disagreement to this retraction. We have kept a record of any response received.

References

[1] W. Yin, "An Artificial Intelligent Virtual Reality Interactive Model for Distance Education," *Journal of Mathematics*, vol. 2022, Article ID 7099963, 7 pages, 2022.

Hindawi
Journal of Mathematics
Volume 2022, Article ID 7099963, 7 pages
https://doi.org/10.1155/2022/7099963

Research Article

An Artificial Intelligent Virtual Reality Interactive Model for Distance Education

Wenjing Yin

Zhengzhou Preschool Education College, Zhengzhou 450000, China

Correspondence should be addressed to Wenjing Yin; wenjing_yin@aliyun.com

Received 2 December 2021; Revised 6 January 2022; Accepted 11 January 2022; Published 14 February 2022

Academic Editor: Naeem Jan

Information and communication technologies play an important role in education. This fact was emphasized even more due to the significant upheavals, globally, caused by the pandemic of COVID-19 and because distance education uses tools of modern technology that prove to be significantly important. Particularly, virtual reality immersion systems, which may include 3D spatial representations, multisensory interaction channels, and real-time intuitive physical interaction, can extend the learning process by providing learners with stimuli that represent a real advanced training environment. In the present work, based on the most modern technologies of computational intelligence, virtual and augmented reality, wireless communications, and space-sensitive positioning applications, an Artificial Intelligent Virtual Reality (AI-VR) interactive model for distance education is presented. This is a case study of escape-room-type educational application, wherewith appropriate practices and methodologies promote individual and collective participation, enhance the active role of the learner, personalize the educational experience, and upgrade the process of participation in distance education, strengthening and assisting role of the educator. Specifically, a Newton polynomial is used for max-polynomials arising from the stereoscopic problem of augmented reality used to indirectly indicate the number of linear regions in order to optimize the problem. The proposed application is related to the training course of agricultural education and methods of modernization of crops, including additional sound, 3D graphics, and short film projection. The history-space-objects relationship takes and evolves with various versions such as the parts of the story to be unlocked as the trainee moves from one tool to the next or the story to guide the trainee to explore the space-time continuum, giving a new dimension to the technological development of agricultural education and the methods of modernization of crops. This finding shows that they learn best when they receive information in a style that incorporates visual, auditory, and kinetic stimuli so that learning improves when learners can examine an idea or concept using a multidimensional approach.

1. Introduction

Following the rapid development of both computer hardware technology and software capabilities in the last decade, a new trend is emerging today that places particular emphasis on human-machine interaction. Virtual reality, which is a key representative of this new trend, is a means for people to visualize, manage, and interact with computer systems as well as extremely complex data in a virtual environment. The result produced by a virtual reality system is called a virtual environment, which is based in part or whole on data generated by a computer system. The goal of the virtual environment is to create to the user the illusion that he is naturally placed in a synthetically produced environment, through his representation (embodiment) by an entity.

Regarding the application of multimedia in education, there is the view that information that circulates in the form of direct experience using different senses, as opposed to reading, which is a purely visual and mental process, maintains and cultivates its correlations. This is one of the reasons that educational multimedia applications manage to convey more quality information to their users, as has been proven in practice. Based on this view, the use of virtual reality systems in educational applications further engages the user in the learning process, offering him various options for exploring the cognitive space and leading to a more efficient educational process.

The main advantage of virtual reality is its ability to facilitate constructive learning activities and to provide alternative forms of learning that can help different types of students (e.g., visual-type students). They also offer the possibility of educational use of shared virtual spaces (or network virtual environments) [1–3] for distance learning and collaborative learning. Such applications can be used as collaboration and training tools, as they can allow students and teachers to take part in virtual meetings, seminars, and lectures in real time.

In general, virtual reality technology can be used in a variety of ways to support the educational process [4], especially in cases where traditional teaching methods are not sufficient, such as the following:

(1) *Simulation of Complex Systems*. The advantage over traditional teaching methods is the ability of learners to observe the operation of the system from many angles using high-quality imaging but also to interact with it.

(2) *Macroscopic and Microscopic Imaging* [5]. The advantage lies in the ability to observe phenomena, systems, objects, and so on, which are too small or too large to become visible or to understand their operation on a normal scale.

(3) *Simulation of Dynamic Events* [6]. The advantage lies in the ability to observe the dynamic event through its different playback speeds. This function is equivalent to the fast forward function on a video device.

Other important features of virtual reality that can be used to support the educational process are the following:

(1) The high level of interaction offered by virtual reality technology: most people learn through practice.

(2) The sense of immersion: in immersive virtual reality environments, users are fully immersed in the virtual world using special input/output devices. This is a useful feature for various applications, like training in architecture where the sense of size is very important for the impact of the design of a building on the external environment and the inhabitants.

(3) The inherent flexibility and adaptability of virtual reality systems: these features come from the nature of the software that supports the virtual environment. A virtual reality system can be used in various ways depending on the software application to be used. So, it can be used for various educational applications.

In addition to the above uses, virtual environments and more specifically the collaborative ones [7–9] offer many useful features to assist the educational process through the following:

(1) Supporting students' social awareness

(2) Increasing the possibility of interaction and active collaboration between students

(3) The up-to-date and varied information available to users and the possibility for collaborative knowledge exchange

(4) The provision of virtual experiences for the perception and understanding of complex concepts

(5) The fusion of aspects and characteristics of direct and indirect learning.

Various proposals have been made related to the use of virtual environments and the exploitation of their advantages in education, some of which are particularly interesting:

(1) The use of avatars [10, 11] to upgrade user presence and collaboration: virtual environments provide a sense of user presence with techniques that shift their focus from the real world to the virtual. Presence is associated with upgrading users' sense of their responsibilities as students in the virtual world, while at the same time feeling more comfortable during the educational process. This is enhanced by the sense of the presence of other users in the virtual environment, through their representation (avatars), which in addition helps the cooperation of users. In addition, the gestures and actions that can represent the avatars of users raise the awareness of other users about their actions.

(2) The design of virtual spaces in correspondence with the real world. Virtual environments place the learning process in a virtual space with a specific purpose. The design of the virtual environment with objects and content similar to a traditional classroom seems to play an important role because of the active interaction with objects familiar to students, like a whiteboard, blackboard, presentations, etc.

Web virtual environments can be the basis for creating educational environments for collaborative distance learning over other technologies, such as video conferencing systems, because of their key advantages over other distance learning technologies. More specifically, they provide important tools for creating communication and collaboration systems with easy access and use at the same time. A fairly large number of users can communicate simultaneously through multiple channels such as voice communication, text messaging, and gestures, without the need to install additional computer hardware.

In addition, avatars provide a set of benefits, offering additional communication channels and helping users to express actions in the virtual environment. At the same time, their use is rather straightforward, which allows users to blend more easily in the general use of the system and not distract them from the educational process.

It should be noted, however, that the existing systems of virtual environments do not take full advantage of their potential in terms of user awareness of the social presence and consequently of the educational function. For this reason, in collaborative distance learning, the term "Educational Virtual Environment" is used.

An educational virtual environment seeks to harness the potential of his online nature to support flexible learning. More specifically, it is based, from a pedagogical point of view, on the concepts that govern collaborative learning and, from a technological point of view, on virtual network environments. A virtual educational environment is therefore a virtual network environment framed with additional functionalities and technologies to effectively support collaborative distance learning communities. Such features include text chat, voice communication, private messaging, application sharing, collaborative text reading, and document management, recognizing the presence of other users and representing users with humanlike avatars that support gestures related to the educational process (e.g., raising hands, pointing, applause, etc.) and observing objects and space from different angles.

Despite these promises, Educational Virtual Environment is still not perfect from technological, organizational, and psychological points of view since it suffers from a number of challenges:

(1) AR is often considered as a game, which is not taken very much seriously—it is fun to play with, but not a real learning process. Students can show the attitude which assists in winning the game but not fully engage their mind to acquire new knowledge and critical thinking.

(2) AR requires intensive graphics capabilities that are not at all times possible with standard computer equipment and it could take significant efforts to achieve smooth implementation and worth.

(3) Immersion and interaction.

(4) AR is often delivered as propriety solutions that could not be matched with similar environments from other developers—many companies offer their own tools to create VR environments that are not compatible with the rest regarding hardware and software.

(5) AR, after its initial adoption as a new technology, will require unified standards for the preparation of professional curriculums that are compatible between different educational institutions regarding content preparation, implementation, and educational result achievement.

(6) AR training time—depending on the size of the organization, cultural characteristics of the workforce, and the existing used methodologies, training time could be minimal or extensive.

(7) AR training could provide participants with a higher level of realism and immersion in comparison to classroom instructions and web-based educational material. However, AR scenarios still lack the direct hands-on experience and face-to-face interactions that real-life exercises provide. The novelty of Educational Virtual Environment requires preliminary training with such environments to enable users to effectively use new systems.

In this work, based on the most modern technologies of computational intelligence, virtual and augmented reality, wireless communications, as well as space-sensitive positioning applications, an AI-VR interactive model for distance education is presented. This is a case study of escape-room-type educational application, wherewith appropriate practices and methodologies promote individual and collective participation, enhance the active role of the learner, personalize the educational experience, and upgrade the process of participation in distance education, strengthening and assisting role of the educator.

The study is organized as follows: Section 2 gives a detailed description of the related review of the topic. Section 3 presents the proposed AI-VR interactive model. Section 4 has a discussion on our study, and finally, the last section draws the conclusions and outlines future research directions.

2. Related Literature

The literature of Artificial Intelligence research in E-Learning, especially in recent years, is becoming more and more frequent because of the great potential of AI in the field of the educational process and especially the personalization aspect.

Montebello [12] presented a comprehensive picture of AI in E-Learning and its future in his substantial work. He aimed to provide answers on how to maximize the contribution of AI to E-Learning through the use of tools, technologies, and approaches. He provided an in-depth examination of multiple future evaluations of various key E-Learning variables, as well as a comprehensive overview of the most recent and relevant technology. The book ended with a foreshadowing of how such a model might manifest in the future, based on the multiple interposing circumstances.

Drozdova and Guseva [13] presented a specific report on E-Learning in the banking industry. The article discusses the characteristics and criteria that should be included in a training course, as well as the outcomes of its implementation. They used Donald Kirkpatrick's four-level training efficiency evaluation approach. The author advocated that the relevant indicators are calculated for each level of this model to give a fuller picture of the overall evaluation of the training course. This method includes objective and accurate efficiency evaluations, faster processing of the collected results, and a clear organization of the outcomes and evaluations.

Holmes and Anastopoulou [14] in their research looked at remote education students' perceptions of the benefits and risks of Artificial Intelligence (AI) technologies, which are rapidly being used in distant education. They presented the preliminary findings of a survey of students from the UK's largest distant institution as a first step toward answering the question of what students at distance universities think about AI.

Cruz-Benito et al. [15] attempted to investigate students' opinions of artificial intelligence and education. They wondered if they would be hesitant to be influenced by

nonhuman actors in a human process like education. This work developed a research model based on the Technology Acceptance Model to answer these issues. They presented the model's many primary structures and variables to describe it, and then they analyzed the model's main implications.

Adamu and Awwalu [16] in their paper covered the components of Adaptive E-Learning Systems (AES), the function of AI in AES content aggregation, potential hazards, and accessible opportunities. They also emphasized the need for Intelligent Tutoring Systems (ITS).

Krendzelak [17] in their research looked into machine learning and how it may be applied in E-Learning frameworks. They attempted to investigate the fact that students must devote a significant amount of time to adjusting their profiles to meet the training's learning objectives.

Finally, Demertzi and Demertzis [18] proposed the Adaptive Educational eLearning System (AEeLS), which can acquire and analyze data from learning repositories and modify it to the educational curriculum based on the student's skills and experience. It is a new hybrid machine learning system that combines a Semisupervised Classification method for ontology matching with a Recommendation Mechanism that employs a hybrid method trying to combine neighborhood-based collaborative and content-based filtering techniques to provide each student with a personalized educational environment.

3. THE Proposed AI-VR Interactive Model

Augmented reality is realized with various devices such as helmets and glasses with more common mobile devices, such as mobile phones and tablets. The built-in cameras of these devices are used to connect the real with the virtual world, giving the user the feeling that he is navigating the real world which has been enhanced with additional objects/information and/or functions as virtual objects are superimposed on the real ones. We note that several augmented reality applications can remove some of the real-world objects. An augmented reality application displays virtual world objects when it recognizes a predefined pattern within the image captured by the device's camera. These patterns are divided into marker-less patterns in which the application displays the virtual world when the camera displays specific parts of the real world and patterns using markers such as a QR (Quick Response) Code. These codes are usually small square images, resembling barcodes and which may include digital information that can be revealed when scanned by appropriate software that accompanies each mobile device, the QR readers.

Specifically, a simple architecture of a network consisting of 2 tropical perceptrons is proposed: the first of which is based on (max; +) and the second on (min; +) algebra, while the total output (maxout) is the sum of the 2 responses. The architecture of this network is summarized in Figure 1.

As shown in the figure above, given an input pattern $x \in R^n$, this network calculates 2 responses, the first of which is a dilation and the second an erosion, respectively:

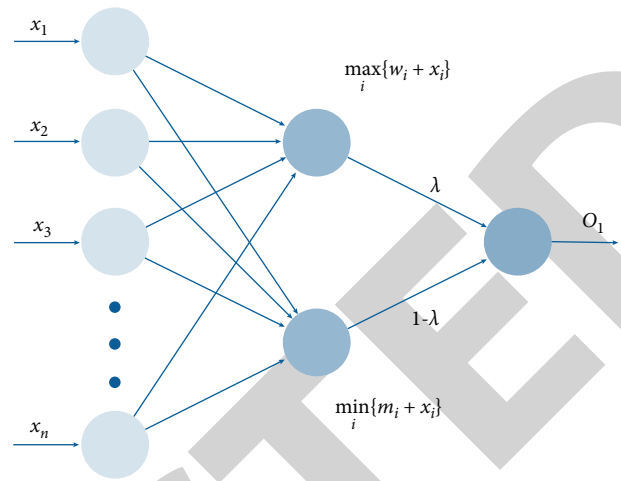

Figure 1: Proposed architecture.

$$\begin{aligned}\delta(x) &= \bigvee_{i=1}^{n} w_i + x_i,\\ \epsilon(x) &= \bigwedge_{i=1}^{n} m_i + x_i,\end{aligned} \tag{1}$$

choosing $a = 1$ and $b = 1$ and vectors $w = Bs$; $m = B$, we end up with the morphological gradient, which is used as an edge detection operator and is defined as

$$\nabla^B I(x) = (I \oplus B) - (I \ominus B). \tag{2}$$

So basically, we have a neural network which at its output calculates the sum of 2 partially continuous convex functions of the form

$$h_i(x) = \max_{j\in 1,2,\ldots,k}\left\{W_{ij}x + b_{ij}\right\} = \bigvee_{k}^{j=1}\left[\left(\sum_{m=1}^{n} W_{ijm}x_m\right) + b_{ij}\right]. \tag{3}$$

For the optimal solution of the resulting polynomial systems, the polytope continuation method is used to divide the original system into simpler problems and to solve them optimally. Specifically, the Newton polynomial is used for max-polynomials arising from the stereoscopic problem of augmented reality used, to indirectly indicate the number of linear regions, to optimize the problem.

A graphical representation of the proposed technique is presented in Figure 2 above, where we illustrate the idea of creating a thinner system by creating polyhedral homeopathy that reduces a polyhedral to a linear system. The lower hull of the polytone Newton causes triangulation, which is used to count the roots while creating homeopathy with as many paths to follow as the volume of the cell, as shown in the following equations:

$$\begin{aligned}P(x_1, x_2) &= \begin{cases} x_1x_2 + c_{11}x_1 + c_{12}x_2 + c_{13} = 0,\\ x_1x_2 + c_{21}x_1 + c_{22}x_2 + c_{23} = 0,\end{cases}\\ \widehat{P}(x_1, x_2, t) &= \begin{cases} x_1x_2t^1 + c_{11}x_1t^0 + c_{12}x_2t^0 + c_{13}t^0 = 0,\\ x_1x_2t^1 + c_{21}x_1t^0 + c_{22}x_2t^0 + c_{23}t^0 = 0.\end{cases}\end{aligned} \tag{4}$$

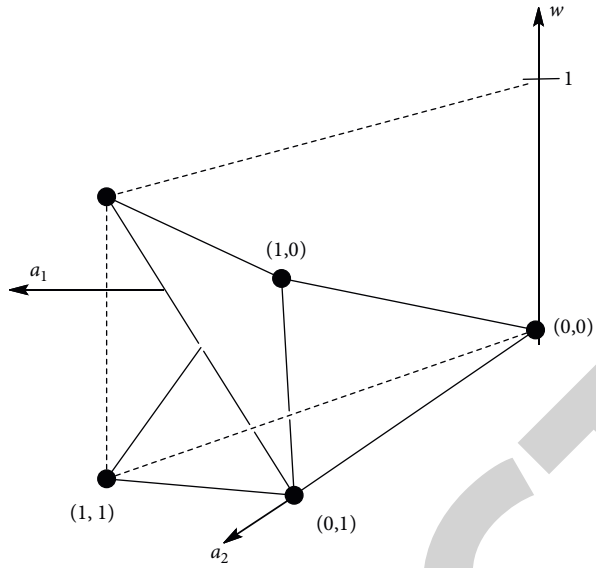

Figure 2: Polyhedral homeopathy proposed technique.

Finally, the calculation follows the extension for the determinant, as it corresponds to the sum of the roots by solving the corresponding linear system:

$$P^{(0)}(x) = \begin{cases} \prod_{i=1}^{4}(x_1 - \alpha_{1i}) \prod_{i=1}^{1}(x_2 - \beta_{1i}) = 0, \\ \prod_{i=1}^{3}(x_1 - \alpha_{2i}) \prod_{i=1}^{2}(x_2 - \beta_{2i}) = 0. \end{cases} \quad (5)$$

Thus, with a relatively simple calculation at the end of the multipath paths, we obtain important structural algebraic information, which is sufficiently utilized by the system. We define this model as follows:

$$g(\mathbf{x}) = \lambda\left(\bigvee_{i=1}^{K_{\max}} c_i + \mathbf{W}_i^T \mathbf{x}\right) + (1-\lambda)\left(\bigwedge_{i=1}^{K_{\min}} d_i + \mathbf{M}_i^T \mathbf{x}\right), \quad (6)$$

$\lambda \in [0, 1]$.

So, the initial problem becomes now

$$\delta(x) = \bigvee_{i=1}^{K_{\max}} c_i + \mathbf{W}_i^T x, \qquad \varepsilon(x) = \bigwedge_{i=1}^{K_{\min}} d_i + M_i^T x. \quad (7)$$

The proposed application is related to the training course of agricultural education and methods of modernization of crops. The application focuses on the evolution of agricultural equipment and in particular the tools used in ancient times for agricultural work. The trainees are connected to a natural space where some natural objects are exhibited. They can read with QR code information about the tools used in the past, as well as about their development history, receiving the relevant information on their device.

Each tool combines multimedia content (photos, videos, etc.) as well as information and comments from the Internet, news, as well as natural exhibition spaces of the wider area, with information on how and when to visit them. Respectively, the implementation of augmented reality systems supports dynamically changing virtual wanderings, offering interactive games, customizable paths during which the learner moves in the virtual space and determines the evolution of the narrative and the projection of the corresponding content. Essentially, with the use of augmented reality, complex images and physical objects are recognized as stimuli to display the selected multimedia content to the user, enhancing his experience. This way learners can use their mobile device, mobile phone, or tablet and get more information about an item.

Based on the virtual reality methodology in question, the learner can choose to play in a virtual escape room based on a story suggested by the application itself based on an AI recommendation system. The virtual escape room is a themed, adventurous game, in which individuals or groups enter a themed virtual era room and are supposedly locked into it. The goal is to escape in a short time, solving a series of puzzles or missions. The time usually varies and ranges from 15 to 60 minutes. Virtual escape rooms can vary and take place in virtual locations depending on the theme.

The creation of the script, which involves learners in a knowledge game, is completed using QR codes, which can accompany the description of an object and can provide the additional information that accompanies the object. Accordingly, the digital augmented reality information that accompanies the object is displayed on the screen of the device when the user focuses with the device on the specific object. This technology includes additional sound, 3D graphics, and short film projection. When the user focuses on a plow exposed to natural space, a digital augmented

reality representation is displayed, with the plow in its traditional form being dragged by oxen.

The history-space-objects relationship takes and evolves with various versions such as the parts of the story to be unlocked as the trainee moves from one tool to the next or the story to guide the trainee to explore the space-time continuum giving a new dimension to the technological development of agricultural education and the methods of modernization of crops.

4. Discussion

According to research and the corresponding case study, individuals learn best when they receive information in their preferred learning style (e.g., auditory, visual, kinetic, and aesthetic). This finding shows that they learn best when they receive information in a style that incorporates visual, auditory, and kinetic stimuli.

The above findings are in full agreement with research that says that learning improves when learners can examine an idea or concept using a multidimensional approach. In this case, synapses and neural circuits develop, and different areas of the brain are activated, depending on the activity and the way the learner performs this activity.

In the context of online learning, the multidimensional approach can be attempted through a variety of teaching and learning approaches. It is important in the design context that the trainer incorporates a range of activities of different strategies. In this way, learners could engage in experiential activities using a variety of technological approaches. In general, a multidimensional approach provides alternative ways for learners to acquire new knowledge, overcome obstacles, and apply this practice in their daily jobs.

In summary, it seems that in the context of online learning, the educator is important to focus on the following: (a) the active participation of learners in the learning process, (b) how he will integrate the evaluation of learners in the educational process, (c) the utilization of tests the trainees undergo, and (d) the multidimensional approach of both his presence and the activities that will be given to the trainees. The teacher has to ensure that the above focal points need to take place in a properly designed educational environment such as the proposed.

5. Conclusions

Modern information and communication technologies in combination with the Internet offer pedagogy, innovative technical solutions for the culmination of the educational experience, and the promotion of the value of distance education. Environments that adopt virtual reality and its technology can provide several possibilities in the way the learner communicates and interacts with the virtual system or with other trainees. Their suitability to facilitate flexible learning as well as their educational applications can be widely used in the field of education as they manage on the one hand to overcome spatial and temporal constraints and on the other hand provide incentives for enjoyable and immediate learning. Given that pedagogy sets the general framework, the features and capabilities of these technologies can enrich the already known and tested practices used, adding an active factor in shaping the educational experience and highlighting the experiential nature of learning. Respectively, the role of technologies and at the same time the developments that they signal is the main springboard that can lead to new practices, which promote participation in actions, cultivate respect for educational practices, emphasize the need to preserve educational diversity, and shape the experience of distance education with new methods, discovering new unexplored aspects of it.

In conclusion, it should be noted that the upgrading of the educational process of distance education is a high-priority creative process. For this reason, it must include an evolving dialectical relationship concept between the achievements and practices of modern technology and the traditional educational goals.

Data Availability

The data used to support and prove the findings of this study are available from corresponding author upon request.

Conflicts of Interest

The authors declare that they have no conflicts of interest regarding the publication of this paper.

Acknowledgments

This work was supported by Henan Province Department of Education 13th Five-Year Plan of Education Science Major Bidding Topic.

References

[1] M. Dergham and A. Gilanyi, "On A system of virtual spaces for teaching kinematics," in *Proceedings of the 2019 10th IEEE International Conference on Cognitive Infocommunications (CogInfoCom)*, pp. 411–414, Naples, Italy, October 2019.

[2] M. Keppell, K. Souter, and M. Riddle, "Physical and virtual learning spaces in higher education: concepts for the modern learning environment," *Information Science Reference*, IGI global, Hershey, PA, USA, 2012.

[3] J. L. Mcbrien, R. Cheng, and P. Jones, "Virtual spaces: employing a synchronous online classroom to facilitate student engagement in online learning," *International Review of Research in Open and Distance Learning*, vol. 10, no. 3, 2009.

[4] J. Hedberg and S. Alexander, "Virtual reality in education: defining researchable issues," *Educational Media International*, vol. 31, no. 4, pp. 214–220, 1994.

[5] A. Saco, J. A. Bombi, A. Garcia, J. Ramírez, and J. Ordi, "Current status of whole-slide imaging in education," *Pathobiology*, vol. 83, no. 2-3, pp. 79–88, 2016.

[6] S. Mittal, U. Durak, and T. Ören, *Guide to Simulation-Based Disciplines: Advancing Our Computational Future*, Springer International Publishing, Cham, Switzerland, 2017.

[7] M. Chang, "Learning by playing: game-based education system design and development," in *Proceedings of the 4th International Conference on E-Learning and Games, Edutainment 2009*, Springer, Banff, Canada, August 2009.

Hindawi
Journal of Mathematics
Volume 2023, Article ID 9830845, 1 page
https://doi.org/10.1155/2023/9830845

Retraction

Retracted: Music Emotion Research Based on Reinforcement Learning and Multimodal Information

Journal of Mathematics

Received 19 December 2023; Accepted 19 December 2023; Published 20 December 2023

This article has been retracted by Hindawi following an investigation undertaken by the publisher [1]. This investigation has uncovered evidence of one or more of the following indicators of systematic manipulation of the publication process:

(1) Discrepancies in scope

(2) Discrepancies in the description of the research reported

(3) Discrepancies between the availability of data and the research described

(4) Inappropriate citations

(5) Incoherent, meaningless and/or irrelevant content included in the article

(6) Manipulated or compromised peer review

The presence of these indicators undermines our confidence in the integrity of the article's content and we cannot, therefore, vouch for its reliability. Please note that this notice is intended solely to alert readers that the content of this article is unreliable. We have not investigated whether authors were aware of or involved in the systematic manipulation of the publication process.

Wiley and Hindawi regrets that the usual quality checks did not identify these issues before publication and have since put additional measures in place to safeguard research integrity.

We wish to credit our own Research Integrity and Research Publishing teams and anonymous and named external researchers and research integrity experts for contributing to this investigation.

The corresponding author, as the representative of all authors, has been given the opportunity to register their agreement or disagreement to this retraction. We have kept a record of any response received.

References

[1] Y. Hu, "Music Emotion Research Based on Reinforcement Learning and Multimodal Information," *Journal of Mathematics*, vol. 2022, Article ID 2446399, 9 pages, 2022.

Hindawi
Journal of Mathematics
Volume 2022, Article ID 2446399, 9 pages
https://doi.org/10.1155/2022/2446399

Research Article

Music Emotion Research Based on Reinforcement Learning and Multimodal Information

Yue Hu [1,2]

[1]*Shanxi Jinzhong Institute of Technology, Taiyuan 030600, China*
[2]*UCSI University, Faculty of Social Sciences and Liberal Arts, Kuala Lumpur, Malaysia*

Correspondence should be addressed to Yue Hu; 1002163449@ucsiuniversity.edu.my

Received 14 December 2021; Revised 14 January 2022; Accepted 18 January 2022; Published 9 February 2022

Academic Editor: Naeem Jan

Music is an important carrier of emotion and an indispensable factor in people's daily life. With the rapid growth of digital music, people's demand for music emotion analysis and retrieval is also increasing. With the rapid development of Internet technology, digital music has been derived continuously, and automatic recognition of music emotion has become the main research focus. For music, emotion is the most essential feature and the deepest inner feeling. Under the ubiquitous information environment, revealing the deep semantic information of multimodal information resources and providing users with integrated information services has important research and application value. In this paper, a multimodal fusion algorithm for music emotion analysis is proposed, and a dynamic model based on reinforcement learning is constructed to improve the analysis accuracy. The model dynamically adjusts the emotional analysis results by learning the user's behavior, so as to realize the personalized customization of the user's emotional preference.

1. Introduction

With the rapid growth of the number of digital music, the traditional music analysis and retrieval methods are more and more difficult to meet people's needs. In the ubiquitous information environment, anyone can connect with the network and obtain personalized information services through appropriate terminal equipment anytime and anywhere [1]. This new environmental change is bound to be accompanied by the changes of information generation mode, information dissemination channels, and information utilization mechanism and also objectively promote the vertical deepening, personalized, and diversified development of users' information needs [2]. For information service organizations, this situation is not only an opportunity but also a challenge. There are massive multimedia data on the vast Internet. How to effectively store, organize, and retrieve such a large amount of information has become an urgent problem to be solved [3]. The purpose of affective computing is to give computers the ability to recognize, understand, and express various emotions similar to humans so that computers can interact with humans more naturally and harmoniously [4]. Music is an emotional medium that conveys the true feelings of human beings. Therefore, music has specific emotional labels, and explicit emotional labels are conducive to the audience to quickly select the songs they want to listen to at the appropriate time and place [5]. In multimodal fusion, decision level fusion is the highest level fusion. The existing decision level fusion first models the multimodal data of decision, and then obtains the linear weighting of decision, so as to generate the decision results [6].

Music is a symbol used by performers to express their thoughts and convey their emotions. It contains rich emotional information. Therefore, emotion-based music retrieval is also one of the key research contents of music information retrieval systems [7]. The characteristics of cross-platform, multisource, heterogeneous, and high-dimensional information and the development trend of dynamic and active services make people pay more attention to the multimodal information fusion theory and technical methods initially applied in the military field and begin to

actively explore possible solutions to extend it to the field of information services [8]. With the development of digital storage technology and mobile Internet, digital music also has a serious problem of information overload [9]. Therefore, the automatic analysis of music emotion has also become one of the hotspots of today's research and has broad application prospects in music retrieval and recommendation [10]. With the gradual expansion of the music scale, the era of digital music has ushered in. At this time, the scientific management of music has attracted much attention [11]. Different from traditional manual retrieval methods, automatic retrieval will save a lot of labor costs. At the same time, compared with manual analysis, improving the accuracy of analysis will be a difficult problem for automatic analysis [12]. As an important means of automatic music retrieval, classifying music according to the expressed emotion is attracting the attention of researchers from different fields.

For music, emotion is the most essential feature and the deepest inner feeling. Music emotion recognition based on computer automation plays a key role in promoting the development of artificial intelligence [13]. For music emotion analysis, the most common method is to analyze the acoustic features extracted from music and get the emotional analysis results. However, the first mock exam is usually not satisfactory. The traditional single-mode research based on can only express some characteristics of the object, just as people observe the world through only one sense, which has considerable limitations [14]. In contrast, multimodal information has richer semantic information, and the information of each mode can complement each other. At the same time, the correlation between different modal data is also helpful to improve the accuracy of analysis results to a certain extent [15]. As an important branch of music labeling, emotion labels can reflect the artistic conception to be expressed by music to a certain extent. People can find music in line with Tun and emotion through emotion labels, which can relieve depression in their hearts and find happy resonance [16]. Compared with other music analysis problems such as genre analysis, emotion analysis is closer to people's perception, and the melody of music often contains the expression of emotion. In this paper, a music emotion analysis algorithm based on multimodal fusion based on reinforcement learning is proposed to improve the analysis accuracy.

In this article, the innovative concept of analysis of music characteristics is studied. Moreover, we discussed the analysis of music features based on lyrics and the music emotion feature analysis method based on multimodal fusion to improve the analysis accuracy. Music feature analysis is a very important step in the process of music emotion analysis and the multimodal music emotion analysis method is to analyze music emotion based on music content and lyrics, respectively, and then combine the two analysis results to get the final music emotion analysis. The relationship between music structured information and human emotion cannot be fully reflected by using existing common features. Therefore, we can further explore the feature extraction method with more musical emotion analysis ability.

The following is a summary of the research: Section 1 contains the introduction; Section 2 discusses the related work and background. Section 3 discusses the analysis of music characteristics. Section 4 discusses the music emotion feature analysis method is based on multimodal fusion; finally, the conclusion brings the paper to a finish in section 5.

2. Related Work

In the task of attribute-level emotion analysis, the literature [17] conducts joint learning through two tasks of attribute extraction and attribute-level emotion analysis, which greatly improves the performance of the attribute-level emotion analysis task. Literature [18] puts forward a joint model, which can simultaneously model the two tasks of emotion analysis and emotion cause recognition and effectively improve the recognition performance of the two tasks. Emotion analysis and emotion analysis are two different subtasks in emotion analysis. Because of the strong relationship between emotion tags and emotion tags, the two tasks are closely related. Literature [19] improves the performance of the two tasks by labeling an extra data set with emotional tags and emotional tags. However, it is difficult to obtain similar data sets in real scenes. Literature [20] adopts integer linear programming (ILP) to study emotion and emotion analysis tasks jointly and obtains the connection between the output of the emotion analyzer and the output of the emotion analyzer through constraints.

Literature [20] shows that music lyrics do contain some special semantic information, including emotion. Therefore, the comprehensive utilization of audio and lyrics modes can effectively improve the accuracy of music emotion analysis. We can analyze the relationship between lyrics, music modes, and human perception and explore the intrinsic relevance between the two modes and complement each other to improve the accuracy of the analysis. Literature [21] has proposed some simple multimodal fusion methods, which comprehensively use the information of lyrics and audio modes to analyze music. The experimental results prove that using multimodal information can improve the accuracy of emotion analysis to a certain extent compared with using only a single mode. Literature [22] preliminarily uses deep neural networks to extract advanced feature representation from original audio data and verifies the effectiveness of deep neural networks in speech emotion recognition. Literature [23] uses a convolution neural network to extract audio features to train audio data, and the accuracy of audio emotion analysis has been greatly improved. Based on reinforcement learning technology, this paper studies the emotional analysis of music from the perspective of audio visualization. According to the demand analysis of music emotion analysis, this paper explores a model framework of music emotion analysis based on multimodal information fusion function and level.

3. Analysis of Music Characteristics

The characteristics of music are sound (overtone, duration, amplitude, pitch, and timbre), melody, rhythm, structure or form, expression, and texture.

3.1. Music Feature Analysis Based on Audio. Music feature analysis is a very important step in the process of music emotion analysis. Different music features may show different emotions. Therefore, the main task of music feature analysis is to find an optimal feature space to represent music [24]. This feature space can not only reflect the emotion of music but also have a certain degree of discrimination, which can distinguish music with different emotions. The framework of multimodal music emotion analysis is shown in Figure 1.

Music is mainly composed of several basic elements, including sound nest, sound length, sound intensity, sound color, and so on [25]. Then, two or more basic elements are integrated to form the basic characteristics of music, mainly including ① rhythm: the rhythm of music reflects the speed and urgency of music tunes, in which the emotion expressed by gentle music is calm and gentle, while the emotion expressed by sudden rhythm music is strong. ② Melody: what people used to call melody actually refers to the melody. It is the most basic element of music. It is a series of organized and rhythmic sequences composed of several musical sounds by artists according to a certain pitch, time value, and volume. Melody can reflect the emotion expressed in music. For example, the emotion expressed by music with a light melody should also be light. ③ Strength: strength can also express the emotion of music. For the same music, the emotion expressed by different degrees is different. Usually, the greater the intensity, the louder and more exciting the music. The smaller the degree, the more soothing and soft the music is. ④ Timbre: timbre refers to people's sensory characteristics of different sounds so that people can distinguish different sounds. Different people or musical instruments produce different timbres.

The choice of music emotion model is the basis of music emotion analysis. Music carries a variety of emotions. The music analyzed by the early music emotion research is mostly classical music. Among them, the vocal content is small, and the emotional characteristics are mostly reflected by the rhythm, melody, pitch, and timbre expressed by musical instruments, and a piece of classical music may contain several completely different emotions. The study of this music needs to intercept a music fragment for analysis. According to the basic and complex characteristics of music, the overall characteristics of music are identified, including music form structure, style, and emotional connotation. The specific structure is shown in Figure 2.

For the music emotion analysis task, the feature extraction method is an important component module, and a good feature extraction method has a great influence on the result of the analysis task. Feature extraction solves the problem of how to better represent the analysis sample set. Usually, samples are converted into feature vector

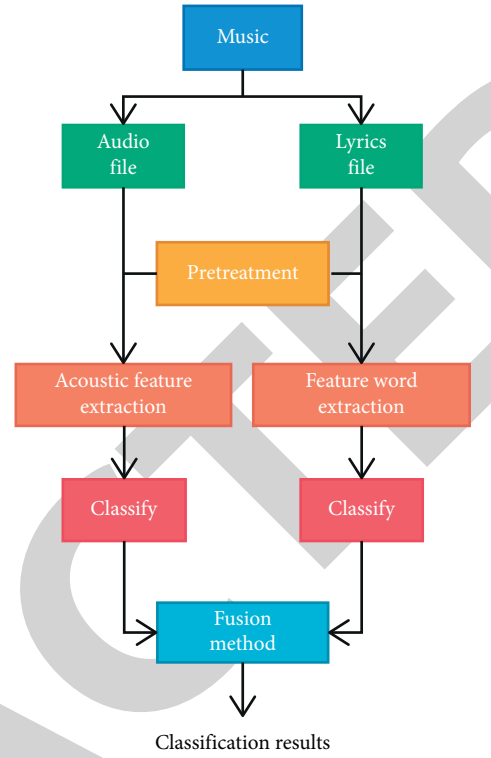

Figure 1: The framework of multimodal music sentiment analysis.

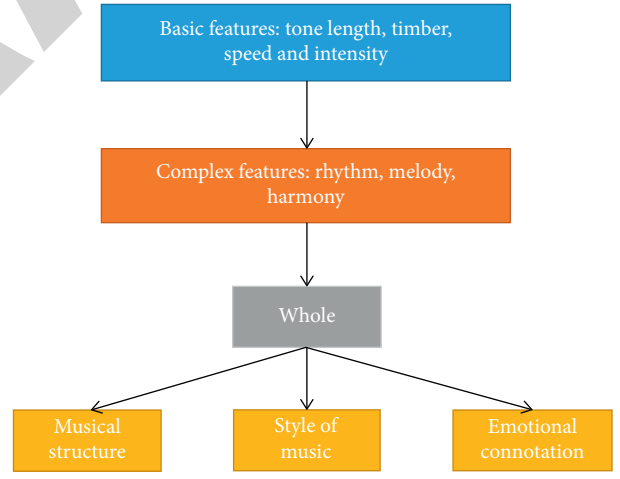

Figure 2: Composition of music form.

representation for the analysis model. Music feature acquisition is an important link in music emotion analysis. Early music acquisition mainly focused on audio attributes of sound killing. The basic audio features of a song, such as a rhythm, timbre, tone, volume, melody, and harmony, can reflect the emotional characteristics of music to varying degrees. Due to the structural heterogeneity between audio features and text features, there is an insurmountable gap between the emotions expressed by the two features. This makes it a serious problem to mine the correlation between the two expressions in emotional expression for multimodal analysis.

Time-domain characteristics of music refer to the time-domain parameters of each post calculated from music signals. Typical time-domain features include short-time energy, short-time average amplitude, short-time average zero-crossing rate, short-time autocorrelation function, and short-time average amplitude difference function.

The short-term energy of the nth frame music signal is defined as follows:

$$E_n = \sum_{m=n-(N-1)}^{n} [x(m)w(n-m)]^2. \tag{1}$$

In the formula, $w(n-m)$ is the moving wins function, N is the effective width of the window, and n is the time position of the window. It can be the starting point of the window or the midpoint or end of the window.

Short-term energy E_n is a time series, from which we can see how the signal energy changes with time. Generally speaking, the short-term energy of voiced sound is much larger than that of unvoiced sound, so it is easy to distinguish voiced sound from unvoiced sound by short-term energy sequence. In addition, the short-time energy sequence can also be used to determine the starting and ending points of music.

The process of extracting the characteristics of pitch and time value of music performance is shown in Figure 3.

Because the calculation of short-time energy needs a square operation, which enlarges the difference between magnitude and amplitude, it cannot accurately reflect the characteristics of signal short-time energy changing with time. Therefore, a short-term average amplitude describing the time-varying characteristics of signal energy is proposed, which is defined as follows:

$$M_n = \sum_{m=n-(N-1)}^{n} |x(m)w(n-m)| = \sum_{m=n-(N-1)}^{n} |x(m)|w(n-m). \tag{2}$$

The different signs of adjacent sampled values are called zero crossing, and the number of zero crossings per unit time is called the zero-crossing rate. The short-term average zero-crossing rate of a frame of music signal is defined as follows:

$$\begin{aligned} Z_n &= \frac{1}{2N} n \sum_{m=n-(N-1)}^{n} \left|\operatorname{sgn}[x(m)w_R(n-m)] - \operatorname{sgn}\{x(m-1)w_R[n-(m-1)]\}\right| \\ &= \frac{1}{2N} \sum_{m=n-(N-1)}^{n} |\operatorname{sgn}[x(m)] - \operatorname{sgn}[x(m-1)]|. \end{aligned} \tag{3}$$

In the formula, $\operatorname{sgm}[x(m)]$ is the symbolic function of $x(m)$, defined as follows:

$$\operatorname{sgn}[x(m)] = \begin{cases} 1, & x(m) > 0, \\ 0, & x(m) = 0, \\ -1, & x(m) < 0. \end{cases} \tag{4}$$

In order to overcome the short-term average zero-crossing rate is very sensitive to noise, the formula (3) can be modified as follows:

$$Z_n = \frac{1}{1N} \sum_{m=n-(N-1)}^{n} \{|\operatorname{sgn}[x(m) - A] - \operatorname{sgn}[x(m-1) - A]| + |\operatorname{sgn}[x(m) + A] - \operatorname{sgn}[x(m-1) + A]|\}. \tag{5}$$

Whether or not it crosses zero is not judged by the different signs of the adjacent sampled value of the signal but judged by the different sign after the adjacent sampled value of the signal exceeds a set appropriate positive and negative limit. This eliminates false zero crossings caused by noise. Normally, the short-term average zero-crossing rate of unvoiced and noise is much larger than that of voiced sounds, so the short-term average zero-crossing rate can be used to distinguish them easily. The short-term autocorrelation function is defined as follows:

$$\begin{aligned} R_n(k) &= \sum_{m=n-(N-1)}^{n} [x(m)w(n-m)]\{x(m+k)w[n-(m+k)]\}, \\ n-m &= m \sum_{m=0}^{N-1-k} [x(m+n)w(m)][x(m+n+k)w(m+k)]. \end{aligned} \tag{6}$$

In the formula, k is the autocorrelation lag time. Equation (6) shows that $R_n(k)$ of each frame of the signal is a sequence with lag time k as an independent variable. The formula of the short-term average amplitude difference function is as follows:

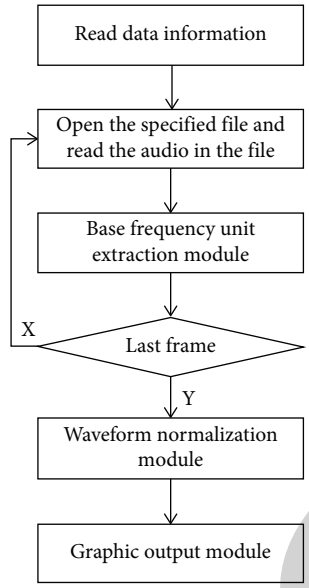

Figure 3: The process of extracting the pitch and time value feature of music performance.

$$\gamma_{k=}\sum_{m=0}^{N-1}\left|x(n+m)w_1(m)-x(n+m+k)w_2(m-k)\right|. \quad (7)$$

In the formula, $w_1(n)$ and $w_2(n)$ are rectangular windows with widths N and $N+K$, respectively, where K is the maximum possible hysteresis value. For any periodic signal, when the lag time is equal to the period or an integer multiple of the period, there will be a short-term average amplitude difference function $\gamma_k = 0$. The voiced signal is approximately a periodic signal, so γ_k will reach its minimum value at a lag time point equal to the pitch period or an integer multiple of the pitch period. Using this property, we can distinguish between voiced and unvoiced sounds based on the γ_k curve and estimate the pitch frequency of voiced sounds.

Pitch depends on the frequency and loudness of sound. Bass gives people a thick and deep feeling, while treble gives people a bright and sharp feeling. Audio features have strong objectivity and can be easily extracted from songs by digital signal processing. The key problem of audio feature extraction is which features are extracted. The results show that the energy, rhythm, melody, and timbre of music are the four characteristics that can best reflect music emotion. Therefore, in the digital signal processing of music, we should focus on these four characteristics. In the existing research, the music characteristics based on audio are usually borrowed from the parameters of speech signals, and the characteristics of speech signals change with time, but the changes are slow. Therefore, it is usually divided into short segments with phase dimensions, and each segment is processed separately by the processing method of a stationary random signal, which is the short-time processing technology of speech signal. The energy characteristics of music are closely related to the degree of motivation that music can bring to people. The higher the energy of music, the stronger the sensory stimulation to the listener. Songs such as metal and rock generally have higher energy value, while songs such as light music generally have lower energy value.

3.2. Analysis of Music Features Based on Lyrics. As an important part of music, lyrics also contain rich emotional information. Therefore, mining emotions from lyrics is a good supplement to music emotional analysis. The core problem of sentiment analysis based on lyrics is how to construct a feature space that can reflect lyrics sentiment, which mainly focuses on the selection of the expression model of lyrics text and the selection of feature selection methods. Lyrics data usually incorporate the expression of the music writer's own emotion, so it has rich semantic information related to emotion. How to extract this emotion from sparse and messy lyrics files will be a great challenge. A typical text emotion recognition system is shown in Figure 4.

Assuming that a document is composed of m feature words, the contribution of each feature word to the document is reflected by its weight. Expressed by a mathematical formula is as follows:

$$D = D(t_1, w_1; t_2, w_2, \ldots, t_m, w_m), \quad (8)$$

where w_i is the weight and $1 \le i \le m$. The similarity of the two documents is expressed by finding the cosine of the angle between the corresponding vectors. The formula is as follows:

$$\mathrm{sim}(D_1, D_2) = \cos\theta = \frac{\sum_{i=1}^{n} w_{1i} \times w_{2i}}{\sqrt{\left(\sum_{i=1}^{n} w_{1i}^2\right)\left(\sum_{i=1}^{n} w_{2i}^2\right)}}. \quad (9)$$

Among them, w_{1i} and w_{1i} represent the weight of the w_{2i} feature item of documents i^{th} and D_1, respectively.

Suppose there is $\mathrm{sim}(D_1, D_2)$, a document set with a total of n documents. After preprocessing, a total of m feature words are extracted, and a matrix of "feature words-documents" can be constructed:

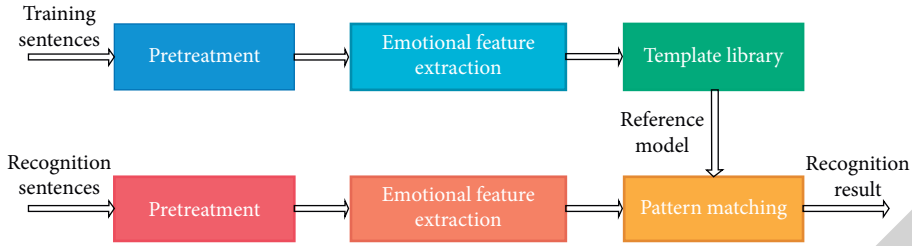

Figure 4: Principles of text emotion recognition.

$$X_{m\times n} = \left[x_{ij}\right]. \tag{10}$$

Among them, x_{ij} represents the weight of the i^{th} feature word in the j^{th} article search. The weight is used to measure the distinguishing ability of the feature word to the document, or the degree of contribution to the analysis. Since the length of each document is different, the weight tends to favor longer documents. In this case, it can be normalized when calculating the weight to avoid this situation. This leads to the following formula:

$$w\left(t_i, d_j\right) = \frac{\left(\log_2\left(1 + tf\left(t_i, d_j\right)\right)\right) \times \log_2\left(N/N_t\right)}{\sqrt{\sum_{t_i \in d_j}\left[\left(\log_2\left(1 + tf\left(t_i, d_j\right)\right)\right) \times \log_2\left(N/N_{t_i}\right)\right]}}. \tag{11}$$

Among them, $w(t_i, d_j)$ represents the weight of feature word t_i in document d_j. $tf(t_i, d_j)$ represents the number of times the feature word t_i appears in the document d_j, and $(1 + tf(t_i, d_j))$ is to prevent the occurrence of $tf(t_i, d_j)$. N represents the number of documents in the document set, and N_{t_i} represents the number of documents in the document set that contain characteristic words.

4. Music Emotion Feature Analysis Method Based on Multimodal Fusion

Multimodal information fusion is an information processing process that comprehensively utilizes natural language processing, semantic analysis, statistical analysis, and other technical methods to detect, correlate, estimate, combine, and analyze multimodal information in multiple levels and dimensions. The multimodal music emotion analysis method is to analyze music emotion based on music content and lyrics, respectively, and then combine the two analysis results to get the final music emotion analysis. If stress is defined as anxiety and happiness, and energy is defined as vitality and calmness, the final analysis result is determined by combining the two analysis results. To study the local form of the melody line, we should not only look at the connection of two notes but at least look at the ups and downs of four or five notes and five or six notes in a bar, so as to see the characteristics of linear form from the harmony interval and disharmony interval in music acoustics and law, for example, Table 1.

The energy of the audio signal changes significantly over time, and its short-term energy analysis gives an appropriate description method to reflect these amplitude changes. For the signal $\{x(n)\}$, the short-term energy is defined as follows:

$$E_n = \sum_{m=-\infty}^{\infty}\left[x(m)w(n-m)\right]^2 = \sum_{m=-\infty}^{\infty} x^2(m)h(n-m) = x^2(n) \times h(n). \tag{12}$$

Among them, $h(n) = w^2(n)$. Equation (12) represents the short-term energy when the window function is started at the nth point of the signal. The short-term energy can be regarded as the output of the square of the audio signal through a linear filter, and the unit impulse response of the linear filter is $h(n)$, as shown in Figure 5.

If $x_w(n)$ is used to represent the signal after $x(n)$ is windowed, the length of the window function is N, and the short-term energy is expressed as follows:

$$E_n = \sum_{m=n}^{n+N-1} x_w^2(m). \tag{13}$$

The requirement of music emotion analysis is based on the multimodal, complex, multisource, and heterogeneous characteristics of music emotion. The service has the quick adaptability of universal access, aggregation on demand, context processing, and seamless application and can realize the interoperability and autonomous cooperation of heterogeneous data across fields and platforms. Through the evaluation of the direction of notes, take the bar as the unit. No matter whether the notes go down or up, as long as a series of notes with the same direction appear continuously, an upward or downward melody line can be generated, which means that the evaluation value is higher.

The feature vector of lyrics is extracted based on the reinforcement learning model, and the feature value of each dimension is calculated. Then labeled lyrics are clustered to get a cluster set, and the similarity between lyrics and each cluster and the similarity of each cluster and the ratio of each category in the cluster are tested. The assignment of melody weights is shown in Table 2. The relationship between melody weight and melody trend is shown in Figure 6.

Table 1: Harmony degree of overtone.

Partial name	Chord vibration length	Degree of concord
1st part	1/10	Absolute concord
2nd part	1/20	Complete concord
3rd part	1/30	Absolute concord
4th part	1/40	Incomplete concord
5th part	1/50	Incomplete concord
6th part	1/60	Disharmony

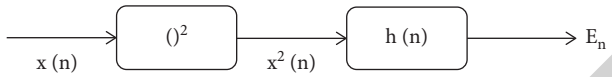

Figure 5: Short-term energy graph.

Table 2: Melody weight data.

Same trend degree of melody	Melody weight
2	0.9
4	0.75
6	0.60
8	0.45
10	0.30
Greater than 10	0.15

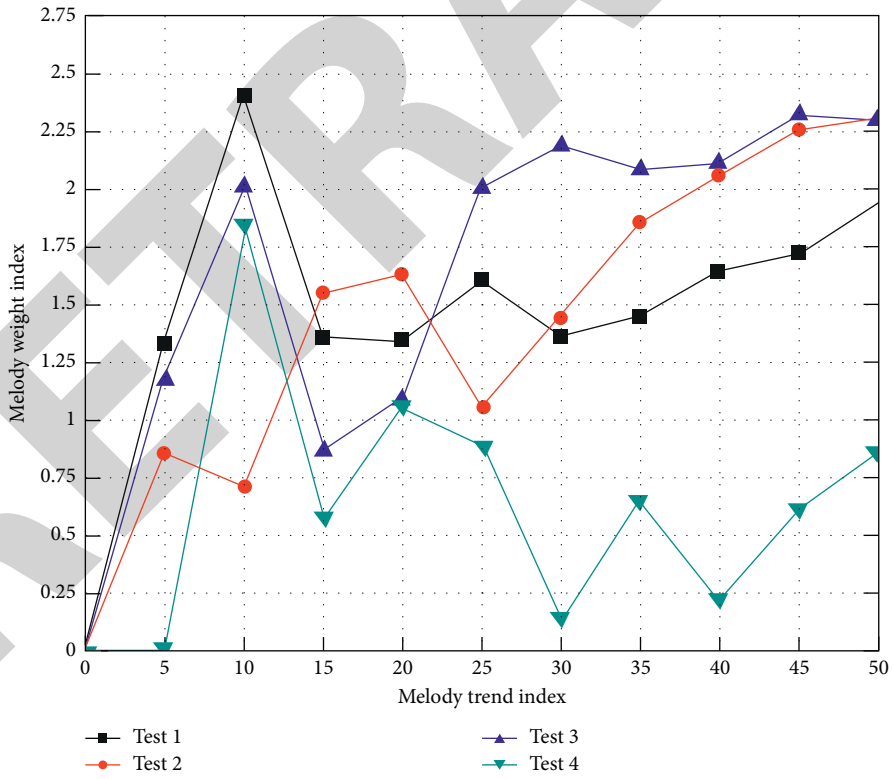

Figure 6: The relationship between the weight of the melody and the degree of the direction of the melody.

Compared with sentence-level emotion classification of automatic encoder, the accuracy of sentiment classification of article-level lyrics based on word vector sentence coding is improved. The dual-mode fusion method based on the neural network has a remarkable effect in audio emotion classification because it can set the weight of each mode. The linear regression curve is calculated according to the stepwise multiple linear regression equation, as shown in Figure 7. The ability of music emotion analysis based on the reinforcement learning

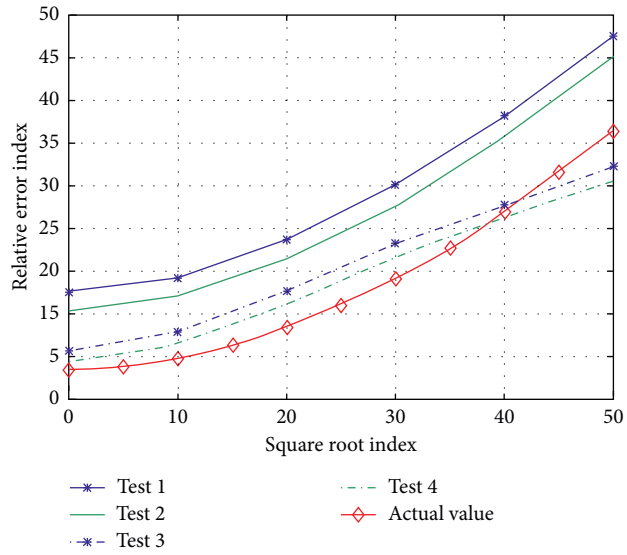

Figure 7: Analysis of the relationship between the error and the number of iterations.

feature extraction model is stronger than that of common multimodal information emotion analysis.

In the speech modality experiment, the method of capturing context information is better than other baseline methods, whether in the main task or the auxiliary task. The above baseline method only uses the phonetic features of the main task or auxiliary task. Due to the weak representation ability of speech modal features and the very small number of samples of "disgust" and "fear" categories, our model cannot predict the corresponding categories, and its performance in individual categories cannot reach the best. Different modes of music data often have a certain correlation in emotional expression; that is, different modes are not independent of each other. This correlation can often enhance the accuracy of sentiment analysis. Because the feature extraction methods used in different modal music data are different from each other, the dimensions and attributes of the obtained features are quite different. This difference makes it impossible for music features of different modes to operate and calculate each other directly, which makes it difficult to fully explore and apply the correlation between music data of different modes. In order to make full use of the temporal correlation of music data of different modes and improve the accuracy of emotion analysis, it is necessary to design an effective mechanism to aggregate music features of different modes and different time scales according to emotion categories.

5. Conclusions

In order to effectively manage music resources and help people efficiently obtain interesting content from massive music, music emotion analysis has always been a hot spot for scholars. Under multimodal fusion, based on the fusion of existing linear weighted decision-making layers, the reinforcement learning method is introduced, which can highly fuse different types of analysis effects of multiple modes, so as to guarantee the overall fusion effect. Based on reinforcement learning technology, this paper studies the emotional analysis of music from the perspective of audio visualization. According to the demand analysis of music emotion analysis, this paper explores a model framework of music emotion analysis based on multimodal information fusion function and level. The experimental results on multimodal emotion analysis data set show that this method can greatly improve the performance of emotion analysis tasks through emotion auxiliary information, and at the same time, the performance of the emotion analysis task is also improved to a certain extent. Music emotion analysis is an important means for automatic music retrieval. The heterogeneity and semantic gap between different modal music data make it a challenging problem to use multimodal information for music emotion analysis. The relationship between music structured information and human emotion cannot be fully reflected by using existing common features. Therefore, we can further explore the feature extraction method with more musical emotion analysis ability.

Data Availability

The data used to support the findings of this study are available from the corresponding author upon request.

Conflicts of Interest

The author declares that he has no conflicts of interest.

References

[1] G. Wang, "Analysis of teaching strategies to strengthen students' emotional experience in middle school music teaching," *Teaching Management and Education Research*, vol. 2, no. 15, pp. 89-90, 2017.

[2] X. Li, L. Han, J. Li, and J. Zhou, "Multimodal music sentiment classification based on optimized residual network," *Computer and Modernization*, vol. 304, no. 12, pp. 87–93, 2020.

[3] K. Chen and L. Han, "Research on music emotion classification based on audio and lyrics," *Electronic Measurement Technology*, vol. 41, no. 22, pp. 15–20, 2018.

[4] Z. Tang, X. Liu, and H. Yang, "Image emotion annotation method based on multimodal information fusion," *Computer Integrated Manufacturing Systems*, vol. 26, no. 1, pp. 134–144, 2020.

[5] Z. Gong and X. Shao, "Multi-modal music recommendation system," *Journal of Nanjing University of Information Technology (Natural Science Edition)*, vol. 59, no. 1, pp. 72–80, 2019.

[6] Y. R. Pandeya and J. Lee, "Deep learning-based late fusion of multimodal information for emotion classification of music video," *Multimedia Tools and Applications*, vol. 80, no. 38, pp. 1–19, 2021.

[7] H. Kaya and A. A. Salah, "Combining modality-specific extreme learning machines for emotion recognition in the wild," *Journal on Multimodal User Interfaces*, vol. 10, no. 2, pp. 139–149, 2016.

[8] X. Wang, "Exploration of music emotion teaching in junior middle schools," *China New Communications*, vol. 18, no. 15, p. 135, 2016.

Hindawi
Journal of Mathematics
Volume 2023, Article ID 9769718, 1 page
https://doi.org/10.1155/2023/9769718

Retraction

Retracted: Application to Biomedical Data: Using the Topp Leone Inverse Lindley Model

Journal of Mathematics

Received 19 December 2023; Accepted 19 December 2023; Published 20 December 2023

This article has been retracted by Hindawi following an investigation undertaken by the publisher [1]. This investigation has uncovered evidence of one or more of the following indicators of systematic manipulation of the publication process:

(1) Discrepancies in scope

(2) Discrepancies in the description of the research reported

(3) Discrepancies between the availability of data and the research described

(4) Inappropriate citations

(5) Incoherent, meaningless and/or irrelevant content included in the article

(6) Manipulated or compromised peer review

The presence of these indicators undermines our confidence in the integrity of the article's content and we cannot, therefore, vouch for its reliability. Please note that this notice is intended solely to alert readers that the content of this article is unreliable. We have not investigated whether authors were aware of or involved in the systematic manipulation of the publication process.

Wiley and Hindawi regrets that the usual quality checks did not identify these issues before publication and have since put additional measures in place to safeguard research integrity.

We wish to credit our own Research Integrity and Research Publishing teams and anonymous and named external researchers and research integrity experts for contributing to this investigation.

The corresponding author, as the representative of all authors, has been given the opportunity to register their agreement or disagreement to this retraction. We have kept a record of any response received.

References

[1] M. A. Aldahlan, "Application to Biomedical Data: Using the Topp Leone Inverse Lindley Model," *Journal of Mathematics*, vol. 2022, Article ID 1985861, 11 pages, 2022.

Hindawi
Journal of Mathematics
Volume 2022, Article ID 1985861, 11 pages
https://doi.org/10.1155/2022/1985861

Research Article

Application to Biomedical Data: Using the Topp Leone Inverse Lindley Model

Maha A. Aldahlan

University of Jeddah, College of Science, Department of Statistics, Jeddah, Saudi Arabia

Correspondence should be addressed to Maha A. Aldahlan; maal-dahlan@uj.edu.sa

Received 14 November 2021; Revised 20 December 2021; Accepted 6 January 2022; Published 8 February 2022

Academic Editor: Naeem Jan

A more flexible two-parameter model named the Topp Leone inverse Lindley model is investigated. Some basic mathematical properties such as quantile, moments, order statistics, and Rényi entropy of the new distribution are considered. Plot analysis for mean, variance, skewness, and kurtosis is performed. The density of the new model can be right skewed and decreasing with unimodal and bimodal shapes. Also, its hazard rate function can be decreasing and upside-down. The maximum likelihood (ML) estimation method is used to estimate the parameters of the distribution. The simulation study is executed to investigate the effectiveness of the estimates. The potential of the distribution is demonstrated through the application of the real biomedical dataset.

1. Introduction

The Topp Leone (TL-G) class of distributions was introduced by Al-Shomrani et al. [1]. A random variable X has TL-G class of distributions if the distribution function (cdf) and probability density function (pdf) are given by

$$F(x) = G(x)^{\alpha}(2 - G(x))^{\alpha} = \left(1 - \overline{G}(x)^2\right)^{\alpha}, \quad x \in \mathbb{R}, \tag{1}$$

and

$$f(x) = 2\alpha g(x)\overline{G}(x)\left(1 - \overline{G}(x)^2\right)^{\alpha-1}, \tag{2}$$

where $\overline{G}(x) = 1 - G(x)$, $G(x)$ is the baseline distribution, and α is a positive shape parameter.

The equation (2) can be rewritten as

$$f(x) = \sum_{i,j=0}^{\infty} W_{i,j} g(x) G(x)^j, \tag{3}$$

where $W_{i,j} = 2\alpha(-1)^{i+j}\binom{\alpha - 1}{i}\binom{i+2}{j}$. The quantile function of TL-G is given by

$$Q(u) = G^{-1}\left(1 - \sqrt{1 - \sqrt[\alpha]{u}}\right), \quad 0 < u < 1. \tag{4}$$

Many distributions have been studied by using TL-G for different baselines. Aryal et al. [2] studied TL Weibull distribution, Abbas et al. [3] introduced and studied TL inverse Weibull, Reyad and Othman [4] studied TL Burr-XII distribution, the TL Nadarajah-Haghighi distribution was proposed by Yousof and Korkmaz [5], the odd Lindley-G was proposed by Gomes et al. [6], Reyad et al. [7] proposed TL generalized inverted Kumaraswamy distribution, TL compound Rayleigh distribution is studied by Rasheed [8], odd Nadarajah-Haghighi-G was proposed by Nascimento et al. [9], Oguntunde et al. [10] introduced TL Lomax distribution, Al-Marzouki et al. [11] studied type II TL power Lomax distribution, Al-Marzouki et al. [12] studied TL odd Fréchet-G family, and Al-Babtain et al. [13] proposed sine TL-G family.

The inverse Lindley (IL) distribution was studied by Sharma et al. [14], and it has the following pdf and cdf, respectively,

$$g(x) = \frac{\theta^2}{1 + \theta}\left(\frac{1 + x}{x^3}\right)e^{-\theta/x}, \quad x > 0, \theta > 0, \tag{5}$$

and

$$G(x) = \left(1 + \frac{\theta}{(1+\theta)x}\right)e^{-\theta/x}, \quad x > 0, \theta > 0. \tag{6}$$

The IL distribution has been generalized by many statisticians in last years: Alkarni [15] introduced a more flexible model named extended IL distribution, Sharma et al. [16] proposed the generalized IL distribution, Barco et al. [17] studied the power IL distribution, Dey et al. [18] introduced alpha power transformed IL distribution, Eltehiwy [19] studied extended exponentiated IL distribution, and logarithmic IL model was studied by Eltehiwy [20].

The main goal of this article is as follows:

(i) To propose a new two-parameter life time model, so called, Topp Leone inverse Lindley (TLIL) distribution

(ii) The density of the new model can be right skewed and decreasing with unimodal and bimodal shapes. Also, it is hazard rate function can be decreasing and upside-down.

(iii) To study some of its various statistical properties such as quantile function, moments, incomplete moments, order statistics, and Rényi entropy

(iv) To discuss the statistical inference of the TLIL model by using the ML method

(v) To investigate a simulation study to show the behavior of the parameters model

(vi) To give leading fits than some known models with favourable results for the TLIL model

The new model is very flexible, and we can get the cdf and pdf by inserting (1) and (2) in (5) and (6) as

$$F(x) = \left(1 - \left(1 - \left(1 + \frac{\theta}{(1+\theta)x}\right)e^{-\theta/x}\right)^2\right)^{\alpha}, \quad x > 0, \theta, \alpha > 0, \tag{7}$$

and

$$f(x) = \frac{2\alpha\theta^2}{1+\theta}\left(\frac{1+x}{x^3}\right)e^{-\theta/x}\left(1 - \left(1 + \frac{\theta}{(1+\theta)x}\right)e^{-\theta/x}\right)\left(1 - \left(1 - \left(1 + \frac{\theta}{(1+\theta)x}\right)e^{-\theta/x}\right)^2\right)^{\alpha-1}. \tag{8}$$

The plots of the pdf and cdf of the TLIL distribution are shown in Figures 1 and 2.

Figure 1 shows the pdf can be decreasing, unimodal, and right skewed.

The remaining part of this article is organized as follows: the reliability analysis of the new distribution is given in Section 2, Section 3 concerns with the linear representation for the new model, the derivation of the mathematical properties of the distribution is proposed in Section 4, the estimation of parameters of the distribution is discussed in Section 5, in Section 6, a simulation study is executed to investigate the performance of the estimates, applications of real-life data to illustrate the potentials of the new distribution is presented in Section 7, and in Section 8, the concluding remarks are presented.

2. The Reliability Analysis

Suppose a random variable X follows the TLIL model, then the reliability function $R(x)$, hazard rate function (hrf) $h(x)$, inverse hazard rate function $\tau(x)$, and cumulative hazard rate function $H(x)$ for the TLIL distribution are given by

$$R(x) = 1 - \left(1 - \left(1 - \left(1 + \frac{\theta}{(1+\theta)x}\right)e^{-\theta/x}\right)^2\right)^{\alpha},$$

$$h(x) = \frac{2\alpha\theta^2/1+\theta\left((1+x)/x^3\right)e^{-\theta/x}\left(1-(1+\theta/(1+\theta)x)e^{-\theta/x}\right)\left(1-\left(1-(1+\theta/(1+\theta)x)e^{-\theta/x}\right)^2\right)^{\alpha-1}}{1-\left(1-\left(1-(1+\theta/(1+\theta)x)e^{-\theta/x}\right)^2\right)^{\alpha}}, \tag{9}$$

$$\tau(x) = \frac{2\alpha\theta^2/1+\theta\left((1+x)/x^3\right)e^{-\theta/x}\left(1-(1+\theta/(1+\theta)x)e^{-\theta/x}\right)}{1-\left(1-(1+\theta/(1+\theta)x)e^{-\theta/x}\right)^2},$$

$$H(x) = -\ln\left(1 - \left(1 - \left(1 - \left(1 + \frac{\theta}{(1+\theta)x}\right)e^{-\theta/x}\right)^2\right)^{\alpha}\right).$$

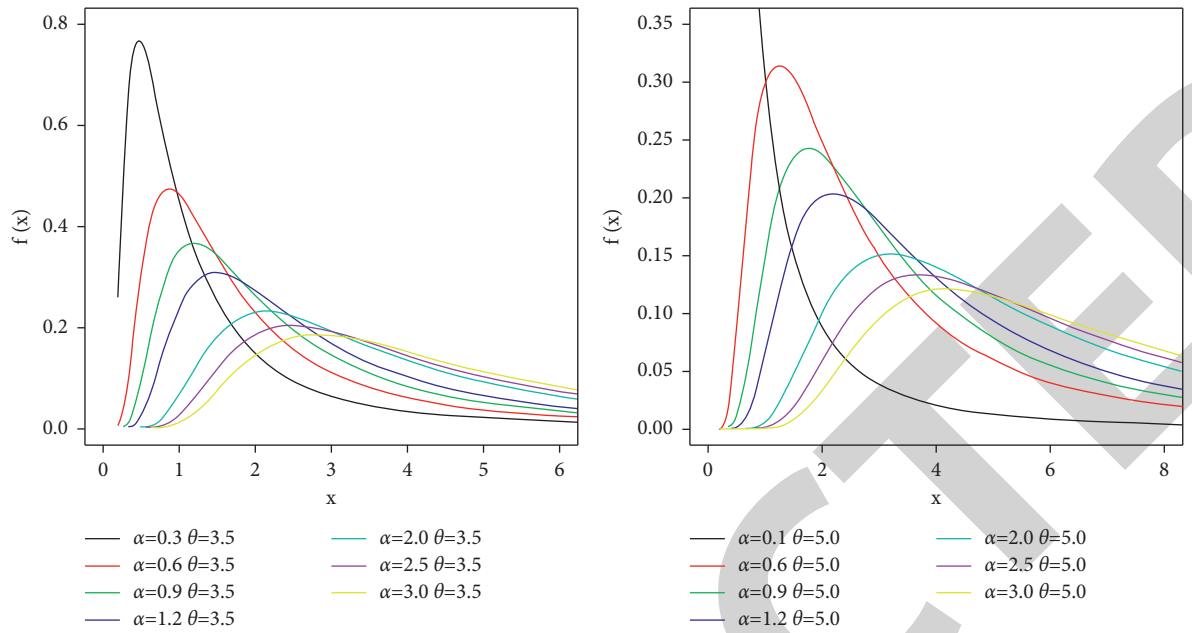

Figure 1: The pdf of the TLIL distribution for different values of parameters.

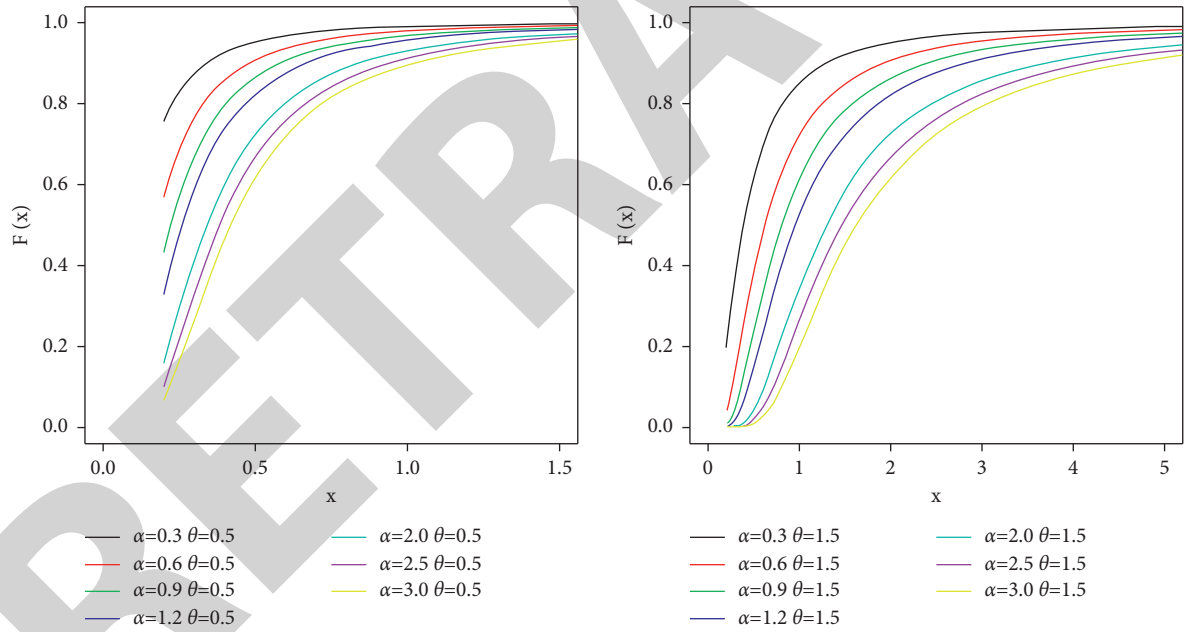

Figure 2: The cdf of the TLIL distribution for different values of parameters.

The plots of the pdf and hrf of the TLIL distribution are shown in Figure 3.

Figure 3 shows some possible shapes including monotone decreasing and right-skewed shapes for hrf.

3. Important Representation

In this section, representations of the pdf for TLIL distribution are calculated.

By using the three equations equation (3), (5), and (6), we can rewrite (8) as

$$f(x) = \sum_{i,j=0}^{\infty} W_{i,j} \frac{\theta^2}{1+\theta} \left(\frac{1+x}{x^3}\right) e^{-\theta(j+1)/x} \left(1 + \frac{\theta}{(1+\theta)x}\right)^j. \tag{10}$$

By applying the binomial expansion in the previous equation, we can rewrite it as

$$f(x) = \sum_{k=0}^{\infty} W_k \left(\frac{1+x}{x^{k+3}}\right) e^{-\theta(j+1)/x}, \tag{11}$$

where $W_k = \sum_{i,j=0}^{\infty} W_{i,j} (j/k) \theta^{k+2} / (1+\theta)^{k+1}$.

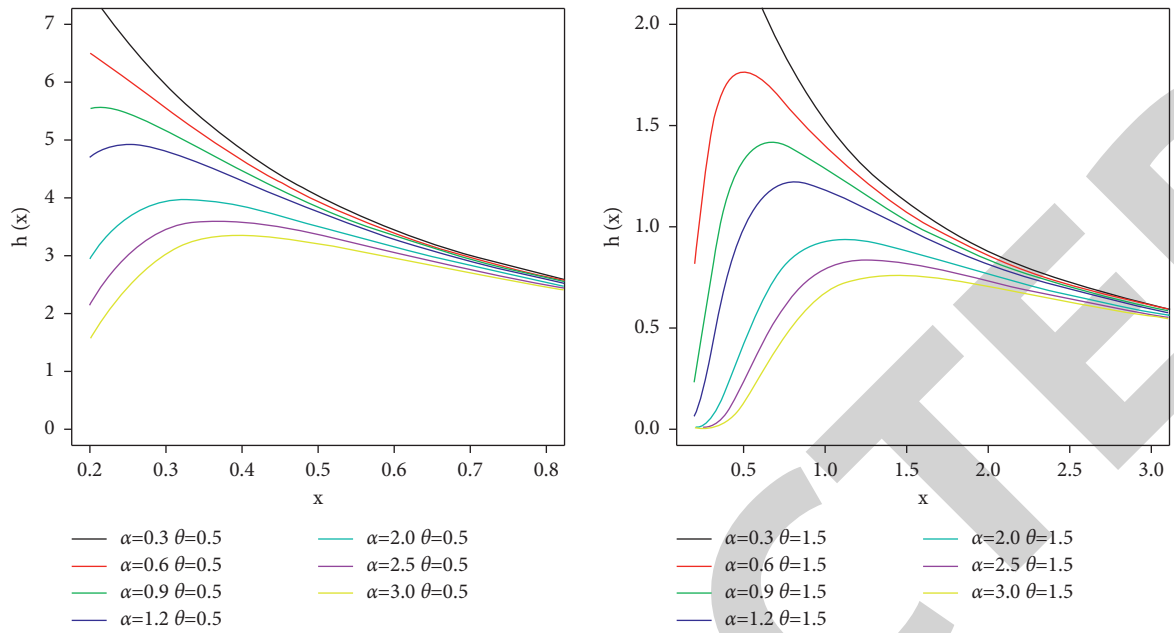

Figure 3: The hrf of the TLIL distribution for different values of parameters.

4. Mathematical Properties

4.1. Quantile Function. Let X has a random variable with pdf (8). The quantile function, say $Q(u)$, defined by $F(Q(u)) = u$ is the root of the equation:

$$\left(1 + \frac{\theta}{(1+\theta)Q(u)}\right)e^{-\theta/Q(u)} = 1 - \sqrt{1 - \sqrt[\alpha]{u}}, \quad 0 < u < 1. \tag{12}$$

By multiplying (12) both sides by $-(1+\theta)e^{-(1+\theta)}$, we get

$$-\left(1 + \theta + \frac{\theta}{Q(u)}\right)e^{-(1+\theta+\theta/Q(u))} = -(1+\theta)e^{-(1+\theta)} \left(1 - \sqrt{1 - \sqrt[\alpha]{u}}\right). \tag{13}$$

By using the Lambert W function which is the solution of the equation $W(z)e^{W(z)} = z$, where z is a complex number, we have

$$W_{-1}\left(-(1+\theta)e^{-(1+\theta)}\left(1 - \sqrt{1 - \sqrt[\alpha]{u}}\right)\right) = -\left(1 + \theta + \frac{\theta}{Q(u)}\right), \tag{14}$$

and then,

$$Q(u) = -\left[1 + \frac{1}{\theta} + \frac{1}{\theta}W_{-1}\left(-(1+\theta)e^{-(1+\theta)}\left(1 - \sqrt{1 - \sqrt[\alpha]{u}}\right)\right)\right]^{-1}. \tag{15}$$

Corollary 1. *If X~TLIL, the median M of X is given by*

$$Q(u) = -\left[1 + \frac{1}{\theta} + \frac{1}{\theta}W_{-1}\left(-(1+\theta)e^{-(1+\theta)}\left(1 - \sqrt{1 - \sqrt[\alpha]{0.5}}\right)\right)\right]^{-1}. \tag{16}$$

4.2. Moments. The r^{th} moments of a random variable having TLIL distribution is defined as

$$\begin{aligned} E(X^r) &= \int_0^\infty x^r f(x)\mathrm{d}x \\ &= \sum_{k=0}^{\infty} W_k \int_0^\infty x^r \left(\frac{1+x}{x^{k+3}}\right)e^{-\theta(j+1)/x}\mathrm{d}x \\ &= \sum_{k=0}^{\infty} W_k \int_0^\infty \left(x^{r-k-3} + x^{r-k-2}\right)e^{-\theta(j+1)/x}\mathrm{d}x. \end{aligned} \tag{17}$$

Letting $y = \theta(j+1)/x$, $x = \theta(j+1)/y\mathrm{d}x = -\theta(j+1)/y^2\mathrm{d}y$ and simplifying further,

$$E(X^r) = \sum_{k=0}^{\infty} W_k \int_0^\infty \left(\left(\frac{\theta(j+1)}{y}\right)^{r-k-3} + \left(\frac{\theta(j+1)}{y}\right)^{r-k-2}\right)e^{-y}\frac{\theta(j+1)}{y^2}\mathrm{d}y$$

$$E(X^r) = \sum_{k=0}^{\infty} W_k (\theta(j+1))^{r-k-2} \int_0^\infty \left(y^{k-r+1} + \theta(j+1)y^{k-r}\right)e^{-y}\mathrm{d}y$$

$$\sum_{k=0}^{\infty} W_k(\theta(j+1))^{r-k-2}(\Gamma(k-r+2)+\theta(j+1)\Gamma(k-r+1)). \tag{18}$$

The moment generating function of the TLIL model can be calculated by

$$M_X(t) = \sum_{r=0}^{\infty}\frac{t^r}{r!}E(X^r) = \sum_{r,k=0}^{\infty}\frac{t^r}{r!}W_k(\theta(j+1))^{r-k-2}$$
$$(\Gamma(k-r+2)+\theta(j+1)\Gamma(k-r+1)), \quad r<k+2. \tag{19}$$

Figure 4 shows the mean, variance, skewness, and kurtosis curves of the TLIL model for numerous values of α and θ.

4.3. Incomplete Moments. The incomplete moments, say $\varpi_s(t)$, is given by

$$\varpi_s(t) = \int_0^t x^s f(x;\varphi)\mathrm{d}x. \tag{20}$$

Using (11), $\varpi_s(t)$ can be taken the next formula:

$$\varpi_s(t) = \sum_{k=0}^{\infty} W_k \int_0^t x^s\left(\frac{1+x}{x^{k+3}}\right)e^{-\theta(j+1)/x}\mathrm{d}x. \tag{21}$$

Then, using the lower incomplete gamma function, we obtain

$$\varpi_s(t) = \sum_{k=0}^{\infty} W_k(\theta(j+1))^{s-k-2}\left(\nu\left(k-s+2,\theta(j+1)t^{-1}\right)\right.$$
$$\left.+\theta(j+1)\nu\left(k-s+1,\theta(j+1)t^{-1}\right)\right), \quad s<k+2, \tag{22}$$

where $\nu(s,t) = \int_0^t x^{s-1}e^{-x}\mathrm{d}x$ is the lower incomplete gamma function.

The Lorenz and Bonferroni curves are given by

$$L_F(x) = \frac{\int_0^t xf(x)\mathrm{d}x}{E(X)} = \frac{\sum_{k=0}^{\infty}W_k(\theta(j+1))^{-k-1}\left(\nu\left(k+1,\theta(j+1)t^{-1}\right)+\theta(j+1)\nu\left(k,\theta(j+1)t^{-1}\right)\right)}{\sum_{k=0}^{\infty}W_k(\theta(j+1))^{-k-1}(\Gamma(k+1)+\theta(j+1)\Gamma(k))},$$
$$B_F(x) = \frac{\int_0^t xf(x)\mathrm{d}x}{E(X)F(x)} = \frac{L_F(x)}{F(x)} = \frac{\sum_{k=0}^{\infty}W_k(\theta(j+1))^{-k-1}\left(\nu\left(k+1,\theta(j+1)t^{-1}\right)+\theta(j+1)\nu\left(k,\theta(j+1)t^{-1}\right)\right)}{\left(1-\left(1-(1+\theta/(1+\theta)x)e^{-\theta/x}\right)^2\right)^{\alpha}\left(\sum_{k=0}^{\infty}W_k(\theta(j+1))^{-k-1}(\Gamma(k+1)+\theta(j+1)\Gamma(k))\right)}. \tag{23}$$

4.4. Order Statistics. Suppose $X_1 < X_2 < \ldots < X_n$ is an order sample from TLIL population, the pdf of the i^{th} ordered statistics is given as

$$f(x_{i:n}) = \frac{n!}{(i-1)!(n-i)!}f(x)F(x)^{i-1}(1-F(x))^{n-i}$$
$$= \frac{n!}{(i-1)!(n-i)!}f(x)\sum_{j=0}^{n-i}(-1)^j\binom{n-i}{j}F(x)^{i+j-1}. \tag{24}$$

Substituting (7) and (8) and applying general binomial series expansion (24) become

$$f(x_{i:n}) = \sum_{j=0}^{n-i}\frac{2\alpha\theta^2(-1)^j\binom{n-i}{j}n!}{(\theta+1)(i-1)!(n-i)!}\left(\frac{1+x}{x^3}\right)e^{-\theta/x}\left(1-\left(1+\frac{\theta}{(1+\theta)x}\right)e^{-\theta/x}\right)\left(1-\left(1-\left(1+\frac{\theta}{(1+\theta)x}\right)e^{-\theta/x}\right)^2\right)^{\alpha(i+j)-1}. \tag{25}$$

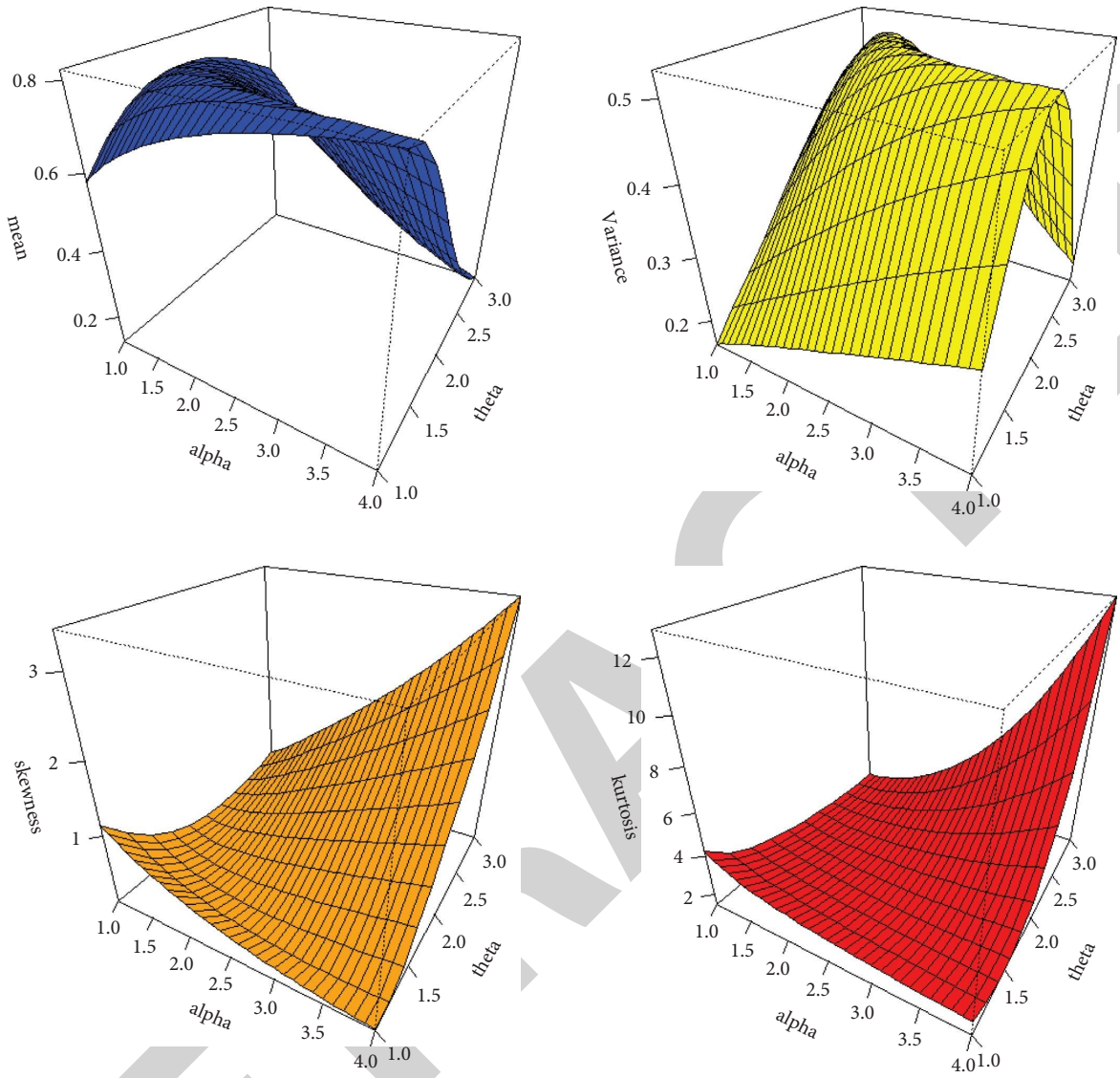

Figure 4: 3D plots of mean, variance, skewness, and kurtosis.

4.5. Rényi Entropy. For a given pdf, the Rényi entropy is defined by

$$I_R(\delta) = \frac{1}{1-\delta}\log\int_0^{\infty} f(x)^{\delta}\mathrm{d}x, \quad \delta > 0, \delta \neq 1. \tag{26}$$

The function $f(x)^{\delta}$ is given by

$$f(x)^{\delta} = \left(\frac{2\alpha\theta^2}{1+\theta}\right)^{\delta}\frac{(1+x)^{\delta}}{x^{3\delta}}e^{-\theta\delta/x}\left(1-\left(1+\left(\frac{\theta}{(1+\theta)x}\right)e^{-\theta/x}\right)\right)^{\delta}\left(1-\left(1-\left(1+\frac{\theta}{(1+\theta)x}\right)e^{-\theta/x}\right)^2\right)^{\delta(\alpha-1)}. \tag{27}$$

By applying the binomial expansion three times in the previous equation, we get

$$f(x)^{\delta} = \frac{(2\alpha)^{\delta}\theta^{2\delta+k}}{(1+\theta)^{\delta+k}} \sum_{i,j,k=0}^{\infty} (-1)^{i+j} \binom{\delta(\alpha-1)}{i} \binom{\delta+2i}{j} \binom{j}{k} x^{-k-3\delta} (1+x)^{\delta} e^{-\theta(j+\delta)/x}. \tag{28}$$

By applying the the binomial expansion to the term $(1+x)^{\delta} = \sum_{l=0}^{\infty} \binom{\delta}{l} x^{l}$, we can write the previous equation as

$$f(x)^{\delta} = \sum_{l=0}^{\infty} t_l x^{l-k-3\delta} e^{-\theta(j+\delta)/x}, \tag{29}$$

where

$$t_l = \frac{(2\alpha)^{\delta}\theta^{2\delta+k}}{(1+\theta)^{\delta+k}} \sum_{i,j,k=0}^{\infty} (-1)^{i+j} \binom{\delta(\alpha-1)}{i} \binom{\delta+2i}{j} \binom{j}{k} \binom{\delta}{l}. \tag{30}$$

Now, we will calculate the integral

$$I = \int_0^{\infty} f(x)^{\delta} \mathrm{d}x = \sum_{l=0}^{\infty} t_l \int_0^{\infty} x^{l-k-3\delta} e^{-\theta(j+\delta)/x} \mathrm{d}x = \sum_{l=0}^{\infty} t_l [\theta(j+\delta)]^{l-k-3\delta+1} \Gamma(k+3\delta-l-1). \tag{31}$$

Then, the Rényi entropy is

$$I_R(\delta) = \frac{1}{1-\delta} \log \sum_{l=0}^{\infty} t_l [\theta(j+\delta)]^{l-k-3\delta+1} \Gamma(k+3\delta-l-1). \tag{32}$$

5. Maximum Likelihood Estimation

Suppose $X_1, X_2, \ldots, X_n$ is a random sample of size n from a population having TLIL pdf, the log-likelihood function is given by

$$\begin{aligned} \mathrm{Log}\, L = {} & n \log(2\alpha) + 2n \log(\theta) - n \log(1+\theta) + \sum_{i=1}^{n} \log\left(\frac{1+x_i}{x_i^3}\right) \\ & - \theta \sum_{i=1}^{n} \frac{1}{x_i} + \sum_{i=1}^{n} \log\left(1 - \left(1 + \frac{\theta}{(1+\theta)x_i}\right) e^{-\theta/x_i}\right) \\ & + (\alpha-1) \sum_{i=1}^{n} \log\left(1 - \left(1 - \left(1 + \frac{\theta}{(1+\theta)x}\right) e^{-\theta/x}\right)^2\right). \end{aligned} \tag{33}$$

The score functions which correspond to equating the first-order partial derivative of the last equation to zero is given by

$$\begin{aligned} \frac{\partial \mathrm{Log}\, L}{\partial \alpha} &= \frac{n}{\alpha} + \sum_{i=1}^{n} \log\left(1 - \left(1 - \left(1 + \frac{\theta}{(1+\theta)x}\right) e^{-\theta/x}\right)^2\right) = 0, \\ \frac{\partial \mathrm{Log}\, L}{\partial \theta} &= \frac{2n}{\theta} - \frac{n}{1+\theta} - \sum_{i=1}^{n} \frac{1}{x_i} + \sum_{i=1}^{n} \frac{Z_i}{N_i} - 2(\alpha-1) \sum_{i=1}^{n} \frac{N_i Z_i}{\left(1-N_i^2\right)} = 0, \end{aligned} \tag{34}$$

where $Z_i = 1/x_i e^{-\theta/x_i}(1+\theta/(1+\theta)x_i + 1/(1+\theta)^2)$ and $N_i = 1 - (1+\theta/(1+\theta)x_i) e^{-\theta/x_i}$. The solutions, say $\widehat{\alpha}$ and $\widehat{\theta}$ of the score functions correspond to the maximum likelihood estimators of TLIL distribution. However, the score functions are nonlinear functions; the numerical values of the maximum likelihood estimates can be obtained using the Newton–Raphson iterative optimisation method.

An approximate confidence interval (CI) of model parameters for TLIL distribution is calculated. It is known that the asymptotic distribution of ML estimates of elements of parameters α and θ is given by

$$((\widehat{\alpha}-\alpha), (\widehat{\theta}-\theta)) \longrightarrow N\left(0, I^{-1}(\alpha,\theta)\right), \tag{35}$$

where I^{-1} is the variance covariance matrix of unknown parameters; hence, the approximate $(1-\nu)$ 100% two-sided CIs for α and θ are, respectively, given by

$$\widehat{\alpha} \pm Z_{\nu/2} \sqrt{\mathrm{var}(\widehat{\alpha})}, \widehat{\theta} \pm Z_{\nu/2} \sqrt{\mathrm{var}(\widehat{\theta})}, \tag{36}$$

where $Z_{\nu/2}$ is the upper $\nu/2^{\text{th}}$ percentile of the standard normal distribution.

6. Simulation

This section provides a simulation study to assess the behavior of the estimators in case of complete samples. Mean square errors (MSEs), biases, lower bound (LB) of CI, upper bound (UB) of CI, and average length (AL) of 90% and 95% are calculated via Mathematica 9. The following algorithm is designed as follows.

(i) 5000 random samples of size $n = 50$, 100, and 200 are generated from TLIL distribution

(ii) Exact values of parameters are choiced

(iii) The ML estimates, MSEs, biases, LB, UB, and AL for selected values of parameters are calculated

(iv) Numerical outcomes are given in Tables 1–5 based on complete

7. Application

The potential of the new model TLIL is illustrated by modelling a real-life dataset. We compare the fits of the TLIL model with five models: IL, generalized IL (GIL),

Table 1: ML estimates, biases, MSE, LB, UB, and AL of the TLIL model for $\alpha = 1.5$, $\theta = 0.5$.

n	ML	Bias	MSE	90%			95%		
				LB	UB	AL	LB	UB	AL
50	1.211	−0.289	0.129	−0.086	2.508	2.594	−0.335	2.756	3.091
	0.574	0.074	0.012	0.239	0.910	0.672	0.174	0.975	0.800
100	1.401	−0.099	0.049	0.462	2.340	1.879	0.282	2.520	2.238
	0.506	0.006	0.004	0.327	0.686	0.359	0.293	0.720	0.427
200	1.441	−0.059	0.018	0.774	2.107	1.333	0.647	2.235	1.589
	0.502	0.002	0.001	0.381	0.623	0.242	0.358	0.646	0.288

Table 2: ML estimates, biases, MSE, LB, UB, and AL of the TLIL model for $\alpha = 1.8$, $\theta = 0.5$.

n	ML	Bias	MSE	90%			95%		
				LB	UB	AL	LB	UB	AL
50	1.194	−0.606	0.532	0.231	2.156	1.925	0.047	2.341	2.294
	0.659	0.159	0.058	0.319	1.000	0.682	0.253	1.065	0.812
100	1.355	−0.445	0.231	0.561	2.148	1.587	0.409	2.300	1.891
	0.558	0.058	0.006	0.380	0.737	0.358	0.345	0.771	0.426
200	1.472	−0.328	0.109	0.739	2.206	1.467	0.598	2.347	1.748
	0.557	0.057	0.004	0.414	0.700	0.286	0.387	0.727	0.340

Table 3: ML estimates, biases, MSE, LB, UB, and AL of the TLIL model for $\alpha = 1.5$, $\theta = 1.2$.

n	ML	Bias	MSE	90%			95%		
				LB	UB	AL	LB	UB	AL
50	1.341	−0.159	0.065	0.031	2.651	2.620	−0.220	2.902	3.121
	1.272	0.072	0.023	0.580	1.964	1.385	0.447	2.097	1.650
100	1.450	−0.050	0.006	0.401	2.498	2.097	0.201	2.699	2.498
	1.189	−0.011	0.002	0.719	1.659	0.940	0.629	1.749	1.120
200	1.498	−0.002	0.000	0.716	2.280	1.565	0.566	2.430	1.864
	1.200	0.000	0.002	0.861	1.538	0.677	0.796	1.603	0.807

Table 4: ML estimates, biases, MSE, LB, UB, and AL of the TLIL model for $\alpha = 1.8$, $\theta = 1.2$.

n	ML	Bias	MSE	90%			95%		
				LB	UB	AL	LB	UB	AL
50	1.296	−0.504	0.285	0.015	2.576	2.560	−0.230	2.821	3.051
	1.420	0.220	0.058	0.629	2.212	1.582	0.478	2.363	1.885
100	1.362	−0.438	0.208	0.467	2.256	1.789	0.296	2.427	2.132
	1.339	0.139	0.030	0.843	1.835	0.993	0.748	1.930	1.183
200	1.500	−0.300	0.090	0.941	2.059	1.118	0.834	2.166	1.333
	1.293	0.093	0.009	1.032	1.553	0.522	0.982	1.603	0.622

Table 5: ML estimates, biases, MSE, LB, UB, and AL of the TLIL model for $\alpha = 1.5$, $\theta = 0.7$.

n	ML	Bias	MSE	90%			95%		
				LB	UB	AL	LB	UB	AL
50	0.993	−0.507	0.478	0.150	1.835	1.685	−0.011	1.996	2.007
	1.034	0.334	0.207	0.439	1.629	1.190	0.325	1.742	1.417
100	1.185	−0.315	0.146	0.380	1.991	1.611	0.226	2.145	1.919
	0.799	0.099	0.016	0.498	1.099	0.601	0.441	1.157	0.716
200	1.336	−0.164	0.070	0.669	2.003	1.334	0.541	2.130	1.589
	0.760	0.060	0.008	0.552	0.968	0.417	0.512	1.008	0.496

Table 6: Descriptive statistics for the both datasets.

	N	Mean	Median	Mode	Var	SK	KU
Data I	20	1.9	1.7	1.7	0.471	1.862	4.185
Data II	72	1.768	1.495	1.08	1.055	1.371	2.225

Table 7: Parameter estimates and the standard error in parentheses for dataset I.

Model	Estimates and MSEs		
TLIL (α, θ)	0.073 (0.043)	853.969 (470.089)	
IL (θ)	60.007 (7.754)		
EIL (α, θ)	3.994 (8.202)	15.696 (30.438)	
GIL (α, θ)	0.786 (0.072)	29.409 (8.237)	
IW (α, β)	0.786 (0.071)	70.962 (12.612)	
EGIL (α, β, θ)	0.784 (0.072)	5.35 (19.465)	6.123 (19.661)

Table 8: Summary of goodness-of-fit statistics for dataset I.

Model	−2LogL	AIC	BIC	KS
TLIL	760.04	764.04	763.567	0.1228
IL	771.4063	773.406	775.467	0.288
EIL	771.492	775.492	780.045	0.2884
GIL	763.2041	767.204	771.325	0.19032
IW	763.1635	767.163	771.284	0.19030
EGIL	763.3393	769.339	775.521	0.191

Table 9: Parameter estimates and the standard error in parentheses for dataset II.

Model	Estimates and MSEs		
TLIL (α, θ)	0.567 (0.24)	3.175 (0.902)	
IL (θ)	1.5767 (0.146)		
EIL (α, θ)	0.6966 (0.993)	2.1041 (2.453)	
GIL (α, θ)	1.0713 (0.076)	1.5487 (0.147)	
IW (α, β)	1.1731 (0.084)	1.0583 (0.113)	
EGIL (α, β, θ)	1.1632 (0.085)	0.0534 (0.079)	20.6388 (29.624)

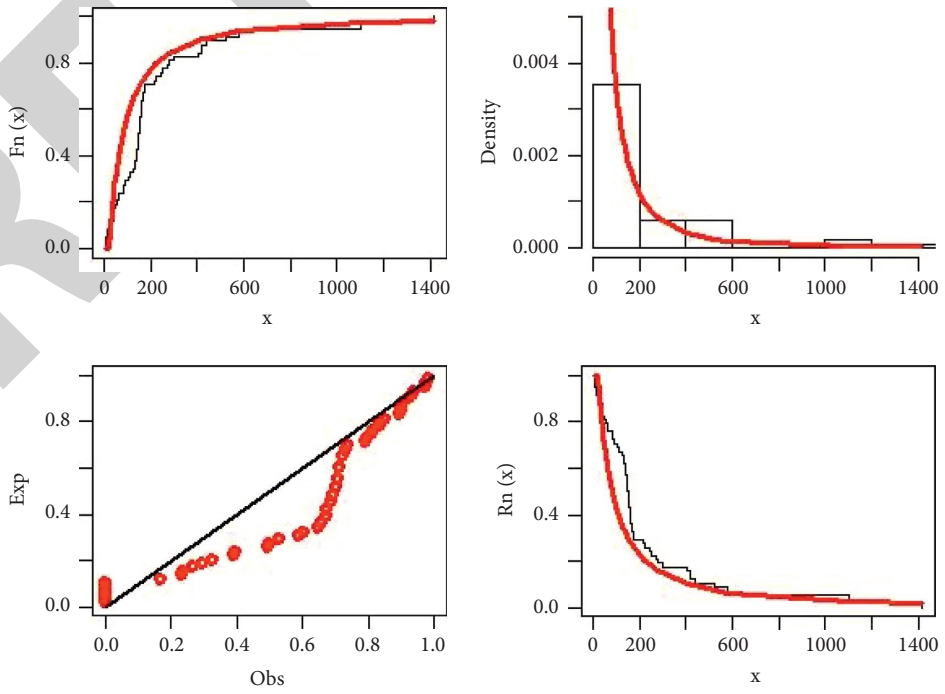

Figure 5: The estimated pdf, ecdf, esf, and pp plots for the TLIL model for dataset I.

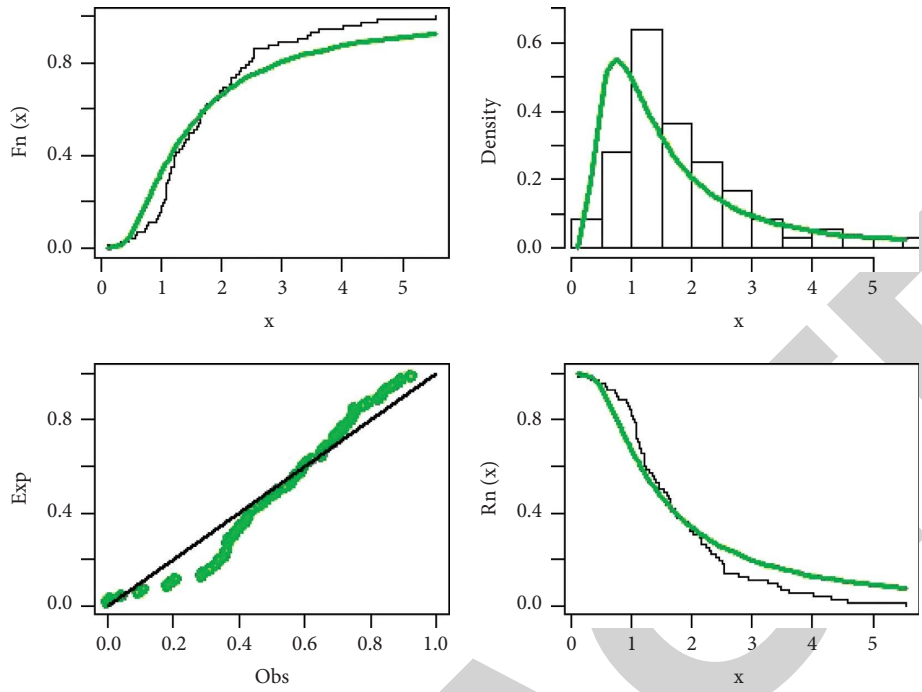

Figure 6: The estimated pdf, ecdf, esf, and pp plots for the TLIL model for dataset II.

Table 10: Summary of goodness-of-fit statistics for dataset II.

Model	−2LogL	AIC	BIC	KS
TLIL	220.527	224.527	224.242	0.179
IL	239.569	241.569	243.846	0.194
EIL	239.494	243.494	247.615	0.199
GIL	238.698	242.698	247.251	0.181
IW	236.332	240.332	244.885	0.183
EGIL	236.501	242.501	249.331	0.184

exponentiated generalized IL (EGIL), exponentiated IL (EIL), and inverse Weibull (IW) distributions. The Kolmogorov–Smirnov (KS) statistic is used to determine how well the distributions fit the dataset. The Akaike information criterion (AIC), Bayesian information criterion (BIC), and the negative two log-likelihood values of the distributions are also computed. The least values of the −2LogL, AIC, BIC, and KS statistics have a better fit.

Dataset I is taken from Sharma et al. [14] and it represents the survival times of a group of patients suffering from head and neck cancer disease. The patients were treated using radiotherapy.

Dataset II is taken from Bjerkedal [21] and it represents the survival times (in days) of 72 guinea pigs infected with virulent tubercle bacilli.

The two datasets are concerned with biomedical data. Many works studied biomedical datasets such as the studies by Alanazi et al. [22], Iskanderani et al. [23], and Antor et al. [24]. Some descriptive analyses of the both datasets are given in Table 6.

Tables 6–9 present the parameter estimates including the standard errors in parentheses and the goodness-of-fit statistics of the competitive distributions, respectively. The values in Tables 7 and 9 indicate that the TLIL distribution has the least values of the goodness-of-fit statistics which imply that it has a better fit among the competitive models.

The graphical fit of the competing distributions on the dataset is shown in Figures 5 and 6. The estimated pdf, ecdf, esf, and pp plots plot of TLIL is closest to the empirical plots. Figures 5 and 6 also confirm the goodness-of-fit statistics values given in Tables 8 and 10 that the TLIL has a better fit.

8. Conclusion

In this study, a new statistical distribution called the Topp Leone inverse Lindley model is introduced. The density of the new model can be right skewed and decreasing with unimodal and bimodal shapes. Also, its hazard rate function can be decreasing and upside-down. Some of the mathematical properties such as quantile function, ordinary moments, incomplete moments, and pdf of the i^{th} ordered statistics are established. The estimation of the parameters of the new distribution using the maximum likelihood method is considered. The simulation study is assessed to investigate the performance of the estimates. The usefulness and potentials of the new distribution are demonstrated by comparing its fit to a real-life dataset with other distributions. The goodness-of-fit statistics indicated that the new distribution has a better fit than other competing distributions.

Data Availability

The dataset used to support the findings of this study are available from the corresponding author upon request.

Hindawi
Journal of Mathematics
Volume 2023, Article ID 9760950, 1 page
https://doi.org/10.1155/2023/9760950

Retraction

Retracted: Intelligent Transportation Design Based on Iterative Learning

Journal of Mathematics

Received 19 December 2023; Accepted 19 December 2023; Published 20 December 2023

This article has been retracted by Hindawi following an investigation undertaken by the publisher [1]. This investigation has uncovered evidence of one or more of the following indicators of systematic manipulation of the publication process:

(1) Discrepancies in scope

(2) Discrepancies in the description of the research reported

(3) Discrepancies between the availability of data and the research described

(4) Inappropriate citations

(5) Incoherent, meaningless and/or irrelevant content included in the article

(6) Manipulated or compromised peer review

The presence of these indicators undermines our confidence in the integrity of the article's content and we cannot, therefore, vouch for its reliability. Please note that this notice is intended solely to alert readers that the content of this article is unreliable. We have not investigated whether authors were aware of or involved in the systematic manipulation of the publication process.

Wiley and Hindawi regrets that the usual quality checks did not identify these issues before publication and have since put additional measures in place to safeguard research integrity.

We wish to credit our own Research Integrity and Research Publishing teams and anonymous and named external researchers and research integrity experts for contributing to this investigation.

The corresponding author, as the representative of all authors, has been given the opportunity to register their agreement or disagreement to this retraction. We have kept a record of any response received.

References

[1] Y. Ma and K. Liu, "Intelligent Transportation Design Based on Iterative Learning," *Journal of Mathematics*, vol. 2022, Article ID 5027412, 7 pages, 2022.

Hindawi
Journal of Mathematics
Volume 2022, Article ID 5027412, 7 pages
https://doi.org/10.1155/2022/5027412

Research Article

Intelligent Transportation Design Based on Iterative Learning

Yinpu Ma[1] and Kai Liu[2]

[1]*School of Mechanical Engineering, Ningxia University, 489 West Helan Mountains Road, Xixia, Yinchuan, China*
[2]*Siemens Mobility Technologies (Beijing) Co., Ltd., No. 7 Wangjing Zhonghuan Nanlu, Chaoyang, Beijing, China*

Correspondence should be addressed to Kai Liu; morton@bjtu.edu.cn

Received 17 November 2021; Revised 14 December 2021; Accepted 17 December 2021; Published 8 February 2022

Academic Editor: Naeem Jan

Most of the existing traffic optimization control methods are based on accurate mathematical models. As an uncertain and complex system, the urban traffic system faces difficulty in accurately calibrating the model parameters. Therefore, the existing methods become very difficult in the actual application process. Based on the massive data contained in the urban traffic system and the repetitive characteristics of traffic flow, this paper proposes a hierarchical traffic signal control method for urban road network based on iterative learning control. The simulation results show that the algorithm can achieve better control effect and can solve the problem of urban traffic congestion more effectively than traditional traffic control methods.

1. Introduction

Traffic signal control is an effective method to change urban road traffic conditions and improve road capacity. Because the current transportation system has the characteristics of complexity, variability, uncertainty, and strong randomness, it is difficult to create an accurate mathematical model [1, 2]. The current control of traffic signals at intersections is to divide the day into several time periods, and the cycle length is fixed in each time period. However, due to the strong randomness of the traffic flow of the road section, the phased traffic congestion is unavoidable, and it cannot be based on specific conditions. It will make real-time adjustments [3]. If the green signal ratio of each phase can be controlled to respond to changes in traffic flow in real time, the waiting time of vehicles will be minimized.

Iterative learning control [4, 5] is a control method for repetitive motion processes. At the same time and place, the traffic flow at the intersection will appear to be approximately repetitive. Ding [6] changed the traffic conditions and selection behaviors in the area according to different road network conditions, established a combined feedforward feedback iterative learning control model, and effectively controlled system interference. Simulation analysis is used to improve the accuracy of tracking error, but the selected traffic model is relatively simple and cannot be applied to complex urban intersections. Jing [7] took the traffic density of main and auxiliary roads as the control target, and the macro-traffic flow model proposed simplifies the store-and-forward model. Iterative learning is applied between the main and auxiliary roads to achieve equilibrium control in local sections, so that the equilibrium control error converges, but the disadvantage is that the model ignores the impact of changing lanes on traffic conditions and cannot be applied to traffic intersections in daily life. In [8], for the entrance of expressway, PD type iterative control law was used to control the traffic flow diffusion model, and then the center of gravity method was used to model and adjust the iterative learning gain, so that the output of the system has better tracking performance. The disadvantage is that it uses 3 types of traffic flow models which are all macroscopic traffic flow models, which will affect the accuracy of the results under microscopic characteristics. Zhou et al. [9] came up with the method of iterative learning control for green signal ratio of single intersection with fixed period. Luo [10] researched iterative control algorithm for

descriptor systems. Lv et al. [11] accelerated the control of random initial state errors through iterative learning control. References [12–17] present the urban intersections, roads, signals verifications, and optimizations problem. Li and Li [18] gave the green wave signal setting and simulation analysis of bus lane. Xiao [19] researched on control group decision and dynamic optimization of arterial round intersection. Wang [20] modelled the traffic control signal optimization. Ge and Zhou [21] worked on the dual-layer hierarchical control solution for traffic signal.

Since iterative learning control is mainly applied to fast intersections with relatively fixed traffic flow and relatively simple vehicle conditions, there are few studies on applying iterative learning control to daily intersection traffic light control. This article first uses the iterative learning control method to determine the best effective green light time for each phase and finally verifies the green signal ratio of a certain road section through simulation. The simulation results show that the control method can effectively reduce the queuing phenomenon of vehicles and play a great role in improving the traffic efficiency. After the introduction and literature review, Section 2 presents the principle of iterative learning control algorithm. Section 3 discusses the timing of traffic signals. In Section 4, the iterative learning was used to design the timing scheme. In Section 5, the simulation research was carried out. Finally, Section 6 concludes the study.

2. The Principle of Iterative Learning Control Algorithm

Assuming t within a certain period of time, the controlled object undergoes multiple iterations from the initial state $x_k(0)$; according to the algorithm, the expected value $y_d(t)$ and the result value of the dynamic process are superimposed continuously. When the number of downscaling approaches infinity, the control of the system will fail. The input function is

$$u_k(t) \longrightarrow u_d(t). \tag{1}$$

The control output function of the system is

$$y_k(t) \longrightarrow y_d(t). \tag{2}$$

When it runs to k times, its expression is

$$\begin{cases} x_k(t) = f\left(x_{k(t)}, u_{k(t)}\right), \\ y_k(t) = g\left(x_{k(t)}, u_{k(t)}\right). \end{cases} \tag{3}$$

Assuming that the expected value $y_d(t)$ of the system is set within the finite time of $[0, T]$, the obtained input signal $u_k(t)$ makes the output signal $y_k(t)$ infinitely approach the output value $y_d(t)$. The error accuracy of system tracking is

$$e_k(t) = y_d(t) - y_k(t). \tag{4}$$

If the number of iterations is $k \longrightarrow \infty$, the tracking error of the system is

$$\lim_{k \longrightarrow \infty} e_k(t) = 0. \tag{5}$$

3. Timing of Traffic Signals

The point control method is often adopted for the signal lights of a single intersection. This article uses the British TRRL method to optimize the signal timing of the current intersection. The number of phases and periods of the point are obtained based on field survey samples, and then the green light duration of each phase is determined separately. This signal timing optimization scheme can minimize the traffic delay time at the intersection, reasonably allocate the traffic flow of each phase to make the control system operate in an orderly manner, and then perform error corrections according to the actual situation to find the most ideal timing plan.

3.1. Optimal Period of Traffic Signal. The formula for calculating the optimal period of signal control is

$$C_0 = \frac{1.5L + 5}{1 - Y}, \tag{6}$$

$$L = \sum_i (l + I - A), \tag{7}$$

where C_0 is the size of the period, L is the time wasted for the system, l is the delay time for signal activation, A is the time for the yellow light, I is the time interval of the signal, i is the number of phases, and Y is the traffic ratio.

Among them, the calculation formula of the flow ratio is as follows:

$$\begin{cases} Y = \sum_{i=1}^{n} Y_i, \\ Y_i = \dfrac{q_i}{S_i}, \end{cases} \tag{8}$$

where Y_i is the flow ratio of the phase, q_i is the traffic flow i of phase, and S_i is the flow threshold of the phase.

3.2. The Best Effective Green Signal Time. According to the obtained signal period, the time of the green signal in each phase needs to be allocated reasonably. Because the green light time is affected by the delay of traffic flow, the traffic flow ratio and the green light signal ratio show a linear relationship; then:

$$\frac{g_1}{g_2} = \frac{Y_1}{Y_2}, \tag{9}$$

where g_1 is the effective time of the first phase green signal, g_2 is the effective time of the second phase green signal, Y_1 is the flow ratio of the first phase, and Y_2 is the flow ratio of the second phase.

From this, it can be deduced that the relational formula with multiple intersection phases is

$$\frac{g_i}{\sum_{i=1}^{n} g_i} = \frac{Y_i}{\sum_{i=1}^{n} Y_i}. \tag{10}$$

Then, the time of each phase of the green light is

$$g_i = \frac{Y_i}{Y}(C_0 - L). \tag{11}$$

The green signal ratio of each phase is

$$\lambda_i = \frac{g_i}{C_0}. \tag{12}$$

The traffic saturation of each phase is

$$x_i = \frac{\max(Y_i)}{\lambda_I}. \tag{13}$$

This article will take the traffic intersection in a certain area as the research object, as shown in Figure 1. After investigating the traffic situation at this intersection, the time lost for each phase is 3.2 s, the saturated flow is 103 veh/h, and the time for all red lights is 2.3 s.

After the actual investigation, the traffic intersection signal light data are statistically analyzed. We optimize the statistical data as parameters, such as the original traffic signal timing plan shown in Table 1 and the traffic data traffic flow statistics in Table 2.

The timing design adopted for the two-phase and three-phase signal control is shown in Figures 2 and 3. The figures assume that the critical saturation flows of the three phases are 600, 300, and 100, respectively. According to formulae (6)–(13), the optimal cycle length, green signal ratio, and saturation are different. The calculation result of the green signal time of the phase is shown in Table 3.

In summary, after the preliminary optimization of the signal lights, the timing scheme with the least delay is derived, and the saturation of each phase is relatively uniform, which further shortens the whole cycle time, ensures the passage of vehicles, and increases the flow per unit time to maximize the application of green light time.

4. Timing Scheme Design Based on Iterative Learning

At each intersection, there is i that presents the phase, suppose the arrival rate of the first phase vehicle is q_i, the waiting distance for this vehicle is x_i, saturated traffic flow rate s_i, the arrival rate of phase i is d_i, and the effective time when the green light is on is g_i. The ultimate goal of the traffic control signal light is to reduce the length of the vehicle queue and pass as many vehicles as possible within a certain period of time, so as to achieve the purpose of intelligent control. For this reason, in a certain signal period, the length of the queue becomes the state quantity of the system, and the dynamic state equation of the system is

$$x_i(t+1) = x_i(t) + C_0 d_i(t+1) - s_i g_i(t). \tag{14}$$

Among them, for the time when the green light is on, the constraint condition is

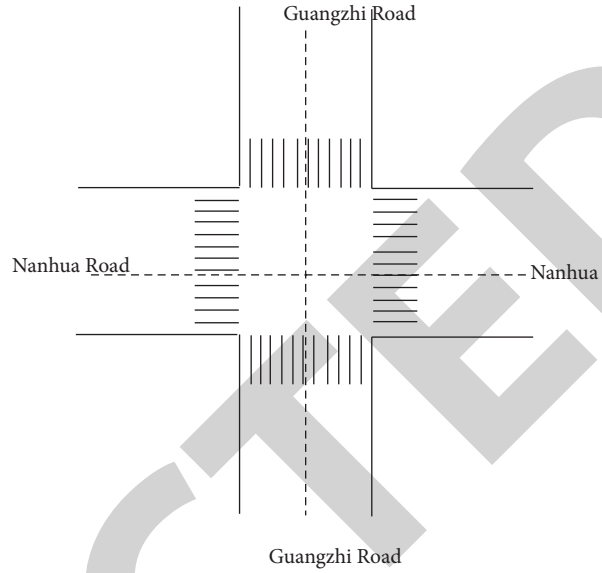

Figure 1: Intersection of Guangzhi Road and Nanhua Road.

Table 1: The original timing plan of traffic lights.

Project	Phase 1	Phase 2	Phase 3
Cycle	120	120	120
Phase time	71	18	24
Red light time	46	103	93
Green light time	70	18	26
Yellow light time	3	3	3

$$\begin{cases} \sum_{i=1}^{3} g_i(t) = C_0 - L \\ g_i(\min) \le g_i(k) \le g_i(\max), \end{cases} \tag{15}$$

where $g_i(\min)$ is the minimum time for the green light to turn on (15 s); $g_i(\max)$ is the maximum time of the first phase (90 s); and L is the total time lost while waiting for the vehicle (15 s).

Control the signal lights to realize that the queue length of each entry vehicle is in a balanced state, that is, control the queue length of different phases. If the queue length is uneven, the green light time will not be fully utilized, which will cause traffic congestion. Therefore, the queuing length difference of each phase becomes the output of this article, and a reference phase needs to be selected here. In this article, the reference phase selects phase 1. Taking the difference between the other two phases and the queue length of phase 1 as the system output $y(t)$, the system output is

$$\begin{aligned} y(t) &= \left[y_{2,1}(t), y_{3,1}(t)\right]^T = \left[x_2(t) - x_1(t), x_3(t) - x_1(t)\right]^T \\ &= \begin{bmatrix} -1 & 1 & 0 \\ -1 & 0 & 1 \end{bmatrix} \left[x_1(t), x_2(t), x_3(t)\right]^T = cx(t), \end{aligned} \tag{16}$$

where $x(t) = [x_1(t), x_2(t), x_3(t)]^T$; $y_{2,1}(t)$ is the output of phase 2; and $y_{3,1}(t)$ is the output of phase 3.

From this, it can be calculated that the queuing length of vehicles at the intersection is

Table 2: Traffic statistics.

Traffic direction	Turn left		Straight		Turn right		Total traffic
	Traffic volume	Number of lanes	Traffic volume	Number of lanes	Traffic volume	Number of lanes	
North import	80	1	214	1	16	1	310
South import	95	1	396	1	242	1	733
West import	88	1	68	1	76	1	232
East import	265	1	66	1	74	1	405

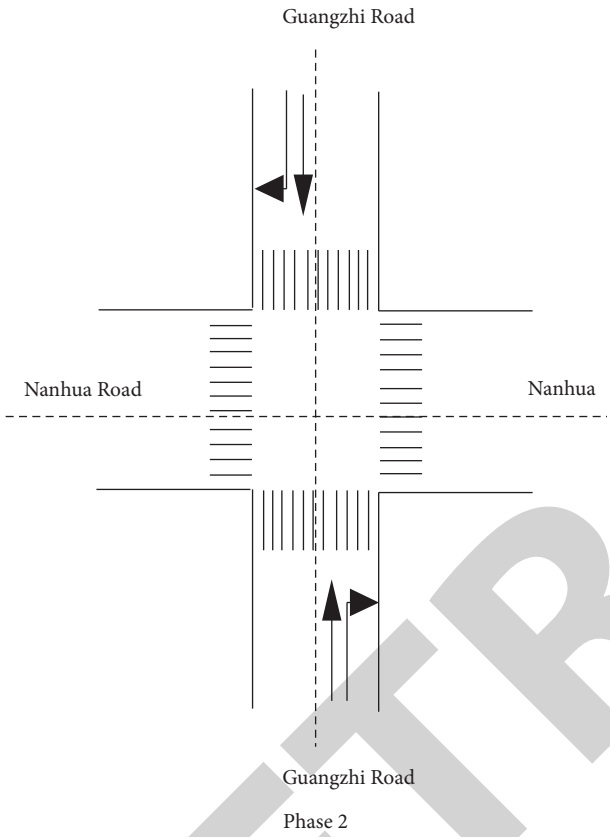

Figure 2: Timing design adopted for two-phase signal control.

$$x(t+1) = x(t) + C_0 d(t+1) - sg(t), \tag{17}$$

where $d(t) = [d_1(t), d_2(t), d_3(t)]^T$, $g(t) = [g_1(t), g_2(t), g_3(t)]^T$, $s = diag\{s_1, s_2, s_3\}$. $d_i(t)$ is the traffic flow for phase i and, $g_i(t)$ is the time when the green light of phase i. It is the time when the green light of phase i is on.

According to the above expression, the vehicle queue length is determined by the vehicle queue length $x(t+1)$ of the current signal cycle, the traffic demand $d(t+1)$ of the next cycle, and the time g when the green light is on in the current cycle. x(t) and d(t) jointly decided the cycle.

According to formula (16), the green time $g_1(t)$ of phase 1 can be obtained from the green time of the other two phases, so formula (17) can be changed to

$$x(t+1) = x(t) + C_0 d(t+1) - sg(t) - (s_1 c_1, 0.0)^T. \tag{18}$$

In the formula (18), c_1, c, and l indicate the period, size of the signal, and the time lost in queuing, respectively.

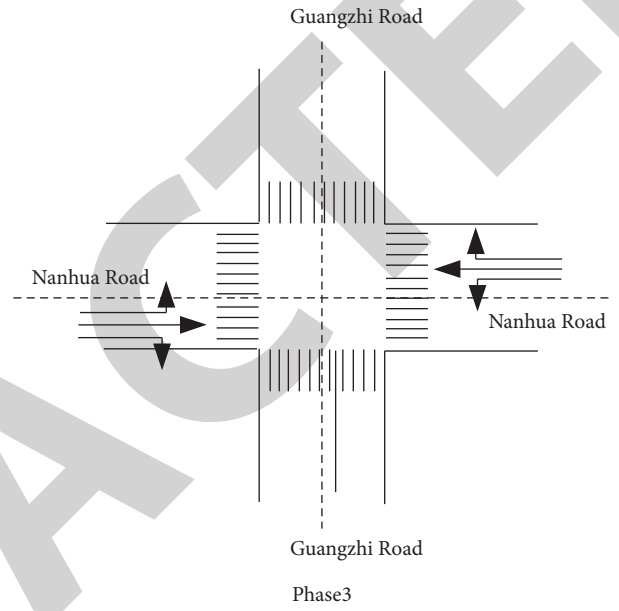

Figure 3: Timing design adopted for three-phase signal control.

$$s = \begin{bmatrix} -s_1 & -s_1 \\ s_2 & 0 \\ 0 & s_3 \end{bmatrix}. \tag{19}$$

After introducing the number of iterations, formula (18) can be changed to

$$x_k(t+1) = x_k(t) + C_0 d_k(t+1) - sg_k(t) - (s_1 c_1, 0.0)^T, \tag{20}$$

where k is the number of iterations.

Because of the large and unstable traffic flow at traffic intersections, the traffic flow has strong repetitiveness. Therefore, this paper adopts iterative learning control to control the periodic signal at each intersection, so as to draw the corresponding laws according to the calculation results.

Assume that in iterative control, the vehicle queue length satisfies the following conditions:

$$x_k(0) = x_0(0). \tag{21}$$

If the traffic volume at the intersection remains constant within a given period, then:

$$d_k(t) = d_0(t). \tag{22}$$

The resulting timing plan for the intersection is

Table 3: Time allocation plan after the intersection signal optimization.

Project	Phase 1 Go straight on Guangzhi Road + turn right	Phase 2 Turn left on Guangzhi Road	Phase 3 Nanhua Road pass
Maximum flow ratio of each phase	0.39	0.11	0.27
Total flow ratio Y		0.75	
Lost time L		16	
Optimal cycle C		114	
Total effective green time		100	
Effective green time for each phase	50	16	35
Yellow light	3	3	3
Red light	62	96	79
Green signal ratio of each phase	0.43	0.13	0.32
Saturation of each phase	0.89	0.78	0.91

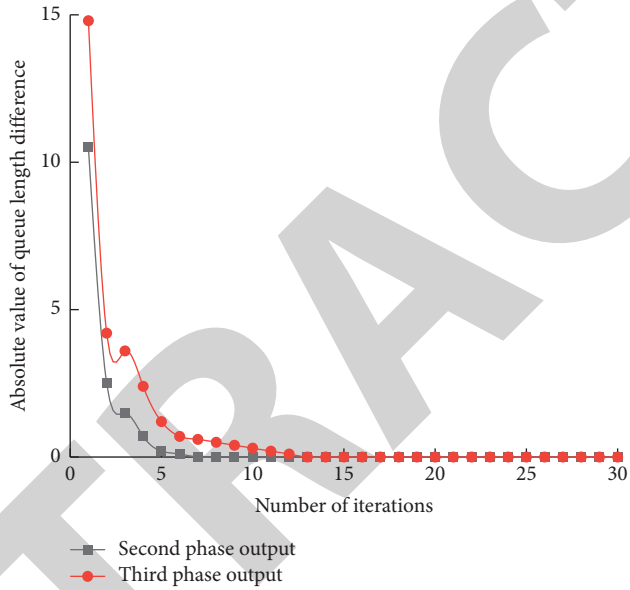

Figure 4: Queue length difference of iterative learning control.

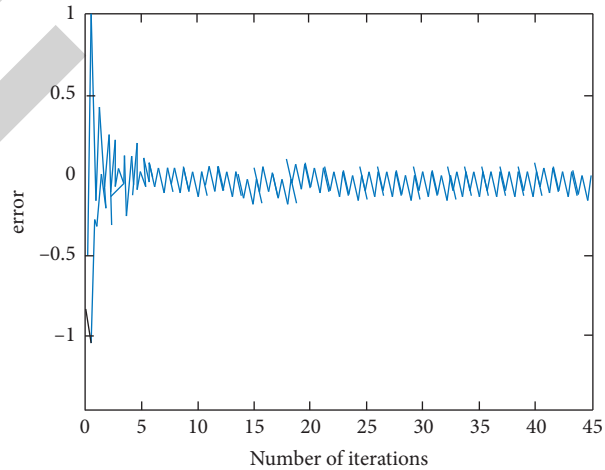

Figure 5: Error caused by the number of iterations.

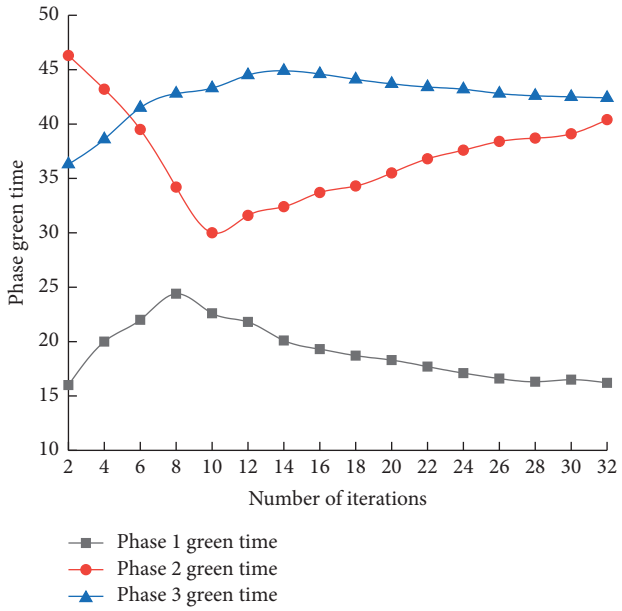

Figure 6: Green light time of each phase after iteration under iterative learning control.

$$g_{k+1}(t) = g_k(t) + \alpha(y_d - y_k(k+1)). \tag{23}$$

where y_d is the expected queuing difference and α is the iterative learning gain matrix.

If the queuing length at the intersection controlled by traffic lights is close to balance, the phase queuing length at each intersection requires $y_d = 0$.

5. Simulation Research

This paper takes the intersection composed of Nanhua East Road and Guangzhi Road as the object of simulation study. There are 3 phases in the intersection. The arrival rates of each phase are, respectively, 0.52 veh/s, 0.16 veh/s, and 0.24 veh/s, and the saturation flow rate of each phase is 0.27 veh/s. The learning gain is −0.83, the loss time of each phase is 2 s, the signal period is 114 s, and the green light time of the three phases is 51 s, 15 s, and 34 s. Considering the complexity of the actual situation, while optimizing the model, the green light time and queue length obtained by MATLAB simulation should be integer values. The simulation results are shown in Figures 4–6.

From the simulation results of Figures 4 and 5, it can be seen that after the number of iterations exceeds 15 times, the difference and error of the queue length almost approach zero, and the timing of the entire traffic signal system is in a uniform distribution state.

Figure 6 shows the time curve of the three-phase green traffic signal lights. After adopting the iterative learning control signal, the green light time of each phase is adjusted in real time according to the specific traffic volume, and reasonable time allocation is carried out, which proves the effectiveness and reliability of the algorithm.

6. Conclusion

In this paper, the controlled object is the traffic light at intersections. The reasonable signal period is determined according to the TRRL method timing plan, and then based on the idea of iterative learning control law, a method to control signal lights is constructed to avoid the establishment of a complex traffic flow model. It can use very few priors. We use real-time traffic flow data to control the traffic lights at intersections. The experimental results of iterative learning control show that the control method of this algorithm is reasonable and can be changed according to the changes of traffic flow. It has the effect of adaptive adjustment and improves the traffic efficiency. The optimization effect of the iterative algorithm is far better than the traditional timed and fixed cycle traffic system. It can adaptively adjust the cycle length and the green light time of each phase. It can pass more vehicles at the same time without additional equipment. Support and additional costs can reduce people's unnecessary waiting time, thereby saving people's travel time and improving work efficiency. However, the scope of application of this article has certain limitations. When there are few or many vehicles at the intersection, the adjustment effect is not obvious.

Data Availability

The data used to support the findings of this study are available from the corresponding author upon request.

Conflicts of Interest

The authors declare that they have no known conflicts of interest or personal relationships that could have appeared to influence the work reported in this paper.

References

[1] W. Ma, *Research on Signal Control Method and Algorithm of Single Intersection Based on Fuzzy Control*, Dalian Maritime University, Dalian, China, 2008.

[2] J. Zhao, *Research on Traffic Light Dynamic Timing Optimization Algorithm Based on Vehicle Guidance*, Shenyang Ligong University, Shenyang, China, 2017.

[3] X. Zhao, *Urban Traffic Congestion Analysis and Governance Strategy Research in Xi'an*, Chang'an University, Xi'an, China, 2018.

[4] S. Arimoto, S. Kawamura, and F. Miyazaki, "Bettering operation of robots by learning," *Journal of Field Robotics*, vol. 1, no. 2, pp. 123–140, 2010.

[5] C. Ronghu, Z. Hou, and B. Huang, "Development of optimal iterative learning control for batch processes: from model-based to data-driven," *Acta Automatica Sinica*, vol. 43, no. 6, pp. 917–932, 2017.

[6] Y. Ding, *Iterative Learning Boundary Control of Urban Traffic Area*, Beijing Jiaotong University, Beijing, China, 2017.

[7] M. Jing, *Research on Model-free Adaptive Iterative Learning Control of Urban Expressway System*, Beijing Jiaotong University, Beijing, China, 2018.

[8] F. Yang, *Research on Iterative Learning Control of Several Types of Expressway Traffic Flow Models*, Guangxi University of Science and Technology, Liuzhou, China, 2015.

Hindawi
Journal of Mathematics
Volume 2024, Article ID 9841684, 1 page
https://doi.org/10.1155/2024/9841684

Retraction

Retracted: Evaluation of Innovation Efficiency of High-Tech Enterprise Knowledge Supply Chain Based on AHP-DEA

Journal of Mathematics

Received 23 January 2024; Accepted 23 January 2024; Published 24 January 2024

This article has been retracted by Hindawi following an investigation undertaken by the publisher [1]. This investigation has uncovered evidence of one or more of the following indicators of systematic manipulation of the publication process:

(1) Discrepancies in scope

(2) Discrepancies in the description of the research reported

(3) Discrepancies between the availability of data and the research described

(4) Inappropriate citations

(5) Incoherent, meaningless and/or irrelevant content included in the article

(6) Manipulated or compromised peer review

The presence of these indicators undermines our confidence in the integrity of the article's content and we cannot, therefore, vouch for its reliability. Please note that this notice is intended solely to alert readers that the content of this article is unreliable. We have not investigated whether authors were aware of or involved in the systematic manipulation of the publication process.

In addition, our investigation has also shown that one or more of the following human-subject reporting requirements has not been met in this article: ethical approval by an Institutional Review Board (IRB) committee or equivalent, patient/participant consent to participate, and/or agreement to publish patient/participant details (where relevant).

Wiley and Hindawi regrets that the usual quality checks did not identify these issues before publication and have since put additional measures in place to safeguard research integrity.

We wish to credit our own Research Integrity and Research Publishing teams and anonymous and named external researchers and research integrity experts for contributing to this investigation.

The corresponding author, as the representative of all authors, has been given the opportunity to register their agreement or disagreement to this retraction. We have kept a record of any response received.

References

[1] H. Han and X. Gu, "Evaluation of Innovation Efficiency of High-Tech Enterprise Knowledge Supply Chain Based on AHP-DEA," *Journal of Mathematics*, vol. 2022, Article ID 3210474, 9 pages, 2022.

Hindawi
Journal of Mathematics
Volume 2022, Article ID 3210474, 9 pages
https://doi.org/10.1155/2022/3210474

Research Article

Evaluation of Innovation Efficiency of High-Tech Enterprise Knowledge Supply Chain Based on AHP-DEA

Huiyuan Han [1] **and Xiaomin Gu** [1,2]

[1]*Glorious Sun School of Business Management, Donghua University, Shanghai, China*
[2]*Shanghai Lixin University of Accounting and Finance, Shanghai, China*

Correspondence should be addressed to Huiyuan Han; huiyuanh@126.com

Received 13 December 2021; Revised 6 January 2022; Accepted 21 January 2022; Published 8 February 2022

Academic Editor: Naeem Jan

This paper introduces a qualitative analysis on the efficiency evaluation of the knowledge supply chain by combining the analytic hierarchy process (AHP) with data envelopment analysis (DEA), drawing on existing literature to determine the index weight through the scoring of industry experts, and selecting appropriate input and output indicators to construct a knowledge supply chain efficiency evaluation system. The system was then applied to the supply chain of a number of high-tech enterprises. The results identified innovation efficiency differences of the knowledge supply chain in these enterprises, along with best practices and suggestions for the current knowledge supply chain efficiency.

1. Introduction

In the supply chain, there is not only logistics, information flow, and capital flow, but also knowledge flow based on products. The intensification of market competition has broken the original competition mode among enterprises and has gradually formed competition among supply chains. Previous academic research has also focused mainly on supply chain management, such as integrating the concept of environmental protection into the supply chain by studying "low-carbon supply chain" [1, 2]; combining natural environmental risks and economic political risks into the supply chain, studying the impact of external factors on the food supply chain [3, 4]; integrating knowledge management into the supply chain and some papers and a conference proceedings previously been published studying the "knowledge supply chain" [5–7].

The supply chain is centered on core enterprises, and it forms a network chain structure model around the R&D, manufacturing, warehousing, logistics, distribution, and sales of commodities. Suppliers not only undertake production and manufacturing operations, but also conduct different types of knowledge exchange and knowledge transfer with customers [8, 9]. In today's rapid digital development of industry, the use of knowledge management to enhance the digital performance of the supply chain plays a crucial role in the digital transformation of the supply chain [10].

The knowledge supply chain was proposed by the "Next Generation Manufacturing Project" in the United States. It refers to the adjacent knowledge nodes in the process of supply, innovation, dissemination [6] and the use of knowledge through the relationship between demand and supply. Link up and convert the concept into a knowledge product and then to a functional network chain for the end user. J. Rechard Hall and Pierpaolo Andfiam put forward the concept of a knowledge chain from the perspective of the supply chain. The knowledge supply chain extends and deepens the traditional physical supply chain.

Compared to the traditional entities that form the supply chain, high-tech enterprises are knowledge-intensive entities. Knowledge-based products and technologies flow through the supply chain upstream and downstream of the enterprise, forming a knowledge supply chain which promotes the supply and dissemination of knowledge and scientific research results. It plays a key role in the landing

transformation of scientific research results [11]. Therefore, improving knowledge conversion, or the efficiency of knowledge flow in the supply chain, and maximizing the benefits of the knowledge economy have become the main problems of enterprises today.

In terms of supply chain performance evaluation, Ramish and Aslam [12] determined indicators for measuring knowledge management in the supply chain, including resource utilization, output measurement, new process performance evaluation, etc. based on the principle of double-loop and three-loop learning. Murata et al. [13] constructed two knowledge supply chain subsystems for Japanese SMEs, including the team building process subsystem and the team management subsystem. The team building process subsystem includes the execution, consulting, and demonstration phases. The team management system includes three steps of management experience accumulation: attention, memorization, and confirmation. Wiig [14] believed that the key to the performance evaluation of the knowledge supply chain lies in the assessment of knowledge management. The indicators should include the promotion of knowledge activities, the infrastructure related to knowledge activities, accumulated knowledge assets, and knowledge learning.

From the perspective of the research index system, there are many ways to evaluate supply chain management and knowledge management, which involve many comprehensive economic indicators. However, the current research aims to build an index system based on the research experience of scholars, which is highly subjective. This study intends to use AHP to screen the efficiency evaluation indicators of the knowledge supply chain. It would effectively draw on the subjective knowledge and experience of experts, while maintaining good objectivity at the same time. In the construction of evaluation models, previous studies mainly used factor analysis and fuzzy synthesis evaluation [15], the entropy method, etc. While using a certain method alone may have certain drawbacks, a combined evaluation method can effectively solve those disadvantages. Thus, it is now trending in comprehensive evaluation research.

Therefore, this study focuses on the efficiency evaluation of the knowledge supply chain, combining the AHP analytic hierarchy process with the DEA data envelopment analysis, and using the authoritative expert scoring method in the industry to determine the key indicators and their weights that need to be considered in the knowledge supply chain efficiency evaluation. Drawing lessons from existing literature research and expert scoring methods, the article screens appropriate input indicators and output indicators, constructs a knowledge supply chain efficiency evaluation system, and further combines supply chain data to calculate the efficiency value. Finally, this article takes the supply chains of high-tech enterprises in four provinces and cities in the Yangtze River Delta as examples to study their innovation efficiency in the process of knowledge and technology innovation, provide certain references for knowledge supply chain management, and put forward relevant policy recommendations.

2. Construction Method of Evaluation Index System

2.1. Knowledge Supply Chain Model. American scholars Holsapple and Singh [16] constructed a systematic knowledge supply chain model from the relationship between organizational knowledge and organizational core competitiveness. The model includes the main part of the knowledge chain and the output of the knowledge chain. The main part of the knowledge chain includes five primary knowledge activities and four advanced high-level activities. The five primary knowledge activities are knowledge acquisition, knowledge selection, knowledge generation, knowledge internalization, and knowledge externalization. The four high-level knowledge activities are leadership, cooperation, control, and measurement. While managing knowledge (output of the knowledge chain) in the supply chain adds additional complexity to the supply chain management process, knowledge sharing between supply chain partners is nonetheless an important element of the supply chain knowledge management (SCKM) system [17].

In the supply chain of high-tech enterprises, the spatial agglomeration effect between enterprises in the industrial park will accelerate the acquisition and generation of knowledge, while the government, financial institutions, and enterprises' own technological R&D investment will promote knowledge transfer, thereby promoting technological innovation and conversion. Once the process of internalization and externalization of knowledge is over, new technologies and processes suitable for the long-term development of the enterprise will be introduced to the consumer, which will bring economic benefits to the enterprise. Therefore, based on the knowledge supply chain model, combined with the process of knowledge acquisition and creation of high-tech enterprises, this study establishes the following knowledge supply chain model (Figures 1 and 2).

2.2. Construction of the Innovation Efficiency Evaluation System of the Knowledge Supply Chain. When selecting supply chain efficiency evaluation indicators, they are usually selected from the two dimensions of input and output. This article will select indicators from the two dimensions of input and output elements based on existing relevant research and evaluation. The input elements include organizational input, human input, and financial input. The output elements include the measurement of innovation output and economic benefits.

Input elements: Since the technological innovation process is an integrated system, all partners involved in this process must group together to establish mutual trust and promote the transfer of tacit knowledge such as experience and technical know-how, thus effectively playing their role in the system. The spirit of collaboration can lead to better acquisition of high-quality tacit and complex knowledge [18]. Therefore, for the supply chain of high-tech enterprises, the spatial agglomeration effect between enterprises in the industrial park can accelerate the acquisition of knowledge

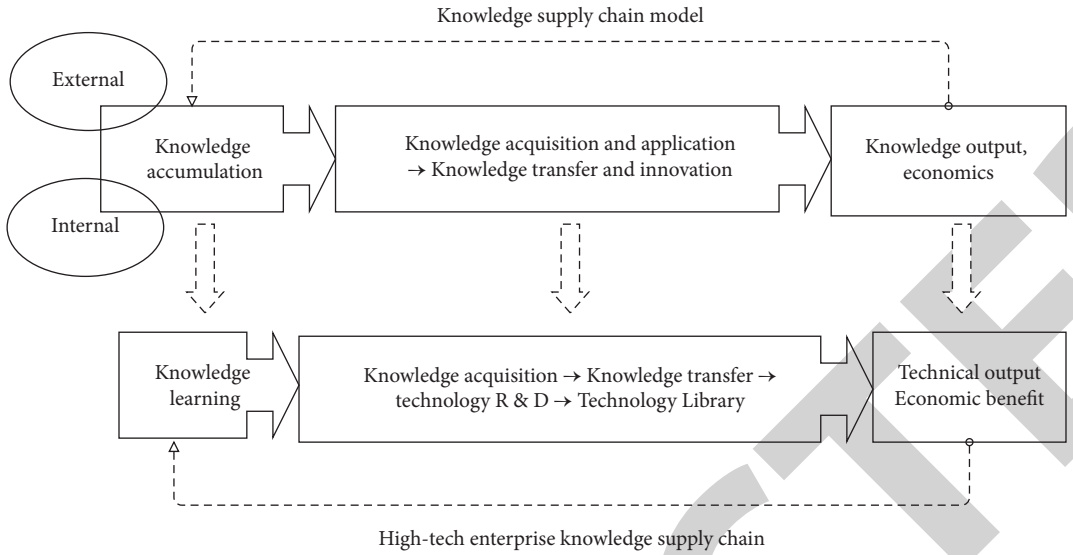

Figure 1: Knowledge supply chain model.

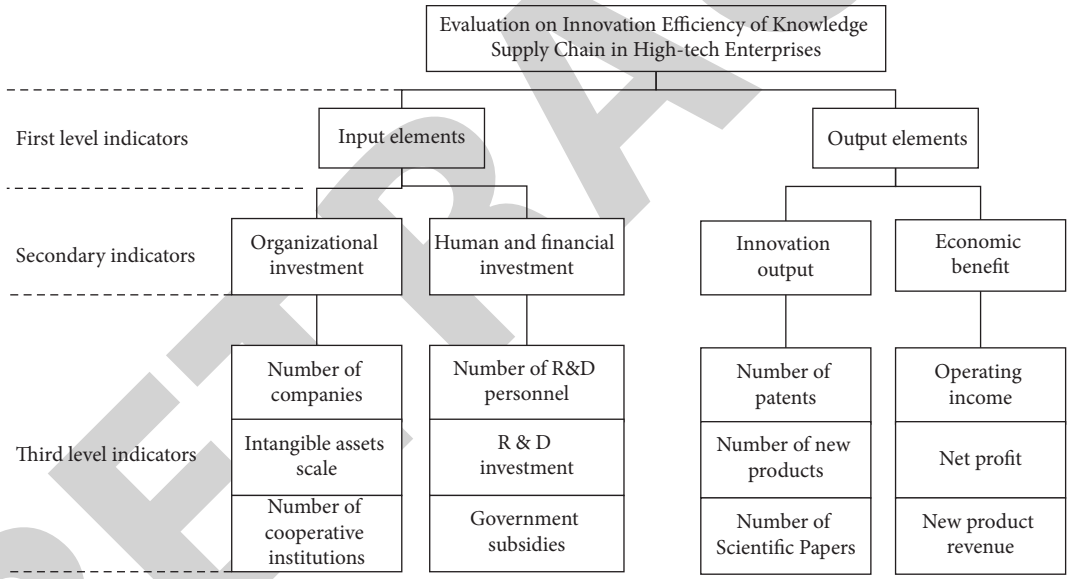

Figure 2: Innovation efficiency evaluation system.

to a certain extent. In addition, cooperation between external institutions and the intangible assets owned by the enterprises within the organization can also accelerate the flow of knowledge. This has an important impact on the dissemination and transformation of knowledge. Carneiro [19] also suggested that, in addition to using financial indicators, organizations can use nonfinancial personnel to measure knowledge management. Based on this, this study considers the number of technical R&D personnel as one of the factors to measure human and financial inputs.

Output elements: In traditional supply chain performance evaluation, financial indicators are often selected to measure economic benefits. However, using only economic benefits to measure performance may lead to bias in the results. In the knowledge supply chain of high-tech industries, the flow of commodities has nothing to do with physical commodities, but with the flow of R&D commodities. R&D products include patents, technologies, research services, and research projects, etc. In high-tech industries, their development and commercialization are considered just as important as real products [20]. Therefore, based on the research of scholars such as Alessandra Alletto, this study uses the number of new patent application and development as the measurement index of knowledge output elements in the measurement of technology output in addition to traditional financial indicators such as the changes in operating income and net profit.

Based on the above analysis, this paper establishes the following level analysis model.

2.3. Calculating Method of Innovation Efficiency of Knowledge Supply Chain. Because there are many supply chain innovation performance evaluation indicators of high-tech enterprises, we needed to ensure the operability of the methods and the simplicity of the indicators and to reduce the complexity of calculations. The many types of indicators present have to be screened and the input and output cover a wide range. The indicators are difficult to screen solely based on the data, so they require the judgment of experts with many years of industry experience. The pairwise comparison method provided by AHP can effectively reduce the difficulty of expert judgment and reduce errors. At the same time, the DEA method has advantages in handling multiinput and multioutput effectiveness evaluation and is widely used in financial resource operation efficiency [21], risk performance evaluation, etc.

Therefore, this study uses the AHP method to screen the established high-tech enterprise knowledge supply chain evaluation indicators and the DEA method to evaluate and rank the innovation efficiency of the knowledge supply chain in the Yangtze River Delta. This calculation method effectively integrates AHP and DEA methods and can reasonably evaluate multiattribute problems. The analytic hierarchy process can fully reflect the preferences of decision makers, while the DEA model can objectively evaluate the efficiency of technological innovation, technological effectiveness, and scale effectiveness. This research uses comprehensive AHP and DEA modeling to evaluate the innovation efficiency of the knowledge supply chain of high-tech enterprises and effectively realize horizontal comparison and sorting, which is beneficial to knowledge management-related research on the supply chain.

3. Model Principles

This article combines analytic hierarchy process (AHP) and data envelopment analysis (DEA) to evaluate and rank the innovation efficiency of the knowledge supply chain. The AHP combines qualitative analysis and quantitative analysis and selects the most representative evaluation indicators by comparing the importance of the elements. The DEA method can be used to calculate the innovation efficiency value based on the objective observation and carry out a numerical evaluation. Therefore, this article first selects representative indicators and then further collects data based on representative indicators, uses data envelopment analysis methods to calculate indicators, and finally calculates the efficiency value comprehensively and realizes the efficiency ranking.

3.1. Principles of Analytic Hierarchy Process. The analytic hierarchy process (AHP) was formally proposed by the American operations researcher T. L. Saaty in the mid-1970s. It is a systematic and hierarchical analysis method that combines both qualitative and quantitative analyses. It compares the importance of each element in pairs, calculates the relative weight of each element through mathematical methods, and finally sorts the importance of the elements based on their relative weight. Because of its practicality and effectiveness in dealing with complex decision-making problems, it quickly gained attention worldwide [22, 23]. Its applications have spread throughout the fields of economic planning and management, energy policy and distribution, behavioral science, military command, transportation, agriculture, education, human resources, medical care, and the environment. The main steps of the analytic hierarchy process are as follows.

3.1.1. Weight Calculations. To establish a quantitative judgment matrix based on input and output indicators, we invited 10 technical field supply chain management experts to compare n indicators at each level in pairs and give a judgment matrix $A = (a_{ij})_{m\times n}$, a_{ij} represents the importance of element i relative to element j, and each element of the judgment matrix satisfies $a_{ij} > 0$, $a_{ij} = 1/a_{ji}, a_{ii} = 1$. The arithmetic average method is used to calculate the maximum eigenvalue λ max of each judgment matrix and its corresponding eigenvector $(W_1, W_2, W_3, \ldots W_n)$, which is the weight of the index.

3.1.2. Consistency Inspection. Calculate the consistency index CI and random consistency ratio CR of each judgment matrix:

$$\begin{aligned} \mathrm{CI} &= \frac{\lambda\max - n}{n-1}, \\ \mathrm{CR} &= \frac{\mathrm{CI}}{\mathrm{RI}}. \end{aligned} \tag{1}$$

RI represents the average consistency index of the judgment matrix. If the consistency ratio is $\mathrm{CR} < 0.10$, the consistency test is passed. The eigenvector obtained above is the weight vector reflecting the relative importance of the indicators. The experts are invited to adjust the judgment against the value of the matrix until satisfactory consistency is achieved.

3.2. Principles of DEA Data Envelopment Analysis. The data envelopment analysis (DEA) method is the most widely used nonparametric performance evaluation method, which was jointly proposed by Charnes and Cooper [24]. The DEA method is widely used in many fields, such as production management of industrial enterprises and efficiency evaluation of scientific research institutions. The DEA algorithm treats each object to be evaluated as a decision-making unit (DMU) and multiple decision-making units together as the evaluated group. The efficiency and effectiveness of each decision-making unit are determined by dividing the indicators into two types of input and output indicators and then using the weight of the input and output indicators as variables to perform optimization calculations.

Commonly used DEA models include the CCR and BCC models. The former is used to evaluate the overall effectiveness of the decision-making unit, and the latter is used to evaluate the technical effectiveness of the decision-making

unit. The use of the CCR model is based on the assumption of constant return to scale (CRS), which assumes that the decision-making unit can increase their output scale return by increasing their input in equal proportions. In practical application, as the input elements increase, the return to scale gradually saturates before entering the stage of diminishing returns to scale. Therefore, this study chooses to incorporate the variable returns to scale (VRS) DEA-BCC model instead.

The basic principle is that, for each decision unit, $\mathrm{DMU}_k\,(k = 1, 2, \ldots, n)$. Each decision-making unit has m inputs and outputs. The i-th input of DMU_k is $X_k = \{X_{ik}, \quad i = 1, 2, \ldots, m\}$, and the j-th output is $Y_k = \{Y_{rk}, \quad r = 1, 2, \ldots, s\}$. The BCC model is established as follows:

$$\begin{cases} \min \Theta = V_{D1} \\ \text{s.t.} \sum_{j=1}^{n} \lambda_j x_j \le \Theta X_0 \sum_{j=1}^{n} \lambda_1 = 1 \lambda_j \ge 0, \, j = 1, 2, \ldots, n. \end{cases} \quad (2)$$

Its dual formula is

$$\begin{cases} \mathrm{Max}\left(u^T Y_0 + u_0\right) = V_{P1} \\ \text{s.t.} w^T X - u^T Y_j - u_0 \ge 0, \, j = 1, 2, \ldots, n \\ w^T X_0 = 1 \\ w \ge 0, u \ge 0 \end{cases}. \quad (3)$$

If there is an efficiency optimal solution $w_0, u_0, \widehat{u}_0$ in the formula which satisfies $V_{P1} = u_0^T Y_0 + \widehat{u}_0 = 1$, it is a weakly valid unit of DEA. If there is $w_0 > 0, u_0 > 0$ in the formula, it is called DMU_{j0} is a fully effective unit of DEA. Finally, after the introduction of non-Archimedean infinitesimal ε, input slack variable S^-, and output slack variable S^+, the final BCC model is as follows:

$$\begin{cases} E_{\mathrm{BCC}} = \min \Theta - \varepsilon\left(s^- + s^+\right) \\ \text{s.t.} \sum_{k=1}^{n} \lambda_k x_k + S^- = \Theta X_0 \\ \sum_{k=1}^{n} \lambda_k x_k - S^+ = Y_0 \\ \sum_{k=1}^{n} = 1 \\ \lambda_k \ge 0, k = 1, 2, \ldots, n \\ s^- \ge 0, s^+ \ge 0 \end{cases}. \quad (4)$$

The goal of the BCC model is to maximize the efficiency of decision-making units. This study uses the BCC model to evaluate the innovation efficiency of multiple decision-making units in the input and output of the high-tech enterprise knowledge supply chain. DEA's comprehensive technical efficiency is composed of pure technical efficiency and scale efficiency. Pure technical efficiency comes from the influence of management and technology on the efficiency of output units, and scale efficiency comes from the influence of scale factors on the efficiency of output units. When the pure technical efficiency is 1, technical efficiency is completely effective. When the scale efficiency is 1, the scale efficiency of the decision-making unit is completely effective. If both are 1, the decision-making unit is a fully effective DEA unit. If only the technical efficiency or scale efficiency is 1, the DEA of the unit is weakly effective. If both are not 1, the DEA of the decision-making unit is invalid.

4. Sample Analysis

This article selects high-tech enterprises in the Yangtze River Delta region of China as the research sample. The Yangtze River Delta region includes four provinces, Shanghai, Jiangsu, Zhejiang, and Anhui, and contains many high-tech enterprises. It is an important strategic economic belt in China, and the integration of the Yangtze River Delta is one of China's national strategies. Therefore, the economic development and various data indicators in this area are representative. As the 2019-nCoV in 2020 will have an impact on the economy, this article selects a sample of knowledge supply chain data from 75 listed high-tech companies in the Yangtze River Delta in 2019 for analysis.

4.1. Expert Scoring and Data Collection. To establish a quantitative judgment matrix based on the input and output element indicators in this study, we invited 10 technical field supply chain management experts to brainstorm and compare indicators at each level in pairs, give a judgment matrix, and calculate the weightage of each index (W represents the weight of the indicator) (Tables 1–3).

Through the weight analysis of the first-level indicators, we can see that, in the measurement of innovation efficiency, the measurement of output elements takes a larger proportion, and the importance of innovation output and economic benefits is equal. In the measurement of input elements, human capital and capital investment are more important. The following is an analysis of the three-level indicator weights contained in the two second-level indicators, as shown in Tables 4–7.

4.2. AHP to Determine the Index Weight. Based on the above index scores, the overall index weights are listed in Table 8.

Based on the results of our analysis, it can be seen that, among the organizational input elements, the weight of the number of enterprises is higher than that of the other indicators, indicating that the greater the number of enterprises in a region, the greater the convergent effect on the acquisition and creation of regional knowledge as well as the rapid flow of knowledge. Among the human and financial input elements, the weight of R&D expenditure and the number of R&D personnel are obviously higher than others, which reflects the importance of human capital and capital investment in knowledge creation. Among the elements of innovation output, the weight of the number of patents is significantly higher than that of new products and papers, indicating that technology creation is an important part of innovation output. Among the indicators of economic benefits at all levels, operating revenue and net profit have a

Table 1: Judgment matrix of primary indicators of knowledge supply chain.

Innovation efficiency	Input elements	Output elements	W
input elements	1	1/2	0.333
Output elements	2	1	0.667

Table 2: Judgment matrix of secondary indicators of knowledge supply chain-input elements.

Input elements	Organizational investment	Human and financial investment	W
Organizational investment	1	1/3	0.25
Human and financial investment	3	1	0.75

Table 3: Judgment matrix of secondary indicators of knowledge supply chain-output elements.

Output elements	Innovation output	Economic benefit	W
Innovation output	1	1	0.50
Economic benefit	1	1	0.50

Table 4: Organizational investment judgment matrix.

Organizational investment	Number of companies	Intangible assets scale	Number of cooperative institutions	W
Number of companies	1	3	5	0.648
Intangible assets scale	1/3	1	2	0.230
Number of cooperative institutions	1/5	1/2	1	0.122
Consistency inspection: CI = 0.0018 < 0.1 CR = 0.0032				

Table 5: Human and financial investment judgment matrix.

Human and financial investment	Number of R&D personnel	R&D investment	Government subsidies	W
Number of R&D personnel	1	1	2	0.387
R&D investment	1	1	3	0.443
Government subsidies	½	1/3	1	0.169
Consistency inspection: CI = 0.0091 < 0.1 CR = 0.0158				

Table 6: Judgment matrix of innovation output.

Innovation output	Number of patents	Number of new products	Scientific papers	W
Number of patents	1	3	5	0.648
Number of new products	1/3	1	2	0.230
Scientific papers	1/5	1/2	1	0.122
Consistency inspection: CI = 0.0018 < 0.1 CR = 0.0032				

Table 7: Judgment matrix of economic benefit.

Economic benefit	Operating income	Net profit	New product revenue	W
Operating income	1	1/2	3	0.309
Net profit	2	1	7	0.582
New product revenue	1/3	1/7	1	0.110
Consistency inspection: CI = 0.0013 < 0.1 CR = 0.0023				

Table 8: Summary of indicator weights.

First-level indicators	*W*	Second-level indicators	*W*	Third-level indicators	*W*	Code
Input elements	0.333	Organizational input	0.083	Number of companies	0.054	X1
				Intangible assets scale	0.019	X2
				Number of cooperative institutions	0.010	X3
		Human and financial investment	0.250	Number of R&D personnel	0.097	**X4**
				R&D investment	0.111	**X5**
				Government subsidies	0.042	X6
Output elements	0.667	Innovation output	0.333	Number of patents	0.216	**Y1**
				Number of new products	0.077	Y2
				Scientific papers	0.041	Y3
		Economic benefit	0.333	Operating income	0.103	**Y4**
				Net profit	0.194	**Y5**
				New product revenue	0.036	Y6

Table 9: Output results of innovation efficiency.

Firm	Crste	Vrste	Scale		Firm	Crste	Vrste	Scale	
1	0.467	0.921	0.507	irs	39	0.489	0.904	0.541	irs
2	0.778	0.903	0.861	irs	40	0.681	0.949	0.717	irs
3	0.447	0.864	0.517	irs	41	0.603	0.899	0.671	irs
4	0.646	0.907	0.712	irs	42	1	1	1	—
5	0.473	0.904	0.523	irs	43	0.837	0.935	0.895	irs
6	0.67	0.918	0.729	irs	44	1	1	1	—
7	0.553	0.961	0.576	irs	45	0.506	0.854	0.592	irs
8	0.777	0.933	0.833	irs	46	0.309	0.844	0.367	irs
9	0.719	0.927	0.776	irs	47	0.424	0.882	0.481	irs
10	0.508	0.85	0.597	irs	48	1	1	1	—
11	0.451	0.9	0.5	irs	49	0.388	0.875	0.444	irs
12	0.712	0.91	0.782	irs	50	0.599	0.863	0.694	irs
13	0.828	0.959	0.863	irs	51	0.461	0.908	0.508	irs
14	0.468	0.871	0.537	irs	52	0.651	0.921	0.707	irs
15	0.07	0.839	0.084	irs	53	0.582	0.921	0.632	irs
16	0.314	0.848	0.371	irs	54	0.942	1	0.942	irs
17	0.531	0.974	0.545	irs	55	0.395	0.929	0.425	irs
18	0.832	0.938	0.887	irs	56	0.591	0.929	0.635	irs
19	0.728	0.95	0.765	irs	57	0.546	0.906	0.603	irs
20	0.506	0.906	0.559	irs	58	0.612	0.921	0.664	irs
21	0.397	0.86	0.462	irs	59	0.758	0.938	0.809	irs
22	0.494	0.899	0.55	irs	60	0.681	0.973	0.7	irs
23	0.592	0.917	0.646	irs	61	1	1	1	—
24	0.827	0.97	0.852	irs	62	0.806	0.934	0.863	irs
25	0.936	1	0.936	irs	63	0.728	0.934	0.78	irs
26	0.105	0.866	0.121	irs	64	0.726	0.901	0.806	irs
27	0.53	0.901	0.588	irs	65	1	1	1	—
28	0.414	0.886	0.467	irs	66	0.553	0.878	0.63	irs
29	0.469	0.883	0.531	irs	67	0.927	0.977	0.948	irs
30	0.408	0.921	0.443	irs	68	0.598	0.885	0.676	irs
31	1	1	1	—	69	0.619	0.887	0.698	irs
32	0.648	0.934	0.694	irs	70	0.783	0.941	0.832	irs
33	0.411	0.887	0.463	irs	71	0.503	0.884	0.569	irs
34	0.703	0.941	0.747	irs	72	0.979	0.981	0.997	irs
35	0.365	0.933	0.391	irs	73	0.448	0.971	0.461	irs
36	0.683	0.925	0.739	irs	74	0.645	0.976	0.661	irs
37	0.744	0.891	0.834	irs	75	0.909	0.953	0.954	irs
38	0.534	0.91	0.587	irs	**Mean**	**0.627**	**0.922**	**0.673**	

Note: irs: increasing benefits of scale, constant benefits of scale, and diminishing returns of scale.

Table 10: The efficiency value of the Yangtze River Delta region.

Region	Code	Crste	Vrste	Scale
Shanghai	D1	0.74	0.938	0.782
Zhejiang	D2	0.828	0.965	0.854
Jiangsu	D3	0.787	0.967	0.808
Anhui	D4	0.963	1	0.963

significantly higher weight. It is not difficult to understand that revenue and profit are the most obvious indicators reflecting the actual capital flow and operating conditions of the supply chain. Therefore, this study selects the economic indicators (X4, X5, Y1, Y4, Y5) with significantly higher weights among all levels of indicators for subsequent DEA analysis.

4.3. Analysis and Evaluation Based on DEA. In actual production activities, input factors can often be controlled artificially, while the output factors are not highly controllable, which makes them more appropriate for the measurement of efficiency values from the perspective of input. Therefore, this study selects an input-oriented DEA model to examine the knowledge supply chain of 75 listed high-tech enterprises in the Yangtze River Delta in 2019, which includes 34 in Shanghai, 20 in Zhejiang, 18 in Jiangsu, and 3 in Anhui. With the help of Deap 2.1 software, we use the input-output indicators selected above to calculate and comprehensively calculate DEA efficiency by province, and the results are as follows. In Table 9, Crste represents the overall efficiency of the knowledge supply chain, Vrste represents pure technical efficiency, and Scale represents scale efficiency.

Further, we grouped and calculated the supply chain of each region to obtain the innovation efficiency of the regional knowledge supply chain (Table 10).

We can see that the overall efficiency (Crste) of the regional knowledge supply chain is ranked as follows: D4 > D2 > D3 > D1. When considering the return to scale (VRS perspective), the order of pure technical efficiency (vrste) is D4 > D3 > D2 > D1. From the overall efficiency level, the indicators of the four regions were higher than the overall average. Anhui's supply chain innovation efficiency is relatively high, while Shanghai's is relatively low. Jiangsu was slightly better than Zhejiang in terms of pure technical efficiency.

5. Conclusions and Policy Recommendations

5.1. Research Conclusion. This paper combines AHP with DEA to introduce qualitative analysis in the efficiency evaluation of the knowledge supply chain by combining relevant research in the existing literature before selecting and determining the appropriate input products through the scoring method of authoritative experts in the industry. After that, the index weights were calculated, and an efficiency evaluation system for the knowledge supply chain was constructed, which was later used to measure the supply chain efficiency of high-tech enterprises in four provinces and cities in the Yangtze River Delta in 2019. The results of this study are as follows:

(1) All indicators in the four regions are higher than the overall average, indicating that the innovation vitality of the Yangtze River Delta region remains at a high level and that there is no significant difference in development between the four provinces and cities.

(2) In terms of specific ranking, Anhui's supply chain innovation efficiency is relatively high, while Shanghai's is relatively low. In terms of overall economic situation, while Shanghai is the leader in the Yangtze River Delta, their innovation efficiency remains low, which could be a reflection on their use of resources or internal limitations in deployment, which requires further attention from relevant management.

(3) In terms of pure technical efficiency, the Jiangsu region is slightly better than the Zhejiang region. Overall, both regions were at the middle level of overall development. Therefore, stabilizing the current development trend and seeking future innovation efficiency improvement is an issue worthy of attention.

5.2. Policy Recommendations. This study focuses on the knowledge supply chain of the Yangtze River Delta, which is an important economic belt in China. The integration of regional talent, technology, capital, and other resources is relatively complete. The problems reflected in the various economic data are forward-looking and reference. Based on the above research conclusions, this article puts forward the following policy recommendations:

First, improvements in innovation efficiency can be achieved by improvement in both input and output elements. In terms of input, attention should be paid to the cooperative innovation and technological exchanges between enterprises in the industrial park and the utilization of upstream and downstream knowledge accumulation in the supply chain. In addition, high-tech talent should also be strengthened. Strengthening the cultivation of knowledge and research investment in important fields can maximize the input of human capital and social capital within the knowledge supply chain. In terms of output, it is necessary to strengthen the assessment model that pays equal attention to the output of technology patents and economic benefits, which can promote the transformation of knowledge and the application of technology.

Hindawi
Journal of Mathematics
Volume 2023, Article ID 9810624, 1 page
https://doi.org/10.1155/2023/9810624

Retraction

Retracted: Analysis of the Resilience of Balance of Payments Using Comprehensive Evaluation

Journal of Mathematics

Received 19 December 2023; Accepted 19 December 2023; Published 20 December 2023

This article has been retracted by Hindawi following an investigation undertaken by the publisher [1]. This investigation has uncovered evidence of one or more of the following indicators of systematic manipulation of the publication process:

(1) Discrepancies in scope

(2) Discrepancies in the description of the research reported

(3) Discrepancies between the availability of data and the research described

(4) Inappropriate citations

(5) Incoherent, meaningless and/or irrelevant content included in the article

(6) Manipulated or compromised peer review

The presence of these indicators undermines our confidence in the integrity of the article's content and we cannot, therefore, vouch for its reliability. Please note that this notice is intended solely to alert readers that the content of this article is unreliable. We have not investigated whether authors were aware of or involved in the systematic manipulation of the publication process.

Wiley and Hindawi regrets that the usual quality checks did not identify these issues before publication and have since put additional measures in place to safeguard research integrity.

We wish to credit our own Research Integrity and Research Publishing teams and anonymous and named external researchers and research integrity experts for contributing to this investigation.

The corresponding author, as the representative of all authors, has been given the opportunity to register their agreement or disagreement to this retraction. We have kept a record of any response received.

References

[1] S. Fan and Y. Liu, "Analysis of the Resilience of Balance of Payments Using Comprehensive Evaluation," *Journal of Mathematics*, vol. 2022, Article ID 4620492, 13 pages, 2022.

Hindawi
Journal of Mathematics
Volume 2022, Article ID 4620492, 13 pages
https://doi.org/10.1155/2022/4620492

Research Article

Analysis of the Resilience of Balance of Payments Using Comprehensive Evaluation

Shixin Fan and Ying Liu

School of Statistics, Dongbei University of Finance and Economics, Dalian 116025, Liaoning, China

Correspondence should be addressed to Ying Liu; yingliu2022@outlook.com

Received 17 December 2021; Accepted 3 January 2022; Published 4 February 2022

Academic Editor: Naeem Jan

Globalization has brought increased attention to the balance of payments situation from a variety of countries. The traditional method of measuring balance of payments may not be applicable in certain situations. This paper draws on the idea of economic resilience, uses the transmission mechanism of balance of payments imbalance, and establishes a system of balance of payments imbalance resilience to provide a complement to the traditional measure. In this article, we establish a system of balance of payments resilience and ensure its reasonableness and effectiveness. The main conclusions are as follows: (1) balance of payments resilience score can be used as a reference and early warning indicator of a country's balance of payments situation and improves the measurement of balance of payments. (2) Improving the country's unemployment rate and boosting adjusted net savings will significantly upgrade the balance of payments situation. Improving foreign capital adequacy and foreign exchange market conditions is more beneficial for improving the country's rank of resilience score.

1. Introduction

Politics, economy, and culture of countries around the globe are becoming increasingly intertwined through globalization and international trade. In such a situation, various countries use the balance of payments (BOP) to measure their gains and losses in international trade. A stable BOP gives a country a competitive edge in international transactions and vice versa. It is common to use the current account balance for the purpose of measuring the BOP internationally [1], and the bounds of the imbalance were set at 5% of GDP [2]. This type of BOP measurement method, however, has some negative aspects. The BOP closely relates to the level of economic development in a country. Having a moderate and stable current account surplus is conducive to a country's economic development, whereas a deficit, especially a large deficit, is strongly unfavorable. We examine the latest data from some countries and find that it conflicts with the above.

2. Literature Review

The literature review of this paper is divided into three parts: (1) we briefly describe the BOP theory and traditional methods of measuring the imbalance. (2) We describe the idea of economic resilience. This article uses this to establish an index system. (3) The rationale for the selection of the BOP imbalance resilience indicators is introduced using the foundation for the selection of the indicators, which is the core portion of the literature review.

2.1. Balance of Payments Theory and Traditional Imbalance Measurement Methods. It should be noted that the BOP does not emphasize the accounts in which the deficit is incurred. According to the sixth edition of *Balance of Payments and International Investment Position Manual* (BPM6) [3], autonomous transactions are recorded in the

current account and capital account, whereas financial accounts have both records, and it is not easy to distinguish between them within the account. As a result, current and capital account deficits should be given greater attention when correcting BOP imbalances. Measures of imbalances have focussed on current accounts and relative deficits in recent years. The most popular method of calculating BOP balance is to utilize the current account balance [1]. The current account is more indicative of the supply and demand situation in the foreign currency market than the capital account [4], and recent Western research has concentrated on current account imbalances [5]. A BOP imbalance exists in industrial nations with a current account balance to GDP ratio of higher than 5%. [2]. As a boundary of imbalance, many international organizations and summits use 5%.

To sum up, the current BOP measure is based on the ratio of current account balance to GDP with 5% as the alert line for imbalance. We consider the use of a single indicator and a fixed alert line to be inappropriate and not helpful in explaining some economic phenomena. Thus, this article constructs an indicator system for the resilience of BOP imbalances, thereby supplementing the existing imbalance measurement methods.

2.2. Economic Resilience. Economic resilience is a relatively new field that involves disciplines such as development economics and regional economics. Holling [6] first proposed the concept of resilience to describe the ability of ecosystems to recover after trauma. Through decades of development, resilience has gradually included ecology, engineering, and economics. In this paper, we adopt the concept of economic resilience in macroeconomics, which describes a country's ability to recover after an external shock to its economy [7]. Briguglio et al. [8] succeeded in developing a system of indicators for estimating economic resilience by looking at four areas: macroeconomic stability, micro market efficiency, better economic governance, and social development. Those areas reflect not only the ability of an economy to resist external shocks, but also the severity of an economic recession resulting from external shocks. As a result, the indicators selected should satisfy two requirements in this paper: (1) This indicator can be used to judge a country's capacity to resist BOP imbalances and its economic strength. (2) Indices will change when a country's BOP imbalances are unbearably high, reflecting the loss and vulnerability of its economy.

2.3. Literature on Unbalanced Resilience System Construction Indicators. In this section, we discuss the criteria that are relevant to resilience indicators selection. Indicators should meet both requirements of Section 2.2 and have literature support. We have finally generated a path of BOP imbalances transmission, containing indicators of resilience.

2.3.1. The Impact of BOP Imbalances on the Domestic Economy. BOP changes may directly impact a country's foreign currency exchange market [9]. The foreign currency reserves, the foreign investment, the exchange rate, and the BOP all interact, according to Lu [10]. The BOP will have an influence on international commerce and investment in addition to foreign money. Foreign direct investment is linked to foreign currency reserves, which in turn is linked to the BOP [11]. Sun [1] and Chen [12] determined that a country's BOP situation is linked to its international trade competitiveness and that the terms of trade index may be used to quantify that competitiveness. As a result, we may deduce that BOP variations have a first-order impact on the foreign exchange and international trade markets and that the BOP limited growth model serves as a link to the domestic economy.

The BOP constrained growth model argues that BOP affects the growth of the domestic economy, especially GDP, through foreign trade and foreign exchange markets. This model, first proposed by Thirlwall [13], considers the impact of BOP on economic growth (GDP). Thirlwall concluded that failure to achieve BOP equilibrium inhibited a country's economic growth, and Thirlwall and Hussain [14] optimized the model to require fewer constraints. Kvedaras et al. [15] analyze new empirical data to demonstrate the current applicability of the model, which means that it is reasonable to apply the model theory in this paper. Scholars have also applied the model to various countries, concluding that the terms of trade index, real interest rate, exchange rate, and other indicators can be affected by the BOP, and using the model to limit GDP growth.

In addition to affecting GDP growth, foreign exchange reserves and exchange rate movements also have an impact on inflation [16]. Li and Ren [17] found that BOP can affect the quality of economic growth by affecting domestic macroeconomic stability; that is, BOP affects macroeconomic stability indicators, such as inflation and employment. The BOP can also reach deep within the macroeconomy and have an impact on fiscal conditions, real interest rates, and economic growth rates [18].

Thus, we can conclude that the BOP affects the foreign exchange rate, foreign trade, domestic economic growth, macroeconomic stability, and other macroeconomic indicators. Some indicators, such as fiscal policy and exchange rate, also affect the BOP.

2.3.2. BOP and Quality of Economic Growth. As clarified above (according to Section 2.3.1), BOP can influence the quality of economic development by affecting the foreign exchange market and the foreign trade market. The quality of economic development itself can be a measure of the economic strength and the ability to resist imbalances, which is precisely what indicators need.

Liu et al. [19] concluded that BOP is conducive to improving the quality of a country's economic growth. Kong et al. [20] conducted research on the relationship between the foreign openness and the quality of economic growth in a changing exchange rate environment from 1994 to 2018 and established a system for measuring the quality of economic growth, the indicators of which could be used to select indicators to construct resilience of BOP. Long and Ji [21] studied the GPI of Chinese provinces and optimized the measure of GPI. The GPI is highly sensitive to the welfare of

people and can be used to complement quality of economic growth.

Thus, we can conclude that indicators such as industrialization level, technical efficiency, TFP growth rates, research expenditures, environmental depletion, and poverty measure will also be added to the system of BOP imbalances resilience indicators.

2.3.3. BOP Crisis Theory and Events. The BOP crisis is a special case of imbalance. By studying the theoretical model of the BOP crisis and the economic variables affected by the crisis, we can choose resilience indicators from another perspective.

Krugman [22] proposed the first generation of BOP crisis model, arguing that when a country's money supply exceeds its money demand for a long period of time, foreign exchange reserves will continue to fall and currency speculators will attack at some point to disintegrate the fixed exchange rate system, causing the country's currency to devalue and the economy to collapse. Obstfeld [23] proposed a second-generation model of BOP crises, noting that when domestic macroeconomics is weak, currency speculation leads governments to abandon fixed exchange rate regimes on their own initiative, which triggers a chain reaction. Third-generation BOP crisis models are more inclined to examine the financial sector, which is called "capital item crisis theory."

Sen [24] optimizes the first generation of the BOP model to make the model's predicted timing of BOP crises more reasonable. Wang [25] examined the third-generation BOP crisis model and concluded that the crisis would result in a significant currency depreciation, which would have a negative impact on macroeconomic stability, and a sharp drop in real investment, which would have a negative impact on the real economy. According to Yin and Li [11], the crisis will result in a massive fiscal deficit. Wang [25] explores the causes of contagions associated with the three BOP crises that have occurred, such as inflation and fiscal conditions.

Studies of this type generally confirm the transmission path of the BOP imbalances derived from Sections 2.3.1 and 2.3.2 from a different angle. As a result, the transmission path obtained in this article will be more reliable.

The paper ultimately briefly describes this component as the transmission path of BOP imbalances, as described below. BOP imbalances will impact the foreign exchange market, resulting in changes in exchange rates, foreign exchange reserves, and foreign investment. As a result of the above-mentioned market changes, the imbalance will further affect domestic macroeconomic growth and stability, as well as inflation, unemployment, and GDP growth rate, which can affect quality of economic growth. Table 1 shows the final results of the election of the BOP imbalance resilience system indicators.

2.4. Summary of the Literature Review. Globally, the ratio of current account deficits to GDP is commonly used rather than large deficits in BOP theory. Using a fixed value as a warning line for imbalances is internationally common, but it also has some disadvantages. Thus, this paper draws on the idea of economic resilience in the macroeconomic field and summarizes two requirements for the selection of imbalance resilience indicators, on the basis of which the transmission path of BOP imbalance is derived to provide reference for the establishment of the resilience system in the next section.

3. Methodology and Data Resources

3.1. Indicator System Construction Method. This article's index system will calculate the BOP resilience score and weighting factors between the basic indicator and resilience score. Thus, the chosen method can express the resilience system in a formula, and the weight coefficients also have economic significance. The gray box-based model cannot give the weight coefficient, so this article does not use this type. Thus, this paper constructs the resilience system using the two-stage weighting evaluation method based on minimum variance. The method first calculates objective weights to the indicators and calculates a resilience score for each year, followed by a time weighting to obtain the total score.

3.2. Data Description. This section introduces the countries, period of time, indicators, and sources of the data.

We began the analysis with Russian Federation's establishment in 1992 and ended it in 2019, making a 28-year-period total. Among them, 2010 is the base year for the relative indicators, so 27 years of data are included in the analysis.

The article aims to analyze as many countries as possible, but for the reliability of the results, the countries included in the analysis must meet the data requirements. The missing value boundary is set at 10%; if a country has more than 3 missing values for an indicator, the country is not selected for analysis, and if only a few countries meet the missing value boundary for an indicator, the indicator is discarded. Table 1 shows the BOP imbalance resilience indicators selected in this article. Table 2 and Figure 1 show the countries that participated in the analysis.

As shown in Figure 1, many African countries did not participate in the analysis, mainly due to data acquisition limitations.

4. Resilience System Results and Reasonableness Analysis and Improvement

4.1. BOP Resilience Results. In this part, the initial weights are first obtained from the entropy value method, the panel data of the resilience scores for each year are obtained using the initial weights, the initial values of the secondary weights are obtained, and the secondary weights are further obtained. Next, the panel score data are weighted by the secondary weights to obtain the final total score of each country, and the initial indicator weights are weighted to obtain the reference weights of the indicators.

4.1.1. Resilience Scores for Each Country by Year. In this paper, we calculated panel data of resilience scores for 37 countries between 1992 and 2019 by entropy method and also calculated the indicators weights for each year. Figures 2 and 3 show the results of the resilience scores and the indicator weights, respectively.

Table 1: Resilience system construction indicators.

Type	Abbreviation	Name	Positive/negative	Data source
Direct economic impact	reer	Real effective exchange rate	Positive	IMF
	tti	Terms of trade index	Positive	IMF
	fera	Foreign exchange reserve adequacy	Positive	IMF
	ftd	Foreign trade dependency	Positive	WB
	fdin/gdp	Foreign direct investment to GDP ratio	Positive	WB
Economic development level	dr	Deficit rate	Positive	IMF
	ti/gdp	Total investment to GDP	Positive	IMF
Economic stability	irc	Inflation rate of change	Negative	IMF
	ir	Inflation rate	Negative	IMF
	u	Unemployment	Negative	IMF
Quality of economic growth	gdpc	GDP growth rate	Positive	IMF
	ans	Adjusted net savings	Positive	WB
	iav/gdp	Industrial value added to GDP	Positive	WB
	nipc	National income per capita	Positive	WB
	tfpc	Total factor productivity of change	Positive	PWT
	wtfpc	Welfare-related total factor productivity of change	Positive	PWT

Direct economic impact refers to the direct impact of the bop on foreign exchange and foreign capital markets. IMF: International Monetary Fund. WB: World Bank. PWT: Penn World Table.

Table 2: Countries participating in the analysis.

Geographic continents	Country code	Country name	Geographic continents	Country code	Country name
Europe	CHE	Switzerland	Asia	CHN	China
	CYP	Cyprus		JPN	Japan
	DEU	Germany		MYS	Malaysia
	DNK	Denmark		PHL	Philippines
	ESP	Spain		SGP	Singapore
	FIN	Finland		IND	India
	FRA	France	America	CHL	Chile
	GBR	United Kingdom		COL	Colombia
	GRC	Greece		CRI	Costa Rica
	HUN	Hungary		DOM	Dominican Republic
	ITA	Italy		MEX	Mexico
	NLD	Netherlands		PRY	Paraguay
	NOR	Norway		CAN	Canada
	POL	Poland		USA	United States
	PRT	Portugal	Africa	MAR	Morocco
	ROU	Romania		TUN	Tunisia
	SVK	Slovak Republic		ZAF	South Africa
	SWE	Sweden	Oceania	AUS	Australia
	RUS	Russian Federation			

As shown in Figure 2, F refers to the resilience score; Figures 2(a), 2(c), and 2(e) show the resilience scores by scatter plots, where the size of the scatter points shows the level of resilience; and Figures 2(b), 2(d), and 2(e) are the kernel density distribution of resilience scores, which is another way of showing the score more visually. We can see visually that countries such as Switzerland (CHE), China (CHN), and Singapore (SGP) have significantly higher resilience scores than other countries, whereas countries like the United States and the United Kingdom are not performing so well.

Figure 3 shows the kernel density distribution of the weights of each indicator, from which it can be seen that most of the indicator weights are relatively concentrated, but the distribution of fdin/gdp is more dispersed, and its change over 27 years is large. *fdin/gdp*, *fera*, and *ftd*, which have relatively large weights, will make the resilience score more differentiated.

4.1.2. Time Weights and Final Total Score. Calculate the initial and final weights at first. In this paper, we present multiple nondimensionalization methods for weight distance data, and the obtained clustering and separation years were all 2001 and 2018. Table 3 shows the time weights of the initial and final weights.

Then, using time weighting, reweigh the panel data of resilience scores for each year and calculate the final score. Figure 4 shows the final resilience score, where the F refers to the resilience score (the F in Figures 5–7 also refers to the resilience score). The resilience score of each country has now been calculated.

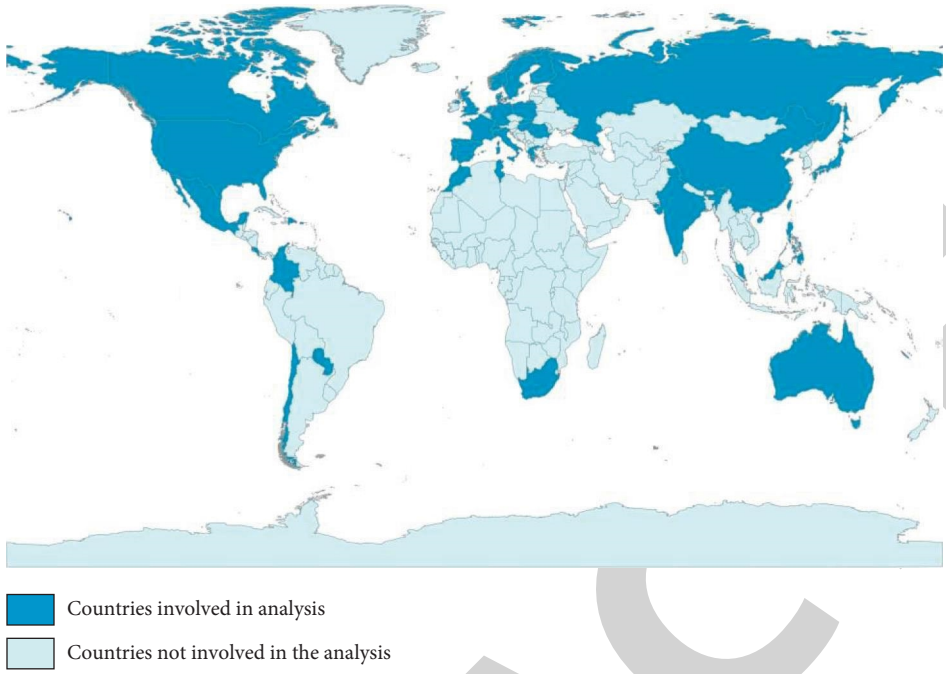

Figure 1: Geographical distribution of participating countries.

4.2. Reasonableness Analysis for Resilience. In this section, we consider the reasonableness of BOP resilience indicators system in three ways: (1) The indicators selected meet the theoretical requirements of the resilience system. (2) There should be a correlation between resilience score and BOP. (3) The resilience score at key points needs to be consistent with history.

4.2.1. The Reasonableness of Indicators Selection. The indicators underlying the construction of the resilience system are all involved in the transmission path of BOP imbalance and meet the two requirements for the selection of indicators (according to Section 2.3). Additionally, the indicator data are obtained from the international organization database after a strict evaluation of missing values and outliers is performed. Countries and indicators with inadequate data are excluded.

4.2.2. Resilience Score and BOP Correlation. The BOP imbalance resilience score should be correlated with the ratio of current account balance to GDP. This is because a country with low resilience will face greater difficulty recovering from a severe shock to its BOP. Similarly, the larger the deficit in a country's current account balance to GDP ratio is, the more the economy suffers, leading to a lower resilience score. In this article, we use the Granger causality test of panel data to see whether the above relationship exists.

The method was proposed by Clive Granger in 1969 and is based on the following idea: if x is a cause of y, but y is not a cause of x, then past values of x can help predict future values of y, but past values of y cannot help predict future values of x. Consider the time series model below:

$$y_t = \gamma + \sum_{m=1}^{p} \alpha_m y_{t-m} + \sum_{m=1}^{p} \beta_m x_{t-m} + \varepsilon_t. \quad (1)$$

In (1), p is the lag order, and the null hypothesis tested is

$$H_0: \beta_1 = \beta_2 = \ldots = \beta_p = 0. \quad (2)$$

The null hypothesis indicates that the past value of x does not predict the future value of y. If the H_0 is rejected, then x becomes the "Granger factor" of y. Changing x and y in (2), we can test whether y is a Granger factor of x. The following models can be applied to panel data:

$$y_{it} = \gamma + \sum_{m=1}^{p} \alpha_m y_{i,t-m} + \sum_{m=1}^{p} \beta_m x_{i,t-m} + u_i + \varepsilon_{it}. \quad (3)$$

In (3), u_i is the heterogeneity of individual i. For dynamic panel models, differenced GMM and system GMM are used for estimation. There are two assumptions when estimating the model. The first is that the cross-section coefficients are the same. The panel data is regarded as stacked data, and a Granger causality test is conducted similarly to that performed on time series data. The second is that coefficients of cross sections are different, and each section member is subjected to the Granger causality test. In this paper, causality tests of up to 6th order were conducted for both assumptions.

The Granger causality test requires that the panel data are stationary. Table 4 demonstrates the results of the panel unit root test.

The results of all four tests are significant, and it can be concluded that the panel data do not have unit roots. Table 5 shows the results of Granger causality tests under two assumptions.

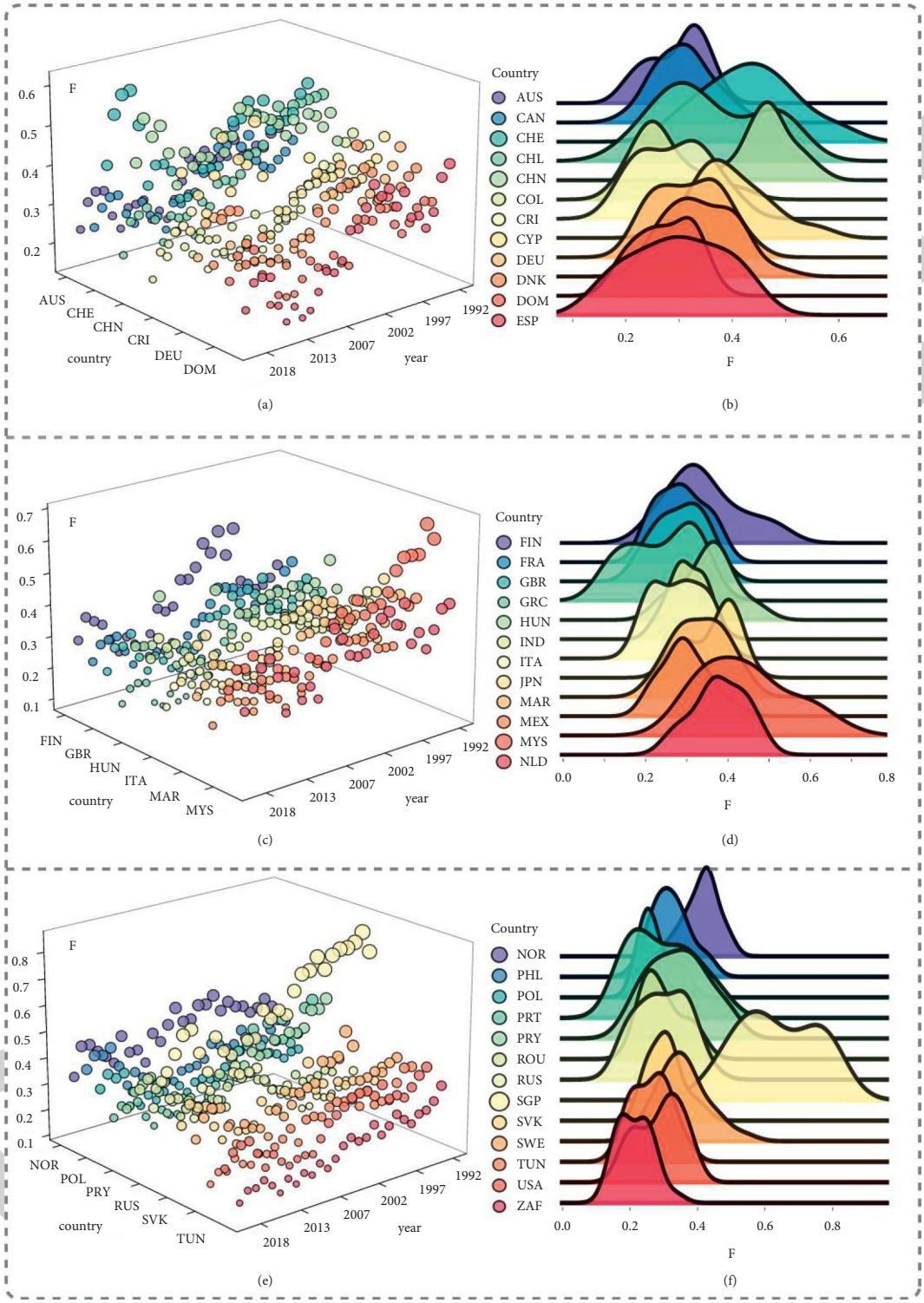

Figure 2: Resilience scores by country by year.

In Table 5, CA refers to the ratio of BOP current account balance to GDP ratio, and F is the resilience score. There is significant evidence that BOP current account balance to GDP ratio and resilience score are causally correlated in the fixed coefficient model. The resilience scores of orders 1, 2, and 4 in the variable coefficient model are the cause of BOP current account balance. Based on the results, it can be shown that the two are causal and that the resilience score correlates with theoretical expectation.

4.2.3. Historical Consistency of Time Points. At the time of the event, BOP imbalance resilience score calculated in this article should fluctuate and trend accordingly. This section

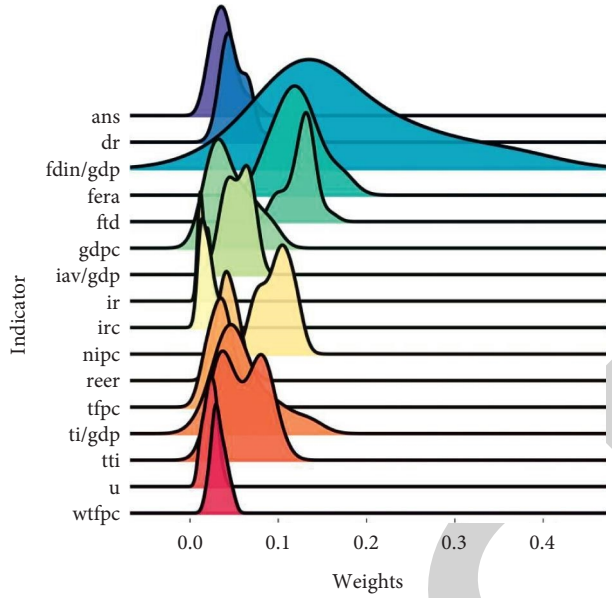

Figure 3: Distribution of indicator weights.

Table 3: Time weights.

year	Initial weights	Final weights	Year	Initial weights	Final weights
1992	0.035783	0	2006	0.032883	0.040212
1993	0.036586	0	2007	0.032281	0.043386
1994	0.038372	0.002116	2008	0.032362	0.046561
1995	0.039552	0.005291	2009	0.036253	0.049735
1996	0.041762	0.008466	2011	0.034754	0.05291
1997	0.041649	0.01164	2012	0.038164	0.056085
1998	0.042268	0.014815	2013	0.039484	0.059259
1999	0.046003	0.017989	2014	0.035973	0.062434
2000	0.050484	0.021164	2015	0.038808	0.065609
2001	0.059982	0.024339	2016	0.031467	0.068783
2002	0.050823	0.027513	2017	0.028217	0.071958
2003	0.04105	0.030688	2018	0	0.075132
2004	0.033153	0.033862	2019	0.027062	0.078307
2005	0.034825	0.037037			

analyzes BOP crisis events, financial crisis events (the financial crisis will damage the country's economy [26, 27], which will affect BOP resilience), and individual country cases.

First is the BOP crisis event. There was the European Monetary System Crisis in 1994–95, the Latin American Debt Crisis in 1995–97, and the 1997 Asian Financial Crisis (actually BOP crisis) during the period covered by this article. These crises relate to the countries involved in the study of this paper as shown in Table 6. Germany and Russia are among the countries affected by the Asian Financial Crisis, so they are also included in the analysis.

Figure 5 illustrates the resilience scores of the countries involved in the crisis events.

In Figure 5, the green shading in Figure 5(a) is the time period of the European Monetary System Crisis, the orange shading is the time period of the Asian Financial Crisis, and Figures 5(b) and 5(c) show their scores specifically, respectively. The countries involved in the European Monetary System Crisis underwent a significant decline in resilience scores starting in 1992, bottoming out in 1994 or 1995 before slowly recovering. Mexico, which is in the midst of a Latin American Debt Crisis, had the same trend. In the Asian Financial Crisis, Russia and Malaysia also experienced a decline in their resilience scores in 1997. Thus, the reflection of the resilience score at BOP crisis is in line with realistic expectations.

The next step is to analyze the resilience score during the financial crisis.

The research period of this paper starts from 1992, so this section examines the international financial crisis in 2007–2011. At the end of our study time period, the high foreign exchange reserves of China and Switzerland may have financial crisis risk [28]. However, this phenomenon is not universal, so it will not be analyzed further.

The crisis (2007–2011) was not prompted by BOP imbalances, but the outburst of the crisis has resulted in huge

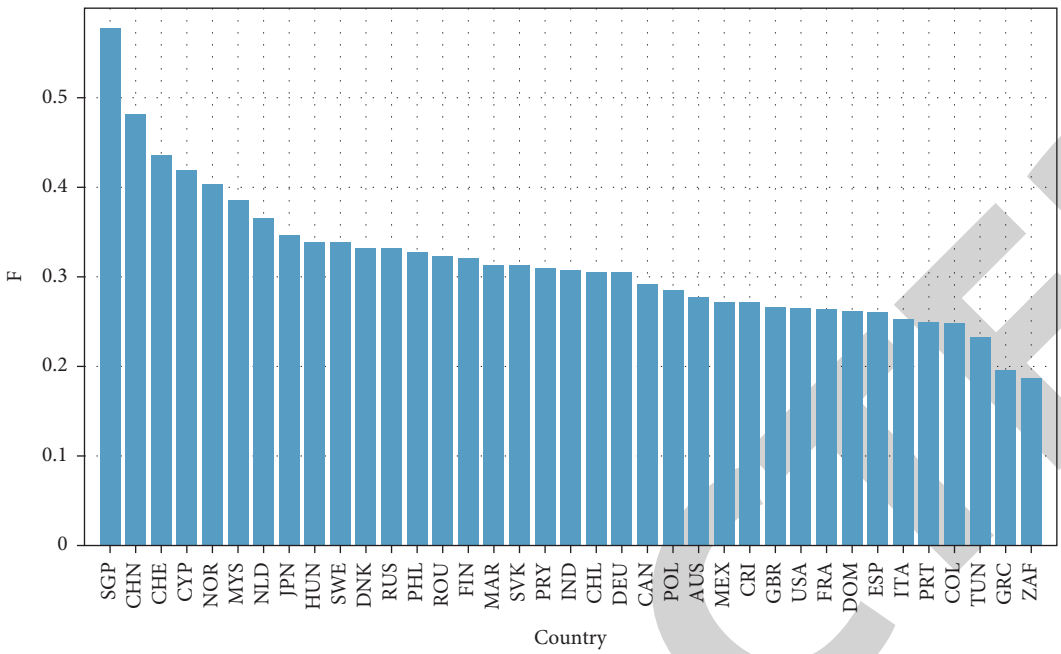

Figure 4: Final resilience scores for each country.

losses, and thus the resilience score should also trend in the same direction. Figure 6 illustrates the change in resilience scores during the financial crisis.

Based on the scores, we can see that most countries had their lowest scores in 2007 and 2009, respectively. Such a score result is consistent with the perception of reality.

Finally, we assess China's and America's BOP resilience separately. Figure 7 shows the resilience scores of the two countries.

In the aftermath of the international financial crisis, the resilience scores of both China and the US trended sharply downward and then upward, with the difference that China's resilience score eventually remained the same as it was before 2007, while the US rarely returned to its previous level. The above scores are consistent with the US focus on its BOP deficit in recent years.

4.3. Improvement of Resilience System. As a result of the limitation of the method for establishing a system, in this paper we propose to use a more appropriate method for determining the importance of resilience system construction indicators.

4.3.1. Limitations in the Construction of the Resilience System. Min–max normalization is particularly sensitive to outliers; if one indicator has a very minor outlier, all other nations' indicators will be near to 0.99. As a result, the indicator's range of fluctuation will be limited. As a consequence, the indicator's weight in the entropy approach will be quite minimal. However, the outlier, not the indication, is to blame for this outcome. The meaning of the indicator weights derived by the entropy technique, in addition to data sensitivity, is "distinctness," which does not entirely match "importance." With a greater weight, the difference between nations in this indicator widens, whereas a lower weight narrows the gap between countries, implying that countries get similar (rather than lower) ratings in this indicator. As a result, the indicator's weight can merely mean that it is more distinct, not that it is more significant or useful in a BOP context. As a result, we choose to utilize the random forest approach to assess the relevance of the indicators and interpret them in conjunction with the weights in this study.

The following is a brief description of the random forest importance score. Random forest method is one of the ensemble methods of decision trees. A decision tree is essentially a collection of judgments, and the input samples are judged layer by layer to form one node of the tree, through which the input space is divided into different regions, and the child nodes continue to divide the regions to get many subregions. The same layer's input and output (leaf nodes) do not overlap, and the final leaf nodes correspond to the areas, so the input and output (leaf nodes) are the same. Ensemble trees are created by combining the outcomes of numerous smaller decision trees and then voting on each class's findings (classification issue) or calculating the mean (regression problem). Although each tree makes errors, making judgments as a group increases accuracy while avoiding the issue of out-of-sample prediction. Each decision tree is given a feature importance score, i.e., the importance of the input variable in making a decision in the tree, with a value between 0 and 1, where 0 means that the variable does not contribute to the decision and 1 indicates a perfect prediction of the target value. In this paper, feature importance is used as a complement to the indicator weights.

Figure 8 shows the results of the indicator importance scores. The time-adjusted importance is the result of weighting the importance scores using the weights above (Table 3).

It can be seen that the importance of the annual average does not change much from the time-adjusted importance,

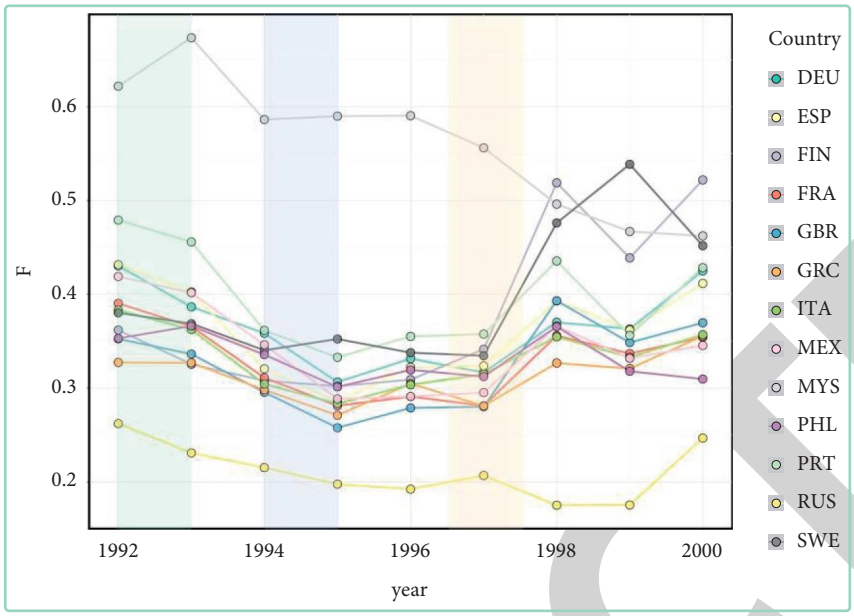

(a)

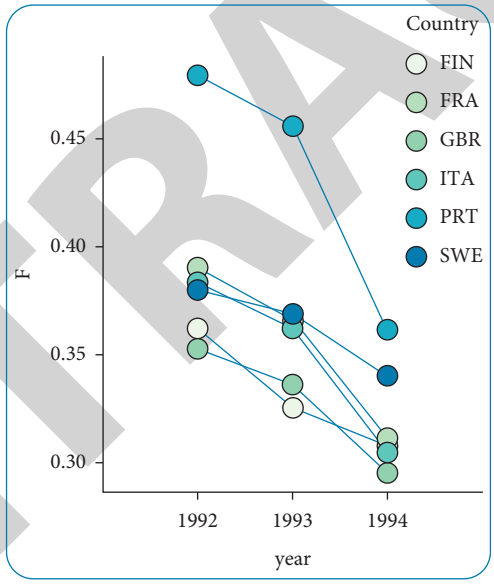

(b)

Figure 5: Continued.

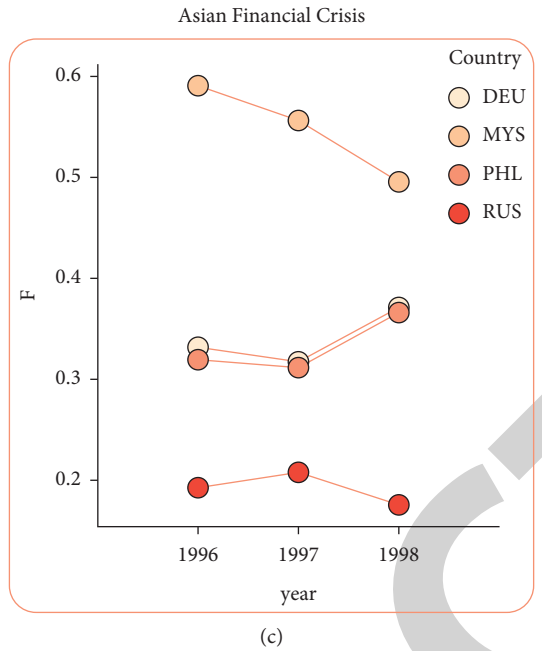

(c)

Figure 5: Resilience scores in BOP crisis.

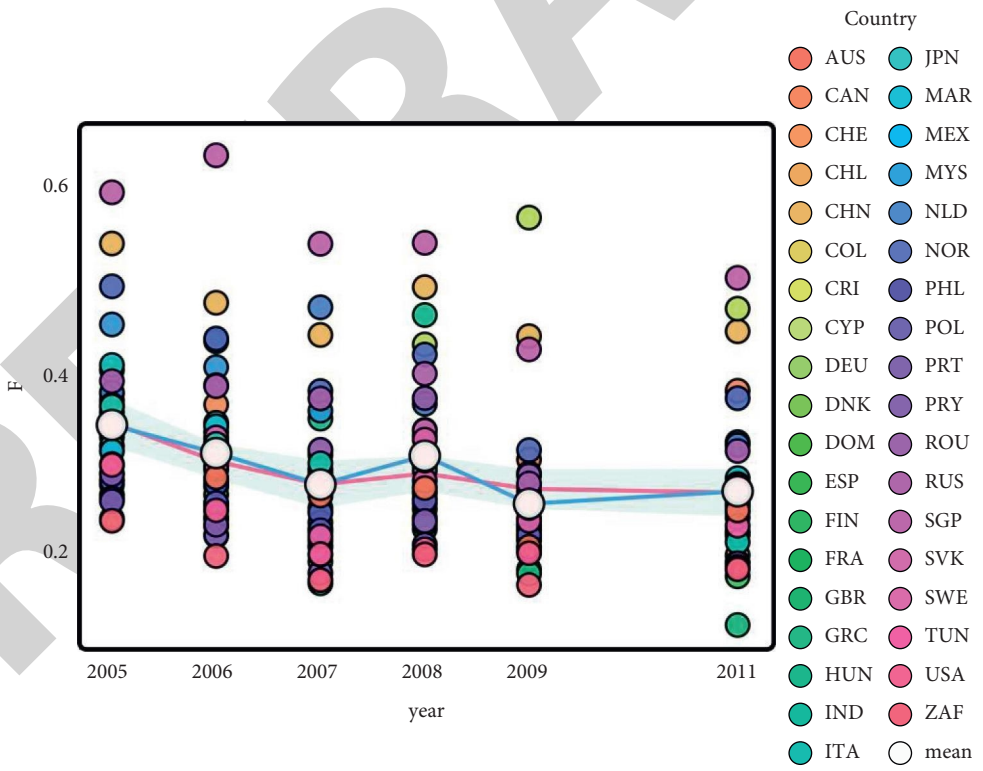

Figure 6: Country resilience scores during the financial crisis.

which means that the importance of the indicators is more stable across years compared to the indicator weights, which has a complementary effect. We can conclude that the unemployment rate and adjusted net savings are more important, while net foreign direct investment to GDP ratio, foreign reserve adequacy, and foreign trade dependence are better at distinguishing between countries' resilience scores.

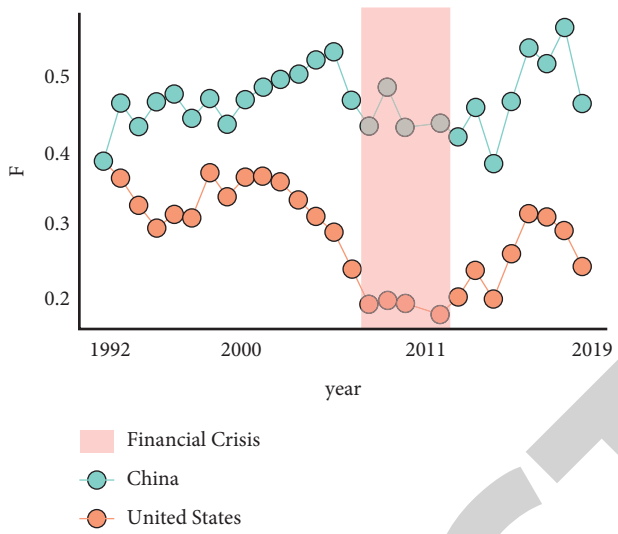

Figure 7: China and US resilience score.

Table 4: Panel unit root test results.

Method	Statistic	Prob.**	Cross sections	Obs
Null: unit root (assumes common unit root process)				
Levin, Lin & Chu t*	−3.26146	0.0006	37	956
Null: unit root (assumes individual unit root process)				
Im, Pesaran and Shin *W*-stat	−4.15204	0.0000	37	956
ADF—Fisher Chi-square	119.654	0.0006	37	956
PP—Fisher Chi-square	115.808	0.0014	37	962

Two asterisks mean that the results are significant at the 0.05 significance level.

Table 5: Results of Granger's causality test.

Fixed coefficient				
Lag order	Null hypothesis	*W*-stat.	Zbar-stat.	Prob.
1	CA does not Granger cause F		25.5178	$5.00E-07$
	F does not Granger cause CA		18.3578	0.00002
2	CA does not Granger cause F		11.5310	0.00001
	F does not Granger cause CA		9.32977	0.0001
3	CA does not Granger cause F		7.09366	0.0001
	F does not Granger cause CA		6.35504	0.0003
4	CA does not Granger cause F		4.54826	0.0012
	F does not Granger cause CA		4.82955	0.0007
5	CA does not Granger cause F		4.10409	0.0011
	F does not Granger cause CA		4.03856	0.0013
6	CA does not Granger cause F		3.91646	0.0007
	F does not Granger cause CA		3.70241	0.0012
Unfixed *coefficient*				
Lag order	Null hypothesis	W-stat.	Zbar-stat.	Prob.
1	CA does not homogeneously cause F	1.49194	1.44778	0.1477
	F does not homogeneously cause CA	2.21510	4.08701	0.00004
2	CA does not homogeneously cause F	2.78540	1.37882	0.168
	F does not homogeneously cause CA	3.28474	2.60133	0.0093
3	CA does not homogeneously cause F	3.99853	1.11452	0.2651
	F does not homogeneously cause CA	4.13998	1.37792	0.1682
4	CA does not homogeneously cause F	5.74697	1.57432	0.1154
	F does not homogeneously cause CA	5.89868	1.79541	0.0726
5	CA does not homogeneously cause F	7.10803	1.10941	0.2673
	F does not homogeneously cause CA	7.01405	1.00483	0.315
6	CA does not homogeneously cause F	9.01583	0.77239	0.4399
	F does not homogeneously cause CA	9.12442	0.85495	0.3926

Table 6: Countries involved in BOP crisis.

	Year	Country
European Monetary System Crisis	1992-1993	Germany, Spain, Finland, France, UK, Greece, Italy, Portugal, Sweden
Latin American Debt Crisis	1994-1995	Mexico
Asian Financial Crisis	1997	Germany, Malaysia, Philippines, Russian Federation

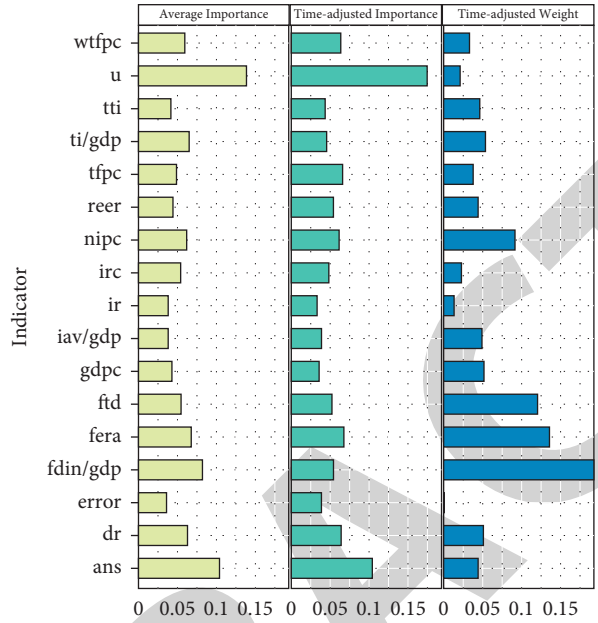

Figure 8: Importance of indicators.

5. Conclusion

5.1. Establishing a System for BOP Imbalance Resilience. This paper draws on the idea of economic resilience and establishes a BOP imbalance resilience score system based on the transmission mechanism of BOP imbalance to measure a country's ability to tolerate BOP imbalance.

The indicator system has been proven to be reasonable in the selection of indicators and the relevance of the result data, and its changes are consistent with historical events and can provide a complement to the traditional measure of BOP imbalance.

5.2. Adjustment of the Balance of Payments. The analysis in this paper concludes that a country that wants to change its disadvantaged BOP position should improve unemployment and increase adjusted net savings, and if it wants to change its resilience ranking among the countries researched, it should improve the net foreign direct investment to GDP ratio, foreign exchange reserve adequacy, and foreign trade dependence.

5.3. The Complementary Effect of Resilience. BOP resilience can provide complementary analysis for countries with surpluses and deficits and can be used as a reference and early warning indicator for BOP position. When the surplus or deficit performance and the resilience score are both good, it is more reliable to conclude that the country is in a positive BOP position.

Introducing categorical variables for further analysis, Asia and Africa have slightly higher resilience scores than Europe and America, and high-development countries perform better than very high-development countries. Asia and Africa are more sensitive to whether they are reserve currency issuers, while in Europe and America, whether they are capital exporters has a greater impact on the score.

Data Availability

The data used to support the findings of this study are included within the article.

Conflicts of Interest

The authors declare that there are no conflicts of interest.

Acknowledgments

This study was funded by the School Research Project of Dongbei University of Finance and Economics (DUFE2020Y09) and Liaoning Provincial Social Science Project (L21BTJ001).

References

[1] G. Sun, "Current account surplus and capital account deficit—options for the evolution of China's balance of payments pattern under the overall balance objective," *Studies of International Finance*, no. 330, pp. 10–22, 2014.

Hindawi
Journal of Mathematics
Volume 2024, Article ID 9872547, 1 page
https://doi.org/10.1155/2024/9872547

Retraction

Retracted: Rough Set Construction and Entropy Weight Evaluation of Urban Higher Education Resource Carrying Capacity Based on Big Data

Journal of Mathematics

Received 23 January 2024; Accepted 23 January 2024; Published 24 January 2024

This article has been retracted by Hindawi following an investigation undertaken by the publisher [1]. This investigation has uncovered evidence of one or more of the following indicators of systematic manipulation of the publication process:

(1) Discrepancies in scope

(2) Discrepancies in the description of the research reported

(3) Discrepancies between the availability of data and the research described

(4) Inappropriate citations

(5) Incoherent, meaningless and/or irrelevant content included in the article

(6) Manipulated or compromised peer review

The presence of these indicators undermines our confidence in the integrity of the article's content and we cannot, therefore, vouch for its reliability. Please note that this notice is intended solely to alert readers that the content of this article is unreliable. We have not investigated whether authors were aware of or involved in the systematic manipulation of the publication process.

Wiley and Hindawi regrets that the usual quality checks did not identify these issues before publication and have since put additional measures in place to safeguard research integrity.

We wish to credit our own Research Integrity and Research Publishing teams and anonymous and named external researchers and research integrity experts for contributing to this investigation.

The corresponding author, as the representative of all authors, has been given the opportunity to register their agreement or disagreement to this retraction. We have kept a record of any response received.

References

[1] L. Wang, C. Liu, and M. Talha, "Rough Set Construction and Entropy Weight Evaluation of Urban Higher Education Resource Carrying Capacity Based on Big Data," *Journal of Mathematics*, vol. 2022, Article ID 7776940, 11 pages, 2022.

Hindawi
Journal of Mathematics
Volume 2022, Article ID 7776940, 11 pages
https://doi.org/10.1155/2022/7776940

Research Article

Rough Set Construction and Entropy Weight Evaluation of Urban Higher Education Resource Carrying Capacity Based on Big Data

Lulu Wang,[1] **Chao Liu**,[1] **and Muhammad Talha**[2]

[1]*Woosuk University, Wanju-gun, Jeollabuk-do 55338, Republic of Korea*
[2]*Department of Computer Science, Superior University Lahore, Lahore, Pakistan*

Correspondence should be addressed to Muhammad Talha; talhashoaibt@yahoo.com

Received 21 December 2021; Revised 7 January 2022; Accepted 12 January 2022; Published 1 February 2022

Academic Editor: Naeem Jan

With the popularization of higher education, the scale of urban higher education continues to expand, and the contradiction between the supply and demand of educational resources becomes increasingly prominent, which restricts the steady development of urban higher education. Based on the rough set theory, this paper constructs a rough set of big data of urban higher education resource carrying capacity from the three levels of higher education core resources, urban economic resources and urban basic resources, and evaluates the entropy weight of the city where the university is located. According to the theoretical knowledge of higher education resource carrying capacity, the system deconstructs and expounds the balance mechanism of higher education resource carrying capacity, which provides solid theoretical support for the development of the paper. The research shows that the agglomeration development of higher education resources can improve the carrying capacity of urban higher education resources. The second section performed well on the whole, and the index distribution was more uniform. The third interval index structure distribution is complex and uneven, and the overall performance is general. The fourth section belongs to the poor section of educational carrying capacity with a low overall index. It can be seen that the carrying capacity of higher education resources varies significantly, which provides a scientific basis for improving the carrying capacity of higher education resources and theoretical and policy basis for realizing rational allocation and sustainable carrying capacity of higher education resources.

1. Introduction

With the acceleration of the modernization of the governance system and the deepening of normalization construction, the construction and development of urban higher education have become a new landmark for different regions to show their new achievements in reform, new progress in economic and social development, and a new level of scientific, technological, and cultural development [1]. In the struggle for urban and regional development, resources, as the foundation supporting the growth of higher education in cities, regions, and nations, play a key role. Higher education resources may easily migrate across areas as a result of economic globalization and regional integration. Cities, as a highly concentrated regional area for human production and living, eventually become the center of higher education resources in the process of free flow of higher education resources [2]. As higher education moves from popularization to popularization, regional center cities progressively become the collecting site for higher education resources, and their capacity to aggregate resources has a significant influence on regional higher education development. For a long time, researchers have been interested in the strategic impact of higher education resource agglomeration on regional higher education growth.

Educational resources refer to the human, material, and financial resources used, occupied and consumed in the course of education, including the human resources of educators and educatees, etc. Material resources include fixed assets, materials, and low-value consumables in the school. Financial resources are the monetary form of human and material resources, including personnel consumption

and public consumption, which are the material basis for the development of education and education work [3]. Educational resources are regarded as the sum total of human resources, financial resources, and material resources. To analyze the attribute of educational resources, we must first understand the connotation of the attribute. The so-called attribute is an abstract description of things, reflecting the homogeneity or difference between things is the attribute. A lot of properties and relations of a thing can be attributed to the attribute of this thing. Therefore, the analysis of the attributes of educational resources is helpful to further distinguish the relationship between educational resources and other resources and then distinguish and separate different core elements in the theory of resource allocation. Scarcity, flexibility, multifunctional, imbalance, and potential are all characteristics of educational resources. Regional imbalances, urban-rural imbalances, and class imbalances are all examples of educational resource imbalances. The difference between imbalance and equilibrium is that the former is absolute and the latter is relative. Bearing capacity is a term adopted from the area of engineering geology. Its initial purpose was to define the strength of a building's foundation bearing capacity, but it has since developed into one of the most often used terms to express the degree of growth limitation. This notion was initially introduced to this field by ecology. Carrying capacity shows the support capacity of ecosystem resources and environment to the benign growth of the human social system, as discussed in the early talks on the interaction between ecosystem resources and environment and human social system [4]. Subsequently, related concepts such as resource carrying capacity, population carrying capacity, and ecological environment carrying capacity are derived. These concepts mainly express the supporting capacity or development limitation of the bearing subject to the growth of the bearing object under certain conditions. In the case of taking a certain region and period as the research scope, if based on the above concepts of "educational resources" and "carrying capacity," the carrying capacity of educational resources is also one of the derivative concepts of carrying capacity. If the research goal is the geographical region where the educational population congregates, the carrying object and main bodies are the educational school-age population and educational resources, respectively. The carrying capacity of educational resources may be separated into two categories based on these two standards: educational resources and specific space. The logical deployment of educational resources and the long-term growth of education are the core of educational resource carrying capacity. However, it is not only a matter of educational resources; it is a multifaceted issue that must take into account a variety of aspects such as population, resources, education, and space. The lower the proportional ratio, the greater the educational resource carrying capacity; the more resources per student, the lower the risk of overloading.

Big data has penetrated into every industry and field and has become an important factor in production. The rapid development of mobile Internet, cloud computing, and the Internet of Things is pushing mankind into the era of big data. The higher education system can be regarded as an ecosystem, which has the same bearing capacity as the natural ecosystem. Once the scale of higher education exceeds the bearing capacity of certain education and the corresponding environment, its resource supply and regeneration capacity will be destroyed, and the system will lose balance [5]. Carrying capacity of educational resources refers to the supporting capacity of existing educational resources for the population of a country or region to receive all kinds of education under the premise of reasonable allocation and quality assurance of various educational resources. The research on education carrying capacity mainly focuses on higher education and vocational education, analyses the concept and elements of education carrying capacity in the higher education system, and analyses the scale of higher education carrying capacity, its relationship with social development and promotion strategies based on the analysis model of ecosystem carrying capacity. It provides useful theoretical reference and measurement methods for the subsequent research on the carrying capacity of compulsory education resources in big cities. The lack of an analytical model and theoretical index system that directly refers to the urban internal connection environmental background, influencing factors, and specific pressure performance provides a new space for the academic development of this study.

This study combines the connotation of educational resources and carrying capacity to produce a stable and logical technique of combining by examining the connotation of educational resources and carrying capacity. The value of educational resource carrying capacity can be maximized to ensure the smooth implementation of educational activities, and social subjects or educational subjects can integrate necessary resources to support the effective operation of educational activities by constructing a rough set of big data of urban higher education resource carrying capacity.

2. Related Work

With the popularization of higher education, the demand for educational resources increases, facing a series of problems such as resource shortage and ecological destruction of education. In this context, it is very important to study the carrying capacity of higher education resources. The resource carrying capacity of higher education is restricted by many factors. Rough set theory is a data mining method that has emerged in recent years, which is mainly used in data simplification, data significance assessment, object similarity or difference analysis, causality, and paradigm mining. Xue et al. discuss the concept, evaluation indexes, and evaluation methods of carrying capacity of educational resources based on the characteristics and influencing factors of educational resources [6]. Ding et al. analyzed the ecological carrying capacity of the education system of overseas students in China from three dimensions of "resource carrying capacity," "environmental carrying capacity," and "ecological elastic force" [7]. Peng et al. define its carrying capacity and, on this basis, put forward three core indicators for

measuring the carrying capacity of resources in the higher education system: the first is the allocation of teachers in colleges and universities. The second is infrastructure and equipment. The third is the government's financial investment in education [8]. Xi et al. constructed the higher education carrying capacity as an evaluation system and screened five key indicators with the support of rough set theory [9]. Shi et al. implemented the construction of an evaluation system related to the resource carrying capacity in higher education and adopted the carrying capacity index model analysis to conduct quantitative analysis on each component of regional higher education resources and their comprehensive carrying capacity [10]. At this time, it is required to strengthen the carrying capacity assessment index system and its evaluation theory.

Education resources bearing capacity is within a specific area with the upper body of production and management role, education resources in maintaining the balance of quantity and quality, education resources reasonable configuration, and effective utiliztation of resources under the premise of complete region for enjoying all educational resources for the population. The level of education of all types are considered as most efficient resource of educations. Shen L. et al. think that educational resource carrying capacity refers to the ability of current resources to sustain the people in the space receiving education at all levels, based on how to distribute and assure the quality of different educational resources in a nation or area [12]. Zhang et al. evaluated the carrying capacity of higher education resources from the perspective of rough set theory [13]. Cao et al. believe that a comprehensive evaluation system including educational, economic, and social indicators should be considered in the evaluation index system of carrying capacity [14]. The evaluation system of higher education resource carrying capacity makes up the higher education resource carrying capacity.

3. Construction of Big Data of Urban Higher Education Resource Carrying Capacity

3.1. PRES Analysis Framework for Education. In view of the carrying capacity of urban higher education resources, the carrying capacity analysis of educational resources based on a variety of constraint factors is a relatively special education system, which is different from the general education system that comprehensively analyses many educational elements within a single education category. It is composed of multiple factors including population, resources, society, and education [15]. Such an analysis perspective not only contains many restrictive factors that affect the resource carrying capacity of urban higher education but also combines these factors with relevant elements within the educational scope, thus establishing a systematic framework analysis perspective and structural relations based on environment and condition constraints.

Educational activities exist in a certain social system and environment and need to use certain resources to carry out education and teaching activities to meet their own educational goals and maintain the existence and development of the education system. With the continuous advancement and development of education, the scale and quality of educational activities are also expanding and improving. Therefore, the educational system with the ultimate goal of human development is becoming more and more extensive, and the connection and influence between the educational system and the social system and other relevant elements are becoming closer and closer. In this context, this paper attempts to construct an educational PRES analysis framework based on the system theory and education system theory and the carrying capacity of educational resources as the core theme and examines and studies the corresponding problems of the carrying capacity of educational resources by analyzing the internal structure and elements of the system.

The structure of the analysis framework refers to the relatively stable way of mutual connection and interaction among various elements of the system, that is, the organizational form, combination mode, and order within the system. According to the simulation, an analysis framework with educational factors as the core and link, social factors, resource factors, and population factors as a whole, and mutual influence and interaction is constructed. The analysis framework of education PRES is shown in Figure 1.

The education PRES analysis framework is made of four fundamental components: education, population, resources, and society [16]. People who are part of the social and educational systems are referred to as demographic factors. In the social system, the population with productive, consumption, and self-management capacity; in the category of education, the educational population, which includes students and faculty, is not only directly related to educational activities and educational resources but also determines its primary status in the educational resource system as a double identity of population and educational population. Educational components are educational activities in the education system, and educational activities in general refer to a wide range of educational activities that influence people's physical and mental development. Educational activities in the limited meaning pertain to school-related activities, but educational activities in this research refer to educational activities in the broadest sense. Educational components are at the heart of the whole system, not only because educational resources are the system's core composition of educational elements but also because the proper operation and development of educational elements ensure the educational resource system's survival and growth [17]. Resource elements refer to all kinds of objective elements related to the development of the social system and educational system, which can support and maintain the development of various activities and system operations. Resource elements refer to various educational resources that can effectively support the development of educational activities, including hardware facilities resources, human resources, financial resources, etc. Resource elements refer to all kinds of material resources in the social system that can effectively support the operation of the educational system and also include other forms of resources that can be transformed into educational resources. Social elements refer to the corresponding value cognition and social

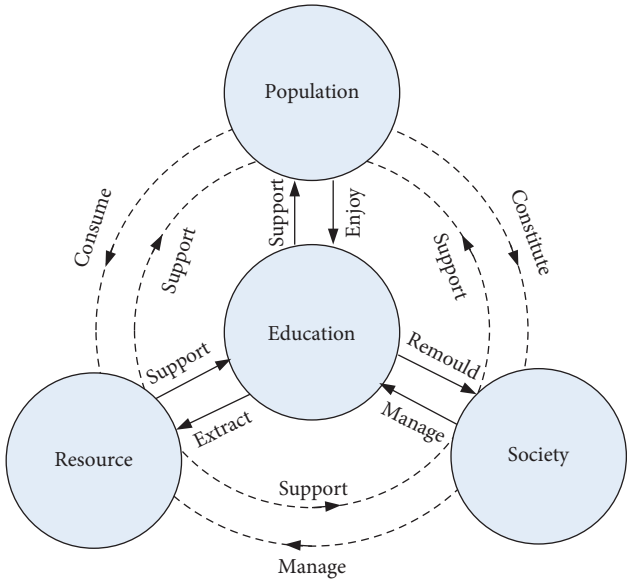

Figure 1: Educational PRES analysis framework diagram.

environment with value concepts that can profoundly influence the educational system and social system. From the macro level, it includes the system, mechanism, system, concept, and culture that can influence the system, and from the microlevel, it includes the policies, regulations, rules, and conditions that specifically guide and regulate the system. Among them, social factors not only invisibly influence and dominate other factors but also receive feedback from other factors for their changes and development.

3.2. Construct Rough Set Evaluation Index System. Index system of design is a comprehensive and systematic scientific research activity; the index system has many characteristics, such as being systematic, comprehensive, scientific; in the collection of many indexes selected appropriate indicators, asking to choose the index can reflect the comprehensive and the internal structure of the system. The resource bearing index of higher education focuses on the supervision index of the education process and monitors the basic operation of higher education by observing and analyzing the dynamic process of each object [18]. Based on relevant theories of higher education resource carrying capacity and strict design principles, this paper selects reasonable evaluation indexes to form a comprehensive, systematic, and scientific evaluation index system of higher education resource carrying capacity.

The bearing capacity of education resources is based on the research methods and research of the indicators used; the existing index to merge similar definition analysis index, remove not related indicators, and define fuzzy index was improved; the index system of comparison and use other types of education at the same time, carefully considering the operability of the system, carefully adheres to the three evaluation index system design principles, and thoroughly examines the idea and connotation of higher education resource carrying capacity. The index system is built from the core resources of higher education, urban economic resources, and urban basic resources, based on a comprehensive reference of some scholars on the construction of educational resource carrying capacity index, in accordance with the principle of scientific, complete, and measurable, and the Angle of data accessibility. Figure 2 depicts the assessment index method for urban higher education resource carrying capacity.

The primary index of core resources of higher education includes four secondary indexes: financial input, number of full-time teachers, number of students, and number of universities, which are mainly used to measure the development foundation, quality level, and sustainable development ability of urban higher education. The first-level indicators of urban economic resources include population density, per capita GDP, the average wage of employees, and regional GDP growth rate, which are mainly used to measure the supporting ability and level of urban economic development to higher education. The first-level indicators of urban basic resources include five second-level indicators: the total amount of urban water supply, the total amount of urban electricity, the number of urban hospital beds, the per capita road area, and the area of urban building land, which are mainly used to measure the auxiliary and supporting role of urban infrastructure and public services on higher education.

3.3. Balance Mechanism of Carrying Capacity of Higher Education Resources. The balance mechanism of higher education resource carrying capacity is a set of operation modes and processes of higher education resource carrying capacity system to maintain the balance of educational resource carrying capacity [20]. For a comprehensive analysis, describe the environment, to understand its relationship with the social development, people created the organizational environment status information of a general framework, using the DPSIR model dynamic analysis of higher education from the perspective of integrity and connecting resources bearing capacity, the depth type structure and describing the content of the preschool education resources bearing capacity of structure system and operation mode, and expressing the resource logic of the development of higher education. According to DPSIR operation logic, this study decomposed the operation mechanism of higher education resource carrying capacity into driving system, bearing system, and response system. The operating mechanism of higher education resource carrying capacity is shown in Figure 3. The three systems are connected and functional according to the operation logic of operation.

3.4. Entropy Weight Method. The entropy weight method is an objective method for determining index weight introduced by information theory. The basic idea is to calculate the entropy weight of an index according to its variability, which is inversely proportional to the variation degree of the index value, the amount of information provided, and its role in comprehensive evaluation [21]. Compared with the qualitative index weight assignment method, the entropy

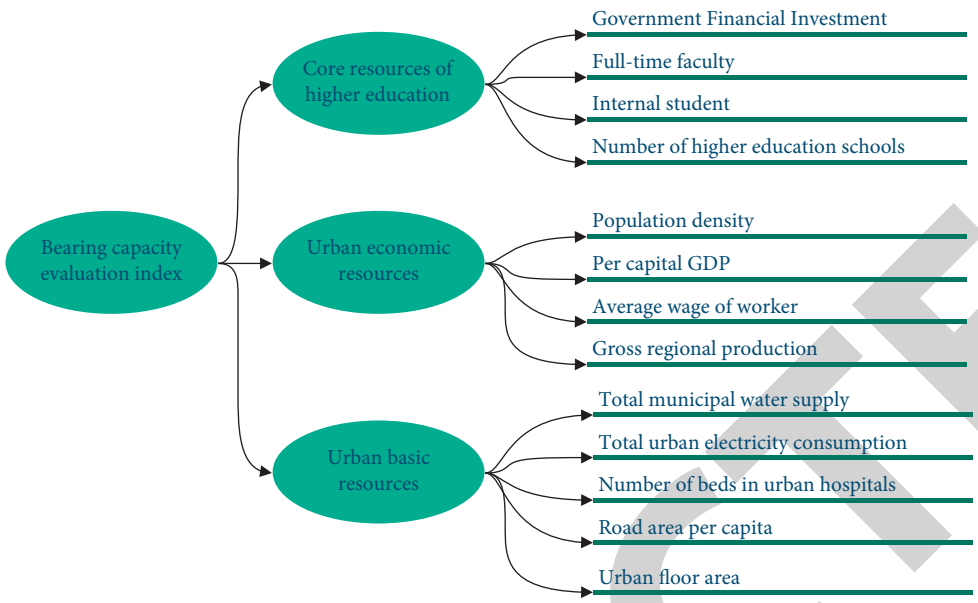

Figure 2: Evaluation index System diagram of urban higher education resource carrying capacity.

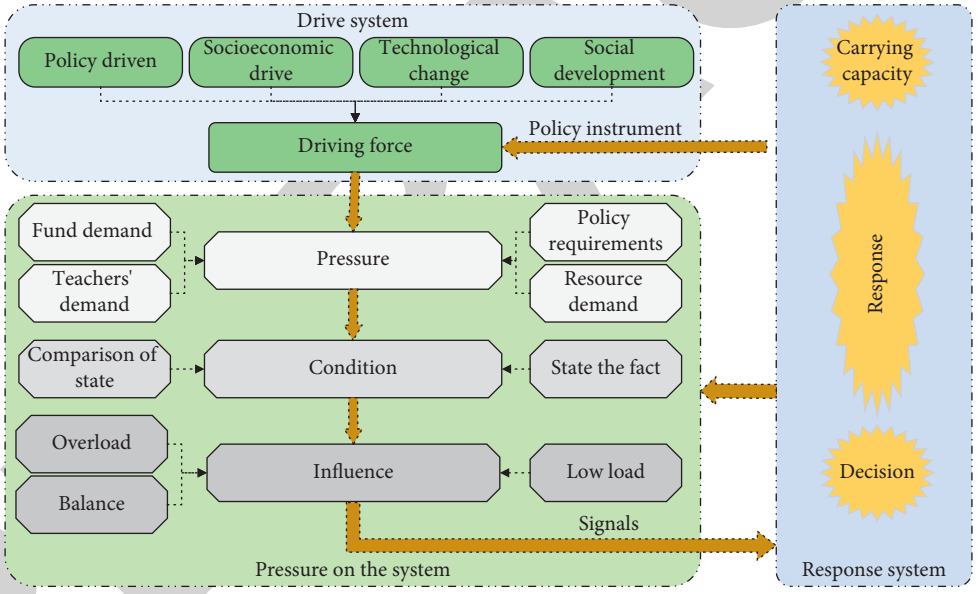

Figure 3: Operation mechanism diagram of higher education resource carrying capacity.

weight method has stronger objectivity and higher accuracy and can better explain the calculated results. The entropy weight method is used for a comprehensive evaluation, and the original matrix is constructed, which includes the evaluated object $m = (m_1, m_2..., m_m)$, evaluation index $D = (D_1, D_2,... D_n)$ raw data matrix.

$$x = \begin{Bmatrix} x_1 & x_2 & \cdots & x_n \\ x_{11} & x_{12} & \cdots & x_{1n} \\ \vdots & \vdots & \cdots & \vdots \\ x_{m1} & x_{m2} & \cdots & x_{mn} \end{Bmatrix}_{m\times n}, \quad (1)$$

where x_{mn} represents the evaluation value of the m item under the n index.

The original matrix is dimensionless. In order to eliminate the dimensionality effects of different indicators, the entropy weight method normalized the original data with different trends. Meanwhile, as the average area of dangerous houses per resident in some provinces, regions, and cities in the original data was zero, the extreme value method was used to standardize different types of indicators to meet the requirement that the real number of logarithmic calculations was greater than zero.

High quality index: positive index, the larger its value, the better the evaluation:

$$V_{mn} = \frac{x_{mn} - \min(x_m)}{\max(x_m) - \min(x_m)} + 1. \quad (2)$$

Low quality index: The higher the reverse index value, the lower the evaluation:

$$V_{mn} = \frac{\max(x_m) - x_{mn}}{\max(x_m) - \min(x_m)} + 1. \tag{3}$$

The characteristic proportion of the m item under the n index is as follows:

$$p_{mn} = \frac{v_{mn}}{\sum_{m=1}^{a} v_{mn}}. \tag{4}$$

The entropy value of the n index is as follows:

$$e_n = -\frac{1}{\ln(a)} \sum_{m=1}^{a} p_{mn} \times \frac{1}{\ln(p_{mn})}. \tag{5}$$

When n is the index of each project, the smaller the entropy value, the greater the difference of the index value, the more information reflected. On the contrary, the larger the entropy value, the larger the difference of the index value, the less information reflected.

The difference coefficient of the n index is as follows:

$$d_n = 1 - e_n. \tag{6}$$

The entropy weight of each indicator is determined as follows:

$$w_n = \frac{d_n}{\sum_{m=1}^{b} d_n}. \tag{7}$$

Positive and negative ideal solutions are determined as follows:

$$\begin{aligned} Z^+ &= \left\{ \max_{1<m<a} v_{mn} | m = 1, 2, \ldots, a \right\} = \{v_1^+, v_2^+, \ldots, v_b^+\}, \\ Z^- &= \left\{ \max_{1<m<a} v_{mn} | m = 1, 2, \ldots, a \right\} = \{v_1^-, v_2^-, \ldots, v_b^-\}. \end{aligned} \tag{8}$$

The distance between each evaluation scheme and positive and negative ideal solutions: The distance of the positive ideal solution is as follows:

$$D_n^+ = \sqrt{\sum_{n=1}^{b} (v_{mn} - v_n^+)^2}, \quad m = 1, 2, \ldots, a. \tag{9}$$

The distance of the negative ideal solution is as follows:

$$D_n^- = \sqrt{\sum_{n=1}^{b} (v_{mn} - v_n^-)^2}, \quad m = 1, 2, \ldots, a. \tag{10}$$

The relative proximity to the optimal scheme is as follows:

$$C_m = \frac{D^-}{D^+ - D^-}, 1 \le m \le a. \tag{11}$$

The larger the C_m, the higher the proximity between m evaluation scheme and the optimal scheme.

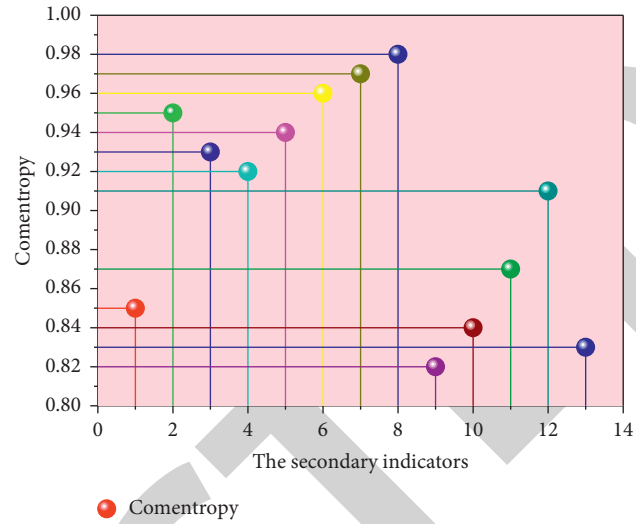

Figure 4: Statistical chart of information entropy of educational carrying capacity index.

4. Result and Analysis

4.1. The Entropy Weight Analysis of Educational Carrying Capacity. Various data were collected on the official website of each school, including financial input, number of full-time teachers, number of students, and number of colleges and universities. Among them, the number of full-time teachers and administrative staff was the number of staff. The index values of urban population density, per capita GDP, average wage of staff and workers, regional GDP growth rate, the total amount of urban water supply, the total amount of urban electricity, the number of urban hospital beds, and per capita road area are collected through this method. Considering that the index caliber of the original data is different and the order of magnitude is greatly different, the original data is standardized. As study samples, this report uses cross section data from 18 institutions. The normalized matrix of the formula style was created after normalization of the original data: Information entropy calculation. The information entropy of 13 educational carrying capacity indicators was estimated using the formula. Figure 4 depicts a statistical representation of the information entropy of educational carrying capacity measures.

The contribution of core resources of higher education, social economic resources, and urban basic resources to the carrying capacity of urban higher education resources is as follows: 40%, 21%, and 39%, fully indicating that the higher education resource carrying capacity is mainly affected by the higher education core resources and urban basic resources, and the impact of urban economic resources indicators on the higher education resource carrying capacity is limited. The carrying capacity of urban higher education resources is not only restricted by the current situation and development of higher education resources but also highlights the supporting role of urban infrastructure and public services to higher education. As a part of the urban system,

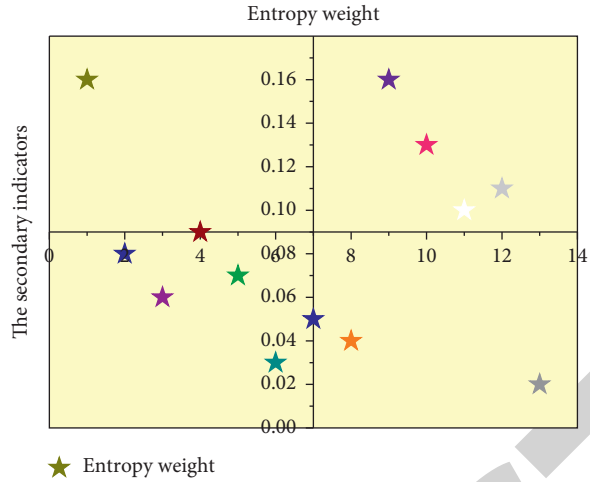

Figure 5: Statistical chart of entropy weight of educational carrying capacity index.

the higher education ecosystem is relatively independent in its operation and development, so it is less affected by the urban economic operation and development. However, the basic resources of the higher education ecosystem need the support of the urban system, so the basic resources become the most important indicator next to the core resources of higher education.

The entropy weights of 13 educational carrying capacity indicators are calculated according to the formula, and the entropy weights statistics of educational carrying capacity indicators are shown in Figure 5.

Financial input, the total amount of urban water supply, and the total amount of urban electricity consumption all contribute significantly to the carrying capacity of urban higher education resources, accounting for nearly half of the total. This fully reflects the main impact of government financial support and urban hydropower infrastructure and service on the carrying capacity of higher education resources. The carrying capacity of urban higher education at the average level is determined by the number of full-time teachers, students, colleges and universities, population density, the number of beds in urban hospitals, and per capita road area, which reflects the status quo of higher education resources. The contribution of urban traffic and medical conditions to the carrying capacity is crucial. The contribution of per capita GDP, average wage, and regional GDP growth rate to urban higher education resource carrying capacity is low. The results of the secondary index are highly consistent with the primary index, which reflects the weak correlation between urban economic development and higher education resource carrying capacity.

The closeness degree of urban higher education resource carrying capacity is calculated according to the formula. The statistical figure of the closeness degree of higher education resource carrying capacity is shown in Figure 6.

As can be seen from the figure, the closer the relevance is to 1, the higher the carrying capacity level of urban higher education is, the stronger the sustainable development capacity of higher education is, and the greater the space and potential of education development is. The closer the degree of closeness is to 0, the vice versa. The ranking results can be divided into four ranges: the first range is 1–6, the comprehensive performance evaluation is "good"; the second range is 7–11, the comprehensive performance evaluation is "good"; the third range is 12–15, indicating "average" overall performance evaluation; the fourth range is that the comprehensive performance evaluation is "poor" after the closeness degree is 16. The grounds for the first section's "excellent" educational carrying capacity can be seen in the figure, which shows that it performs well in terms of full-time teachers, students, and colleges and universities, and the scores of the six cities are comparable to the ranking. As a result, higher education resource agglomeration may increase the carrying capacity of urban higher education resources. Because the overall performance of indicators is better and the distribution of indicators is more uniform, the second interval's overall performance is better. The third segment has a low score, and the structure of the distribution of numerous indicators is complicated and uneven, with general performance. The overall distribution is in the central and western areas, and urban development performance is average. Due to the effect of geographical location or city administrative level, the fourth zone belongs to the weak educational carrying capacity with a low overall index since it cannot compete with the top cities in terms of financial assistance, policy support, and city attractiveness.

4.2. Analysis of Higher Education Resources Concentration Level. Cities with higher education resource concentration levels are distributed in 18 higher education resource concentration indexes. Figure 7 shows the map of cities with higher education resource concentration levels.

As can be seen from the figure, Beijing has the highest concentration index of higher education resources, followed by Shanghai, Wuhan, Nanjing, Guangzhou, Xi 'an, and Chengdu. In addition, the agglomeration level of higher education resources in the eastern, central, and western regions has an obvious trend of stepwise decline. In the eastern region, Beijing is the center, with Shanghai, Nanjing,

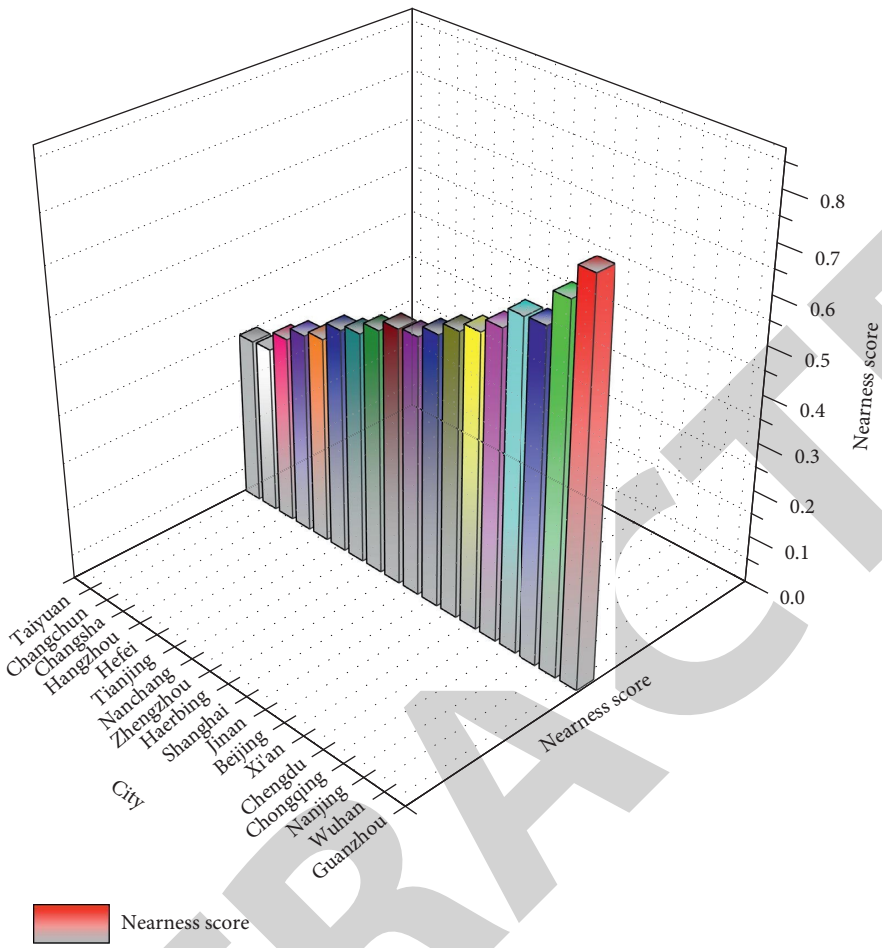

Figure 6: Statistical chart of closeness degree of higher education resource carrying capacity.

and Guangzhou as the three subcenters. In the central region, Wuhan is the center, and Changsha, Zhengzhou, Hefei, and Nanchang are the subcenters. In the western region, Xi 'an and Chengdu are the dual centers, with Chongqing and Kunming as the subcenters. Within each region, the agglomeration ability of urban higher education resources in Fujian province, Guangxi Zhuang Autonomous Region, and Hainan Province is weaker than that of other provincial capitals or subprovincial cities in the east. The capital cities of Shanxi Province and Inner Mongolia Autonomous Region are weak in higher education resources gathering ability. In western China, Qinghai, Gansu, Ningxia, Guizhou, Xizang, and other provinces have a weak ability to gather higher education resources. At the national level, higher education resources are mainly concentrated in the capital cities of municipalities directly under the Central Government, while the higher education resources concentration index of other cities is generally lower than the national average. This shows that China's higher education resources tend to cluster in central cities with larger scale and obvious centrality.

4.3. Analysis of Spatial Distribution Difference of Bearing Capacity. Function core city as the city's economic and political center, known as the owner of the superior quality education resources manpower and material resources, financial resources, the higher education resource bearing capacity should be at a higher level; however, due to its high quality education resources to attract more students to cause a virtuous cycle, the limitation of core area and because of its realistic condition, the students' ability is limited. As a result, the carrying capacity of educational resources is relatively low. The spatial distribution difference of bearing capacity is shown in Figure 8.

According to the figure, the spatial distribution pattern of the comprehensive carrying capacity of higher education resources is analyzed. Specifically, the distribution pattern of human, financial, and material resources is slightly different. The distribution pattern of the carrying capacity of financial resources and material resources is the same as that of comprehensive carrying capacity. The strongest carrying capacity is the ecological conservation and development area, followed by the urban function expansion area; the weakest is the functional core area, and the weakest is the new urban development area. The different distribution patterns are reflected in the human resource carrying capacity, which is still the strongest in ecological conservation development zones, and the second in urban development zones, while the human resource carrying capacity of functional core and functional expansion zones is weak.

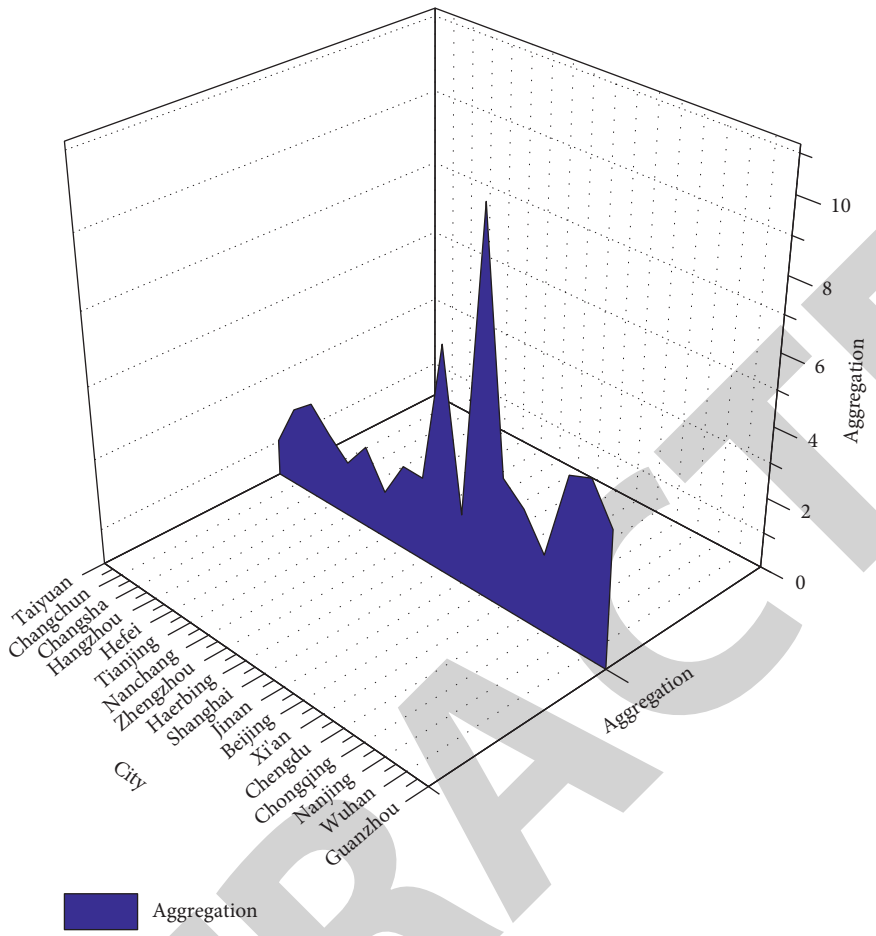

Figure 7: Map of higher education resource concentration level cities.

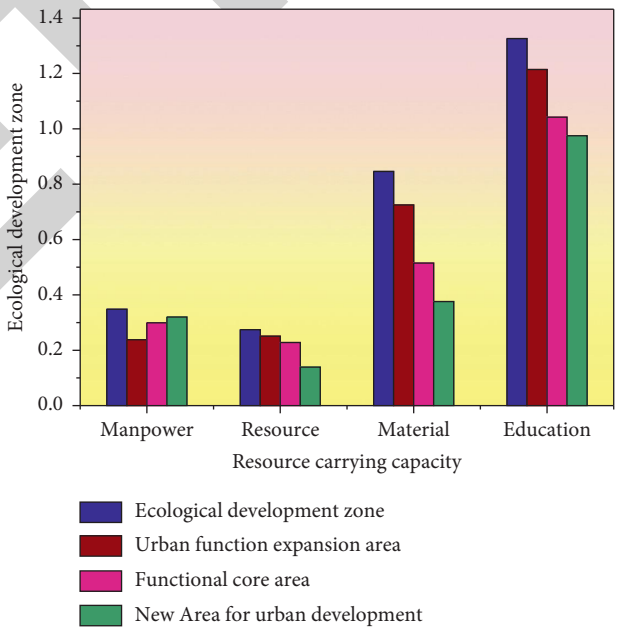

Figure 8: Spatial distribution difference diagram of bearing capacity.

5. Conclusion

Higher education is one of the important components of social development and progress. The level of education determines the quality of a nation's development and affects the basic capabilities of a country and a region. Vigorously developing higher education provides strong support for the realization of sustainable economic and social development. Based on the rough set theory, this paper constructs a rough set of big data of urban higher education resource carrying capacity from the three levels of higher education core resources, urban economic resources, and urban basic resources. This system deeply deconstructs and expounds the balance mechanism of higher education resource carrying capacity and provides solid theoretical support for the development of the thesis. The research shows that the agglomeration development of higher education resources can improve the carrying capacity of urban higher education resources. There are significant differences in the carrying capacity of higher education resources, which provides a scientific basis for improving the carrying capacity of higher education resources and provides theoretical and policy basis for realizing rational allocation and sustainable carrying capacity of higher education resources. From the perspective of education ecology, the evaluation index system of higher education resource carrying capacity is constructed from the three levels of higher education core resources, urban economic resources, and urban basic resources. It is found that the higher education resource carrying capacity is mainly affected by the core resources of higher education and the urban basic resources and has a weak correlation with urban economic development. The impact of financial support and urban hydropower resources on the carrying capacity of higher education resources is prominent. The carrying capacity of urban higher education also has a certain range, so it is necessary to implement an optimal allocation and differentiation strategy to fully tap the potential and concentrate superior resources.

Data Availability

The data are available upon request.

Conflicts of Interest

The authors declare that they have no known competing financial interests or personal relationships that could have appeared to influence the work reported in this paper.

References

[1] Y. Li, M. Sun, G. Yuan, Q. Zhou, and J. Liu, "Study on development sustainability of atmospheric environment in northeast China by rough set and entropy weight method," *Sustainability*, vol. 11, no. 14, p. 3793, 2019.

[2] Y. He, Y. Pang, Q. Zhang, Z. Jiao, and Q. Chen, "Comprehensive evaluation of regional clean energy development levels based on principal component analysis and rough set theory," *Renewable Energy*, vol. 122, pp. 643–653, 2018.

[3] J. Wang, X. Wei, and Q. Guo, "A three-dimensional evaluation model for regional carrying capacity of ecological environment to social economic development: model development and a case study in China," *Ecological Indicators*, vol. 89, pp. 348–355, 2018.

[4] T. Peng and H. Deng, "Comprehensive evaluation on water resource carrying capacity based on DPESBR framework: a case study in Guiyang, southwest China," *Journal of Cleaner Production*, vol. 268, Article ID 122235, 2020.

[5] H. Yan, Y. Huang, G. Wang et al., "Water eutrophication evaluation based on rough set and petri nets: a case study in Xiangxi-River, Three Gorges Reservoir," *Ecological Indicators*, vol. 69, pp. 463–472, 2016.

[6] Q. Xue, X. Yang, and F. Wu, "A three-stage hybrid model for the regional assessment, spatial pattern analysis and source apportionment of the land resources comprehensive supporting capacity in the Yangtze River Delta urban agglomeration," *The Science of the Total Environment*, vol. 711, Article ID 134428, 2020.

[7] L. Ding, Z. Shao, H. Zhang, C. Xu, and D. Wu, "A comprehensive evaluation of urban sustainable development in China based on the TOPSIS-entropy method," *Sustainability*, vol. 8, no. 8, p. 746, 2016.

[8] T. Peng, H. Deng, Y. Lin, and Z. Jin, "Assessment on water resources carrying capacity in karst areas by using an innovative DPESBRM concept model and cloud model," *The Science of the Total Environment*, vol. 767, Article ID 144353, 2021.

[9] X. Xi, S. Wang, L. Yao, Y. Zhang, R. Niu, and Y. Zhou, "Evaluation on geological environment carrying capacity of mining city—a case study in Huangshi City, Hubei Province, China," *International Journal of Applied Earth Observation and Geoinformation*, vol. 102, Article ID 102410, 2021.

[10] Y. Shi, S. Shi, and H. Wang, "Reconsideration of the methodology for estimation of land population carrying capacity in Shanghai metropolis," *The Science of the Total Environment*, vol. 652, pp. 367–381, 2019.

[11] L. He, Y. Du, S. Wu, and Z. Zhang, "Evaluation of the agricultural water resource carrying capacity and optimization of a planting-raising structure," *Agricultural Water Management*, vol. 243, Article ID 106456, 2021.

[12] L. Shen, T. Shu, X. Liao et al., "A new method to evaluate urban resources environment carrying capacity from the load-and-carrier perspective," *Resources, Conservation and Recycling*, vol. 154, Article ID 104616, 2020.

[13] X. Zhang, J. Dai, and Y. Yu, "On the union and intersection operations of rough sets based on various approximation spaces," *Information Sciences*, vol. 292, pp. 214–229, 2015.

[14] X. Cao, Y. Shi, and L. Zhou, "Research on urban carrying capacity based on multisource data fusion-A case study of Shanghai," *Remote Sensing*, vol. 13, no. 14, p. 2695, 2021.

[15] B. Men, H. Liu, W. Tian, and H. Liu, "Evaluation of sustainable use of water resources in Beijing based on rough set and fuzzy theory," *Water*, vol. 9, no. 11, p. 852, 2017.

[16] H. S. Own and H. Yahyaoui, "Rough set based classification of real world Web services," *Information Systems Frontiers*, vol. 17, no. 6, pp. 1301–1311, 2015.

[17] X. Zhang, C. Mei, D. Chen, and J. Li, "Feature selection in mixed data: a method using a novel fuzzy rough set-based information entropy," *Pattern Recognition*, vol. 56, pp. 1–15, 2016.

[18] Q. Duan, Y. L. Yang, and Y. Li, "Rough K-modes clustering algorithm based on entropy," *IAENG International Journal of Computer Science*, vol. 44, no. 1, pp. 13–18, 2017.

Hindawi
Journal of Mathematics
Volume 2023, Article ID 9784351, 1 page
https://doi.org/10.1155/2023/9784351

Retraction

Retracted: Dance Evaluation Based on Movement and Neural Network

Journal of Mathematics

Received 19 December 2023; Accepted 19 December 2023; Published 20 December 2023

This article has been retracted by Hindawi following an investigation undertaken by the publisher [1]. This investigation has uncovered evidence of one or more of the following indicators of systematic manipulation of the publication process:

(1) Discrepancies in scope

(2) Discrepancies in the description of the research reported

(3) Discrepancies between the availability of data and the research described

(4) Inappropriate citations

(5) Incoherent, meaningless and/or irrelevant content included in the article

(6) Manipulated or compromised peer review

The presence of these indicators undermines our confidence in the integrity of the article's content and we cannot, therefore, vouch for its reliability. Please note that this notice is intended solely to alert readers that the content of this article is unreliable. We have not investigated whether authors were aware of or involved in the systematic manipulation of the publication process.

Wiley and Hindawi regrets that the usual quality checks did not identify these issues before publication and have since put additional measures in place to safeguard research integrity.

We wish to credit our own Research Integrity and Research Publishing teams and anonymous and named external researchers and research integrity experts for contributing to this investigation.

The corresponding author, as the representative of all authors, has been given the opportunity to register their agreement or disagreement to this retraction. We have kept a record of any response received.

References

[1] Y. Lei, X. Li, and Y. J. Chen, "Dance Evaluation Based on Movement and Neural Network," *Journal of Mathematics*, vol. 2022, Article ID 6968852, 7 pages, 2022.

Hindawi
Journal of Mathematics
Volume 2022, Article ID 6968852, 7 pages
https://doi.org/10.1155/2022/6968852

Research Article

Dance Evaluation Based on Movement and Neural Network

Yan Lei, Xin Li, and Yi Jiao Chen

Arts College of Sichuan University, Chengdu, Sichuan 610000, China

Correspondence should be addressed to Yan Lei; robert_dials_00@subr.edu

Received 23 November 2021; Revised 8 December 2021; Accepted 13 December 2021; Published 1 February 2022

Academic Editor: Naeem Jan

In terms of music-driven dance movement generation, the music movement matching model and the statistical mapping model have poor fit between the dance generated by the model and the music self. The generated dance movement is incomplete, and the smoothness and rationality of long-term dance sequences are low. The new dance moves and other related issues cannot be generated by the traditional model. In order to address these issues, we design a dance generation algorithm based on movements and neural networks that will extract the mapping between voice and movement features. In the first stage, where the prosody features and audio beat features extracted from music are used as music features, and the coordinates of key points of the human body extracted from dance videos are used as motion features for training. In the second stage, the basic mapping of music and dance movements are realized through the generator module of the model to generate a smooth dance posture; the consistency of dance and music is realized through the discriminator module; the audio characteristics are more possessed through the Autoencoder module representative. In the third and final stage, the modified version of the model transforms the dance posture sequence into a realistic version of the dance. Finally, a realistic version of the dance that fits the music is obtained. The experimental data is obtained from dance videos on the Internet, and the experimental results are analyzed from five aspects: loss function value, comparison of different baselines, evaluation of sequence generation effect, user research, and quality evaluation of real-life dance videos. The results show that the proposed dance generation model has a good effect in transforming into realistic dance videos.

1. Introduction

The two modalities of vision and hearing are strictly related. As long as the object moves, visual changes will inevitably lead to the production of auditory sound. At present, most machine learning still stays in the learning of information in a single mode. In recent years, with the vigorous development of artificial intelligence technology, the transition from single-modal learning to multimodal learning has become the key to a better understanding of machine perception. More and more researchers have begun to pay attention to the learning of multi-modal information, including cross-modal retrieval, multi-modal information joint make a decision, and cross-modal generation. Cross-modal generation aims to synthesize one modal or several modal data based on the information of different modalities. One-way or two-way generation of text to image, text to video, audio to image, and audio to video are all examples of cross-modal generation.

With the development and popularization of deep learning in recent years, artificial neural networks have been successfully applied to the generation of dance movements. The significant advantage of using deep learning for dance generation is that they can directly extract advanced features from raw data. In addition, deep neural networks can create new dance moves. However, the dance generation algorithm based on deep learning also has some problems. For example, due to the end-to-end model, the generated dance may not be smooth before and after the frames, which will make the visualization effect of the generated dance worse; on the other hand, dances directly generated by algorithms are often difficult to match with music. In addition, for the visualization of dance, people often draw the skeleton of the human body or perform animation processing directly according to the coordinates of the key points of the human body, and there is room for further improvement in the visualization effect.

Dance data often comes from the real world. It is necessary to extract continuous dance pose data from a specific dance video using human pose estimation technology, and design a specific audio feature encoder to extract audio features from the music matched by the dance. The dance data reflects the changes in the coordinates of the key points of the human body in different times. It is a typical time series data, so it has the characteristics of multiscale, multidimensional, and dynamic correlation.

Aiming at the characteristics of dance data, this paper constructs a custom music and dance dataset, which contains about 270,000 frames of music and dance movements. The human body pose estimation technology is used to extract the coordinates of the iconic human skeleton key points as the dance pose features, and the design is designed. The specific music feature encoder proposes a model for dance movement generation based on deep learning and performs end-to-end training on the extracted dance features and music features. The model is optimized through quantitative and qualitative experiments, and a dance generation model that best fits music is obtained. Finally, the generated dance is visualized using the improved Pix2Pix model, and a live-action dance video is obtained. Under the premise of no additional labeling of data, an end-to-end dance generation model is obtained through self-supervised learning, which is useful for intelligent dance teaching, game fields, cross-modal generation, and exploring the relationship between audiovisual information a certain value.

2. Related Work

Current Research Status. The cross-modal generation from audio to video can be divided into three categories: body motion generation, audio-driven image generation, and talking face video generation.

Synthesizing the corresponding face video through speech or music is a typical cross-modal generation task. Early research on the generation of talking faces was mainly to synthesize a specific identity from a dataset based on arbitrary speech and audio. Kumar et al. [1] tried to use delayed LSTM [2] to generate key points synchronized to the audio, and then another network generated video frames conditioned on the key points. This is the first network architecture that uses any text as input to generate the corresponding voice and lip-sync video that syncs photos to reality. Unlike other published methods, their method only consists of a fully trainable neural network and does not rely on any traditional computer graphics methods. The model uses three main modules: Char2 Wav-based text-speech network, delayed LSTM for generating voice points synchronized with audio, and Pix2-Pix-based network for generating videos based on these key points. Subsequently, Chung et al. [3] tried to use an Encoder-Decoder CNN model to learn the correspondence between the original audio and video, which used the joint embedding of face and audio to generate synthetic speaking facial video frames. The model inputs the still image and audio voice segment of the target face and outputs the lip-shaped video of the target face synchronized with the audio. Jalalifar et al. [4] combined RNN and GAN [5] to create a sequence of real faces synchronized with the input audio by two networks. One of them is the LSTM network, which is used to create lip landmarks based on audio input. The other is conditional GAN, which is used to generate facial images based on a given set of lip marks. Together, these two networks can generate a natural speaking face sequence synchronized with the input audio track. Borra et al. [6] further proposed a time consistency method for dynamic pixel loss. Compared with the direct audio-to-image method, this cascade method avoids fitting false correlations between audiovisual signals that are not related to speech content. In order to avoid these pixel jitter problems, the authors strengthened the network's attention to audio-visual related areas and proposed a new dynamic and adjustable pixel-level loss attention mechanism. In addition, in order to generate clearer images with well-synchronized facial motion, they proposed a new regression-based discriminator structure that takes into account sequence-level information and frame-level information.

Cross-modal conversion through audio and image is a kind of cross-modal generation problem. Chen et al. [7] first tried to use conditional generation confrontation network to solve this cross-modal generation problem, realized the mutual conversion of music sounds and corresponding playing instrument pictures, and also realized cross-modal audio-visual mutual generation. The researchers, respectively, defined a sound-image network and an image-sound network to generate images and sounds, respectively. Brahmaiah et al. [8] from the Institute of Automation of the Chinese Academy of Sciences and others considered a cross-modal cyclic generation confrontation network and combined different generation subnetworks into one network and proposed a cross-modal generation model based on the cyclic confrontation generation network. The mutual generation effect between music and pictures is enhanced. Recently, there have been some studies trying to reconstruct facial images from speech fragments. Duarte et al. [9] proposed a deep neural network, which is trained from scratch in an end-to-end manner and directly generates faces from the original speech waveform without any additional identity information. Their model is trained in a self-supervised manner by using naturally aligned audio and video features in the video. Another type of cross-modal generation task is to generate corresponding speech videos from voice or text end-to-end without the intervention of specified rules. Some researchers considered combining acoustic analysis with text [10], demonstrating a method of generating 3D virtual humans from audio signals by inferring the acoustic and semantic characteristics of speech. Through prosodic analysis of acoustic signals and linking them with the semantics of the words spoken, dynamic virtual facial expressions and behaviors are generated, including head movements, eye saccades, gesture, blinking, and staring. Research has shown that their technology is superior to the method of generating virtual humans using only phonetic prosody. Some other researchers have realized the speech of any given speaker through self-supervised training in speech video [11], generated the corresponding speech posture without adding any semantic information, and then synthesized realistic speech video.

3. Method

In this section, the proposed method is described in detail. First of all, the long- and short-term memory (LSTM) network is reviewed and then its extensions, promotions, and improvements are discussed. The updated formula is also presented. Further, the deep learning is used as a base for the construction of the dance generation model. Then, the design of prosody feature extraction is presented. It is followed by the representation of training data. Finally, the generator design is given.

3.1. Long- and Short-Term Memory Network. Long- and short-term memory network is usually abbreviated as LSTM, which is a special type of RNN. It is designed to solve the long-term dependence of recurrent neural networks. It was introduced by Hochreiter and Schmidhuber [12]. It was refined and promoted by many people in subsequent work. LSTM has achieved good results on many time series problems and has been widely used.

The first step of LSTM is to decide what information to discard from the cell. This decision is controlled by a sigmoid layer called the "forgotten gate." For each element in the cell state C_{t-1}, the forgetting gate passes input h_{t-1} and x_t and then outputs a number between 0 and 1, which represents the percentage of information retained from the previous cell state C_{t-1} to the current cell f_t. 1 means "keep all this information," and 0 means "discard all this information." The updated formula of f_t is as follows:

$$f_t = \sigma\left(W_f \cdot \left[h_{t-1}, x_t\right] + b_f\right). \tag{1}$$

The next step is to decide what new information the model will store in the cell state. This step is divided into two parts.

$$\begin{aligned} i_t &= \sigma\left(W_i \cdot \left[h_{t-1}, x_t\right] + b_i\right), \\ \widetilde{C}_t &= \tanh\left(W_c \cdot \left[h_{t-1}, x_t\right] + b_c\right). \end{aligned} \tag{2}$$

Then, update the old cell state to the new state.

$$C_t = f_t * C_{t-1} + i_t * \widetilde{C}_t. \tag{3}$$

Finally, after updating the cell state, the final output result needs to be determined according to the input h_t and x_t. The output will be based on the current cell state and some information will be filtered.

$$\begin{aligned} O_t &= \sigma\left(W_0 \cdot \left[h_{t-1}, x_t\right] + b_0\right), \\ h_t &= O_t \cdot \tanh\left(C_t\right). \end{aligned} \tag{4}$$

3.2. Model Overall Design. Figure 1 shows the overall design of a dance generation model based on deep learning. The gray box represents the processing module or the network module, and the red and blue boxes represent music characteristics and dance gesture characteristics, respectively. The light-orange box represents the loss function setting. As shown in the figure, first perform audio feature extraction and action feature extraction on the dance data, and then input the audio features into the dance generator to obtain the predicted dance posture, and make MSE Loss with the real dance posture; the audio features are obtained through the Autoencoder module. The audio features of the structure are constructed, and the loss of audio reconstruction is made; the predicted dance posture and the real dance posture are sent to the discriminator for discrimination, and the model is trained against loss.

3.3. Design of Prosody Feature Extraction. In the field of sound processing, Mel-Frequency cepstrum is a linear transformation of the logarithmic energy spectrum based on the nonlinear Mel scale of the sound frequency. Mel-Frequency Cepstral Coefficients (MFCC) are the coefficients that make up the Mel-frequency Cepstral spectrum. The frequency band division of the Mel-frequency cepstrum is equidistantly divided on the Mel scale, which is closer to the human auditory system than the linearly spaced frequency bands in the normal cepstrum. Such feature representation can provide better characterization of sound signals in many fields, such as audio compression and speech recognition. In summary, we choose the 24-dimensional Mel spectrum feature and the 8-dimensional tempogram feature as the vector representation of the audio melody, as shown in Table 1.

The design of rhythm feature extraction takes into account that all music has a fixed rhythm; that is, each piece of music has a fixed drum beat, so the rhythm feature can be further extracted from the audio feature. When the audio feature vector representing the melody and the rhythm feature vector representing the rhythm of the drums are used as neural network input together, the model is easier to understand the entire audio feature sequence. These beat characteristics are shown in Table 2 and can be used as beat control signals for the dance generation model. By constructing a feature matrix in the form of a three-dimensional arithmetic sequence, the model can add beat information on the basis of audio features, as shown in Table 2. The beat feature vector of the first dimension is the position of each audio frame in the whole piece of music; the beat feature vector of the second dimension is the position of the audio frame within each beat of the music; the beat feature vector of the third dimension is the position of each audio frame in the music.

3.4. Training Data Representation. In summary, the data extracted from the original dance video for training the dance generation model can be expressed as follows.

Audio characteristics:

$$M_i = \langle m_i^1, m_i^2, \ldots, m_i^{32} \rangle. \tag{5}$$

Beat characteristics:

$$B_i = \langle b_i^1, b_i^2, b_i^3 \rangle. \tag{6}$$

Posture feature:

$$P_i = \langle p_i^1, p_i^2, \ldots, p_i^{36} \rangle. \tag{7}$$

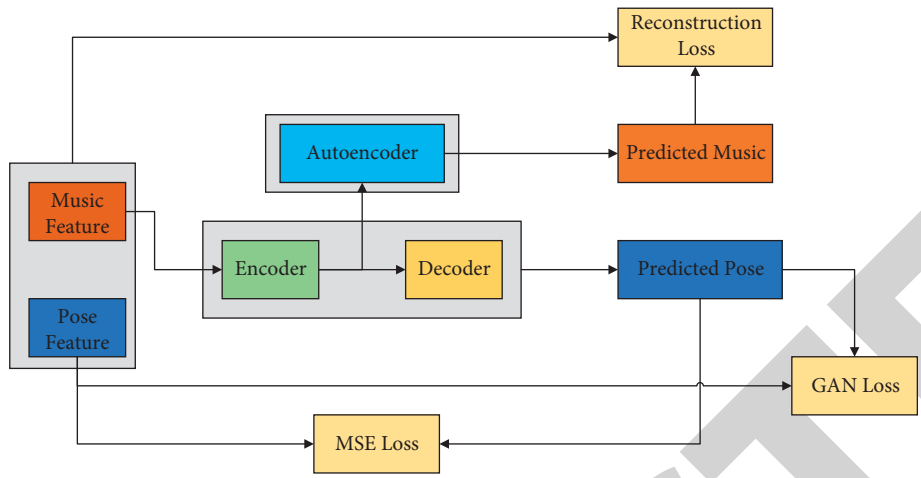

Figure 1: Schematic diagram of the network structure of the dance generative model.

Table 1: Table of music features.

Audio characteristics	Feature dimension
MFCC	$M_1, \ldots, M_{24}$
Tempogram	$M_{24}, \ldots, M_{32}$

Table 2: Table of beats feature.

Rhythmic characteristics	Feature dimension
The position of the entire music audio frame	b_1
The position of the audio frame within the beat	b_2
The relative value of the audio frame within the beat	b_3

Audio data:

$$M = \{M_1, M_2, \ldots, M_n\}. \tag{8}$$

Dance posture data:

$$P = \{P_1, P_2, \ldots, P_n\}. \tag{9}$$

The training data required by the model can be expressed as M and P. Among them, $M = \{M_1, M_2, \ldots, M_n\}$, that is, a total of N frames of audio data; each frame of audio data is represented by M_n; $P = \{P_1, P_2, \ldots, P_n\}$; that is, the dance pose data corresponds to the audio data and the same frame.

3.5. Generator Design. In order to describe the generator design, we classified it into three major phases. The first one is encoder design, which extracts the audio features from the input. Secondly, the process of attention calculation begins. For that reason, a module called attention weight calculation is designed. Lastly, the decoder is designed, which decodes the audio features.

3.5.1. Encoder Design

(1) Encoder Module. In order to extract long-term audio features, the encoder module is composed of multiple layers of LSTM and CNN. The input is the extracted audio feature vector and rhythm feature vector. The output is a music context vector. The specific representation is shown in formulas (10) and (11), where F_1, F_2, F_3 are three convolution kernels, Re LU is the nonlinear activation on each convolution layer, and Encoder Recurrency represents the bidirectional LSTM. The music feature sequence after feature extraction is first sent to a three-layer convolution layer to extract music context information, and then sent to a two-way LSTM to generate the hidden state H of the encoder. As shown in the figure, the input vector $X = \{x_1, x_2, \ldots, x_i\}$. The hidden layer state $H = \{h_1, h_2, \ldots, h_i\}$ in the green box is obtained after coding. After the hidden state of the encoder is generated, it will be sent to the attention network to generate an audio context vector.

$$f_c = \text{Re LU}\left(F_3 * \text{Re LU}\left(F_1 * E(X)\right)\right), \tag{10}$$

$$H = \text{Encoder Recurrency}\left(f_c\right). \tag{11}$$

3.5.2. Design of Attention Calculation Module

(1) Attention Weights Calculation Module. The hidden layer state $H = \{h_1, h_2, \ldots, h_i\}$ and the hidden layer state $S = \{s_1, s_2, \ldots, s_j\}$ can be calculated separately through the encoder module and the decoder module, where H and S are each the hidden state of the encoding layer and the hidden state of the decoding layer at a time step. Then, calculate the Attention Weights and assign the Attention Weights to the music context vector to obtain the audio feature vector after the weight is assigned. Attention calculation occurs at each decoder time step, and the target hidden state and each source state are calculated by a custom score function to generate Attention Weights. In order to reduce potential subsequence duplication or omissions in the decoding process, consider using the cumulative attention weight of the previous decoding process as an additional feature to keep the model consistent when moving forward along the input sequence. So, our model uses a position-sensitive attention mechanism, which is an extension of the previous

attention mechanism. As shown in formula (12), $f_{i,j}$ is the location feature obtained by convolution of the previous Attention Weights, and V_a^T, W, V, U, and B are the parameters to be trained. After the Attention Weights module, the Attention Weights between the hidden state h_j and s_i can be obtained.

$$e_{i,j} = \text{score}\left(s_i, ca_{i-1}, h_j\right) = v_a^T \tanh\left(Ws_i + Vh_j + Uf_{i,j} + b\right). \quad (12)$$

3.5.3. Decoder Design. According to the generated music context vector, the decoding tasks are executed sequentially, and each task focuses on one or several audio feature vectors; that is, different weights are assigned to the audio feature vectors. The encoder part adopts an autoregressive model and uses the predicted value of the dance pose at the previous time step as the input of the next time step to predict the dance pose at the next time step.

In summary, we describe the process of generator training as follows. The music training dataset is $M = \{M_1, M_2, \ldots, M_n\}$, where M_i is a sequence of audio feature vectors. The dance training dataset corresponding to music is $P = \{P_1, P_2, \ldots, P_n\}$, and P_i is the dance posture feature vector corresponding to M_i. The training data of a sample pair composed of $\{M_i, P_i\}$, M, and P are obtained from live dance videos through specific feature extraction schemes. The goal of the model is to train a dance generator G to realize the mapping relationship between M and P. As shown in formula (13), the model is first trained on $\{M_i, P_i\}$, and the MSE Loss is calculated between the dance $G(M_i)$ generated by the model and the real dance P_i. After the training, we input the given music into the training model to get the corresponding dance pose sequence.

$$\mathscr{L}_{\text{MSE}}(G) = \frac{1}{N}\sum_{i=1}^{N}\left\|P_i - G(M_i)\right\|^2. \quad (13)$$

4. Experiments and Discussion

4.1. User Research Results. We mainly conducted user research on the authenticity of the model-generated dance and the consistency between dance and music. First, we investigated whether the dance generated by the model is authentic and credible. We invited 20 observers to conduct a scoring experiment and showed each observer 15 dance fragments generated by five different models according to the dance category. Each observer scored according to the fidelity of the dance. The highest score is 10 points and the lowest score is 0 points. The score of each model is calculated based on the scores of 15 videos by the scorers, and finally the scores of all scorers are averaged to calculate the average value, and then the reality score of each model can be obtained.

According to the data shown in Figure 2, we set the model one to be the LSTM-PCA model, the second model is the LSTM PCA and Discriminator model, the third model is the Generator part of our dance generation model, and the fourth model is the Generator and Discriminator model. The fifth is the Generator and Discriminator and Autoencoder model. As can be seen from the table, in terms of authenticity, our Generator series models are better than other models. Specifically, model one scores 3.61 points, model two scores 5.43 points, model three scores 6.90 points, model four scores 7.85 points, and model five scores 8.52 points.

As can be seen from Figure 3, our Generator series model is better than other models in terms of music consistency. In terms of data, the music consistency of the Kpop dataset is higher than that of other types of dances. This may be due to the large differences in the internal data of the other two dance datasets. For example, the music in the same dance type is quite different. Training is more difficult, but Kpop dance data has no such problem. It also shows that the human body of Kpop dance makes more prominent emotional expressions, and the choreography is more in line with the music. Specifically, model 1 has a score of 4.54 on the Kpop dataset, a score of 2.87 on the Poppin dataset, and a score of 3.19 on the Hiphop dataset; model 2 has a score of 5.61 on the Kpop dataset and a score of 5.61 on the Poppin dataset. The score is 4.32, and the score on the Hiphop dataset is 4.21; the score of model three on the Kpop dataset is 6.54, the score on the Poppin dataset is 5.32, and the score on the Hiphop dataset is 5.39.

The score of model four on the Kpop dataset is 8.01, the score on the Poppin dataset is 7.21, and the score on the Hiphop dataset is 7.45; the score of model five on the Kpop dataset is 9.01 and the score on the Poppin dataset is 7.98; the score in the Hiphop dataset is 7.32. In summary, our model has received the best user reviews compared to other models in terms of dance authenticity and music consistency.

4.2. Image Quality Evaluation Results. As shown in Table 3, using global content discriminator and local time discriminator, even a single frame result, its score is better. Due to the increased lack of attitude perception, the attitude becomes paradoxical, and then the different attitudes are transferred to the frame, which may cause the score to drop. In addition, more significant differences can be observed in our videos.

In order to evaluate the quality of the live-action dance video, BRISQUE [13] is used to evaluate the quality of the live-action dance video. Specifically, different models are used to generate dance poses for the same piece of music, and the same set of live-action generators are used to generate live-action videos. For each live-action video, 100 consecutive video frames are randomly sampled for quality evaluation. According to the quality evaluation results in the table, the effect of adding the Autoencoder module is slightly worse than not adding it. This may be due to the additional loss introduced by Autoencoder, which reduces the generated results.

4.3. Experimental Results. The experimental results of the dance generation model on user research show that for most users, the dance generated by our model exceeds other models in terms of authenticity and musical consistency. This reflects that our model's comprehensive dance generation effect is the best. The experimental results of the dance generation model on the quality of the live-action dance video show that the

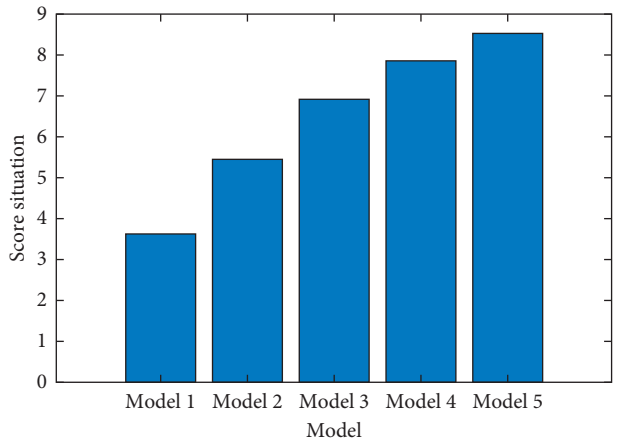

Figure 2: Dance authenticity rating chart.

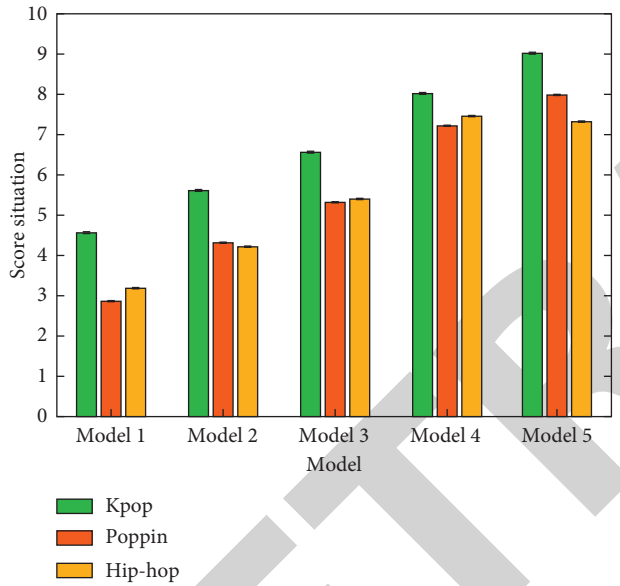

Figure 3: Music consistency rating chart.

Table 3: Image quality assessment score.

Method	BRISQUE
Generator	39.23
Generator-Discriminator	41.40
Generator-Discriminator-Autoencoder	40.37

posture sequence generated by our model is more reasonable, with fewer error or unreasonable posture frames, so the synthesized live-action effect is also the best. This shows that the humanized process we designed is reasonable, and it further reflects that our model has not only achieved good results in sequence generation, but also effective in real human transformation. In summary, our Generator and Discriminator and Autoencoder dance generation model program can effectively extract the characteristics of music, generate dance gesture sequences that fit the music, and transform them into realistic dance videos.

5. Conclusions

The deep leaning-based dance generation algorithm can input music with any type and style. Moreover, it can output the dance posture and real person that the music fits. Researching the related models, this article has completed the following tasks:

It finished reading a large number of domestic and foreign related documents. Furthermore, it understood the current situation and development trend of dance generation algorithms based on deep learning. The combination of the current popular dance generation algorithm and the traditional dance generation algorithm has a couple of problems. The first problem is the difficulty of generating smooth and graceful dance postures. The second problem is the difficulty of matching dance movements with music.

It completed the research on the methods of domestic and foreign dance generation algorithms, combined with the characteristics of music and dance data, and designed audio feature extraction and action feature extraction schemes. The dance generation model is constructed through the extracted audio feature vectors and action feature vectors: in order to achieve a smooth and complete dance sequence, a generator module is designed; in order to achieve a fit between dance and music, a discriminator module is designed; in order to have the extracted audio feature vector, the self-encoder module is designed for better characterization. In order to visualize the effect, the dance posture sequence generated by the dance generation model is transformed into a real person.

The experiments were performed for the purpose of verification in which the dance dataset downloaded from the internet was obtained. It analyzed the five aspects of model loss function value, loss comparison of different models, sequence generation effect, user research, and image generation effect of live-action dance. Experimental results showed that in the feature extraction stage, the use of prosody and rhythm features together as audio features is better than the use of prosody features alone. The use of error frames, missing value differences, and sequence smoothing for dance poses can make the action features smoother. The generation effect is better. In the model building stage, the Generator and Discriminator and Autoencoder model has the strongest generation effect, which can generate a dance posture sequence that is smooth and complete and fits the music. In the stage of live-action dance, the improved Pix2Pix model has also achieved good results in experiments.

The research results play an important reference role for dance generation algorithms. It solves the problem of failure to generate smooth and complete action sequences and dances that fit music in previous studies. It has certain value for intelligent dance teaching, game field, cross-modal generation, and exploring the relationship between audio-visual information. In the future, on the basis of this article, a larger dance dataset can be established to expand the training data to train a more representative and robust dance generation model.

Hindawi
Journal of Mathematics
Volume 2023, Article ID 9812914, 1 page
https://doi.org/10.1155/2023/9812914

Retraction

Retracted: Research on the Integration of Preschool Language Education Resources Based on Metadata Storage

Journal of Mathematics

Received 15 August 2023; Accepted 15 August 2023; Published 16 August 2023

This article has been retracted by Hindawi following an investigation undertaken by the publisher [1]. This investigation has uncovered evidence of one or more of the following indicators of systematic manipulation of the publication process:

(1) Discrepancies in scope

(2) Discrepancies in the description of the research reported

(3) Discrepancies between the availability of data and the research described

(4) Inappropriate citations

(5) Incoherent, meaningless and/or irrelevant content included in the article

(6) Peer-review manipulation

The presence of these indicators undermines our confidence in the integrity of the article's content and we cannot, therefore, vouch for its reliability. Please note that this notice is intended solely to alert readers that the content of this article is unreliable. We have not investigated whether authors were aware of or involved in the systematic manipulation of the publication process.

Wiley and Hindawi regrets that the usual quality checks did not identify these issues before publication and have since put additional measures in place to safeguard research integrity.

We wish to credit our own Research Integrity and Research Publishing teams and anonymous and named external researchers and research integrity experts for contributing to this investigation.

The corresponding author, as the representative of all authors, has been given the opportunity to register their agreement or disagreement to this retraction. We have kept a record of any response received.

References

[1] S. Weiwei, "Research on the Integration of Preschool Language Education Resources Based on Metadata Storage," *Journal of Mathematics*, vol. 2022, Article ID 4802381, 8 pages, 2022.

Hindawi
Journal of Mathematics
Volume 2022, Article ID 4802381, 8 pages
https://doi.org/10.1155/2022/4802381

Research Article

Research on the Integration of Preschool Language Education Resources Based on Metadata Storage

Sun Weiwei

School of Preschool and Art Education, Xinyang Vocational and Technical College, 464000 Xinyang, China

Correspondence should be addressed to Sun Weiwei; xiaolajia@xyvtc.edu.cn

Received 8 December 2021; Accepted 3 January 2022; Published 31 January 2022

Academic Editor: Naeem Jan

Aiming at the problems of high redundancy and slow integration speed in the existing education resource data integration methods, a new preschool language education resource integration method based on metadata warehouse is designed. The metadata warehouse is designed, and the advantages of the integrated database are analyzed. On this basis, the sample data of preschool language education resources are classified with the help of cost matrix, and the constraints of different types of classification are set. The data collector of preschool language education resources is set up by using random forest algorithm to complete the data collection of preschool language education resources. The data of preschool language education resources are processed consistently, and the convergence of the data is calculated by edge function. On this basis, the redundant data in preschool language education data resources are characterized with the help of discourse, and the redundant data are removed to complete the data preprocessing of preschool language education resources. We determine the dimension distance between preschool language education resource data and complete the clustering integration of preschool language education resource data with the help of fuzzy mean clustering algorithm. The experimental results show that the integration method designed in this paper can reduce the redundancy in the integrated data, and the integration speed is fast.

1. Introduction

The early stage of language learning is the key period of human language germination. The habits formed in language learning in this period will affect people's life. As a key tool for human communication, the resource data in the process of language learning have a key impact on it. Preschool language education resources are the first language resources that children come into contact with in their learning. The representation and understanding of these resources play a key guiding role in children's growth [1]. The quantity of data in preschool language instruction materials is expanding as electronic information technology advances; however, there are various data kinds, and fish eyes mistake pearls [2]. The importance of language education in early infancy cannot be overstated. As a result, boosting the quality of instructional materials is beneficial to children's language acquisition. As a result, current research in this sector is focusing on the successful integration of preschool language instruction materials [3], removing unnecessary information from the data to increase its usefulness. A variety of approaches have been tested, and some results have been obtained. Xiao [4] proposed an educational information fusion method based on intelligent data acquisition and processing. This method first represents the relevant education data, then maps the relationship according to different characteristic data, constructs the education information database by Protégé software, and finally effectively fuses the semantic information of education resource data. This method improves the speed of information fusion of educational resources, but the redundancy of data in data fusion is not considered. Wang et al. [5] suggested a machine learning-based parallel integration solution for tiny database datasets. This technique uses a Bayesian algorithm to generate a priori independent hypotheses for relatively unrelated data and then categorizes the educational resource data efficiently. It examines the volatility of data characteristics based on categorization and

utilizes MapReduce parallel processing to finish the integration of education data. This technology has minimal integrated data redundancy and increases the quality of resource data, but the operation procedure is difficult and has certain limitations.

In order to make up for the shortcomings of the above methods, this paper designs a new preschool language education resource integration method based on metadata warehouse. The main technical lines of this method are as follows.

Step 1. Design the metadata warehouse and analyze the advantages of changing the integrated database.

Step 2. Classify the samples of preschool language education resource data with the help of cost matrix, set the constraints of different types of classification, and set the preschool language education resource data collector with random forest algorithm to complete the data collection of preschool language education resources.

Step 3. Perform consistency processing on the data of preschool language education resources and use the edge function to calculate the convergence of the data.

Step 4. On this basis, characterize the redundant data characteristics in preschool language education data resources with the help of discourse, remove the redundant data, and complete the data preprocessing of preschool language education resources. Determine the dimension distance between preschool language education resource data and complete the clustering integration of preschool language education resource data with the help of fuzzy mean clustering algorithm.

Step 5. Conduct experimental analysis.

2. Metadata Storage and Data Integration of Preschool Language Education Resources

2.1. Metadata Warehouse Analysis. This article investigates the use of cloud data warehousing technologies in the integration of preschool language instruction materials. As a result, the metadata warehouse is intended to store the preschool language resource data in the cloud data warehouse database of preschool language education resource integration. It is necessary to extract the metadata of preschool language education resources, deposit the metadata of different preschool language education resources according to certain teaching needs, and store the precipitated data in order to improve the data information of preschool language education resources and collect these resource data into the metadata warehouse [6]. Through excellent integrated retrieval of preschool language education materials, the metadata repository established in this study delivers data services for preschool language instruction.

Metadata warehouse is an effective way to realize the integration of preschool language education resources. Its key role is to store all kinds of basic metadata information of preschool language education resources [7]. The implementation flow of its storage is shown in Figure 1.

The metadata warehouse mainly includes the collection, storage, and integration of preschool language education resource data. By extracting these data and integrating preschool language education resources through the set specific interface, it supports the retrieval and various forms of display of preschool language education resources. The repository supports the mainstream relational preschool language education resource data and the standard of preschool language education resource data through index storage. Preschool language teaching resource data are gathered, preprocessed, and eventually incorporated into the metadata warehouse in a follow-up study to increase the application impact of preschool language teaching resource data [8].

2.2. Data Collection of Preschool Language Education Resources. Based on the metadata warehouse of preschool language education resources designed above, in order to integrate the integrated preschool language education resource data into the database [9], firstly, we need to effectively collect the resource data of preschool language education and take the collected resource data as the basis of the research to realize the research of methods. Because there are many types of preschool language education resource data and the amount of data is complex, these relevant data are classified before data collection of preschool language education resources to reduce the difficulty of data collection [10].

In the data classification of preschool language education resources, firstly, the data samples of preschool language education resources are classified into a category with its cost by means of cost matrix, that is, minimizing the expected generation value [11]. According to the basic original of the matrix, an arbitrary preschool education resource data sample a is divided into the expected cost $Q(j \mid a)$ of class j, yielding

$$Q(j \mid a) = \sum_{j=1} y(j \mid a) \times b(i, j), \tag{1}$$

where $y(j \mid a)$ represents the possibility that any sample of the preschool language education resource can be divided into class j species occurrence.

(1) After determining the probability that preschool language education resource data will be divided, set the divided constraints. After meeting the conditions, classify the qualified preschool language education resource data [12], and the set constraints are as follows.

Conditions that the preschool language education resource data were classified into positive classes were set to

$$q(0 \mid a)c(1, 0) + q(1 \mid a)c(1, 1) \le q(0 \mid a)c(0, 0), \tag{2}$$

where c represents the positive class coefficient of preschool language education resources and q represents the probability estimation coefficient.

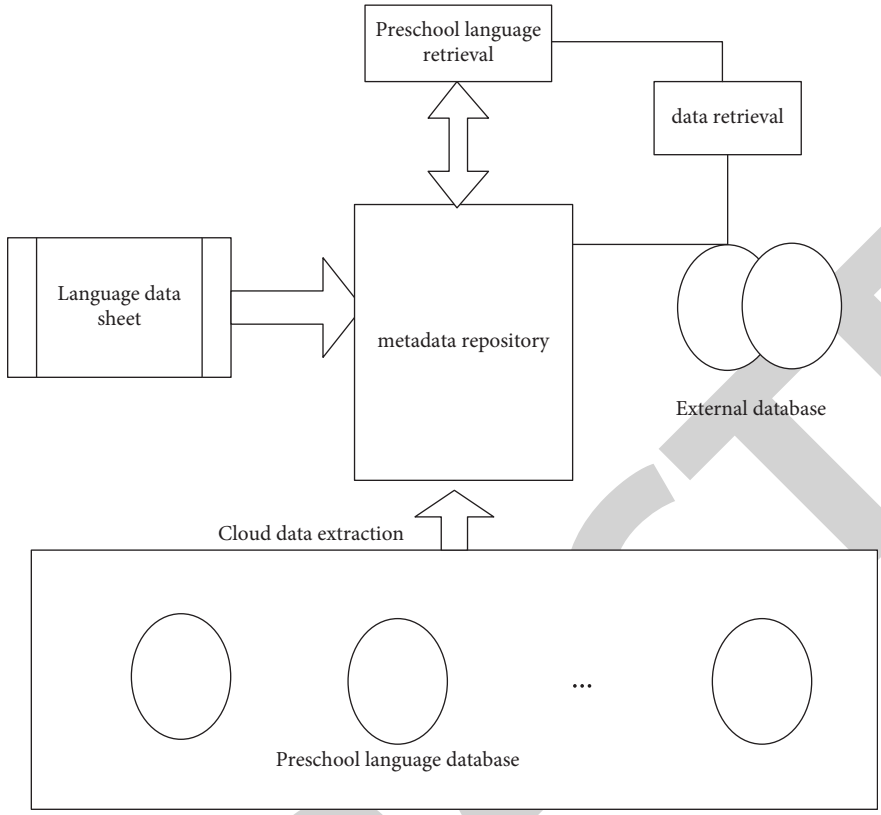

Figure 1: Schematic diagram of implementation process of metadata warehouse of preschool language education resources.

(2) The condition that preschool language education resource data are divided into negative categories is set as

$$q(0\,|\,a)v(1,0) - q(1\,|\,a)c(1,1) \le r(0\,|\,a)c(1,0), \tag{3}$$

where v represents the data resource conversion coefficient and r represents the range of classification proportion, and the value is [0, 1].

After determining the above classification constraints of preschool language education resources, it is necessary to balance the classified preschool language education resources to ensure the effectiveness of data resource collection [13]. The calculation formula of resource data balance is

$$E = \frac{p(1,0)v}{d(1) - d(0)}, \tag{4}$$

where $d(1)$ represents the prior probability of positive class data in the original data of the initial preschool language education data, $d(0)$ represents the prior probability [14] of negative class data in the initial preschool language education data, and c represents the data balance factor. The effective classification process of preschool language education resource data is shown in Figure 2.

On the basis of data classification, through the effective collection of positive data and negative data, presecondary language education data were found. In data collection, the data in different types of datasets are collected through random forest. Through multiple training of data in different types of datasets [15], the data collector is constructed to complete data collection, namely:

$$W(x) = \arg\max \sum_{i=1}^{n} K(h_i), \tag{5}$$

where $W(x)$ represents preschool language education resource data collector, K represents a single base collector, h_i represents the target data acquisition, and arg represents the collection function.

First, the samples of preschool language education resources data are categorized using a cost matrix, and the restrictions of several forms of categorization are established. On this foundation, the data collector for preschool language education resources is set up, and the data collection of preschool language education resources is completed using the random forest method.

In the data collection of preschool language education resources, firstly, the samples of preschool language education resources data are classified with the help of cost matrix, and the constraints of different types of classification are set. On this basis, the data collector of preschool language education resources is set up by using random forest algorithm to complete the data collection of preschool language education resources.

2.3. Data Preprocessing of Preschool Language Education Resources. There are various duplicate data and granularity information conflicting with the integration of the

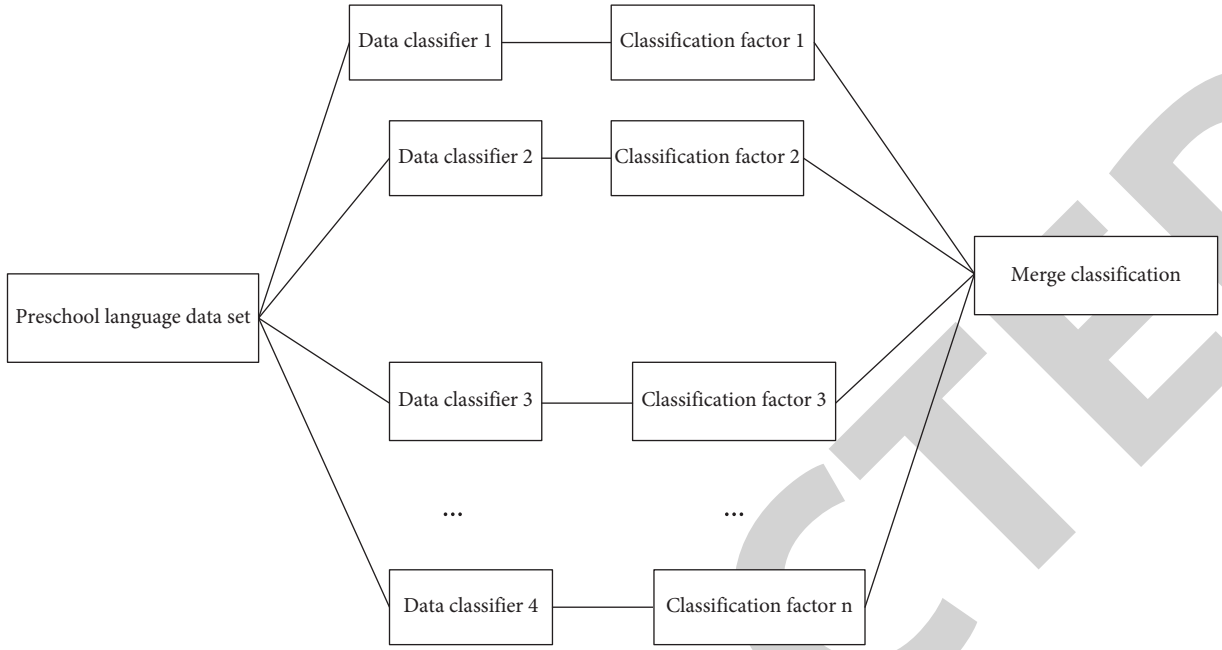

Figure 2: Data classification process of preschool language education resources.

aforementioned obtained preschool language education resource data [16]. To increase the efficacy of the study approach in this work, it is required to properly preprocess the preschool language education resource data. In light of the above-mentioned education resource data convergence, it is required to process the education resource data consistently in order to provide suitable data integration. The edge function is introduced to control the convergence of educational resource data [17], that is:

$$S = t_I \sum \arg h_i \times T, \tag{6}$$

where $\arg h_i$ represents the edge function, T represents the mean function, and t_I represents the degree of the convergence of educational resource data.

The edge function can improve the reliability of preschool language education resource data, but the generalization error needs to be further improved, that is:

$$f = px(L(a,b) < 0), \tag{7}$$

where px represents the probability that preschool language education resource data exist in space.

After solving the consistency of preschool language education resource data, it is necessary to remove the redundant information in the education resource data [18]. The granularity generation process of preschool language education resource data is a kind of granulation process. The redundant data generated in the granulation process become the interference data affecting the integration. At this time, the generated redundant data are regarded as a universe [19] in a space and set as a quadruple, that is:

$$O = \{e, s, H, g\}, \tag{8}$$

where e represents the redundant data attribute values of the educational resource data, s represents the value domain of the redundant data, and H represents the information function.

At this time, the redundant representation of any educational resource data in this domain [20] is

$$U \sum Ra \in e, \quad a \in H, \tag{9}$$

where R represents the redundant database and U represents the information function.

The redundant data of education resource data are reflected by formula (10), and this type of data is removed to obtain

$$Q(x) = \rho \frac{1}{2} |U_i|, \tag{10}$$

where $Q(x)$ represents processed results, U_i represents redundant data features, and the data removal ratio is ρ.

In the preprocessing of preschool language education resource data, firstly, the consistency of preschool language education resource data is processed, and the convergence of data is calculated by edge function. On this basis, with the help of discourse, the redundant data characteristics in preschool language education data resources are characterized, and the redundant data are removed to complete the data preprocessing of preschool language education resources.

2.4. Data Integration of Preschool Language Education Resources. Based on the preprocessing of preschool education resource data after the above preprocessing, the data are effectively integrated. In the integration, first of all, it is necessary to determine the dimensional distance between preschool language education resource data. The effective measurement of this distance is conducive to data integration and improve the speed of integration methods [21].

Set the dataset of preschool language education resources as

$$D = \{d_1, d_2, \ldots, d_n\}, \tag{11}$$

where d_n represents the full space dimension value of the annual data of preschool language education resources and D represents the set of constrained information in the set.

Then, educational resource data in the set dataset are randomly selected to generate a subspace [22]:

$$Z = \left\{z^1, z^2, \ldots, z^B\right\}, \tag{12}$$

where z^B represents the random eigenvalues in the subspace.

At this time, the distance [23] between the subspatial dimension of preschool educational resource data and educational resource data is

$$\mathrm{dis}(a,b) = \sum \frac{D(a_i, b_i)}{|v|}, \tag{13}$$

where $|v|$ represents the data similarity in the subspace set and $D(a_i, b_i)$ represents the constraints.

After determining the dimension distance of preschool language education resource data, the similar data are effectively clustered. This paper completes the clustering integration of preschool language education resource data with the help of fuzzy mean clustering algorithm. The algorithm is a soft clustering algorithm, which replaces the same type of data after effective fuzziness, reduces the difficulty of data integration [24], and can adhere to the influence of uncertain factors on data in the integration process. The integration process is as follows.

Set the preschool education resource dataset to be integrated as

$$M = \{m_1, m_2, \ldots, m_n\}, \tag{14}$$

where M represents the number of data from integrated preschool resources and m_n represents the dimension of data elements.

The above dataset to be integrated is divided into C class clusters, when the set class cluster membership matrix is represented as

$$\gamma = \left[\delta_{ij}\right]_{a\times b}, \tag{15}$$

where γ represents the degree of membership.

All integrated data were summed with a membership value of 1, that is:

$$\sum_{i=1}^{n} \delta_{ij} < k. \tag{16}$$

When the membership value of the calculated integrated data is closer to 1, it represents a higher probability of this type of data being easily integrated.

At this time, set the objective function of preschool education resource data and further determine the key data in the preschool language education resource data integration data through the objective function [25], namely:

$$\varepsilon(a,b) = \sigma \sum_{a=1,b=1}^{n} \left[\delta_{ij}\right]_{a\times b}, \tag{17}$$

where $\varepsilon(a,b)$ represents the objective integration function and σ is the weight factor.

After the objective function determines the data weight of preschool language education resources, the effective data integration is completed. The data integration model is as follows:

$$\vartheta = \sigma \sum_{a=1,b=1}^{n} \left[\delta_{ij}\right]_{a\times b} p + \omega\left(1 - \sum \delta_{ij}\right), \tag{18}$$

where ω represents the Lagrangian multiplier, ϑ represents the final integration result, and p represents the compactness after data integration.

In the data integration of preschool language education resources, the dimensional distance between preschool language education resource data is determined, and the clustering integration of preschool language education resource data is completed with the help of fuzzy mean clustering algorithm.

3. Experimental Analysis

3.1. Experimental Scheme. Following the completion of the design of the preschool language education resource integration approach, a simulation experiment is conducted to confirm the practicality of the proposed technique. The resource database for children's language training in MySQL database is chosen as the study object, with 1000 data selected as the experimental sample data, 300 data having some redundancy, and the other data being unclassified data. The research data are successfully trained to fulfill the experiment's needs in order to assure the experiment's efficacy. SPSS13.0 was used to examine the experimental data statistically.

3.2. Experimental Index Design. In the experiment, the methods in this paper, literature [4], and literature [5] are compared, mainly comparing the redundancy processing of integrated data by different integration methods, the accuracy of data integration, and the time cost of data integration.

3.3. Analysis of Experimental Results. Firstly, the experiment analyzes the redundancy processing of sample preschool language education resource data by this method and the methods in [4, 5]. Among them, the lower the data redundancy after processing, the better the effect of the representative method. On the contrary, the processing effect of the representative method has some shortcomings and needs further improvement. The experimental results are shown in Figure 3.

Using the methodology of this work, literature [4], and literature [5], it is possible to show that there are certain variances in the redundancy in the sample preschool language education resource data in Figure 3. The data redundancy drops dramatically and is always lower than that of the other two approaches when the sample data are integrated using the method described in this research.

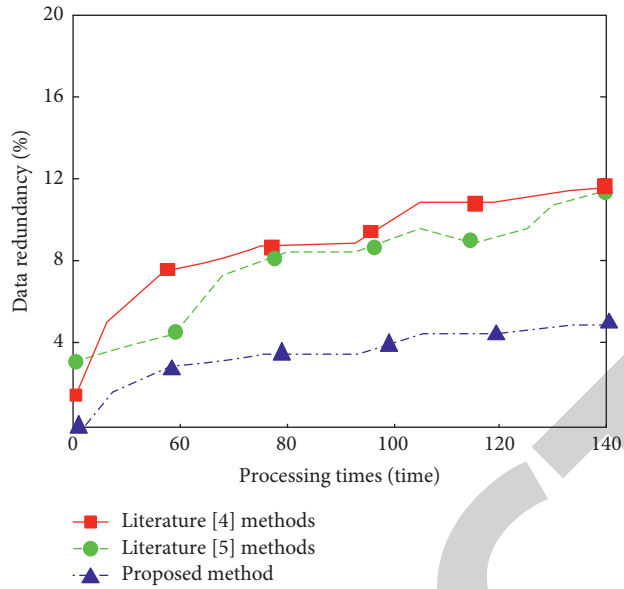

Figure 3: Data redundancy analysis results after integration of different methods.

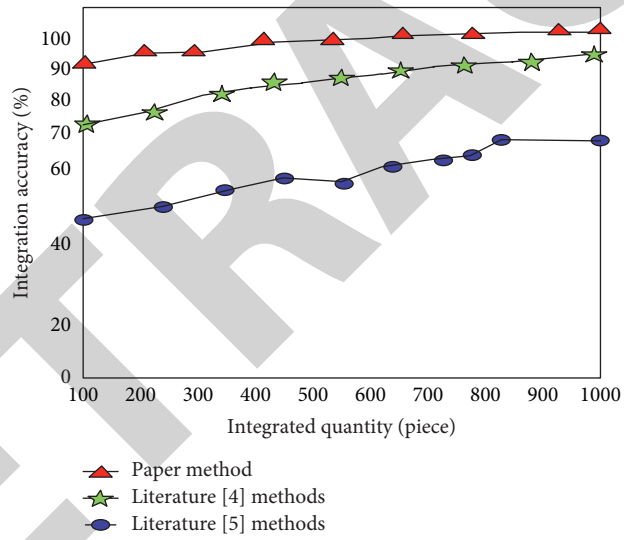

Figure 4: Integration accuracy results of sample data of different methods.

Although the other two approaches' data redundancy is within a respectable range, it is nevertheless larger than that of the method described in this work. This is due to the fact that the data redundancy in this method's dataset is handled in depth, increasing the method's efficacy [31, 32].

The experiment analyzes the accuracy of data integration of sample preschool language education resources by the methods of this paper, literature [4], and literature [5]. The results are shown in Figure 4.

By analyzing the experimental result data in Figure 4, it can be seen that the accuracy of data integration of sample preschool language education resources using this method and the methods in [4] is different. Among them, the data accuracy of this method is always higher than 90%, while the integration accuracy of the other two methods fluctuates greatly and is lower than that of this method. The effectiveness of the proposed method is verified.

In order to further verify the effectiveness of the proposed method, the time cost of data integration of sample preschool language education resources by this method and the methods in literature [4] method and literature [5] method is experimentally analyzed. The results are shown in Table 1.

By analyzing the experimental results in Table 1, it can be seen that with the continuous change of the number of samples, there is a certain gap in the time cost of data integration of sample preschool language education resources by the methods in this paper, literature [4], and literature [5]. Among them, when the data volume is 600, the integration

Table 1: Time cost of data integration of sample preschool language education resources by different methods (s).

Number of samples/bars	The method of this paper	The method in [4]	The method in [5]
200	0.51	1.26	1.34
400	0.53	1.43	1.46
600	0.57	1.62	1.48
800	0.61	1.57	1.66
1000	0.65	1.69	1.87

time overhead of the method in this paper is about 0.57 s, the integration time overhead of the method in literature [4] is about 1.62 s, and the integration time overhead of the method in literature [5] is about 1.48 s. When the amount of data is 1000, the integration time overhead of the method in this paper is about 0.65 s, the integration time overhead of the method in literature [4] is about 1.69 s, and the integration time overhead of the method in literature [5] is about 1.87 s. In contrast, the time cost of data integration in this method is low, which verifies the effectiveness of this method.

4. Conclusion

Preschool is the key period for children to learn language, and the influence of language education resources is more important. In order to solve the problem of poor integration effect in data integration methods, a new method of preschool language education resource integration based on metadata warehouse is designed. The metadata warehouse is designed, and the advantages of changing the integrated database are analyzed. The sample data of preschool language education resources are classified with the help of cost matrix, and the constraints of different types of classification are set. The data collector of preschool language education resources is set up by using random forest algorithm to complete the data collection of preschool language education resources. The data of preschool language education resources are processed consistently, and the convergence of the data is calculated by edge function. With the help of discourse, the characteristics of redundant data in preschool language education data resources are characterized, and the redundant data are removed to complete the data preprocessing of preschool language education resources. We determine the dimension distance between preschool language education resource data and complete the clustering integration of preschool language education resource data with the help of fuzzy mean clustering algorithm. The experimental results show that the integration method designed in this paper can reduce the redundancy in the integrated data, and the integration speed is fast.

Data Availability

The data used to support the findings of this study are included within the article.

Conflicts of Interest

The author declares that there are no conflicts of interest.

References

[1] X. Chen, D. Yang, and J. Lu, "Research on text learning resource recommendation algorithm based on learner model," *Computer Technology and Development*, vol. 30, no. 6, pp. 83–87, 2020.

[2] G. Kortemeyer and S. Drschler, "A user-transaction-based recommendation strategy for an educational digital library," *International Journal on Digital Libraries*, vol. 18, no. 6, pp. 73–88, 2021.

[3] H. Bulat, S. Wela, M. Perez-Ortiz, E. Yilmaz, and J. S. Taylor, "TrueLearn: a family of Bayesian algorithms to match lifelong learners to open educational resources," *Computer Science: Artificial Intelligence*, vol. 66, no. 32, pp. 87–99, 2019.

[4] Z. Xiao, "Research on educational information fusion method based on intelligent data collection and processing," *Modern Electronics Technique*, vol. 43, no. 24, pp. 140–143, 2020.

[5] J. Wang, X.-S. Cheng, and S.-D. Wang, "Parallel integration of small data sets in database based on machine learning," *Science Technology and Engineering*, vol. 19, no. 6, pp. 239–244, 2019.

[6] G. M. Machado, V. Maran, G. M. Lunardi, L. K. Wives, and J. P. Moreira de Oliveira, "Aware: a framework for adaptive recommendation of educational resources," *Journal of Computers*, vol. 12, no. 21, pp. 54–69, 2021.

[7] Y. Chaabi, N. M. Ndiyae, and K. Lekdioui, "Personalized recommendation of educational resources in a MOOC using a combination of collaborative filtering and semantic content analysis," *International Journal of Scientific & Technology Research*, vol. 9, no. 2, pp. 3243–3248, 2020.

[8] D. Shen, "Recommendation of online educational resources based on neural network," in *Proceedings of the 2020 International Conference on Artificial Intelligence and Computer Engineering (ICAICE)*, Beijing, China, October 2020.

[9] Y. Zhang and Y. Chen, "Research on self-help education resource recommendation algorithm based on tag," *Modern Information Technology*, vol. 3, no. 12, pp. 21-22 + 25, 2019.

[10] W. Kang, "Personalized recommendation method of online teaching resources based on spark," *Scientific and Technological Innovation*, vol. 21, no. 25, pp. 86-87, 2019.

[11] J. Zawia, "Artificial intelligence approaches for extracting and recommending online educational resources-systematic review," vol. 32, no. 21, pp. 56–69, 2021.

[12] E. Ossiannilsson, X. Zhang, and J. Wetzler, "From open educational resources to open educational practices for resilient sustainable education," *Distances et Médiations des Savoirs*, vol. 65, no. 31, pp. 78–88, 202.

[13] A. Oliveira, M. Teixeira, and C. Neto, "Recommendation of educational content to improve student performance: an approach based on learning styles," in *Proceedings of the 12th International Conference on Computer Supported Education*, Setúbal, Portugal, January 2020.

[14] K. Nakayama, A. Shimada, and T. Minematsu, "Recommendation of personalized learning materials based on learning history and campus life sensing," in *Proceedings of the Companion Proceedings 10th International Conference on*

Hindawi
Journal of Mathematics
Volume 2024, Article ID 9813159, 1 page
https://doi.org/10.1155/2024/9813159

Retraction

Retracted: Research on the Model of Distance Education Resource Integration from the Perspective of Comparative Education

Journal of Mathematics

Received 23 January 2024; Accepted 23 January 2024; Published 24 January 2024

This article has been retracted by Hindawi following an investigation undertaken by the publisher [1]. This investigation has uncovered evidence of one or more of the following indicators of systematic manipulation of the publication process:

(1) Discrepancies in scope

(2) Discrepancies in the description of the research reported

(3) Discrepancies between the availability of data and the research described

(4) Inappropriate citations

(5) Incoherent, meaningless and/or irrelevant content included in the article

(6) Manipulated or compromised peer review

The presence of these indicators undermines our confidence in the integrity of the article's content and we cannot, therefore, vouch for its reliability. Please note that this notice is intended solely to alert readers that the content of this article is unreliable. We have not investigated whether authors were aware of or involved in the systematic manipulation of the publication process.

Wiley and Hindawi regrets that the usual quality checks did not identify these issues before publication and have since put additional measures in place to safeguard research integrity.

We wish to credit our own Research Integrity and Research Publishing teams and anonymous and named external researchers and research integrity experts for contributing to this investigation.

The corresponding author, as the representative of all authors, has been given the opportunity to register their agreement or disagreement to this retraction. We have kept a record of any response received.

References

[1] Z. Dan, "Research on the Model of Distance Education Resource Integration from the Perspective of Comparative Education," *Journal of Mathematics*, vol. 2022, Article ID 9589394, 8 pages, 2022.

Hindawi
Journal of Mathematics
Volume 2022, Article ID 9589394, 8 pages
https://doi.org/10.1155/2022/9589394

Research Article

Research on the Model of Distance Education Resource Integration from the Perspective of Comparative Education

Zhao Dan

School of Preschool and Art Education, Xinyang Vocational and Technical College, Xinyang 464000, China

Correspondence should be addressed to Zhao Dan; xiaoyy@xyvtc.edu.cn

Received 8 December 2021; Revised 1 January 2022; Accepted 10 January 2022; Published 31 January 2022

Academic Editor: Naeem Jan

In order to solve the problems of high data loss rate, long time-consuming resource integration, large amount of redundant data, and incomplete results of resource integration in traditional methods, a design method of distance education resource integration model from the perspective of comparative education is proposed. Association rules are used to mine resources and get effective resources in the context of comparative pedagogy, with the goal of increasing the impact of resource integration. Then, using a three-tier architecture, a remote education resource integration model is created, and the mining results are combined through the application layer, resource encryption layer, and multicast communication layer to achieve distance education resource integration. Simulation results show that the method of this article has low data loss rate, short resource integration time, less redundant data, and comprehensive integration results, which provides an effective technical support for the development of education.

1. Introduction

With the development and innovation of Internet technology, the network has rapidly penetrated into people's daily life. There are a large number of different types of resources in the network. These resources contain great value. They not only have a variety of expression forms, but they also cover a broad range of topics, including education, medical, trade, military, and economics [1, 2]. The foundation of resource application is resource integration. For example, in the military, integrating and analyzing collected resources can improve the efficiency and scientificity of military analysis and decision-making while also ensuring national security; in education, reasonable resource integration schemes are used to design teaching objectives and plans, which can point out the direction for educational development [3, 4]. Users may examine the market condition in the e-commerce business using integrated data resources, making it easier for them to make consumption choices that are in accordance with their important interests [5]. According to the above analysis, in many fields, the use effect of resources can be improved by reasonably integrating resources. In the field of education, there are a large number of resource integration methods, which provide theoretical and technical support for the development of education.

Reference [6] proposed an information resource integration method based on WLAN. Firstly, a resource integration platform is established. The resources are preliminarily processed via the platform, which comprises a resource acquisition layer, resource integration layer, and application layer; then, the resource integration optimization model is built to further improve the platform preprocessing results. In the optimization process, the integration factor is introduced into the resource integration, and an average rate is set at the same time; finally, the two constraints are combined to realize the integration constraints of information resources. The experimental results show that this method can provide an effective integration method for resource application and improve the effect of resource use. Reference [7] proposed an online integration optimization method of information resources based on clustering algorithm. To begin, the approach calculates the user's interest in relevant information to acquire the keywords of information resources; the forgetting

function is then utilized to characterize the change in user interest, and the user interest model of information resources is created based on the findings. The user interest matrix is created using the established paradigm, and the user types are separated into two categories: core and noncore users. The K-means clustering algorithm and cosine similarity measurement technique are utilized to further segregate the two groups of users and determine their interest weights. Finally, the interest weights are ordered based on the weight calculation findings, and user behavior is projected to achieve online information resource integration and optimization. The experimental results show that this method has high user satisfaction because it fully considers the user's interest in resource integration. Reference [8] designed a large data stream integration system based on multidimensional hierarchical sampling. According to the multidimensional hierarchical sampling strategy, the system was designed. First, the system was separated into modules in the hardware design, such as classifier, CPU, and memory, and the system's stability was enhanced by enhancing module performance. Second, a data hierarchy model is developed in the software architecture, which is utilized to investigate the data flow and realize data quality detection using a clustering technique. Finally, to fulfill the function design of massive data flow integration, the data detection results are merged with the processing results of hardware modules. The testing findings reveal that the system can handle a huge number of data resources and integrate data efficiently in a complex environment, indicating that it has practical application value.

The above traditional methods have played a positive role in resource integration, but with the increase of the number of information resources in the network, they cannot meet the needs of real-time processing of a large number of resources. In the current application process, it is common that the data loss rate in resource integration is too high, the resource integration takes a long time, the amount of redundant data is large, and the results of resource integration are not comprehensive. In order to solve the above problems, this paper proposes a design method of distance education resource integration model from the perspective of comparative education.

2. Research Background

Comparative pedagogy is different from traditional teaching ideas. It mainly advocates education and teaching with a dialectical attitude. Specifically, it refers to discovering the defects and deficiencies in education through the comparison of different educational systems, educational ideas, and educational methods. At the same time, it excavates its advantages and optimizes them in different educational methods so as to promote the reform of the educational model. The development of comparative pedagogy has a certain role in promoting the whole field of education. Analyzing the advantages and disadvantages of different educational models and taking their advantages can improve educational methods. Figure 1 shows the research method system of comparative pedagogy under different principles.

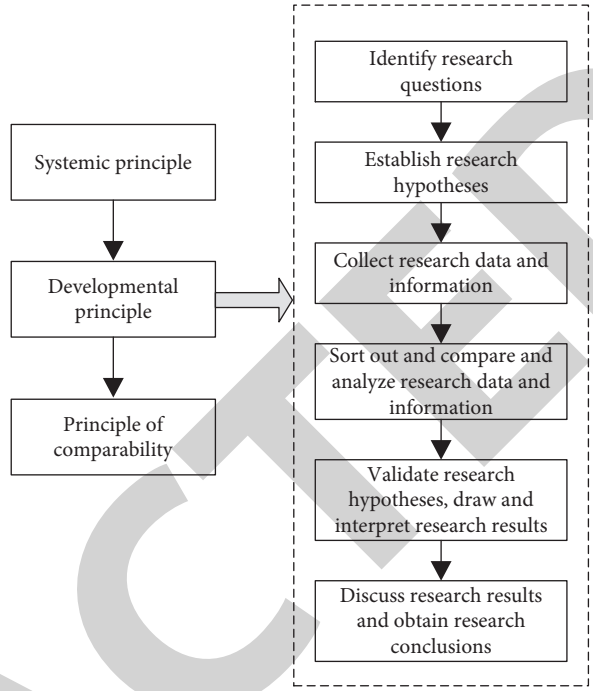

Figure 1: Comparative education research method system.

With the development of comparative pedagogy, education is about enriching educational methods, changing educational thoughts, and improving teaching levels, but more from the perspective of the educated, researching a teaching model of harmony and mutual assistance in various fields. In today's society, the communication between countries in different fields is gradually deepening, and this cultural integration in the field of education is also very obvious. It has certain practical significance to compare the cultural differences between different countries and different ethnic groups in this context. The Internet is mainly used to build communication bridges between various regions and countries in this process. Therefore, a large amount of data resources will be generated on the Internet, and how to effectively process these resources is particularly important. In data processing, resource integration is an effective method that can gather multiple data and resources. Users can find the resources they need in the integrated resources to provide a solid data foundation for education. Therefore, in order to further promote the development of the education field, under the perspective of comparative pedagogy, research on the integration method of distance education resources is the core of the research of this article and its ultimate goal.

3. Distance Education Resource Integration Model

According to the analysis in Section 2, while current educational concepts have gradually become deeply rooted in people's hearts after years of development and have attracted significant attention in related fields, it can be intuitively seen through comparative education theories that while the

depth of the public's research on educational concepts is in a straight line, the depth of the public's research on educational concepts is not. However, the presently developed resource integration techniques need to be enhanced in terms of resource processing impacts. As a result, it is required to investigate an efficient online education resource integration approach against the backdrop of comparative pedagogy development in order to improve the resource processing efficiency. Before that, in order to improve the efficiency of resource integration and avoid the impact of redundant data on the integration results, remote resources should be preprocessed first.

3.1. Distance Education Resource Mining. In order to integrate distance education resources more quickly, first of all, it needs to be mined and analyzed. In the field of resource mining, association rules are a recursive method of frequent set theory, which can scan the resource database many times to obtain the relevant information in the resource database and obtain the attribute association between resources [9, 10].

Under normal circumstances, the association rule method can search the resource library. Assuming that there are N resource sets in the resource library, they are represented in the form of a set:

$$N = \{N_1, N_2, \ldots, N_m\}, \tag{1}$$

where m represents the resource type. The item set corresponding to the resource set N is represented by L:

$$L = \{L_1, L_2, \ldots, L_k\}. \tag{2}$$

In the formula, k represents the number of item sets. The process of using association rules to mine resources is the process of searching different sets of resources through item sets. Item set L_1 is used to search resource set N_1, which is mainly manifested in finding effective resources in resource set N_1; L_2 is used to search resource set N_2, which is mainly manifested in finding effective resources in resource set N_2; by analogy, the resource set L_k is searched through item set N_m, and the process is repeated until the resource set cannot be searched [11, 12]. Finally, the effective resources of all resource sets are obtained through integration to form an integrated resource set G, whose expression is

$$G = \{G_1, G_2, \ldots, G_h\}, \tag{3}$$

where h represents the effective resource type.

In order to facilitate the mining and analysis of distance education resources, two concepts are added to the association rule mining, namely, the natural occurrence probability of attributes and the adjustment support rate of association rules [13]. Among them, the natural occurrence probability P_α of distance education resource attribute α refers to the frequency that the set distance education resource attribute appears in all distance education resources, which is defined as

$$P_\alpha = \frac{C_j(\alpha)}{m}, \tag{4}$$

where $C_j(\alpha)$ represents the attributes of distance education resources.

When mining association rules of different distance education resources, they are independent of each other. The natural occurrence probability $P(\alpha \times \beta)$ of attribute $\alpha + \beta$ represents the product of the occurrence frequency of attributes α and β, which is defined as

$$W_j^k = \frac{\text{sign}P(\alpha \times \beta)\left(\left|C_j(\alpha)\right| + \left|C_j(\beta)\right|\right)}{N_i^k \times M_j^k}, \tag{5}$$

where N_i^k represents the product index of multiattribute object decision-making and M_j^k represents the weighting coefficient of multiattribute object decision-making.

The adjustment support rate T_{ij} of association rules can well reflect the specific connection between different rules [14], which is defined as

$$T_{ij} = \sigma\sqrt{2\ln(N)}\left(1 - \frac{Q_{ij}}{\sum_{i,j=1}^{M} E_{ij}}\right), \tag{6}$$

where $i = 1, 2, \ldots, n$; $j = 1, 2, \ldots, m$; Q_{ij} represents the actual support rate of the association rule; E_{ij} represents the probability of occurrence of all attributes; and σ represents the degree of interest.

When using association rules to mine distance education resources, if $T_{ij} = 0$, it means that there is no specific association between the two resources, and if $T_{ij} = 1$, it means that the two resources have a certain association [15, 16].

According to the analysis results of distance education resources mining based on association rules, the correlation between different distance education resources can be obtained, and the effective resources in the resource library can be mined, which is conducive to the integrated analysis of distance education resources.

Figure 2 shows the remote education resource mining process based on association rules.

3.2. Construction of a Model for the Integration of Distance Education Resources. Based on the distance education resource mining results in Section 3.1, a distance education resource mining model is established. In the process of model construction, with the three-tier architecture as the technical support, the remote education resource mining model designed with the three-tier architecture has the following advantages:

(1) The various levels of the model are independent of each other, and changes in the upper-level business functions do not affect the use of the lower level, and vice versa, which enhances the flexibility of the model

(2) When accessing the resources in the model, the user request can be terminated in time to ensure the safety of the use of the model

(3) All levels can respond to user requests and perform response processing according to specific task assignments, which improves the resource processing efficiency of the model

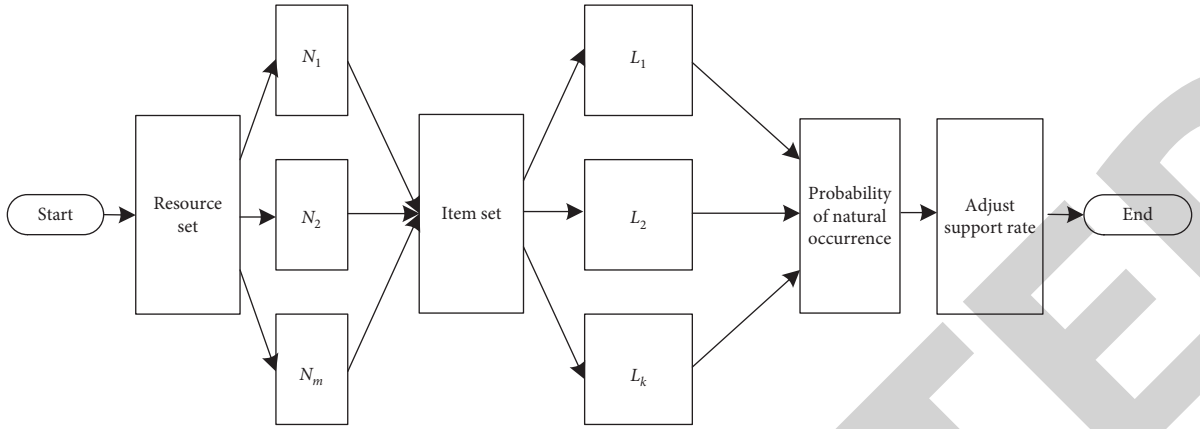

Figure 2: The process of remote education resource mining.

The components of the remote education resource integration model supported by the three-tier structure are shown in Figure 3.

3.2.1. Application Layer. In the process of users accessing the remote education resource integration model, by identifying user service requests, and transferring access control rights to virtualization software, user resource access permissions are formulated according to user role permissions, without affecting the user's application experience. The application layer's major job is to help the resource encryption layer and the multicast communication layer and process user requests. It is the central connection in the distant education resource integration model, which improves resource utilization and the model's overall function [17, 18].

3.2.2. Resource Encryption Layer. Since there are no independent resource nodes in the network, all servers can respond to user requests. Therefore, all servers together form a huge resource cache. In order to improve the security of cache resources, effective management and migration of these resources are required to improve the hit rate of encrypted resources, thereby improving the security of remote education resources [19, 20]. In this step, a key can be added to encrypt the resource, and the key can be expressed as

$$E(r) = \left[e_1(t), e_2(t)\right]^2, \tag{7}$$

where $e_1(t)$ and $e_2(t)$ represent a pair of keys.

3.2.3. Multicast Communication Layer. In order to ensure the consistency of conditions in the integration process of distance education resources, a clustering matrix U is constructed according to the distribution of different resources

$$U = \begin{bmatrix} u_{11} & u_{12} & u_{1n} \\ u_{21} & u_{22} & u_{2n} \\ u_{n1} & u_{n2} & u_{nm} \end{bmatrix}. \tag{8}$$

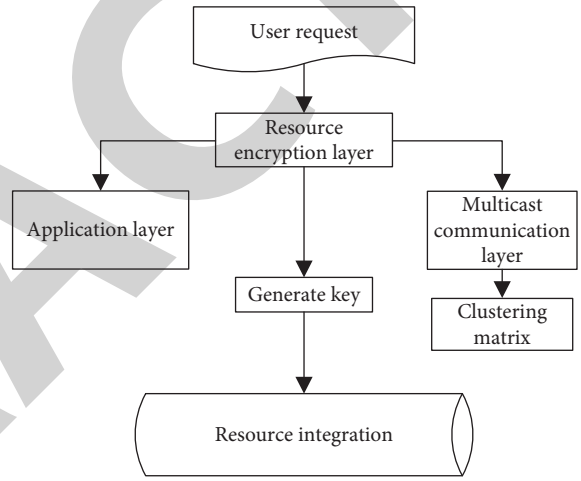

Figure 3: Schematic diagram of remote education resource integration model.

According to the clustering matrix U, the resource structure conditions are constrained and defined, the resource level integration environment is clarified through the condition constraint definition, and the evaluation scale conditions are unified to ensure that the best resource integration results are obtained.

The specific parameters of the multicast communication layer are shown in Table 1.

Construct a remote education resource integration model, use the parameters shown in Table 1 as the standard, discover the effective data in the resource concentration through encryption, clustering, and other steps, and eliminate invalid data, such as interference data and redundant data [21, 22], so as to realize the effective integration of a variety of distance education resources, to ensure that the model is progressive at all levels, and to achieve the goal of resource integration in a comprehensive and real-time manner [23, 24]. The constructed distance education resource integration model is expressed through formulas, specifically as follows:

$$Z = \sqrt{\frac{\left(x_{a1} - x_{a-1}\right)^2 + \left(x_{b1} - x_{b-1}\right)^2 + \left(x_{c1} - x_{c-1}\right)^2}{\sum_{i,j=1}^{M} f(n) F\left(Q_{ij}\right) \times \sigma_{ij}}}. \tag{9}$$

Table 1: Multicast communication layer parameters.

Parameter	Specification
Number of link layers (layer)	12
Transmission rate (Gbps)	8.5
Resource transmission time limit (ms)	24–32 ms
Single-tier resource chain size (TB)	2

In the formula, a, b, and c represent the input items of the model, specifically referring to the resource set, item set, and association rules; $F(Q_{ij})$ represents the distance function between the association rules [25], and its expression is

$$F\left(Q_{ij}\right) = \sum_{i,j=1}^{M} \lambda_1 F\left(\alpha_{ij}\right) + \lambda_2 F\left(\beta_{ij}\right), \tag{10}$$

where λ_1 and λ_2, respectively, represent support and confidence.

Figure 4 is the work flowchart of the remote education resource integration model.

In summary, the design of the distance education resource integration model from the perspective of comparative education is realized at the theoretical level. In order to verify its application effect, the following will proceed from a practical perspective to test the application effect.

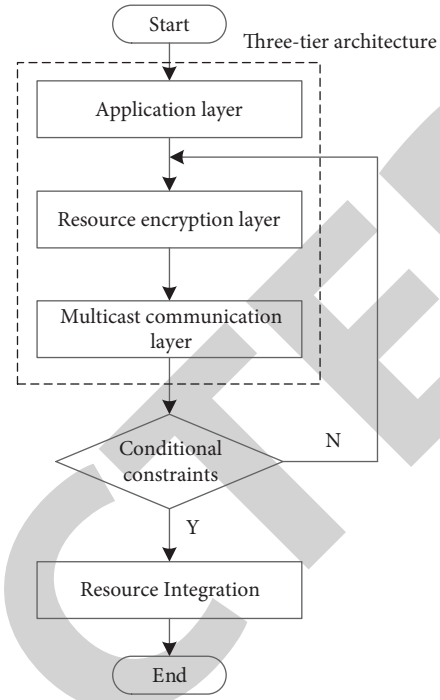

Figure 4: Work flowchart of the remote education resource integration model.

4. Simulation Experiment Analysis

The theoretical design of the remote education resource integration model through the above steps is realized. In order to verify its application value, it is verified by the form of simulation experiment, and its effectiveness is verified from two levels of theory and practice. The method of information resource integration based on wireless local area network and the method of online integration and optimization of information resources based on clustering algorithm are used as comparison methods to compare with the method in this paper and draw specific experimental conclusions through comparison.

4.1. Experimental Dataset. The data used in the experiment are from ERIC educational resources literature database. The platform judges the authority according to the IP address, and the displayed contents are accessible resources. Users can click "EBSCO academic retrieval (whole discipline)" and select subdatabases as needed. The experiment is carried out in the simulation environment of SPSS 9.0.

4.2. Experimental Comparison Indicators. The application effects of resource integration methods are analyzed from the following perspectives:

(1) Data loss rate: this indicator refers to the loss of some data in the process of resource integration, resulting in insufficient resource integration results

(2) Resource integration time-consuming: this indicator mainly reflects the efficiency of resource integration; the shorter the time-consuming, the higher the efficiency.

(3) Redundant data volume: due to a large amount of data, if repeated and redundant data are not effectively processed during resource integration, the amount of redundant data will be too large and affect the effect of resource use.

(4) Comprehensiveness of resource integration results: used to reflect whether the integrated resources can meet the needs of different users.

Taking the above four indicators as the focus of investigation, comparing the application effects of the traditional method and the method in this paper, the comparison results are as follows.

4.3. Experimental Results and Analysis

4.3.1. Data Loss Rate (%). First, using the data loss rate in the process of resource integration as an experimental indicator, the application effects of the three methods are compared, and the results are shown in Figure 5.

According to Figure 5, when the number of iterations is 3, the data loss rate of this article's method is 5.2 percent, the data loss rate of the information resource integration method based on wireless local area network is 7.1 percent, and the data loss rate of the information resource online integration optimization method based on clustering algorithm is 6.4 percent; when the number of iterations is 10, the data loss rate of this article's method is 5.2 percent; and when the number of iterations is 10, according to the data analysis results, the data loss rate of the method of this article in

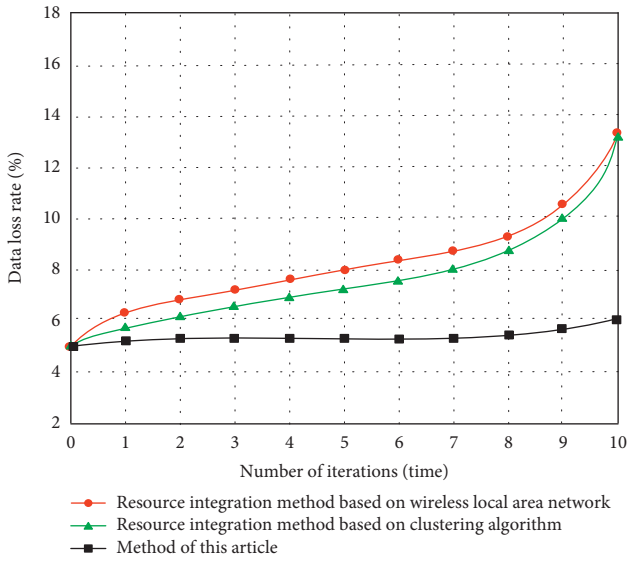

Figure 5: Data loss rate test results.

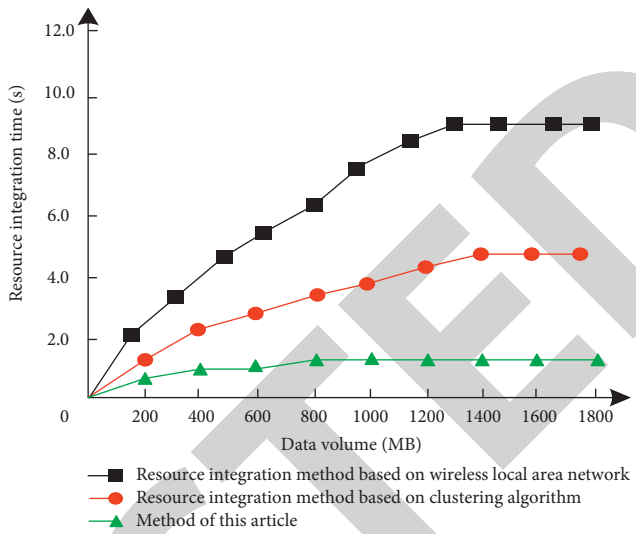

Figure 6: Time-consuming test results of resource integration.

resource integration is low. By analyzing the changing trend of data loss rate under the three methods, it can be seen that with the increase of iteration times, the three methods show a continuous upward trend, but the upward trend of the method of this article is not obvious as that of the traditional method, indicating that the change range of data loss rate of the method of this article is small. Simulation results show that the method of this article can retain data information as much as possible in resource integration and avoid the negative impact of a large amount of data loss on the effect of resource use.

4.3.2. Resource Integration Time (s). To test the time consumed by the resource integration process for different data volumes between the method in this paper and the traditional method, in order to ensure the accuracy of the experimental results, to ensure that the data types and simulation platform parameters are consistent, the test results are shown in Figure 6 under this condition.

Figure 6 shows that the more data there is, the longer the resource integration procedure takes. The resource integration time of the information resource integration method based on wireless local area network and the information resource online integration optimization method based on clustering algorithm are both faster than the method described in this article when dealing with different amounts of data. According to the examination of particular data, the maximum resource integration time of the approach described in this article is 1.2 s, and the time needed for resource integration operation has remained steady when the quantity of data grows to 800 MB. The information resource integration approach based on wireless local area network has a maximum resource integration time of 9.3 seconds. When the quantity of data exceeds 1300 MB, the resource integration time stays constant; the online integration optimization technique of information resources based on clustering algorithm has a maximum resource integration time of 4.8 s. When the data volume hits 1400 MB, the resource integration time stays constant. According to simulation findings, the resource integration efficiency of the approach described in this article is greater when the quantity of data is variable.

4.3.3. Redundant Data Volume (MB). Due to a large number of remote education resources and a large amount of processing business, it is inevitable that there will be duplicate and redundant data, which will affect the effect of resource use, resulting in users not being able to obtain accurate resources. Therefore, the redundant data effect of the resource integration method must be checked. Test to ensure the smooth operation of resource processing tasks. The experiment uses the above three methods to test the amount of redundant data in resource integration, and the test results are shown in Figure 7.

It can be seen from the analysis of Figure 7 that the redundant data ratio reflects the amount of redundant data. The higher the ratio, the more redundant data. When the three methods are used to integrate and process distance education resources, a certain amount of redundant data will be generated. The method of this article has the lowest proportion of redundant data, and the highest value is only 5%. The method of information resource integration based on wireless local area network has the highest proportion of redundant data, with the highest value reaching more than 20%. Although the redundant data ratio of the online information resource integration optimization method based on the clustering algorithm is lower than that of the information resource integration method based on wireless local area network, it is still higher than the method in this article. Simulation experiments prove that the method in this paper can effectively process invalid interference data in resource processing and improve the effect of resource integration. The traditional method is not suitable for resource integration, and it is easy to cause problems for users in resource use. This is because the method of this article

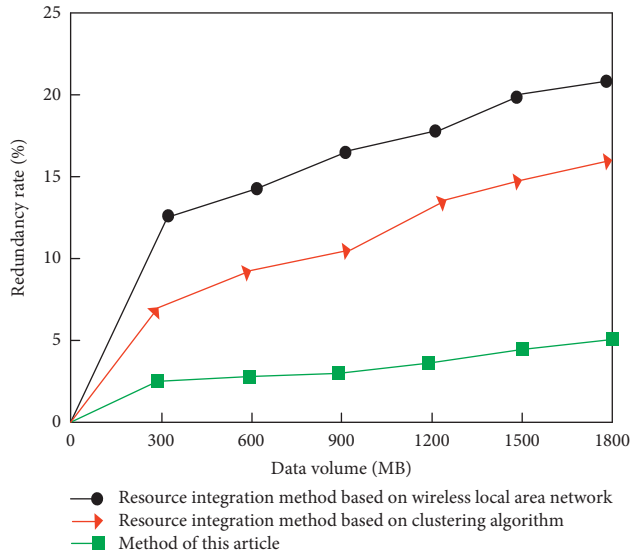

Figure 7: Test results of redundant data volume.

Table 2: Comprehensive comparison results/points of resource integration results.

User ID	Method of this article	Information resource integration method based on wireless local area network	Online integration and optimization method of information resources based on clustering algorithm
1	95.7	89.5	74.2
2	93.2	90.1	76.3
3	90.9	84.2	74.6
4	89.7	87.6	70.2
5	96.3	79.9	79.8
6	98.1	83.3	78.6
7	92.4	82.0	72.3
8	99.0	85.4	77.7
9	97.2	86.3	74.5
10	95.8	90.1	80.9

preprocesses the data in the process of resource integration and obtains effective data in data mining, thus improving the effect of resource integration.

4.3.4. Comprehensiveness of Resource Integration Results. The following is a further analysis of the resource integration effects of different methods. 10 users of online education websites are randomly selected for scoring. The three methods are evaluated in terms of resource comprehensiveness, whether they can meet the user needs, and whether the resources meet the personal needs. The evaluation results are expressed in scores. The score range is 0–100. The higher the score, the more satisfied the users are, that is, resources are more comprehensive. Table 2 shows the comparison results of different methods.

According to the data in Table 2, the overall evaluation score of the method of this article is higher than that of the two traditional methods, and the lowest and highest evaluation scores are 89.7 and 99.0, respectively, while the highest evaluation scores of the information resource integration method based on WLAN and the online information resource integration optimization method based on clustering algorithm are 90.1 and 80.9, respectively. The comparison results fully verify the superiority of the method of this article and show that the integrated resources not only effectively eliminate the interference resources, but also improve the comprehensiveness of resources.

5. Conclusion

Data resource integration is conducive to the healthy and long-term development of various fields. Most researches integrate various types of resources to establish a resource management platform. However, traditional methods have many drawbacks in their applications. In this work, a remote education resource integration model was developed from the viewpoint of comparative education in order to complete the integration of distance education resources better. The experimental findings reveal that the approach described in this article has a low data loss rate in resource integration; the percentage of redundant data is the lowest, and the greatest value is only 5%. The approach described in this article has a higher overall assessment score than the two conventional methods, with the lowest and highest evaluation ratings of 89.7 and 99.0, respectively. The efficiency of resource integration is great, and the maximum time-consuming is just 1.2 s, indicating that the approach described in this article has a better application impact and a higher application value.

Data Availability

The data used to support the findings of this study are included within the article.

Conflicts of Interest

The authors declare that they have no conflicts of interest.

References

[1] G. M. Machado, V. Maran, G. M. Lunardi, L. K. Wives, and J. P. M. D. Oliveira, "AwARE: a framework for adaptive recommendation of educational resources," *Computing*, vol. 16, no. 1, pp. 675–705, 2021.

[2] J. D. Knopf, R. Kumar, M. Barats, P. Klimo, and D. S. Hersh, "Neurosurgical operative videos: an analysis of an increasingly popular educational resource," *World Neurosurgery*, vol. 144, no. 12, pp. 428–437, 2020.

[3] D. Kim, Y. Lee, W. L. Leite, and A. C. Huggins-Manley, "Exploring student and teacher usage patterns associated with student attrition in an open educational resource-supported online learning platform," *Computers & Education*, vol. 156, no. 10, Article ID 103961, 2020.

[4] R. E. K. F. Summers, "Examining the representations of NOS in educational resources: an analysis of lesson plans aligned with the next generation science standards," *Science & Education*, vol. 28, no. 6, pp. 269–289, 2019.

Hindawi
Journal of Mathematics
Volume 2024, Article ID 9817061, 1 page
https://doi.org/10.1155/2024/9817061

Retraction

Retracted: Experiment and Algorithm Research of Coal Direct Liquefaction Residual Oil Pyrolysis and Coking Technology Based on Lumped Kinetic Engineering

Journal of Mathematics

Received 23 January 2024; Accepted 23 January 2024; Published 24 January 2024

This article has been retracted by Hindawi following an investigation undertaken by the publisher [1]. This investigation has uncovered evidence of one or more of the following indicators of systematic manipulation of the publication process:

(1) Discrepancies in scope

(2) Discrepancies in the description of the research reported

(3) Discrepancies between the availability of data and the research described

(4) Inappropriate citations

(5) Incoherent, meaningless and/or irrelevant content included in the article

(6) Manipulated or compromised peer review

The presence of these indicators undermines our confidence in the integrity of the article's content and we cannot, therefore, vouch for its reliability. Please note that this notice is intended solely to alert readers that the content of this article is unreliable. We have not investigated whether authors were aware of or involved in the systematic manipulation of the publication process.

Wiley and Hindawi regrets that the usual quality checks did not identify these issues before publication and have since put additional measures in place to safeguard research integrity.

We wish to credit our own Research Integrity and Research Publishing teams and anonymous and named external researchers and research integrity experts for contributing to this investigation.

The corresponding author, as the representative of all authors, has been given the opportunity to register their agreement or disagreement to this retraction. We have kept a record of any response received.

References

[1] T. Bo and C. Yang, "Experiment and Algorithm Research of Coal Direct Liquefaction Residual Oil Pyrolysis and Coking Technology Based on Lumped Kinetic Engineering," *Journal of Mathematics*, vol. 2022, Article ID 3610246, 8 pages, 2022.

Hindawi
Journal of Mathematics
Volume 2022, Article ID 3610246, 8 pages
https://doi.org/10.1155/2022/3610246

Research Article

Experiment and Algorithm Research of Coal Direct Liquefaction Residual Oil Pyrolysis and Coking Technology Based on Lumped Kinetic Engineering

Tian Bo and Chaohe Yang

School of Chemical Engineering, East China University of Petroleum, No. 66, Changjiang West Road, Huangdao District, Qingdao 266580, China

Correspondence should be addressed to Tian Bo; camhq80@163.com

Received 17 December 2021; Revised 2 January 2022; Accepted 5 January 2022; Published 31 January 2022

Academic Editor: Naeem Jan

With the development of computer operation technology and algorithms, the lumped dynamic model is more practical, and the development and application are more comprehensive. Among them, the direct coal liquefaction residual oil pyrolysis and coking technology, as a coal-to-liquid process, can increase the oil yield of the coal liquefaction process and reduce environmental pollution. The purpose of this paper is to study the experiment and algorithm of coal direct liquefaction residual oil pyrolysis and coking technology based on lumped kinetic engineering. Starting from the lumped kinetic engineering, this paper takes the direct coal liquefaction residual oil pyrolysis and coking technology as the research object. Based on the experiment of small- and medium-sized equipment, the residual oil pyrolysis and coking experiment is carried out. This paper further analyzes the components of the experimental products and explores the factors that affect the yield of residual pyrolysis oil based on the five lumped kinetic model of coking. Experimental data shows that when the pyrolysis temperature is 450°C, the content of liquefied heavy oil HS in the pyrolysis oil is 47.87%, the content of asphaltene A is 44.28%, and the content of preasphaltene PA is 7.85%; the pyrolysis temperature is 500 °C. At this time, the content of liquefied heavy oil HS in the pyrolysis oil is 54.97%, the content of asphaltene A is 40.23%, and the content of preasphaltene PA is 4.8%. It can be seen that, with the increase of pyrolysis temperature, the content of liquefied heavy oil HS increases, and the content of asphaltene A and preasphaltene PA decreases.

1. Introduction

Direct coal liquefaction residual oil pyrolysis and coking technology, as a coal-to-liquid process, effectively provide important technical support for ensuring our country's energy supply and safety, alleviating our country's shortage of petroleum resources and other prominent and sensitive issues [1,2]. However, the existing coal rapid pyrolysis and coking process still faces problems such as low coal utilization, poor tar quality, and reprocessing pyrolysis of the liquefied residue generated at the end of the hydrolysis process [3,4]. The research on the experiment and algorithm of coal direct liquefaction residual oil pyrolysis and coking technology based on lumped kinetic engineering will help to provide a new solution to this type of problem [5,6].

Regarding the research of lumped kinetic engineering, residual oil pyrolysis, and coking technology, many scholars at home and abroad have conducted multidirectional and in-depth research on it. For example, Colantonio [7] conducted a pyrolysis experiment on a synthetic mixture of packaging plastic residues; Wang [8] conducted pyrolysis experiments on wood and forest residues and studied the carbon dioxide gas kinetics of pyrolysis coke; Wang [9] launched a continuous pyrolysis experiment of biomass coal residues and analyzed the results. Chen [10] studied the copyrolysis characteristics and kinetics of furfural residue and oil shale semicoke. It can be seen that since the development of this technology, its innovation and application research have received the attention of the majority of researchers. Therefore, research on the experiment and algorithm of coal

direct liquefaction residual oil pyrolysis and coking technology based on lumped kinetic engineering has important theoretical and practical significance.

The purpose of this paper is to study the experiment and algorithm of coal direct liquefaction residual oil pyrolysis and coking technology based on lumped kinetic engineering. In this paper, starting from the lumped kinetic engineering, the direct coal liquefaction residual oil pyrolysis and coking technology is the research object, and the factors affecting the coal pyrolysis are analyzed. Then, the residual oil pyrolysis is carried out on the basis of the experiment of small- and medium-sized equipment. Finally, the components of the experimental products were analyzed, and the factors affecting the yield of residual pyrolysis oil were explored based on the five lumped kinetic model of coking. In the rest of the paper, the main contents are arranged as follows. Section 2 presents the experiment and the algorithm of coal direct liquefaction residual oil pyrolysis and coking technology has been proposed which is based on lumped kinetic engineering. In Section 3, further experimental research is carried out using the proposed methods. Section 4 presents the analysis of experimental results and experimental data. Lastly, the paper is concluded in Section 5.

2. Experiment and Algorithm of Coal Direct Liquefaction Residual Oil Pyrolysis and Coking Technology Based on Lumped Kinetic Engineering

In this section, the experiments are performed and the algorithm of coal direct liquefaction residual oil pyrolysis and coking technology has been proposed which is based on lumped kinetic engineering. To this end, the factors affecting coal pyrolysis are presented. In addition, the calculation of the rate constant of the coking reaction is carried out.

2.1. Factors Affecting Coal Pyrolysis. The thermogravimetric method is a common method to study the thermal reaction behavior of heavy oil. In a specific reaction device, by using inert gas to isolate the air, you can directly measure the quality of the oil sample and the reaction temperature data and then explore the relationship between the two based on the data. And according to the experimental data, through parameter estimation and optimization methods, the reaction kinetic parameters are obtained.

There are many factors that affect the thermogravimetric method. First of all, the density of the gas is different at different temperatures, which will affect the buoyancy of the gas to be measured in the experiment. In terms of experimental conditions, the heating rate of the reaction will also affect the thermogravimetric curve. According to the related experiments, it is found that an increase in the heating rate will aggravate the difficulty in the production of intermediate products [11]. In addition, the experimental environment and the amount of experimental materials will also affect the measurement results of this research method.

2.1.1. The Influence of Coal Structure. The structure of coal is complex, and there are phenomena of gas, liquid, and solid phases in pyrolysis, leading to many factors that affect coal pyrolysis, for example, coal maturity, high volatile content, and the coalification degree. Among them, the factor that has a greater impact on coal pyrolysis is the coalification degree, that is, the carbon content in coal. The carbon content affects the starting temperature. The higher the carbon content of coal, the higher the incidence of coal pyrolysis [12].

Secondly, the degree of coalification also affects the pyrolysis product and yield. The degree of coalification directly affects the quality of the product, including the size of the coke block, the yield of tar gas, and the strength of the cohesiveness.

The degree of coalification also affects the activity of the coal pyrolysis reaction. The higher the degree of coalification, the lower the reaction activity. Studies have found that, in the process of pyrolysis, different coal ranks have different cross-linking and different maturity. The temperature corresponding to the maximum production of tar and methane will shift. The higher the maturity, the higher the temperature.

2.1.2. The Influence of External Conditions

(1) Temperature. In external conditions, the temperature has a great influence on coal pyrolysis. The specific performance is as follows: as the temperature increases, the degree of coal cracking increases, the volatility increases, the content of coke or semicoke decreases, the pyrolysis temperature is lower, and the gas yield is lower. Finally, as the temperature increases, the gas yield increases, the calorific value decreases, and the coke and tar yield decrease. Therefore, according to the difference in temperature, it is divided into low-temperature pyrolysis, medium-temperature pyrolysis, and high-temperature pyrolysis so as to achieve the required different products.

(2) Heating Rate. The heating rate also has an effect on coal pyrolysis. Specifically, if the heating rate deviates from the gas precipitation temperature and the maximum precipitation temperature, the decomposition of some structures in the coal is too slow, and some of the coal has not been decomposed, which affects the efficiency of coal pyrolysis. Therefore, the rapid heating rate will cause the temperature to shift to the high-temperature direction, so that the volatile components that are decomposed will not be precipitated in time, causing delays.

(3) Change in Heating Rate. The change in heating rate is also an important factor affecting coal pyrolysis. Changing the heating rate will affect the deviation between the starting softening temperature and the starting curing temperature. As the rate changes, the index temperature will move to a higher temperature. In this case, the temperature range of the colloid will be affected and the adhesiveness will change.

(4) Constant Temperature Time. Constant temperature time is also a factor that affects coal pyrolysis. The constant

temperature time will affect the volatilization of the gas; regardless of the temperature, the longer the time, the more thoroughly the volatiles will be removed. But when the temperature is high, the removal of volatiles can be completely removed in a relatively short time at a constant temperature. As the pressure increases during coal pyrolysis, the volatilization of pyrolysis products is limited, and the yield of liquid products increases.

2.2. Calculation of Rate Constant of Coking Reaction. The number of reactions in the coking process is huge, and the calculation methods for different reaction rates are shown as follows:

$$k(T) = \frac{k_B T}{h} \exp\left(\frac{T\Delta S_m - \Delta E}{RT}\right), \quad (1)$$

where k_B is the Boltzmann constant, h is the Planck constant, T is the temperature, R is the ideal gas constant, ΔS_m is the entropy change before and after the reaction, and ΔE is the reaction energy barrier. Therefore, knowing ΔS_m and ΔE, the reaction rate constant at the specified temperature can be calculated.

3. Experimental Research

3.1. Experimental Materials. The original coal liquefaction residue (CHR) sample is a mixture of powdered particles and massive particles. The original mixed particle size sample is crushed and used for analysis and testing to ensure its uniformity. Among them, the CHR material is mixed with quartz sand in different proportions and fed into the pyrolyzer at a feed rate of 50–100 g/h, and the cooling water consumption is about 120 g/h.

3.2. Analysis of Experimental Products

3.2.1. Liquid Product Analysis. The tar product was analyzed by solvent extraction in a Soxhlet extractor using n-hexane and toluene solvents, and n-hexane soluble matter HS, toluene soluble matter—n-hexane insoluble matter A, and tetrahydrofuran soluble—toluene insoluble matter were obtained. The substances PA are, respectively, called liquefied heavy oil HS, asphaltene A, and preasphaltene PA.

3.2.2. Analysis of Solid Products. Morphology characterization of the bonding mixture: FEIQ scanning electron microscopy was used to characterize the morphology of the bond.

3.2.3. Semifocus Analysis. The measurement of semicoke products is directly weighed and measured after the pyrolysis experiment is completed and the temperature is naturally cooled.

3.2.4. Elemental Analysis. The element analysis of the semicoke is determined by an element analyzer to determine the content of C, H, O, N, and S in the semicoke sample.

3.2.5. Tar Separation. There are many methods for separating tar and water, including electrical separation commonly used in the oil refining industry, adsorption separation using lipophilic materials, and gravity separation and centrifugal separation using different oil-water densities.

In this experiment, the tar in the pyrolysis process will produce carbon dioxide. After the protective gas that the carbon dioxide passes into the reactor is diluted, it is discharged through the gas outlet at the bottom of the reactor and is gradually cooled by a three-stage water bath, so the generated pyrolysis water and part of the light oil are condensed in the third stage.

Due to the small scale of this experiment and the small amount of product produced, the mass yields of the experimental liquids are all weighed and measured with a high-precision balance. After each set of experiments is completed, the light oil and pyrolysis water in the third-stage collection bottle are allowed to stand and then separated. It can be seen from the stages divided by the pyrolysis process of coal that most of the pyrolysis water is produced before 350°C. Therefore, under the same experimental environment of the same group of experiments, the final pyrolysis has little effect on the change of temperature on the pyrolysis water output, which reduces the influence of the final temperature on the experiment.

3.3. Pyrolysis Test. A control group is set up, namely, the raw coal and its vitrinite group, and the main weight loss temperature range and maximum weight loss temperature of the two groups are analyzed in the pyrolysis process.

The molecular weight of the raw coal group is 2814, and the element content is C (80.6%), H (6.9%), N (1.00%), and O (11.4%).

The molecular weight of the vitrinite group is 3138, and the element content is C (79.18%), H (4.91%), N (1.00%), and O (14.90%).

3.4. Delayed Coking Experiment. After preheating, the residual oil in the raw material tank is pumped out by the raw material pump. It is first mixed with the high-temperature steam from the steam generator, and after reaching a certain temperature, it is mixed with the circulating oil from the bottom of the fractionation tower and enters the heavy oil heating furnace. After the furnace is heated to the outlet temperature, it quickly enters the coking tower through the oil pipeline for a coking reaction.

The produced coke product stays in the coke tower, and the produced high-temperature oil and gas enter the fractionation tower for fractionation from the top of the tower. Part of the heavy oil is pumped out from the circulating pump at the bottom of the fractionation tower for cyclic reaction, while the light components are cooled from the top of the tower and then enter the distillate oil receiving tank for collection, and the gas products are cooled and then calculated.

After the experiment, the device was cut off from water and power. After the coke tower was cooled, the coke tower was first weighed, the quality of the coke product was

measured, and then the coke removal was started, and the amount of gas and oil produced was calculated.

3.5. All Lumped Codes of the Coking Reaction Process. The lumped code table of the coking reaction process is shown in Table 1.

Among them, the reaction network of five lumped reaction kinetics is shown in Figure 1.

According to Figure 1 and the residue reaction mechanism, the differential form of the five-set total reaction kinetic equation is as follows:

$$\begin{aligned}
\frac{dOC}{dt} &= -(k_1 + k_2 + k_3 + k_4)OC,\\
\frac{DG}{dt} &= k_1 OC,\\
\frac{dGL}{dt} &= k_2 OC,\\
\frac{dDF}{dt} &= k_3 OC,\\
\frac{dCGO}{dt} &= k_4 OC.
\end{aligned} \tag{2}$$

4. Experimental Data Analysis

This section presents the experimental research and analyzes the experimental data. First of all, the extraction analysis of pyrolysis oil is carried out. Then the comparison of solvent extraction composition of CHR pyrolysis oil and residual at different pyrolysis temperatures is proposed. Thirdly, the effects of liquefaction time on liquefaction performance are deliberated. Lastly, the discussion about the total specific surface area and pore volume of copyrolysis semicoke is given.

4.1. Extraction Analysis of Pyrolysis Oil. The results of solvent extraction of pyrolysis oil at different pyrolysis temperatures are shown in Table 2. When the pyrolysis temperature is 450°C, the content of liquefied heavy oil HS in the pyrolysis oil is 47.87% and the content of asphaltene A is 44.28%. The content of asphaltene PA is 7.85%; when the pyrolysis temperature is 500°C, the content of liquefied heavy oil HS in the pyrolysis oil is 54.97%, the content of asphaltene A is 40.23%, and the content of preasphaltene PA is 4.8%; when the pyrolysis temperature is 550°C, the content of liquefied heavy oil HS in the pyrolysis oil is 58.14%, the content of asphaltene A is 30.07%, and the content of preasphaltene PA is 4.67%.

Observing Figure 2, it can be found that as the pyrolysis temperature increases, the content of liquefied heavy oil HS in the oil solution increases and the content of asphaltene A and preasphaltene PA decreases.

Table 1: Delayed coking reaction heavy oil lumped code.

Name	Code	Temperature
Oil and coke	OC	—
Gas	G	—
Gasoline	GL	0~180°C
Diesel fuel	DF	180~350°C
Coker gas oil	CGO	Above 350°C

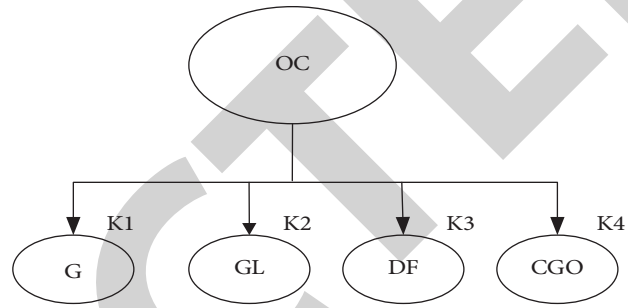

Figure 1: Reaction network diagram of five lumped reaction kinetics.

Table 2: Solvent extraction results of residual pyrolysis oil at different pyrolysis temperatures.

Sample	HS	A	PA
Tar-450°C	47.87	44.28	7.85
Tar-500°C	54.97	40.23	4.80
Tar-550°C	58.14	35.44	6.42
Tar-600°C	65.26	30.07	4.67

4.2. Comparison of Solvent Extraction Composition of CHR Pyrolysis Oil and Residue at Different Pyrolysis Temperatures. The results of the solvent extraction composition of the pyrolysis oil and residue calculated on the basis of CHR are shown in Table 3. The content of the liquefied heavy oil HS in the pyrolysis oil is similar to that of the liquefied heavy oil HS in the residue, but the content of asphaltene A and preasphaltene PA is significantly different.

Observing Figure 3, it can be concluded that most of the liquefied heavy oil HS in the residue during the pyrolysis process is recovered and transferred into the pyrolysis oil, while most of the asphaltene A and preasphaltene PA undergone during the pyrolysis process. Reactions such as polycondensation formed THFIS, an insoluble tetrahydrofuran. In particular, preasphaltene PA undergoes polycondensation at a relatively low pyrolysis temperature, such as 450°C, to form products that are insoluble in tetrahydrofuran solvents, such as pyrolysis semitar and other heavy products. It can be seen that the increase in pyrolysis temperature is conducive to the conversion of asphaltene A in the residue to liquefied heavy oil HS, which may be caused by the enhanced pyrolysis of asphaltene.

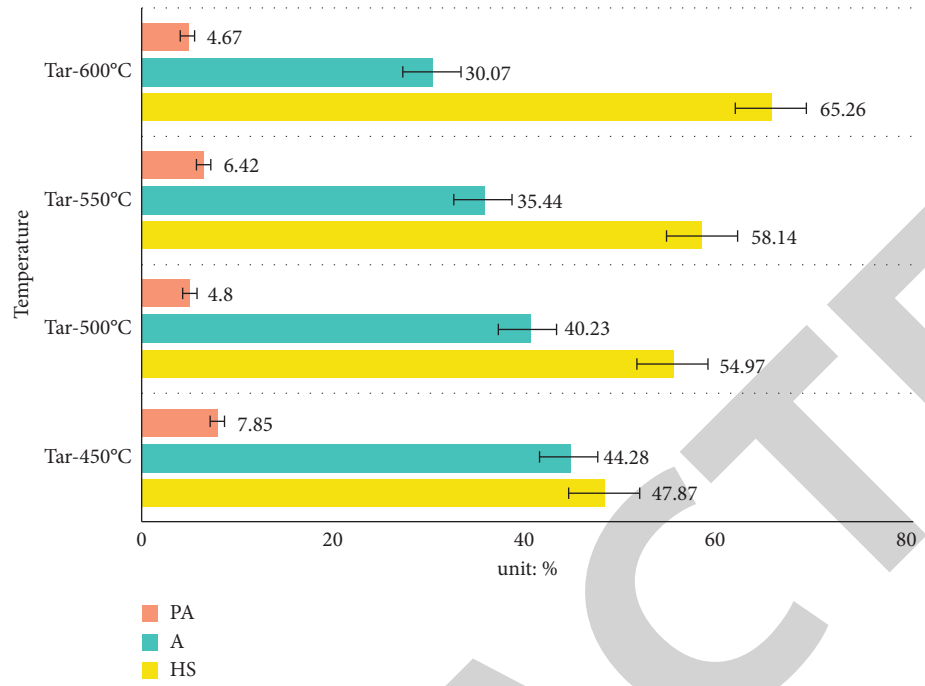

Figure 2: Solvent extraction results of residual pyrolysis oil at different pyrolysis temperatures.

Table 3: Comparison of residue pyrolysis oil and residue solvent extraction composition at different pyrolysis temperatures.

Sample	HS	A	PA
CHR	10.51	37.12	8.69
Tar-450°C	7.03	6.37	0.89
Tar-500°C	10.84	7.62	1.37
Tar-550°C	11.78	7.54	1.26
Tar-600°C	12.51	5.70	1.23

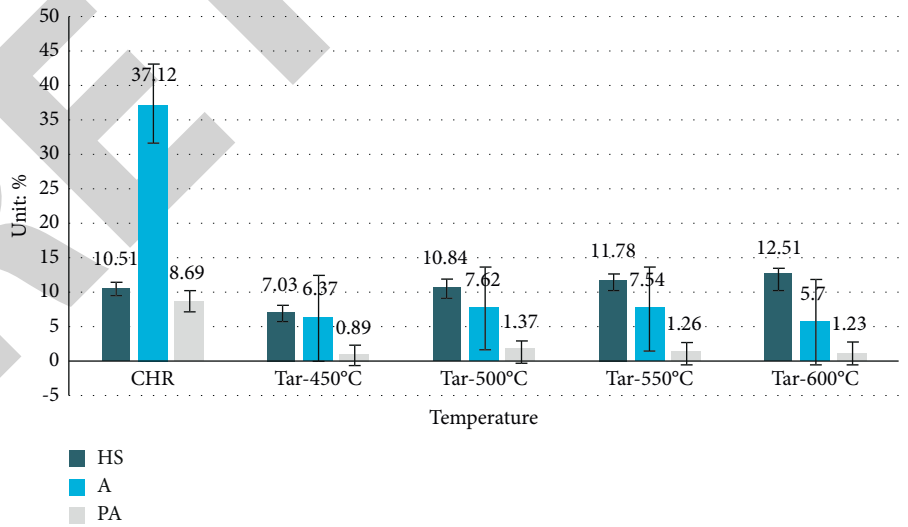

Figure 3: Comparison of residue pyrolysis oil and residue solvent extraction composition at different pyrolysis temperatures.

4.3. Influence of Liquefaction Time on Liquefaction Performance. Coal liquefaction involves the fragmentation of the macromolecular structure of coal, the cracking of chemical bonds, and hydrogenation. It is a complex process. Since these reactions take a certain amount of time to complete, it is necessary to study the effect of reaction time

Table 4: Liquefaction conversion rate and oil yield of raw coal and its vitrinite.

Time (min)	Conversion rate of raw coal	Raw kerosene yield	Vitrinite conversion rate	Vitrinite oil yield
0	74.13	37.16	88.16	28.70
10	78.32	42.41	91.24	62.47
20	80.47	50.07	92.35	67.05
30	82.48	53.47	93.16	69.46
40	83.46	54.79	94.62	70.18
50	84.28	55.16	95.41	73.24
60	85.14	57.24	94.19	74.16

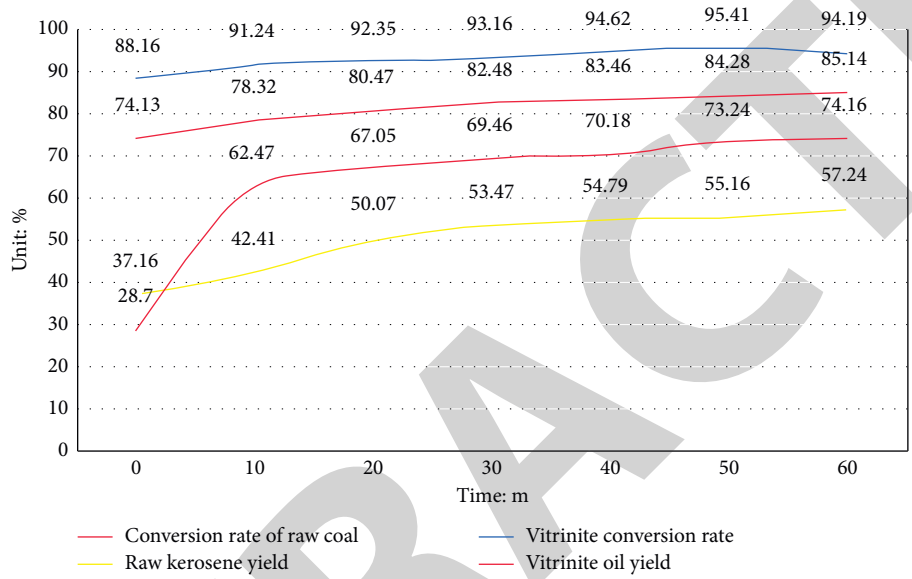

Figure 4: Liquefaction conversion rate and oil yield of raw coal and its vitrinite.

on the result of liquefaction. Table 4 shows the results of liquefaction conversion rate and oil yield of raw coal and its vitrinite at the optimal liquefaction temperature.

It can be seen from Figure 4 that the liquefaction time has an impact on the conversion rate of liquefied coal and the oil yield, but its impact is not as large as that of temperature. With the increase of liquefaction time, the liquefaction conversion rate and oil yield of raw coal and its vitrinite first increase and then become stable. Considering the cost and other issues, the optimal liquefaction temperature (450°C) is determined, and the optimal reaction time is 60 minutes. Under the optimal liquefaction temperature and time, the raw coal liquefaction conversion rate was 85.14%, and the oil yield was 57.24%; the vitrinite liquefaction conversion rate was 94.19%, and the oil yield was 74.16%. It can be seen that the vitrinite group shows a higher liquefaction conversion rate and oil yield.

4.4. Total Specific Surface Area and Pore Volume of Copyrolysis Semicoke. The results of the change of the total specific surface area and pore volume of copyrolysis semicoke are shown in Table 5. When the temperature is 500°C, the total specific surface area of semicoke is 4.1 m^2g and the total pore volume is 5.4 mg; when the temperature is 600°C, the total specific surface area of the semicoke is 4.2 m^2g and the total pore volume is 4.5 mg; when the temperature is 700°C, the total specific surface area of semicoke is 4.5 m^2g and the total pore volume is 6.4 mg; when the temperature is 800°C, the total specific surface area of the semicoke is 7.5 m^2g and the total pore volume is 8.5 mg.

It can be seen from Figure 5 that as the degree of pyrolysis reaction deepens, the total specific surface area and total pore volume of the obtained semicoke will first decrease and then increase with the increase of pyrolysis temperature, reaching the minimum value at 600°C. And the total specific

Table 5: Total specific surface area and pore volume of copyrolysis semicoke.

Temperature (°C)	Total surface area	Total pore volume
HLSHR-char-500°C	4.1	5.4
HLSHR-char-600°C	4.2	4.5
HLSHR-char-700°C	4.5	6.4
HLSHR-char-800°C	7.5	8.5

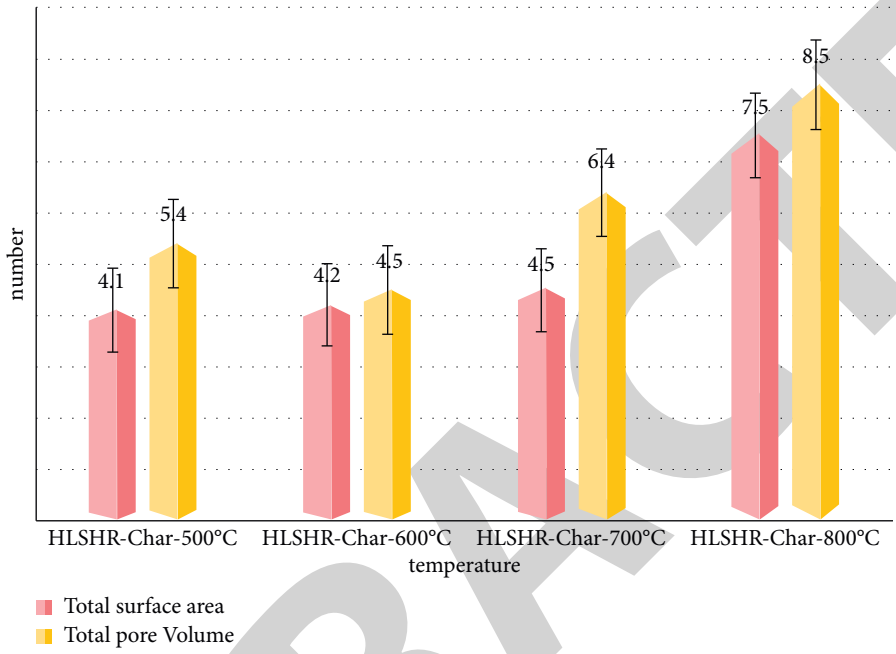

Figure 5: Total specific surface area and pore volume of copyrolysis semicoke.

surface area of copyrolysis semicoke changes slowly when it is between 500 and 600°C, and then as the pyrolysis temperature increases, the total specific surface area increases rapidly.

5. Conclusion

Since our country's national economic development and environmental protection are put under tremendous pressure by the mode of using coal as the main energy consumption. Therefore, the efficient and clean use of coal is a huge test faced by various coal utilization technologies, and it is of great practical significance to develop an efficient and environmentally friendly modern coal chemical industry. This paper carried out the research to complete the following tasks: based on the experiment of small and medium-sized equipment, carried out the residual oil pyrolysis and coking experiment, further carried out the composition analysis of the experimental products, and explored the influence of the residual pyrolysis based on the five-set kinetic model of coking.

Data Availability

The data underlying the results presented in the study are available within the manuscript.

Conflicts of Interest

The authors declare that there are no conflicts of interest.

References

[1] C. Wang, S. Xu, and Y. Feng, "Experiments on pyrolysis of coal hydroliquefaction residue by solid heat carrier technology," *Meitan Xuebao/Journal of the China Coal Society*, vol. 43, no. 12, pp. 3525–3531, 2018.

[2] Z. Guo, F. Guo, Z. Miao et al., "Migration pattern of chlorine during co-pyrolysis for herb residue and coal," *Journal of Environmental Chemical Engineering*, vol. 9, no. 4, Article ID 105196, 2021.

[3] T. Fan, Y. Qu, and Z. Chang, "A TGA investigation to Co-pyrolysis characteristics of shenhua direct coal liquefaction residue and huolinhe lignite and the CO_2 gasification behavior of the derived char," *ChemistrySelect*, vol. 5, no. 39, 2020.

[4] R. Ślefarski, J. Jójka, P. Czyżewski et al., "Experimental and numerical-driven prediction of automotive shredder residue pyrolysis pathways toward gaseous products," *Energies*, vol. 14, no. 6, p. 1779, 2021.

[5] B. Yang and M. Chen, "Py-FTIR-GC/MS analysis of volatile products of automobile shredder residue pyrolysis," *Polymers*, vol. 12, no. 11, p. 2734, 2020.

[6] N. Nigam, K. Shanker, and P. Khare, "Valorisation of residue of mentha arvensis by pyrolysis: evaluation of agronomic and environmental benefits," *Waste and Biomass Valorization*, vol. 9, no. 10, pp. 1909–1919, 2018.

Hindawi
Journal of Mathematics
Volume 2022, Article ID 4346234, 13 pages
https://doi.org/10.1155/2022/4346234

Research Article

Some New Upper Bounds for the Y-Index of Graphs

Durbar Maji,[1] **Ganesh Ghorai**,[1] **and Faria Ahmed Shami**[2]

[1]*Department of Applied Mathematics with Oceanology and Computer Programming, Vidyasagar University, Midnapore 721102, India*
[2]*Department of Mathematics, Bangabandhu Sheikh Mujibur Rahman Science and Technology University, Gopalganj, Bangladesh*

Correspondence should be addressed to Faria Ahmed Shami; fariashami@bsmrstu.edu.bd

Received 25 November 2021; Revised 1 January 2022; Accepted 3 January 2022; Published 30 January 2022

Academic Editor: Naeem Jan

In mathematical chemistry, the topological indices with highly correlation factor play a leading role specifically for developing crucial information in QSPR/QSAR analysis. Recently, there exists a new graph invariant, namely, Y-index of graph proposed by Alameri as the sum of the fourth power of each and every vertex degree of that graph. The approximate range of the descriptors is determined by obtaining the bounds for the topological indices of graphs. In this paper, firstly, some upper bounds for the Y-index on trees with several types of domination number are studied. Secondly, some new bounds are also presented for this index of graphs in terms of relevant parameters with other topological indices. Additionally, a new idea on bounds for the Y-index by applying binary graph operations is computed.

1. Introduction

In this paper, we only consider the molecular graphs (MG) [1], which are simple and connected. In chemical graph theory, molecules or molecular compounds are often modelled by chemical structure as MG. The atoms of a molecular compound are to be represented as the vertices of the MG, whereas the edges represent the chemical bonds. Let $\mathcal{G} = \mathcal{G}(V, E)$ be a MG with $V(\mathcal{G}) = \{\mu_1, \mu_2, \ldots, \mu_n\}$ as the vertex set and $E(\mathcal{G}) = \{e_1, e_2, \ldots, e_m\}$ as the edge set, such that $|V(\mathcal{G})| = n$ and $|E(\mathcal{G})| = m$. The degree of $\mu \in V(\mathcal{G})$, denoted by $\xi(\mu/\mathcal{G})$, is the total number of edges, which are associated with μ. Obviously, $0 \le \delta \le \xi(\mu/\mathcal{G}) \le \Delta \le (n-1)$, where $\delta = \min\{\xi(\mu/\mathcal{G})|\mu \in \mathcal{G}\}$ and $\Delta = \max\{\xi(\nu/\mathcal{G})|\nu \in \mathcal{G}\}$. A set $S \subseteq V(\mathcal{G})$ satisfying the condition $\forall \mu \in V(\mathcal{G}) \setminus S$, $N_{\mathcal{G}}(\mu) \cap S \neq \emptyset\}$ is called a dominating set of $\mathcal{G}$. When $\mathcal{R} \subseteq V(\mathcal{R})$ satisfies the condition $\forall \mu \in V(\mathcal{R}) \setminus \mathcal{R}$, $\xi_{\mathcal{R}}(\mu, \nu) \le \kappa$ for some $\nu \in \mathcal{R}$, where $\xi_{\mathcal{R}}(\mu, \nu)$ denotes the distance between μ and ν, is said to be a distance κ-domination (DD_k) set of $\mathcal{R}$. The (DD_k) number ([2, 3]) of $\mathcal{G}$, denoted by ζ_κ, is the minimum cardinality among all $\mathcal{R}$ sets. The notations $\mathrm{diam}(\mathcal{G}) = \max\{\varepsilon_{\mathcal{G}}(\mu)|\mu \in V(\mathcal{G})\}$ and $\varepsilon_{\mathcal{G}}(\mu) = \max\{\xi_{\mathcal{G}}(\mu, \nu)|\nu \in V(\mathcal{G})\}$ denote the diameter of $\mathcal{G}$ and the eccentricity of μ, respectively. A path P is called a diameter path (DP) of $\mathcal{G}$ when the length of P is equal to $\mathrm{diam}(\mathcal{G})$. We follow the book [4] for the graph theoretical definitions and notations.

The graph invariant (GI) is a number that is uniquely determined by a graph. The subset of (GI) s is topological indices, which are used to predict several properties such as physical, chemical, pharmaceutical, and biological activities of chemical species. In 1947, the great chemist holder Wiener initiated a first-time idea about the topological index (TI). He presented the first TI, namely, Wiener index [5] to search the boiling points of alkanes. After long years, Gutman and Trinajstic [6] investigated two oldest GI s. They are defined as $M_1(\mathcal{G}) = \sum_{\mu \in V(\mathcal{G})} \xi^2(\mu/\mathcal{G})$ and $M_2(\mathcal{G}) = \sum_{\mu\nu \in E(\mathcal{G})} \xi(\mu/\mathcal{G})\xi(\nu/\mathcal{G})$, respectively. The concept of first general ZI was considered by Li and Zheng [7]. It is defined as

$$M_1^{\lambda}(\mathcal{G}) = \sum_{\mu \in V(\mathcal{G})} \xi^{\lambda}\left(\frac{\mu}{\mathcal{G}}\right) = \sum_{\mu\nu \in E(\mathcal{G})} \left[\xi^{\lambda-1}\left(\frac{\mu}{\mathcal{G}}\right) + \xi^{\lambda-1}\left(\frac{\nu}{\mathcal{G}}\right)\right], \tag{1}$$

where $\lambda \in \Re - \{0, 1\}$. For $\lambda = 3$, it becomes forgotten topological index proposed by Furtula et al. [8]. It is presented as

$$F(\mathcal{G}) = \sum_{\mu \in V(\mathcal{G})} \xi^3\left(\frac{\mu}{\mathcal{G}}\right) = \sum_{\mu\nu \in E(\mathcal{G})} \left[\xi^2\left(\frac{\mu}{\mathcal{G}}\right) + \xi^2\left(\frac{\nu}{G\mathcal{G}}\right)\right]. \quad (2)$$

Liu et al. ([9]) introduced the reformulated F-index of $\mathcal{G}$ as follows:

$$\mathrm{RF}(\mathcal{G}) = \sum_{e \in E(\mathcal{G})} \xi^3\left(\frac{e}{\mathcal{G}}\right) = \sum_{e \sim f \in E(\mathcal{G})} \left[\xi^2\left(\frac{e}{\mathcal{G}}\right) + \xi^2\left(\frac{f}{\mathcal{G}}\right)\right]. \quad (3)$$

In [10], Milicevic et al. introduced the first reformulated Zagreb index of a graph $\mathcal{G}$. It is defined as

$$\mathrm{EM}_1(\mathcal{G}) = \sum_{e \in E(\mathcal{G})} \xi^2(e), \quad (4)$$

where $\xi(e) = \xi(\mu/\mathcal{G}) + \xi(\nu/\mathcal{G}) - 2$. Recently, Alameri et al. [11] introduced a GI named Y-index (YI) and defined as

$$Y(\mathcal{G}) = \sum_{\mu \in V(\mathcal{G})} \xi^4\left(\frac{\mu}{\mathcal{G}}\right) = \sum_{\mu\nu \in E(\mathcal{G})} \left[\xi^3\left(\frac{\mu}{\mathcal{G}}\right) + \xi^3\left(\frac{\nu}{\mathcal{G}}\right)\right]. \quad (5)$$

The YI is the special case of the first general Zagreb index for $\lambda = 4$.

In this study, we obtain some new upper bounds (UB) for the YI in terms of different graph parameters, on $\zeta_\kappa(\mathcal{T})$ for tree of vertex n and TI s. We arrange the remaining work as follows: Section 2 contains the UB for the YI on trees with ζ_κ. Section 3 contains some UB for YI in behavior of some relevant parameters. Section 4 collects some UB for YI under several graph operations. Finally, Section 5 presents the conclusions of the obtained results. To know more related to this field, readers are referred to [12–17].

2. Preliminaries

To establish the main results, the following lemmas are required.

Lemma 1. *[18]). Let $\mathcal{T}$ be a $n(>3)$ vertex tree with $e = p_1p_2 \in E(\mathcal{T})$, a nonpendant edge. Suppose the union of $\mathcal{T}_1$ and $\mathcal{T}_2$ is equal to $\mathcal{T} - p_1p_2$, where $p_i \in \mathcal{T}_i$ for $i \in \{1, 2\}$. Let $\mathcal{T}$ be a new tree obtained by taking an edge joining transformation (EJT) of $\mathcal{T}$ on e. It is attained by identifying $p_1 \in T_1$ with $p_2 \in \mathcal{T}_2$ and also joining a pendent vertex s to the $p(= p_1 = p_2)$. In short, we denote $\mathcal{T} = \phi(\mathcal{T}, p_1p_2)$. Then, we get $Y(\mathcal{T}) < Y(\mathcal{T})$.*

Lemma 2. *[19]). If $\mathcal{G}$ is an n vertex MG graph with $n = \kappa + 1$, then $\zeta_\kappa(\mathcal{G}) = \lfloor n/\kappa + 1 \rfloor$.*

Lemma 3. *[20]). Let $\mathcal{H}$ and $\mathcal{T}$ be two trees with n and $(\kappa + 1)n$ vertices, respectively. Then, $\zeta_\kappa(\mathcal{T}) = n$ holds iff at least one of following conditions is satisfied:*

(1) $\mathcal{T}$ is any $(\kappa + 1)$-vertex tree.

(2) $\mathcal{T}$ is equal to $\mathcal{H}^\circ\kappa$ obtained by taking $\mathcal{H}$ and n copies of $P_{\kappa-1}$ and then link with the j^{th} vertex of $\mathcal{H}$ to exactly one end vertex in the j^{th} copy of $P_{\kappa-1}$.

Lemma 4. *[2]). If $\mathcal{G}$ contains the maximum value of the ZI s among all MG s of n-vertices with $\zeta_\kappa(\mathcal{G})$ and $S_\mathcal{G} = \{\mu \in V(\mathcal{G}) | \xi(\mu/\mathcal{G}) = 1, \zeta_\kappa(\mathcal{G} - \mu) = \zeta_\kappa(\mathcal{G})\}$. If $S_\mathcal{G} \neq \emptyset$, then $|N_\mathcal{G}(S_\mathcal{G})| = 1$.*

Lemma 5. *[2]). Suppose μ and ν be two vertices in $\mathcal{G}$ such that $p_1, p_2, \ldots, p_r$ and $q_1, q_2, \ldots, q_t$ pendent vertices adjacent to p and q respectively. Define $\mathcal{G}' = \mathcal{G} - \{qq_1, qq_2, \ldots, q_t\} + \{pq_1, pq_2, \ldots, pq_t\}$ and $\mathcal{G}'' = \mathcal{G} - \{pp_1, pp_2, \ldots, pp_r\} + \{qp_1, qp_2, \ldots, qp_r\}$. Then either $M_i(\mathcal{G}')$ is greater than $M_i(\mathcal{G})$ or $M_i(\mathcal{G}'')$ is greater than $M_i(\mathcal{G}), i = 1, 2$.*

Lemma 6. *[2]). Let $\mathcal{T}$ be a tree of order n with Δ and $\zeta_\kappa \geq 2$. Then $\kappa\zeta_\kappa(\mathcal{T}) \leq (n - \Delta(\mathcal{T}))$.*

Lemma 7. *[21]). Suppose $\mu\nu$ is any edge of $\mathcal{G}$ with n vertices. Then, for any integer $t \geq 2$*

(i) $|\xi(\mu/\mathcal{G}), \xi(\nu/\mathcal{G})|_{S(\mathcal{G},t)} = n^{t-2}(n - \xi(\mu/\mathcal{G}) - \xi(\nu/\mathcal{G}) + \triangleright(\mu, \nu))$

(ii) $|\xi(\mu/\mathcal{G}), \xi(\nu/\mathcal{G}) + 1|_{S(\mathcal{G},t)} = n^{t-2}(\xi(\mu/\mathcal{G}) - \triangleright(\mu, \nu)) - \beta(n)_{t-2}\xi(\mu/\mathcal{G}))$

(iii) $|\xi(\mu/\mathcal{G}) + 1, d(\nu/\mathcal{G})|_{S(\mathcal{G},t)} = n^{t-2}(\xi(\mu/\mathcal{G}) - \triangleright(\mu, \nu)) - \beta(n)_{t-2}\xi(\nu/\mathcal{G}))$

(iv) $|\xi(\mu/\mathcal{G}) + 1, \xi(\nu/\mathcal{G}) + 1|_{S(\mathcal{G},t)} = n^{t-2}((\triangleright(\mu, \nu) + 1) + \beta(n)_{t-2}(\xi(\mu/\mathcal{G}) + \xi(\nu/\mathcal{G}) + 1))$.

Lemma 8. *[22]). (Radon's inequality) Let $x = (x_i)_{i=1}^n$ and $y = (y_i)_{i=1}^n$ be two sequences of positive real numbers. For any $\alpha \geq 0$,*

$$\sum_{i=1}^{n} \frac{x_i^{\alpha+1}}{y_i^\alpha} \geq \frac{\left(\sum_{i=1}^n x_i\right)^{\alpha+1}}{\left(\sum_{i=1}^n y_i\right)^\alpha}. \quad (6)$$

where the equality occurs for $x_i = py_i$ for some constant p, for all $i = 1, 2, \ldots, n$.

3. Main Results and Discussions

3.1. Some UB for the YI on Trees with DD_κ Number. In this section, we establish some sharp UB for the YI of graphs on the trees as to the DD_κ number, ζ_κ. The set of all n vertex trees with ζ_κ and the star of order $(n - \kappa\zeta + 1)$ with $u_1, u_2, \ldots, u_{n-\kappa\zeta_\kappa}$ pendent vertices are denoted as $\mathcal{T}_{n,\kappa,\zeta_\kappa}$ and $S_{n-\kappa\zeta_\kappa+1}$, respectively.

Theorem 1. *Let $\mathcal{T}$ be a tree of order n and it contains $\zeta_\kappa(\mathcal{T}) = 2$; then the UB of $Y(\mathcal{T})$ can be expressed as $Y(\mathcal{T}) \leq (n - 2\kappa)^4 + (n - 2(\kappa + 1)) + (16\kappa + 1) + 16\kappa - 15$. The equality holds for $\mathcal{T} \Leftrightarrow \mathcal{T}^j_{n,\kappa,2}$, where $j \in \{1, 2, \ldots, k\}$.*

Proof. Let $\mathcal{T} \in \mathcal{T}_{n,\kappa,2}$ be a tree with a DP such that P: u_0, $u_1, \ldots, u_d$. For $d \leq 2\kappa$, there exists a DD_κ set $\{\mu_{\lfloor d/2 \rfloor}\}$ of $\mathcal{T}$, a contradiction. In case $d \geq 2\kappa + 2$, also denoted by $\mathcal{T} = \phi(\mathcal{T}, u_iu_{i+1})$ the tree obtained from $\mathcal{T}$ by EJT (Lemma 1) on the edge u_iu_{i+1} for some $i \in \{1, 2, \ldots, d - 2\}$, then $\zeta_\kappa(\mathcal{T}) = 2$; therefore, $\mathcal{T} \in \mathcal{T}_{n,\kappa,2}$. But $Y(\mathcal{T}) > Y(\mathcal{T})$, a contradiction. Thus, it is only s for $d = 2\kappa + 1$.

In this case, we consider a tree $\mathcal{T}^{\alpha}_{n,\kappa,2} \in \mathcal{T}_{n,\kappa,2}$ obtained from the path $P_{2\kappa+2} = w_0w_1 \dots w_{2\kappa+1}$ by attaching $n-2(\kappa+1)$ pendent vertices to w_α, where $\alpha \in \{1, \dots, 2\kappa\}$. Moreover, $\mathcal{T}^{\alpha}_{n,\kappa,2} \cong \mathcal{T}^{d-\alpha}_{n,\kappa,2}$ for $\kappa+1 \le \alpha \le d-1$ and also $Y(\mathcal{T}^{\alpha}_{n,\kappa,2}) = Y(\mathcal{T}^{\beta}_{n,\kappa,2})$ for $1 \le \alpha \ne \beta \le d-1$. Consequently, $\mathcal{T} \cong \mathcal{T}^{\alpha}_{n,\kappa,2}$, for some $\alpha \in \{1, 2, \dots, \kappa\}$. Therefore, the YI for the tree $\mathcal{T}$ can be directly computed as $Y(\mathcal{T}) = Y(\mathcal{T}^{\alpha}_{n,\kappa,2}) = (n-2\kappa)^4 + (n-2(\kappa+1)) + (16\kappa+1) + 16\kappa - 15$. □

Theorem 2. *Consider an n vertex tree $\mathcal{T}$ that belongs to $\mathcal{T}_{n,\kappa,3}$. Then, $Y(\mathcal{T}) \le (n-3\kappa)^4 + (n-3(\kappa+1)) + 2(16\kappa+1) + 16\kappa - 15$. The equality occurs as $\mathcal{T} \Leftrightarrow \mathcal{T}_{n,\kappa,3}$.*

Proof. Given that $\mathcal{T} \in \mathcal{T}_{n,\kappa,3}$. Obviously $n \ge (\kappa+1)\zeta_\kappa$, by Lemma 2. Also, the equality $n = (\kappa+1)\zeta_\kappa$ of Lemma 3 holds the results. Now, we proceed to prove the theorem by induction hypothesis (IH) on n. Assume that $n > 3(\kappa+1)$ and the statement is true for $n-1$. Our main goal is to reach $\mathcal{T} \cong \mathcal{T}_{n,\kappa,3}$.

Let $P = u_0u_1 \dots u_d$ and $\mathcal{D}$ be a DP and minimum DD_κ set of $\mathcal{T}$, respectively. Actually, we have to prove $d \ge 2\kappa+2$. Otherwise, $\{u_\kappa, u_{\kappa+1}\}$ is a DD_κ set, a contradiction. Let us assume that $\{u_\kappa, u_{d-\kappa}\} \subseteq \mathcal{D}$ such that $(\cup_{r=0}^{\kappa} V(\mathcal{T}_r) \setminus \{u_\kappa\}) \cap \mathcal{D} = \varnothing$ and $(\cup_{r=d-\kappa}^{d} V(\mathcal{T}_r) \setminus \{u_{d-\kappa}\}) \cap \mathcal{D} = \varnothing$.

Choose $u_0 (= \alpha_1), u_2, \dots, u_d (= \alpha_t)$ as the pendent vertices of $\mathcal{T}$ and also $\zeta_{\mathcal{T}} = \{\alpha_i | \zeta_\kappa(\mathcal{T} - \alpha_i) = \zeta_\kappa(\mathcal{T})\}$ for $1 \le i \le t$. If $\zeta_{\mathcal{T}} = \varnothing$, then $\zeta_{\mathcal{T}} = \{\alpha_i | \zeta_\kappa(\mathcal{T} - \alpha_i) = \zeta_\kappa(\mathcal{T}) - 1\}$ for $1 \le i \le t$.

When $\xi(u_i/\mathcal{T}) \ge 3$, then $\{\alpha_2, \dots, \alpha_{t-1}\} \cap V(\mathcal{T}_i) \ne \varnothing$. Taking $\{u_\kappa, u_{d-\kappa}\} \in \mathcal{D}$, so $\zeta_\kappa(\mathcal{T} - x) = \zeta_\kappa(\mathcal{T})$ for $x \in \{\alpha_2, \dots, \alpha_{t-1}\} \cap V(\mathcal{T}_i)$, a contradiction. Therefore $\xi(u_i/\mathcal{T}) = 2$ for $i \in \{1, 2, \dots, \kappa, d-\kappa, \dots, d-1\}$. Clearly $\zeta_\kappa(\mathcal{T} - u_0) = \zeta_\kappa(\mathcal{T}) - 1$, since $\xi(u_1/\mathcal{T}) = 2$.

Remark that $\xi_{\mathcal{T}}(u_1, u_{\kappa+1}) = \kappa$ and $(\cup_{r=0}^{\kappa} V(\mathcal{T}_r) v_\kappa) \cap \mathcal{D} = \varnothing$. So, $u_{\kappa+1} \in \mathcal{D}$. Likewise, $u_{d-\kappa-1} \in \mathcal{D}$. For $d > 2\kappa+2$, the vertices $u_\kappa, u_{\kappa+1}, u_{d-\kappa-1}, u_{d-\kappa}$ are distinguished, a contradiction. So, $d = 2\kappa+2$ and $\mathcal{D} = \{u_\kappa, u_{\kappa+1}, u_{d-\kappa}\}$.

On the other side, if $\xi(u_{\kappa+1}/\mathcal{T}) = 2$, then $\mathcal{T} \cong P_{2\kappa+3}$ and $\{u_\kappa, u_{d-\kappa}\}$ is a DD_κ set, which is an inconsistency. Therefore, $\xi(u_{\kappa+1}/\mathcal{T}) \ge 3$ and also $\zeta_\kappa = 3 \le m$. When $m > 3$, then $\zeta_\kappa(\mathcal{T} - \alpha_i) = \zeta_\kappa(\mathcal{T})$ for some $i \in \{1, \dots, m\}$, an impropriety. So, $m = 3$. Thus, $\mathcal{T}_{\kappa+1}$ is a path of which ended vertices are $u_{\kappa+1}$ and α_3. That is, $\xi(u_{\kappa+1}, \alpha_3) = \kappa$. Hence, $|V(\mathcal{T})| = 3(\kappa+1)$, which contradicts $n > 3(\kappa+1)$.

Assume that v is a unique vertex α_i which is a pendent vertex with $\zeta_\kappa(\mathcal{T} - \alpha_i) = \zeta_\kappa(\mathcal{T})$. Note that $\xi(v/\mathcal{T}) \le \Delta \le (n-3\kappa)$, by Lemma 6. So, by the IH and the definition of $Y(\mathcal{T})$, we get

$$\begin{aligned} Y(\mathcal{T}) &= Y(\mathcal{T} - \alpha_i) + 4\xi^3\left(\frac{v}{\mathcal{T}}\right) - 6\xi^2\left(\frac{v}{\mathcal{T}}\right) + 4\xi\left(\frac{v}{\mathcal{T}}\right) \\ &\le (n-1-3\kappa)^4 + (n-1-3(\kappa+1)) + 2(16\kappa+1) + 16\kappa - 15 + 4(n-3\kappa)^3 - 6(n-3\kappa)^2 + 4(n-3\kappa) \\ &= (n-3\kappa)^4 + (n-3(\kappa+1)) + 2(16\kappa+1) + 16\kappa - 15 \end{aligned} \tag{7}$$

Therefore, the equality arrives if and only if $\mathcal{T} - \alpha_i \cong \mathcal{T}_{n-1,\kappa,3}$ and $\xi(v/T) = \Delta = (n-3\kappa)$, that is, $\mathcal{T} \Leftrightarrow \mathcal{T}_{n,\kappa,3}$. □

Theorem 3. *Let $\mathcal{T}$ be a tree having n vertices and $\zeta_k(\mathcal{T}) \ge 3$. If $n = (\kappa+1)\zeta_k$, we have $Y(\mathcal{T}) \le (\zeta_\kappa - 1)^4 + 4(\zeta_\kappa - 1)^3 + (\zeta_\kappa - 1)(6\zeta_\kappa + 5) + 2(8\kappa - 3)\zeta_\kappa - 8$. The equality is attained when $\mathcal{T} \Leftrightarrow \mathcal{T}_{n,\kappa,\zeta_\kappa}$.*

Proof. Given that $n = (\kappa+1)\zeta_\kappa$ for the tree $\mathcal{T}$ of n vertices with DD_κ number, $\zeta_\kappa (\ge 3)$. By Lemma 3, we get $\mathcal{T} = \mathcal{G}^\circ\kappa$ for some tree $\mathcal{G}$ on ζ_κ vertices. Let us consider $V(\mathcal{G}) = \{u_1, u_2, \dots, u_\kappa\}$. Then, $\xi(u_i/\mathcal{G}) = \xi(v_i/T) - 1$. Therefore, $\sum_{i=1}^{\zeta_\kappa} \xi(u_i/\mathcal{G}) = 2(\zeta_\kappa - 1)$ since for every tree (assume $\mathcal{T}'$) containing n-vertices with vertex set $\{x_1, x_2, \dots, x_n\}$ occurs $\sum_{i=1}^{\zeta_\kappa} \xi(x_i/\mathcal{T}') = 2(n-1)$. By the definition of the YI, we can express

$$\begin{aligned} Y(\mathcal{T}) &= \sum_{i=1}^{\zeta_\kappa} \xi^4\left(\frac{u_i}{\mathcal{G}}\right) + \sum_{v_i \in V(\mathcal{T}) \setminus V(\mathcal{G})} \xi^4\left(\frac{v_i}{\mathcal{T}}\right) \\ &= \sum_{i=1}^{\zeta_\kappa} \left(\xi\left(\frac{u_i}{\mathcal{T}}\right) - 1\right)^4 + 4\sum_{i=1}^{\zeta_\kappa} \left(\xi\left(\frac{u_i}{\mathcal{T}}\right) - 1\right)^3 + 6\sum_{i=1}^{\zeta_\kappa} \left(\xi\left(\frac{u_i}{\mathcal{T}}\right) - 1\right)^2 + 4\sum_{i=1}^{\zeta_\kappa} \left(\xi\left(\frac{u_i}{\mathcal{T}}\right) - 1\right) + \zeta_\kappa + 16(\kappa-1)\zeta_\kappa + \zeta_\kappa \\ &= Y(\mathcal{G}) + 4F(\mathcal{G}) + 6M_1(\mathcal{G}) + 8(\zeta_\kappa - 1) + 2\zeta_\kappa + 16(\kappa-1)\zeta_\kappa \\ &\le Y\left(S_{\zeta_\kappa}\right) + 4F\left(S_{\zeta_\kappa}\right) + 6M_1(\zeta_\kappa) + 16\kappa\zeta_\kappa - 6\zeta_\kappa - 8 \\ &= (\zeta_\kappa - 1)^4 + 4(\zeta_\kappa - 1)^3 + (\zeta_\kappa - 1)(6\zeta_\kappa + 5) + 2(8\kappa - 3)\zeta_\kappa - 8 \end{aligned} \tag{8}$$

for equalities $\mathcal{G} \Leftrightarrow S_{\zeta_\kappa}$ that imply $\mathcal{T} \Leftrightarrow \mathcal{T}_{n,\kappa,\zeta_\kappa}$. □

Theorem 4. *Consider $\mathcal{T}$ as an n-vertex tree whose DD_κ number is $\zeta_\kappa \geq 3$. Then, $Y(\mathcal{T}) \leq (n-\kappa\zeta_\kappa)^4 + (n-(\kappa+1)\zeta_\kappa) + (16\kappa+1)(\zeta_\kappa - 1) + 16\kappa - 15$.*

The equality occurs for $\mathcal{T} \Leftrightarrow \mathcal{T}_{n,\kappa,\zeta_\kappa}$.

Proof. Let $\mathcal{T} \Leftrightarrow \mathcal{T}_{n,\kappa,\zeta_\kappa}$ be a tree containing a DP such that $P = u_0u_1 \ldots u_d$ that maximized the YI of graphs. The main goal is to establish the maximization of $Y(\mathcal{T})$ with respect to $\mathcal{T} \cong \mathcal{T}_{n,\kappa,\zeta_\kappa}$. Let us consider $\mathcal{D}$ to be a minimum DD_κ set of $\mathcal{T}$ and also define $\zeta_{\mathcal{T}} = \{x \in V(\mathcal{T}) | \xi(x/\mathcal{T}) = 1 \text{ and } \zeta_\kappa(\mathcal{T} - x) = \zeta_\kappa(\mathcal{T})\}$. If $\Gamma_{\mathcal{T}} = \emptyset$, then $\zeta_\kappa(\mathcal{T} - u_i) = \zeta_\kappa(\mathcal{T}) - 1$ for $i = 0, d$. Also, for $\Gamma_{\mathcal{T}} \neq \emptyset$, by Lemma 4, $|N_{\mathcal{T}}(\Gamma_{\mathcal{T}})| = 1$. In case, $u_0, u_d \in \Gamma_{\mathcal{T}}$, as $d - 1 > 1$, we get $\{u_1, u_{d-1}\} \subseteq |N_{\mathcal{T}}(\Gamma_{\mathcal{T}})|$ that implies $|N_{\mathcal{T}}(\Gamma_{\mathcal{T}})| > 1$, a contradiction. Therefore, we consider that $\zeta_\kappa(\mathcal{T} - u_0) = \zeta_\kappa(\mathcal{T}) - 1$, and thus $\{u_\kappa, u_{\kappa+1}, u_{d-\kappa}\} \subseteq \mathcal{D}$, from Theorem 2.

By Lemma 1, applying EJT of $\mathcal{T}$ on any nonpendent edge of $\mathcal{T}_\alpha$ repeatedly for $\alpha = 1, \ldots, \kappa$, it is to be constructed a tree $\acute{\mathcal{T}}$ from $\mathcal{T}$ such that $\acute{\mathcal{T}}_\alpha \cong S_{|V(\acute{\mathcal{T}}_\alpha)|}$, where $\acute{\mathcal{T}}_\alpha$ is the component of $\acute{\mathcal{T}} - \{u_{\alpha-1}u_\alpha, u_\alpha u_{\alpha+1}\}$ having u_α, for $\alpha = 1, \ldots, \kappa$. Then, we have $\acute{\mathcal{T}} \in \mathcal{T}_{n,\kappa,\zeta_\kappa}$ and also $Y(\mathcal{T}) \leq Y(\acute{\mathcal{T}})$, where the equality holds $\mathcal{T} \Leftrightarrow \acute{\mathcal{T}}$.

Now let $\mathcal{T}^* = \mathcal{T} - \cup_{\alpha \in \{1,\ldots,\kappa\} \setminus (\alpha_r)} \{u_\alpha w | w \in N_{\acute{\mathcal{T}}}(u_\alpha) \setminus \{u_{\alpha-1}, u_{\alpha+1}\}\} + \cup_{\alpha_r \in \{1,\ldots,\kappa\} \setminus (\alpha_r)} \{u_\alpha w || w \in N_{\acute{\mathcal{T}}}(u_\alpha) \setminus \{u_{\alpha-1}, u_{\alpha+1}\}\}$ for some $\alpha_r \in \{1, \ldots, \kappa\}$.

Then, by Lemma 5, we get $Y(\mathcal{T}) \leq \mathcal{T}^*$ with equality if and only if $\mathcal{T} \cong Y(\mathcal{T}^*)$.

Again, define by $\mathcal{T}^\star = \mathcal{T}^* - \{u_{\alpha_r} w | w \in N_{\mathcal{T}^*}(u_{\alpha_r}) \setminus \{u_{\alpha_r-1}, u_{\alpha_r+1}\}\} + \{u_{\kappa+1} w | w \in N_{\mathcal{T}^*}(u_{\alpha_r}) \setminus \{u_{\alpha_r-1}, u_{\alpha_r+1}\}\}$. In fact, let $|N_{\mathcal{T}^*}(u_{\alpha_r}) \setminus \{u_{\alpha_r-1}, u_{\alpha_r+1}\}| = p, p \geq 0$.

Then, $\xi(u_\alpha/\mathcal{T}^\star) = 2$ for $\alpha = 1, \ldots, \kappa$ and also $\mathcal{D}$ will be the minimum DD_κ set of $\mathcal{T}^\star$. It implies that all the vertices in $\cup_{\alpha=0}^{k} N_{\mathcal{T}^\star}^{\alpha}(u_\kappa) \setminus \{u_0, \ldots, u_\kappa\}$ can be determined by $u_{\kappa+1} \in \mathcal{D}$. Therefore, $\mathcal{D} \setminus \{u_\kappa\}$ will be a DD_κ set of $\mathcal{T}^\star - u_0, \ldots, u_\kappa$. Suppose that $PN_{\kappa,\mathcal{D}}(y)$ is the set of all private κ-neighbors of y upon $\mathcal{D}$ in $\mathcal{T}^\star$. Then, $PN_{\kappa,\mathcal{D}}(u_{\kappa+1}) \subseteq V(\mathcal{T}^\star) \setminus u_0, \ldots, u_\kappa$. Thus, $\mathcal{D} \setminus \{u_\kappa\}$ will be a minimum DD_κ set of the tree $\mathcal{T}^\star - \{u_0, \ldots, u_\kappa\}$. Therefore, $\zeta_\kappa(\mathcal{T}^\star - \{u_0, \ldots, u_\kappa\}) = \zeta_\kappa - 1 = \zeta_\kappa(\mathcal{T}^\star - \{u_0, \ldots, u_{\kappa-1}\})$.

So, from the definition of YI, we have

$$\begin{aligned} Y(\mathcal{T}^\star) - Y(\mathcal{T}^\star) &= \left(d\left(\frac{u_{\kappa+1}}{\mathcal{T}^*}\right) + p\right)^4 + 2^4 - \xi^4\left(\frac{u_{\kappa+1}}{\mathcal{T}^*}\right) - (p+2)^4 \\ &= 2p\left(2\xi^3\left(\frac{u_{\kappa+1}}{\mathcal{T}^*}\right) + 3p\xi^2\left(\frac{u_{\kappa+1}}{\mathcal{T}^*}\right) + 2p^2\xi\left(\frac{u_{\kappa+1}}{\mathcal{T}^*}\right) - 4p^2 - 12p - 16\right) \geq 0 \end{aligned} \tag{9}$$

It means that $Y(\mathcal{T}^\star) \geq Y(\mathcal{T}^\star)$, where the equality holds iff either $p = 0$ i.e. $\mathcal{T}^* \cong \mathcal{T}^\star$ or $\xi(u_{\kappa+1}/\mathcal{T}^*) = 2$.

So far, we have proved $Y(\mathcal{T}^\star) \leq (n-\kappa\zeta_\kappa)^4 + (n-(\kappa+1)\zeta_\kappa) + (16\kappa+1)(\zeta_\kappa - 1) + 16\kappa - 15$ with equality iff $\mathcal{T}^\star \cong \mathcal{T}_{n,\kappa,\zeta_\kappa}$ by induction on ζ_k. We have from Theorem 2 that the assertion is mathematics for $n \geq (\kappa+1)\zeta_\kappa$ as well as $\zeta_k = 3$.

Now let us consider the affirmation contains for $\zeta_k - 1$ and all the vertices $n \geq (\kappa+1)(\zeta_\kappa - 1)$.

Because of $\zeta_k(\mathcal{T}^\star - \{u_0, \ldots, u_\kappa\})$ and $|V(\mathcal{T}^\star) - \{u_0, \ldots, u_\kappa\}| = (n - \kappa - 1) \geq (\kappa+1)(\zeta_\kappa - 1)$, we get by the IH

$$\begin{aligned} Y(\mathcal{T}^\star) &= Y(\mathcal{T}^* - \{u_0, \ldots, u_\kappa\}) + 4\xi^3(u_{\kappa+1}) - 6\xi^2(u_{\kappa+1}) + 4\xi(u_{\kappa+1}) - 1 + \sum_{\alpha=0}^{\kappa} \xi_{\mathcal{T}^*}^4(u_\alpha) \\ &= Y\left(\mathcal{T}_{n-\kappa-1,\kappa,\zeta_\kappa-1}\right) + 4(n-\kappa\zeta_\kappa)^3 - 6(n-\kappa\zeta_\kappa)^2 + 4(n-\kappa\zeta_\kappa) + 16\kappa \\ &= (n-\kappa\zeta_\kappa)^4 + (n-(\kappa+1)\zeta_\kappa) + (16\kappa+1)(\zeta_\kappa - 1) + 16\kappa - 15, \end{aligned} \tag{10}$$

where the equality holds iff $\mathcal{T}^\star - \{u_0, \ldots, u_\kappa\} \cong \mathcal{T}_{n-\kappa-1,\kappa,\zeta_\kappa-1}$ and also $\xi_{\mathcal{T}^*}(u_{\kappa+1}) = \Delta = n - \kappa\zeta_\kappa$ and otherwise $\mathcal{T}^* \cong \mathcal{T}_{n,\kappa,\zeta_\kappa}$ with $\xi_{\mathcal{T}^*}(u_\alpha) = 2$ for $\alpha = 1, \ldots, \kappa$. Therefore, we can conclude that $Y(\mathcal{T}) \leq Y(\acute{\mathcal{T}}) \leq Y(\mathcal{T}^*) \leq Y(\mathcal{T}^*) \leq (n-\kappa\zeta_\kappa)^4 + (n-(\kappa+1)\zeta_\kappa) + (16\kappa+1)(\zeta_\kappa - 1) + 16\kappa - 15$ with either equality iff $\mathcal{T} \cong \acute{\mathcal{T}} \cong \mathcal{T}^* \cong \mathcal{T}^\star \cong \mathcal{T}_{n,\kappa,\zeta_\kappa}$ or $\mathcal{T} \cong \acute{\mathcal{T}} \cong \mathcal{T}^*$ with $\xi_{\mathcal{T}^*}(u_{\kappa+1}) = 2$. Besides, $\mathcal{T}^\star \cong \mathcal{T}_{n,\kappa,\zeta_\kappa}$. □

Here, we determine some UB on the YI of trees containing n-vertices with domination number ζ ([23]). The DD_κ number of a graph is said to be the domination number of that graph if $\kappa = 1$. If $\mathcal{T}$ is an n-vertex tree containing a DP such that P: $u_0u_1 \ldots u_d$, then denote by $\mathcal{T}_i$ the component of $\mathcal{T} - \{u_{i-1}u_i, u_iu_{i+1}\}$ containing $u_i, i = 1, 2, \ldots, d-1$. To compute our main outcome, at first, we will focus on the following definition.

Consider $\mathcal{T}_{n,\zeta}$ to be a tree constructed from a star $K_{1,n-1}$ with involvement of a pendant edge to its $\zeta - 1$ pendant vertices. Note that $\mathcal{T}_{n,\zeta} \in \mathcal{T}_{n,\zeta}$, a class of n vertex trees and domination number ζ. Also, $\zeta = 1$ occurs iff $\mathcal{T} \cong \mathcal{T}_{1,n-1}$.

Corollary 1. *If $\mathcal{T} \in \mathcal{T}_{n,\zeta}$, then $Y(\mathcal{T}) \leq (n-\zeta)^4 + (n-2\zeta+1) + 17(\zeta - 1)$ with equality holding for $\mathcal{T} \Leftrightarrow \mathcal{T}_{n,\zeta}$.*

Proof. For $\Delta = 2$, it occurs that $\mathcal{T} \cong P_n (n \geq 2)$. The equality holds for $\mathcal{T} \cong \mathcal{T}_{2,1} (\equiv P_2)$, $\mathcal{T} \cong \mathcal{T}_{3,1} (\equiv P_3)$ and $\mathcal{T} \cong \mathcal{T}_{4,2} (\equiv P_4)$. But for $n \geq 5$, the above inequality is strict. Now, we consider a diameter path $P = u_0, u_1, \ldots, u_d$ and a minimum dominating set $\mathcal{D}$ of $\mathcal{T}$ with $\Delta \geq 3$. To prove the theorem, we will take the way of *IH* on *n*. Let us consider that Theorem 1 is true for $n-1$ and also the statement is to be proved as well as truth by replacing $n+1$ from *n*.When $\zeta(\mathcal{T} - \{u_0\}) = \zeta(\mathcal{T})$, then by the IH we have

$$Y(\mathcal{T}) = Y(\mathcal{T} - \{u_0\}) + 4\xi^3\left(\frac{u_1}{\mathcal{T}}\right) - 6\xi^2\left(\frac{u_1}{\mathcal{T}}\right) + 4\xi\left(\frac{u_1}{\mathcal{T}}\right), \tag{11}$$

$$\begin{aligned} Y(\mathcal{T}) &= Y(\mathcal{T} - \{u_0\}) + 4\xi^3(u_1/\mathcal{T}) - 6\xi^2(u_1/\mathcal{T}) + 4\xi(u_1/\mathcal{T}) \\ &\leq (n-\zeta+1)^4 + (n-2\zeta+3) + 17(\zeta-2) + 16 \\ &= (n-\zeta)^4 + (n-2\zeta+1) + 17(\zeta-1), \end{aligned} \tag{12}$$

where the equality holds iff $\mathcal{T} - \{u_0\} \cong \mathcal{T}_{n-1,\zeta-1}$ and pendant vertex u_0 is adjacent to the vertex u_1 of degree 2, that is, $\mathcal{T} \cong \mathcal{T}_{n,\zeta}$. □

3.2. Some UB for the YI of Graphs with respect to Some Standard Parameters and Others TI. In this section, we establish the some sharp UB for the YI of $\mathcal{G} \cdot w \cdot r$ to some graph parameters such as n, m, δ, Δ and others TI such as $M_1(\mathcal{G}), M_2(\mathcal{G}), F(\mathcal{G}), \mathrm{EF}(\mathcal{G}), \mathrm{EM}_1(\mathcal{G})$. Let $\mathcal{D}(\mathcal{G}) = \{\xi(u_1/\mathcal{G}), \xi(u_1/\mathcal{G}), \ldots, \xi(u_n/\mathcal{G})\}$. If $\mathcal{D}(\mathcal{G}) = \{r\}$, then $\mathcal{G}$ is said to be *r*-regular. If $\mathcal{D}(\mathcal{G}) = \{r, s\}$, then $\mathcal{G}$ is (r, s) biregular and so on. Motivating the proof technique as in [24], we obtain an UB for YI in the following theorem.

Theorem 5. *Consider $\mathcal{G}$ to be a (n, m) graph, i.e., $\mathcal{G}$ contains n vertices and m edges. Then $Y(\mathcal{G}) \leq 2m(\delta+\Delta)(\delta^2+\Delta^2) - n\delta\Delta(\delta^2+\delta\Delta+\Delta^2) + (\delta-t)(\Delta^3+\delta\Delta^2+\delta\Delta) - t(\delta^2+t\delta+t^2)$, where t is the integer defined by relation $2m - n\delta \equiv t - \delta \pmod{\Delta-\delta}$, $\delta \leq t \leq \Delta - 1$ and the equality holds iff at most one vertex of $\mathcal{G}$ has different degree from δ and Δ.*

Proof. Consider x_i as the number of vertices of degree *i* in $\mathcal{G}$. From the definition of YI, we can write

$$Y(\mathcal{G}) = \sum_{i=\delta}^{\Delta} i^4 x_i. \tag{13}$$

Obviously,

$$\begin{aligned} \sum_{i=\delta}^{\Delta} i x_i &= 2m, \\ \sum_{i=\delta}^{\Delta} x_i &= n. \end{aligned} \tag{14}$$

After calculation, we get

$$x_\delta = \frac{1}{\Delta-\delta}\left[n\Delta - 2m + \sum_{i=\delta+1}^{\Delta+1}(i-\Delta)x_i\right], \tag{15}$$

$$x_\Delta = \frac{1}{\Delta-\delta}\left[2m - n\delta + \sum_{i=\delta+1}^{\Delta+1}(\delta-i)x_i\right]. \tag{16}$$

Using (15) and (16), we have

$$\begin{aligned} Y(\mathcal{G}) &= \delta^4 x_\delta + \Delta^4 x_\Delta + \sum_{i=\delta+1}^{\Delta-1} i^4 x_i \\ &= \frac{\delta^4}{\Delta-\delta}\left[n\Delta - 2m + \sum_{i=\delta+1}^{\Delta+1}(i-\Delta)x_i\right] + \frac{\Delta^4}{\Delta-\delta}\left[2m - n\delta + \sum_{i=\delta+1}^{\Delta+1}(\delta-i)x_i\right] + \sum_{i=\delta+1}^{\Delta-1} i^4 x_i. \\ &= \frac{1}{\Delta-\delta}\left[\delta^4(n\Delta-2m) + \Delta^4(2m-n\delta)\right] + \frac{1}{\Delta-\delta}\sum_{i=\delta+1}^{\Delta-1}\left[\delta^4(i-\Delta) + \Delta^4(\delta-i) + i^4(\Delta-\delta)\right]x_i. \end{aligned} \tag{17}$$

Actually, the term $\delta^4(i-\Delta)+\Delta^4(\delta-i)+i^4(\Delta-\delta)$ will be negative for $\delta+1\le i\le\Delta-1$. So, the $Y(\mathcal{G})$ will be maximum if $x_i=0$ for $i=\delta+1,\ldots,\Delta-1$. Therefore, (15) and (16) become to $x_\delta=n\Delta-2m/\Delta-\delta$ and $x_\Delta=2m-n\delta/\Delta-\delta$. These two equations require that

$$2m-n\delta\equiv 0\,(\mathrm{mod}\,(\Delta-\delta)). \tag{18}$$

If the requirement is not true, we choose x_i such that $n_t=1$ and $x_i=0$ for all $i=\delta+1,\ldots,\Delta-1$, except for $i=t$. Then, (15) and (16) become $x_\delta=n\Delta-2m+k-\Delta/\Delta-\delta$ and $x_\Delta=2m-(n-1)\delta/\Delta-\delta$ which satisfy conditions 3 and 4. In [25], there survives a n vertex graph $\mathcal{G}$ of which one vertex with degree 0 when n and δ are both odd. If we add the edges to this graph, the vertex degrees increase one at a time up to Δ. There occurs $2m-n\delta\equiv t-\delta\,(\mathrm{mod}\,(\Delta-\delta))$ that implies that the degree of one more vertex may be increased up to t. Therefore, there exists a graph of order n and size m along with a unique vertex of degree t that different from δ and Δ.

Suppose now that the graph $\mathcal{G}$ contains two vertices of degrees i and k for $\delta+1\le i\le k\le\Delta-1$. If the sum of vertex degrees remains the same by reducing the first vertex degree by 1 and increasing the second vertex degree by 1, the value of the YI is replaced by

$$\begin{aligned}&\Big((\delta-(i-1))\Big(\Delta^3+\delta\Delta^2+\delta^2\Delta-(i-1)\Big(\delta^2+(i-1)\delta+(i-1)^2\Big)\Big)\Big)-(\delta-i)\Big(\Delta^3+\delta\Delta^2+\delta^2\Delta-i\Big(\delta^2+i\delta+i^2\Big)\Big)\\&\quad+(\delta-(k+1))\Big(\Delta^3+\delta\Delta^2+\delta^2\Delta-(k+1)\Big(\delta^2+(k+1)\delta+(k+1)^2\Big)\Big)-(\delta-k)\Big(\Delta^3+\delta\Delta^2+\delta^2\Delta-k\Big(\delta^2+k\delta+k^2\Big)\Big)\\&=(k+1)^3-(i-1)^3+3\Big(k^3-i^3\Big)+3\Big(k^2+i^2\Big)+(k-i)>0.\end{aligned} \tag{19}$$

It means that condition 8 is not true, and it will be the optimal choice of the quantities $x_i=0$ for $\delta+1\le i\le\Delta-1$ such that $x_t=1$ (except for $i=t$). Therefore, we can conclude from (17) that

$$Y(\mathcal{G})\le 2m(\delta+\Delta)\Big(\delta^2+\Delta^2\Big)-n\delta\Delta\Big(\delta^2+\delta\Delta+\Delta^2\Big)+(\delta-t)\Big(\Delta^3+\delta\Delta^2+\delta\Delta\Big)-t\Big(\delta^2+t\delta+t^2\Big). \tag{20}$$

□

Theorem 6. *If $\mathcal{G}$ is a (n,m) graph, then*

$$Y(\mathcal{G})\le EF(\mathcal{G})+6EM_1(\mathcal{G})+12M_1(\mathcal{G})-\frac{3M_1^2(\mathcal{G})}{n}-16m, \tag{21}$$

where the equality holds iff either $\mathcal{G}$ is regular or semiregular bipartite graph.

Proof. Using Lemma 8, for $\alpha=1$, setting $x_i=\xi(j/\mathcal{G})+\xi(k/\mathcal{G})$ and $y_i=1/\xi(j/\mathcal{G})+1/\xi(k/\mathcal{G})$ for the graph $\mathcal{G}$ in (1), we have

$$\sum_{jk\in E(\mathcal{G})}\frac{(\xi(j/\mathcal{G})+\xi(k/\mathcal{G}))^2}{1/\xi(j/\mathcal{G})+1/\xi(k/\mathcal{G})}\ge\frac{\Big(\sum_{jk\in E(\mathcal{G})}\xi(j/\mathcal{G})+\xi(k/\mathcal{G})\Big)^2}{\sum_{jk\in E(\mathcal{G})}(1/\xi(j/\mathcal{G})+1/\xi(k/\mathcal{G}))}, \tag{22}$$

$$i.e.\ \sum_{jk\in E(\mathcal{G})}\xi\Big(\frac{j}{G}\Big)\xi\Big(\frac{k}{G}\Big)\Big(\xi\Big(\frac{j}{G}\Big)+\Big(\frac{k}{G}\Big)\Big)\ge\frac{M_1^2(\mathcal{G})}{n}. \tag{23}$$

Also,

$$\begin{aligned}&\sum_{jk\in E(\mathcal{G})}\xi\Big(\frac{j}{\mathcal{G}}\Big)\xi\Big(\frac{k}{\mathcal{G}}\Big)\Big(\xi\Big(\frac{j}{\mathcal{G}}\Big)+\xi\Big(\frac{k}{\mathcal{G}}\Big)\\&=\frac{1}{3}\left[\sum_{jk\in E(\mathcal{G})}\left(\xi\Big(\frac{j}{\mathcal{G}}\Big)+\xi\Big(\frac{k}{\mathcal{G}}\Big)\right)^3-\sum_{jk\in E(\mathcal{G})}\left(\xi^3\Big(\frac{j}{\mathcal{G}}\Big)+\xi^3\Big(\frac{k}{\mathcal{G}}\Big)\right)\right]\end{aligned}$$

$$= \frac{1}{3}\left[\sum_{e\epsilon E(\mathcal{G})}\left(\xi\left(\frac{e}{\mathcal{G}}\right)+2\right)^3 - Y(\mathcal{G})\right]; \quad \text{where } \xi\left(e=\frac{ij}{\mathcal{G}}\right)=\xi\left(\frac{i}{\mathcal{G}}\right)+\xi\left(\frac{j}{\mathcal{G}}\right)-2.$$

$$= \frac{1}{3}\sum_{e\epsilon E(\mathcal{G})}\xi^3\left(\frac{e}{\mathcal{G}}\right)+2\sum_{e\epsilon E(\mathcal{G})}\xi^2\left(\frac{e}{\mathcal{G}}\right)+4\sum_{e\epsilon E(\mathcal{G})}\xi\left(\frac{e}{\mathcal{G}}\right)+\frac{8}{3}m-\frac{1}{3}\sum_{jk\in E(\mathcal{G})}\left[\xi^3\left(\frac{j}{\mathcal{G}}\right)+\xi^3\left(\frac{k}{\mathcal{G}}\right)\right]$$

$$= \frac{1}{3}EF(\mathcal{G})+2EM_1(\mathcal{G})+4\left(M_1(\mathcal{G})-2m\right)+\frac{8}{3}m-\frac{1}{3}Y(\mathcal{G}). \tag{24}$$

since $\sum_{e\epsilon E(\mathcal{G})}\xi(e/\mathcal{G})=\sum_{i\epsilon V(L(\mathcal{G}))}\xi(i/L(\mathcal{G}))=M_1(\mathcal{G})-2m$.

From (23) and (24), $M_1^2(\mathcal{G})/n \le 1/3EF(\mathcal{G})+2EM_1(\mathcal{G})+4(M_1(\mathcal{G})-2m)+8/3m-1/3Y(\mathcal{G})$. □

Theorem 7. *Suppose a graph $\mathcal{G}$ that contains n vertices and m edges. Then, $Y(\mathcal{G}) \le M_1(\mathcal{G})(F(\mathcal{G})-M_2(\mathcal{G}))$, with equalities $\mathcal{G} \Leftrightarrow P_2$.*

Proof. If $(a), (b), \ldots, (l)$ are positive numbers sets with m elements in each set and $p, q, \ldots, t$ are positive numbers such that $p+q+\cdots+t>1$, then by Jensen's theorem $\sum_{i=1}^m (a_i^p b_i^q \ldots l_i^t) \le (\sum_{i=1}^m a_i)^p (\sum_{i=1}^m b_i)^q \ldots (\sum_{i=1}^m l_i)^t$. We know

$$Y(\mathcal{G}) = \sum_{uv\epsilon E(\mathcal{G})}\left[\xi^3\left(\frac{u}{\mathcal{G}}\right)+\xi^3\left(\frac{v}{\mathcal{G}}\right)\right] = \sum_{uv\epsilon E(\mathcal{G})}\left[\xi\left(\frac{u}{\mathcal{G}}\right)+\xi\left(\frac{v}{\mathcal{G}}\right)\right]\left[\xi^2\left(\frac{u}{\mathcal{G}}\right)+\xi^2\left(\frac{v}{\mathcal{G}}\right)-\xi\left(\frac{u}{\mathcal{G}}\right)\xi\left(\frac{v}{\mathcal{G}}\right)\right]$$

$$\le \sum_{uv\epsilon E(\mathcal{G})}\left[\xi\left(\frac{u}{\mathcal{G}}\right)+\xi\left(\frac{v}{\mathcal{G}}\right)\right]\sum_{uv\epsilon E(\mathcal{G})}\left[\xi^2\left(\frac{u}{\mathcal{G}}\right)+\xi^2\left(\frac{v}{\mathcal{G}}\right)-\xi\left(\frac{u}{\mathcal{G}}\right)\xi\left(\frac{v}{\mathcal{G}}\right)\right]. \tag{25}$$

Setting $a_i=\xi(u/\mathcal{G})+\xi(v/\mathcal{G})$ and $b_i=\xi^2(u/\mathcal{G})+\xi^2(v/\mathcal{G})-\xi(u/\mathcal{G})\xi(v/\mathcal{G})$ and $p=q=1$, then by Jensen's theorem $= M_1(\mathcal{G})(F(\mathcal{G})-M_2(\mathcal{G}))$. □

Theorem 8. *Let $\mathcal{G}$ be a graph of n order and m size. Then, $Y(\mathcal{G}) \le 16m^4/\sqrt[3]{n^{16}}\left\{1/4(\Delta/\delta)^{16/3}+4/3\delta/\Delta\right\}^4$. The equality occurred when $\mathcal{G}$ is regular graph.*

Proof. We prove the theorem using the following inequalities.

If $1<x, y<\infty$, $p_i, q_i \ge 0$ and $\phi q_i^y \le p_i^x \le \varphi q_i^y$ for $1 \le i \le n$, then

$$\left(\sum_{i=1}^n p_i^x\right)^{1/x}\left(\sum_{i=1}^n q_i^y\right)^{1/y} \le c_x(\phi,\varphi)\sum_{i=1}^n p_i q_i, \tag{26}$$

where $c_x(\phi,\varphi)=\max\left\{1/x(\phi/\varphi)^{1/y}+1/y(\varphi/\phi)^{1/x}, 1/x(\varphi/\phi)^{1/y}+1/y(\phi/\varphi)^{1/x}\right\}$ is a constant with some positive constants ϕ, φ. If $p_i>0$ for some $1 \le i \le n$, then the equality holds if and only if $\phi=\varphi$ and $p_i^x=\phi q_i^y$ for every $1 \le i \le n$. Setting $p_i=\xi(u_i/\mathcal{G})$, $q_i=1$ and $x=4, y=4/3$ and also $\phi=\delta^4$, $\varphi=\Delta^4$, we have

$$\left(\sum_{i=1}^n \xi^4\left(\frac{u_i}{\mathcal{G}}\right)\right)^{1/4}\left(\sum_{i=1}^n 1\right)^{4/3} \le \max\left\{\frac{1}{4}\left(\frac{\delta^4}{\Delta^4}\right)^{4/3}+\frac{4}{3}\left(\frac{\Delta^4}{\delta^4}\right)^{1/4}, \frac{1}{4}\left(\frac{\Delta^4}{\delta^4}\right)^{4/3}+\frac{4}{3}\left(\frac{\delta^4}{\Delta^4}\right)^{1/4}\right\}\sum_{i=1}^n \xi\frac{u_i}{\mathcal{G}} \tag{27}$$

so $(Y(\mathcal{G}))^{1/4}n^{4/3} \le 2m\left\{1/4(\Delta/\delta)^{16/3}+4/3\delta/\Delta\right\}$, i.e., $Y(\mathcal{G}) \le 16m^4/\sqrt[3]{n^{16}}\left\{1/4(\Delta/\delta)^{16/3}+4/3\delta/\Delta\right\}^4$. This completes the proof. □

Theorem 9. *For an n vertex graph $\mathcal{G}$, we have $Y(\mathcal{G}) \le (F(\mathcal{G}))^{4/3}$. The equality is satisfied when $\mathcal{G}$ is regular.*

Proof. Let $x_1, x_2, \ldots, x_n$ be n positive real numbers, and let s, t be positive rational numbers. Then, by Jensen's inequality ([26]) $(\sum_{i=1}^n x_i^t)^{1/t} \le (\sum_{i=1}^n x_i^s)^{1/s}$ if $t>s>0$. The equality holds iff $x_1=x_2=\cdots=x_n$. Considering $x_i=\xi(u_i/\mathcal{G})$ for $t=4$, $s=3$, then we have $(\sum_{i=1}^n \xi^4(u_i/\mathcal{G}))^{1/4} \le (\sum_{i=1}^n \xi^3(u_i/\mathcal{G}))^{1/3}$, that is, $Y(\mathcal{G}) \le (F(\mathcal{G}))^{4/3}$. □

Theorem 10. *Let $\mathcal{G}$ be a (n, m) graph. Then, $Y(\mathcal{G}) \le (\delta^2+\Delta^2)M_1(\mathcal{G})-n\delta^2\Delta^2$. The equality is attained when $\mathcal{G}$ is regular.*

Proof. Suppose x_i, y_i, h and H are the positive real numbers such that $hx_i \le y_i \le Hx_i$ for $i=1,2,\ldots,n$. Then, by Diaz-Metacalf inequality [27], $\sum_{i=1}^n y_i^2+hH\sum_{i=1}^n \le (h+H)\sum_{i=1}^n x_i y_i$ ant the equality is attained if and only if $y_i=hx_i$

and $y_i = Ha_i$. Now taking $x_i = 1$ and $y_i = \xi^2(u_i/\mathcal{G})$ and $h = \delta^2$, $H = \Delta$, we get

$$\sum_{i=1}^{n} \xi^4\left(\frac{u_i}{\mathcal{G}}\right) + \delta^2\Delta^2 \sum_{i=1}^{n} 1 \le \left(\delta^2 + \Delta^2\right) \sum_{i=1}^{n} \xi^2\left(\frac{u_i}{\mathcal{G}}\right). \tag{28}$$

Thus, $Y(\mathcal{G}) \le (\delta^2 + \Delta^2)M_1(\mathcal{G}) - n\delta^2\Delta^2$. □

Theorem 11. *Let $\mathcal{G}$ be a graph whose number of vertices is n and edges m. Then,*

$$Y(\mathcal{G}) \le \frac{\beta(n)(\Delta - \delta)^2\left(\Delta^2 + \Delta\delta + \delta^2\right) + 2mF(\mathcal{G})}{n}. \tag{29}$$

The equality is attained iff $x_1 = x_2 = \cdots = x_n$ and $z_1 = z_2 = \cdots = z_n$ and also $\beta(n) = n\lceil n/2\rceil(1 - 1/n\lceil n/2\rceil)$, where $\lceil x\rceil$ is the largest integer greater than or equal to x.

Proof. Let x_i and z_i be positive real numbers for which there exist real constants x, z, X and Z such that $x \le x_i \le X$ and $z \le z_i \le Z$ for $1 \le i \le n$, respectively. Then, we have (discrete) Gruss inequality ([27]) $|n\sum_{i=1}^{n} x_i z_i - \sum_{i=1}^{n} x_i \sum_{i=1}^{n} z_i| \le \beta(n)(X - x)(Y - y)$.

The equality controls iff $x_1 = x_2 = \cdots = x_n$ and $z_1 = z_2 = \cdots = z_n$.

By setting $x_i = \xi^3(u/\mathcal{G})$ and $z_i = \xi(u/\mathcal{G})$ for every $i = 1, 2, \ldots, n$, we have $X = \Delta^3$ and $x = \delta^3$.

Then, the inequality becomes

$$n\sum_{i=1}^{n} \xi^4\left(\frac{u_i}{\mathcal{G}}\right) - \sum_{i=1}^{n} \xi^3\left(\frac{u_i}{\mathcal{G}}\right) \sum_{i=1}^{n} \xi\left(\frac{u_i}{\mathcal{G}}\right) \le \beta(n)\left(\Delta^3 - \delta^3\right)(\Delta - \delta). \tag{30}$$

So, $Y(\mathcal{G}) \le \beta(n)(\Delta - \delta)^2(\Delta^2 + \Delta\delta + \delta^2) + 2mF(\mathcal{G})/n$. This completes our claim. □

Corollary 2. *Since $\beta(n) \le n^2/4$, therefore $Y(\mathcal{G}) \le n^2(\Delta - \delta)^2(\Delta^2 + \Delta\delta + \delta^2) + 8mF(\mathcal{G})/4n$.*

Theorem 12. *Let $\mathcal{G}$ be a (n, m) graph. Then,*

$$\begin{aligned} Y(\mathcal{G}) \le{}& (3\Delta + \delta)F(\mathcal{G}) - \left\{(n-1)(\Delta - \delta) + 3\delta^2 - 3\delta\Delta\right\}M_1(\mathcal{G}) - (n-1)(2m - n\Delta)\delta^2 - 4(n-2)m\delta\Delta \\ &+ 2m\Delta^3 + 6m\delta\Delta^2 - \delta\Delta^3 n \end{aligned} \tag{31}$$

with equality holds if and only if $\mathcal{G}$ is (Δ, δ) biregular.

Proof. We have from [28] that $Y(\mathcal{G}) = (n-1)F(\mathcal{G}) - \overline{Y}(\mathcal{G})$, where $\overline{Y}(\mathcal{G})$ be the Y-coindex of $\mathcal{G}$. From [29], $F(\mathcal{G}) \le M_1(\mathcal{G})(\Delta + 2\delta) - \delta^2(2m - n\Delta) - 4m\delta\Delta$. Define by $X(\mathcal{G}) = (n-1)\sum_{u\in V(\mathcal{G})}(\xi(u/\mathcal{G}) - \Delta)^2 \quad (\xi(u/\mathcal{G}) - \delta) - \sum_{u\in V(\mathcal{G})}(\xi(u/\mathcal{G}) - \Delta)^3(\xi(u/\mathcal{G}) - \delta)$. Since $X(\mathcal{G}) \ge 0$, we have $\overline{Y}(\mathcal{G}) \ge \{(n-1)(\delta + 2\Delta) + 3\Delta^2 + 3\delta\Delta\}M_1(\mathcal{G}) - (3\Delta + \delta)F(\mathcal{G}) - 2m\Delta^2 + \delta\Delta^2 - 4m\delta\Delta - 2m\Delta^3 - 6m\delta\Delta^2 + \delta\Delta^3 n$.

After simplification, we get the required result. □ □

Theorem 13. *Let $\mathcal{G}$ be a (n, m) graph, we have*

$$Y(\mathcal{G}) \le (2x + \Delta + \delta)F(\mathcal{G}) - \left(x^2 + \delta\Delta\right)M_1(\mathcal{G}) + 2mx\{2\delta\Delta + x(\delta + \Delta)\} - x^2\delta\Delta. \tag{32}$$

The equality holds when $\mathcal{G}$ be a (Δ, δ) biregular graph and also $\delta \le x \le \Delta$, where x be a positive real number.

Proof. Define by $F_1(\mathcal{G}) = \sum_{u\in V(\mathcal{G})}[\xi(u/\mathcal{G}) - x]^2[\xi(u/\mathcal{G}) - y][\xi(u/\mathcal{G}) - z]$. Setting $\delta \le x \le \Delta$, $y = \Delta$ and $z = \delta$, then $F_1(\mathcal{G}) \le 0$. Thus,

$$F_1(\mathcal{G}) = \left[Y(\mathcal{G}) - (2x + \Delta + \delta)F(\mathcal{G}) + \left(x^2 + \delta\Delta\right)M_1(\mathcal{G}) - 2mx\{2\delta\Delta + x(\delta + \Delta)\} + x^2\delta\Delta\right] \le 0. \tag{33}$$

□

Theorem 14. *Let $\mathcal{G}$ be a (n, m) graph. Then,*

$$\begin{aligned} Y(\mathcal{G}) \le{}& (4\Delta - 6)F(\mathcal{G}) - \{\Delta(\Delta - 1) + (2\Delta - 1)(2\Delta - 5) + (\Delta - 2)(\Delta - 3)\}M_1(\mathcal{G}) \\ &+ 2m\{(\Delta - 2)(\Delta - 3)(2\Delta - 1) + \Delta(\Delta - 1)(2\Delta - 5)\} - nwxyz. \end{aligned} \tag{34}$$

The equality occurs when $\mathcal{G}$ is a tetra-regular graph.

Proof. Suppose that

$$\begin{aligned} F_2(\mathcal{G}) &= \sum_{u\in V(\mathcal{G})}\left[\xi\left(\frac{u}{\mathcal{G}}\right)-w\right]\left[\xi\left(\frac{u}{\mathcal{G}}\right)-x\right]\left[\xi\left(\frac{u}{\mathcal{G}}\right)-y\right]\left[\xi\left(\frac{u}{\mathcal{G}}\right)-z\right] \\ &= Y(\mathcal{G})-(w+x+y+z)F(\mathcal{G})+\{xw+(w+x)(y+z)+yz\}M_1(\mathcal{G}) \\ &\quad -2m\{(w+x)yz+(y+z)xw\}+wxyz, \end{aligned} \tag{35}$$

where w, x, y, z are the positive real numbers.Setting $w = \Delta, x = \Delta-1, y = \Delta-2$ and $z = \Delta-3$, then $F_2(G) \le 0$. Therefore, we get the required result. The equality is satisfied when $\mathcal{G}$ is a tetra-regular graph. □

Corollary 3. *Let $\mathcal{G}$ be a graph with n vertices and m edges. Then,$Y(\mathcal{G}) \le (3\Delta+\delta)F(\mathcal{G}) - 3\Delta(\Delta+\delta)M_1(\mathcal{G}) + 2m\ \Delta^2(\Delta+3\delta) - \Delta^3\delta n$ and also $Y(\mathcal{G}) \le (3\delta+\Delta)F(\mathcal{G}) - 3\delta(\delta+\Delta)M_1(\mathcal{G}) + 2m\delta^2(\delta+3\Delta) - \delta^3\Delta n$ with equality holding when $\mathcal{G}$ is a (Δ,δ) biregular graph.*

Proof. Consider an auxiliary function $F_3(\mathcal{G}) = \sum_{u\in V(\mathcal{G})}[\xi(u/\mathcal{G})-x]^3[\xi(u/\mathcal{G})-y]$, where x and y are the real numbers. Thus,

$$\begin{aligned} F_3(\mathcal{G}) &= \sum_{u\in V(\mathcal{G})}\left[\xi^4\left(\frac{u}{\mathcal{G}}\right)-(3x+y)\xi^3\left(\frac{u}{\mathcal{G}}\right)+3x(x+y)\xi^2\left(\frac{u}{\mathcal{G}}\right)-x^2(x+3y)\xi\left(\frac{u}{\mathcal{G}}\right)+x^3y\right] = Y(\mathcal{G})-(3x+y) \\ &\quad \cdot F(\mathcal{G})+3x(x+3y)M_1(\mathcal{G})-2mx^2(x+3y)+x^3yn. \end{aligned} \tag{36}$$

Taking $x = \Delta$, $y = \delta$ then $F_3(\mathcal{G}) \le 0$ and $Y(\mathcal{G}) \le (3\Delta+\delta)F(\mathcal{G}) - 3\Delta(\Delta+\delta)M_1(\mathcal{G}) + 2m\Delta^2(\Delta+3\delta) - \Delta^3\delta n$. Also for $x = \delta$ and $y = \Delta$, we have $F_3(\mathcal{G}) \le 0$. Thus, $Y(\mathcal{G}) \le (3\delta+\Delta)F(\mathcal{G}) - 3\delta(\delta+\Delta)M_1(\mathcal{G}) + 2m\delta^2(\delta+3\Delta) - \delta^3\Delta n$. □

Corollary 4. *Let $\mathcal{G}$ be a graph of order n and size m. Then,*

$$\begin{aligned} \overline{Y}(\mathcal{G}) &\le \{(n-1)(3\Delta-1)+3\Delta(2\Delta-1)\}M_1(\mathcal{G}) - (4\Delta-1)F(\mathcal{G}) - 2m(n-1)\Delta(3\Delta-2) - 2m\Delta^2(4\Delta-3) \\ &\quad +\Delta^2(\Delta-1)(n+\Delta-1)n \end{aligned} \tag{37}$$

where the equality is satisfied iff $\mathcal{G}$ is a $(\Delta,\Delta-1)$ biregular graph.

Proof. Define by $F_4(\mathcal{G}) = (n-1)\sum_{u\in V(\mathcal{G})}[\xi(u/\mathcal{G})-\Delta]^2[\xi(u/\mathcal{G})-(\Delta-1)] - \sum_{u\in V(\mathcal{G})}[\xi(u/\mathcal{G})-\Delta]^3[\xi(u/\mathcal{G})-(\Delta-1)]$

$$\begin{aligned} F_4(\mathcal{G}) &= (n-1)\sum_{u\in V(\mathcal{G})}\left[\xi\left(\frac{u}{\mathcal{G}}\right)-\Delta\right]^2\left[\xi\left(\frac{u}{\mathcal{G}}\right)-(\Delta-1)\right] - \sum_{u\in V(\mathcal{G})}\left[\xi\left(\frac{u}{\mathcal{G}}\right)-\Delta\right]^3\left[\xi\left(\frac{u}{\mathcal{G}}\right)-(\Delta-1)\right] \\ &\le (n-1)\left[F(\mathcal{G})-(3\Delta-1)M_1(\mathcal{G})+2m\Delta(3\Delta-2)-\Delta^2(\Delta-1)n\right]-Y(\mathcal{G})+(4\Delta-1)F(\mathcal{G})-3\Delta(2\Delta-1) \\ &\quad \cdot M_1(\mathcal{G})+2m\Delta^2(4\Delta-3)-\Delta^3(\Delta-1)n. \end{aligned} \tag{38}$$

Since $F_4(\mathcal{G}) \le 0$

$$\begin{aligned} \overline{Y}(\mathcal{G}) &\le \{(n-1)(3\Delta-1)+3\Delta(2\Delta-1)\}M_1(\mathcal{G}) - (4\Delta-1)F(\mathcal{G}) - 2m(n-1)\Delta(3\Delta-2) - 2m\Delta^2(4\Delta-3) \\ &\quad +\Delta^2(\Delta-1)(n+\Delta-1)n \end{aligned} \tag{39}$$

□

Corollary 5. *If $\mathcal{G}$ is a graph with n vertices and m edges, the upper bounds of the $\overline{Y}(\mathcal{G})$ are given by $3\Delta(n+2\Delta-1)$ $M_1(\mathcal{G})-4\Delta F(\mathcal{G})+n\Delta^2(n+\Delta-1)\quad -2m\Delta^2(3n+4\Delta-3)$. The equality holds if $\mathcal{G}$ is a regular graph.*

Proof. Similarly, it is to be proved by defining $F_5(\mathcal{G})=(n-1)\sum_{u\in V(\mathcal{G})}[\xi(u/\mathcal{G})-\Delta]^3-\sum_{u\in V(\mathcal{G})}[\xi(u/\mathcal{G})-\Delta]^4$. Obviously, $F_5(\mathcal{G})\le 0$. □

In 2005, Klavzar et al. [30] introduced the generalized Sierpinski graph $gS(\mathcal{G},t)$. It is obtained from $S(\mathcal{G},t)$ by adding a new vertex u, called the special vertex of $gS(\mathcal{G},t)$, and edges joining u with all extreme vertices of $S(\mathcal{G},t)$.

Theorem 15. *Let $\mathcal{G}$ be a graph of order n and size m and let $gS(\mathcal{G},t)$ be its generalized Sierpinski graph with dimension $t\ge 2$. Then, the YI of $gS(\mathcal{G},t)$ is given by*

$$\begin{aligned} Y(gS(\mathcal{G},t)) \le\ & 2m\Delta^3\left(n^{t-1}+4n^{t-2}+4\beta(n)_{t-2}\right) \\ & +2m\left(n^{t-2}+\beta(n)_{t-2}\right)\left(6\Delta^2+4\Delta+1\right). \end{aligned} \tag{40}$$

The upper bound is achieved iff $\mathcal{G}$ is a Δ-regular graph.

Proof. The YI of $gS(\mathcal{G},t)$ can be defined as

$$Y(gS(\mathcal{G},t))=\sum_{uv\in E(\mathcal{G})}\sum_{i,j=0}^{1}\left|\xi\left(\frac{u}{\mathcal{G}}\right)+i,\xi\left(\frac{v}{\mathcal{G}}\right)+j\right|_{S(\mathcal{G},t)}\left(\left(\xi\left(\frac{u}{\mathcal{G}}\right)+i\right)^3+\left(\xi\left(\frac{u}{\mathcal{G}}\right)+j\right)^3\right). \tag{41}$$

By applying Lemma 7, we have

$$\begin{aligned} &=\sum_{uv\in E(\mathcal{G})}\Big[n^{t-2}\left(n-\xi\left(\frac{u}{\mathcal{G}}\right)-\xi\left(\frac{v}{\mathcal{G}}\right)+\triangleright(u,v)\right)\left(\xi^3\left(\frac{u}{\mathcal{G}}\right)+\xi^3\left(\frac{v}{\mathcal{G}}\right)\right) \\ &\quad+\left(n^{t-2}\left(\xi\left(\frac{v}{\mathcal{G}}\right)-\triangleright(u,v)\right)-\beta(n)_{t-2}\xi\left(\frac{u}{\mathcal{G}}\right)\right)\left(\xi^3\left(\frac{u}{\mathcal{G}}\right)+\left(\xi\left(\frac{v}{\mathcal{G}}\right)+1\right)^3\right) \\ &\quad+\left(n^{t-2}\left(\xi\left(\frac{u}{\mathcal{G}}\right)-\triangleright(u,v)\right)-\beta(n)_{t-2}\xi\left(\frac{v}{\mathcal{G}}\right)\right)\left(\left(\xi\left(\frac{u}{\mathcal{G}}\right)+1\right)^3+\xi^3\left(\frac{v}{\mathcal{G}}\right)\right) \\ &\quad+\left(n^{t-2}\left(\triangleright(u,v)+1\right)+\beta(n)_{t-2}\left(\xi\left(\frac{u}{\mathcal{G}}\right)+\xi\left(\frac{v}{\mathcal{G}}\right)+1\right)\right)\left(\left(\xi\left(\frac{u}{\mathcal{G}}\right)+1\right)^3+\left(\xi\left(\frac{v}{\mathcal{G}}\right)+1\right)^3\right)\Big] \\ &\le\sum_{uv\in E(G)}\Big[n^{t-2}(n-2\Delta+\triangleright(u,v))\left(2\Delta^3\right)+2\left(n^{t-2}(\Delta-\triangleright(u,v))-\beta(n)_{t-2}\Delta\right)\left(\Delta^3+(\Delta+1)^3\right) \\ &\quad+\left(n^{t-2}\left(\triangleright(u,v)+1\right)+\beta(n)_{t-2}(2\Delta+1)\right)\left(2(\Delta+1)^3\right)\Big] \\ &=2m\Delta^3\left(n^{t-1}+4n^{t-2}+4\beta(n)_{t-2}\right)+2m\left(n^{t-2}+\beta(n)_{t-2}\right)\left(6\Delta^2+4\Delta+1\right). \end{aligned} \tag{42}$$

□

4. Some UB for YI under Some Graph Operations

In this section, we derive some UB for YI under several graph operations. Let $\mathcal{G}_i$ be a graph with the vertex set $|V(\mathcal{G}_i)|=n_i$ and the edge set $|E(\mathcal{G}_i)|=m_i$ for $i=1,2$. For each $u\in V(\mathcal{G}_1)$ and $v\in V(\mathcal{G}_2)$, we get $\xi(u/\mathcal{G}_1)\le\Delta(\mathcal{G}_1)$ and $\xi(v/\mathcal{G}_2)\le\Delta(\mathcal{G}_2)$.

4.1. Cartesian Product. The Cartesian product ([31]) of $\mathcal{G}_1$ and $\mathcal{G}_2$, denoted by $\mathcal{G}_1\otimes\mathcal{G}_2$, is the graph with vertex set $V(\mathcal{G}_1\otimes\mathcal{G}_2)=V(\mathcal{G}_1)\times V(\mathcal{G}_2)$ and its degree distribution is $\xi((u,v)/\mathcal{G}_1\otimes\mathcal{G}_2)=\xi(u/\mathcal{G}_1)+\xi(v/\mathcal{G}_2)$.

Theorem 16. *The YI of $\mathcal{G}_1\otimes\mathcal{G}_2$ satisfies the following inequality:*
$Y(\mathcal{G}_1\otimes\mathcal{G}_2)\le n_1n_2[\Delta^4(\mathcal{G}_1)+\Delta^4(\mathcal{G}_2)+4\Delta^3(\mathcal{G}_1)\Delta(\mathcal{G}_2)+4\Delta(\mathcal{G}_1)\Delta^3(\mathcal{G}_2)+6\Delta^2(\mathcal{G}_1)\Delta^2(\mathcal{G}_2)]$ *with equality occurring when $\mathcal{G}_1$ and $\mathcal{G}_2$ are regular graphs.*

Proof. By the definition of Y-index, we have

$$Y(\mathcal{G}_1 \otimes \mathcal{G}_2) = \sum_{(u,v)\in V(\mathcal{G}_1\times\mathcal{G}_2)} \left[\xi\left(\frac{(u,v)}{\mathcal{G}_1 \times \mathcal{G}_2}\right)\right]^4$$
$$= \sum_{u\in V(\mathcal{G}_1)} \sum_{v\in V(\mathcal{G}_2)} \left[\xi\left(\frac{u}{\mathcal{G}_1}\right) + \xi\left(\frac{v}{\mathcal{G}_2}\right)\right]^4 \tag{43}$$
$$\le n_1 n_2 \left[\Delta^4(\mathcal{G}_1) + \Delta^4(\mathcal{G}_2) + 4\Delta^3(\mathcal{G}_1)\Delta(\mathcal{G}_2) + 4\Delta(\mathcal{G}_1)\Delta^3(\mathcal{G}_2) + 6\Delta^2(\mathcal{G}_1)\Delta^2(\mathcal{G}_2)\right].$$

The inequality must be equality if $\xi(u_1/\mathcal{G}_1) + \xi(v_1/\mathcal{G}_2) = \xi(u_2/\mathcal{G}_1) + \xi(v_2/\mathcal{G}_2)$ for any $u_1, u_2 \in V(\mathcal{G}_1)$ and $v_1, v_2 \in V(\mathcal{G}_2)$. □

4.2. Join. The degree of a vertex u for the join [32] of $\mathcal{G}_1$ and $\mathcal{G}_2$, denoted by $\mathcal{G}_1 + \mathcal{G}_2$, is given by

$$\xi\left(\frac{u}{\mathcal{G}_1 + \mathcal{G}_2}\right) = \begin{cases} \xi\left(\frac{u}{\mathcal{G}_1}\right) + n_2 & \text{if } u \in V(\mathcal{G}_1) \\ \xi\left(\frac{u}{\mathcal{G}_2}\right) + n_1 & \text{if } u \in V(\mathcal{G}_2) \end{cases} \tag{44}$$

Theorem 17. *The UB on the Y-index of two graphs $\mathcal{G}_1$ and $\mathcal{G}_2$ for join is given by*

$$Y(\mathcal{G}_1 + \mathcal{G}_2) \le 2m_1(\Delta(\mathcal{G}_1) + n_2)^3 + 2m_2(\Delta(\mathcal{G}_2) + n_1)^3 + n_1 n_2\left[(\Delta(\mathcal{G}_1) + n_2)^3 + (\Delta(\mathcal{G}_2) + n_1)^3\right]. \tag{45}$$

The equality holds when $\mathcal{G}_1$ and $\mathcal{G}_2$ are regular graphs.

Proof. By the definition of the YI, we get

$$Y(\mathcal{G}_1 + \mathcal{G}_2) = \sum_{uv\in E(\mathcal{G}_1)} \left[\left(\xi\left(\frac{u}{\mathcal{G}_1}\right) + n_2\right)^3 + \left(\xi\left(\frac{v}{\mathcal{G}_1}\right) + n_2\right)^3\right] + \sum_{uv\in E(\mathcal{G}_2)} \left[\left(\xi\left(\frac{u}{\mathcal{G}_2}\right) + n_1\right)^3 + \left(\xi\left(\frac{v}{\mathcal{G}_2}\right) + n_1\right)^3\right] + \sum_{u\in V(\mathcal{G}_1)} \sum_{v\in V(\mathcal{G}_2)} \left[\left(\xi\left(\frac{u}{\mathcal{G}_1}\right) + n_2\right)^3 + \left(\xi\left(\frac{v}{\mathcal{G}_2}\right) + n_1\right)^3\right]$$
$$\le 2m_1(\Delta(\mathcal{G}_1) + n_2)^3 + 2m_2(\Delta(\mathcal{G}_2) + n_1)^3 + n_1 n_2\left[(\Delta(\mathcal{G}_1) + n_2)^3 + (\Delta(\mathcal{G}_2) + n_1)^3\right]. \tag{46}$$

□

4.3. Composition. For the composition $\mathcal{G}_1[\mathcal{G}_2]$ of two graphs $\mathcal{G}_1$ and $\mathcal{G}_2$ [11], the degree of a vertex $(u, v) \in V(\mathcal{G}_1[\mathcal{G}_2])$ is given by $d((u,v)/\mathcal{G}_1[\mathcal{G}_2]) = n_2\xi(u/\mathcal{G}_1) + \xi(v/\mathcal{G}_2)$.

Theorem 18. *The UB of YI for $\mathcal{G}_1[\mathcal{G}_2]$ is given by $Y(\mathcal{G}_1[\mathcal{G}_2]) \le n_2^5\Delta^4(\mathcal{G}_1) + n_1 n_2\Delta^4(\mathcal{G}_2) + 6n_1 n_2^3\Delta^2(\mathcal{G}_1)\Delta^2(\mathcal{G}_2) + 4n_1 n_2^4\Delta^3(\mathcal{G}_1)\Delta(\mathcal{G}_2) + 4n_1 n_2^2\Delta(\mathcal{G}_1)\Delta^3$. The equality carries for $\mathcal{G}_1$ and $\mathcal{G}_2$ regular graphs.*

Proof. From the definition of Y-index, we have

$$Y(\mathcal{G}_1[\mathcal{G}_2]) = \sum_{u\in V(\mathcal{G}_1)} \sum_{v\in V(\mathcal{G}_2)} \left[n_2\xi\left(\frac{u}{\mathcal{G}_1}\right) + \xi\left(\frac{v}{\mathcal{G}_2}\right)\right]^4 \tag{47}$$
$$\le n_2^5\Delta^4(\mathcal{G}_1) + n_1 n_2\Delta^4(\mathcal{G}_2) + 6n_1 n_2^3\Delta^2(\mathcal{G}_1)\Delta^2(\mathcal{G}_2) + 4n_1 n_2^4\Delta^3(\mathcal{G}_1)\Delta(\mathcal{G}_2) + 4n_1 n_2^2\Delta(\mathcal{G}_1)\Delta^3.$$

□

4.4. Corona Product. For Corona product [33] of $\mathcal{G}_1$ and $\mathcal{G}_2$, denoted by $\mathcal{G}_1 \diamond \mathcal{G}_2$, the degree of a vertex $u \in \mathcal{G}_1 \diamond \mathcal{G}_2$ is given by

$$\xi\left(\frac{u}{\mathcal{G}_1 \diamond \mathcal{G}_2}\right) = \begin{cases} \xi\left(\frac{u}{\mathcal{G}_1}\right) + n_2 & \text{if } u \in V(\mathcal{G}_1) \\ \xi\left(\frac{u}{\mathcal{G}_2}\right) + 1 & \text{if } u \in V\left(\mathcal{G}_{2,i}\right),\ i = 1, 2, \ldots, n_1, \end{cases} \tag{48}$$

where $\mathcal{G}_{2,i}$ is the i-th copy of the graph $\mathcal{G}_2$.

Theorem 19. *Let $\mathcal{G} = \mathcal{G}_1 \diamond \mathcal{G}_2$ be the corona product of $\mathcal{G}_1$ and $\mathcal{G}_2$. $Y(\mathcal{G})$ satisfies the following inequalities $Y(\mathcal{G}) \leq n_1 [\Delta(\mathcal{G}_1) + n_2]^4 + n_1 n_2 [\Delta(\mathcal{G}_2) + 1]^4$. The equality holds when $\mathcal{G}_1$ and $\mathcal{G}_2$ are regular.*

Proof. From definition of YI, we have

$$\begin{aligned} Y(\mathcal{G}_1 \diamond \mathcal{G}_2) &= \sum_{u \in V(\mathcal{G}_1)} \left(\xi\left(\frac{u}{\mathcal{G}_1}\right) + n_2\right)^4 + n_1 \sum_{u \in V(\mathcal{G}_2)} \left(\xi\left(\frac{u}{\mathcal{G}_2}\right) + 1\right)^4 \\ &\leq n_1 \left[\Delta^4(\mathcal{G}_1) + 4n_2\Delta^3(\mathcal{G}_1) + 6n_2^2\Delta^2(\mathcal{G}_1) + 4n_2^3\Delta(\mathcal{G}_1) + n_2^4\right] \\ &\quad + n_1 n_2 \left[\Delta^4(\mathcal{G}_2) + 4\Delta^3(\mathcal{G}_2) + 6\Delta(\mathcal{G}_2) + 4\Delta(\mathcal{G}_2) + 1\right]. \end{aligned} \tag{49}$$

□

4.5. Strong Product. Consider $\xi((u,v)/\mathcal{G}_1 * \mathcal{G}_2) = \xi(u/\mathcal{G}_1) + \xi(v/\mathcal{G}_2) + \xi(u/\mathcal{G}_1)(v/\mathcal{G}_2)$ as a degree distribution of a vertex (u, v) in the strong product [11] $\mathcal{G}_1 * \mathcal{G}_2$.

Theorem 20. *The sharp UB of YI for $\mathcal{G}_1 * \mathcal{G}_2$ is given by*

$$\begin{aligned} Y(\mathcal{G}_1 * \mathcal{G}_2) \leq n_1 n_2 \big[&\Delta^4(\mathcal{G}_1) + \Delta^4(\mathcal{G}_2) + \Delta^4(\mathcal{G}_1)\Delta^4(\mathcal{G}_2) \\ &+6\Delta^2(\mathcal{G}_1)\Delta^2(\mathcal{G}_2)\left(\Delta^2(\mathcal{G}_1) + \Delta^2(\mathcal{G}_2) + 1\right) \\ &+4\Delta(\mathcal{G}_1)\Delta(\mathcal{G}_2)\left(\Delta^3(\mathcal{G}_1) + \Delta^3(\mathcal{G}_2) + \Delta^3(\mathcal{G}_1)\Delta^2(\mathcal{G}_2)\right. \\ &\left.+\Delta^2(\mathcal{G}_1)\Delta^3(\mathcal{G}_2) + \Delta^2(\mathcal{G}_1) + \Delta^2(\mathcal{G}_2)\right) \\ &+12\Delta^2(\mathcal{G}_1)\Delta^2(\mathcal{G}_2)\left(\Delta(\mathcal{G}_1) + \Delta(\mathcal{G}_2) + \Delta(\mathcal{G}_1)\Delta(\mathcal{G}_2)\right)\big]. \end{aligned} \tag{50}$$

The equality occurs when $\mathcal{G}_1$ and $\mathcal{G}_2$ are regular.

5. Application

As an application, we compute the YI of C_{80} Fullerene, by using Theorem 11. Fullerenes are the molecules such as cage-like polyhedra, containing solely carbon atoms. Fullerenes contain the networks of pentagons and hexagons. Here, we consider the fullerene C_{80} such that molecules made up entirely of n (natural number) carbon atoms contain twelve pentagonal sides and $(n/2 - 10)$ hexagonal faces, where $n(\neq 22) \geq 20$. For the graph representing fullerene C_{80} which is given in [34], we have $F(C_{80}) = 2160$. The number of edges(m) in fullerene C_{80} is $m = nr/2 = 80 \times 3/2 = 120$. Thus, by Theorem 11, $Y(\mathcal{G}) \leq \beta(n)(\Delta - \delta)^2(\Delta^2 + \Delta\delta + \delta^2) + 2mF(\mathcal{G})/n = 2 \times 120 \times 2160/80 = 6480$.

6. Conclusion

The YI is one of the new chemical descriptors, which passes the test of having a highly correlation with the physiochemical properties it claims to describe in [11]. It comes as no surprise. Then, we determine some new UBs for the YI using various parameters such as order, size, maximum degree, minimum degree, distance κ-domination number, and some other topological indices. Furthermore, some sharp UB for the YI based on graph binary operations are obtained. At last, we consider an application for YI index of

C_{80} Fullerene. The appeal of computing the UB is of course their generality and simple proofs. Along in this line, determining new lower bounds for YI is considered to be studied in the future.

Data Availability

No data were used to support this study.

Conflicts of Interest

The authors declare that there are no conflicts of interest regarding the publication of this article.

Acknowledgments

The second author acknowledges the support of DST-FIST, New Delhi (India) (Sanction No. SR/FST/MS- I/2018/21) for carrying out this work.

References

[1] N. Trinajstic, *Chemical Graph Theory*, CRC Press, Boca Raton, FL, USA, 1993.

[2] L. Pei and X. Pan, "Extremal values on Zagreb indices of trees with given distance k-domination number," *Journal of Inequalities and Applications*, vol. 2018, p. 16, 2018.

[3] L. Pei and X. Pan, "The minimum eccentric distance sum of trees with given distance k-domination number," *Discret. Math. Algorithms Appl.*vol. 2020, p. 16, 2020.

[4] F. Harary, *Graph Theory*, Addison-Wesley Publishing Co., Boston, MA, USA, 1969.

[5] H. Wiener, "Structural determination of paraffin boiling points," *Journal of the American Chemical Society*, vol. 69, no. 1, pp. 17–20, 1947.

[6] I. Gutman and N. Trinajstić, "Graph theory and molecular orbitals. Total φ-electron energy of alternant hydrocarbons," *Chemical Physics Letters*, vol. 17, no. 4, pp. 535–538, 1972.

[7] X. Li and J. Zheng, "A unified approach to the extremal trees for different indices," *MATCH Communications in Mathematical and in Computer Chemistry*, vol. 54, pp. 195–208, 2005.

[8] B. Furtula and I. Gutman, "A forgotten topological index," *Journal of Mathematical Chemistry*, vol. 53, no. 4, pp. 1184–1190, 2015.

[9] J.-B. Liu, B. Ali, M. A. Malik, H. M. A. Siddiqui, and M. Imran, "Reformulated Zagreb indices of some derived graphs," *Mathematics*, vol. 7, no. 4, p. 366, 2019.

[10] A. Milicevic, S. Nikolic, and N. Trinajstic, "On reformulated Zagreb indices," *Molecular Diversity*, vol. 8, pp. 393–399, 2004.

[11] A. Alameri, N. Al-Naggar, M. Al-Rumaima, and M. Alsharafi, "Y-index of some graph operations," *International Journal of Applied Engineering*, vol. 15, pp. 173–179, 2020.

[12] D. Maji and G. Ghorai, "A novel graph invariant: the third leap Zagreb index under several graph operations," *Discrete Mathematics, Algorithms and Applications*, vol. 11, no. 5, pp. 1–16, 2019.

[13] D. Maji and G. Ghorai, "Computing F-index, coindex and Zagreb polynomials of the kth generalized transformation graphs," *Heliyon*, vol. 6, no. 12, Article ID e05781, 2020.

[14] D. Maji and G. Ghorai, "The first entire Zagreb index of various corona products and their bounds," *Journal of Mathematical and Computational Science*, vol. 11, no. 5, pp. 6018–6044, 2021.

[15] D. Maji, G. Ghorai, M. K. Mahmood, and M. A. Alam, "On the inverse problem for some topological indices," *Journal of Mathematics*, vol. 2021, no. 1, pp. 1–8, 2021.

[16] D. Maji, G. Ghorai, and Y. U. Gaba, "On the reformulated second Zagreb index of graph operations," *Journal of Chemistry*, vol. 2021, no. 5, pp. 1–17, 2021.

[17] F. Hayat, "On extremal results of multiplicative Zagreb indices of trees with given distance k-domination number," 2019, https://arxiv.org/abs/1906.12202.

[18] H. Hua, S. Zhang, and K. Xu, "Further results on the eccentric distance sum," *Discrete Applied Mathematics*, vol. 160, no. 1-2, pp. 170–180, 2012.

[19] A. Meir and J. Moon, "Relations between packing and covering numbers of a tree," *Pacific Journal of Mathematics*, vol. 61, no. 1, pp. 225–233, 1975.

[20] J. Topp and L. Volkmann, "On packing and covering numbers of graphs," *Discrete Mathematics*, vol. 96, no. 3, pp. 229–238, 1991.

[21] M. Imran and M. K. Jamil, "Sharp bounds on certain degree based topological indices for generalized Sierpiński graphs," *Chaos, Solitons & Fractals*, vol. 132, Article ID 109608, 2020.

[22] A. Ali, M. Metajic, M. Matejic, and I. Milovanovic, "Some new upper bounds for the inverse sum indeg index of graphs," *Electronic Journal of Graph Theory and Applications*, vol. 8, no. 1, pp. 59–70, 2020.

[23] B. Borovicanin and B. Furtula, "On extremal Zagreb indices of trees with given domination number," *Applied Mathematics and Computation*, vol. 279, pp. 208–218, 2016.

[24] B. Zhou and I. Gutman, "Further properties of Zagreb indices," *MATCH Communications in Mathematical and in Computer Chemistry*, vol. 54, pp. 233–239, 2005.

[25] P. Erdos and T. Gallai, "Graphs with prescribed degrees of vertices (in Hungarian)," *Mat. Lapok.*vol. 11, pp. 264–274, 1960.

[26] Z. Che and Z. Chem, "Lower and upper bounds of forgotten topological index," *MATCH Communications in Mathematical and in Computer Chemistry*, vol. 76, pp. 635–648, 2016.

[27] S. Hosamani and B. Basavanagoud, "New upper bounds for the first Zagreb index," *MATCH Commun. Math. Comput. Chem.*vol. 74, pp. 97–101, 2015.

[28] A. Alameri, M. Al-Rumaima, and M. Almazah, "Y-coindex of graph operations and its applications of molecular descriptors," *Journal of Molecular Structure*, vol. 1221, Article ID 128754, 2020.

[29] A. Ghalavand, A. Ashrafi, A. Ashrafi, and I. Gutman, "New upper and lower bounds for some degree-based graph invariants," *Kragujevac Journal of Mathematics*, vol. 44, no. 2, pp. 181–188, 2020.

[30] S. Klavar and B. Mohar, "Crossing numbers of Sierpinski-like graphs," *Journal of Graph Theory*, vol. 50, pp. 186–198, 2005.

[31] S. Mondal, N. De, and A. Pal, "On neighborhood Zagreb index of product graphs," *Journal of Molecular Structure*, vol. 1223, Article ID 129210, 2021.

[32] M. Cancan, N. De, M. Alaeiyan, and M. Reza Farahan, "On reformulated narumi-katayama index," *Proyecciones (Antofagasta)*, vol. 39, no. 5, pp. 1333–1346, 2020.

[33] K. Pattabiraman and P. Kandan, "Weighted PI index of corona product of graphs," *Discrete Mathematics, Algorithms and Applications*, vol. 6, no. 4, Article ID 1450055, 2014.

[34] S. Hosamani, *A upper bound for the F1-index and its applications to fullerenes*, 2015.

Hindawi
Journal of Mathematics
Volume 2023, Article ID 9861253, 1 page
https://doi.org/10.1155/2023/9861253

Retraction

Retracted: Film and Television Animation Sensing and Visual Image by Computer Digital Image Technology

Journal of Mathematics

Received 19 December 2023; Accepted 19 December 2023; Published 20 December 2023

This article has been retracted by Hindawi following an investigation undertaken by the publisher [1]. This investigation has uncovered evidence of one or more of the following indicators of systematic manipulation of the publication process:

(1) Discrepancies in scope

(2) Discrepancies in the description of the research reported

(3) Discrepancies between the availability of data and the research described

(4) Inappropriate citations

(5) Incoherent, meaningless and/or irrelevant content included in the article

(6) Manipulated or compromised peer review

The presence of these indicators undermines our confidence in the integrity of the article's content and we cannot, therefore, vouch for its reliability. Please note that this notice is intended solely to alert readers that the content of this article is unreliable. We have not investigated whether authors were aware of or involved in the systematic manipulation of the publication process.

Wiley and Hindawi regrets that the usual quality checks did not identify these issues before publication and have since put additional measures in place to safeguard research integrity.

We wish to credit our own Research Integrity and Research Publishing teams and anonymous and named external researchers and research integrity experts for contributing to this investigation.

The corresponding author, as the representative of all authors, has been given the opportunity to register their agreement or disagreement to this retraction. We have kept a record of any response received.

References

[1] L. Lian and T. Lei, "Film and Television Animation Sensing and Visual Image by Computer Digital Image Technology," *Journal of Mathematics*, vol. 2022, Article ID 6331233, 8 pages, 2022.

Hindawi
Journal of Mathematics
Volume 2022, Article ID 6331233, 8 pages
https://doi.org/10.1155/2022/6331233

Research Article

Film and Television Animation Sensing and Visual Image by Computer Digital Image Technology

Lu Lian and Tong Lei

School of New Media Arts, Xi'an Polytechnic University, Xi'an 710048, Shaanxi, China

Correspondence should be addressed to Lu Lian; 12111852231@stu.wzu.edu.cn

Received 6 December 2021; Revised 24 December 2021; Accepted 28 December 2021; Published 29 January 2022

Academic Editor: Naeem Jan

In order to study the application of computer digital image processing technology in film and television (FAT) animation visual sensing expression, by studying the principle of digital image processing technology and visual sensing technology, a spatial image adaptive steganography image enhancement algorithm by multiscale filters is proposed to carry out enhancement processing of the original image in FAT production. This algorithm can provide more high-quality and refined original materials for FAT animation production, which is convenient for FAT animation postproduction to produce higher-resolution and clear FAT works. Finally, the algorithm is verified. The results show that the spatial image adaptive steganography image enhancement algorithm has high security, and the highest average detection error rate is 25.06%. When $\alpha = 0.4$, the security of the spatial image adaptive steganography image enhancement algorithm is up to 34.62% and the image distortion rate is low. The established image enhancement algorithm can significantly improve the security of the existing spatial image steganography algorithm under different embedding rates, especially at a high embedding rate; the improvement of the spatial domain steganography algorithm is greater. The proposed steganographic image enhancement algorithm by image preprocessing has higher security and better image enhancement effect.

1. Introduction

Computer digital image technology not only builds a new medium and carrier for artistic creation but also connects artistic creation and daily life [1–3]. Film, television, and animation production are closely related to life. As representatives of the cultural industry, film and television (FAT) are becoming more and more popular for daily consumption by the general public. The development of FAT industries has also received more and more attention from consumer groups [4]. Since rich video production experience, how to better serve FAT special effects production and visual communication technology for FAT content is an eternal topic for contemporary FAT producers [5]. In the era of rapid development of FAT animation technology, the visual requirements of movie and television screens have become higher and higher for the movie-watching group. Watching a movie is no longer just about the plot. Aestheticism, shock and other visual effects, and visual impact are also the criteria for the audience to judge the quality of a movie [6]. Computer graphics technology is widely used in FAT production of original pictures and image processing by virtue of its refined image processing capabilities [7].

The advantages of artificial intelligence (AI), machine learning, and deep learning are reflected in image, video processing, natural language processing, and speech recognition. AI algorithms overcome many shortcomings, which help provide state-of-the-art results in computers and other fields. Deeba et al. [8] used artificial neural networks (ANNs) to detect the presence of sensitive information and extract information from the source image. When the appropriate machine learning algorithm is trained, retrained, and adapted to some new applications, the performance is relatively stable. Collins et al. [9] traced the evolution of a series of industries and supporting institutions in the FAT industry in one of the most fringe regions in Europe. Chen

et al. [10] pointed out a stereo calibration method by the correlation of stereo digital images. Because the flexible number of control points has high matching registration accuracy and strong sturdiness, the stereo calibration method that uses the synthetic spot pattern to calibrate the target provides higher calibration accuracy than the calibration accuracy by the calibration target. The target has a limited number of designated functions. The application fields of digital image processing technology are very wide, and there are many research results. However, the previous research content is relatively small in the field of FAT production. The content being studied can fill this technological gap.

The methods of literature research and algorithm verification are adopted. The application of computer image processing technology in the production of FAT animation has been studied. The innovation is that, by the original steganographic image processing algorithm, a spatial image steganography enhancement algorithm by multiscale filters is proposed. Besides increasing the security in the image enhancement process and reducing the distortion, the algorithm also guarantees a higher image resolution, provides high-quality original materials for FAT animation production, and can enhance the visual expression effect of FAT images. The remainder of the paper is organized as follows: Section 2 is about the material and methods where we explained the material, methods, algorithms, and other related topics to our study. In Section 3, the results of different tests are analysed, and the discussion is carried out. In Section 4, the conclusion of our study is presented, and the paper ends with a list of references.

2. Materials and Methods

In this section, we present some of the methods used for image processing. We talk about different aspects of digital image processing, such as its quality, distortion, security, resolution, and filter (smooth image, binary image, sharpened image, and many more). In addition, the materials used for the purposes are also described. To be specific, we shall talk about the cameras and digital camcorders that acquire digital images. Moreover, the animations and videos are also discussed in detail.

2.1. Digital Image Processing. Digital Image Processing (DIP) is a method and technology for removing noise, enhancing, restoring, segmenting, and extracting features of an image through a computer [11]. It contains 5 modules. Image input module refers to image input, also called image acquisition or image digitization. It uses image acquisition equipment (such as digital cameras and digital camcorders) to acquire digital images and digital equipment (such as image scanners) to convert continuous images to be processed into digital images suitable for computer processing [12]. The image storage module is mainly used to store image information. The image output module displays the images before and after processing or saves the processing results permanently. The image communication module is to transmit or communicate image information [13]. Image processing and analysis modules include processing algorithms, implementation software, and digital computers. These modules work together to complete all functions of image information processing [14]. The number of pixels or dots per unit length in an image is the image resolution. The higher the resolution, the more the number of pixels contained in it and the clearer the image display [15]. The digital image processing process is shown in Figure 1.

The amount of information contained in an image can reflect the richness of image information [16]. After the analogue image is discretized, the digital representation of the image is obtained, which is the process of image digitization. Image digitization includes sampling and quantization, where sampling interval and sampling aperture are two important parameters that determine resolution. Sampling is the operation of transforming a spatially continuous image into discrete points with continuous grey levels, and quantization is the process of converting pixel grey levels into discrete integer values. Image enhancement is a very important part of digital image processing. By purposefully emphasizing the overall or partial characteristics of the image (such as improving the colour, brightness, and contrast of the image), the image with low definition can be made clear or emphasize these important features. It can magnify the difference between the features of different types of objects in the image, suppress the uninteresting features, and improve the visual effect of the image.

Traditional image enhancement methods are divided into three categories. The spatial image enhancement method is to directly process the pixel value, such as Histogram Equalization and Gamma Transformation. The frequency domain method is to operate in a certain transform domain, such as wavelet transform. The hybrid domain method is a combination of the spatial domain and the frequency domain. Traditional image enhancement methods are generally simpler and faster, but because the context information in the image cannot be fully considered, the effect is usually very general. Convolutional Neural Networks (CNNs) have made great breakthroughs in many low-level computer vision tasks, including image superresolution, deblurring, dehazing, denoising, and image enhancement. Compared with traditional methods, CNN-based image processing methods greatly improve the quality of image enhancement. Most of the existing methods are supervised learning. For an original image and a target image, the mapping relationship between them is learned to obtain an enhanced image. However, such data sets are relatively small, and many of them are artificially adjusted. Therefore, personal supervision or weak supervision is required to solve this problem.

2.2. Visual Sensing in Movie and TV Animation. Vision sensing technology is one of the sensing technologies. The visual sensor refers to the sensor that calculates the feature quantity of the object by performing image processing on the image taken by the camera and outputs the data and the judgment result [17]. The vision sensor is the direct source of

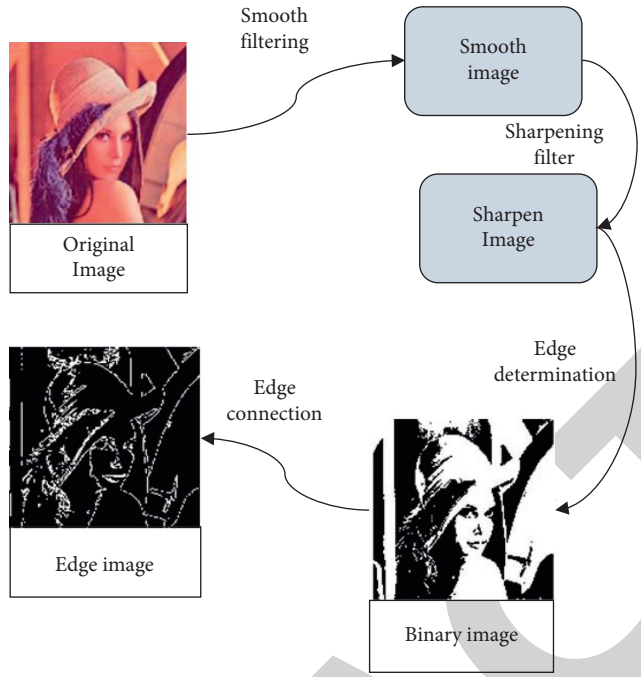

Figure 1: Digital image processing process.

information for the entire machine vision system, which is mainly composed of one or two graphic sensors, sometimes with a light projector and auxiliary equipment [18–20]. The main function of the vision sensor is to obtain enough original images to be processed by the machine vision system. Vision sensors can capture thousands of pixels of light from an entire image. The clarity and fineness of an image are usually measured by resolution, expressed in the number of pixels. After capturing the image, the vision sensor compares it with the reference image stored in the memory for analysis.

During the filming and production of FAT animation, the application of 3D vision sensor technology in vision sensor technology can obtain high-resolution image materials. 3D vision sensing technology combines image acquisition, image processing, and information transmission functions. It integrates image sensors, digital processors, communication modules, and other peripherals into a single camera. Due to this integrated design, the complexity of the system can be reduced, and reliability can be improved. This design provides more high-quality and refined original materials for FAT action production, which is convenient for FAT animation postproduction to produce higher-resolution and clear FAT works. The image acquisition unit of the vision sensor is mainly composed of Charge Coupled Device (CCD) or Complementary Metal-Oxide Semiconductor (CMOS) camera, optical system, lighting system, and image acquisition card. The vision sensor can convert the optical image into a digital image and pass it to the image processing unit. The working process of the visual sensor is shown in Figure 2.

The camera is the eye of the machine vision system. The heart of the camera is the image sensor. The choice of sensor depends on accuracy, output, sensitivity, the cost of the machine vision system, and full understanding of the application requirements. A basic understanding of the main performance of the sensor can help developers quickly narrow the search range and find the right sensor. The dynamic range, speed, and responsiveness of the sensor are indicators of sensor performance. The dynamic range determines the quality of the image that the system can capture and is also called the ability to reflect details. The speed of the sensor refers to the output of the image that the sensor can produce and the image that the system can receive per second. Responsivity refers to the efficiency with which the sensor converts photons into electrons. It determines the brightness level at which the system needs to capture useful images. These indicators determine the quality of FAT output.

2.3. Steganography Enhancement Algorithm for the Spatial Image by Multiscale Filter. Steganography is a means of safely transmitting secret information. Pictures, movies and TV works, audio, and even text on the Internet can all be used as objects to hide secret information. These digital media have a huge amount of data and are a natural carrier library for steganography. The classic model of the steganography algorithm is shown in Figure 3.

The more the positions that are modified to the carrier object are, the easier it is for the hidden object to be detected by the steganography algorithm. The adaptive steganography image enhancement algorithm can embed the complex area and edge area of the image according to the image content of the image carrier itself. It does not embed in flat areas that are relatively easy to model. This process consists of two steps, distortion function calculation and coding embedding. The distortion function can be used to calculate

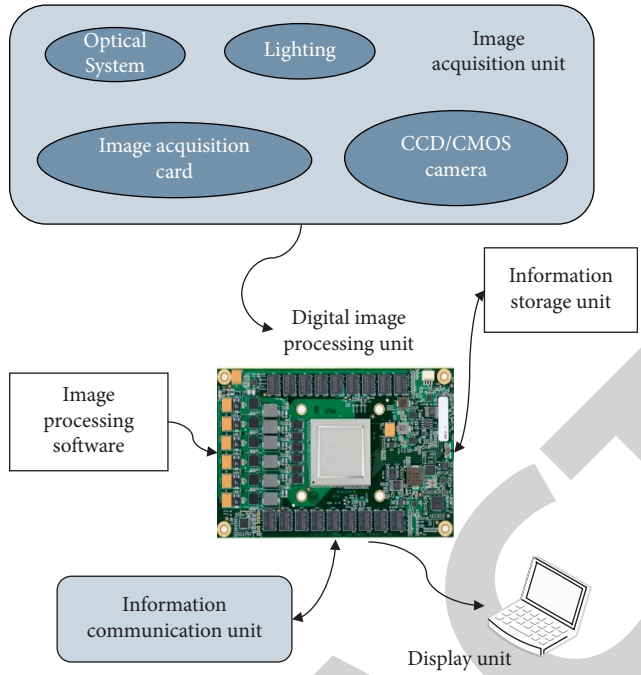

Figure 2: The working process of the visual sensor in the FAT animation production process.

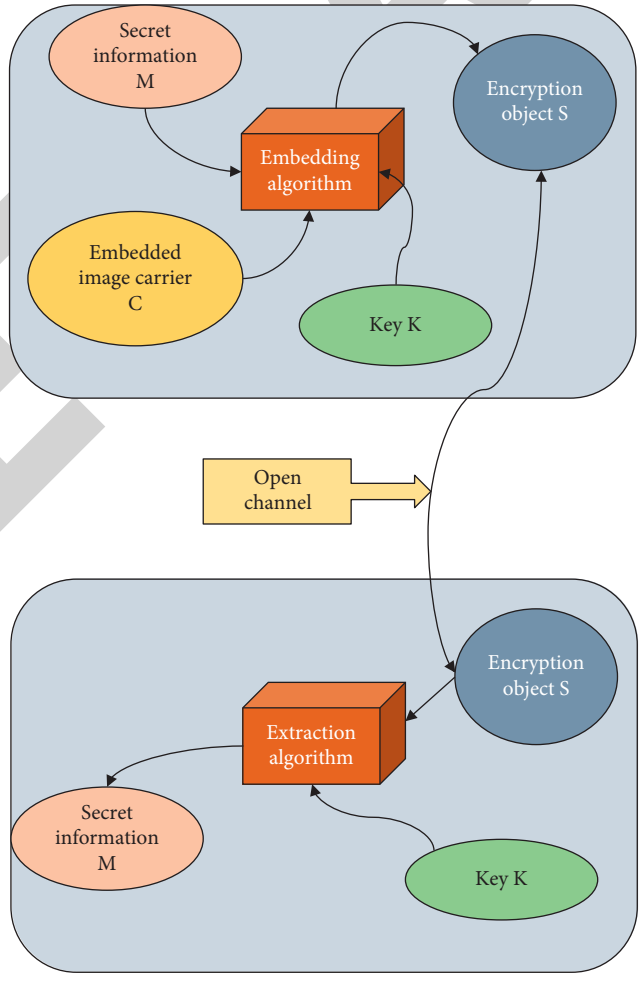

Figure 3: Classic model of steganography algorithm.

the distortion cost value that measures the embedded security of each pixel in the image. The smaller the distortion cost value, the smaller the distortion effect of the modification of this pixel on the image and the smaller the probability of image distortion caused by the modification here. The basic framework of the algorithm is shown in Figure 4. A good distortion function can accurately measure the embedded security of each pixel, making the entire algorithm more secure.

The coding embedding method determines whether it is possible to modify fewer positions to embed as much information as possible and improve the security of the algorithm. Generally, when the distortion function is designed, a smaller distortion cost is given to pixels in a complex texture area and an edge area, and a higher distortion cost is given to a flat area. The adaptive steganography image enhancement algorithm for the spatial image by minimizing distortion can adaptively select these complex texture regions and edge regions. For the additive distortion cost, the calculation method for the sum of the image distortion cost is shown in the following equation:

$$D(X,Y) = \sum_{i=1}^{n}\sum_{j=1}^{n}\rho_{ij}|X_{ij} - Y_{ij}|, \tag{1}$$

where X represents the carrier image cover, Y represents the secret image Stego, and ρ_{ij} represents the distortion cost of the pixel (i, j) at the carrier image.

Most of the distortion functions used in the existing spatial image adaptive steganography image enhancement algorithms are hand-designed heuristic distortion functions. The security measurement method of each pixel is calculated by using the distortion cost of each pixel of the distortion function. However, the hand-designed distortion function cannot well measure the distortion value of each pixel, and it is not accurate enough to capture some pixels. It may appear that there are some pixels in areas with complex textures that have higher distortion costs, but some pixels in flat areas have lower distortion costs; that is, abnormal points of distortion costs appear. This is because the distortion function is not accurate enough to capture the pixels in some areas of the image. To solve the problem of abnormal points and improve the security of adaptive steganography image enhancement algorithm for spatial image, the method of finding these abnormal points can be used to increase the distortion cost of abnormal pixels in flat areas and reduce the distortion cost of abnormal pixels in areas with complex textures so that the embedding is concentrated in the texture complex area.

A multiscale filter obtained by combining a multiscale Gaussian filter and a high-pass filter is proposed. Use this filter to extract image details at different scales. By adjusting the weight value of each filter, it is ensured that while enhancing the complex texture area, the enhancement of the flat area is minimized as much as possible. However, when a filter is used to enhance the image texture area, all the texture areas in the image cannot be enhanced by only one filter. This is because the texture area in the image has a difference in scale; there are large-scale image edges and texture areas

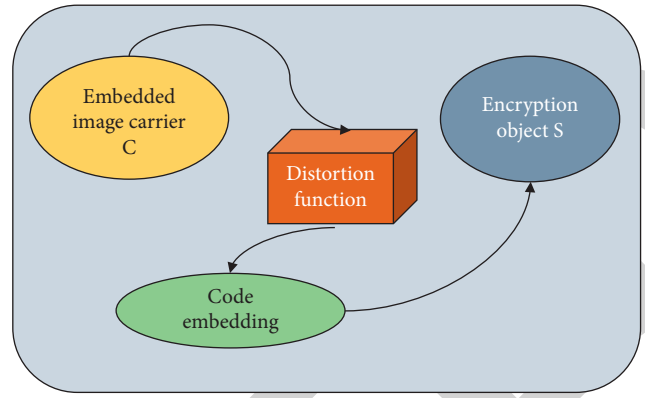

Figure 4: Basic framework of adaptive steganography image enhancement algorithm for the spatial image.

composed of many pixels and small texture areas and noise areas composed of a small number of pixels in the same image. Therefore, multiscale Gaussian filters are used to extract texture details of different scales in the image.

The multiscale Gaussian filter is composed of multiple Gaussian filters of different sizes. These Gaussian filters can extract image details at different scales. When using a multiscale Gaussian filter to enhance an image, the first step is to use 3 Gaussian filters of different sizes to convolve the entire image to obtain a smooth image after 3 filters, expressed as follows:

$$\begin{aligned} L_1 &= G_1 \otimes X, \\ L_2 &= G_2 \otimes X, \\ L_3 &= G_3 \otimes X, \end{aligned} \tag{2}$$

where $\otimes$ represents the convolution operation, G_1, G_2, and G_3 represent 3 Gaussian filters with different sizes, and L_1, L_2, and L_3 represent the smooth image X obtained after filtering the carrier image. Since there may be repeated enhancements to some areas during image enhancement, in order to obtain more precise sharpening details, the difference operation is performed on the three image details obtained by filtering, as shown in the following equations:

$$\begin{aligned} H_1 &= X - L_1, \\ H_2 &= L_1 - L_2, \\ H_3 &= L_2 - L_3, \end{aligned} \tag{3}$$

where H_1, H_2, and H_3 represent image details of different scales. The global details of the carrier image X are composed of the weighted sum of the three image details H_1, H_2, and H_3 as shown in the following equation:

$$h = (1 - \omega \mathrm{sgn}(H_1))H_1 + \omega_2 H_2 + \omega_3 H_3, \tag{4}$$

where ω_1, ω_2, and ω_3 represent the weight of image details of different scales. sgn( ) represents a symbolic function. When $H_1 > 0$, the return value of the function is 1; when $H_1 < 0$, the return value of the function is -1; when $H_1 = 0$, the return value of the function is 0. The multiscale Gaussian filter

integrates the image details of different scales in the form of a weighted sum. The purpose is to extract the details of the image texture area more completely and avoid the enhancement of noise in the flat area as much as possible.

In order to verify the effectiveness of the proposed algorithm, a confirmatory experiment is designed. The 10,000 greyscale images in the Bossbase1.01 image database are selected as the carrier image, and the Subtractive Pixel Adjacency Matrix (SPAM) feature is used as the steganalysis feature. These are compared with the existing mainstream adaptive steganography image enhancement algorithm for spatial image (such as spatial-universal wavelet relative distortion (S-UNIWARD)). The embedding rate is 0.1 bpp and 0.4 bpp, and Maximum Mean Discrepancy (MMD) is used as the measurement standard. The suffix Multiscale Gaussian (MSG) is a spatial image adaptive steganography image enhancement algorithm that uses a multiscale Gaussian filter for image enhancement.

In addition, in order to enhance the texture details of different scales in the image, a spatial image steganography enhancement algorithm by multiscale filters is designed. It consists of two parts: image enhancement and distortion cost calculation. The algorithm flow is divided into six steps:

Step 1: use the multiscale Gaussian filter of equation (4) to enhance the carrier image X to obtain the enhanced part.

Step 2: use a high-pass filter to sharpen the carrier image X to get the sharpened part E_s.

Step 3: get the final enhanced image X_s:

$$X_s = \alpha E_g + (1 - \alpha)E_s + X, \tag{5}$$

where α represents the weight and X represents the carrier image.

Step 4: use the distortion function of the adaptive steganography image enhancement algorithm for spatial image to calculate the distortion cost ρ of the enhanced image X_s.

Step 5: use the mean filter to smooth the distortion cost ρ to obtain the smoothed distortion cost ρ_s.

Step 6: use syndrome trellis codes (STC) to embed the necessary secret information into the carrier image X to obtain the final secret object Stego.

The enhancement algorithm is still verified by experiment, and the sample set and comparison algorithm are the same as the above method. The security of the algorithm here is evaluated using the following equation:

$$P_E = \min_{P_{\mathrm{FA}}} \frac{1}{2}\left(P_{\mathrm{FA}} + P_{\mathrm{MD}}\right), \tag{6}$$

where P_{FA} and P_{MD} represent the false detection rate and the missed detection rate. The false detection rate indicates the probability that the carrier sample is misjudged as a secret sample. The missed detection rate indicates the probability of misjudging a confidential sample as a carrier sample. In order to ensure that the experimental results are valid, the result uses an average of 10 training and testing $\overline{P}_E$.

3. Results and Discussion

3.1. Performance Comparison of Spatial Image Steganography Enhancement Algorithms by Multiscale Filters. The MMD detection results of different adaptive steganography image enhancement algorithm for spatial image are shown in Figure 5.

Figure 5 shows that the existing adaptive steganography image enhancement algorithm for spatial image S-UNIWARD uses a multiscale Gaussian filter for enhancement and has a lower MMD value than that without enhancement. This shows that the enhanced steganography algorithm has more high security.

The value of the 3 Gaussian filters is selected according to the ratio of n, $2n-1$, and $4n-1$. The standard deviations corresponding to the 3 filters are 1.0, 2.0, and 4.0. During the experiment, the embedding rate is set to 0.4 bpp, the parameter is $2 \le n \le 9$ and then the results of the algorithm security test with different values of n are shown in Figure 6.

From Figure 6, it is clear that, for $n = 3$, the average detection error rate is about 25.06%. Thus, it shows that the algorithm currently has the highest security. In subsequent experiments, the value of n is fixed at 3, and the sizes of the corresponding three Gaussian filters are 3×3, 5×5, and 11×11, respectively.

The embedding rate is 0.4bpp, the parameter is $0.2 \le \alpha \le 0.7$, and the value step is set to 0.1. Comparison of the three parameters of the multiscale Gaussian filter $\omega_1 = 0.5$, $\omega_2 = 0.5$, and $\omega_3 = 0.25$, and the changes in the security of the algorithm under different α values are shown in Figure 7.

Figure 7 shows that, at the time of $\alpha = 0.4$, the security of the spatial image adaptive steganography enhancement algorithm by multiscale filters is up to 34.62%, so $\alpha = 0.4$.

In order to compare the performance of the enhanced algorithm and the existing algorithm S-UNIWARD, two mainstreams' spatial steganalysis features, SRM (Spatial Rich Model) and max Spatial Rich Model (max SRM), are used to compare algorithm security. Among them, the suffix Multiscale Gaussian (MSG) represents the spatial image adaptive steganography image enhancement algorithm that uses a multiscale Gaussian filter for enhancement. The suffix MiniMum_Support (MS) represents the MS image enhancement algorithm proposed in literature [21]. The comparison results are shown in Figures 8 and 9.

Figures 8 and 9 show that the established image enhancement algorithm can significantly improve the security of the current spatial image steganography image enhancement algorithm at different embedding rates. Especially under a high embedding rate, the improvement of spatial image steganography image enhancement algorithm is greater. This is because when the embedding rate is high, the texture complex area with lower distortion cost has been embedded. At this time, the spatial image steganography image enhancement algorithm will select some noise points in the flat area for embedding. That is, abnormal points with lower distortion costs in the established flat area will reduce the security of the algorithm. After the carrier image is preprocessed by the proposed enhancement algorithm, the

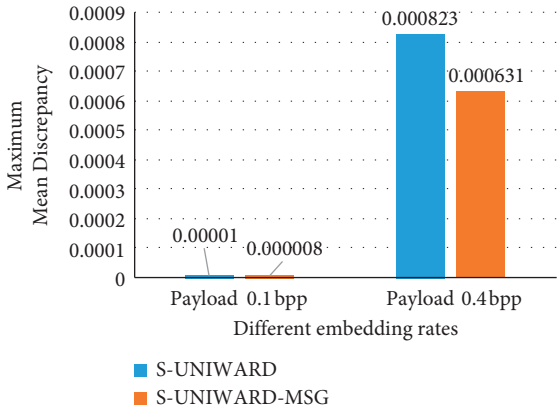

Figure 5: MMD detection results of different adaptive steganography image enhancement algorithm for spatial image.

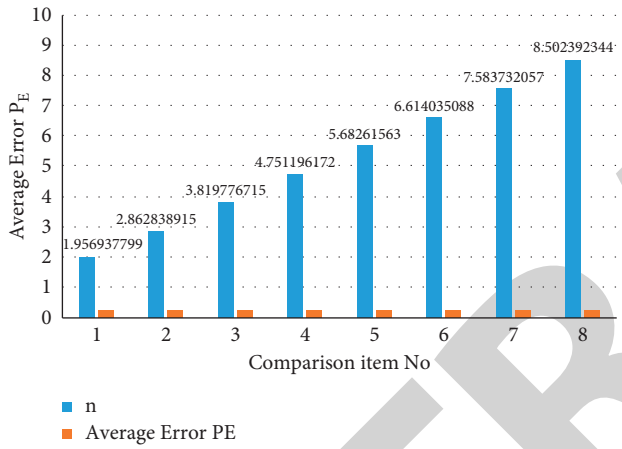

Figure 6: The influence of different values of filter size n on algorithm security.

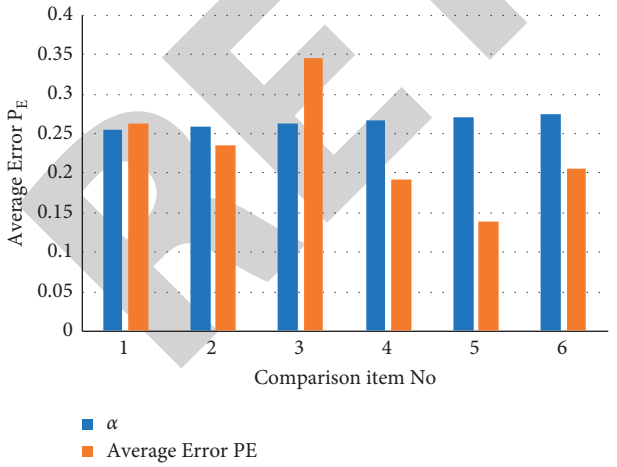

Figure 7: The influence of different values of parameters on the security of the algorithm.

pixels in the complex texture area are enhanced. Meanwhile, it suppresses the noise in the flat area so that the embedding of the spatial image steganography image enhancement algorithm is more concentrated in the embedding of the

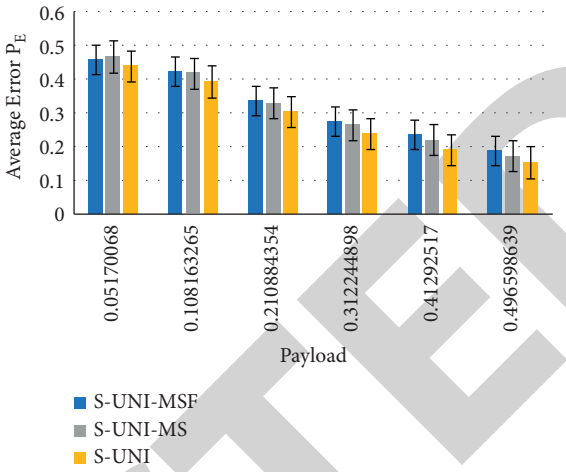

Figure 8: Performance comparison of image enhancement algorithms on feature set SRM.

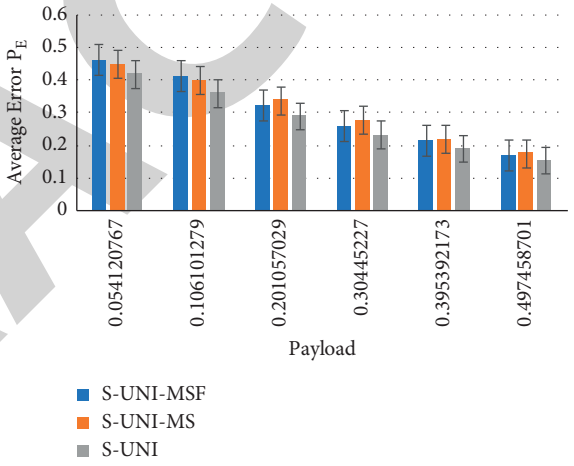

Figure 9: Performance comparison of image enhancement algorithms on feature set max SRM.

texture complex area, and the influence caused by the abnormal points in the flat area is less. The proposed algorithm improves the security of the algorithm, and the image enhancement effect will be better.

4. Conclusions

With the rapid development of computer image processing technology, the scope of Internet information has gradually changed from graphic communication to image communication, creating conditions for network platforms and radio and television platforms to compete. Firstly, advanced computer image processing methods are used in the field of FAT animation production. In view of the current traditional steganography algorithms that do not pay attention to the image content, the generated image quality is low. Aiming at the current situation that there are two types of abnormal points in spatial image steganography, an adaptive steganography algorithm is proposed. In the process of embedding, more fully consider the content of the image

Hindawi
Journal of Mathematics
Volume 2024, Article ID 9894306, 1 page
https://doi.org/10.1155/2024/9894306

Retraction

Retracted: Intelligent Integration Algorithm of National Traditional Sports Culture Resources Based on Big Data

Journal of Mathematics

Received 23 January 2024; Accepted 23 January 2024; Published 24 January 2024

This article has been retracted by Hindawi following an investigation undertaken by the publisher [1]. This investigation has uncovered evidence of one or more of the following indicators of systematic manipulation of the publication process:

(1) Discrepancies in scope

(2) Discrepancies in the description of the research reported

(3) Discrepancies between the availability of data and the research described

(4) Inappropriate citations

(5) Incoherent, meaningless and/or irrelevant content included in the article

(6) Manipulated or compromised peer review

The presence of these indicators undermines our confidence in the integrity of the article's content and we cannot, therefore, vouch for its reliability. Please note that this notice is intended solely to alert readers that the content of this article is unreliable. We have not investigated whether authors were aware of or involved in the systematic manipulation of the publication process.

Wiley and Hindawi regrets that the usual quality checks did not identify these issues before publication and have since put additional measures in place to safeguard research integrity.

We wish to credit our own Research Integrity and Research Publishing teams and anonymous and named external researchers and research integrity experts for contributing to this investigation.

The corresponding author, as the representative of all authors, has been given the opportunity to register their agreement or disagreement to this retraction. We have kept a record of any response received.

References

[1] X.-B. Ai, "Intelligent Integration Algorithm of National Traditional Sports Culture Resources Based on Big Data," *Journal of Mathematics*, vol. 2022, Article ID 8335300, 11 pages, 2022.

Hindawi
Journal of Mathematics
Volume 2022, Article ID 8335300, 11 pages
https://doi.org/10.1155/2022/8335300

Research Article

Intelligent Integration Algorithm of National Traditional Sports Culture Resources Based on Big Data

Xian-Bin Ai [1,2]

[1]*School of P.E., Chaohu University, Hefei, Anhui 238000, China*
[2]*Center for International Education, Philippine Christian University, Manila 1004, Philippines*

Correspondence should be addressed to Xian-Bin Ai; 060054@chu.edu.cn

Received 20 October 2021; Accepted 12 November 2021; Published 28 January 2022

Academic Editor: Naeem Jan

There is an information island between traditional national sports culture resources and realize the efficient real-time interconnection of resources. Therefore, this study proposed an intelligent integration algorithm of traditional national sports culture resources using big data that halts the said information island. Firstly, the complete data set is obtained by determining the time attenuation period of the weighted sample, and the mining parameters are based on the real value to realize the in-depth mining of the resource wisdom of traditional ethnic sports culture. Then, the query set of big data is constructed based on the results of weakly associated data mining, and the query of weakly associated data is completed through data repair. Finally, XML technology is used to run the schema to build a resource integration model. The experimental results show that compared with the traditional integration algorithm, the proposed algorithm can better solve the problem of information island among traditional ethnic sports culture resources at all levels and effectively maintain the stability of the storage environment of traditional ethnic sports culture resources while realizing the real-time interconnection of resources.

1. Introduction

The culture of each nation is formed and developed to adapt to the characteristics of its own nation, with independent national character and social consciousness. In its self-replicating historical origin from generation to generation, it continuously accepts foreign influence and changes, gradually forming and enriching the cultural accumulation of its own nation [1].

China has thousands of years of continuous Chinese traditional culture; traditional national sports culture is a special form of traditional Chinese culture; coupled with a vast land with a large number of ethnic and population, under the influence of traditional Chinese culture, with the passage of time and space changes, ethnic traditional sports have emerged. By 1990, there were 977 traditional ethnic sports. There are a large number of traditional national sports, which provide a resource basis for the development of traditional national sports culture.

The resources of traditional national sports culture include not only the traditional national sports as the mainstream culture of the Chinese nation but also the nonmainstream Han nationality and ethnic minority sports activities. It appears with the development of modern life under the specific regional environment, regional conditions, and regional cultural background. It can take a certain material entity as the carrier but also can be some pure human spiritual culture things, tangible carrier, and intangible spiritual culture content depend on each other, mutual penetration, with obvious characteristics of the times, nationality, and art. Therefore, in the resource connotation of traditional ethnic sports culture, there are not only traditional sports items, sports equipment, equipment, clothing, murals, and unearthed cultural relics in the

material level but also folk culture, organizational culture, and values and rules in traditional ethnic sports activities in the spiritual level [2].

However, in the storage platform of national traditional sports culture resources, there are obvious information islands due to the existence of data coverage, which affects the real-time interconnection between resources. The traditional cloud computing resource integration strategy uses the directory system to integrate traditional national sports culture resources and then uses the portal platform to integrate these information parameters into a new data flow transmission format [3]. However, this method has limited ability to solve the problem of information island, and it is difficult to establish a new real-time resource interconnection relationship.

Therefore, a resource integration algorithm based on online migration is designed in reference [4]. This algorithm takes into account the characteristics of cloud computing; comprehensively considers memory, CPU, and I/O; and proposes an online migration strategy based on the ant colony algorithm. On the basis of analyzing the principle of ant colony algorithm and the integration of cloud platform virtualization resources, the profit incentive is defined as the heuristic information of ant colony algorithm, and then the time difference and migration cost of different virtual machines on the virtual cluster are adjusted to optimize the performance of the virtual cluster and achieve efficient integration of resources. In reference [5], to design a kind of resource integration algorithm based on improved ORM, the algorithm is divided into three parts: first of all, to access the database using the improved ORM technology, extract data resources, and then to preprocess data resources, including cleaning, dimensionality of loading, and finally using KNN algorithm to deal with good classified data resources integration. In reference [6], a data resource integration algorithm based on integrated learning is designed. The algorithm realizes control, regulation, and application by using the administrator operation management operation layer. In the big data analysis layer, the data prediction results fused with multidimensional parameter information were obtained by the parameter single-step prediction method of ELM prediction model, and the high precision strong learning model was obtained by combining ELM prediction model with bagging integrated learning method so as to realize the effective interpretation of differential data resources. The data is integrated by the integration manager and the integration running engine in the integration layer, and the integrated data is fed back to the big data resource layer through the regulation layer, which is stored in the temporary database and metadata database in the layer, and the data in these databases provide data scheduling services for the database.

Based on the above traditional research, in order to break the information island between the data of traditional ethnic sports culture resources at all levels and realize the real-time interconnection of resources, this study proposes an intelligent integration algorithm of traditional ethnic sports culture resources based on big data. Moreover, the association definitions and characteristics of national traditional sports culture resources are described, such as historicity, nationality, blend, and regional. In addition, the resource semantic similarity measurement and integration of ethnic traditional sports culture resources based on XML are explained.

The organization of the rest of the paper is as follows. Section 2 excavates and deals with the resources of national traditional sports culture. Based on big data, Section 3 enquires weakly associated data of ethnic traditional sports culture resources. In Section 4, intelligent integration of national traditional sports culture resources is presented. The experimental studies are carried out in Section 5. Finally, in Section 6, the current article is concluded.

2. Deeply Excavate and Deal with the Resources of National Traditional Sports Culture

The in-depth mining processing of ethnic traditional sports culture resources includes three execution steps: calculating the time attenuation period of weighted samples, data set expression, and parameter setting of real value mining. The specific operation methods are as follows.

2.1. The Time Decay Period of the Weighted Sample. The weighted sample time decay period is a relatively broad physical coefficient index. In the storage space of national traditional sports culture resources, due to the influence of an in-depth mining framework system, the time decay cycle of weighted samples often has a direct impact on the real-time storage behavior of data parameter indexes [7].

For the resources of traditional ethnic sports culture, the larger the actual coverage area of an in-depth mining framework system is, the stronger the application storage capacity of data information parameters will be [8]. To put it simply, the length value of the time decay period of the weighted sample is not completely fixed, and the order of magnitude level of the physical index will also increase with the increase of the amount of traditional sports culture resources of the nationalities to be stored. However, in order not to affect the final integration and sharing results of information parameters, the weighted sample time decay cycle index also contains certain constrained abilities, that is, in a fixed numerical space, the weighted sample time decay cycle index can affect the integration processing results of national traditional sports culture resources [9].

Assuming that s and e represent the sample weight coefficient of the traditional national sports culture resources of two different groups and n represents the sample collection coefficient of the traditional national sports culture resources information, the above physical quantities can be combined together, and the expression of the decay period of the weighted sample time can be defined as follows:

$$J = \sum_{s=1}^{n} \sum_{e=1}^{n} \frac{\left|c_s - c_e\right|^2}{n^2 \cdot |\Delta t|}, \tag{1}$$

where c_s represents the information characteristic value of traditional ethnic sports culture resources when the sample coefficient is s, c_e represents the information characteristic

value of traditional ethnic sports culture resources when the sample coefficient is e, and $|\Delta t|$ represents the unit integration time of traditional ethnic sports culture resources information.

2.2. Data Set Representation. In the process of implementing the information parameter integration and sharing instruction, the data set can include all the undefined national traditional sports culture resource information and change the actual transmission rate of the stored information parameters according to the specific numerical level of the time decay period of the weighted sample.

Data set should be a relatively broad definition condition for information parameters [10]. In order to meet the practical application requirements of an in-depth mining framework more effectively, the remaining data indicators should be integrated into a new transmission form while the parameters of traditional national sports culture resource information should be transferred in a timely manner. On the one hand, the integration and sharing of resource information of the host can be satisfied. On the other hand, it can temporarily alleviate the poor timeliness of information parameter storage caused by the time decay period of weighted samples.

Hypothesis ∂ represents the information-sharing coefficient of ethnic traditional sports culture resources, and simultaneous formula (1) can define the data set expression of ethnic traditional sports culture resources as follows:

$$A = \frac{J}{\varepsilon_1 + \varepsilon_2} \sum_{\partial \longrightarrow 0} x_{\partial}^2, \tag{2}$$

where ε_1 and ε_2, respectively, represent the definition conditions of two different ethnic traditional sports culture resource information parameters and x_{∂} represents the established basis vector of digital resource information integration.

2.3. Set Real Value Mining Parameters. Real value mining parameters setting is one of the key processing steps in deep mining and can be in a known weighted sample attenuation cycle time and the data set expression conditions, on the basis of the national traditional sports culture resources information integration ability in preliminary constraints so that the host of the data parameter query ability get improved [11]. At the same time, the storage platform of national traditional sports culture resources is in charge of a large amount of digital resource information, and the final transmission direction of these information files is also different due to the difference of parameter integration and sharing mode. However, in most cases, its transmission behavior is beneficial to the implementation of parametric deep mining instructions.

It is assumed that $p_{\min}$ represents the minimum value of mining depth value of traditional ethnic sports culture resources and $p_{\max}$ represents the maximum value. In general, the greater the physical difference between the two, the more accurate the setting results of real value mining parameters will be. With the support of the above physical quantities, simultaneous formula (2) can express the setting results of real value mining parameters as follows:

$$L = \frac{f\left(p_{\max} - p_{\min}\right)}{\lambda A} \cdot \sqrt{k_1^2 + k_2^2}, \tag{3}$$

where f represents the depth mining coefficient, λ represents the characteristic value of digital resource information, and k_1 and k_2, respectively, represent the mining permission value of resource information of traditional sports culture of different nationalities.

3. Weakly Associated Data Query of Ethnic Traditional Sports Culture Resources Based on Big Data

Weakly associated data query of national traditional sports culture resources based on big data is the basic link of integration processing. With the support of weakly associated data mining and query set construction, the specific operation methods can be carried out as follows.

3.1. Mining Weakly Linked Data. Weakly associated data mining is the basic operation step of integration algorithm implementation [12]. In the face of the huge amount of original data of traditional ethnic sports culture resources, accurate information characteristic dimension conditions can be determined according to the close connection between adjacent data organizations, and the processed traditional ethnic sports culture resource data can be rearranged according to the constraint conditions. To put it simply, weakly linked data mining is an application processing method to break and rearrange information connections.

The weak correlation attribute becomes the only physical condition that affects the data arrangement when the information association ability of all the traditional sports culture data is unchanged. So-called mining is also called the appropriate link; it is existing in large all the multimedia data in the data network, according to certain relevant influence to carry on the corresponding link, to integrate all the physical structure of complete connection, package it, and set up a special independent organization to store this kind of weak correlation data, waiting for the connection of the next execution processing instruction application [13]. Figure 1 reflects the complete processing principle of weakly associated data mining.

3.2. Building a Big Data Query Set. A big data query set is a mining storage space for weakly associated data, with strong physical carrying capacity and no strict limit on the amount of data information contained in it. Although there is no definite limit on the specific number of weakly associated data of ethnic traditional sports culture resources in the collection, under normal circumstances, the collection structure that meets the requirements of compression must contain three basic data types: mining head information, mining entity information, and mining tail information [14].

The so-called mining header information refers to the big data nodes that directly contact the results of weakly associated data mining, often represented as y_a. Mining entity information is an in-depth explanation of weak association rules and an important component condition that cannot be obtained in big data query sets, which is often expressed as y_b. Tail information mining is the main physical basis for the formulation of the compression method. It has no direct correlation with physical conditions such as the total amount of multimedia data and weak correlation coefficient, which is often expressed as y_c. The big data query set can be expressed as follows:

$$Y = \left\{ T | T = \frac{\mu\lambda \cdot |y_b|^e}{y_c - y_a} \right\}, \tag{4}$$

where T represents any weakly associated data of traditional national sports culture resources in the big data query set; μ and λ, respectively, represent two irrelevant intelligent compression index vectors of big data; in certain cases, $\mu = \lambda$ and $\mu \neq \lambda$ are established at the same time; and e represents the power coefficient related to mining entity information.

3.3. Resource Data Repair. Data repair is a precise limitation on the final intelligent integration result based on a big data query set. Compared with weakly associated data mining, when repairing the resource data of traditional ethnic sports culture, the weak part in the big data environment can be directly targeted and promoted by directional integration [15].

In the process of repairing weakly associated data of ethnic traditional sports culture resources, we should first conduct a preliminary search on the query set of big data and screen out the key information components, and then selectively generate one or more alternative data packets for repairing according to the limitations of weak association rules on integration results. It must contain not only all the information structures selected from the collection of big data queries but also the associated form structures with integrated indexing capabilities. Then, all the information structures are arranged according to the weakly associated data mining rules to ensure that there is no obvious data chaos in the subsequent integration process. Finally, the big data media environment is utilized to repair the data structure that has an obvious weak correlation effect so as to improve the storage and transmission capacity of the data structure of national traditional sports culture resources.

Figure 2 shows the complete data repair process of traditional national sports culture resources.

4. Intelligent Integration of National Traditional Sports Culture Resources

In this section, the characteristics, association definitions, of national traditional sports culture resources are described. In addition, the resource semantic similarity measurement and integration of ethnic traditional sports culture resources based on XML are explained.

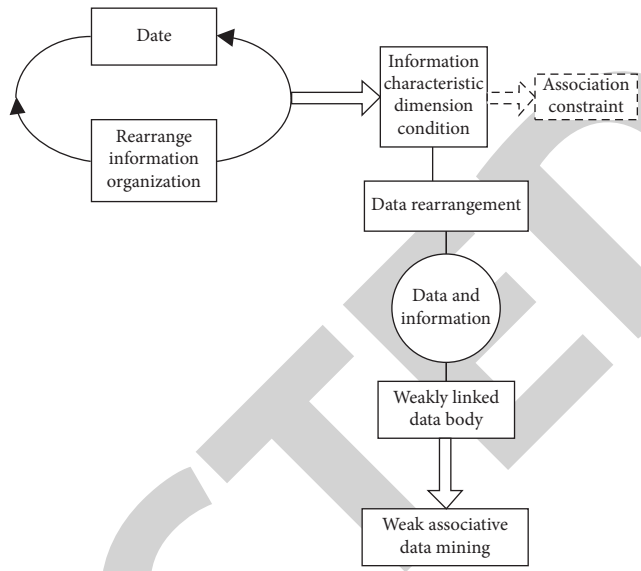

Figure 1: Schematic diagram of weak association data mining for ethnic traditional sports culture resources.

4.1. The Characteristics of National Traditional Sports Culture Resources

(1) Nationality: The so-called nationality refers to the characteristics common to the ethnic groups formed in the process of the development of a national sports culture and different from other national sports cultures. The national character of sports culture can be reflected in the material level, behavior system, and spirit level of sports culture. However, the spiritual level of sports culture can reflect the most intrinsic, the most profound, the most essential national character.

(2) Historicity: Historicity refers to the development of a country's national sports culture in a cycle that spans time and space, and the sports culture system records the formation and development process of national traditional sports culture in this historical period and even interprets it, so that people can understand the traditional national sports culture. In the past, it provides a reference for future research on national traditional sports culture.

(3) Regional: A region is a space that has certain limits and is interconnected with each other with similarities and differences. The regionalism of the national traditional sports culture resources in China means that the national traditional sports culture resources are limited by the geographical environment and show different characteristics. As China is a unified multiethnic country, under the premise of unification, there is a certain correlation between the sports culture of various ethnic regions. However, China is a multiethnic country, the sports culture of each ethnic region cannot be completely the same; they show different distinct characteristics.

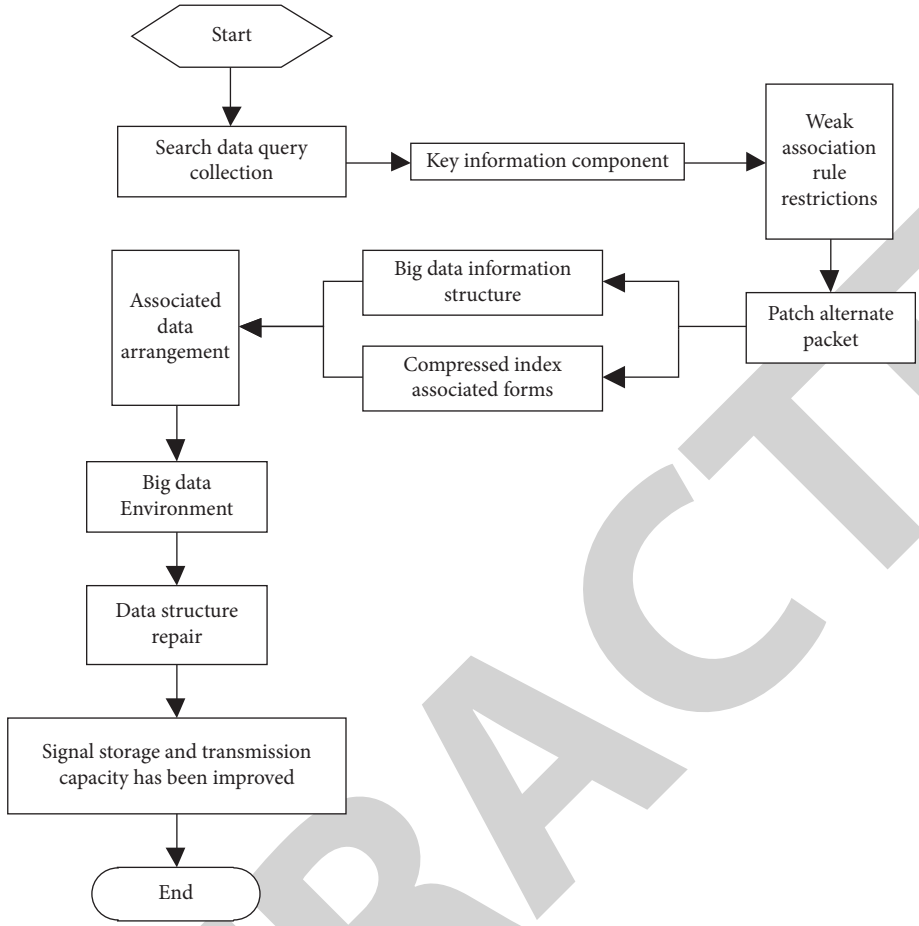

Figure 2: Data repair flow chart of national traditional sports culture resources.

(4) Blend: Integration refers to the process of mutual integration of different countries, national ideas, national cultures, and national economies in the current era of globalization. At present, China's national traditional sports culture is in a diversified economic system. From the cultural level, the national traditional sports culture is in the process of integration, transformation, and development of the global "world culture."

4.2. Association Definition of National Traditional Sports Culture Resources. For the random ethnic traditional sports culture resource ontology A, B, and C, there is $B \neq A, C \neq A, B \neq C$.

(1) If the root entity of C is the child root entity of B, then the description B contains C, and the formulation B contains C, then add association contain (C) to the root entity of B, and add association part − of (B) to the root entity of C.

(2) Add ontology D containing ethnic traditional sports culture resources to make root entities B and C become subroot entities of D, that is, there are associations contain (B) and contain (C) in the root entity of D, so it describes that there are sibling associations between B and C, and associations brother (C) and brother (B) are introduced into root entities B and C, respectively.

(3) If there is no brother layer connection between B and C, specify that b and c represent the sources of the root entities of B and C in the source resource set, respectively. If b and c are the sources of the same category of national traditional sports culture resources, then existed with the connection between B and C, within the root entity B and C, respectively, added associated hom o − course (C) and hom o − course (B).

(4) If there do not have brothers layer connection between B and C, specify that b and c represent the sources of the root entities of B and C in the source resource set, respectively. If b and c is derived from the same category of national traditional sports culture resources, then between B and C will have a same group, within the root entity B and C, respectively, added association hom o − group (C) and hom o − group (B).

(5) If B and C is the traditional sports cultural resource coefficient of different nationalities in the same category, then there is a direct connection between B and C, adding associations in B and C, respectively,

$b-\text{version}(C)$ and $b-\text{version}(B)$. It directly represents the conversion of the old version to the new version.

(6) If B and C have been browsed by the same user, then there is browsing association between B and C. Add association brow(C) and association brow(B) to the root entity of B and C, respectively.

(7) It is proposed that X is the entity set of linked relations existing in the entities in B and C, and Y is the entity set of linked relations existing in the entities in B and C. If at least one of X and Y is empty, then the association describing B and C is an infinitesimal quantity exceeding zero.

4.3. Resource Semantic Similarity Measurement. For the random ethnic traditional sports culture resource noumenon B and C, their semantic similarity is described as $W(B,C)$, which is defined as follows:

Ten meta-resource keywords are collected from traditional ethnic sports culture resources and stored in the attribute set of the real roots X and Y of resource ontology B and C. The similarity of B and C is defined as follows:

$$W(x,y)=\sum_{i=1}^{10}W_i(x,y),$$
$$W_i(x,y)=\frac{\left|\theta_{i,x}\cap\theta_{i,y}\right|/\max\left(\left|\theta_{i,x}\cap\theta_{i,y}\right|\right)+\left|\theta_{i,x}\cap\theta_{i,y}\right|/\min\left(\left|\theta_{i,x}\cap\theta_{i,y}\right|\right)}{(2*9)}, \tag{5}$$

where $\theta_{i,x}$ is the set of the i-th meta-resource in x and $\theta_{i,x}\cap\theta_{i,y}$ represents the total amount of the same value.

4.4. Integration of Ethnic Traditional Sports Culture Resources Based on XML. Based on the above research, this paper makes use of XML (Extensible Markup Language) technology to complete the integration and processing of traditional national sports culture resources.

Unlike traditional structured data, XML data is self-describing and has no fixed form. In practical use, XML is usually used as the framework of data exchange, and the associated database is used as the storage form. In this way, resources in the database can be converted into XML format during use, and files in XML format can also be returned to the associated database [16].

As an open standard, XML has a standard associated with it, as shown in Figure 3.

The essence of national traditional sports culture resource integration is the high combination of digital resources, which is built in XML. Therefore, through such high integration, it cannot only provide an efficient and fast way of resource acquisition and resource retrieval but also lay a foundation for the construction and sharing of national traditional sports culture resources.

Since the traditional ethnic sports culture resources are divided from the server in the network environment during the XML resource integration model, the XNL resource integration model will connect the traditional ethnic sports culture resources with the disk array through the FC (fiber channel) switch. When the resource data integration task appears, The XML resource consolidation model is used to transfer between related servers or disk arrays in the background, and the server can access any node in XML, which greatly improves the availability of the resource consolidation model. The logical topology architecture of a typical XML resource consolidation model is shown in Figure 4.

In Figure 4, the XML resource consolidation model needs to be built from storage media, data servers, disk arrays, fiber channel switches, and tape libraries. A typical integrated media disk array is composed in the form of an all-optical fiber structure rather than a mixture of other devices.

In the XML resource consolidation model, communication between nodes can run simultaneously without interference from each other. Therefore, the bandwidth of national traditional sports culture resources in the switch can reach the sum of the data flow on the port, realizing the long-distance and high-efficiency transmission of optical fiber transmission and realizing the instant storage and retrieval of resource data between different workstations.

Generally speaking, there is a disk array in the information center of ethnic traditional sports and cultural resources, and a converter needs to be introduced when accessing the all-fiber XML resource integration model. According to the previous experiments, it can be proved that the characteristics of fiber high-speed integrated transmission will be lost through the converter, and the converter also has the matching problem with the XML disk array. Therefore, the all-fiber architecture can give full play to the characteristics of the XML resource integration model and Yoshiki, while the original disk array is backed up by the data backup module in the XML resource integration model. At the same time, as the XML resource integration model has formed a storage module, its scalability can support the distributed expansion of storage space, that is, with the continuous improvement of electronic resources, it is integrated into the disk array so as to obtain the optimization of resource construction and investment.

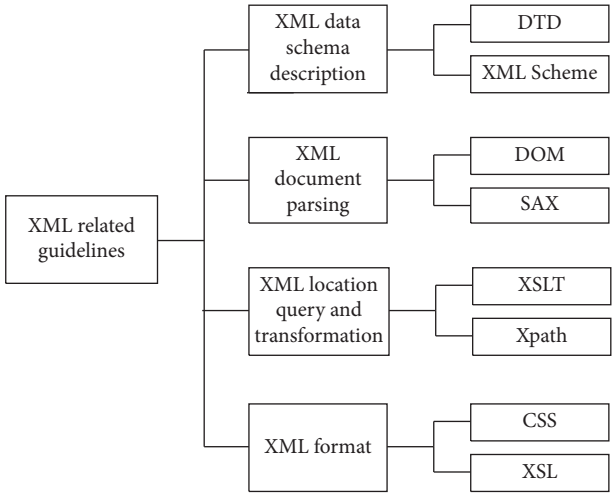

Figure 3: XML association standards.

Due to a large amount of data of national traditional sports culture resources, in order to ensure the operational efficiency of the integration model, this paper integrates multiobjective integration scheduling algorithm, which can select suitable nodes by priority to meet the optimization of operation efficiency. The following parameters are considered:

(1) Completion time: Tthis paper conducts an evaluation based on previous running time, number of requests, and estimated running time. Then the request S_i evaluation implementation time t_c is as follows:

$$t_c = Q_s = \sum_{k=1}^{QL_d} t_{kc},$$
$$t_c = \frac{t_{\text{ini}} + \sum_{n=1}^{\text{Num}} t_n}{\text{Num} + 1}, \quad \text{Num} \neq 0, \tag{6}$$

where QL_d represents the time required in node d, t_c represents the calculation time of S_i, and S_i represents the calculation time of t_{ini}, which is the mean of the calculation time before this request. Num is the number of requests, and t_n is the n-th operation time of S_i. The more S_i is implemented, the closer the value of t_c will be to the actual completion time of the integration. The smaller the value of t_c, the faster the integration can be achieved.

(2) Load balancing: If a load of a node in the XML ethnic traditional sports culture resource integration model exceeds the maximum it can bear, then the performance of the whole model will be greatly reduced. Therefore, it is necessary to schedule the integration to nodes with the light load as far as possible to balance the load. Therefore, a critical value of the integration rejection is proposed for all nodes in this paper. When the node equipment load exceeds the critical value, the following integration requests will be rejected automatically, and the integration requests will be uploaded to facilitate the collection of nodes that do not reach the critical value. The critical value operation equation is as follows:

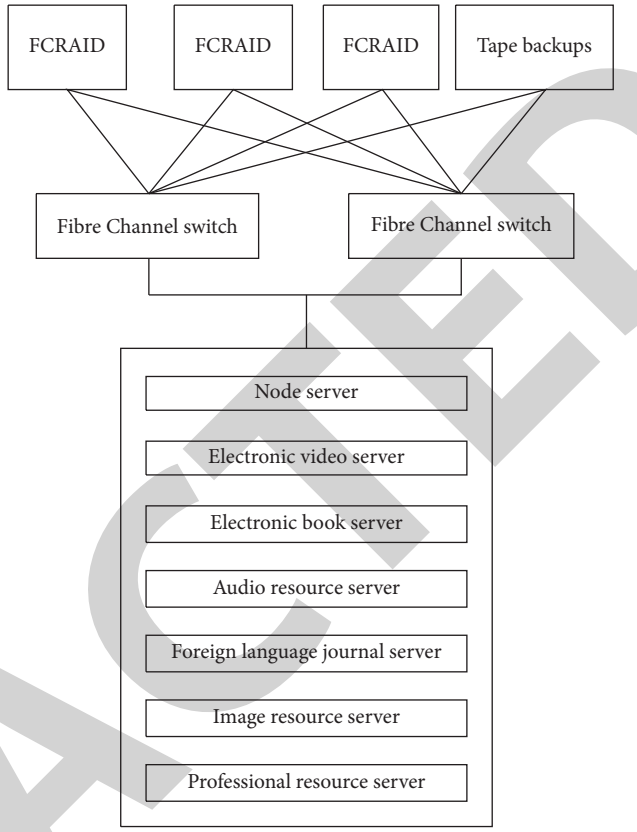

Figure 4: Logical topology of XML resource consolidation model.

$$\text{TLV} = \left\{\text{TLV}_{\text{cpu}}, \text{TLV}_{\text{mem}}, \text{TLV}_{\text{stor}}, \text{TLV}_{\text{net}}\right\}. \tag{7}$$

In the proposed XML integration model, the conversion point of two kinds of fiber converter is proposed between two different nodes. For distributed teaching resources, the fiber converter will transmit from the responding node to the converter in another node. By virtue of this integration method, once the spatial capacity is found in a node, the allocation of national traditional sports culture resources can be integrated together and stored in the node with available capacity.

To sum up, the integration process of national traditional sports culture resources is shown in Figure 5.

5. Experiment and Analysis

The following experiments are designed to verify the effectiveness of the intelligent integration algorithm of national traditional sports culture resources based on big data. The relative resource scheduling model of national traditional sports culture is established.

In order to form an experimental comparison, the processing algorithms of the experimental group and the control group are connected to the resource storage host. The experimental host is equipped with the proposed

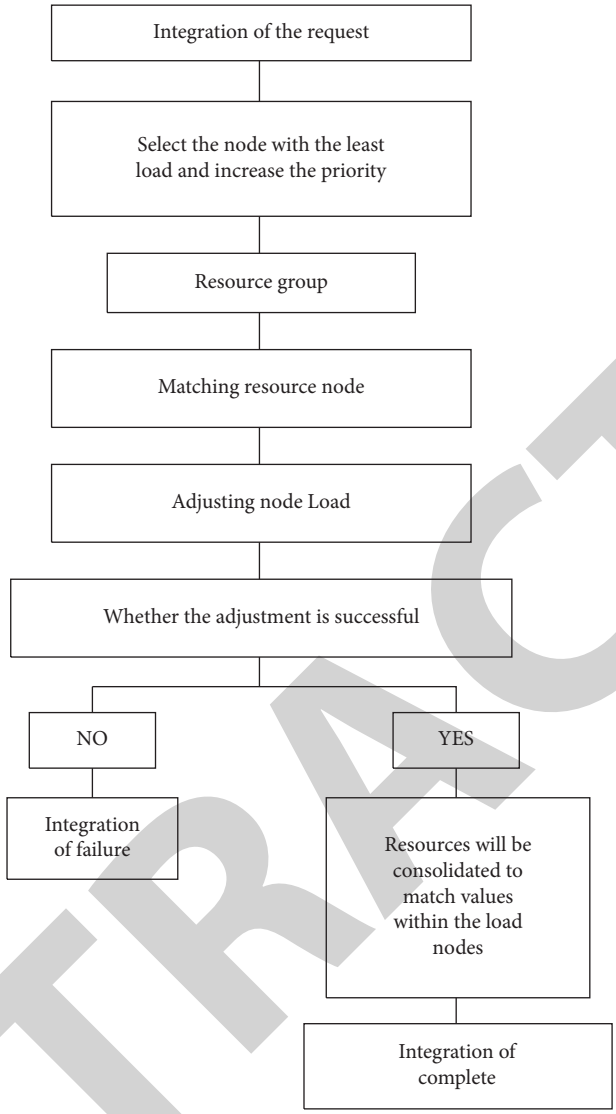

Figure 5: Schematic diagram of integration process of national traditional sports culture resources.

algorithm, while the control host is equipped with the traditional online migration-based resource integration algorithm and the improved ORM-based resource integration algorithm.

Information silos are a serious resource lock-in problem. In general, the more obvious information silos are, the more resources are locked up. It is assumed that indicator A can reflect the occurrence probability of the information island phenomenon of national traditional sports culture resources. The higher the value level of this indicator is, the greater the occurrence probability of the information island phenomenon will be.

Table 1 records the specific changes of index values of the proposed algorithm, the resource integration algorithm based on online migration, and the resource integration algorithm based on improved ORM.

By analyzing Table 1, it can be seen that after the application of the proposed algorithm, the value of index A has always maintained A continuous upward trend, and in the whole experiment, the value of the early period increased significantly more than that of the late period. However, after the application of the two traditional algorithms, the value of index A keeps the trend of increasing first, then stabilizing, and finally decreasing, and there is no significant difference between the increasing range in the early stage and the decreasing range in the late stage. From the perspective of limit value, the maximum value of index A in the experimental group decreased by 26.18% and 34.08%, respectively, compared with that in the control group.

To sum up, the application of the big data-based intelligent integration algorithm of traditional ethnic sports culture resources designed in this study significantly improves the numerical level of index A, solves the information island problem of traditional ethnic sports culture resources to A certain extent, and realizes the stable transmission and sharing of data information parameters.

It is assumed that index B can reflect the real-time interconnection and communication ability of national

Table 1: Comparison of A index values of different algorithms.

Experimental time/min	Index A/%
(a) Algorithm of this paper	
10	10.07
20	10.14
30	10.18
40	10.22
50	10.25
60	10.26
70	10.39
80	10.30
90	10.31
100	10.33
(b) Resource integration algorithm based on online migration	
10	36.46
20	36.48
30	36.50
40	36.53
50	36.57
60	36.57
70	36.56
80	36.55
90	36.51
100	36.51
(c) Resource integration algorithm based on improved ORM	
10	44.36
20	44.38
30	44.40
40	44.43
50	44.47
60	44.46
70	44.46
80	44.46
90	44.31
100	44.21

Table 2: Comparison of B index values of different algorithms.

Experimental time/min	Index B/%
(a) Algorithm of this paper	
10	83.15
20	83.15
30	83.15
40	83.15
50	83.14
60	83.15
70	83.16
80	83.14
90	83.15
100	83.16
(b) Resource integration algorithm based on online migration	
10	62.70
20	62.70
30	62.68
40	62.67
50	62.66
60	62.65
70	62.64
80	62.65
90	62.64
100	62.66

Table 2: Continued.

Experimental time/min	Index *B*/%
(c) Resource integration algorithm based on improved ORM	
10	60.66
20	60.66
30	60.47
40	60.46
50	60.44
60	60.43
70	60.43
80	60.42
90	60.41
100	60.41

traditional sports culture resource information. In the absence of other external influence conditions, the greater the standard value of *B*, the stronger the real-time interconnection and interworking ability of traditional national sports culture resources.

Table 2 records the specific changes of index B of the proposed algorithm, the resource integration algorithm based on online migration, and the improved ORM resource integration algorithm.

By analyzing Table 2, it can be seen that the value of index *B* of the proposed algorithm always maintains an absolutely stable value existence state in the early stage of the experiment, but from the 50 min, the trend of this value gradually tends to be stepped, and the global maximum value reaches 83.16%. The value of index *B* of the two groups of traditional algorithms gradually showed a changing state after a slight decline, and the global maximum value reached 62.70% and 60.66%, respectively, which decreased by 20.46% and 22.50% compared with the maximum value of the experimental group.

To sum up, after the application of the intelligent integration algorithm of traditional ethnic sports culture resources based on big data designed in this study, index *B* shows a significantly increased numerical change state, which proves that the proposed algorithm can improve the real-time interconnection and interworking ability of traditional ethnic sports culture resources.

6. Conclusion

In this study, an intelligent integration algorithm of traditional ethnic sports culture resources based on big data is designed. After in-depth mining of traditional ethnic sports culture resources, weakly associated data is queried through data repair, and a resource integration model is constructed by using XML technology operation mode. The algorithm solves the problem of information island among the traditional national sports culture resources at all levels and effectively maintains the stability of the storage environment of traditional national sports culture resources while realizing the real-time interconnection of resources.

Data Availability

The data used to support the findings of this study are available from the corresponding author upon request.

Conflicts of Interest

The author declares that there are no conflicts of interest.

Acknowledgments

This study was supported by Research Achievements of the Key Discipline of Physical Education in Chaohu University (kj20zdxk01); Research results of the school-level scientific research Project of Chaohu University (XWY-201809).

References

[1] W. Cao and B. Shao, "Analysis of the hot topics of national traditional sports culture research in China based on the co-word analysis," *Journal of Xi'an Institute of Physical Education*, vol. 36, no. 1, pp. 70–81, 2019.

[2] W. Han and J. He, "The functional orientation change and realistic choice of national traditional sports culture," *Sports Culture Guide*, vol. 10, pp. 15–20, 2018.

[3] T. Miller, J. Mckay, G. A. Lawrence, and D. Rowe, "Globalization and sport: playing the world," *IEEE Security & Privacy*, vol. 97, no. 2, pp. 13-14, 2018.

[4] Z. Guan and W. Pang, "Research on virtual resource integration based on online migration," *Automation & Instrumentation*, vol. 3, pp. 59–62, 2018.

[5] X. Xiong, X. Peng, and X. Cao, "Research on oracle database heterogeneous resource integration method based on improved ORM," *Electronic Design Engineering*, vol. 28, no. 21, pp. 44–47, 2020.

[6] Z. Zhang and Y. Tang, "Design of all-cloud health big data integration system based on integrated learning," *Modern Electronics Technique*, vol. 43, no. 22, pp. 181–184, 2020.

[7] H. Yu, "Integration, development and application of informatization resources in continuing education under big data thinking," *Vocational and Technical Education*, vol. 40, no. 14, pp. 18–21, 2019.

[8] S. Hu, J. Mo, and J. Li, "An empirical research on building a performance evaluation index system for integrating public

Hindawi
Journal of Mathematics
Volume 2023, Article ID 9852708, 1 page
https://doi.org/10.1155/2023/9852708

Retraction

Retracted: Analysis and Risk Assessment of Corporate Financial Leverage Using Mobile Payment in the Era of Digital Technology in a Complex Environment

Journal of Mathematics

Received 15 August 2023; Accepted 15 August 2023; Published 16 August 2023

This article has been retracted by Hindawi following an investigation undertaken by the publisher [1]. This investigation has uncovered evidence of one or more of the following indicators of systematic manipulation of the publication process:

(1) Discrepancies in scope

(2) Discrepancies in the description of the research reported

(3) Discrepancies between the availability of data and the research described

(4) Inappropriate citations

(5) Incoherent, meaningless and/or irrelevant content included in the article

(6) Peer-review manipulation

The presence of these indicators undermines our confidence in the integrity of the article's content and we cannot, therefore, vouch for its reliability. Please note that this notice is intended solely to alert readers that the content of this article is unreliable. We have not investigated whether authors were aware of or involved in the systematic manipulation of the publication process.

Wiley and Hindawi regrets that the usual quality checks did not identify these issues before publication and have since put additional measures in place to safeguard research integrity.

We wish to credit our own Research Integrity and Research Publishing teams and anonymous and named external researchers and research integrity experts for contributing to this investigation.

The corresponding author, as the representative of all authors, has been given the opportunity to register their agreement or disagreement to this retraction. We have kept a record of any response received.

References

[1] W. Wei and B. Li, "Analysis and Risk Assessment of Corporate Financial Leverage Using Mobile Payment in the Era of Digital Technology in a Complex Environment," *Journal of Mathematics*, vol. 2022, Article ID 5228374, 9 pages, 2022.

Hindawi
Journal of Mathematics
Volume 2022, Article ID 5228374, 9 pages
https://doi.org/10.1155/2022/5228374

Research Article

Analysis and Risk Assessment of Corporate Financial Leverage Using Mobile Payment in the Era of Digital Technology in a Complex Environment

Wenjing Wei and Bingxiang Li

College of Economic and Management, Xi'an University of Technology, Xi'an, Shaanxi, China

Correspondence should be addressed to Wenjing Wei; wenjingwei@st.btbu.edu.cn

Received 7 December 2021; Accepted 28 December 2021; Published 27 January 2022

Academic Editor: Naeem Jan

The study aims to improve the enterprise's ability to respond to financial crises and find some countermeasures to prevent potential financial risks. The enterprise financial risk is assessed, and the automatic summary function of mobile payment platforms based on long short-term memory (LSTM) is performed to extract the structured data and unstructured texts from its annual report. On this basis, the early warning system model of financial risks is implemented and its accuracy is improved. The structured data and unstructured text in the company's annual report are extracted. The enterprise financial risk early warning system model is constructed. The accuracy of the enterprise financial risk early warning system has been improved. Firstly, we use the convolutional neural network (CNN) to establish a financial risk prediction system using financial data and test various indicators of the system. Secondly, the financial annual report of the listed company is obtained from the Internet. The required financial statements are obtained in two ways. The first is to set high special treatment (ST) sample weights and delete some non-ST samples. The second is to delete punctuation marks, interjections, numbers, and so on and process the collected text data. The financial risk prediction model is established using the financial text, and the LSTM + attention mechanism is used to optimize the model. Finally, combining structured financial data and unstructured financial text to establish a forecasting model, the model uses LSTM. Combined with a single-layer neural network or CNN model, the comparison experiment is carried out in two ways. Experiments show that the CNN or LSTM attention mechanism cannot significantly improve the performance of the system only using financial data or texts. Using the financial data and financial text using the LSTM + CNN model, the $F1$ value reached 85.29%. Financial data and other indicators in the text have also been greatly improved, and the overall performance is the best. In summary, LSTM using financial data and financial texts combined with CNN to establish a risk prediction system can help investors and companies themselves find possible financial crises in listed companies as soon as possible and help companies deal with their financial risks in a timely manner.

1. Introduction

With the rapid development of the global economy, many companies have gone public in various countries. In the expansion of production and operation of the enterprise, a series of problems have followed one after another. Among them, financial risk prediction is a problem that every company must face [1]. From the perspective of investors, the interests of investors are directly related to the financial status of the company. If investors can predict the financial risks of a company in time, they can stop losses in time. As early as 1930, most Western companies had already begun research on financial risk early warning systems. In today's information age, financial analysis methods continue to mature [2].

Scholars have also conducted a lot of research on financial risk prediction systems. In used to collect data through the company's ten-year annual financial report and researched and applied the z-model to study financial performance [3]. With the development of neural network models, various fields have begun to study using neural network models. Wu and Wu established a financial forecasting and early warning model using neural network [4]. Li and Quan showed that the judgment and analysis of

manufacturing financial risks can help promote the healthy development of the real economy. They used improved particle swarm optimization to establish a financial risk early warning model using neural networks [5]. Song and Wu used genetic algorithm, neural network, and principal component analysis methods to collect and process data in order to improve the ability of trade finance companies to deal with the risk of excessive financialization. The risk assessment model of excessive financialization of financial enterprises was constructed in [6]. Malakauskas and Laktutien used logistic regression, artificial neural networks, and random forest techniques to estimate a binomial classifier for financial distress prediction. They used the random forest algorithm with additional factors to achieve the highest prediction accuracy [7]. Matin et al. established a model using convolutional recurrent neural network (RNN) combined with unstructured text data, which provided a statistically significant improvement in the performance of financial distress prediction [8].

Financial issues are the key concern of every listed company. The establishment of a financial risk prediction system can effectively avoid the company's financial crisis and promote the company's sustainable development [9]. If the financial risks that the company will face in the future can be predicted, the company can greatly avoid losses and protect the company's interests. Because of the importance of financial risk control, companies and investors are extremely concerned. It is relatively simple to analyse one's own financial risks from the company's perspective [10]. From the perspective of investors, we extract structured and unstructured information from the annual reports of listed companies, establish financial risk prediction models using neural networks, and compare different models to conduct experiments. The proposed method greatly improves the forecasting effect and provides a reference for investors to discover the financial risks of listed companies in time and avoid losses. For the organization of the paper, we have arranged the paper such that Section 2 constructs the prediction model by using the neural network. In Section 3, the financial data and tests are used to analyse the experimental outcomes. In the end, the paper is concluded in Section 4 which presents the conclusion of the study.

2. Construction of Prediction Model Using Neural Network

2.1. Recurrent Neural Network (RNN). Using the RNN algorithm, a variant algorithm of the RNN is proposed, and research experiments on intrusion detection and knowledge extraction are carried out. When the traditional neural network processes some sequence data, especially when the sequence data have upper and lower connections, it is prone to problems, so the cyclic neural network came into being. The advantage of RNN is that it has a memory mechanism, which can fully analyse the relationship between these data when dealing with these serial data-related problems with upper and lower connections, so that the whole is more optimized [11]. Figure 1 shows the structure of RNN.

x represents the input at the current time h; ? represents the instant hidden node state; ? represents the output (RNN processing), as shown in equations (1) and (2):

$$s_t = f\left(U_{x_h} + W_{s_{h-1}} + b\right) \tag{1}$$

$$o_t = \text{softmax}\left(V_{s_h} + c\right) \tag{2}$$

Sigmoid is an activation function; U, W represent the weight matrix between layers; b, c represent the bias value. The advantage of RNN is that model parameters are shared at different moments and can handle long-term dependence problems; the disadvantage is that model parameter updates are unstable, there are gradients that explode or disappear, and there is only short-term memory.

2.2. Long Short-Term Memory (LSTM). Long short-term memory (LSTM) is an improvement of the RNN model. In terms of structure, a "door" structure has been added. In this way, the problems caused by the long distance can be solved, even if the data sequence length is different [12]. There are four neurons in the LSTM model: the cell state, output gate, input gate, and forget gate. The working method of the forget gate is as follows: the sigmoid function assigns the weighted calculated value of the input p_t at the current time t and the output $n_{t\text{-}1}$ at the time $t\text{-}1$ and uses the above to control the influence of the previous output sequence information on the input stream, as shown in the following equation:

$$g_t = \sigma\left(W_f \bullet [n_{t-1}, p_t]\right) + b_{g.} \tag{3}$$

The sigmoid function is used to weight the input p_t and the output n_{t_1} at the time t_1 to obtain the value s, as shown in equation (4). The new unit state candidate value $\widetilde{A}_t$ is generated by the non-linear tanh function, as shown in equation (5). The new state A_t of the unit only needs to add the two and then pass through the forget gate and the input gate, as shown in equation (6):

$$s_t = \sigma\left(W_i \bullet [n_{t-1}, p_t]\right) + b_s, \tag{4}$$

$$\widetilde{A}_t = \text{tann}\left(W_c \bullet [n_{t-1}, p_t]\right) + b_A, \tag{5}$$

$$A_t = g_t \bullet A_{t-1} + s_t \bullet \widetilde{A_t}. \tag{6}$$

The q_t value of the output gate needs to be weighted to calculate the input p_t and the output n_{t_1} at t_1 using the sigmoid function, as shown in equation (7). The output of the LSTM unit is calculated and controlled by the non-linear tanh function, and finally the output value n_t is obtained, as shown in equation (8). The advantage of LSTM is that it can solve the data problem due to the long distance.

$$q_t = \sigma\left(W_q \bullet [n_{t-1}, p_t]\right) + b_q, \tag{7}$$

$$n_t = q_t \bullet \text{tann}\left(A_t\right) \tag{8}$$

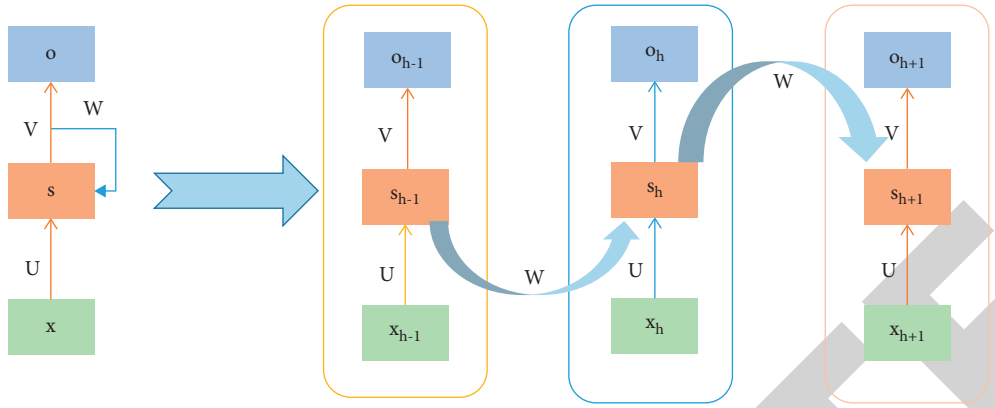

Figure 1: Structure diagram of RNN.

CNN is a feed-forward neural network, which has excellent performance for large-scale image processing [13]. Figure 2 shows the CNN model structure. The picture is first convolved by the convolutional layer, and then the pooling operation is performed. Repeat convolution and pooling and input the obtained feature information into the fully connected layer. Finally, it enters the output layer, and the size of the output layer is determined by the task of the CNN.

2.3. Attention Mechanism. The attention mechanism simulates the attention model of the human brain, which is essentially a resource allocation model. The working principle of the attention mechanism is to allocate the attention resources rationally. More resources should be allocated to the key parts and fewer resources should be given to the rest, reducing or eliminating the adverse effects caused by too many key parts [14]. Commonly used scoring methods: the soft attention scoring function in the hard attention scoring functions are used. Three kinds of weight value calculations are experimented [15]. The first is to input all attention models to score and sum, as shown in the following equation:

$$\alpha_t = \frac{\exp(\text{score}(h_t))}{\sum_{i=1}^{T} \exp(\text{score}(h_t))} \tag{9}$$

where α_t indicates the weight value of the t-th input, h_t indicates the t-th input, and *score* () indicates the score of the input. The second is to calculate and input h_t first. The calculated y_t is input into the model, as shown in the following equation:

$$y_t = \tan h(Wh_t) \tag{10}$$

$$\alpha_t = \frac{\exp(\text{score}(y_t))}{\sum_{i=1}^{T} \exp(\text{score}(y_t))} \tag{11}$$

where y_t is calculated from h_t, W is the output obtained by inputting h_t into a single-layer neural network, and α_t is the input weight value. The first two methods are employed after being figured out and multiplied by, as shown in the following equation:

$$S_t = \sum_{i=0}^{n} \alpha_t h_t \tag{12}$$

where S_t is the output of the h_t-th input model. The third method is obtained by adding the output of the input model of the second method, and its expression is shown in the following equation:

$$S_t = \sum_{i=0}^{n} (\alpha_t h_t + h_t) \tag{13}$$

2.4. Experimental Model Performance Indicators. The performance evaluation indicators for the two-class problem are model prediction accuracy, sensitivity, specificity, precision, and $F1$ [16]. Accuracy: m is the sample size, D is the training set, X_i is the sample, and Y_i is the mark. The prediction accuracy of model f is shown in the following equation:

$$\text{acc}(f: D) = \frac{1}{m} \sum_{i=1}^{m} I(f(x_i) = y_i). \tag{14}$$

Piecewise function: I, $I(1) = 1$, $I(0) = 0$, which indicates the proportion of correctly classified samples to the total number of samples. For a binary classification task, Figure 3 shows a framework diagram of the confusion matrix.

TP refers to true example, FP refers to false positive example, TN refers to true negative example, and FN refers to false negative example; $F1$-score represents the harmonic average of precision and recall [17]. It is one of the main indexes for model evaluation with specificity.

Recall rate:

$$R = \frac{\text{TP}}{\text{TP} + \text{FN}}. \tag{15}$$

Specificity:

$$K = \frac{\text{TN}}{\text{TN} + \text{FP}} \tag{16}$$

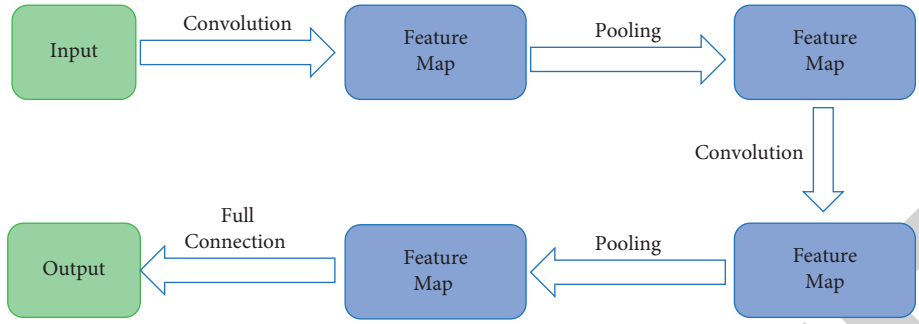

Figure 2: Schematic diagram of the CNN model.

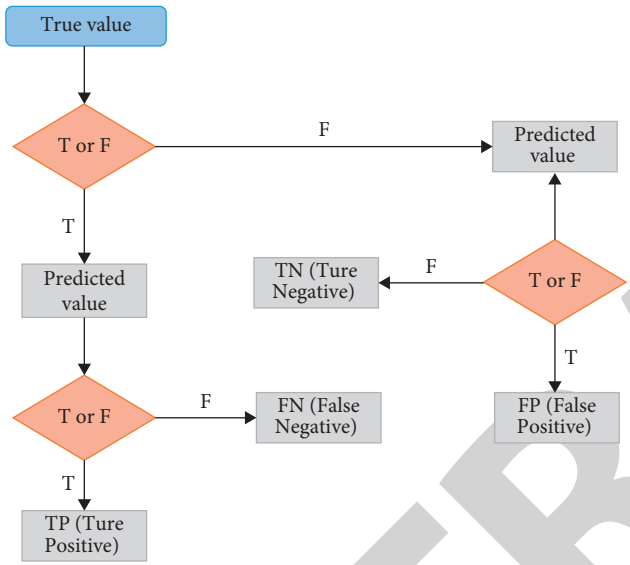

Figure 3: Framework diagram of confusion matrix.

Precision rate:

$$P = \frac{\mathrm{TP}}{\mathrm{TP} + \mathrm{FP}}. \tag{17}$$

$F1$-score:

$$F1 = \frac{2\mathrm{PR}}{P + R}. \tag{18}$$

2.5. Financial Risk Forecast Modelling Using Financial Data. The basic financial status of a company can be understood by analysing financial indicators [18]. In recent years, experts in the financial field generally use computer methods to analyse financial data, establish simple models, and analyse the extracted financial indicators. The CNN model is used to carry out financial risk prediction modelling using financial data, and the listed companies are used as the forecast target to predict the financial risks that exist in these companies. Listed companies are divided into ST companies and non-ST companies.

Index Acquisition. From the JoinQuant database (JQData), the cash flow statement, income statement, and balance sheet of each listed company from 2005 to 2021 are obtained. Meanwhile, 36 financial indicators that are not in the three tables are obtained. Among them, the three basic tables are called financial indicators, and the other 36 are collectively called non-financial indicators.

Data Cleaning. It is the process of re-examining and verifying data with the purpose of removing duplicate information, correcting existing errors, and providing data consistency.

Selecting Data That Meet the Indicators. The missing value of a financial index that reaches more than 30% is cleared. Compensation for missing data: when collecting data by hand, the financial indicators issued by various companies are different, resulting in serious data missing in most companies' financial indicators. According to the distribution of financial index values, replanting is carried out. The specific calculation is shown in the following equation:

$$M = A + R \times A, R \in \{-0.3, 0.3\} \tag{19}$$

where M is a missing value; A is the mean value; and R is a random number. Filtering data: when processing data, set the sample lack threshold, and the threshold is set to 50%; when the missing value exceeds, delete the sample, delete the severely missing data, and ensure the availability of the data [19].

In the end, there are 17,107 data that can be used in the financial measurement standard indicators of each company. In order to ensure the integrity of the financial measurement standard indicators during the experiment, the existing data must be compared with the experiment first. Select all existing companies' public financial measurement standards for experimentation, and there are no missing values for 47 public financial measurement standards of all companies. It is also necessary to continue the experiment to compare and analyse whether the data supplement has an impact on the experimental results. The financial measurement indexes are sorted into two collections, and there are 146 indexes in collection 1 and 47 in collection 2. Using the same model, Figure 4 shows the statistical results of the indicators.

2.6. Construction of Forecasting Model Using Financial Data. Financial risk prediction is a two-class problem. The CNN model performs well on the classification problem [20], so

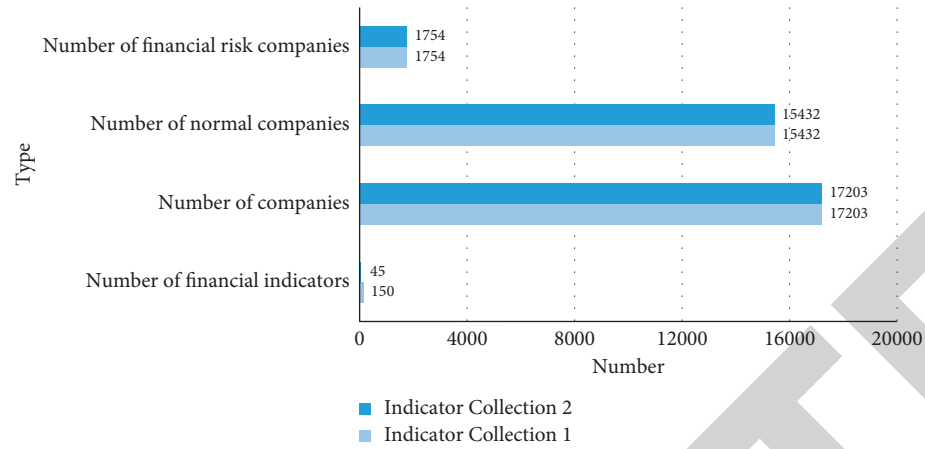

Figure 4: Indicator statistics chart (indicator collection 1 has a complementary value, and indicator collection 2 has no complementary value).

the CNN model is selected to build the model. Figure 5 shows a flowchart of index processing.

After obtaining the financial metrics, the data are cleaned. Financial metrics are converted. After the characteristic representation is converted, a financial vector is established with each financial measurement standard indicator corresponding to each example, and the financial measurement standard indicators are unified and normalized for all the examples, as shown in the following equation:

$$x' = \frac{x - \min(x)}{\max(x) - \max(x)}, \tag{20}$$

where max (x) indicates the maximum value of financial measurement standard indicators in all examples; min (x) indicates the minimum value of financial measurement standard indicators in all examples; x' represents the normalized financial measurement standard indicator value of the example; and x indicates the value of the financial measurement standard before the example is normalized. Meanwhile, due to the good classification effect of the CNN model, the CNN model is used to classify the financial measurement standard indicators.

2.7. Financial Text Processing. First, text data are cleaned, including 2791 samples from 379 ST and 18917 from 2781 non-ST enterprises. Then, two methods are used during the experiment, and some measures are used to balance the dataset distribution. Two ways: set the weight of the loss function category. The weight of ST samples is set to be higher than that of non-ST samples. Some non-ST samples have been deleted, making the ratio of the two samples closer to reasonable. Measures: delete interjections, punctuation marks, tabs, dates, amounts, etc.

After the financial text is obtained, the presentation of the financial text needs to be considered. The financial text needs to be converted into a vector. Then, classify and sort the vectors. It can be divided into word vectors and document vectors. Word vector refers to a vector in which words or phrases from the vocabulary are mapped to real numbers. Text vector is a whole paragraph of text. Word

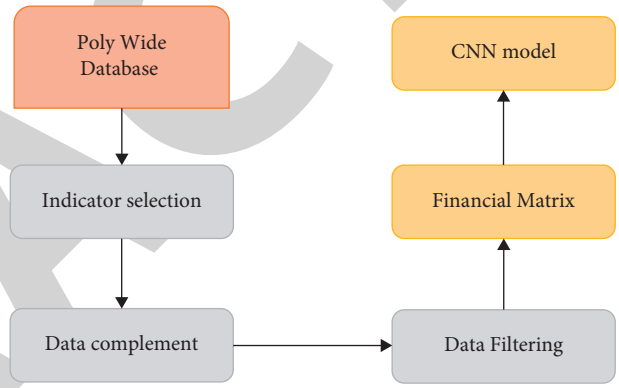

Figure 5: Flowchart of indicator processing.

vectors are all words, so word vectors can form document vectors. In general, the training of the word vector is carried out first, and then the word vector is expressed as a text vector by means of summation [21].

The word2vec model using skip-gram is used for text representation. The advantage of the skip-gram model is that it can predict the relationship between a word and surrounding words.

$$\max \frac{1}{n} \sum_{t=1}^{n} \sum_{j=-c, j \neq 0}^{b} \log p\left(w_{t+j} | w_t\right) \tag{21}$$

where b represents the number of words around the word that needs to be considered now. Here, b takes 5. Log p is calculated using negative sampling, and the subsampling of words is proportional to their inverse frequency. In word2vec, the relationship between words also has an impact. For example, when the semantics are similar, these words all have a high cosine similarity, and vector calculations can also be performed on the words.

2.8. Construction of Forecast Model Using Financial Text. The financial risk prediction model using financial texts uses LSTM as the main body and cooperates with the attention mechanism. Figure 6 shows a basic process diagram.

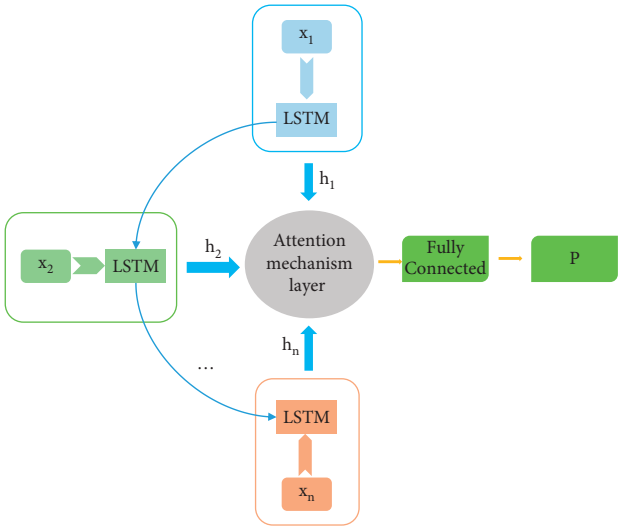

Figure 6: Flowchart using financial text processing.

T_t characterizes the word at the t-th position in the document, T_{wt} embodies the word vector converted from the word at the t-th position, and h_t represents the output of the unit LSTM at the t-th position. The calculation equation selected in the experiment is as follows:

$$y_t = \tanh(Wh_t) \tag{22}$$

$$\alpha_t = \frac{\exp(\text{score}(y_t))}{\sum_{i=1}^{T} \exp(\text{score}(y_t))} \tag{23}$$

$$S_t = \sum_{i=0}^{n} \alpha_t h_t. \tag{24}$$

Score function represents a single-hidden-layer neuron calculation. W stands for the weight of the input h_t. The attention weight α_t of the output h_t of each LSTM unit is obtained by normalizing the scalar by the softmax function. T indicates the step length between step 1 and step t. S_t signifies the final output of the experiment. The experiment uses the attention model mechanism. The attention model can effectively focus the attention on the text and describe not much, but the more important parts of the text can be better described.

2.9. Construction of Forecasting Model Combining Financial Text and Financial Data. Figure 7 shows a framework diagram of the financial data and financial text forecasting model. There are two parts of model input: financial data and financial text. The processing of financial data and financial text in the model is to combine the two, but instead of inputting individual financial data and financial text into the model separately, they are input at the same time.

The right side of Figure 7 shows the processing methods of the two financial measurement standard indicators. The first method: firstly, the financial data $C1$ are processed by the feature engineering into a financial vector $C2$. Then, input a single-layer neural network for processing to obtain a word

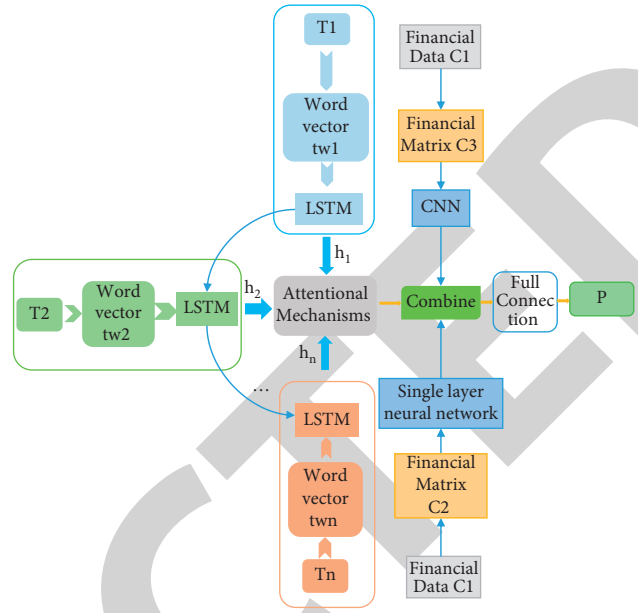

Figure 7: Schematic diagram of financial data combined with financial text model.

vector with the same dimension as the output of the attention model. Finally, it is combined with unstructured information to enter the fully connected layer. The second method: firstly, perform characteristic engineering processing on the financial data $C1$ to obtain a financial matrix $C3$. Then, input the CNN model to summarize and extract the key information. Finally, combine the processed information of the financial text and enter the fully connected layer.

3. Analysis of Experimental Results Using Financial Data and Financial Text

3.1. Experimental Results and Analysis of CNN Model Using Financial Data. The range of CNN model parameters is as follows: convolution kernel (size) $D \in \{3, 4, 5, 6, 7, 8, 9\}$, convolution kernel (number) $H \in \{64, 100, 128, 256, 300, 500, 1000\}$, pooling layer (size) $C \in \{3, 4, 5\}$, CNN (number of layers) $K \in \{2, 3, 4, 5, 6\}$, and fully connected layers (number of neurons) $n \in \{64, 128, 256, 300, 512, 1024\}$. After many experiments, the final parameters are determined: the sizes of the convolution kernel are 4∗4, 5∗5, and 6∗6, respectively, the size of the pooling layer is 4∗4, the number of convolution kernels is 300, and the number of the layers is 4. The numbers of neurons in the fully connected layer are 128 and 64, respectively, and its weight of loss function is 0.6 and 0.4, respectively. Figure 8 shows the experimental results.

The experimental results in Figure 8 show that the accuracy and recall rate of the CNN model are high, but the specificity and $F1$ value are low. In the predictive model, K and $F1$ are more important, so they need to be improved. The CNN model is more likely to overfit the categories with more data when the data are unbalanced, but there is no more in-depth information on the financial indicators. The CNN model's ability to extract information is limited, so in deeper information extraction, it does not bring more benefits.

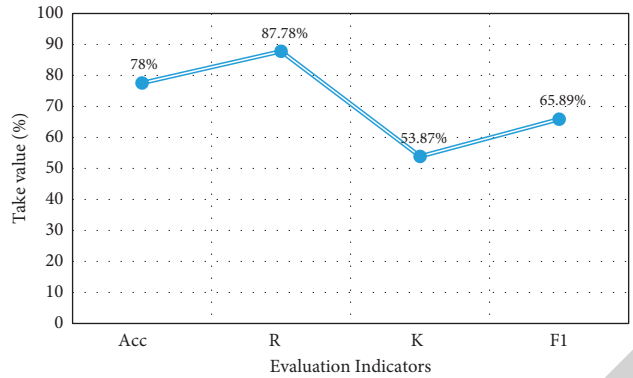

Figure 8: CNN model experimental results.

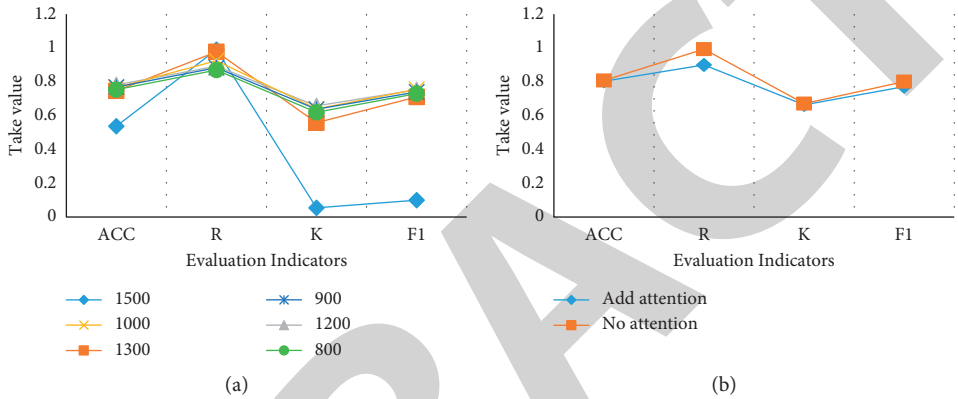

Figure 9: Some parameters after the experiments ((a) 100-word vector dimensions without the attention mechanism; (b) 200-word vector dimensions with the word length of 1200).

3.2. Analysis of Model Experiment Results Using Financial Text. Figure 9 shows the experimental results of selected experimental parameters.

Figure 9 shows that the attention model has a greater effect on improving the *F*1 value. Different word vector dimensions and word lengths have an impact on the results of the experiment. When the word length is 1300 and 1500, the *R* value increases, but the *K* value decreases with a larger amplitude, so the word length 1200 is selected for the attention model experiment. First, make sure the word length is 1200. Then, change the word vector dimension from 100 to 200, and the *R* value and the *K* value are slightly improved, indicating that the improvement of the word vector dimension is helpful. Figure 10 shows a comparison diagram of the experimental results of dimensional changes and attention mechanism changes.

The dotted line in Figure 10(a) indicates that the used word vector has a dimension of 200, and the solid line indicates that the used word vector has a dimension of 100. When the word length is 1200 and the word vector dimension is 200, the experimental results of the attention model and the non-attention model are added in Figure 10(b). When the word length is 1200 and the word vector dimension is 200, after adding the attention model, the accuracy rate, *R*, *K*, and *F*1 are all improved, indicating that the attention model is very helpful for improving the index. Using the above experiments, select the parameters that can produce the best results for the experiment. Figure 11 shows the experimental results of the model.

In Figure 11, the risk prediction model using financial data is not as effective as the model using financial text. There are two reasons for the conclusion: there is interference between individual financial data, and the proportion of non-ST text is too large. Although the overall effect of the financial text-based model is good, *K* is only 66.71%, and the *F*1 value is not high. Continue to conduct model experiments using the combination of financial data and text.

3.3. Model Experiment Results Combining Financial Text and Financial Data. Figure 12 shows the optimal results of the two methods.

Figure 12 shows that adding financial text to the forecasting system, combined with the financial matrix, greatly improves the performance of the CNN model. In terms of accuracy, *R*, *K*, and *F*1 values, CNN model experimental results are higher than those of single-hidden-layer experimental results. There are two reasons for the conclusion: the CNN model is more suitable for the combination of financial matrix and text, and the combination of financial vector and financial text will cause noise interference to part of the data of the vector. The CNN model has better information

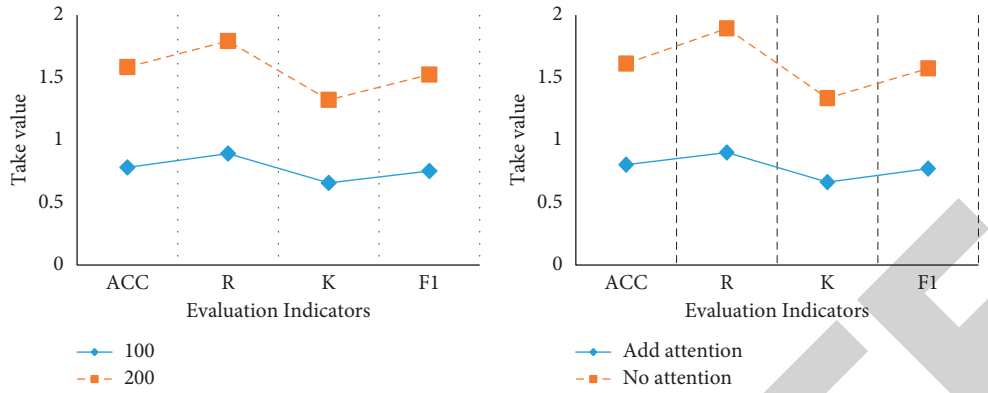

Figure 10: Comparison results ((a) comparison results between 100 and 200 dimensions; (b) comparison between the results with or without the attention mechanism).

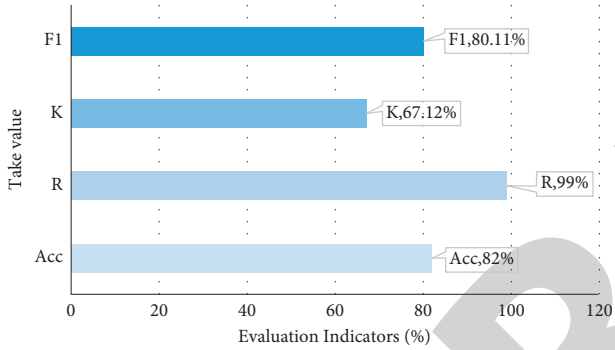

Figure 11: Model prediction results.

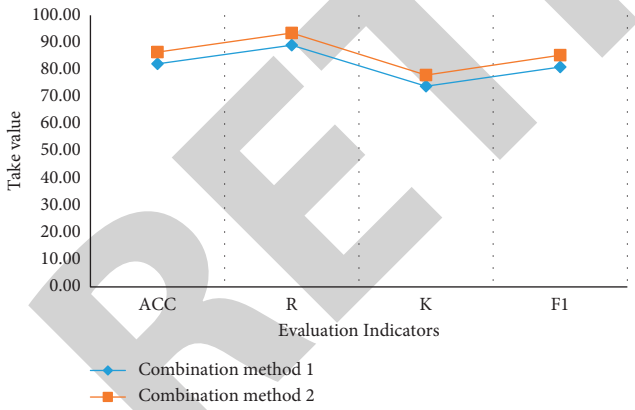

Figure 12: The optimal result of the experiment.

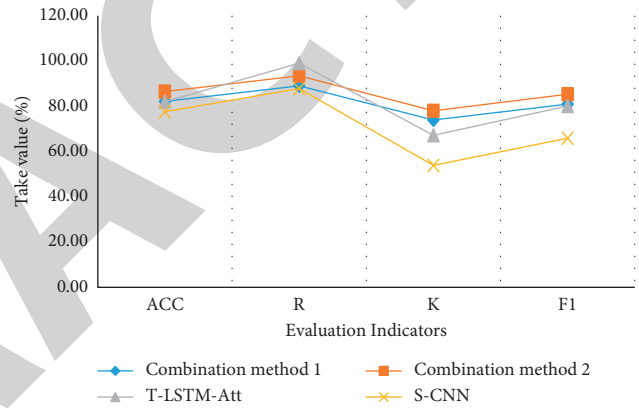

Figure 13: Comparison of experimental results of each model.

extraction effect. Figure 13 shows the final comparison chart of the experimental results of all models.

Figure 13 shows that the performance of the financial matrix combined with the financial text using the CNN model is much higher than that of the financial matrix using the CNN model. Although R is not as good as a model using financial text using LSTM and attention mechanism, it is better in terms of accuracy, K, and $F1$. The results show that the more times the financial text data are trained by the CNN model, the better the performance of the system is, and more important information the system can select. The prediction model based on the combination of financial texts and data has better performance than the model using only financial data or financial texts.

4. Conclusion

On a mobile payment platform, the use of automatic summarization technology on an LSTM network established a financial risk prediction system. In this paper, three methods were used: (i) CNN using financial data to establish a system; (ii) LSTM + attention model, which uses financial documents to establish a system; (iii) a combination of two methods, combining financial data with financial documents. The last method uses CNN + LSTM and a single-hidden-layer neural network + LSTM to establish a system. The system that combines financial documents and financial data has a different improvement over the forecasting system that only uses unstructured text and structured text. Compared with financial data to establish a model, the addition of financial documents increased $F1$ by an average of 14%, which greatly improved the accuracy of the financial risk prediction system. However, only part of the information in the financial report is extracted here, and not all

Hindawi
Journal of Mathematics
Volume 2024, Article ID 9782652, 1 page
https://doi.org/10.1155/2024/9782652

Retraction

Retracted: EM Algorithm for Estimating the Parameters of Quasi-Lindley Model with Application

Journal of Mathematics

Received 23 January 2024; Accepted 23 January 2024; Published 24 January 2024

This article has been retracted by Hindawi following an investigation undertaken by the publisher [1]. This investigation has uncovered evidence of one or more of the following indicators of systematic manipulation of the publication process:

(1) Discrepancies in scope

(2) Discrepancies in the description of the research reported

(3) Discrepancies between the availability of data and the research described

(4) Inappropriate citations

(5) Incoherent, meaningless and/or irrelevant content included in the article

(6) Manipulated or compromised peer review

The presence of these indicators undermines our confidence in the integrity of the article's content and we cannot, therefore, vouch for its reliability. Please note that this notice is intended solely to alert readers that the content of this article is unreliable. We have not investigated whether authors were aware of or involved in the systematic manipulation of the publication process.

Wiley and Hindawi regrets that the usual quality checks did not identify these issues before publication and have since put additional measures in place to safeguard research integrity.

We wish to credit our own Research Integrity and Research Publishing teams and anonymous and named external researchers and research integrity experts for contributing to this investigation.

The corresponding author, as the representative of all authors, has been given the opportunity to register their agreement or disagreement to this retraction. We have kept a record of any response received.

References

[1] M. Kayid and N. S. Al-Maflehi, "EM Algorithm for Estimating the Parameters of Quasi-Lindley Model with Application," *Journal of Mathematics*, vol. 2022, Article ID 8467291, 9 pages, 2022.

Hindawi
Journal of Mathematics
Volume 2022, Article ID 8467291, 9 pages
https://doi.org/10.1155/2022/8467291

Research Article

EM Algorithm for Estimating the Parameters of Quasi-Lindley Model with Application

M. Kayid [1] **and Nassr S. Al-Maflehi** [2]

[1]*Department of Statistics and Operations Research, College of Science, King Saud University, Riyadh 11451, Saudi Arabia*
[2]*Department of Periodontics and Community Dentistry, College of Dentistry, King Saud University, Riyadh, Saudi Arabia*

Correspondence should be addressed to M. Kayid; drkayid@ksu.edu.sa

Received 10 November 2021; Revised 12 December 2021; Accepted 21 December 2021; Published 25 January 2022

Academic Editor: Lazim Abdullah

The quasi-Lindley distribution is a flexible model useful in reliability analysis, management science, and engineering analysis. In this paper, an expectation-maximization (EM) algorithm was applied to estimate the parameters of this model for uncensored and right-censored data. Simulation studies show that the estimates of EM perform better than maximum likelihood estimates (MLEs) for both uncensored and censored data. In an illustrative example, the waiting times of a bank's customers are analyzed and the estimator of the EM algorithm is compared with the MLE. The analysis of the data can be useful for the management of the bank.

1. Introduction

The quasi-Lindley distribution proposed by Shanker and Mishra [1] is a generalization of the Lindley distribution introduced by Lindley [2] and is quite useful in reliability theory and survival analysis. The probability density function (pdf) of the quasi-Lindley distribution is given by

$$f(x) = \frac{\lambda}{\alpha+1}(\alpha+\lambda x)e^{-\lambda x}, x>0, \alpha>0, \lambda>0, \quad (1)$$

and is a mixture of gamma distributions $G(1,\lambda)$ and $G(2,\lambda)$ with weights $\alpha/(\alpha+1)$ and $1/(\alpha+1)$, respectively. The hazard rate function of the quasi-Lindley model is

$$h(x) = \frac{\lambda(\alpha+\lambda x)}{1+\alpha+\lambda x}, x>0, \alpha>0, \lambda>0, \quad (2)$$

which is an increasing function.

An important feature of the quasi-Lindley model is that, unlike the Lindley model and its many other generalizations, it is scale invariant. Nevertheless, it is not complicated but sufficiently flexible. Shanker and Mishra [1] studied some of its basic properties and dynamic reliability measures. They also discussed the maximum likelihood estimator (MLE) for its parameters. The MLE is theoretically consistent and efficient, but in practice, it strongly depends on the initial values and the computational approach, which can be achieved by directly maximizing the log-likelihood function or by solving the likelihood equations. Moreover, the simulation results for the MLE of the quasi-Lindley distribution (especially for α) show extremely large values for the mean square error (MSE) (see Tables 1 and 2). This motivates us to investigate the EM algorithm for estimating the parameters.

In statistics, when the data are collected from a mixture or competing risks model, the EM algorithm is an effective tool for estimating parameters of latent variable models. In their foundational work, Dempster et al. [3] introduced the EM algorithm. Many authors after them have used the idea of EM in their work to provide better estimation of the parameters of the models they are considering. For example, Elmahdy and Aboutahoun [4] and Almhana et al. [5] used the EM algorithm to estimate the parameters for a mixture of Weibull models and a mixture of gamma models, respectively. In addition, Bee et al. [6] applied the EM algorithm to estimate the parameters of Pareto mixture models, Ghosh et al. [7] used the EM algorithm for a mixture of Weibull and Pareto (IV) models, and Balakrishnan and Pal [8] used the EM-based likelihood inference in their work. For detailed discussions of the EM algorithm, we refer the readers to McLachlan and Krishnan [9]

Table 1: Simulation results for MLE and EM estimators of the *QL* distribution for uncensored data (in every cell, the first and second lines are related to α and λ, respectively).

Method	n	100				200			
	α, λ	B	MSE	CP	CILM	B	MSE	CP	CILM
MLE	0.4, 0.02	0.6081	131.03	0.8918	29.48	0.2018	113.33	0.9092	3.20
		0.00005	0.000005	0.954	0.0099	0.00008	0.000002	0.9484	0.0065
	0.5, 0.5	2.9955	2514.5	0.8804	57.31	0.1250	26.72	0.91	4.849
		0.0026	0.0037	0.9472	0.2382	0.00125	0.00181	0.9554	0.1649
	0.7, 0.1	7.9912	5877.70	0.8742	215.57	0.6875	251.728	0.9018	19.197
		0.00041	0.00019	0.9454	0.0540	0.00045	0.00009	0.9574	0.0372
EM	0.4, 0.02	−0.00007	0.01200	0.9868	1.1915	0.00304	0.00599	0.9994	0.8047
		0.00017	0.000002	0.979	0.00917	0.00011	0.000001	0.9936	0.0062
	0.5, 0.5	0.00394	0.01673	0.9872	1.4474	0.00187	0.00863	0.9992	0.9888
		0.00357	0.00164	0.9802	0.2420	0.00155	0.00080	0.9952	0.1664
	0.7, 0.1	0.00767	0.02847	0.9762	2.0985	0.00021	0.01351	0.9976	1.4379
		0.00083	0.00006	0.974	0.0548	0.00051	0.00003	0.9944	0.0378

Table 2: Simulation results for MLE and EM estimators of the *QL* distribution when the censorship rate is $p = 0.2$ (in every cell, the first and second lines are related to α and λ, respectively).

Method	n	100				200			
	α, λ	B	MSE	CP	CILM	B	MSE	CP	CILM
MLE	0.4, 0.02	3.09912	996.321	0.8758	171.84	0.28132	58.7714	0.92	9.9925
		−0.00013	0.000008	0.9452	0.0107	−0.00009	0.000004	0.9588	0.0075
	0.5, 0.5	6.4487	2928.10	0.867	439.53	0.6962	126.6613	0.9054	61.3642
		−0.00363	0.0063	0.939	0.3021	−0.00235	0.00289	0.9604	0.2062
	0.7, 0.1	15.625	6471.68	0.853	958.73	2.6733	556.14	0.8947	215.307
		−0.00139	0.00031	0.9182	0.0699	−0.00099	0.00016	0.9512	0.0498
EM	0.4, 0.02	0.00538	0.01108	0.9812	1.3233	0.00231	0.00557	0.9976	0.8762
		0.00008	0.000003	0.978	0.01113	0.00009	0.0000015	0.994	0.0075
	0.5, 0.5	0.00293	0.01506	0.9698	1.6263	0.00202	0.00752	0.9966	1.1044
		0.00327	0.00193	0.967	0.2993	0.00101	0.00096	0.9944	0.2047
	0.7, 0.1	0.00785	0.02433	0.9452	2.3950	0.00380	0.01193	0.9872	1.6584
		0.00029	0.00007	0.9434	0.06918	0.00038	0.00004	0.9856	0.0482

and Mengersen et al. [10]. In addition, Wu [11] proved some results related to the convergence of the EM algorithm.

In this paper, a specific EM algorithm is developed to obtain a more reliable estimate for the parameters of the quasi-Lindley distribution for uncensored and right-censored data. The paper is organized as follows. Section 2 discusses the EM algorithm for the quasi-Lindley distribution when the data were uncensored. In Section 3, the EM algorithm is extended to right-censored data. Section 4 examines the behavior of the MLE and EM estimates and compares them through simulations. In Section 5, both MLE and EM estimates are computed for a real dataset. Finally, Section 6 draws the conclusions for the paper.

2. Uncensored Data

Assume that $x_1, x_2, \ldots, x_n$ be an independent and identically distributed (iid) random sample from quasi-Lindley distribution with parameters (α, λ), briefly $QL(\alpha, \lambda)$. The log-likelihood function of the parameters is

$$l(\alpha, \lambda; \mathbf{x}) = n \ln \lambda - n \ln(\alpha + 1) + \sum_{i=1}^{n} \ln(\alpha + \lambda x_i) - \lambda \sum_{i=1}^{n} x_i. \tag{3}$$

The likelihood equations can be obtained by partial differentiation of this log-likelihood function with respect to α and λ as follows:

$$\begin{aligned} \frac{\partial}{\partial \alpha} l(\alpha, \lambda; \mathbf{x}) &= \sum_{i=1}^{n} \frac{1}{\alpha + \lambda x_i} - \frac{n}{\alpha + 1} = 0, \\ \frac{\partial}{\partial \lambda} l(\alpha, \lambda; \mathbf{x}) &= \frac{n}{\lambda} + \sum_{i=1}^{n} \frac{x_i}{\alpha + \lambda x_i} - \sum_{i=1}^{n} x_i = 0. \end{aligned} \tag{4}$$

The MLE can be calculated by directly maximizing the log-likelihood function (3) directly or by solving the likelihood equations. Let $l = \ln f(X)$, and the Fisher information matrix of the quasi-Lindley distribution is

$$K = \begin{bmatrix} E\left(-\frac{\partial^2 l}{\partial \alpha^2}\right) & E\left(-\frac{\partial^2 l}{\partial \alpha \partial \lambda}\right) \\ E\left(-\frac{\partial^2 l}{\partial \lambda \partial \alpha}\right) & E\left(-\frac{\partial^2 l}{\partial \lambda^2}\right) \end{bmatrix}. \tag{5}$$

When we have an iid random sample X_i, $i = 1, 2, \ldots, n$ from $QL(\alpha_0, \lambda_0)$, the MLE, $(\widehat{\alpha}, \widehat{\lambda})$, weakly converges to bivariate normal $N((\alpha_0, \lambda_0), n^{-1}K^{-1})$ where K^{-1} is the inverse of the information matrix.

2.1. The EM Algorithm for the Complete Data. Since $QL(\alpha, \lambda)$ is a mixture of two gamma distributions $G(1, \lambda)$ and $G(2, \lambda)$, the EM algorithm can be used to estimate its parameters. Let X_i, $i = 1, 2, \ldots, n$, be an iid random sample of $QL(\alpha, \lambda)$. In the EM approach, for each X_i, we consider one latent random variable Z_i which determines that X_i belongs to $G(1, \lambda)$ or $G(2, \lambda)$. In other words, $X_i | Z_i = j \sim IG(j, \theta)$, $j = 1, 2$, $P(Z_i = 1) = \alpha/(\alpha + 1)$, and $P(Z_i = 2) = 1/(\alpha + 1)$. For a brief representation, take $\theta = (\alpha, \lambda)$. The likelihood function can be written in the following form.

$$L(\theta; \mathbf{x}, \mathbf{z}) = \prod_{i=1}^{n} \prod_{j=1}^{2} \left(g_j(x_i; \theta) P(Z_i = j)\right)^{I(z_i = j)}, \tag{6}$$

where the indicator $I(z_i = j)$ equals 1 when $z_i = j$ and otherwise equals to 0. Also,

$$g_j(x_i; \lambda) = \lambda^j x_i^{j-1} \exp(-\lambda x_i), \tag{7}$$

is the pdf of the underlying gamma distribution and

$$P(Z_i = j) = \frac{1}{\alpha + 1} \alpha^{I(j=1)}. \tag{8}$$

Then, the log-likelihood function is

$$l(\theta; \mathbf{x}, \mathbf{z}) = \ln L(\theta; \mathbf{x}, \mathbf{z}) = \sum_{i=1}^{n} \sum_{j=1}^{2} I(z_i = j) \ln\left(\lambda^j x_i^{j-1} \exp(-\lambda x_i) \frac{1}{\alpha + 1} \alpha^{I(j=1)}\right). \tag{9}$$

The EM algorithm goes through two steps: the expectation step (E) and the maximization step (M). In each iteration, the E step constructs the expected value of the log-likelihood with respect to the current estimate of the conditional latent variable. In the M step, the constructed in the E step is maximized to provide the estimates. The iterative process can be terminated when the improvement in the expectation function falls below a predetermined small value.

2.1.1. The E Step. Given the estimate of the parameters at iteration t, θ_t, the conditional distribution of Z_i is obtained by Bayes theorem:

$$\begin{aligned} p_{ij,t} = P(Z_i = j | X_i = x_i, \theta_t) &= \frac{f(X_i = x_i | Z_i = j, \theta_t) P(Z_i = j | \theta_t)}{f(X_i = x_i | \theta_t)} \\ &= \frac{\lambda_t^j x_i^{j-1} e^{-\lambda_t x_i} (\alpha_t + 1)^{-1} \alpha_t^{I(j=1)}}{\sum_{j=1}^{2} \lambda_t^j x_i^{j-1} e^{-\lambda_t x_i} (\alpha_t + 1)^{-1} \alpha_t^{I(j=1)}}, i = 1, 2, \ldots, n, j = 1, 2, \end{aligned} \tag{10}$$

and after simplification, we have

$$p_{i1,t} = \frac{\alpha_t}{\alpha_t + \lambda_t x_i}, i = 1, 2, \ldots, n, \tag{11}$$

and $p_{i2,t} = 1 - p_{i1,t}$. These probabilities are known as membership probabilities at iteration t and are used to construct the expectation function $Q(\theta | \theta_t)$ as follows:

$$
\begin{aligned}
Q(\theta|\theta_t) &= E_{Z|X,\theta_t}(l(\theta;\mathbf{x},\mathbf{Z})) \\
&= \sum_{i=1}^{n} E_{Z_i|X_i,\beta_t} \sum_{j=1}^{2} I(z_i = j) \ln\left(\lambda^j x_i^{j-1} \exp(-\lambda x_i) \frac{1}{\alpha+1} \alpha^{I(j=1)}\right) \\
&= \sum_{i=1}^{n} P(Z_i = 1|X_i = x_i, \theta_t) \ln\left(\lambda e^{-\lambda x_i} \frac{\alpha}{\alpha+1}\right) \\
&\quad + P(Z_i = 2|X_i = x_i, \theta_t) \ln\left(\lambda^2 x_i e^{-\lambda x_i} \frac{1}{\alpha+1}\right) \\
&= \sum_{i=1}^{n} \left(\left(1 + p_{i2,t}\right) \ln\lambda - \lambda x_i + p_{i2,t} \ln x_i\right) + \sum_{i=1}^{n} \left(p_{i1,t} \ln\alpha - \ln(\alpha+1)\right).
\end{aligned} \tag{12}
$$

The last expressions of (12) show that expectation can be expressed as the sum of two statements, one of which depends only on λ and the other only on α, i.e.,

$$
Q(\theta|\theta_t) = Q_1(\lambda|\theta_t) + Q_2(\alpha|\theta_t), \tag{13}
$$

where

$$
\begin{aligned}
Q_1(\lambda|\theta_t) &= \sum_{i=1}^{n} \left(\left(1 + p_{i2,t}\right) \ln\lambda - \lambda x_i + p_{i2,t} \ln x_i\right), \\
Q_2(\alpha|\theta_t) &= \sum_{i=1}^{n} \left(p_{i1,t} \ln\alpha - \ln(\alpha+1)\right).
\end{aligned} \tag{14}
$$

2.1.2. The M Step. To estimate the parameters at $t+1$ iteration, we maximize the $Q(\theta|\theta_t)$ in terms of θ. So, we have

$$
\theta_{t+1} = \underset{\theta}{\operatorname{argmax}}\, Q(\theta|\theta_t), \tag{15}
$$

which, by (13), reduces to the following separate maximization problems.

$$
\begin{aligned}
\lambda_{t+1} &= \underset{\lambda}{\operatorname{argmax}}\, Q_1(\lambda|\theta_t), \\
\alpha_{t+1} &= \underset{\alpha}{\operatorname{argmax}}\, Q_2(\alpha|\theta_t),
\end{aligned} \tag{16}
$$

where $Q_1(\lambda|\theta_t)$ and $Q_2(\alpha|\theta_t)$ are determined by (14) and (15), respectively. By solving the equation $\partial/\partial\lambda Q_1(\lambda|\theta_t) = 0$, the estimation of λ at $t+1$ iteration is obtained.

$$
\lambda_{t+1} = \frac{n + \sum_{i=1}^{n} p_{i2,t}}{\sum_{i=1}^{n} X_i}. \tag{17}
$$

On the other hand, solving the equation $\partial/\partial\alpha Q_2(\alpha|\theta_t) = 0$, we have

$$
\alpha_{t+1} = \frac{\sum_{i=1}^{n} p_{i1,t}}{\sum_{i=1}^{n} p_{i2,t}}. \tag{18}
$$

The sequence θ_t will converge to θ, and the iterative process can be concluded when for some predefined small $\epsilon > 0$, $Q(\theta_{t+1}|\theta_{t+1}) < Q(\theta_t|\theta_t) + \epsilon$. This means that further iterations do not improve the objective function considerably. For detailed information about convergence of the EM algorithm, see Wu [11].

3. Right-Censored Data

Consider an iid random sample X_i, $i = 1, 2, \ldots, n$, from $QL(\alpha, \lambda)$ which is exposed to right censorship. We say that X_i is censored from the right by a censoring random variable C_i, if $X_i > C_i$, and in this case, the only information about event time is that it is greater than censoring time C_i. The observations consist of $T_i = \min(X_i, C_i)$ and d_i, where $d_i = 1$, when the event has not been censored, $X_i \le C_i$, and $d_i = 0$, when the event has been censored, $X_i > C_i$. Given a right-censored sample (t_i, d_i), $i = 1, 2, \ldots, n$, the log-likelihood function is

$$
l(\alpha, \lambda; \mathbf{t}, \mathbf{d}) = \sum_{i=1}^{n} d_i \ln f(t_i) + \sum_{i=1}^{n} (1 - d_i) \ln R(t_i), \tag{19}
$$

where f and R show the density and the reliability functions of the quasi-Lindley distribution, respectively. The log-likelihood function simplifies to

$$
l(\theta; \mathbf{t}, \mathbf{d}) = n_1 \ln\left(\frac{\lambda}{\alpha+1}\right) + \sum_{i=1}^{n} d_i \ln(\alpha + \lambda t_i) + \sum_{i=1}^{n} (1 - d_i) \ln\left(1 + \frac{\lambda t_i}{\alpha+1}\right) - \sum_{i=1}^{n} \lambda t_i, \tag{20}
$$

where $n_1 = \sum_{i=1}^{n} d_i$ and $\theta = (\alpha, \lambda)$.

3.1. The EM Algorithm for Right-Censored Data. To implement the EM algorithm, we should include the latent variable Z_i, $i = 1, 2, \ldots, n$, defined in the previous section. Then, the likelihood function for the censored data is

$$L(\theta; \mathbf{t}, \mathbf{d}, \mathbf{z}) = \prod_{i=1}^{n} \left(\prod_{j=1}^{2} \left(g_j(t_i; \theta) P(Z_i = j) \right)^{I(z_i = j)} \right)^{d_i} \prod_{i=1}^{n} \left(\prod_{j=1}^{2} \left(\overline{G}_j(t_i; \theta) P(Z_i = j) \right)^{I(z_i = j)} \right)^{1 - d_i}, \tag{21}$$

where g_j shows the gamma pdf considered in the previous section and $\overline{G}_j$ is its corresponding reliability function. By taking logarithm from (21), the log-likelihood function has the following form:

$$\begin{aligned} l(\theta; \mathbf{t}, \mathbf{d}, \mathbf{z}) = & \sum_{i=1}^{n} d_i \left(I(z_i = 1) \ln\left(\lambda e^{-\lambda t_i} \frac{\alpha}{\alpha + 1} \right) + I(z_i = 2) \ln\left(\lambda^2 t_i e^{-\lambda t_i} \frac{1}{\alpha + 1} \right) \right) \\ & + \sum_{i=1}^{n} (1 - d_i) \left(I(z_i = 1) \ln\left(e^{-\lambda t_i} \frac{\alpha}{\alpha + 1} \right) + I(z_i = 2) \ln\left((\lambda t_i + 1) e^{-\lambda t_i} \frac{1}{\alpha + 1} \right) \right). \end{aligned} \tag{22}$$

Similar to the uncensored data, we should iterate two E and M steps to find an improved estimation.

3.1.1. The E Step. Given the estimate of the parameters at iteration t, θ_t, applying the Bayes theorem, we can compute the conditional distribution of Z_i as follows:

$$\begin{aligned} p_{ij,t} &= d_i P(Z_i = j | X_i = t_i, \theta_t) + (1 - d_i) P(Z_i = j | X_i > t_i, \theta_t) \\ &= d_i \frac{f(X_i = t_i | Z_i = j, \theta_t) P(Z_i = j | \theta_t)}{f(X_i = t_i | \theta_t)} + (1 - d_i) \frac{P(X_i > t_i | Z_i = j, \theta_t) P(Z_i = j | \theta_t)}{f(X_i > t_i | \theta_t)} \\ &= d_i \frac{\lambda_t^j t_i^{j-1} e^{-\lambda_t t_i} (\alpha_t + 1)^{-1} \alpha_t^{I(j=1)}}{\sum_{j=1}^{2} \lambda_t^j t_i^{j-1} e^{-\lambda_t t_i} (\alpha_t + 1)^{-1} \alpha_t^{I(j=1)}} \\ &\quad + (1 - d_i) \frac{I(j = 1) e^{-\lambda_t t_i} (\alpha_t / (\alpha_t + 1)) + I(j = 2) (\lambda_t t_i + 1) e^{-\lambda_t t_i} (1 / (\alpha_t + 1))}{e^{-\lambda_t t_i} (\alpha_t / (\alpha_t + 1)) + (\lambda_t t_i + 1) e^{-\lambda_t t_i} (1 / (\alpha_t + 1))} \\ &= d_i \frac{I(j = 1)\alpha_t + I(j = 2)\lambda_t t_i}{\alpha_t + \lambda_t t_i} + (1 - d_i) \frac{I(j = 1)\alpha_t + I(j = 2)\lambda_t t_i + 1}{\alpha_t + \lambda_t t_i + 1}, i = 1, 2, \ldots, n, j = 1, 2. \end{aligned} \tag{23}$$

Specifically, for $j = 1$,

$$p_{i1,t} = d_i \frac{\alpha_t}{\alpha_t + \lambda_t t_i} + (1 - d_i) \frac{\alpha_t}{\alpha_t + \lambda_t t_i + 1}, i = 1, 2, \ldots, n, \tag{24}$$

and $p_{i2,t} = 1 - p_{i1,t}$. Then, using (22), the expectation function at iteration t can be written in the following form.

$$\begin{aligned} Q(\theta | \theta_t) &= E_{Z|t,d,\theta_t}(l(\theta; \mathbf{t}, \mathbf{d}, \mathbf{z})) \\ &= \sum_{i=1}^{n} d_i \left(p_{i1,t} \left(\ln\left(\lambda e^{-\lambda t_i} \frac{\alpha}{\alpha + 1} \right) \right) + p_{i2,t} \left(\ln\left(\lambda^2 t_i e^{-\lambda t_i} \frac{1}{\alpha + 1} \right) \right) \right) \\ &\quad + \sum_{i=1}^{n} (1 - d_i) \left(p_{i1,t} \left(\ln\left(e^{-\lambda t_i} \frac{\alpha}{\alpha + 1} \right) \right) + p_{i2,t} \left(\ln\left((\lambda t_i + 1) e^{-\lambda t_i} \frac{1}{\alpha + 1} \right) \right) \right). \end{aligned} \tag{25}$$

Similar to uncensored case, it is straightforward to check that $Q(\theta|\theta_t)$ can be written as two statements in which one of them just depends on α and the other depends on λ. More precisely,

$$Q(\theta|\theta_t) = Q_1(\lambda|\theta_t) + Q_2(\alpha|\theta_t), \tag{26}$$

where

$$Q_1(\lambda|\theta_t) = \sum_{i=1}^{n} d_i\left(1 + p_{i2,t}\right)\ln\lambda + \sum_{i=1}^{n} d_i p_{i2,t}\ln t_i + \sum_{i=1}^{n}(1-d_i)p_{i2,t}\ln(\lambda t_i + 1) - \lambda\sum_{i=1}^{n} t_i, \tag{27}$$

$$Q_2(\alpha|\theta_t) = \sum_{i=1}^{n}\left(p_{i1,t}\ln\alpha - \ln(\alpha+1)\right) \tag{28}$$

3.1.2. The M Step. In this step, we should maximize the $Q(\theta|\theta_t)$ function to compute the estimations at the $t+1$ iteration.

$$\theta_{t+1} = \arg\max_{\theta} Q(\theta|\theta_t), \tag{29}$$

which, by (26), reduces to the following separate maximization problems.

$$\begin{aligned}\lambda_{t+1} &= \arg\max_{\lambda} Q_1(\lambda|\theta_t),\\ \alpha_{t+1} &= \arg\max_{\alpha} Q_2(\alpha|\theta_t),\end{aligned} \tag{30}$$

in which $Q_1(\lambda|\theta_t)$ and $Q_2(\alpha|\theta_t)$ are determined by (27) and (28), respectively. The likelihood equation $\partial/\partial\lambda Q_1(\lambda|\theta_t) = 0$ which after some algebra can be simplified to

$$\lambda = \frac{\sum_{i=1}^{n} d_i\left(1 + p_{i2,t}\right)}{\sum_{i=1}^{n} t_i} + \frac{\sum_{i=1}^{n}(1-d_i)(\lambda t_i/(1+\lambda t_i))p_{i2,t}}{\sum_{i=1}^{n} t_i} \tag{31}$$

which does not yield to an analytical solution for λ, so the solution can be computed by numerical methods. But, clearly (31) implies that the solution of this equation, namely, λ_{t+1}, satisfies the inequality

$$\lambda_{t+1} > \frac{\sum_{i=1}^{n} d_i\left(1 + p_{i2,t}\right)}{\sum_{i=1}^{n} t_i}. \tag{32}$$

On the other hand, since $1 + p_{i2,t} > (\lambda t_i/(1+\lambda t_i))p_{i2,t}$, one upper bound for the solution is

$$\lambda_{t+1} < \frac{\sum_{i=1}^{n}\left(1 + p_{i2,t}\right)}{\sum_{i=1}^{n} t_i}, \tag{33}$$

and in turn, by (32) and (33), we have

$$\frac{\sum_{i=1}^{n} d_i\left(1 + p_{i2,t}\right)}{\sum_{i=1}^{n} t_i} < \lambda_{t+1} < \frac{\sum_{i=1}^{n}\left(1 + p_{i2,t}\right)}{\sum_{i=1}^{n} t_i}. \tag{34}$$

These bounds can be applied in numerical processes to find optimized answer. The solution for α can be obtained by solving the equation $\partial/\partial\alpha Q_2(\alpha|\theta_t) = 0$ as follows:

$$\alpha_{t+1} = \frac{\sum_{i=1}^{n} p_{i1,t}}{\sum_{i=1}^{n} p_{i2,t}}. \tag{35}$$

Similar to the uncensored case, the iterative process can be concluded when for some predefined small $\epsilon > 0$, $Q(\theta_{t+1}|\theta_{t+1}) < Q(\theta_t|\theta_t) + \epsilon$.

Let $\widehat{\theta}$ and θ_0 be the EM estimator and the real parameter, respectively. Then, $\widehat{\theta} - \theta_0$ converges asymptotically to a bivariate normal distribution $N(0, V)$, where V can be approximated by the inverse of the observed information matrix with respect to the observed data (see Meng and Rubin [12]). It is computed by evaluating the Hessian matrix of the log-likelihood function with respect to the observed data at the point $\widehat{\theta}$, and then calculating the inverse of the obtained Hessian matrix, briefly $V = I_o^{-1}(\widehat{\theta}|\mathbf{x})$. Fortunately, in the case of this study, the log-likelihood function of the observed data is not complicated and can be used to calculate the Hessian matrix and finally the variance approximation. For this purpose, the function "hessian" of the library "pracma" in R is used. Since the asymptotic distribution of the EM estimator is normal, the standard normal quantiles are used to obtain approximate confidence intervals of the parameters.

4. Simulations

In a simulation study, we investigate the behavior of the MLE and EM estimators and compare them. The fact that the quasi-Lindley model is a mixture of gamma distributions is applied to generate random samples. To generate right-censored sample $y_1, y_2, \ldots, y_n$, we assume that the censoring random variable C_i follows the degenerate distribution with mean M. Thus, if p is the censoring rate, we can calculate M by solving the equation $M = F^{-1}(1-p)$ where F^{-1} is the inverse of the distribution function of the quasi-Lindley model. Now, an uncensored sample $x_1, x_2, \ldots, x_n$ is taken from the quasi-Lindley model. Then, the ith instance of the desired right-censored sample is $y_i = \min\{x_i, M\}$.

Each cell of Tables 1 and 2 shows the results of one run. In every run, $r = 5000$ replicates of samples of size $n = 100$ or 200 were generated by the quasi-Lindley model with selected parameters, and in each run, the MLE and EM estimators were calculated. To calculate the MLE, the log-likelihood function was maximized by using the "optim" function built into R with the standard "Nelder–Mead" optimization method. In both the maximum likelihood method and EM, the initial values are generated from a uniform distribution.

Table 3: Waiting times (in minutes) of customers to receive service in a bank.

0.8	0.8	1.3	1.5	1.8	1.9	1.9	2.1	2.6	2.7
2.9	3.1	3.2	3.3	3.5	3.6	4.0	4.1	4.2	4.2
4.3	4.3	4.4	4.4	4.6	4.7	4.7	4.8	4.9	4.9
5.0	5.3	5.5	5.7	5.7	6.1	6.2	6.2	6.2	6.3
6.7	6.9	7.1	7.1	7.1	7.1	7.4	7.6	7.7	8.0
8.2	8.6	8.6	8.6	8.8	8.8	8.9	8.9	9.5	9.6
9.7	9.8	10.7	10.9	11.0	11.0	11.1	11.2	11.2	11.5
11.9	12.4	12.5	12.9	13.0	13.1	13.3	13.6	13.7	13.9
14.1	15.4	15.4	17.3	17.3	18.1	18.2	18.4	18.9	19.0
19.9	20.6	21.3	21.4	21.9	23.0	27.0	31.6	33.1	38.5

Table 4: Results of fitting quasi-Lindley model to dataset of Table 3.

Method	$(\widehat{\alpha}, \widehat{\lambda})$	AIC	KS p value	AD p value	CVM p value
MLE	(0.000002, 0.2025)	638.6014	0.0442 0.9842	0.1914 0.9743	0.0301 0.9621
EM	(0.0118, 0.2013)	—–	0.04198 0.9946	0.1858 0.9938	0.0279 0.9828

Note that checking the termination conditions of the EM process in each EM iteration results in very slow and time-consuming runs. Therefore, the EM algorithm has been tested many times to find a suitable constant for the number of iterations. In this way, we find that 5 iterations are sufficient.

Four measures bias (B), mean squared error (MSE), coverage probability (CP), and confidence interval length mean (CILM) for α and λ have been computed. The B and MSE for α are defined to be

$$\begin{aligned} \mathrm{B} &= \frac{1}{r}\sum_{i=1}^{r}\left(\widehat{\alpha}_i - \alpha\right), \\ \mathrm{MSE} &= \frac{1}{r}\sum_{i=1}^{r}\left(\widehat{\alpha}_i - \alpha\right)^2, \\ \mathrm{CP} &= \frac{1}{r}\sum_{i=1}^{r} I\left(\alpha \in CI_{\alpha}(i)\right), \\ \mathrm{ILM} &= \frac{1}{r}\sum_{i=1}^{r} \text{length of } CI_{\alpha}(i), \end{aligned} \tag{36}$$

where $\widehat{\alpha}_i$ shows the MLE/EM estimator in the run i and $CI_{\alpha}(i)$ shows an approximate asymptotic 95 percent confidence interval for α in the ith iteration (see the last paragraph of Section 3). Also, the indicator function I in (30) equals 1 when the real parameter falls inside the confidence interval and otherwise equals zero. These measures are defined for λ similarly. Tables 1 and 2 present the simulation results for uncensored data and censored data with censorship 0.2, respectively. The main observations from these tables are listed in the following:

(i) The MSE decreases as sample size increases, for both MLE and EM estimators and both uncensored data and censored data which indicates that the MLE and EM estimators are consistent.

(ii) The EM estimator outperforms the MLE in terms of the MSE.

(iii) The results show higher CPs and lower CILMs for EM than MLE. Moreover, the CP increases and CILM decreases as sample size increases.

5. Application

Table 3 shows 100 waiting times of customers of a bank analyzed by Shanker [13]. The quasi-Lindley distribution was fitted to this dataset, and the parameters were estimated using the maximum likelihood method and EM. The "optim" function in the R language was used to calculate the MLE. Table 4 shows the results of the fitting. In terms of the KS, Anderson–Darling (AD), and Cramer–von Mises (CVM) statistics, both methods provide a good fit, but EM outperforms MLE in a close competition. The empirical and the fitted CDFs are shown in Figure 1(a) and also confirm a good fit. The histogram and estimated probability density function are also shown in Figure 1(b). Using the Hessian matrix calculated with the optim function, the variances of the MLE are estimated for the parameters, $\widehat{v}(\widehat{\alpha}) = 4 \times 10^{-12}$ and $\widehat{v}(\widehat{\lambda}) = 0.00020$. Using these variance estimates and standard normal quantiles, the 95% confidence intervals for α and λ are $(0, 0.000006)$ and $(0.1744, 0.2305)$, respectively. The left bound of the α confidence interval was a negative value; by the fact that $\alpha > 0$, it was set to 0.

To find the variances of the EM estimator of the parameters, the bootstrap method is used. In this way, $r = 1000$ samples are derived by the function "sample" of R. Then, for each sample, the EM estimates of the parameters are computed. The estimate of the variance of the EM estimators is approximated by the variance of these estimates which are $\widehat{v}(\widehat{\alpha}) = 0.0015$ and $\widehat{v}(\widehat{\lambda}) = 0.00023$. For each of the parameters, the 2.5% and 97.5% quantiles of the EM estimator can be considered as upper and lower bounds of the 95% confidence intervals. Then, the 95%

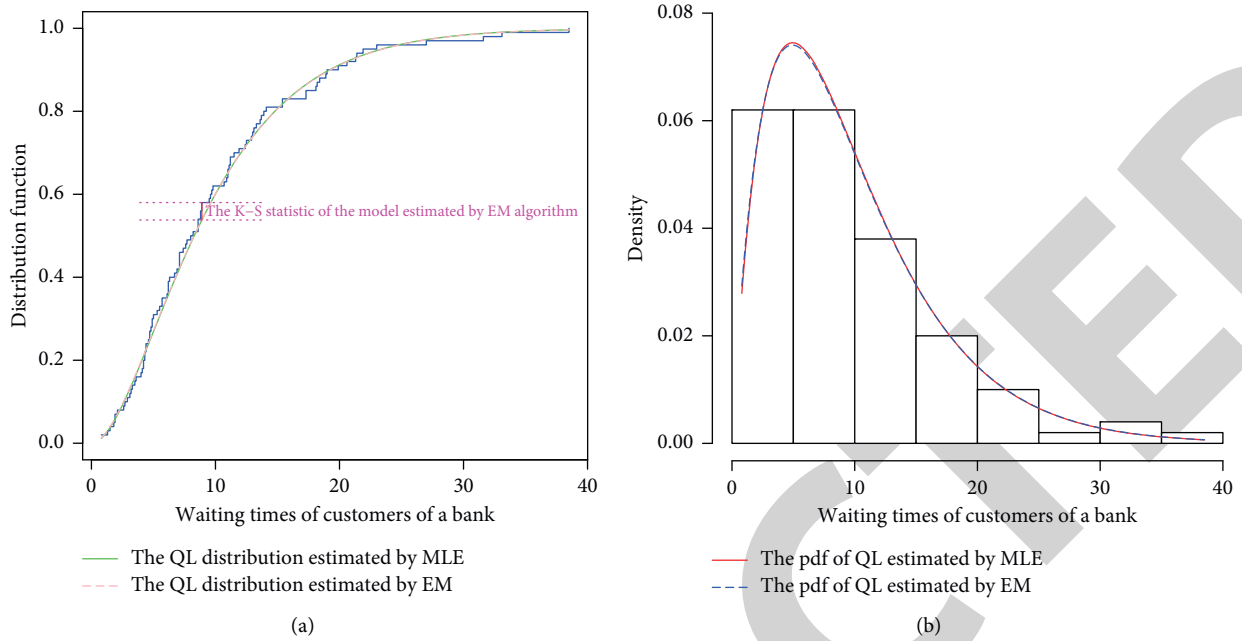

FIGURE 1: (a) The empirical distribution and fitted quasi-Lindley distribution for dataset of Table 3. (b) The histogram and the estimated probability density function for this dataset.

confidence intervals for α and λ are $(0.00024, 0.12845)$ and $(0.1750, 0.2325)$, respectively.

6. Conclusion

The quasi-Lindley distribution is a scale-invariant version of the Lindley distribution with a shape parameter α and a scale parameter λ and is a simple yet flexible model in reliability theory, survival analysis, management science, and many other fields. The MLE and EM approaches were investigated to estimate the parameters of this model. The simulation results show that the EM algorithm is better than the MLE for estimating the parameters for both uncensored and censored data.

Data Availability

The data used to support the findings of this study are included within the article.

Conflicts of Interest

The authors declare that they have no conflicts of interest.

Acknowledgments

This study was supported by Researchers Supporting Project (RSP-2021/392), King Saud University, Riyadh, Saudi Arabia.

Supplementary Materials

Censored-MLE and EM for quasi Lindley. (*Supplementary Materials*)

References

[1] R. Shanker and A. Mishra, "A quasi Lindley distribution," *African Journal of Mathematics and Computer Science Research*, vol. 6, no. 4, pp. 64–71, 2013.

[2] D. V. Lindley, "Fiducial distributions and Bayes' theorem," *Journal of the Royal Statistical Society: Series B*, vol. 20, no. 1, pp. 102–107, 1958.

[3] A. P. Dempster, N. M. Laird, and D. B. Rubin, "Maximum likelihood estimation from incomplete data via the EM algorithm," *Journal of the Royal Statistical Society: Series B*, vol. 39, no. 1, pp. 1–22, 1977.

[4] E. E. Elmahdy and A. W. Aboutahoun, "A new approach for parameter estimation of finite Weibull mixture distributions for reliability modeling," *Applied Mathematical Modelling*, vol. 37, no. 4, pp. 1800–1810, 2013.

[5] J. Almhana, Z. Liu, V. Choulakian, and R. McGorman, "A recursive algorithm for gamma mixture models," in *Proceedings of the IEEE International Conference on Communications ICC 06*, vol. 1, pp. 197–202, Istanbul, Turkey, June 2006.

[6] M. Bee, R. Benedetti, and G. Espa, "On maximum likelihood estimation of a Pareto mixture," *Computational Statistics*, vol. 28, no. 1, pp. 161–178, 2013.

[7] I. Ghosh, G. G. Hamedani, N. Bansal, and M. Maadooliat, "On the mixtures of Weibull and Pareto (IV) distribution: an alternative to Pareto distribution," *Communications in Statistics-Theory and Methods*, vol. 47, no. 9, pp. 2073–2084, 2018.

[8] N. Balakrishnan and S. Pal, "Expectation maximization-based likelihood inference for flexible cure rate models with Weibull lifetimes," *Statistical Methods in Medical Research*, vol. 25, no. 4, pp. 1535–1563, 2016.

[9] G. J. McLachlan and T. Krishnan, *The EM Algorithm and Extensions*, Wiley, New York, NY, USA, 1997.

[10] K. L. Mengersen, C. P. Robert, and D. M. Titterington, *Mixtures: Estimation and Applications*, Wiley, New York, NY, USA, 2011.

Hindawi
Journal of Mathematics
Volume 2023, Article ID 9792569, 1 page
https://doi.org/10.1155/2023/9792569

Retraction

Retracted: Analysis of Intelligent Translation Systems and Evaluation Systems for Business English

Journal of Mathematics

Received 15 August 2023; Accepted 15 August 2023; Published 16 August 2023

This article has been retracted by Hindawi following an investigation undertaken by the publisher [1]. This investigation has uncovered evidence of one or more of the following indicators of systematic manipulation of the publication process:

(1) Discrepancies in scope

(2) Discrepancies in the description of the research reported

(3) Discrepancies between the availability of data and the research described

(4) Inappropriate citations

(5) Incoherent, meaningless and/or irrelevant content included in the article

(6) Peer-review manipulation

The presence of these indicators undermines our confidence in the integrity of the article's content and we cannot, therefore, vouch for its reliability. Please note that this notice is intended solely to alert readers that the content of this article is unreliable. We have not investigated whether authors were aware of or involved in the systematic manipulation of the publication process.

Wiley and Hindawi regrets that the usual quality checks did not identify these issues before publication and have since put additional measures in place to safeguard research integrity.

We wish to credit our own Research Integrity and Research Publishing teams and anonymous and named external researchers and research integrity experts for contributing to this investigation.

The corresponding author, as the representative of all authors, has been given the opportunity to register their agreement or disagreement to this retraction. We have kept a record of any response received.

References

[1] J. Chen, "Analysis of Intelligent Translation Systems and Evaluation Systems for Business English," *Journal of Mathematics*, vol. 2022, Article ID 5952987, 7 pages, 2022.

Hindawi
Journal of Mathematics
Volume 2022, Article ID 5952987, 7 pages
https://doi.org/10.1155/2022/5952987

Research Article

Analysis of Intelligent Translation Systems and Evaluation Systems for Business English

Jianhong Chen

Foreign Languages & International Education College, Quzhou University, Quzhou 324000, Zhejiang, China

Correspondence should be addressed to Jianhong Chen; 33021@qzc.edu.cn

Received 1 December 2021; Revised 24 December 2021; Accepted 27 December 2021; Published 25 January 2022

Academic Editor: Naeem Jan

In order to improve the accuracy of automatic translation of business English, an optimized design of business English translation teaching platform is proposed based on the logistic model combined with deep learning. After using the logistic model to analyze the semantic features of business English translation, the deep learning model is used to segment and mine English images, and the automated lexical feature analysis of business English translation is carried out by using contextual feature matching and adaptive semantic variable finding methods to extract the amount of correlation features between words and vocabulary and to correct the differences in translation in a specific business context to improve the accuracy of English translation. The software design of the platform is carried out under the logistic model, and the platform is mainly divided into a vocabulary database module, an English information processing module, a web interface module, and a human-computer interaction interface module. The test results show that the accuracy of business English translation using this method is good, and the automatic translation capability is strong.

1. Introduction

As machine English translation technology continues to mature, the use of machine English translation for English translation can greatly reduce the time of manual translation and improve translation efficiency [1]. The study of English translation methods based on machine translation has an important role in promoting English education as well as improving the reading efficiency of foreign language literature. In the process of translating business English, the uncertainty and randomness of business English's own context lead to poor accuracy of business English machine translation, which requires the optimal design of a business English translation teaching platform, combined with the improved design of algorithms for business English machine translation, to improve the accuracy and efficiency of business English translation, and the research of related teaching platform design methods has received great attention [2].

The machine algorithm for business English translation currently mainly adopts the limit learning machine algorithm, the machine English translation correction algorithm of support vector machine, and the autoregressive analysis method [3], which combines the semantic features of business English translation for the analysis of language environment and automatic translation feature matching in the translation process to improve the accuracy of business English translation, and uses this as the basis for the teaching platform design of business English translation with high teaching quality [4]. However, the aforementioned methods have a greater problem of contextual interference in conducting large-scale business English translation, resulting in poor accuracy of translation. To address this problem, this paper proposes a design method for a teaching platform for business English translation based on the logistic model, which uses contextual feature matching and adaptive semantic variable finding methods for automated lexical feature analysis of business English translation, and carries out differential correction of translation in specific business contexts to improve the accuracy of English translation [5]. The software development design and simulation experimental analysis of the business English translation teaching

platform were also carried out to draw conclusions on the effectiveness. In the following section, we presented the algorithm design for the translation of the English literature. In Section 3, the deep learning solutions are explained. Section 4 carries out the experimental analysis for the validation of the proposed algorithm and its working. Finally, the paper is concluded in Section 5.

2. English Literature Translation Algorithm Design

In this section, the algorithm for the English literature translation is presented. First, the logistic model is explained which is used for semantic feature analysis of English translation. Then, the optimization of the algorithm for English literature translation is given. On the basis of the logistic model for business English literature translation, the machine algorithm design is realized, which in turn acts as a base for the software development design of translation teaching platform.

2.1. Logistic Model. The logistic model is used for semantic feature analysis of business English translation. As a typical chaos model, the logistic model has the characteristics of randomness and initial feature sensitivity, and it has the advantage of strong environmental adaption for semantic feature analysis in different contexts of business English [6], and the one-dimensional mapping is used to construct the logistic chaos model as follows:

$$x_{n+1} = \lambda x_n(1 - x_n), x \in [0,1], \lambda \in [0,4]. \tag{1}$$

The above equation describes the subcluster Henon attractor for business English translation, and combined with the concept set of English translation output for adaptive context matching, the distribution model of the concept set of textual features for English literature translation is obtained as follows:

$$\begin{cases} \dot{x} = a + by = x^2, \\ \dot{y} = x, \end{cases} a = 1.4, b = 0.3. \tag{2}$$

Lorenz attractors were introduced for semantic revision of business English translations [7], and the Lorenz function was

$$\begin{cases} \dot{x} = -\sigma x + \sigma y, \\ \dot{y} = -xz + rx - y, \\ \dot{z} = xy - bz, \end{cases} \tag{3}$$

where $[\sigma, r, b] = [10, 28, 8/3]$ or $[\sigma,\ r,\ b] = [16,\ 45.92,\ 4]$.

In word clustering feature extraction for business English translation, semantic feature clustering is performed under the logistic chaotic attractor by combining the variability of semantic feature distribution of words [8].

According to the English translation clustering model shown in Figure 1, contextual feature matching and adaptive semantic variable finding methods are used for automated lexical feature analysis of business English translation, assuming that the semantic code sequence of the English utterance to be translated is of length N and the set of semantic distribution concepts is x, which can be represented as an $N \times 1$ column feature vector, $x(n) \in R^N$. Using the associative semantic grouping expression method [9], the clustering model for business English literature translation is obtained as described by

$$x = \sum_{i=1}^{N} s_i \Psi_i = \Psi s. \tag{4}$$

2.2. English Machine Translation Algorithm Optimization. Based on the above semantic feature analysis of business English translation using the logistic model, the machine algorithm design for English translation was carried out, using contextual feature matching and adaptive semantic variable finding [10], and the optimal semantic feature matching results for English translation were obtained as

$$J^*(m) = \max_{\tau}\{J^*(\tau) + D_m(\tau) + C\}, J^*(0) = 0. \tag{5}$$

Based on the semantic discretization of the original text information, parametric adaptive estimation of the semantic text feature quantity Y is performed to obtain the feature matching of the English translation output as

$$p\left(x_1^l \mid \alpha\right) = \prod_{i=1}^{L} p\left(y_i \mid \alpha, r_i, l\right). \tag{6}$$

Automated lexical feature analysis of business English translation was conducted, and the decomposition results of the associated contextual information of the English translation lexicon were obtained as follows [11]:

$$\begin{aligned} E_j &= \sum_{k=1}^{n} E_{j,k,} \\ P_{j,k} &= \frac{E_{j,k}}{E_j}. \end{aligned} \tag{7}$$

The cross-integrated evaluation decision method [12] was used to extract the amount of word-to-word associative features, and the output was obtained as follows:

$$WE_k = -\sum_{j} P_{j,k} \ln\left(P_{j,k}\right). \tag{8}$$

The semantic ontology information of business English translation is thresholded [13], and the empirical modal decomposition method is used to obtain the output similarity and closeness of the translation results as follows:

$$\begin{aligned} S_x &= E\left[x^3(t)\right] + \sqrt{s}\,\mathrm{bu}\left[s(t - \tau_0)\right], \\ K_x &= E\left[x^4(t)\right] - 3E^2\left[x^2(t)\right]\mathrm{bn}. \end{aligned} \tag{9}$$

Figure 1: Real-life English scenario translation target process.

According to the output similarity and closeness feature extraction results, the differential correction of the translation in a specific business context is carried out, and the corrected set of texts of the English literature translation output is obtained as follows:

$$\begin{aligned}\text{Computation}(n_j) &= (E_{\text{elec}} + E_{\text{DF}})l\delta + E_{T_x(l,d_j)} \\ &= (E_{\text{elec}} + E_{\text{DF}})l\delta + lE_{\text{elec}} + l_{\varepsilon_{fs}}d_j^2 \\ &= \left[(E_{\text{elec}} + E_{\text{DF}})\delta + E_{\text{elec}} + \varepsilon_{fs}d_j^2\right]l.\end{aligned} \tag{10}$$

To summarize the above algorithm design, machine algorithm design based on the logistic model for business English literature translation is realized, based on which the software development design of translation teaching platform is carried out [14].

3. Deep Learning Solutions

Through deep learning-based image recognition and machine translation technology, it is possible to make the computer describe the scene presented in the picture in a few short sentences, and then the image recognized by using the computer is accurately described in English and fed to the mobile phone WeChat app in real time. This allows users to translate the pictures taken by their mobile phones into English vocabulary and sentences through the WeChat applet, which not only allows them to learn English anytime and anywhere but also reduces the inconvenience caused by the language barrier when they are in an English-speaking country [15]. Deep learning-based real-world English scene translation mainly lies in the English translation processing of images; the process first requires scene acquisition and image capture by calling the mobile phone camera through the WeChat applet and then image region segmentation, image feature extraction, image target detection, and English description generation for the captured image, i.e., the scene; Figure 1 shows the target flow of the process. The processing of the live image through the target process can produce a more accurate English description of the live scene.

3.1. Image Feature Extraction. After regional segmentation of the image, the image features are extracted. In this paper, we construct a convolutional neural network model to perform image feature extraction [16]. In this paper, we use the VGG-16 architecture, which consists of 13 3×3 convolution layers and 6 2×2 max pooling layers, as shown in Figure 2, so that the extracted input image features $(3\times W\times H)$ generate the corresponding tensor features (where 3 denotes RGB, i.e., the number of channels is 3, W denotes width, and H denotes height) and turn them into $C\times W\times H$. The tensor feature is converted into $C\times W\times H$, where C is a constant number of channels, W is the width, and H is the height. As the pixel image will be converted to a certain level of distortion, the maximum limit of C is set to 512, and the width and height of the image will become 1/16 of the original when C takes the maximum value [17]. The output of the convolutional neural network is positioned at a set of uniformly sampled image locations, and the features of the image are encoded and stored. Extract these features in preparation for target detection.

3.2. Image Target Detection. For target detection, Faster R-CNN [18], a "trendy" technique in the field of target detection, was chosen. The RoI pooling mechanism in Faster R-CNN [20] is replaced by a bilinear interpolation [19] based on Faster R-CNN in order to allow the improved target detection model to propagate the gradient backwards through the coordinates of the prediction region and avoid local optima in target detection. Throughout this paper, the improved neural network is referred to as the "recognition layer."

After receiving the image features extracted in the previous step, when the recognition layer receives an activation tensor of $C\times W\times H$, it internally selects the T regions of interest (T for TOP, merit selection) and returns three output tensors, which give information about these regions [21].

(i) Region coordinates: after merit selection, the T matrix gives the best bounding box coordinates for each output region.

(ii) Region scores: vector of length T gives the confidence score of each output region. Regions with high confidence scores are more likely to be regions of interest.

(iii) Region features: the selected regions are represented by a C-dimensional $X\times Y$ grid, and the image features are bilinearly sampled with the grid to obtain a region feature of size $T\times512\times7\times7$.

The target detection model based on Faster R-CNN is constructed as shown in Figure 3.

3.3. Generate English Descriptions. After the target detection of the image, the English expression of the target features is obtained, and the intermediate output < objects, attributes, activities, scene > is obtained, as shown in Figure 4, and furthermore, the feature words need to form into English sentences according to the scene [22].

In this paper, we use long short-term memory (LSTM) networks to form sentences from real-world features and

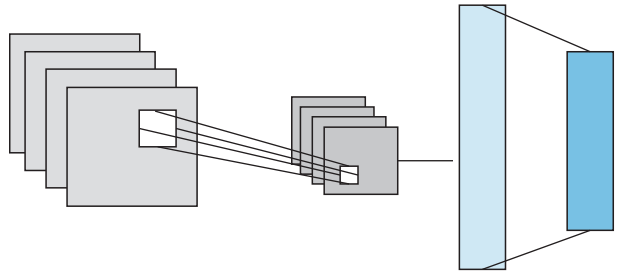

Figure 2: CNN feature extraction model.

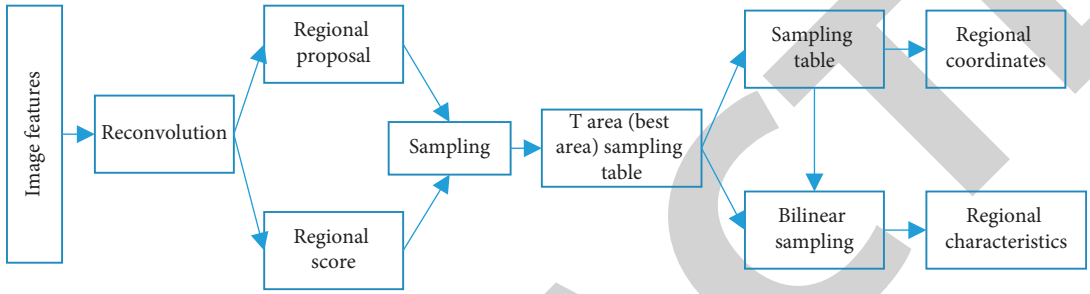

Figure 3: Faster R-CNN-based target detection model.

obtain English descriptions of the scene. The image features extracted by feature extraction, the region features obtained by target detection, and the region coordinates are input into the LSTM neural network to train the sentence formation of real-life words.

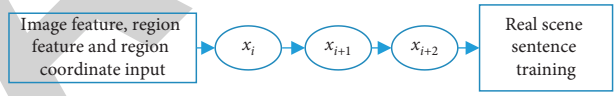

Figure 4: LSTM-based real-world lexical sentence formation model.

4. Experimental Test Analysis

The simulation experiment of the business English translation teaching platform was designed by MATLAB and TinyOS 2.x. The number of data transmission frames for English translation was set to 1200, and the number of English text packets to be translated was 128 Mbit [23]. The number of training samples for business English documents is 12, and the maximum sampling time for semantic features is 24. Based on the above simulation parameter settings, the English translation test was conducted using this method and the traditional method to analyze the correctness of business English translation using this platform. The analysis of Figure 5 shows that the accuracy of business English translation using this method is high, and the output translation error is low.

The time responsiveness of the English translation teaching platform was further tested, and the results were obtained as shown in Figure 5. Analysis of Figure 6 shows that this paper's approach to the design of a business English literature translation teaching platform has a low time overhead in English translation [24].

In order to verify the accuracy of the scene recognition model used in this paper, some images with standard descriptions were selected and put into the training environment for training, as shown in Figure 7, and the one description text with the highest scoring was selected for comparison with the standard description text; it can be seen that the results of this paper can basically and accurately translate the content of the images in the scene.

In a realistic application of the statement, the words "and/or" and "damage or loss" appear in pairs. The word "and/or" is used because the original text indicates "advance freight" and "freight payable at destination." When the two methods are used together or separately, the full amount of the freight must be paid to the carrier. Therefore, it should be translated as "or one of them." With regard to "damage or loss," "damage" refers to an overall loss of value, whereas "loss" refers to a partial loss of overall value. In accordance with the international practice of transport insurance for goods to losses, some policies only cover total loss of goods and some only partial loss, so it is a matter of protection of the interests of the person at the time. Figure 8 shows that, in word cloud analysis, "damage or loss" should be translated as "loss or perish." In order to achieve the effect of euphemism in business English, passive sentences are often used, which are very different from the expression in Chinese. Therefore, there is no ready-made counterpart for translating passive sentences into Chinese, but rather, some appropriate means of expressing the passive meaning of the original text should be selected from a wide range of sentences and auxiliary words according to the customary usage of Chinese [25, 26].

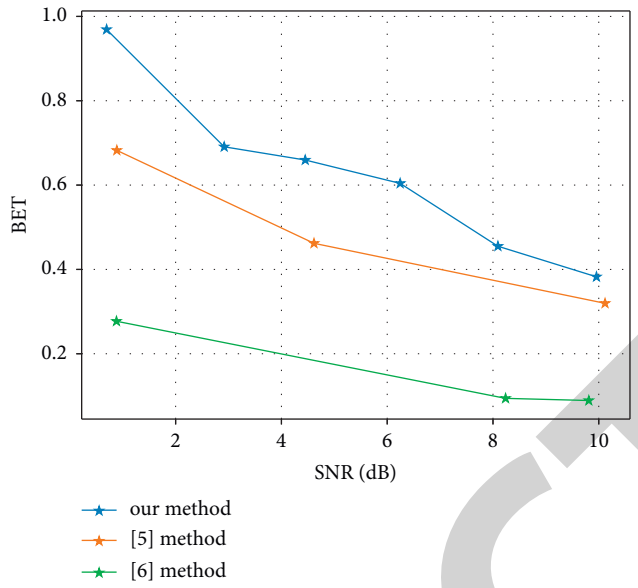

Figure 5: Comparative test of accuracy of English translations.

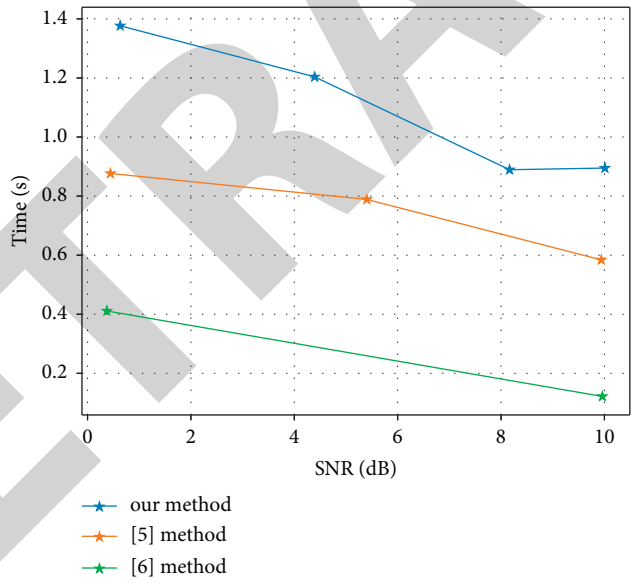

Figure 6: Time performance comparison.

Figure 7: Example of image description results.

Figure 8: Business English word cloud analysis.

5. Conclusions

In the process of translating business English, the uncertainty and randomness of the business English context lead to the poor accuracy of business English machine translation. This paper proposes a design method based on the logistic model for translation. The research has shown that the translation designed in this paper is superior in terms of time responsiveness and accuracy of English translation. There is no ready-made counterpart for translating passive sentences into Chinese, but rather, some appropriate means of expressing the passive meaning of the original text should be selected from a wide range of sentences and auxiliary words according to the customary usage of Chinese.

Data Availability

The datasets used during the current study are available upon request to the author.

Conflicts of Interest

The author declares that he has no conflicts of interest.

References

[1] M. King, "Accuracy and suitability: new challenges for evaluation," *Language Resources and Evaluation*, vol. 39, no. 1, pp. 45–64, 2005.

[2] J. Cadeanes and A. G. Arrieta, "Development of sign language communication skill on children through augmented reality and the MuCy model[J]," *Advances in Intelligent Systems & Computing*, vol. 292, pp. 45–52, 2014.

[3] A. Rocha, H. Adeli, and L. P. Reis, "Advances in intelligent systems and computing trends and advances in information systems and technologies," vol. 2, p. 745.

[4] J. Gutiérrez-Artacho, M.-D. Olvera-Lobo, and I. Rivera-Trigueros, "Human post-editing in hybrid machine translation systems: automatic and manual analysis and evaluation," *Advances in Intelligent Systems and Computing*, pp. 254–263, 2018.

Hindawi
Journal of Mathematics
Volume 2024, Article ID 9825890, 1 page
https://doi.org/10.1155/2024/9825890

Retraction

Retracted: Supply Capability Evaluation of Intelligent Manufacturing Enterprises Based on Improved BP Neural Network

Journal of Mathematics

Received 23 January 2024; Accepted 23 January 2024; Published 24 January 2024

This article has been retracted by Hindawi following an investigation undertaken by the publisher [1]. This investigation has uncovered evidence of one or more of the following indicators of systematic manipulation of the publication process:

(1) Discrepancies in scope

(2) Discrepancies in the description of the research reported

(3) Discrepancies between the availability of data and the research described

(4) Inappropriate citations

(5) Incoherent, meaningless and/or irrelevant content included in the article

(6) Manipulated or compromised peer review

The presence of these indicators undermines our confidence in the integrity of the article's content and we cannot, therefore, vouch for its reliability. Please note that this notice is intended solely to alert readers that the content of this article is unreliable. We have not investigated whether authors were aware of or involved in the systematic manipulation of the publication process.

Wiley and Hindawi regrets that the usual quality checks did not identify these issues before publication and have since put additional measures in place to safeguard research integrity.

We wish to credit our own Research Integrity and Research Publishing teams and anonymous and named external researchers and research integrity experts for contributing to this investigation.

The corresponding author, as the representative of all authors, has been given the opportunity to register their agreement or disagreement to this retraction. We have kept a record of any response received.

References

[1] Q. Quan and Z. Zhang, "Supply Capability Evaluation of Intelligent Manufacturing Enterprises Based on Improved BP Neural Network," *Journal of Mathematics*, vol. 2022, Article ID 8572424, 8 pages, 2022.

Hindawi
Journal of Mathematics
Volume 2022, Article ID 8572424, 8 pages
https://doi.org/10.1155/2022/8572424

Research Article

Supply Capability Evaluation of Intelligent Manufacturing Enterprises Based on Improved BP Neural Network

Quan Quan[1,2] and Zhongqiang Zhang[1]

[1]*China University of Mining and Technology, Xuzhou 221116, China*
[2]*Xuzhou University of Technology, Xuzhou 221018, China*

Correspondence should be addressed to Zhongqiang Zhang; zzq@xzit.edu.cn

Received 23 November 2021; Revised 16 December 2021; Accepted 20 December 2021; Published 21 January 2022

Academic Editor: Naeem Jan

With the rapid development of economy and information technology, traditional manufacturing industry is facing severe challenges. Enterprises need to rectify the traditional manufacturing industry and realize the transformation from traditional manufacturing industry to intelligent manufacturing industry. In order to adapt to market demand, enterprises need to constantly integrate resources to improve the competitiveness of enterprise supply chain. Based on the background of suppliers in intelligent manufacturing enterprises, the evaluation method of supplier efficiency was studied by using machine learning. In this paper, based on the traditional backpropagation (BP) neural network, combined with the improved particle swarm optimization (PSO) algorithm, and on the basis of the supplier evaluation index system, the supplier efficiency evaluation model of intelligent manufacturing enterprises based on DPMPSO-BP neural network is constructed. Through the collected sample data, the network is trained and simulated, and the results are analyzed. Finally, the designed model is applied to a large battery manufacturing enterprise, and the supplier efficiency evaluation method based on DPMPSO-BP neural network is validated and analyzed. Compared with the traditional BP neural network method, the supplier efficiency evaluation method is effective and feasible.

1. Introduction

Manufacturing plays a key role in the economic development of a country or region and reflects the comprehensive strength of a country or region. After the outbreak of the global financial crisis in 2008, the economic growth of all countries in the world is weak, and all developed countries have moved their traditional manufacturing industry closer to the intelligent manufacturing industry, among which the intelligent manufacturing enterprises led by the United States and Germany are developing most rapidly [1, 2].

With the rapid development of intelligent manufacturing, the supply chain of some large manufacturing industries has undergone great changes, and the relationship between enterprises and suppliers has changed from simple "buyer-seller relationship" to "partnership relationship." With the transformation of the relationship between enterprises and suppliers, enterprises have higher and higher requirements on suppliers. How to dig out important value from massive supplier information and apply it to supply chain management is an urgent problem for enterprises. In the supply chain, supplier is the source of supply chain, and the evaluation of supplier is the key problem [3]. Supplier efficiency evaluation is very important in supplier evaluation. Supplier efficiency is an indicator of the rationality of the resources and output value of efficient supplier manufacturing enterprises. Its quality can reflect the carrier of suppliers. Through the study of supplier efficiency hierarchy, on the one hand, it can be used to monitor supplier status and performance. Recognition and translation are related, and it is also the decision basis for selecting supplier incentive strategies. Supplier efficiency evaluation is aimed at efficiency-oriented suppliers, which measures the product quality, cost, and service of such suppliers by establishing appropriate evaluation index system and classifies the efficiency of suppliers by using certain

evaluation criteria. Supplier efficiency evaluation is a key step in the construction of supply chain, which has great influence on the smooth operation of efficient supply chain [4].

Supplier evaluation methods have gone through a process from qualitative to quantitative, a combination of qualitative and quantitative, and a mixed use of quantitative and quantitative. Liu Xiufen adopted the intuitive judgment method in the method of selecting manufacturers, which can quickly and efficiently respond to the intuitive judgment method [5]. When Wang Hao talked about the supplier evaluation method and solution, this method requires both the supplier and the buyer to go through the process. Many times of negotiation to ensure the maximization of the interests of both supply and demand [6], Qiu Min said that in the procurement of materials, choosing the bidding method has a better competitive advantage, but it is cumbersome and unable to deal with emergency procurement [7].

In the quantitative supplier evaluation method, Wang proposed a number of supplier evaluation indicators in view of the characteristics of S Company's petrochemical equipment importing relatively high technology content and used the linear weight method to select appropriate suppliers [8]. Degraeve et al. used the real data generated by Belgian multinational steel companies to build a mathematical model and concluded that the multiobjective mathematical programming model method has great advantages in supplier evaluation and selection [9]. Among quantitative evaluation methods, cost-based methods are the most common, and cost is the easiest indicator to quantify. Taking the reduction of product cost as an example, Zhou Jianzhong proposed the basic ABC cost method and the Analytic Hierarchy Process (AHP) method in the supplier evaluation method for how to select supplier partners, such as the method of using the Analytic Hierarchy Process (AHP) combined with the genetic algorithm. To evaluate suppliers, first use the analytic hierarchy process to evaluate and score, then use genetic algorithm to optimize and sort, and finally use it to evaluate and select suppliers [11]. Dong Shengxu analyzed the characteristics of suppliers of telecom operators and constructed a supplier evaluation indicator system according to their characteristics. Then, he used the traditional BP neural network to train the indicator data collected and finally verified the practicality of BP neural network for supplier evaluation of telecom enterprises [12].

This paper summarizes the research studies of many researchers, who evaluated and selected suppliers in different ways from various angles. Among many evaluation methods, the qualitative method is relatively simple and convenient to operate, but its subjectivity is too strong, which has some hidden dangers for the development of enterprises. The single quantitative evaluation method has too high requirements for quantification of indicators and data collection, and it is rarely used in enterprises because of complicated calculation [13]. The more reasonable supplier evaluation method is the combination of qualitative and quantitative methods, which can not only make up for the strong subjectivity of qualitative evaluation method but also simplify the complex quantitative evaluation. However, it also has limitations. If different evaluation methods are mixed together, problems such as accuracy can be well solved.

In the mixed evaluation method, the method combining BP neural network is more advanced and has the advantages of objective, scientific, easy operation, simple calculation, and so on. Supplier evaluation is a complex nonlinear mapping problem. However, the traditional BP neural network has many shortcomings. Therefore, this paper proposes an improved PSO-BP model by improving particle swarm optimization (PSO) and combining it with the traditional BP neural network and applies the model to the supplier evaluation of a large battery manufacturing enterprise. In Section 2, the discussion is carried out for the intelligent manufacturing enterprises' supplier evaluation index system. Moreover, the BP neural networks are explained with their drawbacks. Further, the improved BP neural networks are deliberated. Also, the steps of DPMPSO-BP algorithm are also given. In Section 3, the experiments are carried out and their outcomes are analyzed. Finally, the paper is concluded in Section 4.

2. Theoretical Basis and Methods

In this section, we propose the main methods. For that reason, first we discuss the intelligent manufacturing enterprises' supplier evaluation index system. Then, BP neural networks are explained with a list of their drawbacks. Further, the improved BP neural networks are deliberated. The steps of DPMPSO-BP algorithm are also given.

2.1. Supplier Evaluation Index System of Intelligent Manufacturing Enterprises. According to the definition of intelligent manufacturing and related documents of intelligent manufacturing enterprise suppliers, the characteristics of intelligent manufacturing enterprise suppliers are summarized as follows: high intelligence level, strong product competitiveness, and good personalized service. This paper collected a large number of domestic and foreign literatures on supplier evaluation and analyzed the quality, cost, delivery, service, and other important indicators in supplier evaluation. By summarizing the research results of domestic and foreign scholars on evaluation index system, analyzing the characteristics of suppliers of intelligent manufacturing enterprises, and constructing the principle of supplier efficiency evaluation index system, the basic indicators are reconstructed from the perspective of supplier efficiency and intelligent manufacturing, and the supplier evaluation index system of intelligent enterprises is formed. The index system consists of three dimensions: product dimension, intelligent dimension, and operation dimension. Each dimension is divided into different categories, and each category is subdivided into different factor domains. Indicators of supplier classification are divided as shown in Table 1.

2.2. BP Neural Network. The most basic component of neural network is neuron, which is connected with other

Table 1: Indicators of supplier classification.

First-level indicator	Secondary indicators	Third-level indicators	Fourth-level indicators
Performance	Quality of the product	Quantitative	Expert scoring
	Cooperation degree	Qualitative	The formula to calculate
	Service level	Quantitative	Expert scoring
	Credit	Qualitative	The formula to calculate
Strategic potential	Technology research and development ability	Quantitative	Expert scoring
	The management level	Quantitative	Expert scoring
	Collaborative innovation capability	Quantitative	Expert scoring
	Level of informatization	Quantitative	Expert scoring

neurons to complete the information transmission between neurons. At present, the neuron receives input signals with n weights. The total input received by the neuron is compared with threshold 0, and then the output value is calculated through activation function processing [14]. The description of the basic structure is shown in Figure 1.

The traditional BP neural network uses the error back-propagation algorithm to update the weights and thresholds of the network structure through error back-propagation to make the error smaller and iterate continuously until the error is smaller than the given expectation [15]. BP neural network also has certain drawbacks which are listed below:

(i) Easy to fall into local minimum values: mathematically, the traditional BP neural network, as a local search optimization method, solves complex nonlinear problems, and the network weight is gradually adjusted through the local improvement direction, so the algorithm can become a local extreme value. Therefore, network training fails. In addition, the BP neural network is very sensitive to the initial weight of the network, and when the network is initialized with different weights, it tends to converge to different local minima, which is the fundamental reason why many scholars get different results every time they train.

(ii) Slow convergence: since BP neural network algorithm is the gradient descent method in essence, the objective function it needs to optimize is very complex. Therefore, "saw-tooth phenomenon" is inevitable, which makes BP algorithm inefficient. In addition, since the optimized objective function is very complex, when the neuron output is close to 0 or 1, some flat areas will inevitably appear. In these regions, the weight error changes very little, making the training process almost stop. In the BP neural network model, in order to make the network perform THE BP algorithm, the step size of each iteration cannot be calculated by the traditional one-dimensional search method, but the step size update rule must be given to the network in advance, which will also cause the algorithm to be inefficient. All of the above result in slow convergence of BP neural network algorithm.

(iii) Sample dependence: the training of BP neural network model requires a large number of training samples, and the small sample data network cannot learn the rules therein, causing problems in accuracy.

Aiming at the disadvantage of the traditional BP neural network easily falling into local minimum, the improved particle swarm optimization algorithm was used to optimize the traditional BP neural network.

2.3. Improved PSO-BP Neural Network Model. The improved particle swarm optimization algorithm is stimulated by the following two operations.

2.3.1. Division Operation. Division operation is to do population division of particle swarm to prepare for mutation operation. In the process of particle optimization, the fitness value of particles is calculated, and the calculated results are divided into molecular populations. Let ε be a sufficiently small integer if the following is true:

$$\frac{\mathrm{fit}\left(X_i^t\right)}{\mathrm{fit}_{\mathrm{avg}}^t} \le \varepsilon, \tag{1}$$

In which, X_i^t represent particle, $\mathrm{fit}_{\mathrm{avg}}^t$ is the average value of the fitness of the first generation of particles, satisfying $\mathrm{fit}_{\mathrm{avg}}^t = (1/m)\sum_{i=1}^{m} \mathrm{fit}(X_i^t)$. Among all outstanding subgroups (ESP), the particle swarm is represented as $X_{EP\_\alpha}^t, \alpha \in (1, 2, \ldots, \theta)$. Through the dynamic setting of values, the division of subpopulations is controlled, and the calculation formula is as follows:

$$\varepsilon = \varepsilon_2 - \frac{\mathrm{MAXITER} - \mathrm{iter}}{\mathrm{MAXITER}} \left(\varepsilon_2 - \varepsilon_1\right), \tag{2}$$

where ε_1 and ε_2 are the initial and final values of $\varepsilon_2 > \varepsilon_1$, MAXITER is the maximum allowable iteration number, and iter is the current iteration number. At the beginning of iteration, the number of particles in ISP is large, that is, the number of mutated particles is large. We increase the diversity of particles. At the end of iteration, the number of variable particles decreases and the particles converge to the optimal solution.

2.3.2. Probability Mutation. The traditional adaptive mutation is to re-initialize some particles with a certain probability [16], but the mutation object and the probability of the mutation object are not reasonably defined, which has

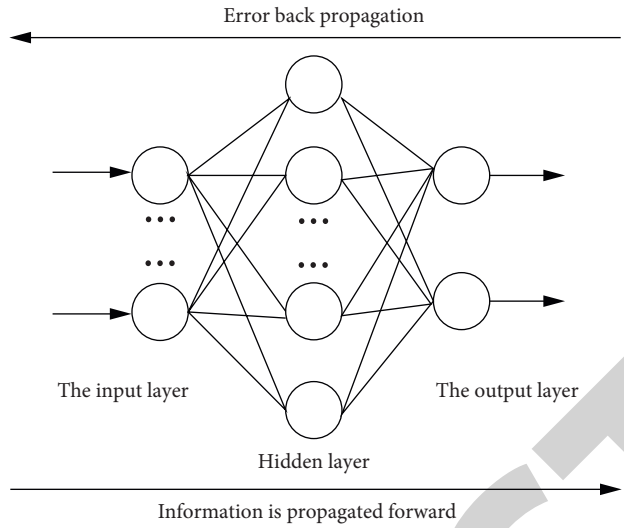

Figure 1: Basic structure of BP neural network.

a certain impact on the result of optimization. New position information will be generated after the particle is mutated, assuming that the position of the newly generated particle is $X^t_{\text{son}\_\beta}$. The mutation operator of $X^t_{\text{son}\_\beta}$ is designed as follows:

$$X^t_{\text{son}\_\beta} = X^t_{IP\_\beta} + P_v \sqrt{\sum_{d=1}^{D} \left(X^t_{\beta\_d} - X^t_{P_{g-}d} \right)^2} \psi \circ V^t_{IP\_\beta}, \quad (3)$$

where $P_v = \text{fit}(X^t_{IP\_\beta}) / \sum_{\beta=1}^{\varphi} \text{fit}(X^t_{IP\_\beta})$, $\sqrt{\sum_{d=1}^{D} (X^t_{\beta\_d} - X^t_{P_{g-}d})^2}$ is the Euclidean distance of the β-th IP position from the global optimal value of the current iteration, and the direction coefficient is a 1xD matrix composed of random numbers within [−1, 1]. At early iterations, the IP and the global optimal solution of the Euclidean distance are large, and the particles will enhance the ability of searching global optimal values. In the iterative process, the particles are in the middle to near the global optimal value, and the optimal value gradually decreases, and the algorithm pays more attention to the search in the later development ability.

The Ackley nonlinear function [17] compares the performance of the original PSO algorithm and the improved PSO algorithm, and the Ackley function is shown as follows:

$$y = -c_1 \exp\left(-0.2 \sqrt{\frac{1}{n} \sum_{j=1}^{n} x_i^2} \right) - \exp\left(\frac{1}{n} \sum_{j=1}^{n} \cos(2\pi x_j) \right) + c_1 + e. \quad (4)$$

Particle swarm optimization combined with BP neural network is mainly used to optimize the threshold and weight in the network structure, so that the prediction model can find the optimal weight and threshold for network training and prediction. The steps of DPMPSO-BP algorithm are as follows:

Step 1: determine BP neural network structure parameters.

Step 2: initialize the particle information and the position and velocity of the particle. Parameters required by PSO algorithm include population size m, particle dimension d, maximum number of iterations MAXITERSIZE, inertial weight initial value and termination value ω_0 and ω_1, learning factors c_1, c_2, and particle maximum and minimum velocity.

Step 3: the synthetic error function of BP neural network was used as the particle swarm fitness function F:

$$F = \frac{1}{P} \sum_{p=1}^{P} \sum_{i=1}^{l} \left(\widehat{y_i^p} - y_i^p \right)^2. \quad (5)$$

Step 4: preliminarily determine the particle individual optimal solution and the population optimal solution.

Step 5**:** call partition algorithm to divide particle swarm into ESP and ISP. ESP enters the next iteration search, and ISP calls probabilistic mutation algorithm to generate new position and speed.

Step 6: search for individual and group extremes of particles. If the current fitness value is better than the individual extreme value, it is updated; if not, the particle speed and position are directly updated. If the particle fitness value is better than the group and volume extreme value, then update.

Step 7: update its speed and position.

Step 8: check whether the particle optimization conditions are met. If so, stop the iteration and map the global optimal value of the particle swarm to the initial

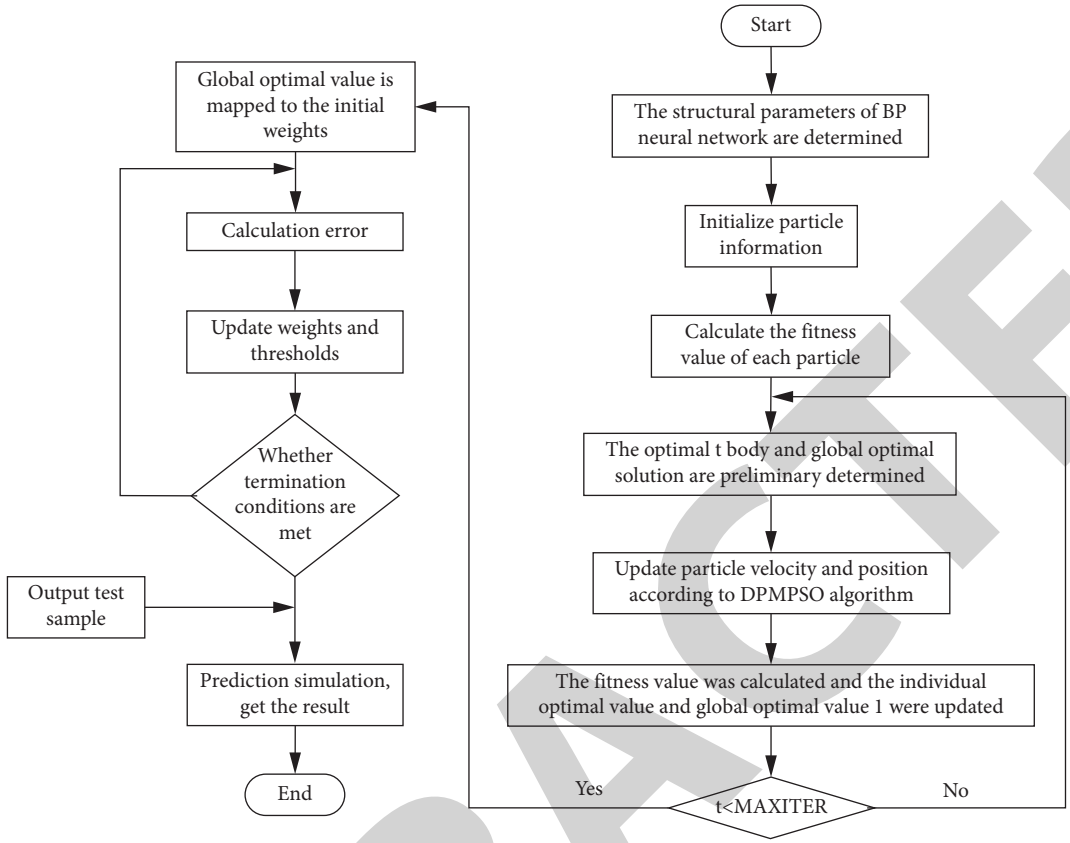

Figure 2: DPMPSO-BP flowchart.

weight and threshold value of the BP neural network; otherwise, return to Step 4 and recalculate the fitness value of the particle.

Step 9: calculate the error of BP neural network, update the weights and thresholds in the network, and check whether the network termination conditions are met. If so, complete the network training and input test samples for prediction simulation. If not, the error is recalculated and the weight and threshold are updated. Figure 2 shows the flowchart.

2.4. General Steps of Supplier Efficiency Evaluation for Intelligent Manufacturing Enterprises

(i) Data collection: the original supplier classification and evaluation datasets were collected by enterprise survey, system data export, and expert and relevant personnel scoring.

(ii) Classification of suppliers: suppliers are classified by Naive Bayes algorithm, and efficient suppliers are output.

(iii) Preprocessing of supplier evaluation data: due to the dimension difference of index data, the data cannot be directly substituted into the model for learning simulation, and the initial data should be standardized. There are positive indicators and negative indicators in the indicator set in this paper, which need to be standardized in different ways according to different properties.

(iv) Network training: with the secondary index in the evaluation index system as the input data and the comprehensive efficiency evaluation value of the supplier as the expected output value, the network is trained by the error backpropagation algorithm.

(v) Result analysis: the results are obtained through experiments, and the results are analyzed. Finally, suggestions for improvement and incentive strategies are put forward for suppliers.

3. Experiments and Results

With the rapid development of the supply chain of intelligent manufacturing enterprises, the evaluation of supplier efficiency has been paid more and more attention by the enterprise management, and more and more researchers have joined in the research of supplier efficiency evaluation. On the basis of the research of experts and scholars, this paper constructed a set of intelligent manufacturing enterprise classification index system and evaluation index system, respectively, through the enterprise field investigation and relying on the school-enterprise cooperation project. The DPMPSO-BP neural network model was used, and the enterprise example was used for simulation verification, and finally the supplier efficiency evaluation model was established.

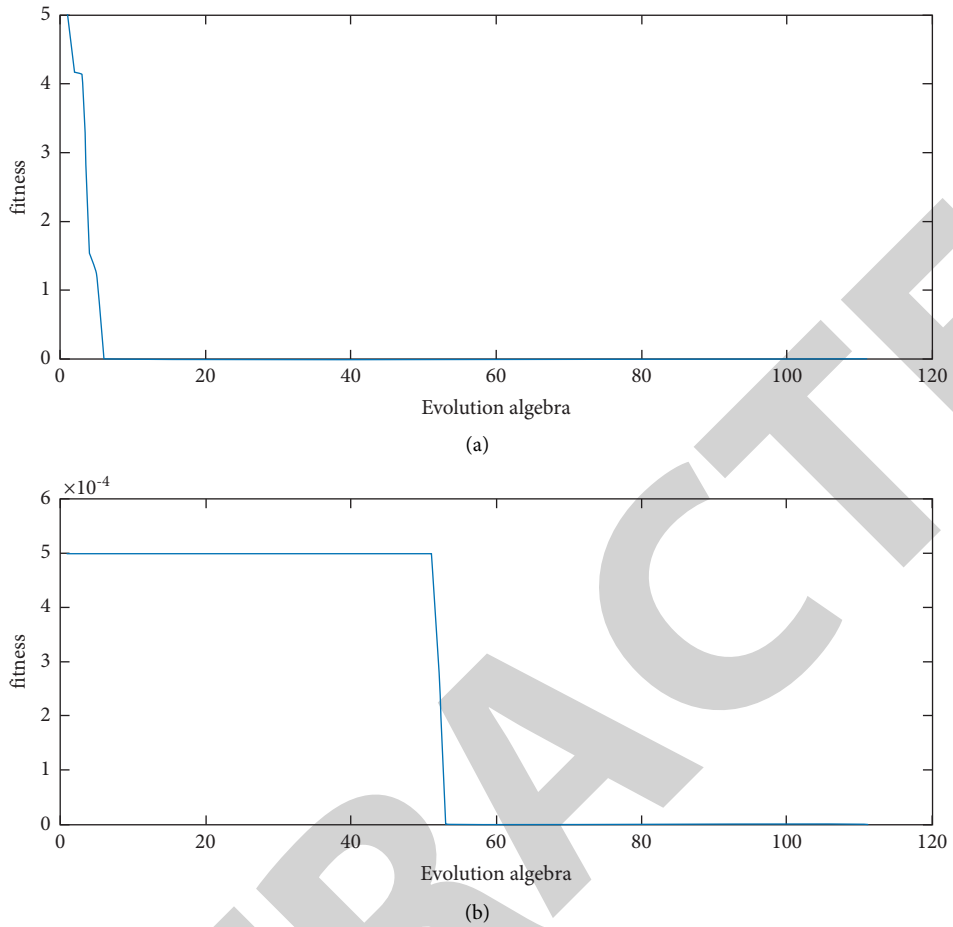

Figure 3: The experimental results of iteration. (a) PSO running effect. (b) DPMPSO running effect.

For a large battery manufacturing enterprise in China, 2,000 suppliers were selected for case analysis. As there are both qualitative and quantitative indicators in the established index system, the qualitative indicators are scored by enterprise managers and experts. For quantitative indicators, classification and evaluation data are collected through systematic data export and formula calculation. Firstly, traditional PSO and improved DPMPSO are compared, where $c_1 = 2$, $e = 2.71282$, and $n = 2$. The experimental results of iteration are shown in Figure 3.

The traditional PSO algorithm obtained the optimal individual fitness value of 0.0095 after 45 iterations, which was close to the actual optimal value of the function, indicating that the PSO algorithm has strong function optimization ability. However, DPMPSO algorithm gets the optimal individual fitness value 0 at iteration 106, which is consistent with the global optimal value of the Ackley function. The experimental results show that DPMPSO algorithm can jump out of the local minimum point and improve the premature convergence of traditional PSO algorithm.

This paper adopts a three-layer neural network structure. The hyperparameters of the BP neural network are set as follows: Inputnum = 25, Hiddennum = 20, Outputnum = 1, use the 'tansig' function from the input layer to the hidden layer, and use purelin activation from the hidden layer to the output layer function, the rest use the trainingda training function, set the maximum number of training to 5000, the learning rate is 0.01, and the error is 0.000010. Parameters of PSO algorithm are set as follows: population size $m = 110$, particle degree $D = 341$, MAXITERSIZE = 100, $\omega_0 = 0.9$, $\omega_1 = 0.4$, $c_1 = c_2 = 1.49445$, $v_{\max} = 1$, and $v_{\min} = -1$. MATLAB R2015b was used to train and test BP, PSO-BP, and DPMPSO-BP models, respectively. The simulation result is shown in Figure 4.

According to the experimental results, the maximum error between the expected output value and predicted value of DPMPSO-BP model is 0.0015, which fully meets the needs of supplier efficiency evaluation of intelligent manufacturing enterprises. When the trained model is stored in the knowledge base, it only needs to input the attribute value matrix of each secondary indicator of the supplier to be evaluated in the supplier management system to obtain the comprehensive evaluation indicator data, which avoids the randomness and human factors in determining the index weight and improves the efficiency of evaluation decision making.

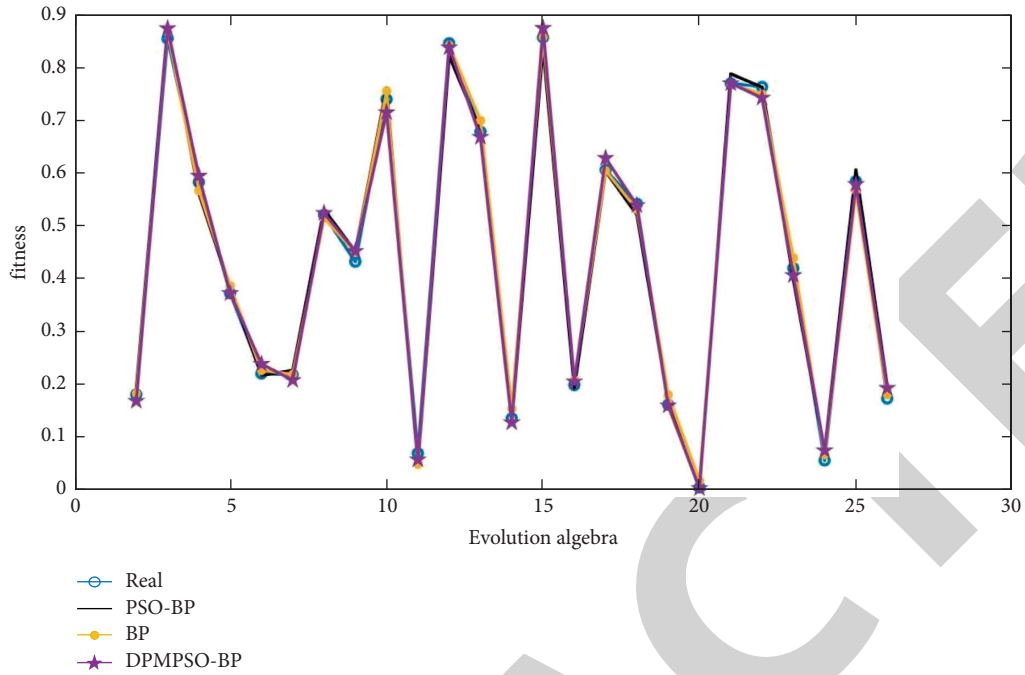

Figure 4: The experimental results of neural network.

4. Conclusion

This paper improved the traditional supplier evaluation method and existing supplier evaluation index system. To this end, the research carried out the analysis of supplier efficiency evaluation index system and supplier evaluation method of intelligent manufacturing enterprises. The current research has theoretical and practical research significances. Machine learning has gradually become a new direction of supplier management research methods, which has obvious value for information mining of massive data. This paper applied the improved PSO-BP neural network model to supplier efficiency evaluation. Use neural network to establish an evaluation model, collect relevant data for analysis and application, and make up for the subjectivity, randomness, and real-time problems of supplier evaluation. It has certain theoretical value for supplier management and supplier scientific innovation research.

Supplier evaluation is an important decision for the operation and production of intelligent manufacturing enterprises. In order to adapt to the development of the new round of industrial revolution, the intelligent reform of enterprises is imperative. The intelligent enterprises are achieved through providing the personalized and intelligent products and services. Based on the background of intelligent manufacturing, this paper puts forward the corresponding supplier evaluation index system and evaluation method, so as to improve the management mode of suppliers, improve production efficiency, point out the direction for the future development of suppliers, and further enhance the core competitiveness of enterprises.

Data Availability

The data used to support the findings of this study are available from the corresponding author upon request.

Conflicts of Interest

The authors declare that they have no conflicts of interest.

References

[1] G. W. Dickson, "An analysis of vendor selection systems and decisions," *Journal of Purchasing*, vol. 2, no. 1, pp. 5–17, 1966.

[2] I. Dobos and G. VörösmartyVörösmarty, "Green supplier selection and evaluation using DEA-type composite indicators," *International Journal of Production Economics*, vol. 157, pp. 273–278, 2014.

[3] W. Song, Z. Xu, and H. C. Liu, "Developing sustainable supplier selection criteria for solar air-conditioner manufacturer: an integrated approach," *Renewable and Sustainable Energy Reviews*, vol. 79, pp. 1461–1471, 2017.

[4] C. Bai and J. Sarkis, "Integrating sustainability into supplier selection with grey system and rough set methodologies," *International Journal of Production Economics*, vol. 124, no. 1, pp. 252–264, 2010.

[5] L. Xiu-Fen, "On the selection and management of suppliers," *Yizhong Technology*, vol. 6, no. Z1, pp. 22-23, 2002.

[6] H. Wang, "Review of supplier selection methods," *Logistics Science and Technology*, vol. 35, no. 11, pp. 87–89, 2012.

[7] M. Qiu, "Research on bidding management of enterprise material procurement," *China Market*, vol. 7, no. 02, pp. 168-169, 2019.

[8] Z. Wang, "Research on petrochemical equipment supplier selection method," *Commodity and Quality*, vol. 5, no. S7, pp. 59-60, 2012.

[9] Z. Degraeve, E. Labro, and F. Roodhooft, "An evaluation of vendor selection models from a total cost of ownership perspective," *European Journal of Operational Research*, vol. 125, no. 1, pp. 34–58, 2000.

[10] J. Zhou, "Evaluation and selection of supply chain partners based on ABC Cost method and AHP," *Economic Research of Coal*, vol. 52, no. 4, pp. 68–71, 2019.

Hindawi
Journal of Mathematics
Volume 2023, Article ID 9842979, 1 page
https://doi.org/10.1155/2023/9842979

Retraction

Retracted: Classification and Analysis of College Students' Skills Using Hybrid AI Models

Journal of Mathematics

Received 19 December 2023; Accepted 19 December 2023; Published 20 December 2023

This article has been retracted by Hindawi following an investigation undertaken by the publisher [1]. This investigation has uncovered evidence of one or more of the following indicators of systematic manipulation of the publication process:

(1) Discrepancies in scope

(2) Discrepancies in the description of the research reported

(3) Discrepancies between the availability of data and the research described

(4) Inappropriate citations

(5) Incoherent, meaningless and/or irrelevant content included in the article

(6) Manipulated or compromised peer review

The presence of these indicators undermines our confidence in the integrity of the article's content and we cannot, therefore, vouch for its reliability. Please note that this notice is intended solely to alert readers that the content of this article is unreliable. We have not investigated whether authors were aware of or involved in the systematic manipulation of the publication process.

Wiley and Hindawi regrets that the usual quality checks did not identify these issues before publication and have since put additional measures in place to safeguard research integrity.

We wish to credit our own Research Integrity and Research Publishing teams and anonymous and named external researchers and research integrity experts for contributing to this investigation.

The corresponding author, as the representative of all authors, has been given the opportunity to register their agreement or disagreement to this retraction. We have kept a record of any response received.

References

[1] H. Tang and Y. Wei, "Classification and Analysis of College Students' Skills Using Hybrid AI Models," *Journal of Mathematics*, vol. 2022, Article ID 4428416, 10 pages, 2022.

Hindawi
Journal of Mathematics
Volume 2022, Article ID 4428416, 10 pages
https://doi.org/10.1155/2022/4428416

Research Article

Classification and Analysis of College Students' Skills Using Hybrid AI Models

Huili Tang and Yanhong Wei

Zhengzhou Preschool Education College, Zhengzhou 450000, China

Correspondence should be addressed to Huili Tang; huilitang92@outlook.com

Received 29 November 2021; Revised 27 December 2021; Accepted 30 December 2021; Published 21 January 2022

Academic Editor: Naeem Jan

Each individual diversifies in the population with certain characteristics. Thus, diversity is a scientifically proven and widely accepted phenomenon when the human being is a concern. One of the areas where the diversity of human beings is mostly paid attention to is called the learning process, since different forms of responses could be observed. For example, each student perceives, assimilates, and uniquely processes the information when being transmitted to him, which confirms the inherited diversity. In this regard, educational systems are required to deal effectively with students and to apply the principles of personalized learning, which is pertinent to learning processes that meet the individual needs and interests of learners. By doing so, taking into account their unique characteristics, talents, skills, inclinations, and desires are satisfied. This manuscript presents an innovative model to classify college students' skills. A hybrid artificial intelligence (AI) system that fully automates the process of personalized training is proposed based on individual skills by taking into account the priority of personalized and fully customized learning systems. The process specifically utilizes the Rasch statistical analysis model and an innovative fuzzy Bayesian network. Higher-level reasoning is generated for the automated and personalized learning process in which college students are automatically classified into a certain category based on their skills.

1. Introduction

Intensive research in both neuroscience and psychology confirms the existence of different ways to obtain [1, 2], assimilate, construct, and reuse the information and knowledge provided to students [3, 4]. However, the learning and training programs implemented by most educational systems are only suitable for one type of student, called visual students [5, 6]. This group of students has a photographic memory and recalls any information exactly as it is presented in books [7]. Otherwise, in the case of acoustic persons, that is, students who learn best by listening to information or kinesthetic formulas, or students who learn by making things themselves manually, these types of students have a lot of difficulty in learning and assimilating knowledge and therefore are very likely to fail to harmonize with the education system provided [8–10].

In this sense, individualized learning is essential for the successful completion of a framework that can cover all areas of intelligence to be beneficial for each type of student. The main features of the personalized learning model are summarized as follows [11–13]:

(1) The adaptive structure of the educational material based on evaluation criteria and the interaction with the aim of its continuous improvement

(2) Giving importance to different learning styles

(3) The student-led participation in the learning process

(4) The emphasis on participation in the learning process through collaborative environments

(5) Accessing technology and the most up-to-date educational resources

All these suggest that the personalized learning model recognizes each student as an individual with a different

style, pace, and way of learning, as well as a different view of learning. It recognizes the value of the involvement of technology in education, providing a variety of options and opportunities so that learning programs are tailored to each learner's skills, needs, and preferences [14, 15].

The aforementioned advantages are fully realized with the holistic introduction of information and communication technologies into education and the rapid spread of the Internet, which altered conventional learning and teaching practices around the world. Especially with the pandemic crisis [16], distance learning has recently adopted advanced learning management systems as a direct and alternative way to access educational resources and services [17]. In general, e-learning can be considered as a means of overcoming the barriers of time, place, and socioeconomic status, which could reduce the access of many individuals and groups to education and knowledge and thus offers great opportunities to improve their social and professional status [8, 18, 19].

However, despite the given penetration of distance education methods (synchronous and asynchronous), the fact that the high dropout rates of the respective programs have been observed in recent years was mainly due to the lack of student satisfaction, since the same static learning was provided for all regardless of their previous knowledge, experience, preferences, and learning objectives during the interaction with the system [2, 20]. Hence, to restructure educational technologies for contemporary needs, teaching methods and the way of constructing educational material are more prominent. Innovative educational systems based on advanced artificial intelligence (AI) methodologies can offer a solution that can be compared with individualized teaching methods [21].

The emerging technologies can improve educational programs and teaching practices in many ways so the technical innovations can be a competitive advantage of the new era. That is the main reason why we need to further examine the involvement of AI, Big Data Analytics, and Machine Learning implementations in education procedures.

This paper presents an innovative model to classify college students' skills based on a hybrid AI system that fully automates the process of personalized learning based on individual skills. Specifically, combining the Rasch statistical analysis model and an innovative fuzzy Bayesian network leads to higher-level reasoning that is produced for the automated and personalized learning process in which the college students are automatically classified into a certain category based on their skills.

The organization of the manuscript is as follows: Section 2 discusses the researches that deal with personalized learning and its implementations based on AI technologies by giving pros and cons concurrently. The proposed method is introduced in Section 3. Section 4 conducts the implementation of the proposed method based on a data set. Section 5 presents the results of the implemented method. The conclusion and discussion are comprehensively provided in Section 6.

2. Related Literature

The literature of AI research in education, especially in recent years, has been increasing at a fast pace because of the great potential of AI in the field of the educational process and especially the personalization aspects. Most researchers conclude that AI in education and particular learning has presented a great potential from both theoretical and pedagogical points of view, but there is still a need to develop a critical stance before fully integrating it into the educational processes. Testing and evaluation of AI in educational processes are essential to avert automated processes and Machine Learning (ML). For example, Sisman-Ugur and Kurubacak [22] presented the future perspectives of AI in various contexts, such as Natural Language Processing, Machine Learning, and Deep Learning. They also utilized Social Network Analysis as a guide for the interpretation of the key concepts in AI research based on an educational perspective. Finally, their research identified three broad themes, adaptive learning, personalization, and learning styles, expert systems, and intelligent tutoring systems. Hence, AI as a future component of educational processes could emerge. However, their research is essentially a general overview of the implementation of AI in the education processes.

Also, Bozkurt et al. [23] analyzed the trend and patterns of AI implementations in education by combining descriptive statistics, t-Distributed Stochastic Neighbor Embedding (t-SNE), Social Network Analysis, and text mining. They concluded an increment of AI in the education publications during recent years.

Klašnja-Milićević and Ivanović [21] aimed to address the research by examining elements of personalized e-learning, intelligent, and interactive technologies. They ultimately have depicted the state-of-the-art online education systems empowered with AI. Their theoretical study also serves as a suggestion to institutions and organizations that want to adopt these new technologies and approaches in education.

Maghsudi et al. [14] provided a brief review of state-of-the-art research and investigated the challenges of AI/ML-based personalized education and discussed potential solutions. They concluded that "personalized education" is one of the most precious merits of AI concerning education because it significantly improves the quality of education in several dimensions by adapting to the distinct characteristics and expectations of each learner such as personality, talent, objectives, and background. Also, online education is of the utmost value under abnormal circumstances such as the COVID-19 outbreak or natural disasters. Indeed, conventional education requires significantly more resources than the online format concerning educational space, scheduling, and human resources, which makes it prone to failure with even a small shift in conditions. As such, emerging alternatives are inevitable. Despite having the potential of a revolutionary transformation from traditional education to modern concepts, personalized education is associated with several challenges.

On the other hand, Krendzelak [18] especially examined ML and its applications in e-learning environments. Also,

the authors in [24] evaluated ML methods to detect and distinguish diverse self-injurious behavior types. Iatrellis et al. [25] provided a complete tool for the optimization and calculation of the offered services by the Higher Educational Institutions in combination with the minimization of respective costs that are enhanced with Machine Learning and semantics. Finally, an improved hybrid ontology-based approach for online learning resource recommendations [1] combining collaborative filtering algorithm and sequential pattern mining techniques was proposed by Shang et al. [26].

From the aforementioned literature, we conclude that the vast majority of the research highlights the great potential of AI in educational processes but there is a lack of proposed schemes to further take advantage from a practical point of view like the current paper does.

3. The Proposed Hybrid AI System

By adopting an eclectic approach to methodological practices [21], a key goal of educational programs is to devise a combination of different methods that aim to involve the learner as actively as possible, which is always based on his particular characteristics and abilities. In this regard, the most important role in the implementation of an adaptive system of personalized learning is the appropriate choice of educational material [18].

The material in question may be digital (study guide, parallel texts, etc.), audiovisual (audio files, digital videos, etc.), practical (exercises and activities, case studies, digital laboratory applications, etc.), and interactive (conversations, video conferencing, etc.). This material should be formulated with a special teaching methodology and function as a preparing process. Accordingly, the variety of elements that a distance learning environment should contain lies in the fact that each of the educational resources should undertake specific objectives in the educational process to create conditions for active participation and learning [2, 21].

In conclusion, it should be suggested that the concept of learning material is related to the designed and transformed synthesis of educational resources, which can devise the right conditions and support the learning process based on each student's skills. The educational material in question concerning the context of education learning is composed of the means of teaching and practicing and like all tools of teaching. Thus, their main function is to support the learning process within the learning environment. The concept of "learning environment" is mainly related to external factors and refers to the whole range of educational and learning materials and how this environment is structured to enable the individualized learning process [14, 15, 22]. Personalization refers to the use of a learner's abilities, sensitivities, and abilities (including emotional ones) to develop his or her skills, abilities, and talents. Individualized teaching is based on carefully prepared educational materials that recognize the different forms of the students' skills and level of knowledge and their ability to learn from different learning environments and to enhance feedback and assessment of their abilities [23, 25].

To devise an intelligent framework whose main features will be easy access to the most up-to-date educational resources, diverse learning environments, personalized rearrangement in the curriculum, and the learner's ability to direct the objectives of the learning process, a hybrid AI system is proposed which aims to intelligently adapt the educational material to the unique skills of each learner.

The specific steps as well as the technical details of how the hybrid system works are presented in the next subsections.

3.1. Preliminary Questionnaire. The proposed system is based on the exploratory statistical analysis that processes questions in questionnaires of different scientific fields as well as their evaluation measure regarding the creation of a reliable measurement scale for the initial classification of the college students and the optimal adaptation of the educational material. The methodology aims at designing a questionnaire and the reliable estimation of the sum of a set of scales that are produced by successive individual measurements, for example, different questions, iterative measurements, and different measurement systems. By applying specific but simple statistical analyses, the various scales are utilized to check whether they contribute to creating a specific evaluation model. Then, the results of the process are forwarded to the next step of the proposed system called the Rasch model [27].

3.2. Rasch Model. The results obtained at the first stage are analyzed based on the Rasch model [28]. The proposed model is inspired by the Item Response Theory [29] and specifically by the peculiarities of Rasch's model, which records the probability of a person answering a question [27, 28]. The responses of the participants are aggregated in a worksheet, in which columns refer to questions and rows to individuals, which is used to generate a final score for each individual. The total score is representative of all the questions and a person with a higher overall score has a higher value position on the scale of the measured variable which is called one-dimensional because of its simplicity of calculation [28].

The application of the Rasch model recommends the creation of a scale to measure questions and the scale of the ability of individuals to respond using special methods. The scale of the questions is approached by a computational process known as item calibration. On this scale, the lower the percentage of correct answers becomes, the higher the difficulty of the questions grows, and consequently the greater the magnitude of the calibrated scale becomes. The scale of the questions is calibrated based on the scale of probabilities (in logit units) and is calibrated as the scale of measuring the responsiveness of individuals in the same way. These two scales create two frequency distributions.

In binary questions, the position of difficulty of a question on the scale corresponds to a responsive position of an individual who correctly answers this question with a defined probability of 0.5. Then, it designates the position on the difficulty of the skill scale. When a person correctly

answers a question whose corresponding position is lower than the corresponding position held by that person, the difficulty occupying a specific position on the skill scale shows a probability of the person answering this question greater than 0.5. Conversely, when the difficulty of the question occupies a position higher than the corresponding position of that person, the probability of the person answering is less than 0.5.

For a better understanding, the Rasch model uses the scale of measurement in the form of a ruler presented in Figure 1. The vertical lines on the scale are the questions that have a special place depending on their degree of difficulty [27–29].

While less difficult questions are answered on the left-hand side of the scale, more difficult ones are on the right-hand side of it. Respondents also take a special position depending on their level of responsiveness: while people with low ability (skills) are located at the left-hand side of the scale, people with a high level of ability are located at the right-hand side of it. Thus, less difficult questions can be easily answered correctly by more capable people. For example, while person B is assessed as having a very low ability after answering only four questions correctly, person *D* is evaluated as an average level of ability because he answers about 50% of the questions correctly. The other person called C has a high response ability because he answers almost all questions successfully. The position of the questions and the individuals along the measurement scale is calculated utilizing the model based on the percentage of the response of each individual to each question.

In general, Rasch's model allows the algebraic separation between the parameters of the question and the parameters of the individual. Therefore, the estimations of the statistical parameters are conducted. The procedure is performed using the dependent maximum probability in which the response dimension is divided into segments concerning the individual's overall score. While the latter provides important information about the individuals concerning the content of the question, the former, which is the overall score of the questions, provides detailed information about the latent characteristics of the individuals [27–29].

The full utilization of the above process and in particular the results of the Rasch model is forwarded to the next step of the framework called the Personalized Classification.

3.3. Personalized Classification. The Personalized Classification process is a methodology used to extract knowledge from the data gathered employing the Rasch model. Each element is assigned to a predefined set of categories to classify the college students into the respective classes that represent their skills and abilities. The process is based on an innovative fuzzy Bayesian network.

Bayesian networks [30] are initially used to generate a probabilistic representation of the data structure derived from the Rasch model and their hypothetical independence through a Directed Acyclic Graph (DAG) in which complete and combined probability distributions are substantiated. The aim is to categorize a sample into one of the predefined

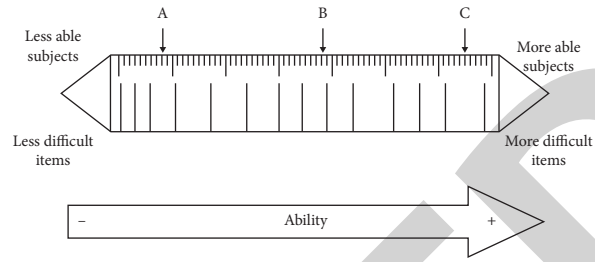

Figure 1: Rasch model rule.

categories represented by C1, C2,.., Cn using a probability model defined by the Bayes theory. In essence, this is an initial categorization process by simply evaluating probabilities and not taking into account forecasts. Its more usefulness and efficiency and quick feature extraction are observed experimentally. Besides, the forecasts have been represented by a degree. The purpose is to minimize the expected costs in the sequel. Each category is characterized by a previous probability. Assume that the given sample belongs to a category Ci. Utilizing the definitions and Bayes theory helps determine the probability [31]. Essentially, the step of the process is related to understanding the dependence between the results of the questionnaire and assigning probabilities to them. Thus, ensuring how the appearance of one event likely occurs is changed when the other is presented. By doing so, the proposed system integrates the previous knowledge gained from the Rasch model into the learning process model through a probabilistic representation of the data structure that emerges from each learner.

Besides, uncertainty has existed in the parameters of the model generated by some sources such as noise, random, or misleading answers. The method uses a gradual assessment that is described with the aid of a membership function in the interval $[0, 1]$. The proposed model introduces the four types of fuzzy set operations between sets, which are the following:

(1) Fuzzy Disjunction:

$$\mu_{\tilde{A}\cup\tilde{B}}(x) = \mu_{\tilde{A}}(x) \vee \mu_{\tilde{B}}(x) = \max\left[\mu_{\tilde{A}}(x), \mu_{\tilde{B}}(x)\right] \forall x \in X. \tag{1}$$

(2) Fuzzy Conjunction:

$$\mu_{\tilde{A}\cap\tilde{B}}(x) = \mu_{\tilde{A}}(x) \wedge \mu_{\tilde{B}}(x) = \min\left[\mu_{\tilde{A}}(x), \mu_{\tilde{B}}(x)\right] \forall x \in X. \tag{2}$$

(3) Fuzzy Product:

$$\mu_{\tilde{A}\bullet\tilde{B}}(x) = \mu_{\tilde{A}}(x) \bullet \mu_{\tilde{B}}(x) \forall x \in X. \tag{3}$$

(4) Fuzzy Complement:

$$\mu_{\tilde{A}}^{-} = 1\mu_{\tilde{A}}(x). \tag{4}$$

3.4. Evaluation. To have an objective evaluation process of the model, both self-evaluation and comparison with corresponding alternative models are needed. The procedure is

validated by content testing based on the original questionnaire that was originally constructed. This process is more suitable in adapting the model to changing problem areas related to the ability to self-adaptive learning, which provides the ability to redefine learning and improve its behavior over time in any iteration process.

Verification is in the form of referring to the personalized learning process. If a measure threshold is activated to allow the accurate calculation of the output vector, it is optimal in the sense of the minimum approach error. In particular, verification refers to the process of achieving the desired behavior through an iterative process of updating the proposed system. It should be emphasized that each algorithm used in the process offers a different way of adapting to the desired result as well as different adaptation techniques which are completely dependent on the problem to be solved. The goal is to systematically and quickly find the appropriate parameters of the system to minimize the error between the actual and the desired outputs.

3.5. Educational Material. When the verification process is completed, it is considered that the educational content has been classified based on the needs and skills of each trainee. The intelligent production process of the educational material proposed is the result of the production of reasoning, that is, knowledge that does not come from an instructor, but is a scientific-technological breakthrough in an environment of uncertainty. For this purpose, the structure and mathematical representation of the educational content which are distributed and disposed of are taken as a fuzzy fact. Defining fuzzy sets is proposed as to how events are combined to produce logical propositions, relationships, and conclusions [32–34].

3.6. Self-Adaptive Fuzzification. Finally, it is possible to perform some additional segmentations and distributions based on the self-adaptive fuzzification process among the ambiguous sets resulting from the previous process [35, 36]. The procedure in question concerns operations between ambiguous sets borrowed from probability theory and concerns the possibility of joining and intersecting two contingencies. A clear distinction between the fuzzy sets and the probability space is then conducted which results in the use of more general expressions for the union and intersection of the sets in question. Specifically, the model produces inference rules that are represented in a logical form or guide consisting of hypotheses that are represented as follows:

(1) Modus Ponens: $\left\{(\tilde{A} \overrightarrow{\ } \tilde{B}) \wedge \tilde{A}\right\} \overrightarrow{\ } \tilde{B}$

(2) Modus Tollens: $\left\{(\tilde{A} \overrightarrow{\ } \tilde{B})\ \tilde{A}\right\} \tilde{B}$

(3) Hypothetical Syllogism: $\left\{(\tilde{A} \overrightarrow{\ } \tilde{B}) \wedge (\tilde{A} \overrightarrow{\ } \tilde{C})\right\} \longrightarrow (\tilde{A} \overrightarrow{\ } \tilde{C})$

With the completion of this step, the educational content has been created and segmented with full evaluation criteria based on the particularities of each trainee. The redefinition process is achieved through the continuous evaluation of the trainees as the process approaches the target as close as possible.

4. Experiments

The scenario developed concerns a preliminary test for the classification of students in respective level departments having similar difficulty and respective courses. A preliminary questionnaire was distributed to a total of 350 college students. The questions are related to their skills and aspirations from the curriculum. Learners were asked to answer the questions using the Likert scale in which the five grades were listed from 1 to 5 whose expressions are as follows: totally disagree, disagree, neither disagree nor agree, agree, and totally agree, respectively.

The processing of the results to assess the reliability of the questionnaire resulted in a total Cronbach index of 0.776, which is a value higher than the generally accepted value of 0.7. This principally suggests that at least some questions are capable of measuring the same composition of anxiety in the pretest process. Cronbach's alpha [37, 38] is not a statistical test, called a coefficient of reliability (or consistency). It measures internal consistency, that is, how a set of items are closely related as a group. It is considered to be a measure of scale reliability. It can be written as a function of the number of test items and the average intercorrelation among the items. Cronbach's alpha is defined in the following equation:

$$a = \frac{N\overline{c}}{\overline{u} + (N-1)\overline{c}}, \tag{5}$$

where N is the number of items, $\overline{c}$ is the average interitem covariance among the items, and $\overline{u}$ is the average variance. As the average interitem correlation increases, Cronbach's alpha increases as well (when the number of items is kept constant).

Note that the process of defining the difficulty and ability parameters is calculated based on the probability of a successful outcome (odds) (quotient of probability p to probability $q = 1 - p$). Its logarithmic version determining the ability of the individual is defined by

$$P(\theta) = \ln\ln \quad \left(\frac{p}{1-p}\right). \tag{6}$$

When the right-hand part of the equation is calculated, $P(\theta) = \theta - \beta$, which expresses that the probability of validation of a question that is equal to the difference between an individual's ability and the difficulty of the question can be calculated. The closer the difference equals 1, the greater the chance of a correct response becomes. Conversely, the smaller the difference grows and the closer it gets to 0, the greater the chance of a wrong answer is. When the capacity scale is measured in units of normal distribution, the response has a 0.50 probability of being correct when the capacity value is $\theta = 1.0$.

The relationship between the successful outcome (correct choice) and the measured latency characteristic (individual capacity) is described in the form of a sigmoid

characteristic curve of the Item Response Function (IRF) [27, 29]. Figure 2 depicts it.

Rasch's model is applied to estimate some characteristics of the sample of students such as individual ability and behavior, which are presented in the form of a latent variable. It is used in the preparation of special questionnaires for the evaluation of the mentioned variables by processing the responses of the participants [27, 28]. The model estimates the probability of responding to the two-parameter function: the "person" and the "question." In particular, it measures the probability of occurrence of the correct answer resulting from the difference between the parameter of the respondent and the question.

Regarding the progress of exams in education, the parameter of the questions is related to the degree of difficulty of each question and the parameter of the student is pertinent to his ability to answer successfully. Thus, the greater a person's ability to respond to a relatively difficult question grows, the more likely he or she is expected to have answered the question correctly. If the magnitude of the difficulty of a question is equivalent to the magnitude of the responsiveness of the individual, then the probability of giving the correct answer is set at 0.5 (50%). Specifically, the outcome of a successful answer to a question is determined by the probability assessment defined by

$$P_r\left(X_i = 1|\theta_j, \beta_i\right) = \frac{e^{\theta_j - \beta_i}}{1 + e^{\theta_j - \beta_i}}, \tag{7}$$

where $X_i = 1$ is the correct answer to question X_i, the condition on the dichotomous variable is denoted by θ_j based on the ability of the trainee j, and β_i is the difficulty of question i.

By applying the logarithm of the student's probability ratio (logit) to the correct answer for a given question, the ratio is equal to $\theta_j - \beta_i$. In addition, this ratio also applies to a correct answer for a second question. It is equal to the difference between the positions of the two questions expressed by

$$o g - o\, d\, d\, s\left(X_i = 1|r_j = 1\right) = \beta_2 - \beta_1, \tag{8}$$

where r_j is the student's overall score regarding the answer to the two questions. It is easy to see that the presentation of the responses using the logarithm ratio in the correct answer provides the estimate of $\beta_2 - \beta_1$ which does not contain the term θ_j. Thus, the dependent maximum probability technique directly serves to calculate the difficulty of the questions.

Thus, Rasch's model takes the model of question response theory where the total score along the questions characterizes exclusively the individual and therefore is calculated based on a single parameter related to the individual (ability) and the other parameter (difficulty) that corresponds to each category of the question and called a threshold [27, 28]. Thus, there exist four thresholds for the five-part questions of the questionnaire under consideration.

By taking into account all the questions of the questionnaire and all the students participating in the exam, we evaluate the answer function of the questions and plot the curve of the IRF questions showing the probability of a correct answer as a result of the students' ability [29]. The IRF graph of the 10 questions in the questionnaire is shown in Figure 3.

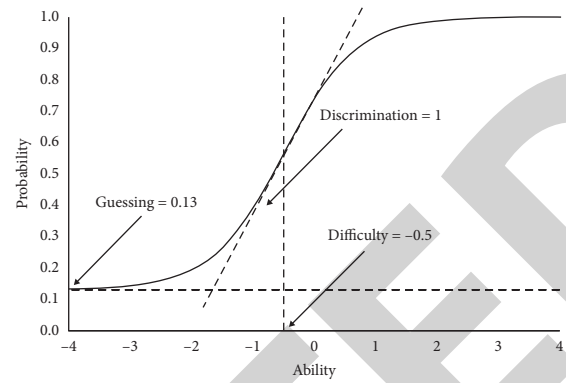

Figure 2: Item Response Function.

Each estimated capacity value is associated with a standard measurement error quantifying the degree of uncertainty of the estimate. The same is true for the estimated values of the questions with a noticeable difference. Thus, the standard errors of the difficult questions are much smaller than those of the individual ability assessment values as the answers to the questions usually outweigh the responses of the individuals. The standard error of individual estimates is narrower in the region where the IRF slope is steeper, that is, in the interval of progress points, since Rasch's model is based on the application of the Poisson distribution [39]. It was experimentally shown and demonstrated that the number of response errors made by an individual is the quotient of the difficulty of the question to the ability to answer by the person. The response estimation measure is based on this assumption.

The results of the aforementioned statistical analysis of the questions and the probabilistic values resulting from the Rasch model process [28] are a basic criterion to map the answers of each student into a pair of variables entering the Bayesian network [31] whose form is denoted by $B = \langle G, \Theta \rangle$, where G is the DAG whose nodes $X_1, X_2, \ldots, X_n$ represent the variables and their probability values resulted from each question in the questionnaire and their edges. Thus, the direct dependencies are represented between these variables (the answers to each question). Graph G encodes independence assumptions. Each variable X_i is independent of the inheritance assumed by G. Θ denotes the set of network parameters. Specifically, this set contains the parameter $\theta_{x_i|\pi_i} = P_B x_i|\pi_i)$ for each x_i implementation of X_i in the condition π_i, for the set of X_i parents in G. Therefore, B defines a unique probability distribution over the variables; namely,

$$P_B = \left(X_1, X_2, \ldots, X_n\right) = \prod_{i=1}^{n} P_B\left(\pi_i\right) = \prod_{i=1}^{n} \theta_{X_i}|\pi_i). \tag{9}$$

The result of the process is to generate a probability value for each variable (answer) that essentially reveals the interdependence of the variable with a class, indicating the

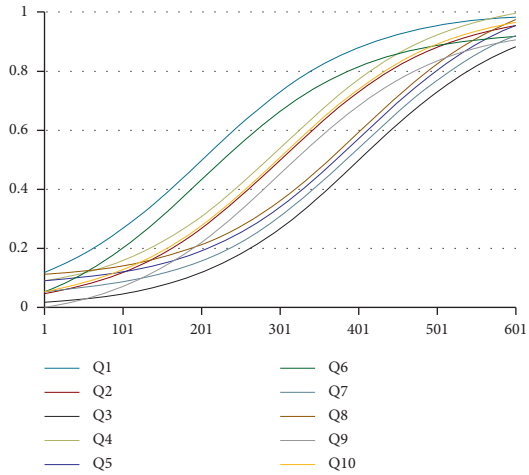

Figure 3: Item characteristic curves.

direction of the influence resulting from each question. An initial categorization of the answers into clear classes can determine the choices and abilities of each student in this way. With this example utilizing the questionnaire, the implemented algorithm of the Bayesian network generates three classes, which are called Theoretical Direction, Positive Direction, and Technological Direction, based on their answers.

5. Results and Discussion

The following criteria were used to evaluate the performance of the hybrid AI system [40–43]:

(1) Overall Accuracy (OA): this measure denotes the number of correctly classified samples divided by the number of test samples.

(2) Average Accuracy (AA): this indicator shows the average of the categorizations of all categories.

(3) Kappa Rate: this is a statistical measurement providing information with the amount of agreement between the truth map and the final classification map, which is calculated by

$$k = \frac{p_0 - p_e}{1 - p_e} = 1 - \frac{1 - p_0}{1 - p_e}, \tag{10}$$

where p_o is the relatively observed agreement among raters and p_e is the hypothetical probability of a chance agreement.

(4) McNemar Test: to assess the importance of classification accuracy resulting from different approaches, a McNemar Test was conducted, which is defined by

$$z_{12} = \frac{f_{12} - f_{21}}{\sqrt{f_{12} + f_{21}}}, \tag{11}$$

where f_{ij} represents the number of samples classified correctly in classification i and incorrectly in classification j.

(5) Coefficient of Determination (R^2): it is used to express the correlation of two variables represented by a percentage. The Coefficient of Determination gives the percentage of variability of Y calculated by X and vice versa and it is defined by

$$R^2 = 1 - \frac{\sum_{i=1}^{n}\left(Y_i - \hat{Y}_i\right)^2}{\sum_{i=1}^{n}\left(Y_i - \underline{Y}_i\right)^2}, \tag{12}$$

where Y_i represents the observed values of the dependent variable, $\hat{Y}_i$ represents the estimated values of the dependent variable, Y is the arithmetic mean of the observed values, and n is the number of observations.

(6) Root Relative Squared Error (RRSE): this function calculates the absolute correlation between actual and predicted values and therefore the absolute success of the model, which is achieved when this is equal to zero, is defined by

$$\text{RRSE} = \frac{\sum_{j=1}^{n}\left(P_{(ij)} - T_j\right)^2}{\sum_{j=1}^{n}\left(T_j - \underline{T}\right)^2}, \tag{13}$$

where $P_{(ij)}$ is the value predicted by the program for a simple hypothesis j, T_j is the target value for the simple hypothesis j, and T is calculated by

$$\underline{T} = \frac{1}{n}\sum_{j=1}^{n} T_j. \tag{14}$$

Table 1 depicts the results of the process.

Table 1 presents accurate results of the proposed method that takes into account the complexity of the implemented scenario. Besides, the proposed method produces a stable environment without recurring issues of unspecified cause. The reliability ($k \geq 0.70$) is found to be high due to the Rasch method allowing the maintenance of the most relevant data for the forthcoming forecasts.

The McNemar test is also presented to show the importance of the difference in the accuracy of the classification of the educational material selected for each student, which is statistically significant when compared to the rest. The result of the simulated process is the devising of completely personalized content for each of the 50 students.

In conclusion, it should be suggested that there were very few cases of students (4 students) with significant content overlap (<85%), while in the number of cases (37 students) the content was different by >30%.

Also, the high reliability and the precision of the model are depicted by the high values of R^2 and the minimum values of the RRSE. On the other hand, various options of the above parameters can lead to various inherent operating standards, so that the firing threshold represents the personalized requirements of each learner. In addition, the integration of the self-adaptive fuzzification mechanism makes it possible to manage multiple intermediate representations. The hybrid approach is based on the individual

Table 1: The outcomes of the assessments.

Class	OA (%)	AA (%)	Kappa	McNemar	$\mathbf{R}^2$	RRSE
1	**99.44**	**98.67**	**0.8992**	**30.172**	**0.989**	**0.0459**
2	**98.37**	**97.52**	**0.8885**	**29.674**	**0.981**	**0.0518**
3	**99.12**	**98.33**	**0.8973**	**30.029**	**0.987**	**0.0479**

needs of each learner, the adaptive structure of the educational material based on evaluation criteria, and the interaction with the aim of its continuous improvement. This leads to high performance even for problems that require student-led participation in the learning process, with emphasis on collaborative environments and access to technology's up-to-date educational resources.

6. Discussion and Conclusions

This paper presented an innovative hybrid AI system that fully automates the process of personalized training based on individual skills. The Rasch statistical analysis model and an innovative fuzzy Bayesian network are used concurrently. Higher-level reasoning is produced for the automated and personalized learning process. By doing so, college students are automatically classified in a certain category based on their skills.

This is an innovative effort to effectively rearrange the educational content of educational systems based on evaluation criteria. Technologically, the proposed system combines a hybrid AI model with statistical methods, Machine Learning algorithms, and fuzzy logic concurrently for the first time. Thus, ensuring the optimal adaptation of the system is conducted for new situations. It offers a high level of generalization, realistically addressing the expectations of those involved, while the application of adaptation and rearrangement rules is done in a completely understandable and clear way.

The process measuring the difficulty and ability parameters of the questions responded to by the students provides probability assessments. Thus, the dependent maximum probability technique directly serves to calculate the difficulty of the questions, which is to generate a probability value for each variable (answer) that essentially reveals the interdependence of the variable with a class, indicating the direction of the influence resulting from each question. An initial categorization of the answers into clear classes can determine the choices and abilities of each student in this way. Then, those values are updated by a fuzzy Bayesian network which results in three classes of Theoretical Direction, Positive Direction, and Technological Direction, based on their answers.

The main future research would be the expansion of the method to use high-level intelligence by sophisticated Machine Learning techniques to model uncertainty aiming at reaching a result of greater accuracy and efficiency.

Abbreviations

α: Cronbach's alpha in [0, 1]
N: The number of items
$\bar{c}$: The average interitem covariance among the items
$\bar{u}$: The average variance
p: Successful outcome
$P(\theta) = \theta - \beta$: The difference between an individual's ability and the difficulty of the question
$P_r(X_i = 1|\theta_j, \beta_i)$: The outcome of a successful answer to a question
θ_j: The ability of trainee j
β_i: The difficulty of question i
$P_B = (X_1, X_2, \ldots, X_n)$: The joint probability density function of the questions
k: Kappa Rate
$\tilde{A}$: Fuzzy set
$\mu_{\tilde{A}}$: Membership function of fuzzy set $\tilde{A}$
R^2: Coefficient of Determination
RRSE: Root Relative Squared Error
Y_i: ith observed value
$\hat{Y}_i$: Estimated ith observation.
$\underline{Y}, \underline{T}$: Average value.

Data Availability

The data used to support and prove the findings of this study are available from corresponding author upon request.

Conflicts of Interest

The authors declare that they have no conflicts of interest.

References

[1] S. Sener and A. Çokçaliskan, "An investigation between multiple intelligences and learning styles," *Journal of Education and Training Studies*, vol. 6, pp. 125–132, 2018.
[2] A. Demetriou, G. Spanoudis, and A. Mouyi, "Educating the developing mind: towards an overarching paradigm," *Educational Psychology Review*, vol. 23, no. 4, pp. 601–663, 2011.
[3] A. Demetriou, 2014, Growing a theory of the developing mind—in and around the ivory tower, In: M. Ibarrola, D. C. Phillips (eds), Leaders in Educational Research, Leaders in Educational Studies, Sense Publishers, Rotterdam, Netherlands.
[4] A. Demetriou, "Mind, Self, and Personality: Dynamic Interactions from late childhood to early adulthood," *Journal of Adult Development*, vol. 10, no. 3, pp. 151–171, 2003.
[5] M. A. Diemer, A. D. Marchand, and R. S. Mistry, "Correction to: charting how wealth shapes educational pathways from childhood to early adulthood: a developmental process model," *Journal of Youth and Adolescence*, vol. 49, no. 5, pp. 1092-1093, 2020.
[6] C. A. Kearney, I. Systemic, and A. Approaches, "Integrating systemic and analytic approaches to school attendance

problems: synergistic frameworks for research and policy directions," *Child and Youth Care Forum*, vol. 50, no. 4, pp. 701–742, 2021.

[7] V. Alfano, *The Forgetting of Symons: Photographic Memory and Formal Reincarnation*, Springer International Publishing, Berlin, Germany, 2017.

[8] M. I. Hernández, D. Couso, and R. Pintó, "The analysis of students' conceptions as a support for designing a teaching/learning sequence on the acoustic properties of materials," *Journal of Science Education and Technology*, vol. 21, no. 6, pp. 702–712, 2012.

[9] A. M. Yorke, J. G. Caron, N. Pukys, E. Sternad, C. Grecol, and C. Shermak, "Foundational reading interventions adapted for individuals who require augmentative and alternative communication (AAC): a systematic review of the research," *Journal of Developmental and Physical Disabilities*, vol. 33, no. 4, pp. 537–582, 2021.

[10] J. Gerlinger, S. Viano, J. H. Gardella, B. W. Fisher, F. Chris Curran, and E. M. Higgins, "Exclusionary school discipline and delinquent outcomes: a meta-analysis," *Journal of Youth and Adolescence*, vol. 50, no. 8, pp. 1493–1509, 2021.

[11] J. A. Chase and R. Houmanfar, "The differential effects of elaborate feedback and basic feedback on student performance in a modified, personalized system of instruction course," *Journal of Behavioral Education*, vol. 18, no. 3, pp. 245–265, 2009.

[12] B. L. Hankin, J. F. Young, R. Gallop, and J. Garber, "Cognitive and interpersonal vulnerabilities to adolescent depression: classification of risk profiles for a personalized prevention approach," *Journal of Abnormal Child Psychology*, vol. 46, no. 7, pp. 1521–1533, 2018.

[13] M. Bassi, P. Steca, A. D. Fave, and G. V. Caprara, "Academic self-efficacy beliefs and quality of experience in learning," *Journal of Youth and Adolescence*, vol. 36, no. 3, pp. 301–312, 2007.

[14] S. Maghsudi, A. Lan, J. Xu, and M. van der Schaar, "Personalized education in the artificial intelligence era: what to expect next," *IEEE Signal Processing Magazine*, vol. 38, no. 3, pp. 37–50, 2021.

[15] L. Tetzlaff, F. Schmiedek, and G. Brod, "Developing personalized education: a dynamic framework," *Educational Psychology Review*, vol. 33, 2020.

[16] T. Szulevicz, "COVID-19 and educational consequences for (vulnerable) children from the perspectives of educational psychologists," *Human Arenas*, 2021.

[17] L. Chen, P. Chen, and Z. Lin, "Artificial intelligence in education: a review," *IEEE Access*, vol. 8, pp. 75264–75278, 2020.

[18] M. Krendzelak, "Machine learning and its applications in e-learning systems," in *Proceedings of the 2014 IEEE 12th IEEE international conference on emerging eLearning technologies and applications (ICETA)*, Stary Smokovec, Slovakia, December 2014.

[19] F. Essalmi, L. J. B. Ayed, M. Jemni, and S. Graf, "Generalized metrics for the analysis of E-learning personalization strategies," *Computers in Human Behavior*, vol. 48, pp. 310–322, 2015.

[20] P. Prinsloo, E. Archer, G. Barnes, Y. Chetty, and D. van Zyl, "Big(ger) data as better data in open distance learning," *International Review of Research in Open and Distance Learning*, vol. 16, pp. 284–306, 2015.

[21] A. Klašnja-Milićević and M. Ivanović, "E-learning personalization systems and sustainable education," *Sustainability*, vol. 13, p. 6713, 2021.

[22] S. Sisman-Ugur and G. Kurubacak: Handbook Of Research on Learning in the Age of Transhumanism: IGI Global, 2019.

[23] A. Bozkurt, A. Karadeniz, D. Baneres, A. E. Guerrero-Roldán, and M. E. Rodríguez, "Artificial intelligence and reflections from educational landscape: a review of AI studies in half a century," *Sustainability*, vol. 13, no. 2, p. 800, 2021.

[24] K. D. Cantin-Garside, Z. Kong, S. W. White, L. Antezana, S. Kim, and M. A. Nussbaum, "Detecting and classifying self-injurious behavior in autism spectrum disorder using machine learning techniques," *Journal of Autism and Developmental Disorders*, vol. 50, no. 11, pp. 4039–4052, 2020.

[25] O. Iatrellis, I. K. Savvas, A. Kameas, and P. Fitsilis, "Integrated learning pathways in higher education: a framework enhanced with machine learning and semantics," *Education and Information Technologies*, vol. 25, no. 4, pp. 3109–3129, 2020.

[26] S. Shanshan, G. Mingjin, and L. Lijuan, "An improved hybrid ontology-based approach for online learning resource recommendations," *Educational Technology Research & Development*, vol. 69, 2021.

[27] J. S. Kreutzer, J. DeLuca, and B. Caplan, *Rasch Modeling, in Encyclopedia of Clinical Neuropsychology*, Springer, New York, NY, USA, 2011.

[28] J. T. Abbitt and W. J. Boone, "Gaining insight from survey data: an analysis of the community of inquiry survey using Rasch measurement techniques," *Journal of Computing in Higher Education*, vol. 33, pp. 367–397, 2021.

[29] F. R. Volkmar, Ed., *Item Response Theory, in Encyclopedia of Autism Spectrum Disorders*, Springer International Publishing, Berlin, Germany, 2021.

[30] I. M. del Águila and J. del Sagrado, "Bayesian networks for enhancement of requirements engineering: a literature review," *Requirements Engineering*, vol. 21, no. 4, pp. 461–480, 2016.

[31] A. B. Mrad, V. Delcroix, S. Piechowiak, P. Leicester, and M. Abid, "An explication of uncertain evidence in Bayesian networks: likelihood evidence and probabilistic evidence," *Applied Intelligence*, vol. 43, no. 4, pp. 802–824, 2015.

[32] T. Chaira, *Fuzzy/Intuitionistic Fuzzy Set Theory, in Fuzzy Set and its Extension: The Intuitionistic Fuzzy Set*, Wiley, Hoboken, NJ, USA, 2019.

[33] A. Imtiaz, U. Shuaib, H. Alolaiyan, A. Razaq, and M. Gulistan, "On structural properties of -complex fuzzy sets and their applications," *Complexity*, vol. 2020, Article ID 2038724, 2020.

[34] M. Jezewski, R. Czabanski, J. Leski, 2017, Introduction to fuzzy sets. In: P. Prokopowicz, J. Czerniak, D. Mikołajewski, D. Ślęzak, (eds) Theory and Applications of Ordered Fuzzy Numbers, Studies in Fuzziness and Soft Computing, vol. 356, Springer, Cham, Switzerland.

[35] Q.-L. Yang, J. Lv, X.-P. Tao, X.-X. Ma, J.-C. Xing, and W. Song, "Fuzzy self-adaptation of mission-critical software under uncertainty," *Journal of Computer Science and Technology*, vol. 28, no. 1, pp. 165–187, 2013.

[36] X.-D. Dai, L.-Q. Gao, and C.-R. Dong, "Self-adaptive fuzzification in fuzzy decision tree induction," in *Proceedings of the 2010 International Conference on Machine Learning and Cybernetics*, vol. 1, pp. 296–301, Qingdao, China, July 2010.

[37] M. Pastore and L. Lombardi, "The impact of faking on Cronbach's alpha for dichotomous and ordered rating scores," *Quality and Quantity*, vol. 48, no. 3, pp. 1191–1211, 2014.

[38] K. Sijtsma, "On the use, the misuse, and the very limited usefulness of cronbach's alpha," *Psychometrika*, vol. 74, no. 1, pp. 107–120, 2008.

[39] T. L. Hung and V. T. Thao, "Bounds for the approximation of Poisson-binomial distribution by Poisson distribution,"

Hindawi
Journal of Mathematics
Volume 2023, Article ID 9851417, 1 page
https://doi.org/10.1155/2023/9851417

Retraction

Retracted: A New Rule-Based Approach for Classical Arabic in Natural Language Processing

Journal of Mathematics

Received 19 December 2023; Accepted 19 December 2023; Published 20 December 2023

This article has been retracted by Hindawi following an investigation undertaken by the publisher [1]. This investigation has uncovered evidence of one or more of the following indicators of systematic manipulation of the publication process:

(1) Discrepancies in scope

(2) Discrepancies in the description of the research reported

(3) Discrepancies between the availability of data and the research described

(4) Inappropriate citations

(5) Incoherent, meaningless and/or irrelevant content included in the article

(6) Manipulated or compromised peer review

The presence of these indicators undermines our confidence in the integrity of the article's content and we cannot, therefore, vouch for its reliability. Please note that this notice is intended solely to alert readers that the content of this article is unreliable. We have not investigated whether authors were aware of or involved in the systematic manipulation of the publication process.

Wiley and Hindawi regrets that the usual quality checks did not identify these issues before publication and have since put additional measures in place to safeguard research integrity.

We wish to credit our own Research Integrity and Research Publishing teams and anonymous and named external researchers and research integrity experts for contributing to this investigation.

The corresponding author, as the representative of all authors, has been given the opportunity to register their agreement or disagreement to this retraction. We have kept a record of any response received.

References

[1] R. Salah, M. Mukred, L. Qadri binti Zakaria, R. Ahmed, and H. Sari, "A New Rule-Based Approach for Classical Arabic in Natural Language Processing," *Journal of Mathematics*, vol. 2022, Article ID 7164254, 20 pages, 2022.

Hindawi
Journal of Mathematics
Volume 2022, Article ID 7164254, 20 pages
https://doi.org/10.1155/2022/7164254

Research Article

A New Rule-Based Approach for Classical Arabic in Natural Language Processing

Ramzi Salah,[1] Muaadh Mukred,[1,2] Lailatul Qadri binti Zakaria,[1] Rashad Ahmed,[3] and Hasan Sari[2]

[1]*Faculty of Information Science and Technology, Universiti Kebangsaan Malaysia, Bangi 43600, Selangor, Malaysia*
[2]*Sana'a Community College, Mareb Street, Hushaishia Road, Sana'a, Yemen*
[3]*ICS Department, King Fahad University of Petroleum and Minerals, Dhahran 31261, Saudi Arabia*

Correspondence should be addressed to Muaadh Mukred; muaadh@scc.edu.ye

Received 13 November 2021; Accepted 29 December 2021; Published 21 January 2022

Academic Editor: Ewa Rak

Named entity recognition (NER) is fundamental in several natural language processing applications. It involves finding and categorizing text into predefined categories such as a person's name, location, and so on. One of the most famous approaches to identify named entity is the rule-based approach. This paper introduces a rule-based NER method that can be used to examine Classical Arabic documents. The proposed method relied on triggers words, patterns, gazetteers, rules, and blacklists generated by the linguistic information about entities named in Arabic. The method operates in three stages, operational stage, preprocessing stage, and processing the rule application stage. The proposed approach was evaluated, and the results indicate that this approach achieved a 90.2% rate of precision, an 89.3% level of recall, and an F-measure of 89.5%. This new approach was introduced to overcome the challenges related to coverage in rule-based NER systems, especially when dealing with Classical Arabic texts. It improved their performance and allowed for automated rule updates. The grammar rules, gazetteers, blacklist, patterns, and trigger words were all integrated into the rule-based system in this way.

1. Introduction

Named entity recognition is a crucial step in numerous natural language processing (NLP) applications such as machine translation, question answering, and information retrieval, to name a few [1, 2]. NER is typically described as a sequence labeling task in which each word in a phrase is given a unique label. Sequence labeling has long been used to model and solve NLP tasks. The input values are often words; however, they can be smaller units like individual characters depending on the task [3].

Arabic is one of the most widely spoken languages in the world, with around 420 million people speaking it. Arabic is the official language of 24 countries [4], most of which are located in the Middle East and North Africa. Due to applications and tools for translation and information retrieval, languages are becoming a crucial aspect of technology. Because of the development in Arabic language presence in the technology and social media landscape, research in Arabic language processing should be prioritized to keep up with modern technologies. There has been extensive research on NER in English text. However, in comparison to English, Arabic language processing research is still in its infancy [5, 6]. Beyond that, there are challenges inherent in the Arabic language and a dearth of annotated corpora and resources. For the Arabic language, extracting named entities is quite challenging due to its morphological structure [7, 8]. Arabic is a morphologically complex language due to its inflectional nature; it has a general form of a word: prefix(es) + stem + suffix(es), with the number of prefixes and suffixes ranging from 0 to many. Another issue is that, depending on its position in the world, an Arabic letter can take up to three different forms [9, 10]. In his paper, we introduce a rule-based NER method that can be used to examine Classical Arabic documents. The proposed method relied on triggers words, patterns, gazetteers, rules,

and blacklists generated by the linguistic information pertaining to entities named in Arabic.

The remainder of this paper is structured as follows. Related work is introduced in Section 2. The linguistic sources used to identify Arabic NEs are listed in Section 3. The rule-based NER method proposed in this study is introduced in Section 4, which outlines the operation, preprocessing, and processing steps incorporated in this method. Each step has been described in the subsections. An evaluation of the proposed method is presented in Section 5. Finally, we conclude our paper in Section 6.

2. Related Work

Name entity recognition, NER, is a common task in the natural language processing fields. Researchers have used three main approaches for NER [1]. They are linguistic rule-based, statistical and machine learning-based, and hybrid approaches. Rule-based approaches require a lexicon of proper names and a set of patterns to match NEs. Matching is achieved by using internal evidence (gazetteers) and external evidence provided by the context in which the NEs appear. Statistical and machine learning approaches are based on a large amount of manually annotated training data. Hybrid methods combine statistical and rule-based approaches [11]. Aboaoga and Ab Aziz [12] proposed a rule-based approach to recognize person names. The developed rules are based on the position of the name. They evaluated their method based on a collected corpus. They reported 92.66, 92.04, and 90.43% performance in terms of F-measure in sports, economic, and political domains. Shaalan and Oudah [13] proposed a rule-based approach that contains a lexicon and a set of grammar rules for NER for the political domain. The proposed approach is evaluated on ANER corpus, and the reported results were 82.76%, 98.3%, and 100% for the person, location, and organization names, respectively.

Shahina [14] used a deep learning-based approach for Arabic NER. The author made use of three well-known architectures, recurrent neural network (RNN), long short-term memory (LSTM), and gated recurrent unit (GRU). The author also experimented on ANERcorp dataset and reported performance of 96.68% in terms of accuracy. Another deep learning-based approach was proposed in [15]. The author introduced a deep learning model that consists of bidirectional long short-term memory and conditional random field. Different network layers such as word embedding, convolutional neural network, and character embedding were used. The proposed method was evaluated by combining two datasets ANERCorp [10] and AQMAR Arabic Wikipedia Named Entity Corpus and Tagger [16]. The reported performance was 76.65% in terms of F1 score for ANER. In [17], the author proposed a machine learning-based approach for Arabic named entity recognition. The author combined radial basis function (RBF) cascaded with a sequential convolutional neural network (CNN) and bidirectional long short-term memory (BiLSTM) in the classification process. The obtained results were 95% in terms of F1 score. Sajadi and Minaei [18] presented a new Classical Arabic corpus and a gazetteer named NoorGazet, about 18000 names. They also developed a new approach based on ensemble learning for named entity extraction. They reported 96.04% in terms of F-measure. Mohammed and Omar [19] conducted a study where they applied a neural network-based approach to identify NER for the Arabic language. The proposed method gave 92% accuracy.

Shaalan and Oudah [13] proposed a hybrid NER that combines rule-based and machine learning-based approaches to recognize 11 types of Arabic named entities. They used decision trees, support vector machines, and logistic regression classifiers. They evaluated their method using the ANERcorp dataset and reported a 94% F-measure for the person name entity. Balgasem and Zakaria [20] proposed a hybrid approach to recognize Arabic names from Hadith. They identified person name candidates using a rule-based method based on keywords that identify the start and the end of the name. The candidate name is fed to a statistical model to identify the possibility of the candidate name. The obtained results were 86% of F-measure for the rule-based method, while LLR has outperformed the other statistical methods by obtaining 85% of precision. Another hybrid model for Arabic named entity recognition was proposed in [21]. The proposed method combines conditional random fields (CRFs), bilingual NE lexicon, and grammar rules to identify named entities. The proposed method is evaluated using the ANERcorp, and the reported results show that their method outperforms the state of the art of Arabic NER in terms of precision with F-measures 83.36% for person, 89.58% for location, and 72.26% for organization. Abdallah et al. [11] integrated machine learning with rule-based approaches for Arabic named entity recognition. The integration is done by using the output of the rule-based system as a feature of the machine learning classifier. Experimental results showed that the proposed approach increases the F-measure by 8 to 14% when compared to the rule-based system and the machine learning approach.

Mohd et al. [8] came up with a way to recognize Quranic text using a convolutional neural network (CNN) and a recurrent neural network (RNN). Because they tested it on many data, they found that it had an accuracy rate of 98% on the validation data. Furthermore, the test data had a 95% WRR and a 99% CRR.

In a related study, Boudjellal [22] presented a BERT-based model to identify biomedical named entities in Arabic text data that investigates the effectiveness of pertaining a monolingual Bidirectional Encoder Representations from Transformers (BERT) model with a small-scale biomedical dataset on enhancing the model understanding of Arabic biomedical text. When the model's performance was compared to that of two state-of-the-art models, it outperformed both with an F1 score of 85%.

3. Linguistic Resources

Rule-based methods, also known as knowledge engineering methods [23], work by applying predefined rules to natural language documents [12, 24–27]. These methods depend on the information provided by linguists that identify NEs [28, 29]. Access to enough domain-relevant texts that can be tested manually is essential [30] if effective rules are to be developed. The expertise and ability of the knowledge engineer are critical to developing an effective system.

The development of an accurate system required repetitive procedures to fine-tune the system. Each procedure begins by creating rules about a set of sample texts. The results of these tests are examined to determine if the rules should be modified [31, 32]. This section discussed the knowledge sources required to identify NEs in classic Arabic texts.

3.1. Dataset. We used the CANERCorpus as our dataset, which is a Classical Arabic NER corpus that is manually annotated by human experts. It contains more than 7,000 Hadiths (Prophet Muhammad's sayings) from Sahih Al-Bukhari book that are annotated using 21 named entity classes. These classes include person (Pers), location (Loc), organization (Org), measurement (Meas), money (Mon), book (Book), date (Date), time (Time), clan (Clan), natural object (NatOb), crime (Crime), day (Day), number (Num), god (Allah), prophet (Prophet), religion (Rlig), sect (Sect), paradise (Para), hell (Hell), month (Month), and others (O). The corpus contains around 72,108 named entities and 258,264 words. Table 1 shows the number of named entities in each tag [33].

In CANERCorpus, as shown in Figure 1, the NE was classified into two main types. The first is the general type covering persons, locations, organizations, measurement, money, book, date, time, natural object, crime, day, and number where you can find this type in many domains such as politics, economy, sport, and crime, and others.

The second type known as the specific domain is related to CA (Islamic domain), including Allah, prophet, religion, sect, paradise, and hell. However, the corpus context that includes general and specific NEs focuses on the Islamic domain. Therefore, there are many differences in the names, meanings, and roles between the Islamic domain and other domains.

3.2. Data Collection. This section is concerned with how the statistical linguistic resources were collected from Islamic texts found in the AL-Shamela library where shamela.ws contains over 6100 books. Table 2 shows the number of improvements made to reinforce the rule-based approach, including grammatical rules, patterns, gazetteers, trigger words, and a blacklist, that were extracted from books in the Al-Shamela library.

3.3. Trigger Words. (TW) Proper names are typically found next to cue or trigger words such as titles. Trigger words were used in the proposed rule-based NER method [12, 27, 29]. The list of trigger words included political, military, and occupational titles such as Dr. or Mr. (الإمام, شيخ). This list also included verbs such as "said" or "declared." The trigger word list used in this study was developed manually using semiautomatic procedures, by finding the most common left and right-hand side and both contexts of known Arabic NEs and by using rules developed using an initial list of seed words to find the context for NEs. A list of 15,215 trigger words was established for use in this study. The trigger words were categorized depending on their position in the classic Arabic texts.

3.4. Trigger Words before and after NE. (TWBA) The trigger words that were found before or after a named entity TWBA included verbs or nouns that introduced a NE. This category of trigger words is the strongest of the three trigger word categories. To the best of our knowledge, this study is the first to mention this subject. Table 3 provides some examples found on the TWBA list.

3.5. Trigger Words before NE Only. (TWB) The TWB list contains words that identify a NE as shown in Table 4. A handful of the words in the introductory verb list (IVL) and introductory word list (IWL) were gathered from earlier studies conducted in [12, 27, 34]. The remaining words were gathered during the corpora analysis phase of this study.

3.6. Trigger Words after NE Only. (TWA) The TWA list is composed of words that identify a NE found after the NEW. A few of these words are shown in Table 5. The words in this list were collected during the corpora analysis phase of this study.

3.7. Gazetteers. (Dictionaries) Another primary linguistic resource is the gazetteer, which is a collection of predefined lists of typed entities. A gazetteer is also known as a dictionary or whitelist [35]. The whitelists were dictionaries of NEs that matched the target texts and that were not dependent on the rules. Whitelists contain complete names that are not found anywhere else, and dictionaries contain single names that can be found in different places [29, 36]. Examples of gazetteers are shown in Table 6.

3.8. Blacklist. (Reject Word) A filtration procedure was completed during the last stage of the NER in the NERA system to create a list of rejected words [36]. Incorrect words used to identify NE were found and filtered out. The filtration process used blacklist dictionaries containing incorrect words to identify NE. The blacklist contained stop words, trigger words, and rejected words.

3.9. Stop Word List. Stop words are non-descriptive common words that cannot be included as an identifying feature of a NE [27]. In this study, 13112 of the most common stop words found in the CA were collected. The resulting list of

Table 1: Word count and percentage of each NE class.

Type	Count	Percentage
Allah	7811	12.95
Prophet	6502	10.77
Pers	39159	64.87
Loc	1349	2.09
Org	9	0.01
Meas	147	0.24
Mon	139	0.23
Book	183	2.24
Date	596	0.95
Time	102	0.17
Rlig	184	0.31
Sect	17	0.03
Clan	674	1.11
NatOb	670	1.11
Crime	212	0.35
Para	294	0.49
Hell	245	0.41
Month	77	0.13
Day	31	0.05
Num	13707	1.51
NamedEntity	72108	100.00

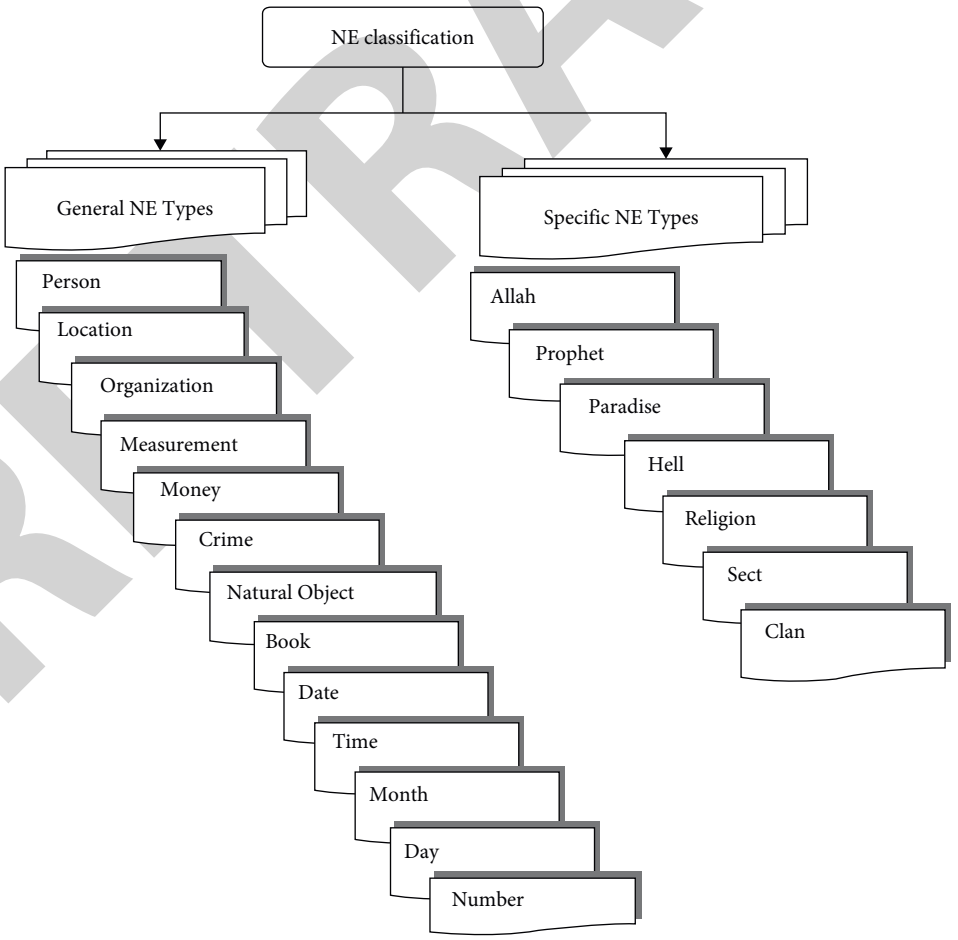

Figure 1: NE classification.

Table 2: Data Resource.

Number of NE type	Grammar rules	Gazetteers	Patterns	Trigger words			Blacklist	
				Before	B&A	After	Stop words	Reject words
Allah (god)	9	115	—	2411	2103	487	13112	31
Prophet	8	29	—	104	413	86		25
Person	11	94115	—	701	686	433		97
Location	4	4418	—	1130	225	131		34
Organization	—	9	—	—	—	—		—
Measurement	4	74	1	72	83	46		14
Money	4	224	1	102	81	73		19
Crime	4	39	—	91	43	67		11
Natural object	4	142	—	485	247	290		21
Book	4	32	—	151	42	70		17
Date	4	55	1	66	34	27		4
Time	5	63	1	31	22	12		5
Month	4	43	1	216	160	77		10
Day	4	7	1	450	338	61		8
Number	6	137	2	63	210	78		12
Paradise	4	17	—	224	242	119		7
Hell	4	18	—	356	283	103		11
Religion	4	12	—	324	219	88		9
Sect	4	73	—	92	50	24		7
Clan	7	35	—	214	93	86		4
All	66	99657	8	7283	5574	2358	13112	159

Table 3: Examples of TWBA.

Type of NE	Before feature	NE	After feature
Allah	ال/said	الله/Allah	لجوزع/almighty
Prophet	المسيح/Jesus	عيسى/Eissa	عليه السلام/peace be upon him
Person	الإمام/Imam	أحمد/Ahmed	رحمه الله/may god have mercy on him
Location	من/from	تهامة/Tahamah	إلى/to
Measurement	فأخذت/I took	القدح/the mug	فجعلت/and made it
Money	بربح/profit	دينار/dinar	لكل for every
Crime	حد/the limit of	السرقة/theft	ونصابه/and its quorum
Natural object	وركب/and he rode	حماراً/donkey	فانطلق so he went
Book	كتاب/book	الرجال/men	للإمام/for the imam
Date	عام/year	1400	هـ/Hijri
Time	وقع/down	الفجر/Al-fajr	فأوتر/Witr prayer
Month	صام/fast	رمضان/Ramadan	إيماناً/faith
Day	يوم/day	الثلاثاء/Tuesday	أو/or
Number	سبع/walk	سبعين/seventy	سنة/year
Paradise	في/in	الفردوس/paradise	أعلى/the higher
Hell	حجبت/hide	النار/hell	بالشهوات/with lusts
Religion	قبل/before	الإسلام/Islam	كان/was
Sect	قال/said	الحنفية/alhanfia	بجواز/with permission

stop words was composed mainly of prepositions, adverbs, verbs, and demonstrative words, as shown in Table 7.

4. The Rule-Based Method's Step by Step Process

This study used a hybrid approach. The new rule-based approach introduced in this study achieved good results as it examined a new domain. The researchers also relied on several other rule-based methods to obtain the best results.

This section describes the proposed rule-based technique for identifying NEs in classic Arabic texts. This method consists of an operational step, preprocessing step, and processing the rule application step. Figure 2 illustrates the framework of the rule-based method proposed for the CANER.

4.1. Operation Stage. The operational stage automatically created system controls and added new dynamic classifications. This stage facilitated the construction process to create a fully automated system. Furthermore, this stage could be generalized and applied to several different domains. The operational stage was followed only once when the system began to identify NE in classic Arabic texts. The steps for the operational stage are shown in Figure 3.

Table 4: Examples of TWB.

Type of NE	Trigger before	NE
Allah	ات‌ق‌ا/fear	الله/Allah
Prophet	ب‌ع‌ث/sent	النبي‌ب/the prophet
Person	ح‌د‌ث‌نا/tell us	ابن عباس‌ا/Ibn Abbas
Location	أهل/the people of	اليمن‌ا/Yemen
Measurement	م‌ق‌دار/the amount of	صاع‌ه/Sa
Money	وينقذه/save him	ديناراً/Dinar
Crime	م‌ج‌اهرة‌ا/in public	الزنا‌ب/prostitution
Natural object	واستاقوا/and they take	الإبل‌ا/the camels
Book	كتاب‌ك/book	صحيح البخاري‌ح/Sahih Bukhari
Date	في‌ف/in	يوم أحد/Ohod day
Time	أنام‌أ/I sleep the	أول الليل‌ل/first night
Month	شهر‌ش/month of	رجب‌ر/Rajab
Day	يوم‌ي/day	الخميس‌ا/Thursday
Number	عاه‌ز/about	ثلاث مائة‌ث/three hundred
Paradise	وبشره‌و/he surprised him	الجنة‌ب/with paradise
Hell	عذاب‌ع/torture of	النار‌ا/hell
Religion	دين‌د/the religion of	الإسلام‌ا/Islam
Sect	مذهب‌م/madhhab	أهل السنة‌س/Sunnah
Clan	مولى‌م/salve	بني حارثة‌ب/Bani Haritha

Table 5: Examples of TWA.

Type of NE	NE	Trigger after
Allah	الله‌ا/Allah	تبارك‌ت/almighty
Prophet	النبي‌ا/prophet	صلى الله عليه وسلم‌ص/peace be upon him
Person	أحمد‌أ/Ahmed	حفظه الله‌ح/may Allah preserve him
Location	مكة‌م/Makkah	إلى‌إ/to
Measurement	مدنا‌م/almada	صاعنا‌و/saae
Money	دينار‌د/Dinnar	أقرضه‌أ/lend it
Crime	بهتان‌ب/falsehood	تفترونه‌ت/defamation
Natural object	جمل‌ج/the camel	فأخاه‌ف/he lowered
Date	عام الفيل‌ع/elephant year	ولد‌و/born
Time	بالعشي‌ب/night-time	والإشراق‌و/Sun rise
Month	رمضان‌م/Ramadan	إيماناً واحتساباً‌إ/faith and anticipation
Day	صام‌ص/he fasts	الإثنين‌ا/Monday
Number	عشرة‌ع/ten	مساكين‌م/poor
Paradise	الجنة‌ا/paradise	دار المتقين‌د/Dar Al Motaqin
Hell	النار‌ا/hell	أجارنا الله‌أ/may Allah keep us out of the hell
Religion	الإسلام‌ا/Islam	دين الحق‌د/true religion
Sect	الشيعة‌ا/Shia	فرقة‌ف/sect
Clan	المهاجرون‌ا/migrants	وأنصار‌و/and supporters

4.1.1. Reading Operation File. Rule-based systems rely on sources that can be used to identify NEs in the operational stage. Consequently, the first operational step is to read the operational files. The reading operation file step was conducted when the system starts to load all files to the data table.

Formally, this step was employed to read the following files:

(i) Operation type.

(ii) A symbol file that contained short words to identify each token.

(iii) A color file that contained the colors that correspond to each NE. Each type of NE was assigned a unique color because the proposed system can visualize the output of the rule-based method.

(iv) A type file composed of the different types of NEs including personal, organizational, and location names. This file was used in the proposed system so that it could be enlarged to include different types of NEs. In addition, this file allows a user to ask the system to identify only some of the NEs.

(v) A blacklist file containing the paths used for each type of NEs in Arabic (refer to Table 8).

4.1.2. Reading Linguistic Resource. The cornerstone for the rule-based method developed for this study was to identify

Table 6: Examples of gazetteers.

Type of NE	NE	Meaning
Allah	الرنمح	Rahman
Prophet	الندمحم يب	The prophet Muhammad
Person	رمع	Omar
Location	ةكم	Makkah
Measurement	أوقية	Awqia
Money	مەرد	Dirham
Crime	اللتق	The kill
Natural object	اللمج	Camel
Book	صمملسم حيح	Sahih Muslim
Date	ةفرع موي	ARAFFA day
Time	الةوحض	Aldahwa
Month	لاوش	Shawwal
Day	السبت	Saturday
Number	ةثالث	Three
Paradise	الةنج	Paradise
Hell	منەج	Hell
Religion	النصرانةي	Christianity
Sect	الصةيفوص	Sufism
Clan	شيرق	Quraysh

Table 7: Examples of stop words.

Categories	Stop word	Translation
Demonstrative nouns	اذه	This
Relative pronoun	الذي	Who, which
Relative pronoun	اليت	
Adverbs	كانه	There

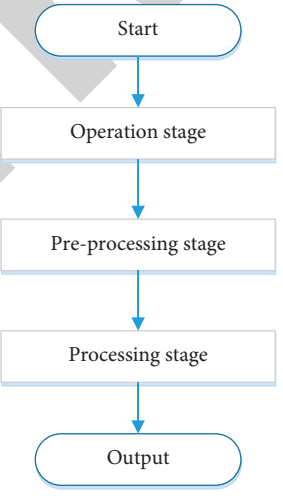

Figure 2: A framework of the CANER.

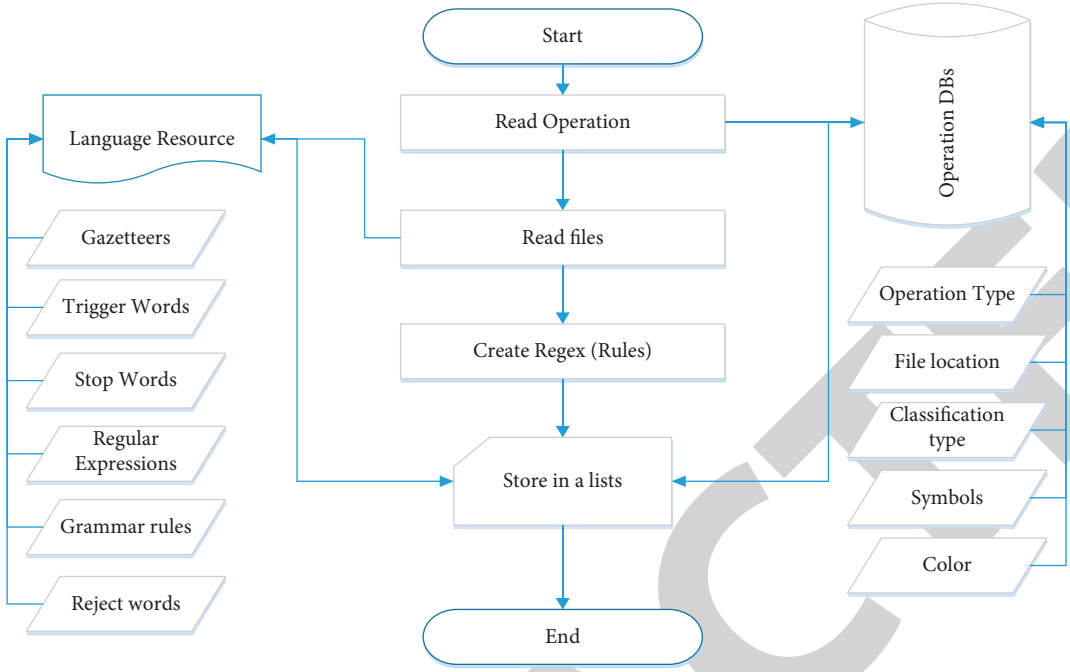

Figure 3: Operation stage of the proposed system.

Table 8: Example of short and color tags.

Type	Short	Color
Person	Pers	Red
Location	Loc	Blue
Organization	Org	Gray

the NEs which were the linguistic resources. The goal of this step is to read the Arabic NER language resources as follows:

(1) Gazetteers.

(2) Rules that contain the following files:

(i) Keywords before NER only.
(ii) Keywords after NER only.
(iii) Keywords before and after NER.

(3) Special rules, such as rules for surnames.

(4) Regular expressions or patterns for CANER, such as date, time, and number.

(5) A blacklist or list of rejecting words that sets out those words that do not identify Nes.

4.1.3. Creating Regex and Rules. Once the operational file was read, the next step for the system was to determine what process would be used for a file and to configure the expression operation for each category. Occasionally, instances occur where a file contains an item that was classified according to the following rules:

(1) Keywords before NER only.

(2) Keywords after NER only.

(3) Keywords before and after NER.

(4) List of names to get direct NER.

4.2. Preprocessing Stage. When used effectively, computerized systems can generate NLP solutions but only after the relevant documents are delimited into meaningful units. For example, many NLP solutions require inputs to be divided into sentences that are further broken down into tokens. Unfortunately, actual documents do not have well-defined structures. As a result, the data from the documents must be prepared and the sentences must be split and tokenized. This can be a challenging process.

A collection of Hadiths is an example of a text without a well-defined structure. These texts typically contain spelling errors, duplicated words, and characters, as well as words that are no longer in use and thus have been omitted from dictionaries. If NLP methods are used without any modifications, they will perform poorly. One way to improve the performance of NLP methods is to start with a data preprocessing step. In this study, the procedures recommended by Saif and Aziz [37] for Arabic texts were applied. The input for the preprocessing step was the raw text that was normalized by extracting the words, removing stop words before stemming the remained words, as shown in Figure 4.

4.2.1. Normalization of Input Text. Before tokenization can take place, normalization must be conducted in the preliminary stage so that the resulting text will be consistent and predictable. In this study, decorative Kashida and all diacritics were removed as they were redundant and misplaced white spaces. These steps meant that the tokenizer was working on a consistent and predictable text. In actual documents, the use of white spaces may be irregular and inconsistent. For example, more than two spaces or a tab may be used instead of a single space. Additionally, spaces may be added before or after punctuation marks. A tool was

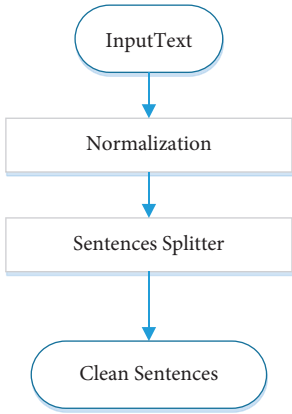

Figure 4: The preprocessing step.

needed to remove inappropriate white spaces so that the tokenization process could identify and analyze words and expressions. In this study, a normalizer was created to review the texts and correct white space errors using the following steps:

(i) Remove the extra spaces between words.

(ii) Delete non-Arabic letters such as English letters or symbols.

(iii) Normalize the different forms for the Arabic letters "Alef." For example أ,إ,ء,ئ were normalized to ا.

(iv) Short vowels diacritics were deleted.

(v) Kashida عـــلـــي was changed to علي.

(vi) Punctuation, numbers, and special characters were removed.

(vii) When a character is repeated to express affirmation or to accentuate meaning, the duplicate characters are replaced.

(viii) The final letter ي was replaced with ى.

(ix) The final letter ة was replaced with ه.

4.2.2. Sentence Splitter. The sentence splitter separated the input text into separate sentences. The boundaries of a sentence are determined by a full stop or other punctuation. Once the sentences were segmented, each sentence and boundary were annotated. However, the proposed system did not use a sentence splitter because texts written in Modern Standard Arabic do not use full stops or punctuation. Instead, the system developed for this study used a tokenizer.

4.2.3. Tokenization. "Tokenization" refers to the process of breaking down a sentence into meaningful units. These meaningful units are called tokens. Identifying tokens is an important initial task because all subsequent tasks are based on the tokens. The tokenizer used in this study split the text into word tokens separated by either a white space or punctuation. Each Hadith was tokenized into multiple tokens separated by white spaces.

4.3. Processing Stage. The rule-based approach used rules that were generated to Arabic linguistic information related to the NEs. The purpose of the processing step was to identify the NEs that were not found in the gazetteers. In this study, the NEs were identified based on trigger words, gazetteers, patterns, and rules.

4.3.1. Trigger Words. In this step, the NEs were identified using the trigger words found either before or after the NE in a sentence. The system begins by checking the first word in the sentence to determine if that word is a trigger word. The terms that occur before and after the trigger words are classified as NEs.

The purpose of this step was to use the trigger words to find the NEs that were not found in the gazetteers. For these NEs, linguistic items such as introductory verbs and words and place names were used to identify the NEs. In the system developed for this study, these items functioned as cues that signaled the presence of NEs in a new text.

4.3.2. Gazetteer Lookup. The gazetteers contained lists of different types of NEs, such as the names of people, places, organizations, and the titles of books. These lists acted as lookup lists to find occurrences of these names in Arabic texts [38]. A word should be an exact match with at least one word in the gazetteer. The sensitive matching means that flexible matching conditions were required. Several NER systems combine gazetteers with rules that consider the surrounding text. In this study, the first step to recognizing NEs in Arabic texts was to use a gazetteer as a lookup list to form a strong feature in the rule-based method. The following techniques were used as part of this method:

(i) Exact match: the Aho–Corasick Algorithm with a linear running time in terms of the input length and the number of matching entries in a gazetteer was used to conduct searches. When a word sequence matched an entry in the gazetteer, EM-GAZ for the first word used the value B-<NE class> where <NE class> was one of the categories of PER, LOC, and ORG. Other words were assigned to the I-<NE class>, where the <NE class> was given the same value as the matched head of the sequence.

(ii) Partial match PM-GAZ: this feature was developed to deal with compound gazetteer entries. If the token was part of a compound name, then this feature was true. For example, if gazetteer contained the compound name "أحمد بن حنبل" "Ahmad ibn Hanbal" and the input text was "أحمد بن حنبل," then Ahmed for the token "أحمد" was set to true. This feature was helpful for PER because it could identify a large list of first names found as part of a compound name.

4.3.3. Regular Expressions. A set of predefined patterns was used to find NEs in Arabic texts. The extraction method exploited the regularities inherent in natural languages.

This study used regular expressions or patterns for numbers, dates, times, and special characters, as seen in Table 9.

Standard Arabic contains an almost unlimited number of patterns, unlike classic Arabic, which contains very few patterns. In classic Arabic, numbers are usually expressed using words, for example, ثلاثة instead of using the numeral 3. Dates are usually described by referring to an event, but there is no specific formula. Time is typically not given as a specific hour; instead, time is defined as night, day, or prayer times.

4.3.4. Grammar Rules. The rule-based approach was composed of linguistic items and rules. The heuristic rules were consistent with Arabic grammatical rules to handle the names. These heuristic rules and linguistic items were used to identify the NEs in new texts. Table 10 presents the statistical information about new grammar rules.

As shown in Table 10, there are 22 new grammar rules most of them for the new types of NE in CA.

(1) General Rules. The general rules were used for all the NEs. The following sections discuss the general rules used in this study.

(i) Conjunctions connect sentences or groups of words. In Arabic, some conjunction may be attached to a word and not separated as they are in English. This can make recognizing NEs challenging. In this study, the conjunctions were separated from the NE by examining words beginning with ك/*k*, ف/*f*, و/w, ل/*l*, and ال/al such as ومكة or Makah. This study also examined words ending with ا/a, for example, اليمن/Yemen. The original word for Yemen was يمن which meant that the last letters were separated from the rest of the word to allow for the application of the rule to arrive at the correct name.

(ii) Categorizing a NE depends on the words found before the NE. For example, King Salman University is the name of an organization. King Salman is a scientific name. When names are linked, the previous words are examined, so when linking names, generally look at the previous word. As an example, King Salman University, the words are classified as the name of organization.

(iii) Sequences (conjunctions) with the letter (ن/an, or و/and) are words that connect sentences or groups of words. For example, (أخبرنا محمد وعلي وصالح/ Mohammed and Ali and Saleh tell us) if the first word belongs to the NE, then all words between the conjunctions are classified as NE.

(iv) If the word occurs next to the letter و/and, it was classified as a NE. For example, in the sentence عبد الجبار وأحمد ومنير ذهبوا إلى المدرسة, which is translated as Abdul Jabbar, Ahmad, and Munir went to school, the names between و/and were classified as the name of a person.

(2) Allah Rules. Allah has 99 names. The 99 names of Allah fall into two categories. The first category contains names that are only used to describe Allah and no one else. If these names are found in a text, they are directly linked to the Allah NE. Names that fall into this category include Allah الله, Ar-Rahman الرحمن, As-Samad الصمد, and Dhu-al-Jalal wa-al-Ikram ذو الجلال و الإكرام. The second category contains names that are not specific to Allah, and that can be used to describe others. Al-Ghani الغني and "The Rich One" are examples of this kind of name. These names are identified by the following:

(i) The name should not include any of the tokens associated with specific names for Allah as discussed above.

(ii) The name should not come after the token Abd, عبد.

(iii) The name should not be preceded by the word "said."

(iv) The name should not come after a token one of the following descriptions سبحانه "subhanah," الج "Gla," or تعالى"taealaa"- Almighty.

(3) Prophets. A NE is labeled as a "Prophet Type" if the names comes before or after one of the following descriptions: "alnnabaya/النبي," "alrrasula/الرسول," "slaa alllah ealayh wasalama/صلى الله عليه وسلم," "elih alssalam/عليه السلام," "sydna/سيدنا," "khatm alnnabyn/خاتم النبيين," "syd almrsalin/سيد المرسلين," "rssul allh/رسول الله," or "syd alrrusul/سيد الرسل."

(4) Person. The entities associated with the names of people are categorized as follows. All words that are found before or after bin/بن or bint/بنت are classified as names of people. Many of the NEs in Classic Arabic are words related to people such as the word for son/بن and daughter/بنت. It is rare to use these words without using a name, for example, Mohammed bin Abdullah and Fatima bint Mohammed. If the word begins with ال/al and ends with ي/ya and is preceded by a Person Name, then ال/al and ي/ya will also be categorized as a person name. For example, رمزي السماوي/ Ramzi Alssamawi contains Ramzi/رمزي, which is the name of a person. This name starts with ال/al and ends with ي/ya السماوي/alssamawi, both of which will now be classified as the name of a person.

(5) Number. A list of numbers recorded as words rather than numbers was added. This is typical in classic Arabic, for example, the 10th of Dhul-Hijjah is recorded as العاشر من ذي الحجة.

(6) Time. Time in classic Arabic is only defined as either night or day or as a time for prayer. If the word أول/first or the word آخر/last is found preceding a word that begins with ال/ala such as the أول الليل/first night or آخر النهار/the last day, then all these words are classified as a time NE. Prayer times were seen as falling into the time NE category, for example, بعد صلاة العصر/after Asr Prayer, which refers to the moment before sunset. The token was also categorized as a time NE if it was قبل/before, بعد/after, or في/in and the next word was one of the following: الضحى/dhaa, ضحوة/ dihwtu, صباح/sibha, الصباح/sibah, الظهر/alzhr, الظهيرة/

Table 9: Example of patterns.

Type of named entity	Pattern
Special characters	return @“\W+“;
Number	return @“\d+“;
Date	return @“((\w+,\s+\d+\s+\w+\s+\d[39][38][37][36][36][36][35][34][33][33][32][32][32][31][30](Ruževičius & Gedminaitė) (|(((\d+) ([.]|[/]|[:]) (\d+) ([.]|[/]|[:]) (\d+)))“;
Time	return @“((?:0?[0–9]|1[0–9]|2[0–3]) () ([0–5][0–9]:[0–5][0–9]))|((?:0?[0–9]|1[0–9]|2[0–3]) () ([0–5][0–9]))“;

Table 10: Statistical information about new grammar rules.

Word	Value
General rules	4
Allah rules	6
Prophet rules	2
Person rules	4
Clan rules	2
Number rules	1
Time rules	3
All	22

alzzahirti, غداة/ghidati, العصر/aliesri, النهار/alnnahar, ’أول النهار/uwl alnnahar, نصف النهار/nisf alnnuhar, آخر النهار/akhur alnnahar, المغرب/almaghrib, مغرب/mighrab, العشاء/alesha’, المساء/almasa’, الليل/alllila, ’أول الليل/awl allili, آخر الليل/akhar allyl, الزوال/alzwal, الغروب/alghrwb, هاجرة/hajr.

4.3.5. Blacklist. Blacklist contains all words that were not related to a NE. In the proposed rule-based system, if any words come as NE and it is one of the blacklist, it will change the rule from NE to others. In the example قال الإمام محمد, Imam Mohammed Said, قال is a trigger word, and according to the rules, the next word should be a person’s name. However, in this case, the next word is الإمام/Imam, which is on the blacklist, and thus this this token was not categorized as a NE.

4.3.6. Integrating Linguistic Resources in the Rule-Based System. In earlier studies, the steps in rule-based methods were separate as some methods relied only on trigger words or grammatical rules. In this study, a rule-based method was devised that would use every available resource before comparing the results (see Figure 5).

Three cases are displayed in Figure 5. If all the features extracted from a token using different resources are false, then the token is not related to any NE. If only one of the features extracted from a token is found on a blacklist, then the token is not related to any type of NE. If the features extracted from a token are found on a blacklist is false and there is more than one feature, the token is related to more than one type of NE.

4.3.7. Annotation Coding. Encoding schemes are required to represent the annotated NEs internally. Encoding scheme tag each token in a text. The most straightforward encoding scheme is IO encoding, which tags each token as either a NE (“I”) or not a NE (“O”). IO encoding does not represent two NEs found next to each other. Another encoding scheme is BIO encoding. BIO encoding is frequently used as it solves the boundary issues found in TO encoding schemes. In BIO encoding, tokens related to NE can be tagged with a “B” indicating that it is the first token or the beginning of the name of a NE or an “I” indicating that this token is also related to a NE. A tag of “O” indicates that the token is not related to a NE.

5. Experimental Results

The attributes of type and span are used to define each NE. Both attributes are essential, but it is more important to use the correct type as the span of a NE can be challenging to determine. The proposed method relied on triggers words, patterns, gazetteers, rules, and blacklists. The first experiment was conducted to determine how using trigger words affected the identification of NEs. The results of not using trigger words are shown in Table 11 and Figure 6.

The gazetteers contained the NEs, and they played an essential role in the identification of NEs in Arabic texts using the proposed rule-based method. Most Arabic NEs were found in the gazetteers, and they were easily recognized in texts. The second experiment conducted in this study examined the effect of not using the gazetteers. The results can be seen in Table 12 and Figure 7.

The third experiment was conducted to investigate how patterns affected the results of the proposed method. Patterns are used to identify NEs by recognizing dates and times in the texts. Table 13 and Figure 8 show the results of not using patterns.

Our proposed method used heuristic rules derived from the Arabic grammatical rules to identify NEs in Arabic texts. The heuristic rules were used to recognize the NEs in new

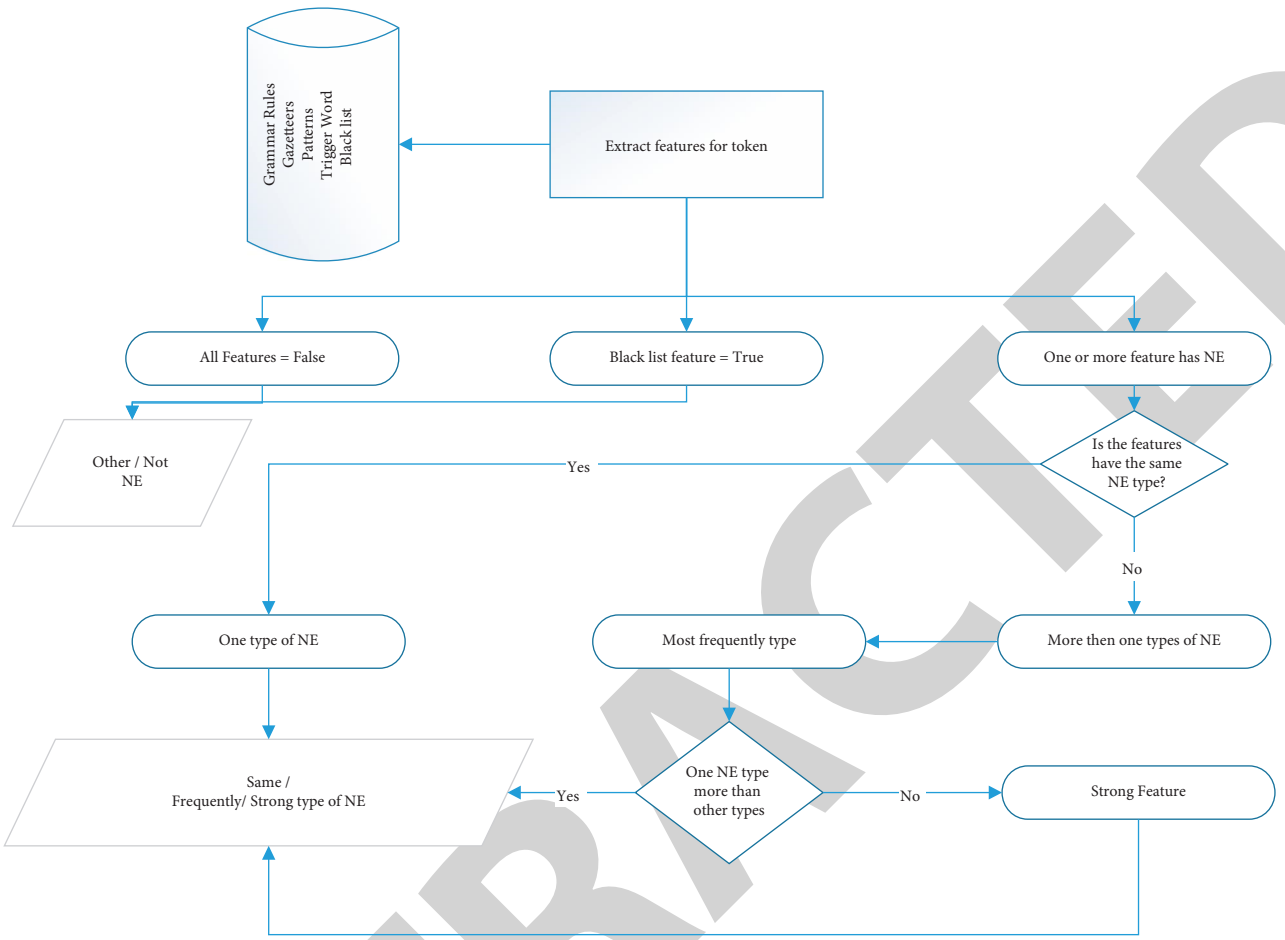

Figure 5: Operational stage for the proposed system.

Table 11: Results of not using trigger words.

NE	Count	TP	FP	FN	Precision	Recall	F-measure
Book	183	103	12	113	0.895652	0.562842	0.691275
Prophet	6502	5932	905	297	0.867632	0.912335	0.889422
Allah	7811	6836	247	796	0.965127	0.875176	0.917953
Pers	39159	27461	2487	621	0.916956	0.701269	0.794739
Org	9	9	0	0	1	1	1
Number	13707	13187	248	444	0.981541	0.962063	0.971704
Date	596	437	2	106	0.995444	0.733221	0.844444
Meas	147	86	23	56	0.788991	0.585034	0.671875
Rlig	184	134	1	24	0.992593	0.728261	0.840125
Sect	17	13	4	2	0.764706	0.764706	0.764706
Loc	1349	897	121	287	0.881139	0.664937	0.757921
NatOb	670	409	61	231	0.870213	0.610448	0.717544
Month	77	63	5	7	0.926471	0.818182	0.868966
Crime	212	141	71	72	0.665094	0.665094	0.665094
Time	102	75	51	27	0.595238	0.735294	0.657895
Clan	674	479	26	109	0.948515	0.710682	0.812553
Hell	245	221	28	22	0.88755	0.902041	0.894737
Para	294	237	20	38	0.922179	0.806122	0.860254
Day	31	24	4	1	0.857143	0.774194	0.813559
Mon	139	121	14	4	0.896296	0.870504	0.883212

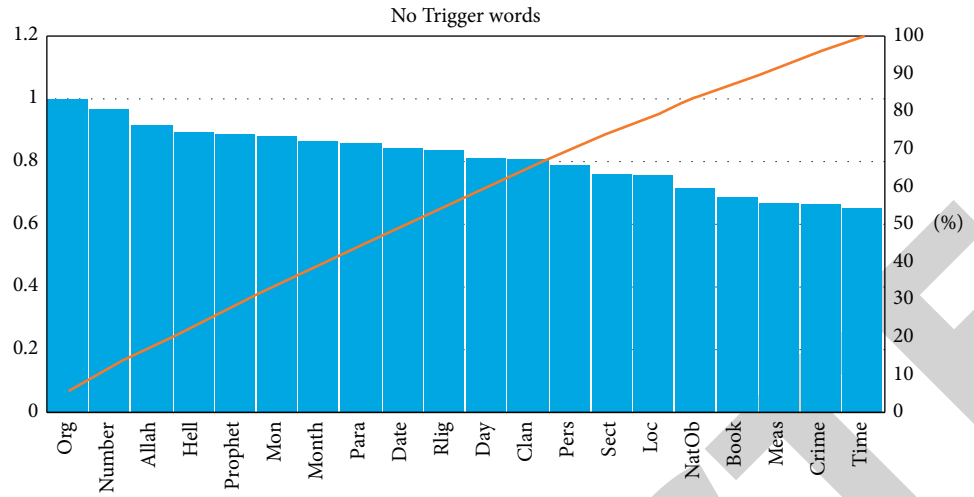

Figure 6: Results of not using trigger words.

Table 12: Results of not using gazetteers.

Key	Count	TP	FP	FN	Precision	Recall	F-measure
Book	183	134	20	113	0.87013	0.73224	0.795252
Prophet	6502	6039	784	186	0.885095	0.928791	0.906417
Allah	7811	6719	73	786	0.989252	0.860197	0.920222
Pers	39159	31581	1701	621	0.948891	0.806481	0.87191
Org	9	0	0	0	0	0	0
Number	13707	13054	145	444	0.989014	0.95236	0.970341
Date	596	437	2	106	0.995444	0.733221	0.844444
Meas	147	74	23	56	0.762887	0.503401	0.606557
Rlig	184	87	2	24	0.977528	0.472826	0.637363
Sect	17	15	4	2	0.789474	0.882353	0.833333
Loc	1349	970	84	287	0.920304	0.719051	0.807324
NatOb	670	601	69	231	0.897015	0.897015	0.897015
Month	77	56	7	7	0.888889	0.727273	0.8
Crime	212	167	39	72	0.81068	0.787736	0.799043
Time	102	59	24	27	0.710843	0.578431	0.637838
Clan	674	398	27	109	0.936471	0.590504	0.724295
Hell	245	157	32	22	0.830688	0.640816	0.723502
Para	294	206	24	38	0.895652	0.70068	0.78626
Day	31	24	9	1	0.727273	0.774194	0.75
Mon	139	101	17	4	0.855932	0.726619	0.785992

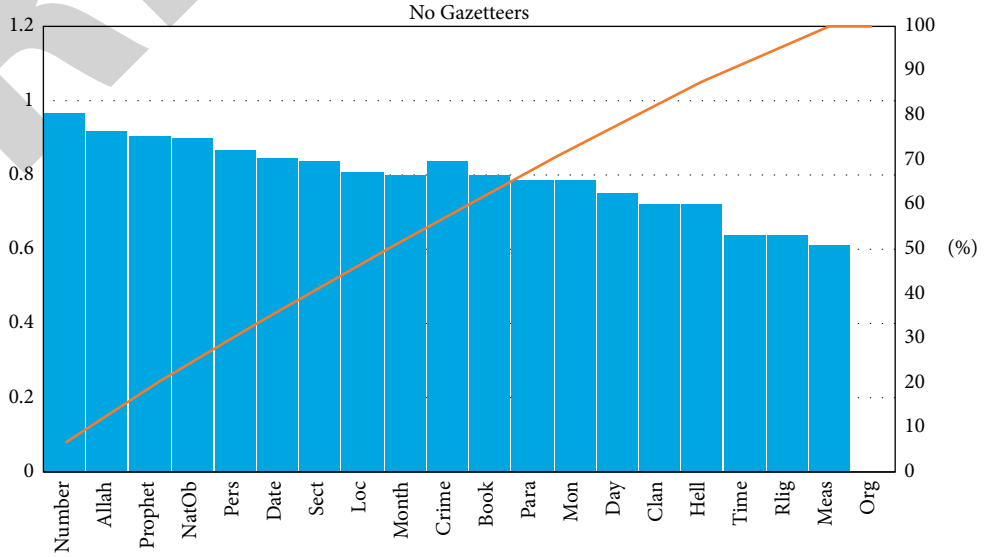

Figure 7: Results of not using gazetteers.

Table 13: Results of not using patterns.

Key	Count	TP	FP	FN	Precision	Recall	F-measure
Book	183	161	20	113	0.889503	0.879781	0.884615
Prophet	6502	6039	1483	186	0.802845	0.928791	0.861238
Allah	7811	7011	385	786	0.947945	0.89758	0.922075
Pers	39159	38149	4054	621	0.90394	0.974208	0.93776
Org	9	9	0	0	1	1	1
Number	13707	404	248	13197	0.619632	0.029474	0.056271
Date	596	437	2	106	0.995444	0.733221	0.844444
Meas	147	118	23	56	0.836879	0.802721	0.819444
Rlig	184	153	2	24	0.987097	0.831522	0.902655
Sect	17	15	4	2	0.789474	0.882353	0.833333
Loc	1349	1090	84	287	0.92845	0.808006	0.864051
NatOb	670	601	69	231	0.897015	0.897015	0.897015
Month	77	72	7	7	0.911392	0.935065	0.923077
Crime	212	181	39	72	0.822727	0.853774	0.837963
Time	102	93	24	27	0.794872	0.911765	0.849315
Clan	674	578	27	109	0.955372	0.857567	0.903831
Hell	245	222	32	22	0.874016	0.906122	0.88978
Para	294	256	24	38	0.914286	0.870748	0.891986
Day	31	30	9	1	0.769231	0.967742	0.857143
Mon	139	131	17	4	0.885135	0.942446	0.912892

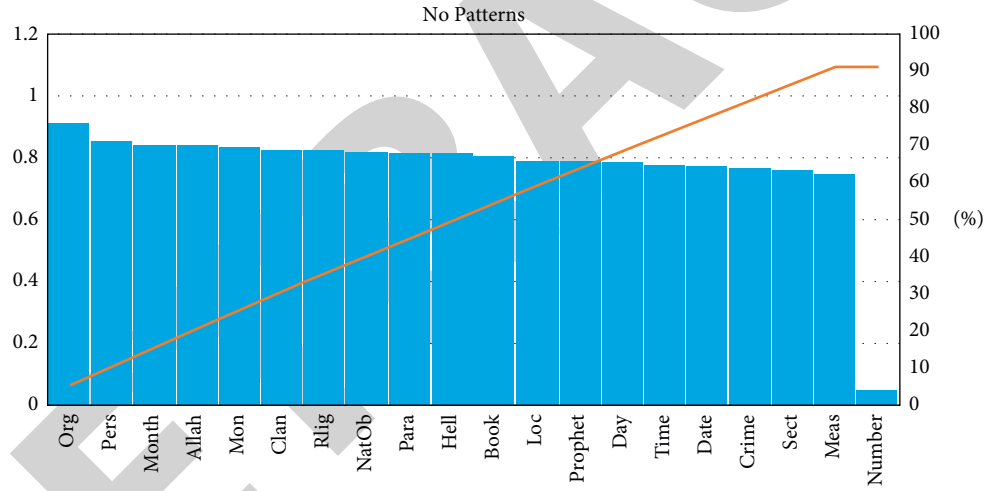

Figure 8: Results of not using patterns.

texts. The next experiment was conducted to determine the effect of not using these grammatical rules. The results are shown in Table 14 and Figure 9.

The blacklists were an important resource for determining the correct type of NE. The results of not using the blacklists to identify NE are shown in Table 15 and Figure 10.

The overall results generated by the Arabic NER proposed in this study for NEs are shown in Table 16. Figure 11 visually represents the results for the five main components: trigger words, patterns, grammar rules, blacklist, and gazetteers.

Table 17 shows the overall results of the integration. A comparison of the results of the method is presented in Figure 12.

When examining Arabic texts, the NEs can be categorized as belonging to either the general domain or the Islamic domain. This study focused on classic Arabic texts, and thus NEs found in the Islamic domain, such as Book, Prophet, Allah, Rlig, Sect, Crime, Clan, Hell, and Para, were considered. Figure 13 describes the performance of the proposed system regarding these NEs.

5.1. Comparison between Baseline and Rule-Based Approach. Since the corpus that is used during this thesis is a new experimental dataset, 10% of this corpus has been evaluated using the existing tools (GATE and the language computer). The results obtained from these tools are baseline results. Therefore, this section introduces a comparison between the baseline results and the results obtained from the rule-based method. In the same dataset that has been used in the baseline results, the proposed rule-based method has been evaluated using the same evaluation measures. Table 18 presents the comparison between the baseline results and the proposed method results.

Table 14: Results of not using grammar rules.

Key	Count	TP	FP	FN	Precision	Recall	F-measure
Book	183	161	20	113	0.889503	0.879781	0.884615
Prophet	6502	5781	675	186	0.895446	0.889111	0.892267
Allah	7811	6547	385	786	0.94446	0.838177	0.88815
Pers	39159	36745	5476	621	0.870302	0.938354	0.903047
Org	9	9	0	0	1	1	1
Number	13707	13187	248	444	0.981541	0.962063	0.971704
Date	596	437	2	106	0.995444	0.733221	0.844444
Meas	147	118	23	56	0.836879	0.802721	0.819444
Rlig	184	153	2	24	0.987097	0.831522	0.902655
Sect	17	12	3	2	0.8	0.705882	0.75
Loc	1349	1090	84	287	0.92845	0.808006	0.864051
NatOb	670	601	69	231	0.897015	0.897015	0.897015
Month	77	72	7	7	0.911392	0.935065	0.923077
Crime	212	181	39	72	0.822727	0.853774	0.837963
Time	102	93	24	27	0.794872	0.911765	0.849315
Clan	674	578	27	109	0.955372	0.857567	0.903831
Hell	245	222	32	22	0.874016	0.906122	0.88978
Para	294	256	24	38	0.914286	0.870748	0.891986
Day	31	30	9	1	0.769231	0.967742	0.857143
Mon	139	131	17	4	0.885135	0.942446	0.912892

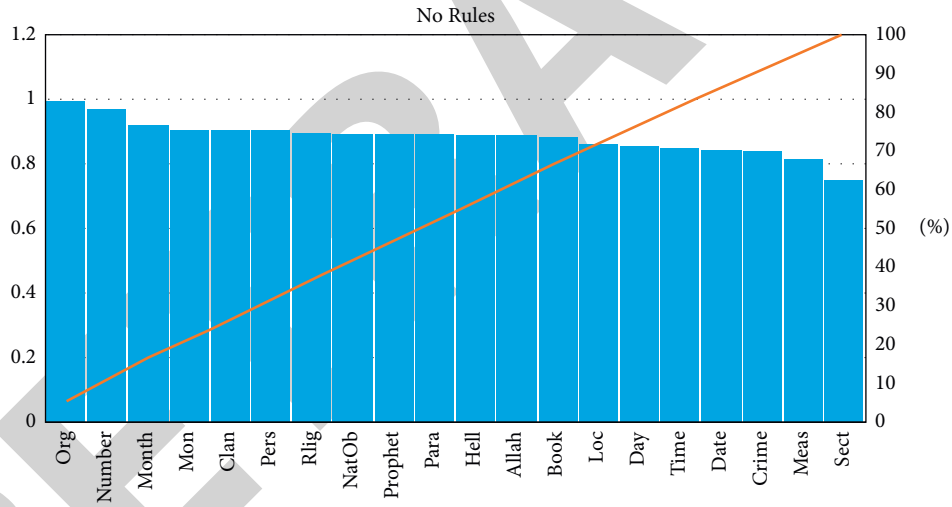

Figure 9: Results of not using grammar rules.

Table 19 presents the comparison between the baseline results and the results of proposed method.

As shown in Table 19 and Figure 14, the GATE and language computer got low results and some of that biased with the 0- values. This is because the language computer could not recognize five NEs and GATE failed to recognize two. Thus, the proposed rule-based method performed better than the GATE and Language computer systems in terms of F-measure.

Table 15: Results of not using blacklist.

Key	Count	TP	FP	FN	Precision	Recall	F-measure
Book	183	161	20	113	0.889503	0.879781	0.884615
Prophet	6502	6039	1475	186	0.8037	0.928791	0.861729
Allah	7811	7011	861	786	0.890625	0.89758	0.894089
Pers	39159	38149	8743	2904	0.81355	0.974208	0.88666
Org	9	9	1	0	0.9	1	0.94736
Number	13707	13187	294	394	0.978192	0.962063	0.97006
Date	596	437	17	106	0.962555	0.733221	0.832381
Meas	147	118	29	56	0.802721	0.802721	0.802721
Rlig	184	153	21	24	0.87931	0.831522	0.854749
Sect	17	15	7	2	0.681818	0.882353	0.769231
Loc	1349	1090	114	287	0.905316	0.808006	0.853897
NatOb	670	601	131	231	0.821038	0.897015	0.857347
Month	77	72	13	9	0.847059	0.935065	0.888889
Crime	212	181	47	72	0.79386	0.853774	0.822727
Time	102	93	31	27	0.75	0.911765	0.823009
Clan	674	578	43	109	0.930757	0.857567	0.892664
Hell	245	222	49	22	0.819188	0.906122	0.860465
Para	294	256	50	38	0.836601	0.870748	0.853333
Day	31	27	9	4	0.75	0.870968	0.80597
Mon	139	131	36	4	0.784431	0.942446	0.856209

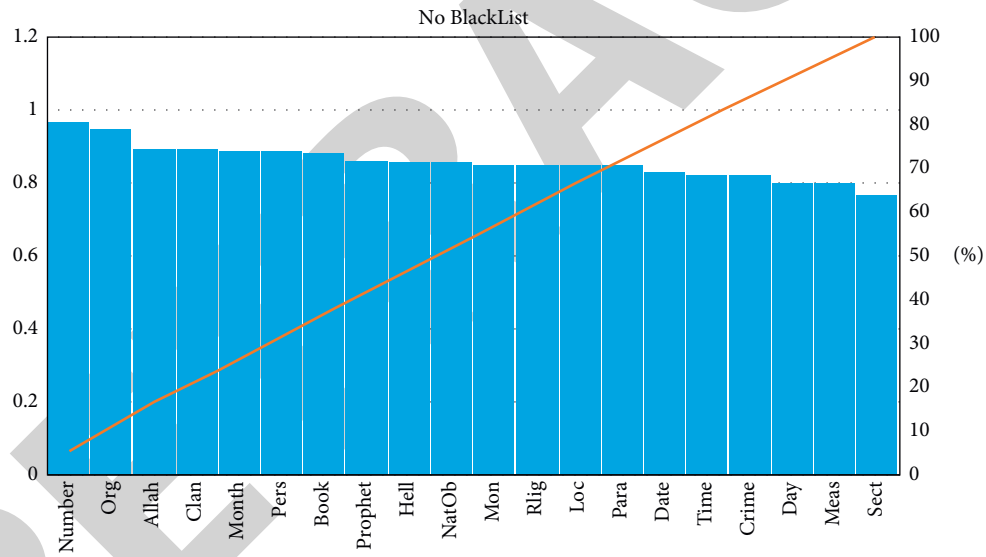

Figure 10: Results of not using blacklist.

Table 16: Overall results for NEs.

Key	Count	TP	FP	FN	Precision	Recall	F-measure
Book	183	161	17	113	0.904494	0.879781	0.891967
Prophet	6502	6039	245	186	0.961012	0.928791	0.944627
Allah	7811	7011	385	786	0.947945	0.89758	0.922075
Pers	39159	37846	4876	621	0.885867	0.96647	0.924415
Org	9	9	0	0	1	1	1
Number	13707	13187	248	444	0.981541	0.962063	0.971704
Date	596	437	2	106	0.995444	0.733221	0.844444
Meas	147	118	23	56	0.836879	0.802721	0.819444
Rlig	184	153	2	24	0.987097	0.831522	0.902655
Sect	17	15	4	2	0.789474	0.882353	0.833333
Loc	1349	1090	84	287	0.92845	0.808006	0.864051

Table 16: Continued.

Key	Count	TP	FP	FN	Precision	Recall	F-measure
NatOb	670	601	69	231	0.897015	0.897015	0.897015
Month	77	72	7	7	0.911392	0.935065	0.923077
Crime	212	181	39	72	0.822727	0.853774	0.837963
Time	102	93	24	27	0.794872	0.911765	0.849315
Clan	674	578	27	109	0.955372	0.857567	0.903831
Hell	245	227	31	22	0.879845	0.926531	0.902584
Para	294	256	24	38	0.914286	0.870748	0.891986
Day	31	30	9	1	0.769231	0.967742	0.857143
Mon	139	131	17	4	0.885135	0.942446	0.912892

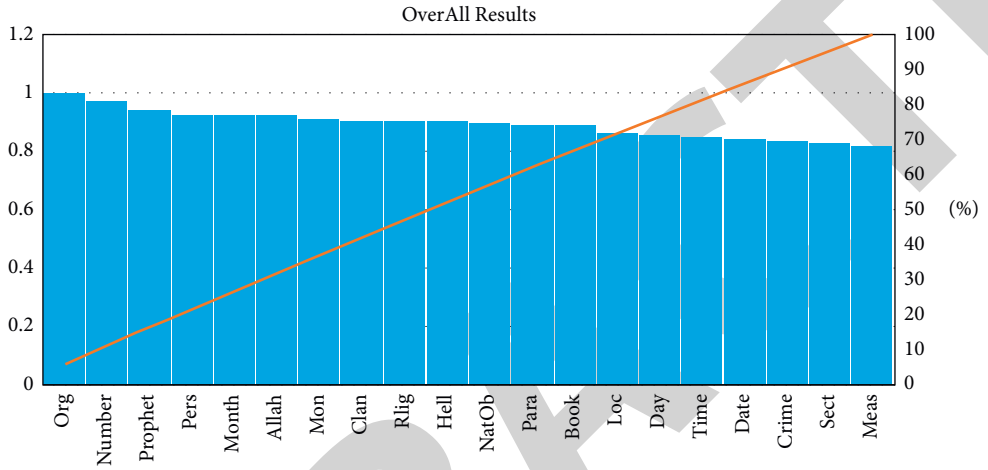

Figure 11: The overall results.

Table 17: The overall results of integration.

Method	Precision	Recall	F-measure
Rule-based method	0.902	0.893	0.895
Without trigger words	0.881	0.769	0.816
Without patterns	0.876	0.845	0.844
Without grammars	0.898	0.877	0.884
Without gazetteers	0.834	0.701	0.755

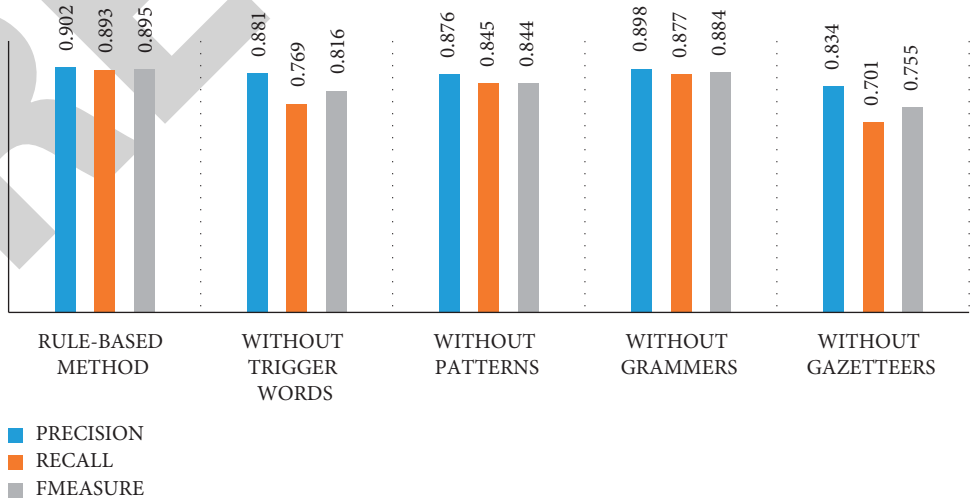

Figure 12: Comparison of versions of the rule-based method.

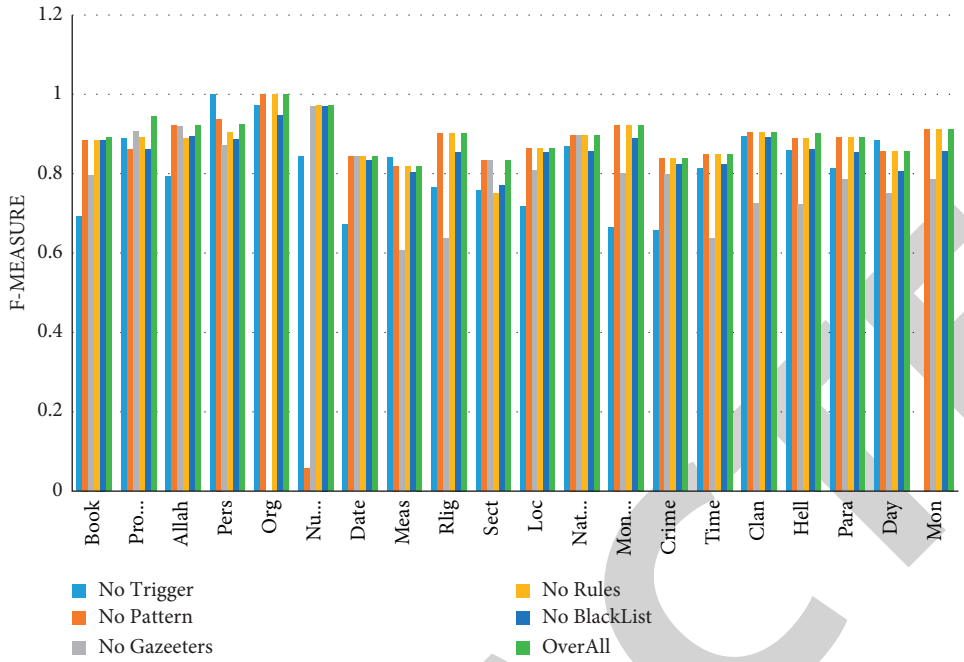

Figure 13: Comparison of features on CA NEs.

Table 18: Evaluation of rule-based method.

NE	Count	TP	FP	FN	Recall	Precision	F-measure
Person	1129	1074	85	41	0.963	0.927	0.945
Location	192	174	7	13	0.930	0.961	0.946
Organization	8	8	1	0	1.000	0.889	0.941
Date	45	37	5	3	0.925	0.881	0.902
Money	33	25	2	3	0.893	0.926	0.909
Book	12	11	1	2	0.846	0.917	0.880
Measurements	19	14	0	4	0.778	1.000	0.875

Table 19: Comparison between baseline analysis and rule-based methods.

NE	GATE	Language computer	Rule-based method
Person	0.4855	0.5767	0.945
Location	0.2418	0.2	0.946
Organization	0.4444	0	0.941
Date/time	0.7399	0	0.902
Money	0.2665	0	0.909
Book	0	0	0.88
Measurements	0	0	0.875

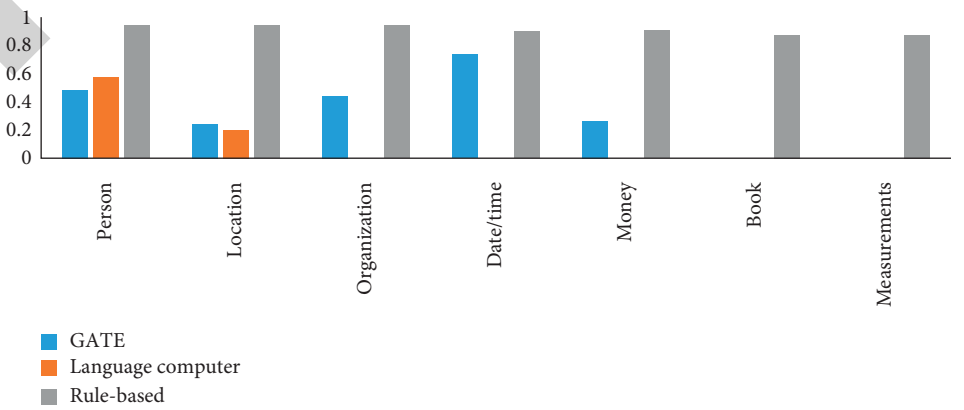

Figure 14: Comparison between baseline analysis and rule-based methods.

6. Conclusion

In this paper, a new rule-based approach was proposed. A description of the linguistic resources used by the new approach was provided before the new approach was explained. Then, the operational contents (read operation file, read linguistic resource, create regex, and rules) were discussed with the preprocessing and processing stages. The new approach proposed by this study used trigger words, gazetteers, regular expressions, grammatical rules, and blacklists, and the methodology was explained in this section. Finally, the rule-based approach was evaluated. The results indicated that this approach achieved a 90.2% rate of precision and an 89.3% level of recall and had an F-measure of 89.5.

NER is a way to extract information, and it is used in several NLP operations, including machine translation and information retrieval. Arabic NER is attracting increasing attention, but the unique nature of Arabic means that using NER can be difficult. The contributions made by this study are essential steps in finding solutions for these issues.

Data Availability

The data used to support the findings of this study are available from the first author and corresponding author upon request.

Conflicts of Interest

The authors declare that they have no conflicts of interest.

References

[1] D. Nadeau and S. Sekine, "A survey of named entity recognition and classification," *Lingvisticæ Investigationes. International Journal of Linguistics and Language Resources*, vol. 30, no. 1, pp. 3–26, 2007.

[2] J. Salminen, M. Hopf, S. A. Chowdhury, S.-g. Jung, H. Almerekhi, and B. J. Jansen, "Developing an online hate classifier for multiple social media platforms," *Human-centric Computing and Information Sciences*, vol. 10, no. 1, pp. 1–34, 2020.

[3] R. E. Salah and L. Qadri binti Zakaria, "A comparative review of machine learning for Arabic named entity recognition," *International Journal of Advanced Science, Engineering and Information Technology*, vol. 7, no. 2, pp. 511–518, 2017.

[4] R. Taquini, K. R. Finardi, and G. B. Amorim, "English as a medium of instruction at Turkish state universities," *Education and Linguistics Research*, vol. 3, no. 2, pp. 35–53, 2017.

[5] N. Alsaaran and M. Alrabiah, "Classical Arabic named entity recognition using variant deep neural network architectures and BERT," *IEEE Access*, vol. 9, pp. 91537–91547, 2021.

[6] A. Ghallab, A. Mohsen, and Y. Ali, "Arabic sentiment analysis: a systematic literature review," *Applied Computational Intelligence and Soft Computing*, vol. 2020, Article ID 7403128, 13 pages, 2020.

[7] R. E. Salah and L. Q. b. Zakaria, "Arabic rule-based named entity recognition systems progress and challenges," *International Journal of Advanced Science, Engineering and Information Technology*, vol. 7, no. 3, pp. 815–821, 2017.

[8] M. Mohd, F. Qamar, I. Al-Sheikh, and R. Salah, "Quranic optical text recognition using deep learning models," *IEEE Access*, vol. 9, pp. 38318–38330, 2021.

[9] S. AbdelRahman, "Integrated machine learning techniques for Arabic named entity recognition," *IJCSI*, vol. 7, no. 4, pp. 27–36, 2010.

[10] Y. Benajiba, P. Rosso, and J. M. Benedíruiz, "Anersys: an Arabic named entity recognition system based on maximum entropy," in *Proceedings of the International Conference on Intelligent Text Processing and Computational Linguistics*, April 2007.

[11] S. Abdallah, K. Shaalan, and M. Shoaib, "Integrating rule-based system with classification for Arabic named entity recognition," in *Proceedings of the International Conference on Intelligent Text Processing and Computational Linguistics*, March 2012.

[12] M. Aboaoga and M. J. Ab Aziz, "Arabic person names recognition by using a rule based approach," *Journal of Computer Science*, vol. 9, no. 7, pp. 922–927, 2013.

[13] K. Shaalan and M. Oudah, "A hybrid approach to Arabic named entity recognition," *Journal of Information Science*, vol. 40, no. 1, pp. 67–87, 2014.

[14] K. Shahina, "A sequential labelling approach for the named entity recognition in Arabic language using deep learning algorithms," in *Proceedings of the 2019 International Conference on Data Science and Communication (IconDSC)*, March 2019.

[15] D. Awad, "Arabic name entity recognition using deep learning," in *Proceedings of the International Conference on Statistical Language and Speech Processing*, October 2018.

[16] B. Mohit, "Recall-oriented learning of named entities in Arabic Wikipedia," in *Proceedings of the 13th Conference of the European Chapter of the Association for Computational Linguistics*, Avignon, France, April 2012.

[17] A. Mousa, "Cascaded RBF-CBiLSTM for Arabic named entity recognition," in *Proceedings of the 2020 International Conference on Communications, Computing, Cybersecurity, and Informatics (CCCI)*, November 2020.

[18] M. B. Sajadi and B. Minaei, "Arabic named entity recognition using boosting method," in *Proceedings of the 2017 Artificial Intelligence and Signal Processing Conference (AISP)*, October 2017.

[19] N. F. Mohammed and N. Omar, "Arabic named entity recognition using artificial neural network," *Journal of Computer Science*, vol. 8, no. 8, p. 1285, 2012.

[20] S. S. Balgasem and L. Q. Zakaria, "A hybrid method of rule-based approach and statistical measures for recognizing narrators name in hadith," in *Proceedings of the 2017 6th International Conference on Electrical Engineering and Informatics (ICEEI)*, November 2017.

[21] E. Hkiri, S. Mallat, and M. Zrigui, "Integrating bilingual named entities lexicon with conditional random fields model for Arabic named entities recognition," in *Proceedings of the 2017 14th IAPR International Conference on Document Analysis and Recognition (ICDAR)*, November 2017.

[22] N. Boudjellal, "ABioNER: a BERT-based model for Arabic biomedical named-entity recognition," *Complexity*, vol. 2021, Article ID 6633213, 21 pages, 2021.

[23] H. L. Chieu, H. T. Ng, and Y. K. Lee, "Closing the gap: learning-based information extraction rivaling knowledge-engineering methods," in *Proceedings of the 41st Annual Meeting on Association for Computational Linguistics*, Association for Computational Linguistics, Sapporo, Japan, July 2003.

Hindawi
Journal of Mathematics
Volume 2024, Article ID 9859646, 1 page
https://doi.org/10.1155/2024/9859646

Retraction

Retracted: A Study on Students' Satisfaction with Classroom Teaching of Independent Adult Universities Based on SERVQUAL and IPA Models, Taking Beijing Haidian Adult University as an Example

Journal of Mathematics

Received 30 January 2024; Accepted 30 January 2024; Published 31 January 2024

This article has been retracted by Hindawi following an investigation undertaken by the publisher [1]. This investigation has uncovered evidence of one or more of the following indicators of systematic manipulation of the publication process:

(1) Discrepancies in scope

(2) Discrepancies in the description of the research reported

(3) Discrepancies between the availability of data and the research described

(4) Inappropriate citations

(5) Incoherent, meaningless and/or irrelevant content included in the article

(6) Manipulated or compromised peer review

The presence of these indicators undermines our confidence in the integrity of the article's content and we cannot, therefore, vouch for its reliability. Please note that this notice is intended solely to alert readers that the content of this article is unreliable. We have not investigated whether authors were aware of or involved in the systematic manipulation of the publication process.

In addition, our investigation has also shown that one or more of the following human-subject reporting requirements has not been met in this article: ethical approval by an Institutional Review Board (IRB) committee or equivalent, patient/participant consent to participate, and/or agreement to publish patient/participant details (where relevant).

Wiley and Hindawi regrets that the usual quality checks did not identify these issues before publication and have since put additional measures in place to safeguard research integrity.

We wish to credit our own Research Integrity and Research Publishing teams and anonymous and named external researchers and research integrity experts for contributing to this investigation.

The corresponding author, as the representative of all authors, has been given the opportunity to register their agreement or disagreement to this retraction. We have kept a record of any response received.

References

[1] X. Wang, Y. Gao, and S. Li, "A Study on Students' Satisfaction with Classroom Teaching of Independent Adult Universities Based on SERVQUAL and IPA Models, Taking Beijing Haidian Adult University as an Example," *Journal of Mathematics*, vol. 2022, Article ID 7744401, 9 pages, 2022.

Hindawi
Journal of Mathematics
Volume 2022, Article ID 7744401, 9 pages
https://doi.org/10.1155/2022/7744401

Research Article

A Study on Students' Satisfaction with Classroom Teaching of Independent Adult Universities Based on SERVQUAL and IPA Models, Taking Beijing Haidian Adult University as an Example

Xiaoya Wang,[1] **Yuanyang Gao**,[2] **and Sumei Li**[1]

[1]*Beijing Haidian Adult University (Zhongguancun College), Beijing 10083, China*
[2]*Beijing University of Aeronautics and Astronautics, Beijing 100191, China*

Correspondence should be addressed to Xiaoya Wang; angelia_xiaoya@163.com

Received 5 November 2021; Revised 17 December 2021; Accepted 21 December 2021; Published 21 January 2022

Academic Editor: Naeem Jan

To some extent, students' satisfaction with classroom teaching reflects the teaching quality of the school. In view of the characteristics of independent adult universities in recent years, which are characterized by great age difference, uneven foundation, and diversified demands, it is necessary to start the research from the perspective of students, through sufficient investigation, forming a survey index, setting up questionnaires, and conducting empirical research on their satisfaction with classroom teaching. In the study, the service quality gap model (SERVQUAL) is introduced; the importance-satisfaction model, importance-performance analysis (IPA), was used to check the consistency of the SERVQUAL research results; the current status of satisfaction was obtained; and countermeasures and suggestions were proposed to improve students' satisfaction with classroom teaching of independent adult universities.

1. Introduction and Literature Review

Independent adult universities play an important role in adult higher education in China. With the influence of China's economic development, the expansion of college enrollment, the decrease of school-age population, and other factors, the mission of independent adult universities has risen from "replenishing academic qualifications" to "permanent education." Therefore, their students are characterized by great age differences, uneven foundation, and personalized needs. Whether teachers can teach students according to their aptitudes, stimulate students' enthusiasm for learning, and get students' recognition plays a crucial role in the sustainable development of schools. Besides, students acquire knowledge and abilities mainly through classroom learning at school. Therefore, it is of great significance to research how to hold classroom teaching and improve students' classroom satisfaction.

The service quality gap model (SERVQUAL) was proposed by Parasuraman, Zeithaml, and Berry [1]. It has good reliability and validity and powerful service quality diagnosis function and is considered as the most typical method of evaluating service quality [2]. However, it also has the disadvantage that the conclusions are not universal and should be revised according to different industries when used [3]. In the education industry, from the end of the 20th century, the revised SERVQUAL model began to attract the attention of higher education researchers [4]. Yu and Han [5] summarized the results of the research on higher education service quality evaluation by experts and scholars at home and abroad in the past 20 years. Zhang [6] introduced the model into the teaching quality evaluation system of higher vocational colleges. Some scholars have also applied this model to classroom teaching. For example, He [7] applied this model to the quality measurement of classroom teaching service in higher education. IPA model is a model proposed by Martila and James to evaluate service quality by forming a quadric chart from the two dimensions of importance and satisfaction. In the field of education, Zhao [8] applied IPA to study the teaching quality of ordinary colleges and universities. Wang [9] studied students' satisfaction with classroom teaching based on IPA model.

In terms of research field, there are few reports on classroom satisfaction of independent adult universities. From the perspective of research methods, some literature studies students' satisfaction with classroom teaching solely based on SERVQUAL model or IPA model, but there are no reports on studying classroom satisfaction by combining the two models. Based on the characteristics of independent adult universities students, this article firstly designed a questionnaire from the perspective of students, through a particular website focusing on questionnaire related items. The questionnaire was distributed to and collected from the students of Beijing Haidian Adult University (an independent adult university, hereinafter referred to as Haizhi). Then, with statistical analysis tools such as SPSS and Excel, the SERVQUAL model was used to analyze the satisfaction of all levels of indicators in the questionnaire and calculate the scores of students' classroom satisfaction, and then the IPA model was used to verify the consistency of the SERVQUAL research results. Therefore, the final conclusions were drawn, and the strategies for improving class satisfaction in independent adult universities were proposed.

2. Application Design and Empirical Analysis of SERVQUAL Model

2.1. Application Design of SERVQUAL Model

2.1.1. Design of Evaluation Index System of Haizhi Students' Classroom Satisfaction. The original SERVQUAL model proposed five dimensions to measure service quality, namely, tangibility, reactivity, assurance, empathy, and reliability. Each dimension was subdivided into 22 indicators to form a scale. This article took Haizhi students as the research object and fully considered the educational objectives of independent adult universities, the characteristics of students, and the problems encountered in the process of teaching supervision in the past three years. The original SERVQUAL scale was revised to retain the original five dimensions, while considering that most of Haizhi students study in their spare time, so students were very concerned about whether the knowledge learned in school can be used to guide their work. Therefore, the practicability dimension was added to the scale to determine whether the knowledge learned in the classroom could provide students with valuable learning support. Consequently, taking the six dimensions above as the first-level indicators, student interviews were organized, and 24 questions were designed as the second-level indicators. Finally, several experts were invited to have a discussion to further confirm the scientificity and rationality of the indicators (refer to Table 1).

2.1.2. Design of Class Satisfaction Evaluation Questionnaire for Haizhi Students. According to the principles and requirements of questionnaire design, the questionnaire set up four parts: basic information, expectation of classroom satisfaction, actual perceived value of classroom satisfaction, and importance. The basic information included gender, age, and major. Likert quantitative index system was used to evaluate the expected value and actual perceived value of classroom satisfaction; each question was given a quantitative score of 1 to 5 points according to the degree of expectation and perceived quality. Likert quantitative index system was also adopted for the degree of importance, and each question was given a quantitative score of 1 to 5 points according to its importance. After the questionnaire design was completed, a small-scale presurvey was conducted by random sampling from all grades and majors. It was found that the factor loads of Q9 and Q10 under the reactivity dimension were less than 0.5, so they were deleted. The remaining 20 indicators had good validity and reliability. Therefore, the final formal questionnaire contains only five dimensions and 20 questions: tangibility, reliability, assurance, empathy, and practicability.

2.1.3. Distribution and Collection of Class Satisfaction Evaluation Questionnaire for Marine Vocational Students. The design, distribution, and collection of the questionnaire are made by the particular website mentioned before, and 312 questionnaires were collected. Due to the setting of the website, only when all the options are completed can the questionnaire be submitted. Therefore, all 312 questionnaires collected were valid questionnaires, which also met the requirements of statistics, valid samples $n \geq 30$ or $n \geq 3*(k+1)$ (k is the number of explanatory variables, and n is the number of samples).

2.1.4. The Reliability and Validity Test of Class Satisfaction Evaluation Questionnaire for Haizhi Students. Reliability test is usually expressed by Cronbach's Alpha Coefficient (α). Generally speaking, if α coefficient is greater than 0.7, the reliability of the questionnaire is relatively high. In this article, KMO and Bartlett's test of sphericity were used to do the validity test. It is generally believed that the validity of the questionnaire can be passed only when the KMO value is greater than 0.7 and the significance level of Bartlett sphericity test is less than 0.05. According to the analysis of SPSS, the α coefficients of the expected value, actual perception, and importance of the five dimensions of the questionnaire were all greater than 0.7; the KMO values were all greater than 0.7; and the significance level is 0.000, indicating that the questionnaire had high reliability and validity (refer to Table 2).

2.2. Empirical Analysis of SERVQUAL Model. The core of SERVQUAL model (service quality gap model) is that service quality (SQ) depends on the degree of difference between customer perceived service level (P) and customer expected service level (E). When $P > E$ and SQ is a positive number, customer satisfaction is generated. When $P = E$ and SQ equals zero, customers feel calm, not better or worse. When $P < E$ and SQ is a negative number, customers are dissatisfied. This paper carried out the empirical analysis according to this principle.

Table 1: Initial indicators of survey on Haizhi students' classroom satisfaction.

Dimensions (first-level indicators)	Questions (second-level indicators)
Tangibility	Q1 Hardware conditions of classroom satisfy teaching needs (desks and chairs, blackboards, multimedia equipment, etc.) Q2 The teacher dresses appropriately, teaches generously, and is full of spirit Q3 The teacher obeys school rules and comes to and leaves class on time Q4 Good classroom learning atmosphere
Reliability	Q5 Teaching objectives and plans are clear Q6 Teaching content is correct and rigorous Q7 Teaching tasks are performed accurately, and teaching plans are completed on time Q8 Electric teaching materials are exquisitely made, or the blackboard design is reasonable and neat
Reactivity	Q9 The teacher pays attention to students' listening status and responds to students' questions in time Q10 The teacher discovers, praises, and gives feedback on students' progress in time
Assurance	Q11 The teacher has profound professional knowledge and is good at stimulating students' interest in learning Q12 The teacher's teaching methods are flexible and adapt to the characteristics of students Q13 The teacher is good at using modern educational technology Q14 The teaching structure is tight and assigned properly Q15 The teacher pays attention to interaction and guides and actively organizes discussions during class time Q16 The teacher treats every student equally
Empathy	Q17 The teacher discovers students' needs initiatively Q18 The teacher helps students kindly, not perfunctorily Q19 The teacher teaches students according to their aptitude and meets their individual needs
Practicability	Q20 The teaching content of the teacher keeps pace with modern times Q21 Students can learn what they want in class Q22 What students learn in class can solve problems in work and life

Table 2: The test result of reliability and validity of the questionnaire.

Dimension	Index number	Cronbach α			KMO		
		Expectations (E)	Actual perceived value (P)	Importance (W)	Expectations (E)	Actual perceived value (P)	Importance (W)
Tangibility	4	0.884	0.863	0.852	0.821	0.822	0.785
Reliability	4	0.943	0.952	0.944	0.855	0.855	0.865
Assurance	6	0.966	0.968	0.962	0.909	0.931	0.901
Empathy	3	0.937	0.939	0.929	0.769	0.766	0.761
Practicability	3	0.941	0.911	0.932	0.748	0.760	0.765

2.2.1. Basic Information Analysis. With the help of Excel, the retrieved data were classified, summarized, and calculated according to the basic information, and the results are represented by graphs (refer to Figures 1 and 2).

According to Figures 1 and 2, from the perspective of gender, male scores were higher than female scores in terms of expectation, actual perception, and importance, and the perceived difference value is positive, indicating that males generally have higher class satisfaction. From the perspective of age, only students aged 31–50 had positive perception difference, while students of other age groups all had negative perception difference, indicating that most students had some dissatisfying feeling with classroom teaching, especially those aged 18–30 and over 51, whose perception difference was over −0.2, indicating low class satisfaction. In addition, students aged 18–30 had the lowest mean score of importance to each question, only 4.392, which indicates that students of lower age group payed less attention to the investigated problems. From the perspective of majors, the perceived difference values of health management, business management, and property management were all positive, which meant students of these three majors had higher satisfaction. However, the perceived difference value of preschool education and hotel management was negative, which resulted in dissatisfaction. In particular, the perceived difference value of preschool education reached −0.17, showing great dissatisfaction. Moreover, the expected value and actual perceived value of this major were generally low. It should be also noticed that the expectations of students majoring in hotel management were relatively high, with an average of 4.960, which was a main reason for their dissatisfaction.

2.2.2. Index Dimension Analysis. With the help of SPSS and Excel, the retrieved data were classified, summarized, and calculated according to the five dimensions of tangibility, reliability, assurance, empathy, and practicability, and the results are presented in Table 3.

The following conclusions can be drawn from Table 3:

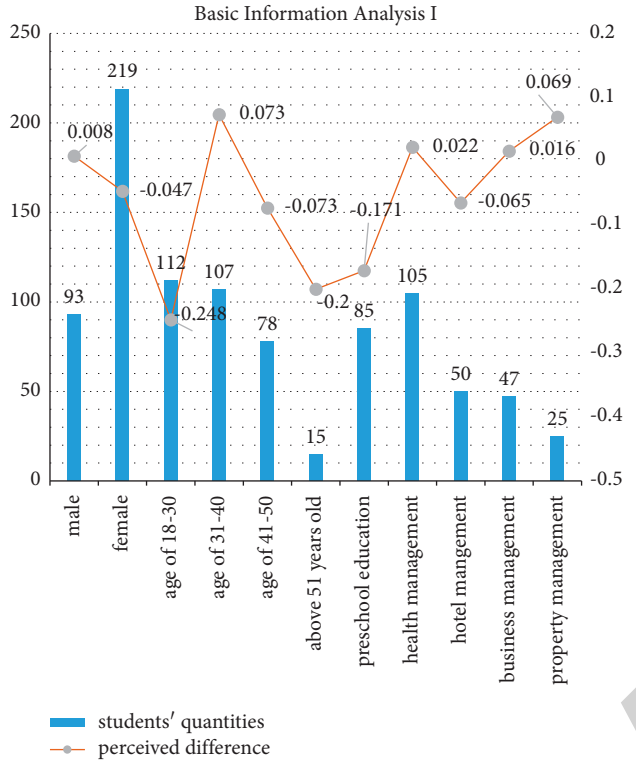

Figure 1: Basic information analysis I.

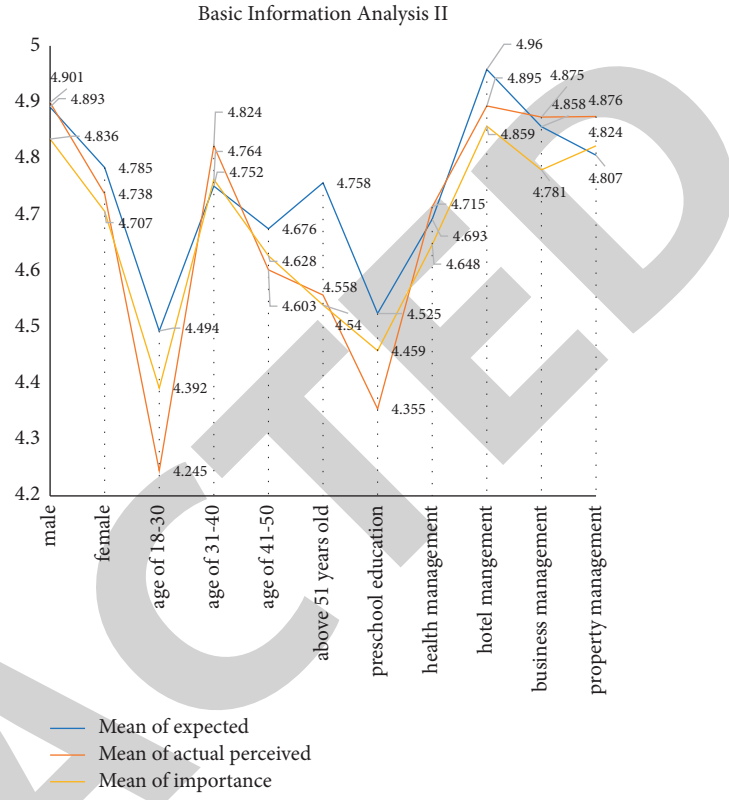

Figure 2: Basic information analysis II.

(i) Students were basically satisfied with all dimensions of classroom teaching.

Although the mean value of perception difference of the five dimensions was negative, they were all very close to zero, indicating that there was no significant difference between students' actual perception and expectation of the five dimensions and 20 questions in the survey, and they were basically satisfied with each dimension of classroom teaching.

(ii) The perception difference and importance of practicability dimension were the largest.

The mean value of perception difference of practicality dimension was -0.065, which is the largest difference among the five dimensions. Therefore, it could be seen that students showed the most dissatisfying emotions with classroom teaching in practicality. Meanwhile, the importance of practicality was considered the highest by students, reaching 4.822. This led to the conclusion that the students in independent adult universities payed the most attention to the practicability of classroom teaching.

(iii) The perception differences of Q2, Q3, Q16, and Q18 were positive.

The perception differences of Q2 and Q3 in tangibility dimension, Q16 in assurance dimension, and Q18 in empathy dimension were positive, which meant that the following aspects were approved by students: "the teacher dresses appropriately, teaches generously, and is full of spirit"; "the teacher obeys school rules and comes to and leaves class on time"; "the teacher treats every student equally"; and "the teacher helps students kindly, not perfunctorily."

(iv) The perception differences of Q6, Q7, Q13, Q15, and Q20 were close to zero.

The perception differences of Q6 and Q7 in reliability dimension, Q13 and Q15 in assurance dimension, and Q20 in practicability dimension were close to zero, which meant that the following aspects were basically recognized by students: "teaching content is correct and rigorous"; "teaching tasks are performed accurately, and teaching plans are completed on time"; "the teacher is good at using modern educational technology"; "the teacher pays attention to interaction and guides and actively organizes discussions during class time"; and "the teaching content of the teacher keeps pace with modern times."

(v) The perception differences of Q1, Q21, and Q22 were the largest.

The largest perception difference among all the second-level indicators was that of Q1 in tangibility dimension, which indicated that the aspect "hardware conditions of classroom satisfy teaching needs" did not achieve students' expectation and that the university did not do well, at least it did not meet the students' expectations. The perception

Table 3: Mean value analysis of each dimension and problem index of student classroom satisfaction.

Dimensions (first-level indicators)	Questions (second-level indicators)	Mean of expected value (E)	Mean of actual perceived value (P)	Mean of perceived difference (P-E)	Mean of importance (W)
Tangibility	Q1	4.747	4.631	−0.115	4.535
	Q2	4.788	4.811	0.022	4.750
	Q3	4.862	4.881	0.019	4.746
	Q4	4.837	4.808	−0.029	4.749
	Mean	4.808	4.783	−0.026	4.695
Reliability	Q5	4.843	4.776	−0.067	4.617
	Q6	4.827	4.817	−0.010	4.824
	Q7	4.830	4.811	−0.019	4.714
	Q8	4.811	4.760	−0.051	4.779
	Mean	4.828	4.791	−0.037	4.733
Assurance	Q11	4.843	4.785	−0.058	4.853
	Q12	4.814	4.782	−0.032	4.821
	Q13	4.808	4.798	−0.010	4.704
	Q14	4.814	4.782	−0.032	4.601
	Q15	4.795	4.782	−0.013	4.801
	Q16	4.846	4.846	0.000	4.746
	Mean	4.820	4.796	−0.024	4.754
Empathy	Q17	4.808	4.769	−0.038	4.708
	Q18	4.817	4.827	0.010	4.840
	Q19	4.821	4.782	−0.038	4.824
	Mean	4.815	4.793	−0.022	4.790
Practicability	Q20	4.821	4.808	−0.013	4.843
	Q21	4.814	4.715	−0.099	4.814
	Q22	4.788	4.705	−0.083	4.808
	Mean	4.808	4.743	−0.065	4.822

differences of Q21 and Q22 in practicability dimension were -0.099 and -0.083, which were relatively a little high, and students were dissatisfied with the aspects "students can learn what they want in class" and "what students learn in class can solve problems in work and life."

2.2.3. Calculation of Students' Classroom Satisfaction Based on SERVQUAL Model

(1) Weight Calculation. There are many methods to calculate the weight. In this paper, the product scale method of analytic hierarchy process was used to calculate the weight of each dimension. According to Table 3, the importance of each dimension from small to large is as follows: tangibility, reliability, assurance, empathy, and practicability. The tangibility is weighted as 1, the reliability is 11.354, the assurance is 11.3541.354, and so on. Through calculation, the weights of each dimension were as follows: $W_{\text{tangibility}} = 9.97\%$, $W_{\text{reliability}} = 13.50\%$, $W_{\text{assurance}} = 18.28\%$, $W_{\text{mobility}} = 24.75\%$, $W_{\text{practicability}} = 33.51\%$.

(2) Satisfaction Calculation. Based on SERVQUAL model, the calculation formula of students' classroom satisfaction is

$$\text{SQ} = \sum_{k=1}^{5} W_k \frac{\sum_{i=1}^{n} (P_i - E_i)}{n}, \text{i} = 1, 2, \ldots 8, 11, 12 \ldots 22. \quad (1)$$

According to (1), SQ = −0.139.

In order to explain the satisfaction more directly, the satisfaction index above SQ can be converted into the percentage status through (2), and the students' classroom satisfaction is 87.99%, which reached a high satisfaction level.

$$\text{SQ}_{(\text{percentage status})} = \frac{\text{SQ} - [\min\ (P_i) - \max\ (E_i)]}{0 - [\min\ (P_i) - \max\ (E_i)]}, \quad \text{i} = 1, 2, \ldots 8, 11, 12 \ldots 22 \quad (2)$$

3. Empirical Analysis of IPA Model

This section used the importance-performance analysis method (IPA model) to analyze the students' evaluation of classroom satisfaction. IPA model is a four-quadrant chart, which, in this article, is drawn with actual perception (satisfaction) as the horizontal axis, importance as the vertical axis, and the mean value of the horizontal axis and vertical axis as the division line, including four areas: advantage area, improvement area, opportunity area, and maintenance area. Based on the data in Table 3 and the principle of IPA, the first-level indicators and the second-level indicators were drawn on the IPA chart with the help of Excel (refer to Figures 3 and 4 for details), and the following conclusions were obtained.

3.1. IPA Analysis of the First-Level Indicators. The dimensions located in the advantage area were empathy and assurance, which showed that teachers' caring for students,

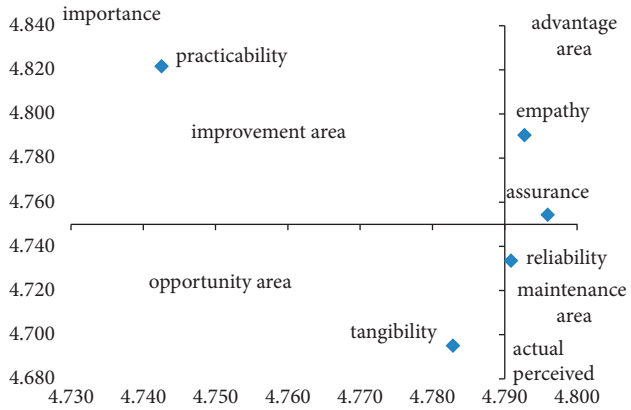

Figure 3: The first-level indicators in IPA.

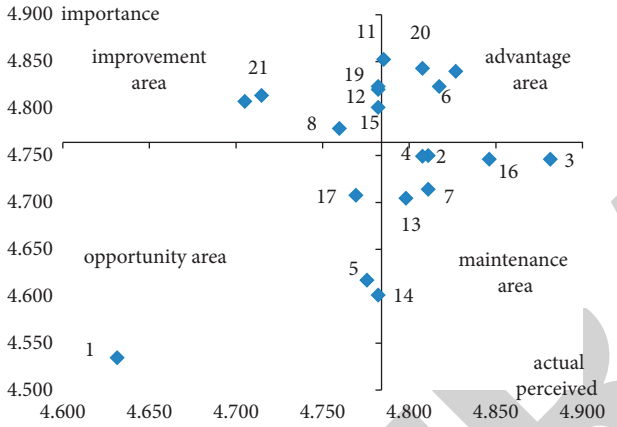

Figure 4: The second-level indicators in IPA.

teachers' personal qualities, and teaching abilities were considered as very significant as well as satisfying aspects, and they were the core competitive advantage of classroom teaching. The dimension located in the improvement area is practicality, which shows that students need to be improved in terms of providing valuable learning support for the knowledge learned in the classroom, because not only the satisfaction is low, but also the students pay special attention to it, and the school must pay great attention to it and improve it as soon as possible. The dimension located in the opportunity area is tangible, which shows that students do not pay attention to the teaching environment and teachers' appearance but are full of opportunities. The dimension located in the maintenance area is reliability, which shows that teachers have been recognized by students in terms of the accurate and reliable implementation of teaching plans and teaching tasks, but students do not pay so much attention to it and can maintain the status quo first.

3.2. IPA Analysis of the Second-Level Indicators

3.2.1. Index Analysis in Advantage Area. There were three indicators in advantage area, Q6, Q18, and Q20. This showed that the three indicators "teaching content is correct and rigorous," "the teacher helps students kindly, not perfunctorily," and "the teaching content of the teacher keeps pace with modern times" were considered by students to be more important and had high satisfaction, which had already achieved students' expectation, so teachers should continue to maintain the strength and make persistent efforts.

3.2.2. Index Analysis in Improvement Area. There were seven indicators in improvement area, which were Q8, Q11, Q12, Q15, Q19, Q21, and Q22. However, the four indicators Q11, Q12, Q15, and Q19 were almost on the dividing line between advantage area and improvement area, indicating that students basically recognized their performance. Therefore, the most concerned indicators were Q8, Q21, and Q22, which had the characteristics of low satisfaction and high attention. In the future, reform should focus on the aspects "electric teaching materials are exquisitely made, or the blackboard design is reasonable and neat," "students can learn what they want in class," and "what students learn in class can solve problems in work and life."

3.2.3. Index Analysis in Opportunity Area. There were four indicators in opportunity area, which were Q1, Q5, Q14, and Q17. The three indicators Q1, Q14, and Q17 were almost on the dividing line between opportunity area and maintenance area, which showed that students were satisfied with them, but they did not pay so much attention to them. Therefore, the most typical indicator in this area is Q1; that is, students neither were satisfied nor payed attention to the aspect "hardware conditions of classroom satisfy teaching needs."

On the other hand, the double low area also had the greatest space for improvement, and the school should also pay attention to it.

3.2.4. Index Analysis in Maintenance Area. There were six indicators in maintenance area, which were Q2, Q3, Q4, Q7, Q13, and Q16. However, the four indicators Q2, Q3, Q4, and Q16 were almost on the dividing line between maintenance area and advantage area, which indicated that students were basically satisfied with them. The area should focus on Q7 and Q16, for the reason that students were satisfied with the aspects "teaching tasks are performed accurately, and teaching plans are completed on time" and "the teacher treats every student equally," but they payed insufficient attention, which was also caused by the typical characteristics of adult university.

4. Consistency Test of SERVQUAL and IPA Models

SERVQUAL and IPA models have different calculation methods and different description methods of satisfaction, but they are based on perceived service quality, and the data sources are the same. Firstly, this study used SERVQUAL model to draw the conclusion that students' overall satisfaction is high and the perception difference of practicability

dimension was the largest one. In order to further verify the effectiveness of the conclusion, this article introduced the IPA model, compared and analyzed the conclusions of the two models, and drew the following conclusions.

4.1. The Analysis Results of the Two Models Were Consistent. The conclusions obtained were consistent with both first-level indicators (dimensions) and second-level indicators.

On the one hand, both models showed that the practicability dimension was the one that needed most attention and improvement, which meant students thought that the knowledge learned in class was not enough to provide them with valuable learning support. The empathy dimension performed best, which meant students recognized teachers' empathy and caring for students.

On the other hand, both models indicated that among the second-level indicators, Q21 and Q22 still needed the most attention, which has been described in detail before and will not be repeated here. Q18 was the best one in all the second-level indicators, which showed that students were most satisfied with the aspect "the teacher helps students kindly, not perfunctorily."

4.2. IPA Model Is a Useful Complement to SERVQUAL Model. Firstly, according to SERVQUAL model, the perceived difference of Q7 "teaching tasks are performed accurately, and teaching plans are completed on time" and Q13 "the teacher is good at using modern educational technology" tended to zero. According to IPA model, they fell in the maintenance area, which pointed out the direction for their improvement, and they could be improved from the perspective of improving students' attention level then pushed into the advantage area.

Secondly, according to SERVQUAL model, Q1 had the largest perception difference. According to IPA model, both Q1 and the tangibility dimension were located in the opportunity area. Improvement of Q1 should not only improve students' perception, but also attract students' attention.

5. Countermeasures and Suggestions on Improving Classroom Satisfaction of Students in Independent Adult Universities

From the perspective of service quality, students' classroom satisfaction can be improved in terms of tangible hardware and intangible software. Based on the empirical study of Haizhi and the conclusions of SERVQUAL and IPA model, this article puts forward some suggestions on how to improve students' classroom satisfaction in independent adult universities.

5.1. Improving Hardware Conditions

5.1.1. Upgrading Classroom Facilities and Equipment. If workers want to do well, they must sharpen their tools first. Since the release of the ten years' development plan for education informatization (2011–2020) [10], the teaching environment of independent adult universities has been greatly improved, the Internet coverage and qualities of multimedia classroom have been significantly improved, high-quality digital education resources are increasingly abundant, and information-based teaching is becoming more and more popular. However, the major setting of adult universities keeps pace with the development of the times, and new majors with strong practicality and practicability keep emerging, which have higher and more professional requirements for classroom hardware facilities and equipment. Therefore, although most independent adult universities have standard desks and chairs and basic multimedia teaching equipment, they still need to combine the characteristics of different majors to improve classroom facilities and equipment. Taking Haizhi as an example, preschool education major should add piano room, practice room, and other training classrooms; health management major should be equipped with sufficient instruments and equipment for students to practice; and teachers should also have sufficient teaching aids for classroom teaching. Once the hardware resources are improved, the perception difference of Q1 will change from negative to positive, which will also make the perception difference of other relevant factors (such as Q21 and Q22 in the practical dimension) positive, so as to improve classroom satisfaction.

5.1.2. Strengthening Informatization Construction. The 13th five-year plan for education informatization [11] issued by the Ministry of Education points out that continuing education should establish a blended teaching and learning mode combining online and offline formats; design the curriculum reform under the background of informatization; and further promote the construction of "three kinds of classrooms," that is, "famous teacher classroom," and "online classroom of famous school." The key points of education informatization and network security in 2019 [12], released by the Ministry of Education, pointed out that new modes and mechanisms of higher continuing education resource construction should be further explored and that the role of digital learning resource opening and online education alliance of higher education should be actively played. Therefore, strengthening information construction and promoting blended teaching are not only the requirements of the Ministry of Education for independent adult universities, but also effective methods to adapt to the development of the times, promote classroom reform, and alleviate the "contradiction between work and study" of adult students. In particular, during the outbreak of COVID-19, information construction has largely solved the problem that "classes suspended but learning continues" for students, providing strong support for the smooth operation of normal teaching. Taking Haizhi as an example, as long as the information platform is well built, teachers can share classroom teaching resources, extracurricular expansion resources, and the latest professional trends on the platform in time. Students who cannot participate in face-to-face teaching can use network learning and communication anytime and anywhere, and the satisfaction of Q13 will be greatly improved.

5.2. Enhancing Soft Power

5.2.1. Strengthening Teaching Management and Improving Service Level. The work of teaching management should be undertaken jointly by the administrative departments and schools. Teaching is the central work of the school, and teaching quality is the lifeline of the school. In order to improve the service level of adult universities, the teaching management of adult universities should strictly comply with the requirements of educational administrative departments and cooperate with other relevant departments. Taking Haizhi as an example, teaching management is not only closely related to the teaching staff department, but also closely related to the publicity of enrollment department, teachers, and head teachers. Therefore, to strengthen teaching management, first of all, it is necessary to avoid overcommitment and avoid artificially raising students' expectations, which will lead to the decline of satisfaction. For example, the average expectation of students majoring in hotel management is as high as 4.96; the head teachers should do a good job in the statistics of students' information, aiming to do a good job of support services, and female students and older and younger students required much more care and help; teachers should follow the principle of "preparing lessons first to prepare students" and have a profound understanding of students' occupation, characteristics, and learning needs through the head teacher before starting classes. During class time, the teaching method and content should be adjusted according to the feedback of students, so that Q21 and Q22 can be improved. In addition, regarding the learning method, younger students should be given more guidance and older students should be given more patience.

5.2.2. Promoting Teachers' Growth Based on Teachers' Training. The outline of national medium and long-term education reform and development plan (2010–2020) explains the teachers training system for continuing education: improve the teachers training system [13], put teachers training funds in the government budget, and implement a five-year cycle for teachers' full-staff training. It also pointed out that it is necessary to attach more importance to the training of counselors and head teachers, deepen teacher education reform, innovate training models, strengthen practice activities, strengthen teacher ethics and teaching abilities, improve the quality of teacher training, encourage universities and enterprises to build a "double-quality teachers" training base, and improve the regular practice system for teachers to get into the enterprise. Therefore, independent adult universities should establish a wholesome system of teachers training and regularly organize diversified teacher training. First, teacher ethics training should be strengthened. Second, the promotion of professional knowledge and skills training should be focused on, and academic exchanges, departmental seminars, and basic skill of teaching competitions should be held regularly. Besides, universities need to encourage teachers to listen to lectures, read reports, learn frontier discipline knowledge, make full use of network resources, study by themselves, and form a good habit of lifelong learning. Finally, the school can also provide teachers with the opportunity to practice in enterprises and prevent "empty talk" in classroom teaching. Taking Haizhi as an example, only when the teachers training is fulfilled sufficiently and properly, can the teaching method of teachers more touch students' spirits and be more suitable for students, so as to improve the transformation ability of classroom knowledge, fundamentally improve Q21 and Q22, and provide valuable learning support for students.

6. Conclusion

Based on the realistic characteristics of independent adult universities and the perspective of students, taking Beijing Haidian Adult University as an example, this article firstly makes a theoretical and empirical study on students' classroom satisfaction by using SERVQUAL model and then uses IPA model to test the consistency of SERVQUAL results. It is concluded that the analysis results of the two models are consistent. Besides, IPA model is a useful supplement to SERVQUAL model. According to the analysis of the two models, this paper draws the following three conclusions: first, students' classroom satisfaction is 87.99%, reaching a high level; second, students are relatively dissatisfied with the practical dimension and think that the knowledge learned in the classroom is not enough to provide valuable learning support for them; third, the satisfaction of male students is higher than that of female students, the satisfaction of older and younger students is relatively lower, and the satisfaction of preschool education students is relatively the lowest. At the same time, in combination with the documents issued by the Ministry of Education in recent years, this paper puts forward improvement measures and suggestions to improve students' classroom satisfaction in independent adult universities from the two aspects of improving hardware conditions and soft power, which has significant practical guidance for independent adult universities.

Data Availability

The data used to support the findings of this study are included within the article.

Conflicts of Interest

The authors declare that they have no conflicts of interest.

Acknowledgments

This manuscript is supported by Key Project of Beijing Adult Education Association in 2020-2021. The project approval number is CRZ2103, and the project title is "Research on Teaching Quality Evaluation and Quality Monitoring Mechanism of Independent Adult Universities—Take Beijing Haidian Adult University for Example."

References

[1] H. Zhang and W. Zhang, *Principle and Practice of Hotel Quality management*, pp. 17–35, Peking University press, Beijing, China, 2015.

Hindawi
Journal of Mathematics
Volume 2024, Article ID 9824283, 1 page
https://doi.org/10.1155/2024/9824283

Retraction

Retracted: Design and Research of the AI Badminton Model Based on the Deep Learning Neural Network

Journal of Mathematics

Received 23 January 2024; Accepted 23 January 2024; Published 24 January 2024

This article has been retracted by Hindawi following an investigation undertaken by the publisher [1]. This investigation has uncovered evidence of one or more of the following indicators of systematic manipulation of the publication process:

(1) Discrepancies in scope

(2) Discrepancies in the description of the research reported

(3) Discrepancies between the availability of data and the research described

(4) Inappropriate citations

(5) Incoherent, meaningless and/or irrelevant content included in the article

(6) Manipulated or compromised peer review

The presence of these indicators undermines our confidence in the integrity of the article's content and we cannot, therefore, vouch for its reliability. Please note that this notice is intended solely to alert readers that the content of this article is unreliable. We have not investigated whether authors were aware of or involved in the systematic manipulation of the publication process.

Wiley and Hindawi regrets that the usual quality checks did not identify these issues before publication and have since put additional measures in place to safeguard research integrity.

We wish to credit our own Research Integrity and Research Publishing teams and anonymous and named external researchers and research integrity experts for contributing to this investigation.

The corresponding author, as the representative of all authors, has been given the opportunity to register their agreement or disagreement to this retraction. We have kept a record of any response received.

References

[1] Y. Chen and H. Hu, "Design and Research of the AI Badminton Model Based on the Deep Learning Neural Network," *Journal of Mathematics*, vol. 2022, Article ID 6739952, 10 pages, 2022.

Hindawi
Journal of Mathematics
Volume 2022, Article ID 6739952, 10 pages
https://doi.org/10.1155/2022/6739952

Research Article

Design and Research of the AI Badminton Model Based on the Deep Learning Neural Network

Yujue Chen[1] and He Hu[2]

[1]*College of Physical Education and Sport Academy, Qinghai Normal University, Qinghai, Xining 810008, China*
[2]*College of Computer Science and Technology, Xi'an University of Science and Technology, Shanxi, Xian 710000, China*

Correspondence should be addressed to He Hu; huhepingzi@163.com

Received 2 December 2021; Revised 19 December 2021; Accepted 22 December 2021; Published 20 January 2022

Academic Editor: Naeem Jan

In view of the fact that it is difficult for existing algorithms to identify the movements of a player in an accurate way, this paper puts forward an artificial intelligence (AI) motion model on the basis of the deep learning neural network instruction set architecture (ISA). Firstly, a mobile neural network (MNN) inference engine was utilized to create a new AI sports project-side intelligent practice model. Under this model, a movement can be segmented into a series of decomposition movements, which are recognized and judged separately for the purpose of measuring the entire movement. In order to test its feasibility, the study compares the MNN inference engine with the traditional reasoning engine in terms of their algorithmic capabilities and compares the results obtained through this algorithm and traditional online motion app. Research shows that, in the MNN of the AI sports project proposed in this paper, the datasets of action recognition exceed the results of other inference engines, characterized by lightweight, high performance, and accessibility. Research also demonstrates that the AI sports project model can adapt to the needs of sports projects with a variety of themes and improve the accuracy of movement recognition details.

1. Introduction

In the sustainable exploration of end intelligence, practice and service empowerment take place in the scenario of healthy life with sports, namely, sports AI project [1]. Projects of this kind contributed greatly to the realization of the core goal of sports digitization and the steady growth of China's sports population, thus becoming a crucial step in intelligence sports [2]. The outbreak of the COVID-19 pandemic has added to the difficulty of traditional offline sports and promoted the development of home-based sports in the context of AI technology. Through technological precipitation, home sports are combined with online sports and further empowered by AI technology, hence intelligent sports or AI sports. With intelligence and movement as their core concept, AI sports are complex that are composed of the process and the conclusion of academic activities [3, 4]. Their ultimate purpose is to create a new, simple, and interesting way for users to exercise at home [5]. To elaborate, one merely needs a mobile phone or a few-square-meter field to do AI sports. As far as badminton is concerned, the user just needs to open the power app, position the phone on the side of the playing field in an appropriate angle, and adjust the phone-subject distance according to the app's automatic voice prompts until the entire image of the player is incorporated in the recognition frame [6].

AI is a marvelous helper for physical training in that it can detect digital features and associations that are not easy to discover through human eyes or the brain, thus making AI sports more exploratory [7, 8]. This paper focuses on the integration of the badminton with AI intelligence and movements and aims to remove mistakes in beginners' movements in a more targeted way and to improve their skills in playing badminton. Firstly, the mobile neural network (MNN) inference engine is utilized to digitize the sport and obtain experimental data. Secondly, a preliminary analysis is made concerning the differences between the data and those obtained through the traditional sports app.

Thirdly, the outcomes show how the badminton players should improve their movements in playing badminton in terms of accuracy, comprehensiveness, movement coordination, and partner cooperation and make their movements approximate professional players. Fourthly, some suggestions are provided as to the application of AI in sports. Moreover, in this study, we first defined the main conceptions and their theoretical foundation in Section 2. Then, we carried out a discussion on the technical supports such as AI and intelligent motion in Section 3. Furthermore, the accuracy is recognized, the consumption of performance is decreased, and the improvement in the efficiency is tested. In addition, the flow of the model of AI sports is given in Section 4 of the paper. In Section 5, the comparative analysis is carried out where we performed the experiments for the stated purpose. Finally, the conclusion of the paper is given in Section 6.

2. Core Concept Definition and Theoretical Foundation

The inference forecast performed in the cloud can then be attempted on the mobile as mobile computing power and deep learning are undergoing rapid development, and small-scale network models are getting all the more mature. The end-side intelligence deploys and runs the AI algorithm at the end. In comparison to server-side intelligence, end-side intelligence has the advantages of low latency, good balance of data privacy, and cloud savings [9, 10].

MNN is a lightweight inference engine based on the deep neutral network (DNN), and loaded on its end side are DNN models. Up to now, MNN has seen wide applications in face detection, gesture recognition, portrait segmentation, and other things [11].

While traditional sports are one-way streamlined, AI sports project is a client-side sports intelligence system that can verify DEMO, systematize various dynamics, and support technical capability transformation. The intelligent sports system realizes terminal inference of the mobile phone through the deep inference engine [12]. Information response and dynamic corrections are made by identifying and analyzing postures and dynamics, sports track, and dynamic angles, and then, the modular combination of technical capabilities is carried out. Currently, the system, which is characterized by an organic integration of sports and AI technology, supports over ten kinds of sports actions and dozens of ways of playing, making online badminton more simple.

3. Technical Supports

The primary technical idea of intelligent motion at the AI sports end is to use the MNN inference engine for reasoning and pose recognition. It includes the following:

(1) Measuring real-time body contour in pictures and videos and finding fourteen important bone points and essential joint parts such as the head, arms, and feet

(2) Connecting the points to form movement images and analyzing body posture, movement angle, and trajectory

(3) Measuring the user's badminton action via the action and posture matching system and carrying out dynamic timing and counting

At the same time, through real-time monitoring and analysis of the standard action, response and interaction are made to improve user experience and interaction.

In traditional badminton training, people can get timely guidance and support from on-site assistants, such as coaches, examiners, relatives, and friends. Smart fitness programs on the AI sports side, nevertheless, allow people to interact directly with mobile apps while making movements. The ability and cognitive level of human-computer interaction will be affected by various factors, including logical reasoning modelling ability, badminton scene complexity, and sports information matching recognition calculation. Some new problems and difficulties appear in the study and execution of remote intelligent human locomotion ability, such as human-computer location matching, insufficiency in bone point recognition, mistakes in joint point identification, two-dimensional distortion, irrelevant user movement, mobile phone shaking, and scene noise.

Badminton dynamic effect evaluation and key algorithm design are conducive to the improvement of matching accuracy of action nodes [13], which is regarded as the cornerstone of human movement. On the premise of enhancing identification efficiency, corresponding measures should be taken to reduce resource consumption of mobile terminals, which are mainly manifested in battery power and heat generation, and improve user experience. In this way, manpower and time consumption involved in mobile terminal testing will be reduced. Additionally, the efficiency of R&D and testing is supposed to be raised to provide strong support for smooth and effective interaction within the team.

3.1. Accuracy Recognition. The most direct and primary exercise experience for users of intelligent badminton is the accuracy of dynamic counting [14]. Once there is a counting error in action recognition, sports users' enthusiasm in using the app will be affected, and their participation initiative will be demotivated. For this reason, counting problems should be avoided in the first place.

The basic principle of the intelligent motion calculation is to decompose an overall action into several decomposition movements and then employ different processes for movement recognition and judgment [15]. After a set of operations is completed, the effects of all dynamics are judged. If it is effective, the count is increased by 1. Otherwise, the steps will be repeated. In short, the recognition and operation in intelligent motion are all state machines. A motion action is discretized and abstracted into N state machines {S (0), S (1), S (2) ..., s (n1)}, which are tested successively. When all state machines are detected, the user has completed the action; then, 1 is added to the calculation

result. In case that a certain state machine is not detected, the system will give feedback and reset the machine. Each condition machine corresponds to a specific automatic trigger condition. The following dynamic matching result can be obtained by detecting the cyclic correspondence between the real-time skeletal point position change and the current state, thus enhancing the stability of the skeletal point and ensuring outcome accuracy. Since the dynamic identification accuracy is closely related to the dynamic collocation calculation, the better the calculation collocation effect, the higher the identification accuracy. To improve the accuracy of badminton motion recognition, the main factors affecting the calculation of motion information matching, such as the skeletal point, state machine, and matching, can be chosen as point cuts. Specific methods are as follows:

(1) Select the action with stable, easily recognizable, and iconic bone points as the state machine.

(2) The frame rate should be able to cover all the state machines of a badminton motion. The accuracy of bone point recognition has a great impact on motion matching.

As is shown in Figures 1 and 2, when an error occurs in the identification of the left arm point, a straight match will get an erroneous result. In this case, it is necessary to utilize the dynamic historical information of badminton users to adjust the dynamic matching result using the dynamic matching algorithm.

3.2. Performance Consumption Reduction. Restricted by physical conditions, the computing power and storage space on the cell phone are limited. Furthermore, deep learning reasoning requires enormous data consumption due to the great deal of complex calculating work. In-depth learning and reasoning will take up a lot of resources of the mobile terminal and CPU, and memory consumption will be increased significantly, leading to overheat and battery overconsumption for the equipment. Therefore, when the intelligent motion device runs on the mobile terminal, performance loss must be avoided so as to improve user experience.

To effectively reduce performance loss of the overall system, it is essential to reduce loss in every step, as is shown in the chart in Figure 3.

These three phases perform different functions. Before logical reasoning, the format conversion is performed; that is, the stream data signals acquired by the camera are converted into various stream data information formats such as YUV format and RGBA format required by the reasoning process (Figure 4). In the inference stage, the input and output skeletal point positions are calculated. The inference engine can perform a series of operations on the input frame number to draw relevant logical inference conclusions. For example, attitude recognition is to convert the RGBA data information of the input image into information of bone point positions. The postreasoning stage involves a series of analyses concerning the performance,

Figure 1: Nodes of swing action.

rendering operations and business-related actions, such as UI display and animation effect display.

The above three stages can be optimized as follows. The optimization of the inference process can be completed by the deep inference engine MNN. Stream data in the prereasoning stage can be converted directly into the required format, without having to rely on intermediate transformation. Raw data in the reasoning stage can be directly converted into the RGBA format, thus reducing unnecessary calculations and alleviating the burden for the terminal. In addition, appropriate rendering methods, such as multibackend abstraction and mixed scheduling, should be selected for the platform bearing the postinference stage to reduce rendering loss. For the IOS platform, metal can be used directly for rendering enhancement.

3.3. Testing Efficiency Improvement. AI intelligent sport is a bold attempt in digitizing sports [16]. Its R&D, particularly the testing process, requires a large amount of investment in terms of time, equipment, and effort to improve the application from various aspects. In addition, the effective detection method for AI motion recognition is greatly influenced by environmental factors, such as light source,

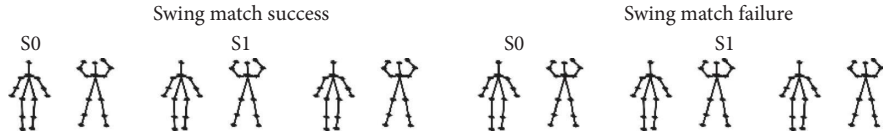

Figure 2: Matching diagram of action nodes.

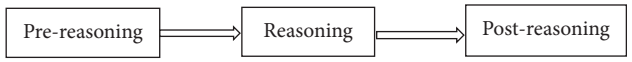

Figure 3: MNN reasoning diagram.

background, motion distance, and the size of a person's image in a shot, putting effective detection methods to the test.

Take the traditional badminton test method as an example. Generally, the detection person has to firstly manually record the real-time actions of real people on the site and make analyses afterwards off the site, as is shown in Figure 5.

In view of the fact that different brands of phones vary in drivers, operating systems, and specific performance parameters, etc., it is quite difficult to take all factors into account when traditional detection methods are employed. This poses great challenges to testers and cannot guarantee detection uniformity and accuracy at the same time. Specific reasons are as follows [17]:

(1) The labour costs are high: a test requires the cooperation of several students, which is time-consuming and exhausting.

(2) The test environment is relatively homogeneous: it cannot adapt to the complex and changing environment on the route.

(3) It is difficult to quantify the test results. It is impossible to quantitatively evaluate model performance, calculation validity, matching accuracy and precision, resource consumption, etc.

(4) Problem location is difficult. The postanalysis and troubleshooting fail to respond to online customer complaints in a targeted way.

The traditional badminton action node testing cannot solve these problems. For this purpose, Shanghai Sports Science and Technology Group has developed an AI sports automatic testing tool and solved the problems commonly found in traditional testing methods. It has realized rapid positioning and regressing badminton nodes online and quantitatively evaluating the calculation accuracy of a model.

The basic processing idea of the automatic testing tool is to simulate the actual situation through batch analysis of video sets, collect bone point data (Figure 6), complete the detection of business results, and automatically form a test report. The specific technical methods are demonstrated in Figure 7.

ISA is an unsupervised learning method with a two-layer network generation model that can effectively simulate the hierarchical response model of simple cells' and complex cells' receptive fields in the V1 region of the human visual system [18]. The most basic implementation method of ISA is to use the first layer of the model to learn the weight W of a linear transformation (L1 is similar to FC) [19, 20]. Next, the same subspace elements are combined in the second layer. Then, a fixed nonlinear transformation V (L2 pooling) is performed to obtain features that are invariant in response to phase changes.

With the introduction of the latest AI testing tool developed by ISA which is introduced, the labour cost is significantly reduced, and the detection performance is greatly improved. It is noteworthy that the effect of the test tool is related to the number of samples tested. The more abundant the models, the better the detection accuracy.

4. The Model Flow of AI Sports

The flow of the model in the diagram in the figure is the overall processing on a mobile terminal of the rear-facing camera on IOS, or Android devices take a front-facing shoot (Figure 8).

First, the system gets the data from the camera as an input to the SDK. Then, the SDK performs the following operations.

Before the MNN engine performs the inference, the original input is processed to guarantee that the face inference in the input data is forward using the AI model. The results are generated based on the key points input to the image coordinate system after preprocessing, and the critical point coordinates are transformed to the same direction as the screen rendering coordinate system to facilitate rendering. The ultimate key points are displayed on the user's screen in the process application, and the front end uses a "canvas" for rendering. The coordinate system of the canvas is called the rendering coordinate system. In the last step of SDK detection, we transform the critical points to the same orientation as the rendering coordinate system and then map the key point coordinates to the coordinates of the rendering coordinate system at an equal scale. After mapping is completed, the results are directly rendered to the canvas.

5. Project Experiment and Comparative Analysis

A comparison between MNN and TVM algorithms is made to test the feasibility of the proposed AI sports with the MNN inference engine.

TVM owns fully automatic search through ML, while the MNN is semiautomatic. It is the biggest and the fatal drawback in terms of refinement and optimization (Figures 9–11).

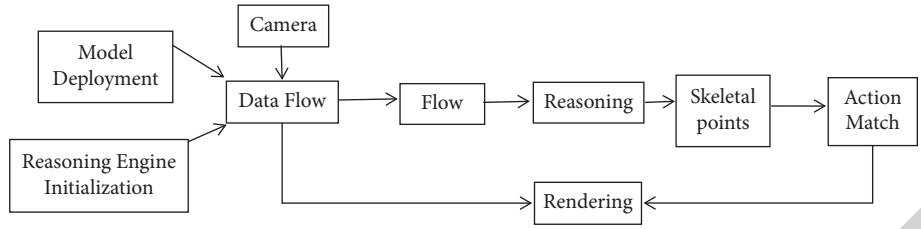

Figure 4: MNN process.

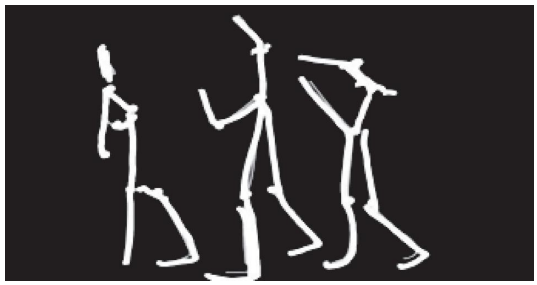

Figure 5: The action node of striking lofty goals of badminton.

5.1. Preinference

5.1.1. Accelerated Scheme Selection. In mobile applications, computation speed and lightness are the primary considerations. Acceleration libraries, such as OpenBLAS [21] and Eigen, cannot be used in mobile applications with a view to alleviating operation burden of the terminal. Therefore, NCNN (Tencent, 2017), MACE (Xiaomi, 2018), and Anakin (Baidu, 2018) opt for a manual search approach that does not rely on any external libraries and implements operators using assembly instructions case by case. This approach makes the reasoning engine lightweight and efficient, but the case-by-case optimization is also time-consuming and difficult to cover for all operators.

Fully automated search is in sharp contrast to manual search. The typical representative is TVM, which solves the problem of redundant dependencies and provides graph-level and operator-level optimizations for both the model and the back end [22]. Hence, TVM has excellent support for the model and device diversity. However, it comes at a cost. The runtime library generated by TVM is model-specific. In other words, when the model needs to be updated, TVM is required to regenerate the runtime library, which is unacceptable for mobile applications. MNN adopts a semiautomatic search approach with enhanced generality and performance.

5.1.2. Calculation Scheme Selection. MNN operates on a cost evaluation mechanism which takes algorithm implementation and backend characteristics into full account so as to find the optimal solution. The following is the cost calculation formula:

$$C_{\text{total}} = C_{\text{algorithm}} + C_{\text{backend}}. \tag{1}$$

To minimize the overall costs, it is crucial to opt for the fastest algorithm and the most efficient backend. Convolution is taken as an example to elucidate the cost of algorithms. There are currently two fastest implementation algorithms—sliding window and Winograd. For a variety of convolution configurations, the algorithm with the lowest computational cost is selected in a dynamic way. The selection method is as follows:

(1) If the kernel size is 1 in a matrix multiplication, the Strassen algorithm is the most appropriate.

(2) If the kernel size exceeds 1, Winograd is recruited to transform the convolution operation into matrix multiplication. Theoretically, the cost of convolution can be expressed by the following formula:

$$C_{(n)} = 2i_c(n+k-1)^3 + i_c o_c (n+k-1)^2 + n(n+k-1)(2n+k-1), \tag{2}$$

$$n = \arg\min C_{(n)}. \tag{3}$$

Based on formulae (2) and (3), the optimal output size can be chosen to minimize the cost. So, the cost for convolution is evaluated as follows.

Scheme = sliding window: if $k > 1$ and $n = 1$,

$$F(n \times n, k \times k) \quad \text{if } k > 1 \text{ and } n > 1. \tag{4}$$

The second problem is how to calculate and minimize the backend cost. That is, the best backend is selected for each operator to ensure the lowest global costs:

$$C_{\text{backend}} = \sum C_{\text{op}}. \tag{5}$$

5.2. Preparation-Execution Decoupling. During the execution of the program, the calculation is typically accompanied by memory requests and releases. For mobile applications, the overhead in memory management is considerable. Considering that the input size is already determined, the engine can execute all the operators virtually to meet the exact memory requirements. In this way, the required memory can be allocated in advance during the preinference stage and reused during the execution stage. The principle is shown in Figure 12.

5.3. Kernel Optimization. A kernel refers to the detailed implementation of an operator [23]. The optimization comes from two primary sources: algorithms and scheduling, i.e., choosing the algorithm with the lowest complexity and taking good advantage of hardware resources.

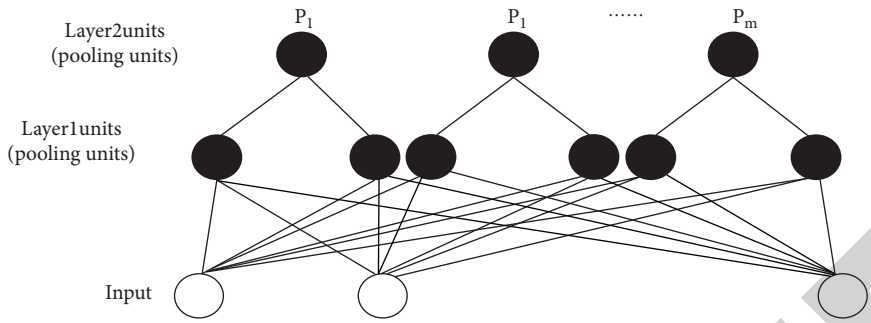

Figure 6: ISA neural network instruction diagram.

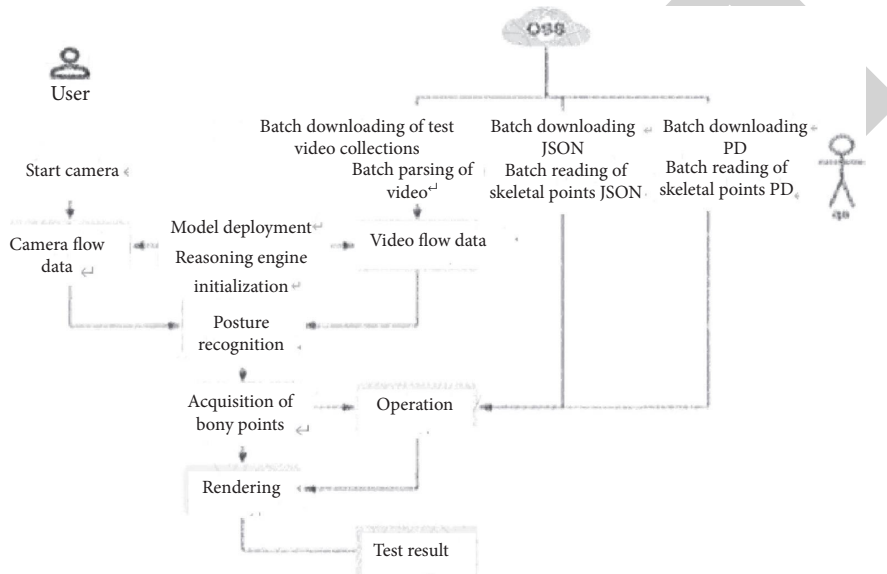

Figure 7: Automatic test flow.

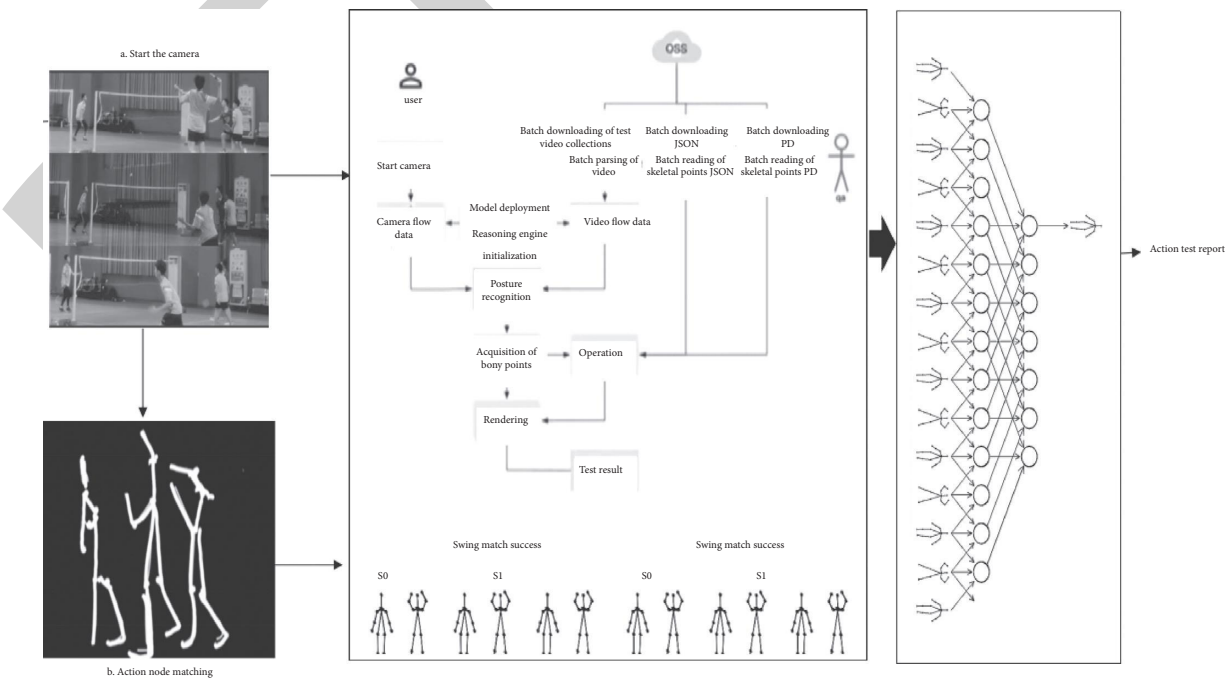

Figure 8: AI sports model.

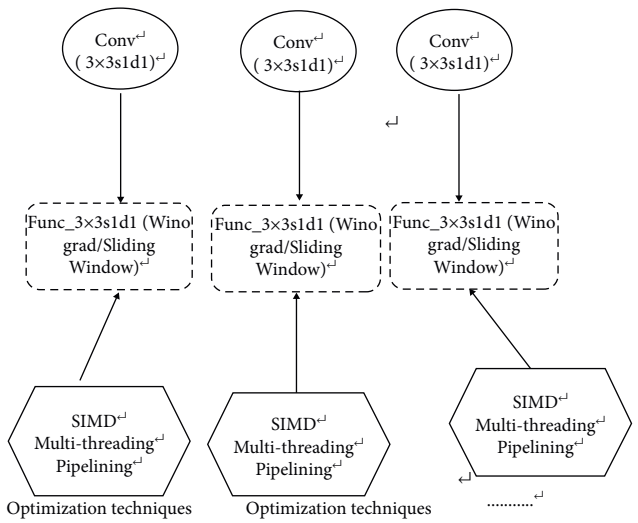

Figure 9: Manual search.

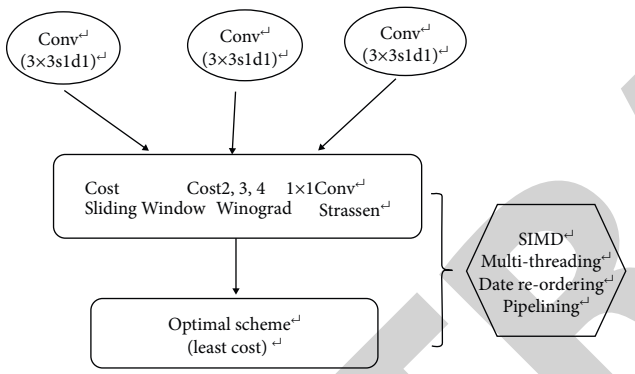

Figure 10: Semiautomatic search (MNN).

5.3.1. Winograd Optimization. The Winograd-based fast convolution algorithm has been widely applied in numerous reasoning frameworks. Different search methods are compared through three processes: (a) the manual search can be optimized by continuous correction, which means that the operators have to perform a case-by-case optimization and error correction. (b) Then, the semiautomatic MNN searches for the optimal action to match in high-performance computing. (c) Finally, the automatic search (TVM) matches the correct action for compiler optimizations through automatic filtering throughout. The Winograd optimization of data outflow in semiautomatic search is as follows:

$$F(2,3) = \begin{bmatrix} d_0 & d_1 & d_2 \\ d_1 & d_2 & d_3 \end{bmatrix} \begin{bmatrix} g_0 \\ g_1 \\ g_2 \end{bmatrix} = \begin{bmatrix} r_0 \\ r_1 \end{bmatrix}. \tag{6}$$

$$\Rightarrow r_0 = (d_0 \cdot g_0)(d_1 \cdot g_1)(d_2 \cdot g_2).$$
$$r_1 = (d_1 \cdot g_0)(d_2 \cdot g_1)(d_3 \cdot g_2).$$

$$F(2,3) = \begin{bmatrix} d_0 & d_1 & d_2 \\ d_1 & d_2 & d_3 \end{bmatrix} \begin{bmatrix} g_0 \\ g_1 \\ g_2 \end{bmatrix} = \begin{bmatrix} m_1 + m_2 + m_3 \\ m_2 - m_3 - m_4 \end{bmatrix}. \tag{7}$$

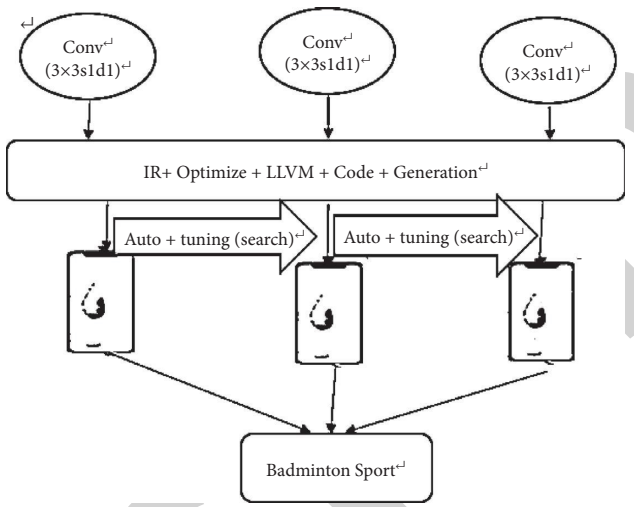

Figure 11: Automatic search (TVM).

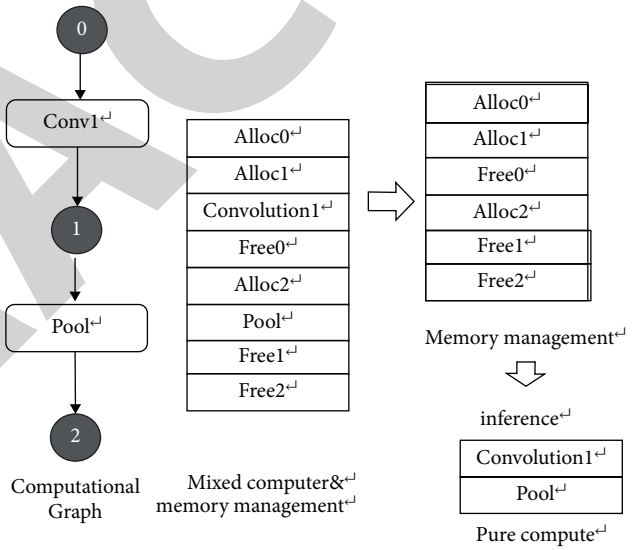

Figure 12: The preinference principle diagram.

$$\Rightarrow m_1 = (d_0 - d_2)g_0 + g_1 + g_2/2.$$
$$m_4 = (d_1 - d_3)g_0 - g_1 + g_2/2.$$

However, Strassen $(O(n3) \longrightarrow O\ (n\log 72))6$.

$$\begin{bmatrix} C_{11} & C_{12} \\ C_{21} & C_{22} \end{bmatrix} = \begin{bmatrix} A_{11} & A_{12} \\ A_{21} & A_{22} \end{bmatrix} \cdot \begin{bmatrix} B_{11} & B_{12} \\ B_{21} & B_{22} \end{bmatrix}. \tag{8}$$

S1 = B12–B22
S2 = A11 + A12
S3 = A21 + A22
S4 = B21–B11
S5 = A11 + A22
S6 = B11 + B22
S7 = A12–A22
S8 = B21 + B22

Table 1: Comparison results of different inference engines.

Mobile inference engine	CPU	GPU				Supported OS
		Metal	OpenGL	OpenGL	Vulkan	
CoreML	110	110	—	—	—	IOS
TF-Lite	92	15	—	—	—	IOS + Android
MACE	62	—	—	29	32	Android
NCNN	67	—	—	—	—	IOS + Android
MNN	93	55	17	32	34	IOS + Android

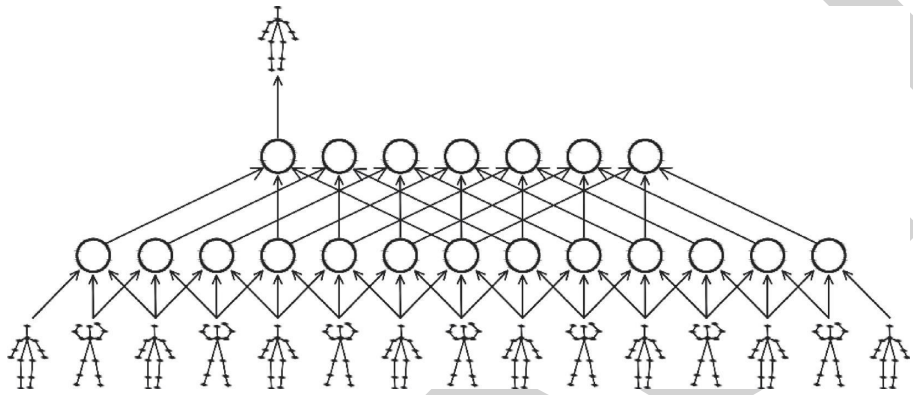

Figure 13: Neural network diagram of the ISA model.

Table 2: Comparison of ISA model results with different command models.

	KTH (%)	UCF (%)	Sports (%)	Hollyword 2 (%)
Best results for other instruction models	92.73	50.3	85.8	71.6
AI sports results	93.9	53.3	86.5	75.8

$$S9 = A11 - A21$$
$$S10 = B11 + B12$$

$$P1 = A11 \cdot S1 = A11 \cdot B12 - A11 \cdot B22$$
$$P2 = S2 \cdot B22 = A11 \cdot B22 + A12 \cdot B22$$
$$P3 = S3 \bullet B11 = A21. \cdot B11 + A22 \cdot B11$$
$$P4 = A22 \cdot S4 = A22 \cdot B21 - A22 \cdot B11$$

$$P5 = S5 \bullet S6 = An \bullet B11 + A11 \bullet B22 + A22 \bullet B11 + A22 \bullet B22$$
$$P6 = S7 \bullet Ss = A12 \bullet B21 + A12 \bullet B22 - A22 \bullet B21 - A22 \bullet B22$$
$$P7 = S9 \bullet S10 = A11 \bullet B11 + A11 \bullet B12 - A21 \bullet B11 - A21 \bullet B12$$

$$C_{11} = P_5 + P_4 - P_2 + P_6$$
$$C_{12} = P_1 + P_2$$
$$C_{21} = P_3 + P_4$$
$$C_{22} = P_5 + P_1 - P_3 - P_7$$

Operator convolution and large-scale matrix multiplication optimization are mainly embodied in the application of two classical algorithms [24, 25]. Many inference frameworks using Winograd are hard-coded, i.e., the three matrices corresponding to the kernel and input sizes are determined, making the scalability poor in the face of new scenarios. On the contrary, the Winograd generator enables Winograd to adapt to arbitrary kernel and input size.

In addition, the Strassen algorithm is used in the MNN to optimize matrix multiplication. MNN is the first mobile inference engine using Strassen algorithm to optimize large matrix multiplication. Strassen replaces several multiplication operations with addition operations. In general, the processor performs the addition operations much faster than the multiplication operations, thus causing a speedup effect. This speedup can be maximized using recursive calls, which requires determining the conditions for the end of the recursion (Table 1).

Furthermore, MNN supports major mobile data devices and has the function setting of hybrid scheduling, which solves the troubles caused by repeated scheduling and facilitates lightweight.

As is shown in Figure 13, a video sequence of the swing action is compressed into a vector as the input value. In AI sports projects, the output of the ISA model is combined as the final output vector to improve the accuracy of movement recognition.

(1) The first layer of the model learns the weight output of the linear transformation.

(2) W between the first and second layers is the weights to be learned. The weight V of the second and third layers of the output layer is fixed and does not need to be learned.

$$p_i\left(x^t; W, V\right) = \sqrt{\sum_{k=1}^{m} V_{ik}\left(\sum_{j=1}^{n} W_{kj} x_j^t\right)^2},$$
$$\min_W i\,\text{mize} \sum_{t=1}^{T}\sum_{i=1}^{m} p_i\left(x^t; W, V\right), \quad (9)$$
$$\text{subject to } \text{WW}^t = I.$$

The AI sports project is formally based on ISA. And it satisfies the weight W orthogonal matrix.

From the above experiments (Table 2), it can be concluded that the MNN solves the problem of redundancy, provides graph-level and operator-level optimization for the model and backend, and enhances versatility and performance of the search approach. In addition, the support of the ISA instruction set structure for neural networks makes MNN more mature and applicable in the AI sports field.

6. Conclusion

Recently, the sports researchers have shifted their focus to AI which, now, has a wide application in sports management. There are many challenges for applications of sports AI projects in sports because the variation of data of sports events, competitions, and teaching led to insufficient resource supply capacity against the backdrop of rapid updating of mobile devices and AI technology development.

AI sports system now supports dozens of badminton sports. In addition, a large number of AI training and learning courses have been developed. Through the modular integration of sports functions, it will contribute much to the expansion of its services in various aspects of sports in the future.

Since the advent of AI intelligent sports technology to date, upper body movements such as straight arm rope and push-up, torso movements such as hip bridge and deep squat, and systemic movements such as badminton games and singles-doubles have been successively launched in various sports-related apps. This enables online sports users to free from time and place constraints and participate in AI sports at any time and place at their will, thereby enhancing its attractiveness and efficiency for users.

Data Availability

The data underlying the results presented in this study are available within the manuscript.

Disclosure

The authors confirm that the content of the manuscript has not been published or submitted for publication elsewhere.

Conflicts of Interest

The authors declare no conflicts of interest.

Authors' Contributions

Both authors saw the manuscript and approved to submit to the journal.

Acknowledgments

This work was supported by the National Natural Science Foundation of China (no. 11551003).

References

[1] A. F. Manfredini, A. M. Malagoni, H. Litmanen et al., "Performance and blood monitoring in sports: the artificial intelligence evoking target testing in antidoping (AR.I.-E.T.T.A.) project," *The Journal of Sports Medicine and Physical Fitness*, vol. 51, pp. 153–159, 2011.

[2] A. C. Lapham and R. M. Bartlett, "The use of artificial intelligence in the analysis of sports performance: a review of applications in human gait analysis and future directions for sports biomechanics," *Journal of Sports Sciences*, vol. 13, no. 3, pp. 229–237, 1995.

[3] R. Bartlett, "Artificial intelligence in sports biomechanics: new dawn or false hope?" *Journal of Sports Science & Medicine*, vol. 5, pp. 474–479, 2006.

[4] P. N. Ramkumar, B. C. Luu, H. S. Haeberle, J. M. Karnuta, B. U. Nwachukwu, and R. J. Williams, "Sports medicine and artificial intelligence: a primer," *The American Journal of Sports Medicine*, Article ID 3635465211008648, 2021.

[5] G. Prabhu, N. E. O'Connor, and K. Moran, "Recognition and repetition counting for local muscular endurance exercises in exercise-based rehabilitation: a comparative study using artificial intelligence models," *Sensors*, vol. 20, 2020.

[6] A. C. N. Rodrigues, A. S. Pereira, R. M. S. Mendes, A. G. Araújo, M. S. Couceiro, and A. J. Figueiredo, "Using artificial intelligence for pattern recognition in a sports context," *Sensors*, vol. 20, 2020.

[7] V. Dhar, "What is the role of artificial intelligence in sports?" *Big Data*, vol. 5, no. 3, pp. 173-174, 2017.

[8] T. Liu, D. Wilczyńska, M. Lipowski, and Z. Zhao, "Optimization of a sports activity development model using artificial intelligence under new curriculum reform," *International Journal of Environmental Research and Public Health*, vol. 18, 2021.

[9] J. Yuan, J. Zhang, L. Shen, D. Zhang, W. Yu, and H. Han, "Massive data management and sharing module for connectome reconstruction," *Brain Sciences*, vol. 10, 2020.

[10] M. R. Schädler, A. Warzybok, S. Hochmuth, and B. Kollmeier, "Matrix sentence intelligibility prediction using an automatic speech recognition system," *International Journal of Audiology*, vol. 54, no. Suppl 2, pp. 100–107, 2015.

[11] P. Palee, B. Sharp, L. Noriega, N. Sebire, and C. Platt, "Heuristic neural network approach in histological sections detection of hydatidiform mole," *Journal of Medical Imaging*, vol. 6, Article ID 044501, 2019.

[12] T. Wang and J. Park, "Design and implementation of intelligent sports training system for college students' mental health education," *Frontiers in Psychology*, vol. 12, Article ID 634978, 2021.

Hindawi
Journal of Mathematics
Volume 2023, Article ID 9840234, 1 page
https://doi.org/10.1155/2023/9840234

Retraction

Retracted: Research on the Construction of Intelligent Media Ideological and Political Learning Platform Based on Artificial Intelligence Technology

Journal of Mathematics

Received 3 October 2023; Accepted 3 October 2023; Published 4 October 2023

This article has been retracted by Hindawi following an investigation undertaken by the publisher [1]. This investigation has uncovered evidence of one or more of the following indicators of systematic manipulation of the publication process:

(1) Discrepancies in scope

(2) Discrepancies in the description of the research reported

(3) Discrepancies between the availability of data and the research described

(4) Inappropriate citations

(5) Incoherent, meaningless and/or irrelevant content included in the article

(6) Peer-review manipulation

The presence of these indicators undermines our confidence in the integrity of the article's content and we cannot, therefore, vouch for its reliability. Please note that this notice is intended solely to alert readers that the content of this article is unreliable. We have not investigated whether authors were aware of or involved in the systematic manipulation of the publication process.

Wiley and Hindawi regrets that the usual quality checks did not identify these issues before publication and have since put additional measures in place to safeguard research integrity.

We wish to credit our own Research Integrity and Research Publishing teams and anonymous and named external researchers and research integrity experts for contributing to this investigation.

The corresponding author, as the representative of all authors, has been given the opportunity to register their agreement or disagreement to this retraction. We have kept a record of any response received.

References

[1] J. Wang and S. Hu, "Research on the Construction of Intelligent Media Ideological and Political Learning Platform Based on Artificial Intelligence Technology," *Journal of Mathematics*, vol. 2022, Article ID 6511962, 11 pages, 2022.

Hindawi
Journal of Mathematics
Volume 2022, Article ID 6511962, 11 pages
https://doi.org/10.1155/2022/6511962

Research Article

Research on the Construction of Intelligent Media Ideological and Political Learning Platform Based on Artificial Intelligence Technology

Jingsheng Wang and Siyuan Hu

Cangzhou Normal University, Cangzhou, Hebei Province 061001, China

Correspondence should be addressed to Siyuan Hu; husiyuan@st.btbu.edu.cn

Received 23 November 2021; Revised 14 December 2021; Accepted 17 December 2021; Published 19 January 2022

Academic Editor: Naeem Jan

Aiming at the problems of slow teaching resource sharing rate, long platform response time, and low student learning efficiency in traditional ideological and political learning platforms, a research on the construction of intelligent media ideological and political learning platforms based on artificial intelligence technology is proposed. We build an artificial intelligence open source development platform framework based on the cloud platform and use the Ceph method to optimize the storage of artificial intelligence training platform data. Under this framework, we design the business process and business module service architecture of the intelligent media ideological and political learning platform. Based on the *K*-means algorithm, the intelligent media ideological and political learning platform resource management module is designed, the teaching resource database is constructed, and the teaching resource sharing model component module is designed to realize the construction of the intelligent media ideological and political learning platform. The experimental results show that the sharing rate of ideological, political, and educational learning resources on the platform is relatively fast. The response time of the platform is 0.08 s when the amount of ideological and political teaching resources is 16000 MB. Students who are interested and very interested in the teaching account for 89% of the total.

1. Introduction

The ideological and political discipline is a relatively theoretical subject, and its teaching content and teaching methods have fewer auxiliary tools that can be used for reference. This makes the ideological and political teaching class more boring, and it cannot better attract the majority of students. The main purpose of the ideological and political course is to convey the mainstream ideology of current social development. This is to help students establish a scientific world outlook, values, and outlook on life [1]. Ideological and political disciplines play an important role in cultivating students' dialectical thinking, logical thinking, and so on and in cultivating students' thinking ability. At the same time, it also meets the requirements of enterprises for talents. The biggest feature of the ideological and political course is its inherent moral education, which can prompt students to successfully complete the transformation of knowledge, affection, faith, intention, and behavior. It has an irreplaceable effect on the development of college students' physical and mental health and plays a decisive role in the entire curriculum system. However, this course has a strong theoretical and slightly less interesting situation. In the current study of ideological and political courses, students' lack of interest in studying ideological and political courses has seriously affected the function of the ideological and political courses. This course involves all aspects of the content, the theoretical system is extensive and complex, college students are very likely to be resistant to studying, students themselves also have some inherent biases and cognitive deviations towards ideological and political courses, and the school's moral education and quality education have not been well received. With the acceleration of people's life rhythm in modern society, how to improve the

efficiency of learning and time utilization has become one of the topics considered in the innovation of current education and teaching methods [2]. Therefore, in order to strengthen college students' interest in learning this course and improve learning efficiency, it is very necessary to effectively adopt teaching methods to cultivate students' interest in ideological and political courses.

Zhang [3] proposed an interactive ideological and political teaching platform based on animation technology. The platform designs different functions for the different needs of teachers and students. Teachers can use the system to maintain the system, enter information, answer questions, and upload course materials; students can use the system to view course schedules and school notices, ask questions, and communicate online with class teachers. The platform can meet the real-time needs of multiple users at the same time and can improve the initiative of students in learning, but there is still room for improvement in learning efficiency. Minmin et al. [4] proposed the design of an auxiliary teaching platform for ideological and political classrooms based on data mining. Using data mining technology and JDT language, an ideological and political classroom teaching auxiliary platform was developed. This platform can provide services such as resource sharing and teaching evaluation for classroom teaching and teaching activities, but the information retrieval time is longer. Based on this, this article proposes an intelligent media ideological and political learning platform based on artificial intelligence technology. In this regard, Section 2 constructs the intelligent media ideological and political learning platform. On the basis of K-means algorithm, Section 3 of this paper presents the design of resource management module of the intelligent media ideological and political learning platform. Then, the experimental analysis is carried out in Section 4 to verify the fluency and strength of the proposed method. In the end, the paper is concluded in Section 5.

2. The Construction of Intelligent Media Ideological and Political Learning Platform

For a long time, the innovation of ideological and political classrooms in colleges and universities has focused on the excavation of the content of ideological and political textbooks and the use of empty theoretical teaching. This not only has great limitations but also is not conducive to the cultivation of students' thinking ability. With the help of existing online teaching methods, it can not only effectively expand the knowledge but also allow students to fully and intensively use ideological and political teaching resources. In order to achieve the above ideological and political teaching goals, a smart media ideological and political learning platform will be constructed.

2.1. Framework of AI Open Source Development Platform Based on Cloud Platform. In order to build a smart media ideological and political learning platform, first build an artificial intelligence open source development platform framework based on the cloud platform to improve the deficiencies in the model training process and improve the development efficiency of the smart media ideological and political learning platform. The framework uses the combination of Docker technology + Kubernetes cluster to build an artificial intelligence open source platform. Using Docker technology, users only need to operate the interface on the page to complete various functions. In cluster deployment, Kubernetes clusters are used for deployment. The Kubernetes cluster is divided into two parts, namely, the master node and the slave node. There are certain differences in the functions of the two. The former mainly completes the management and configuration of the cluster, including the scheduler, API Server, and so on. The calculation process includes service agents, kubelet components, and other basic facilities.

To realize the platform, one is to realize the scheduling of the resource platform, and the other is to realize the optimized storage of data on the artificial intelligence training platform. In traditional scheduling, it is necessary to select an optimal deployment node from the cluster based on the information of resource configuration. Although this scheduling method is relatively simple to implement, it is not highly flexible. It can only complete resource configuration during the first deployment process and cannot be adjusted according to the actual operating state, which will reduce the efficiency of resource utilization, and it is difficult to meet the requirements of actual applications. In addition, this method cannot effectively predict resource usage and ignores the sensitivity of the application to resources, which may cause a certain resource bottleneck on the node. Therefore, an optimization algorithm based on Max Resource Usage Priority is proposed, and a prediction algorithm combining ARIMA and RBF is proposed to better promote the effective scheduling of Kubernetes cluster resources.

2.1.1. The Working Principle of Kubernetes Scheduler. In terms of container management, Kubernetes mainly uses the method of constructing pods. In the entire platform, the Kubernetes scheduler plays a key role, which is equivalent to a hub connecting various parts. It can combine the set scheduling algorithm to establish the association between the pod and the specific host node in the cluster and write the associated information in the etcd, so that each part maintains a normal operating state, so it has the function of connecting the previous and the next. The entire scheduling process is actually to deploy specific pod tasks in the host node using the scheduling algorithm and then use kubelet to detect the pod binding events, and after the event list is obtained, the resources are bound and the corresponding ports are opened, thereby completing the start of the container [5]. The detailed flow of this process is shown in Figure 1.

2.1.2. Max Resource Usage Priority Optimization Algorithm. The Max Resource Usage Priority algorithm is used to improve the computational efficiency of the artificial

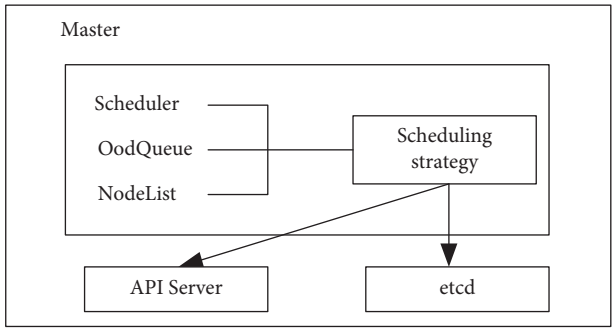

Figure 1: Schematic diagram of Kubernetes scheduler.

intelligence training platform. While increasing the number of tasks, the calculation time can be greatly reduced to meet the requirements of practical applications. However, in the Kubernetes cluster, the weights of the priority function of the scheduling algorithm are the same. Therefore, if the scheduling algorithm uses the primary selected working nodes when assessing the priority, it is difficult to meet the actual production standards. The scoring process of computing nodes is shown in Figure 2. If the weights are about 0 or 1, then it proceeds for further process; otherwise, there is no judgement.

The graphics card information is ignored in the priority function, which is an important aspect of the artificial intelligence training platform. In addition to the process of training the model in the platform, it also involves the process of data storage and processing. Therefore, under the premise of optimal resource utilization, that is, after the pod to be scheduled is scheduled to the host node, the operation of the pod can be minimized by other pods' use of resources. In this regard, the Max Resource Usage Priority algorithm [6] is proposed. The specific process is shown below.

Step 1. Count the number of pods running in the available host nodes. When the number is equal to zero, it means that the corresponding score pod account score is equal to 10 points. If the number is not equal to zero, it needs to be based on the number and running in the cluster. The ratio of the maximum value of the pod is calculated, and the specific rules are as follows.

$$p = \begin{cases} \dfrac{p_{\text{Max}} - p_A}{p_M}, p_A > 0, \\ 10, p_A = 0, \end{cases} \tag{1}$$

where p_{Max} is the maximum number of pods running in the node, p_A is the average number of pods, and p_M is the statistical value of the number of pods.

Step 2. The corresponding weights are set for various resources and need to consider whether to use graphics resources. If the pod needs to use the graphics card, it means that it mainly combines data to obtain the AI model, so CPU resources are more concerned; if the graphics card resources

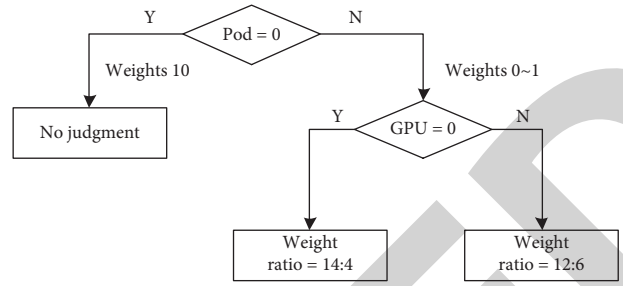

Figure 2: Process of calculating node score.

are not called, it indicates the main data storage and processing process and mainly focuses on memory and CPU resources at this time.

Step 3. Calculate the resource score of each available node. Appropriate weights need to be set during the calculation process, which is generally determined according to the number of pods in the node and whether to schedule graphics card resources, and multiple tests should be performed based on the weights obtained to determine an optimal weight value. Calculate the CPU resource score according to the obtained weight:

$$s = \begin{cases} 1, p > 0, \\ 0, p = 0, \end{cases} \tag{2}$$

$$w_C = \begin{cases} 12, g > 0, \\ 14, g = 0, \end{cases} \tag{3}$$

$$w_M = \begin{cases} 6, g > 0, \\ 4, g = 0, \end{cases} \tag{4}$$

$$m_R = \frac{M - U}{M}, \tag{5}$$

$$C_R = \frac{C - U}{C}, \tag{6}$$

where s is the CPU resource mark amount, w_c is the CPU weight value, w_M is the average CPU weight value, m_R is the weight average calculation score, C_R is the CPU resource mark amount calculation score, M is the total number of nodes, U is the number of nodes used by users, and C is the total amount of CPU resources.

Step 4. Calculate the final score S of the available nodes. The specific formula is shown below.

$$S = U + \frac{(m_R + c_R)}{2}. \tag{7}$$

According to the above calculations, the resource score is directly related to the number of available resources of the host node. If there are more resources, the score tends to be higher. If the number of pods in the node is not equal to zero, the score value is between 0 and 10, and when the number is

equal to zero, the maximum value of 10 can be reached, thus maintaining good consistency with the original design.

2.1.3. Data Optimization Storage Design of Artificial Intelligence Platform. For this platform, it mainly realizes the storage of data. It is proposed to use Ceph to store artificial intelligence training platform data. In the Ceph storage structure, the storage mechanism based on RADOS can ensure that the system can have perfect horizontal expansion capabilities, and the original API is provided in RADOS to perform very detailed operations on the RADOS objects. At the same time, in the hierarchical storage mode, the specific storage scheme is shown in Figure 3.

2.2. The Construction of an Intelligent Media Ideological and Political Learning Platform under the Framework of the Artificial Intelligence Open Source Development Platform. We build an intelligent media ideological and political learning platform under the framework of the above-mentioned cloud platform-based artificial intelligence open source development platform. In the era of smart media, information is created anytime and anywhere, and information is obtained in all aspects. As a result of progressively developing 5G and Internet of Things, the media communication is extending to smart homes, watches, glasses, wearables, and other smart devices including smart TVs and speakers. Now the smart robots that have been successfully researched and have entered thousands of households can automatically search for relevant content through voice control and display them according to equipment requirements. The way to obtain information is convenient and comprehensive. In addition to accessing courses on traditional computers and mobile phones, the smart media ideological and political learning platform can also push learning content to a wider range of scenarios. Learning resources can be obtained anytime and anywhere on any visual device, realizing learning fragmentation.

2.2.1. Business Process. Based on the purpose of system construction and user analysis, a business module composed of teaching resource management business phase and user management business phase is designed to manage resources and users.

(1) Teaching resource management business stage: administrators, teachers, and users are the functional roles of this business. The role of the administrator is to review the uploading of courseware by the teacher; the role of the teacher is to upload, manage, and retrieve resources; users have access restrictions and can only access resources approved by the administrator. The resource management business process of the role of administrator and teacher is shown in Figure 4.

(2) User management business stage: this stage is divided into two parts—registration and management, both of which are realized by the administrator. After the registration information is approved, grouping and role assignment are carried out to complete the registration, viewing, and modification of user information. The process at this stage is shown in Figure 5.

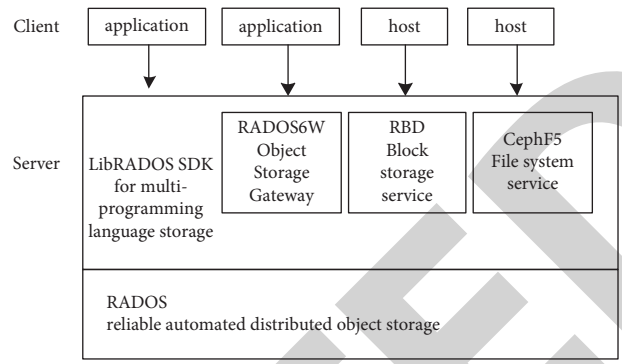

Figure 3: Ceph storage solution.

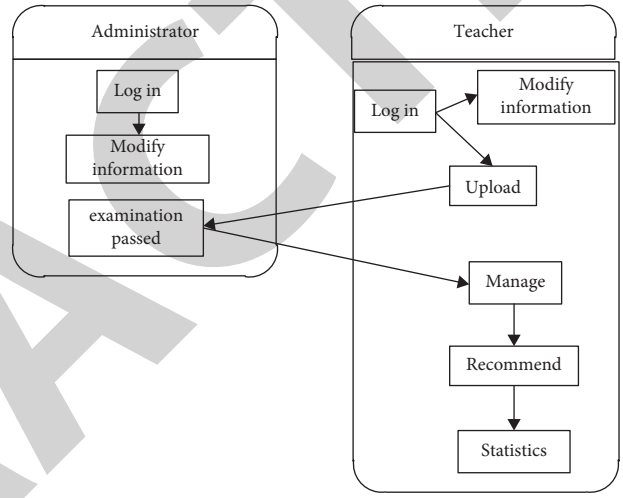

Figure 4: Resource management business flowchart based on the roles of administrators and teachers.

2.2.2. Business Decomposition. Business decomposition is closely related to service development. The former serves as the basis of service discovery, providing users with multiple interfaces, adding services according to functional requirements, and encapsulating resources and services to realize the system's corresponding service business. According to the order from top to bottom, complete the management business decomposition.

(1) Decomposing teaching resource management business: this business consists of two aspects—resource uploading and management. According to Figure 6, the new resource registration and use are hierarchically divided into eight parts; resource registration service, resource package import service, resource audit result submission service, resource status management service, and general retrieval service are each layered into two parts; the

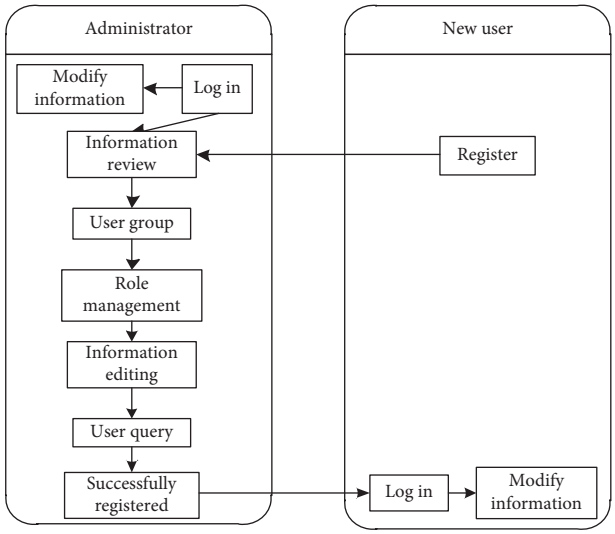

Figure 5: User management business flowchart.

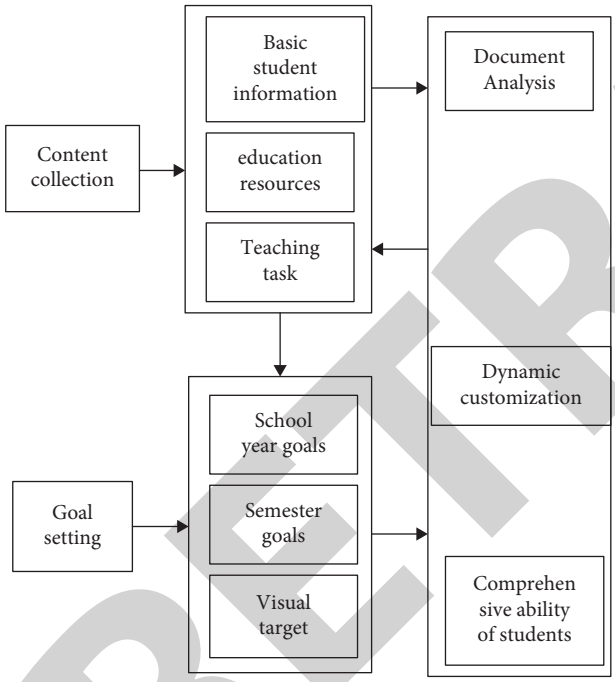

Figure 6: Data collection of ideological and political learning teaching resources.

recommendation list confirms that the service is broken down into three parts.

(2) Decomposition of user management services: the new user registration service consists of eight levels; new user review, user information submission and modification, and role addition each have two parts; there are three levels of grouping lists and submitting audit results.

2.2.3. Business Module Service Architecture. The resource layer in the system service structure is the initial resource information base; the business process layer provides service encapsulation for user registration and management, resource uploading, and management; user registration, resource retrieval, and WEB interface generation are all implemented by the presentation layer. Schematic diagram of service structure is shown in Figure 7.

3. Design of Resource Management Module of Intelligent Media Ideological and Political Learning Platform Based on *K*-Means Algorithm

The push of media information in the era of smart media is not blind, and it will intelligently analyze the user's concerns based on the information of user and then perform accurate push. Users have different learning needs in different positions and different levels. The intelligent media ideological and political learning platform needs to analyze their real needs and push the courses that best meet the users' current learning needs as much as possible within their limited learning time. Informatization, establish user connections through technologies such as recommendation algorithms, user learning profiles, knowledge graph databases, and context-aware computing and intelligently analyze the current professional needs of each user through informatization technology, so that learning content can actively find suitable students and push them achieve intelligent matching of students and content.

3.1. The Construction of the Intelligent Media Ideological and Political Learning Teaching Resource Database. The prerequisite for constructing a smart media ideological and political learning platform is to collect data on ideological and political learning teaching resources required by the platform. The content collection method is shown in Figure 6.

Collect ideological and political learning and teaching resource data to build a database, which can allocate reasonable ideological and political learning and teaching resource data to students. Develop relevant teaching goals and design learning goals according to the actual situation of students. The specific steps are as follows:

Step 1: according to the ideological and political learning needs, design the same teaching goals for all students.

Step 2: based on Step 1, according to the students' own abilities, further design ideological and political teaching goals for them, which must have a certain sense of hierarchy.

Step 3: based on Steps 1 and 2, through the dynamic customization method, according to the differentiation of each student's learning ability, a reasonable learning goal is tailored, and the teaching goal is adjusted in real time while learning to improve the standardization of the teaching goal.

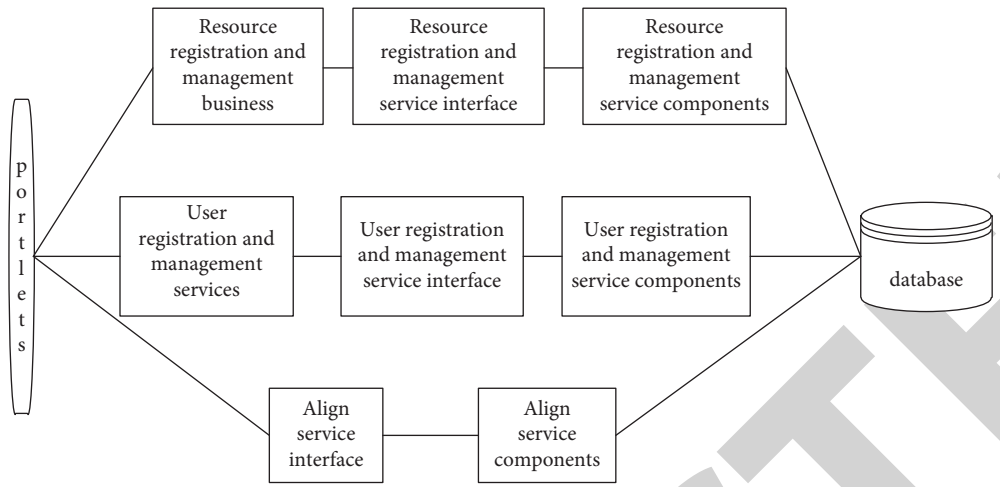

Figure 7: Schematic diagram of service structure.

On the premise of data collection and teaching goals of ideological and political learning teaching resources, the platform database is shaped, and the collected content is stored inside it, and it has the function of retrieval and use [7]. The interactive objects of this module are students, teachers, and administrators. When entering the module, users need to apply for entry first. The module will review the relevant ID card. In the case of user resource matching failure, the module will automatically exit. After the review is passed, users enter different interfaces according to their needs, and the module provides them with the required interfaces according to their needs. The interactive auxiliary function can design different types of same (different) step interactive tools in the module. At the same time, it is closely related to the teaching progress and generates toolbars at various stages, which is helpful for teachers to search for teaching resources and enhance students' understanding of knowledge. Teachers provide communication channels. Presenting the collected student information on the platform is helpful for teachers to design learning plans for them to fill in the knowledge left in the classroom. Teachers fill in the teaching content through a database, which contains multimedia courseware. The specific technology is shown in Table 1.

The multimedia courseware technology in the database can enhance the students' independent learning ability. The students in the database occupy a major position, and valuable teaching activities are arranged for them to ensure that they can search for ideological and political learning resources at any time in the process of students and improve the efficiency of ideological and political learning.

3.2. Ideological and Political Teaching Resource Sharing Model Design

3.2.1. Analysis of Teaching Resource Categories. Use clustering algorithm to classify the collected teaching resources and divide different objects into different clusters. Because the clustering algorithm belongs to unsupervised learning, the class analysis is done under the premise of unknown target conditions [8]. The most famous clustering algorithm is the K-means algorithm [9]. K in the K-means algorithm represents the number of sample classifications. The specific value depends on the actual situation. The implementation process of the algorithm is as follows.

Assume that the given training sample $\{x^{(1)}, x^{(2)}, \cdots, x^{(n)}\}$, each $x^{(i)} \in R^n$ does not include the label information y. Randomly select K cluster centroid points and denote it as $u_1, u_2, \cdots, u_n \in R^n$.

Repeat the following steps until convergence.

Calculate the class to which each sample i belongs:

$$c^{(i)} = \arg\min_j \left\| x^{(i)} - u_j \right\|^2 \tag{8}$$

.

Calculate the similarity between each sample and the centroid. Here, the Euclidean distance is used as the criterion for similarity. Select the centroid points with a small distance from the sample and divide the samples with the same centroid point distance into the same cluster to complete the initial classification of the samples [10].

Recalculate the centroid point of each cluster j:

$$u_j = \frac{\sum_{i=1}^{m} 1\{c^{(i)} = j\} x^{(i)}}{\sum_{i=1}^{m} 1\{c^{(i)} = j\}} \tag{9}$$

.

For the sample data of the same category, recalculate the centroid of the category to complete the data update. This article uses the average value of the sample data of the same category as the basis for the centroid point update [11]. Repeat the above operation until convergence.

3.2.2. Redundant Processing of Teaching Resource Data. An indispensable item in machine learning algorithms is data processing, which directly affects the output results. Data processing generally includes normalization processing, default value processing, and so on [12]. First, remove redundant units from the collected data and convert them

Table 1: Multimedia courseware technology in the database.

Core technologies	Classification	Technical support	Teaching application
Optical technology	Slideshow Projector Broadcast	Based on the principles of light reflection and refraction Expanded application of MP4	Display resources such as text and images, which are more suitable for key and difficult teaching content
Film and television technology	Movie Television Video	Direct application of multimedia technology	Enhance students' interest in learning

into numerical data for later analysis and calculation; in the Euclidean distance, each data index has the same importance. Regarding the collected data, normalize the situation where the values are quite different and control all the values within a reasonable range. The result of maximizing enterprise value is max and the minimum value of each indicator is range = max − min, and after unified naturalization, the result is $x = (x - \min)/\text{range}$, the variable value of each indicator is between 0 and 1.

Most schools have their own independent heterogeneous systems for teaching resources and have not established resource sharing with other schools, forming information islands, and a series of problems have arisen from this. In order to improve this situation, there are currently two solutions:

(i) Abolish all existing resource systems and re-establish a resource sharing system with a unified standard.

(ii) Based on the existing resource system, establish a unified standard, integrate and utilize these resources, and establish a teaching resource sharing model on this basis.

However, the budget of the first method is too high, and the resource system established by each school has its advantages, and it is not feasible to abolish all of it. Therefore, the second method is more in line with actual needs. This article builds an ideological and political teaching resource sharing model based on this. This model is mainly used by teachers and students, and it can provide teachers with modules for improving professional skills in the model, such as resources provided by experts and scholars. The model also contains a large number of high-quality curriculum resources, teachers can refer to and assist teaching, and students can learn independently. It is a platform that combines teaching and learning, as well as resources, interaction, and display.

3.2.3. The Building Blocks of the Teaching Resource Sharing Model. Due to the relatively small amount of data in the resource system and mostly loose coupling methods, a data integration scheme suitable for sharing ideological and political teaching resources is proposed. First, establish a central database, integrate all the data in the shared model into the central database, and then classify the teaching resources in the central database according to certain classification standards to facilitate the search for later teaching materials. The module composition of the teaching resource sharing model is shown in Figure 8.

In order to realize resource sharing and facilitate the implementation in phases and steps, the sharing model is divided into three levels: basic layer, environment layer, and application layer. The functions implemented at each level are as follows:

(i) *Basic Layer*. The basic layer is mainly composed of a shared resource library and various system data that provide data for the shared resource library. In the process of integrating various teaching resources, it is necessary to adapt to the development of students, based on advanced teaching concepts, and ensure the quality and content of the resources in the shared model. After the data enters the sharing model, its main content is first analyzed, and various data for query, analysis, and statistics are extracted and combined into a dataset required by the application theme, which is convenient for the search and application of resources.

(ii) *Environmental Layer*. The environment layer mainly includes streaming media servers, web servers, address servers, and FTP (File Transfer Protocol) servers. The main function is to implement the specific application of the model and execute the operation command after receiving the user's search demand. Store the information entered by the user in the database and receive requests submitted by dynamic web pages. After the server receives the search instruction, it executes the related GUI (graphical user interface) program, performs related operations with the database when conditions permit, and finally feeds the results back to the user through the server.

(iii) *Application Layer*. The application layer is mainly composed of teaching media and teaching environment and is the interface part that feeds back the results to the user. Among them, teaching media refer to graphics library, text library, audio/video, image library, courseware library, and so on; teaching environment refers to teachers and demonstration halls. The application layer realizes the connection between the user and the sharing model and conveys information to the user through the user interface. When the user accesses the shared model, the server directly displays the results required by the user after the operation of the environment layer. In general, the teaching resource sharing model developed by the structure uses three

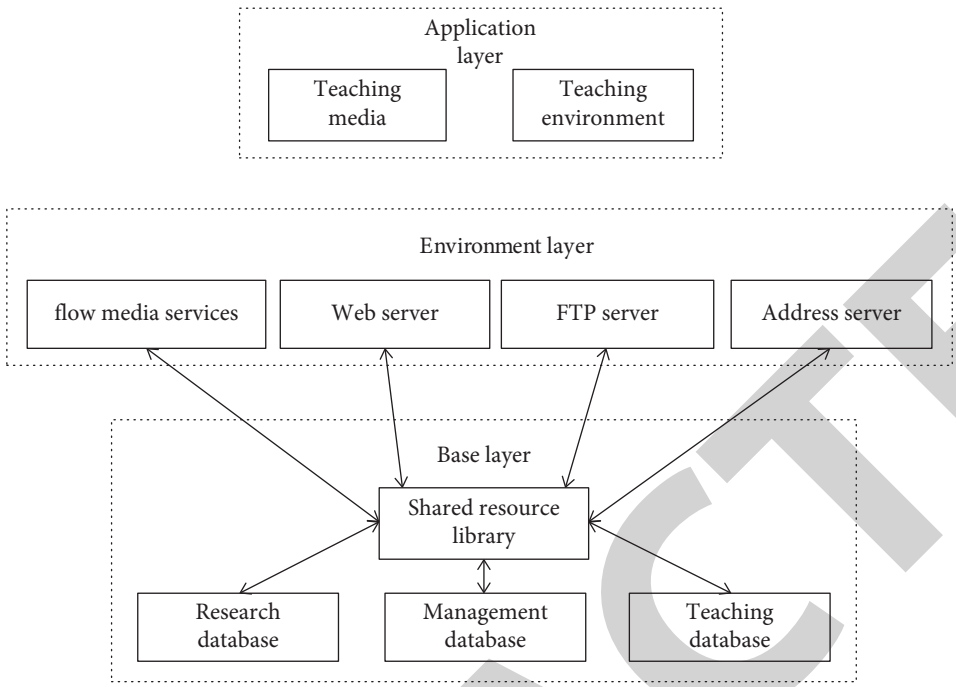

Figure 8: Model building blocks.

levels to realize the classification, storage, and application of resources. It can not only promote the effective use of resources but also make the management of the model easier. The functional modules of the teaching resource sharing model integrate the management, sharing, and release of teaching resources. Based on ideological and political teaching resources, supported by the resource library of each school, use a variety of technical means to achieve the demand for co-construction and sharing of teaching resources. Next, make a specific analysis of each functional module.

(iv) *System Management Module*. In this module, teachers can modify, delete, and update any resource in the model and can divide various resources into groups and set group weights. Resources can be backed up and restored when necessary.

(v) *Standard Management Module*. The unified standard of the model is determined, the basic standard is to select teaching resources, and the inappropriate resources in the model are modified or deleted according to the standard.

(vi) *Media Material Module*. According to the professional ideological and political characteristics, teaching resources are classified level by level according to different classification standards. This is conducive to the centralized management of resources, the formation of a professional management system, and ultimately the formation of the teaching resource management of the subject. According to the type of course, it can be divided into five categories: text, audio/video, animation, and image.

(vii) *Online Course Module*. Network courses are network teaching environments constructed according to different teaching strategies and teaching goals. The online course module has changed the traditional teaching mode in the past, combining the teaching content with the network environment, so that students can independently find resources for online learning. Compared with traditional teaching methods, online courses are more suitable for the relative separation of teachers and students, mainly based on the distance education model of students' self-study and teacher guidance. The two indispensable parts of the online course module are as follows: one is the teaching content formed according to the teaching goals and teaching strategies and the other is the network environment.

(viii) *Test Question Bank Module*. The test question library module is a collection of subject questions realized in a computer system according to a certain educational measurement theory and realizes the functions of searching, entering, deleting, modifying, batching papers, and score statistics. The types of test questions stored in the test question library module should include fill in the blanks, choice, noun explanation, judgement, short answer, question and answer, and multiple choice. Based on the educational measurement theory, the teaching measurement tool is constructed through precise mathematics modules. The test question

library module is more complicated than other modules, which includes not only the management and marking functions of the test questions but also the analysis functions such as score statistics.

(ix) *Courseware Library Module*. Courseware is a very effective "assistant" in the teacher's teaching process. It is formulated by the teacher according to the teaching goal and reflects the teaching content and teaching strategy. When designing courseware library modules, attention should be paid to coherence and systemicity to meet the teaching needs of teachers and facilitate students' understanding.

(x) *Case Library Module*. A reasonable and standardized case is a very important teaching resource in the teaching process of teachers. A complete case should include teaching materials, analysis and evaluation, and teaching opinions. Teachers can select high-quality cases through the case library module to increase students' enthusiasm for learning. The cases in the case library module are mainly provided by experts, scholars, and experienced teachers.

(xi) *Directory Index Module*. The catalog index module matches the keywords entered by the user with the resources in the model and provides the users with more relevant resources and links. This module uses a variety of strategies to synchronize the distributed stored course resources, so as to realize the functions of fast retrieval and positioning of resources in different resource libraries.

4. Experimental Analysis

In this section, the experimental analysis is carried out. Here, the proposed methods are experimentally verified and their performance is proved to be better and flawless. First, the parameters are discussed, and then the outcomes of the experiments are analyzed.

4.1. Experimental Parameters. In order to verify the performance of the designed intelligent media ideological and political learning platform based on artificial intelligence technology, experiments are carried out to verify it. Apply the designed platform to ideological and political teaching in a university. Reference [3] and Reference [4] are used as experimental comparison methods to test the ideological and political learning performance of different methods. Obtain the resource sharing rate of the system when the shared ideological and political teaching resources are in the range of 1000MB–5000 MB as the experimental data.

4.2. Analysis of Experimental Results. In the range of shared ideological and political teaching resources of 1000MB–3000 MB, the experimental data of the resource sharing rate comparison of different methods are shown in Table 2.

According to the resource sharing rate comparison experimental data in Table 2, it can be seen that within the range of 1000MB–5000 MB of shared ideological and political teaching resources, the resource sharing rate of the intelligent media ideological and political learning platform based on artificial intelligence technology is higher than that of the two comparison methods. It can be seen that under different amounts of ideological and political teaching resources, the ideological and political teaching resource management system based on the decision tree algorithm has a higher sharing rate of ideological and political teaching resources, which can better realize the sharing of ideological and political teaching resources.

The evaluation of platform scalability is to test the performance impact of increasing resources on the platform. Taking 1000 MB teaching resources as a starting point, multiplying the resources to 16000 MB, recording the response time of the platform during the increase phase, and evaluating the scalability of the platform, the response time obtained by statistics is shown in Table 3.

It can be seen from the data in Table 3 that the response time of the platform in this paper continues to decrease as the amount of resources increases. When the amount of ideological and political teaching resources is 16000 MB, the response time of the platform is 0.08 s, while the platform response time of Reference [3] and Reference [4] is 0.58 a and 0.64 s, respectively. This is because the intelligent media ideological and political learning platform based on artificial intelligence technology can improve the calculation efficiency of the artificial intelligence training platform by the Max Resource Usage Priority optimization algorithm. Therefore, the increase in the amount of resources does not have a major impact on the system and fundamentally improves the scalability of the platform.

Taking 100 students in the experimental group as an example, three months after the application of this platform, the statistics of the students' interest in ideological and political learning before and after the application of this platform are shown in Figure 9.

It can be seen from Figure 9 that the application of the platform of this article will help increase students' interest in ideological and political learning. After the application, the proportion of students who are very disinterested or not interested in ideological and political learning has dropped to 0%, and the degree of interest in ideological and political learning is average. Compared with the preapplication, the number of students who are interested in the teaching has decreased significantly, and the proportion of students who are interested and very interested in the teaching has

Table 2: Comparison of experimental data of resource sharing rate.

Shared ideological and political teaching resources (MB)	Resource sharing rate (kbps)		
	Intelligent media ideological and political learning platform based on artificial intelligence technology	Reference [3] platform	Reference [4] platform
1000	474.53	341.02	365.20
1500	499.58	333.25	378.20
2000	478.50	351.20	362.01
2500	445.63	333.60	332.01
3000	469.36	358.32	338.90
3500	489.63	384.01	314.20
4000	478.69	336.30	336.25
4500	501.23	335.24	386.14
5000	502.30	339.45	362.02

Table 3: Platform response time (unit: s).

Teaching resources (MB)	Intelligent media ideological and political learning platform based on artificial intelligence technology	Reference [3] platform	Reference [4] platform
1000	0.12	0.52	0.61
2000	0.11	0.56	0.62
4000	0.09	0.53	0.66
16000	0.08	0.58	0.64

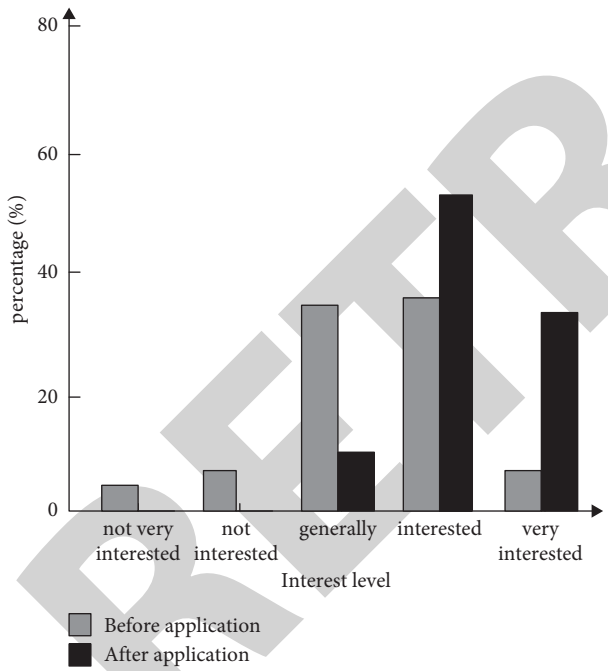

Figure 9: Statistical results of the degree of interest in ideological and political learning.

increased significantly, accounting for a total of 89%. Experimental results prove that the application of this platform can effectively enhance students' interest in ideological and political learning.

5. Conclusion

Using the modern technologies of artificial intelligence, this study built an intelligent media ideological and political learning platform. Furthermore, we carried out an experimental analysis, which showed that the rate of ideological and political teaching resources shared by the proposed platform is faster. It was also proven that the platform response time is short in the proposed platform. The interest of students in ideological and political learning was gained by applying the platform. Hence, a significant improvement had been made in the literature and the related algorithm such as *K*-means algorithm.

Data Availability

The data used to support the findings of this study are available from the corresponding author upon request.

Conflicts of Interest

The authors declare that they have no conflicts of interest.

References

[1] Z. Zhang, X. H. Shan, and S. O. Marxism, "The role of ideological and political education in social governance," *Journal of Central South University*, vol. 25, no. 1, pp. 132–138, 2019.

[2] M. Ding, X. U. Jianjun, S. O. Marxism, C. S. University, and S. O. Marxism, "On the improvement of the efficiency of discourse power in network ideological and political education," *Journal of Central South University*, vol. 25, no. 5, pp. 144–150, 2019.

[3] X. Zhang, "Design and analysis of interactive ideological and political education system based on animation technology," *Modern Scientific Instruments*, no. 5, pp. 169–172, 2019.

[4] L. Minmin, H. Jiang, H.. Yule et al., "A systematic review on botany, processing, application, phytochemistry and pharmacological action of Radix Rehmnniae," *Journal of Ethnopharmacology*, vol. 285, Article ID 114820, 2021.

Hindawi
Journal of Mathematics
Volume 2022, Article ID 9805031, 1 page
https://doi.org/10.1155/2022/9805031

Retraction

Retracted: Research on Intelligent Function Design of Vocational Education System under Mobile Learning Mode

Journal of Mathematics

Received 25 November 2022; Accepted 25 November 2022; Published 27 December 2022

Journal of Mathematics has retracted the article titled "Research on Intelligent Function Design of Vocational Education System under Mobile Learning Mode" [1] due to concerns that the peer review process has been compromised.

Following an investigation conducted by the Hindawi Research Integrity team [2], significant concerns were identified with the peer reviewers assigned to this article; the investigation has concluded that the peer review process was compromised. We therefore can no longer trust the peer review process, and the article is being retracted with the agreement of the Chief Editor.

References

[1] L. Qing, "Research on Intelligent Function Design of Vocational Education System under Mobile Learning Mode," *Journal of Mathematics*, vol. 2022, Article ID 9684363, 10 pages, 2022.

[2] L. Ferguson, "Advancing Research Integrity Collaboratively and with Vigour," 2022, https://www.hindawi.com/post/advancing-research-integrity-collaboratively-and-vigour/.

Hindawi
Journal of Mathematics
Volume 2022, Article ID 9684363, 10 pages
https://doi.org/10.1155/2022/9684363

Research Article

Research on Intelligent Function Design of Vocational Education System under Mobile Learning Mode

Li Qing

School of Preschool and Art Education, Xinyang Vocational and Technical College, 464000 Xinyang, China

Correspondence should be addressed to Li Qing; liqing@xyvtc.edu.cn

Received 28 November 2021; Revised 17 December 2021; Accepted 21 December 2021; Published 19 January 2022

Academic Editor: Lazim Abdullah

Because the traditional vocational education system has intelligent functions, long running time, and low recommendation accuracy of vocational education resources, the vocational education system under mobile learning mode is designed. The system is designed through the registration and login function module, course learning function module, examination and evaluation function module, communication and interaction function module, mobile learning function module, and personalized recommendation function module. In the personalized recommendation function module, the user's preference for vocational education resources is obtained by calculating the user's interest weight, as well as personalized recommendation of vocational education resources. The simulation results show that the intelligent function of vocational education system can operate normally under the designed mobile learning mode, the operation efficiency is high, and the effect of Vocational Education Resource Recommendation is good.

1. Introduction

Despite the fact that vocational education is at the forefront of the nation, innovative classroom reform concepts have played a significant role in its growth. There are still many problems in the cultivation of modern vocational education, particularly secondary vocational education, and the only digital campus network or public network information transmission network courses used in teaching, particularly micro courses, are few and far from meeting the needs [1]. The content of network resources is unappealing, and the building of network resources is inadequate [2]. Network and teaching informatization have received insufficient attention; teaching information resources are organized in their own way; there are no unified norms; teaching information is difficult to share; it cannot adapt to current information technology developments; and it has not been fully applied to classroom teaching. In actuality, the cost of utilizing different kinds of public websites is too expensive, making use uncomfortable; information professionalism is lacking, making use low and inconvenient. Various vocational education application support systems have a poor overall impact, low quality, and inconsistent after-sales service [3]. The use of mobile learning technology, combined with students' own characteristics, and the use of mobile phones, PDA, and other mobile learning terminals can not only obtain the required learning courses. Therefore, it is of great practical significance and practical value to design vocational education system under mobile learning mode and study its intelligent function [4].

Literature [5] designs the vocational education and teaching assistance system based on WeChat public platform. Firstly, the overall architecture of vocational education and teaching assistance system, the system hardware and software under the overall architecture, and the system hardware through PC and server are designed, and then the PC is integrated into WeChat public platform to design the system software function modules, including database and WeChat public platform. According to the system hardware and software design, the design of vocational education teaching assistant system is realized. Finally, the simulation experiment shows that the designed system has good functionality. Literature [6] designs a vocational education auxiliary teaching system based on data mining. The system designs the overall architecture of vocational education auxiliary teaching system through three-tier B/S structure and designs the system

functional structure according to the system architecture, including acquisition function module, storage function module, processing function module, analysis function module, and mining function module. However, the intelligent functions of the above two systems run for a long time, resulting in low system operation efficiency. Literature [7] used the Python framework to create the general structure of a distant teaching aid system for vocational education, as well as the system function modules, which included acquisition, preprocessing, recognition, and query. To obtain student face images, the obtained student face images are preprocessed, the student face images are captured and aligned, and OpenCV technology was used. Facial feature information was extracted and recognized to determine the students' status, and the results were sent to the front end for teachers to view. Teachers may use the query module to look up students' previous learning status to use as a reference for increasing the quality of vocational education. Through the map browsing module, point recording module, data query module, coefficient calculation module, weather viewing module, route preview module, and occurrence survey, literature [8] designed the field geology teaching assistant system on the Android studio platform and verified the overall performance of the system through multiple iterative experiments, in order to lay a good foundation for students' academic performance. However, the above two systems have low accuracy in recommending educational resources, resulting in poor recommendation effect.

In view of the problems existing in the above system, this paper designs the intelligent function of the vocational education system under the mobile learning mode, tests the intelligent function of the system, verifies the effectiveness and timeliness of the system designed in this paper, improves the intelligence and personalization of the vocational education teaching system, and lays a good foundation for the improvement of students' academic performance.

2. Mobile Learning Mode

Information technology and Internet technologies are combined in the mobile learning mode. It is an e-learning-based informal distant learning style. Learners' learning is more convenient and ways are more diverse when a digital multiterminal all media learning platform is established [9]. All learners may log in, view, and download a vast variety of learning materials, whether they are using mobile phones, tablets, PCs, or other terminal devices.

The mobile learning mode builds an information service system serving open education and lifelong education through the system construction of a portal platform and three centers. The structural framework of the mobile learning platform is shown in Figure 1.

In the structure of mobile learning platform, the server needs to build five server clusters: basic platform server cluster, application server cluster, data storage server cluster, data exchange server cluster, and basic application network and security. Three simulation warehouses are established: user data warehouse, application data warehouse, and resource data warehouse [10].

3. Design of Intelligent Function Module of Vocational Education System under Mobile Learning Mode

3.1. System Intelligent Function Architecture. Combined with the mobile learning mode, the intelligent functional architecture of vocational education system is designed, as shown in Figure 2.

The whole vocational education system is logically divided into five layers: customer operation end, logic verification, business logic, data interface, and data resource layer. In the mobile learning mode, the first three layers can be regarded as the function realization of the mobile client, and the last two layers can be regarded as the server-side function [11].

3.2. Design of Registration Function Module. In order to strengthen the management of the mobile learning platform of the vocational education system, learners need to register and establish a personal account before logging in. Before logging in to the learning platform for learning each time, they need to enter personal account, password, and other information. After background verification, if the verification is successful, they can perform specific operations on the platform according to the permissions given by the system [12]. After successful login, the user information is saved in the session. The specific process is as follows:

(i) Log in to the interface of vocational education system and enter user name and password

(ii) Learners click Submit, and the entered user name and password are encapsulated into JSON format, encrypted with 3DES algorithm, and submitted to the web server

(iii) The web server decrypts 3DES and restores the data in JSON format and then parses the JSON data to obtain the user name and password

(iv) Verify the entered user name and password, and process the verification results accordingly

(v) If the user exists in the database server and is legal, the result is returned to the web server [13]

(vi) The web server returns encrypted JSON format data to the mobile client

(vii) Decrypt according to the returned result, obtain the original data, and initialize according to the returned result

(viii) The mobile client prompts that the login is successful, so as to obtain the corresponding operation permission [14]

3.3. Course Learning Function Module Design. The course learning function is divided into my course, popular course, course evaluation, and other specific functions. The details are as follows.

3.3.1. My Course. After successful login, each user has a dedicated personal learning space to record their learning status, learning progress, and relevant course selection

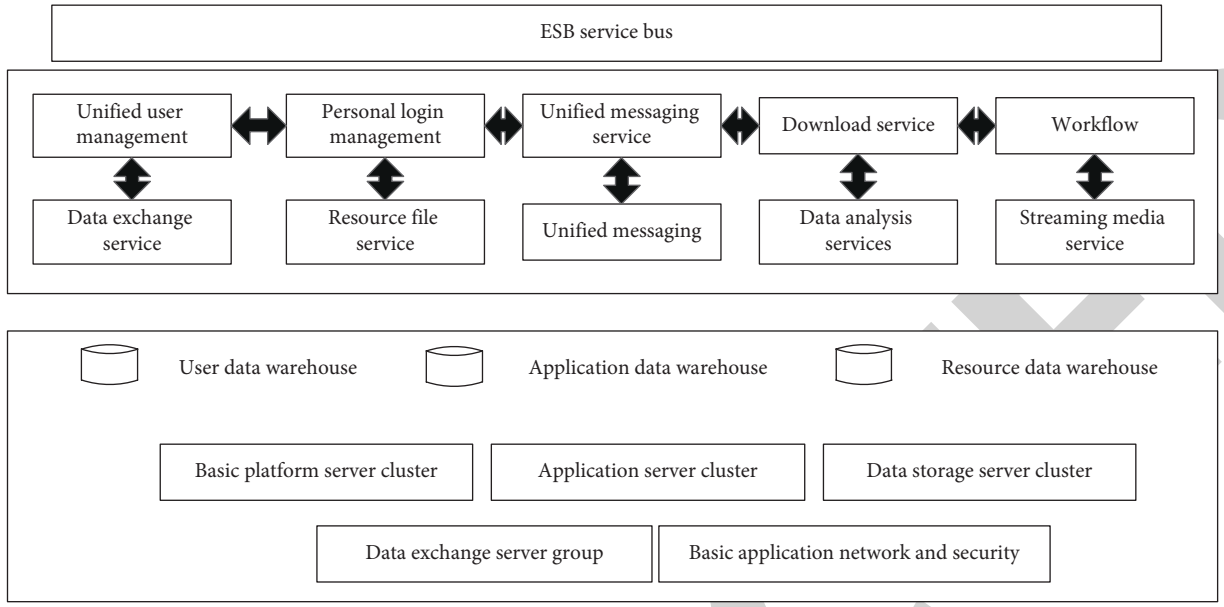

Figure 1: Structural framework of mobile learning platform.

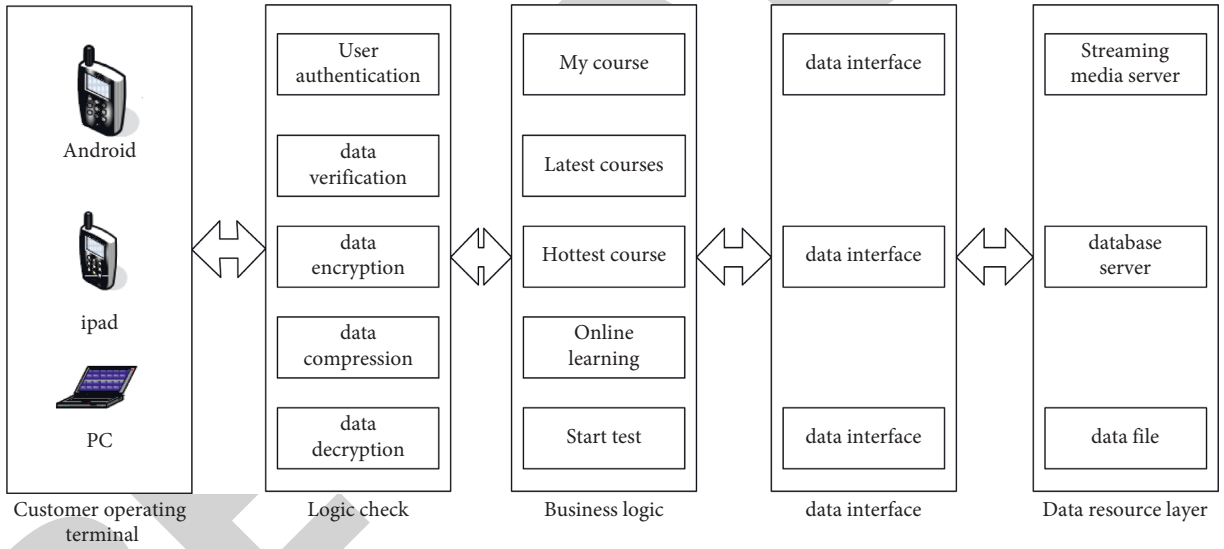

Figure 2: Intelligent functional architecture of vocational education system.

results [15]. Users can query the course selection list in "my courses" to record the courses they are interested in. Here, you need to query the associated vocational education course information in the database according to the user ID and site ID. The specific process is as follows:

(i) On the premise of successful login, the user clicks the "my course" button [16].

(ii) After the client listens to the user's click behavior, it will call the "my course" query interface through HTTP post.

(iii) The web server decrypts and deserializes JSON format data to find out whether there is user login information in the session.

(iv) The web server queries the database for its associated course information according to the user ID and site ID in the session. There may be no or multiple courses [17].

(v) The database returns the course list records according to the query results.

(vi) The web server encapsulates the data into JSON format according to the course list and encrypts it with 3DES.

(vii) The web server returns the encrypted information of my course to the mobile client.

(viii) The mobile client decrypts the data according to the specific format, reads the JSON format data, and initializes the course list.

(ix) The mobile client presents the "my courses" list data in a specific layout and style [18].

3.3.2. Ranking of Popular Courses. Popular courses are vocational education courses with high learning frequency. The more people learn, the higher the ranking, which represents the quality of the course to a certain extent. The specific work flow is as follows:

(i) On the premise of successful login, the user clicks the "popular course ranking" button.

(ii) After the client listens to the user's click behavior, it will call the click ranking query interface through HTTP post.

(iii) The web server decrypts and deserializes JSON format data to find out whether there is user login information in the session [19].

(iv) The web server queries the course information in the database according to the user ID and sorts it in descending order according to the number of clicks; that is, the more popular the course is, the higher it is.

(v) The database returns the course list record.

(vi) The web server assembles JSON format data according to the course list and encrypts it with 3DES.

(vii) The web server returns the encrypted information of the click ranking course to the mobile client [20].

(viii) The mobile client decrypts the data, submits JSON format data, and initializes the ranking list.

(ix) The mobile client displays the list of popular courses to users according to specific layout and style.

3.3.3. Curriculum Evaluation. Mobile terminal users can evaluate the selected courses or courses they study. According to the system regulations, each learner can only evaluate each course once and cannot evaluate it again. The specific process is as follows:

(i) On the premise of successful login, the user clicks "course evaluation"

(ii) After listening to the user's click behavior, the client assembles JSON format data, calls the evaluation interface, and submits the serialized byte stream through HTTP post [21]

(iii) The web server decrypts and deserializes JSON format data to find out whether there is user login information in the session

(iv) The web server adds an evaluation in the evaluation data table according to the evaluation level submitted by the user, user ID, and course ID

(v) The database returned a successful insert

(vi) The web server queries the evaluation table to calculate the average value of the evaluation of this course

(vii) The database server returns the average value of the evaluation

(viii) The web server encapsulates JSON format data according to the course list, adds the average value of the course evaluation, and encrypts it with 3DES

(ix) The web server encapsulates the JSON format data, serializes it, encrypts it, and returns it to the mobile client

(x) The mobile client decrypts the data and submits JSON format data [22]

(xi) The client prompts the user that the evaluation is successful

3.4. Design of Examination and Evaluation Function Module. The function of examination and evaluation is to test the course learning module. The specific interaction is shown in Figure 3.

The specific interaction process is as follows:

(i) Learners enter the examination and evaluation interface and select the evaluation method according to the actual needs.

(ii) The test evaluation interface sends a request to the server, and the server reads the test questions from the database according to the user's request and returns to the test evaluation interface.

(iii) The learner carries out the answer test. After all the questions are answered, the test completion request is submitted to the server. After receiving the learner's request, the server checks the answers according to the extracted questions and generates the evaluation results [23].

(iv) Of course, learners can view the evaluation results or send multiple evaluation results to the server. The server makes comprehensive statistics according to learners' previous answers and responds to the evaluation data statistics report to learners.

3.5. Design of Communication and Interaction Function Module. Communication and interaction are grouped according to learners' interests. Learners can apply for adding groups according to their personal interests or create groups as managers. Members of the group can publish relevant topics or activities, share, and grow together. The specific interaction process is shown in Figure 4.

The whole interaction process is as follows:

(1) Learners may use the interactive interface to look at information such as hot groups, recent themes, and recent actions. If the user picks a popular group in this interface, it will submit a request to the server.

(2) The server handles the request after receiving the command. If it needs to read data from the database, it will make a request to do so [24].

(3) The database replies to the server by retrieving relevant data in response to the server's request.

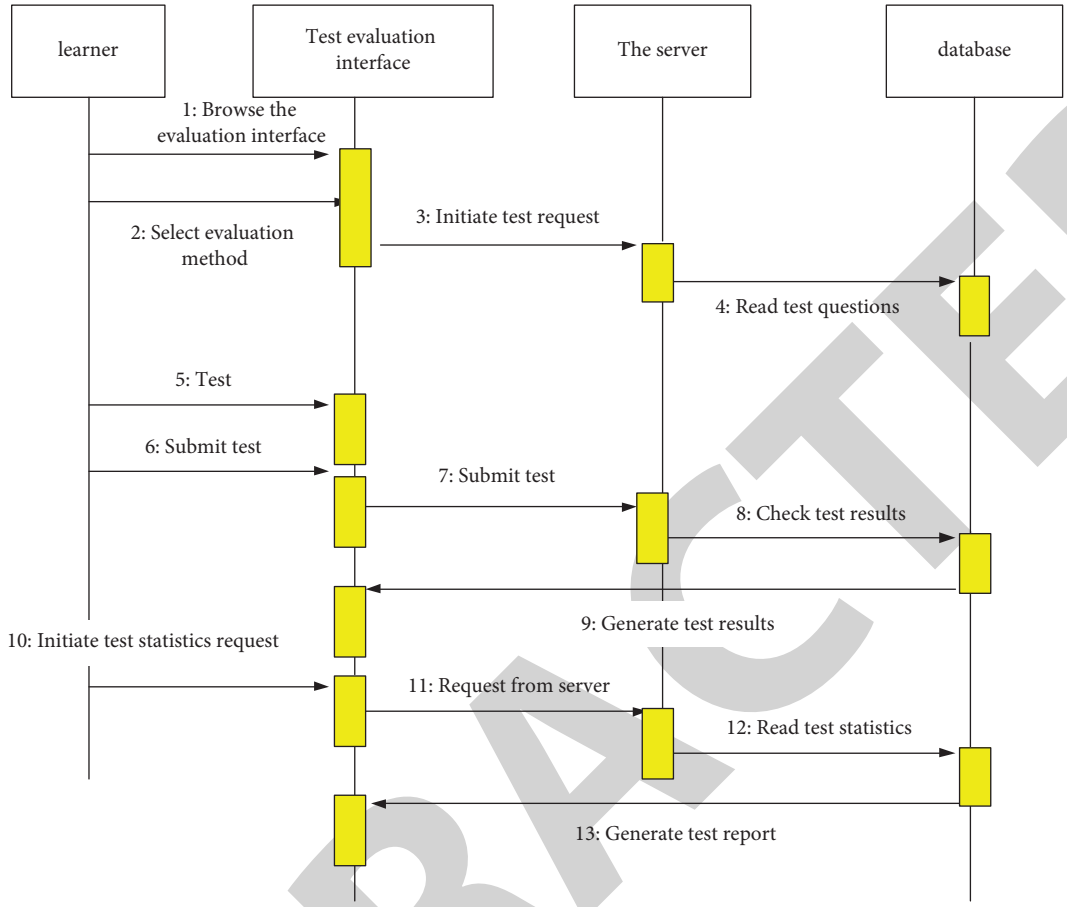

Figure 3: Interaction flow of test module.

(4) The server wraps the data and delivers it in a certain manner in the interactive interface after receiving it.

3.6. Design of Mobile Learning Function Module. The mobile learning module enables students to find learning materials online through mobile terminals, including text, pictures, audio, video, and other forms of resources and can obtain the required materials at any time. You can also customize and obtain relevant learning services through SMS [25]. In addition, learners can also connect to the resource server through the Internet and upload their own resources. The module provides two learning modes, one is live (on-demand) learning and the other is autonomous learning, and also provides a word query service, as shown in Figure 5.

(1) Upload the whole process of the teacher's course explanation in the form of video to the mobile terminal and categorize it according to the course topic so that students may study on-demand.

(2) Students may study on their own by accessing the learning information they need. If students choose synchronous learning as their learning style, the system will automatically supply them with the following sorts of learning materials for each class, based on their learning progress and teaching goals. If students opt to explore freely, the system will provide them with a selection of different resources and assessment levels from which they may pick according to their preferences [26, 27].

3.7. Design of Personalized Recommendation Function Module. For the subject distribution of vocational education resources, $A = \{A_1, A_2, \ldots, A_T\}$ is defined to represent the subject set of vocational education resources. For a vocational education resource l, the posterior probability is $p(A_i|l)$. Therefore, the main part vector of vocational education resources composed of posterior probability is $(p(A_1|l), p(A_2|l), \ldots, p(A_T|l))$, and L represents the number of subject sets of vocational education resources. For the user's interest orientation, suppose that l represents the set of vocational education resources published by the user and then the L-dimensional vector $(w_1, w_2, \ldots, w_L)$ represents the user's interest orientation in vocational education resources, and the calculation formula is

$$w_i = \sum_{j=1}^{d} p\left(A_i|l_j\right). \tag{1}$$

According to the user's interest weight, w_i is improved by personalized adaptive learning, and the following result is obtained:

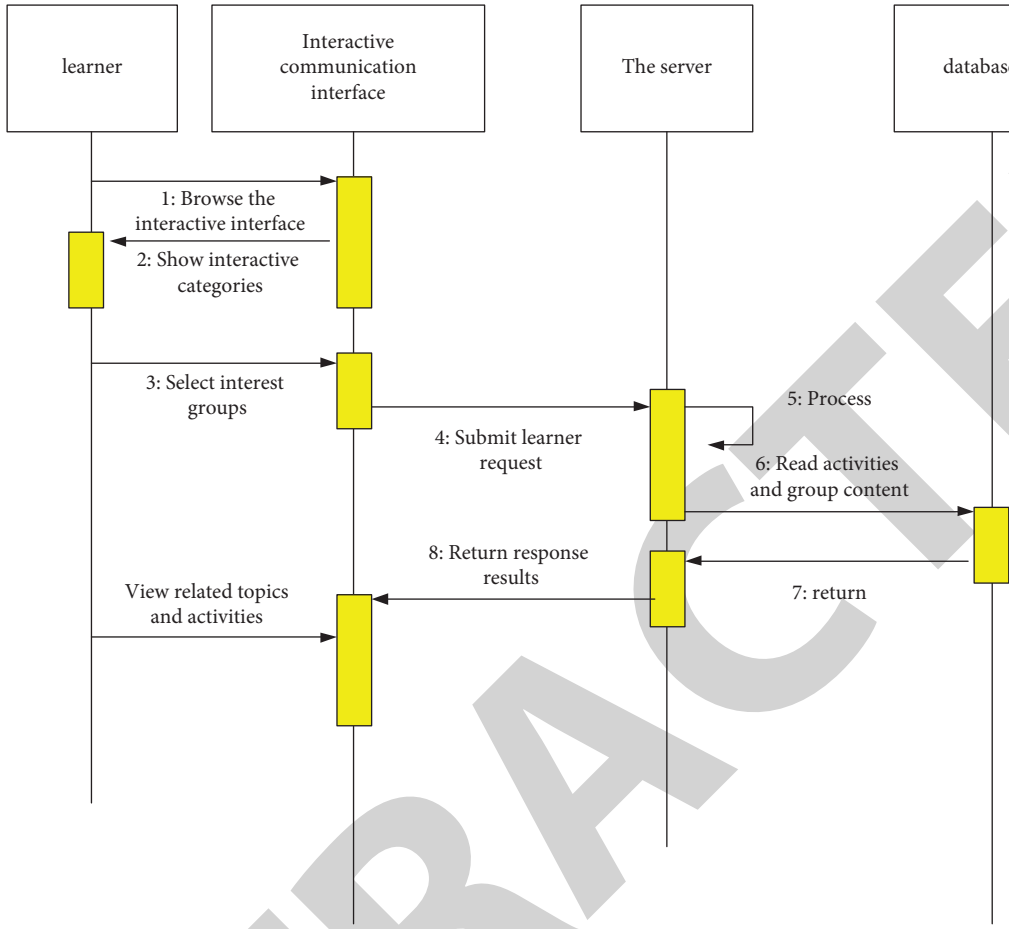

Figure 4: Sequence diagram of communication and interaction module.

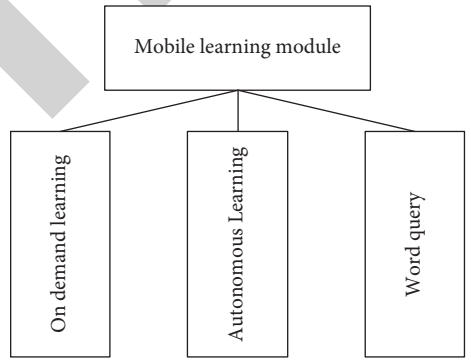

Figure 5: Mobile learning module.

$$w_i = \sum_{j=1}^{d} s_j p\left(A_i | t_j\right), \tag{2}$$

where s_j represents the user's interest weight value in vocational education resources, which can reflect the user's preference set for vocational education resources. The greater the value of s_j, the higher the user's preference for vocational education resources.

Assuming that the vocational education resource l is composed of n words, the n word is marked as w_n, and the subject of w_n is defined as z_{w_n}, and then the probability of z_{w_n} is calculated as

$$P\left(z_{u_i} = j | Z_{t,i}, l, \varphi, s\right) \propto \frac{P\left(z_{w_i} = j, Z_{t,i}, l | \varphi, s\right)}{P\left(Z_{t,i}, l | \varphi, s\right)}. \tag{3}$$

On the basis of formula (3), if the subject distribution of word v_n is $W_{v_n} = (w_1, w_2, \ldots, w_T)$, then the standardization probability of w_i is

Table 1: Test environment.

Testing environment	To configure	Parameter
Hardware environment	CPU	Pentium Quad Processor
Software environment	Memory capacity	2 G
Testing environment	Hard disk capacity	250 G
Hardware environment	Graphics card	Intel integrated graphics card
Software environment	Operating system	Windows XP SP2
	Programing language	Java

$$v_j = \frac{P\left(z_{x_i} = j|Z_{t,i}, l, \varphi, s\right)}{\sum_{j=1}^{L} P\left(z_{u_i} = j|Z_{t,i}, l, \varphi, s\right)}. \quad (4)$$

The probability that vocational education resource l belongs to topic j is

$$\theta_{t,j} = \frac{n(j,l) + s}{n(l) + Ls}. \quad (5)$$

According to $\theta_{t,j}$, the average preference similarity of users in R cycles can be defined:

$$\text{sim}_R = \frac{\sum_{(1/2)}^{R} \text{sim}\left(u_{k-1}, u_k\right)}{R - 1}. \quad (6)$$

In order to facilitate comparison, the user's average preference similarity can be personalized adaptive learning to calculate the user's preference similarity:

$$\text{sim}\left(U_{k-1}, U_k\right) = \cos\,\theta = \frac{\overrightarrow{u_{k-1}} \cdot \overrightarrow{u_k}}{\left\|\mu_{k-1}\right\| \cdot \left|\mu_k\right\|}. \quad (7)$$

4. Simulation Experiment Analysis

In order to verify the effectiveness of the intelligent function of vocational education system in practical application under the mobile learning mode designed in this paper, a simulation test is carried out. The test environment is shown in Table 1.

In the test environment, the network architecture of vocational education system under the mobile learning mode is built, as shown in Figure 6.

Under the above background, the registration and login function module, course learning function module, and examination and evaluation function module are selected for testing.

4.1. Registration and Login Function Module Test

Purpose: to verify whether the module operates according to normal business logic

Test content: whether the user can log in normally

Test results are shown in Table 2.

The test contents and results are shown in Table 3.

4.2. Course Learning Function Module Test. Objective: to verify whether the module displays, plays, and evaluates courses normally.

4.3. Test and Evaluation Function Module Test. Objective: to verify whether the module displays, plays, and evaluates courses normally.

The test contents and results are shown in Table 4.

According to Tables 2–4, the intelligent function of vocational education system under the mobile learning mode designed in this paper can operate normally and the system performance is good.

In order to further verify the effectiveness of the system in this paper, the vocational education system under the mobile learning mode designed in this paper, the vocational education auxiliary teaching system based on data mining designed in literature [28], and the vocational education distance teaching auxiliary system based on facial feature recognition designed in literature [29] are used to compare and analyze the running time of intelligent functions. The comparison results are shown in Table 5.

According to Table 5, the running time of the intelligent function of the vocational education system under the mobile learning mode designed in this paper is within 15.0 s, and the running time of the intelligent function of the vocational education auxiliary teaching system based on data mining designed in literature [30] is within 38.9 s; in literature [31], the running time of the intelligent function of the distance teaching auxiliary system of vocational education based on facial feature recognition is within 28.9 s. Under the mobile learning mode designed in this paper, the running time of the intelligent function of the vocational education system is short and the operation efficiency is high.

In order to further verify the effectiveness of this system, the vocational education system, literature [32] system, and literature system under the mobile learning mode designed in this paper are used to recommend vocational education resources and test the recommendation accuracy of the three systems. The test results are shown in Figure 7.

According to Figure 7, under the mobile learning mode designed in this paper, the accuracy of Vocational Education Resource Recommendation by vocational education system can reach 100%, the accuracy of Vocational Education

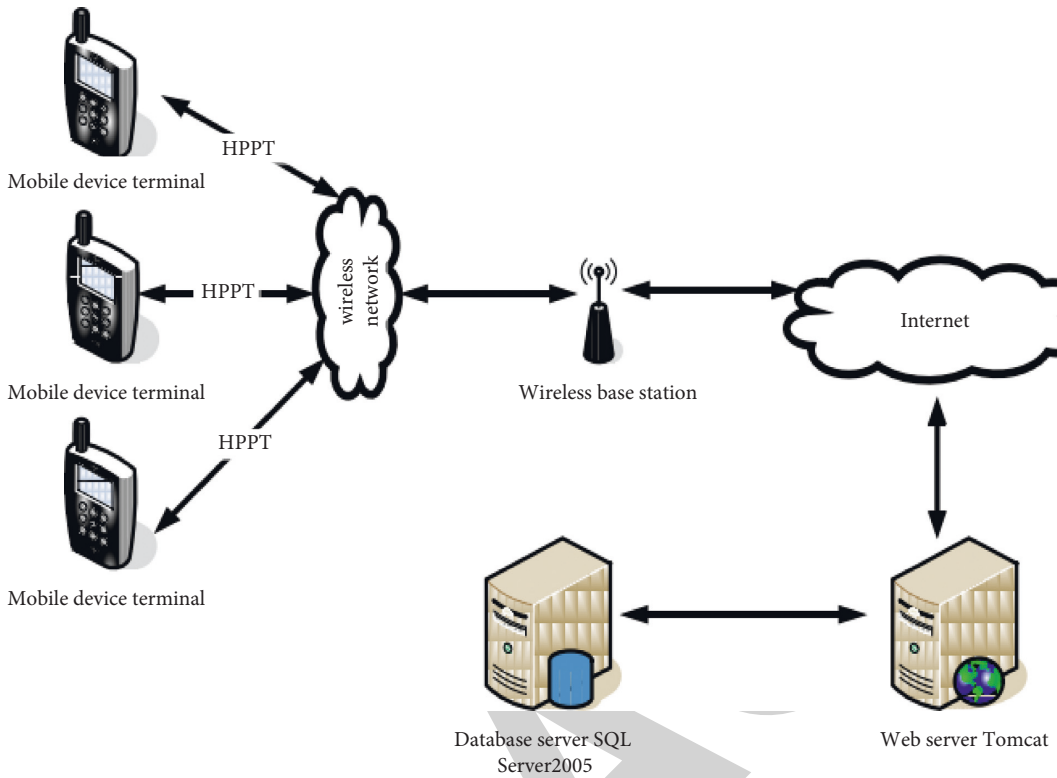

Figure 6: Network architecture of vocational education system under mobile learning mode.

Table 2: Function test results of registration and login function module.

Use case	Test result
Do not enter ID, password, and verification code	Please enter ID, password, and verification code
Enter the wrong user name, password, and verification code	Remind that the ID, password, and verification code entered are incorrect
Close the client's network connection	Please check the system network connection
Shut down the server	Connection timeout, server-side exception, please contact the administrator
The information input is accurate and the network connection is normal	Successfully enter the system main interface

Table 3: Function test results of course learning function module.

Test content	Expected judgment	Test result
Teaching online broadcast	Can I play it online	Video and audio can be played online and according to the learning records
Teaching course download	Can I download the courseware	Video and audio files can be downloaded. The default storage address is memory card
Teaching curriculum evaluation	Can I evaluate the course	Word limit should be set for evaluable courses

Table 4: Function test results of test evaluation function module.

Test content	Expected judgment	Test result
Basic question type training	Is the question type displayed according to the specialty	Initialize the question bank and display the question type according to the selected course
Timing function	Can I time it	The test timing function is enabled, in seconds
Scoring function	Can you score	Enter the test scoring function to score in real time
Collection title	Can I collect topics	Click collect to successfully collect the question
Collection error	Can I collect wrong questions	Answer matching error automatic collection of wrong questions

Table 5: Comparison results of intelligent function running time (s).

Number of experiments/time	Literature [6] system	Literature [7] system	Paper system
10	32.5	21.2	11.2
20	33.6	22.2	11.5
30	34.5	23.1	11.6
40	34.9	23.8	12.5
50	35.1	24.5	12.9
60	36.5	25.0	13.4
70	36.9	25.4	13.5
80	37.0	26.7	14.0
90	37.2	27.2	14.5
100	38.9	28.9	15.0

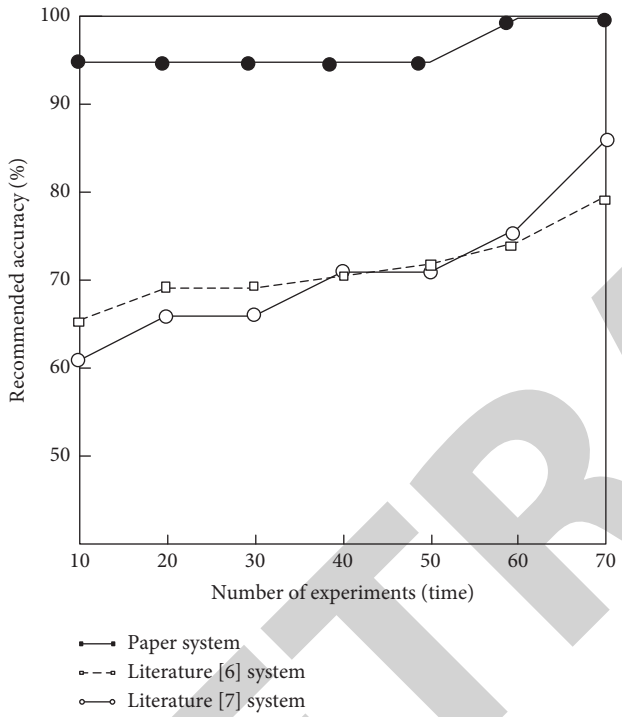

Figure 7: Comparison results of Vocational Education Resource Recommendation accuracy of three systems.

Resource Recommendation by literature [33] system is only 80%, and the accuracy of Vocational Education Resource Recommendation by literature [34] system is only 85%. Under the mobile learning mode, the vocational education system designed in this paper has the highest accuracy and the best recommendation effect.

5. Conclusion

In view of the low efficiency of the intelligent function of the traditional vocational education system and the poor effect of Vocational Education Resource Recommendation, in the mobile learning mode, through the registration and login function module, course learning function module, examination and evaluation function module, communication and interaction function module, mobile learning function module, and personalized recommendation function module, a new vocational education system is designed. Through the personalized recommendation function module, the user's interest weight is calculated by using personalized adaptive learning to obtain the interest weight value of vocational education resources, and the personalized recommendation of vocational education resources is carried out according to the interest weight value. Finally, through the simulation test, the running time of the intelligent function of the vocational education system under the mobile learning mode designed in this paper is within 15.0 s, and the recommendation accuracy of vocational education resources is up to 100%. It is verified that the operation efficiency of this system is high and the recommendation effect of vocational education resources is good.

Data Availability

The data used to support the findings of this study are included within the article.

Conflicts of Interest

The author declares that there are no conflicts of interest.

References

[1] S. Cheng, X. Zhao, and W. Li, "Design and implementation of college teaching assistant system based on bmob back-end cloud," *Computer Programming Skills and Maintenance*, vol. 397, no. 7, pp. 109–113, 2018.

[2] X. Liang, "Design of higher mathematics assistant teaching system based on data mining," *Higher Science Rducation*, vol. 5, pp. 38–43, 2019.

[3] R. Wang and C. Jiang, "Design of the intelligent education system based on the piano introduction," *International English Education Research: English Version*, vol. 2, pp. 3–7, 2019.

[4] W. Gong, L. Tong, W. Huang, and S. Wang, "The optimization of intelligent long-distance multimedia sports teaching system for IOT," *Cognitive Systems Research*, vol. 52, pp. 678–684, 2018.

[5] X. Jiang, "Computer aided teaching system based on wechat public platform," *Modern Scientific Instruments*, vol. 3, pp. 44–49, 2020.

[6] J. Zhou, "Design of computer aided classroom teaching system based on data mining," *Modern Electronic Technology*, vol. 43, no. 2, p. 3, 2020.

[7] H. Liu, Q. Zhu, and T. sun, "Distance teaching assistant system based on facial feature recognition," *Software Engineering and Application*, vol. 10, no. 2, p. 8, 2021.

Hindawi
Journal of Mathematics
Volume 2023, Article ID 9869537, 1 page
https://doi.org/10.1155/2023/9869537

Retraction

Retracted: Teaching Quality Evaluation of Ideological and Political Courses in Colleges and Universities Based on Machine Learning

Journal of Mathematics

Received 15 August 2023; Accepted 15 August 2023; Published 16 August 2023

This article has been retracted by Hindawi following an investigation undertaken by the publisher [1]. This investigation has uncovered evidence of one or more of the following indicators of systematic manipulation of the publication process:

(1) Discrepancies in scope

(2) Discrepancies in the description of the research reported

(3) Discrepancies between the availability of data and the research described

(4) Inappropriate citations

(5) Incoherent, meaningless and/or irrelevant content included in the article

(6) Peer-review manipulation

The presence of these indicators undermines our confidence in the integrity of the article's content and we cannot, therefore, vouch for its reliability. Please note that this notice is intended solely to alert readers that the content of this article is unreliable. We have not investigated whether authors were aware of or involved in the systematic manipulation of the publication process.

Wiley and Hindawi regrets that the usual quality checks did not identify these issues before publication and have since put additional measures in place to safeguard research integrity.

We wish to credit our own Research Integrity and Research Publishing teams and anonymous and named external researchers and research integrity experts for contributing to this investigation.

The corresponding author, as the representative of all authors, has been given the opportunity to register their agreement or disagreement to this retraction. We have kept a record of any response received.

References

[1] L. Qiao, "Teaching Quality Evaluation of Ideological and Political Courses in Colleges and Universities Based on Machine Learning," *Journal of Mathematics*, vol. 2022, Article ID 2835029, 10 pages, 2022.

Hindawi
Journal of Mathematics
Volume 2022, Article ID 2835029, 10 pages
https://doi.org/10.1155/2022/2835029

Research Article

Teaching Quality Evaluation of Ideological and Political Courses in Colleges and Universities Based on Machine Learning

Lijun Qiao

Teaching Department of Ideological and Political Theory Course, Anyang Preschool Education College, Anyang 455000, China

Correspondence should be addressed to Lijun Qiao; qiaolijun@ayyz.edu.cn

Received 25 November 2021; Revised 20 December 2021; Accepted 23 December 2021; Published 19 January 2022

Academic Editor: Naeem Jan

Ideological and political (IAP) education is the soul of socialist construction. As the main position for the cultivation of the "Four Haves" in the cause of socialist construction, colleges and universities shoulder an important educational mission. However, standard, scientific, systematic, and feasible evaluation index system is lacking in the teaching of IAP theory courses. Therefore, it is fervently required to use the modern science and technology for the establishment of a complete, objective, and feasible classroom teaching evaluation system, and the optimization of the evaluation process is also an important issue that needs to be resolved urgently. This paper combines teaching evaluation theory and machine learning methods, analyzes the rationality of evaluation indicators through the acquired evaluation data, and optimizes the evaluation system. By comparing the advantages and disadvantages of traditional machine learning classification algorithms, a classifier based on weighted naive Bayes is analyzed and designed for teaching evaluation, and the specific process of evaluation model construction is introduced. The experimental results show that the classification model based on the weighted naive Bayes algorithm is reasonable and feasible for teaching evaluation. Combined with the weighted Bayesian classification incremental learning principle, the performance of the classification model can be better than the traditional classification model.

1. Introduction

It has always been a top priority for both the party and the country to invest in IAP education programs, as the cornerstone of socialist creation. With the continuous advancement of the reform of the market economy system, my country's spiritual and cultural undertakings are facing unprecedented challenges. A decision was made in this regard at the Sixth Plenary Session of the Seventeenth Central Committee, which met from October 15 to October 18, 2011, and which was titled "Deepening Reform of the Cultural System, Promoting the Development and Prosperity of Socialism Culture." Specifically, the resolution said that, in today's changing social environment, the need of encouraging the development and progress of socialist cultural endeavors, as well as the importance of giving full play to the function of cultural soft power, must be given full consideration. Nowadays, in the primary stage of socialism in our country, due to the imbalance in the construction of material civilization and spiritual civilization, problems such as honesty and morality occur from time to time. There is an urgent need to use the socialist core value system to regulate and guide direction in life. In order to further the cultural system's reform and promote socialist culture's enormous growth and prosperity, skilled builders are required [1]. Therefore, it has become an important task to cultivate the "Four Havings People" who is capable of promoting the growth and development of socialist spirituality.

Colleges and universities are intimately linked to the molding of the "Four Havings People" intellectual and political character as the principal front for growing and creating the socialist "Four Havings People" [2], the reform of the socialist cultural system, and the realization of the goal of cultural prosperity and development. It is the primary method for colleges and universities to educate students on IAP matters [3–5]. The Sixth Meeting of the Seventeenth National Committee of the CPC Central Committee in Canada also clearly put forward the issue of promoting

cultural prosperity. IAP theory courses should be treated seriously as a means of promoting China's development of advanced culture.

There is now a steady advancement in IAP theory courses taught by applying the spirit of several programs suggested by the CPC and basically conforming to the requirements set forth in the central documents. However, there are still some problems. The quality of teaching work is the internal driving force that guarantees the effective development of courses. To improve fundamentally, it is necessary to find out the problems and make targeted improvements on the basis of scientific analysis. On the basis of this, college and university ideology and political theory courses should be thoroughly investigated and evaluated for their teaching quality [6]. However, looking at the existing research results and actual survey results in related fields at this stage, despite the fact that the study on IAP education at colleges and universities has been finished, it is not difficult to come across examples of this. A great deal of work has to be done before IAP theory courses can be considered thorough, and a number of important themes need to be addressed and investigated further.

The research purpose of this topic is to use machine learning methods to solve the problems of traditional classroom teaching evaluation indicators such as fuzzy and relatively single evaluation model [7, 8]. Use data mining technology to explore the internal relationship between various factors that affect teachers' teaching effect and teaching level from the teaching evaluation data and optimize the existing index system. By researching and optimizing machine learning algorithms, construct a teaching evaluation model to reduce subjective factors. Achieve a quick and objective judgment of the quality of teaching and provide effective guidance for teaching management. The study on this topic might hypothetically broaden the use of data mining technologies in education and give new ideas and technical references for the assessment of teaching methods. Solve the issue of too much subjective assessment of teachers in the old manner, try to provide a reliable teaching evaluation method for teaching workers, and improve the efficiency and credibility of evaluation. In Section 2 of this paper, we reviewed the literature related to our work. In Section 3, we explained the different methods and algorithms, including the proposed methods and algorithms. In Section 4, we executed some experiments, which used different algorithms. Then, we compared and analyzed their outcomes and confirmed the perfection of the proposed techniques. Finally, we concluded the study in Section 5.

2. Related Work

It is critical for colleges and universities to teach courses on ideology and politics as part of their overall educational mission. It is to systematically teach IAP morality courses guided by Marxism and its Chinese theoretical results [9]. It is a primary means of acquiring political and ideological knowledge, as well as a significant means of acquiring theoretical knowledge. Its purpose is to cultivate students' socialist personality through teaching activities organized by the school. Through teaching, cultivate the defenders, builders, and successors of socialism that meet the essential requirements of socialism. An essential part of the college and university teaching mission is to teach IAP courses. However, the actual result is that the school does not pay attention to it, the teachers are hard to deal with, the students cannot be interested, and the actual teaching effect is not satisfactory.

Studying the effectiveness of professors who teach courses in political theory and ideologies at colleges and universities relies on theories and practices from both the ancient and modern cultures of China and elsewhere in the world. Chinese academics and professionals have frequently referred to Chinese and foreign traditional theories and practices since the introduction of a new program of IAP theory courses at universities [10, 11]. According to the actual situation of education and teaching of theory courses, different levels of research are carried out on the meaning, function, importance, and initiation of the indication system of the evaluation and evaluation of education and teaching quality of theory courses, accumulated a wealth of ideas, and produced different guiding roles in practice. IAP theory courses in college and university classrooms are rarely studied in terms of their educational and teaching quality. There is still much space for improvement in terms of educational and instructional quality in college and university courses on IAP theory. There is an urgent need to widen the scope of study, whether theoretical or applied.

The following are some example comments on the study's results about the guiding principle for assessing ideology and political theory courses delivered in colleges and universities. The notion of developmental assessment must be included into the evaluation process. IAP theory courses are taught for a variety of reasons, but the ultimate goal is to help students and teachers grow together, which promote the diversification of evaluation methods, the diversification of evaluation subjects, the three-dimensionality of evaluation content, and the dynamic nature of the evaluation process. Continuously realize the promotion of "learning" by evaluation, the promotion of "teaching" by evaluation, and the promotion of development by evaluation. Mei Ping pointed out in "Five Key Points of College IAP Theory Course Teaching Evaluation" that in college IAP theory course teaching evaluation, the evaluation concept of "focusing on the common development of teachers and students" is a developmental evaluation concept. An evaluation system that is based on science and the goal of sustainable human development, as well as an evaluation system that encourages individuals who have been evaluated to participate in evaluations, engage in self-reflection, and pursue professional development and comprehensive quality improvement is positioned [12]. Zhang Sheqiang pointed out in the "Three Questions of Teaching Evaluation of IAP Theory Courses in Colleges and Universities" that the evaluation of the teaching and evaluation of IAP theory courses must also adhere to the scientific development concept to achieve comprehensive, coordinated, and sustainable development of teaching evaluation and better service for education and teaching work.

Current advances in data mining have had a significant impact on education-related research during the last several years, most notably in data collection, storage, analysis, and decision-making. The area of educational data mining has received a lot of interest from academics and researchers alike. It is possible to acquire a huge amount of student information, teacher information, and teaching data during the educational process. However, the information hidden behind these large amounts of data cannot be effectively used. The introduction of data mining technology can dig out more valuable knowledge. Since 2005, the topics of many international conferences have been intelligent mining of educational data. The ongoing evolution of education has also facilitated the progressive expansion of study into the theory and implementation of educational data mining. In 2008, Montreal, Canada hosted the first International Conference on Educational Data Mining. Eight conferences have been successfully hosted to date, as has the Journal of Educational Data Mining (JEMD) [13].

The process of teaching evaluating has changed from a single qualitative assessment to a mix of qualitative and quantitative evaluations as new technologies have been developed. However, it is frequently important to develop a sound data model in order to do quantitative analysis on a variety of data sources. The weighted average approach, expert evaluation technique, AHP analytic hierarchy process [14], fuzzy comprehensive evaluation method [15], neural network model method [16], and Markov chain method [17] are the most extensively used approaches for assessing instruction in the United States and worldwide. Currently, scholars decide the weight of the evaluation index mostly using the fuzzy comprehensive evaluation approach and the analytic hierarchy process [18–20]. For instance, scholars such as Li Xingmin integrated the analytic hierarchy method with fuzzy comprehensive evaluation of teaching quality, resulting in a very scientific quantitative procedure that enhanced the scientificity and reliability of the evaluation outcomes.

The use of rough set theory to overcome the issue of irrational index weights is one aspect of relevant research into integrating machine learning technology into teacher assessment systems [21], the introduction of decision trees to analyze teaching data [22], and an investigation into the effects of teaching quality factors using association rule algorithms. Additional research has found that artificial neural networks can be used to model education in order to evaluate it [23, 24]. Peng Juping, for example, applied artificial neural network theory, developed related mathematical models, quantified the indicators in a comprehensive manner, and then constructed a Bayesian neural network model to obtain a more reasonable evaluation result [25]. It has been proposed in the literature [26] to use wavelet neural networks to construct a mathematical model for evaluating the quality of teaching. There are a lot of disadvantages to using neural networks as an application approach, including a predisposition for falling into local extreme points and a high degree of sample reliance.

To summarize, in recent years, scientists have made significant advances in the field of teacher evaluation research. However, the depth of research on teaching evaluation theory is greater, the content of research on evaluation technique and technology is less, and the technology employed is very straightforward. In order to overcome the shortcomings of qualitative and quantitative evaluation in traditional classroom evaluation, more research in data mining and machine learning is required.

3. Method

The primary focus of this chapter is the development of a methodology for evaluating classroom instruction. To begin, let us have a look at some of the more established methods of classification. The Naive Bayes algorithm is found to have more advantages in teaching evaluation through theoretical and experimental verification. The weighted naive Bayes algorithm incremental learning algorithm is suggested as an evaluation model for teaching.

3.1. Evaluation Method Based on Traditional Classification Algorithm. As part of the supervised learning process, classification is a significant issue. Analyze the training data and identify a model or correct description for each class to summarize its properties. The model may infer the class to which these new data with unknown labels belong using the created class description. This description is then used to categorize future test data in the data set. Learning and classification are the two fundamental processes that make up the classification challenge. A suitable learning approach is utilized to learn a classifier based on the training data set in the learning process. The new input instance is utilized to classify the new input instance in the classification process.

Naive Bayes, support vector machines, K-nearest neighbors, decision trees (DT), neural networks, and so on are all common classification techniques in machine learning. The Nave Bayes (NB) algorithm is a classification approach based on Bayes' theorem among them. A simple classification model is used to introduce the hypothesis of feature condition independence. This type of classification model is known as a support vector machine (SVM). Classifiers are constructed using a linear classifier, which defines the greatest interval in the feature space. Using K-nearest neighbor (KNN), it is assumed that a training data set and an instance category have been established. Suppose you already know the class labels of the k closest training examples and you want to predict the class using majority voting or some other approach. An instance of the DT paradigm is represented by a tree structure, which symbolizes the process of classifying instances based on their qualities. Feature selection, decision tree creation, and decision tree pruning are all common phases in decision tree learning. Nonlinear comprehensive evaluation can be solved by using an artificial neural network. Any complicated nonlinear relationship can be fully approximated, and the nonlinear process can be modelled without knowing the underlying cause of the information.

There are a range of features for each classification technique, and the effect of classification is often determined

by application environment and data properties. It is impossible to find a classifier that works for all kinds of problems and attributes. The following is a side-by-by-side comparison of the several common classification algorithms that were previously mentioned, see Table 1.

Classification algorithms can be used in the teacher evaluation process depending on the requirements. Class labels are based on a sequence of evaluation attribute values, and the evaluation grades are utilized as input. As an evaluation result, the new evaluation attribute's value will be assigned a most likely class label by a classification method. To ensure the validity of the evaluation results, it is essential to select a suitable algorithm for the classifier. Performance can be evaluated by the accuracy of classifiers. A measure of the relationship between the number of samples that the classifier correctly classifies and the total number of samples in a particular test data set. The formula is shown as follows:

$$\text{Acc} = \frac{S_n}{S}. \tag{1}$$

where Acc represents the accuracy rate, S_n represents the number of samples correctly classified, and S is the total number of samples.

3.2. Design of Evaluation Classifier Based on Weighted Naive Bayes. In order to describe the design of evaluation classifier on the basis of WNB, the principle of NB algorithm is given, where we proposed three algorithms which can be combined together to determine the category of the test data. Additionally, evaluation attribute weight determination algorithm is proposed.

3.2.1. Principle of Naive Bayes Algorithm. Bayesian classification, which is derived from the theory, is an example of a classification approach that makes use of Bayes' theorem. To estimate the prior probability of each category in the classification process, a considerable amount of training data must be learned, which is the core premise of classification theory. After that, determine the likelihood that an object X can be classified into multiple groups. In the end, the class with the highest posterior probability is deemed to be the instance. Suppose T is the training data set, $P = \{P_1, P_2, \ldots, P_n\}$ is the attribute variable set, and n is the number of attributes. $Q = \{Q_1, Q_2, \ldots, Q_m\}$ is the set of class variables, and m is the number of categories, then a training sample can be expressed as $\{s_1, s_2, \ldots, s_n, Q_i\}, i \in m$, where Q_i signifies that the sample's class label is well-known. S can be represented as $\{s_1, s_2, \ldots, s_n\}$, and to determine the test sample's chance of being a given type, the formula is

$$p(Q_i|S) = \underset{Q_i}{\text{argmax}} \frac{p(S|Q_i)p(Q_i)}{p(S)}. \tag{2}$$

In the field of Bayesian classification, the Naive Bayes classification algorithm (NB algorithm) is one of the most efficient algorithms. Using a categorization model is advantageous since it is simple to understand, efficient to compute, and stable. When compared to other classifiers, such as decision trees and SVMs, it performs better in some situations. Figure 1 shows the naive Bayes model's simplest mesh structure:

The root node Q is a class variable, and the leaf nodes $P = \{P_1, P_2, \ldots, P_n\}$ are attribute variables. In spite of the fact that the NB classification model is based on the traditional Bayesian classification model, this model does not suffer from the restriction of independence among attributes. When $p(S)$ is a constant in the real world, the calculation formula for the NB method can be written as follows:

$$p(Q_i|S) \propto \underset{Q_i}{\text{argmax}}\, p(S|Q_i)p(Q_i). \tag{3}$$

where $p(Q_i)$ is the class prior probability, which can be learned through training data. The calculation formula is

$$p(Q_i) = \frac{t_j}{t}. \tag{4}$$

where t_j represents the amount of classes, Q_i in the training samples, and t represents the total number of training samples.

It is assumed that all attribute variables are conditionally independent of one another and do not have any relationship in order to ensure the correctness of the NB approach. If the data collection contains a large number of attributes, the computational cost of $p(S|Q_i)$ is extremely high. By introducing the assumption of conditional independence, the computing cost can be reduced while sacrificing some computational accuracy. The computation formula for $p(S|Q_i)$can be simplified as follows:

$$p(S|Q_i) = \prod_{a=1}^{n} p(s_a|Q_i). \tag{5}$$

If the training data is sufficient, $p(s_1|Q_i), p(s_2|Q_i), \ldots, p(s_n|Q_i)$ can all be learned from the training data. It is possible to determine the category of the test data by combining the three algorithms listed above.

3.2.2. Evaluation Attribute Weight Determination Algorithm. Naive Bayes is a computationally efficient method. Conditions are presumed to be unrelated, and the weight assigned to each conditional attribute in the decision classification is set to one, which implies that they are all of equal value. When all weights are set to one, the accuracy of classification is lowered by default. According to this study, the weight allocated to an attribute is determined by how well the attribute contributes in data categorization using the weighted Naïve Bayesian (WNB) approach. As well as maintaining the fast speed of the Naive Bayes algorithm, it minimizes a classifier's reliance on the conditional independence assumption. The formula for the computation is presented as follows:

$$p(Q_i|S) = \underset{Q_i}{\text{argmax}}\, p(Q_i) \prod_{a=1}^{n} p(R_a|Q_i)^{w_a}. \tag{6}$$

During categorization, for example, the weight of the feature R_a is represented by w_a in order to quantify the relevance of different characteristics in the same category. As

Table 1: Comparison and analysis of classification algorithms.

Algorithm	Advantage	Disadvantage
Naive Bayes	Stable classification efficiency	Low efficiency when there are many attributes
Support vector machines	Less training set used	The training speed is slow when many samples
K-nearest neighbor	No need for parameter estimation	Large sample size and high space complexity
Decision tree	Readable and fast classification	Easy to overfit and ignore correlation
BP network	Able to adapt and have certain fault tolerance	Slow convergence speed, strong sample dependence

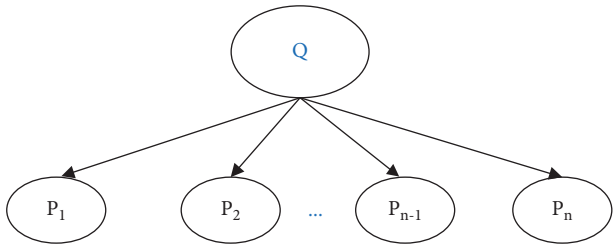

Figure 1: Naive Bayes classification model.

w_a increases, so does the importance of the associated characteristic R_a in categorization. What matters the most in specific applications is determining the weights assigned to each attribute in the weighted naïve model.

Using data from instructional evaluation data to investigate the relationship between each assessment feature of the instructional evaluation data and the overall evaluation value, it was discovered that the value of each index had varying degrees of influence on the evaluation conclusion. This study investigates in detail the approach given in this paper for computing the weight of each assessment characteristic by using the relative probability of the class attribute. Each attribute R_a may have Gdifferent values. Use r_g to indicate its specific value, where $g \in G$. Assuming a specific instance S, when the attribute R_a of S takes the value r_g, for category Q_i, the calculation formulas for the relative probability $p(R_a|Y)$ and irrelevant probability $p(R_a|N)$ of attribute R_a with respect to Q_i are as follows:

$$p(R_a|Y) = \frac{\text{num}(R_a = r_g \wedge Q_i)}{\text{num}(R_a = r_g)}, \quad p(R_a|N) = 1 - p(R_a|Y), \tag{7}$$

where count represents the statistical number. When the value of the attribute R_a is r_g and belongs to the Q_i category, the calculation formula of the attribute weight is as follows:

$$w(R_a, r_g, i) = \frac{p(R_a|Y)}{p(R_a|N)}. \tag{8}$$

As a consequence, the precise calculation formula for the weighted naive Bayes classification method is as follows:

$$p(Q_i|S) = \underset{Q_i}{\text{argmax}}\, p(Q_i) \prod_{a=1}^{n} p(R_a|Q_i)^{w(R_a, r_g, i)}. \tag{9}$$

There are n characteristics in a data collection T if the class labels are m. There are g potential values for each property, hence the total weight of all attributes is $m * n * g$. The particular value and weight of the same property differ. Different categories assign different weights to attributes with the same value. Final step: each characteristic value is converted into a weighted average, and the resulting values are compared across all categories. The result of the categorization is the category that has the across all categories. The result of the categorization is the category that has the maximum number of points.

3.3. Incremental Learning for Weighted Bayesian Classification. With the continuous increase of data, the form of putting all the training sets into the memory for calculation at one time cannot solve practical problems well. The adoption of the principle of incremental learning might therefore minimize the computer's performance needs. Because Bayesian classifiers allow for incremental learning, the algorithm's time consumption can be reduced by a major portion of the calculation process being completed incrementally. Furthermore, the quality of the training data has an impact on the effectiveness of the classification algorithm when it comes to prediction. As a rule, a larger training sample improves both predictive and generalizability abilities. A classifier's training samples cannot be completed all at once in the real world, thus they must be completed progressively.

The classification algorithm in this paper mainly uses the weighted Naive Bayes method. The Bayesian incremental learning process actually updates the original class prior probability $p(Q_i)$ and attribute conditional probability $p(s_a|Q_i)$. Because incremental learning of the classifier does not require retraining the classification model, it is simple to feed the newly collected data into the classification model and to make the necessary adjustments to the model's parameters as needed. The specific correction formula is as follows:

Modification formula of prior probability of Bayesian incremental algorithm:

$$P(Q_i) = \begin{cases} \frac{M}{M+1} \bullet p(Q_i) + \frac{M}{M+1}, \text{when } Q_t = Q_i, \\ \frac{M}{M+1} \bullet p(Q_i), \text{when } Q_t \neq Q_i. \end{cases} \tag{10}$$

Conditional probability modification formula of Bayesian incremental algorithm:

$$P(s_a|Q_i) = \begin{cases} \frac{M_{Q_i}}{M_{Q_i}+1} \bullet p(s_a|Q_i) + \frac{1}{M_{Q_i}+1}, \text{when } Q_t = Q_i \text{ and } s_a = r_g, \\ p(s_a|Q_i), \text{when } Q_t \neq Q_i, \\ \frac{M_{Q_i}}{M_{Q_i}+1} \bullet p(s_a|Q_i), \text{when } Q_t = Q_i \text{ and } s_a \neq r_g, \end{cases} \tag{11}$$

where $P(Q_i)$ and household $P(s_a|Q_i)$ are the updated class prior probability and attribute conditional probability after adding a new sample, M represents the total number of original data records, M_{Q_i} represents the total number of original data records belonging to category Q_i, and r_g represents the value of a certain feature.

It is also necessary to recalculate the attribute value of the newly added sample set in order to account for the number of samples in each category that have been added. In each attribute, update the relevant probability and irrelevant probability values by combining the statistical value of the preceding sample data and then update the weights of each attribute as a result of the update. Using formula (10) and formula (11) and weighted Bayesian formula (9), the probability $P(Q_i|S)$ of the category Q_i of each data record S can be calculated.

4. Experiment and Analysis

In this section, we carried out the experiments for the proposed method and algorithms. The results of these experiments are investigated and analyzed.

4.1. Experimental Results Based on Traditional Classification Algorithms. Experimenting on an existing teaching evaluation data set, this section uses the abovementioned five machine learning classification techniques to evaluate the algorithm's feasibility. The python machine learning skleam package provides an algorithm function that is used to compare the experimental outcomes of each classification method. For the experimental, there are 200 pieces of training data and 100 pieces of test data. After 10 iterations of cross-validation, the average classification accuracy is computed using formula (1). The results of the study are shown in Figure 2.

Figure 3 shows the average time consumption of each algorithm for the same experimental data set.

Because the Naive Bayes method's classification accuracy on this data set is reasonably good, and its running time is the lowest, and the naive Bayes algorithm is employed to design the teaching evaluation model, as demonstrated above in the experimental findings.

4.2. Experimental Results Based on the Weighted Naive Bayes Algorithm. In this section, the experiments are carried out on the Windows10 operating system and on the experimental platform, which is written in the Python3.5 programming language for algorithm development.

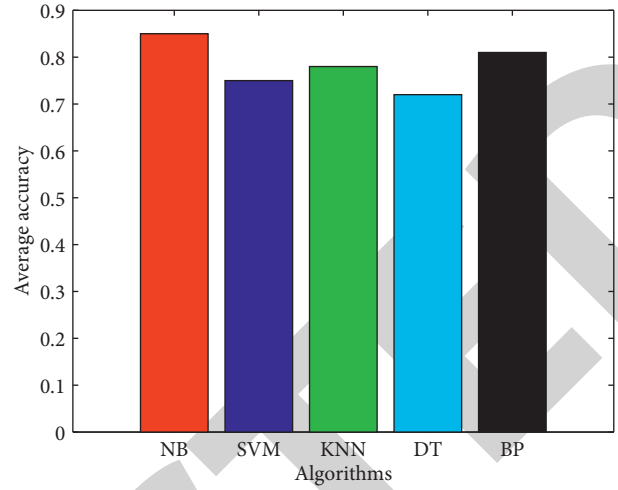

Figure 2: Comparison of classification accuracy of different algorithms.

4.2.1. Comparison of Classification Accuracy between NB and WNB Algorithm. Data from the teaching evaluation database is used for cross-validation studies, with 200 data records selected as the training set and 100 data records selected as the test set. The classification accuracy is evaluated in 10 cross-validation trials. It is shown in Table 2 how each experiment performed.

From Table 2, the classification accuracy comparison between NB algorithm and WNB algorithm is shown in Figure 4.

It was found through the experiments that the average classification accuracy of Naive Bayes technique is 0.81, whereas a similar result was found for the weighted Bayes algorithm, which had an average classification accuracy of 0.84. In general, the weighted naive Bayes algorithm outperforms the regular naive Bayes algorithm when it comes to classifying data from the instructional evaluation data.

4.2.2. Comparison of Classification Accuracy. Back propagation (BP) neural networks are the most commonly used methods in teaching evaluation research nowadays, but for better understanding the teaching evaluation research, this study employs a WNB classifier for the development of an assessment model and the comparison of its efficiency with traditional approaches. Normalization is used to transform a percentage into a decimal in the [0, 1] range when using the BP neural network technique to handle training data. In order to anticipate the evaluation level of fresh data samples, a model is constructed by specifying an error threshold.

For the BP algorithm experiment, 200 data records from the evaluation database are randomly chosen as the training set, and 100 data records from the evaluation database are randomly selected as the test set. According to the results of debugging tests, the most successful experimental parameter settings are as follows: tanh acts as the activation function, the learning rate is 0.005, and the number of cycles is 5000, all of which are depending on the number of characteristics. The input layer, hidden layer, and output layer nodes are set to 8, 6, and 1.

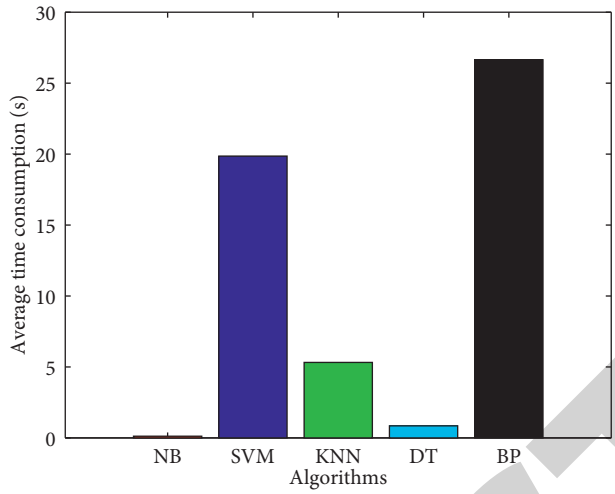

Figure 3: Average running time of different algorithms.

Table 2: Classification accuracy of NB algorithm and WNB algorithm.

Num	1	2	3	4	5	6	7	8	9	10	Average
NB	0.79	0.83	0.78	0.82	0.84	0.81	0.81	0.83	0.79	0.80	0.81
WNB	0.83	0.85	0.87	0.85	0.85	0.81	0.82	0.84	0.86	0.82	0.84

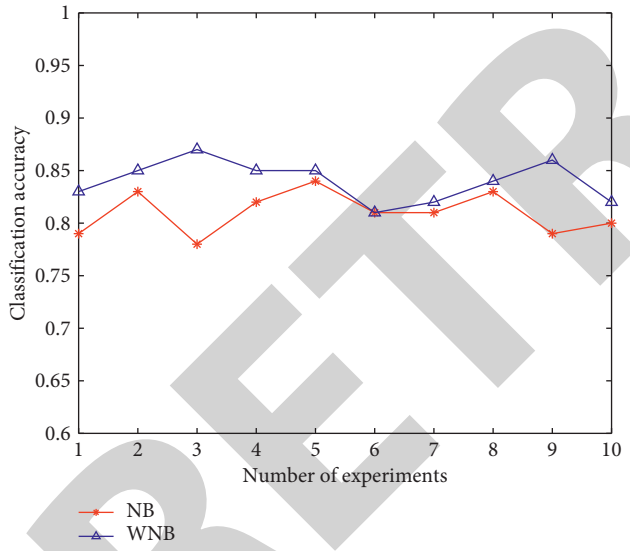

Figure 4: Comparison of classification accuracy between NB and WNB algorithm.

Following the training of the neural network method, the following Table 3 shows the results of the tests that were conducted:

From Table 3, the classification accuracy comparison between NB algorithm and WNB algorithm is graphically depicted in Figure 5.

As a result of the high number of outstanding ratings in the genuine teaching evaluation data set, there are few additional grades available. As a result, when training the classification model with hierarchical data, if the extracted training data sets are different, the experimental findings will have a certain degree of influence. The WNB algorithm had an average classification accuracy of 0.85, whereas the BP method had an average classification accuracy of 0.75. The WNB algorithm has a greater classification effect than the BP method, according to the testing data. This experiment also found that the WNB algorithm consumes less time on average than the BP method, with an average time consumption of 0.15 s compared to 0.63 s. The WNB algorithm, on the other hand, is faster and more accurate. There are many advantages to teaching evaluation using the WNB method.

4.3. Incremental Learning Experiment Results. Create an incremental classification model based on weighted naive Bayes and finish the construction of it. Set the initial training data set at 200 and the test data set to 100 and gradually increase the training sample set. In the accompanying Table 4, the exact computation results of a piece of test data at each stage of the increment are selected at random from a pool of possible outcomes:

As shown in Table 5, when the incremental classifier is used to perform classification, the calculation result is more inclined to the correct category, suggesting that the probability value of belonging to the correct category is increasing. The probability value of other categories is reduced. As the training data gradually increases, the average classification accuracy rate changes as shown in Table 5:

The WNB algorithm with incremental learning uses the same experimental data set to compare the time consumption of the WNB algorithm and the "Add_WNB" algorithm. The running time comparison chart is shown in Figure 6.

Experiments have shown that using an incremental approach improves the classification model. To avoid retraining and calculating a previously trained data set, all that is required of an incremental model is to categorize and

Table 3: Classification accuracy of BP algorithm and WNB algorithm.

Num	1	2	3	4	5	6	7	8	9	10	Average
BP	0.75	0.72	0.73	0.77	0.79	0.74	0.73	0.74	0.78	0.75	0.75
WNB	0.85	0.86	0.88	0.87	0.85	0.83	0.85	0.84	0.82	0.85	0.85

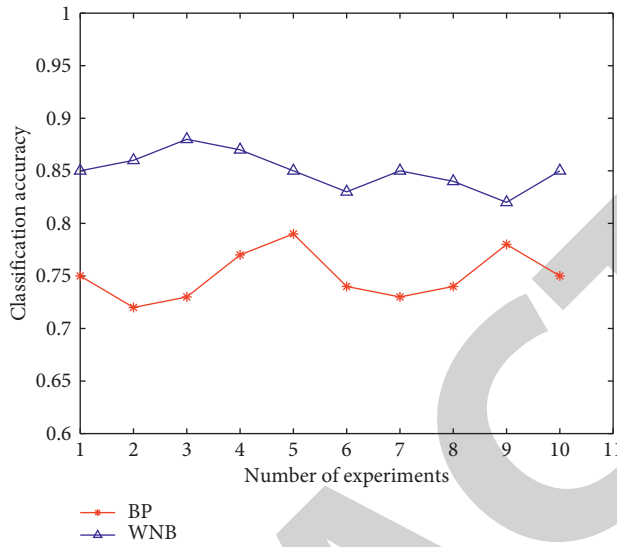

Figure 5: Comparison of classification accuracy between BP and WNB algorithm.

Table 4: The calculation results of certain test data.

Number of increments	Add 50		Add 100		Add 200	
	Before	After	Before	After	Before	After
Level	Excellent		Excellent		Good	
Excellent	$1.2e-08$	$2.0e-08$	$4.0e-07$	$1.8e-07$	$1.5e-06$	$1.4e-06$
Good	$1.6e-10$	$4.5e-15$	$6.4e-13$	$4.8e-12$	$1.6e-07$	$4.2e-07$
Medium	0	0	0	0	$2.4e-08$	$3.2e-08$
Pass	0	0	0	0	0	0
Failed	0	0	0	0	0	0
Judgement	Excellent	Excellent	Excellent	Excellent	Good	Excellent

Table 5: Classification accuracy before and after increment.

Increment value	Before	Add 50	Add 100	Add 200
Average accuracy	0.75	0.77	0.79	0.82

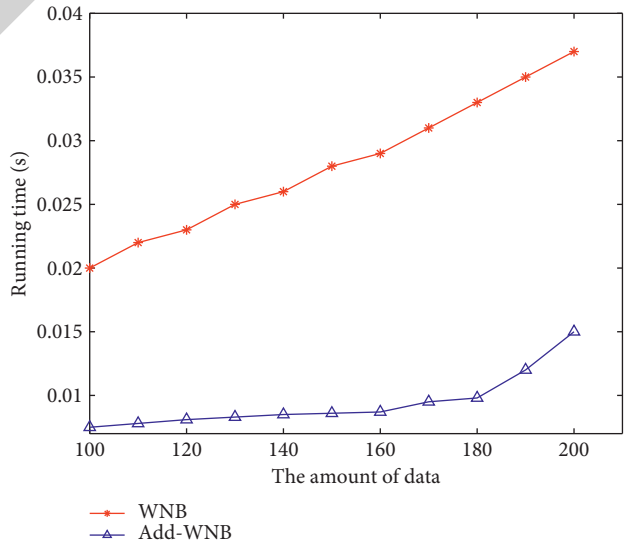

Figure 6: Algorithm runtime comparison.

calculate the new data, integrate it with the past training value, and update the model parameters that are required. As a result, the categorization model gains in terms of time savings and increased productivity.

5. Conclusion

Despite the merits of classical classification algorithms in teaching evaluation models, they also have their drawbacks. In order to assess the educational impact, the weighted Naive Bayes (WNB) method has been incorporated into the evaluation process. We can see that the technique is realistic and feasible for teaching assessment based on the outcomes of the experiments. Lastly, the notion of incremental learning is presented, the classifier is improved, and the experiment is compared to the nonincremental classifier's results. The experiments demonstrated that an incremental learning method increased the performance of a classifier while decreasing the time required for the procedure.

In order to explain the use of data mining and machine learning methods for the analysis and modelling data in the context of teacher assessment, this paper deeply described the classification algorithms and incremental learning methods. The classification method in machine learning is employed in the assessment model development to further increase the scientificity and feasibility of teaching evaluation. The following are the key findings of this study: (1) create a teaching assessment model based on machine learning's classification technique by introducing the weighted Bayes algorithm and proposing the design classifier. As a consequence of extensive data training, each evaluation index is assigned a specific weighting, and the evaluation result value is automatically calculated based on the evaluation data. Running time and classification accuracy show that the weighted naive Bayes method is superior than the classic BP neural network technique for evaluating instructional effectiveness. (2) The weighted Bayesian incremental learning method is used to address the issue of rapidly expanding data sets. The model parameters are constantly modified based on newly added sample data, which enhances the algorithm's effectiveness and reduces the amount of time it takes to process data. Through performing experiments and analyzing the outcomes, we confirmed that the incremental learning method can increase both the time efficiency and the evaluation model when the evaluation data is larger.

Data Availability

The datasets used during the current study are available from the corresponding author on reasonable request.

Conflicts of Interest

The author declares no conflicts of interest.

References

[1] W. B. Chen and Y. C. Zhang, *Principles of IAP Education*, Higher Education Press, Beijing, China, 2nd edition, 2007.

[2] X. G. Liu, *Modern IAP Education Methodology*, People's Publishing House, Beijing, China, 2008.

[3] Y. T. Luo, *Course Theory of IAP Theory in Colleges and Universities*, Wuhan University Press, Wuhan, China, 2006.

[4] Y. X. Shi, *Research on the History of the Course Construction of IAP Theory in Colleges and Universities*, Wuhan University Press, Wuhan, China, 2006.

[5] J. Pei, K. Zhong, J. Li, J. XU, and X. Wang, "ECNN: evaluating a cluster-neural network model for city innovation capability," *Neural Computing and Applications*, pp. 1–3, 2021.

[6] L. S. Zhang, *Discussion on the Teaching Method of IAP Theory Course in the New Era*, Higher Education Press, Beijing, China, 2006.

[7] K. Chen, *Evaluation Model and Analysis of Sustainable Development Capability of Clean Development Mechanism Projects*, Academic Exchange, New York, NY, USA, 2009.

[8] D. C. Zhao and D. Q. Zhang, *New Features and Enlightenment of Current School Evaluation in the United States, Britain and Japan*, pp. 82–6, Comparative Education Research, 2010.

[9] M. S. Wang, *Evaluation of IAP Education*, Social Sciences Press, Beijing, China, 2006.

[10] Z. D. Zhao, *An Introduction to the Evaluation of IAP Education in Colleges and Universities*, Zhejiang People's Publishing House, Zhejiang, China, 2003.

[11] G. Y. Huang, *Educational Measurement and Evaluation,* East China Normal University Press, Shanghai, China, 2003.

[12] J. X. Feng, *Modern Education Evaluation and Surveying*, China Social Sciences Press, Beijing, China, 2005.

[13] X. F. Lei and M. Yang, "Research progress and trends of educational data mining," *Journal of Beijing University of Aeronautics and Astronautics (Social Science Edition)*, vol. 31, no. 4, pp. 108–114, 2018.

[14] T. Emmanuel, D. P. Kumar, P. Konstantinos, I. Goniadis, and A. C. Georgiou, "Evaluating higher education teaching performance using combined analytic hierarchy process and data envelopment analysis," *Journal of the Operational Research Society*, vol. 68, no. 4, pp. 431–445, 2017.

[15] G. F. Yu, X. M. Zhao, and Q. F. Yao, "Based on the multi-level fuzzy comprehensive evaluation method to improve the teaching quality of colleges and universities," *Journal of Hebei Normal University Natural Science Edition*, vol. 34, no. 11, pp. 15–19, 2018.

[16] L. Ma, "Research and development of teacher teaching evaluation system based on neural network," Master thesis, Nanchang Hangkong University, Hangkong, China, 2017.

[17] Q. S. Fang, "Research on Markov chain model of teaching quality evaluation," *Journal of Hebei Normal University Natural Science Edition*, vol. 32, no. 1, pp. 13–17, 2016.

[18] Y. Huang and L. Huang, "Experimental teaching quality evaluation practice based on AHP-fuzzy comprehensive evaluation model," *Intelligent Computing Theories and Technology*, vol. 7996, pp. 94–100, 2013.

[19] X. M. Li, C. Luo, and Z. X. Liu, "Implement fuzzy comprehensive evaluation of MOOC teaching quality in combination with analytic hierarchy process," *Contemporary Continuing Education*, vol. 34, no. 5, pp. 61–64, 2016.

[20] M. F. Zhao, "Application and research of data mining technology in teaching evaluation," pp. 14–43, Ningxia University, Ningxia, China, 2015, Master's thesis.

[21] M. N. Ovando, "Teacher's perceptions of a learner-centered teacher evaluation system," *Journal of Personnel Evaluation in Education*, vol. 15, no. 3, pp. 213–231, 2001.

[22] H.-Y. Ma, J.-K. Chen, N. Yang, and L.-L. Wang, "Application and study of ordinal decision tree in the teaching quality evaluation," *Journal of Applied Sciences*, vol. 13, no. 19, pp. 3903–3908, 2013.

Hindawi
Journal of Mathematics
Volume 2024, Article ID 9819732, 1 page
https://doi.org/10.1155/2024/9819732

Retraction

Retracted: A Convolutional Network-Based Intelligent Evaluation Algorithm for the Quality of Spoken English Pronunciation

Journal of Mathematics

Received 23 January 2024; Accepted 23 January 2024; Published 24 January 2024

This article has been retracted by Hindawi following an investigation undertaken by the publisher [1]. This investigation has uncovered evidence of one or more of the following indicators of systematic manipulation of the publication process:

(1) Discrepancies in scope

(2) Discrepancies in the description of the research reported

(3) Discrepancies between the availability of data and the research described

(4) Inappropriate citations

(5) Incoherent, meaningless and/or irrelevant content included in the article

(6) Manipulated or compromised peer review

The presence of these indicators undermines our confidence in the integrity of the article's content and we cannot, therefore, vouch for its reliability. Please note that this notice is intended solely to alert readers that the content of this article is unreliable. We have not investigated whether authors were aware of or involved in the systematic manipulation of the publication process.

Wiley and Hindawi regrets that the usual quality checks did not identify these issues before publication and have since put additional measures in place to safeguard research integrity.

We wish to credit our own Research Integrity and Research Publishing teams and anonymous and named external researchers and research integrity experts for contributing to this investigation.

The corresponding author, as the representative of all authors, has been given the opportunity to register their agreement or disagreement to this retraction. We have kept a record of any response received.

References

[1] X. Zhan, "A Convolutional Network-Based Intelligent Evaluation Algorithm for the Quality of Spoken English Pronunciation," *Journal of Mathematics*, vol. 2022, Article ID 7560033, 9 pages, 2022.

Hindawi
Journal of Mathematics
Volume 2022, Article ID 7560033, 9 pages
https://doi.org/10.1155/2022/7560033

Research Article

A Convolutional Network-Based Intelligent Evaluation Algorithm for the Quality of Spoken English Pronunciation

Xia Zhan

School of Foreign Languages, Changchun Institute of Technology, Changchun 130012, China

Correspondence should be addressed to Xia Zhan; wy_zx@ccit.edu.cn

Received 30 November 2021; Revised 22 December 2021; Accepted 27 December 2021; Published 18 January 2022

Academic Editor: Naeem Jan

Aiming at the problems of long time consumption and low accuracy of traditional spoken English pronunciation quality assessment algorithms, a convolutional network-based intelligent assessment algorithm for spoken English pronunciation quality is proposed. The convolutional neural network structure is given, the original data of the spoken English pronunciation voice signal are collected by multisensor detection, and the spoken English pronunciation voice signal model is constructed. Based on audio and convolutional neural network learning and training, it realizes the feature selection and classification recognition of spoken English pronunciation. The PID algorithm is used to extract the emotional elements of spoken English at different levels to achieve accurate assessment of the quality of spoken English pronunciation. The experimental results show that the average correct rate of spoken English pronunciation of the algorithm in this paper is 94.58%, the pronunciation quality score is 8.52–9.18, and the detection time of 100 phrases is 2.4 s.

1. Introduction

As a widely used language, English has attracted more and more people's attention. English is becoming more and more important in daily life. People appreciate American TV shows and Hollywood movies. They need to use English when traveling abroad, and they need to use it for import and export transactions. When it comes to English, English is required for academic research communication, and English is also required for industrial production, programming, and viewing technical documents [1]. So, being able to speak English is becoming more and more important for Chinese people. For Chinese people, dumb English has always been the number one problem in learning English. With the development of speech signal processing technology, the use of speech signal recognition methods to intelligently evaluate the quality of spoken English, combined with speech information processing technology to improve the quality of spoken English pronunciation, is of great significance in improving the effectiveness of spoken English teaching. The intelligent assessment of spoken English pronunciation quality evaluates and calculates pronunciation quality and detects pronunciation errors [2]. The related intelligent assessment algorithm of spoken English pronunciation quality has a great role in promoting the standardization of spoken English pronunciation, and it has also received great attention from people.

Wen [3] proposed the design of an automatic correction system for English pronunciation errors based on the dynamic time warping (DTW) algorithm. Relying on the optimized design of the speech recognition sensor and the improved design of the pronunciation recognition processor, the hardware design of the system is completed; the software design of the system is completed based on the design of the English pronunciation acquisition program and the extraction of English pronunciation error signal parameters. This method can accurately assess the pronunciation quality of spoken English, but the assessment takes a long time. Luo et al. [4] proposed an automatic evaluation technology algorithm for spoken English based on deep neural networks. Based on the verification experiment conducted on the real scene data of the large-scale unified oral English test in junior and senior high schools, the proposed automatic evaluation method has a greater performance advantage than the

traditional method based on goodness of pronunciation (GOP). The evaluation of this method takes less time, but the detection accuracy still needs to be improved.

When the user mistakenly pronounces one phoneme into another phoneme in the phoneme set, this hypothesis can be a good approximation to the true posterior probability value, but when the user's pronunciation is different from any standard pronunciation in the phoneme set, maximum number of multiple candidates differs from sum. Therefore, in some cases, this assumption will seriously reduce the accuracy of the confidence calculation. Aiming at the problems of the above methods, this paper proposes an intelligent assessment algorithm for spoken English pronunciation quality based on convolutional networks. Deep learning attempts to learn a better representation of data from large-scale unlabeled data, so deep learning is also called representation learning or unsupervised feature learning algorithm. One of the most commonly used scenarios of deep learning is to use unsupervised or semisupervised algorithms to automatically learn features to replace manually designed features. The convolutional neural network structure in deep learning is used to train the features of spoken English pronunciation signals, and based on audio to realize the screening of spoken English pronunciation features and classification and recognition, the proportional-integral-derivative (PID) algorithm is used to extract the emotional elements of speech, and the quality of spoken English pronunciation can be accurately measured.

The arrangement of the paper is as follows: Section 1 is the introduction and literature review. In Section 2, the structure of the convolutional neural network (CNN) is explained in detail. Moreover, the voice signal model of spoken English pronunciation features is given. Finally, the extraction of spoken English pronunciation features is carried out. Section 3 presents an intelligent assessment algorithm for the quality of spoken English pronunciation. In addition, the screening and classification of spoken English pronunciation features are done. In order to validate the proposed algorithm, Section 4 carries out the experiments and analyses their outcomes for the purpose of comparison. Lastly, Section 5 concludes the paper.

2. Spoken English Pronunciation Feature Extraction Based on the Convolutional Neural Network

In this section, the structure of the convolutional neural network (CNN) is explained in detail. Moreover, the voice signal model of spoken English pronunciation features is given. Finally, the extraction of spoken English pronunciation features is carried out.

2.1. Convolutional Neural Network Structure. The deep convolutional neural network is mainly composed of the input layer, hidden layer, and output layer. The hidden layer is composed of repeated and alternating multilevel convolutional layers and pooling layers, and its structure is shown in Figure 1.

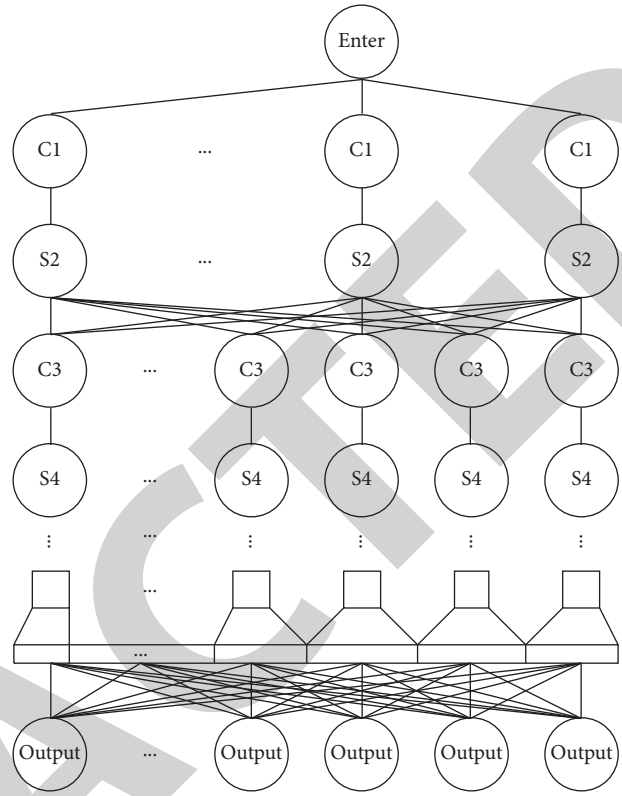

Figure 1: Deep convolutional neural network structure.

The initial data without feature extraction are input into the input layer, the input data are convolved through the convolution kernel in the convolution layer (C1), the corresponding convolution feature map is obtained, and the convolution is pooled through the pooling layer (S2). From the feature map obtained in the layer, the corresponding pooling feature map is obtained [5], and the operation is repeated in the hidden layer (C3, S4) imitating C1 and S2. By setting the convolution and pooling of the network, the extraction of data features can be effectively achieved, and the detection model can improve the degree of tolerance of the image that satisfies the distortion invariance [6]. At the same time, the resolution of the image is reduced, and the feature images are increased to obtain a large amount of feature data. The input information outputs the final detection result through the fully connected layer [7].

2.1.1. Convolutional Layer. The preprocessed acceleration sensor x, y, z data (depth is 3) are taken as the input data. In order to ensure the same size of the input and output, the data need to be filled with 0. During the convolution operation, the transformation of the same convolution kernel does not affect its weight, and the weight is shared with the x-axis data. This feature can effectively reduce the number of parameters of deep convolutional neural networks and accelerate network training [8].

All convolution kernels in the deep convolutional neural network have the function of automatic feature extraction. The acceleration sensor x, y, z data are convolved through

the convolution kernel, and various details can be extracted by each convolution kernel [9].

Let the height and width of the convolution kernel be f_h and f_w, respectively, to obtain a two-dimensional convolution:

$$y_{n,m} = A\begin{Bmatrix} x_{n,m} & x_{n+1,m} & \cdots & x_{n+f_w,m} \\ x_{n,m+1} & x_{n+1,m+1} & \cdots & x_{n+f_w,m+1} \\ \vdots & \vdots & \ddots & \vdots \\ x_{n,m+f_h} & x_{n+1,m+f_h} & \cdots & x_{n+f_w,m+f_h} \end{Bmatrix}. \quad (1)$$

The activation function uses the ReLU function to get the input and output of the total convolutional layer:

$$Y = \mathrm{ReLU}(\sigma(WB + b)). \quad (2)$$

2.1.2. Maximum Pooling Layer. The significance of the existence of the pooling layer is mainly to select and reduce the dimensionality of the output. The maximum pooling strategy is applied, the pooling core is 2×2, let s be the step size, and the height and width of the pooling core are p_h and p_w, respectively, to get the maximum pooling:

$$y_{i,j} = \max\begin{Bmatrix} x_{is,js} & x_{is,js+1} & \cdots & x_{is,js+p_w} \\ x_{is+1,js} & x_{is+1,js+1} & \cdots & x_{is+1,js+p_w} \\ \vdots & \vdots & \ddots & \vdots \\ x_{is+p_h,js} & x_{is+p_h,js+1} & \cdots & x_{is+p_h,js+p_w} \end{Bmatrix}. \quad (3)$$

Through the pooling layer, the dimensionality of the data and the corresponding training parameters can be reduced to a great extent, and the speed of network training can be accelerated.

2.1.3. Fully Connected Layer and Output Layer. The deep convolutional neural network is connected to the fully connected layer below its hidden layer, and the number of connected fully connected layers is greater than or equal to one. The existence of a fully connected layer is equivalent to a multilevel perceptron, in which all neurons of the same level are connected to all neurons in the upper layer, and the difference between the convolutional layer and the pooling layer can also be significant in this layer. Part of the information is fused. Taking the ReLU function as the activation function of the fully connected layer can effectively improve the performance of the deep convolutional neural network structure. The output layer receives the output value from the bottom fully connected layer and connects to different classifiers according to the required target. In order to prevent the overfitting situation in the traditional training of small-scale datasets, regular applications are often applied to the fully connected layer. The randomness of this method leads to the fact that the corresponding network structure of the dataset transmitted every time is not consistent, but the weights of all network structures are shared. This method greatly improves the stability of the detection model and makes every nerve less complicated when the elements adapt to each other [10].

The deep convolutional neural network convolutional layer applies a weight sharing method while reducing the parameters and difficulty of its structure and preventing the model from overfitting in the early stage so that it has better generalization ability, through pooling. To ensure the stability of the model, the network has a variety of characteristics that make it maintain the translation, scaling, and distortion when the transformation occurs. Deep convolutional neural networks have strong expression effects and scalability and can be well applied to various difficult problems.

2.2. The Voice Signal Model of Spoken English Pronunciation. In order to realize the quality assessment of spoken English pronunciation based on the convolutional neural network, firstly, the spoken English pronunciation voice signal model is given, and the multisensor detection method is adopted to collect the original data of spoken English pronunciation voice signals, and then the collected spoken English pronunciation voice signals are collected. Scale decomposition and feature extraction are carried out [11], spoken English pronunciation quality assessment and feature detection are carried out, and the mathematical model expression of the spoken English pronunciation speech signal is given as

$$z(t) = s(t) + js(t) \otimes h(t) = s(t) + j\int_{-\infty}^{+\infty} \frac{s(u)}{t-u}\,\mathrm{d}u. \quad (4)$$

In the formula, $a(t)$ is called the spoken English pronunciation voice signal-received signal amplitude at the nth array element, sometimes called the envelope, $\phi(t)$ is called the phase of the multiuniform linear wideband array, $Z(f)$ can be obtained by the Fourier transform of $S(f)$, and $H(f)$ is the step transfer function of the spoken English pronunciation voice signal. Based on the convolutional neural network, the spoken English pronunciation speech signal modeling and detection and recognition are carried out, and the array element distribution of the speech information sampling is $v_m, m \in [1, n]$. The result of the separation of the phonetic features of spoken English pronunciation is calculated as

$$y(t) = \iint_{a,b} \rho(a,b) f\left(\frac{t-b}{a}\right). \quad (5)$$

In the formula, $f(t - b/a)$ is the instantaneous frequency estimation value of the received spoken English speech signal, $\rho(a, b)$ is the delay component of the broadband signal incident on the array element, a is the high-order statistical characteristic information of the signal, and b is the frequency shift distribution. The feature components of spoken English pronunciation information are calculated as

$$X_p(u) = \int_{-\infty}^{+\infty} K_p(t,u)x(t)\mathrm{d}t. \quad (6)$$

The fusion weight is updated, and the output signal component $\pi/2$ obtained can be expressed as

$$X_p(u) = \begin{cases} x(u), & \alpha = 2n\pi, \\ x(-u), & \alpha = (2n \pm 1)\pi. \end{cases} \tag{7}$$

In the formula, p is the order of the best received polarization vector, which can be any real number, and the phase of voice detection is $\alpha = p\pi/2$. When $\pi/2$ is reached, it rotates to the frequency axis, thus realizing oral English modeling the statistical information of the articulated speech signal.

2.3. Extraction of Spoken English Pronunciation Features. In order to extract the pronunciation features of spoken English, the basic network based on the deep convolutional neural network is ResNet101; in order to better extract the subtle features of spoken English pronunciation, in the middle of the convolutional layer and the pooling layer, batches are added to layer by layer through ResNet. The residual block adjusts the information transmission strategy while accelerating the network training speed and promotes the optimization of the network [12].

The batch normalization algorithm is applied to the batch normalization layer, which integrates the processing operations of the network layer input into the spoken English pronunciation detection and processes the spoken English pronunciation feature samples through microbatch normalization.

The batch normalization is expressed as

$$\widehat{X} = \text{norm}(x, X). \tag{8}$$

In the formula, x describes all the vectors that are input to a certain layer in the deep convolutional neural network, and X represents a certain value for the overall training sample. The output of the batch-normalized network can be judged by using the input vector of the previous layer and the overall value. The network input of each layer of the training set is obtained from the output of the previous layer, and the parameters of the model will also limit the input vector.

When optimizing the network parameters, the backpropagation algorithm is used to obtain the Jacobian matrix corresponding to the batch normalization of the input vector and the overall training sample value. The formula is

$$\frac{\partial norm(x, X)}{\partial x}, \quad \frac{\partial norm(x, X)}{\partial X}. \tag{9}$$

Batch normalization is a big project to process the input of all layers, it needs to calculate the matrix of covariance, and it takes a long time. In this regard, the following two simplified improvement methods are proposed:

(1) The joint normalization processing of each dimension data is replaced with the data of each dimension delivered by the independent batch normalization processing, and the formula is as follows:

$$\widehat{X}(k) = \frac{x_i(k) - E[x(k)]}{\sqrt{[x(k)]}}. \tag{10}$$

In the formula, the k dimension of the input sample is described by $x(k)$, the expectation is described by $E[x(k)]$, and the variance is described by $\text{var}[x(k)]$. Independent batch normalization can effectively speed up the convergence speed of network training, but it does not guarantee the stability of the initial description of each layer of the network, resulting in the initial output characteristics that cannot be fully described by the input. In order to maintain the constant change of the added batch normalization process, parameters $\lambda(k)$ and $\beta(k)$ are added to the k dimension of each input sample to obtain the formula

$$y(k) = \lambda(k)\widehat{X}(k) + \beta(k). \tag{11}$$

In the formula, $\beta(k)$ and $\text{var}[x(k)]$ are equal, both are descriptions of the input standard deviation, which means the k dimension of the input sample after scale transformation, $\beta(k)$ and $E[x(k)]$, is equal, and both are the expected input, which Indicates that the input sample after translation is k. Using this parameter together with each parameter in the model for network training can effectively ensure the description level of the model.

(2) Stochastic gradient training of deep convolutional neural networks is carried out through microbatch samples, the average value and variance of each layer are estimated by calculating each sample, and the aforementioned operation can be used to realize the reverse direction propagation of the gradient.

Suppose the microbatch sample is denoted as B, its sample size is described as m, a certain dimension input to a certain level is denoted as x, and the dimension-wise normalization is expressed as

$$BN_{\lambda,\beta}: x_1, \ldots, x_m \longrightarrow y_1, \ldots, y_m. \tag{12}$$

Through the above content, the feature extraction of spoken English pronunciation based on the convolutional neural network is realized.

3. Intelligent Assessment Algorithm of Spoken English Pronunciation Quality

For the quality of spoken English pronunciation, this section presents an intelligent assessment algorithm. In addition, the screening and classification of spoken English pronunciation features are done.

3.1. Screening and Classification of Spoken English Pronunciation Features. The current spoken English pronunciation assessment algorithms mostly rely on language signals for judgment, ignoring the role of signals in pronunciation error correction. For this reason, an audio-based method for screening and classifying spoken English pronunciation features is proposed. Using the convolutional neural network learning method, the

feature screening and classification of spoken English pronunciation signals are performed. Assuming that the input spoken English pronunciation speech signal is a single-frequency signal $\cos 2\pi f_0 t$, where f_0 is the spoken English pronunciation frequency, the reference component of the spoken English pronunciation signal detected by the first array element is set to construct the error feature screening of the spoken English pronunciation. The model uses the time-frequency feature transformation method for dynamic detection and feature selection of spoken English pronunciation signals, and the mth block sparse feature quantity is

$$s_m(t) = \cos\{2\pi f_0[t + \tau_m(\theta)]\}. \tag{13}$$

The target source signal detection method is used to monitor the characteristics of spoken English pronunciation speech signals, and the characteristic distribution of spoken English pronunciation errors is obtained as

$$l(t) = u_m \cos(2\pi f_0 t) - v_m \sin(2\pi f_0 t), \tag{14}$$

From this, the eigenvalues of spoken English pronunciation speech signals are extracted, and the beam-forming method is used to focus on the characteristics of spoken English speech signals. Therefore, the deep neural network detection method is used to detect the error characteristics of spoken English speech signals. The output is

$$y_1(t) = A_1(t)\exp\{j2\pi[F(t - t_a) - F\ln Dt + f_{e1}t]\}. \tag{15}$$

The output feature quantity of the pronunciation error of harmonic spoken English is expressed as

$$y_2(t) = A_2(t)\exp\{j2\pi[F(t - t_a) - F\ln Dt + f_{e2}t]\}. \tag{16}$$

In the formula, f_{e1} is the beam domain cutoff frequency, and f_{e2} is the harmonic cutoff frequency. The statistical feature analysis method is used to separate the features of spoken English pronunciation errors, and the output information of spoken English pronunciation errors is

$$y(t) = s(t) + n(t). \tag{17}$$

The spectrum of mispronunciation messages in spoken English is

$$\begin{aligned} Y_p(u) &= F^a[y(t)] \\ &= F^a[s(t) + n(t)] \\ &= F^a[s(t)] + F^a[n(t)]. \end{aligned} \tag{18}$$

When the prior probability of the signal satisfies the convergence condition, the time width of the spoken English speech signal is calculated:

$$T^2 = \int_{-\infty}^{+\infty} (t - t_m)^2 |x(t)|^2 \mathrm{d}t. \tag{19}$$

The frequency-domain characteristics of spoken English pronunciation speech signals are described as

$$B^2 = \int_{-\infty}^{+\infty} (v - v_m)^2 |X(v)|^2 \mathrm{d}v. \tag{20}$$

According to the Bayesian formula, the characteristics of the spoken English pronunciation signal are screened, and the detection output is

$$s(t) = \sqrt{s}\, u[s(t - \tau_0)]. \tag{21}$$

3.2. Intelligent Assessment Algorithm of Spoken English Pronunciation Quality. In order to solve the problem that the existing system only considers, intonation and rhythm when evaluating the quality of spoken English pronunciation, but does not take into account the effect of speech emotion, which leads to the poor effect and inefficient evaluation of spoken English pronunciation, the PID algorithm is used to extract the emotional elements of the spoken language at different levels. Taking full account of the imbalance of corpus evaluation data, the data of various elements that affect the pronunciation of spoken English are extracted [13]. Since the traditional system has researched and extracted conventional indicators such as intonation and rhythm, the PID algorithm is used on the basis of the existing methods to extract the emotional elements of spoken English at different levels [14] in order to extract English accurate assessment of the quality of spoken English pronunciation.

PID is the most common algorithm for remote operation. Suppose that the actual output value of the intelligent evaluation algorithm for spoken English pronunciation quality based on the convolutional network is $c(t)$, the fixed value is $r(t)$, and the operation deviation calculation formula of the evaluation algorithm is

$$e(t) = c(t) - r(t). \tag{22}$$

The differential (D), proportion (P), and integral (I) of the scoring deviation of the spoken English pronunciation quality scoring system are linearly combined to form the operation volume of the laboratory experiment remote operating system, and each pronunciation element is scored, which is called the PID algorithm. In the virtual reality-based English-speaking pronunciation quality scoring system, according to the standard rules of spoken English pronunciation and pronunciation characteristics, the P, I, and D operation rules are appropriately combined to complete the extraction of speech emotion elements [15]. The law calculation formula is

$$u(t) = \left[e(t) + T_D + \frac{1}{T_1}\int_0^t e(t)\mathrm{d}t\right] \times K_P. \tag{23}$$

In the formula, K_P represents the proportional coefficient of the emotional elements in the spoken pronunciation; T_1 represents the validity of the voice emotional index; T_D represents the differential time constant for the completion of the operation; t represents the time required for extraction. Since the characteristic data recognized by the traditional scoring system are limited and cannot be operated continuously on the characteristic data, the PID algorithm is used to discretize the information data in the scoring system. The calculation formula for the discretization is

$$u(k) = K_P\left[e(t) + \frac{T}{T_1}\sum_{i=1}^{k} e(i) + \frac{T_D}{T}\right] + u_0. \quad (24)$$

In the formula, u_0 represents the initial value when the score deviation is 0; T represents the sampling period of speech emotion elements. After discretizing the data information through PID algorithm, the continuous operation of the system is realized, and the effective extraction of voice emotion elements is guaranteed [16].

According to the extraction results of speech emotion elements, the quantitative recursive analysis method comprehensively evaluates the quality of spoken English pronunciation and finally obtains the scoring results. The panel data for the evaluation of spoken English pronunciation quality are established, and the method of combining quantitative analysis and fuzzy prediction is used to obtain the statistical regression analysis results of panel data for the evaluation of spoken English pronunciation quality as follows:

$$q^w\left\{\lambda_w \eta^w - D^{-1}\right\} \geq 0. \quad (25)$$

In the formula, w represents the mean value of the feature; η represents the standard deviation of the pronunciation; λ represents the ambiguity feature amount of the speech.

Combining the minimum cost and the best balanced method of teaching quality [17], the game balance control of the English pronunciation quality score is carried out, and the optimization level is selected as the dependent variable, and the statistical detection quantity is obtained as

$$q^A = \frac{(\beta c_n)^2}{16\beta(1-\beta)} + \frac{(1-c_n)^2}{16}. \quad (26)$$

In the formula, β represents the phoneme competition subset; c represents the independent threshold; n represents the voice recording rate.

Therefore, a panel data statistical analysis model for the evaluation of spoken English pronunciation quality is constructed, and a game model for the evaluation of spoken English pronunciation quality is obtained, which is defined as

$$V_i = \frac{X^i_{\max} - X^i}{q^A\left(X^i_{\max} - X^i_{\min}\right)}. \quad (27)$$

In the formula, V represents the factors that affect pronunciation evaluation; X represents the correct vowels and words entered. In summary, the quantitative regression analysis method and the full-sample regression test analysis method are used to achieve the scoring of the quality of spoken English pronunciation.

4. Experimental Analysis

In order to test the performance of the algorithm in this paper in realizing the intelligent evaluation of spoken English pronunciation quality, a simulation experiment was carried out. The experiment was designed with MATLAB 7 simulation software to verify the correct rate of spoken English pronunciation, the score of spoken English pronunciation quality, and the algorithm response time. The effectiveness of the results and the method of Wen [3] and Luo et al. [4] are used as experimental comparison methods.

4.1. Experimental Data Preparation. This study selects the spoken Arabic digit dataset as the experimental dataset, which contains a large amount of spoken English pronunciation data. In order to reduce the difficulty of the experiment, a 16 KHz sampling rate was used to randomly select 13,500 data in the spoken Arabic digit dataset. The specific experimental data information is shown in Table 1.

The number of nodes sampling the spoken English pronunciation signal is 120, the resolution of feature extraction is 200 KHz, the length of the output spoken English pronunciation signal is 1200, the number of sources to be measured is 20, and the interference signal-to-noise ratio is −20 dB.

4.2. Analysis of Experimental Results. Based on the experimental data prepared above and the determined experimental evaluation indicators, an intelligent evaluation experiment for the quality of spoken English pronunciation is carried out. The analysis process of the specific experimental results is shown below.

4.2.1. Analysis of the Correct Rate of Pronunciation Errors in Spoken English. The correct rate data of spoken English pronunciation error detection obtained through experiments are shown in Table 2.

As shown by the comparison of data in Table 2, in the process of 10 experiments on spoken English pronunciation, the algorithm in this paper has a high error detection rate of spoken English pronunciation, the highest is 96.2%, the lowest is 92.5%, and the average is 94.58%, which is much higher than the references' comparison method. Because the method in this paper uses the convolutional neural network to train the spoken English pronunciation data, it improves the correct rate of pronunciation error detection. The experimental results show that the designed intelligent assessment algorithm of spoken English pronunciation quality has better error detection performance.

4.2.2. Analysis of the Quality of Spoken English Pronunciation. After applying the designed intelligent assessment algorithm for spoken English pronunciation quality, the calibrated pronunciation quality score data are shown in Table 3.

Table 1: Experimental data information table.

Experimental data information		
Type of data	Open testing	Close testing
Number of data	4500	9000
Number of speakers	5	10
Proportion of male to female speakers	3 : 2	1 : 1
Data format	16 bit/PCM	

Table 2: Data table of correct rate of pronunciation error detection in spoken English.

Correct rate of pronunciation error detection in spoken English (%)			
Number of experiments	Wen's [3] algorithm	Luo et al.'s [4] algorithm	The proposed algorithm
1	75.2	70.6	92.5
2	73.1	70.5	93.5
3	74.8	69.7	94.5
4	75.6	68.5	95.3
5	74.9	72.2	95.1
6	69.5	71.0	94.8
7	68.4	65.2	95.2
8	72.4	69.3	94.8
9	71.8	68.5	96.2
10	71.6	65.7	93.9

Table 3: Spoken English pronunciation quality score data table.

Number of experiments	Wen's [3] algorithm	Luo et al.'s [4] algorithm	The proposed algorithm
1	6.58	6.31	8.52
2	6.95	6.83	9.01
3	6.78	6.95	9.12
4	6.80	7.09	8.67
5	7.10	7.18	8.95
6	7.08	6.68	8.74
7	6.95	6.95	9.02
8	6.45	7.41	9.15
9	7.01	7.35	8.95
10	6.89	7.25	8.89

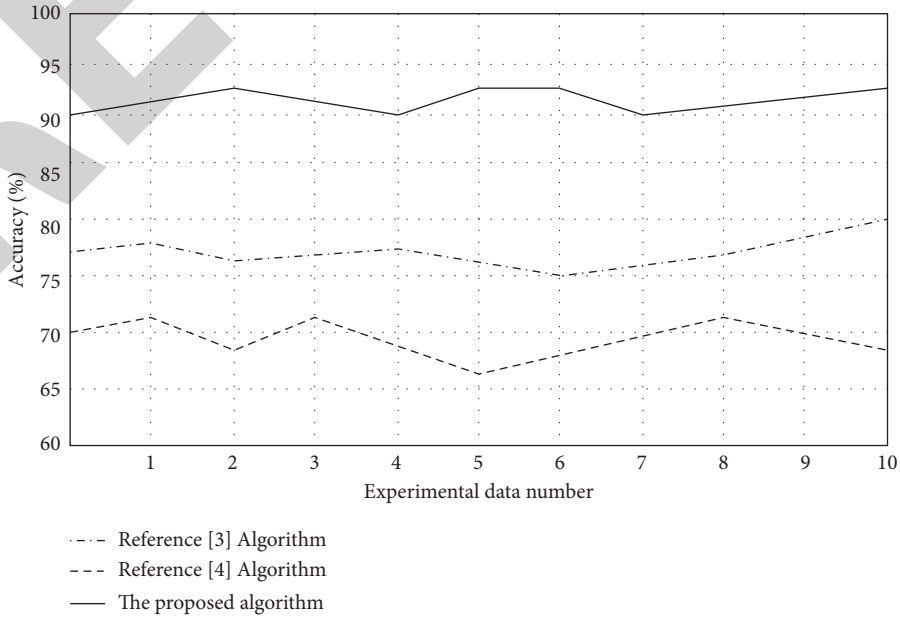

Figure 2: Accuracy rate of the spoken English pronunciation quality score.

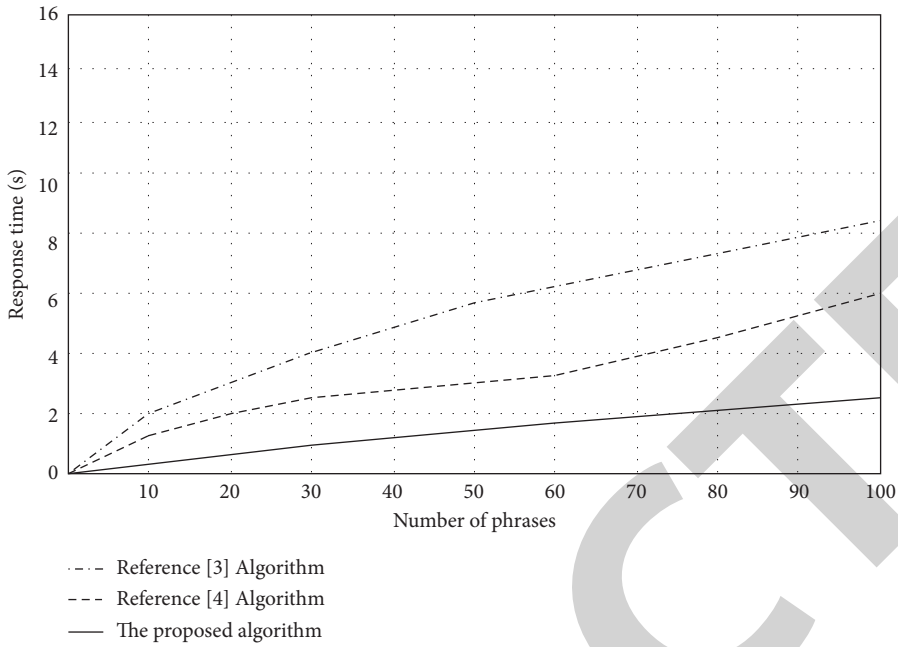

Figure 3: Comparison results of response time.

As shown in Table 3, the pronunciation quality score of the algorithm in this paper is 8.52 points to 9.18 points, the pronunciation quality score of the algorithm in [3] is 6.45 points to 7.10 points, and the pronunciation quality score of the algorithm in [4] is 6.31 points to 7.35 points which shows that the algorithm in this paper has a better effect on scoring spoken English pronunciation quality. The accuracy rate of the spoken English pronunciation quality score is shown in Figure 2.

Analyzing Figure 2 shows that, in the course of 10 spoken English pronunciation quality experiments, the average accuracy rate of the spoken English pronunciation quality score of the algorithm in this paper is 93.5%, and the average accuracy rate of the spoken English pronunciation quality score of the algorithm in [3] is 78.5%. The average accuracy rate of spoken English pronunciation quality scores based on the algorithm in [4] is 71.5%. The experimental results show that the accuracy of the spoken English pronunciation quality score of the algorithm in this paper is higher.

4.2.3. Comparison of Algorithm Response Time. The intelligent assessment algorithm for spoken English pronunciation quality requires extremely high performance for responsive time, and the trainer's pronunciation recording should quickly output the words that need to be corrected. Therefore, the response time is also one of the key indicators of the detection system performance. The experiment uses 100 individual word data as the test data and does not include the collected time. From the initial input to the end of the spoken English pronunciation quality evaluation, the entire process is used. The results of the test comparison are shown in Figure 3.

Analyzing Figure 3, it can be seen that, in the process of the oral English pronunciation test of 100 phrases, the response time of the spoken English pronunciation quality score of the algorithm in this paper is 2.4 s, and the response time of the spoken English pronunciation quality score of the algorithm in [3] is 8.2 s. In [4], the response time of the algorithm's spoken English pronunciation quality score is 6.0 s. The experimental results show that the response time of the algorithm in this paper is shorter, and the accuracy of its spoken English pronunciation quality score is higher, and it can efficiently and accurately realize the intelligent assessment of spoken English pronunciation quality.

5. Conclusion

This paper proposes a convolutional neural network intelligent assessment algorithm for spoken English pronunciation quality, selects a more complex GMM-HMM model than softmax in the original CNN for training and recognition, and builds a CNN-GMM-HMM speech recognition model system. Through audio recognition, the feature screening and classification recognition of spoken English pronunciation are realized, and the PID algorithm is used to extract the emotional elements of spoken English pronunciation, so as to realize the accurate assessment of the quality of spoken English pronunciation. Experiments have proved that the intelligent assessment algorithm of spoken English pronunciation quality based on the convolutional neural network can improve the correct rate of oral English pronunciation error detection and obtain efficient and accurate pronunciation quality assessment results.

Data Availability

The data used to support the findings of this study are available upon request to the author.

Hindawi
Journal of Mathematics
Volume 2023, Article ID 9895762, 1 page
https://doi.org/10.1155/2023/9895762

Retraction

Retracted: Path Optimization of Enterprise Network Innovation Performance Management Based on Deep Learning and Internet of Things

Journal of Mathematics

Received 19 December 2023; Accepted 19 December 2023; Published 20 December 2023

This article has been retracted by Hindawi following an investigation undertaken by the publisher [1]. This investigation has uncovered evidence of one or more of the following indicators of systematic manipulation of the publication process:

(1) Discrepancies in scope

(2) Discrepancies in the description of the research reported

(3) Discrepancies between the availability of data and the research described

(4) Inappropriate citations

(5) Incoherent, meaningless and/or irrelevant content included in the article

(6) Manipulated or compromised peer review

The presence of these indicators undermines our confidence in the integrity of the article's content and we cannot, therefore, vouch for its reliability. Please note that this notice is intended solely to alert readers that the content of this article is unreliable. We have not investigated whether authors were aware of or involved in the systematic manipulation of the publication process.

Wiley and Hindawi regrets that the usual quality checks did not identify these issues before publication and have since put additional measures in place to safeguard research integrity.

We wish to credit our own Research Integrity and Research Publishing teams and anonymous and named external researchers and research integrity experts for contributing to this investigation.

The corresponding author, as the representative of all authors, has been given the opportunity to register their agreement or disagreement to this retraction. We have kept a record of any response received.

References

[1] P. Xiong, "Path Optimization of Enterprise Network Innovation Performance Management Based on Deep Learning and Internet of Things," *Journal of Mathematics*, vol. 2022, Article ID 4932439, 10 pages, 2022.

Hindawi
Journal of Mathematics
Volume 2022, Article ID 4932439, 10 pages
https://doi.org/10.1155/2022/4932439

Research Article

Path Optimization of Enterprise Network Innovation Performance Management Based on Deep Learning and Internet of Things

Peiran Xiong

School of Business Administration, Jiangxi University of Finance and Economics, Nanchang 330013, China

Correspondence should be addressed to Peiran Xiong; 2201810002@stu.jxufe.edu.cn

Received 23 November 2021; Revised 14 December 2021; Accepted 18 December 2021; Published 18 January 2022

Academic Editor: Naeem Jan

In today's global competition environment with rapid changes in market and technology, it is more and more difficult for enterprises to fully grasp the latest knowledge and learn all the technologies by relying on their own strength. It is particularly important for enterprises to establish a network relationship of a certain intensity with other external entities (upstream and downstream enterprises, peer enterprises, scientific research institutions, government departments, financial institutions, and other organizations) for their technological learning and improvement of technological innovation performance. From different perspectives, the academic circles have confirmed that the strength of network relationship does have an impact on the technological innovation performance of enterprises. This paper will explore the measurement scale of technology learning cost, and from the basic perspective of technology learning cost, deeply explore and analyze how enterprise technology innovation performance is affected by the strength of enterprise network relationship. This paper argues that the strength of network relationship can affect the cost of technology learning and therefore the performance of technology innovation. The main contents of this study include the following. (1) Through the collation and review of the related theories of network relationship strength, technological learning cost and technological innovation performance, and the existing research results, the theoretical model of this study is established, and the theoretical assumptions of this study are put forward. (2) A presurvey is carried out first, and the data collected from the presurvey are used to test the reliability and validity of the scale of this study, and the appropriate measurement scales for the strength of network relationship, technology learning cost, and technology innovation performance are determined. (3) Adopt the method of regression analysis combined with the SME method, to verify this paper builds the theoretical model, and further clarify the network relation intensity, technology acquisition cost, and cost of technological learning all dimensions and performance of technological innovation and network strength, technological learning mechanism between cost, and performance of technological innovation.

1. Introduction

In today's society, the market is changing rapidly and technology is changing rapidly. Technological learning becomes a potential source for enterprises to build competitive advantages [1]. Due to the limitation of the enterprise's own resources, it is difficult for the enterprise to fully grasp the latest technical knowledge. Embedded social networks can provide effective channels for enterprises to obtain timely and accurate information for technological learning and can directly provide knowledge resources, information, and complementary resources for technological learning [2]. Both resource-based view and knowledge-based view point out that only by continuously acquiring knowledge resources such as information from the external environment for continuous technical learning can enterprises maintain stable development in the increasingly competitive market. It can be seen from this that enterprise technology learning is closely related to enterprise social network. The process of technology learning needs to consume a certain amount of resources; it is inevitable to produce learning costs. From a certain point of view, the cost of technology learning is

caused by the existence of various obstacles affecting learning, and the cost of overcoming various obstacles is the cost of technology learning. Before the technical learning has reached the fixed goal, the cost of learning directly determines whether the technical learning can be carried out, continued and successful. The cost of technology learning has also become an important issue in the research and practice of technology management. Therefore, whether an enterprise can quickly obtain timely and effective resources from the complex and dynamic social network to overcome the obstacles in technology learning is the key to its success in technology learning. The network relationship of different intensity has different influences on the acquisition, transmission, and absorption of information in the enterprise technology learning, and the cost of technology learning and the performance of technology innovation are closely related to the acquisition, transmission, and absorption of information. Some scholars believe that strong network relationships are conducive to enterprises' access to self-beneficial information and knowledge, which is conducive to enterprises' technical learning. On the contrary, some scholars believe that the network knowledge flow with strong relationship is more frequent, which increases the cost of knowledge transfer and is not conducive to the technological learning of enterprises. Therefore, it is very important for enterprises to maintain a reasonable strength of relationship with social network members.

When studying the relationship between the strength of network relationship and enterprise technological innovation performance, many scholars analyze and study from the angle of knowledge transfer and have obtained rich results. In [3], trust and reciprocity among network members with strong relationships can reduce the level of conflicts between organizations and produce a mechanism for solving problems together, so it is conducive to information transfer between organizations. Andrew C Inkpen pointed out that, in the weak relationship network, the trust between individuals is relatively low and the psychological distance is relatively far, so individuals will show strong self-protection behavior in the process of cooperation, which will obviously limit the transfer and sharing of knowledge. Reagans and McEvily studied the influence of network relationship strength of knowledge source on its tacit knowledge transfer behavior from the perspective of knowledge source. By studying the tacit knowledge transfer behavior among employees within a R&D company, they found that the degree to which a knowledge sender sends knowledge is affected by the knowledge reticence and the strength of network relationship. In addition, compared with the dimension of social network structure, the strength of network relationship is able to reduce the obstacles for knowledge source to transmit knowledge [4]. In [5], it was found that strong network relationship is conducive to the improvement of knowledge transmission and knowledge absorption capacity of the two sides of tacit knowledge transfer, so the more frequent, extensive, and in-depth knowledge sharing and communication between the two sides of knowledge transfer will be strengthened. Schmidt and Roth [6] found through the investigation of pharmaceutical enterprises in Zhejiang, China, that strong Wanfang Data 5 network relationship can play the role of enterprise information channel, and the high-quality information transmitted in this channel is conducive to promoting the transfer of complex knowledge between enterprises, thus significantly improving the technological innovation capability of enterprises. Gu et al. [7] found that the efficiency of interorganizational cooperation is closely related to the strength of interorganizational relations. On the one hand, the higher the intensity, the higher the interaction frequency and the degree of trust, which is conducive to the tacit knowledge transfer between organizations. On the other hand, overdependence on strong relationships may restrict enterprises to a relatively closed network with limited information resources and make it difficult for enterprises to access and obtain information resources outside the closed network, thus restricting the innovation path of enterprises. In [8], the study showed that, compared with networks with weak relationships, the knowledge acquired by groups with close relationships is often highly similar. Therefore, tacit knowledge transfer between closely related groups is not conducive to the development of the group's own innovation activities, and the weak relationship is more conducive to improving the innovation performance than the strong relationship. Huang et al. [9] discussed the influence of cluster network relationship strength on technological innovation from the perspective of inner and outer cluster relationship of core enterprises. They believe that, for an enterprise, the resources needed to maintain internal and external relationships are limited, so the strength of internal and external relationships shows a negative relationship. The strong network relationship is beneficial to the knowledge exchange both inside and outside the cluster, but the weak external relationship provides heterogeneous knowledge and is beneficial to the technological innovation of enterprises. Therefore, there is an inverted U-shaped relationship between the strength of cluster network relationship and technological innovation.

At present, the passive device fingerprint access authentication algorithm generally adopts the method based on shallow feature learning. In [10], protocol types are used as device features to construct the device fingerprint matrix. Based on the feature process of [10], [11] adopts algorithms such as KNN, AdaBoost, and SVM to realize the device access authentication based on passive device fingerprint. The above methods are all shallow feature representation methods. Gupta and Govindaraian [12] proposed a passive fingerprint method that could identify different wireless drivers on network connected devices. McEvily and Zaheer [13] proposed an IOT device identification method that supported a variety of communication connection technologies (including WiFi, ZigBee, Ethernet, and Z-Wave), and tested it on the dataset of communication devices, with good test results. Zander and Kogut [14] proposed a method to identify the type of devices connected to the IP network to realize the identification of device types. Cumming and Teng [3] designed an Internet of Things scanner to identify devices by visualizing media access control (MAC) layer traffic, but regular use to identify devices and compare their

fingerprints to the baseline would increase the processing load. In [4–6], the IAT value is used as the unique feature of the device, and three-layer perceptron is used to implement device access authentication based on the similarity measurement method. The research results show that the IAT value can be used to identify device types and individual devices, but the IAT value for device access authentication depends on a large number of data packets, which will inevitably lead to a long time for device identification in real application scenarios. In view of the above problems, this paper applies the deep learning model to the IoT access authentication scenario based on passive device fingerprint and proposes a deep learning-based IoT device access authentication method. This method uses the bidirectional LSTM (BiLSTM) model to extract features from passive device fingerprints and realize identification of IoT devices. Compared with the traditional LSTM model, the BiLSTM model takes into account the future information and has better recognition effect.

2. Innovation Performance Management

The bucket is divided into mobile terminal, sensor module, wireless communication module, power module, and motor drive module according to functions. The sensor module is equivalent to the "eyes" and "ears" of the smart trash can. It uses infrared sensors, temperature sensors, and pressure sensors, respectively. It is mainly responsible for the security detection part of the smart trash can and provides more human services for the intelligent delivery. The wireless communication module runs through the communication system of the entire intelligent trash can, and the data communication between the mobile terminal and the SCM control is realized through the wireless communication module. The functions of the IoT service system include processing and analyzing the monitoring data transmitted by each sensor on the garbage can, and the server automatically builds the database of relevant monitoring data. Multiple kinds of data collected in all areas can be analyzed, the real-time status of smart garbage cans can be distinguished by mobile terminal monitoring, and the sanitation staff can be reminded to clean the garbage buckets in a timely and effective manner. The overall system design and application of soft and hard can be a different garbage intelligent delivery, from the source to reduce the burden of cleaning personnel. The specific operation process is shown in Figure 1.

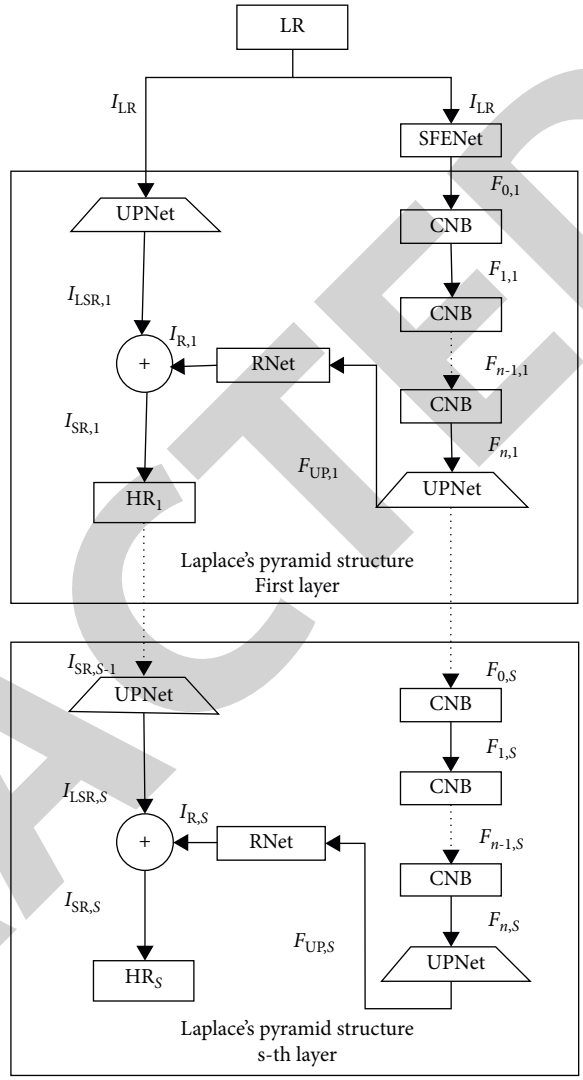

Figure 1: LCN structure.

2.1. Software Design. Considering that if the image recognition module is loaded on hardware, the overall power consumption of the garbage classification system will be greatly increased, and it is difficult to update and upgrade the garbage photo library in the future; the focus will be on the mobile terminal. At present, there are two major mobile platforms, IOS and Android, and each has a huge ecosystem. If we want to adapt them, respectively, the development cost and the increase of the weekly period will bring a great burden to the project. The microchannel small program is lightweight, convenient, spanning two platforms, and a large user base. Based on the above considerations, this paper developed a microchannel small program, named intelligent garbage classification system. The small program was developed by WeChat developer tools at the front end, and the Flash framework with simple core and easy to extend was used to build the server side. The deep learning model deployed in the server was trained on the existing garbage classification dataset using SSD algorithm.

2.1.1. Specific Functions.

(i) Click the search box at the top to enter the search interface. Enter the name of the garbage in the search box, and the corresponding garbage will pop up. Click the garbage with the name similar to the garbage, and click to view the corresponding category of the garbage.

(ii) Click the "Location" button at the top to enter the location interface. The location interface calls the

API of Tencent map, and users can find the location of the nearest intelligent classification trash can and within a certain distance can be automatically connected with the intelligent classification trash can Bluetooth.

(iii) Click the "Camera Recognition" button in the middle to enter the camera interface. In the camera interface, the user can take photos through the mobile phone camera and upload the photos to the server side. The server side will recognize and process the pictures and return to multiple possible categories of items. The user can jump to the corresponding garbage category of the item by selecting and clicking the category of the actual item. If it is connected to the intelligent classification garbage can at this time, the signal will be transmitted to the garbage bucket, and the corresponding category bucket cover will open automatically.

(iv) Click the "Classification" button in the bottom navigation bar to enter the garbage classification guide interface. The garbage classification guide interface contains the introduction of different types of garbage, as well as the classification of common garbage.

(v) Click the "Quiz" button on the side to enter the garbage sorting and answering interface. Ten different kinds of garbage will be randomly given on the garbage sorting answer interface. Users can choose the corresponding garbage type, and the correct answer will be given according to the number of correct answers.

2.2. Hardware Design. The specific hardware modules of the intelligent trash cans are divided into SCM main control board, overfill automatic monitoring module, temperature detection module, voice prompt module, steering gear drive module, wireless communication module, and power module. The main control module of this design plays the logical control role in the whole hardware system. It is the most important part of the whole system and the core of the whole system [15].

(i) **Solar power:** the smart trash can is powered by installed solar batteries and uses batteries to store excess electrical energy obtained on sunny days for use on rainy days. The use of solar battery power not only solves the difficulty of long-distance power supply in the street but also saves energy and protects the local environment. In addition, solar cells made with current technology have a very long life.

(ii) **Voice prompt module:** the module uses infrared sensing technology, which is a technology that uses infrared ray and pyroelectric principle to sense human activity information. When people enter the sensing range, it can accurately identify and detect passively sensing human activity information. The sensor can be rotated 60° to the left and right, easily changing different sensing areas. Furthermore, the TF card equipped with MP3 voice and the battery are inserted into the corresponding position of the trash can, and the indicator light will flash once when the status switch is switched to ON. If there is no operation, the product will be in the waiting state, and the voice will be played when the induction is triggered. When a resident walks near a trash can with a trash bag, the voice prompts automatically play. For example, "it is everyone's responsibility to protect the environment. Please throw the rubbish into the dustbin."

(iii) **The automatic detection module overflows:** the module uses infrared probes and pressure sensors. When the garbage accumulation in the garbage bin reaches a certain height or the weight of the garbage reaches a certain weight, the system will prohibit the lid of the garbage bin from opening and display a red light to indicate that the garbage bin is full. Among them, infrared wave is sent to the garbage box by installing an infrared probe. When the garbage in the garbage bin is full, the garbage blocks the reflected infrared ray reception. At this time, the garbage can be considered to be full and reported to the cloud platform so that the cleaning personnel can be arranged to deal with it in time. The pressure sensor is used to monitor the amount of garbage in the garbage box in real time. When the amount of garbage reaches the preset value, the system will achieve the preset effect. It is forbidden to open the dustbin lid and show the red light. The design of the module prevents environmental pollution caused by garbage overflow, and it does not need the cleaning personnel to repeatedly check whether the garbage is full, which saves a lot of manpower and material resources.

(iv) **Temperature detection module:** the module uses a temperature sensor that sends information to the server when the temperature in the litter exceeds the preset value and is used to monitor the temperature of the garbage box to prevent high temperature and fire phenomenon.

(v) **Wireless communication module:** in the design, the data communication between the mobile terminal and the microcontroller is established by the Bluetooth technology in wireless communication. Bluetooth communication range is large, the cost is low, and its use is targeted, so it is very convenient to set up the relevant data communication, while other wireless communication is not suitable for either the cost or the APP device required for setting up the communication. In addition, the Bluetooth device used in the design has less power consumption, which requires less power consumption in similar communication devices. Because of the limitation of each module of the trash can, it is more reasonable to use the Bluetooth equipment.

(vi) **Steering gear drive module:** steering gear drive module through steering gear rotation simulates the dustbin switch cover. Its working principle is roughly as follows. First of all, the steering gear itself has a control signal and the driving signal is generated by the single chip microcomputer, to achieve the movement of different angles of rotation and to provide effective guarantee for the accurate lid opening of the trash can. This module is based on Bluetooth wireless communication to receive information from the upper computer, so as to determine which part of the steering gear to control the switch cover of the garbage bucket. It is controlled by the high and low level of the I/O output of the single chip microcomputer, and it drives the starting and stopping and reversing of the steering gear through the on-off of the control bridge arm. Then, the system determines which door is always open when no one is operating, and quickly feedback the information to the main control board. The main control board receives the information and controls the work of the steering gear. The steering gear rotates at a certain angle to complete the closing of the bucket cover, and the module basically completes the opening and closing of the trash can cover.

3. Deep Learning Algorithm Model

Super-resolution image reconstruction refers to the technology of converting existing low-resolution images into high-resolution images by means of software algorithms by means of signal processing and image processing [1]. Because high-resolution images have higher pixel density, they have richer texture features and sharper edge features, providing a better visual experience for users. The essence of super-resolution image reconstruction task is to produce corresponding images in high-resolution space as accurately as possible on the premise of providing low-resolution spatial data. In this paper, a deep learning-based approach is used to reconstruct high-resolution images by learning the mapping relationship between low-resolution space and high-resolution space. A Clique network super-resolution image reconstruction algorithm based on Laplace pyramid is the proposed structure, LCN. In order to maximize the communication between the convolution layers, more features are extracted. The Clique Block in CliqueNet was introduced into SR network, and the CliqueNet was further improved. The improved structure was named CNB as the building module of LCN. There are forward and feedback connections between any two convolution layers in the same CNB, and the information between layers is updated alternately so that the information flow and feedback mechanism can be maximized, and the connections between layers are denser. At the same time, the Laplace pyramid structure is used to gradually reconstruct the high-resolution image, and the reconstruction results are optimized step by step. Residual learning is applied to the network to reduce network parameters and avoid gradient explosion. From the experimental results, the super-resolution image reconstruction algorithm proposed in this paper produces good subjective and objective reconstruction results, especially in the reconstruction of edge and line.

3.1. The Clique Network of Laplacian Pyramid Structure. In this paper, a group network of Laplacian pyramid structure is proposed. Laplace pyramid structure has been widely used in image aliasing, texture synthesis, edge sensing and filtering, semantic segmentation, and other fields with good results. Therefore, the network in this paper adopts the Laplace pyramid structure, which can gradually optimize the reconstruction results by the way of gradual reconstruction of high-resolution images. At the same time, the improved group network CNB is used as the building module of Laplacian pyramid structure. Currently, CliqueNet is only used for advanced computer vision tasks (for example, object recognition). The network can maximize the communication between the convolution layers and extract more features. Therefore, this paper improves it and introduces it into SR network.

3.1.1. Overall Network Structure. The overall structure of the network is shown in Figure 1. I_{LR} is taken as the input of the system, and $I_{LR,S}$ is taken as the output of the s-level reconstruction network of the Laplace pyramid structure. Then, $I_{LR,S}$ can be obtained by the following formula:

$$I_{\mathrm{LR},S} = H_{\mathrm{LCN},S}\left(I_{\mathrm{LR},S-1}\right), \tag{1}$$

where $H_{\mathrm{LCN},S}$ represents the process of obtaining the s-level high-resolution image HR of Laplace pyramid, which can be a composite function. More details on LCN are given in Section 3.1.2.

3.1.2. Loss Function. As can be seen from Figure 1, ILR is the input low-resolution image, and it is assumed that θ is the set of network parameters to be optimized. Then, the goal of the network is to learn the mapping function F and generate the estimation image of the real high-resolution image:

$$\widehat{I}_{\mathrm{SR}} = f\left(I_{\mathrm{LR}}; \theta\right). \tag{2}$$

Let IR and S be the residual image of the sth level of the Laplace pyramid, ILSR and S are the low-resolution image directly magnified by the sth level of the Laplace pyramid, and ISR and S are the high-resolution image of the sth level of the Laplace pyramid. Then, at level S of the Laplace pyramid, the expected output high-resolution image can be modeled as follows:

$$I_{\mathrm{SR},S} = I_{\mathrm{LSR},S} + I_{R,S}\,. \tag{3}$$

The loss function of the network can be obtained as follows:

$$L\left(I_{\mathrm{SR}}, I_{\mathrm{SR}}; \theta\right) = \frac{1}{N}\sum_{i=1}^{N}\sum_{s=1}^{L}\rho\left(I_{\mathrm{SR},S}^{(i)} - I_{\mathrm{SR},S}^{(i)}\right), \tag{4}$$

where ρ is the Charbonnier function, N is the number of training samples in each batch, and L is the series of the pyramid. $I_{LR,S}$ is obtained by using the corresponding number of bi-cubic subsamples of real high-resolution images at different levels of the Laplace pyramid. According to formulas (2)–(4), each level has its loss function, and the total loss is the sum of the losses at all levels. This multiloss structure makes the residual of different response levels need to be deeply supervised and guide network training, so the network can predict the residual images of different levels and generate multiscale output images. Therefore, if the model in this paper is trained with an 8x magnification model, the super-resolution results of 2x magnification, 4x magnification, and 8x magnification can be obtained in a feedforward. This feature can be applied to resource-sensitive devices such as mobile devices or network applications.

3.2. Laplacian Pyramid Structure. In this paper, the network adopts Laplacian pyramid structure. As shown in Figure 1, each level of the pyramid structure contains two processes: feature extraction and image reconstruction. Because the low-resolution image and the high-resolution image share a lot of information, only the residual is studied in this paper. In the process of feature extraction, the residual image is obtained, and in the process of image reconstruction, the residual image is added to the low resolution image matrix to obtain the high-resolution image. Thus, the network parameters are reduced, which are advantageous to the gradient transmission and prevents the gradient from disappearing or exploding.

3.2.1. Feature Extraction. For a very deep network, it is difficult and impractical to directly output all the features extracted from each convolutional layer in LR space. Therefore, in this paper, CNB structure is designed as the building block of Laplacian pyramid structure so that more features can be extracted. In each level of the Laplace pyramid, feature extraction is composed of CNB building module, UPNet, and RNet. The input goes through the CNB building module, upsampling network, and residual extraction network in order to predict the residual image at the current pyramid level. The output of each upsampling network is connected to two different layers, one of which is used to extract residual images at the pyramid level, and the other is used as the input for feature extraction at the next level of the pyramid.

Taking $F_{0,S}$ as the s-level input of the Laplace pyramid, assuming that there are n CNB building modules in the s-level of the Laplace pyramid structure, the output of the NTH CNB building module, $F_{n,S}$, can be obtained by the following formula:

$$F_{n,S} = \begin{cases} H_{\mathrm{CNB},n}\left(H_{\mathrm{CNB},n-1}\left(\ldots H_{\mathrm{SFE}}\right)\right) \mathrm{if} S == 1 \\ H_{\mathrm{CNB},n}\left(H_{\mathrm{CNB},n-1}\left(\ldots F_{0,S}\right)\right), \mathrm{otherwise} \end{cases}, \tag{5}$$

where $H_{\mathrm{CNB},n}$ represents the feature extraction of the NTH CNB building module, which can be a composite function. More details on the CNB building blocks are given in Section 2.4. H_{SFE} represents the convolution operation of feature extraction performed by the network input I_{LR} through the shallow feature extraction network (SFENet).

After obtaining the detailed features extracted by the CNB building module, the upsampling network is used to carry out the upsampling. Then, the upsampling feature FUP, S, obtained at the s-level of the image can be obtained by the following formula:

$$F_{\mathrm{UP},S} = H_{\mathrm{UP}}\left(F_{n,S}\right), \tag{6}$$

where $H_{\mathrm{UP}}(\,)$ represents the convolution operation. Input $F_{\mathrm{UP},S}$ is the detailed feature obtained after n CNB building modules in the S level.

After the upsampling feature is obtained, the residual image is obtained by using the residual extraction network. Then, the residual image IR and S generated in the S level of the Laplace pyramid can be obtained by the following formula (7): where $H_R(\,)$ represents the convolution operation. The input is the feature $F_{\mathrm{UP},S}$ obtained by the pyramid s-level image through the upsampling network. So far, the s-level feature extraction of Laplace pyramid is completed:

$$I_{\mathrm{RS}} = H_R F_{\mathrm{UP},S}. \tag{7}$$

3.2.2. Image Reconstruction. In each level of Laplace pyramid, image reconstruction is mainly composed of UPNet and residual fusion. The input first passes through the upsampling network, and then, the upsampling magnified low-resolution image and the residual image obtained from the feature extraction branch are summed in pixels to produce the output image with high resolution. At the same time, the output high-resolution image is used as the input of the next pyramid to reconstruct the high-resolution image of the next pyramid.

At the pyramid $S(S \geq 1)$, when $S = 1$, the upsampling network is used to upsample the input low-resolution image. In addition, the upsampling network is used to upsample the high-resolution images generated at S-1 level. The amplified low-resolution image obtained after upsampling can be obtained by the following formula:

$$I_{\mathrm{LSR},S} = \begin{cases} H_{\mathrm{UP}}\left(I_{\mathrm{LR}}\right), \mathrm{if} S == 1 \\ H_{\mathrm{UP}}\left(I_{\mathrm{SR},S-1}\right), \mathrm{otherwise} \end{cases}, \tag{8}$$

where H_{UP} represents the convolution operation. The input I_{LR} is the low-resolution image, $I_{\mathrm{SR},S-1}$ is the output of the S-1 reconstruction network.

Finally, the low-resolution image $I_{\mathrm{LSR},S}$ obtained from upsampling is combined with the residual IR and S obtained from feature extraction to obtain the high-resolution image $I_{\mathrm{SR},S}$ of s-level pyramid reconstruction. S can be obtained from equations (2) and (3) above. So far, the super-resolution image reconstruction of Laplacian pyramid structure is completed.

3.3. CNB Building Module. Figure 2 shows a Clique Block module with four layers. Except for input nodes $F_{0,n,S}$ any two layers in the same Clique Block are bidirectional connected, that is, any layer is the input and output of another layer. Each Clique Block consists of two stages. The first stage is used to initialize all the layers in the Block. From the second stage, these layers will be extracted repeatedly.

Since this paper is designed specifically for image SR network. So, we are going to refine CilqueNet. First, we remove the batch standardized BN layer that consumes the same amount of GPU memory as the convolution layer, which increases the computational complexity and reduces the generalization performance of the network. Secondly, the existence of the pooling layer will cause the network to discard some pixel-level information, so we removed the pooling layer. Finally, we make full use of the layered features, which are neglected in CliqueNet networks, by using a local feature fusion (LFFNet) network to fuse all the features extracted in the second phase of the network k times. We refer to the improved structure as the CNB building block.

The 5-layer CNB building module designed in this paper is shown in Figure 3, including clique connected network and local feature fusion (LFFNet) network. In a clique connected network, except for input nodes, any two layers in the same CNB are bidirectional connected, and the layers are updated alternately. The first stage is used to initialize all the layers in the block. In the second stage, these layers will be extracted and updated repeatedly. Since more features are extracted in the second stage, in the local feature fusion network, we fuse the features extracted in the second stage for k times in the clique connected network as the input of the next CNB building module. CNB structure is shown in Figure 3.

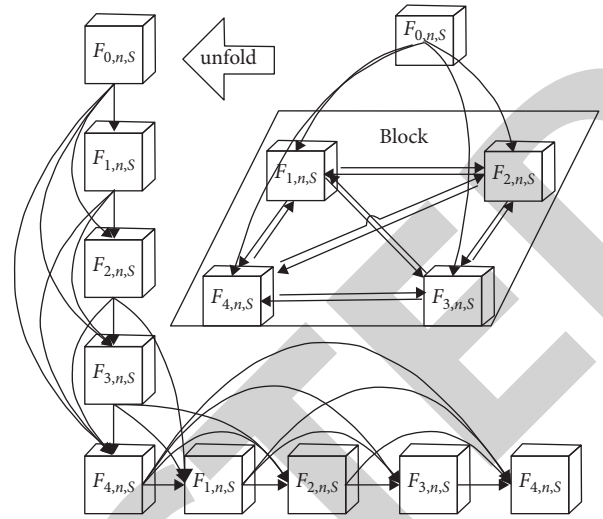

Figure 2: Clique Block structure.

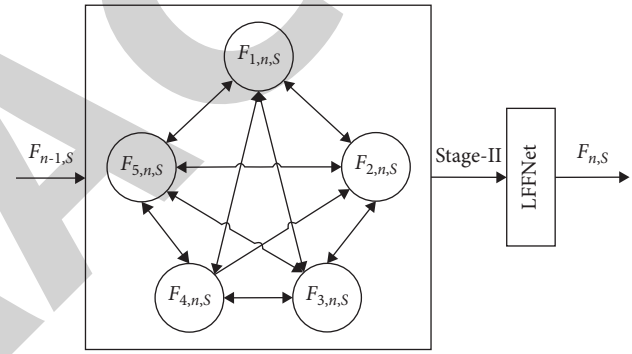

Figure 3: CNB structure.

3.3.1. Clique Connected Network. In the first stage, the input layer $F_{0,n,S}$ initializes all other layers in the CNB building block through a one-way connection, and each updated layer is connected to update the next layer. We set the update layer as the top layer and other layers as the bottom layer, and connect the corresponding parameters of the bottom layer. To facilitate the subsequent derivation of the general formula, we rewrote the input node $F_{n-1,S}$, as $F_{0,n,S}$. In the first stage, the input node in the NTH CNB in the pyramid S level is as follows:

$$F^1_{0,n,S} = F_{n-1,S}. \tag{9}$$

Therefore, in the first stage, the c-layer output of the NTH CNB building module in the pyramid S hierarchy can be obtained by the general formula:

$$F^1_{c,n,S} = \sigma\left(\sum_{l<c} W_{lc,n,S} * F^1_{l,n,S}\right), \tag{10}$$

where σ represents the nonlinear activation function, $*$ represents the convolution operation with parameter, $W_{ij,n,S}$ represents the weight between layers in the newer process, and $W_{ij,n,S}$ is reused in different stages, and each layer will receive feedback from the most recently updated layer.

Starting from the second phase, the layers are updated alternately. We also set the update layer as the top layer and the other layers as the bottom layer and connect the corresponding parameters of the bottom layer. Therefore, at the s-th level of the pyramid, when $c\,(c \geq 1)$ level, the k-th calculation is used. The output in the cycle can be obtained from the general formula:

$$F^k_{c,n,S} = \sum_{l<c} W_{lc,n,S} * F^1_{c,n,S} + \sum_{m>c} W_{lc,n,S} * F^1_{c,n,S}. \tag{11}$$

A delivery with five CNBS is shown in Table 1. It consists of two phases; the first phase is used to initialize all the layers in the block, and the second phase begins; these layers will be extracted repeatedly for k alternate updates.

3.3.2. Local Feature Fusion Network. In the second stage, more features are extracted, so the local feature fusion (LFFNet) network is applied. Local features extracted by cycles. In this paper, the core size of the convolution layer is 1×1 and the output information is adaptively controlled, so the output of the NTH CNB building module after fusion is F_{ns} which can be obtained by the following formula:

Table 1: Control table of policy parameters.

Tacit knowledge party	S knowledge innovation rate	0.05
	S knowledge aging rate	0.02
Knowledge receiver	R knowledge innovation rate	0.02
	R knowledge aging rate	0.02
	R knowledge integration and absorption capacity	(0,0.4)-(36,0.9)
	R network relationship ability level	Test parameters

$$F_{\text{ns}} = H_{\text{LFF}}^{k}\left[F_{c,n,S}^{1}, F_{c,n,S}^{1}, \ldots, F_{c,n,S}^{1}\right], \tag{12}$$

where $H_{\text{LFF}}^{k}(\,)$ represents the convolution operation. So far, feature extraction of the CNB building module is completed.

4. Simulation Experiment

According to the research objectives of this paper, the content of this section can be simulated from three aspects. First, adjust the level parameters of network relational capability to explore the influence on the effect of knowledge flow. The second is to adjust the absorptive capacity of knowledge integration and explore the influence on the effect of knowledge flow. Third, by changing the knowledge innovation rate of knowledge source and knowledge receiver, the law of knowledge flow in innovation market with different structures is explored.

4.1. Simulation Result Analysis of Network Relationship Capability Level. System policy parameters generally refer to constant and LOOKUP function. There are 6 policy parameters in this system, which are S knowledge innovation rate, S knowledge aging rate, R knowledge innovation rate, R knowledge aging rate, R knowledge integration and absorption capacity (denoted by LOOKUP function), and R network relationship ability level. In order to test the influence of the network relationship energy level of the knowledge receiver on the effect of knowledge flow, other policy parameters need to be controlled. Table 1 is the control table of other policy parameters, in which knowledge transfer situation is an auxiliary variable in the model, not an independent policy variable, so it is not specified in the table.

In this experiment, the knowledge innovation rate of S is 0.05, which is higher than that of R. S represents universities and R&D institutions in the collaborative innovation network, while R refers to core enterprises. Therefore, we can understand such an innovation market structure as the innovation market structure with universities and R&D institutions as the main innovation subjects. That is to say, for the core enterprises in our research, their innovative knowledge sources mainly come from universities and R&D institutions. Figure 4 is the simulation curve of the knowledge storage change of the corresponding knowledge receiver under the condition that other parameters remain unchanged and only the capability level parameter of the network relationship is changed.

Figure 5 is the simulation curve of the change of knowledge transferred by the corresponding knowledge receiver (enterprise) under the condition that other

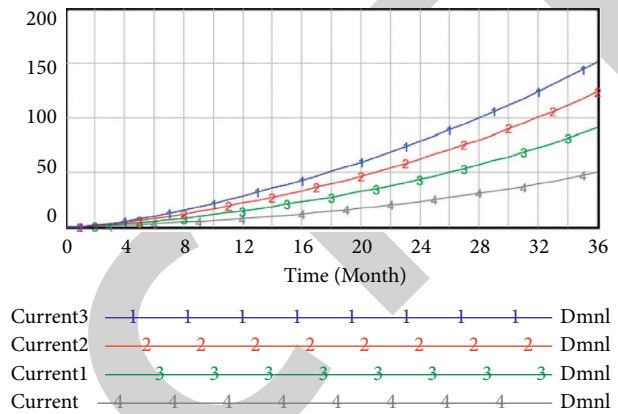

Figure 4: Simulation diagram of the relationship between network relationship capability and knowledge storage of the knowledge receiver.

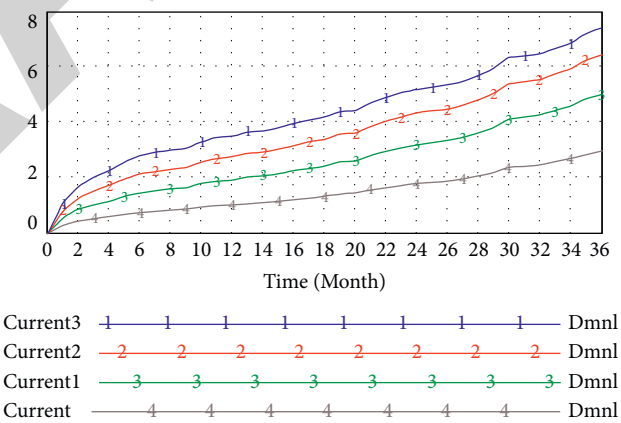

Figure 5: The simulation diagram of the relationship between network relationship capability and knowledge transfer quantity of the knowledge receiver.

parameters remain unchanged and only the network relationship capability level parameter is changed.

Diagram Current3/Current2/Current1/Current is represented by the curve, corresponding to the network relations ability level parameters for 0.8/0.6/0.4/0.2. It can be seen intuitively from the figure that, with the improvement of the network relationship capability level parameter, the r-transferred knowledge amount gradually increases in each period, and the increase of the transferred knowledge amount gradually decreases. For example, in the 18th month, the network relationship capability level parameter changes from 0.2 to 0.4, with an increase of 0.2 units. Knowledge transfer increased by about 0.7 units. When the network relationship capability level parameter changes

from 0.6 to 0.8, it also increases by 0.2 units, but the amount of transferred knowledge only increases by about 0.4 units, that is, the amount of transferred knowledge increases with the improvement of network relationship capability parameter, but it shows the characteristics of marginal decline. This reflects the ability level of the network relationship of the enterprise, which means the opportunity for the enterprise to exchange tacit knowledge with the outside world. This behavior makes the communication range wider, the enterprise knowledge search ability is stronger, and the enterprise is easier to find its own position in the market. However, when the network relationship capability of the enterprise reaches a certain level, with the increase of the number of weak relationships between the recipient enterprise and external knowledge sources, information redundancy will occur. In order to search for effective knowledge, the enterprise may have to pay a greater cost of information screening, which will reduce the efficiency of knowledge transfer of the enterprise. This also indicates that when the number of weak relationships between an enterprise and the outside world increases to a certain extent, it should pay more attention to the maintenance of strong relationships and the improvement of its own innovation ability.

5. Conclusions

In this paper, super-resolution image reconstruction algorithm, image denoising algorithm, and image warping correction algorithm of video preprocessing algorithm were studied and optimized based on deep learning. Later, though good results had been achieved, but also needed to continue to optimize the design, including the following: a Laplacian pyramid structure of the network super-resolution image reconstruction method. The experimental results verified that, in the subjective and objective effect, especially on the reconstruction of edge and line, the algorithm had good reconstruction. However, the network parameters and calculation amount increased, and the super-resolution amplification time was longer for maximum information flow and feedback mechanism and denser connections between layers, so further optimization is needed. Moreover, we also designed a fast image denoising algorithm based on OCT-Net, mainly on the Gaussian noise denoising processing; from the experimental results, the algorithm in different levels of Gaussian noise denoising obtained a good denoising effect and, at the same time, can effectively reduce the network computing resources. However, this algorithm is not effective in real noise removal, so it still needs further optimization. Furthermore, the DewarpNet image warping correction algorithm was optimized, designs the u-net ++ structure to optimize the shape network, and realizes the optimization of network parameters by pruning. However, the optimization algorithm cannot remove the regional shadows produced by the image warping well, so it still needs further optimization. Finally, the super-resolution image reconstruction algorithm was thoroughly studied and optimized and image denoising algorithm and image warping correction algorithm in the video preprocessing algorithm were also optimized. After that, it can add the research and optimization implementation of the algorithms such as fog removal, rain removal, and dither removal.

Data Availability

The data used to support the findings of this study are available from the corresponding author upon request.

Conflicts of Interest

The author declares that he has no conflicts of interest.

References

[1] W. W. Powell, K. W. Koput, and D. L. Smith, "Interorganizational collaboration and the locus of innovation: networks of learning in biotechnology," *Administrative Science Quarterly*, vol. 41, pp. 116–145, 1996.

[2] S. Interorganizational, "Relations in industrial systems: a network approach compared with the transaction cost approach," *International Studies of Management & Organization*, vol. 1, pp. 34–48, 1987.

[3] J. L. Cummings and B. S. Teng, "Transferring R&D knowledge: the key factors affecting knowledge transfer success," *Journal of Engineering and Technology Management*, vol. 20, no. l2, pp. 39–68, 2003.

[4] Y. Chen, H. Fan, and B. Xu, "Drop an octave: reducing spatial redundancy in convolutional neural networks with octave convolution," in *Proceedings of the International Conference on Computer Vision and Pattern Recognition (CVPR)*, pp. 3435–3444, IEEE, Long Beach, CF, USA, November 2019.

[5] K. He, X. Zhang, and S. Ren, "Deep residual learning for image recognition," in *Proceedings of the International Conference on Computer Vision and Pattern Recognition (CVPR)*, pp. 770–778, IEEE, Las Vegas, CF, USA, November 2016.

[6] U. Schmidt and S. Roth, "Shrinkage fields for effective image restoration," in *Proceedings of the International Conference on Computer Vision and Pattern Recognition (CVPR)*, pp. 2774–2781, IEEE, Columbus, OH, USA, September 2014.

[7] S. Gu, L. Zhang, and W. Zuo, "Weighted nuclear norm minimization with application to image denoising," in *Proceedings of the International Conference on Computer Vision and Pattern Recognition (CVPR)*, pp. 2862–2869, IEEE, Columbus, OH, USA, September 2014.

[8] O. Ronneberger, P. Fischer, and T. Brox, "U-net: convolutional networks for biomedical image segmentation," *Lecture Notes in Computer Science*, Springer, Munich, Germany, 2015.

[9] G. Huang, Z. Liu, and L. Van Der Maaten, "Densely connected convolutional networks," in *Proceedings of the International Conference on Computer Vision and Pattern Recognition (CVPR)*, pp. 4700–4708, IEEE, Honolulu, HW, USA, July 2017.

[10] A. Capaldo, "Network structure and innovation: the leveraging of a dual network as a distinctive relational capability," *Strategic Management Journal*, vol. 28, no. 6, pp. 585–608, 2007.

[11] T. E. Smart, "Network positions and propensities to collaborate; an Investigation of strategic alliance formation in a high-technology industry," *Administrative Science Quarterly*, vol. 43, no. 3, pp. 668–698, 1998.

[12] A. K. Gupta and V. Govindarajan, "Knowledge flows within multinational corporations," *Strategic Management Journal*, vol. 21, no. 4, pp. 473–496, 2000.

Hindawi
Journal of Mathematics
Volume 2024, Article ID 9857325, 1 page
https://doi.org/10.1155/2024/9857325

Retraction

Retracted: Digital Effectiveness in Video Conference Methods on Internet Learning Environments of Higher Education

Journal of Mathematics

Received 23 January 2024; Accepted 23 January 2024; Published 24 January 2024

This article has been retracted by Hindawi following an investigation undertaken by the publisher [1]. This investigation has uncovered evidence of one or more of the following indicators of systematic manipulation of the publication process:

(1) Discrepancies in scope

(2) Discrepancies in the description of the research reported

(3) Discrepancies between the availability of data and the research described

(4) Inappropriate citations

(5) Incoherent, meaningless and/or irrelevant content included in the article

(6) Manipulated or compromised peer review

The presence of these indicators undermines our confidence in the integrity of the article's content and we cannot, therefore, vouch for its reliability. Please note that this notice is intended solely to alert readers that the content of this article is unreliable. We have not investigated whether authors were aware of or involved in the systematic manipulation of the publication process.

In addition, our investigation has also shown that one or more of the following human-subject reporting requirements has not been met in this article: ethical approval by an Institutional Review Board (IRB) committee or equivalent, patient/participant consent to participate, and/or agreement to publish patient/participant details (where relevant).

Wiley and Hindawi regrets that the usual quality checks did not identify these issues before publication and have since put additional measures in place to safeguard research integrity.

We wish to credit our own Research Integrity and Research Publishing teams and anonymous and named external researchers and research integrity experts for contributing to this investigation.

The corresponding author, as the representative of all authors, has been given the opportunity to register their agreement or disagreement to this retraction. We have kept a record of any response received.

References

[1] Y. Wei and H. Tang, "Digital Effectiveness in Video Conference Methods on Internet Learning Environments of Higher Education," *Journal of Mathematics*, vol. 2022, Article ID 6996407, 6 pages, 2022.

Hindawi
Journal of Mathematics
Volume 2022, Article ID 6996407, 6 pages
https://doi.org/10.1155/2022/6996407

Research Article

Digital Effectiveness in Video Conference Methods on Internet Learning Environments of Higher Education

Yanhong Wei and Huili Tang

Zhengzhou Preschool Education College, Zhengzhou 450000, China

Correspondence should be addressed to Yanhong Wei; yanhongwei_edu@aliyun.com

Received 27 November 2021; Revised 28 December 2021; Accepted 3 January 2022; Published 17 January 2022

Academic Editor: Naeem Jan

Information and communication technologies, especially modern transmission technologies, for instance, teleconferencing, widely known, provide premium educational and pedagogical opportunities, contributing significantly to the implementation of a collaborative learning environment. That the utilization of video conferencing differs significantly from conventional teaching should be emphasized in a way of leading adaptation to the requirements of the educational environment. In general, the digital efficiency of teleconferencing methods needs to be investigated as a very important factor when it is implemented effectively in online learning environments under the title of modern higher education. This paper has aimed at investigating the ways of effective utilization of video conferencing in an online learning environment and presents a case study following the principles of educational neuroscience and distance education that are related to appropriate utilization of available digital technologies to function as educational and learning means to promote the usage in the framework of higher education.

1. Introduction

Distance education [1] has currently used various digital tools that have been directed to new paths including new principles to meet the needs of contemporary digital life. The most important contribution of the use of technology in learning is the facilitation of communication and the provision of appropriate means so that teachers and learners acquire new communication skills intertwined with modern e-learning environments [2].

Given that communication in the era of digitalization has been transforming educational practices, it is certain that they also affect the learning process by offering more opportunities to exchange ideas, information, and knowledge, but also critical analysis, collaboration, active participation, and access to the worldwide wealth of innovations and ideas. A prerequisite, however, for their effectiveness is the new technologies to be used with a specific design in the learning process, adapted to the personal needs of each learner [3].

One of the most common communication practices in the daily life of modern society, especially in times of pandemics, is teleconferencing [4]. Video conferencing is about real-time audio and video communication between people who are geographically remote and can exchange data, files, and applications. The particular importance for education is the interactive video conference in which participants build knowledge through their active and collaborative participation in a dynamic digital interactive environment.

Teleconferencing resembles the conditions of distance learning that are very close to those of physical learning, providing audiovisual stimuli (verbal and nonverbal) that reduce the isolation of learners. Audiovisual stimuli can enhance the socioemotional interaction of participants with asynchronous ways of communication, promoting their interpersonal relationships and cooperation.

Similar to other ways of e-learning, the application of video conferencing should have a customized and specific

design, utilizing pedagogical criteria to enhance the quality of both learning and teaching processes.

However, teleconferencing has not been particularly investigated either in terms of the pedagogical principles of distance education or at the individual or the group level.

The objective of this paper is to investigate the relationship between theories, principles, and cognitive approaches of audiovisual learning [5]. Besides, perception of the learning process through teleconferencing with the combination of both distance education and learning environments in higher education framework is examined [6]. In particular, both importance of visual perception and learning are highlighted to reduce the perceived interactive distance that enhances the learning process through video conferencing. An appropriate case study examining the practice of the breakout rooms [7, 8] as a tool to optimize participation in terms of knowledge, thoughts, approaches, needs, and feelings for learning is provided.

Therefore, this paper has aimed at investigating the ways of effective utilization of video conferencing in an online learning environment and presents a case study following the principles of educational neuroscience and distance education that are related to appropriate utilization of available digital technologies to function as educational and learning means to promote the usage in the framework of higher education.

The rest of the manuscript is organized as follows: Section 2 is devoted to reviewing the relationship between neuroscience and digital learning concerning the theories developed. Section 3 reviews the issues that existed in the environment of Internet learning concerning the perspective of neuroscience. A case study is presented in Section 4. Section 5 provides a discussion of the findings of the case study. Section 6 presents the conclusion of the research and potential further studies.

2. Neuroscience and Digital Learning

Learning, as a process, has been identified among others by cognitive approaches [9] related to neuroscience that studies the brain and nervous system interdisciplinary, including elements from scientific disciplines such as biology, medicine, psychology, and computer science. Neuroscience combined with the scientific disciplines of education and cognitive psychology forms educational neuroscience [10] that contributes to the comprehensive understanding of the learning process of human beings and leads to the improvement of educational methods and techniques.

The plasticity of the brain is the basic function of the body that serves the learning process in the perspective of neuroscience. The adaptation of the brain to the stimuli of the environment leads to the achievement of learning [11]. More specifically, learning is achieved by devising mental representations through the neuronal activity of the brain. The stimulus of the environment causes the construction of specific synapses in the nerve cells of the brain, which are transformed into movements, senses, emotions, and intellect. This recording of stimuli in connection to neurons is done with both specific pathways and the help of specific organs of the nervous system. The fact that the synapses of nerve cells are altered, additionally or subtractively, also proves the contribution of brain plasticity to human learning.

To achieve learning, specialized centers of the brain work together to coordinate the activities of different neural networks and different brain regions to which different brain functions correspond. Neuroscience approaches learning through perception and memory [12, 13]. Perception is created by transferring sensory stimuli to the brain's memory for processing. Hence, perceptual learning, which refers to the improvement of the individual in distinguishing sensory stimuli, affects his emotions and learning behavior. Ultimately, the stimuli of the environment are filtered by thoughts, ideas, values, habits, attitudes, and feelings to be transformed into perception.

Visual perception, more specifically discussed in [14], is formed through the sensory pathway of vision and refers to the adaptation of the brain to any change in visual reality. It is influenced by specific elements of visual communication such as balance, color, shape, movement, and dimensions of visual elements. It is also governed by specific laws, theories, and principles [15] such as the laws of hierarchy, the Gestalt theory [16], the empiricism theory, the Marr computational theory [17], the Gibson ecological theory, empathy theory [18], and neurophysiological theory. Thus, designing more effective educational learning environments and relevant educational material is contributed by those theories.

The memory of the brain is the focus of the learning process [19] since information is processed and stored or rejected. Information processing theory [20] states that the brain functions in a serial manner like a computer. Sensory information ends up in sensory memory to be transmitted and stored in long-term memory. Shape theory [21] satisfactorily explains the mechanism of information storage in the brain, while contributing to the development of educational techniques that can facilitate learning. "Shapes" are nothing more than cognitive structures (conceptual representations) in which information elements are organized in various ways. While sensory stimuli are processed, the internal representations that the person already has stored in his brain play an important role that defines his psychoemotional state.

The theory of dual coding [22] distinguishes the information that the brain processes into verbal and nonverbal. While verbal stimuli are coded in the form of words, events, ideas, and concepts, nonverbal stimuli are coded as visual, auditory, emotional, and tactile "images." Hence, nonverbal messages can be linked to corresponding verbal messages and construct internal cognitive or mental representations, which are essentially neural circuits created by connections between specific neurons in the brain. The cognitive representations that are created remain inactive until they are activated or consciously connected to some new external information. The result of the variety of connections between verbal and nonverbal information is the empowerment of learning facts, words, and information in the brain. On the other hand, the limited capacity of memory led to the cognitive load theory [23] and the theory of multimedia

learning [24], which suggest ways to maximize its productivity. Cognitive load theory suggests ways to maximize memory productivity while minimizing information that is unrelated to learning objectives or distracting learners. The success of the application of this theory in the learning process depends mainly on the knowledge of the teacher about the cognitive process. Considering the factors affecting negatively the working memory such as the emotional factors and the volume of the teaching material, the appropriate and individualized modification in the types of cognitive loads can be achieved for effective processing of the new information.

The theory of multimedia learning focuses equally on the processing of audiovisual stimuli by the brain. However, it gives special importance to active learning and the involvement of learners in such a way of processing both audiovisual and verbal stimuli during the learning process. This theory suggests that learning becomes more effective when there is a combination of verbal messages and images. Thus, it aims to enhance the cognitive process without overloading the visual or auditory channel through which the corresponding stimuli are processed. The important point is that both theories highlight the importance of proper educational planning and contribute to enhancing learning effectiveness factors that are crucial in distance learning education.

Video conferencing, as a multimedia communication tool, utilizes both audio and video for the interaction of participants. Audiovisual learning theories provide an important medium since teachers can design more effective distance education programs with the help of it. Hence, enhancing audiovisual learning in distance education contributes to the optimal support and guidance of learners and strengthens the learning experience as a way of better knowledge extraction.

The trainer needs to focus on the issues in the context of online learning that can be summarized as follows:

(1) The active participation of the trainees in the learning process

(2) The integration of the evaluation of the trainees in the educational process

(3) The utilization of the teaching barriers of the trainees

(4) The multidimensional approach of both presentation and the activities that will be assigned to the trainees

The teacher's focus on the aforementioned needs should be properly employed when designed and executed in the educational environment.

3. Environments of Internet Learning

The working or learning environment in contemporary e-learning settings plays a crucial role. The findings of educational neuroscience [25–27] suggest that the information captured by the brain is first processed in the parietal system of the brain, which is a neuroanatomical background for the expression and perception of emotional states, mobilization, and the emotional part of the memory process. Long-term memory and learning are significantly affected by this system. Thus, some issues, for instance, stress and threat, in the context of learning have negative effects on learners.

To this end, the learning environment containing positive emotional experiences and connections helps learners contribute to their learning process [28]. The four focused areas were expressed in the previous section, namely, active participation, assessment integration, learning barriers, multidimensional approach. Discussing two more issues related to the work-learning environment became important. While the first issue is called the "speed" with which an online classroom operates, the second concerns the cooperation among learners. The speed with which the online classroom "runs" plays a crucial role in terms of creativity and flexibility. Hence, how learners acquire knowledge from their active participation in the course is thought of significant. The current findings in the field of neuroeducation [29] suggest that working under pressure causes stress and the impression on learners considering that "my mind has stopped working." Therefore, speed affects both learning and the brain.

The research suggests that when learning is undertaken at a fast pace, existing synapses can be strengthened and neural circuits are activated. However, they can weaken just as active participation, integration of assessment, exploitation of didactic barriers are quickly forced. Thus, the multidimensional approach cannot be fully implemented. On the contrary, it seems that learning is enhanced when learners approach concepts and ideas with creativity and flexibility. Therefore, it is suggested that the online learning environment is important to function in such a way of providing learners with the time that they need to be creative. Students need to engage in activities to improve procedural knowledge to reduce the simple reproduction/memorization of information. Thus, lowering the value of speed in online learning is a better approach to take since the development of synapses and neural circuits is a complex and multidimensional process.

Technology contemporarily provides the means for the realization and implementation of online collaborative actions. The ability to utilize virtual rooms is one of the means that can enhance collaboration between learners. In addition, teachers can assign group works by varying the content per group of learners.

In online classrooms, collaborations between learners are important since they allow them to share their concerns and ideas and study the problems successfully that have been assigned. Hence, they help them understand and recognize how other people work. Specifically, a collaboration between learners helps them recognize some or many learning difficulties in the context of learning. Learners will therefore be able to think critically about their learning process and realize how similar or identical problems/obstacles that they experience must be overcome. In addition, learners can make connections and express opinions between ideas, allowing them to explore new ideas and cooperate to solve problems.

The findings in the field of neuroscience [12] suggest that when people work together, the inner cortical cortex and the

frontal cortex network get activated, thus enhancing the development of executive functions. Therefore, these areas of the brain are also referred to as the "social brain" and demonstrate the value of the sociocultural approach to learning and the need to provide students with opportunities for collaboration. Collaboration is, therefore, a complex issue that plays a crucial role in learning, achieving goals, and developing the brain.

Online learning provides a proper framework for collaboration, allowing learners to be split into breakout rooms and assigned teamwork to make decisions and prepare for the virtual plenary presentation. Briefly, the digital effectiveness of the video conference by utilizing breakout rooms in higher education is presented in the following case study.

4. Experiments

Breakout rooms are thought of not as supportive and favorable as imagined previously when a large number of participants attend since several educators consider it as not providing a good level of interaction among the participants of webinars. Thus, reluctance is observed widely among educators. On the other hand, the recent developments of webinar technology have led to various tools specifically designed that aimed at making participants more active. Besides, the breakout room, as a tool, is found to be more superior to what it was thought of.

Breakout rooms represent virtual classrooms like webinar sessions that allow collaboration between a limited number of webinar participants. Therefore, the teacher can develop specific exercises/tasks and divide the webinar sessions into different places where participants can cooperate in some group work and stay away from other groups. The teacher can attend the breakout rooms to supervise the trainees' work or to participate in a specific place when needed by the request of the participants. Breakout rooms can be used to resolve problems, develop arguments on a specific topic, etc. The exercises/tasks assigned to different groups may be different, or the teacher may give a single problem to be tackled and stimulate competitiveness between teams by providing specific incentives for the team who will provide the right solution first.

Then, the results of the work done in the different breakout rooms can be shared with all the other participants in the main webinar session. Therefore, the feature of breakout rooms is the facilitation of the most creative engagement of the participants in the webinar through the interaction with their peers and the promotion of quality teamwork in the virtual environment.

In this particular case study, the instructor uses breakout rooms and other tools available to support the learning process such as private chat, public chat, and private digital board in such a way that learners actively participate and have multiple opportunities to engage with the team. It should be noted that this study was conducted 6 times in an online class of 20 college students who were familiar with the tools of distance learning. Breakout rooms were also devised randomly with a maximum participant of 4 people in each room.

More specifically, the instructor directed the trainees to a question or a problem to explore and ask them to send him/her the answer through private written conversation (the answer was the cooperation of the students of each room). The outcomes of the process result in the following:

(1) All the trainees participate in the activity since they as a group must respond to the trainer

(2) If a group sends the wrong answer through the private written conversation, the instructor asked them to try to solve it again

(3) The trainees are not "exposed" to the whole class, but only to their group

(4) All groups had to submit their answer at a predetermined time as they do not have access to the answers of others

With this approach, the phenomenon of "agree" is eliminated since learners cannot agree with the previous answer. However, it is a common practice in the physical classroom, which is not possible in this setting, since learners hear the answers of others and express their opinions with either agree or disagree. The application of this approach contributes to the enhanced involvement of the trainees and the satisfaction of the latter for active participation in the online course through small groups.

Afterward, the instructor brought the students back to the plenary session to further negotiate a specific issue, utilizing the learners' answers and developing a collaborative framework that further encouraged online collaborative learning after completion of the first task.

In the second task, the trainer asks for the answers of the new groups that were separated in breakout rooms through the written conversation of the group but asks them not to send their answer until he tells them to send it. In this way, all groups participate and must complete the activity independently without being able to see the response of others. In this case, there is a risk of exposure of learners in the group so something needs to be pedagogically managed by the instructor in the classroom, while, on the other hand, each group is allowed to directly compare the answers with the answers of the other groups.

The third task involved the utilization of digital boards in multiple groups (one for each new room). More specifically, each group works on its board, compiling its response and receiving differentiated support from the trainer according to their needs. In this way, the participation of all trainees is achieved without exposure in the classroom.

The above approaches to the operation of the simultaneous online classroom contribute to both the active involvement of all learners and the increase of their participation in small groups. Thus, the possibility of activating synapses and neural circuits is expected based on the result of the opportunities to gain experience and build knowledge increment to a high degree in contrast to a passive process where the learner can hear and/or see with or without multimedia applications such as a simple presentation or lecture.

In the context of constructing, consolidating, storing, and retrieving the new knowledge, the instructor with the offered digital means carried out diagnostic, formative, and final evaluation for each student. Specifically, the instructor using the voting with right/wrong type questions, multiple-choice questions, and matching sentences evaluated the students while allowing them to strengthen their memory to reflect on what they know and what they have understood as well as to identify their personal needs. The evaluation was done in the form of voting where only the instructor sees the students' answers so that there is an attractive framework for participation.

It should be noted that the questions were structured in such a way that consisted of more than one correct answer. Hence, this technique increases the curiosity of the trainees and enhances their participation. The completion of such a process and the answers given by the trainees make the instructor construct new working groups and redefine his teaching practice to meet the needs of the trainees based on more evaluative criteria. In addition, while the development of the brain is further enhanced by making good use of the teaching obstacles, grading has been shown to enhance their interest since the mistakes presented by the instructor resulted in a high degree of grading success. This process was achieved during online learning in which learners needed to be even more actively involved in the learning process to improve or maintain their grades.

Also, the opportunity was given through interactive discussion of the educational subjects to identify failures or mistakes within the group. Hence, the opportunity is given to trainees to review both individual and collaborative mistakes to overcome specific didactic obstacles that lead to misunderstandings. This assessment was made by personal teleconference with the instructor in the form of a press conference for each trainee.

Finally, the trainees were allowed to illustrate how they worked through the presentation. Besides, how each group focuses on their works to identify and correct mistakes by highlighting their strategies was presented. We believe that the strategies identified can be supportive for other learners that allow them to acquire and develop different skills by observing other groups and modeling their behaviors and actions in future respective assessments.

5. Discussion

In this paper, the value and the ways of effective utilization of video conferencing in an online learning environment were presented with a case study following the principles of educational neuroscience and distance education, so that they can function as educational and learning aids appropriate to further examine the objectives of higher education based on the use of available digital technologies. Given the theory of televised proximity that "places" the group of learners in a teleconferencing environment, a successful educational experience with teleconferencing has been shown, which leads to the maximum possible learning outcomes based on the proper coexistence of teleconferencing, televised-teaching, and televised-social presence.

It was also suggested experimentally that the televised-cognitive presence in the televised-learning contains all those elements and actions that activate the cognitive function of the learners. Hence, the proper planning of the educational process and the way of presenting the content are necessary, which is a key conclusion emerging from the case study in this manuscript.

Furthermore, the principles of neuroscience and the theories of audiovisual learning applied to lifelong learning have practically suggested that adaptation to the environment of distance education has many better consequences for learners. The outcomes of the case study highlight the importance of the effect of audiovisual learning on specific pedagogical parameters, such as interactive distance, autonomy, structure, dialogue, communication, but also on emotional expression, learning climate, and knowledge acquisition in a collaborative environment.

In conclusion, proper planning of the educational process can lead to reducing distance issues and enhancing the learning process through appropriate actions related to autonomy, structure, and dialogue. At the same time, the way the content is presented in the video conference brings the transmission of audiovisual messages, participation, and interaction, once the benefits of the software are fully utilized. The educational process can be a springboard for a more effective and efficient learning system. Correspondingly, the audiovisual messages (verbal or nonverbal) through their corresponding presentation activate the appropriate areas of the participants' brains. Therefore, the application of the principles of neuroscience, information processing theory, and the theory of shape can help determine how information is stored in long-term memory achieving more efficient learning. Finally, the audiovisual messages shaping the visual perception, in turn, affect the dialogue and lead to the creation and expression of emotions that might be common to all participants in the teleconference. Hence, the logical thinking of the learners is influenced by the transmission of emotions and imitation of the teacher's thoughts.

The empirical techniques proposed on this basis construct the relationship between the learning process in video conferencing and visual perception. Moreover, the educational process will highlight the value of the audiovisual implementation.

6. Conclusions

What the current research implies is that the proper planning of the educational process and the means used for presenting the content should be devised properly, which is one of the results of the case study in this manuscript. Moreover, the principles of neuroscience and the theories related to audiovisual learning contribute practically to the adaptation of the environment of distance education and result in many better consequences for learners such as interactive distance, autonomy, structure, dialogue, communication, emotional expression, learning climate, and knowledge acquisition in a collaborative environment.

Hindawi
Journal of Mathematics
Volume 2024, Article ID 9807051, 1 page
https://doi.org/10.1155/2024/9807051

Retraction

Retracted: Personalized Education Based on Hybrid Intelligent Recommendation System

Journal of Mathematics

Received 23 January 2024; Accepted 23 January 2024; Published 24 January 2024

This article has been retracted by Hindawi following an investigation undertaken by the publisher [1]. This investigation has uncovered evidence of one or more of the following indicators of systematic manipulation of the publication process:

(1) Discrepancies in scope

(2) Discrepancies in the description of the research reported

(3) Discrepancies between the availability of data and the research described

(4) Inappropriate citations

(5) Incoherent, meaningless and/or irrelevant content included in the article

(6) Manipulated or compromised peer review

The presence of these indicators undermines our confidence in the integrity of the article's content and we cannot, therefore, vouch for its reliability. Please note that this notice is intended solely to alert readers that the content of this article is unreliable. We have not investigated whether authors were aware of or involved in the systematic manipulation of the publication process.

In addition, our investigation has also shown that one or more of the following human-subject reporting requirements has not been met in this article: ethical approval by an Institutional Review Board (IRB) committee or equivalent, patient/participant consent to participate, and/or agreement to publish patient/participant details (where relevant).

Wiley and Hindawi regrets that the usual quality checks did not identify these issues before publication and have since put additional measures in place to safeguard research integrity.

We wish to credit our own Research Integrity and Research Publishing teams and anonymous and named external researchers and research integrity experts for contributing to this investigation.

The corresponding author, as the representative of all authors, has been given the opportunity to register their agreement or disagreement to this retraction. We have kept a record of any response received.

References

[1] F. Zheng, "Personalized Education Based on Hybrid Intelligent Recommendation System," *Journal of Mathematics*, vol. 2022, Article ID 1313711, 9 pages, 2022.

Hindawi
Journal of Mathematics
Volume 2022, Article ID 1313711, 9 pages
https://doi.org/10.1155/2022/1313711

Research Article

Personalized Education Based on Hybrid Intelligent Recommendation System

Fangxia Zheng

Zhengzhou Preschool Education College, Zhengzhou, Henan 450000, China

Correspondence should be addressed to Fangxia Zheng; 20152852@stu.nun.edu.cn

Received 10 November 2021; Accepted 7 December 2021; Published 17 January 2022

Academic Editor: Naeem Jan

Differentiated pedagogy is a flexible and organized adaptation of teaching and learning as it argues that students, even those of the same age, have differences in learning readiness, interests, learning style, experiences, and living circumstances. These differences are important in the determination of requirements of their learning and the way of effective learning. In addition, the foundation for effective learning is the sense of community within the classroom, the authentic learning opportunities of using educational equipment, and the connection of the lesson with the experiences and interests of the students. In essence, the support of a teacher guides the pupils to learn to work on their own during a declining guidance policy, to improve their abilities and skills. Thus, the teachers are asked to modify their teaching methods instead of applying a similar way of teaching for all students. The modified teaching style should meet the different levels of readiness of students, the different ways they learn, and their different interests. In support of this specific task for teachers, the current work presents a personalized education system based on hybrid intelligent recommendations. Specifically, a hybrid framework of artificial intelligence is proposed, which focuses on the way to provide targeted recommendations for the implementation of integrated standard lesson plans, which will be the main tool for creating flexible differentiated pedagogical programs that will perfectly meet the personal needs and particularities of each student.

1. Introduction

Differentiated pedagogy is the adaptation of teaching so that teachers respond to the different needs of students in mixed ability classes considering the differences of students in terms of their interests, their learning style, and their degree of readiness. Each student is treated as a unique entity. Opportunities are offered to demonstrate his/her skills in order to recognize his/her strengths. The choice of a teacher, regarding the form of differentiation, depends on the students that he addresses. In other words, it depends on the context he is dealing with, each time [1]. In addition, the differentiation of teaching is not a recipe to be applied but a method that treats students as biographies and meets the needs of each student. The teacher modifies his teaching method as well as the learning activities to maximize the learning opportunities in the classroom.

Differentiated pedagogy focuses on learning processes, i.e., the way children learn, but does not focus on the results. The teacher aims to form a flexible framework where each student follows his learning path, which provides him with a margin of autonomy, while the goal is common to all [2]. Students are active in the learning process and participate in any way they can, which boosts their self-confidence. They work in groups where everyone contributes according to their levels and interests. However, the fact of permitting the mistakes without punishment provides the students an acceptable feeling which leads them to try new things. At the same time, the teacher who differentiates his teaching utilizes the experiences and interests of the students, encourages them to work independently, but all together enhances the interactions between them. He believes in the potential of all the students and the right to difference. Also, he acts as a facilitator and mediator in the classroom. Similarly, the students in such situations feel that the teacher trusts them, is permissive in their choices and mistakes, and finds motivation and interest in learning [2].

The teacher should also consider the sources of the heterogeneity of his class, i.e., the socio-economic level and cultural background of the parents and the attitude of the children toward the school. In addition, the teacher attempts to create good and strong relationships with his students. He also makes efforts to treat them as individuals and not only as students. He should also be aware that the need of students beyond the learning part is transferred to their emotional need for social interaction and the development of real relationships both with him and with each other. Finally, it is necessary to provide opportunities for meaningful dialogue and discussion. It is also important to strive to develop the feelings of belonging to a group that is governed by meritocracy and transparency [3]. Moreover, the essence is to emphasize that learning to plan as a methodology lets teachers to make decisions with more details such as the process of designing the sequences of learning and teaching activities that are pedagogically oriented and making appropriate use of the respective educational resources and available technologies. Supporting teachers in their role as learning planners is an issue of the research community that has developed around the field as it has been recognized as the key to success and improving the quality of the educational process [4]. In this way, differentiated pedagogy can be the founding stone of knowledge, maximizing motivation mechanisms for the development of individual skills and interests, the promotion of self-action and initiative, the comprehensive development of the individual, and the strengthening of cooperation and social learning. In differentiated teaching, the student tests ideas in practice, sees the correlation between the parts and the whole, and correlates the studied subject with his experiences and other subjects, while he is allowed to participate in the process to experience the joy of desire and learning [5]. Teachers, in such a process, ensure that each student, as he develops, competes with himself and not with his classmates while carrying out continuous evaluation and updating of the educational process. Also, students find the school interesting when it meets their learning ambitions. It is important to mention the fact that, in the context of differentiated pedagogy, the need to recognize the different cultures of students and the provision for its promotion and equal treatment of children from different cultural backgrounds is imperative [6].

In recent decades, differentiated pedagogy has been repeatedly promoted in the relevant research literature. Besides this, it also guides teaching approaches and practices published in the framework of international or national organizations and institutions. In contrast, technology-based approaches that incorporate new methods in the context of diversified pedagogy implementations are minimal in the international literature.

The next section reviews the related literature. In Section 3, the proposed systems are comprehensively explained in stepwise manner. The experimental evaluation is carried out in Section 4. Section 5 presents the discussion, and Section 6 concludes the study.

2. Related Literature

A typical example of the implementation of pedagogical strategies that are adapted to the real individual skills of students is the adaptive educational systems (AES) that adapt their teaching content to the educational needs and skills of students. Demertzi et al. [7] proposed a new adaptive educational e-learning system (AEeLS) that can collect and analyze data from learning repositories and adapt it to the curriculum according to students' skills and experience. It is a new hybrid machine learning system that combines a semi-supervised classification method for matching educational ontologies and a recommendation mechanism that uses a hybrid method of content-based filtering techniques to provide a personalized learning environment for each student. Urdaneta-Ponte et al. [3] in 2021 conducted a systematic review of academic research on recommendation systems that support educational practices to learn more about the types of education and areas addressed, the developmental approach used, and the elements recommended, as well as identifying any gaps in the field for future research. The review included 98 articles, of which it was determined that the majority are geared toward recommending educational resources for users of formal education, with the collaborative approach, content-based approach, and hybrid approach the most common approaches used in recommendation systems, emphasizing the utilization of machine learning in the last two years. Bourkoukou et al. [8] proposed a tailored E-learning system based on Felder and Solomon's psychological model and appropriate collaborative filtering algorithms. They wanted to create an adaptive curriculum that used appropriate learning scenarios to meet each learner's unique needs. They used the idea of making predictions about a learner's preferences or tastes based on the preferences of a group of similar learners.

The system suggests the initial learning technique after determining the learning style using a questionnaire. This occurs when there is a dearth of information about the learners and their preferences, making it unable to offer appropriate recommendations. Gulzar et al. [9] demonstrated a recommendation system that proposes and leads a learner in choosing the appropriate courses for their needs. The goal of this research is to build and construct a hybrid recommender system that can be incorporated to improve the effectiveness of any E-learning system, make the material more accessible, and give learners more personalized experiences.

To obtain important information and produce correct suggestions, the hybrid technique was combined with ontology. Learners may benefit from such an approach if they want to improve their performance and happiness. The outcomes of this study's experiments suggest that using RS to select courses works well. Bourkoukou and Bachari [10] described LearnFitII, an adaptive learning system that can automatically adjust to learners' changing preferences. The goal of this project is to propose a personalized framework that uses a hybrid-based recommendation strategy to provide suitable recommendations and to cope with the cold-

start problem, which occurs when there is a lack of knowledge about a new learner. Through testing the psychological model of learners and mining their server logs, the system recognizes different patterns of learning style and habits. Using the Felder and Silverman model, the device first provided a personalized learning scenario to address the cold-start problem, and then it mined information about learners' activities and interactions to assess the habits and preferences of the learners.

Finally, using a hybrid recommender system based on k-nearest neighbors and association rule mining methods, the learning scenario is examined and revised. The system's findings in real-world settings show that considering the learner's preferences improves learning quality and satisfies the learner. Bhaskaran et al. [11] developed a split and conquer strategy-based clustering to create an intelligent recommender that can adjust to the learners' needs, interests, and levels of expertise automatically. The recommender automatically examines and learns the styles and characteristics of learners. The split and conquer strategy-based clustering is used to process the various learning styles. To extract the learners' functional patterns, the proposed cluster-based linear pattern mining approach is used. The system then makes intelligent recommendations based on the ratings of frequently occurring sequences.

Experiments were carried out on various groups of learners and datasets, and the proposed model recommended essential learning activities to learners based on their learning style, interest classification, and talent characteristics. When compared to learners in the no-recommender cluster category, it was discovered that the suggested cluster-based recommender enhances recommendation performance by resulting in more lessons completed. Based on the gap identified in the ways of implementing integrated standard lesson plans, this article proposes an advanced hybrid artificial intelligence system that optimizes the learning development processes for the implementation of differentiated pedagogical programs. It is a hybrid mechanism of artificial intelligence that focuses on how to provide targeted recommendations for the implementation of integrated standard lesson plans, which will be the main tool for creating flexible diversified pedagogical programs that will best meet the personal needs and particularities of each student.

3. Proposed System

The proposed system recommends to the teacher integrated lesson plans in the form of templates, in the sense that he/she can use a template to intervene in it to create his lesson plan, which will fully meet his abilities, considering the individual needs and learning abilities of each student [3]. The operation of the proposed system, which is based on interaction, is initialized by the completion by the teacher of an indicative preferences questionnaire, which includes relevant data based on thematic, pedagogical method, subject area, level, evaluation model, mode of distribution, and duration. The specific criteria, as it has been proven in the literature, are identified as the most important features that document the learning systems and judge the appropriateness of their reuse framework. The proposed architecture optimally combines multiple technologies in an innovative hybrid system, which is presented step by step below:

Step 1. To determine whether the topic area of a lesson plan is relevant to the topic set by the teacher, lexical analysis is performed based on the keywords related to the topic area in question. For this reason, intelligent natural language processing techniques are used [7]. A key feature of complexity in the process of converting words into concepts is related to the required rearrangements of the words in the original sentence to create the conceptual expression. The process to determine the keywords_matching parameter first involves extracting the entries to create a list (L_{FOL}).

The sentence is analyzed, and considering only words that have an entry are included in the first list, a second list (L_{NL}) is created, which contains the words in the order that they appear in the sentence.

Also, duplicates of a predicate are removed, and only its first occurrence is considered. The predicates from the L_{FOL} list, which were not found in the sentence, are deleted, ensuring that there is the same number of discrete elements in both lists. For each word in the L_{FOL}, its difference from the order in which it appears in the L_{NL} list is calculated. If a word is in position n_1 in the L_{FOL} list and position n_2 in the L_{NL}, then the position difference is defined as $|n_1 - n_2|$. Keywords_matching is the sum of the absolute values of the position differences of all words [12, 13]:

$$\text{Keywords\_Matching} = \sum_{i=1}^{n} \left|\mathrm{pos}_1(x_i) - \mathrm{pos}_2(x_i)\right|, \tag{1}$$

where n is the number of words in the lists and $\mathrm{pos}_1(x_i)$ and $\mathrm{pos}_2(x_i)$ are the functions that return positions n_1 and n_2 of element x in the L_{FOL} and L_{NL} lists, respectively.

Step 2. The evaluation model and the way of distribution for each lesson plan is automatically inferred from the proposed system, which, considering the differentiated pedagogy requested, identifies all the lesson plans that implement the specific pedagogy based on an evaluation measure. The indirect feedback model that uses Jeffrey's adaptation rule is used to find the likelihood that a lesson plan is relevant from the data gathered from the teacher's interactions [14]. This method takes into account the uncertainty of the indirect indications of interest and uses various measures to describe the value or value of the elements of a representation. Jeffrey's model presupposes the existence of a relativity path in a set of mutually exclusive terms in the information space. This relativity path is considered as a new source of information for updating a new possibility.

The following function is used to update the odds based on this new data [14–16]:

$$P'(t) = \left[P(t=1|p_l)\frac{P,(t=1)}{P(t=1)} + P(t=0|p_l)\frac{P'(t=0)}{P_{,}(t=0)}\right] \cdot P(t). \tag{2}$$

The probability of relativity of a lesson plan along the entire length N of the path is denoted P_N and is given by the function [17, 18]:

$$P_N(t) = \sum_{i=1}^{N-1} c_l \cdot I_l \cdot \left[\left(P_l(t=1) p_l \right) \frac{P_{l+1}(t=1)}{P_l(t=1)} + P_l\left(t=0 | p_t\right) \frac{P'_{l+1}(t=0)}{P_l(t=0)} \right) \cdot P_l(t) \Bigg], \tag{3}$$

where a representation in step i on path p is denoted as p_i. Trust in the value of the representation is denoted by c_l, and I_l is the informative value of the representation. Once the odds are updated, they remain constant until the next revision (i.e., the next route of interest).

Step 3. Next, the proposed system identifies groups of similar lesson plans in the sense of similarity in the sequence of activities they include. Specifically, the nearest neighbor algorithm is used to calculate the similarity and produces an estimate considering the weighted average of all ratings [11, 12]. The most numerous groups created in this way reveal the tendency of teachers to implement the specific pedagogy with the specific sequences of learning activities. In each of the more populous groups, the proposed system attempts to identify the lesson plan that satisfies most of the preferences stated by the teacher in the original preferences form and at the same time the one that has gathered the highest preference from the educational community.

Step 4. The lesson plans that are identified are recommended to the teacher. Each proposal is accompanied by comments explaining the rationale behind why it is proposed as relevant studies demonstrate that providing explanations of the recommendations provided can improve the user experience with these systems. The teacher can evaluate the recommendations made to him using a simple voting system [19]. The evaluations made by the teacher influence future recommendations. More specifically, lesson plans that have been rated with fewer votes, as well as the like, are excluded from future lists of recommendations. This recommendation approach takes into account the teacher's interaction process to recommend a range of interactions.

The procedure in question is defined as follows [9, 19, 20]:

$$\text{is}\left(n, N_{S'}\right) = \sum_{n_{i \varepsilon N_{S'}}} \left(\begin{array}{c} \left(lr'\left(n_i\right) \cdot \xi^{l-1} \cdot w \right) | \\ \exists p = n_i \longrightarrow n_j \longrightarrow n \\ w \varepsilon \left\{ n_j, n, w \right\}, l \end{array} \right) = l_{\text{ength}}(p), \quad l < L_{\text{MAX}}, \tag{4}$$

where p is the path between each node n_i and node n, considering the directionality of their connection. N is the path length, having a distance that is less than a maximum length L_{MAX}. Finally, ξ is a length reduction factor, the value of which is determined experimentally. A diagrammatic overview of the above process under flow chart type is presented in Figure 1.

4. Experiments and Evaluation

To investigate the proposed method, an electronic invitation was sent for voluntary participation with the questionnaire methodology, with the final participation of 487 teachers. The Likert 5-point grading method [21] was used ((i) I do not agree at all, (ii) I agree slightly, (iii) I agree moderately, (iv) I strongly agree, and (v) I strongly agree).

As already mentioned, the questionnaire included 10 questions with relevant data based on the topics, the pedagogical method, the topic area, the level, the evaluation model, the method of distribution, and the duration. An indicative statistical analysis of the responses that made up the data set used is presented in Table 1.

The recommendation mechanism implemented for the establishment of lesson plans considering the collection of indirect feedback from the relevant questionnaire was implemented with weights that compose the teacher's answers so that everyone's profile is updated by taking new features thus making the profiles dynamic for reflecting changes in behavior and preference that may be required. Specifically, the information provided by the teacher about his personal preferences is implemented by assigning fixed weighted gradient values so that $W_0 > 0$, $W_A > 0$ for all connections, respectively. Let a_{p_i} also be the level of preference given by the teacher to the term P_i (e.g., it could be 0 or 1, or it could take values from a finite set). Then, the initialization of the weight values is performed in the links [21, 22]:

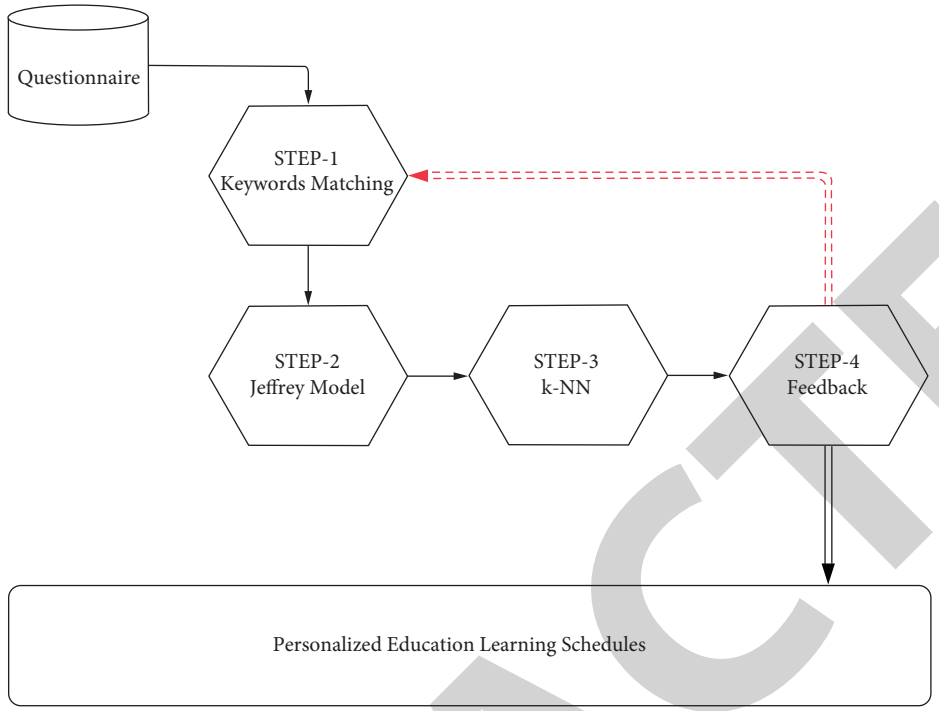

Figure 1: The proposed system.

Table 1: Statistical analysis of the data set used.

	Q1	Q2	Q3	Q4	Q5	Q6	Q7	Q8	Q9	Q10
Avg	49,98	40,73	24,69	35,32	40,30	55,55	36,87	40,96	35,86	45,98
Std	1,06	0,73	0,38	0,90	1,03	1,21	0,92	1,05	0,89	0,88
Med	48	40	25	36	40	56	38	40	37	47
PrevPr	37	22	35	68	35	79	57	64	64	32
MSD	23,49	16,01	8,45	19,92	22,69	26,66	20,20	23,11	19,70	19,37
Kurt	−1,11	−1,23	−1,21	−1,19	−1,18	−1,30	−1,29	−1,23	−1,13	−1,11
Asym	0,11	0,10	−0,06	−0,01	0,00	−0,07	−0,06	−0,06	−0,07	−0,07
Range	83	54	29	48	101	89	51	78	62	73
Min	10	15	10	8	11	10	15	6	18	11
Max	93	69	39	69	79	99	69	79	69	79

Avg = average; Std = standard error; Med = median; PrevPr = prevailing price; MSD = mean square deviation; Kurt = kurtosis; Asym = asymmetry; Min- = minimum; Max = maximum.

$$
\begin{aligned}
W_{P_i} &= a_{P_i} W_0, \quad \forall P_i,\\
W_P^{\max} &= \max_i \{W_{P_i}\},\\
W_{P_i} &\Leftarrow \frac{w_{P_i}}{W_P^{\max}},\\
A_{P_iP_j} &= a_{P_i} a_{P_j} W_A, \quad \forall P_i, P_j,\\
A_P^{\max} &= \max_{i,j} \left\{A_{P_iP_j}\right\},\\
A_{P_iP_j} &\Leftarrow \frac{A_{P_i}P_j}{A_P^{\max}}.
\end{aligned}
\tag{5}
$$

Then the weight value K_u which expresses the sum of all the relativity feedback is calculated as follows [21–23]:

$$
K_u = \frac{R_a^X W_{2a} + R_b^X W_{2b} + R_C^X W_{2c} + R_d^X W_{2d} + R_e^X \text{lev}}{R_a^X + R_b^X + R_c^X + R_d^X + R_e^X}, \tag{6}
$$

where R_a^X is with the significance/weight attached to the indirect feedback mode. Similarly, R_b^X represents the meaning given to the type of pedagogical method, R_C^X is the meaning of feedback, R_d^X is the meaning of enrichment and, finally, the term R_e^X indicates the meaning of explicit feedback. Finally, the similarity is calculated as follows [21, 23]:

$$\text{simil}(x, y) = \frac{\sum_{i \in I_{xy}} \left(r_{x,i} - \bar{r_x}\right)\left(r_{y,i} - \bar{r_y}\right)}{\sqrt{\sum_{i \in I_{xy}} \left(r_{x,i} - \bar{r_x}\right)^2 \sum_{i \in I_{xy}} \left(r_{y,i} - \bar{r_y}\right)^2}}, \tag{7}$$

where I_{xy} is the set of items scored and $r_{x,i}$ is the x user's rating for item i. The items are finally graded according to the above similarity in descending order. Because r ranges from zero to one, collaborative content-based filtering (recommendation) is performed.

To evaluate the above procedure given that there is the feedback that can be provided in stages, the error is calculated in each iteration. The goal is to minimize the cumulative error for all iterations, and by using the square loss function (SLF), the goal is to minimize the empirical error calculated by the function [24, 25]:

$$I_n[w] = \sum_{j=1}^{n} V\left(\langle w, x_j \rangle, y_j\right) = \sum_{j=1}^{n} \left(x_j^T w - y_j\right)^2, \tag{8}$$

where $x_j \in R^d, w \in R^d$, and $y_j \in R$ and X $i \times d$ is a data table and Υ $i \times 1$ is a table of target values after the arrival of the first i data points are assumptions. Assuming that the correlation table $\Sigma_i = X^T X$ is invertible, the optimal solution $f^*(x) = \langle w^*, x \rangle$ for the linear least squares problem is given by the function [17, 18, 24, 25]:

$$w^* = \left(X^T X\right)^{-1} X^T \Upsilon = \sum_{i}^{-1} \sum_{j=1}^{i} x_j y_j. \tag{9}$$

Also, the root mean squared error (RMSE) was used which calculates the average error of the recommendation values relative to the actual preferences, with the following formula [17, 25]:

$$\text{RMSE} = \sqrt{\frac{1}{n} \sum_{j=1}^{n} \left(P_{(ij)} - T_j\right)^2}, \tag{10}$$

where $P_{(ij)}$ is the recommendation value i for a simple hypothesis j and T_j is the target value for the simple hypothesis j. The success of a recommendation model requires extremely small values, while the best case, which implies an absolute correlation between proposals and preferences and therefore the absolute success of the model, is achieved when $P_{(ij)} - T_j = 0$.

The root relative squared error (RRSE) was used accordingly, which is calculated as follows [17, 26]:

$$\text{RRSE} = \frac{\sum_{j=1}^{n} \left(P_{(ij)} - T_j\right)^2}{\sum_{j=1}^{n} \left(T_j - \overline{T}\right)^2}, \tag{11}$$

where $P_{(ij)}$ the predicted value i for a simple hypothesis j, T_j is the target value for the simple hypothesis j, and $\overline{T}$ is calculated from the following relation [18]:

$$\overline{T} = \frac{1}{n} \sum_{j=1}^{n} T_j. \tag{12}$$

The perfect correlation between recommendations and actual preferences is achieved when this is equal to 0. Table 2 presents the results of the process as a 3-class problem where there is a full correlation (class A), partial correlation (class B), and absolute disagreement (class C). Exact errors are presented as performance metrics in the same Table 2.

Respectively, the diagrammatic representations are shown in Figures 2–6. Figures 2–6 show the performance of the model, giving visualized indications of the quality of the model.

Based on the results obtained and presented in detail above, it is obvious that the utilization of the proposed algorithm can find a reliable solution to the extremely difficult problem of creating and sharing lesson plans for the implementation of individualized curricula. The methodology proved that through the widespread use of intelligent methods, important educational tools can emerge so that the teacher can easily manage the student potential of his class and know the specific characteristics of each group, thus offering high-quality education through differentiated approaches considering the special educational needs of each trainee. Undoubtedly, this is a reliable model that can model the problem of differentiated pedagogy with high accuracy.

5. Discussion

As indicated above, in the context of several factors that influence the guidance of an educational policy, the transformation of teaching practices according to the principles of differentiated pedagogy is in many cases closely linked to the expectation of a fair response to student heterogeneity. The specific pedagogical practices, developed in the light of differentiated pedagogy, are often declared to be capable of promoting the principles of pedagogical integration. In the context of the discussion on the development of teaching practices that fall within the logic of inclusive education, it is important to consider, on the one hand, the risk that, in some cases, different interpretations of differentiation are associated with different trends and values of educational policy and, on the other hand, which is a confused and contradictory context, such interpretations can often be combined, thus leading in the opposite direction, i.e., in perpetuating discrimination and exclusion in education. With the conjuncture of the pandemic which changed the ways of education and in parallel with the modern social, economic, and political reality which favors the application of innovations in the educational policy at an international level, the global educational landscape is constantly introducing reformed efforts that focus on the transformation of educational systems according to the rules of the market and competition between students and

Table 2: Performance metrics.

Accuracy	AUC	Recall	Prec.	*F*-score	RMSE	RRSE
0.8908	0.9772	0.8694	0.8920	0.8898	0.8260	0.8273

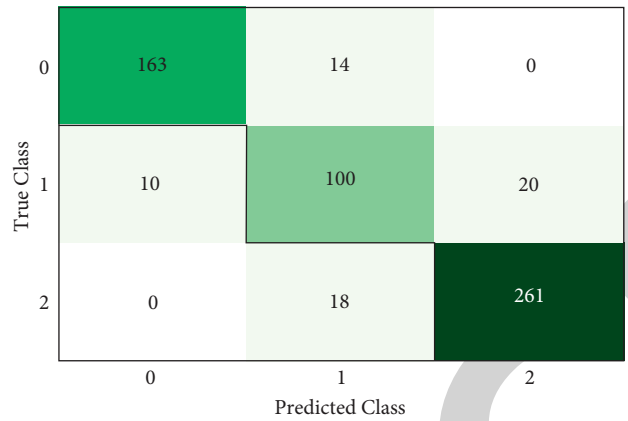

Figure 2: Confusion matrix.

Figure 3: Precision-recall-*F*-score.

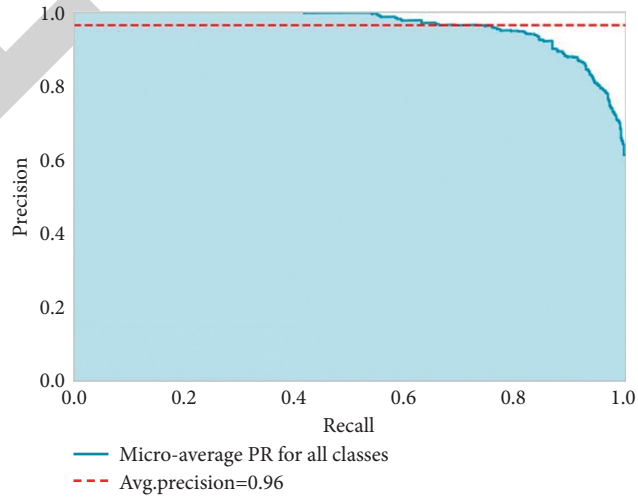

Figure 4: Precision vs. recall.

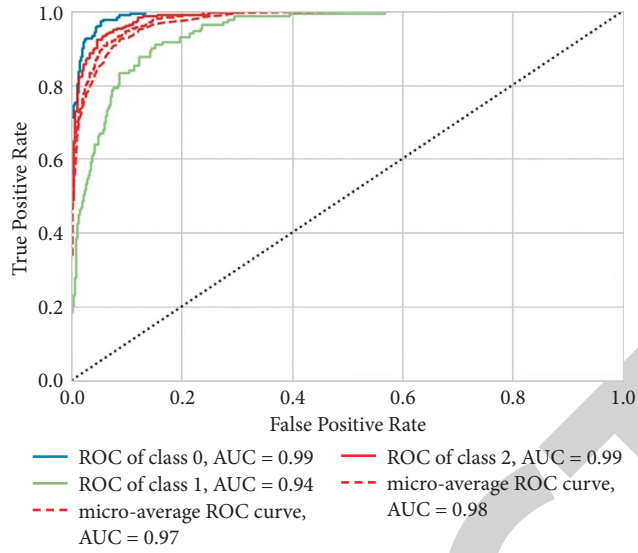

Figure 5: ROC curves.

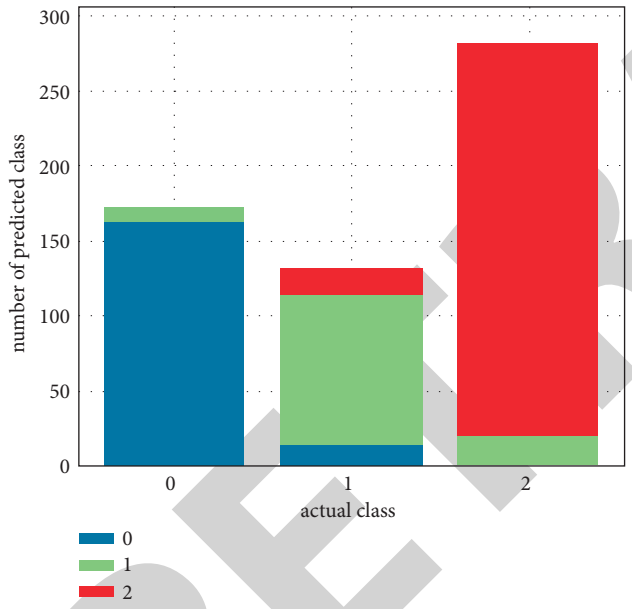

Figure 6: Error by class.

schools. In addition, the promotion of discrimination and unequal access of students to knowledge is taking place. Furthermore, it is often emphasized that if there is a place for differentiated pedagogy in the current socio-political context, it can be ensured through the "political clarity" of all those involved in approaching and analyzing issues of student diversity. Speaking of the advantages of the proposed method, the most important benefit is the diverse application to overcome substantial difficulties arising from institutionalized standards and procedures. Another supporting presumption is that there is no limit to the data that can be accepted as quantitative data, nor to the evaluable factors arising from the multifaceted and holistic evaluation of the curriculum.

6. Conclusion

The proposed algorithmic approach gave realism and went beyond the physical limitations that might arise at the functional levels. From a technical point of view, this study proposed an algorithm for the first time in the literature that showed a higher degree of convergence, which is evidenced by the higher results of recommendations that were achieved and experimentally confirmed. The proposals for the additional research concerns includes the complete automation of the modeling system of the recommendation system, with greater accuracy and efficiency. Moreover, it also embraces the evolution of the system with automatic optimization of the questionnaires with intelligent methods of classification in fields of interest. Finally, an important step for further development is the expansion of the methods to fuzzy logic technologies.

Data Availability

Data sharing does not apply to this article as no data set were generated or analyzed during the current study.

Conflicts of Interest

The author declares no conflicts of interests regarding the publication of the research article.

References

[1] S. Maghsudi, A. Lan, J. Xu, and M. van der Schaar, "Personalized education in the AI era: what to expect next?" *IEEE Signal Processing Magazine*, vol. 38, no. 3, pp. 37–50, 2021.

Hindawi
Journal of Mathematics
Volume 2023, Article ID 9858351, 1 page
https://doi.org/10.1155/2023/9858351

Retraction

Retracted: Optimization Algorithm of Logistics Transportation Cost of Prefabricated Building Components for Project Management

Journal of Mathematics

Received 19 December 2023; Accepted 19 December 2023; Published 20 December 2023

This article has been retracted by Hindawi following an investigation undertaken by the publisher [1]. This investigation has uncovered evidence of one or more of the following indicators of systematic manipulation of the publication process:

(1) Discrepancies in scope

(2) Discrepancies in the description of the research reported

(3) Discrepancies between the availability of data and the research described

(4) Inappropriate citations

(5) Incoherent, meaningless and/or irrelevant content included in the article

(6) Manipulated or compromised peer review

The presence of these indicators undermines our confidence in the integrity of the article's content and we cannot, therefore, vouch for its reliability. Please note that this notice is intended solely to alert readers that the content of this article is unreliable. We have not investigated whether authors were aware of or involved in the systematic manipulation of the publication process.

Wiley and Hindawi regrets that the usual quality checks did not identify these issues before publication and have since put additional measures in place to safeguard research integrity.

We wish to credit our own Research Integrity and Research Publishing teams and anonymous and named external researchers and research integrity experts for contributing to this investigation.

The corresponding author, as the representative of all authors, has been given the opportunity to register their agreement or disagreement to this retraction. We have kept a record of any response received.

References

[1] X. Yang, "Optimization Algorithm of Logistics Transportation Cost of Prefabricated Building Components for Project Management," *Journal of Mathematics*, vol. 2022, Article ID 1460335, 9 pages, 2022.

Hindawi
Journal of Mathematics
Volume 2022, Article ID 1460335, 9 pages
https://doi.org/10.1155/2022/1460335

Research Article

Optimization Algorithm of Logistics Transportation Cost of Prefabricated Building Components for Project Management

Xiaojiang Yang

Department of Planning and Development, Capital University of Physical Education and Sports, Beijing 100091, China

Correspondence should be addressed to Xiaojiang Yang; yangxiaojiang@cupes.edu.cn

Received 30 November 2021; Revised 24 December 2021; Accepted 28 December 2021; Published 17 January 2022

Academic Editor: Naeem Jan

Because the traditional logistics transportation cost optimization algorithm of prefabricated building components has the problems of long transportation time and high transportation cost, a logistics transportation cost optimization algorithm of prefabricated building components for project management is proposed. A project management oriented prefabricated building component management system is built, the logistics and transportation process of prefabricated building components are analyzed, and the logistics vehicles of prefabricated building components under the time window are scheduled. According to the scheduling results, through the waiting unloading time cost, transportation cost, and penalty cost, the total cost objective function is built to obtain the optimal cost. The simulation results show that the proposed algorithm has the shortest logistics transportation time and the lowest transportation cost.

1. Introduction

With the progress of the times and the development of economy, the development of construction industry has ushered in new opportunities and has become an important driving force for China's economic improvement. The traditional cast-in-place construction mode can no longer meet the needs of diversification, high safety, and low energy consumption of current building production, while the energy-saving, labor-saving, safe, and efficient prefabricated buildings gradually replace the traditional production mode [1]. Since 2015, the state has successively issued a series of policies to promote the development of prefabricated buildings. In the same year, the government decided to comprehensively promote prefabricated buildings throughout the country next year and implement unified evaluation standards. It also formulated a series of development plans for prefabricated buildings. It plans to implement prefabricated production in half of the country's construction projects by 2025. In 2016, the government work report further described how to develop prefabricated buildings and proposed that we should not develop blindly. We should fully consider the actual situation, pursue the development of efficient prefabricated buildings, and pay more attention to improving the construction quality of construction projects. The prefabricated construction industry has gradually occupied a certain market share in the construction industry. According to the statistical report in 2019, the proportion of prefabricated buildings in new buildings in China is about 13.4%, with a year-on-year increase of 45% [2].

Prefabricated building refers to the building formed by the unified production and transportation of concrete prefabricated components from the processing plant to the construction site. For construction enterprises, the conditions for selecting suppliers of prefabricated PC components are nothing more than the price, on-time delivery rate, and product qualification rate of PC components. The component price and product qualification rate can be determined according to the industrial and national regulations and the qualification test certificate provided by the component processing factory before selecting suppliers, but the delivery time may depend on weather conditions. The traffic situation changes, which leads to the increase of high logistics cost and becomes an important bottleneck restricting the development of prefabricated buildings in China [3]. The weight of

fabricated PC components can reach up to 3 tons, which is a typical bulk cargo, and its transportation cost can account for 50%–60% of the logistics cost of the whole supply chain. Moreover, the time when the vehicles for prefabricated building components arrive at the construction site directly affects the overall project progress. At present, the transportation of prefabricated building components depends on the experience of the dispatchers in the component processing plant, so it is very likely that the vehicles cannot arrive at the construction site on time due to unreasonable scheduling. This will not only increase the cost of rescheduling the construction at the construction site, but also cause the punishment cost of the component processing plant, so that the cost of the whole prefabricated building component transportation supply chain will increase. Therefore, how to reduce the total cost of logistics transportation has become the research object of many scholars.

The research on logistics transportation cost optimization of prefabricated building components is a process from shallow to deep. Scholars have made relevant exploration in the direction of cost optimization of prefabricated building. Literature [4] proposes the transportation cost optimization algorithm of B2C e-commerce return reverse logistics and divides its cost composition into three categories: transportation cost, inventory cost, and other costs. This paper mainly focuses on the transportation cost of return reverse logistics and constructs the location model of return reverse logistics center of B2C e-commerce enterprises according to its cost composition and influencing factors. Genetic algorithm combined with MATLAB programming is used to solve the model and conduct numerical experiments, select a reasonable return logistics center address, reduce the relevant transportation cost, and then achieve the purpose of optimizing the transportation cost of return reverse logistics under the B2C e-commerce environment. Literature [5] proposed the optimization algorithm of litchi cold chain logistics distribution cost model based on ant colony algorithm. Taking four main factors, i.e., distribution vehicle transportation, cold chain energy consumption, litchi loss, and time window punishment, as the research object, the cost model of each factor is constructed, and the objective optimization function of cost optimization in the process of litchi cold chain logistics distribution is determined. The ant colony algorithm is used to solve the example of cost optimal objective function in the process of litchi cold chain logistics distribution, and the optimization roadmap of litchi cold chain logistics distribution path network is obtained. However, the cost of the above two algorithms for the logistics transportation of prefabricated building components is high. Literature [6] proposed the optimization algorithm of logistics distribution path of fresh food cold chain, established a new cost and constraint model, and gave the optimization method using simulated annealing algorithm. The model considered the influence of vehicle speed and load capacity on transportation energy consumption, distinguished the refrigeration energy consumption of vehicle in transit and loading and unloading stage, and described the deterioration rate of food with exponential function rather than constant. The simulated annealing algorithm is used to solve the example. Paper [7] proposed the container liner transportation stowage optimization algorithm. In the research on the container liner multiport stowage optimization problem, a 0-1 integer optimization mathematical model with the constraint of ship stability and the goal of minimizing the total number of containers in the whole route was established, and the improved adaptive genetic algorithm based on P-1 genome chromosome coding design was used to solve it. The feasibility and effectiveness of the stowage mode are verified by example simulation. However, the above two algorithms consume a long time for the logistics transportation of prefabricated building components, resulting in low transportation efficiency.

Since the above algorithms have certain limitations and issues, these problems led us to introduce the proposed method. Hence, in view of the problems in the above algorithms, this paper proposes a project management oriented logistics transportation cost optimization algorithm for prefabricated building components, and the simulation experiments verify that the algorithm has low cost and high operation efficiency, which lays a foundation for the development of logistics transportation. Following the Introduction, the assembly building component management system for project management is given in Section 2. In Section 3, the logistics and transportation process of prefabricated building components are described. In Section 4, an optimization algorithm which covers the logistics transportation cost of prefabricated building components is explained. In Section 5, the experimental analysis is carried out where the authentication of the proposed algorithm is proved. In the end, the paper is finished with a conclusion in Section 6.

2. Assembly Building Component Management System for Project Management

With the proposal and development of prefabricated building mode, we gradually see the application value of prefabricated building process integration. However, at present, it is still difficult to implement the actual project application. Technology has not been a problem, and the biggest bottleneck is the construction organization and management mode. The ultimate goal of the development of prefabricated buildings is to establish the integrated technology of factory manufacturing, mechanized assembly, and standardized management. What needs to be changed on the surface is the construction process, but what needs to be changed in essence is the management system. As the biggest obstacle to the implementation of cost management, if we follow the traditional cost management mode of taking all the responsibility and cutting in blocks, we cannot realize the real value of the integrated process without taking the overall interests of the project as the goal. To solve this problem, the state has been promoting the general contracting mode to achieve the maximum benefits of construction industrialization [8].

2.1. Prefabricated Building Component Factory in Supply Chain. As a transition, the prefabricated building component factory has stepped onto the historical stage as a

separate party. The positioning of component factories is mainly divided into component factories, single components, and so on including self-supporting mode, self-supporting and joint venture mode, component processing, and integrated nomadic mode of supporting products. Component + type is only responsible for component production and component deepening. Component ++ type plays a role in the scheme design and decision-making stage, and its main functions include R&D, design, production, installation, technical consultation, and management consultation [9].

The component factory under the integrated positioning takes the service general contracting, cost reduction, and efficiency increase as the core, and the key points of management mainly include component demobilization, transportation and stacking, matching of hoisting sequence, optimization of storage yard and stacking scheme, combination of components and finalized formwork, and combination of components and installation.

2.2. Management Process of Prefabricated Building Components. By analyzing the research text of component factories of well-known enterprises in the industry, this paper summarizes the specific management process for prefabricated building components. As can be seen from Figure 1, regarding the subordination of logistics management of prefabricated building components and the relationship with other systems, components are warehoused after passing the finished product inspection standard, and checked and delivered after receiving the transportation instruction, and the marketing management team is responsible for after-sales operation [10]. The problem components shall be handled by the technical management team, repaired and returned to the factory according to the problem size of fabricated building components, and then handed over to the logistics management team for retransportation. It can be seen from Figure 1 that the general transportation service is completed by cooperation between multiple departments. From the signing of the contract through bidding to the completion of transportation delivery, each department is responsible for tracking the components, which are divided into marketing, technology, quality, procurement, production, inventory, and logistics management. Although logistics is rarely mentioned in the structure, it is a main line that runs through the capital flow with the product itself. In order to better manage, many enterprises will establish project management departments independent of the enterprise to coordinate and manage the project.

3. Logistics and Transportation Process of Prefabricated Building Components

Transportation refers to the logistics activities of processing and packaging the goods according to the needs of users within a certain area, and finally transporting them to the location designated by users on time. Transportation is the organic combination of "transportation" and "transportation." Transportation refers to the transportation of users, vehicles, transportation routes, and so on, while "transportation" refers

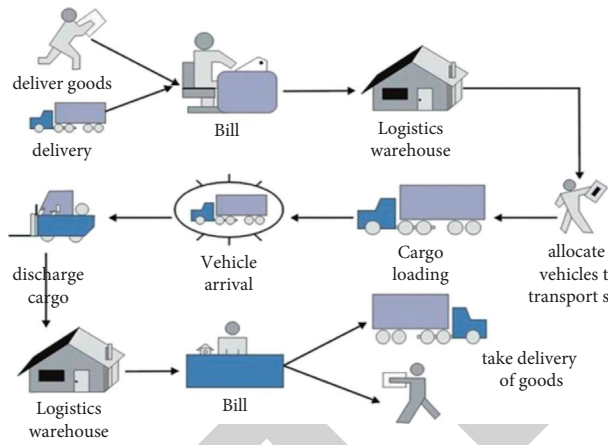

Figure 1: Component management process.

to the transportation of goods. Transportation is the transportation link in the logistics system, and it is the end and last link of the entire logistics system. The biggest difference between transportation and delivery is the extension of transportation and delivery, which is derived from social high-level production for a long time. Transportation is the scientific and reasonable arrangement of transportation tools and routes through the transportation department, which can not only meet the needs of customers, but also reduce the logistics cost. At the same time, scientific transportation can not only enable enterprises to achieve zero inventory, but also alleviate traffic pressure and reduce environmental pollution [11].

According to the prefabricated building component management system for project management, the logistics transportation process of prefabricated building components is analyzed. When transporting according to customer needs, the transportation center will arrange vehicles according to the actual situation. The basic transportation process is shown in Figure 2.

(i) Divide transportation area: in order to make the vehicle transportation route more reasonable and the transportation cost lower, the management personnel of the transportation center need to divide the transportation area according to the customer's area, traffic conditions, and other information before transportation [12].

(ii) Determine user transport sequence: after the area is divided, the delivery sequence is preliminarily arranged according to the time window required by customers in this area, so that customers can enjoy better service [13].

(iii) Arrange vehicles: first, determine the characteristics of the goods to be transported, the number of vehicles, and the vehicle load. Secondly, load the goods according to the user's transportation sequence. Finally, the goods that can be transported by the same vehicle are determined according to the demand of each user and the transportation cost.

(iv) Select transportation route: after determining the goods to be transported by each vehicle, select a

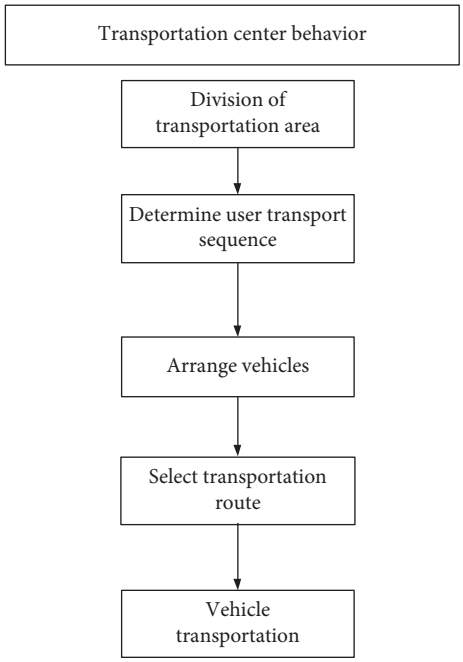

Figure 2: Basic flow chart of transportation.

scientific and reasonable transportation route with short distance and low cost according to the customer's time window, specific location, and other conditions, aiming at obtaining the lowest transportation cost.

(v) Transport goods by vehicle: determine the final vehicle transportation route according to the above determined goods and vehicle arrangement, transportation sequence, and transportation route required by the customer [14].

4. Optimization Algorithm of Logistics Transportation Cost of Prefabricated Building Components

Prefabricated building refers to the building assembled on site by prefabricated components produced by the factory. In terms of structural form, it can be divided into fabricated concrete structure, wood structure, and steel structure. From the perspective of component application specialty, it can be divided into building components, highway components, municipal components, water conservancy components, etc. The components studied in this paper are mainly fabricated reinforced concrete components, such as prefabricated walls, slabs, columns, beams, balcony slabs, and stairs. The logistics transportation cost optimization problem of prefabricated components studied in this paper is a vehicle scheduling problem aiming at logistics transportation cost optimization in logistics transportation management [15].

4.1. Determination of Starting and Ending Vehicle Dispatching Lines. In this section, we determine the starting and ending vehicle dispatching lines. In the process, we first described the starting point of transportation. Then, the final stop position is explained. We give the mathematical description of both positions and provide the best dispatching and terminating positions with respect to time and maximum authority.

4.1.1. Start Scheduling Location. The starting dispatching position refers to the starting point of logistics transportation goods, which can change with the change of multimodal transport network structure. Generally, it is directly affected by the two physical coefficients of multimodal transport network node coverage intensity and vehicle transportation dispatching frequency [16]. The node coverage strength of intermodal network can be expressed as z. In a complete prefabricated building component logistics transportation network, this physical quantity is composed of upper limit value z_l and lower limit value z_0, where l represents the value of transportation vehicle scheduling coefficient per unit time. The vehicle transportation scheduling frequency can be expressed as q. Due to the variability of the logistics transportation network of prefabricated building components, the actual value result of this physical quantity is not completely fixed [17]. The starting dispatching position of logistics transportation vehicles for prefabricated building components can be defined as

$$A_0 = \sqrt{\sum_{z_0}^{z_l} \frac{\left(\max W - q_1 q_2\right)^2}{l^2}}, \tag{1}$$

where q_1 and q_2, respectively, represent the value results of two different vehicle transportation scheduling frequencies, and $\max W$ represents the maximum logistics vehicle scheduling authority value per unit time.

4.1.2. Stop Scheduling Location. The termination scheduling position refers to the end point of logistics transportation goods. It can also change with the change of the structure of multimodal transport network. It is usually directly affected by two physical quantities: vehicle travel distance and logistics network scheduling cycle of prefabricated building components. The vehicle travel distance can be expressed as d. Due to the existence of the initial scheduling position, this physical coefficient always belongs to a dependent variable, and its numerical level cannot be directly affected by the subjective scheduling factors of prefabricated building component logistics transportation vehicles [18]. The logistics network scheduling cycle of prefabricated building components can be expressed as D. Generally, the greater the value of this physical index, the farther the transportation distance that logistics vehicles can reach. According to the joint formula (1), the termination scheduling position of prefabricated building component logistics transportation vehicles can be defined as

$$A_n = \frac{dD \times \sqrt{c_0^2 + c_n^2}}{\eta \cdot A_0}, \tag{2}$$

where c_0 represents the logistics transportation optimization parameters related to the starting dispatching location, c_n represents the logistics transportation optimization parameters related to the ending dispatching location, and η represents the logistics dispatching authority value matching the transportation vehicle [19].

4.2. Transportation Path Grid Model. Based on the learning algorithm of artificial intelligence, the linear programming model of logistics transportation path of prefabricated building components is constructed, and the mathematical problem of transportation path optimization planning of prefabricated building component logistics is expressed as follows:

$$\begin{cases} \min C = \sum_{k=1}^{K}\sum_{i=1}^{V} x_{i,k}C_{i,i+1}^{k} + A_n \sum_{k=1}^{K}\sum_{l=1}^{K}\sum_{i=1}^{V} y_{i,k}C_i^{k,l}, \\ \min T = \sum_{k=1}^{K}\sum_{i=1}^{V} x_{i,k}T_{i,i+1}^{k} + A_n \sum_{k=1}^{K}\sum_{l=1}^{K}\sum_{i=1}^{V} y_{i,k}T_i^{k,l}, \end{cases} \tag{3}$$

where T is the total time spent on transportation; C is the total cost spent; $x_{i,k}$, $y_{i,k}$ are the decision variables; $x_{i,k} = 1$ is the selection of k transportation mode between nodes i and $i + 1$; $y_{i,k} = 1$ is the change of transportation mode k at node i into another transportation mode l; V is the set of transportation nodes, the set of alternative routes; and K is the set of transportation modes. Considering the spatial characteristics, it is found that the number of logistics transportation paths of prefabricated building components is n. The traffic logistics parameter characteristics are linearly fused, and the spatiotemporal parameters of traffic flow data are $L_1, \ldots, L_n$ and $P_1^{\min}, \ldots, P_n^{\min}$. By establishing the adaptive optimization grid distribution model of the logistics transportation path of prefabricated building components, the weight parameter distribution model of the memory unit is obtained, and the weight factor W^T is obtained. According to the traffic flow distribution of the target road section, combined with block matching, the path parameter distribution set of the logistics transportation of prefabricated building components is obtained, and the transportation path grid model is constructed:

$$F = \frac{\sum_{j=0}^{N} c_{ij}x_{ijk}u_{ij}}{\sum_{i=1}^{N} Gy_{ik}}, \tag{4}$$

where i, j are the logistics vehicle transportation stop node and adjacent node, the number of adjacent nodes j of node i is n, c_{ij} is the distance from node i to adjacent node j, u_{ij} is the transportation cost per unit distance, k is the number of transportation vehicles owned by the logistics company, G is the fixed departure cost, $x_{ijk} = 1$ when vehicle k is from node i to adjacent node j, $y_{ik} = 1$ when node k is transported by vehicle i, and x_{ijk}, $y_{ik} = 0$ [20] in other cases.

4.3. Vehicle Scheduling with Time Window. The vehicle scheduling problem is to organically organize and combine several loading points and unloading points to form a series of vehicle routes through the arrangement of vehicle departure sequence when the vehicles of prefabricated building components are limited. The premise of solving this problem is to meet certain constraints, and the ultimate goal is to make the general route of vehicle transportation the shortest, the transportation time the least, and the total cost the lowest [21]. Vehicle scheduling optimization problem is actually to solve the most efficient transportation scheme. The vehicle scheduling problem with time window for prefabricated building components can be described as follows: let $R = (V, A)$ be a complete undirected graph, where V is the node set and A is the edge set. In a fabricated building component processing plant, k vehicles transport the required components to n construction sites. After one transportation trip, the vehicles need to return to the component processing plant for reloading for transportation. If the prefabricated building component transport vehicle does not arrive within the time window required by the construction site, the corresponding penalty cost will be incurred. Considering the distance of the road, the vehicle will exceed the maximum transit time of the vehicle due to long-distance transportation, resulting in the penalty cost. Each construction site can be served by multiple vehicles at the same time, but one vehicle can only serve one construction site at a time, and the needs of customers are random. The goal of vehicle scheduling problem for prefabricated building components is to arrange scientific and reasonable vehicle scheduling time and route, so as to minimize the total cost of vehicle transportation under the condition of meeting the time window and needs of customers [22].

(i) The difference between the driving time of vehicle k and the maximum driving time is

$$TO_i = F\max\left(T_{io} - T_{oi}\right), \tag{5}$$

here o is the component processing plant.

(ii) The penalty cost for vehicle k's failure to arrive within the time window required by construction site n for the i-th transportation is

$$G_{kn} = TO_i\gamma\left(T_{kn} - L_n\right). \tag{6}$$

(iii) The service times of construction site n are

$$CW_{nr} = \frac{N_n}{Q_r}. \tag{7}$$

(iv) The calculation parameters of the i-th transportation of vehicle k serving construction site n are

$$z_{ikn} = \begin{cases} 1, & \text{The } i-\text{th delivery of vehicles } K \text{ serves the construction site } n, \\ 0, & \text{otherwise.} \end{cases} \tag{8}$$

(v) The calculation parameters of vehicle k for transportation are

$$y_k = \begin{cases} 1, & \text{Vehicle } k \text{ is enabled,} \\ 0, & \text{otherwise.} \end{cases} \tag{9}$$

4.4. Cost Objective Function. According to the above vehicle scheduling results with time window, the cost objective function is constructed. According to the characteristics of the transportation form of prefabricated building components, considering the waiting unloading time cost in the transportation process and the penalty cost for failing to meet the soft time constraint, the objective function of the total transportation cost includes not only the transportation cost, but also the waiting unloading time cost and the penalty cost caused by failing to meet the time window requirements of the construction unit. The purpose is to obtain the transportation vehicle arrangement plan when the total transportation cost is the lowest under the constraints of hard time window of each construction unit.

4.4.1. Waiting Time Cost. If the transport vehicles planned by the prefabrication plant need to queue up to unload the fabricated building components after arriving at the construction site, on the one hand, the waiting time will cause the personnel and vehicles to be idle; on the other hand, it may lead to failure to meet the time requirements of other construction sites, thus losing credibility and being subject to the agreed economic punishment. In the waiting time, from the perspective of the supplier, personnel and vehicles will not be used effectively, resulting in a waste of resources and an indirect loss of reputation. A unit waiting time cost coefficient s is proposed by the prefabricated component factory according to the expert's speculation. It is assumed that the tangible and intangible costs of the prefabricated plant caused by waiting increase linearly with the increase of waiting time. The total waiting time cost is

$$U_1 = \sum_{i=1}^{n} s y_i. \tag{10}$$

4.4.2. Transportation Cost. The transportation cost of prefabricated building component vehicles refers to the fuel cost and temporary maintenance cost consumed by vehicles starting from the component processing plant, passing through various construction sites, and finally returning to the component processing plant, which is directly proportional to the total distance traveled by vehicles. The longer the distance, the higher the cost. Therefore, the main factor affecting the transportation cost is the total distance of vehicles, which puts forward requirements for the vehicle dispatcher of the component processing plant to make scientific and reasonable vehicle time and route arrangement before vehicle transportation. Then, the transportation cost generated during vehicle scheduling of prefabricated building components can be expressed as

$$U_2 = \sum_{i=1}^{n} D_{ok} z_{ikn}. \tag{11}$$

4.4.3. Penalty Cost. The normal working time of vehicle drivers is 8 hours; that is, the longest driving time of vehicles is 8 hours. If the working time exceeds 8 hours, it is the driver's overtime, which will produce corresponding overtime expenses, and the driver is prone to fatigue due to driving for a long time, resulting in incalculable consequences, so it will produce corresponding punishment costs. Then, the penalty cost for exceeding the maximum driving time of the vehicle during vehicle scheduling of prefabricated building components can be expressed as

$$U_3 = \sum_{i=1}^{n} G_{kn} TO_i. \tag{12}$$

4.4.4. Total Cost Objective Function. The transportation cost optimization problem of prefabricated building components studied in this paper considers the transportation in the supply process, the waiting time cost caused by unreasonable logistics transportation, and the penalty cost for not reaching the construction site in time. The objective is to realize the lowest logistics transportation related cost of prefabricated component enterprises through reasonable transportation vehicle scheduling. Therefore, the total target cost includes vehicle transportation cost, waiting time cost, and penalty cost, which can be obtained as follows:

$$U = U_1 + U_2 + U_3. \tag{13}$$

5. Simulation Experiment Analysis

In order to verify the effectiveness of the logistics transportation cost optimization algorithm of prefabricated building components for project management in practical application, the experiment was carried out using the following configurations: MATLAB 7.0, VS2010 + OpenCV2.4.13, Windows 10, Intel® Xeon® CPU E5-2603 v4 @2.20 GHz, 32 GB memory. The logistics transportation network structure of prefabricated building components was set as shown in Figure 3.

According to the road network structure of logistics transportation of prefabricated building components, the logistics transportation cost optimization algorithm of prefabricated building components for project management proposed in this paper, the B2C e-commerce return reverse logistics transportation cost optimization algorithm proposed

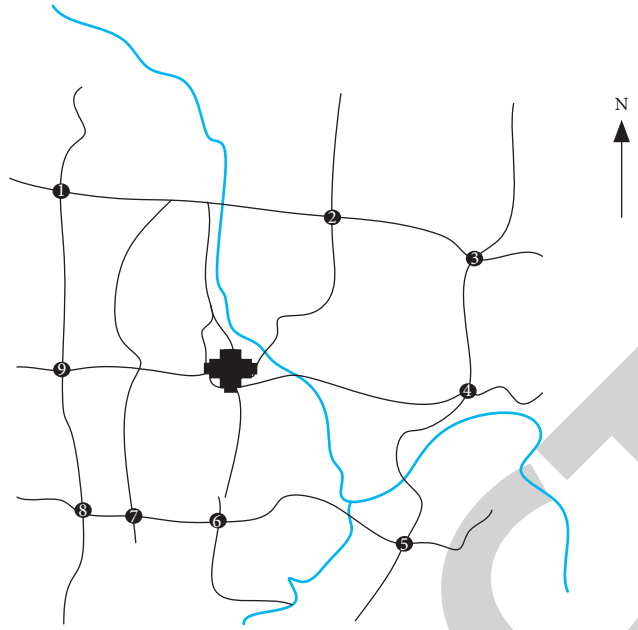

Figure 3: Road network structure diagram of logistics transportation of prefabricated building components.

Table 1: Comparison results of logistics transportation cost error rate of fabricated building components.

Number of experiments/times	Error rate (%)		
	Paper algorithm	Reference [4] algorithm	Reference [5] algorithm
10	4	18	32
20	5	18	34
30	7	18	37
40	8	20	40
50	9	22	42
60	9	24	43
70	10	25	43
80	12	27	44
90	13	32	45
100	15	35	48

in literature [4], and the litchi cold chain logistics distribution cost model optimization algorithm based on ant colony algorithm proposed in literature [5] are adopted; the logistics transportation cost error rate of fabricated building components is compared and analyzed; and the comparison results are shown in Table 1.

According to the data in Table 1, the logistics transportation cost error rate of assembled building components of the logistics transportation cost optimization algorithm of assembled building components for project management proposed in this paper is less than 15%, while the logistics transportation cost error rate of assembled building components of the B2C e-commerce return reverse logistics transportation cost optimization algorithm proposed in [4] is less than 35%. The error rate of logistics transportation cost of prefabricated building components of the optimization algorithm of litchi cold chain logistics distribution cost model based on ant colony algorithm is less than 48%. The logistics transportation cost optimization algorithm of prefabricated building components for project management proposed in this paper has a low cost for logistics transportation of prefabricated building components.

In order to further verify the effectiveness of this algorithm, the logistics transportation cost optimization algorithm of prefabricated building components for project management proposed in this paper, the B2C e-commerce return reverse logistics transportation cost optimization algorithm proposed in literature [4], and the litchi cold chain logistics distribution cost model optimization algorithm based on ant colony algorithm proposed in literature [5] are adopted, The logistics transportation time of fabricated building components is compared and analyzed, and the comparison results are shown in Figure 4.

It can be seen from Figure 4 that the logistics transportation cost optimization algorithm of prefabricated building components for project management proposed in this paper consumes less time (about 7 s) than the B2C e-commerce return reverse logistics transportation cost optimization algorithm proposed in document [4] and document [5]. The proposed optimization algorithm of litchi

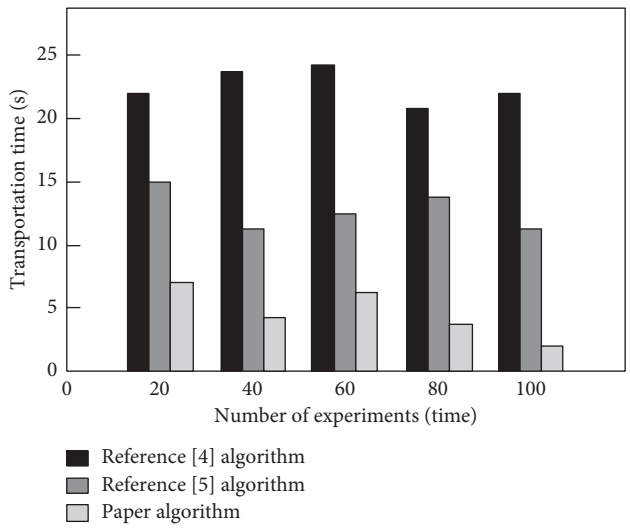

Figure 4: Comparison results of logistics transportation time of three different algorithms.

cold chain logistics distribution cost model based on ant colony algorithm consumes less time for logistics transportation of assembled building components.

6. Conclusion

The system, process, and logistics under the prefabricated construction project management mode are different from those under the traditional mode. The construction process is simplified, the on-site operation time is greatly shortened, and the cost optimization space is transferred to production and transportation, while the cost optimization space of raw materials is limited. PC components are the main products of prefabricated construction. Their transportation cost has become the largest space for cost optimization of assembly enterprises. Although the country has been advocating construction industrialization, the extensive model left over from the early stage of reform and development has not been significantly improved. The logistics cost control of the project needs to be optimized both systematically and technically. Based on the principle of logistics cost management, this paper uses the system optimization method in the field of logistics to optimize the transportation cost. The purpose is to reduce the strategic cost, operation cost, and activity cost of transportation; improve the level of industrialization; and remove obstacles for the development of assembly enterprises. At the same time, this study is conducive to the interdisciplinary intersection of logistics management and construction engineering management and clarifies the shortcomings of the construction industry model compared with the industrialization model. The industrial production scheduling optimization theory is combined with the practice of prefabricated construction engineering to verify its theoretical feasibility. It has certain theoretical significance to provide theoretical reference for the development of architecture to industrialization and lay the foundation for establishing a more perfect theoretical system of PC component transportation.

In this paper, we applied the project oriented management to the research on logistics transportation cost optimization of prefabricated building components. Although some research results have been acquired, due to the restricted exploration level and the absence of in-depth comprehension of model development and solution algorithm, there are still a few deficiencies in this research, which should be additionally improved. Firstly, this paper studied the transportation business between the manufacturer (component factory) and the demander (construction site) of the prefabricated building component, where supply chain transportation cost management was not considered. Considering the common interests of all participants in the prefabricated building component supply chain, including raw material suppliers, the supply chain management of prefabricated building components will be a more practical research. Secondly, the transport vehicles under study had the same model and load, and the demand of each construction site was known. In reality, the vehicles equipped by each prefabricated building component factory might be of multiple models, and the load might also be different to meet different demand. The specifications and requirements for PC components might change dynamically on the construction site due to resource constraints such as changes in manpower, machinery, and traffic conditions and the influence of uncertain factors. The breadth and depth of research need to be further expanded and studied. Thirdly, in the aspect of algorithm improvement, because I am still in the primary stage of mastering the artificial fish swarm algorithm, I slightly improve the field of vision and step size, so that the convergence speed and accuracy of the algorithm have been strengthened. At present, the rapid development of intelligent optimization algorithms such as fish swarm algorithm, tabu search algorithm, genetic algorithm, ant colony algorithm, and particle swarm optimization algorithm needs further research and exploration combining these intelligent algorithms. Moreover, the loading optimization was not fine enough. From the perspective of independent transportation, the transportation cost per unit distance was not a strict linear change. The vehicle fuel consumption after component unloading will fluctuate compared with that before unloading, and the loading link of transportation cost can be further refined. Finally, for the transportation optimization of single vehicle type and single transportation center, more complex multiple vehicle type and multiple center problems may appear in practical engineering. The specific optimization feasibility needs to be analyzed, and the upper and lower bound optimization of scheduling problem need to be studied.

Data Availability

The data used to support the findings of this study are available from the author upon request.

Conflicts of Interest

The author declares that he has no conflicts of interest.

Hindawi
Journal of Mathematics
Volume 2023, Article ID 9841465, 1 page
https://doi.org/10.1155/2023/9841465

Retraction

Retracted: New Types of μ-Proximity Spaces and Their Applications

Journal of Mathematics

Received 17 October 2023; Accepted 17 October 2023; Published 18 October 2023

This article has been retracted by Hindawi following an investigation undertaken by the publisher [1]. This investigation has uncovered evidence of one or more of the following indicators of systematic manipulation of the publication process:

(1) Discrepancies in scope

(2) Discrepancies in the description of the research reported

(3) Discrepancies between the availability of data and the research described

(4) Inappropriate citations

(5) Incoherent, meaningless and/or irrelevant content included in the article

(6) Peer-review manipulation

The presence of these indicators undermines our confidence in the integrity of the article's content and we cannot, therefore, vouch for its reliability. Please note that this notice is intended solely to alert readers that the content of this article is unreliable. We have not investigated whether authors were aware of or involved in the systematic manipulation of the publication process.

Wiley and Hindawi regrets that the usual quality checks did not identify these issues before publication and have since put additional measures in place to safeguard research integrity.

We wish to credit our own Research Integrity and Research Publishing teams and anonymous and named external researchers and research integrity experts for contributing to this investigation.

The corresponding author, as the representative of all authors, has been given the opportunity to register their agreement or disagreement to this retraction. We have kept a record of any response received.

References

[1] R. A. Hosny, T. M. Al-shami, and A. Mhemdi, "New Types of μ-Proximity Spaces and Their Applications," *Journal of Mathematics*, vol. 2022, Article ID 1657993, 10 pages, 2022.

Hindawi
Journal of Mathematics
Volume 2022, Article ID 1657993, 10 pages
https://doi.org/10.1155/2022/1657993

Research Article

New Types of μ-Proximity Spaces and Their Applications

Rodyna A. Hosny,[1] **Tareq M. Al-shami**,[2] **and Abdelwaheb Mhemdi**[3]

[1]*Department of Mathematics, Faculty of Science, Zagazig University, Zagazig, Egypt*
[2]*Department of Mathematics, Sana'a University, Sana'a, Yemen*
[3]*Department of Mathematics, College of Sciences and Humanities in Aflaj Prince Sattam bin Abdulaziz University, Riyadh, Saudi Arabia*

Correspondence should be addressed to Tareq M. Al-shami; tareqalshami83@gmail.com

Received 21 October 2021; Accepted 20 December 2021; Published 17 January 2022

Academic Editor: Lazim Abdullah

Near set theory supplies a major basis for the perception, differentiation, and classification of elements in classes that depend on their closeness, either spatially or descriptively. This study aims to introduce a lot of concepts; one of them is μ-clusters as the useful notion in the study of μ-proximity (or μ-nearness) spaces which recognize some of its features. Also, other types of μ-proximity, termed $R\mu$-proximity and $O\mu$-proximity, on $\mathcal{X}$ are defined. In a μ-proximity space $(\mathcal{X}, \delta_\mu)$, for any subset K of $\mathcal{X}$, one can find out nonempty collections $\delta_\mu[K] = \{G \subseteq \mathcal{X} \mid K \overline{\delta}_\mu G\}$, which are hereditary classes on $\mathcal{X}$. Currently, descriptive near sets were presented as a tool of solving classification and pattern recognition problems emerging from disjoint sets; hence, a new approach to basic μ-proximity structures, which depend on the realization of the structures in the theory of hereditary classes, is introduced. Also, regarding to specific options of hereditary class operators, various kinds of μ-proximities can be distinguished.

1. Introduction

A proximity (or nearness) space is a sort of structured set, that consists of a nonempty set $\mathcal{X}$ and a binary relation between the subsets of $\mathcal{X}$. In constructive mathematics, any one of these relations may be possessed as major, and the others defined utilizing it; thence, we can differentiate, constructively, among a set-set nearness space "δ," a set-set apartness space "$\overline{\delta}$"(negation of δ or nonnear), and a set-set neighborhood space "$\ll$."

Initiatively, descriptive near sets have established to be valuable in an assortment of applications as topology [1, 2], solving a lot of problems that rely on human perception [3, 4] that arises in fields of image analysis [5], image processing [6], face recognition [7], rough set [8, 9], environmental space [10], and information systems [11–13], as well as science problems [14]. Also, Peters and Wasilewski [15] put in an approach to the foundations of information science which are formulated in the context of near sets.

The concept of proximity spaces was introduced by Naimpally and Warrack in [16]. A spatial nearness relation [1] δ is defined by $\delta = \{(A, B) \in P(\mathcal{X}) \times P(\mathcal{X}) \mid clA \cap clB \neq \emptyset\}$. It has ever after proven to be a valuable model in the rating of topological spaces. By introducing f-proximities that depends on certain functions f, Thron [17] created a framework for kinds of proximities. Generalized proximity structures have been widely investigated by several articles including [18, 19]. In [20, 21], several generalized proximities have been established utilizing Ef-proximity and ideals. In [22], Kandil et al. introduced an approach to proximity structures that depend on the recognition of many of the entities important in the theory of ideals. Also, they proposed the concept of g-proximities and showed that, for different choice of "g," one can obtain many of the known types of generalized proximities. Kandil et al. [23] presented approach of proximity and generalized proximity based on the soft sets. Also, they generalized the notions of compact, proximity relation and proximal neighborhood in the multiset context [24].

Many researchers have worked with weaker axioms than those of the fundamental concept ofEfremovic proximity

space [25] enabling them to introduce an arbitrary topology on the underlying set with nice properties, and the theory possesses deep results, rich machinery, and tools. In 2019, Mukherjee et al. [26] constructed a generalized proximity structure, named μ-proximity on set $\mathcal{X}$, which induces a generalized topology(GT) on $\mathcal{X}$. Also, Yildirim [27] constructed a generalized μ–proximity structure by using hereditary class on a set. Császár studies attracted many researchers concentration, inducing their considerable studies which involve an extension of generalized topologies utilizing some specific sort of classes of sets called hereditary classes [28].

In this study, the concept of μ-clusters in the study of μ-proximity (or μ-nearness) spaces is presented and some of its features are investigated. As a generalization of [22], the theory of basic μ-proximities in terms of hereditary classes is developed. A new approach to basic μ-proximity structures, which depend on the realization of the structures in the theory of hereditary classes, is introduced. Also, regarding to specific options of hereditary class operators, various kinds of μ-proximities are distinguished.

2. Preliminaries

To outline this paper as self-sufficient as possible, we recall the next definitions and results which are due to different references.

Definition 1 (see [28]). A nonempty family $\mathcal{H}$ of subsets of $\mathcal{X}$ is called hereditary class if it is closed under subsets. The set of all hereditary classes on $\mathcal{X}$ is denoted by $\mathbb{H}$.

Definition 2 (see [26]). A binary relation δ_μ on the power set $P(\mathcal{X})$ of a set $\mathcal{X}$ is called a μ-proximity (μ-nearness) on $\mathcal{X}$ and $(\mathcal{X}, \delta_\mu)$ is a μ-proximity (μ-nearness) space if, for all $G, K \subseteq \mathcal{X}$, δ_μ satisfies the following axioms:

(1) $G\delta_\mu K \Rightarrow K\delta_\mu G$
(2) $G\delta_\mu K$, $G \subseteq U$, and $K \subseteq V \Rightarrow U\delta_\mu V$
(3) $\{x\}\delta_\mu\{x\}$, $\forall x \in \mathcal{X}$
(4) $G\overline{\delta}_\mu K \Rightarrow \exists E \subseteq \mathcal{X}$ s.t. $G\overline{\delta}_\mu E$, $(\mathcal{X}\backslash E)\overline{\delta}_\mu K$

A relation δ_μ on $\mathcal{X}$ is called a basic μ-proximity if it satisfies only conditions (1), (2), and (3). We denote by $\wp(\mathcal{X})$ the family of all basic μ-proximities on $\mathcal{X}$. Henceforth, we write $x\delta_\mu G$ for $\{x\}\delta_\mu G$.

Several properties of the relation δ_μ on $\mathcal{X}$ have been mentioned with details in [26].

Remark 1 (see [26]). A generalized topology μ is compatible with the μ-proximity relation of sets δ_μ, denoted $\mu_- \sim \delta_\mu$, $\tau_{\delta_\mu} = \mu_-$.

Definition 3 (see [16]). If δ_{μ_1} and δ_{μ_2} are two μ-proximities on a set $\mathcal{X}$, then δ_{μ_2} is called finer than δ_{μ_1} (in symbols $\delta_{\mu_1} \prec \delta_{\mu_2}$) if $G\delta_{\mu_2}K$ implies $G\delta_{\mu_1}K$.

Definition 4 (see [26]). A subset G of a μ-proximity space $(\mathcal{X}, \delta_\mu)$ is a δ_μ nbhood. of a set K if $K\overline{\delta}_\mu(\mathcal{X}\backslash G)$. The set of all δ_μ nbhood. of K with respect to δ_μ is denoted by $\mathcal{N}(\delta_\mu, K)$ or simply, $\mathcal{N}_\mu(K)$, i.e., $\mathcal{N}_\mu(K) = \{G \mid K\overline{\delta}_\mu(\mathcal{X}\backslash G)\}$.

Lemma 1 (see [26]). *For all subsets G, K of a basic μ-proximity space $(\mathcal{X}, \delta_\mu)$, then the following statements hold:*

(1) If $G \subseteq K$, then $\mathcal{N}_\mu(K) \subseteq \mathcal{N}_\mu(G)$
(2) $K \in \mathcal{N}_\mu(G)$ iff $(\mathcal{X}\backslash G) \in \mathcal{N}_\mu(\mathcal{X}\backslash K)$
(3) $\mathcal{N}_\mu(\varnothing) = P(\mathcal{X})$

Proposition 1 (see [26]). *Let $(\mathcal{X}, \delta_\mu)$ be a μ-proximity space and $\tau_{\delta_\mu} = \mu_-$. Then, the μ-closure $c_\mu(G)$ of a set G in $(\mathcal{X}, \mu)$ is given by $c_\mu(G) = \{x: x\delta_\mu G\}$.*

In the following proposition, one can deduce some useful properties of δ_μ.

Proposition 2. *Let $\mathcal{X}$ be a nonempty set. For each $x \in \mathcal{X}$ and $G, K \subseteq \mathcal{X}$,*

(1) $x\delta_\mu G$, $x\delta_\mu K \Rightarrow x\delta_\mu G \cup K$
(2) $x \in G \Rightarrow x\delta_\mu G$
(3) $x\delta_\mu G$, $y\delta_\mu K \forall y \in G \Rightarrow x\delta_\mu K$
(4) If there is a point $p \in \mathcal{X}$ s.t. $G\delta_\mu p$ and $p\delta_\mu K$, then $G\delta_\mu K$

3. On μ-Clusters

Let us consider the concept of μ-cluster from μ-proximity spaces and explore some of its properties.

Definition 5. Let $(\mathcal{X}, \delta_\mu)$ be a μ-proximity space and $G, K \subseteq \mathcal{X}$. A μ-cluster is a nonempty collection σ_μ of subsets of $\mathcal{X}$ s.t.

(1) If $G \in \sigma_\mu$, $K \in \sigma_\mu$, then $G\delta_\mu K$
(2) If $G\delta_\mu K$, for every $K \in \sigma_\mu$, then $G \in \sigma_\mu$

The family of all μ-clusters of $\mathcal{X}$ is denoted by $\aleph_\mu(\mathcal{X})$.

Theorem 1. *If $\sigma_{1\mu}, \sigma_{2\mu}$ are μ-clusters in a μ-proximity space $(\mathcal{X}, \delta_\mu)$ and if $\sigma_{2\mu} \subseteq \sigma_{1\mu}$, then $\sigma_{1\mu} = \sigma_{2\mu}$.*

Proof. Let $G \notin \sigma_{2\mu}$. Then, there exists $B \in \sigma_{2\mu}$ s.t. $B\overline{\delta}_\mu G$. Since $\sigma_{2\mu} \subseteq \sigma_{1\mu}$, then there exists $B \in \sigma_{1\mu}$ s.t. $B\overline{\delta}_\mu G$. By (1) of Definition 5, $G \notin \sigma_{1\mu}$. Hence, $\sigma_{1\mu} \subseteq \sigma_{2\mu}$, so $\sigma_{1\mu} = \sigma_{2\mu}$. □

Remark 2. If $\aleph_\mu(\mathcal{X})$ is a family of finite nested μ-clusters of $\mathcal{X}$, *i.e.*, $\sigma_{n\mu} \subseteq \cdots \subseteq \sigma_{2\mu} \subseteq \sigma_{1\mu}$, then $\aleph_\mu(\mathcal{X}) = \{\sigma_{1\mu}\}$.

In view of Definition 2 and Proposition 2, the following examples are given.

Lemma 2. *Let $(\mathcal{X}, \delta_\mu)$ be a μ-proximity space. A collection σ_μ in $\mathcal{X}$ is a μ-cluster iff all sets $G \in \sigma_\mu$ are near point x. In other words, the collection $\sigma_\mu(x) = \{G \subseteq \mathcal{X} \mid x\delta_\mu G\}$ is a μ-cluster. $\sigma_\mu(x)$ is called a principal μ-cluster or point μ-cluster.*

Remark 3. $G \in \sigma_\mu(x)$ iff $x \in c_\mu(G)$.

Example 1. If δ_μ is defined on $\mathcal{X}$, the family of all natural numbers, as $G\delta_\mu K$ iff both G and K are nonempty sets. Then, the collection $\sigma_\mu = \{G \subseteq \mathcal{X} \mid G \neq \emptyset\}$ is a μ-cluster. Also, $\sigma_\mu = \sigma_\mu(x)$, for every $x \in \mathcal{X}$.

Theorem 2. *If σ_μ is a μ-cluster in a μ-proximity space $(\mathcal{X}, \delta_\mu)$, then*

(1) $\sigma_\mu(x) \neq \emptyset$

(2) $G \in \sigma_\mu$ *and* $G \subseteq K \Rightarrow K \in \sigma_\mu$

(3) $G \in \sigma_\mu$ *iff* $c_\mu(G) \in \sigma_\mu$

(4) If there is a point $x \in \mathcal{X}$ *s.t.* $\{x\} \in \sigma_\mu$, *then* $\sigma_\mu = \sigma_\mu(x)$

(5) $A \in \sigma_\mu$ *iff for all* $G, K \subseteq \mathcal{X}$, $G \in \sigma_\mu$ *and* $(\mathcal{X} \setminus A) \cup K = \mathcal{X} \Rightarrow G\delta_\mu K$

Proof

(1) Obvious.

(2) Let $G \in \sigma_\mu$ and $G \subseteq K$. Suppose $K \notin \sigma_\mu$; then, there exists $B \in \sigma_\mu$ s.t. $B\overline{\delta}_\mu K$. Since $G, B \in \sigma_\mu$, then from (2) of Definition 2 and (1) of Definition 5, $B\delta_\mu G$ and so $B\delta_\mu K$. This is a contradiction. Hence, $K \in \sigma_\mu$.

(3) If $G \in \sigma_\mu$, then, from (1), $c_\mu(G) \in \sigma_\mu$. In the other side, suppose $G \notin \sigma_\mu$. Then, $B\overline{\delta}_\mu G$, for some $B \in \sigma_\mu$. In view of Lemma 2.8 of [26], $c_\mu(B)\overline{\delta}_\mu c_\mu(G)$. So, $B\overline{\delta}_\mu c_\mu(G)$. Then, from (1) of Definition 5, $c_\mu(G) \notin \sigma_\mu$. Hence, the proof has been completed.

(4) Let $G \in \sigma_\mu$. Since $\{x\} \in \sigma_\mu$, then, by (1) of Definition 5, $x\delta_\mu G$. Hence, $G \in \sigma_\mu(x)$, i.e., $\sigma_\mu \subseteq \sigma_\mu(x)$. On the contrary, let $G \in \sigma_\mu(x)$; then, $x\delta_\mu G$. Suppose $G \notin \sigma_\mu$; then, $B\overline{\delta}_\mu G$ for some $B \in \sigma_\mu$. Since $\{x\}, B \in \sigma_\mu$, then $x\delta_\mu B$. According to (4) of Proposition 2, $B\delta_\mu G$. This is a contradiction. Hence, $G \in \sigma_\mu$. Then, $\sigma_\mu(x) \subseteq \sigma_\mu$, so $\sigma_\mu = \sigma_\mu(x)$.

(5) ($\Rightarrow$) Let $A \in \sigma_\mu$ and $G \in \sigma_\mu$; then, $G\delta_\mu A$. Suppose $(\mathcal{X} \setminus A) \cup K = \mathcal{X}$; then, every element of A belongs to K. Hence, from (2), $K \in \sigma_\mu$, so $G\delta_\mu K$. ($\Leftarrow$) Assume that, for all $G, K \subseteq \mathcal{X}$, $G \in \sigma_\mu$ and $(\mathcal{X} \setminus A) \cup K = \mathcal{X}$ imply $G\delta_\mu K$. Choose $K = A$; then, $G\delta_\mu A$, for all $G \in \sigma_\mu$. So, $A \in \sigma_\mu$.

Now, we define a function α from $P(\mathcal{X})$ into a family $\aleph_\mu(\mathcal{X})$ of all μ-clusters of $\mathcal{X}$ by

$$\alpha(G) = \{\sigma_\mu \in \aleph_\mu(\mathcal{X}) \mid G \in \sigma_\mu\}. \quad (1)$$

□

Theorem 3.

(1) $\alpha(\emptyset) = \emptyset$ *and* $\alpha(\mathcal{X}) = \aleph_\mu(\mathcal{X})$

(2) $G \subseteq K \Rightarrow \alpha(G) \subseteq \alpha(K)$

(3) $\alpha(G) \cup \alpha(K) \subseteq \alpha(G \cup K)$ *and* $\alpha(G \cap K) \subseteq \alpha(G) \cap \alpha(K)$

(4) $\alpha(G) \cap \alpha(K) \neq \emptyset$ *iff* $G\delta_\mu K$

Proof

(1) In view of (2) of Theorem 2, $\alpha(\emptyset) = \{\sigma_\mu \in \aleph_\mu(\mathcal{X}) \mid \emptyset \in \sigma_\mu\} = \emptyset$ and $\alpha(\mathcal{X}) = \{\sigma_\mu \in \aleph_\mu(\mathcal{X}) \mid \mathcal{X} \in \sigma_\mu\} = \aleph_\mu(\mathcal{X})$.

(2) Let $\sigma_\mu \in \alpha(G)$; then, $G \in \sigma_\mu$. Since $G \subseteq K$, hence, in view of (2) of Theorem 2, $K \in \sigma_\mu$, so $\sigma_\mu \in \alpha(K)$, i.e., $\alpha(G) \subseteq \alpha(K)$.

(3) It is obvious from (2).

(4) ($\Rightarrow$) Suppose $\alpha(G) \cap \alpha(K) \neq \emptyset$; then, there exists $\sigma_\mu \in \alpha(G) \cap \alpha(K)$. Hence, $\sigma_\mu \in \alpha(G)$ and $\sigma_\mu \in \alpha(K)$ which imply that G and $K \in \sigma_\mu$. From Definition 5, $G\delta_\mu K$. ($\Leftarrow$) Assume that $G\delta_\mu K$ and $\alpha(G) \cap \alpha(K) = \emptyset$; then, $\sigma_\mu \notin \alpha(G)$ for every $\sigma_\mu \in \alpha(K)$. Hence, $G\delta_\mu K$, for every $K \in \sigma_\mu$ which imply that $G \in \sigma_\mu$. It is a contradiction.

Next, we shall introduce an appropriate proximity Φ on $\aleph_\mu(\mathcal{X})$. $\Lambda, \Gamma \subseteq \aleph_\mu(\mathcal{X}) \Lambda \Phi \Gamma \Leftrightarrow \Lambda \subseteq \alpha(G)$ and $\Gamma \subseteq \alpha(K)$ imply $G\delta_\mu K$, for all $G, K \subseteq \mathcal{X}$. □

Theorem 4. *The structure $(\aleph_\mu(\mathcal{X}), \Phi)$ is a μ-proximity space.*

Proof

(1) $\Lambda \Phi \Gamma \Rightarrow \Gamma \Phi \Lambda$.

(2) Suppose $\Omega \overline{\Phi} \Upsilon$, $\Lambda \subseteq \Omega$, and $\Gamma \subseteq \Upsilon$; then, $\Omega \subseteq \alpha(G)$, $\Upsilon \subseteq \alpha(K)$, and $G\overline{\delta}_\mu K$, for some $G, K \subseteq \mathcal{X}$. From hypothesis $\Lambda \subseteq \Omega$ and $\Gamma \subseteq \Upsilon$, hence, $\Lambda \subseteq \alpha(G)$, $\Gamma \subseteq \alpha(K)$, and $G\overline{\delta}_\mu K$, for some $G, K \subseteq \mathcal{X}$. It follows that $\Lambda \overline{\Phi} \Gamma$. Consequently, $\Lambda \Phi \Gamma$, $\Lambda \subseteq \Omega$, and $\Gamma \subseteq \Upsilon$ imply $\Omega \Phi \Upsilon$

(3) Let σ be a μ-cluster of $\mathcal{X}$. If $\{\sigma\} \subseteq \alpha(G)$ and $\{\sigma\} \subseteq \alpha(K)$, then from (4) of Theorem 3, $G\delta_\mu K$, for all $G, K \subseteq \mathcal{X}$. Hence, $\{\sigma\} \Phi \{\sigma\}$.

(4) Suppose $\Lambda \overline{\Phi} \Gamma$; then, $\Lambda \subseteq \alpha(G)$, $\Gamma \subseteq \alpha(K)$, and $G\overline{\delta}_\mu K$, for some $G, K \subseteq \mathcal{X}$. □

Corollary 1. $\Lambda \cap \Gamma \neq \emptyset \Rightarrow \Lambda \Phi \Gamma$.

Proof. Let $\Lambda \cap \Gamma \neq \emptyset$; then, there exists σ s.t. $\sigma \in \Lambda$ and $\sigma \in \Gamma$. Suppose $\Lambda \overline{\Phi} \Gamma$; then, $\Lambda \subseteq \alpha(G)$, $\Gamma \subseteq \alpha(K)$, and $G\overline{\delta}_\mu K$, for some $G, K \subseteq \mathcal{X}$. Hence, $\sigma \subseteq \alpha(G)$ and $\sigma \subseteq \alpha(K)$. According to (4) of Theorem 3, $G\delta_\mu K$. It is a contradiction. So, $\Lambda \Phi \Gamma$. □

4. On μ-Proximity with Hereditary Class

In accordance with principal μ-clusters notion, we will turn to the concept of hereditary classes.

Definition 6. Let $(\mathcal{X}, \delta_\mu)$ be a μ-proximity space and $x \in \mathcal{X}$; then, $\{G \subseteq \mathcal{X} : G \notin \sigma_\mu(x)\}$ is a hereditary class on $\mathcal{X}$.

Remark 4. Let $(\mathcal{X}, \delta_\mu)$ be a μ -proximity space, $G \subseteq \mathcal{X}$ and $x \in \mathcal{X}$. Then,

(1) $\delta_\mu[x] = \{G \subseteq \mathcal{X} : x\overline{\delta}_\mu G\}$

(2) $G \in \delta_\mu[x]$ *iff* $x \in \delta_\mu[G]$

(3) $c_\mu(G) = \{x \in \mathcal{X} \mid x \notin \delta_\mu[G]\}$

In the next section, we introduce the notion $\delta_\mu[K]$ for any subset K of $\mathcal{X}$ as a generalization of $\delta_\mu[x]$ for any $x \in \mathcal{X}$.

Definition 7. Let $(\mathcal{X}, \delta_\mu)$ be a μ-proximity space and $k \subseteq \mathcal{X}$; then, we define

$$\delta_\mu[K] = \left\{G \subseteq \mathcal{X} \mid K \overline{\delta}_\mu G\right\}. \tag{2}$$

Next example shows that $\delta_\mu[K]$ is not an ideal on $\mathcal{X}$, for any set $K \subseteq \mathcal{X}$.

Example 2. Let $\mathcal{X} = \{a, b, c\}$ and let δ_μ be a μ-proximity on $\mathcal{X}$ defined as $G\delta_\mu K \Leftrightarrow G = K$.

If $G_1 = \{a\}, G_2 = \{b\}$, and $K = \{a, b\}$, then $G_1, G_2 \in \delta_\mu[K]$ but $G_1 \cup G_2 \notin \delta_\mu[K]$.

Example 3. Evidently, $\delta_\mu[\varnothing] = P(\mathcal{X})$ and $\delta_\mu[\mathcal{X}] = \{\varnothing\}$.

Next, we reformulate Definition 2 in terms of $\delta_\mu[.]$ as follows:

Definition 8. A binary relation δ_μ on $P(\mathcal{X})$ is called a μ-proximity on $\mathcal{X}$ if, for all $G, K \subseteq \mathcal{X}$, δ_μ satisfies the following axioms:

(1) $G \in \delta_\mu[K] \Rightarrow K \in \delta_\mu[G]$

(2) $U \in \delta_\mu[V]$, $G \subseteq U$, and $K \subseteq V \Rightarrow G \in \delta_\mu[K]$

(3) $\{x\} \notin \delta_\mu[\{x\}]$, $\forall x \in \mathcal{X}$

(4) $G \in \delta_\mu[K] \Rightarrow$ there exists $E \subseteq \mathcal{X}$ s.t. $G \in \delta_\mu[\mathcal{X} \backslash E]$ and $E \in \delta_\mu[K]$

A relation δ_μ is called a basic μ-proximity if it satisfies only conditions (1), (2), and (3). We write $x \in \delta_\mu[K]$ for $\{x\} \in \delta_\mu[K]$ and $\delta_\mu[x]$ for $\delta_\mu[\{x\}]$.

It is clear that (2) in the axiomatical definition of μ-proximity relation δ_μ can be equivalently replaced by $(2)^* \delta_\mu[G \cup K] \subseteq \delta_\mu[G] \cap \delta_\mu[K]$, for every $G, K \subseteq \mathcal{X}$.

In the following, we will display considerable of the properties of $\delta_\mu[.]$.

From Definition 7, the next lemmas follow directly.

Lemma 3. *Let $(\mathcal{X}, \delta_\mu)$ be a μ -proximity space. Then,*

(1) $G_1 \cup G_2 \in \delta_\mu[K] \Rightarrow G_1 \in \delta_\mu[K]$ *and* $G_2 \in \delta_\mu[K] \Rightarrow G_1 \cap G_2 \in \delta_\mu[K]$

(2) $G_r \in \delta_\mu[K]$, $r \in \Lambda \Rightarrow \cap_{r \in \Lambda} G_r \in \delta_\mu[K]$

(3) $G \in \delta_\mu[K] \Rightarrow x \in \delta_\mu[K] \forall x \in G$

(4) $\mathcal{X} \notin \delta_\mu[x]$ *and* $x \notin \delta_\mu[\mathcal{X}]$

Lemma 4. *For all subsets G, K of a μ-proximity space $(\mathcal{X}, \delta_\mu)$, the following statements hold:*

(1) $G \subseteq K \Rightarrow \delta_\mu[K] \subseteq \delta_\mu[G]$

(2) $\delta_\mu[G] \cap \delta_\mu[K] \subseteq \delta_\mu[G \cap K]$

(3) $A \in \delta_\mu[G]$, $B \in \delta_\mu[K] \Rightarrow A \cap B \in \delta_\mu[G \cap K]$

Regarding to hereditary classes on $\mathcal{X}$, one can introduce μ-proximity relations on $\mathcal{X}$ as we show in the following examples.

Example 4. Let $\mathcal{X}$ be a set with any hereditary class $\mathcal{H}$ and $\{x\} \notin \mathcal{H}$. For any subsets G and K of $\mathcal{X}$, we define

$$G \in \delta_\mu[K] \Leftrightarrow G \cap K \in \mathcal{H}. \tag{3}$$

Then, the relation δ_μ is a μ-proximity on $\mathcal{X}$.

Example 5. Let $\mathcal{X}$ be a set with any hereditary class $\mathcal{H}$ and $\{x\} \notin \mathcal{H}$. For any subsets G and K of $\mathcal{X}$, define $G \in \delta_\mu[K] \Leftrightarrow G$ or $K \in \mathcal{H}$.

Then, the relation δ_μ is a μ-proximity on $\mathcal{X}$.

Theorem 5. *Let $(\mathcal{X}, \delta_\mu)$ be a μ-proximity space and $G, K \subseteq \mathcal{X}$. If μ-closures and μ-interiors are taken with respect to $\mu - = \tau_{\delta_\mu}$, then the following properties are true:*

(1) $G \in \delta_\mu[K]$ *implies* $G \cap K = \varnothing$

(2) $G \in \delta_\mu[K]$ *iff* $(\mathcal{X} \backslash G) \in \mathcal{N}_\mu(K)$

(3) K *is* δ_μ *closed WRT* $\mu - = \tau_{\delta_\mu}$ *if* $x \in \delta_\mu[K]$, $\forall x \notin K$

(4) $K \in \tau_{\delta_\mu}$ *WRT* $\mu - = \tau_{\delta_\mu}$ *if* $x \in \delta_\mu[\mathcal{X} \backslash K]$, $\forall x \in K$

(5) $G \in \delta_\mu[K]$ *implies* $c_\mu(G) \in \delta_\mu[K]$ *and* $G \in \delta_\mu[c_\mu(K)]$

(6) $G \in \delta_\mu[K]$ *iff* $c_\mu(G) \in \delta_\mu[c_\mu(K)]$

(7) $x \in \delta_\mu[K]$ *iff* $c_\mu(\{x\}) \in \delta_\mu[c_\mu(K)]$

Proof. Direct to prove. □

Lemma 5. *Let $\delta_{\mu_1}, \delta_{\mu_2}$ be two μ-proximities on a set $\mathcal{X}$. Then, $\delta_{\mu_1} \prec \delta_{\mu_2}$ iff $\delta_{\mu 1}[G] \subseteq \delta_{\mu 2}[G]$, $\forall G \subseteq \mathcal{X}$.*

Proof. Accessible consequence of Definition 3. □

Theorem 6. *Let μ_1 and μ_2 be two μ-completely regular generalized topologies on $\mathcal{X}$ and δ_{μ_1} and δ_{μ_2} be the μ-proximities on $\mathcal{X}$ defined as $G \in \delta_{\mu_j}[K] \Leftrightarrow G$ and* K *are functionally distinguishable WRT μ_j, respectively, $j = 1, 2$.*

Then, $\mu_1 \subseteq \mu_2$ implies $\delta_{\mu_1} \prec \delta_{\mu_2}$

Proof. If $G \in \delta_{\mu_1}[K]$, then there exists a $\mu_1$continuous function $f: (\mathcal{X}, \mu_1) \longrightarrow [0, 1]$, where $[0, 1]$ is endowed with the subspace generalized topology induced by κ on R (where κ is the generalized topology on the set R of reals generated by the base $\beta = \{(-\infty, p): p \in R\} \cup \{(p, \infty): p \in R\})$ s.t. $f(G) = \{0\}$ and $f(K) = \{1\}$. Since $\mu_1 \subseteq \mu_2$, then f is a μ_2 continuous function from $(\mathcal{X}, \mu_2)$ to $[0, 1]$ s.t. $f(G) = \{0\}$ and $f(K) = \{1\}$. So, $G \in \delta_{\mu_2}[K]$. According to Lemma 5, $\delta_{\mu_1} \prec \delta_{\mu_2}$. □

Theorem 7. *Let $\delta_{\mu_1}, \delta_{\mu_2}$ be two μ-proximities on a set $\mathcal{X}$. Then, the following statements are equivalent:*

(1) $\delta_{\mu 1}[x] = \delta_{\mu 2}[x]$, $\forall x \in \mathcal{X}$

(2) $c_{\delta_{\mu 1}}(G) = c_{\delta_{\mu 2}}(G)$, $\forall G \subseteq \mathcal{X}$

(3) $\mathcal{N}_{\delta_{\mu 1}}(\{x\}) = \mathcal{N}_{\delta_{\mu 2}}(\{x\})$, $\forall x \in \mathcal{X}$

Proof. Easy to prove. □

Definition 9. A μ-proximity space $(\mathcal{X}, \delta_\mu)$ is T_0 iff for any two distinct points x, y of $\mathcal{X}$, $x \overline{\delta}_\mu y$.

Utilizing hereditary classes, another equivalent definition of T_0-space is obtained.

Theorem 8. *A μ-proximity space $(\mathcal{X}, \delta_\mu)$ is T_0 iff for any two distinct points x, y of X, $\delta_\mu[x] \neq \delta_\mu[y]$.*

Proof. Let x, y be any two distinct points in a T_0-space $(\mathcal{X}, \delta_\mu)$; then, $x\overline{\delta}_\mu y$. In view of Definition 5, $y \notin \sigma_\mu(x)$ or $x \notin \sigma_\mu(y)$. Suppose $y \notin \sigma_\mu(x)$, which gives $y \in \delta_\mu[x]$, but from (3) of Definition 2 $y \notin \delta_\mu[y]$. Consequently, $\delta_\mu[x] \neq \delta_\mu[y]$. Conversely, let $x, y \in \mathcal{X}$ and $x \neq y$ with $x\delta_\mu y$. Suppose that $\delta_\mu[x] \neq \delta_\mu[y]$; then, there is a subset G of $\mathcal{X}$ s.t. $G \in \delta_\mu[x]$ and $G \notin \delta_\mu[y]$. Then, $G \notin \sigma_\mu(x)$ and $G \in \sigma_\mu(y)$. Hence, $x\overline{\delta}_\mu G$ but $y\delta_\mu G$. Since $x\delta_\mu y$ and $y\delta_\mu G$, then in view of (3) of Proposition 2, $x\delta_\mu G$. It is a contradiction. Thus, $(\mathcal{X}, \delta_\mu)$ is T_0-space. □

Lemma 6. *Let $(\mathcal{X}, \mu)$ be a μ-normal GTS. Then, $c_\mu(G) \cap c_\mu(K) = \varnothing \Leftrightarrow c_\mu(G)$, $c_\mu(K)$ are functionally distinguishable.*

Proof. Suppose $c_\mu(G) \cap c_\mu(K) = \varnothing$; then, by Urysohn's lemma, $c_\mu(G)$ and $c_\mu(K)$ are functionally distinguishable. In the other side, suppose $c_\mu(G) \cap c_\mu(K) \neq \varnothing$. Then, there exists $p \in \mathcal{X}$ s.t. $p \in c_\mu(G) \cap c_\mu(K)$. Since there is no function f s.t. $f(p)$ has distinct values at p; hence, $c_\mu(G)$ and $c_\mu(K)$ are not functionally distinguishable. □

Theorem 9. *Let $(\mathcal{X}, \mu)$ be a μ-normal GTS. For any subsets G and K of $\mathcal{X}$, the relation δ_μ on $\mathcal{X}$ given by $G \in \delta_\mu[K] \Leftrightarrow c_\mu(G) \cap c_\mu(K) = \varnothing$ is a compatible μ-proximity on $\mathcal{X}$.*

Proof. According to Lemma 6, $c_\mu(G) \cap c_\mu(K) = \varnothing$ iff $c_\mu(G)$ and $c_\mu(K)$ are functionally distinguishable. From the features of a μ-continuous function, G and K are functionally distinguishable iff $c_\mu(G)$ and $c_\mu(K)$ are functionally distinguishable. So, $G \in \delta_\mu[K]$ iff $c_\mu(G) \cap c_\mu(K) = \varnothing$ iff G and K are functionally distinguishable. By Urysohn's lemma, every μ-normal GTS is μ-completely regular; then, from Theorem 2.11 of [26], the relation δ_μ is a compatible μ-proximity on $\mathcal{X}$. □

Theorem 10. *If $(\mathcal{X}, \mu)$ is a μ-completely regular, GTS has a compatib1e μ-proximity δ_μ defined by*

$$G \in \delta_\mu[K] \Leftrightarrow c_\mu(G) \cap c_\mu(K) = \varnothing \tag{4}$$

Then, $(\mathcal{X}, \mu)$ is μ-normal GTS.

Proof. Suppose $c_\mu(G), c_\mu(K)$ are disjoint μ-closed sets; then, $G \in \delta_\mu[K]$. Hence, there exists $E \subseteq \mathcal{X}$ s.t. $G \in \delta_\mu[\mathcal{X}\backslash E]$ and $E \in \delta_\mu[K]$. From Corollary 2.7 of [26] and Definition 7, $G \subseteq \mathcal{X}\backslash c_\mu(\mathcal{X}\backslash E) = i_\mu(E)$ and $K \subseteq i_\mu(\mathcal{X}E)$. Since $i_\mu(E)$ and $i_\mu(\mathcal{X}\backslash E)$ are disjoint μ-open sets, so $(\mathcal{X}, \mu)$ is μ-normal. □

5. On Basic μ-Proximity with Hereditary Class

Definition 10. A relation δ_μ is called $O\mu$-proximity on $\mathcal{X}$ if it is a basic μ-proximity on $\mathcal{X}$, and it satisfies the following condition:

$$G\delta_\mu A \text{ and } a\delta_\mu K \forall a \in A \Rightarrow G\delta_\mu K. \tag{5}$$

Example 6. In one of the schools, suppose that G, A, K be parents' council, set of students, and set of teachers, respectively. Evidently, δ_μ satisfies $O\mu$-proximity axioms on $\mathcal{X}$, see Figures 1 and 2.

Definition 11. A relation δ_μ is called $R\mu$-proximity on $\mathcal{X}$ if it is a basic μ-proximity on $\mathcal{X}$, and it satisfies the following condition:

$$x\overline{\delta}_\mu K \Rightarrow \text{there exists } E \subseteq \mathcal{X} \text{ s.t. } x\overline{\delta}_\mu E \text{ and } (\mathcal{X}E)\overline{\delta}_\mu K. \tag{6}$$

Theorem 11. *Let δ_μ be a basic μ -proximity on $\mathcal{X}$. Then, $c_\mu(K) = \cap\{A \mid (\mathcal{X}\backslash A) \in \delta_\mu[K]\}$.*

Proof. Suppose that $L = \cap\{A \mid (\mathcal{X}\backslash A) \in \delta_\mu[K]\}$. We shall prove $L = c_\mu(K)$. Let $x \notin c_\mu(K)$; then, $x \in \delta_\mu[K]$. Hence, $x \notin L$, so $L \subseteq c_\mu(K)$. On the contrary, let $x \notin L$; then, there is a subset A of $\mathcal{X}$ s.t. $x \notin A$ and $(\mathcal{X}\backslash A) \in \delta_\mu[K]$. According to (1) of Lemma 3, $x \in \delta_\mu[K]$. Thus, $x \notin c_\mu(K)$, so $c_\mu(K) \subseteq L$. Hence, $L = c_\mu(K)$ □

Theorem 12. *Let $\delta_\mu \in \wp(\mathcal{X})$. Then, the following are equivalent:*

(1) δ_μ is a μ-proximity on $\mathcal{X}$

(2) If $G \in \delta_\mu[K]$, then $\mathcal{N}_\mu(G) \cap \delta_\mu[K] \neq \varnothing$

(3) If $G \in \mathcal{N}_\mu(K)$, then there exists $E \in \mathcal{N}_\mu(K)$ s.t. $G \in \mathcal{N}_\mu(E)$

Proof

(1) ⇒ (2) Let $G \in \delta_\mu[K]$. In view of (1) and (4) of Definition 7, there exists $E \subseteq \mathcal{X}$ s.t. $(\mathcal{X}\backslash E) \in \delta_\mu[G]$ and $E \in \delta_\mu[K]$. Hence, by (2) of Theorem 5, $E \in \mathcal{N}_\mu(G) \cap \delta_\mu[K]$. Consequently, $\mathcal{N}_\mu(G) \cap \delta_\mu[K] \neq \varnothing$.

(2) ⇒ (3) Let $G \in \mathcal{N}_\mu(K)$; then, $(\mathcal{X}\backslash G) \in \delta_\mu[K]$. Hence, $\mathcal{N}_\mu(\mathcal{X}\backslash G) \cap \delta_\mu[K] \neq \varnothing$ which implies that there exists a set A s.t. $A \in \mathcal{N}_\mu(\mathcal{X}\backslash G)$ and $A \in \delta_\mu[K]$. In view of (2) of Lemma 1 and (2) of Theorem 5, $G \in \mathcal{N}_\mu(\mathcal{X}\backslash A)$ and $(\mathcal{X}\backslash A) \in \mathcal{N}_\mu(K)$. Put $(\mathcal{X}/A)$; then, (3) holds.

(3) ⇒ (1) Let $G \in \delta_\mu[K]$; then, $(\mathcal{X}\backslash G) \in \mathcal{N}_\mu(K)$. According to (3), then there exists $E \in \mathcal{N}_\mu(K)$ s.t. $(\mathcal{X}\backslash G) \in \mathcal{N}_\mu(E)$. Therefore, $G \in \delta_\mu[E]$ and $(\mathcal{X}\backslash E) \in \delta_\mu[K]$, so δ_μ is a μ-proximity on $\mathcal{X}$. □

Theorem 13. *Let $\delta_\mu \in \wp(\mathcal{X})$. Then, the following are equivalent:*

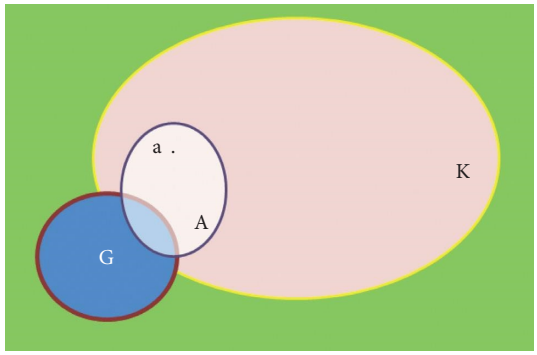

Figure 1: $G\delta_\mu A$ and $a\delta_\mu K \forall a \in A \Rightarrow G\delta_\mu K$.

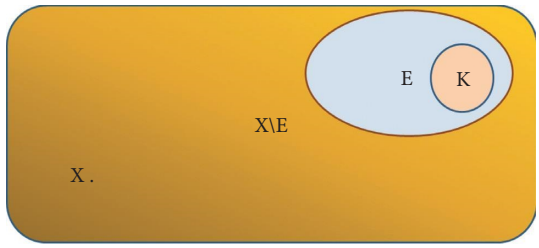

Figure 2: $x\overline{\delta}_\mu K \Rightarrow x\overline{\delta}_\mu E$ and $(\mathcal{X}\setminus E)\overline{\delta}_\mu K$, for some $E \subseteq \mathcal{X}$.

(1) δ_μ is a Rμ-proximity on $\mathcal{X}$

(2) If $x \in \delta_\mu[K]$, then $\mathcal{N}_\mu(x) \cap \delta_\mu[K] \neq \emptyset$

(3) If $K \in \mathcal{N}_\mu(x)$, then there exists $E \in \mathcal{N}_\mu(x)$ s.t. $K \in \mathcal{N}_\mu(E)$

Proof

(1) $\Rightarrow$ (2) Let $x \in \delta_\mu[K]$. From Definition 11, there exists $E \subseteq \mathcal{X}$ s.t. $x \in \delta_\mu[\mathcal{X}\setminus E]$ and $E \in \delta_\mu[K]$. So, $(\mathcal{X}\setminus E) \in \delta_\mu[x]$ and $E \in \delta_\mu[K]$. Hence, $E \in \mathcal{N}_\mu(x) \cap \delta_\mu[K]$. Consequently, $\mathcal{N}_\mu(x) \cap \delta_\mu[K] \neq \emptyset$.

(2) $\Rightarrow$ (3) Let $K \in \mathcal{N}_\mu(x)$; then, $(\mathcal{X}\setminus K) \in \delta_\mu[x]$. Hence, $\mathcal{N}_\mu(\mathcal{X}\setminus K) \cap \delta_\mu[x] \neq \emptyset$ which implies that there exists a set A of $\mathcal{X}$ s.t. $A \in \mathcal{N}_\mu(\mathcal{X}\setminus K)$ and $A \in \delta_\mu[x]$. In view of (2) of Lemma 1 and (2) of Theorem 5, $K \in \mathcal{N}_\mu(\mathcal{X}\setminus A)$ and $(\mathcal{X}\setminus A) \in \mathcal{N}_\mu(x)$. Put $(\mathcal{X}/A)$; then, (3) holds.

(3) $\Rightarrow$ (1) Let $x \in \delta_\mu[K]$; then, $(\mathcal{X}\setminus K) \in \mathcal{N}_\mu(x)$. According to (3), then there exists $E \in \mathcal{N}_\mu(x)$ s.t. $(\mathcal{X}\setminus K) \in \mathcal{N}_\mu(E)$. Therefore, $K \in \delta_\mu[E]$ and $(\mathcal{X}\setminus E) \in \delta_\mu[x]$, so δ_μ is a Rμ-proximity on $\mathcal{X}$. □

Definition 12. Let $\mathcal{H}$ be a hereditary class on a basic μ-proximity space $(\mathcal{X}, \delta_\mu)$. A mapping $\lambda: \wp(\mathcal{X}) \times \mathbb{H} \longrightarrow \mathbb{H}$ is called a hereditary class operator on $\mathcal{X}$ if it identifies to each pair $(\delta_\mu, \mathcal{H})$, a hereditary class $\lambda(\delta_\mu, \mathcal{H})$ on $\mathcal{X}$, satisfying the following conditions: $\lambda(\delta_\mu, \mathcal{H}_1) \subseteq \lambda(\delta_\mu, \mathcal{H}_2)$ whenever $\mathcal{H}_1 \subseteq \mathcal{H}_2$, for every $\mathcal{H}_1$, $\mathcal{H}_2 \in \mathbb{H}$.

Definition 13. Let λ be a hereditary class operator on $\mathcal{X}$. Then, a basic μ-proximity δ_μ on $\mathcal{X}$ is called a λ-μ-proximity if, for every $G \subseteq \mathcal{X}$, $\delta_\mu[G] \subseteq \lambda(\delta_\mu, \delta_\mu[G])$. The family of all λ-μ-proximities is denoted by $\mu\mathcal{P}_\lambda$.

In the next definition, several kinds of hereditary class operators are listed.

Definition 14. For a set $\mathcal{X}$, for all $\delta_\mu \in \wp(\mathcal{X})$ and $\mathcal{H} \in \mathbb{H}$, we define

(1) $e(\delta_\mu, \mathcal{H}) = \mathcal{H}$

(2) $\lambda_0(\delta_\mu, \mathcal{H}) = \{G \subseteq \mathcal{X} \mid \mathcal{N}_\mu(G) \cap \mathcal{H} \neq \emptyset\}$

(3) $\lambda_1(\delta_\mu, \mathcal{H}) = \{G \subseteq \mathcal{X} \mid c_{\delta_\mu}(G) \in \mathcal{H}\}$

(4) $\lambda_2(\delta_\mu, \mathcal{H}) = \{G \subseteq \mathcal{X} \mid \{x\} \in \delta_\mu[G] \cup \mathcal{H}, \forall x \in \mathcal{X}\}$

(5) $\lambda_3(\delta_\mu, \mathcal{H}) = \{G \subseteq \mathcal{X} \mid \mathcal{N}_\mu(\{a\}) \cap \mathcal{H} \neq \emptyset, \forall a \in G\}$

When there is no ambiguity, we will write λ_i for $\lambda_i(\delta_\mu, \mathcal{H}))$, where $i = 0, 1, 2, 3$.

Theorem 14. *For all $\delta_\mu \in \wp(\mathcal{X})$ and $\mathcal{H} \in \mathbb{H}$ and for $\lambda \in \{e, \lambda_0, \lambda_1, \lambda_2, \lambda_3\}$, we have that λ is a hereditary class operator on $\mathcal{X}$.*

Proof

(1) It is understandable; $e(\delta_\mu, \mathcal{H}) = \mathcal{H}$ is a hereditary class operator on $\mathcal{X}$.

(2) Suppose that $\delta_\mu \in \wp(\mathcal{X})$ and $\mathcal{H} \in \mathbb{H}$. Let $G \in \lambda_0 = \lambda_0(\delta_\mu, \mathcal{H})$; then, $\mathcal{N}_\mu(G) \cap \mathcal{H} \neq \emptyset$. If $A \subseteq G$, then according to Lemma 1, $\mathcal{N}_\mu(A) \cap \mathcal{H} \neq \emptyset$ and so $A \in \lambda_0$. Hence, λ_0 is a hereditary class. Now, let $\mathcal{H}_1 \subseteq \mathcal{H}_2$ and $G \in \lambda_0(\delta_\mu, \mathcal{H}_1)$; then, $\mathcal{N}_\mu(G) \cap \mathcal{H}_1 \neq \emptyset$. Therefore, $\mathcal{N}_\mu(G) \cap \mathcal{H}_2 \neq \emptyset$ and so $G \in \lambda_0(\delta_\mu, \mathcal{H}_2)$. Consequently, λ_0 is a hereditary class operator on $\mathcal{X}$.

(3) By using $\delta_\mu$closure operator properties, λ_1 is a hereditary class operator on $\mathcal{X}$.

(4) In view of Lemma 4 (1), λ_2 is a hereditary class operator on $\mathcal{X}$.

(5) By similar manner, λ_3 is a hereditary class operator on $\mathcal{X}$. □

Theorem 15. *Let λ be a hereditary class operator. If $I = \{\lambda \mid \lambda(\delta_\mu, \cap_{r\in\Lambda}\mathcal{H}_r) = \cap_{r\in\Lambda}\lambda(\delta_\mu, \mathcal{H}_r), \delta_\mu \in \wp(\mathcal{X}), \mathcal{H}_r \in \mathbb{H}, \mathcal{H}_r \in \mathbb{H}, r \in \Lambda\}$, thene,$\lambda_1, \lambda_2 \in I$.*

Proof. Straightforward. □

Corollary 2. *Let λ be a hereditary class operator. If $\widetilde{I} = \{\lambda \mid \lambda(\delta_\mu, \mathcal{H}_1 \cap \mathcal{H}_2) = \lambda(\delta_\mu, \mathcal{H}_1) \cap \lambda(\delta_\mu, \mathcal{H}_2), \delta_\mu \in \wp(\mathcal{X}), \mathcal{H}_1, \mathcal{H}_2 \in \mathbb{H}\}$, thene,$\lambda_1, \lambda_2 \in \widetilde{I}$*

Proof. The proof is obvious by using $I \subseteq \widetilde{I}$. □

Remark 5. The following example illustrates that $\lambda_0, \lambda_3 \notin \widetilde{I}$, in general, if $\mathscr{H}_1, \mathscr{H}_2$ are hereditary classes.

Example 7. In Example 2, suppose $\mathscr{H}_1 = \{\varnothing, \{a\}\}$ and $\mathscr{H}_2 = \{\varnothing, \{b\}\}$. Then, $\lambda_0(\delta_\mu, \mathscr{H}_1 \cap \mathscr{H}_2) \neq \lambda_0(\delta_\mu, \mathscr{H}_1) \cap \lambda_0(\delta_\mu, \mathscr{H}_2)$ and $\lambda_3(\delta_\mu, \mathscr{H}_1 \cap \mathscr{H}_2) \neq \lambda_3(\delta_\mu, \mathscr{H}_1) \cap \lambda_3(\delta_\mu, \mathscr{H}_2)$. Hence, $\lambda_0, \lambda_3 \notin \widetilde{I}$

Theorem 16. *Letλ be a hereditary class operator. If* $T = \{\lambda \mid \lambda(\delta_{\mu_1}, \mathscr{H}) = \lambda(\delta_{\mu_2}\mathscr{H})$*with* $c_{\delta_{\mu_1}}(.) = c_{\delta_{\mu_2}}(.), \delta_{\mu_1}, \delta_{\mu_2} \in \wp(\mathscr{X}), \mathscr{H} \in \mathbb{H}\}$*, thene,*$\lambda_1,\lambda_2,\lambda_3 \in T$.

Proof. We shall prove only for λ_2 and the rest of the proof is similar. Let $G \in \lambda_2(\delta_{\mu_1}, \mathscr{H})$; then, $\{x\} \in \delta_{\mu_1}[G] \cup \mathscr{H}, \forall x \in \mathscr{X}$. Hence, $G \in \delta_{\mu_1}[x]$. Since $c_{\delta_{\mu_1}}(.) = c_{\delta_{\mu_2}}(.)$, then, by using Theorem 7, $\delta_{\mu_1}[x] = \delta_{\mu_2}[x]$. Consequently, $G \in \delta_{\mu_2}[x]$ and so $G \in \lambda_2(\delta_{\mu_2}, \mathscr{H})$, i.e., $\lambda_2(\delta_{\mu_1}, \mathscr{H}) \subseteq \lambda_2(\delta_{\mu_2}, \mathscr{H})$. By the same manner, we can prove $\lambda_2(\delta_{\mu_2}, \mathscr{H}) \subseteq \lambda_2(\delta_{\mu_1}, \mathscr{H})$. It follows that $\lambda_2 \in T$.

From Definition 3, one can deduce the following results. □

Lemma 7. *Let $\delta_{\mu_1}, \delta_{\mu_2}$ be two μ-proximities on a set $\mathscr{X}$ and $G \subseteq \mathscr{X}$. If$\delta_{\mu_1} \prec \delta_{\mu_2}$, then*

(1) $c_{\delta_{\mu_2}}(G) \subseteq c_{\delta_{\mu_1}}(G)$
(2) $\mathscr{N}_{\mu_1}(G) \subseteq \mathscr{N}_{\mu_2}(G)$

Theorem 17. *Let λ be a hereditary class operator. If* $U = \{\lambda \mid \lambda(\delta_{\mu_1}, \mathscr{H}) \subseteq \lambda(\delta_{\mu_2}\mathscr{H})$whenever$\delta_{\mu_1} \prec \delta_{\mu_2}, \mathscr{H} \in \mathbb{H}\}$*, then* $e,\lambda_0,\lambda_1,\lambda_2,\lambda_3 \in U$.

Proof. Let $G \in \lambda_0(\delta_{\mu_1}, \mathscr{H})$; then, $\mathscr{N}_{\mu_1}(G) \cap \mathscr{H} \neq \varnothing$. Since $\delta_{\mu_1} \prec \delta_{\mu_2}$, hence by Lemma 7 (2), $\mathscr{N}_{\mu_1}(G) \subseteq \mathscr{N}_{\mu_2}(G)$. Consequently, $\mathscr{N}_{\mu_2}(G) \cap \mathscr{H} \neq \varnothing$. So, $G \in \lambda_0(\delta_{\mu_2}, \mathscr{H})$, i.e., $\lambda_2(\delta_{\mu_1}, \mathscr{H}) \subseteq \lambda_2(\delta_{\mu_2}, \mathscr{H})$. It follows that $\lambda_2 \in U$. The rest of the proof is similar. □

Theorem 18. *$(\mathscr{X}, \delta_\mu)$ is a λ_0 - μ -proximity space iff $\mathscr{N}_\mu(G) \cap \delta_\mu[K] \neq \varnothing$, for every $G \in \delta_\mu[K]$.*

Proof. ($\Rightarrow$) Let $G \in \delta_\mu[K]$. Since δ_μ is a λ_0-μ-proximity on $\mathscr{X}$ and $\delta_\mu[K]$ is a hereditary class on $\mathscr{X}$, then $G \in \lambda_0(\delta_\mu, \delta_\mu[K])$. Hence, by Theorem 12, $\mathscr{N}_\mu(G) \cap \delta_\mu[K] \neq \varnothing$. ($\Leftarrow$) Let $G \in \delta_\mu[K]$; then, $\mathscr{N}_\mu(G) \cap \delta_\mu[K] \neq \varnothing$, which implies that $G \in \lambda_0(\delta_\mu, \delta_\mu[K])$. Consequently, $\delta_\mu[K] \subseteq \lambda_0(\delta_\mu, \delta_\mu[K])$, so δ_μ is λ_0-μ-proximity.

In view of Theorems 12 and 18, the next corollary is verified. □

Corollary 3. *δ_μ is a μ -proximity on $\mathscr{X}$ iff it isλ_0-μ-proximity.*

Theorem 19. *Let $\delta_\mu \in \wp(\mathscr{X})$ and $\mathscr{H} \in \mathbb{H}$; then, $\lambda_0\delta_\mu, \cup_{K \in \mathscr{H}} \delta_\mu[\mathscr{X} \backslash K]$.*

Proof. Suppose that $G \in \lambda_0(\delta_\mu, \mathscr{H})$. Then, $\mathscr{N}_\mu(G) \cap \mathscr{H} \neq \varnothing$. So, there exists $K \in \mathscr{H}$ s.t. $K \in \mathscr{N}_\mu(G)$, i.e., $\mathscr{X} \backslash K \in \delta_\mu[G]$, which leads to $K \in \mathscr{H}$ s.t. $G \in \delta_\mu[\mathscr{X} \backslash K]$. Consequently, $G \in \cup_{K \in \mathscr{H}} \delta_\mu[\mathscr{X} \backslash K]$, so $\lambda_0(\delta_\mu, \mathscr{H}) \subseteq \cup_{K \in \mathscr{H}} \delta_\mu[\mathscr{X} \backslash K]$. By the same manner, $\cup_{K \in \mathscr{H}} \delta_\mu[\mathscr{X} \backslash K] \subseteq \lambda_0(\delta_\mu, \mathscr{H})$ is obtained. □

Theorem 20. *Let $\delta_\mu \in \wp(\mathscr{X})$. If$\delta_\mu \in \mu\mathscr{P}_{\lambda 1}$, then c_{δ_μ} is a μ-closure operator.*

Proof. Certainly, from c_{δ_μ} properties, c_{δ_μ} operator is monotone and extensive. So, we shall prove c_{δ_μ} is an idempotent operator. Obviously, $c_{\delta_\mu}(G) \subseteq c_{\delta_\mu} c_{\delta_\mu}(G)$. Let $G \subseteq \mathscr{X}$ and $x \in c_{\delta_\mu} c_{\delta_\mu}(G)$; then, by Remark 4 (3), $c_{\delta_\mu}(G) \notin \delta_\mu[x]$. Since $\delta_\mu[x]$ is a hereditary class on $\mathscr{X}$, so from Definition 14, $G \notin \lambda_1(\delta_\mu, \delta_\mu[x])$. Since $\delta_\mu \in \mu\mathscr{P}_{\lambda 1}$, i.e., δ_μ on $\mathscr{X}$ is an λ_1-μ-proximity or $\delta_\mu[x] \subseteq \lambda_1(\delta_\mu, \delta_\mu[x])$; then, $G \notin \delta_\mu[x]$, so $x \in c_{\delta_\mu}(G)$. Consequently, $c_{\delta_\mu} c_{\delta_\mu}(G) \subseteq c_{\delta_\mu}(G)$. So, $c_{\delta_\mu} c_{\delta_\mu}(G) = c_{\delta_\mu}(G)$. Hence, c_{δ_μ} is a μ-closure operator. □

Theorem 21. *Let $\delta_\mu \in \wp(\mathscr{X})$. Then, δ_μ is a λ_1-μ-proximity iff $c_{\delta_\mu}(G) \in \delta_\mu[K]$, for every $G \in \delta_\mu[K]$.*

Proof. . Let $G \in \delta_\mu[K]$. Since δ_μ is a λ_1 proximity. Then, $G \in \lambda_1(\delta_\mu, \delta_\mu[K])$ and so $c_{\delta_\mu}(G) \in \delta_\mu[K]$. Conversely, let $K \subseteq \mathscr{X}$ and $G \in \delta_\mu[K]$; then, $c_{\delta_\mu}(G) \in \delta_\mu[K]$. Therefore, $G \in \lambda_1(\delta_\mu, \delta_\mu[H])$, so $\delta_\mu[K] \subseteq \lambda_1(\delta_\mu, \delta_\mu[K])$. Hence, δ_μ is a λ_1-μ-proximity. □

Theorem 22. *Let $\delta_\mu \in \wp(\mathscr{X})$. Then, δ_μ is an Oμ-proximity on $\mathscr{X}$ iff it is λ_1-μ-proximity.*

Proof. ($\Rightarrow$) Let $G \subseteq \mathscr{X}$ and $K \notin \lambda_1(\delta_\mu, \delta_\mu[G])$; then, $c_{\delta_\mu}(K) \notin \delta_\mu[G]$. In view of Definition 8, $G \notin \delta_\mu[c_{\delta_\mu}(K)]$. From the definition of $c_{\delta_\mu}(K)$, then $x \notin \delta_\mu[K], \forall x \in c_{\delta_\mu}(K)$. So, $G \notin \delta_\mu[c_{\delta_\mu}(K)]$, $x \notin \delta_\mu[K]$, and $\forall x \in c_{\delta_\mu}(K)$. Since δ_μ is an $O\mu$-proximity relation on $\mathscr{X}$, then $G \notin \delta_\mu[K]$. So, δ_μ is λ_1-μ-proximity.

($\Leftarrow$) Let $G \notin \delta_\mu[A]$ and $a \notin \delta_\mu[K] \forall a \in A$. Obviously, $A \subseteq c_{\delta_\mu}(K)$, so $G \notin \delta_\mu[c_{\delta_\mu}(K)]$. Hence, $c_{\delta_\mu}(K) \notin \delta_\mu[G]$. Since δ_μ is a λ_1-μ-proximity relation on $\mathscr{X}$, then $K \notin \delta_\mu[G]$, i.e., $G \notin \delta_\mu[K]$, which induces to δ_μ is an $O\mu$-proximity on $\mathscr{X}$. □

Theorem 23. *Let $\delta_\mu \in \wp(\mathscr{X})$ and $\mathscr{H} \in \mathbb{H}$. If $\lambda \in \{e, \lambda_0, \lambda_1, \lambda_3\}$, then $\lambda(\delta_\mu, \mathscr{H}) \subseteq \mathscr{H}$.*

Proof. We prove only for λ_0The rest of the proof follow directly from definitions of e and λ_1.

Let $G \in \lambda_0(\delta_\mu, \mathscr{H})$; then, $\mathscr{N}_\mu(G) \cap \mathscr{H} \neq \varnothing$. Hence, there exists $E \in \mathscr{H}$ s.t. $E \in \mathscr{N}_\mu(G)$. Since $E \in \mathscr{N}_\mu(G)$, then $G \subseteq E \in \mathscr{H}$, so $G \in \mathscr{H}$, i.e., $\lambda_0(\delta_\mu, \mathscr{H}) \subseteq \mathscr{H}$. □

Theorem 24. *Let $\delta_\mu \in \wp(\mathscr{X})$ and $x \in \mathscr{X}$. Then, $\delta_\mu \in \mu\mathscr{P}_{\lambda 2}iff(G \in \delta_\mu[K] \Rightarrow (G \in \delta_\mu[x]orK \in \delta_\mu[x]))$.*

Proof. ($\Rightarrow$) Let $G \in \delta_\mu[K]$. Since $\delta_\mu \in \mu\mathscr{P}_{\lambda 2}$, then $G \in \lambda_2(\delta_\mu, \delta_\mu[K])$, so $\{x\} \in \delta_\mu[G] \cup \delta_\mu[K]$, $\forall x \in \mathscr{X}$. Thus, $G \in \delta_\mu[x]$ or $K \in \delta_\mu[x]$. ($\Leftarrow$) Let $K \in \delta_\mu[G]$ and $x \in \mathscr{X}$; then, $K \in \delta_\mu[x]$ or $G \in \delta_\mu[x]$. Hence, $\{x\}\delta_\mu[G] \cup \delta_\mu[K]$, $\forall x \in \mathscr{X}$; it follows that $K \in h_2(\delta_\mu, \delta_\mu[G])$, $\forall G \subseteq \mathscr{X}$. Hence, $\delta_\mu[G] \subseteq \lambda_2(\delta_\mu, \delta_\mu[G])$. Consequently, $\delta_\mu \in \mu\mathscr{P}_{\lambda 2}$. □

Theorem 25. *$(\mathcal{X}, \delta_\mu)$ is a λ_3 - μ -proximity space iff $\mathcal{N}_\mu(x) \cap \delta_\mu[K] \neq \emptyset$, for every $x \in \delta_\mu[K]$.*

Proof. ($\Rightarrow$) Let $x \in \delta_\mu[K]$. Since δ_μ is a λ_3-μ-proximity on $\mathcal{X}$ and $\delta_\mu[K]$ is a hereditary class on $\mathcal{X}$, then $x \in \lambda_3(\delta_\mu, \delta_\mu[K])$. Hence, by Theorem 13, $\mathcal{N}_\mu(x) \cap \delta_\mu[K] \neq \emptyset$. ($\Leftarrow$) Let $x \in \delta_\mu[K]$, then $\mathcal{N}_\mu(x) \cap \delta_\mu[K] \neq \emptyset$, which implies that $x \in \lambda_0(\delta_\mu, \delta_\mu[K])$. Consequently, $\delta_\mu[K] \subseteq \lambda_3(\delta_\mu, \delta_\mu[K])$, so δ_μ is λ_3-μ-proximity. □

Corollary 4. *δ_μ is a Rμ -proximity on $\mathcal{X}$ iff it isλ_3-μ-proximity.*

Theorem 26. *For all $\delta_\mu \in \wp(\mathcal{X})$ and for all $\mathcal{H} \in \mathbb{H}$, we have*

(1) $\mu\mathcal{P}_{\lambda 0} \subseteq \mu\mathcal{P}_{\lambda 1} \cap \mu\mathcal{P}_{\lambda 3}$

(2) $\mu\mathcal{P}_{\lambda 1} \subseteq \mu\mathcal{P}_{\lambda 2}$

Proof

(1) Let $\delta_\mu \in \mu\mathcal{P}_{\lambda 0}$, i.e., δ_μ is a λ_0-μ-proximity on $\mathcal{X}$. Suppose that $B \in \delta_\mu[G]$; then, $\mathcal{N}_\mu(B) \cap \delta_\mu[G] \neq \emptyset$. Hence, there exists $F \subseteq \mathcal{X}$ s.t. $F \in \mathcal{N}_\mu(B)$ and $F \in \delta_\mu[G]$ and so $\mathcal{X} \backslash F \in \delta_\mu[B]$. According to Theorem 11, $c_{\delta_\mu}(B) \subseteq F$. Since $F \in \delta_\mu[G]$, then $c_{\delta_\mu}(B) \in \delta_\mu[G]$. Hence, $B \in \lambda_1(\delta_\mu, \delta_\mu[G])$. Consequently, $\delta_\mu \in \mu\mathcal{P}_{\lambda 1}$ and so $\mu\mathcal{P}_{\lambda 0} \subseteq \mu\mathcal{P}_{\lambda 1}$. Also, let $\delta_\mu \in \mu\mathcal{P}_{\lambda 0}$. Suppose $G \in \delta_\mu[K]$; then, $\mathcal{N}_\mu(G) \cap \delta_\mu[K] \neq \emptyset$, so $\mathcal{N}_\mu(a) \cap \delta_\mu[K] \neq \emptyset$, for every $a \in G$. Hence, $G \in \lambda_3(\delta_\mu, \delta_\mu[H])$. Hence, $\delta_\mu[K] \subseteq \lambda_3(\delta_\mu, \delta_\mu[H])$. Consequently, $\delta_\mu \in \mu\mathcal{P}_{\lambda 3}$. So, $\mu\mathcal{P}_{\lambda 0} \subseteq \mu\mathcal{P}_{\lambda 3}$.

(2) Let $\delta_\mu \in \mu\mathcal{P}_{\lambda 1}$ and let $G \in \delta_\mu[K]$. Then, by Theorem 21, $c_{\delta_\mu}(G) \in \delta_\mu[K]$. We claim that $G \in \lambda_2(\delta_\mu, \delta_\mu[H])$. Suppose $G \notin h_2(\delta_\mu, \delta_\mu[H])$; then, there exists $x \in X$ s.t. $\{x\} \notin \delta_\mu[G]$ and $\{x\} \notin \delta_\mu[K]$; then, $x \in c_{\delta_\mu}(G)$, $\{x\} \notin \delta_\mu[K]$. However, $\{x\} \subseteq c_{\delta_\mu}(G)$ and $\delta_\mu[K] \in \mathbb{H}$, so $c_{\delta_\mu}(G) \notin \delta_\mu[K]$, a contradiction. Hence, $G \in h_2(\delta_\mu, \delta_\mu[H])$. It follows that $\delta_\mu[K] \subseteq h_2(\delta_\mu, \delta_\mu[H])$. Consequently, $\delta_\mu \in \mu\mathcal{P}_{h2}$ and so $\mu\mathcal{P}_{h1} \subseteq \mu\mathcal{P}_{h2}$. □

Theorem 27. *Let λ be a hereditary class operator. If $E = \{\lambda \mid \lambda(\delta_\mu, \mathcal{H}) \subseteq \lambda(\delta_\mu, \lambda(\delta_\mu, \mathcal{H})), \delta_\mu \in \mu\mathcal{P}_\lambda, \mathcal{H} \in \mathbb{H}\}$, then e , λ_0 , λ_1 , $\lambda_2 \in E$.*

Proof. Let $G \in \lambda_0(\delta_\mu, \mathcal{H})$; then, $\mathcal{N}_\mu(G) \cap \mathcal{H} \neq \emptyset$ which implies that there exists $F \in \mathcal{H}$ s.t. $F \in \mathcal{N}_\mu(G)$. Since $\delta_\mu \in \mu\mathcal{P}_{\lambda_0}$, then, by Theorem 18, there exists $B \in \mathcal{N}_\mu(G)$ s.t. $F \in \mathcal{N}_\mu(B)$ and so $\mathcal{N}_\mu(B) \cap \mathcal{H} \neq \emptyset$. So, $B \in \lambda_0(\delta_\mu, \mathcal{H})$. However, $B \in \mathcal{N}_\mu(G)$; thus, $\mathcal{N}_\mu(G) \cap \lambda_0(\delta_\mu, \mathcal{H}) \neq \emptyset$. Hence, $G \in \lambda_0(\delta_\mu, \lambda_0(\delta_\mu, \mathcal{H}))$. Consequently, $\lambda_0(\delta_\mu, \mathcal{H}) \subseteq \lambda_0(\delta_\mu, \lambda_0(\delta_\mu, \mathcal{H}))$. It follows that $\lambda_0 \in E$.

Next, let $\delta_\mu \in \mu\mathcal{P}_{\lambda_1}$ and let $G \in \lambda_1(\delta_\mu, \mathcal{H})$. Then, $c_{\delta_\mu}(G) \in \mathcal{H}$ and so $c_{\delta_\mu}(G) = c_{\delta_\mu} c_{\delta_\mu}(G) \in \mathcal{H}$ (by Theorem 20). Hence, $c_{\delta_\mu}(G) \in \lambda_1(\delta_\mu, \mathcal{H})$. Hence, $G \in \lambda_1(\delta_\mu, \lambda_1(\delta_\mu, \mathcal{H}))$. Consequently, $\lambda_1(\delta_\mu, \mathcal{H}) \subseteq \lambda_1(\delta_\mu, \lambda_1(\delta_\mu, \mathcal{H}))$. It follows that $\lambda_1 \in E$.

Now, let $G \notin \lambda_2(\delta_\mu, \lambda_2(\delta_\mu, \mathcal{H}))$. Since $\delta_\mu \in \mu\mathcal{P}_{\lambda_2}$, hence, there exists $x \in \mathcal{X}$ s.t. $\{x\} \notin \delta_\mu[G] \cup \lambda_2(\delta_\mu, \mathcal{H})$. This implies that $\{x\} \notin \delta_\mu[G]$ and $\{x\} \notin \lambda_2(\delta_\mu, \mathcal{H})$. It follows that there exists $y \in X$ s.t. $\{y\} \notin \delta_\mu[x] \cup \mathcal{H}$. Then, $y \notin \delta_\mu[x]$ and $y \notin \mathcal{H}$. Since $\{x\} \notin \delta_\mu[G]$, i.e., $G \notin \delta_\mu[x]$, then in view of Theorem 24, $\{y\} \notin \delta_\mu[G] \cup \mathcal{H}$. Hence, $G \notin \lambda_2(\delta_\mu, \mathcal{H})$. Hence, $\lambda_2(\delta_\mu, \mathcal{H}) \subseteq \lambda_2(\delta_\mu, \lambda_2(\delta_\mu, \mathcal{H}))$. Consequently, $\lambda_2 \in E$.

Finally, let $G \in \lambda_3(\delta_\mu, \mathcal{H})$. Since $\delta_\mu \in \mu\mathcal{P}_{\lambda_3}$, then $\mathcal{N}_\mu(a) \cap \mathcal{H} \neq \emptyset$, for every $a \in G$, which implies that there exists $F \in \mathcal{H}$ s.t. $F \in \mathcal{N}_\mu(a)$, for every $a \in G$. Therefore, in

Figure 3: A bit more, punch, 1845 [29].

view of Theorem 13 and Theorem 25, there exists $B \in \mathcal{N}_\mu(a)$ s.t. $F \in \mathcal{N}_\mu(B)$, for every $a \in G$. Hence, $\mathcal{N}_\mu(B) \cap \mathcal{H} \neq \emptyset$, so $\mathcal{N}_\mu(x) \cap \mathcal{H} \neq \emptyset$, for every $x \in B$. It follows that$B \in \lambda_3\delta_\mu$.*Since*$B \in \mathcal{N}_\mu(a)$, so$\mathcal{N}_\mu(a) \cap \lambda_3\delta_\mu \neq \emptyset$. Consequently, $G \in \lambda_3(\delta_\mu, \lambda_3(\delta_\mu, \mathcal{H}))$.Hence, $\lambda_3(\delta_\mu, \mathcal{H}) \subseteq \lambda_3(\delta_\mu, \lambda_3(\delta_\mu, \mathcal{H})))$ and so $\lambda_3 \in E$. □

6. Application

Near sets in mathematics are either spatially close or descriptively close. The classical idea of the nearness of sets is spatial, where sets are near, as long as the sets possess joint elements. Descriptively close sets consist of organs that have matching descriptions, i.e., the set $\mathcal{X}$ with descriptively close sets δ include some of sets that consist of elements, in which every element of them have position and measurable attributes as colour or frequency of apparition.

In the next section, we will display an application about spatially close using $\delta_\mu[.]$ idea.

Remark 6. Obviously, a point μ-cluster $\sigma_\mu(x)$ is spatial nearness collection for any point x.

Example 8. In Example 2 of [29], suppose that $\mathcal{X}$ is the set of points in the picture (see Figure 3). Let $G, K \subseteq \mathcal{X}$ be the set of points in the knights' horse and set of points in the suspended knight, respectively. $G \in \delta_\mu[K]$, since there is no common element between $c_\mu(G)$ and $c_\mu(K)$. So, the subsets G, K are spatially nonnear sets.

7. Conclusion

In this work, we have introduced the concept of μ-clusters to study μ-proximity (or μ-nearness) spaces and investigated main properties. Also, we have defined other types of μ-proximity called $R\mu$-proximity and $O\mu$-proximity on $\mathcal{X}$. Furthermore, we have presented descriptive near sets as a tool of solving classification and pattern recognition problems emerging from disjoint sets; hence, a new approach to basic μ-proximity structures, which depend on the realization of the structures in the theory of hereditary classes, has been introduced.

Finally, we hope this article helps to enrich the near set theory and opens up a door for researchers to conduct further studies in this interesting theory.

Data Availability

No data were used to support this study.

Conflicts of Interest

The authors declare no conflicts of interest.

References

[1] S. A. Naimpally and J. F. Peters, "Topology with applications," *Topological Spaces via Near and Far*, World Scientific, Singapore, 2013.

[2] J. F. Peters, "Topology of digital images - visual pattern discovery in proximity spaces," *Intelligent Systems Reference Library*, Vol. 63, Springer, , Berlin, Germany, 2014.

[3] J. Peters and S. Naimpally, "Applications of near sets," *Notices of the American Mathematical Society*, vol. 59, no. 4, pp. 536–542, 2012.

[4] J. Peters and S. Naimpally, "Approach spaces for near families," *General Mathematics Notes*, vol. 2, no. 1, pp. 159–164, 2011.

[5] A. E. Hassanien, A. Abraham, J. F. Peters, G. Schaefer, and C. Henry, "Rough sets and near sets in medical imaging: a review," *IEEE Transactions on Information Technology in Biomedicine: A Publication of the IEEE Engineering in Medicine and Biology Society*, vol. 13, pp. 955–68, 2009.

[6] S. K. Pal and J. F. Peters, *Rough Fuzzy Image Analysis: Foundations and Methodologies*, CRC Press, Boca Raton, FL, USA, 2010.

[7] S. Gupta and K. Patnaik, "Enhancing performance of face recognition systems by using near set approach for selecting facial features," *Journal of Theoretical and Applied Information Technology*, vol. 4, no. 5, pp. 433–441, 2008.

[8] J. F. Peters, A. Skowron, and J. Stepaniuk, "Nearness of visual objects. Application of rough sets in proximity spaces," *Fundamenta Informaticae*, vol. 128, no. 1–2, pp. 159–176, 2013.

[9] S. Tiwari and P. K. Singh, "Ech rough proximity spaces," *Matematicki Vesnik*, vol. 72, no. 1, pp. 6–16, 2020.

[10] M. F. Worboys, "Nearness relations in environmental space," *International Journal of Geographical Information Science*, vol. 15, no. 7, pp. 633–651, 2001.

[11] T. M. Al-shami, "An improvement of rough sets' accuracy measure using containment neighborhoods with a medical application," *Information Sciences*, vol. 569, pp. 110–124, 2021.

[12] T. M. Al-shami, "Improvement of the approximations and accuracy measure of a rough set using somewhere dense sets," *Soft Computing*, vol. 25, no. 23, pp. 14449–14460, 2021.

[13] T. M. Al-shami and D. Ciucci, "Subset neighborhood rough sets," *Knowledge-Based Systems*, vol. 237, Article ID 107868, 2022.

[14] J. F. Peters, S. Shahfar, S. Ramanna, and T. Szturm, "Biologically-inspired adaptive learning: a near set approach," in *Proceedings of the Frontiers in the Convergence of Bioscience and Information Technologies*, Jeju, Korea, October 2007.

[15] J. F. Peters and P. Wasilewski, "Foundations of near sets," *Information Sciences*, vol. 179, no. 18, pp. 3091–3109, 2009.

[16] S. A. Naimpally and B. D. Warrack, "Proximity spaces," *Cambridge Tracts in Mathematics and Mathematical Physics*, Vol. 59, Cambridge University Press, Cambridge, England, 1970.

[17] W. J. Thron, "Proximity structures and grills," *Mathematische Annalen*, vol. 206, pp. 35–62, 1973.

[18] S. Leader, "On clusters in proximity spaces," *Fundamenta Mathematicae*, vol. 47, no. 2, pp. 205–213, 1959.

[19] M. Lodato, "On topologically induced generalized proximity relations. II," *Pacific Journal of Mathematics*, vol. 17, no. 1, pp. 131–135, 1966.

[20] R. A. Hosny and O. A. Tantawy, "New proximities from old via ideals," *Acta Mathematica Hungarica*, vol. 110, no. 1–2, pp. 37–50, 2006.

[21] R. A. Hosny, "Relations and applications on proximity structures," *Gen*, vol. 11, no. 1, pp. 24–40, 2012.

[22] A. Kandil, S. A. El-Sheikh, M. M. Yakout, and S. A. Hazza, "Proximity structures and ideals," *Matematicki Vesnik*, vol. 67, no. 2, pp. 130–142, 2015.

Hindawi
Journal of Mathematics
Volume 2023, Article ID 9861405, 1 page
https://doi.org/10.1155/2023/9861405

Retraction

Retracted: Intelligent Recommendation Algorithm of Multimedia English Distance Education Resources Based on User Model

Journal of Mathematics

Received 19 December 2023; Accepted 19 December 2023; Published 20 December 2023

This article has been retracted by Hindawi following an investigation undertaken by the publisher [1]. This investigation has uncovered evidence of one or more of the following indicators of systematic manipulation of the publication process:

(1) Discrepancies in scope

(2) Discrepancies in the description of the research reported

(3) Discrepancies between the availability of data and the research described

(4) Inappropriate citations

(5) Incoherent, meaningless and/or irrelevant content included in the article

(6) Manipulated or compromised peer review

The presence of these indicators undermines our confidence in the integrity of the article's content and we cannot, therefore, vouch for its reliability. Please note that this notice is intended solely to alert readers that the content of this article is unreliable. We have not investigated whether authors were aware of or involved in the systematic manipulation of the publication process.

Wiley and Hindawi regrets that the usual quality checks did not identify these issues before publication and have since put additional measures in place to safeguard research integrity.

We wish to credit our own Research Integrity and Research Publishing teams and anonymous and named external researchers and research integrity experts for contributing to this investigation.

The corresponding author, as the representative of all authors, has been given the opportunity to register their agreement or disagreement to this retraction. We have kept a record of any response received.

References

[1] X. Zhang, "Intelligent Recommendation Algorithm of Multimedia English Distance Education Resources Based on User Model," *Journal of Mathematics*, vol. 2022, Article ID 2012700, 8 pages, 2022.

Hindawi
Journal of Mathematics
Volume 2022, Article ID 2012700, 8 pages
https://doi.org/10.1155/2022/2012700

Research Article

Intelligent Recommendation Algorithm of Multimedia English Distance Education Resources Based on User Model

Xiushan Zhang

Chongqing City Vocational College, Yongchuan, Chongqing 402160, China

Correspondence should be addressed to Xiushan Zhang; 20040022@cqwu.edu.cn

Received 23 November 2021; Revised 19 December 2021; Accepted 21 December 2021; Published 13 January 2022

Academic Editor: Naeem Jan

Based on the understanding and comparison of various main recommendation algorithms, this paper focuses on the collaborative filtering algorithm and proposes a collaborative filtering recommendation algorithm with improved user model. Firstly, the algorithm considers the score difference caused by different user scoring habits when expressing preferences and adopts the decoupling normalization method to normalize the user scoring data; secondly, considering the forgetting shift of user interest with time, the forgetting function is used to simulate the forgetting law of score, and the weight of time forgetting is introduced into user score to improve the accuracy of recommendation; finally, the similarity calculation is improved when calculating the nearest neighbor set. Based on the Pearson similarity calculation, the effective weight factor is introduced to obtain a more accurate and reliable nearest neighbor set. The algorithm establishes an offline user model, which makes the algorithm have better recommendation efficiency. Two groups of experiments were designed based on the mean absolute error (MAE). One group of experiments tested the parameters in the algorithm, and the other group of experiments compared the proposed algorithm with other algorithms. The experimental results show that the proposed method has better performance in recommendation accuracy and recommendation efficiency.

1. Preface

With the promotion of the national policy of coconstruction and sharing of educational information resources, the number and types of educational resources are unprecedented rich, and the improvement of people's cognitive ability lags far behind the speed of information diffusion. However, massive educational information resources cause cognitive overload, information trek, and anxiety problems. Learners' access to personalized learning resources is like looking for a needle in a haystack, and learning everywhere has evolved into search everywhere [1–3]. How to reduce the information search cost and annoyance cost of learners, so that learners with different information literacy can obtain information resources suitable for their own needs, and provide educational resource services in line with their personality development needs for learners with different knowledge structures and intelligence types has become an unavoidable practical problem [4, 5].

According to the different types of learning resources, learning objectives, and student groups, designing a flexible personalized recommendation model of learning resources has become a breakthrough to solve this educational problem [6, 7]. This study proposes an intelligent recommendation of educational resources based on user model, which aims to mine educational resources and learning partners that meet the individual needs of learners from massive educational data, recommend learning activities that adapt to learners' cognitive styles, and provide them with adaptive and personalized educational services [8].

2. Algorithm Proposed

Accurate representation of educational resources and effective knowledge organization are necessary prerequisites for the intelligent recommendation of multimedia English distance education resources [9]. To truly realize the coconstruction, sharing, and extensive benefits of

multimedia English distance education resources, on the one hand, it is necessary to accurately and comprehensively describe educational resources; on the other hand, it is necessary to effectively screen and organize educational resources. Collaborative filtering recommendation technology can solve the above problems. It is to find neighbors with similar interests to the target user and predict the preferences of the target user from the interest preferences of the neighbor users, thereby completing the course recommendation for the target user [10].

The basic idea of collaborative filtering recommendation is based on these two assumptions. One is that if two users have very similar hobbies, then the course that one user likes is likely to be liked by the other user; the other is if two courses are very similar, then the user likes one course at the same time; it is very likely that they will also like the other course. Collaborative filtering can be divided into memory-based filtering and model-based filtering. Memory-based collaborative filtering calculates recommendations on all data sets, and each calculation adds new data to the calculation again. With the continuous increase of data, the scalability of this memory-based collaborative filtering recommendation system is greatly reduced. At present, some new technologies, such as clustering, Bayesian networks, machine learning, and association rules, have also been applied to the establishment of the model, in order to better improve the quality of collaborative filtering recommendations. In short, collaborative filtering recommendation is currently attracting the attention and favor of recommendation method researchers [11].

In response to the above problems, Deng [12] used Gaussian distribution method to normalize the score. Yitao et al. [13] proposed a decoupling normalization method and concluded that this method has better performance than Gaussian normalization. This paper uses this decoupling normalization method to process user ratings. The collaborative filtering algorithm proposed in this paper is based on an improved user model. It is called an improved user model because the user score is normalized before modeling with a user score matrix. Many models of collaborative filtering recommendation are established based on user ratings, but user ratings will vary due to the habits of different users. Users who have common interests in the same course may give different ratings to the course. At the same time, referring to the famous Ebbinghaus forgetting curve, a nonlinear logistic function is designed for the algorithm to explore the user's rating forgetting rule more closely, so as to give each normalized rating a different time forgetting weight [14–16]. Considering the influence of the recommendation and the authenticity of the neighbor set, this paper sets an effective weight factor when calculating the user similarity, which helps to improve the accuracy of the recommendation result [17].

3. Improved Collaborative Filtering Algorithm of User Model

The traditional collaborative filtering recommendation calculation of user similarity is based on the original user score data, and the recommendation quality is not very ideal [18]. Based on the basic idea of traditional collaborative filtering recommendation, the collaborative filtering algorithm of improved user model in this paper improves the recommendation efficiency by offline modeling and online recommendation. At the same time, the normalization of user score and the introduction of scoring time weight in the establishment of the model fully consider the different scoring habits of users and the fact that user interests shift with time, so as to ensure the quality of online recommendation in the next step. During online recommendation, the built user model is loaded into memory, and the nearest neighbor set of the target user is generated by calculating the user similarity. These nearest neighbor sets will be used as the reference users who have the most similar interest preferences with the target user, participate in predicting the score of the target user on the nonscored items, and sort the predicted scores. In this way, the collaborative filtering recommendation result based on the improved user model is generated. When calculating the user similarity, this paper fully considers the impact of the number of user common scoring items on the user similarity and excludes the deviation of the recommendation results caused by the fact that there are few items scored by two users and the calculated user similarity is very high. The workflow of the collaborative filtering recommendation algorithm proposed in this paper is shown in Figure 1.

In order to improve the traditional user model, the algorithm in this paper first uses the decoupling method to normalize the user score and then uses the forgetting function to assign different time forgetting weights to the score according to the theory of Ebbinghaus forgetting curve and then processing in this way. The user similarity is calculated on the latter scoring matrix for recommendation.

3.1. Normalized Score. Many collaborative filtering recommendations are based on user rating data, so user rating represents users' real interests and hobbies to ensure the accuracy of recommendations. In the further study of user ratings, this paper finds that the original user rating data show that users with the same interest preferences have differences in ratings:

(i) Different scoring ranges: some users prefer to score in a larger range, while others prefer to score in a smaller range

(ii) Different scoring scales: some users are more "tolerant," it is easier to "show mercy" when scoring, and the score is generally high; on the contrary, some users do not give the highest score even if they like it

Because users have such habit differences in scoring, this paper reduces its impact on the recommendation effect and uses the decoupling method to normalize users' scores. Decoupling normalization is a method of probability mechanism, which is based on two assumptions:

One is that if most of the user's course scores are less than or equal to R, it means that the user is likely to like the course;

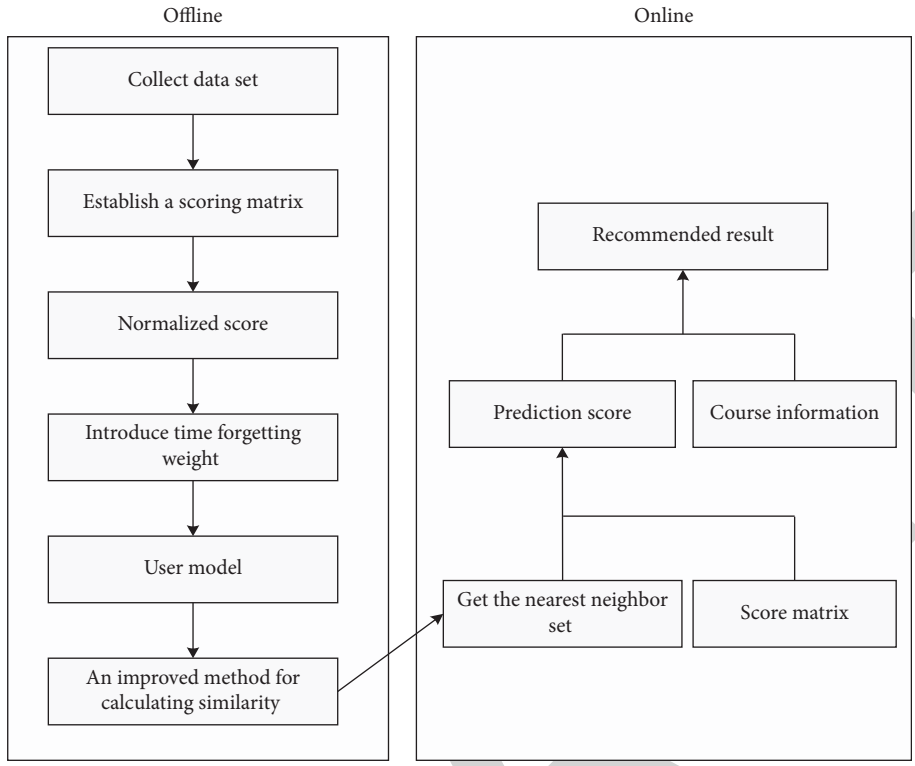

Figure 1: The workflow of collaborative filtering recommendation algorithm with improved user model.

The second is that if user i scores a large part of courses with score R, then the course with score R is less likely to be liked by user i.

Based on these two assumptions, according to the semiaccumulative distribution method, the equation for defining decoupling normalization is as follows:

$$\widetilde{R}_{i,j} = P_i(R \text{ is preferred}) = \frac{P_i(\text{Rating} \le R) - P_i(\text{Rating} = R)}{2}. \tag{1}$$

In the equation, $P_i(R \text{ is preferred})$ is the result of this normalized processing scoring, which represents the probability that the course scored R is liked by the user i. R represents a rating level, $P_i(\text{Rating} \le R)$ and $P_i(\text{Rating} = R)$ respectively represent the probability that the user i will score a course less than or equal to R and equal to R, reflecting the probability that a course rated less than or equal to R and a course equal to R will be liked by the user i. In this way, for the course j scored by the user i as R, we can use $P_i(R \text{ is preferred})$ as the normalized result of the user i which is the rating of the course j and mark it as $\widetilde{R}_{i,j}$.

3.2. Introducing Time Forgetting Weight. With the change of time, users' interests will always shift. Therefore, the scores given by users in different time periods have different reference significance for recommendations. All scores cannot be treated the same without considering the impact of time on the reference value of scores.

To illustrate this problem, let us give an example. Table 1 shows the scoring records of five courses made by four users. It should be noted that the time periods of these scores are somewhat different.

In Table 1, if the time when the score is generated is not considered, then from the score point of view, it is easy to get $SIM(U_1, U_2) > SIM(U_1, U_3) > SIM(U_1, U_4)$, that is, the nearest neighbor of user U_1 is U_2. However, when we consider the time period in which the score was generated, the result has changed. At this time, you will find that it is unreasonable to use U_2 as the nearest neighbor of U_1, because the score of a user in the past time period is used to calculate the similarity with the score of another user in the current time period to explore whether they are similar. Interest preferences are meaningless. Therefore, considering the impact of the scoring time period on the scoring, the nearest neighbor of U_1 in Table 1 should be U_4.

This is an example of considering the impact of time forgetting on scoring between different users, and for a certain user, the user interest shift caused by time forgetting also exists. The user's past preferences will change over time. Past ratings and current ratings cannot be treated the same, and different time weights should be assigned. Next, an appropriate function must be selected to simulate the user's interest shift law to generate time forgetting weights.

In fact, the deviation rule of user interest is very similar to the forgetting rule of people, so the time forgetting function can be given by referring to the forgetting rule. Regarding the study of the law of forgetting, the results of the German psychologist Ebbinghaus are worth learning. The famous Ebbinghaus forgetting curve has been cited in many researches. The Ebbinghaus forgetting curve shows the nonlinear decreasing law of human memory retention. The

Table 1: Scores in different scoring time periods.

	I1	I2	I3	I4	I5	Time period
U_1	2	3	3	4	5	T3
U_2	2	2	3	—	5	T1
U_3	—	3	3	3	4	T2
U_4	1	—	2	4	4	T3

algorithm in this paper uses a logistic function to simulate this curve law [19], reflecting the forgetting shift trend of user interest. The logistic function model is shown in Figure 2.

This logistic function is nonlinearly increasing, which means that the longer the time passes, the more the interest forgetting shifts. However, considering that the deviation of user interests and hobbies is a bit different from forgetting, user interests and hobbies remain relatively stable during a period of time and will not change quickly. The algorithm has made appropriate improvements to the logistic function. Here is a definition: the parameters of the time gap make users' ratings in the same time gap produce the same forgetting function value, which is more in line with the interest shift law. Therefore, the time forgetting function is defined as

$$f\left(t_{i,j}\right) = \frac{1}{1 + e^{-\left(\left(tl - t_{i,j}\right)/T\right)}},$$

$$f\left(t_{i,j}\right) = \frac{1}{(1/K) + b * e^{tl}}, \tag{2}$$

$$b = \frac{e^a}{K},$$

$$b = \frac{e^a}{K},$$

In the function, $t_{i,j}$ represents the time when user i scored course j, which is the independent variable of the function, and tl represents the time when the user scored the last time. T defines a time gap parameter, and its value depends on the result of experimental verification. a, b are constants greater than zero. K is the theoretical limit value. Use the fitting method to solve the parameters; the formula is

$$\phi = \sum_{i=1}^{n}\left(t_{i,j} - \widehat{t}_{i,j}\right)^2 = \sum_{i=1}^{n}\left(t_{i,j} - (a - bT)\right)^2. \tag{3}$$

In the function, n is the number of samples. Calculate the partial derivative of the constant a, b according to the ϕ function and make the partial derivative equal to 0:

$$\frac{\partial \phi}{\partial a} = 0,$$

$$\frac{\partial \phi}{\partial b} = 0. \tag{4}$$

Therefore, the unknown parameter a, b is obtained, and the time forgetting weight can be defined as

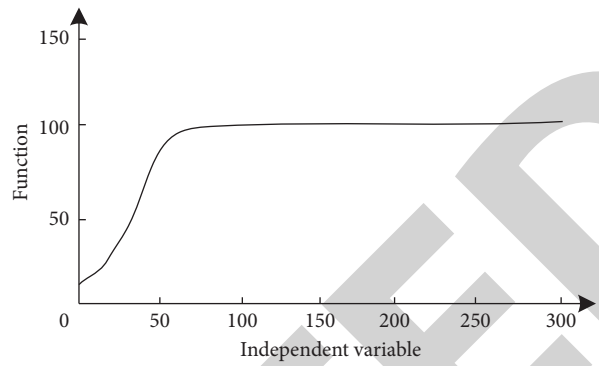

Figure 2: Logistic function model curve.

$$W_{t_{i,j}} = w\left(1 - f\left(t_{i,j}\right)\right). \tag{5}$$

Among them, w is the specification parameter. The time forgetting weight is introduced into the score result of the normalization process, and the processed score is recorded as $R_{i,j}$, which is expressed as

$$R_{i,j} = \widetilde{R}_{i,j} \times W_{t_{i,j}}. \tag{6}$$

So far, the user scoring matrix obtained after processing is the user model established by the algorithm in this paper.

In general, the collaborative filtering recommendation based on the model comprises of the following steps:

Step 1: data collection

Step 2: building the model

Step 3: finding the nearest neighbor collection

Step 4: recommending the forecast

The previous content has discussed the establishment process of the model in the collaborative filtering algorithm to improve the user model. The next work is mainly to recommend based on the model, that is, to find the nearest neighbor set and predict the recommendation.

3.3. Find the Nearest Neighbor Set. The process of finding the set of nearest neighbors of the target user is actually the process of calculating the user similarity between the target user and other users. The two users are similar, which here means that the two users have similar interests and preferences. In the collaborative filtering recommendation based on the user model, the similarity between users is relatively large, and they are more likely to like the same course. Therefore, the user similarity can be used to find the set of nearest neighbors of the target user. Like courses, you can predict which courses the target users are more interested in, so as to make personalized recommendations for the courses.

There are several similarity calculation methods, and there are three widely used in collaborative filtering recommendation algorithm, namely, Pearson correlation coefficient method [20], cosine similarity, and improved cosine similarity method. The algorithm in this paper uses Pearson's correlation coefficient method to calculate user

similarity. The similarity calculation formula of Pearson's correlation coefficient is defined as follows:

$$\operatorname{sim}(a,b)=\frac{\sum_{j\in I_{ab}}\left(R_{a,j}-\overline{R_a}\right)\left(R_{b,j}-\overline{R_b}\right)}{\sqrt{\sum_{j\in I_{ab}}\left(R_{a,j}-\overline{R_a}\right)^2}\sqrt{\sum_{j\in I_{ab}}\left(R_{b,j}-\overline{R_b}\right)^2}},\quad(7)$$

where $\operatorname{sim}(a,b)$ represents the similarity between user a and user b, and $R_{a,j}$ represents user a which is the rating of course j. In this algorithm, this rating is the rating processed in the processing model. Similarly, $R_{b,j}$ represents user b which is the rating of course j. $\bar{R}_a$ represents the average of all ratings of user a, and $\bar{R}_b$ represents the average of all ratings of user b. $I_{a,b}$ refers to the collection of courses that the user a and the user b have jointly rated.

The purpose of calculating the user similarity is to find the real nearest neighbor of the target user. However, when calculating the user similarity according to formula 5, it may occur that the two users only have few common scoring courses, but when calculating the similarity, it happens that the similarity between the two users is large, which overestimates the similarity between the two users. Using such nearest neighbors to predict the courses that target users are interested in, the quality of recommendation after prediction will be affected.

In order to improve the accuracy of similarity calculation and improve the above problems, an effective weight factor is proposed to improve Pearson correlation similarity calculation. This effective weight factor is defined as follows:

$$w=\frac{\operatorname{Min}\left(|I_{a,b}|,\delta\right)}{\delta},\quad(8)$$

where $|I_{a,b}|$ represents the number of courses scored by user a and user b, and δ is an adjustable parameter. Use it to set the threshold for the number of courses scored by user a and user b. In the experiment, we will find one for parameter δ appropriate value. This effective weight factor is to give the similarity value calculated by the Pearson similarity degree. It can be explained in this way. If the number of courses that two users have jointly rated exceeds the set threshold δ, the weight is 1. The user similarity of two users depends on the result of Pearson's correlation similarity calculation; on the contrary, if the number of courses scored by two users does not exceed the threshold, this effective weight will play its role. Obviously, the two users share the same. The fewer the number of courses that have been rated, the smaller the numerator, and the smaller the effective weight factor. That is to say, at this time, the contribution of the Pearson correlation similarity calculation result to the similarity value between the end users will decrease.

By adding this effective weight factor, the final user similarity calculation formula can be expressed as

$$\operatorname{sim}'(a,b)=w\times\operatorname{sim}(a,b).\quad(9)$$

In the above equation, $\operatorname{sim}(a,b)$ represents the similarity between users a and b, w indicates the weight factor, and $\operatorname{sim}'(a,b)$ represents the final similarity after the addition of weight factor's effectiveness. After calculating the similarity between the target user and other users, the score of the target user on historical items is introduced to further revise the similarity formula:

$$\operatorname{sim}_0'(a,b)=\overline{r}+\operatorname{sim}'(a,b),\quad(10)$$

where $\overline{r}$ is the average score of the item that the user has rated. At this time, the top M users with the highest similarity value can be selected as the nearest neighbor set of the target user, and the nearest neighbor set helps the target user predict and recommend courses that may be liked. The size M of the nearest neighbor set here is determined by the specific recommendation background. In the experiment, the optimal value of the collaborative filtering recommendation algorithm of the improved user model in the recommendation background and experimental data environment of this article is also obtained [21].

3.4. Forecast Recommendation. After obtaining the set of nearest neighbors of the target user, this step is to predict the score of the target user for the scoring course based on the set of nearest neighbors. This step uses the traditional collaborative filtering recommendation algorithm. The prediction score is partly determined by the average score of the target user and partly determined by the neighbors of the nearest neighbor set. The formula for predicting user a which is the rating of ungraded course and j is as follows:

$$p(a,j)=\overline{R_a}+\frac{\sum_{i\in UN_a}\operatorname{sim}(a,i)\times\left(R_{i,j}-\overline{R_i}\right)}{\sum_{i\in UN_a}\operatorname{sim}(a,i)},\quad(11)$$

where $\bar{R}_a$ represents the average score of user a and UN_a represents the set of nearest neighbors of user a.

By calculating the target user's score for the scoring course, the obtained top N quotients with higher predicted scores can be recommended to the user as the final personalized recommendation result of the target user.

4. Data Set and Experimental Measurement

4.1. Experimental Data Set. Most of the experimental data sets of collaborative filtering recommendation algorithms are derived from some well-known university multimedia English distance education resource recommendation systems.

The research of many algorithms of collaborative filtering recommendation is based on the data set of the recommendation system. According to the research environment and conditions of the laboratory, this paper uses the ml data set of Northeastern University as the experimental data set. This data set contains 100000 rating records recommended by 943 users for 1682 English-related content, with a rating range of 1–5, and each user has at least 20 rating records. In the experiment, 80% of the data is used as training data, and the remaining 20% is used as experimental verification data.

4.2. Experimental Environment and Tools. The environment of this experiment is Microsoft Windows 7 + Java Develop Kit v1.6.0 + SQL Server 2008, the simulation system runs on the Tomcat 6.0 platform, and the server configuration is Intel(R) Xeon(TM) CPU 2.80 GHz, 2 GB memory.

4.3. Experimental Measurement

4.3.1. Experimental Measurement Standards. There are several standards to measure the accuracy of collaborative filtering algorithm. In this paper, the average absolute error (MAE) is used to measure and verify the accuracy of the algorithm.

The mean absolute error (MAE) calculates the mean absolute error between the predicted score and the real score. The accuracy of the algorithm is judged by the size of the error difference.

If I_a is used to represent the set of courses with both predicted and true ratings for the target user, $p_{a,i}$ is the predicted score of the target user a for the course i, and $r_{a,i}$ is the true score of the target user a for the course i. The calculation method of error (MAE) can be defined as

$$MAE = \frac{\sum_{i \in I_a} \left| p_{a,i} - r_{a,i} \right|}{\left| I_a \right|}. \tag{12}$$

The smaller the calculated MAE value, the higher the accuracy of the algorithm.

The following will take the mean absolute error (MAE) as the measurement standard, divided into two groups of experiments to measure and verify the algorithm proposed in this paper.

4.3.2. Parameter Setting. In the algorithm of this paper, there are two adjustable parameters that need to be set through experiments. One is the time gap parameter T in the logistic function for calculating the time forgetting weight, and the other is the δ threshold in the effective weight factor in the similarity calculation. The experimental results of the influence of these two parameters on the algorithm are shown in Figures 3 and 4.

In the experiment of the test value of the parameter T, the unit of T is taken as time weeks, and the scoring time in the scoring record is seconds. Considering that the user's interest preferences will not change in seconds, the unit of T is converted in the experiment. For a certain user, the experiment changes the value of T to observe the influence of the change of T on the average absolute error (MAE). As shown in the result of Figure 3, under the ml data set of Movie Lens, the best value of T in the algorithm of this paper is 2 weeks. Of course, the value of T will be different in different recommended environments for the algorithm.

For the value of δ in the effective weight factor, the experiment is set to change the value of δ under the condition that the value of T remains the same for a certain user and the value of T is the best value for 2 weeks, and at the same time, the value of δ is obtained for the average absolute error (MAE). The result of the trial value experiment is shown in Figure 4. This result shows that in the algorithm experiment environment of this paper, the best value range of δ is 16 to 20, and the best value of 18 is selected in the comparison experiment. Similarly, when the algorithm is used in different recommendation systems, the value of δ should also be reset.

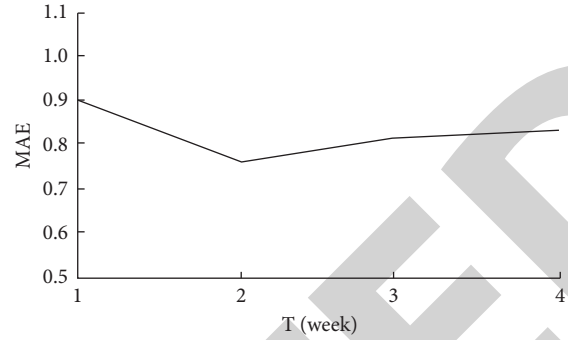

Figure 3: Parameter T test value result.

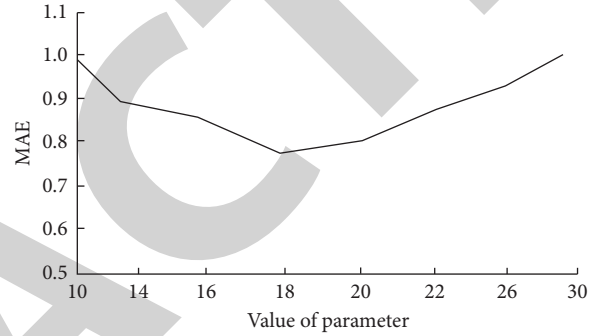

Figure 4: Parameter δ test results.

4.3.3. Comparative Measurement. Next, the proposed collaborative filtering algorithm is compared with the other two algorithms, i.e., the traditional collaborative filtering algorithm, and the collaborative filtering algorithm based on hybrid user model. These algorithms are abbreviated by English initials as follows:

CCF: conventional collaborative filtering is a traditional collaborative filtering algorithm

HUMCF: hybrid user model based collaborative filtering is a collaborative filtering algorithm based on the hybrid user model

IUMCF: improved user model based collaborative filtering is the improvement of the collaborative filtering algorithm of user models

CCF is a classic of collaborative filtering algorithms, so the algorithm in this article is first compared with it; HUMCF is a collaborative filtering method based on a hybrid user model, which is based on such a hybrid user model, which combines user ratings, course features, and demographic information. Weights of feature vectors are learnt using genetic algorithms, so as to calculate the similarity between users to generate a set of nearest neighbors. Experiments have proved that this algorithm also achieves high recommendation accuracy. The author has participated in the research of this algorithm. Therefore, the experiment compared the system filtering algorithm proposed in this paper with the improved user model based on this algorithm.

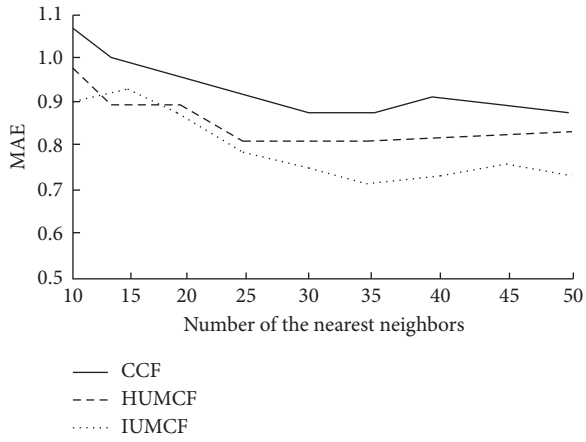

Figure 5: Comparison of MAE results of the same user with different numbers of neighbors.

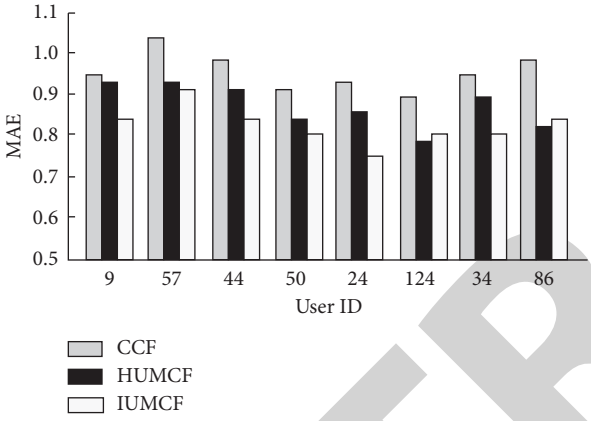

Figure 6: Comparison of MAE results under different users with the same number of neighbors.

IUMCF represents the collaborative filtering algorithm proposed in this paper to improve the user model. The experiment compares the average absolute error (MAE) results of the three algorithms under two different conditions.

First, take the best values for each parameter, and look at the changes in the MAE values of the three algorithms under different numbers of nearest neighbors. After the experiment, the results are shown in Figure 5.

Through experiments, the number of nearest neighbors ranges from 10 to 50. From the results, the collaborative filtering algorithm based on the hybrid model and the collaborative filtering algorithm based on the improved user model in this paper have lower average absolute error (MAE) than the traditional collaborative filtering algorithm. But the algorithm in this paper obviously has a lower MAE value. It can be said that the collaborative filtering algorithm proposed in this paper to improve the user model has better recommendation accuracy.

Secondly, the experiment compares the average absolute error of the three algorithms for different random users. Similarly, all parameters take the best values. The parameter T takes 2 weeks, δ takes 18, and the number of nearest neighbors takes 35. It just selects different users randomly, and different user IDs of different users are randomly selected. The experimental results are shown in Figure 6.

It can be seen from the results in Figure 6 that the MAE values of the algorithm are different for different users, but more importantly, the MAE values of the three algorithms are obviously different for different users. In general, the collaborative filtering algorithm based on hybrid model and the collaborative filtering algorithm of improved user model in this paper can still get lower average absolute error (MAE) than the traditional collaborative filtering algorithm, but the algorithm in this paper has lower MAE value, which further shows that the collaborative filtering algorithm of improved user model proposed in this paper has better performance in recommendation accuracy.

5. Conclusion

The collaborative filtering algorithm of improved user model improves the accuracy of the algorithm at the level of user ratings through the normalization of ratings and the introduction of time forgetting weights. At the same time, the effective weight factor is added when calculating user similarity. On the one hand, it can avoid the impact of data sparsity on the recommendation, and on the other hand, it can make the set of nearest neighbors to be more reasonable, thereby helping to improve the accuracy of the recommendation. The offline modeling of the algorithm and the online recommendation mode save online waiting time for recommendation and improve recommendation efficiency to a certain extent. Experiments have also proved that this improved user model collaborative filtering algorithm has a good performance in recommendation accuracy and recommendation efficiency.

Data Availability

The data used to support the findings of this study are available from the author upon request.

Conflicts of Interest

The author declares that he has no conflicts of interest.

References

[1] L. Li, "Optimal construction of the multimedia distance education resource library based on chinese education," in *Proceedings of the International Conference on Application of Intelligent Systems in Multi-Modal Information Analytics*, Springer, Cham, Switzerland, 2019.

[2] L. F. Lu, "An analysis of influential factors of motivation learning behavior of English learners in distance education," *Journal of YunNan Open University*, vol. 22, no. 1, p. 9, 2020.

[3] P. Branscum and N. Patricio-Agosto, "How children search for health information online: an observational study," *Journal of Nutrition Education and Behavior*, vol. 52, no. 5, pp. 522–527, 2020.

[4] Y. S. Xi, "Development of intelligent english multimedia teaching resources using data mining," *Heimat*, pp. 150–155, Springer, Cham, Switzerland, 2019.

Hindawi
Journal of Mathematics
Volume 2023, Article ID 9834715, 1 page
https://doi.org/10.1155/2023/9834715

Retraction

Retracted: Adaptive Enhancement Algorithm of High-Resolution Satellite Image Based on Feature Fusion

Journal of Mathematics

Received 19 December 2023; Accepted 19 December 2023; Published 20 December 2023

This article has been retracted by Hindawi following an investigation undertaken by the publisher [1]. This investigation has uncovered evidence of one or more of the following indicators of systematic manipulation of the publication process:

(1) Discrepancies in scope

(2) Discrepancies in the description of the research reported

(3) Discrepancies between the availability of data and the research described

(4) Inappropriate citations

(5) Incoherent, meaningless and/or irrelevant content included in the article

(6) Manipulated or compromised peer review

The presence of these indicators undermines our confidence in the integrity of the article's content and we cannot, therefore, vouch for its reliability. Please note that this notice is intended solely to alert readers that the content of this article is unreliable. We have not investigated whether authors were aware of or involved in the systematic manipulation of the publication process.

Wiley and Hindawi regrets that the usual quality checks did not identify these issues before publication and have since put additional measures in place to safeguard research integrity.

We wish to credit our own Research Integrity and Research Publishing teams and anonymous and named external researchers and research integrity experts for contributing to this investigation.

The corresponding author, as the representative of all authors, has been given the opportunity to register their agreement or disagreement to this retraction. We have kept a record of any response received.

References

[1] R. Wang and W. Xiao, "Adaptive Enhancement Algorithm of High-Resolution Satellite Image Based on Feature Fusion," *Journal of Mathematics*, vol. 2022, Article ID 1029247, 9 pages, 2022.

Hindawi
Journal of Mathematics
Volume 2022, Article ID 1029247, 9 pages
https://doi.org/10.1155/2022/1029247

Research Article

Adaptive Enhancement Algorithm of High-Resolution Satellite Image Based on Feature Fusion

Ruizhe Wang[1] and Wang Xiao[1,2]

[1]*Hohai University, College of Hydrology and Water Resources, Nanjing, Jiangsu 210000, China*
[2]*University of Science and Technology of China, National Synchrotron Radiation Laboratory, Hefei, Anhui 230000, China*

Correspondence should be addressed to Wang Xiao; typhoon@ustc.edu.cn

Received 30 November 2021; Revised 22 December 2021; Accepted 27 December 2021; Published 11 January 2022

Academic Editor: Naeem Jan

Since the traditional adaptive enhancement algorithm of high-resolution satellite images has the problems of poor enhancement effect and long enhancement time, an adaptive enhancement algorithm of high-resolution satellite images based on feature fusion is proposed. The noise removal and quality enhancement areas of high-resolution satellite images are determined by collecting a priori information. On this basis, the histogram is used to equalize the high-resolution satellite images, and the local texture features of the images are extracted in combination with the local variance theory. According to the extracted features, the illumination components are estimated by Gaussian low-pass filtering. The illumination components are fused to complete the adaptive enhancement of high-resolution satellite images. Simulation results show that the proposed algorithm has a better adaptive enhancement effect, higher image definition, and shorter enhancement time.

1. Introduction

With the continuous progress of computer electronic technology, human beings have higher and higher requirements for computer applications. In particular, the rapid development of the Internet and multimedia technology is ubiquitous in our lives, which makes the way we obtain information constantly changing. The acquisition of this information must be based on the accurate analysis and processing of the digital image, which is called digital image processing technology. So far, many technologies of digital image processing have been increasingly developed and matured, and their applications have achieved great success in military, industrial research, medicine, and other fields [1].

Satellite remote sensing is a very important part of remote sensing. It takes man-made satellites as a platform. In 1999, the Earth Eye company of the United States successfully launched a satellite named "IKONOS" with a multispectral image resolution of 4 m and a panchromatic image resolution of 1 m, which is called "one of the most important developments in the history of the space age." In 2008, it successfully launched a satellite with a panchromatic image resolution of 0.41 m and a multispectral image resolution of 1.65 m, which is called the "real GeoEye-1;" In 2013, China launched the gaogao-1 satellite. After years of gradual development, satellite remote sensing technology has made great progress. Now, it has entered the era of all-weather information acquisition and observation. In the global earth observation system, the mutual cooperation among large, medium, and small satellites and the mutual compensation between high, medium, and low resolution have been formed. A large number of remote sensing data provided have been widely used in many fields such as the military [2].

According to the statistics provided by the international satellite cloud climate program, it is found that the amount of clouds in the sky accounts for more than 50% over the earth's surface. Therefore, the existence of clouds cannot be avoided in a large number of remote sensing images. In addition, the use of high-resolution satellites plays an important role in the interpretation of small ground objects,

and the image resources are very valuable. Therefore, we need to improve the utilization of available information in the image as much as possible and reduce the waste of data. When the satellite sensor receives the signal, it will inevitably be affected by various factors such as the sensor's own performance, orbit angle, and atmosphere, which are inevitable to be considered in the process of image processing. Therefore, not every remote sensing image obtained through the satellite is qualified in the application [3]. When there are clouds in an image, if the remote sensing image to be used is not preprocessed, it will inevitably cause a great interference to obtain the real information and affect the quantitative analysis and interpretation of remote sensing data, which will reduce the application value of high-score satellite images. Considering the actual situation, that is, the limitations of time and space, it is impossible for the satellite to shoot again, and the shooting cost of high-resolution images is high, so we can only use these images covered by clouds. Therefore, in order to improve the image definition, it is of great significance to realize high-resolution satellite image enhancement.

Reference [4] proposes a haze weather image enhancement algorithm based on the dark channel and multiscale Retinex. Firstly, twice-guided filtering is used to improve the transmittance calculation of the dark primary color prior model. Then, in Hue-Saturation-Value (HSV) space, the brightness V is enhanced by the improved multiscale Retinex algorithm, and the illuminance component is estimated by using a double-edged filter function instead of a Gaussian filter function. The spatial domain convolution is converted to the frequency domain product to reduce the amount of computation. The illuminance of the incident component L is corrected by gamma transform, and the contrast of the reflection component R is stretched by the sigmoid function. Finally, the image is converted to Red-Green-Blue (RGB) space, and the image is simulated by MATLAB. The visual effect and quality evaluation index show that the improved algorithm can effectively restore the color of the fog image and enhance the contrast of the image. Yu and Hao [5] proposed a fog image enhancement algorithm based on the combination of fractional differentiation and multiscale Retinex. Firstly, the original image is processed by the fractional differentiation algorithm to retain the low-frequency information of the image, and the processed image is converted from RGB color space to Hue-Saturation-Intensity (HSI) color space. Then, the Gaussian filter in the multiscale Retinex algorithm is replaced by the guided filter. The luminance component and reflection component are extracted, and the sum of these two components is used as a new luminance layer to enhance the saturation layer using a gamma correction function. Finally, the HSI image is converted into an RGB image to realize image enhancement. However, the accuracy of image enhancement by the above two algorithms is low, resulting in a poor image enhancement effect and poor image definition. Wang et al. [6] proposed a vascular image enhancement algorithm based on the directional adjustable filter. This method takes the machine vision system as the hardware platform, uses a directional adjustable filter to extract venous vessels in all directions, uses wavelet transform for image fusion, obtains venous high-frequency information, and enhances vascular images hierarchically through a nonlinear antisharpening mask. The experimental results show that the proposed method can effectively suppress noise, reduce information loss, and achieve a better enhancement effect. Cui and Yang [7] proposed a single traffic image haze removal algorithm combining histogram equalization (HE) and improved color restoration multiscale Retinex (MSRCR). Firstly, the image is enhanced by HE and MSRCR, respectively. When MSRCR is enhanced, the guiding filter with a smooth-edged preserving function is used to replace the Gaussian function to estimate the illumination component. Then, weighted fusion is performed on the enhanced two images. However, the above two algorithms consume a long time for image enhancement, resulting in low enhancement efficiency.

In view of the problems existing in the above algorithms, this paper proposes a high-resolution satellite image adaptive enhancement algorithm based on feature fusion, and experiments show that the proposed method can carry out high-resolution satellite image adaptive enhancement in the shortest time, with high enhancement accuracy and good image definition, which proves the effectiveness and practicability of the algorithm in this paper. It solves the problems existing in the traditional algorithm. Section 2 of our paper gives a detailed analysis of adaptive enhancement of high resolution satellite images. Section 3 does experiments and studies the final results of the tests. Section 4 is the conclusion of our paper.

2. Adaptive Enhancement of High-Resolution Satellite Images

2.1. A Priori Information Collection. As the sample data before high-resolution satellite image processing, prior information can judge the subsequent uncertainty inference. How to use priori information reasonably is the essence of adaptive enhancement of high-resolution satellite images. Therefore, a priori information is constructed for the background distribution and feature structure of high-resolution satellite images [8].

Acquisition 1: image target individual amplitude distribution prior information.

According to the geometric scattering rules, if the individual length of the target in the high-resolution satellite image is greater than or equal to the incident wavelength, the processed high-resolution satellite image information is composed of multiple independent scattering centers. At this time, a set at frequency i and position angle j, there are p independent scattering centers, and the target individual backscattered field $E_{i,j}$ can be described as follows:

$$E_{i,j} = \sum_{l=1}^{n} S_l \exp\left(a_l \cos j + b_l \sin j\right), \tag{1}$$

where a, b is the spatial azimuth coordinate of scattering center $l = 1, \wedge, n$ and S_k is the mean value of amplitude distribution. If the azimuth scattering value of the target

individual in the high-resolution satellite image is large, the scattering value of the background area is small, as described in the following formula:

$$\begin{aligned} g(x) &\gg 0, \quad x \in T, \\ g(x) &\approx 0, \quad x \notin T, \end{aligned} \tag{2}$$

where T is the target individual coordinate sequence in the sample image [9].

Acquisition 2: image background a priori information.

For most high-resolution satellite images, the background will contain a large number of uneven noise and disorderly clutter, which cannot meet the requirements of equalization hypothesis [10]. In the image adaptive enhancement operation, the individual characteristics of the target are more important, and the background area can ensure the integrity of the light and shadow part and edge details. Therefore, in the nonedge, light and shadow, and target areas, it only needs to approximately meet $|\Delta g| = 0$, that is,

$$\Omega^{\psi} \int (|\Delta g|, |g|) d\Omega = 0, \tag{3}$$

where ψ is used to strengthen the weight of the background area in the limiting conditions, Ω is the central support area of the sample image, and d is the similarity of the edge image. Thus, the weights of regions such as edges and target individuals are reduced [11].

2.2. High-Resolution Satellite Image Preprocessing Based on Histogram Equalization. Histogram equalization is a common algorithm in low-quality image processing. This method is usually used to reflect the size of each gray level in the image and the occurrence probability of corresponding image pixels. The gray range of pixels in a low-quality image is usually small. After histogram equalization, the dynamic range of pixels in the image to be processed is stretched to improve the overall brightness contrast of the original image [12] Therefore, according to the noise removal and quality enhancement regions of high-resolution satellite images determined above, the histogram is used to equalize the high-resolution satellite images.

Assuming that the gray level of the high-resolution satellite image to be processed is m, the total number of pixel points of the image is n, and P_r^k is the probability density function of the occurrence of the image gray level k; the calculation formula of P_r^k is as follows:

$$P_r^k = \frac{n^k}{nE_{i,j}}, \tag{4}$$

where r represents the k-th gray level, n^k represents the gray level of low-quality image, which is the number of pixels, and n is the number of pixels of the whole low-quality image to be processed [13]. The expression of pixel cumulative probability distribution function CDF of histogram equalization algorithm is as follows:

$$s_k = \sum_{j=0}^{k} P_r^k r^k, \tag{5}$$

where s_k represents the histogram equalization formula, which maps the pixels with the gray range of r^k in the low-quality image to the pixel value corresponding to the gray range of s_k in the enhanced image [14].

2.3. Image Feature Extraction. According to the above equalization processing results of the high-resolution satellite image, the local features of the image are extracted by using the local variance theory to obtain the illumination information of the high-resolution satellite image. The application of the local variance algorithm is to judge the pixels containing effective information in the image, obtain the local variance image by calculating the gray variance between the central pixel in one pixel and several adjacent pixels, and realize the comprehensiveness and detail of texture feature extraction of the high-resolution satellite image in combination with the local binary algorithm [15].

Starting from the center point of a pixel, a circular area is planned with a fixed radius, and the regional texture features are expressed as follows:

$$T = \{g_0 - g_b, g_1 - g_b, \cdots, g_{w-1} - g_b\}. \tag{6}$$

In the above formula, T represents the regional texture feature, w represents the number of neighborhood points on the circumference, g represents the gray value, and g_b represents the gray value of the central pixel. Combined with LBP operator, a symbolic function is used to describe regional texture features, and formula (6) is transformed into

$$T = \{t, t, \cdots, t(g_{w-1} - g_b)\}. \tag{7}$$

In the above formula, t represents a symbolic function. The variance calculation results are fused to extract the local texture features of high-resolution satellite images:

$$\begin{aligned} T &= V(\vartheta) \\ &= V(g_0 - g_b, g_1 - g_b, \cdots, g_{w-1} - g_b). \end{aligned} \tag{8}$$

In the above formula, $V(\vartheta)$ represents the variance of the elements in set ϑ [16].

For the effective information contained in the local variance map, the variation function is used to extract and process the image texture features, and its calculation formula is expressed as follows:

$$\alpha(h) = \frac{s_k}{2\gamma(h)} \sum_{i=1}^{\gamma(h)} \left[\frac{g(k_i)}{g(k_i + h)} \right]^2. \tag{9}$$

In the above formula, h represents the step size, $\alpha(h)$ represents the variation function, γ represents the number of pixels meeting the specified step size in set K, q represents the total number of pixels in the set, and k_i represents the i-th pixel in the set [17].

Based on formula (9), it can be seen that the calculation result of the variation function value is often lower than half

of the local variance. If the gray value in the formula is changed to local variance, the variation function formula is changed to

$$\alpha(h) = \frac{1}{2\gamma(h)} \sum_{i=1}^{\gamma(h)} \left[\mathrm{var}(k_i) - \mathrm{var}(k_i + h)\right]^2. \tag{10}$$

In the above formula, $\mathrm{var}(k_i)$ represents the local variance of the element. Considering the continuity of image pixel gray value distribution in space, this continuity will decrease with the distance between pixels. Therefore, in the process of image texture feature extraction, the step size of variogram is always less than half of the pixel length. According to the extracted features, the Gaussian low-pass filtering method is used to obtain the illumination component estimation $i(x, y)$, which contains a large amount of original structure information, which can avoid distortion in the process of high-resolution satellite image enhancement [18].

2.4. Illumination Component Enhancement Based on Feature Fusion. It is usually defined by the product of illumination component and target reflection component. Assuming that the target reflection is r, the mathematical expression of high-resolution satellite image $f(x, y)$ is as follows:

$$f(x, y) = i(x, y) * r(x, y). \tag{11}$$

The light source and target determine the properties of illumination component $i(x, y)$ and image $f(x, y)$ respectively.

Due to the influence of illumination, the edge details of the target are prone to sudden change. Therefore, by separating the incident component and suppressing the interference of the light source, the adaptive gamma function is used to correct the illumination component. The expression of the adaptive gamma correction function is:

$$i_2(x, y) = i(x, y)^{r(x,y)}. \tag{12}$$

Since the variance, gradient, and entropy of the image reflect the image quality, clarity, and richness, respectively, the three parameters of variance, gradient, and entropy are selected to obtain the local features of the image [19]. The calculation methods of variance, gradient, and entropy are as follows:

$$\begin{aligned} Q(x, y) &= \frac{1}{D} \sum_{n=1}^{k} \left(i_2(x, y) - i_p\right)^2, \\ E(x, y) &= \frac{1}{D} \sum_{n=1}^{k} \left(i_p(m+1, n+1) - i_p(m, n)\right), \\ W(x, y) &= \sum_{n=1}^{k} Dp\left(i_p(m, n)\right). \end{aligned} \tag{13}$$

In order to obtain a better illumination correction effect, three image local features of variance, gradient, and entropy are taken to fuse the illumination information of the image [20]. In the fusion process, for each pixel (x, y), the variance, gradient, and entropy of the pixel in its neighborhood are counted as the local features of the pixel, and the weight of the illumination component in the fusion is determined. The expression is as follows:

$$s(x, y) = \frac{Q(x, y)}{\sum_{i=1}^{3} Q(x, y)h + i_2(x, y)}, \tag{14}$$

where h is particularly a small positive number in order to avoid the denominator value of 0 in the above formula (14) [21]. The fused illumination component is the enhanced illumination component $I_e(x, y)$, and its expression is as follows:

$$I_e(x, y) = \sum_{p=1}^{3} s(x, y) + i_p(x, y). \tag{15}$$

The mapping from the membership degree to spatial domain is completed by using the following inverse transformation form of fuzzy domain:

$$x_{ij} = \mu'_{ij} * \left(x_{\max} - x_{\min}\right) + x_{\min} I_e. \tag{16}$$

The HSV (hue-saturation-value) color high-resolution satellite image is transformed into the RGB (red, green, blue) color image to obtain the color of high-resolution satellite image after adaptive enhancement [22].

3. Simulation Experiment Analysis

In this section, we conducted some experiments using custom software and hardware parameter configurations. Moreover, an in-depth analysis of the results is carried out. In this process, we first present the experimental preparation, which is followed by the test of index selection. Then, the image preprocessing process begins. Finally, the results of the experiments are achieved which are then investigated and systematically studied.

3.1. Experimental Preparation. In order to verify the effectiveness of the high-resolution satellite image adaptive enhancement algorithm based on feature fusion in practical applications, a simulation experiment is carried out. The relevant software and hardware configuration of the simulation experiment are shown in Table 1.

In this paper, the high-resolution satellite image is taken as the experimental sample, and the image pixels of the experimental sample are $512 * 512$. The experimental sample is shown in Figure 1.

3.2. Test Index Selection. In order to effectively test the adaptive enhancement performance of high-resolution satellite images, two quantitative indexes, peak signal-to-noise ratio, and entropy are used for relatively objective evaluation. Among them, the peak signal-to-noise ratio index is used to describe the changes of brightness component and chroma component of the image, and the quality of high-resolution satellite image improves with the increase of signal-to-noise ratio. The entropy index is a physical index

Table 1: Experimental software and hardware parameter configuration.

Equipment name	Model parameters
Processor	Intel Core i5-6400
Memory	16 GB
Dominant frequency	3.2 GHz
Operating system	Windows XP
Simulation software	Proteus 7.8
Programing language	C++, C#
Open-source database	OpenCV, OpenGL, etc.

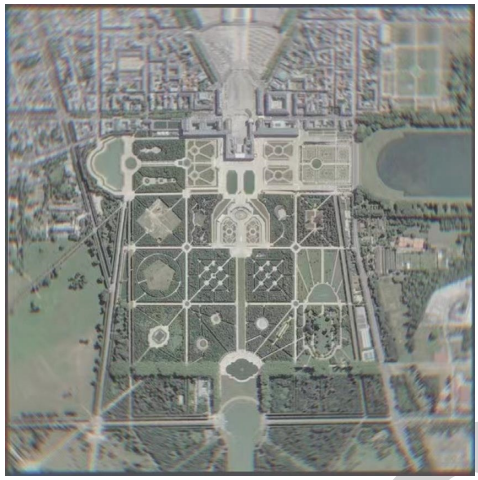

Figure 1: Experimental sample.

based on Shannon information theory to enhance the richness of image information. It is used to describe the average amount of information contained in the image. The outline and texture of the image become clearer with the increase of entropy. The calculation formulas of the two evaluation indexes are as follows:

$$\begin{aligned} \mathrm{PSNR} &= 10\lg\frac{255^2}{\mathrm{MSE}}, \\ E(i) &= -\sum_{u=0}^{Gl(i)-1} C_u * \log(C_u). \end{aligned} \tag{17}$$

In the above formula, C_u is the probability that the pixel gray value of the high-resolution satellite image is u after enhancement. When the gray level occurrence probability of the high-resolution satellite image is $C_u = 1/Gl(i)$ and $E(i)_{\max} = \log[Gl(i)]$, the high-resolution satellite image has a great degree of information value, and the gray level is evenly distributed; when the occurrence probability of gray level of high-resolution satellite image is $C_u = 1$ and $E(i)_{\min} = \log[1] = 0$, there is no information available in the image; MSE in the peak signal-to-noise ratio formula represents the mean square error, which is solved by the following formula:

$$\mathrm{MSE} = \frac{1}{M * N}\sum_{0\le x\le M}\sum_{0\le y\le N}\left(f'(x,y) - f(x,y)\right)^2. \tag{18}$$

3.3. Image Preprocessing. Before the experiment, the image is preprocessed to remove the noise contained in the image. The experimental sample image is described as the histogram shown in Figure 2.

According to the preprocessing method proposed in this paper, the histogram of the above original image is equalized to obtain the preprocessed experimental sample image shown in Figure 3.

According to Figure 3, compared with the original image histogram, the gray value of the preprocessed sample image histogram changes greatly, which promotes the uniformity of image brightness and highlights the image details containing main information. The preprocessed experimental sample image is applied to the image enhancement experiment, which enhances the intuition of the experimental results.

3.4. Experimental Test Results. The high-resolution satellite image adaptive enhancement algorithm based on feature fusion proposed in this paper, the haze weather image enhancement algorithm based on the dark channel and multiscale Retinex proposed in document [4], and the haze image enhancement algorithm based on the combination of fractional differentiation and multiscale Retinex proposed in document [5] are used to test the adaptive enhancement of experimental samples. The test results are shown in Figure 4.

According to Figure 4, the haze image enhancement algorithm based on the dark channel and multiscale Retinex proposed in document [4] and the haze image enhancement algorithm based on the combination of fractional differential and multiscale Retinex proposed in document [5] have not been significantly improved after adaptive enhancement of high-resolution satellite images. The adaptive enhancement algorithm of high-resolution satellite images based on feature fusion proposed in this paper is used to adaptively enhance the high-resolution satellite image. The processed image is clearer, which improves the definition of the high-resolution satellite image and the adaptive enhancement effect of the high-resolution satellite image. The effectiveness of the adaptive enhancement algorithm for high-resolution satellite images based on feature fusion is verified.

The peak signal-to-noise ratio and entropy data are used to evaluate the adaptive enhancement effect of high-resolution satellite images of the three algorithms. After recording the data of each evaluation index, the change trend of each method evaluation index shown in Figure 5 is drawn.

According to Figure 5, the peak signal-to-noise ratio and entropy of the high-resolution satellite image adaptive enhancement algorithm based on feature fusion proposed in this paper are higher than the haze weather image enhancement algorithm based on the dark channel and multiscale Retinex proposed in literature [4] and the haze image enhancement algorithm based on fractional differentiation and multiscale Retinex proposed in literature [5]. It shows that the image obtained by this algorithm contains more information, clearer contour and texture, and higher image quality. The above results further verified the

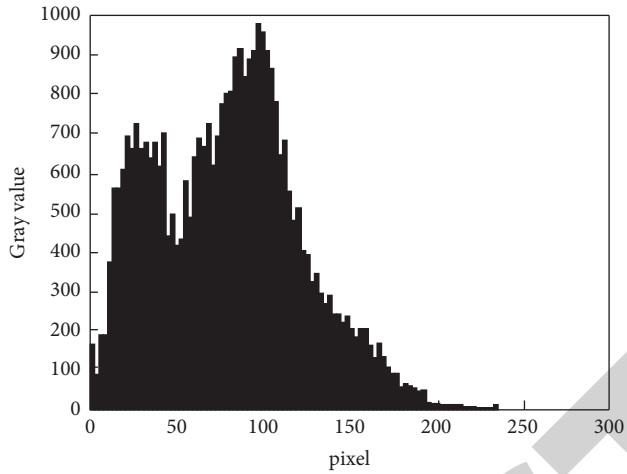

Figure 2: Histogram of original image.

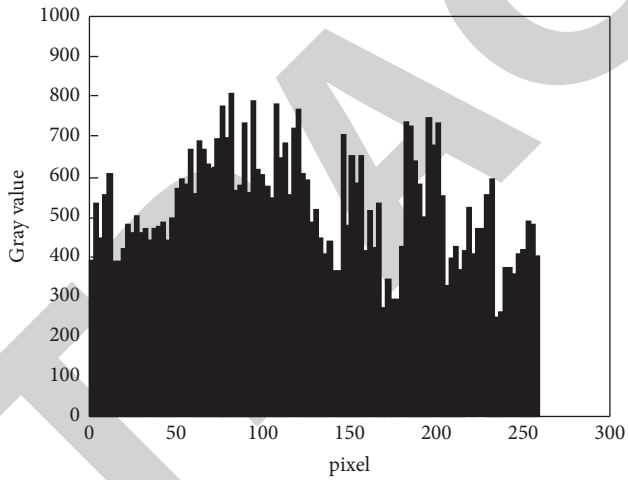

Figure 3: Histogram equalization processing.

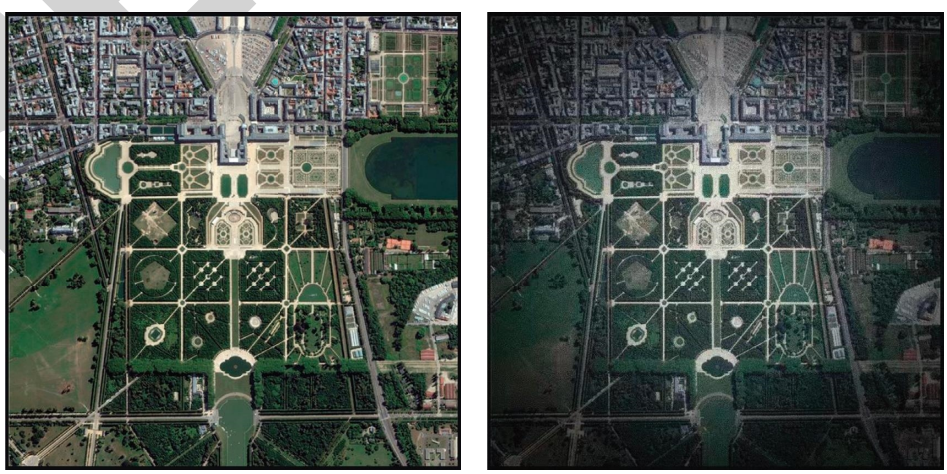

(a) (b)

Figure 4: Continued.

(c)

Figure 4: Image adaptive enhancement results of three algorithms. (a) The adaptive enhancement results of the algorithm in this paper. (b) Adaptive enhancement results of algorithm in reference [4]. (c) Adaptive enhancement results of algorithm in reference [5].

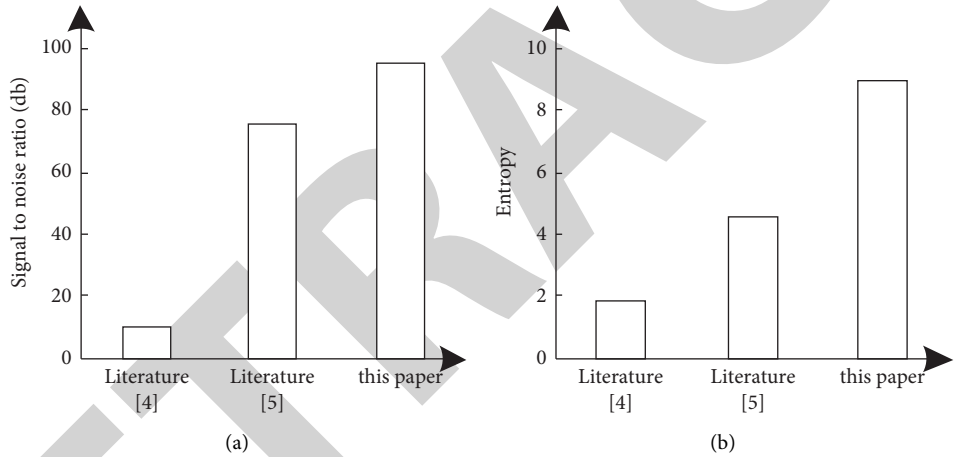

Figure 5: The schematic diagram of evaluation indexes of each algorithm. (a) Peak signal-to-noise ratio. (b) Entropy.

Table 2: Comparison results of image enhancement time of three algorithms (s).

Number of experiments/times	Paper algorithm	Reference [4] algorithm	Reference [5] algorithm
10	5.6	15.2	30.1
20	5.7	15.6	32.5
30	5.9	16.2	33.7
40	6.2	17.5	35.1
50	6.2	18.4	35.8
60	6.8	18.9	36.4
70	7.2	19.2	36.8
80	7.5	19.8	37.8
90	7.9	20.4	38.9
100	8	22.6	39.0

conclusion of the visual effect diagram and reflected the reliability of the index data from the side.

In order to further verify the effectiveness of the algorithm in this paper, the adaptive enhancement time of high-resolution satellite images of the three algorithms is compared and analyzed, and the comparison results are shown in Table 2.

According to Table 2, the time consumed by the high-resolution satellite image adaptive enhancement algorithm based on feature fusion for high-resolution satellite image

enhancement is within 8 s, which is better than the haze weather image enhancement algorithm based on the dark channel and multiscale Retinex proposed in literature [4] and literature [5]. The proposed fog image enhancement algorithm based on the combination of fractional differentiation and multiscale Retinex consumes a short time for high-resolution satellite image enhancement.

4. Conclusion

As we all know, remote sensing is a science and technology that obtains the characteristic information of the observed object through a certain sensor device without direct contact with the studied object and extracts, processes, expresses, and applies this information. A large number of remote sensing images obtained with the help of remote sensing technology have been widely used in various fields of national defense and national economic construction, such as military reconnaissance, crop yield estimation, land resource investigation, oil exploration, geospatial information updating, and other fields, which have produced huge economic and social effects. Satellite remote sensing images can quickly provide information on the earth's surface. The development and use of high-resolution satellite remote sensing images (such as IKONOS, SPOT5, cosmos, and OrbView) have created many new application fields. Due to the limitation of the imaging mechanism of the optical sensor, the quality of the image will be affected by the weather when obtaining the data; for example, it is easy to be affected by clouds and fog. However, atmospheric activities are very frequent, clouds and fog are common in the atmosphere, and a large number of remote sensing images will contain clouds and fog more or less. To obtain high-quality images, you need to select the best time and weather to obtain images. In addition to using aerospace remote sensing to obtain images affected by clouds and fog, common optical photography methods also depend on weather conditions. For example, the images obtained by intersection traffic violation monitors will also be affected by clouds and fog. Especially in foggy weather, the visual distance of the sensor is small, the image contrast obtained is low, and the color also has a certain offset, resulting in the failure of the monitoring system to work normally. Therefore, this paper proposes a high-resolution satellite image adaptive enhancement algorithm based on feature fusion. The experimental results show that the application of this algorithm can improve the quality of the high-resolution satellite image, and the efficiency of high-resolution satellite image adaptive enhancement is high.

Data Availability

The data used to support the findings of this study are available from the corresponding author upon request.

Conflicts of Interest

The authors declare that they have no conflicts of interest.

References

[1] H. Yu, K. Inoue, K. Hara, and K. Urahama, "Saturation improvement in hue-preserving color image enhancement without gamut problem," *ICT Express*, vol. 4, no. 3, pp. 134–137, 2018.

[2] E. Kotoula, D. W. Robinson, and C. Bedford, "Interactive relighting, digital image enhancement and inclusive diagrammatic representations for the analysis of rock art superimposition: the main Pleito cave (CA, USA)," *Journal of Archaeological Science*, vol. 93, pp. 26–41, 2018.

[3] H. Lin, C. Wei, N. Cao et al., "A novel low-signal image enhancement method for multiphoton microscopy," *Journal of Physics D: Applied Physics*, vol. 52, no. 28, pp. 285401–285408, 2019.

[4] C. Zhao and J. Dong, "Haze weather image enhancement algorithm based on dark channel and multi-scale Retinex," *Laser magazine*, vol. 39, no. 1, pp. 104–109, 2018.

[5] P. Yu and C. Hao, "Fog image enhancement algorithm based on fractional differential and multi-scale Retinex," *Progress in laser and Optoelectronics*, vol. 55, no. 1, pp. 6274–6279, 2018.

[6] Y. Wang, G. Deng, and Y. Xia, "Vascular image enhancement algorithm based on directional adjustable filter," *Journal of System Simulation*, vol. 30, no. 6, p. 7, 2018.

[7] X. Cui and Y. Yang, "Traffic haze image enhancement combined with he and improved msrcr," *Journal of Chongqing Normal University: Natural Science Edition*, vol. 35, no. 1, pp. 100–106, 2018.

[8] X. Wu and S. Tang, "Low-light color image enhancement based on NSST," *The Journal of China Universities of Posts and Telecommunications*, vol. 26, no. 5, pp. 45–52, 2019.

[9] H. Talebi and P. Milanfar, "Learned perceptual image enhancement," in *Proceedings of the IEEE International Conference on Computational Photography*, pp. 1–13, IEEE, Pittsburgh, PA, USA, May 2018.

[10] S. Wang and G. Luo, "Naturalness preserved image enhancement using a priori multi-layer lightness statistics," *IEEE Transactions on Image Processing*, vol. 27, no. 2, pp. 938–948, 2018.

[11] S. Park, S. Yu, M. Kim, K. Park, and J. Paik, "Dual autoencoder network for retinex-based low-light image enhancement," *IEEE Access*, vol. 6, pp. 22084–22093, 2018.

[12] P. Ravisankar, T. Sree Sharmila, and V. Rajendran, "Acoustic image enhancement using Gaussian and laplacian pyramid-a multiresolution based technique," *Multimedia Tools and Applications*, vol. 77, no. 5, pp. 5547–5561, 2018.

[13] L. Li and Y. Si, "A novel remote sensing image enhancement method using unsharp masking in nsst domain," *Journal of the Indian Society of Remote Sensing*, vol. 46, pp. 1–11, 2018.

[14] W. Wang, B. Xin, N. Deng, J. Li, and N. Liu, "Single vision based identification of yarn hairiness using adaptive threshold and image enhancement method," *Measurement*, vol. 128, pp. 220–230, 2018.

[15] K. Kim, S. Kim, and K. S. Kim, "Effective image enhancement techniques for fog-affected indoor and outdoor images," *IET Image Processing*, vol. 12, no. 4, pp. 465–471, 2018.

[16] K. G. Dhal and S. Das, "A dynamically adapted and weighted Bat algorithm in image enhancement domain," *Evolving Systems*, vol. 10, no. 2, pp. 1–19, 2018.

[17] M. Toaar, Z. Cmert, and B. Ergen, "Enhancing of dataset using DeepDream, fuzzy color image enhancement and hypercolumn techniques to detection of the Alzheimer's disease stages by deep learning model," *Neural Computing and Applications*, vol. 33, no. 16, pp. 9877–9889, 2021.

Hindawi
Journal of Mathematics
Volume 2022, Article ID 4840964, 8 pages
https://doi.org/10.1155/2022/4840964

Research Article

On Clustering Detection Based on a Quadratic Program in Hypergraphs

Qingsong Tang

College of Sciences, Northeastern University, Shenyang 110819, China

Correspondence should be addressed to Qingsong Tang; tangqs@mail.neu.edu.cn

Received 3 October 2021; Revised 19 November 2021; Accepted 21 December 2021; Published 11 January 2022

Academic Editor: Ewa Rak

A proper cluster is usually defined as maximally coherent groups from a set of objects using pairwise or more complicated similarities. In general hypergraphs, clustering problem refers to extraction of subhypergraphs with a higher internal density, for instance, maximal cliques in hypergraphs. The determination of clustering structure within hypergraphs is a significant problem in the area of data mining. Various works of detecting clusters on graphs and uniform hypergraphs have been published in the past decades. Recently, it has been shown that the maximum $\{1, 2\}$-clique size in $\{1, 2\}$-hypergraphs is related to the global maxima of a certain quadratic program based on the structure of the given nonuniform hypergraphs. In this paper, we first extend this result to relate strict local maxima of this program to certain maximal cliques including 2-cliques or $\{1, 2\}$-cliques. We also explore the connection between edge-weighted clusters and strictly local optimum solutions of a class of polynomials resulting from nonuniform $\{1, 2\}$-hypergraphs.

1. Introduction

Many important phenomena depend on the structures of graphs or hypergraphs, for example, the spread of disease in a society, image segmentation problems in image analysis, or feature extraction in networks. To understand hypergraph structure, we often start with the study of the subhypergraphs with denser relations inside and sparser connections to other subhypergraphs. Thus, detecting such hypergraph clusters of closely related objects remains one of the most interesting problems in the field of bioinformatics, social society, and data mining. Clustering is a process of partitioning a set of objects into meaningful subsets so that all objects in the same group are similar and objects in different groups are dissimilar. It is a method of data exploration and a way of looking for patterns or structure in the data that are of interest. The majority of approaches to clusters available in the literature assume that objects similarities are expressed as pairwise relations in networks in terms of 2-graphs. There is also study of pairwise clustering to edge-weighted and vertex-weighted graphs (see [1–6], respectively). For uniform hypergraphs, there are various works on clustering with applications in different aspects, such as face clustering, perceptual grouping, and parametric motion segmentation, as well as image categorization using high order relations, since approximation of more complicated similarities in terms of pairwise interaction can lead to substantial loss of information (see [7–14]). In real-world cases, similarities in a group of objects may be more appropriate to be modeled in nonuniform weighted edges in general hypergraphs. As an illustration, think of a society of people with different income levels. It makes perfect sense to define similarity measures over one person and two persons that indicate how close they are. To be specific, two persons knowing each other would get pairwise weight 1 and weight 0 otherwise; this pairwise relationship can be modeled by the well-known adjacent matrix in this society; further, for a person labeled i with income bigger than certain amount, say m, we would assign this person weight 1 on a single edge $\{i\}$; for income less than this amount, we would assign this person weight 0 on the single edge $\{i\}$; this situation involving a subset in the society may be denoted by a vector $\overrightarrow{B}$. Naturally, the internal coherency of a cluster can be represented by a maximum optimization problem based on the

society as follows: $\max\left\{\vec{x}^T A\vec{x} + B\vec{x}\right\}$. This optimization is the same as the graph-Lagrangian formed from a nonuniform $\{1,2\}$-hypergraph that models the relationship in this society (the detailed definition is given in the next section). Therefore, it is interesting to detect different types of clusters, say $\{1,2\}$-cliques or 2-cliques. Clearly, this example can be generalized to any model fitting problem, where the deviation of a set of points from the model provides a measure of their dissimilarity. The problem of data clustering using more comprehensive dissimilarity (uniform or nonuniform) is usually referred to as hypergraph clustering, since we can represent any instance of this problem by means of a hypergraph, where vertices are the objects to be clustered and the (edge-weighted) hyperedges (uniform or nonuniform) encode different order similarities.

In 1965, Motzkin and Straus provided a solution to the maximum value of a class of homogeneous quadratic multilinear functions on n variable over the standard simplex of the n-dimension Euclidean space, where the homogeneous quadratic multilinear function is associated with the edge set of a graph with n vertices. Motzkin–Straus' result established a connection between the order of a maximum complete subgraph and the graph-Lagrangian of a graph. This result also provided a new proof of a theorem by Turán who pushed the development of the study of extremal problems in graph theory. In [15], Motzkin and Straus' result was extended to characterization of local maxima in simple graphs. For Motzkin and Straus' type result in nonuniform hypergraphs, recently, in [16], it has been shown that the global maxima of a certain quadratic program are related to the maximum $\{1,2\}$-clique size in $\{1,2\}$-hypergraphs.

In this paper, we extend uniform hypergraph clustering result to nonuniform hypergraphs and provide a solution to the maximum value of a class of nonhomogeneous multilinear functions in n variables over the standard simplex of the n-dimension Euclidean space. Specifically, we first extend this result to relate strict local maxima of this program to certain maximal cliques (either 2-cliques or $\{1,2\}$-cliques or both). We also explore the connection between edge-weighted clusters and strictly local optimum solutions of a class of polynomials in the given hypergraphs. Nonhomogeneous multilinear functions discussed in this paper are associated with nonuniform hypergraphs.

This paper is organized as follows. In Section 2, we give the brief introduction to main concepts, terminology, and related results. In Section 3, we list some useful lemmas. In Section 4, we present the characterization of certain maximal cliques (either 2-cliques or $\{1,2\}$-cliques or both) in terms of strictly local optimum solutions of a class of polynomials formed from unweighted $\{1,2\}$-graphs. In Section 5, we discuss the parametrization graph-Lagrangian and cliques in $\{1,2\}$-graphs. In Section 6, we extend the result in Section 4 to edge-weighted $\{1,2\}$-graphs in some way. Conclusions are given in Section 7.

2. Definitions and Related Results

A hypergraph $H = (V, E)$ consists of a vertex set V and an edge set E, where every edge in E is a subset of V. The set $T(H) = \{|F|\colon F \in E\}$ is called the set of edge types of H. We also say that H is a $T(H)$-graph. For example, if $T(H) = \{1,2\}$, then we say that H is a $\{1,2\}$-graph. If all edges have the same cardinality r, then H is an r-uniform hypergraph. A 2-uniform graph is called a graph. A hypergraph is nonuniform if it has at least two edge types. For any $r \in T(H)$, the rth-level hypergraph H^r is the hypergraph consisting of all edges with r vertices of H and $E(H^r)$ denotes the edge set of H^r. We write H_n^T for a hypergraph H on n vertices with $T(H) = T$. Given a subset $U \subseteq V(H)$, the induced subgraph denoted by $H[U]$ is a hypergraph on U with the edge set $\{F \in E(H)\colon F \subseteq U\}$. An edge $\{i_1, i_2, \ldots, i_r\}$ in a hypergraph is simply written as $i_1 i_2 \cdots i_r$ throughout the paper.

For a positive integer n, let $[n]$ denote the set $\{1, 2, \ldots, n\}$. For a finite set V and a positive integer i, let $\binom{V}{i}$ denote the family of all i-subsets of V. The complete hypergraph K_n^T is a hypergraph on n vertices with edge set $\bigcup_{i\in T}\binom{[n]}{i}$. For example, $K_n^{\{r\}}$ is the complete r-uniform hypergraph on n vertices. $K_n^{[r]}$ is the nonuniform hypergraph with all possible edges of cardinality at most r. The complete graph on n vertices $K_n^{\{2\}}$ is also called a clique. We also let $[k]^{\{r\}}$ represent the complete r-uniform hypergraph on vertex set $[k]$.

For a T-graph $H = (V, E)$, for $r \in T$, we denote the $(r-1)$-neighborhood of a vertex $i \in V$ by $E_i^r = \left\{A \in \binom{V - \{i\}}{r-1}\colon A \cup \{i\} \in E\right\}$. Similarly, we will denote the $(r-2)$-neighborhood of a pair of vertices $i, j \in V$ by $E_{ij}^r = \left\{B \in \binom{V - \{i,j\}}{r-2}\colon B \cup \{i,j\} \in E\right\}$. We denote the complement of E_i^r by $\overline{E_i^r} = \left\{A \in \binom{V - \{i\}}{r-1}\colon A \cup \{i\} \in \binom{V}{r}\right\} \backslash E\}$. Denote $E_{i\backslash j}^r = E_i^r \cap \overline{E_j^r}$.

Definition 1. For an r-uniform graph H with the vertex set $[n]$, edge set $E(H)$, and a vector $\vec{x} = (x_1, \ldots, x_n) \in \mathbb{R}^n$, we associate a homogeneous polynomial in n variables, denoted by $\lambda(H, \vec{x})$, as follows: $\lambda(H, \vec{x}) \coloneqq \sum_{i_1 i_2 \cdots i_r \in E(H)} x_{i_1} x_{i_2} \cdots x_{i_r}$. Let $\Delta \coloneqq \left\{\vec{x} = (x_1, x_2, \ldots, x_n)\colon \sum_{i=1}^n x_i = 1, x_i \geq 0 \text{ for } i = 1, 2, \ldots, n\right\}$. The graph-Lagrangian of H, denoted by $\lambda(H)$, is the maximum of the above homogeneous multilinear polynomial of degree r over the standard simplex S. Precisely,

$$\lambda(H) \coloneqq \max\{\lambda(H, \vec{x})\colon \vec{x} \in \Delta\}. \tag{1}$$

The value x_i is called the weight of the vertex i. A vector $\vec{x} = (x_1, x_2, \ldots, x_n) \in \mathbb{R}^n$ is called feasible weighting for H if and only if $\vec{x} \in S$. A vector $\vec{y} \in S$ is called optimal weighting for H if and only if $\lambda(H, \vec{y}) = \lambda(H)$.

Remark 1. $\lambda(H)$ was called Lagrangian of H in literature [17–20]. The terminology "graph-Lagrangian" was suggested by Franco Giannessi.

The characteristic vector of a set $C \subseteq V$, denoted by $\vec{x}^C = (x_1^C, x_2^C, \ldots, x_n^C)$, is the vector in S defined as

$$x_i^C = \frac{1_{i \in C}}{|C|} \tag{2}$$

where $|C|$ denotes the cardinality of C and 1_P is the indicator function returning 1 if property P is satisfied and 0 otherwise.

In [21], Motzkin and Straus provided the following simple expression for the graph-Lagrangian of a 2-graph.

Theorem 1 (see Theorem 1 in [21]). *If H is a 2-graph with n vertices in which a largest clique has order t then $\lambda(H) = \lambda(K_t^{\{2\}}) = (1/2)(1 - (1/t))$. Furthermore, the characteristic vector of a maximum clique of H is optimal weighting for H.*

This result provided a solution to the optimization problem of this type of quadratic functions over the standard simplex of an Euclidean space.

In [16], Peng et al. generalized the concept of graph-Lagrangian to nonuniform hypergraphs as given below.

Definition 2. For a hypergraph H_n^T with $T(H) = T$ and a vector $\vec{x} = (x_1, \ldots, x_n) \in R^n$, define

$$\lambda'\left(H_n^T, \vec{x}\right) = \sum_{r \in T}\left(r! \sum_{i_1 i_2 \cdots i_r \in E(H^r)} x_{i_1} x_{i_2} \cdots x_{i_r}\right). \tag{3}$$

Let $\Delta = \{\vec{x} = (x_1, x_2, \ldots, x_n)\colon \sum_{i=1}^n x_i = 1, x_i \geq 0 \text{ for } i = 1, 2, \ldots, n\}$. The Lagrangian of H_n^T, denoted by $\lambda'(H_n^T)$, is defined as

$$\lambda'\left(H_n^T\right) = \max\left\{\lambda'\left(H_n^T, \vec{x}\right)\colon \vec{x} \in \Delta\right\}. \tag{4}$$

The value x_i is called the weight of vertex i. A vector $\vec{y} \in S$ is called optimal weighting for H if $\lambda'(H, \vec{y}) = \lambda'(H)$.

In [22], Peng and Yao gave a generalization of Motzkin–Straus result to $\{1, 2\}$-graphs.

Theorem 2 (see Theorem 1.4 in [22]). *If H is a $\{1, 2\}$-graph with n vertices and the order of its maximum complete $\{1, 2\}$-subgraph is t (where $t \geq 2$), then $\lambda'(H) = \lambda'(K_t^{\{2\}}) = 2 - (1/t)$. Furthermore, the characteristic vector of a maximum clique of H is optimal weighting for H.*

In [23, 24], Gu et al. and Tang et al. obtained more Motzkin–Straus results to some uniform hypergraphs.

3. Graph-Lagrangians and Cliques in $\{1, 2\}$-Graphs: Unweighted Case

There is a 1-to-1 connection between strictly local optimum and maximal cliques (2-cliques or $\{1, 2\}$-cliques) in $\{1, 2\}$-graphs.

Theorem 3. *A subset C of vertices in H is a maximum clique of a $\{1, 2\}$-hypergraph H if and only if its characteristic vector $\vec{x}^C$ is a global maximum of optimization problem (4).*

Proof. One direction is immediate from Theorem 2. For the other direction, suppose that $\vec{x}^C$ is a global maximum of optimization problem (4). From (4), $\lambda'(H, \vec{x}^C) = \lambda'(H, \vec{x}^U)$, where U is a maximum clique in H. Let $|C| = c$ and $|S| = s$. From Theorem 2, $\lambda'(H, \vec{x}^C) \leq 2 - (1/c)$ and $\lambda'(x^U) = 2 - (1/u)$. However, $\lambda'(H, \vec{x}^C) = \lambda'(H, \vec{x}^U)$ only if $2 - (1/u) = 2 - (1/c)$. This implies $c = s$. So C must be a clique from Theorem 2 and C is a maximum clique. □

Proposition 1. *Let C be a subset of k vertices of a $\{1, 2\}$-hypergraph H. Then C is a maximal clique of H if and only if its characteristic vector $\vec{x}^C$ satisfies*

$$\frac{\partial \lambda'(H, \vec{x})}{\partial x_j} = \begin{cases} = \dfrac{3k-2}{k}, & \text{if } j \in C, \\ \leq \dfrac{3k-2}{k}, & \text{if } j \notin C. \end{cases} \tag{5}$$

Proof. Suppose that C is a maximal clique. From the definition of maximal clique

$$\frac{\partial \lambda'\left(H, \vec{x}^C\right)}{\partial x_j} = 1 + 2 \sum_{ij \in E^2(C)} x_i^C = 1 + 2\frac{k-1}{k} = \frac{3k-2}{k}, \tag{6}$$

for all $j \in C$; and

$$\frac{\partial \lambda'\left(H, \vec{x}^C\right)}{\partial x_j} = 2 \sum_{ij \in E^2(C)} x_i x_j \leq \frac{3k-2}{k} \tag{7}$$

for all $j \notin C$. Hence $\vec{x}^C$ satisfies (5).

For the other direction, if C is not a clique, then, for some vertex $j \in C$, there exists a vertex $i \in C$ satisfying $i \neq j$ and $ij \notin E^2(C)$ or $i \notin E^1(C)$. Hence,

$$\frac{\partial \lambda'\left(H, \vec{x}^C\right)}{\partial x_j} < 1 + 2 \sum_{ij \in E^2(C)} x_i^C = \frac{3k-2}{k}. \tag{8}$$

This contradicts $\partial\lambda'(H, \overrightarrow{x}^C)/\partial x_j = (3k-2)/k$ for all $j \in C$. So C must be a clique. If C is not a maximal clique, then there must exist a clique C'^C. Let $j \in C' \setminus C$. Then

$$\frac{\partial\lambda'\left(H, \overrightarrow{x}^C\right)}{\partial x_j} = 1 + 2\sum_{ij\in E^2(C)} x_i^C = 3 > \frac{3k-2}{k}. \tag{9}$$

This contradicts $\partial\lambda'(H, \overrightarrow{x}^C)/\partial x_j \le (3k-2)/k$ for $j \notin C$. □

Lemma 1 (KKT necessary condition, [25]). *If feasible weighting $\overrightarrow{x} = (x_1, x_2, \ldots, x_n)$ is a local solution of optimization problem (4), then there exists $\theta \in \mathbb{R}$ such that, for all $j \in [n]$,*

$$\frac{\partial\lambda'(H, \overrightarrow{x})}{\partial x_i} = \begin{cases} = \theta, & \text{if } j \in \sigma(\overrightarrow{x}), \\ \le \theta, & \text{if } j \notin \sigma(\overrightarrow{x}). \end{cases} \tag{10}$$

The following corollary follows from Proposition 1 immediately.

Corollary 1. *If C is a maximal clique of a $\{1,2\}$-hypergraph H, then x^C satisfies the first-order KKT necessarily.*

Definition 3. For a $\{1,2\}$-hypergraph H, a maximal clique C is said to be strictly maximal if, for all $i \in (V\backslash C) \cap E^1$, the number of 2-edges crossing i and C is less than $|C| - 1$.

Note that, for C to be a maximal clique, it suffices that the number of edges crossing i and C be no more than $|C| - 1$ for all $i \in (V\backslash C) \cap E^1$. However, for C to be a strictly maximal clique, this number needs to be strictly less than $|C| - 1$.

Lemma 2. *Consider a $\{1,2\}$-hypergraph H which contains two cliques C and D of equal cardinality $|C| = |D| = k$. Let $m = |C\backslash D| = |D\backslash C| = m \le k$. Then, for every $\alpha_1, \alpha_2 \ge 0$ satisfying $\alpha_1 + \alpha_2 = 1$, we have the following:*

(a) If H has exactly $m(m-1)$ edges crossing $C\backslash D$ and $D\backslash C$, then $\lambda'(H, \alpha_1 \overrightarrow{x}^C + \alpha_1 \overrightarrow{x}^D) = \lambda'(H, \overrightarrow{x}^C)$

(b) If H has fewer than $m(m-1)$ edges crossing $C\backslash D$ and $D\backslash C$, then $\lambda'(H, \alpha_1 \overrightarrow{x}^C + \alpha_1 \overrightarrow{x}^D) < \lambda'(H, \overrightarrow{x}^C)$

The proof of this lemma is similar to the proof of Theorem 6 in [15]. So we omit the details here.

Lemma 3. *Let $\overrightarrow{x}$ be a strict local maximum of optimization problem (4); then, $\forall i, j \in \sigma(\overrightarrow{x})$, there exists an edge $e \in E(H)$ such that $\{i, j\} \subseteq e$.*

Proof. Suppose, for a contradiction, that there exist i and j in $\sigma(\overrightarrow{x})$ such that $\{i, j\} \nsubseteq e$ for any $e \in E(H)$. We define new weighting $\overrightarrow{y}$ for H as follows. Let $\delta < x_j$ be an arbitrarily small positive constant. Let $y_l = x_l$ for $l \ne i, j$, $y_i = x_i + \delta$, and $y_j = x_j - \delta$; then $\overrightarrow{y}$ is clearly legal weighting for H, and

$$\lambda'(H, \overrightarrow{y}) - \lambda'(H, \overrightarrow{x}) = x_j\left(\frac{\partial\lambda'(H, \overrightarrow{x})}{\partial x_i} - \frac{\partial\lambda'(H, \overrightarrow{x})}{\partial x_j}\right) - x_j^2\frac{\partial^2\lambda'(H, \overrightarrow{x})}{\partial x_i \partial x_j} = 0. \tag{11}$$

This contradicts $\overrightarrow{x}$ being a strict local maximum of optimization problem (4). Hence Lemma 3 holds.

Now we are ready to prove the main result of this section. □

Theorem 4. *Let C be a subset of k vertices of a $\{1,2\}$-hypergraph H.*

(a) If $E^1 \cap C \ne \varphi$, then C is a strict maximal $\{1,2\}$-clique of H if and only if $\overrightarrow{x}^C$ is a strict local maximum of optimization problem (4)

(b) If $E^1 \cap C = \varphi$, then C is a strict maximal {2}-clique of H if and only if $\overrightarrow{x}^C$ is a strict local maximum of optimization problem (4)

Proof. (a) Suppose that $\overrightarrow{x}^C$ is a strict local maximum of optimization problem (4); then the KKT conditions (10) hold for some θ. We will show that $\theta = ((3k-2)/k)$, where $k = |C|$. Then, by Proposition 1, C is a maximal clique. Suppose that $\theta \ne ((3k-2)/k)$ for a contradiction. For every two vertices i, j in C, $ij \in E^2$ by Lemma 3. We will show that all the vertices in C are contained in E^1. Then C is a clique and $\theta \ne ((3k-2)/k)$. Assume that there exist some vertices in C not contained in E^1. Since $E^1 \cap C \ne \varphi$, there must exist a vertex $i \in C$ contained in E^1. Assume that $j \in C$ but it is not contained in E^1; then

$$\frac{\partial\lambda'(H, \overrightarrow{x})}{\partial x_i} = 1 + 2 \cdot \frac{k-1}{k}, \qquad \frac{\partial\lambda'(H, \overrightarrow{x})}{\partial x_j} = 2 \cdot \frac{k-1}{k}. \tag{12}$$

This contradicts $(\partial\lambda'(H, \overrightarrow{x})/\partial x_i) = (\partial\lambda'(H, \overrightarrow{x})/\partial x_j)$ by Lemma 1 Hence, all the vertices in C are contained in E^1.

To see C as a strictly maximal clique, suppose to the contrary that $j \in E^1\backslash C$ adjacent to exactly $k-1$ vertex in C, and let i denote the only vertex in C not adjacent to j. Then set $D = j \cup (C\backslash\{i\})$ as a clique of the same cardinality as C. Because $m = |C\backslash D| = |D\backslash C| = 1$, there are no edges crossing CD and $D\backslash C$, since i, j are nonadjacent. From Lemma 2, for all $\alpha \in [0,1]$, we have $\lambda'(H, \overrightarrow{x}^C) = \lambda'(H, \alpha_1 \overrightarrow{x}^C + \alpha_1 \overrightarrow{x}^D)$ which contradicts the hypothesis that $\overrightarrow{x}^C$ is a strict maximum of optimization problem (4). This proves the first part of the theorem.

For the other part, suppose that C is a strictly maximal clique. To prove that x^C is a strict local maximum of optimization problem (4), we apply the second-order sufficiency conditions for constrained optimization. First, from

Corollary 1, x^C satisfies the KKT conditions. Note that, in this case, the Lagrange multipliers μ_i's are given by

$$\mu_i = \frac{3k-2}{k} - 1_{i\in E^1} - \sum_{ij\in E^2} x_j. \tag{13}$$

It remains to be shown that the Hessian of the Lagrangian associated with the optimization in (4) is negative definite on the subspace

$$M = \left\{ \overrightarrow{y} \in R^n, \sum_{i=1}^{n} y_i = 0 \text{ and } y_i = 0, \text{for all } i \in I \right\} \tag{14}$$

where $I = \{i\colon x_i^c = 0 \text{ and } \mu_i > 0\}$. Since C is a strict maximal clique, we have

$$\sum_{ij\in E^2} x_j < \frac{3k-2}{k}, \tag{15}$$

for all $i \notin C$. Now, let $\overrightarrow{y} \in M\backslash\{0\}$; then

$$\begin{aligned} \lambda'(H, \overrightarrow{y}) &= \sum_{i\in E^1} y_j + \sum_{ij\in E^2} y_i y_j = \sum_{i\in C} y_i \left(\sum_{j\in C} y_j - y_i \right) \\ &= -\sum_{i\in C} y_i^2 < 0. \end{aligned} \tag{16}$$

This completes the proof. (b) This is similar to that in (a). We omit the details here. □

4. The Parametrization Lagrangian and Cliques in $\{1,2\}$-Graphs

Definition 4. For a hypergraph H_n^T with H_n^T and a vector $\overrightarrow{x} = (x_1, \ldots, x_n) \in R^n$, define

$$\lambda'\left(H_n^T, \overrightarrow{x}\right) = \sum_{r\in T} \left(r! \sum_{i_1 i_2 \cdots i_r \in E(H^r)} x_{i_1} x_{i_2} \ldots x_{i_r} \right). \tag{17}$$

Let $PS = \{\overrightarrow{x} = (x_1, x_2, \ldots, x_n)\colon \sum_{i=1}^n x_i = 1, \sum_{i=1}^n x_i^2 = 1/s, x_i \geq 0 \text{ for } i = 1, 2, \ldots, n\}$, where s is a real number between $[1, n]$. The parametrization Lagrangian of H_n^T, denoted by $\lambda_s'(H_n^T)$, is defined as

$$\lambda_s'\left(H_n^T\right) \coloneqq \max\left\{\lambda'\left(H_n^T, \overrightarrow{x}\right)\colon \overrightarrow{x} \in PS\right\}. \tag{18}$$

The value x_i is called the weight of vertex i. A vector $\overrightarrow{y} \in PS$ is called optimal weighting for H if $\lambda_s'(H, \overrightarrow{y}) = \lambda_s'(H)$.

Let

$$X(s, C) \coloneqq \{\overrightarrow{x} \mid \overrightarrow{x} \in PS \text{ and } x_u = 0 \forall u \notin C\}. \tag{19}$$

The following is easy to see.

Lemma 4. *The set $X(s, C)$ is nonempty if and only if $1 \leq s \leq |C|$. For $s = |C|$, $X(s, C)$ consists simply of the character vector of C.*

Theorem 5. *Let H be a $\{1,2\}$-hypergraph with clique number ω. Then*

(a) $\lambda_s'(H) = 2 - (1/s)$ for $1 \leq s \leq \omega$

(b) $\lambda_s'(H) \leq 2 - (1/\omega) < 2 - (1/s)$ for $\omega \leq s \leq n$

(c) $\lambda_s'(H) = 2 - (1/s)$ if and only if $s \leq \omega$

(d) $\lambda'(H) = \max_{1\leq s\leq n} \lambda_s'(H) = 2 - (1/\omega)$

(e) For $s \leq \omega$, the set of global optimal solutions of (18) is given by

$$\cup \{(Xs, C) | C \text{ is a clique}, s \leq | \tag{20}$$

(f) The set of global optimal solutions of $\lambda_\omega'(H)$ is $(1_C/\omega)$, where C is an (optimal) $\{1,2\}$-clique of order ω. Hence, there is a one-to-one correspondence between the global optimal solutions of $\lambda_\omega'(H)$ and the optimal cliques in H.

Proof. Proof of (a). Let $s \leq \omega$. Let $\overrightarrow{x}$ be any feasible solution of $\lambda_s'(H)$. Then

$$\begin{aligned} \lambda_s'(H) &= \sum_{i\in E^1} x_i + 2 \sum_{ij\in E^2} x_i x_j \\ &\leq 1 + \left(x_1 + x_2 + \cdots + x_n\right)^2 - \sum_{i=1}^{n} x_i^2 - 2 \sum_{ij\in \overline{E}^2} x_i x_j \\ &\leq 2 - \frac{1}{s}. \end{aligned} \tag{21}$$

On the other side, let C be a clique of size s in H for some $S \geq s$ (note that s is not assumed to be integral). Since $\omega \geq s$, $X(s, C)$ is not empty. Now, for an arbitrary $x \in X(s, C)$,

$$\begin{aligned} \lambda_s'(H) &= \sum_{i\in C} x_i + 2 \sum_{ij\in C} x_i x_j \\ &1 + \left(\sum_{i\in C} x_i \right)^2 - \sum_{i\in C} x_i^2 \\ &2 - \frac{1}{s}. \end{aligned} \tag{22}$$

Hence, $\lambda_s'(H) = 2 - (1/s)$ for $1 \leq s \leq \omega$.

Proof of (b). Let $s > \omega$. Since any $\overrightarrow{x}$ that is feasible for $\lambda_s'(H)$ is also feasible for $\lambda'(H)$, and since $\lambda'(H) = 2 - 1/\omega$, we have $\lambda_s'(H) < \lambda'(H) = 2 - 1/\omega$.

Proof of (c). Since $2 - (1/s)$ is an increasing function of s, (a) and (b) together imply (c).

Proof of (d). Note that the feasible region of $\lambda'(H)$ is the feasible region of $\lambda_s'(H)$ for s in the range $[1, n]$. Combining with (a) and (b) implies (d).

Proof of (e). By equation (22), every $x \in X(s, C)$, where C is a clique of size at least s, satisfies

$$\lambda_s'(H) = 2 - \frac{1}{s}. \tag{23}$$

On the other side, for an arbitrary x of $L(s)$, we have

$$\lambda_s'(H) = 2 - \frac{1}{s} - \sum_{i \in \overline{E}^1} x_i - 2 \sum_{ij \in \overline{E}^2} x_i x_j. \tag{24}$$

Hence, if $\lambda_s'(H) = 2 - 1/s$, then $\sum_{i \in \overline{E}^1} x_i + \sum_{ij \in \overline{E}^2} x_i x_j = 0$. This happens if and only if

$$\begin{aligned} x_i &= 0, \text{whenever } i \in \overline{E}^1, \\ x_i x_j &= 0, \text{whenever } ij \in \overline{E}^2. \end{aligned} \tag{25}$$

So the support $\sigma(\vec{x})$ of $\vec{x}$ forms a clique in H. Let C be this clique. Clearly, $\vec{x} \in X(x, C)$. Lemma 4 implies that $s \le |C|$.

Proof of (f). The result follows from (e) and Lemma 4. □

5. Maximum Vertex-Weighted Cliques in $\{1, 2\}$-Graphs

Given a nonnegative weight vector $\vec{w}_v$, for any subset C of the vertex set, $w_v(C)$ denotes the sum of the weights of vertex in C. The vertex-weighted clique number $\omega(\vec{w}_v, H)$ is the maximum of $w_v(C)$ over all cliques C of G. Note that $\omega(e, H)$ is the usual clique number $\omega(H)$ of the hypergraph. Given a positive weight vector $\vec{w}_v$, define a set of matrices as follows:

$$\mathcal{M}(\vec{w}_v, H) = \left\{ B | B_{ii} = \frac{1}{w_{v_i}} \forall i, B_{ij} + B_{ji} \ge \frac{1}{w_{v_i}} + \frac{1}{w_{v_j}} \forall ij \in \overline{E^2}, B_{ij} = 0 \forall ij \in E^2 \right\}. \tag{26}$$

For a given a matrix $B \in \mathcal{M}(\vec{w}_v, H)$, consider the following optimization problem:

$$L(H, \vec{w}_v) = \min \left\{ -\sum_{i \in E^1} \frac{x_i^2}{w_{v_i}} + 2\vec{x}^T B \vec{x} \mid \vec{x} \in S \right\}. \tag{27}$$

Theorem 6. *Let H be a $\{1, 2\}$-graph. Then $\omega(\vec{w}_v, H) = (1/L(H, \vec{w}_v))$ for any positive weight vector $\vec{w}$, and $B \in \mathcal{M}(\vec{w}, H)$.*

In the Proof of Theorem 6, we will impose an additional condition on a solution $\vec{x} = (x_1, x_2, \ldots, x_n)$ to a global optimum $\vec{x}$ to problem (27): $(*)$ $|\{i: x_i > 0\}|$ is minimal; that is, if $\vec{y}$ is a feasible solution for H satisfying $|i: y_i > 0| < |i: x_i > 0|$, then $L(H, \vec{y}) < L(H)$. We need the following lemmas.

Lemma 5. *Let $\vec{x}$ be a global optimum of optimization problem (27) with minimum support; then there exists an edge $e \in E(H)$ such that $\{i, j\} \subseteq e \forall i, j \in \sigma(\vec{x})$.*

Proof. Let $\vec{x}$ be a global optimum of optimization problem (27) with minimum support. Let $f(\vec{x}) = -\sum_{i \in E^1} x_i^2 / w_{v_i} + 2\vec{x}^T B \vec{x}$. Suppose, for a contradiction, that there exist i and j in $\sigma(\vec{x})$ such that $\{i, j\} \nsubseteq e$ for any $e \in E(H)$. We define a new feasible solution $\vec{y}$ to (27) as follows. Let $y_l = x_l$ for $l \ne i, j$, $y_i = x_i + x_j$, and $y_j = x_j - x_j = 0$; then $\vec{y}$ is clearly a feasible solution (27) with smaller support compared to $\vec{x}$. By KKT necessary condition $(\partial f(\vec{x}) / \partial x_i) = (\partial f(\vec{x}) / \partial x_j)$, and

$$\begin{aligned} f(\vec{y}) - f(\vec{x}) &= x_j \left(\frac{\partial f(\vec{x})}{\partial x_i} - \frac{\partial f(\vec{x})}{\partial x_j} \right) \\ &\quad + 2x_j^2 \left(B_{ii} + B_{jj} - 1_{i \in E^1} \frac{1}{w_{v_i}} - 1_{j \in E^1} \frac{1}{w_{v_j}} - B_{ij} - B_{ji} \right) \\ &= 2x_j^2 \left(B_{ii} + B_{jj} - 1_{i \in E^1} \frac{1}{w_{v_i}} - 1_{j \in E^1} \frac{1}{w_{v_j}} - B_{ij} - B_{ji} \right) \\ &\le 0, \end{aligned} \tag{28}$$

since $B_{ij} + B_{ji} \ge (1/w_{v_i}) + (1/w_{v_i}) \ge B_{ii} + B_{jj} - 1_{i \in E^1} (1/w_{v_i}) - 1_{j \in E^1} (1/w_{v_i})$. This contradicts $\vec{x}$ being a global optimum of optimization problem (27) with minimum support. □

Claim 1. Either $i \in E^1$ for all $i \in \sigma(\vec{x})$ or $i \notin E^1$ for all $i \in \sigma(\vec{x})$.

Proof. Suppose that $i \in E^1$ but $j \notin E^1$ for a contradiction. By the KKT condition, $(\partial f(\vec{x}) / \partial x_i) = (\partial f(\vec{x}) / \partial x_j)$. By Lemma 5, $\forall i, j \in \sigma(\vec{x}), ij \in E^2$; therefore $0 = (2x_j / w_{v_i})$. This is a contradiction.

Now we are ready to prove Theorem 6. □

Proof. of Theorem 6. Let $\vec{x}$ be a global optimum of optimization problem (27) with minimum support. By Lemma 5 and Claim 1, $\sigma(\vec{x})$ induces $\{1, 2\}$-clique or a 2-clique of H.

If $\sigma(\vec{x})$ induces a $\{1, 2\}$-clique, then

$$f(\vec{x}) = -\sum_{i\in E^1}\frac{x_i^2}{w_{v_i}} + 2\vec{x}^T B\vec{x} = \sum_{i\in\sigma(\vec{x})}\frac{x_i^2}{w_{v_i}}, \tag{29}$$

and its minimum over the simplex is at

$$x_i = \begin{cases} \text{if } i \in \sigma(\vec{x}), \\ 0, \qquad\qquad \text{if } i \notin \sigma(\vec{x}). \end{cases} \tag{30}$$

for $i = 1, 2, \ldots, n$. So the optimal value of $f(\vec{x})$ is $1/w_v(\sigma(\vec{x}))$. For the solution to be global optimal, $w_v(\sigma(\vec{x}))$ must be the maximum $\{1,2\}$-clique in H.

If $\sigma(\vec{x})$ induces a 2-clique, then

$$f(\vec{x}) = -\sum_{i\in E^1}\frac{x_i^2}{w_{v_i}} + 2\vec{x}^T B\vec{x} = 2\sum_{i\in\sigma(\vec{x})}\frac{x_i^2}{w_{v_i}}, \tag{31}$$

and the left is similar to the case where $\sigma(\vec{x})$ induces $\{1,2\}$-clique. □

6. Dominant Set for $\{1,2\}$-Graphs

Let $G = (V, E)$ be an edge-weighted graph with edge weight $w_{ij} > 0$ for $ij \in E$. The weighted adjacency matrix $A = (a_{ij})_n$ is defined as $a_{ij} = w_{ij}$ if $ij \in E$ and $a_{ij} = 0$ otherwise. The average weighted degree of i with regard to S is defined as

$$\text{awdeg}_S(i) = \frac{1}{|S|}\sum_{j\in S} a_{ij}. \tag{32}$$

If $j \notin S$, define

$$\varphi_S(i,j) = a_{ij} - \text{awdeg}_S(i). \tag{33}$$

The weight of i with regard to S is defined as

$$W_S(i) = \begin{cases} 1, & \text{if } |S| = 1, \\ \sum_{j\in S\{i\}} \varphi_{S\{i\}}(j,i) w_{S\{i\}}(j), & \text{otherwise}, \end{cases}$$
$$\mathrm{W}(\mathrm{S}) = \sum_{i\in S} w_S(i). \tag{34}$$

Definition 5 (see [4]). A nonempty subset of vertices $S \subseteq V$ such that $W(T) > 0$ for any nonempty $T \subseteq S$ is said to be dominant if

(1) $W_S(i) > 0$ for all $i \in S$

(2) $W_{S*\{i\}}(i) < 0$ for all $i \notin S$

Set the weighted characteristic vector $\vec{x}^S \in \triangle$ as follows:

$$x_i^S = \begin{cases} \dfrac{w_S(i)}{W(S)}, & \text{if } i \in S, \\ 0, & \text{otherwise.} \end{cases} \tag{35}$$

Pavan and Pelillo connect the dominant set to the following quadratic program:

$$\begin{aligned} &\text{maximize } \vec{x}^T A\vec{x} \\ &\text{subject to } \in\triangle, \end{aligned} \tag{36}$$

and establish a correspondence between the global (local) maxima of (36) and the dominant sets of a graph.

Theorem 7 (see [4]). *If S is a dominant subset of vertices, then its weighted characteristic vector $\vec{x}^S$ is a strict local solution of program (36). Conversely, if $\vec{x}^*$ is a strict local solution of program (36), then its support $\sigma = \sigma(\vec{x}^*)$ is a dominant set, provided that $w_{\sigma\cup\{i\}}(i) \neq 0$ for all $i \notin \sigma$.*

Here we consider the quadratic program related to edge-weighted $\{1,2\}$-graph. Let H be a $\{1,2\}$-graph on vertex set $[n]$ with edge sets $E^1 \cup E^2$. Let $\vec{u} \geq 0$ be the edge weight vector of H^1 and let $A \geq 0$ be the edge weight matrix of H^2.

Let $p_i = u_i$ if $\{i\} \in E^1$ and $p_i = 0$ if $\{i\} \notin E^1$; let $q_{ij} = a_{ij} - p_i$ if $ij \in E^2$ and $q_{ij} = -p_i$ if $ij \notin E^2$; that is, $a_{ij} = q_{ij} + p_i$. Consider the following quadratic program:

$$\begin{aligned} &\text{maximize } f(\vec{x}) = \vec{p}^T\vec{x} + \vec{x}^T Q\vec{x} \\ &\text{subject to } \in\triangle, \end{aligned} \tag{37}$$

where $\vec{p} = (p_1, \ldots, p_n)^T$ and $Q = (q_{ij})_n$. A vector $\vec{x} \in \triangle$ satisfies the Karush-Kuhn-Tucker (KKT) conditions for problem (37), that is, the first-order necessary conditions for local optimality, if there exist $n+1$ real constants (Lagrange multipliers) $\mu_1, \ldots, \mu_n$ and λ with $\mu_i \geq 0$ for all $i = 1, \ldots, n$, such that

$$p_i + (Q\vec{x})_i + \theta + \mu_i = 0, \tag{38}$$

for all $i = 1, \ldots, n$, $\sum_{i=1}^n x_i = 1$, and $\sum_{i=1}^n x_i\mu_i = 0$. Note that $\sum_{i=1}^n x_i = 1$ and $a_{ij} = Q_{ij} + p_i$. Equality (38) is equivalent to

$$(A\vec{x})_i + \theta + \mu_i = 0, \tag{39}$$

for all $i = 1, \ldots, n$, $\sum_{i=1}^n x_i = 1$, and $\sum_{i=1}^n x_i\mu_i = 0$. So, if we define the dominant set of H as the dominant set of H^2, then, by Theorem 7, we have the following.

Theorem 8. *If S is a dominant subset of vertices, then its weighted characteristic vector $\vec{x}^S$ is a strict local solution of program (37). Conversely, if $\vec{x}^*$ is a strict local solution of program (37), then its support $\sigma = \sigma(\vec{x}^*)$ is a dominant set, provided that $w_{\sigma\cup\{i\}}(i) \neq 0$ for all $i \notin \sigma$.*

7. Conclusion

In this paper, we study the connection between the local maxima of a class of quadratic program and certain maximal cliques including 2-cliques or $\{1,2\}$-cliques of $\{1,2\}$-hypergraphs. We also explore the connection between edge-weighted clusters and strictly local optimum solutions of a class of polynomials resulting from nonuniform $\{1,2\}$-hypergraphs. In the future, we will try to extend these results to general hypergraphs.

Data Availability

No data were used to support this study.

Conflicts of Interest

The author declares no conflicts of interest.

Acknowledgments

The author thanks Professor Xiangde Zhang and Professor Cheng Zhao for their helpful discussion and also thanks Professor Cheng Zhao for introducing the preliminary version of this work on the 30th Midwestern Conference on Combinatorics and Combinatorial Computing (MCCCC30): https://about.illinoisstate.edu/mcccc30/list-of-participants/. This research was partially supported by Chinese Universities Scientific Fund (no. N180504008).

References

[1] I. M. Bomze, "Evolution towards the maximum clique," *Journal of Global Optimization*, vol. 10, no. 2, pp. 143–164, 1997.

[2] M. Budinich, "Exact bounds on the order of the maximum clique of a graph," *Discrete Applied Mathematics*, vol. 127, no. 3, pp. 535–543, 2003.

[3] S. Busygin, "A new trust region technique for the maximum weight clique problem," *Discrete Applied Mathematics*, vol. 154, no. 15, pp. 2080–2096, 2006.

[4] M. Pavan and M. Pelillo, "Dominant sets and pairwise clustering," *IEEE Transactions on Pattern Analysis and Machine Intelligence*, vol. 29, no. 1, pp. 167–172, 2007.

[5] J. Hou and M. Pelillo, "A simple feature combination method based on dominant sets," *Pattern Recognition*, vol. 46, no. 11, pp. 3129–3139, 2013.

[6] L. E. Gibbons, D. W. Hearn, P. M. Pardalos, and M. V. Ramana, "Continuous characterizations of the maximum clique problem," *Mathematics of Operations Research*, vol. 22, no. 3, pp. 754–768, 1997.

[7] A. K. Jain, "Data clustering: 50 years beyond K-means," *Pattern Recognition Letters*, vol. 31, no. 8, pp. 651–666, 2010.

[8] S. Agarwal, J. Lim, L. Zelnik-Manor, P. Perona, D. Kriegman, and S. Belongie, "Beyond pairwise clustering," in *Proceedings of the IEEE Conference Computer Vision and Pattern Recognition*, vol. 2, pp. 838–845, San Diego, CA, USA, June 2005.

[9] V. M. Govindu, "Tensor decomposition for geometric grouping and segmentation," in *Proceedings of the IEEE Conference Computer Vision and Pattern Recognition*, pp. 1150–1157, San Diego, CA, USA, June 2005.

[10] A. Shashua, R. Zass, and T. Hazan, "Multi-way clustering using super-symmetric non-negative tensor factorization," *Computer Vision-ECCV 2006*, vol. 3954, pp. 595–608, 2006.

[11] Y. Huang, Q. Liu, F. Lv, Y. Gong, and D. N. Metaxas, "Unsupervised image categorization by hypergraph partition," *IEEE Transactions on Pattern Analysis and Machine Intelligence*, vol. 33, no. 6, pp. 1266–1273, 2011.

[12] S. Rota Bulo and M. Pelillo, "A game-theoretic approach to hypergraph clustering," *IEEE Transactions on Pattern Analysis and Machine Intelligence*, vol. 35, no. 6, pp. 1312–1327, 2013.

[13] H. Liu, L. J. Latecki, and S. Yan, "Dense subgraph partition of positive hypergraphs," *IEEE Transactions on Pattern Analysis and Machine Intelligence*, vol. 37, no. 3, pp. 541–554, 2015.

[14] H. Liu, L. J. Latecki, and S. Yan, "Robust clustering as ensembles of affinity relations," in *Proceedings of the 24th Annual Conference on Neural Information Processing Systems 2010*, Vancouver, CanadaAdvances in Neural Information Processing Systems 23, Vancouver, Canada, December 2010.

[15] M. Pelillo and A. Jagota, "Feasible and infeasible maxima in a quadratic program for maximum clique," *Journal of Artificial Neural Networks*, vol. 2, pp. 411–420, 1995.

[16] Y. J. Peng, H. Peng, Q. S. Tang, and C. Zhao, "An extension of Motzkin-Straus theorem to non-uniform hypergraphs and its applications," *Discrete Applied Mathematics*, vol. 200, pp. 170–175, 2015.

[17] P. Frankl and Z. Füredi, "Extremal problems whose solutions are the blowups of the small witt-designs," *Journal of Combinatorial Theory-Series A*, vol. 52, no. 1, pp. 129–147, 1989.

[18] Y. Peng and C. Zhao, "A Motzkin-Straus type result for 3-uniform hypergraphs," *Graphs and Combinatorics*, vol. 29, no. 3, pp. 681–694, 2013.

[19] P. Frankl and V. Rödl, "Hypergraphs do not jump," *Combinatorica*, vol. 4, no. 2-3, pp. 149–159, 1984.

[20] J. M. Talbot, "Lagrangians of hypergraphs," *Combinatorics, Probability & Computing*, vol. 11, no. 2, pp. 199–216, 2002.

[21] T. S. Motzkin and E. G. Straus, "Maxima for graphs and a new proof of a theorem of Turán," *Canadian Journal of Mathematics*, vol. 17, pp. 533–540, 1965.

[22] Y. J. Peng and Y. P. Yao, "On Motzkin-Straus type of results and Frankl-Fúedi conjecture for hypergraphs," 2013, https://arxiv.org/abs/1312.3034.

[23] R. Gu, X. Li, Y. Peng, and Y. Shi, "Some Motzkin-Straus type results for non-uniform hypergraphs," *Journal of Combinatorial Optimization*, vol. 31, no. 1, pp. 223–238, 2016.

[24] Q. Tang, Y. Peng, X. Zhang, and C. Zhao, "On Motzkin-Straus type results for non-uniform hypergraphs," *Journal of Combinatorial Optimization*, vol. 34, no. 2, pp. 504–521, 2016.

[25] D. G. Luenberger and Y. Ye, *Linear and Nonlinear Programming*, Springer Science Business Media, LLC, Berlin, Germany, 3rd edition, 2008.

Hindawi
Journal of Mathematics
Volume 2024, Article ID 9791379, 1 page
https://doi.org/10.1155/2024/9791379

Retraction

Retracted: Research on Clothing Image Database Retrieval Algorithm Based on Wavelet Transform

Journal of Mathematics

Received 23 January 2024; Accepted 23 January 2024; Published 24 January 2024

This article has been retracted by Hindawi following an investigation undertaken by the publisher [1]. This investigation has uncovered evidence of one or more of the following indicators of systematic manipulation of the publication process:

(1) Discrepancies in scope

(2) Discrepancies in the description of the research reported

(3) Discrepancies between the availability of data and the research described

(4) Inappropriate citations

(5) Incoherent, meaningless and/or irrelevant content included in the article

(6) Manipulated or compromised peer review

The presence of these indicators undermines our confidence in the integrity of the article's content and we cannot, therefore, vouch for its reliability. Please note that this notice is intended solely to alert readers that the content of this article is unreliable. We have not investigated whether authors were aware of or involved in the systematic manipulation of the publication process.

Wiley and Hindawi regrets that the usual quality checks did not identify these issues before publication and have since put additional measures in place to safeguard research integrity.

We wish to credit our own Research Integrity and Research Publishing teams and anonymous and named external researchers and research integrity experts for contributing to this investigation.

The corresponding author, as the representative of all authors, has been given the opportunity to register their agreement or disagreement to this retraction. We have kept a record of any response received.

References

[1] X. Cui, "Research on Clothing Image Database Retrieval Algorithm Based on Wavelet Transform," *Journal of Mathematics*, vol. 2022, Article ID 6332592, 8 pages, 2022.

Hindawi
Journal of Mathematics
Volume 2022, Article ID 6332592, 8 pages
https://doi.org/10.1155/2022/6332592

Research Article

Research on Clothing Image Database Retrieval Algorithm Based on Wavelet Transform

Xiaoyue Cui

School of Art&Design, Zhengzhou University of Light Industry, Zhengzhou 450000, China

Correspondence should be addressed to Xiaoyue Cui; cuixiaoyue@zzuli.edu.cn

Received 26 November 2021; Revised 19 December 2021; Accepted 22 December 2021; Published 7 January 2022

Academic Editor: Naeem Jan

Aiming at the problems of low image data retrieval accuracy and slow retrieval speed in the existing image database retrieval algorithms, this paper designs a clothing image database retrieval algorithm based on wavelet transform. Firstly, it represents the color consistency vector of clothing image, reflects the composition and distribution of image color through color histogram, quantifies the visual features of clothing image, aggregates them into a fixed size representation vector, and uses the Fair Value (FV) model to complete the collection of clothing image data. Then, the size of the clothing image is adjusted by using the size transformation technology, and the clothing pattern is divided into four moments with the same size. On this basis, the clothing image is discretized with the help of Hu invariant moment to complete the preprocessing of clothing image data. Finally, the generating function of wavelet transform is determined, and a cluster of functions is obtained through translation and expansion. The wavelet filter is decomposed into basic modules, and then, the wavelet transform is studied step by step. The clothing image data are regarded as a signal, split, predicted, and updated and input into the wavelet model, and the retrieval research of clothing image database is completed. The experimental results show that the design of the retrieval algorithm is reasonable, the retrieval data accuracy is high, and the retrieval speed is fast.

1. Introduction

With the rapid development of the Internet and the popularization of various digital devices, the number of multimedia information in modern society is growing rapidly, which promotes the further prosperity of multimedia information management research. Image data retrieval and management system plays a particularly important role in the research of multimedia information management. Not only is the image the basis of video but also image database technology can be directly applied to many important fields, such as digital library, digital museum, medicine, geographic observation, petroleum geological exploration, public security, and clothing. Image is the main medium for people to communicate with each other and understand the world. It is not only the most intuitive form of important information expression but also the most difficult information content to obtain, transmit, process, realize, and store [1]. Research and statistics show that more than 70% of human information from the outside comes from image information, and the role of image information is difficult to be replaced by other information forms. Image technology covers a wide range and has a close relationship with mathematical physics students' physical psychology, electronics, and computer science. It is widely used in various fields such as scientific research, agricultural production, industrial production, military and national defense, aerospace, culture and entertainment, medical and health care, and traffic management [2].

With the advent of information society, the information people deal with is not only digital and symbolic information but also a large number of image information. Computer image processing technology is a new computer application field developed with the development of computer technology. It is a discipline gradually developed on the basis of achievements in image analysis and research. This technology has been involved in all fields of people's life, study, and work. With the improvement of people's living and

economic standards, they also have their own unique opinions on the pattern requirements in clothing. Using computer technology to identify clothing patterns, so as to improve clothing production efficiency to meet market demand, has become the current trend. In the process of clothing pattern generation, a certain database is designed to generate directly according to people's favorite needs. Therefore, the management and retrieval of clothing pattern database is the key [3].

The traditional management of clothing images is in the form of documents. When users want to query a clothing image, they have to open the file one by one and browse manually to find the target image [4]. Although this manual retrieval method is still in use, with the rapid increase of the number of image files, this query method has been difficult to meet the retrieval requirements of large clothing image database. The retrieval method based on keyword or descriptive text needs to specify the text features or keywords during query, which requires users to describe the text features with certain accuracy and standardization. There are two major problems in this method. One is that manual annotation of images needs to pay a lot of labor cost. Second, image manual annotation is subjective and imprecise, which cannot standardize and accurately describe the rich information contained in the image. Because there is no unified standard for image description, people have different understanding of image content. For example, there is no exact boundary between "big" and "big" of an object [5]. In addition, different language environments, different social conditions, and different nationalities will have different understanding of the same object, which will affect the consistency of image text description. With the passage of time, the things or concepts that people are interested in will also change. The definition of text features of images in the early stage is difficult to adapt to various developments in the later stage.

In order to improve the retrieval efficiency of clothing pattern database, a new clothing image database retrieval algorithm based on wavelet transform is designed in this paper. By collecting and preprocessing the data in the existing clothing pattern database, the wavelet transform method is introduced to design the retrieval scheme of the database and complete the retrieval of clothing image database. The main technical route of this paper is as follows:

Step 1: in Section 2, the process of image data acquisition in the clothing image database is carried out, where we characterize the color consistency vector of the clothing image, reflect the composition and distribution of the image color through the color histogram, quantify the visual features of the clothing image, aggregate them into a fixed size representation vector, and complete the clothing image data acquisition by using the FV model.

Step 2: in the image data preprocessing in the clothing image database also carried out in Section 2, the size of the clothing image is adjusted by using the size transformation technology, and the clothing pattern is divided into four moments of the same size. On this basis, the clothing image is discretized with the help of Hu invariant moment to complete the clothing image data preprocessing.

Step 3: progressing forward in Section 2, in the design of clothing image database retrieval algorithm based on wavelet transform, the generating function of wavelet transform is determined, and a cluster of functions is obtained through translation and expansion. The wavelet filter is decomposed into basic modules, and then, the wavelet transform is studied step by step. The clothing image data are regarded as a signal, split, predicted, and updated and input into the wavelet model. Complete the research of clothing image database retrieval.

Step 4: experimental analysis is performed in Section 3.

Step 5: conclusion is given in Section 4.

2. Image Data Acquisition and Preprocessing in Clothing Image Database

In this section, the image data acquisition in clothing database is described. Moreover, image data preprocessing in clothing image database is explained. Furthermore, the retrieval algorithm of clothing image database based on wavelet transform is proposed.

2.1. Image Data Acquisition in Clothing Image Database. The retrieval work of clothing image database is very different from that of traditional document database. Clothing images are rich in content and unstructured data, so traditional text retrieval methods cannot be directly used for query and retrieval. Therefore, in order to realize the effective retrieval of this paper, key image data are collected in the existing clothing database to provide accurate pattern data for subsequent recognition [6].

In clothing image data acquisition, from the perspective of human vision, color feature is a basic visual feature for human to perceive and distinguish different objects. Therefore, first, the initial dress pattern data are collected according to the color consistency vector of the dress pattern. The color consistency vector not only counts the number of pixels of each color in the whole clothing image but also counts the pixel value of the largest region of each color in the image. Consistent pixels belong to areas with continuous colors in the image. The color consistency vector represents this classification of colors in the image. It makes the consistent pixels in one image cannot be compared with the inconsistent pixels in another image. This is not possible with a simple color histogram. An intuitive way to represent the content of the clothing image is to count the color of pixels to get the color histogram. The color histogram reflects the composition and distribution of colors in the image, that is, the occurrence of colors and the probability of various colors [7]. Color histogram represents a global characteristic of the image.

Assuming that the histogram of the dress pattern has L colors and floats in a certain order and assuming that the

number of pixels of the dress image on the i color is $G(i)$, the cumulative color histogram can be expressed as

$$v(k) = \sum_{i=1}^{k} G(i), \quad k = 1, 2, \ldots, L \tag{1}$$

At this time, the global color histogram of the clothing image only considers the composition distribution of colors, which is easy to ignore the spatial distribution information of various colors in the image. Therefore, it is necessary to quantify the visual features of clothing images and aggregate them into a fixed size representation vector. In this feature quantization, the FV model [8] is used to represent them as a fixed size vector. Generally, the Gaussian mixture model aggregates the normalized cascade gradient vectors of all local descriptors into a unified Fisher variable. In essence, an image is expressed by the gradient vector of the likelihood function. For a clothing image, it is assumed to extract t local descriptors, expressed as

$$R = \{r_i\}, \quad i = 1, 2, \ldots, T. \tag{2}$$

In formula (2), the set of costume image quantification parameters is represented.

On this basis, we make it obey the independent and equal distribution, expressed as follows:

$$L(R|\varphi|) = \frac{1}{N}\sqrt{L}\sum R \tag{3}$$

where $L(R|\varphi|)$ represents the set of costume image quantization parameters.

Assuming that the Y distribution is verified in a Gaussian hybrid model, the quantified costume image parameters and the determined quantified parameters are effectively fit, thus obtaining

$$\psi(v) = \sum_{i=1}^{n} w_k u_k(x) \tag{4}$$

where $\psi(v)$ represents the Gaussian score, u represents the coefficient of linear combinations of costume pattern data, and x represents the covariance matrix.

The quantification process of extracting the costume image data based on the FV model is shown in Figure 1:

After quantizing the above clothing image data, describe its local features, determine the nearest feature point of each local feature, and obtain

$$B(x) = \operatorname{argmin}\left|c_i - x_i\right| \tag{5}$$

According to the determined feature points of clothing pattern data, calculate the residual value of the feature and complete the collection of clothing image data, namely,

$$h_K = \sum_{i=1}^{h} (x - c_i), \tag{6}$$

where c represents the dimension value of the dress pattern feature descriptor and k represents the residual value.

In the process of image data acquisition in clothing image database, the color consistency vector of the clothing image is characterized, the composition and distribution of the image color is reflected through color histogram, and the visual features of clothing image are quantified and aggregated into a fixed size representation vector. The FV model is used to complete the collection of clothing image data.

2.2. Image Data Preprocessing in Clothing Image Database. Image data preprocessing is carried out in clothing image database because there are many interferences in the above collected clothing image data; it cannot be retrieved directly and effectively. Therefore, it is necessary to preprocess the clothing image data. In the process of clothing image processing, the processing effects of clothing image feature extraction, segmentation, recognition, and matching are easily affected by factors such as uneven illumination, image size, rotation, and noise. Therefore, before garment image processing, the image should be preprocessed to eliminate the influence of these irrelevant factors, so as to restore or enhance the useful information in the image and improve the detectability of relevant information [9].

In dress image preprocessing, only when certain conditions are met can the dress image be retrieved by wavelet or contour wave. Therefore, the clothing image is converted to a certain size. Generally, the size transformation technology is used to adjust the size of clothing image, and the size transformation technology usually uses the interpolation method to change the size of the image [10]. The commonly used interpolation algorithms include nearest neighbor interpolation, bilinear interpolation, bicubic interpolation, and wavelet interpolation. Different interpolation algorithms have different processing accuracy, and different interpolation algorithms will also affect the degree of image distortion. The nearest neighbor interpolation method is used to transform the size of $232 * 205$ tire clothing image. In the process of clothing image processing, sometimes, an image with high dimension is divided into nonoverlapping blocks to obtain several subimages with low dimension, and the subimages are used for image analysis [11]. This process is based on the idea of image segmentation. Let the matrix [12] of a discrete two-dimensional clothing image be expressed as

$$P = \begin{bmatrix} p_{11}, p_{12}, \ldots, p_{1n} \\ p_{21}, p_{22}, \ldots, p \\ \cdots \\ p_{m1}, p_{m2}, \ldots, p_{mn} \end{bmatrix} \tag{7}$$

where p represents the number of pixels in the clothing image Assuming that m and n can be divided by 2, the costume image is divided into four pieces without overlap and expressed as

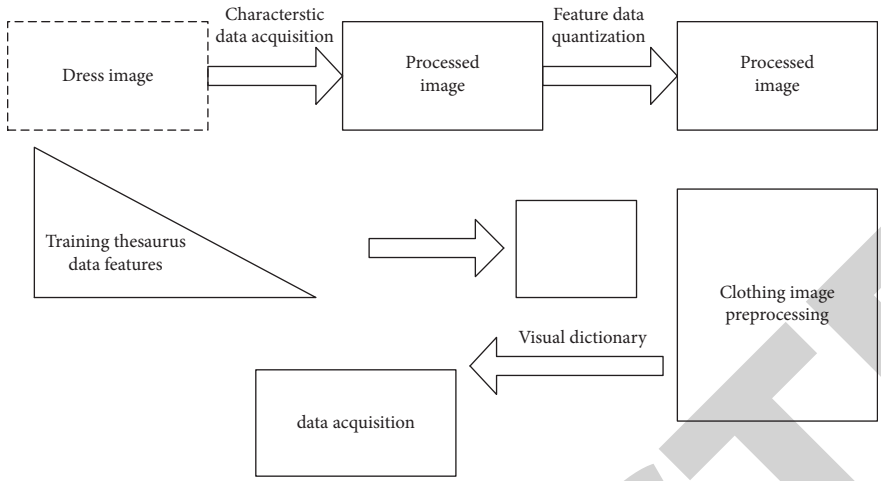

Figure 1: Quantization process of extracting clothing image data based on the FV model.

$$P_1 = \begin{bmatrix} p_{11} \cdots p_{1L} \\ \cdots \\ p_{k1} \quad p_{KL} \end{bmatrix},$$
$$P_2 = \begin{bmatrix} p_{1(L+1)} \cdots p_{1L} \\ \cdots \\ p_{k(L-1)} \quad p_{K(L+1)} \end{bmatrix},$$
$$P_3 = \begin{bmatrix} p_{(K+1)} \cdots p_{1L} \\ \cdots \\ p_{M1} \quad p_{KL} \end{bmatrix}, \tag{8}$$
$$P_4 = \begin{bmatrix} p_{11} \cdots p_{1L} \\ \cdots \\ p_{k1} \quad p_{ML} \end{bmatrix},$$

where the matrix is divided into four submatrices, and each submatrix represents a subblock image. According to the above image blocking method, this technology can be applied in image retrieval technology to establish a new image retrieval database by nonoverlapping segmentation of images. The 128×128 tire image is divided into nonoverlapping blocks to obtain four subclothing images of the same size.

According to the divided image, moment invariants are used for noise reduction [13]. Hu invariant moment is based on the divided image subblock, and the subblock image is discretized to obtain

$$D_{pq} = \sum_x \sum_y x^p y^q f(a,b) \tag{9}$$

where $f(a,b)$ represents a 2-dimensional discrete image, representing the moment.

In the image data preprocessing in the clothing image database, the size of the clothing image is adjusted by using the size transformation technology, and the clothing pattern is divided into four moments of the same size. On this basis, the clothing image is discretized with the help of Hu invariant moment to complete the clothing image data preprocessing.

2.3. Retrieval Algorithm of Clothing Image Database Based on Wavelet Transform. Wavelet transform is the development and upgrading of Fourier transform. It has the local analysis characteristics that Fourier transform does not have. It can transform the time-frequency resolution according to the local regional characteristics of the signal. Wavelet function is a cluster of functions obtained by the translation and expansion of the generating function of wavelet. If it is set as the generating function of wavelet, the derived wavelet function [14] is

$$\eta_{a,b}(t) = |a|^{(1/2)} \phi\left(\frac{t-b}{a}\right) \tag{10}$$

In wavelet transform, not all functions can become generating functions, and they need to meet certain conditions. The conditions to be met are

$$E_\varphi = \int_r \frac{|\phi(w)|^2}{|w|} \mathrm{d}w < \infty \tag{11}$$

where E represents the generating function of wavelet transform and the allowable limiting index. At this time, the wavelet of continuous transformation is expressed as

$$W_f(a,b) = r < f, a > \frac{1}{\sqrt{a}} \int_{-\infty}^{\infty} E_\varphi vt \tag{12}$$

where $W_f(a,b)$ represents wavelet transformation, r represents wavelet inversion transformation, and vt represents the time of wavelet window as a function.

Wavelet transform is a very important artificial intelligence algorithm. Therefore, in the retrieval of clothing image database designed in this paper, the clothing image retrieval model is designed, and then, the above processed clothing image data are input into the model to complete the retrieval of clothing image data.

The wavelet filter is decomposed into several basic modules, and then, the wavelet transform is carried out step

by step, which is the basic idea of lifting wavelet. The lifting algorithm is also relatively simple, mainly to obtain high-frequency components and low-frequency components. High-frequency components can be obtained by polynomial interpolation, and there is a prerequisite for the acquisition of low-frequency components, that is to keep the high-order moment and mean value of the original signal unchanged. The improvement scheme can be divided into the following three steps: splitting, prediction, and updating [15], and the process is shown in Figure 2.

Firstly, the clothing image data are regarded as the signal input into the wavelet model and divided. The presplit costume image data signal is S_n, and the split was set to S_{n-1} and d_{n-1}, respectively. The decomposition process is shown in Figure 3:

Then, the clothing image data are predicted. The significance of prediction is to obtain the detailed information of the signal. First, the filter acts on the even sequence, then takes the obtained value as the predicted value of the odd sequence, and then obtains the detailed information by calculating the difference between the actual value of the odd sequence and the predicted value, that is,

$$d_{n-1} = \text{odd}_{n-1} - P\left(\text{even}_{n-1}\right) \tag{13}$$

Thirdly, the clothing image data are updated. The update is mainly to maintain the global characteristics of the original data in the retrieval. The update algorithm is introduced to obtain the updated clothing image data as follows:

$$S_{n-1} = \text{even}_i + U\left(d_{n-1}\right) \tag{14}$$

where U represents the updated original image data.

Finally, design the wavelet change model, input the updated clothing image data, and complete the retrieval of clothing image data, that is,

$$Q = \int_{-\infty}^{\infty} F(T)\mathrm{d}t < f, \varphi_i > \tag{15}$$

where Q represent costume image data retrieved from the wavelet model.

In the above retrieval, due to some omissions in the retrieved data, it is necessary to reverse transform it and retrieve the clothing image data globally. The results are as follows:

$$l(x, y) = \frac{1}{z} \int_{i=1}^{n} W_f(x, y)\varepsilon \frac{da}{a^3}\mathrm{d}t \tag{16}$$

where z represents the reverse conversion factor, $l(x, y)$ represents the results after retrieval, and ε represents the wavelet base in the vertical direction of the costume image.

In the design of clothing image database retrieval algorithm based on wavelet transform, the generating function of wavelet transform is determined, and a cluster function is obtained through translation and expansion. The wavelet filter is decomposed into basic modules, and then, the wavelet transform is studied step by step. The clothing image data are regarded as a signal, split, predicted, and updated and input into the wavelet model. Complete the research of clothing image database retrieval.

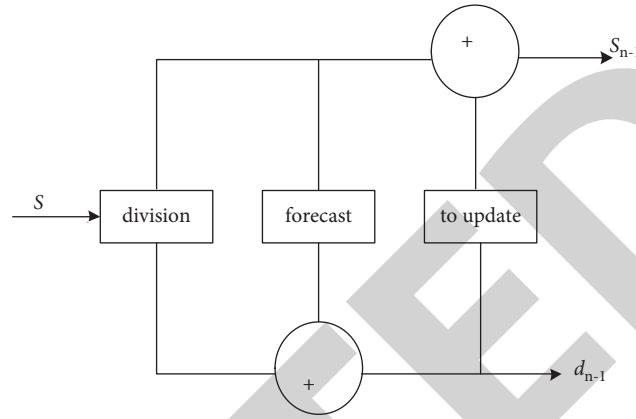

Figure 2: Wavelet transform model scheme.

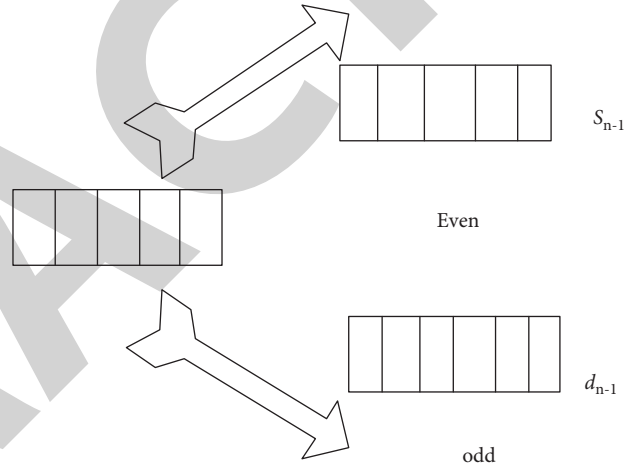

Figure 3: Clothing image data signal classification process.

3. Experimental Analysis

In order to confirm the authenticity of proposed methods, this section performs the experiments and analyses the results. First, we design the experimental scheme, followed by experimental index design, and finally, the analysis of the experimental results is given.

3.1. Experimental Scheme Design. In order to verify the effectiveness of this method, experimental analysis is carried out. In the experiment, 100 experimental retrieved images were selected from the professional "My Structural Query Language" (MySQL) database, these images were set to the size of $256 * 256$, and the images were preprocessed. The processed experimental representative clothing images were used as the experimental sample images to retrieve the colors in the clothing patterns. There were many image colors in the experimental samples. Therefore, in the experiment, the specific recognition color is determined to identify the

Figure 4: Experimental sample image.

(a) (b)

(c) (d)

Figure 5: Comparison of retrieval effects of different retrieval methods. (a) Sample image color retrieval. (b) Proposed method. (c) Image data retrieval based on the block dominant color method. (d) Image retrieval based on joint weighted aggregation depth convolution features.

Table 1: Retrieval time of different methods (s).

Retrieval times	The proposed method	The search of image disorder surge data based on the block primary color method	Image retrieval of jointly weighted aggregate depth convolutional features
20	1.3	1.5	1.6
40	1.3	1.5	1.7
60	1.2	1.6	1.9
80	1.2	1.9	2.1
100	1.2	2.0	2.3

typical clothing pattern color. The experimental sample image is shown in Figure 4:

In Figure 4, the green line box is the color area retrieved in the experiment.

3.2. Experimental Index Design. In order to verify the effectiveness of this method for clothing image retrieval, the experiment is carried out by comparing this method, the image disordered surge data retrieval method based on the block dominant color method, and the image retrieval method based on joint weighted aggregation depth convolution feature. In the experiment, the retrieval accuracy of the color in the sample image and the retrieval time overhead are taken as the experimental indexes. The experimental results obtained in the experiment have been verified for many times and meet the requirements of the experiment.

3.3. Analysis of Experimental Results. Firstly, the experiment analyzes the method in this paper, the image disorderly surge data retrieval method based on block dominant color method, and the image retrieval method combined with weighted aggregation depth convolution feature to retrieve the color in the sample image. The retrieval effect is shown in Figure 5.

By analyzing the retrieval results in Figure 5, it can be seen that there are some differences in the retrieval effects of the method in this paper, the image disorderly surge data retrieval method based on the block main color method, and the image retrieval method combined with weighted aggregation depth convolution feature on the color in the sample image. Among them, the color retrieval accuracy of this method is better; only one part cannot be retrieved, while the color retrieval results of the other two methods are lower than that of this method. In contrast, the retrieval effect of this method is better, which verifies that the retrieval accuracy of this method is higher.

In order to further verify the effectiveness of this method, on the basis of ensuring the retrieval accuracy, the experiment further analyzes the time cost of this method, the image disordered surge data retrieval method based on the block dominant color method, and the image retrieval method combined with weighted aggregation depth convolution feature to retrieve the color in the sample image. The results are shown in Table 1.

By analyzing the data in Table 1, it can be seen that the time cost of color retrieval in the sample image is different by using the method in this paper, the image disordered surge data retrieval method based on the block dominant color method, and the image retrieval method combined with weighted aggregation depth convolution feature. Among them, the retrieval speed of this method is short, up to about 1.3 s, while the image disordered surge data retrieval method based on the block main color method and the image retrieval method based on joint weighted aggregation depth convolution feature have a longer time overhead than this method. In contrast, this method is more effective. It is verified that the work efficiency of this method is faster.

4. Conclusion

In order to solve the problems of low image data retrieval accuracy and slow retrieval speed in the existing image database retrieval algorithms, this paper designed a clothing image database retrieval algorithm based on wavelet transform. Moreover, the characterization of color consistency vector of clothing image is done, in which the color histogram reflects the composition and distribution of image color, which is aggregated into a fixed size representation vector, and the FV model is used to complete the collection of clothing image data. Furthermore, the size of clothing image is adjusted through the use of size transformation technology. In addition, with the aid of Hu invariant moment, the clothing image was discretized to complete the preprocessing of clothing image data. Determine the generating function of wavelet transform, decompose the wavelet filter into basic modules, and then study the wavelet transform step by step. The clothing image data are regarded as a signal, split, predicted, and updated, input into the wavelet model, and complete the retrieval research of clothing image database. The experimental results show that this method has certain retrieval advantages.

Data Availability

The data used to support the findings of this study are available from the corresponding author upon request.

Conflicts of Interest

The author declares that he has no conflicts of interest.

References

[1] J. Wu, J. Wang, Y. Nie, and L. Hu, "Multiple-image optical encryption based on phase retrieval algorithm and fractional Talbot effect," *Optics Express*, vol. 27, no. 24, Article ID 35096, 2019.

Hindawi
Journal of Mathematics
Volume 2023, Article ID 9892024, 1 page
https://doi.org/10.1155/2023/9892024

Retraction

Retracted: Evaluation Algorithm of Labor Legal Effectiveness for Affirmative Action against Gender Discrimination

Journal of Mathematics

Received 19 December 2023; Accepted 19 December 2023; Published 20 December 2023

This article has been retracted by Hindawi following an investigation undertaken by the publisher [1]. This investigation has uncovered evidence of one or more of the following indicators of systematic manipulation of the publication process:

(1) Discrepancies in scope

(2) Discrepancies in the description of the research reported

(3) Discrepancies between the availability of data and the research described

(4) Inappropriate citations

(5) Incoherent, meaningless and/or irrelevant content included in the article

(6) Manipulated or compromised peer review

The presence of these indicators undermines our confidence in the integrity of the article's content and we cannot, therefore, vouch for its reliability. Please note that this notice is intended solely to alert readers that the content of this article is unreliable. We have not investigated whether authors were aware of or involved in the systematic manipulation of the publication process.

Wiley and Hindawi regrets that the usual quality checks did not identify these issues before publication and have since put additional measures in place to safeguard research integrity.

We wish to credit our own Research Integrity and Research Publishing teams and anonymous and named external researchers and research integrity experts for contributing to this investigation.

The corresponding author, as the representative of all authors, has been given the opportunity to register their agreement or disagreement to this retraction. We have kept a record of any response received.

References

[1] L. Juan, "Evaluation Algorithm of Labor Legal Effectiveness for Affirmative Action against Gender Discrimination," *Journal of Mathematics*, vol. 2022, Article ID 4073208, 9 pages, 2022.

Hindawi
Journal of Mathematics
Volume 2022, Article ID 4073208, 9 pages
https://doi.org/10.1155/2022/4073208

Research Article

Evaluation Algorithm of Labor Legal Effectiveness for Affirmative Action against Gender Discrimination

Liao Juan

School of Law in Southwest Minzu University, Chengdu, Sichuan 610041, China

Correspondence should be addressed to Liao Juan; 2016121139@jou.edu.cn

Received 24 November 2021; Revised 17 December 2021; Accepted 20 December 2021; Published 7 January 2022

Academic Editor: Naeem Jan

Aiming at the problems of large evaluation error and low accuracy of determining the key degree of evaluation indicators in the existing evaluation of labor legal effectiveness, this paper designs a labor legal effectiveness evaluation algorithm for affirmative action against gender discrimination. Firstly, using hits degree, the degree of gender discrimination, and social influence, enterprise practice and government supervision and management are determined as the evaluation indexes of labor legal effectiveness in this paper, and on this basis, the labor legal effectiveness evaluation system against gender discrimination is designed. Then, the judgment matrix of the evaluation index of labor legal effectiveness against gender discrimination is constructed. After normalization, the weight of the evaluation index is calculated by entropy method, which lays a foundation for subsequent research. Finally, the tree enhanced Bayesian network is used to classify the labor legal effectiveness evaluation indicators, and the correlation between the indicators is determined through the Spearman rank correlation coefficient. Finally, the labor legal effectiveness evaluation model against gender discrimination is designed through the clustering algorithm, and the labor legal effectiveness evaluation indicators against gender discrimination are input to complete the effective evaluation. The experimental results show that the error of the evaluation algorithm is small, and the accuracy of determining the key degree of the evaluation index is high.

1. Introduction

Throughout history, human society has been plagued by racial, ethnic, and gender discrimination for a long time. Discrimination exists in many areas of social life in different forms, such as gender discrimination, employment discrimination, geographical discrimination, health discrimination, age discrimination, registered residence discrimination, academic discrimination, facial discrimination, religious discrimination, ethnic discrimination, and discrimination in the country [1].

At present, China's domestic academic circles generally believe that gender discrimination is an exclusive unfair treatment based on gender. However, there is no final conclusion on how to define gender discrimination. There are several important understandings: not all gender inequalities are equal to gender discrimination. Differential treatment based on the internal needs of occupation or the special needs of work post and the needs to maintain national security and public order do not belong to the scope of gender discrimination [2]. Gender discrimination is not only discrimination against women but also discrimination against men and discrimination against cross gender groups. Gender politics is essentially the negation and deprivation of women's basic human rights and freedoms. Antigender discrimination has important significance to protect women's human rights. Gender discrimination in employment is a very common problem faced by our society at present. Men and women have different value recognition in the labor market based on gender differences. There is a serious gender stratification in the labor market, the economic income gap between men and women continues to expand, and the vulnerable tendency of women's overall status is also emerging. However, gender differences do not constitute a legitimate reason for gender differential treatment [3]. At present, the important reason why women generally suffer from social discrimination lies in the unfair social division of labor mode of "men outside and women

inside," as well as the social reality that reproductive responsibility is mainly borne by women. The reality requires us to formulate relevant antidiscrimination laws and regulations as soon as possible, recognize the existence of discrimination, deeply understand the harm caused by discrimination to gender equality, promote the development of antigender discrimination work by clearly defining the constituent elements of discrimination and strengthening legislative and judicial practice, accelerate legal reform and innovation, and establish a sound system for the protection of women's rights, change and enhance social values, affirm the social value of women's housework, and establish a sound and perfect maternity security system, so as to change women's disadvantage and development situation caused by childbirth and promote gender equality [4].

Gender equality is a human rights issue, and the essence of gender inequality is the inequality of rights [5]. The pursuit of gender equality is an important part of a harmonious society. Building a harmonious world requires strengthening the protection of human rights, especially the vulnerable groups. In recent years, great progress has been made in the legislative work related to the protection of women's rights and antigender discrimination in China, which has been formed on the basis of the constitution of the People's Republic of China and the law of the People's Republic of China on the protection of women's rights and interests. China's constitution stipulates the fundamental principle of equality before the law and defines that women enjoy equal rights with men in political, economic, cultural, social and family life equal rights [6]. At the level of domestic legal system, China has strengthened relevant legislation against gender discrimination in many social fields such as labor, family life, education, and political participation and is committed to promoting gender equality. The Chinese people's law on the protection of persons with disabilities was adopted in 1990 and revised in 2008 It stipulates that discrimination on the basis of disability and the use of the media or other means to insult, infringe, or belittle the personality of persons with disabilities are prohibited: the labor law was promulgated in 1994, which stipulates that workers shall not be subject to any discrimination in employment on the grounds of nationality, race, gender, and religious belief: in 1995, the government issued the first program of action to promote gender equality. The outline for the development of Chinese women (1995–2000) followed closely with the outline for the development of Chinese women (2001–2010), the second national program of action to promote gender equality in 2001. It has put forward 34 main objectives and 100 strategic measures in six areas: women and the economy, women's participation in decision-making and management, women and education, women and health, women and law, and women and the environment. The marriage law in 2001 explicitly included the prohibition of domestic violence for the first time: the law on the protection of women's rights and interests was newly revised in 2005, emphasizes that women and men have equal rights in politics, economy, culture, and education, gives full play to women's role in socialist modernization, prohibits discrimination, abuse, abandonment, and mutilation of women, and promotes gender equality: the employment promotion law was formulated on the basis of the labor law in 2007; it further clearly requires employers to uniformly provide equal employment opportunities and fair employment conditions to workers and prohibit refusing to hire women on the basis of gender, improving women's employment standards, or setting other discriminatory restrictions.

After the promulgation of these legal provisions, the evaluation of their effectiveness is the key to measure the role of legal provisions. Therefore, this paper designs an evaluation algorithm of labor legal effect.

2. Design of Labor Legal Effectiveness Evaluation Algorithm for Affirmative Action against Gender Discrimination

In this section, we determine the evaluation index of labor legal effectiveness and construct the system against gender discrimination. Next, the weight of labor legal effectiveness evaluation index against gender discrimination is calculated. Then, we also explain the design of the proposed algorithm against gender discrimination.

2.1. Determination of Labor Legal Effectiveness Evaluation Index and System Construction against Gender Discrimination. In order to realize the design of labor legal effectiveness evaluation algorithm in this paper, firstly, we determine the labor legal effectiveness evaluation index against gender discrimination and build an effective evaluation system according to the determined labor legal effectiveness evaluation index against gender discrimination. In this part, according to the existing research, the evaluation indicators of labor legal effectiveness are sorted out, and the four key indicators that can best reflect the legal effectiveness are selected on the basis of advantages and disadvantages of the evaluation indicators, so as to complete the determination of the evaluation indicators of labor legal effectiveness. Among the selected legal effectiveness indicators, the degree of gender discrimination, social influence, enterprise practice, and government supervision and management are determined as the evaluation indicators of industrial legal effectiveness in this paper.

According to the determined legal effectiveness indicators, the authority of these indicators is determined by HITS algorithm to verify that the indicators determined by this method comply with the current evaluation of legal efficiency [7]. The criticality of evaluation indicators is set through HITS algorithm, and the most important indicators are determined among these indicators. These indicators are designed as a root set R, which includes a high proportion of authority assurance. The set is expanded to calculate the authority of new evaluation indicators through continuous iteration [8]. Assume that the indicator set in this set is

$$T = \{t_1, t_2, t_3, \ldots, t_n\}. \quad (1)$$

Each index of authority is a_n, and a higher key index is b_n:

$$a_n = \sum_{i=1}^{m} b_i (i \in b_n(m)). \quad (2)$$

In (2), $b_n(m)$ represents the key degree value of the rating index.

$$b_n = \sum_{i=1}^{n} C_i (i \in R_n(m)). \quad (3)$$

In (3), R_n represents the yield values in the rating index set.

According to the above calculation, the authority degree of legal efficiency of the above four indicators is determined. Based on the four key evaluation indexes, a multilevel evaluation index system is constructed, as shown in Figure 1.

In the key process of calculating the evaluation index by the algorithm, in the determination of the evaluation index of labor legal effectiveness against gender discrimination and the construction of the system, the hits degree is used to determine the degree of gender discrimination, social influence, enterprise practice, and government supervision and management as the evaluation index of labor legal effectiveness studied in this paper. The evaluation system of labor legal effect against gender discrimination is designed.

2.2. Weight Calculation of Labor Legal Effectiveness Evaluation Index against Gender Discrimination. In the above-mentioned evaluation indicators of labor legal effectiveness against gender discrimination and the evaluation process constructed, each indicator plays a different role and influence. In order to ensure the scientificity of the evaluation [6], different weights will be given to the unused indicators. The entropy weight method is used to determine the index weight. The judgment matrix of the evaluation index is defined as r. After normalization, the relative membership function formula of the index is obtained:

$$k_{ij} = \frac{r_{ij} - r_{\min}}{r_{\max} - r_{\min}}. \quad (4)$$

In (4), r_{ij} is the term in the matrix and $r_{\min}$, $r_{\max}$ are the minimum and maximum index values under the same index, respectively.

The entropy of the evaluation index is calculated by the definition of entropy, and the calculation formula can be expressed as

$$H_i = -\frac{1}{Inm} \sum_{j=1}^{m} f_{ij} \mathrm{In} f_{ij}, \quad (5)$$

where f_{ij} represents the ratio of single indicator membership in all index membership. The entropy weight of the i index can be calculated as

$$\omega_i = \frac{1 - H_i}{\left(n - \sum_{i=1}^{n} H_i\right)}, \quad (6)$$

Replacing the calculation results in (5) into formula (6) can calculate the entropy right calculation results of all evaluation indicators, and the sum of all index weights is equal to 1. Replacing the calculation results in (5) into formula (6) can calculate the entropy right calculation results of all evaluation indicators, and the sum of all index weights is 1.

In the weight calculation of labor legal effectiveness evaluation indicators against gender discrimination, the evaluation matrix of labor legal effectiveness evaluation indicators against gender discrimination is constructed. After normalization, the weight [9] of the evaluation indicators is calculated by the entropy method to lay the foundation for subsequent research.

2.3. Design of Evaluation Algorithm of Labor Legal Effect against Gender Discrimination. Based on the weight of the above evaluation index of labor legal effectiveness against gender discrimination, an evaluation algorithm of labor legal effectiveness against gender discrimination is designed. In this paper, Bayesian algorithm is used to design the labor legal effectiveness evaluation algorithm against gender discrimination. Naive Bayesian is a simple technique for constructing classifiers models that assign class labels to problem instances. In this, there is not a single algorithm but a family of algorithms based on a common principle. A naive traditional Bayesian network has great advantages in dealing with complex system state problems, but the assumption of traditional Bayesian network also brings some limitations to its application. The main reason is that Bayesian network is a NP hard problem. When there are many attributes of the research object, the calculation problem of Bayesian network without any learning constraints will become very huge. In order to improve the method, many experts and scholars are studying the Bayesian network method. Friedman transformed the Bayesian network into a tree enhanced naive Bayesian classifier (abbreviated as tree enhanced naive Bayesian) [10]. The tree enhanced Bayesian method is an improvement of the naive Bayesian network method. Compared with the naive Bayesian network, the tree enhanced Bayesian method has a certain relaxation in the requirements of assumptions, which can combine the advantages of the simplicity of naive Bayesian and the ability of Bayesian network to simply and clearly express the dependence between variables. Then, it can improve the classification ability of the method. Tree enhanced naive Bayes is an excellent classification model with good comprehensive performance. It balances the accuracy and learning efficiency in the classification process. The classification performance based on tree enhanced Bayesian network is also significantly higher than that based on traditional naive Bayes [11].

The constrained Bayesian network structure adopted in the labor legal effectiveness evaluation is

$$W = \{x_1, x_2, x_3, \ldots, x_n, f\}. \quad (7)$$

In formula (7), x represents a discrete set of attribute variables, and C represents class variables. There is no parent node for this variable. The class variable is the parent of all the other attribute value variables x, which has at most one attribute variable. That is, any attribute variable other than the class variable C has two parents, and one of the parents is

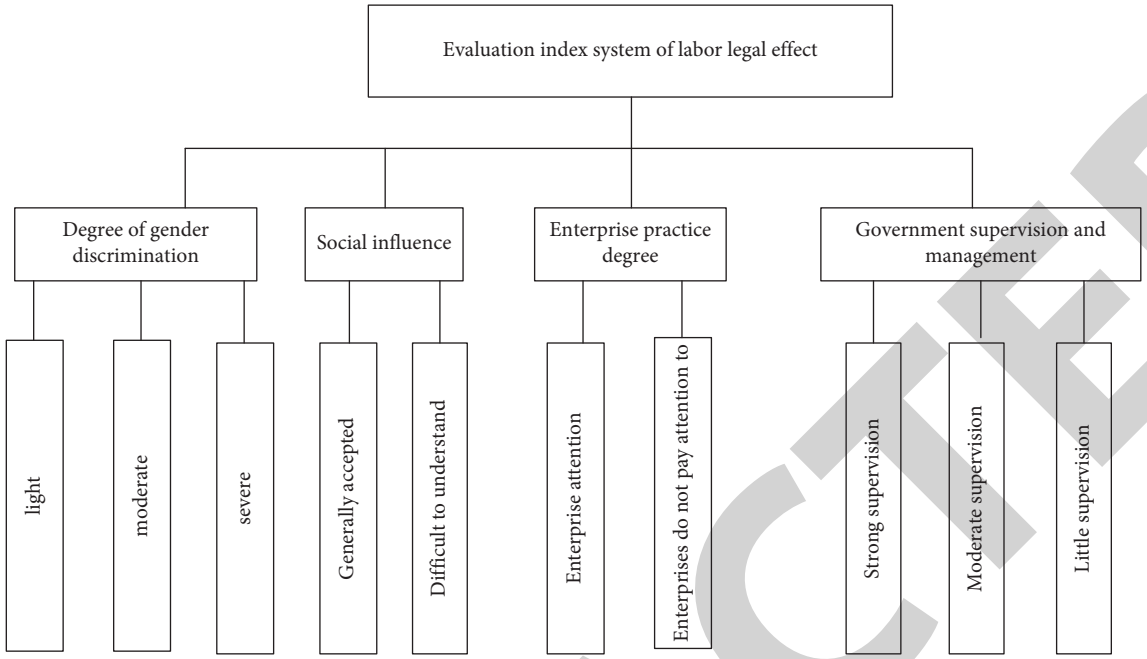

Figure 1: Schematic diagram of labor legal effectiveness evaluation system against gender discrimination.

the class variable [12] C; assuming that $\prod_{x_i}$ represents the parent of an attribute variable x_i, it can be obtained:

$$\prod_f = \alpha, f \in \prod_{x_i}. \tag{8}$$

A naive Bayesian model graph can be enhanced for a basic tree according to the description above, as shown in Figure 2.

Compared with Bayesian network model, tree enhanced naive Bayesian model can only have two parent nodes at most for each node, except the inner node, of which only one parent node can be a nonclass variable, and the class variable must be the parent node of other variables. This is mainly to reduce the search space and solve the problem of "state explosion" to a certain extent. In Bayesian network, the conditional probability table will increase with the increase of the number of parent nodes, which may become a "state explosion" problem. Limiting the number of parent nodes to less than 2 can effectively solve the "state explosion" problem caused by the large number of parent nodes [13].

For any unknown category, the evaluation index examples that need to be classified are

$$v_i = <v_{i1}, v_{i2}, v_{i3}, \ldots, v_{in}>. \tag{9}$$

The legal effectiveness indexes to be evaluated are classified by tree enhanced Bayesian method. If the largest class label is determined according to the formula calculated by Yebes, there is

$$p = \arg\max \frac{p(v_{i1}, v_{i2}, v_{i3}, \ldots, v_{in})}{p} p(c_i). \tag{10}$$

Among them, the evaluation set can be deduced according to the structure of tree enhanced naive Bayes.

Based on the classification of labor legal effectiveness evaluation indexes according to the tree enhanced Bayesian algorithm, the correlation of each evaluation index is analyzed to realize the design of the algorithm. Correlation analysis is to measure the correlation of two or more variables. In the research of microblog influence evaluation algorithm, the correlation coefficient in statistical method is often used to measure the correlation and difference of the algorithm. This paper selects Spearman rank correlation coefficient to measure the correlation between crank algorithm and existing microblog influence algorithm [14].

Spearman's rank correlation coefficient is an index to measure the dependence between two parameters, which was proposed by Charles Spearman. The biggest feature of Spearman's rank correlation coefficient is that the correlation can be calculated regardless of the distribution of parameters and the size of samples. The calculation formula is as follows: assuming that there are data sets X and Y, then

$$E = \frac{\sum_i (x_i - \overline{x})(y_i - \overline{y})}{(x_i - \overline{x})(y_i - \overline{y})^2}. \tag{11}$$

In (11), x_i represents the key degree ranking of x in the evaluation index set, and y_i represents the y secondary degree ranking of u in the data set, the $\overline{x}$ represents the mean of the critical degree in the set of evaluation metrics, and the $\overline{y}$ represents the secondary degree in the data set. To simplify the computational simplicity of the evaluation index phase, the formula is reduced to

$$E' = \frac{2\sum_i d_i}{n(n-1)}. \tag{12}$$

In (12), d_i represents the range of values. When the larger the value represents the greater the degree of association

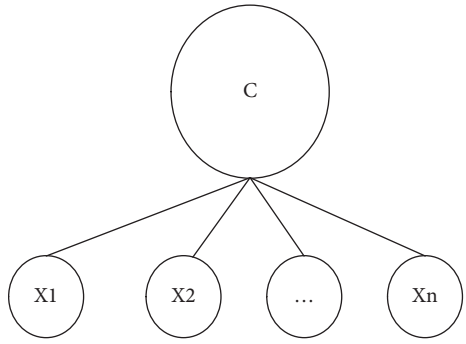

Figure 2: Basic tree enhanced naive Bayesian model.

between the evaluation index, the correlation of the evaluation index reflects the simplicity of the evaluation.

Based on the determination of the correlation of the above evaluation indexes, this paper designs an evaluation model of labor legal effectiveness against gender discrimination with the help of clustering algorithm and inputs the determined evaluation indexes with high correlation into it to achieve the final effective evaluation. The main principle of K-means clustering algorithm is as follows: randomly select k points as the particles of the initial clustering, then calculate the distance from each data point to the k particles, collect the data point to the nearest particle, traverse all data objects, and get the k categories of the first clustering. Calculate the new class center according to the last clustering result. If the distance between the class center and the class center of the last clustering is small, it indicates that the algorithm has converged. Otherwise, recalculate the distance from each data point to the new k particles and classify each point into a new particle class and continue the iteration. When the distance between all new particles and the last particle is less than a given initial value, it means that all particle classes have converged and a local optimal solution is obtained, then the iteration is stopped.

In a given set of evaluation metrics, each set e_i represents an evaluation indicator element, where each element includes the attributes of multiple evaluation metrics. Fuzzy clustering is to determine the evaluation index as class C, setting

$$U = e_i\{u_1, u_2, u_3, \ldots, u_n\}. \tag{13}$$

The formula represents the centroid distance of the evaluation index. In the fuzzy division, each evaluation index cannot be rigidly divided or belong to a class. It needs to be classified according to the evaluation membership degree. The unified results obtained at this time are

$$G_m(e_i) = \sum_{i=1}^{n}\sum_{c}^{f} u_i^m d_i, \tag{14}$$

where G_m represents the centroid of mass distance between the data after unification and u_i indicates the fuzzy index.

Based on this basis, we design the labor legal effectiveness evaluation model against gender discrimination. First, initialize the category of the evaluation index and set the fuzzy number to M, and the calculation of the iterative stop threshold, when the maximum number of iterations is L and the fuzzy partition matrix is U, is obtained:

$$H_{ij}^{(I+1)} = \frac{1}{\left(\sum_{k=1}^{c} d_{ij}/d_{kj}\right)/n}. \tag{15}$$

Then, the results of this model evaluation are updated and the results are

$$h = \frac{1}{\sum_{i=1}^{c} H_{ij}/\left(d_{ij}/d_{kj}\right)}. \tag{16}$$

In (16), the h output is the final effectiveness evaluation.

Based on the above analysis, the design of labor legal effectiveness evaluation algorithm against gender discrimination is realized. The overall evaluation process is shown in Figure 3.

Figure 3 explains the evaluation algorithm of labor legal effectiveness. Initialize evaluation index and calculate the index weight through fuzzy unified index membership. If the clustering model of evaluation has been successfully constructed, it gives the results and stops the process. If clustering model has not been constructed successfully, repeat the process again to get the effective output. In the design of labor legal effectiveness evaluation algorithm against gender discrimination, firstly, the tree is used to enhance the Bayesian network to classify the labor legal effectiveness evaluation indicators, and the correlation between the indicators is determined by Spearman's rank correlation coefficient. Finally, the labor legal effectiveness evaluation model against gender discrimination is designed by clustering algorithm. Input the evaluation index of labor legal effectiveness against gender discrimination into it to complete the effective evaluation.

3. Experimental Analysis

The purpose of this section is to verify the productivity and validation of the proposed work. First, the environment and the conditions are described in which the experiment is performed. Then, experimental index design is talked about. Lastly, the outcomes of the experiment are analyzed and investigated.

3.1. Experimental Environment. In order to verify the effectiveness of the algorithm designed in this paper,

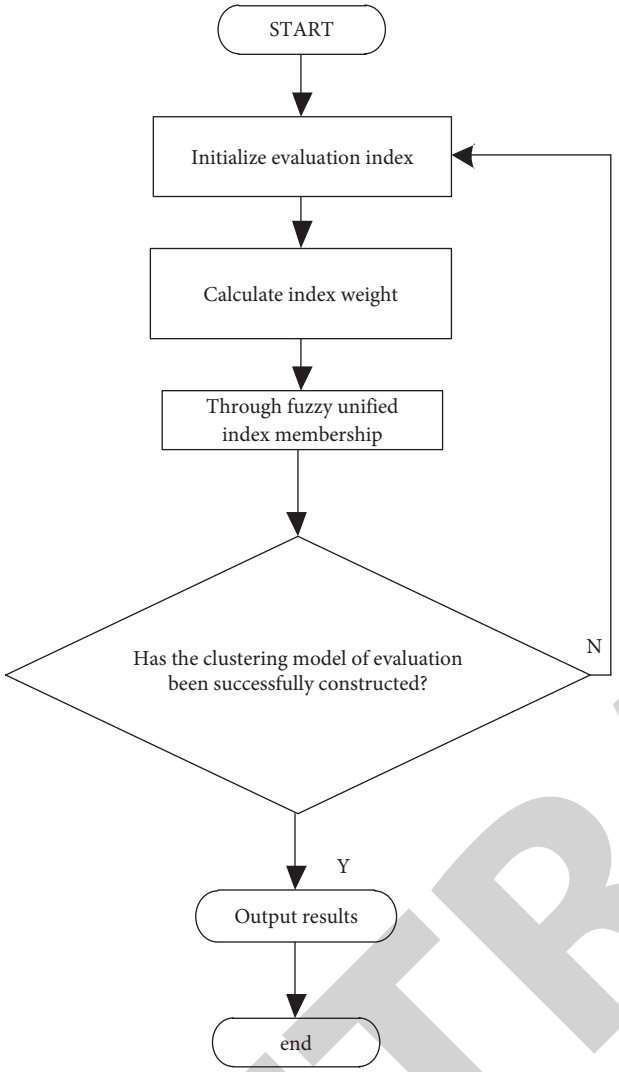

Figure 3: Design process of labor legal effectiveness evaluation algorithm against gender discrimination.

experimental analysis is carried out. In the experiment, the data of complaints about gender discrimination in enterprise recruitment in 2020 were collected through the network and the amount of data collected was 1000. In the experiment, 1000 pieces of data were collected on a local government website because of insufficient supervision of gender discrimination and through the form of online questionnaire to determine the relevant data of 1000 work-related gender discrimination. The sample training data set is 3000, in which 2000 pieces of positive energy data are selected. In the experiment, the experimental results are integrated by data statistics software. The type of data collected is shown in Figure 4.

3.2. Experimental Index Design. Based on the experimental sample data set determined above, the experiment compares and analyzes the effectiveness evaluation method based on system simulation big data, the statistical data reliability evaluation method based on robust principal component regression, and the method in this paper. In the experiment, the evaluation error and the accuracy of the key degree of the evaluation index are taken as the indexes.

3.3. Analysis of Experimental Results. In order to verify the effectiveness of this method in the evaluation of labor legal effectiveness against gender discrimination based on the sample data, the experiment compares and analyzes the effectiveness evaluation method based on system simulation big data, the statistical data reliability evaluation method based on robust principal component regression, and the evaluation error of this method in the sample data. The results are shown in Figure 5.

By analyzing the experimental results in Figure 5, it can be seen that with the continuous increase of the evaluated sample data, there are some differences in the evaluation errors of the sample data using the efficiency evaluation method based on system simulation big data, the statistical data reliability evaluation method based on robust principal component regression, and the method in this paper. When the sample data size is 500, the error of the evaluation method in this paper is about 2.9%, the evaluation error of the efficiency evaluation method based on system simulation big data is 6.9%, and the evaluation error of the statistical data reliability evaluation method based on robust principal component regression is about 8.9%. When the sample data size is 1000, the error of the evaluation method in this paper is about 1.3%, the evaluation error of the efficiency evaluation method based on system simulation big data is 5.1%, and the evaluation error of the statistical data reliability evaluation method based on robust principal component regression is about 6.1%. From the evaluation result curve, it can be seen that the evaluation error of this method is low, which verifies that this method is feasible.

In order to further verify the effectiveness of the proposed method, the effectiveness evaluation method based on system simulation big data, the statistical data reliability evaluation method based on robust principal component regression, and the accuracy of the method in determining the key degree of the evaluation index of sample data are experimentally analyzed. The results are shown in Figure 6.

By analyzing the result data in Figure 6, it can be seen that with the increase of the number of samples to determine the accuracy of the evaluation index of sample data, the efficiency evaluation method based on system simulation big data is adopted. There are some differences between the statistical data reliability evaluation method based on robust principal component regression and the method in this paper. Among them, the highest accuracy of using this method to determine the key degree of evaluation indicators is about 98%, while the accuracy of the other two methods is lower than this method although it is within a reasonable range. Therefore, the effectiveness of this method is verified.

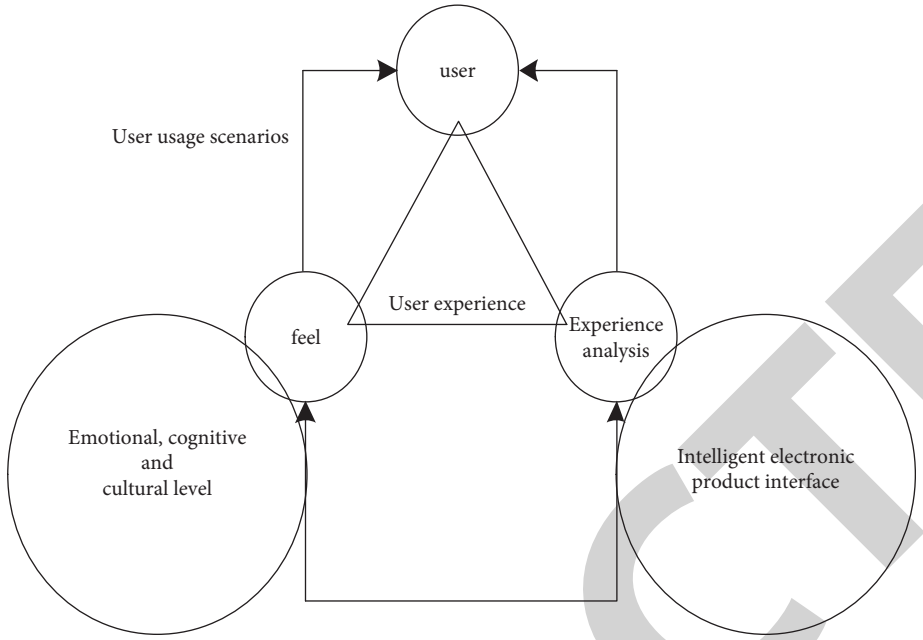

Figure 4: Experimental sample data collection mode.

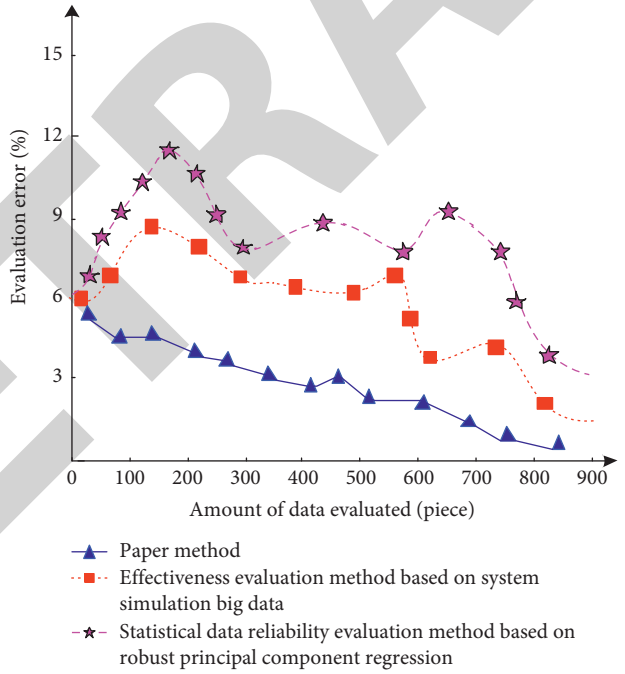

Figure 5: Analysis of evaluation error results of different algorithms.

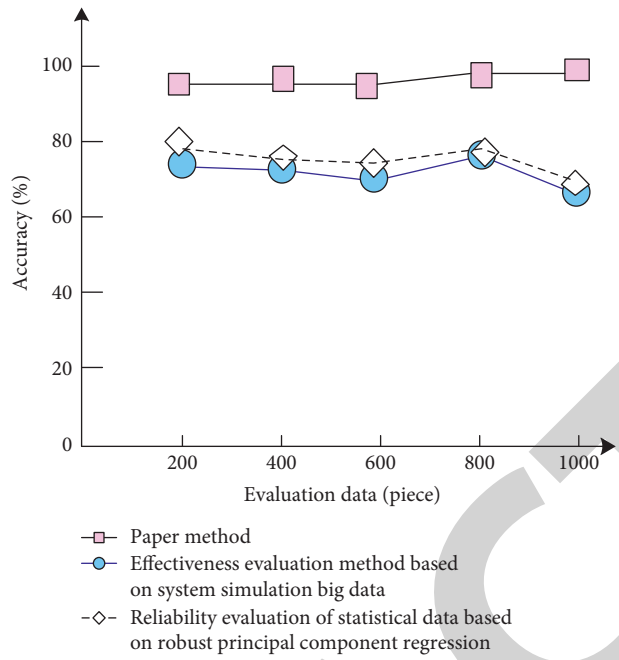

Figure 6: Accuracy analysis of key degree determination of indicators in different methods.

4. Conclusion

In order to improve the evaluation effect of the existing productiveness legal effectiveness assessment, this paper designed a labor felony effectiveness evaluation algorithm for affirmative action against gender discrimination. The proposed method used hits degree for the determination of the degree of gender discrimination, social influence, enterprise practice, and government supervision and management as the evaluation indexes of labor legal effectiveness in this paper. On this basis, an evaluation system of labor legal effectiveness against gender discrimination was designed, which is composed of constructing the judgment matrix of the evaluation index of labor legal effectiveness against gender discrimination. After normalization, the entropy method was used to calculate the weight of the evaluation index, so as to lay the foundation for subsequent research. The tree enhanced Bayesian network was used to classify the labor legal effectiveness evaluation indexes, and the correlation between the indexes was determined through the Spearman rank correlation coefficient. Finally, the labor legal effectiveness evaluation model against gender discrimination was designed through the clustering algorithm, and the labor legal effectiveness evaluation indexes against gender discrimination were input to complete the effective evaluation. This algorithm gave more advanced and better results. Indexes in this system evaluated more precisely and reduced the chances of uncertainty. The experimental results showed that the error of the evaluation algorithm was small, whereas the accuracy of determining the key degree of the evaluation index was high and accurate.

Data Availability

The data used to support the findings of this study are available from the author upon request.

Conflicts of Interest

The author declares that he has no conflicts of interest.

Acknowledgments

This paper was sponsored by State Scholarship Fund: "Young Backbone Teachers Study Abroad Project" (File No. 201900850007).

References

[1] J. Heymann, J. K. Levy, B. Bose et al., "Improving health with programmatic, legal, and policy approaches to reduce gender inequality and change restrictive gender norms," *The Lancet*, vol. 393, no. 10190, pp. 2522–2534, 2019.

[2] I. Anna-Karin, G. En Rique, and L. Marisol, "Does country-level gender equality explain individual risk of intimate partner violence against women? a multilevel analysis of individual heterogeneity and discriminatory accuracy (MAIHDA) in the European Union," *European Journal of Public Health*, vol. 30, no. 2, pp. 293–299, 2019.

[3] P. Passas, S. Natsiavas, and E. Paraskevopoulos, "Numerical integration of multibody dynamic systems involving non-holonomic equality constraints," *Nonlinear Dynamics*, vol. 5, pp. 1–21, 2021.

[4] L. Wang, "Reconstruction the standard of judicial review for gender discrimination in employment," *Collection of Women's Studies*, vol. 6, no. 2, pp. 55–66, 2019.

[5] M. Zhou, "How signing labor contract affect social security coverage? an empirical study based on China urban labor survey," *Economic Issues in China*, vol. 5, no. 15, pp. 107–122, 2019.

[6] J. N. Erdman and R. J. Cook, "Decriminalization of abortion - a human rights imperative," *Best Practice & Research Clinical Obstetrics & Gynaecology*, vol. 62, pp. 11–24, 2020.

Hindawi
Journal of Mathematics
Volume 2023, Article ID 9876921, 1 page
https://doi.org/10.1155/2023/9876921

Retraction

Retracted: Design of Enterprise Economic Information Management System Based on Big Data Integration Algorithm

Journal of Mathematics

Received 19 December 2023; Accepted 19 December 2023; Published 20 December 2023

This article has been retracted by Hindawi following an investigation undertaken by the publisher [1]. This investigation has uncovered evidence of one or more of the following indicators of systematic manipulation of the publication process:

(1) Discrepancies in scope

(2) Discrepancies in the description of the research reported

(3) Discrepancies between the availability of data and the research described

(4) Inappropriate citations

(5) Incoherent, meaningless and/or irrelevant content included in the article

(6) Manipulated or compromised peer review

The presence of these indicators undermines our confidence in the integrity of the article's content and we cannot, therefore, vouch for its reliability. Please note that this notice is intended solely to alert readers that the content of this article is unreliable. We have not investigated whether authors were aware of or involved in the systematic manipulation of the publication process.

Wiley and Hindawi regrets that the usual quality checks did not identify these issues before publication and have since put additional measures in place to safeguard research integrity.

We wish to credit our own Research Integrity and Research Publishing teams and anonymous and named external researchers and research integrity experts for contributing to this investigation.

The corresponding author, as the representative of all authors, has been given the opportunity to register their agreement or disagreement to this retraction. We have kept a record of any response received.

References

[1] X. Liu, "Design of Enterprise Economic Information Management System Based on Big Data Integration Algorithm," *Journal of Mathematics*, vol. 2022, Article ID 3257748, 9 pages, 2022.

Hindawi
Journal of Mathematics
Volume 2022, Article ID 3257748, 9 pages
https://doi.org/10.1155/2022/3257748

Research Article

Design of Enterprise Economic Information Management System Based on Big Data Integration Algorithm

Xiao Liu

Middlesex University, London NW4 4BT, UK

Correspondence should be addressed to Xiao Liu; b20160202424@stu.ccsu.edu.cn

Received 18 November 2021; Revised 8 December 2021; Accepted 13 December 2021; Published 7 January 2022

Academic Editor: Naeem Jan

In economic growth, the gradual increase in the effect of information technology makes the enterprise economic information management increasingly important for the survival and development of the enterprises. This paper designs an enterprise economic information management system for the complex internal economic information management business and process of enterprises. It provides daily office, information access, document preview, and transmission. The proposed design (i) copes with the inconsistency and irregularity of enterprise economic information data, (ii) quickly obtains valuable information from these massive high-frequency data, and (iii) improves the economic benefits of data assets and data management efficiency. The printing function systematizes the information management for departments such as enterprise economic information, personnel, and production. The main focus of this research includes the mode, framework, and function of the whole system software. Moreover, it also comprises of the use of Internet platform big data technology to realize the practicality, stability, and security of the system database algorithm, which has been practically used by enterprises to improve office efficiency and meet the needs of daily management of enterprises. Based on the analysis of the current status of enterprise big data application, this paper constructs an enterprise economic informational management system based on big data and also describes in detail the key technologies of enterprise economic informational data management from three aspects: NoSQL-based big data storage management, Hadoop-based economic informational big data informational and economic informational big data analysis, and mining algorithm. Provide theoretical basis and basic technical support for online decision analysis.

1. Introduction

The competition among enterprises in today's market is no longer limited to the traditional sense of simple market competition behavior. In order to better adapt to the new form of business competition, people have started to explore the application of some new technologies in the construction of enterprise information systems in business management, especially the application of big data technology and cloud computing technology in it, which is popular research among scholars at present [1].

With the rapid development of Internet technology and data analysis technology, the information storm brought by big data is profoundly changing people's production, life, and way of thinking. In the era of big data, the degree of informational in management functions is deepening, and the existing means of enterprise economic informational management is facing serious challenges [2]. How to apply information technology to the process of enterprise economic information management, improve its operational efficiency, and effectively promote the healthy, stable, and rapid development of the enterprise economic information management system has become the worthiest of in-depth consideration of enterprise economic information management personnel. Management informational refers to the development of information technology productivity with computers and other intelligent tools as the main medium, on the basis of the integration of advanced management concepts, the transformation of enterprise business processes, business methods, and other traditional management tools, and re-integration of enterprise strategic planning and management tools to achieve corporate goals and processes.

At present, enterprise economic informational management has gone through three stages: accounting computerization, enterprise economic informational management network, and group enterprise economic informational management. Accounting computerization mainly refers to the combination of accounting knowledge and information technology means, the daily accounting processing of various information as management information resources, the use of computers, and network communications based information technology means to obtain, process, and transmit information related to enterprise economic information [3]. Accounting computerization can solve the problems brought by manual bookkeeping such as bookkeeping errors, long data aggregation time, and much energy consumed by accountants in watchmaking, significantly improving the efficiency of enterprise economic information management and the speed and efficiency of data sharing. However, accounting computerization does not have the function of enterprise economic information management, and human factors have a greater impact on enterprise economic information management [4]. For example, to provide effective information for the purpose of management, accounting had to spend a lot of energy to a variety of data processing and deep analysis, and the processing of a lot of basic work greatly distracted the management accountant's main energy.

At present, state-owned enterprises have established enterprise economic information systems, but most of them are still in the stage of networked enterprise economic information management, that is, the stage of docking the construction of accounting information systems with other business information ports. The degree of economic informatization is not high, and related business modules have not been integrated to form data sharing and control sharing, and management coordination has not been formed [5]. Group enterprise economic informational management has largely improved the efficiency and effectiveness of enterprise economic informational data processing and realized enterprise economic informational management and data processing automation and intelligence. Nowadays, the management has gradually noticed that business processes and enterprise economic informational are inseparable. Enterprises should integrate enterprise economic informational with business processes and realize the complete sharing of resources with core business as the axis through the "five streams" of decision flow, capital flow, information flow, business flow, and logistics for the purpose of enterprise strategic management and goal-oriented management [6].

In this paper, Section 2 presents the demand analysis. Section 3 proposes the system design. In Section 4, the experimental verification has been given for the proposed methods. And Section 5 concludes the study.

2. Demand Analysis

Enterprise economic informational construction is a new technology in enterprise management that has emerged in recent years, and the application of big data technology has a crucial impact on the improvement of enterprise management, especially the application of big data technology in economic informational construction is strongly promoting the speed of economic informational construction, so it is necessary to discuss the foundation of economic informational construction in the big data environment [7]. The development stages of domestic and foreign enterprises' economic management systems are shown in Table 1. Its informational basis contains two aspects: one is the information basis of big data, big data has a specific definition of data information, the volume of information in big data is very huge, it is difficult for ordinary economic software to do effective capture, management, and application analysis and processing of economic information of big data and so on; second is the technical conditions of economic informational in the big data environment [8]. As we all know, cloud computing and big data have an inseparable relationship, and the technical conditions of economic informational in the big data environment are the distribution of processing cloud computing technology. In a sense, with only the use of big data "big," it is difficult to promote the process of economic information technology construction and the need for cloud computing cloud, in order to achieve the effective use of data and to provide the basis for enterprise management decisions [9].

The general practice of economic management of the company is to accurately account for the economic situation and business data of the company in a certain period of time according to the period specified in the plan. However, in this form, the collection of economic information may be delayed due to various circumstances. Now that we are in the era of big data management, we can make better use of big data for timely accounting and summary information in the economic management of the company [10]. It also simplifies the work of economic personnel in the aggregation of complicated information and can be completed in a shorter period of time to organize and analyze economic information. This can also reduce the unnecessary loss to the company because of the lag of information acquisition. In the past, the main content of the economic information of the company was according to the economic ratio and its three groups of tables for accounting [11]. However, due to the development of the times, this accounting method is no longer applicable to the economic management of the company and may hinder the long-term development of the company. To enable companies to obtain economic information more timely and accurately and to ensure the relevance of various types of information, companies must establish dynamic software analysis capabilities. Instead of using traditional forms of accounting, it is necessary to use the information management technology of big data.

3. System Design

The advancement and widespread use of big data management technology have led to a change in the old mode of operation forced by most industry sectors, including, of course, the economic management within the company [12]. The prerequisite for the use of big data is to ensure the

Table 1: Enterprise economic management system development stage.

Time	Development stage	Key technology	Stage characteristics
Before 1992	Monolithic financial software	DOS development platform	Simple accounting function
1993 to 1997	Accounting-based financial software	Local area network (LAN)-based sharing, limited expansion	Not conducive to long-term development
1998 to 2001	Structured financial software	C/S-based structure	Network-based information management
2002 to 2005	Structured financial system	Internet-based B/S structure	More comprehensive functions and more powerful interactivity
2006 to present	Intelligent financial management system	Integrated architecture	Data mining capability, integrated management, high level of information sharing

necessary correlation and timeliness between various information so as to avoid the economic information from lagging too much in the process of collection and collation and to help reflect directly the actual operating conditions of the company in that period through the company's economic information [13]. It also helps the top management of the company to find out the problems in the process of operation through economic information and give timely solutions. Therefore, the managers of enterprises should adapt to the development of big data era and put the technology into economic management, change the old economic information management methods, and require the company's economic personnel to master this advanced technology, to ensure the timely effectiveness of economic work. In addition, as big data technology is widely used in the current era, companies have more diverse types of index data in their daily operations. In order to better promote the reform of the company's economic management, it is necessary to set up a professional economic information management team within the company to ensure that the process of obtaining economic information can be timelier and more effective, so as to help the top management of the company to better use the data to make scientific decisions. First of all, the economic management personnel of the enterprise must have professional technical ability and high overall quality. Moreover, each employee responsible for economic work should learn from each other's strengths and merits and make a clear division of labor to improve efficiency in the process of accounting for economic information. The company should make a perfect system charter for the work of economic information management and regulate the behavior of economic management staff. And the company managers should also raise the status of economic management to strategic decision-making, so as to attract the attention of all employees and in the daily work can better help economic personnel to organize and analyze the economic information management [14].

The proposed system architecture is shown in Figure 1. Due to the current technological requirements of big data, the company has various indicators in terms of economic information. Therefore, in order to ensure that the company organizes and analyzes economic information in a timely and accurate manner, a real-time dynamic forecasting system must be designed [15]. First of all, it is required to divide the data of economic information according to the developed classification system and make clear the actual role and meaning of each economic data. This helps the company to make decisions and improve efficiency in its daily operations.

The use of advanced big data management technology can also help companies to collect comprehensive economic information. The information is then integrated and analyzed according to certain rules to provide the company's top management with a data base and basis for decision-making. In addition, different management models can be constructed based on economic information to help managers understand the actual economic situation of the company in a more intuitive way and to help the company's employees clarify the actual development goals and directions of the company. Because the development of big data management technology is relatively short, so many domestic enterprises still do not have a good grasp of this technology and apply it to the actual operation of the company. Therefore, the top management of the company can apply the big data technology to the economic management of the company through the following ways. First, a cloud computing economic information management platform is established. This platform is initially established in accordance with the principle of systemic and articulation-based. The use of big data management technology is ensured to integrate and analyze the economic information of the enterprise, and it can be timely and accurate. Second, the applicability of the cloud computing service platform is enhanced. The company's managers and employees in charge of economic management should be clear about their responsibilities. And the economic information management system process to achieve a good grasp of the relevant system should also be established in the company for the protection of economic information security mechanism in order to promote the actual benefits of the service platform. Third, the economic control platform is improved in the business model. This must ensure the transparency and interoperability of information between the company's economic information and the economic management platform of cloud computing. And the company's economic personnel should have a certain understanding of the company's daily operation mode and the related production process. Then, before establishing the economic control platform, the cloud computing technology and economic information should be used as the basis. The ultimate goal is to improve the efficiency and mode of the company in its daily operations.

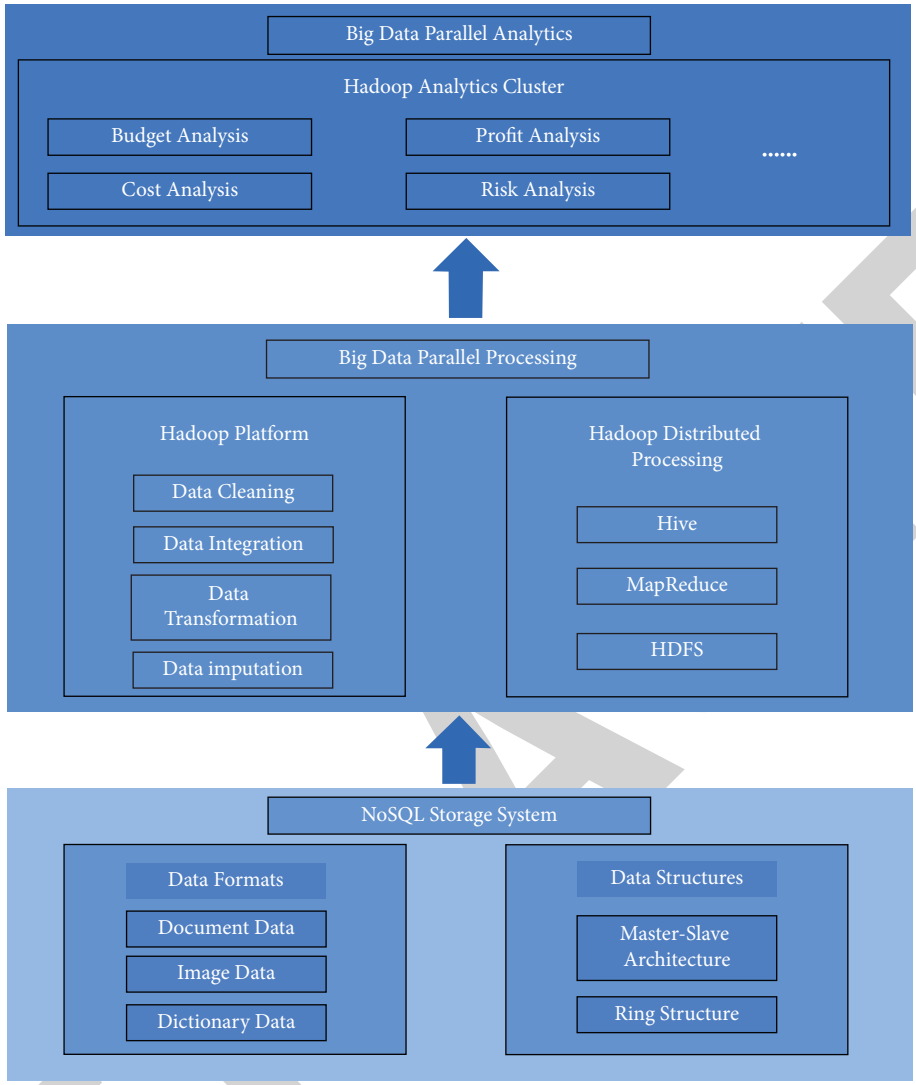

Figure 1: System architecture.

There are six main characteristics of big data: massive volume, complex and diverse data types, high timeliness, high variability, high data quality, and the search for high-quality value. (1) Hadoop ecosystem: HDFS is a distributed file system with high fault tolerance, high throughput, and so on, ideal for applications on large-scale data sets; H-base is a tool for fast access to NoSQL databases; Hive is a database framework that transforms structured data files into database tables and provides SQL-like query functions to convert user-written SQL statements into Map-Reduce tasks; Flume is a log collection system with high efficiency and high reliability. (2) NoSQL is a nonrelational database, which has the advantages of high scalability, large capacity, high performance, shareable, and high flexibility and can solve various challenges brought by massive and complex data, especially the problem of big data applications. Data mining methods are classified according to different mining perspectives, and the following are several common data mining methods. Association rules reflect the existence of a certain association between one thing and other things and mine valuable data items through this association. Find out the characteristics of the data objects in the database through algorithms, then combine and classify the data in the database according to the specified characteristics, classify the data in the database into a given category, and then perform characteristic analysis. Clustering classifies data according to similarity, with as much similarity as possible in the same class and as little similarity as possible in different classes. Regression analysis maps the attribute values of data to some connection due to changes in time and maps the characteristics of the connection to the actual predicted function to analyze the relationship that exists between its data, mainly applied to feature prediction and analysis of data series.

The streaming data cleaning architecture is shown in Figure 2. The system involves multiple data sources, including Excel, monitoring logs, and relational databases. The data sources are pushed into the distributed message queue Kafka after unified encapsulation by the unified data access module. The computing cluster consumes the data and performs cleaning operations and finally outputs the cleaned

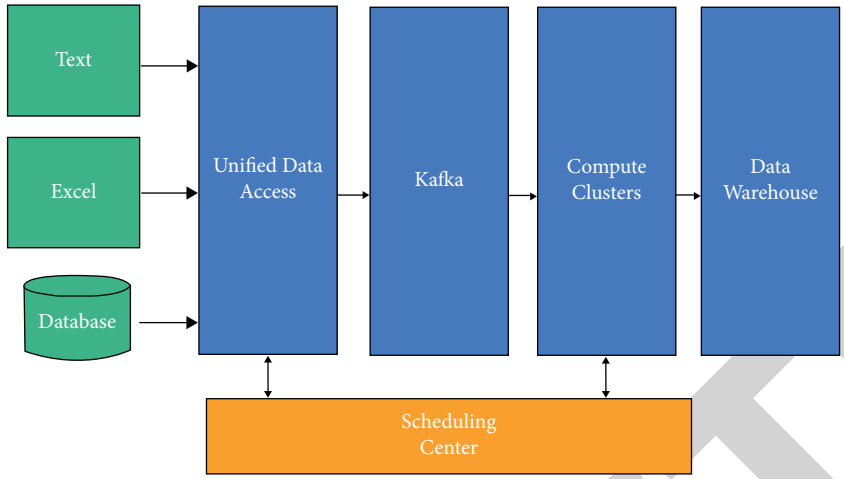

Figure 2: Stream data cleansing architecture.

results to the data warehouse. This architecture has the following main advantages:

(i) It converts all the different types of data into stream form so that different data are unified in form. The computational nodes for cleaning data only need to care about the specific data and do not need to deal with the data source.

(ii) The cleaning data are processed in a parallel and distributed manner, which improves the performance of data cleaning. The computing nodes can be scaled according to the actual load, which is highly scaled.

(iii) The interactive scheduling center can visually configure the cleaning process according to the demand, which reduces the complexity of data cleaning.

3.1. Unified Data Access Architecture Design. The unified data access module mainly includes three submodules: timer, file monitoring, and SQL execution. Following is the brief explanation for each of these submodules:

(i) *Timer Module.* The timer module provides timing function for the file monitoring module and SQL execution module. Through timing, it also controls the data collection rate. It enables the users to configure the timer through the interface. Additionally, it also allows the user to customize the execution period for each data source [13].

(ii) *File Monitoring.* The file monitoring module is designed for log file collection. The file monitoring module reads the new file which is added to the monitored folder. Further, it parses the file according to the agreed parsing rules. It also generates the specified uniform data protocol and finally pushes it to Kafka.

(iii) *SQL Execution.* SQL execution module implements the collection of relational databases such as MySQL, Oracle, and SQL-Server. The SQL execution module regularly reads a batch of data from the database and pushes it to Kafka. The SQL execution module regularly reads a batch of data from the database and converts it into a unified data protocol and pushes it to Kafka.

3.2. Uniform Data Protocol Design. As shown in Table 2, the data protocol mainly has the following fields. Uid is the unique id of each data dynamically generated, name-id is the unique id of the data source, and timestamp is the time when these data are produced. Fields are a string array that holds the field names of relational databases or column names of Excel. Dates hold the specific data values.

3.3. Calculation Cluster Module Design. As shown in Figure 3, the computing cluster consists of several computing nodes:

(i) *Interface Module.* The interface module is used to communicate with the scheduling center module and the unified data access module, including data source configuration interface, cluster management interface, process scheduling interface, and other interfaces. The interface module adopts RPC interface protocol, which is Remote Produce Call remote process call protocol, a computer communication protocol. The protocol allows a program running on one computer to call a subroutine on another computer without the programmer having to additionally program this interaction.

(ii) *Synchronization Module.* The synchronization module is used to synchronize with the scheduling jobs in the database. This module keeps the real-time status of the job operation and reads the last running status of the job after the job restarts to ensure the correct operation of the cleaning job.

(iii) *Metadata Module.* The metadata module keeps information about the data structure of the data

Table 2: Field table.

Fields	Name	Category	Required
Uid	Unique ID	String	False
Name-id	Data source name	String	True
Timestamp	Timestamp	Long	True
Fields	Field name	List<Field>	True
Datas	Loaded data	List<Field>	True

source and caches the dictionary code table information of the cleaning data.

(iv) *Process Parser Module*. The process parser module reads the configuration information of the job cleaning process through the interface module and parses the configuration information into data the corresponding directed acyclic graph for cleaning.

(v) *Operator Executor*. The operator executor reads the configured cleaning parameters and invokes the cleaning method in the operator for cleaning. The operator executor does not need to care about the specific cleaning process but only needs to focus on the cleaning method in the operator, which makes data cleaning scalar.

3.4. Scheduling Center Module Design. The scheduling center module serves as a window for system user interaction, providing users with a visual interface for cleaning process configuration, which facilitates the configuration of various complex cleaning processes. The scheduling center module has functional modules such as data source management, cluster configuration, operator management, cleaning dictionary management, and cleaning process management [14].

(i) *Data Source Management Module*. The data source management module provides unified configuration management functions for different data sources. The module provides access rules for data sources, mainly including timing cycles, monitoring folders, extracting SQL statements, and unified data protocols, and interacts with the unified data access module to control the start and stop of the unified data access module.

(ii) *Cluster Management*. The cluster management module provides management and monitoring functions for the unified access module clusters and computing clusters, such as monitoring the online and offline of clusters and monitoring the cluster. The cluster management module provides management and monitoring functions for the unified access module clusters and computing clusters, such as monitoring the online and offline of clusters, monitoring the utilization of resources, monitoring the execution of cleaning jobs, and providing early warning functions for erroneous jobs.

(iii) *Computation Operator*. The computation operator is divided into computation operator and output operator. The computation operator is used for data cleaning, and the output operator is used for the output of cleaning results. Commonly used output operators include Elasticsearch output operator, Hive output operator, database output operator, and Kafka output operator. When adding the operator, you need to configure the execution function, operator description, parameter name, and parameter type.

(iv) *Cleaning Operator Dictionary Management*. The cleaning operator dictionary management module is designed for dictionary replacement operators. This module provides dictionary configuration functions and caches the mapping relationships in Redis. The dictionary replacement operator reads the Redis cache and does the dictionary mapping.

(v) *Cleaning Process Management*. The cleaning process management module provides users with interactive cleaning process configuration functions. The user can drag and drop the cleaning operators on the canvas through the Web interface, configure the cleaning parameters corresponding to each cleaning operator, and connect them according to the cleaning rules to form a flow chart from the starting point to the output. This visual configuration gives users intuitive control of the cleaning process and reduces the complexity of data cleaning.

3.5. Integration of Map-Reduce-Based Canopy + K-Means Algorithm. Although the K-means algorithm is efficient, the randomness of the clustering parameters and the uncertainty of the initial clustering center are two drawbacks of the K-means algorithm, thus leading to unstable optimal values of clustering. In order to improve the stability and accuracy of the clustering effect, the Canopy + K-means algorithm is proposed. Using the Canopy algorithm to coarsely process the data, the processed data are used as the initial data of K-means, which can solve the problems of K-means and improve the efficiency of the K-means algorithm. In order to improve the efficiency of the Canopy + K-means algorithm, the combination with the Hadoop ecological Map-Reduce framework is used, and the multiserver deployment further improves the timeliness of the algorithm, which is also the core of the enterprise financial management system. The implementation process has mainly two stages:

(i) *Canopy Clustering Stage*. The map process groups the data sets, and each group is clustered using the Canopy algorithm to get multiple Canopy clusters.

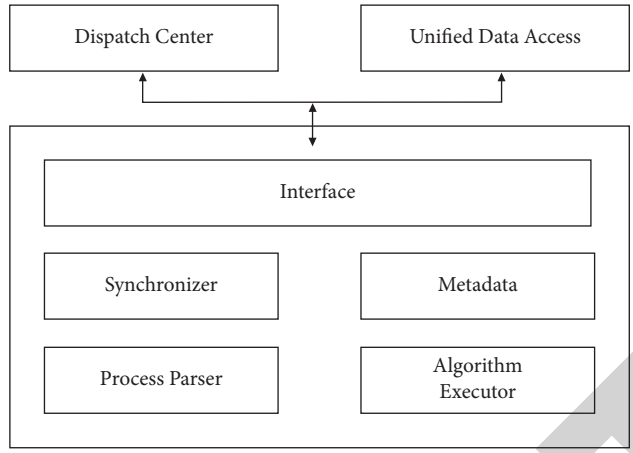

Figure 3: Calculation node module structure diagram.

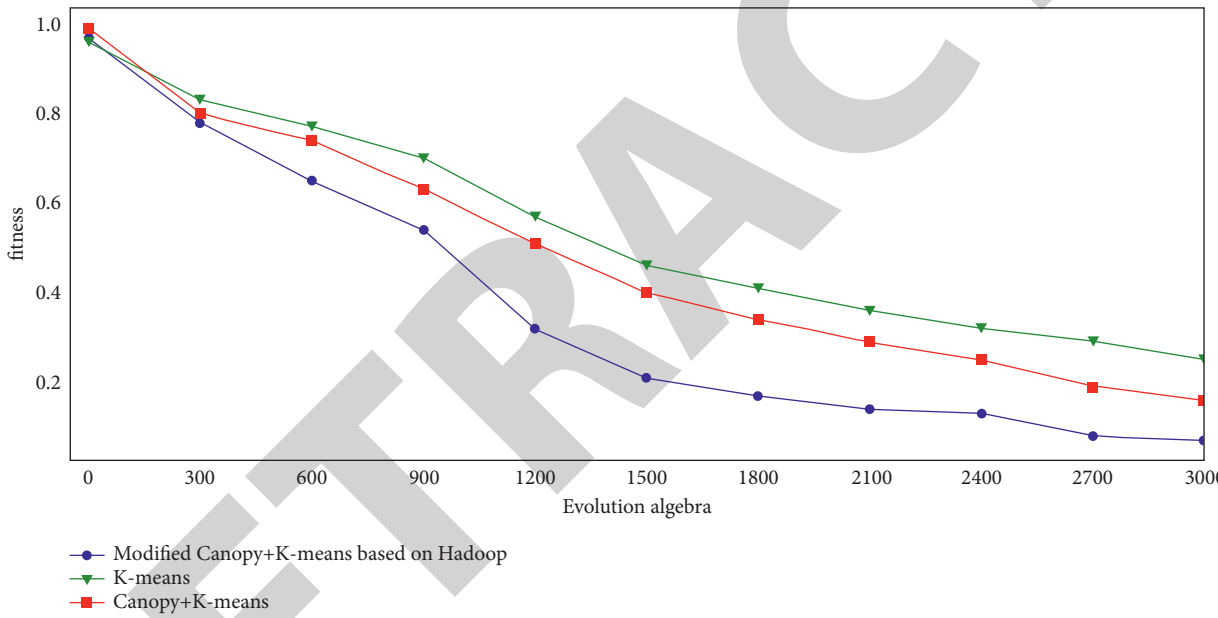

Figure 4: Algorithm comparison.

Table 3: Evaluation of clustering effect when setting the number of K-means clusters to 10.

Fields	Modified Canopy + K-means based on Hadoop	Canopy + K-means	K-means
REK	7	4	11
K	3	39	10
DB	1.39	1.79	1.69
SC	0.28	0.12	0.23
AMI	0.89	0.39	0.71
ARI	0.91	0.13	0.66
JC	0.016	0.078	0.005
TD	0.0015	0.0060	0.021

Reduce process merges multiple Canopy centers into one group and reprocess Hadoop platform data to obtain new Canopy center data.

(ii) *K-Means Clustering Phase*. The Canopy center is used as the initialized clustering center for K-means, and one task in Map-Reduce is one iteration of K-means. The Map-Reduce function records the distance from each sample element to the cluster center and the result of each cluster and then recalculates it using the Reduce function. The steps are repeated until the clustering results are the most convergent and stable.

4. Experimental Verification

In order to verify the effectiveness of the enterprise economic information management system based on the big data integration algorithm, this paper selects one dataset, compares them with traditional Canopy + K-means and K-means algorithms, and evaluates the clustering effect based on clustering evaluation indexes such as DB, SC, and AMI.

First of all, the three algorithms are compared, i.e., Modified Canopy + K-means based on Hadoop, Canopy + K-means, and K-means. Then, their convergence is compared at the same iteration step, as shown in Figure 4. By analyzing Figure 4, it is found that the convergence speed and performance of Modified Canopy + K-means based on Hadoop significantly outperform the other two methods when we output the performance once every 300 iteration steps.

In Table 3, the evaluation of the clustering effect is shown for 10 numbers of K-means clusters. Table 3 describes that the clustering effect of the Canopy + K-means algorithm is significantly better than that of the K-means algorithm for each filed, i.e., DB, SC, AMI, ARI or JC, and TD. The K-means algorithm needs to set the parameter k in advance, while the optimized algorithm does not need to set the value of k in advance. However, it is capable of getting better initial clustering center, whose result is closer to the true value. The optimized algorithm does not need to set the k value in advance, but it can get better initial clustering center, which results in more realistic clustering results, and the combined Canopy + K-means clustering with Hadoop is better than the traditional Canopy + K-means algorithm.

5. Conclusion

In this paper, the information management technology was reasonably used to control the enterprise economic information management information under the environment of big data. Thus, the information management work was improved. Moreover, the foundation for the good development of the enterprise was laid. Furthermore, an enterprise economic data management system based on big data was constructed, using the Canopy optimized K-means algorithm combined with Hadoop platform and NoSQL database management in the background, to improve the standardization and efficiency of enterprise financial management and achieve the purpose of increasing economic benefits. At the same time, in order to achieve good development of enterprises, both the top management and front-line managers of enterprises should pay enough attention to the information informational construction work, control the current level of information management of enterprises, and strive to solve the problems faced by the information construction work. In addition, advanced management technology should be continuously introduced to optimize the management mode under the big data environment, so as to improve the quality of enterprise information management work.

Data Availability

The data used to support the findings of this study are available upon request to the author.

Conflicts of Interest

The author declares that he has no conflicts of interest.

References

[1] Y. Li, "Research on enterprise economic management mechanism based on decision process," in *Proceedings of the 2019 4th International Symposium on Management, Economics, E-Business and Marketing (ISMEEM 2019)*, pp. 511–519, Hanoi, Vietnam, October 2019.

[2] Y. Li, "Analysis of enterprise economic management optimization strategy based on improved ant colony algorithm," in *Proceedings of the 2019 7th International Conference on Machinery, Materials and Computing Technology (ICMMCT 2019)*, Chongqing, China, May 2019.

[3] G. Yuping, "Research on effective innovation measures of enterprise economic management based on innovation ability training," in *Proceedings of the 2019 5th International Conference on Economics, Business, Finance, and Management (ICEBFM 2019)*, Shenzhen, China, July 2019.

[4] G. E. Krokhicheva, V. V. Lesnyak, E. M. Selezneva, and E. S. Arakelyants, "Adaptive engineering management tools of enterprise economic security," *Management Science Letters*, vol. 8, no. 6, pp. 605–618, 2018.

[5] T. Teng, "Research on enterprise economic management system based on computer big data technology," *Journal of Physics: Conference Series*, vol. 1865, no. 4, Article ID 042078.

[6] Y. Jin, "On the innovation of enterprise economic management under the new situation," *International Journal of Social Sciences in Universities*, vol. 180, 2019.

[7] W. Ding, "Research on enterprise economic management innovation under the new situation of value management," in *Proceedings of the 2019 5th International Conference on Education Technology, Management and Humanities Science ETMHS 2019*, Xi'an, China, June 2019.

[8] N. Caihong, "Research on application of target cost management in enterprise economic management," in *Proceedings of the 2019 5th International Conference on Economics, Management and Humanities Science (ECOMHS 2019)*, Krasnodar, Russia, October 2019.

[9] Q. Meng and Y. Zhou, "Enterprise economic performance evaluation based on 5 G network and embedded processing system," *Microprocessors and Microsystems*, vol. 80, Article ID 103603, 2021.

Hindawi
Journal of Mathematics
Volume 2024, Article ID 9854275, 1 page
https://doi.org/10.1155/2024/9854275

Retraction

Retracted: Study on Driver Gaze Characteristics in Sight Distance Limited Section of Mountain Highway Based on Visual Information

Journal of Mathematics

Received 23 January 2024; Accepted 23 January 2024; Published 24 January 2024

This article has been retracted by Hindawi following an investigation undertaken by the publisher [1]. This investigation has uncovered evidence of one or more of the following indicators of systematic manipulation of the publication process:

(1) Discrepancies in scope

(2) Discrepancies in the description of the research reported

(3) Discrepancies between the availability of data and the research described

(4) Inappropriate citations

(5) Incoherent, meaningless and/or irrelevant content included in the article

(6) Manipulated or compromised peer review

The presence of these indicators undermines our confidence in the integrity of the article's content and we cannot, therefore, vouch for its reliability. Please note that this notice is intended solely to alert readers that the content of this article is unreliable. We have not investigated whether authors were aware of or involved in the systematic manipulation of the publication process.

In addition, our investigation has also shown that one or more of the following human-subject reporting requirements has not been met in this article: ethical approval by an Institutional Review Board (IRB) committee or equivalent, patient/participant consent to participate, and/or agreement to publish patient/participant details (where relevant).

Wiley and Hindawi regrets that the usual quality checks did not identify these issues before publication and have since put additional measures in place to safeguard research integrity.

We wish to credit our own Research Integrity and Research Publishing teams and anonymous and named external researchers and research integrity experts for contributing to this investigation.

The corresponding author, as the representative of all authors, has been given the opportunity to register their agreement or disagreement to this retraction. We have kept a record of any response received.

References

[1] Y. Tang, X. Peng, S. Xu, M. Bai, L. Lin, and H. Sun, "Study on Driver Gaze Characteristics in Sight Distance Limited Section of Mountain Highway Based on Visual Information," *Journal of Mathematics*, vol. 2022, Article ID 9482875, 8 pages, 2022.

Hindawi
Journal of Mathematics
Volume 2022, Article ID 9482875, 8 pages
https://doi.org/10.1155/2022/9482875

Research Article

Study on Driver Gaze Characteristics in Sight Distance Limited Section of Mountain Highway Based on Visual Information

Yuzhou Tang,[1] **Xiaodang Peng**,[2] **Shiyong Xu**,[2] **Mingju Bai**,[2] **Lifang Lin**,[3] **and Haihan Sun**[1]

[1]*School of Civil Engineering, Chongqing Jiaotong University, Chongqing 400074, China*
[2]*Duyun Management Bureau, Duyun 558000, Guizhou, China*
[3]*Zhongke Luheng Engineering Design Co., Ltd., Taiyuan 030000, China*

Correspondence should be addressed to Yuzhou Tang; pengpengdang@outlook.com

Received 17 November 2021; Revised 25 November 2021; Accepted 29 November 2021; Published 6 January 2022

Academic Editor: Naeem Jan

In order to study the gaze behavior characteristics of drivers in mountainous road sections with limited sight distance, the real vehicle test is carried out by using Smart Eye Pro 5.7 noninvasive eye tracker. Combined with the sight distance change rate theory, 6 typical test representative mountainous sections are selected to study the gaze distribution law and gaze duration of drivers in different mountainous sections. The research shows that when the driver drives on the test section with the most unfavorable sight distance of 44 m, 50 m, and 56 m, the fixation characteristics of "from far to near" are significant, and the long fixation duration accounts for a large proportion of the driver. When the driver drives on the section with the most unfavorable sight distance of more than 70 m, i.e., the sight distance change rate of less than 1.33, the fixation characteristics of "from far to near" disappear. The driver's fixation stability increases, the fixation freedom increases, and the proportion of medium and long fixation duration decreases. The data analysis provides a theoretical basis for drivers to pass safely in mountainous sections.

1. Introduction

Sight distance is a necessary basis to ensure driving safety. In mountainous areas, due to poor linear balance and vegetation influence, the incidence of sight distance limited sections is high. Insufficient sight distance can easily lead to insufficient depth of driver's field of vision, a sharp rise in driving tension, and then, it is easy to take abnormal driving behaviors such as sharp turning and sharp deceleration, making the road section with limited sight distance a high-risk road section. Potts et al. [1] analyzed the impact of sight distance on road traffic safety and concluded that sight distance is an important index affecting road traffic accident rate. At present, the problems related to sight distance have received the attention of scholars at home and abroad.

First, scholars at home and abroad have carried out more research on highway driving sight distance. Based on people's research on kinematics theory, Yuan et al. [2] have developed a new calculation method of parking sight distance. Du and Fang [3] have proposed a new method of calculating sight distance by segmented h-order parabola. The original sight distance calculation method has been improved. Based on the road environment perception technology, Li et al. [4] established the ranging model of driving sight distance by extracting effective feature points and using the small hole imaging model. Bassani et al. [5] analyzed the longitudinal behavior of drivers on rural roads with limited sight distance and obtained the relevant impact of sight distance on driving behavior. Yang et al. [6] and others obtained the nonlinear relationship between spatial sight distance and expected velocity by using the method of regression analysis and experiment. Li [7] modelled and analyzed the driver gaze behavior on the basis of drivers while crossing urban roads. Qiao et al. [8] investigated the movement of drivers' eyes while crossing roads. Wu and Yan [9] studied the distribution characteristics of viewpoint of a driver on the crosswalks. Wuhong et al. [14] studied transportation systems that are smart and connected.

In terms of the impact of horizontal curve design elements on highway traffic safety, Jia and Wang [10] put forward the corresponding improvement scheme of safety

guarantee technology through the evaluation of intersection angle, road conditions, traffic safety facilities, and other factors and combined with the research on its safety influencing factors. Robertson [11] analyzed the impact of geometric design indexes such as curvature radius, truck sight distance, turning radius, and longitudinal slope on truck operation safety. Ibrahim et al. [12] found that the occurrence of adverse combination of alignment will greatly improve the incidence of traffic accidents, among which the adverse combination of horizontal and vertical curves with small radius has the greatest impact;

At present, the research status at home and abroad mainly focuses on the calculation method of highway sight distance and the impact of horizontal curve design elements on highway safety in mountainous areas. The research on drivers' eye movement characteristics mainly focuses on intersections, urban sections, and urban roads. There is less research on drivers' gaze characteristics with limited sight distance in mountainous roads, Therefore, this study intends to carry out real vehicle eye movement test on the road section with limited sight distance in mountainous areas and study the driver's gaze characteristics in the road section, so as to provide theoretical reference for the road element design and the setting of traffic safety facilities in the road section with limited sight distance in mountainous areas.

In the following sections, Section 2 presents the scheme of the test. The fixation distribution characteristics are discussed in Section 3. Further, the analysis of fixation distribution characteristics is given in Section 4. Section 5 ends the study with a conclusion.

2. Test Scheme

2.1. Test Section. This time, g319 Chongqing Bishan Tongliang section is selected as the test section. This section is a class II mountain highway with a design speed of 40 km/h. It has good technical conditions, complex topographic conditions along the line, many small radius flat curve line sections, and prominent problems of limited sight distance.

Relevant research shows that the greater the sight distance change rate, the worse the driving safety of the road section [13]. Take the sight distance change rate as the basis for the selection of sight distance limited sections, and calculate the entry sight distance value, the most unfavorable sight distance value, and sight distance change rate of each curve section, respectively, as shown in the following equation:

$$I_S = \frac{(S_1 - S_2)}{L}, \tag{1}$$

where I_S is the sight distance change rate (%), indicating the turning sight distance value of the road section; S_1 and S_2 are the most unfavorable sight distance values; and L is the length of sight distance transition section.

Seven typical test sections are selected for the real vehicle test, and the alignment parameters are given in Table 1:

The selected road section is shown in Figure 1.

Table 1: Selection of alignment parameters of experimental sections.

No.	R (m)	S_1 (m)	S_2 (m)	L (m)	Rate of change, I_S
1	62	65	44	10	2.1
2	80	75	50	15	1.67
3	100	70	56	10	1.4
4	162	90	70	18	1.33
5	260	102	90	11	1.09
6	360	120	106	14	1.00

2.2. Test Personnel. Five drivers with more than 3 years of driving experience are selected, with an average age of 35 years and driving ages of 10, 6, 15, 5, and 6 years, respectively. It is required to have normal physical function, good driving habits, and no previous driving experience on the test section.

2.3. Test Process. Install eye tracker and other test instruments for the test driver, drive the test vehicle to the starting point of the test section, stop, adjust the most comfortable driving position, turn on the host, and try to turn on each instrument synchronously on the premise of ensuring that each test instrument can operate normally, and let the camera record the accurate time of turning on the instrument, and start the test from the starting point of the test section, as shown in Figure 2:

3. Analysis of Fixation Distribution Characteristics

3.1. Characteristic Analysis during Driving. Select the driver's gaze point coordinate data of the two sections with great difference in the severity of sight distance restriction and analyze the difference in the distribution characteristics of the driver's gaze point from entering to leaving the corner.

Figure 3 shows the driver's gaze characteristics during driving in the section with a sight distance of 44 m; when the driver is about to drive into the section with limited sight distance from the general section, the driver's gaze is mainly focused on the landscape at the end of the far field of vision on the right side of the front and the roadside guardrail. At this time, due to the limited sight distance, drivers need to constantly pay attention to the changing road information in the blind area of the right field of vision to adjust their driving behavior.

When the vehicle has just entered the road section with limited sight distance and has not yet passed the midpoint of the curve, because the driving sight distance is seriously limited at this time, the distribution law of fixation points begins to show the characteristics of "from far to near." At this time, the driver mainly focuses on the obstacles near the right side, and the distance between the vehicle and the obstacles needs to be controlled on the one side. On the other hand, the steering wheel needs to be adjusted through the collected visual information, and the visual load will increase to a certain extent.

When the driver passes the midpoint of the curve, with the gradual improvement of sight distance, the driver's gaze

Figure 1: Test section.

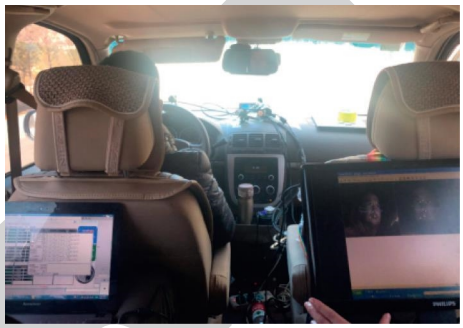

Figure 2: Data acquisition during test.

area shifts from the near obstacles on the right to the road, landscape, and guardrail far away on the right. At this time, the driver's attention to the far road landscape increases and the attention to the near obstacles decreases.

Figure 4 shows the driver's gaze characteristics during driving in the road section with a sight distance of 106 m; compared with the gaze characteristics of the road section with a sight distance of 44 m, the driver's gaze points are basically concentrated in the far area from the incoming road section to the midpoint of the curve, and the gaze characteristics of "from far to near" disappear. After passing the midpoint of the curve, due to the further improvement of the sight distance, the driver looked at the increased degree of freedom and began to pay attention to the vehicle driving on the left. It shows that the driver's gaze stability is higher in the section with small sight distance change.

3.2. Driver's Gaze Distribution under Different Sight Distance Conditions. The fixation point coordinate data of eye movement data are selected to study the distribution law of drivers' fixation points in the road section with limited sight distance under different sight distance conditions.

According to the actual vehicle test (Figure 5), the driver's eye movement data on the road section with sight distance of 44 m are screened and analyzed. It can be seen that when the driver is driving on this road section, the fixation points are mainly focused on the far ahead (right), far right, and near right, and the fixation frequencies are 65%, 20%, and 5%, respectively. At this time, in addition to focusing on the far ahead (right) to adjust the driving direction, due to the limited sight distance on the right side, the driver also needs to pay attention to the obstacles on the right side to ensure that there is sufficient safety distance between the vehicle and the obstacles. During the whole process from entering the curve to driving out of the curve, the driver's gaze characteristics show the characteristics of "from far to near."

Figure 3: Distribution of drivers' injection points from entering to leaving the corner in the road section with the most unfavorable sight distance of 44 m.

Figure 4: Distribution of drivers' injection points from entering to leaving the corner in the road section with the most unfavorable sight distance of 106 m.

According to the actual vehicle test (Figure 6), the driver's eye movement data on the road section with a sight distance of 50 m are screened and analyzed. It can be seen that when the driver is driving on this road section, the fixation points are mainly focused on the far ahead (right), far right, and near right, and the fixation frequencies are 71%, 10%, and 8%, respectively. Compared with the road section with a sight distance of 44 m, although the driver's fixation frequency on the near right is reduced at this time, the distribution of gaze in the whole curve driving process still shows the characteristics of "from far to near."

According to the actual vehicle test, the driver's eye movement data on the road section with sight distance of 56 m are screened and analyzed (Figure 7). It can be seen that when the driver is driving on this road section, the fixation point position does not change greatly due to the small increase of sight distance. At this time, the driver's fixation points are also concentrated in the far ahead (right), far right, and near right, and the fixation frequencies are 73%, 18%, and 4%, respectively. The fixation characteristics of "from far to near" are still significant.

According to the actual vehicle test, the eye movement data of the driver on the road section with the sight distance of 70 m are screened and analyzed (Figure 8). It can be seen that when the driver is driving on this road section, the distribution of fixation points has changed to a certain extent

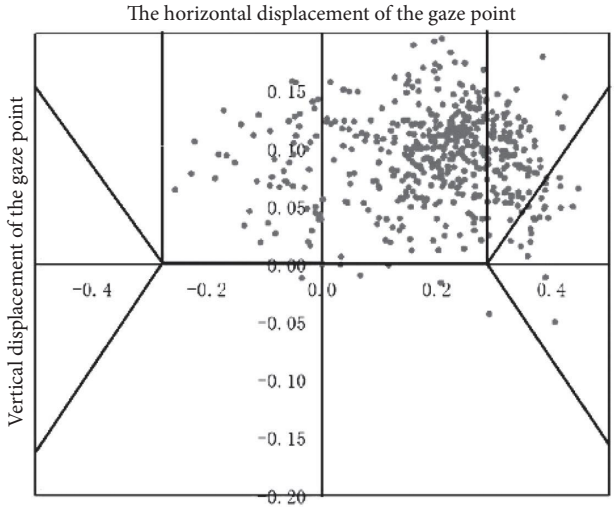

Figure 5: Distribution of driver's fixation points in 44 m sight distance section.

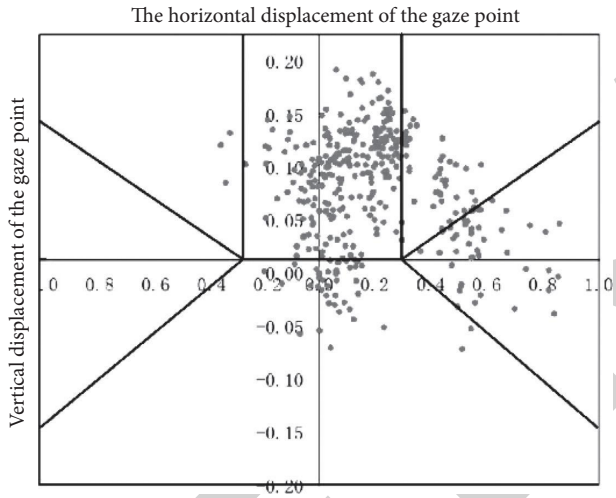

Figure 6: Distribution of driver's fixation points in the road section with sight distance of 50 M.

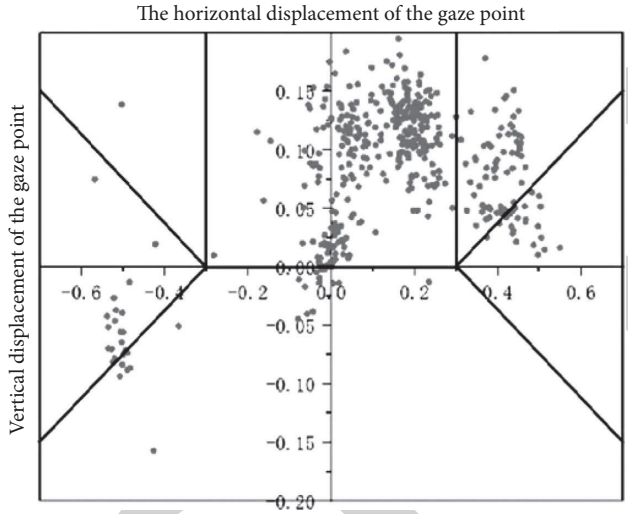

Figure 7: Distribution of driver's fixation points in 56 m sight distance section.

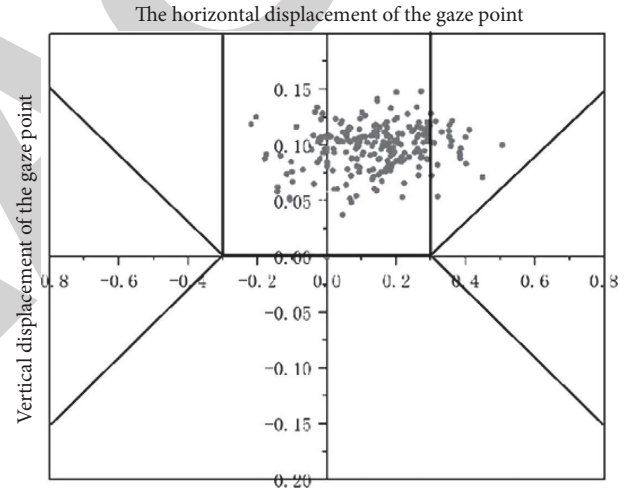

Figure 8: Distribution of driver's fixation points in the road section with sight distance of 70 m.

with the increase of sight distance. The fixation points are mainly concentrated in the far ahead and the far right, and the video injection rates are 84% and 16%, respectively; the driver basically focused on the distant landscape, roads, and obstacles. Due to the improvement of sight distance, the lack of depth of vision caused by insufficient sight distance has been improved, and the "from far to near" gaze characteristics have disappeared.

For the test section with a sight distance of 90 m (Figure 9), the driver's main focus area is still far ahead. Compared with the section with a sight distance of 70 m, the driver's frequency of paying attention to the far ahead (left side) increases, indicating that in the right turn section with a wide sight distance, the driver has a greater degree of freedom to pay attention to the road traffic information not on the right side.

When the sight distance value of the test section reaches 106 m (Figure 10), due to the continuous improvement of sight distance, the driver has a higher degree

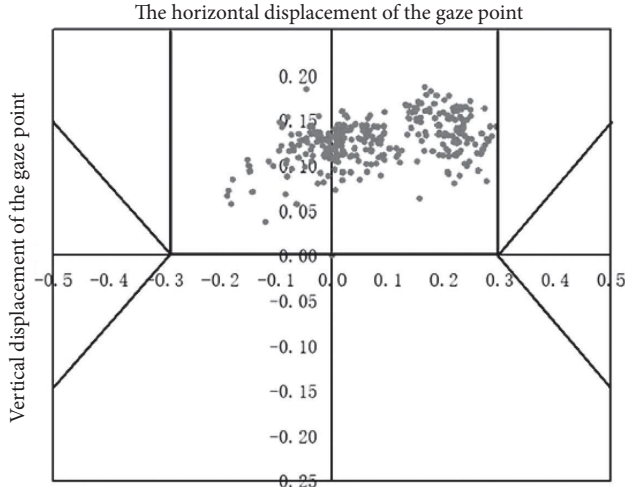

Figure 9: Distribution of driver's fixation points in 90 m sight distance section.

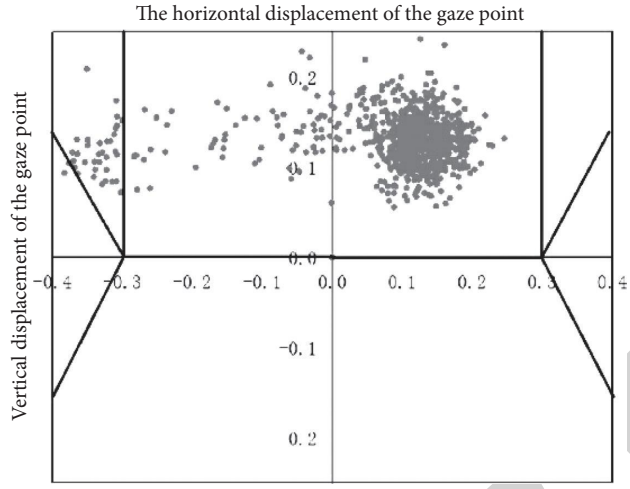

Figure 10: Distribution of driver's fixation points in 106 m sight distance section.

of freedom to pay attention to the road traffic information in other directions, and the attention to the road landscape and traffic information in the distance is much higher than that in the near.

When the driver is driving on the road with limited sight distance, the gaze characteristics change with the gradual increase of sight distance. When the sight distance restriction is serious, the gaze characteristics of "from far to near" are significant (Tables 2 and 3). Although the main gaze area is far ahead (right side), due to the serious sight distance restriction, it is necessary to focus part of his energy on nearby things such as roadside obstacles, compared with the general road section with good sight distance, the visual load will accumulate, and the psychophysiological intensity load of long-term driving and driving on this road section will accumulate, which is not conducive to the driving safety of the road section. When the sight distance value reaches 70 m and the sight distance change rate is close to 1.33, the driver's attention to the road landscape and traffic information in the distance is much greater than that in the near, the "from far to near" gaze characteristics disappear, and the gaze stability increases. With the further increase of sight distance value and the further decrease of sight distance change rate, the driver's gaze freedom increases.

4. Fixation Duration Analysis

In the process of driving, different objects carry different amounts of information, which also leads to differences in the difficulty of drivers in identifying different objects. The difficulty of drivers in identifying objects can be measured by gaze duration. The shorter the gaze duration, the less difficult it is to process traffic information, and the easier it is for drivers to identify objects. When the driver's gaze time is too long, it is considered that it is difficult for the driver to process the traffic information, or the driver is interested in the area. In this section, the relevant data of the driver's gaze duration under the sight distance of 44 m, 50 m, 56 m, and 106 m are selected for analysis, as given in Table 4.

It can be seen from Table 4 that in sections with limited sight distance, the driver's gaze duration is mostly less than 50 ms. With the gradual increase of sight distance, the driver's gaze duration will focus more on short gaze, and the longer gaze will gradually decrease. It shows that with the continuous improvement of sight distance, the difficulty for drivers to obtain the road information in front is gradually reduced, and there is no need to look for a long time to obtain the driving information.

(i) In the right turn section with a distance of 44 m, the driver's gaze duration is mostly concentrated within 100 ms. However, due to the serious restriction of sight distance in the section, the driver needs to pay constant attention to the information such as obstacles near the right side and roadside dangerous objects to ensure his driving safety. Therefore, the proportion of driving gaze duration exceeding 100 ms exceeds 30%. It reflects that the driver needs to constantly pay attention to the changing road traffic information when driving under the sight distance condition. Compared with the road section with better sight distance condition, it is easier to accumulate visual load.

(ii) In the right turn section with a distance of 50 m, the proportion of drivers' gaze duration exceeding 100 ms is still high, reaching about 25%

(iii) In the right turn section with sight distance value of 56 m, the proportion of drivers with gaze duration less than 100 ms reaches 78.14%, and the proportion of drivers with gaze duration less than 50 ms reaches 52.79%. Compared with the first two sections, such short note video rate increases, but the proportion of gaze duration more than 150 ms still exceeds 10%.

(iv) When driving on a right turn section with a plane sight distance of 70 m, the proportion of drivers' gaze duration less than 100 ms has reached 85%, the proportion of longer gaze duration has been greatly reduced, and the proportion of gaze duration greater than 300 ms has changed to 0%, indicating

Table 2: Proportion of fixation distribution 1.

Proportion of fixation point distribution under different sight distance conditions	44 m	50 m	56 m
Far ahead	65%	71%	73%
Near the front	0	0	0
Far right	25%	10%	18%
Near the right	5%	8%	4%
Far left	0	0	0
Near the left	0	0	0

Table 3: Proportion statistics of fixation point distribution 2.

Proportion of fixation point distribution under different sight distance conditions	70 m	90 m	106 m
Far ahead	84%	100%	86%
Near the front	0	0	0
Far right	16%	0%	0
Near the right	0%	0%	0
Far left	0	0	13%
Near the left	0	0	1%

Table 4: Analysis of driver gaze duration in different sight distance limited sections.

Fixation duration t (ms)	Percentage of corresponding fixation time under different sight distances (%)					
	44 m	50 m	56 m	70 m	90 m	106 m
$0 < t < 50$	47.37	52.84	57.79	70	71.24	77.14
$50 \le t < 100$	20	23.07	20.35	15	21.43	14.29
$100 \le t < 150$	11.16	10.53	11.16	7.5	4.15	2.86
$150 \le t < 200$	5.26	3.85	2.38	0	0	1.43
$200 \le t < 250$	5.26	2.52	3.22	0	1.72	1.43
$250 \le t < 300$	7.9	5.39	3.1	7.5	0	0
$t \ge 300$	3.05	1.89	2	0	1.28	2.86

that when the sight distance is increased to 70 m, the driving field of vision increases, and the proportion of short gaze duration increases. The proportion of longer gaze duration is small, the difficulty of obtaining road traffic information is reduced, and the driving visual load is reduced.

(v) When the plane sight distance reaches 106 m, the proportion of the driver's fixation duration less than 100 ms has exceeded 90%, and the proportion of the driver's fixation duration more than 150 ms has decreased to 3%, indicating that the driver's visual load intensity accumulation speed has decreased to a great extent, and the psychological tension will be reduced accordingly.

5. Conclusion

In this study, we found that the distribution of drivers' fixation points in the road with limited sight distance is affected by the sight distance change rate. In the case of larger change rate of sight distance, the driver gradually transfers his gaze energy from the far right to the obstacles near the right due to the lack of depth of field of vision, and the gaze characteristic of "from far to near" is significant. On the other hand, when the sight distance change rate is decreased, the fixation characteristics of fixation point "from far to near" gradually weakened, disappeared when the sight distance change rate was close to 1.33, and the fixation freedom increased. Moreover, in the road section with limited sight distance, the driver's gaze is mainly short gaze. With the gradual increase of sight distance, the proportion of short gaze increases and the proportion of medium and long gaze decreases. In addition, the driver is prone to the visual load accumulation effect in the road section with severe sight distance restriction. Reasonable safety guarantee measures shall be arranged to induce the driver to adopt reasonable running speed to safely pass through the road section with limited sight distance.

Data Availability

The data supporting the findings of this study are included within the article.

Disclosure

The authors confirm that the content of the manuscript has not been published or submitted for publication elsewhere.

Conflicts of Interest

The authors declare that they have no conflicts of interest.

Authors' Contributions

All authors have read the manuscript and approved the study.

Hindawi
Journal of Mathematics
Volume 2023, Article ID 9878209, 1 page
https://doi.org/10.1155/2023/9878209

Retraction

Retracted: Research on the Spread Path and Evolution Causes of Oral Language in the Digital Era

Journal of Mathematics

Received 19 December 2023; Accepted 19 December 2023; Published 20 December 2023

This article has been retracted by Hindawi following an investigation undertaken by the publisher [1]. This investigation has uncovered evidence of one or more of the following indicators of systematic manipulation of the publication process:

(1) Discrepancies in scope

(2) Discrepancies in the description of the research reported

(3) Discrepancies between the availability of data and the research described

(4) Inappropriate citations

(5) Incoherent, meaningless and/or irrelevant content included in the article

(6) Manipulated or compromised peer review

The presence of these indicators undermines our confidence in the integrity of the article's content and we cannot, therefore, vouch for its reliability. Please note that this notice is intended solely to alert readers that the content of this article is unreliable. We have not investigated whether authors were aware of or involved in the systematic manipulation of the publication process.

Wiley and Hindawi regrets that the usual quality checks did not identify these issues before publication and have since put additional measures in place to safeguard research integrity.

We wish to credit our own Research Integrity and Research Publishing teams and anonymous and named external researchers and research integrity experts for contributing to this investigation.

The corresponding author, as the representative of all authors, has been given the opportunity to register their agreement or disagreement to this retraction. We have kept a record of any response received.

References

[1] Z. Li, "Research on the Spread Path and Evolution Causes of Oral Language in the Digital Era," *Journal of Mathematics*, vol. 2022, Article ID 2325711, 9 pages, 2022.

Hindawi
Journal of Mathematics
Volume 2022, Article ID 2325711, 9 pages
https://doi.org/10.1155/2022/2325711

Research Article

Research on the Spread Path and Evolution Causes of Oral Language in the Digital Era

Zhiqiang Li

Anhui Radio, Film and Television Vocational and Technical College, Hefei 230000, China

Correspondence should be addressed to Zhiqiang Li; 2011010221@st.btbu.edu.cn

Received 20 November 2021; Revised 6 December 2021; Accepted 9 December 2021; Published 5 January 2022

Academic Editor: Naeem Jan

Visual orientation seems to indicate the decline of oral communication, but oral communication has its own living space under the new media ecology. Research has found that in the digital media era, voice communication is manifested as a single-level feature that simulates current interaction and information communication. Although voice communication is a lie constructed by individuals, the interaction between the subject's discourse and the actual field of interaction separate the emotional distance, but the situation is harmonious and inclusive. The following voice communication and new media technologies are still trustworthy. Aiming at multifactor evolutionary algorithm (MFEA), the most classical multifactor evolutionary algorithm in multitask computation, we theoretically analyze the inherent defects of MFEA in dealing with multitask optimization problems with different subfunction dimensions and propose an improved version of the multifactor evolutionary algorithm, called HD-MFEA. In HD-MFEA, we proposed heterodimensional selection crossover and adaptive elite replacement strategies, enabling HD-MFEA to better carry out gene migration in the heterodimensional multitask environment. At the same time, we propose a benchmark test problem of multitask optimization with different dimensions, and HD-MFEA is superior to MFEA and other improved algorithms in the test problem. Secondly, we extend the application scope of multitask evolutionary computation, and for the first time, the training problem of neural networks with different structures is equivalent to the multitask optimization problem with different dimensions. At the same time, according to the hierarchical characteristics of neural networks, a heterodimensional multifactor neural evolution algorithm HD-MFEA neuro-evolution is proposed to train multiple neural networks simultaneously. Through experiments on chaotic time series data sets, we find that HD-MFEA neuro-evolution algorithm is far superior to other evolutionary algorithms, and its convergence speed and accuracy are better than the gradient algorithm commonly used in neural network training.

1. Introduction

`Spoken language has changed from the stage of mimicry to the formation of conventional language symbols, from the vagueness of information to the clarity of consensus, and from the narrow tribal communication to the social communication with both depth and breadth. Oral communication plays a key role in the interactive communication between individuals and society. Oral communication can not only cultivate individual consciousness but also participate in the shaping process of social development. The effectiveness of spoken language is not only in simple information interaction but also in knowledge transmission, cultural production, and emotional maintenance. Socrates' sitting and discussing the Dao sowed the seeds of wisdom to the audience in the form of oral communication, and knowledge inheritance depended on the listener's self-realization. The recitation and poetry culture generated by spoken language makes up for the impoverishment of individual spiritual culture. The oral language integrates with visual symbols in the form of presence to realize the experience of emotional integration.

1.1. The Balance Theory Crisis of Oral Communication under the Mapping of Internet. The emergence of written language makes language shift from oral tradition to secular power, resulting in the emphasis on spatial relations over temporal relations [1]. The interactive communication of spoken language between individuals could not be preserved in the

past. The recording of human voice originated from the development of modern science and technology. The invention of the phonograph made the recording of voice no longer a myth. Recording sound has been a very popular behavior, and individuals also enjoy the sensory experience of hearing. Oral communication can be preserved under the construction of Internet technology, and the vertical communication of oral language can be realized in the dimension of time. McLuhan put forward the concept of a global village, and the distance of oral communication is no longer a problem. With the help of Internet technology, oral communication has broken through the bondage of distance and realized the horizontal leap of the spatial dimension of oral communication. Oral communication has broken through the limitations of time and space dimensions. Under the dominant discourse system of information and knowledge sharing, the monopolistic behavior of knowledge inheritance caused by oral communication tends to solidify. The popularization of knowledge is a normalized behavior. The Internet aggregates all kinds of knowledge, and individuals' search for information on demand is a daily presentation. The monopoly of knowledge inheritance constructed by oral communication has been questioned in the new context. Similarly, the effect of oral communication in space diffusion is no less than that of paper, which plays a key role in the process of civilization because of its portability.

1.2. The Real and Virtual Distinction in the Field of Oral Interactive Communication. Traditionally, relying on written means (rather than eyes and ears), and visual art, architecture, sculpture, painting and other means (rather than relying on time and space) to express [2] under the influence of the media, the reality of oral decay seems to be impossible to verify, especially facing the visual era in the era of printed text and images. But in fact, oral communication has not died out. Oral communication and other media on which information transmission depends have created the same space of discourse expression. The existence of new media is not based on the premise of sacrificing the existence of spoken language but enables them to combine and form a harmonious situation. Spoken language is one of the modes of multi-information expression, and its practical utility still plays an important role in the daily life of individuals. The perceived happiness of communication is not limited to the acquisition of the latest information but to the emotional comfort of communicating with each other. The ways of information interaction and dissemination are diversified, and the ideographic nature of visual standard is highlighted in the presentation of diversified information. Real spoken interaction is actually quite different from virtual spoken interaction. The characteristics of present and nonpresent are as follows: in real oral interaction, people participate in the same field of communication mode, and the subjects and objects of communication can perceive each other's subtle details and psychological changes. The spoken language interaction in the virtual space presents the surreal simulation of the communication field. In the local framing of the horizon, the individual cannot perceive the changes of objects outside the horizon. However, in the real oral communication environment, the oral communication environment is flexible, and the intervention of information transmission can be flexible in the face of unexpected situations. From the perspective of relationship composition, it is not difficult to construct the relationship between subject and object in real field communication, while the relationship construction of oral communication in a virtual environment has distinct directivity.

1.3. The Synergy and Information Heterogeneity of Nonverbal Symbols Are Reduced. "Nonverbal communication" refers to the process in which people exchange information with "nonverbal" behavior consciously or thought to be consciously in a specific environment [3]. As a medium, oral communication is not a single ideographic process but a clear description of the same object together with nonverbal symbols. These nonverbal signs include individual actions and expressions, and their main function is to facilitate the clarification of meaning. The coordination of oral communication and nonverbal signs builds a complete system together. The main body of information transmission is often different in explaining something or even blurring the fact itself, which affects the effect of interactive oral communication. Individual differences are shown on the basis of familiar semantic code, and their own grasp of semantic code cannot explain the fact itself, familiar semantics! When code blocks are in heterogeneous areas, nonverbal symbols play a key role with their unique advantages. Under the Internet media ecology, nonverbal symbols show the characteristics of richness. In the past, information circulation was transmitted through multiple levels. In the process of circulation, different levels of audiences interpreted information in various self-interpretation processes. In the process of interpretation, there are a lot of misinterpretations and misinterpretations. This phenomenon is the key factor that causes the deviation between oral communication and actual intention.

At present, a large number of literature works have promoted, improved, applied to multitask evolutionary computing, and achieved good results. The research on multitask evolutionary computing can be divided into four categories: extending multitask framework to a wider range of evolutionary algorithms, applying multitask evolutionary computing to multiobjective problems, applying multitask evolutionary computing to practical optimization problems, and proposing improved multitask evolutionary algorithms based on MFEA. For the study of the first type of problem, Wen and Ting [4] extended the concept of multitasking evolutionary computation to genetic programming (GP) and proposed multifactorial genetic programming (MFGP). Feng et al. [5] proposed multifactorial particle swarm optimization (MFPSO) and multifactorial difference algorithm (MFDE) algorithms based on PSO and DE. Yokoya et al. [6] proposed the multifactorial artificial bee colony algorithm (MFABC) and applied it to the optimization of automobile structure design. In view of the research of multitasking evolutionary

computation in multiobjective problems, Fogel et al. [7] first proposed the multiobjective and multitask evolutionary algorithm (MO-MFEA) and verified the effectiveness of the algorithm in multiobjective optimization problems in reality. Gupta et al. [8] modeled the operation index optimization problem in the beneficiation process as a multiobjective and multitask problem and solved this problem by using improved MO-MFEA. For the third type of problems, multitask evolutionary computation has obtained good results in symbolic regression problem [9], biological network module identification problem [10], shortest path tree problem [11], and combinatorial optimization problem [12]. The fourth type of research is defect improvement of MFEA, mainly focusing on two major problems in MFEA: (i) how to adjust gene migration adaptively according to the similarity between tasks. Denoising autoencoders proposed [13] should be used to automatically construct mappings between tasks and complete gene migration through mapping. MFEA is based on the decomposition method [14] and resource allocation mechanism, which can dynamically adjust gene migration according to the similarity between tasks. (ii) How to make gene migration in MFEA play a role when the optimal solutions between tasks differ greatly. Bali et al. [15] proposed an adaptive strategy to solve this problem. Assuming that the algorithm simultaneously processes two optimization tasks of different difficulties, the strategy maps the optimization space of the low difficulty task to the optimization space of the high difficulty task, and the mapping and the similarity of the latter two tasks become higher, which can amplify the effect of gene migration. Gustafson and Burke [16] proposed the strategy of decision variable transformation, whose basic idea is to map individuals in different tasks to the same position in the normalized search interval before gene transfer.

This paper systematically introduces the multifactor evolutionary algorithm (MFEA), in 2 sections, gives the basic properties of MFEA in the multitask environment, and systematically analyzes the entire algorithm flow of MFEA. In Section 3, the benchmarking problems used in multitasking optimization are introduced in detail, and the performance of MEFA is analyzed by comparing MFEA with SOMA in benchmarking problems. Through the analysis, we found that MFEA could not solve the test problems with different subfunction dimensions well. In Section 3, we proposed an improved version of MFEA for such dimensional multitask optimization problems and applied it to the prediction problem of chaotic time series.

2. Multifactor Evolutionary Algorithm

This section focuses on multitask evolutionary computing. Multitask evolutionary computing is a new direction of evolutionary computing that has attracted much attention in recent years. When there is a similarity between tasks, evolutionary algorithms can be used to simultaneously optimize multiple tasks and achieve better results than single-task algorithms by sharing information between tasks through gene transfer. This section mainly introduces the first multitask evolutionary algorithm and multifactorial evolutionary algorithm. In Section 2, firstly, the mathematical definition of multitask optimization and the special properties of the evolutionary algorithm in multitask environment are given. Then, the whole algorithm flow of MFEA is analyzed in detail, and the selective intersection algorithm (assortative) in MFEA introduces mating and selective imitation in detail. In Section 2, MFEA is verified experimentally. Firstly, the benchmark test in multitask optimization is introduced, and then, the results of MFEA on the benchmark function are analyzed. Section 2 summarizes the content of Section 2.

2.1. Algorithm Analysis. The multifactor evolutionary algorithm (MFEA) is the first multitask evolutionary algorithm that can simultaneously optimize multiple problems through a single population. In this section, we first introduced the basic definition of MFEA and then analyzed the whole process of MFEA in detail.

2.1.1. Basic Definition. Here, we first define multitask optimization: consider K optimization tasks, denoted by $T_1, T_2, \ldots, T_k$, the objective function of the jth task T_j is f_j: $X_j \longrightarrow \mathfrak{R}$, where $X_j \in \mathfrak{R}^{D_j}$ is the domain after the function. The purpose of multitask optimization can be expressed as $\{x_1, x_2, \ldots, x_k\} = \arg\min\{f_1(x), f_2(x), \ldots, f_K(x)\}$, wherein $x_i \in X_i$. MFEA regards each task as a factor and defines the population P scale as N. In order to make the algorithm apply to multitask problems, MFEA defines three basic properties for individual p_i and $i \in \{1, 2, \ldots, N\}$ in population P.

Definition 1 (factorial rank). The adaptive values of all individuals in population P on task T_j form an adaptive array $[f_j^1(x), f_j^2(x), \ldots, f_j^N(x)]$, where N represents the population number and f represents the adaptive values of individual p_i on task T_j. The array of adaptive values is sorted in ascending order. The factor level of individual p_i on task T_j is the subscript value of F in the sorted array, denoted as r_{ij}.

According to the definition, we can know $r_{ij} \in N^+$ and $1 < r_{ij} < N$, and factor grade r_{ij} represents the quality of individual p_i on task T_j. The smaller the factor grade r_{ij} is, the better the individual p_i performs on task T_j. When $r_{ij} = 1$, it means that individual p_i is optimal on task T_j. The factor levels of all individuals in the population on all tasks constitute the factor level matrix R of the population.

Definition 2 (standard adaptive value, scalar fitness). The standard adaptive value is the evaluation standard for the quality of an individual in a multitask environment. The standard adaptive value of individual p_i is denoted as φ_i, which can be obtained from the following equation:

$$\varphi_i = \frac{1}{\min_{j \in \{1,2,\ldots,k\}} r_{ij}}. \tag{1}$$

From the definition, we can see that $\varphi_i \in (0, 1]$, the larger the φ_i, the better the individual. In a single-task environment, the value of an individual on the objective function

can be directly taken as the adaptive value, but in a multitask environment, there are K objective functions, and a single individual will have K adaptive values. How to evaluate the merits and disadvantages of an individual in a multitask environment becomes a problem? It can be seen from Formula (1) that as long as the individual is optimal in a task (factor level is equal to 1), the individual's standard fitness value will be the largest.

Definition 3 (optimal factor, skill factor). The optimal factor of individual p_i is denoted as φ_i. Task T_j is the task in which p_i performs best out of all K tasks.

$$\tau_i = \arg\min_{j\in\{1,2,\ldots,k\}} r_{ij}. \tag{2}$$

Standard fitness can help us measure the merits and disadvantages of individual p_i in multitask environment, but we still need to know the standard fitness φ_i of p_i is generated by the task of p_i. Therefore, MFEA introduces the concept of individual optimal factor, which is used to represent the task in which an individual is optimal.

From the above three definitions, we can know that, different from a single-objective optimization problem, multitask optimization does not require an individual to obtain the optimal solution on all tasks. As long as an individual obtains the optimal solution on one task, the individual will achieve the optimal solution in the multitask environment. Multifactor evolutionary algorithm introduces the concept of multitask optimization to describe the above situation.

Definition 4 (multitask optimal). The adaptive value of individual p on K tasks is $\{f_j^*(x), f_j^*(x), \ldots, f_K^*(x)\}$. If $j \in \{1, 2, \ldots, K\}$ makes $f_j^*(x) \le f_j(x_j)$ valid for all feasible $x_i \in X_i$, p is said to be multitask optimally.

To test and verify the effectiveness of the above improvements, choose Sphere, Rosenbrock, Griewank, Ackley, and Rastrigin experiment the five classical test functions, and the function definition and variable scope are as follows:

(i) Sphere:

$$\min f(x) = \sum_{i=1}^{n} x_i^2, \quad x_i \in [-20, 20], \quad i = 1, 2, \ldots, n. \tag{3}$$

(ii) Rosenbrock:

$$\min f(x) = \sum_{i=1}^{n-1}\left[100\left(x_{i+1} - x_i^2\right)^2 + \left(x_i - 1\right)^2\right], \quad x_i \in [-10, 10], \quad i = 1, 2, \ldots, n. \tag{4}$$

(iii) Griewank:

$$\min f(x) = \frac{1}{4000}S(x) - U(x) + 1,$$
$$S(x) = \sum_{i=1}^{n}(x_i - 100),$$
$$U(x) = \prod_{i=1}^{n}\cos\left(\frac{x_i - 100}{\sqrt{i}}\right),$$
$$x_i \in [-300, 300], \quad i = 1, 2, \ldots, n. \tag{5}$$

(iv) Ackley:

$$\min f(x) = -20\exp[U(x)] - \exp[V(x)] + 20 + e,$$
$$U(x) = -0.2\sqrt{\frac{1}{n}\sum_{i=1}^{n}x_i^2},$$
$$V(x) = \frac{1}{n}\sum_{i=1}^{n}\cos 2\pi x_i^2,$$
$$x_i \in [-32, 32], \quad i = 1, 2, \ldots, n. \tag{6}$$

(v) Rastrigin:

$$\min f(x) = \sum_{i=1}^{n}\left[x_i^2 - 10\cos(2\pi x_i) + 10\right], \quad x_i \in [-5.12, 5.12], \quad i = 1, 2, \ldots, n. \tag{7}$$

2.1.2. Algorithm Flow. The traditional single-objective evolutionary algorithm (SOEA) uses real or binary encoding. The main process of the algorithm is to generate offspring through crossover and mutation and then select excellent individuals for the next generation through selection operation. MFEA takes the traditional genetic algorithm as the prototype algorithm and extends the encoding mode and generation mode of offspring.

(1) Encoding-Decoding Method. Evolutionary algorithm is used in the vector to represent the individual in the population, and individual elements of vector are called "gene," and in the same way, we will be a single vector called "chromosome." MFEA uses single species and optimizes all tasks at the same time, but for different tasks, the search space of different dimensions may be different, and new coding methods need to be designed to map individuals to multiple tasks. Multifactor evolutionary algorithm adopts a new code-decoding method to solve this problem. In the coding stage, the search space of different tasks is linearly

mapped to the uniform interval Y. It means that, in each dimension, the search space of different tasks is linearly compressed to the range of [0, 1]; if the dimensions between tasks are different, the highest dimension in all tasks is taken as a dimension D_m of the unified interval Y. The decoding phase refers to the decoding of the individual encoded in the unified interval Y into the value in the actual search space corresponding to the task when the individual is evaluated for its adaptation value. For example, suppose that the real variable y on the ith dimension of the task corresponds to the real search space $[L, U]$, and the corresponding variable on the unified interval Y is X. The decoding process refers to the process of obtaining Y from X so that the decoding of a single variable can be completed. For task T, its dimension is D, so we only need to decode the first D variables of the vector on the unified interval Y. The reason why the multifactor evolutionary algorithm adopts this coding-decoding method is that the search space of different tasks is compressed into a unified interval, and then, the gene transfer between tasks can be carried out well through crossover operation.

(2) Traditional Single-Objective Genetic Algorithm. It generates offspring through crossover mutation operator, but the generation mode of offspring is different in the multifactor evolutionary algorithm. The core of the multifactor evolutionary algorithm is to make use of the similarity between tasks and carry out implicit gene transfer between different tasks through crossover operators to speed up the convergence of tasks. Assortative mating is used to generate offspring in the multifactor evolutionary algorithm. The pseudocodes of the assortative mating algorithm are shown in Table 1.

Selective crossover algorithm is the core of multitask evolutionary computing, which uses crossover operators to transfer genes between different tasks. Let the optimal factor of an individual P be t, indicating that P is optimal on task T. All individuals in population P whose optimal factor is 1 together constitute the candidate solution of task T. The purpose of selecting a crossover algorithm is to communicate with other tasks on the premise that the distribution of the candidate solution of task T will not change too much. In the selection crossover algorithm, if the two parent optimal factors are the same or rand $(0, 1)$ & gt, in RMP, the offspring generation is directly generated through crossover or mutation operator, and the distribution of the offspring will be basically consistent with that of the parent generation. Only if the rand $(0, 1)$ & lt, in RMP, the parents with different optimal factors were crossed to complete implicit gene transfer. RMP stands for random mating probability, which is used to control the size of gene migration. As can be seen from the pseudocode of the selection crossover algorithm, if the RMP is too small, the migration between tasks will be less, and the multitask evolutionary algorithm will degenerate into the traditional single-task evolutionary algorithm. If RMP is too large, the distribution of candidate solutions for a single task will change greatly, and the algorithm will over explore, and convergence will slow down. After the generation of the offspring, it is necessary to determine the optimal factor attribute of the offspring. The adaptation value of the offspring can be evaluated on all K tasks, and then, the optimal factor of the offspring can be determined according to formula (2). However, such an operation is time-consuming when the value of K is very large. Selective imitation is used in multifactor evolutionary algorithms to solve this problem. Selective imitation means that the offspring directly inherit the optimal factor from the parent and only perform decoding and fitness evaluation on the task corresponding to the optimal factor. When the optimal factors of two parent generations are different, the offspring randomly choose one parent to inherit its optimal factor. The specific flow of the selective imitation algorithm is shown in Table 2.

Other operations of the multifactor evolutionary algorithm are the same as those of the traditional genetic algorithm, and the pseudocodes of the overall algorithm are shown in Table 3. Firstly, the population is randomly generated, and the adaptive value is evaluated on all tasks to obtain the individual factor grade and optimal factor attribute. The above steps are the initialization steps. After initialization, the algorithm iteration begins. Firstly, children are generated according to the selective crossover algorithm. In RMP, two parents with different optimal factors complete gene transfer between different tasks through crossover operators. Then, selective imitation operation was carried out on the generated progeny in order to determine the optimal factor of the progeny individual according to the parent. After determining the optimal factor of the offspring, only the adaptive value of the offspring is calculated on the optimal factor task, and then, the parent and offspring are combined to form the intermediate generation. At this point, the adaptive value of the individuals in the intermediate generation is known, and the factor grade, optimal factor, and standard adaptive value attribute of the individuals in the intermediate generation are updated. The standard adaptive value is taken as the measurement, and the optimal individuals are selected from the intermediate generation to enter the next cycle. Finally, the algorithm is iterated until the end of the algorithm.

3. Experimental Results

In this section, the performance of multifactor evolutionary algorithm is verified by experiments. Firstly, the benchmark test problem used in the experiment is introduced, and then, the performance of multifactor evolutionary algorithm on the test problem is analyzed.

3.1. Benchmarking Issues. Different from the existing single-task optimization and multiobjective optimization problems, multitask optimization needs to design a new test problem. Reference [13] pointed out that the degree of overlap of global optimal values between tasks and the correlation between tasks had the greatest influence on the multitask problem. Multitask optimization problems can be divided into the complete intersection (CI), partial intersection (PI), and no intersection (ND) according to the degree of overlap of global optimal values between tasks.

Table 1: Selecting the cross algorithm pseudocodes.

Algorithm 1: select the crossover algorithm
Input: two parents p_a and p_b randomly selected from the current population; random cross probability RMP. (1) if $\tau_a = \tau_b$ or rand$(0, 1) <$ rmp then Parent p_a and p_b produce two children C1 and C2 by crossing operators (2) else Parent p_a directly produces a child C1 through the mutation operator Parent p_b directly produces a child C2 by the mutation operator (3) end if Output: children C1 and C2

Table 2: Pseudocodes of selective imitation algorithms.

Algorithm 2: selective imitation algorithm
Input: child individual C generated by two parents p_a and p_b or single parent p (1) if C is generated by two parents then (i) if rand$(0, 1) > 0.5$ then C directly inherits the optimal factor of parent p_a (ii) else C directly inherits the optimal factor of parent p_b (iii) end if C directly inherits the optimal factor of its parent p (2) else C directly inherits the optimal factor of its parent p (3) end if Output: child C with the optimal factor attribute

Table 3: Pseudocode of multifactor evolutionary algorithm.

Algorithm 3: multifactor evolutionary algorithm (MFEA)
(1) Initialize population P and calculate individual fitness on all tasks (2) Calculate individual factor grade (R) and optimal factor (T) (3) While (termination condition not met) do (i) Selecting cross-generation progeny population C (Algorithm 1) (ii) Run selective imitation algorithm in progeny population C (Algorithm 2) (iii) Only on task T, the adaptation value of offspring population C is calculated (iv) Generate intermediate generation population R, where $R = PUC$ (v) Update factor grade (R), optimal factor (T), and standard fitness (P) of individuals in intermediate population R (vi) According to the standard adaptive values, the optimal individuals in the intermediate population R were selected to form the next generation population P

According to the correlation between tasks, it can be divided into three types: high similarity (HS), middle similarity (MS), and low similarity (LS). Single-objective multitask benchmarking problems are shown in Table 4.

Spearman's rank correlation coefficient was used as a measure of similarity between tasks. It was assumed that individual X was decoded as y_1 and y_2 on task T_1 and T_2 on the uniform interval y. $R(y_1)$ and $R(y_1)$, respectively, represent individual factor grades on the two tasks. We randomly generate 1×10^6 individuals on the unified interval y to form the sequence x, decode the sequence on task T_1 and T_2, respectively, and generate new sequences y_1 and y_2. Then, the similarity between T_1 and T_2 can be expressed by R:

$$R_s = \frac{\operatorname{cov}\left(r\left(y_1\right), r\left(y_2\right)\right)}{\operatorname{std}\left(r\left(y_1\right)\right) \times \operatorname{std}\left(r\left(y_1\right)\right)}. \tag{8}$$

According to the overlap degree and R_s value of global optimal values between tasks, several common single-objective test functions were rotated and shifted, and then combined into three types of 9 benchmark test problems [13], as shown in Table 3. More detailed information on benchmarking issues is available in the original paper [13].

3.2. Result Analysis. In this section, the results of multifactor evolutionary algorithm (MFEA) and single-objective genetic algorithm (SOMA) are compared. The population size of MFEA is equal to 100, the final number of cycles is equal to 1000, and the random crossover probability is RMP-0.3. The crossover operation is selected to simulate a simulated binary crossover operator (SBX), and polynomial mutation operator is selected for mutation operation. Since MFEA optimizes two tasks simultaneously while SOMA optimizes

Table 4: Single-objective multitask benchmarking problems.

Problem category	Function	dim	Global optimal degree of overlap	R_s
CI + HS	T = Griewank	50	Coincide	1
	T = Rastrigin_	50		
CI + MS	T = Ackley	50	Coincide	0.2261
	T = Rastrigin	50		
CI + LS	T = Ackley	50	Coincide	0.0002
	T = Schwefei	50		
PI + HS	T = Rastrigin	50	Part of the overlap	0.867
	T = Sphere	50		
PI + MS	T = Ackley	50	Part of the overlap	0.2154
	T = Rosenbrock	50		
PI + LS	T = Ackley	50	Part of the overlap	0.0725
	T = Weierstrass	25		
NI + HS	T = Rosenbrock	50	No overlap at all	0.9434
	T = Rastrigin	50		
NI + MS	T = Griewank	50	No overlap at all	0.3669
	T = Weierstrass	50		
NI + LS	T = Rastrigin	50	No overlap at all	0.0016
	T = Schwefel	50		

Table 5: Results of MFEA and SOMA on the multitask benchmark problem.

Problem category	MFEA		SOMA	
	T_n	T_2	T_n	T_2
CI + HS	0.3493 (0.0480)	189.5901 (39.2992)	0.9014 (0.05675)	419.7629 (61.8293)
CI + MS	4.6468 (0.5185)	229.8366 (49.5841)	5.4119 (1.7629)	424.9846 (56.8671)
CI + LS	20.1471 (0.0528)	3884.6405 (427.5915)	21.1944 (0.0934)	4240.0025 (517.8067)
PI + HS	557.7668 (73.8933)	8.7799 (1.4670)	425.6852 (51.1415)	86.7612 (21.0913)
PI + MS	3.5587 (0.4635)	704.5293 (261.5528)	5.0311 (0.6787)	29158.8343 (14301.4714)
PI + LS	20.0767 (0.0646)	20.5621 (3.0864)	5.0346 (0.8623)	12.2019 (2.3042)
NI + HS	755.7619 (316.9677)	233.2365 (70.0560)	25339.6592 (11111.8147)	434.1805 (54.4270)
NI + MS	0.4018 (0.0452)	25.9959 (3.2959)	0.9162 (0.0521)	38.2774 (3.6352)
NI + LS	670.0172 (169.6736)	3858.2066 (470.5808)	435.0968 (51.5959)	4364.407 (611.3337)

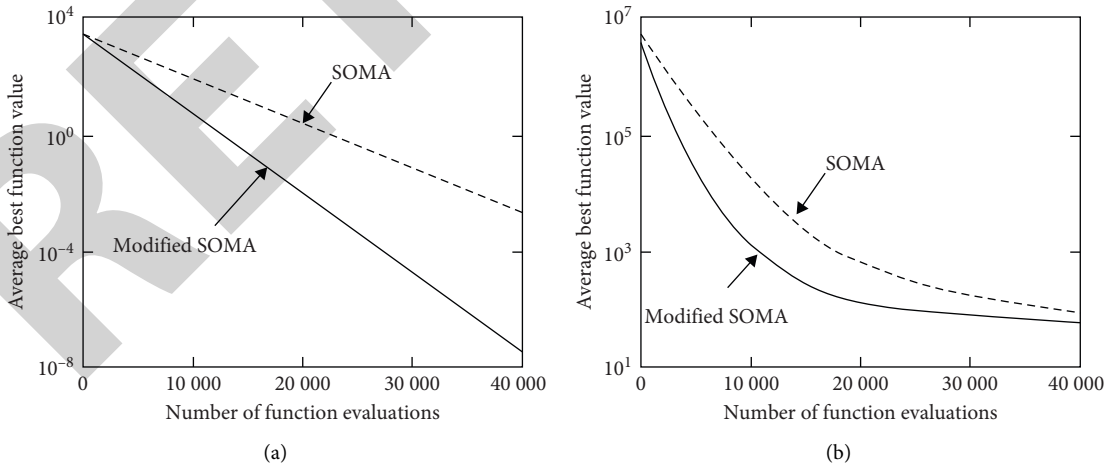

Figure 1: Convergence curves of modified SOMA and SOMA on the problem of full coincidence of global optimal values (CI).

only one task, the maximum number of iterations of SOMA is set to 500 to ensure the fairness of comparison, and other parameters are consistent with MFEA. Each algorithm is independently run for 50 times to eliminate the randomness of the results, and the final results are shown in Table 5. Convergence curves of modified SOMA and SOMA on the problem of full coincidence of global optimal values (CI) are shown in Figure 1.

As can be seen from Table 5 and the convergence diagram, MFEA has an excellent performance in 6 questions

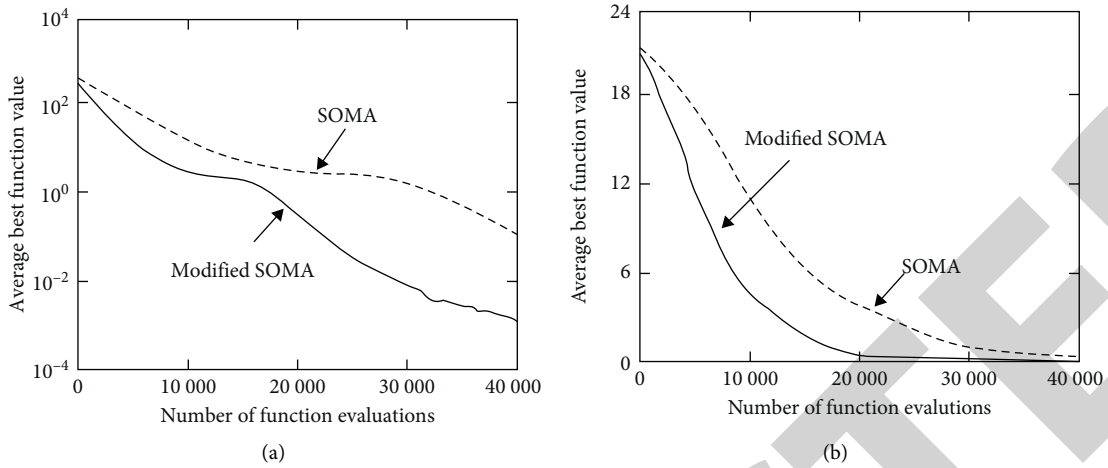

Figure 2: Convergence curves of modified SOMA and SOMA on global optimal partial coincidence (PI).

(CI + HS, CI + MS, CI + LS, PI + MS, NI + HS, and NI + MS) and is superior to SOMA in terms of accuracy and convergence speed. In terms of PI + LS and NI + LS, MFEA does not perform well. Reference [13] certainly states that when the similarity between tasks becomes low, the effect of MFEA will become worse. As can be seen from Figure 1, modified SOMA is slightly worse than SOMA in NI + LS problem, and MFEA is far worse than SOMA in PI + LS problem. However, the R of Pi-LS problem is greater than that of NI + LS problem, so the performance of MFEA is not only affected by the similarity between tasks. It can be seen from Table 5 that the dimensions of the two tasks in PI + LS problem are different, and MFEA performs poorly in the multitask optimization problem with different dimensions. Convergence curves of modified SOMA and SOMA on global optimal partial coincidence (PI) are shown in Figure 2.

The improved ant colony algorithm (IVRS + 20PT), ant colony algorithm combined with 20PT (AC0 + 20PT), and ant colony algorithm combined with artificial bee colony algorithm (ACO + ABC) with excellent results in recent years were selected as the comparison to verify the effectiveness of discrete lion colony algorithm. Table 4 shows the comparison results on six TSP problems. "__" indicates that there are no data in the original literature, and the boldface number indicates the best performance among the four algorithms. As can be seen from Table 4, the discrete lion colony algorithm is superior to the other three algorithms in both optimal and average solutions. For ACO + ABC algorithm, the discrete lion colony algorithm can improve the quality of solution within the range of [1%, 5%]. For ACO + 20PT algorithm, discrete lion group algorithm can improve the quality of Eil51, KroA100, and D198 problems, and especially for KroA100 problem, discrete lion group algorithm can improve the accuracy of about 10%. For IVRS + 20PT algorithm, discrete lion swarm algorithm can improve the solution accuracy by about 0.5% for Ei151, KroA100, and D198 problems.

4. Conclusion

This paper focused on the multifactor evolutionary algorithm (MFEA) and introduced the improved version of MEFA that is HD-MFEA. In the process, the basic properties of MFEA in the multitask environment were given. Meanwhile, a systematic analysis was carried out for the entire algorithm flow of MFEA. Moreover, the detailed introduction of benchmarking problems used in multitasking optimization was given. In addition, the comparison between MFEA and SOMA was carried out to evaluate their performances in benchmarking problems. As a result, MFEA was found to be unable to efficiently solve the test problems with different subfunction dimensions. To this end, i.e., for such dimensional multitask optimization problems, the improved version of MFEA was proposed. Finally, it was applied for the prediction problem of chaotic time series.

Data Availability

The data used to support the findings of this study are available from the corresponding author upon request.

Conflicts of Interest

The author declares that he has no conflicts of interest.

Acknowledgments

This study was supported by (1) Research Achievements of "Li Zhiqiang Technical Skills Master Studio" of Anhui Provincial School of Learning (Project no.: 2019dsgzs32) and (2) 2019 Linkage Report Research on Traditional Media and New Media under the Background of Media Integration on Humanities and Social Sciences in Anhui University (Project no.: SK2019A0966).

Hindawi
Journal of Mathematics
Volume 2024, Article ID 9838430, 1 page
https://doi.org/10.1155/2024/9838430

Retraction

Retracted: Recursive Neural Network-Based Market Demand Forecasting Algorithm for Calligraphy Practice Products

Journal of Mathematics

Received 23 January 2024; Accepted 23 January 2024; Published 24 January 2024

This article has been retracted by Hindawi following an investigation undertaken by the publisher [1]. This investigation has uncovered evidence of one or more of the following indicators of systematic manipulation of the publication process:

(1) Discrepancies in scope

(2) Discrepancies in the description of the research reported

(3) Discrepancies between the availability of data and the research described

(4) Inappropriate citations

(5) Incoherent, meaningless and/or irrelevant content included in the article

(6) Manipulated or compromised peer review

The presence of these indicators undermines our confidence in the integrity of the article's content and we cannot, therefore, vouch for its reliability. Please note that this notice is intended solely to alert readers that the content of this article is unreliable. We have not investigated whether authors were aware of or involved in the systematic manipulation of the publication process.

Wiley and Hindawi regrets that the usual quality checks did not identify these issues before publication and have since put additional measures in place to safeguard research integrity.

We wish to credit our own Research Integrity and Research Publishing teams and anonymous and named external researchers and research integrity experts for contributing to this investigation.

The corresponding author, as the representative of all authors, has been given the opportunity to register their agreement or disagreement to this retraction. We have kept a record of any response received.

References

[1] Y. Xue, "Recursive Neural Network-Based Market Demand Forecasting Algorithm for Calligraphy Practice Products," *Journal of Mathematics*, vol. 2022, Article ID 8086789, 10 pages, 2022.

Hindawi
Journal of Mathematics
Volume 2022, Article ID 8086789, 10 pages
https://doi.org/10.1155/2022/8086789

Research Article

Recursive Neural Network-Based Market Demand Forecasting Algorithm for Calligraphy Practice Products

Yi Xue

Jilin University of Architecture and Technology, Jilin, Changchun 130000, China

Correspondence should be addressed to Yi Xue; 2016121641@jou.edu.cn

Received 17 November 2021; Revised 30 November 2021; Accepted 6 December 2021; Published 5 January 2022

Academic Editor: Naeem Jan

In today's society, calligraphy, which reflects one's basic writing skills, is becoming more and more important to people. People are influenced by calligraphy in their studies, work, etc. Improving calligraphy writing skills has become one of the key directions for developing one's abilities at this stage. As an important means of improving writing skills, calligraphy practice products are attracting more and more attention and purchases. In particular, in recent years, as the market economy has developed in a deeper direction, people's demand for calligraphy practice products has diversified and calligraphy practice product companies have launched a variety of products to meet the public's calligraphy practice needs in order to adapt to the reality of consumer demand. However, with the development of the Internet culture industry and influenced by objective factors such as school holidays and seasons, the current market demand for calligraphy practice products is rapidly and dynamically changing, making market changes difficult to grasp and leading to poor sales, which directly affects the profits of calligraphy practice product-related companies. The artificial intelligence neural network method realizes the nonlinear relationship between the input and output of sample data through the self-learning ability of each neuron and has a certain nonlinear mapping ability in prediction, which plays a great role in the market demand prediction of many commercial products. Based on this, this paper proposes a recursive neural network-based algorithm to predict the future demand and development trend of calligraphy practice products through extensive and in-depth research, so as to provide positive and beneficial guidance for enterprises' future production and sales.

1. Introduction

China has been a cultural power since ancient times, and after more than a thousand years of historical evolution, the major ancient Chinese civilizations have long influenced each other and merged. Today, a China with a splendid culture stands in the East of the world with its colorful cultural elements. An important part of Chinese culture is writing, and the different aesthetic forms of writing form the art of calligraphy [1]. The art of Chinese calligraphy, with its long and unbroken history, has attracted generations of calligraphers to cultivate and tread the paths of the ancients, to experience the essence of the culture that has been precipitated for thousands of years, and on the other hand, to read ten thousand books, travel ten thousand miles, capture the world, cultivate their bodies, and express it in their brushstrokes, creating a style of calligraphy appropriate to the times. Together with other forms of art, they form a vast sea of Chinese culture. The art of calligraphy has always been respected by the nation as an elegant, erudite, and nurturing art form. The art of Chinese calligraphy is a manifestation of Chinese culture and is one with the spirit of the Chinese nation. The spirit of Chinese culture is the unity of heaven and man, the valuing of harmony, and the shunning of center. The Chinese culture's value of "harmony is precious" is perfectly embodied through the beauty of harmony in the art of calligraphy [2]. Calligraphy practice products collection is shown in Figure 1.

Chinese calligraphy, with its ability to express the richness and complexity of human thought and emotion in the simple shape of lines, has great aesthetic value. The study of Chinese calligraphy is a great help in understanding Chinese art and culture. Calligraphy exists alongside the written word and is concerned with brushwork, strokes, and strokes of meaning. With the help of Chinese characters, calligraphy is an expression of sentiment and sentimentality

Figure 1: Calligraphy practice products collection.

and has a strong national character and high artistic taste. Chinese calligraphy has been steeped in thousands of years and is ubiquitous in Chinese life. It is closely related to residential culture, landscape culture, educational culture, religious culture, political culture, coin culture, folk ritual customs, and the arts of painting, architecture, dance, arts, and crafts [3]. As shown in Figure 1, Chinese calligraphy is a unique visual art that still exudes a fascinating artistic charm after thousands of years. The artistic beauty of Chinese calligraphy is composed of two elements: form and spirit. The beautiful and distinct artistic effects and infectious power of calligraphy reflect a unique national style. The composition of traditional painting and calligraphy requires the author not only to make a subjective and rational judgment but also to take the various elements of the picture and to achieve a dialectical unity between the whole and the parts so that the picture can achieve balance and harmony, which can be regarded as the earliest theory of composition in Chinese painting [4]. The aesthetic value of the art of calligraphy has many applications in home decoration, where its content has a subtle effect on the human spirit, gaining knowledge and culture, drawing inspiration and strength. At the same time, calligraphy with its unique means of art life and service life is widely used in the design of patterns for product packaging. The art of Chinese calligraphy, which on the surface appears to be very common, is nothing more than taking a brush and dipping it in ink to write Chinese characters on paper (of course, other writing carriers are sometimes used), but it is this extreme simplicity and richness of variation that has made calligraphy less attractive in contemporary times due to the advancement of modern science and technology, especially the spread of computers and the reduction of handwriting. It has become one of the most popular art forms in contemporary China, with the largest number of participants and the widest audience. Calligraphy is widely recognized for its ability to cultivate the body and nourish the mind. Calligraphy is indeed a great source of health benefits, allowing the whole body to move, the waist and arm strength and eye strength to be harmonized, and the rigidity and flexibility to be combined with movement and stillness, as well as strengthening the body and brain, eliminating fatigue, regulating the psyche, and quieting the mind. Calligraphers and calligraphy education work have also become a highly respected profession in society. The Chinese Calligraphers Association, which consists of national calligraphers, seal carvers, calligraphy theorists, calligraphy educators, and calligraphy activity organizers and management workers, has become a national professional organization and a group member of the Chinese Federation of Literary and Art Circles. Calligraphy enthusiasts have relatively good social recognition. This intangible social recognition and support provide great assistance in the spread, learning, and development of calligraphy [5].

Chinese calligraphy has always been an excellent traditional culture that we are proud of, with thousands of years of history. As life has improved, many parents have begun to pay attention to the cultural development of their children. Learning calligraphy can lay the foundation for children's writing and can improve their overall quality. China's contemporary design started late, and so did the stationery industry's design system, with a large proportion of domestic stationery manufacturers borrowing or directly copying foreign stationery products in the early days. However, as a local cultural product, it is difficult to find a mature product from abroad that is worth learning from. With the rapid development of the Internet culture industry, calligraphy practice products are now combined with modern design to create new developments that shine in a different light [6]. As a representative of traditional culture, the calligraphy practice product industry is also facing unprecedented impact, challenges, and opportunities in the Internet era,

and it is worthwhile to deeply explore the artistic value of calligraphy and promote it, thus creating economic value and prosperity for the calligraphy industry. In recent years, with the rapid development of computer technology, the Internet is deeply integrated with various traditional industries. The Internet economy, represented by the booming e-commerce, has become an important engine of economic development. This will provide great development potential and broader development space for the rise of the Internet economy. The Internet has changed people's lifestyles and brought more possibilities for consumption upgrading and industrial development. The further integration of the Internet with traditional industries has changed the way the original industries produce, sell, and communicate, bringing new opportunities for development. As a typical representative of traditional industries, the calligraphy practice product industry is also integrating Internet technology, quietly undergoing the biggest change in thousands of years. Artificial intelligence is a new technical science that studies and develops theories, methods, technologies, and application systems used to simulate, extend, and expand human intelligence. Artificial intelligence-based market demand forecasting method refers to the method of using artificial intelligence techniques, mainly machine learning and deep learning, etc., to simulate industry experts for market demand forecasting, which differs from fundamental analysis and technical analysis methods in terms of modeling methods, and focuses on the use of artificial intelligence techniques to uncover potential connections between data from various sources in the market and market movements. In order to adapt to the new environment of the Internet culture industry, it is necessary to design and study new intelligent field demand forecasting algorithms for the calligraphy practice product market using artificial intelligence techniques.

In this paper, we start by presenting related works in Section 2; then, in Section 3, we discuss an artificial intelligence neural network method that has certain nonlinear mapping ability in prediction; and for the concerned method, we do experiments in Section 4 and evaluations and finally put a conclusion in Section 5.

2. Related Work

2.1. Calligraphy Practice Products Market Analysis. As an important part of art and culture, calligraphy has gradually moved from the study to the marketplace, forming the basic chain of industrialization, the emergence of specialized calligraphic art dealers and collectors, and the involvement of merchants in the operation of calligraphic artwork that has to some extent further guided the development of calligraphy in the direction of industrialization. At the same time, the development of a related industrial chain plus the framing of calligraphic works and the trading of the Four Treasures of calligraphy market gradually took shape. As the national economy is developing rapidly and people's consumption levels are increasing, the art of calligraphy is also seeing better opportunities for development. People have more time and money for calligraphy-related consumption. First, consumables such as ink, paper, and inkstone are relatively inexpensive compared to other hobbies, such as musical instruments and photography equipment. The vast majority of consumers can afford them. Beginners can basically get all the materials they need to learn calligraphy for under $1,000. With the rise of productivity and the economy, the cost of consumables for calligraphy practice is no longer an issue that hinders the spread of calligraphy learning. Secondly, the calligraphy training industry is also in full swing with economic development. As more and more families reach the well-off level and have a relatively good income, parents have the funds and ability to send their children to calligraphy training courses to learn calligraphy. The cost of calligraphy education is in the middle of the range of hobby learning costs and is becoming more and more acceptable to parents and families. The good economic development and the increase in consumption power have created a good development environment and opportunity for the calligraphy training industry. In addition, economic development has led to the development of the Internet and online education, and payment for knowledge has become the consensus of the times. Online education and online paid courses in calligraphy are also being accepted by more and more adult learners, all of which have brought great prosperity and opportunities to the calligraphy practice products market. Practitioners of calligraphy practice products have also enjoyed the dividends of economic development, and calligraphy, an important art form, has gradually become a leisurely and elegant way of life for the general public after the majority of people have solved the problem of food and clothing [7].

With the development of society and the advancement of technology and culture, the calligraphy industry has also seen unprecedented growth. Various calligraphy practice products have become abundant, the four treasures of calligraphy supplies continue to innovate, and new teaching models and online classes have become popular with the advancement of video and live streaming technology. Online shopping, online payments, and interpersonal trust have taken calligraphy practice products from offline to online. It can be said that the calligraphy industry has also enjoyed the great convenience of the Internet and technological advances, and the dissemination of calligraphy has become easier and more convenient. However, the calligraphy market still has its limitations [8]. Calligraphy is a niche industry with a small group of learners, and although calligraphy can be found everywhere in life, it is still a minority of people who actually learn and come into contact with calligraphy, so the small consumer base and low degree of consumer demand are the biggest obstacles to building a calligraphy industry chain. Compared to the entertainment and leisure industries, such as movies, music, dance, and food, which have a high degree of popularity, calligraphy is still relatively inactive. Calligraphy is a quiet art, limited to the line and visual appreciation, lacking auditory and gustatory stimulation, with limited impact and limited influence, and with the popularity of computer fonts, the practicality of calligraphy is even weaker. Many people are not involved, making market activity and demand

lukewarm. The cycle of production (creation), sales, and consumption of calligraphy are slow, circulation is tiny, age groups are large, and innovation is slow. Calligraphy products are also nondepleting; many calligraphy products can be used for years, and many calligraphy paintings can be preserved for years, which makes the replacement of new calligraphy products slow, and low consumption and low attrition make it difficult for demand for calligraphy products to rise. Calligraphy is an elegant, high-end, spiritual art with a high skill threshold, requiring a certain level of practice, cultural heritage, and knowledge to resonate, love, and appreciate. Calligraphy also has regional and cultural limitations, limited to a few countries such as China and Japan, and from an international perspective, it lacks global demand and circulation. All of this has hindered the rapid development of the calligraphy market. The calligraphy industry is a more stable, long-term lukewarm state of development, with an overall stable Baidu search index and information index with a slight increase. Calligraphy is a traditional culture of thousands of years, and even with the impact of the Internet and artificial intelligence, it will continue to be relatively stable and will not experience major ups and downs [9]. The calligraphy industry is inactive, and the calligraphy auction industry is relatively sluggish, with fewer influential calligraphy works and calligraphy masters, although precious calligraphy works can fetch high prices. The calligraphy industry is in disarray, with small calligraphy practice product manufacturers stealing and evading taxes, and calligraphers with low tax capacity or conducting private transactions without paying taxes. Numerous small and scattered calligraphy training institutions are popping up, and paying taxes is not regulated enough. The state does not have much revenue to spend on the calligraphy industry, and there is no major investment. In the calligraphy industry analysis, the competition in the same industry for sales of calligraphy products also needs to be mastered. Offline competition can be judged by market research; whether there are local calligraphy training institutions, calligraphy galleries, and calligraphy stores, etc., and how the customer flow and sales are can be investigated. Competition on online e-commerce platforms can be obtained through big data analysis tools on e-commerce platforms, allowing for a clear, accurate, real-time grasp of competition in the same industry. The Internet and big data provide tremendous and convenient help for marketing analysis and business decisions. In conclusion, calligraphy practice products have enjoyed the dividends of the Internet technology era, but there are also great limitations and space, which requires the joint efforts of every calligraphy lover and calligraphy industry practitioners to pioneer and innovate and constantly explore to make it prosperous and strong.

Calligraphy practice is often easy to start and difficult to become a master, or it is easy for beginners to practice calligraphy through text posters. China's calligraphy post industry according to user classification is mainly divided into the K12 calligraphy post market (the main users are kindergarten to high school), adult calligraphy post market, and professional calligraphy post market (the main users with certain career characteristics, such as doctors, civil servants, etc.). K12 calligraphy post is the largest segment of the entire calligraphy post industry, accounting for more than 60% of the market. At present, China's character post industry is mainly led by several well-known calligraphers, and there are mainly two types of calligraphy practice character post usage forms, one is the tracing character post, and the other is the water writing character post. Their common drawback is the lack of interaction, the use of a single mode, the use of boring, and not being able to write a variety of fonts. It is based on the lack of interaction between the existing handwriting posters and the practitioner where the laser projection technology and VBK keyboard technology are integrated into the interactive laser projection calligraphy practice product, which has the advantages of easy writing, strong interactivity, and assistance in correcting posture. It has three practice modes. First, learning mode: the laser emitter projects the trajectory and strokes of calligraphy on the paper, visually demonstrating the writing technique; second, copying mode: the laser emitter projects the outer outline of the font on the paper, and the user can directly copy the practice; third, practice mode: the laser emitter projects the meter grid on the paper, and the user can practice writing, and after the writing is completed, the product's intelligent scoring function will rate and voice correct the user's writing. After writing, the product's intelligent scoring function will rate the user's writing and voice correction. At the same time, the system is set up with a library of different types of fonts, so users can choose different types of fonts for practice. The interactive laser projection calligraphy practice product makes up for the shortcomings of the existing calligraphy posters while enriching the functions of the calligraphy practice tool to better meet the needs of consumers. In terms of product functionality, the interactive laser projection calligraphy practice product has a great advantage in that it allows for good human-computer interaction and can meet the requirements of users with different fonts, while being able to detect and correct the words written by the user, preserving a realistic writing experience. In terms of functionality, this product is the equivalent of a calligraphy postcard with thousands of fonts in one and a calligraphy teacher at the same time, providing a one-stop service for learning, practicing, and correcting calligraphy, which is not possible with the calligraphy practice products currently available on the market. The interactive projection calligraphy practice product has advanced technical support to ensure that its function is achieved. The product uses the currently mature laser projection technology and VBK keyboard technology, with a built-in laser emitter to project the interface information on the surface of any paper and then track the finger movements through infrared technology to finally complete the acquisition of input information. High-tech products are a trend for future product development, and consumer enthusiasm for high-tech products is always growing. When high-tech elements are incorporated into a product, then the product can stand out among similar products. The interactive laser projection calligraphy practice product is precisely the integration of laser projection technology and VBK keyboard technology that makes the product stand out

among calligraphy practice products. With the increasing popularity of high-tech products, interactive laser projection calligraphy practice products will be favored by many consumers. According to the "Guideline for Primary and Secondary School Calligraphy Education" published on the website of the Ministry of Education, elementary school grades 3 to 6 are required to schedule one class period per week for brush writing study. According to statistics released by the National Bureau of Statistics on February 24, 2015, it can be seen that 93.6 million students were enrolled in general elementary schools nationwide in 2015. There is such a huge group of calligraphy practitioners among children. The latest survey results released by Regus, a world-renowned office solutions provider, said that the stress suffered by office workers in mainland China in the past year ranked first in the world. Nowadays, office workers' life is accelerated and their work life is irritating; they are also eager to seek a new way to reduce stress. Practicing calligraphy can cultivate the mind, practice qi, and benefit the brain, nurture respect, and greatly reduce the stress from life. With the development of society and the aging of the population, more and more elderly people are experiencing "retirement syndrome" because they do not know how to organize their lives after retirement. In addition to considering retirement as a rest, the elderly should also maintain a certain level of tension so that life does not become boring. This shows that there is a huge demand for calligraphy practice tools. In this regard, we did an interview survey, by interviewing some parents, teachers, students, office workers, and retired elderly people, the survey results show that primary and secondary school students have the need to practice calligraphy, and it is very important for the development of students. Working people have to sign contracts, agreements, examinations for titles, etc., and they need to improve their writing skills urgently, and the demand for word practice is also great. Secondly, retired seniors: surveys show that many retired seniors prefer to read and write then to play cards and watch TV and other similar activities. So according to the survey results, the target market for calligraphy practice products should be basically located in primary and secondary school students, office workers, and retired seniors [10].

2.2. Recursive Neural Networks. Artificial neural network (ANN) has been named deep learning at the time of rapid development of computer storage, communication, and computing power and has set off the third artificial intelligence boom in the world's history with unprecedented scale. "Deep" gives neural networks the ability to abstract information in a hierarchical way, giving them the "intuition" that people have [11]. Overnight, many fields that had been firmly dominated by fine-grained mathematical models let go of their previous obsession with equations and their prejudice against the inscrutable black box and jumped into the deep learning bandwagon. In this transformation, a recursive neural network (RNN) is responsible for modeling sequential data. Common serial data include signals, text, video image sequences, and serial data such as stock prices that characterize trends. In daily applications, RNN models are widely used in tasks such as speech recognition and machine translation, bringing convenience to people's lives. In the biomedical field, sequence data are even more diverse and large in scale, in which RNNs are widely used for tasks such as health monitoring, auxiliary diagnosis, and information extraction, making great contributions to medical development as well as human health. Most biomedical signals are time-varying (time-variant) nonlinear signals, including electrocardiogram (ECG), electroencephalogram (EEG), and electromyogram (EMG). Based on ECG signals, RNN can be used for arrhythmia diagnosis. Based on EEG signals, RNN can be used for sleep signal classification. In addition, in the brain-computer interface, RNN can be used to decode EEG signals and improve the grasping accuracy of neural prostheses. In recent years, the multimodal (multimodal) biomedical signal utilization approach has become a trend. For example, RNN can simultaneously utilize EEG signals as well as functional near-infrared spectroscopy (f NIRS) for epilepsy monitoring. Text in biomedicine is even more complex and diverse, and it is natural that RNNs can perform natural language processing (NLP) on such data [12]. For example, RNN-based biomedical named entity recognition (BNER) technology can help researchers extract useful information from massive biomedical texts. In clinical practice, medical images including ultrasound images, CT images, and MRI images are an important basis for disease diagnosis. Based on ultrasound image sequences, RNN models can significantly improve the detection accuracy of prostate cancer. In computer-aided detection (CAD), RNN can improve the accuracy of early breast cancer detection using current X-ray scans as well as previous scans. At the microscopic scale, RNNs have also been successful in the task of target tracking in time-lapse cell image sequences. In the clinical setting, electronic health record (EHR) data contains sequences of different modalities, which is typical of multimodal data. Based on EHR, RNN can perform disease prediction and also predict the risk of readmission of discharged patients over a period of time, providing the possibility of early initiation of targeted intervention programs for patients at risk of readmission, effectively reducing the probability of readmission, and controlling the cost of care. In recent years, dynamic treatment recommendation systems based on large-scale electronic health records have emerged as the key to the successful improvement of actual clinical outcomes. However, these successes do not conceal a series of problems that arise during the backpropagation of error signals in the depth structure when training RNN models with gradient descent, mainly including the vanishing and exploding gradient problem and the gradient conflict. The former is the most common problem in the general feed-forward neural system. The former is also frequently mentioned in general feed-forward neural network (FNN) research [13]. Before the popularization of Rectified Linear Unit (ReLU), FNNs with deeper structures were often difficult to train due to these problems (especially the gradient vanishing problem). Unlike FNNs, the depth structure of RNNs is inherent, because even an RNN model that contains only a single layer of hidden units in space

becomes very deep when it is expanded in time. RNN models have the ability to remember, are turing complete, and can theoretically learn dependencies at any time interval in a sequence. However, the long-time memory capability of RNNs is not reliable due to the aforementioned problems. Specifically, it is very difficult to rely on gradient descent to train RNN models to learn long-time dependencies, and early RNN models with simple structures are often deep in the quagmire of gradient disappearance. The Long Short-Term Memory (LSTM) proposed at the end of the last century largely alleviated the gradient disappearance problem, which made RNNs shine in this century's boom, and the LSTM structure itself became the standard configuration of most RNN models. However, LSTM has not fundamentally changed the dilemma that the RNN family is in, and gradients still vanish in the face of longer time series. On the other hand, the gradient explosion problem has never been properly solved. At the time of writing this paper, the third wave of neural networks is still going on. The amount of data available for learning by various neural models is increasing dramatically, and new sequence data and their corresponding learning tasks are emerging. The long-time dependencies embedded in the sequence data are becoming richer, longer in time span, and more obscure in presentation, and capturing these long-time dependencies efficiently and accurately is the key to dealing with such problems. On the other hand, neural network models are increasing day by day. Increasing the network size by stacking model layers and increasing link lengths usually accelerates the decline of model memory. In this context and historical trend, it is urgent to investigate the RNN architecture and related algorithms with long-time memory capability. The method proposed in this paper is the market demand prediction of calligraphy practice products with long- and short-term memory network architecture.

3. Method

The Internal structure of neurons in recurrent neural networks is shown in Figure 2.

A neural network is a model with strong learning ability, especially effective in dealing with pattern recognition, intelligent control, and other problems. In recent years, with the booming development of computer science and technology and hardware devices, neural networks have gradually become a hot research topic in the field of artificial intelligence [14]. However, Full Connected Neural Network (FCNN) has the limitation that the nodes of the same layer are not connected to each other, and FCNN cannot be used when the information of the previous moments of the sequence is needed. Since FCNNs cannot share features between different locations of a sequence, they can only handle one input individually, i.e., there is no relationship between the previous input and the next input, and they cannot handle inputs that are related back and forth in time or space. However, many learning tasks need to deal with sequential information, such as time series prediction and task-based dialogues, which require the model to learn from sequential inputs. Recursive Neural Network (RNN) was

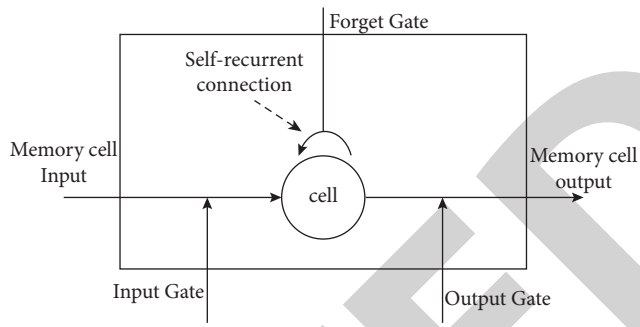

Figure 2: Internal structures of neurons in recurrent neural networks.

created to address the need for sequential inputs. Long Short-Term Memory (LSTM) is essentially a specific form of recursive neural network (RNN). In addition to containing a memory module, LSTM solves the RNN long-term dependency problem by adding a threshold (Gated RNN) to solve the problem that the LSTM adds input gate, output gate, and forget gate to the basic structure of RNN [15]. Each of these three logic control units is connected to a multiplication element (see Figure 2), and the input and output of the information flow and the state of the memory cell are controlled by setting the weights at the edges where the memory cell of the neural network is connected to the other parts. The specific structure is shown in Figure 2.

To note, the input gate denoted as i_t controls whether information flows into the memory cell whereas the forget gate controls whether the information in the memory cell at the previous moment accumulates into the memory cell at the current moment, and it is denoted as f_t . The output gate denoted as o_t controls whether the information in the memory cell at the current moment flows into the currently hidden state h_t. We recall also the cell "memory cell", which represents the memory of the neuron state and makes the LSTM cell have the ability to save, read, reset, and update the long history information, denoted as c_t . At moment t, the LSTM neural network is defined by the following equation:

$$\begin{aligned} f_t &= \text{sigmoid}\left(W_f \cdot \left[h_{t-1}, x_t\right] + b_f\right), \\ i_t &= \text{sigmoid}\left(W_i \cdot \left[h_{t-1}, x_t\right] + b_i\right), \\ o_t &= \text{sigmoid}\left(W_o \cdot \left[h_{t-1}, x_t\right] + b_o\right), \\ \widetilde{c}_t &= \tanh\left(W_c \cdot \left[h_{t-1}, x_t\right] + b_c\right), \\ c_t &= f_t * c_{t-1} + i_t * c_t, \\ h_t &= o_t * \tanh\left(c_t\right). \end{aligned} \tag{1}$$

The recursive neural network timing diagram is shown in Figure 3.

In addition to the previously mentioned i_t f_t, o_t, and c_t, W^* represent the recursive connection weights of their corresponding gates, and sigmoid and tanh are the two activation functions. In the training process of the LSTM neural network, firstly, the data features at moment t are input to the input layer and the results are output through the excitation function. The output results, the output of the hidden layer at moment $t-1$, and the information stored in

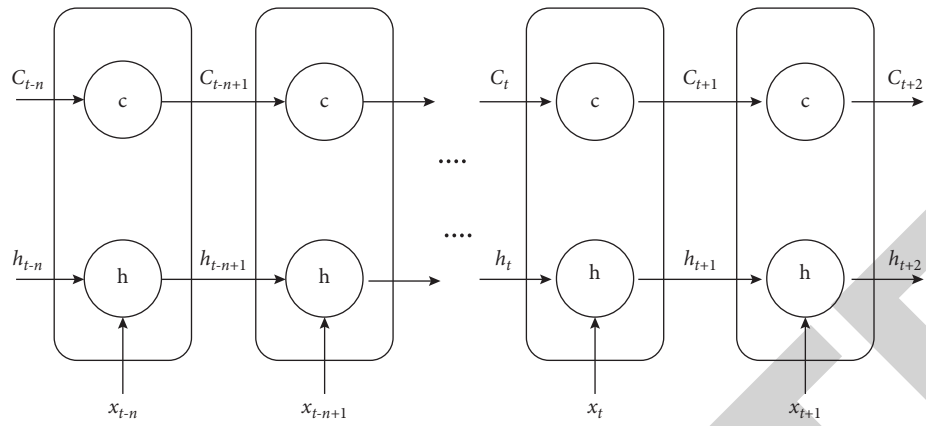

Figure 3: Recursive neural network timing diagram.

the cell unit at moment $t-1$ are input into the nodes of the LSTM structure, and the data are output to the next hidden layer or output layer through the processing of input gate, output gate, forget gate, and cell units, the results of the nodes of the LSTM structure are output to the neurons of the output layer, and the calculation of backpropagation error updates each weight. The overall structure is shown in Figure 3.

A simple recursive neural network consists of an input layer, a hidden layer, and an output layer. For a given input sequence $x = [X_1, X_2, \ldots, X_t]$, at moment t, the hidden layer state is s_t and the output value is z_t, as follows:

$$z_t = \sigma(V \cdot s_t), \tag{2}$$

$$s_t = \delta(U \cdot x_t + W \cdot s_{t-1}), \tag{3}$$

where V is the weight matrix of the output layer; σ is the output layer activation function; U is the weight matrix of the input x; W is the weight matrix of the hidden layer state s_{t-1} at moment $t-1$ as the input at moment t; g is the hidden layer activation function. Looping equation (3) into equation (2), we get

$$z_t = V * \delta(U * x_t + W * \delta(U * x_{t-1} + W * \delta(U * x_{t-2} + W * \delta(U * x_{t-3} + \cdots)))). \tag{4}$$

The LSTM differs from the RNN in that it adds a "processor" to the algorithm to determine whether the information is useful or not. A cell has three gates, called input gate, forget gate, and output gate. When a message enters the LSTM network, it can be judged as useful or not according to the rules. Only information that meets the algorithm's certification is left behind, while information that does not match is forgotten through the forgetting gate. It is just a one-in-two-out working principle, but it can solve the long-standing big problems in neural networks with iterative operations. It has been shown that LSTM is an effective technique to solve the long-order dependence problem and the generalization of this technique is very high, leading to a great variety of possibilities brought about.

LSTM networks are trained using a backpropagation algorithm with the following steps: (1) forward computation of each neuron output value, for LSTM, i.e., five vectors i_t f_t, o_t, c_t, and h_t, which have been described in the previous section; (2) backward computation of the error term for each neuron; as with recursive neural networks, the backward propagation of LSTM error terms consists of two directions: the first is the backward propagation along time, i.e., calculating the error term at each moment starting from the current moment; the second is propagating the error term one layer up; (3) calculating the gradient of each weight according to the corresponding error term.

4. Experimentation and Evaluation

4.1. Datasets. In this paper, the daily sales volume data of a brand company's calligraphy exercise products in each market of a region within three consecutive years were selected, and the brand company had 78 retail stores in the region, and 78 sets of 1096 sales volume time series were obtained after statistical collation; one set of sales data and data format are listed in Table 1. The data in Table 1 can be used as a random time series for different outlets according to the synchronous series sorted from January 1, 2015, to December 31, 2017.

By observing the data characteristics of the sales volume of the enterprise's products and then the above data as a unit of weekly statistics sales data, extracting the more representative three groups of data for comparative analysis shows the sales volume of the enterprise's products in the period 2015–2017; there are obvious fluctuations; with time, sales data show a more obvious downward trend and a certain seasonal pattern and the existence of randomness, mainly as part of the seasonal trend and the overall decline in

Table 1: Daily sales volume statistics of calligraphy practice products of a company from 2015 to 2017.

	1	2	3	4	5	6	7	8	9	10	11	12	13	14	...
2015	6	8	11	7	4	5	6	6	5	4	11	6	10	4	...
2016	15	13	10	9	8	4	5	9	6	13	4	6	4	7	...
2017	13	15	5	5	7	3	8	16	7	5	11	9	5	6	...

sales volume of mixed trends, and the local existence of large fluctuation characteristics.

4.2. Model Combinations. In order to fully utilize the advantages of the Prophet model and LSTM neural network model, this paper proposes an optimal combined forecasting model based on Prophet and LSTM neural network for sales time series forecasting of calligraphy exercise products. In February 2019, Drotár et al. open-sourced a set of time series forecasting tools Prophet. Unlike traditional time series forecasting models (ARIMA, etc.), the Prophet model is essentially a curve fit to time series data, while having excellent adaptability to holiday effects and trend change points (change points) in the data, especially robust to missing values, shifts in trends, and a large number of outliers, and is currently mainly applied to traffic forecasting on Facebook social networking sites. Prophet itself is a model based on a self-additive model to predict time series data, the model as a whole consists of growth (trend term), seasonality (period term), and holidays (holiday term) 3 parts superimposed, and the basic form is as follows:

$$P(t) = g(t) + s(t) + h(t) + \varepsilon, \tag{5}$$

Here, the trend term $g(t)$ is the core component of the whole Prophet model, containing parameters with different degrees of assumptions and adjusting smoothness, which is used to fit the nonperiodic changes in the time series and select the change point (change point) from the data to detect the trend direction. Firstly, the Prophet model and the LSTM network model with high prediction accuracy are constructed separately for the sales data, the prediction value of the Prophet model at time t is set as $P(t)$, the prediction value of the LSTM network model is $L(t)$, $t = 1, 2, ..., N$, and the two models are assigned dynamic weights w_1 and w_2, respectively. t, this point, defines the integrated Prophet-LSTM combined prediction model as

$$Y(t) = w_1 P(t) + w_2 L(t), \quad w_1 + w_2 = 1, t = 1, 2, \ldots, N, \tag{6}$$

where t is the time when the predicted value appears and $Y(t)$ is the result of summing the predicted data of the Prophet model and LSTM network by weights. The Prophet-LSTM neural network sales volume forecasting model is obtained by calculating the optimal weights composed of the two models after integration. The Prophet model can transform the time series by certain functions into combined patterns of different time dimensions such as daily, weekly, quarterly, and yearly with overall trends. The Prophet-LSTM model is first initialized and empirically set change point = 0.15 to make the growth trend more sensitive to changes. The forecast interval is specified as September 2017–December 2017, and the forecast frequency is "days". In order to predict the value of sales change in the future period, the original sales volume time series data was divided into a training set and a test set according to 9 : 1 as a whole, the training set was input into the model for training, and the Prophet model was used to analyze and predict the results of the sales volume data, which will theoretically decline gradually in fluctuations over time. In order to optimize the update rate of the LSTM model parameters, the learning rate (Learning Rate) needs to be further controlled. The Adam algorithm combines the advantages of Ada Grad and RMS Prop algorithms to dynamically adjust the learning rate of each parameter by using the first-order moment estimation and second-order moment estimation of the gradient. It is an effective gradient-based stochastic optimization method, which makes the update of parameters smoother and takes less storage resources.

4.3. Experimental Results. In order to find the optimal weight coefficients w_1 and w_2 in the integrated model Prophet-LSTM model, we take the coefficients w_1 to be 11 values in [0.0, 1.0] increments, $w_1 + w_2 = 1$ and then the corresponding weight coefficients w_2 to be 11 values in [1.0, 0.0] decrements and multiply the 11 sets of weight coefficients w_1 and w_2 with the sales volume forecasts of the respective models at each moment. After the above process, the 11 sets of weighted integrated sales forecasts are obtained as

$$Y(t_i), \quad i = 1, 2, \ldots, 11, ti = 1, 2, \ldots, n. \tag{7}$$

In order to find the specific values of the weight coefficients w_1 and w_2, the root mean square error equation (RMSE) and the mean absolute error (MAE) are used as the criteria to evaluate the effect of the Prophet-LSTM combined sales forecasting model for each group of weight coefficients, and the expressions are as follows: where x is the actual value of product sales in week i. According to Table 2, the root mean square error of the prediction results is minimized when the weight coefficients $w_1 = 0.6$ and $w_2 = 0.4$, and the mean absolute error of the prediction results is minimized when the weight coefficients $w_1 = 0.4$ and $w_2 = 0.6$. The results show that the prediction results of the Prophet-LSTM model are improved compared with the Prophet and LSTM models, and its prediction accuracy is generally better than the other two single prediction models, indicating that the prediction results of the Prophet-LSTM combined prediction model are relatively effective and more applicable than the single prediction model in the sales forecast of this enterprise. The weight coefficients corresponding to the evaluation metrics of the model are shown in Table 3.

In order to further verify the application performance of the Prophet-LSTM model, Holt–Winters (exponential smoothing model), ARIMA model, Prophet model, LSTM, and Prophet-LSTM combined model were used as comparison models in this paper to model the prediction of another new set of sales data, and the evaluation results of each model are listed in Table 3. The evaluation results show

Table 2: Comparison of the performance of different models.

Models	Evaluation metrics	
	RMSE	MAE
Holt–Winters	35.273	16.976
ARIMA	23.457	13.650
Prophet	3.465	2.143
LSTM	5.746	3.254
Prophet-LSTM ($w_1 = 0.6$, $w_2 = 0.4$)	2.645	1.645
Prophet-LSTM ($w_1 = 0.4$, $w_2 = 0.6$)	7.103	3.635

Table 3: The weight coefficients correspond to the evaluation metrics of the model.

w_1	0.0	0.1	0.2	0.3	0.4	0.5	0.6	0.7	0.8	0.9	0.0
w_2	1.0	0.9	0.8	0.7	0.6	0.5	0.4	0.3	0.2	0.1	0.0
RMSE	3.700	3.427	3.274	3.153	3.059	3.022	3.010	3.050	3.139	3.253	3.490
MAE	2.514	2.380	2.300	2.274	2.269	2.297	2.351	2.453	2.524	2.605	2.778

that Prophet and LSTM single models have comparable forecasting performance, and both are significantly better than Holt–Winters and ARIMA classical time series models; Prophet-LSTM combined forecasting model has further optimized the forecasting accuracy based on the single model and has the best forecasting effect.

5. Conclusion

Calligraphy is the art of writing Chinese characters. The Chinese people love calligraphy and practice it. In a general sense, the art of calligraphy is the art of writing; writing can only meet the aesthetic requirements of the art of calligraphy if it is pursued in an aesthetically pleasing way and sublimated to art. From the practice of calligraphy education, learning calligraphy has many functions. The market for calligraphy practice products is vast, but in the face of a complex and dynamic market, it is important to predict the market demand for calligraphy practice products in a timely and accurate manner, to analyze the characteristics and patterns of sales volume data, and to improve the accuracy of sales volume forecasting, so that calligraphy practice product enterprises can develop timely and effective marketing strategies. This paper proposes a combined model prediction method based on recursive neural network model based on the pattern of sales volume time series data of a calligraphy practice product enterprise, constructs a weighted Prophet-LSTM combined prediction model, and conducts comparison experiments with the model under each weight coefficient, the single model before combination, and two classical time series models. The experimental results show that the forecasting performance of the Prophet and LSTM neural network models is significantly higher than that of the typical time series forecasting models, and the combined Prophet-LSTM model has better forecasting performance. Overall, based on the verification that the Prophet model and the LSTM model have obvious advantages in forecasting the sales volume of calligraphy practice products, this paper further improves the model prediction performance by weighted combination, maximizing the advantages of both prediction models. In this paper, only a combined forecasting model combining two single forecasting models is designed, on which new forecasting models can be introduced for further combination in the future to pool the advantages of more models and thus obtain more accurate forecasting results. Besides, further experiments can be done on the parameter preferences of LSTM neural networks in the follow-up work to seek a better modeling method. In the future, in order to analyze the sales volume time series data more deeply, further research on the influencing factors of sales volume can be targeted.

Data Availability

The data used to support the findings of this study are available from the corresponding author upon request.

Conflicts of Interest

The author declares that he has no conflicts of interest.

References

[1] S. Lin and X. Ban, "Study on cultural and creative design of traditional chinese calligraphy tools in digital era," in *Proceedings of the 6th International Conference on Arts, Design and Contemporary Education (ICADCE 2020)*, pp. 427–430, Jaipur, India, Febraury 2021.

[2] A. Ahmad Zarnuji, H. Hanif Amrulloh, and I. N. Isnaini Nur Azizah, "Utilization of rice husk waste for paper raw materials as an Arabic calligraphy media," *Engage: Jurnal Pengabdian Kepada Masyarakat*, vol. 3, no. 1, pp. 43–54, 2019.

[3] Y. Dai, "Research on the application of computer multimedia in calligraphy education," *Journal of Physics: Conference Series*, vol. 1915, no. 3, Article ID 032019, 2021.

[4] L. Xiang and L. L. S. Gee, "The importance of lines: the modern calligraphy of wang dongling and qiu zhenzhong," in *Proceedings of the 2nd International Conference on Interdisciplinary Arts & Humanities (ICONARTIES) 2020*, Yogyakarta, IndonesiaAvailable at SSRN 3800559, 2021, Yogyakarta, Indonesia, March 2021.

[5] R. Long, C. Sun, and H. Pan, "Research on the design and application of persuasive game in calligraphy learning," in *Proceedings of the International Conference on Applied Human*

Hindawi
Journal of Mathematics
Volume 2024, Article ID 9791314, 1 page
https://doi.org/10.1155/2024/9791314

Retraction

Retracted: Research on Sports Training Action Image Recognition Based on SDN

Journal of Mathematics

Received 23 January 2024; Accepted 23 January 2024; Published 24 January 2024

This article has been retracted by Hindawi following an investigation undertaken by the publisher [1]. This investigation has uncovered evidence of one or more of the following indicators of systematic manipulation of the publication process:

(1) Discrepancies in scope

(2) Discrepancies in the description of the research reported

(3) Discrepancies between the availability of data and the research described

(4) Inappropriate citations

(5) Incoherent, meaningless and/or irrelevant content included in the article

(6) Manipulated or compromised peer review

The presence of these indicators undermines our confidence in the integrity of the article's content and we cannot, therefore, vouch for its reliability. Please note that this notice is intended solely to alert readers that the content of this article is unreliable. We have not investigated whether authors were aware of or involved in the systematic manipulation of the publication process.

In addition, our investigation has also shown that one or more of the following human-subject reporting requirements has not been met in this article: ethical approval by an Institutional Review Board (IRB) committee or equivalent, patient/participant consent to participate, and/or agreement to publish patient/participant details (where relevant).

Wiley and Hindawi regrets that the usual quality checks did not identify these issues before publication and have since put additional measures in place to safeguard research integrity.

We wish to credit our own Research Integrity and Research Publishing teams and anonymous and named external researchers and research integrity experts for contributing to this investigation.

The corresponding author, as the representative of all authors, has been given the opportunity to register their agreement or disagreement to this retraction. We have kept a record of any response received.

References

[1] D. Wang and L. Shen, "Research on Sports Training Action Image Recognition Based on SDN," *Journal of Mathematics*, vol. 2022, Article ID 3668647, 10 pages, 2022.

Hindawi
Journal of Mathematics
Volume 2022, Article ID 3668647, 10 pages
https://doi.org/10.1155/2022/3668647

Research Article

Research on Sports Training Action Image Recognition Based on SDN

Dianhai Wang and Lianmei Shen

Chuzhou Polytechnic, Chuzhou, Anhui 239000, China

Correspondence should be addressed to Dianhai Wang; s01280660@acad.tri-c.edu

Received 26 November 2021; Revised 20 December 2021; Accepted 23 December 2021; Published 5 January 2022

Academic Editor: Naeem Jan

Current image recognition methods cannot combine the transmission of image data with the interaction of image features, so the steps of image recognition are too independent, and the traditional methods take longer time and cannot complete the image denoising. Therefore, a recognition method of sports training action image based on software defined network (SDN) architecture is proposed. The SDN architecture is used to integrate the image data transmission and interactive process and to optimize the image processing centralization. The network architecture is composed of application layer, control layer, and infrastructure layer. Based on this, the dimension of image sample set is reduced, and the edge detection operator in any direction is constructed. The image edge filter is realized by calculating the response and threshold of image edge by using lag threshold and nonmaximum suppression (NMS). The Hough transform algorithm is improved to optimize the detection range. Extracting the neighborhood feature of sports training action, the recognition of sports training action image based on SDN architecture is completed. Simulation results show that the proposed method takes less time and the image denoising effect is better. In addition, the F1 test results of the proposed method are higher than those of the literature, and the convergence is better. Therefore, the performance of the proposed method is better.

1. Introduction

A large number of sports videos are collected in the process of sports training and teaching. Accurate recognition of sports action in the video can prevent accidental injury and protect athletes' health. In the sports movement recognition aspect, the computer image processing technology has obtained the widespread application. But at present, there are all kinds of complex movements in sports training. It is difficult to judge the wrong movements simply by traditional contour detection methods, which results in that athletes cannot get correct movements in time [1]. In [2], relevant scholars summarized the research progress and significance of motion recognition and summarized it into two processes: motion capture and motion classification based on deep learning. First, three mainstream motion capture methods based on video, depth camera, and inertial sensor are introduced in detail, and the commonly used motion datasets are listed. Second, motion recognition based on depth learning is described from two aspects: automatic feature extraction and multimodal feature fusion. Reference [3] proposes an automatic tracking method based on image recognition to recognize human actions under high-intensity motion. First, the double convolution theory is used to segment the image of human action under high intensity, and the feature of human action is extracted. Then, combined with the Gaussian distribution model, the obtained human motion image target and background and foreground information are processed to obtain the Gaussian distribution model of human motion image background, and the tracking trajectory of human motion image is obtained by Kalman filter. Finally, the Bayesian classification theory is applied to construct the target model for the gray information of human motion image, solve the optimal peak point of human motion image, and realize the segmentation and tracking of multiple targets. Reference [4] extracts pose

features from local areas of the image and depth features from the overall image to explore their complementary role in motion recognition. First, a pose representation method is introduced. The pose of each limb component is represented by a set of poselet detection scores describing the pose of the component. In order to suppress detection errors, a component-based model is designed as the basis of detection. In order to train CNN network from a limited number of datasets, the methods of pretraining and fine adjustment are used.

However, the previously mentioned methods cannot combine the transmission of image data with the interaction of features, which leads to the independence of the steps of image recognition, which takes longer time and has higher noise. Therefore, a recognition method of sports training action image based on SDN architecture is proposed. In Section 2 of this paper, we propose the method for recognition of sports training action image on the basis of SDN architecture. In Section 3, the simulation test design is proposed, and the results of the tests are analyzed for the validation of proposed techniques. At the end, the paper is concluded in Section 4.

2. Sports Training Action Image Recognition Method Based on SDN Architecture

This section proposed the method for recognition of sports training action image on the basis of SDN architecture. In the process, we first define the SDN network. Then, the reduction of image dimensions is talked about. Through adaptive threshold, the edges of images are filtered. Moreover, the Hough transformation algorithm is improved. Lastly, the sports training action's neighborhood feature is extracted.

2.1. SDN Network. SDN is a software-defined network, and it is an architecture that simplifies and optimizes the traditional network. SDN combines data transfer or interaction between devices and application services to control centralized networks, primarily applications that interact between devices and the data information they transmit [5, 6]. The SDN network architecture is shown in Figure 1.

As shown in Figure 1, the existing network architecture is rooted in traditional network devices. Traditional networks control each device individually in the form of distributed control and tightly couple the forwarding layer and the control layer. Because the manager cannot control and forward the data center directly, the network protocol needs to be configured, which has an impact on the forwarding behavior through the network protocol. This impact is fixed mode, so it is relatively closed and uncontrollable compared with the traditional network equipment and the traditional network architecture. In other words, it is difficult to manage and control the existing network.

The traditional network architecture of SDN is composed of application layer, control layer, and infrastructure layer. It uses the east-west interface to communicate to keep the consistency of flow table between controllers.

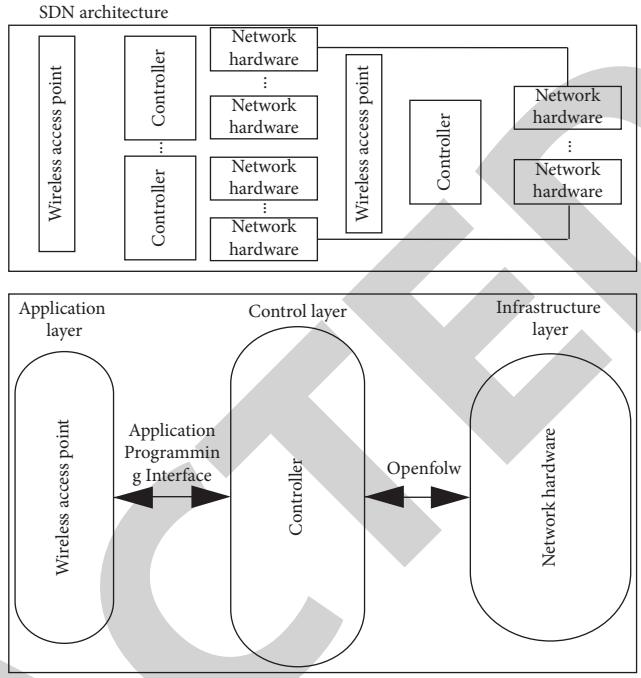

Figure 1: Existing network architecture and SDN network architecture.

2.2. Image Dimensionality Reduction. Set $Q = [q_1, q_2, \ldots, q_n]$ to represent the sample set to be processed and reduce the dimension of the sample set. Specific sports training images are easily affected by equipment parameters, illumination, time, and other factors in the process of collection, and there are more useless data and information in the sports training images, which leads to a longer time for recognizing local changeable features of the images. The method of recognizing local changeable features of specific sports training images removes the useless data and information in the images through dimensionality reduction [7]. First, the global discrete matrix can be reduced by solving the problem of global discrete matrix. The global optimal discrete matrix J is obtained by using PCA algorithm.

$$J = Y\left(J_{\text{in}} + J_{\text{out}}\right), \tag{1}$$

where Y represents the weighting factor; J_{out} represents interclass discrete matrix; and J_{in} represents in class discrete matrix.

The intraclass discrete matrix is weighted by the following formula to update the global discrete matrix. The result is

$$J' = \frac{\left(J_{\text{in}} + J_{\text{out}}\right)}{\delta \cdot Y}. \tag{2}$$

In the expression, δ is the global discrete coefficient.

In order to realize the conversion between linear discriminant analysis (LDA) reduction and principal component analysis (PCA) reduction in space, the following formula is used to calculate the second update result J'' of the in-class discrete matrix:

$$J'' = \frac{\sum_{i=1}^{n}\sum_{j=1}^{n}\left(q_j^{(i)} - g^{(i)}\right)\left(q_j^{(i)} - g^{(i)}\right)}{Q}. \tag{3}$$

In the formula, Q represents the total number of samples corresponding to clustering number i, $g^{(i)}$ represents the cluster center corresponding to clustering number i, and $q_j^{(i)}$ represents the number j samples in clustering number i.

The principle of PCA is to realize the projection of correlated variables in the principal component space, and the projection Q' of Q is obtained by PCA mapping in the PCA subspace to complete the dimensionality reduction of specific sports training images [8].

2.3. Image Edge Filtering Based on Adaptive Threshold. Sports training image edge filtering is an image edge detection operator in any direction, which uses lag threshold and NMS to realize image edge filtering [9, 10]. It mainly has two parts: calculating image edge response and selecting threshold.

2.3.1. Select Adaptive Threshold. After the edge response intensity of the sports training image is calculated by the edge detection operator, it is necessary to locate the edge of the sports training image. When locating the image edge, the lag threshold method can connect the image edges according to the spatial information of the gradient image. In the lag threshold method, it is necessary to set the high threshold and low threshold. The larger the threshold, the stronger the anti-interference ability of image edge detection, but the edge of the image is easy to be lost. When selecting the size of the filter, when the size of the filter is smaller, the small edge of the image can be detected, but the phenomenon of poor anti-interference ability will appear.

Through the previously mentioned analysis, it can be seen that when using a small-size filter to detect the edge of sports training image, a large threshold should be selected to locate the image edge shape, which can improve the anti-interference ability of image edge filtering. When a larger size filter is selected, a small threshold should be selected to locate the image edge shape to avoid the loss of image edge, and the lag threshold method should be used to determine [11].

Set the high threshold and low threshold as $T_{\max}$ and $T_{\min}$, respectively, and the size of the image edge detection filter is $\mathfrak{R}$. The size of this value determines the value of the threshold, and then

$$T' = \begin{cases} \max\left(T_1, T_2, \ldots, T_n\right), \mathfrak{R} = \mathfrak{R}_{\max}, \\ \min\left(T_1, T_2, \ldots, T_n\right), \mathfrak{R} = \mathfrak{R}_{\min}, \end{cases} \tag{4}$$

where T' represents the candidate threshold, $1 \le i \le n$, when $\mathfrak{R} = \mathfrak{R}_{\max}$, and T selects the maximum candidate threshold. In order to make the image edge filtering have better real-time performance, two threshold selection methods are used to determine the candidate threshold, namely, the image gradient histogram and the image edge threshold determination method of Canny operator [12].

Among the existing image edge threshold calculation methods, the more common method is to determine the image edge response threshold according to the image gradient probability. Let the gradient of sports training image I be normalized so that the number of pixels is N, the gray range of the image is $[1, L']$, the gray level is $1 \le j' \le L'$, the number of pixels is n', and the probability is

$$p_j = \frac{n'}{N}. \tag{5}$$

Then,

$$\sum_{j=1}^{n} p_j = 1. \tag{6}$$

The gradient histogram $h(I)$ of the sports training image can be obtained through p_j, in which the kurtosis χ and skewness X relative to the gray level are, respectively,

$$\begin{aligned} \chi &= \frac{\mathfrak{F}_4}{\mathfrak{F}_2^2}, \\ \mathrm{X} &= \frac{\mathfrak{F}_3}{\mathfrak{F}_2^2}, \end{aligned} \tag{7}$$

where $\mathfrak{F}_n$ represents the n-order center distance relative to the first j gray levels of $h(I)$.

The gradient of sports training image can be expressed as

$$\mathrm{K} = \sqrt{\sum^{n} \mathrm{X}_{\theta_{i'}}^2}, \tag{8}$$

where n represents the number of image edge angles $\theta_{i'}$. According to relevant regulations, the angles are 0°, 45°, 90°, and 135°. When using formula (8) to calculate the image edge response, it is necessary to determine the value of φ in $G_{x'}$ and $G_{y'}$. There is a close correlation between Gaussian distribution and Gaussian function. For Gaussian distribution, the probability distribution outside $[-6\varphi, 6\varphi]$ range is less than 0.05. Let the size of filter template window be $\mathfrak{R} \times \mathfrak{R}$, $\mathfrak{R} \ge 3$ be odd, $\mathfrak{R} = 6\varphi + 1$, and filter size $\mathfrak{R}$ be important parameters. The shape of functions $G_{x'}$ and $G_{y'}$ is determined by this parameter.

In order to determine the edge threshold of the image through ROI, Otsu is used to calculate the interclass variance of the gray value of the sports training image in ROI, and the image gray value with the maximum variance is selected as the image edge threshold. Set the ROI relative histogram gray value between $[L_1', L_2']$, and calculate the interclass variance of each gray level $L_1' \le T \le L_2'$ of the image. The calculation formula is as follows:

$$\sigma = \mathfrak{R}_0\mathfrak{R}_1\left(\mu - \mu'\right)^2, \tag{9}$$

of which

$$\mathfrak{R}_0 = \sum_{j=1}^{n} p_j,$$

$$\mathfrak{R}_1 = 1 - \mathfrak{R}_0,$$

$$\begin{cases} \mu = \dfrac{\varphi}{\mathfrak{R}_0} \sum_{j=1}^{n} p_j, \\ \mu' = \dfrac{\varphi}{\mathfrak{R}_1} \sum_{j=1}^{n} p_j. \end{cases} \tag{10}$$

When $L_1' \le T \le L_2'$, the maximum image gray level of φ is the image edge candidate threshold. Generally, the image edge threshold of Canny operator is determined according to the total number of nonedge points in the sports training image pixels. Set the total number of pixels as N and the proportion of nonedge points as r. When the number of image points is accumulated to $N \times r$, the gradient value of the image is the image edge candidate threshold. When there is noise in the sports training image, the selection of lag threshold and filter size directly affects the image edge filtering effect. The large-size filter can reduce the noise and improve the image edge filtering effect by changing the filter size.

Suppose that the proportion of nonedge pixels relative to B_{min} and B_{max} in the image is r_{min} and r_{max}, so that

$$\Delta r = r_{max} - r_{min}. \tag{11}$$

Assuming that the filter size is within the range of $[\mathfrak{R}_{max}, \mathfrak{R}_{min}]$, when the initial value is $\mathfrak{R}_{init}$, the value of $\mathfrak{R}$ is determined according to Δr iteration. After the calculation of image edge response and adaptive selection of threshold, the morphological composite filtering of sports training image edge is finally realized. The expression is as follows:

$$Q = \Delta r + \mathfrak{R} \cdot (B_{min} - B_{min}) \cdot p. \tag{12}$$

2.3.2. Edge Shape Response Calculation. In the process of image processing, Gaussian function has good filtering performance and is widely used in image filtering and image restoration. Generally, Gaussian operator $G(x', y', \ell)$ has the following expression:

$$G(x', y', \sigma') = \exp\left(\frac{\left(x'^2 + y'^2\right)}{\ell}\right). \tag{13}$$

The differential operator along the two axes can be obtained by differentiating the Gaussian operator along the x' and y' axes. The expressions are as follows:

$$G_{x'} = \ell \cdot \exp\left(\frac{\left(x'^2\right)}{\ell}\right), \tag{14}$$

$$G_{y'} = \ell \cdot \exp\left(\frac{\left(y'^2\right)}{\ell}\right). \tag{15}$$

Based on formulas (14) and (15), the edge morphology detection operator of sports training image is established:

$$G_{\theta'}(x', y') = G_{x'} \cos\phi + G_{y'} \sin\phi, \tag{16}$$

where ϕ represents the image edge angle, and $G_{x'}$ and $G_{y'}$ represent the linear operator. Convolute the input sports training image with formula (13) to obtain the edge response of the sports training image in the image edge angle direction, and the expression is:

$$G(x', y') \otimes I(x', y') = R_{x'}' \cos\phi + R_{y'}' \sin\phi, \tag{17}$$

where $\otimes$ is the convolution calculation, and there are $R_{x'}' = G_{x'} \otimes I(x', y')$ and $R_{y'}' = G_{y'} \otimes I(x', y')$. After solving the edge response of sports training images in different directions, the total image edge response can be obtained.

2.4. Improved Hough Transform Algorithm. If there is a straight line with intercept ϖ and slope σ in the plane coordinate system, the straight line equation is as follows:

$$Y = \sigma X + \varpi. \tag{18}$$

The following functional formula with intercept and slope as parameters is derived from the previously mentioned formula:

$$\varpi = Y - \sigma X. \tag{19}$$

According to the formula, based on the plane coordinate system, the formula describes Y straight line with intercept a and negative slope X.

Based on the previously mentioned two straight line equations, two key points are obtained: a point (X_1, Y_1) in the plane corresponds to a straight line $\varpi = Y_1 - \sigma X_1$ in the plane. The point cluster contained in the line $y = \mu_1 x + \xi_1$ in the plane corresponds to the line cluster in the plane. The line cluster is composed of lines composed of each slope and each intercept. All lines have a common intersection point (σ_1, ϖ_1).

Therefore, the polar coordinate equation is used to define the straight line in the plane; that is, the vertical distance D between the straight line and the origin and the included angle α between the normal line and the horizontal axis are used to determine any image point (X, Y) in the image space. The expression is as follows, in which the direction of the straight line is determined by the included angle α:

$$D = X \cos\alpha + Y \sin\alpha. \tag{20}$$

By using the linear equation and the expression of the perpendicular distance from the origin, the point (X_i, Y_i) in the image space is mapped to the accumulator $HT(\sigma_i, \varpi_i)$ in the Hough space, and all points in the image space where the two formulas are true are numerically added to the corresponding accumulator to realize the calculation of the Hough transform algorithm [13, 14]. If there is a line in the image, then the accumulator has a

local maximum. Compared with the preset threshold, the existence of the line is determined. When the threshold is greater than the local maximum, the straight line does not exist; otherwise, the straight line exists. Linear parameters can be obtained according to the peak value of parameter space.

Since the parameter space in the current Hough transform algorithm mostly adopts D and α parameters, which limits the detection range of the image to a certain extent, it is optimized. The specific process is described as follows.

Step 1. Preset global threshold τ and tolerance z.

Step 2. Selection of no. 1 seed point seed_1: if the size of a binary image is $m * n$ and the number of feature points is K, these feature points can be used to form no. 1 seed point set $\text{seed}_1' = \{(x_i, y_i) | i = 1, 2, \ldots, K\}$. In the no. 1 seed point set seed_1', select the feature points in order as the no. 1 seed point seed_1. If the current seed point has been processed, remove the feature point, and the no. 1 seed point is represented by the next feature point until the untreated seed point is obtained. Based on the no. 1 seed point, a set $\text{seed}_2' = \{(x_i, y_i) | i = 1, 2, \ldots, M\}$ storing the no. 2 seed point is constructed. In the initial stage of the set, the feature point contains a no. 1 seed point seed_1 less than seed_1'.

Step 3. Selection and solution of seed point seed_2 no. 2: in the same way, seed point $\text{seed}_2 = (x_2, y_2)$ no. 2 is obtained from seed point seed_2', and it is paired with seed point $\text{seed}_1 = (x_1, y_1)$ no. 1 to obtain a straight line in Figure 1. The length of the straight line to the origin is ρ, and the angle between the vertical line and the transverse axis is β. The calculation formula is shown as follows:

$$\beta = \tan^{-1} \frac{X_2 - X_1}{Y_2 - Y_1}, \quad \rho = \left(\frac{Y_2 - Y_1}{X_2 - X_1} \right) - \sin \beta. \tag{21}$$

Determination of straight line by feature point pair is shown in Figure 2.

Step 4. Accumulative Hough space: suppose S is zero initial accumulator which can get a straight line as shown in formula (3) according to the angle values between each characteristic point (X, Y) and the obtained image, as shown in Figure 2. If there is a difference between the origin and the length of the line q and ρ, and the range of variation of the difference is less than tolerance z, then the selected feature point is located on the line which is defined by the seed point pairs. Add 1 to the accumulator S, and then remove the feature point:

$$|\rho - q| \leq z. \tag{22}$$

Feature points and included angle determination line are shown in Figure 3.

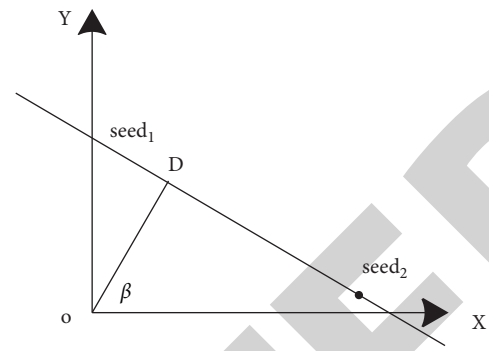

Figure 2: Determination of straight line by feature point pair.

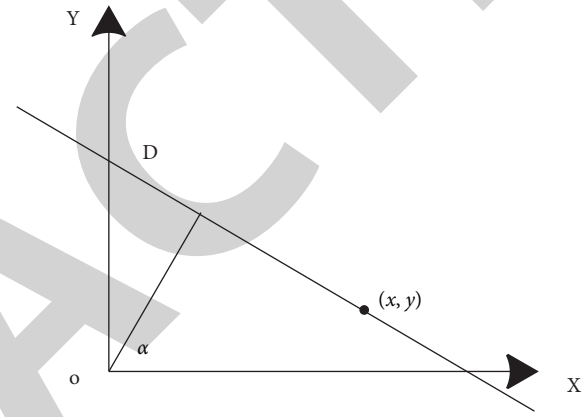

Figure 3: Feature points and included angle determination line.

Step 5. For the iteration operation step 4 of the next feature point, the iteration shall be terminated upon the completion of all the feature points.

Step 6. Retention of results: if the global threshold is greater than the value of the accumulator, then the straight line does not exist, jumping to step 8; otherwise, the straight line exists, and the detected linear parameters and D are calculated using formulas (4) and (5);

Step 7. Removal of feature points contained in a line: the detected feature points contained in a line are removed from the no.1 seed point set to reduce the calculation complexity.

Step 8. Seed point update no. 1 and no. 2: remove the selected seed points from the set of seed points, select the next feature point as the seed point, and perform the next iteration until the termination conditions are met.

2.5. Neighborhood Feature Extraction of Sports Training Action. Because of the difference of data acquisition equipment, the collected data may be in different coordinate system. Therefore, the following Frankfurt coordinate system is used to measure the human body contour coordinate unity. After unifying the coordinate, normalization of the scale is needed. Setting the distance between human contour

curves to 1 requires scaling the 3D contour lines. When the mannequin is filled and normalized, the maximum curvature of the surface of the human body needs to be set as the center of the sphere to draw a sphere for the radius, and the region contained in the sphere is the effective region [15].

Because there are obvious differences between the restored 3D facial model and the real human model, this paper mainly uses morphological feature points to judge. Among them, the following two factors shall be considered in the selection of feature points.

(1) The feature points are obvious and easily demarcated.

(2) It is relatively stable and does not change greatly with the expression or weight.

First, the nasal tip coordinates are obtained, the intervals between different coordinate points are analyzed, and the body profile is set perpendicular to the body and face. At the same time, in practical application, it is necessary to judge whether the vertex is in the set cutting plane. If it is, then the distance between the vertex and the plane is 0; otherwise, it is necessary to extract the section of the adjacent point as the vertex, and judge the distance between the vertex and the cutting plane with the help of the set threshold.

In the process of 3D model processing, all the neighborhood of feature points in the 3D model are set as discrete scale parameters by multiscale method, and the number of neighborhood is calculated to ensure the descriptive feature of the algorithm is effectively improved. In addition, the size of the neighborhood scale will also have a significant impact on the effectiveness of the whole algorithm. Among them, the size of neighborhood needs to be completed through the relevant prior knowledge and human–computer interaction [16].

Adaptive neighborhood needs to analyze the intrinsic characteristics of the image first, and then obtain the dynamic changes of different neighborhood points. Because of different composing feature structure, the neighborhood points of the image are different, but they all have multiscale. In the process of practical application, it is not necessary to consider the number of neighborhood points [17]. Among them, the first order neighborhood corresponding to feature point P_i is selected to participate in the calculation of the feature point, and the formula for calculating the difference in average curvature $\mathbb{N}$ between feature point q_j and feature point P_i is shown as follows:

$$\mathbb{N} = \left| \frac{k_1(q_j) + k_2(q_j) - k_1(P_i) + k_2(P_i)}{2} \right|. \tag{23}$$

In the previously mentioned formula, k_1 and k_2 represent the maximum curvature and the minimum curvature, respectively.

The covariance descriptor is constructed by the corresponding feature points of the sports training image, and the 3D human model is transformed into covariance descriptor sequence. Among them, the similarity problem of 3D human model can also be transformed into the similarity problem of different descriptor sequences. In the practical application, RM is used to represent the restored human model, M is used to represent the real human model, and the similarity between the restored human model and the real human model is used to describe the similarity between different descriptors. The following measures are mainly based on logarithmic Euclidean Riemann, and then, the neighborhood features are established. The specific calculation formula is as follows:

$$\Theta(RM, M) = \sum_{i=1}^{n} \left(\left\| In\left(RM_{P_i}\right) + In\left(M_{P_i}\right) \right\| \right). \tag{24}$$

In the previously mentioned formula, RM_{P_i} represents the feature descriptor of the restored manikin feature point P_i; M_{P_i} represents the feature descriptor of the feature point P_i corresponding to the real manikin; δ represents the logarithm of the matrix.

The expression formula of geometric feature variance descriptor of feature point P_i is

$$S = \sum_{i=1}^{N} \left(F_{P_i} - \bar{\partial} \right) \left(F_{P_i} + \bar{\partial} \right). \tag{25}$$

In the previously mentioned formula, $\bar{\partial}$ represents the average value of geometric feature vector corresponding to feature points of 3D manikin; N represents the number of nodes participating in neighborhood calculation; S stands for symmetric matrix.

3. Simulation Test Design and Result Analysis

Experiments on sports training images are carried out under the environment of Intel Core 2 Duo cpu2.33ghz/2gb, Windows Vista Business and MATLAB 2020. The multimodal human motion recognition method based on depth camera proposed in [2], image motion recognition method based on pose feature proposed in [4], and the proposed method are tested, respectively. Compare the time taken by the three methods to identify the local changeable features of the image. The test results are shown in Figure 4.

By analyzing Figure 4, it can be seen that the recognition time of the proposed method is less than that of the multimodal human motion recognition method based on depth camera proposed in [2] and the image motion recognition method based on attitude feature proposed in [4]. Because the local polytropic feature recognition method of a specific sports training image reduces the dimension of the specific sports training image by adjusting the interclass discrete matrix and the intraclass discrete matrix before identifying the local polytropic feature of the image, removes the useless information and data in the specific sports training image, and reduces the amount of data to be calculated for identifying the local polytropic feature of the image, it shortens the time used to identify the local changeable features of specific sports training images.

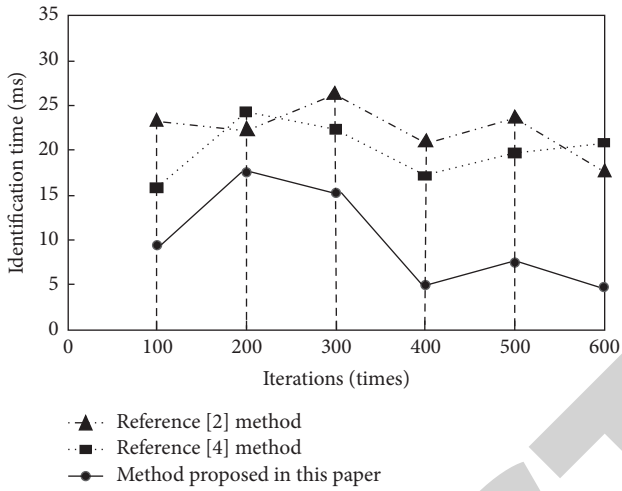

Figure 4: Identification time of different methods.

The multimodal human motion recognition method based on depth camera proposed in [2] and the image motion recognition method based on pose feature proposed in [4] do not remove the redundant and useless information in specific sports training images and spend more time calculating a large amount of data. Through the previously mentioned analysis, it can be seen that the local changeable feature recognition method of specific sports training image can realize the recognition of local changeable features in a short time, and it is verified that the recognition efficiency of the local changeable feature recognition method of specific sports training image is high.

Based on the previously mentioned experimental results, the multimodal human motion recognition method based on depth camera proposed in [2] and the image motion recognition method based on pose features proposed in [4] are used as the control methods. The denoising effect of the proposed method is compared with that of the proposed method. The test results are shown in Figures 5–8.

According to the experimental results in Figures 6–8, the proposed method has better denoising effect on the image. Under the comparison of various methods, the multimodal human motion recognition method based on depth camera proposed in [2] and the image motion recognition method based on pose features proposed in [4] still have noise in the processed sports training image, and the incomplete noise removal will directly affect the accuracy of image recognition. Therefore, the experimental results show that the application effect of the proposed method is better for the application of image noise removal and image quality improvement.

Taking F1 value as an index to measure the performance of sports training image recognition, if you want to show that the method has strong performance, the higher F1 value should be. A comparative experiment is designed. The multimodal human motion recognition method based on depth camera proposed in [2] and the image motion recognition method based on posture features proposed in [4] are selected as the comparison methods of this method. The F1 value results of sports training image recognition of the three methods under different sample numbers are described in Figure 9.

Analysis of Figure 9 shows that the F1 value of the method in this paper is always higher than that of the other two methods, and when the number of samples continues to increase, the F1 value shows an upward trend, and the method performance is gradually improved. The F1 value of the multimodal human motion recognition method based on depth camera proposed in [2] is close to the method in this paper, but when the number of samples increases to 300–500, the F1 value shows a downward trend and the performance stability of the method is poor. The F1 value of the image motion recognition method based on attitude features proposed in [4] is greatly affected by the number of samples, fluctuates violently, and is always at the lowest value. Compared with these data, this method has excellent sports training image recognition performance and good stability.

Test the convergence characteristics of sports training image recognition method, and the test results are shown in Figure 10.

According to Figure 10, the convergence of the proposed method is better than the depth camera based multimodal human motion recognition method proposed in [2] and the image motion recognition method based on attitude features proposed in [4], and the convergence characteristics of the proposed method are relatively stable. The SDN architecture is used to closely combine the image data transmission and interaction process, and optimizing the centralization of image processing can extract the global features of the image, so the algorithm can still obtain the best convergence characteristics when the image resolution is reduced, so the convergence characteristics of the algorithm are good.

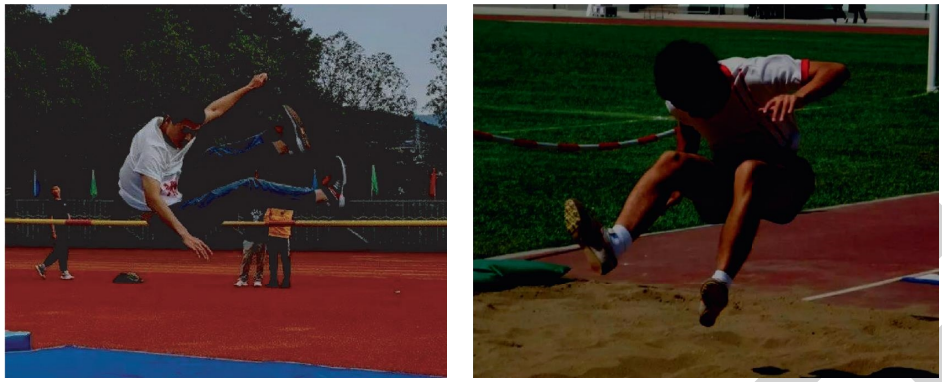

(a) (b)

Figure 5: Experimental sample image. (a) Image sample 1. (b) Image sample 2.

(a) (b)

Figure 6: The method proposed in this paper. (a) Image sample 1. (b) Image sample 2.

(a) (b)

Figure 7: Multimodal human motion recognition method based on depth camera. (a) Image sample 1. (b) Image sample 2.

(a) (b)

Figure 8: Image action recognition method based on attitude features. (a) Image sample 1. (b) Image sample 2.

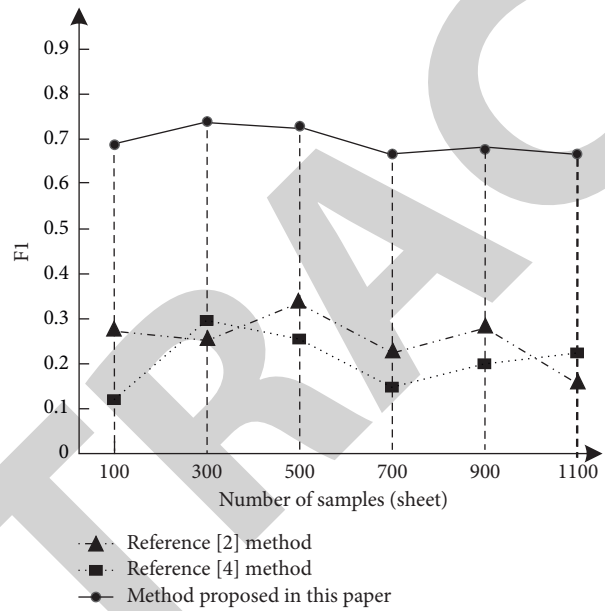

Figure 9: Comparison of F1 value results of sports training image recognition.

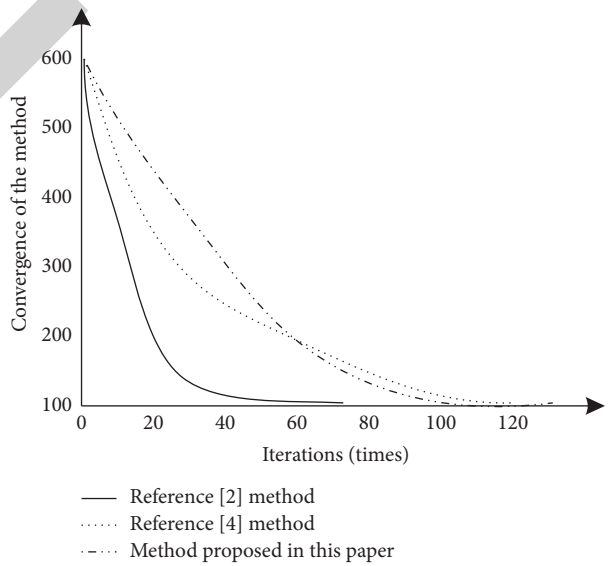

Figure 10: Convergence test results of different methods.

Hindawi
Journal of Mathematics
Volume 2024, Article ID 9782496, 1 page
https://doi.org/10.1155/2024/9782496

Retraction

Retracted: Research on Fast Compensation Algorithm for Interframe Motion of Multimedia Video Based on Manhattan Distance

Journal of Mathematics

Received 23 January 2024; Accepted 23 January 2024; Published 24 January 2024

This article has been retracted by Hindawi following an investigation undertaken by the publisher [1]. This investigation has uncovered evidence of one or more of the following indicators of systematic manipulation of the publication process:

(1) Discrepancies in scope

(2) Discrepancies in the description of the research reported

(3) Discrepancies between the availability of data and the research described

(4) Inappropriate citations

(5) Incoherent, meaningless and/or irrelevant content included in the article

(6) Manipulated or compromised peer review

The presence of these indicators undermines our confidence in the integrity of the article's content and we cannot, therefore, vouch for its reliability. Please note that this notice is intended solely to alert readers that the content of this article is unreliable. We have not investigated whether authors were aware of or involved in the systematic manipulation of the publication process.

Wiley and Hindawi regrets that the usual quality checks did not identify these issues before publication and have since put additional measures in place to safeguard research integrity.

We wish to credit our own Research Integrity and Research Publishing teams and anonymous and named external researchers and research integrity experts for contributing to this investigation.

The corresponding author, as the representative of all authors, has been given the opportunity to register their agreement or disagreement to this retraction. We have kept a record of any response received.

References

[1] N. Li and S. Wan, "Research on Fast Compensation Algorithm for Interframe Motion of Multimedia Video Based on Manhattan Distance," *Journal of Mathematics*, vol. 2022, Article ID 3468475, 10 pages, 2022.

Hindawi
Journal of Mathematics
Volume 2022, Article ID 3468475, 10 pages
https://doi.org/10.1155/2022/3468475

Research Article

Research on Fast Compensation Algorithm for Interframe Motion of Multimedia Video Based on Manhattan Distance

Ning Li and Shuai Wan

School of Electronics and Information, Northwestern Polytechnical University, Xi'an, Shaanxi 710072, China

Correspondence should be addressed to Ning Li; ning_li@mail.nwpu.edu.cn

Received 18 November 2021; Revised 6 December 2021; Accepted 10 December 2021; Published 5 January 2022

Academic Editor: Naeem Jan

To improve the video quality, aiming at the problems of low peak signal-to-noise ratio, poor visual effect, and low bit rate of traditional methods, this paper proposes a fast compensation algorithm for the interframe motion of multimedia video based on Manhattan distance. The absolute median difference based on wavelet transform is used to estimate the multimedia video noise. According to the Gaussian noise variance estimation result, the active noise mixing forensics algorithm is used to preprocess the original video for noise mixing, and the fuzzy C-means clustering method is used to smoothly process the noisy multimedia video and obtain significant information from the multimedia video. The block-based motion idea is to divide each frame of the video sequence into nonoverlapping macroblocks, find the best position of the block corresponding to the current frame in the reference frame according to the specific search range and specific rules, and obtain the relative Manhattan distance between the current frame and the background of multimedia video using the Manhattan distance calculation formula. Then, the motion between the multimedia video frames is compensated. The experimental results show that the algorithm in this paper has a high peak signal-to-noise ratio and a high bit rate, which effectively improves the visual effect of the video.

1. Introduction

In recent years, with the rapid development of multimedia and network technology, video, image, computer vision, multimedia database, and computer network technology are increasingly integrated, covering all aspects of the national economy and social life. Video processing, video coding, and video communication, which are in the core position, have become the frontier fields and hot topics of information and communication engineering [1]. Among them, with the gradual penetration of multimedia, the boundaries among videos, graphics, computer vision, multimedia database, and computer network become blurred, making video processing a multi-disciplinary research field [2]. At present, video processing has been at the core of multimedia technology [3]. At the same time, with the rapid development of video technology, the research of motion compensation between multimedia video frames is very important and necessary. Therefore, video interframe motion compensation plays an important role in many technologies included in video processing [4].

As one of the classic problems in the field of image and video processing, video interframe motion compensation is widely used in video frame rate improvement, slow video production, and virtual view synthesis. At present, the commonly used interframe motion compensation method of the video image is to intensively match the input image pairs based on the optical flow field estimation algorithm and interpolate the input image pixel by pixel using the obtained dense matching information to synthesize the intermediate frame image. As the optical flow field estimation itself is an ill-conditioned problem, especially in the case of weak image texture or occlusion, the effect is poor, and the peak signal-to-noise ratio is low. The existing methods often face difficulties in practical application. In recent years, the method based on deep learning has attracted extensive attention and has achieved remarkable results in many computer vision problems, such as target

classification, face recognition, and so on. However, the key to the success of this method is to use a large number of training samples to train the appropriate depth neural network, which has the problems of long compensation time and low bit rate. In addition, reference [5] proposes a deep convolution neural network algorithm to realize image interframe compensation. Firstly, the image interframe compensation model is constructed according to the deep convolution neural network. Secondly, the image features of the compensation model are extracted by sparse self-coding and linear decoding. Then, the image features are mapped by a multilayer convolution neural network. Finally, the image frame resolution is reconstructed according to the sparse algorithm to compensate for the image frame. The experimental results show that the image frame compensation method based on a deep convolution neural network can effectively solve the problem of image loss, however, the bit rate is low and the application effect is poor.

To improve the peak signal-to-noise ratio, the visual effect, and the bit rate of multimedia video images, a fast interframe motion compensation algorithm based on the Manhattan distance is proposed in this paper. Section 2 of this paper presents the processing of the multimedia video. In Section 3, the multimedia video interframe motion fast compensation algorithm is presented. Section 4 proposes the simulation experiments that verify the strength of our method, and the conclusion is given in Section 5.

2. Multimedia Video Preprocessing

2.1. Gaussian Noise Variance Estimation. For the noise level mixed in the multimedia video, this paper adopts the variance to measure. Use the absolute median difference based on the wavelet transform [6] to estimate the Gaussian noise standard deviation of a noisy multimedia video A:

$$\widehat{\partial} = \mathrm{MAD}(x_a) * \left(1 - \frac{S_y}{S}\right). \tag{1}$$

x_a represents the first-level fine-scale wavelet coefficients of the multimedia video A. The MAD operator is defined as follows:

$$\mathrm{MAD}(x_a) = \frac{\mathrm{Med}(E_1)}{K_w W_1}. \tag{2}$$

$\mathrm{Med}(\cdot)$ represents the median of the input vector. The fast wavelet transform ensures the high execution rate of the MAD operator, making it suitable for the batch estimation of the Gaussian noise variance of video frames [7]. The specific Gaussian noise variance estimation formula is as follows:

$$\sigma_a^2 = \frac{I_r \sqrt{\left(R_r/\widehat{\partial}\right)^2}}{\omega_s}. \tag{3}$$

I_r represents the high frequency information of the video. R_r represents the low frequency information of the video. ω_s represents the amount of noise in the video.

2.2. Active Noise Mixing Forensics Algorithm. According to the results of the Gaussian noise variance estimation, this paper proposes an active noise mixing forensics algorithm. Firstly, preprocess the original video for noise mixing, i.e., use a pseudo-random sequence to generate Gaussian noise with a standard deviation of s^2 and add it to each pixel of the video sequence. Then, the processed video will be tampered with by Frame Rate Up-Conversion (MC-FRUC) to generate an up-converted video, and attacks such as denoising and compression may also be implemented. Finally, analyze the Gaussian noise distribution of the suspicious video to identify whether there is MC-FRUC tampering. The following specifically introduces the core of the proposed algorithm: noise mixing, forensics, and detection.

Assume that the original video sequence is composed of K video frames of size $n \times m$. The pseudo-random sequence can be used to generate 0-mean Gaussian noise with a standard deviation of s^2, and the pixels of the original video sequence are added as

$$h_k(i, j) = e_k(i, j) + l_k(i, j). \tag{4}$$

$e_k(i, j)$ and $h_k(i, j)$, respectively, represent the original frame of the k^{th} frame and the pixel value of the noisy frame at position (i, j). $l_k(i, j)$ represents the value of the mixed Gaussian noise. When the original video sequence encounters MC-FRUC tampering, the combination of the two original frames r_{k-1} and r_{k+1} must insert the current frame $\widehat{r_k}$, and formula (4) is derived to obtain

$$\widehat{h_k}(i, j) = \widehat{e_k}(i, j) + \widehat{l_k}(i, j). \tag{5}$$

Of which,

$$\widehat{e_k}(i, j) = \prod_{i=1}^{N} \prod_{j=1}^{N} P_{ij}(1 - P_\alpha), \tag{6}$$

$$\widehat{l_k}(i, j) = \prod_{i=1}^{N} \prod_{j=1}^{N} \left(U_{ij} \times \ln\left(1 - P_\beta\right)\right). \tag{7}$$

P_{ij} represents the adjacent frames. P_α and P_β represent the threshold. U_{ij} represents the corner points of the video frame.

It is observed from formula (7) that the interpolated frame noise term $\widehat{l_k}$ is obtained by the weighted summation of the noise term l_{k-1} of the $k-1^{\text{th}}$ frame and the noise term l_{k+1} of the $k+1^{\text{th}}$ frame along the motion trajectory. Since the components of the noise term are independent of each other, the variance of both ends of formula (5) can be obtained at the same time.

$$\sigma_k^2 = W\left[\widehat{l_k}(i, j)\right] = W\left[C_{k,1}^{(i,j)}, C_{k,2}^{(i,j)}\right]. \tag{8}$$

Since each pixel in h_{k-1} and h_{k+1} is premixed with 0-mean Gaussian noise with a standard deviation of s^2, it can be seen that

$$s^2 = W_{k-1}\left[C_{k,1}^{(i,j)}, C_{k,2}^{(i,j)}\right] \times W_{k+1}\left[C_{k,1}^{(i,j)}, C_{k,2}^{(i,j)}\right]. \tag{9}$$

Substituting formula (9) into formula (8), we can get

$$\sigma_k^2 = \frac{s^2}{2}. \tag{10}$$

According to formula (10), it can be known that the variance σ_k^2 of the interpolated frame $\widehat{I}_k$ is half of the variance s^2 of the mixed noise. MC-FRUC tampering will periodically insert the interpolated frames. Therefore, the noise standard deviation of the fake video will show periodic sudden changes, as shown in Figure 1 (the unforged video is the original 30 fps video, and the fake video is the 15 fps original video up to 30 fps). The standard deviation is premixed into the video Gaussian noise of 5. Using the MAD method to estimate the noise standard deviation of the unforged and forged videos, it can be seen that the noise standard deviation curve of the unforged video changes smoothly and slowly, while the noise standard deviation curve of the forged video changes rapidly and periodically. It can be seen that the periodicity of the noise standard deviation curve can be used as a strong piece of evidence to discriminate the tampering of MC-FRUC.

2.3. Smooth Processing of Noisy Multimedia Video. To improve the accuracy of motion compensation between multimedia video frames, the fuzzy C-means clustering method [8] is used to smoothly process noisy multimedia videos. Use the gray-scale cluster membership matrix to transform the membership tensor in the noisy multimedia video. The detailed process is as follows:

Step1: The determination of the iteration error, the maximum number of iterations, and the number of clustering categories is followed by the obtaining of a segmented initial membership degree θ_z, for which the calculation formula is as follows:

$$\theta_z = \sum_{j=1}^{N} \frac{U_j - P_j}{1 - P_j}. \tag{11}$$

U_j represents the fuzzy compactness function of the global interval value. P_j represents the fuzzy mean value of the local interval.

Step 2: Calculate the label value of the noisy frame in the noisy multimedia video according to the degree of membership θ_z.

$$G(\theta_z) = Q_z - \sum_{j=1}^{N} u_j. \tag{12}$$

Step 3: Perform step t iterative processing based on the tag value, and update the membership tag value.

Step 4: For the new label value of the membership degree, mark according to the principle of maximum membership degree.

Step 5: Obtain the iteration error according to the maximum membership degree of the mark. The calculation formula is as follows:

$$\varepsilon^2 = \left|\theta_{z(t+1)} - \theta_{zt}\right|^2. \tag{13}$$

$\theta_{z(t+1)}$ represents the maximum membership error produced by the $t + 1^{\text{th}}$ iteration. θ_{zt} represents the maximum membership error produced by the t^{th} iteration.

On this basis, the obtained gray-scale cluster membership degree is converted into the membership degree tensor corresponding to the multimedia video. After the membership degree tensor is subjected to mean filtering processing, the label value is obtained, and the smooth processing result of the noisy multimedia video can be realized. Figure 2 is a flow chart of the smoothing processing of noisy multimedia videos.

2.4. Extraction of Significant Information from Multimedia Video. It can be seen from the characteristics of the human visual system that the human eye usually notices first the target or the area of interest in the scene, while the remaining noninteresting parts or repetitive content are easily overlooked. The saliency map model is a selective attention model that simulates the visual attention mechanism of organisms. In this paper, the residual spectrum method is used to extract the visual saliency map of the multimedia video [9], which can be expressed as follows:

$$X(d) = Y(d) - Z(d). \tag{14}$$

$Y(d)$ represents the original video logarithmic amplitude spectrum. $Z(d)$ represents the general logarithmic amplitude spectrum after mean filtering. $X(d)$ represents the remaining spectrum. The following is a detailed analysis of the significant information extraction steps of multimedia videos:

Step 1: Perform a two-dimensional Fourier transform on the multimedia video image.

Step 2: Obtain the amplitude spectrum by calculating the absolute value of the transformed video image. Also, calculate the phase spectrum.

Step 3: Obtain the difference amplitude spectrum by subtracting the filtered amplitude spectrum from the amplitude spectrum of the original video image.

Step 4: Reconstruct the video image by two-dimensional inverse Fourier transform using the difference amplitude spectrum and phase spectrum.

Step 5: Obtain the saliency map of the video image by performing the Gaussian filtering and normalization on the reconstructed video image.

Compared with the high-frequency information of the video image, the saliency map of the video image can not only reflect the details of the video image but also extract the

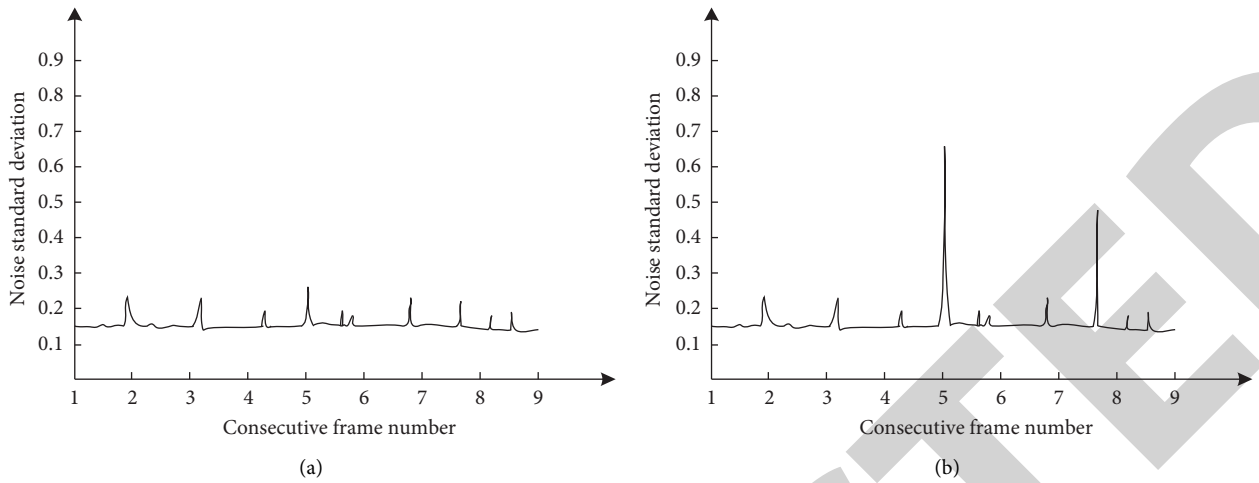

Figure 1: Standard deviation spectrum of unforged noise and forged noise. (a) Unforged noise. (b) Forged noise.

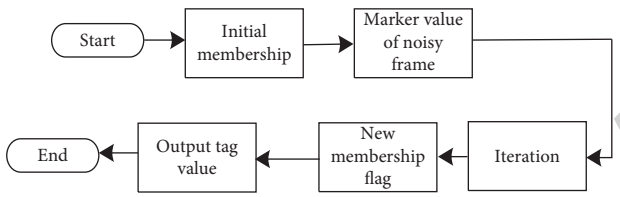

Figure 2: Flow chart of the smoothing processing of a noisy multimedia video.

areas that can attract the attention of the human eye. Therefore, using the saliency map of the video image to represent the details of the video image is more in line with the visual characteristics of the human eye.

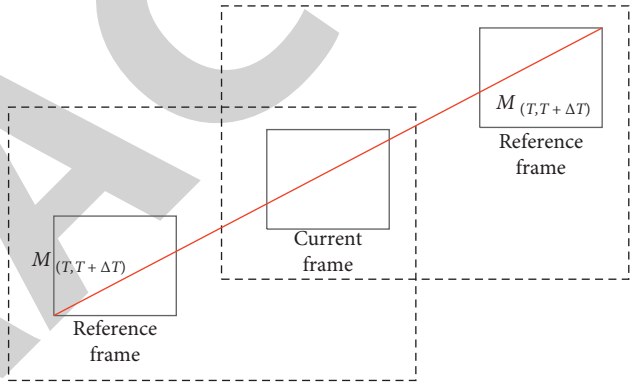

Figure 3: Schematic diagram of motion estimation.

3. Multimedia Video Interframe Motion Fast Compensation Algorithm

In the multimedia video preprocessing link, the smooth processing of noisy multimedia video is realized, and the significant information of multimedia video is obtained, which provides a stable basic condition for the fast compensation of multimedia video interframe motion. Next, the fast compensation processing of multimedia video interframe motion will be carried out.

3.1. Multimedia Video Motion Estimation. Extracting object motion information from video images is called motion estimation. The basic principle of general motion estimation is as follows: assume that the video frame $g(x, y)$ at time T represents the current frame, and the video frame $g'(x, y)$ at time T' represents the reference frame. When the reference frame is the previous frame of the current frame, i.e., when $T' = T + \Delta T$, it is called backward motion estimation [10]. When the best position of the block in the current frame $g(x, y)$ is searched in the reference frame $g'(x, y)$, the corresponding motion field $M_{(T,T+\Delta T)}$ can be obtained to obtain the motion vector of the current frame as shown in Figure 3.

Motion estimation generally adopts block-based motion estimation. The basic idea of block-based motion is to divide each frame of the video sequence into nonoverlapping macroblocks and find the best position of the block corresponding to the current frame in the reference frame according to the specific search range and specific rules, i.e., find the matching block. The relative displacement between the matching block and the current block is the motion vector [11].

The whole implementation process of block matching motion estimation is to find the most matched motion vector, and it reduces the time redundancy of motion compensation by eliminating the time correlation between the current frame and the reference frame. The basic principle of block matching motion estimation is to take the prediction unit as the basic unit, find the corresponding prediction unit in the reference frame for each prediction unit of the current frame in a certain order, and determine the relative displacement between them using the found prediction unit, i.e., the search of the motion vector is completed. The importance of the motion vector cannot be ignored. The more accurate the motion vector prediction, the better the effect of motion estimation.

The ultimate goal of motion estimation is to transmit the motion vector and prediction error to the video decoding end. Motion compensation is to subtract the prediction unit from the current prediction unit based on motion estimation to obtain the residual unit. Such residual unit contains little information. Carry out quantization transformation and entropy coding to obtain the code stream. Therefore, the accuracy of motion estimation directly affects the effect of fast motion compensation between multimedia video frames [12].

Figure 4 shows the basic process of motion estimation. In the figure, time T corresponds to the g^{th} frame image, and time $T-1$ corresponds to the $g-1^{\text{th}}$ frame image. In the $g-1$ frame, find a part that most closely matches the g frame. It is called searching for the best block, and it is judged that the position of the matching block in the $g-1$ frame is the previous position of the block in the g frame, and the displacement of this movement is called the motion vector.

3.2. Realization of Fast Motion Compensation between Multimedia Video Frames

3.2.1. Manhattan Distance. Manhattan distance refers to the distance between the two points strictly based on a horizontal or vertical path, rather than a diagonal line or a distance similar to a straight broken line [13]. It is a simple superposition of the distance between the horizontal and vertical components.

M-dimensional space is a set of points. Each point e of it can be expressed as $\{e(1), e(2), \ldots, e(n)\}$, where $e(i)$ is called the i^{th} coordinate of e, and $i = 1, 2, \ldots, n$. The Manhattan distance between two points $P = \{p(1), p(2), \ldots, p(n)\}$ and $Q = \{q(1), q(2), \ldots, q(n)\}$ can be expressed as

$$D_{pq} = \sum_{i=1}^{N} \|p(i) - q(i)\|^2. \tag{15}$$

The Manhattan distance is applied to the video image. The background image is also the background template. The Manhattan distance is the sum of the Manhattan distances of each pixel:

$$\text{MDB} = \sum_{i=1}^{n} \sum_{j=1}^{n} P_{ij}. \tag{16}$$

The Manhattan distance between the background template and the current frame (MDFB) is the sum of the relative distances between the background image and the corresponding pixels of the current frame:

$$\text{MDFB} = \sum_{i=1}^{n} \sum_{j=1}^{n} P_{ij} - Q_{ij}. \tag{17}$$

The calculation formula of the relative Manhattan distance RMD between the background template and the current frame to the background is,

$$\text{RMD} = \frac{\text{MDB}}{\text{MDFB}}. \tag{18}$$

In the above formula, MDB represents the Manhattan distance of the background template itself. MDFB represents the Manhattan distance between the background template and the current frame. RMD represents the relative Manhattan distance of the current frame to the background.

3.2.2. Fast Compensation of Motion between Multimedia Video Frames. The Manhattan distance calculation formula is used to obtain the relative Manhattan distance between the current frame of the multimedia video and the background, and the motion between the multimedia video frames is compensated.

(1) Basic Idea. Firstly, judge whether the current frame is a background frame or a target frame according to RMD. Secondly, if it is a background frame, i.e., RMD < TH1, then the current frame is used as the background image. Thirdly, if the change is small, i.e., TH1 ≤ RMD ≤ TH2, the median operation is performed with the adjacent four frame images. The fourth point is that if TH2 ≤ RMD ≤ TH3 is satisfied, then the target frame is subjected to the median operation. The median operation is carried out with the background frame, and the final result is taken as the new background frame. The fifth point is that if there is a large difference, i.e., RMD ≥ TH3, then the target frame is judged as the object starts moving from rest, and the current frame is used as the background frame. The specific implementation formulas are shown in formulas (19) and (20).

$$\begin{cases} \text{RMD} < \text{TH1}, \\ \text{TH1} \le \text{RMD} \le \text{TH2}, \\ \text{TH2} \le \text{RMD} \le \text{TH3}, \\ \text{RMD} \ge \text{TH3}, \end{cases} \tag{19}$$

$$V(t) = \{v(t), v(t-1), v(t-2), v(t-3), v(t-4)\}. \tag{20}$$

In the above formula, $V(t)$ represents the background model at time t. $v(t)$ represents the current target frame. $v(t-1)$, $v(t-2)$, $v(t-3)$, and $v(t-4)$ are the first four frames immediately adjacent to $v(t)$.

Since the motion of different pixels in the current multimedia video is related to the motion of the candidate block, the motion compensation prediction in the merge mode is not accurate enough. To make full use of the motion correlation between pixels as the distance changes, this section proposes a weighted prediction based on Manhattan distance as an additional candidate for the merge mode [14]. The specific steps are as follows:

(i) Detecting neighbor merge candidate blocks: firstly, the neighbor merge candidate block is detected. Figure 5 is a schematic diagram of the position of the merge mode candidate block.

As shown in the position of the candidate block in the merge mode in Figure 5, the candidate blocks in different positions are detected in the order of α_1, α_2,

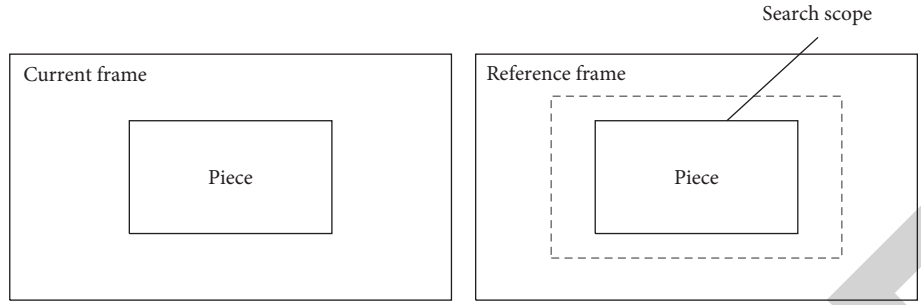

Figure 4: Schematic diagram of motion estimation.

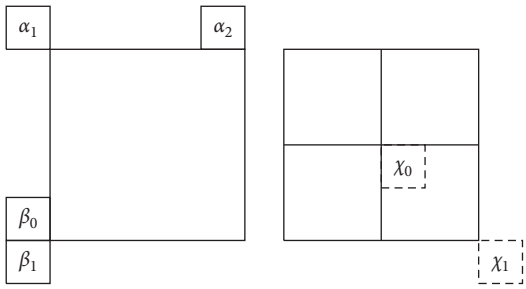

Figure 5: Schematic diagram of the position of candidate blocks in the merge mode.

β_0, χ_0, β_1, and χ_1, and the corresponding motion vector is generated. If the number of generated motion vectors is less than 2, then the algorithm of this paper is not executed. Otherwise, the algorithm of this paper is executed.

(ii) Motion compensation: use the motion vector generated in Step 1 to perform motion compensation prediction to obtain the corresponding prediction block, which is denoted as $P_k(x, y)$. In the algorithm proposed in this paper, a macroblock with a size of $16 * 16$ pixels is used for motion compensation. Each macro block in the current frame adopts the minimum SAD (Sum of Absolute Differences) criterion, and searches in the previous frame to find the macro block corresponding to the current macro block with the smallest SAD value. This macro block corresponds to the previous frame. The macro block with the most matching current macro block is called the reference macro block, and its definition is shown in formula (21).

$$\mathrm{SAD} = \sqrt{\left|\varpi_{ij} - \vartheta_{ij}\right|}. \tag{21}$$

ϖ_{ij} represents the gray value of each pixel in the current macro block, and ϑ_{ij} represents the gray value of each pixel in the reference macro block. Using the motion compensation technology based on the minimum SAD, in the fixed search range of the previous frame, the most matching reference macroblock corresponding to the current macroblock can be found. The current macroblock and the reference macroblock constitute the motion trajectory of the current macroblock in the time domain, and the current macroblock can be filtered in the time domain along the motion trajectory.

To overcome the "tailing" phenomenon of the fast-moving objects easily caused by pure time-domain filtering, motion intensity detection technology is adopted. For objects with different motion intensities, the filter adopts different filtering intensities, which effectively avoids the phenomenon of "tailing" of fast-moving objects. Since the algorithm is processed with a macro block as the smallest unit in the algorithm, a motion intensity detection operator τ is defined to detect the motion intensity of the current macro block on the motion trajectory. The definition of τ is shown in formula (22).

$$\tau = \sum_{i=1}^{n}\sum_{j=1}^{n}\varpi_{ij} - \sum_{i=1}^{n}\sum_{j=1}^{n}\vartheta_{ij}. \tag{22}$$

By the test of a large number of motion sequences, two empirical values for measuring the motion intensity of the macroblock are determined, namely the high and low thresholds h_1 and h_2 of the motion intensity of the macroblock. By detecting the operator τ and the two high and low thresholds h_1 and h_2 determined by experiments, the motion intensity of the current macroblock on the motion trajectory can be determined [15].

The motion intensity of each macro block is defined as three cases. If the value of the detection operator τ of the current macro block is less than the low threshold value h_1, it indicates that the current macro block is a steady and slow motion on the motion trajectory with low motion strength. In this case, the filter intensity of the filter can be set higher, which can effectively remove noise, and at the same time, because of the low motion intensity of the current block, it will not cause the phenomenon of "tailing." When the value of the detection operator τ is higher than the high threshold value h_2, it indicates that the current macroblock is violently moving on the motion trajectory and has a strong motion intensity. At this time, the filter strength should be adjusted to a lower level so that the filtered macroblock keeps the information of the current macroblock as much as possible to avoid the "tailing" phenomenon. When the value of the detection operator τ is between h_1 and h_2, it indicates that the motion intensity of the current macroblock is in an intermediate state, and the filtering intensity of the filter will also be adjusted to an intermediate level. The filter strength

of the filter is adjusted by the corresponding weight λ. The definition of λ is as shown in formula (23).

$$\begin{cases} \lambda = 0.35, & \tau \le h_1, \\ \lambda = 0.6, & h_1 < \tau < h_2, \\ \lambda = 0.8, & h_1 \le \tau. \end{cases} \tag{23}$$

According to the motion intensity of the macroblock, the rapid compensation of the motion between the multimedia video frames can be realized by adjusting the weight of the filter intensity.

4. Simulation Experiment

To verify the effectiveness of the fast interframe motion compensation algorithm of the multimedia video based on the Manhattan distance proposed in this paper, the compensation algorithm based on depth learning and the compensation algorithm based on depth convolution neural network are used as comparison methods, and the application effects of different methods are judged according to the experimental results.

4.1. Experimental Platform and Parameter Settings. The working platform parameters of this experiment are as follows: the processor is Intel Pentium(R) Dual-core CPU E6500 2.93 GHz, the memory is 2 GB, and the operating system is Windows XP Professional. In the experiment, the JVT-released H.264 standard JM12.4 version of the official codec software was compiled and implemented on the Visual C++ software platform, and the JCT-VC-released HEVC standard HM9.0 version test model was compiled and implemented on the Visual Studio 2008 software platform. In the experiment, four official test sequences with different characteristics were used to complete the comparative experiment, as shown in Table 1.

To comprehensively compare the performance differences between various methods, four groups of the test video sequences with different motion amplitudes, motion directions, and numbers, as well as the size of the moving objects are selected as the experimental data objects. These four groups of video sequences have different objects and different motion modes. Sequence 1 is mainly vertical movement, and the moving objects are small, and also, the range of motion is small. Sequence 2 mainly shows horizontal movement, however, the moving objects are larger and the movement range is small, especially the movement of large cargo ships. Sequence 3 mainly reflects the movement of the coast guard motorboats and yachts in the horizontal direction, and the motorboats have a larger range of motion, while the yacht movement range is small. Sequence 4 is mainly reflected in the horizontal direction of the car movement, and the movement range is relatively large. At the same time, because of the lack of vertical motion changes in the standard video sequence, this article took two pictures. The characteristics of these two video sequences are that there are different amplitudes of motion in the vertical direction in the image. Self-portrait 2 is larger than self-portrait 1.

For the above four test sequences, the compensation effects of different methods are counted and compared. The experimental results are shown below.

4.2. Analysis of Experimental Results

4.2.1. Peak Signal-to-Noise Ratio PSNR. PSNR is an objective evaluation method that can reflect the actual visual effect of the video in general. The calculation process is relatively simple, and it is widely used in the fields of video coding and image processing. The calculation formula of PSNR is as follows:

$$\mathrm{PSNR} = 10\lg\frac{(2^n - 1)^2}{\mathrm{MSE}}. \tag{24}$$

MSE (Mean Square Error) is the mean square error between the original video image and the processed video image. The unit of PSNR is expressed in decibels (dB). Under normal circumstances, the greater the PSNR value, the closer the quality of the processed video image will be to the original video image. In some special cases, the PSNR value is too large and the actual effect of the video image is poor. The peak signal-to-noise ratio comparison results of different methods are shown in Table 2.

By analyzing the data in Table 2, it can be seen that the peak signal-to-noise ratio of the video image is higher than that of the depth learning algorithm and depth convolution neural network algorithm after using this method to compensate the application between video frames in different test sequences. Although the peak signal-to-noise ratio of the depth convolution neural network algorithm is better than that of the depth learning algorithm, it still has a certain distance from this algorithm. Therefore, after using this algorithm to compensate for the motion between the video frames, the quality of the video image has been effectively improved, which shows that this method has a better application effect.

4.2.2. Visual Effect Evaluation. Firstly, evaluate the results of the interframe motion compensation of the video image by the algorithm in this paper, the deep learning algorithm, and the deep convolutional neural network algorithm from the perspective of visual effects. Figure 6 shows the effect of the three algorithms for motion compensation on the representative images of test sequence 1 to generate interpolated frames.

According to Figure 6, it can be seen that the three algorithms perform motion interpolation on the input video image well. Note that the deep convolutional neural network algorithm has a slight loss in image details. Although the deep learning algorithm maintains more video image details than the deep convolutional neural network algorithm, there are some errors in interpolation. Compared with the two traditional algorithms, the visual effect of the algorithm in this paper is better. There is no loss of details, and the clarity is higher. From the visual effect evaluation results, the

Table 1: Characteristic parameters of comparative experimental test sequence.

Test sequence	Resolution	Total number of frames	Video characteristics		
			Details	Color	Movement
1	352 × 288	300	Average	Average	Small
2	352 × 288	500	Average	Average	Small
3	416 × 240	400	Less	Average	More
4	416 × 240	500	Less	Average	Average

Table 2: Peak signal-to-noise ratio.

Test sequence	Peak signal-to-noise ratio/dB		
	The algorithm of this article	Deep learning algorithm	Deep convolutional neural network algorithm
1	12.08	9.56	10.21
2	25.47	21.37	23.67
3	51.39	46.25	47.52
4	9.70	6.94	7.26

(a) (b) (c)

Figure 6: Visual effect evaluation. (a) Deep learning algorithm. (b) Deep convolutional neural network algorithm. (c) The algorithm of this paper.

algorithm in this paper can perform correct motion interpolation on the video image sequence, which shows that the algorithm in this paper has good generalization ability.

4.2.3. Execution Time. The execution time of video motion compensation is used as an experimental indicator, and different methods are compared. The results are shown in Figure 7.

Analyzing Figure 7 shows that when using the algorithm in this paper to perform motion compensation on multimedia video images, the execution time is always less than 0.5 s, and the minimum is only 0.25 s, while deep learning algorithms and deep convolutional neural network algorithms are used to perform motion compensation on multimedia video images. The execution time is much higher than the calculation time of the algorithm proposed in this paper. It can be seen that the execution time of the algorithm in this paper is shorter, and the motion compensation of the video image can be realized at a faster speed.

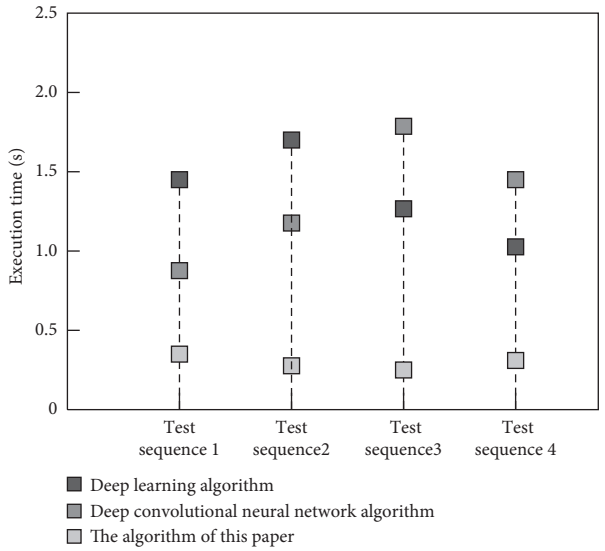

Figure 7: Comparison results of execution time.

4.2.4. Bit Rate. The higher the bit rate, the better the video image quality and the smaller the distortion. Taking test sequence 3 and test sequence 4 as examples, the bit rate is used as an experimental indicator to compare the video compensation effects of different methods. The results are shown in Figure 8.

According to Figure 8, it can be seen that in the test of test sequence 3 and test sequence 4, the code rate of this algorithm is higher than that of the deep learning algorithm

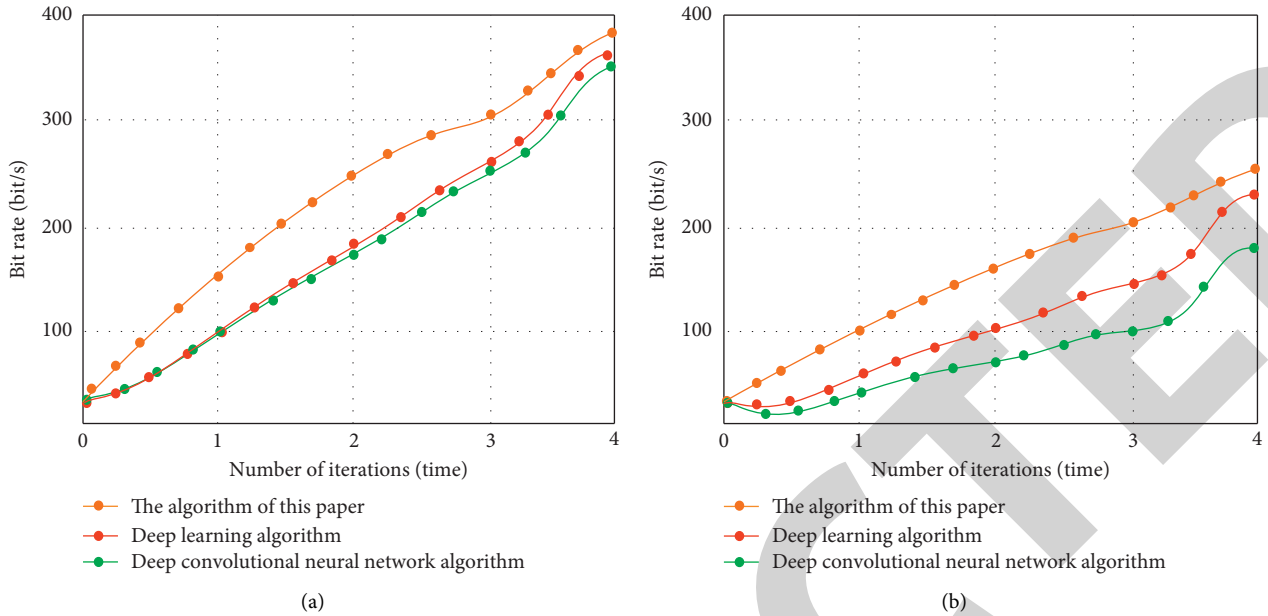

Figure 8: Code rate comparison result. (a) Test sequence 3. (b) Test sequence 4.

and deep convolutional neural network algorithm. It shows that the better the video image quality of the algorithm in this paper, the smaller the distortion, which further verifies the application value of the algorithm in this paper.

5. Conclusion

To solve the problems of low peak signal-to-noise ratio, poor visual effect, and low bit rate in traditional methods, this paper proposed a fast compensation algorithm for motion between multimedia video frames based on Manhattan distance. The purpose of denoising and extracting significant information from the video image was achieved by the preprocessing of the video image. To this end, the block-based motion idea was the division of each frame of the video sequence into nonoverlapping macroblocks. Moreover, the best position of the block corresponding to the current frame was found. Furthermore, the current frame of the multimedia video was obtained with the Manhattan distance calculation formula. Then, the compensation of the relative Manhattan distance between the backgrounds was pushed forward for the motion between the multimedia video frames. Finally, the experimental results were analyzed, which verified that the proposed algorithm has a high peak signal-to-noise ratio, a higher bit rate, and a better video visual effect.

Data Availability

The data used to support the findings of this study are available from the corresponding author upon request.

Conflicts of Interest

The authors declare no conflicts of interest.

Acknowledgments

The paper did not receive any financial support.

References

[1] A. J. Hussain and Z. Ahmed, "A survey on video compression fast block matching algorithms," *Neurocomputing*, vol. 335, no. 28, pp. 215–237, 2019.

[2] B. Veerasamy and S. Annadurai, "Video compression using hybrid hexagon search and teaching–learning-based optimization technique for 3D reconstruction," *Multimedia Systems*, vol. 27, no. 12, pp. 1–15, 2021.

[3] M. N. Sadat, R. Dai, L. Kong, and J. Zhu, "QoE-aware multi-source video streaming in content centric networks," *IEEE Transactions on Multimedia*, vol. 22, no. 9, pp. 2321–2330, 2019.

[4] P. Maniotis, E. Bourtsoulatze, and N. Thomos, "Tile-based joint caching and delivery of 360° videos in heterogeneous networks," *IEEE Transactions on Multimedia*, vol. 22, no. 9, pp. 2382–2395, 2020.

[5] S. L. Yang, J. Sun, Z. Yan, and X. L. Li, "Research on image interframe compensation based on deep convolutional neural network," *Computer Simulation*, vol. 37, no. 1, pp. 452–455, 2020.

[6] A. Rezapour, A. Ortega, and M. Sahimi, "Upscaling of geological models of oil reservoirs with unstructured grids using lifting-based graph wavelet transforms," *Transport in Porous Media*, vol. 127, no. 3, pp. 661–684, 2019.

[7] J. Montalvo, "Noise variance estimation through joint analysis of intrinsic dimension and differential entropy," *IEEE Signal Processing Letters*, vol. 26, no. 9, pp. 1330–1333, 2019.

[8] H. M. Hossein-Abad, M. Shabanian, and I. A. Kazerouni, "Fuzzy c-means clustering method with the fuzzy distance definition applied on symmetric triangular fuzzy numbers," *Journal of Intelligent and Fuzzy Systems*, vol. 38, no. 3, pp. 1–15, 2020.

[9] Y. Zhu, G. Zhai, X. Min, and J. Zhou, "The prediction of saliency map for head and eye movements in 360 degree

Hindawi
Journal of Mathematics
Volume 2023, Article ID 9814165, 1 page
https://doi.org/10.1155/2023/9814165

Retraction

Retracted: Design of Sports Image Contour Feature Acquisition System Based on the Background Subtraction Method

Journal of Mathematics

Received 19 December 2023; Accepted 19 December 2023; Published 20 December 2023

This article has been retracted by Hindawi following an investigation undertaken by the publisher [1]. This investigation has uncovered evidence of one or more of the following indicators of systematic manipulation of the publication process:

(1) Discrepancies in scope

(2) Discrepancies in the description of the research reported

(3) Discrepancies between the availability of data and the research described

(4) Inappropriate citations

(5) Incoherent, meaningless and/or irrelevant content included in the article

(6) Manipulated or compromised peer review

The presence of these indicators undermines our confidence in the integrity of the article's content and we cannot, therefore, vouch for its reliability. Please note that this notice is intended solely to alert readers that the content of this article is unreliable. We have not investigated whether authors were aware of or involved in the systematic manipulation of the publication process.

Wiley and Hindawi regrets that the usual quality checks did not identify these issues before publication and have since put additional measures in place to safeguard research integrity.

We wish to credit our own Research Integrity and Research Publishing teams and anonymous and named external researchers and research integrity experts for contributing to this investigation.

The corresponding author, as the representative of all authors, has been given the opportunity to register their agreement or disagreement to this retraction. We have kept a record of any response received.

References

[1] Z. Xiong, "Design of Sports Image Contour Feature Acquisition System Based on the Background Subtraction Method," *Journal of Mathematics*, vol. 2022, Article ID 3859795, 9 pages, 2022.

Hindawi
Journal of Mathematics
Volume 2022, Article ID 3859795, 9 pages
https://doi.org/10.1155/2022/3859795

Research Article

Design of Sports Image Contour Feature Acquisition System Based on the Background Subtraction Method

Zhichao Xiong

Ezhou Vocational University, Ezhou 436000, China

Correspondence should be addressed to Zhichao Xiong; 631605030229@mails.cqjtu.edu.cn

Received 18 November 2021; Revised 30 November 2021; Accepted 7 December 2021; Published 4 January 2022

Academic Editor: Naeem Jan

Moving target detection (MTD) is one of the emphases and difficulties in the field of computer vision and image processing. It is the basis of moving target tracking and behavior recognition. We propose two methods are improved and fused, respectively, and the fusion algorithm is applied to the complex scene for MTD, so as to improve the accuracy of MTD in complex and hybrid scenes. Using the main idea of the three-frame difference image method, the background difference method and the interframe difference method are combined to make their advantages complementary to overcome each other's weaknesses. The experimental results show that the method can be well adapted to the situation of periodic motion interference in the background, and it can adapt to the situation of sudden background changes.

1. Introduction

In recent years, although the methods of video moving target detection (MTD) have been deeply studied and some problems existing in algorithms have been improved, most of these algorithms are for specific applications [1]. It is the follow-up tracking and recognition of moving objects and the basis of semantic understanding of moving object sequences [2–4]. For applications such as encoding and decoding of key information in the video, the moving target of interest in the video sequence needs to be extracted from the background, so as to achieve compressed storage of the video image [5–7]. Intelligent video surveillance [8] is one of the most typical applications of video MTD at home and abroad in recent years, and MTD has been applied to video surveillance, UAV target detection, and other fields [9–11].

In foreign intelligent video surveillance system developed earlier, as early as the 1960s, many universities and research institutions in the United States engaged in MTD, tracking, and abnormal behavior recognition and other fields to carry out research. One of the most representative is the developed at Carnegie Mellon University, and other well-known colleges and universities in the United States dedicated to the detection, identification, and analysis of human behavior and can realize the prediction of human action; according to the forecast results, we judge the abnormal behavior of pedestrian is going to happen and give warning and prompt the use of such as public surveillance system. At the same time, VSAM (visual surveillance and monitoring) is mainly used for unmanned operations in hostile environments, such as severe disasters, long-term battlefield monitoring, and effective detection and tracking of enemy moving targets in military situations [12]. Subsequently, the University of Maryland in the United States independently developed a real-time visual monitoring system W4 (Who? When? Where? What?) [13] to achieve the positioning, segmentation, and multitarget tracking of the moving human body and to simply judge the next human behavior by detecting whether the human body is carrying other items. The Defense Advanced Research Agency's Airborne Video Surveillance (AVS) program uses target detection technology to capture static or dynamic moving target information from video in real time and then combines moving target tracking and recognition technology to obtain moving target speed, position, and trajectory information. Using such moving target information can improve the real-time detection function of UAV for specific environment [14].

Domestic universities and key research institutes have gradually studied the intelligent video surveillance system since the 1990s. There are many foreign experimental projects that are only under simulated conditions. Now many of them have been transformed into products, and they are widely used. The domestic market is not to be outdone. Now some fields can be independently innovated, and many products are gradually put into use. From automation, the Chinese Academy of Sciences, institute of independent research, develops a set of traffic monitoring prototype system [15] to detect moving vehicles, based on the license plate number, and automatically identifies and analyzes if there is any cause to track the vehicle, and then, tracking the identified vehicle, even anomalies cases can be predicted. It can detect moving vehicles in real time and is insensitive to changes in light conditions, so it has strong robustness to occlusion phenomenon.

The classification method of MTD [16, 17] can be classified according to the principle of MTD and whether it is based on pixel-level features. The classification of MTD methods and their advantages and disadvantages are as follows:

(1) Frame difference method [18–20] is based on the difference in the gray value. The difference results are distinguished into background and moving foreground by the preset threshold value. At the same time, when the color of the moving target is similar to that of the background, the detected moving target considers the information in the moving target as a part of the background information.

(2) Background subtraction method [21, 22] is to obtain the latest back image through background modeling. According to the different modeling methods of the Gaussian model, it can be divided into different kinds of background subtraction, among which the most common and most effective is the single Gaussian background model. The advantage of the background subtraction method is that the background modeling method is the most effective method to detect and extract moving objects.

(3) Optical flow method [23] calculates the optical flow direction and size of each pixel point between adjacent frames at a certain time, uses the optical flow field correlation equation to distinguish whether the image sequence in the scene is the background or the moving target, and takes the obvious optical flow field area as the foreground in the scene.

(4) A variety of combination of MTD algorithm frame differential method through the above analysis, the advantages, and disadvantages of the background modeling method and the optical flow method, can use a variety of MTD algorithm combining MTD algorithm under complicated background and improve the MTD algorithm adaptability to different scenarios; this also is the central idea of this paper.

In this paper, passing to Section 2, we start by recalling some concepts that we will use throughout this study; then, in Section 3, we discuss different MTD methods. We analyze using experiments and results in Section 4 and then put our main conclusion in Section 5.

2. Concept Review

2.1. Extraction of Background. There are usually three methods to obtain background images: manual rendering, statistical method, and Surendra background update algorithm.

(1) The manual background method requires people to start the camera to obtain the background image when no foreground object is observed. This method of background extraction increases the demand of manpower and material resources, and the background image without the foreground is hard to obtain, such as the vehicle monitoring system of highway.

(2) Statistical methods: background images can be summed up as in a specific time period of pixel grayscale average and use this as a background image corresponding to the pixel point of the average gray; when read in a video of a pixel point observation, we will find that there is no prospect; through a moving target point gray value which remained stable, the change is very small; only when it prospects through a moving target, the grayscale of the point will change dramatically.

(3) Surendra background update algorithm: we can adaptively obtain the background image; the algorithm to extract the background idea is to find the movement of objects through the current poor Zhen image area; movement area on the background remains the same, rather than the sports area with the background of the current frame to replace updates. The algorithm steps are shown below:

(1) Image 1 of frame 1 is taken as background B.
(2) Select I value T, the number of generations $m = 1$, MAX STEPS.
(3) Find the frame difference image of the current frame:

$$D = \begin{cases} 1, \left|I_i - I_{i-1}\right| \geq T, \\ 0, \left|I_i - I_{i-1}\right| < T, \end{cases} \tag{1}$$

where we denote I_i to be the i^{th} frame.
(4) Update background image B from binary image D:

$$B(m,n) = \begin{cases} B_{i-1}(m,n), D(m,n) = 1, \\ \alpha I_i + (1-\alpha) B_{i-1}(m,n), D(m,n) = 0, \end{cases} \tag{2}$$

where B_i denotes the current background which is set to be the weighted average of the instantaneous background and previous background and α is a background update coefficient.

2.2. Detection of Moving Targets. Under normal circumstances, there is a great difference between the foreground and the gray value of the background, while the gray value of moving objects itself will not be very different. Thus, the current frame image is I and background image is B; the background differential binary image is

$$\mathrm{DB}(m,n)=\begin{cases}255, I(m,n)-B(m,n)\geq T,\\ 0, I(m,n)-B(m,n)<T,\end{cases} \tag{3}$$

where we denote by T to be the threshold which is given by the corresponding pixel value of searching toward increasing pixel intensity. In this way, pixels with the gray value of 255 in the differential binary image can be regarded as moving target points in the foreground.

2.3. Image Postprocessing. Due to the influence of noise, some points belonging to the background will be wrongly detected as moving targets in the foreground. Meanwhile, due to the slight disturbance of objects in the background, these background points will also be wrongly identified as moving target points. In order to eliminate these influences, it is necessary to process the difference images of foreground and background. For example, the mathematical morphology method is used to process the difference images.

Because the shadow pixels and the pixels of the moving target is the same visual feature, the background of the direct reduction method cannot distinguish between moving objects and shadows; normally, the shadow will be wrongly judged to be moving targets; in RGB space, people's perception of the difference and the consistency of the calculated difference are very poor. Calculate the color similarity between images. Therefore, shadow detection is suitable for HSV color space. When a pixel is covered by shadow, its brightness value changes greatly, while chromaticity signal changes little. In this way, the following method can be used for discrimination:

$$S(x,y)=\begin{cases}1, & \alpha\leq\dfrac{I(x,y)}{B(x,y)}\leq\beta\cap(I(x,y)-B(x,y)),\\ 0, & \text{other},\end{cases} \tag{4}$$

where $I(x,y)$ is the current frame, $B(x,y)$ is the background image, $S(x,y)$ is the shaded pixel point, and A is set as the influence coefficient of the light source. The stronger the light source is, the smaller the value of " A" is. B is set to remove the influence of noise.

3. Frame Difference MTD and Improved Algorithm

For video image sequence, there is continuity between adjacent frames, so it can be considered that the illumination of the two frames is basically unchanged in the case of a very short time interval. By calculating the difference of adjacent frames, the amount of the gray value change between corresponding pixels of adjacent frames can be calculated. Because of the moving object in video before and after the two frames relative to the movement of background image pixel values of the same as a prime spot for two frames of pixel values before and after the change amount is larger, we exercise background pixel values of a point. In the case where the pixel values of the two frames before and after the volume change are small, we can separate the moving target and the background according to the frame difference method. The frame difference method is the simplest MTD method among all the current MTD methods.

3.1. Two-F Difference Method. First of all, two consecutive frames of images obtained after filtering are represented by $I_{k-1}(x,y)$ and $I_k(x,y)$, respectively, from the extracted video sequence.

Secondly, the obtained two adjacent video sequence images are used to carry out difference operation to obtain the difference images $D(x,y)$:

$$D(x,y)=\left|I_{k-1}(x,y)-I_k(x,y)\right|. \tag{5}$$

If the threshold value T is small, the background information will be regarded as a part of the moving target, reducing the accuracy of MTD. In this paper, according to the dynamic adaptive generation of multiple segmentation thresholds for each frame of the video sequence, segmentation thresholds are obtained by adapting to the changes of foreground and background contrast. The binarization process can be expressed by

$$T_k(x,y)=\begin{cases}0, & D(x,y)<T,\\ 1, & D(x,y)\geq T.\end{cases} \tag{6}$$

The principle block diagram of two-FDM is shown in Figure 1:

Below is the experiment of two-FDM using laboratory video dataset, as shown in Figure 2:

In Figure 2, (a) is frame 97 of the video sequence, (b) is frame 98 of the video sequence, and (c) is the difference between frame 97 and frame 98 of the picture. Through the experimental results, we can see the simple algorithm and fast detection speed and other characteristics. Disadvantages: when the time interval is long or the object moves too fast, the phenomenon of "double shadow" appears in (c) in Figure 2. At the same time, if the moving target moves too slowly or the time interval is too short, the pixel values of the two frames before and after cannot be changed, resulting in the difference of pixel values basically unchanged.

3.2. Three-Frame Difference Method (TFDM). The moving target area obtained by the two-FDM is larger than the actual target, resulting in the phenomenon of "double shadow". The binarization method of two-FDM can be used, as shown in formula (6) above, to obtain the final three-frame difference in the middle frame, as shown in formula (7).

Principle block diagram of TFDM is shown in Figure 3.

The specific process of MTD by TFDM is as follows.

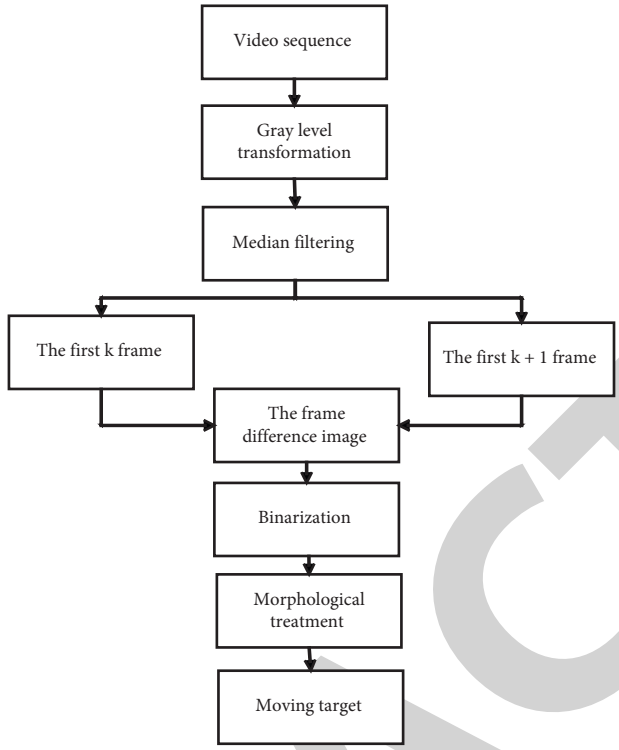

Figure 1: Block diagram of two-FDM.

(a) (b) (c)

Figure 2: Experimental results of two-frames difference. (a) Frame 97. (b) Frame 98. (c) Two frames of differential images.

First of all, Figure 3 shows that two difference images are obtained by difference operation on three consecutive frames of images.

Secondly, the two difference images obtained are thresholding by using formula (6), respectively, through the selected threshold value.

Finally, the binary foreground image $T(m, n)$ and $T(m, n)$ are calculated.

Laboratory video dataset was used for the experiment of TFDM, and the result is shown in Figure 4:

3.3. Canny Edge Detection. The common principle of edge detection is to use the discrete gradient approximation function to find the points with great changes in the gray value in the image, and we connect these points with great changes to form the edge information of the image.

The common steps of edge detection are as follows:

(1) The applied edge detection of the filter is realized by the derivative of image intensity, and the derivative is greatly affected by voice. Therefore, it is necessary to reduce the influence of voice on the derivative of image intensity through filtering, so as to improve the performance of edge detection and reduce the amount of calculation.

(2) Image enhancement is to realize the effect of image enhancement by enhancing the intensity value of pixel points that have obvious changes in the neighborhood of image gray points (the gradient

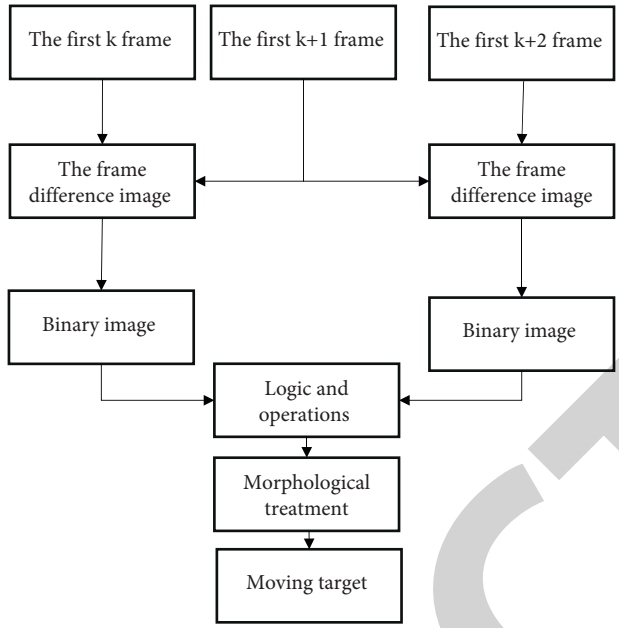

Figure 3: Principle block diagram of TFDM.

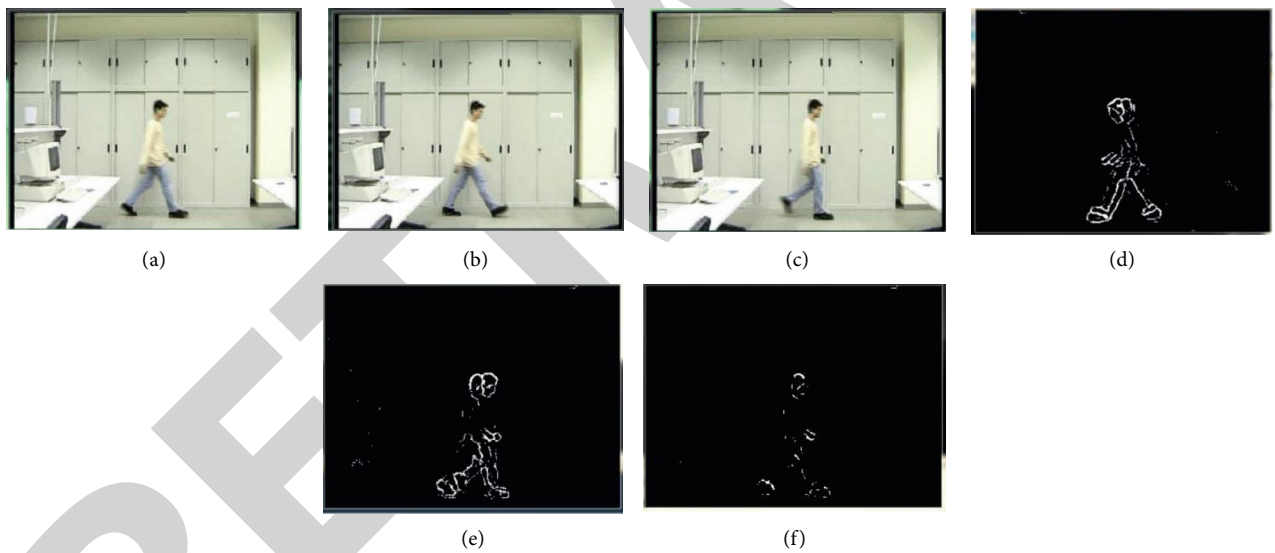

Figure 4: Three-frame difference experiment results. (a) Frame 97. (b) Frame 98. (c) Frame 99. (d) Frames 97 and 98, (e) Frame 98 and frame 99. (f) Three-frame.

amplitude of the image can be calculated to determine which points have obvious changes and need to be enhanced) and determine the pixel points in the candidate region of the image edge.

(3) The image edge detection, due to image enhancement, will make the neighborhood within many of the gradient value bigger, so we get to the edge pixels than the actual real; we are looking for more edge pixels, we can use the threshold method to select the points, while only keeping the real pixels at the edge of the image.

3.3.1. Gaussian Filtering. Since the result of edge detection is easily affected by image noise. In order to make the image smooth, a Gaussian filter is used to process the image to achieve the purpose of noise reduction.

3.3.2. Calculate Gradient Amplitude and Direction. The gray gradient value of the image can be approximately replaced by the first-order finite difference score. The gradient and direction of the edge can be obtained.

The partial derivatives of x and y directions used by Canny algorithm to calculate the convolution template are as follows:

$$A_m = \begin{bmatrix} -1 & 1 \\ -1 & 1 \end{bmatrix}, \; B_n = \begin{bmatrix} 1 & 1 \\ -1 & -1 \end{bmatrix}. \tag{7}$$

The first-order partial derivative matrix of the image gray gradient value in the x direction can be obtained as

$$\alpha[m,n] = \frac{(f[m,n+1] - f[m,n] + f[m+1,n+1] - f[m+1,n])}{2}. \tag{8}$$

The first-order partial derivative matrix of the image gray gradient value in the y direction can be obtained as

$$\beta[m,n] = \frac{(f[m,n] - f[m+1,n] + f[m,n+1] - f[m+1,n+1])}{2}. \tag{9}$$

Formulas (8) and (9) can obtain the gradient amplitude of the edge:

$$X[m,n] = \sqrt{\alpha[m,n]^2 + \beta[m,n]^2}. \tag{10}$$

With formulas (8) and (9), the gradient direction of the edge can be obtained:

$$Y[m,n] = \arctan\left(\frac{\alpha[m,n]}{\beta[m,n]}\right). \tag{11}$$

$M[i, j]$ and $A[i, j]$ can be obtained by calculating the first-order partial derivative matrix of x direction and y direction. If the angle obtained is not within these several ranges, the formula can be converted to between 0° and 360°.

3.4. Background Modeling Method. As the scene environment changes slightly over time, the background model needs to be updated in real time for the background subtracting method so that a good background model can accurately detect the moving target from the image.

At present, most background modeling methods are based on the improvement and optimization of the original algorithm. Common modeling methods are as follows:

(1) Single Gaussian background modeling: Gaussian background modeling is mainly used in complex scene environments, such as leaves shaking or camera shaking. The principle of the method is, respectively, for each pixel point in the original image to a single modeling, assumes that each pixel in the image for a period of time has nothing to do with other pixels, and is independent, and the characteristic value of the background pixels' fluctuation in a period of time satisfies the Gaussian distribution, according to the reasonable hypothesis for background modeling.

(2) Mean method background modeling: if the video image sequence scene is not too complex, the mean method can be used for background modeling. In essence, the mean method is an idea of statistical filtering, which is realized by summing up the multiple frames captured by the camera within a period of time, dividing the cumulative value by the number of captured frames, and finally obtaining the average value, which is used as the background reference model.

4. Experimental Results and Analysis

The software environment of the experiment is windows7, combined with VS2010 and Opencv. Video sequences from frames 81 to 115 of laboratory dataset are used to select representative moving objects of frames 97, 98, and 99 from 35 frames to conduct the experiment of improving the TFDM, as shown in Figure 5.

In Figure 5, figures (a), (b), and (c) represent sequential video sequences from the Laboratory dataset. Figure (a) is frame 97 of the video sequence. Figure (b) is frame 98 of the video sequence. Figure (c) is frame 99 of the video sequence. Figure (d) is frame 98 and frame 97 difference diagram. Figure (e) is frame 99 and frame 98 difference diagram. Figure (f) is frame three difference diagram.

Analysis of experimental results is as follows:

(1) Figures (d) and (e) represent that the two-frame difference method shows that moving targets detected by the two-FDM have "double shadow" phenomenon. Figure (f) is the traditional TFDM. It performs the logical "and" operation on the two-frame difference images by making the difference between the front and back frames of the three adjacent frames and takes the common part of the moving target of the two-FDM. Figure (f) is the MTD result of the traditional TFDM.

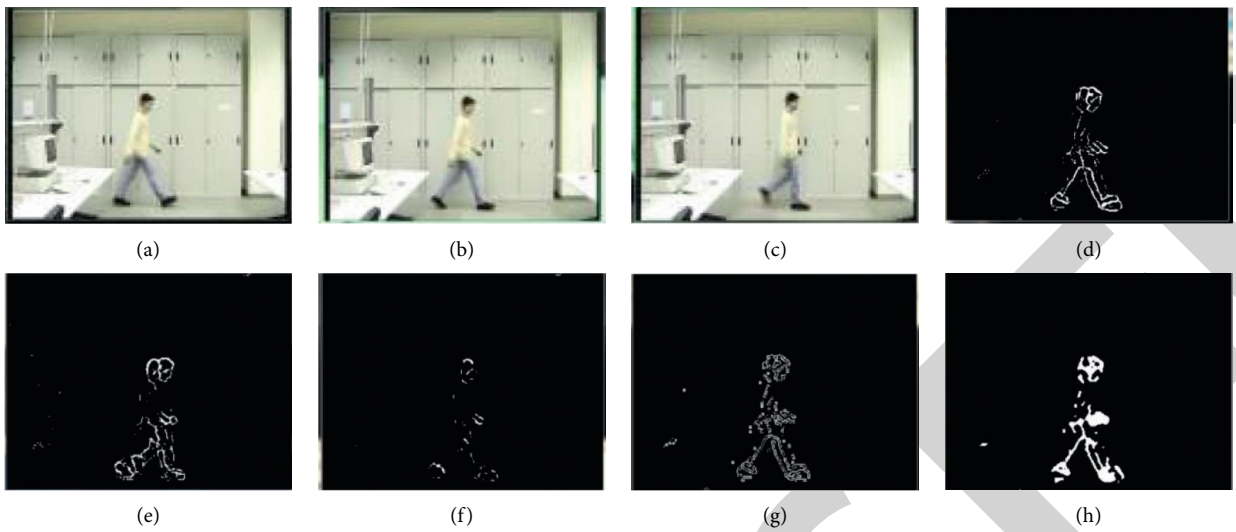

Figure 5: Experimental results of improved TFDM

Table 1: Comparison of detection accuracy between TFDM and the improved TFDM algorithm.

Video sequence	Detection rate	
	Traditional TFDM (%)	Improved TFDM (%)
Intelligent room	89.86	94.93
Laboratory	85.71	91.43

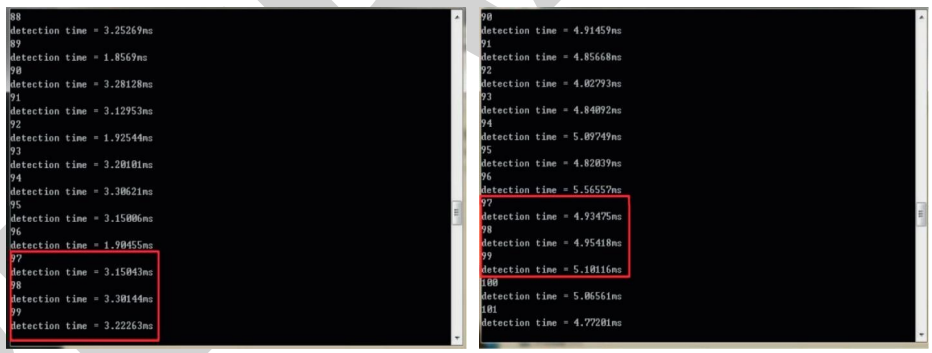

Figure 6: Running time of the frame difference method before and after improvement.

Table 2: Comparison of processing time between the traditional TFDM and the improved TFDM.

Current frame picture		Traditional TFDM (ms)	Improved TFDM (ms)
Laboratory	The 97th frame	3.15043	4.93475
	The 98th frame	3.30144	4.95418
	The 99th frame	3.22263	5.10116

(2) It can be seen from Figure (g) that a relatively complete contour of the moving target can be obtained by using Canny edge detection algorithm. This method can not only obtain more complete contour information but also obtain part of the internal information of the moving target.

Table 1 compares the accuracy of MTD between the traditional TFDM and the improved frame difference method. Through experimental results and comparison experiments, we can see that the improved algorithm can get more accurate moving targets compared with the traditional TFDM.

The laboratory dataset of three consecutive frames at frame 97, 98, and 99 were improved by the frame difference method before and after running time statistics, and the experimental results are shown in Figure 6:

In Figure 6, the right and the left images represent the running time of the traditional frame difference method and the improved frame difference method, respectively. Since the improved frame difference method performs Canny edge detection based on the moving target image obtained by the two-frame difference method and then performs "or" operation with the traditional TFDM, the increased running time is the Canny edge detection time and "or" operation time based on the two-frame difference method. Therefore, after the improvement, the time increase is relatively small, but the experimental accuracy has achieved a high improvement.

Table 2 shows the comparison of processing time between the traditional TFDM and the improved TFDM. When the processing time is increased little, the detection accuracy improved the frame difference.

Both intelligent room and laboratory datasets are due to the similarity between moving target and moving background in complex scenes, so the improved frame difference method detects more complete contour of the moving target than the traditional frame difference method, and the frame difference method is less affected by illumination changes.

5. Conclusion

Through the study of Canny edge algorithm, we can know that Canny edge detection can detect more complete edge information according to the small difference between the color value of the moving target and complex scene when the color of the moving target and the background is similar. Background model-based moving target detection is a very effective detection technology, which subtracts the current frame image from the existing background model image. If a pixel value in the difference image is greater than the threshold, it belongs to the moving target; otherwise, it belongs to the background region. From the above introduction and simulation test, it can be seen that background subtraction method is simple in operation, accurate in detection position, and fast in speed, and the results obtained after threshold operation directly give the location, size, shape, and other information of the target, which has a good application prospect. In this study, simulation experiments verify that the improved frame difference method is better than the traditional TFDM when the moving target color is similar to the background color in complex background.

Data Availability

The data used to support the findings of this study are available upon request to the author.

Conflicts of Interest

The author declares that he has no conflicts of interest.

Acknowledgments

This paper was supported by Outstanding talented person cultivation projects 2019 colleges and universities (Item no. gxyq201XXX2), the 2017 Anhui finance & trade.

References

[1] L. Najman, "Using mathematical morphology for document skew estimation," in *Proceedings of the Electronic Imaging 2004. International Society for Optics and Photonics*, pp. 182–191, San Jose, CA, USA, January 2004.

[2] E. Jayabalan and A. Krishnan, "Detection and tracking of moving object in compressed videos," *Computer Networks and Information Technologies*, vol. 142, pp. 39–43, 2011.

[3] X. Li, Q. Chen, and H. Chen, "Detection and tracking of moving object based on PTZ camera," in *Proceedings of the 2012 IEEE Fifth International Conference on Advanced Computational Intelligence (ICACI)*, pp. 493–497, Nanjing, China, October 2012.

[4] D. Parikh and C. L. Zitnick, "The role of image understanding in contour detection," in *Proceedings of the IEEE Conference on Computer Vision & Pattern Recognition*, pp. 622–629, Washington, NJ, USA, June 2012.

[5] X. Liu, H. Yao, R. Ji, P. Xu, and X. Sun, "Bidirectional-isomorphic manifold learning at image semantic understanding & representation," *Multimedia Tools and Applications*, vol. 64, no. 1, pp. 53–76, 2012.

[6] T. Y. Lee, S. H. Nam, and J. S. Baek, "A motion estimation VLSI architecture for video image compression[J]," *Aesthetic Surgery Journal*, vol. 33, no. 3, pp. 456-457, 2013.

[7] H. Ke, H. Sun, and L. Gao, "A video image compression method based on visually salient features," *Journal of Digital Information Management*, vol. 12, no. 5, pp. 333–339, 2014.

[8] C. Held, J. Krumm, P. Markel, and R. P. Schenke, "Intelligent video surveillance," *Computer*, vol. 45, no. 3, pp. 83-84, 2012.

[9] J. Kim, D. Yeom, and Y. Joo, "Fast and robust algorithm of tracking multiple moving objects for intelligent video surveillance systems," *IEEE Transactions on Consumer Electronics*, vol. 57, no. 3, pp. 1165–1170, 2011.

[10] D. Conte, P. Foggia, and M. Petretta, "Meeting the application requirements of intelligent video surveillance systems in MTD," *Pattern Recognition and Image Analysis*, vol. 46, no. 4, pp. 180–187, 2011.

[11] N. Chen and F. Ding, "Flame object segmentation by an improved frame difference method," in *Proceedings of the 2012 Third International Conference on Digital Manufacturing and Automation (ICDMA)*, pp. 422–425, IEEE, Guilin, China, August 2012.

[12] L. L. Xia, X. Y. Pan, and X. D. Yang, "MTD method based on three-frame difference and improved by markowitz portfolio model," *Journal of Chinese Inertial Technology*, vol. 22, no. 2, pp. 200–204, 2014.

[13] L. I. Qiu lin and H. E. Jia feng, "Vehicles detection based on three-frame-difference method and cross-entropy threshold method[J]," *Computer Engineering*, vol. 37, no. 4, pp. 172–174, 2011.

[14] B. Karasulu and S. Korukoglu, "Moving object detection and tracking by using annealed background subtraction method in videos: performance optimization," *Expert Systems with Applications*, vol. 39, no. 1, pp. 33–43, 2012.

[15] H. Sang and C. Xu, "MTD based on background subtraction of block updates," in *Proceedings of the 2013 6th International*

Hindawi
Journal of Mathematics
Volume 2024, Article ID 9836324, 1 page
https://doi.org/10.1155/2024/9836324

Retraction

Retracted: The Impact of Convention and Exhibition Industry on Regional Economic Development Based on Grey Relational Model

Journal of Mathematics

Received 23 January 2024; Accepted 23 January 2024; Published 24 January 2024

This article has been retracted by Hindawi following an investigation undertaken by the publisher [1]. This investigation has uncovered evidence of one or more of the following indicators of systematic manipulation of the publication process:

(1) Discrepancies in scope

(2) Discrepancies in the description of the research reported

(3) Discrepancies between the availability of data and the research described

(4) Inappropriate citations

(5) Incoherent, meaningless and/or irrelevant content included in the article

(6) Manipulated or compromised peer review

The presence of these indicators undermines our confidence in the integrity of the article's content and we cannot, therefore, vouch for its reliability. Please note that this notice is intended solely to alert readers that the content of this article is unreliable. We have not investigated whether authors were aware of or involved in the systematic manipulation of the publication process.

Wiley and Hindawi regrets that the usual quality checks did not identify these issues before publication and have since put additional measures in place to safeguard research integrity.

We wish to credit our own Research Integrity and Research Publishing teams and anonymous and named external researchers and research integrity experts for contributing to this investigation.

The corresponding author, as the representative of all authors, has been given the opportunity to register their agreement or disagreement to this retraction. We have kept a record of any response received.

References

[1] X. Yang, "The Impact of Convention and Exhibition Industry on Regional Economic Development Based on Grey Relational Model," *Journal of Mathematics*, vol. 2022, Article ID 9752636, 8 pages, 2022.

Hindawi
Journal of Mathematics
Volume 2022, Article ID 9752636, 8 pages
https://doi.org/10.1155/2022/9752636

Research Article

The Impact of Convention and Exhibition Industry on Regional Economic Development Based on Grey Relational Model

Xiaoning Yang [1,2]

[1]*Guangdong Vocational College of Hotel Management, Dongguan, China*
[2]*Macau University of Science and Technology, Taipa, China*

Correspondence should be addressed to Xiaoning Yang; 18098535bt20003@student.must.edu.mo

Received 24 November 2021; Revised 16 December 2021; Accepted 20 December 2021; Published 4 January 2022

Academic Editor: Naeem Jan

Since the exhibition is an exhibition industry, it has got so much importance by many countries. In China, the development of the said industry is wonderful. Therefore, we use the grey relational model to study the impact of convention. Moreover, the exhibition industry on regional economic development is proposed, and the concept and characteristics of exhibition industry, exhibition economy, and the research results of exhibition industry at home and abroad are expounded in detail. Then, according to the influence mechanism of exhibition industry on regional economy, the grey relational model is used to analyze the economic development of Changsha from 2012 to 2016. The analysis disclosed that the exhibition industry remained the main driving force of Changsha's economic development in these five years, which effectively promoted the economic development and the benign growth of various industries in Changsha.

1. Introduction

With the rapid development of global trade and the acceleration of global economic integration, the exhibition industry is one of the important manifestations of the tertiary industry, and it has attracted more and more attention from all over the world [1]. In economy, the exhibition industry has been out of commodity trading patterns, evolved into the comprehensive information gathering of information, technology, goods and talents, and the comprehensive business activity that promotes trade, investment, services, forums, and cultural exchanges [2]. After hundreds of years of development, the operation mode of convention and exhibition industry has become very mature. In today's world, Europe and the United States are in a leading position, and Europe becomes a well-deserved exhibition industry leader with technological, transportation, communications, and other technical advantages [3]. With the long period of continuous reform and opening up in China, the economy has long been in a state of rapid development, the exhibition industry as a comprehensive business activity has begun to gradually active, and its scale has continued to grow at an annual rate of more than 20% and showed a very good development. According to the related research and statistics, our country has formed the exhibition economic zone in the Yangtze River Delta, Pearl River Delta, Bohai Rim, Northeast China, and the Midwest, and the exhibition industry has been becoming one of the main driving forces of China's economic growth [4]. It is precisely because the Ministry of Commerce will begin to cultivate the exhibition industry to make it become China's strategic pilot industry of the tertiary industry from the government level.

According to relevant data statistics, in the global GDP total, the convention and exhibition industry directly produces GDP already accounted for 1%, and if GDP of the surroundings of the convention and exhibition area is also included, it accounts for 8% of the total, and the direct economic gain is as high as 20% [5]. The exhibition industry brings direct economic benefits and leads to the flow of talent, goods, information, and funds, so the relevant scholars call exhibition industry as "the bread of the city" [6]. As an important part of the commercial activities of the tertiary industry, the exhibition industry has the effect of

strong economic agglomeration and diffusion, which can effectively promote the economic and trade growth in the region, and bring great promotion to regional manufacturing, production factors, and resource allocation optimization [7]. The exhibition venue can also promote the development of related service industries, promote the communication between regional culture and external world, and bring direct or indirect huge economic benefits. Due to the important role of exhibition industry, it is precise, and the world gives excessive importance to its development. It is made an important form of international trade [8]. The influence of exhibition industry on the regional economy has also become an important subject of the research of relevant scholars. Therefore, this article would study the influence of exhibition industry on regional economic development through the grey relational model and take C city as an example. In this article, the concept, characteristics, and other related research associated with industry and economy of exhibition and convention are discussed in Section 2. Then in Section 3, the influence mechanism of exhibition industry on regional economy and grey relational model were presented. In Section 4, the impact of convention and exhibition industry on Changsha's economic growth was proposed, and finally, the concluding remarks are given in Section 5.

2. The Concept, Characteristics, and Related Research of Industry and Economy of Convention and Exhibition

2.1. The Concept and Characteristics of Industry and Economy of Convention and Exhibition. The exhibition industry, as a kind of commercial activity under the economic globalization, has been widely regarded and studied by all countries. According to the definition of convention and exhibition industry of China's Statistics Bureau, the exhibition industry is a large-scale industrial chain, which includes commodity display, promotion and circulation, economic and trade talks, business and civil exchanges, and international exchanges [9]. In the whole exhibition industry, the core content is exhibition and conference, its carrier is the related industries, and the complete infrastructure and related services of region are utilized to operate [10]. Therefore, from the industrial point of view, the exhibition industry belongs to the tertiary industry. According to the current operational situation, the exhibition industry involves various economic and trade cultural exchanges, such as attracting investment, cultural and technical exchanges, international exchanges, and commodity exhibitions [11]. Such a large number of contents also give the exhibition industry more extensive features. As the exhibition industry and a variety of industries have a greater relevance, it shows the characteristics of comprehensiveness and relevance. The ability of the exhibition industry to integrate buyers, sellers, products, information, and technology in a certain area in a short period of time also makes it to have a clustering effect, coupled with its large number of industries to exchange information and promote development in a short time, logistics, people, and information flow around the globe; therefore, it has interactive and open characteristics. These characteristics and advantages of the exhibition industry make it possible to promote the economic development of a country or a country under the circumstances of economic globalization, and also form a unique economic effect [12].

The economic development takes the exhibition industry as the core, and the relevant experts and scholars call such an economic development as the exhibition economy [13]. Through the exhibition activities (Figure 1), the exhibition economy promotes the development of regional industries and brings huge social and economic benefits for the region. To sum up, the economic effect of the exhibition economy, which takes the exhibition as the core, has four major effects. The first is the direct economic effects of the exhibition activities, which include exhibition organizers, participants, related services, media costs, and corporate salaries; the second is the economic benefits derived, such as hotels, catering, transportation, and tourism; the third is the economic and trade transactions produced by the exhibition itself, such as commodity trading, regional investment, and investment and economic and trade talks; and the fourth is the economic and social effects brought by the exhibition to the region. As the exhibition activities cannot be separated from the support of the related industries and infrastructure, the convention and exhibition activities will greatly enhance the economy, influence, reputation, infrastructure construction, related services, and tourism in the host country. It is precisely because the convention and exhibition industry can bring about such enormous economic effects on the economic development of cities and regions, each country, and region or city attaches great importance to the development of the exhibition industry in the region.

2.2. Related Research on Exhibition Industry and Exhibition Economy. In the economic globalization today, the huge economic effect of the exhibition industry has become increasingly important. Countries and regions around the world attach great importance to the development of their own exhibition industry, so the relevant research is also closely following the pace of the times [14]. In the related research of exhibition industry, developed countries in Europe and America have mature experience with their own advantages, the related research is also leading the research in China, the research content is more mature and in-depth research, and the exhibition industry has a greater reference in China [15]. In the early 80s of the last century, in Hanlon A's book "Trades Shows in the Marketing Mix," the development, significance, cost, and related economic benefits of exhibition were described in great detail, and this book regarded the exhibition as an efficient marketing tool and had made a very important contribution and inspiration to the related research of the exhibition industry [16]. Christinc Christman conducted a systematic study of the preparation and operation of the exhibition, and discussed the market objectives of the different stages, so his theory was currently in the leading position in the exhibition industry. After

Figure 1: Various forms of exhibition activities.

entering the new century, JcAnnaAbbott and Agne SDe Franco, who cowrote the "exhibition management," the book made a full range of dissection and analysis of the exhibition industry and gave detailed advice and guidance. In addition to the theoretical research on the convention and exhibition industry, foreign scholars have also conducted extensive research on the choice of the venue and the urban economic development of the convention and exhibition industry, and achieved more results.

Compared with foreign counterparts in the field of exhibition industry, domestic research in this area is relatively backward. In addition to backwardness, the domestic research methods are also quite different from those in other countries. At present, the domestic research on exhibition industry is mainly divided into two directions: qualitative and quantitative research [17]. Qualitative research mainly focuses on the economic benefits, industry promotion, and regional impact of the exhibition industry from a macropoint of view [18]. In this aspect, the research of the scholar Yu Xiangping and Wang Dongmei had a good representation, and these two people carried on a more thorough research separately from the perspective of industry leading effect, the conference, and exhibition for the city development. While the quantitative analysis is based on the direction of the industry-driven coefficient, research on this aspect is relatively more, and the results are relatively rich, and scholars Hu Ping, Li Zirong, Wang Haiyu, and Tian Jinxin are the excellent figures on these researches. Ye Kai, Tian Jinxin, and Shi Min used Granger cointegration analysis and causality to study the exhibition industry and pointed out that the exhibition industry could promote the optimization of urban industrial structure. Apart from the research on the exhibition industry itself, the domestic exhibition industry is also studied. These studies were mainly concentrated on the impact of tourism, such as Yu Yonghai, Kong Qingfu, and other scholars put forward research and suggestions on the cooperation between exhibition industry and tourism industry [19]. The scholar Wang Yajing put forward the problems and revelation between the exhibition industry and the hotel industry through the research on the exhibition industry in Jinan. Today, the exhibition industry plays a more and more important role in China's regional economic development (Figure 2), and the related research is also more and more thorough, and in the near future, the gap between convention and exhibition industry of China and foreign counterparts will shrink, which provides an advanced and solid theoretical basis for the development of convention and exhibition industry in China [20].

3. The Influence Mechanism of Exhibition Industry on Regional Economy and Grey Relational Model

3.1. The Influence Mechanism of Exhibition Industry on Regional Economy. Convention and exhibition activities are the interaction and the business platform and the intermediary between enterprises, and between the enterprise and the public; therefore, the exhibition activities will inevitably make business, product, technology and information, and other elements gathered in a specific period of time; and in the promotion and exchange of new technologies and new products, information, knowledge, and ideas are spread, and economic, trade, and investment promotion among regions are promoted. The agglomeration effect of the integrated economy is called the agglomeration effect of geographical space, which means that the exhibition

Figure 2: Exhibition industry has been paid more and more attention by domestic scholars.

industry has a agglomeration effect on urban development, so it can form a strong agglomeration effect. Because the industries of the participants during the exhibition activities are different from each other, the influencing factors of the agglomeration effect of the exhibition industry are also different, and each factor also has a mutual influence; Therefore, the exhibition industry is a very complex system, as shown in Table 1.

In the exhibition industry cluster effect, hardware and software facilities and exhibition environment have favorable effects on the exhibition industry, logistics, transportation, exhibition services, and basic industries play a positive role in the exhibition industry. While the adjustment of regional industrial structure and the attraction of other regions have adverse effects on the convention and exhibition industry, and form negative feedback, construction of infrastructure, finance, and media advertising in the city have become the influence factors of the exhibition.

Besides the strong agglomeration effect, the convention and exhibition industry also has obvious multiplier effect; the specific manifestation is that the exhibition industry itself will develop a large number of related industries in the process of development of itself. In the multiplier effect, the multiplier in a conference and exhibition industry generally refers to multiples, which represents the ratio between income changes and the inputs that cause change. The multiplier effect is that public spending and investment are effective incentives for demand, and the increase in public spending and investment will lead to a multiple growth in the region's economy. Cairns made it clear that macroeconomic investment, income, and unemployment were closely linked between in his economic thinking, and the increase in investment would inevitably increase income and the scope of employment; otherwise, income decreased and employment scope shrunk. Under certain conditions, the addition of a certain amount of investment in a region will inevitably lead to a multiple increase in the national income in the region. If a sector increases its investment and raises its own income, it will lead to an increase in departmental income and further lead to an increase in investment in these sectors and a new increase in revenue. The increment of national income was assumed to be ΔY, the investment multiplier was K, and the increment of government investment was ΔI. Then, the following formula can represent the multiplier formula of investment:

$$\Delta Y = \Delta I \cdot K. \tag{1}$$

In the multiplier effect, the marginal propensity to consume determined the investment multiplier, the consumption increment was assumed to be a, and then, the following formula could be obtained:

$$\Delta Y = \Delta C + \Delta I. \tag{2}$$

Formula (2) was substituted into formula (1), and then, the following formula could be is obtained:

$$K = \frac{\Delta Y}{\Delta Y - \Delta C} = \frac{1}{1 - (\Delta C/\Delta Y)}. \tag{3}$$

The above formula represented the marginal propensity to consume $\Delta C/\Delta Y$, and then by formula (3), the following formula could be derived:

$$\Delta Y = \frac{\Delta I}{1 - (\Delta C/\Delta Y)}. \tag{4}$$

Through formula (4), we can know that the increase in national income is ΔY, which has not only a great relationship with the implementation of incremental government investment ΔI, but also a great relationship with the marginal propensity to consume $\Delta C/\Delta Y$, and when the amount of government investment ΔI is fixed, the greater the marginal propensity to consume $\Delta C/\Delta Y$ is, and the greater the increase in national income ΔY will be. When the marginal propensity to consume is fixed, the greater the amount of government investment ΔI is, the greater the national income ΔY will be. Therefore, we can see that the increment of national income is proportional to the amount of government investment and marginal propensity to consume; marginal propensity to consume also determines the investment multiplier. According to Keynes's argument, the marginal propensity to consume is between [0, 1].

The amount of government investment in a region was assumed $\Delta I = 100$, and the marginal propensity to consume was assumed $\Delta C/\Delta Y = b$; among them, B1 = 2/3 and B2 = 1/2. The values of B1 and B2 were substituted into formula (4); thus the national income of the region was increased to $\Delta Y_1 = 300$. Those means the total national income in the region was 3 times of the amount of government investment. We can see $Y\varepsilon$ and Y_2 trend in Figure 3. From this inference, we can draw that the total amount of national

Table 1: Exhibition industry agglomeration factor statistics.

Exhibition industry cluster	Exhibition facilities	Exhibition area
		Concentration degree
		Modernization degree
	Exhibition service provider	Enterprise quantity
		Brand quantity
		Advertising media
		Financial insurance
		Accommodation catering
	The exhibition environment	Exhibition talents
		Natural condition
		Popularity
		Geographical position
		City foreign trade level
		Urban infrastructure
		Logistics transportation
		Basic industry
		Industrial structure adjustment
		Regional attraction

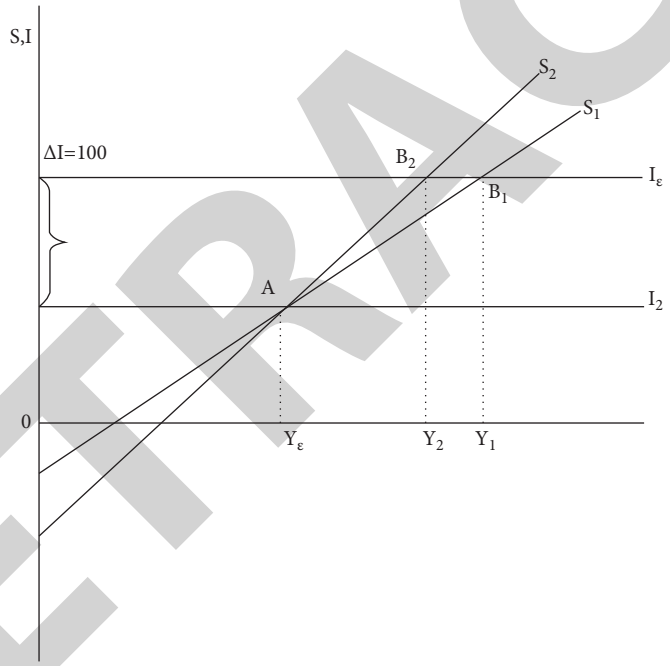

Figure 3: The equilibrium between the savings function curve and the investment curve.

income ΔY brought by an equal amount of government investment ΔI is not the same, and the main reason is that the slope of the savings function is different; that is, the multiplier effect is different, which leads to the result.

3.2. Grey Relational Model. Through the agglomeration effect and the multiplier effect, the convention and exhibition industry promotes the interactive development of the related industries and affects the development of regional economy. Therefore, we can analyze the impact of the convention and exhibition industry on the regional economy through the grey relational model. The grey relational analysis model mainly described the relationships among the objects, the strength, the size, and the order of the factors through the grey relational grade. Through the grey correlation degree, the influence degree of the object or the contribution degree of the factor to the object of study was expounded. The basic idea is that in the process of development of the object of study, the changes of the two factors are basically the same, which means that the correlation between the two is larger, or the correlation is less related. The main basis of the judgment is the geometry of the curve. If the two approaches, it indicates that the degree of association is higher; otherwise, it is smaller. In this article, the grey relational model was used to study the impact of convention and exhibition industry on regional economic development, and Changsha was chosen as the research object. Changsha, as an important component of the triangle area of Changsha Zhuzhou Xiangtan, its exhibition industry develops early,

the scale of convention and exhibition industry is relatively large, and its level of development is relatively mature, In 2014, it won the "the gold five stars" in the national exhibition—the "excellent exhibition city award." Therefore, the development level of convention and exhibition industry in Changsha is highly representative of the economic impact of Changsha region. The grey relational model was used to study the impact of the convention and exhibition industry on the economic development of Changsha. The specific steps are as follows:

First of all, through the network and other platforms, the exhibition industry, industrial production, and other related raw data of convention and exhibition industry in the Changsha region were statistically counted to establish the grey relational set and determine the dependent variables and independent variables. A sequence consisting of variables was set as a reference sequence, and a sequence of independent variables was a comparison sequence, which was set to $\{X_i\}$. Table 2 is the related raw data of Changsha from 2012 to 2016.

Secondly, the raw data of the statistics were processed by a nondimensional method. There are many methods for dimensionless processing, such as averaging and initialization. In this article, the mean processing method was chosen, and the results are shown in Table 3. The method is mainly that all the original data in that series is divided by the average of each sequence. The formula is given as follows:

$$Xi = \frac{xi(k)}{(1/n)\sum_i^n xi(k)}. \tag{5}$$

Moreover, the sequence difference, the maximum difference, and the minimum difference were obtained. The sequence difference formula was $\Delta O_i(k) = |x_0(k) - x_i(k)|$, the two largest difference formula of two grades was $\max_i \max_k \Delta O_i(k)$, and the minimum difference formula of two grades was $\min_i \min_k \Delta O_i(k)$.

The third step is to find the correlation coefficients, the correlation coefficient reflects the correlation degree between the reference sequence and the comparison sequence at a certain time, and the value is generally between 0 and 1. The correlation coefficient is greater, the correlation degree will be greater, conversely, the correlation degree will be smaller, and its formula for calculation is

$$\gamma(x_0(k); x_i(k)) = \frac{\min_i \min_k \Delta O_i(k) + \xi \max_i \max_k \Delta O_i(k)}{\Delta O_i(k) + \xi \max_i \max_k \Delta O_i(k)}. \tag{6}$$

The fourth step is to calculate the correlation degree and the rank of correlation degree. Among them, the correlation degree reflects the relation between the comparative sequence and the reference sequence, and the formula of the correlation degree is as follows:

$$\gamma(x_0, x_i) = \frac{1}{n}\sum_{k-1}^{n} \gamma(x_0(k), x_i(k)). \tag{7}$$

The final is to analyze the results. According to the above steps, after calculating the correlation degree, the relation between the reference sequence and the comparative sequence was analyzed by the correlation degree. Relevance was used to sort, and sorting could reflect the impact of convention and exhibition industry on urban economic development, which meant the impact of the convention and exhibition industry on the elements of urban economic development is greater, and then the ranking would be more upfront and vice versa.

4. The Impact of Convention and Exhibition Industry on Changsha's Economic Growth

By using the grey relational grade model, this article calculated the total value of convention and exhibition industry and GDP, and correlation coefficient and correlation degree of three industries of Changsha in 5 years from 2012 to 2016 in Hunan, Changsha. Detailed results are shown in Table 4.

From the calculation results of Table 4, the influence of convention and exhibition industry on the economic development of Changsha was analyzed. The exhibition industry has a very strong correlation. According to the GDP of Changsha, the correlation degree of exhibition industry and GDP is 0.6871 and ranks first. The calculation results show that during 2012 to 2016, a total of 5 years, convention and exhibition industry and economic development in Changsha is very strong, and the convention and exhibition industry becomes the main driving force of economic development in the region of Changsha. The rapid development of convention and exhibition industry is closely related to the regional economic development of Changsha. The convention and exhibition industry has promoted the economic development and promoted the transformation and upgrading of the industrial structure in Changsha, and the changes of the exhibition area and regional economic growth in Changsha also confirm this result, as can be seen in Figure 4, which is a scatter diagram of the relationship between the convention and exhibition industry and GDP in Changsha. The convention and exhibition industry of Changsha has become a leader in economic development in the past 5 years; this is inseparable from the strong support of the Hunan provincial government. In 2013, the Hunan provincial government promulgated *The plan for the development of convention and exhibition industry in Hunan province (2013–2020).* The planning provides the direction and policy basis for the development of convention and exhibition industry in Hunan province. Data from 2012 to 2016 show the effectiveness of this policy support is very good.

Apart from the correlation between GDP and exhibition industry in Changsha, the output value of tertiary industry and exhibition industry is the most relevant in Changsha, and the correlation degree is 0.6809. This result is consistent with the tertiary industry, so the overall trend of the tertiary industry is consistent with the development trend of the exhibition industry. In addition to strong policy support, the rapid development of convention and exhibition industry and the tertiary industry is benefited from that Changsha's own cultural tourism resources are very rich. Changsha is the cradle of Chu culture, and its history can be traced back

Table 2: Changsha exhibition and output statistics in 2012~2016.

	2012	2013	2014	2015	2016
Exhibition area (ten thousand m^2)	135.00	190.7	180.18	197	203.33
Gross product (billion Yuan)	6399.91	7153.13	7824.81	8510.13	9323.7
Primary industry (billion Yuan)	272.31	291.15	318.04	341.78	370.95
The secondary industry (billion Yuan)	3592.52	3946.97	4245.68	4478.20	4513.23
The service sector; the tertiary industry (billion Yuan)	2535.08	2915.01	3261.09	3690.15	4439.52

Table 3: The result of dimensionless processing of raw data.

	2012	2013	2014	2015	2016
Exhibition area (ten thousand m^2)	0.7432	1.0499	0.9920	1.0956	1.1194
Gross product (billion Yuan)	0.8161	0.9121	0.9978	1.0852	1.1889
Primary industry (billion Yuan)	0.8540	0.9131	0.9975	1.0719	1.1634
The secondary industry (billion Yuan)	0.8646	0.9499	1.0217	1.0777	1.0861
The service sector; the tertiary industry (billion Yuan)	0.7527	0.8655	0.9682	1.0956	1.3181

Table 4: The correlation coefficient, correlation degree, and ranking of convention and exhibition industry in Changsha.

	2012	2013	2014	2015	2016	Correlation degree	Sort
Gross product	0.5771	0.4191	0.9450	0.9055	0.5886	0.6871	1
Primary industry	0.4728	0.4209	0.9477	0.8081	0.6932	0.6685	3
The secondary industry	0.4503	0.4985	0.7695	0.8479	0.7494	0.6631	4
The service sector; the tertiary industry	0.9135	0.3502	0.8074	1.0000	0.3334	0.6809	2

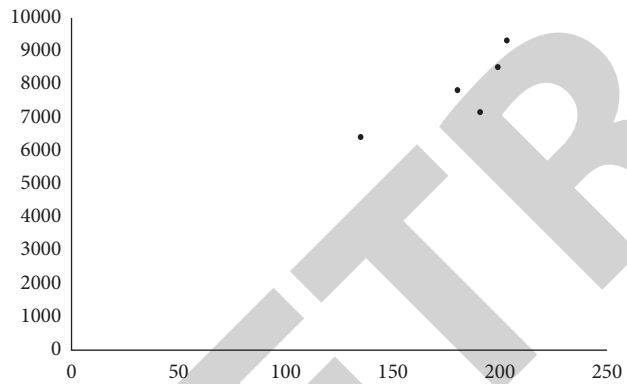

Figure 4: Changsha convention and exhibition industry and the relationship between the total outputs of the scattered map.

to the spring and autumn periods and the Warring States period, and in ancient times, Changsha is known as "the hometown of Jia Yi and Qu Yuan" and "famous city of Chu and Han"; the entertainment and catering of the contemporary Hunan have become very developed, and a batch of entertainment industries which have influenced the whole country and even the whole world have appeared, such as the "Hunan army on TV" in Hunan TV. Unique historical, geographical, and cultural background also provides very favorable factors for the development of convention and exhibition industry and indirectly promotes the economic growth of the tertiary industry in Changsha.

The correlation of the convention and exhibition industry, the primary industry, and the secondary industry is analyzed in Table 4. The relevancy between Changsha convention and exhibition industry and the primary industry is 0.6685, and the difference of correlation degree of exhibition industry in Changsha between the primary industry and the secondary industry is very small. This result is very similar to the development of Changsha itself, and Changsha is located in the lower reaches of Xiangjiang, and not only an important grain production base, but also an important base of equipment manufacturing industry in our country. Therefore, the industry and agriculture in Changsha are much developed. Table 2 shows the statistics of the output value of the primary industry and the secondary industry in Changsha from 2012 to 2016, and the results show that the growth of the two is in line with the development of the convention and exhibition industry.

5. Conclusions

The economy of China has rapidly developed with the deepening of international exchanges between China and the rest of the world. The government is giving increasing attention to the exhibition industry. Therefore, the grey relational model used to study the impact of the exhibition industry on regional economic development was put forward. Changsha region was taken as an example, a statistical analysis of the exhibition industry and GDP in Changsha in a total of 5 years from 2012 to 2016 was made, and then, the grey relational analysis method was used to analyze. The analysis shows that the exhibition industry has the most significant correlation with the GDP of Changsha and is the main driving force for economic development in Changsha; the relation between the exhibition industry and the tertiary industry is inferior to that of GDP; this coincides with the result of the exhibition industry belonging to the tertiary industry. Through the analysis of the Changsha region, it can be seen that the exhibition industry has a great influence on the regional economic development, which can bring huge

Hindawi
Journal of Mathematics
Volume 2024, Article ID 9820467, 1 page
https://doi.org/10.1155/2024/9820467

Retraction

Retracted: Research on Automatic Classification Method of Ethnic Music Emotion Based on Machine Learning

Journal of Mathematics

Received 23 January 2024; Accepted 23 January 2024; Published 24 January 2024

This article has been retracted by Hindawi following an investigation undertaken by the publisher [1]. This investigation has uncovered evidence of one or more of the following indicators of systematic manipulation of the publication process:

(1) Discrepancies in scope

(2) Discrepancies in the description of the research reported

(3) Discrepancies between the availability of data and the research described

(4) Inappropriate citations

(5) Incoherent, meaningless and/or irrelevant content included in the article

(6) Manipulated or compromised peer review

The presence of these indicators undermines our confidence in the integrity of the article's content and we cannot, therefore, vouch for its reliability. Please note that this notice is intended solely to alert readers that the content of this article is unreliable. We have not investigated whether authors were aware of or involved in the systematic manipulation of the publication process.

Wiley and Hindawi regrets that the usual quality checks did not identify these issues before publication and have since put additional measures in place to safeguard research integrity.

We wish to credit our own Research Integrity and Research Publishing teams and anonymous and named external researchers and research integrity experts for contributing to this investigation.

The corresponding author, as the representative of all authors, has been given the opportunity to register their agreement or disagreement to this retraction. We have kept a record of any response received.

References

[1] Z. Wu, "Research on Automatic Classification Method of Ethnic Music Emotion Based on Machine Learning," *Journal of Mathematics*, vol. 2022, Article ID 7554404, 11 pages, 2022.

Hindawi
Journal of Mathematics
Volume 2022, Article ID 7554404, 11 pages
https://doi.org/10.1155/2022/7554404

Research Article

Research on Automatic Classification Method of Ethnic Music Emotion Based on Machine Learning

Zijin Wu

College of Humanities and Management, Guilin Medical University, Guilin 541199, China

Correspondence should be addressed to Zijin Wu; wuzijin@glmc.edu.cn

Received 21 November 2021; Revised 7 December 2021; Accepted 11 December 2021; Published 4 January 2022

Academic Editor: Naeem Jan

With the development of the country's economy, there is a flourishing situation in the field of culture and art. However, the diversification of artistic expressions has not brought development to folk music. On the contrary, it brought a huge impact, and some national music even fell into the dilemma of being lost. This article is mainly aimed at the recognition and classification of folk music emotions and finds the model that can make the classification accuracy rate as high as possible. The classification model used in this article is mainly after determining the use of Support Vector Machine (SVM) classification method, a variety of attempts have been made to feature extraction, and good results have been achieved. Explore the Deep Belief Network (DBN) pretraining and reverse fine-tuning process, using DBN to learn the fusion characteristics of music. According to the abstract characteristics learned by them, the recognition and classification of folk music emotions are carried out. The DBN is improved by adding "Dropout" to each Restricted Boltzmann Machine (RBM) and adjusting the increase standard of weight and bias. The improved network can avoid the overfitting problem and speed up the training of the network. Through experiments, it is found that using the fusion features proposed in this paper, through classification, the classification accuracy has been improved.

1. Introduction

With the development of information and multimedia technology, people's demand in the entertainment industry has increased. Particularly, the increase in demand for music has promoted the vigorous development of the music market. As of June 2019, the number of online music users in my country reached 583 million, an increase of 29.76 million from the end of 2018, accounting for 68.8% of the total Internet users. Music has become an indispensable part of our lives. Folk music takes root under the nourishment of local cultures. It contains the characteristics of local cultures and presents various forms of expression. It combines the excellent and unique cultural connotations of various places and uses stage performances and other performance methods to show the people's pursuit of various aspects of living conditions, lifestyles, and ideals of life. Through its performance, it reveals the cultural ecology of each place, shows the unique culture of each place, and constitutes a vivid road map of life. Folk music is an important cultural resource. It contains people's understanding of life, views of things, and evaluation of characters. It is of great significance to the study of the humanities and ecology of the region. Through folk music, we can have a preliminary understanding of the ideology and life beliefs of the people in the region. Folk music is the embodiment of the core values of the Chinese nation, and it contains the essence of the traditional Chinese culture, which is a pursuit of morality and beauty, and is an important part of our cultural core competitiveness. The in-depth study of folk music is an interpretation of the life, world, and values of drama creators. Through the performance of historical figures and the recurrence of historical events, folk music adopts a way of expression that is easy for people to accept, expressing the mainstream values of the people of our country, showing our traditional virtues, and condensing our cultural core competitiveness.

Emotion in music [1] is an important attribute of music, and the use of music emotion is reflected in all aspects of our lives. When scoring film and television works, a series of music works are often created because of their specific themes and emotional needs. This music not only brings the

auditory enjoyment to the audience, but also a suitable soundtrack which helps to express the emotion of film and television works and describe the story. In terms of psychotherapy, the right music can soothe the patient's inner trauma. The selection of these music often does not care about the style and age but pays more attention to the expressions of emotions in the music. All this shows that people are more or less inseparable from the influence of music emotions. It is this unique attribute of music that makes music spread widely. And folk music also has the basic attributes of emotional expression, so it is necessary and meaningful to carry out recognition and classification research on the emotion of folk music. The motivation behind carrying out this research work includes several factors, such as the need for cultural protection, the support of national policies, the emotional needs of people, and the use of science and technology. These factors make the research on the identification and classification of folk music emotions not only necessary, but also meaningful and feasible. In fact, the recognition and classification systems are basically the same, whether it is the recognition and classification of the folk music emotions or the recognition and classification of popular music emotions. In the rest of the paper, Section 2 highlights some of the related literatures. In Section 3, the proposed methods are presented, involving DBN and SVM. In Section 4, the experimental analysis has been carried out to verify the strength of proposed methods. Finally, the conclusion is given in Section 5.

2. Related Work

With the rapid development of economy and society, audio resources are becoming more and more abundant, and people's demand and taste for music are gradually improving. Some methods of categorizing music are gradually emerging. Early music classification methods originated in the 1990s and were mainly used to distinguish the differences between speech, music, and environmental sounds. This is easier than distinguishing music styles. As the field of music classification continues to innovate, many pioneering research results have been produced. The subject of music style classification has gradually obtained more progress and results in practice and theory [2–4]. Music classification task is currently an important research direction based on content music retrieval, and it has received extensive attention from Music Information Retrieval (MIR) at home and abroad. In the MIR community, since 2004, most of the advanced tasks of the Music Information Retrieval Evaluation Exchange (MIREX) competition held every year are related to music classification, including music sentiment classification and genre classification. In the review of music classification in 2011 [5], through the investigation of music classification task, the current music classification task model is usually disassembled into two structures: feature extractor and classifier. Audio feature extraction is the most critical step in music classification. Whether the relevant features of the classification target can be extracted from the complex music signal is the key to improving the accuracy of the final classification. From the perspective of music comprehension, audio features can be divided into low-level, intermediate-level, and high-level features. Low-level characteristics refer to timbre characteristics and time characteristics. Tone characteristics capture the tonal quality of sounds related to different instruments, such as zero-crossing rate, spectral centroid, and Mel Frequency Cepstrum Coefficient (MFCC). The time feature captures the change and evolution of timbre over time, such as average, variance, and covariance. Low-level features can generally be directly obtained through signal extraction and processing techniques, which are easy to extract, and show good performance in almost all music classification tasks. Therefore, the current low-level features are important audio features of the audio classification system. But these low-level features are the basic attribute values of the signal, which is not closely related to people's perception. Therefore, compared with low-level features, intermediate features such as rhythm, pitch, and harmony are more in line with the musical attributes that people understand. These features can also be further extracted from low-level features through technology. High-level features currently refer to content-based semantic tags, such as genre, mood, genre, etc., and the attributes of intermediate features are more in line with people's direct perception of music. But this is an abstract concept because it is difficult to obtain directly from low-level and intermediate features.

In 2002, Tzanetakis and Cook [6] began to focus on the classification of music genres and provided a GTZAN data set containing 10 genres, which laid the foundation for future research on music genre classification. This article solves the problem of automatic music genre classification by using three sets of audio features (timbre, pitch, and rhythm). This research laid the foundation for music classification and labeling. Many researchers devote themselves to the study of manual extraction of combined features. MFCC is a single-tone low-level feature widely used in genre classification. Compared with other complex feature combinations, only MFCC features can produce a good classification effect. Currently, in content-based music classification, the common choices of classifiers are k-nearest neighbor [7], Support Vector Machine (SVM) [8], and Gaussian Mixture Models (GMM) classifier [9]. With the development of technology, such as logistic regression [10], Artificial Neural Network (ANN) [11], decision tree [12], Linear Discriminant Analysis (LDA) [13, 14], Gaussian mixture model, hidden Markov [15, 16], and other more advanced models have also been used for different music tasks. In recent years, deep learning has achieved remarkable results in both image and text fields, and more and more researchers have begun to explore the application of deep learning in the field of music. Convolutional neural network, as a typical neural network in deep learning, has begun to be widely used in music classification and labeling tasks. Unlike traditional classifiers that use complex music feature combinations, using Convolution Neural Network (CNN) as a classifier can use simple input features, such as MFCC, spectrogram, and audio signals. MFCC is still a lossy structure as an effective audio input form in low-level features, and the completely lossless original audio does not

show better performance than the spectrogram. So, the spectrogram retains more information than MFCC. However, the dimensionality is lower than that of the original audio, and the information in the audio signal is fully utilized, which is more suitable for the classification task with CNN as the classifier [17]. In 2009, Kim et al. [18] first applied CNN to improve the accuracy of music genre and artist classification. In 2016, the CNN network designed by Choi et al. [19] showed excellent performance on the task of music classification. However, the spectrogram is not exactly the same as the traditional image. To some extent, the convolution of the spectrogram along the frequency axis seems to be unreasonable in the interpretation of music. Therefore, in 2014, Dieleman [20] introduced the 1D-CNN structure to deal with the spectrogram in the music category.

In the development process, convolutional neural networks have derived a variety of structures to greatly improve the performance of image recognition. The residual network ResNet [21] launched by He et al. in 2015 has made great innovations in convolutional neural networks. By introducing shortcut connections to solve the problem of network degradation, deeper networks can be effectively trained. Since ResNet was put forward, the variant networks of ResNet have emerged in an endless stream, each with its own characteristics, and the network performance has also been improved to a certain extent. The dense connection network DenseNet [22] realizes feature reuse through dense connection, which not only absorbs the advantages of ResNet, but also improves the model effect and has better performance. In 2018, Kim et al. [23] used the original audio signal as input and successfully applied the ResNet structure to automatic music labeling. Other commonly used deep learning models such as convolutional neural networks are usually based on large-scale label data. Due to the lack of current music emotion classification data, in addition to using enhanced data, the concept of transfer learning proposed in recent years can effectively solve such problems. Transfer learning is a new machine learning method, and it is a hot research topic now. There are extensive researches on images and texts. The parameters trained in the source domain are transferred to the target domain so that a small amount of sample data can be effectively learned. In 2017, Choi et al. [24] used the CNN method for source domain training, which use the trained parameters in other music classification tasks by transfer learning.

3. Method

In the study of the emotional classification of folk music in this paper, the establishment of a musical emotional model must first be combined with the expression characteristics of the music itself and related psychology knowledge. Because there are currently no publicly available data sets on folk music, it is necessary to collect and sort out music data sets before classification. And before obtaining the music features required for classification, it is also necessary to perform preprocessing operations on the music fragments. Because the deep belief network can perform feature extraction on sample data through autonomous learning, it can be well suited for tasks that require highly abstract and complex features. And compared to the convolutional neural network that is good at processing two-dimensional images, it can handle one-dimensional data well, and music signals are typical three-dimensional data. In order to achieve a better classification effect of folk music emotions, consider using the DBN structure model to extract music features and achieve classification. In this section, in the research on the recognition and classification of folk music emotions, through the exploration of the DBN network training and fine-tuning process, the DBN and SVM algorithms are combined to achieve classification.

3.1. Music Sentiment Classification Based on DBN and SVM Algorithm

3.1.1. Classification Model Based on DBN and SVM. Considering that DBN can learn more abstract and comprehensive features that characterize music attributes, this paper combines the algorithms of DBN and SVM to achieve classification. The deep belief network is used to extract the features, and then the SVM classifier is used for classification. That is to say, the output of the last hidden layer of DBN is used as the input of the SVM classifier to build a new classification model. First, the extracted music features are used as the input of the DBN network model. DBN obtains the music features extracted by DBN by learning the input feature data. Then, use the feature data extracted by DBN to train the SVM classification model. Finally, the test samples are classified through the trained classification model to realize the recognition and classification of folk music emotions. Therefore, the new classification model abstracts the input features of the network to obtain high-level features that are more conducive to classification and can retain the original features, while also having the advantages of the SVM classifier.

Figure 1 is a flow chart of using a combined algorithm to achieve emotional classification of folk music. As can be seen from the figure, the function of the algorithm is divided into two categories: feature extraction and classification. First, input the extracted folk music features into DBN. Each RBM in the DBN network is used to learn the original features layer by layer, and the output of the last hidden layer of the DBN is extracted as the audio feature for classification. Then, the classifier is trained by using the training samples corresponding to the feature samples extracted by DBN. Then, use the trained SVM classifier to test the test sample data, and finally get the accuracy of the classification.

In the research on the recognition and classification of folk music emotion based on the combined algorithm of DBN and SVM, the main factors that affect the classification result are (1) input feature parameters in the DBN network; (2) features extracted by the DBN network structure model; and (3) the training of the classifier when the SVM classifier implements mult-classification. The classifier used in the study of music sentiment classification in this chapter is still SVM, so the next step is to study the DBN network structure model.

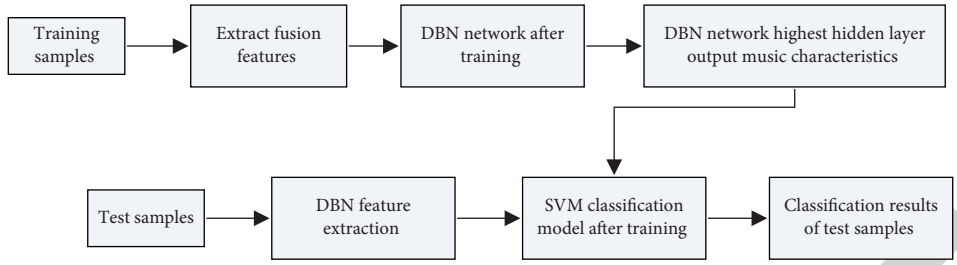

Figure 1: The flow chart of DBN and SVM combined algorithm to achieve classification.

3.1.2. The Training Process of DBN. In extracting the features of the audio signal using the deep belief network, the fusion feature of folk music fragments is used as the original feature input of the deep belief network, and the original input feature is only this one. When it is input into the entire network through the input layer, through the learning of the first RBM, the output of the hidden layer is used as the input of the second RBM visible layer. The hidden layer is mainly to ensure that the input feature vector is mapped to different feature spaces to retain as much feature information as possible. By decomposing and reconstructing the output features of the previous layer, more abstract new features can be used to realize the characterization of the original features. After multiple RBM learning, the output of the last hidden layer is the feature extracted by the DBN network. Each node of the hidden layer in the network uses the output of the visible layer as the input of the current layer. The activation function can be used to express the functional relationship between the input and output of the two layers of nodes. In this chapter, the sigmoid function is mainly used in the construction of the DBN structure model. The function expression is as follows:

$$f(x) = \frac{1}{1 + e^{-x}}. \tag{1}$$

The training process of the deep belief network is mainly divided into the unsupervised pretraining process of forward propagation and the supervised reverse tuning process of back propagation. In the experiment using DBN to achieve feature extraction, pretraining is to implement unsupervised training for each RBM network separately. And it is necessary to ensure that after the original features of folk music have been mapped many times, the final output abstract high-level features can still contain as many original features as possible.

In fact, the most important thing in RBM training is to find the increments of weights and biases. The specific pretraining process of RBM is as follows:

Step 1. Initialize the weight W and bias a and b. Among them, both a and b are set to 0, and the initial value of W is close to 0; set the initial learning rate of the network, and set it to 0.001 based on experience.

Step 2. Input the characteristics of various music emotion sample data into the DBN network. The input of the experiment in this chapter is the fusion feature extracted in this article.

Step 3. The input original music feature is used as the input of the visible layer of the DBN network, and the input data sample is used as the initial state of the visible layer.

Step 4. According to the initial state of each node in the visible layer, the binary state of all hidden layer nodes can be obtained through the forward propagation of the network.

Step 5. When the state of each node in the hidden layer is determined, calculate the binary state of the visible layer.

Step 6. Steps 4 and 5 are a reconstruction of the visible layer, using the log-likelihood function to obtain partial derivatives of the weights and biases to obtain the corresponding likelihood gradients.

Step 7. Calculate the increment of the weight and the offset to update the corresponding offset value $m' = m + \Delta m, n' = n + \Delta n$, weight in the DBN network $W' = W + \Delta W$.

DBN training is based on the RBM training process. When the RBM in the network is trained layer by layer from bottom to top to the highest layer, then the optimal bias and weight corresponding to each RBM will be obtained, but this kind of optimal is only a local optimal. If the optimization of each RBM is only considered separately, and the overall network is not considered, the final feature extraction may fall into a local optimal situation. In the process of extracting the characteristics of folk music, in the reverse tuning part, according to the label information of the training samples, this paper uses the network weights and bias optimal values obtained in the pretraining stage as input to achieve self-topping.Finally, by comparing the size of the error between the target output and the actual output, according to the predetermined error range, it is determined whether the tuning should be terminated.

3.2. Classification Model Based on Improved DBN and SVM. Similar problems often arise when using deep learning network models for classification testing. That is, when the classification test is performed on the data test sample, the prediction accuracy of its classification is very low. However, in the model training process, the prediction accuracy of the data training sample classification is actually relatively high.

Considering the fact that it may be due to the overfitting problem caused by the lack of training data samples during the training process, overfitting is a common problem in many machines learning. This article is in the process of using the classification model based on the combination of DBN and SVM to classify folk music. Since the RBM in the DBN structure model can prevent overfitting of training to a certain extent, the overall classification result is not bad. However, consider the fact that the overfitting problem may make the trained model almost ineffective. In order to further prevent overfitting and alleviate the problem of low prediction accuracy brought by overfitting to the network, in this paper, a "Dropout" layer is added to each RBM in the DBN network to make the model's generalization ability stronger. When using neural networks to solve practical problems, they often encounter the problem of long network training time. In the process of using DBN to extract the abstract features of folk music, this paper frequently encounters the problems of long training time and slow convergence speed. In order to alleviate the network pressure caused by time complexity, the momentum coefficient is introduced.

3.2.1. Dropout Layer. "Dropout" means that when the network model is being trained, some nodes are not functioning and do not participate in the learning process of features, and we can temporarily think that these nonfunctioning nodes do not exist. Because they are only considered temporarily that they do not exist, these nodes may play a role in subsequent training, so the weight matrix corresponding to these nodes still needs to be retained. Simply put, it is to stop certain neural nodes from working during the forward propagation stage of the neural network, which avoids the network from relying too much on some local features and effectively avoids the problem of overfitting. "Dropout" is currently used extensively in fully connected networks. In this article, when improving the DBN model, in each RBM of the DBN, "Dropout" is added between the visible layer and the hidden layer. Compared with the previous network, after adding "Dropout," the training process of DBN will have a little change. Suppose the probability of the node working after joining "Dropout" is α. Then, in the training model stage, first, randomly select $(1-\alpha)$ times the node in the visible layer and temporarily delete it. Then, the input data samples are forwarded and back-propagated in the network; this step is the same as the training process of RBM. Then, update the weights and biases corresponding to the neural nodes that are not deleted, and finally restore the deleted neural nodes.

Figure 2 shows the corresponding node information of the visible layer and the hidden layer in the forward propagation process of the network before and after adding "Dropout." It can be seen that before adding "Dropout," the calculation formula for the visible layer to transfer the output value to the hidden layer is as follows:

$$\begin{aligned} p_i^{(n+1)} &= W_i^{(n+1)} q^{(n)} + c_i^{(n+1)}, \\ q_i^{(n+1)} &= f\left(p_i^{(n+1)}\right). \end{aligned} \tag{2}$$

By the adoption of "Dropout" network, the calculation formula becomes

$$\begin{aligned} \widetilde{q}^n &= s^{(n)} * q^n, \\ p_i^{(n+1)} &= W_i^{(n+1)} \widetilde{q}^n + c_i^{(n+1)}, \\ q_i^{(n+1)} &= f\left(W_i^{(n+1)} \widetilde{q}^n + c_i^{(n+1)}\right), \end{aligned} \tag{3}$$

where n represents the number of layers of the network, which is the visible layer in the network of this article. $n+1$ denotes the hidden layer. $q_i^{(n)}$ is the node of the visible layer, $\widetilde{q}_i^{(n)}$ is the node with the addition "Dropout"; $s^{(n)}$ is a random 0, 1 vector with "Dropout" added, and the value of the vector indicates the existence state of the corresponding node. Generally, it is generated by Bernoulli's function $s_j^{(n)} \sim \text{Bernouli}\, p(\alpha)$, where α is the probability of neural nodes working in the network. In this article, the value of p after adding "Dropout" is mainly obtained based on experience and experiments. The working probability p for the input layer node is set to 0.9, and the working probability for other hidden layer nodes is set to 0.5.

3.2.2. Momentum Coefficient. The momentum coefficient is mainly used to update the weight and bias in DBN. In RBM, the weight and bias are determined by first setting the initial state of the visible layer. After forward and reverse calculations, the binary states of all nodes in the hidden layer and the visible layer are obtained, and the visible layer is reconstructed. Then, by maximizing the log-likelihood function, the partial derivatives of the weights and biases are obtained, respectively, and the likelihood gradients corresponding to the weights and the biases are obtained. Finally, use formulas to calculate the increments of weights and biases to complete the update. In the update of the relevant parameters W, m, and n of the DBN network, this paper increases the dependence on the offset increment and weight increment produced by the previous iteration. The improved formula for weight and bias is as follows:

$$\begin{aligned} \Delta W_{ij(t+1)} &= \eta\left(x_i y_{j\text{data}} - x_i y_{j\text{model}}\right) + \lambda \Delta W_{ij(t)}, \\ \Delta m_{(t+1)} &= \eta\left(x_{i\text{data}} - x_{i\text{model}}\right) + \lambda \Delta m_{i(t)}, \\ \Delta n_{j(t+1)} &= \eta\left(y_{j\text{data}} - y_{j\text{model}}\right) + \lambda \Delta n_{j(t)}, \end{aligned} \tag{4}$$

where t represents the t-th iteration, which, respectively, corresponds to the tth increment of the weight and bias. η is the learning rate, and λ is the weight corresponding to the increase dependence, which is in the range of 0 to 1. Because every time the weight and bias are updated, it will affect the performance of the network. By increasing their dependence on the original increment, the weights and biases can be accelerated to change in the direction they changed in the

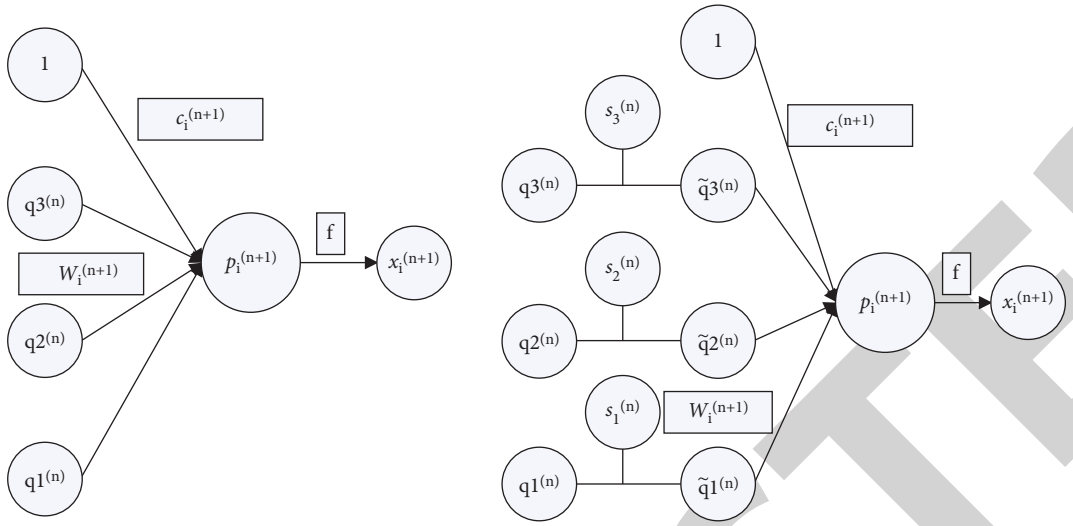

Figure 2: Corresponding information before and after adding the "Dropout" node.

Table 1: Specific information of the music clips used in the experiment.

Number	Music emotion category	Number of training clips	Number of test clips	Number of verify clips
1	Happy	600	200	200
2	Woeful	600	200	200
3	Eager	600	200	200
4	Peaceful	600	200	200

previous iteration. These speeds up the convergence process, thereby alleviating the problem of long network training time. When improving DBN in this paper, it is found through parameter tuning that when λ is set to 0.1, the overall performance of the network is improved, so this paper sets the weight λ to 0.1.

4. Experiment and Analysis

In this experiment, in order to ensure the fairness of classification, 1000 pieces of music are randomly selected for each kind of music emotion for experiment. Table 1 lists the number of music fragments used in the study of music sentiment classification in this article.

The emotion model in this paper uses participation and value orientation to describe emotions as a whole. The music emotion is divided into four parts, and adjectives are added to each part to describe the corresponding emotion. But just using these 3 words cannot mark all the musical emotions. In order to describe music emotions more comprehensively, four similar adjectives with the same dimension range are added to each category. These adjectives are all from the Hevner's emotional ring model. See Table 2 for specific categories and descriptions.

The experimental results directly compare the classification performance of each classification algorithm under different feature extraction methods; that is, analyze the recognition and classification effect and misjudgment rate of the corresponding music emotion category under different algorithms.

This chapter mainly studies the classification of music emotion based on DBN extracted features. And through the improvement of DBN, the classification effect of the combined algorithm of DBN and SVM is improved. Therefore, the experiment mainly discusses from two aspects of the original feature extraction method and the classification algorithm. The original feature extraction methods mainly include MFCCs feature parameters and the fusion feature parameters proposed in this paper. The classification algorithm involves the combination of SVM, DBN and SVM, and the improved combination of DBN and SVM. Through the combination of features and classification algorithms, comparative experiments are realized. Table 3 shows the comparative experiments of using different classification algorithms to achieve classification under different feature extraction methods.

It can be seen from the table that when the classifiers are all SVMs, the accuracy of using MFCCs feature parameters to identify and classify folk music emotions is only 52.5%, which is because of the diversity of music features. If only considering the problem of music emotion classification from the inverse frequency domain of music, the extracted music features are relatively monotonous and do not have good distinguishability. In contrast, the abstract features obtained by learning the feature parameters of MFCCs using deep belief networks can more accurately recognize music emotions. This is because DBN can learn independently and extract abstract features that can better distinguish the emotions of ethnic music.

Table 2: Descriptive words corresponding to text sentiment classification.

Number	Music emotion category	Descriptive words
1	Happy	Longing, awe-inspiring, lyrical
2	Woeful	Heavy, dark, miserable
3	Eager	Satisfied, calm, gentle
4	Peaceful	Passionate, humored, victorious

Table 3: Classification accuracy of different classification algorithms.

Extract features	MFCCs (%)	Fusion feature (%)
SVM	52.5	58.6
DBN + SVM	68.3	76.5
Improved DBN + SVM	72.1	79.4

When the classification algorithm combining DBN and SVM is used, and the fusion feature is input into the DBN network as the original feature, the classification accuracy rate reaches 76.5%. This not only proves the ability of DBN to learn features, but also shows that the fusion features proposed in this paper can be effectively used for the classification of folk music emotions. Particularly, after making improvements to DBN, when the fusion feature is used as the network input, the classification accuracy has increased by 2.9%. Mainly because this article adds Dropout to each RBM, overfitting can be prevented, and the update method of weights and biases is changed, which makes their update direction clearer, improve the efficiency of determining weights and biases, and realize the optimization of DBN.

Figure 3 is based on MFCCs feature parameters, using SVM to achieve the classification accuracy and error of folk music emotion recognition classification. It can be seen from the figure that only using MFCCs features for classification, the accuracy of music sentiment classification is very low, and the classification misjudgment rate is mostly relatively high. In particular, the misjudgment rate of music clips that peaceful emotion is up to 66%, and the overall best recognition and classification rate is only 62%.

Figure 4 is the classification result of folk music emotion recognition classification based on fusion features. It can be seen from the figure that compared to extracting MFCCs features for classification, the overall accuracy of classification using fusion features has increased, and the misjudgment rate of emotion categories has also decreased. The overall best classification accuracy is for music samples in an eager mood, with a classification accuracy of 68%.

Figure 5 shows the classification accuracy and error of the folk music emotion recognition classification based on the MFCCs parameter characteristics, using the classification algorithm combining DBN and SVM. It can be seen from the figure that compared to only using the SVM classification model for classification, the classification accuracy of the model that uses the DBN to learn features is improved. And it showed a trend of overall increase in classification accuracy and overall decrease in misjudgment rate. This shows that DBN has a high learning ability for the original feature data of folk music input into the network.

Figure 6 is based on improved DBN and SVM combined algorithm classification, using MFCCs feature parameters as the original network input, to achieve the classification accuracy and error of folk music emotion recognition classification. It can be seen from the figure that, compared to using the abstract features of DBN for classification, the accuracy of classification using the abstract features learned by the improved DBN network has not changed much overall. However, the classification accuracy of calm and desire emotions has improved.

Figure 7 is the classification accuracy and error of folk music emotion recognition classification based on the fusion features proposed in this paper and using the classification algorithm combining DBN and SVM. It can be seen from Figure 7 that, compared to only using the MFCCs feature parameters as the input features of the DBN network, the fusion feature more comprehensively represents the emotion of the national music itself. Particularly, for music clips with eager emotions, the classification accuracy rate reaches 83%, and the probability of misjudgment of eager emotions has decreased. And compared with other combinations of feature extraction and classification algorithms, the probability that music clips of other emotions are misjudged as anxiety emotions become lower.

Figure 8 is the classification accuracy and error of folk music emotion recognition classification based on the fusion features proposed in this paper and using the improved DBN and SVM combined classification algorithm. It can be seen from the figure that compared to the combination of other classification algorithms and features, when the fusion features proposed in this paper are used, the overall classification accuracy is the best through the algorithm based on the combination of improved DBN and SVM. Among them, the classification accuracy of calm emotions is the highest, reaching 87%, and the classification rate of desire emotions has also increased a lot. It further illustrates the efficiency of the fusion feature proposed in this paper and also proves that this paper improves the effectiveness of the DBN network by adding "Dropout" to the DBN network and using momentum coefficients to adjust the increment of weights and biases.

Through the overall analysis of the six simulation results, it is found that among all the classification models, the classification of folk music with eager emotions has the best

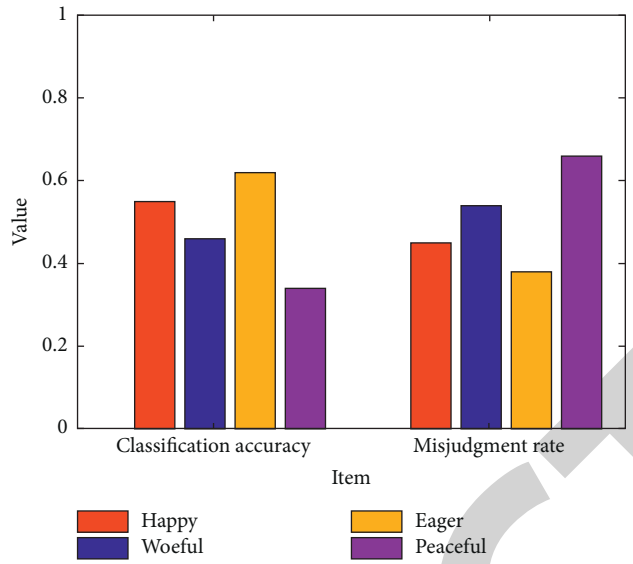

Figure 3: Comparison of classification results based on the characteristics of MFCCs.

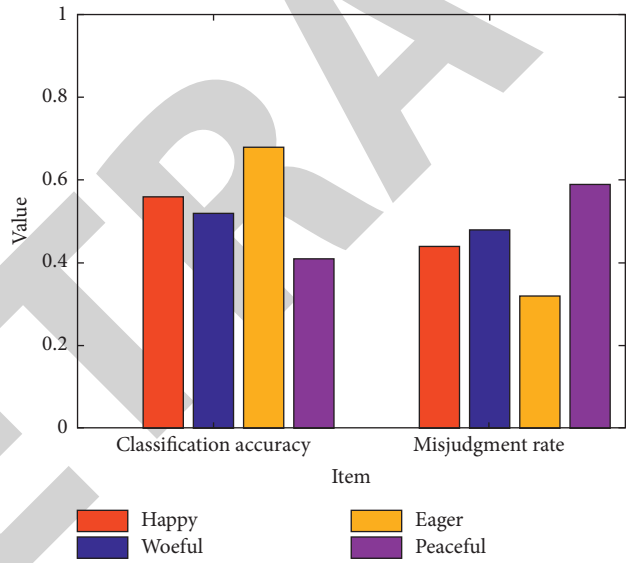

Figure 4: Comparison of classification results based on fusion features.

effect, and the classification of music with peaceful for emotions has the worst effect. The analysis shows that in the music emotion model of this article, peaceful represents a high degree of participation. But generally woeful or happy music can also indicate a high degree of participation to a certain extent. Therefore, there may be a slight deviation in the classification process of music fragments. And eager emotions represent low participation, and relatively speaking, the discrimination is high, so the overall classification accuracy is also high. Although the accuracy of music classification of peaceful for emotion is relatively low, the fusion feature is extracted, and then the fusion feature is used as the input of DBN for learning, and finally the DBN is improved. Every time the feature extraction method and the improvement of the classification algorithm are improved, the classification accuracy has been improved. It illustrates the superiority of using DBN to extract features to achieve classification, the effectiveness of improved DBN network, and the feasibility and efficiency of fusion feature classification.

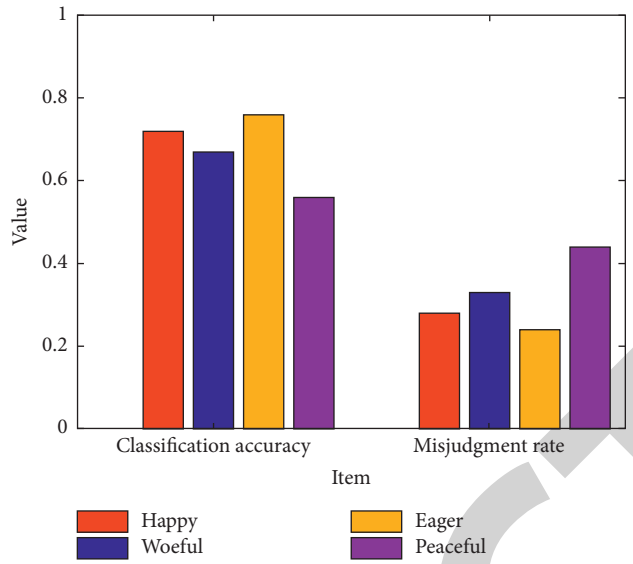

Figure 5: Classification result of MFCCs feature parameters used as DBN network input.

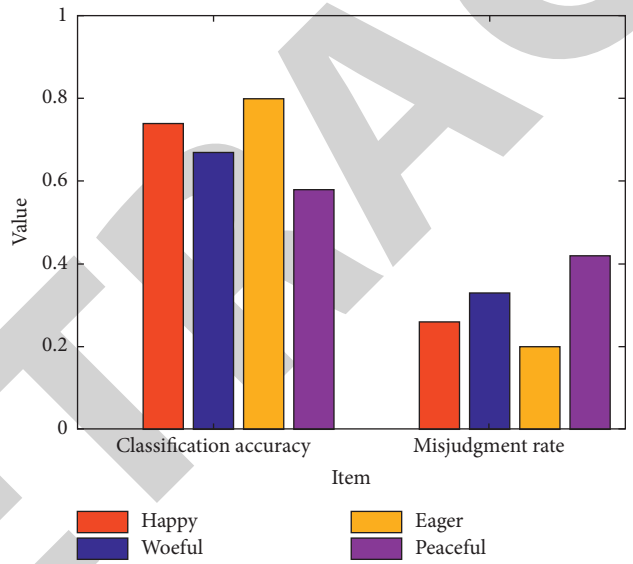

Figure 6: Classification result of fusion feature used as DBN network input.

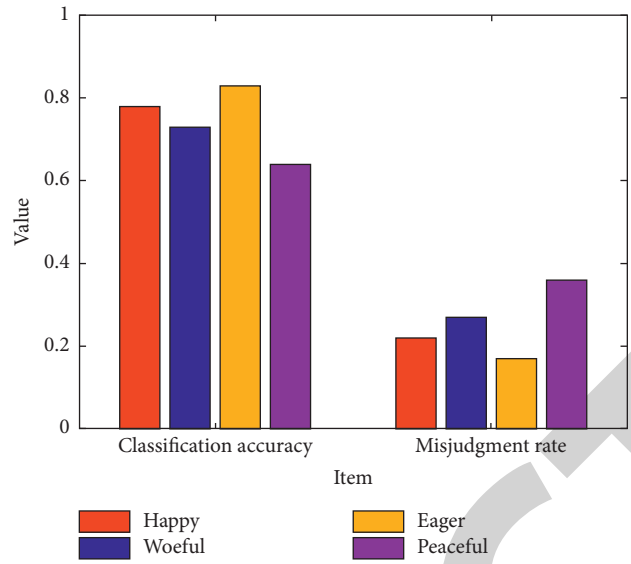

Figure 7: Classification result of MFCCs parameters used as improved DBN input.

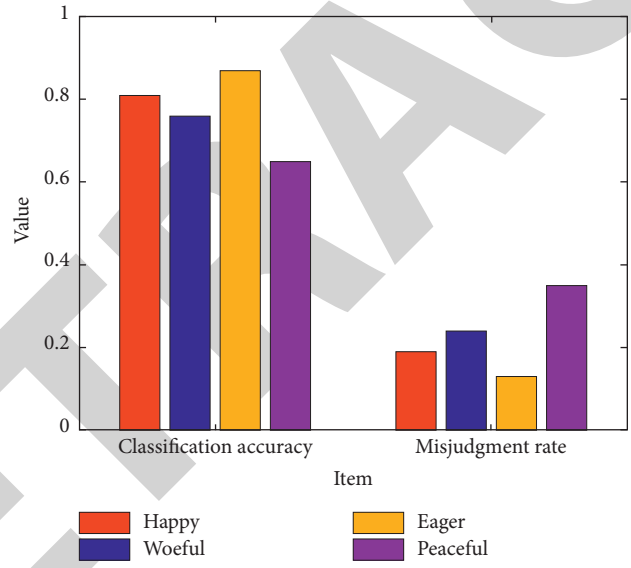

Figure 8: Classification result of fusion feature used as improved DBN network input.

5. Conclusion

With the steady development of the national economy, various art forms have also emerged in large numbers. As a result, the protection and inheritance of folk music has suffered a huge impact and faces the danger of loss. How to use science and technology to realize the digital protection and research of national music is a problem that needs to be solved urgently. On the other hand, with the maturity of deep learning related technologies, deep learning has been used in various aspects such as feature extraction, classification, and recognition, and achieved good results. This article tries to combine the research of folk music with deep learning knowledge. First, customize the fusion features of music and extract them, and use the features obtained from network learning as the input of the classifier to realize the emotional classification of ethnic music. The research of this article has realized the digital protection of national music resources to a certain extent and has achieved certain results in the research of emotion classification. Therefore, the study of folk music in this article is not only an attempt, but also a breakthrough. In the research on the classification of folk music emotions, this paper uses fusion features as network input, uses deep belief networks to extract features, and improves the update standard of weights and biases by adding Dropout to the restricted Boltzmann machine. Through experiments, it is found that the accuracy of ethnic music sentiment classification based on DBN extracted features is better than the classification results of traditional classification algorithms. And the use of improved DBN to extract features for classification not only ensures the improvement of classification accuracy, but also reduces the

Hindawi
Journal of Mathematics
Volume 2024, Article ID 9890519, 1 page
https://doi.org/10.1155/2024/9890519

Retraction

Retracted: Evaluation Method of IT English Blended Teaching Quality Based on the Data Mining Algorithm

Journal of Mathematics

Received 23 January 2024; Accepted 23 January 2024; Published 24 January 2024

This article has been retracted by Hindawi following an investigation undertaken by the publisher [1]. This investigation has uncovered evidence of one or more of the following indicators of systematic manipulation of the publication process:

(1) Discrepancies in scope

(2) Discrepancies in the description of the research reported

(3) Discrepancies between the availability of data and the research described

(4) Inappropriate citations

(5) Incoherent, meaningless and/or irrelevant content included in the article

(6) Manipulated or compromised peer review

The presence of these indicators undermines our confidence in the integrity of the article's content and we cannot, therefore, vouch for its reliability. Please note that this notice is intended solely to alert readers that the content of this article is unreliable. We have not investigated whether authors were aware of or involved in the systematic manipulation of the publication process.

In addition, our investigation has also shown that one or more of the following human-subject reporting requirements has not been met in this article: ethical approval by an Institutional Review Board (IRB) committee or equivalent, patient/participant consent to participate, and/or agreement to publish patient/participant details (where relevant).

Wiley and Hindawi regrets that the usual quality checks did not identify these issues before publication and have since put additional measures in place to safeguard research integrity.

We wish to credit our own Research Integrity and Research Publishing teams and anonymous and named external researchers and research integrity experts for contributing to this investigation.

The corresponding author, as the representative of all authors, has been given the opportunity to register their agreement or disagreement to this retraction. We have kept a record of any response received.

References

[1] L. Shao, "Evaluation Method of IT English Blended Teaching Quality Based on the Data Mining Algorithm," *Journal of Mathematics*, vol. 2021, Article ID 3206761, 8 pages, 2021.

Hindawi
Journal of Mathematics
Volume 2021, Article ID 3206761, 8 pages
https://doi.org/10.1155/2021/3206761

Research Article

Evaluation Method of IT English Blended Teaching Quality Based on the Data Mining Algorithm

Lin Shao

Dalian University of Foreign Languages, Dalian, Liaoning 116044, China

Correspondence should be addressed to Lin Shao; shaolin@dlufl.edu.cn

Received 24 November 2021; Revised 14 December 2021; Accepted 17 December 2021; Published 31 December 2021

Academic Editor: Naeem Jan

As the mixed education model gradually becomes widespread in various universities in Japan, the evaluation of the quality of IT English mixed education has become a very important issue, and it is worth considering the corresponding evaluation method. In this paper, we use a data mining algorithm to implement an evaluation method for the interconversion of quantitative data and qualitative concepts and use the IT English mixed teaching model to evaluate and analyze the teaching quality of the course. The evaluation method is feasible and provides a mixing method. Evaluation of the quality of education. Reference method.

1. Introduction

With the progress of educational reform in universities, the IT English mixed education model is attracting more and more attention from various universities, and many university teachers conduct practical education and topic research aimed at reforming mixed curriculum education [1, 2]. Blended teaching is becoming more and more important, which is welcomed by the majority of teachers and students. Therefore, what is the quality of education in the IT English mixed education model and how to evaluate the quality of education in this education model are the important issues faced by domestic universities in monitoring the quality of education [3–5]. This requires the establishment of an effective and comprehensive evaluation system for the IT English mixed education model, and we are actively considering various educational quality evaluation methods under the mixed education model. At universities, there are many reference methods for daily class quality evaluation, and from the perspective of fuzzy data processing, there are rough set theory and fuzzy evaluation methods, but they have drawbacks. For example, the rough set theory adopts the idea of removing redundant data, so the reduced information is relatively incomplete. The fuzzy evaluation method has a strong subjectivity in acquiring the fuzzy evaluation matrix, so the rigor of the evaluation result is low. Due to the randomness and ambiguity of the educational evaluation itself, it is necessary for our evaluation method to be able to reflect the randomness and ambiguity of this evaluation so that the evaluation results are more consistent with the actual situation. In addressing these issues, Thoma et al. used a reverse cloud generator to achieve qualitative and quantitative transformation of evaluation reviews and a virtual cloud algorithm to obtain a comprehensive evaluation cloud model [6–10]. Ye Yong proposed a cloud model-based classroom quality data mining method to estimate the nonlinear relationship between classroom quality and metrics. With the advent of data mining algorithms, data mining algorithms have been applied to various qualitative evaluations of the system and achieved specific results. The application of data mining algorithms in qualitative evaluations can accurately reflect the actual situation of the evaluated object and reflect the randomness and ambiguity of the evaluation itself. This article explores its application in the quality assessment of mixed education using the relevant theory of data mining algorithms. Section 2 of this paper describes data mining. On the basis of this data mining, Section 3 proposes a model evaluation method. Section 4 presents the design of the proposed model. In Section 5, the experimental design and experimental analysis are carried out. In Section 6, the conclusion is given.

2. Description of Data Mining

Data mining generally refers to the process of finding hidden information in large amounts of data using a variety of methods such as statistics, online analytics, and intelligence searches. Education data mining refers to the application of multiple disciplines of theory and methods for describing data so that people can quickly distinguish data. Through data mining processes such as clustering and associations, we provide students with video viewing tools for education, research, and solving time problems. For example, teachers can find student learning rules based on student learning data and teach them to effectively improve their teaching methods. This improves educational efficiency and builds effective explanatory models to predict and analyze future education, as shown in Figure 1.

Theoretical methods of data mining models are used to teach evaluation. It mainly uses the three digital feature values of the data mining model (expectations E_x, entropy E_n, and superentropy H_e) to characterize the results of the evaluation and analyze more detailed information to teach the evaluation. In expectations, E_x represents the center point of the evaluation value which indicates the definite value of the comment, where expectations E_x value falls within which comment value range of the evaluation result belongs to the comment level. Entropy E_n reflects the ambiguity of the comment result, E_n bigger explains that the comment level is more blurred, superentropy H_e reflects the degree of dispersion of the evaluation result from the evaluation curve, E_n explains that the uncertainty of the evaluation result is higher. The three digital feature values of the data mining model can be calculated using the data mining model reverse cloud generator method; that is, the digital feature values of the data mining model for each rating index are obtained from a large number of quantitative ratings. The specific calculation process is as follows: you can get the calculation steps of the reference.

3. Model Evaluation Method Based on Data Mining

Data mining models can achieve effective transformations between quantitative and qualitative concepts, thus transforming large amounts of specific evaluation data into corresponding natural comments. According to the evaluated index data, the inverse cloud generator of the data mining model is used to calculate the digital feature values of the data mining model of each index and analyze the meaning of the digital feature values [11, 12]. Because IT English mixed education involves independent learning of online courses and classroom education, the entire teaching process includes many online and offline links. Therefore, in addition to assessing the quality of teachers' traditional classroom education, students should be assessed online. The status of self-learning and the quality of online learning resources are assessed. Due to limited space, this article evaluates and analyzes the learning situation of the school's open course "College English" from the student's perspective and describes the process of applying a data mining model in educational evaluation. The specific process for applying for an educational evaluation is as follows [13, 14].

3.1. Specific Evaluation Indicators for Curriculum Design. In order to better reflect the actual situation of the course education and improve the quality of the course education evaluation, it is necessary to combine the educational practices of specific courses to develop the evaluation index corresponding to the course. If the course is a theoretical course or a hands-on course with a high percentage of hands-on operation, the corresponding metrics should be different to emphasize the characteristics of the course [15]. For example, the training direction of a university's open English course is to pay more attention to the student's language proficiency, and the corresponding content should be reflected in the designed metrics. In addition, the design of the metric system not only considers the comprehensiveness of the metric but also analyzes the importance of each metric in the overall metrics and reasonable weights each metric [16]. Two grades of metrics are set according to the teaching method of the "College English" course. One-step indicators are set up for online learning, learning resources, and classroom learning. Second-level indicators of "online learning" can be set as a result of self-learning attitudes, video viewing progress, and online testing. Second-level indicators under "learning resources" can be set as course video resources, course exercise resources, and course experiment resources. Second-level indicators under "learning in the classroom" can be set as teacher teaching attitudes, teacher teaching abilities, and module test scores [17, 18].

3.2. Scoring Various Indicators. Surveys are designed and published, students and related personnel are organized to score various metrics, these scoring data are collected, and some invalid data are processed according to the metrics set summarizing valid data.

3.3. Calculating the Digital Feature Value of the Data Mining Model of Various Indicators. Based on the scoring data for each metric, the data mining model reverse cloud generator is used to calculate the data for each metric to get the low-level digital feature values for the data mining model for each metric. These numerical characteristic values reflect the score distribution of each particular indicator.

3.4. Calculating the Comprehensive Evaluation. According to the digital function values of the cloud model of the low-level indicator, the data mining calculation method can be used to calculate the data mining model parameters of the high-level indicator layer by layer, and finally, the comprehensive evaluation parameters can be calculated and obtained. The overall assessment is used as the final outcome of this assessment and as a reference for measuring the comment level of the quality of education assessment [19].

3.5. Set Comment Collection. According to the practice of daily education evaluation of the school, the final comment

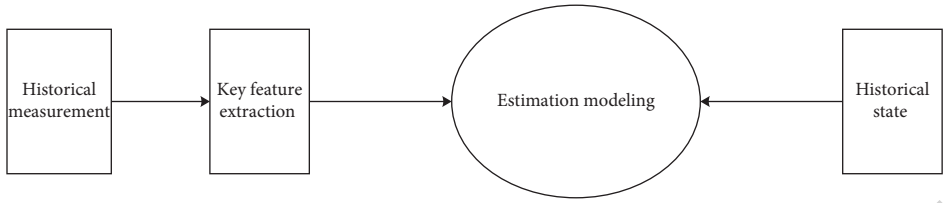

Figure 1: Modeling estimation driven by data.

set of the evaluation of the quality of education is set to four levels of "excellent, good, medium, and bad," and the division interval corresponding to each evaluation level is set and increased. The corresponding "excellent" level score is 9–10 points, the "good" level is 8–9 points, the "medium" level is 6–8 points, and the corresponding score is "bad." The level is 6–8 points. Values are 0–6 minutes. If the expected value of the overall rating is within the score range corresponding to the "excellent" level, the result of this rating is "excellent."

3.6. Drawing a Cloud Map. Rooting and rendering are simulated and analyzed by MATLAB, etc. The method is similar to the observation point and distribution shape, intuitive judgment, combined conclusion result, etc.

3.7. Analysis and Evaluation Results. As comprehensive evaluation combines the cloud digital feature values and the cloud drop distribution state of the cloud map, the evaluation results are analyzed, and more detailed information on educational evaluation is unearthed. Using the cloud model evaluation method, the digital characteristic of each index in each layer of the index can be analyzed concretely, and the evaluation result of each index in the evaluation can be obtained. If the expected value of a certain magical index is low, further improvement is needed in the future, and educational reform can be carried out appropriately. A low module test score in the classroom indicates that the ability to apply knowledge comprehensively is inadequate and that comprehensive content training can be conducted during normal hours. If the expected value of a certain magical index is too high, it means that the magical index is highly recognized. For example, the test shows that the expected value of the teacher's teaching attitude score is the highest of all indicators, indicating that the student is aware of the teacher's teaching attitude. If the superentropy value of the indicator is too large, it means that the metric's score has high volatility, which means that the gap between most scores is large.

4. Model Design

4.1. Dynamic Time Warping Algorithm. Data processing and analysis must rely on education. Due to different educational situations, the particle size of the collection time for different mixed education data is different. This causes the time dimension to accumulate different data formats, making it impossible to unify the time period. In this scenario, it is difficult for a typical data mining model to deliver its own performance, so this white paper presents a dynamic time warping (DTW) algorithm for data processing and analysis. The basic principles are as follows:

Suppose the test dataset is R, the training dataset is T, and the dimensions of each dataset sample are m and n. For supervised learning algorithms, we need to compare the similarities between the test and training datasets. At this time, the similarity of the samples can be measured by calculating the Euclidean distance D between the samples. If $n = m$,

$$D[T,R] = \sqrt{\sum_{i=1}^{M} (D[T(i),R(i)])^2}, \tag{1}$$

when $n \neq m$ needs to introduce the idea of dynamic programming to calculate D.

As shown in Figure 2, the test sample serial numbers are marked on the x-axis of the Cartesian coordinate system, and the training samples are marked on the y-axis. At this time, a cross grid can be formed on the coordinate axes, and the intersection of the grid becomes the intersection of the test sample and the training sample. At the same time, you need to find a path from the lower-left corner to the upper right corner of the axes. The i-th point that passes through this path is written as (n_i, m_i), and the path function is written. Thatis why

$$\begin{aligned} m_i &= \varphi(n_i), n = i, \\ \varphi(1) &= 1, \varphi(N) = M. \end{aligned} \tag{2}$$

When searching for a path, you need to limit the gradient to ensure the direction of the path. The slope usually varies from 0.5 to 2. If the point of the path that passes through at this time is n_{i-1}, m_{i-1}, then all possible situations at the next point are

$$\begin{aligned} (n_i, m_i) &= (n_{i-1} + 1, m_{i-1} + 2), \\ (n_i, m_i) &= (n_{i-1} + 1, m_{i-1} + 1), \\ (n_i, m_i) &= (n_{i-1} + 1, m_{i-1}). \end{aligned} \tag{3}$$

At this time, the above equation is used as the constraint condition, the best path in equation (1) is solved, the shortest path is taken as the optimization objective, and the objective function is obtained as follows:

$$\sum_{\substack{n_i=1 \\ m_i=F(n_i)h}}^{N} D(n_i, m_i) = \min_{F(n_i)} \sum_{\substack{n_i=1 \\ m_i=F(n_i)}}^{N} D(n_i, m_i). \tag{4}$$

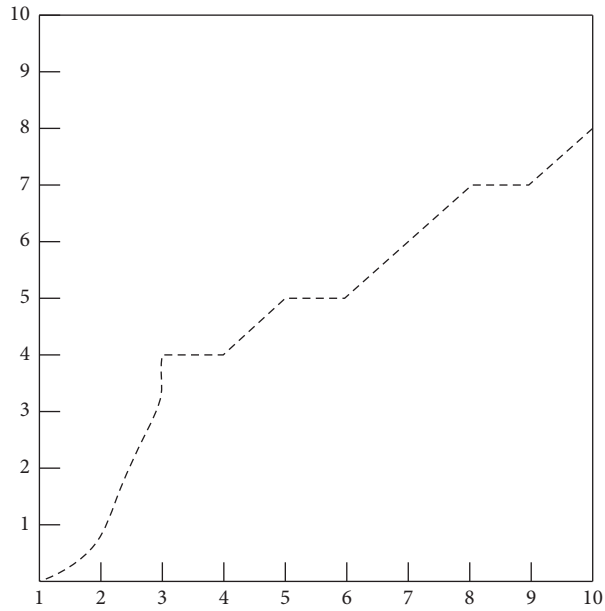

Figure 2: DTW algorithm path search principle.

At any point on the axes, only one path can eventually be passed during the path search process. So, for (n_i, m_i), there are only three cases (n_{i-1}, m_i), (n_{i-1}, m_{i-1-1}), or (n_{i-1}, m_{i-2}) at the previous point on the path. At this time, you need to select the point with the shortest distance from point (n_i, m_i) to the two points in these three cases as the previous node on the path. At this point, the total distance of the path can be obtained as follows:

$$D[(n_{i-1}, m_{i-1})] = \min\left\{\begin{array}{l} D[(n_{i-1}, m_i)] \\ D[(n_{i-1}, m_{i-1} - 1)] \\ D[(n_{i-1}, m_i - 2)] \end{array}\right\}. \quad (5)$$

4.2. Improved DTW Algorithm Based on Dynamic Bending. In the above equation, the DTW algorithm limits the slope of the path bend during the path search process. However, there are some points where this limitation cannot be met in the actual iterative process. Taking Figure 3 as an example, if the diamonds in Figure 3 perform distance matching, it is not necessary to calculate the distance outside the grid points. Due to the geometric properties of the diamond, it is not necessary to store the cumulative distance of every step in the calculation.

In Figure 3, the actual bend is divided into three path segments: $(1, X_a)$, $(X_a + 1, X_b)$, and $(X_b + 1, N)$, and the coordinates have the following relationship:

$$\left\{\begin{array}{l} X_a = \dfrac{1}{3}(2M - N), \\ \\ X_b = \dfrac{2}{3}(2N - M). \end{array}\right. \quad (6)$$

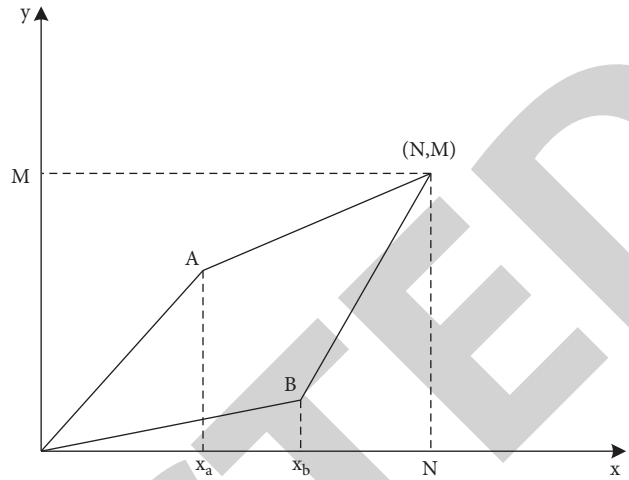

Figure 3: Schematic diagram of algorithm path constraint.

Taking X_a and X_b as close integers, the constraint conditions for dynamic bending matching can be obtained at this time:

$$\left\{\begin{array}{l} 2M - N \geq 3, \\ 2N - M \geq 2. \end{array}\right. \quad (7)$$

After introducing dynamic bending, there is no need to compare the X-axis feature vector with the feature vector corresponding to the Y-axis point. All you have to do is to compare it to the eigenvectors of $[y_{\min}, y_{\max}]$. The calculation method of the endpoints of this section is as follows:

$$\begin{array}{l} y_{\min} = \left\{\begin{array}{l} \dfrac{1}{2}x, 0 \leq x \leq X_b, \\ \\ 2x + (M - 2N), X_b \leq x \leq N, \end{array}\right. \\ \\ y_{\max} = \left\{\begin{array}{l} 2x, 0 \leq x \leq X_a, \\ \\ \dfrac{1}{2}x + \left(M - \dfrac{1}{2}N\right), X_a \leq x \leq N. \end{array}\right. \end{array} \quad (8)$$

At this time, the update method of distance accumulation is as follows:

$$D(x, y) = d(x, y) + \min\left[\begin{array}{c} D(x-1), y \\ D(x-1, y-1) \\ D(x-1, y-2) \end{array}\right]. \quad (9)$$

According to the above equation, if the X-axis time label advances gradually, you only need to pay attention to the cumulative distance in the previous column. Therefore, the algorithm does not have to store all the distance matrices, thereby achieving the goal of saving the memory required for the operation. Figure 4 shows the specific update method.

5. Experimental Design and Analysis

5.1. Experimental Design. To evaluate the performance of the algorithm, you need to collect and analyze the data. In this article, we will select relevant data for mixed education at the

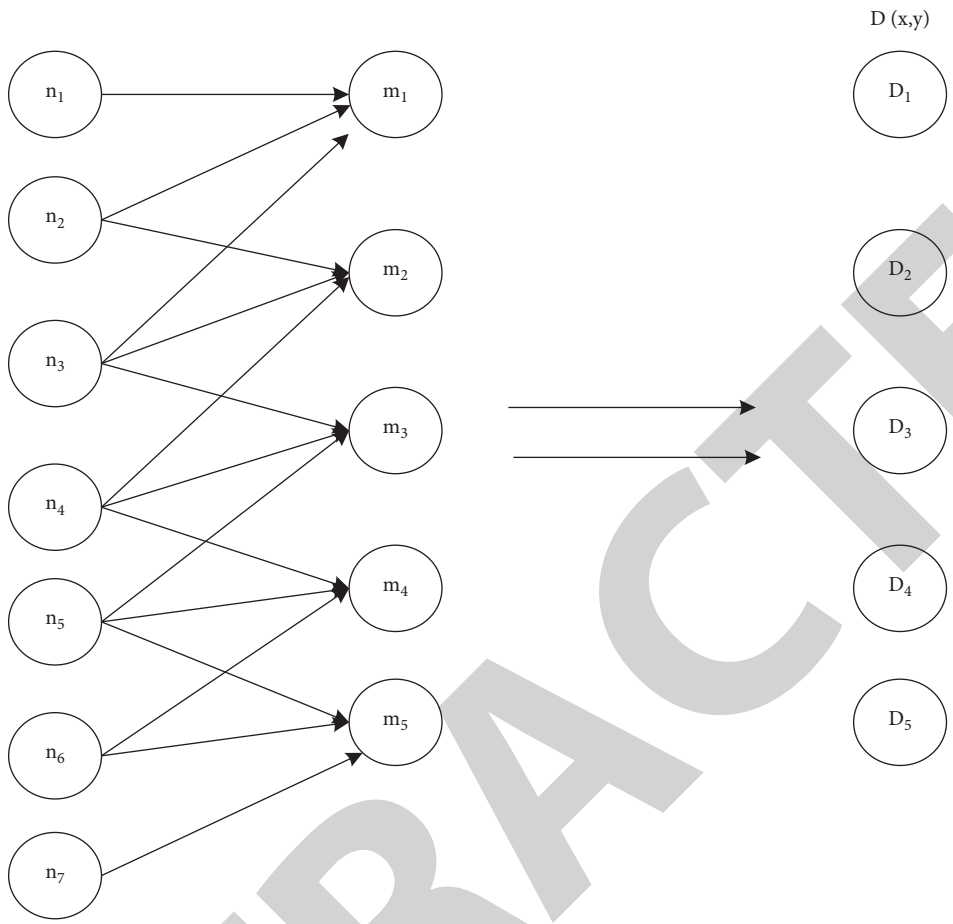

Figure 4: Cumulative distance update method.

university. The bibliography [4] method (method 1), bibliography [5] method (method 2), and bibliography [6] method (method 3) are used to test and compare the detection rates of the various methods. The description of the recall rate is as follows: the percentage of anomalous data detected in the overall anomaly of the correct information sample is calculated as follows:

$$\text{detection rate} = \frac{\text{true positive}}{\text{true positive}} + \text{false negative}. \tag{10}$$

In the above formula, true positive represents the true positive rate and true negative represents the true negative class. Recall rate of an abnormal dataset is shown in Figure 5.

From the data in Figure 5, it can be seen that the recall rate of the abnormal points in Method 1 is higher than that in Methods 2 and 3, and the recall rate in Method 1 is as high as 98% or more. 1 is in the diagnostic information for COPD. Prior to the automatic mining of sensitive data, we used an unsupervised step-by-step learning method to clean up sensitive data in COPD diagnostic information. This has reduced a large amount of duplicate data in the database and improved the recall rate. To further verify the overall effectiveness of this method, the method above is used to test the automatic mining of sensitive data for COPD diagnostic information and compare the time spent of the three methods with the same amount of data, Figure 6.

Analyzing Figure 6 shows that with the same amount of data, Method 1 consumes less time than Methods 2 and 3. This is because Method 1 is based on the data cleaning framework for sensitive data in COPD diagnostic information. The cleaning process eliminated erroneous data in COPD diagnostic data, reduced the time required for automatic mining of sensitive data in COPD diagnostic information, and verified the efficiency of Method 1. The error data detection rates of the above three methods are compared. The detection rate of incorrect data can be calculated by the following formula:

$$\text{detection accuracy} = \frac{\text{TN} + \text{TP}}{\text{FN} + \text{TN} + \text{FP} + \text{TP}}. \tag{11}$$

In the above formula, TP represents that the wrong data is judged wrong data, TN represents that the correct data is judged correct data, FP represents that the correct data is judged wrong, and FN represents that the wrong data is judged correct data.

The detection capabilities of the three methods for erroneous data are shown in Figure 7.

As the amount of data increases, the ability to detect incorrect data decreases. Analyzing Figure 7 shows that the error detection rate for Method 1 decreases with increasing data volume, but all exceeds 80%. It automatically resolves and records the optimal boundary function for sensitive data

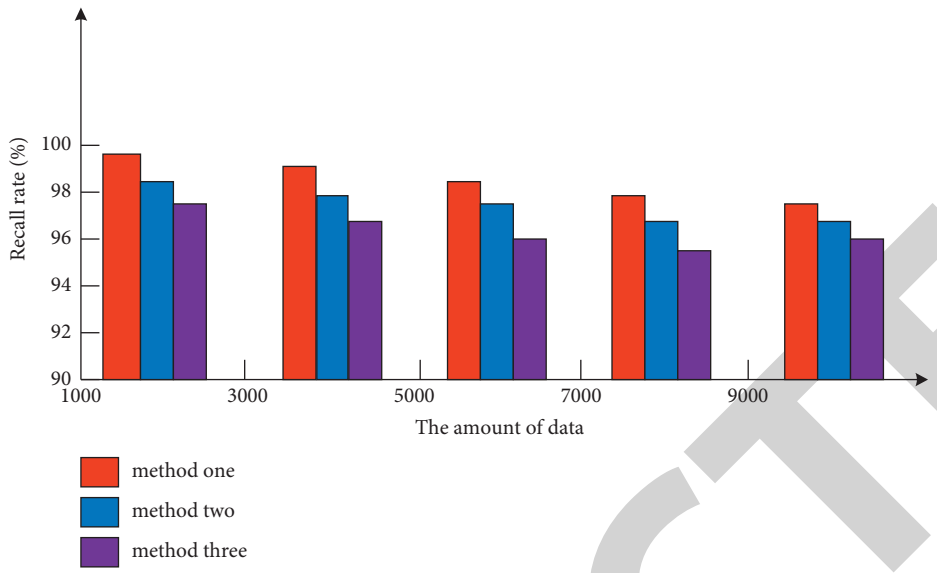

Figure 5: Recall rate of abnormal dataset.

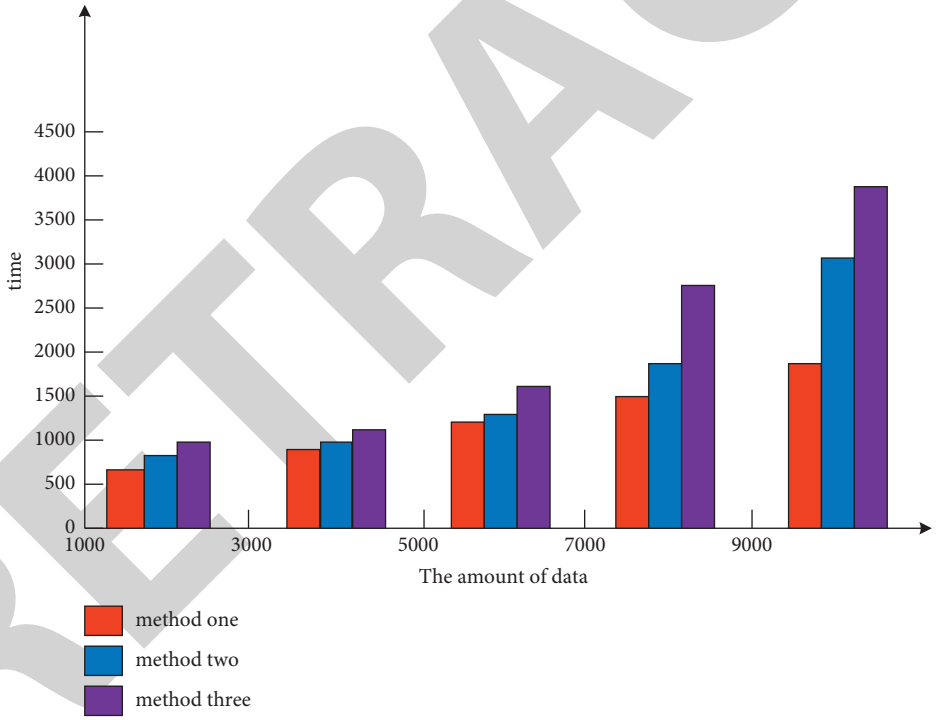

Figure 6: Time consumption.

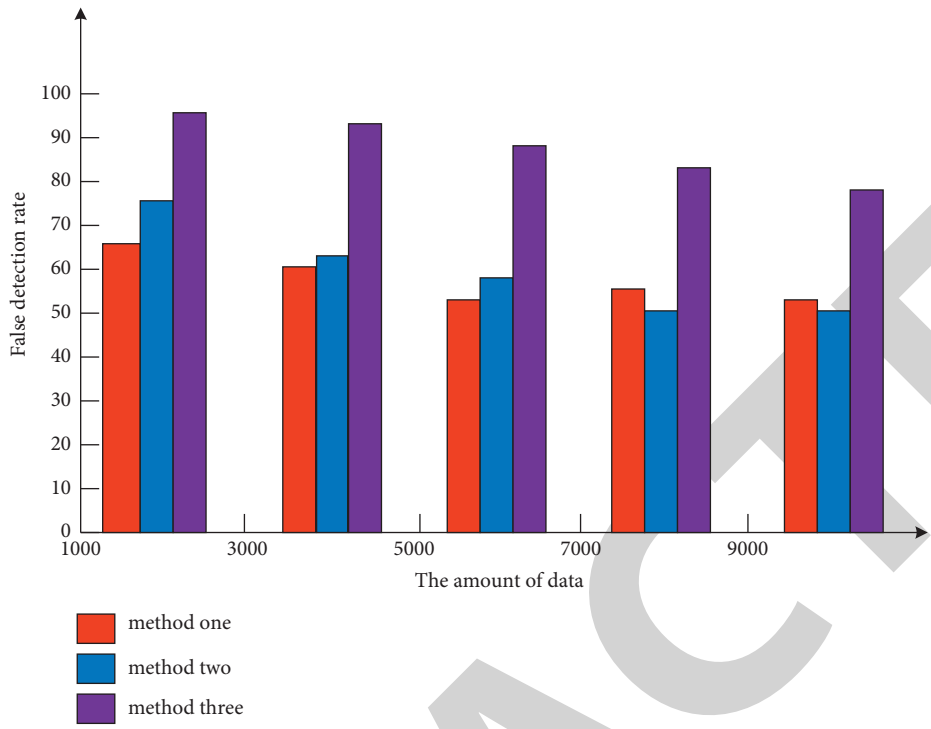

Figure 7: Detection rate of wrong data.

in mined COPD diagnostic information, processes large numbers of unlabeled data records, and detects all incorrect data in the database to avoid data nonuniformity. Other useless data improves your ability to detect false data.

6. Conclusion

Data mining models can enable the conversion of quantitative data to qualitative assessments and are an effective tool for teaching quality assessments. The data mining model has certain advantages in dealing with mixed educational quality assessments. It can not only get the results of a comprehensive assessment but also reflects the ambiguity and randomness of the assessment data, reflecting the reliability and rationality of the assessment process. In addition, the data mining model method can be used to mine the meaning contained in the evaluation data and obtain more detailed evaluation information so that it is possible to find specific problems in education that are convenient for teachers and improve education in a targeted way, thereby improving educational effectiveness. Of course, when assessing education using a data mining model, there are some issues that make the computational process more complex, and the evaluator must have specific computer application capabilities.

Data Availability

The data used to support the findings of this study are available from the corresponding author upon request.

Conflicts of Interest

The author declares that he has no conflicts of interest.

Acknowledgments

This paper was supported in 2017 by the Basic Scientific Research Projects of Colleges and Universities in Liaoning Province "A Practical Study on Microlecture Assisted Teaching Model of College English Course Based on ESP Concept" (Project No. 2017JYT22).

References

[1] Y. Zhou, "The application of data mining based on Rough set in teaching evaluation," *Journal of Chongqing University of Posts and Telecommunications:Natural Science Edition*, vol. 20, no. 5, pp. 627–629, 2008.

[2] B. Zhang, L. Sun, L. Ma, and H. Xu, "Fuzzy evaluation of university teachers' teaching quality based on analytic hierarchy process," *Journal of Liaoning Radio & TV University*, vol. 5, no. 3, pp. 1–4, 2016.

[3] Y. Zhang, D. Jin, and S. An, "Qualitative evaluation based on cloud model and its application in teaching evaluation," *Computer Engineering and Applications*, vol. 48, no. 31, pp. 210–215, 2012.

[4] Y. Ye, "Data mining of classroom teaching quality based on cloud model," *Computer Simulation*, vol. 29, no. 8, pp. 373–376, 2012.

[5] C. Liu, F. Mang, X. Dai, and D. Li, "A new reverse cloud algorithm based on cloud X information," *Journal of System Simulation*, vol. 16, no. 11, pp. 2417–2420, 2004.

[6] Y. Thoma, A. Dassatti, D. Molla, and E. Petraglio, "FPGA-GPU communicating through PCIe," *Microprocessors and Microsystems*, vol. 39, no. 7, pp. 565–575, 2015.

[7] Z. Zhao and C. Qian, "Financial crisis based on data envelopment and data miningResearch on computer prediction model," *Computer Science*, vol. 43, no. S2, pp. 461–465, 2016.

Hindawi
Journal of Mathematics
Volume 2023, Article ID 9831759, 1 page
https://doi.org/10.1155/2023/9831759

Retraction

Retracted: Deep Learning-Based Economic Forecasting for the New Energy Vehicle Industry

Journal of Mathematics

Received 19 December 2023; Accepted 19 December 2023; Published 20 December 2023

This article has been retracted by Hindawi following an investigation undertaken by the publisher [1]. This investigation has uncovered evidence of one or more of the following indicators of systematic manipulation of the publication process:

(1) Discrepancies in scope

(2) Discrepancies in the description of the research reported

(3) Discrepancies between the availability of data and the research described

(4) Inappropriate citations

(5) Incoherent, meaningless and/or irrelevant content included in the article

(6) Manipulated or compromised peer review

The presence of these indicators undermines our confidence in the integrity of the article's content and we cannot, therefore, vouch for its reliability. Please note that this notice is intended solely to alert readers that the content of this article is unreliable. We have not investigated whether authors were aware of or involved in the systematic manipulation of the publication process.

Wiley and Hindawi regrets that the usual quality checks did not identify these issues before publication and have since put additional measures in place to safeguard research integrity.

We wish to credit our own Research Integrity and Research Publishing teams and anonymous and named external researchers and research integrity experts for contributing to this investigation.

The corresponding author, as the representative of all authors, has been given the opportunity to register their agreement or disagreement to this retraction. We have kept a record of any response received.

References

[1] B. Cai, "Deep Learning-Based Economic Forecasting for the New Energy Vehicle Industry," *Journal of Mathematics*, vol. 2021, Article ID 3870657, 10 pages, 2021.

Hindawi
Journal of Mathematics
Volume 2021, Article ID 3870657, 10 pages
https://doi.org/10.1155/2021/3870657

Research Article

Deep Learning-Based Economic Forecasting for the New Energy Vehicle Industry

Bowen Cai

Beijing Jiaotong University, Beijing 100044, China

Correspondence should be addressed to Bowen Cai; brooven@cumt.edu.cn

Received 22 November 2021; Revised 8 December 2021; Accepted 11 December 2021; Published 31 December 2021

Academic Editor: Naeem Jan

Recently the issues of insufficient energy and serious air pollution around the world have been rising. Henceforth, there is a need to carry out a research of new energy. Soon, new energy vehicles will be the mainstream trend, which can not only reduce the burden of consumers due to rising fuel prices but also solve the air pollution problem caused by the exhaust emissions of fuel vehicles. With the rapid development of science and technology, deep learning continues to make breakthroughs, and, in the field of economy with huge information data, we have more powerful weapons available to predict and research important economic data with infinite value, which can not only provide reference information to policy makers but also help enterprises and even economic markets to develop more healthily and sustainably. Therefore, this article uses deep learning algorithms to forecast and analyze the new energy industry, starting from the financial information released by new energy vehicle companies in their annual reports, in order to make basic judgments and help policy makers and enterprises in the new energy vehicle industry.

1. Introduction

Since the industrial revolution, a series of ecological and environmental problems [1] brought about by excessive human production and consumption [2] have come to a point where we have to pay attention to them and take measures to remedy and correct them. In this context, the concept of low-carbon development [3], which balances environmental protection and development, has gradually emerged and become a global trend. From personal lifestyles to government policies, the shadow of low-carbon development can be seen everywhere. Economic and social development and environmental protection have always been a dilemma for human beings [4], especially after the industrialization era. After years of practical exploration, mankind has finally found the road to low-carbon development, which is to integrate development into the construction of ecological civilization and environmental protection into economic development. From the current energy production and consumption situation, the development of new energy and energy-efficient technologies and products is an important step to ensure the sustainable development of the global economy.

The automotive industry is not only a pillar industry driving the national economy [5] but also a high-consumption and high-emission industry [6], which plays an important role in macroeconomic development and low-carbon economic transformation. The rapid development of China's economy and market has attracted many automobile manufacturers from developed countries to come to China, not only bringing advanced products and technologies but also making China face huge pressure of environmental protection, such as the oil crisis, urban environmental pollution, and traffic deterioration. The traditional development mode of automobile industry has obvious obstructive effect on economic sustainability, so the automobile industry must transform to low carbon with technological innovation as the core. New energy vehicles

are the inevitable product of the development of the times, and the development of new energy vehicles is the inevitable path for the global automotive industry.

The industrial change triggered by the development of new energy vehicles will be a complete reshuffle; however, the development of the new energy vehicle industry will also be accompanied by a lot of uncertainty, especially because new energy vehicle companies have significant differences from the traditional automobile industry. For this reason, both the policy makers of the new energy industry and the practitioners of the new energy vehicle enterprises always need to assess and control the industry accurately. In the current fast-moving 21st century, scientists and researchers have provided us with many new techniques and analytical tools to study the industrial economy. Not only has deep learning become one of the most important key technologies in the field of AI, but also it has attracted a lot of attention from researchers in related business economies [7]. Deep learning has a wide range of applications in various fields and industries [8], driving industrial innovation and breakthrough development. In the field of economy and finance, people are also increasingly aware of the importance of economic data to enterprises, which determines the development and future of enterprises [9]. As the volume of economic data increases dramatically and the forms of data become more and more diversified, the approach of deep learning provides a new research idea of finding patterns from big data and learning the potential features behind the data through deep learning models [10]. So it is of great importance to apply deep learning to the field of economy and finance.

The main theme and focus of this article are on the use of deep learning methods to analyze and predict the corporate financial reports of new energy vehicle companies, especially the net profit of a company and the net cash flow from operating activities. The end-product of the operations of an enterprise is the net profit, that is, the principle sign of the working productivity of the enterprise. Net profit is utilized to replicate the operation and profitability of the enterprise. However, the value of the revenues should be evaluated along with other comprehensive factors. The most significant factor is the net cash flow from operating activities in the cash flow statement. Free income is created in the business exercises based on guaranteed normal operation and consistent/reliable reinvestment of the enterprise, which guarantees the free circulation and investment in a safe situation and is the actual fund that can be called by the enterprise, and operating cash flow is the most important part that constitutes free cash flow. The analysis of net income and net cash flow from operating activities not only reflects a company's ability to operate on a sustainable basis but also conveys information about the possible existence of abnormalities in the long-term operation of the company. By analyzing the matching ratio between net profit and operating cash flow, we can make a basic judgment on the sustainable operating ability and competitiveness of the new energy vehicle company.

The organization of the rest of the paper is as follows: Section 2 reviews some of the related literature. In the third section, the deep learning prediction models are build, which are based on GRU and CNN. Section 4 presents the experimental analysis and the results achieved by the trials. In Section 5, the final results and achievements are deliberated as a conclusion.

2. Related Work

2.1. Data Resources. Nowadays, both business operators and ordinary investors attach great importance to the data of economic and financial fields such as company annual reports, stocks, and funds, and, accordingly, major financial websites collect and display various announcements and data information. In this paper, we need to obtain the annual reports of companies in the new energy automobile industry and crawl them to further process and analyze the important information in the annual reports.

The process of crawling PDF financial statements from financial websites is roughly as follows: (1) Using crawler technology, we obtain the IDs of all companies, generate Uniform Resource Locators (URLs) for the main pages of all company information, and put them into the queue of URLs to be crawled. (2) The crawler reads from the queue of URLs to be crawled in turn, resolves the URLs through a domain name resolver (DNS), and converts the link addresses to the IP address of the web server, and then the web page can be downloaded. (3) We use Python's Request module to crawl to the main page of the company's information, and the URL of the company's annual report in PDF format is in the web page content. According to the characteristics of the annual report URL, generate a regular expression, and then use the Re module to search for the company's annual report URL. (4) Finally, use the Request module to download the annual report in PDF format, and use the company ID as the file name for storage for subsequent use.

2.2. PDF Analysis and Table Data Extraction. In this article, we want to study the sustainability of new energy vehicle companies, and the important economic data needed are net profit and net cash flow from operating activities, so we need to extract the income statement and cash flow statement from the PDF annual reports of listed companies for subsequent research and analysis. We need to get a number of companies as well as multiple years of data, so you want to efficiently and accurately analyze the PDF, and you need to crop a long PDF, according to keywords to get the specific location of the target form, making the analysis more convenient. As shown in Figure 1, the specific steps will be explained in detail below.

2.2.1. Location Information Based on Keywords. In order to streamline and intercept PDF to obtain more accurate positioning and analysis, to improve efficiency, the first step is the need to get the target data according to the keyword page number and location. This paper uses Java to write ITextpdf method to locate the target data. When we provide the PDF file path, store the target location information to get the file path, and match the content of the target with keywords of

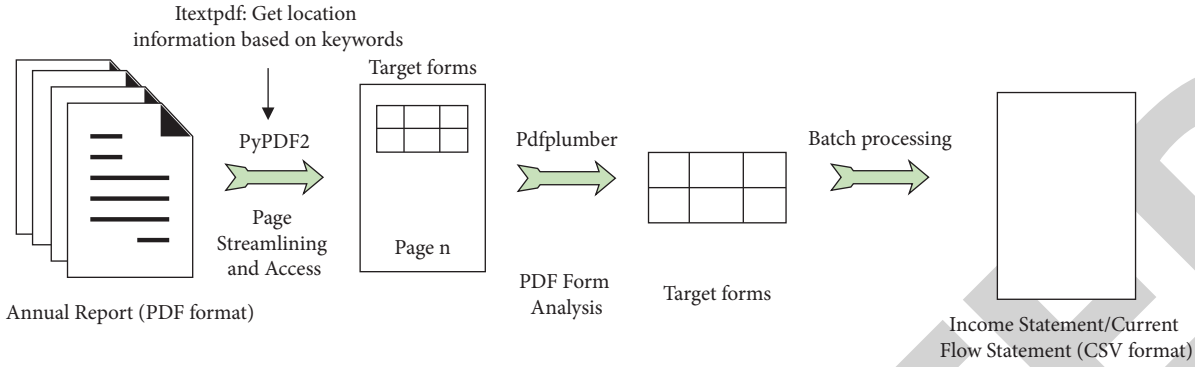

Figure 1: Data extraction process.

the three parameters, we can achieve the target location and page number, and batch management for subsequent use.

2.2.2. PDF Page Streamlining and Interception. In this paper, we use the Python library PyPDF2 to streamline and intercept the pages of the annual reports of listed companies with a large number of pages. According to the previous section of the method to obtain the target location and page number, call addPage() and other methods to add the loop to the object created by the PdfFileWriter class, in the output stream to add PDF pages; finally, we want to streamline and intercept the target page written to a new PDF file and want to achieve batch operations and management in order to follow the analysis of the work.

2.2.3. PDF Form Parsing and Data Batch Grabbing. After obtaining the streamlined PDF, we were able to target the important economic data in the tables and use the Pdfplumber technique in the Python third-party library to parse the PDF and extract the income statements and cash flow statements of several new energy companies and multiple years. Finally, the extracted results were modified and collated to obtain the income statements and cash flow statements for the annual reports of the new energy companies needed for this study and sorted by company and chronological order according to the different industries and collated into an easy-to-use CSV file.

2.3. Experimental Data Preprocessing and Sample Generation. After parsing and extracting the data from the PDF annual reports of the new energy vehicle companies, the data is obtained in a convenient CSV format for use. In order to obtain the dataset for the final model requirements, this paper also requires preprocessing of the data, including various data cleaning, normalization, feature selection, and finally sample generation for the experimental requirements.

2.3.1. Data Cleaning. Data cleaning is an essential and critical step in data analysis [11], and the quality of the data obtained after cleaning will directly affect the subsequent model effects and experimental conclusions. In the first step of missing value cleaning, the proportion of missing values for each feature is firstly counted. If there are too many missing values, the validity of the features is lost, so the feature columns with more than 80% missing values are directly deleted in this paper. Then the missing values are filled in. As each economic indicator has a certain standard, if it is filled in randomly, it may cause the data to be unrealistic, and there are many 0 values in many features, so, according to experience, this paper fills in the missing values with 0. The second step is to clean the formatted content. The format of the data will affect the data import as well as the experimental process; for example, in this paper, the accounting time in the income statement and cash flow statement is cleaned in format.

2.3.2. Normalization. In real data, different features have different ranges of values, and thus it may happen that individual features with larger values in the feature space have a dominant effect on the sample. In order to have all features in the same scale, it is important to map them to the same scale so that the accuracy of the model can be improved as well as the speed of the fit, so this experiment is to normalize the sample [12]. We use the maximum-minimum normalization method, which scales the dataset equally and ends up being represented as a value between [0, 1], as shown in the following equation:

$$X_{\text{scale}} = \frac{x - \min}{\max - \min}. \tag{1}$$

2.3.3. Feature Selection. Feature selection is a very important step in the actual processing of data [13]. Not only does it help to further understand the characteristics and relationships between data features but it also reduces feature dimensionality, reduces overfitting to improve model generalization, and improves the performance of algorithms and models. We have experimentally chosen the Randomized Lasso algorithm of the top-level feature selection algorithm, which is a kind of stability selection. Lasso regression means that the penalty function used in solving the objective function of the regression coefficients is the L1 parametrization, as shown in the following equation:

$$\widehat{\beta}_{\text{Lasso}} = \arg\min_{\beta \in R^d} \left(\|Y - X\beta\|^2 + \lambda \sum_{j=1}^{d} \left|\beta_j\right| \right). \tag{2}$$

2.3.4. Sliding Sample Generation. Through the above data preprocessing, the effective features are selected using the feature selection algorithm; this paper uses a time span of 2 years as a sample and sliding order to select samples, with each company individually divided for sample generation. The 2-year time span is the best time span to be tested. Through analysis, if the time span is too small, it will not be easy to grasp the trend pattern, and if the time span is too large, the number of samples will be too small, which will make the prediction effect poor. The specific operation process is shown in Figure 2, and finally a dataset sample with multiple characteristics over multiple time spans can be obtained. As our aim is to study the data in the annual reports of new energy vehicle companies, not only are there a limited number of new energy vehicle companies, but also a limited number of years of annual reports can be obtained, so a sliding approach to sample generation not only allows for a more detailed delineation of features while maintaining the time-series characteristics but also increases the number of samples and is suitable for smaller datasets.

3. Building Deep Learning Prediction Models Based on GRU and CNN

Deep learning is applied to the annual reports of new energy vehicle companies, the prediction and analysis of the net profit in the income statement, which reflects the operation and profitability of the enterprise, and the net cash flow from operating activities in the cash flow statement, which reflects the quality of profitability. Finally the basic judgment of the sustainability of individual enterprises and the industry as a whole is of certain research and practical significance.

For the prediction of important economic data with time-series characteristics, this paper first uses machine learning models that have the advantages of being simple, efficient, and stable, such as the MLR model [14], which is the simplest multiple linear regression model that can handle linear relationships well, and the SVR model [15], which has multiple kernel functions that can be applied to data with a variety of characteristics. However, as they do not adequately consider and reflect the time-series characteristics of the data nor can they extract the underlying features between the data in depth, the prediction results are rather mediocre. However, these two problems that arise can be well improved using deep learning methods. The GRU model [16], a variant of the recurrent neural network (RNN) gated recurrent unit [17], is particularly suitable for time-series data and also addresses the long-time dependence problem that is important for predictive regression results, coupled with the convolutional neural network (CNN) model that can effectively extract potentially important features between data. The combination of GRU and CNN models [18] is therefore ideally suited to our prediction and regression of corporate financial reports.

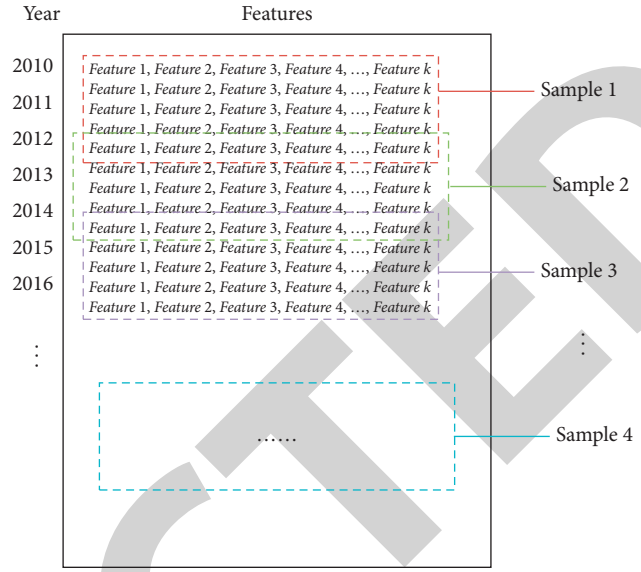

Figure 2: Sliding sample generation.

3.1. CNN Model. CNNs have great advantages in extracting local high-level abstract features due to their local perception, weight sharing, and pooling layer downsampling [19]. CNN uses forward propagation to calculate the output values and gradient descent and backpropagation to train the model, adjusting the weights, biases, and so forth. The forward calculation formula for the convolutional layer of the CNN is as follows:

$$X_j^l = f\left(\sum_{i \in M_j} X_i^{l-1} * K_{ij}^l + b_j^l \right), \tag{3}$$

where K is the convolution kernel, which contains $n * m$ weights. The feature mapping map of layer $L-1$ is convolved with K in a dot product operation and then summed and a bias is added to prevent overfitting. Finally, the activation function is used to obtain the feature map of the Lth layer. In order to reduce the computational complexity and extract the main features, the feature mapping map needs to be compressed, so the downsampling formula for the pooling layer is as follows:

$$X_j^l = f\left(\beta_j^l \text{down}\left(X_i^{l-1}\right) + b_j^l\right), \tag{4}$$

where down() is a function that samples the feature values of layer $L-1$, for example, to find the maximum value and the average value, and then adds a bias to the activation function to obtain a feature map of the specified size after compression of the Lth layer. When training in the training set using the backpropagation algorithm, weights and biases are obtained, which are continuously adjusted to meet the training objectives. These set weights and biases can then be used to obtain regression predictions when the test set is tested.

The exact operation of a CNN is roughly shown in Figure 3.

In the input layer, each feature in the input sample is treated as a neuron. After setting the number of convolutional kernels, size, convolutional move step, and so

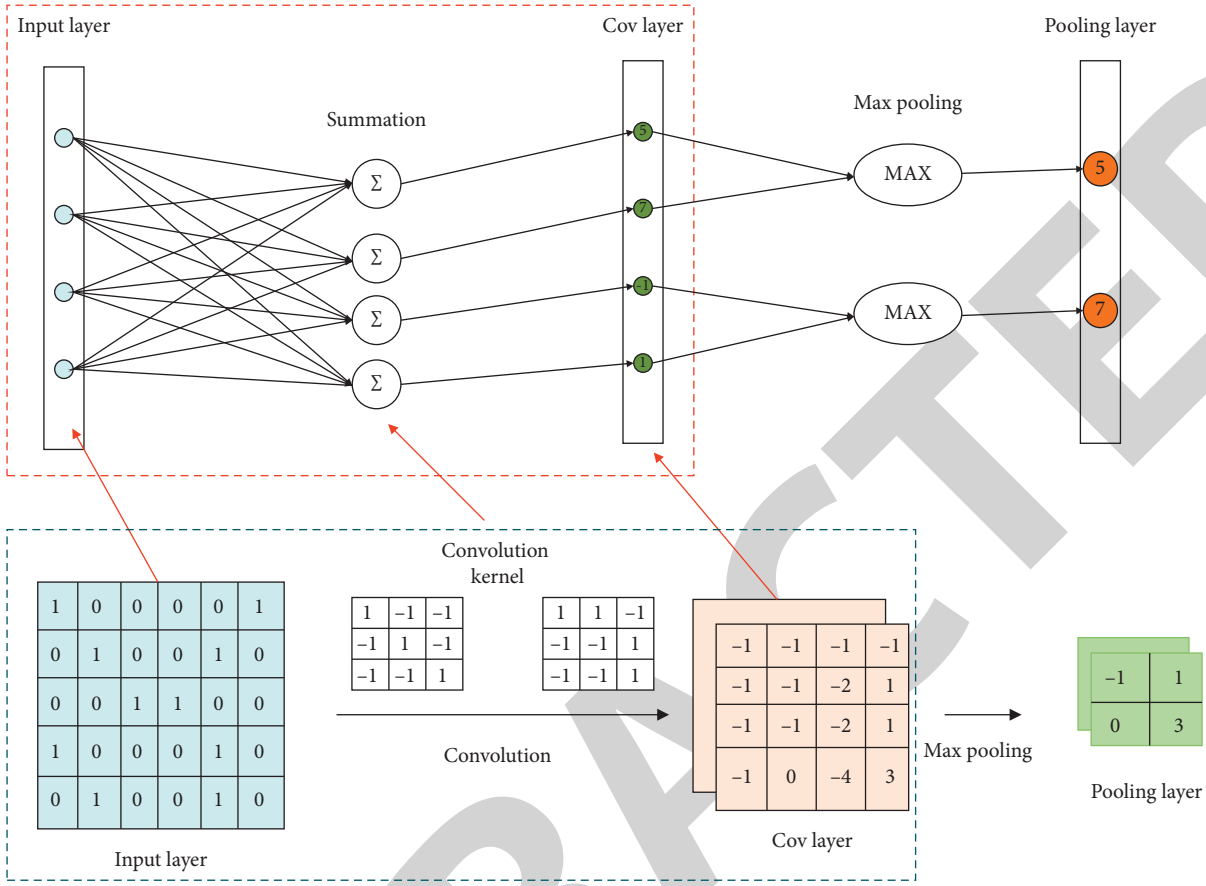

Figure 3: The schematic diagram of CNN.

forth and using the weight parameters of the convolutional kernels calculated by the backpropagation algorithm, the convolutional operations and summation are performed with the neurons in the input layer to obtain the feature maps of the convolutional layer composed of the feature values. For the pooling layer, we use the maximum pooling algorithm, which sets the size of the pooling kernel and the sliding step to calculate the new feature values and form the compressed feature maps of the pooling layer.

3.2. GRU Model. The GRU model not only has the power of an RNN for time-series data but also has the advantage of an LSTM network that is good at dealing with long- and short-term dependencies. The GRU model works as shown in Figure 4 and equations (5) to (12).

GRU has two important gates, the Update Gate and the Reset Gate. As shown in Figure 4, z_t represents the Update Gate. Equation (5) connects input x_t and the two vectors of h_{t-1} of the previous hidden layer and then performs a dot product with the weight matrix W_z. Finally, the result is compressed between 0 and 1 by the sigmoid activation function. The closer z_t is to 0, the more information from the previous hidden layer should be forgotten in that hidden layer, and the closer it is to 1, the more information needs to be retained in that hidden layer. r_t represents the Reset gate, which is similar to z_t, except that the weight matrix is W_r, as shown in equation (6). The more r_t is closer to 0, the more information from the previous hidden layer should be forgotten in the current memory content, and the closer it is to 1, the more information needs to be retained in the current memory content. The closer it is to 1, the more information needs to be in the current memory content that will continue to be retained.

$$z_t = \sigma(W_z \bullet [h_{t-1}, x_t]), \tag{5}$$

$$r_t = \sigma(W_r \bullet [h_{t-1}, x_t]). \tag{6}$$

In Figure 4, $\tilde{h}_t$ represents the candidate hidden layer state (Candidate Activation), which is expressed by multiplying the previous moment hidden layer h_{t-1} with the Reset gate r_t, which is used to determine how much of the previous moment hidden state is to be forgotten in the current memory content. This is then linked to the input x_t matrix, dotted with the weight matrix $W_{\tilde{h}}$, and finally scaled to −1 to 1 by the tanh activation function. $\tilde{h}_t$ finally stores all the important information recorded by GRU by calculating the important information in the hidden layer at the previous moment as well as the important information in the current input, as shown in the following equation:

$$\tilde{h}_t = \tanh\left(W_{\tilde{h}} \bullet [r_t * h_{t-1}, x_t]\right). \tag{7}$$

Finally, it is necessary to calculate the current moment hidden layer h_t, as expressed in equation (8) by multiplying

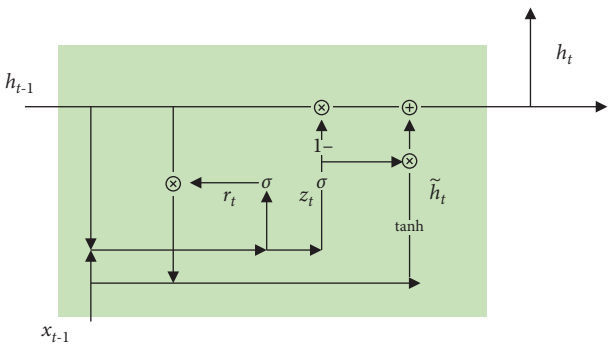

Figure 4: The structure diagram of GRU.

all the important information $\tilde{h}_t$ in the candidate hidden layer state with the Update gate to obtain the updated important information that needs to be obtained. The information that continues to be retained with the hidden layer at the previous moment is summed to obtain the hidden layer h_t. Finally, by dotting the product with the weight matrix W_o and then inputting the sigmoid activation function, result y_t is obtained, as shown in equation (9).

$$h_t = (1 - z_t) * h_{t-1} + z_t * \tilde{h}_t, \tag{8}$$

$$y_t = \sigma(W_o \bullet h_t). \tag{9}$$

The above process is the GRU forward propagation process, where W_r, W_z, $W_{\tilde{h}}$, and W_o are the parameters to be trained, and W_r, W_z, and $W_{\tilde{h}}$ are stitched together by two vector matrices, respectively. This is shown in the following equations:

$$W_r = W_{rx} + W_{rh}, \tag{10}$$

$$W_z = W_{zx} + W_{zh}, \tag{11}$$

$$W_{\tilde{h}} = W_{\tilde{h}x} + W_{\tilde{h}h}. \tag{12}$$

Then the model is trained by backpropagation algorithm and gradient descent regularization. The parameters, such as weights and biases, are adjusted, updated, and iterated until the loss converges; that is, the training is completed, and the test set data can be fed into the GRU for prediction.

3.3. CNN-GRU Model Construction. Taking advantage of the efficient extraction of potential relationships between features by CNN and the powerful ability of GRU to handle long- and short-term dependencies of time-series data, the construction process of CNN-GRU [20], the first model combining CNN and GRU in this paper, is shown in Figure 5.

The first input sample size is a matrix of $5 * k$, where 5 represents a sample of 5 years as a time step. k represents the number of features of the sample after feature selection. 25 features from the income statement of the listed company are selected for training when predicting net profit, so k is 25. When predicting net cash flow from operating activities, the cash flow statement is used to obtain 29 features after feature selection. After feature selection, 29 features are available, so k is equal to 29 currently.

Then the sample data is input into CNN for abstraction of local features, and the CNN of Convolution2D is selected. Firstly, the first convolutional layer is entered for training, in which the convolutional kernel size is set to $2 * 3$ rectangle, and the number of convolutional kernels filters is set to 32, which can get 32 layers of feature maps, used to extract different kinds of potential relationships and features; the convolutional step strides are equal to 1. By sliding the convolution from top to bottom in left-to-right order, the padding attribute is set to same, because the boundary information is chosen to be discarded when padding is equal to another valid value. When set to same, the boundary information is preserved, and the input and output sizes are kept consistent because the boundary is complemented by adding 0. This layer is learned using the ReLU activation function, which is easier to learn to optimize, and is then fed to the second convolutional layer in order to extract the features in more depth. In this layer, the convolutional kernel size is set to a rectangle of $3 * 5$, and the number of filters is set to a larger 64 to store the extracted features, resulting in thicker 64-layer feature maps, with the convolutional step length strides still equal to 1. In the pooling layer, the window size of the pooling kernel is set to a $2 * 2$ rectangle, the window sliding steps are set to 2, and the ReLU activation function is used. After pooling, the number of layers of 64 is unchanged but the features are compressed to obtain the feature maps, and, finally, a dropout mechanism is used to temporarily disable the neurons in the hidden layer at a random rate of 0.25 to effectively alleviate the overfitting situation.

After the features of the samples are extracted by the CNN network, the extracted features can be tiled in temporal order by the TimeDistributed(Flatten()) layer to preserve the temporal order of the features. The features are then fed to the GRU layer, which takes advantage of the GRU's ability to process temporal features efficiently and to handle long- and short-term dependency problems. Finally, a dense fully connected layer is connected, and the final prediction results are output using linear activation function.

3.4. CNN + GRU Fusion Model Construction. The last column of features in the sample of this paper is called direct features, and the other columns of features are called indirect features. In other words, when forecasting net profit through the past income statements of new energy vehicle companies, the last column of characteristics is the net profit of previous years, and the other columns are the indirect characteristics of operating income and sales expense of previous years. When forecasting the operating cash flow from operating activities through the cash flow statement, the last column of features is the operating cash flow of previous years, and the other columns are indirect features such as tax refunds received in previous years and net increase in cash and cash equivalents. Since different features have different potential characteristics, in this paper, we

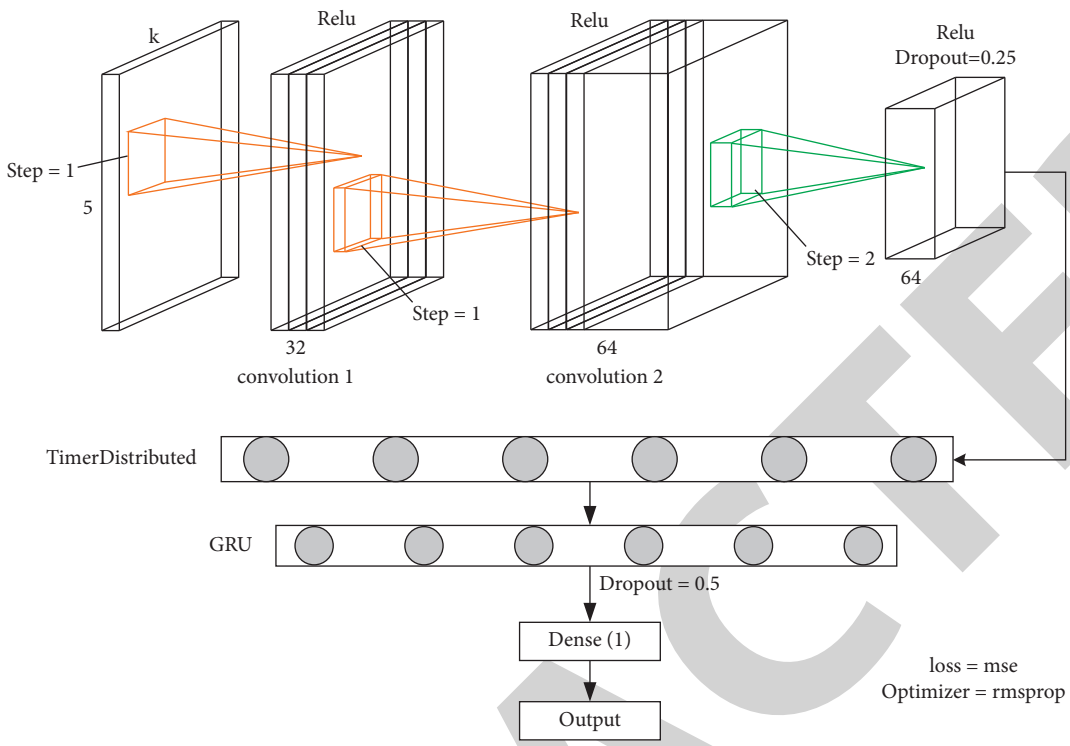

Figure 5: The overview of CNN-GRU.

build different models for each of the different characteristics for training and then finally merge and splice the different abstract features obtained from each training and then carry out the next training together to achieve better and more ideal prediction results. The construction process of our second model combining CNN and GRU, that is, CNN + GRU with CNN and GRU fusion [21], is shown in Figure 6.

First, the sample of size $5 * k$ matrix is input, 5 still represents the best time step of 5 years after experimental validation, k represents the number of effective features after feature selection, k takes 25 when predicting net profit, and k equals 29 when predicting operating cash flow. Then the samples have to be divided into samples, and the first $k - 1$ indirect features are input into the CNN model as shown in the left-dashed box for training, and the last column of direct features FEATURE k is input into the GRU model as shown in the right-dashed box for training.

In the left CNN model, in order to extract the potential high-level abstraction relationship between indirect features, firstly enter the first convolution layer Convolution2D, set the size of convolution kernel as a rectangle of $2 * 3$, and perform the convolution operation sequentially in the order of top to bottom, left to right, and step size of 1. The number of 32 convolution kernels is set to extract different kinds of features, and finally the feature map of 32 layers can be obtained in this layer. Then we enter the second convolution layer of Convolution2D, the size of the convolution kernel in this layer is $3 * 5$, and the number of convolution kernels is increased to 64 to store the extracted features. The activation functions of both convolutional layers use the efficient ReLU activation function. In order to reduce the parameters to extract more important and higher-level features and relationships, a pooling layer is connected next, using a maximum pooling algorithm, each time selecting the maximum value in a matrix with a pooling kernel size of $2 * 2$, with the aim of reflecting the extraction of the most important features in it. Then use Dropout mechanism, and set the parameter to 0.5, which randomly makes some neurons in the hidden layer of the neural network fail, in order to improve the model generalization ability and other effects. Finally, the flatten layer is used to tile the feature information extracted by the CNN for subsequent training.

In the GRU model on the right, for the predicted values of previous years, they are directly input into the GRU model that is very suitable for processing time-series data and extracting the long- and short-term dependencies in the time-series data enables better analysis of this part of the features. So the last column of direct features of the sample is input to the GRU with 128 neurons, and the input shape is set to (5,1), where 5 represents a time step of 5 years and 1 represents a column of features. The return sequence is set to False to ensure that only the last target value is input at the end after training according to the whole time step. The same Dropout mechanism with parameter of 0.5 is used after the GRU training is completed. Finally, the important features extracted by the GRU model are obtained.

After the CNN and GRU models are trained to extract different kinds of features, respectively, it is necessary to use the most critical Merge fusion mechanism provided by Keras to stitch the two models together and set the parameter as concat to get all features after the whole sample extraction.

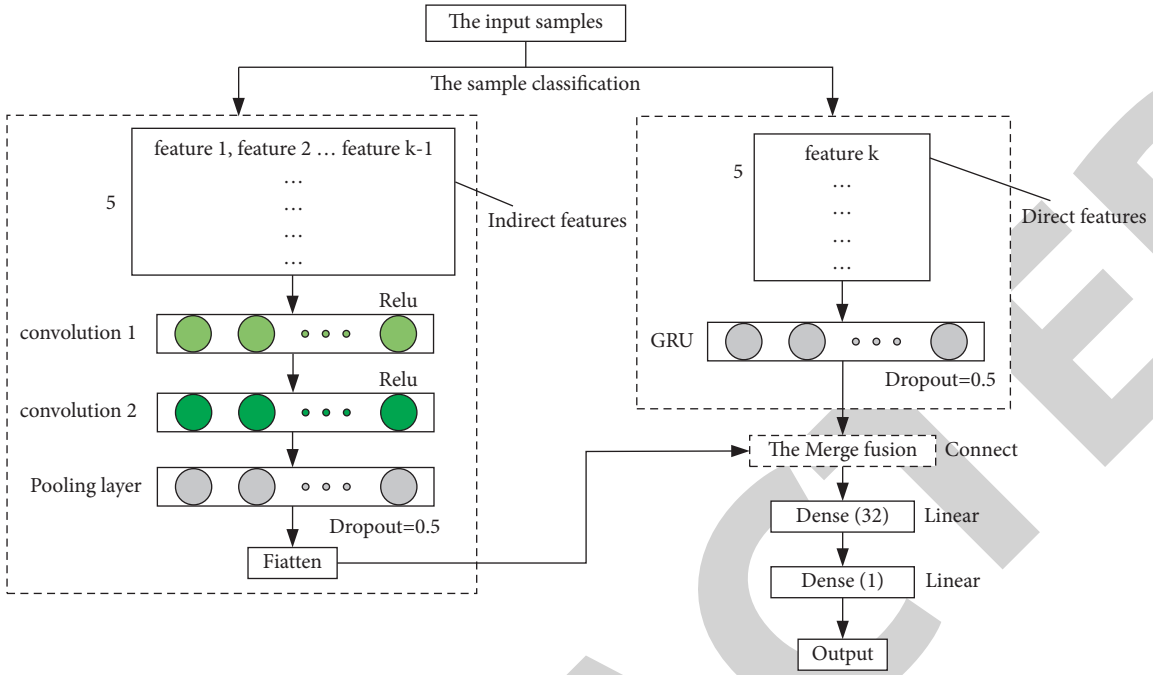

Figure 6: The overview of CNN + GRU.

Then all features are input to the dense fully connected layer for training together and finally input to a fully connected layer for final regression prediction using the linear activation function.

4. Experimental Results and Analysis

4.1. Evaluation Criteria. In this paper, in order to evaluate the experimental results, RMSE and *R*2 are firstly selected as evaluation criteria. Both of these rubrics are common criteria for judging the results of prediction and regression analysis.

Root Mean Square Error (RMSE) is the value obtained after the root of the variance between the predicted value and the true value, and the RMSE is a clearer measure of the prediction result than the MSE and better represents the deviation between the true value and the predicted value, because the root of the error unit can be kept constant. The calculation formula is shown in (13), where $\hat{y}_i$ represents the predicted value and y_i represents the true value.

$$\text{RMSE} = \sqrt{\frac{1}{m}\sum_{i=1}^{m}(y_i - \hat{y}_i)^2}. \tag{13}$$

The coefficient of determination (*R*-squared, *R*2), also known as goodness of fit, is an indicator that varies between 0 and 1. *R*2 reflects the predictive effect by the change in the data, comparing the predicted value to the actual mean value only, as shown in the following equation:

$$R2 = 1 - \frac{\sum_i (\hat{y}_i - y_i)^2}{\sum_i (\overline{y_i} - y_i)^2}. \tag{14}$$

The numerator represents the predicted value minus the sum of the true values squared, like the mean squared, that is, all errors in the trained model prediction. The denominator is the mean value minus the sum of the squares of the true values, which is similar to the variance, that is, the guess is the mean of the true values. *r*2 takes the value range [0,1]; when the result is 0, it means that the model prediction deviates a lot; if *r*2 is 1, it means that the fit is quite accurate, so the closer *r*2 is to 1, the better the model prediction result is. In addition, the larger *R*2 means that the model prediction results are closer to the true value.

4.2. Model Experimental Results. In this paper, we built models and conducted experiments based on Python 3.6 using the high-level neural network module Keras, with Theano as its back end. We built the MLR and support vector regression (SVR) models of the deep learning approach and the NN, CNN, RNN, LSTM, and GRU models of the general neural network, convolutional neural network, recurrent neural network, long short-term memory network, and gated recurrent unit of the deep learning approach as comparison models for experimental comparison. When building the machine learning model, the third-party module Sklearn is used, and, in the MLR model, the samples are tiled and input to the model LinearRegression() for training. In the SVR model, the SVR is initialized using the radial basis kernel function. When building the deep learning model, the Sequential() model is used, and the specific model is created by adding the add() function and

Table 1: Experimental results of forecasting net profit.

Dataset	Model	*R*2	RMSE
Net income dataset	MLR	0.6048	0.0987
	SVR	0.6900	0.0759
	NN	0.7241	0.0203
	CNN	0.7907	0.0575
	RNN	0.8046	0.0230
	LSTM	0.8731	0.0195
	GRU	0.9104	0.0180
	CNN-GRU	0.8919	0.0161
	CNN + GRU	**0.9059**	**0.0150**

passing a series of different layers. In the NN model, the samples are tiled and fed to only one fully connected layer for training. In the CNN model, two convolutional layers and one maximum pooling layer are used. In the RNN model, it is created by a layer of SimpleRNN (128). The LSTM model and the GRU model are created by LSTM/GRU (128, input_shape, return_sequences = False), respectively. These comparison models were trained and tested with the CNN-GRU model and CNN + GRU fusion model constructed in this paper, using the same training and test sets. The experimental results are shown specifically in Tables 1 and 2.

The following summary can be made through Tables 1 and 2 evaluation index results data:

(1) From the overall view of each evaluation index, machine learning MLR and SVR fit the least well, but SVR is slightly better than MLR in general. Among the deep learning algorithms, the general neural network (NN) performs generally, and CNN and RNN have improved significantly, while LSTM and GRU can achieve more satisfactory results in general. However, the CNN-GRU and CNN + GRU fusion models constructed in this paper basically achieve the most desirable results in each evaluation index; in particular, the CNN + GRU fusion model has the best overall performance in each dataset.

(2) From the *R*2 goodness-of-fit evaluation index, the CNN-GRU and CNN + GRU models can reach 0.8 or even 0.9 or more on both datasets, which also has about 5% improvement over the best results in other comparison models; and the *R*2 value of the CNN + GRU model will be about 2% higher than that of CNN-GRU in general.

(3) From the Root Mean Square Error (RMSE), the CNN-GRU and CNN + GRU models can reach about 0.015 on each dataset and achieve the lowest RMSE value.

4.3. Analysis of Model Results. In order to carry out the comparison, we analyzed the actual data of a new energy company and proposed CNN + GRU fusion model for prediction. Figure 7 portrays the graphical comparison between the net income, net profit, and the proposed forecasted net profit. The data in Tables 1 and 2 and the following graphs show that the net income is greater than 0,

Table 2: Experimental results of forecasting operating cash flow.

Dataset	Model	*R*2	RMSE
Operating cash flow dataset	MLR	0.4298	0.1357
	SVR	0.3113	0.1983
	NN	0.8902	0.0203
	CNN	0.8619	0.0239
	RNN	0.7405	0.0266
	LSTM	0.8939	0.0197
	GRU	0.9104	0.0173
	CNN-GRU	0.9202	0.0158
	CNN + GRU	**0.9452**	**0.0114**

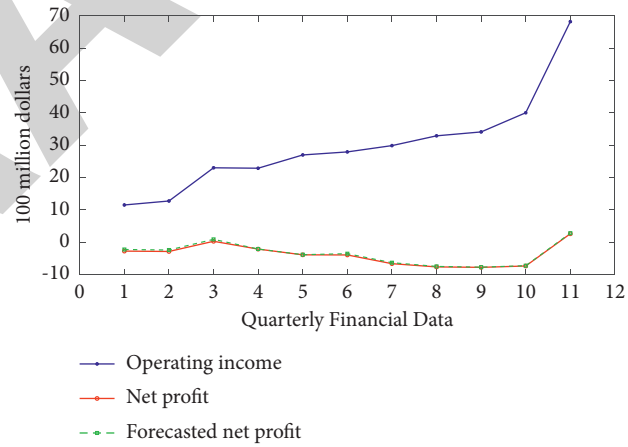

Figure 7: Financial real value and forecast of a new energy vehicle company.

the net profit gradually changes from negative to positive, and the overall trend is up. The net profit predicted by the CNN + GRU fusion model also fits well with the actual net profit and can predict the trend well. This new energy vehicle enterprise has more room for development.

5. Conclusion

In this paper, we firstly parse the annual reports of listed companies in PDF format, through ITextpdf, PyPDF2, and Pdfplumber technologies, to parse and extract PDF tables in a more standardized and accurate way and achieve the target data in batch for multiple years. Then the data is cleaned and normalized, and the Randomized Lasso algorithm is used for feature stability selection. We study the financial statements of new energy vehicle companies, and the data available to

Hindawi
Journal of Mathematics
Volume 2024, Article ID 9871350, 1 page
https://doi.org/10.1155/2024/9871350

Retraction

Retracted: Optimisation of Driver's Traffic Literacy Evaluation Index from the Perspective of Information Contribution Sensitivity

Journal of Mathematics

Received 23 January 2024; Accepted 23 January 2024; Published 24 January 2024

This article has been retracted by Hindawi following an investigation undertaken by the publisher [1]. This investigation has uncovered evidence of one or more of the following indicators of systematic manipulation of the publication process:

(1) Discrepancies in scope

(2) Discrepancies in the description of the research reported

(3) Discrepancies between the availability of data and the research described

(4) Inappropriate citations

(5) Incoherent, meaningless and/or irrelevant content included in the article

(6) Manipulated or compromised peer review

The presence of these indicators undermines our confidence in the integrity of the article's content and we cannot, therefore, vouch for its reliability. Please note that this notice is intended solely to alert readers that the content of this article is unreliable. We have not investigated whether authors were aware of or involved in the systematic manipulation of the publication process.

In addition, our investigation has also shown that one or more of the following human-subject reporting requirements has not been met in this article: ethical approval by an Institutional Review Board (IRB) committee or equivalent, patient/participant consent to participate, and/or agreement to publish patient/participant details (where relevant).

Wiley and Hindawi regrets that the usual quality checks did not identify these issues before publication and have since put additional measures in place to safeguard research integrity.

We wish to credit our own Research Integrity and Research Publishing teams and anonymous and named external researchers and research integrity experts for contributing to this investigation.

The corresponding author, as the representative of all authors, has been given the opportunity to register their agreement or disagreement to this retraction. We have kept a record of any response received.

References

[1] L. Wang and K. Tian, "Optimisation of Driver's Traffic Literacy Evaluation Index from the Perspective of Information Contribution Sensitivity," *Journal of Mathematics*, vol. 2021, Article ID 9503037, 10 pages, 2021.

Hindawi
Journal of Mathematics
Volume 2021, Article ID 9503037, 10 pages
https://doi.org/10.1155/2021/9503037

Research Article

Optimisation of Driver's Traffic Literacy Evaluation Index from the Perspective of Information Contribution Sensitivity

Lingzhi Wang[1] **and Kang Tian**[2]

[1]*School of Mechanical and Electrical Engineering, Guangxi Science & Technology Normal University, Laibin, Guangxi, China*
[2]*School of Management and Economics, North China University of Water Resources and Electric Power, Zhengzhou, Henan, China*

Correspondence should be addressed to Kang Tian; tiankang@stu.ncwu.edu.cn

Received 22 October 2021; Accepted 16 December 2021; Published 31 December 2021

Academic Editor: Naeem Jan

The practice has proven that relying solely on large-scale transportation facilities cannot fundamentally alleviate urban transportation problems. Since the motor vehicle drivers are the main participants of transportation, they should improve their knowledge of transportation. Moreover, the drivers should equally cope with transportation problems. This paper establishes an evaluation index system for traffic literacy of urban drivers. In addition, it proposes a method of information contribution sensitivity to optimise the index system. The main results and achievement of this paper include the following: (1) A traffic literacy evaluation index system including 13 evaluation indexes such as traffic rules and general knowledge of machinery has been constructed. (2) Based on the calculation results of the sensitivity of the information contribution, the first 10 indexes that satisfy the cumulative information contribution rate's value of greater than 90% are retained and 3 indexes with lower contribution rates are eliminated. This study provides a theoretical framework and basic methods to evaluate the traffic literacy of urban drivers.

1. Introduction

With the rapid development of urbanisation, the total demand for transportation and motor vehicles has continued to increase. However, road congestion is also becoming more serious, traffic accidents occur frequently, and violations of traffic regulations are continually occurring. According to estimates by the World Health Organization (WHO), about 1.35 million people die from road traffic injuries, which means that 3,700 people die from road traffic accidents every day (2018) [1]. Other studies have proved that human factors cause more than 90% of traffic accidents [2, 3]. The practice has proven that relying solely on large-scale transportation facilities cannot fundamentally alleviate urban transportation problems. As the main participants of transportation, motor vehicle drivers should improve their transportation literacy and jointly cope with transportation problems. To this end, this article attempts to establish and optimise a model for evaluating urban driver traffic literacy to create a theoretical foundation to evaluate the traffic literacy of urban drivers.

Research on traffic literacy evaluation indexes at home and abroad is scarce, and most literature has focused on researching the factors that affect traffic accidents [4–6]. Most traffic accidents occur because traffic participants have a relatively poor understanding of safe traffic, and many scholars have evaluated their status by constructing safe traffic evaluation index systems. For example, Zhang et al. [7] took the status of local transportation system safety management as the evaluation object and divided the indexes that reflect safe traffic conditions into three categories, veto indexes, qualitative indexes, and quantitative indexes, to build safe traffic evaluation index systems. Guo et al. [8] constructed a rail transit safety evaluation index system model composed of 14 evaluation indexes from three aspects: the train's safety, the interface between the train and other systems, and the safety guarantee system. Scholars have carried out systematic research on the evaluation index

systems of green transportation [9, 10], intelligent transportation [11], and harmonious transportation [12]. Many studies have also been conducted on the impact of traffic safety, such as drivers' attitudes and behaviours towards traffic safety [13], the use of safety devices during driving [14], and drivers' traffic violations [15].

However, none of those abovementioned studies has been researched from the perspective of drivers' traffic literacy. Traffic literacy can better reflect a person's necessary driving qualities and gradually reduce the probability of traffic safety incidents under the joint influence of knowledge acquisition, skill mastery, safety awareness, and driving safety behaviour. At present, the concept of transportation literacy is still in the exploratory stage. Based on the existing literature analysis, this paper sorts out the factors that affect the driver's traffic literacy and uses an improved mathematical method to screen the indexes, hoping to lay a theoretical foundation for the further evaluation and improvement of the driver's traffic literacy.

Studying whether the evaluation index system of traffic literacy is reasonable will directly affect the evaluation results' scientificity. At present, research on the optimisation methods of evaluation indexes is relatively extensive. The principal component analysis method is often used to select the original indexes. For example, Tung and Lee [16] used principal component analysis to reduce the dimensionality of many enterprises' financial indexes based on the grey theory method. Zheng et al. [17] used the principal component analysis method to optimise the comprehensive evaluation index system of reservoirs after an earthquake, reduced 15 risk factors to two principal components, and eliminated redundant information indexes. A variety of other methods are also used to screen and optimise the original indexes. Liu et al. [18] conducted nonparametric Bayesian discrimination for the first round of screening for all credit indexes and nonparametric clustering for the second round of screening for retained credit indexes and provided a set of nonparametric methods for screening credit evaluation indexes with unknown index distributions. Xu et al. [19] used a combination of correlation analysis, frequency analysis, principal component analysis, grey correlation analysis, membership function analysis, cluster analysis, and stepwise regression analysis to complete the selection of drought resistance indexes. Zhu et al. [20] used the Memetic Algorithm to optimise the index parameters extracted by the 3D wavelet transform to obtain distinct and parsimonious feature sets and perform accurate classification. The main problems in the existing research are as follows. First, the indexes are screened and optimised using various research methods, the dimensions of the indexes cannot be reduced, and the original indexes have not changed. Second, the selected method can only optimise the index, but it cannot determine the index's weight after optimisation.

This paper establishes an index selection and weighting method based on the sensitivity of information contribution, which retains the significant and low information overlap indexes and weights the indexes according to the sensitivity of information contribution. First, through the definition of the concept of traffic literacy and by combining the factors that affect traffic literacy, the formation mechanism, the purpose of evaluation, etc., a traffic literacy evaluation index system was proposed, and a questionnaire was designed based on the initially established evaluation index system to obtain the original data. Second, the concept of the sensitivity of index information contribution, which is the sum of the difference between the main component and the cumulative contribution rate of the corresponding principal component variance, is proposed. Indexes with less sensitive information contribution are excluded; the retained indexes can reflect most of the original indexes' information. Finally, all indexes are weighted according to the proportion of each index's information contribution sensitivity to the sum of all indexes' information contribution sensitivities. The weight of the indexes reflects the relative information content of different indexes.

2. Theory

2.1. Definition of the Concept of Driver Traffic Literacy. By analysing the literature and drawing on previous research experience, we believe that the concept of literacy can be introduced to the study of driver traffic behaviour, and the current traffic problem can be regarded as a "human action." Therefore, the prerequisite for solving such problems is to improve the traffic action literacy of drivers, that is, their "traffic literacy." We draw lessons from the definition of literacy by Ritchhart [21] of Harvard University: an acquired behaviour pattern that includes multiple behaviours and is subjectively active. In the development process of a specific situation, these behaviours are dynamic and exceptional and must be combined with necessary abilities. Another definition of thinking literacy is that it is not merely a subjective desire or tendency to think critically in a specific situation. Simultaneously, it is necessary to form habits to use skills or actively believe and choose to use their abilities [22].

Traffic literacy is a kind of professional literacy with practical significance. It refers to the traffic behaviours or tendencies that traffic participants gradually develop in long-term driving activities and the awareness, attitude, and control ability to drive activities. It mainly refers to a comprehensive quality that people gradually accumulate due to coping with various road traffic conditions, the awareness of traffic, the relationship between people and the traffic environment, and the treatment of traffic conditions by individuals. It is the sum of specific transportation knowledge and experience, reasonable method skills, and people-oriented green awareness. The formation of traffic literacy begins with the grasp of traffic knowledge by individuals and develops through the cultivation and formation of a healthy traffic awareness; eventually, the traffic knowledge is mastered, and a sound awareness of traffic safety is established and converted into a skill that is used to guide actions.

2.2. Basic Components of Driver Traffic Literacy. This part draws on previous studies on driver prevention of traffic accidents, combined with the author's research experience,

and explores the factors that affect drivers' traffic literacy levels from four dimensions: knowledge, awareness, skills, and behaviour.

2.2.1. Driver's Traffic Knowledge. Some studies believe that changes in knowledge will reduce traffic safety accidents [23, 24]. Driver's traffic knowledge means that traffic participants need to master the corresponding rules, such as traffic rules, mechanical common sense, and knowledge of laws and regulations. The first task of traffic literacy is to make the road participants understand their environment to determine the appropriate driving means accurately. According to an analysis of statistical data from a United Nations survey in 2016, the fatality rate of traffic accidents in developed countries was less than 4%, and the death toll was 1.2–1.7 people per 10,000 vehicles, while the fatality rate in China was as high as 22%, and the death toll was approximately 3.3 people per 10,000 vehicles. Both of China's evaluation indexes are higher than those of developed countries. Most of the causes of accidents are the driver's insufficient traffic experience and noncompliance with traffic laws [25, 26]. In today's rapidly developing traffic environment, mastering sufficient traffic knowledge and experience will lay the foundation for driving in traffic. For example, only by understanding the road signs' information can the driver know the road conditions they are driving on. Studies have proved that a better understanding of traffic signs will promote good traffic behaviour [27] so that it will not be easy to conflict with other traffic participants and avoid unnecessary disputes.

2.2.2. Driver's Traffic Awareness. Driver traffic awareness is an inherent extension of traffic literacy, reflecting the driver's moral cultivation and reflecting how people treat others and deal with the traffic environment. A cautious driving attitude should be formed, and a correct road traffic concept should be established, mainly in terms of safety awareness, kindness to others, values, and situation foresight. Changing people's attitudes towards traffic laws is crucial in preventing traffic accidents [28]. When drivers have strong traffic risk perception capabilities, they will take the initiative to take certain protective traffic behaviours [29]. For traffic drivers, safety and equality need to be considered in establishing traffic awareness [30, 31], and the main emphasis is on traffic safety awareness. Values are also the main representation of the level of traffic awareness. They give the driver a subjective judgment, drive behaviour standards, and shape their driving behaviour [32–34]. In recent years, personal moral issues related to transportation have gradually attracted people's attention [35–37]. The concept of traffic ethics will affect traffic participants' consciousness to comply with laws and regulations and determine whether they can correctly view the position of traffic participants in the transportation society and their relationships with other participants. Correct traffic concepts and attitudes should lead to the establishment of the concepts of "safety first" and "treat others" and the further formation of an attitude of "driving cautiously," "obeying orders," and "being polite to others."

2.2.3. Driver's Traffic Skills. Driving is a complex task that relies on different skills [38]. The perception of traffic skills can affect self-regulation behaviours during driving and prevent unnecessary driving behaviours [39]. Traffic skills are a further manifestation of traffic awareness and a specific means to reflect traffic knowledge. It is divided into two dimensions: perception of motor skills and safety skills [40]. The driver's traffic skills can transform the knowledge he already knows into skills, be proficient in manipulating the vehicle, and take timely action in response to sudden road conditions. Skills are the prominent ability to make correct judgments and operations based on knowledge and experience. If the driver overestimates his driving skill level, potential hazards will occur [41]. By investigating the status of people involved in traffic accidents, it was found that participants with relatively low skills accounted for a relatively high proportion of the accident group [42]. Only transforming traffic knowledge into a driving ability and gradually forming traffic skills that can be directly used in manipulating vehicles and then positively intervening in driving behaviour will reduce driving safety incidents. Some studies have also proved that skills are closely related to behaviour and accidents [43, 44].

2.2.4. Driver's Traffic Behaviour. Traffic knowledge, traffic awareness, and traffic skills are all directly established at the traffic participants' level, which indirectly affects drivers' traffic literacy level. Driver traffic behaviour is aimed at the driver's actual action level, which is the most direct reflection of driver traffic literacy. Studies have shown that traffic accidents' leading cause is the driver's improper behaviour (76.1%) [45]. The driver's traffic behaviour is a process of continuously receiving, analysing, and responding to the surrounding environment and changes. The external environment's quality may increase the probability of violations [46]. For example, when drivers believe that the external environment is normal, they will often show more dangerous driving behaviours [47].

On the contrary, the driver cannot be affected by the external environment, make certain self-management behaviours, and safely control the vehicle, effectively reducing the possibility of traffic accidents. As a kind of cognitive behaviour, safe and civilised behaviour can reduce driving aggression caused by angry and risky driving behaviours [48, 49]. Therefore, focusing on cultivating drivers' safe and civilised behaviour will directly affect every link of the driving process and reduce traffic accidents.

2.3. Construction of the Driver Traffic Literacy Index System. The construction of a driver traffic literacy evaluation system is a multi-index and multilevel comprehensive evaluation problem, which contains more content, involves a broader range, and is more complicated. There are many problems related to transportation literacy, and the corresponding influencing factors can be divided into dozens or hundreds of factors. For the convenience of research and the operability of the evaluation model, combined with the influencing factors, formation mechanism, evaluation purpose,

and index selection principles of traffic literacy, the traffic literacy evaluation index system is constructed according to the four dimensions of knowledge, awareness, skills, and behaviour. There are 13 indexes in the specific subjective index layer, including traffic rules, common sense of machinery, knowledge of laws and regulations, safety awareness, kindness to others, values, situation foresight, vehicle control, precautionary measures, emergency measures, self-management behaviour, driving control behaviour, and safe and civilised behaviour, as shown in Table 1.

3. Material and Empirical Analysis

3.1. Data Sources and Analysis. Based on the Likert five-level scale, this study designed a questionnaire to assess "evaluation of traffic literacy of motor vehicle drivers" with a total of 17 questions. To ensure the data integrity of individual indexes, we consulted experts in related fields on the design ratio of questionnaire questions. Finally, it is determined that the four indexes of traffic rules, safety awareness, vehicle control, and self-management behaviour each correspond to 2 questions, and the other indexes correspond to 1 question. The survey respondents selected persons with driving experience within the administrative area of Zhengzhou City and issued a total of 550 questionnaires to eliminate complete questionnaires (for example, the online questionnaire has a short response time, and more than 80% of the questions are answered for the same option; the questionnaire is not completed completely). Finally, 393 valid questionnaires were obtained, and the sample efficiency was 71.45%. The preliminary analysis of the questionnaire data shows that the Cronbach's α coefficient of the questionnaire is 0.821, which indicates that the overall questionnaire has good reliability. Through the KMO test on the questionnaire data, the questionnaire's KMO value was 0.854, and the significance p value of the Bartlett sphere test is less than 0.05. The cumulative variance contribution rate of the common factor was 63.311%. Each entry's load value on a common factor was greater than 0.4, and the load values of other common factors were below 0.4, indicating that the questionnaire for traffic literacy of motor vehicle drivers has a higher validity.

3.2. Empirical Analysis Results

3.2.1. Screening of Indexes Based on Information Contribution Sensitivity. According to the data collected from the questionnaire survey, the data of each index are first standardized to obtain a standardized matrix Z, and the standardized matrix is solved for the correlation coefficient matrix R:

$$R = \left[r_{ij}\right]_{13\times 13} = X^T X \tag{1}$$

as shown in Table 2.

The correlation coefficient matrix R is brought into the formula $|R - \lambda_i E_n| = 0$, where E_n is a n-order identity matrix, and the eigenvalue λ_i is obtained. The obtained eigenvalue λ_i is brought into the formula $\omega_i = \lambda_i / \sum_{i=1}^{n} \lambda_i$, and the variance contribution ratio of principal component Z_i to ω_i is calculated (Z_i is the i-th principal component, $i = 1, 2, \ldots, k$, and k is the number of retained principal components). ω_i is the proportion of the i-th principal component Z_i explaining the total variation of all 13 original indexes and reflecting the proportion of the information content of the i-th principal component Z_i that occupies the information content of all indexes. The larger this value is, the more the original information of the main component Z_i is carried by $X_1, X_2, \ldots, X_{13}$.

Based on the variance contribution rate of each principal component, the proportion of the sum of the information content of each principal component in the former k to the information content of all original indexes is calculated, that is, the cumulative variance contribution rate $U_k = \sum_{i=1}^{k} \omega_i$. The cumulative variance contribution ratios of the first k principal components are arranged from the largest to the smallest. In general, when the eigenvalues of the indexes are greater than 1 and the cumulative variance contribution rate exceeds 60%, these principal components contain the main information of most measurement indexes [50]. In this study, if the first three principal components' cumulative variance contribution rate is retained, the first three principal components with the largest variance contribution ratio are retained. The calculation results are shown in Table 3.

The eigenvector p_i^T that is orthogonally unitized by the correlation coefficient matrix R is obtained from the basic solution system of the following linear equations with the formula $(R - \lambda_i E_n)x = 0$. The initial matrix and eigenvalues formed by all the data are brought into the formula to obtain the eigenvectors of the three principal components. The calculation results of the orthogonalization of the eigenvectors to the absolute value are shown in Table 4.

The main information of the original index is expressed by a few principal components Z_i, and its expression formula is as follows:

$$Z_i = p_{i1}X_1 + p_{i2}X_2 + \cdots p_{ij}X_j + \cdots p_{in}X_n. \tag{2}$$

Based on this result, the sensitivity α_{ij} of the i-th principal component affected by the size change of the j-th index is calculated as follows:

$$\alpha_{ij} = \left|\frac{Z_i^* - Z_i}{X_j^* - X_j}\right| = \left|p_{ij}\right|. \tag{3}$$

In this paper, the result of the difference operation is approximated to the orthogonalization of the eigenvectors to determine the absolute value. The calculated data are shown in Table 4.

The sensitivity β_{ij} of the information of all original indexes through the i-th principal component, which is affected by the change of the size of the j-th index and the information contribution sensitivity β_j of the fourth index, is calculated.

Table 1: Structure of the evaluation indexes for transportation literacy.

Evaluation goals	Evaluation index	Main connotation
Traffic literacy X	Traffic rules X_1	To maintain road traffic order, prevent and reduce traffic accidents, protect personal safety, protect the property and other legitimate rights and interests of citizens, legal persons, and other organisations, and improve traffic efficiency and other related rules.
	Knowledge of laws and regulations X_2	Knowledge of road traffic safety-related laws, administrative regulations, and departmental rules and regulations.
	Mechanical common sense X_3	Understand the vehicle's basic structure and be proficient in its correct operation and each component's performance.
	Safety consciousness X_4	In production activities, a state of alertness and alertness to the external environment may cause harm to the driver.
	Values X_5	Values, which are acquired via the dominant social context and the unique experiences of the person, can result in an action, giving it direction and emotional intensity while also designating standards for judging and justifying action.
	Treat others well X_6	Drivers are always grateful for the unexpected things that happen during driving, and they have more understanding and tolerance.
	Situation foresight X_7	In driving, grasp possible future situations and make scientific predictions on complex problems.
	Vehicle control X_8	The driver drives the vehicle through the steering system and the steering wheels' direction (straight or corner). When exposed to external disturbances (uneven roads, crosswinds, cargo, or passengers being eccentrically loaded), the vehicle can resist interference and maintain everyday driving.
	Precaution X_9	The driver takes response measures to eliminate potential emergencies or other potentially undesirable emergencies.
	Emergency measures X_{10}	The handling method is adopted when an emergency occurs, which mainly includes the handling method.
	Driving control behaviour X_{11}	The behaviours of controlling vehicle operation and monitoring the driving environment include driving control operation sensitivity, driving control activity intensity, and driving control state stability.
	Self-management behaviour X_{12}	Self-teaching and restraint. The driver's self-management of goals, thoughts, psychology, and behaviour during driving.
	Safe civilised behaviour X_{13}	Drivers drive in a safe and civilised driving life and can calmly face complicated traffic conditions, to avoid illegal behaviours.

$$\beta_{ij} = \omega_i \left| \frac{Z_i^* - Z_i}{X_j^* - X_j} \right| = \omega_i \left| p_{ij} \right|,$$
$$\beta_j = \sum_{i=1}^{k} \omega_i \left| \frac{Z_i^* - Z_i}{X_j^* - X_j} \right| = \sum_{i=1}^{k} \omega_i \left| p_{ij} \right|, \tag{4}$$

β_j reflects the degree of influence of index X_j on the evaluation results. The greater the value of β_j, the more important the index X_j. Indexes with a higher contribution sensitivity to the overall evaluation are retained. The calculation results are shown in Table 4.

Based on the calculations of the above model, indexes with a low sensitivity of information contribution are eliminated, and the obtained values of β_j $(j = 1, 2, \ldots, 13)$ are arranged in order from large to small. The ratio γ_m of the sum of the β_j values of the top m indexes to the sum of all 13 indexes β_j indicates the information volume of the selected indexes for all indexes, which is called the sensitivity of the cumulative information contribution. The calculation formula is

$$\gamma_m = \frac{\sum_{j=1}^{m} \beta_j}{\sum_{j=1}^{13} \beta_j}. \tag{5}$$

In the principal component analysis theory, when the cumulative information contribution sensitivity reaches 70% ~ 90%, the principal components can reflect most of the information of all the original indexes. Based on this, to ensure the maximum information contribution and prevent the omission of information from individual indexes, the first m indexes that meet the value of the cumulative information contribution rate γ_m at a level of 90% or greater are selected and retained. The specific calculation data are shown in Table 5. The cumulative information contribution sensitivity of the 10th line is 90.00%. Therefore, the first 9 indexes are retained, and the 3 indexes with lower contribution rates such as X_6, X_3, and X_{12} are excluded.

3.2.2. Index Weighting Based on Information Contribution Sensitivity. The core idea of index weighting is to divide the sensitivity of each index's information contribution by the sum of the sensitivity of the information contribution of all indexes. The formula is

$$w_r = \frac{\beta_r}{\sum_{j=1}^{n} \beta_j}, \ (r = 1, 2, \ldots, n). \tag{6}$$

This article presents the weighting results based on index selection, as shown in Table 5. It should be noted that after the index selection is completed, the problems corresponding to the elimination index shall be deleted, and the reserved indexes shall be reempowered. The specific process is not shown in detail.

Table 2: Correlation coefficient matrix of the original index.

Index	X_1	X_2	X_3	X_4	X_5	...	X_{13}
X_1	1.0000	0.457	0.612	0.526	0.320	...	0.222
X_2	0.457	1.000	0.589	0.527	0.275	...	0.127
X_3	0.612	0.589	1.000	0.628	0.387	...	0.237
X_4	0.526	0.447	0.527	1.000	0.628	...	0.234
X_5	0.320	0.275	0.387	0.628	1.000	...	0.218
...	...	...	...	...	...	...	...
X_{13}	0.222	0.127	0.237	0.234	0.218	...	1.000

Table 3: Characteristic values and contribution rates of principal components.

Number/item	Eigenvalues	Variance contribution rate	Cumulative variance contribution rate
	λ_i	ω_i (%)	U_k (%)
1	6.697	51.518	51.518
2	1.173	9.025	60.543
3	1.074	7.494	68.037
4	0.839	6.455	74.492
5	0.608	4.680	79.172
6	0.531	4.084	83.256
7	0.469	3.605	86.861
8	0.395	3.035	89.896
9	0.345	2.655	92.551
10	0.329	2.528	95.078
11	0.264	2.033	97.112
12	0.243	1.871	98.983
13	0.132	1.017	100.000

4. Discussion

The influencing factors of driver's traffic literacy are discussed from four dimensions through the analysis of the existing literature. Literacy is a collection of preferences, attitudes, intentions, and the related ability to reflect preferences in a specific way [51]. Therefore, we believe that the driver's literacy should include knowledge, awareness, skills, and behaviour. These four dimensions comprehensively reflect the driver's overall quality in the entire driving process from basic theory to behaviour implementation. Based on these four dimensions, the representative indexes in each size (such as traffic knowledge including traffic rules, laws, and regulations) are further screened out. The driver's traffic literacy level can be evaluated more scientifically and comprehensively. Government departments or organisations can also take some targeted measures based on these indexes to guide drivers to improve their traffic literacy continuously. Implementing some positive measures will help reduce the occurrence of traffic accidents, make urban traffic more orderly, and meet the needs of social and economic development and people's lives.

The rationality of indexes directly affects the results of the evaluation. In many studies, relying on indexes' relative importance can only reflect the importance of the amount of information reflected by an index relative to the evaluation results [52–55]. However, in the era of big data, the dimensions of index sets presented by different evaluation systems are becoming more and more complex, and there will inevitably be information overlap between indexes. Screening indexes based on relative importance cannot determine the collinearity between indexes and whether there is an overlap of information. Some scholars have adopted principal component dimensionality reduction methods to reduce information overlap [56, 57], but only using the size of the load factor cannot effectively reflect the information content of the index and cannot determine the weight of the index. From the perspective of information contribution sensitivity, this study uses improved principal component analysis methods to prioritize the retention of indexes with greater information contribution sensitivity. The research results ensure that the retained evaluation indexes carry more information from the original data set and achieve a low degree of information overlap between the indexes, guaranteeing the rationality of the evaluation system and at the same time getting the weight of each index.

The research results obtained by using this research method show that the knowledge of laws and regulations in the traffic knowledge, the kindness to others in the traffic awareness, and the driving control behaviour in the traffic behaviour are deleted. These three indexes carry a small amount of information (information contribution rates are 4.32%, 3.1%, and 2.23%) and overlap with the amount of information carried by other indexes. For example, the "traffic rules" in traffic knowledge will include part of the knowledge of traffic laws and regulations, which will lead to overlap of information; another example is that there is an inevitable overlap of information between the indexes "be kind to others" and "values." Kaçan et al. [34] believe that traffic values are obtained through dominant social background and unique personal experience. The direction and emotional intensity of behaviour can be given, and standards can be specified to judge and prove the rationality of actions. A driver with good traffic values will reasonably control the

Table 4: The results of orthogonal normalization of the first three principal component eigenvectors to determine the absolute values.

Serial number	Index	Eigenvector orthogonal normalization to determine the absolute value			Information contribution sensitivity
		$\lvert p_{1j}\rvert$	$\lvert p_{2j}\rvert$	$\lvert p_{3j}\rvert$	β_j
1	X_1	0.2280	0.5124	0.0231	0.1654
2	X_2	0.3917	0.1167	0.0328	0.2148
3	X_3	0.0996	0.0876	0.0342	0.0618
4	X_4	0.3678	0.2321	0.0239	0.2122
5	X_5	0.6317	0.4582	0.0625	0.3715
6	X_6	0.1565	0.0287	0.0375	0.0860
7	X_7	0.2302	0.5372	0.0096	0.1678
8	X_8	0.1289	0.2220	0.1862	0.1004
9	X_9	0.1537	0.1769	0.6955	0.1473
10	X_{10}	0.1748	0.2200	0.6737	0.1604
11	X_{11}	0.1772	0.1047	0.1287	0.1104
12	X_{12}	0.0896	0.0066	0.0484	0.0504
13	X_{13}	0.2502	0.1513	0.0033	0.1428

Table 5: Index screening and weighting based on cumulative information contribution sensitivity.

Serial number (1)	Index (2)	Metrics are sorted by the value of β_j	Cumulative information contribution sensitivity γ_m	Retained and removed indexes	Weights
1	X_1	X_5 (0.3715)	18.66%	Retained X_5	0.0831
2	X_2	X_2 (0.2148)	29.44%	Retained X_2	0.1079
3	X_3	X_4 (0.2122)	40.10%	Retained X_4	0.0310
4	X_4	X_7 (0.1678)	48.53%	Retained X_7	0.1066
5	X_5	X_1 (0.1654)	56.84%	Retained X_1	0.1866
6	X_6	X_{10} (0.1604)	64.89%	Retained X_{10}	0.0432
7	X_7	X_9 (0.1473)	72.29%	Retained X_9	0.0843
8	X_8	X_{13} (0.1428)	79.46%	Retained X_{13}	0.0504
9	X_9	X_{11} (0.1104)	85.00%	Retained X_{11}	0.0740
10	X_{10}	X_8 (0.1004)	90.05%	Retained X_8	0.0806
11	X_{11}	X_6 (0.086)	94.37%	Removed X_6	0.0554
12	X_{12}	X_3 (0.0618)	97.47%	Removed X_3	0.0253
13	X_{13}	X_{12} (0.0504)	100.00%	Removed X_{12}	0.0717

Note. The weights in the last column correspond to the indexes in the second column.

implementation of his own emotions and behaviours in the traffic interaction with others, take the initiative to treat others kindly, and effectively avoid traffic injuries. As a subjective behaviour of the driver, driving control behaviour occurs during the entire driving process. However, as the number of vehicles on the road gradually increases, the degree of automation is getting higher and higher [58], and different countries and regions have aligned their driving licenses. The standards for examinations have gradually increased, and the driver's driving control knowledge and skills have been improved in driving training [59, 60], making the driver more instinctively focused on behaviour in the actual driving process. As a result, this index's impact on traffic literacy is relatively low during the investigation process.

The research results show that the weights of the three mechanical knowledge indexes, safety awareness, and values are relatively high, all greater than 0.1. "Mechanical knowledge" can better reflect the driver's understanding of the vehicle, master the driving tool's performance and operation instructions, and enhance the interaction between the driver and the vehicle information [61], which guarantees the driver a prerequisite for safe driving. Safety awareness and values belong to traffic awareness. Studies have shown that changing people's attitudes towards traffic is essential to prevent traffic accidents. When drivers have a solid ability to perceive traffic risks, they will take the initiative to take certain protective behaviours [28]. Schwartz [62] believes that values are universal, but their importance varies from person to person and is a dynamically changing emotional state. Values exist in the individual at different levels, thereby affecting the individual's real-life behaviour [63]. When applied to the driving environment, they interact with their knowledge reserves and master skills, thereby affecting their driving behaviour. Driving behaviour as a direct factor that affects the driver's traffic literacy does not show a greater weight, which may be related to the behaviour as an actor in the driver's daily driving activities and has not attracted the driver's attention.

5. Conclusions

Through an analysis and induction, a traffic literacy evaluation index system was constructed based on the concept of traffic literacy. This system includes thirteen indexes, such as safety awareness, traffic rules, vehicle control, emergency

measures, being kind to others, values, driving control behaviour, situation foresight, common sense regarding machinery, precautionary measures, knowledge of laws and regulations, self-management behaviour, and safe and civilised behaviour. Through combining various texts, this article summarizes the indexes that can comprehensively reflect the level of driver traffic literacy and lay a specific theoretical basis for further research on the evaluation index system of driver traffic literacy.

The research method proposed in this paper excludes the indexes with overlapping information. During the index screening process, the concept of information contribution sensitivity was proposed. Its value is obtained by calculating the sum of the difference operation result of the retained principal component to an index and the cumulative contribution rate of the principal component variance corresponding to this index. Each index is weighted by the ratio of the information contribution sensitivity of one index to the sum of the information contribution sensitivity of all indexes, so the index's weight can genuinely reflect the corresponding index's information content. It overcomes the shortcomings that existing research cannot use the principal component analysis method to complete the empowerment and makes the weights of various indexes more objective and expands scientific methods other than subjective empowerment.

Data Availability

The data that support the findings of this study are available from the corresponding author upon reasonable request.

Conflicts of Interest

The authors declare that there are no conflicts of interest.

Acknowledgments

This research was supported by the Doctoral Student Innovation Fund of North China University of Water Resources and Electric Power (NCWU).

References

[1] Y Üzümcüoğlu, T Özkan, C Wu, and H Zhang, "Traffic climate and driver behaviors: the moderating role of driving skills in Turkey and China," *Journal of Safety Research*, vol. 75, pp. 87–98, 2020.

[2] L. S. Nangana, B. Monga, N. R. Ngatu, E. P. Mbelambela, L. H. Mbutshu, and K. F. Malonga, "Frequency, causes and human impact of motor vehicle-related road traffic accident (RTA) in Lubumbashi, Democratic Republic of Congo," *Environmental Health and Preventive Medicine*, vol. 21, no. 5, pp. 350–355, 2016.

[3] K. Rumar, "The role of perceptual and cognitive filters in observed behavior," *Human Behavior and Traffic Safety*, Springer, Boston, MA, USA, pp. 151–170, 1985.

[4] H. Lu, X. F. Xi, W. C. Yang, and C. Y. Hu, "Cause analysis of traffic accidents in plateau and mountain highway environment," *Journal of Chinese Safety Science*, vol. 29, no. 05, pp. 44–49, 2019, in Chinese.

[5] Z. Yan, X. Lu, and W. Hu, "Analysis of factors affecting traffic accident severity based on heteroskedasticity ordinal Logit," in *ICTE 2019*, pp. 422–435, American Society of Civil Engineers, Reston, VA, USA, 2020.

[6] T. O. Nævestad, R. O. Phillips, and B. Elvebakk, "Traffic accidents triggered by drivers at work–A survey and analysis of contributing factors," *Transportation Research Part F: Traffic Psychology and Behaviour*, vol. 34, no. 8, pp. 94–107, 2015.

[7] Y. Zhang, Z. W. Chen, and Q. S. Zhang, "Building of assessment index system of safe transport," *Journal of Transportation Research*, vol. 1, no. 6, pp. 8–13, 2015, in Chinese.

[8] Z. Guo, X. Shang, and H. Li, "AHP-based safety assessment model for rail transit system," *Zhong Guo Tie Dao Ke Xue*, vol. 32, no. 3, pp. 123–125, 2011.

[9] G. X. Liu, ""Research on evaluation method and index system of green transportation in small cities," China science and technology association, ministry of transport of the people's Republic of China, Chinese academy of engineering," in *Proceedings of the 2019 World Transportation Conference (Part 2)*, pp. 820–830, China Highway Society, 2019, in Chinese.

[10] P. Y. Long and C. N. Gao, "Study on evaluation index system of green city traffic based on tourism development," *Technology of Highway and Transport*, vol. 33, no. 3, pp. 116–120+125, 2017.

[11] Y. X. Yu, X. C. Wang, H. Zhang, and X. Chen, "Reconfiguration DEA′ s optimal in ITS evaluation," *Journal of Shandong Jiaotong University*, vol. 18, no. 1, pp. 17–21, 2010.

[12] J. J. Fan, "Construction and empirical analysis of Beijing harmonious transportation evaluation index system," PHD thesis, Beijing Jiaotong University, Beijing, China, 2010.

[13] Y.-H. Huang, P.-L. P. Rau, B. Zhang, and M. Roetting, "Chinese truck drivers' attitudes toward feedback by technology: A quantitative approach," *Accident Analysis & Prevention*, vol. 40, no. 4, pp. 1553–1562, 2008.

[14] Y.-H. Huang, W. Zhang, L. Murphy, G. Shi, and Y. Lin, "Attitudes and behavior of Chinese drivers regarding seatbelt use," *Accident Analysis & Prevention*, vol. 43, no. 3, pp. 889–897, 2011.

[15] G. Zhang, K. K. W. Yau, and X. Gong, "Traffic violations in Guangdong Province of China: Speeding and drunk driving," *Accident Analysis & Prevention*, vol. 64, pp. 30–40, 2014.

[16] C.-T. Tung and Y.-J. Lee, "A novel approach to construct grey principal component analysis evaluation model," *Expert Systems with Applications*, vol. 36, no. 3, pp. 5916–5920, 2009.

[17] H. Y. Zheng, J. B. Sheng, X. H. Peng, and D. W. Yang, "Earth-rock dam risk consequence's comprehensive evaluation under drought condition," *Procedia Earth and Planetary Science*, vol. 5, pp. 237–240, 2012.

[18] Y. M. Liu, Z. J. Li, and W. Yin, "Credit index selection model based on Bayesian discriminant and cluster analysis under non-parameters," *Statistics & Decisions*, vol. 22, no. 5–10, in Chinese, 2018.

[19] Y. P. Xu, Y. D. Pan, Q. D. Liu et al., "Drought resistance identification and drought resistance indexes screening of barley resources at mature period," *Acta Agronomica Sinica*, vol. 46, no. 3, pp. 448–461, 2019.

[20] Z. Zhu, S. Jia, S. He, Y. Sun, Z. Ji, and L. Shen, "Three-dimensional Gabor feature extraction for hyperspectral imagery classification using a memetic framework," *Information Sciences*, vol. 298, pp. 274–287, 2015.

[21] R. Ritchhart, *Intellectual Character: What it Is, Why it Matters, and How to Get it*, Academic Press, John Wiley & Sons, San Francisco, CA, USA, 2004.

[22] S. P. Norris, "Testing for the disposition to think critically," *Informal Logic*, vol. 14, no. 2, pp. 157–164, 1992.

[23] S. Miccoli, G. Giraldi, A. Boccia, and G. La Torre, "School teachers' knowledge, attitudes and behaviors towards road safety: results from a multicenter cross-sectional study in Italy," *Annali di Igiene: Medicina Preventiva e di Comunita*, vol. 24, no. 4, pp. 289–299, 2012.

[24] R. Mirzaei, N. Hafezi-Nejad, M. Sadegh Sabagh et al., "Dominant role of drivers' attitude in prevention of road traffic crashes: A study on knowledge, attitude, and practice of drivers in Iran," *Accident Analysis & Prevention*, vol. 66, pp. 36–42, 2014.

[25] D. Shinar and R. Compton, "Aggressive driving: an observational study of driver, vehicle, and situational variables," *Accident Analysis & Prevention*, vol. 36, no. 3, pp. 429–437, 2004.

[26] M. A. Machin and K. S. Sankey, "Relationships between young drivers' personality characteristics, risk perceptions, and driving behaviour," *Accident Analysis & Prevention*, vol. 40, no. 2, pp. 541–547, 2008.

[27] P. Hardini and E. W. Indriyati, "Pengetahuan Dan Pengaruhnya Terhadap Perilaku Berlalu Lintas; Tinjauan Terhadap Pelaku Lalu Lintas Usia Remaja Di Smk Ypt 1 Purbalingga," *Journal of Indonesia Road Safety*, vol. 1, no. 3, pp. 138–146, 2018.

[28] L. M. Martinussen and C. G. Prato, "Facilitating improved road safety based on increased knowledge about driving behaviour and profiling sub-groups of drivers," PhD thesis, Technical University of Denmark, Denmark, Europe, 2013.

[29] H. A. Deery, "Hazard and risk perception among young novice drivers," *Journal of Safety Research*, vol. 30, no. 4, pp. 225–236, 1999.

[30] H. Safarpour, D. Khorasani-Zavareh, and R. Mohammadi, "The common road safety approaches: a scoping review and thematic analysis," *Chinese Journal of Traumatology*, vol. 23, no. 2, pp. 113–121, 2020.

[31] F. Di Ciommo and Y. Shiftan, "Transport equity analysis," *Transport Reviews*, vol. 37, no. 2, pp. 139–151, 2017.

[32] S. H. Schwartz, "Beyond individualism/collectivism: new cultural dimensions of values," in *Individualism and Collectivism: Theory, Method, and Applications*, U. Kim, H. C. Triandis, Ç. Kâğitçibaşi, S.-C. Choi, and G. Yoon, Eds., pp. 85–119, Sage Publications, Inc, Thousand Oaks, CA, USA, 1994.

[33] T. Özkan and T. Lajunen, "Person and environment: traffic culture," in *Handbook of Traffic Psychology*, pp. 179–192, Academic Press, Middle East Technical University, Ankara, Turkey, 2011.

[34] B. Kaçan, G. Fındık, Y. Üzümcüoğlu et al., "Driver profiles based on values and traffic safety climate and their relationships with driver behaviors," *Transportation Research Part F: Traffic Psychology and Behaviour*, vol. 64, pp. 246–259, 2019.

[35] D. Husak, "Vehicles and Crashes," *Social Theory and Practice*, vol. 30, no. 3, pp. 351–370, 2004.

[36] S. O. Hansson, "Making road traffic safer: reply to Ori," *Philosophical Papers*, vol. 43, no. 3, pp. 365–375, 2014.

[37] M. Ori, "Why not road ethics?" *Theoria*, vol. 86, no. 3, pp. 389–412, 2020.

[38] M. Hatakka, E. Keskinen, N. P. Gregersen, A. Glad, and K. Hernetkoski, "From control of the vehicle to personal self-control; broadening the perspectives to driver education," *Transportation Research Part F: Traffic Psychology and Behaviour*, vol. 5, no. 3, pp. 201–215, 2002.

[39] A. Siren and A. Meng, "Older drivers' self-assessed driving skills, driving-related stress and self-regulation in traffic," *Transportation Research Part F: Traffic Psychology and Behaviour*, vol. 17, pp. 88–97, 2013.

[40] T. Lajunen and H. Summala, "Driving experience, personality, and skill and safety-motive dimensions in drivers' self-assessments," *Personality and Individual Differences*, vol. 19, no. 3, pp. 307–318, 1995.

[41] F. P. McKenna and M. S. Horswill, "Risk taking from the participant's perspective: the case of driving and accident risk," *Health Psychology*, vol. 25, no. 2, pp. 163–170, 2006.

[42] T. Pan and R. F. Wang, "Based on the traffic quality of drivers to the city's traffic safety management research," *Journal of Technical Economics & Management*, vol. 2, pp. 76–78, 2007, in Chinese.

[43] L. M. Martinussen, M. Møller, and C. G. Prato, "Assessing the relationship between the driver behavior questionnaire and the driver skill inventory: revealing sub-groups of drivers," *Transportation Research Part F: Traffic Psychology and Behaviour*, vol. 26, pp. 82–91, 2014.

[44] Y Üzümcüoğlu, T Özkan, C Wu, and H Zhang, "Traffic climate and driver behaviors: the moderating role of driving skills in Turkey and China," *Journal of Safety Research*, vol. 75, pp. 87–98, 2020.

[45] A. A. Redhwan and A. J. Karim, "Knowledge, attitude and practice towards road traffic regulations among university students, Malaysia," *IIUM Medical Journal Malaysia*, vol. 9, no. 2, 2010.

[46] W. Chu, C. Wu, C. Atombo, H. Zhang, and T. Özkan, "Traffic climate, driver behaviour, and accidents involvement in China," *Accident Analysis & Prevention*, vol. 122, pp. 119–126, 2019.

[47] T. Gehlert, C. Hagemeister, and T. Özkan, "Traffic safety climate attitudes of road users in Germany," *Transportation Research Part F: Traffic Psychology and Behaviour*, vol. 26, pp. 326–336, 2014.

[48] J. L. Deffenbacher, "A review of interventions for the reduction of driving anger," *Transportation Research Part F: Traffic Psychology and Behaviour*, vol. 42, pp. 411–421, 2016.

[49] S. Q. Shen, "The associated factors and psychological intervention of driving anger and aggression for plateau military truck drivers east," PhD thesis, China Normal University, Shanghai, China, 2013.

[50] L. B. Wang, *Multivariate Statistical Analysis: Model Cases and Application of SPSS*, Economic Science Press, Beijing, China, 2010, in Chinese.

[51] G. Salomon, *Interaction of Media, Cognition, and Learning*, Psychology Press, London, UK, 1994.

[52] M. Kazemi, "Partial correlation screening for varying coefficient models," *Journal of Mathematical Modeling*, vol. 8, no. 4, pp. 363–376, 2020.

[53] D. Fouskakis, G. Petrakos, and I. Rotous, "A Bayesian longitudinal model for quantifying students' preferences regarding teaching quality indicators," *Metron*, vol. 78, no. 2, pp. 255–270, 2020.

[54] J. Rezaei, W. S. van Roekel, and L. Tavasszy, "Measuring the relative importance of the logistics performance index indicators using Best Worst Method," *Transport Policy*, vol. 68, pp. 158–169, 2018.

[55] W. N. K. Wan Ahmad, J. Rezaei, S. Sadaghiani, and L. A. Tavasszy, "Evaluation of the external forces affecting the sustainability of oil and gas supply chain using Best Worst Method," *Journal of Cleaner Production*, vol. 153, pp. 242–252, 2017.

Hindawi
Journal of Mathematics
Volume 2023, Article ID 9798076, 1 page
https://doi.org/10.1155/2023/9798076

Retraction

Retracted: Research on Community Public Service Information Collaborative Governance Based on Deep Learning Model

Journal of Mathematics

Received 19 December 2023; Accepted 19 December 2023; Published 20 December 2023

This article has been retracted by Hindawi following an investigation undertaken by the publisher [1]. This investigation has uncovered evidence of one or more of the following indicators of systematic manipulation of the publication process:

(1) Discrepancies in scope

(2) Discrepancies in the description of the research reported

(3) Discrepancies between the availability of data and the research described

(4) Inappropriate citations

(5) Incoherent, meaningless and/or irrelevant content included in the article

(6) Manipulated or compromised peer review

The presence of these indicators undermines our confidence in the integrity of the article's content and we cannot, therefore, vouch for its reliability. Please note that this notice is intended solely to alert readers that the content of this article is unreliable. We have not investigated whether authors were aware of or involved in the systematic manipulation of the publication process.

Wiley and Hindawi regrets that the usual quality checks did not identify these issues before publication and have since put additional measures in place to safeguard research integrity.

We wish to credit our own Research Integrity and Research Publishing teams and anonymous and named external researchers and research integrity experts for contributing to this investigation.

The corresponding author, as the representative of all authors, has been given the opportunity to register their agreement or disagreement to this retraction. We have kept a record of any response received.

References

[1] Y. Liu, "Research on Community Public Service Information Collaborative Governance Based on Deep Learning Model," *Journal of Mathematics*, vol. 2021, Article ID 4727617, 9 pages, 2021.

Hindawi
Journal of Mathematics
Volume 2021, Article ID 4727617, 9 pages
https://doi.org/10.1155/2021/4727617

Research Article

Research on Community Public Service Information Collaborative Governance Based on Deep Learning Model

Yajing Liu

School of Business Management, Suzhou Industrial Park Institute of Services Outsourcing, Suzhou 215123, China

Correspondence should be addressed to Yajing Liu; liuyj@siso.edu.cn

Received 9 November 2021; Revised 14 December 2021; Accepted 16 December 2021; Published 31 December 2021

Academic Editor: Naeem Jan

The communities have significantly increased in number and the environment has become complex. There are problems such as poor information collection in community public service information governance, lack of relevant analysis standards and models, and unreliable prediction results. In order to forecast and manage the risk information of the community, this research analyzes the public information of the community through the collaborative deep learning model. First of all, the information characteristic factors are selected that affect social risks based on the correlation analysis theory. Secondly, the convolutional neural network is used in deep learning for simulation of the community risk prediction model. Finally, through the comparative analysis of the model prediction results, it can be concluded that the accuracy rate of the proposed prediction model reaches 92.5%. An effective collaborative deep learning model is used to govern community public service information.

1. Introduction

The analysis and research of community public service information directly affects the governance of community public security. Only a good community safety management environment can effectively protect the interests of the broad masses of the people. Our party attaches great importance to this. In the report of the 19th national congress, it proposed to sink social governance to the grass-roots level [1] and published the opinions on strengthening the construction of community public security prevention and control system on relevant government websites, emphasizing the importance of community public security prevention and control [2]. An intuitive indicator of community risk quantification is the number of community public security cases. Through the research on community public service information, accurate prediction of the number of community cases can not only effectively prevent and reduce the number of community public security cases, but also provide auxiliary support for relevant public security organs [3], so as to improve the ability to crack down on relevant illegal and criminal acts, reduce the risk of community governance, and make more effective use and analysis of community public service information. At present, most of the research related to community public service information governance takes the risk event of theft as the measurement standard [4]. Theft occurs most frequently in the community, and it is generally considered that theft is the most typical case type in the community. However, based on the actual situation, other case types are also very important for the result prediction of risk governance [5]; at the same time, most of the existing prediction models are based on convolutional neural networks, but the existing analytical neural networks are basically single channel prediction models [6]. In this paper, the existing single channel prediction model is improved and the multichannel convolution neural network prediction model is used to improve the accuracy of the prediction model. It better adapts to the characteristics of too many characteristic factors and various types of community public security cases. At the same time, the impact of natural disasters is added to the overall risk prediction, which greatly improves the accuracy of the model prediction. Therefore, this paper comprehensively considers all kinds of case types, takes all kinds of case types as a whole, and makes model prediction through multichannel convolutional neural network.

To conclude, it is stated that a large correlation exists between the predicted and the actual values of CART regression tree prediction model. As a result, the prediction performance was better. Moreover, the correlation between the actual and predicted values of the comprehensive prediction model is good. The comprehensive prediction is higher than the single prediction model, and its prediction's accuracy is also higher.

Initially, this study organizes and examines the collected data. The characteristic factors affecting social security are preliminarily selected by using relevant analysis theory. Irrelevant factors are removed through data cleaning to establish a reliable data source. Secondly, the convolutional neural network prediction model based on deep learning is finally established by the improvement of the single channel convolutional neural network and use of the multichannel convolutional neural network to expand the data acceptance and prediction ability of the neural network. The experimental results show that the accuracy of the prediction model reaches 92.5% which is higher than the single prediction model. Compared with the first mock exam model, the integrated prediction model has higher accuracy and robustness. Finally, the collaborative depth model is realized to calculate the community public service information and manage the community risk.

The rest of the paper is organized as follows:

(i) Section 2 provides some fine points of the related works

(ii) Section 3 presents the proposed method in detail

(iii) Section 4 analyzes and discusses the results

(iv) Section 5 concludes the paper

2. Related Work

Community public service information analysis and governance is a very complex project, and the information is often massive. However, in the process of information processing, there are often problems such as insufficient manpower, high operation cost, and being unable to respond quickly to the processing results [7]. However, the emergence and development of deep learning algorithms in recent years show their strong prediction ability. Therefore, in recent years, deep learning technology is widely used at home and abroad to analyze and predict community public service information, so as to realize the collaborative governance of public service information [8]. For example, the Memphis police department analyzed and predicted the community public service information by using the in-depth learning model, which has greatly reduced the violent crime in the past five years. At the same time, it was found that the accuracy of big data analysis and prediction based on in-depth learning is much higher than that of traditional methods [9]. Based on the deep learning model, the prediction of community public service information in China started a little later than that in foreign countries, but it has also made great progress in recent years. For example, Tianjin University undertakes the research on building a smart and safe community, which is to predict the community public service information based on the in-depth learning model and improve the governance efficiency of the community [10].

Chinese scholars An Simin and others combined community information data and related crime data to build a community crime rate analysis and prediction system based on data mining method [11]. On this basis, Li and Li [12] proposed a crime prediction model and algorithm based on deep learning model big data analysis. At present, the common algorithm is the random forest algorithm. Xiao and Yong [13] proposed the degradation decision tree algorithm based on the random algorithm to obtain accurate prediction conclusions. Taking Shanghai as an example, Yun and Shi others established the quantitative relationship between crime susceptibility and community public service information characteristic factors based on deep learning algorithm and analyzed the action equation of influencing factors [14]. In the analysis and research of some community spatial location data and crime space-time, He and others identified and analyzed the theft spatial aggregation area through community personal location data clustering and clustering with the help of GIS data analysis software and spatial analysis tools based on the nearest neighbor index analysis method [15]. According to the different types of community public service information obtained and the predicted objects and technologies, the in-depth learning network models used are also different. For example, the fuzzy backpropagation (BP) neural network model is usually used to predict the number of community risk events. The time prediction technology of community events is usually based on Support Vector Machine (SVM) prediction model. The prediction technology of crime time of relevant risk cases is based on Autoregressive Integrated Moving Average-Least Square Support Vector Machine (ARIMA-LSSVM) hybrid model. At the same time, relevant scholars applied this theoretical knowledge to reality, carried out research on big data + smart policing, and built smart cities with AI and big data. Among them, the war epidemic Golden Shield Project has demonstrated excellent scientific and technological achievements of the reporting system in the fight against epidemic diseases. At the same time, it has covered the health information of nearly 40,000 residents and real-time data of enterprises in 56 communities under the jurisdiction of Beijing Economic Development Zone, providing a strong guarantee for the collaborative management of community public service information.

Through the above research on the current situation at home and abroad, in terms of community public service information analysis technology, we usually use big data analysis to quickly and efficiently analyze massive data based on deep learning network model and conduct risk assessment on the community based on the existing big data model. However, at present, there are relatively single evaluation characteristic factors. When collecting the risk factor characteristics of community public information services, most researchers only consider the characteristic factors of a single risk event, such as theft cases, and ignore the characteristic factors of various types of public security

cases in the community, resulting in the imperfect level of community public service information collection, which affects the subsequent risk assessment, prediction, and governance. In addition, the first mock exam model is the single model formed by many weak learning devices. Although homogeneous or heterogeneous learning in single channel is higher than that in traditional prediction models, the integration of multichannel learning and weak learning has never been carried out.

3. Method

Compared with the deep learning model, the traditional machine learning algorithm has worse learning effect when the number of multichannel training bases is large, but at the same time, the traditional machine learning algorithm performs better when the number of trainings is low. Most of the data sets used in this paper come from community public information and involve certain confidentiality. Therefore, the data and base are not large, and the performance will be better than that of traditional machine learning algorithms. Therefore, our prediction model here selects the decision tree model. The decision tree model is one of the classical model algorithms used for prediction in traditional machine learning. It has low requirements for the amount of data, easy construction, and high operation efficiency. In the decision tree model, this paper selects Classification And Regression Tree (CART) decision tree algorithm, whose algorithm structure is dichotomy. CART is basically a classification algorithm which builds a decision tree on the basis of Gini's impurity index as splitting criterion. This algorithm operates repetitively in three steps: (i) finding the best split of each feature; (ii) finding the best split of node; (iii) using the best node split from the first two steps to split the node until stopping criterion is satisfied. The whole algorithm is in the shape of a binary tree, involving classification and regression. Therefore, the algorithm can be used for both classification and regression, which depends on the target task of decision-making. When the prediction result expected by the decision task is discrete data, the Classification And Regression Trees (CART) algorithm automatically generates the classification decision tree. On the contrary, when the large prediction result required by the decision task is continuous data, the CART algorithm automatically generates the classification decision tree. At the same time, when CART generates a classification decision tree, the inflection point of its prediction result is the Gini value according to node splitting. When CART generates a regression decision tree, the inflection point of its prediction result, i.e., node splitting, is based on Mean Squared Error (MSE) (standard variance of prediction result). Since the final prediction result of this paper is the risk degree of the community, and its quantitative index is expressed as a continuous value by the number of community cases, CART regression algorithm is selected here. The specific algorithm is as follows:

$$\mathrm{MSE}(D) = \frac{1}{M}\sum_{1}^{M}\left(y_m - \overline{Y}\right)^2. \tag{1}$$

Firstly, the optimal feature selection method of the algorithm is determined. According to the number and type of prediction data sets, CART regression tree and mean square error are used for model measurement. In formula (1), y_m is the actual observation value in the prediction process, and $\overline{Y}$ is the model prediction value. Then, a CART regression tree is established based on the decision tree. By inputting the training set D, it is necessary to determine the threshold of the number of samples to avoid affecting the prediction results due to the size of the data set and output the decision tree T:

$$\min_{j,s}\left[\min_{C_1}\sum_{\chi_1\in R_1(j,s)}\left(y_1 - c_1\right)^2 + \min_{C_2}\sum_{\chi_1\in R_2(j,s)}\left(y_1 - c_2\right)^2\right]. \tag{2}$$

In formula (2), the training set is recursively divided into two subregions by constructing a binary decision tree, and the output value is obtained. In this process, the variable j can be traversed to obtain the minimum value pair (j, s). By continuously calling in the two subdomains divided by the dichotomy, the output values $R_1(j, s)$ and $R_2(j, s)$ satisfying the conditions are found. Then the input control is divided into M regions according to $R_1(j, s)$ and $R_2(j, s)$ to generate decision tree T. Note that, during the application of the formula, if the input features are used up, that is, there are no features available for use, the output values $R_1(j, s)$ and $R_2(j, s)$ will be stopped during splitting operation. If the input characteristic elements are of the same class, the output results have been divided completely, and the dichotomy operation is no longer carried out to distinguish, the splitting decision will be stopped. If all samples have been used up in the final child node, the node no longer has samples to divide and stop splitting.

However, the decision tree has overfitting phenomenon when executing the decision algorithm for result prediction. In order to solve the problem of overfitting phenomenon caused by training, we regularize the prediction results of CART regression number (pruning of regression tree). Through regularization, the learning ability of CART decision model for sample data set can be effectively increased. The CART regularization used in this paper adopts the postpruning method. After generating the CART regression tree through formula (2), the cross validation method is used to verify the pruning effect of the CART regression tree, so as to select the pruning strategy with the strongest effect. The whole process can be roughly divided into two steps. Firstly, the generated CART regression tree is regularized through different pruning strategies; secondly, the efficiency and performance of CART pruning strategy are verified by cross validation method. Finally, the CART regression tree with the best effect and performance is selected as the final prediction algorithm model. The specific algorithm formula is as follows:

$$C_a(T_t) = C(T_t) + \alpha|T_t|, \tag{3}$$

$$C_a(T) = C(T) + \alpha, \tag{4}$$

$$\alpha = \frac{C(T) - C(T_t)}{|T_t| - 1}. \tag{5}$$

Formula (3) indicates that if there is no pruning process, any subtree T_1 located in a child node T is the loss value of the input data value in the prediction process. Formula (4) indicates that, in the process of regularization, if only the number of children T_1 is cut, the loss value of the root node is retained. At the same time, when α is zero or infinitely approaches zero, the index T_1 is cut off, and the loss value of the reserved root node is greater than the loss value of T_t under any index of t for any child node. When α continues to increase, the inequality is reversed, and the loss value satisfies formula (5) according to the size of α. α is the regularization degree parameter, and $C(T_t)$ represents the ground error between the predicted value of the deep learning model algorithm and the input actual value. In this paper, MSE (square error) is selected to measure the fitting degree of the algorithm training data. C is the number of T leaf nodes in the subtree of the regression tree. $|T_t|$ is the number of T leaf nodes in the subtree of the dichotomy regression tree. When α is zero, the regularization degree parameter is zero; that is, the prediction process is not regularized; then the generated cart regression number is the optimal subtree. When α tends to infinity, it means that the degree of regularization is infinitely close to the maximum. At this time, the regularization intensity is the maximum, and the number composed of the root node of the CART regression number is the optimal index. To sum up, between zero and infinity, the greater the α value, the greater the degree of regularization and the stronger the pruning, and the smaller the error of the generated optimal index compared with the initial CART number. When the α value is constant, the loss function is the smallest when there are unique subnumbers. Formula (5) can calculate the threshold value of whether each subtree needs pruning and then judge. Finally, through cross validation, the optimal regularization α value is selected as the final result. The overall structural frame is shown in Figure 1.

After determining the algorithm based on deep learning model, we also need to formulate risk identification and evaluation criteria, so as to judge whether the risk event is or not. The risk assessment here refers to the analysis and research on the risk based on the collected and analyzed community public service information through the in-depth learning model algorithm to evaluate the probability of risk events and provide the basis for the follow-up evaluation and processing methods according to the prediction results. Common risk assessment methods include fuzzy analytic hierarchy process, Delphi method, D-S evidence theory method, and fuzzy comprehensive evaluation method. The risk assessment method adopted in this paper is the disaster risk assessment model proposed in the report "coexistence with risk" of the United Nations Bureau for international strategy for disaster reduction (ISDR). Its specific assessment algorithm is shown in formula (6).

$$R = H \times \frac{V}{C}, \tag{6}$$

where R represents risk degree, H represents vulnerability, V represents disaster risk degree, and C represents emergency capacity. Formula (6) evaluates the risk from three aspects: vulnerability, disaster risk degree, and emergency response capacity, making the risk model more suitable for the management of community public service information and evaluating the possible risks. The three dimensions of the assessment model also correspond to the three aspects of community disaster causing factors, community vulnerability, and community emergency response capacity of community risk assessment. Among them, the risk degree of disaster causing factors is positively correlated with the overall risk of the community. The higher the risk degree of disaster causing factors, the greater the overall risk of the community. Vulnerability is also positively correlated with the degree of risk. The higher the vulnerability, the greater the risk. The capacity of disaster reduction is negatively correlated with the total risk of the community. The stronger the capacity of disaster reduction, the smaller the risk.

After determining the algorithm prediction model and relevant risk assessment standards, we began to extract the community security risk factors from the community public service information based on the deep learning model. The data source of this time is mainly the public service information of N community in M city (hereinafter referred to as N community) as the main source, and the acquisition method is reference online materials. The data referred to in this paper are mainly the public security prevention and control data of M city from 2017 to 2019, the weather and climate data of M city from 2017 to 2019, the second-hand house price data of N community from 2017 to 2019, etc. After desensitization and simple analysis of the existing data, we can see that, in the occurrence of community risk events, the main time is theft, but there are still other case types, and the other 73 case types also account for a certain proportion every day. It can be inferred that they also have a certain impact on the final prediction results. Therefore, in the process of collaborative governance of community public service information based on deep learning model, we must consider the impact of the overall case types and consider the case types other than theft, rather than only considering the case types with a large proportion and ignoring the prediction and analysis of other cases. At the same time, according to psychologists' experimental research, weather has a great impact on people's mood. In the criminal environmental determinism, it is also mentioned that the quality of the environment not only affects people's health, but also has an impact on social harmony and stability beyond our imagination. Therefore, in the process of public service information collection and analysis based on depth model, this paper will also consider the great impact of climate on people's mood and add climate characteristic factors to the final result prediction. Finally, we captured the

historical weather data of *M* city from the historical weather website. Capture dimensions include date, weather, wind direction, wind force, maximum and minimum temperature, city, etc. In addition, housing is a major event related to the national economy and the people's livelihood, and house prices are also crucial to social stability. At the same time, house prices are usually used to measure the environment around the community and to some extent reflect the quality of life of community residents, community supporting facilities, and security conditions. After climbing the second-hand house price in *M* city on the second-hand trading house data website and comparing the number of cases at relevant time, we find that there is a certain correlation between the second-hand house price and the number of community risk events, which fluctuated within a certain range from March 2018 to December 2019, and the fluctuation trend is similar. In addition to the above data, we also investigated the area of the community and the number of registered residents in the community through community property, the geographical location information of the community, and other publicly available information on the Internet. 2017 to 2019 years of housing price changes is shown in Figure 2.

In the process of collecting data, there may be problems such as data missing or wrong value in the process of data statistical transmission, which greatly affects the final prediction effect. Therefore, after data collection, data preprocessing is very important. This paper mainly does missing value filling and deletion processing, data normalization processing, and generating derived data items for the collected community public service information.

The preprocessing of missing values depends on the magnitude and nature of missing values. For missing values that will not affect the objectivity and effectiveness of the prediction results, the deletion method is usually used directly. Due to the large amount of data, deleting individual missing value data has little impact on the overall prediction results of the case, which ensures the objectivity and accuracy of the prediction results to the greatest extent. For the missing values with less missing magnitude but more important and certain impact on the prediction results, the method of manual supplement is usually adopted, which is confirmed and filled manually through secondary collection of information. For the data that has absolute influence on the case and cannot be collected again, regardless of its magnitude, this paper uses the moving window mean filling method to fill the missing value. If the number of community risk events is missing on a certain day, the missing data of risk events is defined as the average value of risk events in the first three days and the next three days of the event, which is used as the number of risk events on that day and filled in. The algorithm is as follows:

$$\chi_m = \frac{1}{6}\left(\chi_{m-3} + \chi_{m-2} + \chi_{m-1} + \chi_{m+3} + \chi_{m+2} + \chi_{m+1}\right). \tag{7}$$

In the process of analyzing characteristic factors, the unit and magnitude of each characteristic factor are different. For example, the house price of second-hand houses is usually calculated in 10000 units, while the occurrence of community risk events is usually calculated in single digits. At this time, in the analysis of relevant factors, the second-hand house price with larger magnitude usually masks the impact of less magnitude, such as the occurrence of risk events. Therefore, the difference between the unit magnitudes of different characteristic factors needs to be normalized. The processing algorithm is as follows:

$$\begin{aligned} y &= \frac{\chi - \mathrm{Min}}{\mathrm{Max} - \mathrm{Min}}, \\ Y &= \alpha + \frac{\chi - \mathrm{Min}}{\mathrm{Max} - \mathrm{Min}} \times (\beta - \alpha). \end{aligned} \tag{8}$$

In addition, in the subsequent model construction process, there are some characteristics that cannot be directly reflected by data, and a series of preprocessing should also be carried out, such as weather characteristic factors, which are usually displayed as sunny or rainy days, rather than intuitive data quantification. Here, we use scoring processing. The worse the weather, the higher the score. Similarly, the quantization and feature selection of holidays are processed, and the algorithm is as follows:

$$\begin{aligned} \rho &= \frac{P_1 + P_2 + \cdots + P_n}{S}, \\ R &= \frac{\sum_1^n (\chi_i - \overline{X})(Y_i - \overline{Y})}{\sqrt{\sum_1^n (Y_i - \overline{Y})^2}\sqrt{\sum_1^n (X_i - \overline{X})^2}}, \\ R_m &= \frac{\sum_1^n (\chi_i - M_i)(Y_i - \overline{Y})}{\sqrt{\sum_1^n (Y_i - \overline{Y})^2}\sqrt{\sum_1^n (X_i - M_i)^2}}, \\ \alpha &= \frac{R(a) - R(A_a)}{\left|N_{A_a}\right| - 1}, \\ R(a) &= r(a) \times p(a). \end{aligned} \tag{9}$$

4. Result Analysis and Discussion

Through the correlation analysis method to analyze the factor characteristics of the original input data, we finally get that the correlation between the actual data and the predicted data in the first seven days is 0.978. In the data of the first six days, the correlation between the actual data and the predicted data is 0.982. From this, we can see that the predicted data in the first seven days and the data in the first six days are more accurate and have a high correlation. In order to enrich the amount of input data, we changed the structure tree in the dichotomy and set the maximum tree depth as 4 and the minimum leaf node as 5. The experimental results are shown in Figure 3.

Figure 3 through the comparison between the predicted results on the data set and the actual input results, it can be seen that the CART regression tree prediction model performs well. The abscissa is the date and the ordinate is the amount of community risk events. The blue solid line is the

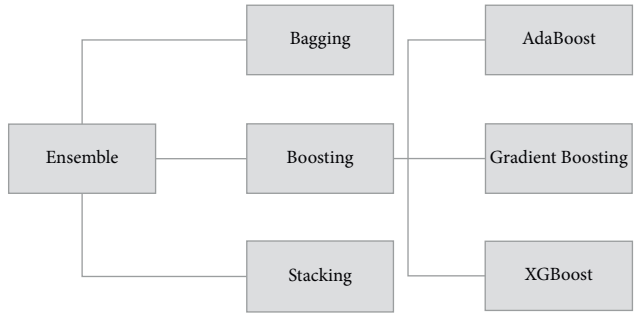

Figure 1: Ensemble model structural framework.

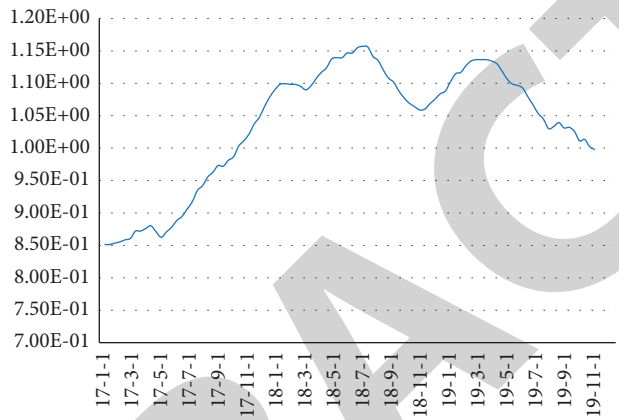

Figure 2: 2017 to 2019 years of housing price changes.

input data set, M is the real number of cases per day in a year, and the orange is the prediction result of CART regression tree model, that is, the number of community risk events per day in that year. It can be seen that the trend of the orange line is basically consistent with that of the blue line. The final results show that the correlation coefficient is 86.2%, the error coefficient is 74.3%, and the variance is 0.971. To sum up, we can think that there is a large correlation between the predicted value and the actual value of CART regression tree prediction model, and the prediction performance is good.

Neural network model is a very powerful model to calculate and simulate the nonlinear relationship. It has strong applicability no matter what the relationship between variables is. In the first mock exam, traditional convolution neural network is used to predict the results. The deep learning framework is constructed by building multiple single models and integrating into multichannel convolution neural networks. Multiple single network models do not need complex relationships between them, and the multichannel deep learning model can integrate different information sources. Each connected information source has a parameter called weight, and the information is converted and learned between different neurons according to different weights. In the multilayer sensing mechanism, layers are fully connected, and each neuron in the upper layer is connected with all neurons in the lower layer. In the multilayer sensing mechanism, the bottom layer is the input layer and the data to be trained. In the middle is the hidden layer data, which is continuously transmitted and learned between the hidden layers. Finally, the output layer outputs the final result. The specific structure is shown in Figure 4.

Finally, the prediction results are analyzed based on the comprehensive prediction model, and the results are shown in Figure 5. The data is based on the granularity of one day, the abscissa is the date, and the ordinate is the occurrence of community risk events. The blue solid line is m, which is the real amount of risk events in the community every day in 2019, and the orange is the prediction result of the comprehensive prediction model. It can be seen that the change trend of blue solid line is basically the same as that of orange solid line. At the same time, compared with the single prediction model, it can be seen that the result of the comprehensive prediction model is significantly better than that of the single prediction model. The final results show that the correlation coefficient between the actual data and the predicted data of the comprehensive prediction model is 92.5%, the error value is 85.5%, and the variance is 0.703. To sum up, the correlation between the actual value and the predicted value of the comprehensive prediction model is good, which is higher than that of the single prediction model, and the accuracy of the prediction results is also higher, which is higher than that of the single prediction model. Comparison of results of comprehensive prediction model is shown in Figure 5.

To conclude, it is stated that a large correlation exists between the predicted and the actual values of CART

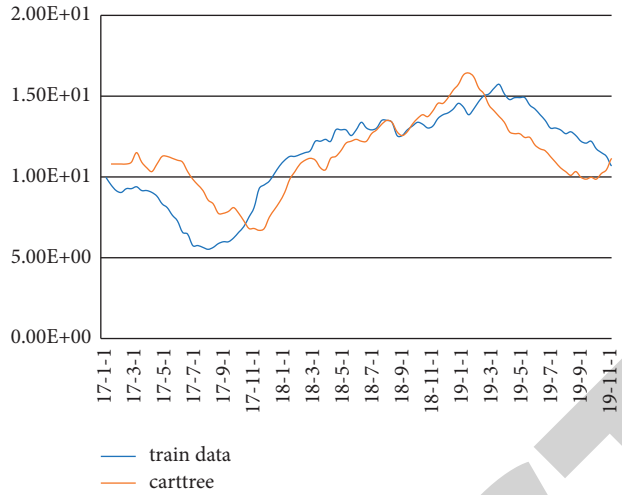

Figure 3: Comparison diagram of prediction results of CART regression tree model.

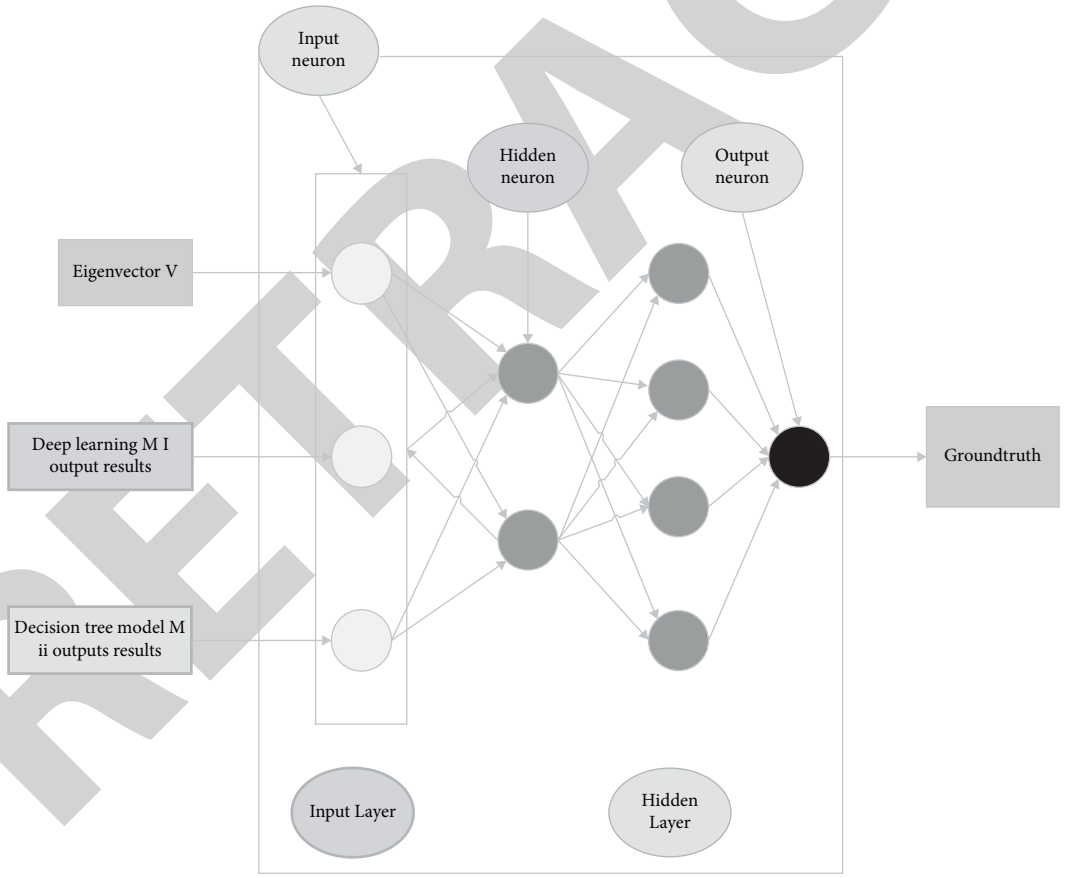

Figure 4: Neural network structure of synthetic prediction model.

regression tree prediction model. As a result, the prediction performance was better. Moreover, the correlation between the actual and predicted values of the comprehensive prediction model is good. The comprehensive prediction is higher than the single prediction model, and its prediction's accuracy is also higher.

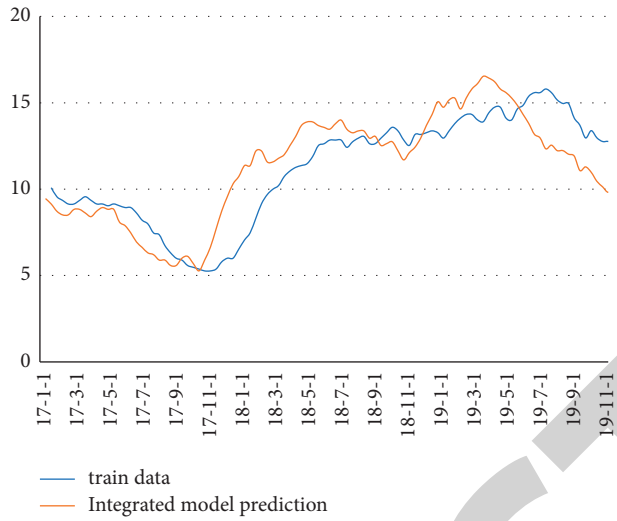

Figure 5: Comparison of results of comprehensive prediction model.

5. Conclusion

This paper carried out the research on the basis of deep learning model. The proposed study could be explained into a few major stepwise points as follows: (i) initially, the screening of characteristics of community related risk factors was carried out, (ii) then, the construction models took place, i.e., CART regression tree prediction model and multichannel convolution neural network model, respectively; breaking the traditional prediction method, multiple single channel models were integrated into multichannel prediction model; (iii) finally, the experimental verification showed that the multichannel prediction model can not only improve the processing ability of community public service information, but also well predict the occurrence of community public service security governance problems. Although the model greatly improved the prediction accuracy and processing speed of risk events, in the processing algorithm, more consideration was given to the time-dependent sequence model. Further, no more in-depth analysis was made on the impact of spatial factors on the prediction accuracy of the model. Therefore, the impact of community spatial location will be considered in the next stage. At the same time, it is hoped that this research will provide some ideas and methods for the current community public service information collaborative governance on the basis of deep learning model.

Data Availability

The data used to support the findings of this study are available upon request to the author.

Conflicts of Interest

The author declares that he has no conflicts of interest.

Acknowledgments

This research was supported by Project of Philosophy and Social Science Research in Colleges and Universities in Jiangsu Province, Research on the integrated development path of community public services under the background of urban-rural integration (2021SJA1439).

References

[1] R. Lu and L. Li, "Crime prediction model based on Random Forest," *Journal of China Interpol Academy*, vol. 5, no. 3, pp. 108–112, 2019.

[2] L. Chen, L. Yin, T. Yu, and K. Wang, "Short-term load forecasting of power system based on deep forest algorithm," *Power Engineering Set*, vol. 39, no. 11, pp. 42–50, 2018.

[3] W. Lin and J. Chen, "Evaluation and prediction of spatial and temporal pattern of population in Chaoyang district of Beijing based on multi-source data," *Journal of Geo-Information Science*, vol. 20, no. 10, pp. 1467–1477, 2018.

[4] T. Bi, "A review of single image depth estimation based on supervised learning," *Journal of Computer-Aided Design & Computer Graphics*, vol. 30, no. 8, pp. 1383–1393, 2018.

[5] L. Duan, L. Dang, T. Hu, X. Zhu, and X. Ye, "Prediction of suspect social activity location based on Historical Crime Data," *Journal of Geo-Information Science*, vol. 20, no. 7, pp. 929–938, 2018.

[6] L. Liu, W. Liu, W. Liao et al., "Comparison of prediction of crime hotspots in different cycles based on random forest and temporal and spatial kernel density methods," *Progress in Geography*, vol. 37, no. 6, pp. 761–771, 2018.

[7] J. Ye, L. Sun, B. Du, Y. Fu, F. Tong, and H. Xiong, "Co-prediction of multiple transportation demands based on deep spatio-temporal neural network," in *Proceedings of the 25th ACM SIGKDD International Conference*, Anchorage, AK USA, August 2019.

[8] N. Tam and Y. Keiji, "Visualizing crime clusters in a space-time cube: an exploratory data-analysis approach using space-

Hindawi
Journal of Mathematics
Volume 2023, Article ID 9787535, 1 page
https://doi.org/10.1155/2023/9787535

Retraction

Retracted: Weather Radar Image Superresolution Using a Nonlocal Residual Network

Journal of Mathematics

Received 19 December 2023; Accepted 19 December 2023; Published 20 December 2023

This article has been retracted by Hindawi following an investigation undertaken by the publisher [1]. This investigation has uncovered evidence of one or more of the following indicators of systematic manipulation of the publication process:

(1) Discrepancies in scope

(2) Discrepancies in the description of the research reported

(3) Discrepancies between the availability of data and the research described

(4) Inappropriate citations

(5) Incoherent, meaningless and/or irrelevant content included in the article

(6) Manipulated or compromised peer review

The presence of these indicators undermines our confidence in the integrity of the article's content and we cannot, therefore, vouch for its reliability. Please note that this notice is intended solely to alert readers that the content of this article is unreliable. We have not investigated whether authors were aware of or involved in the systematic manipulation of the publication process.

Wiley and Hindawi regrets that the usual quality checks did not identify these issues before publication and have since put additional measures in place to safeguard research integrity.

We wish to credit our own Research Integrity and Research Publishing teams and anonymous and named external researchers and research integrity experts for contributing to this investigation.

The corresponding author, as the representative of all authors, has been given the opportunity to register their agreement or disagreement to this retraction. We have kept a record of any response received.

References

[1] H. Yuan, Q. Zeng, and J. He, "Weather Radar Image Superresolution Using a Nonlocal Residual Network," *Journal of Mathematics*, vol. 2021, Article ID 4483907, 11 pages, 2021.

Hindawi
Journal of Mathematics
Volume 2021, Article ID 4483907, 11 pages
https://doi.org/10.1155/2021/4483907

Research Article

Weather Radar Image Superresolution Using a Nonlocal Residual Network

Haoxuan Yuan[1,2] **Qiangyu Zeng**[1,2] **and Jianxin He**[1,2]

[1]*College of Electronic Engineering, Chengdu University of Information Technology, Chengdu 610225, China*
[2]*CMA Key Laboratory of Atmospheric Sounding, Chengdu 610225, China*

Correspondence should be addressed to Qiangyu Zeng; zqy@cuit.edu.cn

Received 26 October 2021; Revised 30 November 2021; Accepted 3 December 2021; Published 30 December 2021

Academic Editor: Naeem Jan

Accurate and high-resolution weather radar images reflecting detailed structure information of radar echo are vital for analysis and forecast of extreme weather. Typically, this is performed by using interpolation schemes, which only use several neighboring data values for computational approximation to get the estimated value regardless of the large-scale context feature of weather radar images. Inspired by the striking performance of the convolutional neural network (CNN) applied in feature extraction and nonlocal self-similarity of weather radar images, we proposed a nonlocal residual network (NLRN) on the basis of CNN. The proposed network mainly consists of several nonlocal residual blocks (NLRB), which combine short skip connection (SSC) and nonlocal operation to train the deep network and capture large-scale context information. In addition, long skip connection (LSC) added in the network avoids learning low-frequency information, making the network focus on high-level features. Extensive experiments of ×2 and ×4 super-resolution reconstruction demonstrate that NLRN achieves superior performance in terms of both quantitative evaluation metrics and visual quality, especially for the reconstruction of the edge and detailed information of the weather radar echo.

1. Introduction

Doppler weather radar with high temporal and spatial resolution e.g., China Next Generation Weather Radar (CINRAD) provides measurements with high temporal (approx. 6 minutes) and spatial (approx. 1 × 1 km) resolution and have been widely applied in operational research and forecasts on medium-scale and intense precipitation weather phenomena.

However, single weather radar is susceptible to beam blocking, ground clutter, and reduced resolution at long distances due to beam broadening and averaging. As shown in Figure 1, the beam width increases with the detection distance which leads to a loss of information on sudden changes in radar echoes such as velocity changes in tornadoes and mesocyclones, as well as information on extreme precipitation intensity and gradients when detection target occurs at a distance from the observing radar [1, 2]. It is, therefore, worthwhile to improve the resolution of weather radar data by upgrading the observation equipment and by postprocessing the observation data such as interpolation or superresolution reconstruction. Due to the long cycle and high cost of the first scheme, many scholars have conducted a lot of research on the second scheme.

In terms of interpolation methods, Ruzanski and Chandrasekar [3] proposed a kernel-based Fourier interpolation method, which effectively improves the spatial and temporal resolution of weather radar by adding windows to screen the effective input data to be interpolated. Sharifi et al. [4] proposed a downscaling method based on spline interpolation to address the problem of too coarse spatial-temporal resolution when satellite precipitation estimates are applied to small areas, which effectively improves the resolution of precipitation data products while accurately capturing detailed precipitation patterns and information. Considering the non-Gaussian and locally coherent structure of weather radar reflectivity data in the wavelet domain, Kou et al. [5] proposed an interpolation method to improve

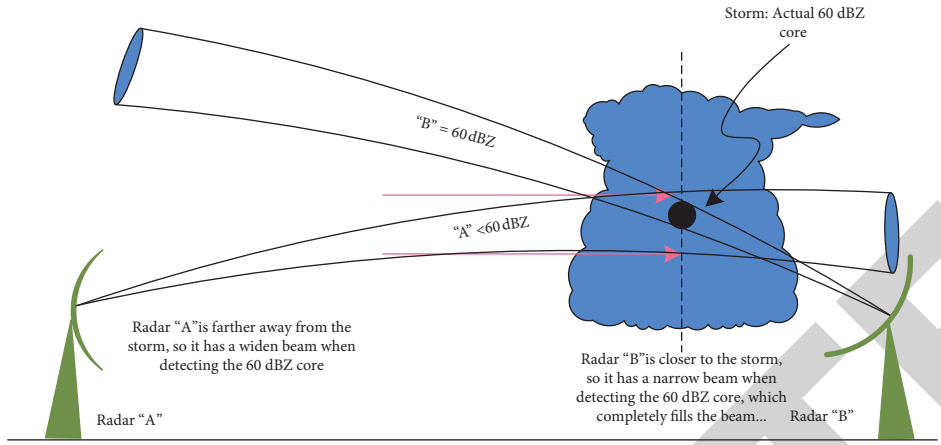

Figure 1: The effect of beam broadening.

the resolution of radar reflectivity data, which effectively use the hidden Markov tree (HMT) model as priority information to well capture the multiscale statistical characteristics of radar reflectivity data in small-scale intense precipitation condition.

Inspired by the sparsity of weather radar precipitation images in the wavelet domain, dictionary-based sparse regularization methods have been applied to statistical down scaling, converting coarse observation data into more refined [6, 7]. Based on sparse regularization, Zhang et al. [8] further proposed a nonlocal self-similar sparse representation (NSSR) model, which effectively uses the nonlocal self-similarity of weather radar echo during the reconstruction process. Similarly, in the research article, Yuan et al. [9] proposed adaptive regularized sparse representation for weather radar echo super-resolution reconstruction. Based on dictionary learning, Xu et al. [10] proposed a downscale method to obtain more refined short-duration precipitation data.

With the rapid progress of deep learning, the atmospheric research community has already taken advantage of the convolutional neural network (CNN)'s ability [11], such as the application of super resolution is related to the statistical downscaling of climate data. Vandal et al. [12] first applied CNN to climate data downscalling and improved the accuracy of precipitation data from 1° (100 km) to 1/8° (12.5 km) by stacking CNN-based super-resolution models. Cheng et al. [13] innovatively integrated the residual dense block (RDB) [14] with the Laplacian pyramid super-resolution network (LapSRN) [15] to exploit hierarchical features from all convolutional layers and generate a more refined climate image than Vandal's method. Geiss and Hardin [16] combined the classic "up-net" [17] with the "dense network" [18] and proposed a new deep convolutional neural network to learn large-scale precipitation features in weather radar images. The reconstructed weather radar image is superior to the traditional interpolation method in terms of both objective evaluation metrics and visual quality. Stengel et al. [19] also used adversarial learning to significantly enhance the resolution of wind and solar data, which shows the notable performance of the generative adversarial network (GAN) in downscaling climate data.

However, there is an issue existing in most CNN-based super-resolution models. These networks use local convolutional operations to extract features, which result in a relatively small receptive field size of the network and the inability to capture the large-scale context information of weather radar image, such as the recurrence features of small-scale organized precipitation within and across different storm environments.

To address this issue, we proposed a nonlocal residual network (NLRN) on the basis of CNN, which increases the depth of the network and the efficiency in exploiting the large-scale context information of the weather radar image by applying residual learning and nonlocal operation.

The main contributions of this work are as follows:

(i) According to the nonlocal self-similarity of weather radar images, this research endowed the network's ability that allows them to fuse nonlocal information by stacking the nonlocal residual block (NLRB). In order to achieve a nonlocal operation, it embeds the nonlocal block (NLB).

(ii) The outstanding performance of residual learning has inspired us to introduce the long and short skip connections in the overall structure of the network and NLRB, respectively. It trains a deeper network, which effectively facilitates the flow of information and solves the gradient vanishing problems.

(iii) This study conducted loads of experiments on reflectivity data under different weather conditions. They justified that weather radar images reconstructed by NLRN achieved better quantitative results and visual quality by the proposed method than other SR methods mentioned in the experimental section.

The remaining part of the article proceeds as follows: Section 2 gives a brief introduction to the background that is related to the article. The framework and details of the proposed NLRN are described in Section 3. Section 4 presents the implementation details of NLRN. Several experimental results and discussions are presented to validate the effectiveness of the proposed NLRN in Section 5. Section 6 concludes the article.

2. Background

First, this section gives a concise overview of the SR methods that are related to the article. Second, we discuss the characteristic of a weather radar image. Finally, to facilitate the understanding of subsequent experimental parts by readers without a background in meteorology, we give a brief introduction to the hook echo.

2.1. Image Super-Resolution Methods. According to the means of implementation, the image super-resolution methods can be divided into three types: interpolation-based, reconstruction-based, and learning-based image super-resolution methods.

2.1.1. Methods Based on Interpolation. The basic idea of classical interpolation methods such as nearest interpolation, bilinear interpolation, and bicubic interpolation [20] is to approximate the lost image information by using the basis function or interpolation kernel, which only exploits the neighboring information. These methods often result in blurred edges and loss of high-frequency detail while reducing computational complexity.

2.1.2. Methods Based on Reconstruction. Reconstruction-base methods apply prior knowledge of image as constraint terms to the process of super-resolution reconstruction, which effectively solves the ill-posed problem of super-resolution reconstruction. Classical reconstruction-based methods are iterative back projection (IBP) [21], maximum a posterior estimation (MAP) [22], etc.

2.1.3. Methods Based on Shallow Learning. Before the deep learning is applied to image super resolution, the most learning-based methods are proposed on the basis of sparse representation such as nonlocally centralized sparse representation (NCSR) [23] and structure-modulated sparse representation (SMSR) [24], which mainly includes dictionary learning and sparse coding.

2.1.4. Methods Based on Deep Learning. In recent years, with the rapid progress of deep learning, learning methods represented by convolutional neural networks (CNNs) quickly dominate the computer vision field and have been widely applied in the fields of image recognition and segmentation [25–29]. Deep learning methods based on CNN have been popularly applied to the image super-resolution (SR) field since Dong et al. first proposed to combine CNN and super-resolution reconstruction (SRCNN) [30]. Dong et al. [31] replaced the large convolution kernel with more and smaller convolutional layers on the basis of SRCNN and introduced a deconvolution layer at the end of the network to greatly improve the training speed of the model. Benefiting from the increasing depth and complexity of networks, super-resolution networks possess increasingly better performance. The structure of the residual network (ResNet) [32] has been widely applied to effectively solve the gradient vanishing and gradient exploding problems faced by deep networks. The network proposed by Kim et al. (VDSR) [33] increases the convolutional layers to 20 layers, which apply global skip connection as well as adjustable gradient cropping strategy to solve the problem of difficult convergence of deep networks and achieve striking reconstruction results. An enhanced deep super-resolution network (EDSR) [34] further improves the results by removing the unnecessary batch normalization modules. Haris et al. proposed a deep back-projection network (DBPN) [35] exploiting iterative up-and-down sampling layers, which effectively use the interdependence of LR and HR images.

2.2. Weather Radar Image Characteristic. Statistics show that the weather radar image contains much redundant information. As shown in Figure 2, the red box in the left PPI (Plane Position Indicator) and the black box in the right PPI indicate the given patch and the patches that are nonlocally similar to it, respectively. Many similar and redundant structures can be observed between two patches (the example data are the reflectivity data of the first layer elevation angle of CINRAD-SA radar (Yancheng, Jiangsu, China, 11: 48, June 23, 2016). These data have 360 radials, and each radial has 460 range bins. This nonlocal redundant information has the effect of improving the quality of weather radar image reconstructed. As discussed above, limited by the size of the local receptive field, the convolution operation has deficiencies in the fusion of nonlocal information, resulting in the failure to effectively capture the long-range dependencies. Therefore, the network that can better fuse the nonlocal information of weather radar images has better super-resolution reconstruction performance.

2.3. Hook Echo. The Hook Echo is a well-researched radar reflectivity signature that must involve descending precipitation curtains as hydrometeors fall relative to the ambient air. As shown on the left part of Figure 3, the falling precipitation occurs on the back side of the updraft, which can be regarded as the low-level "extension of the bounded weak echo region (BWER)" [36]. It is commonly believed that the falling precipitation interacts with the mesocyclone of the storm, so it descends along an arc [37]. The right part of Figure 3 shows the radar reflectivity signatures of the hook echo. A common belief is that the hook echo is the area where tornadoes may occur in supercell thunderstorms [38, 39]. Therefore, capturing as much detailed information as possible about the hook echo can help in tornado detection and early warning forecasting.

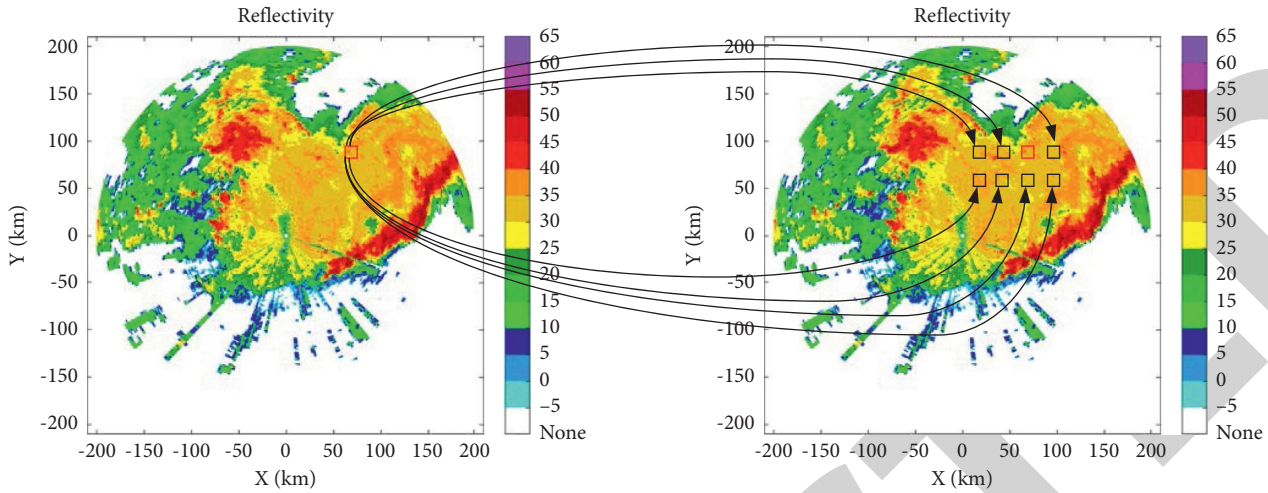

Figure 2: Example of nonlocally similar weather radar image patches.

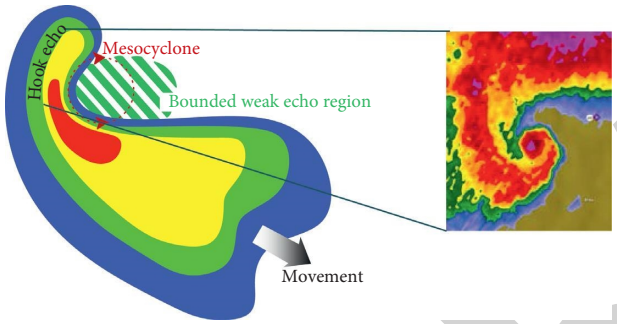

Figure 3: Conceptual model and radar reflectivity signature of hook echo.

3. Network Structure

The architecture of NLRN is illustrated in Figure 4(a), which consists of four parts: shallow feature extraction, deep feature extraction, upsampling, and reconstruction layer. I_{LR} and I_{SR} denote the input and output of NLRN. The first part extracts the shallow features F_0 from the input LR image I_{LR}.

$$F_0 = H_{SF}(I_{LR}), \tag{1}$$

where H_{SF} denotes the two convolution operation, each followed by an activation function. To effectively solve the vanishing gradients and dying ReLU problem, we choose leaky rectified linear unit (LReLU) as the activation function. The shallow features F_0 are then used as input to the nonlinear mapping network part that consists of G nonlocal residual blocks (NLRBs) to learn mapping relations with sufficient representational ability. The structure of NLRB will be given in detail later. We formulate the deep feature-extraction process as follows:

$$F_g = H_{RNAB,g}\left(F_{g-1}\right), \quad g = 1, \ldots, G, \tag{2}$$

where $H_{RNAB,g}(\cdot)$ represents the operation of g_{th} NLRB, F_{g-1} and F_g denote the input and output of g_{th} NLRB, respectively. To make the network more focused on high-frequency information, we avoid learning low-frequency information by adding long skip connection (LSC), which also effectively fuses shallow and deep features. The process is expressed as follows:

$$F_{G+1} = H(F_G) + F_0, \tag{3}$$

where H represents a convolution operation and F_{G+1} as the input to the upscale module. As the previous work [34], we apply ESPCNN [40] to upscale the deep features and then use one final convolution layer with three filters to provide the final reconstructed images. The output of NLRN can be obtained by

$$I_{SR} = H_R(H_{UP}(F_{G+1})) = H_{NLAN}(I_{LR}), \tag{4}$$

where H_{UP} and H_R denote the upsampling and the convolution operation, respectively. H_{NLAN} denotes the function of our NLRN.

3.1. Nonlocal Residual Block. Restricted by the local receptive field size, most CNN-based SR methods have deficiencies in the fusion of nonlocal information, which result in low-efficiency utilization of self-similarity properties in images. Inspired by the classical nonlocal means [41], Wang et al. [42] proposed a nonlocal block (NLB) to fuse the nonlocal information of the image by using the self similarity of the nonlocal patches of the image, which obtain promising results in image recognition. Returning to the task of super-resolution reconstruction, in order to fully exploit the input information through the network, we propose a nonlocal residual block (NLRB). As shown in Figure 4(b), the first part of the NLRB is three convolutions with a size of 3×3, each of them is followed by LReLU. The input of NLRB and output of NLB are combined by residual learning through a short skip connection (SSC), which also effectively solves the vanishing gradient problems faced by the deep network and facilitates the flow of information.

3.2. Nonlocal Block. Now, we present details about NLB. Nonlocal operations can transform the response of the current position into the weighted sum of all position features in the

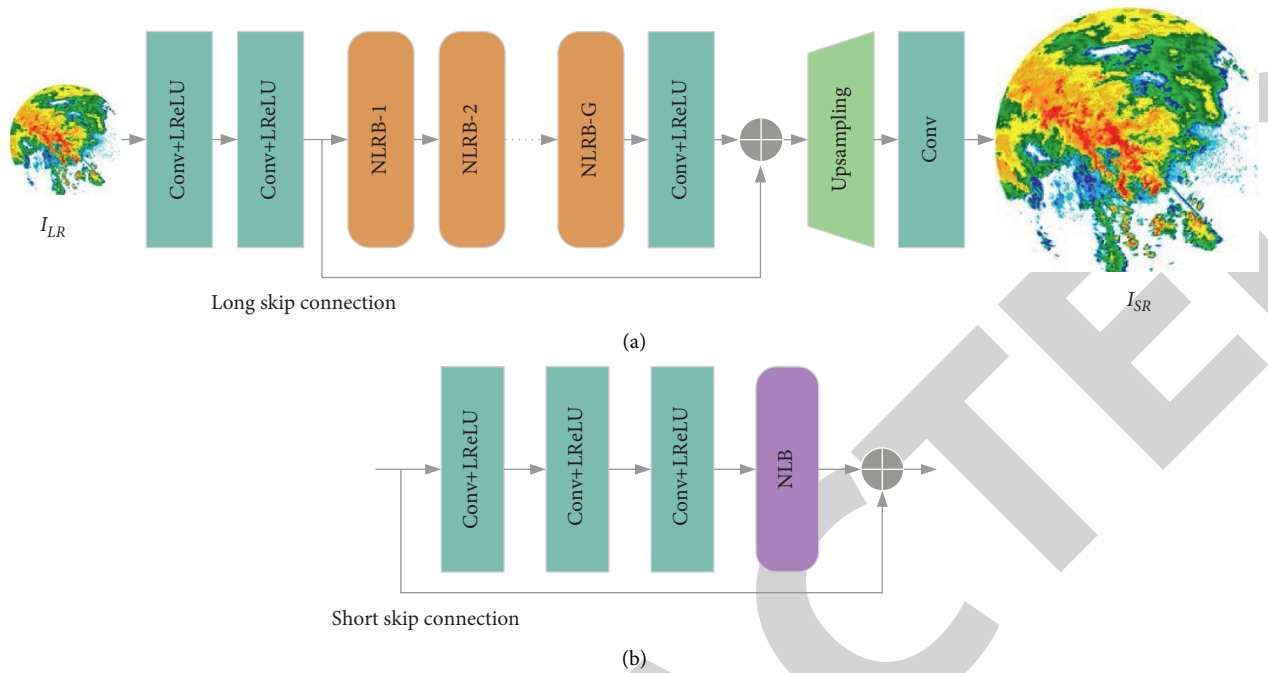

FIGURE 4: (a) The overall architecture of the proposed nonlocal residual network (NLRN). (b) The inner structure of nonlocal residual block (NLRB).

input feature map, so the nonlocal mean can fuse the nonlocal information of the image by using the self similarity of the local patch of the image. The generalization formula of the nonlocal operation in neural networks is defined as

$$y_i = \frac{\sum_{\forall j} f(x_i, x_j) g(x_j)}{\sum_{\forall j} f(x_i, x_j)}, \tag{5}$$

where i is the location index of the target output y, j is the index of all possible positions in this operation. x is the input feature mapping; y is the output feature mapping, and x and y have the same size. $f(x_i, x_j)$ represents the scalar relationship between the positions i and j. The unary function $g(x_j)$ represents the eigenvalues of the feature mapping x at the position index j. Inspired by nonlocal means and bilateral filters, we use embedded Gaussian functions to compute similarity.

$$f(x_i, x_j) = \exp\left(u(x_i)^T v(x_j)\right), \tag{6}$$

where $u(x_i) = W_u x_i$, $v(x_j) = W_v x_j$, W_u and W_v denote the weight matrices. This can be seen from the fact that for a given i, $(1/\sum_{\forall ?j} f(x_i, x_j)) f(x_i, x_j)$ becomes the SoftMax computation along the dimension j. So, we have $y_i = \text{softmax}(x_i^T W_u^T W_v x_j) g(x_j)$. For simplicity, we consider a linear embedding for $g(x_j)$: $g(x_j) = W_g x_j$, and W_g denotes the weight matrix. We further transform nonlocal operations into a nonlocal block (NLB). The definition of NLB is as follows:

$$z_i = W_z y_i + x_i, \tag{7}$$

where y_i has been given in equation (5), $+x_i$ represents a residual connection, which allows us to embed a new NLB in any pretraining model without changing its original structure. Then, the output z at the position i of the (NLB) is calculated as follows:

$$z_i = W_z y_i + x_i = W_z \text{softmax}\left(x_i^T W_\theta^T W_\phi x_j\right) g\left(x_j\right) + x_i, \tag{8}$$

where W_z denotes the weight matrix and is initialized as zeros. The structure of NLB is illustrated in Figure 5.

3.3. Loss Function. When training NLRN, the optimal set of network parameters is obtained by minimizing the loss between training samples. To show the effectiveness of our NLRN, we choose l_1 loss function for our network optimization to provide better convergence [40]. Now, for a batch of N training images i.e. $\{I_{\text{SR}}^i, I_{\text{LR}}^i\}_{i=1}^N$, the aim is to minimize the l_1 loss function as

$$L(\theta) = \frac{1}{N} \sum_{i=1}^{N} \left\| I_{\text{HR}}^i - I_{\text{SR}}^i \right\|_1, \tag{9}$$

where θ denotes the parameters to be learned by the network. The Adam algorithm is applied to optimize the loss function.

4. Implementation Details

The implementation details on datasets, degradation process, training details, and evaluation metrics are presented in this section.

4.1. Datasets. We use reflectivity data from China's New Generation Weather Radar (CINRAD-SA) as a dataset. For the elevation of each layer, there are 360 radials, 460 range bins reflectivity data for each radial, and the range resolution

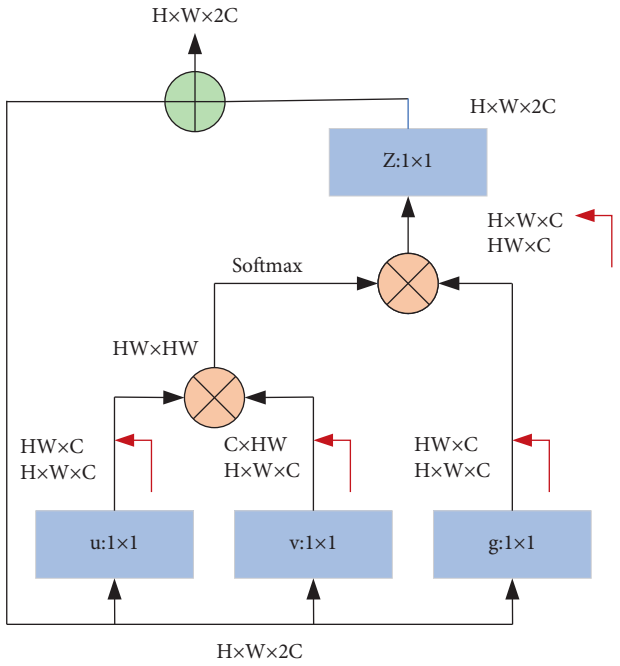

Figure 5: The framework of nonlocal block. Red solid line denotes matrix reshaping. $H \times W \times C$ means C features with height H and width W, and $\otimes$ denotes the matrix multiplication. $\oplus$ denotes element-wise addition.

of 1 km. To enable NLRN to learn large-scale precipitation features and small-scale extreme weather features, we use the precipitation experimental data of South China in Guangdong on May-June, 2016, the tornado and hail data of Yancheng in Jiangsu on May 27, 2008, the tornado data of Yancheng in Jiangsu on June 23, 2016 and Nantong in Jiangsu on July 06, 2016, and the typhoon data of Xuzhou in Jiangsu in August 2018. The total number of high resolution (HR) datasets with a size of 512×512 is 1800, of which 1600 images are used for training, 20 images for validation, and 180 images for testing. We mainly study the super-resolution reconstruction performance of NLRN under ×2 and ×4 conditions, so low resolution (LR) images with a size of 256×256 and 128×128 are obtained as input of NLRN by applying the degradation method to HR images.

4.2. Degradation Process. The weather radar image degradation process includes three processes: blurring, downsampling, and system noise. The degradation process can be formulated by the equation as follows:

$$\mathbf{y} = \mathbf{A}\mathbf{x} + \mathbf{n}, \tag{10}$$

where $\mathbf{A}$ represents the degradation operation (e.g., blurring kernel and downsampling operation), and $\mathbf{n}$ represents the weather radar receiver noise, which obeys the zero-mean Gaussian distribution.

4.3. Parameter Settings. During the training, common data enhancement methods are also used in training, such as random horizontal rotations of 90°, 180°, and 270°. For every training batch, 16 LR patches with the size of 20×20 are randomly extracted as inputs. The convolutional kernels present in the network are all 3×3 in size and 64 in number of filters. To explore the most appropriate number of G, we have counted the average PSNR under different weather conditions (e.g., the large weather system, small weather system, and cloudless) with different parameter G. As shown in Figure 6, when $G \geq 4$, the growth of PSNR becomes slow or even decreases. For balancing performance and computational complexity, we set the number of G as 4. The negative slope of leaky rectified linear units (LReLUs) is 0.1. The Adam algorithm with $\beta_1 = 0.9, \beta_2 = 0.09, \varepsilon = 10^{-8}$ is adopted to optimize the network. The initial learning rate is 10^{-4} and decreases by half for every 200 epochs. Training a NLRN on PyTorch (1.01) framework roughly takes two days with two Tesla P40 GPUs for 500 epochs.

4.4. Evaluation Metrics. In order to test the effectiveness of the proposed NLRN, we compare NLRN with several SR methods, including Bicubic, IBP, NCSR, VDSR, and EDSR. Bicubic is a classic interpolation method. IBP is a classical reconstruction method based on gradual iteration. NCSR is a traditional learning method based on sparse dictionary learning. VDSR and EDSR are CNN-based deep learning methods. Peak-signal-to-noise ratio (PSNR) (dB) and structural similarity (SSIM) [43] are used to quantitatively evaluate the SR methods.

5. Experimental Results and Analysis

In this section, we compare NLRN with other SR methods in terms of the training process, visual quality, and quantitative results.

5.1. Training Comparison. To further compare the convergence and accuracy when training VDSR, EDSR, and NLRN, the training loss curves of three networks are plotted in Figure 7(a). From Figure 7(a), it can be seen that after 100 epochs, the loss function loss decreases more slowly with iterations increasing and finally stabilizes between 6.0 and 7.0, indicating that the network has converged on the training dataset. It can be seen that NLRN has both faster convergence and better accuracy than VDSR and EDSR when training. Figure 7(b) represents the validation PSNR values of several SR methods mentioned above during the training. It can be seen that NLRN exhibited considerable advantages over the conventional methods (Bicubic, IBP, and NCSR) and CNN-based methods (EDSR and VDSR).

5.2. Visual Quality Comparison. In order to test the performance of NLRN under the large-scale weather system, we choose precipitation and typhoon reflectivity data as test data. For weather radar reflectivity data, the intense precipitation convective cells are often embedded in a lower intensity region, which shows high aggregation and sparse correlation. Figure 8 shows some of the visual results of the different SR methods under an intense precipitation

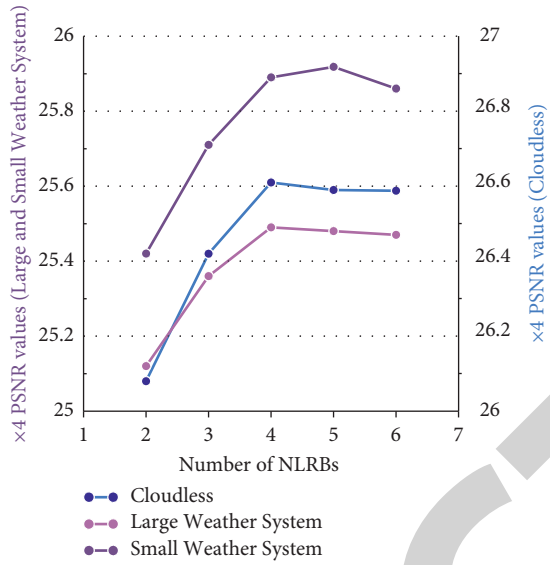

Figure 6: The average PSNR performance of NLRN on validation set with different parameter G (the total numbers of NLRB).

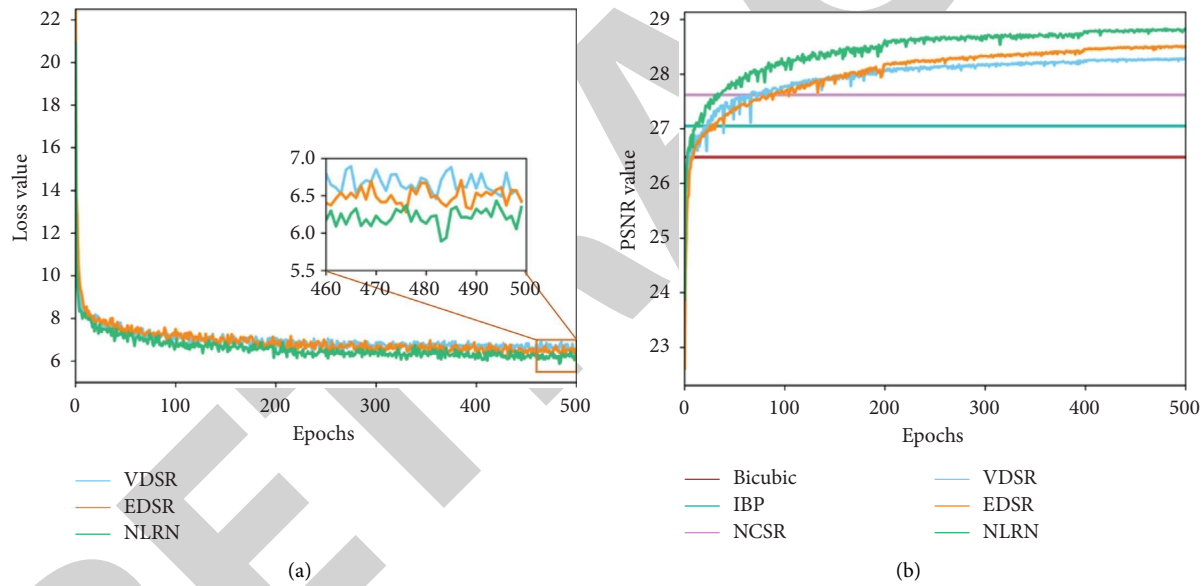

Figure 7: (a) Training l_1 loss of VDSR, EDSR, and NLRN for scale ×4. (b) Validation PSNR values of Bicubic, IBP, NCSR, VDSR, EDSR, and NLRN during training for scale ×2.

condition (Heyuan, Guangdong, China, 11:48, June 15, 2016). The deep learning-based output is subjectively superior to the conventional methods. The approach is not able to recover all of the very fine-scale precipitation structure that is lost when the original weather radar image is degraded. However, the deep leaning methods preserve more of the fine-scale structure and is notably better at preserving sharp edges associated with the larger features. Compared with VDSR and EDSR, NLRN effectively exploits the self similarity of radar precipitation images through the nonlocal operation, which is very useful for the identification and monitoring of intense convective precipitation echo by reconstructing high-frequency details that are prone to variability in the map, making the echo structure more refined and highlighting the location of intense echo. As shown in Figure 9, NLRN also achieves the best subjective output under the typhoon condition

(Xuzhou, Jiangsu, China, 09:30, August 18, 2018) by reconstructing more intense echo information. To test the performance of NLRN under the small-scale weather system, we choose tornado data (Yancheng, Jiangsu, China, 14:08, June 23, 2016) as test data. From Figure 10, it can be seen that although both the conventional methods and the deep learning methods can reconstruct most of the hook echo detail information, the hook echo reconstructed by the NLRN is closer to the original hook echo, which helps forecasters to analyze small- and medium-scale extreme weather and make timely forecast and warning condition (Xuzhou, Jiangsu, China, 09:30, August 18, 2018) by reconstructing more intense echo information.

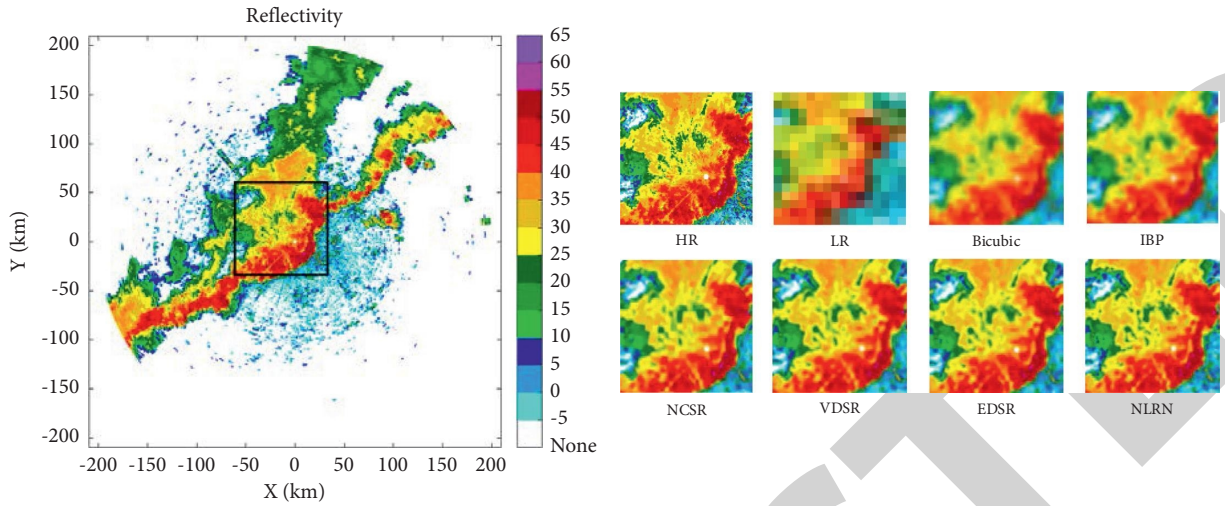

Figure 8: Visual comparison of ×4 super-resolution reconstruction results of intense precipitation data. The best results are in bold.

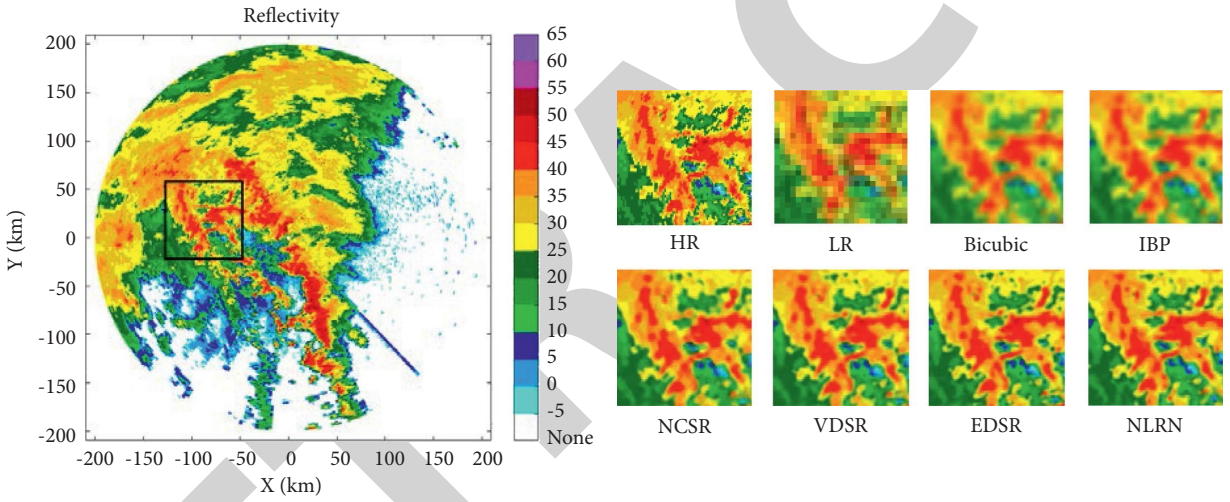

Figure 9: Visual comparison of ×4 super-resolution reconstruction results of typhoon data. The best results are in bold.

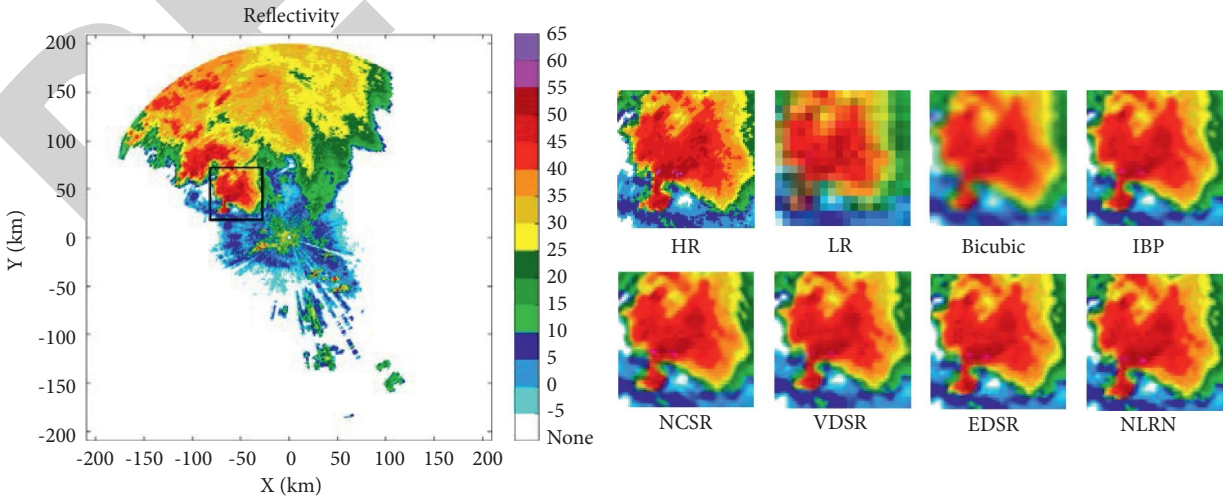

Figure 10: Visual comparison of ×4 super-resolution reconstruction results of tornado data. The best results are in bold.

Table 1: Average PSNR (dB) of VDSR, EDSR, and NLRN for ×4 super-resolution reconstruction on test set.

Network	VDSR	EDSR	NLRN
Long skip Connection (LSC)	√	√	√
Short skip Connection (SSC)	×	√	√
Nonlocal operation	×	×	√
PSNR	25.17	25.38	**25.45**

Table 2: Quantitative results of the compared methods on different weather conditions.

Method	Scale	Large weather system		Small weather system		Cloudless	
		PSNR	SSIM	PSNR	SSIM	PSNR	SSIM
Bicubic	×2	26.18	0.7933	26.56	0.8012	27.89	0.8458
IBP	×2	26.67	0.7935	27.13	0.8079	28.45	0.8562
NCSR	×2	27.28	0.8233	27.65	0.8263	28.98	0.8749
VDSR	×2	28.05	0.8496	28.11	0.8492	29.31	0.8961
EDSR	×2	28.26	0.8531	28.48	0.8569	29.42	0.9013
NLRN	×2	**28.41**	**0.8546**	**28.57**	**0.8612**	**29.53**	**0.9042**
Bicubic	×4	23.21	0.6739	23.66	0.6743	25.12	0.7268
IBP	×4	23.77	0.6784	24.13	0.6803	25.43	0.7327
NCSR	×4	24.69	0.6898	24.51	0.7078	25.81	0.7513
VDSR	×4	24.83	0.7325	24.92	0.7405	26.22	0.7857
EDSR	×4	24.98	0.7382	25.08	0.7487	26.41	0.7893
NLRN	×4	**25.11**	**0.7421**	**25.19**	**0.7498**	**26.48**	**0.8013**

The best results are in bold.

5.3. Quantitative Result Comparison. Average PSNR (dB) comparison of VDSR, EDSR, and NLRN is listed in Table 1. It can be seen from the result that both EDSR and NLRN can achieve PSNR more than 0.2 dB higher than VDSR, which indicates that EDSR and NLRN with SSC have better performance in feature fusion compared with VDSR only using LSC. Furthermore, NLRN achieves better performance in exploiting large-scale context information by adding the nonlocal operation, which leads to the PSNR gain of NLRN over EDSR up to 0.07 dB. To further validate the effectiveness of NLRN, we compare the proposed NLRN with various SR methods on degraded weather radar images under different weather conditions (e.g., large- and small-scale weather system, and cloudless). All the results on ×2 and ×4 reconstruction are shown in Table 2, from which we can see that the NLRN proposed in this article can get the highest PSNR and SSIM values compared with other SR methods. Especially under the small-scale weather system, the PSNR gain of NLRN over Bicubic is up to 2 dB under ×2 reconstruction.

6. Conclusion

In this article, we proposed a nonlocal residual network (NLRN) for weather radar image super resolution, where the nonlocal residual block (NLRB) allows NLRN to integrate the nonlocal dependencies and structural information (e.g., the local and nonlocal correlations of intense precipitation echo) by inserting nonlocal blocks (NLBs) in the network. Extensive experiments on different weather conditions show the effectiveness of our NLRN in terms of quantitative and visual results. Although NLRN cannot reconstruct exactly the same echo geometry, it can recover more accurate echo edges and details than other SR methods listed in the experimental part and highlight the structure, location, and development of intense echo, which contributes to fine detection and prediction of small- and medium-scale intense convection processes. It is worth noting that the deep learning-based super resolution of weather radar image relies not only on an excellent model structure but also on the completeness and diversity of the dataset, and that both the NLRN and the training dataset need to be further optimized to meet the increased demand for monitoring and forecasting of severe convective weather events.

Data Availability

The datasets used during the current study are available from the corresponding author on reasonable request.

Conflicts of Interest

The authors declare that there are no conflicts of interest.

Acknowledgments

The authors gratefully acknowledge the CMA Key Laboratory of Atmospheric Sounding for providing the experimental data. This work was supported by the National Key R&D Program of China (2018YFC01506100), the National Natural Science Foundation of China (U20B2061), and the Department of Science and Technology of Sichuan Province (2020ZYD051).

References

[1] G. Ge, J. Gao, K. Brewster, and M. Xue, "Impacts of beam broadening and earth curvature on storm-scale 3D variational data assimilation of radial velocity with two Doppler radars," *Journal of Atmospheric and Oceanic Technology*, vol. 27, no. 4, pp. 617–636, 2010.

[2] Y. Averyanova, A. Averjanov, and F. Yanovsky, "Doppler polarization radar methods for meteorological applications," *IEEE Aerospace and Electronic Systems Magazine*, vol. 29, no. 7, pp. 64–73, 2014.

[3] E. Ruzanski and V. Chandrasekar, "Weather radar data interpolation using a kernel-based Lagrangian now casting technique," *IEEE Transactions on Geoscience and Remote Sensing*, vol. 53, pp. 3073–3083, 2014.

[4] E. Sharifi, B. Saghafian, and R. Steinacker, "Downscaling satellite precipitation estimates with multiple linear regression, artificial neural networks, and spline interpolation techniques," *Journal of Geophysical Research: Atmospheres*, vol. 124, no. 2, pp. 789–805, 2019.

[5] L. Kou, Y. Jiang, A. Chen, and Z. Wang, "Statistical modeling with a hidden Markov tree and high-resolution interpolation for spaceborne radar reflectivity in the wavelet domain," *Advances in Atmospheric Sciences*, vol. 37, no. 12, pp. 1359–1374, 2020.

[6] A. M. Ebtehaj, E. Foufoula-Georgiou, and G. Lerman, "Sparse regularization for precipitation downscaling," *Journal of Geophysical Research: Atmospheres*, vol. 117, 2012.

[7] E. Foufola-Giorgiou, A. M. Ebtehaj, S. Q. Zhang, and A. Y. Hou, "Downscaling satellite precipitation with emphasis on extremes: a variational ℓ1-norm regularization in the derivative domain," *Surveys in Geophysics*, vol. 35, no. 3, 2014.

[8] X. Zhang, J. He, Q. Zeng, and Z. Shi, "Weather radar echo super-resolution reconstruction based on nonlocal self-similarity sparse representation," *Atmosphere*, vol. 10, no. 5, p. 254, 2019.

[9] H. Yuan, Q. Zeng, and J. He, "Adaptive regularized sparse representation for weather radar echo super-resolution reconstruction," in *Proceedings of the 2021 International Conference on Electronic Information Engineering and Computer Science (EIECS)*, pp. 33–38, IEEE, Changchun, China, September 2021.

[10] M. Xu, Q. Liu, D. Sha et al., "PreciPatch: a dictionary-based precipitation downscaling method," *Remote Sensing*, vol. 12, no. 6, p. 1030, 2020.

[11] M. Reichstein, G. Camps-Valls, B. Stevens et al., "Deep learning and process understanding for data-driven Earth system science," *Nature*, vol. 566, no. 7743, pp. 195–204, 2019.

[12] T. Vandal, E. Kodra, S. Ganguly, A. Michaelis, R. Nemani, and A. R. Ganguly, "Generating high resolution climate change projections through single image super-resolution: an abridged version," in *Proceedings of the 27th International Joint Conferences on Artificial Intelligence Organization(IJCAI-2018)*, pp. 5389–5393, Stockholm, Sweden, July 2018.

[13] J. Cheng, Q. Kuang, C. Shen, J. Liu, X. Tan, and W. Liu, "ResLap: Generating high-resolution climate prediction through image super-resolution," *IEEE Access*, vol. 8, pp. 39623–39634, 2020.

[14] Y. Zhang, Y. Tian, Y. Kong, B. Zhong, and Y. Fu, "Residual dense network for image super-resolution," in *Proceedings of the 2018 IEEE/CVF Conference on Computer Vision and Pattern Recognition*, pp. 2472–2481, Salt Lake City, UT, USA, June 2018.

[15] W. S. Lai, J. B. Huang, N. Ahuja, and M. H. Yang, "Deep laplacian pyramid networks for fast and accurate super-resolution," in *Proceedings of the 2017 IEEE Conference on Computer Vision and Pattern Recognition (CVPR)*, pp. 624–632, Honolulu, HI, USA, July 2017.

[16] A. Geiss and J. C. Hardin, "Radar super resolution using a deep convolutional neural network," *Journal of Atmospheric and Oceanic Technology*, vol. 37, no. 12, pp. 2197–2207, 2020.

[17] O. Ronneberger, P. Fischer, and T. Brox, "U-net: convolutional networks for biomedical image segmentation," in *Proceedings of the 18th International Conference on Medical Image Computing and Computer-Assisted Intervention*, pp. 234–241, Springer, Munich, Germany, October 2015.

[18] G. Huang, Z. Liu, L. Van Der Maaten, and K. Q. Weinberger, "Densely connected convolutional networks," in *Proceedings of the 2017 IEEE Conference on Computer Vision and Pattern Recognition (CVPR)*, pp. 4700–4708, Honolulu, HI, USA, July 2017.

[19] K. Stengel, A. Glaws, D. Hettinger, and R. N. King, "Adversarial super-resolution of climatological wind and solar data," *Proceedings of the National Academy of Sciences*, vol. 117, no. 29, pp. 16805–16815, 2020.

[20] X. Xin Li and M. T. Orchard, "New edge-directed interpolation," *IEEE Transactions on Image Processing*, vol. 10, no. 10, pp. 1521–1527, 2001.

[21] P. Rasti, H. Demirel, and G. Anbarjafari, "Iterative back projection based image resolution enhancement," in *Proceedings of the 2013 8th Iranian Conference on Machine Vision and Image Processing (MVIP)*, pp. 237–240, IEEE, Zanjan, Iran, September 2013.

[22] C. Ce Liu and D. Deqing Sun, "On bayesian adaptive video super resolution," *IEEE Transactions on Pattern Analysis and Machine Intelligence*, vol. 36, no. 2, pp. 346–360, 2014.

[23] W. Dong, L. Zhang, G. Shi, and X. Li, "Nonlocally centralized sparse representation for image restoration," *IEEE Transactions on Image Processing*, vol. 22, pp. 1620–1630, 2012.

[24] Y. Zhang, J. Liu, W. Yang, and Z. Guo, "Image super-resolution based on structure-modulated sparse representation," *IEEE Transactions on Image Processing*, vol. 24, no. 9, pp. 2797–2810, 2015.

[25] K. Zhang, Y. Huang, Y. Du, and L. Wang, "Facial expression recognition based on deep evolutional spatial-temporal networks," *IEEE Transactions on Image Processing*, vol. 26, no. 9, pp. 4193–4203, 2017.

[26] O. Oktay, E. Ferrante, K. Kamnitsas et al., "Anatomically constrained neural networks (ACNNs): Application to cardiac image enhancement and segmentation," *IEEE Transactions on Medical Imaging*, vol. 37, pp. 384–395, 2017.

[27] D. Nie, L. Wang, E. Adeli, C. Lao, W. Lin, and D. Shen, "3-D fully convolutional networks for multimodal isointense infant brain image segmentation," *IEEE Transactions on Cybernetics*, vol. 49, pp. 1123–1136, 2018.

[28] D. Liu, B. Cheng, Z. Wang, H. Zhang, and T. S. Huang, "Enhance visual recognition under adverse conditions via deep networks," *IEEE Transactions on Image Processing*, vol. 28, no. 9, pp. 4401–4412, 2019.

[29] R. He, J. Cao, L. Song, Z. Sun, and T. Tan, "Adversarial cross-spectral face completion for NIR-VIS face recognition," *IEEE Transactions on Pattern Analysis and Machine Intelligence*, vol. 42, pp. 1025–1037, 2019.

[30] C. Dong, C. C. Loy, K. He, and X. Tang, "Image super-resolution using deep convolutional networks," *IEEE Transactions on Pattern Analysis and Machine Intelligence*, vol. 38, pp. 295–307, 2015.

[31] C. Dong, C. C. Loy, and X. Tang, "Accelerating the super-resolution convolutional neural network," in *Proceedings of the European Conference on Computer Vision-ECCV 2016*, pp. 391–407, Springer, Amsterdam, The Netherlands, October 2016.

[32] K. He, X. Zhang, S. Ren, and J. Sun, "Deep residual learning for image recognition," in *Proceedings of the 2016 IEEE Conference on Computer Vision and Pattern Recognition (CVPR)*, pp. 770–778, Las Vegas, NV, USA, June 2016.

[33] J. Kim, J. K. Lee, and K. M. Lee, "Accurate image super-resolution using very deep convolutional networks," in *Proceedings of the 2016 IEEE Conference on Computer Vision and Pattern Recognition (CVPR)*, pp. 1646–1654, Las Vegas, NV, USA, June 2016.

[34] B. Lim, S. Son, H. Kim, S. Nah, and K. Mu Lee, "Enhanced deep residual networks for single image super-resolution," in *Proceedings of the 2017 IEEE Conference on Computer Vision and Pattern Recognition Workshops (CVPRW)*, pp. 136–144, Honolulu, HI, USA, July 2017.

[35] M. Haris, G. Shakhnarovich, and N. Ukita, "Deep back-projection networks for super-resolution," in *Proceedings of the 2018 IEEE/CVF Conference on Computer Vision and Pattern Recognition*, pp. 1664–1673, Salt Lake City, UT, USA, June 2018.

[36] E. C. Bruning, W. D. Rust, D. R. MacGorman, M. I. Biggerstaff, and T. J. Schuur, "Formation of charge structures in a supercell," *Monthly Weather Review*, vol. 138, no. 10, pp. 3740–3761, 2010.

Hindawi
Journal of Mathematics
Volume 2022, Article ID 9858146, 1 page
https://doi.org/10.1155/2022/9858146

Retraction

Retracted: Badminton Backcourt Stroke Route Planning Method Based on Deep Learning

Journal of Mathematics

Received 25 November 2022; Accepted 25 November 2022; Published 25 December 2022

Journal of Mathematics has retracted the article titled "Badminton Backcourt Stroke Route Planning Method Based on Deep Learning" [1] due to concerns that the peer review process has been compromised.

Following an investigation conducted by the Hindawi Research Integrity team [2], significant concerns were identified with the peer reviewers assigned to this article; the investigation has concluded that the peer review process was compromised. We therefore can no longer trust the peer review process, and the article is being retracted with the agreement of the Chief Editor.

References

[1] Y. Ma, "Badminton Backcourt Stroke Route Planning Method Based on Deep Learning," *Journal of Mathematics*, vol. 2021, Article ID 6407049, 6 pages, 2021.

[2] L. Ferguson, "Advancing Research Integrity Collaboratively and with Vigour," 2022, https://www.hindawi.com/post/advancing-research-integrity-collaboratively-and-vigour/.

Hindawi
Journal of Mathematics
Volume 2021, Article ID 6407049, 6 pages
https://doi.org/10.1155/2021/6407049

Research Article

Badminton Backcourt Stroke Route Planning Method Based on Deep Learning

Yanping Ma

Taiyuan University of Technology, Taiyuan 030024, China

Correspondence should be addressed to Yanping Ma; mayanping@tyut.edu.cn

Received 4 November 2021; Revised 23 November 2021; Accepted 24 November 2021; Published 29 December 2021

Academic Editor: Naeem Jan

In order to improve the planning ability of the badminton backcourt stroke line, this study designs a badminton backcourt stroke line planning method based on deep learning. Firstly, the trajectory adaptive learning method of motion primitives is used to design the hitting line nodes and path space, so as to construct the shortest distributed grid structure model of the hitting line. Then, the constraint parameters of hitting route planning are analyzed, and then the hitting position and player posture are controlled according to node positioning and shortest path optimization deployment. Finally, the adaptive optimization of the route planning process is realized by combining the deep learning method. The simulation results show that this method has good learning control ability and good convergence performance and improves the reliability of badminton backcourt hitting line planning.

1. Introduction

With the popularization of badminton training, higher requirements are put forward for the efficient training and pertinence of badminton. The key factor for the improvement of effects of badminton training is the badminton backcourt stroke line planning. It is necessary to build an optimized badminton backcourt stroke line planning model, combined with the optimization control method of the badminton backcourt stroke line, adopt artificial intelligence learning algorithm, realize the planning and design of the badminton backcourt stroke line, and improve the stability and reliability of the badminton backcourt stroke, and the design of the relevant badminton backcourt stroke line planning model is of great significance in guiding the optimal training ability of badminton [1].

With the steady improvement of the national economic development level and the continuous progress of the society, badminton is increasingly loved by the masses. Badminton has great sporting advantages. It is not restricted by the site. In addition, it does not require any sports cost investments. Any open place can facilitate people's sports, as long as a pair of rackets and a ball. In addition, badminton is also very helpful to exercise people's endurance and control. It can also move a variety of joints of the human body, which is very beneficial to enhance physique. However, although badminton has become a popular fitness sport in China and has no sports requirements for ordinary badminton lovers, professional badminton athletes are required to have strong professional skills. They are found through many investigations and practices. The use of multiball training can greatly promote the improvement of badminton players' professional skills [1].

In the traditional methods, the intelligent planning methods for the badminton backcourt stroke line mainly include the badminton backcourt stroke line planning method based on the small-world model [2]. By constructing the grid model of badminton backcourt stroke line planning, combined with spatial grid optimization, the badminton backcourt stroke line planning and design are realized. Based on the method of badminton backcourt stroke line based on ant colony optimization [3], the intelligent planning and design of the badminton backcourt stroke line are based on the node positioning and path optimization control of the badminton backcourt stroke line, and the design is realized through the intelligent planning algorithm. And the badminton backcourt stroke line planning method based on fuzzy PID [4] uses the shortest path optimization and spatial

parameter estimation, combined with the double programming method, to realize the badminton backcourt stroke line planning. Josue et al. [5] studied the movement pattern of top international male and female badminton players during BMF World Championships. Hung et al. [6] applied the landing strategies in badminton footwork training. Eason et al. [7] analyzed the effects of proactive interference on the learning of backhand strokes.

However, the adaptive optimization ability of the above traditional methods for badminton backcourt stroke line planning is not good, and the spatial positioning ability is not strong. Therefore, aiming at the above problems, this paper proposes a method based on deep learning for the planning of the badminton backcourt stroke route. First of all, the motion primitive trajectory adaptive learning method is used for the planning and designing of badminton backcourt hitting line nodes and path space. Furthermore, the segmented route optimization control method is used for the node positioning and shortest path optimization deployment of the badminton backcourt hitting line. Then, by the use of vertical model measurement and modeling method, the figure model design of the badminton backcourt hitting line is realized. Additionally, the badminton backcourt hitting position and athlete's posture are followed to carry out the linear iterative optimal control. Combined with the deep learning method, the adaptive optimization of badminton backcourt hitting route planning and the motion path planning and design of the target position are apprehended. Finally, the simulation test analysis is carried out which shows the superior performance of the proposed method in improving the ability of badminton backcourt stroke line planning.

2. Badminton Backcourt Hitting Line Distribution Grid Model and Parameter Analysis

2.1. Grid Model of Badminton Backcourt Hitting Line Distribution. In order to realize the badminton backcourt stroke line planning based on deep learning, the motion primitive trajectory adaptive learning method is used to plan and design the badminton backcourt stroke line nodes and path space. Firstly, the badminton backcourt stroke line distribution grid model is constructed [8, 9], and the location node distribution of the badminton backcourt stroke is obtained, as shown in Figure 1.

According to the location node distribution of the badminton backcourt stroke shown in Figure 1, the shortest path optimization parameter analysis model of badminton backcourt stroke line planning is constructed by using the spatial path-distributed reorganization and optimization control method. According to the geometric description of athletes and the environment [10], the target node optimization of badminton backcourt stroke line planning is carried out [11]; according to the intelligent planning of the badminton backcourt hitting line, the node transmission load is

$$[\nabla F(x)]_j = F(x) \cdot \mathrm{Rot}[v_i(x) - F(x)], \tag{1}$$

where $F(x)$ represents the objective function of badminton backcourt stroke line planning and $v_i(x)$ is the local optimal parameter set of badminton backcourt stroke line distribution. Using the Newton gradient descent algorithm, the parameter estimation and optimization design of badminton backcourt stroke line intelligent planning are carried out [12]. It is obtained that the distribution of random parameters in the badminton backcourt stroke line configuration space is

$$\left[\nabla^2 F(x)\right]_{kj} = \frac{1}{\partial F(x)} - 2\sum_{j=1} [\nabla F(x)]_j \cdot v_i(x). \tag{2}$$

Combined with the random parameter distribution results, the shortest path optimization parameters from the initial node to the target node are analyzed, and the linear programming model of path parameters is obtained:

$$l(v_v) = \mathrm{Tran}(P_e - P_0) + \frac{1}{\left[\nabla^2 F(x)\right]_{kj}}, \tag{3}$$

where $\mathrm{Tran}(P_e - P_0)$ represents the translation amount of the path position of the target node. On the differential manifold, according to the analysis of random parameters in the shape space, the path optimization of badminton backcourt hitting line intelligent planning is carried out, and the path optimization equation is

$$T(t) = \int_0^{\infty} l(v_v)\mathrm{d}v + \mathrm{Tran}(P_e - P_0). \tag{4}$$

The shortest path optimization method is used to design the adaptive spatial parameters of badminton backcourt stroke line planning, and the optimal solution in the distribution nodes v_a, v_b, and v_c of the badminton backcourt stroke line is expressed as

$$l(v_a) = \left\| v_a + v_b + v_c \right\|^2 - \sum_{t=1} T(t) - l(v_v). \tag{5}$$

The segmented route optimization control method is adopted to design the badminton backcourt hitting line distribution grid model, and the shortest path planning design is adopted to obtain the badminton backcourt hitting line shortest distribution grid structure model, as shown in Figure 2.

To sum up, taking the shortest path as the optimization objective function and using the motion primitive trajectory adaptive learning method, the badminton backcourt hitting line node and path space planning and designing are realized in the grid structure model, so as to improve the ability of route planning.

2.2. Analysis on Constraint Parameters of Badminton Backcourt Hitting Route Planning. The visual servo moving route optimization control method is adopted to carry out the node positioning and shortest path optimization deployment of the badminton backcourt hitting route. Under the node coordinate system, the constraint parameter

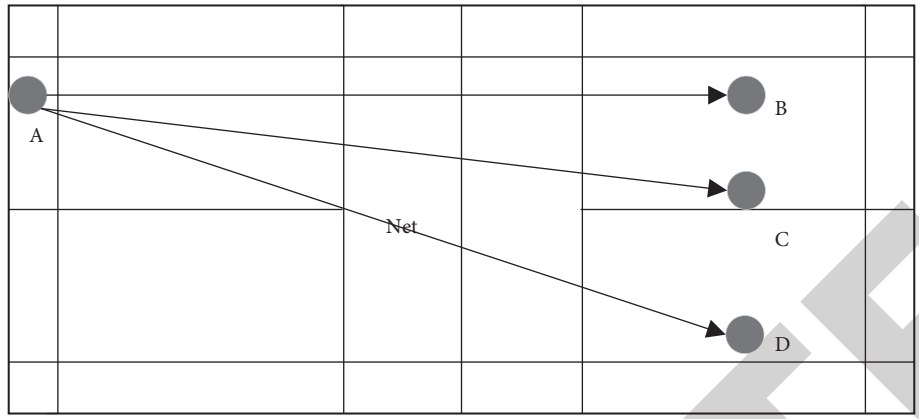

Figure 1: Location node distribution of the badminton backcourt stroke.

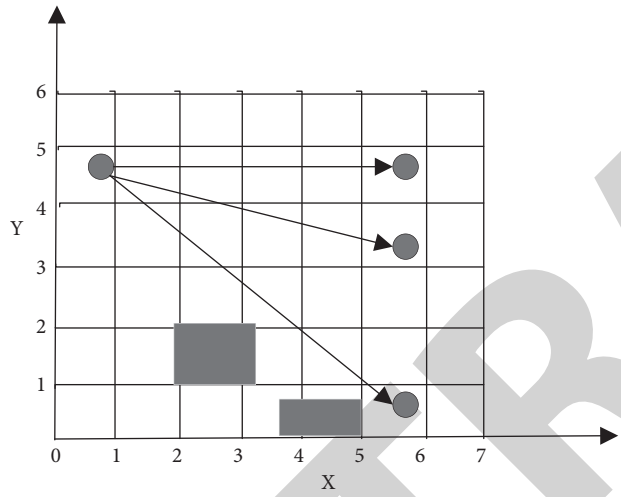

Figure 2: The shortest line distribution grid structure model of the badminton backcourt stroke.

optimization distribution of badminton backcourt hitting route planning is $X_i(t)$. In the configuration space starting from the initial posture of badminton backcourt hitting, the line parameter estimation model of badminton backcourt hitting is obtained. Its expression is

$$\Delta S(t) = \sum_{a-1} l(v_a) + \left(\frac{T_0 - U_0}{X_i(t)}\right), \tag{6}$$

where T_0 and U_0, respectively, represent the shortest distribution distance and pose distance of the badminton backcourt hitting line obtained by using the depth camera.

$$V_0 = \left\|p^1\right\| + \sqrt{T_6^1 + \Delta S(t)}. \tag{7}$$

where T_6^1 represents the deep learning fusion feature distribution set for badminton backcourt stroke line optimization and $p^1 = (p_x^1, p_y^1, p_z^1)^T$ represents the shortest line fusion parameter of the badminton backcourt stroke line.

Combined with the spatial three-dimensional information sampling method, the depth learning gradient function of badminton backcourt hitting route planning is

$$\mathrm{Rr} = \sqrt{\Delta T + \Delta U} + \min V_0, \tag{8}$$

where ΔT and ΔU represent the shortest distribution distance and average position distance of the badminton backcourt hitting line, respectively. Using the method of three-dimensional model measurement and modeling, the figure model design of the badminton backcourt hitting circuit is realized [13]. The characteristic distribution function of the badminton backcourt hitting circuit is x_i, y_i, and z_i. According to each depth projection corresponding to a programmable badminton backcourt stroke line, the fuzzy control equation of line space planning is obtained:

$${}^{i-1}T_i = \frac{\mathrm{Rr} - \sum_0^i x_i + y_i + z_i}{s + c}, \tag{9}$$

where s represents the positioning error of the badminton backcourt hitting line and C represents the optimization parameters of badminton backcourt hitting line planning.

In the process of badminton backcourt stroke line movement, the starting point of the badminton backcourt stroke line is $P_0, P_1, P_2, \ldots, P_n$, and the normal vector of each point is T.

According to the above analysis, the optimization parameters of badminton backcourt stroke line planning are obtained, so as to locate the nodes of the badminton backcourt stroke line and deploy the shortest path optimization.

3. Optimization of the Badminton Backcourt Stroke Route Planning Model

3.1. Deep Learning of Badminton Backcourt Stroke Route Planning. According to the analysis results of constraint parameters of badminton backcourt stroke line planning, combined with the deep learning method, the intelligent planning and design of the badminton backcourt stroke line are carried out. Given the spatial planning matrix of the badminton backcourt stroke line [14], according to the three-dimensional point cloud information of the scene, the error measurement parameter of badminton backcourt stroke line planning is

$$l = \frac{x(t) - 1}{h(t,u)} + P_d, \tag{10}$$

where $x(t)$ represents the three-dimensional point cloud information points of the badminton backcourt scene and $h(t,u)$ represents the evaluation parameters of the line planning response.

On any $M \times N$-dimensional matrix A, combined with iterative optimization and moving parameter analysis, the in-depth learning control of badminton backcourt stroke line planning is carried out, and the in-depth learning quadratic programming model of badminton backcourt stroke line planning composed of N decision variables is obtained, which is expressed as

$$F(x) = l \cdot \sqrt{A + h(t,u)}. \tag{11}$$

An adaptive optimization model of the badminton backcourt hitting line is constructed by using the method of double linear programming, which is expressed as

$$\eta = \sqrt{E(MA) + E(MB)} \cdot \int_0^{\infty} F(x)\mathrm{d}x, \tag{12}$$

where $E(MA)$ represents the fuzzy membership function value of badminton backcourt stroke line planning and $E(MB)$ represents the inner product parameter of the badminton backcourt stroke line orientation vector.

Through experimental analysis, the stability parameters of the badminton backcourt stroke are estimated, and the optimization function of the equilibrium point position is obtained, which is expressed as

$$K = f^2 + \frac{\tau}{2} \cdot \left|\eta^* t\right|^2, \tag{13}$$

where τ is the location information in the process of badminton backcourt stroke line planning, f is the fuzzy state characteristic quantity of badminton backcourt stroke line distribution, and t is the time interval of badminton backcourt stroke line optimization.

Based on the optimization results of the equilibrium point position, the optimized depth learning planning function is obtained as

$$E[VA] = \left|\sqrt{1 + K}\right| + \int_0^{\infty} f(t)\mathrm{d}t. \tag{14}$$

To sum up, the in-depth learning optimization design of badminton backcourt hitting line planning is realized, and on this basis, the optimization control design is carried out.

3.2. Optimal Control of Badminton Backcourt Stroke Route Planning. Based on the deep learning spatial parameter fusion model of badminton backcourt stroke line planning, the deviation parameter analysis model of the badminton backcourt stroke line is analyzed, and the entity prediction sequence distribution of badminton backcourt stroke line planning is expressed as

$$Q_i = 2\sqrt{K} + \sum_{A=1} (E[VA] - 1)^2. \tag{15}$$

In the process of continuous optimization of the badminton backcourt hitting line, the adaptive learning approximation control function for line optimization is obtained:

$$L_i = \left\| Q_i - E\left[V_A\right]^2 \right\| + \frac{1}{2}. \tag{16}$$

Based on the trajectory optimization and parameter fusion method, the characteristic parameters of the badminton backcourt stroke line planning optimization process are described as

$$y = \frac{\sqrt{Q_i - L_i}}{2}. \tag{17}$$

Combined with the results of characteristic parameters, discuss according to the method of trajectory learning and data fusion, and the degree of freedom trajectory of the badminton backcourt hitting line is expressed as

$$y(t) = [G + 1] \cdot y\left(\sqrt{Q_i - L_i}\right), \tag{18}$$

where G is the global transfer matrix. Using the two-degree-of-freedom learning model, the depth learning function of the badminton backcourt stroke is

$$f(x,y) = \int_0^{\infty} \frac{y(t)}{\varepsilon(x,y)}\mathrm{d}t + \frac{L_i - y}{g(x,y)}, \tag{19}$$

where $g(x,y)$ and $\varepsilon(x,y)$ represent the independent variables and constraint variables of badminton backcourt stroke path optimization control, respectively.

Through the fusion decision, the fuzzy decision coefficient is σ_n^2. Under the single degree of freedom, the inertial tracking parameter model of the badminton backcourt hitting path is

$$g_i^* = \sum_i^{s_j} \frac{f(x,y) + g_i}{R} + \sigma_n^2, \tag{20}$$

where I represents the point set of badminton backcourt stroke path distribution, R represents a normative constant, x represents the reliability constraint parameter of badminton backcourt stroke path optimization, and y represents the two-dimensional spatial planning set of the badminton backcourt stroke path. Its calculation formula is

$$g_i = \sqrt{1 - \sigma_n^2} \cdot \frac{1}{R}. \tag{21}$$

It is assumed that the spatial distribution of the badminton backcourt hitting path is $M \times N$. M and N correspond to the length and width of the spatial distribution of the badminton backcourt hitting path, and the optimal control function of badminton backcourt hitting path planning is

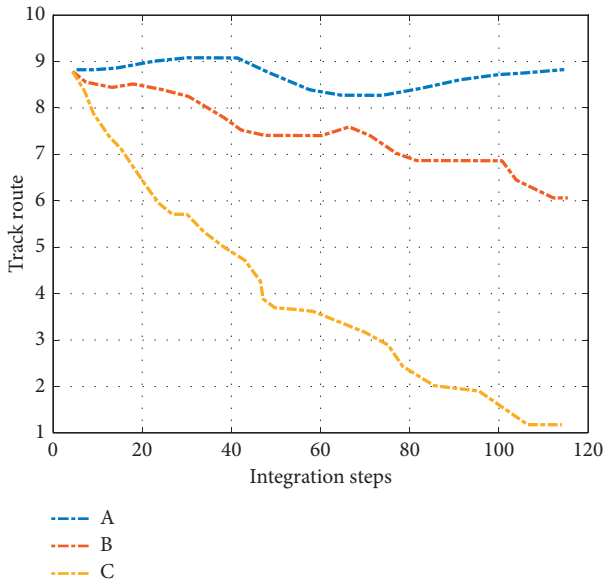

Figure 3: Original path of the badminton backcourt stroke.

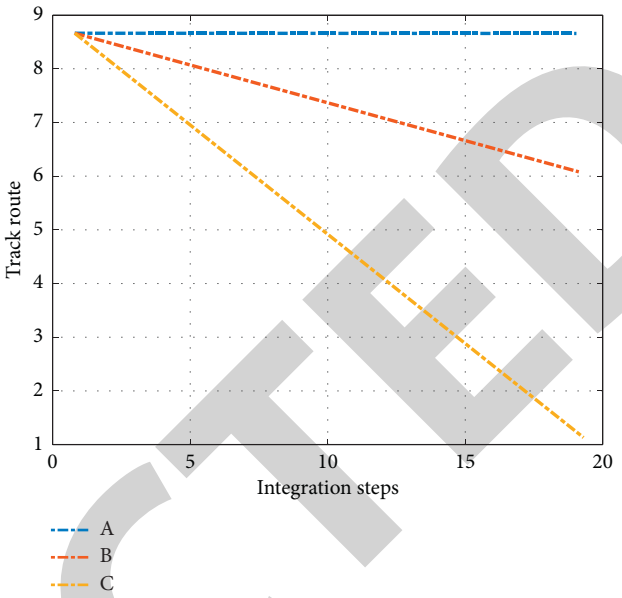

Figure 4: Optimized badminton backcourt stroke path planning results.

$$V(M_{mi}) = \frac{\sum_{j=1}^{i}(M \times N)}{\Delta u - 1} + g_i^*. \tag{22}$$

Among them, ΔU is the gradient parameter of badminton backcourt stroke path planning. Combined with the deep learning method, the optimal path planning control convergence formula is obtained:

$$F = \frac{p(x, y) + g_i}{V(M_{mi})}, \tag{23}$$

where $p(x, y)$ represents the convergence parameter set.

To sum up, the linear iterative optimal control is carried out according to the badminton backcourt hitting position and player posture, so as to realize the adaptive optimization of badminton backcourt hitting route planning and the motion path planning and design of the target position.

4. Simulation Experiment

In order to test the performance of this method in realizing badminton backcourt stroke path planning, the simulation test is carried out. The parameters are set as that the spatial parameters of the badminton backcourt stroke are $200 * 300$, the number of entities of backcourt stroke path planning is $n = 300$, the maximum number of iterations of deep learning is 250, and the coefficient of adaptive learning is 0.37. The original path of badminton backcourt hitting in different groups is obtained, as shown in Figure 3.

Taking the original path in Figure 3 as the experimental data, this method is used to optimize the badminton backcourt hitting position and player posture, and the optimized path planning results are shown in Figure 4.

According to the analysis of Figure 4, the route planning and adaptive optimization of the badminton backcourt stroke can be effectively realized by using this method, and the optimization effect is obvious.

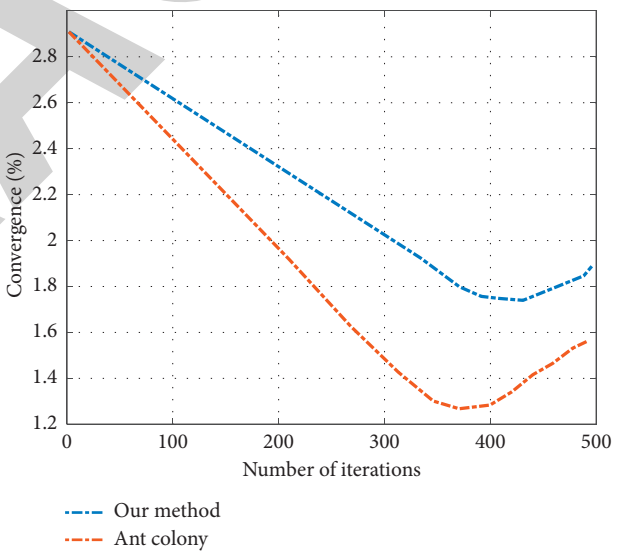

Figure 5: Comparison of convergence of badminton backcourt hitting route planning.

In order to further verify the superior performance of this method, the badminton backcourt stroke route planning method based on the small-world model, the badminton backcourt stroke route planning method based on ant colony optimization, and the badminton backcourt stroke route planning method based on fuzzy PID are used as comparison methods to test the convergence ability of badminton backcourt stroke route planning under different methods. The comparison results are shown in Figure 5.

The analysis of the above simulation results shows that the convergence performance of this method for badminton backcourt stroke path planning is better, which is obviously better than other methods. It shows that this method has strong adaptive planning ability for badminton backcourt

Hindawi
Journal of Mathematics
Volume 2024, Article ID 9802386, 1 page
https://doi.org/10.1155/2024/9802386

Retraction

Retracted: Evaluation Algorithm of Ecological Energy-Saving Effect of Green Buildings Based on Gray Correlation Degree

Journal of Mathematics

Received 23 January 2024; Accepted 23 January 2024; Published 24 January 2024

This article has been retracted by Hindawi following an investigation undertaken by the publisher [1]. This investigation has uncovered evidence of one or more of the following indicators of systematic manipulation of the publication process:

(1) Discrepancies in scope

(2) Discrepancies in the description of the research reported

(3) Discrepancies between the availability of data and the research described

(4) Inappropriate citations

(5) Incoherent, meaningless and/or irrelevant content included in the article

(6) Manipulated or compromised peer review

The presence of these indicators undermines our confidence in the integrity of the article's content and we cannot, therefore, vouch for its reliability. Please note that this notice is intended solely to alert readers that the content of this article is unreliable. We have not investigated whether authors were aware of or involved in the systematic manipulation of the publication process.

Wiley and Hindawi regrets that the usual quality checks did not identify these issues before publication and have since put additional measures in place to safeguard research integrity.

We wish to credit our own Research Integrity and Research Publishing teams and anonymous and named external researchers and research integrity experts for contributing to this investigation.

The corresponding author, as the representative of all authors, has been given the opportunity to register their agreement or disagreement to this retraction. We have kept a record of any response received.

References

[1] C. Wang, "Evaluation Algorithm of Ecological Energy-Saving Effect of Green Buildings Based on Gray Correlation Degree," *Journal of Mathematics*, vol. 2021, Article ID 6705220, 10 pages, 2021.

Hindawi
Journal of Mathematics
Volume 2021, Article ID 6705220, 10 pages
https://doi.org/10.1155/2021/6705220

Research Article

Evaluation Algorithm of Ecological Energy-Saving Effect of Green Buildings Based on Gray Correlation Degree

Chongyu Wang

Urban and Rural Construction Institute, Hebei Agricultural University, Baoding, Hebei 071000, China

Correspondence should be addressed to Chongyu Wang; chjwchy@hebau.edu.cn

Received 23 November 2021; Revised 8 December 2021; Accepted 13 December 2021; Published 28 December 2021

Academic Editor: Naeem Jan

The environmental protection attribute and energy-saving level of green buildings cannot be described by the traditional evaluation model. In order to solve the above problems, a new ecological energy-saving effect evaluation algorithm of green buildings based on gray correlation degree is designed. Based on the framework of building energy-saving index system, the environmental protection evaluation standards are divided and the results are used to screen the energy-saving indexes, so as to complete the establishment of green building ecological energy-saving index system and standards. Then, the evaluation set is established, and the evaluation scale of each layer of indicators is accurately located according to the weight value of each index. On this basis, the membership matrix is constructed. By calculating the index weight and determining the fuzzy synthesis operator, the rating process of the algorithm is improved and the analysis of the evaluation algorithm of environmental protection and energy conservation indicators of green building materials based on gray correlation degree is realized. The experimental results show that the designed algorithm has good stability of the fitting curve, can save energy, and has low cost.

1. Introduction

Energy consumption is large all over the world. Developing green and energy-saving buildings is the only way to reduce building energy consumption [1]. With the wide spread of "green culture," green buildings have emerged accordingly [2]. The purpose of green building is to give green concept to architecture, connect architecture with sustainable development, and connect architecture with ecosystem. Only by vigorously developing green buildings can we meet the needs of the development of modern urban ecological construction and realize the coordination and unity of man, architecture, and nature. Most construction units use traditional building materials such as cement, concrete, glass, and ceramics [3]. Although these materials have the advantages of good durability and high environmental adaptability, from the perspective of sustainable development, most of these materials belong to nonrenewable resources [4]. Excessive utilization of this type of materials will not only have a serious impact on the total amount of environmental resources, but also make the overall environmental level show a downward trend year by year. Green materials are the general name of all building materials without pollution. This type of resource material has the application advantages of no pollution, no toxicity, and no radioactivity. With the gradual increase of service life, the building materials after reaching the service cycle can still be recycled, which not only is conducive to the comprehensive implementation of the concept of sustainable development, but also provides a certain guarantee for people's health. The definition of green building materials mainly focuses on the four links of raw material application, product manufacturing, use, and waste treatment. On the premise of ensuring the rational utilization of materials, how to realize the common development of many concepts such as environmental protection and health on the basis of reducing environmental load has become the primary goal of the construction industry at this stage.

The study in [5] considers water ecological issues and uses monetary valuation to establish a quantitative climate model for urban green buildings. The need to respect environmental factors in terms of resource consumption and

harmful production has led to the formulation of green building regulations. Environmental water attitude was added to Madad's green building model, which is completely developed based on environmental and climatic factors. The model of each city is a function of its climate and population conditions and is implemented according to expert recommendations and analytic hierarchy process (AHP) method. The results of currency valuation research are used to improve the selection of indicators and accurately determine their weight in the model. The index in current research is to reduce runoff, water consumption, and reuse of gray water. The evaluation results of the study area show that only 11% of the green building capacity is used. The study in [6] uses the benefit transfer method to improve the current energy conservation in cooling and lighting in the green building sector in Malaysia. The Malaysian government has shifted from increasing energy supply to meet the demand for reducing energy consumption by promoting green building practices. Malaysia's eleventh plan includes three indicators to monitor the performance of green buildings, including power consumption. Therefore, the study aims to monitor the progress of energy conservation in Malaysia's green building industry by reviewing the current energy conservation performance and quantifying the economic prospect of future energy conservation improvement. It is of great significance to promote Malaysia to become a country with sustainable development through insight into the formulation of future sustainable development roadmap and green building implementation and development strategy. Therefore, residential and industrial buildings in Malaysia have great potential to save energy to the greatest extent. It is strongly recommended that vegetation green envelopes are implemented in green buildings in Malaysia. The study in [7] proposed the governance mechanism for the transformation of building materials industry to green building materials industry from the perspective of green building. Firstly, the evolutionary game theory is used to establish the three-party dynamic game model of building materials enterprises, government, construction developers, and construction consumers. Secondly, based on the model derivation and the theoretical analysis of green transformation, the multistage governance mechanism of green transformation is studied by using numerical simulation experimental algorithm. The numerical simulation results show that the green building infrastructure construction project is an important governance mechanism for the rapid development of GBMI and that the green innovation subsidy is the core governance mechanism for the high-quality development of GBMI. The pollution and fraud compensation punishment for green BME, green innovation subsidy, tax incentive for green BD, and purchase subsidy for green BC are conducive to promoting the transformation of green production and consumption concept. The above mechanisms and infrastructure construction help to promote the production of green building materials in BME through the development and purchase of green buildings. Infrastructure construction and green innovation subsidies play a key role in the high-quality development of GBMI.

Based on the above research, an evaluation algorithm of ecological energy-saving effect of green buildings based on gray correlation degree is proposed. On the one hand, the gray correlation degree is mainly constructed by reflecting the similarity of development process or magnitude between the two sequences. On the other hand, it is constructed by reflecting the similarity of the development trend or curve shape of the two sequences; that is, it mainly describes the proximity of the relative change trend of the ecological energy-saving effect of green buildings between the sequence curves. The research shows that the evaluation algorithm has a good effect on the ecological results of green buildings. In Section 2, the ecological energy-saving index system and the standard of green buildings are established. In Section 3, the proposed evaluation algorithm based on system standard is analyzed. In Section 4, the experimental analysis is carried out. In Section 5, the paper is finally concluded.

2. Establishment of the Ecological Energy-Saving Index System and Standard of Green Buildings

Green building ecological energy-saving index system and standard are the application basis of the new evaluation algorithm. With the support of three links: framework construction, grade division, and index screening, the specific establishment algorithm can be carried out according to the following steps.

2.1. Construction of Green Building Ecological Energy-Saving Index System Framework. Deeply implementing the architectural concept of people-oriented and harmonious coexistence of man and environment and building an environmental protection and energy-saving index system of green building materials can effectively coordinate the relationship between human economic and social development and ecological and environmental protection. A healthy ecological energy-saving index system of green buildings is the dialectical unity of the natural attribute of ecological environment [8] and the evaluation service attribute. It is not only the material basis for ensuring the good development of ecological environment, but also the key link to promote the rapid development of building environmental protection theory. According to the connotation of the concept of environmental protection and energy conservation [9], a perfect index system should be able to accurately describe the application status, construction environment level, material application direction, expected building effect, and other indicators of green buildings, and each index is an independent individual without being affected by other external conditions. With the support of the above theoretical basis, the framework structure of green building ecological energy conservation index system is shown in Figure 1.

2.2. Classification of Environmental Protection Evaluation Standards. The grade of environmental protection evaluation standard is the key index to measure the accuracy of

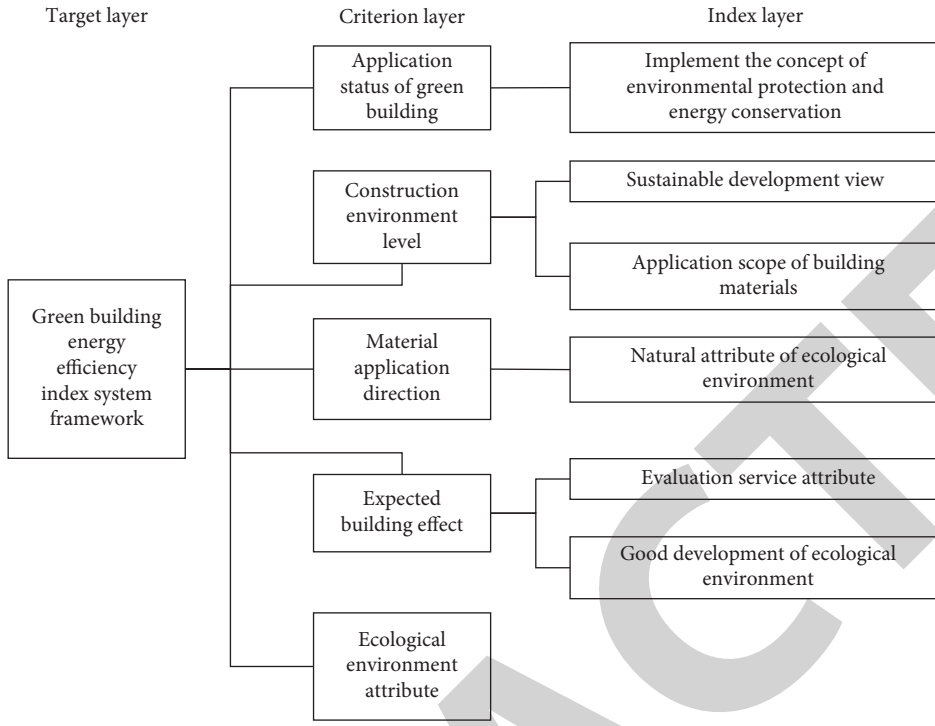

Figure 1: Frame structure of the ecological energy-saving index system of green buildings.

green building measurement results. Based on the ecological energy-saving index system of green buildings, the abstract grade index can be transformed into specific environmental protection evaluation standards by comparing the eigenvalues and standard values of the evaluated object in terms of parameter difference. The main source [4], strength and toughness, pollution intensity, pressure bearing capacity, and pricing range of green building materials are selected as the grading variables of the five environmental protection evaluation standards. In the green building ecological energy-saving index system, the above five indexes correspond to one or more frame structures, and there will be no obvious interaction between them. The four indexes of main source, strength and toughness, pollution intensity, and pressure bearing capacity are only affected by the properties of building materials, which belong to the main evaluation grade classification standard. The pricing range is affected by many factors such as season, output, and sales area, which belongs to the secondary evaluation grade classification standard. On the premise of ensuring that green building materials can maintain a low energy consumption level, the classification results of specific environmental protection evaluation standards are shown in Table 1.

2.3. Screening of Green Environmental Protection and Energy-Saving Indicators. There are many factors in the evaluation algorithm of green building ecological energy efficiency index, and the interaction between the factors makes the model complex. The construction of the index system cannot be applied to all factor conditions, but the most representative characteristic indexes that can best reflect the evaluation function of the model are selected. This selection process is the screening of green environmental protection and energy-saving indexes. The new index evaluation algorithm is a composite structure composed of multiple elements, so all the indexes involved must be able to reflect the environmental protection and energy-saving attributes of green building materials independently. In green buildings, energy-saving thermal insulation materials are widely used. Because of the cold climate in winter, the application of energy-saving and environmental protection materials not only has the function of general thermal insulation materials, but also can reduce energy consumption and environmental pollution and has strong market competitiveness. Therefore, the following environmental protection assessment indicators of the model are selected: one level-1 indicator, three level-2 indicators, and 12 level-3 indicators, as shown in Table 2. Due to the different ecological energy-saving thermal insulation materials of green buildings, the selection of evaluation indicators is not fixed, and appropriate indicators need to be selected according to the evaluation focus.

According to Table 2, the principal component analysis method is used to establish the evaluation index set.

The primary indicator set is

$$P = \{p_1, p_2, p_3\}. \tag{1}$$

In (1), p_1, p_2, and p_3 represent the energy consumption, resource consumption, and environmental impact, respectively.

The secondary indicator set is

Table 1: Classification of environmental protection evaluation standards.

Division of primary and secondary factors of evaluation	Environmental protection evaluation index	Evaluation criteria and equivalent division results
Main evaluation grade classification criteria	Main sources	Subsidiary indicators affecting the evaluation results of the model
	Strength and toughness	The key index affecting the evaluation results of the model is second only to the pollution intensity of green building materials
	Pollution intensity	The key indicators affecting the evaluation results of the model are much more important than other factors
	Bearing capacity	Subsidiary indicators affecting the evaluation results of the model
Classification criteria for secondary evaluation	Pricing range	On the premise of the change of environmental protection evaluation standards, the pricing range of green building materials also changes

Table 2: Selection results of evaluation indicators.

Primary index	Secondary index	Tertiary index
Environmental performance	Energy consumption	Energy consumption
		Energy type
		Energy recovery rate
		Proportion of energy use
	Resource consumption	Raw material consumption
		Raw material recovery
		Raw material reuse rate
		Raw material substitution ratio
	Environmental effect	Air pollution
		Water environment pollution
		Solid waste pollution
		Radioactive contamination

$$P_1 = \{p_{11}, p_{12}, p_{13}, p_{14}\}. \quad (2)$$

In (2), p_{11}, p_{12}, p_{13}, and p_{14} represent energy consumption, type of energy, energy recovery rate, and proportion of energy use, respectively.

$$P_2 = \{p_{21}, p_{22}, p_{23}, p_{24}\}. \quad (3)$$

In (3), p_{21}, p_{22}, p_{23}, and p_{24} represent raw material consumption, recovery rate of raw materials, reuse rate of raw materials, and raw material substitution ratio, respectively.

$$P_3 = \{p_{31}, p_{32}, p_{33}, p_{34}\}. \quad (4)$$

In (4), p_{31}, p_{32}, p_{33} and p_{34} represent atmospheric environmental pollution, water environment pollution, solid waste pollution, and radioactive contamination, respectively.

In order to ensure the authenticity of the algorithm evaluation results, the screening of relevant index data must maintain a certain advance, and the official parameters issued by relevant departments shall be applied in data calculation as far as possible. Although some unofficial energy conservation and environmental protection indicators can greatly promote the evaluation accuracy of the algorithm [10], due to the failure to accurately grasp the attribute parameters of green building materials, the evaluation results will be distorted in the subsequent application of the algorithm, resulting in a certain type of green environmental protection and energy conservation indicators that cannot be included by the algorithm [7]. Then, it affects the accuracy of environmental protection attribute description of building materials. In order to avoid the above situation, it is set to represent the average value of all green environmental protection and energy-saving indicators, and the specific screening results can be expressed as follows:

$$F = \frac{\sqrt{\overline{n} + (S_s + D_d)^2}}{G_g \times K - L_j}. \quad (5)$$

In (5), F represents the screening results of green environmental protection and energy conservation indicators, S_s represents the environmental protection and energy conservation attribute parameters of green building materials, D_d represents the composite structure factor of the algorithm, G_g represents the official parameters of energy conservation and environmental protection indicators, K represents the characteristic indicators of the evaluation function of the algorithm, and L_j represents the stable constant quantity of the ecological energy conservation index system of green buildings.

3. Analysis of Evaluation Algorithm Based on System Standard

The effect evaluation algorithm is used to judge the degree to which something plays a role. At present, the evaluation of green building materials focuses on economic and environmental benefits without considering other attributes, resulting in one-sidedness in the results of the evaluation algorithm. Therefore, this study will focus on not only the environmental attributes of building materials, but also the

resource attributes and energy attributes of building materials [11], so as to build a comprehensive environmental performance evaluation algorithm. Based on the establishment of green building ecological energy-saving index system and standard, the smooth application of the new green building ecological energy-saving effect evaluation algorithm is realized through the steps of calculating index weight and fuzzy synthesis operator.

3.1. Weight Calculation of the Green Building Ecological Energy-Saving Index. In the process of building the new green building ecological energy-saving effect evaluation algorithm, the green building ecological energy-saving index weight is an important index to determine the evaluation strength of the algorithm. Most index evaluation and decision-making processes must be applied to the index weight. Building ecological energy-saving index weight is the importance measurement unit between the index itself and the subject to be evaluated. Determining the index weight is of great significance to the evaluation of green building ecological energy-saving level, and it is an important link in the whole comprehensive evaluation process. The impact of each lower level indicator on the upper level indicator is different. Therefore, in order to objectively evaluate the environmental protection performance of green buildings, it is necessary to give each evaluation index a corresponding weight value. The greater the impact of the evaluation index on the model, the greater the weight value. In fact, general evaluation problems can be transformed into weight value calculation problems. Since the ecological energy-saving effect evaluation of green buildings involves many evaluation indexes, in order to reduce the amount of calculation, the most widely used analytic hierarchy process is used to determine the weight coefficient value of each index [12].

Analytic hierarchy process, referred to as AHP for short, is applied to the index weight calculation of the evaluation algorithm in this study. It refers to the method of decomposing each evaluation index related to the comprehensive environmental protection performance evaluation layer by layer, and then performing qualitative and quantitative analysis on each evaluation index on this basis. Its basic operation process is shown in Figure 2.

As shown in Figure 2, different index weight values will lead to different evaluation results [13]. For green buildings, the weighting of indicators reflects a kind of randomness to a great extent. Due to different environmental protection concepts adhered to by different construction units, the importance given to the same type of buildings is different. Therefore, under the concept of environmental protection and energy conservation, calculating the index weight of green building materials based on gray correlation degree is the primary link in the construction of new evaluation algorithm. The weight of building ecological energy conservation index can be expressed as

$$I = \frac{H_h - \left(X_g \times K_i - M_u\right)}{F} \times \theta. \tag{6}$$

In (6), H_h represents the measurement coefficient of the index, X_j represents the evaluation effect produced by the algorithm, K_i represents the environmental protection concept factor, and M_u represents the decision-making processing limit value of energy-saving index.

3.2. Determination of the Fuzzy Evaluation Synthesis Operator. The fuzzy evaluation synthesis operator of green building ecological energy-saving index can reflect the index weight and enhance the comprehensive evaluation degree of the evaluation algorithm. Without considering the influence of other external conditions, a single environmental protection and energy-saving index is not enough to judge the evaluation results of the algorithm, and when the upper limit of green building resources is limited, the energy-saving level of building materials cannot be clearly described by the algorithm. The fuzzy evaluation synthesis operator calculates the average binding coefficient of all indicators by using the weight of building ecological energy-saving indicators and then obtains the accurate operator synthesis result by combining a number of environmental protection and energy-saving level parameters. The upper limit value of green building material resources and the lower limit value of green building material resources are set. Let α represent the upper limit value of green building material resources and β represent the lower limit value of green building material resources. Using α and β, the energy consumption factor of the index can be expressed as

$$H_n = \alpha \times \beta\left(\left(\frac{Q_q}{P_p}\right)^2 + a \times b\right). \tag{7}$$

In (7), P_p represents the energy-saving level factor of green building materials, Q_q represents the comprehensive evaluation degree of the algorithm, a represents the judgment coefficient of the evaluation result of the algorithm, and b represents the comprehensive judgment coefficient. Let $\overline{T}$ represent the average value of environmental protection and energy conservation level parameters; simultaneous formula (7) can express the fuzzy evaluation synthesis operator of green building ecological energy conservation index algorithm as

$$E = \frac{H_n}{\sqrt{Z_{\tilde{y}} \times Z_e}} \times m_1 \times n_1 \times \overline{T}. \tag{8}$$

In (8), m_1 represents the target fuzzy evaluation parameter, n_1 represents the original fuzzy evaluation parameter, Z_y represents the average evaluation synthesis time, and Z_e represents the periodic frequency of operator synthesis.

3.3. Implementation of Evaluation Algorithm Process. The evaluation process of green building ecological energy-saving effect evaluation algorithm takes the determination of comprehensive environmental factors as the starting link. Based on the gray correlation degree, the overall evaluation level of the algorithm can reach the expected standard

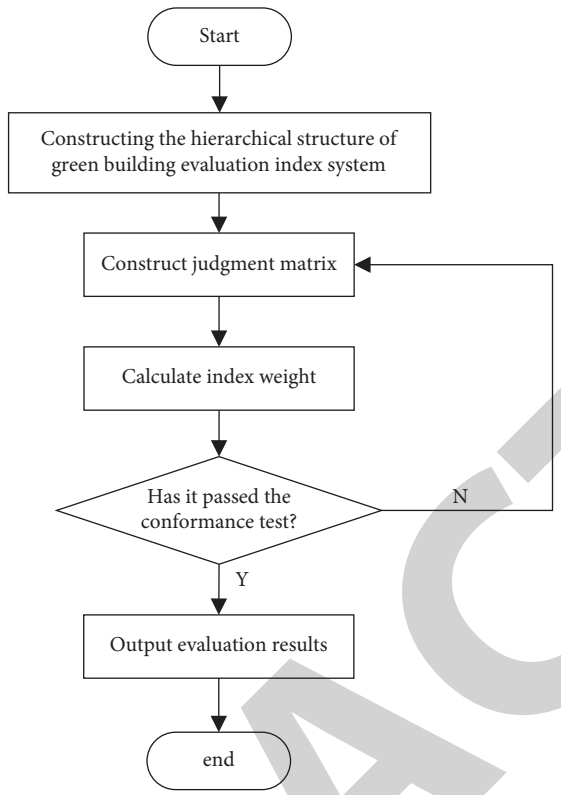

Figure 2: Operation process of analytic hierarchy process.

through the simultaneous establishment of environmental protection and energy-saving factors many times. Under the condition of ensuring the stability of the construction environment, there will be no obvious difference between the actual consumption and the target consumption of green building materials, but the related environmental protection and energy-saving indicators will fluctuate significantly with the increase of construction time. In order to avoid the influence of unstable indexes on the evaluation results of the algorithm, the actual consumption of green building materials is used as the evaluation basis, the actual consumption of materials is used as the main evaluation criterion, and the construction time is used as the operation cycle of the algorithm. On the premise that the framework of green building ecological energy-saving index system is stable, the grade of green building materials is divided by using environmental protection evaluation standards, and the accurate grade division results are used as the target operator to screen the environmental protection and energy-saving indexes that meet the evaluation standards. Based on the above operations, the index weight and fuzzy synthesis operator are calculated, and the above calculation results are used as the evaluation criteria of the algorithm to complete the evaluation and analysis of the ecological energy-saving index of green buildings. The detailed algorithm evaluation process is shown in Figure 3.

Under the influence of subjective factors, everyone's evaluation of something cannot be exactly the same. Therefore, in order to evaluate the performance of ecological energy conservation of green buildings, it is assumed that the i evaluation index makes the possible degree of the j evaluation scale. This possible degree is called subordination degree and recorded as Z_{ij}. Membership reflects the degree to which an object has a certain fuzzy property or belongs to a certain fuzzy concept. There are three evaluation scale subsets in the established comment set, and the membership vector obtained by each subset is

$$Z_i = (z_1, z_2, z_3), \quad i = 1, 2, 3. \tag{9}$$

Therefore, the established membership matrix is

$$Z = \begin{bmatrix} z_1 \\ z_2 \\ z_3 \end{bmatrix} = \begin{bmatrix} z_{11} & z_{12} & z_{13} \\ z_{21} & z_{22} & z_{23} \\ z_{31} & z_{32} & z_{33} \end{bmatrix}. \tag{10}$$

This membership matrix is a fuzzy relationship between the evaluation index and the comment set. Based on the known index weight C_n and membership matrix Z, the comprehensive evaluation vector of ecological energy-saving effect of green buildings is obtained as follows:

$$O = C_n \times Z = (C_{n1}, C_{n2}, \ldots, C_{ni}) \begin{bmatrix} z_{11} & z_{12} & z_{13} \\ z_{21} & z_{22} & z_{23} \\ z_{31} & z_{32} & z_{33} \end{bmatrix} = (o_1, o_2, \ldots, o_i). \tag{11}$$

In (11), $o_1, o_2, \ldots, o_i$ represent the comprehensive evaluation vector of each index.

To sum up, the comprehensive evaluation results of the algorithm are as follows:

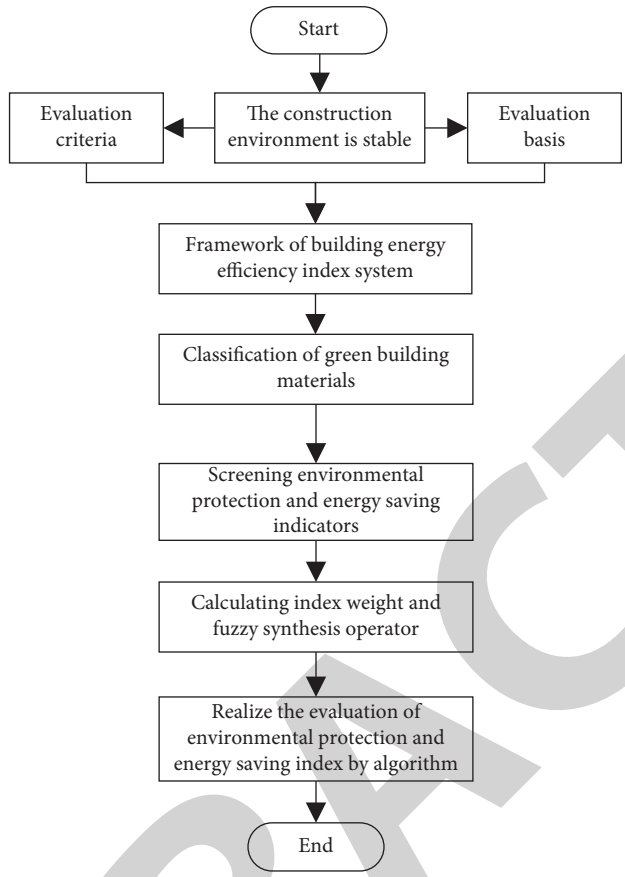

Figure 3: Flow chart of algorithm evaluation.

$$S = O \times P = \left(f_1, f_2, \ldots f_3, f_i\right)\begin{pmatrix} p_1 \\ p_2 \\ p_3 \end{pmatrix}. \quad (12)$$

According to the above process, the research on the evaluation algorithm of ecological energy-saving effect of green buildings based on gray correlation degree is completed.

4. Experimental Analysis

In order to evaluate the effect and feasibility of the green building ecological energy-saving effect evaluation algorithm based on gray correlation degree, a simulation experiment is set up. In the experiment, a wood structure building covering an area of 185 m^2 is selected, its simulation structure is constructed on the Simulink platform, and the structure is used to test the ecological energy-saving effect of the green building under the proposed algorithm. The internal effect of wood structure is shown in Figure 4.

The evaluation results of ecological energy conservation are not fixed and low, have great fuzziness, and are easily affected by human factors. Therefore, they are usually described by a degree word rather than specific values, such as "good," "bad," "average," "poor," or "very poor." Therefore, this model can also be used to evaluate the ecological energy-saving effect of green buildings, using fuzzy set theory and digital quantification to determine its energy-saving effect. Therefore, the comments on the energy-saving effect can be expressed through the following set:

$$J = \{j_1, j_2, j_3\}. \quad (13)$$

In (13), J, j_1, j_2, and j_3 represent the comment set, "excellent," "medium," and "inferior," respectively. Generally, the numerical interval is used to determine the grade. For example, when its weight C_n is 1, the comment set for the comprehensive evaluation of ecological energy-saving effect of green buildings can be established as follows: excellent $(C_n \geq 0.90)$, medium $(0.60 \leq C_n \leq 0.90)$, inferior $(C_n \leq 0.60)$. Therefore, the weight value can be obtained according to each index, and the ecological energy-saving effect of green buildings based on gray correlation degree can be accurately positioned according to the above evaluation criteria.

The energy consumption factor H_n is set, and the energy consumption factor H_n is taken in the interval [0, 1]. The higher the value of energy consumption factor H_n, the worse the energy-saving performance of external maintenance structure of green building; On the contrary, the smaller the value of energy consumption factor H_n, the better the energy-saving performance of maintenance structure outside the building. The algorithm in this paper, the algorithm in [6], and the algorithm in [7] are used for testing, and the energy-saving performance of the three different algorithms is compared. The test results are shown in Figure 5.

Figure 4: Internal structure of wooden building.

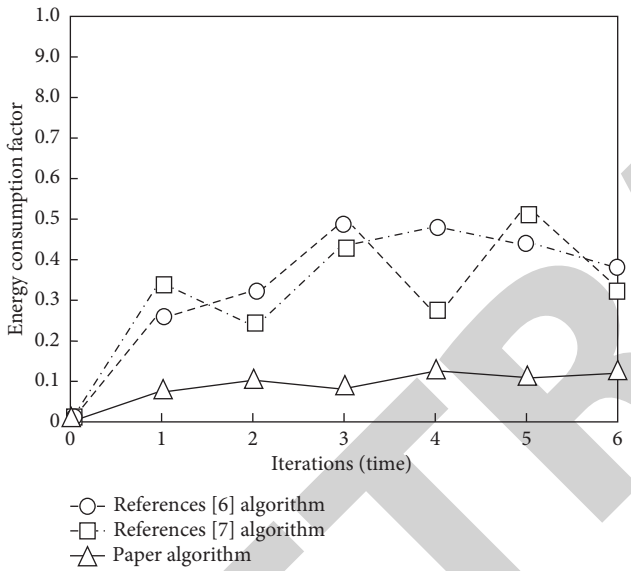

Figure 5: Comparison of energy consumption factors of three different methods.

It can be seen from Figure 5 that the energy consumption factors obtained by this method in multiple iterations are less than those of the algorithm in [6] and the algorithm in [7]. Because the algorithm calculates the weight of the ecological energy-saving index of green buildings and determines the comprehensive fuzzy evaluation operator, it is helpful to stabilize the influence of the external maintenance structure of the green building to a certain extent. According to the analysis results, the algorithm constructs an energy-saving optimization design target algorithm, reduces the energy consumption of the external maintenance structure of the green building, and verifies that the algorithm has good energy-saving performance.

The experimental index is set as the fitting degree between the simulated structure and the actual energy-saving results. The evaluation results before and after the application of this algorithm are shown in Figure 6.

By analyzing the experimental results in Figure 6, it can be clearly seen that in terms of the degree of fitting with the actual energy saving, the fitting degree curve of the actual energy-saving effect fluctuates continuously before the application of the designed algorithm, while the energy-saving effect after the application of the green building ecological energy-saving effect evaluation algorithm based on gray correlation degree is better than that before the application, and the fitting degree curve has good stability and long-term fitting.

After determining that the fitting degree meets the requirements of energy-saving effect, the following two evaluation indexes are established to determine the advantages and disadvantages of the proposed algorithm: the maximum energy-saving effect and the maximum cost increment. At the same time, the design effects of the algorithms in [6] and [7] are compared, and the comparison results are shown in Figures 7 and 8:

(i) Maximum energy-saving effect: the calculation formula for the maximum energy-saving effect that the design algorithm can achieve is as follows:

$$W_{\max} = \frac{(R_{\max} - R_r)}{R_r}. \tag{14}$$

(ii) Maximum cost increment: the economic benefits shown by the transformation design algorithm are described by the following formula:

$$K_{\max} = \frac{(B_{\max} - B_r)}{B_r}. \tag{15}$$

In (15), $W_{\max}$ and $K_{\max}$, respectively, represent the maximum energy-saving rate and cost increment; $R_{\max}$ represents the maximum annual energy consumption; R_r represents the average annual energy consumption of the target building; $B_{\max}$ represents the highest construction cost in the design algorithm; and B_r represents the reconstruction cost of the building.

As can be seen from Figures 7 and 8, the maximum energy-saving effect is most obvious in winter and summer. The proposed design algorithm can save more power. Through the transformation and design of the roof, ground, and windows of green buildings, it can make the indoor warm in winter and cool in summer, reduce the use time of air conditioning in winter and summer, and achieve the purpose of energy conservation and environmental protection. In addition, the cost increment of the algorithm is also the lowest, because this algorithm simulates and constructs the overall structure of the green building and carries out similarity analysis, so as to transform the design on the basis of ensuring the maximum similarity of the original building and reduce the cost consumption.

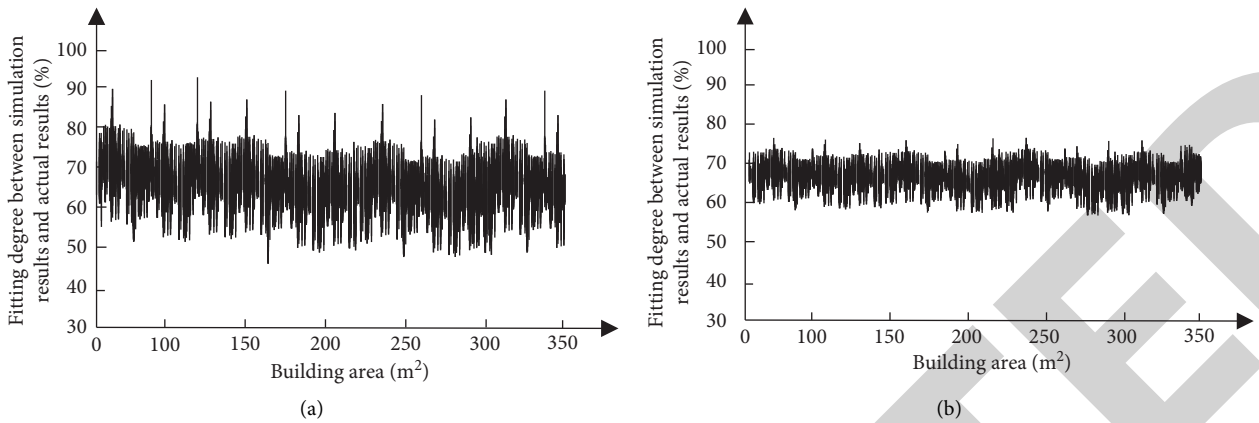

Figure 6: Comparison of fitting degree between different designs and actual energy saving before (a) and after (b) applying the algorithm in this paper.

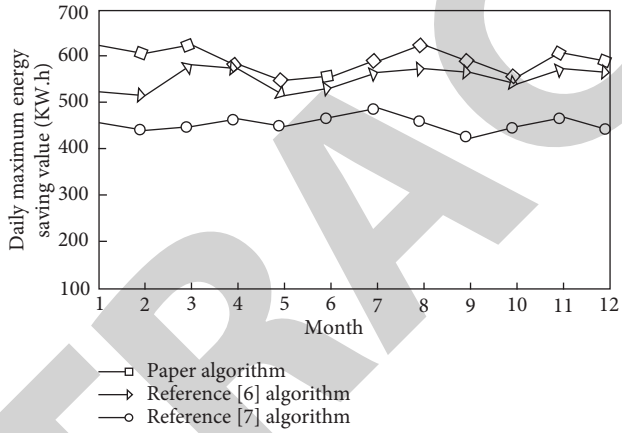

Figure 7: Comparison results of the maximum energy-saving effects of different algorithms.

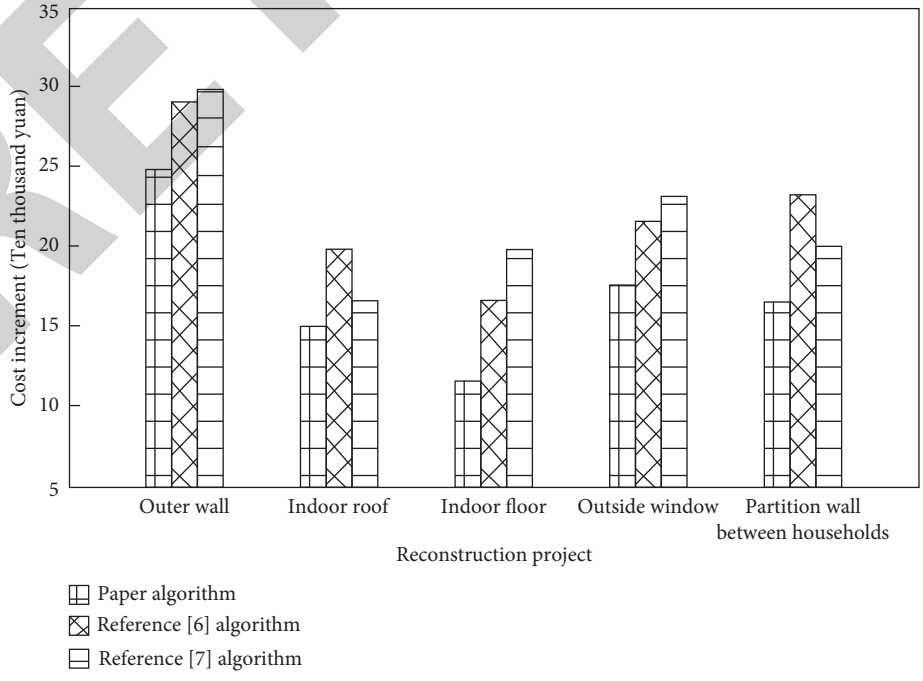

Figure 8: Comparison results of the cost increment of different algorithms.

Hindawi
Journal of Mathematics
Volume 2024, Article ID 9896547, 1 page
https://doi.org/10.1155/2024/9896547

Retraction

Retracted: Research on Design and Application of National Fitness System

Journal of Mathematics

Received 23 January 2024; Accepted 23 January 2024; Published 24 January 2024

This article has been retracted by Hindawi following an investigation undertaken by the publisher [1]. This investigation has uncovered evidence of one or more of the following indicators of systematic manipulation of the publication process:

(1) Discrepancies in scope

(2) Discrepancies in the description of the research reported

(3) Discrepancies between the availability of data and the research described

(4) Inappropriate citations

(5) Incoherent, meaningless and/or irrelevant content included in the article

(6) Manipulated or compromised peer review

The presence of these indicators undermines our confidence in the integrity of the article's content and we cannot, therefore, vouch for its reliability. Please note that this notice is intended solely to alert readers that the content of this article is unreliable. We have not investigated whether authors were aware of or involved in the systematic manipulation of the publication process.

In addition, our investigation has also shown that one or more of the following human-subject reporting requirements has not been met in this article: ethical approval by an Institutional Review Board (IRB) committee or equivalent, patient/participant consent to participate, and/or agreement to publish patient/participant details (where relevant).

Wiley and Hindawi regrets that the usual quality checks did not identify these issues before publication and have since put additional measures in place to safeguard research integrity.

We wish to credit our own Research Integrity and Research Publishing teams and anonymous and named external researchers and research integrity experts for contributing to this investigation.

The corresponding author, as the representative of all authors, has been given the opportunity to register their agreement or disagreement to this retraction. We have kept a record of any response received.

References

[1] S. Wang, "Research on Design and Application of National Fitness System," *Journal of Mathematics*, vol. 2021, Article ID 5178550, 10 pages, 2021.

Hindawi
Journal of Mathematics
Volume 2021, Article ID 5178550, 10 pages
https://doi.org/10.1155/2021/5178550

Research Article

Research on Design and Application of National Fitness System

Shengyou Wang

Huanghe S & T University, Zhengzhou 450052, China

Correspondence should be addressed to Shengyou Wang; wsy@hhstu.edu.cn

Received 19 November 2021; Revised 6 December 2021; Accepted 9 December 2021; Published 26 December 2021

Academic Editor: Naeem Jan

In order to improve the physical quality of the national people, a national fitness system is designed and applied to practice. Design the overall architecture of the national fitness system, including the perception layer, network layer, and application layer. The perception layer mainly uses Internet of Things gateway, central machine, wireless perception node, and fitness data dashboard to obtain fitness data. The network layer mainly uses WiFi, 4G, Ethernet, and other public networks to transmit fitness data, fitness guidance data, and equipment operation and maintenance data. The application layer provides data storage, device management, user management, and client services. On this basis, through the collection of users' fitness data rating data, the data are transformed into fitness data rating matrix, and the matrix is analyzed and calculated to realize the intelligent recommendation of fitness data and complete the design of national fitness data recommendation algorithm. The test results show that the system can meet the requirements of normal use, good compatibility, and user score is high and has high practical application value.

1. Introduction

With the rapid development of Internet technology, big data technology, machine learning, and other emerging technologies, the era of "Internet +" and big data has come. The penetration of Internet technology and big data technology into various traditional industries in the society subverts the original market operation mode and industrial pattern, and all traditional industries begin to upgrade and transform to adapt to the new market demand, so does the sports industry [1, 2].

With the improvement of people's living standards, people pay more attention to health, so the national fitness craze rises. National fitness refers to the strengthening of strength and flexibility, endurance, coordination, and control of all parts of the body by all people, regardless of age [3]. Bodybuilding offers people a way of life that improves their quality of life. Regular exercise can prevent various diseases, such as heart disease, stroke, hypertension, arterial embolism, obesity, cholelithiasis, diabetes, and osteoporosis, eliminate tension and pressure, relax the body and mind, improve sleep, make people happy, enhance self-confidence and self-esteem, and make people easier to communicate with others [4]. Regular exercise can not only improve the basic activities of the body but also delight the body and mind, regulate emotions, relieve psychological pressure, and enhance people's physical and mental health. The fitness movement advocates the fashionable fitness concept, the purpose of fitness is no longer a simple physical fitness; its ultimate purpose is "heart." When a person is in a happy mood, the state of mind will be peaceful; the body can get a full range of relaxation. It is easy to complete every day's work efficiently and successfully when the body relaxes, feels happy, and improves its physical quality [5]. Therefore, fitness is an upward way of life, which will bring high-quality life enjoyment and spiritual experience to modern people [6]. Therefore, this paper designs a national fitness system and applies it to the practice to verify the practical application effect of the system.

The contents of this paper follow the following pattern; Section 2 discusses the national fitness system design which is composed of system architecture and fitness material recommendation algorithm design. In Section 3, the application effect of national fitness system is analyzed through carrying out the compatibility and pressure tests. Finally, the results of the study are summarized in Section 4, conclusion.

2. National Fitness System Design

In this section, the design for national fitness system is explained. To this end, we first describe the complete architecture of the system. The system has three layers, that is, perception layer, network layer, and application layer. Secondly, the fitness material recommendation algorithm design is deliberated which is based upon decomposition of matrices.

2.1. Overall System Architecture. The perception layer of the system obtains the data information of each fitness exercise, and the specific equipment includes Internet of Things gateway, central machine, wireless perception node (fitness client), and fitness equipment dashboard (data transmission unit). The network layer of the system is used to transmit fitness data, fitness guidance data, and equipment operation and maintenance data, mainly using WiFi, 4G, Ethernet, and other public networks [7]. The main functions of the system application layer include storage and maintenance of fitness data, fitness equipment management and control, user rights management, and extended interface service. Extended interface service mainly provides application interfaces and data query services for the expansion requirements of third-party application systems. Through further analysis of system requirements, the overall structure diagram of the national fitness system is designed as shown in Figure 1.

Among them, because the network layer uses the public network, the network layer is not discussed too much, so focus on the analysis and design of the perception layer and the application layer.

2.1.1. Perception Layer. The perceptive layer device is used to collect the operating parameters of the equipment and the physical parameters of fitness and send the data to the central machine, which integrates and calculates the data and uploads it to the remote server. The perception layer of the fitness system of the Internet of Things plays the role of the fitness information collector and is compatible with various types of fitness equipment of the Internet of Things through the central machine and gateway of the perception layer, so as to achieve all-weather LAN access and system access of various fitness equipment [8]. In the perception layer, there are two types of perception devices: data transmission units for their own dashboards and fitness terminals suitable for wireless sensors. A national fitness system based on the Internet of Things is designed and implemented by designing and implementing the central machine to support data transmission unit and fitness terminal [9]. In the deployment of perception-layer equipment, appropriate fitness equipment should be selected according to the application situation of fitness, so as to design the corresponding data transmission unit or wireless sensor and fitness terminal, and connect it to the center. The central machine has functions such as data acquisition and processing, network communication [10], authority management, and man-machine interface, and its functional block diagram is shown in Figure 2.

The essence of the central computer is a microcomputer system, which is specially used for fitness information management. When designing the system hardware, it is necessary to choose the appropriate processor chip according to the application background [11]. From the point of view of hardware functions, the central machine has such basic functions as data collection, data display, data storage, data network transmission and local download, QR code decoding, NFC label reading and writing, Mifare card reading and writing, and human-computer interaction, so the schematic diagram of the hardware structure of the central machine is shown in Figure 3.

The software system of central computer consists of serial port driver, NFC driver, and application software. FTDI company provides API for serial port program, and NFC also has corresponding API. Therefore, serial port driver and NFC driver only need to be familiar with program flow [12] and make API call. This paper mainly designs application software of central computer to realize functions such as data collection, identity verification, and network communication. The overall software structure of the central computer is shown in Figure 4.

The sports and fitness data acquisition module is used to collect all kinds of sports and fitness parameter information, including the identity information of the fitness users, physiological parameter information, and equipment operation parameters. In order to support a variety of fitness, the module needs to design different submodules for different data transmission units and fitness terminals [13]. The equipment management module is mainly used for the statistics of fitness equipment warehousing, warehousing, running status and equipment activation, deactivation, opening, closing, and exercise prescription implementation. The sports and fitness data storage and query module is mainly used for local storage and remote server storage of fitness data, as well as extracting historical data from remote server or local files, and realizing visualization. The authentication module is mainly used for NFC Tag and QR code information collection [14] and then connects to the remote server through Ethernet for authentication. The human-computer interaction module is mainly used for data query, data graphical display, equipment management, personnel management, and parameter configuration.

The application software flow of central computer is as follows:

(1) Administrator authentication, enter the interface;

(2) initialize the NFC interface and UART interface to open a thread to receive identity information;

(3) initialize communication program, start SOCKET server, wait for device connection, and open thread for data collection [15];

(4) initialize human-computer interaction configuration, obtain information of each fitness equipment, and monitor data upload instructions; and

(5) wait for thread data.

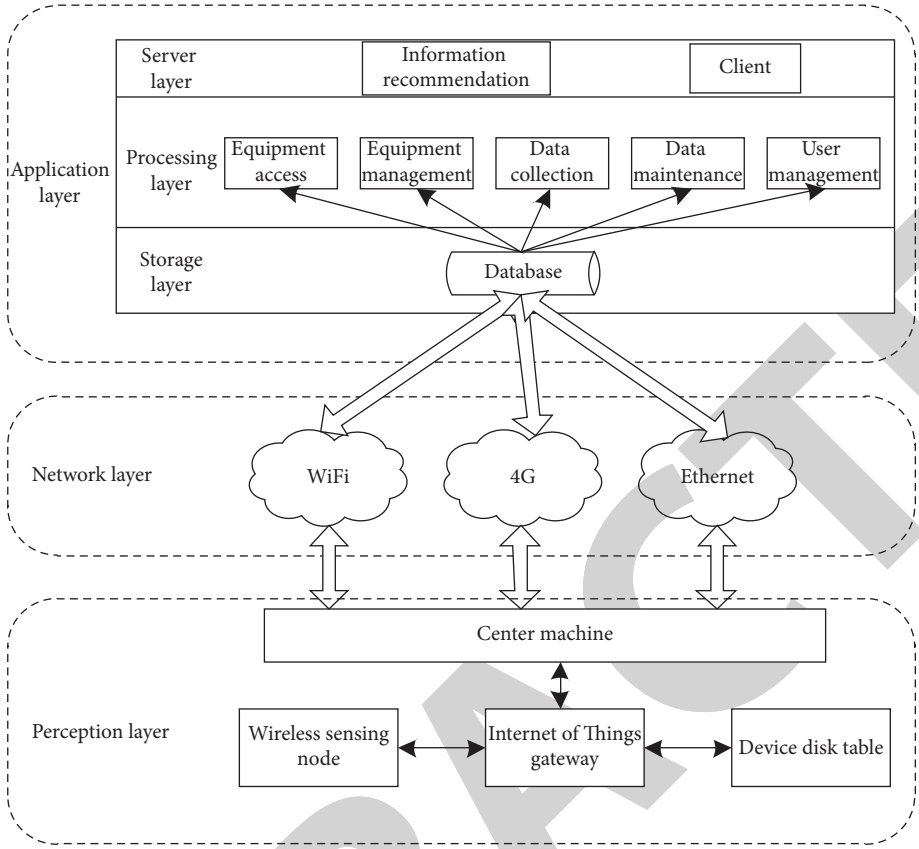

Figure 1: System structure diagram.

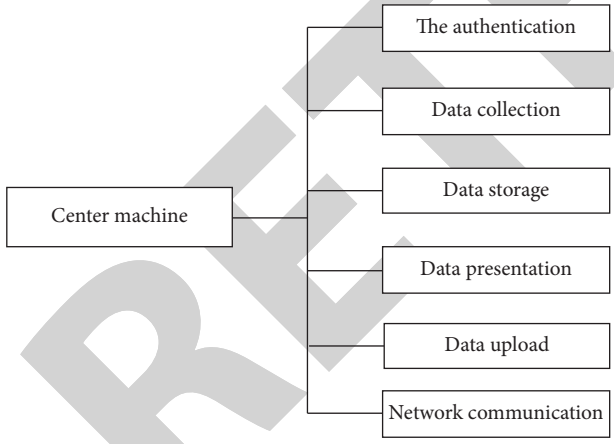

Figure 2: Functional block diagram of central computer.

2.1.2. Application Layer. The application layer of the system consists of storage layer, processing layer, and service layer.

The storage layer is responsible for data storage, including device information, user information, fitness data, and so on. The user information table contains user names, passwords, gender, age, permissions, profile pictures, and other information for user information storage, adding data during user registration. The user information is shown in Table 1.

In user movement record form records are added after a user exercises, including user name, height, time, abscissa value, ordinate value, and heat consumption, and are used to draw movement curves. The user movement record is shown in Table 2.

The heat consumption meter includes fields username, date, and heat consumed. The heat consumption meter is shown in Table 3.

In fitness equipment list users record equipment name, number, and other information, as shown in Table 4.

The system processing layer is responsible for data maintenance, including user management, equipment management, and fitness data calculation and update.

Authentication: According to the system design requirements, the system authentication in this paper is implemented in the form of Mifare card and QR code hardware decoding. The flow chart of authentication is shown in Figure 5.

The QR code hardware decoder is connected to the central machine through serial port, and the NFC card reader is connected to the central machine through USB. The main difference of the whole process is reflected in the module initialization. The initialization of QR code module is mainly through serial port connection. The basic process is as follows:

(1) Enumerates connected serial port devices;

(2) access to communicate with peripherals;

(3) configure parameters such as baud rate for the serial port; and

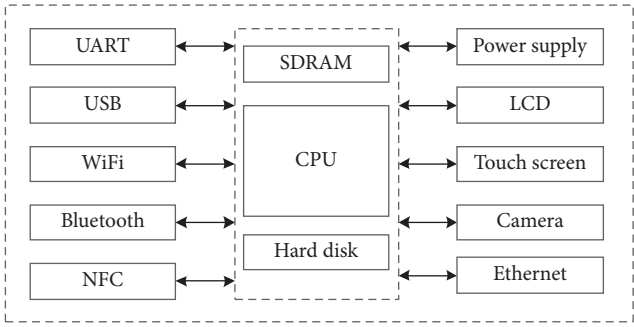

Figure 3: Hardware structure of central machine.

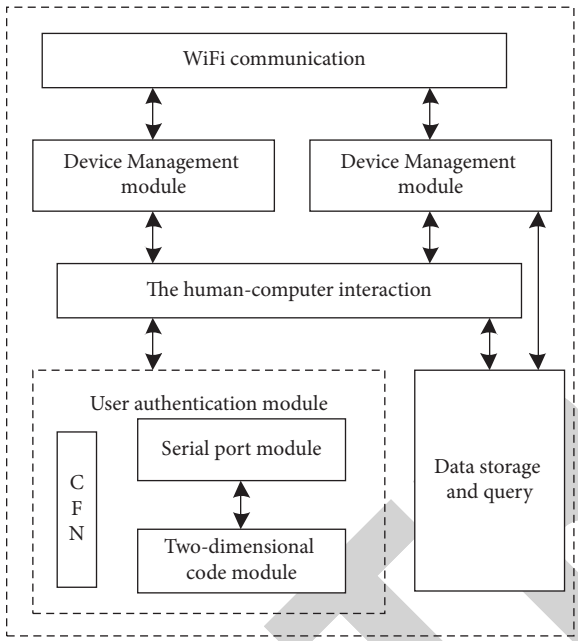

Figure 4: Overall structure of central computer software.

(4) communicate with peripherals to obtain identity information.

In the user authentication program, open up a thread for serial communication, each scans a QR code, through the regular expression to extract the user name and password, and then communicate with the remote server, request authentication, and return the results; the authentication passes the jump to the relevant page, otherwise prompted to reauthentication.

User management: The device management module is designed for device managers. Therefore, users must be authenticated before entering the device management module. The main function is to realize the maintenance and visualization of fitness equipment table, including the addition, deletion, activation, deactivation of equipment, editing and viewing of equipment information, and the maintenance and management of equipment information, such as daily maintenance, remote warranty, and so on. As the data and logic of this module are intricate, the specific design and programming implementation are not described.

Human-computer interaction: The man-machine interaction module provides various man-machine interfaces. Fitness coaches and other managers can manage equipment, personnel, and data through the central machine. At the same time, the central machine provides a friendly interface for ordinary fitness users to query data, exercise prescriptions, and other fitness information.

Data collection and update: Whenever the central computer receives data, it first writes the data into the database, and then searches the fitness equipment table according to the IP address of the current socket connection, and then adds or statistics the use record of the equipment according to the data type [16, 17]. The data acquisition and update flow chart is shown in Figure 6.

The client in the service layer is the direct medium of the interaction between the system and the user. We adopt the intelligent client technology and deploy the function modules of the client through the network. The main interface includes the main interface, registration interface, login interface, and heat consumption query interface. When the system starts, the login page is displayed. There is a registration button on the login page. After you click the button, the registration page is displayed. It should be said that interface design is more important because it is the first impression the software leaves on the user. This paper adheres to the design principles of graphical user interface, which is intuitive and transparent to users. Users can see the corresponding functions on the interface at a glance after contacting the software and can easily use this system without much training. Use a uniform composition layout, with a uniform tone, contrast, color levels, and image style. The design of the interface follows the principle of conciseness and clarity. No unnecessary menus, buttons, and other components are set. As long as it can realize various functions of calling software, it is convenient for users to use. The flow of using the client interface is shown in Figure 7.

2.2. Fitness Material Recommendation Algorithm Design Based on Matrix Decomposition. The matrix decomposition model is a collaborative filtering method, which takes advantage of users' preference data for goods and converts these data into a two-dimensional matrix with users as rows and goods as columns. This paper collects the rating data of users' fitness data, converts the data into the rating matrix of fitness data, analyzes and calculates the matrix, and realizes the intelligent recommendation of fitness data.

Assuming that the actual "user-item" scoring matrix is S and dimension is $u * e$, it is decomposed into $u * k$-dimension user factor matrix A and $e * k$-dimension item factor matrix B; then the loss function is shown in formula (1).

$$C = \sum_{i=1}^{u} \sum_{j=1}^{e} \left(S_{i,j} - A_i \cdot B_j^T\right)^2, \tag{1}$$

wherein i and j represent the i-th row and j-th column of the scoring matrix and $S_{i,j}$ cannot be the missing value. By minimizing the loss function, the predicted matrix is as close as possible to the original scoring matrix. However, when the

Table 1: User information table.

Field names	Data type	Length
User name	Char	10
Password	Varchar	50
Salt	Varchar	50
Gender	Char	10
Age	Char	10
Permissions	Char	10
Head portrait	Char	10

Table 2: User movement record table.

Field names	Data type	Length
User name	Char	10
Highly	Int	4
Time	Decimal	9
Abscissa values	Int	4
Ordinate values	Int	4
Consumption quantity of heat	Decimal	9
ID	Int	4
Heart rate	Nchar	10
Distance travelled	Nchar	10

Table 3: Heat consumption meter.

Field names	Data type	Length
User name	Char	10
Date of	Decimal	9
Consumption quantity of heat	Decimal	9

Table 4: Fitness equipment list.

Field names	Data type	Length
Key	VARCHAR	10
Devname	VARCHAR	2
Devid	VARCHAR	9
Devtype	VARCHAR	5
Devvision	VARCHAR	4
Sportstype	VARCHAR	10
Duration	VARCHAR	12
Devip	VARCHAR	6
Devbrand	VARCHAR	4
Fixdate	VARCHAR	10
Bitmap	VARCHAR	2
State	VARCHAR	6

matrix is sparse, over-fitting may occur. The method of over-fitting is to use regularization, which is to add the binary norm of user factor matrix and data factor matrix to the loss function. The loss function after introducing regularization is shown in formula (2) below.

$$C = \sum_{i=1}^{u}\sum_{j=1}^{e}\left(S_{i,j} - A_i \cdot B_j^T\right)^2 + \lambda\left(\left\|A_i\right\|^2 + \left\|B_j\right\|^2\right). \tag{2}$$

The user factor matrix A and data factor matrix B can be obtained by optimizing the loss function to the minimum value, so that their product approximates the original score matrix. Since both user factor matrix and data factor matrix

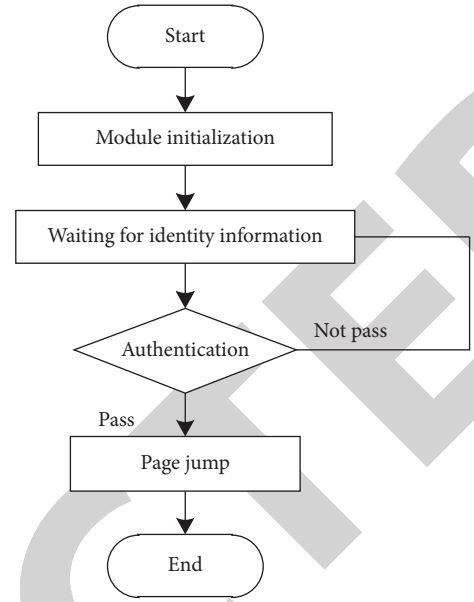

Figure 5: Authentication process.

are changing here, it is difficult to calculate, so the cross least square method is adopted to fix one of the two factor matrices to update the other and keep iterating until the model converges or reaches the set number of iterations. The steps are as follows:

(1) Generate a user factor matrix $A^{(0)}$ randomly.

(2) Fix $A^{(0)}$ and obtain the optimal $B^{(0)}$ by taking partial derivative of data factor matrix B. The partial derivative of loss function C is taken with respect to B_j, as shown in formula (3).

$$\begin{aligned}
\frac{\partial C}{\partial B_j} &= \frac{\partial}{\partial B_j}\left(\sum_{i=1}^{u}\left(S_{i,j} - A_i \cdot B_j^T\right)^2 + \lambda\left(\left\|A_i\right\|^2 + \left\|B_j\right\|^2\right)\right),\\
&= \sum_{i=1}^{u}\left[2\left(S_{i,j} - A_i^{(0)} \cdot B_j^T\right) \cdot \frac{\partial\left(-A_i^{(0)} \cdot B_j^T\right)}{\partial B_j} + 2\lambda B_j\right]\\
&= \sum_{i=1}^{u}\left[2\left(S_{i,j} - A_i^{(0)} \cdot B_j^T\right) \cdot \left(-A_i^{(0)}\right) + 2\lambda B_j\right]\\
&= \sum_{i=1}^{u}\left[2S_{i,j} \cdot \left(-A_i^{(0)}\right) + 2B_j \cdot A_i^{(0)} + 2\lambda B_j\right]\\
&= 2\sum_{i=1}^{u}\left[B_j\left(\left(A_i^{(0)}\right)^T \cdot A_i^{(0)} + \lambda - S_{i,j} \cdot A_i^{(0)}\right)\right].
\end{aligned} \tag{3}$$

1 The above partial derivative formula uses the vector derivative rule and the exchange law of matrix multiplication. The vector derivative rule and matrix penalty exchange law are shown in formula (4) and formula (5), respectively.

2 Vector derivative rule:

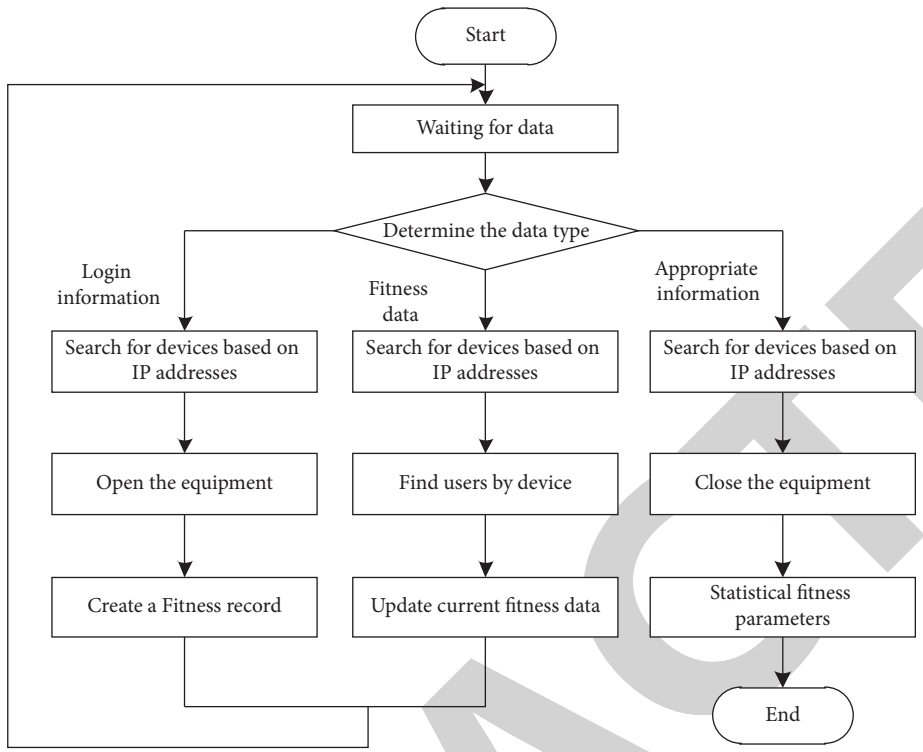

Figure 6: Data collection and update process.

$$\frac{\partial\left(-A_i^{(0)} \cdot B_j^T\right)}{\partial B_j} = -A_i^{(0)}. \tag{4}$$

3 Commutative law of matrix multiplication:

$$2B_j \cdot \left(A_i^{(0)}\right)^T \cdot A_i^{(0)} = B_j\left(\left(A_i^{(0)}\right)^T \cdot A_i^{(0)}\right). \tag{5}$$

(3) Let the partial derivative of loss function C with respect to B_j be 0, and it can be obtained:

$$\sum_{i=1}^{u}\left[B_j\left(\left(A_i^{(0)}\right)^T \cdot A_i^{(0)} + \lambda\right) - S_{i,j} \cdot A_i^{(0)}\right] = 0. \tag{6}$$

There are

$$\sum_{i=1}^{u} B_j\left(\left(A_i^{(0)}\right)^T \cdot A_i^{(0)} + \lambda\right) = \sum_{i=1}^{u} S_{i,j} \cdot A_i^{(0)}. \tag{7}$$

That is,

$$B_j\left(A^T A + \lambda E\right) = A^T S_j^T. \tag{8}$$

If $M_1 = (A^T A + \lambda E), M_2 = A^T S_j^T$, then

$$B_j = \frac{M_2}{M_1}. \tag{9}$$

The data factor matrix B can be obtained by calculating $B_1, B_2, \ldots, B_e$ in turn.

(4) Fixed data factor matrix B and solved user factor matrix A.

$$\begin{aligned}
\frac{\partial C}{\partial A_i} &= \frac{\partial}{\partial A_i}\left(\sum_{j=1}^{e}\left(S_{i,j} - A_i \cdot B_j^T\right)^2 + \lambda\left(\|A_i\|^2 + \|B_j\|^2\right)\right), \\
&= \sum_{j=1}^{e}\left[2\left(S_{i,j} - A_i \cdot B_j^T\right) \cdot \frac{\partial\left(-A_i \cdot B_j^T\right)}{\partial B_j} + 2\lambda A_i\right] \\
&= \sum_{j=1}^{e}\left[2\left(S_{i,j} - A_i \cdot B_j^T\right) \cdot \left(-B_j\right) + 2\lambda A_i\right] \\
&= \sum_{i=1}^{u}\left[2S_{i,j} \cdot \left(-B_j\right) + 2A_i \cdot B_j^T \cdot B_j + 2\lambda A_i\right] \\
&= 2\sum_{j=1}^{e}\left[A_i\left(B_j^T \cdot B_j + \lambda\right) - S_{i,j} \cdot B_j\right].
\end{aligned} \tag{10}$$

Let formula (10) be 0 and get

$$2\sum_{j=1}^{e}\left[A_i\left(B_j^T \cdot B_j + \lambda\right) - S_{i,j} \cdot B_j\right] = 0. \tag{11}$$

There are

$$\sum_{j=1}^{e} A_i\left(B_j^T \cdot B_j + \lambda\right) = \sum_{j=1}^{e} S_{i,j} \cdot B_j. \tag{12}$$

That is,

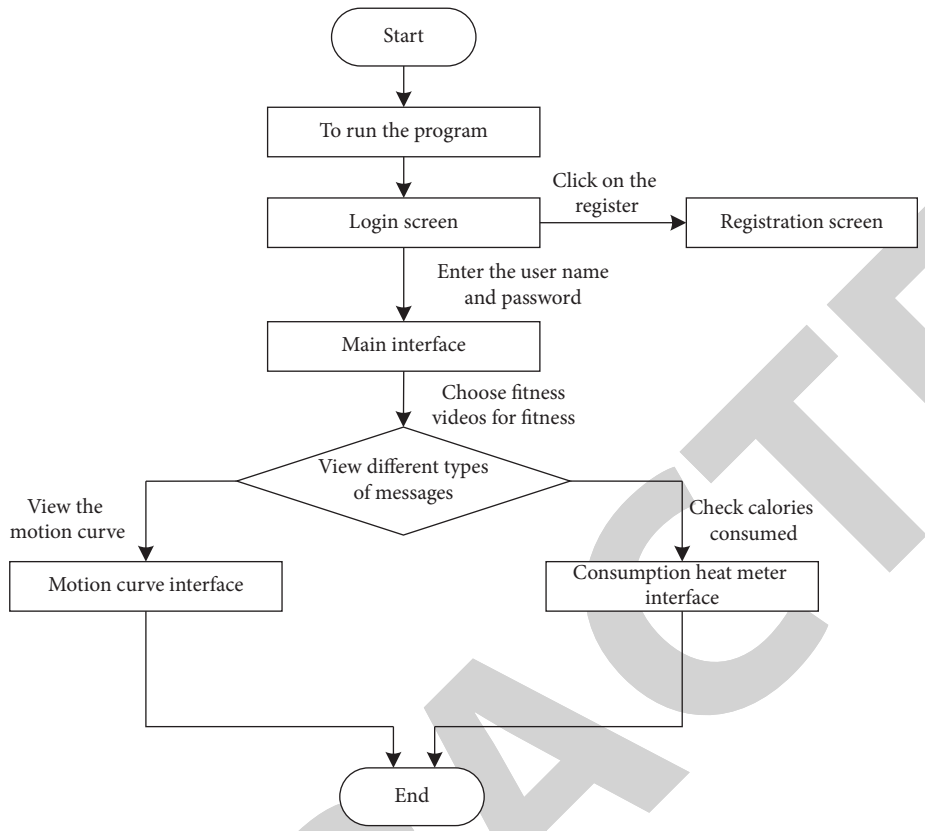

Figure 7: Client usage flow.

$$A_i\left(B^TB+\lambda E\right)=B^TS_i^T. \tag{13}$$

If $M_1=(B^TB+\lambda E), M_2=B^TS_i^T$, then

$$A_i=\frac{M_2}{M_1}. \tag{14}$$

The data factor matrix A can be obtained by calculating $A_1, A_2, \ldots, A_u$ in turn.

(5) The steps (3) and (4) are cyclically executed successively until the loss function C converges or the number of cycles reaches the set value. Then the optimal user factor matrix A and data factor matrix B are obtained.

(6) Build a recommendation model to realize the recommendation of fitness materials. The specific description of the model is as follows:

$$G=\frac{\sum_{(i,j)\in R}\left(S_{i,j}-J_{i,j}\right)^2}{A+B}. \tag{15}$$

In the above formula, 1 represents the scoring approximation matrix.

3. Analysis of the Application Effect of National Fitness System

3.1. Establishment of Development and Operation Environment. According to the analysis and description of the national fitness system design above, the Wamp (Windows + Apache + My SQL + PHP) framework is adopted in the development environment based on Windows, and the concept of continuous integration is integrated to facilitate the maintenance and expansion of the system in the later stage. After the development of this system is basically completed, it will be deployed on the WEB application server of a key laboratory of a university, and stage tests will begin.

1 Development environment: in this paper, the national fitness system is developed using Wamp architecture, the language is object-oriented PHP5.5.12, and the development editor is Net Beans8.1; Net Beans is open source software development integration environment, is an open framework, extensible development platform, and can be used for Java, C/C++, PHP, and other language development. In terms of database management, the graphical management tool phpMyAdmin is used, version 4.1.14.

2 Operating environment:

1 web server: Apache 2.4.9;
2 database: My SQL 5.6.17; and
3 operating system: Windows XP/7/Vista/8/10.

3.2. Application Test

3.2.1. Pressure Test. In this paper, the system tested the high concurrency test and big data test of the system through the pressure test tool ab of the Apache server. By simulating the access of users, the system continuously submitted requests

to verify the bearing capacity of the system. Apache server pressure test tool ab is a relatively popular professional system test tool and has been widely praised in the industry.

The specific test steps are as follows:

(1) Open the Apache server installation directory. An executable program ab.exe is displayed in the bin directory.

(2) On the CLI of Windows, go to the directory where the ab.exe program resides and run the ab.exe program.

(3) Start the ab stress test and input the command line to access the script 5000 times, 200 concurrent (simulate 200 users access at the same time).

The pressure test results are shown in Table 5.

According to the test results of the system, when the number of online visitors increases, the average response time of the system, the throughput per minute of the system, and the offset given by the system increase correspondingly. For the system in this paper, considering the actual situation after the system goes online, the system can still meet the requirements of normal use in extreme cases.

3.2.2. Compatibility Tests. The stability of a system running flawlessly and perfectly on different platforms is known as the compatibility of the system. In this subsection, the compatibility test system under different operating systems will be carried out mainly through the test system. It will be evaluated that whether the browsers display effect is good or bad. Moreover, the tests will be run in different operating systems and browsers.

The compatibility test tool used by the system in this paper is Browser-shots, a popular online test. Browser-shots is an excellent tool on the market to detect the compatibility of websites or systems. It tests the compatibility of websites or systems by rendering web pages in different browsers under different operating systems and then obtaining screenshots. And its service is completely free.

The specific steps of using Browser-shots to test the compatibility of the system in this paper are as follows.

Start by going to Browser-shots' official website, https://browsershots.org/ and selecting a variety of browsers for the different operating systems you want to test. There are four operating systems, Linux, Windows, Mac OS, and Free BSD, as well as various browser versions. Detailed test parameters are available at the bottom. Then enter the URL of the web page to be tested and finally select the platform and browser version. Click Submit to start making effect screenshots. The final test screen will be shown in screenshots and show the compatibility test results for different operating systems and browsers. The results are shown in Table 6.

Table 5: Pressure test results.

The number of threads	20	50	100
Number of samples	200	500	1000
Average response time (ms)	112	409	2876
Offset	65	447	3215
Throughput per minute	356 M	906 M	905 M

Table 6: Compatibility test results.

Browser compatibility testing	IE7	Test pass
	IE8	Test pass
	IE9	Test pass
	IE10	Test pass
	Chrome	Test pass
	Firefox	Test pass
	Google Chrome	Test pass
Server compatibility test	Windows server 2019	Test pass
	Windows 7	Test pass
	Windows 8	Test pass
	Windows 10	Test pass
	Linux	Test pass

As can be seen from the above table, the system in this paper can run stably in different operating systems and browsers, so the compatibility test of the system in this paper shows that the system has good compatibility.

3.3. Application Effect. After 10 months of experiment, the evaluation results of the system in this paper were obtained. The full score was 100, and the lowest score was 0. The user evaluation results are shown in Table 7.

By analyzing the data in Table 7, it can be seen that with the increase of the experiment time, the score of the testers for the fitness system designed in this paper increases, and the user score reaches the maximum value at the 12th month, indicating that the testers are very satisfied with the system designed in this paper, thus proving that the system has a good application effect.

On the basis of the above, a questionnaire survey was conducted among 1000 subjects at the end of the experiment. The results are shown in Table 8.

By analyzing the data in Table 7, it can be seen that with the increase of the experiment time, the score of the testers for the fitness system designed in this paper increases, and the user score reaches the maximum value at the 10th month, indicating that the testers are very satisfied with the system designed in this paper, thus proving that the system has a good application effect.

On the basis of the above, a questionnaire survey was conducted among 1000 subjects at the end of the experiment. The results are shown in Table 8.

By analyzing the data in Table 8, it can be seen that most testers are satisfied with the fitness effect, novelty, lasting attraction, entertainment, and recommendation

Table 7: User evaluation results.

Experimental time	Evaluation results
1 month	85.35
2 months	87.47
3 months	89.52
4 months	92.63
5 months	94.31
6 months	95.74
7 months	96.18
8 months	96.57
9 months	97.34
10 months	97.64

Table 8: Questionnaire survey results.

Project	Satisfaction		Dissatisfaction	
	Number of people	Proportion (%)	Number of people	Proportion (%)
Effect of fitness	9725	97.25	275	27.5
Novelty	9816	98.16	184	18.4
Lasting appeal	9732	97.32	268	26.8
Entertaining	9274	92.74	726	7.6
Recommend effect	9536	95.36	464	46.4

effect of the system. In particular, the novelty of the system has been highly praised by most testers. At the same time, the tester also gave many good suggestions, such as increasing the playability of the system and the fineness of the interface, so as to improve the application effect of the system.

4. Conclusion

The development and implementation of the national fitness program is a systematic project and an open, dynamic, and self-organizing system. To maintain the stability of the national fitness system, it must be an open system. It needs to constantly exchange material, energy, and information with the external environment; that is, it needs to constantly attract all sectors of society to participate and invest, introduce excellent sports instructors, and absorb advanced management experience and technology. With the improvement of scientific and technological level and quality of life, people also put forward higher requirements for the professionalism of fitness and pay more and more attention to the information construction of fitness industry. At the same time, the development of massive data management technology and micro service architecture provides an opportunity for the technical transformation of fitness system. Therefore, this paper designs a new national fitness system and proves that the system has good application effect through practical application, which can be further popularized in practice. However, there are still the following aspects to be improved.

(1) Due to the tight time, the business consideration of the system is not perfect. This paper only realizes the basic business functions, but there are other functions, such as online fitness course management, coach recommendation, and so on.

(2) With the continuous popularity of mobile devices, we will study how to expand the fitness system business to the mobile terminal in the future and provide corresponding data interfaces for Android, IOS, and other mobile terminals.

Data Availability

The data used to support the findings of this study are available from the corresponding author upon request.

Conflicts of Interest

The author declares that he has no conflict of interest.

Acknowledgments

The paper did not receive any financial support.

References

[1] A. G. Khan, S. Banik, M. A. Uddin, and S. Moudud-Ul-Huq, "Unlocking the relationship between talent management practices and performance sustainability in the sports industry," *International Journal of Asian Business and Information Management*, vol. 12, no. 3, pp. 366–380, 2021.

[2] J.-H. Yu, H.-H. Lin, J.-M. Huang, C.-H. Wu, and K.-C. Tseng, "Under industry 4.0, the current status of development and trend sports industry combining with cloud technology," *Mathematical Problems in Engineering*, vol. 2020, no. 11, pp. 1–16, 2020.

[3] D. Min, "Perceived service quality, image, trust and word-of-mouth recommendation among participants of National Fitness Awards in South Korea," *Korean Journal of Sport Management*, vol. 26, no. 1, pp. 31–48, 2021.

[4] Q. Z. He, "Mechanism design of bodybuilding and entertainment rehabilitation equipment based on the spatial fixed

Hindawi
Journal of Mathematics
Volume 2024, Article ID 9809684, 1 page
https://doi.org/10.1155/2024/9809684

Retraction

Retracted: Statistical Inferences of Burr XII Lifetime Models under Joint Type-1 Competing Risks Samples

Journal of Mathematics

Received 23 January 2024; Accepted 23 January 2024; Published 24 January 2024

This article has been retracted by Hindawi following an investigation undertaken by the publisher [1]. This investigation has uncovered evidence of one or more of the following indicators of systematic manipulation of the publication process:

(1) Discrepancies in scope

(2) Discrepancies in the description of the research reported

(3) Discrepancies between the availability of data and the research described

(4) Inappropriate citations

(5) Incoherent, meaningless and/or irrelevant content included in the article

(6) Manipulated or compromised peer review

The presence of these indicators undermines our confidence in the integrity of the article's content and we cannot, therefore, vouch for its reliability. Please note that this notice is intended solely to alert readers that the content of this article is unreliable. We have not investigated whether authors were aware of or involved in the systematic manipulation of the publication process.

Wiley and Hindawi regrets that the usual quality checks did not identify these issues before publication and have since put additional measures in place to safeguard research integrity.

We wish to credit our own Research Integrity and Research Publishing teams and anonymous and named external researchers and research integrity experts for contributing to this investigation.

The corresponding author, as the representative of all authors, has been given the opportunity to register their agreement or disagreement to this retraction. We have kept a record of any response received.

References

[1] T. A. Abushal, A. A. Soliman, and G. A. Abd-Elmougod, "Statistical Inferences of Burr XII Lifetime Models under Joint Type-1 Competing Risks Samples," *Journal of Mathematics*, vol. 2021, Article ID 9553617, 16 pages, 2021.

Hindawi
Journal of Mathematics
Volume 2021, Article ID 9553617, 16 pages
https://doi.org/10.1155/2021/9553617

Research Article

Statistical Inferences of Burr XII Lifetime Models under Joint Type-1 Competing Risks Samples

Tahani A. Abushal,[1] **A. A. Soliman**,[2] **and G. A. Abd-Elmougod**[3]

[1]*Department of Mathematical Science, Faculty of Applied Science, Umm AL-Qura University, Mecca, Saudi Arabia*
[2]*Department of Mathematics, Sohag University, Sohag, Egypt*
[3]*Department of Mathematics, Faculty of Science, Damanhour University, Damanhour, Egypt*

Correspondence should be addressed to Tahani A. Abushal; taabushal@uqu.edu.sa

Received 24 September 2021; Accepted 10 November 2021; Published 24 December 2021

Academic Editor: Naeem Jan

The problem of statistical inference under joint censoring samples has received considerable attention in the past few years. In this paper, we adopted this problem when units under the test fail with different causes of failure which is known by the competing risks model. The model is formulated under consideration that only two independent causes of failure and the unit are collected from two lines of production and its life distributed with Burr XII lifetime distribution. So, under Type-I joint competing risks samples, we obtained the maximum likelihood (ML) and Bayes estimators. Interval estimation is discussed through asymptotic confidence interval, bootstrap confidence intervals, and Bayes credible interval. The numerical computations which described the quality of theoretical results are discussed in the forms of real data analyzed and Monte Carlo simulation study. Finally, numerical results are discussed and listed through some points as a brief comment.

1. Introduction

The failure times which are obtained from life testing experiments are exposed in complete or censored data. Therefore, the word complete data is used when the failure time of all units under the test is observed but, under some restrictions of time and cost, the failure time of some not all units is observed. Then, we used the word censoring data when the available lifetime data are taken from some units under the test. Censoring scheme can be done under different forms, and the commonly ones are known by Type-I and Type-II censoring schemes (CSs). In Type-I CS, the test has a prefixed time and random number of failure units. However, in Type-II CS, the test time is random and has prefixed number of failure units. Each of Type-I CS and Type-II CS does not allow to remove unit from the test other than the final point. The availability of removed units from the test at any stage is known by progressive censoring scheme (see Balakrishnan and Aggarwala [1]). Under consideration that units of product are taken from different lines of production under the same facility, the joint censoring scheme appeared. Censoring schemes under joint sample are called joint censoring scheme (JCS). Therefore, we combine the joint censoring scheme with Type-I and Type-II censoring schemes to obtain the Type-I and Type-II joint censoring schemes (Type-I and Type-II JCSs).

The product produced from the different lines of production under the same facilities needs some tests to measure the relative merits in a competing duration. In practice, JCSs are applied on random selection taken from lines of production. Different authors exposed to this problem, for early discussion, such as Rao et al. [2] developed the rank order theory under two-sample censoring scheme, Basu [3] presented and discussed the statistics of rank sets from two-sample scheme called Savage statistic, Johnson and Mehrotra [4] used two-sample problem to preset the locally most powerful rank tests under censored data, Bhattacharyya and Johnson [5] applied two-sample censored situation for asymptotic sufficiency and asymptotically most powerful tests, Mehrotra and Bhattacharyya

[6] measured the equality of two exponential distributions testing under Type-II censoring, and Mehrotra and Bhattacharyya [7] discussed under jointly Type-II censored samples the confidence intervals from two exponential distributions. Also, Balakrishnan and Rasouli [8] presented exact likelihood inferences under jointly censoring schemes, Rasouli and Balakrishnan [9] discussed the exact likelihood inference under joint progressive Type-II censoring for two exponential populations, and Shafay et al. [10] discussed the Bayes inference under joint Type-II censored sample for two exponential populations. And, this problem is handled recently by Al-Matrafi and Abd-Elmougod [11], Momenkhan and Abd-Elmougod [12], Mondal and Kundu [13], and Mondal andKundu [14]. The problem of statistical inference under jointly censoring schemes with the competing risks model is recently discussed by Almarashi et al. [15].

Under Type-I JCS, a sample of size N is randomly selected from two lines of production η_1 and η_2 to satisfy that S_1 is selected from the first line η_1 and S_2 is selected from the second line η_2, and the ideal test time τ is given. The sample of size S_1 taken from the line η_1 has $T_1, T_2, \ldots, T_{S_1}$ lifetimes distributed with PDF and CDF given, respectively, by $f_1(\cdot)$ and $F_1(\cdot)$. Also, S_2 from the line η_2 has $\mathbf{T}_1, \mathbf{T}_2, \ldots, \mathbf{T}_{S_2}$ lifetimes with PDF and CDF given, respectively, by $f_2(\cdot)$ and $F_2(\cdot)$. Under given the test time τ, the ordered life times $\{X_1, X_2, \ldots, X_J\}$, $1 \le J \le N$, obtained from the joint sample $\{T_1, T_2, \ldots, T_{J_1}, \mathbf{T}_1, \mathbf{T}_2, \ldots, \mathbf{T}_{J_2}\}$, $J = J_1 + J_2$, present the Type-I JCS. Therefore, under Type-I JCS, the failure time and the corresponding type of failure (mean from the line η_1 or η_2) are recorded. Hence, the Type-I JCS is given by

$$\mathbf{X} = \{(X_1, v_1), (X_2, v_2), \ldots, (X_J, v_J)\}, \tag{1}$$

where $v_i = 1$ or 0 dependent on the failure from the line η_1 or the line η_2, respectively. Suppose that the integer numbers denoted the number of failure from the line η_1 given by $n_1 = \sum_{i=1}^{J} v_i$ and number of failure from the line η_2 given by $n_2 = \sum_{i=1}^{J} (1 - v_i)$. Hence, the joint likelihood function under $\mathbf{X}$, Type-I JCS, is formulated by

$$L_{1,2,\ldots,J}(\mathbf{X}|\boldsymbol{\omega}) = \frac{S_1! S_2!}{(S_1 - n_1)!(S_2 - n_2)!} \left(\prod_{i=1}^{J} [f_1(x_i)]^{v_i} [f_2(x_i)]^{1-v_i} \right) R_1^{S_1 - n_1}(x_J) R_2^{S_2 - n_2}(x_J), \tag{2}$$

where $R_i(\cdot)$, $i = 1, 2$, mean the reliability functions and ω presents the parameters vector.

In a real-life testing, commonly the failure times of units/individuals may be reported under different causes of failure which is known by the competing risks model. In this problem, our aim is measuring the risk of one cause of failure with respect to other causes. Early, this problem was discussed under exponential populations by Cox [16] and some properties of the competing risks model by Crowder [17], Balakrishnan and Han [18], Modhesh and Abd-Elmougod [19], and Bakoban and Abd-Elmougod [20]. Recently, the properties of the competing risks model under the accelerated life test model were discussed by Ganguly and Kundu [21], Hanaa and Neveen [22], and Algarn et al. [23]. The competing risk problem under Type-I censoring scheme can be described as follows.

Suppose that N unit is put under life testing experiment and the ideal test τ is given under consideration that only two independent causes of failure exist. The failure time and the corresponding cause of failure are recorded, say $\mathbf{X} = \{(X_1, \delta_1), (X_2, \delta_2), \ldots, (X_J, \delta_J)\}$ and $1 \le J \le N$. The joint likelihood function under competing risks Type-I,$\mathbf{X}$, is formulated by

$$L(\mathbf{X}|\boldsymbol{\omega}) = \frac{n!}{(n-J)!} \left(\prod_{i=1}^{J} [h_1(x_i)]^{\mu(\delta_i = 1)} [h_2(x_i)]^{\mu(\delta_i = 2)} R_1(x_i) R_2(x_i) \right) \left(R_1(x_J) R_2(x_J) \right)^{(N-J)}, \tag{3}$$

where

$$\mu(\delta_i = l) = \begin{cases} 1, & \delta_i = l, \\ 0, & \delta_i \ne l, \end{cases} \quad l = 1, 2, \tag{4}$$

$$0 < x_1 < x_2 < \cdots < x_J < \infty. \tag{5}$$

Early, the Burr system is introduced as a system that includes twelve types of cumulative distribution functions (see Burr [24]). Also, the Burr system present a variety of density shapes that are applied in different branches of sciences such as chemical engineering, medical and reliability studies, business, and quality control. The Burr XII distribution which is member of this system has different application in life testing models. The random variable X is called Burr XII random variable if it has cumulative distribution function (CDF) given by

$$F(x) = 1 - \left(1 + x^{\beta}\right)^{-\alpha}, \quad x > 0. \tag{6}$$

Burr XII distribution has unimodal or decreasing failure rate function. Also, the shape of failure rate function is not affected by shape parameters α and has unimodal curve when $\beta > 1$. Also, it has decreasing failure rate function when $\beta \le 1$. Therefore, the shape parameter β is more effective in distribution. Different authors discussed Burr XII such as Rodriguez [25], Lee et al. [26], and recently Hassan and Nada [27].

The product coming from different lines of production is tested under the type of testing known by comparative life tests. When population units or individuals fail under different causes of failure, we have joint competing risks' data as an important source of data. Our aims in this paper are building the statistical inferences of Burr XII life populations based on this competing risk Type-I JCS. Then, we give a complete description for the model formulation considering only two independent causes of failure and the unit life distributed with Burr XII lifetime distribution. The collected data observed under this model are used to estimate the model parameters with maximum likelihood estimation for point and corresponding confidence interval. Also, two confidence intervals with bootstrap-p and bootstrap-t are formulated. The Bayes approach is used to construct the point and credible interval estimations. Different tools are used to measure the quality performance of these estimators. The point estimations were measured under mean squared errors (MSEs). And, the interval estimations were measured under interval length (IL) and probability coverage (PC) through the Monte Carlo simulation study. Also, we analyze the real data set to illustrate our purpose.

The paper is planned as follows. Section 2 discusses general assumptions and modeling. Estimation with MLE, point, and asymptotic confidence intervals is presented in Section 3. Bootstrap confidence intervals are discussed in Section 4. Bayes estimation is presented in Section 5. The real example is used and analyzed in Section 6. Assessment and comparing the numerical results with simulation study are presented in Section 7. The brief comments are summarized in Section 8.

2. Model Formulation

Let a sample of size $N = S_1 + S_2$ be selected from two lines η_1 and η_2 (S_1 from η_1 and S_2 from η_2) for a life testing experiment, and the ideal test time τ is proposed. When the experiment is running, the failure time X and the corresponding type υ as well as cause of failure δ are reported. The experiment is continual until τ is observed; then, we can say $(X_i, \upsilon_i, \delta_i)$, $i = 1, 2, \ldots, J$, are observed. Therefore, the random set $\mathbf{X} = \{(X_1, \upsilon_1, \delta_1), (X_2, \upsilon_2, \delta_2), \ldots, (X_J, \upsilon_J, \delta_J)\}$, and $1 \le J \le N$ is called Type-I joint competing risks sample (Type-I JCRS). Therefore, under Type-I JCRS, we have the following assumption:

(1) The number $n_1 = \sum_{i=1}^{J} \upsilon_i$ present number of failure from the line η_1.

(2) The number $n_2 = \sum_{i=1}^{J} (1 - \upsilon_i)$ present number of failure from the line η_2.

(3) The number $m_{1j} = \sum_{i=1}^{J} \upsilon_i * \mu(\delta_i = j)$ present number of failure from the line η_1 and cause j.

(4) The number $m_{2j} = \sum_{i=1}^{J} (1 - \upsilon_i) * \mu(\delta_i = j)$ present number of failure from the line η_2 and cause j. Hence, the joint likelihood function of Type-I JCRS $\mathbf{X} = \{(X_1, \upsilon_1, \delta_1), (X_2, \upsilon_2, \delta_2), \ldots, (X_J, \upsilon_J, \delta_J)\}$ is formulated by

$$
\begin{aligned}
L_{1,2,\ldots,J}(\mathbf{X}|\boldsymbol{\omega}) \propto \prod_{i=1}^{J} \Big\{ \Big[[h_{11}(x_i)]^{\mu(\delta_i=1)} [h_{12}(t_i)]^{\mu(\delta_i=2)} R_{11}(x_i) R_{12}(x_i) \Big]^{\upsilon_i} \\
\times [h_{21}(x_i)]^{\mu(\delta_i=1)} [h_{22}(t_i)]^{\mu(\delta_i=2)} R_{21}(x_i) R_{22}(x_i) \Big\}^{1-\upsilon_i} \\
\times \left[R_{11}(x_J) R_{12}(x_J) \right]^{S_1 - n_1} \left[R_{21}(x_J) R_{22}(x_J) \right]^{S_2 - n_2},
\end{aligned}
\tag{7}
$$

where $\mu(\delta_i = l)$ is given by (4).

(5) If k defines the unit type, then the observed failure time $x_i = \min\{x_{ik1}, x_{ik2}\}$, $i = 1, 2, \ldots, J$.

(6) The CDF of random variable X_{ikj} of Burr XII lifetime distribution is given by

$$
F_{kj}(x) = 1 - \left(1 + x^{\beta_k}\right)^{-\alpha_{kj}}, \quad x > 0, \beta_k, \alpha_{kj} > 0, k, j = 1, 2. \tag{8}
$$

(7) The minimum value has distribution given by $F_{k1}(\cdot) + F_{k2}(\cdot) - F_{k1}(\cdot) * F_{k2}(\cdot)$. Therefore, the latent failure time is distributed with Burr XII distributions with shape parameters β_k and $\alpha_{k1} + \alpha_{k2}$.

(8) The discrete random variables m_{1j} and m_{2j} have the binomial distributions given by

$$
\begin{aligned}
m_{1j} &\longrightarrow \text{binomial}\left(n_j, \frac{\alpha_{k1}}{\alpha_{k1} + \alpha_{k2}} \right), \\
m_{2j} &\longrightarrow \text{binomial}\left(n_j, \frac{\alpha_{k2}}{\alpha_{k1} + \alpha_{k2}} \right).
\end{aligned}
\tag{9}
$$

3. Maximum Likelihood Estimation

The model parameters in this section are discussed under given Type-I JCRS from Burr XII distribution. The joint likelihood function (7) is reduced to

$$L(\boldsymbol{\omega}|\mathbf{X}) \propto \prod_{i=1}^{J}\left[x_i^{\beta_1-1}\left(1+x_i^{\beta_1}\right)^{-(\alpha_{11}+\alpha_{12}+1)}\right]^{v_i}\left[x_i^{\beta_2-1}\left(1+x_i^{\beta_2}\right)^{-(\alpha_{21}+\alpha_{22}+1)}\right]^{1-v_i} \times \left(1+x_J^{\beta_1}\right)^{-(S_1-n_1)(\alpha_{11}+\alpha_{12})}\left(1+x_J^{\beta_2}\right)^{-(S_2-n_2)(\alpha_{21}+\alpha_{22})} \times \beta_1^{n_1}\beta_2^{n_2}\alpha_{11}^{m_{11}}\alpha_{12}^{m_{12}}\alpha_{21}^{m_{21}}\alpha_{22}^{m_{22}}x_J^{\beta_1-1}x_J^{\beta_2-1}, \tag{10}$$

where $\omega = \{\beta_1, \beta_2, \alpha_{11}, \alpha_{12}, \alpha_{21}, \alpha_{22}\}$ and $\mathbf{X}$ be Type-I JCRS. Function (10) after taking the natural logarithm is reduced to

$$\begin{aligned}\ell(\boldsymbol{\omega}|\mathbf{X}) &= n_1\log\beta_1 + n_2\log\beta_2 + m_{11}\log\alpha_{11} + m_{12}\log\alpha_{12} + m_{21}\log\alpha_{21} + m_{22}\log\alpha_{22} \\ &+ (\beta_1-1)\sum_{i=1}^{J} v_i\log x_i - (\alpha_{11}+\alpha_{12}+1)\sum_{i=1}^{J} v_i\log\left(1+x_i^{\beta_1}\right) \\ &+ (\beta_2-1)\sum_{i=1}^{J}(1-v_i)\log x_i - (\alpha_{21}+\alpha_{22}+1)\sum_{i=1}^{J}(1-v_i)\log\left(1+x_i^{\beta_2}\right) \\ &- (S_1-n_1)(\alpha_{11}+\alpha_{12})\log\left(1+x_J^{\beta_1}\right) - (S_2-n_2)(\alpha_{21}+\alpha_{22})\log\left(1+x_J^{\beta_2}\right).\end{aligned} \tag{11}$$

3.1. Point Estimation. From the log-likelihood function, we obtain the likelihood equations by taking the first partially derivatives respective to the model parameters as follows:

$$\begin{aligned}\frac{\partial\ell(\boldsymbol{\omega}|\mathbf{X})}{\partial\alpha_{1j}} &= \frac{m_{1j}}{\alpha_{1j}} - \sum_{i=1}^{J} v_i\log\left(1+x_i^{\beta_1}\right) - (S_1-n_1)\log\left(1+x_J^{\beta_1}\right) = 0, \\ \frac{\partial\ell(\boldsymbol{\omega}|\mathbf{X})}{\partial\alpha_{2j}} &= \frac{m_{2j}}{\alpha_{2j}} - \sum_{i=1}^{J}(1-v_i)\log\left(1+x_i^{\beta_2}\right) - (S_2-n_2)\log\left(1+x_J^{\beta_2}\right) = 0,\end{aligned} \tag{12}$$

which reduced to

$$\widehat{\alpha}_{1j}(\beta_1) = \frac{m_{1j}}{\sum_{i=1}^{J} v_i\log\left(1+x_i^{\beta_1}\right) + (S_1-n_1)\log\left(1+x_J^{\beta_1}\right)}, \tag{13}$$

$$\widehat{\alpha}_{2j}(\beta_2) = \frac{m_{2j}}{\sum_{i=1}^{J}(1-v_i)\log\left(1+x_i^{\beta_2}\right) + (S_2-n_2)\log\left(1+x_J^{\beta_2}\right)}. \tag{14}$$

And the derivatives with respect to β_k are reduced to the likelihood equations as follows:

$$\frac{\partial\ell(\boldsymbol{\omega}|\mathbf{X})}{\partial\beta_k} = 0, \quad k = 1, 2, \tag{15}$$

which reduced to

$$\frac{n_1}{\beta_1} + \sum_{i=1}^{J} v_i\log x_i - (\alpha_{11}+\alpha_{12}+1)\sum_{i=1}^{J}\frac{v_i x_i^{\beta_1}\log x_i}{1+x_i^{\beta_1}} - \frac{(S_1-n_1)(\alpha_{11}+\alpha_{12})x_J^{\beta_1}\log x_J}{1+x_J^{\beta_1}} = 0, \tag{16}$$

$$\frac{n_2}{\beta_2} + \sum_{i=1}^{J}(1-v_i)\log x_i - (\alpha_{21}+\alpha_{22}+1)\sum_{i=1}^{J}\frac{v_i x_i^{\beta_2}\log x_i}{1+x_i^{\beta_2}} - \frac{(S_2-n_2)(\alpha_{21}+\alpha_{22})x_J^{\beta_2}\log x_J}{1+x_J^{\beta_2}} = 0. \tag{17}$$

Equations (13) to (17) have shown that the problem of obtaining the ML estimate of model parameters needs to solve two nonlinear equations (16) and (17) to obtain $\widehat{\beta}_k$, $k = 1, 2$. Different iteration methods can be applied such as

Newton–Raphson or fixed point iteration with initial value can be obtained from the profile log-likelihood (11) after replacing the parameters α_{kj} of equations (13) and (14) as follows:

$$\begin{aligned} f(\beta_1,\beta_2|\mathbf{X}) &= n_1\log\beta_1 + n_2\log\beta_2 + m_{11}\log\widehat{\alpha}_{11}(\beta_1) + m_{12}\log\widehat{\alpha}_{12}(\beta_1) \\ &+ m_{21}\log\widehat{\alpha}_{21}(\beta_2) + m_{22}\log\widehat{\alpha}_{22}(\beta_2) + (\beta_1-1)\sum_{i=1}^{J} v_i\log x_i \\ &- (\widehat{\alpha}_{11}(\beta_1) + \widehat{\alpha}_{12}(\beta_1) + 1)\sum_{i=1}^{J} v_i\log\left(1+x_i^{\beta_1}\right) + (\beta_2-1) \\ &\times \sum_{i=1}^{J}(1-v_i)\log x_i - (\widehat{\alpha}_{21}(\beta_2) + \widehat{\alpha}_{22}(\beta_2) + 1)\sum_{i=1}^{J}(1-v_i) \\ &\times \log\left(1+x_i^{\beta_2}\right) - (S_1-n_1)(\widehat{\alpha}_{11}(\beta_1) + \widehat{\alpha}_{12}(\beta_1))\log\left(1+x_J^{\beta_1}\right) \\ &- (S_2-n_2)(\widehat{\alpha}_{21}(\beta_2) + \widehat{\alpha}_{22}(\beta_2))\log\left(1+x_J^{\beta_2}\right). \end{aligned} \tag{18}$$

Also, the ML estimate of parameters $\widehat{\alpha}_{kj}$ is obtained from (13) and (14) after replacing β_k by $\widehat{\beta}_k$.

Remark 1. The equations from (13) to (17) showed that the conditional estimators of the model parameters depend on the discrete random variable m_{kj}. Hence, the estimate $\widehat{\alpha}_{1j}$ and $\widehat{\alpha}_{2j}$ does not exist for $m_{1j} = 0$ or J and $m_{2j} = 0$ or J, respectively. And, the problem of exact distributions for estimators $\widehat{\alpha}_{1j}$ and $\widehat{\alpha}_{2j}$ is defined as mixture of discrete and continuous distributions, hence as given in Kundu and Joarder [28] is difficult to obtain.

3.2. Interval Estimation. The asymptotic confidence intervals of model parameters depend on the second partial derivative of the log-likelihood function (11) and hence information matrix (see Salah [29]). And, the Fisher information matrix of the model parameters is defined as the minus expectation of the second partial derivatives which is presented as follows:

$$\begin{aligned} \frac{\partial^2\ell(\boldsymbol{\omega}|\mathbf{X})}{\partial\beta_1^2} &= \frac{-n_1}{\beta_1^2} - (\alpha_{11}+\alpha_{12}+1)\sum_{i=1}^{J} v_i\frac{x_i^{\beta_1}(\log x_i)^2}{\left(1+x_i^{\beta_1}\right)^2} \\ &- \frac{(S_1-n_1)(\alpha_{11}+\alpha_{12})x_J^{\beta_1}\left(\log x_J\right)^2}{\left(1+x_J^{\beta_1}\right)^2}, \\ \frac{\partial^2\ell(\boldsymbol{\omega}|\mathbf{X})}{\partial\beta_2^2} &= \frac{-n_2}{\beta_2^2} - (\alpha_{21}+\alpha_{22}+1)\sum_{i=1}^{J}(1-v_i)\frac{x_i^{\beta_2}(\log x_i)^2}{\left(1+x_i^{\beta_2}\right)^2} \\ &- \frac{(S_1-n_1)(\alpha_{21}+\alpha_{22})x_J^{\beta_2}\left(\log x_J\right)^2}{\left(1+x_J^{\beta_2}\right)^2}, \\ \frac{\partial^2\ell(\boldsymbol{\omega}|\mathbf{X})}{\partial\alpha_{kj}^2} &= \frac{-m_{kj}}{\alpha_{kj}^2}\Big|_{k,j=1,2}, \\ \frac{\partial^2\ell(\boldsymbol{\omega}|\mathbf{X})}{\partial\alpha_{kj}\partial\alpha_{il}} &= 0, \quad \text{For each } kj \neq il, \\ \frac{\partial^2\ell(\boldsymbol{\omega}|\mathbf{X})}{\partial\beta_1\partial\alpha_{1j}} &= \frac{\partial^2\ell(\boldsymbol{\omega}|\mathbf{X})}{\partial\alpha_{1j}\partial\beta_1} = -\sum_{i=1}^{J}\frac{v_i x_i^{\beta_1}\log x_i}{1+x_i^{\beta_1}} - \frac{(S_1-n_1)x_J^{\beta_1}\log x_J}{1+x_J^{\beta_1}}, \quad j=1,2, \\ \frac{\partial^2\ell(\boldsymbol{\omega}|\mathbf{X})}{\partial\beta_2\partial\alpha_{2j}} &= \frac{\partial^2\ell(\boldsymbol{\omega}|\mathbf{X})}{\partial\alpha_{2j}\partial\beta_2} = -\sum_{i=1}^{J}\frac{(1-v_i)x_i^{\beta_2}\log x_i}{1+x_i^{\beta_2}} - \frac{(S_2-n_2)x_J^{\beta_2}\log x_J}{1+x_J^{\beta_2}}, \quad j=1,2, \\ \frac{\partial^2\ell(\boldsymbol{\omega}|\mathbf{X})}{\partial\beta_1\partial\alpha_{2j}} &= \frac{\partial^2\ell(\boldsymbol{\omega}|\mathbf{X})}{\partial\beta_2\partial\alpha_{1j}} = \frac{\partial^2\ell(\boldsymbol{\omega}|\mathbf{X})}{\partial\alpha_{2j}\partial\beta_1} = \frac{\partial^2\ell(\boldsymbol{\omega}|\mathbf{X})}{\partial\alpha_{1j}\partial\beta_2} = \frac{\partial^2\ell(\boldsymbol{\omega}|\mathbf{X})}{\partial\beta_1\partial\beta_2} \\ &= \frac{\partial^2\ell(\boldsymbol{\omega}|\mathbf{X})}{\partial\beta_2\partial\beta_1} = 0. \end{aligned} \tag{19}$$

Suppose that the fisher information matrix is defined by $\Psi(\beta_1, \beta_2, \alpha_{11}, \alpha_{12}, \alpha_{21}, \alpha_{22})$, where

$$\Psi(\beta_1, \beta_2, \alpha_{11}, \alpha_{12}, \alpha_{21}, \alpha_{22}) = -E\left(\frac{\partial^2 \ell(\boldsymbol{\omega}|\mathbf{X})}{\partial \omega_i \partial \omega\ l}\right), \quad i, l = 1, 2, \ldots, 6, \tag{20}$$

where $\omega = (\beta_1, \beta_2, \alpha_{11}, \alpha_{12}, \alpha_{21}, \alpha_{22})$ be the model parameters. Equation (19) has shown that the expectations of the second derivative of the log likelihood function are more serious. Therefore, we applied the approximate information matrix $\widehat{\Psi}_0(\widehat{\beta}_1, \widehat{\beta}_2, \widehat{\alpha}_{11}, \widehat{\alpha}_{12}, \widehat{\alpha}_{21}, \widehat{\alpha}_{22})$ defined by

$$\widehat{\Psi}_0\left(\widehat{\beta}_1, \widehat{\beta}_2, \widehat{\alpha}_{11}, \widehat{\alpha}_{12}, \widehat{\alpha}_{21}, \widehat{\alpha}_{22}\right) = \left(\frac{\partial^2 \ell(\boldsymbol{\omega}|\mathbf{X})}{\partial \omega_i \partial \omega\ l}\right)\Bigg|_{\widehat{\beta}_1, \widehat{\beta}_2, \widehat{\alpha}_{11}, \widehat{\alpha}_{12}, \widehat{\alpha}_{21}, \widehat{\alpha}_{22}}, \quad i, l = 1, 2, \ldots, 6. \tag{21}$$

Therefore, $\widehat{\Psi}_0^{-1}(\widehat{\beta}_1, \widehat{\beta}_2, \widehat{\alpha}_{11}, \widehat{\alpha}_{12}, \widehat{\alpha}_{21}, \widehat{\alpha}_{22})$ exists with nonzero values of the elements of diagonal. Under normal properties of $(\widehat{\beta}_1, \widehat{\beta}_2, \widehat{\alpha}_{11}, \widehat{\alpha}_{12}, \widehat{\alpha}_{21}, \widehat{\alpha}_{22})$, the approximate $(1 - 2\theta)\%$ confidence intervals of the parameters $\beta_1, \beta_2, \alpha_{11}, \alpha_{12}, \alpha_{21}$, and α_{22} are given by

$$\begin{cases} \widehat{\beta}_1 \mp z_\theta \epsilon_{11}, & \widehat{\beta}_2 \mp z_\theta \epsilon_{22}, \\ \widehat{\alpha}_{11} \mp z_\theta \epsilon_{33}, & \widehat{\alpha}_{12} \mp z_\theta \epsilon_{44}, \\ \widehat{\alpha}_{21} \mp z_\theta \epsilon_{55}, & \widehat{\alpha}_{22} \mp z_\theta \epsilon_{66}, \end{cases} \tag{22}$$

where ϵ_{il} is the element of diagonal of the invariance approximate information matrix $\widehat{\Psi}_0^{-1}(\widehat{\beta}_1, \widehat{\beta}_2, \widehat{\alpha}_{11}, \widehat{\alpha}_{12}, \widehat{\alpha}_{21}, \widehat{\alpha}_{22})$ with significant level θ.

4. Bootstrap Confidence Intervals

In this section, we discussed a bootstrap technique in statistical inference problem about parameters estimation. This technique is a commonly resembling method not only in parameter estimation but also used to estimate bias and variance of an estimator or calibrate hypothesis tests. The bootstrap technique is defined in parametric and nonparametric methods (see Davison and Hinkley [30] and Efron and Tibshirani [31]). Therefore, we adopted parametric bootstrap technique to build two different confidence intervals, percentile bootstrap technique, and bootstrap-t technique. For more details, see Efron [32] and Hall [33]. The following algorithms are used to describe the procedure that is used to build different two bootstrap confidence intervals:

(1) Under consideration that the original observed Type-I JCRS $\mathbf{X} = \{(X_1, \upsilon_1, \delta_1), (X_2, \upsilon_2, \delta_2), \ldots, (X_J, \upsilon_J, \delta_J)\}$, the estimates are obtained and given by $\widehat{\omega} = (\widehat{\beta}_1, \widehat{\beta}_2, \widehat{\alpha}_{11}, \widehat{\alpha}_{12}, \widehat{\alpha}_{21}, \widehat{\alpha}_{22})$.

(2) For given $\widehat{\omega}$ and integer values of $N, S_1\ S_2$, and time τ, generate a sample of size S_1 from Burr XII distribution with shape parameters $\widehat{\beta}_1$ and $\widehat{\alpha}_{11} + \widehat{\alpha}_{12}$ and a sample of size S_2 from Burr XII distribution with shape parameters $\widehat{\beta}_2$ and $\widehat{\alpha}_{21} + \widehat{\alpha}_{22}$. The τ-bootstrap Type-I JCRS is obtained from the generated joint sample as a small J satisfies that $X_J < \tau$ denoted by $\mathbf{X} = \{(X_1^*, \upsilon_1, \delta_1), (X_2^*, \upsilon_2, \delta_2), \ldots, (X_J^*, \upsilon_J, \delta_J)\}$.

(3) From Step 2, the two numbers n_1^* and n_2^* (number of failure taken from line η_1 and η_2, respectively) are obtained.

(4) The four numbers m_{1j}^* and m_{2j}^*, $j = 1, 2$, are randomly generated from binomial distribution with size $J - n_{3-k}^*$ and probability $(\widehat{\alpha}_{kj}/(\widehat{\alpha}_{k1} + \widehat{\alpha}_{k2}))$, $k, j = 1, 2$.

(5) The bootstrap estimate sample $\widehat{\omega}^* = (\widehat{\beta}_1^*, \widehat{\beta}_2^*, \widehat{\alpha}_{11}^*, \widehat{\alpha}_{12}^*, \widehat{\alpha}_{21}^*, \widehat{\alpha}_{22}^*)$ is obtained.

(6) Repeat Steps 2 to 5 $\mathbf{M}$ times.

(7) The values $(\widehat{\beta}_1^{[i]*}, \widehat{\beta}_2^{[i]*}, \widehat{\alpha}_{11}^{[i]*}, \widehat{\alpha}_{12}^{[i]*}, \widehat{\alpha}_{21}^{[i]*}, \widehat{\alpha}_{22}^{[i]*})$, $i = 1, 2, \ldots, \mathbf{M}$, are arranged in ascending order to obtain $\widetilde{\omega}^* = (\widehat{\beta}_1^{(i)*}, \widehat{\beta}_2^{(i)*}, \widehat{\alpha}_{11}^{(i)*}, \widehat{\alpha}_{12}^{(i)*}, \widehat{\alpha}_{21}^{(i)*}, \widehat{\alpha}_{22}^{(i)*})$.

4.1. Percentile Bootstrap Confidence Interval (PBCI). Suppose that the ordered sample described by distribution $\Phi(x) = P(\widetilde{\omega}_l^* \le x)$, $l = 1, 2, 3, 4, 5, 6$, be cumulative distribution function of $\widetilde{\omega}_l^*$, where $\widetilde{\omega}_1^*$ mean $\widetilde{\beta}_1^*$ and others. So, the point bootstrap estimate is defined by

$$\widehat{\boldsymbol{\omega}}_l^* = \frac{1}{\mathbf{M}} \sum_{i=1}^{\mathbf{M}} \widetilde{\boldsymbol{\omega}}_l^{(i)*}. \tag{23}$$

Also, the $100(1 - 2\theta)\%$ PBCIs are given by

$$\left(\widetilde{\boldsymbol{\omega}}_{l\text{boot}(\theta)}^*, \widetilde{\boldsymbol{\omega}}_{l\text{boot}(1-\theta)}^*\right), \tag{24}$$

where $\widetilde{\omega}_{l\text{boot}}^* = \Phi^{-1}(x)$.

4.2. Bootstrap-t Confidence Interval (PTCI). From the order sample $\widetilde{\omega}^* = (\widehat{\beta}_1^{(i)*}, \widehat{\beta}_2^{(i)*}, \widehat{\alpha}_{11}^{(i)*}, \widehat{\alpha}_{12}^{(i)*}, \widehat{\alpha}_{21}^{(i)*}, \widehat{\alpha}_{22}^{(i)*})$, we built the order statistics values $\Phi_l^{*(1)} < \Phi_l^{*(2)} < \cdots < \Phi_l^{*(\mathbf{M})}$, where

$$\Phi_l^{*[i]} = \frac{\widetilde{\boldsymbol{\omega}}_1^{(i)*} - \widehat{\boldsymbol{\omega}}_1}{\sqrt{\mathrm{var}\left(\widetilde{\boldsymbol{\omega}}_1^{(i)*}\right)}}, \quad i = 1, 2, \ldots, \mathbf{M}, l = 1, 2, 3, 4, 5, 6. \tag{25}$$

The $100(1-2\theta)\%$ PTCIs are given by

$$\left(\widetilde{\boldsymbol{\omega}}^*_{l\mathrm{boot}-t(\theta)}, \widetilde{\boldsymbol{\omega}}^*_{l\mathrm{boot}-t(1-\theta)}\right), \tag{26}$$

where the value $\widetilde{\omega}^*_{l\mathrm{boot}-t}$ is given by

$$\widetilde{\boldsymbol{\omega}}^*_{l\mathrm{boot}-t} = \widehat{\boldsymbol{\omega}}^*_l + \sqrt{\mathrm{Var}\left(\widehat{\boldsymbol{\omega}}_l\right)}\Phi^{-1}(x), \tag{27}$$

and $\Phi(x) = P(\widetilde{\omega}^*_l \le x)$ be the cumulative distribution function of $\widetilde{\omega}^*_l$.

5. Bayesian MCMC Estimation

In this section, we adopted Bayesian approach to estimate the model parameters under Type-I JCRS (see Ullah and Aslam [34]). So, we suppose that the prior information available about the parameters are independent Gamma prior distributions. Therefore, for parameters vectors $\omega = (\beta_1, \beta_2, \alpha_{11}, \alpha_{12}, \alpha_{21}, \alpha_{22})$, the prior information is defined by

$$P_i^*(\omega_i) = \frac{b_i^{a_i}}{\Gamma(a_i)}\omega_i^{a_i-1}\exp(-b_i\omega_i), \quad \omega_i > 0, (a_i, b_i > 0), i = 1, 2, 3, 4, 5, 6. \tag{28}$$

And the corresponding density is defined by

$$P^*(\boldsymbol{\omega}) \propto \prod_{i=1}^{6}\omega_i^{a_i-1}\exp\left(-b_{i\boldsymbol{\omega}_i}\right). \tag{29}$$

Therefore, the posterior distribution can be formulated by using (10) and (29) as follows:

$$\begin{aligned} P(\omega|\mathbf{X}) \propto{}& \beta_1^{n_1+a_1-1}\beta_2^{n_2+a_1-1}\alpha_{11}^{m_{11}+a_1-1}\alpha_{12}^{m_{12}+a_1-1}\alpha_{21}^{m_{21}+a_1-1}\alpha_{22}^{m_{22}+a_1-1}x_J^{\beta_1-1}x_J^{\beta_2-1}\exp\{-b_1\beta_1 \\ &- b_2\beta_2 - b_3\alpha_{11} - b_4\alpha_{12} - b_5\alpha_{21} - b_6\alpha_{22} + (\beta_1-1)\sum_{i=1}^{J}v_i\log x_i \\ &- (\alpha_{11}+\alpha_{12}+1)\sum_{i=1}^{J}v_i\log\left(1+x_i^{\beta_i}\right) + (\beta_2-1)\sum_{i=1}^{J}(1v_i)\log x_i \\ &- (\alpha_{21}+\alpha_{22}+1)\sum_{i=1}^{J}(1-v_i)\log\left(1+x_i^{\beta_2}\right) - (S_1-n_1)(\alpha_{11}+\alpha_{12}) \\ &\times\log\left(1+x_J^{\beta_1}\right) - (S_2-n_2)(\alpha_{21}+\alpha_{22})\log\left(1+x_J^{\beta_2}\right)\}. \end{aligned} \tag{30}$$

The full conditional distributions are obtained from the joint posterior distribution (29), as follows:

$$\begin{aligned} P_1(\beta_1|\omega_{-1}, \mathbf{X}) \propto{}& \beta_1^{n_1+a_1-1}\exp\left\{-b_1\beta_1 + (\beta_1-1)\sum_{i=1}^{J}v_i\log x_i - (\alpha_{11}+\alpha_{12}+1)\right. \\ &\left.\times\sum_{i=1}^{J}v_i\log\left(1+x_i^{\beta_1}\right) - (S_1-n_1)(\alpha_{11}+\alpha_{12})\log\left(1+x_J^{\beta_1}\right)\right\}, \end{aligned} \tag{31}$$

$$\begin{aligned} P_2(\beta_2|\omega_{-1}, \mathbf{X}) \propto{}& \beta_2^{n_1+a_2-1}\exp\left\{-b_2\beta_2 + \beta_2\sum_{i=1}^{J}(1-v_i)\log x_i - (\alpha_{21}+\alpha_{22}+1)\right. \\ &\left.\times\sum_{i=1}^{J}(1-v_i)\log\left(1+x_i^{\beta_2}\right) - (S_2-n_2)(\alpha_{21}+\alpha_{22})\log\left(1+x_J^{\beta_2}\right)\right\}, \end{aligned} \tag{32}$$

and the full conditional distributions of parameters α_{kj} are gamma distributions given as

$$P_3\left(\alpha_{1j}|\omega_{-1},\mathbf{X}\right)\propto \text{Gamma}\left[m_{1j}+a_{j+2},b_{j+2}+\sum_{i=1}^{J}v_i\log\left(1+x_i^{\beta_1}\right)+\left(S_1-n_1\right)\log\left(1+x_J^{\beta_1}\right)\right],\quad j=1,2, \tag{33}$$

$$P_4\left(\alpha_{2j}|\omega_{-1},\mathbf{X}\right)\propto \text{Gamma}\left[m_{2j}+a_{j+4},b_{j+4}+\sum_{i=1}^{J}\left(1-v_i\right)\log\left(1+x_i^{\beta_2}\right)+\left(S_2-n_2\right)\log\left(1+x_J^{\beta_2}\right)\right],\quad j=1,2, \tag{34}$$

where the conditional value $\omega_i|\omega_{-1}$ means that the conditional i-th parameter for given the parameter vector ω without the i-th parameter ω_i. The point and interval estimate of model parameters under MCMC methods depend on the forms of full conditional distributions and the subclass of MCMC that can be applied. Therefore, full conditional distribution given by (31) to (34) has shown that we can use the algorithms of Gibbs and generally Metropolis Hasting (MH) under Gibbs (for more details, see [35]) described in Algorithm 1.

The problem of generation under the MCMC method needs to determine the number of iteration needed to reach stationary distribution (burn-in) which is defined by $\mathbf{M}^*$. Therefore, the point estimate is reduced to

$$\widetilde{\omega}_{lB}=E_P\left(\omega_l|X\right)=\frac{1}{\mathbf{M}-\mathbf{M}^*}\sum_{i=\mathbf{M}^*+1}^{\mathbf{M}}\omega_l^{(i)},\quad l=1,2,3,4,5,6, \tag{35}$$

and the corresponding variance is reduced to

$$\widehat{V}\left(\omega_l|X\right)=\frac{1}{\mathbf{M}-\mathbf{M}^*}\sum_{i=\mathbf{M}^*+1}^{\mathbf{M}}\left(\omega_l^{(i)}-\widetilde{\omega}_{lB}\right)^2. \tag{36}$$

Also, $100\left(1-2\theta\right)\%$ credible intervals are obtained from ordered vectors given by

$$\left(\omega_{l\theta(\mathbf{M}-\mathbf{M}^*)},\omega_{l(1-\theta)(\mathbf{M}-\mathbf{M}^*)}\right). \tag{37}$$

6. Real Data Analysis

In this section, we analyzed a real data set presented by Hoel [36] to present the failure times and the corresponding cause of failure for two groups of strain male mice under laboratory experiment received a radiation dose of 300r at an age of 5-6 weeks. The life data are presented in Table 1, and let η_1 be considered as the first group which lived in a conventional laboratory environment, but η_2 be the second group lived in a germ-free environment. The data are classified into two causes of failure: thymic lymphoma with reticulum cell sarcoma as the first cause of death (failure) and the second cause is presented by other causes of death (failure); more details are presented by Koley and Kundu [37]. For simplicity, the data are divided by 1000.

Therefore, the observed Type-I JCRS is taken from two lines of production η_1 and η_2 under censoring scheme $N=181, S_1=99, S_2=82$, and $\tau=0.50$ and is reported in Table 2. The data given in Table 2 show that $(n_1,n_2)=(50,30)$, $(m_{11},m_{12},m_{21},m_{22})=(26,24,25,5)$, and $J=80$. Figure 1 shows the joint profile log-likelihood function (18), and the value (2, 2) is a suitable initial value needed in the iteration method. The point estimate under ML, bootstrap, and Bayes estimators for noninformative prior information (mean $a_i=b_i=0.0001$, $i=1,2,3,4,5,6$) is reported in Table 3. And, the corresponding 95% approximate ML, two bootstrap confidence (Bootstrap-p and Bootstrap-t), and credibly intervals are, respectively, reported in Table 4. The generation results of full conditional distribution as a generation from posterior distribution and its convergence for Bayesian approach under MCMC methods are described in Figures 2 to 7 which have shown the quality of posterior generation.

7. Simulation Studies

The proposed model and its theoretical results in section are assessed and compared through the Monte Carlo study. So, we built this study to measure the effect of changing each of random sample size $N=S_1+S_2$, the test time τ, and parameters values. The values of sample size and the corresponding test time used in simulation study are reported in Tables 5 to 8. However, for the parameter values choosing, we used two sets, $\omega=\{2.0,1.2,1.3,1.8,2.0,2.0\}$ and {1.0, 2.0, 3.0, 2.0, 2.5, 1.0}. In our studying, we generate 1000 simulated data sets. The prior parameters are selected to satisfy the property that $E\ (\omega_i)\simeq(a_i/b_i)$ and information presented with two cases noninformative defined by P_0^* and informative prior P_1^*. The informative prior P_1^* is taken to be (a, b) = {(3, 0.8), (2, 1.5), (2, 2), (2, 1), (3, 1.5), (4, 2)} for the first selected parameter values. And the informative prior information for the second selection of the parameters values is (a, b) = {(2, 2), (2, 2), (3, 1.2), (4, 2), (4, 1.5), (1, 1)}. Also, through this problem, mean estimate (ME) and the corresponding mean squared error (MSE) are used to measure the

(1) Put $\xi = 1$ and $\omega^{(0)} = (\widehat{\beta}_1, \widehat{\beta}_2, \widehat{\alpha}_{11}, \widehat{\alpha}_{12}, \widehat{\alpha}_{21}, \widehat{\alpha}_{22})$ as initial values
(2) The parameters α_{kj} are generated from Gamma distributions (32) and (33)
(3) With normal proposal distribution with the accepted rejection method with mean $\beta_k^{(\xi-1)}$ and variances ϵ_i, generate $\beta_i^{(\xi)}$, $i = 1, 2$
(4) Put $\xi = \xi + 1$
(5) Steps 2 to 4 are repeated M times and report the vector $\omega^{(\xi)} = (\beta_1^{(\xi)}, \beta_2^{(\xi)}, \alpha_{11}^{(\xi)}, \alpha_{12}^{(\xi)}, \alpha_{21}^{(\xi)}, \alpha_{22}^{(\xi)})$

Algorithm 1: MH under Gibbs algorithms.

Table 1: Time-to-failure of male mice which received a radiation dose at age 5-6 weeks.

η_1	Thymic lymphoma	159	189	191	198	200	207	220	235	245	250	256
		261	265	266	280	343	356	383	403	414	428	432
		317	318	399	495	525	536	549	552	554	557	558
	Reticulum cell sarcoma	571	586	594	596	605	612	621	628	631	636	643
		647	648	649	661	663	666	670	695	697	700	705
		712	713	738	748	753						
	Other cases	40	42	51	62	163	179	206	222	228	249	252
		282	324	333	341	366	385	407	420	431	441	461
		462	482	517	517	524	564	567	586	619	620	621
		622	647	651	686	761	763					
η_2	Thymic lymphoma	158	192	193	194	195	202	212	215	229	230	237
		240	244	247	259	300	301	321	337	415	434	444
		485	496	529	537	624	707	800				
	Reticulum cell sarcoma	430	590	606	638	655	679	691	693	696	747	752
		760	778	821	986							
	Other cases	136	246	255	376	421	565	616	617	652	655	658
		660	662	675	681	734	736	737	757	769	777	800
		807	825	855	857	864	868	870	873	882	895	910
		934	942	1015	1019							

Table 2: Type-I JCRS from heal data with $\tau = 0.5$.

Data	0.040	0.042	0.051	0.062	0.136	0.158	0.159	0.163	0.179	0.189
	0.191	0.192	0.193	0.194	0.195	0.198	0.200	0.202	0.206	0.207
	0.212	0.215	0.220	0.222	0.228	0.229	0.230	0.235	0.237	0.240
	0.244	0.245	0.246	0.247	0.249	0.250	0.252	0.255	0.256	0.259
	0.261	0.265	0.266	0.280	0.282	0.300	0.301	0.317	0.318	0.321
	0.324	0.333	0.337	0.341	0.343	0.356	0.366	0.376	0.383	0.385
	0.399	0.403	0.407	0.414	0.415	0.42	0.421	0.428	0.430	0.431
	0.432	0.434	0.441	0.444	0.461	0.462	0.482	0.485	0.495	0.496
(η_1 or η_2)	1	1	1	1	0	0	1	1	1	1
	1	0	0	0	0	1	1	0	1	1
	0	0	1	1	1	0	0	1	0	0
	0	1	0	0	1	1	1	0	1	0
	1	1	1	1	1	0	0	1	1	0
	1	1	0	1	1	1	1	0	1	1
	1	1	1	1	0	1	0	1	0	1
	1	0	1	0	1	1	1	0	1	0
(δ_1 or δ_2)	2	2	2	2	2	1	1	2	2	1
	1	1	1	1	1	1	1	1	2	1
	1	1	1	2	2	1	1	1	1	1
	1	1	2	1	2	1	2	2	1	1
	1	1	1	1	2	1	1	1	1	1
	2	2	1	2	1	1	2	2	1	2
	1	1	2	1	1	2	2	1	1	2
	1	1	2	1	2	2	2	1	1	1

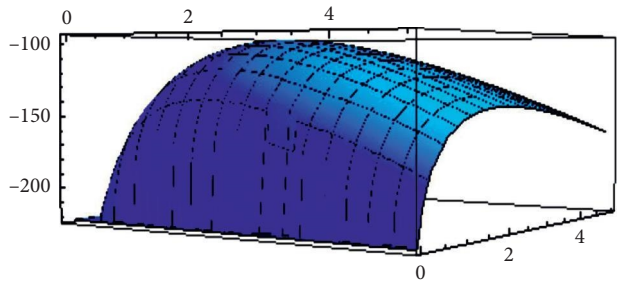

Figure 1: The profile loglikelihood of α_1 and α_2.

Table 3: The point ML, bootstrap, and Bayes estimate.

Method	β_1	β_2	α_{11}	α_{12}	α_{21}	α_{22}
$(\cdot)_{ML}$	1.864 9	1.947 3	1.495 7	1.380 6	1.691 1	0.338 2
$(\cdot)_{Boot}$	2.001 3	1.854 1	1.625 4	1.564 2	1.745 2	0.625 4
$(\cdot)_{B-MCMC}$	1.751 4	1.821 7	1.303 3	1.202 5	1.456 4	0.291 0

Table 4: 95% ML, bootstrap, and Bayes interval estimate.

Pa.	ACI	Length	Boo-p		Boot-t		CI	Length
β_1	(1.577, 2.153)	0.577	(1.474, 2.65)	1.180	(1.452, 2.274)	0.822	(1.343, 2.232)	0.889
β_2	(1.665, 2.064)	0.397	(1.212, 2.845)	1.633	(1.275, 2.414)	1.138	(1.273 7, 2.448)	1.174
α_{11}	(1.066, 1.926)	0.860	(0.422, 2.854)	2.433	(0.748, 2.184)	1.436	(0.754, 2.147)	1.393
α_{12}	(0.955, 1.806)	0.851	(0.425, 2.321)	1.396	(0.692, 2.066)	1.374	(0.675, 1.969)	1.294 06
α_{21}	(1.298, 2.084)	0.786	(0.215, 2.965)	1.896	(0.746, 2.624)	1.878	(0.757, 2.521)	1.765
α_{22}	(0.062, 0.615)	0.553	(0.001, 0.966)	0.964	(0.020, 0.659)	0.639	(0.085, 0.645)	0.559

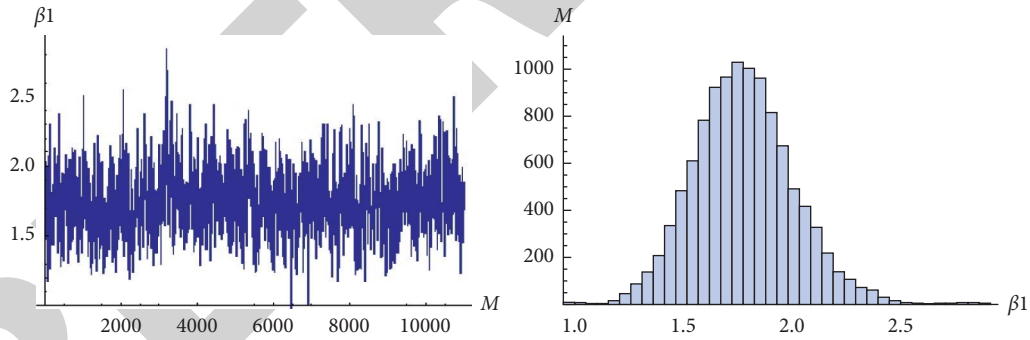

Figure 2: Simulation MCMC generated number/histogram of the parameter α_1.

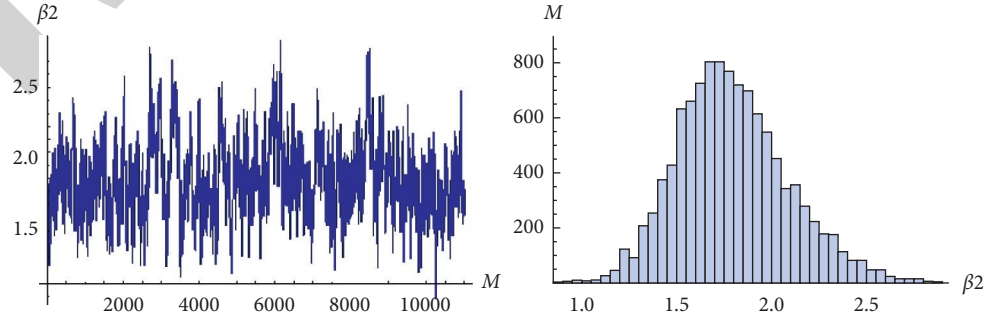

Figure 3: Simulation MCMC generated number/histogram of the parameter α_2.

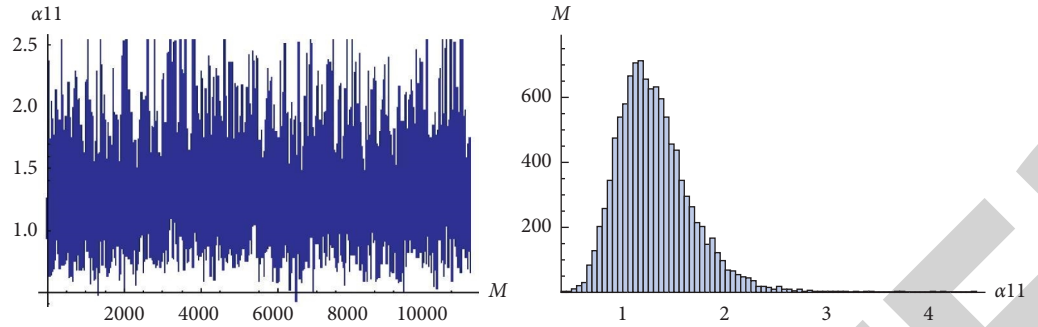

Figure 4: Simulation MCMC generated number/histogram of the parameter β_{11}.

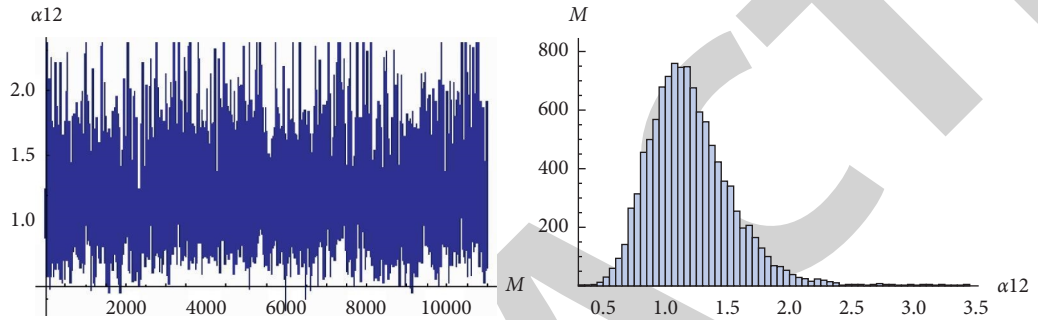

Figure 5: Simulation MCMC generated number/histogram of the parameter β_{12}.

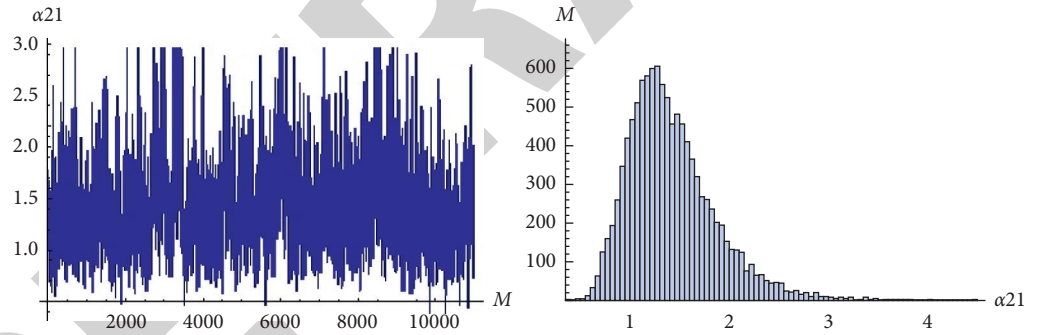

Figure 6: Simulation MCMC generated number/histogram of the parameter β_{21}.

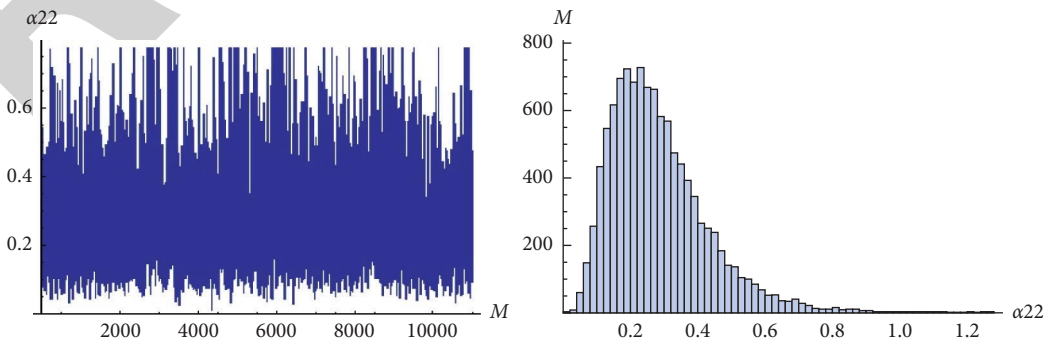

Figure 7: Simulation MCMC generated number/histogram of the parameter β_{21}.

(1) Two samples of size S_1 and S_2 are generated form Burr XII distribution with parameters β_k and $\alpha_{k1} + \alpha_{k2}$, $k = 1, 2$, respectively. Hence, the joint sample of size $N = S_1 + S_2$ is generated.
(2) For given τ, the Type-I JCRS and its size J are determined.
(3) The integers n_1 and n_2 are computed from the Type-I JCRS.
(4) The random integers m_{kj} are generated from binomial distributions.
(5) Steps 1 to 4 are repeated 1000 times to obtain 1000 Type-I JCRS.
(6) The MLE, bootstrap, and Bayes point and intervals estimates are computed for each sample.
(7) The values of each ME, MSEs, MILs, and PCs are computed and reported in Tables 5–8.

Algorithm 2: General steps used to generate Type-I joint competing risk samples and the corresponding estimate (see Almarashi et al. [15]).

Table 5: The ME and MSEs of ML, boot, and Bayes methods under $\omega = \{2.0, 1.2, 1.3, 1.8, 2.0, 2.0\}$.

(τ, S_1, S_2)		β_1		β_2		α_{11}		α_{12}		α_{21}		α_{22}	
		ME	MSE	ME	MSE	ME	MSE	ME	MSE	ME	MSE	ME	MSE
(0.2, 30, 30)	ML	2.542	0.454	1.423	0.423	1.524	0.421	2.352	0.632	2.457	0.489	2.397	0.500
	Boot	2.577	0.481	1.625	0.488	1.599	0.502	2.387	0.689	2.499	0.532	2.421	0.552
	Bayes P_0	2.537	0.452	1.414	0.411	1.517	0.411	2.341	0.618	2.442	0.481	2.387	0.492
	Bayes P_1	2.425	0.355	1.317	0.318	1.427	0.357	2.240	0.518	2.314	0.392	2.301	0.380
(0.2, 50, 30)	ML	2.521	0.428	1.419	0.442	1.481	0.395	2.329	0.601	2.449	0.483	2.390	0.492
	Boot	2.555	0.452	1.627	0.493	1.548	0.481	2.365	0.661	2.481	0.528	2.417	0.553
	Bayes P_0	2.519	0.424	1.418	0.421	1.478	0.392	2.318	0.585	2.445	0.484	2.379	0.487
	Bayes P_1	2.407	0.321	1.313	0.313	1.403	0.331	2.215	0.481	2.307	0.387	2.303	0.371
(0.2, 40, 60)	ML	2.525	0.431	1.379	0.404	1.488	0.391	2.325	0.598	2.407	0.452	2.361	0.459
	Boot	2.551	0.449	1.600	0.458	1.539	0.483	2.354	0.663	2.438	0.490	2.275	0.511
	Bayes P_0	2.522	0.418	1.378	0.381	1.479	0.388	2.321	0.579	2.409	0.449	2.341	0.451
	Bayes P_1	2.403	0.317	1.281	0.279	1.297	0.327	2.219	0.480	2.278	0.351	2.269	0.339
(0.2, 80, 80)	ML	2.500	0.400	1.362	0.292	1.429	0.358	2.300	0.563	2.298	0.447	2.354	0.451
	Boot	2.512	0.411	1.591	0.441	1.512	0.448	2.318	0.618	2.430	0.483	2.270	0.501
	Bayes P_0	2.477	0.281	1.371	0.373	1.441	0.339	2.292	0.543	2.397	0.432	2.337	0.444
	Bayes P_1	2.275	0.282	1.275	0.270	1.263	0.300	2.189	0.439	2.267	0.338	2.254	0.328
(0.8, 30, 30)	ML	2.507	0.407	1.371	0.296	1.441	0.365	2.308	0.571	2.301	0.452	2.362	0.457
	Boot	2.518	0.418	1.598	0.447	1.518	0.457	2.315	0.624	2.447	0.489	2.279	0.514
	Bayes P_0	2.481	0.293	1.377	0.375	1.453	0.351	2.299	0.555	2.405	0.438	2.347	0.457
	Bayes P_1	2.279	0.285	1.281	0.277	1.269	0.308	2.161	0.449	2.278	0.345	2.263	0.341
(0.8, 50, 30)	ML	2.481	0.380	1.374	0.292	1.407	0.328	2.274	0.538	2.307	0.450	2.360	0.449
	Boot	2.489	0.385	1.593	0.441	1.475	0.414	2.281	0.571	2.441	0.491	2.271	0.510
	Bayes P_0	2.455	0.261	1.372	0.370	1.411	0.304	2.254	0.514	2.401	0.433	2.342	0.458
	Bayes P_1	2.244	0.285	1.284	0.279	1.219	0.172	2.147	0.404	2.281	0.342	2.260	0.338
(0.8, 40, 60)	ML	2.487	0.385	1.331	0.263	1.411	0.331	2.274	0.541	2.279	0.418	2.328	0.411
	Boot	2.493	0.387	1.479	0.404	1.479	0.422	2.289	0.578	2.408	0.458	2.237	0.471
	Bayes P_0	2.459	0.264	1.338	0.318	1.418	0.314	2.260	0.525	2.369	0.404	2.315	0.411
	Bayes P_1	2.248	0.289	1.224	0.232	1.221	0.183	2.151	0.413	2.234	0.300	2.218	0.300
(0.8, 80, 80)	ML	2.415	0.341	1.311	0.245	1.390	0.290	2.215	0.502	2.255	0.402	2.302	0.292
	Boot	2.425	0.359	1.452	0.381	1.462	0.382	2.227	0.514	2.401	0.441	2.218	0.449
	Bayes P_0	2.411	0.241	1.314	0.301	1.390	0.271	2.211	0.500	2.354	0.292	2.301	0.395
	Bayes P_1	2.207	0.242	1.200	0.214	1.200	0.144	2.114	0.351 3	2.218	0.271	2.202	0.281

Table 6: The MILs and CPs of ML, boot, and Bayes methods under $\omega = \{2.0, 1.2, 1.3, 1.8, 2.0, 2.0\}$.

(τ, S_1, S_2)		β_1		β_2		α_{11}		α_{12}		α_{21}		α_{22}	
		MIL	CP	MIL	CP	MIL	CP	MIL	CP	MIL	CP	MIL	CP
(0.2, 30, 30)	ML	4.142	0.85	3.211	0.87	3.512	0.88	4.215	0.89	5.413	0.88	5.124	0.88
	Boot	4.314	0.88	3.415	0.88	3.688	0.89	4.389	0.89	5.598	0.89	5.311	0.88
	Bayes P_0	4.101	0.89	3.178	0.89	3.481	0.90	4.182	0.90	5.389	0.89	5.047	0.90
	Bayes P_1	3.245	0.91	3.001	0.90	3.214	0.91	4.007	0.90	5.217	0.90	4.874	0.91

Table 6: Continued.

(τ, S_1, S_2)		β_1		β_2		α_{11}		α_{12}		α_{21}		α_{22}	
		MIL	CP	MIL	CP	MIL	CP	MIL	CP	MIL	CP	MIL	CP
(0.2, 50, 30)	ML	3.850	0.90	2.901	0.89	3.012	0.90	3.841	0.90	5.211	0.90	5.109	0.90
	Boot	3.950	0.90	3.080	0.90	3.130	0.90	4.007	0.89	5.417	0.89	5.214	0.89
	Bayes P_0	3.811	0.91	2.920	0.90	3.011	0.92	3.700	0.92	5.198	0.89	5.001	0.90
	Bayes P_1	3.124	0.93	2.710	0.91	2.910	0.96	3.507	0.94	4.987	0.92	4.780	0.94
(0.2, 40, 60)	ML	3.899	0.89	2.725	0.89	3.025	0.90	3.871	0.91	5.003	0.90	4.952	0.91
	Boot	3.981	0.90	2.895	0.91	3.142	0.91	4.019	0.89	5.274	0.92	5.001	0.91
	Bayes P_0	3.861	0.92	2.701	0.90	3.019	0.92	3.722	0.90	5.000	0.91	4.890	0.92
	Bayes P_1	3.190	0.91	2.503	0.93	2.927	0.90	3.531	0.91	4.711	0.93	4.520	0.91
(0.2, 80, 80)	ML	3.601	0.90	2.610	0.91	2.911	0.91	3.590	0.91	4.802	0.91	4.815	0.91
	Boot	3.690	0.92	2.781	0.94	3.000	0.93	3.811	0.90	5.003	0.92	5.912	0.91
	Bayes P_0	3.570	0.92	2.590	0.90	2.890	0.90	3.530	0.92	4.779	0.90	4.715	0.91
	Bayes P_1	2.854	0.93	2.401	0.94	2.711	0.94	3.224	0.93	4.490	0.92	4.412	0.95
(0.8, 30, 30)	ML	3.654	0.89	2.680	0.90	2.978	0.91	3.610	0.89	4.875	0.90	4.864	0.90
	Boot	3.697	0.90	2.775	0.90	3.069	0.90	3.882	0.90	5.069	0.92	5.949	0.90
	Bayes P_0	3.630	0.90	2.640	0.91	2.945	0.90	3.591	0.90	4.819	0.92	4.760	0.93
	Bayes P_1	2.915	0.90	2.501	0.92	2.774	0.91	3.305	0.92	4.500	0.92	4.445	0.92
(0.8, 50, 30)	ML	3.418	0.91	2.671	0.90	2.760	0.91	3.401	0.91	4.879	0.89	4.871	0.90
	Boot	3.498	0.90	2.754	0.93	2.879	0.93	3.670	0.92	5.085	0.91	5.939	0.90
	Bayes P_0	3.401	0.91	2.621	0.91	2.847	0.92	3.402	0.94	4.804	0.91	4.748	0.91
	Bayes P_1	2.721	0.92	2.491	0.90	2.576	0.94	3.115	0.94	4.503	0.94	4.445	0.93
(0.8, 40, 60)	ML	3.441	0.89	2.451	0.91	2.772	0.91	3.424	0.90	4.610	0.96	4.623	0.90
	Boot	3.514	0.90	2.524	0.97	2.881	0.90	3.679	0.91	4.850	0.92	5.790	0.91
	Bayes P_0	3.422	0.92	2.405	0.92	2.842	0.91	3.414	0.90	4.579	0.94	4.624	0.91
	Bayes P_1	2.738	0.92	2.213	0.92	2.495	0.92	3.008	0.91	4.280	0.95	4.215	0.94
(0.8, 80, 80)	ML	3.150	0.93	2.178	0.92	2.684	0.92	3.314	0.92	4.390	0.90	4.398	0.93
	Boot	3.241	0.92	2.290	0.90	2.701	0.92	3.450	0.91	4.512	0.93	5.588	0.90
	Bayes P_0	3.110	0.93	2.154	0.94	2.629	0.92	3.375	0.93	4.370	0.94	4.401	0.93
	Bayes P_1	2.415	0.95	2.001	0.95	2.478	0.95	3.000	0.93	4.003	0.93	4.005	0.96

Table 7: The ME and MSEs of ML, boot, and Bayes methods under $\omega = \{1.0, 2.0, 3.0, 2.0, 2.5, 1.0\}$.

(τ, S_1, S_2)		β_1		β_2		α_{11}		α_{12}		α_{21}		α_{22}	
		ME	MSE	ME	MSE	ME	MSE	ME	MSE	ME	MSE	ME	MSE
(0.1, 30, 30)	ML	1.234	0.234	2.421	0.421	3.342	0.645	2.324	0.402	2.842	0.495	1.321	0.255
	Boot	1.335	0.238	2.542	0.426	3.452	0.648	2.426	0.405	2.890	0.498	1.435	0.291
	Bayes P_0	1.229	0.233	2.418	0.420	3.302	0.644	2.314	0.400	2.834	0.493	1.313	0.243
	Bayes P_1	1.198	0.224	2.370	0.411	3.201	0.634	2.280	0.390	2.790	0.484	1.280	0.242
(0.1, 50, 30)	ML	1.217	0.217	2.408	0.403	3.264	0.627	2.305	0.387	2.829	0.477	1.304	0.237
	Boot	1.319	0.221	2.528	0.409	3.401	0.621	2.407	0.391	2.875	0.481	1.421	0.278
	Bayes P_0	1.208	0.215	2.404	0.401	3.255	0.627	2.293	0.385	2.817	0.472	1.300	0.225
	Bayes P_1	1.181	0.209	2.367	0.382	3.185	0.613	2.261	0.369	2.777	0.468	1.266	0.222
(0.1, 40, 60)	ML	1.223	0.222	2.365	0.367	3.272	0.631	2.314	0.395	2.780	0.441	1.285	0.209
	Boot	1.325	0.227	2.451	0.371	3.415	0.627	2.412	0.397	2.831	0.449	1.370	0.251
	Bayes P_0	1.214	0.218	2.361	0.362	3.267	0.635	2.299	0.388	2.777	0.447	1.275	0.201
	Bayes P_1	1.193	0.213	2.322	0.348	3.192	0.621	2.274	0.374	2.731	0.415	1.214	0.191
(0.1, 80, 80)	ML	1.175	0.187	2.314	0.328	3.231	0.561	2.272	0.351	2.735	0.407	1.251	0.172
	Boot	1.286	0.192	2.407	0.347	3.370	0.588	2.350	0.362	2.800	0.415	1.361	0.199
	Bayes P_0	1.269	0.179	2.321	0.327	3.229	0.564	2.264	0.347	2.722	0.401	1.254	0.162
	Bayes P_1	1.144	0.152	2.279	0.301	3.151	0.541	2.217	0.322	2.680	0.362	1.182	0.127
(0.5, 30, 30)	ML	1.211	0.214	2.407	0.401	3.324	0.615	2.285	0.284	2.815	0.476	1.309	0.241
	Boot	1.310	0.217	2.531	0.409	3.428	0.619	2.404	0.292	2.867	0.481	1.424	0.279
	Bayes P_0	1.203	0.212	2.400	0.397	3.287	0.617	2.289	0.271	2.807	0.482	1.304	0.231
	Bayes P_1	1.175	0.205	2.356	0.394	3.180	0.601	2.260	0.362	2.766	0.461	1.271	0.228

Table 7: Continued.

(τ, S_1, S_2)		β_1		β_2		α_{11}		α_{12}		α_{21}		α_{22}	
		ME	MSE	ME	MSE	ME	MSE	ME	MSE	ME	MSE	ME	MSE
(0.5, 50, 30)	ML	1.200	0.200	2.397	0.385	3.244	0.600	2.284	0.365	2.801	0.455	1.292	0.222
	Boot	1.302	0.204	2.510	0.397	3.381	0.593	2.391	0.373	2.849	0.463	1.409	0.266
	Bayes P_0	1.185	0.197	2.389	0.387	3.237	0.601	2.273	0.367	2.790	0.454	1.291	0.210
	Bayes P_1	1.160	0.192	2.351	0.362	3.161	0.586	2.244	0.351	2.751	0.449	1.252	0.214
(0.5, 40, 60)	ML	1.207	0.201	2.347	0.349	3.251	0.603	2.292	0.376	2.751	0.424	1.252	0.189
	Boot	1.303	0.204	2.438	0.355	3.400	0.601	2.394	0.380	2.802	0.430	1.358	0.238
	Bayes P_0	1.191	0.200	2.347	0.341	3.244	0.607	2.281	0.369	2.748	0.418	1.263	0.187
	Bayes P_1	1.181	0.192	2.307	0.329	3.175	0.590	2.255	0.359	2.703	0.400	1.200	0.177
(0.5, 80, 80)	ML	1.162	0.170	2.300	0.309	3.214	0.534	2.249	0.335	2.708	0.389	1.239	0.160
	Boot	1.271	0.173	2.394	0.328	3.352	0.559	2.329	0.347	2.771	0.401	1.350	0.184
	Bayes P_0	1.252	0.158	2.302	0.307	3.207	0.537	2.241	0.322	2.700	0.381	1.241	0.151
	Bayes P_1	1.129	0.134	2.262	0.282	3.133	0.515	2.200	0.301	2.653	0.341	1.170	0.114

Table 8: The MILs and CPs of ML, boot, and Bayes methods under $\omega = \{1.0, 2.0, 3.0, 2.0, 2.5, 1.0\}$.

(τ, S_1, S_2)		β_1		β_2		α_{11}		α_{12}		α_{21}		α_{22}	
		MIL	CP	MIL	CP	MIL	CP	MIL	CP	MIL	CP	MIL	CP
(0.1, 30, 30)	ML	2.514	0.88	4.521	0.89	5.985	0.87	3.985	0.90	5.234	0.90	2.451	0.90
	Boot	2.674	0.89	4.654	0.89	6.124	0.89	4.231	0.89	5.385	0.90	2.562	0.91
	Bayes P_0	2.485	0.90	4.492	0.90	5.941	0.89	3.937	0.90	5.201	0.90	2.414	0.90
	Bayes P_1	2.350	0.90	4.320	0.91	5.752	0.91	3.813	0.90	5.025	0.90	2.285	0.91
(0.1, 50, 30)	ML	2.465	0.90	4.472	0.90	5.944	0.90	3.941	0.90	5.192	0.91	2.400	0.90
	Boot	2.627	0.91	4.601	0.89	6.051	0.91	4.188	0.90	5.341	0.90	2.523	0.90
	Bayes P_0	2.441	0.90	4.451	0.91	5.900	0.91	3.900	0.92	5.154	0.91	2.366	0.94
	Bayes P_1	2.304	0.93	4.275	0.92	5.707	0.92	3.762	0.92	4.955	0.93	2.241	0.92
(0.1, 40, 60)	ML	2.454	0.90	4.439	0.90	5.936	0.90	3.939	0.90	5.155	0.91	2.360	0.92
	Boot	2.631	0.89	4.569	0.92	6.061	0.91	4.175	0.92	5.311	0.93	2.481	0.91
	Bayes P_0	2.447	0.90	4.418	0.91	5.903	0.92	3.909	0.90	5.119	0.91	2.328	0.93
	Bayes P_1	2.314	0.90	4.245	0.94	5.715	0.91	3.769	0.93	4.921	0.94	2.207	0.96
(0.1, 80, 80)	ML	2.407	0.90	4.401	0.92	5.902	0.91	3.903	0.92	5.111	0.94	2.360	0.92
	Boot	2.582	0.92	4.515	0.93	6.024	0.92	4.132	0.92	5.271	0.93	2.481	0.90
	Bayes P_0	2.400	0.94	4.375	0.91	5.871	0.92	3.861	0.92	5.062	0.93	2.328	0.94
	Bayes P_1	2.267	0.95	4.208	0.96	5.674	0.94	3.715	0.94	4.874	0.94	2.187	0.95
(0.5, 30, 30)	ML	2.485	0.89	4.502	0.89	5.955	0.89	3.961	0.91	5.205	0.91	2.436	0.92
	Boot	2.641	0.90	4.635	0.89	6.101	0.89	4.209	0.90	5.344	0.91	2.544	0.91
	Bayes P_0	2.449	0.90	4.474	0.91	5.915	0.90	3.915	0.90	5.145	0.90	2.400	0.92
	Bayes P_1	2.324	0.90	4.301	0.91	5.727	0.91	3.800	0.91	5.000	0.92	2.271	0.91
(0.5, 50, 30)	ML	2.441	0.91	4.456	0.90	5.919	0.90	3.918	0.92	5.151	0.91	2.378	0.90
	Boot	2.600	0.91	4.580	0.90	6.024	0.92	4.161	0.92	5.302	0.92	2.502	0.92
	Bayes P_0	2.415	0.91	4.433	0.91	5.875	0.91	3.882	0.92	5.115	0.91	2.341	0.92
	Bayes P_1	2.274	0.93	4.257	0.93	5.691	0.92	3.744	0.92	4.912	0.92	2.221	0.92
(0.5, 40, 60)	ML	2.427	0.91	4.418	0.90	5.914	0.92	3.925	0.92	5.114	0.91	2.339	0.92
	Boot	2.607	0.90	4.550	0.92	6.032	0.91	4.151	0.92	5.311	0.93	2.460	0.94
	Bayes P_0	2.421	0.90	4.401	0.91	5.274	0.93	3.892	0.90	5.066	0.92	2.309	0.93
	Bayes P_1	2.288	0.92	4.227	0.93	5.894	0.91	3.751	0.93	4.869	0.94	2.191	0.96
(0.5, 80, 80)	ML	2.381	0.93	4.384	0.92	5.877	0.92	3.877	0.93	5.070	0.92	2.339	0.92
	Boot	2.555	0.92	4.500	0.92	5.982	0.94	4.114	0.92	5.239	0.93	2.455	0.94
	Bayes P_0	2.274	0.92	4.362	0.91	5.850	0.92	3.851	0.92	5.030	0.95	2.307	0.94
	Bayes P_1	2.231	0.95	4.189	0.94	5.644	0.95	3.703	0.92	4.835	0.94	2.179	0.94

point estimate. And, mean interval length (MIL) and probability coverage (PC) are used to measure interval estimate. The Monte Carlo study is done with respect to Algorithm 2.

8. Conclusions

Recently, the joint censoring scheme is more widely used in a comparative life testing specially for products coming from different lines of production. The problem of comparative life testes under different causes of failure has been discussed recently under the joint censoring scheme of competing risks exponential lifetime model by Almarashi et al. [15]. In this paper, we adopted this problem when units or individual is distributed with Burr XII distributions. The unknown model parameters are estimated with classical methods (ML and bootstrap) and Bayes method with noninformative and informative prior. Numerical computation is exposed with real data analysis and Monto Carlo simulation study to assess and discuss the developed results. The numerical result discusses changing of sample size, test time, and available information. Therefore, we observed the following points:

(1) The proposed model under Type-I JCRS serves well for all choice of censoring schemes and parameters choices

(2) The Bayes estimation under noninformative prior P_0 is more close to maximum likelihood estimation

(3) The informative priors P_1 serve better than noninformative prior and maximum likelihood estimations

(4) The increasing effect of sample size $S_1 + S_2$ reduces the MSE and MIL

(5) The large value of test time τ serves well than small value of τ

Data Availability

The used data are the real data set presented by Hoel (1972) in [36].

Conflicts of Interest

The authors declare that they have no conflicts of interest.

Acknowledgments

The authors would like to thank the Deanship of Scientific Research at Umm Al-Qura University for supporting this work by grant no. 19-SCI-1-03-0011.

References

[1] N. Balakrishnan and R. Aggarwala, *Progressive Censoring-Theory, Methods, and Applications*, Birkhäuser, Basel, Switzerland, 2000.

[2] U. V. R. Rao, I. R. Savage, and M. Sobel, "Contributions to the theory of rank order statistics: the two-sample censored case," *The Annals of Mathematical Statistics*, vol. 31, no. 2, pp. 415–426, 1960.

[3] A. P. Basu, "On a generalized savage statistic with applications to life testing," *The Annals of Mathematical Statistics*, vol. 39, no. 5, pp. 1591–1604, 1968.

[4] R. A. Johnson and K. G. Mehrotra, "Locally most powerful rank tests for the two-sample problem with censored data," *The Annals of Mathematical Statistics*, vol. 43, no. 3, pp. 823–831, 1972.

[5] K. G. Mehrotra and R. A. Johnson, "Asymptotic sufficiency and asymptotically most powerful tests for the two sample censored situation," *Annals of Statistics*, vol. 4, pp. 589–596, 1976.

[6] G. K. Bhattacharyya and K. G. Mehrotra, "On testing equality of two exponential distributions under combined type-IIcensoring," *Journal of the American Statistical Association*, vol. 76, no. 376, pp. 886–894, 1981.

[7] K. G. Mehrotra and G. K. Bhattacharyya, "Confidence intervals with jointly type-II censored samples from two exponential distributions," *Journal of the American Statistical Association*, vol. 77, no. 378, pp. 441–446, 1982.

[8] N. Balakrishnan and A. Rasouli, "Exact likelihood inference for two exponential populations under joint type-II censoring," *Computational Statistics & Data Analysis*, vol. 52, no. 5, pp. 2725–2738, 2008.

[9] A. Rasouli and N. Balakrishnan, "Exact likelihood inference for two exponential populations under joint progressive type-II censoring," *Communications in Statistics -Theory and Methods*, vol. 39, no. 12, pp. 2172–2191, 2010.

[10] A. R. Shafay, N. Balakrishnan, and Y. Abdel-Aty, "Bayesian inference based on a jointly type-II censored sample from two exponential populations," *Journal of Statistical Computation and Simulation*, vol. 84, no. 11, pp. 2427–2440, 2014.

[11] B. N. Al-Matrafi and G. A. Abd-Elmougod, "Statistical Inferences with jointly type-II censored samples from two rayleigh distributions," *Global Journal of Pure and Applied Mathematics*, vol. 13, pp. 8361–8372, 2017.

[12] F. A. Momenkhan and G. A. Abd-Elmougod, "Stimations in partially step-stress accelerate life tests with jointly type-II censored samples from rayleigh distributions," *Transylvanian Review*, vol. 28, pp. 7609–7616, 2018.

[13] S. Mondal and D. Kundu, "Bayesian inference for weibull distribution under the balanced joint type-II progressive censoring scheme," *American Journal of Mathematical and Management Sciences*, vol. 39, no. 1, pp. 56–74, 2019.

[14] S. Mondal and D. Kundu, "Inferences of weibull parameters under balance two sample type-II progressive censoring scheme," *Quality and Reliability Engineering International*, vol. 36, no. 1, pp. 1–17, 2020.

[15] A. M. Almarashi, A. Algarni, A. M. Daghistani, G. A. Abd-Elmougod, S. Abdel-Khalek, and M. Z. Raqab, "Inferences for joint hybrid progressive censored exponential lifetimes under competing risk model," *Mathematical Problems in Engineering*, vol. 2021, Article ID 3380467, 12 pages, 2021.

[16] D. R. Cox, "The analysis of exponentially distributed lifetimes with two types of failures," *Journal of the Royal Statistical Society: Series B (Methodological)*, vol. 21, no. 2, pp. 411–421, 1959.

[17] M. J. Crowder, *Classical Competing Risks*, Chapman and Hall, London, UK, 2001.

[18] N. Balakrishnan and D. Han, "Exact inference for a simple step-stress model with competing risks for failure from exponential distribution under type-II censoring," *Journal of*

Hindawi
Journal of Mathematics
Volume 2024, Article ID 9865089, 1 page
https://doi.org/10.1155/2024/9865089

Retraction

Retracted: Few Samples of SAR Automatic Target Recognition Based on Enhanced-Shape CNN

Journal of Mathematics

Received 23 January 2024; Accepted 23 January 2024; Published 24 January 2024

This article has been retracted by Hindawi following an investigation undertaken by the publisher [1]. This investigation has uncovered evidence of one or more of the following indicators of systematic manipulation of the publication process:

(1) Discrepancies in scope

(2) Discrepancies in the description of the research reported

(3) Discrepancies between the availability of data and the research described

(4) Inappropriate citations

(5) Incoherent, meaningless and/or irrelevant content included in the article

(6) Manipulated or compromised peer review

The presence of these indicators undermines our confidence in the integrity of the article's content and we cannot, therefore, vouch for its reliability. Please note that this notice is intended solely to alert readers that the content of this article is unreliable. We have not investigated whether authors were aware of or involved in the systematic manipulation of the publication process.

Wiley and Hindawi regrets that the usual quality checks did not identify these issues before publication and have since put additional measures in place to safeguard research integrity.

We wish to credit our own Research Integrity and Research Publishing teams and anonymous and named external researchers and research integrity experts for contributing to this investigation.

The corresponding author, as the representative of all authors, has been given the opportunity to register their agreement or disagreement to this retraction. We have kept a record of any response received.

References

[1] M. Huang, F. Liu, and X. Meng, "Few Samples of SAR Automatic Target Recognition Based on Enhanced-Shape CNN," *Journal of Mathematics*, vol. 2021, Article ID 9141023, 16 pages, 2021.

Hindawi
Journal of Mathematics
Volume 2021, Article ID 9141023, 16 pages
https://doi.org/10.1155/2021/9141023

Research Article

Few Samples of SAR Automatic Target Recognition Based on Enhanced-Shape CNN

Mengmeng Huang, Fang Liu, and Xianfa Meng

Automatic Target Recognition Key Lab, National University of Defense Technology, Changsha, Hunan Province 410005, China

Correspondence should be addressed to Fang Liu; smartlf@sina.com

Received 29 October 2021; Accepted 25 November 2021; Published 23 December 2021

Academic Editor: Naeem Jan

Synthetic Aperture Radar (SAR), as one of the important and significant methods for obtaining target characteristics in the field of remote sensing, has been applied to many fields including intelligence search, topographic surveying, mapping, and geological survey. In SAR field, the SAR automatic target recognition (SAR ATR) is a significant issue. However, on the other hand, it also has high application value. The development of deep learning has enabled it to be applied to SAR ATR. Some researchers point out that existing convolutional neural network (CNN) paid more attention to texture information, which is often not as good as shape information. Wherefore, this study designs the enhanced-shape CNN, which enhances the target shape at the input. Further, it uses an improved attention module, so that the network can highlight target shape in SAR images. Aiming at the problem of the small scale of the existing SAR data set, a small sample experiment is conducted. Enhanced-shape CNN achieved a recognition rate of 99.29% when trained on the full training set, while it is 89.93% on the one-eighth training data set.

1. Introduction

High-resolution radar images in range and azimuth can be obtained by Synthetic Aperture Radar (SAR), which includes synthetic aperture principle, pulse compression technology, and signal processing technology. Compared with optical and infrared sensors, SAR has the advantages of day-and-night, all-weather, and the ability to penetrate obstacles such as clouds and vegetation [1–6]. With the increasing SAR imaging resolution, SAR has been diversely utilized in military and civilian fields, such as marine, land monitoring [7], and weapon guidance [8]. Therefore, SAR automatic target recognition (SAR ATR) is becoming a meaningful and challenging research field.

The MIT Lincoln Laboratory proposed to divide SAR ATR into three subsystems: detection, discrimination, and classification [9]. The task of target detection is to determine whether the image contains the target of interest and find the target's position in the image. In the discrimination stage, a discriminator is designed to solve a two-class (target and clutter) classification problem, and the probability of false alarm can be significantly reduced. And then the true target is categorized in the classification and recognition stage.

This paper only focuses on the classification and recognition stage and does not include detection and discrimination. There are three mainstream methods for recognition: template-based, model-based, and deep learning. For template matching, the test sample is matched with certain matching criteria from the template library, which is constructed from the labeled training set [10, 11]. Template-based method is simple but needs to build a large number of template libraries, and the quality of the template library has a great influence on the recognition results.

Due to the unrobustness of the template matching method, a model-based method is proposed. The method extracts the effective features of the training samples and test samples, and then the features extracted from SAR images are fed into the classifier for recognition [12–15]. The features of SAR images primarily include geometric features, transformation features, and electromagnetic features. The geometric features describe the shape and structure of target, such as contour, edge, size, and area. Principal component

analysis (PCA) [16], kernel principal component analysis (KPCA) [17], linear discriminant analysis (LDA) [18], independent component analysis (ICA) [19], and other means are all transformation features that are also applied for SAR target recognition. Due to the unique mechanism of SAR imaging, SAR images have the unique electromagnetic features [20, 21] including polarization mode and scattering centers. After feature extraction, the classifiers are necessary for feature. K-nearest neighbor (K-NN), support vector machine (SVM), and sparse representation-based classification (SRC) are frequently used as classifiers in SAR recognition.

While deep learning is well applied in various fields over years, a great quantity of deep learning methods have also emerged in SAR ATR. Chen et al. [22] proposed that the fully connected layer in convolutional neural network (CNN) is replaced with convolutional layer, which effectively suppresses the overfitting problem and reduces the number of parameters. Since the SAR images are highly sensitive to azimuth angle, Zhou et al. [23] combined three continuous azimuth images of the same target as a pseudocolor image inputting, which are input into CNN. Wang et al. [24] designed a multiview convolutional neural network and long short term memory network (CNN-LSTM) to extract and fuse the features from different adjacent azimuth angles. Zhang et al. [25] utilized CNN with CBAM, which is an attention mechanism to improve recognition rate. The deep-learning method can extract the deep semantic information of the target. Compared with the model-based method, it does not need to extract features manually and has achieved a high recognition rate in the field of SAR target recognition.

More recently, there is a viewpoint that CNN, which is different from human, is more inclined to learn the texture and surface features of the target but pays less attention to deep semantic features such as contour and shape. Contour and shape are the most reliable information in human and biological vision. Geirhos et al. [26] demonstrated that Image Net-trained CNNs are strongly biased towards recognizing textures rather than shapes, which is in stark contrast to human behavioral evidence and reveals fundamentally different classification strategies. Hermann et al. [27] indicated that, on out-of-distribution test sets, the performance of models that like to classify images by shape rather than texture is better than baseline.

Therefore, this paper proposes an enhanced-shape CNN, whose network structure is shown in Figure 1. First, the enhanced-shape CNN strengthened the shape features of the target at the input, constructing a three-channel pseudocolor image as data set, so that the convolutional neural network can tend to pay more attention to target shape. Second, the pooling commonly use in CNNs is maximum pooling and average pooling, and the target information is easily lost when downsampling the feature maps. Thus, we use the SoftPool [28] instead of max pooling to improve the network. Meanwhile, in the above literatures, some attention mechanisms combined with CNNs have been applied to SAR recognition. The channel attention module mechanism, i.e., Squeeze-and-Excitation (SE) module [30], can effectively increase the channel weights that are beneficial for recognition and suppress feature that are less useful in CNNs. However, SE module distributes channel weights more evenly in target recognition, such that there is essentially the same as CNN, as noted in paper [29]. Therefore, SoftPool is utilized by replacing global pooling, which can obtain unbalanced channel weights. Third, it is still troublesome to acquire SAR image data sets with relatively rich conditions of imaging, despite the fact that the acquisition of high-resolution SAR images has become easier. Over these years, a great quantity data sets of SAR ships and vehicles have emerged, but their resolution is not enough to be recognized; hence, the data sets are used for detection. At present, most research of SAR target recognition is based on the Moving and Stationary Target Acquisition and Recognition (MSTAR) [31] data set. From the perspective of less samples, this paper designs experiments to verify that this method has a higher recognition rate compared to existing methods under limited data sets.

The main contributions of this paper are as follows:

(1) Constructing a three-channel pseudocolor image, which is formed by extracting the features of the target and shadow from the original SAR data set, filtering the original SAR images, and the original SAR images. The pseudocolor three-channel images are input to the CNN, enhancing the model to use the shape information of the image.

(2) Improving the pooling of the network and the global pooling of the attention module. Using SoftPool in the network can increase the information of the feature map during the pooling. At the same time, the pooling in the SE module is improved to make the weight distribution of the channel more different, instead of balance.

(3) Training in the full training set, one-half of the training set, one-quarter of the training set, and one-eighth of the training set and testing in full test set based on the MSTAR data set. It is proved that the method proposed in this paper can obtain a higher recognition rate with a few samples.

The remainder of this paper is organized as follows: Section 2 describes the principles of the method, including the extraction method of target and shadow, the principle of lee filter, and the fusion of three-channel pseudocolor image. and a novel pooling method (SoftPool), the Squeeze and Excitation module and Enhanced SE module. Section 3 presents the experimental results to validate the effectiveness of the proposed network, and Section 4 concludes the paper.

2. Methodology

In this section, we will describe some of the principles and structures used in our model.

2.1. Extraction of Target and Shadow. Unlike optical images, SAR images are side-view imaging, so there are shadows in the image in addition to the target. The shadow is the result

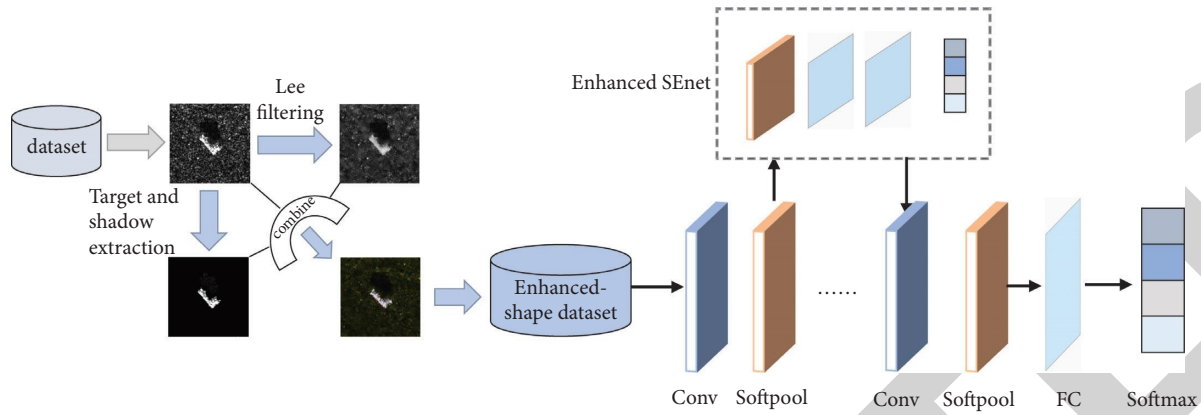

Figure 1: Structure of the enhances-shape network.

of the mutual coupling between the target and the background environment under a specific radar line of sight, and its shape reflects the physical size and shape distribution of the target, so combining joint features of the target and shadow is more helpful for the recognition.

There are many existing segmentation algorithms to extract target and shadow. The focus of our model is not the segmentation algorithm; therefore, the simplest threshold method is used to segment the target and the shadow area. Our threshold setting is based on the threshold proposed by the paper [32]. The main steps are as follows:

(1) Equalize the original SAR image histogram;

(2) Use mean filtering to smooth the result of step 1, and transform the gray dynamic range to [0, 1];

(3) Set the thresholds of the shadow and target area to 0.2 and 0.8, the pixels greater than 0.8 are the target area, and those less than 0.2 are the shadow areas;

(4) Remove the area of total pixels less than 25 to reduce the influence of background noise;

(5) Utilize the morphological closing operation to connect the target area and the shadow area, which obtain a smooth target and shadow contour.

It can be seen that the simple threshold method can achieve good segmentation results and remove a lot of background noise and clutter. However, in real world situations, the common segmentation algorithm may not be able to segment the target and the shadow well, so we set the thresholds 0.1 and 0.9, and 0.3 and 0.7, respectively, to verify that a slightly biased segmentation algorithm works better.

Figure 2 demonstrates the target and shadow images obtained with different segmentation thresholds. (a) is the original image. (b) describes the morphological image of the target and shadow when the threshold is set to 0.8 and 0.2. The target and shadow extracted in (c) are relatively complete, and the pixel value of the shadow is too low to be clear. Relatively, the target area extracted in (d) is redundant, and in (e) it is incomplete.

2.2. Lee Filtering. Due to its special imaging mechanism, SAR images contain more coherent speckle noise. After filtering the SAR image, the shape characteristics of the target can be enhanced, and the texture, especially the interference of noise, can be reduced.

For speckle noise, many filtering methods for the speckle noise of SAR images have been proposed. Our model utilizes lee filtering, which is a classic SAR filtering strategy. The two key aspects of noise suppression are, on the one hand, establishing a true backscatter coefficient estimation mechanism, and on the other hand, formulating a selection plan for pixel samples in homogeneous regions.

Lee filtering is one of the typical methods of image speckle filtering using the local statistical characteristics. It is based on a fully developed speckle noise model. First, a window of a certain length is selected as the local area. Then, it is assumed that the prior mean $\overline{x}$ and variance $\mathrm{var}(x)$ can be calculated by calculating the local mean $\overline{y}$ and the variance $\mathrm{var}(y)$.

$$\hat{x} = a\overline{x} + by, \tag{1}$$

$$\begin{aligned} a &= 1 - \frac{\mathrm{var}(x)}{\mathrm{var}(y)}, \\ b &= \frac{\mathrm{var}(x)}{\mathrm{var}(y)}, \end{aligned} \tag{2}$$

$$\hat{x} = \overline{y} + b(y - \overline{y}), \tag{3}$$

$$\begin{aligned} \mathrm{var}(x) &= \frac{\mathrm{var}(y) - \sigma_v^2 \overline{y}^2}{1 + \sigma_v^2}, \\ \sigma_v^2 &= \frac{1}{N}, \end{aligned} \tag{4}$$

where y signifies the value in the selected window. The window size N selected in this paper is 7.

It can be observed from Figure 3 that the speckle noise in the image is significantly reduced, and the texture features of the target and shadow parts are reduced, but the contour shape is more obvious after lee filtering.

2.3. Fusion. Typically, SAR images are gray images. When recognizing SAR images with CNN, the gray-scale image is generally converted into a three-channel image input. In this

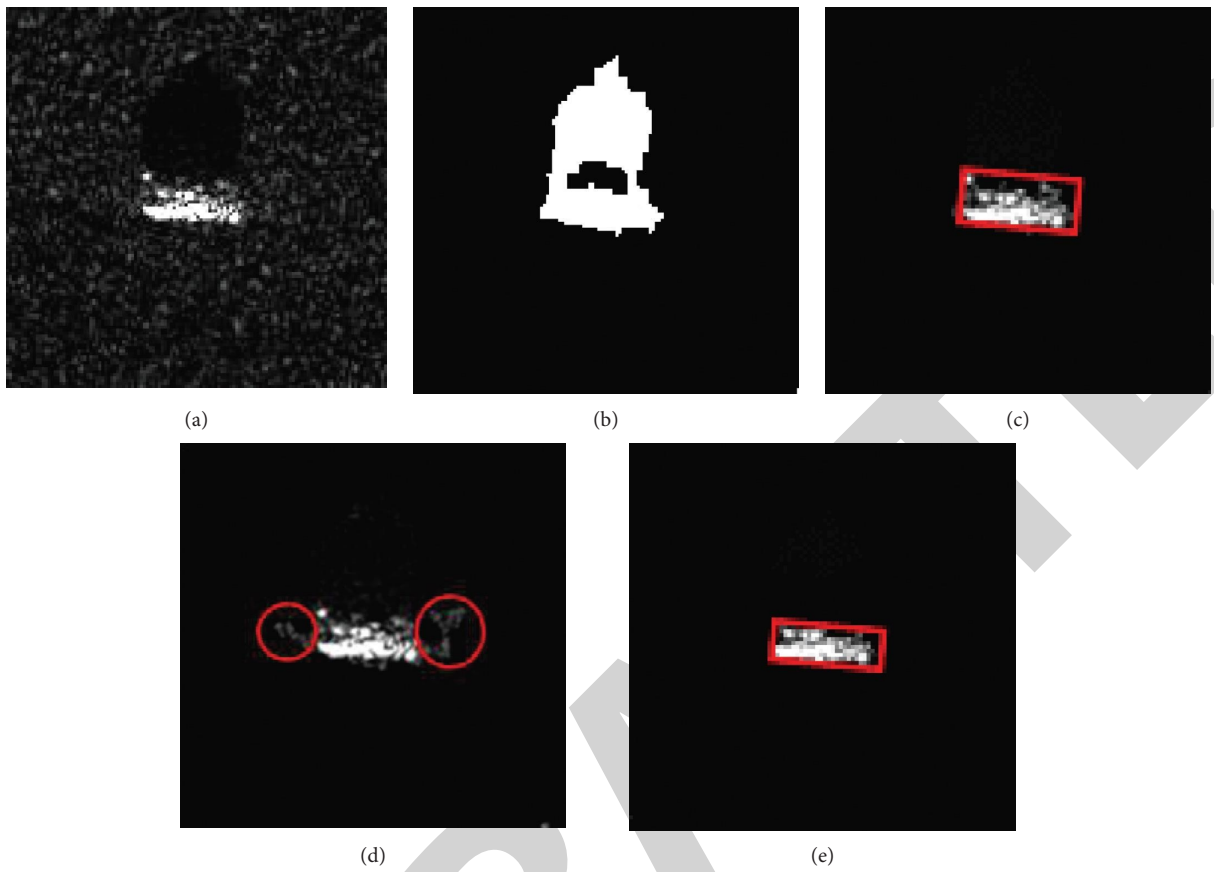

Figure 2: The segmentation of the target and shadow. (a) The original image. (b) Morphological image of target and shadow. (c) Target and shadow when setting the thresholds 0.2 and 0.8. (d) Target and shadow when setting the thresholds 0.1 and 0.8. (e) Target and shadow when setting the thresholds 0.3 and 0.7.

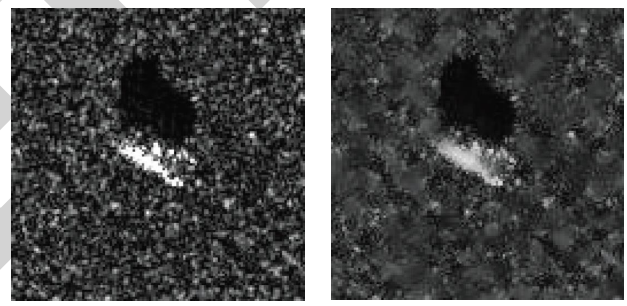

Figure 3: (a) The original image. (b) Image after lee filtering.

paper, the original image is combined with the image of target and shadow and the filtered image in RGB mode to form a three-channel pseudocolor image, as shown in Figure 4. The original image can contain complete target information including shape, contour, and texture, while the image of target and shadow and filtered image can enhance the target shape characteristics. Using pseudocolor images as network input can acquire global information and deep semantic information instead of focusing on texture information.

2.4. SoftPool. The SoftPool is used by us in the network to reduce the loss of target information. Pooling is used in CNN to reduce the size of feature maps to achieve local space invariance and increase convolutional receptive fields. At present, the most commonly used in neural networks is max pooling and average pooling, which will lose the information mapped in the feature map. Therefore, paper [28] proposed SoftPool to reduce the loss of information, while limiting the calculation and memory overhead.

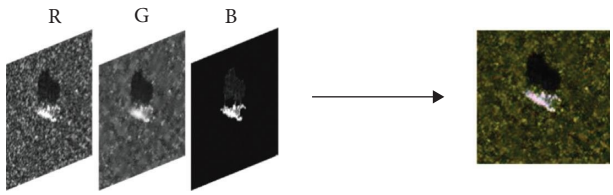

Figure 4: The fusion of multifeature images.

The SoftPool is differentiable. For the pooling kernel $k * k$, we suppose that the output of the pooling operation is $\widetilde{a}_R$, the corresponding gradient is $\Delta\widetilde{a}_i$, R is the maximum approximation in the activation area, and each activation a_i with index i corresponds to a weight w_i. The weight w_i is the ratio of the natural index of the activation to the sum of the natural indices of all activations in the neighborhood R:

$$w_i = \frac{e^{a_i}}{\sum_{j\in R} e^{a_j}}. \tag{5}$$

The weight together with the corresponding activation value is used as a nonlinear transformation. Higher activation is more dominant than lower activation. The output value after the SoftPool is obtained by summing all the weighted activation criteria in the kernel neighborhood R:

$$\widetilde{a} = \sum_{i\in R} w_i * a_i. \tag{6}$$

In the training update phase of SoftPool, the gradient update is proportional to the weight calculated in the forward propagation process, namely, $\nabla a_i = w_i * \nabla\widetilde{a}$. It is realized that the gradient update of the smaller activation is smaller than the gradient update of the larger activation. The forward propagation and backward update of SoftPool are shown in Figure 5.

Compared to max pooling and average pooling, the SoftPool can balance the influence of average pooling and max pooling, while average pooling reduces the effect of activations in the area, and max pooling selects only the highest activation in the area. For SoftPool, all activations in this area contribute to the final output, and higher activations dominate the lower activations. Therefore, in the pooling of CNN, a larger activation value has a greater impact on the output, and the significant details of the feature map can be retained to the greatest extent.

Figure 6 gives the effect of different pooling. The first column is the original image, the second column is the image after max pooling, the third column is the image after average pooling, and the fourth column is the image after SoftPool. The comparison shows that the max pooling activates the pixel points with large gray values in the region, highlighting the target, as well as highlighting scattered noise. The average pooling approximates filtering, reducing the effect of noise, but weakening the structural shape information of the target with it. SoftPooling, on the other hand, retains the relatively intact structural information of the target while removing the effect of scattered noise, making the shape more prominent.

2.5. SE Module and Enhanced SE Module. The core of typical CNN is the convolution operator, and the input feature map is mapped to the new feature map through the convolution kernel. In the convolutional layer, the feature maps of the previous layer are considered to have the same weight for the next layer, but research [30] illustrates that this is not the case. The equal mechanism limits the convolutional neural network to obtain more information. Therefore, paper [30] proposed SE module, which focuses on the relationship between channels and hopes that the model can automatically learn the importance of different channel features.

The network structure of SE module is shown in Figure 7. For input feature map tensor X: $X \in R^{W\times H\times C}$, where $W \times H$ represents the length and width of the feature map, and C represents the number of input channels, and SE module performs a squeeze operation on X to obtain the channel-level global features and then performs an excitation operation on the global features to learn the relationship between each channel and get the weights of different channels. Finally, the output feature map $\widetilde{X}$ is calculated by multiplying the weights and the input feature map X.

As mentioned above, the SE module consists of two steps: squeeze and excitation. For the squeeze F_{sq}, global average pooling is applied to encode the entire spatial feature on a channel as a global feature. The input of average pooling is the feature map tensor X, and the output after a squeeze operation is $z_c \in R^C$, denoting the cth value in the vector z. The mapping relationship between X and z_c is as follows:

$$z_c = F_{sq}(x_c) = \frac{1}{H\times W}\sum_{i=1}^{H}\sum_{j=1}^{W} x_c(i,j), \tag{7}$$

where x_c represents the feature map tensor of the cth channel of input X. The squeeze operation gets the global description feature, and then the excitation operation is performed.

$$s = F_{ex}(z,W) = \sigma(g(z,W)) = \sigma\left(W_2\mathrm{ReLU}\left(W_1 z\right)\right), \tag{8}$$

where $W_1 \in R^{(C/r)\times C}$, $W_2 \in R^{C\times(C/r)}$, r is a fixed hyperparameter, σ is the sigmoid activation function, and s indicates the learning weight of different channels. The first FC layer plays the role of dimensionality reduction, and the final FC layer restores the feature map to the original dimensions. After squeeze and excitation, the channel weight is obtained, and finally, the weight is multiplied by the original feature tensor.

$$\widetilde{x}_c = F_{\mathrm{scale}}\left(x_c, s_c\right) = s_c \cdot x_c, \tag{9}$$

where s_c represents the weight of x_c and $F_{\mathrm{scale}}(x_c, s_c)$ represents the product of them.

Essentially, the SE module performs attention operations in the channel dimension. This attention mechanism allows the model to pay more attention to the channel features with the most information, while suppressing those unimportant channel features. However, this advantage is not directly reflected in the experiment on the SAR data set MSTAR. It can be seen from the paper [29] that the channel weights

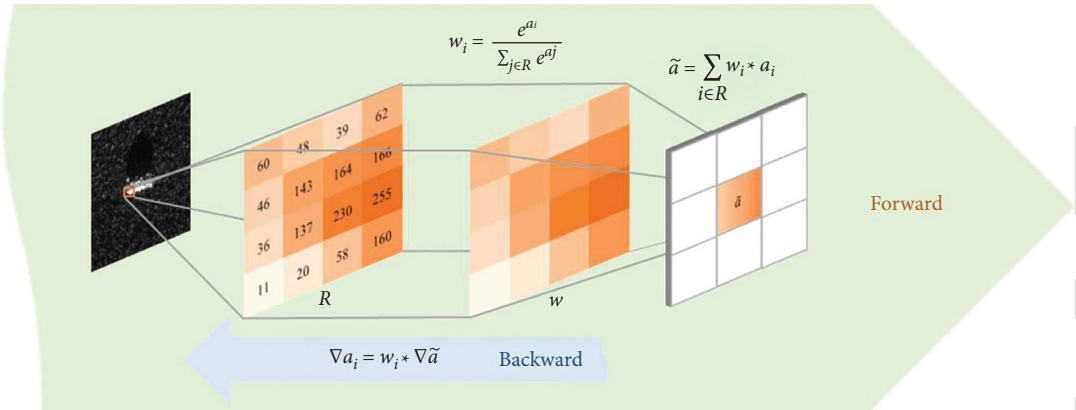

Figure 5: The green part represents forward propagation. The output of pooling is the product of the weights and activation values in region R. The blue part represents backward propagation, and the update of the activation value is also related to the weight.

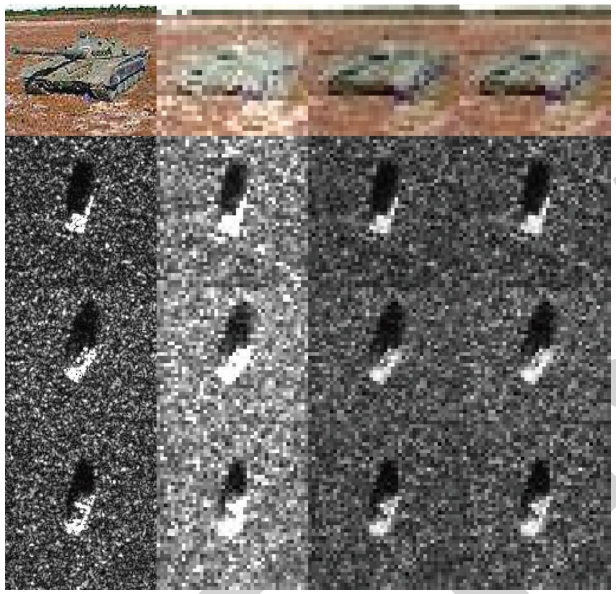

Figure 6: Results for different pooling.

calculated by the SE module are close to 1, which does not reflect the importance of the channel.

Global pooling performs max pooling or average pooling on the entire feature map to obtain a $1 \times 1 \times C$ vector, but this also will lose feature information. Therefore, we think of replacing the global pooling of the SE module with SoftPool to ensure that the dominant feature map has a high weight. Figure 8 gives the calculation results of the two feature matrices under global pooling and soft pooling. (1) can represent the edge information of the target and contains more information amount than (2), but both matrices have the same calculation result, both 4, under global pooling, and cannot distinguish the importance of the channels. When the weight matrix is multiplied with the feature matrix after using soft pooling, the output of (1) is 5.724, and the output of (2) is 3.69, which can make the feature matrix containing more information have greater channel weights and solve the problem of uniform weight distribution of SE module.

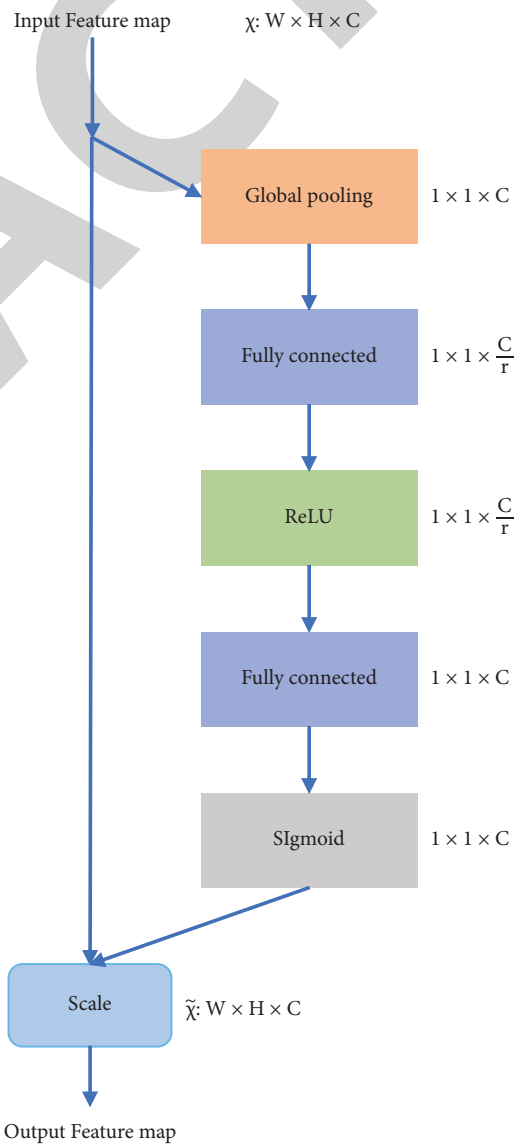

Figure 7: The fusion of multifeature images. The structure of the SE module [30].

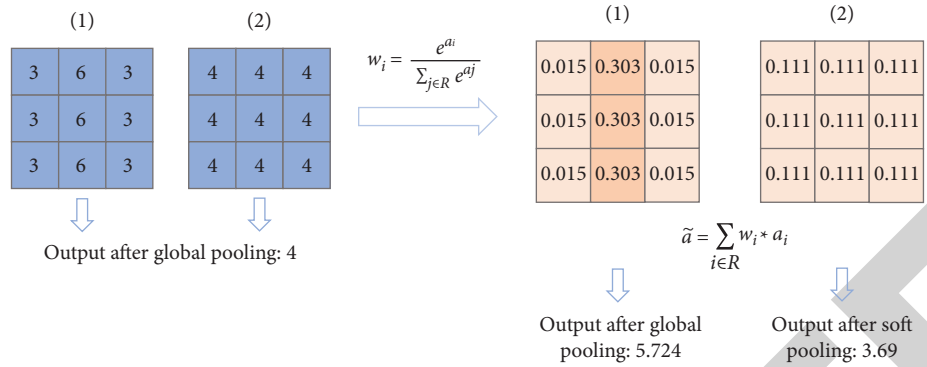

Figure 8: Calculation of global average pooling and soft pooling.

2.6. Analysis with Channel-Wise Activation Maps. Because the deep network will easily lead to overfitting when doing training and recognition with few samples, this paper builds a simple CNN. The structure of the network is designed as Figure 9. (a) is the basic CNN network, and (b) is the shape enhancement network used in this paper.

Figure 10 illustrates the visualization of the features map from the network using the SE module and using the SoftPool-SE module respectively. SoftPool-SEnet clearly highlights certain channels compared to the SE module.

Figure 11 shows the 16 maps of adding different modules in the first convolutional layer. Compared with feature map in (a), that in (b) obviously removes the texture information brought by the background noise and enhances the network's attention to the target's shape. The feature map in (c) adds a lot of information, where SoftPool is used in the network. The network in (d) uses ordinary SE module, but compared with feature map of (d), there are more dark pixels, and more information is lost. The bright pixels of the target in (e) are increased because of the use of enhanced SE module.

2.7. Configuration Specifics in the Enhanced-Shape CNN. The convolutional layer maps the input to a new feature map with a convolutional kernel to perform local perception of the target. Pooling layer is a subsampling to reduce trainable parameters. In order to prevent the problems such as declined convergence speed and poor generalization performance due to the different distributions of the training set and the test set, we adopted batch normalization in the network.

For all convolutional layers, the stride is set to 1, and no spatial zero padding is used in the convolution layer. Meanwhile, the activation function adopts ReLU nonlinearity. Each of the first three convolutional layers is followed by a soft pooling layer with a pooling size of 2×2 and a stride of 1. The size of the input enhance-shape image is $128 * 128$. After the first convolutional layer, where the size of convolution kernel is 5×5, the size of output feature map is $124 * 124$, and their size becomes 62×62 after the first layer of pooling layer. The 62×62 input image was filtered by convolution kernel of size 6×6 in the second convolutional layer, resulting in feature map of size 57×57. After the second pooling, the feature map becomes of size 28×28. At this time, the 28×28 feature map is input into the SoftPool-SE module, and the learning channel has different weights while the output feature map size is still $28 * 28$. The filter kernel of the third convolutional layer is of size 7×7, producing feature map of size 22×22, which becomes 11×11 after pooling and SoftPool-SE module. The convolution kernel of the last layer is $7 * 7$, which brings out 5×5 feature map. Finally, through two fully connected layers and a softmax classifier, 10 vectors are obtained, corresponding to the class probabilities.

In this paper, the loss function is cross entropy loss, and the optimization algorithm uses stochastic gradient descent, with the momentum parameter of 0.9 and the weight decay parameter of 0.005. Subsequently, the learning rate is initially 0.001 and is reduced by a factor of 0.5 after 20 epochs, where epoch denotes the number of times each example has used during training. Finally, batch size is set to 8.

3. Experiments on MSTAR Dataset

3.1. Dataset Description. The experiment data set in this paper is the MSTAR public data set, where the resolution of all images is $0.3\ \text{m} \times 0.3\ \text{m}$, and the polarization mode used is HH polarization mode. The data set contains hundreds of thousands SAR images, covering military targets of different categories, aspect angles, and depression angles, of which only a small part is publicly available. They were collected by *X* band, full aspect coverage (in the range of 0° to 360°).

The disclosed data set includes ten types of ground vehicle targets: armored personnel carrier (BMP-2, BRDM-2, BTR-60, and BTR-70); tank (T-62, T-72); rocket launcher (2S1); air defense unit (ZSU-234); truck (ZIL-131); bulldozer (D7). Figure 12 shows examples of ten types of targets and their corresponding optical images.

When the MSTAR data set is used in SAR ATR, it is often divided into standard operating conditions (SOC) and extended operating conditions (EOC). SOC means that the target configuration and serial number of the test set and training set are the same, and depression angles are different but close. EOC indicates that there is a big difference between the test set and the training set, including target configuration and image clarity.

SOC is a dataset that consists of images with an imaging condition of 17° depression angle as the training set, and 15°

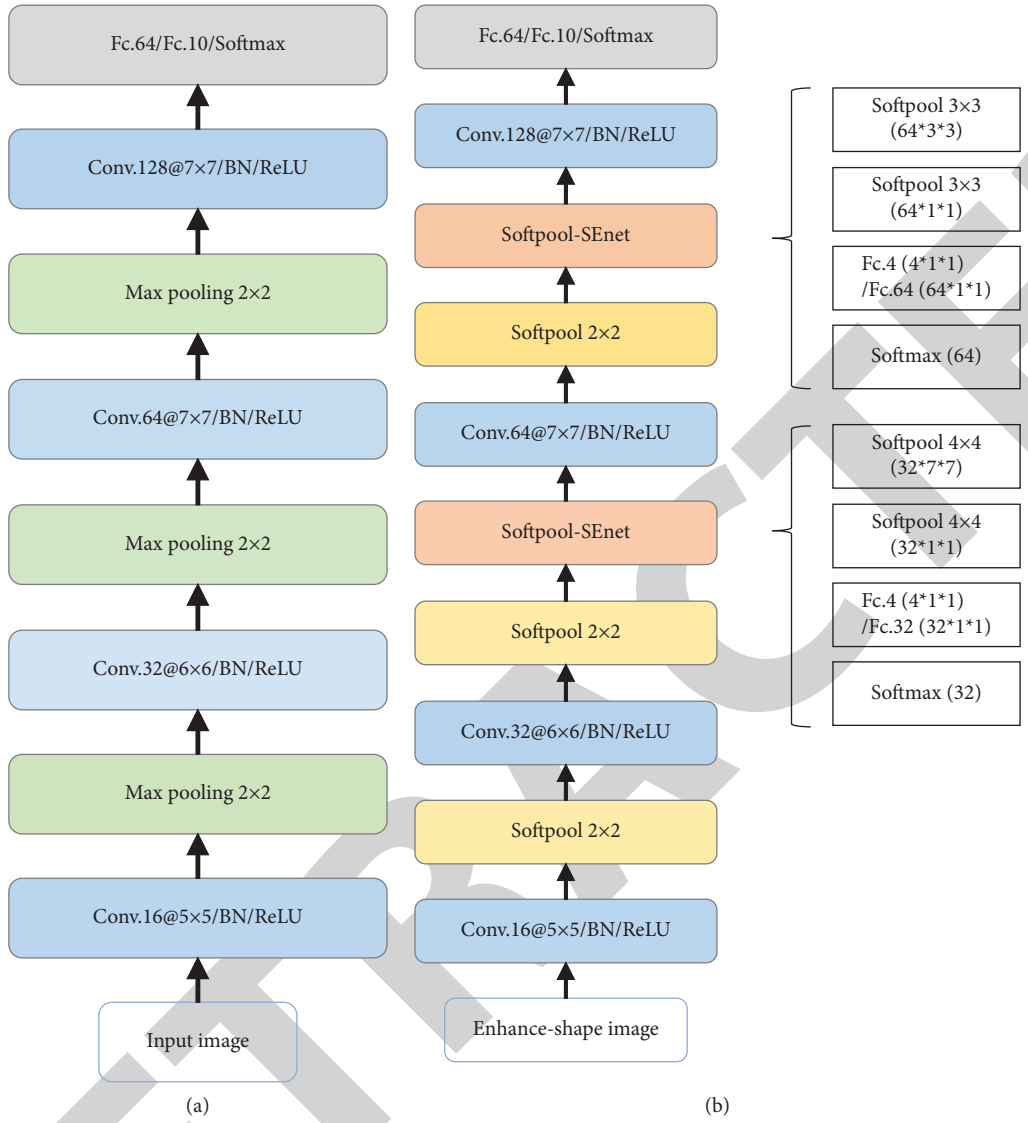

Figure 9: Network structure. Next to the network structure is the size of the feature map. (a) CNN. (b) Enhanced-shape CNN.

depression angle as the test set. The number of test and training samples for each category and the total number of samples are shown in Table 1.

In addition to SOC dataset, we have also set up several EOC datasets. Configuration change refers to the addition or removal of some parts on the vehicle, such as whether the T72 has an oil tank behind the vehicle. In this paper, these two changes are referred to as EOC-1 and EOC-2, i.e., configuration variants and version variants. The specific information of the EOC-1 and EOC-2 data set is listed in Tables 2 and 3. The training set is BMP2, BRDM-2, BTR-70, and T72 with 17° depression, and the test set only includes variants of T72 with 15° depression and 17° depression. The training set of EOC-2 is the same as EOC-1. The test set contains variants of T72 and BMP-2.

Moreover, the image signal-noise ratio of MSTAR is as high as 30 dB, but most images in actual situations contain noise. We set EOC-3 dataset, which adds noise to the MSTAR data [33] to simulate a noisy situation. The method of adding noise is as follows:

$$\mathrm{SNR} = 10\log_{10} f\left[\frac{\mathrm{var}(\text{original image})}{\mathrm{var}(\text{error image})}\right], \tag{10}$$

where var is a variance operator. The result is shown in Figure 13.

3.2. Result of SOC. Table 4 shows a confusion matrix, whose row represents the actual target category, and column represents the predicted target category. It is observed that the recognition rate of all targets has reached more than 96%, and the overall recognition rate has reached 99.29%. The recognition rate of each method is listed in Table 5. Compared with other methods, our method got the highest recognition rate, verifying the effectiveness of the proposed method.

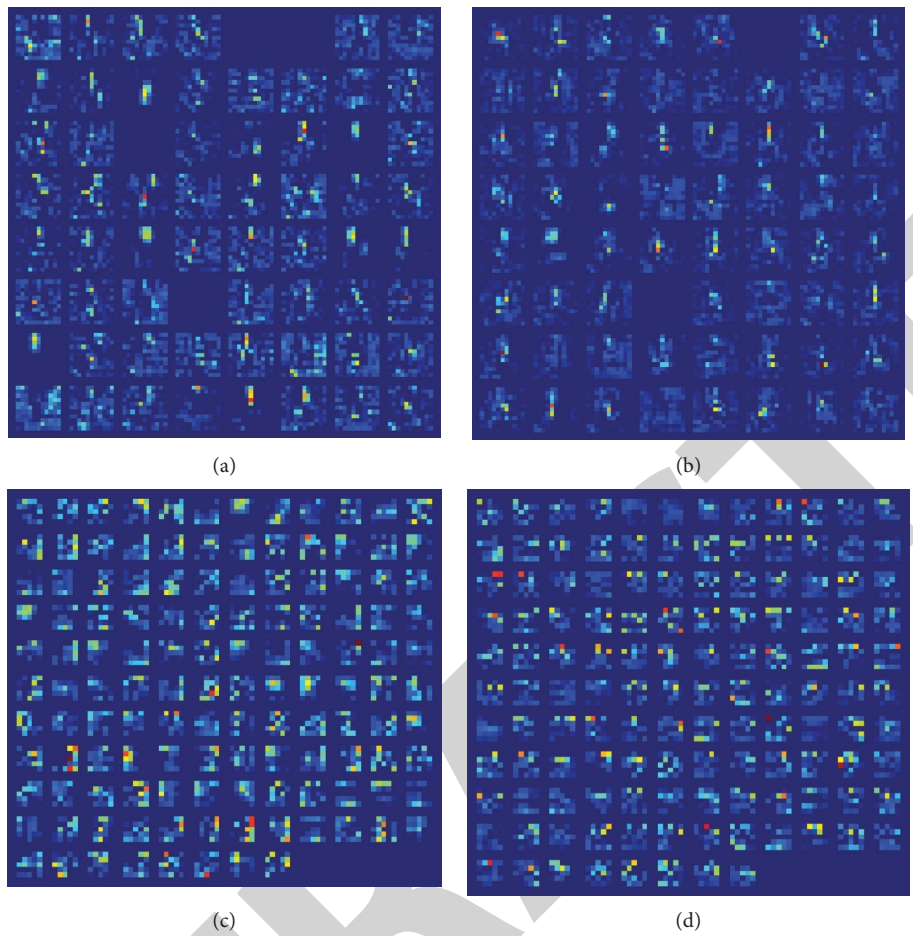

(a) (b) (c) (d)

Figure 10: Visualization of feature maps: (a) output by first SE module; (b) output by first SoftPool-SE module; (c) output by second SE module; (d) output by second SoftPool-SE module.

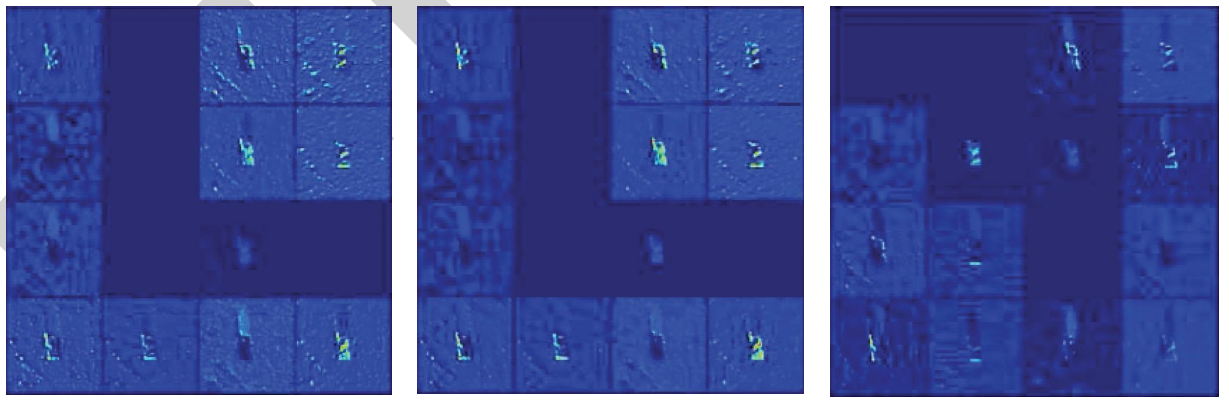

(a) (b) (c)

Figure 11: Continued.

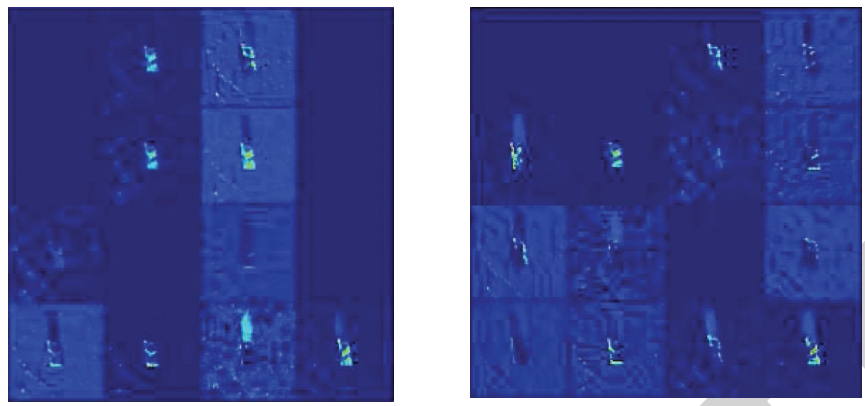

(d) (e)

Figure 11: (a) The basic network. (b) Basic network using enhanced-shape data set. (c) SoftPool is used on the basic network, where enhanced-shape dataset is inputted. (d) SoftPool and SE module are used on the basic network, where enhanced-shape data set is inputted. (e) SoftPool and enhanced SE module are used on the basic network, where enhanced-shape data set is inputted.

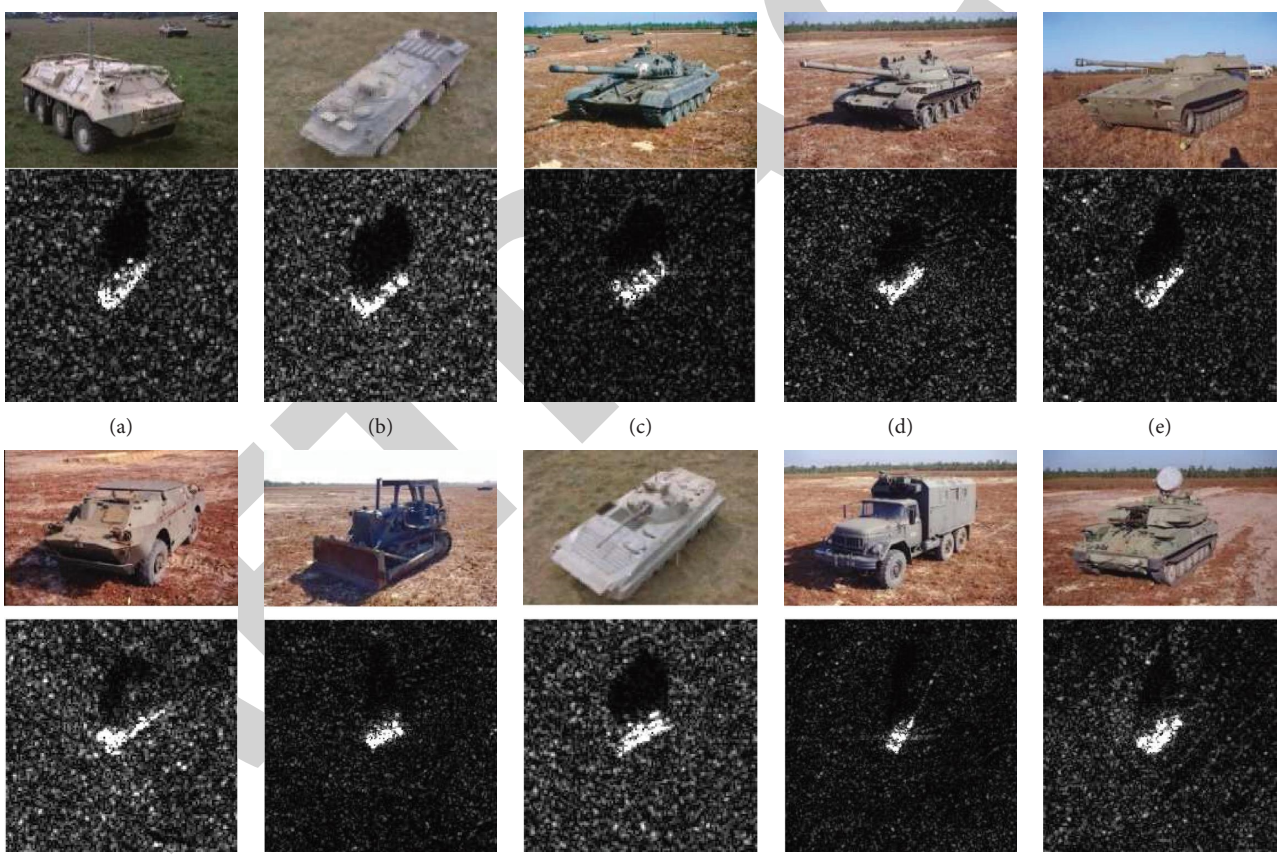

(a) (b) (c) (d) (e)

(f) (g) (h) (i) (j)

Figure 12: Optical image (top) and SAR image (bottom) of ten types of vehicle targets.

In order to verify that enhanced-shape CNN can also achieve better recognition on a few-sample data set, we set training sets of 100%, 50%, 25%, and 12.5%, respectively, while the size of the testing set remains the same to calculate the recognition rate. The comparison network we used is the basic CNN network pointed out in Figure 9.

As shown in Table 6, in the case of the full training set, the enhanced-shape CNN has reached a recognition rate of more than 99%, which is not much improvement compared to the basic CNN. When we only use 50%, 25%, and 12.5% training sets separately, there will be a corresponding increase of 1.18%, 2.23%, and 4.56%. Compared with the

Table 1: Number of training and test samples for SOC.

Class	Train		Test	
	Depression	Number	Depression	Number
BRDM2	17°	298	15°	274
BTR60	17°	256	15°	195
T72	17°	232	15°	196
2S1	17°	299	15°	274
D7	17°	299	15°	274
BMP2	17°	232	15°	196
ZIL131	17°	299	15°	274
ZSU23/4	17°	299	15°	274
BTR70	17°	233	15°	196
T62	17°	299	15°	273

Table 2: Number of training and test samples for EOC-1 (configuration variants).

	Train			Test	
Class	Depression	Number	Class	Depression	Number
BMP2(9563)	17°	233	T-72(S7)	15° 17°	419
BRDM-2(E71)	17°	298	T-72(S32)	15° 17°	572
BTR-70(c71)	17°	233	T-72(S62)	15° 17°	573
T-72(132)	17°	232	T-72(S63)	15° 17°	573
			T-72(S63)	15° 17°	573

Table 3: Number of training and test samples for EOC-2 (version variants).

	Train			Test	
Class	Depression	Number	Class	Depression	Number
BMP2(9563)	17°	233	T-72(812)	15° 17°	426
BRDM-2(E71)	17°	298	T-72(A04)	15° 17°	573
BTR-70(c71)	17°	233	T-72(A05)	15° 17°	573
T-72(132)	17°	232	T-72(A07)	15° 17°	573
			T-72(A10)	15° 17°	567
			BMP-2/9566	15° 17°	428
			BMP-2/C21	15° 17°	429

experimental results of other methods under small sample data sets, the method proposed in this paper is also far superior to other methods.

Due to the standard of the MSTAR data set, it is relatively simple to segment the target and the shadow area, but the actual situation is often more complicated, so the target and the shadow may not be completely segmented. In order to verify the robustness of our algorithm, we can make a slight deviation when doing threshold segmentation. The deviation image has been given in Figures 2(c) and 2(e), corresponding to set the segmentation threshold to 0.1 and 0.9, and 0.3 and 0.7, respectively.

It can be seen in Figure 14 that even when the segmentation algorithm is not ideal, our method still has a higher recognition rate than CNN on a small number of samples. The shape and shadow area are extracted to highlight the target and enhance the network's learning of target information. Therefore, even when the segmentation algorithm is slightly deviated, it can still achieve better recognition results than the original data.

3.3. Result of EOC. This paper tests the recognition accuracy on two types of data sets, EOC-1 and EOC-2, to further test the effectiveness of the proposed method for refined recognition. The tested confusion matrix is shown in Tables 7 and 8. According to the experimental results, the methods proposed on the EOC-1 and EOC-2 data sets both have achieved good recognition results. The recognition rate reached 99.3% under EOC-1, while it reached 98.85% under EOC-2. It illustrates that when the target changes slightly, such as the addition or removal of fuel tanks, the network can achieve better recognition results.

Figure 15 shows the comparison curves of the recognition rates obtained by the two networks on training sets of different sizes under different noises. It can be seen that our proposed method has achieved a higher recognition rate than ordinary CNN on different data quality. When the signal-to-noise ratio is −5 dB and −10 dB, the recognition rate in enhanced-shape CNN, which uses the 12.5% training set, is improved by nearly 20% compared to that in CNN.

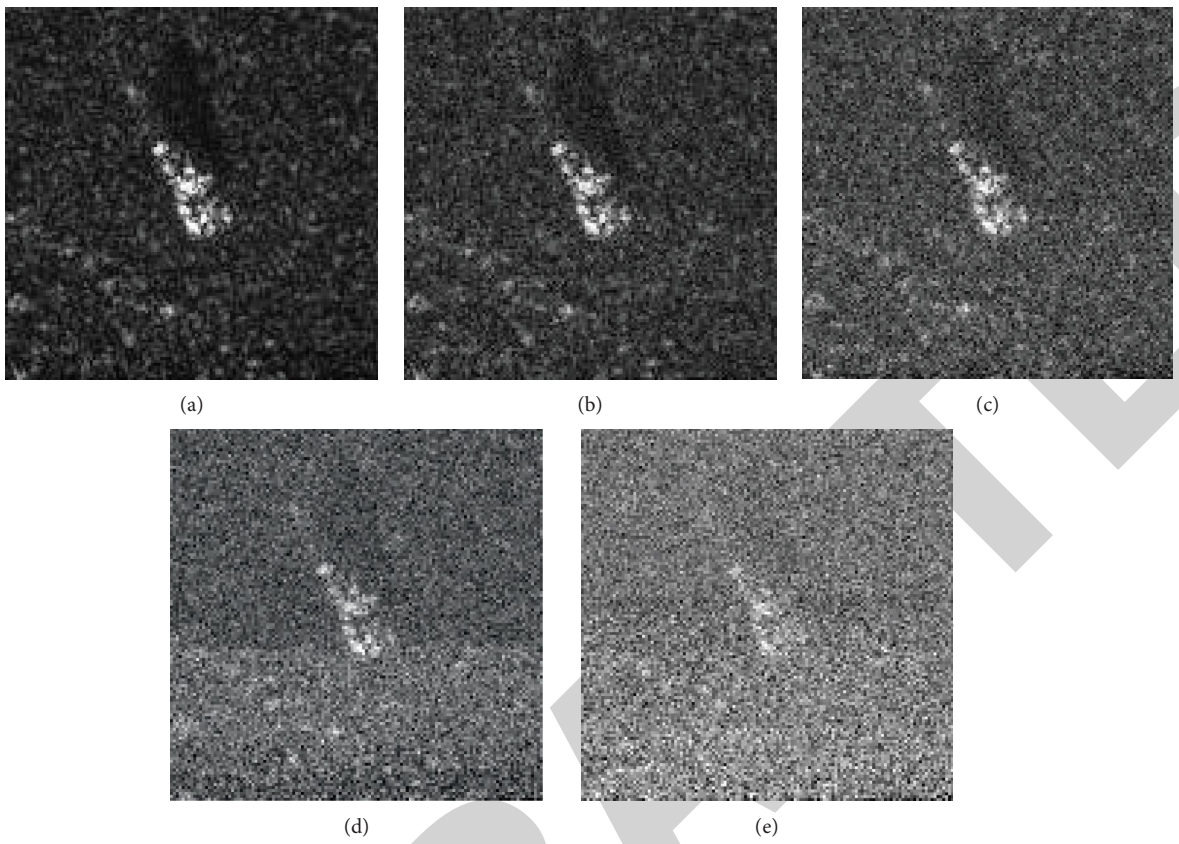

Figure 13: Image after adding different noises.

Table 4: Confusion matrix of Enhanced-shape CNN.

Class	BRDM2	BTR60	T72	2S1	D7	BMP2	ZIL131	ZSU23/4	BTR70	T62	P_{cc} (%)
BRDM2	**272**	0	0	0	0	0	1	1	0	0	99.27
BTR60	4	**189**	0	1	0	0	0	1	0	0	96.92
T72	0	0	**196**	0	0	0	0	0	0	0	100
2S1	0	0	0	**271**	0	0	0	0	0	3	98.91
D7	0	0	0	0	**272**	0	2	0	0	0	99.27
BMP2	0	0	2	0	0	**194**	0	0	0	0	98.98
ZIL131	0	0	0	0	0	0	**274**	0	0	0	100
ZSU23/4	0	0	0	0	1	0	0	**273**	0	0	99.64
BTR70	0	0	0	0	0	0	0	0	**196**	0	100
T62	0	0	0	1	0	0	0	0	0	**272**	99.63
Overall											99.29

Table 5: Performances of different methods.

Method	Accuracy (%)
ACS [34]	95.54
CNN-LSTM [24]	98.78
Multiview-DCNN [35]	98.52
CHU-Net [36]	99.09
A-Convnet [22]	99.13
Enhanced-shape CNN	99.29

Table 6: Recognition rate on different sizes of training set.

Method	Training dataset size			
	100%	50%	25%	12.5%
CNN	99.11	97.65	95.92	85.37
Enhanced-shape CNN	99.29	**98.83**	**98.15**	**89.93**
ARGN [37]	98	97.28	—	—
DS-AE Net [38]	**99.30**	98.06	95.42	—
TAI-SARNET [39]	97.97	93.22%	88.69	76.27

Table 7: Confusion matrix of Enhanced-shape CNN under EOC-1 (configuration variants).

Class	Variants	BMP-2	BTR-70	T-72	BRDM-2	P_{cc} (%)
T-72	S7	6	7	406	0	96.897
	A32	2	0	570	0	99.65
	A62	0	0	573	0	100
	A63	0	0	572	1	99.83
	A64	3	0	570	0	99.48
Total						99.30

Table 8: Confusion matrix of Enhanced-shape CNN under EOC-2 (version variants).

Class	Variants	BMP-2	BTR-70	T-72	BRDM-2	P_{cc} (%)
BMP-2	9566	414	5	7	2	96.73
	c21	420	0	7	2	97.90
T-72	812	2	11	413	0	96.95
	A04	0	0	572	1	99.83
	A05	0	0	573	0	100
	A07	1	0	571	1	99.65
	A10	2	0	565	0	99.65
Total						98.85

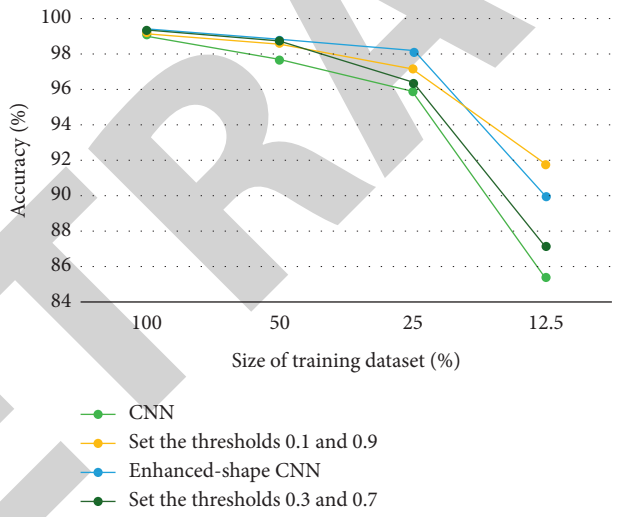

Figure 14: Recognition results under different segmentation thresholds.

3.4. Ablation Experiment. In order to verify the influence of different modules on the performance of the model, ablation experiments are also carried out in this paper. We set up different inputs, respectively, selecting the original image, filtering the image, and extracting the target and shadow image, and the fusion image, to verify that the data enhancement of the fusion of multiple features is effective.

Figure 16 shows the recognition rates obtained for several inputs. The recognition rate of a single filtered image and segmented image is lower than that after fusion. When only the segmented image is input, it is found that the recognition rate is lower than that of the original image input. This is because we extract the target and shadow area only to strengthen the network's attention to the target and shadow. If only the target and shadow are input, the target information will be incomplete owing to the segmentation algorithm, so the recognition rate without inputting the original data is high.

Figure 17 shows the recognition rate using a single module. It can be seen that the different modules used in this

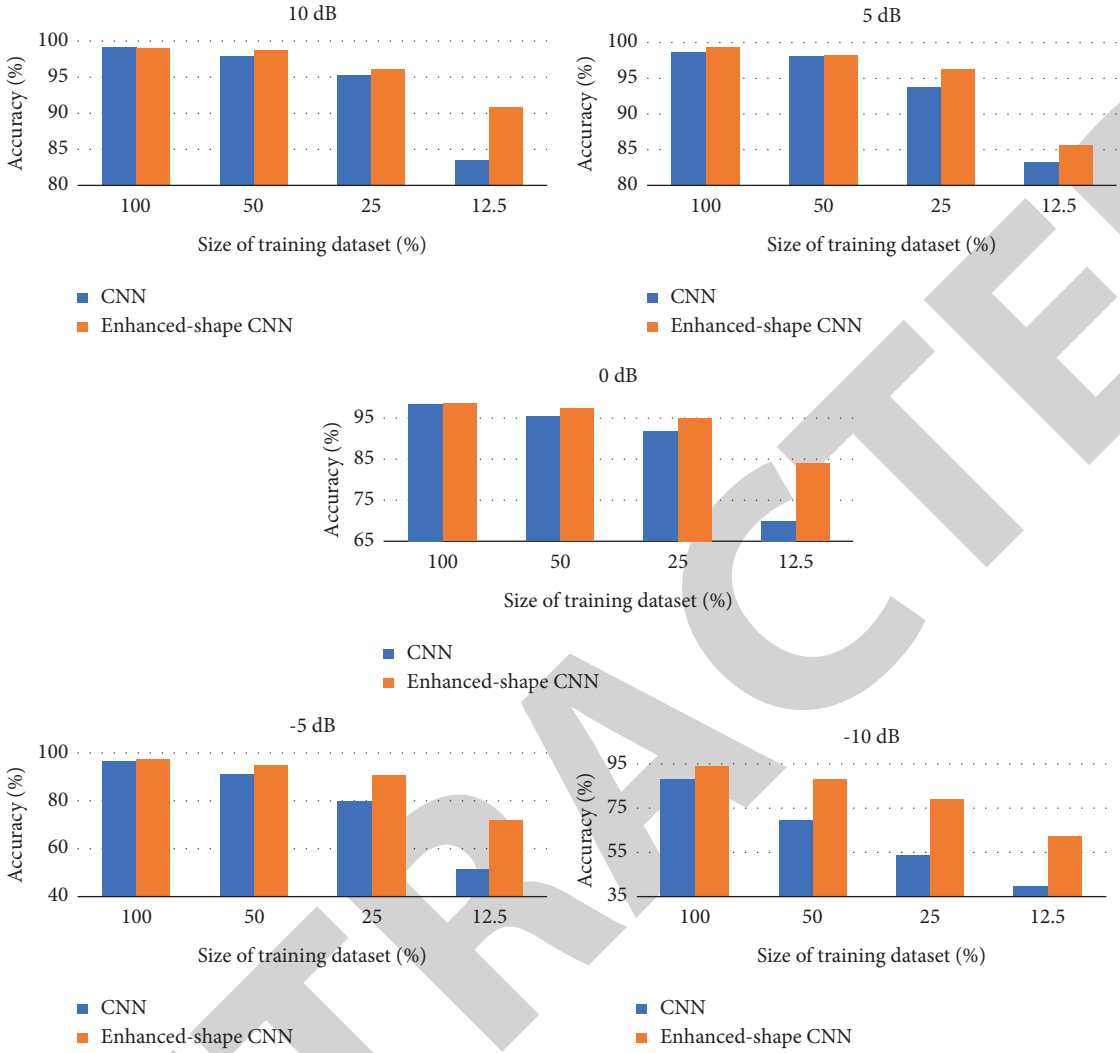

Figure 15: Performance comparison of enhanced-shape CNN and CNN under different signal-to-noise ratios.

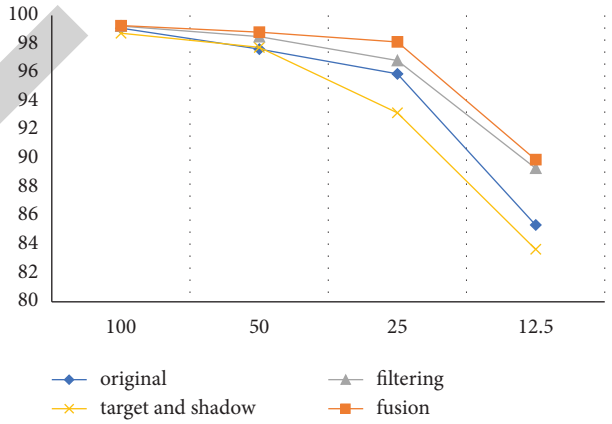

Figure 16: Recognition rate under different input.

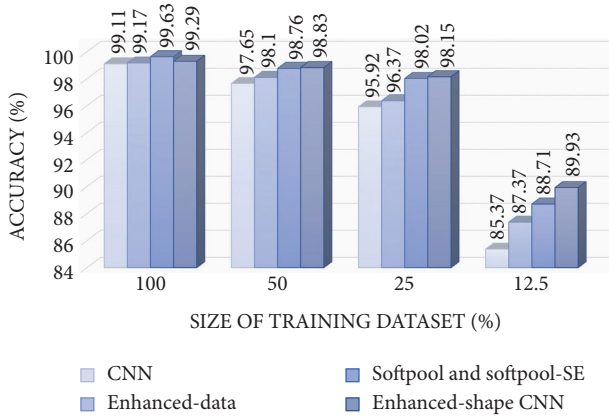

Figure 17: Results of ablation experiments.

paper have an effect on the recognition accuracy of the model.

4. Conclusions

SAR ATR has become an important and promising field of remote sensing image processing. This paper proposed a method from the perspective of shape enhancement with filtering and enhancing target area at the input and synthesizing to strengthen the connection between channels. Simultaneously, the information loss due to ordinary pooling is reduced by the application of SoftPool in CNN. Moreover, the SE module has been improved to highlight the prominent channels for recognition results. As a result, more target information is obtained on a few samples. The experiments verified the accuracy of proposed method, which can achieve an accuracy of 99.29% on ten types of targets, and when the segmentation effect is not good, which is closer to the actual situation, it also has higher performance than CNN. This paper also proved the robustness of the method under noise. In the case of varying degrees of noise, the proposed method is greatly improved compared to CNN when there are few samples. The basic approach proposed in this paper can continue in the future to explore the method of balancing texture features and shape features and guide the directional training of the network based on the attention mechanism.

Data Availability

The data used to support the findings of this study are included within the article.

Conflicts of Interest

The authors declare that they have no competing interest.

Acknowledgments

The authors did not receive specific funding.

References

[1] X. Bai, R. Xue, L. Wang, and F. Zhou, "Sequence SAR image classification based on bidirectional convolution-recurrent network," *IEEE Transactions on Geoscience and Remote Sensing*, vol. 57, no. 11, pp. 9223–9235, 2019.

[2] H. Xu, Z. Yang, M. Tian, Y. Sun, and G. Liao, "An extended moving target detection approach for high-resolution multichannel SAR-GMTI systems based on enhanced shadow-aided decision," *IEEE Transactions on Geoscience and Remote Sensing*, vol. 56, pp. 715–729, 2017.

[3] C. Clemente, L. Pallotta, D. Gaglione, A. De Maio, and J. J. Soraghan, "Automatic target recognition of military vehicles with krawtchouk moments," *IEEE Transactions on Aerospace and Electronic Systems*, vol. 53, no. 1, pp. 493–500, 2017.

[4] P. Tait, *Introduction to Radar Target Recognition*, Vol. 18, IET, , London, UK, 2005.

[5] Y. Zhai, W. Deng, T. Lan et al., "MFFA-SARNET: deep transferred multi-level feature fusion attention network with dual optimized loss for small-sample SAR ATR," *Remote Sensing*, vol. 12, no. 9, p. 1385, 2020.

[6] O. Kechagias-Stamatis, "Automatic target recognition on synthetic aperture radar imagery: a survey," 2020, https://arxiv.org/abs/2007.02106.

[7] A. Moreira, P. Prats-Iraola, M. Younis, G. Krieger, I. Hajnsek, and K. P. Papathanassiou, "A tutorial on synthetic aperture radar," *IEEE Geoscience and Remote Sensing Magazine*, vol. 1, no. 1, pp. 6–43, 2013.

[8] P. Wang, W. Liu, J. Chen, M. Niu, and W. Yang, "A high-order imaging algorithm for high-resolution spaceborne SAR based on a modified equivalent squint range model," *IEEE Transactions on Geoscience and Remote Sensing*, vol. 53, pp. 1225–1235, 2014.

[9] R. L. Dudgeon, "An overview of automatic target recognition," *Lincoln Laboratory Journal*, vol. 6, pp. 3–10, 1993.

[10] L. Novak, G. Owirka, W. Brower, and A. Weaver, "The automatic target-recognition system in SAIP," *Lincoln Laboratory Journal*, vol. 10, pp. 187–201, 1997.

[11] G. Owirka, S. Verbout, and L. Novak, "Template-based SAR ATR performance using different image enhancement techniques," *Proceedings of SPIE*, vol. 3721, pp. 302–319, 1999.

[12] C. Clemente, L. Pallotta, I. Proudler, A. De Maio, J. J. Soraghan, and A. Farina, "Pseudo-Zernike-based multi-pass automatic target recognition from multi-channel synthetic aperture radar," *IET Radar, Sonar & Navigation*, vol. 9, no. 4, pp. 457–466, 2015.

[13] Y. Sun, L. Du, Y. Wang, Y. Wang, and J. Hu, "SAR automatic target recognition based on dictionary learning and joint dynamic sparse representation," *IEEE Geoscience and Remote Sensing Letters*, vol. 13, no. 12, pp. 1777–1781, 2016.

[14] L. M. Novak, G. R. Benitz, G. J. Owirka, and L. A. Bessette, "ATR performance using enhanced resolution SAR," in *Algorithms for Synthetic Aperture Radar Imagery III*, pp. 332–337, International Society for Optics and Photonics, Bellingham, WA, USA, 1996.

[15] K. El-Darymli, E. W. Gill, P. McGuire, D. Power, and C. Moloney, "Automatic target recognition in synthetic aperture radar imagery: a state-of-the-art review," *IEEE Access*, vol. 4, pp. 6014–6058, 2016.

[16] Z. He, J. Lu, and G. Kuang, "A Fast SAR target recognition approach using PCA features," in *Proceedings of the*

Hindawi
Journal of Mathematics
Volume 2023, Article ID 9891376, 1 page
https://doi.org/10.1155/2023/9891376

Retraction

Retracted: Popular Song Composition Based on Deep Learning and Neural Network

Journal of Mathematics

Received 19 December 2023; Accepted 19 December 2023; Published 20 December 2023

This article has been retracted by Hindawi following an investigation undertaken by the publisher [1]. This investigation has uncovered evidence of one or more of the following indicators of systematic manipulation of the publication process:

(1) Discrepancies in scope

(2) Discrepancies in the description of the research reported

(3) Discrepancies between the availability of data and the research described

(4) Inappropriate citations

(5) Incoherent, meaningless and/or irrelevant content included in the article

(6) Manipulated or compromised peer review

The presence of these indicators undermines our confidence in the integrity of the article's content and we cannot, therefore, vouch for its reliability. Please note that this notice is intended solely to alert readers that the content of this article is unreliable. We have not investigated whether authors were aware of or involved in the systematic manipulation of the publication process.

Wiley and Hindawi regrets that the usual quality checks did not identify these issues before publication and have since put additional measures in place to safeguard research integrity.

We wish to credit our own Research Integrity and Research Publishing teams and anonymous and named external researchers and research integrity experts for contributing to this investigation.

The corresponding author, as the representative of all authors, has been given the opportunity to register their agreement or disagreement to this retraction. We have kept a record of any response received.

References

[1] J. Kuang and T. Yang, "Popular Song Composition Based on Deep Learning and Neural Network," *Journal of Mathematics*, vol. 2021, Article ID 7164817, 7 pages, 2021.

Hindawi
Journal of Mathematics
Volume 2021, Article ID 7164817, 7 pages
https://doi.org/10.1155/2021/7164817

Research Article

Popular Song Composition Based on Deep Learning and Neural Network

Jun Kuang and Tingfeng Yang

Music Education, Hunan Normal University, Changsha, China

Correspondence should be addressed to Tingfeng Yang; 14684@hunnu.edu.cn

Received 26 October 2021; Accepted 24 November 2021; Published 22 December 2021

Academic Editor: Naeem Jan

For the general public, composition appears to be professional and the threshold is relatively high. However, automatic composition can improve this problem, allowing more ordinary people to participate in the composition, especially popular music composition, so the music becomes more entertaining, and its randomness can also inspire professionals. This article combines deep learning to extract note features from the demonstration audio and builds a neural network model to complete the composition of popular music. The main work of this paper is as follows. First, we extract the characteristic notes, draw on the design process of mel-frequency cepstral coefficient extraction, and combine the characteristics of piano music signals to extract the note characteristics of the demonstration music. Then, the neural network model is constructed, using the memory function of the cyclic neural network and the characteristics of processing sequence data, the piano notes are combined into a sequence according to the musical theory rules, and the neural network model automatically learns this rule and then generates the note sequence. Finally, the ideal popular piano music scores are divided into online music lover scores and offline professional ratings. The score index is obtained, and each index is weighted by the entropy weight method.

1. Introduction

tThe spiritual and cultural needs of the people have grown rapidly due to the development of our country's economy and society and the improvement of material living standards. It shows that the characteristics of multi-level, multi-form and diversified, cultural consumption ability have been greatly enhanced, and the level of appreciation has been continuously improved. Music art reflects the real emotions of human beings. It helps people find the connotation of their thoughts. Moreover, it brings the sincerest resonance and power. Thus, the art of music plays an important role in people's spiritual world.

The piano has a magnificent sound, a wide range, full of variation, and strong expressiveness. The piano occupies an important position in music creation and rehearsal due to its rich musical theory expression ability. At present, people's work music requires professional knowledge of basic music theory, musical style, harmony, etc., in order to create music scores marked with basic content such as speed and chords. Composers often do not think out of thin air when they are composing music. Most composers like to use guitar or piano to create while playing. The finished product is usually sheet music, which will be marked with basic content such as speed and chords as well as the arrangement of the music and some basic ideas of style [1]. For ordinary users, the professionalism and threshold of composition are too high.

After more than 60 years of evolution, driven by new theories and technologies such as mobile Internet, big data, supercomputing, brain science, and social development needs, artificial intelligence has accelerated its development, showing new features such as deep learning and cross-border integration [2, 3]. In recent years, artificial intelligence has developed rapidly in the field of composition, breaking through the constraints of human work music, so human needs to master profound music theory. Artificial intelligence is capable of creating fresh music and improving the efficiency of music creation and the performance of music. Domestic and foreign technology giants have also significantly commercialized the practices in this field, and

some of their works can pass the Turing test, reaching a level that ordinary users cannot distinguish.

The significance of this article's topic selection is as follows:

(i) First and foremost, promote music learners to have a better understanding of the field of popular music. This can be achieved through the analysis of popular music piano creation.

(ii) Secondly, the combination of popular music and deep learning establishes an artificial neural network piano automatic composition method. This will give song creators certain inspirations, so that people in general can participate in the creation of popular music, accumulate the amount of popular music piano pieces, give it to popular music, and bring more possibilities for music creation.

(iii) Thirdly, the qualified and capable piano educators should make more creations and try more. To this end, they have to master and learn from the piano creation techniques of popular music, integrate popular music piano creation into one's own piano teaching, and enhance students' interest in piano learning and musical creativity. In addition, their overall musical quality, cooperation, and communication skills will improve [4].

The following section highlights some of the related works. Section 3 describes the methods of the proposed study. In Section 4, the experimental results are analyzed, and Section 5 concludes the research.

2. Related Work

At present, searching for the keyword "popular music" related to this topic, we have obtained more than 1,000 related documents on CNKI; Wan F database collected more than 400 relevant art articles. The author believes that the "popular" here is not simply defined by the broad masses, and its premise comes from the division of regions [5]. Whether it is American jazz or Chinese pop music and whether it is Gershwin's "Rhapsody in Blue" or Li J H's "Drizzle," this belongs to the category of popular music. Popular music includes pop music, light music, jazz music, rock music, and so on. By reviewing the related literature of popular music, the authors found that the field of popular music has its unique charm. The authors believe that music has no borders, but popular music has its own borders. According to literature research, the development of popular music in modern China began with the "school music and songs" promoted in schools. In the 1920s and 1930s, popular anti-Japanese mass songs that inspired the people's fighting spirit played a huge role in the war. At the same time, the creation of urban music represented by Li J H has also been greatly developed, which has promoted the development of the field of modern popular music in our country. Although the notation technology and media of that era were relatively backward, most of them were appreciated in the form of radio, but as a symbolic product of the era, its existence itself was communicative. Nowadays, the development of popular music is very rapid, and the forms of dissemination and programs are also diversified. Music from all over the world can be communicated with each other through television, the Internet, and other means, and it is spread widely. While preserving the classics, the repertoire is updated very quickly. From the perspective of current music culture, it can also be found that popular music repertoires have also come to the fore in various competitions and are loved by the masses.

As early as the 1960s, there were attempts to combine computers with traditional music. In 1956, Hiller and Isaacson created the world's first string quartet that was completely computer-generated [6]. The famous music intelligence system EMI was developed by Professor David Cope. It uses a pattern matching algorithm to extract music sequence features in music works and assigns corresponding weights according to the frequency of feature appearance. The final generated music style is similar to the original work style [7]. Markov chain has Markov properties in probability theory and mathematical statistics [8]. Many scholars used Markov chains to study algorithmic composition. Visell used hidden Markov chains to implement a manual tuning real-time music system [9]. Genetic algorithm is a computational model in biological evolution, which can be used for reference in artificial music creation [10]. Many related studies have used genetic algorithms to achieve music composition. The GenJam system constructed by Biles selects a chord. Based on this chord, a jazz solo melody can be created. This system has the function of interactive improvisation [11].

Artificial neural network is a computational model that imitates neurology and biology. It is widely used in music creation systems and has achieved certain success. Eck and Schmidhebuer used LSTM to initially explore the creation of music. Compared with the previous music creation with RNN that can only capture the local structure of the music, LSTM can capture and reproduce the long-term music structure, and the final generated music can follow the chord law [12]. Franklin used LSTM to learn music knowledge; taking into account the coordination of music structure, the final model can improvise a piece of music [13]. Smith and Garnett used the deep neural network reinforcement learning model to generate music and improve the quality of music works through creativity [14].

3. Method

In this section, the methods of the proposed study are explained, such as audio file feature extraction and automatic composition neural network model construction.

3.1. Audio File Feature Extraction. The audio file feature extractions are illuminated separately. The classification is based on the features.

3.1.1. Mel-Frequency Cepstral Coefficient (MFCC). Music signals and speech signals have similarities. In the field of speech recognition and speech reconstruction, mel-frequency cepstral coefficient (MFCC) is commonly used to extract the characteristics of speech signals [15]. MFCC takes into account the auditory characteristics of the human ear but does not take into account the music and the music theory characteristics. Short-time Fourier transform is used in MFCC extraction. Short-time Fourier transform is the most commonly used time-frequency analysis method, which can be used to process nonstationary signals whose frequency changes with time. Specifically, the original signal is divided into many time periods with a window function, and Fourier transform is performed on it in each time period [16]. The short-time Fourier transform (STFT) was proposed by Gabor in 1946. For a continuous signal $x(t)$, the STFT is defined as follows:

$$\mathrm{STFT}(t, w) = \int_{-\infty}^{+\infty} x(\tau) w(\tau - t) e^{-jw\tau} \mathrm{d}\tau, \tag{1}$$

where $x(t)$ is the window function. The choice of the length of the window function affects the time resolution and frequency resolution. The longer the length of the window function, the worse the time resolution and the higher the frequency resolution after Fourier transform; on the contrary, the shorter the length of the window function, the better the time resolution and the worse the frequency resolution [17].

3.1.2. Cepstral Coefficient Extraction. Figure 1 shows a flowchart of the entire MFCC extraction, each step of which will be explained below. In the first step, the input original signal $x(t)$ is divided into frames, and then each frame of signal is processed to obtain each frame of signal $x(t)$ and then the Fourier transform is performed:

$$X(k) = \sum_{n=0}^{N-1} x(n) e^{-j2\pi k/N}, \quad 0 \le n, k \le N - 1. \tag{2}$$

A series of transformations are performed on the above equation, and the MFCCs are extracted:

$$C(n) = \sum_{n=0}^{M-1} S(m) \cos\left(\frac{\pi n(m + 0.5)}{M}\right), \quad 0 \le n \le M. \tag{3}$$

3.1.3. Note Feature Extraction. This paper extracts piano note features, referring to the process of MFCC feature extraction, and uses a filter-based algorithm to extract the fundamental frequency. The design principle of the filter refers to the twelve-average law because each key of the piano is tuned according to the twelve-average law [18]. The extraction flowchart is shown in Figure 2.

3.2. Automatic Composition Neural Network Model Construction. The section is subdivided into two parts, i.e., the recurrent neural network structure and automatic composition neural network model.

3.2.1. Recurrent Neural Network Structure. Compared with the general feedforward neural network, the structure of recurrent neural network increases the feedback link from hidden layer to hidden layer [19]. The recurrent neural network will have an input x_t at every moment, then calculate a new state $t - 1$ according to the hidden layer state s_{t-1} at s_t, and finally output O_t. The calculation formula of the output layer O_t is as follows:

$$O_t = \varphi(\mathrm{Vf}(\mathrm{Ux}_t + \mathrm{Wf}(\mathrm{Ux}_{t-1} + \mathrm{Wf}(\mathrm{Ux}_{t-2} + \mathrm{Wf}(\mathrm{Ux}_{t-3} + \mathrm{Ws}_{t-4}))))). \tag{4}$$

It can be seen from the equation that the output value of the neural network depends on the previous input values, and it also shows that the cyclic neural network has memory capabilities. Therefore, the cyclic neural network is chosen as the basic unit of the neural network model of piano automatic composition.

3.2.2. Automatic Composition Neural Network Model. A piano music is a sequence composed of multiple notes according to certain musical theory rules. The neural network can learn this hidden rule and then predict and generate the note sequence to realize automatic composition. From the previous analysis, it can be seen that the cyclic neural network has a memory function. In theory, it can establish dependencies between states at long intervals. However, there is a problem of gradient explosion or disappearance in the actual training. It is difficult for a simple neural network to model such a length dependency. The piano automatic composition process is divided into two steps: the first step is to use the note sequence dataset to train the neural network model, and after multiple rounds of learning and training, a good note prediction network model is obtained. The second step is to use the note prediction network model to generate a note sequence, match it with the piano sound source, and get a piano music in audio format. The training process will not be described in detail. After the training process of the automatic composition neural network model is completed, a good note prediction network model will be obtained. The note prediction network model can be used to generate a specified number of note sequences. The note value predicted by the note prediction network model is also used for calculation by the softmax function, and the note category with the largest probability value is selected as the final actual predicted note

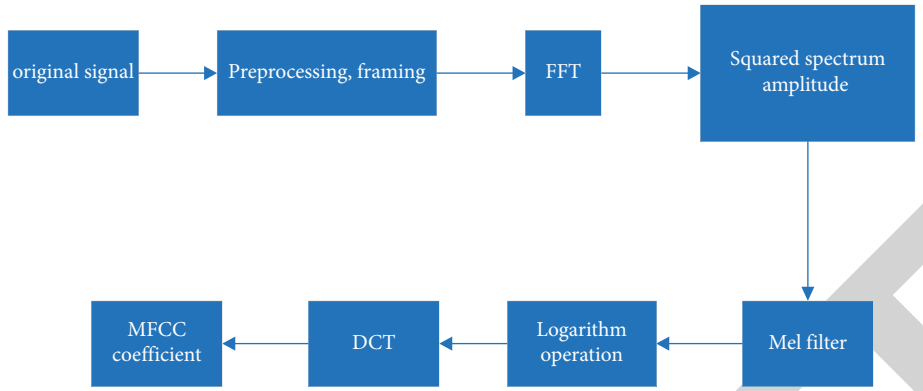

Figure 1: MFCC extraction flowchart.

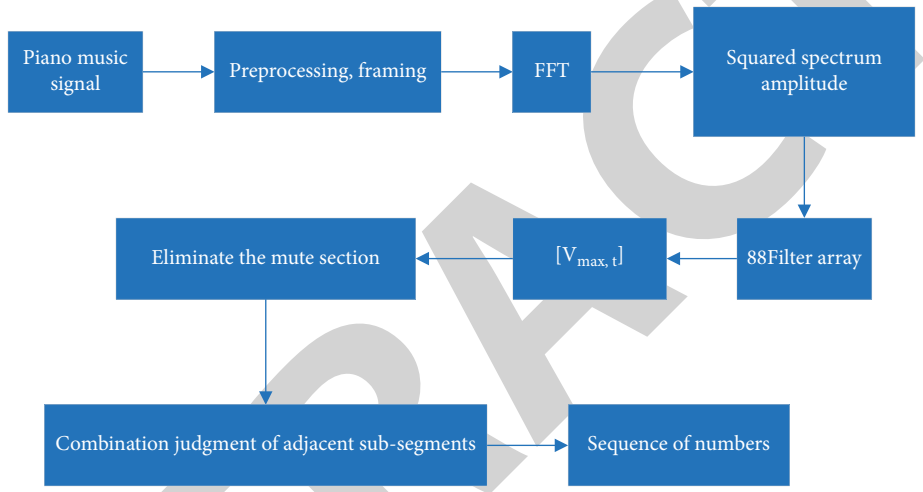

Figure 2: Note feature extraction flowchart.

output [20]. The note prediction network model generates the note set X as follows:

$$X = \begin{bmatrix} note\_pre_1 \\ note\_pre_2 \\ note\_pre_3 \\ \cdots \\ note\_pre_m \end{bmatrix}. \quad (5)$$

The entire composition process is to first specify the input note sequence of the input layer of the note prediction network model. The note prediction network model generates a note, arranges the predicted notes of m times in order to obtain a set of generated note sequences, and assigns the musical instrument to the note sequence. For the piano, the sound source is dubbed at the same time, and finally the piano music is obtained in audio format. The composition process is shown in Figure 3.

4. Experiments and Results

All data in this study are from the ADNI1 dataset. This section introduces in detail the construction process of the neural network model of automatic composition in this paper, the training rules, and the process of automatically generating piano music. Combining with the characteristics of this demonstration audio set, after many experimental results comparisons, the final automatic composition neural network model will need to use specific parameter values. In the process of automatically generating piano music, the note prediction network model will generate a note every time, arrange the 400 notes generated by the 400 predictions in order to obtain a set of generated note sequences, assign the musical instrument to the note sequence as the piano, equip the piano sound source at the same time, and finally get the piano music in audio format.

4.1. Results of Online Audition Evaluation. The online audition effect scoring platform adopts a development method that separates the front and back ends. The front end is developed with React, and the back end uses Java [21]. After the development of the platform is completed, 20 test piano songs are placed on the platform, of which five are from the audio collection of the demo composer one. Five are from the music website, and ten are generated by the automatic composition neural network model [22]. The duration of each piano piece is intercepted for 30 seconds to avoid auditory fatigue of the auditors. We invited testers to listen

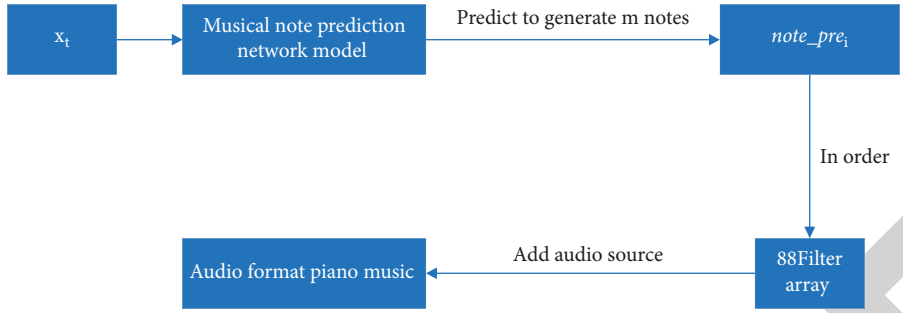

Figure 3: Automatic composition neural network model composition process.

Table 1: The scoring standards.

5 points	4 points	3 points	2 points	1 point
Very beautiful	Not bad	General	Barely able to hear	Very bad

Table 2: Top 10 online scores.

Rank	Test music name	Creation method	Composer	Score
1	Demo_10	Artificial composition	Famous composer	4.50
2	Demo_08	Artificial composition	MS	4.20
3	Demo_17	Automatic composition	GRU	4.10
4	Demo_01	Artificial composition	MS	4.07
5	Demo_11	Automatic composition	GRU	3.80
6	Demo_06	Automatic composition	GRU	3.74
7	Demo_04	Artificial composition	MS	3.74
8	Demo_09	Automatic composition	GRU	3.60
9	Demo_15	Artificial composition	Famous composer	3.42
10	Demo_12	Automatic composition	GRU	3.34

to 10 piano music online and score and evaluate them according to their subjective listening feelings. The scoring standards are shown in Table 1.

A total of 20 music lovers were invited to participate in this test, the scores of each piano song were counted and the average score was calculated, and the final score ranking is shown in Table 2.

Among the aforementioned final evaluation score results, the piano music Demo_17 generated by automatic composition entered the top three, and the scores of Demo_11 and Demo_06 also ranked in front of the two work songs. The next score is the piano music automatically generated in this article, which shows that the quality of automatically generated piano music is different, and the network model of automatic composition has room for further optimization. The comparison of scores above 3 is shown in Figure 4, and the comparison of scores above 4 is shown in Figure 5.

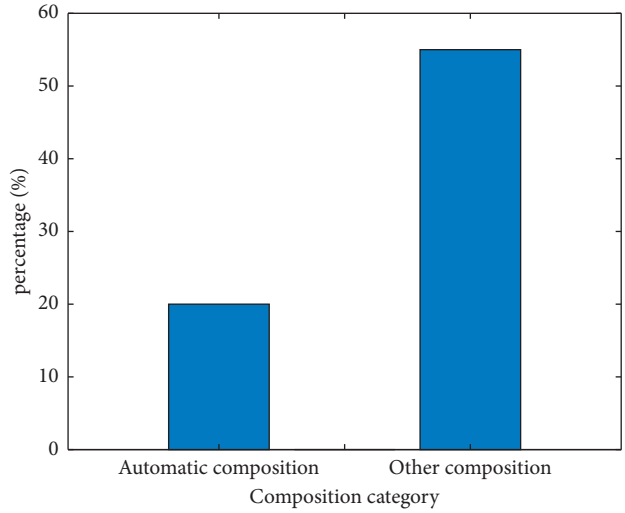

Figure 4: Percentage with a score of 3 or more.

4.2. Results of Offline Audition Evaluation. The offline performance evaluation invites professionals who have rich experience in piano performance. Professionals have designated 5 indicators for this evaluation, namely, "melody, texture, harmony, tension, and aesthetics." The full score for each indicator is 100 points. Then, 10 piano songs are performed and the scores of 5 indicators for piano songs are recorded. In the end, the top ten scores of each piano song are shown in Table 3. The comparison of scores above 80 is shown in Figure 6, and the comparison of scores above 60 is shown in Figure 7.

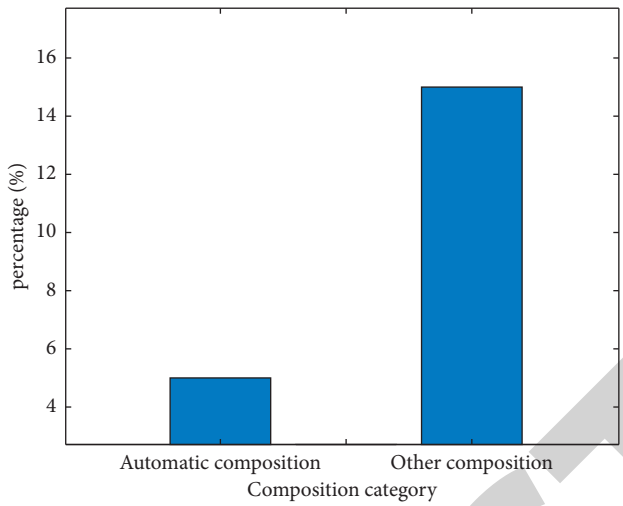

Figure 5: Percentage with a score of 4 or more.

Table 3: Top ten evaluation rankings for offline audition.

Rank	Test music name	Creation method	Composer	Score
1	Demo_10	Artificial composition	Famous composer	95.4
2	Demo_15	Artificial composition	Famous composer	90.7
3	Demo_13	Artificial composition	MS	85.6
4	Demo_01	Artificial composition	MS	82.4
5	Demo_11	Automatic composition	MS	81.9
6	Demo_06	Automatic composition	GRU	80.1
7	Demo_04	Artificial composition	GRU	79.9
8	Demo_14	Automatic composition	MS	77.6
9	Demo_07	Artificial composition	MS	77.4
10	Demo_12	Automatic composition	MS	75.4

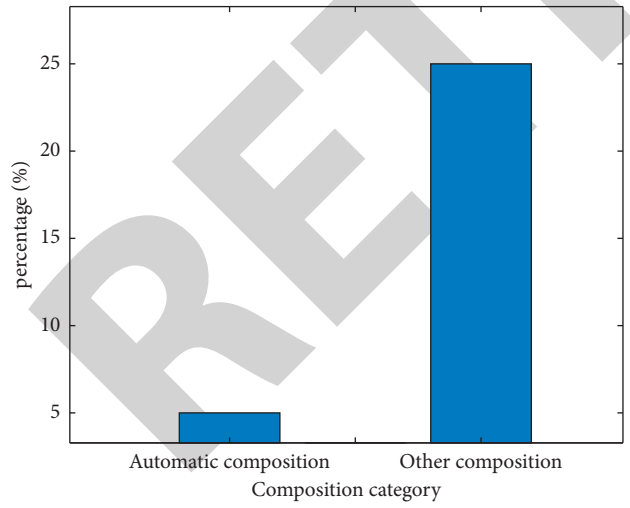

Figure 6: Percentage with a score of 80 points or more.

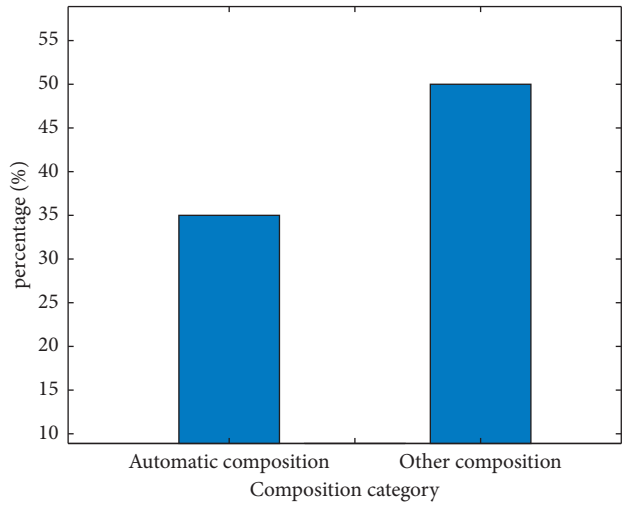

Figure 7: Percentage with a score of 60 points or more.

Judging from the final scoring situation, 5 of the automatically generated piano songs in this article have entered the top 10, indicating that the automatically generated piano music in this article can reach the level of general manual creation, but compared with the works of the famous composer Schumann, the score is the gap is large. The two lowest scores are also automatically generated piano music in this article, which shows that the quality of automatically generated piano music is different, and the network model of automatic composition needs to be further optimized. Professionals also commented on the spot that the piano music automatically created in this article is monotonous, without complicated variations, and lacking "rhythm."

Hindawi
Journal of Mathematics
Volume 2023, Article ID 9760327, 1 page
https://doi.org/10.1155/2023/9760327

Retraction

Retracted: A Computational Offloading Method for Edge Server Computing and Resource Allocation Management

Journal of Mathematics

Received 19 December 2023; Accepted 19 December 2023; Published 20 December 2023

This article has been retracted by Hindawi following an investigation undertaken by the publisher [1]. This investigation has uncovered evidence of one or more of the following indicators of systematic manipulation of the publication process:

(1) Discrepancies in scope

(2) Discrepancies in the description of the research reported

(3) Discrepancies between the availability of data and the research described

(4) Inappropriate citations

(5) Incoherent, meaningless and/or irrelevant content included in the article

(6) Manipulated or compromised peer review

The presence of these indicators undermines our confidence in the integrity of the article's content and we cannot, therefore, vouch for its reliability. Please note that this notice is intended solely to alert readers that the content of this article is unreliable. We have not investigated whether authors were aware of or involved in the systematic manipulation of the publication process.

Wiley and Hindawi regrets that the usual quality checks did not identify these issues before publication and have since put additional measures in place to safeguard research integrity.

We wish to credit our own Research Integrity and Research Publishing teams and anonymous and named external researchers and research integrity experts for contributing to this investigation.

The corresponding author, as the representative of all authors, has been given the opportunity to register their agreement or disagreement to this retraction. We have kept a record of any response received.

References

[1] M. Al-Razgan, T. Alfakih, and M. M. Hassan, "A Computational Offloading Method for Edge Server Computing and Resource Allocation Management," *Journal of Mathematics*, vol. 2021, Article ID 3557059, 11 pages, 2021.

Hindawi
Journal of Mathematics
Volume 2021, Article ID 3557059, 11 pages
https://doi.org/10.1155/2021/3557059

Research Article

A Computational Offloading Method for Edge Server Computing and Resource Allocation Management

Muna Al-Razgan,[1] Taha Alfakih ,[2] and Mohammad Mehedi Hassan[2]

[1]*Department of Software Engineering, College of Computer and Information Sciences, King Saud University, Riyadh 11345, Saudi Arabia*
[2]*Department of Information Systems, College of Computer and Information Sciences, King Saud University, Riyadh 11345, Saudi Arabia*

Correspondence should be addressed to Taha Alfakih; talfakih@ksu.edu.sa

Received 24 October 2021; Accepted 22 November 2021; Published 21 December 2021

Academic Editor: Naeem Jan

The emerging technology of mobile cloud is introduced to overcome the constraints of mobile devices. We can achieve that by offloading resource intensive applications to remote cloud-based data centers. For the remote computing solution, mobile devices (MDs) experience higher response time and delay of the network, which negatively affects the real-time mobile user applications. In this study, we proposed a model to evaluate the efficiency of the close-end network computation offloading in MEC. This model helps in choosing the adjacent edge server from the surrounding edge servers. This helps to minimize the latency and increase the response time. To do so, we use a decision rule based Heuristic Virtual Value (HVV). The HVV is a mapping function based on the features of the edge server like the workload and performance. Furthermore, we propose availability of a virtual machine resource algorithm (AVM) based on the availability of VM in edge cloud servers for efficient resource allocation and task scheduling. The results of experiment simulation show that the proposed model can meet the response time requirements of different real-time services, improve the performance, and minimize the consumption of MD energy and the resource utilization.

1. Introduction

There are more issues facing mobile devices such as smart phones, reconnaissance planes (drones), robots, patient monitoring devices, and wireless sensors, due to limited specifications of these devices (like storage, memory, CPU, battery), and intensive applications (e.g., real-time translation, video processing, image processing) require supercomputing. Mobile devices with limited resources are not efficient or opportune to process those applications. Therefore, mobile cloud computing (MCC) emerged as a solution to overcome the resource limitation of mobile devices by using computation offloading.

Computation offloading is a transfer mechanism of software application processes from limited resource devices to resource-rich platforms. Mobile cloud is the well-known module for MD computation offloading. MCC is becoming a popular technique for mobile services (MS), e.g., video streaming, mobile video games, social networking, education, mobile healthcare services, and instant messaging [1].

Wireless communication limitations like disconnection, low bandwidth, security issues, latency, and mobility are considered the key barriers to offloading computation in cloud computing (CC) [2]. Real-time services are extremely latency sensitive and thus require computing data in close proximity to MDs. Therefore, a proximity cloud like MEC, fog computing, and cloudlet can be an efficient and appropriate module for computation offloading.

Edge computing (EC) is an emerging technique, which is currently being standardized in ETSI Industry Specification Group (ISG). EC offers a service of IT environment and capabilities of CC at the mobile network edge, within the Radio Access Network (RAN), and in close proximity to mobile users (MU). The aims are to minimize the services

delay, confirm effective network operation and service delivery, and offer an enhanced user experience [3]. There are some challenges facing the MEC [4], like the service synchronization and orchestration between the cloud servers and edge server (ES) (the central cloud), in addition to "seamless service delivery" as the connectivity at the EC infrastructure may be intermittent with mobility. Additionally, the standard IP based operations become infeasible to address the interactions between MD and servers, considering that the problem is more emphasized in the services of edge computing facility. The other challenges to the services of edge computing may not always assume the availability of the local infrastructure.

MEC is a distributed system that provides features such as low latency, distributed analytics, real-time interaction, geographical distribution, mobility support, and context awareness, which are not supported by centralized CC paradigm [5].

We considered the mobile devices aiming to perform own intensive applications interacting with many edge cloud computing infrastructures, through different wireless connections or Wi-Fi, in order to distribute the computation load to one or more edge computing infrastructures (MEC, cloudlet, and remote cloud) and receive data results, to perform the computation offloading [6]. MEC, e.g., computation offloading of heavy tasks to EC in the communication network (or cellular network), has become a promising technique for the next generation of the cellular networks. Therefore, there is a need for enhancing a model of distributed computation offload, so that not only the computational servers are applied at their superlative capacity, but also the response time of user's restrictions is achieved [7].

The essential components of the computation offloading model are a client running on the client device and a server running on the edge server, regardless of the surrounding devices or remote cloud. The component of client has three main functions: firstly, monitoring and predicting the performance of the MD network; secondly, predicting and tracking the requirements of computation of client services in terms of input and output requirements of data and time of execution on both the client and the ES; thirdly, using such information to select some partition of the computation to perform in the cloud so that the total execution time is reduced. The components of the server immediately execute offloaded portions after receiving them and return back the results to the client components, so the application can be continued on the mobile device. Our objective in this paper is to reduce latency of the processes (i.e., offloading the process and receiving the results) by proposing an evaluation model to evaluate the efficiency of near-end network computation offloading in mobile edge computing (MEC). This model helps in choosing the adjacent edge server from the surrounding edge servers. This helps to reduce the latency and increase the response time. To do so, we use a decision rule based Heuristic Virtual Value (HVV). The HVV is a mapping function dependent on the feature of the edge server like the performance and workload. Additionally, in this paper, we propose a VM resource availability algorithm (AVM) that optimizes resource allocation and task assignment based on VM availability in the edge cloud servers. The simulation results show that the proposed model satisfies the requirements of response time of real-time applications, improves the performance, and minimizes the MD power consumption.

The rest of the paper is organized as follows: In Section 2, we present the related work review. In Section 3, we outline the computation offloading in MEC. In Section 4, resource allocation model is given. Then, in Section 5, we describe our proposed model results and analysis, followed by the conclusion in Section 6.

2. Related Work

In [8], the performance ability or capability is enhanced to leverage the available computing of edge servers and capacity, by the proposing a system which provides a collection of colocated devices as cloud service at the edge and enables leveraging multiple clients into a coordinated cloud computing service despite churn in participation of mobile devices. On the other hand, the study in [9] proposed a framework and a model used a holistic approach to bond context adaptation and computation offloading (cloud aware), to help app's developers to design scalable and flexible edge depending on mobile applications.

The cloud RAN (C-RAN) service is exploited to propose a decision algorithm of offloading that makes decisions about computation offloading from the client to the cloud remote radio heads (RRHs), to save power consumption and keep a satisfying user QoE by reducing app's time of response [10]. Lyapunov optimization algorithm is proposed to take the decisions of the offloading, frequencies of the cycle of CPU for mobile application execution, and energy of the communication for computation offloading [11].

A scheme of opportunistic computation offloading for the MECC systems is provided to execute tasks of data mining in client devices and edge servers (ES), to reduce time of execution and energy consumption [12]. In [13], a distributed computation offloading model that can achieve a Nash equilibrium is proposed to fulfil the superior performance of computation offloading and scale well as the user size increases. In study [7], the authors used minority games theory to analyze the statistical characteristics of the offloading delay for the users' requests and channel quality by using a distributed algorithm to solve efficient servers selection issues. In [14], the authors assess a performance and investigate the computation offloading from the MD's to the small cell cloud (SCC). In the scenario of a cooperative MEC server [15], the authors analyze the problem of joint task offloading and resource distribution. Furthermore, IoT resource fairness should begin by taking the user experience into account. Additionally, the authors propose a two-level heuristic: the first, inspired by evolutionary algorithms, searches for superior offloading schemes globally; the second, considering fairness among all tasks, generates resource allocation modules, making use of the server's resources as efficiently as possible [15].

The proposed method is formatted as an optimization problem to reduce the consumption of MD energy, due the overhead of the MEC capacity. The priority of offloading for each device depends on its power consumption and channel gain. Complete offloading is performed for a high priority, while minimum offloading is performed for a low priority [16].

A modern framework for computation offloading from a mobile device as a client to an edge server as a host, with availability of highest CPU, is presented. The main idea is to estimate RTT value between mobile device and edge server according to signal quality of the RAN as an application programming interface (API) to make the mobile device decision to offload or not computing tasks for application. Additionally, a novel algorithm of computation is proposed; it depends on the estimated RTT connected with other parameters (e.g., consumption of power) to take a decision as to when to offload application computation tasks of mobile device to the mobile edge computing server [17].

Proposing computation offloading in a multicell system, the authors considered multiple users requests with multiple inputs and multiple outputs (MIMO). Additionally, the researchers expressed the problem using the radio joint optimization and presence of the intercellular interference with the resources of computational for computation offloading in an applications intensive deployment [18]. The preceding research works did not deal with the process of evaluation pre-decision to the unloading process. When used, this technology needs to be handled with caution, and more research should be done on such issues such as confidentiality, authenticity, and integrity [19]. In this study, an evaluation model is proposed to evaluate the efficiency of near-end network computation offloading in MEC.

Max–Min algorithm [20] is one of the popular, very simple, and easy to implement cloud scheduling algorithms, because it has very few control variables, and we use it in the edge cloud computing. All the small tasks are allocated to faster resources, and large tasks are allocated to slower resources. Hence, it minimizes the waiting time average of shorter jobs, by assigning them to faster resources, and our large tasks are executed by slower resources. Therefore, this algorithm improves simultaneous implementation of tasks on resources. Therefore, algorithm of Minimum Completion Time (MCT) allocates offloaded tasks to resources or VMs based on the best expected completion time for these tasks in random order. Each task is allocated to the resource or VM that has the closest completion time. In the MCT algorithm, some tasks are assigned to resources or VMs that do not have minimum processing time [21].

Round Robin algorithm (RR) [22] is considered one of the easiest process scheduling algorithms. It gives equal time for each process, dealing with all processes without priority for any of them. The RR scheduling is characterized by its simplicity and ease of implementation, as well as being free from starvation, which means that the process does not have the resources needed to complete it at all or after a long period.

In the study, the vertical collaboration of mobile devices, mobile edge servers, and mobile cloud servers, as well as the horizontal cooperation of edge nodes in computation, is examined in relation to cooperative computation task offloading and resource assignment in the MEC. It is formulated to make decisions regarding computation offloading, cooperative selection, power allocation, and CPU cycle frequency assignment. In order to minimize latency, energy consumption, transmission power, and CPU cycle frequency should be reasonably constrained [23].

3. Computation Offloading in ES

The computation offloading is the technique used to raise the performance of the mobility of devices and minimize the power consumption by offloading the intensive tasks which need urgent and accurate processing to the remote resources that are able to compute these tasks and return the results immediately, for example, real-time and intensive applications like image processing.

The major objective of our research is the concurrent offloading of the offloadable processes (partitioned tasks) to proximate resources EC (L-ESs) as shown in Figure 1, to make the appropriate decision based on the results of the profile examination of each resource (i.e., L-ESs, ECC, or RC). In other words, we decide the computation offloading of the process to EC resources (L-ESs, ECC, and remote cloud), mobility management, and effective allocation of the computation resources, for exploiting the moving users within each resource.

3.1. Edge Server Computing Architecture. Figure 2 portrays the high-level overview of the edge server and the mobile devices, such as smart phones, tablets, robots, and drones. The base station communicates with the network of the local ES before entering the Internet. At the ES, the components of network having super computation and storage capabilities are collected to create a virtual server (VS) offering mobile ES. If a workload demands resources beyond what the ES can support, the request can be redirected over the core network until reaching the cloud services on the other side of the network [24].

ME is the complementary edge computing model especially prototyped for unified and latency-aware MS. The offloading decision depends on the following parameters: performance, energy consumption, latency, and cost. The proposed model automatically selects the computing source based on the following parameters: performance, signal strength, radio bandwidth, and workload. We relied on these criteria to choose the suitable edge server.

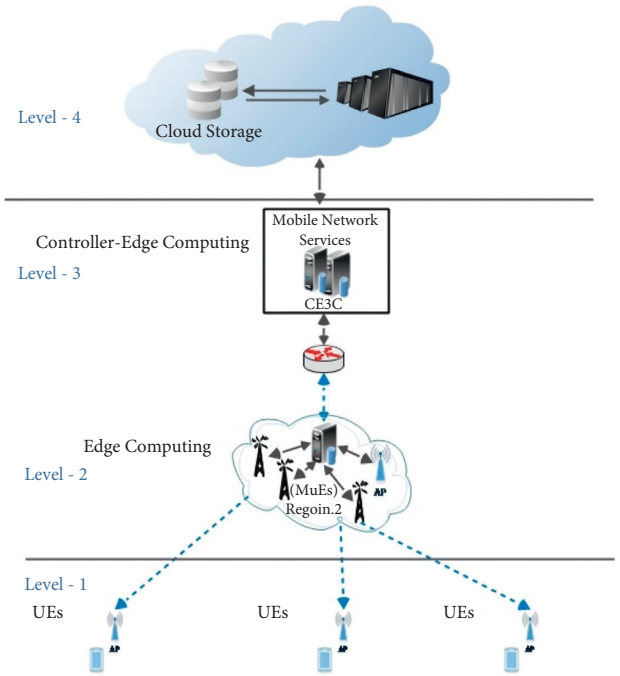

Figure 1: A high-level overview of edge server computing.

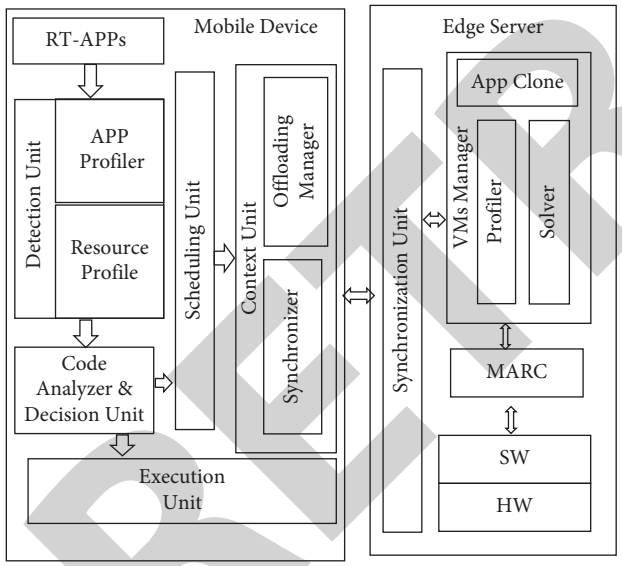

Figure 2: Mobile edge computing system architecture.

Figure 2 illustrates the MECS architecture. The MECS on the edge server consists of the synchronization unit, which is responsible for maintaining the synchronization between mobile devices and edge server; management allocation resource control (MARC) unit; and virtual management unit, which consists of profiler to monitor the VM workload and edge server performance. Additionally, the solver executes the task or the application clone.

MECS architecture on the mobile device consists of five units: the detection unit detects the tasks and the available resources; the code analyzer divides the task into subtasks and determines whether a subtask is offloadable or nonoffloadable; the scheduling unit places subtasks in the waiting queue if they are offloadable and assigns them to local execution otherwise; the context unit is responsible for synchronization between the client and edge server and management of offloading to distribute the subtasks.

3.2. Offloading Decision Rule. Since computation offloading migrates the intensive tasks to more resourceful computing, it involves decision making as to whether and what computation should be migrated. The decisions of offloading to remote resources are divided into improving performance and saving energy [25]. However, other problems emerged, especially for the sensitive computational tasks, including latency, mobility, bandwidth bottleneck, resource management, privacy, and security.

We consider an ECC consisting of a pool of edge servers (L-ES) denoted by **s** that is connected through the LTE and AP, edge server control (ESC) denoted by S, and a set of mobile devices (MDs) denoted by M in each zone Z. Each mobile device has some sensitive computational processes $\mathscr{C}$ to be accomplished in successive periods (time) $\mathscr{T}$. Each process P may be partitioned into several tasks c, according to the tasks performed by this process. T is the time consumed to compute the task on the MD, while T' is the time consumed to complete task on the edge server. The consumed energy to compute the task on the MDs is denoted by E, and the consumed energy to process the task on the edge server is denoted by E'.The workload for each edge server is denoted by $\mathbf{s_W}$.

The execution time of the task on the edge server (**S**) is

$$T = \frac{\mathscr{C}}{M_p}, \tag{1}$$

where $\mathbf{M_p}$ the performance of the mobile device and $\mathbf{s_p}$ represents the performance of the edge server. The offloading process will improve the response time in processing tasks, as it reduces the response time due to the ES close to the user. The total time of responsiveness is calculated using the following:

$$\text{Total time} = \text{time of communication} + \text{time of computation},$$

$$T' = \frac{c_i}{b} + \frac{\mathscr{C}}{s_p}, \tag{2}$$

The offloading performance (latency) improves if the following condition holds:

$$\begin{aligned} T > T' &\Rightarrow \frac{\mathscr{C}}{M_p} > \left(\frac{c_i}{b} + \frac{\mathscr{C}}{s_p}\right) \\ &\Rightarrow \mathscr{C}\left(\frac{1}{M_p} - \frac{1}{s_p}\right) > \frac{c_i}{b}, \end{aligned} \tag{3}$$

where c_i indicate the size of task that needs to be sent and b is the bandwidth.

The consumed energy to execute the task within the mobile device system is given by

$$E = e_m \times \frac{\mathscr{C}}{M_p}, \tag{4}$$

where e_m represents the energy on the mobile system. The total consumed power considering the computation and transmission is determined by

$$E' = e_w \times \frac{c_i}{b} + e_c \times \frac{\mathscr{C}}{s_p}, \tag{5}$$

where e_c indicates the power required for communication between mobile device and server edge over the network, e_w refers to the power required to wait for the result, c_i is the size of task that needs to be offloaded, and b is the bandwidth. The offloading power is saved if the following condition holds:

$$\begin{gathered} E > E' \Rightarrow e_m * \frac{\mathscr{C}}{M_p} > e_w * \frac{c_i}{b} + e_c * \frac{\mathscr{C}}{s_p}, \\ \mathscr{C}\left(\frac{e_m}{M_p} - \frac{e_c}{s_p}\right) > e_w * \frac{c_i}{b}. \end{gathered} \tag{6}$$

Saving offloading power will be computation process $\mathscr{C}$, and light communication of the each task c_i is considered.

3.3. Decision Rule. We have several edge servers and we need to offload tasks to one of them (where). In other words, we need to choose the optimal edge to compute the offloadable task depending on our proposed Heuristic Virtual Value (HVV) and signal strength (s_{ss}) of the edge servers. The HVV is a mapping function dependent on the features of the edge server like the performance and workload. Each server independently decides whether to be in active mode (to accept computation task, $s_M = 1$) or inactive mode (not to accept computation task, $s_M = 0$). Therefore, we proposed the Heuristic Virtual Value (HVV) for each server, and we need to calculate it. The HVV depends on some parameters (like performance $\mathbf{s}_\mathrm{p}$, workload s_W, mode $\mathbf{s_M}$) for each edge server $\mathbf{s} \in \mathbf{S}$. The edge server depends on the HVV to connect to the mobile devices. Let $\mathbf{s_i}(\mathbf{t})$ be the server that decides to be ready to receive the task at the time $\mathbf{t}$ if the server mode is active ($\mathbf{s_M} = 1$), so that the HVV for each server is given by

$$\mathrm{HVV}_{s_i}(t) = \mathscr{F}\left[s_p, s_W\right]. \tag{7}$$

The $\mathbf{HVV}_{\mathbf{s_i}}(\mathbf{t})$ is a mapping function that receives the values of $\mathbf{s_p}$ edge server performance and $\mathbf{s_w}$ edge server workload as percentage and converts them into categorical values between one and four as shown in Table 1.

$$\begin{gathered} \mathscr{F}\left[s_p, s_W\right] = \frac{S_p}{S_w}, \\ \mathrm{HVV}_{s_i}(t) = \frac{S_p}{S_w}, \\ S_M = \begin{cases} 0, & 0 < \mathrm{HVV}_{s_i}(t) < 1, \\ 1, & \text{Otherwise.} \end{cases} \end{gathered} \tag{8}$$

The resulting potential values of such HVV (t) function receive the result of division edge server performance $\mathbf{s_p}$ over edge server workload $\mathbf{s_W}$. The edge server mode $\mathbf{s_M}$ depends on the value of the $\mathbf{HVV}_{\mathbf{s_i}}(t)$; for instance, in the best cases the value of $\mathbf{HVV}_{\mathbf{s_i}}(t)$ is 4, which makes the edge server in active mode $\mathbf{s_M} = 1$; in contrast, in the worst cases the $\mathbf{HVV}_{\mathbf{s_i}}(t)$ is 25, which makes the edge server in inactive mode $\mathbf{s_M} = 0$, as illustrated in Algorithm 1.

Figure 3 illustrates the processes of the computation offloading; before making a computation offloading decision, each client detects the signals for each surrounding edge server and makes an ordered list of signal strength degrees for edge servers. The client receives the strength of signal as a percentage and converts it into a categorical value between one and four like the values of $\mathbf{s_p}$ as shown in Table 1. The client selects the edge server that has a maximum S_{ss} and starts to communicate with it by sending acknowledgment ack (t). $\mathbf{T_n}$ represents the threshold value for the offloadable task. If the edge server receives the ack(t), the server calculates the $\mathrm{HVV}_{s_i}(t)$; if $\mathbf{s_M} = 1$, the edge server replies to the client that it is active and assigns each mobile device a unique ID. Then, the client starts to offload the task $c(t)$ to the edge server and receive the result.

In contrast, if the edge server returns $S_M = 0$, this means that the server is unable to serve the client and meet time requirements; in this situation, the client finds an alternative server by checking the order list $[S_{ss}]$, choosing the Next Max$[S_{ss}]$, starting to communicate with it, and so on. Otherwise, it is the client. If the client fails to communicate with the alternative server, they have to communicate with the remote cloud.

4. Resource Allocation Management in the MEC Based on VM Resource Availability

Figure 4 illustrates the system model, which consists of the following units: The monitoring and migration unit as a core unit is responsible for the resource management of ES. The profiling module unit works to acquire the tasks features and its computing requirements to compare them with the ES capabilities and determine whether it can serve them. Then, the VMs control unit works to create VMs according to the offloaded tasks' computation requirements. The scheduling unit distributes these tasks to the available VMs. In the UE mobility, if the UE is out of coverage service of ES, the aggregation unit, in collaboration with the other units in the system model, distributes the tasks to adjacent ES, as well as balancing the resources between VMs.

4.1. VM Availability Evaluation. VM availability directly impacts the scheduling tasks in the edge cloud platform; therefore, the evaluation of VMs availability is considered when managing task scheduling. Additionally, VM resource availability is the capacity of providing functional services within required time after the task is offloaded to VMs.

We can measure the capacity of available task processing $\mathbf{q}_{ij}$ of VMs using completion time (τ), completion rate (t_c), and task arrival rate (t_r). We calculate the capacity of VMs

Table 1: Values of server's performance and workload.

Range (%)	Mapping value (s_P, s_W)
0–25	1
26–50	2
51–75	3
76–100	4

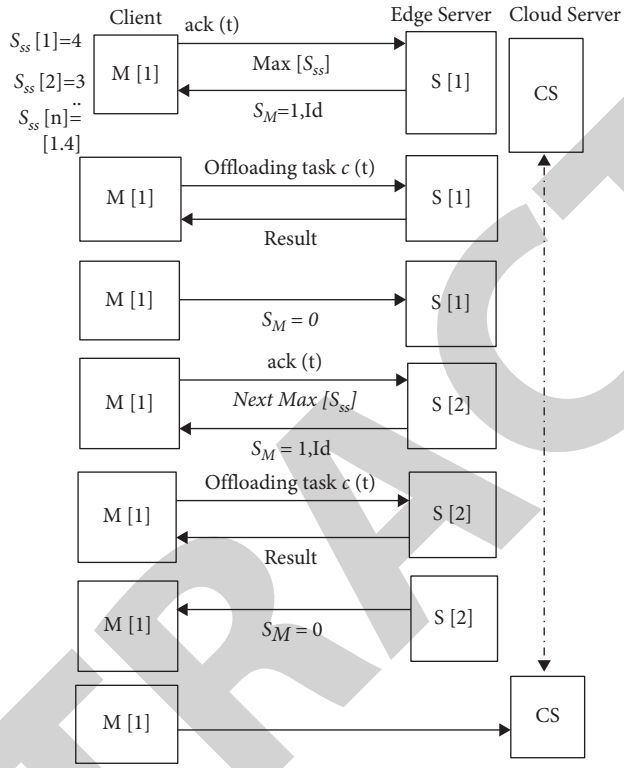

Figure 3: Processes of the computation offloading to the edge server.

(1) Input: s_P, s_W
(2) Output: s_M
(3) Begin
    //Mapping s_P, and s_W into their corresponding category.
(4) if s_P & s_W, in [0% –25%] then
(5) $s_P = 1$; $s_W = 1$;
(6) elseif s_P & s_W, in [26% –50%] then
(7) $s_P = 2$; $s_W = 2$
(8) elseif s_P, in [51% –75%] then
(9) $s_P = 3$; $s_W = 3$;
(10) else
(11) $s_P = 4$; $s_W = 4$;
(12) End if
(13) $\mathrm{HVV}_{s_i}(t) = S_p/S_w$
(14) if $(0 < \mathrm{HVV}_{s_i}(t) < 1)$ then
(15) $s_M = 0$;
(16) else
(17) $s_M = 1$;
(18) Return s_M
(19) End

Algorithm 1: Heuristic Virtual Value algorithm-based decision rule.

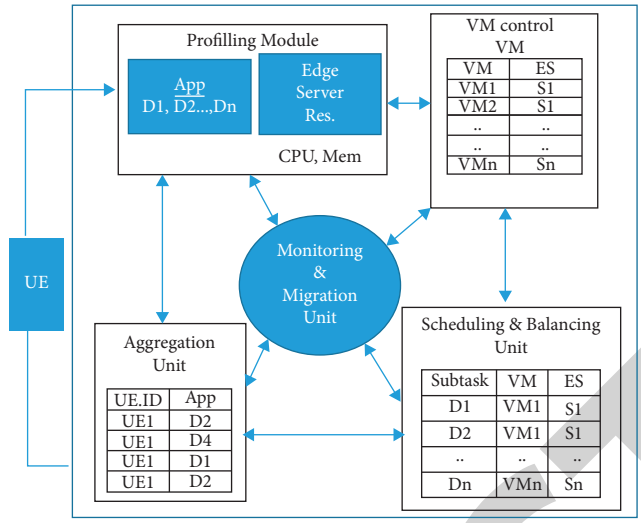

Figure 4: System model of resource allocation management.

available to task processing (q_{ij}^{V}) of the VM_j in the S_i edge server after receiving the task $\{c_i, i = 1, \ldots, n\}$, as follows:

$$q_{ij}^{V} = \frac{P_{ij}\alpha}{t_c}, \tag{9}$$

where P_{ij} is the probability that the VM_j in the S_i edge server receives a task and α is rate of task arrival in the edge cloud platform.

Task completion time τ refers to the difference between task time of arrival t_r and task completion rate t_c, namely,

$$\tau = t_r - t_c. \tag{10}$$

Therefore, the capacity of available task processing q_{ij}^{S} of each S_i edge server is the sum of processing capacities of all VMs in the edge server.

$$q_{ij}^{S} = \frac{\sum_{j=1}^{n} P_{ij}\alpha}{t_{cij}}. \tag{11}$$

The available capacity of S to tasks processing ($\mathbf{q}_{ij}$) of the VM_j in the S_i edge server gives the model strength and ability to compute the most significant number of tasks. Therefore, we can calculate the resource utilization ($\mathcal{R}_u$) as follows:

$$\mathcal{R}_u = \frac{q_{ij}^{S}}{q_{ij}^{V}}, \quad \text{where } q_{ij}^{V} \subset q_{ij}^{S}. \tag{12}$$

4.2. Scheduling Algorithm. We assume that the task requirements are already acquired. We measure each VM workload (V_W) and workload of edge server (S_W) as follows:

$$V_W = \frac{f_{Vi}}{T}, \tag{13}$$

where

$$S_W = \sum_{i=1}^{n} V_W \quad , \forall V_i \in S, \tag{14}$$

where T is the execution time of the task on the edge server ($\mathbf{S}$).

Measurement of the VM availability and allocation of VMs to accommodate the offloaded tasks constitute one of the most important issues that edge servers face in order to be able to schedule tasks for computation and meet time requirements [26]. We proposed a task scheduling algorithm based on the availability of VMs (abbreviated to AVM), Algorithm 2, and their dynamic evaluation. The choice is made among the most available resources, which avoids slowing down the tasks computing. The module of task scheduler manages the scheduling of tasks based on requests of task resources $\{c_i, i = 1, \ldots, n\}$ The purpose of the task scheduling is to maximize available differential of VMs, and VMs with relatively small workloads on the edge server where they are located are selected, which can improve task computation time as shown in Algorithm 2.

5. Simulation and Result Analysis

This study used the Cloudsim tool [27] to evaluate the proposed decision rule, VM resources availability, and resource allocation management. The CloudSim is an open-source package that is obtainable for public use. In this section, we will verify two aspects: (1) offloading decision making; (2) resource allocation management and task scheduling based on availability of VM.

5.1. Offloading Decision Making. There are some factors that influence offloading decision making: First (when to offload), predict execution time and power consumption in the mobile devices and remote cloud and compare them. If the e_m, $t_m > e_c, t_c$, the offloading is active, where e_m indicates the mobile energy consumption, t_m mobile time execution, e_c cloud energy consumption, and c_m cloud time execution.

(1) **Input**: A set of tasks $\{c_i, i = 1, \ldots, n\}$, $S = \{S_1, S_2, \ldots, S_n\}$, and VM = $\{v_1, v_2, \ldots, v_n\}$
(2) **Output**: Scheduling tasks and resource allocation
(3) Compute available of the VM for computing capabilities to meet processing time requirement based on (9)
(4) Initialize VM available capabilities of task processing
(5) for all tasks $\{c_i, i = 1, \ldots, n\}$ do
(6) for all VMs = $\{v_1, v_2, \ldots, v_n\}$ do
(7) Assigned tasks c_i into v_i
(8) Compute v_i available task processing capabilities based on (9)
(9) end for
(10) for all tasks $\{c_i, i = n + 1, \ldots\}$ do
(11) Assigned tasks c_i into v_i
(12) add a new VM
(13) end for

Algorithm 2: Task scheduling algorithm of VM available differential maximization (AVM).

Second, the decision depends on network features like the bandwidth and signal strength. Third (where to offload and which edge server is selected), selecting the appropriate server depends on the performance and workload of the edge server. In this research, we focus on the third factor. We suppose that we have offloadable task, it is divided into subtasks, and some of the subtasks (blocks) are offloadable but the others are executed locally. Additionally, we suppose that the feature of the network is appropriate to offloading. We suppose that we have several edge servers and we need to offload tasks to one of them (where to offload). Each server independently decides whether to be in active mode (to accept computation task $s_M = 1$) or in inactive mode (not to accept computation task $s_M = 0$) based on the Heuristic Virtual Value (HVV) for each server. The edge server depends on the HVV to connect to the mobile devices. Let $\mathbf{s_i}$ (**t**) be the server that decides to be ready to receive the task at the time **t** if the server mode is active ($\mathbf{s_M} = 1$); otherwise, the server mode is inactive ($\mathbf{s_M} = 0$).

We can compare the performance of the sample topologies in many aspects, such as the service time and power consumption. However, we want to highlight the results, which can be only provided by our simulation. Figure 5 shows that the average of service time (performance) is shown with respect to the number of offloadable subtasks (blocks). In the simulation, we note that the execution time when offloading subtasks to the edge server in case it is active is much less than that in case it is inactive, assuming that the offloading processes are done whether the edge server is active or inactive.

Figure 6 shows the average of power consumption with respect to the number of offloadable subtasks (blocks). We notice that the power consumption of subtasks when offloading is active is much less than that when offloading process is inactive, under the assumption that offloading processes are done whether the edge server is active or inactive.

5.2. Task Scheduling Based on VM Availability. To evaluate the effectiveness of the algorithm, we configure the simulation environment setting by computer configuration as follows: CPU: 1,500–3,000 MIPS, octa-core; memory: 32,000–64,000 MB; storage: 2 TB. Experimental parameters are set as follows: 2 edge servers, 40 VMs, range of offloaded tasks from 20 to 300. We simulated many offloaded tasks using LCG data for VMs in each ES, assuming that the ES provides edge cloud services to the VMs [28].

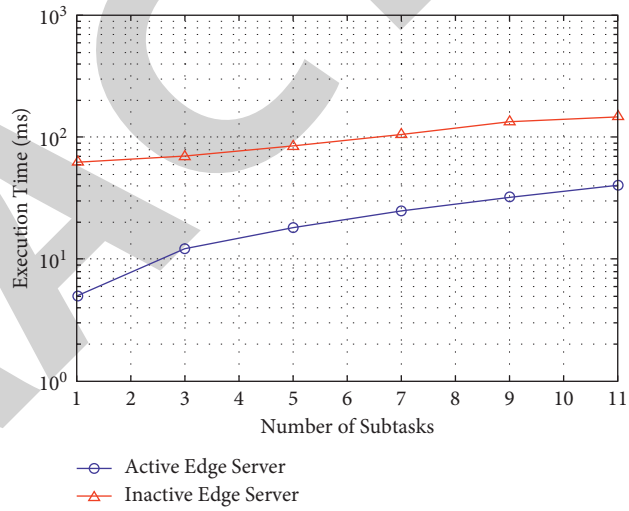

Figure 5: Average of execution time.

To evaluate the proposed algorithm AVM, we compare its results with other scheduling algorithms, namely, Round Robin (RR) and Minimum Completion Time (MCT) algorithm. We adopted three important parameters for comparison, which are awaiting time, resource utilization, and response time. The experimental results show that the AVM is superior to the other two algorithms. In the experiment, we measure the response time in milliseconds. Figure 7 illustrates the differential of the response time of each task. The number of tasks ranges between 20 and 300. Therefore, the results of the AVM are better than those of the other algorithms, as AVM improved the response time for each task.

In Figure 8, we measure the resource utilization by calculating the amount of resources remaining after serving

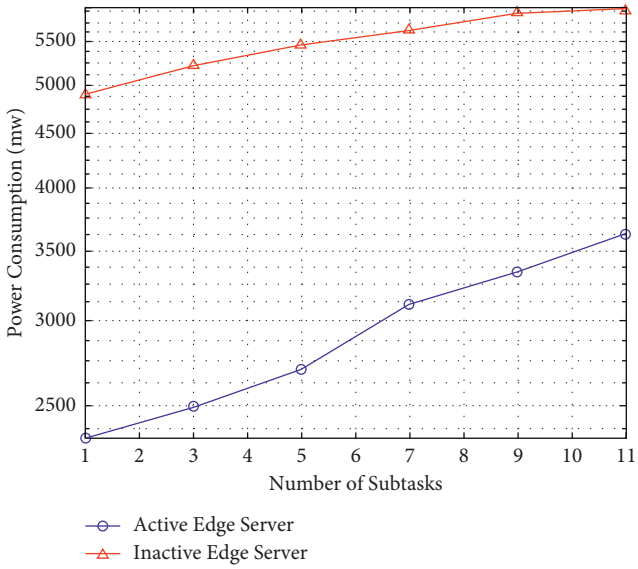

Figure 6: Average of power consumption.

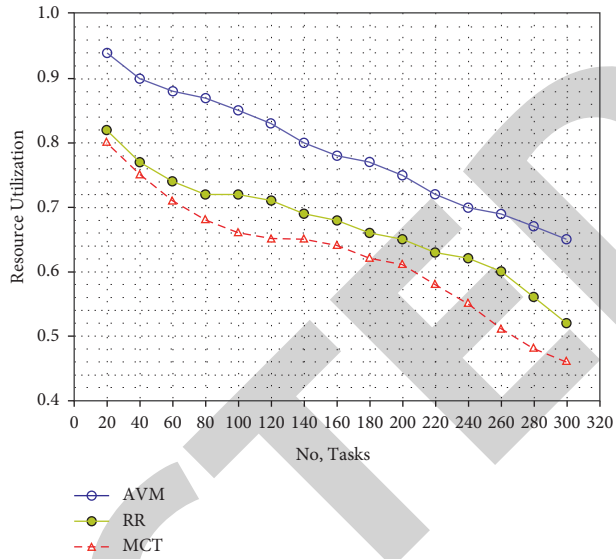

Figure 8: VM resource utilization.

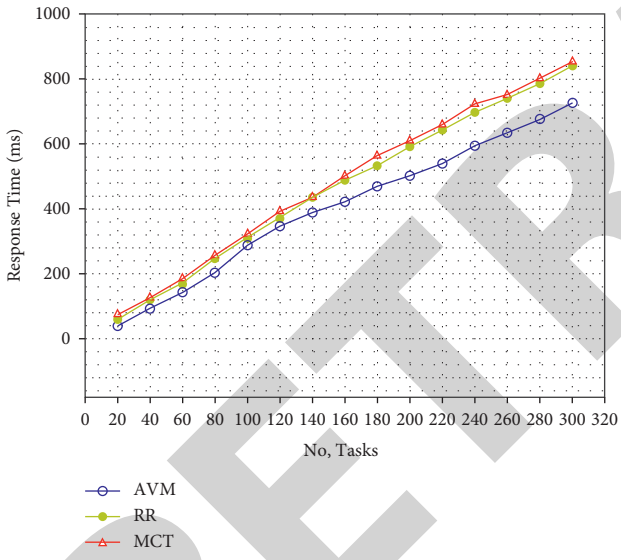

Figure 7: Response time per task.

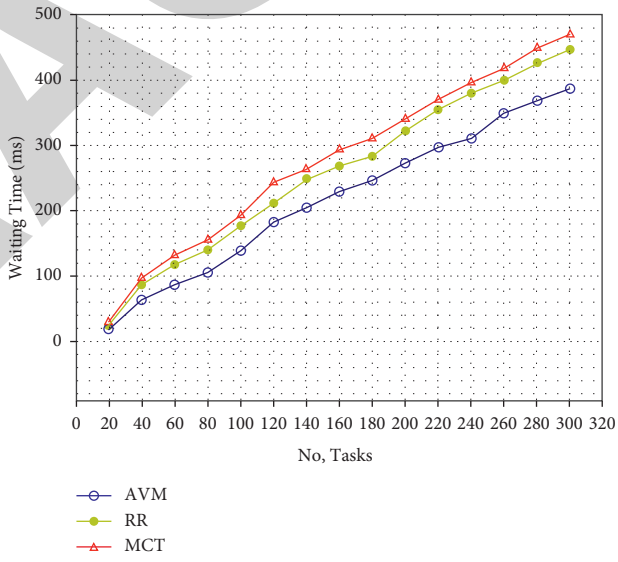

Figure 9: Task waiting time.

the tasks; for example, in our experiment, based on (14), the percentage of the remaining resources is measured.

Average waiting time is measured by computing the difference between the task offloaded time to the edge server and the starting time of the execution of the task. Figure 9 shows that the waiting time when applying the proposed algorithm was less compared to the other algorithms. Figure 9 depicts the average waiting time depending on the number of tasks when the number of VMs ranges between 20 and 300. The waiting time was affected by the number of offloaded tasks at the edge server (ES), as the waiting time gradually increased based on the number of tasks.

6. Conclusions

The edge computing technology promises an opportunity to overcome the constraints of mobile devices by offloading resource intensive and time sensitive applications to a nearby server. Until now, the concept of edge computing is not standardized, and it is hard to develop different and various architectures or scenarios of application. In this research, we proposed an evaluation module to evaluate the efficiency of the close-end network computation offloading in MEC. This model helps in choosing the adjacent edge server from the surrounding edge servers. This helps to decrease the latency and increase the response time. To do

so, we use a decision rule based Heuristic Virtual Value (HVV). The HVV is a mapping function based on the features of the ES like the performance and workload. Additionally, in this study, we proposed AVM algorithm to address the resource balancing, resource allocation, and task scheduling. The results of simulation show that the proposed model satisfies the latency requirements of time sensitive applications, enhances the performance, and minimizes the energy consumption of mobile devices. Furthermore, the experiment of the proposed AVM algorithm showed improvement in task response time and efficiency in resource utilization compared to the other similar algorithms.

Data Availability

The data used to support the findings of this study are available from the corresponding author upon request.

Conflicts of Interest

The authors declare no conflicts of interest regarding the publication of this paper.

Acknowledgments

This research was supported by King Saud University (Project no. RSP-2021/206), Riyadh, Saudi Arabia.

References

[1] N. Fernando, S. W. Loke, and W. Rahayu, "Mobile cloud computing: a survey," *Future Generation Computer Systems*, vol. 29, no. 1, pp. 84–106, 2013.

[2] G. H. Forman and J. Zahorjan, "The challenges of mobile computing," *Communications of the ACM*, vol. 36, no. 7, pp. 75–84, 1993.

[3] Y. C. Hu, M. Patel, D. Sabella, N. Sprecher, and V. Young, "Mobile edge computing—a key technology towards 5G," *ETSI white paper*, vol. 11, no. 11, pp. 1–16, 2015.

[4] A. C. Baktir, A. Ozgovde, and C. Ersoy, "How can edge computing benefit from software-defined networking: a survey, use cases & future directions," *IEEE Communications Surveys & Tutorials*, vol. 19, 2017.

[5] F. Bonomi, R. Milito, J. Zhu, and S. Addepalli, "Fog computing and its role in the internet of things," in *Proceedings of the First Edition of the MCC Workshop on Mobile Cloud Computing*, pp. 13–16, Helsinki, Finland, August 2012.

[6] D. Mazza, D. Tarchi, and G. E. Corazza, "A cluster based computation offloading technique for mobile cloud computing in smart cities," in *Proceedings of the IEEE International Conference on Communications (ICC), 2016*, pp. 1–6, Kuala Lumpur, Malaysia, October 2016.

[7] S. Ranadheera, S. Maghsudi, and E. Hossain, "Computation offloading and activation of mobile edge computing servers: a minority game," *IEEE Wireless Communications Letters*, vol. 7, no. 5, pp. 688–691, 2018.

[8] K. Habak, M. Ammar, K. A. Harras, and E. Zegura, "Femto clouds: leveraging mobile devices to provide cloud service at the edge," in *Proceedings of the IEEE 8th International Conference on Cloud Computing (CLOUD), 2015*, pp. 9–16, Nice, France, March 2015.

[9] G. Orsini, D. Bade, and W. Lamersdorf, "Computing at the mobile edge: designing elastic android applications for computation offloading," in *Proceedings of the 8th IFIP Wireless and Mobile Networking Conference (WMNC)*, pp. 112–119, Munich, Germany, June 2015.

[10] O. Chabbouh, S. B. Rejeb, Z. Choukair, and N. A. Ueve, "Computation offloading decision algorithm for energy saving in 5G/HetNets C-RAN," in *Proceedings of the 2016 5th International Conference on Multimedia Computing and Systems (ICMCS)*, pp. 284–289, Marrakech, Morocco, September 2016.

[11] Y. Mao, J. Zhang, and K. B. Letaief, "Dynamic computation offloading for mobile-edge computing with energy harvesting devices," *IEEE Journal on Selected Areas in Communications*, vol. 34, no. 12, pp. 3590–3605, 2016.

[12] M. H. ur Rehman, C. Sun, T. Y. Wah, A. Iqbal, and P. P. Jayaraman, "Opportunistic computation offloading in mobile edge cloud computing environments," in *Proceedings of the 17th IEEE International Conference on Mobile Data Management (MDM)*, vol. 1, pp. 208–213, Porto, Portugal, June 2016.

[13] X. Chen, L. Jiao, W. Li, and X. Fu, "Efficient multi-user computation offloading for mobile-edge cloud computing," *IEEE/ACM Transactions on Networking*, vol. 24, no. 5, pp. 2795–2808, 2016.

[14] J. Dolezal, Z. Becvar, and T. Zeman, "Performance evaluation of computation offloading from mobile device to the edge of mobile network," in *Proceedings of the 2016 IEEE Conference on Standards for Communications and Networking (CSCN)*, pp. 1–7, Berlin, Germany, October 2016.

[15] J. Zhou and X. J. Zhang, "Fairness-aware task offloading and resource allocation in cooperative mobile edge computing Z," *IEEE Internet of Things Journal*, 2021.

[16] C. You and K. Huang, "Multiuser resource allocation for mobile-edge computation offloading," in *Proceedings of the Global Communications Conference (GLOBECOM)*, pp. 1–6, Washington, NJ, USA, March 2016.

[17] F. Messaoudi, A. Ksentini, and P. Bertin, "On using edge computing for computation offloading in mobile network," in *Proceedings of the Globecom 2017-IEEE Global Communications Conference*, Singapore, December 2017.

[18] S. Sardellitti, G. Scutari, and S. Barbarossa, "Joint optimization of radio and computational resources for multicell mobile-edge computing," *IEEE Transactions on Signal and Information Processing over Networks*, vol. 1, no. 2, pp. 89–103, 2015.

[19] T. M. Alfaqih and J. J. Al-Muhtadi, "Internet of things security based on devices architecture," *MEC Compation*, vol. 133, no. 15, pp. 19–23, 2016.

[20] M. Derakhshan and Z. Bateni, "Optimization of tasks in cloud computing based on MAX-MIN, MIN-MIN and priority," in *Proceedings of the 2018 4th International Conference on Web Research (ICWR)*, pp. 45–50, Tehran, Iran, April 2018.

[21] S. H. H. Madni, M. S. Abd Latiff, M. Abdullahi, S. i. M. Abdulhamid, and M. J. Usman, "Performance comparison of heuristic algorithms for task scheduling in IaaS cloud computing environment," *PLoS One*, vol. 12, no. 5, Article ID e0176321, 2017.

[22] M. Sanaj and P. J. Prathap, "An enhanced Round robin (ERR) algorithm for effective and efficient task scheduling in cloud environment," in *Proceedings of the 2020 Advanced Computing and Communication Technologies for High Performance Applications (ACCTHPA)*, pp. 107–110, Cochin, India, July 2020.

Hindawi
Journal of Mathematics
Volume 2023, Article ID 9868607, 1 page
https://doi.org/10.1155/2023/9868607

Retraction

Retracted: Evaluation of the Effect of Ideological and Political Education on Psychological Crisis Intervention for University Students Based on Data Mining Algorithm

Journal of Mathematics

Received 15 August 2023; Accepted 15 August 2023; Published 16 August 2023

This article has been retracted by Hindawi following an investigation undertaken by the publisher [1]. This investigation has uncovered evidence of one or more of the following indicators of systematic manipulation of the publication process:

(1) Discrepancies in scope

(2) Discrepancies in the description of the research reported

(3) Discrepancies between the availability of data and the research described

(4) Inappropriate citations

(5) Incoherent, meaningless and/or irrelevant content included in the article

(6) Peer-review manipulation

The presence of these indicators undermines our confidence in the integrity of the article's content and we cannot, therefore, vouch for its reliability. Please note that this notice is intended solely to alert readers that the content of this article is unreliable. We have not investigated whether authors were aware of or involved in the systematic manipulation of the publication process.

Wiley and Hindawi regrets that the usual quality checks did not identify these issues before publication and have since put additional measures in place to safeguard research integrity.

We wish to credit our own Research Integrity and Research Publishing teams and anonymous and named external researchers and research integrity experts for contributing to this investigation.

The corresponding author, as the representative of all authors, has been given the opportunity to register their agreement or disagreement to this retraction. We have kept a record of any response received.

References

[1] H. Yao and M. D. H. A. Malek, "Evaluation of the Effect of Ideological and Political Education on Psychological Crisis Intervention for University Students Based on Data Mining Algorithm," *Journal of Mathematics*, vol. 2021, Article ID 9504247, 8 pages, 2021.

Hindawi
Journal of Mathematics
Volume 2021, Article ID 9504247, 8 pages
https://doi.org/10.1155/2021/9504247

Research Article

Evaluation of the Effect of Ideological and Political Education on Psychological Crisis Intervention for University Students Based on Data Mining Algorithm

Hexia Yao[1,2] and Mohd. Dahlan Hj. A. Malek[3]

[1]*Faculty of Psychology and Education, University Malaysia Sabah, Kota Kinabalu, Sabah, Malaysia*
[2]*Student Affairs Department, Hebei University of Engineering, Handan, Hebei, China*
[3]*Faculty of Islamic Studies, University Malaysia Sabah, Kota Kinabalu, Sabah, Malaysia*

Correspondence should be addressed to Mohd. Dahlan Hj. A. Malek; dahlanam@ums.edu.my

Received 16 November 2021; Revised 30 November 2021; Accepted 6 December 2021; Published 21 December 2021

Academic Editor: Naeem Jan

The mental health level of university students not only directly affects their own growth, but also affects the stability of the campus, which in turn affects the harmony of society and the improvement of the quality of all people. The combination of ideological education and mental health education is an important educational project in contemporary universities. To enhance the quality of psychological health education of college students can promote the overall development of students' comprehensive quality; the two are closely integrated together, so as to successfully promote the effective combination of ideological education and psychological education, thus realizing the role of ideological education and psychological health education in promoting the physical and mental health development of contemporary college students. This paper explains the technology of data mining and the current situation of the psychological impact of Civic Education on college students and analyzes in depth the feasibility of introducing data mining technology in Civic Education to intervene in the psychological crisis of college students. The results show that the application of the technology provides a new idea for the mental health education of college students and a new way for the construction of a preventive college student mental health education model.

1. Introduction

At present, major institutions are paying increasing attention to the ideological education in order to ensure the psychological health of students. In the process of conducting Civic Education [1, 2], teachers should fully grasp the concept of education, make their own educational tools further improve, make the content of education more diversified, be able to give effective solutions to different mental health problems, ensure the stable and healthy growth of students through Civic Education, so that students can carry out effective logical analysis when facing problems, and put forward the correct solution strategy, for the overall development of the university. This will provide strong support for the overall development of the university. The ideological education is guided by Marxism-Leninism and other ideological theories, focusing on the needs of the contemporary state and society, and guiding students to establish the correct three views. Mental health education in higher education is based on students' individual psychological needs, focusing on their psychological development and personality development to promote good psychological quality. There is an inevitable link between ideological education and mental health education, and it is only through the organic integration of the two that the practical needs of contemporary university students can be addressed. Therefore, combining the two together can, in a broad sense, promote the development of moral education in contemporary colleges and universities, expand the teaching objectives of moral education by improving the way of education development, thus enriching the content contained in moral education in contemporary colleges and universities and improving the effectiveness of the curriculum teaching of moral education in colleges and

universities. In actual life, it realizes the integration between Civic Education and Mental Health Education, improves students' social adaptability, and perfects their personality qualities [2].

The ideological education is responsible for the development of students' inner potential and pays more attention to the cultivation of students' ideology and morality. Mental health education, as an important part of contemporary university curriculum construction, promotes the overall development of students' comprehensive quality, enhances students' psychological tolerance, and improves their psychological quality. Therefore, we can see that mental health education is an important part of ideological and political education, and there is unity in the cultivation objectives between the two. Mental health teachers in colleges and universities can use the ideology education approach to guide students to establish a correct world view and outlook on life and values. They can also introduce psychological health education into the classroom teaching process, so that students have the ability to solve problems on their own and face the pressures of life in a more positive way. The mental health development of university students has gradually begun to mature, and university teachers should combine scientific and systematic ideological education guidance with psychological guidance for students, which will have a profound impact on their daily work and life. At present, there are many undesirable factors and temptations in society that have a negative impact on the psychological health of students, resulting in a higher rate of truancy. Teachers need to keep an eye on students' psychological state, enhance their self-confidence, and encourage them to form a correct and perfect outlook and personality.

At present, most universities have incorporated mental health education into their ideological and political construction education system. They have set up special institutions, offered courses on mental health education, carried out psychological counselling for school students, and established mental health files for students. Most universities conduct psychological tests on students every year, and the tests are mostly conducted in the traditional way; i.e., students are given questionnaires and then the results are collected on basis of which a database is established. A database is capable of providing a simple statistical and overall grasp of the students' psychological problem situation. However, these traditional data analysis methods can only obtain superficial information about psychological data, making it difficult to analyze the data at a deeper level. In addition, the prediction of the future trends based on the available data also becomes hard, i.e., they would not be able to gain essential and scientific knowledge. As a result, the prediction accuracy rate becomes relatively low. Although many data mining tools have emerged which have their own purpose and focus, these mining tools are demanding on the user and not much user friendly; i.e., they require the help of various professionals to achieve the purpose of use.

In this paper, data mining technology is applied to the psychological intervention of college students in Civic and Political Education. The aim is to uncover the useful knowledge veiled under the data of college students' psychological problems through the application of data mining technology, using this valuable knowledge to predict the mental health of college students more accurately, providing a scientific basis for the planning and decision-making of mental health education, making mental health education more targeted and effective, and truly improving the level of mental health education. This will make mental health education more relevant and effective and truly improve the level of mental health education. The following section discusses the data mining and its different techniques including the classification and methods. In third section, the design and implementation of an ideological and political psychological data management system for university students are presented. Finally, the paper is concluded in the fourth section.

2. Data Mining Techniques

This section classifies the systems of data mining with respect to some criteria into database technology, information science, visualization, machine learning, statistics, and many more. Further, the important data mining methods are explained such as decision trees, genetic algorithms, neural networks, rough set, fuzzy set, and statistical analysis. Then the process of data mining is given. Finally, the classification in the mining data is explained in detail.

2.1. Classification of Data Mining Systems. Data mining is the process of extracting from large, incomplete, noisy, fuzzy, random data, information, and knowledge that is implicit in it and not known beforehand but is potentially useful. To put it more bluntly, data mining is the mining of knowledge from data [3]. The raw data can be structured or semi-structured, or heterogeneous and distributed over the network. The discovered knowledge is presented in the form of concepts, rules, laws, patterns, etc. It can be used for process control, query optimization, information management, decision support, and maintenance of own data.

Data mining techniques originate from a number of disciplines [4], all of which have an impact on data mining, as illustrated in Figure 1.

Because data mining is a cross-cutting discipline, data mining gives rise to many different types of data mining systems. A clear classification of data mining systems can provide a scientific basis for the user to select the most appropriate data mining system. Based on different classification criteria, the classification of data mining systems is shown in Table 1.

2.2. Main Methods of Data Mining

2.2.1. Decision Trees. In data mining, decision trees are mainly used for classification [6, 7]. The decision tree model generated using this method looks like an upside-down tree, where the root node at the top level represents a dataset, and each node represents a classification problem. And each branch represents a classification result, and each leaf node at the bottom level represents a category or class distribution. The decision tree represents the classification in a tree-like structure according to

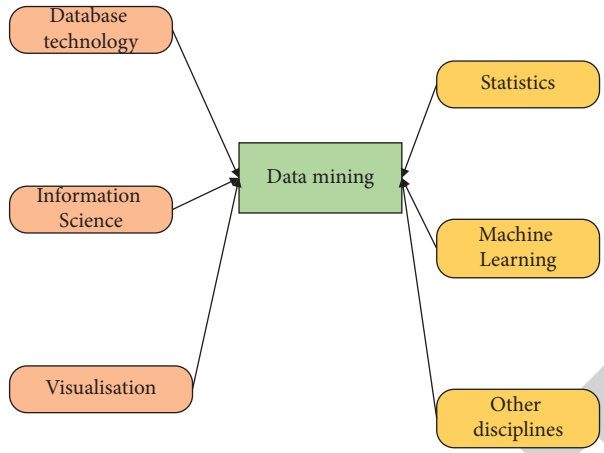

Figure 1: Multiple disciplines influence data mining.

Table 1: Classification of data mining systems [5].

Classification criteria	Category
According to the type of database mined	Relational, transactional, object-relational or data warehouse mining systems, etc.
According to the type of data being processed	Spatial, time series, textual, streaming data, multimedia data mining systems or web mining systems, etc.
Depending on the type of knowledge to be mined	Association rule mining, feature rule mining, classification rule mining, clustering rule mining, etc.
Depending on the type of technology used	Discovery-driven data mining, machine learning data mining, interactive data mining, statistical analysis data mining, etc.
By application area	Data mining for retail, data mining for finance, data mining for telecoms, data mining for internet, etc., data mining, internet data mining, etc.

different characteristics and is used as a basis for generating rules. The main advantages of decision trees are that they are simple to describe, are fast to classify, generate models that are easy to understand and have a high accuracy, and are widely used in various data mining systems. Its main disadvantage is that it is difficult to construct a decision tree based on a combination of variables.

2.2.2. Genetic Algorithms. Genetic algorithms simulate the natural evolutionary process of "survival of the fittest" and are based on the principles of biogenetics [8, 9]. The algorithm is easily parallelized and excels at data clustering. However, it is an algorithm that is not easy to understand, and it is used to solve problems by encoding the problem to be solved first symbolically and discretely. To improve the ease of understanding of the model at a higher level, genetic algorithms are often used in conjunction with neural network algorithms.

2.2.3. Neural Networks. Neural networks are a widely used and very important method in data mining [10]. It is a computational model based on the theory of neurobiology that mimics the working mechanism and structure of neural networks in the human brain. Neural networks exhibit many of the characteristics of the human brain, consist of many interconnected neurons, are capable of performing nonlinear operations and more complex logical operations, and have some of the functions of the human brain. As neural networks are a distributed matrix structure, the neural units are highly parallel and distributed, enabling parallel computation and distributed storage of data, making them highly adaptive, self-organizing, and self-learning.

2.2.4. Statistical Analysis. There are functional relationships between database fields (deterministic relationships that can be expressed in function formulas) and correlation relationships (relevant deterministic relationships that cannot be expressed in function formulas). The analysis of the two relationships can be used by statistical methods, that is, the use of statistical principles of the data warehouse or database information for analysis and processing. The main methods of statistical analysis are shown in Table 2.

2.2.5. Rough Set. Rough set methods can be used for classification, to deal with imprecise, uncertain, inconsistent, and incomplete information, to simplify information as well as to derive knowledge from experience, and as a means of mathematical analysis [12]. Rough sets can also be used for correlation analysis and attribute subset selection. The basic principle of rough sets is based on the idea of equivalence classes, where the elements of an equivalence class are considered indistinguishable. The basic method of rough sets is to discretize the values of the attributes in a relationship using the rough set approximation, classifying each attribute into equivalence.

Table 2: Statistical analysis methods [11].

Method	Function
Common statistics	Sum, mean, maximum, minimum, etc.
Correlation analysis	Correlation coefficients are used to measure the degree of correlation between variables
Analysis of variance	Use the value of a sample statistic to determine the difference between overall parameters
Regression analysis	Expressing the quantitative relationship between variables using linear or nonlinear regression equations
Discriminant analysis	Establishing a discriminant function and specifying the discriminant criteria and then using the discriminant function to assign the object of study to a category
Cluster analysis	Comparing the distances between samples in a sample set and grouping those that are closer together into one category, while those that are further apart cannot be grouped into one category

Based on the equivalence relation of the set, the reduction of the relation is carried out and the minimum decision relation is obtained, thus making it easy to obtain rules. The main advantage of rough sets is that no initial information about the data or additional information is required.

2.2.6. Fuzzy Sets. Fuzzy sets are based on fuzzy set theory for fuzzy evaluation of practical problems, fuzzy cluster analysis, fuzzy pattern recognition, and fuzzy decision-making. In data mining classification, fuzzy set methods enable us to deal with high abstraction levels and provide a means to deal with imprecise measures of data. More importantly, fuzzy sets are able to deal with fuzzy or imprecise facts.

2.3. The Main Processes of Data Mining. Data mining is seen by some as a key step in the knowledge discovery process. The knowledge discovery process is shown in Figure 2. The data warehouse in the figure is the basis for data mining. Because data mining uncovers hidden patterns, it is more commonly equated with knowledge discovery from a pattern processing perspective.

2.4. Classification in Data Mining. Data classification is a very important function of data mining [13]. Data classification has become an important feature of many data mining systems. Classification is the construction of a classification model or classification function (also known as a classifier) based on a given piece of data and the use of this model to classify unknown data records in a database, i.e., for prediction purposes. Data classification can usually be grouped into two steps: building a model and using the model for classification, as shown in Figure 3.

3. Design and Implementation of an Ideological and Political Psychological Data Management System for University Students

The collection and analysis of students' ideological and political psychological assessment data is a basic task necessary for the development of mental health education in colleges and universities, and as the number of students enrolled in colleges and universities increases and the connotation of psychological data analysis increases, more and more psychological data needs to be analyzed and processed in greater depth. This paper adopts a B/S model of psychological data management system for university students based on data mining technology to improve the efficiency of psychological assessment data collection and increase the depth of psychological data analysis. The data mining function of this system can be used to successfully detect the presence or absence of psychological symptoms in students and to achieve the prediction of potential possible psychological symptoms. According to the general steps of data mining, the business process of data mining of university students' ideology and political psychology is designed as shown in Figure 4.

3.1. Data Collection. In order to obtain the required data, 1,700 students in 5 departments, 29 majors, and 42 classes at a university were measured. The students were aged between 17 and 24 years. 1700 self-assessment scales were distributed and 1640 were returned. The collected "symptom self-assessment scales" were used to calculate the scores of each student for each ideological and psychological factor. The data required for the analysis of psychological issues is managed using the database management system SQL Server 2008. The "psychology" database is created in the SQL Server Management Studio of SQL Server 2008 under the graphical interface. Create the "Personal Psychological Problems" and "Personal Profile" tables in the "psychology" database. Table 3 gives the definition of the table structure of the "Personal Psychological Problems" table.

In this paper, 2/3, i.e., 1066 records, were randomly selected from the data set used for the analysis of university students' psychological problems after data preprocessing as the training sample set for decision tree mining, and the other 1/3, i.e., 533 records, were used as the test sample set for decision tree testing. The whole process of constructing a decision tree model of whether students have ideological and political psychological disorders based on the C4.5 algorithm is presented comprehensively below, with the following steps. Equations (1)–(5) were used to calculate the training the information gain rate for each split attribute in the training sample set.

$$\text{Info}(D) = -\sum_{i=1}^{m} p_i \log_2(p_i), \tag{1}$$

where p_i is the probability that any sample in D belongs to C_i and is calculated using $(|C_{i,D}|/|D|)$. In practice, the above equation is simply the number of samples per class as a proportion of the total number of samples utilized. $\text{Info}(D)$

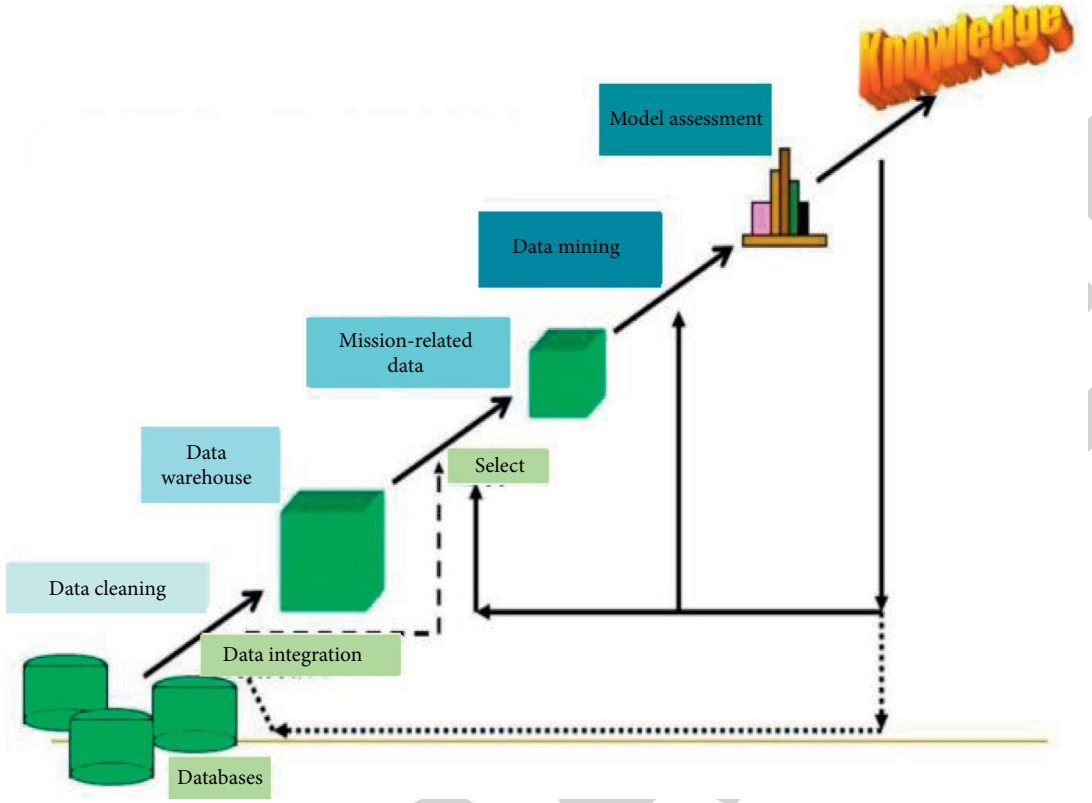

Figure 2: Data mining as a key step in knowledge discovery.

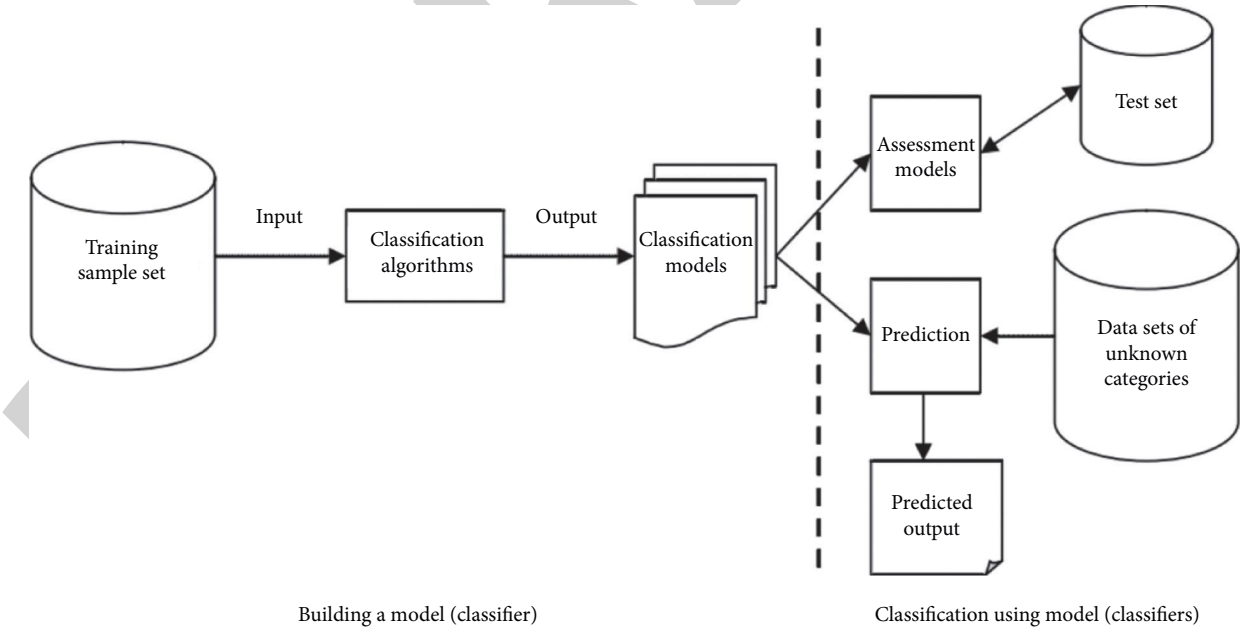

Figure 3: Steps in classification.

is also known as the entropy of D. Entropy is a statistic that measures the degree of disorder in a system.

$$\text{Info}_A(D) = \sum_{j=1}^{v} \frac{D_j}{|D|} \times \text{Info}\left(D_j\right), \tag{2}$$

where $(D_j/|D|)$ is the weight of the subset of values on attribute A that take the value a_j. $\text{Info}_A(D)$ is the desired information needed to classify the samples on D based on the classification by attribute A. This reduction in entropy due to the knowledge of the value of attribute A can be derived from

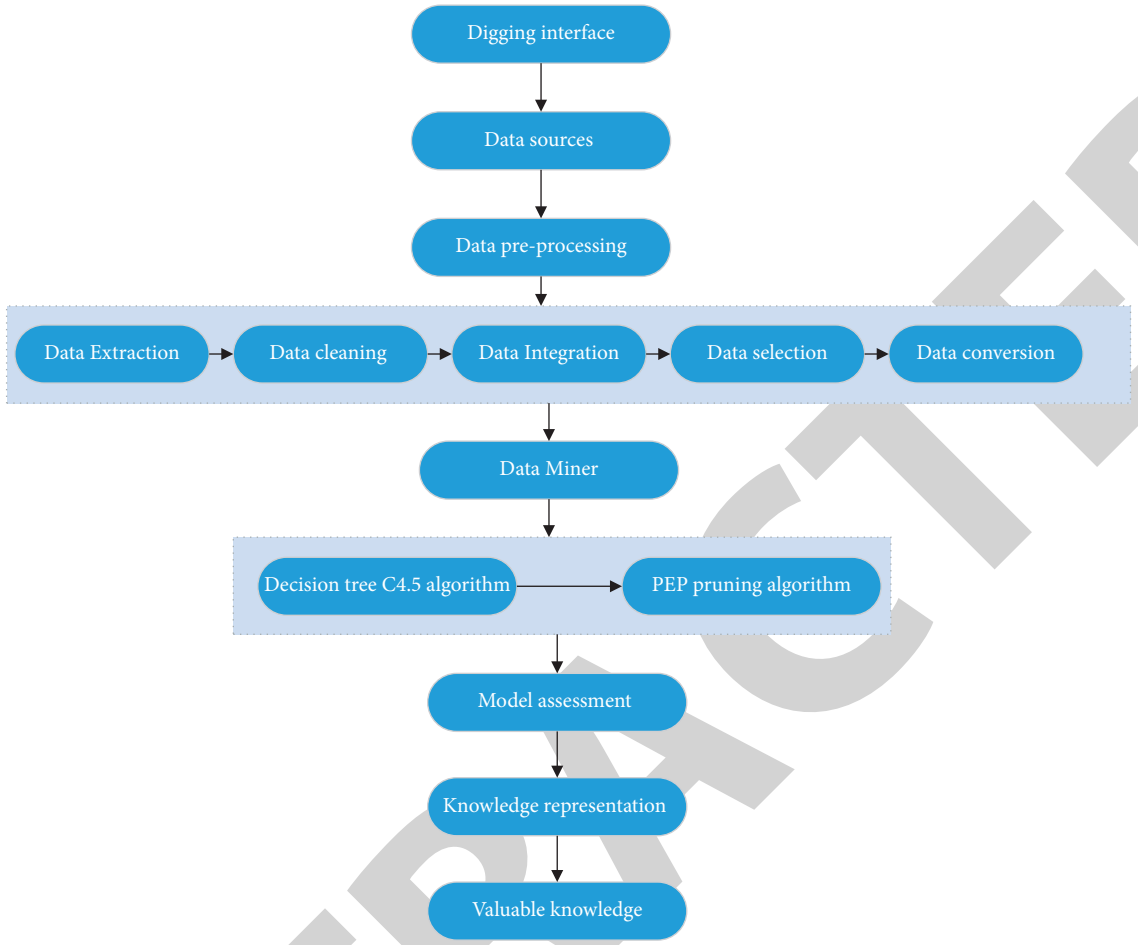

Figure 4: Business process of psychological data mining for university students.

Table 3: Definition of the structure of the "personal psychological problems" table.

Field name	Type	Maximum length	Meaning
XH	C	10	Academic number
Q	N	4	Somatization
QP	N	4	Obsessive compulsive
MG	N	4	Interpersonal sensitivity
YY	N	4	Depression
JL	N	4	Anxiety
DD	N	4	Hostility
KB	N	4	Terror
PZ	N	4	Paranoia
JS	N	4	Psychotic

$$\text{Gain}(A) = \text{Info}(D) - \text{Info}_A(D). \tag{3}$$

Classification actually extracts information from the system to reduce the level of chaos in the system, thus making the system more regular, more orderly, and more organized. The more chaotic the system is, the greater the entropy will be. Clearly, the splitting scheme that results in the greatest reduction in entropy is the optimal splitting scheme. Therefore, the C4.5 algorithm selects the attribute A with the maximum information gain $\text{Gain}(A)$ as the splitting attribute on node N.

$$\text{GainRatio}(A) = \frac{\text{Gain}(A)}{\text{SplitInfo}(A)}. \tag{4}$$

This is the definition of information gain rate. Split information is used in the above equation for the purpose of normalizing the information gain; split information is similar to $\text{Info}(D)$, defined as

$$\text{SplitInfo}_A(D) = -\sum_{j=1}^{v} \frac{|D_j|}{|D|} \times \log 2 \frac{|D_j|}{|D|}. \tag{5}$$

$\text{SplitInfo}_A(D)$ represents the information generated by splitting the training sample set D into v plans corresponding to the v outputs of the attribute A test.

3.2. System Architecture. The system uses the B/S model and the architecture of the system is shown in Figure 5.

According to the analysis and design of the psychological data management system for university students, the student function module and the administrator function module are implemented. When the system is running, the login interface opens first, through which the user enters the account number and password, selects the identity (student or administrator), and after verification, can enter the system. The system login screen is shown in Figure 6.

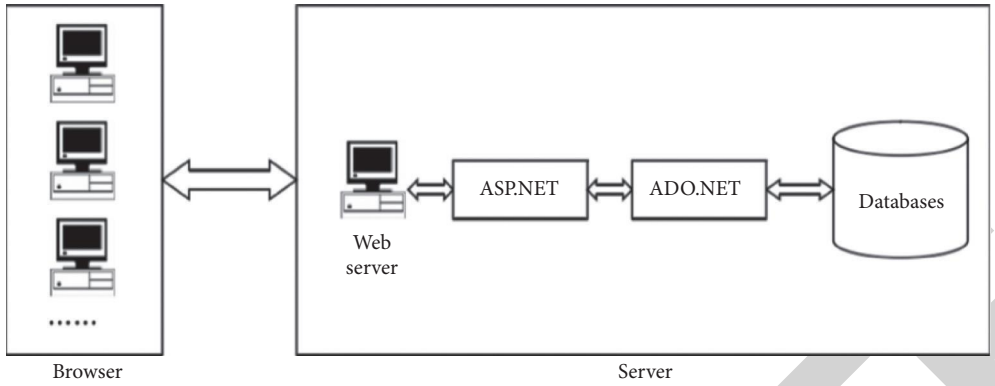

Figure 5: System structure of the ideological and psychological data management system for university students.

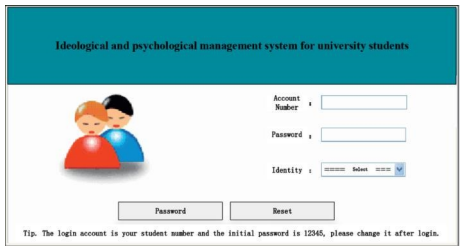

Figure 6: Main system interface.

The process of assessing ideological and psychological interventions for university students using data mining is as follows:

(1) Data preparation: Preprocessing of raw data to provide a data source for the data mining module.

(2) Decision tree generation: The C4.5 algorithm [14] is used to mine the preprocessed data for classification and generate a decision tree model that is pruned using the PEP pruning algorithm.

(3) Generating classification rules: Extracting classification rules from the final decision tree model.

(4) Psychological problem prediction: It predicts which ideological and political psychological symptoms a given student is likely to have by entering the values taken for the attributes of that student.

4. Conclusion

This paper investigated the application of data mining technology in the analysis of the ideological and political psychological problems of college students. The analysis of important techniques of data mining was carried out. Also, a basis was provided for the application of decision tree algorithm for the analysis of political and ideological psychological problems of college students. We applied decision trees for the construction of a classification model for university students' psychological problems. Moreover, a set of B/S structure has been independently developed which is based on data mining, psychological data management system for university students. The paper realized the automation of the collection of basic information and psychological assessment information of college students and increased the depth of data analysis of psychological problems through the application of data mining technology. The application of data mining technology has increased the depth of data analysis of psychological problems.

There are still some limitations in the mining of university students' psychological data. In the actual implementation process, some unexpected problems were encountered, which are not elaborated in detail due to the limited space of this paper. In order for this study to play a greater role in supporting decision-making in mental health education, a great deal of work needs to be done in future research, mainly in the following areas:

(1) When preprocessing the data, missing values in the dataset were simply replaced with a constant, an approach that is too simplistic and could actually try to use more data cleaning strategies.

(2) Since there is no single classification method that is suitable for all classification problems, a comprehensive in-depth study and comparison of various classification methods is a valuable research direction for application.

(3) The focus was the application of classification techniques in data mining, but other techniques of data mining can be tried to analyze the data of university students' psychological problems, such as using the Apriori algorithm of association rules to analyze some intrinsic connection between the data of students' attributes that affect each other. A variety of methods can also be used to analyze the data on students' psychological problems in a comprehensive manner, with a view to providing a more accurate and comprehensive basis for decision-making in mental health education work.

Data Availability

The data used to support the findings of this study are available from the corresponding author upon request.

Conflicts of Interest

The authors declare that there are no conflicts of interest.

Hindawi
Journal of Mathematics
Volume 2024, Article ID 9894065, 1 page
https://doi.org/10.1155/2024/9894065

Retraction

Retracted: Economic Benefit Evaluation and Analysis Based on Intelligent Agriculture Internet of Things

Journal of Mathematics

Received 23 January 2024; Accepted 23 January 2024; Published 24 January 2024

This article has been retracted by Hindawi following an investigation undertaken by the publisher [1]. This investigation has uncovered evidence of one or more of the following indicators of systematic manipulation of the publication process:

(1) Discrepancies in scope

(2) Discrepancies in the description of the research reported

(3) Discrepancies between the availability of data and the research described

(4) Inappropriate citations

(5) Incoherent, meaningless and/or irrelevant content included in the article

(6) Manipulated or compromised peer review

The presence of these indicators undermines our confidence in the integrity of the article's content and we cannot, therefore, vouch for its reliability. Please note that this notice is intended solely to alert readers that the content of this article is unreliable. We have not investigated whether authors were aware of or involved in the systematic manipulation of the publication process.

Wiley and Hindawi regrets that the usual quality checks did not identify these issues before publication and have since put additional measures in place to safeguard research integrity.

We wish to credit our own Research Integrity and Research Publishing teams and anonymous and named external researchers and research integrity experts for contributing to this investigation.

The corresponding author, as the representative of all authors, has been given the opportunity to register their agreement or disagreement to this retraction. We have kept a record of any response received.

References

[1] S. Liu and Y. Wu, "Economic Benefit Evaluation and Analysis Based on Intelligent Agriculture Internet of Things," *Journal of Mathematics*, vol. 2021, Article ID 9499197, 7 pages, 2021.

Hindawi
Journal of Mathematics
Volume 2021, Article ID 9499197, 7 pages
https://doi.org/10.1155/2021/9499197

Research Article

Economic Benefit Evaluation and Analysis Based on Intelligent Agriculture Internet of Things

Shu Liu and Yuting Wu

Sichuan Railway College, Chengdu, Sichuan 610097, China

Correspondence should be addressed to Shu Liu; panyzhou98@email.swu.edu.cn

Received 17 November 2021; Revised 30 November 2021; Accepted 6 December 2021; Published 20 December 2021

Academic Editor: Naeem Jan

There has been a consensus on the development of ecological agriculture to promote the leap from traditional agriculture to ecological agriculture, but the unavoidable fact is that the development of ecological agriculture is still relatively slow at the present stage and has not formed a major climate and great influence. The rise of the Internet is a technology that has promoted the transformation and upgrading of modern agriculture, changed the traditional agricultural production mode, and accelerated the scientific and technological integration of information. In view of the characteristics and difficulties of agriculture, this paper builds an Agricultural Internet of Things (IoT) management system to realize the integrated management of Internet equipment and realize the management of environmental data, video data, and agricultural expert knowledge. Then from perception technology, transmission technology, and the perspective of three intelligent information processing technologies, this paper introduces the present state of agricultural IoT, analyzes the Internet of Things to the economic benefits of agricultural production, to research the problems of China's agricultural development of the Internet of Things, and puts forward China's agricultural Internet of the future research emphasis and direction of development.

1. Introduction

The Internet of Things is an important symbol of the global information age. Its basic connotation includes the following two points. First, the Internet of Things is the expansion and extension of the Internet, telecommunications network, and broadcasting network, while the three networks provide technical support for the generation and development of the Internet of Things. Second, information exchange between traditional users has expanded to interactive communication between users and objects and between objects, with further development of intelligent objects [1, 2]. Agriculture is the primary industry and is an important part of the national economy; the narrow sense of agriculture refers to the planting industry. Nowadays, the international agricultural product market is a complex combination of commercialization, scale, science and technology, and internationalization. The development of Chinese agriculture is of great significance to the international agricultural product market. Traditional agriculture relies on manpower and experience in the process of work, many problems in the process of work cannot be accurately answered, and the control of the process of work is also very difficult. Agricultural Internet of Things can realize parametric control to automatic control in the planting process through equipment and instruments, providing a scientific basis for the planting process of crops while reducing manpower and material resources, and it can increase at the same time.

Smart agriculture is a process of intelligent management such as agricultural visual remote diagnosis, remote control, and disaster warning by fully applying modern information technology achievements and integrating computer and network technology, Internet of Things technology, audio and video technology, 3S technology, wireless communication technology, and expert wisdom and knowledge [3]. Smart agriculture integrates the agricultural ecosystem, uses modern science and technology, realizes energy recycling,

saves labor costs, realizes intensive utilization of resources, and improves the quality of agricultural products to a certain extent. It is a new agricultural development model [4]. In the early 1980s, smart agriculture first emerged in the United States and gradually spread to all continents with the development of informatization and intelligence [5]. Although smart agriculture started late in China, the government attaches great importance to the introduction of high and new technologies. By 2013, the industrial scale of smart agriculture in China has reached 400 billion yuan [6]. From the 13th Five-Year Plan of National Science and Technology Innovation, smart agriculture has become a key part of the construction of efficient, safe, and ecological modern agricultural technology. However, in a strict sense, China's smart agriculture is still in its infancy and exploration stage [7]. As a big agricultural country, smart agriculture is an important way to transform the agricultural production mode at this stage by gradually replacing the traditional production mode.

The Agricultural Internet of Things (IoT) improves the speed and quality of agricultural products by addressing problems in extensive agricultural production, transportation, and marketing. It plays a great role in promoting and promoting the development of agriculture. In terms of economic benefits, the role of agricultural IoT is mainly reflected in the following aspects [8]:

(i) The first aspect is agricultural productivity and production efficiency that has been greatly developed and improved: agriculture accounts for a large proportion in the development of the national economy. How to optimize agricultural productivity and improve production efficiency has been attached importance to by governments of all countries. Agricultural IoT can improve the speed and precision of data collection and information processing, make overall planning of agricultural production, transportation, and sales process, reduce the input of human, material, and financial resources, improve the operation efficiency of agricultural enterprises, and improve economic benefits.

(ii) The second aspect is to reduce agricultural production expenditure and improve the utilization efficiency of funds: agricultural production, transportation, and sales require coordination from all aspects of society, which will consume a lot of human resources and capital costs. How to reduce costs and improve economic benefits is the focus of Agricultural Internet of Things research. Agricultural IoT can optimize the agricultural management of the whole process from production to sales, on the premise of ensuring that the quality of agricultural products will maximize cost at each stage of compression. Every step is closely focused on production, logistics, marketing resources, and so on to make reasonable allocations to avoid unnecessary waste of resources. Production, transportation, and sales are coordinated with each other, and the cost will also be greatly reduced. In addition, the real-time change and sharing of information in the agricultural supply chain also enable all parties to grasp the production, transportation, and sales situation in a timely manner, facilitating timely adjustment for problems, realizing the circular flow of resources in the transaction process, and making win-win cooperation easier for all parties in the supply chain.

(iii) The third aspect is to save resources and improve the efficiency of resource use: resource conservation and environmental friendliness are widely recognized by the world's mainstream ideas, traditional agricultural production methods and ideas are relatively old, there is a lot of unreasonable use of resources, and the most common is the unreasonable fertilization and irrigation methods. Traditional agriculture has been far from the concept of resource conservation advocated in modern society, while the Agricultural Internet of Things can accurately calculate and reasonably allocate resources in the agricultural production process, which is conducive to reducing or even eliminating resource waste. Taking the aquaculture industry of European and American developed countries as an example, the oxygenation and feed delivery in the traditional aquaculture process completely depend on the experience of workers. With the introduction of the Agricultural Internet of Things, the scale of breeding has been continuously expanded, and the whole process of breeding has realized the intelligent increase of oxygen and feed delivery. Through the real-time monitoring of oxygen content and feed residue in the water, relevant technicians can remotely control the oxygenation pump and feed delivery equipment from the mobile phone terminal. Compared with the traditional experience and a lot of human resources, the whole breeding process is more scientific, the cost of human and related resources is lower, and agriculture is truly unmanned, automated, and intelligent.

At present, the development of the Agricultural Internet of Things is still in the initial stage. The Agricultural Internet of Things architecture is not perfect, the threshold of building the underlying perception system is high, and the sharing of the Internet of Things resources is poor, presenting a fragmented state [9, 10]. Therefore, based on the Internet of Things technology, combined with wireless sensor network technology and data fusion technology, this paper designed a farmland environment monitoring and early warning system based on the Internet of Things to realize the real-time dynamic control of agricultural production factors information, so as to effectively promote the development of agriculture in the direction of refinement and intelligence. Then the advantages of the application of Internet of Things technology in agricultural informatization are explored, and the economic benefits of the application of Internet of Things technology in agriculture are analyzed by using the budget model. The experimental

results show that the input of Agricultural Internet of Things technology can improve the economic benefits of farms, agricultural machinery stations, and agricultural machinery households to varying degrees, and the equipment has an obvious price advantage, which has a good prospect of popularization and application.

Throughout this paper, we present in Section 2 a system designed in a way that reduces cost and needs less power, then analyze in Section 3 the method used, but to go forward for the effectiveness of methods, we need to do experiments and have results and that is what we do in Section 4, and finalize this paper by a conclusion in Section 5.

2. Agricultural IoT Architecture

Unlike greenhouse or other types of monitoring, farmland environmental monitoring does not require the real-time collection of environmental data. Therefore, some data transmission methods with low cost and low power consumption can be selected. Secondly, real-time acquisition technology also has a long data transmission cycle. In general, soil monitoring systems can monitor various soil data information every few months or longer [11]. Therefore, as long as the data upload cycle is set in advance, automatic monitoring and management can be realized.

2.1. Overall System Design. This system is mainly applied in farmland environment to collect soil temperature, degree, humidity, PH value, light, and other data [12]. By monitoring these data, we can provide a scientific basis for precise control of agricultural production so as to improve yield, economic benefit, and quality. Based on the consideration of the actual farmland environment, the system adopts ZigBee technology and 4G network to design an intelligent monitoring system suitable for the farmland environment [13]. The overall requirements of the system are as follows:

(1) Cover 150 mu of farmland, set sensor nodes every 50 m, and set sink nodes every 20 mu on average.

(2) Monitor soil temperature, humidity, PH value, air temperature, and light.

(3) Sensor nodes require small size, low cost, simple installation and deployment, waterproof, and dustproof and are suitable for outdoor operations.

(4) Data transmission is stable, the upload cycle is automatically set, and the node battery is required to work continuously for more than 3 months.

The system mainly designs two modules of data acquisition and data monitoring [14]. The overall structure of the system is shown in Figure 1. Data are collected by the sensor terminal, uploaded to the sink node in the ZigBee network, and then transmitted to the PC end of the monitoring system platform through the 4G network for data display and analysis. In addition, the monitoring end provides WEB services to facilitate users to connect to the monitoring system in B/S mode to query real-time data.

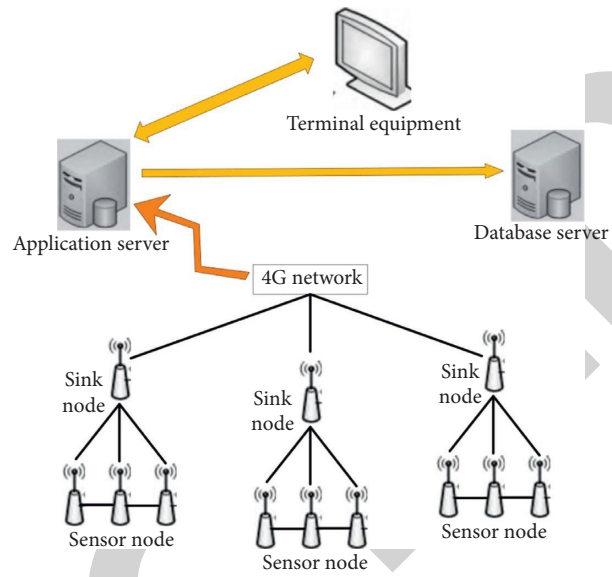

Figure 1: Overall system structure drawing.

The overall network structure of the system is divided into perception layer, network layer, and application layer from bottom to top [15]. The perception layer mainly collects and obtains information by using various sensors such as temperature and humidity sensors and sends the collected data to the transmission layer through the ZigBee transmission protocol [16]. The transmission layer mainly exchanges and shares the data collected by the equipment with the help of the 4G network. In the application layer, the system can provide a basis for intelligent and information management of agricultural production through data processing.

2.2. Data Acquisition Module. The data acquisition module in the system mainly completes the acquisition of farmland environmental parameters. The module consists of two parts: sensor and circuit. The acquisition nodes in the system mainly include air temperature and humidity sensor, soil temperature and humidity sensor, and light intensity sensor. Through ZigBee technology and 4G communication technology sensor and system communication, the ZigBee chip used in the system is TI's CC2530 chip, which uses an enhanced 8.51CPU, has the characteristics of ultralow power consumption, and can achieve multifunctional, high-efficiency wireless data transmission. Among them, the output data of the ZigBee wireless sensor network needs to be sampled. After digitization, the serial port data transmission between the collected data and the gateway is carried out. The hardware framework of the system is shown in Figure 2.

(1) Air temperature and humidity sensor: the sensor is a composite sensor, its main application is digital acquisition technology, temperature sensing technology, and humidity sensing technology, and the main characteristics are strong anti-interference ability, small size, low power consumption, and cost-effectiveness

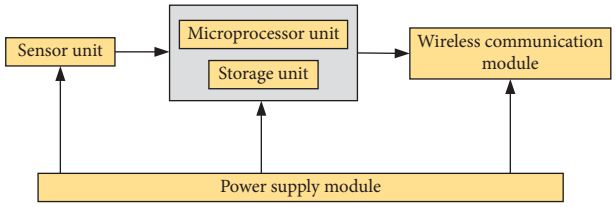

Figure 2: System hardware framework diagram.

(2) Soil temperature and humidity sensor: soil stability and moisture content were measured by embedding thermistors in farmland

(3) Light intensity sensor: the light intensity signal can be converted into an electrical signal and transmitted to the monitoring platform for analysis and summary

2.3. Wireless Communication Module. ZigBee technology is a two-way wireless communication technology with low power consumption, simple technology, and relatively low networking cost. Its main feature is that it is suitable for short-distance transmission ZigBee data communication rate, which is generally 250 kB/s, which does not require high data transmission rate. In the communication transmission process of the system, it is necessary to add a 4G transmission module in the ZigBee network to carry out data transmission, and all indirect interfaces of the 4G network are open. The physical network layer, intermediate environment layer, and application environment layer can provide wireless services with seamless and high data rate. The system separates the acquisition module and monitoring system in space through the mobile network of operators. ZigBee antennas generally require omnidirectional radiation and use inverted F antennas.

2.4. Functional Design. The farmland environment monitoring system is designed and developed in this paper. The monitoring system uses Eclipse as the development tool platform, and the system uses B/S architecture. The function of the whole system monitoring platform is divided into five modules, namely, news notification, farmland management, pest prevention, statistical analysis, and user management, as shown in Figure 3. The data fusion algorithm based on BP neural network is used to fuse the data collected in the system.

2.5. Database Design. In view that the traditional relational database cannot better solve the data storage problems of the Internet of Things, the system adopts the method of mixed data storage; MySQL and NoSQL databases are selected. NoSQL, a nonrelational database, selects MongoDB, a database of schema-free, collective-oriented storage and easy storage object type. It is a product between a relational database and a nonrelational database. The advantage of this database is that the

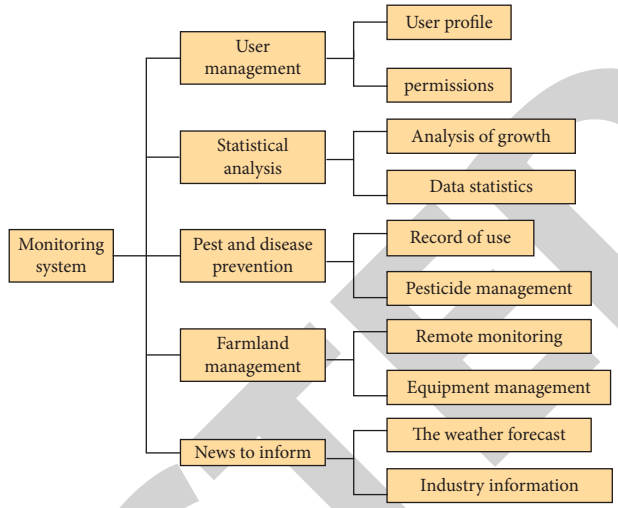

Figure 3: Schematic diagrams of system function modules.

structure of the table is variable, there are no strict requirements for the data structure, there is no need to predefine the structure image of the table, which is completely different from the relational database. The disadvantage is that there is no uniform query syntax. Therefore, the data obtained from sensors are first stored in MongoDB database, summarized after big data analysis, and then transferred to MySQL database, which provides users with data query service, thus improving the response speed and query quality of data service in the system.

3. Method of Economic Benefit Evaluation

The principle of the partial budget method is when a certain measurement index changes, it may lead to changes in some or all of the four aspects of cost reduction, low output, cost increase, and income. The net economic benefit will change as a positive change, and the cost will be reduced. Increasing revenue is a negative economic benefit (reducing revenue and costs). This method can be used to evaluate projects after certain indicators of the economy change, such as expansion projects and renovation projects (buying new machines to replace labor or old machines). This method of comparing expected costs with changes in benefits involves all direct and indirect factors that affect profits. Calculating the change caused by a certain action is the core part. When calculating the cost of some equipment with a useful life of more than one year, the total cost is converted into the annual cost. This method is suitable for analyzing the operation economic benefits of the Beidou navigation system from the perspective of large-scale agricultural production in the Yellow Sea.

The investment analysis method can also be used to analyze the economic benefits of Beidou navigation agricultural machinery automatic driving technology, including static analysis and dynamic analysis. The static analysis does not consider the time factor, and the evaluation index is the

income data of a certain year in the service life, such as the internal rate of return and investment payback period. Dynamic analysis needs to consider the economic effects of the project over its lifetime. Project investment analysis is based on the analysis of the cash flow statement, sorting the project investment, production costs, income, and so on into a cash flow statement in the form of a tabular arrangement and calculating and evaluating various evaluation indicators, net present value, and internal rate of return. Investment payback period and investment payback period are commonly used indicators. The higher the internal rate of return, the greater the difference between the investment in the industry and the greater the average level of return, that is, the greater the profit margin of a new investment project. This method is applicable to the economic benefit analysis of the Beidou navigation automatic driving system and its supporting equipment from the perspective of large-scale agricultural machinery operation of state-owned agricultural machinery stations (agricultural machinery cooperatives).

The quantitative indexes to measure the economic feasibility of agricultural IoT projects are mainly economic benefit evaluation indexes. The feasibility of the project is evaluated by comparing the specific indicators of the project with the benchmark (reference) indicators issued by the state and industry. There are two kinds of evaluation indexes: dynamic indexes and static indexes.

Dynamic indicators are mainly used to evaluate the time value of funds. Through the analysis of project cash flow, the inflow and outflow of cash are determined, the statement of project cash flow is formulated, and the internal recovery rate and the net present value of the project are calculated according to the principle of the time value of funds: 0 internal rate of return (IRR) refers to the discount rate when the cumulative net cash flow value of the project is zero during the calculation period; that is to say, IRR is the discount rate when the following formula is established:

$$\sum_{t=1}^{n} (\mathrm{CI} - \mathrm{CO}) t \, (1 + \mathrm{IRR})^{-1} = 0. \tag{1}$$

In the formula, CI represents cash inflow; CO represents cash outflow; (CI-CO) represents the net cash flow in the t year; n is the number of years calculated for the project. The project plan is feasible if the IRR is not less than the set judgment benchmark (commonly known as the benchmark rate of return); otherwise, it is not feasible. Net present value (NPV) refers to the sum of the present value of the net cash flows of the project during the calculation period calculated according to the set discount rate (generally using the benchmark rate of return I), which is calculated by the following formula:

$$\mathrm{NPV} = \sum_{t=1}^{n} (\mathrm{IC} - \mathrm{CO})_t \left(1 + i_c\right)^{+}. \tag{2}$$

In the formula, IC represents the set discount rate (the same as the benchmark rate). When the net present value calculated according to the set discount rate (generally set at present IC = 10%) is not less than zero, the project scheme can accept; otherwise, it cannot accept. This model only lists the total rate of return on investment and the payback period. 0 total returns on investment (RQI) represents the profit rate of total investment; that is, the annual EBIT in normal years after the project reaches the designed production capacity or the average annual EBIT in operation period and the total investment of the project are being identified and translated online. The total return on investment should be calculated according to E:

$$\mathrm{ROI}(\%) = \frac{\mathrm{EBIT}}{\mathrm{TI}} \times 100. \tag{3}$$

In the formula, EBIT represents the annual EBIT of the project in normal years or the average annual EBIT of the project during the operating period; TI represents the total investment of the project. The total return on investment exceeds the reference rate of return in the same industry, indicating that the profitability calculated by the total return on investment meets the requirements. The payback period is the time required to recover the total investment of the project based on the net income of the project. It can be calculated by the following formula:

$$\sum_{t=1}^{n} (\mathrm{CI} - \mathrm{CO})_t = 0. \tag{4}$$

The project investment cash flow statement can be used to calculate the recovery of project investment. The payback period of a project is the point at which the accumulated net cash flow in the calculation of the project investment cash flow statement changes from negative to zero. The payback period can be calculated by the following formula:

$$P_t = T - 1 + \frac{\left|\sum_{i=1}^{T-1} (\mathrm{CI} - \mathrm{CO})\right|}{(\mathrm{CI} - \mathrm{CO})^T}. \tag{5}$$

In the formula, T represents the number of years in which cumulative net cash flow is positive or zero for the first time in each year. The short payback period indicates that the project has a fast recovery and strong risk resistance.

Uncertainty analysis is a process of hypothesizing the uncertainty factors that affect the project, calculating the influence of its change on the project benefit, finding out the most sensitive factors that affect the project, identifying the risk factors, and giving an early warning of the project risk. Break-even analysis (BEP) is to analyze the balance relationship between project cost and revenue by using the break-even point when the project meets the conditions of design production capacity. The break-even point is between the profit and loss of the project in the agricultural machinery business. When industry revenue is equal to the total cost, there is no profit or loss, which can be used to test the adaptability and antirisk ability of the project to change in agricultural machinery operations. The lower the break-even point, the greater the ability of the project to adapt to changes in agricultural machinery operations and the stronger the ability to resist risks. The break-even point of capacity utilization is often used in project evaluation.

Table 1: Prediction of profit from investment in Agricultural Internet of Things projects.

Project	Total money	Total period					
		1	2	3	4	5–9	10
Operating income	4000	400	400	400	400	2000	400
Business taxes and surcharges	0	0	0	0	0	0	0
Total cost and expenses	2770.7	277.07	277.07	277.07	277.07	277.07	277.07
Subsidizing income	102	34	0	0	34	34	0
Total profit	1569.3	156.93	156.93	156.93	156.93	784.65	156.93
Income tax payable	1569.3	156.93	156.93	156.93	156.93	784.65	156.93
Net profit	1569.3	156.93	156.93	156.93	156.93	784.65	156.93

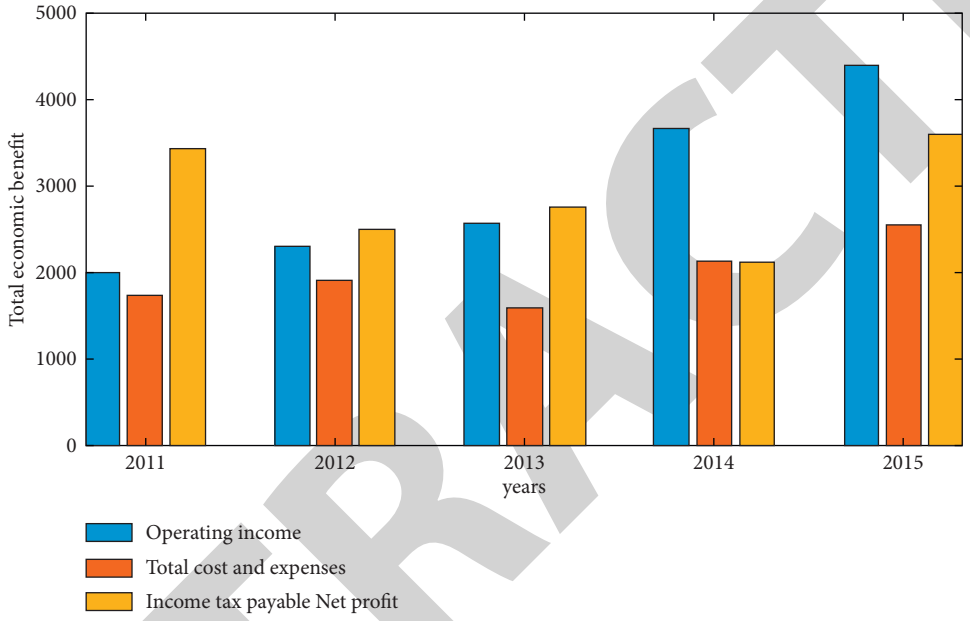

Figure 4: Schematic diagrams of economic benefit changes.

4. Experiments and Results

Assuming that an agricultural machinery station currently has 40 sets of equipment, calculated as 100,000 yuan/set, which is mainly engaged in farm field operations and transportation services of machinery and tools, it is estimated that only 20 sets of Agricultural Internet of Things can meet all farm machinery operations, and the annual operating income is expected to be 4 million yuan/year. A total of 2,400 square meters will be occupied, with 800 square meters for hangar and offices. 1.2 million yuan was invested in the purchase of Agricultural Internet of Things equipment (20 sets in total, 60,000 yuan per set); 800,000 yuan has been invested to construct hangar and office buildings. The total investment of the site occupation cost is 500,000 yuan, and the occupation time is 30 years. Operating capital needs 500,000 yuan. A total of 7 million yuan was invested in the project, of which 6.5 million yuan was invested in construction and 500,000 yuan was used for operation. The project is expected to have an annual operating income of 4 million yuan, mainly from agricultural operations. According to the current national policy, the income from the Agricultural Internet of Things industry is not subject to business tax. See Table 1 for profits from agricultural IoT projects.

According to the calculation of other cost items, 63.17% is the break-even point of the project, and 36.83% is the profit area of the project. The break-even point is relatively low, and the ability to resist risks is relatively strong. 18.08% is the internal rate of return of the project, and 12% is the reference rate of return of the industry. This scheme is feasible. 5.3498 million yuan is the net present value of the project (IC-10%), which is acceptable. 4.22 years is the payback period of the project investment. The payback period is relatively short, and the project has relatively high economic benefits. 17.78% is the total investment rate of the project, which meets the requirements. Operating income is the income change of the Agricultural Internet of Things and is a sensitive factor for project operation. Special attention should be paid to operating income during project operation.

According to the above calculation results, the input of the Internet of Things in the agricultural network conforms to the situation that both net income and variable input have increased, and it is necessary to determine whether to adopt new technology according to the rate of return. Assuming an

Hindawi
Journal of Mathematics
Volume 2023, Article ID 9789820, 1 page
https://doi.org/10.1155/2023/9789820

Retraction

Retracted: A Study of English Informative Teaching Strategies Based on Deep Learning

Journal of Mathematics

Received 19 December 2023; Accepted 19 December 2023; Published 20 December 2023

This article has been retracted by Hindawi following an investigation undertaken by the publisher [1]. This investigation has uncovered evidence of one or more of the following indicators of systematic manipulation of the publication process:

(1) Discrepancies in scope

(2) Discrepancies in the description of the research reported

(3) Discrepancies between the availability of data and the research described

(4) Inappropriate citations

(5) Incoherent, meaningless and/or irrelevant content included in the article

(6) Manipulated or compromised peer review

The presence of these indicators undermines our confidence in the integrity of the article's content and we cannot, therefore, vouch for its reliability. Please note that this notice is intended solely to alert readers that the content of this article is unreliable. We have not investigated whether authors were aware of or involved in the systematic manipulation of the publication process.

Wiley and Hindawi regrets that the usual quality checks did not identify these issues before publication and have since put additional measures in place to safeguard research integrity.

We wish to credit our own Research Integrity and Research Publishing teams and anonymous and named external researchers and research integrity experts for contributing to this investigation.

The corresponding author, as the representative of all authors, has been given the opportunity to register their agreement or disagreement to this retraction. We have kept a record of any response received.

References

[1] Y. Guo, "A Study of English Informative Teaching Strategies Based on Deep Learning," *Journal of Mathematics*, vol. 2021, Article ID 5364892, 8 pages, 2021.

Hindawi
Journal of Mathematics
Volume 2021, Article ID 5364892, 8 pages
https://doi.org/10.1155/2021/5364892

Research Article

A Study of English Informative Teaching Strategies Based on Deep Learning

Yaojun Guo

School of Applied Foreign Languages, Xinyang Vocational & Technical College, Xinyang 464000, China

Correspondence should be addressed to Yaojun Guo; guoyaojun@xyvtc.edu.cn

Received 16 November 2021; Revised 30 November 2021; Accepted 3 December 2021; Published 17 December 2021

Academic Editor: Naeem Jan

The rapid development of artificial intelligence brings new development opportunities and challenges to English teaching university. This paper explores the concept of "smart education" and the path of building an ecological information-based teaching model of English college by interpreting the concepts of artificial intelligence, deep learning, ecological linguistics, and language education. Artificial intelligence, especially deep learning, will be promising in many aspects, such as the analysis of individual differences of language learners, customized learning content, diversified and three-dimensional teaching media, the role of teachers as smart classroom designers, and multidimensional and dynamic formative assessments. By relying on the data mining technology of deep learning to analyze learners' characteristics, the smart classroom design, the promotion of language learners' independent learning, and the establishment of dynamic and complete learner profiles, the language learning process is no longer a linear process but an evolving open loop, ultimately forming a harmonious development of various ecological niches in the language learning process. In this paper, we study and design a deep learning-based English informatics teaching system to develop a deep learning-based scoring prediction model. The model incorporates deep learning models based on word embedding and text convolutional networks, which can uncover the hidden interest features of academics for English. The experimental research results prove that the online e-learning service platform cannot only effectively meet the diverse and personalized English learning needs of university students, but also improve the learning efficiency of teachers and students.

1. Introduction

The application of deep learning techniques can show a unique advantage in the field of English learning and play an important supporting role in students' learning and teachers' teaching. Its role in promoting the reform of English language teaching is explored in terms of writing, translation, listening, and speaking. Concerning the writing, [1] includes deep learning for teaching English professional writing, where the application is mainly about English composition content criticism. The automatic correction system on the deep learning platform can analyze students' English compositions very comprehensively, make basic judgments on the structure of students' essays, make timely corrections to spelling errors and grammatical errors in students' essays, and propose timely corrections. Teachers can also use the system's automatic feedback mechanism to manually correct students' essays for a second time and provide further feedback to students. At the same time, the teacher can also grasp the students' learning situation according to the assessment report given by the system and implement reasonable curriculum improvement, which is important for the improvement of teaching methods and upgrading of the teaching system [2]. For the role explored in the form of translation, we mention deep learning for teaching English professional translators, which made significant achievements and breakthroughs in the field of English translation and has achieved certain pedagogical results in teaching English translation. First, the use of deep learning-assisted translation systems for English translation can significantly optimize the basic process of English translation. This is especially important for students to be able to translate English proficiently in the future and to apply their learning. Secondly, the English translation software and platform based on cloud services can help students solve many difficult translation points, which can

enhance students' confidence to a certain extent and stimulate their interest in learning English at a deeper level. Finally, the translation tasks set by the intelligent cloud platform can use artificial intelligence to track each student's translation and form evaluation reports, which can grasp the students' translation characteristics and problems in a timely and accurate manner and realize personalized teaching guidance and improvement of teaching courses. In in-depth study of college English listening instruction, listening training is of great importance to the development of students' English literacy [3]. However, many students are resistant to listening to English due to the boring content of listening materials and the difficulty of listening. The deep learning language platform can provide students with a large amount of listening materials with a wide variety of difficulty and topics to meet the different needs of different students for English listening. In such an environment, not only can students choose the corresponding English learning materials according to their interests for in-depth learning, but also deep learning can automatically match students with suitable listening materials and learning contents through the analysis of their basic information. Finally, the assessment of spoken English for majors is an important aspect. The purpose of learning a language is to achieve better communication and exchange. Therefore, in the actual teaching process, it is necessary to strengthen students' learning as well as mastery of spoken English to help them improve their English speaking skills [4]. Deep learning has a great advantage in teaching English as a foreign language, as the English communication environment becomes more colorful because of educational robots, and real-time conversations help students to use English. Educational robots can be accompanied by students and interact with them to create a continuous and natural environment for using English, and this process can help students to improve their English speaking skills by relieving their nervousness when talking with real people.

2. Related Works

In this section, strategies for learning languages are discussed; some used techniques, processes, and evaluations.

2.1. English Informatics Teaching Strategies. With the deepening of AI in multiple perspectives of teaching such as English teaching assessment, teaching platform optimization, and teaching tutoring, it has brought new creativity to the teaching space for students and teachers, greatly improving teaching efficiency and optimizing students' learning experience at the same time [5]. Firstly, in the preclass preparation stage, the introduction of AI teaching platform brings teachers a natural free resource bank, and at the same time, teachers can share lesson plans at any time and any place across time and space intervals to achieve the optimal use of resources. Finally, in the after-school evaluation stage, the AI teaching end does not need to worry about face, whether it is the teacher to students or students to the teacher's summary evaluation. Evaluation should be more fair and just, and it is also more conducive to both parties to discover and correct problems in a timely manner [6]. Personalized education is more inclined to export more innovative and personalized talents to the society than the traditional education of "uniform production," which contradicts the limited energy of teachers. The personalization of education requires teachers to develop targeted development strategies by understanding students' psychological characteristics and interests. This conflict is also solved by the large database of the AI-enabled education system [7]. The database will make judgments based on the students' own set learning preferences, learning abilities, and the actual learning status of the students and make a series of learning plans according to the different situations of each student. Based on this, the database will also collect the learning dynamics of each student and adjust the curriculum according to their learning dynamics so as to truly tailor the teaching to the student's needs and achieve personalized development [8]. Regarding the nonstandardized examination and evaluation system before the introduction of artificial intelligence system into the teaching evaluation, the daily test questions were given by one or more teachers, but such a way of giving questions has a great human factor. On the one hand, the teachers do not fully grasp the difficulty level of the test questions, and there is lack of standardization; on the other hand, because different teachers have different teaching styles and teach students with different emphasis on knowledge points, it is difficult to take into account. On the other hand, it is difficult to take into account the learning progress of all students because different teachers have different teaching styles and teach students with different emphasis. After the introduction of the intelligent system, the test questions are combined by the system database, basically based on the requirements of the syllabus, and the test methods are diversified so that the test questions can be intelligently composed according to the online learning records of different students, and the students can be monitored purposefully so that the students can find out what they have not yet mastered in the process of the test, which is more conducive to checking the gaps and playing the evaluation role of the test. In addition, the AI system can mark the papers by itself after the students finish the exams, reducing the teachers' workload. Data-driven effective promotion of teaching work quantification behind the AI teaching end is based on a rich database of data resources, providing information to teaching while also designing programs that play a good role in supporting teachers' teaching work. For example, teachers can use the mobile terminal to sign in students so as to judge students' classroom attendance, use the data terminal to issue practice questions, which can effectively view students' answering thinking based on their answering records, and prevent behaviors such as copying homework and students' late or even nonsubmission of homework that exist in traditional education, and release the daily essential word quantity through the mobile terminal to view students' word reserve. This is equivalent to dividing the teacher's responsibilities more clearly. The teaching work and the amount of students' learning are quantified in chunks, which provides a good

quantitative reference for the later evaluation of teaching work. Synergistic human-machine development artificial intelligence is, after all, a software system developed by human beings. From the perspective of science and technology, AI education has both its human side and its limited side. Therefore, the use of AI in teaching usually reflects a clear human-machine synergy, with the teacher still playing a major role in education and AI serving as a supporting role for meeting the teacher's daily teaching needs [9]. As shown in Figure 1, AI can perform data mining by recording and analyzing learners' historical data and integrate the data through deep machine learning in order to do further in-depth analysis and research. Specifically, AI can form a basic modeling of English learners based on their basic profiles (e.g., age, gender, learning experience, and cognitive level) and then refine their learner types based on their English learning profiles, social profiles, and other profiles to provide technical support for creating a personalized English teaching model [10].

2.2. Teaching Process and Evaluation. Teaching process and assessment is shown in Figure 2.

Modern education focuses more on the personalized development of students and their overall development. To achieve individualized development of students, the first step is to guide them to master individualized learning methods [11]. The prerequisite of so-called personalization is to combine different students' learning situations and not to generalize, but to differentiate education for different students. Under traditional education conditions, a teacher needs to face dozens of students, making the realization of differentiated teaching fraught with difficulties. But with the artificial intelligence platform, each student's learning dynamics can be recorded on the system in real time, and teachers can understand the learning level of each student based on his or her learning record so as to guide students to conduct targeted practice. For example, a student's learning record shows that he often makes mistakes in the passive voice, so the teacher can understand it in time through the record on the teaching side and at the same time can send relevant exercises through the mobile side to give him one-on-one guidance. At the same time, the actual situation of different students in the system is used to establish different methods of teaching, which is conducive to the improvement of teaching efficiency. As shown in Figure 2, the LMS software based on artificial intelligence technology can provide technical support for the whole teaching process [12].

Language skills include the four skills of listening, speaking, reading, and writing as well as the ability to use these four skills together. Listening is one of the ways for learners to input a large amount of language knowledge, and speaking is the main channel for language expression. Therefore, listening and speaking skills are the basis of language use ability, and listening and speaking lessons are also an important type of lesson in the English curriculum. For most primary school students in China, elementary school is the beginning stage of English learning. In elementary school English teaching [13], developing students' listening and speaking skills plays a crucial role in the development of students' comprehensive language skills. However, there are still some problems in primary English listening and speaking teaching; for example, some teachers still focus more on cultivating students' test-taking ability and ignore cultivating students' listening and speaking ability; the English classroom lacks real language context, plus the influence of the mother tongue, making the English language communication environment relatively lacking; some teachers still rely on mechanical drills, and the classroom listening and speaking activities lack interest and variety, which cannot effectively stimulate students' willingness to participate in listening and speaking activities; students receive knowledge passively in the classroom, and their higher-order thinking is not effectively developed. The concept of deep learning originated in the field of artificial neural networks and has been gradually applied to the field of education [14]. Traditional shallow learning is a more mechanical and passive way of learning, ignoring the internal connection and transfer of knowledge. In contrast, deep learning refers to students' use of multistep analysis and processing strategies, such as conceptual transformation, cognitive structure development, resource interaction, and reflective reconsideration, in order to gain a deeper understanding of knowledge. In essence, deep learning is an active, inquiry-based, and comprehension-based learning style that requires learners to use higher-order thinking wisely to achieve effective transfer and application of knowledge. Deep learning advocates that students learn on the basis of understanding and then connect old and new knowledge and realize the transfer and application of knowledge, thus helping students develop their creative thinking, critical thinking, and other higher-order thinking skills. The necessity of practicing deep learning in listening and speaking teaching English curriculum standards points out the fact that cultivating students' observation, memory, thinking, imagination, and creative spirit is one of the basic tasks of the English curriculum at the basic teaching stage, which coincides with the essence of deep learning. The whole teaching process can be supervised with the help of AI, and structural and indicator assessments of teaching activities can be made and fed back to the teaching and learning terminals of teachers and students in a timely manner to promote the construction of the whole ecological teaching activities scientifically and effectively. It can be said that AI plays a decisive role in the whole teaching session (including the formulation of teaching contents, the development of teaching activities, and learning and process assessment). Deep learning makes the teaching link no longer a closed system but evolves into an open loop in an evolving spiral. Nevertheless, we need to recognize that the AI platform only creates a new environment for the ecological teaching of college English. After all, language teaching is a human-centered activity, and ecological college English teaching must comply with the law of second language acquisition and coordinate the relationship between teachers and students and their interaction with the teaching environment to ensure a dynamic and balanced relationship for its benign

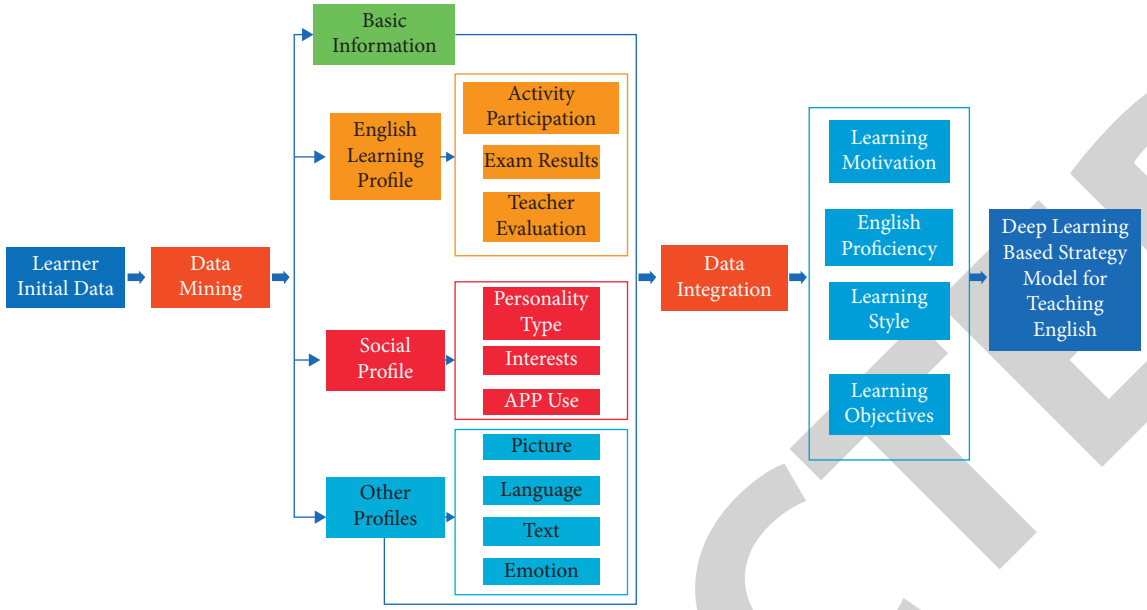

Figure 1: English informatization teaching strategy framework.

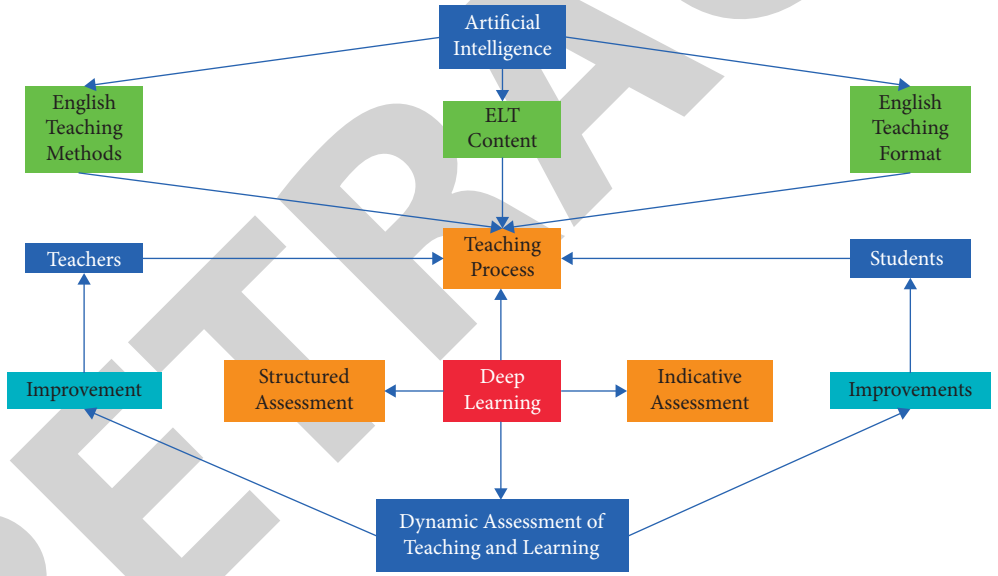

Figure 2: Teaching process and assessment.

development. The intervention of artificial intelligence enables teachers and students to interact and collaborate on an intelligent platform and build an open, holistic, and sustainable virtuous language learning ecology, allowing students to generate knowledge and skills in a dynamic way and to perceive and internalize them in the process of interactive experience. Although the powerful technology supports us in sketching the future picture of college English teaching, how to make it a reality remains to be further thought and explored. In general, we need to follow the following "changes" and "constants" in university English teaching integrated with AI: the way English learners learn changes (i.e., more emphasis on "contextual" and "interactive" learning, "interaction," "experience") and the realization of a native language environment or near-native language environment on top of the platform created by technology; English learning is moving towards ubiquitous learning. The role of English teachers needs to be changed to become intelligent classroom designers, organizers, and leaders of activities; their practical knowledge needs to be updated to become a lifelong learner with subject content knowledge and pedagogical knowledge and adept at using technology for blended teaching. Their practical knowledge needs to be updated to become lifelong learners who have subject content knowledge and pedagogical knowledge, and are adept at using technology to carry out blended learning; their assessment methods change; that is, they no longer use the "one-test-for-life" summative assessment, but fully use

the real-time monitoring function of big data to model and profile learners so that assessment becomes both the temporary end of the learning task and the new starting point of the next task. In the AI-assisted classroom ecosystem, what remains unchanged is the "learner-centered" approach, with the teacher being the guide and the technology being the intermediary; the ultimate goal is to equip learners with independent learning, self-directed learning, and problem-solving skills through "scaffolding." The ultimate goal is to equip learners with the awareness and ability to learn independently and solve problems through the role of "scaffolding."

3. System Analysis and Design

In this section, a deep learning-based English informatics teaching system is designed to develop a deep learning-based scoring prediction model. Where we analyze this system, we discuss the framework design besides the system functional design and finally the overall model design.

3.1. System Analysis. With the increasing number of courses published on the English informatics teaching system, users are easily overwhelmed by the large number of course resources, which raises the difficulty of obtaining the resources they need. The deep learning-based English IT teaching intelligent strategy system can significantly improve the above problems. The system is based on deep learning intelligent recommendation technology that can extract the required information from the complicated information and also make user recommendations based on log information. To date, recommendation systems have received a lot of attention and have a wide range of applications. Although traditional recommendation methods can accomplish the recommendation task, they have limited effect on the problem of cold-start and Xi-number matrix. The hybrid recommendation method that incorporates multiple heterogeneous information can alleviate the above problems, but it also faces challenges when the auxiliary information is large-scale, multimodal, data heterogeneous, data sparse, and unevenly distributed. There are users with different rights in the English education information system: administrators and learners. Different users have different transparency to the system. Learners can register to learn, select and browse courses and online experimental cases, and post and reply to posts in the forum. The administrator has the highest authority role. The corresponding functions are key information management (management of students, main course information), user management (user rights and information), learning resource management (course resources, video resources), background management, and information analysis.

3.2. Overall System Framework Design. The deep learning-based English informatics teaching strategy system contains various subsystems and business functions, which are also divided into many modules and components according to the componentization and modularization idea of Vue.js. The coupling between the various functions of the componentized system is reduced, and there is a qualitative change in reusability. The system consists of four layers, namely, the system portal layer, the application module layer, the functional module layer, and the data storage layer.

(1) System portal layer: it provides different services for different users. Learners can learn video, browse course materials, and ask questions online; administrators can manage learning information, course resources, and answer questions. (2) Application module layer: it describes the implementation steps of each module operation: vue.js for front-end development, vue-video-player open source plug-in for video playback, Axios for HTTP requests, and deep learning model for data processing and analysis. (3) Functional module layer: it expresses and divides the submodules with different functions and work with data model for data processing and analysis. Deep learning model is for data processing and analysis. (4) Functional module layer: it expresses and divides the submodules with different functions and connects with the data layer to provide information transfer services for the operation of the data storage layer. (5) Data storage layer: it stores information about different users and the system's information. It includes student information, forum information, course information, and management information.

3.3. Overall System Functional Design. The system is based on B/S architecture, using MVC model, with the front-end implemented by Vue.js framework and the back-end built with Spring Boot. The online learning system is developed around the design of networked, diversified, and intelligent student learning. (1) Student personalized learning recommendation module through the collection of student learning content, grades, course preferences, disadvantaged courses, learning records and other characteristics of information, information processing analysis, and for learners to recommend personalized learning courses. (2) Student learning evaluation module through the learning preferences (mainly learning). (3) Online video learning module where the administrator can upload their own learning course videos, students can learn through the online learning system, and the system records the user's playback and other functions. (4) Online program practice module through the online program practice platform to achieve the relevant course program development practice, to improve the students' hands-on ability. (5) User management submodule control user login, caching of logged-in information and registration of new users and storage of user information. (6) Course materials management module in this subsystem, teacher users upload course materials, which include PDF, PPT, Word documents, and lab guides. Student users can download these course materials, which is an indispensable part of online learning. (7) Online communication submodule learning communication and experience sharing with classmates and teachers by posting replies in the forum, and so on. (8) Knowledge map display module constructing course knowledge maps to facilitate students' intuitive learning and querying of materials. This learning system

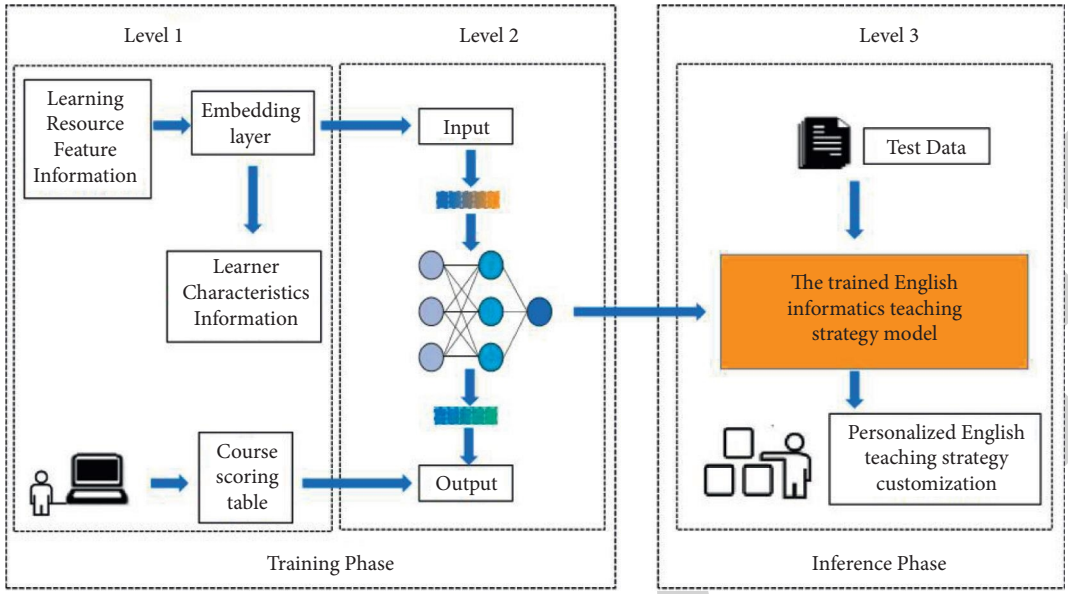

Figure 3: English informatics teaching strategy model.

involves a variety of modules: user login and registration, online learning, online experiment, resource sharing, online communication, and other functions. Among them, online learning includes online video learning, course materials such as PPT, Word documents, and lab guide learning, which can meet students' various personalized needs and improve learning efficiency.

3.4. Overall Model Design. English informatics teaching strategy model is shown in Figure 3.

In this paper, a neural network-based rating prediction model is designed. This model incorporates a deep learning model based on word embedding and text convolutional networks, makes improvements in the feature vector with users as well as learning resources, and uses deep learning to mine hidden interest features on this basis. The model is also trained with the help of the user's historical rating information, and the scores are used to express a potential association between the user and the learning resource. Finally, the performance of the recommendation effect is improved, and the user experience is enhanced. The model is divided into two parts: training and recommendation (Figure 3).

The extraction of the learner feature vector and the learning resource vector is performed during the training process. The learner feature vector is extracted using word embedding's to take the user's ID, name, and preferences as input to form a vector that can model a user's features. After this, the user feature vector is trained through a two-layer fully connected layer to extract the potential relationships between each user feature. The extraction of the learning resource feature vector is performed through a text convolutional network to obtain the course noun vector, the course id and course type are passed through an embedding layer to model the feature vectors of different attributes, and finally the link integration of the attribute vectors is performed using a fully connected layer. The first layer of the text convolutional network is the input layer, and this layer is a matrix of words in sentences arranged in the corresponding top and bottom order, establishing the sentence matrix:

$$\mathbf{A} = [x_1, x_2, \ldots, x_m, \ldots, x_n]. \tag{1}$$

The second layer of the network is the convolution layer, and each word in this layer forms an overall embedding matrix through the individual vectors of the embedding layer. By the dot product of the input matrix and the filter plus the compilation term, the convolution operation is formulated as follows:

$$h_i = f\left(W_1 \cdot x_{i*j+l-1} + b\right). \tag{2}$$

Finally, the output is performed using the activation function, which is as follows:

$$f(x) = \begin{cases} x, & x \geq 0, \\ 0, & x < 0. \end{cases} \tag{3}$$

The third layer is the pooling layer, which uses the Max-over-time-Pooling method. This method extracts the one-dimensional features processed in the previous step and extracts the largest value in the convolution window as the feature value of this window:

$$\hat{s} = \max\left[h_1, h_2, h_3, \ldots, h_{n-l+1}\right]. \tag{4}$$

The fourth layer is the fully connected + softmax layer, which controls the training fit by using the properties of the Dropout technique and restricts the weight parameters of this layer with L2 regularization. This is done to prevent the fit from being reduced due to the adaptive nature of the hidden units:

$$\hat{y} = \arg\max\left[W_2 \cdot \hat{s} + b_1\right]. \tag{5}$$

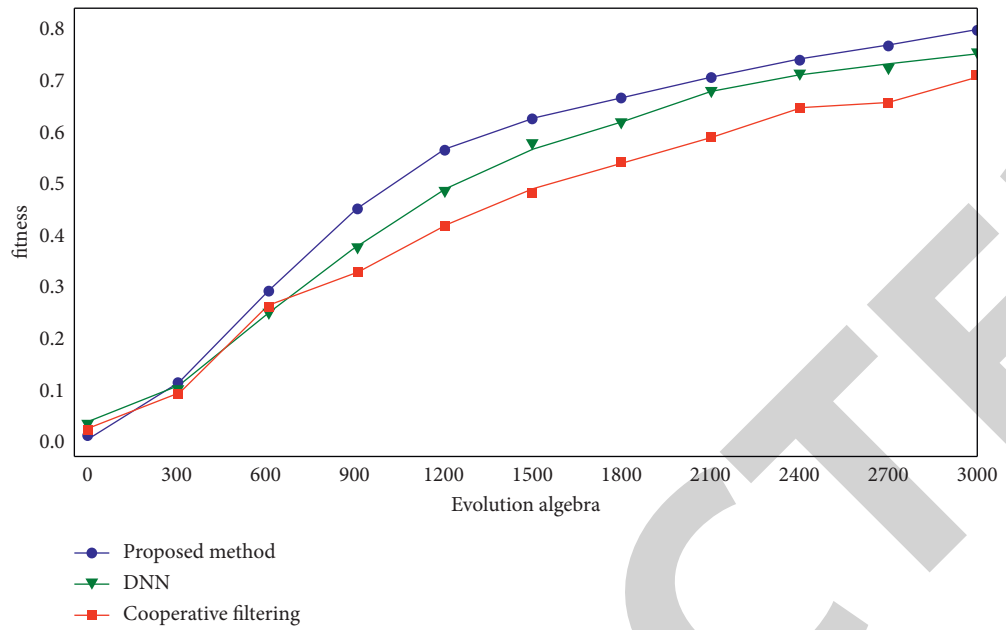

Figure 4: The experimental results of iteration.

Table 1: Training results table.

Data set category	Number of datasets	Accuracy rate (%)	Recall rate (%)	$F1$ (%)
edX	26000	78.34	77.56	77.95
Online learning system	10000	72.71	71.96	72.33

After four layers of processing, the vector features of the learning resource title are obtained.

4. Experimental Results

To verify the effectiveness of any algorithm or model, experiments must be done. So, in this paper, we use this section for the experimental results.

4.1. Experimental Data. This paper uses the Open edX dataset, which contains data related to 16 ELT courses offered by Harvard University and MIT on the edX platform from 2012 to 2013. Dozens of attributes are provided, including course data, learner information, and learner behavior characteristics.

4.2. Experimental Results. In order to further verify the effectiveness and optimization performance of the proposed deep learning algorithm for the English informatics teaching strategy model, this paper conducts a comparison analysis of the quality recognition error MSE of three algorithms, a comparison analysis of the convergence under the same number of iterations and initialization parameters, and a comparison analysis of the accuracy of the quality recognition of the algorithms. The convergence curves are shown in Figure 4.

A portion of the test set was taken as the validation set for verification, and the course ratings were compared with the target values, and the ratings of the contents in the rating scale of the data set were compared, with a final accuracy of 78.34%, a recall of 77.56%, and an $F1$ value of 78.56% (Table 1).

5. Conclusion

The deep learning-based English teaching strategy system is based on big data analysis and intelligent processing to study the behavior and personality characteristics of students in the process of learning English and make personalized recommendations based on the intelligent guidance function in the system. This system takes the most basic information about students and their own learning conditions as the basis for deep excavation so as to build a model of English learning behavior and experience, and through the personalized analysis of learning conditions, it can also make students' enthusiasm for learning English rekindled. The online English learning and teaching recommendation system can recommend more in-depth learning methods and content to students and specific classes and generate an intuitive image of learning changes after the teaching is completed so as to achieve accurate and high-quality teaching.

Data Availability

The data used to support the findings of this study are available from the corresponding author upon request.

Hindawi
Journal of Mathematics
Volume 2023, Article ID 9879807, 1 page
https://doi.org/10.1155/2023/9879807

Retraction

Retracted: Early Warning System for Penalty Constrained Financial Risks of Enterprises under Diversified Investment

Journal of Mathematics

Received 31 October 2023; Accepted 31 October 2023; Published 1 November 2023

This article has been retracted by Hindawi following an investigation undertaken by the publisher [1]. This investigation has uncovered evidence of one or more of the following indicators of systematic manipulation of the publication process:

(1) Discrepancies in scope

(2) Discrepancies in the description of the research reported

(3) Discrepancies between the availability of data and the research described

(4) Inappropriate citations

(5) Incoherent, meaningless and/or irrelevant content included in the article

(6) Peer-review manipulation

The presence of these indicators undermines our confidence in the integrity of the article's content and we cannot, therefore, vouch for its reliability. Please note that this notice is intended solely to alert readers that the content of this article is unreliable. We have not investigated whether authors were aware of or involved in the systematic manipulation of the publication process.

Wiley and Hindawi regrets that the usual quality checks did not identify these issues before publication and have since put additional measures in place to safeguard research integrity.

We wish to credit our own Research Integrity and Research Publishing teams and anonymous and named external researchers and research integrity experts for contributing to this investigation.

The corresponding author, as the representative of all authors, has been given the opportunity to register their agreement or disagreement to this retraction. We have kept a record of any response received.

References

[1] Y. Zhu, "Early Warning System for Penalty Constrained Financial Risks of Enterprises under Diversified Investment," *Journal of Mathematics*, vol. 2021, Article ID 4153774, 9 pages, 2021.

Hindawi
Journal of Mathematics
Volume 2021, Article ID 4153774, 9 pages
https://doi.org/10.1155/2021/4153774

Research Article

Early Warning System for Penalty Constrained Financial Risks of Enterprises under Diversified Investment

Yongyong Zhu

Faculty of Management of Chuzhou Polytechnic, Chuzhou, Anhui 239000, China

Correspondence should be addressed to Yongyong Zhu; zhuyongyong@chzc.edu.cn

Received 16 November 2021; Revised 30 November 2021; Accepted 3 December 2021; Published 17 December 2021

Academic Editor: Naeem Jan

Based on the understanding of the main types and purposes of enterprise diversification investment, this paper conducts an in-depth analysis of the environmental, structural, and scale risks of enterprise diversification investment and uses this as the basis for the effective construction of a risk prevention model. It can help enterprises effectively avoid investment risks, avoid bringing huge economic losses to enterprises, and help lay a good foundation for the positive development of enterprises. With the rapid development of social economy, enterprises must realize diversified investment if they want to improve their market economy status. However, due to many factors, they face greater economic risks and even cause serious economic losses to enterprises. Therefore, effective measures must be taken to prevent risks and promote the sustainable development of enterprises so as to obtain more economic benefits.

1. Introduction

Enterprise diversification investment can be broadly classified into the following types [1]: (1) concentric diversification type [2], which refers to the development of investment and operation in a diffuse direction with the existing main business as the core, with correlation and noncorrelation characteristics; (2) vertical integration type [3], which can be divided into two forms: forward integration refers to the promotion of enterprises to expand their business scope and develop in the direction of the end market, and backward integration is the development of the upstream supply chain end; (3) the horizontal integration type, which refers to market-centered product sales, overlapping or spreading on the original basis, is also a relevant diversification; and (4) the overall diversification type, which has a strong mixed nature, diversifying investments in technology, markets, and other aspects, both relevant and irrelevant. The main purpose of diversification is to avoid over-reliance on a single market, to diversify business risks and thus reduce the risks faced by unilateral investments, to increase revenue opportunities for the enterprise, and to promote the process of sustainable development.

The main focus of this study is the early warning system for financial risks in corporate diversification. The selection of indicators is dependent on the selection of financial indicators that reflect the risks of corporate financing, investment, capital operation, and earning distribution. On the basis of theoretical analysis combined with specific cases of companies, the early warning system of financial risks is thoroughly studied. The analytical framework diagram for this paper is shown in Figure 1. The following flowchart explains the methodology and the complete process of the proposed method by classifying it into three major portions.

The rest of the article is organized as follows: Section 2 highlights some of the theoretical foundations such as the definition of risk and its classification and the content and placement of financial risk warnings. In Section 3, the construction of financial risk early warning is described. First, we determined the early warning index weight and then calculated the values of financial warning. Finally, the study is winded up in Section 4, which presents the conclusion.

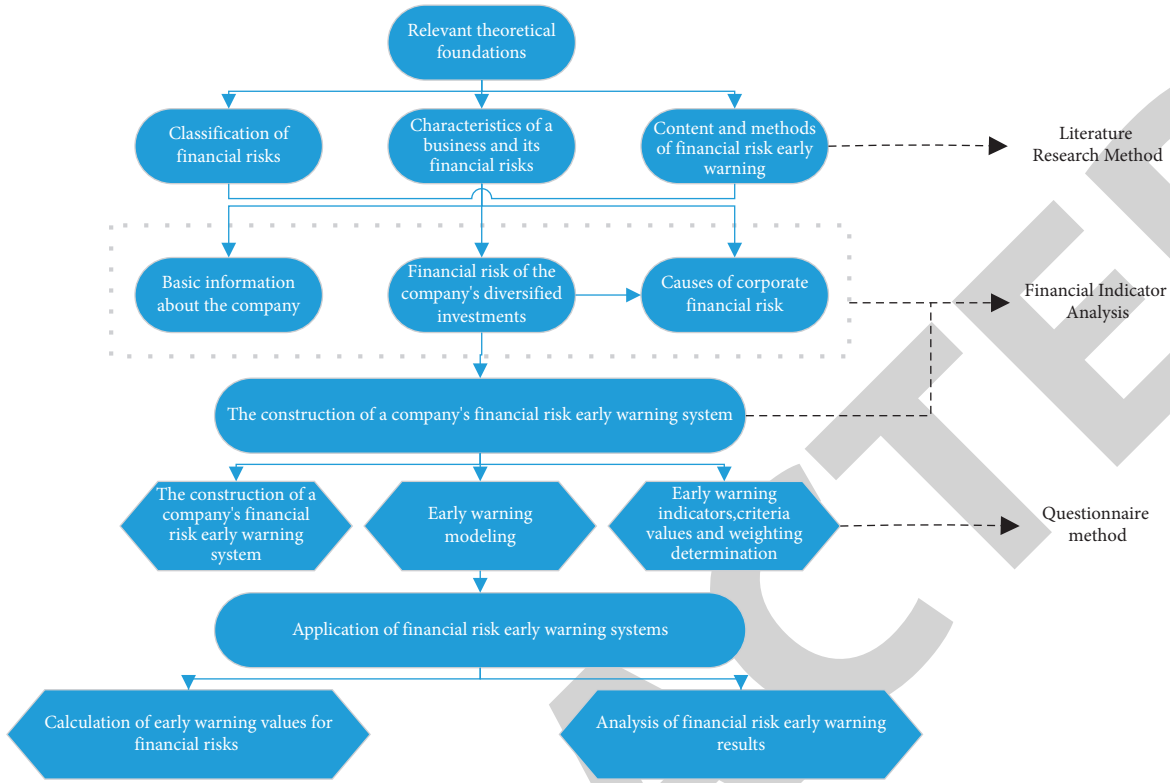

Figure 1: Analysis framework diagram.

2. Relevant Theoretical Foundations

2.1. Financial Risk Definition and Classification. The financial activities of an enterprise include financing activities, investment activities, capital operation activities, and allocation activities, which exist throughout the cycle of the enterprise's business operations. Financial risks are divided into the following risks: financing risk, investment risk, capital operation risk, and revenue distribution risk.

2.1.1. Financing Risks. Financing activities are the most fundamental source of capital for a business in its day-to-day operations [4]. From the moment a company starts operating, its capital becomes the product or service that it produces and through which it generates more capital. In the process, the ratio of equity to debt will bring risks to the subsequent operation of the enterprise; for example, if the enterprise's debt financing is too large, it will make the enterprise's financial leverage high, although it is possible to expand the enterprise's revenue, but the pressure to repay the capital and interest later will be great. The pressure of repaying the debt will be very high, which will bring great financial risks to the overall operation of the enterprise, and if there are problems with the working capital of the enterprise, the enterprise may also face a direct break in the capital chain, which may lead to bankruptcy in serious cases.

If you cannot raise capital, you cannot do well. Most companies now raise capital by issuing shares, bonds, attracting investment, and so on. At the same time, the company has to pay dividends, interest, or repay the principal of loans and sometimes other related costs. Only with the right decisions and efficient management a can company achieve its predetermined goals. In practice, however, the market environment is quite complex, and there is a high risk of errors in decision making, which can affect the allocation of funds and thus the actual profitability of the company, thus increasing the likelihood of financing risks.

For companies, financing risk is one of the most likely financial risks in their business development process [5], as all companies need to expand and grow, and the direct impact of this is an increase in the financial risk. First of all, if an enterprise wants to expand its own financial strength, financing is an important method. Most enterprises raise funds by issuing shares or bonds, thus obtaining some capital income, which in turn means that the enterprise has to bear the capital payments for various operations in the process or needs to repay loans. In its own development process, an enterprise can only ensure the achievement of its business development goals if it makes the right decisions. However, nowadays, the market environment is highly variable, and the market competition is uncontrollable. If an enterprise is affected by changes in market information, it will make incorrect judgements and even make errors in major decisions, which will result in unreasonable business development configurations and lead to serious financial risks as the enterprise is unable to achieve its own expected financial objectives.

2.1.2. Investment Risk. Investment activities are an important part of an enterprise's operation [6]. The funds obtained in the financing activities will be used for new production or

investment in new industries through investment activities, and the success of the investment activities will determine the recovery of the enterprise's funds, including the efficiency and quality of the recovery; if the investment activity fails, it will not be able to recover the funds directly, which will cause the financial risk of the enterprise, causing financial losses. At the same time, from the perspective of the enterprise's investment projects, the type of assets formed will also have an impact on the enterprise's financial risk. Therefore, it is important to carry out a feasibility study beforehand to assess the possible investment risks faced by the company, as well as to assess the company's risk tolerance, and to select investment projects that match the company's risk tolerance so as to prevent the financial risks that may be brought about by the company's financial investment activities [7].

Investment risk refers to the risk that during or after the investment process, the investor will not be able to recover the funds in time due to losses and will not be able to achieve the expected returns, thus affecting the profitability and solvency of the enterprise; in other words, the risk that the enterprise may encounter in the process of its investment activities [8]. In the course of the various investment activities of the enterprise, if the investment income is not well controlled, the capital will not be recovered in the expected manner, which will result in the enterprise encountering financial risks in its financial activities, thus failing to ensure the profitability and repayment level of the enterprise [9]. There are several aspects of investment risk in the enterprise. Firstly, in the course of business, the enterprise may not have a comprehensive understanding of the market environment, which may lead to poor sales of products and a build-up of inventory, thus affecting the capital problems of the enterprise. Secondly, in the process of investment in the enterprise, the enterprise's various production technologies and so on are not up to standard, and the final production results will not achieve the expected results. Then, in the case of enterprises increasing the scale of investment, the internal management of enterprises cannot keep up, resulting in internal management chaos, forming a situation beyond the control of enterprises. Then, with large investments, the debt burden of the enterprise increases, eventually leading to a result that the enterprise cannot afford. Finally, one of the major characteristics of the market economy is that it is highly uncontrollable. If an enterprise cannot keep pace with the development of the market and cannot upgrade its product technology and research and development capabilities, it will be in a disadvantaged position in the market competition, resulting in the enterprise failing to achieve its expected financial objectives.

2.1.3. Liquidity Risk. Capital operations are a production activity that follows the investment activities of an enterprise. The flow of funds from capital operations will affect the liquidity of the enterprise and affect the liquidity risk of the enterprise [10]. If the enterprise's account payable cycle is short, while the account receivable cycle is long, it will directly affect the enterprise's liquidity, greatly reducing the enterprise's liquidity; at this time, if the relevant loans from banks and other financial institutions cannot be provided in a timely manner, it may have to use the enterprise's long-term funds to supplement the needs of liquidity, which does not seem to exist in the case of capital risk. Related long-term loan data need to be updated dynamically. The rate of return of the relevant long-term loans will be significantly reduced, thus affecting the efficiency of the enterprise's use of funds.

In the course of production and operation activities, there may be an increase in the price of purchased materials, forced production stoppages, and a reduction in orders. Once these circumstances change, the enterprise's capital will change accordingly, affecting the value of the enterprise, resulting in increased costs and reduced profits.

2.1.4. Revenue Distribution Risk. The issue of how dividends are distributed is a highly sensitive one from the perspective of the enterprise's stakeholders [11]. From the perspective of creditors, they would like the company to distribute as little dividend as possible to ensure that creditors' debts are repaid first; from the perspective of shareholders, they would like the company to distribute as much dividend as possible and to recover their investment as soon as possible to achieve the expected financial goals; from the perspective of managers, they would like the company to retain more retained earnings to obtain further capital income and thus increase management salaries. With the need to balance the needs of all parties, the business has to make a comprehensive choice, taking into account the overall interest. Revenue allocation risk refers to the possibility that the financial position will be at risk due to an unreasonable allocation of revenue. If the income distribution policy is not reasonable, the solvency of the enterprise will be weakened, causing the investors and employees of the enterprise to lose motivation, raising the risk of the enterprise's capital operation and thus increasing the possibility of financial risk. The specific manifestation of earning distribution risk lies in balancing the contradiction between dividend payout and accumulation.

2.2. The Content and Placement of Financial Risk Warning

2.2.1. Building a Database of Alert Information and Establishing Alert Coverage. The early warning information database is the result of the conversion of raw warning source information to warning information [12]. The sources of this database include the investment transaction processing system, the management information systems, decision support systems, executive information systems, financial information systems, and other systems' output information. The establishment of an early warning information base is to be based on the early warning of financial risks. The scope of the warning is established by the early warning information base, which is the premise of the early warning of financial risks of the enterprise. Setting the scope of early warning requires clarifying the types and contents of financial risks. The financial risks of enterprises are mainly financing risks, investment risks, capital operation risks, and revenue allocation risks. In addition, the early warning information base should be updated and maintained in a timely manner.

2.2.2. Selecting Early Warning Indicators. Another important part of establishing an early warning system for financial risks in an enterprise is the selection of early warning indicators [13]. Based on the good or bad selection of early warning indicators, you can judge whether the early warning system for the financial risks of an enterprise is scientific enough. According to the characteristics of the enterprise, the early warning system of the financial risk should be established by selecting indicators reflecting the risk of financing, indicators reflecting the risk of investment, indicators reflecting the risk of capital operation, and indicators reflecting the risk of revenue distribution, which together constitute the early warning indicator system of the enterprise's financial risk.

2.2.3. Setting Early Warning Values for Early Warning Indicators. When setting up an early warning system for the financial risk of an enterprise, the most crucial thing is to set the early warning value of the early warning indicator, which is an important link to ensure the effectiveness of the early warning system. For the determination of the early warning value, the first thing is to reflect the scientific nature of the early warning value; that is to say, the establishment of the early warning value must have a certain scientific basis; the second one is to reflect the overall coordination of the early warning; that is, the process of determining the early warning value must take into account the coordination of the relationship between the various indicators; again, to reflect the stability of the early warning value, the early warning value is to maintain a relatively stable, not in a constantly changing situation. In the early warning analysis of enterprise financial risk, the range of early warning values should be determined in the context of the enterprise's industry.

2.2.4. Building an Early Warning Response Library. A warning response library is a set of contingency responses developed in various risk situations. When a financial risk early warning system issues a risk warning glance, it is necessary to find the corresponding countermeasures to address such warning alerts based on the glance information, the nature of the warning and the level of the warning. The countermeasures in the early warning response library are generally well thought out and inspiring. When the financial risk early warning system issues an alert, the company follows the tips in the early warning response library and analyzes the specific situation of the company before seeking more effective solutions and countermeasures.

The main financial early warning methods currently available can generally be divided into qualitative and quantitative analyses:

Qualitative analysis method: the qualitative analysis method of financial risk early warning refers to the analysis and investigation of the company's situation, which can identify the potential factors and causes of financial risks so that the relevant personnel of the company can arrange risk prevention measures in advance to avoid the occurrence of the financial crisis. Qualitative analysis methods include standard survey method, "four-stage symptom" analysis method, "four-stage risk" analysis method, the three-month capital turnover table analysis method, and the capital movement flowchart method. In this paper, we mainly use the first two survey methods such as Table 1 and 2 for the standardized questionnaire and the "four-stage symptom" analysis method, respectively.

The qualitative analysis method of financial risk early warning is highly subjective. Therefore, in order to overcome this subjective influence, most researchers began to turn their attention to the quantitative analysis of financial early warning.

Quantitative analysis method: quantitative analysis of financial risk early warning refers to the calculation of financial indicators by selecting specific financial data of the enterprise, using corresponding digital processing methods to digitally process the financial data or nonfinancial data of the enterprise, and then establishing related models. And this model is used to predict the financial risk of the enterprise [14]. A series of variable early warning indicators include indicators that reflect the company's solvency status, profitability status, asset operating capacity status, development capacity status, and cash flow status, and use these indicators to establish a multivariate early warning model [15]. The specific indicators are shown in Figure 2.

3. Construction of Financial Risk Early Warning System

3.1. Early Warning Index Weight Determination. According to the relevant requirements of the expert scoring method, by issuing questionnaires, the questionnaire surveys senior managers and experts in the financial risk field of the enterprise on the four aspects of financing risk, investment risk, capital operation risk, and profit distribution risk studied in this article. The indicators are scored. Figure 3 shows the scoring results of the first level of financing risk, investment risk, capital operation risk, and profit distribution risk.

After the weighting process, the weighting values of the first-tier indicators are 28% for funding risk, 24% for investment risk, 25% for capital operation risk, and 23% for return distribution risk.

The weights of the secondary indicators under the funding risk indicator weights are shown in Figure 4.

After the weighting process, the weighting values of the funding risk indicators were obtained as cash flow debt ratio 9.66%, quick ratio 9.80%, and gearing ratio 8.54%.

The weights of the secondary indicators under the investment risk indicator weights are shown in Figure 5.

After the weighting process, the weighting values of the investment risk indicators were obtained as 4.32% for the growth rate of total assets, 6.00% for the operating profit margin, 7.20% for the return on total assets, and 6.48% for the return on net assets.

The results of the risk indicator weighting of the capital operation are shown in Figure 6.

Table 1: Standardized questionnaire.

Project	Content of the Survey
Performance	1. Current status: bad/fair/good 2. Outlook: stable/growth/decline/unknown 3. Trading partners: growth/stable/decline/unknown 4. External creditworthiness: low/average/high/unknown
Peer group comparison	1. Size and status: small/medium/large/independent. 2. Competition among peers: Fierce/general/none 3. Sales base: sales route, customer trademark, and advertising special sales method 4. Production base: special technology, special equipment, special materials, special products, and special production organization
Financial management problems and causes	1. Problems: poor return on sales turnover, high costs, low productivity, and insufficient manpower 2. Reasons for low sales: fierce competition, industry decline, weak sales capacity, slow product development, and low productivity 3. Reasons for low revenue: low prices and high interest rates 4. Reasons for low production: low efficiency, insufficient human resources, poor management, and low modernization 5. Reasons for high costs: high material costs, inadequate start-ups, and high corporate expenses
Prospects	1. Guidance: expansion to maintain status quo conversion unclear 2. Direction of expansion: overall scale range of personnel 3. Specific methods: diversification of new products and new marketing specialization 4. Key foundations: product development and design, equipment technology, and sales force personnel cost quality

Table 2: The "four-stage symptom" analysis.

Crisis Incubation period	Crisis onset period	Crisis worsening	Crisis realization
1. Blind expansion	1. Insufficient own capital	1. The operator is unmotivated and preoccupied with financially weak assets	1. Liabilities more than assets and insolvency
2. Ineffective marketing	2. Over-reliance on externally funded business and heavy interest burden	2. Liquidity difficulties	2. Closure announced
3. Neglect of risk management	3. Lack of early warning function	3. Nonpayment of debts due	
4. No effective management system	4. Delaying instigation		
5. Ignoring significant changes in the environment			

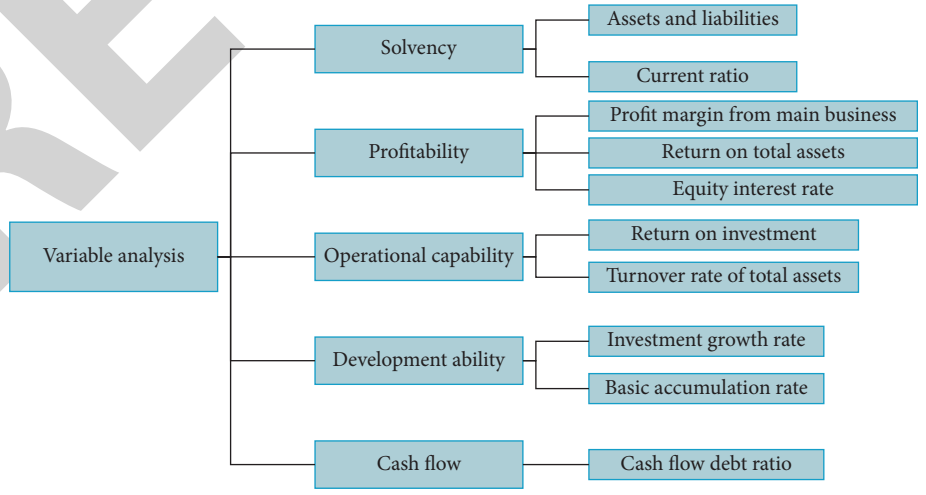

Figure 2: Variable analysis index diagram.

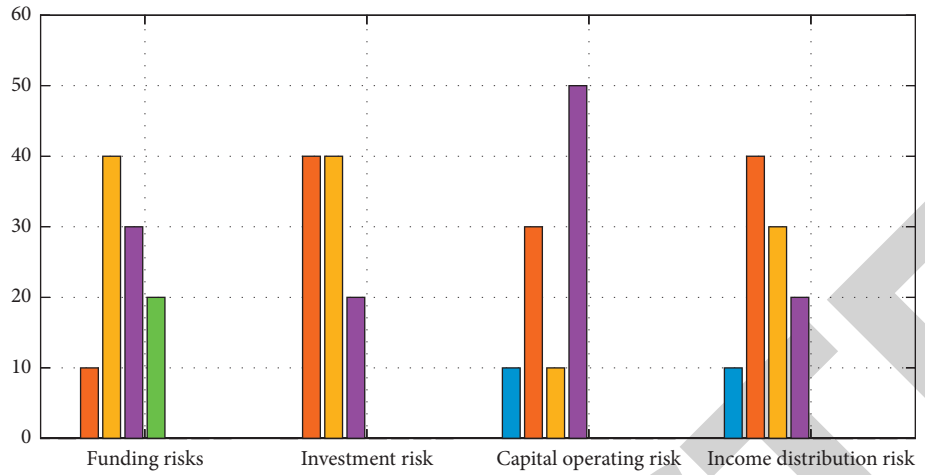

Figure 3: Histogram of the results of the first indicator tier scores.

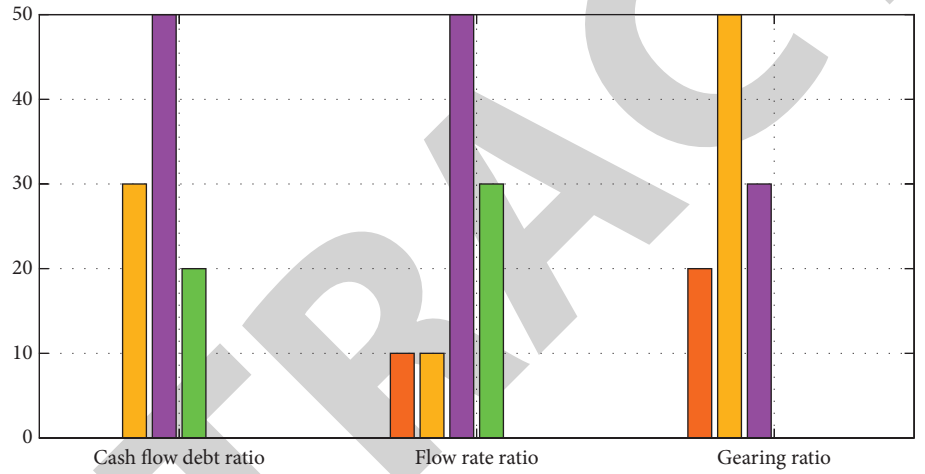

Figure 4: Histogram of funding risk indicator score results.

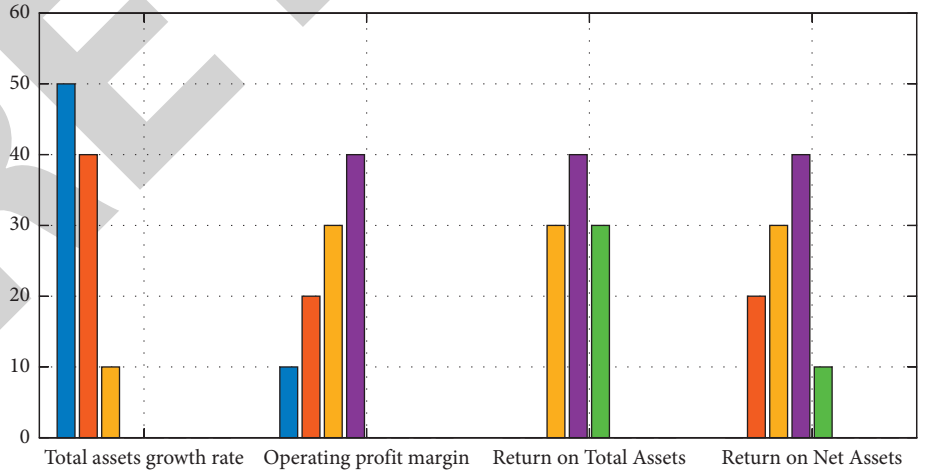

Figure 5: Histogram of investment risk indicator score results.

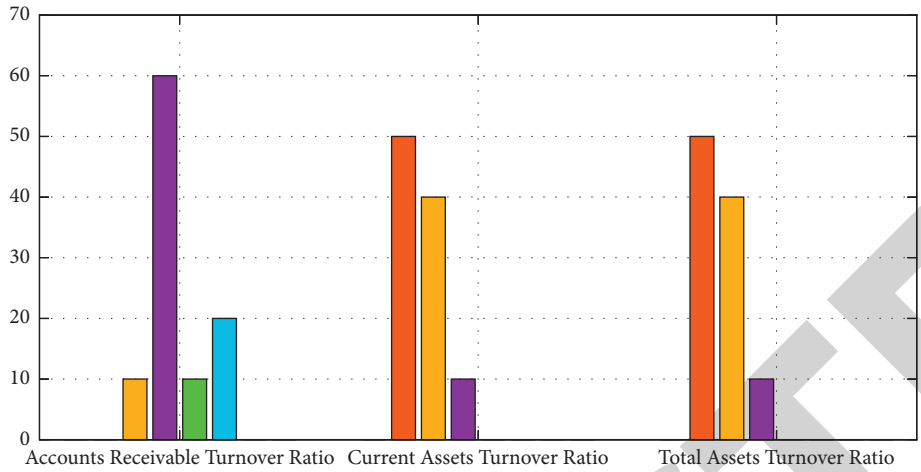

Figure 6: Histogram of the results of the scoring of the capital operation risk indicators.

After the weighting process, the weighting values of capital operation risk indicators were 8.00% for account receivable turnover, 5.75% for current asset turnover, and 5.75% for total asset turnover.

The resultant statistics for the weighting of revenue allocation risk indicators are shown in Figure 7.

After the weighting process, the weighting values of the income distribution risk indicators were obtained as 9.43% of the surplus cash guarantee multiple, 7.25% of the operating profit growth rate, and 6.32% of the asset cash recovery rate.

3.2. Calculation of Financial Warning Values. The score calculation of the efficiency coefficient method is divided into basic scores and adjustment scores. Generally, the proportions of basic scores and adjustment scores are relatively fixed at 60 points and 40 points, respectively. However, this division is not precise enough, and it is not conducive to enterprises to obtain the most accurate scores for financial risks. So the calculation formula is adjusted accordingly in the following:

$$\begin{aligned}
\text{single basic index score} &= \text{basic score of this file} + \text{adjustment score},\\
\text{the basic score of this crotch} &= \text{index weight} \times \text{standard coefficient of this file},\\
\text{upgrading basic score} &= \text{index weight} \times \text{upgrading standard coefficient},\\
\text{adjustment score} &= \text{efficacy coefficient} \times (\text{basic score for the upper file} - \text{basic score for this file}),\\
\text{efficacy coefficient} &= \frac{\text{actual value} - \text{standard value of this file}}{(\text{standard value of the previous file} - \text{standard value of this file})},\\
\text{comprehensive index score} &= \text{sum}\ \ (\text{individual index score}).
\end{aligned} \tag{1}$$

If the actual value is excellent, the efficiency coefficient method is 1.

Initially, the early warning interval is required to be determined because it contains the financial situation. The enterprise is located according to its score. The clarification of the financial warning situation of the enterprise at this stage will enable the users of relevant information to clearly identify the risks faced by the enterprise's financial situation. Moreover, the determination of the severity of the financial risks will also be allowed. The specific early warning intervals are determined as shown in Table 3.

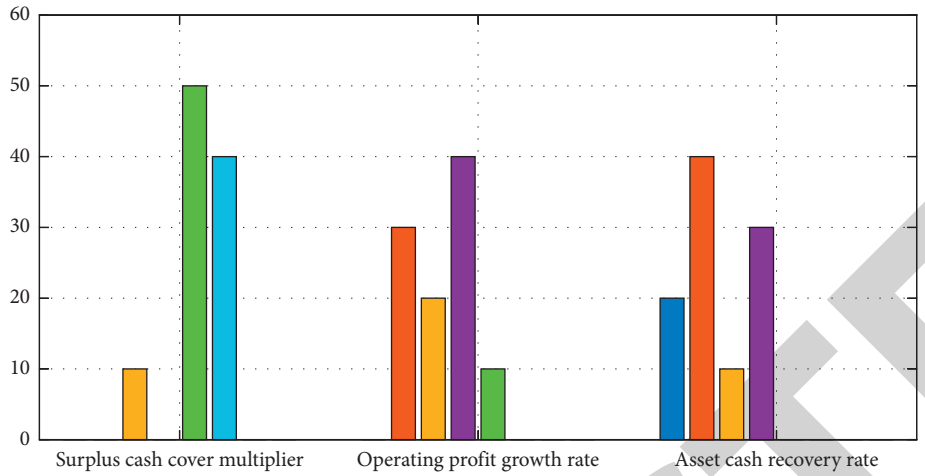

Figure 7: Histogram of the results of the revenue allocation risk indicator scores.

Table 3: Classification of the company's financial risk warning level.

Early warning level	Early warning interval	Risk status	Description
No warning	(80–100)	No risk	The company is operating in good condition, and there is almost no financial risk
Light warning	(60–80)	Risks of concern	The enterprise is running normally, some financial indicators are abnormal, and risk of concern may occur
Moderate warning	(40–60)	Less risky	There are problems with the operation of the business, some indicators are clearly abnormal, and there is a high possibility of financial risk
Severe warning	(20,–40)	Greater risk	Difficult business operations, with most indicators clearly abnormal and a high probability of financial risk
Serious warning	(0, 20)	Serious risks	The business is operating in extreme difficulty, with almost all indicators deteriorating and the business facing bankruptcy

4. Conclusion

In the process of corporate diversification investment, it is necessary to clarify the content of risks and their impact and use this as a basis to establish financial risk awareness and achieve effective judgment of corporate investment opportunities. In order to effectively improve the investment efficiency of enterprises, it is necessary to actively construct a financial risk prevention model in a diversified investment environment to actually prevent possible financial risks.

When enterprises want to make industrial investments according to the actual situation, they need to understand and analyze the investment environment, the scale and structure of diversified investments, and make use of effective means to optimize and adjust them. At the same time, in the process of building the model, the degree of resource sharing and the complementarity of investment factors should be fully considered, and the actual and ideal states should be compared and integrated at this stage. Through the construction of multiple systems such as investment systems and actual industrial systems, a diversified and multiattribute financial early warning model can be established.

To sum up, in the process of enterprise development, increasing attention to the prevention of financial risks of diversified investment of enterprises is an inevitable trend to meet the development of modern enterprises, and it is also an important content of improving the market economy status of enterprises and expanding market development space. Therefore, it is necessary to deepen the awareness of risk prevention and optimize the risk prevention model so as to achieve the harmony and unity of enterprise benefits and investment scale.

Data Availability

The data used to support the findings of this study are available from the corresponding author upon request.

Conflicts of Interest

The author declares that there are no conflicts of interest.

References

[1] Z. Li, "A study of Chinese A-share listed companies: effect of corporate valuation on the investment level," *International Journal of Science and Business*, vol. 5, 2021.

[2] R. Rijamampianina, R. Abratt, and Y. February, "A framework for concentric diversification through sustainable competitive advantage," *Management Decision*, vol. 41, no. 4, pp. 362–371, 2003.

[3] S. D. Giannatale, I. Curiel-Cabral, and J. Chacón, "Monitoring decisions in vertical integration," *Economia e Politica Industriale*, vol. 48, no. 3, pp. 1–22, 2021.

[4] I. A. Bradea and C. Delcea, "Early warning system framework for financial risk event in hospitals," *Journal Studii si Cercetari*

Hindawi
Journal of Mathematics
Volume 2023, Article ID 9761056, 1 page
https://doi.org/10.1155/2023/9761056

Retraction

Retracted: Data Mining and Analysis of the Compatibility Law of Traditional Chinese Medicines Based on FP-Growth Algorithm

Journal of Mathematics

Received 19 December 2023; Accepted 19 December 2023; Published 20 December 2023

This article has been retracted by Hindawi following an investigation undertaken by the publisher [1]. This investigation has uncovered evidence of one or more of the following indicators of systematic manipulation of the publication process:

(1) Discrepancies in scope

(2) Discrepancies in the description of the research reported

(3) Discrepancies between the availability of data and the research described

(4) Inappropriate citations

(5) Incoherent, meaningless and/or irrelevant content included in the article

(6) Manipulated or compromised peer review

The presence of these indicators undermines our confidence in the integrity of the article's content and we cannot, therefore, vouch for its reliability. Please note that this notice is intended solely to alert readers that the content of this article is unreliable. We have not investigated whether authors were aware of or involved in the systematic manipulation of the publication process.

Wiley and Hindawi regrets that the usual quality checks did not identify these issues before publication and have since put additional measures in place to safeguard research integrity.

We wish to credit our own Research Integrity and Research Publishing teams and anonymous and named external researchers and research integrity experts for contributing to this investigation.

The corresponding author, as the representative of all authors, has been given the opportunity to register their agreement or disagreement to this retraction. We have kept a record of any response received.

References

[1] S. Zhou, "Data Mining and Analysis of the Compatibility Law of Traditional Chinese Medicines Based on FP-Growth Algorithm," *Journal of Mathematics*, vol. 2021, Article ID 1045152, 10 pages, 2021.

Hindawi
Journal of Mathematics
Volume 2021, Article ID 1045152, 10 pages
https://doi.org/10.1155/2021/1045152

Research Article

Data Mining and Analysis of the Compatibility Law of Traditional Chinese Medicines Based on FP-Growth Algorithm

Shuchun Zhou

Affiliated Nanhua Hospital, University of South China, Health School of Nuclear Industry, Hengyang 421002, Hunan Province, China

Correspondence should be addressed to Shuchun Zhou; 631505040131@mails.cqjtu.edu.cn

Received 26 October 2021; Accepted 23 November 2021; Published 17 December 2021

Academic Editor: Naeem Jan

The compatibility law of prescriptions is the core link of TCM theory of "theory, method, prescription and medicine," which is of great significance for guiding clinical practice, new drug development and revealing the scientific connotation of TCM theory, and is also one of the hot spots and difficulties of TCM modernization research. How to efficiently analyze the frequency of drug use, core combination, and association rules between drugs in prescription is a basic core problem in the study of prescription compatibility law. In this paper, a systematic study was made on the compatibility rules of traditional Chinese antiviral classical prescriptions and the mechanism of traditional Chinese medicine molecules. FP-growth algorithm was used to analyze association rules of 961 classical prescriptions collected and to explore the compatibility rules of traditional Chinese antiviral classical prescriptions. In terms of compatibility law of traditional Chinese antiviral prescriptions, this paper studied the compatibility law of traditional Chinese antiviral prescriptions based on the FP-growth algorithm and made exploratory research on the compatibility law information of 961 traditional classical antiviral prescriptions. Firstly, FP tree was constructed based on the classic recipe data set. Then, frequent item set rules were established, and association rules contained in FP tree were extracted. Finally, the frequency and association rules of antiviral TCM prescriptions were analyzed according to dosage forms (decoction, pill, paste, and ingot). The results show that the FP-growth algorithm adopted in this paper has excellent algorithm performance and strong generalization and robustness in the screening and mining of large-scale prescription data sets, which can provide important processing tools and technical methods for the study of the compatibility rule of traditional Chinese medicine prescriptions.

1. Introduction

In recent years, infectious diseases present a high incidence trend, among which more than 75% are caused by viruses. With the continuous variation of viruses and the enhancement of drug resistance, the treatment of viral diseases has become one of the world's difficult problems. In the aspect of prevention, control, and treatment of virus infectious diseases, traditional classic antiviral prescription, such as MaXingShi sweet soup, hot disease, Fructus Forsythiae and scattered, small Bupleurum decoction, and Sang Ju Yin, because of its adjustable immunity, can interfere with viral DNA or RNA replication, suppress the virus proliferation, and have the effect that protect cells against the virus damage [1]. It has played a pivotal role in the treatment of epidemic viral diseases such as SARS; AIDS; hand, foot, and mouth disease; and H7N9. The traditional Chinese medicine antiviral prescription plays an important role, promotes new prescription antiviral herbs and new drug research and development to dig deeper into the traditional classic antiviral prescription information, has become a new drug development of traditional Chinese medicine study the compatibility of the law, an important subject in the field of it to study the internal relations and characteristics of the prescription system, and also has the very vital significance [2, 3].

Data mining is a processing technology to search for information with special relevance hidden in a large amount of data, which has played an important role in the basic

theory of traditional Chinese medicine, traditional Chinese medicine prescription, traditional Chinese medicine philology, and clinical research of traditional Chinese medicine. As an important branch of data mining, the association rule can describe the potential relationship between data items in the database. Moreover, the said method discovers the relationship between variables of interest in the database [1]. Some important results have been obtained in the dose-effect study of traditional Chinese medicine based on association rule method, which has played an important role in promoting the study of traditional Chinese medicine formulations. For example, in terms of clustering analysis [4], such as using the *K*-means clustering analysis method for treating diabetes, analysis of prescription drugs, and learned of diabetes prescription drug law and basic medicine, Radix Rehmanniae, prepared Rhizome of Rehmannia, Radix Trichosanthis, Rhizoma Anemarrhenae, Rhizoma Alismatis, and Radix Ophiopogonis, for prescriptions of traditional Chinese medicine theory research and new drug development to provide the reference information. Reference [5] used the clustering method to automatically divide the fuzzy interval of drug dose in dot-effect analysis of drug pairs and then analyzed the association rules of drug pairs by combining the fuzzy association rules. The mined knowledge had a high accuracy. Using frequency and frequent term set method, reference [6] used frequency statistical analysis to explore the compatibility methods of reducing toxicity and increasing efficiency of toxic Chinese traditional medicine *Pinellia ternata*. It was concluded that the compatibility of soothing poison, dampening to prevent dryness, cold to make heat, and phase killing to make poison could reduce the toxicity of *Pinellia ternata*. The authors in [3] used frequency analysis and association rule method to analyze and study the compatibility rules of TCM prescriptions for the clinical treatment of senile dementia by physicians of all dynasties and obtained the compatibility rules of common prescriptions for the clinical treatment of senile dementia. Reference [7] analyzed the prescription law of Chinese herbal compound oral treatment of ulcerative colitis and excavated 60 core combination prescriptions and 23 new prescriptions. Using association rule technology, [8] explored the compatibility rule and core drug use of Chinese medicine prescription of Chai Songyan in the treatment of premature ovarian failure based on syndrome differentiation and found 45 pairs of commonly used 2 drug combinations. Data mining was conducted [9] on the compatibility rule of the drugs with the strongest correlation of TCM antiemea prescription and obtained that ginger, *Pinellia ternata* and *Poria cocos* were the most commonly used drug combinations in TCM antiemea prescription, and confirmed that *Pinellia ternata* plus *Poria cocos* decoction created by Zhang Zhongjing was the core drug group of TCM antiemea prescription. Based on the apriori association rule algorithm, [8] analyzed the real-world clinical rules of the combined application of compound *Sophora* flaveseed injection and Chinese and Western drugs in the treatment of malignant tumors, providing useful reference for clinical treatment ideas and reasonable reference for the clinical application of compound *Sophora* flaveseed injection. The medicinal properties were processed [10] and efficacy of 365 flavors in Shennong Materia Medica Classic to find frequent patterns and strong association rules between qi, flavor, and efficacy, providing new methods and ideas for theoretical research on the medicinal properties of the four qi and five flavors of Traditional Chinese medicine. Liver fibrosis antiviral drugs, such as Liuwei Wupian combined with Ganoderma lucidum, have certain advantages in the antiviral treatment of chronic hepatitis B liver fibrosis virus-like meta-analysis. A systematical evaluation of the effectiveness and safety of *Astragalus* was carried out based on the TCM compound in the treatment of diabetic nephropathy in 488 patients and conducted a meta-analysis, concluding that *Astragalus*-based TCM compound may be a relatively safe and effective drug in the treatment of diabetic nephropathy.

Data mining is the extraction or "mining" of knowledge from large amounts of data. Through data mining, valuable knowledge, rules or high-level information can be extracted from the relevant data set of the database. And, display from different angles, so that the large database or data warehouse as a rich and reliable resource for decision-making services. In data mining, the discovery of rules is based on the statistical rules of large samples. When the confidence reaches a certain threshold, rules can be considered to be established. The core methods of data mining are association rules and sequential pattern mining, classification, and clustering. Association rule analysis is a very important research topic in the field of data mining, and it is also one of the most mature research methods. The purpose is to mine the association rules that meet the minimum support and minimum confidence between transaction features from the given data. Minimum support and minimum confidence are two measures reflecting the value of association rules, representing the usefulness and reliability of rules, respectively. Rules are considered meaningful only if they satisfy both minimum support and minimum confidence. We believe that there is some form of association in the compatibility of Chinese medicines. According to the theory of traditional Chinese medicine, there are the following five relationships between Chinese medicines, that is, the seven must, cause, fear, kill, and have nothing to do with each other. For example, in Buzhong and Yiqi decoction, the combination of Bupleurum and Hoshoi can draw seven liters of qi tonic from ginseng, Qi qi, shu, and grass. Together to achieve the effect of beneficial qi rising trap, this combination is the role of phase. We can find meaningful combination patterns of traditional Chinese medicine from common prescriptions. The tool used in this study is the algorithm of extracting association rules from data mining—FP-growth algorithm.

Demand for new antiviral medicine of Chinese medicine research and development, using the experience of the study, in order to improve the effectiveness and accuracy of association rules analysis algorithm, this study intends to use the FP-growth algorithm to the traditional Chinese medicine classical prescription data screening for large-scale data set mining, aim to do exploratory research antiviral herbs prescription compatibility of the law, and verify the

effectiveness of the algorithm and explore the law of traditional classical antiviral prescription and potential useful information.

2. Association Rule Data Mining

2.1. Mining Association Rules. Data mining is a new research field gradually developed in recent 30 years. It is the product of the combination of multidisciplines and technology, which is widely used in various fields such as government decision-making, enterprise management, scientific discussion, and medical research, and plays an important role in promoting the development of all aspects of society. Association rule mining is one of the most typical knowledge types in data mining. In the medical field, it has a wide range of applications.

Association rules are used to represent the association degree of many attributes (item sets) in OLTP database. They are used to find the correlation of attributes by the association algorithm using a large amount of data in the database. The problems of association rule mining are described as follows.

Let $I = \{I_1, I_2, \ldots, I_m\}$ is the set of data items, $D = \{T_1, T_2, \ldots, T_n\}$ is a transaction database, where each transaction T is a subset of data item set I, namely, $T \subseteq I$, and each transaction T has an identifier TID associated with it. Transaction T is said to contain item set X if a subset X of I satisfies $X \subseteq T$. An association rule is something like "$X => Y$." The meaning is that the occurrence of some items in a transaction leads to the occurrence of other items in the same transaction, where "=>"; called the "association" operation, X is the prerequisite for the association rule, and Y is the result of the association rule. For example, in the compatibility of Chinese medicine prescriptions, more than 90% of prescriptions using Chinese medicine A must has to use the Chinese medicine B at the same time. So, the association rule R can be expressed as $R : A = > B$. Support and confidence are important concepts in association rules.

Support is similar to the percentage of prescriptions using both A and B in the total prescriptions. Confidence is the percentage of the prescriptions of all Chinese medicine A and B to the prescriptions of Chinese medicine A, which is called regular confidence. The former is used to measure the statistical importance of association rules in the whole data set, while the latter is used to measure the credibility of association rules. Their formulas are formulas (1) and (2), respectively:

$$\text{Support}(A \Rightarrow B) = P(A \cup B) = \frac{B}{A}, \tag{1}$$

$$\begin{aligned}\text{Confidence}(X = Y) &= P(Y|X) \\ &= \frac{P(X \cup Y)}{P(X)} = \frac{\text{Support}(X \cup Y)}{\text{Support}(X)}.\end{aligned} \tag{2}$$

In practical applications, associations with high support and confidence can be used as useful association rules, which are called minimum support threshold (min_ sup) and minimum confidence threshold (min-conf). Min-sup indicates the lowest statistical importance of data items. Only data item sets that meet min-sup appear in association rules, which are called frequent item sets. The minimum confidence is the lowest reliability of the association rule. Rules that meet the requirements greater than min-sup and min-conf are called strong rules. The task of association rule mining is to discover all frequent item sets and dig out all strong rules in transaction database D.

Association rule mining is actually frequent pattern mining. According to the following criteria, frequent pattern mining has multiple classification methods:

2.1.1. Classification according to the Completeness of Mined Patterns. Given the minimum support threshold, the complete, closed, and extremely frequent item sets of frequent item sets can be mined. It is also possible to mine constrained frequent itemsets (that is, frequent itemsets that satisfy a set of constraints specified by the user), approximate frequent itemsets (that is, only the approximate support count of the mined frequent itemsets is derived), near-matched frequent itemsets (that is, itemsets that conform to the support count of close or nearly matched itemsets), and mostK frequent itemsets (that is, k most frequent itemsets for user-specified K), and so on [12].

2.1.2. Classify according to the Abstraction Layer Involved in the Rule Set. Some methods of mining association rules can discover different abstraction layer rules. For example, suppose the mined association rule set contains the following rules:

$$\begin{aligned}&\text{buys}(X, \text{“computer”}) \Rightarrow \text{buys}(X, \text{“HP\_printer”}), \\ &\text{buys}(X, \text{“laptop\_computer”}) \Rightarrow \text{buys}(X, \text{“HP\_printer”}).\end{aligned} \tag{3}$$

2.1.3. If the Item or Attribute in an Association Rule Involves Only One Dimension, It Is a Single-Dimensional Association Rule.

$$\begin{aligned}&\text{buys}(X, \text{“computer”}) \Rightarrow \text{buys}(X, \text{“antivirus\_software”}), \\ &\text{age}(X, \text{“30} \ldots \text{39”}) \Rightarrow \text{buys}(X, \text{“high\_resolutionTV”}).\end{aligned} \tag{4}$$

2.2. Improving FP-Growth Algorithm. FP-growth algorithm is a famous algorithm based on FP-growth tree proposed by Han Jiawei et al. This algorithm provides a good frequent pattern mining process without generating candidate set, and its performance is improved compared with apriori algorithm. However, FP-growth algorithm generates more and more conditional FP-trees with the deepening of recursive calls. Especially in the case of shared prefixes, FP-growth algorithm is very time-consuming. In order to solve this

problem, this paper proposes the improvement of FP-growth algorithm, FP-growth* algorithm.

The idea of FP-growth algorithm is to reduce the time of searching shared prefixes to reduce the time of generating FP tree to improve mining efficiency. That is, if there is a shared prefix, the shared prefix is found by traversing the first child node of the node. Its mining steps are as follows.

2.2.1. Ranking of Frequent L Item Set. Describe the transaction database *D* once, generate frequent *L* item set and the support degree of each frequent item set, sort by descending support degree, and the result is L.

2.2.2. Transaction Item Reordering. The transaction database items are sorted according to the order of frequent item table *L* to generate transaction database *D*.

2.2.3. Transaction Set Reordering. The whole data set of *D* is reordered according to the order of *L*, that is, the first column of the transaction set is sorted according to the order of L. Then, the second columns of the transaction set are sorted in the order of *L*, and the final columns of the data set are analogized to get sorted data set *D*.

2.2.4. Construct FP-Tree Condition. Create root node marked with "NULL," scan *D*, call insert—Tree (P, T1) procedure for each transaction in it. Generate the FP tree.

2.2.5. Mining FP Tree. Recursively call FP-growth algorithm to mine FP tree and obtain frequent item sets.

2.3. Research on FP-Growth Algorithm in Mining Compatibility Rules of Traditional Chinese Medicine Prescriptions. In the fact of more than 100,000 TCM prescriptions, spleen and stomach prescriptions were selected as the data source of association mining in this paper. All prescriptions were from the clinical prescriptions of Hua Tuo Hospital of Traditional Chinese Medicine and the Database of TCM Prescriptions of Shanghai TCM Data Center. As the hometown of the magical doctor Hua Tuo, Bozhou has long been known as the "peony flowers outside the city of Xiaohuang, producing the morning clouds for miles and five miles." It is a well-known center for the planting and processing of Chinese medicinal materials in the world. There are hao peony, hao chrysanthemum, hao mulberry bark, and hao pollen in the real estate medicinal materials included in the Pharmacopoeia. With a planting area of 1 million mu, it is known as the "Chinese medicine Capital." A large number of traditional Chinese medicine resources provide natural conditions for the development of traditional Chinese medicine prescriptions. Huatuo traditional Chinese medicine hospital has a large number of clinical prescriptions: "TCM Prescription database" of Shanghai TCM data center contains l90,000 TCM prescriptions and extracts the prescriptions contained in the literature. The data items include the name, composition, dosage, indications, and other information of prescriptions.

2.3.1. Data Processing of TCM Prescriptions. The original data expression of the existing prescription database is not standardized, so it is necessary to transform the descriptive language of the prescription into the data information that can be processed by the computer, so as to make it standard and standard, so as to realize the correct expression and reasonable organization of prescription data in the computer system. Using computer data to express is not only helpful for in-depth analysis and operation of data. It is also an important way to realize data normalization and standardization. The data preprocessing method in this paper is as follows:

(1) Standardized Data. The purpose is to standardize the semantic ambiguity and expression of the concept words, polysemy monosyllabic word, multiword monosyllabic word lexicalization. The split expression of multiconcept combination words such as dizziness refers to symptoms such as dizziness, which are different from simple dizziness, blood dizziness, motion sickness, etc., such as fever, severe fever, and night fever which are treated as a single concept of fever.

(2) Structured Data. The purpose is to refine and organize the original data of prescription reasonably, so as to meet the requirements of data mining and to realize the orderly arrangement of key concepts and the formation of the associated structure between data.

Prescription data have multiple associations, such as between drugs, between drugs and symptoms, and between efficacy and indications. "Syndrome, medicine and prescription" is the core, and "medicine" is the key element in the core. Their relationship is as follows: select "medicine" and "prescription" for "syndrome." "Syndrome" is composed of syndrome sets, "medicine" contains different taste and quantity, etc., and "prescription" has complex matching relations and the problem of adding or subtracting prescription.

(3) Digitize Data. Numbers are easy to represent the structure and mutual relationship between data, while data described by other characters or symbols is not easy to do, so as far as possible to use numbers to replace the characters or symbols containing some knowledge. If the dose is described in grams, the drug taste and virulence are also represented by numbers. If flatness is set to 0, the corresponding value of skewness is shown in Table 1.

2.3.2. Mining Compatibility Rules of TCM Prescriptions Based on FP-Growth Algorithm.* A total of 106 spleen-stomach prescriptions with symptom frequency greater than 25 were screened out of 338 prescriptions collected, and each prescription was considered as a transaction with the marker code TID : T001, T002...T106, the code of each Chinese medicine in the formula is $I_i(I = l, 2, 3, ...)$

The collected spleen and stomach prescriptions and their components are as follows:

Table 1: Digital representation of data.

Very hot	Hot	Wen	Lukewarm	Flat	Cool	Slight cold	Cold	Severe cold
1.2	0.9	0.6	0.3	0	0.3	0.6	0.9	1.2

Two Chen soup flavor (F001): atractylodes, *Glycyrrhiza* glycyrrhiza, tangerine peel, *Magnolia officinalis*, *Poria cocos*, *Pinellia ternata*, rhizoma SPP

Sijunzi decoction (T002): atractylodes, glycyrrhiza, ginseng, *Poria cocos*, sweet sand

Liujunzi decoction (TO03): atractylodes, *Glycyrrhiza* glycyrrhiza, ginseng, tangerine peel, *Poria cocos*, xylobacter, *Pinellia ternata*, *Amomum amomum*, ginger

Qinlianping, Weitang (T004): liquorice, tangerine peel, magnolia bark, *Scutellaria baicalensis*, *Coptis chinensis*, *Atractylodes atractylodes*

Huoxiang Fupi drink (T005): liquorice, tangerine peel, wood incense, *Magnolia officinalis*, *Pinellia ternata*, Huoxiang, Malt

Shipi drink (T006): atractylodes, *Glycyrrhiza*, *Magnolia officinalis*, *Poria cocos*, xylobacter, papaya, grass fruit, areca nut, ginger, monkshood fruit, jujube

Guipi decoction (T007): atractylodes, licorice, ginseng, xylobacter, *Poria cocos*, angelica, *Astragalus membranaceus*, *Polygenus longan*, jujube seed

Yigong powder (T008): atractylodes, *Glycyrrhiza*, tangerine peel, ginseng, *Poria cocos*

Lizhong pill (T009): atractylodes, licorice, ginseng, ginger

Baoyuan soup (TO10): atractylodes, ginseng, angelica, cassia twig, *Astragalus membranaceus*, raw aconite

The main codes of prescriptions are as follows: atractylodes I1, *Glycyrrhiza* I2, tangerine peel I3, ginseng I4, *Magnolia officinalis* I5, aucklanoides I6, *Poria cocos* I7, codonopsis I8, *Pinellia ternata* I9, angelica I10, Quanyi peony I12, ginger I selected ginseng I14, Su stem I15 amomum I16, almond I17, *Coptis coptidis* I18, *Astragalus membranaceus* I19, cinnamon I20, jujube I21, polygonum I22, yam I23, lentil I24, *Solanum solanum* I25, *Lobelia* I26, cardamom I27, *Corni ruyu* I28, black aconite I29, *Atractylodes atractylodes* I30, nutmeg I31, papaya I32, cardamom I33, preparation of aconite I34, longan meat I34, weak, sour jujube seed I36, patchouli I37, selected ginseng I38, *Scutellaria baicalensis* I39.

The establishment of spleen and stomach agent transaction database (part) D is shown in Table 2:

FP-tree tree was constructed according to transaction database *D* (FP tree was omitted due to limited space), and the corresponding support degree of the frequency of the occurrence of traditional Chinese medicine in the prescription was set at the minimum of 30. FP-growth improved algorithm was used to obtain frequent sets by establishing conditional pattern library, mining all frequent item sets, and the compatibility rules of spleen and stomach prescription were found as follows.

(1) Prescription Core Drugs. Liquorice (97), dried tangerine or orange peel, atractylodes (93) (92), ginseng (78), thick ~ *b* (56), combination (48), angelica (36), the 7 of TCM to occur more often than other drugs in the prescription but also can get the ingredients are: sijunzi decoction, different work loose and sweet sand six main medicine soup, namely, is Lord of the spleen and prescription drugs.

(2) Prescription Structure. After the above analysis, results prove that the spleen and stomach fangfang looks complex. There is a basic structure.

The decoction of invigorating qi and invigorating spleen represented by Sijunzi Tang is the most basic prescription. The second is the combination of qi medicine + qi medicine prescription, such as Xiangsha Liujunzi Decoction, Yigong powder prescription. Replenishing qi medicine + regulating qi medicine + disease medicine (or humidification medicine) compatible prescription, such as Shenling Baizhu Powder, six gentleman decoction and other prescriptions. Supplementing qi medicine + warm medicine compatibility of prescriptions, such as Bao Yuan soup, li Zhong pills and other prescriptions.

In order to improve the efficiency of apriori algorithm, Han Jiawei et al. proposed a FP-growth algorithm based on growth tree structure to generate frequent item sets [27].The basic idea of the algorithm is to scan the database only twice: the first time scans the number of the occurrence of a single item in the data set and filters out the items that do not meet the minimum support.

In the second scan, the frequent pattern tree (FP-tree) structure is established, and then the FP tree is recursively grown into a large item set, and then the test is carried out on the whole data set. This algorithm does not generate candidate item sets, avoids multiple scanning of the original database, and can directly compress the database to generate a FP tree, and finally form association rules. Studies have shown that FP-growth algorithm is one order of magnitude faster than apriori algorithm in finding large item sets.

3. Study on Compatibility Rule of Chinese Medicine Antiviral Prescription Based on FP-Growth Algorithm

3.1. Data Source of Chinese Medicine Antiviral Prescription. In order to study the compatibility rules of traditional and classical antiviral prescriptions, the research group designed and developed the TCM prescription management system in advance. The system is based on web B/S architecture mode, using Java development language and access database management software, and can run in Windows/Linux system. It adopts top-down overall planning, top-down application development strategy, standardized framework structure, and easy to operate import mode. TCM

Table 2: Transaction database D (Part).

TID	Items
T001	I1, I2, I3, I5, I7, I9
T002	I1, I2, I3, I7
T003	I1, I2, I3, I4
T004	I2, I3, I5, I18, I30, I39
T005	I1, I2, I3, I5, I6, I9, I37, I40
T006	I2, I3, I5, I7, I6, I15, I21, I32
T007	I1, I2, I4, I6, 17, I10, I19, I22, I35, I36
T008	I1, I2, I3, I4, I7
T009	I1, I2, I4, I15
T0010	I1, I4, I10, I19, I41, I4
.....	.....

prescription management system can meet the basic import, export, retrieval, and other operations and simple statistical functions. Through the TCM prescription management system, all the books on epidemic diseases collected in the First Part of Wen's Disease Dacheng (2007, Fujian Science and Technology Publishing House) are selected.

3.2. Data Preprocessing. Literature data sources of classical antiviral prescriptions are diverse, and drug names are not standardized. Therefore, according to the traditional Chinese medicine name standard in the Dictionary of Traditional Chinese Medicine, the collected prescriptions were cleaned and the names of medicines were standardized. In the process of this study, examples of traditional Chinese medicine name standardization are shown in Table 3.

3.3. Application Process of FP-Growth Algorithm. The following uses a specific example to illustrate the implementation process and characteristics of the FP-growth algorithm.

Step 1. According to the FP-growth algorithm, the sample data set was scanned first, and the traditional Chinese medicines meeting the minimum support threshold were arranged in the descending order according to the frequency of occurrence in the data set.

Step 2. Arrange formula data in the example in the descending order of frequency and select TCM with frequency greater than 3. According to the result of reordering, FP tree is established.

In Figure 1, root is the empty set used to build the subsequent FP tree. The structure of FP tree itself is represented by solid arrow head, and the count at the node represents the frequency of occurrence of this item in the data set. For example, Gardenia and Scutellaria in the first branch on the right of the tree correspond to the ninth prescription, while Gardenia and Scutellaria in the second branch on the right correspond to the seventh and eighth prescriptions, so the count at the node is 2. The whole FP tree can be obtained by analogy. The title table on the left of the figure shows the frequency of TCM meeting the minimum support in the data set, in the descending order. Dotted arrows connect the title table to the tree structure and join items with the same name together for easy traversal of the tree structure. The sum of counts of items with the same name in the figure corresponds to the item support in the title table. After the FP tree is obtained, the reverse recursive processing tree can get the gradually increasing item set, and the association rules can be further calculated. It is worth noting that, in the process of establishing FP tree, the traditional Chinese medicine that does not meet the minimum support in the example will not be inserted into the FP tree. Therefore, the FP-growth algorithm can effectively remove the terms less than the support and enable multiple prescriptions to share the most frequent traditional Chinese medicine and finally achieve a high compression effect in the root of the tree. The designed experimental algorithm flow is shown in Figure 2, Algorithm flow of FP-growth is shown in Figure 3.

4. Experimental Results and Analysis

Chinese medicine prescription is not a random combination of drugs but has potential compatibility law and processing technology. According to the characteristics of drugs and the needs of clinical syndrome treatment, in order to give full play to the effect of drug therapy, TCM prescriptions are often made into various dosage forms such as decoction, wine, tea, dew, pill, powder, paste, dan, tablet, ingot, glue, striping agent, and line agent for internal and external use. Due to the low quantity of some dosage forms in the research data, this study mainly analyzed the four dosage forms of decoction, pill, ointment, and spindle and obtained the core drug use and corresponding association rules of the corresponding dosage forms of antiviral prescriptions. Among them, the occurrence frequency of glycyrrhiza uralensis "with all kinds of drugs, cure all kinds of poison" was up to 480 in 961 antiviral prescriptions, and the occurrence frequency of glycyrrhiza uralensis was too high with other drugs, so that part of the analysis results were not valuable. In order to make the association rules mined more meaningful. In the experimental process, except for the ointment (only 15 pieces), the item sets with drug combinations greater than (including) 3 traditional Chinese medicines were selected for study and analysis.

4.1. Medicinal Broth. The top ten frequently used drugs in decoction antiviral prescription were glycyrrhiza, *Scutellaria baicalensis*, rhubarb, angelica, orange stem, ginger, shengdi, mint, Rhizoma chinensis, and *Poria cocos*, which were the main drugs in decoction antiviral prescription. Drug combination is greater than 3 taste traditional Chinese medicine (TCM), the frequency is more than 10, and confidence is more than 90% of a total of 32 groups, the association rules in the combination of the frequency highest with liquorice—Gardenia—Radix scutellariae and mint—*Platycodon grandiflorum*—licorice root, rhubarb—mint—Radix scutellariae and mint—even become warped, licorice, mint—St. John's wort, Radix scutellariae, all is one common combination of antiviral prescription. Some of them had strong association rules. For example,

Table 3: Sample table of drug name normalization.

The specification before	After the specification
Cicada, cicada skin, cicada slough, cicada shell	Cicada
Dried reed root, dried reed root, reed root	Reed root
Tender osmanthus, sichuan osmanthus, liugui, osmanthus tip, osmanthus tip, osmanthus section	*Cassia* twig
Wolfberry, sweet wolfberry, red wolfberry, western	Medlar
Thousand lily, southern lily, large lily, xuan lily, new lily, du lily, sweet lily, white lily, white flower lily, lily slice	Lily
Bright sulfur, yellow fluid, stone sulfur, ship sulfur	Sulfur
.....	.....

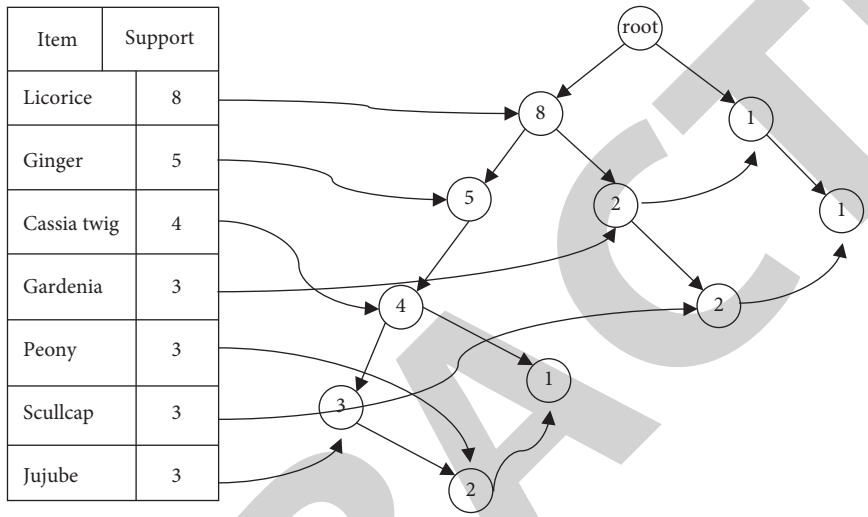

Figure 1: Diagram of FP tree of 9 prescriptions.

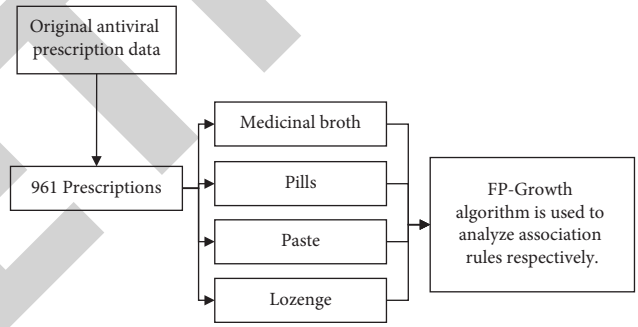

Figure 2: Algorithm flow of compatibility rule of TCM antiviral prescription based on the FP-growth algorithm.

when *Scutellaria baicalensis* and cicada slua appeared simultaneously, the occurrence probability of coptis was 100%. When *Scutellaria baicalensis*—silkworm—Rhizoma coptidis appears simultaneously in one prescription, cicada exuvium will inevitably appear in the prescription, which vividly excavate the internal relationship between the drugs in the prescription and provide the basis for clinical doctors to use medicine. Frequency and probability of the top ten drugs used in decoction is shown in Table 4.

4.2. Pills. The frequency and probability of the top ten Chinese medicines in pill antiviral prescriptions are shown in Table 5. There were 30 association rules with drug combinations greater than 3 traditional Chinese medicines, frequency higher than 25, and confidence greater than 80%. The combinations with the highest frequency were ginger—jujube—glycyrrhiza, glycyrrhiza—Rhizoma coptidis—Scutellariae, glycyrrhiza—forsythia—Scutellariae, which were the core combinations of pill antiviral TCM prescriptions. There are strong association rules among some Chinese medicines, which can provide theoretical support for new drugs. For example, in a formula, when jujube—ginseng appeared at the same time, ginger appeared in the probability of 97.06%. When Scutellariae and cicada slits appeared at the same time, the probability of silkworm emergence was 97.06%.

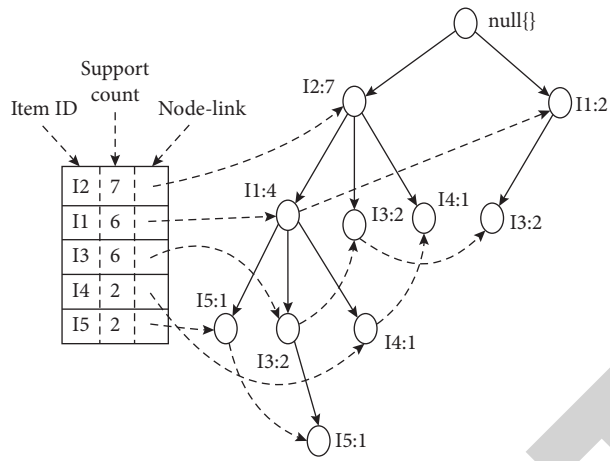

Figure 3: Algorithm flow of FP-growth.

Table 4: Frequency and probability of the top ten drugs used in decoction.

Medicines	Frequency	Probability
Licorice	81	46.55
Scullcap	49	28.16
Rhubarb	34	19.54
Angelica	27	15.52
Platycodon grandiflorum	27	15.52
Ginger	26	14.94
Radix rehmanniae	26	14.94
Mint	23	13.22
Rhizoma coptidis	23	13.22
Poria cocos	23	13.22

Table 5: Frequency and probability of the top ten drugs used in pills.

Medicines	Frequency	Probability
Licorice	350	52.87
Scullcap	201	30.36
Ginger	143	21.60
Radix rehmanniae	105	15.86
Rhubarb	103	15.56
Jujube	96	14.50
Ginseng	92	13.90
Peony	91	13.75
Gypsum	91	13.75
Rhizoma coptidis	83	12.54

4.3. Medicinal Extract. The collection of cream antiviral prescriptions is relatively small, only 15. Chinese medicines with frequencies greater than 3 were scutellaria baicalensis, licorice, mint, Sichuan rhizome, rhubarb, shengdi, and rhino horn, which were the main drugs used in ointment antiviral prescriptions. The specific frequency and probability of occurrence are shown in Table 6. Table 7 shows the association rules of TCM frequency greater than 3. It is easy to know that there are strong association rules between the drugs in the ointment, such as the prescription of scutellaria, raw ground, and rhinoceros horn at the same time any two drugs, another medicine will also appear.

4.4. Experimental Analysis of FP-Growth Algorithm.* In the same computer software and hardware system, with the increase of the number of data sets, the time of FP-tree generation by the improved algorithm decreases obviously. According to the experimental analysis, when the number of data sets is large, the mining efficiency of FP-growth* algorithm is increased by about 20%, as shown in Figure 4:

4.5. Algorithm Analysis and Comparison. FP-growth* algorithm is improved on the basis of FP-growth algorithm, and it retains the efficient characteristics of FP-growth algorithm and adds support for the mining of numerical data, support for interdimensional association mining, mining maximum frequent itemsets instead of mining all frequent patterns. This method can greatly save the space and time cost of producing all frequent patterns and also meet the needs of traditional Chinese medicine mining. From the perspective of time complexity, the FP-growth* algorithm is better than FP-growth algorithm.

(i) FP-growth* algorithm finally mined the maximum frequent item set, which is more than one order of magnitude different from all frequent item sets. Therefore, when FP-growth* algorithm generates conditional pattern tree and maximum frequent item set, it takes much less time than FP-growth algorithm.

(ii) FP-growth* algorithm adopts an optimized search strategy, omits a certain number of item searches, and does not need to generate conditional modular basis, conditional pattern tree, and longest frequent item set for these items, saving considerable time. Performance comparison in time of *c* and FP-growth is shown in Figure 5.

Therefore, the FP-growth* algorithm proposed by the author can not only deal with numerical interdimensional rules in mining function but also outperforms FP-growth algorithm in running time efficiency. Through the analysis of the mining results of this algorithm, it is obvious that the interdimensional maximum frequent item set is really meaningful for the FP-

Table 6: Frequency and probability of drugs with frequency greater than 3 in the ointment.

Medicines	Frequency	Probability
Scullcap	5	33.33
Licorice	4	26.67
Mint	3	20.00
Chuanlian	3	20.00
Rhubarb	3	20.00
Radix rehmanniae	3	20.00
Rhinoceros horn	3	20.00

Table 7: List of ointment association rules.

Pharmaceutical compositions	Frequency	Support	Confidence (%)
Chuan lian => Scutellaria	3	0.20	100.00
Rhizome of rehmannia => Scutellaria	3	0.20	100.00
Rhinoceros horn => Scutellaria	3	0.20	100.00
Rhinoceros horn => rhizome of rehmannia	3	0.20	100.00
Rhizome of rehmannia => rhinoceros horn	3	0.20	100.00
Scutellaria, rhizome of rehmannia => rhinoceros horn	3	0.20	100.00
Rhinoceros horn, rhizome of rehmannia => Scutellaria	3	0.20	100.00

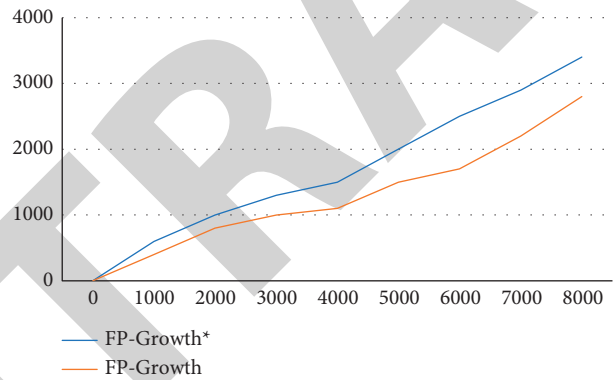

Figure 4: Comparison between FP-growth * and FP-growth algorithm to generate FP tree.

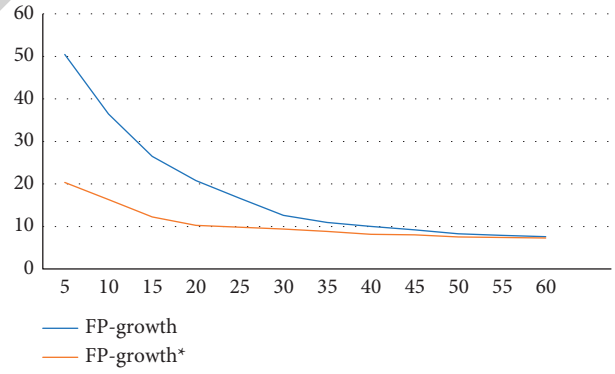

Figure 5: Performance comparison in time of c and FP-growth.

Hindawi
Journal of Mathematics
Volume 2023, Article ID 9810127, 1 page
https://doi.org/10.1155/2023/9810127

Retraction

Retracted: The Application of "Internet+" in the Ageing Adaptation of Elderly People with Disabilities at Home

Journal of Mathematics

Received 19 December 2023; Accepted 19 December 2023; Published 20 December 2023

This article has been retracted by Hindawi following an investigation undertaken by the publisher [1]. This investigation has uncovered evidence of one or more of the following indicators of systematic manipulation of the publication process:

(1) Discrepancies in scope

(2) Discrepancies in the description of the research reported

(3) Discrepancies between the availability of data and the research described

(4) Inappropriate citations

(5) Incoherent, meaningless and/or irrelevant content included in the article

(6) Manipulated or compromised peer review

The presence of these indicators undermines our confidence in the integrity of the article's content and we cannot, therefore, vouch for its reliability. Please note that this notice is intended solely to alert readers that the content of this article is unreliable. We have not investigated whether authors were aware of or involved in the systematic manipulation of the publication process.

Wiley and Hindawi regrets that the usual quality checks did not identify these issues before publication and have since put additional measures in place to safeguard research integrity.

We wish to credit our own Research Integrity and Research Publishing teams and anonymous and named external researchers and research integrity experts for contributing to this investigation.

The corresponding author, as the representative of all authors, has been given the opportunity to register their agreement or disagreement to this retraction. We have kept a record of any response received.

References

[1] H. Juan, L. Li, M. Jiasong, Z. Lifang, and H. Baoying, "The Application of "Internet+" in the Ageing Adaptation of Elderly People with Disabilities at Home," *Journal of Mathematics*, vol. 2021, Article ID 6074643, 6 pages, 2021.

Hindawi
Journal of Mathematics
Volume 2021, Article ID 6074643, 6 pages
https://doi.org/10.1155/2021/6074643

Research Article

The Application of "Internet+" in the Ageing Adaptation of Elderly People with Disabilities at Home

Huang Juan,[1] **Li Li**,[1] **Mai Jiasong**,[2] **Zhang Lifang**,[3] **and Huang Baoying**[1]

[1]*Department of Special Education, Guangxi College for Preschool Education, Nanning, Guangxi 530022, China*
[2]*People's Hospital of Yongning District, Nanning City, Nanning, Guangxi 530299, China*
[3]*Nursing School, Youjiang Medical University for Nationalities, Baise, Guangxi 533000, China*

Correspondence should be addressed to Huang Juan; hj@ymun.edu.cn

Received 16 November 2021; Revised 30 November 2021; Accepted 4 December 2021; Published 16 December 2021

Academic Editor: Naeem Jan

This paper focuses on the role of the Internet in empowering social work to intervene in ageing-in-place services for the disabled elderly in terms of time, space, and resources. Through the practical analysis of home care service providers, the advantages and characteristics of the "Internet" for ageing-in-place services for the disabled elderly are identified, as well as some of the problems that exist in the current intelligent home care service platform. This paper proposes to improve and optimize the "Internet+" by fully enhancing the technical empowerment of the Internet, improving the integration and spanning of space, and giving full play to the role of social work on the Internet. This paper proposes to improve and optimize the "Internet+" elderly home care services for the disabled, so as to solve to a certain extent the practical problems faced by the "Internet+" elderly home care services in the early stage of development. The significance of this paper is that, through the study of the "Internet+" home care services for the elderly with disabilities, the process of the services is sorted out and summarized, and suggestions and measures are put forward for its shortcomings, providing practical methods and feasible paths for future generations, which are of great significance for other social work agencies using Internet tools.

1. Introduction

By the end of 2019, China had 176 million elderly people aged 65 and above, accounting for 12.6 percent of the total population. As the population ages, the number of disabled elderly people in China is increasing year by year. The 2016 data show that there are 40.63 million disabled elderly people in China, and the size of the disabled elderly population will expand to 61.68 million in 2030. With this, the demand for daily care for the disabled elderly is on the rise, and long-term care services in China are in short supply, making long-term care for the elderly a serious social problem [1, 2].

The rapid onset of ageing has led to a dramatic weakening of the family's elderly care function in China at this stage [3], with families themselves finding it difficult to take on the role of caring for the elderly, especially the disabled. At the same time, however, China's entire public elderly care industry is still in its infancy, the market for elderly care is still being explored, resources for nursing homes are scarce and costs are high, and the traditional Chinese concept that elderly people prefer to spend their old age at home and are less willing to go to nursing homes has led to a more obvious home-based nature of the elderly care sector in China. However, for the disabled elderly, ageing in place faces many challenges such as lack of care, lack of attention, and unmet spiritual needs. Along with the development of social services, especially professional social services, and with the continuous promotion of relevant government policies, more and more people, enterprises, and nonprofit organizations are joining the home care service, gradually becoming the main force of home care in China now.

Based on the intervention of social work, this paper uses Internet technology as a working vehicle to broaden the scope of social support networks for the disabled elderly, improve the efficiency of social support networks, and expand the social and environmental resources needed by the

disabled elderly. This study is of great theoretical value to the study of social work intervention in the home care of the elderly with disabilities. At the same time, the integration of the professional, humanistic, and ethical nature of social work with the timeliness, instrumentality, and extensibility of Internet technology is also of some significance to the research on the integration of social work services with the Internet.

The breakthroughs in technological tools on the Internet and the integration of these breakthroughs with existing services offer new possibilities for addressing the diverse needs of older people, especially those who are disabled [4, 5]. Likewise, this high degree of integration will lead to the satisfaction of the needs of the elderly with disabilities, the achievement of organizational efficiency, and operational goals, as well as the realization of the professional value of social work in helping people to help themselves, which will become a key focus point for the industry to break through the barriers to development and will give a strong impetus to the development of the elderly services industry. This will provide a new solution to the current and future problem of home care services for China's large elderly population, especially the rapidly growing number of disabled elderly people. In Section 2, some of the basic concepts and technologies related to our study are reviewed. In Section 3, the main theme of the paper is discussed, which comprises of the problems that elderly people with disabilities have to face. Moreover, the provision of their needs is also discussed. Section 4 presents the application of "Internet+" in the ageing adaption of elderly people with disabilities at home. In Section 5, the paper is concluded.

2. Related Technologies and Concepts

2.1. "Internet+" Concept. The concept of "Internet+" has not been around for very long, and different scholars have different views on its definition, so it is easy to see that it is still a concept that is constantly being discussed and explored. The first aspect is to emphasize the impact of the Internet in the economic sphere, which is usually referred to as "Internet+traditional industries," which in fact means that traditional industries are combined with the Internet in a deeper way by relying on new technologies and developing new forms of innovation [6, 7]. It is a new way of combining traditional industries with the Internet in a more profound way, innovating and developing new forms to further enhance the transformation of traditional industries. The other side of the coin focuses on the infinite power of the Internet+ in the social sphere, as the main grip of information technology today. It is not only a tool for communication, but it has even reshaped the links and roles of traditional political, social, and economic relations. The "Internet+" is driving the deepening of new models of relationships, whether as governments, societies, or markets, which need to emerge with innovative organizational models to adapt to the new environment.

The "Internet+" technology is a new kind of information technology developed on the basis of computer technology. It consists of software, hardware, and applications. Software refers to a variety of software that can collect, retain, search, analyses, apply, and evaluate information. Hardware refers to the mainframe and network communication facilities where data are stored, processed, and transmitted. Applications refer to the use of software or supporting technologies such as ERP to assist decision makers in developing strategies. However, some professionals combine "Internet+" technologies with hardware and software to refer to the preservation, processing, and delivery of information, while applications are the use of information. However, some professionals also combine applications with software, often ignoring the applications, but in reality, only by using information sufficiently can the capabilities of Internet+ technology be demonstrated and truly connected to the information age.

2.2. Community Public Service. Community public services refer to nonexclusive ones. The main providers of community public services (usually the government) use certain organizations and methods to achieve the needs of community life and work and provide noncompetitiveness in a certain area or a larger area [8, 9]. Welfare goods and services are social public services given to the community as a whole. Community public services in our country have always been a combination of nonprofit and commercial services, a combination of comprehensive and regional services, and the services of cities, streets, and neighborhood committees complement each other.

3. The Main Problems and Needs of the Disabled Elderly in Providing for the Aged

3.1. The Main Problems in Providing for the Disabled Elderly

3.1.1. Life Care Issues. For the disabled elderly at home, their daily life, including food, clothing, shelter, and transportation, must rely on the help of others to complete. With the continuous degradation of their physiological functions and the relatively weak welfare system and life service facilities in rural areas, their daily care problems have become the first serious problem they have to face at home without the care of their children [10, 11]. Especially, in emergencies and acute diseases, it is difficult to get a timely response, which leads to the expansion of the consequences of the accident and the inability to treat the disease in time, thereby threatening the health and safety of the disabled elderly. Figure 1 shows the difference in the care time of the family members of the disabled elderly at home with different levels of disability. It can be clearly seen that severely disabled people are mostly taken care for 4 hours, while the mildly incapable people get the least care as compared to the other two cases.

3.1.2. Emotional Deficit Issues. As a social animal, sociality is the basic attribute that distinguishes man from animals. In traditional societies, the family, as the basic unit of social composition, carries the most basic function of social interaction and is also the most stable and convenient place for

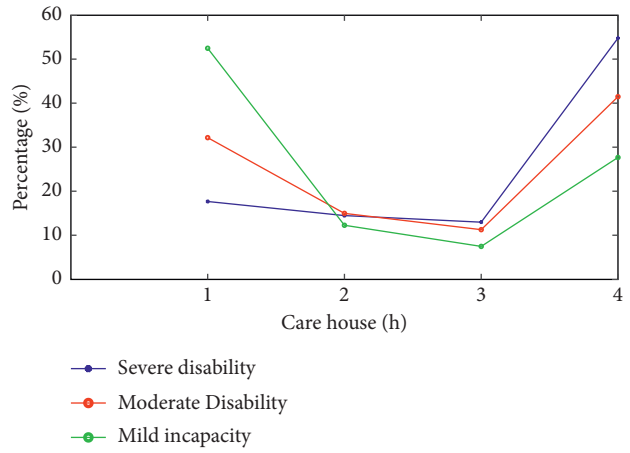

Figure 1: Differences in family caregiving time for older people with different levels of disability at home.

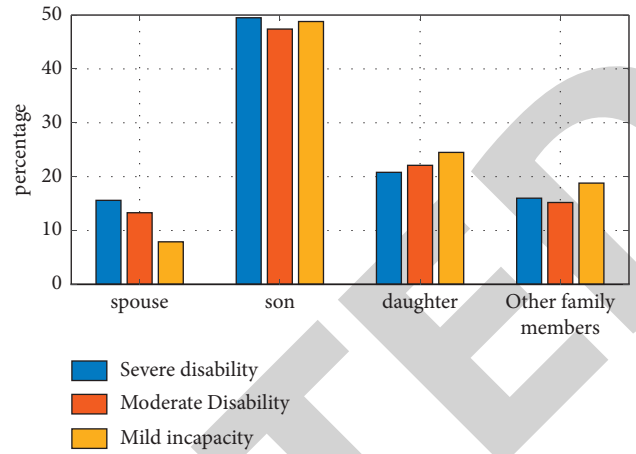

Figure 2: Differences in sources of emotional support for older people with different levels of disability at home.

individual people to obtain emotional support. The traditional family structure, where children and even grandchildren live with the elderly, provides great emotional support and satisfaction for the elderly through long lasting interaction and a multilayered family composition. With the continuous development of social and economic development, especially in modern society where the pace of work and life is accelerating, young people are under greater mental and financial pressure and are less and less willing to communicate with the elderly, and the time and frequency of communication are decreasing, which determines that the traditional emotional support function of the family is being weakened. The most direct consequence of this weakening is a greater lack of emotional support for the elderly. Figure 2 shows the differences in the sources of emotional support for older people with different levels of disability at home.

3.1.3. Mental Illness Issues. Long-term emotional deprivation, loneliness, and frustration caused by living alone, coupled with a range of emotions triggered by unexpected events, leaves older people without emotional outlet and communication for a long time. This coupled with the fact that the elderly is in a period of transition and adjustment from social life and work and the psychological discomfort caused by the change in social role can easily lead to psychological disorders in the disabled elderly if these problems remain unresolved for a long time.

4. The Application of "Internet+" in the Ageing Adaptation of Elderly People with Disabilities at Home

In this section, the "Internet+" has been applied to study the services and gadgets that elderly people with disabilities adapt at the home. The main topics covered in this section are the analysis of structure of "Internet+" home care service model, running through the home care services by the "Internet+" social workers for the elderly disabled people, and safeguard measures for the applications of "Internet+."

4.1. Structural Analysis of the "Internet+" Home Care Service Model. In the 21st century and especially in recent years, as mobile Internet technology has matured and infrastructure has been improved, various internet-based interactive platforms have been built to provide panoramic coverage of various life scenarios of the general public. For the elderly sector, Internet-based support platforms have also emerged and are becoming an important tool to support the market expansion and daily business development of elderly institutions today. The relevant roles and institutional components of the Internet+application are shown in Figure 3. It comprises of seven components, i.e., operators, service centers, service providers, family members, doctor, community standards, and volunteers. Figure 4 shows some of the Internet health component devices for elderly people with disabilities. Five different gadgets have been listed that are blood pressure and blood glucose meters, oximeters, urine testers, smart watches, and smart mattresses.

We prefer to define traditional services for the elderly as labor intensive. The labor-intensive nature of the service industry is characterized by the need to invest a lot of manpower and time, low service efficiency, and relatively low input and output, which in turn makes it impossible for most of the organizations involved in elderly services to make a sustainable profit, let alone expand the scale of services and the industrial chain. Traditional services for the elderly with disabilities also have problems such as untimely information transmission, difficulties in optimizing the allocation of service resources, low effectiveness of continuous services, and weak support networks. However, with the introduction of an intelligent elderly service platform, the convenience, immediacy, and comprehensive resources of Internet technology have provided a new way and path to solve the traditional problems of home services for the elderly with disabilities.

4.1.1. Support the Multidirectional Extension of the Network. Through the construction of the "Internet+" intelligent home care service platform, each disabled home elderly person who participates in the platform does not just

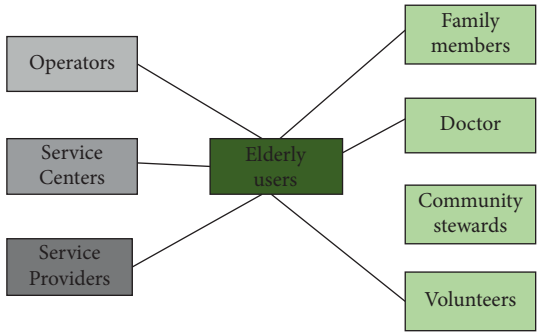

Figure 3: Composition of relevant players and institutions in "Internet+" applications.

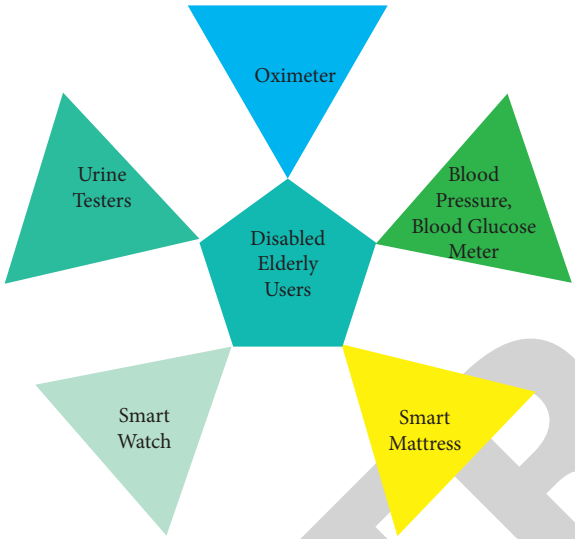

Figure 4: Some of the Internet health component devices for elderly people with disabilities.

become a basic member of the elderly service center, but more meaningful is the huge social support network that is accessed behind this membership network [12, 13]. The eight service areas of mobility, medical care, meals, family support, shopping, emergency assistance, and fun and travel assistance allow the disabled elderly to access a rich network of professional resources at home with just a smartphone and a mobile web platform. This network provides access to the resources they need, and through the continuity of membership, they continue to benefit from a stable, rich, and diverse network of support.

A stable, rich, and diverse network of support (Figure 5) shows the "Internet+" application model diagram.

4.1.2. Round-the-Clock Emergency and Response. Being alone at home is the biggest safety hazard for elderly people with disabilities who age at home. On the contrary, even if the information is passed on, traditional elderly care services or relatives of the elderly cannot provide timely feedback and assistance. The 24-hour emergency response system of the intelligent elderly care platform provides a strong guarantee for solving emergency emergencies for elderly people who

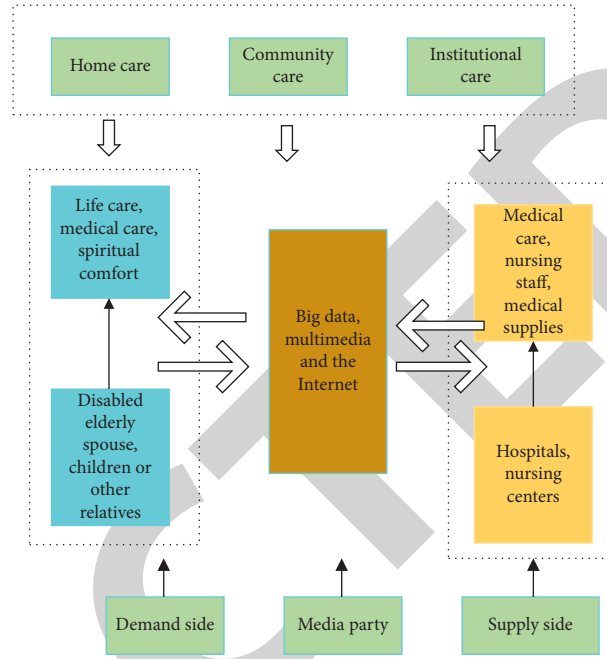

Figure 5: Map of the "Internet+" application model.

are living at home [14, 15]. Through the intelligent senior care service platform, the disabled elderly can transmit information through the mobile software and receive assistance within a limited period of time. The intelligent senior care service platform allows the elderly empty nesters to transmit information via mobile software and receive feedback and services within a limited period of time.

4.1.3. Service Efficiency Improvements. The most distinctive feature of the "Internet+"-based senior care service platform is the high level of integration and refined allocation of resources, which, based on a large user base, can continuously reduce marginal costs and deepen the rational allocation of resources. Once the planning effect is formed, the original service links and processes will be changed, which will also bring about an increase in efficiency. It can effectively solve the drawbacks of high-service costs and the inability to achieve scale development due to the scattered living and diversified needs of elderly people living at home. At the same time, through the rational deployment and use of the online platform, the resources of the organization can be maximized and optimized.

4.2. Practice of Home Care Services for the Disabled Elderly by the "Internet+" Social Workers. The application of "Internet+" to long-term care for older people with disabilities requires the use of artificial intelligence, big data, and the Internet of Things to build this comprehensive service platform. It is designed to meet the needs of the elderly as far as possible and to receive, store, and feedback information about the disabled elderly via the Internet. Figure 6 shows the design of the service platform for the "Internet+" application.

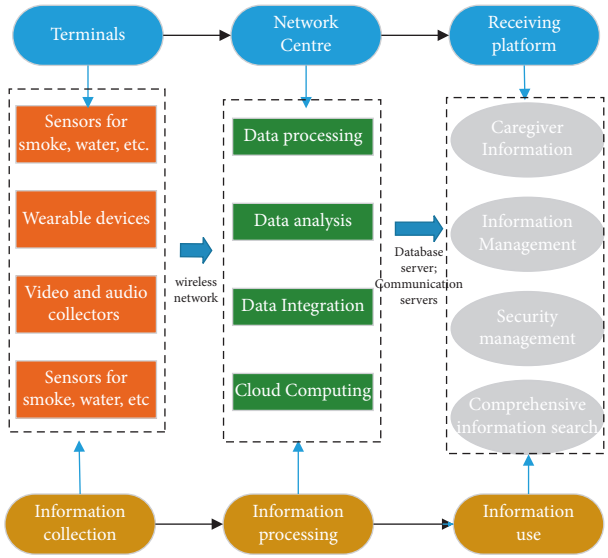

Figure 6: Design of the service platform for "Internet+" applications.

The terminals are used to capture the needs of older people, to sense their behavior, and to sense their surroundings. The care services are mainly provided by the elderly care service center, which provides the caregiver with a positioning device, such as a simple positioning bracelet or mobile phone, so that once the elderly person requests care, the service center can select the nearest person to the elderly person's home for notification based on the positioning. With the development of intelligent networking, personal information needs to be fully grasped and protected against leakage. Firstly, there is a need to register all care service center staff and the elderly with disabilities in their real names. Secondly, the service center can analyse the time, number, and content of calls from the elderly to find out what the elderly need and what they are potentially looking for so that they can change from a passive service to an active one. Finally, the children of the elderly can check the health and living conditions of the elderly at anytime and anywhere through their registered accounts so that they can work outside without worries.

The biggest difference and innovation between the Internet and the traditional network are that a virtual space has been constructed through network technology. In this space, everyone can connect across space with those who can be connected within the network through the network factor, while people who were originally distributed relatively far apart in physical space can quickly gain access to each other through the network platform of the Internet. Similarly, in another dimension, people from different spaces can form a kind of fork in the network and rely on this integration of different dimensions and the formation of various fork connections, forming a complete system similar to the offline one. However, unlike the offline system, this Internet-based virtual platform also virtualizes the space requirements, solving the inconvenience and problems caused by space, which is the weakest part of the service system for the elderly with disabilities. For the intelligent ageing-in-place service platform, the service status has been changed from the original point-to-point offline space to a point-to-point mode with virtual vouchers on the Internet, which has greatly improved the efficiency and timeliness of social worker services. More importantly, the integration of this space allows social workers to take the first step in transforming their identity. Through the construction of a virtual space and in the virtual network space, social workers have the opportunity to build an online domain containing various elements such as psychological counselling, spiritual solace, daily life information enquiry, daily care, and accident response. Within this space, the social worker coordinates the space of all parties involved in the field in a timely manner to ensure that the daily services for the elderly with disabilities are met. Free from spatial constraints in some respects, the integration of the multidimensional space provides a solid foundation for the services for the elderly with disabilities.

4.3. Safeguard Measures for "Internet+" Applications. Solving the problem of elderly people with disabilities is a matter of social development and stability, and it is a necessary path for our entire social system to self-improvement, self-growth, and self-healing. Due to their physiological, psychological, social, and family characteristics, most of the social support networks of the disabled elderly are in a state of extinction and disintegration. Under such circumstances, helping the disabled elderly to reconstruct their external social support networks to replace their own internal support networks and thus to meet the needs of the empty nesters, is one of the most important aspects of home care services for the empty nesters nowadays. As Internet technology continues to mature and Internet platforms continue to innovate, a wide range of organizations involved in the elderly care industry have begun to actively embrace the Internet, giving full play to the Internet's tool attributes and resource integration capabilities to continuously optimize the model of home care for the elderly with disabilities, in order to solve the problem of home care services for the elderly with disabilities.

4.3.1. Improving the Technological Empowerment of the Internet. As a technology tool, the Internet is essentially a platform for sharing information and connecting multiple parties through the construction of an online contact platform, a connection that transcends time and especially physical space. In addition, the Internet itself has the functions of resource integration, process management, and optimal allocation of resources. These attributes of technology have solved many of the problems previously faced by social work in the process of home care services for the elderly with disabilities and have improved the entire home care service system. It provides a scientific, reasonable, and sustainable solution for solving the challenges of the elderly with disabilities, improving the happiness index of the elderly with disabilities in their twilight years, and safeguarding their immediate survival interests and living

Hindawi
Journal of Mathematics
Volume 2024, Article ID 9814325, 1 page
https://doi.org/10.1155/2024/9814325

Retraction

Retracted: An English Online Homework Tutoring System Supported by Internet Database

Journal of Mathematics

Received 30 January 2024; Accepted 30 January 2024; Published 31 January 2024

This article has been retracted by Hindawi following an investigation undertaken by the publisher [1]. This investigation has uncovered evidence of one or more of the following indicators of systematic manipulation of the publication process:

(1) Discrepancies in scope

(2) Discrepancies in the description of the research reported

(3) Discrepancies between the availability of data and the research described

(4) Inappropriate citations

(5) Incoherent, meaningless and/or irrelevant content included in the article

(6) Manipulated or compromised peer review

The presence of these indicators undermines our confidence in the integrity of the article's content and we cannot, therefore, vouch for its reliability. Please note that this notice is intended solely to alert readers that the content of this article is unreliable. We have not investigated whether authors were aware of or involved in the systematic manipulation of the publication process.

In addition, our investigation has also shown that one or more of the following human-subject reporting requirements has not been met in this article: ethical approval by an Institutional Review Board (IRB) committee or equivalent, patient/participant consent to participate, and/or agreement to publish patient/participant details (where relevant).

Wiley and Hindawi regrets that the usual quality checks did not identify these issues before publication and have since put additional measures in place to safeguard research integrity.

We wish to credit our own Research Integrity and Research Publishing teams and anonymous and named external researchers and research integrity experts for contributing to this investigation.

The corresponding author, as the representative of all authors, has been given the opportunity to register their agreement or disagreement to this retraction. We have kept a record of any response received.

References

[1] H. Hao, "An English Online Homework Tutoring System Supported by Internet Database," *Journal of Mathematics*, vol. 2021, Article ID 5960185, 12 pages, 2021.

Hindawi
Journal of Mathematics
Volume 2021, Article ID 5960185, 12 pages
https://doi.org/10.1155/2021/5960185

Research Article

An English Online Homework Tutoring System Supported by Internet Database

Huanxiang Hao

School of International Education, Jiaxing Nanyang Polytechnic Institute, Jiaxing 314001, China

Correspondence should be addressed to Huanxiang Hao; 11603029@zju.edu.cn

Received 29 October 2021; Revised 23 November 2021; Accepted 24 November 2021; Published 14 December 2021

Academic Editor: Naeem Jan

College English tutoring is an important content of current research, and how to provide more effective methods for teaching tutoring is currently a hot research topic. Therefore, this paper designs an Internet-based online tutoring platform for college English teaching, which is accelerated by using the K-means clustering algorithm. The data processing efficiency and processing methods to improve user satisfaction require more practical experience to summarize. In the business logic layer, the uploaded information is mined through the K-means clustering algorithm to form an online tutoring university English database to provide platform data support, realize the business logic judgment of the data, convert the data in the database, and return to the user interface of other formats, to provide users with browsing and consulting. In the data access layer, the data from the business logic layer is processed. After the processing is completed, data can be added, deleted, modified, and checked in the database. Finally, the operation result of the database is fed back to the business logic layer for processing. Experimental results show that the designed platform has good data mining performance, low connection speed and low response delay, good compatibility, low CPU usage, fast resource sharing speed, and high user satisfaction. It can be connected to different operating systems.

1. Introduction

In traditional English education, teachers are the source of knowledge, and students learn English by receiving the information provided by teachers. As a teaching recipient, students are only in a passive position to accept knowledge in English teaching, and their initiative cannot be fully mobilized. The quality of teaching is usually evaluated by students' English learning achievements, which leads to an overemphasis on scores and only paying attention to the education of a few top-notch students, which hurts the self-esteem of most students and ignores the development and cultivation of most students' abilities [1]. From this point of view, this is a great waste of educational resources and strangles students' personalities and creativity.

As early as the 19th century, Issac Pittman proposed the first generation of Network Teaching—correspondence education. With the rapid development of multimedia technology, multimedia classrooms have been widely established in many colleges and universities. Many courses are carried out in multimedia classrooms. The teaching mode of English courses has changed from traditional classroom teaching to computer-aided teaching based on multimedia classrooms. In the process of English teaching, teachers use multimedia equipment to show students the English teaching content of pictures, texts, sounds, and images through multimedia courseware and other multimedia materials, so that students can be influenced by them and receive information in an all-round way, to achieve good English teaching effect. However, there are some shortcomings in this teaching mode: firstly, multimedia English teaching has a large amount of information dissemination, students have to listen carefully in class, many students do not have the habit of taking notes, and some students try to take notes but often cannot keep up with the progress of teachers' lectures, which is not conducive to students' self-study review after class. Secondly, by using multimedia English teaching, class teachers have to put the required teaching courseware and other materials on a mobile storage device, which is portable and very inconvenient. Thirdly,

there is no improvement in interaction with students [2–4]. In view of the above problems, some teachers make personal home pages to provide students with English learning materials after class, answer students' questions, and regularly update the content of personal home pages. Every time they update the home page's content, they must use HTML editing tools to modify the home page, which is very inconvenient.

In recent years, the rapid development of Internet technology has declared that human beings have entered the "information age." "Global village" has been accepted by most people. With the rapid development of multimedia technology and network technology, network learning has become possible. It breaks the boundaries of the traditional campus and can create a broader and diversified learning environment without time and space constraints. The network can make learners more actively participate in and enhance their interest in learning and achieve non-real-time teaching. Therefore, with the development of network technology, online teaching platforms based on the Internet are an effective auxiliary teaching tool and the best way to achieve information exchange and resource sharing. From this aspect, Luo Xian studied the university's SPOC-based public curriculum information teaching platform, and Jia et al. designed the Android-based physics mobile learning platform of the university, but they had obvious pertinence [5, 6]. Meanwhile, security and online communication are also important issues in the field of online teaching. Thus, we have to strictly protect data communication network maintenance and security management during online teaching to ensure that the learning platform is safe and efficient. In the face of the development of English education for online education, it is necessary to develop a more personalized online tutoring teaching platform for college English. With the help of the online tutoring teaching platform of college English, students can change their passive learning into active learning of English at any time in the network environment. In this platform, students are the center of teaching. Students carry out personalized learning so that teachers and students break through the limitations of time and place in the communication process. In the network English teaching, the contradiction between fewer class hours and a substantial increase in teaching information is well solved. The contradiction between a substantial increase in the number of students and few teaching staff members is solved. The online tutoring teaching platform of college English can cultivate students' ability to acquire knowledge by using the network and promote the cultivation of students' independent spirit and cooperative quality. Recently, mobile learning has grown in popularity and complexity with the proliferation of mobile devices and online video services [7]. New challenges include the multitude of mobile devices with different characteristics and limitations and the exponential growth in educational multimedia content. While several adaptive m-learning systems have been previously proposed, none of these has thoroughly addressed the adaptation of educational multimedia content. Moldovan and Muntean [8] propose the novel DQAMLearn framework to support mobile learners' seamless access to educational multimedia content from various mobile devices with different characteristics. Meanwhile, mobile devices have become more affordable and powerful, and an increasing range of rich media applications could offer mobile users a highly realistic and immersive experience. However, this comes at the cost of very stringent Quality of Service (QoS) requirements, putting significant pressure on the underlying networks. Comşa et al. [9] propose an innovative machine learning-based scheduling solution that supports increased quality for live omnidirectional (360°) video streaming to accommodate this new rich media application and overcome its associated challenges.

For online tutoring, the data objects of college English are divided into k clusters based on the K-means clustering algorithm, which is conducive to the formation of each group in line with the conditions that the objects in the same collection are very close and the things in different clusters are completely different. The clustering algorithms can be conducted to form each group in line with the conditions that the objects in the same collection are very close and the things in different clusters are completely different. The main assumption of DBSCAN [10] is that two dense regions are separated by one sparse region. Since DBSCAN works with density, it can easily model nonglobular structures. In addition, DBSCAN is better suited for datasets with disproportional cluster sizes and whose data can be separated in a nonlinear fashion.

However, existing models have a bottleneck of low efficiency in transmitting large amounts of data, which has a terrible effect on the quality of online tutoring. To improve the teaching effect of English tutoring, this paper designs an Internet-based online tutoring platform for college English teaching to speed up data processing efficiency and improve user satisfaction. The K-means clustering algorithm at the business logic layer is utilized to form an online tutoring college English database to provide data support for the platform. Meanwhile, it can realize the business logic judgment of the data, convert the data in the database, return to the user interface of other formats, and provide users with browsing and consulting. The main contributions of this work are as follows:

(i) An Internet-based online tutoring platform for college English teaching is designed to speed up data processing efficiency and improve user satisfaction

(ii) The K-means clustering algorithm at the business logic layer is utilized to form an online tutoring college English database to provide data support for the platform

The rest of this paper is organized as follows. The framework and technical details of our proposed system are described in Section 2. In Section 3, we present extensive experimental results to demonstrate the effectiveness of the proposed model. Finally, we conclude our work in Section 4.

2. Web-Based Online Tutoring Platform

In this section, different components of online tutoring platforms are described such as their basic structure, functional structure, database, and data mining and its algorithms.

2.1. Basic Structure of the Platform. In this paper, the development of online tutoring platform of college English is based on .NET three-tier architecture, namely, user interface layer, business logic layer, and data access layer. The user layer is at the top layer, and the user is the operator of this layer. This layer has a visible and user-friendly interface, through which users can safely operate the layer, and they cannot consider the implementation of this layer. The business logic layer of the platform is in the middle. In the operation interface, the data input by the user will be reflected in the business logic layer, and the obtained data will be judged by business logic. On the other hand, the data in the database will be converted into other formats by calculating the data. After returning to the user interface, it can facilitate user's browsing and consulting. What the function of the operation interface can realize can be explained by the business logic layer of the platform; the data access layer is at the bottom of the platform. After the data processing in the business logic layer is completed, the data in the database can be added, deleted, modified, or queried, and other operations can be performed. It needs to return the final database operation results to the business logic layer and then transfer the data operation results to the middle layer for processing [11, 12]. As shown in Figure 1, the overall architecture of the online tutoring platform of English teaching is shown.

Online tutoring platform of English teaching adopts .NET three-tier framework, mainly because it has the following advantages: the client and the system servers are directly connected, and there is no need to connect through other parts, so the response time of the system will be very short; the user interface is friendly and beautiful, and the interface style is changeable, which can meet the various needs of users; the transaction processing ability is relatively strong, and the complex business process can also be realized [13].

The separation of each layer is the biggest advantage of this framework, which can reduce the coupling between the functional modules to the maximum and fully practice the viewpoint of "low coupling, high cohesion" in software engineering [14]. According to the developer's point of view, this method is helpful to the change of business requirements of the system. When there is a change, there is no need to modify all the code, and the business logic can be adjusted accordingly. Therefore, the development efficiency of the program can be improved, and the development cost of the system can be reduced.

2.2. Design of Platform Functional Structure. In this paper, the role of online English tutoring platform for colleges and universities is divided into students, teachers, and administrators. There are four main function modules of the platform, which are teaching support, resource management, educational administration management, and platform management. After that, users can log in to the online English tutoring platform for colleges and universities according to their permissions. Figure 2 shows the main functional structure of the platform.

Among them, the role of the teaching support module is mainly teachers and students. After users log in to the platform, English teachers can manage the courseware online, arrange and modify the homework, and upload the relevant information of the courseware. Students can browse English course content, complete homework online, and address questions to teachers. The module mainly includes two submodules: course teaching and communication between teachers and students. The course teaching submodule has the functions of courseware browsing, course announcement, tutoring and answering, VOD on-demand, homework review, and so on. It can centrally manage the courseware resources that have been developed and formed. Students can browse the courseware according to the corresponding courseware address provided by the selected course, while teachers can browse the courseware according to the corresponding courseware address provided by the course and release an instant message about the course. Teachers upload auxiliary teaching documents, classic cases, and common questions and answers related to English courses for students to download and learn, and provide excellent teaching video resources of English for students and teachers; teachers arrange, correct, and analyze course assignments and browse the overall situation of assignments; students modify and submit assignments online and can browse teachers' comments to understand the mastery of knowledge points; teachers can input English test questions and answers through the platform, and students can choose the corresponding chapters to test. After the user logs on to the online tutoring teaching platform of college English, the platform will automatically track the user's operation and provide detailed attendance records and log reports at any time [15–17]. The submodule of the teacher-student exchange platform has the functions of classroom discussion and academic forum. Users can discuss and express their opinions on problems related to English courses, as the submodule provides a powerful online communication tool for teachers and students.

The resource module contains shared software resources and teaching material resources. The shared software resources are for all users and provide rich shared software resources for users. The teaching material resources are mainly for teachers and provide rich and diversified multimedia material resources to meet the teaching needs of teachers in developing network courseware [18, 19]. The module mainly consists of four parts: resource storage submodule, resource type management submodule, resource modification submodule, and resource retrieval submodule. The resource type management submodule is for system maintenance personnel, and the administrator can establish the resource directory according to the type and also has the operation authority to add, delete, and modify the resource directory; the resource storage submodule is for teachers and system maintenance personnel and can add various types of teaching resources to the resource database. The resource modification submodule is for teachers and system maintenance personnel. The author and administrator of the resource can modify the attributes of the resource, including description, type, author, size, and

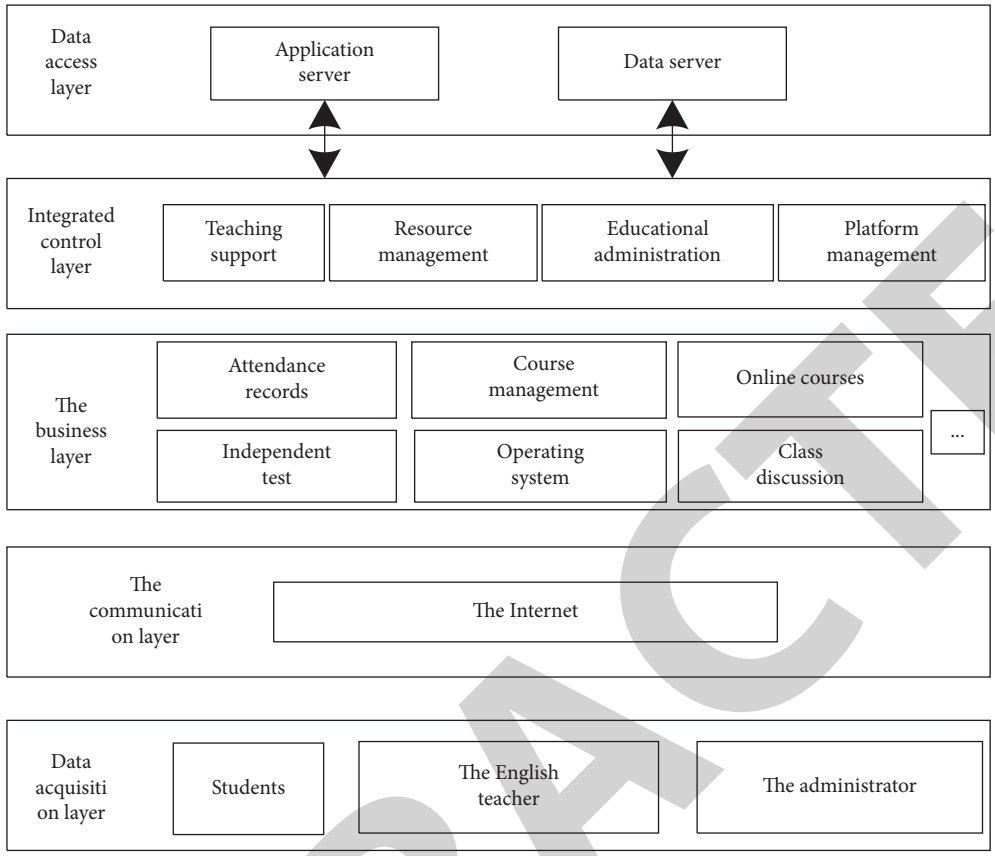

Figure 1: The overall structure of the Internet-based online tutoring platform of college English teaching.

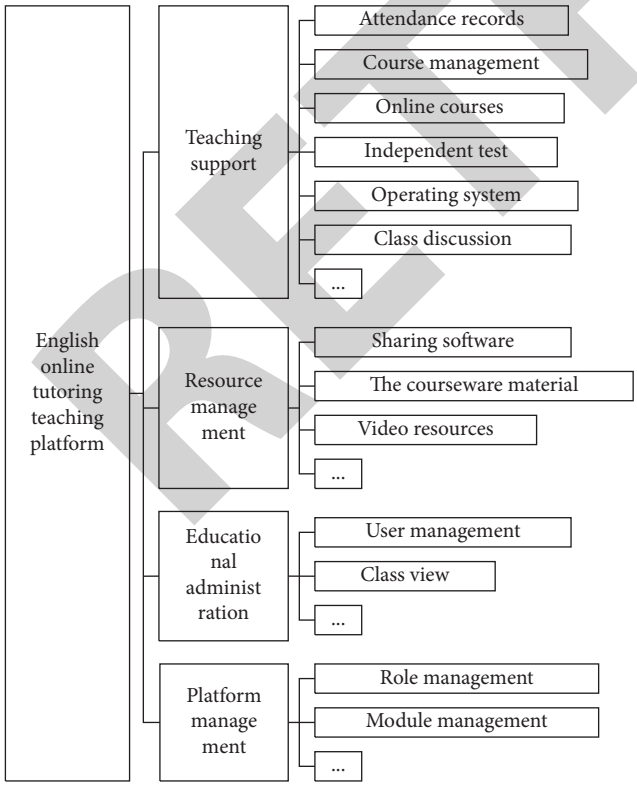

Figure 2: Main function structure of platform.

other related information or delete a resource record. The resource retrieval submodule searches the shared software resources for all users, and the teaching material resources are mainly for teachers. Full text retrieval based on representation is adopted in the retrieval, which has a variety of combination retrieval methods according to keywords and resource types.

Teaching management module mainly provides English teaching related management functions, including user management, course management, classroom observation, and other submodules. User management submodule is object-oriented for educational administrators and system administrators. User management is the management of system user information and permissions. The system includes user role management, user authority management, user role authority management, user password maintenance, and other functions [20]. The content of user management includes viewing the basic information of users and course selection, suspending the activation of an account, and resetting the user's password. The course resource management submodule includes adding and modifying new courses, setting course charges, and checking the payment of the students of the course. In the classroom observation submodule, the educational administrators can check the traditional classroom teaching arrangements of English courses after logging in.

The platform management module is for platform administrators, and its main functions include customizing system interface, customizing user permissions, and managing various function submodules, providing powerful functions for platform management and upgrading.

2.3. Design of Platform Database. In the database design work, platform developers abstract the relational database structure and internal relationship of the platform by establishing the E-R database model of the platform. The relationship correspondence between entities in the E-R model graph is the correspondence between parameters and the data table in the database, which can be divided into three types (1 : 1, 1 : M, M : N) [21] from the mathematical model. On the basis of E-R model, with the determination of each specific data table in the database, it can further get the detailed model of platform database composed of platform data table and its dependency. The platform database model composed of main data tables and their dependencies is shown in Figure 3.

2.4. Data Mining. For online tutoring, the data objects of college English are divided into k clusters based on the K-means clustering algorithm, which is conducive to the formation of each group in line with the conditions that the objects in the same collection are very close and the things in different clusters are completely different.

2.4.1. Framework of K-Means Clustering Algorithm. After users input data in the operation interface of the platform, K-means clustering algorithm is applied to mine data in the business logic layer to provide data support for the Internet-based online tutoring platform of college English teaching. This paper takes the number of clusters k of online tutoring data of college English as the goal of K-means and divides the data into k clusters, so that the data objects in the cluster are close to each other, while the data outside the cluster are far from each other. K-means clustering algorithm is to select k points as the initial cluster center, then calculate the distance between each sample and the cluster center, put the data object into the cluster center nearest to the data, and finally calculate the adjusted cluster center. If the two adjacent cluster centers do not change, the sample adjustment is completed, and the clustering criterion function has converged [22]. K-means clustering is simply a division of the set of data objects into nonoverlapping subsets (clusters) such that each data object is in exactly one subset, while hierarchical clustering is a set of nested clusters that are arranged as a tree. DBSCAN solves some of the problems of K-means by working with the density of points. This is a density-based method. The main assumption of DBSCAN is that two dense regions are separated by one sparse region. Since DBSCAN works with density, it can easily model nonglobular structures. Furthermore, DBSCAN is better suited for datasets that have disproportional cluster sizes and whose data can be separated in a nonlinear fashion.

K-means clustering algorithm belongs to dynamic clustering algorithm. The algorithm completes the iterative process by batch modification. Each iteration needs to reclassify data objects, and then use the adjusted classification to calculate a new clustering center and implement the next iteration. If all data objects are classified correctly in a certain iteration, it is not necessary to continue to implement the adjustment, and the clustering center is not changed, indicating that the algorithm has been completed and the clustering criterion function has converged [23]. The mathematical description of K-means clustering algorithm is as follows.

When clustering, the sample dataset $\{x_1, x_2, x_3, \ldots, x_n\}$ and the number of clusters k are determined, the initial data cluster center $\{c_1, c_2, c_3, \ldots, c_k\}$ is randomly selected in the sample dataset of k online tutoring data objects of college English, and the distance $D\{x_i, c_j\}$ between the remaining data objects and each cluster center is calculated $\{i = 1, 2, \ldots, n; j = 1, 2, \ldots, k\}$.

The Euclidean distance method is used to calculate the distance, and the equation is

$$D(x_i, c_j)' = \sqrt{(x_{i1} - c_{j1})^2 + (x_{i2} - c_{j2})^2 + \cdots + (x_{im} - c_{jm})^2}, \tag{1}$$

where $D\{x_i, c_j\}$ denotes the distance, x_i denotes the i-th sample, and c_j denotes the j-th cluster center.

If $D(x_i, c_j)$ satisfies the following equation:

$$D(x_i, c_j) = \min\{D(x_i, c_j)'\}, \tag{2}$$

Then the data object x_i of online tutoring of college English is classified into c_j clustering.

After the data objects are classified into the corresponding clusters, the new cluster center is recalculated according to the adjusted cluster, and the equation is

$$c_j^* = \frac{1}{n_j} \sum_{i=1}^{n_j} x_i^j, \tag{3}$$

where the number of online tutoring data objects of college English in c_j -cluster is n_j.

The criterion function J of the sum of squares of errors is calculated as follows:

$$J^* = \sum_{k=1}^{n_j} \sum_{j=1}^{k} \left\| x_k^j - c_j^* \right\|^2. \tag{4}$$

If $|J^* - J| < \xi$, the clustering criterion function converges, and the final clustering result is obtained; if $|J^* - J| > \xi$, the distance between the remaining data objects and each clustering center is calculated iteratively until $|J^* - J| < \xi$ is satisfied.

2.4.2. Process of K-Means Clustering Algorithm. The central idea of K-means clustering algorithm is to divide n online tutoring data objects of college English into k clusters, which is conducive to the formation of each cluster in line with the conditions that the objects in the same cluster are very close

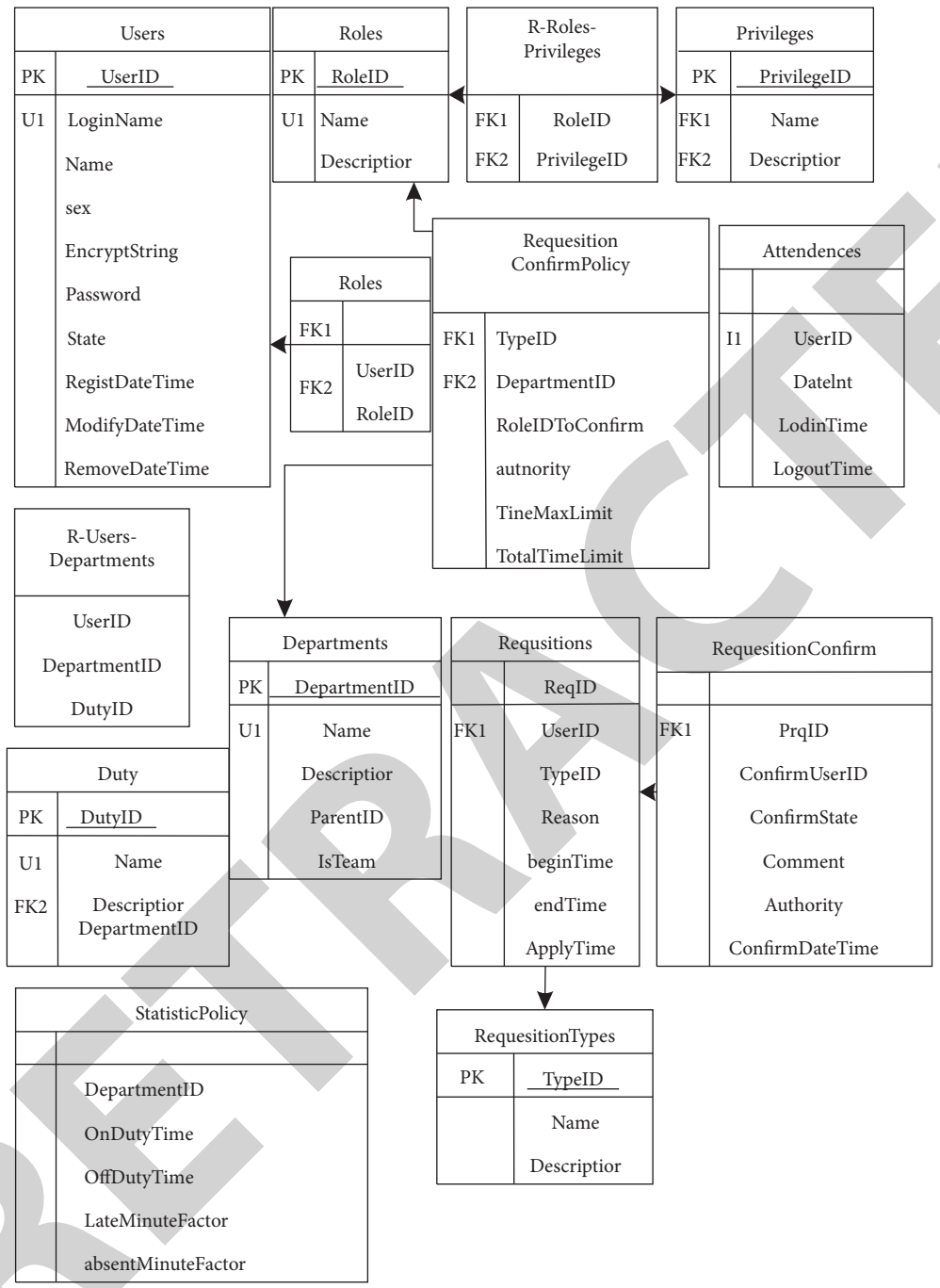

Figure 3: Diagram of platform database model.

and the objects in different clusters are completely different [24]. The input of K-means clustering algorithm is k clusters, in which the dataset has n objects; the output is k clusters where the final clustering center and data objects are located; Figure 4 illustrates the workflow of K-means clustering algorithm.

The processing steps of K-means clustering algorithm are as follows:

Step 1: the initial clustering center is k objects randomly selected in the sample dataset of n data objects

Step 2: calculate the distance between the remaining data objects and each cluster center, and assign the data objects to the nearest cluster

Step 3: after all data objects are allocated, recalculate the cluster center according to the new cluster

Step 4: compare the two adjacent cluster centers; if the cluster center changes, go back to step 2; if the cluster center does not change, continue to step 5

Step 5: output the cluster with k final clustering centers and data objects, that is, the final clustering result

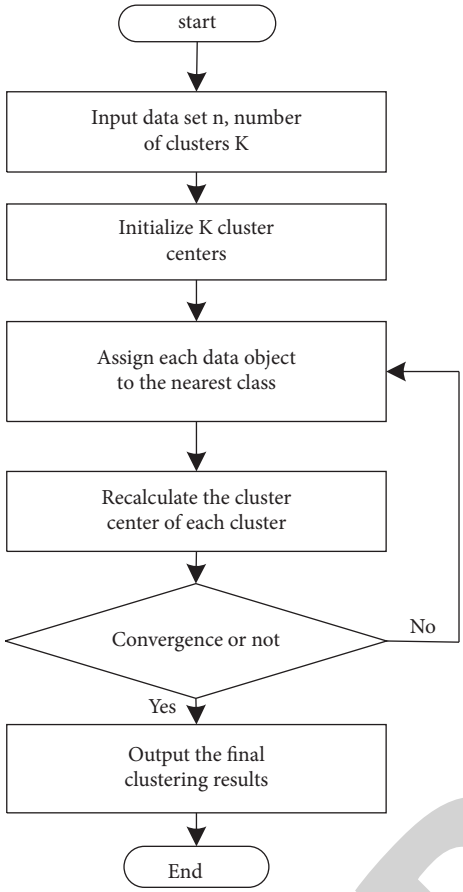

Figure 4: Workflow of K-means clustering algorithm.

3. Experimental Analysis

Taking a university in a province as the experimental object, this paper tests the function of the platform and transmits data through the Internet. There are 36887 English teachers and students in this university. The platform is put into use on March 1, 2019. Experiments are carried out using one GPU (GeForce GTX 1050 Ti) and an Intel Core i7 with 16 GB RAM system.

In order to verify the data mining ability of the platform in this paper, the following experiments are carried out. The collection time interval of online tutoring information features of college English is set as 100 s, the training set size as 500, the big data distribution length as 2000, and the code width of intelligent scheduling of online tutoring information of college English as 0.15 ms. The original data mined by this platform is shown in Figure 5.

As can be seen from Figure 5, the time-amplitude and frequency-amplitude fluctuations of this platform are relatively stable, which indicates that the platform in this paper can stably mine online tutoring information data of college English and has good data mining performance.

The connection speed delay response test of the platform can reflect the server configuration, the platform coding optimization, and the comprehensive performance of the platform running network environment. Three users are randomly selected to operate the platform, and the connection speed delay response of the platform is measured by testing the throughput of the user's operation process. The test results are shown in Figure 6.

Here, we conducted comparative experiments on the effect of platform connection delay response 8 times (as shown in Figure 6, Test1–Test8). It can be seen from Figure 6 that the throughput of the platform in this paper is above 1200/byte in 8 tests of 3 users, which is much better than the baseline models. This indicates that this platform's connection speed delay response is small and can meet the actual application requirements.

The time of HTTP timeout of the interface is set as 900 s, the execution time of the whole test is 44 minutes, the maximum number of users of the platform is 200, and the number of hits is 130606. Figure 7 shows the pressure curve of the platform. In the test, all cases of the platform are successful, and none of them fails. It can be seen from the pressure curve that the operating parameters of the platform conform to and meet the requirements of the Internet-based online tutoring platform of college English teaching.

Because the framework selected in the development process is universal, in order to ensure the maximum compatibility of the platform in this paper, the client access test of this platform is carried out through Windows XP, Windows 7, Linux kernel's Ubuntu, Red Hat, Debian, Apple's iOS, and other operating systems. Table 1 shows the compatibility test instructions.

According to the analysis of Table 1, the platform can be accessed normally through the browser on the above operating systems, and the platform compatibility is good, so there is no problem in the operating system test of the platform client.

The platform of this paper, university's public course information teaching platform based on SPOC and university's physics mobile learning platform based on Android are used to collect data and verify the accuracy of data collection results. The comparison platform is represented by the platform in [5]; the platform in [6], which is based on the analysis of the current situation of college physics teaching and the needs of students learning (a college-based physical mobile learning platform based on Android system is designed and developed in this paper, and it is also applied to the curriculum to be carried out in the teaching practice); the platform in [7], which is a type of Fab Lab-based learning system; and the platform in [8]. The data collection results of all platforms are shown in Table 2. It should be noted that the parameters of the baseline models are obtained from the corresponding papers. Meanwhile, we implement all models under the same hardware environment for guaranteeing fairness.

It can be seen from Table 2 that the data acquisition results of all platforms are different at different times. The data acquisition results of the platform in this paper are always higher than those of the other four platforms. Meanwhile, there is little difference between the data output and the input results, while there is a big difference between the input and output results of the other four platforms, which proves that the data acquisition results of this platform are effective and accurate.

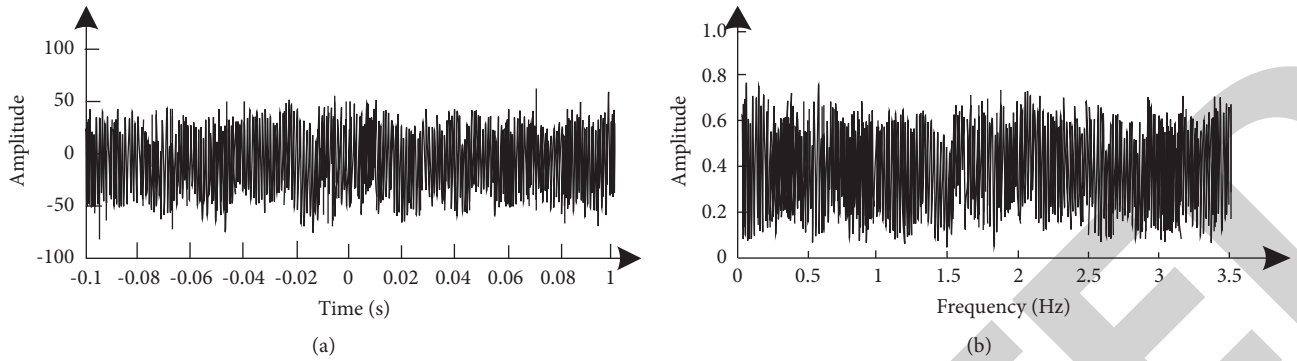

Figure 5: Results of innovation and entrepreneurship information mining: (a) time amplitude; (b) frequency amplitude.

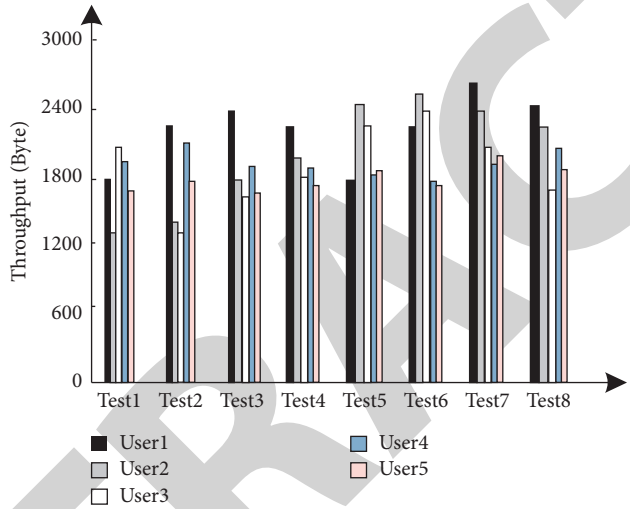

Figure 6: Test effect of platform connection delay response.

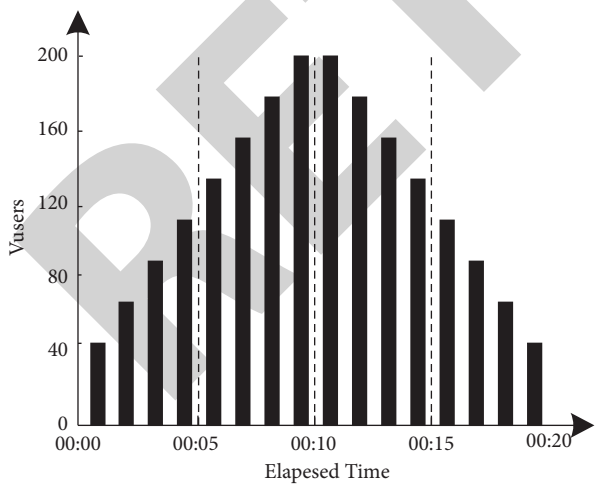

Figure 7: Pressure curve of platform operation.

To verify the stability of the platform, the CPU occupancy and network flow rate of the four platforms are compared. The results are shown in Tables 3 and 4.

According to Tables 3 and 4, the CPU occupancy range of [5] is 0.5~0.7, and the network flow rate range is 2800 kb/s~4000 kb/s; the CPU occupancy range of [6] is 0.4~0.5, and the network flow rate range is 1000 kB/s ~ 2500 kb/s; the CPU occupancy range of [7] is 0.3~0.5, and the range of network flow rate is 2500 kb/s~3700 kb/s; the CPU occupancy range of [8] is 0.4~0.5, and the network flow rate range is 1700 kb/s~3100 kb/s; and the CPU occupancy range of the platform in this paper is 0.3~0.4, and the network flow rate range is 5000 kb/s~6000 kb/s. Specifically, there are still problems of subjective ways and little entirely reasonable sampling in the model of [7], which results in a lower flow rate. The method in [8] is a kind of multiview based method, which has high computational complexity. Thus, the high requirements of the hardware in the synchronization method of [8] result in a lower flow rate. The CPU occupancy rate of the platform in this paper is the lowest among all platforms, the network flow rate is the highest, and the change range of this platform is small, which proves that the CPU occupancy rate of this platform is small and the resource sharing speed is fast and stable.

In order to test the practical application effect of the platform, six months after the platform was put into use, a questionnaire survey was started according to the voting function of the platform's personalized service. The four aspects of teaching support, resource management,

Table 1: Compatibility test description.

Use case number	D001	D002	D003	D004	D005
Use case description	IE6 + browses the system	Firefox browses the system	Safari browses the system	Chrome browses the system	Opera browses the system
Operation	Run the system using Internet Explorer 6	Run the system using the Firefox browser	Run the system using the Safari browser	Run the system using the Chrome browser	Run the system using the Opera browser
Expected	Normal operation display	Normal operation display	Normal operation display	Normal operation display	Normal operation display

Table 2: Data acquisition results of all platforms.

Time (min)	Bytes per second (k)									
	Platform of this article		Platform of literature [5]		Platform of literature [6]		Platform of literature [7]		Platform of literature [8]	
	Input	Output	Input	Output	Input	Output	Input	Output	Input	Output
5	179	189	121	101	59	71	135	125	156	114
10	250	250	201	209	238	238	215	215	178	158
15	255	182	131	151	90	180	196	180	221	215
20	265	265	112	120	15	15	169	172	236	226
25	270	270	78	150	15	15	202	15	239	229
30	280	220	158	99	161	101	223	220	252	248
35	285	300	260	240	261	301	256	251	261	258
40	285	280	180	150	250	240	198	198	268	225
45	290	280	250	300	285	180	253	256	285	270
50	295	295	133	170	200	265	156	153	298	299
55	300	300	300	240	300	299	256	256	299	299
60	300	300	190	158	299	300	163	163	300	300

Table 3: Comparison of CPU occupancy of all platforms.

Time (min)	CPU share				
	Platform of this article	Literature [5] platform	Literature [6] platform	Literature [7] platform	Literature [8] platform
5	0.361	0.500	0.412	0.374	0.422
10	0.363	0.550	0.421	0.431	0.431
15	0.363	0.570	0.418	0.454	0.438
20	0.362	0.568	0.416	0.466	0.436
25	0.363	0.568	0.408	0.458	0.438
30	0.363	0.568	0.405	0.465	0.435
35	0.364	0.600	0.400	0.463	0.430
40	0.364	0.653	0.454	0.454	0.454
45	0.363	0.651	0.459	0.459	0.459
50	0.364	0.622	0.460	0.460	0.460

Table 4: Comparison of network flow rates of all platforms.

Time (min)	Network flow rate (kb/s)				
	Platform of this article	Literature [5] platform	Literature [6] platform	Literature [7] platform	Literature [8] platform
5	5000	3000	1236	2582	1789
10	5125	2988	1651	2652	1982
15	5210	3250	2210	2556	2156
20	5182	3530	1000	2665	2262
25	5223	2800	1346	2685	2265
30	5734	3076	2500	2688	2568
35	5742	3561	1500	2788	2685
40	6000	3010	2100	2960	2695
45	5993	4000	1700	3652	2890
50	6000	3500	1800	3650	3006

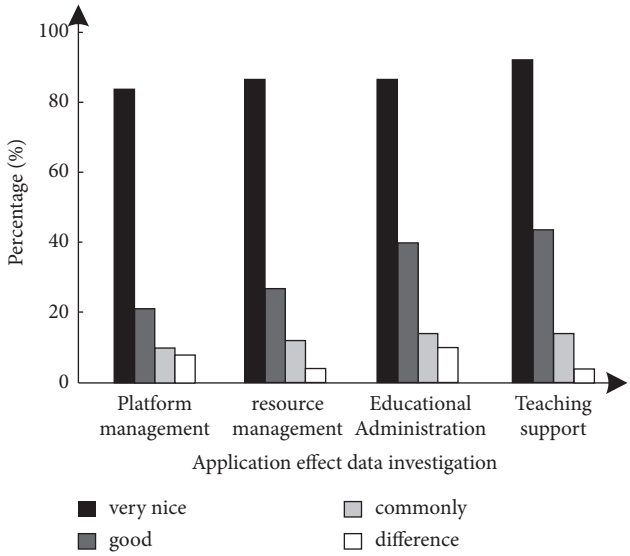

Figure 8: Investigation of application effect.

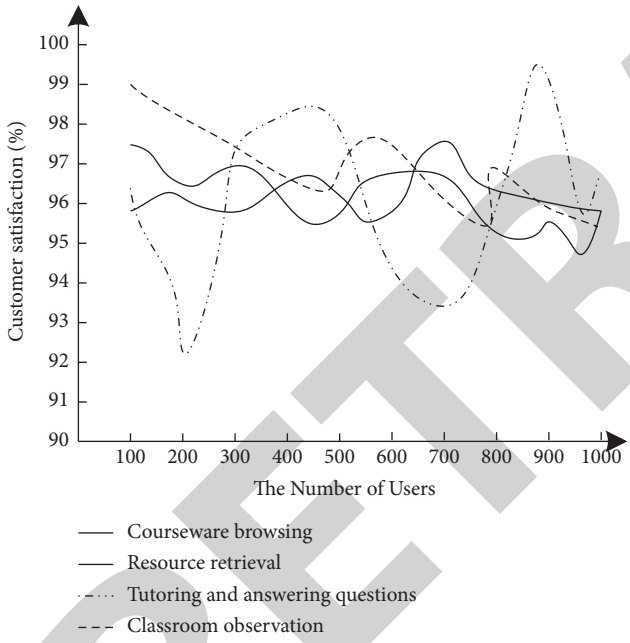

Figure 9: Customer satisfaction survey.

educational administration management, and platform management were investigated. The four voting options of "very good, good, average, and poor" were set. 300 users were randomly selected to conduct the questionnaire survey. The survey results are shown in Figure 8.

As can be seen from Figure 8, 89% of the users think that the teaching support module is "very good" and "good," only 5% think that it has no effect at present, and the other indicators of "very good" and "good" are more than 80%. Generally speaking, the Internet-based online tutoring platform of college English teaching is widely praised by users and has very good applicability; in particular, the teaching support module is the most recognized by users.

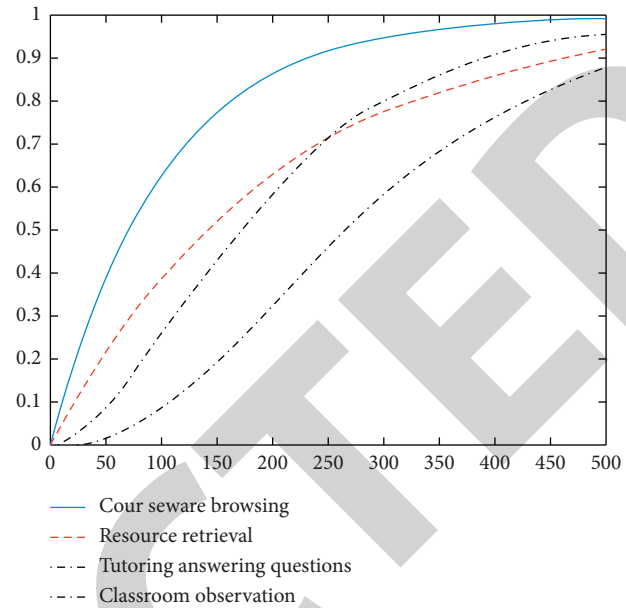

Figure 10: The cumulative distribution function of the user satisfaction.

The satisfaction with the platform function is investigated. To verify the superiority of the proposed model, we select 100 users to score the satisfaction with the platform after the operation. Certainly, the satisfaction with the platform scored by the users can help us to further perfect the accuracy and reliability of the system design. The satisfaction with the functions represented by courseware browsing, tutoring and answering, resource retrieval, and classroom observation is tested. The test results are shown in Figures 9 and 10.

The experiment investigates the users' satisfaction with the platform functions. The results show that the satisfaction of 100 users with the courseware browsing, tutoring and answering, resource retrieval, and classroom observation functions of the platform in this paper is more than 93%, indicating that the users are satisfied with this information service platform. Finally, according to the experimental results and the satisfaction with the platform scored by the users, we will make a great adjustment to the mode to perfect the structure of the mode so that it can be used easily by users in practice.

4. Conclusion

The focus of the current discussion is college English teaching. How to realize the function of online English tutoring and solve the problems that students and teachers may encounter in English learning and teaching has become a hot topic for scholars. Further optimization of the online tutoring platform for English teaching, under the premise of ensuring the stability of the platform, can also enhance the security of communication, data transmission, and data storage; vigorously promote the networked online tutoring platform for college English teaching to help students and teachers get rid of the traditional classroom; and improve the

subjective initiative of students and teachers in the process of work and learning. Since the experimental data is only the test data in the laboratory environment, more standardized and stricter network optimization and server deployment connection tests should be carried out after the platform is officially deployed to ensure that the response delay time of the platform is as short as possible. In addition, our method is to use data communication networks to maintain data security. However, our model also has some limitations. For example, our system lacks query functions and erased data recovery functions. Therefore, it is very important to improve system functions in the future.

Data Availability

The datasets used and/or analyzed during the current study are available from the author on reasonable request.

Conflicts of Interest

The author declares that he has no conflicts of interest.

Acknowledgments

This work was supported by the First Batch of Teaching Reform Projects in the 13th Five-Year Plan of Zhejiang Province Higher Education, "Research on the Evaluation System of International Ability in Higher Vocational Teaching of Chinese as a Foreign Language" (Grant no. jg20180821), and by Jiaxing Nanyang Polytechnic Institute, "Smart Teaching of College English Based on the Cultivation of International Innovative Talents Model Construction" (Grant no. p30017jg101) and "Testing to Promote Learning: Research on the Improvement of Vocational Students' Deep Learning Ability in the Realm of National Talent Examination" (Grant no. p30018ky011).

References

[1] F. H. Wang, "An exploration of online behaviour engagement and achievement in flipped classroom supported by learning management system," *Computers & Education*, vol. 114, pp. 79–91, 2017.

[2] R. A. Sottilare, R. S. Baker, A. C. Graesser, and J. C. Lester, "Special issue on the generalized intelligent framework for tutoring (gift): creating a stable and flexible platform for innovations in aied research," *International Journal of Artificial Intelligence in Education*, vol. 28, no. 2, pp. 139–151, 2018.

[3] Y. I. Dimitrienko, E. A. Gubareva, K. M. Zubarev et al., "Open BMSTU platform and teachers training in online courses development and implementation areas," *ITM Web of Conferences*, vol. 35, no. 2, Article ID 03015, 2020.

[4] E. A. Tarim and H. C. Tekin, "Performance evaluation of webrtc-based online consultation platform," *Turkish Journal of Electrical Engineering and Computer Sciences*, vol. 27, no. 6, pp. 4314–4327, 2020.

[5] Y. Jia and L. Zhang, "Research and application of online SPOC teaching mode in analog circuit course," *International Journal of Educational Technology in Higher Education*, vol. 18, no. 1, pp. 1–14, 2021.

[6] Y. Yu, "Design of mobile learning service platform based on data mining," *Journal of Physics: Conference Series*, vol. 1757, no. 1, Article ID 012134, 2021.

[7] M. A. Togou, C. Lorenzo, G. Cornetta, and G.-M. Muntean, "Assessing the effectiveness of using Fab lab-based learning in schools on K-12 students' attitude toward STEAM," *IEEE Transactions on Education*, vol. 63, no. 1, pp. 56–62, 2020.

[8] A. N. Moldovan and C. H. Muntean, "DQAMLearn: device and QoE-aware adaptive multimedia mobile learning framework," *IEEE Transactions on Broadcasting*, vol. 67, no. 1, pp. 185–200, 2020.

[9] I. S. Comşa, G. M. Muntean, and R. Trestian, "An innovative machine-learning-based scheduling solution for improving live UHD video streaming quality in highly dynamic network environments," *IEEE Transactions on Broadcasting*, vol. 67, no. 1, pp. 212–224, 2020.

[10] Y. Chen, L. Zhou, N. Bouguila, C. Wang, Y. Chen, and J. Du, "BLOCK-DBSCAN: fast clustering for large scale data," *Pattern Recognition*, vol. 109, Article ID 107624, 2021.

[11] X. Wang, Q. Tan, and M. Goh, "Attention-based deep neural network for internet platform group users' dynamic identification and recommendation," *Expert Systems with Applications*, vol. 160, no. 5, Article ID 113728, 2020.

[12] K. Xu, T. Li, H. Wang et al., "Errata to "modeling, analysis, and implementation of universal acceleration platform across online video sharing sites"," *IEEE Transactions on Services Computing*, vol. 11, no. 4, p. 740, 2018.

[13] W. Sheng, Y. Jing, and M. Qiang, "Design and implementation of learning platform based on MOOC model—take anhui sanlian university as an example," *China Computer & Communication*, vol. 11, 2019.

[14] D. Baneres and C. Robert, "Evaluation of a new self-study platform for introductory digital systems," *International Journal of Engineering Education*, vol. 35, no. 1, pp. 286–303, 2019.

[15] M. Mohd Yusof, N. Lee Wah, R. Mohamed, and M. Othman, "E-learning tutoring system for Sijil Pelajaran Malaysia (SPM) English," *MATEC Web of Conferences*, vol. 150, no. 5, Article ID 05001, 2018.

[16] X. Zhou, J. Wang, M. Guo, and Z. Gao, "Cross-platform online visualization system for open BIM based on WebGL," *Multimedia Tools and Applications*, vol. 78, no. 20, pp. 28575–28590, 2019.

[17] S. Benatti, F. Montagna, V. Kartsch, A. Rahimi, D. Rossi, and L. Benini, "Online learning and classification of emg-based gestures on a parallel ultra-low power platform using hyperdimensional computing," *IEEE Transactions on Biomedical Circuits and Systems*, vol. 13, no. 3, pp. 516–528, 2019.

[18] V. M. Ribeiro and L. Bao, "Professionalization of online gaming? theoretical and empirical analysis for a monopoly-holding platform," *Journal of Theoretical and Applied Electronic Commerce Research*, vol. 16, no. 4, pp. 682–708, 2021.

[19] W. Y. Liang, "The design of flash network courseware," *Advanced Materials Research*, vol. 933, pp. 720–722, 2014.

[20] B. Schiemer, S. Elke, and G. Grabher, "Collaborative innovation online: entanglements of making content, skills, and community on a songwriting platform," *Research in the Sociology of Organizations*, vol. 64, no. 293, p. 316, 2019.

[21] S. Chen, "Design of internet of things online oral English teaching platform based on long-term and short-term memory network," *International Journal of Continuing Engineering Education and Life Long Learning*, vol. 31, no. 1, p. 1, 2021.

Hindawi
Journal of Mathematics
Volume 2023, Article ID 9852630, 1 page
https://doi.org/10.1155/2023/9852630

Retraction

Retracted: A New Algorithm for Extracting Winter Wheat Planting Area Based on Ownership Parcel Vector Data and Medium-Resolution Remote Sensing Images

Journal of Mathematics

Received 19 December 2023; Accepted 19 December 2023; Published 20 December 2023

This article has been retracted by Hindawi following an investigation undertaken by the publisher [1]. This investigation has uncovered evidence of one or more of the following indicators of systematic manipulation of the publication process:

(1) Discrepancies in scope

(2) Discrepancies in the description of the research reported

(3) Discrepancies between the availability of data and the research described

(4) Inappropriate citations

(5) Incoherent, meaningless and/or irrelevant content included in the article

(6) Manipulated or compromised peer review

The presence of these indicators undermines our confidence in the integrity of the article's content and we cannot, therefore, vouch for its reliability. Please note that this notice is intended solely to alert readers that the content of this article is unreliable. We have not investigated whether authors were aware of or involved in the systematic manipulation of the publication process.

Wiley and Hindawi regrets that the usual quality checks did not identify these issues before publication and have since put additional measures in place to safeguard research integrity.

We wish to credit our own Research Integrity and Research Publishing teams and anonymous and named external researchers and research integrity experts for contributing to this investigation.

The corresponding author, as the representative of all authors, has been given the opportunity to register their agreement or disagreement to this retraction. We have kept a record of any response received.

References

[1] H. Xie, Q. Wu, T. Zhang et al., "A New Algorithm for Extracting Winter Wheat Planting Area Based on Ownership Parcel Vector Data and Medium-Resolution Remote Sensing Images," *Journal of Mathematics*, vol. 2021, Article ID 1860160, 16 pages, 2021.

Hindawi
Journal of Mathematics
Volume 2021, Article ID 1860160, 16 pages
https://doi.org/10.1155/2021/1860160

Research Article

A New Algorithm for Extracting Winter Wheat Planting Area Based on Ownership Parcel Vector Data and Medium-Resolution Remote Sensing Images

Huaming Xie,[1,2] Qianjiao Wu ,[2,3] Ting Zhang,[1,2] Zhende Teng,[1] Hao Huang,[1,2] Ying Shu,[1,2] Shaoru Feng,[1,2] and Jing Lou[4]

[1]*School of Environment and Energy Engineering, Anhui Jianzhu University, Hefei 230601, China*
[2]*Institute of Remote Sensing and Geographic Information Systems, Anhui Jianzhu University, Hefei 230601, China*
[3]*School of Public Policy & Management, Anhui Jianzhu University, Hefei 230601, China*
[4]*Remote Sensing Application Center, Ministry of Agriculture, Hefei Branch, Hefei 230601, China*

Correspondence should be addressed to Qianjiao Wu; qianjiaowu@ahjzu.edu.cn

Received 29 October 2021; Revised 22 November 2021; Accepted 24 November 2021; Published 14 December 2021

Academic Editor: Naeem Jan

In the complex planting area with scattered parcels, combining the parcel vector data with remote sensing images to extract the winter wheat planting information can make up for the deficiency of the classification from remote sensing images simply. It is a feasible direction for precision agricultural subsidies, but it is difficult to collect large-scale parcel data and obtain high spatial resolution or time-series remote sensing images in mass production. It is a beneficial exploration of making use of existing parcel data generated by the ground survey and medium-resolution remote sensing images with suitable time and spatial resolution to extract winter wheat planting areas for large-scale precision agricultural subsidies. Therefore, this paper proposes a new algorithm to extract winter wheat planting areas based on ownership parcel data and medium-resolution remote sensing images for improving classification accuracy. Initially, the segmentation of the image is carried out. To this end, the parcel data is used to generate the region of interest (ROI) of each parcel. Second, the homogeneity of each ROI is detected by its statistical indices (mean value and standard deviation). Third, the parallelepiped classifier and rule-based feature extraction classification methods are utilized to conduct the homogeneous and nonhomogeneous ROIs. Finally, two classification results are combined as the final classification result. The new algorithm was applied to a complex planting area of 103.60 km^2 in central China based on the ownership parcel data and Gaofen-1 PMS and WFV remote sensing images in this paper. The experimental results show that the new algorithm can effectively extract winter wheat planting area, eliminate the problem of salt-and-pepper noise, and obtain high-precision classification results (kappa = 0.9279, overall accuracy = 96.41%, user's accuracy = 99.16%, producer's accuracy = 93.39%, commission errors = 0.84%, and omission errors = 6.61%) when the size of ownership parcels matches the spatial resolution of remote sensing images.

1. Introduction

Accurate extraction of crop planting structure is fundamental to understanding the information of crop growth and yield and agricultural disasters, which have great value in formulating national agricultural policies and guaranteeing national food security [1–3]. With controllable costs, obtaining accurate crop planting areas of small peasant households for every season through remote sensing and geographic information technology is important to improve the precision and directivity of agricultural planting subsidies in the complex planting area [4].

There are numerous approaches for extracting crop planting areas using advanced remote sensing images from multiple sensors [5–10]. These approaches can be categorized as pixel-based, object-based, or a combination of the two [11]. Pixel-based methods consist of maximum likelihood classification [12–14], spectral angle mapper [15, 16], random forest classifier [17–20], support vector machine [21–23], tassel cap brightness–greenness–wetness [24, 25],

decision tree algorithm [26, 27], phenological algorithm [28–30], and machine learning algorithm [31–33]. Object-based methods include hierarchical image segmentation software [11, 34, 35] and rule-based feature extraction [36, 37]. Combining methods using object-based and pixel-based methods has been proposed to classify crops planting areas [38–40]. However, these methods are difficult to achieve breakthroughs in automatic classification and visual recognition of crop planting areas simply from the spectral information of remote sensing images in the scattered and small planting areas [41–44]. Combining the parcel data with remote sensing image to extract the structure information of crop planting can make up for the deficiency of the classification from remote sensing images simply and obtain better classification accuracy. It provides a simple and effective method to resolve the problems of spectral variation and spectral mixing in pixel-based classification methods and is a feasible direction for remote sensing of large-scale precision agricultural subsidies [45–49].

The idea of parcel-based crop planting classification originated by Derenyi [50], which is still a research hotspot in the field of remote sensing information extraction of crop planting. Recently, parcel-based crop planting classification research has focused on parcels obtained by vectorization or image segmentation [51–54]. Previous studies on parcel-based classification usually use digitization or image segmentation to extract the parcel data and use multispectral images or time-series images to carry out the crop planting classification with a variety of classifiers. It is difficult to collect large-scale parcel data. Moreover, incorporating high spatial resolution or time-series remote sensing images and parcel data is difficult to obtain remote sensing image in mass production and is not conducive to promotion and application. Recently, confirming and registering the contracted management rights of rural land in China have accumulated an amount of ownership parcel data, which provide an ideal data source for the parcel-based classification methods. It is a beneficial exploration of making use of existing parcel data generated by the ground survey and medium-resolution remote sensing images with suitable time and spatial resolution to extract crop planting information for large-scale precision agricultural subsidies [53–56].

Moreover, remote sensing images with different spatial resolutions have their own applicability and limitations in the crop planting classification [57, 58]. Remote sensing images with low spatial resolution have high temporal resolution and can cover a large region, but limited by the spatial resolution, there are many mixed pixels, and they can only be applied to extract crop planting areas roughly. Remote sensing images with high spatial resolution provide more abundant information about structure, texture, and geometry but generally have a low temporal resolution, making it challenging to obtain key phenological period images of different crops. In addition, using them multiplies the workload of data processing. Remote sensing images with medium spatial resolution have better accuracy and target recognition reliability. However, applied to mountains, hills, and other complex terrain regions with numerous mixed pixels, crop planting structures are insufficiently expressed and have low interpretation accuracy. It is possible to overcome this shortcoming if we combine the vector boundary information of the parcel with medium spatial resolution remote sensing images to extract crop planting areas.

Therefore, this study proposes a new algorithm for extracting winter wheat planting areas based on ownership parcel vector data and medium-resolution remote sensing images to improve the extraction accuracy. To verify its feasibility, accuracy, and applicability, the new algorithm was applied to a complex planting area of 103.60 km^2 in central China in 2018. Moreover, the matching relationship between the size of parcels and the spatial resolution of remote sensing images was discussed in this paper.

The paper is organized as follows: Section 2 describes the study area and data. The methods are presented in Section 3. The experimental results and discussion are given in Section 4. Section 5 concludes the paper and indicates directions for further research.

2. Materials and Methods

In this section, the methodology of the study and essential tools are elaborated.

2.1. Study Area. We selected a complex planting area of 103.60 km^2 in central China as the study area. The study area covers the 19 administrative villages of Fengle Town, in Feixi County, Hefei City, Anhui Province, China. It extends from 31°32′34.77″ to 31°39′29″ N and 117°2′10″ to 117°12′23″ E. The area's terrain is relatively flat, with a general trend of being lower from north to south. It is in a subtropical monsoon climate zone with the characteristics of remarkable monsoon climate, mild climate, moderate rainfall with an annual average of 1020.6 mm, adequate light, and a long frost-free period. It had a total population of 45,726 in 2017. The study area was registered as arable land with a total area of 6317.95 hectares in 2018. Because it is near the capital city of Anhui Province, there are more economic agricultural crops in the region. Production mainly uses small agricultural machinery and artificial operation modes. The structure of crop planting is more complex in the region, which is distributed in a scattered and discontinuous mode. Wheat, rice, and other food products are the main crops in this region, accounting for about 70% of the total crop planting area. There are also other crops, such as rape, cotton, vegetables, melons, and fruits. It is a typical region with a hilly landform and complex planting structure in the Yangtze River delta region. Extracting the winter wheat planting area in this region has certain representativeness and typicality by combining vector boundaries of ownership parcels and remote sensing images. Figure 1 displays the map of study area.

2.2. Data Processing. The components of data processing are described in this section.

2.2.1. Ownership Parcel Data. In January 2015, the Chinese Ministry of Agriculture, Ministry of Finance, and four other departments jointly issued their "opinions on earnestly

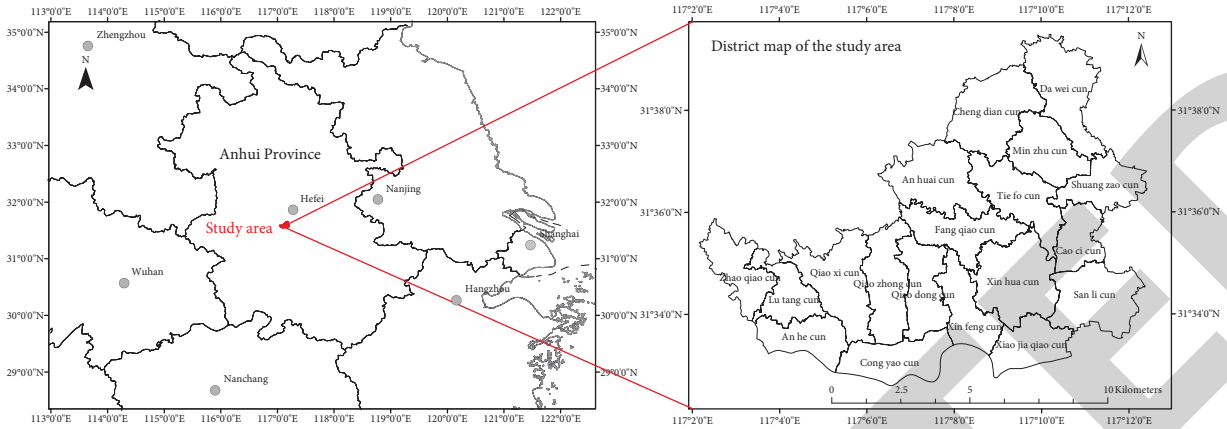

Figure 1: Location map of the study area.

confirming, registering, and certifying the contracted management rights of rural land" and required that the following be completed by the end of 2017: (1) carrying out a comprehensive inventory of land contract files and materials to find out the status of contracted fields; (2) mastering the situation of contracted peasant households, checking contractor representatives and family members, and collecting their changes and other information; and (3) investigating contracted field management rights to find out the ownership rights of contracted fields. The survey of contracted field status completed the geospatial information of all agricultural planting parcels and the corresponding contractor information. The survey of geospatial information and corresponding contractor information for all agricultural parcels was completed to investigate contracted field status. Figure 2 illustrates the ownership parcel map of the study area.

The land contractual management rights confirmation and registration database of the study area was collected from the Agriculture and Rural Affairs Bureau of Feixi County on December 31, 2017. Aerial remote sensing orthophoto images with 0.5 m spatial resolution were obtained at the end of 2017 and were matched with the collected data, as shown in Figure 2. This database contains class files of parcel elements and an attribute table of contracted parcels in shape (shp) format, the information of contractors in the table and access library, and other information. A unified query of "parcel code" and "contractor code" fields can obtain the spatial vector positions of all parcels and the ownership information of contracted farmers. The spatial vector and ownership information can be derived from the database. There was a total of 71,869 parcels, among which the minimum area was 10.98 m^2, the maximum area was 21,604.77 m^2, the average area was 879.09 m^2, and the standard deviation of the area was 850.37.

2.2.2. Medium Spatial Resolution Remote Sensing Images. We selected Gaofen-1 satellite panchromatic multispectral sensor (PMS) images with a spatial resolution of 8 meters from March 11, 2018, and wide field view (WFV) images with a spatial resolution of 16 meters from February 23, 2018. They are shown in Figure 3.

The Gaofen-1 satellite carries two 2 m panchromatic and 8 m multispectral cameras and four 16 m multispectral cameras. The sensor parameter information is shown in Table 1. PMS and WFV have four bands: red, green, blue, and near-infrared. The spectral reflectance of the green and near-infrared bands is sensitive to winter crops and can be beneficial in effectively identifying winter wheat. Images with 8 m and 16 m resolution are typical medium-resolution images, commonly applied to extract the structure information of winter wheat plantings in large regions.

We selected the most recognizable growing period of winter wheat in the Jianghuai region from February to March for the time phase of remote sensing images. In this region, winter wheat is sown in early November and harvested in mid-June. The seedling stage is from mid-December to mid-January. From early February to early April, the winter wheat returns to green for the jointing and heading stages. This is the time when it is the easiest to differentiate winter wheat in remote sensing images.

Gaofen-1 satellite images can be downloaded from the China Resources Satellite Ground Application Center (http://36.112.130.153:7777/DSSPlatform/index.html) for free. The data preprocessing of the two images included the following:

(i) Orthorectifying RPC points combined with 30 m DEM

(ii) Converting the coordinate system from the WGS-84 geographic coordinate system (GCS_WGS_1984) to the CGCS2000 geodetic coordinate system with a 3-degree Gaussian kriging projection coordinate system under a central longitude of 117′ E (CGCS2000_3_Degree_GK_CM_117E)

(iii) Utilizing accurately calibrated aerial remote sensing orthophoto images with 0.5 m spatial resolution, whose coordinate system is also CGCS2000_3_Degree_GK_CM_117E, to perform geometric precision correction of PMS and WFV images in order to keep the local error to less than 2 pixels and the average error less than 1 pixel

(iv) Clipping the two remote sensing images using the vector administrative region data of the study area

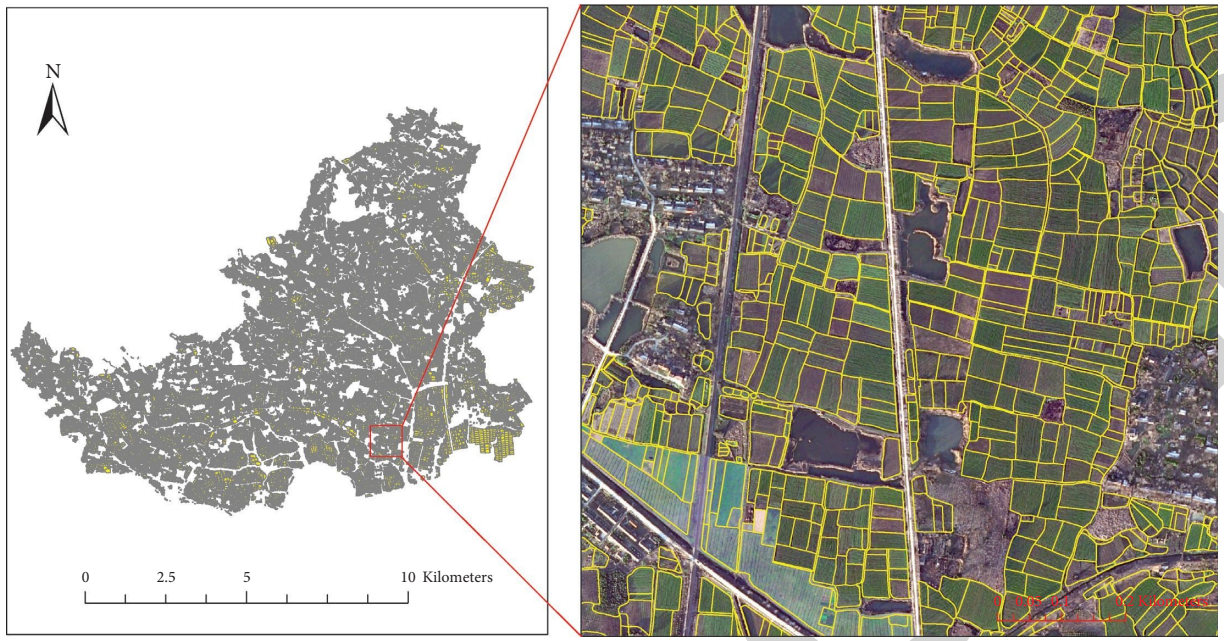

Figure 2: Ownership parcel data of the study area.

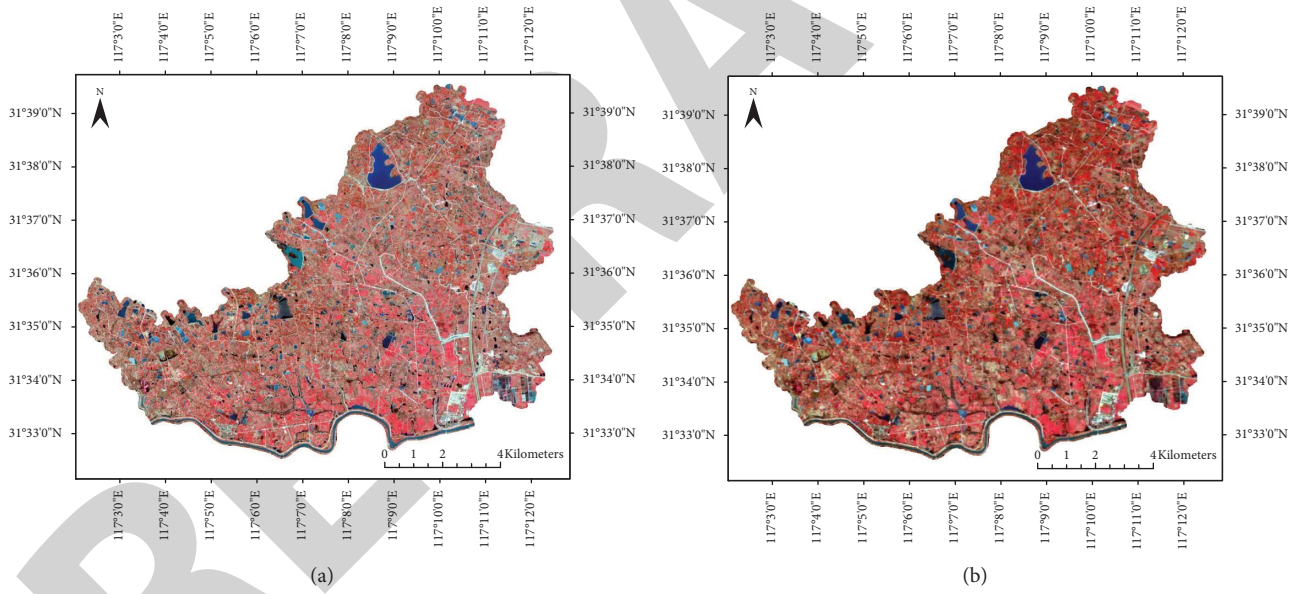

Figure 3: Remote sensing satellite images selected in this paper: (a) Gaofen-1 (GF-1) satellite PMS image with 8 m spatial resolution. (b) GF-1 satellite WFV image with 16 m spatial resolution.

Table 1: Sensor parameter information of Gaofen-1 satellite PMS and WFV images.

	Spectrum (μm)	Spectrum range	Spatial resolution (m)	Breadth (km)	Swinging ability	Revisit time (days)
Panchromatic multispectral camera	1	0.45~0.90	2	60 (two combination cameras)	±35°	4
	2	0.45~0.52	8			
	3	0.52~0.59				
	4	0.63~0.69				
	5	0.77~0.89				
Multispectral camera	6	0.45~0.52	16	800 (four combination cameras)		2
	7	0.52~0.59				
	8	0.63~0.69				
	9	0.77~0.89				

2.2.3. Sample Data of Crop Planting Conditions. There were 1,038 parcels or nonagricultural cropping samples for spring crop plantings in 2018 by field investigation. These parcels include 524 samples of winter wheat and 514 samples of other crops, noncrops, and noncrop nonagricultural plantings. There were 253 winter wheat samples used for information extraction of remote sensing images and 271 winter wheat samples for accuracy verification. There were 240 samples of other crops or noncrops used for classification and 274 samples for accuracy verification. The statistical data are shown in Table 2.

2.2.4. Relationship between the Size of Parcels and Spatial Resolution of Remote Sensing Images. There are some differences between the ownership parcel of small peasant households and those parcels obtained by vectorization or image segmentation. If the area of ownership parcels is small, there are the same crops of one season planted in the ownership parcels basically. The overall distribution of the size of parcels also affects the optimal spatial resolution of remote sensing images, because there should be enough pixels in the parcel. Thus, the optimal matching relationship between them needs to be further discussed.

There is a certain matching relationship between the size of parcels and the spatial resolution of remote sensing images. In general, if a parcel has purer pixels except for the boundary pixels, it is beneficial to classify different crops. However, if the parcel area is too large, it may have mixed cropping; there will be multiple crops within the parcel, which is not conducive to the winter wheat classification.

As shown in Figure 4 and Table 3, parcels of 200–500, 500–1,000, and 1,000–1,500 m^2 in the study area accounted for 28.82, 33.08, and 15.92%, respectively. Parcels with less than 1,500 m^2 accounted for 86.04%. This demonstrates that the parcels in this region were generally small and fragmented.

From Table 3, we can see that, for GF-PMS images, parcels with an area less than 200 m^2, accounting for 8.22% of the total, have a large majority of mixed pixels. Parcels with an area of 200–500 m^2, accounting for 28.82% of the total, have more mixed pixels. Parcels with an area of 500–3,500 m^2, accounting for 61.46% of the total, have purer pixels, and the pixels are relatively appropriate in these parcels.

For GF-WFV images, parcels with an area less than 1,000 m^2, accounting for 70.12% of the total, have a large majority of mixed pixels, which is not conducive to classification. Parcels with an area of 1,000–1,500 m^2, accounting for 15.92% of the total, have more mixed pixels. Parcels with an area of 1,500–3,500 m^2, accounting for 12.46% of the total, have purer pixels, and the pixels are appropriate to the parcels. For the two images, parcels with an area of more than 3,500 m^2, accounting for 1.50% of the total, have large areas and may be planted with mixed crops.

In theory, the GF-PMS (8 m) remote sensing image has a higher matching degree with the size of parcels in the study area, and the classification accuracy should be higher. The GF-WFV (16 m) image has a relatively low matching degree, which cannot reflect the advantages of combination classification. These are further validated later.

3. Methods

This research aimed to utilize ownership parcel data and medium spatial resolution remote sensing images to classify the winter wheat in the complex planting area accurately. The methodology adopted for this paper had 6 parts: (1) building the region of interest (ROI) to obtain the statistical indices; (2) detecting and determining the homogeneity of each ROI; (3) classifying the winter wheat within the homogeneous ROIs; (4) classifying the winter wheat within the nonhomogeneous ROIs; (5) selecting comparison classification methods; and (6) evaluating the classification accuracy. The specific steps of the combination classification are illustrated in Figure 5. IDL language and Envi software were implemented for coding and data processing.

3.1. Building the Region of Interest (ROI) to Obtain Statistical Indices. Due to the abundant spectral and textural features of different crops in remote sensing satellite images, these features are typically explored to design statistical indices to monitor winter wheat classes. However, classification results based on remote sensing images cannot focus on the ownership and management of crop planting regions. The ownership parcel data can make up for this deficiency.

Therefore, the ownership parcels were combined with the remote sensing images to build the regions of interest (ROIs), which have the spectral and textural features of the remote sensing images and all of the information of the ownership parcels. The remote sensing images were logically segmented by the ownership parcels, and a corresponding ROI was obtained for each parcel. The statistical indices of each ROI were extracted from the band spectrum digital number (DN) value of its corresponding remote sensing images and written into the attribute table of parcels. The statistical indices express the mean value and standard deviation of the DN values.

3.2. Detecting and Determining the Homogeneity of Each ROI. In general, the same crops may be planted in ROIs with a small area and belong to the same ownership contractor. There may be different crops planted in ROIs with a large area or in special cases. Thus, it is essential to detect whether the same crop is the winter wheat planted in the ROI. If it is determined that the same crop is planted, it can be considered in its entirety to judge whether it is the winter wheat. Otherwise, it is necessary to classify different crops to extract the planting area of the winter wheat.

Generally speaking, if the crop type of the ROI is consistent, its spectral value should be basically consistent. Therefore, it can be detected by the standard deviation of the spectral value. If the standard deviation of the spectral value of the ROI to be detected is less than K times the standard deviation of the sample, both the crop type and ROI are considered to be homogeneous. Otherwise, the parcel is regarded as a nonhomogeneous ROI. The detection formula is as follows:

Table 2: Statistical data for samples of crop planting conditions.

	Winter wheat (parcels)	Others (parcels or region)	Total
Classification samples	253	240	493
Accuracy verification samples	271	274	545
Total	524	240	1,038

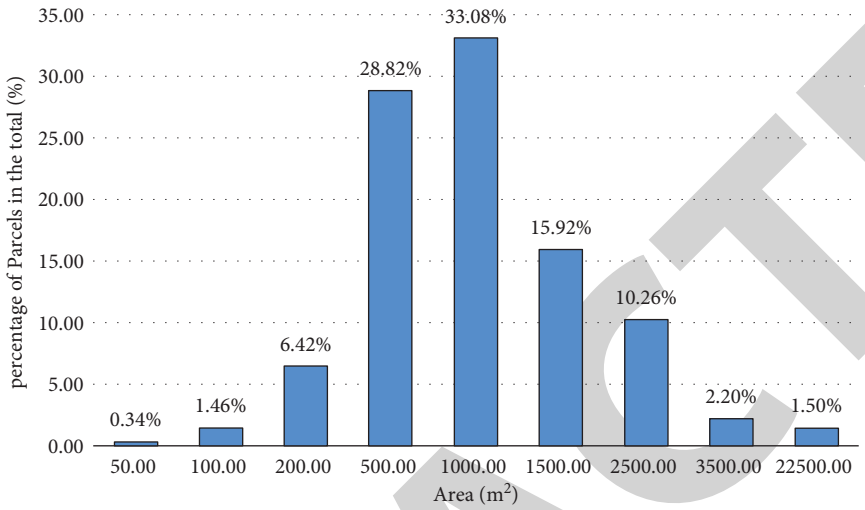

Figure 4: Histogram of the proportion of areas of ownership parcels.

Table 3: Matching between the area of ownership parcels and GF-PMS and GF-WFV images.

Parcel area (m^2)	Parcel number	Proportion (%)	GF-PMS (8 m) Parcel number	GF-PMS (8 m) Applicable situation	GF-PMS (8 m) Proportion sum (%)	GF-WFV (16 m) Parcel number	GF-WFV (16 m) Applicable situation	GF-WFV (16 m) Proportion sum (%)
0~50	241	0.34	1	Large majority of mixed pixels	8.22	1	Large majority of mixed pixels	70.12
50~100	1,052	1.46	1-2			1		
100~200	4,616	6.42	2–4			1		
200~500	20,715	28.82	4–8	More mixed pixels	28.82	1-2		
500~1,000	23,771	33.08	8–16			2–4		
1,000~1,500	11,443	15.92	16–24	More pure pixels (number of pixels in parcel is appropriate)	61.46	4–6	More mixed pixels	15.92
1,500~2,500	7,373	10.26	24–40			6–10	More pure pixels (number of pixels in parcel is appropriate)	12.46
2,500~3,500	1,583	2.20	40–55			10–14		
>3,500	1,075	1.50	55–352	Large area (there may be mixed crops)	1.50	14–88	Large area (there may be mixed crops)	1.50
Total	71,869	100	—	—	100	—	—	100

$$\left\{\begin{array}{l} B1i_{\text{stdDev}} \le K * B1s_{\text{stdDev}} \\ B2i_{\text{stdDev}} \le K * B2s_{\text{stdDev}} \\ B3i_{\text{stdDev}} \le K * B3s_{\text{stdDev}} \\ B4i_{\text{stdDev}} \le K * B4s_{\text{stdDev}} \end{array}\right\}, \quad (1)$$

where $B1i_{\text{stdDev}}$ denotes the standard deviation of band 1 for the ith ROI, $B1s_{\text{stdDev}}$ denotes the standard deviation of band 1 for the sample, and K denotes the threshold value of detecting the homogeneity of the ROI, regarded as a coefficient, which depends on the actual situation.

Because different ground features have different standard deviations, it is difficult to use a series of threshold values to examine the homogeneity of all ground features. A series of threshold values can only examine the homogeneity of one type of ground feature. In this paper, the threshold value of detecting the homogeneity of ROIs for GF-PMS and GF-WFV images was obtained by using K times the standard deviation of the classified samples, and K was tried with two numbers, 1.5 and 2. The detailed information is shown in Table 4.

3.3. Classifying the Winter Wheat within the Homogeneous ROIs. For homogeneous ROIs, it is only necessary to determine whether the planted crop is winter wheat. The parallelepiped classifier is utilized to classify the winter wheat for homogeneous ROIs in this paper. It calculates the mean value of each band of the ROI to be classified and then judges whether it is within the range of K times the mean value of the

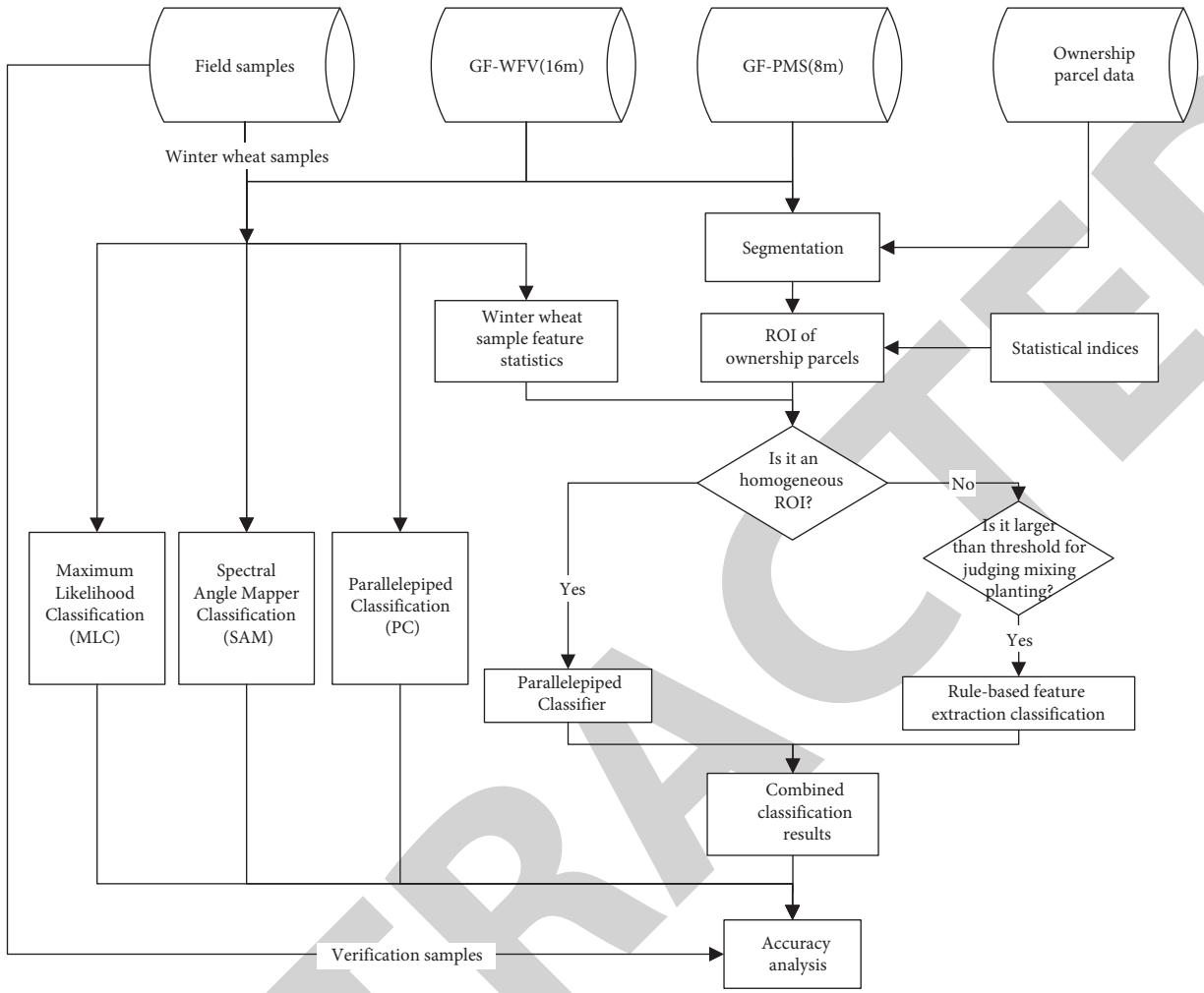

Figure 5: Flowchart of the new algorithm for extracting winter wheat planting area in this paper.

Table 4: Threshold of detecting homogeneity of ROIs for GF-PMS and GF-WFV images.

Band	Sample for GF-PMS		Threshold value	Sample for GF-WFV		Threshold value
	Mean	Std. dev.		Mean	Std. dev.	
B1 (blue)	387.87	16.28	ROUNDUP[2] (K ∗ 16.28, 0)	275.27	9.71	ROUNDUP (K ∗ 9.71, 0)
B2 (green)	378.81	24.53	ROUNDUP (K ∗ 24.53, 0)	252.90	16.83	ROUNDUP (K ∗ 16.8, 0)
B3 (red)	254.94	28.46	ROUNDUP (K ∗ 28.46, 0)	220.35	20.08	ROUNDUP (K ∗ 20.08, 0)
B4 (near-infrared)	553.54	69.87	ROUNDUP (K ∗ 28.46, 0)	339.84	37.91	ROUNDUP (K ∗ 37.91,0)

ROUNDUP (n, 0) indicates rounding up and keeping 0 decimal places.

standard deviation of the crop sample, shown as equation (2). If the mean value of all bands for the ROI is within the preset range, it is regarded as a homogeneous ROI.

$$\left\{\begin{array}{l} B1s_{\text{mean}} - K * \text{stdDev} \le B1i_{\text{mean}} \le B1s_{\text{mean}} + K * \text{stdDev} \\ B2s_{\text{mean}} - K * \text{stdDev} \le B2i_{\text{mean}} \le B2s_{\text{mean}} + K * \text{stdDev} \\ B3s_{\text{mean}} - K * \text{stdDev} \le B3i_{\text{mean}} \le B3s_{\text{mean}} + K * \text{stdDev} \\ B4s_{\text{mean}} - K * \text{stdDev} \le B4i_{\text{mean}} \le B4s_{\text{mean}} + K * \text{stdDev} \end{array}\right\}, \quad (2)$$

where $B1i_{\text{mean}}$ denotes the mean value of the standard deviation of band 1 for the ith parcel, $B1s_{\text{mean}}$ denotes the mean value of the standard deviation of band 1 for the sample, and K denotes the threshold for detecting the homogeneity of the ROI.

Figure 6 shows the spectral curves of the maximum value, sum of mean value and standard value, mean value, the difference between the mean value and standard value, and minimum value of the four bands of the samples for GF-PMS and GF-WFV images. It can be seen that the standard deviation is not large, although the maximum and minimum values of the wheat samples vary greatly in each band. The values of each pixel in the ROI are close to the mean value, so it is feasible to use the parallelepiped classifier to process homogeneous ROIs for the winter wheat classification.

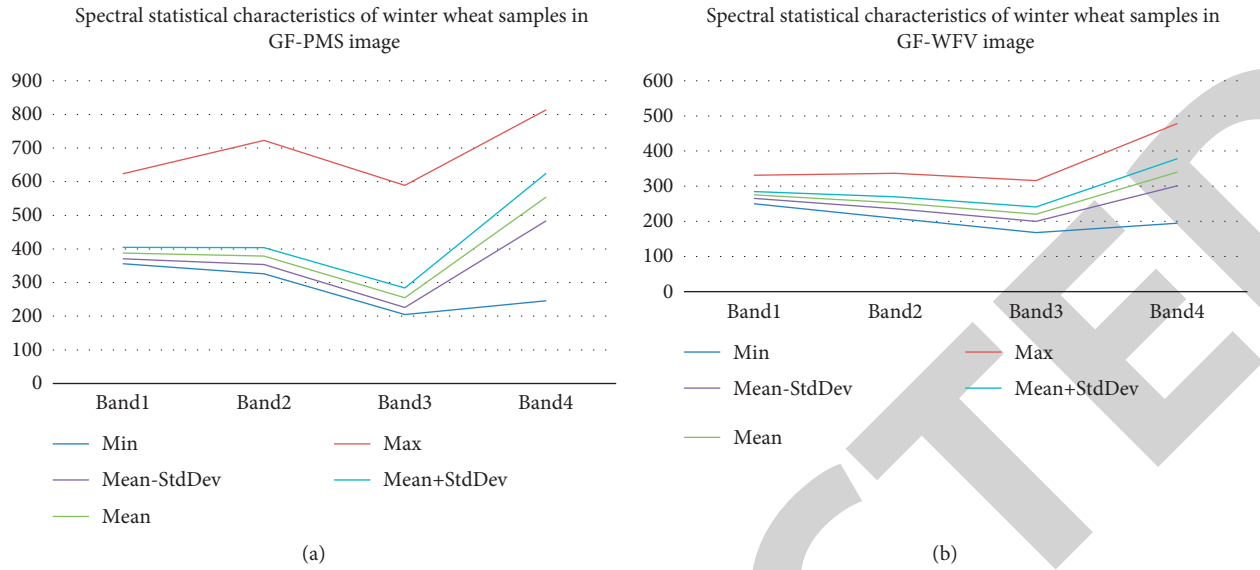

Figure 6: Statistical indices of various spectral bands of remote sensing images of winter wheat sample region: (a) GF1 PMS image; (b) GF1 WFV image.

3.4. Classifying the Winter Wheat within the Nonhomogeneous ROIs. Nonhomogeneous ROIs indicate that the planting area cannot be planted with the same crop. There are two cases to be discussed in this context. One case is that the area of the ROI is smaller than the threshold value (S_t) for judging mixing planting. There is a low probability of mixing planting, and it is directly judged like the other crops. The other case is that the area of the ROI is larger than the threshold value (S_t) for judging mixing planting. The ROI may be planted with different crops, and it is necessary to regard it as an independent image for pixel-based classification. The rule-based feature extraction classification method is adopted to deal with nonhomogeneous ROIs in this paper. Finally, the classification results for homogeneous and nonhomogeneous ROIs are combined as the final classification result. The threshold value for judging mixing planting (S_t) is used as the parameter and input in the specific operation.

In the study area of this paper, S_t is 3500 m^2 which has been analyzed through Section 2.3.2. The rule-based feature extraction method directly invokes the ENVI_FX_RULE-BASED_DOIT module in Envi ver. 5.3. The rule file is defined by the range of K times of the standard deviation of the mean value of the spectral value from winter wheat samples, similar to equation (2), which judges the mean value of the spectrum of the ROI, while it also judges every pixel in the ROI.

3.5. Selecting Comparison Classification Methods. In order to compare the accuracy of the new algorithm, this study selected the maximum likelihood classification (MLC), spectral angle mapper (SAM) classification, and parallelepiped classification (PC) methods for the GF-PMS and GF-WFV images in the study area. Different combinations of input parameters were also adopted for each method, as shown in Table 5.

3.6. Evaluating the New Algorithm's Crop Planting Classification Accuracy. The stratified sampling method was employed to evaluate the new algorithm's crop planting classification accuracy. A total of 271 samples of wheat planting parcels and 274 samples of other ground features were used to verify the accuracy in this study. The kappa, overall accuracy, user's accuracy, producer's accuracy, and commission and omission errors [59, 60] were calculated from the established error matrix of each classification method.

Because the 253 classified wheat samples could comprehensively cover the actual surface state of wheat parcels, it was difficult for the 240 other samples to fully cover images on the entire actual surface state of non-wheat parcels due to their numerous actual feature states, and in the accuracy evaluation, the unclassified category in the classification results is also classified as "other" before the accuracy evaluation.

4. Results and Discussion

The entire study area in this research is 103.60 km^2 and the total area of the ownership parcels is 6317.95 hectares. According to the statistics from the agricultural department, the sowing area of winter wheat in the spring of 2018 was 1226.90 hectares. This was approximated by the proportion of winter wheat acreage planted in several sampled small regions and is regarded as the reference area.

Field survey samples were used to classify GF-PMS and GF-WFV images in the study area using the four methods with ten parameters. Figures 7 and 8 show the best classification results on the GF-PMS and GF-WFV images for each method. The classification accuracy and planting areas of winter wheat from different classification methods were calculated and are shown in Table 6.

Table 5: Threshold of detecting homogeneity of ROIs for GF-PMS and GF-WFV images.

Classification method	Corresponding parameters
Maximum likelihood classification (MLC)	Probability threshold 0.8 (single value)
	Probability threshold 0.9 (single value)
Spectral angle mapper (SAM) classification	Maximum angle 0.1 (single value)
	Maximum angle 0.15 (single value)
Parallelepiped classification (PC)	Max std. dev. from mean 1.5 (single value)
	Max std. dev. from mean 2 (single value)
	Max std. dev. from mean 1.5, 0 (multiple value: 1.5 for wheat, 0 for others)
	Max std. dev. from mean 2, 0 (multiple value: 2 for wheat, 0 for others)
New algorithm	$K = 1.5$; $S_t = 3500\,m^2$
	$K = 2.0$; $S_t = 3500\,m^2$

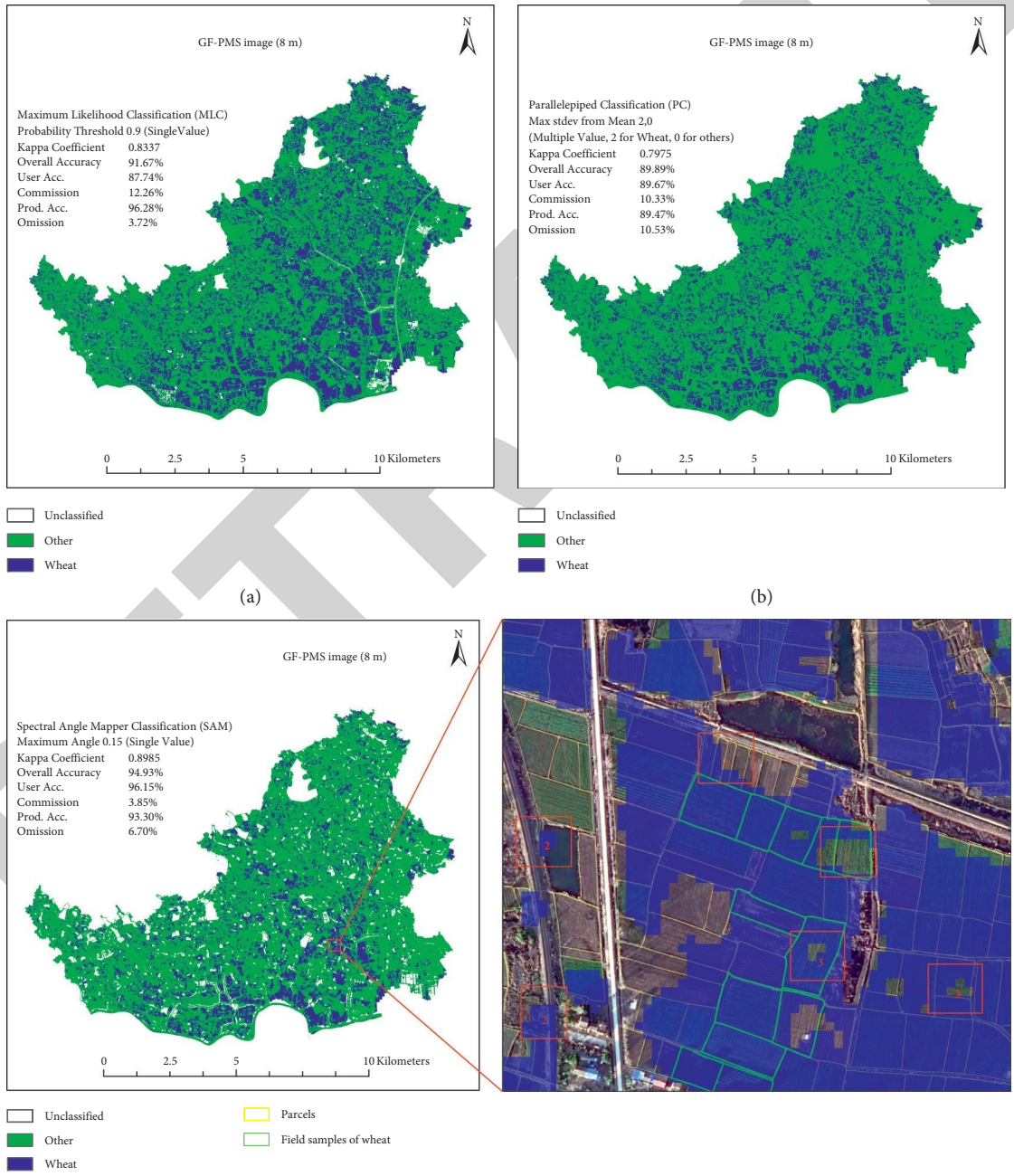

Figure 7: Continued.

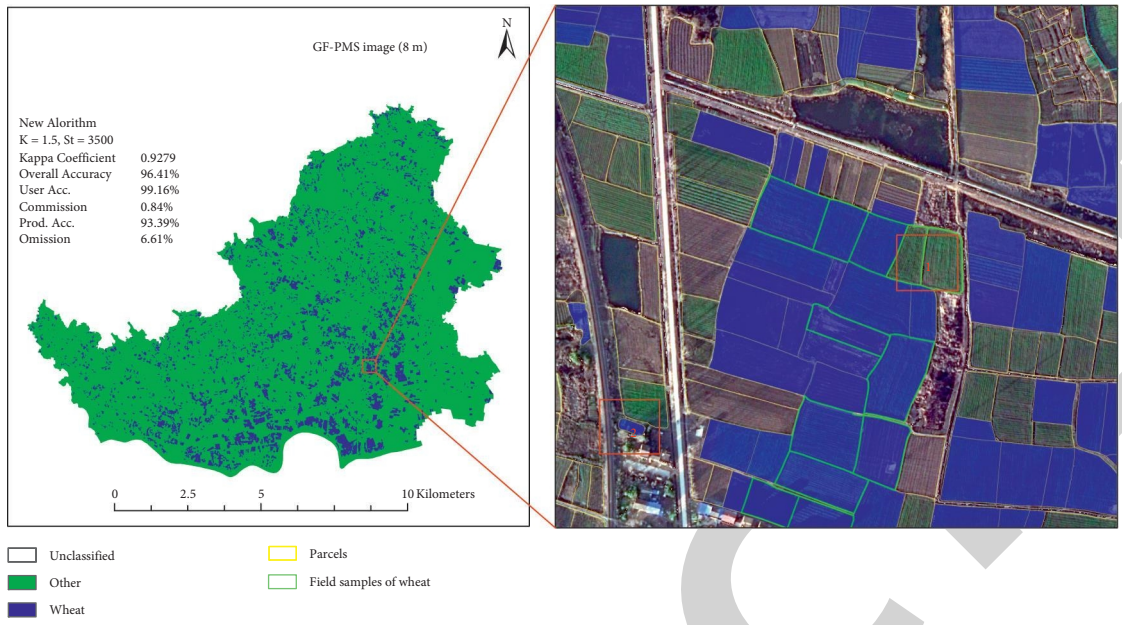

(d)

Figure 7: Best classification results on GF-PMS images in the study area from different methods. (a) MLC. (b) PC. (c) SAM. (d) New algorithm.

4.1. Accuracy Analysis. This section explains the accuracy of the results and carries out an analysis of the matter.

4.1.1. Overall Accuracy of Classification Results. From Table 6, we know that the winter wheat planting area varied greatly among the different methods. Taking the GF-PMS image as an example, according to the MLC, SAM, PC, and new methods, the winter wheat planting area reached 3063.60, 1812.13, 2406.76, and 1018.77 hectares, respectively, showing a threefold difference between them.

There are also significant differences in accuracy between the four classification methods under different parameters from Table 6. On the GF-PMS image, the accuracy of the new algorithm was the highest with K of 1.5 and kappa coefficient, overall accuracy, user's accuracy, commission error, producer's accuracy, and omission error of 0.9279, 96.41%, 99.16%, 0.84%, 93.39%, and 6.61%, respectively. For the PC method, the best classification accuracy was with kappa coefficient, overall accuracy, user's accuracy, commission error, producer's accuracy, and omission error of 0.7975, 89.89%, 89.67%, 10.33%, 89.47%, and 10.53%, respectively, showing a difference from the new method. The worst classification accuracy for the PC method was with kappa coefficient, overall accuracy, user's accuracy, commission error, producer's accuracy, and omission error of 0.2636, 63.98%, 99.91%, 0.09%, 25.83%, and 74.17%, respectively.

It should be noted that a small difference in accuracy can result in a large difference in detecting the winter wheat planting area. Taking the GF-PMS image as an example, the classification results with the highest accuracy detected a wheat planting area of 1028.77 hectares and the classification results with second-highest accuracy detected 1812.13 hectares. This difference is nearly double. It can be seen that, in regions with complex sporadic planting, different parameters in the classification methods have a significant impact on the results. What seems like good classification accuracy could turn out to be extremely different from the actual situation.

4.1.2. Comparative Analysis with the Traditional Classification Method. The study selected the best classification results from the other methods to compare the results from Table 6. We can see that the MLC method has lower accuracy than the new algorithm. The area extracted from the GF-PMS and GF-WFV images is about 3,063 and 4,015.56 hectares, respectively, which are much larger than the reference area (1226.90 hectares). Figures 7(a) and 8(a) also indicate that the MLC method tends to overidentify winter wheat and has a higher commission error, which may be caused by the underrepresentation of classification samples from other categories. The parallelepiped classification method has lower accuracy than the proposed algorithm, but the area it extracted (1,194.73 hectares) is closer to the reference area on the GF-PMS image. In addition, the parallelepiped classification method has high omission and low commission error.

Although the SAM method has the highest accuracy among the algorithms on the two images, the kappa coefficient, overall accuracy, user's accuracy, and producer's accuracy are lower than those of the new algorithm, and the omission and commission errors are higher on the GF-PMS image. Compared to the SAM method, the winter wheat planting area with the new method is closer to the reference

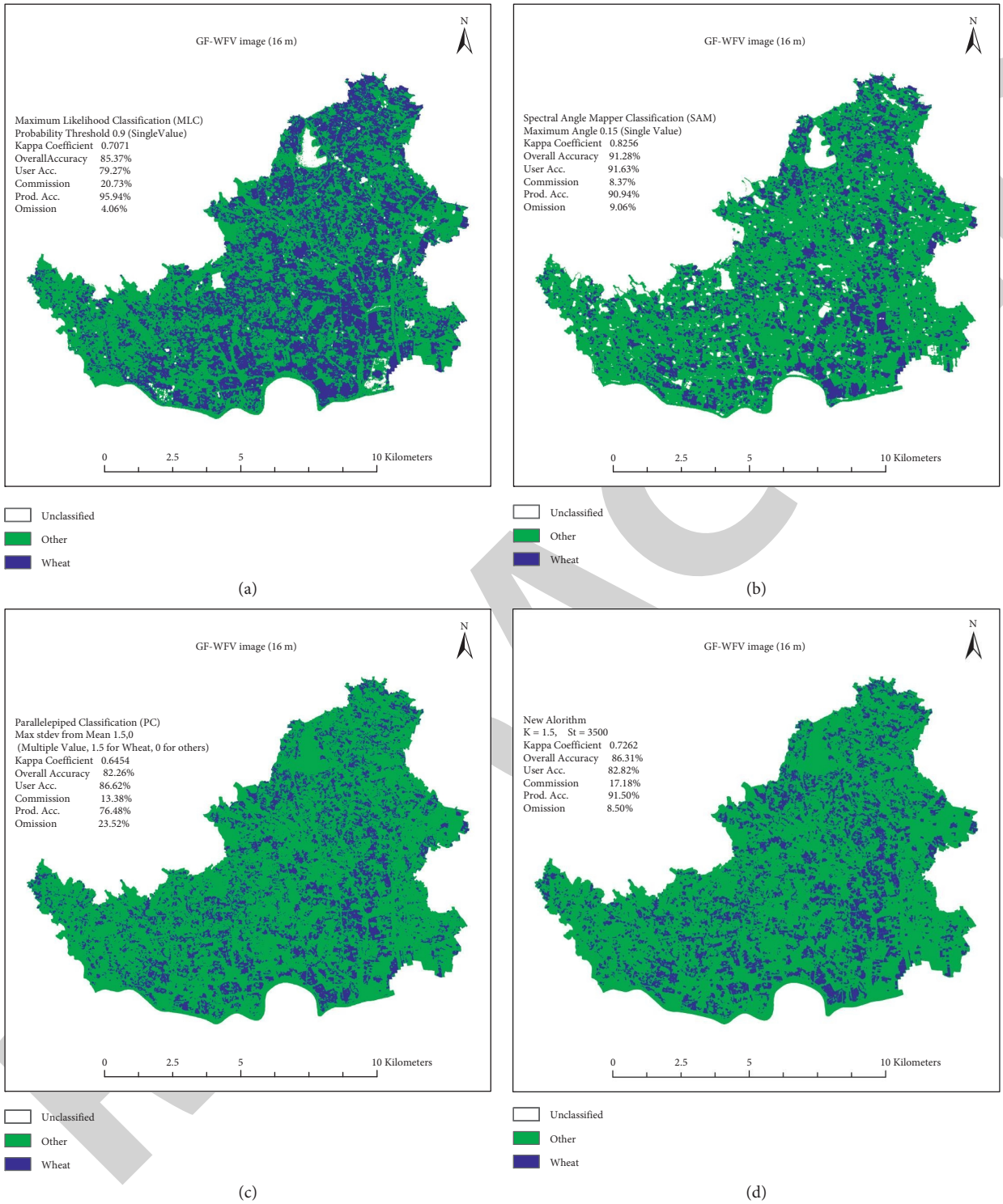

Figure 8: Best classification results on GF-WFV images in the study area from different methods. (a) MLC. (b) SAM. (c) PC. (d) New algorithm.

area. The SAM method has slightly higher accuracy on the GF-WFV image than the new algorithm, but compared to the new method, the winter wheat planting area with the SAM method (2257.02 hectares) is larger than the reference area.

Figures 7(c) and 7(d) demonstrate that (1) the classification results from the SAM method cannot match the actual natural boundaries affected by the mixed pixels leading to the overidentification and omission of winter wheat, as shown in the locations within the red boxes marked 1; (2) the SAM method misclassifies the ROIs due to the phenomenon of different objects having the same spectrum, as shown in the locations within the red boxes

Table 6: Classification results of 4 methods with 10 parameters in the study area.

Images	Methods	Parameters	Area of winter wheat (hectares)	Kappa	Classification accuracy				
					Overall accuracy (%)	User's accuracy (%)	Commission errors (%)	Producer's accuracy (%)	Omission errors (%)
GF-PMS (8 m)	MLC	0.8	3063.69	0.8337	91.67	87.74	12.26	96.28	3.72
		0.9	3063.60	0.8337	91.67	87.74	12.26	96.28	3.72
	SAM	0.1	1378.51	0.8559	92.82	97.82	2.18	87.16	12.84
		0.15	1812.13	0.8985	94.93	96.15	3.85	93.30	6.70
	PC	1.5	416.01	0.6316	81.79	99.90	0.10	62.54	37.46
		2	134.70	0.2636	63.98	99.91	0.09	25.83	74.17
		1.5, 0	1194.73	0.7951	89.82	98.24	1.76	80.46	19.54
		2, 0	2406.76	0.7975	89.89	89.67	10.33	89.47	10.53
	New algorithm	1.5	1018.77	0.9279	96.41	99.16	0.84	93.39	6.61
		2	2014.61	0.8028	90.16	91.22	8.78	88.28	11.72
GF-WFV (16 m)	MLC	0.8	4015.56	0.7071	85.37	79.27	20.73	95.94	4.06
		0.9	4015.56	0.7071	85.37	79.27	20.73	95.94	4.06
	SAM	0.1	2243.74	0.8058	90.29	91.46	8.54	88.97	11.03
		0.15	2257.02	0.8256	91.28	91.63	8.37	90.94	9.06
	PC	1.5	305.64	0.2047	60.11	95.09	4.91	21.65	78.35
		2	99.58	0.0434	51.99	96.06	3.94	4.55	95.45
		1.5, 0	2256.72	0.6454	82.26	86.62	13.38	76.48	23.52
		2, 0	4523.14	0.5095	75.51	68.86	31.14	93.48	6.52
	New algorithm	1.5	1975.18	0.7262	86.31	82.82	17.18	91.50	8.50
		2	3637.73	0.4550	72.71	64.88	35.12	98.62	1.38

marked 2; and (3) its classification results have the problem of salt-and-pepper noise, as shown in the locations within the red boxes marked 3.

4.1.3. Accuracy Analysis of the New Algorithm under Different Spatial Resolutions. From Table 6, we can find that the new method has the best accuracy on the GF-PMS image with 8 m spatial resolution with a K of 1.5. It has high and balanced user's and producer's accuracy, but low omission and commission error. The performance of the new method on the GF-WFV image with 16 m spatial resolution is average, and the kappa coefficient and overall accuracy are even worse than those of the spectral angle mapper classification method. This is consistent with the analysis from Table 3, because 70.12% of the total number of ROIs with an area less than 1000 m^2 in the study area result in the occurrence of more mixed pixels, making the image resolution not match the overall distribution of the size of ROIs on the 16 m image. So, the new algorithm cannot exploit its advantages.

In this paper, the parallelepiped classification method is used to process homogeneous ROIs. Although this method is not suitable for pixel-based classification, it obtains good results in classifying ROIs as a whole, reflecting the superiority of the new algorithm. Whether using other classification methods, such as spectral angle mapper, to deal with homogeneous ROIs could further improve the accuracy is worth further study.

From Figure 7(d), we can see that, by detecting the homogeneity of ROIs, the new method can well control the mixing problem of a small amount of spectral variation at the boundaries and inside the ROIs to solve the problem of salt-and-pepper noise effectively. The new algorithm does not need to rely on the spatial information of remote sensing images and only uses the images to obtain spectral information of ROIs. This makes it possible to obtain high-precision classification results by using medium-resolution remote sensing images, and the classification results correspond well with ground reality, so they have high practical value. In reality, the vector boundaries of the ownership parcel data will not change greatly in a short period (such as 3–5 years), so continuous observation and comparison of the parcels or regions can be achieved by using the new method. The prerequisite is the high-precision geometric correction of remote sensing images.

4.1.4. Matching Degree Analysis between the Size of Parcels and Spatial Resolution of Remote Sensing Images. Combining Table 6 with Figures 7 and 8, we find that the accuracy of the new algorithm on the GF-PMS (8 m) and GF-WFV (16 m) images of the study area was completely different. It can always get high accuracy from high-spatial-resolution images, which is suitable for the other methods. However, different methods are sensitive to different spatial resolution. The SAM method shows a small difference in accuracy between the two images. The new algorithm has a relatively large difference in accuracy between images with different spatial resolution and needs to match the spatial resolution of remote sensing images with the size of ownership parcels. It is also worth studying whether the classification accuracy of the new algorithm can be greatly enhanced by further improving the spatial resolution of remote sensing images in scattered growing region with small ROIs.

4.2. Applicability Analysis. Food stability is the foundation of social stability and agricultural subsidies. At present, subsidies for agricultural planting are based on the area of farmers' contracted fields instead of actually measured crop planting areas in practice. This makes the direction of subsidies unclear and imprecise, which is contrary to the practice of encouraging farmers to grow grain. Because the target of subsidies is not precise enough, farmers' enthusiasm to grow grain decreases, leading to the tendency of nongrain farmland becoming more serious. Therefore, it is urgent to improve the precision of agricultural subsidies by exploring and obtaining precise crop planting areas of peasant households for every season.

The experimental results in this paper demonstrate that it is feasible to extract crop planting areas based on medium-resolution remote sensing images and ownership parcel vector data. Moreover, under the condition that the spatial resolution of remote sensing images matches the size of ROIs, the classification accuracy is high, and the results can be associated with the ownership of field contract operations, which is a research direction for the realization of precise subsidies for agricultural planting in the future.

4.3. Limits. The new algorithm was implemented on the secondary development platform of Envi 5.3 using the IDL language. The ownership parcel vector data has 71,869 parcels. The GF-PMS and GF-WFV images are composed of $2{,}027 \times 1{,}591$ and $1{,}014 \times 796$ grid cells, respectively. During the process of implementing the new algorithm, it was necessary to use the parcel data to segment the raster image logically and to detect the homogeneity of each ROI corresponding to each parcel.

Due to a large amount of data, the computational efficiency is lower than that of other comparison methods on a desktop computer with an i7-7600 CPU, 16 GB RAM, and Microsoft Windows 10 using the 64-bit option. At present, the proposed algorithm is implemented on a single-core CPU and has the characteristics of large amounts of data, low coupling, and high computational density, which is suitable to be parallelized. Its computational efficiency can be improved by parallel computing, such as MPI, OpenMP, cloud computing, and Compute Unified Device Architecture (CUDA). Therefore, parallelization of the proposed algorithm based on parallel computing is also worth further research.

5. Conclusions

This paper proposed a new algorithm for extracting winter wheat planting areas based on ownership parcel vector data and medium-resolution remote sensing images to enhance the winter wheat classification accuracy in complex planting areas. First, the region of interest (ROI) of each parcel was generated by using the parcel data to segment the image. Then, the homogeneity of each ROI was detected by its statistical indices (mean value and standard deviation), calculated from the spectral information of the image to get homogeneous and nonhomogeneous ROIs. The parallelepiped classifier and rule-based feature extraction classification methods were utilized to extract winter wheat planting areas from homogeneous and nonhomogeneous ROIs, respectively. Finally, in order to achieve the final classification result, the two classification results were combined.

The experiments verified that the new algorithm could extract the winter wheat planting areas by combining a GF-PMS image with 8 m spatial resolution and the ownership parcels (71869 parcels) in a complex planting area of 103.60 km^2 in central China, which covers the 19 administrative villages of Fengle Town, in Feixi County, Hefei City, Anhui Province, China. The kappa coefficient and overall accuracy of the new algorithm reached 0.9279 and 96.41%, respectively. The new algorithm can effectively control the mixing of a few spectral variations within the boundary and interior of parcel and solve the problem of salt-and-pepper noise. It does not rely on the use of remote sensing images to extract spatial location information and only uses images for the spectral information of ROIs, which makes the classification results have high accuracy with remote sensing images with medium spatial resolution. It has high user's and producer's accuracy, which were higher than those of maximum likelihood, spectral angle mapper, and parallelepiped classification methods.

The new algorithm needs to match the spatial resolution of the image with the size of the ROIs to ensure that each ROI has a majority of pure pixels but not mixed pixels. If they do not match, the advantages of the proposed classification algorithm cannot be realized, and the accuracy of the classification results is worse than that with the traditional pixel-based classification methods. A GF-WFV image with 16 m spatial resolution was utilized in the scattered growing region with small parcels; thus, it requires high-precision geometric correction of remote sensing images.

In this study, a parallelepiped classification was utilized to process the homogeneous ROIs. Whether other classification methods can further improve the accuracy of the new method deserves further study. It is also worth studying whether the classification accuracy of the new algorithm can be greatly enhanced by further improving the spatial resolution of images in scattered growing regions with small parcels. Research could also focus on inserting parallel computing into the new algorithm to improve its computational efficiency.

Data Availability

The satellite image with 8 m spatial resolution from Gaofen-1 carrying a panchromatic multispectral sensor (PMS) and the satellite image with 16 m spatial resolution from GF1 carrying a wide field view (WFV) were downloaded from http://36.112.130.153:7777/DSSPlatform/index.html. The ownership parcel vector data are confidential.

Conflicts of Interest

The authors declare no conflicts of interest.

Acknowledgments

The authors thank the Agriculture and Rural Bureau of Feixi County, Anhui Province, China, for data support. This research was funded by the Natural Science Research Project of University in Anhui Province (grant nos. KJ2018A0509 and KJ2019A0763) and the Natural Science Foundation of Anhui Province (2108085QD151).

References

[1] N.-T. Son, C.-F. Chen, C.-R. Chen, and H.-Y. Guo, "Classification of multitemporal sentinel-2 data for field-level monitoring of rice cropping practices in taiwan," *Advances in Space Research*, vol. 65, no. 8, pp. 1910–1921, 2020.

[2] L. Xun, P. Wang, and L. Li, "Identifying crop planting areas using fourier-transformed feature of time series MODIS leaf area index and sparse-representation-based classification in the north China plain," *International Journal of Remote Sensing*, vol. 40, no. 5–6, pp. 2034–2052, 2019.

[3] J. Zhang, X. Li, and Y. Wu, "Object oriented estimation of winter wheat planting area using remote sensing data," *Transactions of the Chinese Society of Agricultural Engineering*, vol. 24, no. 5, pp. 156–160, 2008.

[4] J. Schmedtmann and M. Campagnolo, "Making the use of remote sensing for agricultural subsidy control more effective: automatizing photo interpretation of Satellite Imagery over Southern Portugal in the Context of the European CAP," in *Proceedings of the AGU Fall Meeting, Session: Earth Observations for National to Global Agricultural and Rangeland Monitoring (GEOGLAM)*, San Francisco, CA, USA, 2014.

[5] M. K. Gumma, P. S. Thenkabail, K. C. Deevi et al., "Mapping cropland fallow areas in Myanmar to scale up sustainable intensification of pulse crops in the farming system," *GIScience and Remote Sensing*, vol. 55, no. 6, pp. 926–949, 2018.

[6] Y. Guo, H. Xia, and L. Pan, "Development of a new phenology algorithm for fine mapping of cropping intensity in complex planting areas using sentinel-2 and google earth engine," *ISPRS International Journal of Geo-Information*, vol. 10, no. 587, 2021.

[7] P. Teluguntla, D. Ryu, B. George, J. Walker, and H. Malano, "Mapping flooded rice paddies using time series of MODIS imagery in the krishna river basin, India," *Remote Sensing*, vol. 7, no. 7, pp. 8858–8882, 2015.

[8] W. Li, D. Fu, and F. Su, "Spatial-temporal evolution and analysis of the driving force of oil palm patterns in Malaysia from 2000 to 2018," *ISPRS International Journal of Geo-Information*, vol. 9280 pages, 2020.

[9] S. Wu, H. Lu, and H. Guan, "Optimal bands combination selection for extracting garlic planting area with multi-temporal sentinel-2 imagery," *Sensors*, vol. 21, no. 5556, 2021.

[10] A. Nasrallah, N. Baghdadi, and M. Mhawej, "A novel approach for mapping wheat areas using high resolution sentinel-2 images," *Sensors*, vol. 18, no. 2089, 2018.

[11] P. Teluguntla, P. S. Thenkabail, A. Oliphant et al., "A 30-m landsat-derived cropland extent product of Australia and China using random forest machine learning algorithm on google earth engine cloud computing platform," *ISPRS Journal of Photogrammetry and Remote Sensing*, vol. 144, pp. 325–340, 2018.

[12] M. H. Asad and A. Bais, "Weed detection in canola fields using maximum likelihood classification and deep convolutional neural network," *Information Processing in Agriculture*, vol. 7, no. 4, pp. 535–545, 2020.

[13] A. Ozdarici-Ok, A. Ok, and K. Schindler, "Mapping of agricultural crops from single high-resolution multispectral images-data-driven smoothing vs. Parcel-based smoothing," *Remote Sensing*, vol. 7, no. 5, pp. 5611–5638, 2015.

[14] A. Moiane and A. M. L. Machado, "Class-based affinity propagation for hyperspectral image dimensionality reduction and improvement of maximum likelihood classification accuracy," *Bulletin of Geodetic Sciences*, vol. 25, no. 1, Article ID e2019004, 2019.

[15] O. B. Özdemir and Y. Y. Çetin, *Improved Hyperspectral Vegetation Detection Using Neural Networks with Spectral Angle Mapper*, San Francisco, CA, USA, 2017.

[16] G. Randazzo, M. Cascio, and M. Fontana, "Mapping of Sicilian pocket beaches land use/land cover with sentinel-2 imagery: a case study of messina Province," *Land*, vol. 10678 pages, 2021.

[17] K. Tatsumi, Y. Yamashiki, and C. L. R. Taipe, "Crop classification of upland fields using random forest of time-series landsat 7 ETM+ data," *Computers and Electronics in Agriculture*, vol. 115, pp. 171–179, 2015.

[18] J. Wang, Y. Zhao, C. Li, L. Yu, D. Liu, and P. Gong, "Mapping global land cover in 2001 and 2010 with spatial-temporal consistency at 250m resolution," *ISPRS Journal of Photogrammetry and Remote Sensing*, vol. 103, pp. 38–47, 2015.

[19] F. Zhang and X. Yang, "Improving land cover classification in an urbanized coastal area by random forests: the role of variable selection," *Remote Sensing of Environment*, vol. 251112105 pages, 2020.

[20] L. Loosvelt, J. Peters, H. Skriver, B. De Baets, and N. E. C. Verhoest, "Impact of reducing polarimetric SAR input on the uncertainty of crop classifications based on the random forests algorithm," *IEEE Transactions on Geoscience and Remote Sensing*, vol. 50, no. 10, pp. 4185–4200, 2012.

[21] G. Mountrakis, J. Im, and C. Ogole, "Support vector machines in remote sensing: a review," *ISPRS Journal of Photogrammetry and Remote Sensing*, vol. 66, no. 6, pp. 247–259, 2011.

[22] J. M. Guerrero, G. Pajares, M. Montalvo, J. Romeo, and M. Guijarro, "Support vector machines for crop/weeds identification in maize fields," *Expert Systems with Applications*, vol. 39, no. 12, pp. 11149–11155, 2012.

[23] F. Camacho de Coca, B. Fuster, and W. Li, "Crop specific algorithms trained over ground measurements provide the best performance for GAI and FAPAR estimates from landsat-8 observations," *Remote Sensing of Environment*, vol. 260112453 pages, 2021.

[24] G. Tana, H. Letu, Z. Cheng, and R. Tateishi, "Wetlands mapping in north America by decision rule classification using MODIS and ancillary data," *IEEE Journal of Selected Topics in Applied Earth Observations and Remote Sensing*, vol. 6, no. 6, pp. 2391–2401, 2013.

[25] W. B. Cohen and S. N. Goward, "Landsat's role in ecological applications of remote sensing," *BioScience*, vol. 54, no. 6, pp. 535–545, 2004.

[26] M. Ozdogan and G. Gutman, "A new methodology to map irrigated areas using multi-temporal MODIS and ancillary data: an application example in the continental US," *Remote Sensing of Environment*, vol. 112, no. 9, pp. 3520–3537, 2008.

[27] A. Asgarian, A. Soffianian, and S. Pourmanafi, "Crop type mapping in a highly fragmented and heterogeneous agricultural landscape: a case of Central Iran using multi-temporal landsat 8 imagery," *Computers and Electronics in Agriculture*, vol. 127, pp. 531–540, 2016.

[28] Z. Pan, J. Huang, Q. Zhou et al., "Mapping crop phenology using NDVI time-series derived from HJ-1 A/B data,"

International Journal of Applied Earth Observation and Geoinformation, vol. 34, pp. 188–197, 2015.

[29] L. Zhong, L. Hu, L. Yu, P. Gong, and G. S. Biging, "Automated mapping of soybean and corn using phenology," *ISPRS Journal of Photogrammetry and Remote Sensing*, vol. 119, pp. 151–164, 2016.

[30] L. G. J. Van Bussel, E. Stehfest, S. Siebert, C. Müller, and F. Ewert, "Simulation of the phenological development of wheat and maize at the global scale," *Global Ecology and Biogeography*, vol. 24, no. 9, pp. 1018–1029, 2015.

[31] D. C. Duro, S. E. Franklin, and M. G. Dubé, "A comparison of pixel-based and object-based image analysis with selected machine learning algorithms for the classification of agricultural landscapes using SPOT-5 HRG imagery," *Remote Sensing of Environment*, vol. 118, pp. 259–272, 2012.

[32] X. E. Pantazi, D. Moshou, T. Alexandridis, R. L. Whetton, and A. M. Mouazen, "Wheat yield prediction using machine learning and advanced sensing techniques," *Computers and Electronics in Agriculture*, vol. 121, pp. 57–65, 2016.

[33] D. Paudel, H. Boogaard, and A. de Wit, "Machine learning for large-scale crop yield forecasting," *Agricultural Systems*, vol. 187, no. 103016, 2021.

[34] J. Peña, P. Gutiérrez, and C. Hervás-Martínez, "Object-based image classification of summer crops with machine learning methods," *Remote Sensing*, vol. 6, pp. 5019–5041, 2014.

[35] J. C. Tilton, Y. Tarabalka, P. M. Montesano, and E. Gofman, "Best merge region-growing segmentation with integrated nonadjacent region object aggregation," *IEEE Transactions on Geoscience and Remote Sensing*, vol. 50, no. 11, pp. 4454–4467, 2012.

[36] M. Chellasamy, R. T. Zielinski, and M. H. Greve, "A multievidence approach for crop discrimination using multitemporal WorldView-2 imagery," *IEEE Journal of Selected Topics in Applied Earth Observations and Remote Sensing*, vol. 7, no. 8, pp. 3491–3501, 2014.

[37] Y. Kang and L. Zhou, "RubE: rule-based methods for extracting product features from online consumer reviews," *Information & Management*, vol. 54, no. 2, pp. 166–176, 2017.

[38] J. Xiong, P. Thenkabail, and J. Tilton, "Nominal 30-m cropland extent map of continental africa by integrating pixel-based and object-based algorithms using sentinel-2 and landsat-8 data on google earth engine," *Remote Sensing*, vol. 91065 pages, 2017.

[39] G. Chen, J.-C. Thill, S. Anantsuksomsri, N. Tontisirin, and R. Tao, "Stand age estimation of rubber (hevea brasiliensis) plantations using an integrated pixel- and object-based tree growth model and annual landsat time series," *ISPRS Journal of Photogrammetry and Remote Sensing*, vol. 144, pp. 94–104, 2018.

[40] T. Zhou, J. Pan, P. Zhang, S Wei, and T Han, "Mapping winter wheat with multi-temporal SAR and optical images in an urban agricultural region," *Sensors*, vol. 171210 pages, 2017.

[41] A. I. De Castro, J. Six, and R. E. Plant, "Mapping crop calendar events and phenology-related metrics at the parcel level by object-based image analysis (OBIA) of MODIS-NDVI time-series: a case study in central California," *Remote Sensing*, vol. 101745 pages, 2018.

[42] J. Huang, H. Wang, Q. Dai, and D. Han, "Analysis of NDVI data for crop identification and yield estimation," *IEEE Journal of Selected Topics in Applied Earth Observations and Remote Sensing*, vol. 7, no. 11, pp. 4374–4384, 2014.

[43] P. Li, C. Xiao, and Z. Feng, "Mapping rice planted area using a new normalized EVI and SAVI (NVI) derived from landsat-8 OLI," *IEEE Geoscience and Remote Sensing Letters*, vol. 15, no. 12, pp. 1822–1826, 2018.

[44] M. Wei, B. Qiao, J. Zhao, and X. Zuo, "The area extraction of winter wheat in mixed planting area based on sentinel-2 a remote sensing satellite images," *International Journal of Parallel, Emergent and Distributed Systems*, vol. 35, no. 3, pp. 297–308, 2020.

[45] R. D'Andrimont, G. Lemoine, and M. Van der Velde, "Targeted grassland monitoring at parcel level using sentinels, street-level images and field observations," *Remote Sensing*, vol. 101300 pages, 2018.

[46] M. J. Falkowski and J. A. Manning, "Parcel-based classification of agricultural crops via multitemporal landsat imagery for monitoring habitat availability of western burrowing owls in the imperial valley agro-ecosystem," *Canadian Journal of Remote Sensing*, vol. 36, no. 8, pp. 750–762, 2010.

[47] M. Ebadian, M. E. Shedden, E. Webb et al., "Impact of parcel size, field shape, crop yield, storage location, and collection equipment on the performance of single-pass cut-and-chip harvest system in commercial shrub willow fields," *Bioenergy Research*, vol. 11, no. 2, pp. 364–381, 2018.

[48] J. C. Foltête, "A parcel-based graph to match connectivity analysis with field action in agricultural landscapes: is node removal a reliable method," *Landscape and Urban Planning*, vol. 178, pp. 32–42, 2018.

[49] P. Zhang, S. Hu, W. Li, and C. Zhang, "Parcel-level mapping of crops in a smallholder agricultural area: a case of Central China using single-temporal VHSR imagery," *Computers and Electronics in Agriculture*, vol. 175, Article ID 105581, 2020.

[50] E. Derenyi, "A small crop information system," *Proceedings of Remote Sensing for Natural Resources*, vol. 1, pp. 78–87, 1979.

[51] F. Levavasseur, P. Martin, C. Bouty et al., "RPG Explorer: a new tool to ease the analysis of agricultural landscape dynamics with the Land Parcel Identification System," *Computers and Electronics in Agriculture*, vol. 127, pp. 541–552, 2016.

[52] L. Deng, Z. Shen, and Y. Ke, "Winter wheat planting area extraction using multi-temporal remote sensing images based on field parcel," *Transactions of the Chinese Society of Agricultural Engineering*, vol. 34, no. 21, pp. 157–164, 2018.

[53] C. Zhu, J. Luo, and Z. Shen, "Winter wheat planting area extraction using multi-temporal remote sensing data based on field parcel characteristic," *Transactions of the Chinese Society of Agricultural Engineering*, vol. 27, no. 9, pp. 94–99, 2011.

[54] Q. Huang, Z. Zeng, and G. Xie, "Investigation on crop planting structure based on synergy of high spatial-temporal resolution remote sensing data," *Journal of Southern Agriculture*, vol. 48, no. 3, pp. 552–560, 2017.

[55] Y. Sun, J. Luo, L. Xia et al., "Geo-parcel-based crop classification in very-high-resolution images via hierarchical perception," *International Journal of Remote Sensing*, vol. 41, no. 4, pp. 1603–1624, 2020.

[56] X. Gu, Y. Pan, and X. He, "Measurement of sown area of winter wheat based on per-field classification and remote sensing imagery," *Chineise Journal of Remote Sensing*, vol. 14, no. 4, pp. 789–805, 2010.

[57] F. Löw and G. Duveiller, "Determining suitable image resolutions for accurate supervised crop classification using remote sensing data," *SPIE, Remote Sensing, Earth Resources & Environmental Remote Sensing/gis Applications IV*, vol. 8893, 2013.

[58] M. Fauvel, J. A. Palmason, and J. A. A. Benediktsson, "Classification of remote sensing imagery with high spatial

Hindawi
Journal of Mathematics
Volume 2023, Article ID 9765832, 1 page
https://doi.org/10.1155/2023/9765832

Retraction

Retracted: Predicting the Link between Stock Prices and Indices with Machine Learning in R Programming Language

Journal of Mathematics

Received 19 December 2023; Accepted 19 December 2023; Published 20 December 2023

This article has been retracted by Hindawi following an investigation undertaken by the publisher [1]. This investigation has uncovered evidence of one or more of the following indicators of systematic manipulation of the publication process:

(1) Discrepancies in scope

(2) Discrepancies in the description of the research reported

(3) Discrepancies between the availability of data and the research described

(4) Inappropriate citations

(5) Incoherent, meaningless and/or irrelevant content included in the article

(6) Manipulated or compromised peer review

The presence of these indicators undermines our confidence in the integrity of the article's content and we cannot, therefore, vouch for its reliability. Please note that this notice is intended solely to alert readers that the content of this article is unreliable. We have not investigated whether authors were aware of or involved in the systematic manipulation of the publication process.

Wiley and Hindawi regrets that the usual quality checks did not identify these issues before publication and have since put additional measures in place to safeguard research integrity.

We wish to credit our own Research Integrity and Research Publishing teams and anonymous and named external researchers and research integrity experts for contributing to this investigation.

The corresponding author, as the representative of all authors, has been given the opportunity to register their agreement or disagreement to this retraction. We have kept a record of any response received.

References

[1] M. Cao, "Predicting the Link between Stock Prices and Indices with Machine Learning in R Programming Language," *Journal of Mathematics*, vol. 2021, Article ID 1275637, 10 pages, 2021.

Hindawi
Journal of Mathematics
Volume 2021, Article ID 1275637, 10 pages
https://doi.org/10.1155/2021/1275637

Research Article

Predicting the Link between Stock Prices and Indices with Machine Learning in R Programming Language

Mengya Cao

Olin Business School, Washington University in St. Louis, St. Louis 63130, MO, USA

Correspondence should be addressed to Mengya Cao; c.mengya@wustl.edu

Received 9 November 2021; Revised 20 November 2021; Accepted 26 November 2021; Published 10 December 2021

Academic Editor: Naeem Jan

This paper provides an in-depth analysis machine study of the relationship between stock prices and indices through machine learning algorithms. Stock prices are difficult to predict by a single financial formula because there are too many factors that can affect stock prices. With the development of computer science, the author now uses many computer science techniques to make more accurate predictions of stock prices. In this project, the author uses machine learning in R Studio to predict the prices of 35 stocks traded on the New York Stock Exchange and to study the interaction between the prices of four indices in different countries. Further, it is proposed to find the link between stocks and indices in different countries and then use the predictions to optimize the portfolio of these stocks. To complete this project, the author used Linear Regression, LASSO, Regression Trees, Bagging, Random Forest, and Boosted Trees to perform the analysis. The experimental results show that the MRDL deep multiple regression model proposed in this paper predicts the closing price trend of stocks with a mean square error interval [0.0043, 0.0821]. Additionally, 80% of the proposed DMISV, KDJSV, MACDV, and DKB stock buying and selling strategies have a return greater than 10%. The experimental results validate the effectiveness of the proposed buying and selling strategies and stock price trend prediction methods in this paper. Compared with other algorithms, the accuracy of the algorithm in this study is increased by 15%, and the efficiency of prediction is increased by 25%.

1. Introduction

A stock is a certificate of ownership issued by a joint-stock company to raise funds, which allows the shareholder to receive dividends and bonuses. With the development of China's economy, the stock market has become a bigger and bigger part of our economic market, even becoming a "barometer" of our economic development [1]. The stock market is a very complex and sizeable financial system, so various economic and political factors affect the changes in the stock market at every moment. Changes in stock price trends are of the utmost concern to stockholders in the stock market. In our stock market, stock prices are influenced by numerous factors, such as policy adjustments, economic environment, and international situation. Therefore, making reasonable forecasts of stock price trends has been a critical difficulty for economists to study [2]. Suppose one can make a good prediction of the stock price trend. In that case, he or she can reduce the investment risk and combine the predicted stock price trend with the stock buying and selling strategy to help investors make a reasonable adjustment to their investment structure and maximize the return.

At present, there are numerous indicators for judging stock quotes in the stock market, such as MACD (Exponential Smoothed Moving Average), KDJ (Stochastic Indicator), and DMI (Movement Indicator or Tendency Indicator). It is impossible to take all of them into account when making a judgment on the stock market. The selection of one or more of these indicators as a reference, combined with the market environment to judge the stock market, is what we call a buying and selling strategy. Choosing the right buying and selling strategy can help us choose the most desirable stocks from among many and determine when to buy and when to sell the stock so that the shareholder's investment risk is reduced [3].

Machine learning techniques include many different methods to do analysis. A deeper understanding of how the different methods work can help make predictions more robust and more accurate. Therefore, machine learning is an essential tool that can be used in the financial world. In this project, the author used Linear Regression, LASSO, Regression Trees, Bagging, Random Forest, and Boosted Trees to do the analysis. The author will give a brief description of each method in the following section.

The linear regression model is a linear approach to do the analysis, and the model can be written specifically as

$$y_i = \beta_0 + \beta_1 x_1 + \beta_2 x_2 +, , , + \beta_p x_p + \varepsilon_1. \quad (1)$$

As it can be seen from the model formulation, the linear regression model is easy to interpret. β_0 is the intercept. β_2 is the slope of the variable x_2. The linear regression model uses the least-squares method to estimate the parameters [4].

The LASSO model is a more modern alternative analysis. Traditionally, models like linear regression models and ridge regression models would include all variables in the results. However, the LASSO model can force some coefficients to be zero, which makes it easier to interpret. LASSO estimation $\widehat{\beta}_j$ is done by minimizing the following equation:

$$\sum_{i=1}^{n} \left(y_i - \beta_0 - \sum_{i=1}^{p} \beta_j x_{ij} \right)^2. \quad (2)$$

The regression tree model has many advantages over the first two approaches. First, regression tree models are easy to use, and the resulting rules are easy to interpret and implement. Second, the selection and reduction of variables in regression tree models are automatic and do not require statistical model assumptions. Finally, regression tree models do not require a large amount of task delivery data to be used. However, regression tree models can have high variance.

The Bagging (Bootstrap Aggregating) model is a solution to the problem of high variance generated by regression tree models. The Bagging model is also a simple analysis method, but with powerful ideas. It uses averaging to reduce variance and bootstrap to ensure a large training data set [5]. However, since the Bagging process involves the random selection of a subset of observations, interpreting the results can be difficult. This problem can be solved by using relative impact plots. This paper is mainly focusing on the U.S. stock market. The follow-up research will consider more local stock markets.

The random forest model and the boosted tree model are only models that build on the bag method. Partial dependency graphs and relative importance graphs are important ways to interpret these models.

With these machine learning methods, the author can make better forecasts of stock prices, and one can have a deep understanding of the connections between index prices in different countries. After the prediction, the author will use the naive heuristic to do portfolio optimization. How to obtain valuable information from the massive stock history data? The author researched stocks' buying and selling points, combined deep learning methods to predict stock price trends, dug out stocks with their investment value, and assisted stock investors in making investment decisions. These researches are of theoretical and practical significance.

The rest of the paper will proceed as follows. The author reviewed historical literature in Section 2. In Section 3, the author introduced the methodology and analysis used in the paper. The author discussed the influence of the forecast and the result of portfolio optimization in Section 4. In Section 5, the author concluded the paper.

2. Literature Review

2.1. Machine Learning and Optimization. Machine learning techniques and optimization mathematics are interactive. Machine learning techniques are a solid foundation for optimization—however, machine learning and optimization focus on different areas of development. Machine learning focuses on more straightforward mathematics and generates robust general optimization codes [6]. But optimization focuses more on accuracy, speed, and robustness.

LASSO is a handy model selection tool for large-scale predictors. Traditional methods such as OLS regression and stepwise regression are subject to random errors. Moreover, when real-world datasets are analyzed in *R*, the results show that LASSO performs better and more accurately than other traditional methods. On the other hand, based on the forecast curve fit and the mean squared error of the forecast results, the highest accuracy is obtained using the MRDL_4 model to forecast the 30-day trend of stocks. Next, the author compared the MRDL_4 model with the traditional multiple regression model (MLRM). The experiments show that the MRDL_4 model fits the prediction curve better than the multiple regression model, which verifies the effectiveness of the proposed method. However, the different parameter settings in the MRDL model have an impact on the prediction results. The next step will be to adjust the model's parameters and try to train the MRDL model using different optimization functions to improve the prediction accuracy [7].

2.2. Determinants of Stock Price Movements. Jothimani used regression methods to analyze the SSE Composite Index and predict stock prices [8]. Asghar used partial least squares to make a simple prediction of stock prices [9]. Cao et al. used the least-squares trained regression model to select the price of the gold spot as an influencing factor to predict the trend of gold stocks [10]. Livieris used the one-dimensional linear regression method combined with least-squares training regression coefficients to analyze and predict the movements of per capita GDP and per capita consumption in 31 provinces [11]. Atkins et al. used the least-squares training regression model to analyze the trend of rebar prices [12].

Predicting stock price movements is a central and challenging issue in the financial world. There are thousands of factors that can affect the direction of stock prices. The cash flow of a company is an essential factor in predicting stock price movements [13]. The second significant predictor

is diversification. Qing Jiang et al. proposed using an extended short-term memory network (LSTM) to predict stock prices [14]. Gao et al. predicted future market prices based on a deep belief network consisting of multiple layers of random hidden variables [15]. Huck et al. predicted stock prices based on the structure of the restricted Boltzmann machine algorithm in deep belief networks [16]. Ghazanfar et al. predicted stock prices based on recurrent neural networks with a multifactor training model [17]. Parikh et al. expect stock prices based on multiplex recurrent neural networks combined with extracted stock-related news text features [18]. Weihua Chen et al. combined deep learning methods with stock forum data to study stock market volatility accuracy prediction [19].

2.3. Predicting Stock Prices by Machine Learning. A basic approach is to focus on the patterns generated in the stock market and extract knowledge from these patterns to predict the future behavior of the stock market. A necessary process is to make the data easily classifiable. All methods in machine learning can be used to predict the stock market, and most of them are adequate and easy to do analysis.

Due to the numerous factors affecting stock price fluctuations and the high complexity of financial markets, most scholars in past academic studies of stock markets have chosen to use complex techniques or methods to predict stock price movements to judge stock buying and selling points [20]. These theoretically involved stock buying and selling trading models have primarily enriched the theoretical knowledge in the field of finance, but as the complexity of the models increases, the time consumed by their training models increases. If investors are not familiar with stock movements, they can easily suffer losses from the stock market. The use of machine learning for stock price prediction is becoming more critical as increased stocks are entering the market. Artificial neural networks can perform better in predicting stock prices. And decision trees can provide some rules to describe the prediction. Combining these two methods can give us a comprehensive knowledge of stock price prediction.

3. Methodology and Analysis

3.1. Collecting and Processing Data in Excel. All prices for these thirty-five stocks and four smaller companies have been collected from Yahoo Finance. The timeline is from March 7, 2018, to March 5, 2021. When the prices were downloaded from Yahoo Finance, there were some stocks and small companies with null values, and these null values were replaced with the average of the respective stock prices. In addition, in this project, the author has used the percentage change as a predictor, that is, the following formula:

$$y = h\left(x_i^2\right), \quad i = m + 1, \ldots, M. \tag{3}$$

In addition, the author created a lagged variable of percentage change to eliminate the effect of time differences between countries. Each layer of the DenseNet network is connected to any other layer in the form of feedforward, and the input of any layer is the output of all the previous layers, and the output of the layer itself is the input of all the subsequent layers so that each layer is connected to the input data, which reduces the error of input information transfer between multiple layers and optimizes the gradient and information transfer [21]. This optimizes the gradient and the flow of information and enhances the transmission of data features. More importantly, the DenseNet network has the effect of regularization, which alleviates the problem of overfitting the data set to a certain extent and utilizes the data features more effectively, as shown in Figure 1.

In addition, the DenseNet network is different from the residual network (ResNet) where each layer has its weight and the number of parameters is huge. In addition, the DenseNet network does not acquire new network architecture by deepening the number of network layers but improves the utilization of parameters by reusing features, so it requires fewer parameters and is easier to train the network. In both forward and backward propagation neural networks, the ReLU function has only a linear relationship, so it takes less time to train the model. On the other hand, the ReLU function does not produce gradient saturation if the input z is a real number greater than 0. Therefore, the ReLU function is chosen as the activation function of the neural network in this paper.

The depth regression model MRDL objective function is to minimize the mean squared error between the predicted and true values of the closing price and is calculated as follows:

$$\text{loss} = \frac{1}{k}\sum_{i}^{i+k}\frac{1}{2}\left(y_i + h\left(x_i^2\right)\right). \tag{4}$$

Figure 2 shows the time required to train the MRDL_4 model with the different number of neurons in the hidden layer and its training loss. Therefore, in this section, the MRDL_4 model uses 64 neurons in the implicit layer, and the output of 64 neurons in MRDL_4 implicit layer H1 is used as the input of implicit layer H2, and the implicit layer H2 is adjusted by the small-batch gradient descent method. The output of 64 neurons of implicit layer H2 is used as the input of the output layer, and the weight of each input data is also determined using the small-batch gradient descent method.

DMI is a medium to long-term indicator used to analyze the trend of stock prices. Most of the existing stock analysis indicators are calculated by using the closing price of each day of the stock to calculate each index, ignoring the real difficulties of the stock on that day. For example, when a stock's opening and closing prices for the day are the same as the previous day's opening and closing prices, but the highest (lowest) price for the day is different, then this stock's up and down quotes for the two days are not the same. In most other indicators, this is very difficult to reflect. The DMI indicator is composed of two sets of four parameters: a long/short indicator that includes upward movement +DI and

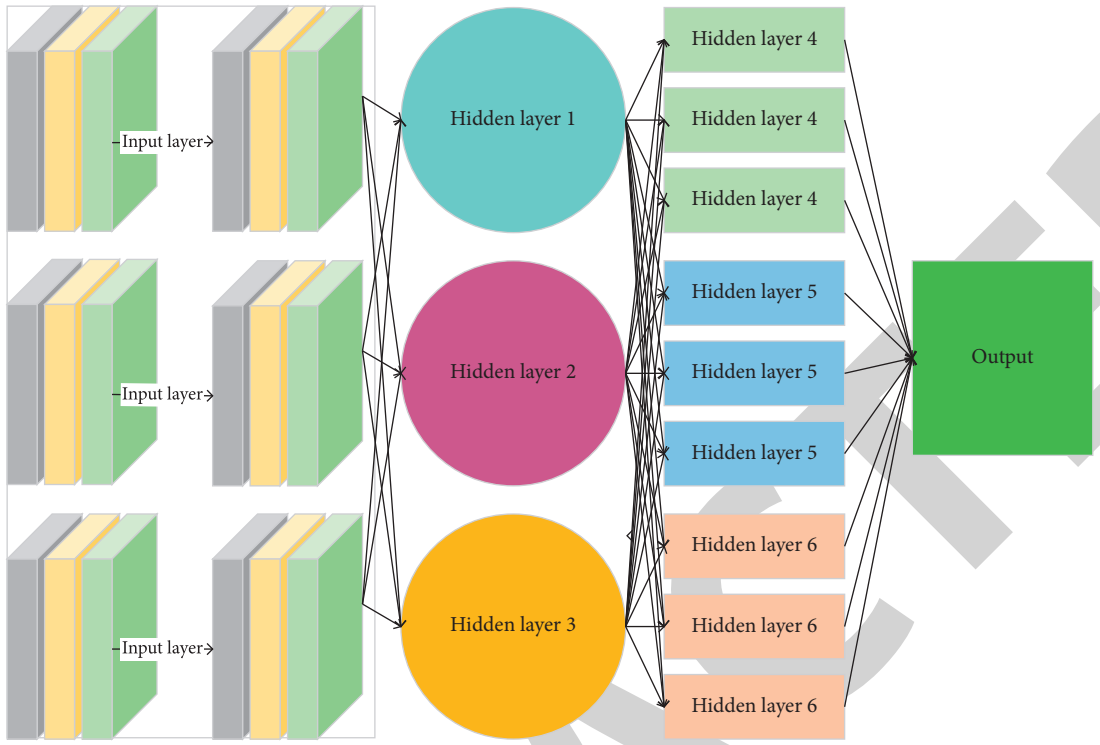

Figure 1: DenseNet network structure.

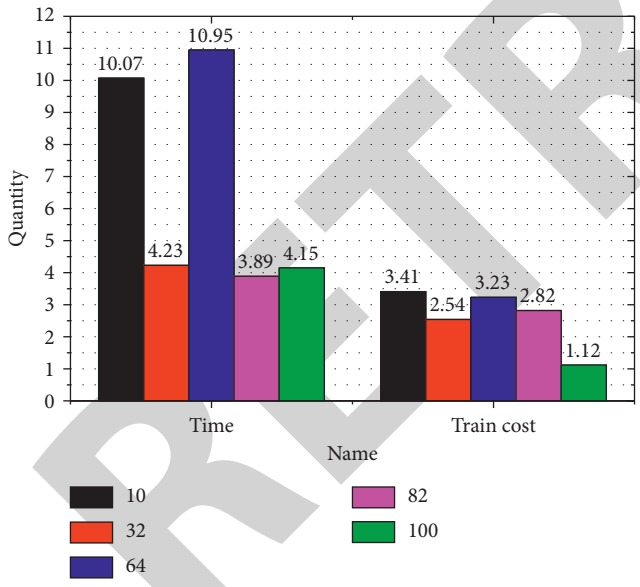

Figure 2: Training loss and time required for MRDL_4 model with different number of neurons in the hidden layer.

downward movement −DI and a trend indicator that includes ADX and ADXR. Given a stock X, the parameters of the DMI indicator are defined and calculated as follows. This method is a compressed estimation. It obtains a more refined model by constructing a penalty function, which makes it compress some regression coefficients, that is, force the sum of absolute values of coefficients to be less than a certain fixed value; at the same time, set some regression coefficients to zero. Therefore, the advantage of subset shrinkage is retained, and it is a biased estimate for processing data with multicollinearity.

$$\begin{aligned} +DM_i &= H_i + H_{i-1}, \\ -DM_i &= L_i - L_{i-1}. \end{aligned} \tag{5}$$

The long/short indicators +DI and −DI represent the strength of the upward and downward trend of the stock price. A larger +DI means a stronger uptrend, while a larger −DI, on the contrary, means a stronger downtrend. If +DI rises and −DI falls, and if +DI crosses −DI, then the stock price will have an upward wave and the buyer's power will be increasing; on the contrary, if +DI falls and −DI rises, and +DI crosses −DI, then there will be a downward wave and the seller's power will be increasing, representing a partial fall in the stock price.

In general, the movement indicators +DI and −DI are most accurate in predicting short-term stock buying and selling operations, and when the stock is in an oscillating uptrend, because in an oscillating downtrend, the rally up is short, and the movement indicators +DI and −DI take longer to respond, so it is impossible to accurately predict whether the uptrend can continue at this time, and the same problem exists in consolidation trends. In addition, it should be noted that when the rising indicator +DI rises from 20 or below to above 50, the stock is likely to have an intermediate upward wave, and similarly, when the falling indicator −DI rises from 20 or below to above 50, the stock is likely to have an intermediate downward wave. If both +DI and −DI fluctuate above and below the benchmark line of 20, then the stock is mostly in a box, and the stock market is balanced between long and short forces.

3.2. Descriptive Analysis. To better understand the data set, the author has divided the thirty-five stocks into four categories. Airline-related stocks: DAL, UAL, ALK, SKYW, ALGT, SAVE, CPA, JBLU; transportation and coordination: UPS, FDX, NM, EGLE, TK, EXPD, HUBG, DSX; transportation stocks: KEX, CHRW, ODFL, KNX, ASTG, ASIA, KSU, LSTR, *R*, OSG, JBHT, STNG, RAIL, NSC, CSX, UNP, MRTN, and others. After the classification step, the distribution, correlations, linear relationships, and seasonal effects are analyzed.

First, the distribution of the percentage changes in stock prices and Indigo prices was seen. For some stocks and small-cap stocks, the percentage changes varied greatly. For example, stocks related to aviation changed more than other stocks. It can be seen in Figure 3 that we chose four stocks related to aviation and plotted box plots to see the distribution. The percentage change ranges from -40% to 40%.

If the ADX crosses the ADXR, the cross formed at this point is called a golden cross, as marked by the solid line in Figure 3. This indicates a period of upward movement for the stock. If the ADX and ADXR move up to above 50 at the same time, the stock market will have an intermediate or higher upward movement, and if it moves up to above 80, the stock market will have a more than doubling of the market. If the ADX and ADXR move down to about 20, the stock market is in a consolidation phase and there is no market. When the distance between ADX, ADXR, +DI, and −DI lines is shortened, the stock market is also in consolidation, but the difference is that the method of using the DMI index to determine the stock market is distorted.

Furthermore, it was found that the percentage change in the price of indices is smaller than the percentage change in the price of stocks. Most of the percentage changes in indices prices are between -10% and 20%.

For the daily data of a given stock, the DMISV buy-sell strategy algorithm is used to calculate the output buy-sell points, and the buy-sell operation is performed based on the buy-sell points, and the stock return is calculated by equation (6), thus verifying the effectiveness of the DMISV buy-sell strategy.

$$D_b = \{DM_i, DM_{i+1}, DM_{i+2}, \ldots, DM_{i+k}\}. \quad (6)$$

Second, the correlation and linear relationship between the percentage changes in stocks were checked. The result is that there is a positive relationship between stocks in the same classification. However, this relationship may not be linear. Let me use the shipping and coordination category as an example. Figure 4 shows a scatter plot of these stocks; we can see that there are some positive linear relationships, such as UPS and FDX.

In addition, the relationship between indices from different countries is not clear through the scatter plot. It can be seen from Figure 5 that only SPX and NDX have a strong positive relationship because they are both indices from the United States.

The scope of stock market linkage can be the tendency to have common movements between stock indices of various countries or between various segments of a country's stock market and between the prices of various stock assets within each segment.

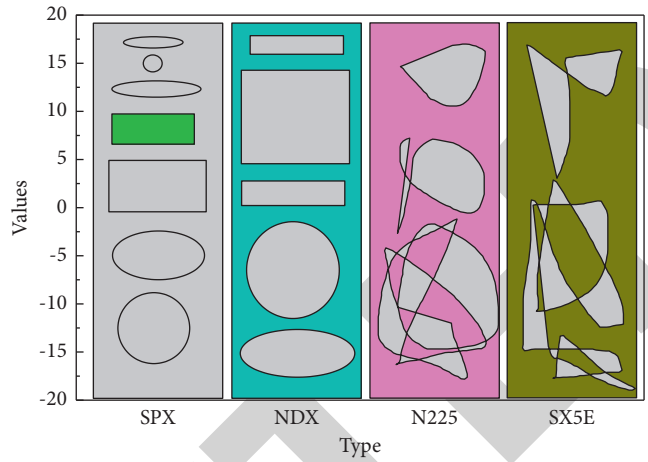

Figure 3: Box plot of percentage change in airline-related stocks.

Based on the principle of the regional scope and market scope of stock indices and stocks from large to small, the main four aspects of stock market linkage are described in terms of linkage among stock indices in the world, linkage among different stock indices between the same countries, linkage among various sections of the same stock market and different industries, and linkage among individual stocks in the same section [22]. Thirdly, the seasonality effect was analyzed. The result is that only some stocks related to airlines have a strong seasonality effect. We can see in Figure 6 that the stock price of Delta Airlines increased from October to December 2018. The seasonal effect may be caused by the holiday season. The economic fundamentals hypothesis is based on the efficient market hypothesis, which asserts that the linkage between stock markets comes from the linkage of fundamental factors between economies. Economic fundamentals as intrinsic causes drive the transmission of shocks between different markets mainly include the microstructure of the market, economic system, industrial structure, macroeconomic policies, and cultural background.

In addition, it is found that airline-related stocks are most affected by COVID-19. As can be seen in Figure 7, the price of Delta Air Lines is relatively stable until COVID-19, and there is significant volatility from COVID-19 onward. When one country's stock market is hit by a capital shock, investors in another country's stock market cannot accurately determine whether the capital shock is the result of an economic risk outbreak or a systemic error based on available information. In addition, coupled with geographical differences, policy differences, and institutional differences, this leads to irrational decisions at the economic level, that is, portfolio adjustments, resulting in stock market volatility in the invested stock market and so contagion to the next stock market. This is reflected in the fact that the opening prices of the stock markets with different opening times have an impact on the opening prices of the stock markets that opened earlier; moreover, the closing prices of

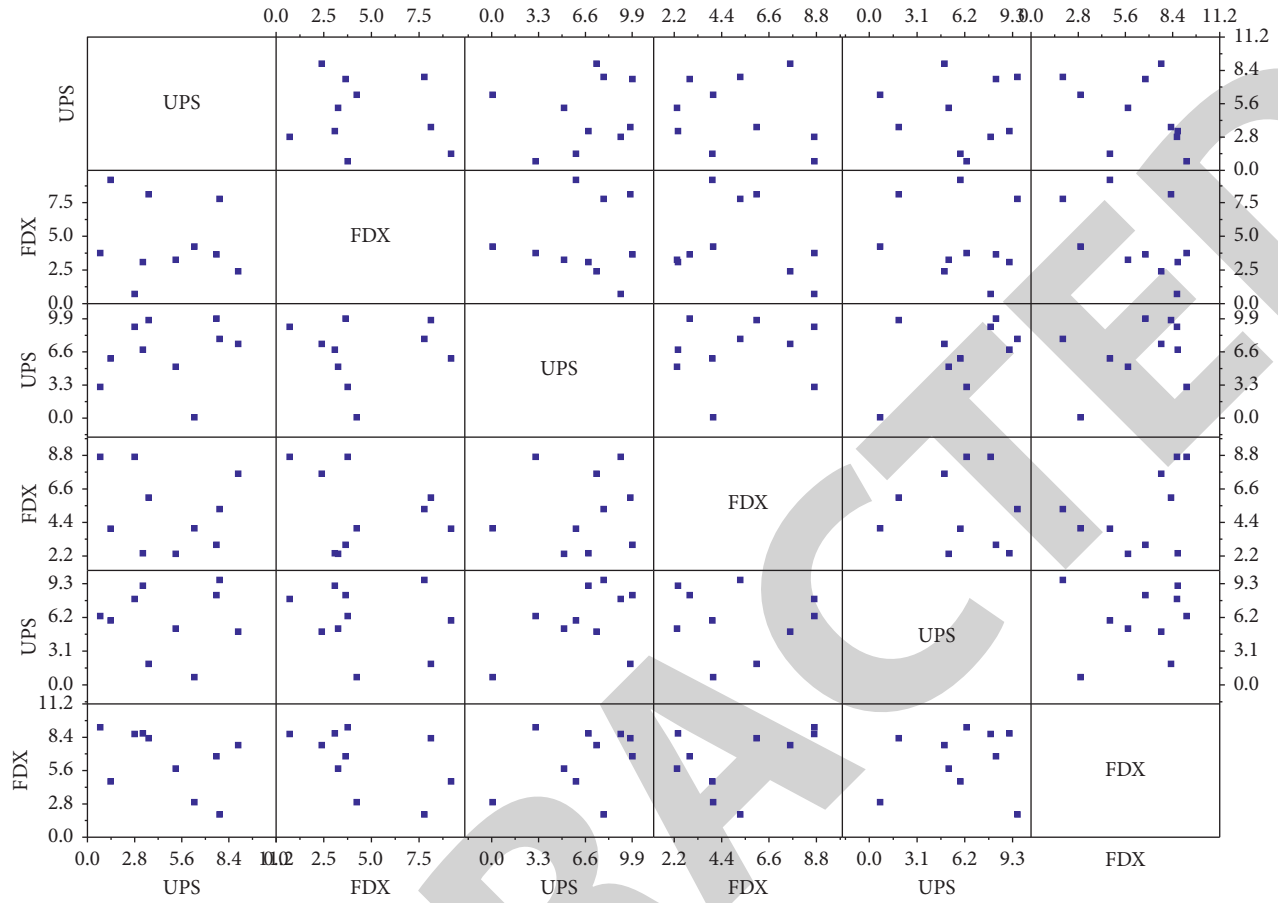

Figure 4: Scatter plot of shipping and coordination categories.

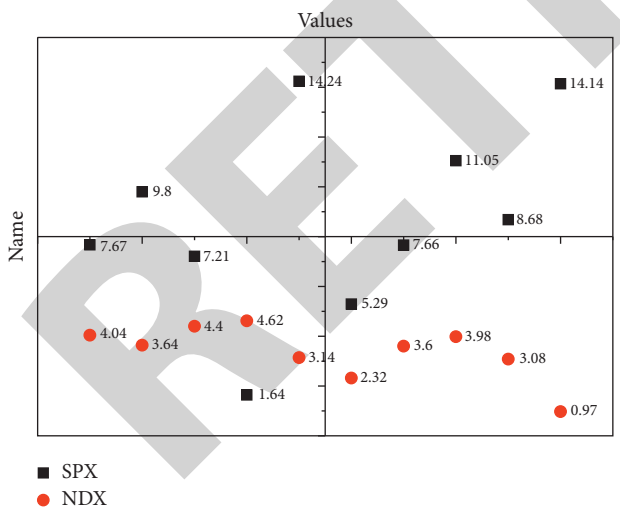

Figure 5: Scatter plot of indices.

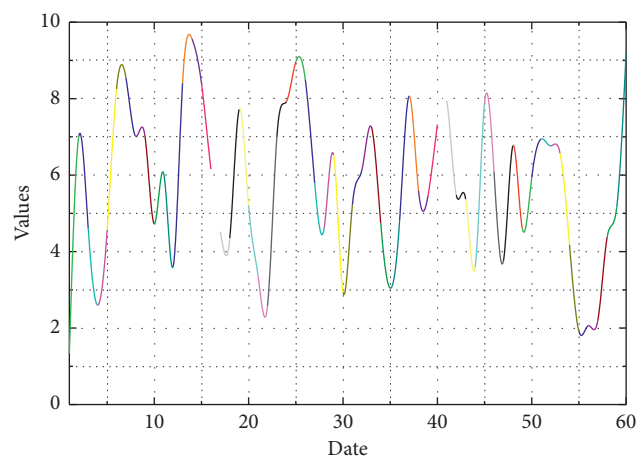

Figure 6: Time series plot of DAL stock prices.

the stock markets on the same day have an impact on the opening prices of the stock markets on the following day. The linkage effect of stock market contagion is more pronounced during the financial crisis.

Financial liberalization is becoming increasingly widely accepted in the economics world, and at the same time, a series of deregulation measures are gradually being implemented in many countries, further breaking down the barriers between financial markets, in which investors can allocate their assets to multiple markets as they wish, and cross-investment scenarios are gradually emerging. The stock and money markets of a country are influenced by the capital flows of these trading agents in the stock and money markets, thus creating a linkage between the two markets. At the same time, due to the gradual breaking down of the barriers to the flow of funds between the various financial

markets, trading entities can interoperate across financial markets for the financing of funds. In the current situation in China, the main trading entities in the stock market, such as securities companies, trust companies, and fund companies, can use the interbank lending market or the interbank bond market for short-term financing, and such financing activities will lead to a certain degree of capital flow from the money market to the capital market, and it is this flow of funds in the financial market that makes the intermarket. It is this flow of funds in the financial markets that make the linkage between the markets even closer.

4. Result Analysis

4.1. Forecast Analysis of Stock Prices and Printing and Dyeing Prices. Each stock and indices were analyzed by using Linear Regression, LASSO, Regression Trees, Bagging, Random Forest, and Boosted Trees. For each stock, the author used the percentage change in U.S. indices and the lagged variables of indices, as well as the lagged variables of percentage change for all stocks. Let me use the KNX stock as a specific example to illustrate my predictive analysis.

The linear regression model is the simplest. From the linear regression model, only the lagged variables of percentage change of SPX, a percentage change of ODFL, lagged variables of percentage change of SKYW, lagged variables of percentage change of MRTN, and lagged variables of percentage change of ALGT are significant. The R-squared is only 0.3105 and the MSE is 4.2346. When there are too many predictors, the linear regression is inadequate and difficult to interpret [23].

The LASSO model will give a more convenient result because it allows some coefficients to be zero. In addition, the cross-validation of the LASSO model shows that when we obtain the lowest MSE, the regression tree model results in 17 terminal nodes. We can see this result in Figure 8.

Most of the terminal nodes are on the right side of the tree, that is, when the percentage change in SPX closing price is greater than −0.64185. In the first two levels, the regression tree model uses only the percentage change in the closing price of SPX. Finally, Bagging, Random Forest, and Boosted Trees are used. There are too many predictors in the model; so to understand the results, one can look at the significance plot. Figure 9 shows the importance plot for Boosted Trees, as shown in Figure 9.

The first two predictors are the percentage changes in the SPX and NDX. In fact, for most stock prices, the percentage changes in SPX and NDX are the most important predictors.

The study of stock market linkage theory considers stock market linkage mainly as a common trend of change in the prices of multiple stock assets in the stock market. The study of this common trend of stock market changes is usually examined from the two perspectives of return and volatility of stock indices. The specific scope of the study refers to four aspects of stock market linkage: linkage among stock indices in the world, linkage among different stock indices between the same countries, linkage among sectors and different industries in the same stock market, and linkage among individual stocks in the same sector. The most authoritative definition of market contagion theory from a methodological point of view refers to the significant increase in linkages between stock markets in a country or a region after a financial crisis. This theory is consistent with the theory of increased stock market linkages in the wake of a financial crisis. Market contagion theory suggests that the crisis is mainly transmitted between stock markets of different countries through spillover effects, monsoon effects, and net contagion effects, and the corresponding mechanisms of contagion are trade spillover, financial spillover, industrial linkage, and net contagion. The relationship between linkage and market contagion is complementary; that is, the linkage between stock markets is established through different contagion channels, while the occurrence of financial crisis breaks the original linkage between markets, and the crisis strengthens the linkage between stock markets in the process of market contagion.

4.2. Naive Heuristics and Portfolio Optimization. This paper determines the lag order of Johansen cointegration based on the SC and AIC criteria and uses the Pantula principle to determine whether the tested model has a deterministic trend term, a linear deterministic trend term, and a quadratic trend term. The Johansen cointegration test shows that there is a long-run equilibrium relationship between European and US stock markets, both in the prefinancial crisis period and during the subprime and European debt crises. This indicates that mature and developed capital markets such as the European and American stock markets have gradually developed economic base level linkages in the context of economic and financial globalization, and although the contagion effect caused by the international financial crisis will weaken the economic base level linkages, it is impossible to completely offset them, so the European and American stock markets will show long-term linkages. In addition, the widespread and rapid spread of technology has gradually increased the interdependence of European and American economies and strengthened the international economic coordination mechanism, and the globalization of the economy has continuously led to the globalization of finance; thus, the linkage between European and American stock markets has rapidly increased.

For portfolio optimization, the Naïve Heuristics method is used. Naïve Heuristics is based on stock price forecasts, ranking stocks based on potential returns and allocating an equal percentage of capital to each stock. Moreover, the stock price forecast is calculated from the formula generated by LASSO. And the potential return is today's closing price minus the previous day's closing price. Here are some recommendations for 10 stocks from March 8 to March 12, 2021, as shown in Figure 10.

For the daily data of a given stock, the KDJSV buy/sell strategy algorithm is used to calculate the output buy-sell points and perform buy and sell operations based on the buy and sell points. The effectiveness of the KDJSV buy/sell strategy is verified by calculating the stock return. The highest stock return is achieved when the long-short indicator growth rate was equal to the threshold $c = 4$. The experimental results are shown in column R8. Using the

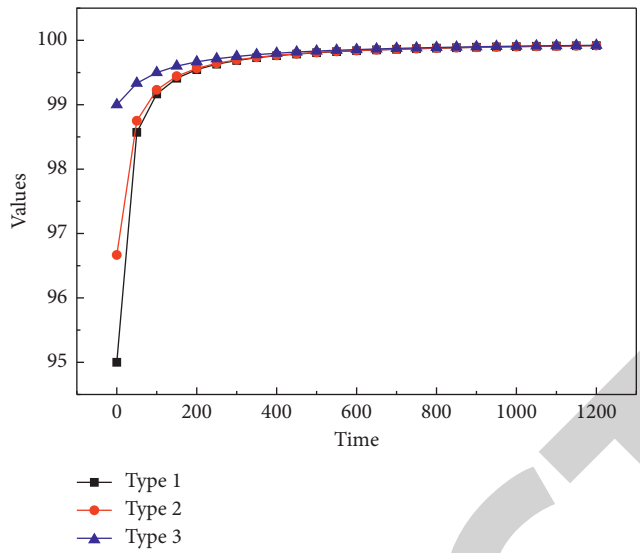

Figure 7: Time series plot of the percentage change of DAL.

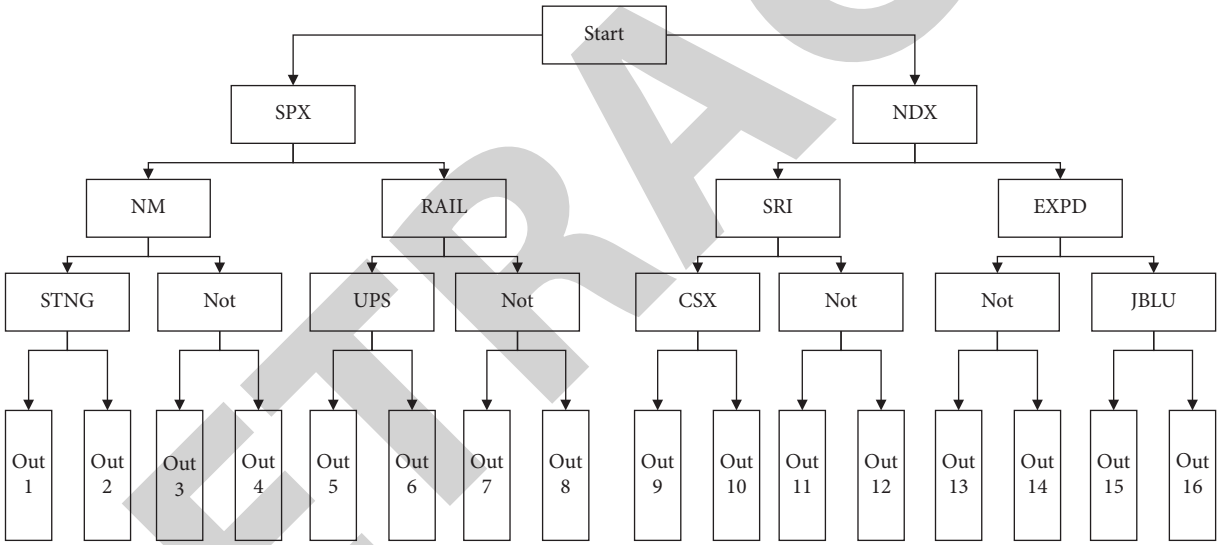

Figure 8: Regression tree model.

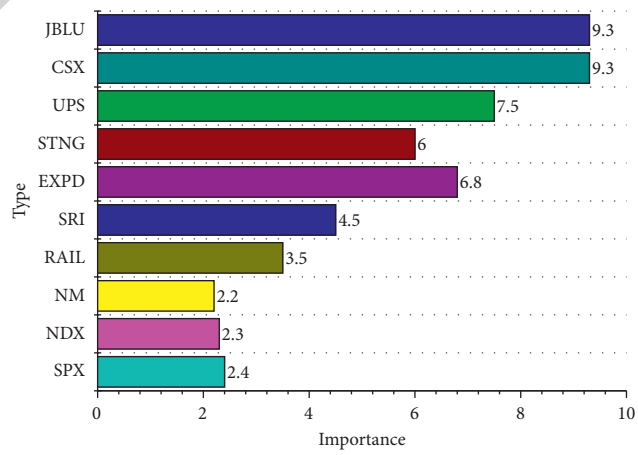

Figure 9: Importance of lifting tree diagram.

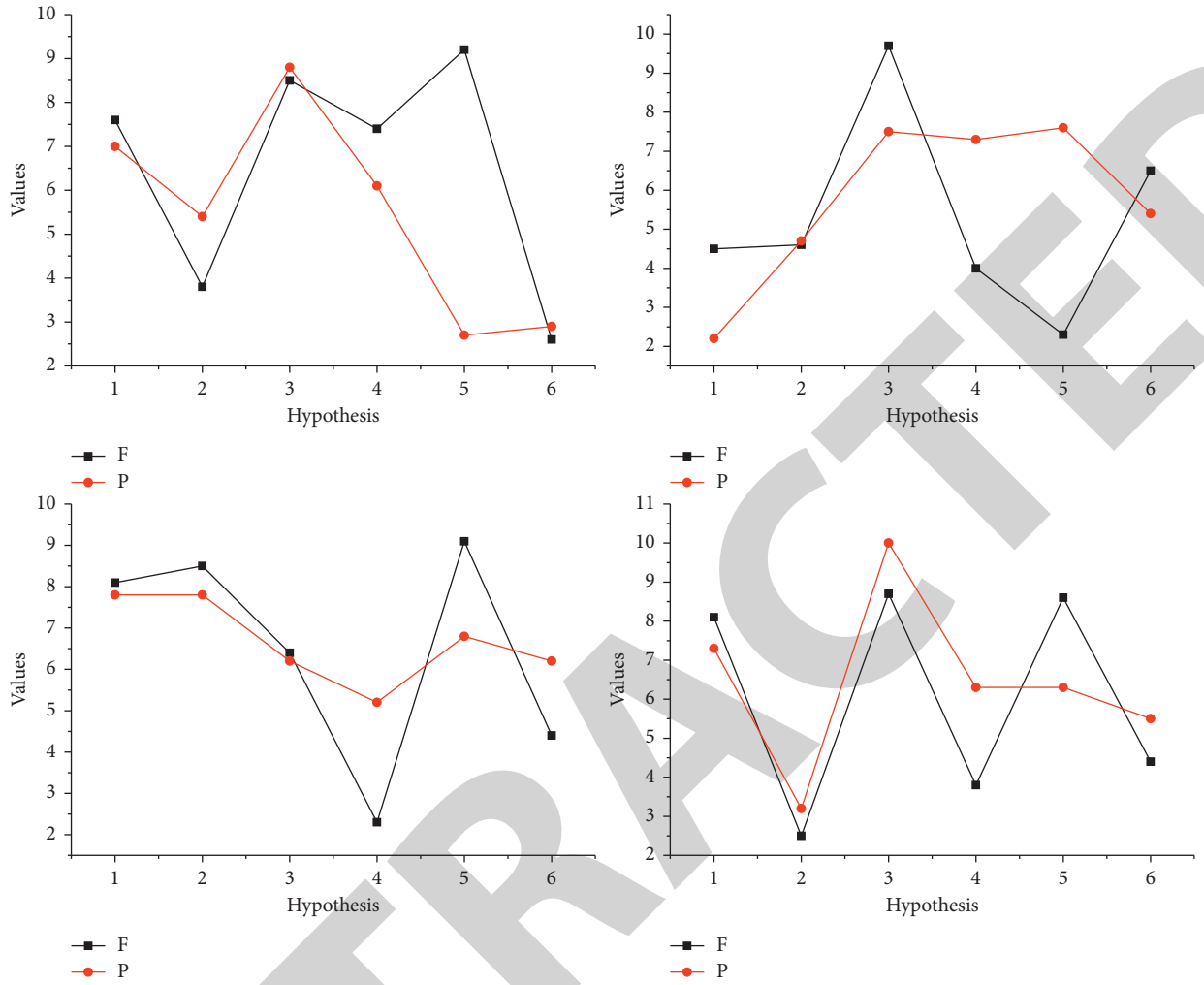

Figure 10: Causality test results.

KDJSV buy and sell strategy algorithm, 78.86% of the stocks had a return greater than 30% when $c = 4$ and 5.76% of the stocks had a negative return.

5. Conclusion

Since the stock examples are all from the US market, the results show that their prices are highly correlated with SPX and NDX prices. The link between different stocks is not obvious. It is difficult to use other stocks to predict prices. However, stocks in the same area tend to move in the same direction. In addition, stock prices and indices prices tend to move in the same direction. However, the movement of indices prices will be smaller than the movement of stock prices. Stock returns are highest when the long-short indicator grows at a rate iDK threshold. Focusing on 52 representative stocks in different sectors of the Shanghai and Shenzhen stock markets, buying and selling points were calculated using daily data from 2013.10.1 to 2018.10.17, and the KDJSV buying and selling strategy algorithm was used. 78.86% of stocks with $c = 4$ had returns greater than 30%, and 5.76% of stocks had negative returns. The DMISV buying and selling strategy is based on the DMI indicator. The KDJSV buying and selling strategy is based on the KDJ indicator. The MACDV buying and selling strategy is based on MACD indicator. The DKB buying and selling strategy is proposed based on DMI, KDJ, and MACD indicators. The stock system is complex, and there are many influencing factors. In this paper, only the stock opening price, closing price, and other factors of the stock itself are selected, but other economic factors related to the stock such as macroeconomic and financial policies are not considered; therefore, the selection of other factors affecting the stock price fluctuation as independent variables to judge the stock price trend is one of the contents to be studied in the future.

Data Availability

The data used to support the findings of this study are available from the corresponding author upon request.

Conflicts of Interest

The author declares that there are no conflicts of interest regarding the publication of this paper.

Hindawi
Journal of Mathematics
Volume 2024, Article ID 9854294, 1 page
https://doi.org/10.1155/2024/9854294

Retraction

Retracted: Multiple Collaborative Supervision Pattern Recognition Method within Social Organizations Based on Data Clustering Algorithm

Journal of Mathematics

Received 23 January 2024; Accepted 23 January 2024; Published 24 January 2024

This article has been retracted by Hindawi following an investigation undertaken by the publisher [1]. This investigation has uncovered evidence of one or more of the following indicators of systematic manipulation of the publication process:

(1) Discrepancies in scope

(2) Discrepancies in the description of the research reported

(3) Discrepancies between the availability of data and the research described

(4) Inappropriate citations

(5) Incoherent, meaningless and/or irrelevant content included in the article

(6) Manipulated or compromised peer review

The presence of these indicators undermines our confidence in the integrity of the article's content and we cannot, therefore, vouch for its reliability. Please note that this notice is intended solely to alert readers that the content of this article is unreliable. We have not investigated whether authors were aware of or involved in the systematic manipulation of the publication process.

Wiley and Hindawi regrets that the usual quality checks did not identify these issues before publication and have since put additional measures in place to safeguard research integrity.

We wish to credit our own Research Integrity and Research Publishing teams and anonymous and named external researchers and research integrity experts for contributing to this investigation.

The corresponding author, as the representative of all authors, has been given the opportunity to register their agreement or disagreement to this retraction. We have kept a record of any response received.

References

[1] W. Zhang and L. Pang, "Multiple Collaborative Supervision Pattern Recognition Method within Social Organizations Based on Data Clustering Algorithm," *Journal of Mathematics*, vol. 2021, Article ID 7890658, 12 pages, 2021.

Hindawi
Journal of Mathematics
Volume 2021, Article ID 7890658, 12 pages
https://doi.org/10.1155/2021/7890658

Research Article

Multiple Collaborative Supervision Pattern Recognition Method within Social Organizations Based on Data Clustering Algorithm

Wei Zhang[1,2] **and Lili Pang**[3]

[1]*School of Public Administration, Hohai University, Nanjing, Jiangsu 210098, China*
[2]*College of Economic and Management, Nanjing Institute of Technology, Nanjing, Jiangsu 211167, China*
[3]*Development and Planning Division, Nanjing Xiaozhuang University, Nanjing, Jiangsu 211171, China*

Correspondence should be addressed to Wei Zhang; zhangwei@njit.edu.cn

Received 21 October 2021; Revised 5 November 2021; Accepted 10 November 2021; Published 8 December 2021

Academic Editor: Naeem Jan

This paper proposes a multiple collaborative supervision pattern recognition method within social organizations based on data clustering algorithm to realize diversified supervision within social organizations and improve the effect of the said pattern recognition. Firstly, the characteristics and functions of social organizations are analyzed, and the definition of social organizations is given. Further, this paper studies the meaning and characteristics of social organization supervision, analyzes the failure of internal supervision of social organizations, and then determines the internal governance elements of social organizations. In addition, the basic steps of pattern recognition are given. Finally, multiple collaborative supervision patterns recognition within social organizations is realized based on data clustering algorithm. Experiments show that this method can improve the recognition accuracy of multiple collaborative supervision patterns and reduce the recognition time.

1. Introduction

Social organizations are the operating subjects of public welfare undertakings, and their credibility determines the rapid development of public welfare undertakings. In recent years, there have been frequent negative public welfare news in China, such as the "Renrenhui" and "Shanxinhui" scam, zhihu goddess fraudulent donation, public welfare worker thunder incident, "Luo Er," and other incidents, which have caused an unprecedented crisis of confidence in China's public welfare undertakings, resulting in a lack of public trust in social organizations. Through in-depth interviews, it is found that there are many problems in the development of social organizations, such as incomplete legal system, lack of transparent information disclosure, and lack of professional talents [1]. Further investigations show that all these problems are caused by the imperfect internal governance structures of social organizations, which affects the healthy development and benign operation of organizations. The outline of the 13th Five-Year Plan clearly proposes to "improve the management system of social organizations, and form a modern social organization system in which government and social organizations are separated, rights and responsibilities are clearly defined, and autonomy is implemented in accordance with the law." In relevant documents issued by the Ministry of Civil Affairs, it is pointed out that measures such as party building, financial audit, and third-party evaluation should be strengthened, which puts forward higher requirements for internal supervision of social organizations [2]. Zhang et al. [3] proposed the refinement recognition algorithm of power load model based on kernel density clustering, Fan et al. [4] worked on spherical data clustering and used nonparametric Bayesian mixture models for feature selection, and Liu et al. [5] described the pattern recognition of power consumption. For more on pattern recognition and cluster analysis, we refer the reader to [7–12] and [6, 9–13], respectively.

The description and classification of a sequence of events are called the pattern recognition, whose research object is summarized into two categories: the intuitive image and the nonintuitive image. Moreover, the four main parts of the proposed method are as follows: (i) acquisition of information: attaining data by analyzing the topic of interest, (ii) processing: eliminating the noise to achieve the object perfect for computer to deal with it, (iii) feature extraction: processing and analyzing the data to eliminate false, retain true, and extract the features that reflect the essence of things, and (iv) classification decision: using algorithms to identify and classify the information.

Social organization is the third sector outside the government and market, and it is a new form of organization in the process of social and economic development. Whether social organizations can develop in a healthy and orderly manner, the internal governance of social organizations is the key. This paper introduces data clustering algorithm to identify multiple collaborative supervision modes in social organizations and promote diversified supervision strategies in internal governance of social organizations, in order to solve the internal governance dilemma of social organizations and promote the standardized development of social organizations.

This paper is organized as follows: Section 1 presents the introduction and literature review. Section 2 defines the social organization. In Section 3, the meaning and characteristics of social organization supervision are explained. The multiple cooperative supervision patterns recognition method in social organizations based on data clustering algorithm is given in Section 4. Section 5 contains the experimental analysis and Section 6 concludes the paper.

2. The Definition of Social Organization

Globally, every country or region has its own cultural and social environment, so social organizations have different types and forms of appellation in various countries. There is no substantial difference between these appellations, but they are different in expression. China also has different degrees of expression for social organizations, including "civil organizations," "intermediary organizations," and "mass organizations" [3]. The concept of "social organization" began to appear at the sixth Plenary Session of the 16th CPC. After 2006, official documents began to use the more appropriate title "social organizations" instead of "non-governmental organizations." In essence, the "social organization" used in China is no different from the "non-governmental organization" and "non-profit organization" commonly used around the world. It is a concept with more Chinese characteristics. According to Wang Ming, NPS are actually organizations that adhere to the goal of "non-profit," uphold the concept of mutual benefit, adhere to the nature of public welfare, and are independent of the party and government system.

2.1. Characteristics of Social Organization. Social organizations do not belong to the government, nor are they composed of the market, but they have independent "third parties." Their characteristic is usually distinct, concrete performance is nongovernmental, public welfare, and sociality. One is nongovernmental. Social organizations are actually folk groups formed based on voluntary behaviors [4]. Therefore, they are quite different from national organizations and have extremely outstanding characteristics of nongovernment. Based on the decision-making mechanism, social organizations are full of autonomy, which can reduce constraints and improve efficiency in decision-making. Based on the operating mechanism, social organizations always adhere to the concept of survival of the fittest and have a sense of competition. Once social organizations lose the quality of service, they will inevitably be questioned by the public and face difficulties. On the other hand, government departments have the important feature of administrative monopoly, so they can exist forever without worrying about elimination [5]. In addition, social organization comes from the masses. The organizational structure is relatively simple and flat. As a result, they often have more flexibility as activities progress. Second, public welfare, namely, nonprofit, has always been an important feature of social organizations' independence from the market [6]. First of all, being nonprofit is the fundamental principle of social organization. Social organizations are not prohibited from engaging in business-related activities, but their income is used exclusively for public services. Members of social organizations shall be prohibited from seeking personal gains. Secondly, social organizations tend to have more rigorous and strict self-control systems. Finally, social organizations always uphold the concept of property preservation, and their income is mostly in the form of social donation. Its property rights are not based on national property rights or private property rights but are derived from public resources and have the nature of public property rights [7]. There is no doubt that social organizations have undeniable characteristics of public welfare. Third is sociality. Social organizations work in relatively fixed areas, that is, education, charity, poverty alleviation, and other works, with a significant social nature. Moreover, social organizations also focus on the public. Based on this, it is identified as having social characteristics. The core characteristic of social organizations is being nonprofit, their material resources are mostly from donations, and their staff rely on voluntary participation of volunteers. Moreover, output also has a certain sociality. The purpose of all kinds of services provided by social organizations is to provide better life enjoyment to the public rather than applying them to themselves, so they are public-welfare-oriented [8]. Finally, accountability is also social. One is to establish a complete internal supervision and undertake various forms of supervision from the public. These three characteristics are the characteristics by which social organizations are distinguished. Indeed, with the sustainable development of society, the three characteristics of nongovernment, public welfare, and sociality will be adjusted accordingly [9]. However, it always exists and is an important guarantee that social organizations can be independent from government and enterprises.

2.2. The Role of Social Organization. With their own advantages, social organizations play an irreplaceable role in the appeal of public interests, the adjustment of social contradictions, the provision of public goods and services, the provision of employment opportunities, the enrichment of old-age services, the protection of vulnerable groups, the promotion of public spirit, and other aspects.

2.2.1. Make Up for Government Failure and Market Failure. If the efficiency of government departments is difficult to improve, resource utilization rate is too low and is bound to lead to resource waste. Moreover, the market system suffers from monopoly, which also leads to excessive rigidity in the distribution of goods and services, resulting in social development that is difficult to meet expectations. The advantage of social organization lies in its characteristics of being nongovernment and nonprofit. Therefore, it has an ideal performance in dealing with government failure and market failure [10].

First, social organizations can share government functions to a certain extent. Looking around the world, although the form of single government governance can maintain the authority of the government, its cost support is high and the operation efficiency is not optimistic. In addition, the government often lacks internal supervision, which leads to failure, which is contrary to the concept of interest diversification. If the performance is not up to expectations, public opinion will become worse and the government's recognition will be greatly reduced. Social organizations have unique advantages in the category of fair products. The government and social organizations give full play to their advantages and try to cooperate, helping to provide the public with more diversified forms of services.

Second, the existence of social organizations also provides important carriers for communication and interaction between the government and the public. Under the previous model, there was no buffer between the government and the public. If there is a dispute between the two, due to the lack of interest integration mechanism, serious opposition and other events often occur. If the public believes that the government's policies are too extreme, they lack the necessary communication system and mechanism and even take extreme measures to resist, threatening the stability of the social structure [11]. As nongovernmental organizations, social organizations can become a platform for the government to communicate with the public, effectively deliver government policies to the public, and organize and negotiate the interests of different groups. Moreover, social organizations can also conform to norms and express corresponding interests. Therefore, social organizations promote the effective communication between the government and the public, alleviate social contradictions, and create a stable social environment for social construction.

Third, social organizations also help to allocate social resources. Social organizations have the important feature of being nonprofit. As a result, they are very different from the market companies focused on competition. The corresponding social resources of social organizations can be divided into two categories: one is the resource reserves obtained by charitable donations from different channels and the other is volunteer groups that are dedicated and do not ask for anything. The rational and scientific allocation of social resources ensures that social organizations can express their service objectives and gain public recognition. This will also enable them to supplement more substantial charitable resources and expand their volunteer ranks. It has positive benefits in the field of public welfare activities and can effectively control the negative crisis caused by market failure [12].

2.2.2. Promote Social Harmony and Stability. One of the significances of social organizations is to provide corresponding public services to the society. For example, we will support the poor, improve medical conditions, and promote employment. Social organizations play an irreplaceable role in the development of people's living standards and are also a key link to buffer social contradictions and promote social harmony.

First, social organizations can play a role in alleviating social problems. Social organizations can provide corresponding support for public interest expression. In addition, they can also actively allocate social resources to ensure that the social vulnerable groups get spiritual care, as well as the necessary material support, to solve the urgent need, to ensure that their living needs are guaranteed.

Second, social organizations ensure the diversity of public life [13]. As China's reform and opening-up policy continues to unfold, cultures from all over the world are becoming more and more integrated. Based on this, the public's cultural needs are also colorful. The emergence of social organizations makes it possible for the public to find their favorite social organizations to participate in various social activities based on their own needs. This can also bring about a flowering of social life.

Third, social organizations can promote the harmonious development of man and nature. The report of the 18th National Congress of the Communist Party of China once explained the scientific discussion of "five-in-one," and the construction of ecological civilization is increasingly valued and respected [14]. For example, environmental protection social organizations are committed to assisting the government in formulating policies related to environmental protection and providing professional advice. Education and promotion of environmental protection knowledge and concept play a vital role in promoting the harmonious development of man and nature.

3. The Meaning and Characteristics of Social Organization Supervision

Supervision of social organizations is a process in which the subject of supervision supervises and manages the work of social organizations. This paper defines the supervision of social organizations as follows: the supervision subject of social organizations carries out follow-up supervision and corresponding management of the rules and regulations of

legally registered social organizations, members' daily organizational behavior, and financial situation. Their characteristics are as follows.

First are institutionalization and rule of law. In short, it is the system composition in the supervision of social organizations, namely, the system composition that social organizations should strictly abide by when implementing supervision and management [15]. Based on the cases of developed countries, we can clearly realize that the institutionalization of supervision can provide essential legal guarantee for the supervision of social organizations. Australia's Public Service Act and Japan's Government Policy Evaluation Act are all based on legislation to ensure that the government can meet the requirements of norms and conduct orderly supervision on social organizations. In the category of social organization legislation in China, there is a certain degree of lag. In fact, until the current stage, China has not set up systematic and mature supervision laws for social organizations. Relevant requirements and opinions are scattered in other laws and regulations [16].

Second are openness and transparency. Information disclosure of social organizations is conducive to public supervision, and it is also a prerequisite for social organizations to perform their public welfare duties and can provide reliable support for the protection of public rights and interests. In recent years, government information disclosure has also been actively explored in various parts of China, which is conducive to organization members and the public to understand information related to activities of social organizations, improve social credibility, influence, and cohesion, and implement industry self-discipline [17].

Third is mechanism diversification. The regulation of social organizations is analyzed: whether it comes from the government regulation of external regions, or is a form of self-supervision that develops within the organization. They all have the characteristics of rich levels, diversified subjects, and extensive channels. On the one hand, there is the government supervision, and, on the other hand, there is the public opinion supervision from the public or the news media. Internal supervision and management are also abundant, and the corresponding supervision from the system and members is of great value [18]. It also includes the oversight provided by the organization's stakeholders. Fourth is target responsibility. Fayol once regarded power and responsibility as the components of management principles, indicating that power and responsibility are interdependent and complementary to each other. Responsibility goes hand in hand with power, and if it has power, it also has to bear the corresponding responsibility. Social organizations are public welfare, so their public social responsibility is highly valued. Unfortunately, the accountability system set up based on the supervision and management of social organizations still needs continuous improvement and supplement: for the first time, the ethnic composition of the responsible subject is known, followed by the detailed responsibility inspection steps and finally strengthening accountability.

3.1. The Content of Social Organization Regulation

3.1.1. Supervision over Registration of Social Organizations. In addition to the supervision of social organizations, our country adheres to the form of "preventive system." In short, the state has raised the threshold requirements for the registration of social organizations and strictly upheld the requirement of permission registration. If NGOs fail to meet the needs and obtain permissions, they will naturally find it difficult to register and will become illegal. The advantage lies in that the state can effectively grasp the legitimacy and compliance of social organizations and complete strict restrictions on illegal organizations [19]. According to the relevant regulations on the registration of social organizations and foundations, the registration of social organizations should strictly abide by three conditions. Social activities should first conform to the purpose and have the characteristics of public welfare, second have independence and autonomy, and third have the asset composition that meets the demand, as well as the fund supplement that conforms to the law. Moreover, the appellation of social groups should not be arbitrary but conform to the legal norms and avoid violating moral customs. When naming a social group, it should strictly follow the business category, membership configuration, operation interval, and other factors, and it should clearly grasp the characteristics of the organization.

3.1.2. Daily Supervision of Social Organizations. The government's daily management of social organizations focuses on two levels. The first is the construction of laws and regulations. In fact, the daily management of social organizations is complicated, and many behaviors are too chaotic to be controlled. Therefore, in addition to daily management, administrative regulations are often attached importance. The second is the annual inspection system. The regulation on the registration and management of social organizations says strict annual inspections must be carried out around social organizations, with the authorities responsible for corresponding preliminary audit tasks. In addition, major activity reporting mechanism and corresponding examination and approval system are among the key components of daily management.

3.1.3. Financial Supervision of Social Organizations. The Chinese government's financial supervision of social organizations is reflected in three aspects: The first aspect is the requirements for being nonprofit. The Regulations on the Registration and Administration of Social Organizations (2016) clearly instruct social organizations to prohibit profit-based activities. The second aspect is in view of the proportion of expenditure of donated property requirements. The Public Welfare Donation Law of the People's Republic of China clearly states that the fund expenditure in public welfare should meet the specific proportion required by the state. The third aspect is practice financial disclosure system. The Regulations on the Registration and Administration of Societies provide instructions for financial disclosure, and

relevant behaviors such as accepting or applying donations need to be made public in accordance with the regulations.

3.2. Classification of Supervision of Social Organizations. In terms of type division, social organizations focus on their own characteristics. Social organizations have outstanding characteristics of independence and have the important characteristics of nongovernment. This determines that a public service is not a government welfare, nor is it a corresponding private product derived from a for-profit organization. Social organizations are engaged in precisely the public work that the government and profit-making institutions, for some reason, resist, find difficulty to accomplish, or are rarely able to accomplish. In order to grasp the basis and significance of the classification of supervision types of social organizations, the first task is to understand the classification of social organizations. Before the third Plenary Session of the 18th CPC Central Committee, based on traditional thinking, China pointed out that social organizations are actually composed of four categories: industrial and commercial economy, social welfare, charity, and social service. Based on the trend of The Times, the third Plenary Session of the 18th CPC Central Committee was redistributed into six categories, namely, industry associations and chambers of commerce, public welfare charities, science and technology, urban and rural community services, interest and volunteer service organizations, and religious organizations. In the classification of social organization supervision, the corresponding classification methods of social organization should not be strictly adhered to.

3.3. Determine the Internal Governance Elements of Social Organizations

3.3.1. Multiple Supervision Subjects within the Organization. The subject of supervision is the one or several parties that shoulder the responsibility of internal supervision of social organizations. According to the logic model of axial coding and responsive regulatory perspective of pluralistic social organization coordinated regulatory path, in the social organization management regulation, use of the government, the self-regulation, the public, and the four elements of the third-party institutions coordinated regulation, to contribute to the improvement of the social organization management, make its management specification, to enable sustainable development to the organization.

(i) Government: centralized supervision of organization operation. The government is responsible for centralized administrative management of social organizations, so it plays the main supervision role of internal governance. Its supervision of social organizations is manifested in the formulation and implementation of rules for the registration and management of social organizations, the implementation of supervision of social organizations according to law, and the supervision and guidance of local social organization registration and management. In the narrow sense, the supervision responsibility is the daily supervision of the operation of social organizations, such as the conduct and result supervision of the managers, council, secretariat, and ordinary members of social organizations under the constraints of laws and regulations. It is also the main content of daily supervision for social organizations to receive classified guidance and periodic inspection from centralized management departments; and this is taken as an important measure to normalize the supervision of the daily operation process of social organizations.

(ii) Self-regulation: the regulation of improving internal governance. In order to improve the internal management level of social organizations, social organizations can also carry out self-regulation and improve the ability of self-discipline and autonomy. Therefore, self-regulation is also the main supervision subject of the internal governance of social organizations. Through a large number of media surveys on charitable activities with public welfare corruption and severe damage to the credibility of social organizations, it can be found that there is an urgent need to establish and improve the self-discipline and supervision mechanism of social organizations to improve their management level and improve operational efficiency. At the present stage, the internal governance of social organizations in China has some problems, such as insufficient supervision consciousness, lack or imperfect supervision system, insufficient supervision executive force, and weak self-discipline mechanism. It is easy to make self-supervision become a mere form of self-justification, resulting in the failure of supervision. The mutual supervision mechanism from outside social organizations has not yet been formed. The establishment of the internal management and supervision mechanism of social organizations should be based on laws and regulations and on the premise of abiding by the rules of the industry, and the responsibilities and powers of decision-making organs, executive organs, and supervision organs should be clearly defined, and various activities of the organizations should be carried out within the regulatory framework.

(iii) Public: strengthen the consciousness of subject supervision responsibility. The conditions for the public to be the subject of supervision come from three aspects. The first is the donation or service purchase behavior of the public directly to social organizations. As a principle of reciprocity in real right transaction, social organizations naturally have the obligation to accept the supervision of the public, which has the attribute of market. The second is that social organizations provide services

to the public as an important undertaking subject. For example, the government purchases public services from social organizations, but, as the served party, the public can make joint and several claims to social organizations, thus forming an obligation of indirect supervision. The third is that, in view of the public welfare nature of social organizations, every public that cares about the organization or has doubts about the vision and behavior of the organization can, as taxpayers, enjoy the natural right to supervise the social organizations approved by the government and registered with qualifications. Therefore, the public supervision with extensive participation consciousness can urge social organizations to strengthen self-discipline.

(iv) Third-party evaluation agencies: strengthening supervision during and after the event. The government transfers part of its regulatory authority through certain authorization or service outsourcing so that more other institutions become regulatory subjects. The supervision authority of third-party evaluation institutions on social organizations mainly comes from the transfer of government power. Internal governance of the third-party supervision that refers to the social organization has the qualification of the interest related third parties under the principle of laws and regulations, scientific design review procedures, and inspection standards, to organize society including but not limited to financial audit, operation management, achievement and performance appraisal, and specified aspects of assessment and grading and issue the evaluation report. As a useful supplement and correction of government supervision, third-party supervision with professional and independent characteristics and basic requirements plays an important role in the modernization of China's internal governance system and governance capacity of social organizations. Its importance is reflected in the following aspects: First, it promotes the transformation of government functions and desalinizes the compulsory administrative color in the evaluation process. Second, it promotes the social transformation of the service-oriented government. This is not only because third-party supervision can divert the burden of the government but also because third-party supervision and evaluation can play a greater role in strengthening the in-process and post-process supervision. Third, third-party evaluation focuses on the significance of social forces in the coordinated supervision of social organizations and enhances the credibility of social evaluation.

3.3.2. Multiple Regulatory Contents within the Organization. In the process of using the supervision of social organizations, in the link of internal governance, the four important contents of the supervision of the mission and voluntary spirit of the organization, the sound evaluation mechanism and supervision mechanism, the quality of the leaders, and the structure of the organization are realized, so as to expand and improve the internal governance of social organizations.

(i) Organizational mission and volunteerism. The board structure can make the organization's mission more clear, can make the organization's decision-making strategy more reasonable and feasible, can make the supervision more comprehensive, and can achieve self-assessment. The mission is the direction of an organization, which needs to be defined at the beginning of its establishment and gradually adjusted with the development. The primary responsibility of the Board of Directors is to define the mission of the organization, ensure that the members of the organization are loyal to the mission, and put forward specific provisions and constraints on the goals, activity areas, and development modes of the organization. The establishment of the organization's mission to correspond to the situation of national development, in terms of development at the present stage in China, the need to address the education, grassroots governance, and related problems such as poverty and environmental governance, because of these problems is crucial in the field of society; the government needs to pay attention to these important issues, to solve these problems to improve the public satisfaction. The government can provide policy and financial support to social organizations, and it is also required that the government further strengthen the mission, voluntary spirit, and supervision of social organizations.

(ii) Sound evaluation mechanism and supervision mechanism. The rapid development of the social organization brought a great challenge for the regulatory system, improves and perfects the system of social organization regulation, and must introduce the social institutions of the third-party evaluation and objective evaluation on the performance on the development of social organizations, to strengthen social organization registration, financial content, project activities, organization development, and matter, and afterwards supervision has become the important content of social organization internal governance. 19th National Party Congress pointed out the direction of the future development path of social organization and also put forward more specific requirements, social organization regulation according to ZhengShe separation reform train of thought, not only at the time of registration review stage, and to improve the existing evaluation system as soon as possible, set up in advance, matter and afterwards whole process supervision system, to perfect innovative ways and means and ensure the orderly progress of supervision over social organizations.

(iii) Leadership qualities. Council members, administrative staff above the middle level, and those responsible for major projects are considered to be the leadership of the social organization. The quality of leaders is the key to the existence and development of social organizations and the fate of organizations. This is especially true for social organizations. Due to their special organizational structure and governance mode, the quality of leaders is very important for the realization of social organizations' goals, activities, development trajectory, and organizational performance. Leaders of social organizations should not only have strong professional qualities like corporate executives but also take into account the particularity of social organizations and possess high political quality and moral accomplishment, so as to guide members to practice the mission and core socialist values of social organizations.

(iv) Personnel structure. Human resources are the foundation and guarantee for the development of social organizations, while personnel structure is the key factor restricting the effect of internal governance of organizations. Through the investigation, it is found that part-time workers account for a relatively high proportion of social organizations, and the uneven quality of staff is also a common problem. Therefore, we must strictly implement the basic requirements of the personnel structure in social organizations: First, the proportion of full-time staff in social organizations is higher than that of part-time staff. Second, in the total number of staff in social organizations, those with bachelor's degrees or above account for more than half. Full-time staff refers to those who have established formal social labor relations with social organizations and those who are specialized in the work of social organizations, excluding administrative staff, labor dispatch personnel, and part-time staff and those who are rehired after retirement. Therefore, to strengthen the construction of personnel in social organizations, we should not only ensure the number of staff, especially the number of full-time staff, but also pay attention to the quality of staff and optimize the personnel structure of social organizations.

3.3.3. Analysis of the Failure of Internal Supervision in Social Organizations

(i) Policies and regulations lag behind. A sound legal system is the institutional guarantee for the good operation of society, and the legal operation and supervision of social organizations are the fundamental prerequisite for the governance of social organizations. The improvement of relevant policies and regulations can guide and standardize the governance of social organizations, facilitate the connection between the two regulatory parties, and provide a framework for the dialogue and consultation on regulatory matters. At the present stage, the legal system of internal governance and supervision of social organizations in China is not perfect. In the survey, many social organizations mentioned that local administrative departments are ineffective in publicizing and promoting laws and regulations or fail to formulate corresponding implementation rules in time, resulting in social organizations having no basis for improving internal supervision. It also affected the enthusiasm of social organizations to implement standardized supervision and improve. On the contrary, the imperfection of policies and regulations has become the main problem restricting the internal governance and supervision of social organizations.

(ii) The management mechanism fails. The internal system design of social organizations should fully ensure the achievement of social organizations' goals and visions and the efficiency of daily operation and provide a performance-related supervision and accountability mechanism for implementation. At present, in the investigation, it is found that the human resource management system, volunteer system, and financial management system of many social organizations are not perfect. Due to the inefficiency or ineffectiveness of the internal management system of social organizations, the operation and development of social organizations cannot be orderly and then the supervision efficiency of the internal governance of social organizations is affected.

(iii) The internal governance structure is not sound. The internal governance structure and management mechanism of social organizations complement each other. It is the carrier of social organization system and the institutional entity for social organizations to realize various operational practices. The redundancy and lack of internal governance institutions will have a negative impact on supervision. However, they appear on different occasions. In the current supervision system of social organizations, institutional redundancy often exists in various administrative supervision subjects, while the content of social organizations is often manifested as the lack of institutions due to the imperfect construction, so that they cannot exercise and complete the docking of supervision functions. Only when social organizations achieve organic structural cohesion can they release organizational efficiency to the greatest extent.

(iv) The application of network technology lags behind. For a long time, because of the uniqueness of administrative mechanism, government agencies have tended to lag behind those outside the system in terms of operation efficiency and new technology application. In addition, it is also necessary for the

public to use Internet technology to participate in the internal governance and supervision of social organizations. With the rapid development of modern information technology and Internet of Things technology and the increase of social organization activities, it is necessary to use network technology to complete the supervision information exchange, supervision policy formulation, and supervision form research and judgment. It has become a general trend to transform traditional application fields including internal governance and supervision of social organizations with the concept of "Internet plus" and big data analysis technology.

4. Multiple Cooperative Supervision Patterns Recognition Method in Social Organizations Based on Data Clustering Algorithm

Pattern recognition refers to the classification and description of a series of processes or events. The processes or events to be classified can be a series of physical objects or some relatively abstract psychological states. Processes or events that have some similar properties fall into one category. The research object of pattern recognition can be basically summarized into two categories: One is intuitive image, such as image, graph, text, remote sensing image, cell, or other biological slices, etc. The other type of image is nonintuitive, such as language, ECG pulse waveform, object detection waveform, and seismic wave. The general components of a pattern recognition system are shown in Figure 1. There are four main components.

The first part is the acquisition of information, which is equivalent to the investigation and understanding of the object of study, from which data and materials are obtained. The second part is preprocessing; its purpose is to remove interference, noise, and difference and turn the original object into a form suitable for computer feature extraction. The third part is feature extraction. Its function is to process, sort out, analyze, and summarize the data materials learned from the investigation to eliminate the false and retain the true, remove the dross, and extract the essence, as well as extracting the features that can reflect the essence of things. Of course, what features are extracted and retained has a lot to do with what kind of judgment is adopted. The fourth part is the classification decision, that is, according to the extracted characteristic parameters, using a classification discrimination algorithm (such as fuzzy clustering analysis method) and discrimination rules, to classify and identify the information and get the recognition results, of course, in the classification decision, must consider the validity of the classification.

4.1. The Basic Steps of Pattern Recognition. In practical applications, the design of a single pattern recognition system is a complex task and is often a recycling process. It is impossible to try to provide a comprehensive algorithmic process but considering the intrinsic relevance of pattern recognition, probably to describe the basic steps of pattern recognition system is feasible; therefore, the basic implementation steps of a pattern recognition system can be described as follows:

Step 1: Consider possible description; we study pattern recognition, including quantification of pattern structure and estimation of probabilistic description, possible intra- and interclass similarity measurement, distortion of pattern, invariance of noise source, and description.

Step 2: Identify utilized characteristics and measurement data.

Step 3: Consider the expected system operating indicators and computing resource constraints, such as running speed and classification accuracy.

Step 4: Consider available training data.

Step 5: Consider the appropriate pattern recognition techniques available (e.g., fuzzy clustering analysis, etc.) and consider the overall pattern recognition system structure.

Step 6: Establish a pattern recognition system simulation implementation, including the selection of model, semantic or network structure.

Step 7: Train the system built.

Step 8: Simulate the execution of the system.

Step 9: Repeat the above steps until the desired results of the system are achieved.

The realization steps of fuzzy set recognition algorithm are as follows.

The algorithm for pattern recognition of fuzzy sets can be described as follows: Suppose that there are n fuzzy sets $A_1, A_2, \ldots, A_n$, where $A_i = (i = 1, 2, \ldots, n)$ represents n types.

When a recognition algorithm acts on object x, membership degree $\mu_{Ai}(x)(i = 1, 2, \ldots, n)$ is generated, indicating the degree to which object x belongs to set A_i. If a clear description of a recognition algorithm has been given, this algorithm is called explicit. If the algorithm is not clearly described, this algorithm is called ambiguous. People directly recognize object x through ambiguous algorithm, and pattern recognition is to convert an ambiguous algorithm into explicit algorithm, from identifying the object itself to identifying its pattern.

In principle, the implementation of fuzzy set recognition algorithm is divided into three steps:

Step 1: Feature extraction: extract various features related to recognition from object x, measure the specific data of x on each feature, and convert x into pattern $p(x) = \{x_1, x_2 \ldots, x_n\}$. This step is the basis. Whether the feature extraction is appropriate will directly affect the recognition results. However, this work involves the background of specific problems and the knowledge and skills of recognizers, so it is difficult to make a general discussion.

Step 2: Establish the membership function and establish a clear algorithm to generate the membership function

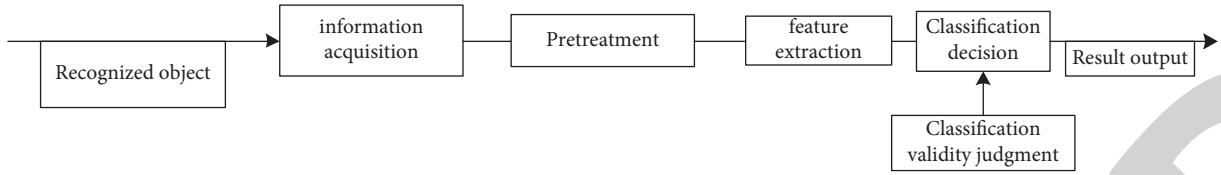

Figure 1: Structural block diagram of pattern recognition system.

$\mu_{Ai}(x)$, $i = 1, 2, \ldots, n$, x is the membership degree; $\mu_{Ai}(x)$ belonging to A_i depends on $x_1, x_2 \ldots, x_n$. There is no general or universal principle to determine the membership function, and many methods in application also have subjective and empirical components.

Step 3: Identification decision: judge the identified object x according to a certain attribution principle and point out which type it should belong to and the effectiveness of classification. Some of the common recognition and decision methods are maximum membership principle recognition method, proximity principle recognition method, and fuzzy cluster analysis recognition method. When choosing different fuzzy set theory knowledge and using different recognition algorithms, different implementation steps will be obtained.

4.2. Multiple Collaborative Supervision Patterns Recognition within Social Organizations Based on Data Clustering Algorithm. Data clustering algorithm is a classical hard clustering algorithm. It is based on within-group sum of squared errors and minimum criterion, which can classify data sets with hyperellipsoid distribution.

The sample set to be classified is $X = \{X_1, x_2 \ldots, X_n\}^T \subset R^{n\times p}$, n is the number of elements in the data set, $c\,(2 \le c \le n)$ is the classification number of samples, and the data clustering algorithm can be expressed as the mathematical problem of the minimum objective function J_1; that is,

$$\min J_1(X, \mu, v) = \sum_{i=1}^{c}\sum_{j=1}^{n}\mu_{ij}\left\|v_i - X_j\right\|^2 = \sum_{i=1}^{c}\sum_{j=1}^{n}\mu_{ij}{d_{ij}}^2. \quad (1)$$

$J_1(X, \mu, v)$ is the classical objective function of sum of squares of within-class errors, d_{ij} is Euclidean distance, which represents the similarity measure between sample X_j and cluster center v_i. The calculation formula of d_{ij} is as follows:

$$d_{ij} = \left\|v_i - X_j\right\| = \sqrt{\sum_{l=1}^{p}\left(v_{ij} - x_{jl}\right)^2}, \quad 1 \le i \le c, 1 \le j \le n. \quad (2)$$

The clustering criterion is to obtain the appropriate partition matrix $\mu = \{\mu_{ij}\}$ and a group of clustering centers v_i so that the objective function J_1 reaches the minimum. According to the Lagrange multiplier method, μ_{ij} and v_i are

$$\mu_{ij} = \begin{cases} 1, & d_{ij} = \min\limits_k\{d_{kj}\}, \\ 0, & d_{ij} \ne \min\limits_k\{d_{kj}\}, \end{cases} \quad 1 \le i \le c, 1 \le j \le n. \quad (3)$$

$$v_i = \frac{\sum_{j=1}^{n}\mu_{ij}X_j}{\sum_{j=1}^{n}\mu_{ij}}, \quad 1 \le i \le c. \quad (4)$$

The calculation flow of data clustering algorithm is as follows:

Step 1: Set the number of cluster categories c, initialize the partition matrix T_c, $\mu_{(0)} = \{\mu_{1i(0)}, \mu_{2i(0)}, \ldots, \mu_{ci(0)}\}^T$, $1 \le i \le n$ according to the three constraints (4)–(6), and set an arbitrarily small iterative cut-off error value $\varepsilon > 0$, and the maximum number of iterations of the algorithm $T_{\max}$ $t = 0, 1, 2, \ldots, T_{\max}$.

Step 2: From $\mu(t) = \{\mu_{1i(t)}, \mu_{2i(t)}, \ldots, \mu_{ci(t)}\}^T$, calculate the cluster center according to equation (4).

$$v_i(t) = \frac{\sum_{j=1}^{n}\mu_{ij(t)}X_j}{\sum_{j=1}^{n}\mu_{ij(t)}}, \quad 1 \le i \le c. \quad (5)$$

Step 3: Calculate the submatrix of data clustering algorithm according to the following equation:

$$\mu_{ij\,(t)} = \begin{cases} 1, & d_{ij(t)} = \min\limits_k\{d_{kj(t)}\}, \\ 0, & d_{ij(t)} \ne \min\limits_k\{d_{kj(t)}\}, \end{cases} \quad 1 \le i \le c, 1 \le j \le n. \quad (6)$$

Step 4: If $\|\mu_{(t+1)} - \mu_{(t)}\| \le \varepsilon$, when the system reaches a stable state, the iteration is terminated to obtain the required clustering center v_i and data clustering algorithm partition matrix $\mu = \{\mu_{ij}\}$. Otherwise, make $t = t + 1$ and turn $\mu_{(t)} = \mu_{(t+1)}$ to Step 2 to continue.

The above algorithm can also use the initialization cluster center v as the initial state, and its basic idea and implementation steps are basically similar to the above method.

Dunn extends the data clustering algorithm to the fuzzy situation according to the fuzzy division concept of set defined by Ruspini and weights the membership degree; that is, μ_{ij} in the data clustering algorithm becomes μ_{ij}^2. Therefore, Dunn gives the following recognition process of multiple collaborative supervision patterns within social organizations of the data clustering algorithm:

$$\min J_2(X,\mu,v) = \sum_{i=1}^{c}\sum_{j=1}^{n}\mu_{ij}^2\left\|v_i - X_j\right\|^2 = \sum_{i=1}^{c}\sum_{j=1}^{n}\mu_{ij}^2 d_{ij}^2. \quad (7)$$

The above expression is extended to a more general case, and a general description of data clustering algorithm is given:

$$\min J_m(X,\mu,v) = \sum_{i=1}^{c}\sum_{j=1}^{n}\mu_{ij}^m\left\|v_i - X_j\right\|^2 = \sum_{i=1}^{c}\sum_{j=1}^{n}\mu_{ij}^m d_{ij}^2, \quad (8)$$

where μ_{ij} satisfies three constraints, that is, (7)–(9), $m \in [1,\infty)$ is a weighting coefficient, and $J_m(X,\mu,v)$ is the objective function of the weighted sum of squares of the in-class error.

The clustering criterion is to obtain the appropriate fuzzy partition matrix $\mu = \{\mu_{ij}\}$ and fuzzy clustering center v_i, so that the objective function $J_m(X,\mu,v)$ reaches the minimum. According to the Lagrange multiplier method, the fuzzy partition matrix μ_{ij} and fuzzy clustering center v_i are

$$v_i = \frac{\sum_{j=1}^{n}\mu_{ij(t)}^m X_j}{\sum_{j=1}^{n}\mu_{ij(t)}^m}, \quad 1 \le i \le c, \quad (9)$$

$$\mu_{ij} = \frac{1}{\sum^{c}\left(d_{ij}/d_{kj}\right)^{2/m-1}}, \quad 1 \le i \le c, 1 \le j \le n. \quad (10)$$

The implementation steps of data clustering algorithm are as follows:

Step 1: Set the number of clustering categories c, initialize the fuzzy partition matrix and partition matrix $\mu_{(0)} = \{\mu_{1i(0)}, \mu_{2i(0)}, \ldots, \mu_{ci(0)}\}^T$, $1 \le i \le n$ according to three constraints in (5) and (6), and set an arbitrarily small iterative cut-off error value $\varepsilon > 0$, as well as the maximum number of iterations of the algorithm $T_{\max}$, $t = 0, 1, 2, \ldots, T_{\max}$.

Step 2: From $\mu(t) = \{\mu_{1i(t)}, \mu_{2i(t)}, \ldots, \mu_{ci(t)}\}^T$, the fuzzy clustering center $v_{(t)}$, $1 \le i \le c$ is calculated according to equation (9).

Step 3: The fuzzy partition matrix $\mu_{ij(t)}, 1 \le i \le c, 1 \le j \le n$ is calculated according to equation (10).

Step 4: If $\|\mu_{(t+1)} - \mu_{(t)}\| \le \varepsilon$ and the system reaches a stable state, terminate the iteration to obtain the required fuzzy clustering center v_i and fuzzy sub matrix $\mu = \{\mu_{ij}\}$; otherwise, make $t = t + 1$ and turn $\mu_{(t)} = \mu_{(t+1)}$ to Step 2 to continue.

Note that, for data clustering algorithm, the clustering problem is transformed into a nonlinear optimization problem with constraints, which is generally difficult to obtain its global minimum. In order to obtain better clustering results, the usual method is to use the iterative algorithm of alternately optimizing the fuzzy partition matrix μ and the clustering center matrix v_i to obtain a local minimum. The implementation method of the above data clustering algorithm is actually an offline learning method without supervision information. The data set x to be classified is all input at one time for clustering analysis.

5. Experiment

5.1. Analysis of Pattern Recognition Accuracy. In order to verify the effectiveness of multiple collaborative supervision patterns recognition method within social organizations based on data clustering algorithm, the accuracy of multiple collaborative supervision patterns recognition needs to be verified. The recognition accuracies of multiscale clustering analysis method, multidimensional feature fusion method, kernel density clustering method, and data clustering algorithm are compared. The results are shown in Table 1.

According to Table 1, the effectiveness of multiple collaborative supervision patterns recognition methods within social organizations is different under different methods. When the number of experimental iterations is 50, the accuracy of multiscale cluster analysis method is 67.65%, that of multidimensional feature fusion method is 65.67%, that of kernel density clustering method is 54.55%, and that of data clustering algorithm is 97.45%. When the number of experimental iterations is 150, the accuracy of multiscale cluster analysis method is 71.65, that of multidimensional feature fusion method is 70.30%, that of kernel density clustering method is 59.32%, and that of data clustering algorithm is 93.32%. The recognition accuracy of multiple collaborative supervision patterns within social organizations of this method is significantly higher than those of the other methods, which shows that the recognition effectiveness of this method is better.

5.2. Pattern Recognition Efficiency. In order to verify the efficiency of this method in multiple collaborative supervision patterns recognition within social organizations, the recognition times of multiscale clustering analysis method, multidimensional feature fusion method, kernel density clustering method, and data clustering algorithm are compared. The results are shown in Table 2.

According to the analysis of Table 2, when the number of iterations is 100, the time for multidimensional collaborative supervision pattern recognition of multiscale clustering analysis method is 57.75 s, the time for multidimensional collaborative supervision pattern recognition of multidimensional feature fusion method is 60.60 s, the time for multidimensional collaborative supervision pattern recognition of kernel density clustering method is 54.56 s, and the time for multidimensional collaborative supervision pattern recognition of data clustering algorithm is 17.73 s. When the number of iterations is 300, the multiscale cluster analysis method takes 186.78 s for multidimensional collaborative supervision pattern recognition, the multidimensional feature fusion method takes 143.43 s for multidimensional collaborative supervision pattern recognition, the kernel density clustering method takes 132.43 s for multidimensional collaborative supervision pattern recognition, and the data clustering algorithm takes 36.43 s for multidimensional collaborative supervision pattern recognition. According to the above results, the time of recognition of multiple collaborative supervision patterns in this method is obviously short, which shows that the pattern recognition efficiency of this method is high.

Table 1: Effectiveness of multiple collaborative supervision patterns recognition methods within social organizations.

Iterations/time	Recognition accuracy of multiple collaborative supervision patterns (%)			
	Multiscale cluster analysis method	Multidimensional feature fusion method	Kernel density clustering method	Data clustering algorithm
50	67.65	65.67	54.55	97.45
100	69.85	69.64	58.54	89.98
150	71.65	70.30	59.32	93.32
200	77.46	73.39	60.76	95.54
250	74.31	72.53	67.54	97.42
300	66.22	73.35	68.34	96.43

Table 2: Identification time of multiple collaborative supervision modes within social organizations.

Iterations/time	Time for recognition of multiple collaborative supervision patterns			
	Multiscale cluster analysis method	Multidimensional feature fusion method	Kernel density clustering method	Data clustering algorithm
50	32.50	38.76	36.54	12.54
100	57.75	60.60	54.56	17.73
150	89.75	85.54	86.63	21.65
200	129.43	98.62	99.54	26.89
250	154.54	110.53	102.43	32.53
300	186.78	143.43	132.43	36.43

6. Conclusion

This paper proposes a recognition method of multiple collaborative supervision patterns within social organizations based on data clustering algorithm. Firstly, it analyzes the characteristics and functions of social organizations and gives the definition of social organizations. Secondly, it analyzes the failure of internal supervision of social organizations and determines the internal governance elements of social organizations. Finally, the data clustering algorithm is introduced to realize the pattern recognition of multiple collaborative supervision within social organizations. The following conclusions are drawn through experiments:

(i) When the number of experimental iterations is 150, the accuracy of multivariate collaborative supervision pattern recognition of data clustering algorithm is as high as 93.32%. This shows that the recognition effectiveness of this method is better.

(ii) When the number of iterations is 300, the time of multivariate collaborative supervision pattern recognition of data clustering algorithm is 36.43 s, which shows that the pattern recognition efficiency of this method is high.

Data Availability

The data used to support the findings of this study are available from the corresponding author upon request.

Conflicts of Interest

The authors declare that there are no conflicts of interest.

Acknowledgments

The study was supported by "Jiangsu Social Science Foundation, China" (Grant no. 20SHD005).

References

[1] W. Yun, "Improved simulation of large-scale hybrid network database fuzzy query algorithm," *Computer Simulation*, vol. 37, no. 5, pp. 251–254, 2020.

[2] Y. Liu, Y. Wang, and H. Liu, "Study on temporal distribution of precipitation in Beijing city during flood period based on dynamic cluster analysis and fuzzy pattern recognition," *Journal of China Hydrology*, vol. 39, no. 1, pp. 74–77, 2019.

[3] T.-h. Zhang, D. U. Xin-hui, and S. Wang, "Research on refinement recognition algorithm of power load model based on kernel density clustering," *Mathematics in Practice and Theory*, vol. 49, no. 8, pp. 155–164, 2019.

[4] W. Fan and N. Bouguila, "Spherical data clustering and feature selection through nonparametric Bayesian mixture models with von Mises distributions," *Engineering Applications of Artificial Intelligence*, vol. 94, no. 4, pp. 773–781, 2020.

[5] X. Liu, J. Lu, and Q. Zhou, "The research of pattern recognition of heterogeneous residential power consumption based on multi-dimensional features," *Power Demand Side Management*, vol. 128, no. 6, pp. 95–100, 2020.

[6] A. Yang, "Deep data mining and trend analysis of students' teaching evaluation based on multi-scale cluster analysis," *China University Teaching*, vol. 1, no. 12, pp. 65–68, 2019.

[7] M. Gong, F. Wang, and W. Liu, "Pattern recognition receptor-mediated innate immune responses in seminal vesicle epithelial cell and their impacts on cellular function," *Biology of Reproduction*, vol. 12, no. 4, pp. 4–16, 2019.

Hindawi
Journal of Mathematics
Volume 2021, Article ID 4800499, 11 pages
https://doi.org/10.1155/2021/4800499

Research Article

A Novel Description on Vague Graph with Application in Transportation Systems

Zheng Kou,[1] **Saeed Kosari**,[1] **and Maryam Akhoundi**[2]

[1]*Institute of Computing Science and Technology, Guangzhou University, Guangzhou 510 006, China*
[2]*Clinical Research Development Unit of Rouhani Hospital, Babol Univetsity of Medical Sciences, Babol, Iran*

Correspondence should be addressed to Saeed Kosari; saeedkosari38@gzhu.edu.cn

Received 14 October 2021; Revised 11 November 2021; Accepted 16 November 2021; Published 2 December 2021

Academic Editor: Lazim Abdullah

Fuzzy graph (FG) models embrace the ubiquity of existing in natural and man-made structures, specifically dynamic processes in physical, biological, and social systems. It is exceedingly difficult for an expert to model those problems based on a FG because of the inconsistent and indeterminate information inherent in real-life problems being often uncertain. Vague graph (VG) can deal with the uncertainty associated with the inconsistent and determinate information of any real-world problem, where FGs many fail to reveal satisfactory results. Regularity definitions have been of high significance in the network heterogeneity study, which have implications in networks found across biology, ecology, and economy; so, adjacency sequence (AS) and fundamental sequences (FS) of regular vague graphs (RVGs) are defined with examples. One essential and adequate prerequisite has been ascribed to a VG with maximum four vertices is that it should be regular based on the adjacency sequences concept. Likewise, it is described that if ζ and its principal crisp graph (CG) are regular, then all the nodes do not have to have the similar AS. In the following, we obtain a characterization of vague detour (VD) g-eccentric node, and the concepts of vague detour g-boundary nodes and vague detour g-interior nodes in a VG are examined. Finally, an application of vague detour g-distance in transportation systems is given.

1. Introduction

The graph concept stands as one of the most dominant and widely employed tools for the multiple real-world problem representation, modeling, and analyses. To represent the objects and the relations between them, the graph vertices and edges are applied, respectively. FG-models are beneficial mathematical tools for addressing the combinatorial problems in various fields involving research, optimization, algebra, computing, environmental science, and topology. Thanks to the natural existence of vagueness and ambiguity, fuzzy graphical models are strikingly better than graphical models. Rosenfeld [1] proposed the idea of FG in 1975. Akin to the set theory, the historical past of the FG theory is the fuzzy set theory developed by Zadeh [2] in 1965. The notion of vague set theory, the generalization of Zadeh's fuzzy set theory, was introduced by Gau and Buehrer [3] in 1993. The VSs describe more possibilities than fuzzy sets. VS is more effective for the existence of the false membership degree. Kauffman [4] represented FGs based on Zadeh's fuzzy relation [5, 6]. Akram et al. [7, 8] described several concepts and results of FGs. Samanta et al. [9, 10] represented fuzzy competition graphs and some remarks on bipolar fuzzy graphs. Gani et al. [11, 12] investigated on irregular and regular fuzzy graphs. Sunitha et al. [13, 14] studied complement of a fuzzy graph. VG notion was introduced by Ramakrishna in [15]. Borzooei et al. [16, 17] investigated new concepts of VGs. Gary Chartrand [18] discussed the concepts of detour center of a graph. The notion of detour number, detour set, detour nodes, and detour basis in a graph were established by Gary Chatrand, G. L. Johns, and P. Zhang [19]. Interior nodes and boundary nodes are discussed by G. Chatrand, D. Erwin, G. L. Johns, and P. Zhang [20]. Fuzzy detour g-distance was given by J. P. Linda and M. S. Sunitha [21]. Ghorai et al. [22, 23] defined detour g-interior nodes in bipolar fuzzy graphs and characterization of regular bipolar fuzzy graphs. The idea of strong arcs in FG was given by Bhutani and Rosenfeld [24], and types of arc in FG were given by Mathew and Sunitha [25]. The notion of bridge, trees, cycles,

and end nodes were described by Rosenfeld [1]. Rosenfeld and Bhutani [24] represented the notion of g-distance in FG. Also, the notions of g-boundary node, g-interior node, and g-eccentric node were defined by Linda and Sunitha [26].

A VG is referred to as a generalized structure of an FG that conveys more exactness, adaptability, and compatibility to a system when coordinated with systems running on FGs. Also, a VG is able to concentrate on determining the uncertainly coupled with the inconsistent and indeterminate information of any real-world problem, where FGs may not lead to adequate results.

The concepts of regularity play an important part in both graph theory and application in the vague environment. The highly regular graphs characterization has also been applied to the question of heterogeneity, yet all of these fail to shed enough light on real-world situations; hence, in this paper, AS and FS of RVGs are defined with examples. One essential and adequate prerequisite has been ascribed to a VG with maximum four vertices is that it should be regular based on the AS concept. Detection of nodes on the network boundary is necessary for correct operation in many wireless applications. Also, nodes close to network boundary are often assumed to provide the best candidate for beacon nodes in virtual co-ordinate construction. Focusing on these applications, a research is carried out for boundary nodes and interior ones in vague graph. A characterization of vague detour g-eccentric node and the concepts of vague detour g-boundary nodes and vague detour g-interior nodes in a VG are examined. Finally, an application of vague detour g-distance in transportation systems is given. Recently, some research has been conducted by the authors in the continuation of previous works related to VGs, bipolar fuzzy graphs, and intuitionistic fuzzy graphs which are mentioned in [27–38]. Shoaib et al. [39] introduced new concepts of pythagorean fuzzy graphs.

2. Preliminaries

A graph denotes a pair $G^* = (V, E)$ satisfying $E \subseteq V \times V$. The elements of V and E are the nodes and edges of the graph G^*, correspondingly. An FG has the form of $G = (\lambda, \nu)$, where λ: $V \longrightarrow [0,1]$ and ν: $V \times V \longrightarrow [0,1]$ as is defined by $\nu(ab) \leq \lambda(a) \wedge \lambda(b)$ and $\forall a, b \in V$ and ν is a symmetric fuzzy relation on λ and $\wedge$ denotes the minimum.

The FS of an FG $G = (\lambda, \nu)$ ([40]) is described as follows:

$$f_S(G) = \{\lambda(a) > 0, a \in V\} \cup \{\nu(a,b) > 0, a, b \in V\}, \quad (1)$$

in which the elements are taken from the interval $[0,1]$.

Definition 1 (see [3]). A VS M is a pair (t_M, f_M) on set V that t_M and f_M are real-valued functions which can be defined on $V \longrightarrow [0,1]$, so that $t_M(a) + f_M(a) \leq 1$, $\forall a \in V$.

Definition 2 (see [15]). A pair $\zeta = (M, N)$ is called to be a VG on a CG G^*, where $M = (t_M, f_M)$ is a VS on V and $N = (t_N, f_N)$ is a VS on $E \subseteq V \times V$ so that $t_M(ab) \leq \min(t_M(a), t_M < (b))$ and $f_N(ab) \geq \max(f_M(a), f_M(b))$, for every edge $ab \in E$.

Definition 3 (see [16]). The complement of a VG ζ is a VG $\overline{\zeta} = (\overline{M}, \overline{N})$, where $\overline{M} = M$ and $\overline{N} = (\overline{t_N}, \overline{f_N})$ are defined by the following:

$$\overline{t_N}(ab) = \min(t_M(a), t_M(b)) - t_N(ab),$$
$$\overline{f_N}(ab) = f_N(ab) - \max(f_M(a), f_M(b)), \quad \text{for all } ab \in E. \quad (2)$$

Definition 4 (see [17]). Let $\zeta = (M, N)$ be a VG.

(i) Then, OND of $a \in V$ is defined by $\deg(a) = (\deg^t(a), \deg^f(a))$, that $\deg^t(a) = \sum_{\substack{a \neq b \\ ab \in E}} t_N(ab)$ and $\deg^f(a) = \sum_{\substack{a \neq b \\ ab \in E}} f_N(ab)$. If all the nodes of ζ have the same OND (m_1, m_2), then, ζ is called to be (m_1, m_2)-regular.

(ii) The CND of $a \in V$ in ζ is denoted as $\deg[a] = (\deg^t[a], \deg^f[a])$, where $\deg^t[a] = \deg^t(a) + t_M(a)$ and $\deg^f[a] = \deg^f(a) + f_M(a)$. If every node of ζ has equal closed neighborhood degree (n_1, n_2), then ζ is called to be (n_1, n_2)-totally regular.

Definition 5 (see [17]). Let ζ be a VG. If $t_N(ab) = \min\{t_M(a), t_M(b)\}$ and $f_N(ab) = \max\{f_M(a), f_M(b)\}$, $\forall a, b \in V$, then ζ is called a complete-VG and if $t_N(ab) = \min\{t_M(a), t_M(b)\}$ and $f_N(ab) = \max\{f_M(a), f_M(b)\}$, $\forall ab \in E$, then, ζ is called a strong-VG of the CG $G^* = (V, E)$.

Definition 6 (see [7]). Let $L(G^*) = (Y, Z)$ be a line graph of a CG G^*. Suppose $\zeta = (M, N)$ be a VG of G^*. Then, a vague line graph $L(\zeta) = (M_1, N_1)$ of ζ is described as follows:

(i) M_1 and N_1 are vague subsets of Y and Z, respectively

(ii) $t_{M_1}(R_m) = t_N(m) = t_N(u_m v_m)$

(iii) $f_{M_1}(R_m) = f_N(m) = f_N(u_m v_m)$

(iv) $t_{N_1}(R_m R_n) = \min\{t_N(m), t_N(n)\} = \min\{t_N(u_m v_m), t_N(u_n v_n)\}$

(v) $f_{N_1}(R_m R_n) = \max\{f_N(m), f_N(n)\} = \max\{f_N(u_m v_m), f_N(u_n v_n)\}$, $\forall R_m, R_n \in Y$ and $R_m R_n \in Z$

Definition 7 (see [16]). Let ζ be a VG and $a, b \in V$.

(i) A path P: $a = a_0, a_1, \ldots, a_k = b$ in ζ is a sequence of distinct nodes so that $t_N(a_{i-1}a_i) > 0$, $f_N(a_{i-1}a_i) > 0$, $i = 1, 2, \ldots, k$ and the length of the path is k.

(ii) If P: $a = a_0, a_1, \ldots, a_k = b$ be a path of length k between a and b, then, $(t_N(ab))^k$ and $(f_N(ab))^k$ are defined as $(t_N(ab))^k = \sup\{t_N(aa_1) \wedge t_N(a_1a_2) \wedge \cdots \wedge t_N(a_{k-1}b)\}$ and $(f_N(ab))^k = \inf\{f_N(aa_1) \vee f_N(a_1a_2) \vee \cdots \vee f_N(a_{k-1}b)\}$. $(t_N^\infty(ab), f_N^\infty(ab))$ is said to be the strength of connectedness between two nodes a and b in ζ, where $t_N^\infty(ab) = \sup(t_N^k(ab))$ and $f_N^\infty(ab) = \inf(f_N^k(ab))$. If $t_N(ab) \geq t_N^\infty(ab)$ and $f_N(ab) \leq f_N^\infty(ab)$, then, the arc ab is said to be a

strong arc. A path $a-b$ is strong path if all arcs on the path are strong.

Definition 8 (see [16]). A connected-VG ζ is said to be a vague tree if ζ has a vague spanning subgraph $S = (A, E)$ which is also a vague tree and for all arcs (a, b) not in S, $t_N(ab) < t_N^{\infty}(ab)$ and $f_N(ab) > f_N^{\infty}(ab)$. The vague spanning subgraph S of ζ is a maximum spanning subgraph of ζ if ζ has no vague spanning subgraph different from S contains S.

Notations are shown in Table 1.

3. New Concepts in Regular Vague Graphs

Definition 9. The AS of a node a in a VG ζ is described by $AS(a) = (AS(a)_t, AS(a)_f)$, where $AS(a)_t = (t_1, t_2, \ldots, t_n)$ and $AS(a)_f = (f_1, f_2, \ldots, f_n)$ signify the sequence of TMVs and FMVs of the edges neighbor to a arranged in ascending order, respectively.

Example 1. Consider the VG ζ as Figure 1. The AS of the nodes are

$$\begin{aligned} AS(a) &= \left(AS(a)_t, AS(a)_f\right) = ((0.1, 0.2), (0.5, 0.7)),\\ AS(b) &= \left(AS(b)_t, AS(b)_f\right) = ((0.1, 0.2, 0.2), (0.5, 0.6, 0.6)),\\ AS(c) &= \left(AS(c)_t, AS(c)_f\right) = ((0.1, 0.1), (0.6, 0.7)),\\ AS(d) &= \left(AS(d)_t, AS(d)_f\right) = ((0.1, 0.2, 0.2), (0.6, 0.7, 0.8)),\\ AS(e) &= \left(AS(e)_t, AS(e)_f\right) = ((0.1, 0.2), (0.7, 0.8)). \end{aligned} \tag{3}$$

Remark 1

(i) The elements number in $\mathrm{AS}(a)_t$ or $\mathrm{AS}(a)_f$ is the degree of a in G^*.

(ii) The sum of all elements in $\mathrm{AS}(a)_t$ and the sum of all elements in $\mathrm{AS}(a)_f$ is $\deg(a)$ in VG ζ, i.e.,

$$\deg(a) = \left(\sum_{t_i \in AS(a)_t} t_i, \sum_{t_i \in AS(a)_f} f_i\right). \tag{4}$$

Remark 2. If ζ is a RVG, then G^* does not have to be regular and all the nodes do not need to have the same AS.

Now, we present an example that proves the correctness of the above remark.

Example 2. Consider the VG ζ in Figure 2.

In this example, ζ is a $(0.4, 0.8)$-RVG, but G^* is not regular and the nodes in ζ do not share the same AS.

$$\begin{aligned} \mathrm{AS}(b) &= ((0.1, 0.1, 0.2), (0.2, 0.2, 0.4)) \neq \mathrm{AS}(a)\\ &= ((0.2, 0.2), (0.4, 0.4)). \end{aligned} \tag{5}$$

Table 1: Some basic notations.

Notation	Meaning
FG	Fuzzy graph
VS	Vague set
VG	Vague graph
AS	Adjacency sequence
FS	Fundamental sequence
RVG	Regular vague graph
CG	Crisp graph
OND	Open neighborhood degree
CND	Closed neighborhood degree
TMV	True membership value
FMV	False membership value
FFS	First fundamental sequence
SFS	Second fundamental sequence
VLG	Vague line graph
CVG	Connected vague graph
RG	Regular graph
MV	Membership value
VEN	Vague end node
VD	Vague detour

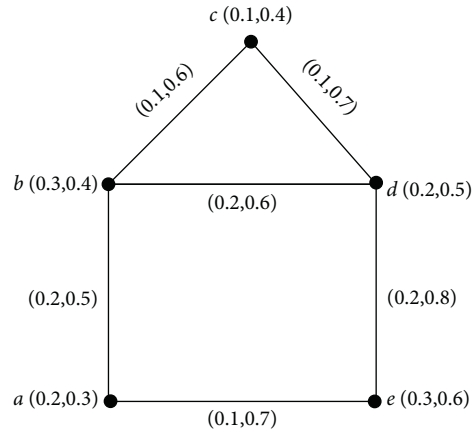

Figure 1: Vague graph ζ and its AS.

Hence, in a RVG, all the nodes do not need to have the similar AS.

Remark 3. If ζ and ζ^* are RGs, then all the nodes do not need to have the similar AS.

Example 3. Consider the VG ζ as Figure 3.

Here, $\deg(a) = \deg(b) = \deg(c) = \deg(d) = \deg(e) = (0.4, 1.5)$. So, ζ is a RVG. Correspondingly, we observe that G^* is regular. But $\mathrm{ads}(a) = ((0.1, 0.1, 0.2), (0.4, 0.5, 0.6)) \neq \mathrm{ads}(f) = ((0.1, 0.1, 0.2), (0.4, 0.4, 0.7))$.

Definition 10. The FS of a VG ζ is defined as $f_s(\zeta) = (F_{s^t}(\zeta), f_{s^f}(\zeta))$, where

$$\begin{aligned} f_{s^t}(\zeta) &= \{t_M(a) > 0; a \in V\} \cup \{t_N(ab) > 0: a, b \in V\},\\ f_{s^f}(\zeta) &= \{f_M(a) > 0; a \in V\} \cup \{f_N(ab) > 0: a, b \in V\}. \end{aligned} \tag{6}$$

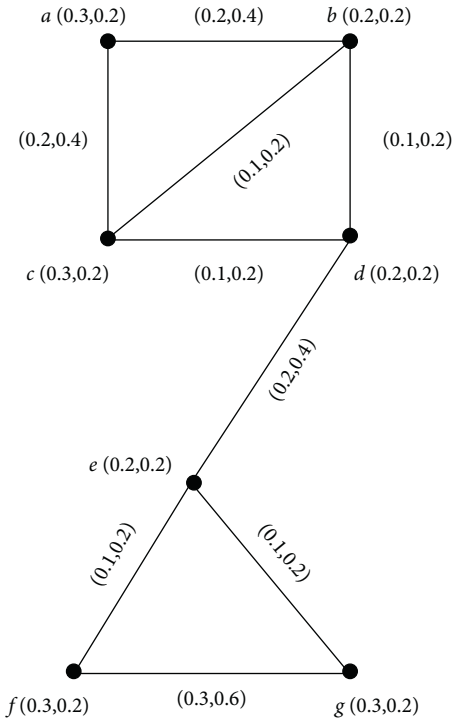

Figure 2: Rvg ζ.

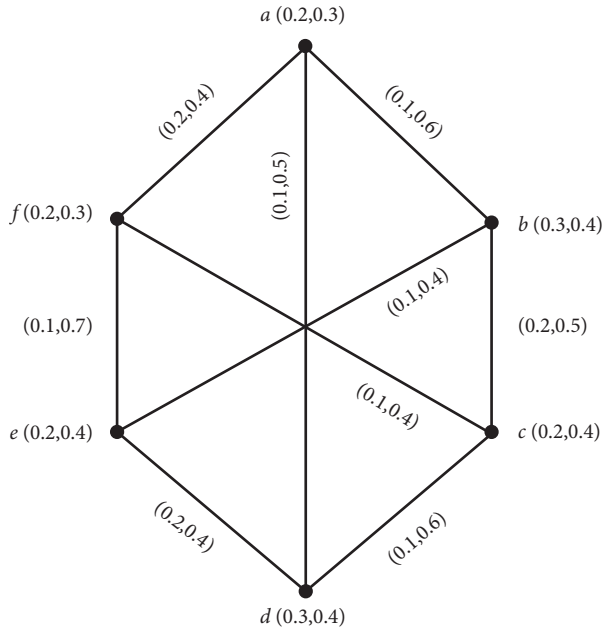

Figure 3: Regular graphs ζ and G^* with different adjacency sequence.

The elements of $f_{s^t}(\zeta)$ and $f_{s^f}(\zeta)$ are ordered in descending and ascending order, respectively. The node part of the FS is characterized as the FFS and the edge part of the FS is labeled as the SFS and described by $ffs(\zeta)$ and $sfs(\zeta)$, respectively.

Theorem 1. *Let ζ be a VG. If $n \leq 4$, then ζ is a RVG iff G^*, i.e., RG and all the nodes have the similar AS, n being the number of nodes in ζ.*

Proof. Suppose G^* is a RG and all the nodes have the similar AS. Then, ζ is a RVG.

On the contrary, let ζ be a $d = (d_1, d_2)$-RVG. If there is no edge among the nodes or if the number of nodes is one, then there is nothing to prove. Thus, we suppose that $E \neq \emptyset$. Then, $p > 1$ and $d \neq 0$. Consider the three cases for $n = 2, 3, 4$.

Case 1. If $n = 2$, then, ζ have two nodes a_1 and a_2. So, G^* is 1-regular, and a_1 and a_2 have the same AS $AS(a_1) = (t_N(a_1a_2), f_N(a_1a_2))$.

Case 2. If $n = 3$, then there are three nodes a_1, a_2, a_3 with edges a_1a_2, a_2a_3, a_1a_3 in ζ (see Figure 4). Let the edge-MV a_1a_2, a_2a_3, and a_1a_3 be $(t_N(a_1a_2), f_N(a_1a_2))$, $(t_N(a_2a_3), f_N(a_2a_3))$, and $(t_N(a_1a_3), f_N(a_1a_3))$, respectively.

Since ζ is $d = (d_1, d_2)$-RVG, $d(a_i) = (d_1, d_2)$, for $i = 1, 2, 3$. Hence, we have

$$\begin{aligned} t_N(a_1a_2) + t_N(a_2a_3) &= d_1, \\ t_N(a_2a_3) + t_N(a_1a_3) &= d_1, \\ t_N(a_1a_2) + t_N(a_1a_3) &= d_1, \\ f_N(a_1a_2) + f_N(a_2a_3) &= d_2, \\ f_N(a_2a_3) + f_N(a_1a_3) &= d_2, \\ f_N(a_1a_2) + f_N(a_1a_3) &= d_2. \end{aligned} \tag{7}$$

Simplifying the above equations, we have

$$\begin{aligned} t_N(a_1a_2) = t_N(a_2a_3) = t_N(a_1a_3) &= \frac{d_1}{2}, \\ f_N(a_1a_2) = f_N(a_2a_3) = f_N(a_1a_3) &= \frac{d_2}{2}. \end{aligned} \tag{8}$$

So, each node has the similar AS, i.e., $AS(a_i) = ((d_1/2, d_1/2), (d_2/2, d_2/2))$, for $i = 1, 2, 3$ and G^* is 2-RG. Here, G^* is a cycle and each edge has the MV $(d_1/2, d_2/2)$.

Case 3. If $n = 4$, then, there are four nodes a_1, a_2, a_3, a_4 of ζ with edges $a_1a_2, a_1a_4, a_1a_3, a_2a_3, a_2a_4, a_3a_4$ (see Figure 5). Suppose the MV of the edges is $(t_N(a_1a_2), f_N(a_1a_2))$, $(t_N(a_1a_4), f_N(a_1a_4))$, $(t_N(a_1a_3), f_N(a_1a_3))$, $(t_N(a_2a_3), f_B(a_2a_3))$, $(t_N(a_2a_4), f_N(a_2a_4))$, and $(t_N(a_3a_4), f_N(a_3a_4))$, respectively. Since ζ is (d_1, d_2)-RVG, $d(a_i) = (d_1, d_2)$, for $i = 1, 2, 3, 4$. Hence, we have

$$\begin{aligned} t_N(a_1a_2) + t_N(a_1a_3) + t_N(a_1a_4) &= d_1, \\ t_N(a_2a_1) + t_N(a_2a_3) + t_N(a_2a_4) &= d_1, \\ t_N(a_3a_1) + t_N(a_3a_2) + t_N(a_3a_4) &= d_1, \\ t_N(a_4a_1) + t_N(a_4a_2) + t_N(a_4a_3) &= d_1, \\ f_N(a_1a_2) + f_N(a_1a_3) + f_N(a_1a_4) &= d_2, \\ f_N(a_2a_1) + f_N(a_2a_3) + f_N(a_2a_4) &= d_2, \\ f_N(a_3a_1) + f_N(a_3a_2) + f_N(a_3a_4) &= d_2, \\ f_N(a_4a_1) + f_N(a_4a_2) + f_N(a_4a_3) &= d_2. \end{aligned} \tag{9}$$

On simplification, we obtain

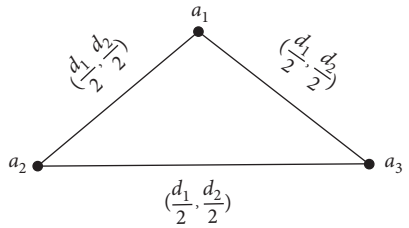

FIGURE 4: ζ is a (d_1, d_2)-regular vague graph with G^* cyclic and 2-RG.

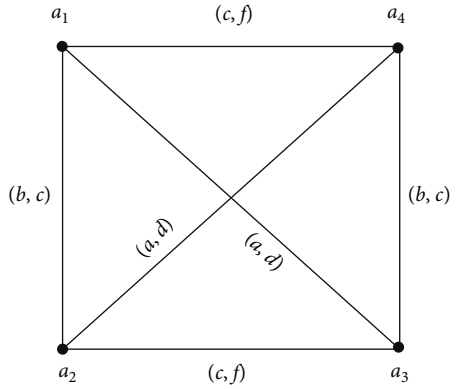

FIGURE 5: ζ is a (d_1, d_2)-regular vague graph with G^* 3-RG or 2-RG or 1-RG.

$$\begin{aligned} t_N(a_1a_3) &= t_N(a_2a_4), t_N(a_1a_2) = t_N(a_3a_4), t_N(a_1a_4) \\ &= t_B(a_2a_3), \\ f_N(a_1a_3) &= f_N(a_2a_4), f_N(a_1a_2) = f_N(a_3a_4), f_N(a_1a_4) \\ &= f_N(a_2a_3). \end{aligned} \tag{10}$$

Let $t_N(a_1a_3) = t_N(a_2a_4) = a$, $t_N(a_1a_2) = t_N(a_3a_4) = b$, $t_N(a_1a_4) = t_N(a_2a_3) = c$, and $f_N(a_1a_3) = f_N(a_2a_4) = d$, $f_N(a_1a_2) = f_N(a_3a_4) = e$, and $f_N(a_1a_4) = f_N(a_2a_3) = f$.

Since that $E \neq \emptyset$, at least one of the edges-MV should be nonzero. If all the edges-MVs are non-zero, then G^* is 3-RG and every node of AS has the elements $((a, b, c), (d, e, f))$ in ascending order.

If any two edges-MVs are nonzero, then G^* is 2-RG and each node AS has those two nonzero MVs in the ascending order. If one edge-MVs is nonzero, then G^* is 1-RG and each node AS has that nonzero MV.

Theorem 2. *Let $\zeta = (M, N)$ be a (d_1, d_2)-RVG of the q-regular CG G^* and every node has the same AS $((r_1, r_2, \ldots, r_q), (s_1, s_2, \ldots, s_q))$, $r_i \in [0, 1]$ and $s_i \in [0, 1]$, $i = 1, 2, \ldots, q$. Then, the VLG $L(\zeta)$ of ζ is regular iff either N is constant or N has exactly three values so that $r_1 = r_2 = \cdots = r_{q-1}$, $r_i < r_q \leq 1$, for $i = 1, 2, \ldots, q-1$ and $s_2 = s_3 = \cdots = s_{q-1} = s_q$, $0 \leq s_1 < s_i$, for $i = 2, \ldots, q-1$.*

Proof. Let the VLG $L(\zeta)$ of ζ be (t_1, t_2)-regular. Let $N(e) = (r_i, s_i)$ for some $i = 1, 2, \ldots, q$, where $e = ab$ be any edge of ζ. Then, every a and b is neighbor with $(q-1)$ edges with MVs $(r_1, s_1), (r_2, s_2), \ldots, (r_{i-1}, s_{i-1}), (r_{i+1}, s_{i+1}), \ldots, (r_q, s_q)$. So, the node e in $L(\zeta)$ is neighbor with $2(q-1)$ edges with MVs $(r_1 \wedge r_i, s_1 \vee s_i), (r_2 \wedge r_i, s_2 \vee s_i), \ldots, (r_{i-1} \wedge r_i, s_{i-1} \vee s_i), (r_{i+1} \wedge r_i, s_{i+1} \vee s_i), \ldots, (r_q \wedge r_i, s_q \vee s_i)$, each appearing twice. So, $d_{L(\zeta)}(e) = (d^t_{L(\zeta)}(e), d^f_{L(\zeta)}(e))$, where

$$\begin{aligned} d^t_{L(\zeta)}(e) &= 2\sum_{j \neq i} r_j \wedge r_i \\ &= 2\sum_{j=1}^{i-1} r_j \wedge r_i + 2\sum_{j=i+1}^{q} r_j \wedge r_i \\ &= 2\sum_{j=1}^{i-1} r_j + 2\sum_{j=i+1}^{q} r_i, \quad \left(\text{since } r_1 \leq r_2 \leq \cdots \leq r_q\right) \\ &= 2\sum_{j=1}^{i-1} r_j + 2(q-i)r_i, \end{aligned} \tag{11}$$

and

$$\begin{aligned} d^f_{L(\zeta)}(e) &= 2\sum_{j \neq i} s_j \vee s_i \\ &= 2\sum_{j=1}^{i-1} s_j \vee s_i + 2\sum_{j=i+1}^{q} s_j \vee s_i \\ &= 2\sum_{j=1}^{i-1} s_i + 2\sum_{j=i+1}^{q} s_j, \quad \left(\text{since } s_1 \leq s_2 \leq \cdots \leq s_q\right) \\ &= 2(i-1)s_i + 2\sum_{j=i+1}^{q} s_j. \end{aligned} \tag{12}$$

This holds for every edge e of ζ. Since $L(\zeta)$ is (t_1, t_2)-regular, $d_{L(\zeta)}(e) = (t_1, t_2)$ for each node set e in $L(\zeta)$. Thus, $2\sum_{j=1}^{i-1} r_j + 2(q-i)r_i = t_1$ and $2(i-1)s_i + 2\sum_{j=i+1}^{q} s_j = t_2$, i.e.,

$$\begin{aligned} \sum_{j=1}^{i-1} r_j + (q-i)r_i &= \frac{t_1}{2} \\ (i-1)s_i + \sum_{j=i+1}^{q} s_j &= \frac{t_2}{2}, \quad \text{for all } i = 1, 2, \ldots, q. \end{aligned} \tag{13}$$

By equation (13), we have

$$\begin{aligned} (q-1)r_1 &= \frac{t_1}{2} \\ \sum_{j=2}^{q} s_j &= \frac{t_2}{2}, \end{aligned} \tag{14}$$

$$\begin{aligned} r_1 + (q-2)r_2 &= \frac{t_1}{2} \\ s_2 + \sum_{j=3}^{q} s_j &= \frac{t_2}{2}, \end{aligned} \tag{15}$$

$$\begin{aligned} r_1 + r_2 + (q-3)r_3 &= \frac{t_1}{2} \\ 2s_3 + \sum_{j=4}^{q} s_j &= \frac{t_2}{2}, \end{aligned} \tag{16}$$

$$\begin{aligned} r_1 + r_2 + \cdots + r_{q-2} + r_{q-1} &= \frac{t_1}{2} \\ (q-2)s_{q-1} + s_q &= \frac{t_2}{2}, \end{aligned} \tag{17}$$

$$\begin{aligned} \left(r_1 + r_2 + \cdots + r_{q-1}\right) &= \frac{t_1}{2} \\ (q-1)s_q &= \frac{t_2}{2}. \end{aligned} \tag{18}$$

Simplifying equations (13)–(18), we have the following:

$$\begin{aligned} r_1 &= r_2 = \cdots = r_q \\ s_2 &= s_3 = s_{q-1} = s_q. \end{aligned} \tag{19}$$

If $r_1 = r_q$ and $s_1 = s_q$, then N is constant; otherwise, N has three values so that $r_1 = r_2 = \cdots = r_{q-1}$ and $s_2 = s_3 = \cdots = s_{q-1} = s_q$.

On the contrary, suppose N is constant or N have just three values so that $r_1 = r_2 = \cdots = r_{q-1}$, $r_i < r_q \le 1$, for $i = 1, 2, \ldots, q-1$, and $s_2 = s_3 = \cdots = s_{q-1} = s_q$, $0 \le s_1 < s_i$, for $i = 2, \ldots, q-1$. If N is constant, let $N(ab) = (k_1, k_2)$, $\forall\, ab \in E$. Then, $k_1 = r_i$ and $k_2 = s_i$, $\forall\, i = 1, 2, \ldots, q$. So, $r_j \wedge r_i = k_1$ and $s_j \vee s_i = k_2$, $\forall\, j \ne i$. Otherwise, suppose $r_j = k_1, \forall\, j = 1, 2, \ldots, q-1$ and $s_j = k_2, \forall\, j = 2, \ldots, q$. Next, $r_j = k_1 < r_q$ and $s_1 < s_j = k_2$.

So, $r_j \wedge r_i = k_1$ and $s_j \vee s_i = k_2$, $\forall\, j \ne i$. Therefore, in all the cases, $r_j \wedge r_i = k_1$ and $s_j \vee s_i = k_2$, $\forall\, j \ne i$. Thus, for any node $e = ab \in L(\zeta)$, we have

$$\begin{aligned} d_{L(\zeta)}(e) &= \left(d^t_{L(\zeta)}(e), d^f_{L(\zeta)}(e)\right) \\ &= \left(2\sum_{j\ne i} r_j \wedge r_i, 2\sum_{j\ne i} s_j \vee s_i\right) \\ &= \left(2\sum_{j\ne i} k_1, 2\sum_{j\ne i} k_2\right) \\ &= \left(2(q-1)k_1, 2(q-1)k_2\right). \end{aligned} \tag{20}$$

Hence, $L(\zeta)$ is a $(2(q-1)k_1, 2(q-1)k_2)$-regular. □

Remark 4. The RVG complement does not have to be regular. This can be observed in the following example.

Example 4. Consider the VG ζ as Figure 6.

Here, $\deg(a) = \deg(b) = \deg(c) = (0.2, 1.2)$. So, ζ is $(0.2, 1.2)$-regular. But in its complement $\overline{\zeta}$, $\deg(a) = (0.6, 0.4)$, $\deg(b) = (0.4, 0.5)$, $\deg(c) = (0.6, 0.5)$.

So, $\overline{\zeta}$ is not regular.

4. Vague Detour g-Distance and Vague Detour g-Periphery

Definition 11. The length of a $x - y$ strong path p between x and y in a CVG $\zeta = (M, N)$ is said to be a vague detour (VD) g-distance if there is no other strong path longer than p between x and y, and we show this by $VD_g(x, y)$. Any $x - y$ strong path whose length is $VD_g(x, y)$ is named a $x - y$ vague g-detour.

Example 5. Let $\zeta = (M, N)$ be a CVG of the graph G^*, where $V = \{x, y, z, w, k\}$ and $E = \{(x, y), (z, w), (y, z), (x, w), (x, z), (x, k), (k, w)\}$. For the VG ζ in Figure 7, it is seen that all arcs except (k, w) and (y, w) are strong arcs and the VD g-distance of two nodes are given as follows:

$$\begin{aligned} VD_g(x, y) &= 1, \\ VD_g(y, k) &= 1, \\ VD_g(w, k) &= 4, \\ VD_g(z, w) &= 2, \\ VD_g(x, z) &= 2, \\ VD_g(x, w) &= 2, \\ VD_g(y, w) &= 3, \\ VD_g(k, z) &= 4, \\ VD_g(y, z) &= 3, \\ VD_g(k, x) &= 2. \end{aligned} \tag{21}$$

Definition 12. The length of any smallest strong path from x to y is named the vague geodesic distance, described by $Vd_g(x, y)$.

The VD g-eccentricity $e_{VD_g}(a)$ for a node a is $\max(V \cdot D_g(a, x))$, $\forall x \in \zeta$. The set of all VD g-eccentricity nodes of a, described by $a^*_{V \cdot D_g}$. The VD g-radius of ζ, denoted by $\mathrm{rad}_{V \cdot D_g}(\zeta)$, is defined as $\min\,(e_{V \cdot D_g}(x))$, $\forall x \in \zeta$. If $e_{V \cdot D_g}(a) = \mathrm{rad}_{V \cdot D_g}(\zeta)$, then the node a is the VD g-central node of ζ. The VD g-diameter of ζ, denoted by $\mathrm{diam}_{V \cdot D_g}(\zeta)$, is defined as $\max(e_{V \cdot D_g}(x))$, $\forall x \in \zeta$. If $e_{V \cdot D_g}(a) = \mathrm{diam}_{V \cdot D_g}(\zeta)$, then the node a is named the VD g-peripheral node of ζ.

Example 6. For the connected-VG ζ in Figure 7, $e_{V \cdot D_g}(x) = 2$, $e_{V \cdot D_g}(y) = 3$, $e_{V \cdot D_g}(k) = 4$, $e_{V \cdot D_g}(w) = 4$, $e_{V \cdot D_g}(z) = 4$, and $\mathrm{rad}_{V \cdot D_g}(\zeta) = 1$, $\mathrm{diam}_{V \cdot D_g}(\zeta) = 4$.

Definition 13. The vague subgraph of the VG $\zeta = (M, N)$, whose nodes are only the VD g-peripheral nodes is named a VD g-periphery of ζ, and it is denoted by $\mathrm{Per}_{V \cdot D_g}(\zeta)$.

Definition 14. If every node of a CVG $\zeta = (M, N)$ is a VD g-eccentric node, then ζ is said to be a VD g-eccentric vague

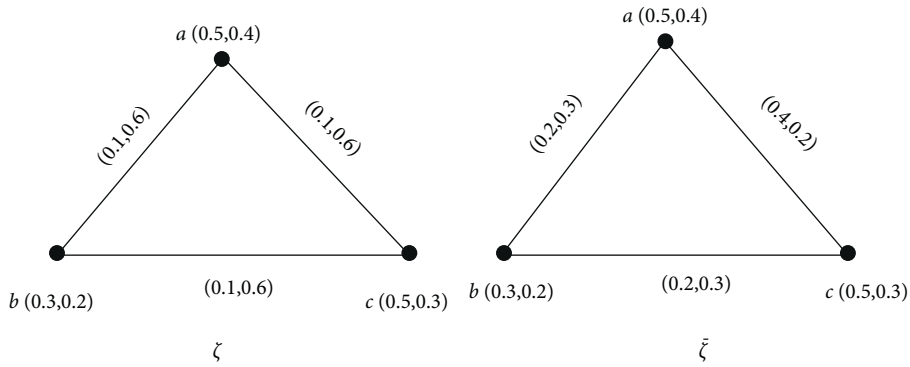

FIGURE 6: Vague graph ζ and its complement $(\overline{\zeta})$.

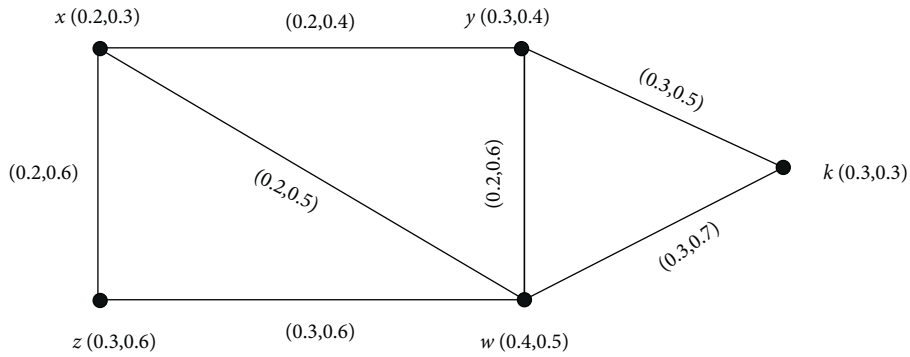

FIGURE 7: Connected vague graph ζ.

graph. The vague subgraph of ζ formed by the set of all vague g-eccentric nodes of ζ is named a VD g-eccentric vague subgraph of ζ, it is described by $E_{CC_{V\cdot D_g}}(\zeta)$

Example 7. For the VG of Figure 8, all nodes x, y, z, and w are VD g-periphery nodes since $e_{V\cdot D_g}(x) = e_{V\cdot D_g}(y) = e_{V\cdot D_g}(z) = e_{V\cdot D_g}(w) = 2$, $\text{diam}_{V\cdot D_g}(\zeta) = 2$. Also, we have

$$\begin{aligned} x^*_{V\cdot D_g} &= \{y\}, \\ y^*_{V\cdot D_g} &= \{x\}, \\ z^*_{V\cdot D_g} &= \{w\}, \\ w^*_{V\cdot D_g} &= \{z\}. \end{aligned} \tag{22}$$

Theorem 3. *A VG ζ is a VD g-self-centered if and only if each node of ζ is a VD g-eccentric.*

Proof. Assume ζ is a VD g-self centered graph and let y be a node in ζ. Let $x \in y^*_{V\cdot D_g}$. So, $e_{V\cdot D_g}(y) = V \cdot D_g(x, y)$. Since ζ is a VD g-self centered vague graph, $e_{V\cdot D_g}(x) = e_{V\cdot D_g}(y) = V \cdot D_g(x, y)$, and this implies that $y \in x^*_{V\cdot D_g}$. So, y is a VD g-eccentric vertex of ζ. Conversely, let each vertex of ζ is a VD g-eccentric node. If possible, suppose ζ be not VD g-self-centered vague graph. Then, $\text{rad}_{V\cdot D_g}(\zeta) \neq \text{diam}_{V\cdot D_g}(\zeta)$, and there exists a node $s \in \zeta$ so that $e_{V\cdot D_g}(s) = \text{diam}_{V\cdot D_g}(\zeta)$. Also, let $p \in s^*_{V\cdot D_g}$ Let u be a $s - p$ VD in ζ. So, there must have a node q on u for which the

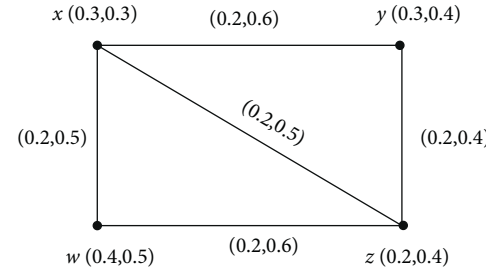

FIGURE 8: Connected vague graph ζ.

node q is not a VD g-eccentric node of u. Also, q cannot be a VD g-eccentric node of each other node. Again, if q be a VD g-eccentric node of a node x (say), it means $q \in x^*_{V\cdot D_g}$. Then, there exists an extension of a $x - q$ vague g-detour up to s or up to p. But this contradicts the facts that $q \in x^*_{V\cdot D_g}$. Therefore, $\text{rad}_{V\cdot D_g}(\zeta) = \text{diam}_{V\cdot D_g}(\zeta)$ and ζ is a VD g-self centered vague graph. □

Theorem 4. *If ζ is a VD g-self-centered graph, then $rad_{V\cdot D_g}(\zeta) = diam_{V\cdot D_g}(\zeta) = n - 1$, where n is the number of nodes of ζ.*

Proof. Let ζ be a VD g-self-centered graph. If possible, let $\text{diam}_{V\cdot D_g}(\zeta) = l < n - 1$. Let u_1 and u_2 be two distinct VD g-peripheral path. Let $r \in u_1, s \in u_2$. So, there exists a strong path between r and s because of connectedness of ζ. Then, there exists nodes on u_1 and u_2, whose *eccentricity* $> l$, but

this is impossible because $\text{diam}_{V\cdot D_g}(\zeta) = l$. Hence, u_1 and u_2 are not distinct. Since u_1 and u_2 are arbitrary, so there exists a node t in ζ such that t is a common in all VD peripheral paths. So, $e_{V\cdot D_g}(t) < l$, which is impossible, because ζ is a VD g-self-centered. Therefore, $\text{diam}_{V\cdot D_g}(\zeta) = n - 1 = \text{rad}_{V\cdot D_g}(\zeta)$. □

Corollary 1. *For a CVG ζ, $per_{V\cdot D_g}(\zeta) = \zeta$ if and only if the VD g-eccentricity of every node of ζ is $n-1$, n = number of nodes in ζ.*

Proof. Let $\text{Per}_{V\cdot D_g}(\zeta) = \zeta$. Then, $e_{V\cdot D_g}(p) = \text{diam}_{V\cdot D_g}(\zeta)$, $\forall p \in \zeta$. So, each node of ζ is a VD g-periphery node of ζ. So, ζ is a self-centered vague graph and $\text{diam}_{V\cdot D_g}(\zeta) = \text{rad}_{V\cdot D_g}(\zeta) = n - 1$. Therefore, the VD g-eccentricity of every node of ζ is $n - 1$.

Conversely, let the VD g-eccentricity of every node of ζ is $n - 1$. So, $\text{diam}_{V\cdot D_g}(\zeta) = \text{rad}_{V\cdot D_g}(\zeta) = n - 1$. All nodes of ζ are VD g-peripheral nodes, and hence $\text{Per}_{V\cdot D_g}(\zeta) = \zeta$. □

Corollary 2. *For a CVG ζ, $E_{CC_{V\cdot D_g}}(\zeta) = \zeta$ if and only if the VD g-eccentricity of every node of ζ is $n-1$, n = number of nodes in ζ.*

Proof. Let $E_{CC_{V\cdot D_g}}(\zeta) = \zeta$. So, all nodes of ζ are VD g-eccentric node. Hence, ζ is self-centered vague graph and $\text{diam}_{V\cdot D_g}(\zeta) = n - 1$. So, the VD g-eccentricity of every node of ζ is $n - 1$.

Conversely, let the VD g-eccentricity of every node of ζ is $n - 1$. So, $\text{rad}_{V\cdot D_g}(\zeta) = \text{diam}_{V\cdot D_g}(\zeta) = n - 1$. Therefore, all nodes of ζ are VD g-peripheral nodes as well as VD g-eccentric node. So, $E_{CC_{V\cdot D_g}}(\zeta) = \zeta$. □

Theorem 5. *In a CVG ζ, a node x is a VD g-eccentric node if and only if x is a VD g-peripheral node.*

Proof. Let x be a VD g-eccentric node of ζ and let $x \in y^*_{V\cdot D_g}$. Let z and w be two VD g-peripheral nodes, then $V \cdot D_g(z, w) = \text{diam}_{V\cdot D_g}(\zeta) = k$ (say). Let p_1 and p_2 be any $z - w$ and $y - x$ vague g-detour in ζ, respectively. There arise two cases:

Case 1**:** if x is not internal node in ζ, i.e., there is only one node, say s which is adjacent to x. So, $s \in P_2$. Since ζ is connected, s is connected to a node of p_1, say $p\prime$. Therefore, either $s\prime \in p_2$ or $s\prime \in (p_1 \cap p_2)$. Thus, in any case, the path from y to z or y to w through s and $s\prime$ is longer than p_2. But it is impossible, since x is a VD g-eccentric node of y. So, $e_{V\cdot D_g}(y) = \text{diam}_{V\cdot D_g}(\zeta)$, i.e., b is a VD g-peripheral node of ζ.

Case 2**:** if x is an internal node in ζ, then $\exists$ a connection between x to z and x to w because of connectedness of ζ. Then, $y - x$ vague g-detour can be extended to z or w. This is impossible because x is a VD g-eccentric node of y. Hence, $e_{V\cdot D_g}(y) = \text{diam}_{V\cdot D_g}(\zeta)$, i.e., x is a VD g-peripheral node of ζ. Conversely, we suppose that x be a VD g-peripheral node of ζ. So, $\exists$ a VD g-peripheral node, say y (distinct from x). Therefore, x is a VD g-eccentric node of y. □

Definition 15. In a CVG ζ, a node y is said to be a VD g-boundary node of a node x, if $V \cdot D_g(x, y) \geq V \cdot D_g(x, z)$, for each z in ζ, where z is a neighbor of y.

The set of all VD g-boundary nodes of x described by $x_{V\cdot D_g}{}'$.

Example 8. Consider the CVG ζ in Figure 9.

In this example, we have

$$\begin{aligned} x'_{V\cdot D_g} &= \{t, s\}, \\ y'_{V\cdot D_g} &= \{x, t, s\}, \\ z'_{V\cdot D_g} &= \{x, t, s\}, \\ w'_{V\cdot D_g} &= \{x, t, s\}, \\ t'_{V\cdot D_g} &= \{x, s\}, \\ s'_{V\cdot D_g} &= \{x, t\}. \end{aligned} \tag{23}$$

Here, x, t, and s are the VD g-boundary nodes of ζ.

Theorem 6. *A CVG ζ is a vague tree if and only if ζ is a vague g-detour graph.*

Proof. Let ζ be a vague tree. Then, between any two nodes in ζ, there is exactly one vague strong path. So, $V \cdot D_g(x, y) = V \cdot d_g(x, y)$, for any two nodes x, y in ζ. Hence, ζ is a vague g-detour graph.

On the contrary, let ζ be a vague g-detour graph, which has n nodes. Then, $V \cdot D_g(x, y) = V \cdot d_g(x, y)$, for any two nodes x, y in ζ. If $n = z$, then ζ is a vague tree. Let $n \geq 3$. If possible, let ζ be not a vague tree. So, there exists two nodes s, t in ζ for which there is at least two strong paths between s and t. Let Q_1 and Q_2 be two $s - t$ vague strong paths. So, $Q_1 \cup Q_2$ has a cycle C (say) in ζ. If nodes x and y are adjacent nodes in ζ, then we have $V \cdot d_g(x, y) = 1$ and $V \cdot D_g(x, y) > 1$. This contradicts the fact that $V \cdot D_g(x, y) = V \cdot d_g(x, y)$. Hence, ζ is a vague tree. □

Definition 16. A node x in a VG ζ is called a VEN of ζ if y is the only strong neighbor of x, where $y \in \zeta$.

Example 9. For the VG ζ in Figure 9, the nodes x, t, and s are VENs of ζ.

Theorem 7. *A node y in a vague tree ζ is a VD g-boundary node if and only if y is a VEN.*

Proof. Let a node y be a VD g-boundary node for a node x in a vague tree ζ. Let E be a maximum vague spanning tree in ζ, which is unique in ζ. □

5. Application of Vague Detour g-Distance in the Transportation System

Today, the issue of transportation plays a very important role in human life. If this is done faster and easier, then it can affect the quality of life and human health. Unfortunately, in the past, due to the lack of sufficient vehicles and bad road

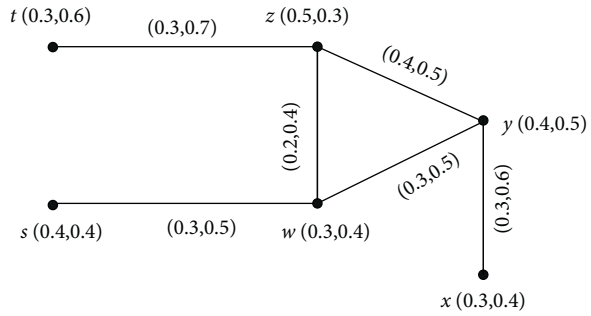

Figure 9: Connected vague graph ζ.

Table 2: Weight of nodes.

	A	B	C	D	E
t_A	0.2	0.2	0.3	0.5	0.4
f_A	0.2	0.3	0.5	0.2	0.3

Table 3: Weight of edges.

ζ	A – Yahya Nejad	A – Beheshti	A – Mehregan
(t_B, f_B)	(0.2, 0.5)	(0.1, 0.8)	(0.2, 0.4)
ζ	A – Rouhani	Beheshti – Mehregan	Mehregan – Rouhani
(t_B, f_B)	(0.2, 0.4)	(0.3, 0.7)	(0.3, 0.7)
ζ	Yahya Nejad – Beheshti		
(t_B, f_B)	(0.2, 0.7)		

conditions, many problems were created for human beings, one of the most important of which is the lack of timely transfer of patients to private hospitals and clinics for treatment. Therefore, in this paper, we intend to express the importance and application of vague detour g-distance in the transportation of a patient to the most appropriate hospital in the shortest possible time. For this purpose, we consider four hospitals in Iran (Babol City) named Yahya Nejad (B), Beheshti (C), Mehregan (D), and Rouhani (E), which are shown in the graph with the symbols of B, C, D, and E. Suppose that a patient lives in location A and must be transported by ambulance to one of these four hospitals in the shortest possible time. In this vague graph, the nodes represent the hospitals and the edges also shows the amount of traffic generated at a certain hour of the day. The weight of the nodes and edges is shown in Tables 2 and 3. The location of hospitals is shown in Figure 10.

The node $D(0.5, 0.2)$ shows that this hospital has 50% of the medical facilities and equipment needed to treat a patient, but does not have 20% of the necessary tools. The edge $A\ D$ indicates that 40% of this route has traffic and congestion caused by vehicles, but 20% of it is free of cars and vehicles. The vague detour g-distance for Figure 11 is as follows:

$$\begin{aligned} VD_g(A,B) &= 4,\\ VD_g(A,C) &= 3,\\ VD_g(A,D) &= 3,\\ VD_g(A,E) &= 4,\\ VD_g(B,C) &= 4,\\ VD_g(B,D) &= 3,\\ VD_g(B,E) &= 3,\\ VD_g(C,D) &= 4,\\ VD_g(C,E) &= 3,\\ VD_g(D,E) &= 4. \end{aligned} \tag{24}$$

It is clear that $VD_g(A,D)$ has the lowest value, so we conclude that it can be the best choice because, firstly, Mehregan hospital has the most medical equipment and facilities compared to other hospitals, and secondly, A-Mehregan route has the most empty space for patient transfer to medical centers by ambulance. Therefore, governments should provide conditions for patients to be transported to hospitals without stress due to the congestion of roads and intercity traffic, so that they can be treated as soon as possible.

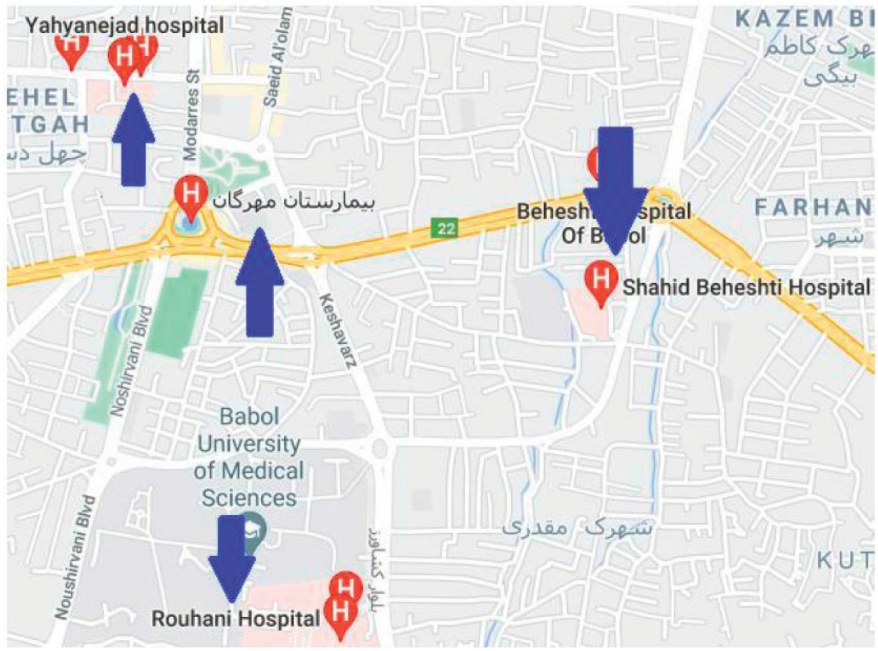

Figure 10: Location of hospitals in Babol City.

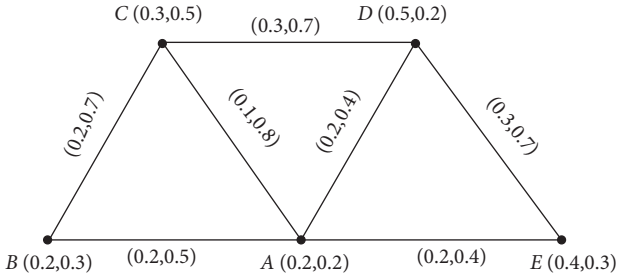

Figure 11: Vague graph ζ.

6. Conclusion

A VG is an indiscriminately comprehensive structure of an FG that offers higher precision, adaptability, and compatibility to a system when coordinated with systems running on FGs. VGs are so useful tool to examine many issues such as networking, social systems, geometry, biology, clustering, medical science, and traffic plan. Eccentric nodes and g-boundary nodes are a practical interest in several areas. In wireless networking, boundary nodes are used to find efficient routes within ad hoc mobile networks. They have also been used in document summarization and in designing secure systems for electrical grids. Hence, in this paper, the adjacency sequence of RVGs is defined with examples. Also, a characterization of vague detour g-eccentric node and the concepts of vague detour g-boundary nodes, vague detour g-interior nodes in a VG are examined. In our future work, we will introduce vague incidence graphs and study the concepts of perfect dominating set, regular perfect dominating set, and independent perfect dominating set on vague incidence graph. Likewise, we will try to define the average connectivity index, parameter and the new concepts of vague connectivity-enhancing node, vague detour g-interior node, and vague detour g-boundary node of a vague incidence tree using maximum vague spanning tree.

Data Availability

No data were used to support this study.

Conflicts of Interest

The authors declare no conflicts of interest.

References

[1] A. Rosenfeld, *Fuzzy Graphs, Fuzzy Sets and Their Applications*, L. A. Zadeh, K. S. Fu, and M. Shimura, Eds., Academic Press, New York, NY, USA, pp. 77–95, 1975.

[2] L. A. Zadeh, "Fuzzy sets," *Information and Control*, vol. 8, no. 3, pp. 338–353, 1965.

[3] W.-L. Gau and D. J. Buehrer, "Vague sets," *IEEE Transactions on Systems, Man, and Cybernetics*, vol. 23, no. 2, pp. 610–614, 1993.

[4] A. Kauffman, "Introduction a la theories des sous-emsembles 503 ous," *Masson Cie*, vol. 1, pp. 607–618, 1973.

[5] L. A. Zadeh, "Similarity relations and fuzzy orderings," *Information Sciences*, vol. 3, no. 2, pp. 177–200, 1971.

[6] L. A. Zadeh, "Is there a need for fuzzy logic?" *Information Sciences*, vol. 178, no. 13, pp. 2751–2779, 2008.

[7] M. Akram, W. A. Dudek, and M. Murtaza Yousof, "Regularity in vague intersection graphs and vague line graphs," *Abstract and Applied Analysis*, vol. 2014, Article ID 525389, 10 pages, 2014.

[8] M. Akram, A. N. Gani, and A. B. Saeid, "Vague hypergraphs," *Journal of Intelligent and Fuzzy Systems*, vol. 26, no. 2, pp. 647–653, 2014.

[9] S. Samanta and M. Pal, "Irregular bipolar fuzzy graphs," *International Journal of Fuzzy System Applications*, vol. 2, pp. 91–102, 2012.
[10] S. Samanta and M. Pal, "Fuzzy k-competition graphs and p-competition fuzzy graphs," *Fuzzy Information and Engineering*, vol. 5, no. 2, pp. 191–204, 2013.
[11] A. Nagoorgani and S. R. Latha, "On irregular fuzzy graphs," *Applied Mathematical Sciences*, vol. 6, pp. 517–523, 2012.
[12] A. Nagoorgani and K. Radha, "On regular fuzzy graphs," *Journal of Physical Science*, vol. 12, pp. 33–44, 2008.
[13] M. S. Sunitha and S. Mathew, "Fuzzy graph theory: a survey, Ann," *Pure and Applied Mathematics Journal*, vol. 4, pp. 92–110, 2013.
[14] M. S. Sunitha and A. Vijayakumar, "Complement of a fuzzy graph," *Indian Journal of Pure and Applied Mathematics*, vol. 33, pp. 1451–1464, 2002.
[15] N. Ramakrishna, "Vague graphs," *International Journal of Cognitive Computing*, vol. 7, pp. 51–58, 2009.
[16] R. Borzooei and H. Rashmanlou, "Domination in vague graphs and its applications," *Journal of Intelligent and Fuzzy Systems*, vol. 29, no. 5, pp. 1933–1940, 2015.
[17] R. A. Borzooei and H. Rashmanlou, "Degree of vertices in vague graphs," *Journal of applied mathematics & informatics*, vol. 33, no. 5_6, pp. 545–557, 2015.
[18] G. Chatrand, H. Escuadro, and P. Zhang, "Detour distance in graph," *Journal of Combinatorial Mathematics and Combinatorial Computing*, vol. 53, pp. 75–94, 2005.
[19] G. Chatrand, G. L. Johns, and P. Zhang, "Detour number of a graph," *Utilitas Mathematica*, vol. 64, pp. 97–113, 2003.
[20] G. Chatrand, D. Erwin, G. L. Johns, and P. Zang, "Boundary vertices in graphs," *Discrete Math*, vol. 263, no. 1-3, pp. 25–34, 2003.
[21] J. P. Linda and M. S. Sunitha, "Fuzzy detour g-centre in fuzzy graphs, Ann," *Fuzzy Math Informa*, vol. 7, no. 2, pp. 219–228, 2014.
[22] G. Ghorai, "Characterization of regular bipolar fuzzy graphs," *Afrika Matematika*, vol. 32, no. 5-6, pp. 1043–1057, 2021.
[23] S. Poulik and G. Ghorai, "Detour g-interior nodes and detour g-boundary nodes in bipolar fuzzy graphs with applications," *Hacettepe Journal of Mathematics and Statistics*, vol. 49, no. 1, pp. 106–119, 2020.
[24] K. R. Bhutani and A. Rosenfeld, "Strong arcs in fuzzy graphs," *Information Sciences*, vol. 152, pp. 319–322, 2003.
[25] S. Mathew and M. S. Sunitha, "Types of arcs in a fuzzy graph," *Information Sciences*, vol. 179, no. 11, pp. 1760–1768, 2009.
[26] J. P. Linda and M. S. Sunitha, "On g-eccentric nodes g-boundary nodes and g-interior nodes of a fuzzy graph," *International Journal of Mathematical Sciences & Applications*, vol. 2, no. 2, pp. 697–707, 2012.
[27] S. Banitalebi and R. A. Borzooei, "2-Domination in vague graphs," *Algebraic Structures and Their Applications*, vol. 8, no. 2, pp. 203–222, 2021.
[28] P. K. Kishore Kumar, Y. Talebi, H. Rashmanlou, A. A. Talebi, and F. Mofidnakhaei, "New concept of cubic graph with application," *Journal of Multiple-Valued Logic and Soft Computing*, vol. 33, pp. 135–154, 2019.
[29] S. Kosari, Y. Rao, H. Jiang, X. Liu, P. Wu, and Z. Shao, "Vague graph structure with application in medical diagnosis," *Symmetry Plus*, vol. 12, no. 10, p. 1582, 2020.
[30] K. Radha and N. Kumaravel, "Some properties of edge regular fuzzy graphs," *Jamal Academic Research Journal*, pp. 121–127, 2014.
[31] H. Rashmanlou, S. Samanta, M. Pal, and R. A. Borzooei, "Intuitionistic fuzzy graphs with categorical properties," *Fuzzy Information and Engineering*, vol. 7, no. 3, pp. 317–334, 2015.
[32] S. Samanta, M. Pal, and A. Pal, "New concepts of fuzzy planar graph," *International Journal of Advanced Research in Artificial Intelligence*, vol. 3, no. 1, pp. 52–59, 2014.
[33] S. Samanta and M. Pal, "Fuzzy tolerance graphs," *International Journal of Latest Trends in Mathematics*, vol. 1, no. 2, pp. 57–67, 2011.
[34] S. Sahoo, M. Pal, H. Rashmanlou, and R. A. Borzooei, "Covering and paired domination in intuitionistic fuzzy graphs," *Journal of Intelligent and Fuzzy Systems*, vol. 33, no. 6, pp. 4007–4015, 2017.
[35] A. A. Talebi, N. Mehdipoor, and H. Rashmanlou, "Some operations on vague graphs," *Journal of Advanced Research in Pure Mathematics*, vol. 6, no. 1, pp. 61–77, 2014.
[36] S. Zeng, M. Shoaib, S. Ali, Q. Abbas, and M. S. Nadeem, "Complex vague graphs and their application in decision-making problems," *IEEE Access*, vol. 8, pp. 174094–174104, 2020.
[37] S. Zeng, M. Shoaib, S. Ali, F. Smarandache, H. Rashmanlou, and F. Mofidnakhaei, "Certain properties of single-valued neutrosophic graph with application in food and agriculture organization," *International Journal of Computational Intelligence Systems*, vol. 14, no. 1, pp. 1516–1540, 2021.
[38] S. Zeng, Z. Ali, and T. Mahmood, "Novel complex T-spherical dual hesitant uncertain linguistic muirhead mean operators and their application in decision-making," *Computer Modeling in Engineering and Sciences*, vol. 129, no. 2, pp. 849–880, 2021.
[39] M. Shoaib, S. Kosari, H. Rashmanlou et al., "Notion of complex pythagorean fuzzy graph with properties and application," *Journal of Multiple-Valued Logic and Soft Computing*, vol. 34, pp. 553–586, 2020.
[40] W. L. Craine, "Characterizations of fuzzy interval graphs," *Fuzzy Sets and Systems*, vol. 68, no. 2, pp. 181–193, 1994.

Hindawi
Journal of Mathematics
Volume 2023, Article ID 9845696, 1 page
https://doi.org/10.1155/2023/9845696

Retraction

Retracted: Research on the Risk Measurement Algorithm of Supply Chain Order Financing Based on Insurance Actuarial

Journal of Mathematics

Received 19 December 2023; Accepted 19 December 2023; Published 20 December 2023

This article has been retracted by Hindawi following an investigation undertaken by the publisher [1]. This investigation has uncovered evidence of one or more of the following indicators of systematic manipulation of the publication process:

(1) Discrepancies in scope

(2) Discrepancies in the description of the research reported

(3) Discrepancies between the availability of data and the research described

(4) Inappropriate citations

(5) Incoherent, meaningless and/or irrelevant content included in the article

(6) Manipulated or compromised peer review

The presence of these indicators undermines our confidence in the integrity of the article's content and we cannot, therefore, vouch for its reliability. Please note that this notice is intended solely to alert readers that the content of this article is unreliable. We have not investigated whether authors were aware of or involved in the systematic manipulation of the publication process.

Wiley and Hindawi regrets that the usual quality checks did not identify these issues before publication and have since put additional measures in place to safeguard research integrity.

We wish to credit our own Research Integrity and Research Publishing teams and anonymous and named external researchers and research integrity experts for contributing to this investigation.

The corresponding author, as the representative of all authors, has been given the opportunity to register their agreement or disagreement to this retraction. We have kept a record of any response received.

References

[1] G. Li and M. Yin, "Research on the Risk Measurement Algorithm of Supply Chain Order Financing Based on Insurance Actuarial," *Journal of Mathematics*, vol. 2021, Article ID 5344205, 9 pages, 2021.

Hindawi
Journal of Mathematics
Volume 2021, Article ID 5344205, 9 pages
https://doi.org/10.1155/2021/5344205

Research Article

Research on the Risk Measurement Algorithm of Supply Chain Order Financing Based on Insurance Actuarial

Gushuo Li and Menglin Yin

Business School, University of Sydney, Sydney, New South Wales 2006, Australia

Correspondence should be addressed to Menglin Yin; hej20@mails.tsinghua.edu.cn

Received 15 October 2021; Revised 8 November 2021; Accepted 10 November 2021; Published 1 December 2021

Academic Editor: Lazim Abdullah

In today's globalized economy, all the links of supply chain are interlinked. Most of the upstream raw material manufacturers or producers in the said chain are small- and medium-sized enterprises (SMEs) that provide the basis for the efficient operation of the whole supply chain. However, SMEs in China, especially those playing a pivotal role in China's export-oriented economy at this stage, do not have access to the corresponding financial treatment. Supply chain finance provides a new perspective to solve this contradiction. Henceforth, this paper introduces modern financial engineering risk measurement tools to measure the financial risk in supply chain finance, specifically while evaluating the single financing business. Moreover, the chief objective of this paper will be the analysis of the characteristics and connotations of order financing business model. In addition, the focus will be to analyze the risk of order financing from the perspective of banks and other financial institutions. Additionally, this paper will use the CreditRisk + model based on insurance actuarial principles to manage credit risk in order financing business based on foreign currency settlement, in conjunction with the characteristics of supply chain finance and multinational supply chain. Furthermore, a risk measurement method for the application of order financing in multinational supply chains will be provided. Ultimately, the experiments show that the solution of this paper defines and analyzes the financial risks brought by order financing business to bank financing.

1. Introduction

The globalization of economy brings the globalization of manufacturing, and with the globalization of production, investment, and market, the transnational supply chain is formed by the collaboration, exchange, and operation of information flow, logistics, and capital flow among international organizations around the nuclear enterprises in transnational trade, and the whole supply chain starts from the upstream procurement of raw materials from one or more countries and makes intermediate and final products, and finally the global sales network sells the products to consumers all over the world. Finally, the products are sold to consumers all over the world by the global sales network. China's manufacturing industry is still in the status of "world factory" in this supply chain, and a large number of small- and medium-sized enterprises are responsible for the important production and manufacturing functions in this functional chain, but they have not received the corresponding financial treatment, many small- and medium-sized enterprises are facing the problem of difficult financing, supply chain finance can solve the problem of providing these enterprises with a new perspective, and at the same time, it also brings a huge potential market for banks and other financial enterprises. The supply chain finance can provide a solution for these enterprises from a new perspective and also bring a huge potential market for banks and other financial companies. For this reason, in recent years, especially after the financial crisis, supply chain finance business has developed rapidly and became a new business growth point for banks and other financial institutions.

However, commercial banks in China should not only see the huge benefits brought by the supply chain finance business, but also ignore the potential risks in this business, such as the risk of price changes of inventory goods in

movable warehouse receipts pledge financing, the risk of supervision of logistics enterprises in the process of warehouse receipts financing, or the risk of interperiod exchange rate in the financing of orders in cross-border trade, etc. In the whole business process, banks, logistics enterprises, and manufacturing, only after understanding the mechanism of risk formation can we avoid the risk in a timely and effective way in the actual business [1].

The customer base of China's supply chain finance is mainly SMEs, and in order to avoid the higher credit risk of SMEs, its risk control methods differ greatly from traditional bank financing when conducting business. Traditional bank financing focuses on the credit rating and financial status of individual enterprises, which sets a high threshold for SMEs, while some large state-owned enterprises that do not lack capital can easily obtain financing, resulting in an unreasonable distribution of bank credit; i.e., financing is not provided according to the actual capital box needs of enterprises [2, 3]. As a financing method based on supply chain, supply chain Gimblee pays more attention to the operation status of the whole supply chain and whether the trade background is true, while the requirements for the qualification of the main body can be appropriately reduced [4, 5].

The existing financing methods involve the risk prevention and control methods such as verification and also enterprise credit bundling, control of the right of goods, and claims of the financing enterprise (i.e., chattel pledge) and emphasize the self-repayment of repayment sources. These methods effectively avoid some of the risks in financing, but the current risk prevention and control methods of supply chain financing are still not perfect [6].

Especially for the more advanced order financing business model in the actual case of supply chain finance, the theoretical research on its business risk identification, measurement, and later risk control is still far from meeting the real business development [7, 8]. Coupled with the advanced and operational nature of the order financing business and its application, this business model will become the main business model in the supply chain finance business model, and its business scope and business volume will account for a larger and larger proportion of the supply chain finance business, and its importance to the financing needs of SMEs and business development will become more and more prominent.

Based on the importance of order financing business, this paper will apply the principle of Jin Christmas engineering, use the modern Jin Christmas engineering risk measurement model, analyze and discuss the operational risk, credit risk, and exchange rate risk factors of coincidental order financing in tracing country trade, analyze the problem of risk identification and measurement of supply chain finance in multinational supply chain from the bank's point of view, and calculate the risk measurement for coincidental order financing by means of calculation examples and the analysis and calculation of the risk measurement of the supply chain finance from the bank's perspective [9]. Also, the modern tools for measuring the financial engineering risk are introduced, which are used to measure the supply chain finance's financial risk. This paper specifically focuses on the analysis of the characteristics and connotations of order financing business model. Further, the paper also emphasizes the analysis of order financing's risk from banks' and other financial institutions' perspectives. Moreover, the CreditRisk + model based on insurance actuarial principles is used to manage credit risk in order financing business based on foreign currency settlement. Furthermore, a method is provided that measures risk for the application of order financing in multinational supply chains. In addition to the said objectives, this paper also presents the experiments that verify the point that financial risks brought by order financing business to bank financing are defined and analyzed through the proposed solution. The identification, avoidance, and control of the risk led to the evaluation of the order financing business's risks. Through this article, the author proposes numerous suggestions for risk prevention and control from the banks' perspective. The intentions are to help the Chinese banks to carry out risk prevention in order financing business.

The organization of the paper is as follows:

Section 1 contains the introduction to the article. Section 2 discusses some related works. Section 3 talks about the risk measurement of order financing based on foreign currency settlement. Section 4 presents the experimental results. The discussion of the article is given in Section 5. Finally, in Section 6, the article is concluded.

2. Related Work

First of all, through the study of foreign literature on supply chain finance, we know that supply chain finance was called logistics finance in the early stage of development, and some banks and financial institutions collectively called it supply chain finance; commercial banks and other financial institutions with this business, combined with the financing requirements of financing enterprises, gradually developed, from the beginning of logistics finance to cover a wider range of supply chain finance, from the initial logistics finance to the broader scope of supply chain finance, until the development of a series of innovative financial services due to the needs of enterprise management.

Compared with the traditional supply chain finance, order financing has become a hot spot for research because of its special advantages, and in the actual bank financing cases, order financing also accounts for a significant proportion of them, including the French Bank of Zurich, the Netherlands Wanbay Bank, and the United States Citibank; and some foreign financial institutions have also set up special logistics banks, such as the United States in 1999 Morgan Stanley which invested $350 million to Redwood Trust, a listed logistics company, in 1999, to carry out supply chain finance business, while United Parcel (UP) acquired the First International Bank of the United States and set up a special UPS finance company, so as to provide customers with a full range of supply chain financial services, to achieve its logistics, information flow, and capital flow with high degree of synchronization.

When it comes to the financial risk of supply chain finance, more foreign related literature can be retrieved, but

most of them are rather broad. Among them, Shearer and Diamond (999) point out that the risk rating approach has played an important role in traditional commercial financing, but with the increase of competition and changes in the market environment, the risk rating approach is no longer sufficient for commercial financing.

Barsky and Catanach (2005) argue that commercial finance business control should change from a subject access-based risk control concept to a process control-based risk management concept. [10] It is worth noting that foreign scholars believe that supply chain finance itself is a means and method to reduce risk, and the research on risk is mostly focused on the use of supply chain finance technology to achieve automation and visualization through supply chain financial regulation technology for the purpose of reducing supply chain risk. For example, Martin Christopher and Hau Lee (2004) point out that one of the key factors to reduce supply chain risk is to improve the visibility of "end-to-end." Visualization of physical supply chain metrics can certainly reduce the risk of supply chain financing significantly.

Bemabucci D. Robert (2006) argues that supply chain visibility has changed the form of trade force financing and reduced the risk of trade finance. A report by W. A. Berdeen (2007) highlights the importance of supply chain gold knockout technology platforms, which provide features such as visualization that can improve risk management and reduce costs [11]. Allen N Berger (2007) introduces supply chain finance as a new form of financing and argues that the automation of procurement, invoicing, and the use of visual trade platforms will effectively reduce supply chain finance risk. Further, they will also provide a platform where the parties to a commodity transaction and a financing transaction are interfaced, which makes key events in the supply chain transparent and provides several transaction completion markers as "financing triggers" [12].

Domestic scholars' research on the financial risk of supply chain finance is mainly based on the traditional business model of supply chain finance, mainly including quantitative and qualitative levels, among which quantitative analysis is reflected in the following aspects:

The first is the credit risk of supply chain finance. Xiao Junhong (2007) constructed an evaluation system for credit risk of SMEs in supply chain finance, evaluated the system by using multilevel gray comprehensive evaluation method, and proposed the principle and idea of using credit spread option method to transfer and manage credit risk in supply chain finance. He Tao (2007) also proposed the use of carry option method to transfer and manage supply chain finance credit risk [13]. Lou, Qiao, and Qian, Zhi-Xin (2008) predicted the repayment risk of loaning enterprises by using the technique of plain Bayesian for the credit risk of SME loans in supply chain finance.

Zhang Zhen (2009) used hierarchical analysis to determine the weights, combined with the characteristics of supply chain finance to construct a credit rating model for SMEs based on supply chain finance.

Wang Qi coincidentally used the method of decision tree in data mining to construct a credit risk assessment model for supply chain finance. The credit risk in the three financing modes of supply chain finance is analyzed in depth, and the credit risk evaluation system is constructed, and the KMV model is used to measure the credit risk of supply chain financing [14].

The second is the research on the market risk, liquidity risk, and pledge rate setting of inventory financing mode of supply chain finance. At present, many scholars in domestic theoretical circles have used VaR for risk measurement of inventory pledge financing; for example, Li Yixue (2010) studied the setting of inventory advisory pledge rate and inventory financing market risk [9]; Chen Baofeng et al. (2009) studied inventory financing liquidity risk. Then there is a study on the risk of accounts receivable financing model. Bending Hongdi (2008) argues that the risk avoidance mechanism relied on by supply chain finance has the possibility of failure by analyzing the risk model of accounts receivable financing model.

The results of a game theoretic differentiation analysis of moral hazard in the receivables financing model by Zhou Bo (2010) show that moral analysis is influenced not only by the willingness of the nucleus to repay and the compliance of the borrower's use of loan funds, but also by the dual influence of the relationship between the borrower and the nucleus and the relationship between the nucleus and the bank.

3. Risk Measurement of Order Financing Based on Foreign Currency Settlement

In the following, this paper will analyze the financial risks in the process through a typical business case of coincident order financing based on foreign currency settlement and the modeling of CreditRisk + to return to the setting of financing rates of banks and other financial institutions for order financing business based on foreign currency settlement, adjusting the probability of occurrence of risks in the financing process at each stage of the financing process, and the calculation of default rate and default loss rate to analyze the risk analysis path of banks in the order financing process.

We assume that there is a typical financing SME C company, which is engaged in export trade, which has a large customer, A company from North America; today C company received an order worth 100 million US dollars from A company, to start production, in order to alleviate the financial pressure, W purchases raw materials to arrange production, and contacts local bank B for loan matters, and B handles overseas matters through company C. Through background investigation, Bank B decided to join hands with logistics company W to cooperate with Company C H in a supply chain financing project; the brief business process is shown in Figure 1.

At the starting time t, Company C receives the order, finances to Bank B, and sets up a special account in Bank B. Bank B simply lends the total amount of Company C's order to Company C's special account to purchase raw materials and make production arrangements, etc. At time t_1, Company C completes the production of the coincidental order, and the goods are delivered to the W logistics company designated by Bank B. The W logistics company

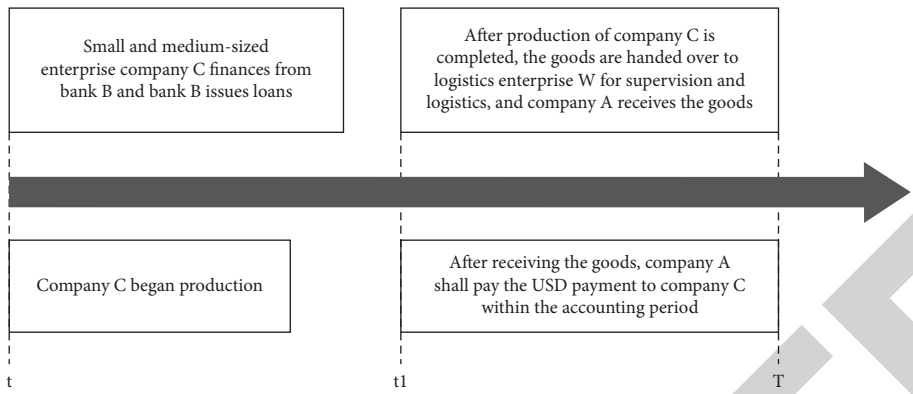

Figure 1: Business process of order financing based on foreign currency settlement.

makes shipping arrangements despite the W and finally at time T. Company A, after receiving the goods delivered by Company C according to the order, completes the payment for the order (in US dollars) to the special account set up by Company C in Bank B before the arrival date, and Bank B receives the payment and completes the clearing of various costs with Company C. By the design of the business process on W, according to the identification of risk factors in supply chain finance listed in the previous article, we can see that its main risk points are as follows.

First, credit risk, that is, Company C is unable to return the loan principal and interest to the bank in accordance with the time listed in the loan contract due to various unforeseen reasons in objective fact.

Second, the operational risk for C company after receiving the loan from Bank B; although it is a dedicated account operation, and through the W logistics company to purchase raw materials, it does not exclude the C company and W company collusion and misappropriation of earmarked funds; sent is the operational risk faced by Bank B. In addition, with the completion of the coincidental single shipment in Company C, its customer A company in the account period on time, full payment is also another risk factor based on credit risk.

There is another situation; when Company C starts production, it will not be able to deliver the order on time or deliver it with unacceptable quality problems because of its own factory operation, management, W, and production technology capability.

Here, because Company A pays Company C in US dollars, and at the moment when Company C receives the order and starts to start, after the production, delivery, and transportation, to the moment when Company A receives the goods and has a certain billing period arrangement, the exchange rate fluctuation of US dollars to RMB must be considered, which is the market risk in this case. To facilitate our assessment of risk, we can use a binomial tree model to define the nodes in this supply chain financing. Sequential default process of order financing is shown in Figure 2.

In this, P1, P2, and P3 are the probability of default in their respective links, but according to the Hexer concordance in commercial banks facing the risk of default, we also need to take into account the default loss rate, as default occurs, the extent of losses faced by the bank's debt, and the recovery rate, and the sum of 1 and emphasize that the estimated default rate of loss refers to economic losses, rather than accounting book losses; economic losses must take into account the cost of recovery and the time value of money, that is, the use of a suitable discount rate to calculate the present value of the recovery cash flow; we generally use the following formula to calculate the default loss rate:

$$\mathrm{LGD} = 1 - \frac{\sum\left[\left(\text{recovery amount} - \text{recovery cost}\right)_t / \left(1 + \text{discount rate}\right)^t\right]}{\text{default exposure}}. \tag{1}$$

The model construction of LGD has always been a difficult task for banks, and the key obstacle is that the data deficiency of LGD has been serious to the local level. The lack of data in the probability of default (PD) model is mainly the lack of data required for the calculation of the independent variables, and the quality of the dependent variable data is relatively good, but the lack of data in both aspects of the LGD model is relatively serious.

In applying the above formula to calculate LGD, we will find in a more empirical scope that LGD presents a bimodal distribution, where P3 shows that if Company A is willing to pay for the order, regardless of the time duration, it will eventually pay Company C for most of the goods, which means that LGD is relatively low, the peak at the lower end of the bimodal peak, and if Company A does not subjectively have the will or ability to pay for the goods, then, since the full amount cannot be paid, it is better to completely default; that is to say, Company C will not get any money, presenting as the higher peak in the bimodal peak, but in general, it is still the majority of companies that keep their word; using the graph to represent the bimodal distribution, LGD bimodal distribution is shown in Figure 3.

The LGD is corresponding to the default node in the binomial tree model; according to the new capital agreement of Hexel, the default rate is Beta distributed, and we know that Beta distribution is the distribution of a few values in a certain space, and there are two parameters that affect the Beta distribution, and the change of parameters can lead to a great change in the graph of Beta distribution; assuming that we take the value (a, |3) for these six groups of numbers, (1, 1); (1, 2); (3, 2); (4, 2); (1, 1/2); (1/2, 1/3), the graphs of the

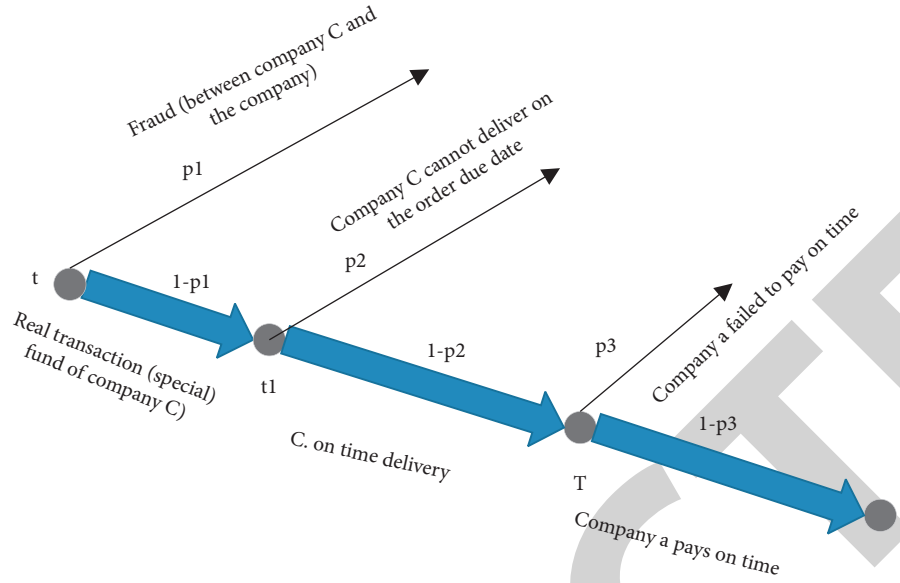

Figure 2: Sequential default process of order financing.

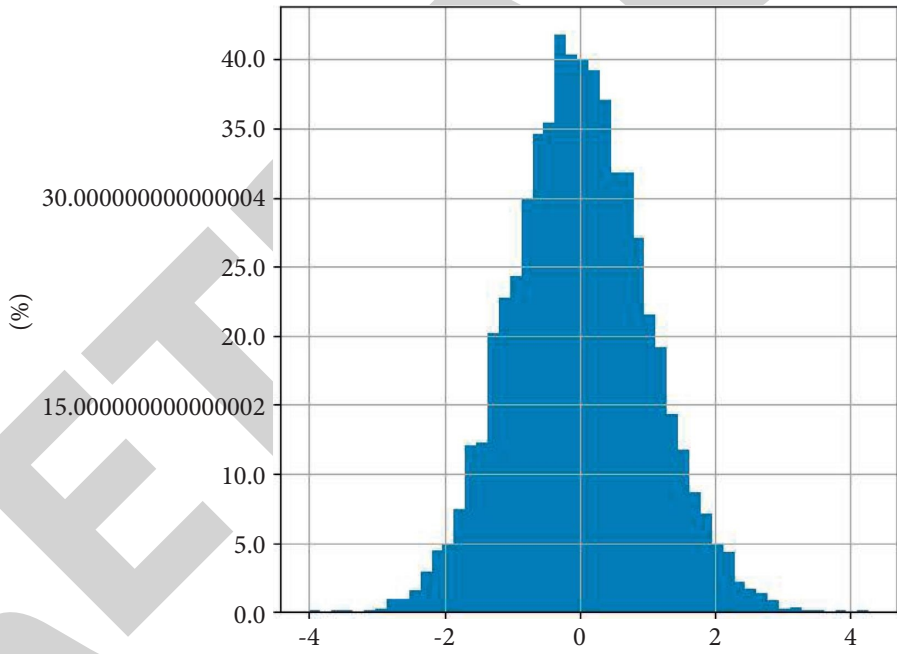

Figure 3: LGD bimodal distribution.

Beta distribution will also be plotted as curves 1 to 6, respectively; Beta distribution (corresponding to (a, P) taking different values) is shown in Figure 4.

In this example, we empirically set the parameters of the Beta distribution of LGD as (4, 2), (1, 1/2), and (6.3) for the default of P1, P2, and P3, respectively. In addition, given that the coincident payments in this business are based on foreign currency settlement, while Bank B settles in local currency, i.e., RMB, when extending credit to Company C, the exchange rate fluctuations in the period from t_1 to T will unquestionably bring exchange rate risk to Bank B. The general exchange rate risk refers to the possibility of on- and off-balance sheet losses of commercial banks due to exchange rate changes, which can be divided into transaction risk, translation risk, and asset-liability mismatch risk. In this particular case, transaction risk is the most important risk factor, because in recent years, with the continuous appreciation of the RMB, commercial banks have rapidly increased the number of USD loans issued. Joining the commercial banks without actively adjusting the interest rates of USD loans with the changes of the exchange rate of RMB against USD will lead to a large transaction risk for the commercial banks.

According to the VaR model of the internal model, which is a probabilistic estimate of potential losses, the

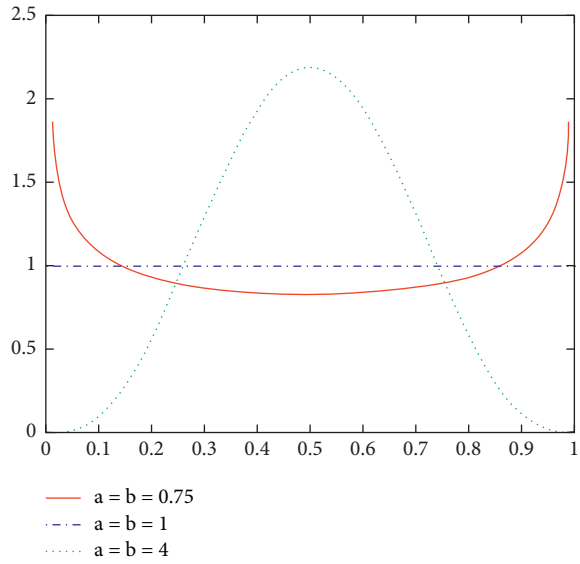

FIGURE 4: Beta distribution (corresponding to (a, P) taking different values).

general requirements of the Hexel Committee for the internal model approach are as follows.

(i) Banks are required to calculate VaR values and meet capital requirements on a daily basis

(ii) The capital requirement is the higher of the two under W; the VaR value of the previous day and the average VaR value of the previous 60 business days X (multiplier factor + additional value), and the formula for measuring market wind pickup capital is

$$\mathrm{MRC} = \max\left\{k\frac{1}{60}\sum_{i=1}^{60}\mathrm{VaR}_{i-1}, \mathrm{VaR}_{t-1}\right\} + \mathrm{SRC}_t, \quad (2)$$

where k is the correction factor multiplier and SRC is the special risk accrual capital.

The method on W, by analyzing the characteristics of each risk factor, and through the method of model calculation, can provide certain quantitative analysis methods in giving commercial banks in making order financing business decisions, so as to further decide the relevant financing ratio and cost.

We know that according to the Black Turbine-Scholes pricing model, the distribution of the forward exchange rate can be obtained by applying the pricing formula to

$$S_T = S_t \exp\left[\left(\mu - \frac{1}{2}\sigma^2\right)(T-t) + \xi\sigma\sqrt{T-t}\right], \quad (3)$$

where ξ is the normal distribution, and then the agreed exchange rate is S_t; we set it to 6.3, with μ with an expected exchange rate increase of -0.02, T-t of 0.5, and σ with 8 percent.

In addition, at moment t to T, we assume a time duration of six months for the default loss rate of the whole supply chain process, according to its characteristics:

(i) The value of LGD is limited to [0, I], and the empirical study shows that its distribution is Beta or bimodal, but not normal.

(ii) LGD takes the value on [0, 1] continuously; we use Beta distribution to simulate LGD here; we set the bank at the beginning according to the order quota (100 million US dollars) according to the agreement exchange rate issued to the C company's RMB loan of Ao RMB, and the corresponding default loss rate of P_1, P_2, P_3, respectively, is LGD_1, LGD_2, LGD_3, and in the whole supply chain operation process time of the interest rate is fixed at r. Then the revenue distribution of Bank B in the business of sending a supply chain Jinlan, that is, the corresponding formula for calculating the risk exposure, is

$$R' = E\left\{\frac{A_0(1+r)}{F_0}(1-\mathrm{LGD})P_1 + \left\{\left[\frac{A_0(1+r)}{F_0}(1-\mathrm{LGD})P_3 + \frac{A_0(1+r)}{F_0}(1-P_3)\right](1-P_2) + \frac{A_0(1+r)}{F_0}P_2(1-\mathrm{LGD})\right\}(1-P_1)S_T\right\}, \quad (4)$$

where work is 0.04 (set interest rate constant) (equation (3)).

Combining the key H default nodes, $P1$, $P2$, $P3$, we can follow the definition of the CreditRisk + model:

$$P(n) = \frac{(\mu t)^n e^{-\mu t}}{n} \quad n = 1, 2, 3, \ldots. \quad (5)$$

4. Experiment

Within a time length of 1 year (t is 1), we first assume that the average default among 1000 SMEs in need of financing is 50 ($i = 50$) in the first link of the binomial tree (P1), which is distributed as follows: the first ten groups of the (1000) data set are taken as an example.

Bringing P1, P2, P3 and LGD1, LGD2, LGD3 into equation (1), respectively, we calculate the value of R in this example in the interval [0.988104, 1.05418] scraping, below we use the graph to visualize the distribution frequency of R in this interval, and we go up in this interval and divide it into 3 0 partitions, so that the distribution frequency histogram of the final R value can be made. Distribution frequency histogram 1 is shown in Figure 5.

Similarly, we do a sensitivity analysis for the average number of defaults M per unit of time for the distribution of bank returns min; we take H corresponding to $P1$, $P2$, and $P3$ as (40, 30, 50) and (30, 50, 40), respectively. LGD1, LGD2,

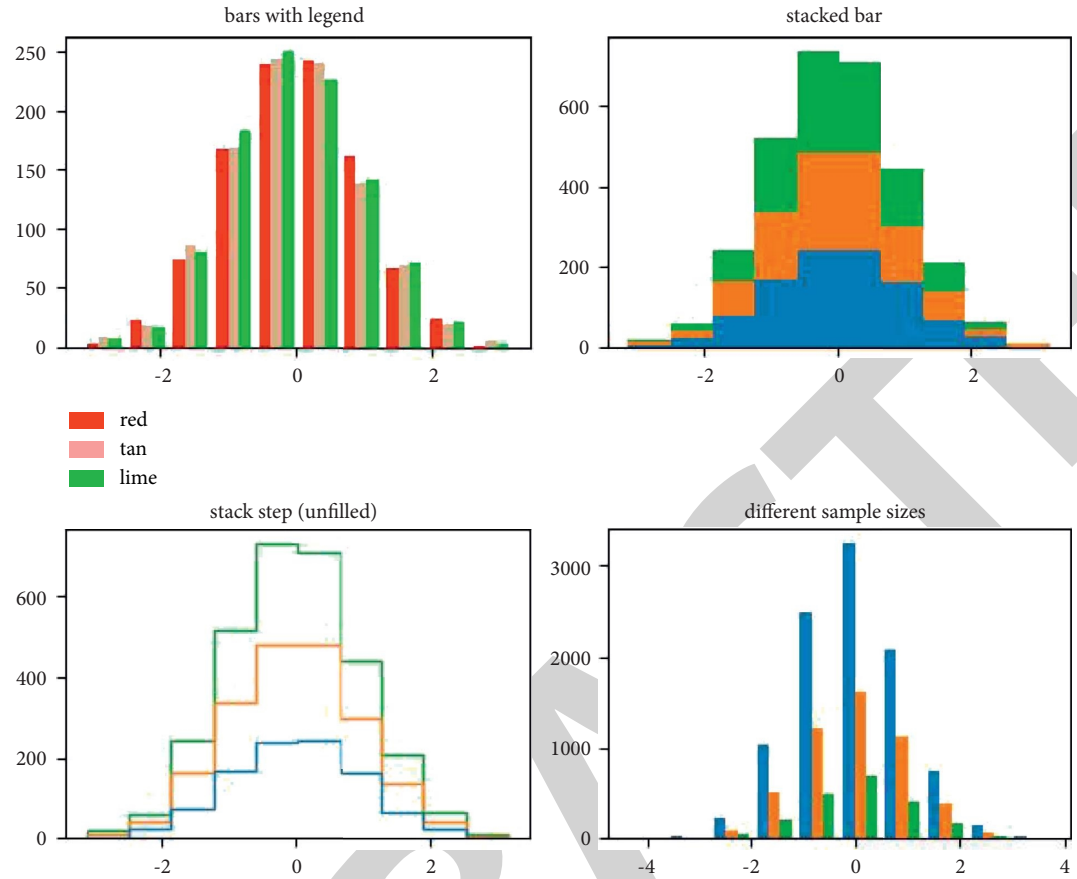

Figure 5: Distribution frequency histogram. (a) Bar with legends. (b) Stacked bar. (c) Stack step (unfilled). (d) Different sample sizes.

and LGD3 still keep the parameters unchanged, and the histograms of different distribution frequencies of the min obtained by BEA are shown in Figure 6.

In our hypothetical business process, the smaller the probability of a risk factor (e.g., $P1$), the smaller the standard deviation of LGD1, LGD2, LGD3, and finally the distribution of returns in the bank, and the more concentrated the distribution is, the larger the expected value of W and returns is. The smaller the standard deviation, the more concentrated the distribution, and the larger the expected value of W and return, and vice versa.

We now only use $P1$, $P2$, $P3$ to do a limited stochastic distribution of the value of the measurement, according to the needs of the bank credit line; we can also do a more comprehensive distribution of this default probability analysis and deduce the credit line and $P1$, $P2$, $P3$ in the sensitivity analysis. This provides a theoretical basis for banks to control their risk exposures more accurately.

The above statistical analysis, by means of modeling examples, first verifies that when a bank conducts order financing business, when the probability of a certain risk factor becomes smaller and larger, after the financing business is completed, the interval of the bank's earnings distribution will also become larger and the distribution will be more spread out, which means that the bank's exposure to risk will also be larger.

5. Discussion

The ultimate purpose of evaluating the risks of order financing business is to identify, avoid, and control the risks. Through the research and coincidental evaluation of the risks of order financing business on W, combined with the current situation of order financing business in China, the author puts forward several suggestions for risk prevention and control from the perspective of banks, hoping that it can be helpful for Chinese banks to carry out risk prevention in order financing business.

5.1. Strengthen the Monitoring Capacity of Third-Party Professional Logistics Enterprises Themselves. In the order financing business, although the partners with the bank are quite strong and have a good business reputation and related technical capabilities, the guarantors of the logistics enterprises need a strong sense of responsibility, are more active to cooperate with the bank, and constantly improve their monitoring capabilities. Logistics enterprises should have a perfect warehouse management system, a standardized inlet and outlet management system, internal control system and business operation process, and a more complete training system; warehouse managers should have rich professional experience and have the ability to identify the specifications,

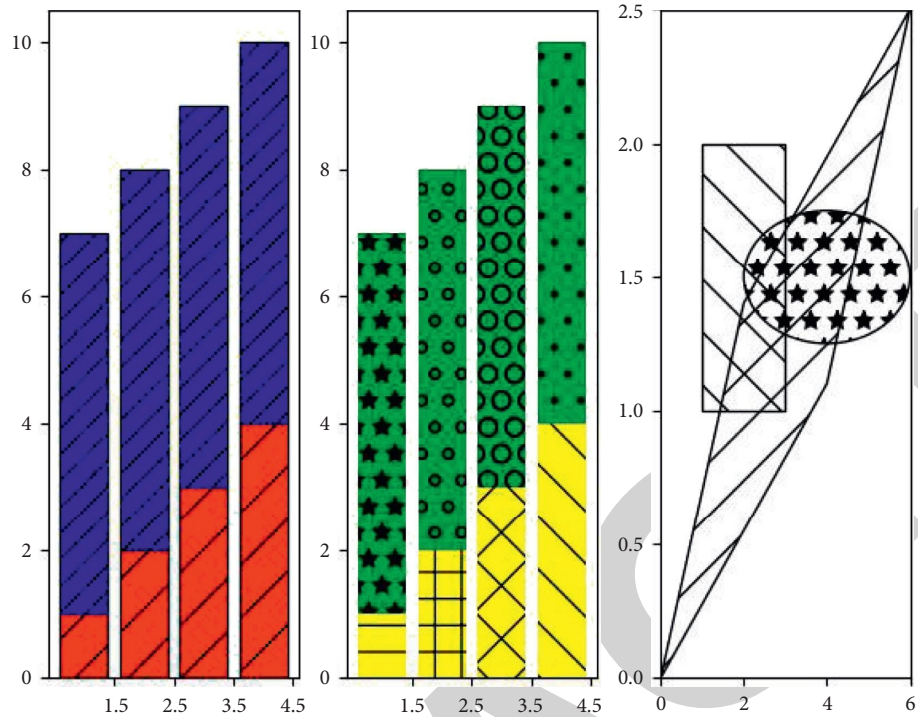

Figure 6: Distribution frequency histogram.

quality, and grade of the goods of the financing enterprises under their supervision. In addition, logistics enterprises should also improve commodity inspection, laboratory testing, testing technology, and equipment or related channels and strengthen enterprise software and hardware facilities, including information systems and network security and other aspects of the construction.

5.2. Strengthen the Monitoring of the Process of Order Realization by Financing Companies. The monitoring of the financing company's order fulfillment process is the focus of the bank and the logistics company's risk control. The financing enterprise will hand over the purchased raw materials to the H-party logistics enterprise for storage and supervision, and the logistics enterprise will assist in the full range of logistics services and distribution of final products, thus making the logistics enterprise integrate into the order fulfillment process of the financing enterprise, helping the floating enterprise to relieve capital pressure and reduce the risk of its order fulfillment process. In the process of sending some, logistics enterprises should standardize the registration system for the receipt of raw materials required by financing enterprises, the quantity received, the number of raw materials, the recipient, and the time of receipt; the approver and the issuer must be registered in accordance with the regulations. In the capital flow business, it should also contact the bank in a timely manner to obtain confirmation and permission from the bank according to the relevant business requirements. At the same time, the products produced by the floating enterprises should be delivered to the logistics enterprises for storage, and the products should be registered in the warehouse. Logistics companies can also collect market information for evaluation, using statistical data, to understand the product market capacity and other related situations, in product refinement management.

5.3. Focus on the Audit of Nuclear Tunnels and Enterprises. When banks carry out order financing business with logistics enterprises, they need to review the creditworthiness of the downstream NEAs that issue orders. In this process, banks and logistics enterprises should consider the industry category of the NEAs, the industry status of the NEAs, their creditworthiness, and credit history. Moreover, the bank should make an assessment of the strength of the noninstitutionalized credit bundle the relationship between core companies and financing companies, and this is to control the risk. For example, it can examine the situation related to the strictness and enforceability of the system of access, exit, incentives, and penalties in the supply chain.

6. Conclusions

This paper introduces modern financial engineering risk measurement tools to measure the risk of financial risks in supply chain finance, especially in order financing business. Specifically, this paper has analyzed the characteristics and connotations of order financing business model. Moreover, we also analyzed the risk of order financing from the perspective of banks and other financial institutions. Furthermore, CreditRisk + model based on insurance actuarial principles was used to manage credit risk in order financing business based on foreign currency settlement. Additionally, a method for the measurement of risk for the application of order financing in multinational supply chains was delivered.

Hindawi
Journal of Mathematics
Volume 2021, Article ID 9411696, 8 pages
https://doi.org/10.1155/2021/9411696

Research Article

On the Inverse Problem for Some Topological Indices

Durbar Maji,[1] **Ganesh Ghorai**,[1] **Muhammad Khalid Mahmood**,[2] **and Md. Ashraful Alam**[3]

[1]*Department of Applied Mathematics with Oceanology and Computer Programming, Vidyasagar University, Midnapore 721102, India*
[2]*Department of Mathematics, University of the Punjab, Lahore 54590, Pakistan*
[3]*Department of Mathematics, Jahangirnagar University, Savar, Dhaka, Bangladesh*

Correspondence should be addressed to Md. Ashraful Alam; ashraf_math20@juniv.edu

Received 11 September 2021; Revised 20 October 2021; Accepted 22 October 2021; Published 30 November 2021

Academic Editor: Lazim Abdullah

The study of the inverse problem (IP) based on the topological indices (TIs) deals with the numerical relations to TIs. Mathematically, the IP can be expressed as follows: given a graph parameter/TI that assigns a non-negative integer value (g) to every graph within a given family $(\mathcal{G})$ of graphs, find some $G \in \mathcal{G}$ for which $\mathrm{TI}(G) = g$. It was initiated by the Zefirov group in Moscow and later Gutman et al. proposed it. In this paper, we have established the IP only for the Y-index, Gourava indices, second hyper-Zagreb index, reformulated first Zagreb index, and reformulated F-index since they are closely related to each other. We have also studied the same which is true for the molecular, tree, unicyclic, and bicyclic graphs.

1. Introduction

Throughout the paper, we consider Ł = (V(Ł), E(Ł)) as a simple (without loops and multiple edge loops) finite graph that contains $|V(Ł)| = n$ vertices and $|E(Ł)| = m$ edges, respectively. The notation $d(u/Ł)$ denotes the degree of a vertex $u \in V(Ł)$. All other notations and terminologies used but not clearly stated in this paper may be followed from [1].

In chemical graph theory, a TI, usually known as a molecular descriptor, can be expressed by a real number calculated from a chemical/molecular graph which is the representation of a chemical compound by replacing atoms with vertices and bonds with edges. The TI is calculated for evaluating the information about the atomic constitution and bond characteristics of a molecule/chemical compound. The TI of a molecular graph is a numerical number that enables us to collect information about the concerned chemical structure. It helps us to know its hidden properties without performing experiments [2–4]. The TIs also correlate and predict several physical, chemical, biological, pharmaceutical, pharmacological activities/properties from molecular structures of graphs corresponding to real-life situations. The IP is defined as the feasibility of finding/modeling the chemical structure represented by a graph whose index value is equal to a given non-negative integer for the integer-valued problem. In the QSAR and QSPR studies [5], a method by which it is possible to predict the properties of a given molecular structure is called a forward problem. The inverse problem is concerned that, one can design the exact molecular structure that satisfies the given target properties by applying the forward problem solution.

The most popular as well as the oldest degree-based graph indices are the first and second Zagreb indices. Gutman et al. introduced the first Zagreb index $M_1(Ł)$ in [6] and second Zagreb index $M_2(Ł)$ in [7]. They are defined, respectively, as

$$M_1(Ł) = \sum_{u \in V(Ł)} d^2\left(\frac{u}{Ł}\right) = \sum_{uv \in E(Ł)} \left[d\left(\frac{u}{Ł}\right) + d\left(\frac{v}{Ł}\right)\right],$$
$$M_2(Ł) = \sum_{uv \in E(Ł)} d\left(\frac{u}{Ł}\right) d\left(\frac{v}{Ł}\right). \tag{1}$$

In 2016, Farahani et al. [8] defined the second hyper-Zagreb index as follows:

$$HM_2(Ł) = \sum_{uv \in E(Ł)} \left[d\left(\frac{u}{Ł}\right) d\left(\frac{v}{Ł}\right) \right]^2. \quad (2)$$

Kulli [9] introduced the first and second Gourava indices, defined, respectively, as

$$\begin{aligned} GO_1(Ł) &= \sum_{uv \in E(Ł)} \left[d\left(\frac{u}{Ł}\right) + d\left(\frac{v}{Ł}\right) + d\left(\frac{u}{Ł}\right) d\left(\frac{v}{Ł}\right) \right], \\ GO_2(Ł) &= \sum_{uv \in E(Ł)} \left[\left(d\left(\frac{u}{Ł}\right) + d\left(\frac{v}{Ł}\right) \right) d\left(\frac{u}{Ł}\right) d\left(\frac{v}{Ł}\right) \right]. \end{aligned} \quad (3)$$

Milicevic proposed the reformulated first Zagreb index $EM_1(Ł)$ in [10], defined as

$$EM_1(Ł) = \sum_{e \in E(Ł)} d^2\left(\frac{e}{Ł}\right); \quad d\left(\frac{e}{Ł}\right) = d\left(\frac{u}{Ł}\right) + d\left(\frac{v}{Ł}\right) - 2. \quad (4)$$

Liu et al. [11] put forward the reformulated F-index, and it is defined as follows:

$$RF(Ł) = \sum_{e \in E(Ł)} d^3\left(\frac{e}{Ł}\right) = \sum_{e \sim f \in E(Ł)} \left[d^2\left(\frac{e}{Ł}\right) + d^2\left(\frac{f}{Ł}\right) \right]. \quad (5)$$

Alameri et al. [12] introduced Y-index, and it is defined by

$$Y(Ł) = \sum_{u \in V(G)} d^4\left(\frac{u}{Ł}\right) = \sum_{uv \in E(Ł)} \left[d^3\left(\frac{u}{Ł}\right) + d^3\left(\frac{v}{Ł}\right) \right]. \quad (6)$$

Graph theory, a branch of mathematics, provides the tools for solving problems of information theory, computer sciences, physics, and chemistry [13–15]. The study of the IP is encountered in various fields of science, especially in mathematics and chemistry. The IP for a TI is defined as follows: for a given TI and a non-negative integer value (x), find (chemical) graph $(Ł)$ for which $TI(Ł) = x$. Also, the inverse existence problem [16] for the pair (G, Γ) can be asked as follows: given $(\mathcal{G})$ a class of graph and function Γ: $\mathcal{G} \longrightarrow H$, for which $g \in H$ there is $G \in \mathcal{G}$ with $\Gamma(G) = g$? The idea of the IP based on TIs was initiated by the Zefirov group in Moscow [5, 17, 18] and was first proposed by Gutman et al. in [19]. The IP for Wiener index was solved in [20]. In [21], the IP was studied for sigma index as well as for acyclic, unicyclic, and bicyclic graphs. The same problem for the Steiner Wiener index was also solved in [22]. This type of problem for the Zagreb indices, forgotten Zagreb index, and the hyper-Zagreb index was studied in [23]. Tavakoli et al. [24] addressed the IP for first Zagreb index. Also, the IP for some graph indices was investigated in [25]. In [26], Czabarka et al. solved the IP for certain tree parameters. To study more about the inverse problems and the topological indices of graph operations, one can see these references [27–32].

There are so many benefits in the solution of IP. It helps to design of combinatorial libraries for drug discovery in combinatorial chemistry [33]. It may be helpful in speeding up the discovery of lead compounds with desired properties [34]. Also, the IP plays its significance in the application of trees [35] such as the field of algorithms, chemical graph theory, signal processing, and electrical circuits.

2. Preliminaries

To study the IP for Y-index, we will use the following crucial observation.

Let Ł be a graph having u and v as vertices which are adjacent to each other. We subdivide each edge (uv) by introducing a new vertex (w) (of degree 2) to construct a new graph Ł* (see Figure 1).

Here, the Y-index of the new graph Ł* will be sixteen which is more than the graph Ł.

Lemma 1. *By applying the transformation Ł ⟶ Ł*, the Y-index value will be increased by 16. That is, $Y(Ł^*) = Y(Ł) + 16$.*

Proof. Let us consider the graph Ł with vertices u and v of degrees x and y, respectively. Since in the new constructed graph Ł*, a new vertex w is inserted between u and v,

$$\begin{aligned} Y(Ł^*) - Y(Ł) &= d^4\left(\frac{u}{Ł^*}\right) + d^4\left(\frac{w}{Ł^*}\right) + d^4\left(\frac{v}{Ł^*}\right) \\ &\quad - d^4\left(\frac{u}{Ł}\right) - d^4\left(\frac{v}{Ł}\right) \\ &= x^4 + 16 + y^4 - x^4 - y^4 \\ &= 16. \end{aligned} \quad (7)$$

□

Lemma 2. *If either $d(u/Ł) = 2$ or $d(v/Ł) = 2$ (or both), then by the means of the above transformation Ł ⟶ Ł*, the value of the first Gourava index increases by 8. That is,*

$$GO_1(Ł^*) = GO_1(Ł) + 8. \quad (8)$$

Similarly, the value of the second Gourava index increases by 16. Thus,

$$GO_2(Ł^*) = GO_2(Ł) + 16. \quad (9)$$

Lemma 3. *If either $d(u/Ł) = 2$ or $d(v/Ł) = 2$ (or both), then by means of the above transformation Ł ⟶ Ł*, the value of the second hyper-Zagreb index increases by 16. That is,*

$$HM_2(Ł^*) = HM_2(Ł) + 16. \quad (10)$$

Lemma 4. *If either $d(u/Ł) = 2$ or $d(v/Ł) = 2$ (or both), then by applying the transformation Ł ⟶ Ł*, the values of the reformulated first Zagreb index and reformulated F-index of the graph Ł increase by 4 and 8, respectively. Thus,*

$$\begin{aligned} EM_1(Ł^*) &= EM_1(Ł) + 4, \\ RF(Ł^*) &= RF(Ł) + 8. \end{aligned} \quad (11)$$

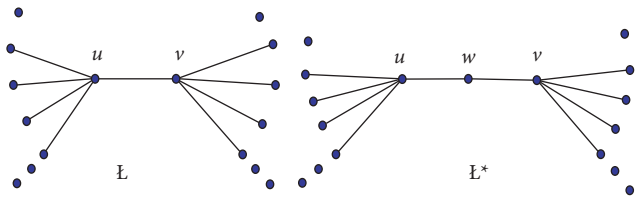

Figure 1: The graphs (a) Ł and (b) Ł* used in auxiliary Lemmas 1–4.

3. Main Results and Discussion

In graph theory, the IP based on the TIs is an interesting one among the problems associated with the estimation of different graph invariants/TIs such as chromatic number, connectivity, girth, and number of independent sets. The IP plays a crucial role in many areas of science, especially in mathematics. In this section, we have investigated the IP for Y-index, Gourava indices, second hyper-Zagreb index, reformulated first Zagreb index, and reformulated F-index. Additionally, we have developed the same problem for molecular, tree, acyclic, unicyclic, and bicyclic graphs.

3.1. The IP for Y-Index. Here we will discuss the IP for Y-index.

Theorem 1. *The Y-index for connected graphs can take all positive even integers, except for* $4, 6, 8, 10, 12, 14, 16, 2(8i+2), 2(8j+3), 2(8k+4), 2(8m+5), 2(8n+6), 2(8p+7)$ *where* $i = 1, 2, \ldots, 4$; $j = 1, 2, \ldots, 9$; $k = 1, 2, \ldots, 14$; $m = 1, 2, \ldots, 19$; $n = 1, 2, \ldots, 24$; *and* $p = 1, 2, \ldots, 29$.

Proof. Proof. To prove the theorem, we establish a set of graphs $Y_0, Y_2, Y_4, Y_6, Y_8, Y_{10}, Y_{12}, Y_{14}$ whose Y-index values are 48, 2, 84, 166, 248, 330, 412, and 494, respectively. These numbers are congruent to 0, 2, 4, 6, 8, 10, 12, and 14 (mod 16), respectively.

Consider the cyclic graphs C_n for $n \geq 3$. Clearly, in Figure 2(a), $Y(Y_0 = C_3) = 48$, $Y(C_4) = 64$, $Y(C_5) = 80$, and $Y(C_n) = 16n$ for $n \geq 3$. Now we apply Lemma 1 for each graph in Figure 2. Thus, $Y(Y_0)$ takes all those even positive integer values which are divisible by 16, except 16 and 32.

In Figure 2(b), $Y(P_2) = 2$. By applying the transformation in Lemma 1, we arrive at graphs whose Y-index values are 18, 34, 50, 66, and so on. There are the path graphs. Thus, Y (Ł) takes all positive even integer values which are congruent to 2 (mod 16).

Now consider the graph in Figure 2(c) with $Y(Y_4) = 84$. By applying Lemma 1, we can obtain graphs with Y-index values 100, 116, 132, 148, …. Here, $Y(Y_4)$ contains all positive even integer values $\equiv 4 \pmod{16}$, except the integers 20, 36, 52, and 68.

The graph is depicted in Figure 2(d) with $Y(Y_6) = 166$, and then by using Lemma 1, we can take the graphs with Y-index values 182, 198, 214, 230, …, and so on. Therefore, $Y(Y_6)$ covers all positive even integer values $\equiv 6 \pmod{16}$ and ≥166. Obviously, the integers $6, 22, \ldots, 134, 150$ are not covered by the construction.

In Figure 2(e), we have $Y(Y_8) = 248$, and then by using Lemma 1, we can take the graphs with Y-index values 264, 280, 296, 314, …, and so on. So, $Y(Y_8)$ takes all positive even integer values $\equiv 8 \pmod{16}$ and ≥248. Obviously, the integers $24, 40, \ldots, 216, 232$ are not covered by the construction.

The graph in Figure 2(f) contains $Y(Y_{10}) = 330$. Again by Lemma 1, $Y(Y_{10})$ goes to all those positive even integer values $\equiv 10 \pmod{16}$ and ≥330 giving 330, 348, 364, 380, …, and so on.

From Figure 2(g), we have $Y(Y_{12}) = 412$. By applying Lemma 1, $Y(Y_{12})$ takes all positive even integer values $\equiv 12 \pmod{16}$ and also ≥412 having 412, 428, 444, 460, …, and so on.

The graph in Figure 2(h) has $Y(Y_{14}) = 494$. By applying Lemma 1, $Y(Y_{14})$ takes all positive even integer values $\equiv 14 \pmod{16}$ and also ≥494 taking 494, 510, 526, 542, …, and so on. There exist no connected graphs with the Y-indices mentioned in Table 1. □

Corollary 1. *The Y-index of a tree (or molecular) graph can take all positive even integers, except for* $4, 6, 8, 10, 12, 14, 16, 2(8r+2), 2(8s+3), 2(8t+4), 2(8w+5), 2(8x+6), 2(8y+7)$ *where* $r = 1, 2, 3, 4$; $s = 1, 2, \ldots, 9$; $t = 1, 2, \ldots, 14$; $w = 1, 2, \ldots, 19$; $x = 1, 2, \ldots, 24$; *and* $y = 1, 2, \ldots, 29$.

Corollary 2. *Let Ł be a connected unicyclic or bicyclic graph. Then, there exists the Y-index of the form* $16h + 2k$ *for all non-negative integers where* $h \neq 0$ *and* $1 \leq k \leq 7$.

Proof. Proof. Let $Ł_1$ be a unicyclic graph which is obtained by adding a path of length two to any vertex u of the cyclic graph C_n for $n = 5$. Thus, $Y(Ł_1) = 162 = 16 \times 10 + 2 \times 1$. Similarly, the unicyclic graph $Ł_2$ is obtained by adding another path of length two to one of the two adjacent vertices to u that lie on $Ł_1$ (see Figure 3). We get $Y(Ł_2) = 244$.

The bicyclic graph $Ł_3$ is obtained by gluing two cyclic graphs with one side of both, and we have $Y(Ł_3) = 306$ which also can be expressed in the said form. Similarly, another bicyclic graph $Ł_4$ is obtained by adding a path with length two to any vertex u of $Ł_3$. Thus, $Y(Ł_4) = 388$ is of the form $16h + 2k$ for $h = 24, k = 2$. □

3.2. The IP for Gourava Indices. Here we study the IP for Gourava indices.

Theorem 2. *The first Gourava index of a connected graph can take any positive integer except for 1, 2, 4, 5, 6, 7, 8, 9, 11, 12, 13, 14, 15, 16, 17, 19, 20, 22, 23, 25, 27, 28, 29, 31, 33, 35, 41, 44, 49, 57, and 73.*

Proof. By applying Lemma 2, we construct eight series of graphs $(G_j, j = 0, 1, 2, \ldots, 7)$ containing at least one vertex of degree 2, whose GO_1-values are of the form $8s + t$ for $t = 0, 1, 2, \ldots, 7$. These graphs are drawn in Figures 4(a)–4(h).

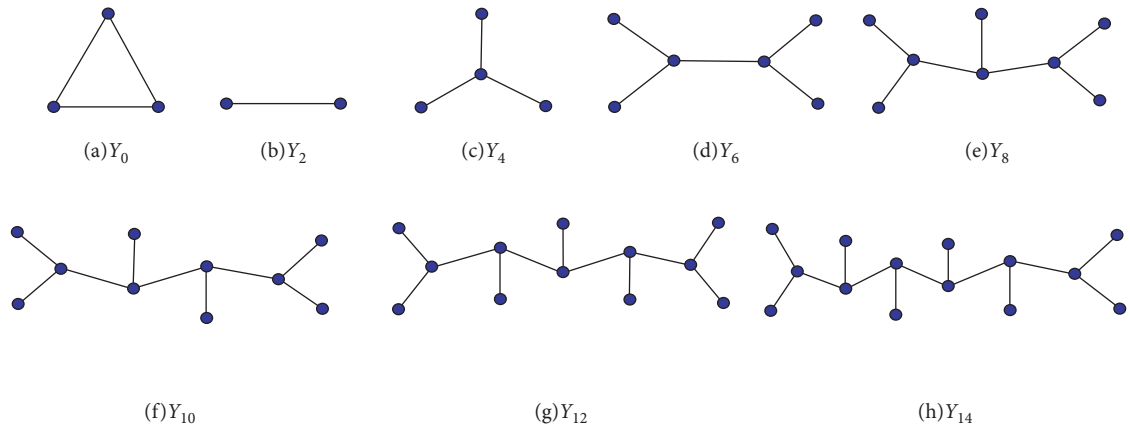

FIGURE 2: The graphs Y_i, for $i = 0, 2, 4, 6, 8, 10, 12$, and 14: (a) Y_0, (b) Y_2, (c) Y_4, (d) Y_6, (e) Y_6, (f) Y_8, (g) Y_{10}, (h) Y_{12}, and (i) Y_{14}.

TABLE 1: Y-index values which do not exist.

Y_0	Y_4	Y_6	Y_8	Y_{10}	Y_{12}	Y_{14}
	4	6	8, 24	10, 26	12, 28, 44	14, 30, 46
16	20	22	40, 56	42, 58	60, 76, 92	62, 78, 94
32	36	38	72, 88	74, 90	108, 124, 140	110, 126, 142
	52	54	104, 120	106, 122	156, 172, 188	158, 174, 190
	68	70	136, 152	138, 154	204, 220, 236	206, 222, 238
		86	168, 184	170, 186	252, 268, 284	254, 270, 286
		102	200, 216	202, 218	300, 316, 332	302, 318, 334
		118	232	234, 250	348, 364, 380	350, 366, 382
		134		266, 282	396	398, 414, 430
		150		298, 314		446, 462, 478

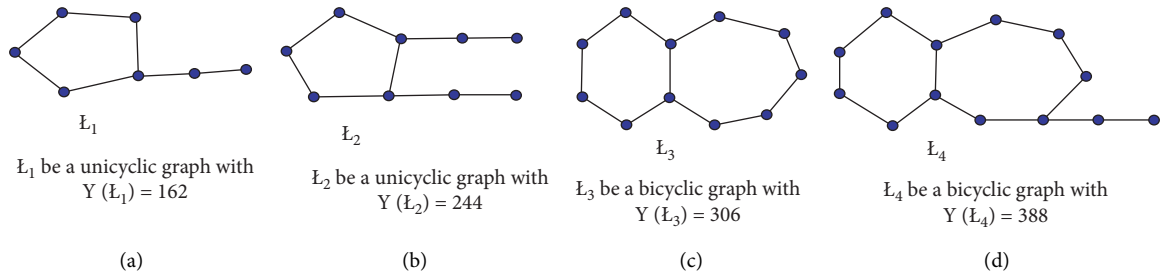

FIGURE 3: The graphs Ł$_1$, Ł$_2$, Ł$_3$, and Ł$_4$ with Y-index values: (a) let Ł$_1$ be a unicyclic graph with Y (Ł$_1$) = 162, (b) let Ł$_2$ be a unicycle graph with Y (Ł$_3$) = 244, (c) let Ł$_3$ be a bicyclic graph with Y (Ł$_3$) = 306, and (d) let Ł$_4$ be a bicyclic graph with Y (Ł$_4$) = 388.

Consider a cycle graph C_n with $n \geq 3$. Clearly, $GO_1(C_n) = 8n$. Therefore, GO_1 (Ł) can take all those positive integer values which are divisible by 8. From the graph G_0 (Figure 4) and Lemma 2, we obtain the graphs with GO_1 (Ł)-values 32, 40, 48, 56, 64, ... Thus, GO_1 (Ł) takes all positive integers $\equiv 0 \pmod 8$ and ≥ 24.

Consider the graph G_1 in Figure 4 with GO_1 (Ł) = 81, i.e., GO_1 (Ł) implies all positive integer values $\equiv 1 \pmod 8$. Then, by Lemma 2, we obtain graphs with GO_1 (Ł) = 89, 97, 105, 113, 121, ... Again for the graph G_2, GO_1 (Ł) = 10. Thus, we can arrive at graphs whose GO_1 values are 18, 26, 34, 42, 50, 58, 66, 74, 82, ... Similarly, by applying Lemma 2 to the graphs G_3, G_4, G_5, G_6, and G_7, we get the graphs with GO_1 = 59, 67, 75, 83, 91, 99, 107, 115, . . ., 60, 68, 76, 84, 92, 100, 108, . . ., 45, 53, 61, 69, 77, 85, . . ., 38, 46, 54, 62, 70, 78, . . ., and 47, 55, 63, 71, 79, 87, . . ., respectively. The star graphs S_4, S_5 and examples depicted in Figures 2(d) and 5(b) show that there exist graphs with GO_1 (Ł) as 21, 36, 43, and 65, respectively. There exist no connected graphs with first Gourava index as listed in Table 2. □

Corollary 3. *The first Gourava index of a tree (or molecular) graph can take any positive integer, except for 1, 2, 4, 5, 6, 7, 8, 9, 11, 12, 13, 14, 15, 16, 17, 19, 20, 22, 23, 25, 27, 28, 29, 31, 33, 35, 41, 44, 49, 57, and 73.*

Now we study to settle the IP for the second Gourava index.

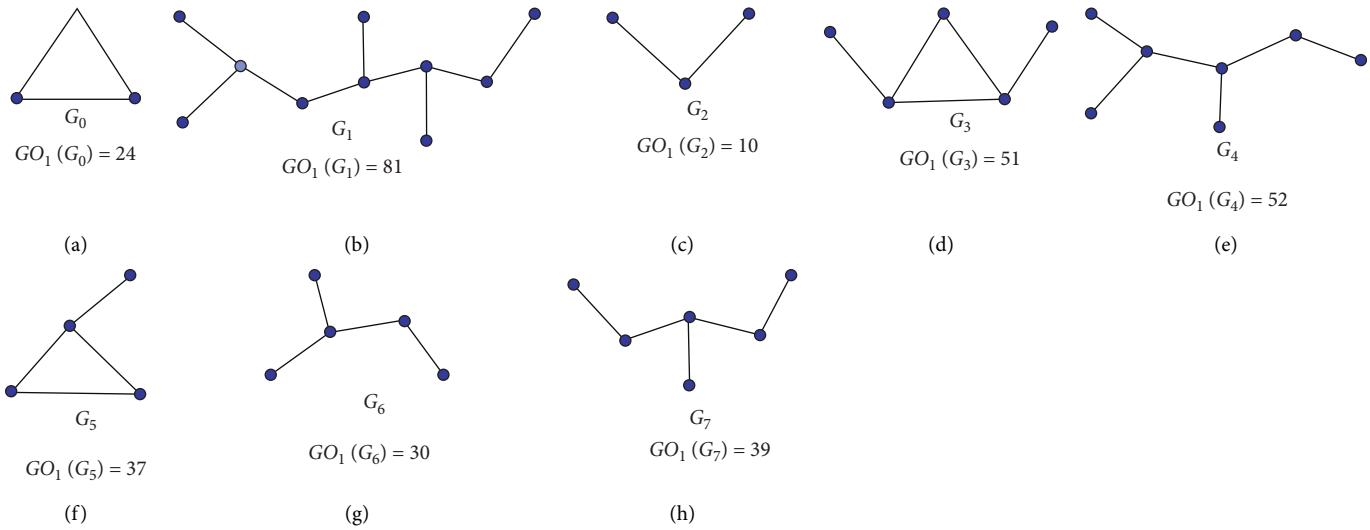

FIGURE 4: The graphs G_j, for $j = 0, 1, 2, \ldots, 7$ with first Gourava index values: (a) G_0 $\mathrm{GO}_1(G_0) = 24$, (b) G_1 $\mathrm{GO}_1(G_1) = 81$, (c) G_2 $\mathrm{GO}_1(G_2) = 10$, (d) G_3 $\mathrm{GO}_1(G_3) = 51$, (e) G_4 $\mathrm{GO}_1(G_4) = 52$, (f) G_5 $\mathrm{GO}_1(G_5) = 37$, (g) G_6 $\mathrm{GO}_1(G_6) = 30$, and (h) G_7 $\mathrm{GO}_1(G_7) = 39$.

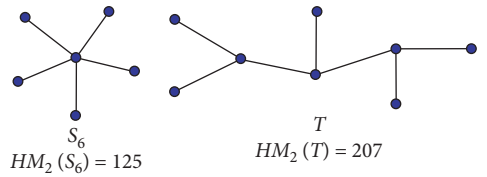

FIGURE 5: The star graph (a) S_6 and tree (b) T with second hyper-Zagreb index values.

TABLE 2: The first Gourava index values which do not exist.

G_0	G_1	G_2	G_3	G_4	G_5	G_6	G_7
	1	2		4	5	6	7
8	9		11	12	13	14	15
16	17, 25		19	20		22	23
	33, 41		27	28	29		31
	49, 57		35				
	73			44			

Theorem 3. *The second Gourava index of a connected graph can take any positive even integer except for 4, 6, 8, 10, 14, 16, 20, 22, 24, 26, 30, 32, 34, 38, 40, 42, 46, 50, 52, 54, 56, 58, 62, 66, 68, 70, 72, 74, 78, 82, 86, 90, 94, 98, 102, 106, 110, 118, 122, and 134.*

Proof. Consider first path graphs P_n for $n \geq 2$. It is clear that $\mathrm{GO}_2(P_2) = 2$ and $\mathrm{GO}_2(P_3) = 12$. By Lemma 2, since $\mathrm{GO}_2(P_n) = 16n - 36$ for $n \geq 3$, we obtain the graphs whose GO_2-values are 28, 44, 60, 76, 92, 108, ... which are congruent to 12 (mod 16). If we consider a cyclic graph C_n with n vertices, then $\mathrm{GO}_2(C_n) = 16n$ for $(n \geq 3)$. Clearly, we get the graphs with GO_2-values 48, 64, 80, 96, 112, ... Now the graph G_7 drawn in Figure 4 has $\mathrm{GO}_2(Ł) = 84$. Therefore, by applying Lemma 2, we obtain the graphs with second Gourava index values 100, 116, 132, 148, 164, ... The graphs G_4 and G_5 in Figure 4 contain $\mathrm{GO}_2(Ł) = 126$ and $\mathrm{GO}_2(Ł) = 88$, respectively. Therefore, by Lemma 2, $\mathrm{GO}_2(Ł)$ obtains all those even integer values 126, 142, 158, 174, 190, 206, 222, ... and 104, 120, 136, 152, ..., respectively. In same procedure, from Figure 4, we get the graph G_3 with $\mathrm{GO}_2(Ł) = 138$. So, it follows the GO_2-values 154, 170, 186, 202, 218, ...

In Figure 6, by Lemma 2, we have $GO_2(G_8) = 150$ and $GO_2(G_9) = 114$ with. Then by using the Lemma 2, we can take the graphs with 166, 182, 198, 214, ... and 130, 146, 162, 178, 194, ..., respectively. The integers not covered by the above transformation for the second Gourava index are listed in Table 3. □

Corollary 4. *The second Gourava index of a tree (or molecular) graph can take any positive even integer, except for 4, 6, 8, 10, 14, 16, 20, 22, 24, 26, 30, 32, 34, 38, 40, 42, 46, 50, 52, 54, 56, 58, 62, 66, 68, 70, 72, 74, 78, 82, 86, 90, 94, 98, 102, 106, 110, 118, 122, and 134.*

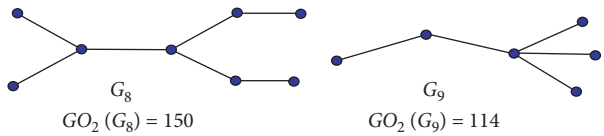

Figure 6: The graphs (a) G_8 and (b) G_9 with second Gourava index values.

Table 3: The second Gourava index values which do not exist.

G_0	G_2	G_4	G_6	G_8	G_{10}	G_{14}
		4	6	8	10	14
16		20	22	24	26	30
32	34		38	40	42	46
	50	52	54	56	58	62
	66	68	70	72	74	78
	82		86		90	94
	98		102		106	110
			118		122	
			134			

3.3. The IP for Second Hyper-Zagreb Index

Theorem 4. *The second hyper-Zagreb index of a connected graph can be any positive integer, except 2, 3, 4, 5, 6, 7, 9, 10, 11, 12, 13, 14, 15, 16, 17, 18, 19, 20, 21, 22, 23, 25, 26, 28, 29, 30, 31, 32, 33, 34, 35, 36, 37, 38, 39, 41, 42, 43, 44, 45, 46, 47, 49, 50, 51, 52, 53, 54, 55, 57, 59, 60, 61, 62, 63, 65, 66, 67, 68, 69, 70, 71, 73, 75, 76, 77, 78, 79, 81, 82, 83, 84, 85, 86, 87, 91, 92, 93, 94, 95, 98, 99, 100, 101, 102, 103, 107, 109, 110, 111, 114, 115, 118, 119, 123, 126, 127, 130, 131, 133, 134, 135, 141, 142, 143, 146, 147, 149, 150, 151, 157, 158, 159, 163, 165, 167, 173, 174, 175, 181, 183, 190, 191, 199, 206, 215, 222, 223, 231, 239, 255, and 271.*

Proof. We construct a series of sixteen graphs such as $H_0, H_1, H_2, \ldots, H_{15}$. The HM_2 values of these graphs can be expressed in the form $16h + i$ for $i = 0, 1, 2, \ldots, 15$. In Figure 7, we construct the graphs H_k for $k = 2, 3, 4, 5, 6, 7$ and $11, 12, 13, 14, 15$. Note that the graphs $H_0, H_1, H_8, H_9, H_{10}$ are similar to Figures 4(a), 4(f), 4(c), 4(h), and 4(g) respectively. We have $HM_2\ (H_0) = 48$. Then by using Lemma 3, we can take the graphs with HM_2 values 64, 80, 96, 112, ... which are congruent to 0 (mod 16). Secondly, consider the graph H_1 which generates the HM_2-values $97, 113, 129, 145, 161, \ldots$, and all these are congruent to 1 (mod 16).

Since $HM_2(H_2) = 162$, by mean of the construction method upon the graph H_2 from the Lemma 3, we get the graphs with HM_2 values 178, 194, 210,226, ... which are congruent to 2 (mod 16). For H_3, the HM_2-values cover the integers $179, 195, 211, 227, \ldots$ which are $\equiv 3$ (mod 16). Analogously, the HM_2 values for the graph H_4 cover all the integers $116, 132, 148, \ldots$., and all these numbers are congruent to 4 (mod 16). For H_5, it provides the HM_2 values $197, 213, 229, \ldots$ which are $\equiv 5$ (mod 16). For H_6 there exist HM_2 values $166, 182, 198, \ldots$ which are $\equiv 6$ (mod 16). It follows $247, 263, 379, \ldots$ for the graph H_7, and these integers are congruent to 7 (mod 16). Similarly by Lemma 3, we get for the graphs $H_8, H_9, H_{10}, H_{11}, H_{12}, H_{13}, H_{14}, H_{15}$ with Now, using the construction method in Lemma 3 to $H_8, H_9, H_{10}, H_{11}, H_{12}, H_{13}, H_{14}$, and H_{15}, we can generate the graphs with HM_2 values 8, 24, 40, ... congruent to 8 (mod 16); 89, 105, 121, ... congruent to 9 (mod 16); 58, 74, 90, ... congruent to 10 (mod 16); 139, 155, 171, ... congruent to 11 (mod 16); 108, 124, 140, ... congruent to 12 (mod 16); 189, 205, 221, ... congruent to 13 (mod 16); 238, 254, 270, ... congruent to 14 (mod 16); and 257, 303, 319, ... congruent to 15 (mod 16), respectively.

The examples drawn in the Figures 2(c), 2(d), 5(a), and 5(b) have HM_2 values $117, 27, 125$, and 207, respectively. These numbers are congruent to 5, 11, 13, and 15 (mod 16), chronologically. There exist no connected graphs with the HM_2-indices mentioned in Table 4. □

Corollary 5. *The second hyper-Zagreb index of a tree (or molecular) graph can be any positive integer, except 2, 3, 4, 5, 6, 7, 9, 10, 11, 12, 13, 14, 15, 16, 17, 18, 19, 20, 21, 22, 23, 25, 26, 28, 29, 30, 31, 32, 33, 34, 35, 36, 37, 38, 39, 41, 42, 43, 44, 45, 46, 47, 49, 50, 51, 52, 53, 54, 55, 57, 59, 60, 61, 62, 63, 65, 66, 67, 68, 69, 70, 71, 73, 75, 76, 77, 78, 79, 81, 82, 83, 84, 85, 86, 87, 91, 92, 93, 94, 95, 98, 99, 100, 101, 102, 103, 107, 109, 110, 111, 114, 115, 118, 119, 123, 126, 127, 130, 131, 133, 134, 135, 141, 142, 143, 146, 147, 149, 150, 151, 157, 158, 159, 163, 165, 167, 173, 174, 175, 181, 183, 190, 191, 199, 206, 215, 222, 223, 231, 239, 255, and 271.*

3.4. The IP for Reformulated First Zagreb Index

Theorem 5. *The first reformulated Zagreb index of a connected graph can take all positive even integer values except for 4 and 8.*

Proof. At first, we consider the path P_n with $n \geq 3$. The Rez-value for P_3 is equal to 2. By Lemma 4, we obtain graphs with Rez-values 6, 10, 14, 18, ..., and so on. Also, since $\mathrm{Rez}(S_3) = 12$, by means of the construction described in Lemma 4, we have the graphs whose Rez-values are 16, 20, 24, 28, 32, 36, 40, ... Hence, Rez(Ł) covers all positive even integers except 4 and 8. □

Corollary 6. *The first reformulated Zagreb index of a tree (or molecular) graph can take all positive even integer values, except for 4 and 8.*

3.5. The IP for Reformulated F-Index

Theorem 6. *The reformulated F-index of a connected graph can be any positive even integer, except for 4, 6, 8, 12, 14, 16, 20, 22, 28, 30, 36, 38, 46, 54, and 62.*

Proof. For the path graphs P_3, we get $\mathrm{RF}(P_3) = 2$. Thus, by applying Lemma 4, we obtain graphs with RF(Ł)-values equal to 10, 18, 26, 34, ... Similarly, for the cyclic graph C_3, we have $\mathrm{RF}(C_3) = 24$ and next obtained graphs having RF(Ł)-values 32, 40, 48, 56, ... In an analogous manner,

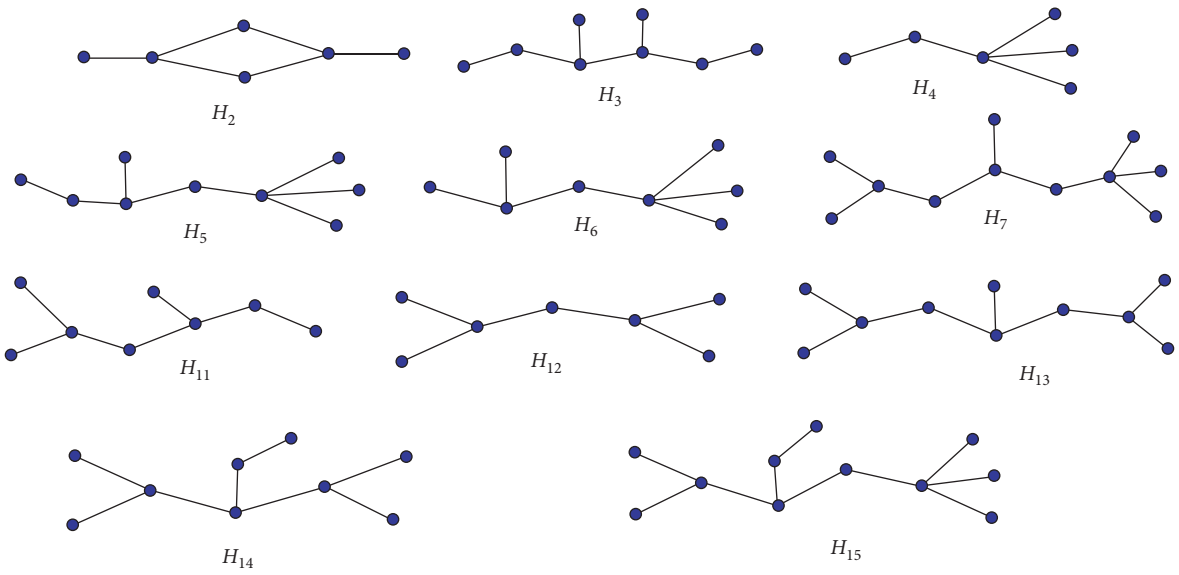

Figure 7: The graphs H_k, for $k = 2, 3, 4, 5, 6, 7$ and $11, 12, 13, 14, 15$.

Table 4: HM_2 values which do not exist.

H_0	H_1	H_2	H_3	H_4	H_5	H_6	H_7	H_9	H_{10}	H_{11}	H_{12}	H_{13}	H_{14}	H_{15}
		2	3	4	5	6	7	9	10	11	12	13	14	15
16	17	18	19	20	21	22	23	25	26		28	29	30	31
32	33	34	35	36	37	38	39	41	42	43	44	45	46	47
	49	50	51	52	53	54	55	57		59	60	61	62	63
	65	66	67	68	69	70	71	73		75	76	77	78	79
	81	82	83	84	85	86	87			91	92	93	94	95
		98	99	100	101	102	103			107		109	110	111
		114	115			118	119			123			126	127
		130	131		133	134	135					141	142	143
		146	147		149	150	151					157	158	159
			163		165		167					173	174	175
					181		183						190	191
							199						206	223, 239
							215, 231						222	255, 271

starting with G_5 and G_6 in Figure 4, we obtain the graphs with RF-values 78, 86, 94, 102, ... and 52, 60, 68, 76, ..., respectively. □

Corollary 7. *The reformulated F-index of a tree (or molecular) graph can be any positive even integer, except for 4, 6, 8, 12, 14, 16, 20, 22, 28, 30, 36, 38, 46, 54, and 62.*

4. Conclusion

The inverse problem is one of the recent problems of graph theory related to the applicative area. Here, we have studied the IP based on some topological graph indices such as Y-index, Gourava indices, second hyper-Zagreb index, reformulated first Zagreb index, and reformulated F-index. We have studied the inverse problems for the aforesaid indices since they are closely related to each other. We have also investigated the results for tree, molecular, unicyclic, and bicyclic graphs. The inverse problem is still open for other graph indices and other molecular structures.

Data Availability

No data were used to support this study.

Conflicts of Interest

The authors declare that there are no conflicts of interest regarding the publication of this article.

References

[1] H. Wiener, "Structural determination of paraffin boiling points," *Journal of the American Chemical Society*, vol. 69, no. 1, pp. 17–20, 1947.

[2] Y. C. Kwun, M. Munir, W. Nazeer, S. Rafique, and S. Min Kang, "M-Polynomials and topological indices of V-Phenylenic Nanotubes and Nanotori," *Scientific Reports*, vol. 7, no. 1, pp. 8756–8759, 2017.

[3] M. Munir, W. Nazeer, S. Rafique, and S. Kang, "M-polynomial and degree-based topological indices of polyhex nanotubes," *Symmetry*, vol. 8, no. 12, p. 149, 2016.

[4] M. Munir, W. Nazeer, S. Rafique, and S. Kang, "M-polynomial and related topological indices of nanostar dendrimers," *Symmetry*, vol. 8, no. 9, p. 97, 2016.

[5] E. V. Gordeeva, M. S. Molchanova, and N. S. Zefirov, "General methodology and computer program for the exhaustive restoring of chemical structures by molecular connectivity indexes. Solution of the inverse problem in QSAR/QSPR," *Tetrahedron Computer Methodology*, vol. 3, no. 6, pp. 389–415, 1990.

[6] I. Gutman and N. Trinajstić, "Graph theory and molecular orbitals. Total φ-electron energy of alternant hydrocarbons," *Chemical Physics Letters*, vol. 17, no. 4, pp. 535–538, 1972.

[7] I. Gutman, B. Rucic, N. Trinajstic, and C. F. Wilcox, "Graph theory and molecular orbitals. XII. Acyclic polyenes," *The Journal of Chemical Physics*, vol. 62, no. 9, pp. 3399–3405, 1975.

[8] M. R. Farahani, M. R. Rajesh Kanna, and R. P. Kumar, "On the hyper-Zagreb indices of some nanostructures," *Asian Academic Research Journal of Multidisciplinary*, vol. 3, no. 1, pp. 115–123, 2016.

[9] V. R. Kulli, "The Gourava indices and coindices of graphs," *Annals of Pure and Applied Mathematics*, vol. 14, no. 1, pp. 33–38, 2017.

[10] A. Milicevic, S. Nikolic, and N. Trinajstic, "On reformulated Zagreb indices," *Molecular Diversity*, vol. 8, pp. 393–399, 2004.

[11] J.-B. Liu, B. Ali, M. A. Malik, H. M. A. Siddiqui, and M. Imran, "Reformulated Zagreb indices of some derived graphs," *Mathematics*, vol. 7, no. 4, p. 366, 2019.

[12] A. Alameri, N. Al-Naggar, M. Al-Rumaima, and M. Alsharafi, "Y-index of some graph operations," *International Journal of Applied Engineering Research*, vol. 15, pp. 173–179, 2020.

[13] F. Asif, Z. Zahid, and S. Zafar, "Leap Zagreb and leap hyper-Zagreb indices of Jahangir and Jahangir derived graphs," *Engineering and Applied Science Letters*, vol. 3, no. 2, pp. 1–8, 2020.

[14] M. Numan, S. I. Butt, S. I. Butt, and A. Taimur, "Super cyclic antimagic covering for some families of graphs," *Open Journal of Mathematical Sciences*, vol. 5, no. 1, pp. 27–33, 2021.

[15] A. Tabassum, M. A. Umar, M. A. Umar, M. Perveen, and A. Raheem, "Antimagicness of subdivided fans," *Open Journal of Mathematical Sciences*, vol. 4, no. 1, pp. 18–22, 2020.

[16] A. B. Dainyak and A. D. Kurnosov, "On an extremal inverse problem in graph theory," *Journal of Applied and Industrial Mathematics*, vol. 9, no. 2, pp. 157–164, 2015.

[17] I. I. Baskin, E. V. Gordeeva, R. O. Devdariani, N. S. Zefirov, V. A. Palyulin, and M. I. Stankevich, "Methodology for solving the inverse problem of structure-property relationships for the case of topological indexes," *Doklady Akademii Nauk SSSR*, vol. 307, pp. 613–617, 1989.

[18] N. S. Zefirov, V. A. Palyulin, and E. V. Radchenko, "Problem of generation of structures with given properties solution of inverse problem for the case of centric Balaban index," *Doklady Akademii Nauk SSSR*, vol. 316, pp. 921–924, 1991.

[19] I. Gutman and Y. Yeh, "The sum of all distances in bipartite graphs," *Mathematica Slovaca*, vol. 45, no. 4, pp. 327–334, 1995.

[20] S. G. Wagner, "A class of trees and its wiener index," *Acta Applicandae Mathematica*, vol. 91, no. 2, pp. 119–132, 2006.

[21] I. Gutman, M. Togan, A. Yurttas, A. S. Cevik, and I. N. Cangul, "Inverse problem for sigma index," *MATCH Communications in Mathematical and in Computer Chemistry*, vol. 79, pp. 491–508, 2018.

[22] X. Li, Y. Mao, and I. Gutman, "Inverse problem on the steiner wiener index," *Discussiones Mathematicae Graph Theory*, vol. 38, pp. 83–95, 2018.

[23] A. Yurtas, M. Togan, V. Lokesha, I. N. Cangul, and I. Gutman, "Inverse problem for Zagreb indices," *Journal of Mathematical Chemistry*, vol. 57, no. 2, pp. 609–615, 2019.

[24] M. Tavakoli and F. Rahbarnia, "Note on properties of first Zagreb index of graphs, Iran," *Journal of Mathematical Chemistry*, vol. 3, no. 1, pp. 1–5, 2012.

[25] X. Li, Z. Li, and L. Wang, "The inverse problems for some topological indices in combinatorial chemistry," *Journal of Computational Biology*, vol. 10, no. 1, pp. 47–55, 2003.

[26] É. Czabarka, L. Székely, and S. Wagner, "The inverse problem for Certain tree parameters," *Discrete Applied Mathematics*, vol. 157, no. 15, pp. 3314–3319, 2009.

[27] D. Maji and G. Ghorai, "A novel graph invariant: the third leap Zagreb index under several graph operations," *Discrete Mathematics, Algorithms and Applications*, vol. 11, no. 5, pp. 1–16, 2019.

[28] D. Maji and G. Ghorai, "Computing F-index, coindex and Zagreb polynomials of the k th generalized transformation graphs," *Heliyon*, vol. 6, no. 12, Article ID e05781, 2020.

[29] D. Maji and G. Ghorai, "The first entire Zagreb index of various corona products and their bounds," *Journal of Mathematical and Computational Science*, vol. 11, no. 5, pp. 6018–6044, 2021.

[30] M. I. Skvortsova, I. I. Baskin, I. I. Baskin, O. L. Slovokhotova, V. A. Palyulin, and N. S. Zefirov, "Inverse problem in QSAR/QSPR studies for the case of topological indexes characterizing molecular shape (Kier indices)," *Journal of Chemical Information and Computer Sciences*, vol. 33, no. 4, pp. 630–634, 1993.

[31] M. Togan, A. Yurttas, U. Sanli, F. Celik, and I. Cangual, "Inverse problem for Bell index," *Filomat*, vol. 34, no. 2, pp. 615–621, 2020.

[32] M. Togan, A. Yurttas, and I. N. Cangul, "Inverse problem for the first entire Zagreb index," *Advanced Studies in Contemporary Mathematics*, vol. 29, pp. 161–169, 2019.

[33] D. Goldman, S. Istrail, G. Lancia, A. Piccolboni, and B. Walenz, "Algorithmic strategies in combinatorial chemistry," in *Proceedings of the 11th ACM-SIAM Syposium on Discrete Algorithms*, pp. 275–284, Philadelphia, PA, USA, 2000.

[34] Z. Du and A. Ali, "The inverse Wiener polarity index problem for chemical trees," *PLoS One*, vol. 13, Article ID e0197142, 2018.

[35] J. V. Kureethara, A. Asok, and I. N. Cangul, "Inverse problem for the forgotten and the hyper Zagreb indices of trees," *Communications in Combinatorics and Optimization*, pp. 1–7, 2021.

Hindawi
Journal of Mathematics
Volume 2024, Article ID 9847963, 1 page
https://doi.org/10.1155/2024/9847963

Retraction

Retracted: Morphological Bias of Ancient Artifacts: A Case Study of Incense Burners in Ming and Qing Dynasties

Journal of Mathematics

Received 30 January 2024; Accepted 30 January 2024; Published 31 January 2024

This article has been retracted by Hindawi following an investigation undertaken by the publisher [1]. This investigation has uncovered evidence of one or more of the following indicators of systematic manipulation of the publication process:

(1) Discrepancies in scope

(2) Discrepancies in the description of the research reported

(3) Discrepancies between the availability of data and the research described

(4) Inappropriate citations

(5) Incoherent, meaningless and/or irrelevant content included in the article

(6) Manipulated or compromised peer review

The presence of these indicators undermines our confidence in the integrity of the article's content and we cannot, therefore, vouch for its reliability. Please note that this notice is intended solely to alert readers that the content of this article is unreliable. We have not investigated whether authors were aware of or involved in the systematic manipulation of the publication process.

In addition, our investigation has also shown that one or more of the following human-subject reporting requirements has not been met in this article: ethical approval by an Institutional Review Board (IRB) committee or equivalent, patient/participant consent to participate, and/or agreement to publish patient/participant details (where relevant).

Wiley and Hindawi regrets that the usual quality checks did not identify these issues before publication and have since put additional measures in place to safeguard research integrity.

We wish to credit our own Research Integrity and Research Publishing teams and anonymous and named external researchers and research integrity experts for contributing to this investigation.

The corresponding author, as the representative of all authors, has been given the opportunity to register their agreement or disagreement to this retraction. We have kept a record of any response received.

References

[1] Y.-F. Chen and J. Wei, "Morphological Bias of Ancient Artifacts: A Case Study of Incense Burners in Ming and Qing Dynasties," *Journal of Mathematics*, vol. 2021, Article ID 7859189, 9 pages, 2021.

Hindawi
Journal of Mathematics
Volume 2021, Article ID 7859189, 9 pages
https://doi.org/10.1155/2021/7859189

Research Article

Morphological Bias of Ancient Artifacts: A Case Study of Incense Burners in Ming and Qing Dynasties

Yu-Fu Chen and Jie Wei

School of Design, Jiangnan University, 1800 Lihu Avenue, Wuxi City, Jiangsu Province, China

Correspondence should be addressed to Yu-Fu Chen; yu_fu_chen@126.com

Received 6 October 2021; Revised 20 October 2021; Accepted 1 November 2021; Published 30 November 2021

Academic Editor: Naeem Jan

This study verifies the relevance of the combination of traditional Chinese artifacts and perceptual semantic research. It provides new research ideas to study the Chinese artifact culture. Moreover, it helps people to understand the cultural spirit better and design crystallization of traditional artifacts. This study considered Chinese traditional incense burners in Ming and Qing dynasties to adopt morphological analysis and affinity diagram to select representative experimental samples. Furthermore, this research applied the perceptual engineering theory to explore the relation between design group's description of perceptual semantics and the shape of incense burners. The focuses were the design group on the shape and style of ancient artifacts in aesthetic consideration. According to the results of semantic principal component analysis, the perceptual semantic bias of the design group towards incense burners was concentrated, which is related to the style acceptance of incense burners. Among these related incense burner styles, the design group paid more attention to the proportional design of "incense burner foot" in the perceptual bias of incense burner shape and preferred the proportional incense burner shape of "long foot."

1. Introduction

Chinese incense burners became one of the popular artifacts in Tang and Song dynasties [1]. Under the rule of ritual system in the Ming Dynasty, a large number of porcelain incense burners became necessary products in the life of palace nobles and people [2]. The Qing Dynasty, following the development of incense burner technology in the Ming Dynasty, became another golden period in the history of Chinese incense burner development [3]. The culture of incense burners is closely related to people's aesthetic consciousness at that time. Aesthetic consciousness is the active reflection of the subject to the aesthetic attribute of the objective image, including people's aesthetic feeling, experience, viewpoint, and ideal [4]. Aesthetic consciousness comes from the process of interaction between humans and nature, which is a psychological process of grasping aesthetics through perceptual intuition to achieve rational essence. Active aesthetic feelings rather than passive perceptions have both thinking and emotional reflection and recognition [5]. Aesthetic consciousness is related to the level of social development and restricted by the society, but at the same time, it develops into aesthetics with individual characteristics [6]. The essence of aesthetic contemplation is a kind of perceptual activity state in which the subject concentrates on the object and forgets the existence of other things, which is the starting point of all artistic activities [7].

Perception is the most direct reaction of human beings to external things in practice. Moreover, it is also the inevitable existence of people's understanding of things and behavior reaction. It has a great influence and guiding effect on people's various behaviors [8]. In the perceptual research of incense burners, the so-called perception refers to the audience's subjective evaluation of the size, color, shape, pattern, and other artifact attributes of incense burners [9]. Perception is not determined by the attribute of a single thing and can hardly be measured [10]. There are many uncertainties in people's perception of artifacts, which leads to ups and downs in people's aesthetic cognition of artifacts [11]. However, the core idea is still to quantify people's

feelings about things [12]. Perceptual thought is an internal thing, while the material world is an external thing. The transformation from perceptual thought to the material world is "externalization" [13]. The core idea of ancient artifact design also comes from an "externalization" form produced by people's perceptual needs on artifacts. Gestalt theory of Gestalt Psychology emphasizes the integrity of objects and the role of human psychology in the organizational structure and integration of objects [14]. In addition to understanding things through perceptual perception, people also perceive, distinguish, and confirm them, which is called shape recognition or pattern recognition [15].

Kansei Engineering studies people's psychological needs and determines the relationship between perceptual perception and shape recognition [16]. Such needs are people's intuitive psychological and perceptual reflections, which are contained in spirit or physiology [17]. People perceive perceptual information from incense burner objects through external shape recognition. Furthermore, they employ their own knowledge and experience to explain the characteristics and attributes of incense burner objects. This way they obtain the Gestalt meaning of incense burner objects. The principle of "simplification" in Gestalt Psychology holds that under specific conditions, shape recognition will be presented in the simplest structure and the generated "shape" has clear and strong stimulation [18]. People's perceptual psychology will produce some special images due to visual shape recognition, because "shape" is the most important basic object in visual phenomena [19]. The form of incense burners has the principle of simplification and a complete shaping system, which enables people to better grasp the characteristics of shape recognition and produce a deep visual impression. In modern design, audiences' perceptual needs are often the focus of designers' attention, while aesthetics is a psychological activity that affects the audience's perceptual needs. Kansei Engineering can explore the factors of audience perception level and transform perceptual needs and images into elements of design details [20].

2. Research Method and Procedures

Step 1. Subgroup between morphological groups

R. Faulkner pointed out that "appearance, block and structure are narrow words, but shape is the most comprehensive. We use shape to describe the internal structure and visual shape, and even the block that defines outline and shape" [21]. Shape is the form of human thinking, which is of objectivity and subjectivity, can include the appearance, form, and internal structure of morphological objects. The main core of morphology is to discuss the essence and composition of things, and at the same time, it also emphasizes the discussion of the composition structure of things at the connotation level [22]. In the process of morphological analysis, the morphological classification is carried out by the link between the shape characteristic attributes of incense burners in Ming and Qing dynasties and the hierarchical membership relationship of each level, showing systematic induction and coding [23]. According to the "style" characteristics of incense burners in Ming and Qing dynasties as the classification standard, incense burner styles such as Li-type tripod incense burner, Gui-shaped incense burner, Ding-shaped tripod incense burner, incense burner in the shape of square Ding, polyhedral-type incense burner, tall tripod incense burner, cylindrical tripod incense burner, incense burner with animal handles, incense burner with ring handles, alms-bowl-shaped incense burner, and square-shaped incense burner can be drawn (Figure 1).

The research of traditional creation relies on literature and inference analysis, and it is difficult to provide objective and reasonable inference for the crux of the problem. The affinity diagram rule can integrate the majority opinions of experts and audiences, sum up various facts from scattered arguments in a structured way, and explore "creative skills" with new meanings. The classification principle of the affinity diagram was adopted. In the classification, five professional professors with more than 5 years of teaching experience in ancient artifact research, shape design, and other related disciplines and relevant background in shape research were invited to select representative incense burner images that met the feature level to obtain experimental samples through shape analysis according to the aesthetic intuitive perception evaluation of incense burner shape feature attributes (Figure 2). Then, they were divided into two experimental groups: Ming Dynasty incense burners and Qing Dynasty incense burners.

Step 2. Semantic Survey

Semantic analysis was put forward by American psychology professor C. E. Osgood in 1942. It is a research method of "common feeling." It uses a semantic subscale to study the meaning of things and is used as a manifestation of the psychological scale [24]. The generation of common sensation is a phenomenon in human sensation. When any sensory system is stimulated, other sensory systems resonate in series at the same time, which is called the "synesthesia" phenomenon in psychology [25]. The semantic subscale consists of three parts: concept, scale and subject. It is used to study cultural comparison, differences between individuals and groups, and people's attitudes and views on the surrounding environment or things [26]. The semantic difference method is the cornerstone of perceptual image research, which reflects the correlation between the overall aesthetic image tendency by reducing the dimension of the subjects' multidimensional aesthetic image space [27]. The semantic subscale of incense burners in Ming and Qing dynasties mainly selected images first and used Likert 5-point and other scales for evaluation. The evaluation scale consists of pairs of adjectives (Table 1) [28].

The subjects of the experiment were 200 designers or professional teachers with design-related backgrounds. Subjects have certain design professional reserve knowledge and aesthetic level and have more than 3 years of experience in design-related work as semantic survey samples. The design group chose concepts and images for concrete or abstract objects and showed the appropriate evaluation scale through multiple sets of extremely opposite paired adjectives [29].

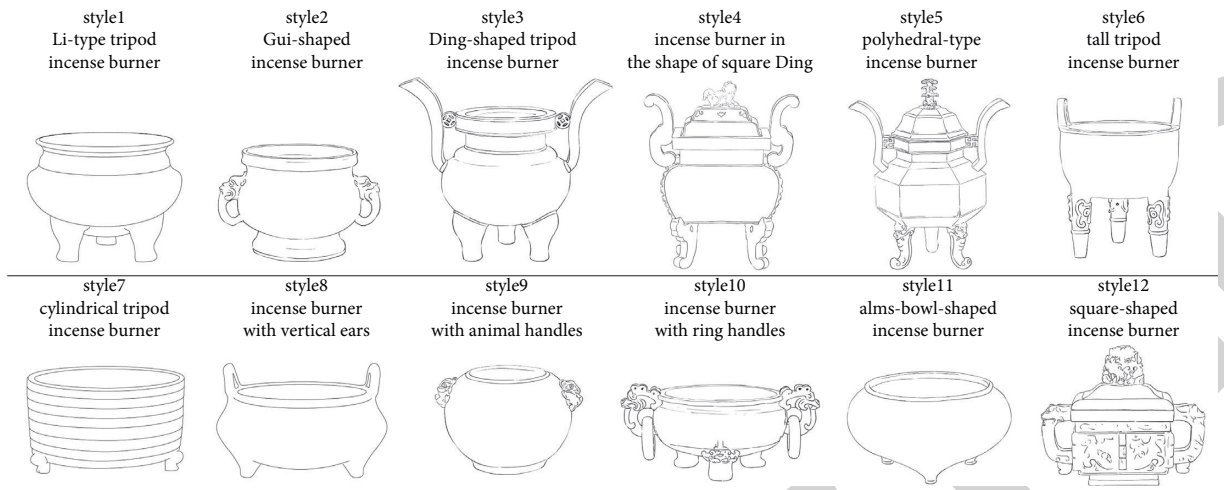

Figure 1: Incense burner style in the Ming and Qing dynasties.

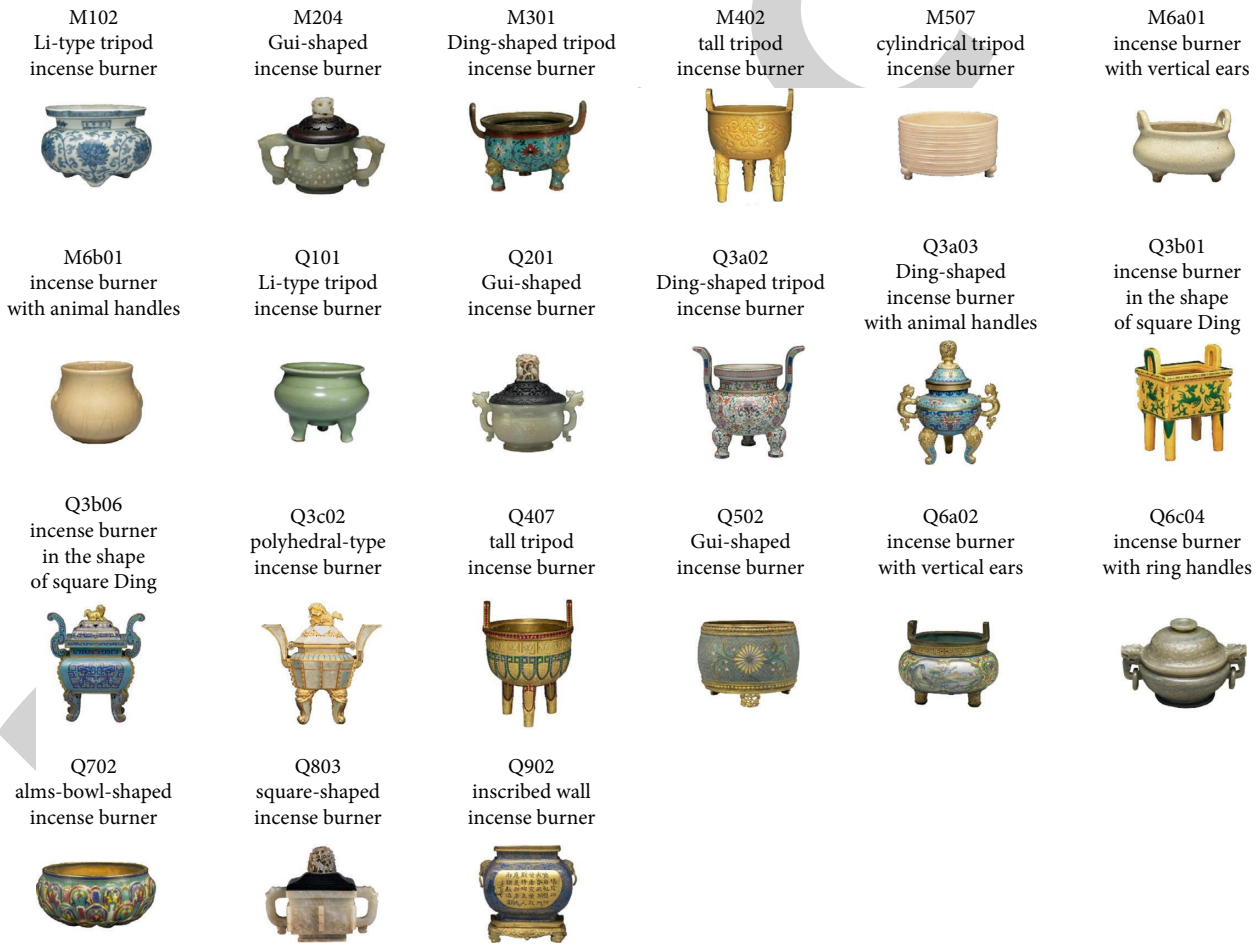

Figure 2: Experimental samples of incense burners in the Ming Dynasty (M) and Qing Dynasty (Q).

Table 1: Incense burner Kansei description semantic group.

Strange-ordinary	Special-plain	Rich-monotonous	Heavy-light	Colorful-dim
Gentle-stiff Regular-messy	Luxurious-simple Artistic-superficial	Concrete-abstract Amazing-plain	Traditional-fashionable	Simple-complex

Step 3. Principal component analysis

Principal component analysis was proposed by K. Pearson in 1901. It is a statistical method that can simplify huge data and find out the main direction of variation [30]. Principal component analysis is used to linearly combine the original P variables (assumed to be P) in the data to obtain K new variables (assumed to be K). In the principle of data simplification, the K value is usually less than the *P* value and the K new variables must have the ability to explain the covariable structure of the original variables [31]. By calculating the correlation between the data, the P variables that have correlation with each other are linearly combined to make the component variation reach the maximum. The largest individual difference that is highlighted on the original data is K variables, and K value is the number of principal components [32]. Principal component analysis enables researchers to obtain information that is not easy to observe on the surface and generates new data combinations through coordinate axes to improve the overall variance and express data differences [33]. In addition to the equivalence between variance and data difference, it is also necessary to consider the pointer of message volume. There are many types of new variables formed by linear combination. New variables containing as much pointer information as possible should be selected as far as possible. According to relevant statistical theories, variance is generally considered as an index reflecting the amount of information contained in variables [34]. The higher the value of the global variance, the more information may be obtained.

3. Results

In this section, the principal components of correlation analysis are described.

3.1. Principal Component Correlation of Incense Burners in the Ming Dynasty. The KMO and Bartlett test of factor analysis showed that KM0 was 0.972, which indicated that the obtained data were suitable for factor analysis. Bartlett's spherical test showed significant *P* values of $0.000 < 0.05$, which also indicated that the data were suitable for factor analysis, indicating that the questionnaire had a structural effect [35]. The principle of extracting the number of principal components is the first *m* principal components whose corresponding eigenvalues are greater than 1 [36]. To some extent, the eigenvalue can be regarded as an index indicating the influence strength of the principal component. If the eigenvalue is less than 1, it means that the interpretation strength of the principal component is not as strong as the average interpretation strength of directly introducing an original variable. Therefore, the eigenvalue greater than 1 can generally be used as the inclusion standard [37].

From the total variance explanation (Table 2), four principal components with eigenvalues greater than 1 were extracted and the four eigenvalues are 4.846, 3.267, 2.722, and 1.205, respectively. According to the analysis of Figure 3, the eigenvalues of common factor 1, common factor 2, common factor 3, and common factor 4 are all greater than 1, indicating that the influence index is large, so it shows that there are four principal components that have important influence on the shape of the censer in the Ming Dynasty.

The variance contribution of the first principal component is 37.278%, the variance contribution of the second principal component is 25.134%, the variance contribution of the third principal component is 20.935%, and the variance contribution of the fourth principal component is 9.267%. After rotating the load, it can be known that the contribution rate of the four principal component variances has changed, but the total cumulative variance contribution rate has not changed and it is still arranged in descending order. The contribution rate of the first principal component variance is 34.018%. The contribution rate of the second principal component variance is 28.342%, the contribution rate of the third principal component variance is 18.064%, and the contribution rate of the fourth principal component variance is 12.192%. Its total cumulative variance contribution is 92.615% (Table 2), which is higher than the standard index of 85%, indicating that these four principal components contain all the information in the pointer.

Through in-depth calculation of the importance of each perceptual vocabulary to the design of incense burners in the Ming Dynasty, the component matrix of four common factors for perceptual image vocabulary was obtained and the principal components 1, 2, 3, and 4 were set as E_1, E_2, E_3, and E_4. The component coefficient matrix of four principal components corresponds to each perceptual phrase. Factor scores of E_1, E_2, E_3, and E_4 in each incense burner sample were calculated in SPSS and expressed with b, b_2, b_3, and b_4. Component coefficient scores in equation (1) and Table 3 were used to calculate the comprehensive factor score of the samples, which was denoted by B (Table 4) [38].

$$B = \left(\left(\frac{34.018\%}{92.615\%}\right) \times b_1 + \left(\frac{28.342\%}{92.615\%}\right) \times b_2 + \left(\frac{18.064\%}{92.615\%}\right) \times b_3 + \left(\frac{12.192\%}{92.615\%}\right) \times b_4\right). \tag{1}$$

In equation (1), b_1 is the first common factor score of the sample; b_2 is the second common factor score of the sample; b_3 is the third common factor score of the sample; and b_4 is the fourth common factor score of the sample.

Rotation matrix analysis showed that "gentle," "traditional," and "artistic" were closely related to principal component 1; "strange," "characteristic," "gorgeous," and "concrete" are closely related to principal component 2; "heavy" and "luxurious" are closely related to principal component 3; "rich" and "simple" are closely related to principal component 4, which are greater than the default extraction standard of 0.6, indicating that they meet the perceptual needs of design groups. Table 4 shows that the Ming Dynasty incense burner shapes of M402 (tall tripod incense burner), M6a01 (incense burner with vertical ears), M6b01 (incense burner with animal handles), and M204

Table 2: Explanation of total variance of incense burners in the Ming Dynasty.

	Total variance explanation								
	Initial eigenvalue of component			Extracting the sum of squares of loads			Sum of squares of rotating loads		
	Total variance	%	Accumulated %	Total variance	%	Accumulated %	Total variance	%	Accumulated %
1	4.846	37.278	37.278	4.846	37.278	37.278	4.422	34.018	34.018
2	3.267	25.134	62.413	3.267	25.134	62.413	3.684	28.342	62.359
3	2.722	20.935	83.348	2.722	20.935	83.348	2.348	18.064	80.424
4	1.205	9.267	92.615	1.205	9.267	92.615	1.585	12.192	92.615
5	0.689	5.300	97.915						
6	0.271	2.085	100.000						
7	$7.035e^{-16}$	$5.411e^{-15}$	100.000						
8	$2.162e^{-16}$	$1.663e^{-15}$	100.000						
9	$4.998e^{-17}$	$3.844e^{-16}$	100.000						
10	$-3.698e^{-17}$	$-2.844e^{-16}$	100.000						
11	$-1.806e^{-16}$	$-1.389e^{-15}$	100.000						
12	$-2.834Ee^{-16}$	$-2.180e^{-15}$	100.000						
13	$-3.645e^{-16}$	$-2.804e^{-15}$	100.000						

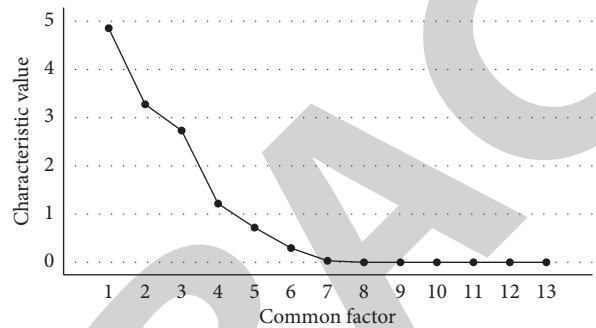

Figure 3: Factor analysis of the incense burner in the Ming Dynasty gravel map.

Table 3: Component matrix and composition score coefficient matrix of censers after rotation in the Ming Dynasty.

	Rotated component matrix				Component score coefficient matrix			
	Component				Component			
	1	2	3	4	E_1	E_2	E_3	E_4
Strange	−0.594	0.728	0.214	0.112	−0.110	0.176	0.131	0.122
Characteristic	−0.076	0.983	−0.084	−0.111	0.029	0.274	−0.064	−0.108
Rich	−0.020	−0.214	−0.075	0.970	−0.027	-0.074	0.158	0.681
Heavy	−0.265	0.220	0.912	−0.091	−0.061	0.049	0.424	0.118
Gorgeous	0.252	0.850	−0.293	−0.061	0.101	0.250	−0.157	−0.117
Gentle	0.927	−0.159	0.007	0.050	0.209	-0.004	0.004	0.026
Luxurious	0.393	−0.128	0.831	−0.105	0.079	-0.018	0.375	0.087
Concrete	−0.116	0.885	0.413	0.029	0.007	0.242	0.204	0.093
Traditional	0.975	0.121	0.122	0.136	0.230	0.075	0.075	0.106
Simple	0.405	0.436	−0.430	0.625	0.109	0.132	−0.087	0.349
Regular	−0.799	0.497	−0.027	−0.060	−0.163	0.104	−0.017	−0.044
Artistic	0.874	0.214	−0.097	−0.058	0.216	0.100	−0.068	−0.077
Amazing	−0.621	0.220	−0.549	0.419	−0.135	0.029	−0.175	0.196

Table 4: Sample factors of incense burners in the ming dynasty.

Sample number	b_1	b_2	b_3	b_4	B
M402	1.27531	0.72821	−1.33460	1.05498	0.5698
M6a01	0.54095	−0.54175	1.43287	0.67021	0.4005
M6b01	1.12827	−0.00153	0.52503	−1.63890	0.3006
M204	−0.98950	1.89180	0.34106	−0.36379	0.2341
M102	−0.09300	−0.68950	0.11236	0.46126	−0.1625
M507	−1.13915	−0.41104	0.23024	0.74174	−0.4017
M301	−0.72288	−0.97618	−1.30695	−0.92550	−0.9409

(Gui-shaped incense burner) can be more accepted by the perceptual psychology of the design group, especially the "three-legged incense burner" shape of M402 can be more recognized by designers. However, the scores of comprehensive factors of M102 (Li-type tripod incense burner), M507 (cylindrical tripod incense burner), and M301 (Ding-shaped tripod incense burner) are lower, which indicates that the shape characteristics of incense burners are not the styles expected by the design group in perceptual aesthetics.

3.2. Principal Component Correlation of Incense Burners in the Qing Dynasty. The KMO and Bartlett test of factor analysis showed that KM0 was 0.921 which indicated that the obtained data were suitable for factor analysis. Bartlett's spherical test showed significant P values of $0.000 < 0.05$ which also indicated that the data were suitable for factor analysis, indicating that the questionnaire had structural effect. Four principal components with eigenvalues greater than 1 were extracted from the total variance interpretation (Table 5), and the four eigenvalues were 6.245, 2.353, 1.443, and 1.150, respectively. According to scree plot (Figure 4) analysis, the eigenvalues of common factor 1, common factor 2, common factor 3, and common factor 4 are all greater than 1, indicating that the influence index is relatively large and there are four principal components that have important influence on the shape of censers in the Qing Dynasty.

The variance contribution of the first principal component is 48.038%, the variance contribution of the second principal component is 18.097%, the variance contribution of the third principal component is 11.101%, and the variance contribution of the fourth principal component is 8.849%. After rotating the load, it can be known that the contribution rate of the four principal component variances has changed, but the total cumulative variance contribution rate has not changed, with an arrangement in descending order. The contribution rate of the first principal component variance is 35.473%. The contribution rate of the second principal component variance is 22.497%, the contribution rate of the third principal component variance is 17.976%, and the contribution rate of the fourth principal component variance is 10.138%. Its total cumulative variance contribution is 86.084% (Table 5), which is higher than the standard index of 85%, indicating that these four principal components contain the information contained in all pointers.

Through in-depth calculation of the importance of each perceptual vocabulary to the design of incense burner in the Qing Dynasty, the component matrix of four common factors for perceptual image vocabulary was obtained and the principal components 1, 2, 3, and 4 were set as E_1, E_2, E_3, and E_4. The component coefficient matrix of four principal components corresponds to each perceptual phrase. Factor scores of E_1, E_2, E_3, and E_4 in each incense burner sample were calculated in SPSS and expressed with b_1, b_2, b_3, and b_4. Component coefficient scores in equation (2) and Table 6 were used to calculate the comprehensive factor score of the samples, which was denoted by B (Table 7).

$$B = \left(\left(\frac{35.473\%}{86.084\%}\right) \times b_1 + \left(\frac{22.497\%}{86.084\%}\right) \times b_2 + \left(\frac{17.976\%}{86.084\%}\right) \times b_3 + \left(\frac{10.138\%}{86.084\%}\right) \times b_4\right). \tag{2}$$

In equation (2), b_1 is the first common factor score of the sample; b_2 is the second common factor score of the sample; b_3 is the third common factor score of the sample; and b_4 is the fourth common factor score of the sample.

Rotation matrix analysis showed that "characteristic," "rich," "gorgeous," and "artistic" are closely related to principal component 1; "strange," "heavy," and "concrete" are closely related to principal component 2; "amazing" is closely related to principal component 3; and "gentle" and "traditional" are closely related to principal component 4, which are greater than the default extraction standard of 0.6, indicating that they meet the perceptual needs of the design group (Table 7). It indicates the incense burner shapes of Q3a03 (Ding-shaped incense burner with animal handles), Q902 (inscribed wall incense burner), Q3b06 (incense burner in the shape of square Ding), Q3a02 (Ding-shaped tripod incense burner), Q702 (alms-bowl-shaped incense burner), Q6a02 (incense burner with vertical ears), Q3c02 (polyhedral-type incense burner), and Q407 (tall tripod incense burner) can be more accepted by the perceptual psychology of the design group. Especially, Q3a03 (Ding-shaped incense burner with animal handles) incense burner can be more recognized by the design group. However, Q3b01 (incense burner in the shape of square Ding), Q502 (Gui-shaped incense burner), Q201 (Gui-shaped incense burner), Q803 (square-shaped incense burner), Q101 (Li-type tripod incense burner), and Q6c04 (incense burner with ring handles) have lower comprehensive factor scores, indicating that their shape characteristics are not what the design group expects in perceptual aesthetics.

According to the results obtained from the component matrix after the rotation matrix, the incense burner shapes of the tall tripod incense burner, incense burner with vertical ears, and incense burner with animal handles in the Ming Dynasty and the Ding-shaped incense burner with animal handles, inscribed wall incense burner, and incense burner in the shape of square Ding in the Qing Dynasty were accepted by the design group. In terms of incense burner shape characteristics, tall tripod incense burner, Ding-shaped incense burner with animal handles, and incense burner in the shape of square Ding all belong to the incense burner shape with a long proportion of incense burner feet. Ding-shaped tripod incense burner, cylindrical tripod incense burner, and Li-type tripod incense burner in the Ming Dynasty and incense burner with ring handles, Li-type tripod incense burner, and square-shaped incense burner in the Qing Dynasty were rejected by designers. The comprehensive results showed that most of the incense burners with higher acceptance belong to a large proportion of incense burners, while the incense burners with lower acceptance belong to the incense burners with short or no incense feet. "Incense

Table 5: Explanation of total variance of incense burners in the Qing Dynasty.

	Total variance explanation								
	Initial eigenvalue of component			Extracting the sum of squares of loads			Sum of squares of rotating loads		
	Total variance	%	Accumulated%	Total variance	%	Accumulated%	Total variance	%	Accumulated%
1	6.245	48.038	48.038	6.245	48.038	48.038	4.611	35.473	35.473
2	2.353	18.097	66.134	2.353	18.097	66.134	2.925	22.497	57.970
3	1.443	11.101	77.235	1.443	11.101	77.235	2.337	17.976	75.947
4	1.150	8.849	86.084	1.150	8.849	86.084	1.318	10.138	86.084
5	0.691	5.313	91.397						
6	0.518	3.981	95.378						
7	0.283	2.180	97.558						
8	0.186	1.430	98.988						
9	0.061	0.471	99.459						
10	0.051	0.395	99.854						
11	0.014	0.109	99.963						
12	0.003	0.022	99.986						
13	0.002	0.014	100.000						

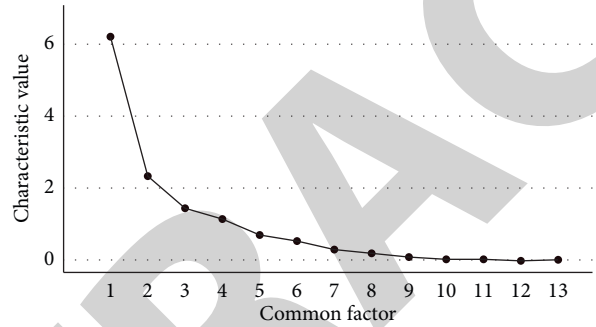

Figure 4: Factor analysis of incense burners in the Qing Dynasty gravel map.

Table 6: Component matrix and composition score coefficient matrix of censers after rotation in the Qing Dynasty.

	Rotated component matrix				Component score coefficient matrix			
	Component				Component			
	1	2	3	4	E_1	E_2	E_3	E_4
Strange	0.386	0.874	0.121	0.052	−0.044	0.375	−0.119	−0.022
Characteristic	0.949	0.273	0.094	−0.026	0.225	−0.039	−0.021	0.001
Rich	0.946	0.292	0.003	-0.050	0.221	−0.008	-0.074	-0.020
Heavy	0.020	0.899	0.156	0.051	−0.156	0.447	−0.099	−0.043
Gorgeous	0.843	0.130	0.284	0.268	0.231	−0.164	0.114	0.240
Gentle	0.051	0.333	0.284	0.818	−0.009	0.036	0.091	0.610
Luxurious	0.786	0.379	−0.152	−0.161	0.156	0.111	−0.173	−0.124
Concrete	0.313	0.745	0.223	0.140	-0.039	0.289	-0.036	0.056
Traditional	−0.119	-0.197	−0.596	0.676	0.044	−0.029	−0.270	0.533
Simple	−0.403	−0.446	−0.718	0.142	−0.019	−0.037	−0.286	0.127
Regular	-0.278	−0.358	−0.647	−0.020	−0.007	−0.011	−0.269	−0.001
Artistic	0.972	-0.028	0.127	−0.038	0.285	−0.212	0.057	0.022
Amazing	−0.197	−0.016	0.866	0.211	−0.058	−0.170	0.472	0.164

burner foot" appeared to be a characteristic attribute that the design group paid special attention to in perceptual aesthetics, and the design group had a high degree of favor for "considerable." Theoretical research has showed that the attributes of artifacts constitute human visual aesthetic experience and have perceptual differences and strong morphological associations between individuals. In the process of people's cognition of artifacts, the treatment of special shape parts and descriptive semantics determines how to present a part of perceptual aesthetics [39].

Table 7: Sample factors of incense burners in the Qing Dynasty.

Sample number	b_1	b_2	b_3	b_4	B
Q3a03	0.68242	0.60728	0.67548	0.90831	0.6880
Q902	0.23002	0.32095	2.00044	−0.47288	0.5406
Q3b06	0.35624	0.46543	0.67200	0.51144	0.4690
Q3a02	0.47644	0.66711	−0.08006	0.95894	0.4669
Q702	0.68874	−0.08793	0.23433	1.00962	0.4287
Q6a02	0.64958	0.53015	−0.58051	0.57706	0.3530
Q3c02	0.54753	0.74535	0.92145	−2.55006	0.3124
Q407	0.72761	−0.00571	−1.09237	0.68502	0.1510
Q3b01	0.63330	0.32102	−1.82842	−1.06727	−0.1626
Q502	0.11062	−2.53479	0.55518	0.33232	−0.4617
Q201	−0.75881	0.12591	−0.99831	−0.65870	-0.5658
Q803	−0.14069	−1.39021	−0.83919	−0.69636	−0.6785
Q101	−2.63087	1.23969	−0.16109	0.52327	−0.7322
Q6c04	−1.57213	−1.00427	0.52109	−0.06070	−0.8086

4. Conclusion

In this study, Kansei Engineering theory was used to explore modern people's perceptual thinking about traditional implements, which is a tentative, cross-disciplinary, and innovative way. Furthermore, this study discussed the perceptual thinking of design groups on traditional artifacts through perceptual engineering. Moreover, the aesthetic intersection of design groups was explored among different groups and different styles of artifacts through descriptive vocabulary. This is a practical application of ancient artifacts in modern design. The results of this investigation showed that there is a correlation between the perceptual aesthetic semantic bias and the shape of the artifacts. It probed into the design group's emphasis on the characteristics of the shape of the artifacts. In addition, it reflected the differences in people's perceptual cognition of the artifacts in different periods. It was also shown that the design group paid more attention to the proportion of "incense burner foot" in incense burner style and preferred the incense burner shape with a longer proportion of "incense burner foot."

Data Availability

The data used in this study are available at request from the corresponding author.

Ethical Approval

The authors confirm that all the research meets ethical guidelines and adheres to the legal requirements of the study country.

Conflicts of Interest

The authors declare no conflicts of interest.

Acknowledgments

This study was supported by the 2019 National Social Science Fund Art Category under Grant no. 19BG130 and the Fundamental Research Funds for the Central Universities under Grant no. JUSRP121105.

References

[1] J. Wei, *Lightness of Incense Burner: Design Research of Incense Burner in Tang and Song Dynasties*, China Light Industry Press, Beijing, China, 2019.

[2] Q. H. Yu, *Research on the Art of Incense Burner Creation*, Beijing Arts and Crafts Publishing, Beijing, China, 2012.

[3] J. Rawson, "The Chinese hill censer, boshan lu: a note on origins, influences and meanings," *Arts Asiatiques*, vol. 61, no. 1, pp. 75–86, 2006.

[4] J. Loesberg, "Idleness and aesthetic consciousness, 1815–1900 by richard adelman (review)," *Victorian Studies*, vol. 62, no. 2, pp. 341-342, 2020.

[5] K. M. Kim, "The aesthetic turn in everyday life in korea," *Open Journal of Philosophy*, vol. 03, no. 03, pp. 359–365, 2013.

[6] V. Papushyna, "Forming pedagogical aesthetic culture of students in British experience," *Comparative Professional Pedagogy*, vol. 7, no. 3, pp. 49–54, 2017.

[7] L. A. Rule, "Approaches to teaching fitzgerald's the great gatsby edited by jackson R. Bryer and nancy P. VanArsdale," *The F. Scott Fitzgerald Review*, vol. 7, no. 1, pp. 155–158, 2009.

[8] J. F. Zhang, "The application of color psychological effect on fashion design," *Advanced Materials Research*, vol. 796, pp. 474–478, 2013.

[9] Q. H. Yu, "Chairman of the international conference on computer aided industrial design and conceptual design. Integration of tradition and fashion: decoration, usage and philosophy of incense burner—the current situation of censer design in the city of jingdezhen," in *Proceedings of the 2011 IEEE 12th International Conference on Computer-Aided Industrial Design & Conceptual Design*, Beijing, China, July 2011.

[10] S. M. Smith and I. Krajbich, "Mental representations distinguish value-based decisions from perceptual decisions," *Psychonomic Bulletin & Review*, vol. 16, pp. 1–10, 2021.

[11] A. Zhou, J. Ouyang, J. Su, S. Zhang, and S. Yan, "Multimodal optimisation design of product forms based on aesthetic evaluation," *International Journal of Arts and Technology*, vol. 12, no. 2, p. 128, 2020.

[12] M. Nagamachi and A. S. Imada, "Kansei Engineering: an ergonomic technology for product development," *International Journal of Industrial Ergonomics*, vol. 15, no. 1, pp. 1–74, 1995.

[13] G. W. F. Hegel, *The Philosophy of Fine Arts*, Commercial Press, Shanghai, China, 1817.

Hindawi
Journal of Mathematics
Volume 2023, Article ID 9783817, 1 page
https://doi.org/10.1155/2023/9783817

Retraction

Retracted: Probability Density Evolution Algorithm for Stochastic Dynamical Systems Based on Fractional Calculus

Journal of Mathematics

Received 15 August 2023; Accepted 15 August 2023; Published 16 August 2023

This article has been retracted by Hindawi following an investigation undertaken by the publisher [1]. This investigation has uncovered evidence of one or more of the following indicators of systematic manipulation of the publication process:

(1) Discrepancies in scope

(2) Discrepancies in the description of the research reported

(3) Discrepancies between the availability of data and the research described

(4) Inappropriate citations

(5) Incoherent, meaningless and/or irrelevant content included in the article

(6) Peer-review manipulation

The presence of these indicators undermines our confidence in the integrity of the article's content and we cannot, therefore, vouch for its reliability. Please note that this notice is intended solely to alert readers that the content of this article is unreliable. We have not investigated whether authors were aware of or involved in the systematic manipulation of the publication process.

Wiley and Hindawi regrets that the usual quality checks did not identify these issues before publication and have since put additional measures in place to safeguard research integrity.

We wish to credit our own Research Integrity and Research Publishing teams and anonymous and named external researchers and research integrity experts for contributing to this investigation.

The corresponding author, as the representative of all authors, has been given the opportunity to register their agreement or disagreement to this retraction. We have kept a record of any response received.

References

[1] Y. Yan and X. Yu, "Probability Density Evolution Algorithm for Stochastic Dynamical Systems Based on Fractional Calculus," *Journal of Mathematics*, vol. 2021, Article ID 9218857, 9 pages, 2021.

Hindawi
Journal of Mathematics
Volume 2021, Article ID 9218857, 9 pages
https://doi.org/10.1155/2021/9218857

Research Article

Probability Density Evolution Algorithm for Stochastic Dynamical Systems Based on Fractional Calculus

Yang Yan[1] and Xiaohong Yu[2]

[1]*Jinzhong College of Information, Taigu, Shanxi 030805, China*
[2]*Shanxi Agricultural University, Taigu, Shanxi 030805, China*

Correspondence should be addressed to Xiaohong Yu; yuxiaohong@sxau.edu.cn

Received 14 October 2021; Accepted 12 November 2021; Published 29 November 2021

Academic Editor: Naeem Jan

With the increasing load and speed of trains, the problems caused by various random excitations (such as safety and passenger comfort) have become more prominent and thus arises the necessity to analyze stochastic dynamical systems, which is important in both academic and engineering circles. The existing analysis methods are inadequate in terms of computational accuracy, computational efficiency, and applicability in solving complex problems. For that, a new efficient and accurate method is used in this paper, suitable for linear and nonlinear random vibration analysis of large structures as well as static and dynamic reliability assessment. It is the direct probability integration method, which is extended and applied to the random vibration reliability analysis of dynamical systems. Dynamical models of the dynamic system and coupled system "three-car vehicle-rail-bridge" are established, the time-varying differential equations of motion are derived in detail, and the dynamic response of the system is calculated using the explicit Newmark algorithm. The simulation results show the influence of the number of representative points on the smoothness of the image of the probability density function and the accuracy of the calculation results.

1. Introduction

Railroad transportation is one of the major modes of transportation in the world today, and the mileage of high-speed railroad in China has reached 38,000 km, and it is planned to realize the "eight horizontal and eight vertical" high-speed railroad network by 2030. China is a vast country with many mountains and rivers, and bridge structures occupy a high proportion in the lines. The three subsystems of train, track, and bridge are coupled into a large system through wheel-rail contact forces and bridge-rail interactions, and the dynamic response of the vehicle, track, and bridge structures is triggered by the system excitation [1]. The train operation will have a dynamic impact on the track and bridge structure, causing the track and bridge to vibrate, affecting its working condition and service life; the vibration of the track and bridge structure will in turn affect the train operation smoothness and passenger comfort [2, 3]. This train-track-bridge dynamic interaction problem is a typical large system dynamics problem, which is usually called vehicle-track-bridge coupled vibration [4]. At present, this latter problem has received wide attention from the engineering and academic communities.

With the development of railroad transportation tending to be high speed and lighter, it is necessary to ensure high smoothness, stability, and reliability of the line in order to ensure the safety and stability of high-speed train operation as well as passenger comfort [5]. The stochastic uncertainties are widely present in the vehicle-rail-bridge coupled system (stochastic dynamical system), such as bridge (track) uneven excitation, wind load and seismic action, wheel geometry deviation, and wheel pair serpentine motion, which are directly related to whether the train can run safely and smoothly [6]. The scale of railways is getting bigger and bigger, and there is a strong interest in theory and application. Therefore, studying the dynamic interaction of the "car-iron-bridge" coupling system, as well as stochastic dynamic analysis, correct evaluation of the safety of vehicle operation, etc. have become the focus of research.

The existing methods for the analysis of the dynamics of stochastic dynamic systems such as Monte Carlo simulation, probability density evolution method, and diffusion process method have different degrees of defects, such as low computational accuracy and efficiency, difficult to solve, large computational cost, and insufficient applicability to compute complex problems [8]. Therefore, it is important to find a more accurate and efficient method to evaluate the stochastic vibration and bridge dynamics reliability of the coupled vehicle-rail-bridge system and to study the trend and statistical law of the representative stochastic response of the coupled vehicle-rail-bridge system under the joint action of deterministic load and stochastic excitation, which is important for vehicle dynamics performance evaluation and vehicle bridge maintenance. It is of great significance for the evaluation of vehicle dynamics performance and vehicle bridge maintenance. Guohai Chen and Dixiong Yang proposed a general and efficient method for structural linear and nonlinear stochastic vibration and hydrodynamic reliability analysis: the direct probability integration method (DPIM) [9]. The probability density integral equation for the propagation of randomness in static and dynamic systems is derived uniformly based on the principle of probability conservation [10]. Using probability space dissection and Dirac function smoothing techniques, an efficient solution of the probability density integral equation is achieved, and the probability density functions of the stochastic response of the static and dynamic systems as well as the reliability are obtained by decoupling the calculation from the deterministic dynamics equations. In this paper, the coupled vehicle-bridge and three-car vehicle-rail-bridge systems are modeled, respectively, and the stochastic dynamics of the dynamic system is analyzed by using the direct probability integral method and compared with the Monte Carlo simulation results to analyze the change trend and statistical law of the stochastic dynamics response of the coupled system and to verify the accuracy and efficiency of the direct probability integral method [11]. The results are compared with Monte Carlo simulations to analyze the change trend and statistical law of the coupled system stochastic dynamics response, to verify the accuracy and efficiency of the direct probability integration method, and to provide new ideas and methods for the stochastic dynamics analysis of the power system [12].

2. Related Works

Stochastic dynamic system vibration analysis is mainly used to analyze the impact of system parameters and external environment on the safety and comfort of the train by solving the statistical law of the system response of interest and to provide guidance for safer, smoother, and high-speed operation of the train. The dynamic reliability of a bridge structure represents its probability of not breaking or failing in a given time under the action of internal and external random excitation of the system. The failure criteria commonly used for bridge dynamic reliability analysis are the first beyond failure criterion and the fatigue failure criterion. Among them, fatigue failure refers to the structural response under cyclic random loading, and the structural damage occurs when the structural response is repeated in the threshold range until the damage accumulates to a certain limit value, and its complex fatigue damage mechanism limits the development and application of this method [13]. The first time beyond failure criterion considers that the structural dynamic response (this paper mainly consider the bridge span displacement) first exceeds a given threshold value when the structure is damaged. This criterion is concise and widely used, and the dynamic reliability assessment of the bridge structure in the vehicle-bridge coupled system and the vehicle-rail-bridge coupled system is also based on the first time beyond failure criterion [14].

The methods of analyzing stochastic dynamical system are equally divided into the time domain method and the frequency domain method. The latter method takes the power spectral density function as the core of analysis and is mainly applicable to the analysis of stochastic dynamics of linear vehicle-rail-bridge coupled systems. Zeng Sanyuan and Wu Yingxuan derived the influence of suspension parameters on the vehicle vertical vibration amplitude as well as bridge structural safety by studying the rail excitation function and its application to vehicle stochastic vibration calculation. By solving the dynamic response of the simple vehicle model and the vehicle-track coupled system model, Chen Guo et al. analyzed their power spectra and found that the agreement is better in the low-frequency region, but there will be a large gap in the high-frequency region. Lin Jiahao proposed the virtual excitation method to transform the complex random track upset into simple harmonic virtual track upset, which can improve the calculation accuracy and efficiency, gave a new method to evaluate the train operation comfort based on the elastic vehicle model [15], combined the virtual excitation method and the fine integration method to analyze the nonsmooth stochastic response of a bridge system under the action of random track upset, and concluded that the root mean square of the system response would be doubled for each level of track upset. Zeng et al. used the virtual excitation method to calculate the vehicle-bridge coupled system under the assumption of wheel-rail close connection and the wheel-rail transverse creep rate; considering the vehicle moving load, the random dynamic response of the coupled vehicle-bridge system under the combined effect of vehicle moving load, random uneven excitation of the bridge deck and ground vibration load was calculated using the virtual excitation method and its statistical law was analyzed. The effect of train speed, track irregularity, etc., on the system dynamic response amplitude and driving safety by calculating the amplitude-frequency transfer function between track irregularity and vehicle vertical acceleration is analyzed [16].

The probability density evolution method proposed by Jie Li and Jianbing Chen is a more common method for the dynamics analysis of stochastic dynamical systems, which has higher computational efficiency compared to MCS. Xu and Zhai calculated the three-dimensional probability

density evolution surface of the response of the vehicle body transverse displacement, transverse acceleration, and wheel-rail force by establishing a detailed vehicle-rail (plate rail) coupled system dynamics model. Yu et al. established a vertical vehicle-bridge coupled system and used PDEM to calculate the effect of the randomness of vehicle suspension parameters on the dynamic response of the system. However, Goller et al. pointed out that the probability density evolution method has a complicated solution process, not applicable to cases of large number of random variables [17].

As railroad transportation becomes more and more developed, the number of traffic safety accidents caused by wheel-rail nonlinear contact and various stochastic excitations during vehicle travel is increasing. However, the existing analysis methods have problems such as insufficient computational accuracy, low efficiency, and complex solutions. Therefore, there is a need to develop more accurate, efficient, simple, and universal methods for analyzing the stochastic dynamics of coupled vehicle-rail-bridge systems. The direct probabilistic integration method (DPIM) [9], which is based on the integral formulation of the probability conservation principle, is a new method for linear and nonlinear stochastic vibration analysis of large complex structures, static and dynamic reliability assessment of structures, with significant computational accuracy and efficiency advantages. It is of great academic and theoretical significance and engineering application value.

3. Differential Equations for Vibration of Rail Structures

In practical engineering problems, the infinite-length Euler beam model for steel rails is often simplified to a finite-length simply supported beam model [10]. When a vehicle crosses the bridge, the higher-order modes in the structural system of the track and the bridge are not easily excited, and usually only a few lower modes will be excited, besides to a few modes with lower self-oscillation frequencies that are superimposed to express the vibration state of the structure. This paper uses the vibration superposition method to solve the midpoint displacement of the track and the span displacement of the bridge.

We start our study by deriving a basic form second-order ordinary differential equation for rail vertical vibration so that, at the end of this section, we have all calculations done by steps, and as a result of this, we can follow the same way to derive the differential equation form of the vertical vibration of a bridge.

The vertical, lateral, and torsional vibrations of the track structure under the moving vehicle load are given by the following formula:

$$\begin{aligned} EI_Y\frac{\partial^4 z_r(x,t)}{\partial x^4}+m_r\frac{\partial^2 z_r(x,t)}{\partial t^2}&=-\sum_{i=1}^{N_s}F_{rvi}(t)\delta(x-x_i)+\sum_{j=1}^{N_w}P_{vj}(t)\delta\left(x-x_{wj}\right),\\ EI_Z\frac{\partial^4 y_r(x,t)}{\partial x^4}+m_r\frac{\partial^2 y_r(x,t)}{\partial t^2}&=-\sum_{i=1}^{N_s}F_{rHi}(t)\delta(x-x_i)+\sum_{j=1}^{N_w}P_{Hj}(t)\delta\left(x-x_{wj}\right),\\ \rho I_0\frac{\partial^2 \phi_r(x,t)}{\partial t^2}+GI_t\frac{\partial^2 \phi_r(x,t)}{\partial x^2}&=-\sum_{i=1}^{N_s}F_{rTi}(t)\delta(x-x_i)+\sum_{j=1}^{N_w}P_{Tj}(t)\delta\left(x-x_{wj}\right), \end{aligned} \tag{1}$$

where E and G represent Young's modulus of elasticity and shear modulus of the rail, respectively, m_r represents the mass of the rail, which is equal to the product of the cross-sectional area of the rail A_r and the mass density ρ_r, I_y and I_z represent the moments of inertia of the rail section with respect to the horizontal and vertical axes, respectively, I_0 and I_t represent the extreme moments of inertia and torsional moments of inertia of the rail section, respectively, N_s and N_w represent the number of fastener nodes and the number of vehicle axles, respectively, F_{rvi}, F_{rHi}, and F_{rTi} denote the vertical, lateral, and torsional reaction forces at the ith pivot point of the rail, respectively, P_{vj}, P_{Hj}, and P_{Tj} denote the vertical, lateral, and torsional forces on the rail by the jth wheel, respectively, and x_i and x_{wj} denote the x-coordinate of the ith pivot point of the rail and the x-coordinate of the jth wheel pair, respectively.

Equation (1) is a fourth-order partial differential equation, which needs to be transformed into a second-order ordinary differential equation in order to solve it. The regular vibration coordinate $qk(t)$ of the rail is introduced, and the modal order of the interception is M. According to the regular vibration function of the simply supported beam, the vertical vibration of the rail is expressed as

$$Z_k(x)=\sqrt{\frac{2}{m_r l}}\sin\frac{k\pi x}{l}, \tag{2}$$

and the solution of equation (1) can be expressed as

$$Z_r(x,t)=\sum_{k=1}^{M}Z_k(x)q_k(t). \tag{3}$$

Now, substituting (3) in equation (1),

$$\sum_{k=1}^{M} EI_Y \frac{\mathrm{d}^4 Z_k(x)}{\mathrm{d}x^4} q_k(t) + \sum_{k=1}^{M} m_r Z_k(x) \ddot{q}_k(t) = -\sum_{i=1}^{N_s} F_{rvi}(t)\delta(x - x_i) + \sum_{j=1}^{N_w} P_{vj}\delta\left(x - x_{wj}\right). \tag{4}$$

Then, multiplying both sides of equation (4) by $Z_h(x)$ $(h = 1, 2, \ldots, M)$ and integrating x from 0 to l using orthogonality of modes, we obtain

$$\int_0^l Z_h(x) Z_k(x) \mathrm{d}x = 0, \quad (h \neq k). \tag{5}$$

Thus,

$$\int_0^l EI_Y \frac{\mathrm{d}^4 Z_k(x)}{\mathrm{d}x^4} Z_k(x) q_k(t) \mathrm{d}x + \int_0^l m_r Z_k(x) Z_k(x) \ddot{q}_k(t) \mathrm{d}x = -\sum_{i=1}^{N_s} \int_0^l F_{rvi}(t) Z_k(x) \delta(x - x_i) \mathrm{d}x + \sum_{j=1}^{Nw} \int_0^l P_{vj}(t) Z_k(x) \delta\left(x - x_{wj}\right) \mathrm{d}x, \quad (k = 1 \sim M), \tag{6}$$

and by the nature of the Dirac δ function, equation (6) can be organized as

$$m_r \ddot{q}_k(t) \int_0^l Z_k^2(x) \mathrm{d}x + EI_Y q_k(t) \int_0^l Z_k(x) \frac{\mathrm{d}^4 Z_k(x)}{\mathrm{d}x^4} \mathrm{d}x = -\sum_{i=1}^{N_s} F_{rvi}(t) Z_k(x_i) + \sum_{j=1}^{Nw} P_{vj}(t) Z_k\left(x_{wj}\right), \quad (k = 1 \sim M). \tag{7}$$

Moreover, using

$$\int_0^l Z_k^2(x) \mathrm{d}x = \frac{1}{m_r} \int_0^l Z_k(x) \frac{\mathrm{d}^4 Z_k(x)}{\mathrm{d}x^4} \mathrm{d}x = \int_0^l \frac{2}{m_r l} \left(\frac{k\pi}{l}\right)^4 \sin^2 \frac{k\pi x}{l} \mathrm{d}x = \left(\frac{k\pi}{l}\right)^4 \int_0^l Z_k^2(x) \mathrm{d}x = \frac{1}{m_r} \left(\frac{k\pi}{l}\right)^4, \tag{8}$$

equation (7) is reduced to

$$\ddot{q}_k(t) + \frac{EI_Y}{m_r} \left(\frac{k\pi}{l}\right)^4 q_k(t) = -\sum_{i=1}^{N_s} F_{rvi}(t) Z_k(x_i) + \sum_{j=1}^{N_w} P_{vj}(t) Z_k\left(x_{wj}\right), \quad (k = 1 \sim M), \tag{9}$$

where formula (9) is the basic form of the second-order ordinary differential equation for rail vertical vibration.

4. Dynamics Analysis of Stochastic Dynamical Systems Based on the Direct Probability Integration Method

In this section, a vertical vehicle-bridge coupled system is established, in which a multirigid body model is used for the vehicle and a planar beam unit finite element model is used for the bridge, as shown in Figure 1. Assuming elastic contact between the wheels and the bridge deck, a spring with a stiffness of 2k can be used for the simulation.

The equations of motion of the vehicle and bridge systems can be expressed, respectively, as

$$\begin{aligned} M_v \mathbf{Y}_v + \mathbf{C}_v \dot{\mathbf{Y}}_v + \mathbf{K}_v \ddot{\mathbf{Y}}_v &= L_v F(t), \\ M_b \mathbf{Y}_b + \mathbf{C}_b \dot{\mathbf{Y}}_b + \mathbf{K}_b \ddot{\mathbf{Y}}_b &= L_b(x)[-F(t) + G], \end{aligned} \tag{10}$$

where M_v, $\mathbf{C}_v$, and $\mathbf{K}_v$ and M_b, $\mathbf{C}_b$, and $\mathbf{K}_b$ denote the mass matrix, damping matrix, and stiffness matrix of the vehicle-bridge system, respectively, $\mathbf{Y}_v$, $\dot{\mathbf{Y}}_v$, and $\ddot{\mathbf{Y}}_v$ and $\mathbf{Y}_b$, $\dot{\mathbf{Y}}_b$, and $\ddot{Y}_b$ denote the displacement vector, velocity vector, and acceleration vector of the considered system, respectively, $F(t)$ and G denote the transient contact force between the wheels and the bridge deck and the vehicle self-weight, respectively, and L_v and $L_b(x)$ denote the positioning vectors of $F(t)$ and $[-F(t) + G]$, respectively.

When solving the equations of motion for the coupled vehicle-bridge system, the displacement compatibility condition between the wheels and the bridge deck should also be considered:

$$y_v(t) - y_b(x, t) - r(x) = -\frac{F(t)}{k_2}, \tag{11}$$

where $y_v(t)$ represents the vertical displacement of the wheel, $y_b(x, t)$ represents the vertical displacement of the contact point between the wheel and the bridge deck, and $r(x)$ represents the unevenness of the bridge deck.

4.1. Stochastic Dynamical System Modeling and Dynamic Response Solving. The system parameters are taken from the literature: bridge span $L = 40$ m, linear density $\rho A = 6067$ (kg/m), flexural stiffness $EI = 2658069$ kN/m^2, without considering bridge damping, body mass $m_1 = 12000$ kg, wheel mass $m_2 = 500$ kg, body suspension stiffness factor $k_1 = 280$ (kN/m), damping factor $c_1 = 2\xi\sqrt{m_1 k_1}$, $\xi = 0.1$, wheel stiffness $k_2 = 156$ (kN/m), and vehicle travel speed is $v = 20$ (m/s).

The differential equations of motion for the bridge, vehicle body, and wheels in the vehicle-bridge coupled system are

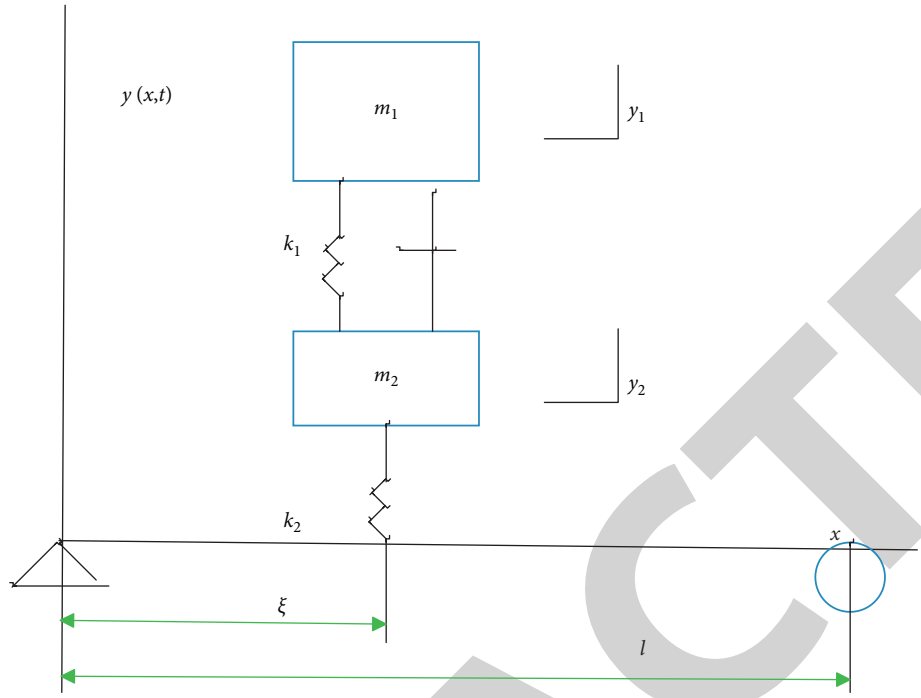

Figure 1: Dynamics model of the train-bridge coupling system.

$$\begin{aligned} &EIy^{(4)}(x,t) + c\dot{y}(x,t) + \rho A\ddot{y}(x,t) = -\{m_1\ddot{y}_1(t) + m_2\ddot{y}_2(t) + (m_1 + m_2 g)\}\delta(x-\xi) \\ &m_1\ddot{y}_1(t) + c_1\dot{y}_1(t) - c_1\dot{y}_2(t) + k_1 y_1(t) - k_1 y_2(t) = 0, \\ &m_2\ddot{y}_2(t) - c_1\dot{y}_1(t) + c_1\dot{y}_2(t) - k_1 y_1(t) + (k_1 + k_2)y_2(t) - k_2 y(\xi,t) = k_2\eta(\xi), \end{aligned} \tag{12}$$

where $y_1(t)$, $y_2(t)$, and $y(x,t)$ represent the vertical displacement response of the vehicle, wheels, and bridge at position x, respectively, ξ represents the distance of the vehicle through the bridge and ξ is a function of time t, and η represents the unevenness of the bridge deck and η is also a function of ξ. Known bridge vibration function is

$$\varphi_i(x) = \sqrt{2}\sin\frac{i\pi x}{l}, \tag{13}$$

and has the orthogonal property

$$\int_0^l \rho A\varphi_i(x)\varphi_j(x)\mathrm{d}x = m_b\delta_{ij}, \tag{14}$$

where ρAl is the total bridge mass and δ_{ij} is the Kronecker symbol.

The ith order inherent frequency of the bridge is

$$\omega_i = \left(\frac{i\pi}{l}\right)^2\sqrt{\frac{EI}{\rho A}}, \quad i = 1,2,\ldots. \tag{15}$$

The relationship between the bridge vibrational function and the intrinsic frequency and flexural stiffness is as follows:

$$EI\frac{\mathrm{d}^4\varphi_i(x)}{\mathrm{d}x^4} = \omega_i^2\rho A\varphi_i(x). \tag{16}$$

The bridge displacement response $y(x, t)$ is solved by the vibration superposition method by taking the first n orders of the modal response of the bridge:

$$y(x,t) = \sum_{i=1}^{n}\varphi_i(x)q_i(t), \tag{17}$$

where $q_i(t)$ is the modal response corresponding to the oscillation function $\varphi_i(x)$.

The mass matrix of the coupled system is

$$\mathbf{M}(t) = \begin{bmatrix} 1 & 0 & 0 & \cdots & 0 & \frac{m_1}{m_b}\varphi_1(\xi) & \frac{m_2}{m_b}\varphi_1(\xi) \\ 0 & 1 & 0 & \cdots & 0 & \frac{m_1}{m_b}\varphi_2(\xi) & \frac{m_2}{m_b}\varphi_2(\xi) \\ \cdots & \cdots & \cdots & \cdots & \cdots & \cdots & \cdots \\ 0 & 0 & 0 & \cdots & 1 & \frac{m_1}{m_b}\varphi_n(\xi) & \frac{m_2}{m_b}\varphi_n(\xi) \\ 0 & 0 & 0 & \cdots & 0 & m_1 & 0 \\ 0 & 0 & 0 & \cdots & 0 & 0 & m_2 \end{bmatrix}. \tag{18}$$

Using the explicit Newmark algorithm to solve the differential equations of motion of the coupled vehicle-bridge system, the vector to be solved $\mathbf{q} = [q_1 \ q_2 \cdots q_n \ y_1 \ y_2]^T$ is calculated, and the time analysis step is taken $\Delta T = 0.01$ s, so the total number of time steps $S = (T/\Delta T)$.

5. Stochastic Vibration Simulation Analysis of Stochastic Dynamical Systems

The differential equations of motion of the coupled vehicle-bridge system are derived above, and the deterministic response of the system is calculated under the action of the moving vehicle load. However, in the actual process of vehicle crossing the bridge, it is inevitable that it will be subjected to random uneven excitation of the bridge deck, which has a great impact on the driving safety and passenger comfort. Therefore, it is important to analyze the stochastic dynamics of the coupled vehicle-bridge system under the joint action of vehicle moving load and bridge deck uneven excitation and to study the trend and statistical law of the stochastic response of the system in the process of vehicle crossing the bridge.

5.1. Generate Bridge Deck Unevenness Time Domain Samples. Assuming that the bridge unevenness field is a uniform random field with zero mean, the power spectral density function is considered as

$$S_r(\omega) = \frac{1}{\pi} \frac{4\gamma\alpha\beta\omega_0^2}{\left(\omega_0^2 - \omega^2\right)^2 + 4\alpha^2\beta^2}, \tag{19}$$

where $\omega_0^2 = \alpha^2 + \beta^2$, $\alpha = 0.1$ (rad/m), $\beta = 0.1$ (rad/m), and $\gamma = 1$ (cm^2 · m/rad) and the frequency is in the range [−10, 10] rad/m.

Since the stochastic dynamics analysis of the vehicle-bridge coupled system belongs to the ultra-high-dimensional problem, in order to facilitate the solution, the original D-dimensional space is firstly decomposed into $D/2$-dimensional subspaces using the stratified sampling method, and then, the bridge deck stochastic uneven time domain samples are generated according to the Fourier inverse transform method, and the simulated values of the power spectrum are compared with the analyzed values to verify the correctness of the samples, as shown in Figures 2 and 3, respectively.

5.2. Random Vibration Analysis of Coupled Vehicle-Bridge System Based on the Direct Probability Integration Method. The random excitation caused by the bridge deck irregularities is obtained by multiplying the time domain samples of the bridge deck irregularities generated in the previous section with the wheel stiffness. Using the direct probability integration method, the probability density function of the response of the coupled vehicle-bridge system under the combined effect of the vehicle moving load and the bridge deck upset excitation can be solved and its mathematical statistical law can be analyzed.

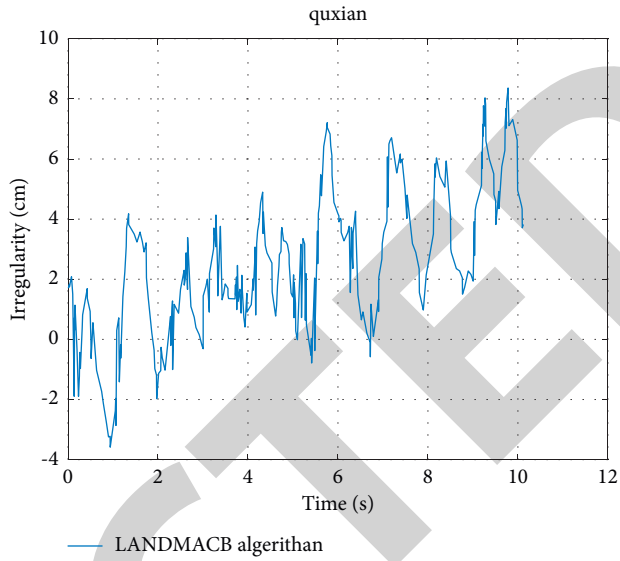

Figure 2: Time domain sample of bridge deck unevenness.

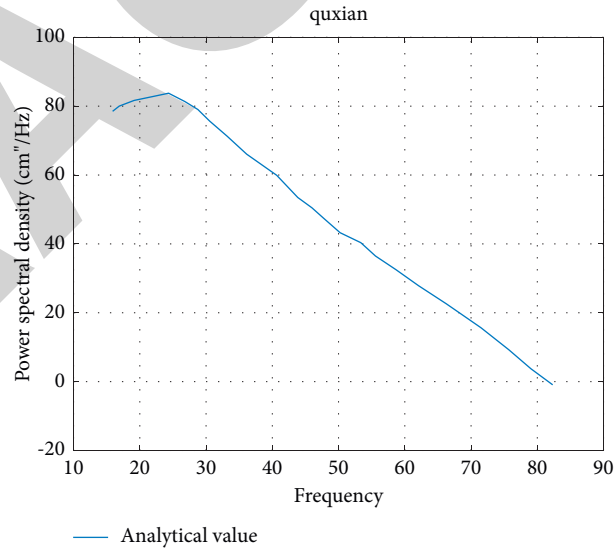

Figure 3: Simulated and resolved power spectrum of bridge deck irregularities.

Taking the number of representative points, $N = 984$, the representative responses of N bridge span displacements and vehicle accelerations are shown in Figures 4 and 5, respectively.

Analysis of Figure 5 shows that the variability of the bridge span displacement is very small until the vehicle reaches the midbridge position, after which the variability increases slightly, but overall the variability is small. Analysis of Figure 6 shows that the variability of the vehicle acceleration response is consistently higher throughout the bridge crossing process, with greater variability near the midspan position and when the vehicle is about to exit the bridge. Comparing the bridge span displacement and vehicle acceleration representative response, it is obvious that the variability of the N-body acceleration response is greater for

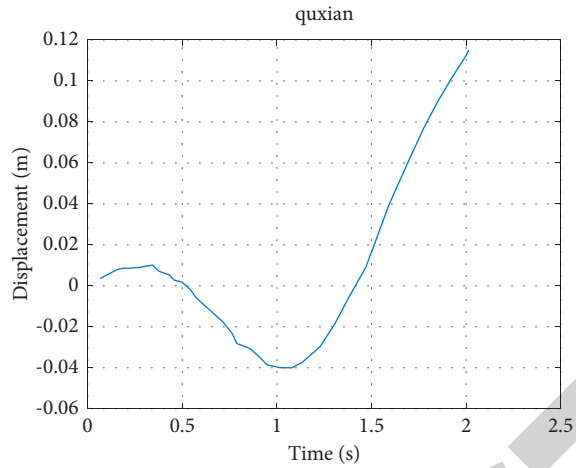

Figure 4: Midspan displacement of the bridge ($N = 984$).

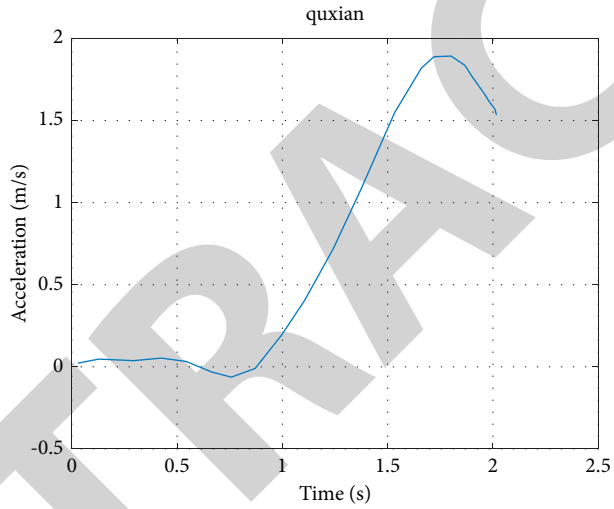

Figure 5: Vehicle acceleration of the simply supported girder bridge ($N = 984$).

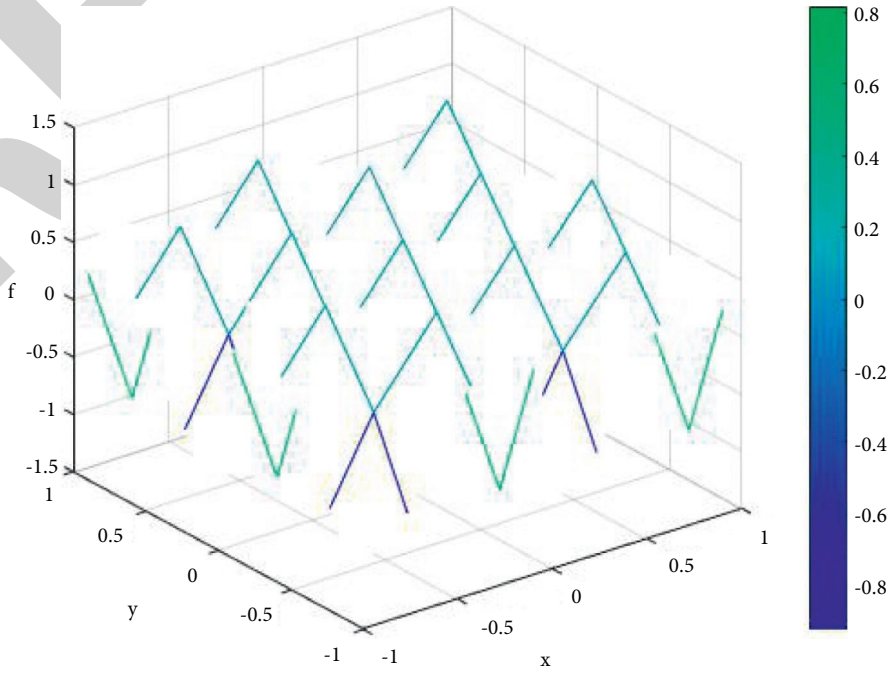

Figure 6: Probability density function surface of bridge midspan displacement.

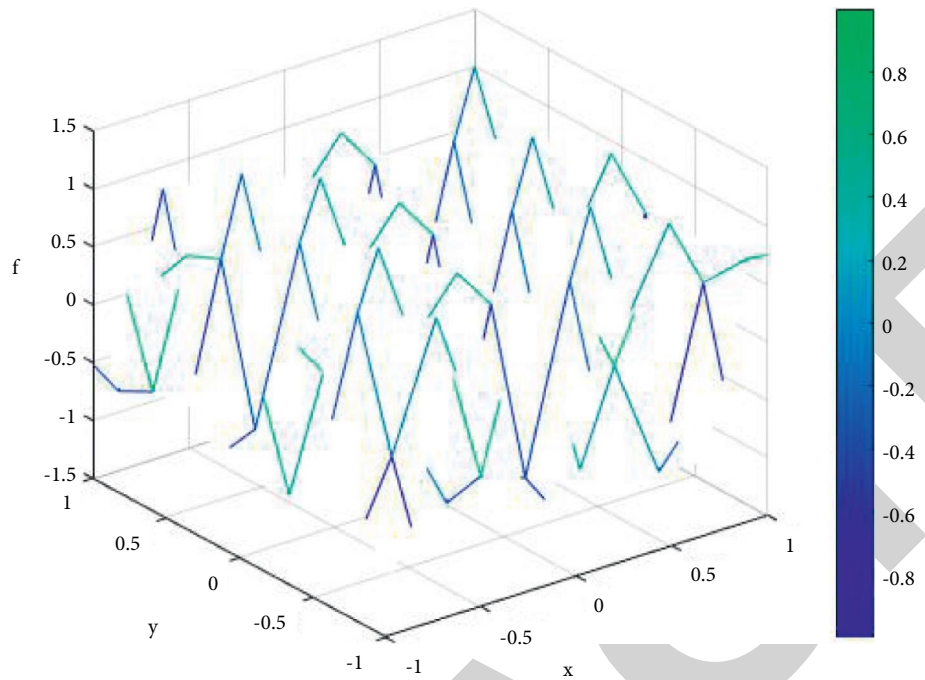

Figure 7: Body acceleration probability density function surface.

the bridge span displacement response, i.e., the vibration of the vehicle is more complex than that of the bridge. This is because the random uneven excitation of the bridge deck acts directly on the vehicle and then acts on the bridge structure through the wheel-bridge contact force. If the number of representative points is reduced by taking $N = 607$ or $N = 374$, the statistical laws of the bridge midspan displacement and vehicle acceleration response are similar to those for $N = 984$ and will not be repeated. Body acceleration probability density function surface is shown in Figure 7.

The 3D probability density function surfaces of the bridge span displacement and vehicle acceleration response can be obtained by substituting the obtained representative responses of the bridge span displacement and vehicle acceleration into equation (19), as shown in Figures 6 and 7, respectively. Based on the probability density function surfaces, the statistical patterns of the bridge span displacement and vehicle acceleration responses can be seen more intuitively. At the initial moment, the variability of the response is very small, and the peak value of PDF image is very high, and then, the peak value of PDF decreases as the variability of response increases gradually.

Intercepting the three-dimensional probability density function surface with the time plane at any moment which can be obtained at that moment of the two-dimensional probability density function curve, we choose $t = 0.7$ s, $t = 1.1$ s, and $t = 1.5$ s three planes to intercept the bridge span displacement three-dimensional PDF image of the results shown in Figure 7; choose $t = 0.8$ s, $t = 1.1$ s, and $t = 1.4$ s three planes to intercept the three-dimensional acceleration of the car body PDF images. It can be seen that the PDF curves of the bridge span displacement and vehicle acceleration response at different moments show different evolutionary patterns. The peak values of the PDF images of the span displacements of the bridge differed greatly at different moments, and the peak values of the PDF images decreased gradually as the train traveled on the bridge; the PDF images of the vehicle acceleration showed a high peak value except for the initial moment, and the peak values of the PDF images differed less at each moment afterwards. Overall, the peak of the probability density function curve of the bridge span displacement is two orders of magnitude higher than that of the vehicle acceleration, and the variability of the bridge span displacement response is relatively small and the probability density function curve is smoother.

6. Conclusions

In this paper, the direct probability integral method is applied to the stochastic vibration reliability analysis of the dynamical system. A dynamical model of the dynamic system and the coupled system "three-car vehicle-rail-bridge" is established, where its time-varying differential equations of motion are derived in detail, and the dynamic response of the system is calculated using the explicit Newmark algorithm. The simulation results show the influence of the number of representative points on the smoothness of the image of the probability density function and the accuracy of the calculation results.

Data Availability

The data used to support the findings of this study are available from the corresponding author upon request.

Conflicts of Interest

The authors declare that they have no conflicts of interest.

Hindawi
Journal of Mathematics
Volume 2024, Article ID 9814834, 1 page
https://doi.org/10.1155/2024/9814834

Retraction

Retracted: A New Neutrosophic Negative Binomial Distribution: Properties and Applications

Journal of Mathematics

Received 23 January 2024; Accepted 23 January 2024; Published 24 January 2024

This article has been retracted by Hindawi following an investigation undertaken by the publisher [1]. This investigation has uncovered evidence of one or more of the following indicators of systematic manipulation of the publication process:

(1) Discrepancies in scope

(2) Discrepancies in the description of the research reported

(3) Discrepancies between the availability of data and the research described

(4) Inappropriate citations

(5) Incoherent, meaningless and/or irrelevant content included in the article

(6) Manipulated or compromised peer review

The presence of these indicators undermines our confidence in the integrity of the article's content and we cannot, therefore, vouch for its reliability. Please note that this notice is intended solely to alert readers that the content of this article is unreliable. We have not investigated whether authors were aware of or involved in the systematic manipulation of the publication process.

Wiley and Hindawi regrets that the usual quality checks did not identify these issues before publication and have since put additional measures in place to safeguard research integrity.

We wish to credit our own Research Integrity and Research Publishing teams and anonymous and named external researchers and research integrity experts for contributing to this investigation.

The corresponding author, as the representative of all authors, has been given the opportunity to register their agreement or disagreement to this retraction. We have kept a record of any response received.

References

[1] R. A. K. Sherwani, S. Iqbal, S. Abbas, M. Aslam, and A. H. AL-Marshadi, "A New Neutrosophic Negative Binomial Distribution: Properties and Applications," *Journal of Mathematics*, vol. 2021, Article ID 2788265, 12 pages, 2021.

Hindawi
Journal of Mathematics
Volume 2021, Article ID 2788265, 12 pages
https://doi.org/10.1155/2021/2788265

Research Article

A New Neutrosophic Negative Binomial Distribution: Properties and Applications

Rehan Ahmad Khan Sherwani,[1] Sadia Iqbal,[1] Shumaila Abbas,[1] Muhammad Aslam ,[2] and Ali Hussein AL-Marshadi[2]

[1]*College of Statistical and Actuarial Sciences, University of the Punjab Lahore, Lahore, Pakistan*
[2]*Department of Statistics, Faculty of Science, King Abdulaziz University, Jeddah 21551, Saudi Arabia*

Correspondence should be addressed to Muhammad Aslam; aslam_ravian@hotmail.com

Received 22 September 2021; Revised 3 November 2021; Accepted 8 November 2021; Published 26 November 2021

Academic Editor: Ewa Rak

Many problems in real life exist that are full of confusion, vagueness, and ambiguity. The quantification of such issues in a scientific way is the need of time. The negative binomial distribution is an important discrete probability distribution from the account of classical probability distribution theory. The distribution was used to study the chance of kth success in n trials before $n-1$ failures for crisp data. The literature lacks in dealing with the situations for interval-valued data under negative binomial distribution. In this research, the neutrosophic negative binomial distribution is proposed to generalize the classical negative binomial distribution. The generalized proposed distribution considers the indeterminacy and crisp form from interval-valued. Several properties of the proposed distribution, such as moment generating function, characteristic function, and probability generating function, are also derived. Furthermore, the derivation of reliability analysis properties such as survival, hazard rate, reversed hazard rate, cumulative hazard rate, mills ratio, and odds ratio are also presented. In addition, order statistics for the proposed distribution, including w^{th}, joint, median, minimum, and maximum order statistics are part of the paper. The proposed distribution is discussed from the real data applications perspective by considering the different case studies. This research opens the way to deal with the problems that follow conventional conveyances and include nonprecisely determined details simultaneously.

1. Introduction

The term neutrosophy was introduced by Smarandache [1], a modern philosophical branch inspired by famous fuzzy logic. It is a generalization of intuitionistic fuzzy logic [2]. The term is based on the logic of vague, unclear, blurred, fuzzy realms (problems, circumstances, and ideas) that are common in today's era. The fuzzy logic is a limiting case of precise reasoning used to quantify the imprecise modes of reasoning [3]. The theory helps articulate decisions for decision-making problems under an imprecise and uncertain environment [4, 5]. Zadeh recently presented the fuzzy logic theory and applications in a precise way [6].

Further extensions in fuzzy logic and its applications can be seen in [4,7–11]. The standard fuzzy sets deal with the exact values, and there are many situations in real-life data where it is hard to find single values data. In such situations, interval-valued fuzzy sets were introduced by [12]. Smarandache claimed both neutrosophic sets and neutrosophic statistics to generalize fuzzy logic [13, 14]. Neutrosophic statistics deals with the interval-valued data as the classical statistical methods are helpless in dealing with the situations that generate indefinite data in interval form. Some methodological and applied forms of neutrosophic statistics have been discussed in [15–18].

Probability is among the classical statistical methods that deal with the quantification of random phenomena. The techniques available in the literature paid less attention to uncertainty-related problems under the fuzzy environment. The classical probability ignored serious, aberrant, ambiguous values, so a new suitable instrument was used. Smarandache [19] introduced the basic definition of

neutrosophic sets in his well-defined book in 2014 purely in the statistical scenario, which provides a new basis containing indeterminate data to deal with many problems. The primary objective of neutrosophic logic is to define any logical argument of a statement under consideration in a 3-D neutrosophic space where each dimension represents truth (T), false (U), and indeterminacy (I), respectively. The symbols T, I, and U are the standard, a nonstandard real subset of $(-0, 1+)$ without any specific connection. Many researchers have extended the classical distributions under neutrosophic logic that includes neutrosophic binomial distribution and neutrosophic normal distribution [20, 21], neutrosophic multinomial distribution [19], neutrosophic Poisson, neutrosophic exponential, and neutrosophic uniform distribution [22], neutrosophic gamma distribution [23], neutrosophic Weibull distribution and its several families [24], and neutrosophic beta distribution [25]. In this paper, we extended the concept of two parameters negative binomial distribution to neutrosophic negative binomial distribution using neutrosophic logic.

2. Neutrosophic Negative Binomial Distribution (NNBD)

The classical negative binomial distribution is generalized neutrosophically, which ensures some indeterminacy related to the probabilistic experiment. Suppose each trial of an experiment results in an outcome, labeled as success (S) and failure (U) and also with some indeterminacy (I). For example, tossing a coin on an unbalanced surface may have cracks, a coin may fall on its edge inside the crack, and one may get neither head nor tail but some indeterminacy.

The neutrosophic negative binomial random variable is defined as a variable number of trials to obtain the fixed number of successes. It is known as a neutrosophic negative binomial distribution. First, obtaining indeterminacy for every trial means there will be indeterminacy for all trials. Secondly, obtaining indeterminacy for no trial means no indeterminacy for all trials. There may exist a situation when we get indeterminacy for a few trials and determinacy for other trials. In that case, we introduce an indeterminacy threshold. Let th^* be the number of trials that result in indeterminacy and $\mathrm{th}^* = \{0, 1, 2, \ldots, \infty\}$. Cases where threshold $> \mathrm{th}^*$ will belong to indeterminate part, and when threshold $< \mathrm{th}^*$, those cases will belong to a determinate part.

For $x = \{ś, ś + 1, ś + 2, \ldots\}$, Np_r (occurrences of a fixed number of successes for a variable number of trials) $= (T_x, U_x, I_x)$, probability mass function and cumulative distribution function of neutrosophic negative binomial distribution are, respectively, given as

$$T_x = (p_r(S))^{ś} \sum_{t=0}^{\mathrm{th}^*} \binom{x - ś}{t} (p_r(I))^t (p_r(U))^{x-ś-\mathrm{t}}. \tag{1}$$

Similarly,

$$U_x = \sum_{\substack{y=ś \\ y \neq x}}^{\infty} T_y = (p_r(S))^{ś} \sum_{\substack{y=ś \\ y \neq x}}^{\infty} \sum_{t=0}^{\mathrm{th}^*} \binom{y - ś}{t} (p_r(I))^t (p_r(U))^{y-ś-\mathrm{t}}, \tag{2}$$

$$I_x = (p_r(S))^{ś} \sum_{z^*=\mathrm{th}^*+1}^{x-ś} \binom{x - ś}{z^*} (p_r(I))^{z^*} \sum_{x=ś}^{\infty} \sum_{t=0}^{x-ś-z^*} \binom{x - ś - \mathrm{z}^*}{t} (p_r(U))^{x-ś-\mathrm{z}^*-\mathrm{t}}. \tag{3}$$

The CDF corresponding to (1) is given by

$$F(x) = 1 - (p_r(S))^{ś} (p_r(U))^{x-ś+1} \sum_{m'=1}^{\infty} \binom{x - ś + \mathrm{m}'}{m' - 1} (p_r(I))^{m'-1}. \tag{4}$$

The CDF corresponding to (3) is given by

$$F(x) = 1 - (p_r(S))^{ś} \sum_{m'=1}^{\infty} \binom{x - ś + \mathrm{m}'}{m'} (p_r(I))^{m'} \sum_{m'=0}^{\infty} \binom{x - ś}{m'} (p_r(U))^{x-ś-\mathrm{m}'}. \tag{5}$$

2.1. A Special Case of Neutrosophic Negative Binomial Distribution (NNBD). The neutrosophic geometric distribution is a special case of NNBD when the number of successes $ś = 1$.

2.2. Physical Conditions

(i) Each trial results in three mutually exclusive and exhaustive outcomes such as success, failure, and indeterminacy

(ii) All the trials must be independent

(iii) The probability of success remains fixed or constant for each trial

(iv) An experiment is repeated a variable number of times to produce a fixed number of successes

2.3. Case Studies

2.3.1. Case Study 1. Assume that you are surveying individuals existing at the polling booth and asking them if they voted independently. It was observed that 20% of people voted independently, 60% did not vote independently, and 10% were unsure whether they voted independently or not. What is the probability of eight people, you must ask before you find three people who voted independently?

Using the information in the problem mentioned above, we compute the probability for all three parts of pmf.

$X \longrightarrow$ number of people who voted

ś $\longrightarrow$ number of people who voted independently will be considered a success

So, $X = 3, 4, \ldots, 8$ and ś $= 3$

Let the threshold $\text{th}^* = 2$

p_r (people voted independently) $= p_r(S) = 0.2$

(i) p_r (people not voted independently) $= p_r(U) = 0.6$

(ii) p_r (people not sure about their voting) $= p_r(I) = 0.1$

$$
\begin{aligned}
T_x = T_3 &= (0.2)^3 \sum_{t=0}^{2} \binom{8-3}{t} (0.1)^t (0.6)^{8-3-t} \\
&= (0.2)^3 \left\{ \binom{5}{0} (0.1)^0 (0.6)^5 + \binom{5}{1} (0.1)^1 (0.6)^4 + \binom{5}{2} (0.1)^2 (0.6)^3 \right\} \\
&= (0.2)^3 \{0.7776 + 0.0648 + 0.0216\} \\
&= 0.0013132, \\
I_3 &= (0.2)^3 \sum_{z^*=3}^{8-3=5} \frac{(8-3)!}{z^*!} (0.1)^{z^*} \sum_{t=0}^{5-z^*} \frac{(0.6)^{5-z^*-t}}{t!(5-z^*-t)!} \\
&= (0.2)^3 \left[\left\{ \frac{5!}{3!} (0.1)^3 \sum_{t=0}^{2} \frac{(0.6)^{2-t}}{t!(2-t)!} \right\} + \left\{ \frac{5!}{4!} (0.1)^4 \sum_{t=0}^{1} \frac{(0.6)^{1-t}}{t!(1-t)!} \right\} + \left\{ \frac{5!}{5!} (0.1)^5 \sum_{t=0}^{0} \frac{(0.6)^{0-t}}{t!(0-t)!} \right\} \right] \\
&= (0.2)^3 \left\{ 1.28 + 8 \times 10^{-4} + 0.1^5 \right\} \\
&= 0.010246.
\end{aligned}
\tag{6}
$$

U_3 can be easily calculated in the following way rather than using combinational formula.

As we know that

$$T_x + I_x + U_x = \left(p_r(S) + p_r(I) + p_r(U)\right)^n, \tag{7}$$

here instead of n, we will use x, as x is the number of trials.

$$T_x + I_x + U_x = \left(p_r(S) + p_r(I) + p_r(U)\right)^x. \tag{8}$$

So, we may compute U_3 as given below:

$$
\begin{aligned}
U_3 &= \left(p_r(S) + p_r(I) + p_r(U)\right)^x - T_3 - I_3 \\
&= (0.2 + 0.1 + 0.6)^8 - 0.0013132 - 0.010246 \\
&= 0.41891.
\end{aligned}
\tag{9}
$$

If the computed vector is normalized,

$$(T_3, I_3, U_3) = (0.0013132, 0.41891, 0.010246), \tag{10}$$

by dividing each component of a vector with their total sum

$$0.0013132 + 0.41891 + 0.010246 = 0.4304692. \tag{11}$$

Hence, we get

$$(T_3, I_3, U_3) = (0.0030506, 0.023802, 0.973147). \tag{12}$$

2.3.2. Case Study 2. A specified location has 35% rain on any specific day, 70% chances that day will be sunny, and 15% indeterminacy that neither the day will be sunny nor rainy.

What is the probability that there will be rain on three specific days in a week?

Using the information in the problem mentioned above, we compute the probability for all three parts of pmf.

$X \longrightarrow$ number of days in a week

ś $\longrightarrow$ number of rainy days

So, $X = 3, 4, 5, 6, 7$ and ś $= 3$. Let the threshold be 3, i.e., $\text{th}^* = 3$

p_r (the day will be rainy) $= p_r(S) = 0.35$

(i) p_r (the day will be sunny) $= p_r(U) = 0.7$

(ii) p_r (the day will be neither rainy nor sunny) $= p_r(I) = 0.15$

$$
\begin{aligned}
T_x = T_3 &= (0.35)^3 \sum_{t=0}^{3} \binom{7-3}{l} (0.15)^t (0.7)^{7-3-t} \\
&= (0.35)^3 \left\{ \binom{4}{0} (0.15)^0 (0.7)^4 + \binom{4}{1} (0.15)^1 (0.7)^3 + \binom{4}{2} (0.15)^2 (0.7)^2 + \binom{4}{3} (0.15)^3 (0.7)^1 \right\} \\
&= (0.35)^3 \{0.2401 + 0.2058 + 0.06615 + 0.00945\} \\
&= 0.022359, \\
I_3 &= (0.35)^3 \sum_{z^*=4}^{7-4=3} \frac{(7-4)!}{z^*!} (0.15)^z \sum_{t=0}^{4-z^*} \frac{(0.7)^{4-z^*-t}}{t!(4-z^*-t)!} \\
&= (0.35)^3 \cdot \sum_{z^*=4}^{4} \frac{3!}{4!} (0.15)^4 \sum_{t=0}^{0} \frac{(0.7)^{4-4-t}}{t!(4-4-t)!} \\
&= (0.35)^3 \left\{ \frac{3!}{4!} (0.15)^4 (1) \right\} \\
&= 5.42636 \times 10^{-6}, \\
U_3 &= \left(p_r(S) + p_r(I) + p_r(U)\right)^x - T_3 - I_3 \\
&= (0.35 + 0.15 + 0.7)^7 - 0.022359 - 5.42636 \times 10^{-6} \\
&= 3.560816.
\end{aligned}
\tag{13}
$$

If the computed vector is normalized,

$$
\left(T_3, I_3, U_3\right) = \left(0.022359, 5.42636 \times 10^{-6}, 3.560816\right), \tag{14}
$$

by dividing each component of a vector with their total sum

$$
0.022359 + 5.42636 + 3.560816 = 3.583180. \tag{15}
$$

Hence, we get

$$
\left(T_3, I_3, U_3\right) = \left(0.0062399, 1.51440 \times 10^{-6}, 0.99376\right). \tag{16}
$$

2.3.3. Case Study 3. Jackson is a football player. His success rate of hitting the goal is 70%, the failure rate is 40%, and 15% chance that the situation may provide no clear evidence about the goal whether hitting or not. What is the probability that Jackson hits 2nd goal on his fifth attempt? Using the information in the problem mentioned above, we compute the probability for all three parts of pmf.

$$
\begin{aligned}
&\text{ś} = 2, \\
&X = 2, 3, 4, 5.
\end{aligned}
\tag{17}
$$

Let the threshold be 1; $\text{th}^* = 1$.

p_r (goal hit) $= p_r(S) = 0.7$

p_r (goal not hit) = $p_r(U) = 0.4$

p_r (no evidence about hitting or not hitting of goal) = $p_r(I) = 0.15$

$$
\begin{aligned}
T_x = T_2 &= (0.7)^2 \sum_{t=0}^{1} \binom{5-2}{t} (0.15)^t \cdot (0.4)^{5-2-t} \\
&= (0.7)^2 \left\{ \binom{3}{0} (0.15)^0 (0.4)^3 + \binom{3}{1} (0.15)^1 (0.4)^2 \right\} \\
&= (0.7)^2 \{0.064 + 0.072\} \\
&= 0.06664, \\
I_2 &= (0.7)^2 \sum_{z^*=2}^{5-2=3} \frac{3!}{z^*!} (0.15)^{z^*} \sum_{t=0}^{3-z^*} \frac{(0.4)^{3-z^*-t}}{t!(3-z^*-t)!} \\
&= (0.7)^2 \left[\left\{ \frac{3!}{2!} (0.15)^2 \cdot \sum_{t=0}^{1} \frac{(0.4)^{1-t}}{t!(1-t)!} \right\} + \left\{ \frac{3!}{3!} (0.15)^3 \cdot \sum_{t=0}^{0} \frac{(0.4)^{0-t}}{t!(0-t)!} \right\} \right] \\
&= (0.7)^2 \left\{ 0.0945 + (0.15)^3 \right\} \\
I_2 &= 0.047959, \\
U_2 &= \left(p_r(S) + p_r(I) + p_r(U)\right)^x - T_2 - I_2 \\
&= (0.7 + 0.15 + 0.4)^5 - 0.06664 - 0.047959 \\
&= 2.937159.
\end{aligned}
\tag{18}
$$

If the computed vector is normalized,

$$(T_2, I_2, U_2) = (0.06664, 0.047959, 2.937159), \tag{19}$$

by dividing each component of a vector with their total sum

$$0.06664 + 0.047959 + 2.937159 = 3.051758. \tag{20}$$

Hence, we get

$$(T_2, I_2, U_2) = (0.021836, 0.962448, 0.015715). \tag{21}$$

3. Main Properties of NNBD

3.1. Moment Generating Function. Moment generating function (m.g.f) of $X \sim \mathrm{NNBD}(x; ś, \mathrm{p_r(S)})$ for true part of pmf is given by

$$M_0(t) = \left(\frac{p_r(S)}{p_r(U)}\right)^{ś} \left(1 - \frac{p_r(U)}{p_r(U)}\right)^{-1} \sum_{m'=0}^{\infty} \left(p_r(U)e^t\right)^{ś+m'}, \tag{22}$$

for indeterminate part of pmf is given as

$$M_0(t) = A^* \left(p_r(S)\right)^{ś} \left(\sum_{n=1}^{\infty} -\frac{(p_r(I))^n}{n}\right) \left(\sum_{m'=0}^{\infty} \left(p_r(U) \cdot e^t\right)^{ś+m'}\right), \tag{23}$$

where

$$A^* = -\frac{(p_r(U))^{-(ś+1)}}{1!} + \frac{(p_r(U))^{-(ś+3)}}{2!} - \frac{(p_r(U))^{-(ś+5)}}{2!3!} + \cdots. \tag{24}$$

3.2. Characteristic Function. The characteristic function of $X \sim \mathrm{NNBD}(x; ś, \mathrm{p_r(S)})$ for true part of pmf is given by

$$\phi_i(t) = \left(\frac{p_r(S)}{p_r(U)}\right)^{ś} \left(1 - \frac{p_r(I)}{p_r(U)}\right)^{-1} \sum_{m'=0}^{\infty} \left(p_r(U)e^{it}\right)^{ś+m'}, \tag{25}$$

for indeterminate part of pmf is given as

$$\phi_i(t) = A^* \left(p_r(S)\right)^{ś} \cdot \left\{ \sum_{n=1}^{\infty} -\frac{(P(I))^n}{n} \right\} \left\{ \sum_{m'=0}^{\infty} \left(p_r(U)e^{it}\right)^{ś+m'} \right\}. \tag{26}$$

3.3. Probability Generating Function. Probability generating function of $X \sim \mathrm{NNBD}(x; ś, \mathrm{p_r(S)})$ for true part of pmf is given by

$$G(\theta) = \left(\frac{p_r(S)}{p_r(U)}\right)^{ś}\left(1 - \frac{p_r(I)}{p_r(U)}\right)^{-1} \sum_{m'=0}^{\infty} \left(p_r(U)\cdot\theta\right)^{ś+m'}, \tag{27}$$

for indeterminate part of pmf is given as

$$G(\theta) = A^*\left(p_r(S)\right)^{ś}\left\{\sum_{n=1}^{\infty} -\frac{\left(p_r(I)\right)^n}{n}\right\}\left\{\sum_{m'=0}^{\infty}\left(p_r(U)\cdot\theta\right)^{ś+m'}\right\}. \tag{28}$$

4. Reliability Analysis

This section finds various reliability properties like survival function, hazard rate function, reversed hazard rate function, and cumulative hazard rate function. In addition, the mills ratio and odds ratio for the new proposed distribution are derived.

4.1. Survival Function. Survival function of r.v $X \sim \mathrm{NNBD}(x; ś, \mathrm{p_r(S)})$ for true part of pmf is given as

$$S(x) = \left(p_r(S)\right)^{ś}\left(p_r(U)\right)^{x-ś+1} \sum_{m'=1}^{\infty}\binom{x-ś+m'}{m'-1}\left(p_r(I)\right)^{m'-1}. \tag{29}$$

The indeterminate part of pmf is given as

$$S(x) = \left(p_r(S)\right)^{ś} \sum_{m'=1}^{\infty}\binom{x-ś+m'}{m'}\left(p_r(I)\right)^{m'} \sum_{m'=0}^{\infty}\binom{x-ś}{m'}\left(p_r(U)\right)^{x-ś-m'}. \tag{30}$$

4.2. Hazard Rate or Failure Rate Function. Hazard rate function of r.v $X \sim \mathrm{NNBD}(x; ś, \mathrm{p_r(S)})$ for true part of pmf is given as

$$h(x) = \frac{\sum_{t=0}^{th^*}\binom{x-ś}{t}\left(p_r(I)\right)^t\left(p_r(U)\right)^{x-ś-t}}{\left(p_r(U)\right)^{x-ś+1}\sum_{m'=1}^{\infty}\binom{x-ś+m'}{m'-1}\left(p_r(I)\right)^{m'-1}}. \tag{31}$$

The indeterminate part of pmf is given as

$$h(x) = \frac{\sum_{z^*=\mathrm{th}^*+1}^{x-ś}\binom{x-ś}{z^*}\left(p_r(I)\right)^{z^*}\sum_{x=ś}^{\infty}\sum_{t=0}^{x-ś-z^*}\binom{x-ś-z^*}{t}\left(p_r(U)\right)^{x-ś-z^*-t}}{\sum_{m'=1}^{\infty}\binom{x-ś+m'}{m'}\left(p_r(I)\right)^{m'}\sum_{m'=0}^{\infty}\binom{x-ś}{m'}\left(p_r(U)\right)^{x-ś-m'}}. \tag{32}$$

4.3. Reversed Hazard Rate Function. Reversed hazard rate function (RHRF) of r.v $X \sim \mathrm{NNBD}(x; ś, \mathrm{p_r(S)})$ for true part of pmf is given as

$$\partial(x) = \frac{\left(p_r(S)\right)^{ś}\sum_{t=0}^{\mathrm{th}^*}\binom{x-ś}{t}\left(p_r(I)\right)^t\left(p_r(U)\right)^{x-ś-t}}{1-\left(p_r(S)\right)^{ś}\left(p_r(U)\right)^{x-ś+1}\sum_{m'=1}^{\infty}\binom{x-ś+m'}{m'-1}\left(p_r(I)\right)^{m'-1}}. \tag{33}$$

For the indeterminate part of pmf, RHRF is given as

$$\partial(x) = \frac{(p_r(S))^{ś} \sum_{z^*=\mathrm{th}^*+1}^{x-ś} \binom{x-ś}{z^*} (p_r(I))^{z^*} \sum_{x=ś}^{\infty} \sum_{t=0}^{x-ś-z^*} \binom{x-ś-\mathrm{z}^*}{t} (p_r(U))^{x-ś-z^*-\mathrm{t}}}{1-(p_r(S))^{ś} \sum_{m'=1}^{\infty} \binom{x-ś+\mathrm{m}'}{m'} (p_r(I))^{m'} \sum_{m'=0}^{\infty} \binom{x-ś}{m'} (p_r(U))^{x-ś-\mathrm{m}'}}. \tag{34}$$

4.4. Cumulative Hazard Rate Function. Cumulative hazard rate function (CHRF) of r.v $X \sim \mathrm{NNBD}(x; ś, \mathrm{p_r(S)})$ for true part of pmf is given as

$$H(x) = -\ln\left\{ (p_r(S))^{ś} (p_r(U))^{x-ś+1} \sum_{m'=1}^{\infty} \binom{x-ś+\mathrm{m}'}{m'-1} (p_r(I))^{m'-1} \right\}. \tag{35}$$

For the indeterminate part of pmf, CHRF is given as

$$H(x) = -\ln\left\{ (p_r(S))^{ś} \sum_{m'=1}^{\infty} \binom{x-ś+\mathrm{m}'}{m'} (p_r(I))^{m'} \sum_{m'=0}^{\infty} \binom{x-ś}{m'} (p_r(U))^{x-ś-\mathrm{m}'} \right\}. \tag{36}$$

4.5. Mills Ratio. Mills ratio of r.v $X \sim \mathrm{NNBD}(x; ś, \mathrm{p_r(S)})$ for true part of pmf is given as

$$m(x) = \frac{(p_r(U))^{x-ś+1} \sum_{m'=1}^{\infty} \binom{x-ś+\mathrm{m}'}{m'-1} (p_r(I))^{m'-1}}{\sum_{t=0}^{\mathrm{th}^*} \binom{x-ś}{t} (p_r(I))^{t} (p_r(U))^{x-ś-\mathrm{t}}}. \tag{37}$$

For indeterminate part of pmf, mills ratio is given as

$$m(x) = \frac{\sum_{m'=1}^{\infty} \binom{x-ś+\mathrm{m}'}{m'} (p_r(I))^{m'} \sum_{m'=0}^{\infty} \binom{x-ś}{m'} (p_r(U))^{x-ś-\mathrm{m}'}}{\sum_{z^*=\mathrm{th}^*+1}^{x-ś} \binom{x-ś}{z^*} (p_r(I))^{z^*} \sum_{x=ś}^{\infty} \sum_{t=0}^{x-ś-\mathrm{z}^*} \binom{x-ś-\mathrm{z}^*}{t} (p_r(U))^{x-ś-z^*-\mathrm{t}}}. \tag{38}$$

4.6. Odds Ratio. The odds ratio of r.v $X \sim \mathrm{NNBD}(x; ś, \mathrm{p_r(S)})$ for true part of pmf is given as

$$\varphi(x)=\frac{1-(p_r(S))^{ś}(p_r(U))^{x-ś+1}\sum_{m'=1}^{\infty}\binom{x-ś+m'}{m'-1}(p_r(I))^{m'-1}}{(p_r(S))^{ś}(p_r(U))^{x-ś+1}\sum_{m'=1}^{\infty}\binom{x-ś+m'}{m'-1}(p_r(I))^{m'-1}}. \tag{39}$$

For the indeterminate part of pmf, the odds ratio is given as

$$\varphi(x)=\frac{1-(p_r(S))^{ś}\sum_{m'=1}^{\infty}\binom{x-ś+m'}{m'}(p_r(I))^{m'}\sum_{m'=0}^{\infty}\binom{x-ś}{m'}(p_r(U))^{x-ś-m'}}{(p_r(S))^{ś}\sum_{m'=1}^{\infty}\binom{x-ś+m'}{m'}(p_r(I))^{m'}\sum_{m'=0}^{\infty}\binom{x-ś}{m'}(p_r(U))^{x-ś-m'}}. \tag{40}$$

5. Order Statistics

In this section, we derived the order statistics for the new proposed distribution NNBD, such as the w^{th} order statistics, joint, largest, and smallest order statistics, maximum and minimum, and median order statistics, as well as smallest and largest order statistics.

5.1. w^{th} Order Statistics. Let $X_1, X_2, \ldots, X_w$ be the random sample from NNBD and let $X_{(1)}, X_{(2)}, \ldots, X_{(w)}$ be the corresponding order statistics. w^{th} order statistics for the true part of NNBD can be given as

$$f_{w:n}(x)=\frac{n!}{(w-1)!(n-w)!}(p_r(S))^{ś+n-w}\sum_{t=0}^{\text{th}^*}\binom{x-ś}{t}(p_r(I))^{t}(p_r(U))^{x-ś-t}\left[1-(p_r(S))^{ś}(p_r(U))^{x-ś+1}\sum_{m'=1}^{\infty}\binom{x-ś+m'}{m'-1}(P(I))^{m'-1}\right]^{w-1}$$
$$\left[(p_r(U))^{x-ś+1}\sum_{m'=1}^{\infty}\binom{x-ś+m'}{m'-1}(p_r(I))^{m'-1}\right]^{n-w}. \tag{41}$$

w^{th} order statistics for the indeterminate part of NNBD can be given as

$$f_{w:n}(x)=\frac{n!}{(w-1)!(n-w)!}(p_r(S))^{n+ś-w}$$
$$\sum_{z^*=th^*+1}^{x-ś}\binom{x-ś}{z^*}(p_r(I))^{z^*}\sum_{x=k}^{\infty}\sum_{t=0}^{x-ś-z^*}\binom{x-ś-z^*}{t}(p_r(U))^{x-ś-z^*-t}$$
$$\left[1-(p_r(S))^{ś}\sum_{m'=1}^{\infty}\binom{x-ś+m'}{m'}(p_r(I))^{m'}\sum_{m'=0}^{\infty}\binom{x-ś}{m'}(p_r(U))^{x-ś-m'}\right]^{w-1} \tag{42}$$
$$\left[\sum_{m'=1}^{\infty}\binom{x-ś+m'}{m'}(p_r(I))^{m'}\sum_{m'=0}^{\infty}\binom{x-ś}{m'}(p_r(U))^{x-ś-m'}\right]^{n-w}.$$

5.2. Joint Order Statistics. Joint order statistics of $y_{1:\,b}$ and $y_{u:\,b}$ for true part of NNBD is derived as follows:

$$f_{a:\,u:\,b}(x) = \frac{b!}{(a-1)!\,(u-a-1)!\,(b-u)!}\left(p_r(S)\right)^{\acute{s}(b-a+1)}\left(\sum_{t=0}^{th^*}\binom{y-\acute{s}}{t}\left(p_r(I)\right)^t\left(p_r(U)\right)^{y-\acute{s}-t}\right)$$
$$\left(\sum_{t=0}^{th^*}\binom{z-\acute{s}}{t}\left(p_r(I)\right)^t\left(p_r(U)\right)^{z-\acute{s}-t}\right)\left[1-\left(p_r(S)\right)^{\acute{s}}\left(p_r(U)\right)^{y-\acute{s}+1}\sum_{m'=1}^{\infty}\binom{y-\acute{s}+m'}{m'-1}\left(p_r(I)\right)^{m'-1}\right]^{a-1}$$
$$\left[\left(p_r(U)\right)^{y-\acute{s}+1}\sum_{m'=1}^{\infty}\binom{y-\acute{s}+m'}{m'-1}\left(p_r(I)\right)^{m'-1}-\left(p_r(U)\right)^{z-\acute{s}+1}\sum_{m'=1}^{\infty}\binom{z-\acute{s}+m'}{m'-1}\left(p_r(I)\right)^{m'-1}\right]^{u-a-1} \tag{43}$$
$$\left[\left(p_r(U)\right)^{y-\acute{s}+1}\sum_{m'=1}^{\infty}\binom{y-\acute{s}+m'}{m'-1}\left(p_r(I)\right)^{m'-1}\right]^{b-u}.$$

Joint order statistics for the indeterminate part of NNBD is given as

$$f_{a:\,u:\,b}(x) = \frac{b!}{(a-1)!\,(u-a-1)!\,(b-u)!}\left(p_r(S)\right)^{\acute{s}(b-a+1)}$$
$$\left\{\sum_{z^*=th+1}^{y-\acute{s}}\binom{y-\acute{s}}{z^*}\left(p_r(I)\right)^{z^*}\sum_{x=\acute{s}}^{\infty}\sum_{t=0}^{y-\acute{s}-z^*}\binom{y-\acute{s}-z^*}{t}\left(p_r(U)\right)^{y-\acute{s}-z^*-t}\right\}$$
$$\left\{\sum_{z^*=th^*+1}^{z-\acute{s}}\binom{z-\acute{s}}{z^*}\left(p_r(I)\right)^{z^*}\sum_{z=\acute{s}}^{\infty}\sum_{t=0}^{z-\acute{s}-z^*}\binom{z-\acute{s}-z^*}{t}\left(p_r(U)\right)^{z-\acute{s}-z^*-t}\right\}$$
$$\left[\sum_{m'=1}^{\infty}\binom{y-\acute{s}+m'}{m'}\left(p_r(I)\right)^{m'}\sum_{m'=0}^{\infty}\binom{y-\acute{s}}{m'}\left(p_r(U)\right)^{y-\acute{s}-m'}-\sum_{m'=1}^{\infty}\binom{z-\acute{s}+m'}{m'}\left(p_r(I)\right)^{m'}\sum_{m'=0}^{\infty}\binom{z-\acute{s}}{m'}\left(p_r(U)\right)^{x-\acute{s}-m'}\right]^{u-a-1}$$
$$\left[\sum_{m'=1}^{\infty}\binom{y-\acute{s}+m'}{m'}\left(p_r(I)\right)^{m'}\sum_{m'=0}^{\infty}\binom{y-\acute{s}}{m'}\left(p_r(U)\right)^{y-\acute{s}-m'}\right]^{b-u}. \tag{44}$$

5.3. Largest Order Statistics. For $= \acute{\eta}$ the largest order statistics for the true part of NNBD is given as

$$f_{\acute{\eta}:\,\acute{\eta}}(x) = \acute{\eta}\left(p_r(S)\right)^{\acute{s}}\sum_{t=0}^{th^*}\binom{x-\acute{s}}{t}\left(p_r(I)\right)^t\left(p_r(U)\right)^{x-\acute{s}-t}\left[1-\left(p_r(S)\right)^{\acute{s}}\left(p_r(U)\right)^{x-\acute{s}+1}\sum_{m'=1}^{\infty}\binom{x-\acute{s}+m'}{m'-1}\left(p_r(I)\right)^{m'-1}\right]^{\acute{\eta}}-1. \tag{45}$$

Largest order statistics for an indeterminate part of NNBD is given as

$$f_{\eta}: \eta(x) = \eta(p_r(S))^{ś} \sum_{z^*=\text{th}^*+1}^{x-ś} \binom{x-ś}{z^*} (p_r(I))^{z^*} \sum_{x=ś}^{\infty} \sum_{t=0}^{x-ś-z^*} \binom{x-ś-z^*}{t} (p_r(U))^{x-ś-z^*-t}$$

$$\left[1-(p_r(S))^{ś} \sum_{m'=1}^{\infty} \binom{x-ś+m'}{m'} (p_r(I))^{m'} \sum_{m'=0}^{\infty} \binom{x-ś}{m'} (p_r(U))^{x-ś-m'}\right]^{\eta} - 1. \tag{46}$$

5.4. Smallest Order Statistics. For $u = 1$, smallest order statistics for the true part of NNBD is given as

$$f_{1:n}(x) = n(p_r(S))^{nś} \sum_{t=0}^{\text{th}^*} \binom{x-ś}{t} (p_r(I))^{t} (p_r(U))^{x-ś-t}$$

$$\left[(p_r(U))^{x-ś+1} \sum_{m'=1}^{\infty} \binom{x-ś+m'}{m'-1} (p_r(I))^{m'-1}\right]^{n-1}. \tag{47}$$

The smallest order statistics for the indeterminate part of NNBD is given as

$$f_{1:n}(x) = n(p_r(S))^{nś} \sum_{z^*=\text{th}^*+1}^{x-ś} \binom{x-ś}{z^*} (p_r(I))^{z^*} \sum_{x=ś}^{\infty} \sum_{t=0}^{x-ś-z^*} \binom{x-ś-z^*}{t} (p_r(U))^{x-ś-z^*-t}$$

$$\left[\sum_{m'=1}^{\infty} \binom{x-ś+m'}{m'} (p_r(I))^{m'} \sum_{m'=0}^{\infty} \binom{x-ś}{m'} (p_r(U))^{x-ś-m'}\right]^{n-1}. \tag{48}$$

5.5. Median Order Statistics. For $u = m + 1$, median order statistics for true part of NNBD is given as

$$f_{m+1:n}(x) = \frac{(2m+1)!}{m!n!} (p_r(S))^{ś(m+1)} \left[1-(p_r(S))^{ś} (p_r(U))^{x-ś+1} \sum_{m'=1}^{\infty} \binom{x-ś+m'}{m'-1} (p_r(I))^{m'-1}\right]^{m}$$

$$\left[(p_r(U))^{x-ś+1} \sum_{m'=1}^{\infty} \binom{x-ś+m'}{m'-1} (p_r(I))^{m'-1}\right]^{m} \sum_{t=0}^{\text{th}^*} \binom{x-ś}{t} (p_r(I))^{t} (p_r(U))^{x-ś-t}. \tag{49}$$

Median order statistics for the indeterminate part of NNBD is given as

$$f_{m+1:n}(x) = \frac{(2m+1)!}{m!n!} (p_r(S))^{ś(m+1)} \left[1-(p_r(S))^{ś} \sum_{m'=1}^{\infty} \binom{x-ś+m'}{m'} (p_r(I))^{m'} \sum_{m'=0}^{\infty} \binom{x-ś}{m'} (p_r(U))^{x-ś-m'}\right]^{m}$$

$$\left[\sum_{m'=1}^{\infty} \binom{x-ś+m'}{m'} (p_r(I))^{m'} \sum_{m'=0}^{\infty} \binom{x-ś}{m'} (p_r(U))^{x-ś-m'}\right]^{m}$$

$$\sum_{z^*=\text{th}^*+1}^{x-ś} \binom{x-ś}{z^*} (p_r(I))^{z^*} \sum_{x=ś}^{\infty} \sum_{t=0}^{x-ś-z^*} \binom{x-ś-z^*}{t} (p_r(U))^{x-ś-z^*-t}. \tag{50}$$

5.6. Minimum and Maximum Joint Order Statistics. Minimum and maximum joint order statistics for the true part of NNBD is given as

$$f_{1:\,a:a}(y) = n(n-1)\,(p_r(S))^{a\acute{s}}\left\{\sum_{t=0}^{\mathrm{th}^*}\binom{y-\acute{s}}{t}(p_r(I))^t\,(p_r(U))^{y-\acute{s}-\mathrm{t}}\right\}$$
$$\left\{\sum_{t=0}^{\mathrm{th}^*}\binom{z-\acute{s}}{t}(p_r(I))^t\,(p_r(U))^{z-\acute{s}-\mathrm{t}}\right\} \tag{51}$$
$$\left[(p_r(U))^{y-\acute{s}+1}\sum_{m'=1}^{\infty}\binom{y-\acute{s}+\mathrm{m}'}{m'-1}(p_r(I))^{m'-1}-(p_r(U))^{z-\acute{s}+1}\sum_{m'=1}^{\infty}\binom{z-\acute{s}+\mathrm{m}'}{m'-1}(p_r(I))^{m'-1}\right]^{a-2}.$$

Minimum and maximum joint order statistics for the indeterminate part of NNBD is given as

$$f_{1:\,a:a}(y) = a(a-1) = n(n-1)\,(p_r(S))^{a\acute{s}}$$
$$\left\{\sum_{z^*=\mathrm{th}^*+1}^{y-\acute{s}}\binom{y-\acute{s}}{z^*}(p_r(I))^{z^*}\sum_{x=\acute{s}}^{\infty}\sum_{t=0}^{y-\acute{s}-z^*}\binom{y-\acute{s}-z^*}{t}(p_r(U))^{y-\acute{s}-z^*-\mathrm{t}}\right\}$$
$$\left\{\sum_{z^*=\mathrm{th}^*+1}^{z-\acute{s}}\binom{x-\acute{s}}{z^*}(p_r(I))^{z^*}\sum_{x=\acute{s}}^{\infty}\sum_{t=0}^{z-\acute{s}-z^*}\binom{z-\acute{s}-z^*}{t}(p_r(U))^{z-\acute{s}-z^*-\mathrm{t}}\right\} \tag{52}$$
$$\left[(p_r(U))^{y-\acute{s}+1}\sum_{m'=1}^{\infty}\binom{y-\acute{s}+\mathrm{m}'}{m'-1}(p_r(I))^{m'-1}-(p_r(U))^{z-\acute{s}+1}\sum_{m'=1}^{\infty}\binom{z-\acute{s}+\mathrm{m}'}{m'-1}(p_r(I))^{m'-1}\right]^{a-2}.$$

6. Conclusion

This paper proposes a discrete neutrosophic negative binomial probability distribution using the neutrosophic logic. We have discussed various case studies under the proposed distribution. Several mathematical properties, including mgf, characteristics function, and probability generating function of the proposed distribution, have been derived and presented. On reliability review, we have presented characteristics such as survival function, hazard rate function, reversed hazard rate function, cumulative hazard rate function, mills ratio, and odds ratio. Furthermore, we have obtained the order statistics for the proposed distribution. The proposed NNBD was useful in modeling the k th successes in a sequence of n independent trials before a specified number of failures took place.

Data Availability

The data is given in the paper.

Disclosure

This research is part of the thesis with Turnitin similarity report ID: 1481816761 dated December 29, 2020, submitted to Punjab University Library, Lahore

Conflicts of Interest

The authors declare no conflicts of interest.

Acknowledgments

The research was funded by the Deanship of Scientific Research, King Abdulaziz University.

References

[1] F. Smarandache, *Neutrosophy: Neutrosophic Probability, Set, and Logic: Analytic Synthesis & Synthetic Analysis*, American Research Press., Rehoboth, MA, USA, 1998.
[2] K. T. Atanassov, "Intuitionistic fuzzy sets: theory and applications," *Studies in Fuzziness and Soft Computing*, Physica-Verl, New York, NY, USA, 2002.
[3] L. A. Zadeh, "Fuzzy sets," *Information and Control*, vol. 8, no. 3, pp. 338–353, 1965.
[4] M. Akram and K.-P. Shum, "A survey on single-valued neutrosophic K-algebras," vol. 40, 2020.
[5] L. A. Zadeh, "Is there a need for fuzzy logic?" *Information Sciences*, vol. 178, no. 13, pp. 2751–2779, 2008.
[6] L. A. Zadeh and R. A. Aliev, *Fuzzy Logic Theory and Applications: Part I and Part II*, World Scientific Publishing, Singapore, 2018.

Hindawi
Journal of Mathematics
Volume 2024, Article ID 9796040, 1 page
https://doi.org/10.1155/2024/9796040

Retraction

Retracted: A Relevant Customer Identification Algorithm Based on the Internet Financial Platform

Journal of Mathematics

Received 23 January 2024; Accepted 23 January 2024; Published 24 January 2024

This article has been retracted by Hindawi following an investigation undertaken by the publisher [1]. This investigation has uncovered evidence of one or more of the following indicators of systematic manipulation of the publication process:

(1) Discrepancies in scope

(2) Discrepancies in the description of the research reported

(3) Discrepancies between the availability of data and the research described

(4) Inappropriate citations

(5) Incoherent, meaningless and/or irrelevant content included in the article

(6) Manipulated or compromised peer review

The presence of these indicators undermines our confidence in the integrity of the article's content and we cannot, therefore, vouch for its reliability. Please note that this notice is intended solely to alert readers that the content of this article is unreliable. We have not investigated whether authors were aware of or involved in the systematic manipulation of the publication process.

In addition, our investigation has also shown that one or more of the following human-subject reporting requirements has not been met in this article: ethical approval by an Institutional Review Board (IRB) committee or equivalent, patient/participant consent to participate, and/or agreement to publish patient/participant details (where relevant).

Wiley and Hindawi regrets that the usual quality checks did not identify these issues before publication and have since put additional measures in place to safeguard research integrity.

We wish to credit our own Research Integrity and Research Publishing teams and anonymous and named external researchers and research integrity experts for contributing to this investigation.

The corresponding author, as the representative of all authors, has been given the opportunity to register their agreement or disagreement to this retraction. We have kept a record of any response received.

References

[1] G. Yangyudongnanxin, "A Relevant Customer Identification Algorithm Based on the Internet Financial Platform," *Journal of Mathematics*, vol. 2021, Article ID 9770471, 9 pages, 2021.

Hindawi
Journal of Mathematics
Volume 2021, Article ID 9770471, 9 pages
https://doi.org/10.1155/2021/9770471

Research Article

A Relevant Customer Identification Algorithm Based on the Internet Financial Platform

Guo Yangyudongnanxin

Business School, Hunan International Economics University, Hunan, Changsha 410205, China

Correspondence should be addressed to Guo Yangyudongnanxin; 201914040036@zknu.edu.cn

Received 1 October 2021; Accepted 29 October 2021; Published 23 November 2021

Academic Editor: Lazim Abdullah

In order to improve the intelligent search capabilities of Internet financial customers, this paper proposes a search algorithm for Internet financial data. The proposed algorithm calculates the customers corresponding to the two selected financial platforms based on the candidate customer set selected from the seed dataset and combined with the restored social relationship. Moreover, it also calculates the similarity of each field between the pairs. Furthermore, this article proposes an entity customer classification model based on logistic regression. Through the SNC model, threshold propagation, and random propagation, the model is transformed into an algorithm that identifies the associated customers, eliminates redundant customers, and realizes associated user identification. Experimental results verify that pruning increases the accuracy of identifying related customers by 8.44%. The average sampling accuracy of the entire customer association model is 79%, the lowest accuracy is 40%, and the highest is 1. From the sampling results, the overall recognition effect of the model reaches the expected goal.

1. Introduction

In recent years, IT has benefited from the increasing development of the Internet and the in-depth development of financial disarmed. The Internet finance has rapidly and finally evolved into a global financial phenomenon and become one of the most popular financial topics. Internet finance is a new financial business model for traditional financial institutions and Internet enterprises to realize funds, payments, investments, and information intermediary services. On the one hand, the Internet finance has played a role of traditional financial institution to replace the active role in promoting direct financing, improving the efficiency of financial services and resident financial services, and fully excavating and catering the market demand. It is called "squid effect" and contributing positive energy [1]. Though there will be some drawbacks, due to the relative lack of supervision norms, the industry has led to its development, which is characterized by "good, slime," highlighting in some market participation, the main motive is not pure, high interest, etc. For the scorpion, the scam is implemented, and the scandal of misappropriation of customer funds or even the curved running road is constantly occurring [2].

Basically, the term "Internet finance" is used for the funding achieved by traditional financial institutions and Internet companies through using the Internet and information communication technologies. The sellers on the platform characterize the features of the Internet financial platform. That means, the higher number of buyers attract the sellers to that very platform. Henceforth, the buyers and the sellers are attracted to the platform by following the operational models, specifically the pure platform mode and guarantee mode. Furthermore, the information regulations are essential parts of financial markets. The selection and configuration of the information regulatory tool is obligatory to be emphasized on the crucial links of Internet financial platform information regulation. There is a direct regulation and indirect regulation, mandatory regulation, and excitation regulations, and the information tools hidden by different types of information regulations are naturally different. In our experiments, we filtered data. 838 customers

were chosen for manual matching and labeling in a financial platform; thus, the training and testing of logical regression models took place. Furthermore, the data were processed to get similarity feature vector which is actually the input data of the model. The total data were divided into the training and test sets. Then, the remaining data were decomposed into 4 training sets and a testing set. In 5 groups of data, 1760 customers were chosen which were randomly paired to find the positive and negative cases for acquiring the initial classification model. Next, the semisupervised learning method was adopted for the calculation process. Finally, the results are used for superposition training of the model.

First, this article is designed with a cloud protocol based on a cookie single sign-on, used to implement cross-platform, cross-domain storage of customers. According to the design of the storage protocol, the personalized recommendation system proposed herein needs to meet the requirements of efficient return recommendations. Conventional content-based personalized recommendation algorithm first maintained all customers' configuration files. Each recommended traversing all products or pages to get the best recommendation. This is a cross-platform cloud personalized recommendation and related clients proposed in this article. The identification system is not applicable.

Finally, this paper applies the recommended algorithm to the Internet actual system, performing data mining and verifying personalized recommendation algorithms and customer identification from accuracy and efficiency angles. This paper puts forward a cloud storage identification designed from the customer's personal demand and associated customer identification and designs the associated data processing algorithm that matches it. While considering the actual system requirements, the algorithm also reflects the characteristics of the customer's class and realizes the integration of accuracy. It has a certain value for enhancing the Internet customer experience, identifying associated customer information, and implementing the Internet business integration.

2. Literature Review

Recently, a continuous development is being made in the fields of information and technology. Moreover, the information technology also gained attention due to the growing use of Internet and financial disarmed. As a result, the Internet finance has come up as a global financial phenomenon. It is actually an innovative business model for financial institutions as described earlier. Lu et al. [3] proposed a new and rapid SimRank algorithm, He and Yao [4] came with a structural regularization in a quadratic logistic regression model, Yao et al. [5] studied the resources trading in blockchain based on industrial IoT, Zhuang and Zhang [6] worked on the legal and risk prevention of third-party payment in Internet finance, and Wv and Dh [2] discussed the characteristics and consensus of blockchain in modern business processes. Guan et al. [7] worked on the sharing of demand information in competing supply chains with manufacturer provided service, and Pang and Yang [8] presented a loss model with its application in the Internet financial platform. Later in 2020, Peng [9] wrote an article on the Internet financial platform based on 5G network. Ju et al. [10] explained the effective fault localization of evolution software which is based on the multivariate logistic regression model, Wang et al. [11] adopted the forward local push with its parallelization for accurate and fast SimRank computation, Chang et al. [12] worked for the person reidentification and proposed a transductive semisupervised metric learning. Deng et al. [13, 14] proposed some enhanced and evolutionary algorithms for optimization problems.

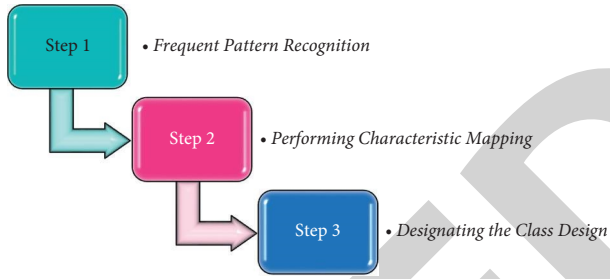

Figure 1: Methodology.

With the implication of technical methods for financing, the threats and risks became a challenge. Thus, the researchers also came forward to solve the issue by proposing the security techniques and risk analysis. Han [15] worked on the legal regulations of the price war of the security company's brokerage business under the Internet finance, Yang et al. [16] proposed an identification algorithm of a high-breaching-risk member of the Internet financial platform, and Zhang et al. [17] researched the risk management of the Internet financial platform. Furthermore, Qu et al. [1] gave the idea of two-factor cross-domain authentication schemes such as biometric and password based on the technology of blockchain. Han et al. [18] described a method for dynamically assessing credit risk of the Internet financial platform, and Yu et al. [19] proposed privacy protection as a base for the multiparty secure computing financial shared platform.

3. Methodology

For the efficient return requirements, this paper proposes a personalized recommendation algorithm based on associated rules, using three steps to meet the real-time requirements of the cloud personalized recommendation system. The first step is using a frequent pattern recognition algorithm for non-real-time update, establishing a frequent mode library based on the customer's previous cloud data. In the second step, in order to reduce the difficulty of personalized recommendation in real time, the characteristic mapping based on frequent mode libraries is performed, and the clustering algorithm is designed and analyzed. In the third step, according to the result of clustering, the specific criteria for designing the class are designated, and the frequent mode of each type of customer is obtained, thereby completing the design of personalized recommendation and customer identification algorithm. Figure 1 illustrates the methodology of the proposed algorithm.

4. Internet Financial Platform

The historical process in the Internet era has been advanced from the depth, and people not only no longer satisfy the breakthroughs of Internet technology but also pay more attention to the application of Internet thinking. Due to Weibo, WeChat, social networking sites, and the "Taobao" representative of C2C (personal and personal) e-commerce websites, individuals in all sides are free to exchange information on the network platform, for low-cost trading of goods. With the development of the times, people exchange the content or will not be limited to information, and people trading should no longer stop in the goods. In recent years, Internet thinking has gradually penetrated into the field of funding and capital markets, and as a sign in the emerging Internet finance industry, it is a "detriment" nature of the Internet financial platform [7].

My country's official document has defined "Internet Finance." On July 14, 2015, the Top Ten Committee of the State Council's Guidance Opinions on Promoting Internet Financial Development (hereinafter referred to as "Guiding Opinions") pointed out that Internet finance refers to "traditional financial institutions and Internet companies use Internet technology and information communication technology to achieve funding." New financial business models for financing, payment, investment, and information intermediary services are introduced. "In this analysis, it was not difficult to find that "Guidance Opinions" did not remove traditional financial institutions to the Internet financial industry, and the business main body of the Internet financial industry can be both traditional financial institutions or an Internet buccaneering. Obviously, this is a quite ambient definition. It is also because "Guidance Opinions" has adopted a broad sense of Internet finance. Subsequently, there are six kinds of activities of Internet finance: Internet payment, network borrowing, equity crowdfunding financing, Internet fund sales, Internet insurance, Internet trust, and Internet consumption finance. However, the author believes that Internet fund sales, Internet insurance, Internet trust, and Internet consumption finance, although carried out on the Internet platform, are still "one-to-many" online sales models of traditional financial institutions, and the end of the field belongs to the Internalization of traditional financial institutions or is the upgraded version of traditional finance [8]. Although "Guidance Opinions" incorporate it into a scope of generalized Internet finance, it is not an Internet finance in the true sense. Insufficient production capacity and high requirements on personnel bring inevitably high costs [19]. Due to the inability to get rid of basic business such as accounting, enterprises are gradually reforming their financial strategies and organizational structures and starting to build Financial Shared Service Centers. Bryan Bergeron first summarized the concept of financial sharing in Essentials of Shared Services as a semiautonomous approach that integrates operational functions of existing business units into a centralized new business unit [5]. The Internet payment is a business of Internet finance, but it does not have a distinct platform attribute. The essence of the Internet financial platform is "It is to build a trading platform, let all needs and materials search and match on this platform by themselves, and turn centralized matching into a distributed "point-to-point" transaction state." Go to center, low-cost trading ecology [17].

4.1. Operation Mode. The operation mode of the Internet financial platform fundamentally determines the legal attributes and risk levels of the platform. "In the platform, both sides (or more) interact on a platform. The characteristics of this model are characterized by the seller on the platform. The greater the attraction of the buyer, the more the seller is considering whether to use this platform, the more the buyers on the platform, and the more attractive it is to the seller. "In order to attract the buyer and the seller to the platform, my country's Internet financial platform is constantly evolving out the following operational models [9].

4.1.1. Pure Platform Mode. In the pure platform mode, the platform strictly positions itself as a pure information intermediary, does not interfere in the essence of the transaction, but only provides investors and financiers with technical services such as information release, information matching, credit rating, "one-to-one" matching, and capital settlement. Equity crowdfunding financing platforms belong to the pure platform model because in equity crowdfunding financing activities, financiers share benefits and risks with investors and financiers do not promise to repay principal and interest. Therefore, the platform does not play any form of credit intermediary role, but pure information intermediary [16]. However, in contrast, in the field of P2P, the pure platform mode is very small. In 2007, the "shooting loans" established in Shanghai is China's first information intermediary service platform for China's information providing P2P-free network borrowing and is also a P2P platform that is not much more purely charged for a profit model. "Loan" is not guaranteed, does not set up a fund pool, always standalone, ans the role of third-party platforms, and the risk is borne by the borrowing transactions. The borrowing process of "shooting loans" is as follows: borrowers release borrowings, borrowers compete for bidding, borrowers are successful, borrowers get borrowings, and borrowers are repayable on time. In order to control the borrowing risk on the platform to attract more investors, "shooting" is based on the wind control model of the big data, and a risk score is given to each borrowing to reflect the forecast of overdue rates. Each score interval will be displayed to the borrower and the lender in the form of a letter rating, such as from AAA to F, and rising in turn. In order to protect the interests of investors, "shooting" is implemented, and when the "Overdue payment" is dealt, the platform extraction is placed in the "risk spare gold account." Once a borrowing is overdue for more than 30 days, the platform will pay the remaining borrowing of this borrow from the investors through the risk spare gold.

4.1.2. Guarantee Model. Since the equity crowdfunding financing platform does not have a guaranteed space, the Internet financial platform for the warranty mode is also

limited to the P2P platform. In recent years, there have been many guaranteed P2P platforms in China, and it can be divided into two types of self-guarantees and third-party guarantees in accordance with the guarantee main body. Platform self-warrants means that the properties of the platform have changed fundamentally, and the platform evolved into a guarantee mechanism, not a simple information intermediary organization, and credit risk is borne by the platform. This type of nature transform has been banned by the current regulatory policy. As early as the disposal of illegal fundraising, the relevant person in charge of the China Banking Regulatory Commission clearly pointed out four boundaries of the P2P network lending platform: first, it is necessary to clarify the mediation properties of the platform; second, it is necessary to clarify the platform itself must not provide guarantees; the third is to return the funds; and the four is to not illegally absorb public funds [18].

4.2. Information Regulation. The financial market is a typical information market. The analysis paradigm of information is an analysis of financial institutional analysis, which is of course applicable to the legal regulation of Internet financial platforms. From the state of view, Internet technology helps to simplify financial transaction processes and improve financial regulation efficiency and plays a unique role in creating money flow and information disclosure so that information is asymmetrical in the Internet finance market and credit risk issues. In this context, the introduction of the information regulation concept and the necessity of the system are highlighted [6]. At present, the concept of information regulation is widely used in the field of environmental protection, food safety, consumer rights relief, legal control, and legal governance of shared economy, but its connotation is different in different contexts. According to the authority of Anthony Ogs, the information regulation mainly includes two aspects. The first is the information disclosure; that is, the supplier is obliged to provide information about the price, identity, ingredient, and quantity or quality of the goods, and the other is to control errors or distortion information. The descriptive definition is clearly defined from the perspective of consumer rights protection and cannot be the basis for this article. Some scholars believe that the information regulation refers to the detailed and accurate information of the goods or services to the information or service to provide information or service to the information of the government's announcement of the government announcement information or the provisions of the government, in order to reduce the negative impact of information bias. There are also scholars who believe that the connotation of information regulation includes "regulation of information" and "regulation of information." The former is to adjust the information in accordance with the legal means to achieve the orderly flow of information and ensure the accuracy and effectiveness of information collection and reduce the overall operation cost of the society, and the latter is to adjust the social relationship with information as a regulatory tool to provide support for the country to moderate and effectively intervene and achieve effective implementation of social political economic decision making [15]. Information regulations are collectively referred to using various information tools to boot, specification, and governance of the Internet financial platform, pointing to "regulation of information rather than" regulation of information. About this concept, it is necessary to emphasize that the key link of Internet financial platform information regulation is the selection and configuration of the information regulatory tool. There is a direct regulation and indirect regulation, mandatory regulation, and excitation regulations, and the information tools hidden by different types of information regulations are naturally different. For example, the tool for mandatory information includes mandatory information disclosure, forced information storage, and forced information sharing, and the tools such as the excitation information include information exchange and information protection. Different types of information regulatory tools should be properly configured to promote timely replacement and benign interactions, thereby increasing the effectiveness of Internet financial platform legal regulation.

5. Related Customer Information Identification

This section presents the discussion about the customer information identification.

5.1. Introduction to the Cross-Network Customer Relationship Model

5.1.1. Logic Regression. The candidate customer set according to the seed dataset is used, combined with the reduced social relationship; first, the similarity of the two financial platforms corresponding to each field between the two financial platforms is calculated, combining the similarity of the field into similarity feature vectors as follows:

$$\overrightarrow{S} = \langle V_0, V_1, V_2, V_3, V_4, V_5, V_6, V_7, V_8, V_9 \rangle, \quad (1)$$

where V0 represents the similarity of the customer's nickname, V1 represents the similarity of customer gender, etc., and different dimensions represent the similarity between different attributes. When conducting customer confirmation, the confirmation classification is considered to be a two-point issue; that is, it is confirmed that the same entity customers are a two-point issue. The logistic regression (LR) [10] model is a commonly used classification model. Binomial logistic regression is commonly used in logistic regression, and there are only two classifications. Therefore, in this paper, the customer association confirmation selects the logistic regression model for classification. The results belong to positive examples (represented by 1) and negative examples (represented by 0), and the conditional probability of binomial logistic regression is

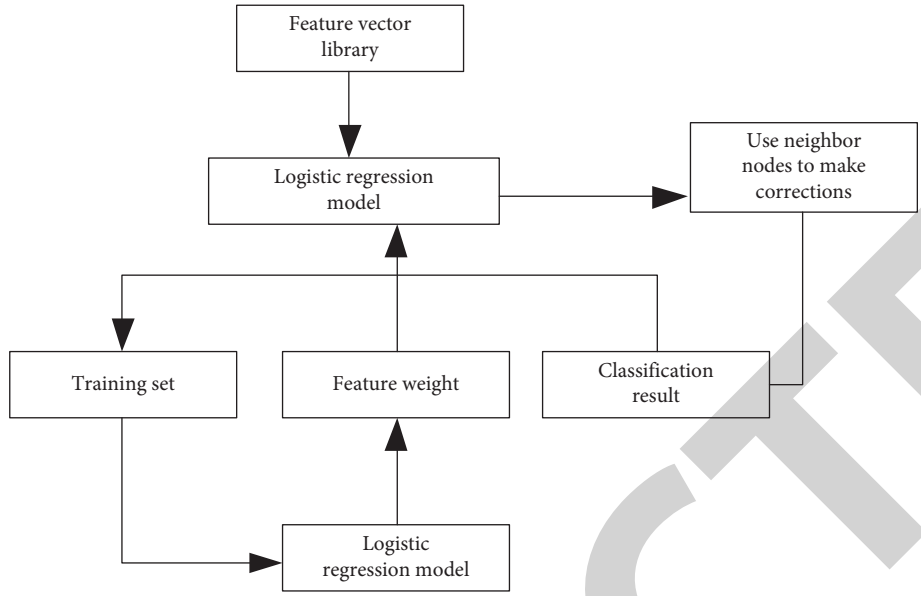

Figure 2: Classification model flow.

$$P(Y = 1|x, w) = \frac{e^{w^T+b}}{1 + e^{w^T+b}} = \frac{1}{1 + e^{-(w^T+b)}}, \quad (2)$$

$$P(Y = 0|x, w) = \frac{1}{1 + e^{w^T+b}}. \quad (3)$$

In formulae (2) and (4), xRN is an input, representing the characteristics of an example; Y {0, 1} indicates the output, which is of only two types, simple representation or no. xRN and PR represent parameters, where w represents the weight vector, and its corresponding value represents the weight of the input feature; b expresses the offset. During classification, according to formulae (2) and (4), $P\ (Y = 1X, w)$ and $P\ (Y = 0x, w)$ can be obtained, respectively, and logic regression compares the size of these two conditional probability and divides the entered instance into the kind of probability value relatively large. The classification model flow is shown in Figure 2.

To use the model to classify the predictive determination requires training to train the model, obtain the feature weight parameters, and then, calculate the input feature vector according to the feature weight and compare the comparative determination according to the calculated results [4]. When the logic regression calculation result is greater than the threshold, the result is divided into a correct case, indicating that the client of the two platforms belongs to the same entity customer; otherwise, the result is divided into a negative, indicating that it is not to point to the same entity customer.

5.1.2. SNC Algorithm. Simrank [11], originally proposed by the MIT Lab Glen Jeh and Jennifer Widom in 2002, is a model of the topology information that uses the map to measure the similarity of the two objects. The core idea is if the two objects are referenced (in the social network is expressed as a similar neighbor), the two objects are similar. There is a strong homogeneity in the social network, which is gathered by a class, and people in a population who have the same symbol or interest become friends. During the customer discovery, if most of the friends have similarity, then you can think that this is the same customer, and this law and Simrank are consistent, so it is widely used in the study of social networks. To eliminate these excess customers, Simrank's [3] neighbor similarity ideas are used to learn from, and the Simneighbor-Cut (SNC) algorithm of the neighbor node is proposed to make the mossil.

The algorithm involves the following formula:

$$s = \frac{1}{n}\sum_{i=1}^{n}\left(\frac{1}{m}\sum_{m=1}^{m} u_m\right), \quad (4)$$

$$I_i = \otimes s_u - s \otimes . \quad (5)$$

In formula (5), n represents the number of direct neighbor nodes that the customer matches and m means that if a direct neighbor is also present in set A, there is a plurality of correct classification results, and then, taking the result, the adjacent variance is taken in the formula as a neighbor similarity value. In formula (5), s u represents the predicted value calculated by the logic regression function, I_i is an absolute value of the predicted value and the neighbor similarity, and the final output customer pair is the lower value of the predicted value and the neighbor similarity difference.

6. Experimental Research

In this section, the experimental research is discussed. Moreover, the tests and their results are also illustrated.

6.1. Training Model and Test. When filtering data, 838 customers in a financial platform are selected for manual labeling and matching, for the training and testing of logical

Input: Determination of the predictive result set A, user pairing set B, seed user relationship matrixM_r, candidate set matrixM_h;
Output: Best Paired Combination $U_r - U_k$ in Collection B;
The specific steps are as follows:
(1) Extract the pairing user in B, divide users into u_r and u_h;
(2) Search all direct neighbors of u_r in M_r, labeled, deposits set S_r;
(3) Search all direct neighbors of u_h in M_h, labeled, deposits set S_h;
(4) Use the user in S_r and S_h to combine the collection A, find a common neighbor of $u_r$and u_h, and label;
(5) The similarity s of u_r and u_h is calculated by the following formula;
(6) The absolute difference l_i is calculated by the following formula;
(7) Repeat the above steps until all the pairing users in the collection B are complete;
(8) Take the l_i value to the user output, the pairing user $U_r - U_h$ corresponding to $l = \mathrm{Min}(l_i)$.

Algorithm 1: SNC algorithm.

regression models. Processing data get the similarity feature vector, namely, the input data of the model. The 838 customers' data are divided into training sets and test sets, and 38 isolated nodes are removed to reduce the impact on the relationship between friends. The remaining 800 customers are then divided into 5 groups in the proportion of 4 to 1, of which 4 are used for training and 1 set is used for testing. In 5 groups of data, 1760 customers were selected from which 1760 customers were selected and then randomly paired with customers in the seed dataset as a negative example in the training. The proportion of positive cases and negative cases in each group is different, which is used for training to obtain the initial classification model. After obtaining the initial model, the semisupervised learning method [12] is adopted in the subsequent calculation process, and the final customer association results are used for superposition training of the model. After completing the data packet, it is trained with the number of iterations, and packet training, incremental training, and combined training, respectively. Grouping training is to train models by four packets, producing four models, corresponding to training sets, numbered M1 (training set 1), M2 (training set 2), M3 (training set 3), and M4 (training set 4); incremental training uses four groups to enter the model in turn, producing a model, numbered M5; during combined training, all four groups are synthesized to train, and a model is generated, numbered M6. Table 1 is a comparison of the determination result of the input test set after the completion of the training (proportion of training concentration and negatives).

From the test results of M1, M2, M3, and M4 in Table 2, the number of negatives added during the training process has little effect on the prediction results; the results of comparison M1 to M4 and M5 and M6 have found that the number of original training concentrations will affect the final result; the more accurate it is, the higher will be the final result. The accuracy of model M5 and M6 is higher than that of the other models, and the accuracy of the two is different, but the recall rate of the model M6 is relatively high, so model M6 of combined training is used to classify the associated customers. At the time of statistics on the final test results, there is a pair of multiphenomena discussed in the classification result, and the SNC algorithm is used to score, and the results after the twig are shown in Table 2.

As can be seen from the results of the correction in Table 2, the number of positive numbers in the posttwig decrease is 31, the number of negatives increases by 31, the number of correct classifications has increased by 27, the correct number of correct classifications decreased to 4, there is an error in the twig process, a small amount of correct classification is determined as an error classification, and the correct result is deleted, resulting in a slight decrease in the correct number of normal number and the recall rate. The result of pruning is 8.44% higher than that of the original logistic regression model. The purpose of pruning is to delete the wrong classification in the positive example and keep the correct classification as far as possible. The more matched the customers, the more obvious the pruning effect. The larger the number of positive examples of correct classification retained in the positive example, the higher the final accuracy of the model.

6.2. Customer Association Experiment. There are a total of 100 in the seed dataset in this paper, which is recorded as a seed dataset. The two target datasets used to screen are a certain financial platform customer dataset (recorded as So) and the second financial platform customer dataset (recorded SW). The SW has 5,448,509 client data, and all customers are combined with data fusion. The customer's behavior data are used to fill the partial fields, and the SW will retain 5,428,959 customers after processing. The So contains 24,950,474 customer data. After completing the data, the joint filtering vector and threshold in the client filter module are selected, the 73-tested amount of the 2.2 knit is used, whose value is (0.4, 0.3, 0.2, 0.1), and the screening threshold is set to 0.36. The logic regression model selects the logical regression model M6 of combined training. This experiment mainly uses cross-network customers to associate an overall model, from customers in seed data, and uses the proliferation inspiration to discover and identify customers. The entire customers' associated model is running 11 rounds, and its output is shown in Figure 3.

The number of matching customers in Figure 3 represents the total number of associated customers that run each round; each round increases the number of clients representing the number of related clients in each round; the original customer

Table 1: Judgment result.

Results	M1(1 : 1)	M2(1 : 1)	M3(1 : 2)	M4(1 : 3)	M5(2 : 5)	M6(2 : 5)
Number of positive cases	183	188	185	177	182	199
Correct number of classifications	115	126	121	117	156	151
Correct number of positive examples	69	77	73	67	89	95
Accuracy	0.3592	0.3935	0.3745	0.3652	0.4851	0.4756
Recall rate	0.4311	0.4874	0.4512	0.4156	0.5563	0.5968

Table 2: Decision results of the test set.

Results	Original result set	The result set after pruning
Number of positive cases	199	168
Correct number of classifications	121	152
Correct number of positive examples	151	178
Accuracy	95	91
Recall rate	0.4752	0.5569
Number of positive cases	0.5938	0.5688

represents the number of customers in the seed customer concentrated in the model. In addition to the first round, each round of input is a direct friend of the previous round of identification results. According to the "six-degree space" theory, everyone can connect with 6 people to establish a friend relationship with 6 people. However, after the study of social networks is 13, that is, after connecting with 13 people, customer relationships can form a loop. At this time, the number of friends will not increase. After the model is running 11 rounds, the number of friends (i.e., the original customer) increases; that is, the social network restriction has been reached, and the operation is stopped and output. Since the number of initial customers is small, after the first two rounds of slow start, the model starts from the third round, and the new customer volume starts to increase rapidly, but after running 3 rounds, the number of new customers starting from the 6th round is rapidly reduced, because the average path of the social network is 3.6, there are many shorter paths than the actual path length, and there is a high coarability. After 3 rounds, many customers have formed a loop, resulting in a decrease in new customers. After the model runs 11 rounds, I finally discovered 53,351 to the associated customers. From the number of customers from the entire dataset, the dataset included 5,428,959 customers, the identification ratio was 1%, the proportion of customers identified is very low, and the integrity of primary and customer personal data is very big. Many fields in a large number of customers are blank, and they can be complete and "serious" to fill in the number of customers, which causes this inevitable randomness leading to a low ratio. In order to evaluate the associated customers in the 53, 351 discoveries, from these 53, 351, 1,000 to the customer randomly, they are divided randomly into 100 groups, 10 customers per group, using artificial manual determination.

6.3. Determination Results Experiment. When the manual determination is used to determine the character of the customer avatar, the customer behavior information and the determination results are shown in Figure 4.

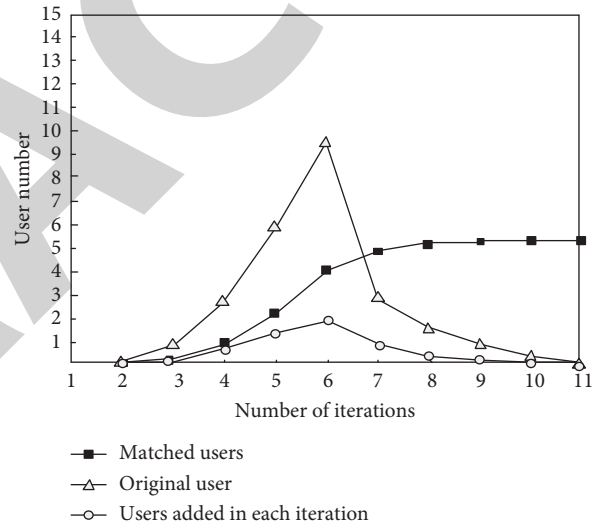

Figure 3: User association model operation results.

As can be seen from the accuracy distribution in Figure 4, the average accuracy of the entire customer's association model is 79%, the minimum accuracy is 40%, the highest is 1, and from the sample result, the overall identification effect of the model can be achieved the expected goal. In order to evaluate the customer's recognition ability, the customers in the final result set are sorted in similar degree, and the customers who are ranked 1000 are manually determined.

6.4. Judgment Results Experiment. They are also randomly divided into 100 groups, each set having 10 customers, and their judgment results are shown in Figure 5.

As can be seen from the accuracy distribution in Figure 5, the correct rate is 0.5, the highest is 1, the average correct rate is 0.855, and the correct rate of most of the packets is higher than the average value; note that the recognition capacity of the association model is strong; i.e., the probability of customers having similar characteristics in the dataset is high.

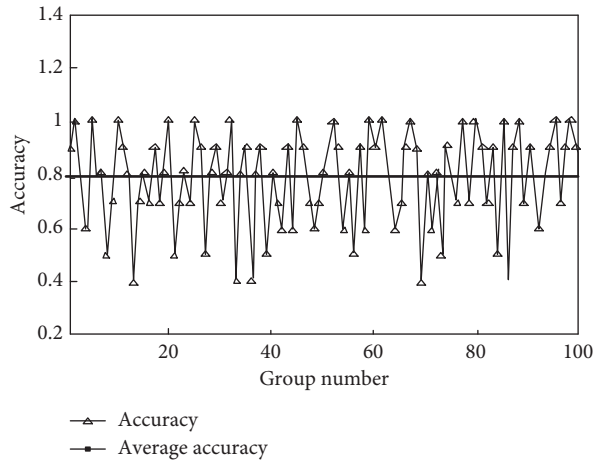

Figure 4: Distribution of user-associated random sampling accuracy.

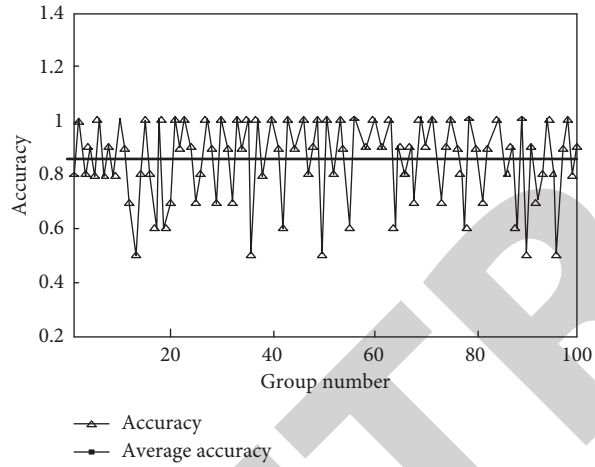

Figure 5: Distribution of user recognition accuracy in the top 1000.

7. Conclusions

This paper selects two Internet financial platform networks that have not been studied in China. Henceforth, this paper studies the client technologies related to Internet finance through these selected networks. Moreover, it proposes a cross-network client correlation model. The model uses the relationship between the associated customer network and the customer's candidate set and restores the customer relationship network. Furthermore, it uses the logical regression model to determine whether the customer belongs to the same entity. Finally, the SNC algorithm is used to make a result reduction correction, delete the repeated classification result, and thus, improve the accuracy of the model. Ultimately, this paper discovered 53351 related customers through experiments and proved that the model can effectively associate customers between Internet financial platforms across networks, thereby facilitating the associated certification and behavioral difference analysis of online customer entities. It is helpful to streamline customer information and improve the efficiency of public opinion supervision. However, we still need to design a more realistic model for practical application.

Data Availability

The data used to support the findings of this study are available from the corresponding author upon request.

Conflicts of Interest

The author declares no conflicts of interest.

Acknowledgments

This paper was supported by the Provincial Soft Science Key Project (2013ZK2024 and 2014GK3147) of the Science and Technology Department of Hunan Province.

References

[1] Q. Qu, C. Liu, and X. Bao, "E-commerce enterprise supply chain financing risk assessment based on linked data mining and edge computing," *Mobile Information Systems*, vol. 2021, Article ID 9938325, 9 pages, 2021.

[2] L. Wang, M. Gao, and Z. Liang, "Application of data envelopment and internet of things technology for asset value evaluation," *Mobile Information Systems*, vol. 2021, Article ID 9934090, 8 pages, 2021.

[3] J. Lu, Z. Gong, and X. Lin, "A novel and fast SimRank algorithm," *IEEE Transactions on Knowledge and Data Engineering*, vol. 29, no. 3, pp. 572–585, 2017.

[4] J. He and D. Yao, "Structural regularization in quadratic logistic regression model," *Knowledge-Based Systems*, vol. 163, pp. 842–857, 2019.

[5] H. Yao, T. Mai, J. Wang, Z. Ji, C. Jiang, and Y. Qian, "Resource trading in blockchain-based industrial internet of things," *IEEE Transactions on Industrial Informatics*, vol. 15, no. 6, pp. 3602–3609, 2019.

[6] W. Zhuang and X. Zhang, "Legal risk and prevention of third-party payment in internet finance," *Journal of Anhui Radio & TV University*, 2019.

[7] Z. Guan, X. Zhang, and M. Zhou, "Demand information sharing in competing supply chains with manufacturer-provided service," *International Journal of Production Economics*, vol. 220, 2020.

[8] X. Yu, J. Yang, and Z. Xie, "Training SVMs on a bound vectors set based on Fisher projection," *Frontiers of Computer Science*, vol. 8, no. 5, pp. 793–806, 2014.

[9] H. Peng, "Research on credit evaluation of financial enterprises based on the genetic backpropagation neural network," *Scientific Programming*, vol. 2021, Article ID 7745920, 8 pages, 2021.

[10] X. Ju, J. Qian, Z. Chen, C. Zhao, and J. Qian, "Mulr4FL: effective Fault localization of evolution software based on multivariate logistic regression model," *IEEE Access*, vol. 8, pp. 207858–207870, 2020.

[11] Y. Wang, Y. Che, and X. Lian, "Fast and accurate SimRank computation via forward local push and its parallelization," *IEEE Transactions on Knowledge and Data Engineering*, vol. 99, p. 1, 2020.

[12] T. Ouyang and X. Lu, "Clustering analysis of risk divergence of China government's debts," *Scientific Programming*, vol. 2021, Article ID 7033597, 9 pages, 2021.

Hindawi
Journal of Mathematics
Volume 2024, Article ID 9767958, 1 page
https://doi.org/10.1155/2024/9767958

Retraction

Retracted: An Effective Approach for Modular Community Detection in Bipartite Network Based on Integrating Rider with Harris Hawks Optimization Algorithms

Journal of Mathematics

Received 23 January 2024; Accepted 23 January 2024; Published 24 January 2024

This article has been retracted by Hindawi following an investigation undertaken by the publisher [1]. This investigation has uncovered evidence of one or more of the following indicators of systematic manipulation of the publication process:

(1) Discrepancies in scope

(2) Discrepancies in the description of the research reported

(3) Discrepancies between the availability of data and the research described

(4) Inappropriate citations

(5) Incoherent, meaningless and/or irrelevant content included in the article

(6) Manipulated or compromised peer review

The presence of these indicators undermines our confidence in the integrity of the article's content and we cannot, therefore, vouch for its reliability. Please note that this notice is intended solely to alert readers that the content of this article is unreliable. We have not investigated whether authors were aware of or involved in the systematic manipulation of the publication process.

Wiley and Hindawi regrets that the usual quality checks did not identify these issues before publication and have since put additional measures in place to safeguard research integrity.

We wish to credit our own Research Integrity and Research Publishing teams and anonymous and named external researchers and research integrity experts for contributing to this investigation.

The corresponding author, as the representative of all authors, has been given the opportunity to register their agreement or disagreement to this retraction. We have kept a record of any response received.

References

[1] B. Fahad Alkhamees, M. A. A. Mosleh, H. AlSalman, and M. Azeem Akbar, "An Effective Approach for Modular Community Detection in Bipartite Network Based on Integrating Rider with Harris Hawks Optimization Algorithms," *Journal of Mathematics*, vol. 2021, Article ID 9511425, 16 pages, 2021.

Hindawi
Journal of Mathematics
Volume 2021, Article ID 9511425, 16 pages
https://doi.org/10.1155/2021/9511425

Research Article

An Effective Approach for Modular Community Detection in Bipartite Network Based on Integrating Rider with Harris Hawks Optimization Algorithms

Bader Fahad Alkhamees,[1] **Mogeeb A. A. Mosleh**,[2] **Hussain AlSalman**,[3] **and Muhammad Azeem Akbar**[4]

[1]*Department of Information Systems, College of Computer and Information Sciences, King Saud University, Riyadh 11543, Saudi Arabia*
[2]*Faculty of Engineering and Information Technology, Taiz University, Taiz 6803, Yemen*
[3]*Department of Computer Science, College of Computer and Information Sciences, King Saud University, Riyadh 11543, Saudi Arabia*
[4]*Lappeenranta-Lahti University of Technology (LUT), Department of Software Engineering, Lappeenranta 53851, Finland*

Correspondence should be addressed to Mogeeb A. A. Mosleh; mogeebmosleh@taiz.edu.ye

Received 29 August 2021; Accepted 28 October 2021; Published 16 November 2021

Academic Editor: Naeem Jan

The strenuous mining and arduous discovery of the concealed community structure in complex networks has received tremendous attention by the research community and is a trending domain in the multifaceted network as it not only reveals details about the hierarchical structure of multifaceted network but also assists in better understanding of the core functions of the network and subsequently information recommendation. The bipartite networks belong to the multifaceted network whose nodes can be divided into a dissimilar node-set so that no edges assist between the vertices. Even though the discovery of communities in one-mode network is briefly studied, community detection in bipartite networks is not studied. In this paper, we propose a novel Rider-Harris Hawks Optimization (RHHO) algorithm for community detection in a bipartite network through node similarity. The proposed RHHO is developed by the integration of the Rider Optimization (RO) algorithm with the Harris Hawks Optimization (HHO) algorithm. Moreover, a new evaluation metric, i.e., h-Tversky Index (h-TI), is also proposed for computing node similarity and fitness is newly devised considering modularity. The goal of modularity is to quantify the goodness of a specific division of network to evaluate the accuracy of the proposed community detection. The quantitative assessment of the proposed approach, as well as thorough comparative evaluation, was meticulously conducted in terms of fitness and modularity over the citation networks datasets (cit-HepPh and cit-HepTh) and bipartite network datasets (Movie Lens 100 K and American Revolution datasets). The performance was analyzed for 250 iterations of the simulation experiments. Experimental results have shown that the proposed method demonstrated a maximal fitness of 0.74353 and maximal modularity of 0.77433, outperforming the state-of-the-art approaches, including h-index-based link prediction, such as Multiagent Genetic Algorithm (MAGA), Genetic Algorithm (GA), Memetic Algorithm for Community Detection in Bipartite Networks (MATMCD-BN), and HHO.

1. Introduction

Naturally, the complex systems are deemed to be divided into multiple communities or modules. Usually, in order to represent the networks, the said communities or modules are labeled as clusters of compactly linked nodes with scarce links to the nodes of other clusters. Complex network models have several representations, including one-mode network, bipartite network, and multimode network, but the existence of a bipartite network is very close to a natural phenomenon when especially modeling association relations between two different classes of real-world objects. In a

bipartite network, there are two different kinds of nodes. The existence of the edges between nodes is conditional such that if connecting nodes are associated with other types. Bipartite networks maintain rich information regarding the entire network being modeled and share important statistical properties like clustering coefficient as their single-mode form. Many real-world applications include the P2P network, entertainment and audience network, research coordination network, and items lending network.

Community detection holds an essentially significant contribution in many complex networks, especially an important class, i.e., bipartite networks. Community identification and dichotomy characteristics in a bipartite network not only reveal details about the hierarchical structure of a multifaceted network but also assist in better understanding of the core functions of the network and subsequently information recommendation. The bipartite networks belong to the multifaceted network whose nodes can be divided into a dissimilar node-set so that no edges assist between the vertices. Even though the discovery of communities in one-mode networks is briefly studied, community detection with bipartite networks is not studied.

Community detection is a trending research domain in the field of network science that poses the ability to offer vision to the fundamental structure and provides impending functions to the networks. Numerous real-world models like the Internet, food webs, social relationships, and biological systems are considered complex networks [1, 2]. The community is represented as a complex network which is described as the collection of nodes which are sturdily linked to one another but sporadically linked to nodes that are present external to the set [3]. The algorithms based on community detection are developed for recognizing the nodes, modules, or clusters inside the network that are more likely to interrelate among themselves than with the other network. This process is carried out when the nodes belong to the same community whereas it performs differently when the node belongs to other communities [4]. The social network using the attribute nodes is given by the bipartite graph and the extracted bicommunities are revealed later like other communities in bipartite bibliographic network which is employed for citation recommendation [4, 5]. The bipartite network is also known as two-mode network or the affiliation network wherein the nodes are divided into two different collections that involved upper and lower nodes. Here, each edge is adapted to connect the upper nodes to the lower nodes. Here, no edges exist between the two upper nodes and no edges lie between lower nodes [6]. The bipartite network offers an insight exemplification between two disjoint groups using the applications that range between the citation networks, disjoint groups, collaboration networks, and ecological networks. Here, the bipartite graph contains specific coverage property also termed as maximum matching [7].

Bipartite networks can be epitomized in the real-world scenarios considering two different categories of objects that involved movie-actor relation and paper-reference relation. The dichotomy physiognomies of the target network assist in disclosing more details than the single model networks [5]. The bipartite networks provide statistical properties in their single-mode form which helps to define nodes of two parts of single model network and the original bipartite network offers the degree distribution and clustering coefficient to handle more information using the real network being modeled with single model version [4]. The network model is broadly employed in the reality, and the researchers provided bipartite network-related research using real-time application, cooperation network, and P2P exchange network [8]. There exist two ways for curving the relation of different object classes which involved projection method and nonprojection method [8]. The projection method projects the two parts of bipartite network considering certain nodes to evaluate further study. Similarity-based strategies are the frequently employed link prediction strategies wherein each pair of nodes considers proximity score, described based on network structure which implies that two nodes are similar if they pose higher structural similarities [9]. The proposed approach [10] is a heuristic method based on modularity optimization and demonstrated high quality of the community detection in terms of modularity in bipartite networks. The efficiency and effectiveness of Louvain algorithm had been proved by several applications.

Numerous techniques of community detection are designed to recognize the community structure. The near-optimal or optimal values of some criteria are generated by good partition. Moreover, the good separation also reveals the organization using community structure with different resolutions [11]. Conventionally, hierarchical clustering and graph partitioning strategies like agglomerative algorithms and disruptive counterparts are used for solving the issues of community detection [12]. In [13], modularity is delineated to measure the quality of partitions. Corrêa et al. [14] followed a complex network approach for word sense disambiguation. Through community detection in input-output bipartite graphs (BGs), Tang and Daoutidis [15] proposed the network decomposition for distributed control. In order to discover the necessary patterns in the IP traffic, Viard et al. [16] used cliques in bipartite link streams. Huang et al. [17] presented a novel link prediction for large scale miRNA-lncRNA interaction network in the BG. Rechner et al. [18] introduced the uniform sampling of the BGs with degrees in suggested intervals. Based on theory of complex network, Guan et al. [19] offered a service-oriented deployment policy of end-to-end network slicing. Bian and Deng [20] carried out the research to identify the influential nodes in complex networks. Gao et al. [21] wrote a paper; titled "an adaptive optimal-Kernel time-frequency representation-based complex network method for characterizing fatigued behavior using the SSVEP-based BCI system." Huang et al. [22] carried out a survey on techniques of community detection in multilayer networks. Rostami et al. [23] presented a genetic algorithm for feature selection that is based on a novel community detection, Li et al. [24] proposed the convex relaxation techniques for community detection, and Joo et al. [25] utilized the community detection for studying the stream gauge network grouping. The modularity is employed to reflect the fraction of edges using the communities related to the amount of edges developed using communities. Here, the method devised a null model, which utilizes the nodes degree for computing the uncertainty of edges that are established between the nodes.

Moreover, the modularity with high value specifies good partition, thereby maximizing the standard using optimization method [26]. However, it is obstinate to determine the precise optimal solution for the issues. Thus, many approximate techniques are designed for community detection. In [13], greedy method was devised for community detection. The algorithm showed effective performance and is considered as an efficient algorithm for detecting the nodes similarities. The Louvain algorithm contained two important processes. In the initial phase, using the community of each node, the modularity is optimized locally. The node with the same communities is aggregated and is considered as supernode and forms the novel coarse-grained network. The process is repeatedly performed using concentrated networks considering modularity to devise the node movement contained in network. Even though Louvain algorithm and modularity-based strategies pose certain drawbacks, they are still extensively utilized to evaluate real-world issues [27].

The principal purpose of this research is to devise a technique for community detection in bipartite network based on the node similarity. Here, the h-Tversky Index (h-TI) measure is newly designed by modifying h-index based on Tversky index for computing node similarity. This method is based on the similarity measures between nodes that exploit the bipartite networks. The algorithm holds the cycles for connection to maximize the similarity between nodes in order to define the communities. Then, the community detection is performed based on the proposed Rider-Harris Hawks Optimization algorithm (RHHO) and modularity. The RHHO introduced in this study is developed by integrating Rider Optimization (RO) algorithm with the Harris Hawks Optimization (HHO) algorithm. In addition, the fitness is newly devised considering modularity and proposed h-Tversky Index (h-TI) for evaluating the node similarity. The aim of modularity is to enumerate the integrity of specific division of network to evaluate the accuracy of the proposed community detection.

The major contributions are enlisted as follows:

(i) Proposing RHHO for community detection: the proposed RHHO algorithm is a novel derivation which is achieved by the combination of RO and HHO algorithms, for community detection

(ii) Proposing h-Tversky Index (h-TI) for node similarity: the similarity between the nodes is evaluated by integrating h-index and Tversky similarity index

Rest of the sections of this article is arranged as follows. Section 2 describes the strategies of conventional community detection that are used in the literature and challenges faced, which motivated developing the proposed technique. The objective model of community detection using bipartite graph is illustrated in Section 3. The method introduced for community detection through proposed RHHO is described in Section 4. The results of the introduced RHHO are compared with other techniques in Section 5 and finally, Section 6 provides the conclusion.

2. Motivations

The problem of community detection is NP-hard, since people have utilized different techniques to address the optimization problem. Therefore, precise algorithms like swarm evolutionary algorithms (EAs) and intelligence algorithms are employed for community detection, but the convergence of the global optimal solution needs more time. The limitation linked with modularity is identified, which is termed as resolution limits. Moreover, the modularity fails to determine the community structure for fewer nodes. The aforementioned limitations stood as the motivation for designing a novel community detection model in bipartite networks.

2.1. Literature Survey. The techniques based on eight existing community detection algorithms using bipartite network are illustrated. Zhou et al. [9] designed two h-index-based link prediction techniques using the citation network. Here, the h-type index was adapted for computing the significant nodes using the citation network. Moreover, the accuracy of prediction was found better but the method was inapplicable with other types of networks to enhance the performance of system. Gmati et al. [4] designed Fast-Bi community detection (FBCD) for detecting the community in social network using the node attributes. The goal of the model is to discover the maximum matching using bipartite graph for minimizing the complication. The method failed to use other kinds of bipartite network like directed, weighted, or dynamic network for determining the community structure. Che et al. [28] devised memetic algorithm, namely, MATMCD-BN for community detection using two-mode networks. The method employed conventional string-driven representation strategy for chromosome representation. Here, population initialization method was devised using bipartite network for enhancing the convergence rate. Moreover, the density-based bipartite modularity function was devised using the fitness function. However, the method failed to determine more than one node. Chang et al. [7] designed overlapping community detection strategy considering complete bipartite graph using microbipartite network Bi-EgoNet (CBG and BEN), which combined the benefits of both bipartite graph and the Bi-EgoNet for generating the best community structure. However, the method failed to evaluate associated issues faced by the bipartite network considering Bi-EgoNet. Sun et al. [29] designed BiAttracter for determining the two-mode communities using bipartite networks. The method was computed on the basis of distance dynamics attractor model. Even though the method precisely determined the two-mode communities of bipartite network in less time, it failed to discover community detection considering heterogeneous network, multilevel network, and temporal network. Li et al. [3] designed quantitative function for determining the community structures considering bipartite network. Moreover, the Heuristic and Adapted Label Propagation Algorithm (BiLPA) was devised to optimize the

quantitative function using huge scale bipartite networks. However, some of the data of bipartite network were missing in the obtained proposed network. Zhou et al. [10] designed a method for community detection using the bipartite network. Here, the expansion of bipartite modularity was designed and Louvain algorithm was devised. The Louvain algorithm adapted indigenous moving heuristic to unfold the complete hierarchical structure of the network. In addition, the Laplacian dynamics was considered for analyzing the constancy of community structure but failed to develop community-enabled recommendation model. Xue et al. [30] designed a method for addressing the cold start issue for community detection considering bipartite graph. At first, the decoupled normalization strategy was used to extract the inclination patterns considering the ratings. Moreover, two incremental community detection methods were devised for capturing the interesting shifts based on missing method of rating. However, the technique was unsuccessful in using the pairwise constraints for semisupervised learning for the enhancement of system's performance.

2.2. Challenges. The challenges confronted by the conventional techniques for developing a method for effective community detection are portrayed as follows:

(i) Another drawback confronted by the community detection method is weighted modularity. Here, the weighted modularity was only effective on networks in which all connections are positive. However, these methods failed to create modules in weighted networks for devising negative and positive link strengths [26].

(ii) Determining the structure of networks is beneficial for illustrating their formulation function and performance and is considered a significant issue in community detection [1].

(iii) In [30], the Incremental Group-Specific model was designed for community detection. However, the empirical analysis was not performed for offering a reasonable explanation to simplify the grouping method and failed to combine valuable topological information.

(iv) In [9], h-index-based link prediction method was developed using the citation network. Still, it did not consider the h-index and Tversky similarity indices and the Salton to improve performance.

(v) Bipartite networks fit in the category of complicated networks, whose vertices are distributed into two alienated collections of vertices, such that there do not exist any edges between vertices of the same collections/set, and edges only subsist between nodes of different collections. Even though, in one-mode networks, the community discovery is widely studied, the community detections in bipartite networks have not been studied due to the fact that the projection loses important information of the original bipartite network.

3. Objective Model for Community Detection

Community detection is a fundamental tool employed for discovering valuable information that is hidden over complex networks. Numerous community detection techniques for bipartite networks are devised considering different viewpoints. However, the efficiency of these techniques worsens when the community structure turns ambiguous. Improving the community structure is a complicated task. The bipartite network is an essential class of complex networks in real-world systems, wherein each node is of different types, and no two nodes are the same type. For example, a bipartite network that has three communities is shown in Figure 1.

As bipartite networks pose community structure and the communities are independent of one another, that helped to expose indefinite functional modules. The analysis and detection of these communities from the bipartite network offer a means for functional classification of the bipartite network. Community detection is a challenging task considering bipartite networks due to the fact that the community detection problem is NP-hard. The algorithm makes the issue of community detection into a combinatorial optimization issue.

Modularity is widely applied for the evaluation of the quality of a specific partition of a network into communities. Moreover, modularity reflects the extent, relative to a null model network, to which edges are formed within communities instead of between them. Further, the bipartite modularity measures are proposed, which could be useful in the recognition of communities in bipartite networks. In turn, the model is newly devised that would have the same number of nodes and degree distribution as that of the original network while the edges of the node are replaced.

Assume a bipartite graph which is modeled as an undirected graph $G = (D, I)$ where D represents set of nodes and I indicates a set of edges. The node-set D is expressed as $D = \{X \cup W\}$ where X and W indicate the types of node X and type W. The set of edges is represented as I. The edges pose the ability to connect different types of nodes, which are modeled as edges $n_{ef} \in I\,(b_e \in X; s_f \in W)$, and $|I|$ indicate the number of edges in a bipartite graph. The detection of community in a bipartite graph is expressed as $G = (D, I) = (X \cup W, I)$ which is employed to partition G into subgraphs, modeled as $G_e = (X_e \cup W_e, I_e)$ where $e = \{1, 2, \ldots, o\}$ and o is a total number of communities.

3.1. Bipartite Modularity for Detecting Similarity between Nodes. The modularity [31] is devised to quantify the integrity of a specific part in the provided network and is considered as a widespread benchmark index to compute the accuracy in community detection. The community structure is defined as a model that arranges the edges in a statistically surprising manner. Assume g_j represents the degree of node j and E indicates a total number of edges. The probability of edge being presented between node j and node q is represented as $(g_j g_q / 2E)$. The modularity quantifying the number of edges based on newly devised model can be expressed as

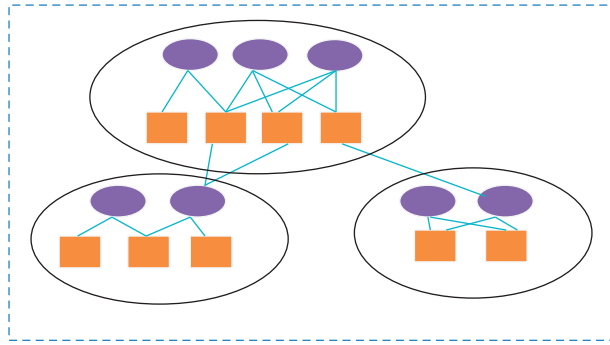

Figure 1: A bipartite network having three communities.

$$M = \frac{1}{2E}\sum_{j=1}^{S}\sum_{q=1}^{S}\left(T_{j,q} - \frac{g_j g_q}{2E}\right)\eta\left(r_j r_q\right), \tag{1}$$

where M represents the sum of difference over all groups, S indicates network size, $T_{j,q}$ indicates the adjacent relation between node j and node q, g_j indicates the degree of node j, and g_q represents the degree of node q, η represents a function that acquires a value 1 if $r_j = r_q$ and receives value 0 otherwise, E indicates the number of edges, and r_q indicates the group of node q. Here, the value of M varies between -1 and 1, and the larger value of Q indicates a more precise division of network in communities. A bipartite network with S nodes can be represented as duality $(x, y) \ni x + y = S$ where x and y indicate two types of nodes such as $\{1, 2, \ldots, x, x+1, \ldots, S\}$, where leftmost x indicates one type of node and rightmost x indicates other types of nodes. The bipartite modularity that considers a community of specific type of node in the network is given as

$$M_r = \frac{1}{E}\sum_{j=1}^{q}\sum_{q=x+1}^{S}\left(T_{jq} - \frac{g_j g_q}{E}\right)\eta\left(r_j r_q\right). \tag{2}$$

The unipartite network can be expressed as a bipartite one, and the bipartite network can recover the modularity of the given network. If each node j is represented by two nodes K_j and L_j and each edge $j - q$ is represented by two nodes $K_j - L_q$ and $K_q - L_j$ then the unipartite network with S nodes and E edges is converted into a corresponding bipartite network with $2S$ nodes and $2E$ edges. Moreover, the bipartite network is considered a massive class of networks that offers a solution for dealing with community structure detection. The bipartite modularity is served as a standardized goal for detecting communities using optimization.

3.2. Proposed h-Tversky Index (h-TI) for Node Similarity. In this research, a novel h-Tversky similarity index is proposed by combining the Tversky index with h-index [9] for computing the similarity between two nodes. The Tversky index is a similarity measure used for comparing the variant with respect to the prototype. The Tversky index is considered as a generalization of the Dice coefficient and Tanimoto coefficient. On the other hand, the h-index is a term utilized for discovering the significance of a node considering a citation network. The h-index is also termed as lobby index, which is devised on the basis of Schubert's h-index. The nodes with high degree neighbors are strengthened by h-index, which has been discovered. Thus, the combination of Tversky index and h-index is defined to evaluate the similar nodes in order to improve the network performance. The proposed h-Tversky similarity index is represented as

$$G_{jq} = \frac{\theta\left|\Gamma_j \cap \Gamma_q\right|}{\theta\left|\Gamma_j \cap \Gamma_q\right| + \alpha\left|\Gamma_j \backslash \Gamma_q\right| + \beta\left|\Gamma_q \backslash \Gamma_j\right|}. \tag{3}$$

The values of the similarity function in the above form are bounded to unit interval $[0, 1]$. This formula generalizes numerous common similarity functions for suitable values of parameters, θ, α, β, and choice of the interval scale function. For instance, if $\theta = \alpha = \beta = 1$ Tversky index is the same as Jaccard index or Jaccard similarity coefficient. When $\theta = 1$ and $\alpha = \beta = 0.5$, Tversky's formula turns out to be the same as the Dice similarity coefficient, Here, $\alpha = t_j$ and $\beta = t_q$, $\Gamma_j \cap \Gamma_q$ represents a set of common neighbors of nodes j and q, α corresponds to the weight of prototype and β denotes the weight of variant, t_j represents the h-index of a node j, and t_q specifies the h-index of a node q. Here, the h-index of a node j is expressed as

$$t_j = Y\left(C_{j1}g_1, \ldots, C_{jq}g_q, \ldots, C_{qS}g_S\right), \tag{4}$$

where S indicates a total number of nodes, C_{jq} represents the adjacency matrix, and g_q indicates the degree of node j neighbors.

4. Proposed Rider-Harris Hawk Optimization (RHHO) for Community Detection

The goal of community detection is to generate high quality community structures. To attain the goal, a novel h-Tversky Index (h-TI) is used, which combines h-index and Tversky similarity index for determining the nodes similarity. Based on the similarities, the community detection is performed considering the proposed RHHO algorithm. The proposed RHHO is designed by integrating RO [32] and HHO [33]. Here, the proposed RHHO algorithm is employed to determine the communities in multifaceted networks, which are done on the basis of optimizing the network modularity.

The proposed RHHO is a novel population initialization method, which is useful for accelerating population convergence. In addition, the fitness function, namely, h-Tversky similarity index, is newly devised for computing the individuals from the population.

4.1. Bipartite Graph. Consider a bipartite graph which is represented as a graph $G = (D, I)$ where D represents nodes' set and I indicates edges' set. The nodes' set D is expressed as $D = \{X \cup W\}$ where X and W indicate the node of type X and type W. The set of edges is represented by I. The edges pose the ability to connect different types of nodes, which are modeled as edges $n_{ef} \in I\,(b_e \in X; s_f \in W)$ and $|I|$ indicates the number of edges in a bipartite graph. The detection of community in a bipartite graph is expressed as $G = (D, I) = (X \cup W, I)$, which is employed to partition G into subgraphs, which are modeled as $G_e = (X_e \cup W_e, I_e)$ where $e = \{1, 2, \ldots, o\}$ and o is the total number of communities.

4.2. Determination of Node Similarity. The similarity is defined as a metric utilized for computing the amount of closeness between two pairs of nodes. Numerous node similarity measures based on the local information are described in the literature, which showed a different performance for determining the community structure from the complicated networks. However, the proposed method computes the node similarity in the network using a fitness function derived by the bipartite modularity and h-Tversky similarity index. Here, the fitness function is considered as a maximization function and is expressed as

$$F = \frac{M_a + M_G}{2}, \tag{5}$$

where M_a indicates a bipartite modularity and M_G represents the proposed h-Tversky similarity index considering a specific community structure. The proposed h-Tversky similarity index that considers a community of specific type of node in the network is given as

$$M_G = \frac{1}{E}\sum_{j-1}^{q}\sum_{q=x+1}^{S}\left(G_{jq}\right)\eta\left(r_j r_q\right), \tag{6}$$

where E represents a number of edges and η represents a function that acquires value 1 if $r_j = r_q$ and acquires value 0 otherwise, G_{jq} represents proposed h-Tversky similarity index, r_j indicates a group of node j, and r_q indicates a group of the node q.

4.3. Algorithmic Steps of Proposed Rider-Harris Hawk Optimization (RHHO) Algorithm. The HHO [33] is modified using the RO algorithm [32] wherein the update rule of HHO is updated based on the update rule of bypass rider in RO algorithm, thus obtaining the new algorithm, an RHHO, which is used to perform the community detection optimally. Basically, HHO is inspired by the chasing behavior of Harris hawks. The HHO provides a smoother transition among the exploitation and exploration and helps to boost the exploratory behavior. Moreover, the quality of solutions is improved during a number of iterations. The HHO algorithm is effective in handling the difficulties of search space with local optimal solutions. On the other hand, the RO algorithm is inspired by riders racing to reach a particular destination. Simultaneously, the usual RO algorithm displays good global optimal convergence. Based on the imaginary ideas and thoughts, nothing like the other nature-inspired and artificial computing algorithms, RO algorithm works in the fictional computing platform. In RO algorithm, the optimization behavior depends on four groups of riders, each presenting particular characteristics. The overtaking rider derives the new update rule in the HHO algorithm by using the RO algorithm. The advantages of bypass include the faster convergence with greater global neighborhoods. Hence, in the current RHHO, the optimal global convergence is enhanced at the maximal iteration. The algorithmic steps of the introduced RHHO are defined as follows.

4.3.1. Step 1: Initialization. First is initialization of population that is denoted as Z with total d rabbits, where $1 \le c \le d$,

$$Z = \{Z_1, Z_2, \ldots, Z_c, \ldots, Z_d\}, \tag{7}$$

where d is total solution, and Z_c indicates the cth solution.

4.3.2. Step 2: Determination of Fitness Function. The success rate or fitness of the solution is computed on the basis of bipartite modularity and proposed h-Tversky similarity index, which is elaborated in Section 4.2. Hence, the solution's fitness is depicted in equation (3).

4.3.3. Step 3: Determination of Update Position. The scheme of selection in an HHO [33] algorithm helps to progressively update the position to attain an improved position. Moreover, Harris' hawks enclose the anticipated prey by updating their places. In such circumstances, the current place updates the solution space as

$$Z(v+1) = Z_{\text{rab}}(v) - H|\Delta Z(v)|, \tag{8}$$

where $z(v+1)$ indicates the position of hawks in next iteration, $Z_{\text{rab}}(v)$ indicates the position of rabbit, $\Delta Z(v)$ specifies the difference between position vector of rabbit and current location of prey, and H represents the energy of prey.

$$Z(v+1) = Z_{\text{rab}}(v) - H\left|Z_{\text{rab}}(v) - Z(v)\right|, \tag{9}$$

where $Z(v)$ indicates the current position vector. Assuming $Z_{\text{rab}}(v)$ as positive, the above equation is represented as

$$Z(v+1) = Z_{\text{rab}}(v) - H\left(Z_{\text{rab}}(v) - Z(v)\right). \tag{10}$$

Here, the updated position of the bypass rider according to RO algorithm [32] is utilized in the process of update for maximizing the rate of success by finding the position of bypass rider. The bypass riders trail a common route without

stalking the foremost rider. The bypass rider's equation given by riders is represented as

$$Z(v+1) = \mu[Z(v) * \gamma(w) + Z(v) * [1 - \gamma(w)]], \quad (11)$$

where ϑ and ℓ denote the random digits between 0 and 1, inclusive, κ and μ are random digits, and k indicates the iterations. Assume $\mu = r$; the equation is rewritten as

$$Z(v+1) = \mu Z(v) * \gamma(w) + \mu Z(v)[1 - \gamma(w)], \quad (12)$$

$$Z(v+1) = Z(v)[\mu\gamma(w) + \mu[1 - \gamma(w)]], \quad (13)$$

$$Z(v) = \frac{Z(v+1)}{[\mu\gamma(w) + \mu[1 - \gamma(w)]]}. \quad (14)$$

Substituting equation (14) in (10), the update equation derived is

$$\begin{aligned} Z(v+1) &= Z_{\text{rab}}(v) - H\left(Z_{\text{rab}}(v) - \frac{Z(v+1)}{[\mu\gamma(w) + \mu[1 - \gamma(w)]]}\right), \\ Z(v+1) - \frac{HZ(v+1)}{\mu\gamma(w) + \mu[1 - \gamma(w)]} &= Z_{\text{rab}}(v) - H\left(Z_{\text{rab}}(v)\right), \\ Z(v+1)\left[1 - \frac{H}{\mu\gamma(w) + \mu[1 - \gamma(w)]}\right] &= Z_{\text{rab}}(v) - H\left(Z_{\text{rab}}(v)\right), \\ Z(v+1)\frac{\mu\gamma(w) + \mu[1 - \gamma(w)] - H}{\mu\gamma(w) + \mu[1 - \gamma(w)]} &= Z_{\text{rab}}(v) - H\left(Z_{\text{rab}}(v)\right). \end{aligned} \quad (15)$$

The final equation is given by

$$Z(v+1) = \frac{\mu}{\mu - H}\left[Z_{\text{rab}}(v) - H\left(Z_{\text{rab}}(v)\right)\right]. \quad (16)$$

4.3.4. Step 4: Determining the Best Solution. If the solution acquired the minimal fitness value, then it is the best solution. Furthermore, the parameters of the update of a rider are crucial in order to conclude the best solution.

4.3.5. Step 5: Termination. Repeat the steps in anticipation of the iteration reaching the maximum count.

5. Results and Discussion

The analysis of the community detection model using the proposed RHHO is demonstrated in this section with an effective comparative analysis to prove the effectiveness of the proposed model.

5.1. Experimental Setup. The proposed method is executed in a system running Windows 8 OS with 4 GB of RAM, Intel core i-3 processor, and the implementation is carried out in Python.

5.2. Database Description. The nodes for the experimentation are taken from the datasets, namely, the citation networks dataset [34] and the bipartite network dataset [35]. The description for each is given below.

5.2.1. Citation Networks Dataset. The experimentation is performed on a citation network dataset wherein the node denotes papers and edges denote citations. The citation network dataset can be employed for clustering the network and for studying the influence of citation networks to determine the most influential papers. Here, cit-HepPh and cit-HepTh are the two datasets used for performing the community detection:

(a) Analysis based on cit-HepPh: the cit-HepPh network is an instance of citation network dataset data that can be temporal, directed, or labeled with 34,546 nodes and 421,578 edges. The cit-HepPh network data is employed in the Arxiv High Energy Physics paper citation network.

(b) Analysis based on cit-HepTh: the cit-HepTh network data can be directed, temporal, or labeled with 27,770 nodes and 352,807 edges. The cit-HepTh network data is employed in the Arxiv High Energy Physics paper citation network.

5.2.2. Bipartite Network Dataset. The experimentation is performed on a bipartite network dataset wherein the network consists of two distinct node types, and all edges connect a node of the first type with a node of the second type. Here, Movie Lens 100 K was acquired from the official website (https://grouplens.org/datasets/movielens/), and the American Revolution network was obtained from the website (http://konect.cc/networks/brunson_revolution/) with two public datasets employed for performing the community detection.

(a) Analysis based on Movie Lens 100 K: this bipartite network consists of ten million movie ratings wherein the left nodes are users, and the right nodes are movies. An edge connecting the user and a movie represents the user who has rated the movie with the rating value attached to the edge.

(b) Analysis based on American Revolution: the bipartite network consists of membership information of thirty-six people in five organizations considering the period before the American Revolution. The list consists of well-known people like American activist Paul Revere. Here, the left nodes indicate persons, and the right nodes denote organizations. Here, the edge linking the person and the organization reveals that the person is a member of the organization.

5.3. Simulation Results. The simulation results of proposed community detection model considering citation network dataset and bipartite network dataset are illustrated in Figures 2 and 3.

5.3.1. Citation Networks Dataset. In this section, we analyze the simulation results of community detection based on citation networks datasets. Figure 2 elaborates the simulation results of the proposed community detection model using citation network dataset considering cit-HepPh and cit-HepTh datasets.

Figure 2(a) describes the original network using the cit-HepPh dataset and the communities identified considering the original network with the cit-HepPh dataset described in Figure 2(b). In Figure 2(b), green, red, and blue are the nodes representing different communities. Figure 2(c) elaborates the original network using the cit-HepTh dataset, and the communities detected by the original network using the cit-HepTh dataset are described in Figure 2(d). In Figure 2(d), green, red, and blue are the nodes with different communities present in the original network.

5.3.2. Bipartite Network Dataset. This section explains the simulation results of community detection based on bipartite networks datasets. Figure 3 elaborates the simulation results of the proposed community detection model using a bipartite network dataset considering Movie Lens 100 K and American Revolution datasets.

Figure 3(a) describes the original network using the Movie Lens 100 K dataset and the communities identified considering the original network with Movie Lens 100 K dataset described in Figure 3(b). In Figure 3(b), green, red, and blue represent different communities. Figure 3(c) elaborates the original network using the American Revolution dataset, and the communities detected by the original network using the American Revolution dataset are described in Figure 3(d). In Figure 2(d), green, red, and blue are the nodes with different communities' present in the original network.

5.4. Performance Analysis. The performance analysis of the proposed RHHO considering citation network dataset and bipartite network dataset is illustrated considering fitness and modularity measures.

5.4.1. Performance Analysis Based on Citation Networks Dataset Using cit-HepPh. Figure 4 illustrates the performance analysis of RHHO method using the cit-HepPh based fitness and modularity measures. The analysis of RHHO based on the fitness metric is portrayed in Figure 4(a). When the iteration is 1, the corresponding fitness values computed by the proposed RHHO with population = 5, 10, 15, 20, 25, and 30 are 6.628186, 0.000010, 0.000014, 0.000018, 0.000024, and 0.000035. Likewise, when the iteration is 250, then the corresponding fitness values computed by the proposed RHHO with population = 5, 10, 15, 20, 25, and 30 are 0.0059, 0.0182, 0.8430, 0.8771, 0.9431, and 0.9958, respectively. The analysis of the RHHO based on the modularity metric is illustrated in Figure 4(b). When the iteration is 1, the corresponding modularity values computed by proposed RHHO with population = 5, 10, 15, 20, 25, and 30 are 0.00038, 0.00113, 0.00274, 0.00327, 0.00422, and 0.00455. Likewise, when the iteration is 250, then the corresponding modularity values computed by proposed RHHO method with population = 5, 10, 15, 20, 25, and 30 are 6 0.62139, 0.65143, 0.65208, 0.65385, 0.66975, and 0.67397, respectively.

5.4.2. Performance Analysis Based on Citation Networks Dataset Using cit-HepTh. Figure 5 illustrates the performance analysis of the proposed RHHO using cit-HepTh based fitness and modularity measures. The analysis of the proposed RHHO based on the fitness metric is portrayed in Figure 5(a). When the iteration is 1, the corresponding fitness values computed by proposed RHHO with population = 5, 10, 15, 20, 25, and 30 are 8.7459, 0.000012, 0.000018, 0.000030, 0.000031, and 0.000068. Likewise, when the iteration is 250, then the corresponding fitness values computed by proposed RHHO with population = 5, 10, 15, 20, 25, and 30 are 0.0011, 0.0020, 0.9203, 0.9586, 0.9681, and 0.9932, respectively. The analysis of the proposed RHHO based on the modularity metric is illustrated in Figure 5(b). When the iteration is 1, the corresponding modularity values computed by proposed RHHO with population = 5, 10, 15, 20, 25, and 30 are 0.00146, 0.00177, 0.00211, 0.00346, 0.00361, and 0.00390. Likewise, when the iteration is 250, then the corresponding modularity values computed by proposed RHHO with population = 5, 10, 15, 20, 25, and 30 are 0.5954, 0.6006, 0.6270, 0.6306, 0.6391, and 0.6855, respectively.

5.4.3. Performance Analysis Based on Bipartite Network Dataset Using Movie Lens 100 K. Figure 6 illustrates the performance analysis of the proposed RHHO using Movie Lens 100 K-based fitness and modularity measures. The analysis of the proposed RHHO based on the fitness metric is portrayed in Figure 6(a). When the iteration is 1, the

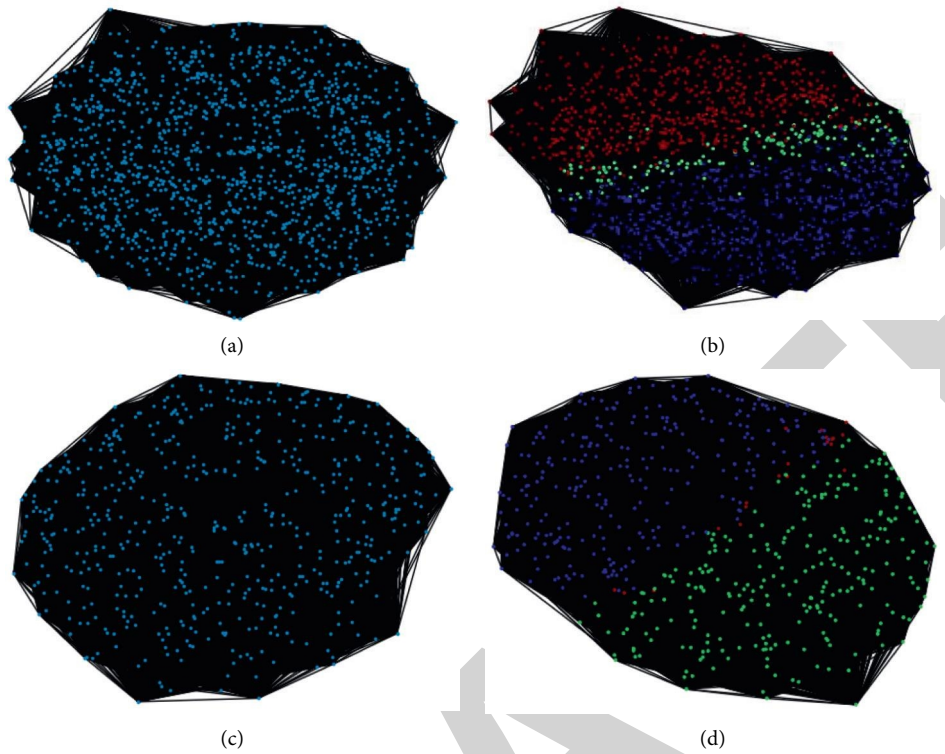

Figure 2: Analysis based on citation networks dataset using (a) original network using cit-HepPh dataset; (b) community detection using cit-HepPh dataset; (c) original network using the cit-HepTh dataset; (d) community detection using the cit-HepTh dataset.

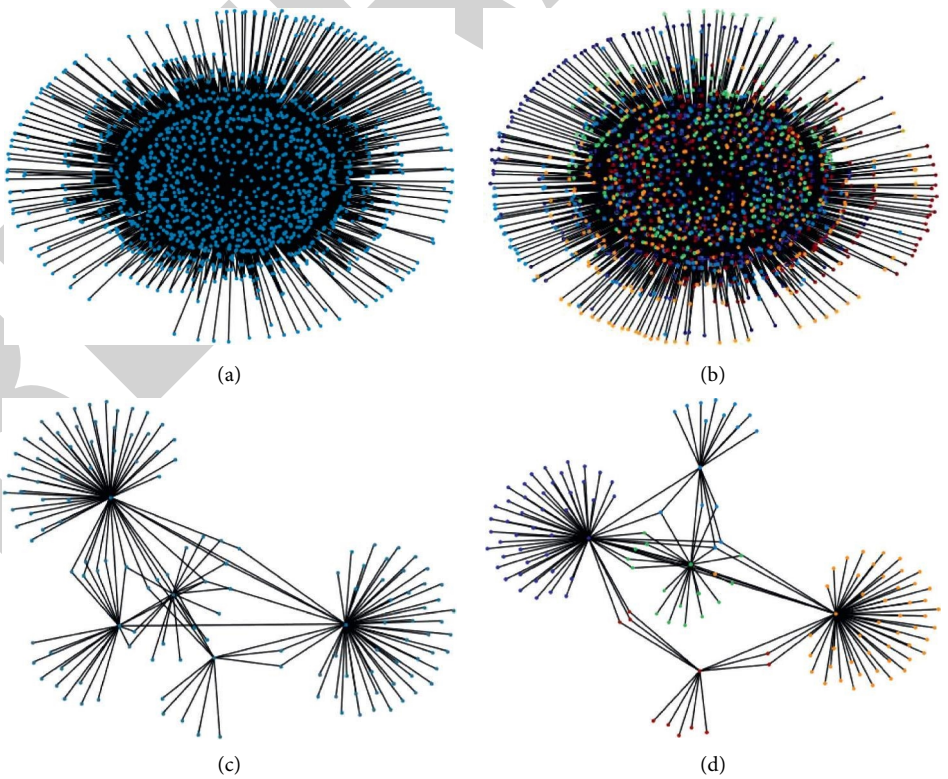

Figure 3: Analysis based on bipartite networks datasets using (a) original network using the Movie Lens 100 K dataset; (b) community detection using the Movie Lens 100 K dataset; (c) original network using the American Revolution dataset; (d) community detection using the American Revolution dataset.

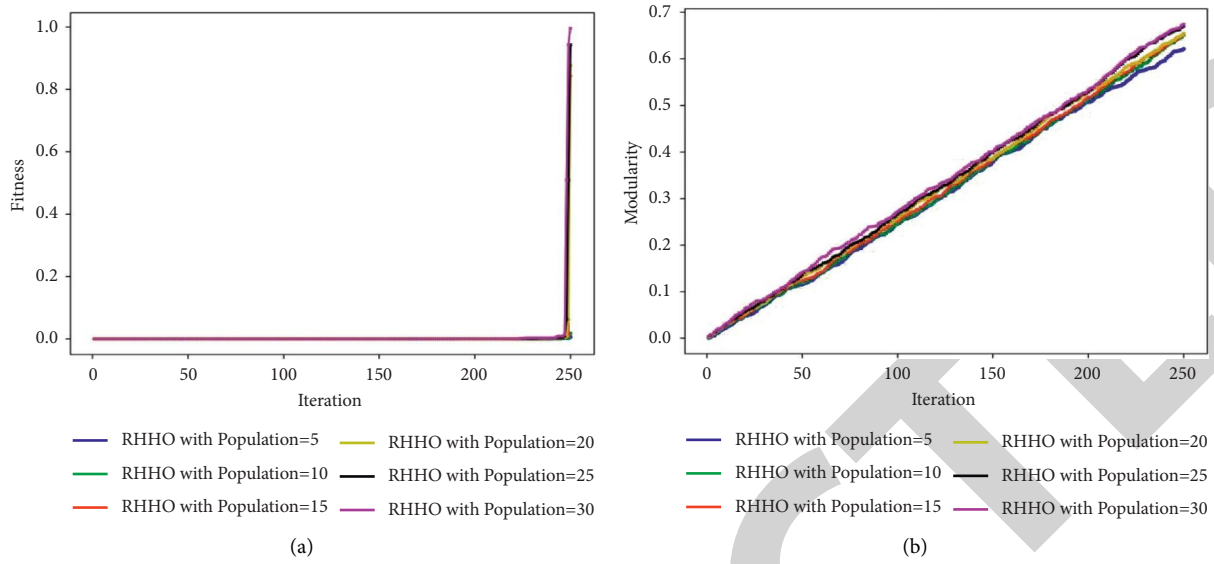

Figure 4: Performance analysis of proposed RHHO method using the cit-HepPh considering (a) fitness and (b) modularity.

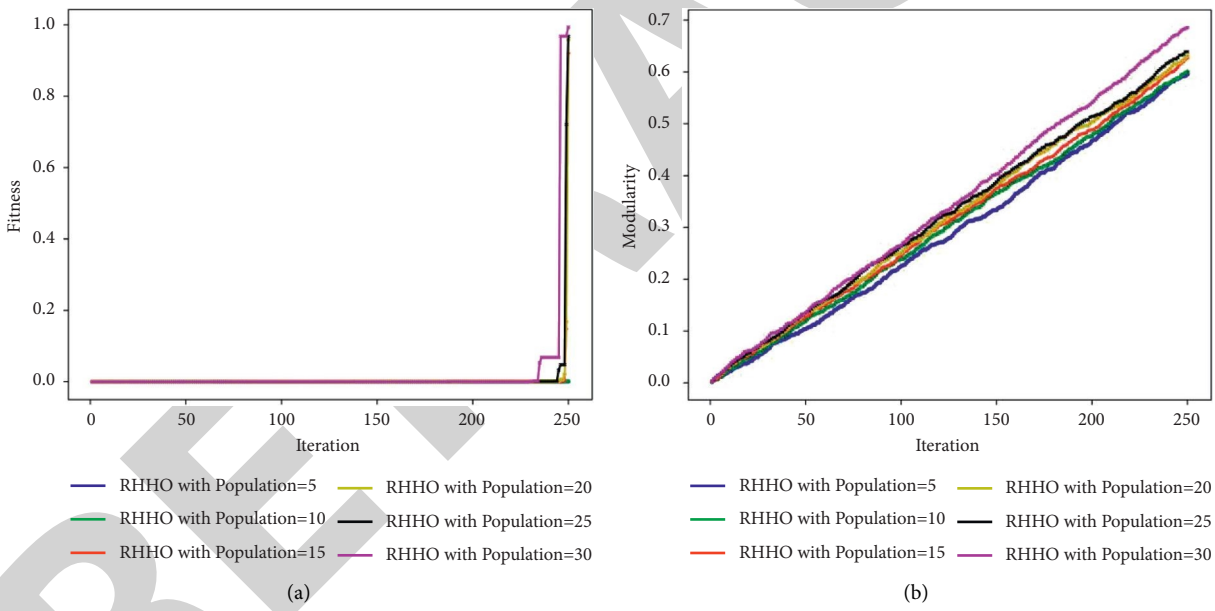

Figure 5: Performance analysis of proposed RHHO using the cit-HepTh considering (a) fitness and (b) modularity.

corresponding fitness values computed by proposed RHHO with population = 5, 10, 15, 20, 25, and 30 are 0.0000061, 0.000010, 0.000012, 0.000016, 0.000031, and 0.000063. Likewise, when the iteration is 250, then the corresponding fitness values computed by proposed RHHO with population = 5, 10, 15, 20, 25, and 30 are 0.00076, 0.00576, 0.07740, 0.88287, 0.97519, and 0.99201, respectively. The analysis of the proposed RHHO based on the modularity metric is illustrated in Figure 6(b). When the iteration is 1, the corresponding modularity values computed by proposed RHHO with population = 5, 10, 15, 20, 25, and 30 are 0.000419, 0.00204, 0.00213, 0.00284, 0.00303, and 0.00376. Likewise, when the iteration is 250, then the corresponding modularity values computed by proposed RHHO with population = 5, 10, 15, 20, 25, and 30 are 0.6069, 0.6205, 0.6398, 0.6404, 0.6542, and 0.6790, respectively.

5.4.4. Performance Analysis Based on Bipartite Network Dataset Using American Revolution. Figure 7 illustrates the performance analysis of the proposed RHHO using American Revolution-based fitness and modularity measures. The analysis of the proposed RHHO based on the fitness metric is portrayed in Figure 7(a). When the iteration is 1, the corresponding fitness values computed by proposed RHHO with population = 5, 10, 15, 20, 25, and 30 are

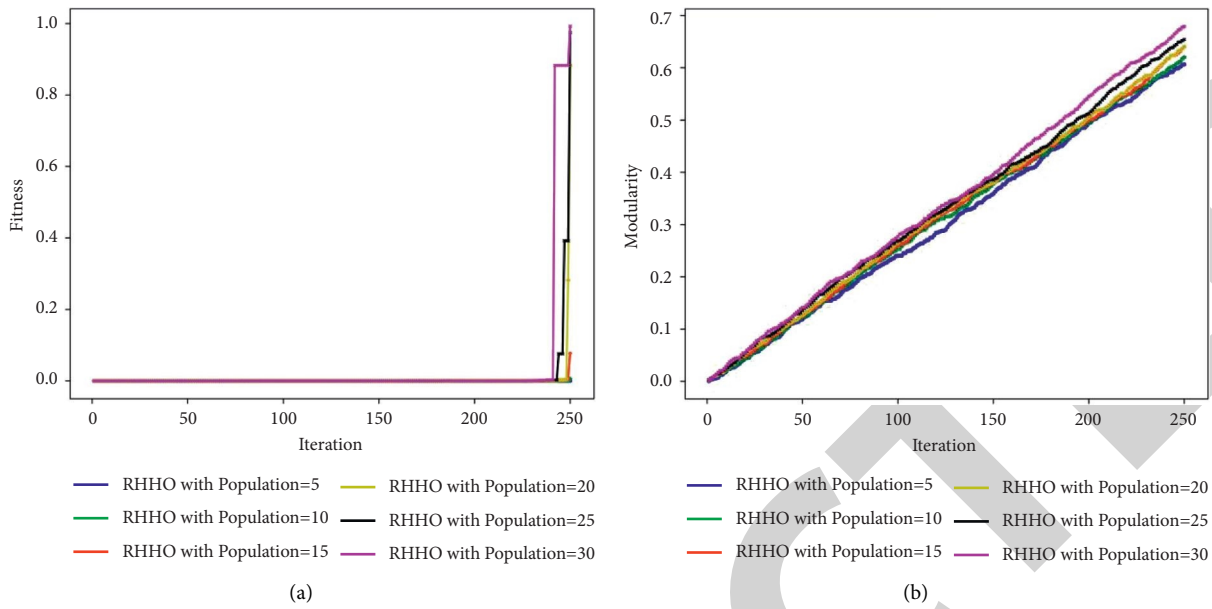

Figure 6: Performance analysis of proposed RHHO using Movie Lens 100 K considering (a) fitness and (b) modularity.

0.000021, 0.000026, 0.000036, 0.000044, 0.000051, and 0.00040. Likewise, when the iteration is 250, then the corresponding fitness values computed by proposed RHHO with population = 5, 10, 15, 20, 25, and 30 are 0.0016, 0.0017, 0.0069, 0.5085, 0.9140, and 0.9962, respectively. The analysis of the proposed RHHO based on the modularity metric is illustrated in Figure 7(b). When the iteration is 1, the corresponding modularity values computed by proposed RHHO population = 5, 10, 15, 20, 25, and 30 are 0.00023, 0.00300, 0.00311, 0.00327, 0.00436, and 0.00496. Likewise, when the iteration is 250, then the corresponding modularity values computed by proposed RHHO with population = 5, 10, 15, 20, 25, and 30 are 0.57925, 0.61982, 0.64765, 0.65844, 0.66412, and 0.67721, respectively.

5.5. Competing Methods. The methods, such as h-index-based link prediction [9], MAGA [31], GA [36], MATMCD-BN [28], and HHO [33], are employed for the comparison with the proposed RHHO.

5.6. Comparative Analysis. The comparative analysis of the proposed model is performed by evaluating the performance of other techniques based on fitness and modularity. The analysis is conducted by varying the number of iterations.

5.6.1. Analysis Based on Citation Networks Dataset Using cit-HepPh. Figure 8 illustrates the analysis of the methods using cit-HepPh based fitness and modularity measures. The analysis of the methods based on the fitness metric is portrayed in Figure 8(a). When the iteration is 1, the corresponding fitness values computed by h-index-based link prediction, MAGA, GA, MATMCD-BN, HHO, and proposed RHHO are 0.0000513, 0.00183, 0.47324, 0.48179, 0.50100, and 0.51568. Likewise, when the iteration is 250, the corresponding fitness values computed by h-index-based link prediction, MAGA, GA, MATMCD-BN, HHO, and proposed RHHO are 0.130475, 0.574730, 0.59360, 0.60131, 0.64708, and 0.66048, respectively. The analysis of methods based on modularity metric is illustrated in Figure 8(b). When the iteration is 1, the corresponding modularity values computed by h-index-based link prediction, MAGA, GA, MATMCD-BN, HHO, and proposed RHHO are 0.000759, 0.00109, 0.00138, 0.00190, 0.00211, and 0.00285. Likewise, when the iteration is 250, the corresponding modularity values computed by h-index-based link prediction, MAGA, GA, MATMCD-BN, HHO, and proposed RHHO are 0.36686, 0.37422, 0.37475, 0.38952, 0.39476, and 0.77560, respectively.

5.6.2. Analysis Based on Citation Networks Dataset Using cit-HepTh. Figure 9 illustrates the analysis of the methods using cit-HepTh based fitness and modularity measures. The analysis of the methods based on the fitness metric is portrayed in Figure 9(a). When the iteration is 1, the corresponding fitness values computed by h-index-based link prediction, MAGA, GA, MATMCD-BN, HHO, and proposed RHHO are 0.000118, 0.00095, 0.36191, 0.40654, 0.43435, and 0.48270. Likewise, when the iteration is 250, the corresponding fitness values computed by h-index-based link prediction, MAGA, GA, MATMCD-BN, HHO, and proposed RHHO are 0.36032, 0.51114, 0.54192, 0.55247, 0.63780, and 0.69778, respectively. The analysis of the methods based on modularity metric is illustrated in Figure 9(b). When the iteration is 1, the corresponding modularity values computed by h-index-based link prediction, MAGA, GA, MATMCD-BN, HHO, and proposed RHHO are 0.000375, 0.00083, 0.00101, 0.00120, 0.00134, and 0.00298. Likewise, when the iteration is 250, the corresponding modularity values computed by h-index-based

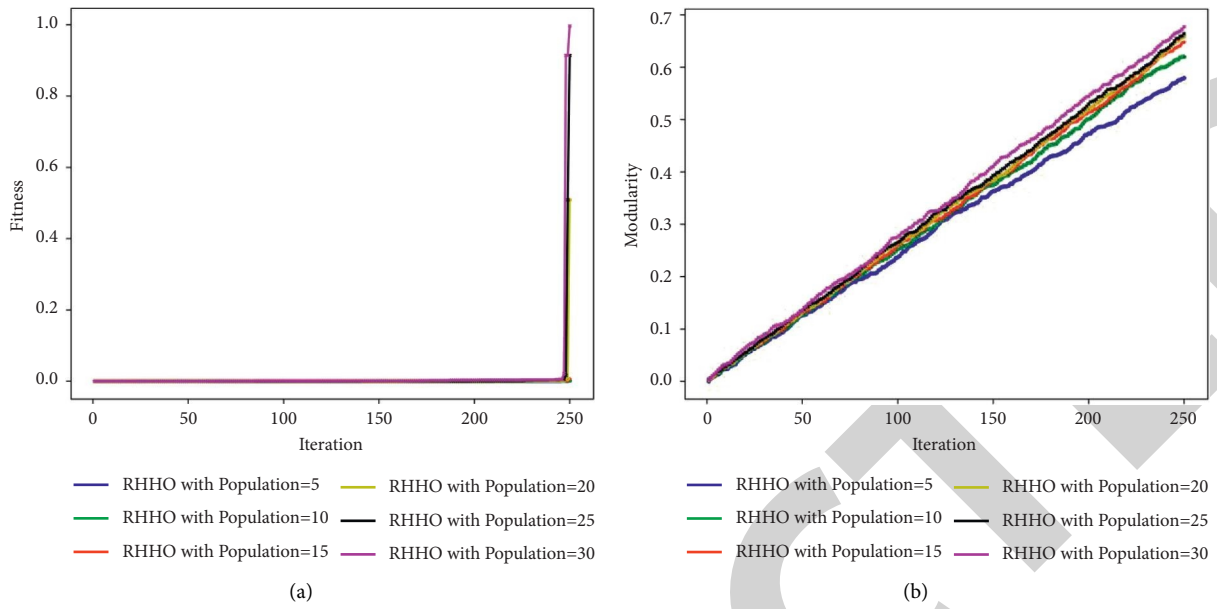

Figure 7: Performance analysis of proposed RHHO method using the American Revolution considering (a) fitness and (b) modularity.

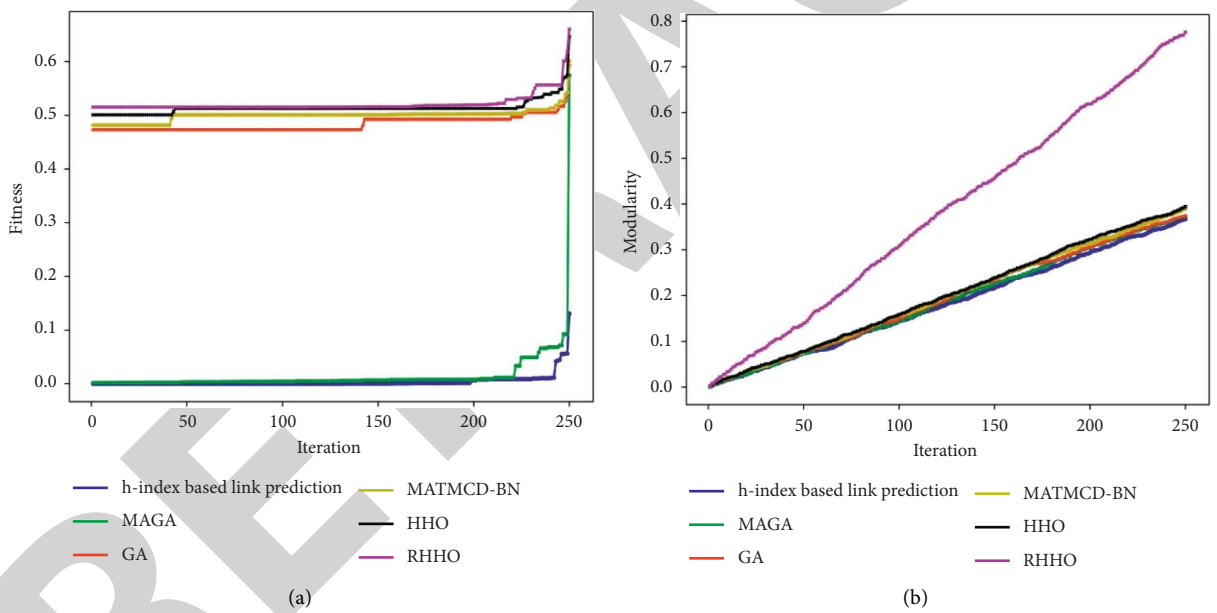

Figure 8: Analysis of methods using the cit-HepPh considering (a) fitness and (b) modularity.

link prediction, MAGA, GA, MATMCD-BN, HHO, and proposed RHHO are 0.34853, 0.37638, 0.37948, 0.38210, 0.38734, and 0.77807, respectively.

5.6.3. Analysis Based on Bipartite Network Dataset Using Movie Lens 100 K. Figure 10 illustrates the analysis of the methods using Movie Lens 100 K-based fitness and modularity measures. The analysis of the methods based on the fitness metric is portrayed in Figure 10(a). When the iteration is 1, the corresponding fitness values computed by h-index-based link prediction, MAGA, GA, MATMCD-BN, HHO, and proposed RHHO are 0.000035, 0.00069, 0.39608, 0.41400, 0.41713, and 0.49527. Likewise, when the iteration is 250, then the corresponding fitness values computed by h-index-based link prediction, MAGA, GA, MATMCD-BN, HHO, and proposed RHHO are 0.04802, 0.31454, 0.52216, 0.58928, 0.64062, and 0.68944, respectively. The analysis of the methods based on modularity metric is illustrated in Figure 10(b). When the iteration is 1, the corresponding modularity values computed by h-index-based link prediction, MAGA, GA, MATMCD-BN, HHO, and proposed RHHO are 0.00035, 0.00129, 0.00163, 0.00168, 0.00196, and 0.00553. Likewise, when the iteration is 250, then the corresponding modularity values computed by h-index-based link prediction, MAGA, GA, MATMCD-BN, HHO, and

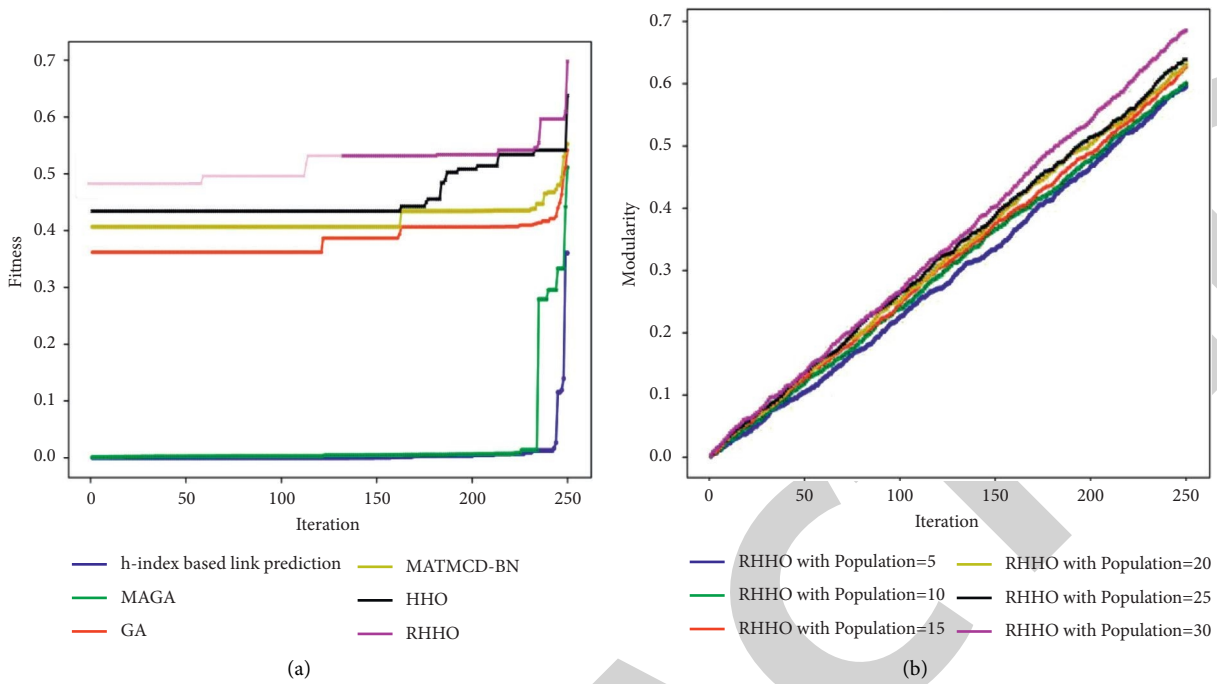

Figure 9: Analysis of methods using the cit-HepTh considering (a) fitness and (b) modularity.

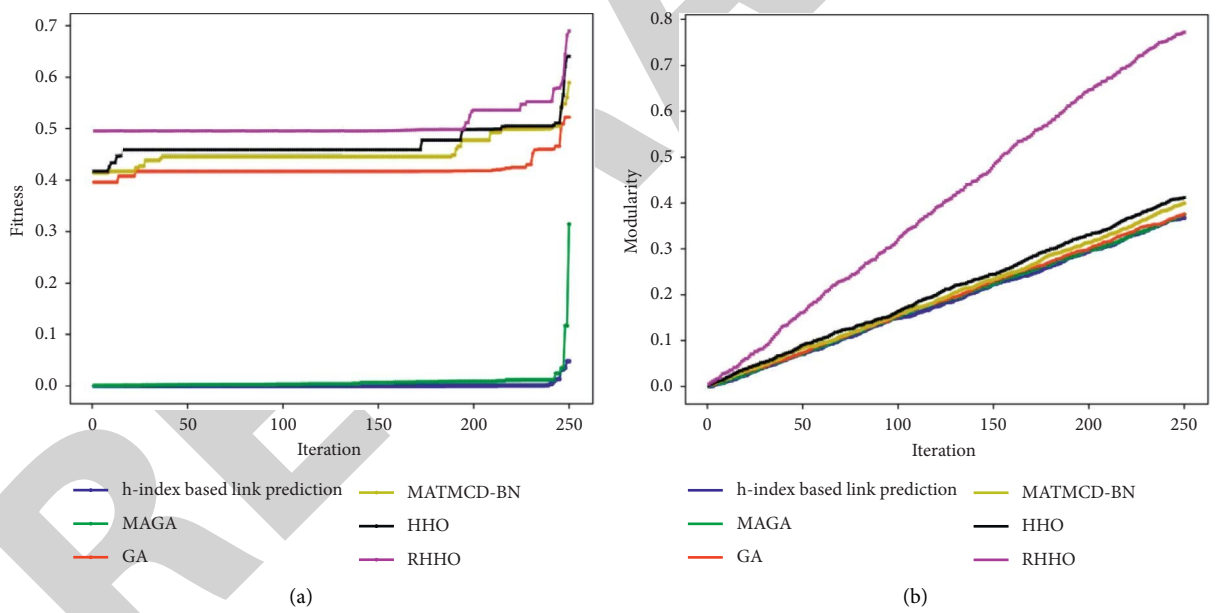

Figure 10: Analysis of methods using the Movie Lens 100 K considering (a) fitness and (b) modularity.

proposed RHHO are 0.36727, 0.37546, 0.37596, 0.39952, 0.41170, and 0.77191, respectively.

5.6.4. Analysis Based on Bipartite Network Dataset Using American Revolution. Figure 11 illustrates the analysis of the methods using Movie Lens 100 K-based fitness and modularity measures. The analysis of the methods based on the fitness metric is portrayed in Figure 11(a). When the iteration is 1, the corresponding fitness values computed by h-index-based link prediction, MAGA, GA, MATMCD-BN, HHO, and proposed RHHO are 0.00053, 0.00142, 0.23572, 0.26296, 0.3476, and 0.4756. Likewise, when the iteration is 250, then the corresponding fitness values computed by h-index-based link prediction, MAGA, GA, MATMCD-BN, HHO, and proposed RHHO are 0.31137, 0.36367, 0.47276, 0.64272, 0.73190, and 0.74353, respectively. The analysis of the methods based on modularity metric is illustrated in Figure 11(b). When the iteration is 1, the corresponding modularity values computed by h-index-based link

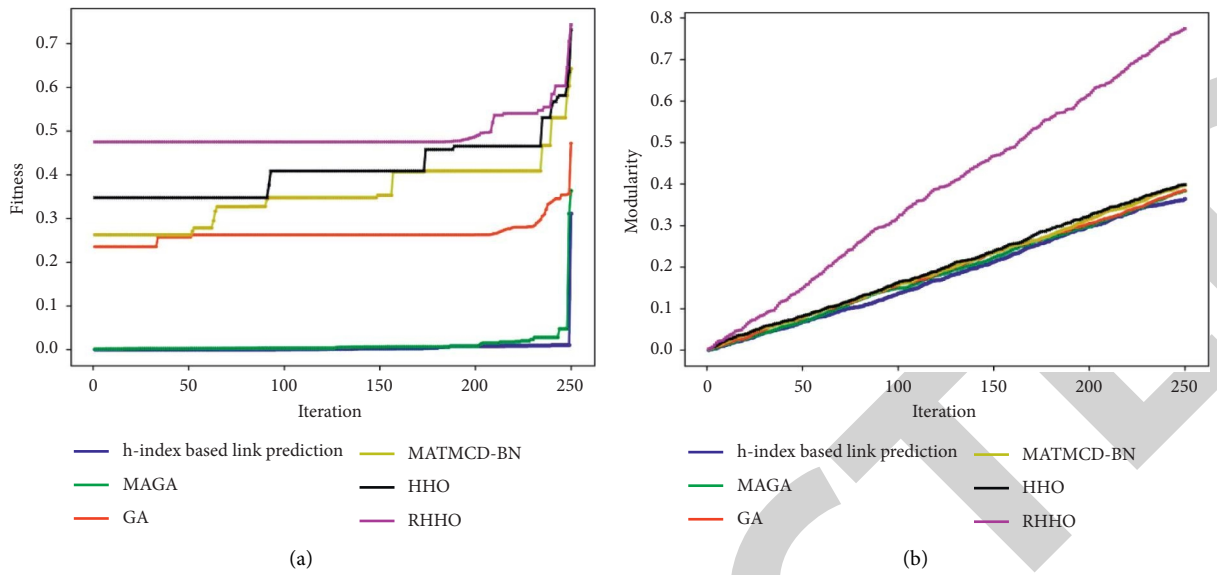

Figure 11: Analysis of methods using the American Revolution considering (a) fitness and (b) modularity.

Table 1: Comparative results of proposed RHHO method with other existing methods in terms of modularity and fitness.

Dataset	Metrics	h-index-based link prediction	MAGA	GA	MATMCD-BN	HHO	Proposed RHHO
cit-HepPh	Fitness	0.130475	0.574730	0.59360	0.60131	0.64708	0.66048
	Modularity	0.36686	0.37422	0.37475	0.38952	0.39476	0.77560
cit-HepTh	Fitness	0.36032	0.51114	0.54192	0.55247	0.63780	0.69778
	Modularity	0.34853	0.37638	0.37948	0.38210	0.38734	0.77807
Movie Lens 100 K	Fitness	0.04802	0.31454	0.52216	0.58928	0.64062	0.68944
	Modularity	0.36727	0.37546	0.37596	0.39952	0.41170	0.77191
American Revolution	Fitness	0.31137	0.36367	0.47276	0.64272	0.73190	0.74353
	Modularity	0.36400	0.38391	0.38523	0.39717	0.39896	0.77433

prediction, MAGA, GA, MATMCD-BN, HHO, and proposed RHHO are 0.000207, 0.00116, 0.00190, 0.00217, 0.00224, and 0.00275. Likewise, when the iteration is 250, then the corresponding modularity values computed by h-index-based link prediction, MAGA, GA, MATMCD-BN, HHO, and proposed RHHO are 0.36400, 0.38391, 0.38523, 0.39717, 0.39896, and 0.77433, respectively.

5.7. Comparative Discussion. Table 1 deliberates the comparative analysis of proposed RHHO with other existing methods in terms of modularity and fitness. The analysis is done by considering citation network and bipartite network dataset. Considering cit-HepPh, the maximal fitness is computed by proposed RHHO with 0.66048 whereas the fitness values of existing h-index-based link prediction, MAGA, GA, MATMCD-BN, and HHO are 0.130475, 0.574730, 0.59360, 0.60131, and 0.64708. The maximal modularity is computed by proposed RHHO with 0.77560 whereas the modularity values of existing h-index-based link prediction, MAGA, GA, MATMCD-BN, and HHO are 0.36686, 0.37422, 0.37475, 0.38952, and 0.39476, respectively. Likewise, considering cit-HepTh, the maximal fitness is 0.69778, and maximal modularity is 0.77807. Based on Movie Lens 100 K, the maximal fitness is 0.68944, and maximal modularity is 0.77191. Similarly, considering American Revolution, the maximal fitness is 0.74353 and maximal modularity is 0.77433. It is also observed that the proposed RHHO outperformed other methods with maximal fitness of 0.74353 and maximal modularity of 0.77433 considering American Revolution network, respectively.

6. Conclusion

In the complex network structure, including bipartite networks, community detection is a major critical task. Community identification in a bipartite network not only reveals details about hierarchical structure of multifaceted network but also assists in better understanding of the core functions of the network and subsequently information recommendation. This paper presents a community detection method in a bipartite network considering the node similarity measure. In order to check the similarity of nodes, the h-Tversky measure is newly designed by modifying h-index based on Tversky index. In addition, a novel algorithm Rider-Harris Hawks Optimization (RHHO) is devised for community detection and developed by integrating RO and HHO algorithms to speed up the rate of convergence in the algorithm. The fitness is newly devised considering modularity and proposed h-Tversky index for

evaluating the node similarity. The purpose of incorporating modularity in the fitness function is to quantify the goodness of specific division of network to compute the precision of the proposed community detection. The proposed method showed effective performance with maximal fitness of 0.74353 and maximal modularity of 0.77433 using American Revolution network from bipartite network dataset. It can be utilized in machine learning discipline to detect groups with similar characteristics and properties inside a stock market or a social network like a bipartite network and then extract these groups for different reasons. In future, the MapReduce approach can be employed for determining the overlapping communities where more than one node is shared between the communities.

Data Availability

The Movie Lens 100 K dataset is publicly available at https://grouplens.org/datasets/movielens/ and American Revolution network dataset is publicly available at http://konect.cc/networks/brunson_revolution/.

Conflicts of Interest

The authors declare no conflicts of interest about the publication of this research article.

Acknowledgments

This research was supported by the Researchers Supporting Project number (RSP-2021/244), King Saud University, Riyadh, Saudi Arabia.

References

[1] S. Zhang, G. Jin, X.-S. Zhang, and L. Chen, "Discovering functions and revealing mechanisms at molecular level from biological networks," *Proteomics*, vol. 7, no. 16, pp. 2856–2869, 2007.

[2] S. Zhang, J. Zhao, and X.-S. Zhang, "Common community structure in time-varying networks," *Physical Review E*, vol. 85, no. 5, 2012.

[3] Z. Li, R.-S. Wang, S. Zhang, and X.-S. Zhang, "Quantitative function and algorithm for community detection in bipartite networks," *Information Sciences*, vol. 367-368, no. 1, pp. 874–889, 2016.

[4] H. Gmati, A. Mouakher, A. Gonzalez-Pardo, and D. Camacho, "A new algorithm for communities detection in social networks with node attributes," *Journal of Ambient Intelligence and Humanized Computing*, pp. 1–13, 2018.

[5] D. Chen, W. Zhao, D. Wang, and X. Huang, "Similarity-based local community detection for bipartite networks," *Filomat*, vol. 32, no. 5, pp. 1559–1570, 2018.

[6] L. Xiong, G.-Z. Wang, and H.-C. Liu, "New community estimation method in bipartite networks based on quality of filtering coefficient," *Scientific Programming*, vol. 2019, Article ID 4310561, 12 pages, 2019.

[7] F. Chang, B. Zhang, Y. Zhao, S. Wu, and K. Yoshigoe, "Overlapping community detecting based on complete bipartite graphs in micro-bipartite network bi-egonet," *IEEE Access*, vol. 7, pp. 91488–91498, 2019.

[8] C. Carusi and G. Bianchi, "Scientific community detection via bipartite scholar/journal graph co-clustering," *Journal of Informetrics*, vol. 13, no. 1, pp. 354–386, 2019.

[9] W. Zhou, J. Gu, and Y. Jia, "h-index-based link prediction methods in citation network," *Scientometrics*, vol. 117, no. 1, pp. 381–390, 2018.

[10] C. Zhou, L. Feng, and Q. Zhao, "A novel community detection method in bipartite networks," *Physica A: Statistical Mechanics and Its Applications*, vol. 492, pp. 1679–1693, 2018.

[11] L. Feng, C. Zhou, and Q. Zhao, "A spectral method to find communities in bipartite networks," *Physica A: Statistical Mechanics and Its Applications*, vol. 513, pp. 424–437, 2019.

[12] M. Girvan and M. E. J. Newman, "Community structure in social and biological networks," *Proceedings of the National Academy of Sciences*, vol. 99, no. 12, pp. 7821–7826, 2002.

[13] V. D. Blondel, J.-L. Guillaume, R. Lambiotte, and E. Lefebvre, "Fast unfolding of communities in large networks," *Journal of Statistical Mechanics: Theory and Experiment*, vol. 2008, no. 10, Article ID P10008, 2008.

[14] E. A. Corrêa Jr., A. A. Lopes, and D. R. Amancio, "Word sense disambiguation: a complex network approach," *Information Sciences*, vol. 442-443, pp. 103–113, 2018.

[15] W. Tang and P. Daoutidis, "Network decomposition for distributed control through community detection in input-output bipartite graphs," *Journal of Process Control*, vol. 64, pp. 7–14, 2018.

[16] T. Viard, R. Fournier-S'niehotta, C. Magnien, and M. Latapy, "Discovering patterns of interest in IP traffic using cliques in bipartite link streams," in *Proceedings of the 2018 International Workshop on Complex Networks*, Boston, MA, USA, March 2018.

[17] Z.-A. Huang, Y.-A. Huang, Z.-H. You, Z. Zhu, and Y. Sun, "Novel link prediction for large-scale miRNA-lncRNA interaction network in a bipartite graph," *BMC Medical Genomics*, vol. 11, no. S6, pp. 17–27, 2018.

[18] S. Rechner, L. Strowick, and M. Müller-Hannemann, "Uniform sampling of bipartite graphs with degrees in prescribed intervals," *Journal of Complex Networks*, vol. 6, no. 6, pp. 833–858, 2018.

[19] W. Guan, X. Wen, L. Wang, Z. Lu, and Y. Shen, "A service-oriented deployment policy of end-to-end network slicing based on complex network theory," *IEEE Access*, vol. 6, pp. 19691–19701, 2018.

[20] T. Bian and Y. Deng, "Identifying influential nodes in complex networks: a node information dimension approach," *Chaos: An Interdisciplinary Journal of Nonlinear Science*, vol. 28, no. 4, Article ID 043109, 2018.

[21] Z. Gao, K. Zhang, W. Dang et al., "An adaptive optimal-Kernel time-frequency representation-based complex network method for characterizing fatigued behavior using the SSVEP-based BCI system," *Knowledge-Based Systems*, vol. 152, pp. 163–171, 2018.

[22] X. Huang, D. Chen, T. Ren, and D. Wang, "A survey of community detection methods in multilayer networks," *Data Mining and Knowledge Discovery*, vol. 35, no. 1, pp. 1–45, 2021.

[23] M. Rostami, K. Berahmand, and S. Forouzandeh, "A novel community detection based genetic algorithm for feature selection," *Journal of Big Data*, vol. 8, no. 1, pp. 1–27, 2021.

[24] X. Li, Y. Chen, and J. Xu, "Convex relaxation methods for community detection," *Statistical Science*, vol. 36, no. 1, pp. 2–15, 2021.

[25] H. Joo, M. Lee, J. Kim, J. Jung, J. Kwak, and H. S. Kim, "Stream gauge network grouping analysis using community

Hindawi
Journal of Mathematics
Volume 2024, Article ID 9852879, 1 page
https://doi.org/10.1155/2024/9852879

Retraction

Retracted: Music Segmentation Algorithm Based on Self-Adaptive Update of Confidence Measure

Journal of Mathematics

Received 23 January 2024; Accepted 23 January 2024; Published 24 January 2024

This article has been retracted by Hindawi following an investigation undertaken by the publisher [1]. This investigation has uncovered evidence of one or more of the following indicators of systematic manipulation of the publication process:

(1) Discrepancies in scope

(2) Discrepancies in the description of the research reported

(3) Discrepancies between the availability of data and the research described

(4) Inappropriate citations

(5) Incoherent, meaningless and/or irrelevant content included in the article

(6) Manipulated or compromised peer review

The presence of these indicators undermines our confidence in the integrity of the article's content and we cannot, therefore, vouch for its reliability. Please note that this notice is intended solely to alert readers that the content of this article is unreliable. We have not investigated whether authors were aware of or involved in the systematic manipulation of the publication process.

Wiley and Hindawi regrets that the usual quality checks did not identify these issues before publication and have since put additional measures in place to safeguard research integrity.

We wish to credit our own Research Integrity and Research Publishing teams and anonymous and named external researchers and research integrity experts for contributing to this investigation.

The corresponding author, as the representative of all authors, has been given the opportunity to register their agreement or disagreement to this retraction. We have kept a record of any response received.

References

[1] J. Li, "Music Segmentation Algorithm Based on Self-Adaptive Update of Confidence Measure," *Journal of Mathematics*, vol. 2021, Article ID 8329088, 9 pages, 2021.

Hindawi
Journal of Mathematics
Volume 2021, Article ID 8329088, 9 pages
https://doi.org/10.1155/2021/8329088

Research Article

Music Segmentation Algorithm Based on Self-Adaptive Update of Confidence Measure

Jianhua Li

School of Music and Dance, Huaihua University, Huaihua, Hunan 418000, China

Correspondence should be addressed to Jianhua Li; ljh@hhtc.edu.cn

Received 9 October 2021; Revised 23 October 2021; Accepted 27 October 2021; Published 8 November 2021

Academic Editor: Naeem Jan

To improve the accuracy of music segmentation and enhance segmentation effect, an algorithm based on the adaptive update of confidence measure is proposed. According to the theory of compressed sensing, the music fragments are denoised, and thus the denoised signals are subjected to short-term correlation analysis. Then, the pitch frequency is extracted, and the music fragments are roughly classified by wavelet transform to realize the preprocessing of the music fragments. In order to calculate the confidence measure of the music segment, the SVM method is used, whereas the adaptive update of the confidence measure is studied using reliable data selection algorithm. The dynamic threshold notes are segmented according to the update result to realize music segmentation. Experimental results show that the recall and precision values of the algorithm reach 97.5% and 93.8%, respectively, the segmentation error rate is low, and it can achieve effective segmentation of music fragments, indicating that the algorithm is effective.

1. Introduction

The audio signal in a music clip is a complex mixture of multiple sound signals (voice, music, environmental sound, etc.) intertwined. When converting from one type of audio signal to another, some auditory features will change, and the difference between the front and back is large, just like the visual features in the image sequence [1]. The purpose of music segmentation is to distinguish different audio signals according to audio characteristics in preparation for subsequent audio processing, such as classification [2]. Through music segmentation, different processing methods can be adopted for different types of audio signals to reduce the search space for further processing. Besides, the results of this segmentation reflect the high-level semantic features of audio content, especially the features of audio clips, which are of great importance for music retrieval and understanding music content [3].

At present, the commonly used music segmentation methods mainly include real-time audio segmentation method based on adaptive threshold adjustment, audio segmentation algorithm based on hierarchical entropy detection, audio segmentation algorithm based on credibility change trend, and audio segmentation algorithm based on fixed-length window hierarchical detection. Among them, the real-time audio segmentation method based on threshold adaptive adjustment mainly aims at real-time audio applications, takes the environmental factor as the measurement of external environment detection, and uses it to adaptively adjust the segmentation threshold. Finally, the table lookup method is used to judge the segmentation type through state transition to achieve a balance between efficiency and accuracy, so as to realize music segmentation. The audio segmentation algorithm based on hierarchical entropy detection uses the fixed length analysis window hierarchical structure to traverse the audio stream, and the jump points are detected according to the entropy change trend in the window. Experimental results show that the algorithm is an effective audio segmentation method. The audio segmentation algorithm based on the change trend of credibility adopts the fixed length sliding window detection structure to reduce the cumulative error, calculates the credibility of each audio frame in the window, and detects the jump point according to the change trend of credibility,

so as to avoid the false detection caused by threshold selection and hard threshold decision. Experimental results show that the algorithm has good segmentation performance. The audio segmentation algorithm based on fixed-length window layered detection uses fixed-length window sliding to traverse the audio stream, and the detected jump points are calculated from top to bottom in the window. Finally, the detected candidate jump points are verified by local extreme value determination method. Experimental results show that the processing speed of this algorithm is greatly improved compared with other segmentation algorithms.

Although the above methods can realize music segmentation because the noise interference is not considered, the error rate of segmentation results is high, and the accuracy needs to be improved. Therefore, this paper proposes a music segmentation algorithm based on an adaptive update of confidence measure.

In this paper, we classify the musical fragments following some methods and theories in Section 2. Further research on the segmentation algorithm to achieve accurate music segmentation is presented in Section 3. Additionally, experimental verifications on the effectiveness of the music segmentation algorithm based on the adaptive update of the confidence measure are done in Section 4. A conclusion is presented in Section 5 that includes a summary of the methods used to solve the problem of low accuracy of music segmentation.

2. Music Preprocessing

In this section, the accuracy of segmentation is taken into consideration, where we use vocal and nonvocal attributes of music segments. To avoid the noise signals that occur in this situation, the compressed sensing theory is used. The classification of music by wavelet transform to realize if the music fragments are ready to be processed is also presented.

2.1. Music Segment Presegmentation. Music signal has short-term stationary characteristics; that is, the signal characteristics are basically stable in a limited short time period. According to different music signal characteristics, the duration of stationary segments ranges from hundreds of milliseconds to several seconds. Segment presegmentation is to divide the continuous nonstationary signal flow into a series of short-term stationary segments. At present, the commonly used presegmentation methods can be divided into fixed-length segmentation and indefinite length segmentation. The former directly divides the processed signal into several equal length segments according to the characteristics of the processed signal and assumes that each segment contains only one kind of sound source. In the latter, the whole signal stream is predivided into several short segments by the signal spectrum breakpoint detection algorithm. These two presegmentation algorithms are difficult to avoid presegmentation errors; that is, a segment may contain different sound sources, resulting in segmentation errors.

In an effort to become more precise, this paper used to break music segments into small forms of vocal and nonvocal model training because of their quality that directly affects the accuracy of music segment presegmentation. Suppose that there is a set $A = \{a_1, a_2, \ldots, a_n\}$ such that a_i either belongs to a vocal or to a nonvocal music segment. Let $\{b_{11}, b_{12}, \ldots, b_{1m}\}$ be the m-frame feature vector of the a_i segment. φ_c and φ_{nc} are the vocal and nonvocal presegmentation models, respectively. The log likelihood rates of the two are

$$\begin{aligned} \varphi_c(a_i) &= \mathrm{net}_i(k) \times m_1(k) \quad i = 1, 2, \ldots, N, \\ \varphi_{nc}(a_i) &= \mathrm{net}_i(k) \times m_2(k) \quad i = 1, 2, \ldots, N. \end{aligned} \tag{1}$$

In the previous formula, $\mathrm{net}_i(k)$ represents the music piece to be divided; $m_1(k)$ represents the vocal music model that matches the music piece to be divided; $m_2(k)$ represents the nonvocal music model that matches the music piece to be divided. If $\varphi_c(a_i) > \varphi_{nc}(a_i)$, then a_i is vocal music; otherwise, it is nonvocal music.

Due to the many types and genres of music and songs, the instruments used, the way of playing, the singer's voice, and singing are all very different. In order to fully characterize different music characteristics as much as possible, a large amount of music is often needed as training data to establish φ_c and φ_{nc}. On the one hand, this increases the complexity of the model. On the other hand, it increases the mismatch between the model and a particular piece of music to be segmented. Therefore, reducing the complexity of the model while making it closer to each piece of music to be processed is the key to improving the segmentation accuracy.

2.2. Music Signal Denoising. According to Section 2.1, the vocal and nonvocal attributes of music segments can be preliminarily obtained. Although it provides a certain basis for music segmentation, due to the influence of external interference conditions, there will be a lot of noise in music segments [4], which will affect the effect of music segmentation. Therefore the compressed sensing theory will be used to denoise the noise signals in music segments [5].

The core idea of compressed sensing theory [6] is to use nonadaptive linear projection of the collected signal and then reconstruct the original signal from the measured value according to the corresponding reconstruction algorithm. Given a measurement matrix as $\Psi \in E^{m \times n}$ $(m \ll n)$, and define the linear measurement value as F, $F \in E^m$, of the signal $f(n) \in E^n$ under the measurement matrix, namely:

$$F = \Psi f(n). \tag{2}$$

Now consider reconstructing $f(n)$ from F. Obviously, since the dimension of F is much lower than that of $f(n)$, the above equation has infinite solutions. The theory proves that the signal $f(n)$ can be accurately calculated from the measured value F by solving the optimal norm. Refactor

$$\widehat{F} = \arg\min \|F\| \tag{3}$$

or

$$\widehat{F} = \arg\min\|F - \Psi f(n)\|_2^2. \tag{4}$$

On the basis of signal reconstruction, considering that the wavelet coefficients of noise signals at various scales do not have sparseness [7], compressed sensing theory can be used to restore the sparseness of wavelet coefficients, so as to achieve the purpose of signal noise reduction. The denoising process is shown in Figure 1.

In the denoising process, the random measurement matrix Ψ needs to satisfy the principle of uniform uncertainty, that is, for any sparse vector h, if

$$0.6\frac{M}{N}\|h\|_2^2 \le \|\Psi h\|_2^2 \le 1.4\frac{M}{N}\|h\|_2^2. \tag{5}$$

It is said that $\Psi_{M\times N}$ satisfies the principle of unanimous uncertainty and the music signal can be denoised.

2.3. Pitch Frequency Extraction. Perform short-term correlation analysis on the denoised music signal, and define the autocorrelation function of a certain frame of signal as

$$x_i(k) = \sum_{i=1}^{N} u(k)u_i(k+g). \tag{6}$$

In the formula, $u(k)$ represents a certain music signal, $u_i(k)$ represents a section of windowed and framed signal, and g represents a lag.

The autocorrelation function will have a peak at an integer multiple of the pitch period, so the pitch period value can be extracted by detecting the position of the peak. To ensure that the pitch is extracted correctly, the window length is set to be greater than 2 pitch periods when framing, and the median smoothing method is used to remove the "outliers" caused by the pitch extraction process:

$$R(n) = w(n) - r(m) \times p_i. \tag{7}$$

In the formula, $w(n)$ represents the input signal, $r(m)$ represents the output of the median filter, and p_i represents the smoothing window, which satisfies

$$\sum_{i=1}^{l} p_i = 1. \tag{8}$$

In the formula, l represents the length of the smooth window.

The pitch of each frame of the music signal is extracted to form a pitch frequency string. Since the change of the pitch string value can correspond to the pitch change, it is convenient to search and classify music according to the pitch change.

2.4. Rough Classification of Music Fragments. In the rough classification of music fragments, a comprehensive processing method is adopted in this paper. This method combines gene recognition and chord recognition in an algorithm to process simultaneously, which improves computational efficiency [8]. The basic idea is to first analyze the music data structure through wavelet transform, then screen the part with the largest amplitude as the comparison item, and time the pronunciation time of adjacent candidate items. Finally, compare the adjacent data one by one to find out the large amplitude change point and record the duration of large and small amplitude domain; thus, the desired rough classification effect can be obtained.

Figure 2 is a schematic diagram of the frequency-amplitude of the note comparison item of a mixed note measure. Among them, F_1 is the single note comparison item with frequency t_1, Y_1 is the amplitude; F_2, F_3, and F_4 are the triad note comparison items with the frequency of the consonant components being t_2, t_3, and t_4, respectively, and Y_2, Y_3, and Y_4 are the corresponding amplitudes; F_5 is a single note comparison item with frequency t_5, and Y_5 is its amplitude. The elements with the smaller amplitude in the middle are not marked. These elements have little significance for the rough classification of music and can be ignored by the given selection threshold. The frequency-amplitude diagram of the note comparison item is shown in Figure 2.

In order to achieve a rough classification of music, a number sequence $W_j = \{w_{j1}, w_{j2}, \ldots, w_{jn}\}$ can be defined, where w_{ji} represents the note included in the selected j-th note comparison item. If it is a single note, then $i = 1$. If it is a chorus, then $i = n$. In addition, a number sequence $D_{W_j} = \{d_{wj1}, d_{wj2}, \ldots, d_{wjn}\}$ can be defined, where d_{wji} represents the note strength contained in the filtered j-th note comparison item, $j = 1, 2, \ldots, i = 1, 2, \ldots$. Let the comparison coefficient be D_j, and its calculation formula is

$$D_j = \frac{D_{z+1}}{D_z} \quad z = 0, 1, 2, \ldots. \tag{9}$$

In the formula, D_z represents the average energy of the z-th note comparison item. The note comparison item can be a single sound or a consonant. The expression is

$$D_z = \overline{D_{W_j}} = \sum_{j=1}^{n} \frac{d_{wji}}{n}. \tag{10}$$

When the note comparison item is monophonic, $j = n = 1$, its balance energy $D_j = D_{W_j} = D_{wj1}$.

The value of D_j can be used to judge the changes in the comparison items of adjacent notes. If the value of D_j is in the closed interval [0.6, 1.4] (the value is an empirical value), the change can be approximated as a small change in the same set of coarse emotional domains. If the value of D_j exceeds this range, its change can be approximated as a jump in the coarse emotional domain. However, a common situation arises in this comparison, namely,

$$\begin{aligned} d_1, d_2, \ldots, d_{j-1} &\in [0.6, 1.4] \\ d_j, d_{j+1}, \ldots, d_{j+m} &\notin [0.6, 1.4] \\ d_{j+m+1}, \ldots &\in [0.6, 1.4]. \end{aligned} \tag{11}$$

For example, $m = 1$ or $m = 2$; this occasional single or several jumps, based on experience, are not enough to show

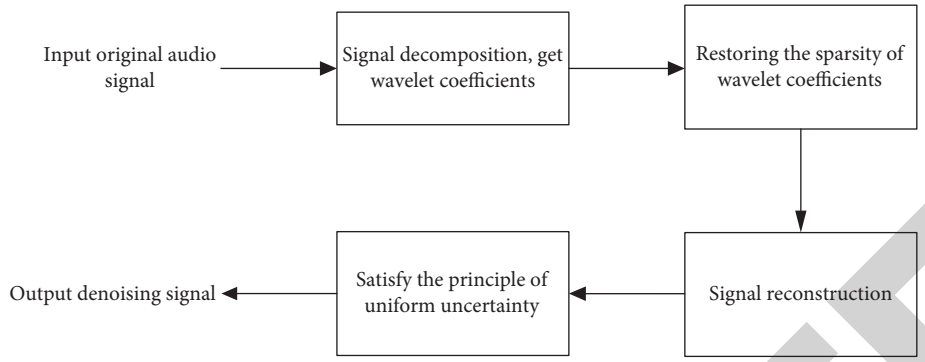

Figure 1: Music denoising process.

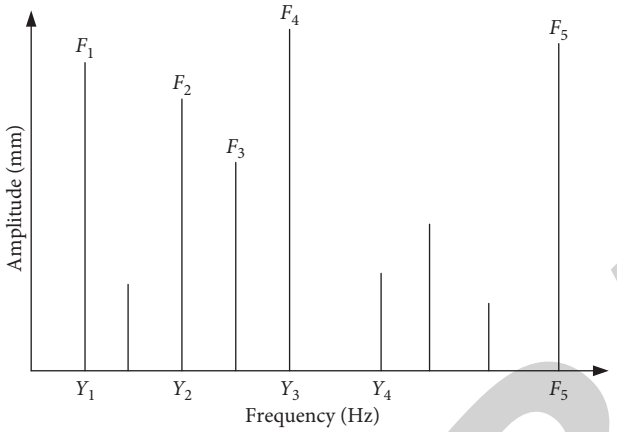

Figure 2: The frequency-amplitude diagram of the note comparison item.

that the emotion of music has jumped in different coarse emotional domains, so certain restrictions on m need to be made. m can be set within a certain range according to the actual situation of the music, so as to ensure that the music with emotional changes can stably stay in its emotional domain for a period of time, so that the emotional information of this music segment can be fully displayed. Otherwise, it needs to be regarded as an invalid emotional expression segment, so the whole music can be roughly classified according to the local intensity and rhythm of the music.

3. Realization of Music Segmentation

The presegmentation of music segments, music signal denoising, pitch frequency extraction, and rough classification of music segments are realized through the preprocessing of music segments. The processing results provide a solid foundation for music segmentation. On this basis, in order to achieve accurate music segmentation, further research is conducted on the segmentation algorithm.

3.1. Music Segment Processing Based on Adaptive Update of Confidence Measure

3.1.1. Calculation of Confidence Measure of Music Fragment. In this paper, the SVM method [9] is used to calculate the confidence measure of music fragments. First, the confidence measure feature vector is extracted for each syllable according to the information in the candidate. Assuming that μ is a keyword composed of N_w syllables, its corresponding candidate μ_w can be decomposed for N'_w syllable candidates, and syllable v_i^w corresponds to candidate $\mu_{v_i^w}$. The SVM classifier is used to obtain the classification score $S(\mu_{v_i^w})$ of the confidence measure feature vector corresponding to the candidate $\mu_{v_i^w}$, and then the confidence measure $S_{\mathrm{SVM}}(\mu_{v_i^w})$ of the syllable candidate is calculated according to the classification score.

The specific calculation steps are as follows: first, use the Sigmoid function to normalize the score of the SVM classifier to (1, 1); then, take the logarithm of the normalized result. The above process is similar to the process of calculating factor-level confidence measures. The specific calculation formula is

$$S_{\mathrm{SVM}}\left(\mu_{v_i^w}\right) = \ln \frac{1}{1 + \exp\left(\vartheta \times S\left(\mu_{v_i^w}\right)\right)}. \tag{12}$$

In the formula, ϑ represents a constant that controls the smoothness of the Sigmoid function.

Next, according to the classification score of each syllable candidate, the confidence measure of the entire keyword candidate can be calculated. The simplest way is to use the classification score to take the average [10]:

$$\overline{S} = \frac{1}{\mu_{v_i^w}} \sum_{i=1}^{n} S\left(\mu_{v_i^w}\right). \tag{13}$$

As with the phoneme-based weighted confidence measure, if the syllable-level confidence measure distribution is considered different, different weights can be used to weigh the syllable-level confidence measure. As a result, a syllable-based weighted confidence measure is obtained, namely,

$$O_{\mathrm{SVM}}\left(\mu_{v_i^w}\right) = \frac{1}{\mu_{v_i^w}} \left[\alpha_i + \beta_j\right]. \tag{14}$$

In the formula, α_i and β_j, respectively, represent the linear weighting coefficient and the offset. These two parameters can be obtained according to the weighting coefficient training method.

3.1.2. Confidence Measure Adaptive Update Data Selection. Due to the different training data, the pretrained vocal and nonvocal models cannot accurately characterize the acoustic characteristics of the music signal to be segmented. The mismatch between the model and the processed data will lead to serious errors in the segmentation results. If vocal and nonvocal signals are extracted from the music signals to be segmented and the corresponding model is updated adaptively, the matching degree between the model and the processed data can be improved. Since the vocal and nonvocal parts of music signals are known, a reliable data selection algorithm is proposed for adaptive updating of confidence measure.

Based on the presegmentation of music clips, use φ_c and φ_{nc} to divide music clips into two categories, namely,

$$\begin{aligned}\widehat{R}_{ri} &= \varphi_c\left(W_1^0, W_2^0\right),\\ \widehat{R}_{rj} &= \varphi_{nc} \times \overline{R}_{ij}\left(W_j^0\right).\end{aligned} \tag{15}$$

In the formula, W_1^0 represents the pure music and voice segments, W_2^0 represents the music mixed segments, and W_j^0 represents the music climax segments.

Due to the mismatch between the model and the processed data, there are misidentified data in $\widehat{R}_{ri}$ and $\widehat{R}_{rj}$, that is, fragments containing opposite classes. Confidence measures δ_1 and δ_2 are used to judge the reliability of the segments in $\widehat{R}_{ri}$ and $\widehat{R}_{rj}$, respectively, which are defined as

$$\begin{aligned}\delta_1 &= \frac{1}{\mu_1}\frac{\left|\omega_{r1}(k)\right|^2}{\sigma_1(k)^2},\\ \delta_2 &= \frac{1}{\mu_2}\frac{\left|\omega_{r2}(k)\right|^2}{\sigma_2(k)^2}.\end{aligned} \tag{16}$$

The larger the δ_1 and δ_2, the greater the possibility that the segment is correctly identified as vocal or nonvocal. Research shows that δ_1 and δ_2 are approximately normally distributed. The reliable data selection criteria adopted in this study are as below.

Let χ_1 and χ_2 be the mean and standard deviation of δ_i, respectively. For each segment W_{ij}, if its confidence measure $\delta_i > \chi_1 - l\chi_2$, then W_{ij} is reliable data, which can be used for the model update. Through analysis, it is found that the optimal segmentation result can be obtained when the value of l is around 1. Therefore, this paper takes $l = 1$ and then updates the confidence measure δ_i to obtain the data update result.

3.2. Dynamic Threshold Note Segmentation. The traditional amplitude difference note segmentation algorithm will affect the average value of the fundamental frequency due to the inaccurate calculation of the note occupancy frame or affect the number of notes due to the wrong segmentation and thus affect the segmentation accuracy. Therefore, based on the adaptive update of the confidence measure, this paper uses the amplitude difference function to dynamically set the threshold to obtain the position of the segmentation line and set the constraint conditions to determine the segmentation line to improve the adaptability and accuracy of the algorithm.

3.2.1. Determine the Split Point. Scan the category label sequence obtained by the rough classification to find all adjacent point pairs with different categories. Each such point pair corresponds to an audio clip with a length of 12 s [11]. There is a suitable segmentation point, which is called the segmentation point boundary area.

In the boundary area of a segmentation point, the problem of accurately locating the segmentation point can be transformed into a series of two types of audio classification problems at a small scale. The specific category is determined by the category transition point pair (p, q). The boundary region of the segmentation point is divided into several continuous small audio clips, and a 17-dimensional feature vector is extracted from each small audio clip. Each small audio clip is divided into class p or class q by the corresponding two kinds of classifiers. The length of each small audio clip is 1 second, and there is no overlap between adjacent clips. After classifying these small audio clips one by one, a category label sequence about the boundary area of the segmentation point will be obtained, in which there are only category labels of class p and class q.

After adjusting the correction rules, in this category label sequence, all reasonable category jump point pairs will be used as the final segmentation point decision point pair. The so-called "reasonable" category jump point pair means that if there is a category jump point pair (p, q) in the rough segmentation sequence, those point pairs consistent with the category jump direction determined in the rough segmentation are reasonable in the process of determining the last segmentation point accordingly.

In order to ensure the accuracy of segmentation points, multiple final segmentation points are allowed in the boundary area of a segmentation point. If a reasonable category jump point pair cannot be found in the boundary region of a segmentation point, the algorithm will give up locating the segmentation point in the boundary region of the segmentation point, which may remove some false segmentation point boundary regions determined by the coarse segmentation algorithm.

3.2.2. Amplitude Difference Function. The amplitude of the music signal will change drastically over time; especially, the amplitude of the note segmentation has a significant gap. The amplitude function in the traditional segmentation algorithm is defined as follows:

$$F(e) = \sum_{i=1}^{n} a_i(\alpha) W^i. \tag{17}$$

In the formula, $F(e)$ represents the waveform amplitude function, $a_i(\alpha)$ represents the amplitude of the sampling point, and W^i represents a certain frame of the input signal. Then, the amplitude difference function of $F(e)$ is

$$O_{F(e)} = F(e+1) - F(e). \tag{18}$$

Applying $O_{F(e)}$ is more obvious than applying $F(e)$ alone to the dividing line of a single note, which is convenient for subsequent processing.

3.2.3. Determination of Dividing Line. In order to find the dividing line, a threshold κ must be determined (usually, κ is a percentage of the mean $O_{F(e)}$); τ_i is the note start frame, τ_j is the note end frame [12], and the expressions of the two are

$$\tau_i = \underset{O_{F(e)} \geq \kappa}{\arg} O_{F(e)},$$
$$\tau_j = \underset{O_{F(e)} < \kappa}{\arg} O_{F(e)}. \tag{19}$$

After analysis, it can be seen that, after fixing κ, the adaptability to different music segments is poor. Even if κ changes with $O_{F(e)}$, since only the overall signal properties are considered and the local peak characteristics are ignored, errors will inevitably be caused. Therefore, each segment is calculated after a fixed percentage of the mean of the notes, and a set of dynamically changing κ is obtained:

$$\kappa = \Delta L \times \frac{\lambda_l}{L(x)}. \tag{20}$$

In the formula, ΔL represents the step length of the change and λ_l represents a certain segment divided by the variable step length.

Since κ changes in a local range, a set of dynamic segmentation values can be obtained.

In a cluster of dividing lines, there is only the only optimal division. According to the two characteristics of the note, the finiteness of the note length and the fixedness of the music rhythm, the restriction conditions are set and the optimal solution is found [13]. The judgment conditions are as follows:

(1) The number of frames occupied by notes is appropriate. The minimum and maximum frames are set through experiments to remove that obviously inappropriate segmentation.

(2) Note segmentation is uniform. Because the beat of a piece of music is certain, the notes segmented by the segmentation line are uniform. When a single note is greater than or less than 1.5 times the number of frames occupied by the adjacent note, the division is determined to be invalid.

3.3. The Realization Process of Music Segmentation. In the process of music segmentation, the length of the audio file has certain restrictions on the segmentation result. When the audio is too long, the segmentation process consumes more time. Considering the possibility of data loss due to segmentation failure, the segmented speech segment should not be too long; when the segmented speech segment is too short, it will increase the number of times the segmentation engine is called and reduce the segmentation efficiency. This article chooses to divide the length of the audio file to about 30 s. If the audio is directly divided into a length of 30 s, it will cause part of the music and voice to be divided into the same segment, which will interfere with the segmentation of the audio segment, which will inevitably cause data loss or music segmentation errors. In this paper, when audio segmentation is performed, the coarse segmentation is performed first; that is, the audio length after the initial segmentation is set to more than 5 s, and then the audio files are merged after the segmentation to obtain an audio file that meets the needs and has an appropriate length. The algorithm is summarized as follows:

(1) Read in the audio file and normalize the audio [14].

(2) Filter the normalized signal [5].

(3) Starting from the starting position of the audio stream, find the audio segment with signal strength greater than 0.2 and length greater than 0.3 s. If it exists, record the start and end positions of the audio segment, enter step 4, if it does not exist, the audio segment is music or noise, and end the process.

(4) Framing, adding windows, seeking short-term energy.

(5) Calculate the average short-term energy of the mute section from the start and end positions in step 3.

(6) The audio stream is finely divided, and the duration of the silent segment between the two audio segments is set to 0.2 s in this article.

(7) Calculate the effective segment ratio and silent ratio of each audio segment after segmentation, find the classification factor value, determine the type of each audio segment based on this value, and finally realize the music segmentation.

Table 1: Scale and frequency comparison.

Scale	1	2	3	4
Notation	1	2	3	4
Frequency	260	279	324	337
Scale	$g1$	$a1$	$b1$	$d1$

4. Simulation Experiment

In order to verify the effectiveness of the music segmentation algorithm based on the adaptive update of the confidence measure, simulation experiments are carried out.

4.1. Experimental Parameter Settings. The proposed algorithm is tested. In the experiment, the input music signal is sampled in 11.025 kHz/8 bits/monc format through a microphone and filtered by a bandpass filter. The upper and lower cut-off frequencies are fH = 3400 Hz and fL = 60 Hz–100 Hz, respectively. Use a first-order digital filter $H(Z) = 1-\mu z^{-1}$ to perform high-frequency enhancement processing on the humming signal, where the value of μ is 0.98. Using Hamming window to window and frame the humming signal segment, the window length is 128, and the overlap length between frames is set to 64. The segmentation algorithm proposed in this paper is tested in an audio stream containing 4 types of audio (piano music 1, symphony 2, Beijing opera 3, pop song 4) with a total length of 1 hour. There are 56 real segmentation points in this audio stream. Table 1 is a comparison of audio stream scale and frequency.

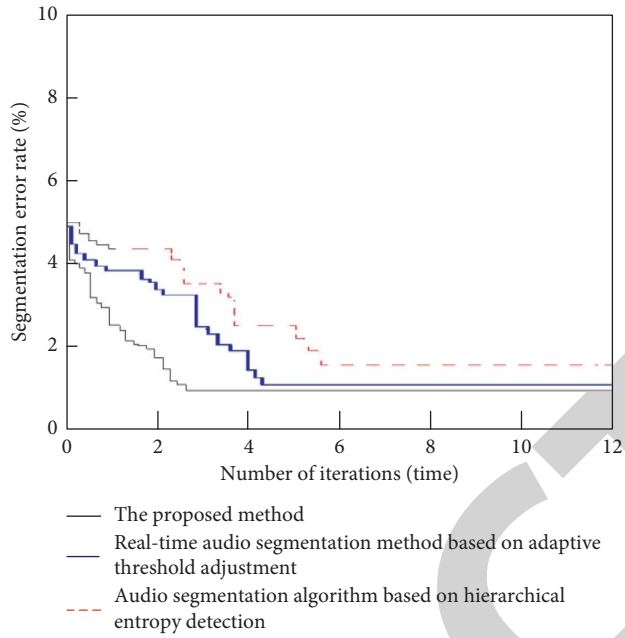

Figure 3: Comparison of music segmentation error rate.

Table 2: Comparison of recall and precision values.

Index	Method of this article	Real-time audio segmentation method based on adaptive threshold adjustment	Audio segmentation algorithm based on hierarchical entropy detection
Recall value	97.5	87.3	80.5
Precision value	93.8	85.6	79.9

Based on the information shown in Table 1, the real-time audio segmentation method based on adaptive threshold adjustment and the audio segmentation algorithm based on hierarchical entropy detection are used as comparison methods to compare with the method in this paper. The results are analyzed as follows.

4.2. Experimental Results and Analysis

4.2.1. Music Segmentation Error Rate (%). Figure 3 shows the corresponding segmentation error rates after different methods of segmentation, where the error rate is defined as the percentage of the length of the music signal that is incorrectly segmented to the total signal length.

It can be seen from Figure 3 that, as the number of iterations increases, the music segmentation error rate of different methods generally shows a trend of first decline and then stable change. Among them, the music segmentation algorithm proposed in this paper based on the adaptive update of the confidence measure reaches 3 iterations. After the second time, the error rate of music segmentation was significantly reduced. It not only has advantages in the iterative cycle but also has more obvious advantages in the error rate method of music segmentation, indicating that the segmentation results of the method in this paper are more reliable. However, the real-time audio segmentation method based on adaptive threshold adjustment and the audio segmentation algorithm based on hierarchical entropy detection has consistently higher music segmentation error rates than this method, and the segmentation effect is not good.

4.2.2. Comparison of Recall and Precision Values. In order to further verify the accuracy of the segmentation of the method in this paper, the recall and the precision values are used as comparison indicators, and the three methods are further compared and analyzed. The calculation formulas for the two parameters are

$$\text{recall} = \frac{N_d}{N_d + N_m}, \qquad \text{precision} = \frac{N_d}{N_d + N_k}. \tag{21}$$

In the formula, N_d represents a correctly segmented audio scene, N_m represents a missing segmented audio scene, N_k represents an incorrectly segmented audio scene.

Obtain the recall and the precision values according to the above formula, and the results are shown in Table 2.

According to the data in Table 2, the recall and precision values of this method reached 97.5% and 93.8%, respectively, while the recall and precision values of the real-time audio segmentation method based on adaptive threshold adjustment are 87.3% and 85.6%, respectively. Lower than the method in this paper, the audio segmentation algorithm

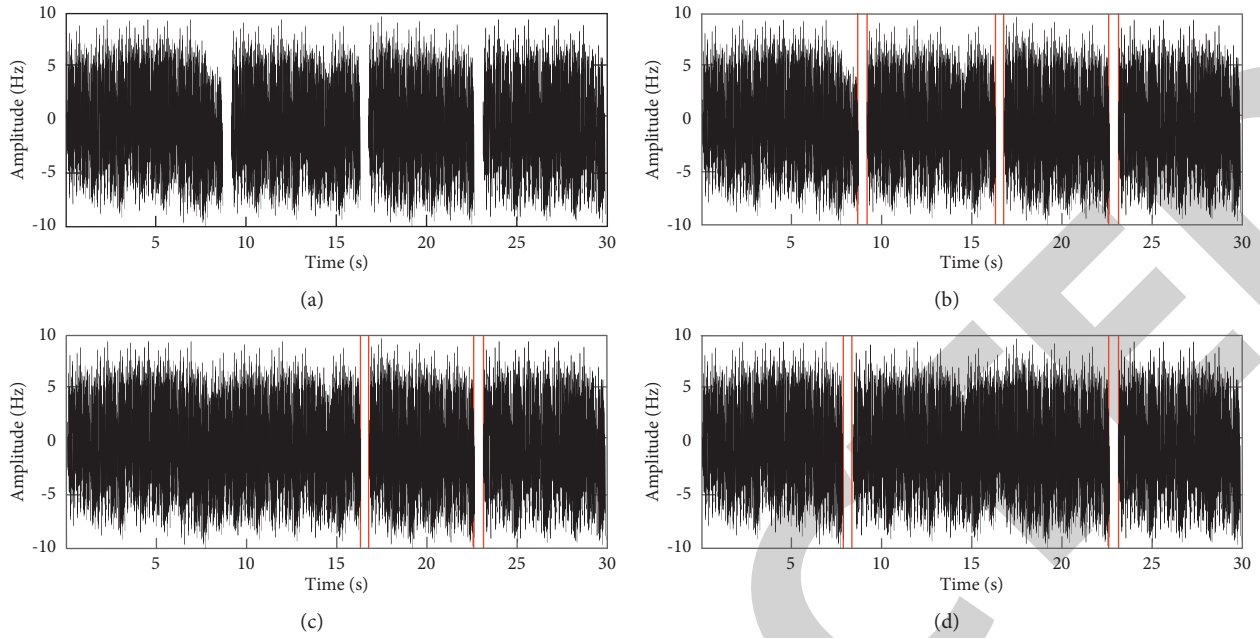

Figure 4: Comparison of segmentation results. (a) Original waveform. (b) The method of this paper. (c) Real-time audio segmentation method based on adaptive threshold adjustment. (d) Audio segmentation algorithm based on hierarchical entropy detection.

based on hierarchical entropy detection has lower recall and precision values. It can be seen that the segmentation results of this method have high accuracy, which shows the effectiveness of the segmentation method.

4.2.3. Audio Clip Segmentation Effect. Choose a piece of audio arbitrarily; the audio has pauses at 9 s, 16 s, and 23 s. Three methods are used to segment it, and the segmentation results obtained are shown in Figure 4.

By analyzing Figure 4, it can be seen that the audio file can be accurately segmented in the 9 s, 16 s, and 23 s by the proposed method, and three pause points can be obtained. The real-time audio segmentation method based on adaptive threshold adjustment can only segment the 16 s and 23 s pauses. The audio segmentation algorithm based on hierarchical entropy detection can only segment the 23 s pause, and there is a segmentation error; that is, the segmentation is performed in the 8 s, but in fact, there is no pause at that time. Therefore, the segmentation effect of this method is better, which shows that its application value is higher.

5. Conclusion

In order to solve the problem of low accuracy of music segmentation and poor segmentation effect in traditional methods, a music segmentation algorithm based on a self-adaptive update of confidence measure is proposed. The following is a summary of the innovative points of the methods in this article:

(1) Denoise the music fragment based on the theory of compressed sensing and performing short-term correlation analysis on the denoised music signal to obtain the pitch frequency

(2) Use the wavelets transform method to roughly classify the music fragments, obtain the classification results, and realize the preprocessing of the music fragments

(3) Use the SVM method to calculate the confidence measure of the music segment, and adaptively update the confidence measure

(4) According to the update results, the dynamic threshold notes are segmented to achieve music segmentation

The analysis of the experimental results shows that compared with the traditional method, the segmentation effect of the algorithm is better, which is specifically manifested in the recall and precision values, the segmentation error rate, and the segmentation effect, which fully verifies the practical application value of the algorithm.

Data Availability

The data used to support the findings of this study are available from the corresponding author upon request.

Conflicts of Interest

The author declares that there are no conflicts of interest regarding this paper.

References

[1] S. Sun, "A college music teaching system designed based on android platform," *Scientific Programming*, vol. 2021, Article ID 7460924, 16 pages, 2021.

[2] H. Purwins, B. Sturm, B. Li, J. Nam, and A. Alwan, "Introduction to the issue on data science: machine learning for

Hindawi
Journal of Mathematics
Volume 2024, Article ID 9793567, 1 page
https://doi.org/10.1155/2024/9793567

Retraction

Retracted: Inverted Length-Biased Exponential Model: Statistical Inference and Modeling

Journal of Mathematics

Received 23 January 2024; Accepted 23 January 2024; Published 24 January 2024

This article has been retracted by Hindawi following an investigation undertaken by the publisher [1]. This investigation has uncovered evidence of one or more of the following indicators of systematic manipulation of the publication process:

(1) Discrepancies in scope

(2) Discrepancies in the description of the research reported

(3) Discrepancies between the availability of data and the research described

(4) Inappropriate citations

(5) Incoherent, meaningless and/or irrelevant content included in the article

(6) Manipulated or compromised peer review

The presence of these indicators undermines our confidence in the integrity of the article's content and we cannot, therefore, vouch for its reliability. Please note that this notice is intended solely to alert readers that the content of this article is unreliable. We have not investigated whether authors were aware of or involved in the systematic manipulation of the publication process.

Wiley and Hindawi regrets that the usual quality checks did not identify these issues before publication and have since put additional measures in place to safeguard research integrity.

We wish to credit our own Research Integrity and Research Publishing teams and anonymous and named external researchers and research integrity experts for contributing to this investigation.

The corresponding author, as the representative of all authors, has been given the opportunity to register their agreement or disagreement to this retraction. We have kept a record of any response received.

References

[1] W. Almutiry, "Inverted Length-Biased Exponential Model: Statistical Inference and Modeling," *Journal of Mathematics*, vol. 2021, Article ID 1980480, 8 pages, 2021.

Hindawi
Journal of Mathematics
Volume 2021, Article ID 1980480, 8 pages
https://doi.org/10.1155/2021/1980480

Research Article

Inverted Length-Biased Exponential Model: Statistical Inference and Modeling

Waleed Almutiry

Department of Mathematics, College of Science and Arts in Ar Rass, Qassim University, Ar Rass, Saudi Arabia

Correspondence should be addressed to Waleed Almutiry; wkmtierie@qu.edu.sa

Received 17 September 2021; Revised 29 September 2021; Accepted 11 October 2021; Published 26 October 2021

Academic Editor: naeem jan

This research article proposes a new probability distribution, referred to as the inverted length-biased exponential distribution. The hazard rate function (HZRF) and density function (PDF) in the new distribution allow additional flexibility as well as some desired features. It provides a more flexible approach that may be used to represent many forms of real-world data. The quantile function (QuF), moments (MOs), moment generating function (MOGF), mean residual lifespan (MRLS), mean inactivity time (MINT), and probability weighted moments (PRWMOs) are among the mathematical and statistical features of the inverted length-biased exponential distribution. In the case of complete and type II censored samples (TIICS), the maximum likelihood (MLL) strategy can be used to estimate the model parameters. An asymptotic confidence interval (COI) of parameter is constructed at two confidence levels. We perform simulation study to examine the accuracy of estimates depending upon some statistical measures. Simulation results show that there is great agreement between theoretical and empirical studies. We demonstrate the new model's relevance and adaptability by modeling three lifespan datasets. The proposed model is a better fit than the half logistic inverse Rayleigh (HLOIR), type II Topp–Leone inverse Rayleigh (TIITOLIR), and transmuted inverse Rayleigh (TRIR) distributions. We anticipate that the expanded distribution will attract a broader range of applications in a variety of fields of research.

1. Introduction

Length-biased exponential (LBE) or moment exponential (ME) distribution is considered as one of the most important univariate and parametric models. It is commonly utilized in the analysis of data collected throughout a lifespan and in problems connected to the modeling of failure processes. There is much to be said for a flexible lifespan distribution model, and this one may be a suitable fit for some sets of failure data. Reference [1] proposed the LBE with the following PDF and distribution function (CDF):

$$g(x;\alpha) = \alpha^2 x e^{-\alpha x}; \quad x \geq 0,\ \alpha > 0, \tag{1}$$

$$G(x;\alpha) = 1 - (1 + \alpha x)e^{-\alpha x}; \quad x \geq 0,\ \alpha > 0, \tag{2}$$

where α is the scale parameter. Different values of the shape parameter lead to different shapes of density function.

Many authors extended new models from the LBE distribution such as exponentiated ME [2], generalized exponentiated ME [3], and Marshall–Olkin (MO) LBE (MOLBE) distributions [4]. MO Kumaraswamy ME model was discussed in [5].

Several univariate continuous distributions have been extensively used in environmental, engineering, financial, and biomedical sciences, among other areas for modeling lifetime data. However, there is still a strong need for a significant improvement of the classical distributions through different techniques for modeling several data lifetime. In this regard, the inverted (or inverse) (I) distribution is one procedure that explores extra properties of the phenomenon which cannot be produced from noninverted distributions. Applications of inverted distributions include econometrics as well as the engineering sciences as well as biology and survey sampling as well as medical research among others. In the literature, several studies related to

inverted distributions have been handled by several researchers; for instance, Reference [6] introduced the I Weibull distribution. Reference [7] studied the I Pareto type 1 distribution. Reference [8] investigated the I Pareto type 2 distribution. Reference [9] handled exponentiated I Weibull distribution. Reference [10] provided the I Lindley distribution. Reference [11] suggested the I Kumaraswamy model. Reference [12] presented the I Nadarajah-Haghighi model. Reference [13] studied the I power Lomax model. Reference [14] suggested I exponentiated Lomax model. Reference [15] discussed the Weibull I Lomax model. Reference [16] suggested the power transmuted I Rayleigh model. Reference [17] investigated the I Topp–Leone distribution, and half logistic I Topp–Leone distribution was studied in [18].

Our motivation here is (i) introducing a new distribution, referred to as the inverted length-biased exponential (ILBE), (ii) studying some of the main properties, (iii) providing point and interval estimators for the model parameter from complete and censored samples, and (iv) examining its applicability using three real datasets.

The inverted LBE (ILBE) distribution is constructed by using the random variable $T = 1/X$ where X follows (2). The ILBE distribution's CDF is described as

$$F(t;\alpha) = \left(1 + \frac{\alpha}{t}\right)e^{-\alpha/t}; \quad t \geq 0, \alpha > 0. \tag{3}$$

The ILBE distribution's PDF is specified as

$$f(t;\alpha) = \frac{\alpha^2}{t^3}e^{-\alpha/t}; \quad t \geq 0,\ \alpha > 0. \tag{4}$$

The survival function (SRF) and HZRF of the ILBE distribution are provided by

$$\begin{aligned} \overline{F}(t;\alpha) &= 1 - \left(1 + \frac{\alpha}{t}\right)e^{-\alpha/t}, \\ h(t;\alpha) &= \frac{\alpha^2 e^{-\alpha/t}}{t^3\left[1 - (1 + \alpha/t)e^{-\alpha/t}\right]}. \end{aligned} \tag{5}$$

Figure 1 depicts PDF and HZRF plots for the ILBE distribution. According to Figure 1, the density of the suggested distribution is highly flexible in nature and can take on a number of forms, including positively skewed and unimodal. Through the parameter space, the HZRF can take on many forms, such as decreasing, rising, or upside down.

This paper is organized as follows. In Section 2, the basic characteristics of the ILBE distribution are obtained. The MLL estimators for the ILBE model are described in Section 3 and are established on complete and censored samples, accompanied by a simulation analysis. The application to actual data collection is covered in Section 4. Section 5 concludes the paper with some remarks.

2. Fundamental Mathematical Properties of ILBE Distribution

Here, we give some essential properties of the ILBE distribution, like QuF, MOs, PRWMOs, incomplete MOs, and inverse MOs.

2.1. Quantile Function. A generated random number from the ILBE distribution is obtained by solving the following equation numerically:

$$Q(u) = \frac{\alpha}{-1 - W_{-1}\left(-e^{-1}u\right)}, \quad 0 < u < 1, \tag{6}$$

where W_{-1} denotes the negative branch of the Lambert W function (i.e., the solution of the equation $W(Z)e^{W(Z)} = z$. The median, say Q_2, is achieved by adjusting $u = 0.5$ in (6), and the first quartile and third quartile, denoted by Q_1 and Q_3, are obtained by setting $u = 0.25$ and 0.75, respectively, in (6). Note that equation (6) is solved numerically by using Mathematica 9.

$$\begin{aligned} Q_1 &= \frac{\alpha}{-1 - W_{-1}\left(-0.25e^{-1}\right)}, \\ Q_2 &= \frac{\alpha}{-1 - W_{-1}\left(-0.5e^{-1}\right)}, \\ Q_3 &= \frac{\alpha}{-1 - W_{-1}\left(-0.75e^{-1}\right)}. \end{aligned} \tag{7}$$

2.2. Moments. Due to its relevance in any statistical study, we shall give the n-th MO of the ILBE distribution here. For the ILBE model, the n-th MO of T about the origin is computed as follows:

$$\mu_n' = E(T^n) = \int_0^\infty t^n \frac{\alpha^2}{t^3}e^{-\alpha/t}\mathrm{d}t = \alpha^n\Gamma(2-n), \quad n < 2. \tag{8}$$

The following formula may be used to determine the MOGF of the ILBE distribution:

$$M_x(t) = \sum_{n=0}^{\infty}\frac{t^n}{n!}\mu_n' = \sum_{n=0}^{\infty}\frac{t^n}{n!}\alpha^n\Gamma(2-n), \quad n < 2. \tag{9}$$

The incomplete (IN) MO, say $\varsigma_n(x)$, is

$$\varsigma_n(t) = \alpha^2 t\int {}^0t^{n-3}e^{-\alpha/t}\mathrm{d}t = \alpha^n\gamma\left(2-n, \frac{\alpha}{t}\right), \quad n < 2, \tag{10}$$

where, $\gamma(.,t)$ is the upper IN gamma function.

Further, the conditional MO, say $\varpi_s(x)$, is

$$\varpi_s(t) = \alpha^2\int_t^\infty t^{\alpha-3}e^{-\alpha/t}\mathrm{d}t = \alpha^n\Gamma\left(2-n, \frac{\alpha}{t}\right), \quad n < 2, \tag{11}$$

where $\Gamma(.,t)$ is the lower IN gamma function.

For the ILBE distribution, the n-th inverse MO is calculated on the basis:

$$\tau_k(x) = \alpha^2\int_0^\infty t^{-n-3}e^{-\alpha/t}\mathrm{d}t = \alpha^{-k}\Gamma(n+2). \tag{12}$$

For $n = 1$, we get the harmonic mean of the ILBE distribution.

The Lorenz and Bonferroni curves are obtained as follows.

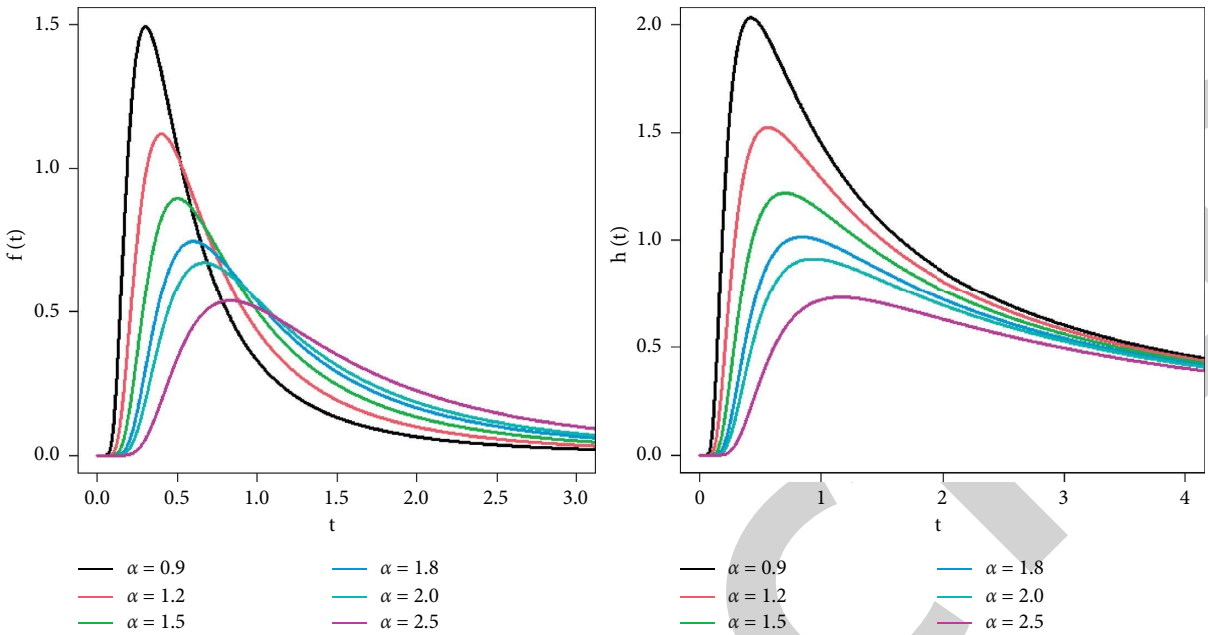

Figure 1: Plots of PDF and HZRF for the ILBE distribution.

$$L_F(t) = \frac{\varsigma_1(t)}{E(T)} = \gamma\left(1, \frac{\alpha}{t}\right), \tag{13}$$

$$B_F(t) = \frac{L_F(t)}{F(t)} = \frac{\gamma(1, (\alpha/t))}{(1 + (\alpha/t))e^{-\alpha/t}}. \tag{14}$$

2.3. Order Statistics. Let $T_1, T_2, \ldots, T_n$ be r samples from the ILBE model with order statistics $T_{(1)}, T_{(2)}, \ldots, T_{(n)}$. The PDF of $T_{(k)}$ of order statistics is given by

$$f_{T_{(k)}}(t) = \frac{n!}{(k-1)!(n-k)!} F^{k-1}(t) f(t) (1 - F(t))^{n-k}. \tag{15}$$

The PDF of $T_{(k)}$ can be expressed as

$$f_{T_{(k)}}(t) = \frac{n!\alpha^2}{(k-1)!(n-k)!} t^{-3}\left(1 + \frac{\alpha}{t}\right)^{k-1} e^{-k\alpha/t}\left(1 - \left(1 + \frac{\alpha}{t}\right)e^{-\alpha/t}\right)^{n-k}. \tag{16}$$

Particularly, PDF of the first and largest order statistics can be calculated as

$$f_{T_{(1)}}(t) = n\alpha^2 t^{-3} e^{-\alpha/t}\left(1 - \left(1 + \frac{\alpha}{t}\right)e^{-\alpha/t}\right)^{n-1}, \tag{17}$$

$$f_{T_{(n)}}(t) = n\alpha^2 t^{-3}\left(1 + \frac{\alpha}{t}\right)^{n-1} e^{-n\alpha/t}, \tag{18}$$

respectively.

2.4. Mean Residual Life Function. It has an important application of the MOs of residual lifetime function. The MRLS of ILBE distribution is

$$v(t) = E(T - t | T > t) = \frac{1}{\overline{F}(t)} \int_t^\infty x f(x) dt - t = \alpha\Gamma\left(1, \frac{\alpha}{t}\right)\left[1 - \left(1 + \frac{\alpha}{t}\right)e^{-\alpha/t}\right]^{-1} - t. \tag{19}$$

The MINT represents the amount of time that has passed after an item has failed, assuming that this failure has occurred. The MINT of ILBE distribution is

$$\varpi(t) = E(T - t | T \le t) = t - \frac{1}{F(t)} \int_0^t x f(x) dx = t - \alpha\gamma\left(1, \frac{\alpha}{t}\right)\left(1 + \frac{\alpha}{t}\right)^{-1} e^{\alpha/t}. \tag{20}$$

2.5. Probability Weighted Moments. The PRWMOs are often used to investigate additional aspects of the probability distribution. The PRWMOs of the random variable T, denoted by $\mathbb{S}_{r,p}$, are defined as

$$\mathbb{S}_{r,p} = \int_{-\infty}^{\infty} t^r f(t) [F(t)]^p dt, \tag{21}$$

where r and p are positive integers. Substituting (3) and (4) into (21) yields the PRWMOs of the ILBE distribution as follows:

Table 1: MLE, $\wp$, $\mathfrak{F}$, $\mathcal{O}$, $\mathfrak{H}$, and $\sqsupset$ of the ILBE distribution for $\alpha = 1.2$ under TIIC.

n	t_r (%)	MLE	$\wp$	$\mathfrak{F}$	90%			95%		
					$\mathcal{O}$	$\mathfrak{H}$	$\sqsupset$	$\mathcal{O}$	$\mathfrak{H}$	$\sqsupset$
100	60	1.6091	0.4091	0.2111	1.3068	1.9113	0.6045	1.2489	1.9692	0.7203
	80	1.3548	0.1548	0.0546	1.0803	1.6294	0.5490	1.0278	1.6819	0.6542
	100	1.2316	0.0316	0.0263	0.9700	1.4931	0.5231	0.9199	1.5432	0.6233
200	60	1.5648	0.3648	0.1575	1.3372	1.7924	0.4552	1.2937	1.8360	0.5424
	80	1.3195	0.1195	0.0319	1.1125	1.5266	0.4142	1.0728	1.5663	0.4935
	100	1.1993	0.0007	0.0146	1.0020	1.3965	0.3946	0.9642	1.4343	0.4701
300	60	1.5777	0.3777	0.1551	1.4154	1.7399	0.3245	1.3844	1.7710	0.3866
	80	1.3307	0.1307	0.0256	1.1831	1.4784	0.2953	1.1548	1.5067	0.3519
	100	1.2097	0.0097	0.0071	1.0690	1.3504	0.2814	1.0420	1.3773	0.3353

Table 2: MLE, $\wp$, $\mathfrak{F}$, $\mathcal{O}$, $\mathfrak{H}$, and $\sqsupset$ of the ILBE distribution for $\alpha = 1.5$ under TIIC.

n	t_r (%)	MLE	$\wp$	$\mathfrak{F}$	90%			95%		
					$\mathcal{O}$	$\mathfrak{H}$	$\sqsupset$	$\mathcal{O}$	$\mathfrak{H}$	$\sqsupset$
100	60	1.9815	0.4815	0.2846	1.6091	2.3538	0.7447	1.5378	2.4251	0.8873
	80	1.6720	0.1720	0.0666	1.3332	2.0107	0.6775	1.2683	2.0756	0.8073
	100	1.5196	0.0196	0.0313	1.1969	1.8423	0.6454	1.1351	1.9041	0.7690
200	60	1.9785	0.4785	0.2638	1.6907	2.2664	0.5757	1.6356	2.3215	0.6859
	80	1.6695	0.1695	0.0544	1.4075	1.9315	0.5240	1.3573	1.9817	0.6243
	100	1.5170	0.0170	0.0215	1.2674	1.7665	0.4991	1.2196	1.8143	0.5946
300	60	1.9562	0.4562	0.2273	1.7550	2.1573	0.4023	1.7165	2.1958	0.4793
	80	1.6486	0.1486	0.0359	1.4656	1.8315	0.3659	1.4306	1.8666	0.4359
	100	1.4988	0.0012	0.0114	1.3245	1.6731	0.3487	1.2911	1.7065	0.4154

$$\begin{aligned}\mathbb{S}_{r,p} &= \alpha^2 \int_0^\infty t^{r-3}\left(1+\frac{\alpha}{t}\right)^p e^{-(p+1)\alpha/t} \\ &= \sum_{j=0}^{p}\binom{p}{j}\alpha^{j+2}\int_0^\infty t^{r-3-j}e^{-(p+1)\alpha/t}\mathrm{d}t.\end{aligned} \tag{22}$$

As a result of the simplification, the PRWMOs of the ILBE distribution assume the following structure:

$$\mathbb{S}_{r,p} = \sum_{j=0}^{p}\binom{p}{j}\alpha^r\frac{\Gamma(j-r+2)}{(p+1)^{j-r+2}}. \tag{23}$$

3. Statistical Inference

3.1. MLL Estimator Based on TIIC. Assume $T_{(1)}, T_{(2)}, \ldots, T_{(n)}$ are the recorded TIICS of size r, whose lifetimes have the ILBE distribution with PDF (4), and the experiment is completed once the r-th object fails for just some fixed values of r. The log-likelihood function (LLF), according to TIIC, is provided by

$$\begin{aligned}\ln l_2 &= \ln C + 2r\ln\alpha - 3\sum_{i=1}^{r}\ln t_i - \sum_{i=1}^{r}\frac{\alpha}{t_i} \\ &\quad + (n-r)\ln\left[1-\left(1+\frac{\alpha}{t_r}\right)e^{-\alpha/t_r}\right],\end{aligned} \tag{24}$$

and for the sake of simplification, we abbreviate t_i rather than $t_{(i)}$. As a result, the partial derivatives of the LLF with regard to the component of the score $U(\alpha) = \partial \ln l_2/\partial\alpha$ may be computed as follows:

$$U(\alpha) = \frac{2r}{\alpha} - \sum_{i=1}^{r}\frac{1}{t_i} + \frac{(n-r)\alpha e^{-\alpha/t_r}}{t_r^2\left[1-\left((1+(\alpha/t_r))e^{-\alpha/t_r}\right)\right]}. \tag{25}$$

The model parameters' MLL estimator is produced by numerically solving equation (18) after assigning it to zero. In the case of a complete sample, we acquire the MLL estimators of the model parameters for $r = n$.

3.2. Simulation Results. A simulation is used to evaluate the estimators' behavior considering a set of parameter choices. Mean square error ($\wp$), bias ($\mathfrak{F}$), lower limit ($\mathcal{O}$) of the COIs, upper bound ($\mathfrak{H}$) of the COIs, and average length ($\sqsupset$) of 90% and 95% are among the metrics computed. All numerical calculations are made using the R programming (R 4.1.1). The following algorithm are used:

(i) On aggregate, the ILBE distribution produces 1000 random samples with sizes of $n = 100$, 200, and 300.

(ii) Values for a few parameters are $\alpha = 1.2$ and $\alpha = 1.5$.

(iii) There are three degrees of censorship: $r = 60\%$, 80% (TIIC), and 100% (complete sample).

(iv) $\wp$, $\mathfrak{F}$, $\mathcal{O}$, $\mathfrak{H}$, and $\sqsupset$ of estimates are computed.

Tables 1 and 2 include the numerical findings for the complete and TIIC measurements, respectively.

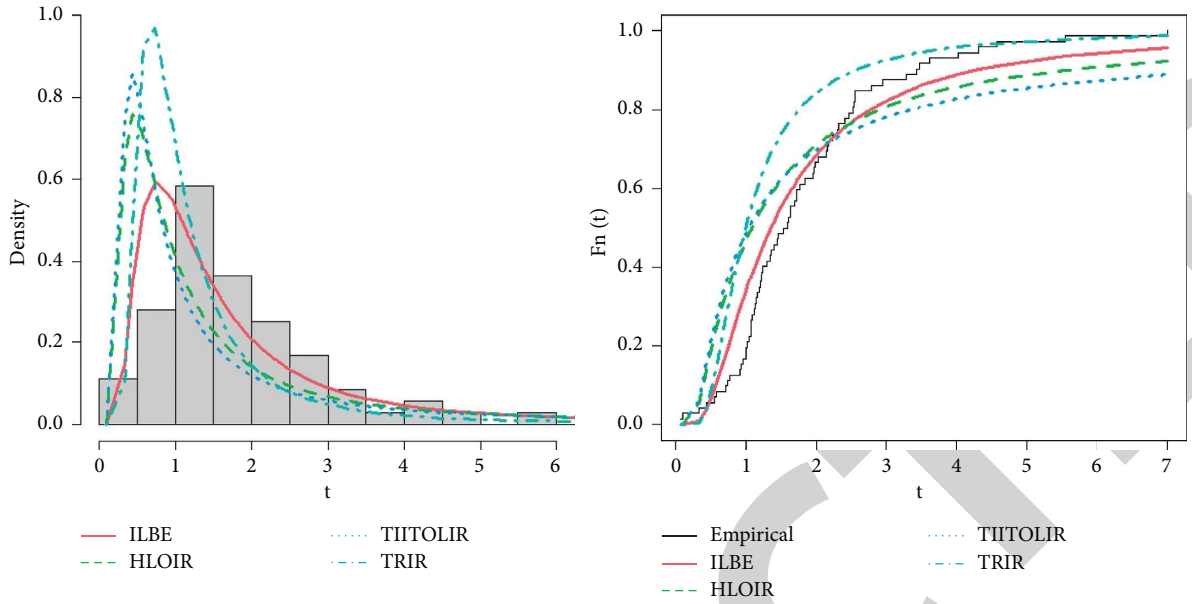

Figure 2: Fitted PDFs and CDFs of comparison models for the first dataset.

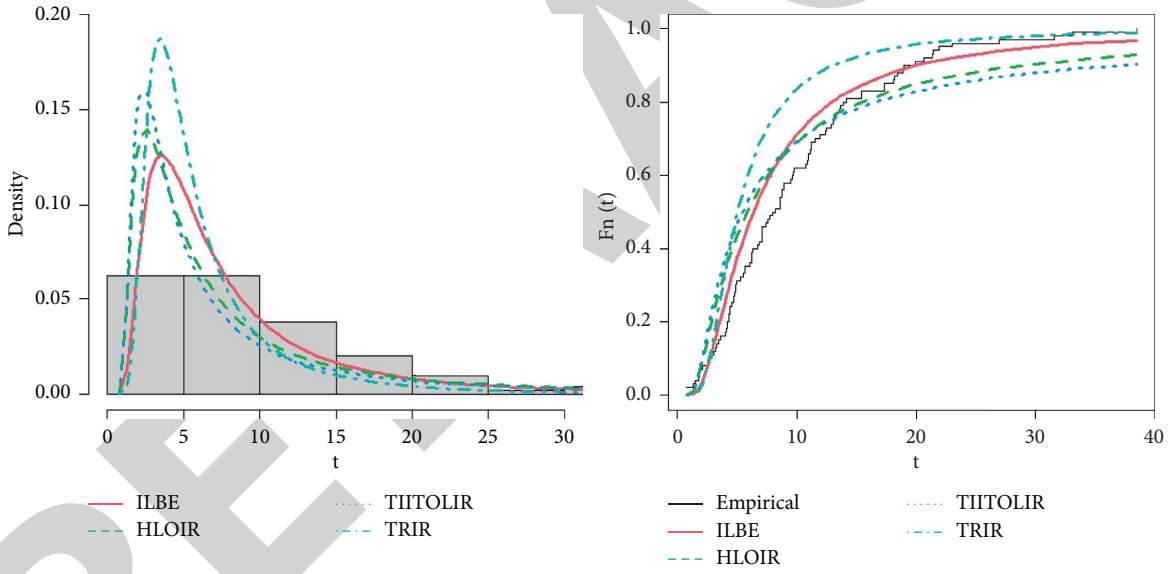

Figure 3: Fitted PDFs and CDFs of comparison models for the second dataset.

From these tables, we conclude the following:

(i) As the sample size grows, $\wp, \Im$, and $\sqsupset$ of all estimates decrease.

(ii) $\wp, \Im$, and $\sqsupset$ of all estimates decrease as r decreases.

(iii) $\sqsupset$ of the COIs increases as the confidence levels increase from 90% to 95%.

4. Applications to Real Data

In this part, we demonstrate the ILBE model's adaptability by examining three real-world datasets. Comparing the fit of the ILBE model with known distributions such as the HLOIR [19], TIITOLIR [20], and TRIR [21] distributions, the ILBE model performs better. The PDFs of competitive models are

$$f_{HLOIR}(t) = \frac{4\lambda\alpha^2 t^{-3}\exp\left(-(\alpha/t)^2\right)\left(1-\exp\left(-(\alpha/t)^2\right)\right)^{\lambda-1}}{\left(1+\left(1-\exp\left(-(\alpha/t)^2\right)\right)^{\lambda}\right)^2},$$

$$f_{TIITOLIR}(t) = 4\theta\alpha^2 t^{-3}\exp\left(-2(\alpha/t)^2\right)\left(1-\exp\left(-2(\alpha/t)^2\right)\right)^{\theta-1}, \tag{26}$$

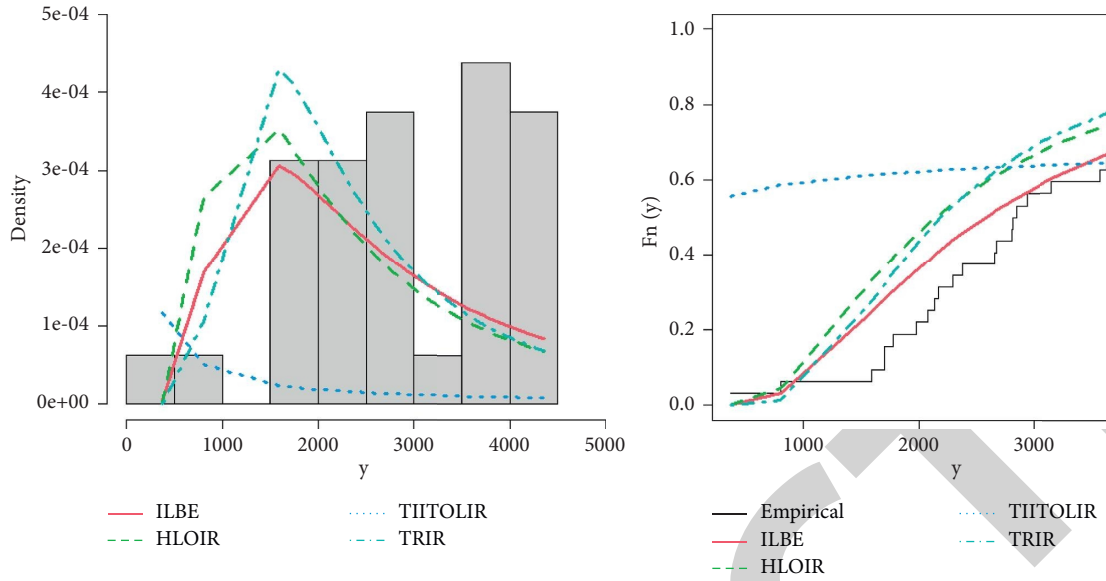

Figure 4: Fitted PDFs and CDFs of comparison models for the third dataset.

Table 3: Numerical results of MLE, SE, ∧**1**, ∧**2**, ∧**3**, ∧**4**, and ∧**5** for the first dataset.

Model	MLEs and SE		∧1	∧2	∧4	∧5	∧3
ILBE (α)	2.272 (0.189)		224.111	226.111	225.969	227.018	226.168
HLIR (α,λ)	0.436 (0.05)	0.579 (0.07)	260.586	264.586	264.301	266.399	264.76
TIITLIR (α,λ)	0.325 (0.036)	0.404 (0.058)	280.492	284.492	284.207	286.305	284.666
TIR (α,λ)	0.352 (0.426)	−0.942 (0.351)	280.538	284.538	284.253	286.351	284.712

Table 4: Numerical results of MLE, SE, ∧**1**, ∧**2**, ∧**3**, ∧**4**, and ∧**5** for the second dataset.

Model	MLEs and SE		∧1	∧2	∧4	∧5	∧3
ILBE (α)	10.696 (0.7563)		664.794	666.794	666.794	667.848	666.834
HLIR (α,λ)	2.404 (0.226)	0.589 (0.06)	680.806	684.806	684.806	686.915	684.93
TIITLIR (α,λ)	1.824 (0.162)	0.43 (0.051)	700.214	704.214	704.214	706.323	704.338
TIR (α,λ)	9.978 (1.136)	−0.812 (0.085)	720.665	724.665	724.665	726.774	724.706

Table 5: Numerical results of MLE, SE, ∧**1**, ∧**2**, ∧**3**, ∧**4,** and ∧**5** for the third dataset.

Model	MLEs and S.E		∧1	∧2	∧4	∧5	∧3
ILBE (α)	4326 (540.7191)		567.141	569.141	568.647	569.627	569.275
HLIR (α,λ)	1237 (184.326)	0.866 (0.172)	575.242	579.242	578.252	580.214	579.656
TIITLIR (α,λ)	0.069 (0.041)	0.049 (0.0091)	716.204	720.204	719.214	721.176	720.618
TIR (α,λ)	1821000 (346600)	−0.859 (0.126)	575.303	579.303	578.313	580.275	579.717

$$f_{TRIR}(t) = 2\theta t^{-3}\exp\left(-\frac{\theta}{t^2}\right)\left(1+\lambda-2\lambda\exp\left(-\frac{\theta}{t^2}\right)\right). \tag{27}$$

In order to make a comparison between various models, some information criteria (INC) like maximized likelihood (**?1**), Akaike INC (**?2**), consistent Akaike INC (**?3**), Bayesian INC (**?4**), and Hannan–Quinn INC (**?5**) are used. According to the given data, the optimal model is one with the lowest value of **?1**, **?2**, **?3**, **?4**, and **?5**.

The first dataset [22]: it describes 72 guinea pigs infected with highly pathogenic tubercle bacilli and their survival periods (in days).

The second dataset: acquired and documented in [23], the dataset comprises the waiting times (in minutes) of 100 bank clients.

The third dataset [24]: it offers 32 observations on the failure time for vertical boring machines.

Figures 2–4 indicate the fitted PDFs, fitted CDFs of the ILBE distribution, and those of the comparison models (HLOIR, TIITOLIR, and TRIR) for the three datasets.

It can be observed from Figures 2–4 that the ILBE distribution exhibits good matches, attesting its applicability for the three datasets.

Tables 3–5 show the ML estimates (MLEs) and standard errors (SEs) for the ILBE model when compared to various known distributions such like HLOIR, TIITOLIR, and TRIR. They also include the relevant measures of fit statistic.

Furthermore, Tables 3–5 show that the ILBE distribution is the best match among the other models for the three datasets, since the ILBE distribution has the lowest values of the suggested metrics.

5. Conclusions

This paper developed a new one-parameter lifetime distribution, named as inverse length-biased exponential distribution. The new model is quite flexible in nature and can acquire a variety of shapes of density and hazard rate functions. MOs, PRWMOs, inverse MOs, incomplete MOs, MRLS, and MINT are all explored as key characteristics of the new distribution. In both complete and censored samples, the maximum likelihood methodology is developed to calculate the parameters of the new distribution. To investigate the conduct of estimations, a simulation analysis is discussed. Three real-world examples show that the inverse length exponential distribution gives a pretty good fit and may be used as a competitive model to fit real-world data. It is hoped that this distribution would be helpful to scholars in a variety of disciplines. In the future, we plan to use the new proposed model to study the statistical inference of it under different censored schemes, using various methods of estimation to assess the performance of its parameters. Also, researchers can extend and generalized it because this model is very simple and has more flexibility to fitting more datasets.

Data Availability

Interested parties can reach out to the author in order to receive the numerical dataset used to perform the research described in the paper.

Conflicts of Interest

The author declares that there are no conflicts of interest.

Acknowledgments

The author would like to thank the Deanship of Scientific Research, Qassim University, for funding the publication of this project.

References

[1] S. T. Dara and M. Ahmad, *Recent Advances in Moment Distribution and their Hazard Rates*, Lap Lambert Academic Publishing GmbH KG, Sunnyvale, CA, USA, 2012.

[2] S. A. Hasnain, *Exponentiated Moment Exponential Distributions*, National College of Business Administration & Economics, Lahore, Pakistan, 2013.

[3] Z. Iqbal, S. A. Hasnain, M. Salman, M. Ahmad, and G. Hamedani, "Generalized exponentiated moment exponential distribution," *Pakistan Journal of Statistics*, vol. 30, no. 4, pp. 537–554, 2014.

[4] M. A. u. Haq, R. M. Usman, S. Hashmi, and A. I. Al-Omeri, "The Marshall-Olkin length-biased exponential distribution and its applications," *Journal of King Saud University Science*, vol. 31, no. 2, pp. 246–251, 2019.

[5] A. Ali, H. Ahmadini, A. S. Hassan, R. E. Mohamed, S. S. Alshqaq, and H. F. Nagy, "A New four-parameter moment exponential model with applications to lifetime data," *Intelligent Automation & Soft Computing*, vol. 29, no. 1, pp. 131–146, 2021.

[6] A. Keller and A. R. R. Kamath, "Alternative reliability models for mechanical systems," in *Proceedings of the Third International Conference on Reliability and Maintainability*, Toulse, France, October 1982.

[7] R. I. Abd EL-Kader, G. R. AL-Dayian, and S. A. AL-Gendy, "Inverted Pareto type I distribution: properties and estimation," *Journal of Faculty of Commerce AL-Azhar University*, vol. 21, pp. 19–40, 2013.

[8] G. R. AL-Dayian, "Inverted Pareto type II distribution: properties and estimation," *Journal of Faculty of Commerce AL-Azhar University Girls' Branch*, vol. 22, pp. 1–18, 2004.

[9] A. Aljuaid, "Estimating the parameters of an exponentiated inverted Weibull distribution under type-II censoring," *Applied Mathematical Sciences*, vol. 7, no. 35, pp. 1721–1736, 2013.

[10] V. K. Sharma, S. K. Singh, U. Singh, and V. Agiwal, "The inverse Lindley distribution: a stress-strength reliability model with application to head and neck cancer data," *Journal of Industrial and Production Engineering*, vol. 32, no. 3, pp. 162–173, 2015.

[11] A. M. Abd AL-Fattah, A. A. EL-Helbawy, and G. R. AL-Dayian, "Inverted Kumaraswamy distribution: properties and estimation," *Pakistan Journal of Statistics*, vol. 33, no. 1, pp. 37–61, 2017.

[12] M. H. Tahir, G. M. Cordeiro, S. Ali, S. Dey, and A. Manzoor, "The inverted Nadarajah-Haghighi distribution: estimation methods and applications," *Journal of Statistical Computation and Simulation*, vol. 88, no. 14, pp. 2775–2798, 2018.

[13] A. S. Hassan and M. Abd-Allah, "On the inverse power Lomax distribution," *Annals of Data Science*, vol. 6, no. 2, pp. 259–278, 2019.

[14] A. S. Hassan and R. E. Mohamed, "Parameter estimation for inverted exponentiated Lomax distribution with right censored data," *Gazi University Journal of Science*, vol. 32, no. 4, pp. 1370–1386, 2019.

[15] A. S. Hassan and R. E. Mohamed, "Weibull inverse Lomax distribution," *Pakistan Journal of Statistics and Operation Research*, vol. 15, no. 3, pp. 587–603, 2019.

[16] A. S. Hassan, S. M. Assar, and A. M. Abd Elghaffar, "Statistical properties and estimation of power-transmuted inverse Rayleigh distribution," *Statistics in Transition new series*, vol. 21, no. 3, pp. 1–20, 2020.

[17] A. S. Hassan, M. Elgarhy, and R. Ragab, "Statistical properties and estimation of inverted Topp-Leone distribution," *Journal of Statistics Applications & Probability*, vol. 9, no. 2, pp. 319–331, 2020.

[18] R. A. Bantan, M. Elsehetry, A. S. Hassan et al., "A two-parameter model: properties and estimation under ranked sampling," *Mathematics*, vol. 9, pp. 1–16, 2021.

Hindawi
Journal of Mathematics
Volume 2021, Article ID 7330385, 9 pages
https://doi.org/10.1155/2021/7330385

Research Article

Estimation of Sine Inverse Exponential Model under Censored Schemes

M. Shrahili,[1] I. Elbatal,[2] Waleed Almutiry,[3] and Mohammed Elgarhy[4]

[1]*Department of Statistics and Operations Research, College of Science, King Saud University, P.O. Box 2455, Riyadh 11451, Saudi Arabia*
[2]*Department of Mathematics and Statistics, College of Science Imam Mohammad Ibn Saud Islamic University (IMSIU), Riyadh, Saudi Arabia*
[3]*Department of Mathematics, College of Science and Arts in Ar Rass, Qassim University, Ar Rass, Saudi Arabia*
[4]*The Higher Institute of Commercial Sciences, Al Mahalla Al Kubra 31951, Algharbia, Egypt*

Correspondence should be addressed to Mohammed Elgarhy; m_elgarhy85@sva.edu.eg

Received 21 August 2021; Revised 30 September 2021; Accepted 7 October 2021; Published 21 October 2021

Academic Editor: Naeem Jan

In this article, we introduce a new one-parameter model, which is named sine inverted exponential (SIE) distribution. The SIE distribution is a new extension of the inverse exponential (IE) distribution. The SIE distribution aims to provide the SIE model for data-fitting purposes. The SIE distribution is more flexible than the inverted exponential (IE) model, and it has many applications in physics, medicine, engineering, nanophysics, and nanoscience. The density function (PDFu) of SIE distribution can be unimodel shape and right skewed shape. The hazard rate function (HRFu) of SIE distribution can be J-shaped and increasing shaped. We investigated some fundamental statistical properties such as quantile function (QFu), moments (Mo), moment generating function (MGFu), incomplete moments (ICMo), conditional moments (CMo), and the SIE distribution parameters were estimated using the maximum likelihood (ML) method for estimation under censored samples (CS). Finally, the numerical results were investigated to evaluate the flexibility of the new model. The SIE distribution and the IE distribution are compared using two real datasets. The numerical results show the superiority of the SIE distribution.

1. Introduction

In the recent years, inverse and half-inverse problems are studied in general operator theory [1–3], numerous authors have attracted the attention of generated families of distributions such as Kumaraswamy-G by [4], sine generated (S-G) by [5], Kumaraswamy Type-I half-logistic-G [6], Weibull-G [7], odd Fréchet -G by [8], the Burr type X-G by [9], Kumaraswamy Kumaraswamy-G [10], truncated Cauchy power-G by [11], generalized odd half-Cauchy-G by [12], and among others.

The cumulative distribution function (CDFu) and PDFu of S-G are

$$F(x;\xi) = \sin\left[\frac{\pi}{2}G(x;\xi)\right], \quad x \in R, \tag{1}$$

$$f(x;\xi) = \frac{\pi}{2}g(x;\xi)\cos\left[\frac{\pi}{2}G(x;\xi)\right], \quad x \in R. \tag{2}$$

Letting $g(x;\xi)$ and $G(x;\xi)$, the PDFu and CDFu of IE distribution, it has the following form:

$$g(x) = \theta x^{-2}e^{-(\theta/x)}, \quad \theta > 0,\ x > 0, \tag{3}$$

$$G(x) = e^{-(\theta/x)}, \quad \theta > 0,\ x > 0. \tag{4}$$

The main idea for this paper was to introduce a new one-parameter model that is more flexible than the IE model by using the S-G family. The new model is called the SIE model. The SIE model is more flexible than the IE model and it has

many applications in physics, medicine, nanophysics, and nanoscience [13–16]. This manuscript is arranged as follows. Section 2 presents materials and methods. In Section 3, statistical inference of the SIE model under the censored scheme is studied. Section 4 presents results and discussion. At the end of article, conclusions are discussed.

2. Materials and Methods

2.1. The New SIE Model. Letting random variable X to have SIE distribution, then the CDFu, PDFu, survival function (SFu), and HRFu of X are

$$F(x) = \sin\left[\frac{\pi}{2}e^{-(\theta/x)}\right], \quad x>0,\ \theta>0, \tag{5}$$

$$f(x) = \frac{\pi\theta}{2x^2}e^{-(\theta/x)}\cos\left[\frac{\pi}{2}e^{-(\theta/x)}\right], \quad x>0,\ \theta>0, \tag{6}$$

$$R(x) = 1-\sin\left[\frac{\pi}{2}e^{-(\theta/x)}\right], \tag{7}$$

$$h(x) = \frac{\left(\pi\theta/2x^2\right)e^{-(\theta/x)}\cos\left[(\pi/2)e^{-(\theta/x)}\right]}{1-\sin\left[(\pi/2)e^{-(\theta/x)}\right]}, \tag{8}$$

where θ is a scale parameter.

Figures 1–3 show the plots of PDFu, CDFu, and HRFu of the SIE model. The PDFu of the SIE model can be right skewed and unimodal shaped, while the HRFu of the SIE model can be increasing or J-shaped.

2.2. Quantile and Median. If X~ SIE, then the QFu of SIE is as follows:

$$Q(u) = \theta\left[\ln\left(\frac{\pi}{2\mathrm{Arcsin}(u)}\right)\right]^{-1}, \tag{9}$$

and by taking $u=0.5$, we get the median (M) as $M=\theta[\ln(3)]^{-1}$.

MacGillivray's skewness function is defined in [17] as

$$\mathrm{MGS} = \frac{Q(u)+Q(1-u)-2M}{Q(u)-Q(1-u)}. \tag{10}$$

Figure 4 plots MGS for all values of the parameter θ.

2.3. Moments

Theorem 1. *Letting X be a r.v. from the SIE model, then its r^{th} Mo is*

$$\theta_r' = \sum_{i=0}^{\infty}\frac{\theta^{r-1}\Lambda\Gamma(1-r)}{(2i+1)^{1-r}}. \tag{11}$$

Proof. Let X be a r. v. with pdf equation (6). The r^{th} Mo of SIE distribution is computed as follows:

$$\theta_r' = \int_0^{\infty}x^r f(x)\,\mathrm{d}x = \frac{\pi\theta}{2}\int_0^{\infty}x^{r-2}e^{-(\theta/x)}\cos\left[\frac{\pi}{2}e^{-(\theta/x)}\right]\mathrm{d}x. \tag{12}$$

By inserting the expansion $\cos[G(x)] = \sum_{i=0}^{\infty}((-1)^i/(2i)!)G(x)^{2i}, n$ to the previous equation, then

$$\theta_r' = \sum_{i=0}^{\infty}\frac{\theta(-1)^i}{(2i)!}\left(\frac{\pi}{2}\right)^{2i+1}\int_0^{\infty}x^{r-\delta-1}e^{-(2i+1)(\theta/x)}\,\mathrm{d}x. \tag{13}$$

The last equation can be rewritten as follows:

$$\theta_r' = \sum_{i=0}^{\infty}\Lambda\int_0^{\infty}x^{r-2}e^{-(2i+1)(\theta/x)}\,\mathrm{d}x, \tag{14}$$

where $\Lambda = \sum_{i=0}^{\infty}(\theta(-1)^i/(2i)!)(\pi/2)^{2i+1}$.

Let $y=(\theta/x)$; then,

$$\theta_r' = \sum_{i=0}^{\infty}\theta^{r-1}\Lambda\int_0^{\infty}y^{-r}e^{-(2i+1)y}\,\mathrm{d}y. \tag{15}$$

Then,

$$\theta_r' = \sum_{i=0}^{\infty}\frac{\theta^{r-1}\Lambda\Gamma(1-r)}{(2i+1)^{1-r}}. \tag{16}$$

The MGFu of X is

$$M_X(t) = \sum_{r=0}^{\infty}\frac{t^r}{r!}\theta_r' = \sum_{r,i=0}^{\infty}\frac{t^r\theta^{r-1}\Lambda\Gamma(1-r)}{r!(2i+1)^{1-r}}. \tag{17}$$

The ICMo, denoted by $\varphi_s(t)$, of the SIE distribution is

$$\varphi_s(t) = \int_0^{t}x^s f(x)\,\mathrm{d}x = \frac{\pi\theta}{2}\int_0^{t}x^{s-2}e^{-(\theta/x)}\cos\left[\frac{\pi}{2}e^{-(\theta/x)}\right]\mathrm{d}x. \tag{18}$$

By using equation (18), $\varphi_s(t)$ will be as

$$\varphi_s(t) = \sum_{i=0}^{\infty}\frac{\theta^{r-1}\Lambda\gamma(1-r,(\theta/t))}{(2i+1)^{1-r}}, \tag{19}$$

where $\gamma(s,t) = \int_0^t y^{s-1}e^{-y}\,\mathrm{d}y$ is the lower ICGFu where ICGFu is incomplete gamma function.

The CMo, denoted by $\tau_s(t)$, of the SIE distribution is

$$\tau_s(t) = \int_t^{\infty}x^s f(x)\,\mathrm{d}x = \frac{\pi\theta}{2}\int_t^{\infty}x^{s-2}e^{-(\theta/x)}\cos\left[\frac{\pi}{2}e^{-(\theta/x)}\right]\mathrm{d}x. \tag{20}$$

By using equation (20), $\tau_s(t)$ will be as given

$$\tau_s(t) = \sum_{i=0}^{\infty}\frac{\theta^{r-1}\Lambda\Gamma(1-r,(\theta/t))}{(2i+1)^{1-r}}, \tag{21}$$

where $\Gamma(s,t) = \int_t^{\infty}y^{s-1}e^{-y}\,\mathrm{d}y$ is the upper ICGFu. □

2.4. Order Statistics. Let $X_1, X_2, \ldots, X_n$ be random sample from the SIE distribution with order statistics (OS) $X_{(1)}, X_{(2)}, \ldots, X_{(n)}$. The pdf of $T_{(m)}$ of OS is

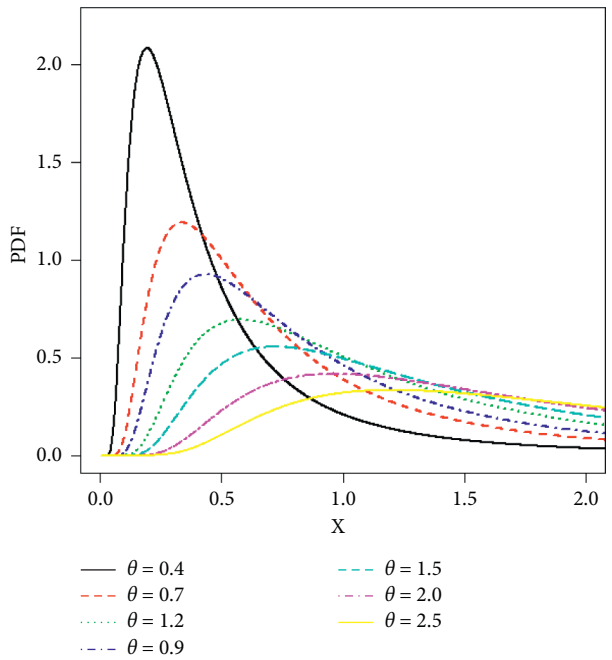

Figure 1: Plots of PDFu for the SIE model.

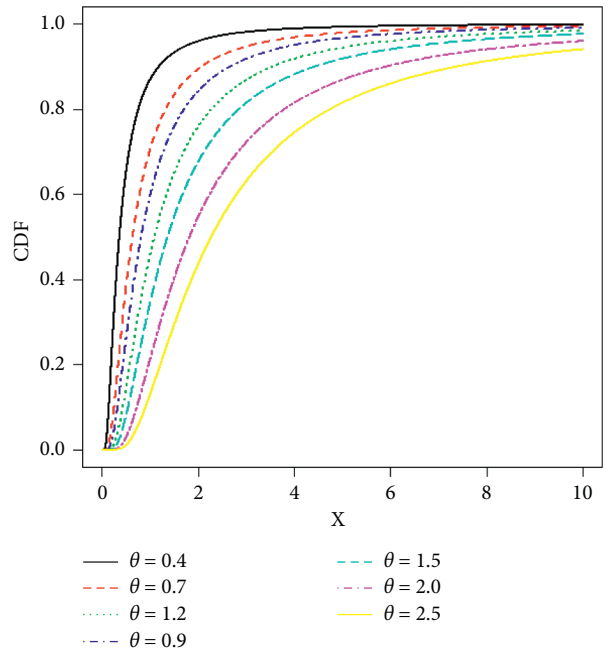

Figure 2: Plots of CDFu for the SIE model.

The pdf of $X_{(m)}$ can be expressed as

$$f_{X_{(m)}}(x) = \frac{n!}{(m-1)!(n-m)!} F^{m-1}(x) f(x) (1 - F(x))^{n-m}. \tag{22}$$

$$f_{X_{(m)}}(x) = \frac{n!\pi\theta}{2(m-1)!(n-m)!} x^{-2} e^{-(\theta/x)} \sin^{m-1}\left[\frac{\pi}{2} e^{-(\theta/x)}\right] \cos\left[\frac{\pi}{2} e^{-(\theta/x)}\right] \left(1 - \sin\left[\frac{\pi}{2} e^{-(\theta/x)}\right]\right)^{n-m}. \tag{23}$$

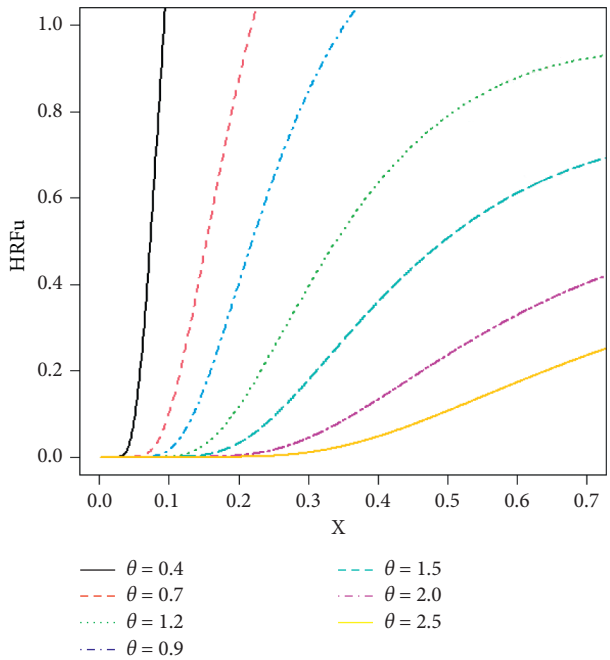

Figure 3: Plots of HRFu for the SIE model.

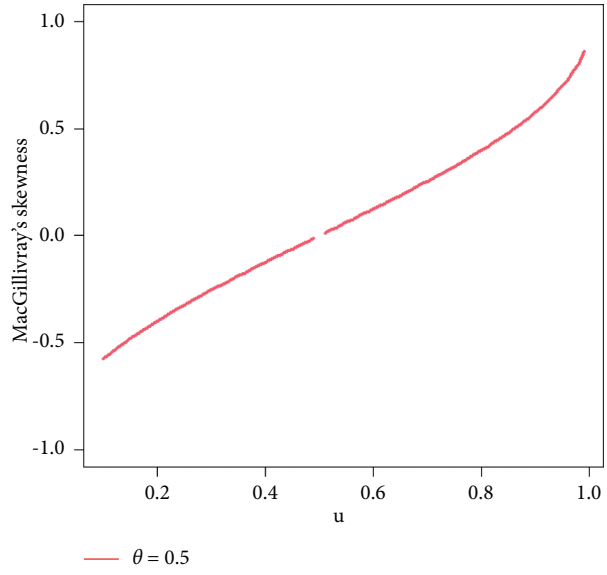

Figure 4: Plots of MGS for the SIE model.

Specially, the pdfs of the lowest and greatest OS can be computed as

$$f_{X_{(1)}}(x) = \frac{n\pi\theta}{2}x^{-2}e^{-(\theta/x)}\cos\left[\frac{\pi}{2}e^{-(\theta/x)}\right]\left(1-\sin\left[\frac{\pi}{2}e^{-(\theta/x)}\right]\right)^{n-1}, \tag{24}$$

$$f_{X_{(n)}}(x) = \frac{n\pi\theta}{2}x^{-2}e^{-(\theta/x)}\sin^{n-1}\left[\frac{\pi}{2}e^{-(\theta/x)}\right]\cos\left[\frac{\pi}{2}e^{-(\theta/x)}\right]. \tag{25}$$

3. Statistical Inference under Censored Samples

For different reasons, such as time constraints, money, or other resources, reliability or lifespan testing trials are typically censored. Generally speaking, there are two types of censorship schemes: Type-I and Type-II CS. Estimation using these two censoring techniques will be discussed in this section of the paper. If we use type-I censoring, we have a set time, say X, but the amount of things that fail during the trial is completely random. Type-II censoring, on the contrary, is a process that continues until the stated number of failures is reached.

3.1. ML Estimation under Type-I Censor. Assume that $X_1, X_2, \ldots, X_r$ be a type-I CS of size r obtained from lifetime testing experiment on k items whose lifetime follows the PDFu for SIE. The likelihood function (LLFu) of type-I CS is given as

$$L = \frac{n!}{(n-r)!}\left[1 - F(x_0)\right]^{n-r}\left\{\prod_{i=1}^{r}\left[f(x_i)\right]\right\}. \tag{26}$$

The log-LLFu corresponding to equation (26) is given by

$$\ln(L) = \ln\left(\frac{n!}{(n-r)!}\right) + (n-r)\ln\left(1 - \sin\left[\frac{\pi}{2}e^{-(\theta/x_0)}\right]\right) + r\ln\frac{\pi}{2} + r\ln\theta - 2\sum_{i=1}^{r}\ln(x_i) - \sum_{i=1}^{r}\frac{\theta}{x_i} + \sum_{i=1}^{r}\ln\left(\cos\left[\frac{\pi}{2}e^{-(\theta/x_i)}\right]\right). \tag{27}$$

The ML equations for the SIE distribution are as follows:

$$\frac{\partial \ln L}{\partial\theta} = \frac{(n-r)\pi e^{-(\theta/x_0)}\cos\left[(\pi/2)e^{-(\theta/x_0)}\right]}{2x_0\left[1 - \sin\left[(\pi/2)e^{-(\theta/x_0)}\right]\right]} + \frac{r}{\theta} - \sum_{i=1}^{r}\frac{\theta}{x_i} + \frac{\delta\pi}{2\theta}\sum_{i=1}^{r}\left(\frac{\theta}{x_i}\right)^{\delta} e^{-(\theta/x_i)^{\delta}}\left(\tan\left[\frac{\pi}{2}e^{-(\theta/x_i)^{\delta}}\right]\right). \tag{28}$$

Then, the ML estimators for the parameter θ are computed by putting $(\partial \ln L/\partial\theta) = 0$ and solving.

3.2. ML Estimation under Type-II Censor. Let $X_1, X_2, \ldots, X_r$ be a type-II CS of size r observed from lifetime testing experiment on k items whose lifetime has the PDFu for SIE. The LLFu of type-II CS is

$$L = \frac{n!}{(n-r)!}\left[1 - F(x_r)\right]^{n-r}\left\{\prod_{i=1}^{r}\left[f(x_i)\right]\right\}. \tag{29}$$

The log-LLFu corresponding to equation (29) is given by

$$\ln(L) = \ln\left(\frac{n!}{(n-r)!}\right) + (n-r)\ln\left(1 - \sin\left[\frac{\pi}{2}e^{-(\theta/x_r)}\right]\right) + r\ln\frac{\pi}{2} + r\ln\theta - 2\sum_{i=1}^{r}\ln(x_i) - \sum_{i=1}^{r}\frac{\theta}{x_i} + \sum_{i=1}^{r}\ln\left(\cos\left[\frac{\pi}{2}e^{-(\theta/x_i)}\right]\right). \tag{30}$$

The ML equations for the SIE distribution are as follows:

$$\frac{\partial \ln L}{\partial\theta} = \frac{(n-r)\pi e^{-(\theta/x_r)}\cos\left[(\pi/2)e^{-(\theta/x_r)}\right]}{2x_r\left[1 - \sin\left[(\pi/2)e^{-(\theta/x_r)}\right]\right]} + \frac{r}{\theta} - \sum_{i=1}^{r}\frac{\theta}{x_i} + \frac{\delta\pi}{2\theta}\sum_{i=1}^{r}\left(\frac{\theta}{x_i}\right)^{\delta} e^{-(\theta/x_i)^{\delta}}\left(\tan\left[\frac{\pi}{2}e^{-(\theta/x_i)^{\delta}}\right]\right). \tag{31}$$

Then, the ML estimators for the parameter θ is calculated by putting $(\partial \ln L/\partial\theta) = 0$ and solving.

3.3. Simulation Outcomes. Numerical outcomes are given in this section to examine how the estimators behave in cases of full, TIC, and TIIC estimations. With the help of Mathematica 9, you can compute the mean square errors ($A1$) as well as the lower limit ($L1$) and upper bound ($U1$) of the confidence interval, as well as the average length (AvLe) for 90 percent and 95 percent. The following is a description of how the following algorithm works:

(i) SIE distribution generates 5000 random samples with size $n = 30$, 50, 100, 200, 300, 500, 1000, and 2000.

(ii) True parameter θ values are taken.

(iii) The termination time is set to $T = 1.5$ in the event of TIC and 3 in the absence of TIC. Three levels of censorship are chosen: $r = 80\%$, $r = 90\%$ (TIIC), and $r = 100\%$ (complete sample).

(iv) The ML estimates, $A1$, $L1$, $U1$, and AvLe for various parameter values are computed.

(v) Tables 1–6 include numerical outputs based on completeness and TIIC, while Tables 7–10 contain TIC-based simulation findings.

From Tables 1–10, we can note that when n increases, the MLE and AvLe are decreased.

Table 1: MLEs, estimates, $A1$, $L1$, $U1$, and AvLe of the SIE model under TIIC for $x_r = 0.8$ and $\theta = 0.8$.

n	MLE	$A1$	90%			95%		
			$L1$	$U1$	AvLe	$L1$	$U1$	AvLe
30	0.6394	0.0336	0.4777	0.8010	0.3233	0.4467	0.8320	0.3853
50	0.6410	0.0327	0.5152	0.7667	0.2515	0.4911	0.7908	0.2997
100	0.6454	0.0295	0.5474	0.7235	0.1761	0.5305	0.7403	0.2098
200	0.6519	0.0294	0.5700	0.6939	0.1238	0.5582	0.7057	0.1476
300	0.6530	0.0286	0.5824	0.6836	0.1013	0.5727	0.6933	0.1207
500	0.6630	0.0284	0.5938	0.6722	0.0785	0.5863	0.6797	0.0935
1000	0.6720	0.0282	0.6043	0.6597	0.0554	0.5990	0.6650	0.0660
2000	0.6813	0.0276	0.6118	0.6509	0.0391	0.6080	0.6546	0.0466

Table 2: MLEs, estimates, $A1$, $L1$, $U1$, and AvLe of the SIE model under TIIC for $x_r = 0.9$ and $\theta = 0.8$.

n	MLE	$A1$	90%			95%		
			$L1$	$U1$	AvLe	$L1$	$U1$	AvLe
30	0.7151	0.0161	0.5501	0.9000	0.3500	0.5165	0.9336	0.4170
50	0.7203	0.0125	0.5856	0.8550	0.2694	0.5598	0.8808	0.3210
100	0.7270	0.0099	0.6222	0.8119	0.1897	0.6040	0.8301	0.2260
200	0.7344	0.0090	0.6476	0.7813	0.1337	0.6348	0.7941	0.1592
300	0.7359	0.0085	0.6594	0.7685	0.1090	0.6490	0.7789	0.1299
500	0.7446	0.0079	0.6723	0.7569	0.0845	0.6642	0.7650	0.1007
1000	0.7448	0.0076	0.6849	0.7447	0.0598	0.6791	0.7504	0.0713
2000	0.7536	0.0056	0.6925	0.7347	0.0422	0.6885	0.7388	0.0503

Table 3: MLEs, estimates, $A1$, $L1$, $U1$, and AvLe of the SIE model under TIIC for $x_r = 1$ and $\theta = 0.8$.

n	MLE	$A1$	90%			95%		
			$L1$	$U1$	AvLe	$L1$	$U1$	AvLe
30	0.8200	0.0129	0.6229	0.9972	0.3743	0.5871	1.0330	0.4459
50	0.8157	0.0073	0.6616	0.9498	0.2882	0.6341	0.9774	0.3434
100	0.7893	0.0040	0.6983	0.9003	0.2021	0.6789	0.9197	0.2408
200	0.7965	0.0017	0.7271	0.8699	0.1428	0.7134	0.8835	0.1701
300	0.8024	0.0013	0.7438	0.8610	0.1171	0.7326	0.8722	0.1396
500	0.7986	0.0008	0.7544	0.8448	0.0904	0.7457	0.8535	0.1077
1000	0.8011	0.0004	0.7690	0.8331	0.0641	0.7629	0.8392	0.0763
2000	0.8005	0.0002	0.7778	0.8231	0.0453	0.7735	0.8274	0.0539

Table 4: MLEs, estimates, $A1$, $L1$, $U1$, and AvLe of the SIE model under TIIC for $x_r = 0.8$ and $\theta = 1.5$.

n	MLE	$A1$	90%			95%		
			$L1$	$U1$	AvLe	$L1$	$U1$	AvLe
30	0.6394	0.0336	0.4777	0.8010	0.3233	0.4467	0.8320	0.3853
50	0.6410	0.0327	0.5152	0.7667	0.2515	0.4911	0.7908	0.2997
100	0.6454	0.0295	0.5474	0.7235	0.1761	0.5305	0.7403	0.2098
200	0.6519	0.0294	0.5700	0.6939	0.1238	0.5582	0.7057	0.1476
300	0.6530	0.0286	0.5824	0.6836	0.1013	0.5727	0.6933	0.1207
500	0.6630	0.0284	0.5938	0.6722	0.0785	0.5863	0.6797	0.0935
1000	0.6720	0.0282	0.6043	0.6597	0.0554	0.5990	0.6650	0.0660
2000	0.6813	0.0276	0.6118	0.6509	0.0391	0.6080	0.6546	0.0466

4. Results and Discussion

4.1. Application. In this section, two real datasets are analyzed to explain the benefit of the SIE model compared to the IE model. To compare the competitive models, we suggested some information criterion (ICr) as minus two log-LLFu ($D1$), Akaike ICr ($D2$), the correct Akaike ICr ($D3$), Bayesian ICr ($D4$), and Hannan–Quinn ICr ($D5$).

The first data are known as ball bearing data, and it represents the number of rotations before ball bearing failure obtained [18]. The second data set consists of 100 observations of breaking stress of carbon fibres (in Gba) given by

Table 5: MLEs, estimates, $A1$, $L1$, $U1$, and AvLe of the SIE model under TIIC for $x_r = 0.9$ and $\theta = 1.5$.

n	MLE	$A1$	90%			95%		
			$L1$	$U1$	AvLe	$L1$	$U1$	AvLe
30	0.7151	0.0161	0.5501	0.9000	0.3500	0.5165	0.9336	0.4170
50	0.7203	0.0125	0.5856	0.8550	0.2694	0.5598	0.8808	0.3210
100	0.7270	0.0099	0.6222	0.8119	0.1897	0.6040	0.8301	0.2260
200	0.7344	0.0090	0.6476	0.7813	0.1337	0.6348	0.7941	0.1592
300	0.7359	0.0085	0.6594	0.7685	0.1090	0.6490	0.7789	0.1299
500	0.7446	0.0079	0.6723	0.7569	0.0845	0.6642	0.7650	0.1007
1000	0.7448	0.0076	0.6849	0.7447	0.0598	0.6791	0.7504	0.0713
2000	0.7536	0.0056	0.6925	0.7347	0.0422	0.6885	0.7388	0.0503

Table 6: MLEs, estimates, $A1$, $L1$, $U1$, and AvLe of the SIE model under TIIC for $x_r = 1$ and $\theta = 1.5$.

n	MLE	$A1$	90%			95%		
			$L1$	$U1$	AvLe	$L1$	$U1$	AvLe
30	0.8200	0.0129	0.6229	0.9972	0.3743	0.5871	1.0330	0.4459
50	0.8157	0.0073	0.6616	0.9498	0.2882	0.6341	0.9774	0.3434
100	0.7893	0.0040	0.6983	0.9003	0.2021	0.6789	0.9197	0.2408
200	0.7965	0.0017	0.7271	0.8699	0.1428	0.7134	0.8835	0.1701
300	0.8024	0.0013	0.7438	0.8610	0.1171	0.7326	0.8722	0.1396
500	0.7986	0.0008	0.7544	0.8448	0.0904	0.7457	0.8535	0.1077
1000	0.8011	0.0004	0.7690	0.8331	0.0641	0.7629	0.8392	0.0763
2000	0.8005	0.0002	0.7778	0.8231	0.0453	0.7735	0.8274	0.0539

Table 7: MLEs, estimates, $A1$, $L1$, $U1$, and AvLe of the SIE model under TIC for $T = 1.5$ and $\theta = 0.2$.

n	MLE	$A1$	90%			95%		
			$L1$	$U1$	AvLe	$L1$	$U1$	AvLe
30	0.1671	0.0040	0.1252	0.2090	0.0838	0.1172	0.2170	0.0998
50	0.1672	0.0033	0.1350	0.1995	0.0645	0.1288	0.2056	0.0769
100	0.1674	0.0027	0.1444	0.1898	0.0455	0.1400	0.1942	0.0542
200	0.1685	0.0018	0.1533	0.1857	0.0324	0.1502	0.1888	0.0386
300	0.1688	0.0017	0.1557	0.1820	0.0263	0.1531	0.1845	0.0314
500	0.1696	0.0012	0.1575	0.1778	0.0203	0.1555	0.1797	0.0242
1000	0.1714	0.0010	0.1641	0.1787	0.0146	0.1627	0.1801	0.0174
2000	0.1719	0.0008	0.1667	0.1771	0.0103	0.1658	0.1781	0.0123

Table 8: MLEs, estimates, $A1$, $L1$, $U1$, and AvLe of the SIE model under TIC for $T = 3$ and $\theta = 0.2$.

n	MLE	$A1$	90%			95%		
			$L1$	$U1$	AvLe	$L1$	$U1$	AvLe
30	0.1898	0.0051	0.1447	0.2349	0.0902	0.1360	0.2435	0.1075
50	0.1913	0.0032	0.1591	0.2295	0.0704	0.1523	0.2362	0.0839
100	0.1923	0.0024	0.1668	0.2159	0.0491	0.1621	0.2206	0.0585
200	0.1925	0.0021	0.1760	0.2110	0.0350	0.1727	0.2143	0.0417
300	0.1931	0.0019	0.1788	0.2073	0.0285	0.1761	0.2100	0.0340
500	0.1939	0.0016	0.1828	0.2050	0.0222	0.1807	0.2071	0.0264
1000	0.1940	0.0016	0.1828	0.2050	0.0222	0.1807	0.2071	0.0264
2000	0.1942	0.0012	0.1864	0.2020	0.0157	0.1849	0.2035	0.0186

Table 9: MLEs, estimates, $A1$, $L1$, $U1$, and AvLe of the SIE model under TIC for $T = 1.5$ and $\theta = 0.8$.

n	MLE	$A1$	90%			95%		
			$L1$	$U1$	AvLe	$L1$	$U1$	AvLe
30	0.6316	0.0335	0.4710	0.7921	0.3211	0.4403	0.8229	0.3826
50	0.6323	0.0314	0.5081	0.7565	0.2484	0.4843	0.7803	0.2959
100	0.6382	0.0311	0.5408	0.7156	0.1748	0.5241	0.7324	0.2083
200	0.6403	0.0306	0.5684	0.6922	0.1238	0.5565	0.7040	0.1475
300	0.6481	0.0302	0.5777	0.6784	0.1007	0.5680	0.6881	0.1200
500	0.6494	0.0294	0.5903	0.6685	0.0782	0.5828	0.6760	0.0931
1000	0.6578	0.0288	0.6003	0.6554	0.0551	0.5950	0.6607	0.0657
2000	0.6583	0.0276	0.6088	0.6478	0.0390	0.6050	0.6515	0.0465

Table 10: MLEs, estimates, $A1$, $L1$, $U1$, and AvLe of the SIE model under TIC for $T = 3$ and $\theta = 0.8$.

n	MLE	$A1$	90%			95%		
			$L1$	$U1$	AvLe	$L1$	$U1$	AvLe
30	0.7492	0.0117	0.5783	0.9400	0.3617	0.5437	0.9747	0.4310
50	0.7575	0.0080	0.6099	0.8852	0.2753	0.5835	0.9115	0.3280
100	0.7639	0.0063	0.6470	0.8409	0.1939	0.6284	0.8594	0.2310
200	0.7646	0.0045	0.6760	0.8133	0.1373	0.6629	0.8264	0.1635
300	0.7738	0.0041	0.6878	0.7998	0.1120	0.6771	0.8105	0.1334
500	0.7748	0.0040	0.6878	0.7998	0.1120	0.6771	0.8105	0.1334
1000	0.7807	0.0039	0.6994	0.7860	0.0866	0.6911	0.7943	0.1031
2000	0.7820	0.0037	0.7115	0.7726	0.0611	0.7056	0.7785	0.0729

Table 11: MLEs, $D1$, $D2$, $D3$, $D4$, and $D5$ for ball bearing data.

Models	MLE and SE	$D1$	$D2$	$D3$	$D4$	$D5$
SIE	73.586 (11.48)	243.07	245.07	245.252	244.45	245.382
IE	20.403 (2.55)	253.927	255.927	256.109	255.307	256.24

Table 12: MLEs, $D1$, $D2$, $D3$, $D4$, and $D5$ for carbon fibres' data.

Models	MLE and SE	$D1$	$D2$	$D3$	$D4$	$D5$
SIE	2.817 (11.48)	348.384	350.384	350.404	350.384	351.438
IE	2.135 (2.55)	397.956	399.956	399.977	399.956	401.011

[19]. According to Tables 11 and 12, our new model is better suited than the IE model and has the lowest values for all statistics.

4.2. Discussion. From the modelling to ball bearing and carbon fibres datasets, we see that the SIE model provides the greatest fit for the both datasets. The numerical values in Tables 11 and 12 are proposed; the both datasets supported the superiority of the SIE model.

5. Conclusion

In this study, we proposed a new one-parameter model, which is called the SIE model. Some basic statistical properties of the SIE model are also proposed. Estimation of the SIE parameter was assessed by using the ML method of estimation censored and complete samples. Application to carbon fibres datasets were used to explain the importance of SIE model against the IE model. The SIE model as we see is very flexible and simple model, so many authors can use it in the future articles. The authors can use Bayesian estimation under complete and various censored schemes to estimate its parameters. Also, ranked set sampling papers can apply the new model. Also, the authors which are interested in distribution theory can generalize more extensions of this model by many different ways.

Data Availability

The data used to support the findings of the study are available from the corresponding author upon request.

Conflicts of Interest

The authors declare no conflicts of interest.

Acknowledgments

This study was supported by King Saud University, Deanship of Scientific Research, College of Science Research Center.

References

[1] R. Amirov, A. Ergun, and S. Durak, "Half-inverse problems for the quadratic pencil of the Sturm-Liouville equations with impulse," *Numerical Methods for Partial Differential Equations*, vol. 37, no. 1, pp. 915–924, 2021.

[2] R. K. Amirov and A. Ergun, "Half inverse problems for the impulsive singular diffusion operator," *Turkish Journal of Science*, vol. 5, no. 3, pp. 186–198, 2020.

[3] A. Ergün, "A half-inverse problem for the singular diffusion operator with jump conditions," *Miskolc Mathematical Notes*, vol. 21, no. 2, pp. 805–821, 2020.

[4] G. M. Cordeiro and M. de Castro, "A new family of generalized distributions," *Journal of Statistical Computation and Simulation*, vol. 81, no. 7, pp. 883–898, 2011.

[5] D. Kumar, U. Singh, and S. K. Singh, "A new distribution using sine function- its application to bladder cancer patients data," *Journal of Statistics Applications & Probability*, vol. 4, no. 3, pp. 417–427, 2015.

[6] S. A. Elsherpieny and M. Elsehetry, "Kumaraswamy type I half logistic family of distributions with applications," *Gazi University Journal of Science*, vol. 32, no. 1, pp. 333–349, 2019.

[7] M. Bourguignon, R. B. Silva, and G. M. Cordeiro, "The Weibull–G family of probability distributions," *Journal of Data Science*, vol. 12, pp. 53–68, 2014.

[8] M. A. Haq and M. Elgarhy, "The odd Fréchet-G family of probability distributions," *Journal of Statistics Applications and Probability*, vol. 7, pp. 185–201, 2018.

[9] H. M. Yousof, A. Z. Afify, G. G. Hamedani, and G. Aryal, "The burr X generator of distributions for lifetime data," *Journal of Statistical Theory and Applications*, vol. 16, pp. 1–19, 2017.

[10] A. A. Mohamed, R. M. Mahmoud, and S. A. ElSherbini, "The new Kumaraswamy Kumaraswamy family of generalized distributions with application," *Pakistan Journal of Statistics and Operation Research*, vol. 11, no. 2, pp. 159–180, 2015.

[11] M. A. Aldahlan, F. Jamal, C. Chesneau, M. Elgarhy, and I. Elbatal, "The truncated Cauchy power family of distributions with inference and applications," *Entropy*, vol. 22, pp. 1–25, 2020.

[12] G. M. Cordeiro, M. Alizadeh, T. G. Ramires, and E. M. M. Ortega, "The generalized odd half-Cauchy family of distributions: properties and applications," *Communications in Statistics—Theory and Methods*, vol. 46, no. 11, pp. 5685–5705, 2017.

[13] P. E. Oguntunde, A. O. Adejumo, and E. A. Owoloko, "Exponential inverse exponential (EIE) distribution with applications to lifetime data," *Asian Journal of Scientific Research*, vol. 10, no. 3, pp. 169–177, 2017.

[14] P. E. Oguntunde, M. A. Khaleel, A. O. Adejumo, H. I. Okagbue, A. A. Opanuga, and F. O. Owolabi, "The Gompertz inverse exponential (GoIE) distribution with applications," *Cogent Mathematics & Statistics*, vol. 5, no. 1, Article ID 1507122, 2018.

[15] P. E. Oguntunde, A. O. Adejumo, and E. A. Owoloko, "Application of Kumaraswamy inverse exponential distribution to real lifetime data," *International Journal of Applied Mathematics & Statistics*, vol. 56, no. 5, pp. 34–47, 2017.

[16] M. A. Aldahlan, "The inverse Weibull inverse exponential distribution with application," *International Journal of Contemporary Mathematical Sciences*, vol. 14, no. 1, pp. 17–30, 2019.

[17] H. L. MacGillivray, "Skewness and asymmetry: measures and orderings," *Annals of Statistics*, vol. 14, pp. 994–1011, 1986.

[18] M. J. Crowder, A. C. Kimber, R. L. Smith, and T. J. Sweeting, *Statistical Analysis of Reliability Data*, Chapman & Hall, London, UK, 1991.

[19] M. D. Nichols and W. J. Padgett, "A bootstrap control chart for Weibull percentiles," *Quality and Reliability Engineering International*, vol. 22, no. 2, pp. 141–151, 2006.

Hindawi
Journal of Mathematics
Volume 2021, Article ID 3071765, 8 pages
https://doi.org/10.1155/2021/3071765

Research Article

On Soft Quantum B-Algebras and Fuzzy Soft Quantum B-Algebras

Xiongwei Zhang,[1] Sultan Aljahdali,[2] and Ahmed Mostafa Khalil[3]

[1]*School of Mathematics and Statistics, Yulin University, Yulin 719000, China*
[2]*Department of Computer Science, College of Computers and Information Technology, Taif University, P. O. Box 11099, Taif 21944, Saudi Arabia*
[3]*Department of Mathematics, Faculty of Science, Al-Azhar University, Assiut 71524, Egypt*

Correspondence should be addressed to Ahmed Mostafa Khalil; a.khalil@azhar.edu.eg

Received 20 August 2021; Accepted 15 September 2021; Published 16 October 2021

Academic Editor: Naeem Jan

This paper aims to make a combination between the quantum B-algebras (briefly, $\mathscr{X}$-As) and two interesting theories (e.g., soft set theory and fuzzy soft set theory). Firstly, we propose the novel notions of soft quantum B-algebras (briefly, $\mathbb{SQB}$-As), a soft deductive system of $\mathbb{QB}$-As, and deducible soft quantum B-algebras (briefly, $\mathbb{DSQB}$-As). Then, we discuss the relationship between $\mathbb{SQB}$-As and $\mathbb{DSQB}$-As. Furthermore, we investigate the union and intersection operations of $\mathbb{DSQB}$-As. Secondly, we introduce the notions of a fuzzy soft quantum B-algebras (briefly, $\mathbb{FSQB}$-As), a fuzzy soft deductive system of $\mathbb{QB}$-As, and present some characterizations of $\mathbb{FSQB}$-As, along with several examples. Finally, we explain the basic properties of homomorphism image of $\mathbb{FSQB}$-As.

1. Introduction

In 1999, Molodtsov [1] introduced the notion called soft sets (briefly, $\mathbb{SS}$) (i.e., which reduce the uncertainty and vagueness of knowledge). Maji et al. [2] presented the fuzzy soft sets (briefly, $\mathbb{FSS}$). Since then, many researchers studied further on $\mathbb{SS}$ and $\mathbb{FSS}$ as in the following published articles (e.g., [3–9]).

In 2014, Rump and Yang [10] proposed the notion of $\mathbb{QB}$-As (i.e., a partial ordered implication algebras). Rump [11, 12] investigated many implication algebras (for example, pseudo-BCK-algebras, po-groups, BL-algebras, MV-algebras, GPE-algebras, and resituated lattices). Botur and Paseka [13] studied filters on integral $\mathbb{QB}$-As, and Zhang et al. [14] established the quotient structures by using q-filters in $\mathbb{QB}$-As and investigated the relation between basic implication algebras and $\mathbb{QB}$-As. Han et al. [15] constructed the unitality of $\mathbb{QB}$-As and explained the injective hulls of $\mathbb{QB}$-As in [16]. By the framework of $\mathbb{QB}$-As, there are many published papers on $\mathbb{QB}$-As (e.g., [17–23]).

Regarding these developments, as the motivation of this paper, we will combine $\mathbb{QB}$-As with $\mathbb{SS}$ and $\mathbb{FSS}$ (i.e., enrich the previous work on hybrid soft set and fuzzy soft set theories algebras with quantum structures). We introduce the notions of $\mathbb{SQB}$-As and the soft deductive system of $\mathbb{QB}$-As and consider the relation between $\mathbb{SQB}$-As and $\mathbb{DSQB}$-As. Furthermore, some conditions are given to ensure the operations union and intersection holds of soft deductive of $\mathbb{QB}$-As. Then, we investigate the homomorphism image of deductive $\mathbb{SQB}$-As. Lastly, we define $\mathbb{FSQB}$-As and fuzzy soft deductive system of $\mathbb{QB}$-As and give an example to illustrate its derive properties.

In the following, we have arranged the sections as follows. In Section 2, we briefly recall many notions related to $\mathbb{QB}$-As, $\mathbb{SS}$, and $\mathbb{FSS}$ as indicated in Definitions 1–7, which are used in the sequel. In Section 3, we propose the notions of $\mathbb{SQB}$-As, soft deductive system of $\mathbb{QB}$-As, and $\mathbb{DSQB}$-As. In Section 4, we present the notions of $\mathbb{FSQB}$-As and a fuzzy soft deductive system of $\mathbb{QB}$-As and discuss the homomorphism image of $\mathbb{FSQB}$-As. The conclusions are explained in Section 5.

2. Preliminaries

We give some basic notions of $\mathbb{QB}$-$\mathbb{A}$s, $\mathbb{SS}$, and $\mathbb{FSS}$ before defining $\mathbb{SQB}$-$\mathbb{A}$s in Section 3.

Definition 1 (cf. [10]).

(1) $\mathbb{QB}$-$\mathbb{A}$s is a partially ordered set $(\mathscr{X}, \leq)$ with two binary operations $\longrightarrow$ and $\rightsquigarrow$ which satisfy $(\forall x, y, z \in \mathscr{X})$:

$$\begin{aligned} y \longrightarrow z \leq (x \longrightarrow y) \longrightarrow (x \longrightarrow z),\\ y \rightsquigarrow z \leq (x \rightsquigarrow y) \rightsquigarrow (x \rightsquigarrow z),\\ y \leq z \Longrightarrow x \longrightarrow y \leq x \longrightarrow z,\\ x \leq y \longrightarrow z \Longleftrightarrow y \leq x \rightsquigarrow z. \end{aligned} \tag{1}$$

(2) $\mathbb{QB}$-$\mathbb{A}$ is a commutative (briefly, $\mathbb{CQB}$-$\mathbb{A}$) if $x \longrightarrow y = x \rightsquigarrow y$ $(\forall x, y \in \mathscr{X})$.

(3) A subset $\mathscr{Y}$ of a $\mathbb{QB}$-$\mathbb{A}$ $\mathscr{X}$ is a subalgebra if $x \longrightarrow y, x \rightsquigarrow y \in \mathscr{Y}$ $(\forall x, y \in \mathscr{X})$.

In what follows, denote by $\mathscr{X}$ a $\mathbb{QB}$-$\mathbb{A}$ unless otherwise specified.

Definition 2 (cf. [10]). Let $\mathscr{X}_1$ and $\mathscr{X}_2$ be two $\mathbb{QB}$-$\mathbb{A}$s. Then, $\psi: \mathscr{X}_1 \longrightarrow \mathscr{X}_2$ is a morphism of $\mathbb{QB}$-$\mathbb{A}$s if it satisfies $(\forall x, y \in \mathscr{X}_1)$:

$$\begin{aligned} \psi(x \longrightarrow y) \leq \psi(x) \longrightarrow \psi(y),\\ \psi(x \rightsquigarrow y) \leq \psi(x) \rightsquigarrow \psi(y). \end{aligned} \tag{2}$$

We say morphism ψ is exact if the inequalities become equations.

Definition 3 (cf. [1]). Assume that $\mathscr{X}$ be a set and $\mathscr{K}$ be a set of parameters. $\mathcal{S}_{\mathscr{K}}$ (called $\mathbb{SS}$) is a mapping given by $\mathcal{S}: \mathscr{K} \longrightarrow 2^{\mathscr{X}}$ (i.e., $2^{\mathscr{X}}$ is the power set of $\mathscr{X}$).

Definition 4 (cf. [3]). Assume that $\mathcal{S}_{\mathscr{K}_1}$ and $\mathcal{S}_{\mathscr{K}_2}$ are two $\mathbb{SS}$ over $\mathscr{X}$. $\mathcal{S}_{\mathscr{K}_1}$ is a subset of $\mathcal{S}_{\mathscr{K}_2}$ (denoted by $\mathcal{S}_{\mathscr{K}_1} \widetilde{\subset} \mathcal{S}_{\mathscr{K}_2}$) if

(1) $\mathscr{K}_1 \subset \mathscr{K}_2$

(2) For every $k \in \mathscr{K}_1$, $\mathcal{S}_{\mathscr{K}_1}(k)$ and $\mathcal{S}_{\mathscr{K}_2}(k)$ are identical approximations

Definition 5 (cf. [3]). Assume that $\mathcal{S}_{\mathscr{K}_1}, \mathcal{S}_{\mathscr{K}_2}$, and $\mathcal{S}_{\mathscr{K}_3}$ are three $\mathbb{SS}$ over $\mathscr{X}$. $\mathcal{S}_{\mathscr{K}_3}$ is the intersection of $\mathcal{S}_{\mathscr{K}_1}$ and $\mathcal{S}_{\mathscr{K}_2}$ (denoted by $\mathcal{S}_{\mathscr{K}_3} = \mathcal{S}_{\mathscr{K}_1} \widetilde{\cap} \mathcal{S}_{\mathscr{K}_2}$) if

(1) $\mathscr{K}_3 = \mathscr{K}_1 \cap \mathscr{K}_2$

(2) $\forall k \in \mathscr{K}_3$, $\mathcal{S}_{\mathscr{K}_3}(k) = \mathcal{S}_{\mathscr{K}_1}(k)$ or $\mathcal{S}_{\mathscr{K}_2}(k)$ (as both are same sets)

Definition 6 (cf. [3]). Assume that $\mathcal{S}_{\mathscr{K}_1}, \mathcal{S}_{\mathscr{K}_2}$, and $\mathcal{S}_{\mathscr{K}_3}$ are three $\mathbb{SS}$ over $\mathscr{X}$. $\mathcal{S}_{\mathscr{K}_3}$ is called the union of $\mathcal{S}_{\mathscr{K}_1}$ and $\mathcal{S}_{\mathscr{K}_2}$ (denoted by $\mathcal{S}_{\mathscr{K}_3} = \mathcal{S}_{\mathscr{K}_1} \widetilde{\cup} \mathcal{S}_{\mathscr{K}_2}$) if

(1) $\mathscr{K}_3 = \mathscr{K}_1 \cup \mathscr{K}_2$.

(2) $k \in \mathscr{K}_3$,

$$\mathcal{S}_{\mathscr{K}_3}(k) = \begin{cases} \mathcal{S}_{\mathscr{K}_1}(k), & k \in \mathscr{K}_1 \backslash \mathscr{K}_2\\ \mathcal{S}_{\mathscr{K}_2}(k), & k \in \mathscr{K}_2 \backslash \mathscr{K}_1,\\ \mathcal{S}_{\mathscr{K}_1}(k) \cup \mathcal{S}_{\mathscr{K}_2}(k), & k \in \mathscr{K}_1 \cap \mathscr{K}_2 \end{cases} \tag{3}$$

Definition 7 (cf. [2]). $\mathbb{FSS}$ (called $\mathbb{FSS}$) $\widehat{\mathcal{S}}_{\mathscr{K}}$ is a mapping given by $\widehat{\mathcal{S}}: \mathscr{K} \longrightarrow I^X$ (i.e., I^X is the set of all fuzzy sets [24] of $\mathscr{X}$).

3. $\mathbb{SQB}$-$\mathbb{A}$s

We define the $\mathbb{SQB}$-$\mathbb{A}$s and give several examples based on $\mathbb{SQB}$-$\mathbb{A}$s. Also, we will study the union and intersection operations between two $\mathbb{SQB}$-$\mathbb{A}$s as follows .

Definition 8. $\mathcal{S}_{\mathscr{K}}$ is a $\mathbb{SQB}$-$\mathbb{A}$s over $\mathscr{X}$ if $\mathcal{S}_{\mathscr{K}}(x)(\forall x \in \mathscr{K})$ are subalgebras of $\mathscr{X}$ (i.e., in case $\mathscr{K} = \mathscr{X}$).

Example 1

(1) Suppose $\mathscr{X}$ (i.e., $\mathscr{X} = \{k_1, k_2, k_3, 1\}$) with the order $k_2, k_3 < k_1 < 1$. Now, we show, by Table 1, the binary operation $\longrightarrow$.

Clearly, $\mathscr{X}$ is a $\mathbb{CQB}$-$\mathbb{A}$. We define $\mathcal{S}_{\mathscr{K}}(\forall x \in \mathscr{K})$ (i.e., $\mathscr{K} = \mathscr{X}$) by

$$\mathcal{S}_{\mathscr{K}}(x) = \{y \in \mathscr{X} \mid (x \longrightarrow y) \longrightarrow y \in \{k_1, 1\}\}. \tag{4}$$

From Table 1, we can get on $\mathcal{S}_{\mathscr{K}}(k_1) = \mathscr{X}$, $\mathcal{S}_{\mathscr{K}}(k_2) = \mathcal{S}_{\mathscr{K}}$, $(k_3) = \{k_1, k_3, 1\}$, and $\mathcal{S}_{\mathscr{K}}(1) = \mathscr{X}$, and then, $\mathcal{S}_{\mathscr{K}}(x)(x \in \mathscr{K})$ are all subalgebras of $\mathscr{X}$. Consequently, $\mathcal{S}_{\mathscr{K}}$ is a $\mathbb{SQB}$-$\mathbb{A}$s over $\mathscr{X}$.

(2) Suppose $\mathscr{X}$ (i.e., $\mathscr{X} = \{k_1, k_2, k_3, 1\}$) with the order $k_1 < k_2 < k_3 < 1$. Now, we show, by Table 2, the binary operation $\longrightarrow$.

Clearly, $\mathscr{X}$ is a $\mathbb{CQB}$-$\mathbb{A}$. We define $\mathcal{S}_{\mathscr{K}}(\forall x \in \mathscr{K})$ (i.e., $\mathscr{K} = \mathscr{X}$) by

$$\mathcal{S}_{\mathscr{K}}(x) = \{y \in \mathscr{X} | x \mathscr{R} y \Longleftrightarrow x \longrightarrow (x \longrightarrow y) \in \{k_3, 1\}\}. \tag{5}$$

From Table 2, we can get on (HTML translation failed), and then, $\mathcal{S}_{\mathscr{K}}(x)(x \in \mathscr{K})$ are all subalgebras of $\mathscr{X}$. Consequently, $\mathcal{S}_{\mathscr{K}}$ is a $\mathbb{SQB}$-$\mathbb{A}$s over $\mathscr{X}$.

We ensure the operations (i.e., union and intersection) are holding on $\mathbb{SQB}$-$\mathbb{A}$s by the following suggested theorem.

Theorem 1. *Assume that $\mathcal{S}_{\mathscr{K}_1}$ and $\mathcal{S}_{\mathscr{K}_2}$ are $\mathbb{SQB}$-$\mathbb{A}$s over $\mathscr{X}$. Then,*

(1) If $\mathscr{K}_3 = \mathscr{K}_1 \cap \mathscr{K}_2$, then $\mathcal{S}_{\mathscr{K}_3} = \mathcal{S}_{\mathscr{K}_1} \widetilde{\cap} \mathcal{S}_{\mathscr{K}_2}$ is called a $\mathbb{SQB}$-$\mathbb{A}$ over $\mathscr{X}$

(2) If $\mathscr{K}_1 \cap \mathscr{K}_2 = \emptyset$, then $\mathcal{S}_{\mathscr{K}_1} \widetilde{\cup} \mathcal{S}_{\mathscr{K}_2}$ is called a $\mathbb{SQB}$-$\mathbb{A}$ over $\mathscr{X}$

Table 1: The binary operation $\longrightarrow$.

$\longrightarrow$	k_1	k_2	k_3	1
k_1	1	k_1	k_1	1
k_2	1	1	k_1	1
k_3	1	1	k_1	1
1	k_1	k_2	k_3	1

Table 2: The binary operation $\longrightarrow$.

$\longrightarrow$	k_1	k_2	k_3	1
k_1	1	1	1	1
k_2	k_1	k_2	1	1
k_3	k_1	k_1	1	1
1	k_1	k_1	k_3	1

Proof

(1) If $\mathscr{K}_3 = \mathscr{K}_1 \cap \mathscr{K}_2$ and by Definition 5, we obtain $\mathcal{S}_{\mathscr{K}_3}(x) = \mathcal{S}_{\mathscr{K}_1}(x)$ or $\mathcal{S}_{\mathscr{K}_3}(x) = \mathcal{S}_{\mathscr{K}_2}(x)$, for all $x \in \mathscr{K}_3$. Since $\mathcal{S}_{\mathscr{K}_1}$ and $\mathcal{S}_{\mathscr{K}_2}$ are $\mathbb{SQB}$-$\mathbb{A}$s over $\mathscr{X}$, which implies that $\mathcal{S}_{\mathscr{K}_3}$ is a $\mathbb{SQB}$-$\mathbb{A}$s over $\mathscr{X}$, that is, $\mathcal{S}_{\mathscr{K}_3}(x) = \mathcal{S}_{\mathscr{K}_1}(x)$ or $\mathcal{S}_{\mathscr{K}_3}(x) = \mathcal{S}_{\mathscr{K}_2}(x)$ are both subalgebras of $\mathscr{X}(\in \mathscr{K}_3)$, therefore, $\mathcal{S}_{\mathscr{K}_3} = \mathcal{S}_{\mathscr{K}_1} \widetilde{\cap} \mathcal{S}_{\mathscr{K}_2}$ is a $\mathbb{SQB}$-$\mathbb{A}$ over $\mathscr{X}$.

(2) If $\mathscr{K}_3 = \mathscr{K}_1 \cup \mathscr{K}_2$ and by Definition 6, we obtain

$$\mathcal{S}_{\mathscr{K}_3}(x) = \begin{cases} \mathcal{S}_{\mathscr{K}_1}(x), & x \in \mathscr{K}_1 \backslash \mathscr{K}_2, \\ \mathcal{S}_{\mathscr{K}_2}(x), & x \in \mathscr{K}_2 \backslash \mathscr{K}_1, \\ \mathcal{S}_{\mathscr{K}_1}(x) \cup \mathcal{S}_{\mathscr{K}_2}(x), & x \in \mathscr{K}_1 \cap \mathscr{K}_2 \end{cases} \tag{6}$$

For $x \in \mathscr{K}_1 \backslash \mathscr{K}_2$ and since $\mathcal{S}_{\mathscr{K}_1}$ is a $\mathbb{SQB}$-$\mathbb{A}$, then we have $\mathcal{S}_{\mathscr{K}_3}(x) = \mathcal{S}_{\mathscr{K}_1}(x)$ is a subalgebra of $\mathscr{X}$. Similarly, for $x \in \mathscr{K}_2 \backslash \mathscr{K}_1$, then $\mathcal{S}_{\mathscr{K}_3}(x) = \mathcal{S}_{\mathscr{K}_2}(x)$ is a subalgebra of $\mathscr{X}$ due to $\mathcal{S}_{\mathscr{K}_2}$ is a $\mathbb{SQB}$-$\mathbb{A}$. Again, for $\mathscr{K}_1 \cap \mathscr{K}_2 = \emptyset$, so $x \in \mathscr{K}_1 \cap \mathscr{K}_2$ or $x \in \mathscr{K}_2 \cap \mathscr{K}_1$, for all $x \in \mathscr{K}_3$. Thus, $\mathcal{S}_{\mathscr{K}_3} = \mathcal{S}_{\mathscr{K}_1} \widetilde{\cup} \mathcal{S}_{\mathscr{K}_2}$ is a $\mathbb{SQB}$-$\mathbb{A}$ over $\mathscr{X}$. □

Remark 1. If $\mathscr{K}_1 \cap \mathscr{K}_2 \neq \emptyset$, then Theorem 1 (2) does not hold by the following example.

Example 2. Suppose $\mathscr{X}$ (i.e., $\mathscr{X} = \{0, k_1, k_2, k_3, k_4, 1\}$). Now, we show, by Tables 3 and 4, the binary operations $\longrightarrow$ and $\rightsquigarrow$, respectively.

Clearly, $\mathscr{X}$ is a $\mathbb{CQB}$-$\mathbb{A}$. Then,

(i) We define $\mathcal{S}_{\mathscr{K}_1}(\forall x \in \mathscr{K}_1)$ (i.e., $\mathscr{K}_1 = \mathscr{X}$) by

$$\mathcal{S}_{\mathscr{K}_1}(x) = \{y \in \mathscr{X} | x \mathscr{R} y \Longleftrightarrow x \longrightarrow (x \longrightarrow y)x \rightsquigarrow (x \rightsquigarrow y) \in \{k_3, k_4, 1\}\}. \tag{7}$$

From Table 3, we can get $\mathcal{S}_{\mathscr{K}_1}(0) = \mathscr{X}$ and $\mathcal{S}_{\mathscr{K}_1}(k_1) = \mathcal{S}_{\mathscr{K}_1}(k_2) = \mathcal{S}_{\mathscr{K}_1}(k_3) = \mathcal{S}_{\mathscr{K}_1}(k_4) = \mathcal{S}_{\mathscr{K}_1}(1) = \{k_3, k_4, 1\}$, and then, $\mathcal{S}_{\mathscr{K}_1}(x)(x \in \mathscr{K}_1)$ are all subalgebras of $\mathscr{X}$. Consequently, $\mathcal{S}_{\mathscr{K}_1}$ is a $\mathbb{SQB}$-$\mathbb{A}$s over $\mathscr{X}$.

Table 3: The binary operation $\longrightarrow$.

$\longrightarrow$	0	k_1	(HTML translation failed)	k_3	k_4	1
0	1	1	1	1	1	1
k_1	0	k_2	0	k_4	1	1
k_2	0	0	k_2	k_4	k_4	1
k_3	0	0	0	1	1	1
k_4	0	0	0	k_4	1	1
1	0	0	0	k_4	k_4	1

Table 4: The binary operation $\rightsquigarrow$.

$\rightsquigarrow$	0	k_1	k_2	k_3	k_4	1
0	1	1	1	1	1	1
k_1	0	0	0	1	1	1
k_2	0	k_1	k_2	k_3	k_4	1
k_3	0	0	0	1	1	1
k_4	0	0	0	1	1	1
1	0	0	0	k_3	k_4	1

(ii) We define $\mathcal{S}_{\mathscr{K}_2}(\forall x \in \mathscr{K}_2)$ (i.e., $\mathscr{K}_2 = \{k_2\}$) by

$$\mathcal{S}_{\mathscr{K}_2}(x) = \{y \in \mathscr{K}_2 | x \mathscr{R} y \Longleftrightarrow x \longrightarrow y = k_2,\ x \rightsquigarrow y = k_2\}. \tag{8}$$

From Table 4, we can get $\mathcal{S}_{\mathscr{K}_2}(k_2) = \{k_2\}$ is the subalgebra of $\mathscr{X}$. Consequently, $\mathcal{S}_{\mathscr{K}_2}$ is a $\mathbb{SQB}$-$\mathbb{A}$s over $\mathscr{X}$.

From (i) and (ii) and $\mathscr{K}_1 \cap \mathscr{K}_2 = \{k_2\} \neq \emptyset$, then we have $\mathcal{S}_{\mathscr{K}_3}(k_2) = \mathcal{S}_{\mathscr{K}_1}(k_2) \cup \mathcal{S}_{\mathscr{K}_2}(k_2) = \{k_3, k_4, 1\} \cup \{k_2\} = \{k_2, k_3, k_4, 1\}$ is not a subalgebra over $\mathscr{X}$. Thus, $\mathcal{S}_{\mathscr{K}_3}$ is not a $\mathbb{SQB}$-$\mathbb{A}$.

3.1. Soft Deductive Systems of $\mathbb{SQB}$-$\mathbb{A}$s. Based on Definition 8, we will propose the notion of soft deductive systems of $\mathbb{SQB}$-$\mathbb{A}$s as indicated below.

Definition 9. Assume that $\mathscr{X} = (\mathscr{X}, \longrightarrow, \rightsquigarrow, \leq)$ be a $\mathbb{SQB}$-$\mathbb{A}$. A nonempty subset $\mathscr{D} \subseteq \mathscr{X}$ is a deductive system of $\mathscr{X}$ if it satisfies

(1) $\forall x \in \mathscr{D}$, $x \longrightarrow x \in \mathscr{D}$, $x \rightsquigarrow x \in \mathscr{D}$

(2) $\forall x, y \in \mathscr{X}$, $x \in \mathscr{D}$, $x \longrightarrow y \in \mathscr{D} \Longrightarrow y \in \mathscr{D}$

Definition 10. Let $\mathscr{X}$ be a $\mathbb{SQB}$-$\mathbb{A}$ and $\mathscr{Y}$ a subalgebra of $\mathscr{X}$. A subset $\mathscr{D}$ of $\mathscr{X}$ is a deductive system of $\mathscr{X}$ related to $\mathscr{Y}$ (i.e., $\mathscr{Y}$-deductive system of $\mathscr{X}$), denoted by $\mathscr{D} \bowtie \mathscr{Y}$, and satisfies the following two conditions:

(1) $\forall x \in \mathscr{D}$, $x \longrightarrow x \in \mathscr{D}$, $x \rightsquigarrow x \in \mathscr{D}$

(2) $\forall y \in \mathscr{Y}$, $x \in \mathscr{D}$, $x \longrightarrow y \in \mathscr{D} \Longrightarrow y \in \mathscr{D}$

Remark 2. According to Definitions 9 and 10, we obtain that any deductive system of $\mathscr{X}$ is $\mathscr{Y}$-deductive system if $\mathscr{Y}$ is a subalgebra of $\mathscr{X}$.

The converse of Remark 2 does not hold by Example 3 (i.e., $\mathscr{Y}$ is a subalgebra of $\mathscr{X}$ and $\mathscr{Y}$-deductive system is not a deductive system).

Example 3. Suppose $\mathscr{X}$ (i.e., $\mathscr{X} = \{0, k_1, k_2, k_3, 1\}$) with partial order $0 < k_1 < k_3 < 1$ and $0 < k_1 < k_2 < 1$. Now, we show, by Tables 5 and 6, the binary operations $\longrightarrow$ and $\rightsquigarrow$, respectively.

Clearly, $\mathscr{X}$ is a $\mathbb{CQB}$-$\mathbb{A}$. Consider a subalgebra $\mathscr{Y} = \{k_1, 1\}$ and a subset $\mathscr{D} = \{k_1, k_2, 1\}$; we can see that $\mathscr{D} \bowtie \mathscr{Y}$. However, $\mathscr{D}$ is not a deductive system of $\mathscr{X}$ since $k_3 \longrightarrow 1 = 1 \in \mathscr{D}$ and $k_3 \notin \mathscr{D}$.

Definition 11. Assume that $\mathcal{S}_{\mathscr{K}}$ is a $\mathbb{SQB}$-$\mathbb{A}$ over $\mathscr{X}$. $\mathcal{S}_{\mathscr{D}}$ (i.e., $\mathbb{SS}$) over $\mathscr{X}$ is a soft deductive system of $\mathcal{S}_{\mathscr{K}}$, denoted by $\mathcal{S}_{\mathscr{D}} \widetilde{\triangleright\triangleleft} \mathcal{S}_{\mathscr{K}}$, and satisfies the following two conditions:

(1) $\mathscr{D} \subseteq \mathscr{K}$

(2) $\forall x \in \mathscr{D}$, $\mathcal{S}_{\mathscr{D}}(x) \triangleright\triangleleft \mathcal{S}_{\mathscr{K}}(x)$

Now, we will give an example to illustrate Definition 11 as follows.

Example 4. Suppose $\mathscr{X}$ (i.e., $\mathscr{X} = \{k_1, k_2, k_3, k_4, 1\}$) with partial order $k_1 < k_2 < k_3 < k_4 < 1$. Now, we show, by Tables 7 and 8, the binary operations $\longrightarrow$ and $\rightsquigarrow$, respectively.

Clearly, $\mathscr{X}$ is a $\mathbb{CQB}$-$\mathbb{A}$. We define $\mathcal{S}_{\mathscr{K}}(\forall x \in \mathscr{K})$ (i.e., $\mathscr{K} = \mathscr{X}$) by

$$\mathcal{S}_{\mathscr{K}}(x) = \{y \in \mathscr{X} | x \mathscr{R} y \Longleftrightarrow (x \longrightarrow y) \rightsquigarrow y = 1\}. \tag{9}$$

From Tables 7 and 8, we can get on $\mathcal{S}_{\mathscr{K}}(k_1) = \mathcal{S}_{\mathscr{K}}(k_2) = 1$, $\mathcal{S}_{\mathscr{K}}(k_3) = \{k_2, 1\}$, $\mathcal{S}_{\mathscr{K}}(k_4) = \{k_2, k_3, 1\}$, and $\mathcal{S}_{\mathscr{K}}(1) = \mathscr{X}$, and then, $\mathcal{S}_{\mathscr{K}}(x)(x \in \mathscr{K})$ are all subalgebras of $\mathscr{X}$. Consequently, $\mathcal{S}_{\mathscr{K}}$ is a $\mathbb{SQB}$-$\mathbb{A}$s over $\mathscr{X}$.

Next, for a subset $\mathscr{D} = \{k_2, k_4\}$, we define $\mathcal{S}_{\mathscr{D}}(\forall x \in \mathscr{D})$ by

$$\mathcal{S}_{\mathscr{D}}(x) = \{1\} \cup \{y \in \mathscr{X} | y \leq x\}. \tag{10}$$

Then, we obtain $\mathcal{S}_{\mathscr{D}}(k_2) = \{k_1, k_2, 1\} \triangleright\triangleleft \{1\} = \mathcal{S}_{\mathscr{K}}(k_2)$ and $\mathcal{S}_{\mathscr{D}}(k_4) = \mathscr{X} \triangleright\triangleleft \{k_2, k_3, 1\} = \mathcal{S}_{\mathscr{K}}(k_4)$. Consequently, $\mathcal{S}_{\mathscr{D}}$ is a soft deductive system of $\mathcal{S}_{\mathscr{K}}$.

Theorem 2. *Assume that $\mathcal{S}_{\mathscr{K}}$ is a $\mathbb{SQB}$-$\mathbb{A}$ over $\mathscr{X}$ and $\mathcal{S}_{\mathscr{D}_1}$ and $\mathcal{S}_{\mathscr{D}_2}$ are two $\mathbb{SS}$. Then,*

(1) If $\mathscr{D}_1 \cap \mathscr{D}_2 \neq \varnothing$, then $\mathcal{S}_{\mathscr{D}_1} \widetilde{\triangleright\triangleleft} \mathcal{S}_{\mathscr{K}}, \mathcal{S}_{\mathscr{D}_2} \widetilde{\triangleright\triangleleft} \mathcal{S}_{\mathscr{K}} \Longrightarrow \mathcal{S}_{\mathscr{D}_1} \widetilde{\cap} \mathcal{S}_{\mathscr{D}_2} \widetilde{\triangleright\triangleleft} \mathcal{S}_{\mathscr{K}}$

(2) If $\mathscr{D}_1 \cap \mathscr{D}_2 = \varnothing$, then $\mathcal{S}_{\mathscr{D}_1} \widetilde{\triangleright\triangleleft} \mathcal{S}_{\mathscr{K}}, \mathcal{S}_{\mathscr{D}_2} \widetilde{\triangleright\triangleleft} \mathcal{S}_{\mathscr{K}} \Longrightarrow \mathcal{S}_{\mathscr{D}_1} \widetilde{\cup} \mathcal{S}_{\mathscr{D}_2} \widetilde{\triangleright\triangleleft} \mathcal{S}_{\mathscr{K}}$

Proof

(1) Follow from Definition 5.

(2) If $\mathcal{S}_{\mathscr{D}_1} \widetilde{\triangleright\triangleleft} \mathcal{S}_{\mathscr{K}}, \mathcal{S}_{\mathscr{D}_2} \widetilde{\triangleright\triangleleft} \mathcal{S}_{\mathscr{K}}$, then, by Definition 6, we have $\mathscr{D}_3 = \mathscr{D}_1 \cap \mathscr{D}_2$ (i.e., $x \in \mathscr{D}_3$), $\mathcal{S}_{\mathscr{D}_1} \widetilde{\cup} \mathcal{S}_{\mathscr{D}_2} = \mathcal{S}_{\mathscr{D}_3}$, and

Table 5: The binary operation $\longrightarrow$.

$\longrightarrow$	0	k_1	k_2	k_3	1
0	1	1	1	1	1
k_1	0	1	k_2	1	1
k_2	k_1	k_1	1	1	1
k_3	0	k_1	k_2	1	1
1	0	k_1	k_2	k_3	1

Table 6: The binary operation $\rightsquigarrow$.

$\rightsquigarrow$	0	k_1	k_2	k_3	1
0	1	1	1	1	1
k_1	k_2	1	k_2	1	1
k_2	0	k_1	1	1	1
k_3	0	k_1	k_2	1	1
1	0	k_1	k_2	k_3	1

Table 7: The binary operation $\longrightarrow$.

$\longrightarrow$	k_1	k_2	k_3	k_4	1
k_1	1	1	1	1	1
k_2	k_3	1	1	1	1
k_3	k_2	k_2	1	1	1
k_4	k_2	k_2	k_c	1	1
1	k_1	k_2	k_3	k_4	1

Table 8: The binary operation $\rightsquigarrow$.

$\rightsquigarrow$	k_1	k_2	k_3	k_4	1
k_1	1	1	1	1	1
k_2	k_4	1	1	1	1
k_3	k_2	k_2	1	1	1
k_4	k_1	k_2	k_3	1	1
1	k_1	k_2	k_3	k_4	1

$$\mathcal{S}_{\mathscr{D}_3}(x) = \begin{cases} \mathcal{S}_{\mathscr{D}_1}(x), & x \in \mathscr{D}_1 \backslash \mathscr{D}_2 \\ \mathcal{S}_{\mathscr{D}_2}(x), & x \in \mathscr{D}_2 \backslash \mathscr{D}_1, \\ \mathcal{S}_{\mathscr{D}_1}(x) \cup \mathcal{S}_{\mathscr{D}_2}(x), & x \in \mathscr{D}_1 \cap \mathscr{D}_2 \end{cases} \tag{11}$$

Since $\mathscr{D}_1 \cap \mathscr{D}_2 = \varnothing$, we obtain either $x \in \mathscr{D}_1 \backslash \mathscr{D}_2$ or $x \in \mathscr{D}_2 \backslash \mathscr{D}_1$. Then, we have the following:

Case 1: if $x \in \mathscr{D}_1 \backslash \mathscr{D}_2$, since $\mathcal{S}_{\mathscr{D}_1} \widetilde{\triangleright\triangleleft} \mathcal{S}_{\mathscr{K}}$, then $\mathcal{S}_{\mathscr{D}_3}(x) = \mathcal{S}_{\mathscr{D}_1}(x) \triangleright\triangleleft \mathcal{S}_{\mathscr{K}}(x)$

Case 2: if $x \in \mathscr{D}_2 \backslash \mathscr{D}_1$ and $\mathcal{S}_{\mathscr{D}_2} \widetilde{\triangleright\triangleleft} \mathcal{S}_{\mathscr{K}}$, then $\mathcal{S}_{\mathscr{D}_3}(x) = \mathcal{S}_{\mathscr{D}_2}(x) \triangleright\triangleleft \mathcal{S}_{\mathscr{K}}(x)$

Consequently, for all $x \in \mathscr{D}_3$, we have $\mathcal{S}_{\mathscr{D}_3}(x) \triangleright\triangleleft \mathcal{S}_{\mathscr{K}}(x)$, which implies that $\mathcal{S}_{\mathscr{D}_1} \widetilde{\cup} \mathcal{S}_{\mathscr{D}_2} = \mathcal{S}_{\mathscr{D}_3} \widetilde{\triangleright\triangleleft} \mathcal{S}_{\mathscr{K}}$. □

Remark 3. If $\mathscr{K}_1 \cap \mathscr{K}_2 \neq \varnothing$, then Theorem 2 (2) does not hold by the following example.

Example 5. Suppose $\mathscr{X}$ (i.e., $\mathscr{X} = \{0, k_1, k_2, k_3, k_4, 1\}$). Now, we show, by Table 9, the binary operations $\longrightarrow$.

Table 9: The binary operation $\longrightarrow$.

$\longrightarrow$	0	k_1	k_2	k_3	k_4	1
0	1	1	1	1	1	1
k_1	k_3	1	k_2	k_3	k_2	1
k_2	k_4	k_1	1	k_2	k_1	1
k_3	k_1	k_1	1	1	k_1	1
k_4	k_2	1	1	k_2	1	1
1	0	k_1	k_2	k_3	k_4	1

Clearly, $\mathscr{X}$ is a $\mathbb{CQB}$-$\mathbb{A}$. Then,

(i) We define $\mathcal{S}_{\mathscr{K}}(\forall x \in \mathscr{K})$ (i.e., $\mathscr{K} = \mathscr{X}$) by

$$\mathcal{S}_{\mathscr{K}}(x) = \{y \in \mathscr{X} | x\mathscr{R}y \Longleftrightarrow (x \longrightarrow y) \longrightarrow y \in \{k_1, k_2, 1\}\}. \tag{12}$$

From Table 9, we can get $\mathcal{S}_{\mathscr{K}}(0) = \{k_1, k_2, 1\}$, $\mathcal{S}_{\mathscr{K}}(k_1) = \mathscr{X}$, $\mathcal{S}_{\mathscr{K}}(k_2) = \mathcal{S}_{\mathscr{K}}(k_3) = \{k_1, 1\}$, and $\mathcal{S}_{\mathscr{K}}(k_4) = \{k_1, k_2, k_3, 1\}$, $\mathcal{S}_{\mathscr{K}}(1) = \mathscr{X}$, and then, $\mathcal{S}_{\mathscr{K}}(x)(\forall x \in \mathscr{K})$ are all subalgebras of $\mathscr{X}$. Consequently, $\mathcal{S}_{\mathscr{K}}$ is a $\mathbb{SQB}$-$\mathbb{A}$s over $\mathscr{X}$.

(ii) We define $\mathcal{S}_{\mathscr{K}_1}(\forall x \in \mathscr{K}_1)$ (i.e., $\mathscr{K}_1 = \{k_1, k_2, k_3\}$) by

$$\mathcal{S}_{\mathscr{K}_1}(x) = \{y \in \mathscr{X} | x\mathscr{R}y \Longleftrightarrow x \longrightarrow y = 1\}. \tag{13}$$

Then, we can get $\mathcal{S}_{\mathscr{K}_1}(k_1) = \{k_1, 1\} \triangleright\triangleleft X = \mathcal{S}_{\mathscr{K}}(k_1)$, $\mathcal{S}_{\mathscr{K}_1}(k_2) = \{k_2, 1\} \triangleright\triangleleft \{a, 1\} = \mathcal{S}_{\mathscr{K}}(k_2)$, and $\mathcal{S}_{\mathscr{K}_1}(k_3) = \{k_2, k_3, 1\} \triangleright\triangleleft \{k_1, 1\}$. Therefore, $\mathcal{S}_{\mathscr{K}_1}$ is a soft deductive system over $\mathcal{S}_{\mathscr{K}}$.

(iii) We define $\mathcal{S}_{\mathscr{K}_2}(\forall x \in \mathscr{K}_2)$ (i.e., $\mathscr{K}_2 = \{k_1\}$) by

$$\mathcal{S}_{\mathscr{K}_2}(x) = \{y \in \mathscr{X} | x\mathscr{R}y \Longleftrightarrow y \longrightarrow x = k_1\}. \tag{14}$$

Then, we can get $\mathcal{S}_{\mathscr{K}_2}(k_1) = \{k_2, k_3, 1\} \triangleright\triangleleft X = \mathcal{S}_{\mathscr{K}_2}(k_1)$. Therefore, $\mathcal{S}_{\mathscr{K}_2}$ is a soft deductive system over $\mathcal{S}_{\mathscr{K}}$.

From (i)–(iii), we have $\mathcal{S}_{\mathscr{K}_3} = \mathcal{S}_{\mathscr{K}_1} \widetilde{\cup} \mathcal{S}_{\mathscr{K}_2}$ which is not a soft deductive system of $\mathcal{S}_{\mathscr{K}}$, where $\mathcal{S}_{\mathscr{K}_3}(k_1) = \mathcal{S}_{\mathscr{K}_1}(k_1) \cup \mathcal{S}_{\mathscr{K}_2}(k_1) = \{k_1, k_2, k_3, 1\}$ is not a $\mathcal{S}_{\mathscr{K}}(a)$-deductive system because $k_2 \longrightarrow k_4 = k_1 \in \{k_1, k_2, k_3, 1\}$ and $k_4 \notin \{k_1, k_2, k_3, 1\}$.

3.2. $\mathbb{DSQB}$-$\mathbb{A}$*s.* We will give the notion of $\mathbb{DSQB}$-$\mathbb{A}$s and investigate homomorphism image of $\mathbb{DSQB}$-$\mathbb{A}$s as indicated below.

Definition 12. Assume that $\mathcal{S}_{\mathscr{K}}$ is a $\mathbb{SQB}$-$\mathbb{A}$ over $\mathscr{X}$. If $\mathcal{S}_{\mathscr{K}}(x)(\forall x \in \mathscr{K})$ is a deductive system of $\mathscr{X}$, then $\mathcal{S}_{\mathscr{K}}$ is called a $\mathbb{DSQB}$-$\mathbb{A}$ over X.

Example 6 (continued from Example 1 (2)). Clearly, $\mathcal{S}_{\mathscr{K}}$ is $\mathbb{DSQB}$-$\mathbb{A}$ over $\mathscr{X}$.

Definition 13

(1) Suppose $\mathscr{X}$ be a $\mathbb{QB}$-$\mathbb{A}$ with the greatest element 1 (i.e., $\mathscr{X}$ just only a poset); for any $x \in \mathscr{X}$, the order of element x is defined as

$$\mathcal{O}(x) = \min\left\{p, q \in N | x \overset{p}{\longrightarrow} x = 1,\ x \overset{q}{\rightsquigarrow} x = 1\right\}, \quad (i), \tag{15}$$

where N is a natural number and $x \overset{p}{\longrightarrow} x = (((x \longrightarrow x) \longrightarrow \cdots) \longrightarrow x)$, $x \overset{q}{\rightsquigarrow} x = (((x \rightsquigarrow x) \rightsquigarrow \cdots) \rightsquigarrow x)$.

(2) If $p, q \in N$ does not exist to satisfy the above condition (i), then $x(\forall x \in \mathscr{X})$ is called infinite order.

Remark 4. Assume that $\mathcal{S}_{\mathscr{K}}$ and $\mathcal{S}_{\mathscr{K}_1}$ be two $\mathbb{SQB}$-$\mathbb{A}$s over $\mathscr{X}$ such that $\mathscr{K}_1 \subseteq \mathscr{K} \subseteq \mathscr{X}$. If $\mathcal{S}_{\mathscr{K}}$ is a $\mathbb{DSQB}$-$\mathbb{A}$ over $\mathscr{X}$, then $\mathcal{S}_{\mathscr{K}_1}$ is a $\mathbb{DSQB}$-$\mathbb{A}$.

The converse of Remark 4 does not hold by the following Example 7.

Example 7 (continued from Example 2). We define $\mathcal{S}_{\mathscr{K}}(\forall x \in \mathscr{K})$ (i.e., $\mathscr{K} = \mathscr{X}$) by

$$\mathcal{S}_{\mathscr{K}}(x) = \{y \in \mathscr{X} | \mathcal{O}(x) = \mathcal{O}(y)\}. \tag{16}$$

Then, we get on $\mathcal{S}_{\mathscr{K}}(0) = \mathcal{S}_{\mathscr{K}}(k_3) = \mathcal{S}_{\mathscr{K}}(k_4) = \mathcal{S}_{\mathscr{K}}(k_1) = \{0, k_3, k_4, 1\}$, $\mathcal{S}_{\mathscr{K}}(k_1) = \{k_1\}$, and $\mathcal{S}_{\mathscr{K}}(k_2) = \{k_2\}$. However, $k_3 \longrightarrow k_1 = 0 \in \{0, k_3, k_4, 1\}$ and $k_1 \notin \{0, k_3, k_4, 1\}$ imply that $\mathcal{S}_{\mathscr{K}}$ is not $\mathbb{DSQB}$-$\mathbb{A}$. If we take $\mathscr{K}_1 = \{k_3, k_4, 1\} \subseteq \mathscr{K}$ and we define $\mathcal{S}_{\mathscr{K}_1} = \{y \in \mathscr{X} | \mathcal{O}(x) = \mathcal{O}(y)\}(\forall x \in \mathscr{K}_1)$, then $\mathcal{S}_{\mathscr{K}_1}$ is $\mathbb{DSQB}$-$\mathbb{A}$.

Definition 14. Assume that $\mathcal{S}_{\mathscr{K}}$ is $\mathbb{SQB}$-$\mathbb{A}$ over $\mathscr{X}$ with the greatest element 1. If $\mathcal{S}_{\mathscr{K}}(x) = \mathscr{X}(\forall x \in \mathscr{K})$, then $\mathcal{S}_{\mathscr{K}}$ is called whole $\mathbb{DSQB}$-$\mathbb{A}$.

Example 8. Suppose $\mathscr{X}$ (i.e., $\mathscr{X} = \{0, k_1, k_2, 1\}$) with partial order $0 < k_1 < k_2 < 1$. Now, we show, by Tables 10 and 11, the binary operations $\longrightarrow$ and $\rightsquigarrow$, respectively.

Clearly, $\mathscr{X}$ is a $\mathbb{CQB}$-$\mathbb{A}$. We define $\mathcal{S}_{\mathscr{K}}(\forall x \in \mathscr{K})$ (i.e., $\mathscr{K} = \mathscr{X}$) by

$$\mathcal{S}_{\mathscr{K}}(x) = \{y \in \mathscr{X} | \mathcal{O}(x) = \mathcal{O}(y)\}. \tag{17}$$

From Tables 10 and 11, we can get on $\mathcal{S}_{\mathscr{K}}(x) = \mathscr{X}(\forall x \in \mathscr{K})$. Thus, $\mathcal{S}_{\mathscr{K}}$ is a whole $\mathbb{DSQB}$-$\mathbb{A}$ over $\mathscr{X}$.

Now, we will study homomorphism image of $\mathbb{DSQB}$-$\mathbb{A}$s by the following two theorems.

Theorem 3. *Assume that ψ: $\mathscr{X} \longrightarrow \mathscr{Y}$ be a surjective exact morphism of $\mathbb{QB}$-$\mathbb{A}$ and $\mathscr{X}$ is a $\mathbb{QB}$-$\mathbb{A}$s. If $\mathcal{S}_{\mathscr{K}}$ is a $\mathbb{DSQB}$-$\mathbb{A}$ over $\mathscr{X}$, then $\psi(\mathcal{S}_{\mathscr{K}})$ is also$\mathbb{DSQB}$-$\mathbb{A}$ over $\mathscr{Y}$.*

Proof. Since $\mathcal{S}_{\mathscr{K}}(x)(x \in \mathscr{K})$ is a deductive system of $\mathscr{X}$ and ψ is surjective, then $\psi(\mathcal{S}_{\mathscr{K}})(x) = \psi(\mathcal{S}_{\mathscr{K}}(x))$ is a deductive system of $\mathscr{Y}$ which implies that $\psi(\mathcal{S}_{\mathscr{K}})$ is a $\mathbb{DSQB}$-$\mathbb{A}$ over $\mathscr{X}$. □

Theorem 4. *Assume that ψ: $X \longrightarrow Y$ be a surjective exact morphism of $\mathbb{QB}$-$\mathbb{A}$ and $\mathcal{S}_{\mathscr{K}}$ a $\mathbb{DSQB}$-$\mathbb{A}$ over $\mathscr{X}$. Then,*

Table 10: The binary operation $\longrightarrow$.

$\longrightarrow$	0	k_1	k_2	1
0	1	1	1	1
k_1	k_1	1	1	1
k_2	k_1	k_1	1	1
1	0	k_1	k_2	1

Table 11: The binary operation $\rightsquigarrow$.

$\rightsquigarrow$	0	k_1	k_2	1
0	1	1	1	1
k_1	k_2	1	1	1
k_2	0	k_1	1	1
1	0	k_1	k_2	1

(1) *If $\mathcal{S}_{\mathcal{K}}(x) = ker(\psi)$, for all $x \in \mathcal{K}$, then $\psi(\mathcal{S}_{\mathcal{K}})$ is the whole $\mathbb{DSQB}$-$\mathbb{A}$ over $\mathcal{Y}$*

(2) *If is whole $\mathbb{DSQB}$-$\mathbb{A}$ over $\mathcal{X}$, then $\psi(\mathcal{S}_{\mathcal{K}})$ is the whole $\mathbb{DSQB}$-$\mathbb{A}$ over $\mathcal{Y}$*

Proof

(1) Assume that $\mathcal{S}_{\mathcal{K}}(x) = \ker(\psi)$, where $\ker(\psi) = \{x \in \mathcal{X} | \psi(x) = x \longrightarrow x, \quad \psi(x) = x \rightsquigarrow x\}$. Since ψ is surjective, then, from Theorem 3, we have $\psi(\mathcal{S}_{\mathcal{K}})(x) = \psi(\mathcal{S}_{\mathcal{K}}(x)) = \psi(\mathcal{X}) \quad = \mathcal{Y}(x \in \mathcal{K})$. Thus, $\psi(\mathcal{S}_{\mathcal{K}})$ is the whole $\mathbb{DSQB}$-$\mathbb{A}$ over $\mathcal{Y}$.

(2) Clearly, $\mathcal{S}_{\mathcal{K}}(x) = \mathcal{X}$ since $\mathcal{S}_{\mathcal{K}}$ is whole $\mathbb{DSQB}$-$\mathbb{A}$ over $\mathcal{X}(x \in \mathcal{K})$. Thus, $\psi(\mathcal{S}_{\mathcal{K}})(x) = \psi(\mathcal{S}_{\mathcal{K}}(x)) = \psi(\mathcal{X}) = \mathcal{Y}(x \in \mathcal{K})$. By Theorem 3, we have $\psi(\mathcal{S}_{\mathcal{K}})$ is the whole $\mathbb{DSQB}$-$\mathbb{A}$ over $\mathcal{Y}$ □

4. FSQB-As

We give the definition of $\mathbb{FSQB}$-$\mathbb{A}$s; a concrete example is given to illustrate its derive properties. Furthermore, we study the homomorphism image and preimage of $\mathbb{FSQB}$-$\mathbb{A}$s. Now, we first propose the definition of fuzzy quantum B-algebra (briefly, $\mathbb{FQB}$-$\mathbb{A}$) as indicated below.

Definition 15. We call $\mathbb{FQB}$-$\mathbb{A}$ (or a fuzzy set $\widehat{\mu}$ in $\mathbb{QB}$-$\mathbb{A}$) if it satisfies ($\forall x, y \in \mathcal{X}, \mathcal{X}$ is $\mathbb{QB}$-$\mathbb{A}$):

$$\begin{aligned} \widehat{\mu}(x \longrightarrow y) &\geq \min\{\widehat{\mu}(x), \widehat{\mu}(y)\}, \\ \widehat{\mu}(x \rightsquigarrow y) &\geq \min\{\widehat{\mu}(x), \widehat{\mu}(y)\}. \end{aligned} \tag{18}$$

Definition 16. We call $\widehat{\mu}$ is a fuzzy deductive system of $\mathcal{X}$ if it satisfies ($\forall x, y \in \mathcal{X}$):

$$\begin{aligned} &\widehat{\mu}(x \longrightarrow x) \geq \widehat{\mu}(x), \\ &\widehat{\mu}(x \rightsquigarrow x) \geq \widehat{\mu}(x), \\ &\widehat{\mu}(y) \geq \min\{\widehat{\mu}(x \longrightarrow y), \widehat{\mu}(x)\}. \end{aligned} \tag{19}$$

Definition 17. Assume that $\widehat{\mathcal{S}}_{\mathcal{K}}$ be a $\mathbb{FSS}$ over $\mathcal{X}$. Then,

(1) If there exists $\widehat{\mu} \in \mathcal{K}$ such that $\widehat{\mathcal{S}}_{\mathcal{K}}[\mu]$ is a $\mathbb{FQB}$-$\mathbb{A}$ (i.e., fuzzy deductive system) in a $\mathbb{QB}$-$\mathbb{A}$ over $\mathcal{X}$, then $\widehat{\mathcal{S}}_{\mathcal{K}}$ is called a $\widehat{\mathcal{S}}_{\mathcal{K}}$-$\mathbb{A}$ (i.e., fuzzy soft deductive system $\mathbb{FSDS}$) which depends on a parameter set $\widehat{\mu}$ over $\mathcal{X}$

(2) If $\widehat{\mathcal{S}}_{\mathcal{K}}[\mu]$ is a $\mathbb{FQB}$-$\mathbb{A}$ (i.e., fuzzy deductive system) of $\mathcal{X}$ based on all parameters, then we say that $\widehat{\mathcal{S}}_{\mathcal{K}}$ is a $\mathbb{FSQB}$-$\mathbb{A}$ (i.e., $\mathbb{FSDS}$) of $\mathcal{X}$

In the following, a concrete example is given to illustrate Definition 17.

Example 9. Suppose that there are five-class cars:

$$X = \{\text{BMW, Audi, Toyota, Jeep, Cadilac}\}. \tag{20}$$

Let $\oplus$ and $\otimes$ be two soft machines to characterize two cars, defined by the following manner.

BMW$\oplus x$ = Cadilac, forall $x \in \mathcal{X}$,

$$\text{Audi}\oplus y = \begin{cases} \text{Jeep}, & y = \text{BMW}, \\ \text{Cadilac}, & y \in \{\text{Audi, Toyouta, Jeep, Cadilac}\}, \end{cases}$$

$$\text{Toyota}\oplus z = \begin{cases} \text{Toyota}, & z = \text{BMW}, \\ \text{Jeep}, & z = \text{Audi}, \\ \text{Cadilac}, & z \in \{\text{Toyota, Jeep, Cadilac}\}, \end{cases}$$

$$\text{Jeep}\oplus s = \begin{cases} \text{Toyota}, s = \text{BMW}, \\ \text{Jeep}, s \in \{\text{Audi, Toyoya}\}, \\ \text{Cadilac}, s \in \{\text{Jeep, Cadilac}\}, \end{cases}$$

$$\text{Cadilac}\oplus t = \begin{cases} \text{BMW}, t = \text{BMW}, \\ \text{Audi}, t = \text{Audi}, \\ \text{Toyota}, t = \text{Toyota}, \\ \text{Jeep}, t = \text{Jeep}, \\ \text{Cadilac}, t = \text{Cadilac}, \end{cases} \tag{21}$$

$\text{BMW} \otimes x = \text{Cadilac forall } x \in \mathcal{X}$,

$$\text{Audi} \otimes y = \begin{cases} \text{Jeep}, & y = \text{BMW}, \\ \text{Cadilac}, & y \in \{\text{Audi, Toyouta, Jeep, Cadilac}\}, \end{cases}$$

$$\text{Toyota} \otimes z = \begin{cases} \text{Jeep}, & z \in \{\text{BMW, Audi}\}, \\ \text{Cadilac}, & z \in \{\text{Toyouta, Jeep, Cadilac}\}, \end{cases}$$

$$\text{Jeep} \otimes s = \begin{cases} \text{Audi}, & s = \text{BMW}, \\ \text{Jeep}, & s \in \{\text{Audi, Toyouta}\}, \\ \text{Cadilac}, & s \in \{\text{Jeep, Cadilac}\}, \end{cases}$$

$$\text{Cadilac} \otimes t = \begin{cases} \text{BMW}, & t = \text{BMW}, \\ \text{Audi}, & t = \text{Audi}, \\ \text{Toyota}, & t = \text{Toyota}, \\ \text{Jeep}, & t = \text{Jeep}, \\ \text{Cadilac}, & t = \text{Cadilac}. \end{cases} \tag{22}$$

Then, $(\mathscr{X}, \oplus, \otimes, \leq)$ is a $\mathbb{QB}$-$\mathbb{A}$. Now, we consider a set of parameters: $\widehat{\mu}$ =(Excellent, Good, Moderate)$\in\in\mathscr{K}$. Then, we have the following:

(1) We define $\widehat{\mathcal{S}}_{\mathscr{K}}[\widehat{\mu}]$ over $\mathscr{X}$ (i.e., $\widehat{\mathcal{S}}_{\mathscr{K}}$[Excellent], $\widehat{\mathcal{S}}_{\mathscr{K}}$[Good], and $\widehat{\mathcal{S}}_{\mathscr{K}}$[Moderate] are fuzzy sets) by Table 12.

Therefore, we can see that $\widehat{\mathcal{S}}_{\mathscr{K}}$[Excellent], $\widehat{\mathcal{S}}_{\mathscr{K}}$[Good], and $\widehat{\mathcal{S}}_{\mathscr{K}}$[Moderate] are all $\mathbb{FSQB}$-$\mathbb{A}$s based on parameters "Excellent," "Good," and "Moderate" over $\mathscr{X}$. Thus, $\widehat{\mathcal{S}}_{\mathscr{K}}$ is a $\mathbb{FSQB}$-$\mathbb{A}$ over $\mathscr{X}$.

(2) We define $\widehat{\mathcal{S}}_{\mathscr{K}_1}[\widehat{\mu}]$ over $\mathscr{X}$ (i.e., $\widehat{\mathcal{S}}_{\mathscr{K}_1}$[Excellent], $\widehat{\mathcal{S}}_{\mathscr{K}_1}$[Good], and $\widehat{\mathcal{S}}_{\mathscr{K}_1}$[Moderate] are fuzzy sets) by Table 13.

However, $\widehat{\mathcal{S}}_{\mathscr{K}_1}[\widehat{\mu}]$ is not a $\mathbb{FSQB}$-$\mathbb{A}$ based on a parameter "Excellent" over (HTML translation failed), where $\widehat{\mathcal{S}}_{\mathscr{K}_1}$[Excellent](Toyota$\oplus$BMW) = $\widehat{\mathcal{S}}_{\mathscr{K}_1}$[Excellent](Toyota) = $0.1 \not\geq 0.2 = \min\{0.2, 0.4\} = \min\{\widehat{\mathcal{S}}_{\mathscr{K}_1}$[Excellent] (Audi), $\widehat{\mathcal{S}}_{\mathscr{K}_1}$[Excellent](BMW)$\}$. Also, we obtain that $\widehat{\mathcal{S}}_{\mathscr{K}_1}[\widehat{\mu}]$ is a $\mathbb{FSQB}$-$\mathbb{A}$ based on both the parameter "Good" and "Moderate" over $\mathscr{X}$.

(3) We define $\widehat{\mathcal{S}}_{\mathscr{K}_2}[\widehat{\mu}]$ over $\mathscr{X}$ (i.e., $\widehat{\mathcal{S}}_{\mathscr{K}_2}$[Excellent] and $\widehat{\mathcal{S}}_{\mathscr{K}_2}$ [Good] are fuzzy sets) by Table 14.

Then, $\widehat{\mathcal{S}}_{\mathscr{K}_2}[\widehat{\mu}]$ is a $\mathbb{FSDS}$ on parameters "Excellent." However, $\widehat{\mathcal{S}}_{\mathscr{K}_2}[\mu]$ is not a fuzzy deductive system of $\mathscr{X}$ based on parameter "Good," where $\widehat{\mathcal{S}}_{\mathscr{K}_2}$[Good](Toyota)= $0.3 < 0.5 = \min\{\widehat{\mathcal{S}}_{\mathscr{K}_2}$[Good](Jeep$\oplus$Toyota), $\widehat{\mathcal{S}}_{\mathscr{K}_2}$[Good](Jeep)$\}$.

(4) We define $\widehat{\mathcal{S}}_{\mathscr{K}_3}[\widehat{\mu}]$ over $\mathscr{X}$ (i.e., $\widehat{\mathcal{S}}_{\mathscr{K}_3}$[Excellent] and $\widehat{\mathcal{S}}_{\mathscr{K}_2}$[Moderate] are fuzzy sets) by Table 15.

Then, $\widehat{\mathcal{S}}_{\mathscr{K}_3}[\widehat{\mu}]$ is a $\mathbb{FSDS}$ of $\mathscr{X}$.

Now, we will present several characterizations of $\mathbb{FSQB}$-$\mathbb{A}$s.

By Definition 17, if $\widehat{\mathcal{S}}_{\mathscr{K}}$ is a $\mathbb{FSQB}$-$\mathbb{A}$ of $\mathbb{QB}$-$\mathbb{A}$ over $\mathscr{X}$ based on all parameters, then we say that $\widehat{\mathcal{S}}_{\mathscr{K}}$ is a $\mathbb{FSQB}$-$\mathbb{A}$ of $\mathscr{X}$, that is,

$$\begin{aligned}\widehat{\mathcal{S}}_{\mathscr{K}}[\widehat{\mu}](x \longrightarrow y) &\geq \min\left\{\widehat{\mathcal{S}}_{\mathscr{K}}[\widehat{\mu}](x), \widehat{\mathcal{S}}_{\mathscr{K}}[\widehat{\mu}](y)\right\},\\ \widehat{\mathcal{S}}_{\mathscr{K}}[\widehat{\mu}](x \rightsquigarrow y) &\geq \min\left\{\widehat{\mathcal{S}}_{\mathscr{K}}[\widehat{\mu}](x), \widehat{\mathcal{S}}_{\mathscr{K}}[\widehat{\mu}](y)\right\}.\end{aligned} \tag{23}$$

Proposition 1. *Assume $\mathscr{X}$ be a $\mathbb{QB}$-$\mathbb{A}$. If $\widehat{\mathcal{S}}_{\mathscr{K}}$ is $\mathbb{FSQB}$-$\mathbb{A}$ over $\mathscr{X}$, then, for all $t \in [0,1]$, $(\widehat{\mathcal{S}}_{\mathscr{K}})_t \neq \varnothing$ is the subalgebra of $\mathscr{X}$, in which*

$$\left(\widehat{\mathcal{S}}_{\mathscr{K}}\right)_t = \left\{\left(\widehat{\mathcal{S}}_{\mathscr{K}}[\widehat{\mu}]\right)_t | \widehat{\mu} \in \mathscr{K}\right\}. \tag{24}$$

Proof. Let $(\widehat{\mathcal{S}}_{\mathscr{K}}[\widehat{\mu}])_t \neq \varnothing$. Then, $\forall x, y \in (\widehat{\mathcal{S}}_{\mathscr{K}}[\widehat{\mu}])_t$; since $\widehat{\mathcal{S}}_{\mathscr{K}}$ is a $\mathbb{FSQB}$-$\mathbb{A}$, then $\widehat{\mathcal{S}}_{\mathscr{K}}[\widehat{\mu}](x) \geq t$, $\widehat{\mathcal{S}}_{\mathscr{K}}[\widehat{\mu}](y) \geq t$. So,

Table 12: Fuzzy sets $\widehat{\mathcal{S}}_{\mathscr{K}}[\widehat{\mu}]$ over $\mathscr{X}$.

$\widehat{\mathcal{S}}_{\mathscr{K}}$	BMW	Audi	Toyota	Jeep	Cadilac
Excellent	0.2	0.2	0.5	0.6	0.8
Good	0.1	0.2	0.3	0.5	0.7
Moderate	0.1	0.1	0.4	0.4	0.6

Table 13: Fuzzy sets $\widehat{\mathcal{S}}_{\mathscr{K}_1}[\widehat{\mu}]$ over $\mathscr{X}$.

$\widehat{\mathcal{S}}_{\mathscr{K}_1}$	BMW	Audi	Toyota	Jeep	Cadilac
Excellent	0.4	0.2	0.1	0.6	0.8
Good	0.2	0.2	0.3	0.5	0.7
Moderate	0.1	0.1	0.4	0.5	0.9

Table 14: Fuzzy sets $\widehat{\mathcal{S}}_{\mathscr{K}_2}[\widehat{\mu}]$ over $\mathscr{X}$.

$\widehat{\mathcal{S}}_{\mathscr{K}_2}$	BMW	Audi	Toyota	Jeep	Cadilac
Excellent	0.2	0.2	0.2	0.2	0.6
Good	0.2	0.2	0.3	0.5	0.7

Table 15: Fuzzy sets $\widehat{\mathcal{S}}_{\mathscr{K}_3}[\widehat{\mu}]$.

$\widehat{\mathcal{S}}_{\mathscr{K}_3}$	BMW	Audi	Toyota	Jeep	Cadilac
Excellent	0.3	0.3	0.3	0.3	0.3
Moderate	0.1	0.1	0.1	0.1	0.7

$$\begin{aligned}\widehat{\mathcal{S}}_{\mathscr{K}}[\widehat{\mu}](x \longrightarrow y) &\geq \min\left\{\widehat{\mathcal{S}}_{\mathscr{K}}[\widehat{\mu}](x \longrightarrow y), \widehat{\mathcal{S}}_{\mathscr{K}}[\widehat{\mu}](x \rightsquigarrow y)\right\}\\ &\geq \min\left\{\widehat{\mathcal{S}}_{\mathscr{K}}[\widehat{\mu}](x), \widehat{\mathcal{S}}_{\mathscr{K}}[\widehat{\mu}](y)\right\} \geq t.\end{aligned} \tag{25}$$

Similarly, we have $\widehat{\mathcal{S}}_{\mathscr{K}}[\widehat{\mu}](x \rightsquigarrow y) \geq t$. Therefore, $x \longrightarrow y, x \rightsquigarrow y \in (\widehat{\mathcal{S}}_{\mathscr{K}}[\widehat{\mu}])_t$. This implies that $(\widehat{\mathcal{S}}_{\mathscr{K}}[\widehat{\mu}])_t$ is the subalgebra of $\mathscr{X}$.

Analogously, we can get Proposition 2 as follows. □

Proposition 2. *Assume that $\mathcal{S}_{\mathscr{K}_1}$ and $\mathcal{S}_{\mathscr{K}_2}$ are two $\mathbb{FSQB}$-$\mathbb{A}$ over $\mathscr{X}$. Then, $\mathcal{S}_{\mathscr{K}_1} \widetilde{\cap} \mathcal{S}_{\mathscr{K}_2}$ and $\mathcal{S}_{\mathscr{K}_1} \widetilde{\cup} \mathcal{S}_{\mathscr{K}_2}$ are $\mathbb{FSQB}$-$\mathbb{A}$s over $\mathscr{X}$.*

Definition 18. Let (α, β) be a fuzzy soft map from $\mathbb{QB}$-$\mathbb{A}$ over $\mathscr{X}$ to $\mathbb{QB}$-$\mathbb{A}$ over $\mathscr{Y}$. Then,

(1) If α is an exact morphism from $\mathscr{X}$ to $\mathscr{Y}$, then (α, β) is called a $\mathbb{FSQB}$-$\mathbb{A}$ exact morphism from $\mathscr{X}$ to $\mathscr{Y}$

(2) If α is an isomorphism from $\mathscr{X}$ to $\mathscr{Y}$ and β is a bijective from $\mathscr{K}_1$ to $\mathscr{K}_2$, then (α, β) is a called an isomorphism between $\mathbb{FSQB}$-$\mathbb{A}$s

Proposition 3. *Let $\mathscr{X}$ and $\mathscr{Y}$ be two $\mathbb{QB}$-$\mathbb{A}$s. $\mathcal{S}_{\mathscr{K}}$ is a $\mathbb{FSQB}$-$\mathbb{A}$ over $\mathscr{Y}$ and (α, β) a $\mathbb{FSQB}$-$\mathbb{A}$ exact morphism from $\mathscr{X}$ to $\mathscr{Y}$; then, $(\alpha, \beta)^{-1}\mathcal{S}_{\mathscr{K}}$ is $\mathbb{FSQB}$-$\mathbb{A}$ over $\mathscr{X}$.*

Proof. For $\widehat{\mu} \in \beta^{-1}(\mathscr{K})$,

$$\begin{aligned}
&\alpha^{-1}(\mathcal{S}_{\mathscr{K}})[\widehat{\mu}](x \longrightarrow y)\\
&\quad = \mathcal{S}_{\mathscr{K}}\beta[\widehat{\mu}](\alpha(x \longrightarrow y))\\
&\quad = \mathcal{S}_{\mathscr{K}}\beta[\widehat{\mu}](\alpha(x) \longrightarrow \alpha(y))\\
&\quad \geq \min\{\mathcal{S}_{\mathscr{K}}\beta[\widehat{\mu}]\alpha(x),\ \mathcal{S}_{\mathscr{K}}\beta[\widehat{\mu}]\alpha(y)\}\\
&\quad = \min\left\{\alpha^{-1}(\mathcal{S}_{\mathscr{K}})[\widehat{\mu}](x),\ \alpha^{-1}(\mathcal{S}_{\mathscr{K}})[\widehat{\mu}](x)\right\}.
\end{aligned} \tag{26}$$

Consequently, $(\alpha, \beta)^{-1}\mathcal{S}_{\mathscr{K}}$ is a $\mathbb{FSQB}$-$\mathbb{A}$ over $\mathscr{X}$.
Similarly, we can get Proposition 4 as follows. □

Proposition 4. *Let $\mathscr{X}$ and $\mathscr{Y}$ be two $\mathbb{QB}$-$\mathbb{A}$s. $\mathcal{S}_{\mathscr{K}}$ is a $\mathbb{FSQB}$-$\mathbb{A}$s over $\mathscr{X}$ and (α, β) a $\mathbb{FSQB}$-$\mathbb{A}$s isomorphism from $\mathscr{X}$ to $\mathscr{Y}$; then, $(\alpha, \beta)\mathcal{S}_{\mathscr{K}}$ is the $\mathbb{FSQB}$-$\mathbb{A}$s over $\mathscr{Y}$.*

5. Conclusions

In this paper, we introduce the concept of $\mathbb{SQB}$-$\mathbb{A}$s, and some examples are given to illustrate this definition. Also, we investigate the union and intersection operations between two $\mathbb{SQB}$-$\mathbb{A}$s and give some conditions for the operation holds. With the help of the definition of $\mathbb{SQB}$-$\mathbb{A}$s, we define soft deductive systems of $\mathbb{SQB}$-$\mathbb{A}$s and then investigate the relation between them. As a further step, we define $\mathbb{DSQB}$-$\mathbb{A}$s and investigate the homomorphism image of $\mathbb{DSQB}$-$\mathbb{A}$s. Moreover, we define $\mathbb{FSQB}$-$\mathbb{A}$s. Finally, a concrete example is given to illustrate its derive properties; besides, homomorphism image and preimage of $\mathbb{FSQB}$-$\mathbb{A}$s are discussed.

As a future work, it makes sense to apply $\mathbb{SQB}$-$\mathbb{A}$s to medical diagnosis (for example, [25, 26]) in practice. Furthermore, it would be interesting if we study hybrid soft lattice-ordered quantum B-algebras.

Data Availability

No data were used to support this study.

Conflicts of Interest

The authors declare that they have no conflicts of interest.

Acknowledgments

Sultan Aljahdali acknowledges Taif University Researchers Supporting Project (no. TURSP2020/73), Taif University, Taif, Saudi Arabia. This work was supported by the science and technology project of Yulin City (CXY-2020-007).

References

[1] D. Molodtsov, "Soft set theory-first results," *Computers & Mathematics with Applications*, vol. 37, no. 4-5, pp. 19–31, 1999.
[2] P. K. Maji, R. Biswas, and A. R. Roy, "Fuzzy soft sets," *Journal of Fuzzy Mathematics*, vol. 9, no. 3, pp. 589–602, 2001.
[3] P. K. Maji, R. Biswas, and A. R. Roy, "Soft set theory," *Computers & Mathematics with Applications*, vol. 45, no. 4-5, pp. 555–562, 2003.
[4] N. Cagman and S. Enginoglu, "Soft set theory and unit decision making," *European Journal of Operational Research*, vol. 207, no. 2, pp. 848–855, 2010.
[5] A. M. Khalil, S.-G. Li, H.-X. Li, and S.-Q. Ma, "Possibility m-polar fuzzy soft sets and its application in decision-making problems," *Journal of Intelligent and Fuzzy Systems*, vol. 37, no. 1, pp. 929–940, 2019.
[6] A. M. Khalil and N. Hassan, "Inverse fuzzy soft set and its application in decision making," *International Journal of Information and Decision Sciences*, vol. 11, no. 1, pp. 73–92, 2019.
[7] A. M. Khalil, S.-G. Li, H. Garg, H. Li, and S. Ma, "New operations on interval-valued picture fuzzy set, interval-valued picture fuzzy soft set and their applications," *IEEE Access*, vol. 7, pp. 51236–51253, 2019.
[8] H. Lu, A. M. Khalil, W. El-Gayar, and M. A. El-Gayare, "A new type of generalized picture fuzzy soft set and its application in decision making," *Journal of Intelligent and Fuzzy Systems*, vol. 40, no. 6, pp. 12459–12475, 2021.
[9] C. Cheng, Z. Cao, and F. Xiao, "A generalized belief interval-valued soft set with applications in decision making," *Soft Computing*, vol. 77, no. 24, pp. 9339–9350, 2020.
[10] W. Rump and Y. C. Yang, "Non-commutative logical algebras and algebraic quantales," *Annals of Pure and Applied Logic*, vol. 165, no. 2, pp. 759–785, 2014.
[11] W. Rump, "Quantum B-algebras," *Central European Journal of Mathematics*, vol. 11, pp. 1881–1899, 2013.
[12] W. Rump, "Quantum B-algebras: their omnipresence in algebraic logic and beyond," *Soft Computing*, vol. 21, no. 10, pp. 2521–2529, 2017.
[13] M. Botur and J. Paseka, "Filters on some classes of quantum B-algebras," *International Journal of Theoretical Physics*, vol. 54, no. 12, pp. 4397–4409, 2015.
[14] X. Zhang, R. Borzooei, and Y. Jun, "Q-Filters of quantum B-algebras and basic implication algebras," *Symmetry*, vol. 10, no. 11, p. 573, 2018.
[15] S. Han, X. Xu, and F. Qin, "The unitality of quantum B-algebras," *International Journal of Theoretical Physics*, vol. 57, no. 5, pp. 1582–1590, 2018.
[16] S. Han, R. Wang, and X. Xu, "On the injective hulls of quantum B-algebras," *Fuzzy Sets and Systems*, vol. 369, no. 15, pp. 114–121, 2019.
[17] W. Rump and Y. Yang, "Hereditary arithmetics," *Journal of Algebra*, vol. 468, pp. 214–252, 2016.
[18] F. Pan, "Dual quantum B-algebras," *Soft Computing*, vol. 23, no. 16, pp. 6813–6817, 2019.
[19] L. C. Ciungu, "Monadic classes of quantum B-algebras," *Soft Compting*, vol. 25, pp. 1–14, 2021.
[20] C. Xia, "On the finite embeddability property for quantum B-algebras," *Mathematica Slovaca*, vol. 69, no. 4, pp. 721–728, 2019.
[21] Q. Zhan, "Some operators on quantum B-algebras," *Symmetry*, vol. 13, no. 8, p. 1381, 2021.
[22] S. Han and X. Xu, "A few notes on quantum B-algebras," *Studia Logica*, 2021.
[23] S. Han and Z. Bao, "Locally unital quantum B-algebras," *Journal of Algebra and Its Applications*, 2021.
[24] L. A. Zadeh, "Fuzzy sets," *Information and Control*, vol. 8, no. 3, pp. 338–353, 1965.
[25] A. M. Khalil, S. G. Li, Y. Lin, H. X. Li, and S. G. Ma, "A new expert system in prediction of lung cancer disease based on fuzzy soft sets," *Soft Computing*, vol. 24, pp. 14179–14207, 2020.
[26] N. Hassan, O. R. Sayed, A. M. Khalil, and M. A. Ghany, "Fuzzy soft expert system in prediction of coronary artery disease," *International Journal of Fuzzy Systems*, vol. 19, no. 5, pp. 1546–1559, 2017.